Physical Properties of Polymers Handbook

Second Edition

Physical Properties of Polymers Handbook

Second Edition

Edited by

James E. Mark

Polymer Research Center and
Department of Chemistry
University of Cincinnati
Cincinnati, Ohio

Springer

Editor:
James E. Mark
Distinguished Research Professor
Department of Chemistry
Crosley Tower, Martin Luther King Drive
University of Cincinnati
Cincinnati, OH 45221-0172
markje@email.uc.edu

Library of Congress Control Number: 2005938500

ISBN-13: 978-0-387-31235-4 eISBN-13: 978-0-387-69002-5
ISBN-10: 0-387-31235-8 eISBN-10: 0-387-69002-6

Printed on acid-free paper.

10 9 8 7 6 5 4 3 2 1

springer.com

Contents

Contributors

R. G. Alamo *Department of Chemical and Biomedical Engineering, Florida Agricultural and Mechanical University, and Florida State University College of Engineering, Tallahassee, FL 32310-6046, alamo@eng.fsu.edu*

Anthony L. Andrady *Engineering and Technology Division, RTI International, Research Triangle Park, NC 27709, andrady@rti.org*

Pamela A. Arnold *Chemistry Department, Gettysburg College, Gettysburg, PA 17325, parnold@gettysburg.edu*

Rodney Andrews *University of Kentucky Center for Applied Energy Research, 2540 Research Park Dr, Lexington, KY 40511, andrews@caer.uky.edu*

Nitash P. Balsara *Department of Chemical Engineering, University of California at Berkeley, Berkeley, CA 94720, nbalsara@cchem.berkeley.edu*

Gary W. Beall *Center for Nanophase Research, Southwest Texas State University, San Marcos, TX 78666, gb11@txstate.edu*

Richard A. Blatchly *Chemistry Department, Keene State College, Keene NH 03435, rblatchly@keene.edu*

Witold Brostow *Department of Materials Science and Engineering and Department of Physics, University of North Texas, PO Box 305310, Denton, TX 76203-5310, brostow@unt.edu*

Donald J. Buckley *General Electric Global Research Center, One Research Circle, Niskayuna, NY 12309, buckley@crd.ge.com*

V. Castelletto *Department of Chemistry, University of Reading, Reading, RG6 6AD, UK.*

Edward S. Clark *Department of Materials Science and Engineering, The University of Tennessee, Knoxville, TN 37996, eclark2@utk.edu*

R. H. Colby *Materials Science and Engineering, Penn State University, University Park, PA 16802, rhc@plmsc.psu.edu*

Mohamed Daoud *Laboratoire Leon Brillouin (CEA-CNRS), CE Saclay, Gif-sur-Yvette, Cedex, France, daoud@llb.saclay.cea.fr*

K. Dawes *Department of Materials Science and Engineering, North Carolina State University, Campus Box 7907, Raleigh, NC 27695, keith_dawes@ncsu.edu*

A. E. Dowrey *Miami Valley Innovation Center, 11810 E. Miami River Rd., Cincinnati, OH 45242, dowrey.ae@pg.com*

Hany B. Eitouni *Department of Chemical Engineering, University of California at Berkeley, Berkeley, CA 94720, superhany@gmail.com*

Arthur J. Epstein *Department of Physics and Department of Chemistry, The Ohio State University, Columbus, OH 43210-1117, epstein@mps.ohio-state.edu*

Afshin Falsafi *3 M Company, 3M Center, 260-2B-12, St. Paul, MN 55144, afalsafi@mmm.com*

Lewis J. Fetters *School of Chemical Engineering, Cornell University, Ithaca, NY 14853, ljf25@cheme.cornell.edu*

Joel R. Fried *Department of Chemical and Materials Engineering, Mail Location #0012, The University of Cincinnati, Joel.Fried@uc.edu*

Richard H. Friend, F. R. S., *Optoelectronics Group, Cavendish Laboratory, Madingly Road, Cambridge, CB3 OHE, UK, rhf10@cam.ac.uk*

Harry L. Frisch *Department of Chemistry, State University of New York at Albany, Albany, NY 12222, hlf04@albany. Edu*

Vassilios Galiatsatos *Equistar Chemicals, LP, 11530 Northlake Dr., Cincinnati, OH 45249, vgaliatsatos@worldnet.att.net, Vassilios.Galiatsatos@Equistarchem.com*

Varun Gauba *Department of Chemistry and Bioengineering, 6100 Main Street, Rice University, Houston, TX 77005, vgauba@rice.edu*

Harry W. Gibson *Department of Chemistry, Virginia Polytechnic & State University, Blacksburg, VA 24061, hwgibson@vt.edu*

L. C. Glover *Tyco Electronics, 305 Constitution Dr, Menlo Park, CA 94025, lglover@tycoelectronics.com*

N. C. Greenham *Optoelectronics Group, Cavendish Laboratory, Madingly Road, Cambridge, CB3 OHE, UK, email address not available*

Ian W. Hamley *Department of Chemistry, University of Reading, Reading, RG6 6AD, UK. i.w.hamley@reading.ac.uk*

Jeffrey D. Hartgerink *Department of Chemistry and Bioengineering, 6100 Main Street, Rice University, Houston, TX 77005, jdh@rice.edu*

J. L. Haynes *The Procter & Gamble Company, Beckett Ridge Technical Center, 8611 Beckett Road, West Chester, OH 45069, haynes.jl@pg.com*

Gert Heinrich *Leibniz Institut für Polymerforschung Dresden e. V., Hohe Strasse 6, D-01069 Dresden, Germany, gheinrich@ipfdd.de*

Carin A. Helfer *Institute of Polymer Science, The University of Akron, Akron, OH 44325-3909, chelfer@uakron.edu*

Ferenc Horkay *National Institutes of Health, National Institute of Child Health and Human Development, Laboratory of Integrative and Medical Biophysics, Section on Tissue Biophysics and Biomimetics,, Bethesda, Maryland 20892, horkay@helix.nih.gov*

Feihe Huang *Department of Chemistry, Virginia Polytechnic & State University, Blacksburg, VA 24061, fhuang@chem.utah.edu*

Vladyslav Kholodovych *Department of Pharmacology, University of Medicine & Dentistry of New Jersey (UMDNJ), Robert Wood Johnson Medical School and the UMDNJ Informatics Institute, Piscataway, NJ 08854, kholodvl@umdnj.edu*

Andrzej Kloczkowski *L.H. Baker Center for Bioinformatics and Biological Statistics, Iowa State University, Ames, IA 50011, kloczkow@iastate.edu*

Manfred Klüppel *Deutsches Institut für Kautschuktechnologie e. V., Eupener Straße 33, D-30519 Hannover, Germany, Manfred.Klueppel@dikautschuk.de*

Andrzej Kolinski *Faculty of Chemistry, University of Warsaw, Pasteura 1, 02-093 Warsaw, Poland,* kolinski@chem.uw.edu.pl

F. Kremer *Universitat Leipzig, Fakultat f. Physik u. Geowissenschaften, Leipzig, Germany, kremer@physik.uni-leipzig.de*

Chandima Kumudinie Jayasuriya *Department of Chemistry, University of Kelaniya, Sri Lanka, jayasuc@kln.ac.lk*

Kwang-Sup Lee *Department of Polymer Science and Engineering, Hannam University, Daejeon 306-791, Korea, kslee@mail.hannam.ac.kr*

Qinghuang Lin *IBM Thomas J. Watson Research Center, 1101 Kitchawan Rd, Route 134/PO Box 218, Yorktown Heights, NY 10598, qhlin@us.ibm.com*

Chuanjun Liu *Department of Chemistry, Tsinghua University, Beijing 100084, P. R. China, chuanjunliu@yahoo.com.cn*

D. J. Lohse *ExxonMobil Research and Engineering Company, Annandale NJ 08801-0998, david.j.lohse@exxonmobil.com*

George Makhatadze *Department of Biochemistry and Molecular Biology, Penn State University College of Medicine, Hershey, PA 17033, makhatadze@psu.edu*

L. Mandelkern *Department of Chemistry and Biochemistry, Florida State University, Tallahassee, FL 32306-3015, mandelker@chem.fsu.edu*

Subu Mangipudi *Medtronic Corporation, 6800 Shingle Creek Parkway, Brooklyn Center, MN 55430, subu.mangipudi@medtronic.com*

C. Marcott *Miami Valley Innovation Center, 11810 E. Miami River Rd., Cincinnati, OH 45242, marcott.ca@pg.com*

J. E. Mark *Department of Chemistry, Crosley Tower, Martin Luther King Drive, The University of Cincinnati, Cincinnati, OH 45221-0172, markje@email.uc.edu*

Wayne L. Mattice *Institute of Polymer Science, The University of Akron, Akron, OH 44325-3909, wlm@polymer.uakron.edu*

Gregory B. McKenna *Department of Chemical Engineering, Texas Tech University, Lubbock, TX 79409-3121, greg.mckenna@ttu.edu*

Khaled Mezghani *Mechanical Engineering Department, King Fahd University of Petroleum & Minerals, Box 169, Dhahran 31261, Saudi Arabia, mezghani@kfupm.edu.sa*

Antonios G. Mikos *Department of Bioengineering, PO Box 1892, MS-142, Rice University, Houston, TX 77005-1892, mikos@rice.edu*

Sheila A. Moore *Department of Bioengineering, PO Box 1892, MS-142, Rice University, Houston, TX 77005-1892, samoore@rice.edu*

Kia L. Ngai *Code 6807, Naval Research Laboratory, Washington, DC 20375-5320, ngai@estd.nrl.navy.mil*

Isao Noda *The Procter & Gamble Company, Beckett Ridge Technical Center, 8611 Beckett Road, West Chester, OH 45069, noda.i@pg.com*

Robert A. Orwoll *Department of Chemistry, College of William and Mary, Williamsburg, VA 23187-8795, raorwo@wm.edu*

Michael J. Owen *Dow Corning Corporation, Midland, MI 48686-0994, michaelowen01@Chartermi.net*

Guirong Pan *Department of Chemical and Materials Engineering, The University of Cincinnati, Cincinnati, OH 45221-0012, pang@email.uc.edu*

Yi Pang *Department of Chemistry, University of Akron, Akron, OH 44325-3601, yp5@uakron.edu*

Rahul Patki *Department of Chemical and Materials Engineering, The University of Cincinnati, Cincinnati, OH 45221-0012, patkirp@email.uc.edu*

Adam M. -P. Pederson *Department of Chemistry, Virginia Polytechnic & State University, Blacksburg, VA 24061, adamp@vt.edu*

Paul J. Phillips *Department of Chemical and Materials Engineering, The University of Cincinnati, Cincinnati, OH 45221-0012, pphillip@alpha.che.uc.edu*

Donald J. Plazek *Department of Materials Science and Engineering, University of Pittsburgh, Pittsburgh, PA 15261, plazek@engrng.pitt.edu*

Aphonsus V. Pocius *3 M Corporate Research Materials Laboratory, St. Paul, MN 55144-1000, avpocius1@mmm.com*

Clois E. Powell *Center for Nanophase Research, Southwest Texas State University, San Marcos, TX 78666, cp21@txstate.edu*

P. N. Prasad *Department of Chemistry, The State University of New York at Buffalo, Buffalo, NY 14260-3000, pnprasad@acsu.buffalo.edu*

Jagath K. Premachandra *Department of Chemical and Process Engineering, University of Moratuwa, Sri Lanka, jagath@cheng.mrt.ac.lk*

T. Rantell *University of Kentucky Center for Applied Energy Research, 2540 Research Park Dr, Lexington, KY 40511, terry@caer.uky.edu*

Andreas Schröder *Rheinchemie Rheinan GmbH, Düsseldorfer str. 23–27, D-68219 Mannheim, Germany*

Taner Z. Sen *Department of Biochemistry, Biophysics, and Molecular Biology, Iowa State University, Ames, IA 50011, taner@iastate.edu*

Weiqing Shi *Department of Chemistry, Tsinghua University, Beijing 100084, P. R. China, shiwqzx@mail.tsinghua.edu.cn*

Annette D. Shine *Department of Chemical Engineering, University of Delaware, Newark, DE 19716, shine@donald.che.udel.edu*

Moitreyee Sinha *General Electric Global Research Center, One Research Circle, Niskayuna, NY 12309, sinha@crd.ge.com*

Morris Slutsky *Department of Polymer Science and Engineering, University of Massachusetts, Amherst, MA 01003, mslutsky@umich.edu*

H. Eugene Stanley *Center for Polymer Studies and Department of Physics, Boston University, Boston, MA 02215, hes@buphy.bu.edu*

Dietrich Stauffer *Institute of Theoretical Physics, Cologne University, D-50923 Koln, Euroland, stauffer@thp.Uni-Koeln.DE*

S. Alexander Stern *Department of Biomedical and Chemical Engineering, Syracuse University, Syracuse, NY 13244, USA, sasternou@aol.com*

Laura J. Suggs *Department of Biomedical Engineering, University of Texas at Austin, Austin, TX 78712, Laura.Suggs@engr.utexas.edu*

P. R. Sundararajan *Department of Chemistry, Carleton University, 1125 Colonel By Drive, Ottawa, Ontario, Canada K1S 5B6, sundar@Carleton.ca*

Gregory N. Tew *Department of Polymer Science and Engineering, University of Massachusetts, Amherst, MA 01003,* tew@mail.pse.umass.edu

Archibald Tewarson *FM Global, Research, 1151 Boston Providence Turnpike, Norwood, MA 02062, archibald.tewarson@fmglobal.com*

Donald A. Tomalia *Dendritic Nanotechnologies Inc./Central Michigan University, 2625 Denison Drive, Mt. Pleasant, MI 48858, tomalia@dnanotech.com*

Alan E. Tonelli *Fiber & Polymer Science Program, North Carolina State University, Raleigh, NC 27695, alan_tonelli@ncsu.edu*

Thomas Vilgis *Max Planck Institut fur Polymerforschung, Postfach 3148, D-6500, Mainz, Germany 55021, vilgis@mpip-mainz.mpg.de,*

D. A. Vroom *Tyco Electronics, 305 Constitution Dr, Menlo Park, CA 94025, david.vroom@sbcglobal.net*

Shuhong Wang *DuPont Performance Elastomers L.L.C., DuPont Experimental Station, P.O. Box 80293, Wilmington, DE 19880, shuhong.wang@dopontelastomers.com*

M. C. Weisenberger *University of Kentucky Center for Applied Energy Research, 2540 Research Park Dr, Lexington, KY 40511, matt@caer.uky.edu*

William J. Welsh *Department of Pharmacology, University of Medicine & Dentistry of New Jersey (UMDNJ), Robert Wood Johnson Medical School and the UMDNJ Informatics Institute, Piscataway, NJ 08854, welshwj@UMDNJ.EDU*

Jianye Wen *ALZA Corp., 1900 Charleston Rd., Mountain View, CA 94039, jhmwen@hotmail.com, jwen3@alzus.jnj.com*

Jeffery L. White *Department of Chemistry, Department of Chemistry, Oklahoma State University, jeff.white@okstate.edu*

George D. Wignall *Center for Neutron Scattering, Condensed Matter Sciences Division, Oak Ridge National Laboratory, Oak Ridge, TN 37831-6393, wignallgd@ornl.GOV, gdw@ornl.gov*

W. M. K. P. Wijekoon *Applied Materials, 3303 Scott Blvd; M/S 10852, Santa Clara, CA 95054, kapila_wijekoon@amat.com*

Ping Xu *W.L. Gore & Associates, Inc., Cherry Hill Division, 2401 Singerly Road, P.O. Box 1220, Elkton, MD 21922-1220, Pxu@aol.com, pxu@wlgore.com*

Yong Yang *Benjamin Moore and Co., Flanders, NJ 07836, Yong.Yang@Benjaminmoore.com*

Wanxue Zeng *Albany NanoTech, CESTM Building, 251 Fuller Road, Albany, NY 12203, wanxue@rocketmail.com*

Xi Zhang *Department of Chemistry, Tsinghua University, Beijing 100084, P. R. China,* xi@mail.tsinghua.edu.cn

Preface to the Second Edition

As before, the goal of this handbook is to provide concise information on the properties of polymeric materials, particularly those most relevant to the areas of physical chemistry and chemical physics. The hope is that it will simplify some of the problems of finding useful information on polymer properties.

All of the chapters of the first edition were updated and 11 entirely new chapters added. Four of them focus on novel polymeric structures, specifically dendrimers, polyrotaxanes, foldamers, and supramolecular polymers in general. Another group of chapters covers reinforcing phases in polymers, including carbon black, silica, clays, polyhedral oligomeric silsesquioxanes (POSS), carbon nanotubes, and relevant theories. The final new chapter describes experiments on single polymer chains.

It is a pleasure to acknowledge with gratitude the encouragement, support, and technical assistance provided by Springer, particularly David Packer, Lee Lubarsky, Felix Portnoy, and, earlier, Hans Koelsch. The editor also wishes to thank his wife Helen for the type of understanding and support that helps get one through book projects of this complexity.

James E. Mark
Cincinnati, Ohio

December 2006

Preface to the First Edition

This handbook offers concise information on the properties of polymeric materials, particularly those most relevant to the areas of physical chemistry and chemical physics. It thus emphasizes those properties of greatest utility to polymer chemists, physicists, and engineers interested in characterizing such materials. With this emphasis, the more synthetic–organic topics such as the polymerization process and the chemical modification of polymers were considered beyond its scope.

The contributors to this handbook have endeavored to be highly selective, choosing and documenting those results considered to have the highest relevance and reliability. There was thus no attempt to be exhaustive and comprehensive. The careful selection of the results included, however, suggests it should nonetheless provide the great majority of topics and data on polymer properties likely to be sought by members of the polymer community. Extensive indexing should facilitate locating the desired information, and it is hoped that the modest size of the handbook will give it considerable portability and wide availability.

Every attempt has been made to include modern topics not covered in a convenient handbook format elsewhere, such as scaling and fractal dimensions, computational parameters, rotational isomeric state models, liquid–crystalline polymers, medical applications, biodegradability, surface and interfacial properties, microlithography, supercritical fluids, pyrolyzability, electrical conductivity, nonlinear optical properties, and electroluminescence.

All contributions to this volume were extensively reviewed by a minimum of two referees, to insure articles of the highest quality and relevance. Many of the reviewers were chosen from the Editorial Board of the *AIP Series in Polymers and Complex Materials*, of which this handbook is a part. Their important contributions are gratefully acknowledged, as are those of the Editors-in-Chief of the Series, Ronald Larson and Philip A. Pincus. One Editorial Board member, Robert E. Cohen, deserves special acknowledgment and sincere thanks. He not only originated the idea of doing a handbook of this type, but also contributed tremendously to its realization. Charles H. Doering and Maria Taylor (and earlier, Zvi Ruder) also provided unfailing support and encouragement in this project. It has been a distinct pleasure working with them and other members of the AIP Press: K. Okun, K. S. Kleinstiver, M. Star, and C. Blaut. The editor also wishes to thank his wife Helen for the type of understanding and support that is not always easy to put into words.

Both the editor and contributors to this volume would feel well rewarded if this handbook helps relieve some of the problems of finding useful information on polymer properties in the ever-growing scientific literature.

James E. Mark
Cincinnati, Ohio

November 1995

CHAPTER 1

Chain Structures

P. R. Sundararajan

Department of Chemistry, Carleton University, 1125 Colonel By Drive, Ottawa, Ontario, Canada K1S 5B6

1.1 INTRODUCTION

It is known that the physical properties of a polymer depend not only on the type of monomer(s) comprising it, but also on the secondary and tertiary structures, i.e., the stereochemistry of the linkage, the chain length and its distribution, its ability to crystallize or remain amorphous under various conditions, and the shape or distribution of the shapes of the chain in the crystalline and amorphous states. Through advances in polymer chemistry, in most cases polymers can be designed with specific properties. Control of the microstructure, e.g., the tacticity and molecular weight distribution of vinyl polymers, has been the focus of a number of papers in the last two decades.

In most applications, a polymer, once designed as a product, has to be stable and maintain its structure and morphology under various temperatures and other environmental conditions during the lifetime of the product. However, the recent interest is also in changing the shape or morphology of the molecule instantaneously and reversibly, without any memory or hysteresis effects, with electrical, optical or mechanical stimulus. These "smart" materials are aimed towards such applications as information processing, storage, and retrieval, and molecular recognition similar to the biological systems. Synthetic efforts on *in situ* devices such as the photonic molecular wire, electronic molecular wire, and molecular shuttle have been the focus of several research groups (see below). The intent is to acquire the ability to control the material at the atomic/molecular level, i.e., on the nano scale [1–5].

This chapter gives an overview of the literature on microstructures, "photonic" polymers, fullerence-based polymers, cyclics, rotaxanes, and dendrimers. The properties of polymers with other architectures and morphologies are discussed in various other chapters of this handbook.

Please note that in this chapter, in the previous edition of this handbook, we had listed examples from published articles in Tables 1.1–1.8. Most of the topics discussed at that time were new and emerging. Since that time, publications in each of these topics have been numerous and cannot be accommodated within the scope and size of this chapter. The original tables are kept, however, since these include the initial work in these areas.

1.2 MICROSTRUCTURE

Since the stereospecific polymerization of polyolefins pioneered by Natta, an extensive literature has developed in the synthesis, characterization, and utilization of polymers of defined microstructure. Although x ray diffraction could confirm the existence or absence of regular

microstructure, and infrared spectroscopy could be used to estimate the isotactic or syndiotactic content of a polymer, it was not until the development of NMR spectroscopy for microstructure analysis that the isotactic, syndiotactic, or atactic perpetuation extending to pentads and hexads could be determined quantitatively and accurately. This is dealt with in detail in the chapter by Tonelli in this handbook.

A schematic for defining the tacticity of vinyl polymers of the type $[(CH_2)—(CHR)]_n$ is shown in Fig. 1.1. If, as shown in Fig. 1.1(a), the skeletal bonds are in the *trans* conformation and lie in the plane of the paper, the *R* groups on successive asymmetric carbons projecting on the same side (up in this figure) defines a meso diad and perpetuation of this configuration leads to an isotactic polymer. Assignment of a configuration *d* to the asymmetric carbons in this figure is arbitrary. If, by a 180° rotation of the chain, all the *R* groups are rendered to lie below the plane of the paper, the carbon centers are assigned an *l* configuration. The stereochemistry of the chain would not differ, however, if the chain ends are indistinguishable. Thus, an "all *d*" or "all *l*" chain is isotactic in character. If one of the asymmetric carbons of the diad is in the *d* configuration and the other is in *l*, the diad is racemic (Fig. 1.1b) and regular alternation of the *d* and *l* centers along the chain defines a syndiotactic polymer. Random occurrence of *d* and *l* centers along the chain leads to an atactic polymer, as shown schematically in Fig. 1.1c. The convenience of defining the tacticity of a vinyl polymer in this manner and its application to developing the matrix methods for calculating the configurational average properties of these chains have been discussed by Flory [6].

The effect of tacticity on the properties of polymers has long been recognized, with such basic differences as in the glass transition temperature. Lemieux *et al*. [7] studied the effect of the tacticity of poly(methyl methacrylate) (PMMA) on its miscibility with poly(vinyl chloride) (PVC), chlorinated PVC and Saran. In a series of papers, Beaucage and Stein [8] and Beaucage *et al*. [9] examined the effect of the tacticity of poly(vinyl methyl ether) on its blend characteristics with polystyrene. Many of the "regular" or isotactic polymers have been studied in terms of the crystalline structure, crystal growth, and morphology [10,11]. These studies also prompted development of theories on chain folding, nucleation, and growth, etc., to model the experimental observations, as well as to predict the properties of these

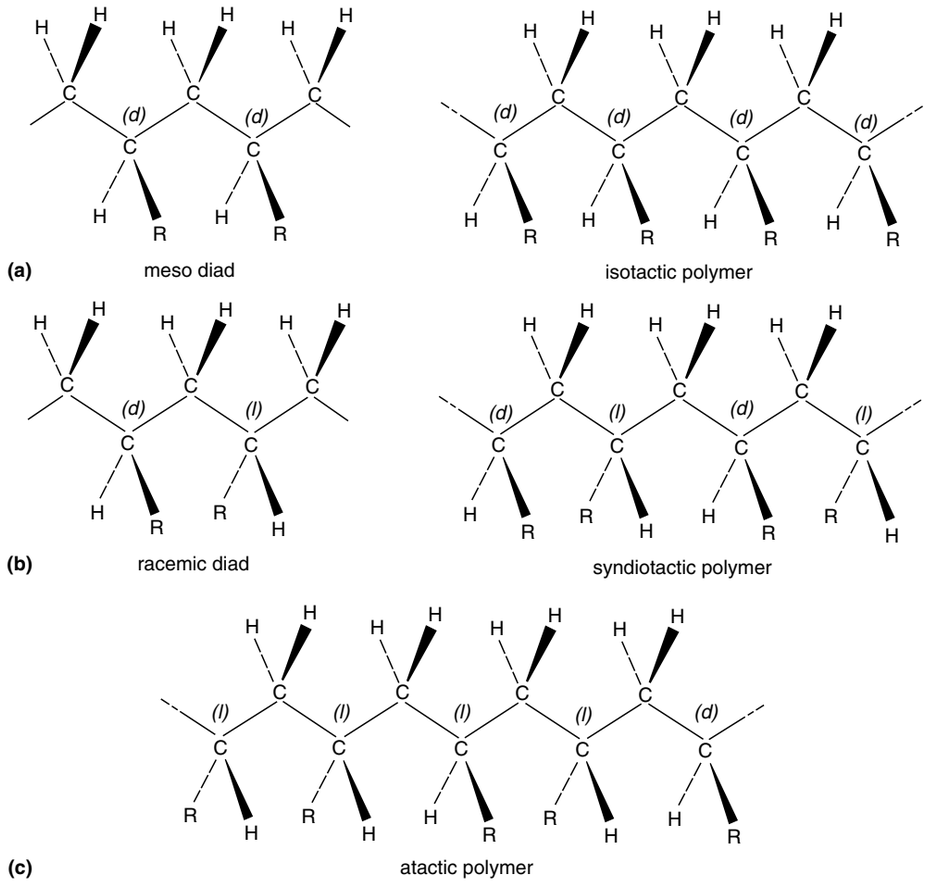

FIGURE 1.1. Schematic of the definition of tacticity of an asymmetric chain of the type $[(CH_2)(CHR)]_n$.

polymers. Solution properties of these isotactic chains could in most cases be interpreted in terms of the local conformation of the chain segments using the rotational isomeric state schemes. However, the rationalization of these properties for stereoirregular or syndiotactic chains was impeded to some extent by the lack of experimental results on polymer samples with precisely tailored microstructure. In a highly isotactic chain, the stereo defects can be not only an isolated *r* diad, but a short perpetuation of it. Zhu *et al*. [12], from ^{13}C NMR analysis of highly isotactic polypropylene, concluded that isolated racemic units can occur up to a pentad (*rrrr*) sequence.

Whereas most of the early work on crystallization, etc., were concerned with predominantly isotactic chains, the recent developments in synthetic methodologies have enabled the preparation of highly syndiotactic polymers [13,14]. Since the high stereoregularity of these syndiotactic polymers facilitates their crystallization, several papers have been published on the x-ray crystal structure and polymorphism of syndiotactic polystyrene [15–18]. The chain conformation in the crystalline state has also been analyzed using NMR [19]. Similarly, the crystal structure of syndiotactic polypropylene has also been studied by a number of authors [20–22].

Liquori *et al*. [23] first discovered that isotactic and syndiotactic PMMA chains form a crystalline stereocomplex. A number of authors have since studied this phenomenon [24]. Buter *et al*. [25,26] reported the formation of an "*in situ*" complex during stereospecific replica polymerization of methyl methacrylate in the presence of preformed isotactic or syndiotactic PMMA. Hatada *et al*. [24] reported a detailed study of the complex formation, using highly stereoregular PMMA polymers with narrow molecular weight distribution. The effect of tacticity on the characteristics of Langmuir-Blodgett films of PMMA and the stereocomplex between isotactic and syndiotactic PMMA in such monolayers at the air-water interface have been reported in a series of papers by Brinkhuis and Schouten [27,27a]. Similar to this system, Hatada *et al*. [28] reported stereocomplex formation in solution and in the bulk between isotactic polymers of *R*-(+)- and *S*-(−)-α-methylbenzyl methacrylates.

1.3 ARCHITECTURE

In addition to the tacticity, the molecular weight and its distribution are also major factors which influence the ultimate properties of these chains. Whereas a wide molecular weight distribution can even be a merit for some commodity resin applications, consistent control of the distribution is obviously a requirement for commercial applications. With a wide molecular weight distribution, factors of concern are the internal plasticization of the high molecular weight component by the low molecular weight fraction and the resultant effects on properties such as the T_g. Recent synthetic efforts focus on controlling not only the tacticity but the molecular weight distribution as well.

Anionic living polymerization was used by Hatada *et al*. [29,30] to prepare narrow molecular weight, highly stereoregular poly(methyl methacrylate). These authors also discussed isolation of stereoregular oligomers of PMMA using a preparative supercritical fluid chromatography method [31]. Preparation of heterotactic-rich poly(methyl methacrylate) and other alkyl methacrylates has also been described [32,33]. The living anionic polymerization of methacrylic esters and block copolymers with low dispersity has been discussed by Teyssié *et al*. [34,35], Bayard *et al*. [36], and Baskaran [36a]. Diblock copolymers of styrene and *t*-Bu acrylate with $M_w/M_n = 1.05$ have been obtained. Wang *et al*. [37] presented an extensive set of results on the effect of various types of ligands and different solvents and solvent mixtures on the stereochemistry of anionically polymerized poly (methyl methacrylate). Predominantly isotactic or syndiotactic polymers, with narrow polydispersity or bimodal or multimodal distribution of molecular weights were obtained depending on the synthetic conditions. Using different types of catalysts, Asanuma *et al*. [38] prepared iso- and syndiotactic poly(1-butene), poly(1-pentene), poly(1-hexene), and poly(1-octene) with narrow molecular weight distribution.

Whereas the authors cited above employed anioinic polymerization to control the molecular weight distribution, Georges *et al*. [39–42] developed a living, stable-free radical polymerization process that can be performed in solution, bulk, or suspension. This was also extended to emulsion polymerization of block copolymers [43a]. Since then, there has been a burst of activity on several polymerization methods such as atom transfer radical polymerization (ATRP) [43b–e], living metal catalyzed radical polymerization [43f], and living cationic polymerization [43g]. Designing novel polymer topologies using living ROMP methods has also been developed [43h].

Table 1.1 summarizes some of the work on the control of tacticity and molecular weight distribution with common polymers such as the PMMA and polystyrene.

In addition to the occurrence of defects in a stereoregular vinyl polymer in terms of a diad of alternate tacticity, the head-to-head/tail-to-tail (H-H/T-T) defect is also of interest [44]. This type of defect is shown schematically in Fig. 1.2. Different types of polymerization conditions which would introduce these defects have been summarized by Vogl and Grossman [45]. The H-H content has been known to vary from about ∼4% in PVC to ∼30% in polychlorotrifluoroethylene. Such a linkage would no doubt affect the properties of the chain to different extents. Indirect synthetic methods (e.g., hydrogenation of polydienes) have been developed to specifically prepare H-H polymers and compare their properties with regular head-to-tail (HT) counterparts. For example, Földes *et al*. [46] have developed a synthetic route to prepare H-H polystyrene, with molecular weights ranging from 240 000 to 1 200 000, and close to

TABLE 1.1. *Microstructure.*

Polymer	Tacticity (%) and remarks	Reference
Atactic poly(alkyl methacrylate)s	Methyl methacrylate: $rr = 64\%$, $mr = 31\%$, $mm = 5\%$; $M_n = 33,000$; $M_w/M_n = 1.14$ Ethyl methacrylate: $rr = 66\%$, $mr = 28\%$, $mm = 6\%$ Isobutyl methacrylate: $rr = 66\%$, $mr = 28\%$, $mm = 6\%$; $M_n = 30,000$; $M_w/M_n = 1.31$ Langmuir Blodgett monolayer behavior with tacticity discussed.	[27]
Heterotactic poly(aklyl methacrylate)s	Ester group: -CH_2CH_3: $mr = 87.2\%$; $M_n = 7010$; $M_w/M_n = 1.08$ -$CH_2CH_2CH_2CH_3$: $mr = 87.1\%$; $M_n = 9300$; $M_w/M_n = 1.07$ -$CH_2CH(CH_3)_2$: $mr = 78.4\%$; $M_n = 6350$; $M_w/M_n = 1.07$ -$CH(CH_3)_2$: $mr = 69.2\%$; $M_n = 4730$; $M_w/M_n = 1.07$ Tacticity variation of poly(ethyl methacrylate) with synthetic conditions discussed in detail.	[33]
Isotactic poly(alkyl methacrylate)s	Methyl methacrylate: mm>97%; $M_n = 36,000$; $M_w/M_n = 1.17$ Ethyl methacrylate: $mm = 95\%$; $M_v = 115,000$ Isobutyl methacrylate: $mm = 95\%$; $M_n = 3200$; $M_w/M_n = 4.8$ Langmuir Blodgett monolayer behavior with tacticity discussed.	[27a]
Syndiotactic poly(alkyl methacrylate)s	rr content with side group: C_2H_5: 90% $CH(CH_3)_2$: 92% $(CH_2)_3CH_3$: 92% CH_2-$CH(CH_3)_2$: 93% $C(CH_3)_3$: $rr = 57\%$, $mr = 33\%$ M_n: 6000−8690; M_w/M_n: 1.06−1.64	[139]
Syndiotactic poly(alkyl methacrylate)s	Various types of side chain ester groups. rr: 82–92% DP 31–421; $M_w/M_n = 1.07-1.43$ Stereocomplex with iso-PMMA discussed.	[24]
Syndiotactic poly(alkyl methacrylate)s	Methyl methacrylate: $rr = 85\%$, $mr = 14\%$; $M_n = 46,000$; $M_w/M_n = 1.2$ Ethyl methacrylate: $rr = 88\%$, $mr = 9\%$; $M_v = 93{,}000$ Isobutyl methacrylate: $rr = 97\%$, $mr = 3\%$; $M_n = 16{,}000$; $M_w/M_n = 1.09$ Langmuir Blodgett monolayer behavior with tacticity discussed.	[27a]
Isotactic poly(2-N-carbazolylethyl acrylate)	$m = 87$–97%; $M_n = 0.56 \cdot 10^4$ to 5.10^4; $M_w/M_n = 4.0-4.8$ Hole mobility is discussed.	[140]
Poly(cyclobutyl methacrylate)	rr: 65%, ($mr+rm$): 32%; $M_w = 13.9.10^4$; $M_w/M_n = 1.3$; $T_g = 78\,^\circ$C	[141]
Poly(cyclodecyl methacrylate)	rr: 67%, ($mr+rm$): 30%; $M_w/M_n = 1.7$; $T_g = 58\,^\circ$C	[141]
Poly(cyclododecyl methacrylate)	rr: 63%, ($mr+rm$): 34%; $M_w = 9.8 \cdot 10^4$; $M_w/M_n = 1.4$; $T_g = 56\,^\circ$C	[141]
Poly(cycloheptadecyl methacrylate)	$rr = 67\%$, ($mr+rm$): 31%; $M_w/M_n = 1.6$; $T_g = 56\,^\circ$C	[141]
Poly(cyclooctyl methacrylate)	rr: 63%, ($mr+rm$): 34%; $M_w = 12.1 \cdot 10^4$, $M_w/M_n = 1.4$; $T_g = 73\,^\circ$C	[141]
Poly(cyclopentyl methacrylate)	rr: 66%, ($mr+rm$): 32%; $M_w = 11{:}0 \cdot 10^4$, $M_w/M_n = 1.2$; $T_g = 75\,^\circ$C	[141]
Isotactic poly(ethyl methacrylate)	$mm = 97\%$	[142]
Isotactic oligo(methyl methacrylate)	mm:mr:rr = 96.1:3.9:0 19–29-mer isolated by preparative supercritical fluid chromatography; $\overline{DP} = 28.6$; $M_w/M_n = 1.15$; T_g of 28mer = 34.5 °C; Stereocomplex with syndiotactic oligo(methyl methacrylate) discussed.	[31]
Syndiotactic oligo(methyl methacrylate)	mm:mr:rr = 0.3:7.6:92.1 isolated by preparative supercritical fluid chromatography; $\overline{DP} = 26.8$; $M_w/M_n = 1.09$; stereocomplex with isotactic oligo(methyl methacrylate) discussed.	[31]
Atactic poly(methyl methacrylate)	$mm = 6\%$, $mr = 36\%$, $rr = 58\%$; $M_w = 124{,}000$; $M_w/M_n = 2.8$;	[143]
Atactic poly(methyl methacrylate)-d_2	FTIR spectroscopic analysis of the conformational energy differences between rotational isomeric states is presented.	[32]
Heterotactic poly(methyl methacrylate)	$mr = 67.8\%$, $rr = 20.6\%$, $mm = 11.6\%$; $M_n = 11640$; $M_w/M_n = 1.09-1.14$; $T_g = 102.2\,^\circ$C; Various mr and rr contents result depending on the synthetic conditions.	[32]
Isotactic poly(methyl methacrylate)	mm>98%; $M_w = 115\,000$; $M_w/M_n = 2.8$	[143]

TABLE 1.1. *Continued.*

Polymer	Tacticity (%) and remarks	Reference
Isotactic poly(methyl methacrylate)-d_2	FTIR spectroscopic analysis of the conformational energy differences between rotational isomeric states is presented.	
Isotactic poly(methyl methacrylate)	$mm = 96\%$; $M_w/M_n = 1.1$	[30]
Isotactic poly(methyl methacrylate)	$mm = 97\%$, $mr = 2\%$; $rr = 1\%$; $M_n = 33030$, $M_w/M_n = 1.25$ Stereocomplexation with syndiotactic methacrylates discussed.	[24]
Isotactic poly(methyl methacrylate)-*b*-poly (ethylmethacrylate)	*DP*: 59/59, 97/151, 64/182; $mm = 95$–97%; $M_w/M_n = 1.29-2.11$	[142,144]
Isotatic poly(methyl methacrylate)-*b*-poly (ethylmethacrylate)-*b*-poly (methyl methacrylate)-*b*-Poly(methylmethacrylate-*b*-ethylmethacrylate)	*DP*: 35/50/200, 25/28/25; *mm* 95–97%; $M_w/M_n = 1.17$, 1.42 *rr*: 89–91% ($mm = 0$, $mr = 9$–11%); M_n 8900–12,300; $M_w/M_n = 1.07-1.25$	[142,144] [139]
Isotactic poly(methyl methacrylate)-*co*-poly(ethylmethacrylate)	$mm = 96$–97%; MMA/EMA 78/22 to 26/74; $M_w/M_n = 1.53-3.57$	[142]
Poly(iso-MMA-*b*-syndio-MMA)	Stereoblock polymer with isotactic and syndiotactic blocks. $M_w/M_n = 1.27$; Isotactic block: $mm = 97\%$, $mr = 2\%$, $rr = 1\%$ Syndiotactic block: $mm = 7\%$, $mr = 17\%$, $rr = 76\%$ Stereocomplex between the block polymer and iso or syndiotactic PMMA discussed.	[24]
Syndiotactic poly(methyl methacrylate)	$rr = 76\%$, $mr = 22\%$, $mm = 2\%$; $M_w = 152{,}000$; $M_w/M_n = 2.0$; FTIR	[143]
Syndiotactic poly(methyl methacrylate)-d_2	Spectroscopic analysis of the conformational energy differences between rotational isomeric states is presented.	
Syndiotactic poly(methyl methacrylate)	Two samples with *rr*: 89.5 and 91.5%. $M_w = 2.6 \cdot 10^5$ to $5.5 \cdot 10^5$; $M_w/M_n = 1.3-1.4$ Aggregation process in *n*-butyl acetate discussed.	[145]
Syndiotactic poly(methyl methacrylate)	Two samples (i) $mm = 2\%$, $mr = 8.5\%$, $rr = 89.5\%$ (ii) $mm = 3\%$, $mr = 31\%$, $rr = 66\%$ (i) $M_n = 145{,}000$; $M_w/M_n = 1.6$ (ii) $M_n = 45{,}000$ NMR, IR studies of aggregation in solution; IR and x-ray studies of crystallinity. Sample (i) crystallinity 27–32%, crystallite size 46–57 Å *rr* up to 96%.	[146]
Syndiotactic poly(methyl methacrylate)	Anionic living polymerization; $M_n = 2000-14500$; $M_w/M_n = 1.13-5.5$; effect of synthetic variables on tacticity, molecular weight and distribution and yield discussed.	[139,147]
Syndiotactic poly-1,2-(4-methyl-1,3-pentadiene)	More than 88% 1,2 content; amorphous; hydrogenation produced crystalline syndiotactic poly(4-methyl-1-pentene) with $T_m = 186\,^\circ$C.	[148] [for the crystal structure of the hydrogenated polymer, poly (4-methyl-1-pentene), see 149]
Isotactic poly(1-pentene)	*mmmm* (pentad) = 90%; $M_w = 17\,000$; $M_w/M_n = 2.3$; $T_m = 64\,^\circ$C; x ray and NMR data.	[150]
Syndiotactic poly(1-pentene)	*rrrr* (pentad) = 85%; $M_w = 65000$; $M_w/M_n = 3.0$; $T_m = 42\,^\circ$C; $T_g = -22.7\,^\circ$C; crystallinity 30%; x ray and NMR data.	[150]
Syndiotactic polypropylene	*rrrr* 74–86%; $M_w = 52 \cdot 10^3$ to $777 \cdot 10^3$, $M_w/M_n = 1.8-2.4$	[151]
Syndiotactic polypropylene	$rrrr = 91.5\%$; $M_w = 1.5 \cdot 10^5$; $M_w/M_n = 1.9$; crystalline structure of the zig-zag form is reported.	[152]

TABLE 1.1. *Continued.*

Polymer	Tacticity (%) and remarks	Reference
Syndiotactic polypropylene	*rrrr* pentads 81.4–94.5% $M_w = 9.6 \cdot 10^4 - 17.3 \cdot 10^4$; T_m: 135–186 °C; thermal behavior discussed.	[153] [for the crystal structure using one of these samples, see 22]
Polypropylene	Five samples, mm = 92.2–94.9% (NMR); M_w = 22 000–947 000; fractionation according to stereoregularity; crystallization and melting behavior with IR tacticity studied.	[154]
Syndiotactic polystyrene	rr>98%, $rrrrrr$>94%; NMR, IR and x ray diffraction results discussed; $T_m \approx 270$ °C.	[13,155]
Syndiotactic polystyrene	rr>98%	[14]
Syndiotactic polystyrene	$rrrr$>96%; T_m = 260–270 °C; IR and Raman spectroscopic studies of local chain conformation in glass and gels.	[156,157]
Isotatic polystyrene	m>95%; T_m = 230 °C; IR and Raman spectroscopic studies of local chain conformation in glass and gels.	[157]
Heterotactic poly(vinyl alcohol)	mr = 67%; mm = 18%; rr = 15%	[158]
Isotactic poly(2-vinyl pyridine)	mm>98% Cystallization and melt behavior discussed. M_v = 400000; maximum spherulite growth rate at T_c = 165 °C; $T_m{}^\circ$ = 212.5 °C.	[159]

100% conversion. The synthesis and properties of H-H polymers have been reviewed by Vogl [47] and Vogl and Grossman [45]. The chain flexibility of a H-H polymer either increases or decreases as compared to the H-T chain, depending on the nature of the side group. A comparison [45,47] of the glass transition temperatures of some of the polymers is given in Table 1.2. Arichi *et al*. [48] found that the theta temperature of H-H polypropylene in isoamylacetate was about 9° higher than that of atactic H-T polypropylene (34 °C). On the other hand, a study of dilute solution properties of H-H polystyrene by Strazielle *et al*. [49] showed that the theta temperature in cyclohexane was 19 °C, which is lower by 16° than the theta temperature of H-T polystyrene in the same solvent. Hattam *et al*. [50] studied the solution properties of H-H polypropylene (see chapter on ''Theta Temperatures'').

Another type of specificity that can occur is the chirality. Isotactic poly(triphenylmethyl methacrylate) is the first known case in which the helicity of the polymer leads to chirality and optical activity [51,52]. A conformational analysis of this polymer has been reported by Cavallo *et al*. [53].

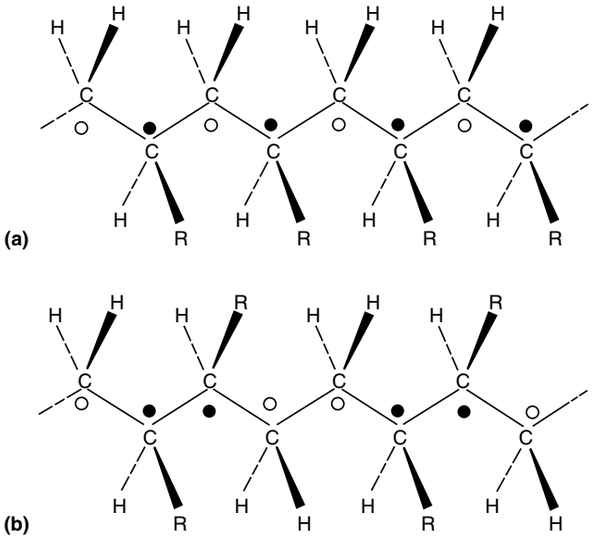

FIGURE 1.2. Schematic of the (a) head-to-tail and (b) head-to-head/tail-to-tail placements. Note the sequence of the "markers", ○●○●○● in (a) versus ●●○○●● in (b).

TABLE 1.2. *Glass transition temperatures of some head-to-head and head-to-tail polymers.*

Polymer	Head-to-Head (°C)	Head-to-Tail (°C)
Poly(isobutylene)	87	−61
Poly(methyl acrylate)	40	12
Poly(methyl crotonate)	107	80
Poly(methyl cinnamate)	210	190
Poly(methyl methacrylate)	160–170	100
Poly(propylene)	−39	−17
Poly(styrene)	97	98
Poly(vinyl cyclohexane)	88	138
Poly(vinyl chloride)	91	83

Taken in part from Ref. 45.

Apart from the carbon chain polymers discussed above, the silicon chain polymers have also been investigated extensively in terms of microstructure. The stereochemistry of polysilanes has been studied using ^{29}Si-*NMR* spectroscopy [54,55]. Wolff *et al*. [56] concluded that for a poly (phenylmethyl silane), the ratio of mm:rr:mr(rm) to be 3:3:4 and that the spectra of poly(1,2,2-trimethyl -1-phenyldisilane) are consistent with approximately equal amounts of head-to-head and head-to-tail sequences and an atactic configuration.

1.4 POLYMERS WITH MACROCYCLIC AND OTHER PHOTOACTIVE GROUPS

Synthetic efforts in designing polymers with functional moieties in the main chain or the side chain to impart photoconductivity, eletro-optic, nonlinear optical properties, etc., has been an active area in recent years [57,58]. Covalent tagging of chromophores to polymers in order to study the conformational dynamics and to study charge transfer complexes has been reported by a number of authors [59–61]. A summary of the work on π and σ conjugated oligomeric tetrathiafulvalenes for increasing the dimensionality of electrical conduction was presented by Adam and Müllen [62]. In searching for polymers with photorefractivity, photoconductivity and optical nonlinearity, metalloporphyrins, and metallophthalocyanines have been candidate materials for inclusion in the main chain or the side chain. A brief overview of this area was discussed by Allcock [63]. For example, initial designs on the *molecular electronic* wires, with backbone-linked porphyrins have been reported by Crossley and Burn [64]. Following this analogy, a *molecular photonic* wire was announced by Wagner and Lindsey [65]. In the latter, a boron-dipyrromethene dye provides an optical input at one end of the chain, a linear array of three zinc porphyrins serves as a signal transmission element and a free base porphyrin provides an optical output at the other end of the chain.

In the case of main chain porphyrin or phthalocyanine polymers, (1) the central metal atoms are covalently linked by a single atom such as O such that the porphyrin (porph) or phthalocyanine (Pc) macrocyclic rings are cofacial, as shown in Fig. 1.3a or (2) the central metal atoms are linked by a flexible or rigid spacer. In the case of side chain polymers, polymerization is performed via side chains attached to the macrocyclic using an acrylic or methacrylic polymer as the backbone. This is illustrated in Fig. 1.3b. (The designs of Crossley and Burn [64], and Wagner and Linsey [65] are different from these general classes.) Intra- or inter-molecular π overlap of these macrocyclics dictate the ultimate properties. It is known from the work on small molecule analogues that the extent of π overlap of these macrocyclics influence the photoconductivity, absorption wavelength, etc. [66]. The flexible spacers as well as the side groups attached to these macrocyclics improve their

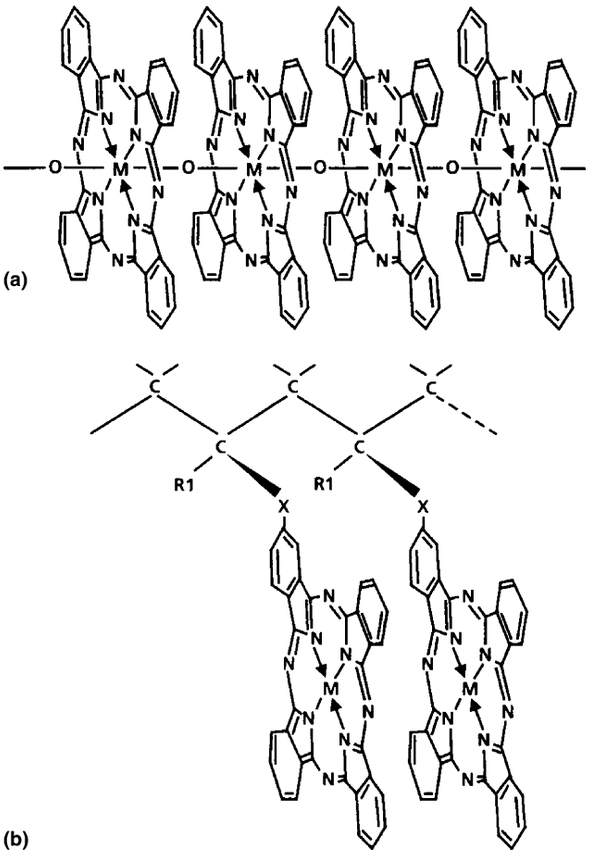

FIGURE 1.3. The main chain and side chain polymers incorporating metallophthalocyanines are shown schematically. (a) The main chain formed by linking the metallo-PC units, with an oxygen atom, leading to a cofacial arrangement of the macrocyclic rings. Flexible spacers can also be used instead of a single oxygen atom. (b) The metallo-Pc is attached to a side group of a chain such as PMMA. Although two adjacent Pc's are shown here in the cofacial arrangement, such an intramolecular overlap would depend on the tacticity and the conformation of the chain. The metal *M* can be Cu, Al, Si, Ge, etc.

solubility and processibility. It is well known that phthalocyanines, without any flexible side groups, are notoriously insoluble in any convenient solvent. A summary of some of these activities are presented in Table 1.3. Phthalocyanine-containing polymers [66a] and conjugated polymer-based chemical sensors [66b] have been discussed.

The asymmetrically substituted porphyrins or phthalocyanines exhibit isomerism. A theoretical treatment of this aspect was published by Knothe [67].

With the emergence of photonics for telecommunication applications, there have been extensive activities related to the development of polymeric materials to this end. Several reviews are available on the synthesis and fabrication of polymer-based molecular wires and switches [67a–g]. In addition, a number of studies on azobenzene-containing

TABLE 1.3. *Polymers with macrocyclic photoactive groups.*

Polymer	Remarks	Reference
Poly(5-[4-(acryloyloxy)phenyl]-10,15,20-triphenylporphyrin) Poly(5-[4-(methacryloyloxy)phenyl]-10,15,20-triphenylporphyrin) Poly(methylmethacrylate-*co*-5-[4-(methacryloyloxy)phenyl]10,15,20-triphenylporphyrin)	Polyacrylate or methacrylate polymers with pendant porphyrin units; hypochromism and hyperchromism discussed.	[160]
Poly[porph-O-CH_2-](I) Poly[porph-O-$(CH_2)_6$-](II) Poly[porph-O-$(CH_2)_8$-](III) Poly[porph-O-$(CH_2)_8$-](IV)	Main chain porphyrin polymers; meso-tetraarylporphyrins used; I, II, III with CH_3 substituted Porph; IV with CH_2CH_3 substitution; III and IV also with Co, Mn, and Zn transition metals.	[161]
Poly[(O-porph-O-CH_2)$_x$-*co*-(O-bisph-O-CH_2)$_y$] Poly[(porph-O-CH_2-O)$_x$-*co*-(bisph-O-CH_2-O)$_y$]	Main chain porphyrin polymers; various copolymer compositions; M_w up to 125 000; Co and Cu transition metal inclusion with some copolymers.	[161a]
(Porph-Ph-porph)$_3$ 1,4-*phenylene bridged porphyrins*	Metal free and Zn; several types of substitutions on the porphyrin.	[162]
Poly(porph-phenylenevinylene)	Main chain porphyrin polymers; 68% yield; metallized with Zn, Cu, or Ni; NMR, FTIR and cyclic voltammetric results.	[163]
Tetrakisporphyrin and oligomeric porphyrin	An approach to molecular electronic wire; Tetrakisporphyrin ($C_{322}H_{370}N_{28}$) is about 65 Å long. The tert-butyl groups along the backbone provide an insulating sheath around the conjugated core and enables solubility.	[64]
Boron-dipyrromethene dye-(ZnPorph)$_3$-Porph	An approach to photonic molecular wire. Absorption and emission spectra discussed.	[65]
Poly(*N*-vinyl-2-pyrrolidone-Porph)	Poly(N-vinyl-2-pyrrolidone) with metal free or Mg porphyrin side group; spectroscopic behavior discussed.	[164]
Poly[(AlPc)–F] Poly[(GaPc)-F] Poly[(CrPc)-F] Poly[(SiPc)-O] Poly[(GePc)-O] Poly[(SnPc)-O]	Co-facial packing of Pc rings; spectroscopy, electrical conductivity, electron microscopy, effect of doping discussed.	[165]
Poly[(SiPc)-O] Poly[(GePc)-O] Poly[(SnPc)-O]	DP = 120 with SiPc (density $\rho = 1.432$), 70 with GePc ($\rho = 1.512$) and 100 with SnPc ($\rho = 1.719$). Cofacial structure of Pc rings. Crystal structure discussed based on powder x ray diffraction data and modeling.	[166,167]
Poly(CuPc) Poly(CoPc) Poly(NiPc)	Sheet polymers of metal phthalocyanines; insoluble; electronic spectra, magnetic susceptibility, electrical conductivity, x ray diffraction discussed.	[168]
Poly(AlPc-F) Poly(SiPc-O)	Main chain metallized phthalocyanine (Pc) polymers; electron microscopy and electron diffraction; both AlPc and SiPc are cofacial.	[169]
Poly[octakis(decyloxy)SiPc-O]	Substituted SiPc main chain, soluble polymer; $M_w = 118\ 000$ and 250 000 by SAXS of heptane solutions; rod length 219 and 472 A for the two samples.	[170]
Poly(CH_2-CHCOOROPc) *R*: C_8H_{17} or $C_{12}H_{25}$	Side chain phthalocyanine polymers; Pc substituted with various groups; metal free, Cu and Ni Pc's; M_w up to 47 000; liquid crystalline; absorption and fluorescence spectroscopy.	[171]
Poly[(SiPc)-O] Poly[(SiPc)-O-$(CH_2)_4$-Si$(C_6H_5)_2$-$(CH_2)_4$-O] Poly[(SiPc)-O-$(CH_2)_4$-Si$(CH_3)_2$-C_6H_4-Si$(CH_3)_2$-$(CH_2)_4$-O] Poly[(SiPc)-O-$(CH_2)_4$-Si$(CH_3)_2$-(O-Si$(CH_3)_2)_4$-$(CH_2)_4$-O] Poly[(SiPc)-(Si$(CH_3)(C_6H_5)$)$_n$] ($n \approx 6.6$)	Main chain Pc polymers; symmetric and unsymmetric alkyl substituted Si phthalocyanines; absorption and emission spectroscopy, optical properties, cyclicvoltammetry are discussed in terms of packing and interactions of phthalocyanines.	[172]

TABLE 1.3. *Continued.*

Polymer	Remarks	Reference
Tetra(methoxy)-tetra(octyloxy)-phthalocyaninato-polysiloxane	Langmuir-Blodgett film properties studied.	[173]
Poly[(SiPc)-O]	SAXS from dilute solutions.	[174]
Poly[acrylamide-CuPc$(NO)_2$]	Side chain phthalocyanine polymer; water soluble; also doped with iodine; photoconductivity discussed.	[175]
Poly[vinylcarbazole-CuPc$(NO)_2$]	Copolymer with vinyl carbazole and dinitro CuPc covalently attached to the carbazole moiety. 21 mol % CuPc$(NO)_2$ bonded to PVK. The polymer shows better photoconductivity than monomeric CuPc or CuPc$(NO_2)_4$.	[176]
Poly[2-[[11-(methacryloyloxy)undecyl]oxy]-3-methoxy9,10,16,17,23,24, hexakis (dodecyloxy)phthalocyanine] (*polyundecyloxy methacrylate with side chain metal-free phthalocyanine*)	Langmuir-Blodgett monolayer formation studied with IR, ellipsometry, electron diffraction; effect of adding 1-arachidic acid discussed.	[177]
Poly(perylene imide): Poly(perylene-*R*) *subtituted perylenes*; *R*: *Linkage*: $(CH_2)_9$ or Ph-O-Ph or Ph-CH_2-Ph	Main chain perylene polyimide; M_w up to 64 100; soluble in various solvents; absorption, fluorescence spectra discussed.	[178]
Poly(4′-dialkylamino-4-nitrostilbene acrylate-*b*-methyl methacrylate) Poly(4′-dialkylamino-4-nitrostilbene methacrylate-*b*-methyl methacrylate) Poly(4′-dialkylamino-4-nitroazobenzene methacrylate-*b*-methyl methacrylate)	Polyacrylates with NLO active side chains; wide range of M_w up to 186 000; many soluble in methylene chloride or THF; two samples show liquid crystallinity; microscopy and thermal analysis discussed.	[179]
Poly[(R,R)-dibenzo-19-crown-6] Poly[(S,S)-dibenzo-19-crown-6]	Polymeric chiral crown ethers; hostguest complexation discussed.	[180]

polymers have been reported [67h,i], including the fabrication of light driven organized layered materials [67j]. Advances in polymerization methods have played a key role in recent efforts to design materials with specific properties. As an example, the ATRP technique mentioned in Sect. 1.3 has recently been used to tailor the photochromic performance of polymer-dye conjugates [67k].

1.5 POLYMERS WITH FULLERENE AND CARBON NANOTUBE

Summarizing the research activities on fullerenes, Baum [68] wrote "*... the question most commonly asked of fullerenè researchers has been very simple: What is it good for? The answer to that question has generally gone something like this: We don't yet know what applications will be discovered for* C_{60} *and the other fullerenes. However, the remarkable properties of these new forms of carbon will inevitably lead to many new products that will range from new types of polymers ...*" Fullerenes have been incorporated into polymeric backbones as "pearl necklace" or as side chains ("charm bracelet"). The synthesis of dendrimers with C_{60} has also been reported [69]. A brief summary of polymer related fullerene work was given by Hirch [70]. Chemical derivitization of C_{60} has been described by Petrie *et al*. [71]. A summary of the initial work on polymers incorporating C_{60} is given in Table 1.4.

Various forms of polymeric fullerenes have been prepared in the past decade: side chain polymers, main chain polymers, dendritic fullerenes, star-shaped polymers, fullerene endcapped polymers, etc. [71a–d]. With the invention of the carbon nanotubes [71e,f] and the development of methods to functionalize them [71g–i], their applications in the area of polymers range from opto-electronic devices to biosensors [71j–m].

1.6 CYCLIC POLYMERS

The cyclic polymers or oligomers are distinct in their physical properties from the corresponding linear chains. There has been considerable interest in the synthesis, isolation, characterization, and utilization of polymeric cyclics, although in a number of cases, they are at best oligomeric. A collection of reviews on various aspects of cyclic polymers has been published and an introduction to this area has been given [72–74a–c].

Chromatographic methods are normally used experimentally to determine the population of the cyclics which may coexist with the corresponding linear chains. Three methods have been reviewed by Semlyen [73] to

TABLE 1.4. *Polymers with fullerenes.*

Polymer	Remarks	Reference
Polyarenefullerenes	Reaction with benzene and toluene led to C_{60}-$(C_6H_6)_{12}$ and $C_{60}(C_6H_5\text{-}CH_3)_{12}$, respectively.	[181]
C_{60}-*p*-xylylene copolymer	Cross-linked; insoluble; xylylene/C_{60} rato: 3.4:1.0 Solid state NMR spectra discussed.	[182]
Poly(4,4′-diphenyl-C_{61} sebacate)	Side chain C_{60} polymer; 61% yield; soluble in nitrobenzene, benzonitrile; NMR, IR, cyclic voltammetry are discussed.	[183]
Poly(bisphenol *A* hexamethyleneurethane-C_{61})		[183]
Poly(ethylene imine-C_{60})	Side chain C_{60} polymer; molar mass 35 000 $gmol^{-1}$; molar ratio polymer/C_{60}: 18/1.	[184]
Poly(ethylene propylene)terpolymer-C_{60} (amine functionalized)	Side chain C_{60} polymer.	[185]
Poly[4-[[(2-aminoethyl)imino]methyl] styrene-C_{60}]	Side chain C_{60} polymer; molar mass 20 000 $gmol^{-1}$; molar ratio polymer/C_{60}: 19/1; soluble in toluene, carbon disulfide.	[184]
$C_{60}(=C=C=C_{58})_n$	Solid state photopolymerization; soluble in boiling isodurene.	[186]
Poly[(styrene)-co-(styrene/C_{60})]	Side chain C_{60} polymer; polymers made with 5.5% ($T_g = 112\,^\circ$C), 21% ($T_g = 142\,^\circ$C) and 29% ($T_g = 166\,^\circ$C) (w/w) of C_{60}; $M_w = 38500$; single T_g; soluble in methylenechloride, THF.	[187]
Poly(RbC_{60}) and poly(KC_{60})	Lattice parameters and x ray data.	[188]
Polyether dendrimer-C_{60}	A deuteriated fourth generation azide dendrimer[138] with C_{60} as the core; 68% yield; extremely soluble; $T_g = 52\,^\circ$C (13° higher thanstarting dendrimer).	[69]

theoretically calculate the population of the cyclics in cyclic-chain equilibrium [75–80]. The molar cyclization equilibrium constants have been determined both experimentally and by calculations for a number of cases such as dihydrogen siloxanes [81], dimethyl siloxanes [76,81–86], and sodium metaphosphates [87], cyclic nylon 6 [88], poly(ethylene terephthalate) [89], and liquid sulphur [90].

Cyclics offer a wide range of opportunities for polymer synthesis, processing, and modification. Ring opening polymerization of cyclics leads to high molecular weight polymers. This was demonstrated using octamethylcyclotetrasiloxane to synthesize long chain polysiloxanes [91]. This process of involving the cyclics has also been used to control the block length of polysiloxane in the preparation of siloxane-styrene-siloxane or siloxane-isoprene-siloxane triblock copolymers [92] and styrene-dimethylsiloxane diblock copolymers [93]. The cyclics offer the advantage of the ease of processing due to their low viscosity at the product fabrication temperature. Hence, in applications such as injection molding, the cyclics can be used for postpolymerization to achieve high molecular weight polymer end products [94]. Macrocyclic oligmers of bisphenol A polycarbonate have been used to prepare polycarbonates of very high molecular weight ($M_w = 200\,000$–$400\,000$), by ring-opening polymerization which avoids the creation of byproducts. Cyclics with 2–21 monomer units have been prepared and the cyclics yield can be varied from 0% to over 85% by manipulating the synthetic conditions [95–97]. Synthesis and polymerization of cyclic oligomeric arylates [98] and cyclic ether ketones, ether sulfones, and ether imides have also been reported [99].

Mark and Semlyen, in a series of papers, have studied the mechanism and the effect of trapping cyclics in end-linked elatomeric networks [100–103]. Sharp fractions of cyclics of poly(dimethylsiloxane) (PDMS), varying in size from 31 to 517 skeletal atoms, were mixed with linear chains for different periods of time and the linear chains were then end-linked using a tetrafunctional silane. The untrapped cyclics were extracted to determine the amount trapped. It was found that while cyclics with less than 38 skeletal atoms were not at all trapped, for $n>38$, the percentage of cyclics trapped increased with size, with 94% trapped in the case of the cyclic with 517 skeletal atoms. In effect, the system of trapped cyclics in the end linked PDMS network is a polymeric catenane. It is thus possible to control the elastomeric properties of the network by incorporating the appropriate sized cyclics. This study has been extended to cyclic PDMS in poly(2,6-dimethyl-1,4-phenylene oxide) [104,105] and cyclic polyesters in PDMS [106].

Percec and coworkers [107–110] have synthesized liquid crystalline cyclic oligomeric polyethers based on 1-(4-hydroxy-4′-biphenyl)-2-(4hydroxyphenyl)butane with dibromoalkanes. Rings varying from 2 to 5 monomer units were prepared and show isotropic-nematic transition. The nematic order is modeled to arise from the collapse of the rings in the form of a ''folded chain'' structure, as shown schematically in Fig. 1.4. This is similar to the case of chain folded crystallization of cyclic alkanes (with 34–288 CH_2 groups) and cyclic urethanes [111–114].

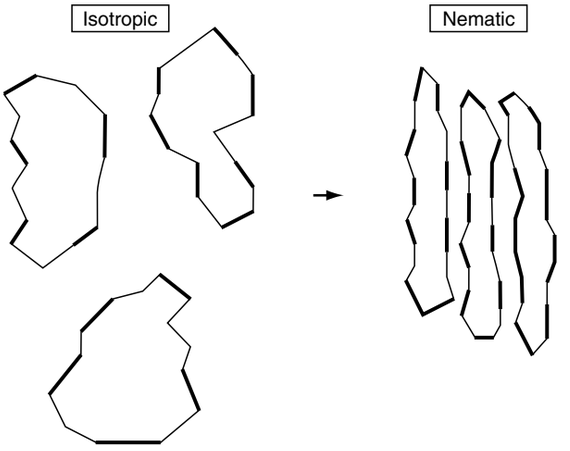

FIGURE 1.4. A model of the isotropic → nematic transition in cyclic oligomeric polyethers via intramolecular collapse of the cyclic.

Table 1.5 summarizes the studies on cyclics of poly(dimethyl siloxane) and derivatives, and Table 1.6, those of other polymers. In these tables, K_x refers to the molar cyclization equilibrium constant and RIS, to the rotational isomeric state scheme to analyze chain conformations.

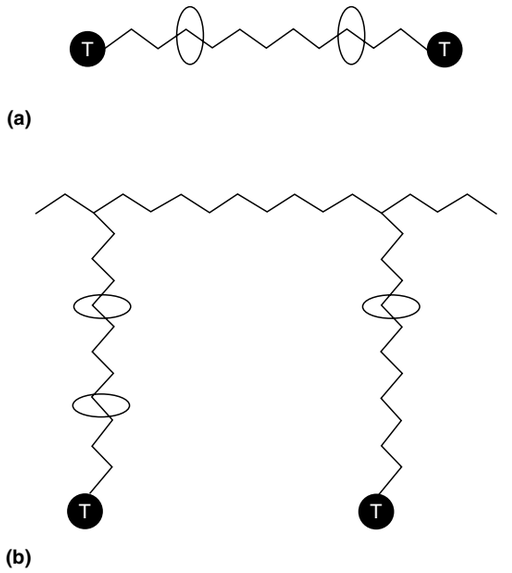

FIGURE 1.5. A schematic representation of the (a) main chain and (b) side chain rotaxanes. The *T* represents a large terminal group which may be used to prevent dethreading of the cyclic from the chain.

1.7 ROTAXANES

Polyrotaxanes (the name derived from Latin words for wheel and axle) are essentially *in situ* molecular composites consisting of a linear chain threaded through a cyclic molecule. The interior diameter of the cyclic must be large enough to accommodate the linear chain. Large end groups might be necessary to prevent the unthreading of the chain from the cyclic.

Two principal approaches have been used in the synthesis of polyrotaxanes. In the statistical method, no specific interaction exists between the linear and the cyclic species. The equilibrium for threading is driven by entropic factors. This hence provides a wide choice of pairs of cyclics and linear chains. However, the resulting yield is often low. In the template or directed method, specific attractive interaction (such as metal chelation, charge transfer interactions, etc.) between the cyclic and the linear species is taken advantage of.

The polyrotaxanes can be of the ''main chain'' or the ''side chain'' type [115], as illustrated schematically in Fig. 1.5, along with a bulky terminal group to prevent dethreading. In the former, the cyclic is threaded through a linear chain and is free to glide along the chain as the steric interactions would permit. In the case of side chain rotaxanes, the cyclic is threaded through a long side chain of a polymer. Thus, a wide range of options and architectures are possible.

Rotaxanes have also been part of dendrimers, i.e., dendritic molecules containing rotaxane-like bonds to link their components, either at the core, termini, or branches [115a].

Comprehensive reviews of the history, chemistry, and physical chemistry of rotaxanes and the related architecture, the catenanes, have been published [115–120]. Joyce *et al.* [121] reported a molecular modeling study of cyclics of poly(dimethylsiloxane) to understand the energetics of the threading process of linear chains with particular reference to rotaxanes. Of relevance is also the exhaustive review by Wenz [122] on the role of cyclodextrins in the building of supramolecular structures. Cyclodextrins are cyclics of D-glucose, with α-1,4′ linkages. The common ones are α,β,γ-cyclodextrins, with 6, 7, and 8 D-glucose units, respectively.

The rotaxanes offer a plethora of possibilities in terms of supramolecular architecture [115, 116, 122a]. Applications toward molecular machines, motors, and switches have been extensively explored [122b–e].

Table 1.7 lists the examples of different types of rotaxanes reported in the literature. Some of the early work on the chemistry is omitted but can be found in the reviews cited above. In naming the rotaxanes in this table, we follow the nomenclature of Gibson and Marand [115]: polymer-*rotaxa*-cyclic.

1.8 DENDRIMERS

Dendrimers (Greek) or arborols (arbor: tree+alcohol = arborol) are tree-like macromolecular structures topologically controlled during the synthesis. Starting from

TABLE 1.5. *Cyclics of poly(dimethyl siloxane) and its derivatives.*

Polymer	Number of monomers in cyclics	Remarks	Reference
Poly(*n*-butyl methylsiloxane)		K_4: 0.37; K_5: 0.19	[189]
Poly(dimethyl siloxane)	4–200	K_x determined.	[82]
Poly(dimethyl siloxane)	4–40	K_x determined with bulk and solution equilibrates; characteristic ratio measured. Calculations with RIS models.	[83]
Poly(dimethyl siloxane)		K_4: 0.19; K_5: 0.09	[189]
Poly(dimethyl siloxane)	4–200	K_x measured; dilute solution behavior and RIS treatment discussed.	[84]
Poly(dimethyl siloxane)	3–6	$[\eta]$-M_w relationships.	[190]
Poly(dimethyl siloxane)	up to approx. 650 (number average number of skeletal bonds 1300)	Construction of a preparative GPC for isolating sharp fractions of cyclics; $M_w/M_n = 1.05$; viscosity of fractions measured.	[191]
Poly(dimethyl siloxane)	65–275	Neutron scattering measurements of chain dimensions.	[192]
Poly(dimethyl siloxane)	16–259	Used in trapping experiments with linear chains; effect of ring size on trapping and elastic properties of the network studied.	[100–103, 106]
Poly(dimethyl siloxane)	92	Cyclics trapped to form catenanes with poly(2,6-dimethyl-1,4-phenylene oxide). 26% w/w cyclics permanently captured in network. 1μ phase domains seen after extraction; mechanical and thermal properties discussed.	[104]
Poly(dimethyl siloxane)	33–122	Trapped to form catenanes with poly(2,6-dimethyl-1,4-phenylene oxide); weight fraction of cyclics trapped increases with their DP. Two T_g's observed; phase separated domains form.	[105]
Poly(dimethyl siloxane-b-styrene-*b*-dimethylsiloxane)	4–8	Solution equilibrates; short styrene and DMS blocks, M_w approx 1.1×10^4.	[193]
Poly(ethyl methyl siloxane)	4–20	Equilibrated in bulk and in toluene; 25.8% w/w cyclics; K_x measured	[194]
Poly(ethyl methyl siloxane)		K_4: 0.25; K_5: 0.16.	[189]
Poly(hydrogen methyl siloxane) [-H(CH_3)SiO-]	4–15	Equilibrated in bulk and in toluene; 12.5% w/w cyclics; K_x measured.	[194]
Imide-disiloxane			[98]
Paraffin-siloxanes			[195]
Paraffin siloxane [-(CH_3)$_2$ Si-(CH_2)$_4$-(CH_3)$_2$Si-O-]	2–10	K_x measured for $x = 1-6$.	[81]
Poly(phenyl methylsiloxane)	3–50	30% w/w undiluted, 90% with toluene; $K_4 = 0.25$; K_5: 0.16; populations of configurational isomers for $x = 3-5$.	[189]
Poly(n-propylmethyl siloxane)	4–8	Equilibrated in bulk and in toluene; 31% w/w cyclics; K_x measured.	[194]
3,3,3-trifluoropropyl methyl siloxane	3–13	>80% (w/w) population.	[196]
Poly(3,3,3-trifluoropropylmethyl siloxane)	4–20	Equilibrated in bulk and in cyclohexanone; 82.7% w/w cyclics; K_x measured.	[194]
Poly(vinylmethyl siloxane)	4–23	K_x, dilute solution viscosity, melt viscosity, T_g measured.	[197]

a single branch cell, repeat units or branch cells are iteratively added, to produce ''star-burst'' structures, one generation after another (STARBURST is a registered trademark of Dow Chemical Company) [123]. During such multiplicative growth, the polymer adopts a spherical shape, free of chain entanglements, as shown schematically

TABLE 1.6. *Cyclics of other polymers.*

Polymer	Number of monomers in cyclic	Remarks	Reference
Cycloalkane	34	X ray crystal structure.	[111]
Cycloalkane	12–84	Thermal behavior studied; entropy of fusion/unit increases with chain length; melting temperatures discussed.	[198]
Cycloalkane	36	X ray crystal structure	[113]
Cycloalkane	24–288	T_m, LAM frequencies. Discussion of chain folding.	[114]
Cyclic amides		Prepared with dodecanedioyl dichloride and pure isomers of 4,4′-methylenedicyclohexylamine; NMR, IR, x ray diffraction discussed.	[199]
Amide-imides			[98]
Bisphenol-A-*co*-4,5-bis(p-hydroxyphenyl)-2-(p- nitrophenyl)-oxazole		Macrocycles for NLO copolycarbonates; T_g increases with 2nd component.	[200]
Polycarbonate		Up to 95% yield of cycllcs; large cyclics with M_w more than 100,000.	[201]
Polycarbonate	2–21	Cyclics content (0–85%) depends on catalyst.	[95, 97]
Polycarbonate		Dimer 5%; trimer 18%; tetramer 16%; pentamer 12%; hexamer 9%; higher oligomers 25%.	[202]
Polycarbonate	2,4	X ray crystal structure.	[203]
Poly(decamethylene adipate)			[75a]
Poly(decamethylene adipate)	1–5	K_x measured and compared with theory; RIS treatment discussed.	[204]
Poly(1,3-dioxolane)	2–9	K_x measured; RIS treatment discussed.	[205]
2,2′-dithiobis(2-methyl propionaldehyde	ester tetramer	95% yield, $T_m = 182\,^\circ$C	[206]
Polyester [-$(CH_2)_{10}$COO-]	5–15	Trapping experiments with linear PDMS chains; molecular modeling of the phenomenon.	[106]
Polyethers with 1-(4-hydroxy-4′-biphenyl)-2-(4- hydroxyphenyl) butane and dibromoalkanes	2–5	Exhibit nematic mesophase; chiral cyclics display cholesteric phase.	[107,109,110]
Ether imides		25–75% yield.	[99]
Ether ketones		40–52% yield.	[99]
Ether sulphones		40–52% yield.	[99]
Ethylene terephthalate	3–9	Extracted from PET; K_x given.	[207]
Tris(ethylene terephthalate)	3	Synthesized.	[208]
Tris(ethylene terephthalate)	3	Synthesized; 46% yield.	[209]
2-Norbornene	2–7		[210]
Nylon-6	1–6	2% w/w cyclics; melt equilibrates; K_x measured.	[88,211]
Oligo(cyclooctene)s	2–10		[212,212a]
1,3,6-*trio*xacyclooctane	1–9	T_m for $x = 2$: 60 °C $x = 4$: 35 °C $x = 6$: 40 °C K_x given.	[213]
(2R,5R,8R,11R)-2,5,8,11-tetra-tertbutyl-1,4,7,10- tetraoxa cyclododecane	4	$T_m = 168\,^\circ$C NMR, conformation discussed.	[214]
1,3,6,9,12,15-hexa oxacycloheptadecane	1–5		[213]
1,3,6,9,12-penta oxacyclotetradecane	1–7	T_m for $x = 2$: 44 °C $x = 4$: 61 °C	[213]
1,3,6,9-tetra oxacycloundecane	2–8		[215]

TABLE 1.6. *Continued.*

Polymer	Number of monomers in cyclic	Remarks	Reference
1,3,6,9-tetra oxacycloundecane	1–8	T_m for $x = 2$: 88 °C $x = 4$: 54 °C $x = 6$: 39 °C K_x given.	[213]
Poly(phenyl methyl silane)	6	Two isomers characterized by NMR; crystal structure determined for one.	[216]
N-methylated oligo(p-phenyleneterephthal amide)	3–6		[217]
Polyphosphate $[NaPO_3]_x$	3–7	10 w/w cyclics	[218]
Polystyrene	M_w: 4 500−20 000	Yields from 10 to 45%	[219]
Polystyrene		Synthesis and fractionation described; M_w of rings 5×10^3 to 4.5×10^5; yield decreases with M_w from 55% to 18%	[220]
Polystyrene		M_w 11 100 to 181 500, $M_w/M_n < 1.2$; quasi elastic light scattering experiments to determine translational diffusion coefficients and compare with linear chains.	[221]
Polystyrene		M_w12 000−22 000 SANS experiments to determine mean square radii of gyration and second virial coefficient for cyclic and linear chains.	[222]
Polystyrene		Macrocyclic fractions with $11{,}500 \leq M_w \leq 181\,000$; thermodynamic and hydrodynamic properties in dilute solution and melt viscosity studied and compared with corresponding linear fractions.	[223, 224]
Polystyrene		Macrocyclic fractions with $1.9 \times 10^4 \leq M_w \leq 3.9 \times 10^5$ viscoelastic properties measured and compared with theory.	[225]
Poly(trimethylene succinate)	1–7	K_x measured, compared with theory; RIS treatment discussed.	[204]
Poly(sulphur)	>8		[90]
Poly(sulphur)	6 to 26		[73]
Cyclo(oligourethane)s	1–7	Melting temperatures, long periods, x ray diffraction and structure discussed.	[112]
Poly(tetra hydrofuran)	4–6		[226]

in Fig. 1.6. However, theory predicts [124] a limit of 10 generations beyond which the reaction rates decrease significantly and defects begin to predominate. Extensive reviews of advances in this field have been published [123,125–128].

The synthesis of ''cascade molecules'' or arborols as spherical micelles has been described by Newkome *et al*. [129,130] who also proposed a nomenclature for such structures. A designation [*m*]-[*n*]-[*p*] would refer to a case in which *m* and *p* represent the number of surface groups and *n* denotes the bridge size.

The conventional synthesis of dendrimers involves the ''divergent'' method, in which branch cells are constructed *in situ* around the initiator core or preformed branch cells are attached to the core. Successive generations are then built. On the other hand, in the ''convergent'' method [131–133] the dendritic fragments are prepared by starting from fragments which would ultimately comprise the periphery and progressing inward. The resulting dendritic wedges, after several generations of growth, are coupled to a polyfunctional core. A double-stage convergent growth approach has also been described by Wooley *et al*. [134], which enables synthesis of a dendrimer with a ''hypercore'' made of flexible segments and a rigid outer layer or vice versa. Dendrimers have also been used as macroinitiators for forming hybrid linear-globular AB block copolymers [135]. A summary of all known synthetic strategies to dendrimers has been given by Tomalia [127]. Self-aggregation of certain dendrimers into lyotropic and thermotropic mesophases has been reported [108, 136, 137].

In particular, the review by Tomalia *et al*. [124] traces the similarities and scope of the dendrimer designs to biological systems tailored by Mother Nature and the prospects and applications of supramolecular mimetics via man-made

TABLE 1.7. *Poly(rotaxanes).*

Poly(rotaxane)	Remarks	Reference
Poly(amide)-*rotaxa*-β-cyclodextrin	Rotaxane becomes insoluble; no melting observed in DSC before decomposition.	[227]
Poly(ethylene glycol)-*rotaxa*-α-cyclodextrin	PEG M_w from 400 to 10 000 studied; complexation in aqueous solution at room temperature; maximum complexation with $M_w = 1000$; two ethylene glycol units/α-CD cavity; x ray study leads to an extended columnar structure.	[228]
Poly(ethylene glycol) bisamine-*rotaxa*-α-cyclodextrin	PEG end capped with 2,4-dinitrofluorobenzene after complexation in aqueous solution; 20–23 alpha-CD molecules entrapped on each chain; rotaxane is insoluble in water; hydrogen bonds between entrapped alpha-CD's suggest alternating face-to-face, back-to-back arrangement of the CD's.	[229,230]
Poly(iminoundecamethylene)-*rotaxa*-α-cyclodextrin	A nicotinoyl group was used for endcapping to prevent dethreading.	[231]
Poly(iminoundecamethylene)-*rotaxa*-heptakis(2,6-di-O-methyl)-β-cyclodextrin		
Poly(iminotrimethylene-iminodecamethylene)-*rotaxa*-α-cyclodextrin		
Poly(iminotrimethylene-iminodecamethylene)-*rotaxa*-heptakis(2,6-di-O-methyl)-β-cyclodextrin		
Poly(isobutylene)-*rotaxa*-β-cyclodextrin	Complex formed in water although PIB is insoluble in it;	[232]
Poly(isobutylene)-*rotaxa*-γ-cyclodextrin	complexation with β-and γ-CD's show opposite dependence on M_w of PIB. More than 90% yield with γ-CD and PIB M_w between 800 and 1350.	
Poly(propylene glycol)-*rotaxa*-β cyclodextrin Poly(propylene glycol)-*rotaxa*-α cyclodextrin	96% yield with PPG $M_w = 1000$ and beta-CD and decreases with increasing M_w. Two PPG repeat units per β-CD. More than 70% yield with PPG M_w 400–1000 and γ-CD. Complexation in aqueous solution at room temperature.	[233]
Polyvinylidene chloride-*rotaxa*-β cyclodextrin	*In situ* polymerization; x ray diffraction of the inclusion compound discussed.	[234,235]
Poly(azomethine)-*rotaxa*-42-crown-14	*p*-tri(*p*-*t*-butylphenyl) derivatives used as blocking groups; liquid crystalline; T_m is 67 °C, and smectic between 67 and 73 °C. $T_i = 123$ °C. Parent polymer is insoluble; polyrotaxane is soluble in chloroform, acetone, etc.	[236]
Poly(butylene sebacate)-*rotaxa*-(30-crown-10)	With and without a triarylmethyl derivative as blocking group; efficiency of threading depends on	[237]
Poly(butylene sebacate)-*rotaxa*-(60-crown-20)	size of the macrocycle; blocking group is not always needed for stability.	
Poly(decamethylene sebacate)-*rotaxa*-(30-crown-10)		[238]
Polystyrene-*rotaxa*-bisparaphenylene-34-crown-10	With a triphenyl blocking group; free-radical and anionic polymerizations.	[239]
Polystyrene-*rotaxa*-30-crown-10	Two T_g's observed.	
Poly(triethyleneoxy sebacate)-*rotaxa*-(30-crown-10)	With and without a triarylmethyl derivative as blocking group; efficiency of threading depends on size of the macrocycle;	[237]
Poly(triethyleneoxy sebacate)-*rotaxa*-(60-crown-20)	blocking groups is not always needed for stability.	
Poly(urethane-*rotaxa*-bis(*p*-phenylene)-34-crown-10	Segmented polyurethane; host-guest complexation approach; 80% threading efficiency.	[240]
Poly(urethane)-*rotaxa*-(60-crown-20)	Statistical threading approach; threading efficiency 57% with	[241]
Poly(urethane)-*rotaxa*-(36-crown-12)	60Cr20 and 16% with 36Cr12. T_g of rotaxanes (-28 °C for 60Cr20 and 19 °C for 36Cr12) lower than the parent polymer (51 °C).	

m-crown-*n* refers to a crown ether containing *m* backbone atoms, with *n* oxygen atoms. α,β,γ- cyclodextrins: cyclics with 6, 7, and 8 α-1, 4′-*D*-glucose units, respectively.

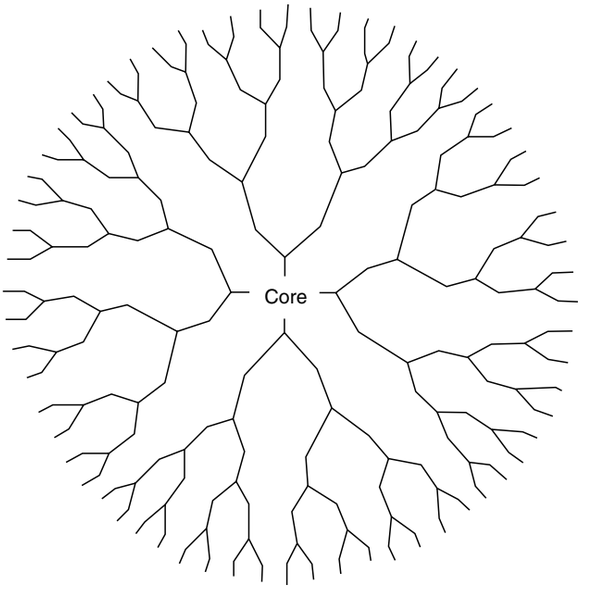

FIGURE 1.6. A schematic representation of a symmetric dendrimer.

dendrimer structures. Tomalia *et al*. [123] and Fréchet [128] also discuss the similarities and differences between starburst dendrimers and other starbranched or hyperbranched systems. While they are similar in terms of a core, radial branches, and perhaps telechelic functionality, the structure of hyperbranched polymers is neither regular nor highly symmetrical. The branch-segment densities decrease from the core in a concentric radial fashion in the case of starbranched systems. On the other hand, in the case of starburst dendrimers with symmetrical branch cells and topologies, the density increases with generations and it remains constant for the asymmetrically branched starburst dendrimers.

Other physical properties which contrasts them with linear polymers are [126] (1) the radius of gyration of a dendrimer is larger than that of a linear chain with the same M_w; (2) the T_g depends on the terminal groups as well as on the nature of the repeat unit blocks; (3) the high degree of branching prevents any interchain entanglements; and (4) the Mark-Houwink type relationship between M_w and intrinsic viscosity does not apply. The hydrodynamic radius increases more rapidly with generations than the radius of gyration.

Wooley *et al*. [138] made a systematic study of the glass transition temperatures of several types of dendrimers. They also derived an equation to relate the T_g of a dendrimer to $T_{g\infty}$ corresponding to infinite molecular weight:

$$T_g = T_{g\infty} - K'(n_e/M), \tag{1.1}$$

here n_e is the number of chain ends per molecule, M is the molecular weight, and K' includes several parameters such as the free volume per chain end, etc. It was found that the nature of the chain ends dramatically affects the T_g and that the latter increases with the polarity of the chain ends. The internal composition, as in the case of block copolymer dendrimers, also influences the T_g.

A summary of various published dendritic structures is given in Table 1.8.

TABLE 1.8. *Polymeric dendrimers.*

Dendrimer	Remarks	Reference
Acid-terminated dendrimers	*Z*- cascade:methane[4]:(3-oxo-6-oxa-2-azaheptylidyne):(3-oxo-2-azapentylidyne):propanoic acids. Five generations; pH dependence of hydrodynamic radii discussed.	[242]
Ammonium ion dendrimers		[243]
Aramid dendrimers	Fully aromatic amide dendrimers; 1,3,5-benzenetricarboxamide core; 3,5-dicarboxamidophenyl repeat units; phenyl or 3,5-dit-butyl isophthalate termini. Molecular modeling showed that the conformations of the isophthalate segment lead to the either open or conjested structure.	[244]
Aryl ester dendrimers	Based on symmetrically substituted benzenetricarboxylic acid esters; convergent synthesis; four generations.	[245]
Carbosilane dendrimers	Tetravinylsilane as the core; dichloromethylsilane as the propagating unit; four generations; M_w,[η] discussed.	[246]
"Comb burst" dendrimer	Backbone: styrene/divinylbenzene copolymer; teeth: triethanolamine; ion exchange material (anionic: core and branch points, cationic: termini).	[247]
Crown ether dendrimers	Based on *N*-benzyloxycarbonyl-1,4,10,13-tetraoxa-7,16 diazacyclooctadecane and with trichloroformyl mesitylene as core.	[248]
Dendrimer-*b*-polyethyleneglycol-*b*-dendrimer	Third and fourth generation polyether dendrimers used; DP of PEG from 24 to 447: M_w of copolymers 3600–20 300; $M_w/M_n \leq 1.1$; size and shape of the block copolymers discussed.	[249, see also 250 for further characterization]

TABLE 1.8. *Continued.*

Dendrimer	Remarks	Reference
Dendrimer-*b*-polyethyleneoxide-*b*-dendrimer Dendrimer-*b*-polyethyleneglycol-*b*-dendrimer	Polyether dendrimers from Hawker and Fréchet [132] used; reactivities in the melt and solution discussed.	[2, 49, 250]
Phosphonium dendrimers	Based on tris(*p*-methoxymethylphenyl)phosphine.	[250a, see also 250]
Phenylene dendrimers	1,3,5-phenylene based hydrocarbon dendrimers; $M_w/M_n = 1.08$; soluble in common organic solvents; spectroscopy, thermal analysis described.	[253]
Phenyl acetylene dendrimer	94 monomer units ($C_{1134}H_{1146}$); 3,5-di-*tert*-butylphenyl peripheral group; $M_w = 14776$; $M_w/M_n = 1.03$; soluble in pentane.	[254,255]
Propylene imine dendrimers	Method for large scale (several Kg) synthesis presented; diaminobutane as the core; NH_2 or CN end groups; five generations; T_g, viscosity discussed.	[256]
Quaternary ammonium ion dendrimer	36 terminal trimethylammonium groups, catalysis applications discussed.	[257]
Trimethylene imine dendrimers	Ammonia as the initiator core; nitrile or amine end groups; five generations.	[258]
Aromatic polyamide dendrimers	Lyotropic.	[136]
Polyamide dendrimers	Three polyamides with the same internal hierarchical architectures but with either acidic, neutral or basic terminal functionality; 5 generations, 972 terminal groups in 5th gen.; the polymers shrink or swell upon pH change (“smart behavior”).	[259]
Polyamido amine dendrimers	Ethylenediamine or ammonia core, *N*-(2-aminoethyl)acrylamide repeat units, seven generations; $M_w = 43\,451$ with ammonia core, 57 972 with ethylenediamine core.	[260, 261]
	With CO_2Me or NH_2 head groups; hydrodynamic radii ($[\eta]$-M_w measurement), and surface area with generations discussed.	[262–264]
Polyarylamines	Based on 2,4-dinitrofluorobenzene and anilines. Complexation with iodine; T_m and cyclic voltammetry discussed.	[265]
Polyester dendrimers	Based on 3,5-bis(trimethylsiloxy) benzoyl chloride; M_w from 30 000 to 200 000; M_w and dispersity depend on temperature; 55 to 60% branching.	[266]
Polyester dendrimers	Hyperbranched aromatic polyesters based on 5-acetoxyisophthalic acid ($T_g = 239\,^\circ$C) and 5-(2-hydroxyethoxy)isophthalic acid ($T_g = 190\,^\circ$C); Carboxylic acid terminal groups; degree of branching: 50%; $[\eta]$, polyelectrolyte properties discussed.	[267]
Polyether dendrimer	3,5-dihydroxybenzyl alcohol monomer unit reacted with benzylic bromide; 1, 1, 1-tris(4′ hydroxyphenyl)ethane core; six generations; $M_w = 154\,000$; $M_w/M_n = 1.02$.	[131, 132]
Polyether dendrimer	Size exclusion chromatography, $[\eta]$-M_w relationship; linear dependence of hydrodynamic radii on generation; a characteristic maximum in $[\eta]$ observed; samples from Hawker and Fréchet [131, 132] used.	[268]
Polyether dendrimer (thermotropic)	Dibromalkanes with 1-(4-hydroxy-4′-biphenylyl-2-(4-hydroxyphenyl); 6–10 methylene units as flexible spacers; those with 6, 8, and 10 CH_2 units or with benzyl chain end exhibit nematic mesophase.	[108]
Polyether dendrimers (thermotropic)	Monomers: 6-bromo-1-(4-hydroxy-4′-biphenylyl)-2-(4-hydroxyphenyl)hexane (TPH); 13-bromo-1-(4-hydroxyphenyl)-2- [4-(6-hydroxy-2-naphthalenylyl)-phenyl]tridecane (BPNT); 13- bromo-1-(4-hydroxyphenyl)-2-(4-hydro-4″-*p*- terphenylyl)tridecane (TPT); Chain ends: benzyl or allyl or alkyl. TPH and BPNT show narrow nematic meosphase; TPT nematic mesophase extends over 82 °C. Degree of branching for TPT with allyl end is 0.82.	[137]

TABLE 1.8. *Continued.*

Dendrimer	Remarks	Reference
Polyether-*b*-polyester dendrimer	3,5-dihydroxybenzyl alcohol as monomer for ether-linked fragments and 2,2,2-trichloroethyl 3,5-dihydroxybenzoate for ester linked fragments; radially alternating the dendritic segments produced segmented-block polymer and concentric alternation gave layer-block polymer; spectroscopy, thermal characterization described.	[269]
Polyether dendrimer-styrene copolymer	Copolymer of the type poly[$(\text{styrene})_y$-co-$(\text{styrene-G-4})_x$] where the fourth generation dendrimer is *p*-linked to styrene.	[270]
Polyether dendrimer-C_{60}	A deuteriated fourth generation azide dendrimer [138], with C_{60} as the core; 68% yield; extremely soluble: $T_g = 52\,^{\circ}\text{C}$ (13° higher than starting dendrimer).	[69]
Polyphenylene dendrimer	Carboxylate form is water soluble. complexation with *p*-toluidine reported.	[271]
Polyphenolic dendrimers	A double stage convergent synthesis is described; a 'hypercore' based on 4,4- bis(4′-hydroxyphenyl)pentanol.	[134]
Silane dendrimers	Tetraallylsilane as the zeroth generation; five generations synthesized ($C_{4368}H_{7764}Si_{485}$).	[272, 273]
Silicone dendrimers		[274]
Polysiloxysilane dendrimers		[275]
Polysiloxane dendrimers	Tris-[(phenyldimethylsiloxy) dimethylsiloxy]methylsilane core; bis[(phenylimethylsiloxy)methyl siloxy] dimethylsilanol as the building block; Three generations; $[\eta]$-M_w relationship/Mark-Houwink constants, NMR, molecular diameter discussed; $M_w/M_n \leq 1.1$.	[276]
Siloxane starburst dendrons and dendrimers	Allylbis[4-(hydroxydimethylsily)phenyl]-methylsilane as the building block; Four generations; $[\eta]$-M_w relationship and T_g reported.	[277]

1.9 SUPRAMOLECULAR POLYMERS

Using molecular recognition and self-assembly to construct macromolecules and to design devices using macromolecules is emerging as a fertile area of research. Both covalent and noncovalent bonding are used to this end. Along with interactions such as hydrogen bonding, charge transfer complex, ionic bonding, etc. the secondary and tertiary structures can be designed in a controlled and reversible manner [278–285]. Chain folding as a precursor to self-assembly has also been realized. Sequences of rigid hydrophobic chromophores, linked by flexible hydrophilic segments, fold and unfold [286]. While the intramolecular interaction between the chromophores leads to chain folding, intermolecular attractions favor self-assembly. Incorporating a specific "foldamer" [287] to cause, for example, a U turn in the polymer structure has been accomplished [288,289]. The possibilities for molecular architectures are thus endless.

ACKNOWLEDGMENTS

Financial support by the Natural Sciences and Engineering Research Council of Canada (NSERC) is gratefully acknowledged.

REFERENCES

1. D. H. Reneker, W. L. Mattice, and R. P. Quirk, Smart Mater. Struct. **1,** 84 (1992).
2. M. V. Gandhi and B. S. Thompson, *Smart materials and Structures* (Chapman & Hall, London, 1992).
3. B. C. Crandall and J. Lewis, Eds. *Nanotachnology: Research and Perspectives* (The MIT Press, Cambridge, MA, 1992).
4. "*New Macromolecular Architectures*," Macromol. Symp., vol. 77, 1994.
5. *Abstracts of the 35th IUPAC International Symposium on Macromolecules*, Akron, Ohio, July 11–15, 1994.
6. P. J. Flory, *Statistical Mechanics of Chain Molecules* (John Wiley, NY, 1969), Chapter VI (republished by Hanser Publishers, 1988).
7. E. Lemieux, R. E. Prud'homme, R. Forte, *et al*., Macromolecules **21,** 2148 (1988).
8. G. Beaucage and R. S. Stein, Macromolecules **26,** 1609, 1617 (1993).
9. G. Beaucage, R. S. Stein, and R. Koningsveld, Macromolecules **26,** 1603 (1993).
10. B. Wunderlich, *Macromolecular Physics*, Volume 1 (Academic Press, New York, 1973).
11. H. Tadokoro, *Structure of Crystalline Polymers* (John Wiley & Sons, New York, 1979).
12. S.-N. Zhu, T. Asakura, and R. Chûjô, Polym. J. **16,** 895 (1984).
13. N. Ishihara, T. Seimiya, M. Kuramoto, *et al*., Macromolecules **19,** 2464 (1986).
14. C. Pellecchia, P. Longo, A. Grassi, *et al*., Makromol. Chem., Rapid Commun. **8,** 277 (1987).
15. P. Corradini, G. Natta, P. Ganis, *et al*., J. Polym. Sci., Part C **16,** 2477 (1967).
16. A. Immirzi, F. de Candia, P. Iannelli, *et al*., Makromol. Chem., Rapid Commun. **9,** 761 (1988).

16a. O. Greis, Y. Xu, T. Asano, *et al*., Polymer **30,** 590 (1989).

17. V. Vittoria, Makromol. Chem., Rapid Commun. **9,** 765 (1988).
17a. V. Vittoria, R. Russo, and F. de Candia, J. Macromol. Sci., Phys. **B28,** 419 (1989).
18. P. Corradini, R. Napolitano, and B. Pirozzi, Eur. Polym. J. **26,** 157 (1990).
18a. G. Guerra, V. M. Vitagliano, C. De Rosa, *et al*., Macromolecules **23,** 1539 (1990).
18b. Z. Sun and R. L. Miller, Polymer **34,** 1963 (1993).
19. M. A. Gomez and A. E. Tonelli, Macromolecules **23,** 3385 (1990).
20. A. J. Lovinger, B. Lotz, and D. D. Davis, Polymer **31,** 2253 (1990).
21. A. J. Lovinger, B. Lotz, D. D. Davis, *et al*., Macromolecules **26,** 3494 (1993).
22. C. De Rosa and P. Corradini, Macromolecules **26,** 5711 (1993).
23. A. M. Liquori, G. Anzuino, V. M. Coiro, *et al*., Nature (London) **206,** 358 (1965).
24. K. Hatada, T. Kitayama, K. Ute, *et al*., Macromol. Symp. **84,** 113 (1994).
25. R. Buter, Y. Y. Tan, and G. Challa, J. Polym. Sci., Part A-1 **10,** 1031 (1972).
26. R. Buter, Y. Y. Tan, and G. Challa, J. Polym. Sci., Polym. Chem. Ed. **11,** 1003, 1013 (1973).
27. R. H. G. Brinkhuis and A. J. Schouten, Langmuir **8,** 2247 (1992).
27a. R. H. G. Brinkhuis and A. J. Schouten, Macromolecules **25,** 2717, 2725, 2732 (1992).
28. K. Hatada, S. Shimizu, Y. Terawaki, *et al*., Polym. J. **13,** 811 (1981).
29. K. Hatada, K. Ute, K. Tanaka, *et al*., Polym. J. **17,** 977 (1985).
30. K. Hatada, K. Ute, K. Tanaka, *et al*., Polym. J. **18,** 1037 (1986).
31. K. Ute, N. Miyatake, T. Asada, *et al*., Polym. Bull. **28,** 561 (1992).
32. T. Kitayama, Y. Zhang, and K. Hatada, Polym. Bull. **32,** 439 (1994).
33. T. Kitayama, Y. Zhang, and K. Hatada, Polym. J. **26,** 868 (1994).
34. Ph. Teyssié, R. Fayt, J. P. Hautekeer, *et al*., Makromol. Chem., Macromol. Symp. **32,** 61 (1990).
35. Ph. Teyssié, R. Fayt, C. Jacobs, *et al*., Polym. Preprints **32**(1), 299 (1991).
36. P. Bayard, R. Jérôme, Ph. Teyssié, *et al*., Polym. Bull. **32,** 381 (1994).
36a. D. Baskaran, Prog. Polym. Sci. **28**, 521 (2003).
37. J. S. Wang, R. Jérôme, and Ph. Teyssié, Macromolecules **27,** 4902 (1994).
38. T. Asanuma, Y. Nishimori, M. Ito, *et al*., Polym. Bull. **25,** 567 (1991).
39. M. K. Georges, R. P. N. Veregin, P. M. Kazmaier, *et al*., TRIP **2,** 66 (1994).
40. M. K. Georges, R. P. N. Veregin, P. M. Kazmaier, *et al*., Macromolecules **26,** 2987 (1993).
41. M. K. Georges, R. P. N. Veregin, P. M. Kazmaier, *et al*., Macromolecules **27,** 7228 (1994).
42. R. P. N. Veregin, M. K. Georges, P. M. Kazmaier, *et al*., Macromolecules **26,** 5316 (1993).
43a. A. Szkurhan and M. K. Georges, Macromolecules **37**, 4776 (2004).
43b. K. Matyjaszewski, Chem. Eur. J. **5**, 3095 (1999).
43c. K. Matyjaszewski and J. Xia, Chem. Rev. **101**, 2921 (2001).
43d. V. Coessens, T. Pintauer, and K. Matyjaszewski, Prog. Polym. Sci. **26**, 337 (2001).
43e. K. Matyjaszewski and J. Spanswick, Materials Today (Elsevier) March 2005, pp. 26
43f. M. Kamigaito, T. Ando, and M. Sawamoto, Chem. Rev. **101**, 3689 (2001).
43g. M. Sawamoto and M. Kamigaito, New Methods Polym. Synth. (Blackie) 37 (1995)
43h. D. Grande, J.-L. Six, S. Breunig, V. Heroguez, M. Fontanille, and Y. Gnanou, Polym. Adv. Technol. **9**, 601 (1998).
44. P. J. Flory, *Principles of Polymer Chemistry* (Cornell University Press, Ithaca, NY, 1953), Chapter VI.
45. O. Vogl and S. Grossman, in: *Encyclopedia of Polymer Science and Engineering* (John Wiley & Sons, New York, 1987), Vol. **7,** pp. 626.
46. E. Földes, G. Deak, F. Tüdös *et al*., Eur. Polym. J. **29,** 321 (1993).
47. O. Vogl, J. Macromol. Sci., Chem. **A21,** 1725 (1984).
48. S. Arichi, M. Y. Pedram, and J. M. G. Cowie, Eur. Polym. J. **15,** 107, 113 (1979).
49. C. Strazielle, H. Benoit, and O. Vogl, Eur. Polym. J. **14,** 331 (1978).
50. P. Hattam, S. Gauntlett, J. W. Mays, *et al*., Macromolecules **24,** 6199 (1991).
51. Y. Okamoto, K. Suzuki, K. Ohta, *et al*., J. Am. Chem. Soc. **101,** 4763 (1979).
52. Y. Okamoto, I. Okamoto, and H. Yuki, J. Polym. Sci., Polym. Lett. Ed. **19,** 451 (1981).
53. L. Cavallo, P. Corradini, and M. Vacatello, Polym. Commun. **30,** 236 (1989).
54. R. D. Miller and J. Michl, Chem. Rev., **89,** 1359 (1989).
55. F. C. Schilling, F. A. Bovey, A. J. Lovinger, *et al*., in *Silicon-Based Polymer Science*, J. M. Zeigler and F. W. Fearon, Eds., Am. Chem. Soc., Adv. Chem. Ser. **224,** pp. 341 (1990).
56. A. R. Wolff, I. Nozue, J. Maxka, *et al*., J. Polym. Sci., Polym. Chem. Ed. **26,** 701 (1988).
57. W.-K. Chan, Y. Chen, Z. Peng, *et al*., J. Am. Chem. Soc. **115,** 11735 (1993).
58. S. R. Marder and J. W. Perry, Science **263,** 1706 (1994).
59. A. V. Tkachev, V. A. Tverskoi, and V. P. Zubov, New Polymeric Mater. **3,** 187 (1992).
60. E. V. Anufrieva, O. V. Tcherkasskaya, M. G. Krakovyak, *et al*., Macromolecules **27,** 2623 (1994).
61. M. A. Winnik, in *Cyclic Polymers*, J. A. Semlyen, Ed. (Elsevier, London, 1986), Chapter 9.
62. M. Adam and K. Müllen, Adv. Mater. **6,** 439 (1994).
63. H. R. Allcock, Chem. Eng. News, March **18,** 22 (1985).
64. M. J. Crossley and P. L. Burn, J. Chem. Soc., Chem. Commun., 1569 (1991).
65. R. W. Wagner and J. S. Lindsey, J. Am. Chem. Soc. **116,** 9759 (1994).
66. E. Hädicke and F. Graser, Acta Crystallogr., Sect. C **42,** 189, 195 (1986).
66a. N. B. McKeown, J. Mater. Chem. **10**, 1979 (2000).
66b. D. T. McQuade, A. E. Pullen, and T. M. Swager, Chem. Rev. **100**, 2537 (2000).
67. G. Knothe, Makromol. Chem., Theory Simul. **2,** 503 (1993).
67a. H. Segawa, N. Nakayama, F. Wu, and T. Shimidzu, Synth. Met. **55**, 966 (1993).
67b. T. Shimidzu, Pure Appl. Chem. **67**, 2039 (1995); J. Jortner, M. Ratner, Eds. *Molecular Electronics*, (1997), pp. 381; *Photonic and Optoelectronic Polymers*, ACS Symposium Series, **672**, 460 (1997).
67c. B. Jiang, S. W. Yang, S. L. Bailey, L. G. Hermans, R. A. Niver, M. A. Bolcar, and W. E. Jones, Jr., Coord. Chem. Rev. **171**, 365 (1998).
67d. W. E. Jones, Jr., L. Hermans, and B. Jiang, Mole. Supramol. Photochem. **4**, 1 (1999).
67e. J. Roncali, Acc. Chem. Res. **33**, 147 (2000).
67f. J. M. Tour, in *Stimulating Concepts in Chemistry,* F. Voegtle, J. F. Stoddart, and M. Shibasaki, Eds. (Wiley-VCH Verlag GmbH & Co. KGaA, Weinheim, Germany, 2000), pp. 237–253.
67g. J. M. Tour, Polym. News **25**, 329 (2000).
67h. A. Natansohn and P. Rochon, Chem. Rev. **102**, 4139 (2002).
67i. Z. Sekkat and W. Knoll, Eds. *Photoreactive Organic Thin Films* (Academic Press, San Diego, CA, 2002)
67j. T. Seki, S. Nagano, Y. Kawashima, and N. Zettsu, Mol. Cryst. Liq. Cryst. **430**, 107 (2005).
67k. G. K. Such, R. A. Evans, and T. P. Davis, Mol. Cryst. Liq. Cryst. **430**, 273 (2005).
68. R. M. Baum, Chem Eng. News **November 22,** 8 (1993).
69. C. J. Hawker, K. L. Wooley, and J. M. J. Fréchet, J. Chem. Soc., Chem. Commun., 925 (1994).
70. A. Hirsch, Adv. Mater. **5,** 859 (1993).
71. S. Petrie, G. Javahery, and D. K. Bohme, J. Am. Chem. Soc. **115,** 1445 (1993).
71a. L. Dai, Polym. Adv. Technol. **10**, 357 (1999).
71b. P. C. Eklund and A. M. Rao, Eds. *Fullerene Polymers and Fullerene Polymer Composites*. Springer Ser. Mater. Sci. (Springer, Berlin, 2000).
71c. J.-F. Nierengarten, Top. Curr. Chem. **228**, 87 (2003); J.-F. Nierengarten, New J. Chem. **28**, 1177 (2004); J.-F. Nierengarten, M. Guttierez-Nava, S. Zhang, P. Masson, L. Oswald, C. Bourgogne, Y. Rio, G. Accorsi, N. Armaroli, and S. Setayesh, Carbon **42**, 1077 (2004).
71d. C. Wang, Z.-X. Guo, S. Fu, W. Wu, and D. Zhu, Prog. Polym. Sci. **29**, 1079 (2004).
71e. S. Iijima, Nature **354**, 56 (1991); S. Iijima and T. Ichihashi, Nature **363**, 603 (1993).
71f. D. S. Bethune, C. H. Klang, M. S. de Vries, G. Gorman, R. Savoy, J. Vazquez, and R. Beyers, Nature **363**, 605 (1993).
71g. A. Hirsch, Angew. Chem. Int. Ed. **41**, 1853 (2002).
71h. A. Carrillo, J. A. Swartz, J. M. Gamba, R. S. Kane, N. Chakrapani, B. Wei, and P. M. Ajayan, Nano Lett. **3**, 1437 (2003).

71i. C. A. Dyke and J. M. Tour, J. Phys. Chem., Part A, **108**, 11151 (2004).
71j. P. M. Ajayan, L. S. Schadler, and P. V. Braun, *Nanocomposite Science and Technology*. (Wiley-VCH Verlag GmbH & Co., Germany, 2003).
71k. L. Dai, Smart Mater. Struct. **11**, 645 (2002).
71l. A. M. Fennimore, T. D. Yuzvinsky, W.-Q. Han, M. S. Fuhrer, J. Cuming, and A. Zettl, Nature **424**, 408 (2003).
71m. A. Star, J.-C. Gabriel, K. Bradley, and G. Grüner, Nano Lett. **3**, 459 (2003).
72. J. A. Semlyen, Adv. Polym. Sci. **21,** 41 (1976).
73. J. A. Semlyen, in: *Cyclic Polymers*, J. A. Semlyen, Ed. (Elsevier, London, 1986), pp 1.
74. J. A. Semlyen, in: *Siloxane Polymers*, S. J. Clarson and J. A. Semlyen, Eds. (PTR Prentice Hall, NJ, 1993), Chapter 3.
74a. J. A. Semlyen, in *Cyclic Polymers*, second edition, J. A. Semlyen, Ed. (Kluwer Academic Publ., Netherlands, 2000), pp. 1.
74b. C. W. Bielawski, D. Benitez, and R. H. Grubbs, Science **297,** 2041 (2002).
74c. N. Hadjichristidis, M. Pitsikalis, S. Pispas, and H. Iatrou, Chem. Rev. **101,** 3747 (2001).
75. H. Jacobson and W. H. Stockmayer, J. Chem. Phys. **18,** 1600 (1950).
75a. H. Jacobson, C. O. Beckman, and W. H. Stockmayer, J. Chem. Phys. **18,** 1607 (1950).
76. P. J. Flory and J. A. Semlyen, J. Am. Chem. Soc. **88,** 3209 (1966).
77. J. A. Semlyen, Trans. Faraday Soc. **63,** 2342 (1967).
78. P. J. Flory, *Statistical Mechanics of Chain Molecules* (John Wiley, New York, 1969; republished by Hanser Publishers, 1988), Appendix D.
79. M. A. Winnik, R. E. Trueman, G. Jackowski, *et al*., J. Am. Chem. Soc. **96,** 4843 (1974).
80. P. J. Flory, U. W. Suter, and M. Mutter, J. Am. Chem. Soc. **98,** 5733 (1976).
81. M. S. Beevers and J. A. Semlyen, Polymer **13,** 523 (1972).
82. J. F. Brown and G. M. J. Slusarczuk, J. Am. Chem. Soc. **87,** 931 (1965).
83. J. A. Semlyen and P. V. Wright, Polymer **10,** 543 (1969).
84. P. V. Wright, J. Polym. Sci., Polym. Phys. Ed. **11,** 51 (1973).
85. L. E. Scales and J. A. Semlyen, Polymer **17,** 601 (1976).
86. U. W. Suter, M. Mutter, and P. J. Flory, J. Am. Chem. Soc. **98,** 5740 (1976).
87. D. R. Cooper and J. A. Semlyen, Polymer **13,** 414 (1972).
88. J. M. Andrews, F. R. Jones, and J. A. Semlyen, Polymer **15,** 420 (1974).
89. U. W. Suter and M. Mutter, Makromol. Chem. **180,** 1761 (1979).
90. J. A. Semlyen, Polymer **12,** 383 and ref. therein (1971).
91. M. Morton and E. E. Bostick, J. Polym. Sci., Part A **2,** 523 (1964).
92. M. Morton, A. A. Rembaum, and E. E. Bostick, J. Appl. Polym. Sci. **8,** 2707 (1964).
93. J. C. Saam, D. J. Gordon, and S. Lindsey, Macromolecules **3,** 1 (1970).
94. D. J. Brunelle, E. P. Boden, and T. G. Shannon, J. Am. Chem. Soc. **112,** 2399 (1990).
95. D. J. Brunelle, T. L. Evans, T. L. Shannon, *et al*., Polym. Preprints **30,** (2), 569 (1989).
96. T. L. Evans, C. B. Berman, J. C. Carpenter, *et al*., Polym. Preprints **30**(2), 573 (1989).
97. D. J. Brunelle and E. P. Boden, Makromol. Chem., Macromol. Symp. **54/55,** 397 (1992).
98. T. L. Guggenheim, S. J. McCormick, J. J. Kelly, *et al*., Polym. Preprints **30**(2), 579 (1989).
99. J. A. Cella, J. J. Talley, and J. M. Fukuyama, Polym. Preprints **30**(2), 581 (1989).
100. L. Garrido, J. E. Mark, S. J. Clarson, *et al*., Polym. Commun. **25,** 218 (1984).
101. L. Garrido, J. E. Mark, S. J. Clarson, *et al*., Polym. Commun. **26,** 53 (1985).
102. S. J. Clarson, J. E. Mark, and J. A. Semlyen, Polym. Commun. **27,** 244 (1986).
103. S. J. Clarson, J. E. Mark, and J. A. Semlyen, Polym. Commun. **28,** 151 (1987).
104. T. J. Fyvie, H. L. Frich, J. A. Semlyen, *et al*., J. Polym. Sci., Polym. Chem. Ed. **25,** 2503 (1987).
105. W. Huang, H. L. Frisch, Y. Hua, *et al*., J. Polym. Sci., Polym. Chem. Ed. **28,** 1807 (1990).
106. B. R. Wood, S. J. Joyce, G. Scrivens, *et al*., Polymer **34,** 3052, 3059 (1993).
107. V. Percec and M. Kawasumi, Adv. Mater. **4,** 572 (1992).
108. V. Percec and M. Kawasumi, Macromolecules **25,** 3843 (1992).
109. V. Percec and M. Kawasumi, Macromolecules **26,** 3663, 3917 (1993).
110. V. Percec, M. Kawasumi, P. L. Rinaldi, *et al*., Macromolecules **25,** 3851 (1992).
111. B. A. Newman and H. F. Kay, J. Appl. Phys. **38,** 4105 (1967).
112. W. Heitz, H. Höcker, W. Kern, *et al*., Makromol. Chem. **150,** 73 (1971).
113. T. Trzebiatowski, M. Drager, and G. R. Strobl, Makromol. Chem. **183,** 731 (1982).
114. K. S. Lee and G. Wegner, Makromol. Chem., Rapid Commun. **6,** 203 (1985).
115. H. W. Gibson and H. Marand, Adv. Mater. **5,** 11 (1993).
115a. J. W. Lee and K. Kim, Top. Curr. Chem. **228,** 111 (2003).
116. S. Yu. Lipatov, T. E. Lipatova, *et al*., Adv. Polym. Sci. **88,** 49 (1989).
117. H. W. Gibson, C. Wu, Y. X. Shen, *et al*., Polym. Preprints **32**(3), 593 (1991).
118. H. W. Gibson, C. Wu, Y. X. Shen, *et al*., Polym. Preprints **32**(3), 637 (1991b).
119. H. Marand, A. Prasad, C. Wu, *et al*., Polym. Preprints **32**(3), 639 (1991).
120. P. L. Anelli, P. R. Ashton, R. Ballardini, *et al*., J. Am. Chem. Soc. **114,** 193 (1992).
121. S. J. Joyce, R. E. Hubbard, and J. A. Semlyen, Eur. Polym. J. **29,** 305 (1993).
122. G. Wenz, Angew. Chem. Int. Ed. Engl. **33,** 803 (1994).
122a. R. A. Bissell, E. Cordova, A. E. Kaifer, and J. F. Stoddart, Nature, London **369,** 133 (1994).
122b. M.-J. Blanco, J. M. Consuelo, J.-C. Chambron, V. Heitz, M. Linke, and J.-P. Sauvage, Chem. Soc. Rev. **28,** 293 (1999).
122c. M. Gomez-Lopez and J. F. Stoddart, in *Handbook of Nanostructured Materials and Nanotechnology*, H. S. Nalwa, Ed. (Academic Press, San Diego, CA, 2000), Vol. 5, pp. 225.
122d. J.-P. Collin, J.-M. Kern, L. Raehm, and J.-P. Sauvage, in *Molecular Switches*, B. L. Feringa, Ed. (Wiley-VCH, Germany, 2001), pp. 249.
122e. F. M. Raymo and J. F. Stoddart, in *Molecular Switches*, B. L. Feringa, Ed. (Wiley-VCH, Germany, 2001), pp. 219.
123. D. A. Tomalia, A. M. Naylor, and W. A. Goddard III, Angew. Chem. Int. Ed. Engl. **29,** 138 (1990).
124. P. G. de Gennes and H. J. Hervet, J. Phys. Lett. **44,** 351 (1983).
125. H. B. Mekelburger, W. Jaworek, and F. Vögtle, Angew, Chem., Int. Ed. Engl. **31,** 1571 (1992).
126. Y. H. Kim, Adv. Mater. **4,** 764 (1992).
127. D. A. Tomalia, Adv. Mater. **6,** 529 (1994).
127a. D. A. Tomalia and I. Majoros, in *Supramolecular Polymers*, A. Ciferri, Ed. (Marcel Dekker, Inc., NY, 2000), pp. 359.
127b. D. A. Tomalia, Aldrichim. Acta **37,** 39 (2004).
127c. D. A. Tomalia, Materials Today (Elsevier), March 2005, pp. 34.
128. J. M. J. Fréchet, *Science*, **263,** 1710 (1994).
128a. S. M. Grayson and J. M. J. Fréchet, Chem. Rev. **101,** 3819 (2001).
128b. D. C. Tully and J. M. J. Fréchet, Chem. Commun. 1229 (2001).
129. G. R. Newkome, G. R. Baker, M. J. Saunders, *et al*., J. Chem. Soc., Chem. Commun., 752 (1986).
130. G. R. Newkome, Z-q. Yao, G. R. Baker, *et al*., J. Am. Chem. Soc. **108,** 849 (1986).
131. C. J. Hawker and J. M. J. Fréchet, J. Chem. Soc., Chem. Commun., 1010 (1990).
132. C. J. Hawker and J. M. J. Fréchet, J. Am. Chem. Soc. **112,** 7638 (1990).
133. T. M. Miller and T. X. Neenan, Chem. Mater. **2,** 346 (1990).
134. K. L. Wooley, C. J. Hawker, and J. M. J. Fréchet, J. Am. Chem. Soc. **113,** 4252 (1991).
135. I. Gitsov, P. T. Ivanova, and J. M. J. Fréchet, Macromol. Rapid Commun. **15,** 387 (1994).
136. Y. H. Kim, J. Am. Chem. Soc. **114,** 4947 (1992).
137. V. Percec, P. Chu, and M. Kawasumi, Macromolecules **27,** 4441 (1994).
138. K. L. Wooley, C. J. Hawker, J. M. Pochan, *et al*., Macromolecules **26,** 1514 (1993).

139. T. Kitayama, T. Shinozaki, T. Sakamoto, *et al*., Makromol. Chem., Supplement **15,** 167 (1989).
140. T. Uryu, H. Ohkawa, and R. Oshima, Macromolecules **20,** 712 (1987).
141. J. W. Mays, E. Siakali-Kioulafa, and N. Hadjichristidis, Macromolecules **23,** 3530 (1990).
142. T. Kitayama, K. Ute, M. Yamamoto, *et al*., Polym. J. **22,** 386 (1990).
143. J. M. O'Reilly, D. M. Teegarden, and R. A. Mosher, Macromolecules **14,** 602, 1693 (1981).
144. T. Kitayama, K. Ute, and K. Hatada, Brit. Polym. J. **23,** 5 (1990).
145. B. Sedláček, J. Spěváček, L. Mrkvičková, *et al*., Macromolecules **17,** 825 (1984).
146. J. Spěváček, B. Schneider, J. Dybal, *et al*., J. Polym. Sci., Polym. Phys. Ed. **22,** 617 (1984).
147. T. Kitayama, T. Shinozaki, E. Masuda, *et al*., Polym. Bull. **20,** 505 (1988).
148. A. Zambelli, P. Ammendola, and A. Proto, Macromolecules **22,** 2126 (1989).
149. C. De Rosa, V. Venditto, G. Guerra, *et al*., Macromolecules **25,** 6938 (1992).
150. M. Galimberti, G. Balbontin, I. Camurati, *et al*., Macromol. Rapid Commun. **15,** 633 (1994).
151. J. A. Ewen, R. L. Jones, A. Razavi, *et al*., J. Am. Chem. Soc. **110,** 6255 (1988).
152. Y. Chatani, H. Maruyama, K. Noguchi, *et al*., J. Polym. Sci., Polym. Lett. Ed. **28,** 393 (1990).
153. G. Balbontin, D. Dainelli, M. Galimberti, *et al*., Makromol. Chem. **193,** 693 (1992).
154. R. Paukkeri and A. Lehtinen, Polymer **34,** 4075 (1993).
155. N. Ishihara, M. Kuramoto, and M. Uoi, Macromolecules **21,** 3356 (1988).
156. M. Kobayashi, T. Nakaoki, and N. Ishihara, Macromolecules **22,** 4377 (1989).
157. M. Kobayashi, T. Nakaoki, and N. Ishihara, Macromolecules **23,** 78 (1990).
158. S. Nozakura, S. Ishihara, Y. Inaba, *et al*., J. Polym. Sci., Polym. Chem. Ed. **11,** 1053 (1973).
159. G. O. R. Alberda van Ekenstein, Y. Y. Tan, and G. Challa, Polymer **26,** 283 (1985).
160. M. Kamachi, X. S. Cheng, T. Kida, *et al*., Macromolecules **20,** 2665 (1987).
161. E. Scamporrino and D. Vitalini, Macromolecules **25,** 1625 (1992).
161a. D. Vitalini and E. Scamporrino, Macromolecules **25,** 6605 (1992).
162. D. Hammel, P. Erk, B. Schuler, *et al*., Adv. Mater. **4,** 737 (1992).
163. Z. Bao, Y. Chen, and L. Yu, Macromolecules **27,** 4629 (1994).
164. H. Kamogawa, S. Miyama, and S. Minoura, Macromolecules **22,** 2123 (1989).
165. P. M. Kuznesof, R. S. Nohr, K. J. Wynne, *et al*., J. Macromol. Sci., Chem. **A16,** 299 (1981).
166. C. W. Dirk, E. A. Mintz, K. F. Schoch, Jr., *et al*., J. Macromol. Sci., Chem. **A16,** 275 (1981).
167. C. W. Dirk, T. Inabe, K. F. Schoch, Jr., *et al*., J. Am. Chem. Soc. **105,** 1539 (1983).
168. B. N. Achar, G. M. Fohlen, J. A. Parker, and J. Keshavayya, J. Polym. Sci., Polym. Chem. Ed. **25,** 443 (1987).
169. J. R. Fryer and M. E. Kenney, *Macromolecules*, **21,** 259 (1988).
170. W. Caseri, T. Sauer, and G. Wegner, Makromol. Chem., Rapid Commun. **9,** 651 (1988).
171. J. F. van der Pol, E. Neeleman, R. J. Nolte *et al*., Makromol. Chem. **190,** 2727 (1989).
172. T. Sauer, W. Caseri, and G. Wegner, Mol. Cryst. Liq. Cryst. **183,** 387 (1990).
173. T. Sauer, T. Arndt, D. N. Batchelder *et al*., Thin Solid Films **187,** 357 (1990).
174. T. Sauer and G. Wegner, Macromolecules **24,** 2240 (1991).
175. H. Z. Chen, M. Wang, L. X. Feng, *et al*., J. Appl. Polym. Sci. **46,** 1033 (1992).
176. H. Z. Chen, M. Wang, L. X. Feng, and S. L. Yang, J. Appl. Polym. Sci. **49,** 679 (1993).
177. C. F. van Nostrum, R. J. M. Nolte, M. A. C. Devillers, *et al*., Macromolecules **26,** 3306 (1993).
178. D. Dotcheva, M. Klapper, and K. Müllen, Makromol. Chem. Phys. **195,** 1905 (1994).
179. D. R. Robello, J. Polym. Sci., Polym. Chem. Ed. **28,** 1 (1990).
180. H. Hashimoto, T. Kakuchi, O. Haba, *et al*., Macromolecules **25,** 1828 (1992).
181. G. A. Olah, I. Bucsi, C. Lambert, *et al*., J. Am. Chem. Soc. **113,** 9387 (1991).
181a. Z. Sun and R. L. Miller, Polymer **34,** 1963 (1993).
182. D. A. Loy and R. A. Assink, J. Am. Chem. Soc. **114,** 3978 (1992).
183. S. Shi, K. C. Khemani, Q. C. Li, *et al*., J. Am. Chem. Soc. **114,** 10656 (1992).
184. K. E. Geckeler and A. Hirsch, J. Am. Chem. Soc. **115,** 3850 (1993).
185. A. O. Patil, G. W. Schriver, B. Carstensen, *et al*., Polym. Bull. **30,** 187 (1993).
186. A. M. Rao, P. Zhou, K-A. Wang, *et al*., Science **259,** 955 (1993).
187. C. J. Hawker, Macromolecules **27,** 4836 (1994).
188. P. W. Stephens, G. Bortel, G. Faigel, *et al*., Nature (London) **370,** 636 (1994).
189. M. S. Beevers and J. A. Semlyen, Polymer **12,** 373 (1971).
190. K. Dodgson and J. A. Semlyen, Polymer **18,** 1265 (1977).
191. K. Dodgson, D. Sympson, and J. A. Semlyen, Polymer **19,** 1285 (1978).
192. J. S. Higgins, K. Dodgson, and J. A. Semlyen, Polymer **20,** 553 (1979).
193. F. R. Jones, Eur. Polym. J. **10,** 249 (1974).
194. P. V. Wright and J. A. Semlyen, Polymer **11,** 462 (1970).
195. W. A. Piccoli, G. G. Haberland, and R. L. Merker, J. Am. Chem. Soc. **82,** 1883 (1960).
196. E. D. Brown and J. B. Carmichael, J. Polym. Sci., Polym. Lett. Ed. **3,** 473 (1965).
197. T. R. Formoy and J. A. Semlyen, Polym. Commun. **30,** 86 (1989).
198. H. Höcker and K. Riebel. Makromol. Chem. **178,** 3101 (1977).
199. G. E. Hahn, P. Kusch, V. Rossbach, *et al*., Makromol. Chem. **186,** 297 (1985).
200. J. J. Kulig, W. J. Brittain, S. Gilmour, *et al*., Macromolecules **27,** 4838 (1994).
201. A. Horbach, H. Vernaleken, and K. Weirauch, Makromol. Chem. **181,** 111 (1980).
202. E. P. Boden, D. J. Brunelle, and T. G. Shannon, Polym. Preprints **30**(2), 571 (1989).
203. D. J. Brunelle and M. F. Garbauskas, Macromolecules **26,** 2724 (1993).
204. F. R. Jones, L. E. Scales, and J. A. Semlyen, Polymer **15,** 738 (1974).
205. J. M. Andrews and J. A. Semlyen, Polymer **13,** 142 (1972).
206. K. Hayashi, Macromolecules **3,** 5 (1970).
207. D. R. Cooper and J. A. Semlyen, Polymer **14,** 185 (1973).
208. E. Meraskentis and H. Zahn, J. Polym. Sci. **4,** 1890 (1966).
209. F. L. Hamb and L. C. Trent, J. Polym. Sci., Polym. Lett. Ed. **5,** 1057 (1967).
210. L. Reif and H. Höcker, Makromol. Chem., Rapid Commun. **2,** 183 (1981).
211. J. A. Semlyen and G. R. Walker, Polymer **10,** 597 (1969).
212. H. Höcker and R. Musch, Makromol. Chem. **175,** 1395 (1974).
212a. L. Reif and H. Höcker, Macromolecules **17,** 952 (1984).
213. Y. Yamashita, J. Mayumi, Y. Kawakami *et al*., Macromolecules **13,** 1075 (1980).
214. A. Sato, T. Hirano, M. Suga, *et al*., Polym. J. **9,** 209 (1977).
215. C. Rentsch and R. C. Schulz, Makromol. Chem. **178,** 2535 (1977).
216. J. Maxka, F. K. Mitter, D. R. Powell, *et al*., Organometallics **10,** 660 (1991).
217. G. P. Lorenzi, L. Tomasic, and U. W. Suter, Macromolecules **26,** 1183 (1993).
218. J. F. McCullough, J. R. van Wazer, and E. J. Griffith, J. Am. Chem. Soc. **78,** 4528 (1956).
219. G. Hild, A. Kohler, and P. Rempp, Eur. Polym. J. **16,** 525 (1980).
220. J. Roovers and P. M. Toporowski, Macromolecules **16,** 843 (1983).
221. M. Duval, P. Lutz, and C. Strazielle, Makromol. Chem., Rapid. Commun. **6,** 71 (1985).
222. M. Ragnetti, D. Geiser, H. Höcker, *et al*., Makromol. Chem. **186,** 1701 (1985).
223. G. Hadziioannou, P. M. Cotts, G. ten Brinke, *et al*., Macromolecules **20,** 493 (1987).
224. G. B. McKenna, G. Hadziioannou, P. Lutz, *et al*., Macromolecules **20,** 498 (1987).
225. G. B. McKenna, B. J. Hostetter, N. Hadjichristidis, *et al*., Macromolecules **22,** 1834 (1989).
226. J. M. McKenna, T. K. Wu, and G. Pruckmayr, Macromolecules **10,** 877 (1977).

227. N. Ogata, K. Sanui, and J. Wada, J. Polym. Sci., Polym. Letters Ed. **14,** 459 (1976).
228. A. Harada and M. Kamachi, Macromolecules **23,** 2821 (1990).
229. A. Harada, J. Li, and M. Kamachi, Nature (London) **356,** 325 (1992).
230. A. Harada, J. Li, and M. Kamachi, Macromolecules **26,** 5698 (1993).
231. G. Wenz and B. Keller, Angew. Chem. Int. Ed. Engl. **31,** 197 (1992).
232. A. Harada, J. Li, S. Suzuki, *et al*., Macromolecules **26,** 5267 (1993).
233. A. Harada and M. Kamachi, J. Chem. Soc., Chem. Commun., 1322 (1990).
234. M. Maciejewski, J. Macromol. Sci., Chem. **A13,** 77, 1175 (1979).
235. M. Maciejewski, A. Gwizdowski, P. Peczak, *et al*., J. Macromol. Sci., Chem. **A13,** 87 (1979).
236. J. Y. Sze and H. W. Gibson, Polym. Preprints **33**(2), 331 (1992).
237. C. Wu, M. C. Bheda, C. Lim *et al*., Polym. Commun. **32,** 204 (1991).
238. H. W. Gibson, P. Engen, and P. LeCavalier, *Polym. Preprints*, **29**(1), 248 (1988); H. W. Gibson, M. C. Bheda, and P. T. Engen, "Rotaxanes, catenanes, polyrotaxanes, polycatenanes, and related materials," Prog. in Polym. Sci. **19,** 843 (1994).
239. P. T. Engen, P. R. LeCavalier, and H. W. Gibson, Polym. Preprints **31**(2), 703 (1990).
240. Y. X. Shen, C. Lim, and H. W. Gibson, Polym. Preprints **32**(1), 166 (1991).
241. Y. X. Shen and H. W. Gibson, Macromolecules **25,** 2058 (1992).
242. G. R. Newkome, J. K. Young, G. R. Baker, *et al*., Macromolecules **26,** 2394 (1993).
243. K. Rengan and R. Engel, J. Chem. Soc., Chem. Commun., 757 (1992).
244. S. C. E. Backson, P. M. Bayliff, W. J. Feast, *et al*., Polym. Preprints **34** (1), 50 (1993).
245. T. M. Miller, E. W. Kwock, and T. X. Neenan, Macromolecules **25,** 3143 (1992).
246. L-L. Zhou and J. Roovers, Macromolecules **26,** 963 (1993).
247. A. Cherestes and R. Engel, Polymer **35,** 3343 (1994).
248. T. Nagasaki, M. Ukon, S. Arimori, *et al*., J. Chem. Soc., Chem. Commun., 608 (1992).
249. I. Gitsov, K. L. Wooley, and J. M. J. Fréchet, *Angew. Chem. Int. Ed. Engl*., **31,** 1200 (1992).
250. I. Gitsov and J. M. J. Fréchet, Macromolecules **26,** 6536 (1993).
250a. I. Gitsov, K. L. Wooley, C. J. Hawker, *et al*., Macromolecules **26,** 5621 (1993).
251. K. Rengan and R. Engel, J. Chem. Soc., Chem. Commun., 1084 (1990).
252. K. Rengan and R. Engel, J. Chem. Soc., Perkin Trans. **I,** 987 (1991).
253. T. M. Miller, T. X. Neenan, R. Zayas, *et al*., J. Am. Chem. Soc. **114,** 1018 (1992).
254. J. S. Moore and Z. Xu, Macromolecules **24,** 5893 (1991).
255. Z. Xu and J. S. Moore, Angew. Chem. Int. Ed. Engl. **32,** 246 (1993).
256. E. M. M. de Brabander-van den Berg and E. W. Meijer, Angew. Chem. Int. Ed. Engl. **32,** 1308 (1993).
257. J-J. Lee, W. T. Ford, J. A. Moore, *et al*., Macromolecules **27,** 4632 (1994).
258. C. Wörner and R. Mülhaupt, Angew. Chem. Int. Ed. Engl. **32,** 1306 (1993).
259. J. K. Young, G. R. Baker, G. R. Newkome, *et al*., Macromolecules **27,** 3464 (1994).
260. D. A. Tomalia, H. Baker, J. Dewald, *et al*., Polym. J. **17,** 117 (1985).
261. D. A. Tomalia, H. Baker, J. Dewald, *et al*., Macromolecules **19,** 2466 (1986).
262. D. A. Tomalia, V. Berry, M. Hall, *et al*., Macromolecules **20,** 1164 (1987a).
263. D. A. Tomalia, M. Hall, and D. M. Hedstrand, J. Am. Chem. Soc. **109,** 1601 (1987b).
264. L. R. Wilson and D. A. Tomalia, Polym. Preprints **30**(1), 115 (1989).
265. H. K. Hall and D. W. Polis, Polym. Bull. **17,** 409 (1987).
266. C. J. Hawker, R. Lee, and J. M. G. Fréchet, J. Am. Chem. Soc. **113,** 4583 (1991).
267. S. R. Turner, F. Walter, B. I. Voit, *et al*., Macromolecules **27,** 1611 (1994).
268. T. H. Mourey, S. R. Turner, M. Rubinstein, *et al*., Macromolecules **25,** 2401 (1992).
269. C. J. Hawker and J. M. J. Fréchet, J. Am. Chem. Soc. **114,** 8405 (1992b).
270. C. J. Hawker and J. M. J. Fréchet, Polymer **33,** 1507 (1992a).
271. Y. H. Kim and O. W. Webster, J. Am. Chem. Soc. **112,** 4592 (1990).
272. A. W. van der Made and P. W. N. M. van Leeuwen, J. Chem. Soc., Chem Commun., 1400 (1992).
273. A. W. van der Made, P. W. N. M. van Leeuwen, J. C. de Wilde, *et al*., Adv. Mater. **5,** 466 (1993).
274. H. Uchida, Y. Kabe, K. Yoshino *et al*., J. Am. Chem. Soc. **112,** 7077 (1990).
275. L. J. Mathias and T. W. Carothers, J. Am. Chem. Soc. **113,** 4043 (1991).
276. A. Morikawa, M. Kakimoto, and Y. Imai, Macromolecules **24,** 3469 (1991).
277. A. Morikawa, M. Kakimoto, and Y. Imai, Macromolecules **25,** 3247 (1992).
278. J.-M. Lehn, *Supramolecular Chemistry: Concepts and Perspectives* (VCH Publishers, 1995).
279. S. I. Stupp, S. Son, L. S. Li, H. C. Lin, and M. Keser, J. Am. Chem. Soc. **117,** 5212 (1995); Science **276,** 384 (1997).
280. A. Ciferri, Ed. *Supramolecular Polymers*. (Marcel Dekker, NY, 2000).
281. O. Ikkala and G. ten Brinke, Science **295,** 2407 (2002).
282. Y. Guan, S.-H. Yu, M. Antonietti, C. Böttcher, and C. F. J. Faul, Chem. Eur. J. **11,** 1305 (2005).
283. K. V. Gothelf and R. S. Brown, Chem. Eur. J. **11,** 1062 (2005).
284. G. B. W. L. Ligthart, H. Ohkawa, R. P. Sijbesma, and E. W. Meijer, J. Am. Chem. Soc. **127,** 810 (2005).
285. S. Hecht, Materials Today (Elsevier) March 2005, pp. 48.
286. A. D. Q. Li, W. Wang, and L.-Q. Wang, Chem Eur. J. **9,** 4594 (2003).
287. S. H. Gellman, Acc. Chem. Res. **31,** 173 (1998).
288. P. D. Yarborough and D. Y. Sogah, Polym. Mater. Sci. Eng. **76,** 395 (1997); **77,** 601 (1997).
289. C. Kübel, M. J. Mio, J. S. Moore, and D. C. Martin, J. Am. Chem. Soc. **124,** 8605 (2002).

CHAPTER 2

Names, Acronyms, Classes, and Structures of Some Important Polymers

Chandima Kumudinie Jayasuriya* and Jagath K. Premachandra†

**Department of Chemistry, University of Kelaniya, Dalugama, Kelaniya, Sri Lanka*; *†Department of Chemical and Process Engineering, University of Moratuwa, Katubedda, Moratuwa, Sri Lanka*

Common name	Acronym, alternate name	Class	Structure of repeat unit
Amylose		Polysaccharide	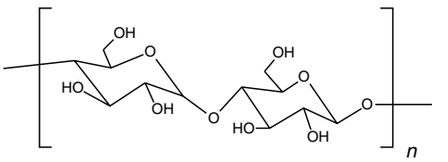
Bisphenol A polysulfone		Polysulfone	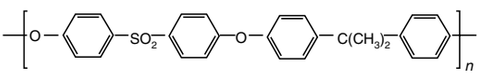
Cellulose	Rayon, cellophane, regenerated cellulose	Polysaccharide	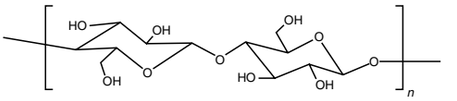
Cellulose acetate	CA	Cellulose ester	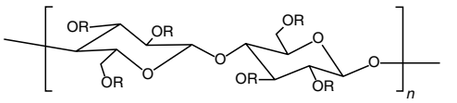 R = –$COCH_3$
Cellulose nitrate	CN	Cellulose ester	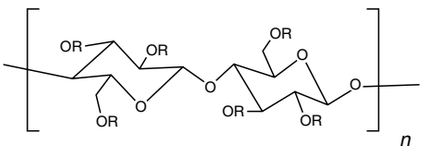 R = –NO_2

Continued.

Common name	Acronym, alternate name	Class	Structure of repeat unit
Hydroxypropyl cellulose	HPC	Cellulose ester	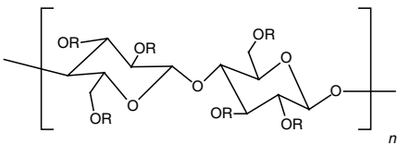 R = –$(CH_2)_3$–OH
Ladder polymer	Double-strand polymer		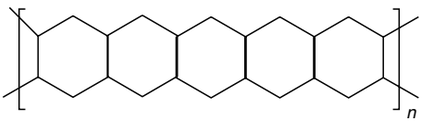
Polyacetal		Polyether	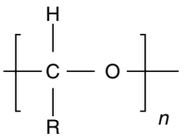
Polyacetaldehyde		Polyether	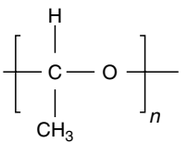
Polyacetylene		Polyalkyne	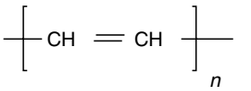
Polyacrylamide		Vinyl polymer, acrylic polymer	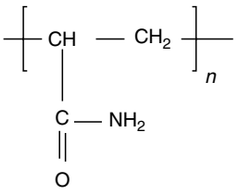
Poly(acrylic acid)		Vinyl polymer, acrylic polymer	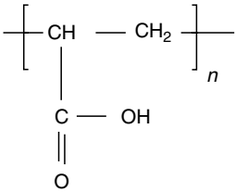

Continued.

Common name	Acronym, alternate name	Class	Structure of repeat unit
Polyacrylonitrile	PAN	Vinyl polymer, acrylic polymer	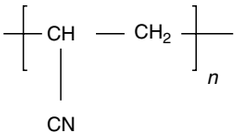
Poly(L-alanine)		Polypeptide	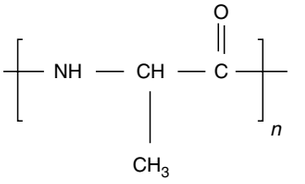
Polyamide	Nylon	Polyamide	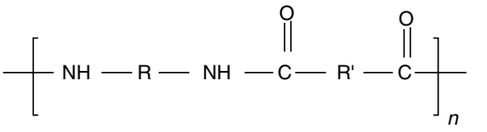
Polyamide imide	PAI		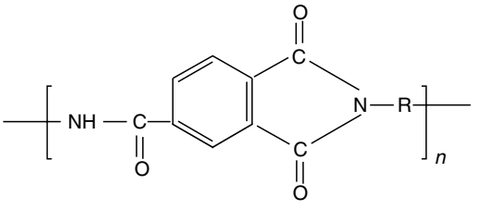
Polyaniline		Polyamine	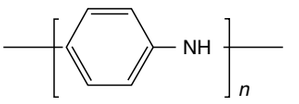
Polybenzimidazole	PBI	Polyheteroaromatic	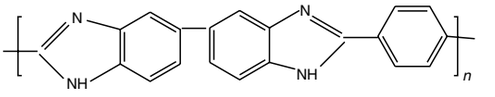
Polybenzobisoxazole	PBO	Polyheteroaromatic	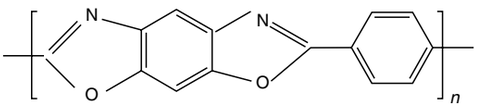
Polybenzobisthiazole	PBT	Polyheteroaromatic	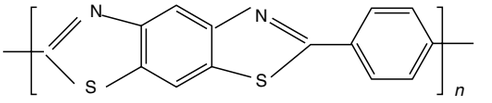

Continued.

Common name	Acronym, alternate name	Class	Structure of repeat unit
Poly(γ-benzyl-L-glutamate)	PBLG	Polypeptide	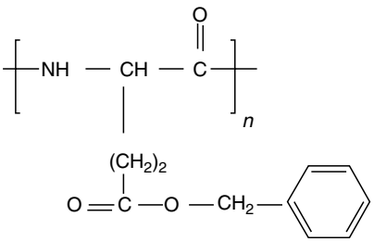
1,2-Polybutadiene	PBD	Diene polymer	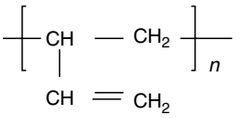
cis-1,4-Polybutadiene	PBD	Diene polymer	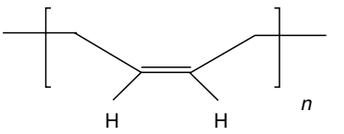
trans-1,4-Polybutadiene	PBD	Diene polymer	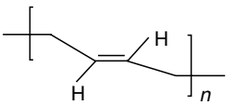
Poly(1-butene)	PB-1	Polyolefin	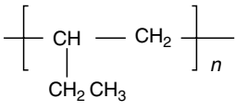
Polybutylene terephthalate	PBT	Polyester	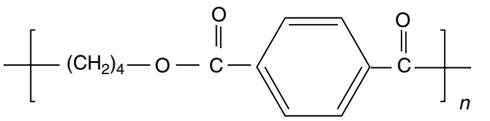
Poly(ε-caprolactam)	Nylon 6	Polyamide	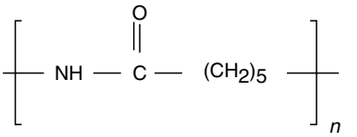
Poly(ε-caprolactone)		Polyester	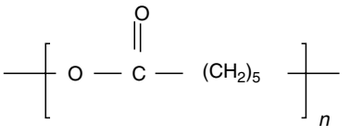

Continued.

Common name	Acronym, alternate name	Class	Structure of repeat unit
Polycarbonate	PC	Polyester	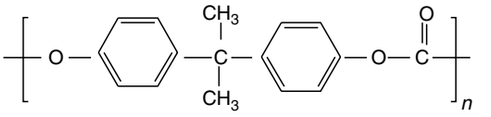
cis-1,4-Polychloroprene	Neoprene	Diene polymer	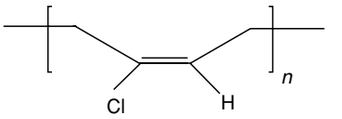
trans-1,4-Polychloroprene	Neoprene	Diene polymer	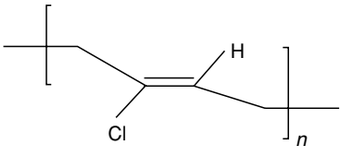
Polychlorotrifluoroethylene	PCTFE	Vinyl polymer, Fluoro polymer	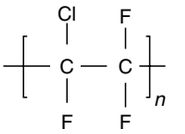
Poly(10-decanoate)		Polyester	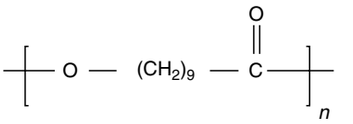
Poly(diethyl siloxane)	PDES	Polysiloxane	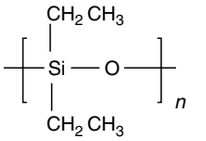
Poly(dimethyl siloxane)	PDMS	Polysiloxane	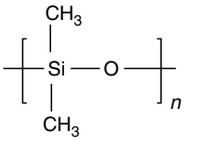

Continued.

Common name	Acronym, alternate name	Class	Structure of repeat unit
Poly(diphenyl siloxane)	PDPS	Polysiloxane	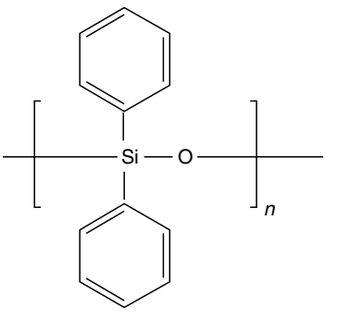
Polyester			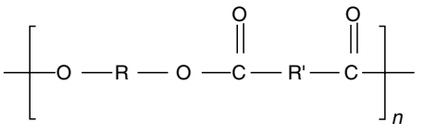
Polyether ketone	PEK	Polyketone	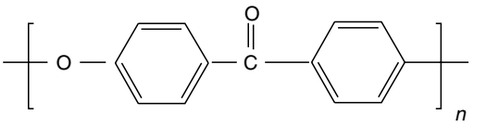
Polyether etherketone	PEEK	Polyketone	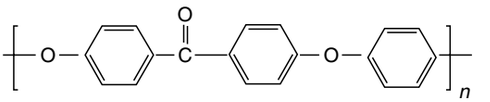
Polyether sulfone	PES		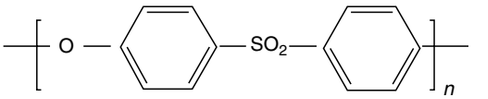
Polyethylene	PE	Polyolefin	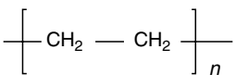
Poly(ethylene imine)		Polyamine	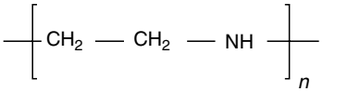
Poly(ethylene oxide) [Poly(ethylene glycol)]	PEO [PEG]	Polyether	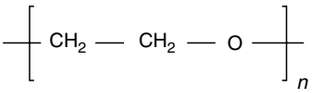

Continued.

Common name	Acronym, alternate name	Class	Structure of repeat unit
Poly(ethylene terephthalate)	PET	Polyester	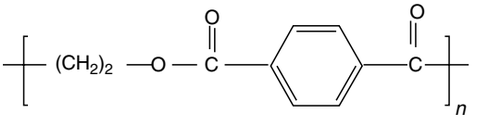
Polyglycine		Polypeptide	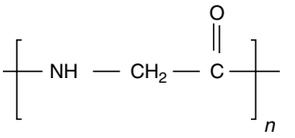
Poly(hexamethylene adipamide)	Nylon 6,6	Polyamide	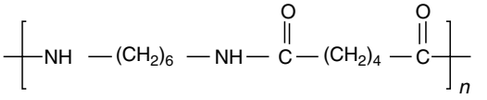
Poly(hexamethylene sebacamide)	Nylon 6,10	Polyamide	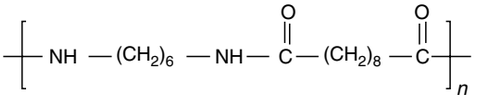
Polyhydroxybutyrate	PHB	Polyester	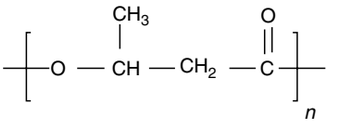
Polyimide	PI	Polyimide	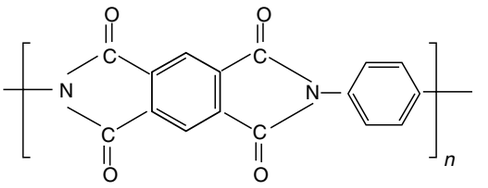
Polyisobutylene	Butyl rubber	Vinylidine polymer	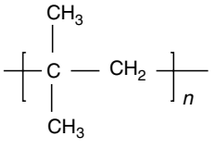
Polyisocyanate	PIC	Polyamide	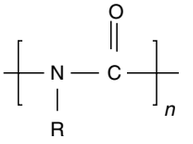

Continued.

Common name	Acronym, alternate name	Class	Structure of repeat unit
Polyisocyanide		Polyisocyanide	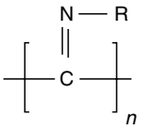
cis-1,4-Polyisoprene	*cis*-PIP, natural rubber	Diene polymer	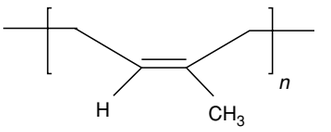
trans-1,4-Polyisoprene	*trans*-PIP Gutta percha	Diene polymer	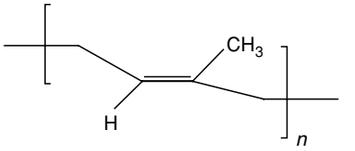
Polylactam		Polyamide	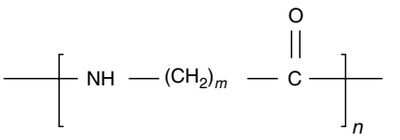
Polylactone		Polyester	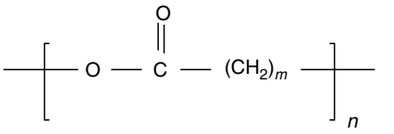
Poly(methacrylic acid)		Vinyl polymer, acrylic polymer	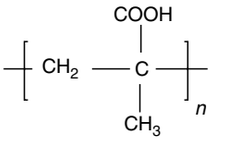
Poly(methyl acrylate)	PMA	Vinyl polymer, acrylic polymer	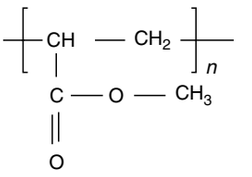

Continued.

Common name	Acronym, alternate name	Class	Structure of repeat unit
Poly(methyl methacrylate)	PMMA	Vinylidene polymer, acrylic polymer	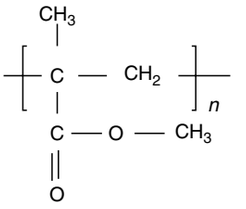
Poly(4-methyl pentene)		Polyolefin	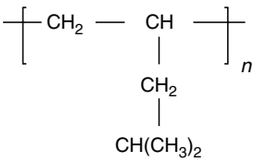
Poly(α-methyl stryrene)		Vinylidene polymer	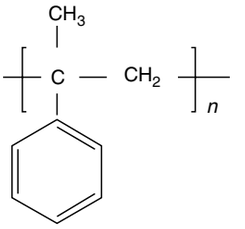
Poly(methylene oxide)	PMO Polyformaldehyde	Polyether	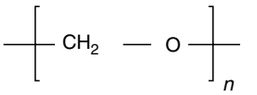
Poly(methyl phenyl siloxane)	PMPS	Polysiloxane	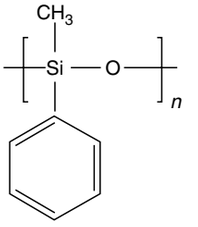
Poly(*m*-phenylene terephthalamide)	Nomex	Polyaramid	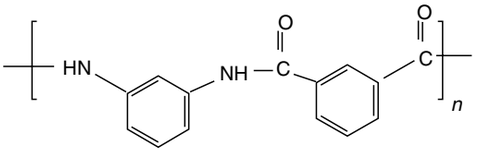

Continued.

Common name	Acronym, alternate name	Class	Structure of repeat unit
Poly(*p*-phenylene terephthalamide)	Kevlar	Polyaramid	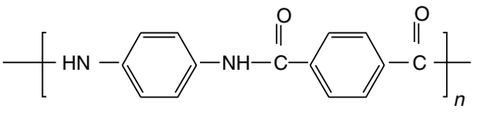
Polynitrile		Polyimine	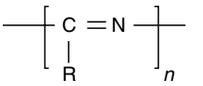
Polynucleotide		Polynucleotide	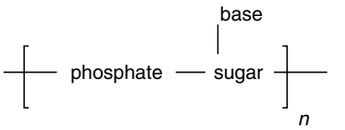
Poly(*n*-pentene-2)		Poly(α-olefin)	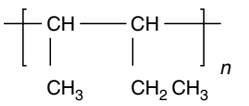
Poly(*n*-pentene-1)	Poly (1-pentene)	Poly(α-olefin)	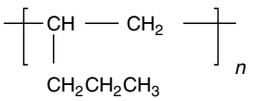
Polypeptides [Poly(α-amino acid)]		Polypeptide	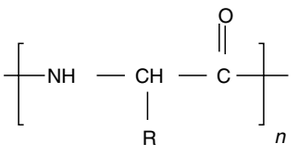
Poly(*p*-methyl styrene)		Vinyl polymer	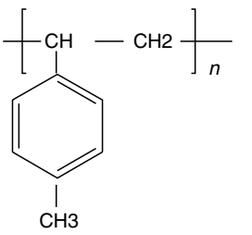
Poly(*p*-phenylene)	PP	Polyaromatic	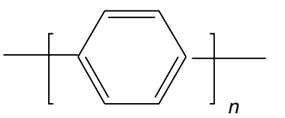

Continued.

Common name	Acronym, alternate name	Class	Structure of repeat unit
Poly(*p*-phenylene oxide)	PPO	Polyether	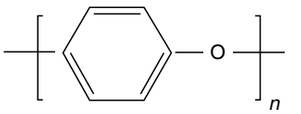
Poly(*p*-phenylene sulfide)	PPS	Polysulfide	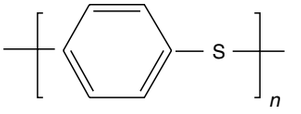
Poly(*p*-phenylene vinylene)		Polyaromatic	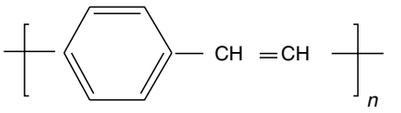
Polyphenylsulfone		Polysulfone	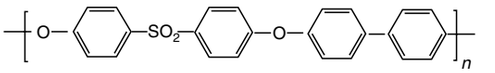
Polyphosphate		Inorganic polymer	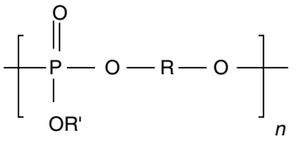
Polyphosphazene		Inorganic polymer	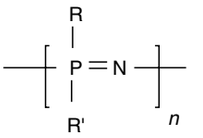
Polyphosphonate		Inorganic polymer	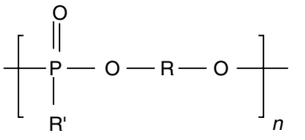
Poly(3-propionate)	Poly(β-propiolactone)	Polyester	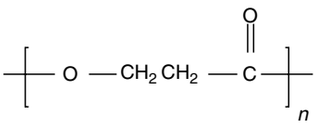
Polypropylene	PP	Poly(α-olefin)	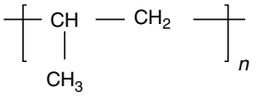

Continued.

Common name	Acronym, alternate name	Class	Structure of repeat unit
Poly(propylene glycol)	PPG	Polyether	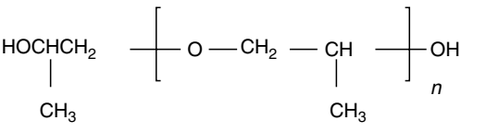
Poly(propylene oxide)	PPO	Polyether	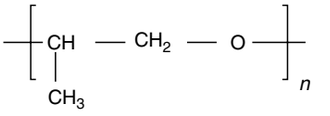
Polypyrazine		Heterocyclic polymer	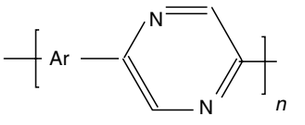
Polypyrazole		Heterocyclic polymer	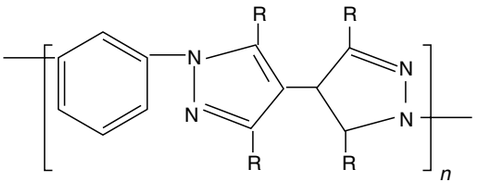
Poly(pyromellitimide-1,4-diphenyl ether)	Kapton	Polyimide	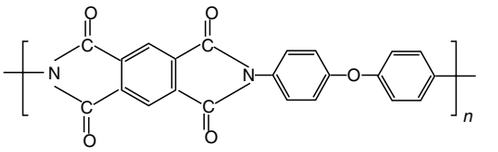
Polypyrrole		Heterocyclic polymer	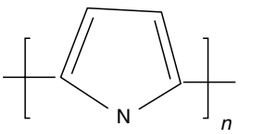
Polyquinoxaline		Heterocyclic polymer	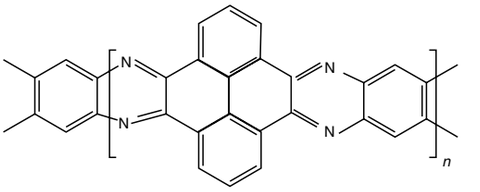
Polysilane		Inorganic polymer	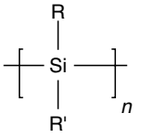

Continued.

Common name	Acronym, alternate name	Class	Structure of repeat unit
Polysilazane		Inorganic polymer	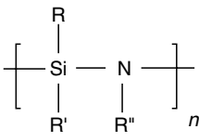
Polysiloxane	Silicone	Inorganic polymer	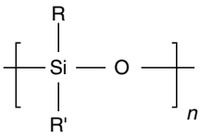
Polystyrene	PS, styrofoam	Vinyl polymer	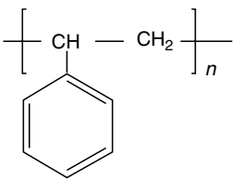
Polysulfide	Thiokol	Polysulfide	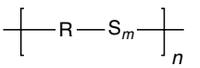
Polysulfur		Polysulfur	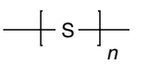
Polytetrafluoroethylene	PTFE, Teflon	Poly(α-olefin)	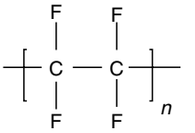
Poly(tetramethylene oxide)	PTMO	Polyether	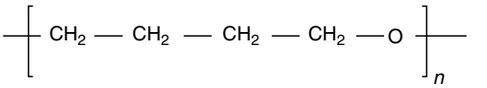
Polythiazyl			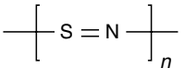
Polythienyl vinylene			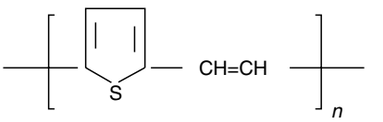

Continued.

Common name	Acronym, alternate name	Class	Structure of repeat unit
Polythiopene		Polyheterocyclic	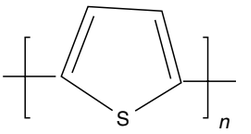
Poly(trimethylene ethylene urethane)			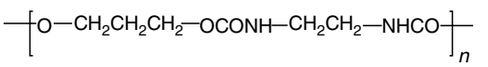
Polyurea		Polyurea	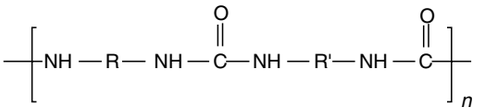
Polyurethane	Adiprene	Polyurethane	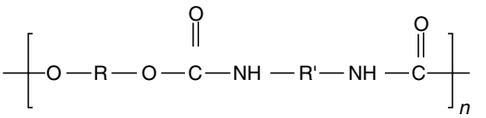
Poly(L-valine)		Polypeptide	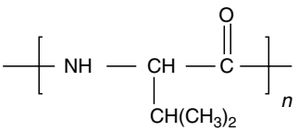
Poly(vinyl acetate)	PVAc	Vinyl polymer	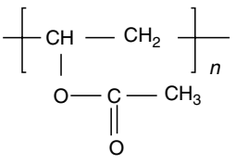
Poly(vinyl alcohol)	PVA	Vinyl polymer	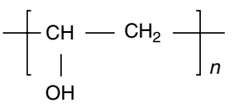
Poly(vinyl butyral)	PVB	Vinyl polymer	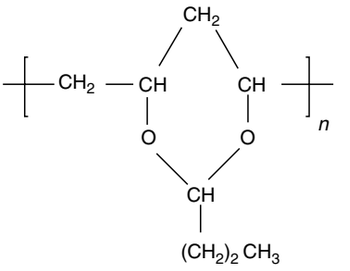

Continued.

Common name	Acronym, alternate name	Class	Structure of repeat unit
Poly(vinyl carbazole)			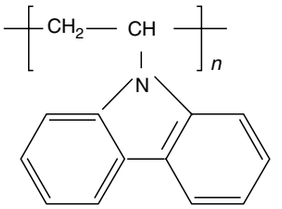
Poly(vinyl chloride)	PVC	Vinyl polymer	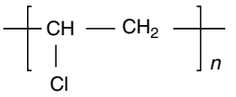
Poly(vinyl fluoride)	PVF	Vinyl polymer, fluoro polymer	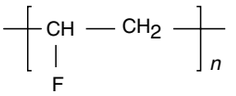
Poly(vinyl formal)		Vinyl polymer	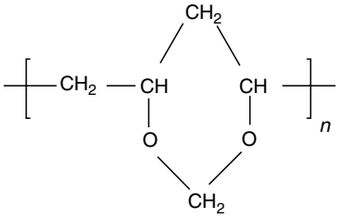
Poly(2-vinyl pyridine)	PVP	Vinyl polymer	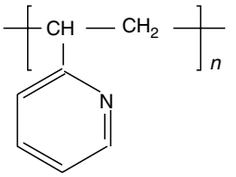
Poly(*N*-vinyl pyrrolidone)		Vinyl polymer	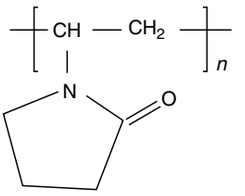
Poly(vinylidene chloride)	PVDC	Vinylidene polymer	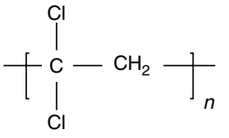

Continued.

Common name	Acronym, alternate name	Class	Structure of repeat unit
Poly(vinylidene fluoride)	PVDF	Vinylidene polymer	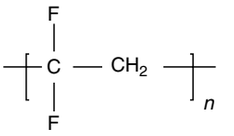
Poly(*p*-xylylene)			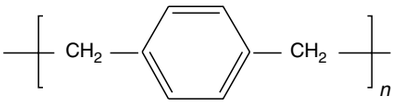
Vinyl polymer		Vinyl polymer	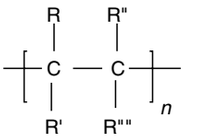

ACKNOWLEDGEMENT

The authors wish to acknowledge the contribution of W. Zhao, formerly of SRI International, to this chapter.

CHAPTER 3

The Rotational Isomeric State Model

Carin A. Helfer and Wayne L. Mattice

Institute of Polymer Science, The University of Akron, Akron, OH 44235-3909

3.1 INTRODUCTION

Flexible macromolecules populate an enormous number of conformations at ordinary temperature, T. If ν stable conformations are available to each internal bond in a chain of n bonds, the chain can access ν^{n-2} conformations. When $\nu = 3$, as is appropriate for many simple polymers, the number of distinguishable conformations exceeds 10^{100} when $n > 211$. This number is achieved by polyethylene at the relatively low molecular weight of 2,984. Scientists and engineers need information about the average properties of specific chains with much larger values of n, where the conformation-dependent physical properties of interest depend on an appropriate average over a truly enormous number of conformations. Among the several models that have been proposed for averaging over this ensemble of conformations, the rotational isomeric state (RIS) model is unique in its combination of structural detail with computational efficiency. It incorporates as much structural detail (bond lengths, l, bond angles, θ, torsion angles, ϕ, differences in energy for conformations produced by rotation about a bond or pair of bonds) as most chemists are likely to desire. Figure 3.1 defines the values of θ and ϕ that are associated with bond i. This detailed description of the local chain structure is presented in a mathematical framework that often permits extremely fast calculation of the average values of many conformation-dependent physical properties of individual polymer chains in the amorphous bulk state and in dilute solution in a solvent chosen so that the excluded volume effect is negligible. The speed of the calculation follows from the formulation of the problem as the serial product of n matrices. Computers are easily trained to rapidly, and accurately, compute this serial product.

The most commonly calculated property is the mean square unperturbed dimension. It is usually represented by the mean square unperturbed end-to-end distance, $\langle r^2 \rangle_0$, obtained by averaging the square of the length of the end-to-end vector, $\mathbf{r}$, over all conformations under conditions where the chain is unperturbed by long-range interactions.

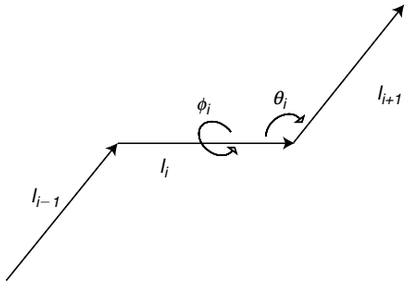

FIGURE 3.1. The definitions of θ_i and ϕ_i associated with bond *i*.

$$\mathbf{r} = \sum_{i=1}^{n} \mathbf{l}_i, \tag{3.1}$$

$$\langle r^2 \rangle_0 = \langle \mathbf{r} \cdot \mathbf{r} \rangle_0 = \sum_{i=1}^{n} l_i^2 + 2 \sum_{i=1}^{n-1} \sum_{j=i+1}^{n} \langle \mathbf{l}_i \cdot \mathbf{l}_j \rangle_0. \tag{3.2}$$

The double sum in Eq. (3.2) can be handled efficiently by matrix methods when the chain is in its unperturbed, or $\boldsymbol{\Theta}$, state. The result for $\langle r^2 \rangle_0$ is usually presented as the dimensionless characteristic ratio, C_n.

$$C_n = \frac{\langle r^2 \rangle_0}{nl^2}. \tag{3.3}$$

As defined in Eq. (3.3), C_n is the ratio of the mean square unperturbed end-to-end distance to the value expected for the freely jointed chain with the same number of bonds, of the same length. If the bonds in the chain are of different lengths, as in polyoxyethylene, l^2 in the denominator is replaced by the mean square bond length. For any flexible unperturbed chain, C_n approaches a limit, C_∞, as $n \to \infty$. The final approach to this limit is usually from below, but it can sometimes be from above. The latter situation can be encountered when C_n passes through a maximum at finite n [1].

The mean square unperturbed radius of gyration, $\langle s^2 \rangle_0$, is accessible by similar methods that rapidly evaluate and sum the mean square end-to-end distances for all of the subchains, denoted by $\langle r_{ij}^2 \rangle_0$, where i and j identify the chain atoms at the ends of the subchain. If all $n + 1$ chain atoms, indexed from 0 to n, can be taken to have the same mass, $\langle s^2 \rangle_0$ is given by the expression in Eq. (3.4).

$$\langle s^2 \rangle_0 = \frac{1}{(n+1)^2} \sum_{i=0}^{n-1} \sum_{j=i+1}^{n} \left\langle r_{ij}^2 \right\rangle_0. \tag{3.4}$$

If the chain is flexible, the RIS calculations produce $\langle s^2 \rangle_0 = \langle r^2 \rangle_0 / 6$ in the limit as $n \to \infty$, as expected [2]. The ratio $\langle r^2 \rangle_0 / \langle s^2 \rangle_0$ may differ from 6 at finite n because $\langle r^2 \rangle_0$ and $\langle s^2 \rangle_0$ do not have the same approach to their limiting behavior [1]. For many real chains, $\langle r^2 \rangle_0 / \langle s^2 \rangle_0 > 6$ at finite n, although $\langle r^2 \rangle_0 / \langle s^2 \rangle_0 \to 6$ as $n \to \infty$. The RIS model has no peer for the calculation of $\langle s^2 \rangle_0$ or $\langle r^2 \rangle_0$ as a function on n because it combines speed with structural detail. Numerous other conformation-dependent physical properties are accessible also from this model. This chapter will describe the RIS method, present a few illustrative results, and cite many of the RIS models for specific polymers that have been presented in the literature.

3.2 HISTORY AND NOTEWORTHY REVIEWS

The speed of calculations using the RIS model arises from its formulation of the problem as a serial product of matrices. The generator matrix technique, which lies at the heart of the calculation, predates the appearance of the RIS model by 10 years [3]. The application of the RIS technique to polymers is now over five decades old [4], although its appearance in the polymer literature did not begin to mushroom until a decade after its first appearance [5–9]. Because computers at that time did not have nearly the speed and widespread availability that is seen today, there was a strong motivation for formulation of the problem in a manner that allowed efficient calculation. With today's computers, the most popular calculations require no more than a few seconds of cpu time.

The first important general work on the RIS model is Flory's classic book, which first appeared in 1969 [10]. His book was followed 5 years later by an excellent review in *Macromolecules* that presented a more general and concise formulation of the RIS method [11]. Another book on the RIS model appeared during the year of the 25th anniversary of the first publication of Flory's original text [12]. It was soon followed by an exhaustive compilation, in a standardized format, of the RIS models presented in the literature over the four decades that ended in the mid-1990s [13].

3.3 RELATIONSHIP TO SIMPLER MODELS

The information incorporated in the RIS model and several simpler models is summarized in Table 3.1. The freely jointed chain has n bonds of length l, with no correlation whatsoever in the orientations of any pair of bonds. The contribution of the double sum in Eq. (3.2) is nil, and $C_n = 1$ at all values of n. Fixing the bond angle, but allowing free rotation about all bonds, produces the freely rotating chain. If $\theta \neq 90°$, C_n will depend on n. The asymptotic limit as $n \to \infty$ is $(1 - \cos\theta)/(1 + \cos\theta)$. If $\theta > 90°$, as is usually the case with real polymers, the freely rotating chain model yields $C_\infty > 1$. Energetic information, in the form of a torsional potential about the internal bonds, $E(\phi)$, is incorporated in the third model in Table 3.1. If the same symmetric torsion potential is applied independently to all internal bonds, the characteristic ratio depends on the average value of the cosine of the torsion angle. The term from the freely rotating chain is retained, and it is multiplied by another term that arises from the symmetric hindered rotation, $C_\infty = [(1-\cos\theta)/(1+\cos\theta)]\,[(1-\langle\cos\phi\rangle)/(1+\langle\cos\phi\rangle)]$.

TABLE 3.1. *Information incorporated in the RIS model and in several simpler models.*

Model	Geometric information[a]	Energetic information
Freely jointed chain	n, l	None
Freely rotating chain	n, l, θ	None
Simple chain with symmetric hindered rotation	n, l, θ,ϕ	First-order interactions (independent bonds, symmetric torsion)
RIS model	n, l, θ,ϕ	First- and higher-order interactions (interdependent bonds, torsion need not be symmetric)

[a]All bonds are assumed to be identical in the usual implementations of the first three models. The assumption of identical bonds is easily discarded in the RIS model.

Since $\langle\cos\phi\rangle$ depends on T, $\langle\cos\phi\rangle = \{\int \exp[-E(\phi)/kT]\, d\phi\}^{-1} \int \cos\phi \exp[-E(\phi)/kT]\, d\phi$, this model is the only one in this paragraph that explicitly says the mean square unperturbed dimensions are temperature dependent. The Boltzmann constant is denoted by k. All of the results in this paragraph assume that the bonds are identical.

In general, it is difficult or impossible to write the results for C_∞ with such simple closed-form expressions when the torsions become interdependent and the bonds are not all identical. However, Nature asks that we take account of the interdependence of the torsions, because nearly all of the real-world polymers have bonds that are subject to interdependent torsions. And many important polymers are made up of bonds with different lengths. The closest one can come to a general and simple expression is something of the form given in Eq. (3.5).

$$C_\infty = \lim_{n\to\infty} \frac{\boldsymbol{G}_1\boldsymbol{G}_2\cdots\boldsymbol{G}_n}{\mathbf{U}_1\mathbf{U}_2\cdots\mathbf{U}_n} = \lim_{n\to\infty} \frac{1}{Z_n}\boldsymbol{G}_1\boldsymbol{G}_2\cdots\boldsymbol{G}_n. \qquad (3.5)$$

As we shall see below, the denominator in Eq. (3.5) is the conformational partition function, Z_n, for the RIS model of the chain. It is constructed as a sum of Boltzmann factors that depend on T and the energies of the first- and higher-order interactions present in all of the conformations of the chain. Structural information does not appear explicitly in Z_n. However, a wealth of structural information (l, θ, ϕ) can appear in the numerator of Eq. (3.5). The numerator also contains all of the thermal and energetic information from Z_n. The combination of this information allows a rapid estimation of C_n, even at large n, because computers can rapidly calculate the serial matrix products that appear in the numerator and denominator of Eq. (3.5).

$\mathbf{U}_1 \ldots \mathbf{U}_n$ is a simpler serial product than $\boldsymbol{G}_1 \ldots \boldsymbol{G}_n$, because it does not include structural information explicitly. For this reason, the easiest introduction to the RIS model is to focus first on Z_n, rather than $\boldsymbol{G}_1 \ldots \boldsymbol{G}_n$.

3.4 THE ROTATIONAL ISOMERIC STATE APPROXIMATION

The basis for the RIS model is most easily seen if we consider a chain where the torsion angles at internal bonds are restricted to a small set of values. For many simple polymers, the RIS models use $\nu = 3$, but the model is sufficiently robust so that it can be used with other choices also. The number of conformations of a chain of n bonds is ν^{n-2}, which becomes enormous when n is large enough so that the molecule becomes of interest to polymer scientists. A pair of two consecutive bonds, bonds $i-1$ and i, has ν^2 conformations. The ν^2 conformations can be presented in tabular form, where the columns represent the ν conformations at bond i, and the rows represent the ν conformations at bond $i-1$. Each entry in the table corresponds to a specific choice of the conformations at these two bonds. In the RIS model, this table becomes a matrix. The elements in the matrix represent contributions to the statistical weights for the conformation adopted at bond i (which depends on the column in the matrix), for a specific choice of the conformation at the preceding bond (which depends on the row in the matrix).

3.5 THE STATISTICAL WEIGHT MATRIX

The statistical weight matrix for bond i, denoted $\mathbf{U}_i$, is usually formulated as the product of two matrices.

$$\mathbf{U}_i = \mathbf{V}_i\mathbf{D}_i. \qquad (3.6)$$

Interaction energies that depend only on the torsion at bond i are responsible for the statistical weights that appear along the main diagonal in $\mathbf{D}_i$. These interactions are termed first-order interactions because they depend on a single degree of freedom, ϕ_i. For the example of a polyethylene-like chain with a symmetric three-fold torsion potential, the rotational isomeric states are t, g^+, g^- (*trans*, *gauche*$^+$, *gauche*$^-$). In the approximation that all bonds are of the same length, all bond angles are tetrahedral, and the torsion angles for the t and $g^\pm$ states are 180° and $\pm 60^\circ$, the separation of the terminal atoms in a chain of three bonds is $(19/3)^{1/2}l$ in the t state, but this separation falls to $(11/3)^{1/2}l$ in the $g^\pm$ states. This change in separation usually produces different energies in the t and $g^\pm$ states. The influence of these energies on the conformation of the chain is taken into account in $\mathbf{D}$. Often a statistical weight is calculated from the corresponding energy as a Boltzmann factor, $w = \exp(-E/RT)$. The t state is usually taken as the reference point, with $E_t = 0$

and a statistical weight of one, and the g states have a statistical weight of $\sigma = \exp[-(E_g - E_t)/RT]$ if the torsion is symmetric, with $E_{g+} = E_{g-}$. A pre-exponential factor may also be necessary if the t and $g^{\pm}$ wells have significantly different shapes. When the order of indexing of the rows and columns is t, g^+, g^-, this diagonal matrix takes the form shown in Eq. (3.7).

$$\mathbf{D}_i = \text{diag}(1,\sigma,\sigma) = \begin{bmatrix} 1 & 0 & 0 \\ 0 & \sigma & 0 \\ 0 & 0 & \sigma \end{bmatrix}, \quad 1 < i < n. \tag{3.7}$$

Real chains often have $\sigma < 1$, as in polyethylene [14], but a few chains, such as polyoxymethylene, have $\sigma > 1$ [15].

The second-order interactions depend jointly on ϕ_{i-1} and ϕ_i. For a simple chain with $\nu = 3$ and symmetric torsion about its internal bonds, the second-order interactions in the tg^+, tg^-, g^+t, and g^-t states are identical, as are the interactions in the g^+g^+ and g^-g^- states, and the interactions in the g^+g^- and g^-g^+ states. The general form of $\mathbf{V}_i$ under these conditions appears in Eq. (3.8), where the order of indexing is t, g^+, g^- for both rows and columns, and the reference point for the second-order interactions is any of the four conformations where one bond is t and the other is g.

$$\mathbf{V}_i = \begin{bmatrix} \tau & 1 & 1 \\ 1 & \psi & \omega \\ 1 & \omega & \psi \end{bmatrix}, \quad 2 < i < n. \tag{3.8}$$

The state at bond $i-1$ indexes the rows, and the state at bond i indexes the columns.

Figure 3.2 depicts the four possible separations of the terminal atoms in a chain of four bonds when all bonds are of the same length, bond angles are tetrahedral, and the torsion angles for the t and $g^{\pm}$ states are 180° and ±60°. By far the shortest separation is seen when the two internal bonds adopt g states of opposite sign. This short distance causes most real chains to have severely repulsive second-order interactions in the g^+g^- and g^-g^+ conformations, producing $\omega < 1$, as in both polyethylene and polyoxyethylene. Often the other second-order interactions are weak enough so that little error is introduced if they are ignored, which frequently leads to the approximation $\tau = \psi = 1$.

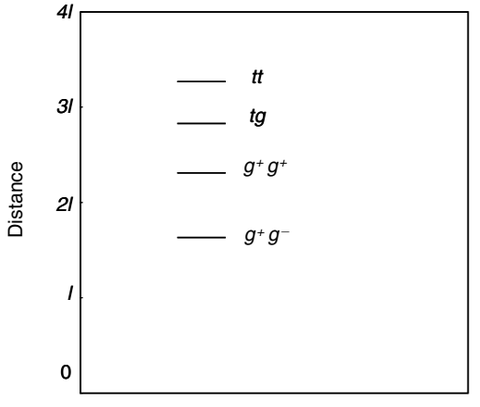

FIGURE 3.2. The four distinguishable separations of the terminal atoms in a chain of four bonds when all bonds are of the same length, l, all bond angles are tetrahedral, and the three states at each internal bond have torsion angles of 180° (t) or ± 60° (g^+ and g^-).

The statistical weight matrix incorporates the first- and second-order interactions, according to Eq. (3.6). For the chain with a symmetric three-fold torsion potential and pairwise interdependent bonds, $\mathbf{U}_i$ adopts the form in Eq. (3.9).

$$\mathbf{U}_i = \begin{bmatrix} \tau & \sigma & \sigma \\ 1 & \sigma\psi & \sigma\omega \\ 1 & \sigma\omega & \sigma\psi \end{bmatrix}, \; 2 < i < n. \tag{3.9}$$

The first rotatable bond in the chain, with $i = 2$, is a special case because there is no preceding rotatable bond for use in defining the statistical weights to be incorporated in $\mathbf{V}_2$. This situation is handled by formulating $\mathbf{U}_2$ using only the statistical weights for first-order interactions, which is achieved by using a value of 1 for every element in $\mathbf{V}_2$.

For the simple chain considered in the examples presented in Eqs. (3.7)–(3.9), all of the $\mathbf{U}_i$ are square and identical [14]. In polyoxymethylene, all of the $\mathbf{U}_i$ are square, but there are two square $\mathbf{U}_i$ with distinctly different numerical values of the elements [15]. Half of the statistical weight matrices for polyoxymethylene incorporate second-order interactions between pairs of oxygen atoms, and the other half incorporate second-order interactions between pairs of methylene groups. For other polymers, such as the polycarbonate of bisphenol A [16], some of the $\mathbf{U}_i$ may be rectangular but not square, because there is a different number of rotational isomeric states at bonds $i-1$ and i. The RIS model does not require that all bonds adopt the same value for ν.

3.6 THE CONFORMATIONAL PARTITION FUNCTION, Z_n

The conformational partition function, in the RIS approximation, is the sum of the statistical weights for the ν^{n-2} conformations in the RIS model. The terminal row and column vectors must be formulated so that they will extract the desired sum of the statistical weights of all conformations from $\mathbf{V_2D_2} \ldots \mathbf{V}_{n-1}\mathbf{D}_{n-1}$.

$$\begin{aligned} Z_n &= \mathbf{J}^*\mathbf{V}_2\mathbf{D}_2\mathbf{V}_3\mathbf{D}_3 \ldots \mathbf{V}_{n-1}\mathbf{D}_{n-1}\mathbf{J} \\ &= \mathbf{J}^*\mathbf{U}_2\mathbf{U_3} \ldots \mathbf{U}_{n-1}\mathbf{J}. \end{aligned} \tag{3.10}$$

$\mathbf{J}^*$ denotes a row of ν elements in which the first element is 1 and all following elements are 0, and $\mathbf{J}$ denotes a column of ν elements in which every element is 1. The statistical weight matrix $\mathbf{U}_i$, $1 < i < n$, is the product $\mathbf{V}_i\mathbf{D}_i$. Often $\mathbf{J}^*$ and $\mathbf{J}$ are written instead as $\mathbf{U}_1$ and $\mathbf{U}_n$ [11].

$$Z_n = \mathbf{U}_1\mathbf{U}_2\mathbf{U}_3 \ldots \mathbf{U}_{n-1}\mathbf{U}_n = \prod_{i=1}^{n} \mathbf{U}_i. \tag{3.11}$$

As a specific example, Z_n for a polyethylene chain can be calculated by the combination of Eqs. (3.9) and (3.11), in the approximation where $\tau = \psi = 1$ [14].

$$Z_n = [1 \quad 0 \quad 0] \begin{bmatrix} 1 & \sigma & \sigma \\ 1 & \sigma & \sigma \\ 1 & \sigma & \sigma \end{bmatrix} \begin{bmatrix} 1 & \sigma & \sigma \\ 1 & \sigma & \sigma\omega \\ 1 & \sigma\omega & \sigma \end{bmatrix}^{n-3} \begin{bmatrix} 1 \\ 1 \\ 1 \end{bmatrix} = \mathbf{J}^* \begin{bmatrix} 1 & \sigma & \sigma \\ 1 & \sigma & \sigma\omega \\ 1 & \sigma\omega & \sigma \end{bmatrix}^{n-2} \mathbf{J}. \tag{3.12}$$

For ethyl terminated polyoxyethylene, the main portion of the calculation employs a repetition of three distinct statistical weight matrices, containing two distinct σ's and two distinct ω's [15].

$$Z_n = \mathbf{J}^* \begin{bmatrix} 1 & \sigma_a & \sigma_a \\ 1 & \sigma_a & \sigma_a \\ 1 & \sigma_a & \sigma_a \end{bmatrix} \left(\begin{bmatrix} 1 & \sigma_a & \sigma_a \\ 1 & \sigma_a & \sigma_a\omega_a \\ 1 & \sigma_a\omega_a & \sigma_a \end{bmatrix} \begin{bmatrix} 1 & \sigma_b & \sigma_b \\ 1 & \sigma_b & \sigma_b\omega_b \\ 1 & \sigma_b\omega_b & \sigma_b \end{bmatrix} \begin{bmatrix} 1 & \sigma_a & \sigma_a \\ 1 & \sigma_a & \sigma_a\omega_b \\ 1 & \sigma_a\omega_b & \sigma_a \end{bmatrix} \right)^{(n-4)/3} \begin{bmatrix} 1 & \sigma_a & \sigma_a \\ 1 & \sigma_a & \sigma_a\omega_a \\ 1 & \sigma_a\omega_a & \sigma_a \end{bmatrix} \mathbf{J}. \tag{3.13}$$

Here σ_a and σ_b denote the statistical weights for the first-order interaction of two methylene groups and two oxygen atoms, respectively, in g states. The statistical weights for the second-order interactions of two methylene groups and a methylene group with an oxygen atom in $g^{\pm}g^{\mp}$ states are denoted by ω_a and ω_b, respectively.

Table 3.2 summarizes RIS models for several chains with pair-wise interdependent bonds subject to a symmetric three-fold torsion potential, such that $\mathbf{U}$ is given by Eq. (3.9). The torsion angles are 180° and $\pm(60^\circ + \Delta\phi)$. Every entry has $E_\omega < 0$. This energy is listed as being infinite when the population of the g^+g^- and g^-g^+ states is so small that it can be ignored. In contrast with E_ω, the table contains entries for E_σ that are of either sign.

Table 3.3 summarizes selected literature citations for RIS models for homopolymers with 1–7 bonds per repeat unit, with all bonds subject to symmetric torsions. The list in Table 3.3 terminates with poly(6-aminocaproamide), nylon 6, although RIS models for chains with much longer repeat units have been reported in the literature [13]. The selection of entries in Table 3.3 is based in part on recognizing contributions of historical interest, and in part on more recent models that exploit computational methods and experiments that were not readily available during the early days of the development of RIS models. It does not include all applications of the RIS model to a given polymer. In some cases this number would be huge. For example, there are well over 100 applications of RIS models for polyethylene in the literature.

TABLE 3.2. *RIS models for several chains with pair-wise interdependent bonds subject to a symmetric threefold torsion potential and $E_\tau = E_\psi = 0$. Lengths in nm, angles in degrees, energies in kJ/mol.*

Polymer	Bond	l	θ	$\Delta\phi$	E_σ	E_ω	Reference
Polymethylene	C–C	0.153	112	7.3±3	1.1–1.9	5.4–6.7	[14]
Polymethylene	C–C	0.153	112	0±3	1.8–2.5	7.1–8.0	[14]
Polyoxymethylene	C–O	0.142	112	5	−5.9	∞	[15]
	O–C	0.142	112	5	−5.9	6.3	
Polydimethylsilmethylene	Si–C	0.190	115	0	0	∞	[17]
	C–Si	0.190	109.5	0	0	0.80	
Polydimethylsiloxane	Si–O	0.164	143	0	3.6	∞	[18]
	O–Si	0.164	110	0	3.6	4.2	
Polyoxyethylene	C–O	0.143	111.5	10	−1.7 to −2.1	1.7	[15]
	O–C	0.143	111.5	10	−1.7 to −2.1	∞	
	C–C	0.153	111.5	10	3.8	1.7	
Poly(trimethylene oxide)	O–C	0.143	111.5	10	3.8	∞	[15]
	C–C	0.153	111.5	0	−1.7	∞	
	C–C	0.153	111.5	0	−1.7	2.5	
	C–O	0.143	111.5	10	3.8	∞	

TABLE 3.3. *Selected literature citations for RIS models of polymers without rings in the backbone and with bonds subject to symmetric torsions. x denotes the number of chain atoms in the repeat unit. For a given value of x, the models are listed in the order of increasing molecular weight of the repeat unit specified in the third column.*

x	Polymer	Repeat unit	References
1	Polymethylene, polyethylene	$-CH_2-$	[14,19]
	Polysilane	$-SiH_2-$	[20]
	Polymeric sulfur	–S–	[21–23]
	Polytetrafluoroethylene	$-CF_2-$	[24–26]
	Polydimethylsilylene	$-Si(CH_3)_2-$	[20]
	Polymeric selenium	–Se–	[21–23, 27]
2	Polyoxymethylene	$-CH_2-O-$	[15,28,29]
	Polysilylenemethylene	CH_2SiH_2	[30]
	Polydihydrogensiloxane	$OSiH_2$	[31]
	Polyisobutylene	$-CH_2-C(CH_3)_2-$	[32–35]
	Polyvinylidene fluoride	$-CH_2-CF_2-$	[36,37]
	Polydimethylsilylenemethylene	$-CH_2-Si(CH_3)_2-$	[17,30,38]
	Polydimethylsiloxane	$-O-Si(CH_3)_2-$	[18,39]
	Polyphosphate	$-O-PO_2-$	[40]
	Polyvinylidene chloride	$-CH_2-CCl_2-$	[41]
	Polydichlorophosphazene	$-N-PCl_2-$	[42]
	Polyvinylidene bromide	$-CH_2-CBr_2-$	[36]
	Polydiphenylsiloxane	$-O-Si(C_6H_5)_2-$	[43]
3	Polyoxyethylene	$-O-CH_2-CH_2-$	[15,44–46]
	Polyglycine	$-NH-CH_2-CO-$	[47]
	Polythiaethylene	$-S-CH_2-CH_2-$	[48,49]
	Poly(oxy-1,1-dimethylethylene)	$-O-CH_2-CH(CH_3)_2-$	[50]
4	Poly(1,4-*cis*-butadiene)	$-CH_2-CH=CH-CH_2-$	[51–54]
	Poly(1,4-*trans*-butadiene)	$-CH_2-CH=CH-CH_2-$	[53–56]
	Poly(trimethylene oxide)	$-CH_2-CH_2-CH_2-O-$	[15]
	Poly(1,4-*cis*-isoprene)	$-CH_2-CH=C(CH_3)-CH_2-$	[51,52,57]
	Poly(1,4-*trans*-isoprene)	$-CH_2-CH=C(CH_3)-CH_2-$	[53,55,56]
	Poly(trimethylene sulfide)	$-CH_2-CH_2-CH_2-S-$	[58]
	Poly(3,3-dimethyloxetane)	$-O-CH_2-C(CH_3)_2-CH_2-$	[59,60]
	Poly(3,3-dimethylthietane)	$-S-CH_2-C(CH_3)_2-CH_2-$	[61]
5	Poly(tetramethylene oxide)	$-CH_2-CH_2-CH_2-CH_2-O-$	[15]
	Poly(1,3-dioxolane)	$-CH_2-CH_2-O-CH_2-O-$	[62]
6	Poly(pentamethylene sulfide)	$-S-CH_2-CH_2-CH_2-CH_2-CH_2-$	[63]
	Poly(thiodiethylene glycol)	$-O-CH_2-CH_2-S-CH_2-CH_2-$	[64]
7	Poly(hexamethylene oxide)	$-O-CH_2-CH_2-CH_2-CH_2-CH_2-CH_2-$	[65]
	Poly(6-aminocaproamide)	$-NH-CH_2-CH_2-CH_2-CH_2-CH_2-CO-$	[66]

3.7 THE STEREOCHEMICAL SEQUENCE IN VINYL POLYMERS

Vinyl polymers, for which polypropylene serves as a prototype, present some additional issues not encountered in chains with symmetric torsions. The physical properties of these chains depend on the stereochemical composition and stereochemical sequence of the chain, and this dependence must be reflected in Z. Two equivalent methods have been used for description of the stereochemistry of vinyl polymers. One approach uses pseudoasymmetric centers [67]. Although the fragment denoted by $-CH_2-CHR-CH_2-$ does not contain a chiral center, it can be treated as though it were chiral if one CH_2 group is distinguished from the other. This distinction is drawn when the bonds in the chain are indexed from one end to the other, because then the CH_2-CHR bond preceding the pseudoasymmetric center bears a different index from the following $CHR-CH_2$ bond. The –CHR-group is defined here to be in the d (l) configuration if the z component of the nonhydrogen substituent is positive (negative) in a local coordinate system for the $CHR-CH_2$ bond. This local coordinate system is defined as follows: The x-axis for the $CHR-CH_2$ bond is parallel with the bond and oriented from CHR to CH_2. The y-axis is in the plane of the chain atoms in $-CH_2-CHR-CH_2-$, and oriented with a positive projection on the x-axis for the preceding CH_2-CHR bond, which points from CH_2 to CHR. The z-axis completes a right-handed Cartesian coordinate system. Alternatively (and equivalently), the stereochemical sequence can be described

as sequences of *meso* diads (two successive identical pseudoasymmetric centers) and/or *racemo* diads (two successive nonidentical pseudoasymmetric centers) [67].

Statistical weight matrices that include all first- and second-order interactions can be formulated using Eq. (3.6) and the additional matrix defined in Eq. (3.14).

$$\mathbf{Q} = \begin{bmatrix} 1 & 0 & 0 \\ 0 & 0 & 1 \\ 0 & 1 & 0 \end{bmatrix}. \tag{3.14}$$

$\mathbf{Q}$ has the useful property that $\mathbf{Q}^2 = \mathbf{E}$, where $\mathbf{E}$ denotes the identity matrix. For a vinyl polymer with a nonarticulated side chain (such as a halogen atom), the $-$CHR$-$CH$_2-$ bond immediately following a pseudoasymmetric center has a $\mathbf{D}$ matrix that is either

$$\mathbf{D}_d = \text{diag}(\eta,1,\tau) \tag{3.15}$$

or

$$\mathbf{D}_l = \text{diag}(\eta,\tau,1) = \mathbf{Q}\mathbf{D}_d\mathbf{Q}, \tag{3.16}$$

depending on whether the CHR is a *d* or *l* pseudoasymmetric center. The three-rotational isomeric states are t,g^+, and g^-, in that order. The conformation weighted by τ has two first-order interactions, which occur between the underlined pairs of atoms in $\underline{\text{C}}\text{H}_2-\text{CHR}-\text{CH}_2-\underline{\text{C}}$ and $\text{CH}_2-\text{CH}\underline{\text{R}}-\text{CH}_2-\underline{\text{C}}$ (this τ is different from the one used in Eq. (3.9)). The conformation with only the second of these first-order interactions is weighted by η, and the conformation with only the first of these first-order interaction is the reference point, with a statistical weight of 1. The most important second-order interactions are independent of the configuration of the side chain because they only involve atoms in the main chain.

$$\mathbf{V}_d = \mathbf{V}_l = \begin{bmatrix} 1 & 1 & 1 \\ 1 & 1 & \omega \\ 1 & \omega & 1 \end{bmatrix}. \tag{3.17}$$

The complete statistical weight matrices for this bond in the two stereochemical configurations are obtained as $\mathbf{VD}$, from Eq. (3.6).

$$\mathbf{U}_d = \mathbf{Q}\mathbf{U}_l\mathbf{Q} = \begin{bmatrix} \eta & 1 & \tau \\ \eta & 1 & \tau\omega \\ \eta & \omega & \tau \end{bmatrix}. \tag{3.18}$$

Proceeding in the same manner, there are four possible statistical weight matrices for the CH$_2-$CHR bond immediately before a pseudoasymmetric center, depending on the stereochemistry at this center and the preceding pseudoasymmetric center. If both pseudoasymmetric centers have the same chirality, the two possibilities, $\mathbf{U}_{dd}$ and $\mathbf{U}_{ll}$, can be interconverted using $\mathbf{Q}$.

$$\mathbf{U}_{dd} = \mathbf{Q}\mathbf{U}_{ll}\mathbf{Q} = \begin{bmatrix} \eta\omega_{\text{RR}} & \tau\omega_{\text{CR}} & 1 \\ \eta & \tau\omega_{\text{CR}} & \omega_{\text{CC}} \\ \eta\omega_{\text{CR}} & \tau\omega_{\text{CC}}\omega_{\text{RR}} & \omega_{\text{CR}} \end{bmatrix}. \tag{3.19}$$

The double subscript on ω shows whether the second-order interaction is between two groups in the backbone, ω_{CC}, two side chains, ω_{RR}, or a side chain and a group in the backbone, ω_{CR}. If the two pseudoasymmetric centers have opposite chirality, the two possibilities are given in Eq. (3.20).

$$\mathbf{U}_{dl} = \mathbf{Q}\mathbf{U}_{ld}\mathbf{Q} = \begin{bmatrix} \eta & \omega_{\text{CR}} & \tau\omega_{\text{RR}} \\ \eta\omega_{\text{CR}} & 1 & \tau\omega_{\text{CC}} \\ \eta\omega_{\text{RR}} & \omega_{\text{CC}} & \tau\omega_{\text{CR}}^2 \end{bmatrix}. \tag{3.20}$$

When pseudoasymmetric centers are used for the description of the stereochemical sequence, six distinct statistical weight matrices, Eqs. (3.18)–(3.20), are required. They can be replaced by a total of three statistical weight matrices, denoted by $\mathbf{U}_p$,$\mathbf{U}_m$, and $\mathbf{U}_r$, if the stereochemical sequence is described instead as a sequence of *meso* and *racemo* diads.

$$\mathbf{U}_p = \mathbf{Q}\mathbf{U}_d = \mathbf{U}_l\mathbf{Q}, \tag{3.21}$$

$$\mathbf{U}_m = \mathbf{U}_{dd}\mathbf{Q} = \mathbf{Q}\mathbf{U}_{ll}, \tag{3.22}$$

$$\mathbf{U}_r = \mathbf{U}_{dl} = \mathbf{Q}\mathbf{U}_{ld}\mathbf{Q}. \tag{3.23}$$

The conformational partition function for a vinyl polymer of specified stereochemical sequence is formulated as a string of matrices where every second matrix is $\mathbf{U}_p$, and the intervening matrices are either $\mathbf{U}_m$ or $\mathbf{U}_r$, depending on the sequence of the diads in the chain. The definitions of the rotational isomeric states must change also when Eqs. (3.21)–(3.23) are used. Instead of using the t,g^+, and g^- states that are appropriate for *d* and *l* pseudoasymmetric centers, one uses t, g, and $\bar{g}$ states for *meso* and *racemo* diads. The *gauche* state that has τ in its statistical weight is denoted by $\bar{g}$, and the other *gauche* state is denoted simply by g. Indexing of rows and columns in $\mathbf{U}_p$,$\mathbf{U}_m$, and $\mathbf{U}_r$ is in the sequence t, g, $\bar{g}$.

Several vinyl polymers, such as polystyrene, have statistical weights such that τ and all of the ω's are much smaller than 1. Under these circumstances little error may be introduced if the $\bar{g}$ state is ignored because its statistical weight always includes $\tau\omega$. This simplification allows construction of Z with 2×2 matrices where the rows and columns are indexed t, g [68].

$$\mathbf{U}_p = \begin{bmatrix} 1 & 1 \\ 1 & \omega \end{bmatrix}, \tag{3.24}$$

$$\mathbf{U}_m = \begin{bmatrix} \eta^2\omega_{\text{RR}} & \eta \\ \eta & \omega_{\text{CC}} \end{bmatrix}, \tag{3.25}$$

$$\mathbf{U}_r = \begin{bmatrix} \eta^2 & \eta\omega_{\text{CR}} \\ \eta\omega_{\text{CR}} & 1 \end{bmatrix}. \tag{3.26}$$

In these three equations, all of the statistical weights for first-order interactions in the diad have been placed in $\mathbf{U}_m$ and $\mathbf{U}_r$. The $\mathbf{U}_p\mathbf{U}_m$ sequence shows that an isotactic chain can avoid conformations weighted by ω (a very small number in most polymers) if it adopts an ordered sequence that is either *tg* or *gt*, which is consistent with the commonly observed chain conformation in crystalline isotactic

polymers. In contrast, the $\mathbf{U}_p\mathbf{U}_r$ sequence shows that a syndiotactic chain is more likely to crystallize in either the *tt* or *gg* conformation, because these conformations do not require weighing with ω.

Literature citations for RIS models for several vinyl polymers, as well as related polymers for which stereochemical compositions and stereochemical sequences are issues, are summarized in Table 3.4.

3.8 EXTRACTION OF USEFUL INFORMATION FROM Z_n

The conformational partition function is subject to the same types of manipulations as are other partition functions encountered in statistical mechanics. Thus the average conformational energy of the chain is obtained from the temperature dependence of Z_n.

$$\langle E\rangle - E_0 = kT^2\left(\frac{\partial \ln Z_n}{\partial T}\right). \tag{3.27}$$

Z_n depends on T because the elements of the statistical weight matrices are Boltzmann factors. The conformational entropy is obtained from this result and $\ln Z_n$.

$$S = \frac{\langle E\rangle - E_0}{T} + k\ln Z_n. \tag{3.28}$$

The same approach can be used to deduce average conformations of local portions of the chain. The probability that bond i is in a particular rotational isomeric state, η, is obtained by dividing Z_n into the sum of the statistical weights of all conformations where this bond is in the desired state.

$$p_{\eta;i} = Z^{-1}\mathbf{U}_1\mathbf{U}_2\cdots\mathbf{U}_{i-1}\mathbf{U}'_{\eta;i}\mathbf{U}_{i+1}\cdots\mathbf{U}_n. \tag{3.29}$$

The modified statistical weight matrix denoted by $\mathbf{U}'_{\eta;i}$ is obtained by zeroing all columns of $\mathbf{U}_i$ except the column that indexes the desired state, η. This operation has the effect of ignoring the statistical weights of all conformations of the chain where bond i is not in the desired state, while keeping intact the statistical weights of all chain

Table 3.4. *RIS models for selected vinyl polymers and related polymers for which stereochemical composition and stereochemical sequence are issues. Chains are listed in the order of the molecular weight of their repeat unit.*

Polymer	Repeat unit	References
Polypropylene	$-CH_2-CH(CH_3)-$	[69–72]
Poly(vinyl alcohol)	$-CH_2-CH(OH)-$	[73,74]
Poly(vinyl fluoride)	$-CH_2-CHF-$	[75]
Poly(1-butene)[a]	$-CH_2-CH(C_2H_5)-$	[76]
Polysilapropylene	$-CH_2-SiH(CH_3)-$	[77]
Poly(propylene oxide)	$-O-CH_2-CH(CH_3)-$	[78,79]
Poly(vinyl methyl ether)[a]	$-CH_2-CH(OCH_3)-$	[80]
Poly(vinyl chloride)	$-CH_2-CHCl-$	[81,82]
Poly(methyl vinyl ketone)	$-CH_2-CH(COCH_3)-$	[83]
Poly(propylene sulfide)	$-S-CH_2-CH(CH_3)-$	[79,84,85]
Poly(trifluoroethylene)	$-CF_2-CHF-$	[75]
Head-to-head, tail-to-tail polypropylene[b]	$-CH_2-CH(CH_3)-CH(CH_3)-CH_2-$	[86]
Poly(vinyl acetate)	$-CH_2-CH(OCOCH_3)-$	[87]
Poly(methyl acrylate)	$-CH_2-CH(COOCH_3)-$	[88–90]
Poly(tert-butyl vinyl ketone)	$-CH_2-CH[COC(CH_3)_3]-$	[91]
Poly(methyl methacrylate)	$-CH_2-C(CH_3)(COOCH_3)-$	[92–94]
Poly(methyl phenyl siloxane)	$-O-Si(CH_3)(C_6H_5)-$	[95]
Polystyrene	$-CH_2-CH(C_6H_5)-$	[68,96,97]
Poly(2-vinylpyrridine)	$-CH_2-CH(C_5NH_4)-$	[98]
Poly(vinyl bromide)	$-CH_2-CHBr-$	[99]
Poly(*N*-vinyl pyrrolidone)	$-CH_2-CH(C_4NOH_6)-$	[100]
Poly(α-methylstyrene)	$-CH_2-C(CH_3)(C_6H_5)-$	[101]
Polysilastyrene	$-SiH_2-SiH(C_6H_5)-$	[102,103]
Poly(*p*-chlorostyrene)	$-CH_2-CH(C_6H_4Cl)-$	[104]
Poly(phenyl acrylate)	$-CH_2-CH(COOC_6H_5)-$	[105]
Poly(*N*-vinyl carbazole)	$-CH_2-CH(C_{12}NH_8)-$	[106,107]
Poly(methylphenylsilylene)	$-Si(CH_3)(C_6H_5)-$	[102,108]
Asymmetrically substituted polysilylenemethylene[a]	$-CH_2-Si(CH_3)[O(CH_2)_3OC_6H_4C_6H_5]-$	[109]

[a] These articulated side chains require more elaborate methods that are extensions of the simpler ones described in this Chapter.
[b] Hydrogenated poly(2,3-dimethylbutadiene).

conformations where this bond is in state η. The $p_{\eta;i}$ are useful in the interpretation of conformation-dependent properties of polymers that are highly local in origin. Examples are the coupling constants in NMR spectra [110], as evaluated by a Karplus relationship [111–114], and the optical activity of chiral vinyl polymers [115].

An extension of this approach yields the probability that bonds $i-1$ and i are simultaneously in states ξ and η, respectively.

$$p_{\xi\eta;i} = Z^{-1}\mathbf{U}_1\mathbf{U}_2\cdots\mathbf{U}_{i-1}\mathbf{U}'_{\xi\eta;i}\mathbf{U}_{i+1}\cdots\mathbf{U}_n. \tag{3.30}$$

The matrix $\mathbf{U}'_{\xi\eta;i}$ is obtained from $\mathbf{U}_i$ by zeroing every element except the one in the row and column indexed by ξ and η, respectively.

A useful method for calculating the probabilities for longer sequences of bonds, in the approximation where there is interdependence of nearest-neighbor pairs of bonds, makes use of another probability that can be calculated from the results of Eqs. (3.29) and (3.30).

$$q_{\xi\eta;i} = p_{\xi\eta;i}/p_{\xi;i-1}. \tag{3.31}$$

This term is the probability that bond i is in state η, given that bond $i-1$ is in state ξ. (This restriction on the state at bond $i-1$ was absent in the definition of $p_{\xi\eta;i}$.) The differences in $q_{\xi\eta;i}$ and $p_{\xi\eta;i}$ are apparent from examination of the types of summations that must be performed in order to achieve unit probability.

$$\sum_{\xi=1}^{\nu}\sum_{\eta=1}^{\nu} p_{\xi\eta;i} = 1, \tag{3.32}$$

$$\sum_{\eta=1}^{\nu} q_{\xi\eta;i} = 1. \tag{3.33}$$

The normalization is achieved differently for $p_{\xi\eta;i}$ and $q_{\xi\eta;i}$. If $\sigma = 0.543$ and $\omega = 0.087$, a C–C bond in the middle of a long polyethylene chain has the following values for these probabilities, where each set of probabilities is presented in the form of a 3×3 matrix with rows and columns indexed in the order t, g^+, g^-.

$$\mathbf{p}_{\xi\eta;i} = \begin{bmatrix} 0.321 & 0.138 & 0.138 \\ 0.138 & 0.0591 & 0.00516 \\ 0.138 & 0.00516 & 0.0591 \end{bmatrix}, \tag{3.34}$$

$$\mathbf{q}_{\xi\eta;i} = \begin{bmatrix} 0.538 & 0.231 & 0.231 \\ 0.682 & 0.292 & 0.026 \\ 0.682 & 0.026 & 0.292 \end{bmatrix}. \tag{3.35}$$

The elements in Eq. (3.34) illustrate the importance of the interdependence of the bonds in polyethylene. The probability for a pair of bonds in g states depends strongly on whether they are of the same or opposite sign. The interdependence of the bonds is also apparent in Eq. (3.35). If the bonds were independent, all rows of $\mathbf{q}_{\xi\eta;i}$ would be identical.

The probability that bonds $i-2$, $i-1$, and i are in states ζ, ξ, and η, respectively, is given by $p_{\zeta;i-2}q_{\zeta\xi;i-1}q_{\xi\eta;i}$, which results from the logical extension of Eq. (3.30). This approach can be extended to the probabilities for observations of longer sequences of bonds in specified states.

3.9 VIRTUAL BONDS

Many important chains contain bonds that are locked into a single conformation due to restrictions imposed by ring formation, as in the benzene ring of poly(ethylene terephthalate), or electronic structures (as in the amide unit of nylon-6, which strongly prefers the planar *trans* conformation). These rigid units are often treated with virtual bonds, where a single virtual bond spans the rigid unit. Several instances where virtual bonds have been used are summarized in Table 3.5.

3.10 MATRIX EXPRESSION FOR THE DIMENSIONS OF A SPECIFIED CONFORMATION

The geometry for a specified conformation of a chain of n bonds is formulated in a manner that will facilitate averaging of the result with the aid of the information contained in Z_n. We will defer the averaging process until the next section, and focus here on a single conformation. The statistical weight of this conformation is irrelevant in the present section, but it will become highly relevant in the next section.

The local Cartesian coordinate system depicted in Fig. 3.3 is affixed to each bond in the chain. Bond i runs from chain atom $i-1$ to chain atom i. The x-axis for this bond is parallel with the bond, and oriented from chain atom $i-1$ to chain atom i. The y-axis is in the plane of bonds i and $i-1$, and oriented with a positive projection on bond $i-1$. The z-axis completes a right-handed Cartesian coordinate system. Since the first bond does not have a previous bond for use in defining the y-axis, an imaginary zeroth bond is used. This bond is oriented such that it produces a *trans* state

TABLE 3.5. *Examples of the use of virtual bonds in the construction of RIS models.*

Rigid unit	Examples	References
Aromatic ring	Polybenzoxazine	[116]
	Polycarbonates	[16,117]
	Polyesters	[118–120]
	Polypyrrole	[121]
Aliphatic ring	Polysaccharides	[122–124]
	Nucleic acids	[125]
Amide group	Poly(amino acids)	[126–128]
Ester group	Poly(lactic acid)	[129]
$CH_2CH{=}CHCH_2$unit	Polybutadiene	[51]

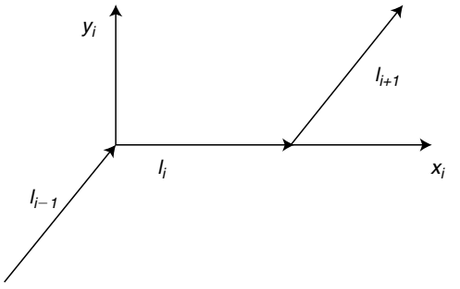

FIGURE 3.3. Local coordinate system for bond *i*. The *x* and *y* axes are drawn on the figure. The *z*-axis (not drawn) completes a right-handed Cartesian coordinate system.

at the first bond. With these definitions of the local coordinate systems, a bond vector in its own coordinate system can be quickly written.

$$\mathbf{l}_i = \begin{bmatrix} l \\ 0 \\ 0 \end{bmatrix} \tag{3.36}$$

The matrix that transforms a vector from its representation in the coordinate system of bond $i+1$ into its representation in bond i is denoted $\mathbf{T}_i$. It depends on the angle made by these two bonds and the torsion at bond i.

$$\mathbf{T}_i = \begin{bmatrix} -\cos\theta & \sin\theta & 0 \\ -\sin\theta\cos\phi & -\cos\theta\cos\phi & -\sin\phi \\ -\sin\theta\sin\phi & -\cos\theta\sin\phi & \cos\phi \end{bmatrix}. \tag{3.37}$$

The expression for $\mathbf{l}_{i+1}$ in the coordinate system of bond i is $\mathbf{T}_i\mathbf{l}_{i+1}$. With this notation, the end-to-end vector in a specified conformation can be written as a serial product of n matrices constructed from $\mathbf{T}$ and $\mathbf{l}$ [11].

$$\begin{aligned} \mathbf{r} &= [\,\mathbf{T}_1 \quad \mathbf{l}_1\,] \begin{bmatrix} \mathbf{T}_2 & \mathbf{l}_2 \\ \mathbf{0} & 1 \end{bmatrix} \cdots \begin{bmatrix} \mathbf{T}_{n-1} & \mathbf{l}_{n-1} \\ \mathbf{0} & 1 \end{bmatrix} \begin{bmatrix} \mathbf{l}_n \\ 1 \end{bmatrix} \\ &= \mathbf{A}_1\mathbf{A}_2\cdots\mathbf{A}_{n-1}\mathbf{A}_n. \end{aligned} \tag{3.38}$$

All of the geometric information (l_i, θ_i, ϕ_i) pertinent to bond i appears in $\mathbf{A}_i$. The squared end-to-end distance and squared radius of gyration can be calculated using exactly the same information, but with the information presented in larger matrices.

$$r^2 = [\,1 \quad 2\mathbf{l}_1^{\mathrm{T}}\mathbf{T}_1 \quad l_1^2\,] \begin{bmatrix} 1 & 2\mathbf{l}_2^{\mathrm{T}}\mathbf{T}_2 & l_2^2 \\ \mathbf{0} & \mathbf{T}_2 & \mathbf{l}_2 \\ 0 & \mathbf{0} & 1 \end{bmatrix} \cdots \begin{bmatrix} 1 & 2\mathbf{l}_{n-1}^{\mathrm{T}}\mathbf{T}_{n-1} & l_{n-1}^2 \\ \mathbf{0} & \mathbf{T}_{n-1} & \mathbf{l}_{n-1} \\ 0 & \mathbf{0} & 1 \end{bmatrix} \begin{bmatrix} l_n^2 \\ \mathbf{l}_n \\ 1 \end{bmatrix} = \mathbf{G}_1\mathbf{G}_2\cdots\mathbf{G}_{n-1}\mathbf{G}_n. \tag{3.39}$$

The expression for s^2 is written in the approximation where all of the chain atoms can be taken to be of the same mass.

$$s^2 = (n+1)^{-2}\mathbf{H}_1\mathbf{H}_2\ldots\mathbf{H}_{n-1}\mathbf{H}_n. \tag{3.40}$$

Matrices $\mathbf{H}_1$ and $\mathbf{H}_n$ are written as the first row and last column, respectively, of the general expression for $\mathbf{H}_{i,1} < i < n$, as was true also for $\mathbf{G}$ [11].

$$\mathbf{H}_i = \begin{bmatrix} 1 & 1 & 2\mathbf{l}_i^{\mathrm{T}}\mathbf{T}_i & l_i^2 & l_i^2 \\ 0 & 1 & 2\mathbf{l}_i^{\mathrm{T}}\mathrm{T}_i & l_i^2 & l_i^2 \\ \mathbf{0} & \mathbf{0} & \mathbf{T}_i & \mathbf{l}_i & \mathbf{l}_i \\ 0 & 0 & \mathbf{0} & 1 & 1 \\ 0 & 0 & \mathbf{0} & 0 & 1 \end{bmatrix}, \quad 1 < i < n. \tag{3.41}$$

The squared dipole moment, μ^2, of polar chains such as polyoxymethylene can be treated using a simple modification of Eq. (3.39). The bond vector, $\mathbf{l}_i$, for bond i is replaced by the dipole moment vector, $\mathbf{m}_i$, for the same bond [15]. For polyoxymethylene, the bond vectors are connected in a head-to-tail fashion, but the bond dipole moment vectors are connected in a head-to-head, tail-to-tail fashion, with the oxygen atom being at the negative end of $\mathbf{m}_i$. Extension to polyoxyethylene requires that some of the $\mathbf{m}_i$ be null vectors, as would be the case for the CH_2–CH_2 bond [15]. In some chains, such as poly(vinyl chloride), the important $\mathbf{m}_i$ are not aligned with the $\mathbf{l}_i$ [130].

3.11 AVERAGING THE DIMENSIONS OVER ALL THE CONFORMATIONS IN $\mathbf{Z_n}$

The matrices denoted by $\mathbf{A}_i$, $\mathbf{G}_i$, and $\mathbf{H}_i(1 < i < n)$ in Eqs. (3.38)–(3.40) depend on the rotational isomeric state assigned to bond i through the appearance of ϕ_i in $\mathbf{T}_i$. The states at this bond also index the columns of $\mathbf{U}_i$. We now seek a pairing of the appropriate statistical weight from $\mathbf{U}_i$ with the geometry in $\mathbf{T}_i$. This objective is achieved by expansion of each element in $\mathbf{U}_i$ through multiplication of each of its elements by the appropriate $\mathbf{A}_i$, $\mathbf{G}_i$, or $\mathbf{H}_i$, depending on whether the target of the calculation is $\langle\mathbf{r}\rangle_0$, $\langle r^2\rangle_0$, or $\langle s^2\rangle_0$. As an example, the calculation of $\langle r^2\rangle_0$ can be written as a serial product of n $\mathbf{G}$ matrices [11].

$$\langle r^2\rangle_0 = Z^{-1}\boldsymbol{G}_1\boldsymbol{G}_2\ldots\boldsymbol{G}_{n-1}\boldsymbol{G}_n. \tag{3.42}$$

The internal $\boldsymbol{G}_i$ are constructed by expansion of each element in $\mathbf{U}_i$, denoted $u_{\xi\eta}$, by $\boldsymbol{G}_\eta$, such that $\boldsymbol{G}_i$ becomes a $5\nu \times 5\nu$ matrix, whereas $\mathbf{U}_i$ was a $\nu \times \nu$ matrix. The terminal $\boldsymbol{G}_i$ are either a row or column of 5ν elements. When $\nu = 3$, the $\mathbf{G}$ matrices take the forms shown in Eqs. (3.43)–(3.45).

$$\boldsymbol{G}_1 = \begin{bmatrix} 1 & 2l_1^T\mathbf{T}_1 & l_1^2 & 0 & \cdots & 0 \end{bmatrix}, \tag{3.43}$$

$$\boldsymbol{G}_i = \begin{bmatrix} u_{11}\boldsymbol{G}_t & u_{12}\boldsymbol{G}_{g^+} & u_{13}\boldsymbol{G}_{g^-} \\ u_{21}\boldsymbol{G}_t & u_{22}\boldsymbol{G}_{g^+} & u_{23}\boldsymbol{G}_{g^-} \\ u_{31}\boldsymbol{G}_t & u_{32}\boldsymbol{G}_{g^+} & u_{33}\boldsymbol{G}_{g^-} \end{bmatrix}, \quad 1 < i < n, \quad (3.44)$$

$$\boldsymbol{G}_n = \begin{bmatrix} l_n^2 \\ \mathbf{l}_n \\ 1 \\ l_n^2 \\ \mathbf{l}_n \\ 1 \\ l_n^2 \\ \mathbf{l}_n \\ 1 \end{bmatrix}. \quad (3.45)$$

3.12 USE OF C_n FOR CALCULATION OF C_∞

The results of an illustrative calculation are depicted in Fig. 3.4. The chain has $\theta = 112°$, $\nu = 3$, and $\phi = 180°$ and $\pm 60°$. The statistical weight matrix for all internal bonds is given by Eq. (3.9) with $\tau = \psi = 1$. When σ and ω are also 1, the chain has the same C_n as the freely rotating chain with the same bond angle. Imposition of a symmetric torsional potential that penalizes the g states, with $\sigma = 0.4$, increases the C_n. Introduction of a pair-wise interdependence, via $\sigma = 0.4$ and $\omega = 0.1$, produces a further increase in C_n. Obviously, the interdependence of the bonds can have a strong effect on the unperturbed dimensions of the chain.

The value of C_∞ can be reliably determined from the results depicted in Fig. 3.4 if $\sigma = \omega = 1$, but the limiting value is less reliably defined when $\sigma = 0.4$ and $\omega = 0.1$. This problem is alleviated by plotting the same data in another manner, as shown in Fig. 3.5. The linear extrapolation of the data to $1/n = 0$ leads unambiguously to the value for C_∞. This linear extrapolation is theoretically justified both for $\langle r^2 \rangle_0 / nl^2$ and for $\langle s^2 \rangle_0 / nl^2$ [1] and also for the corresponding ratio constructed from the mean square unperturbed dipole moment, $\langle \mu^2 \rangle_0 / nm^2$ [131].

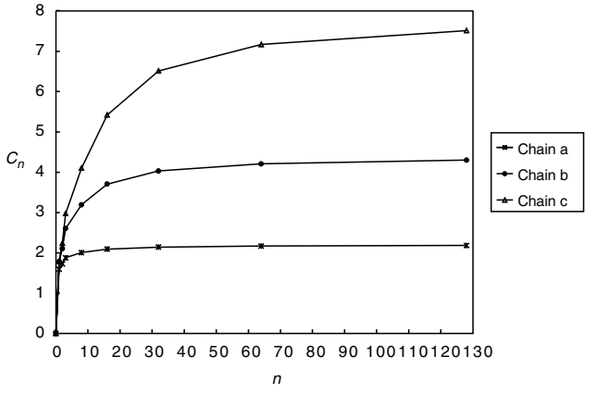

FIGURE 3.4. C_n vs. n for chains with $\theta = 112°$, $\nu = 3$, and $\phi = 180°$ and $\pm 60°$. **U** for all internal bonds is given by Eq. (3.9) with $\tau = \psi = 1$. The other statistical weights are (a) $\sigma = \omega = 1$, (b) $\sigma = 0.4$, $\omega = 1$, and (c) $\sigma = 0.4$, $\omega = 0.1$.

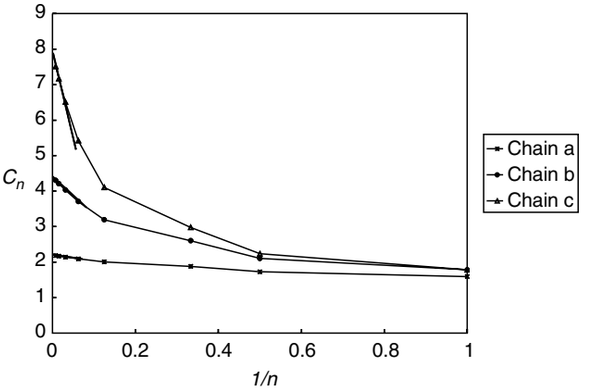

FIGURE 3.5. The data in Fig.3. 4 plotted as C_n vs. $1/n$, along with linear extrapolations to $1/n = 0$. The values of C_∞, which are (a) 2.198, (b) 4.396, and (c) 7.869, can be estimated with an error no larger than 1% by linear extrapolation of the data for n no larger than 128. The linear extrapolation shown, which uses C_{64} and C_{128}, leads to estimates for C_∞ of (a) 2.198, (b) 4.393, and (c) 7.858.

3.13 OTHER APPLICATIONS OF THE RIS MODEL

The previous portion of this chapter has focused primarily on the use of the RIS model for the computation of the mean square unperturbed dimensions, because that is the most frequent application of the model. This section describes briefly many other applications of the RIS model. All of these applications employ the conformational partition function, but the additional information incorporated in the calculation, and the manipulation of Z, depend on the application.

3.13.1 Applications That Depend Only on the Energetic Information Contained in Z

The calculation of $p_{\eta;i}$ as a function of i provides an estimate of the distance that end effects penetrate into a long unperturbed chain. This calculation shows that end effects for polyethylene are confined to the first few bonds at the end of the chain [10]. The end effects can extend much further into the chain when the second-order interactions become more severe, as is frequently the case for the probability of a helical conformation, $p_{h;i}$, in a long homopolypeptide near the midpoint of its helix-coil transition [132]. In proton NMR, the values of $p_{\eta;i}$ are helpful in understanding the values of the spin–spin coupling constants, using the Karplus relationship [111–114], and in understanding the γ effect on the chemical shift in ^{13}C NMR spectra [110,133]. The values of $p_{\eta;i}$ have also been used to interpret the optical activity exhibited by chiral poly(α-olefins) [115] and other polymers [134,135].

The combination of p_η and $p_{\xi\eta}$ gives the number of bonds in a run of state η. An illustrative use is in the determination of the average number of residues in a helical segment in a homopolypeptide as $p_h/p_c h$, where h denotes the helical state, and c denotes any other state [10,132].

The stereochemical composition of vinyl polymers after epimerization to stereochemical composition can be determined from the information contained in a more elaborate form of Z that takes account of the conformations of all stereochemical sequences, with all sequences weighted with respect to the same definition for the zero point of the conformational energy [136,137].

3.13.2 Applications That Use Properties Accessible From Z and the Geometry of the Chains

The higher even moments of the unperturbed dimensions, $\langle r^{2p}\rangle_0$ and $\langle s^{2p}\rangle_0$, $p > 1$, are accessible through an appropriate expansion in the dimensions of the generator matrices used for the simpler cases where $p = 1$ [11]. Dimensionless ratios formed from appropriate combinations of these even moments provide information about the shape of the distribution functions. Thus $\langle r^2\rangle_0$ measures the average value of r^2,$\langle r^4\rangle_0/\langle r^2\rangle_0^2$ measures the width of the distribution for r^2, and $\langle r^6\rangle_0/\langle r^2\rangle_0^3$ measures the skewness of this distribution function. All flexible homopolymers will approach the Gaussian limit of $\langle r^4\rangle_0/\langle r^2\rangle_0^2 = 5/3$ as $n \to \infty$, but narrower distributions (smaller $\langle r^4\rangle_0/\langle r^2\rangle_0^2$) are typical at finite n [138]. Macrocyclization equilibria can be understood in terms of these dimensionless ratios, via an elaboration of the Jacobson–Stockmayer approach [139,140]. More accurate results, particularly for rather short chains, are obtained when the $\langle r^{2p}\rangle_0/\langle r^2\rangle_0^p$ are supplemented by additional terms, calculated from the RIS model, that monitor the angular correlation between bonds 1 and n in the unperturbed chain as $r^2 \to 0$ [141,142].

Although the averages of many conformation-dependent physical properties of interest can be extracted rapidly from the RIS model by a matrix multiplication scheme of the type shown in Eq. (3.42), with $\boldsymbol{G}_i$ defined as appropriate for the specific property of interest, there are numerous other properties that cannot be evaluated by this simple device. For these other properties, an efficient Monte Carlo (MC) simulation can often be constructed, using the information in the RIS model. The information in Z allows rapid computation of the $p_{\eta;2}$ and $q_{\xi\eta;i}$, $2 < i < n$. These normalized probabilities and a random number generator allow rapid generation of a representative sample of unperturbed chains. If the sample is sufficiently large, the simple average of r^2 over all chains in the sample will approach the value of $\langle r^2\rangle_0$ specified by Eq. (3.42). The MC simulation is less efficient than Eq. (3.42) in the calculation of $\langle r^2\rangle_0$, but it offers the opportunity for the calculation of other physical properties that cannot be formulated as a serial matrix product. An example is provided by the angular scattering function, $P(q)$, where q is related to the scattering angle, θ, and wavelength of the radiation, λ, by Eq. (3.47).

$$P(q) = \frac{1}{(n+1)^2}\sum_{i=0}^{n}\sum_{j=0}^{n}\left\langle\frac{\sin(qr_{ij})}{qr_{ij}}\right\rangle, \tag{3.46}$$

$$q = \frac{4\pi}{\lambda}\sin\left(\frac{\theta}{2}\right). \tag{3.47}$$

An illustrative example is provided by the use of this approach to determine how the scattering function of unperturbed poly(methyl methacrylate) depends on the stereochemical composition of the chains [143]. The method can also be employed to generate accurate distribution functions for the end-to-end distance in unperturbed chains that are sufficiently short so that there are strong departures from the Gaussian distribution which would be achieved in the limit as $n \to \infty$ [144].

The representative sample of unperturbed chains can be edited to generate other useful ensembles. One of the most common examples is to discard chains with r larger than a specified cutoff. As this cutoff becomes smaller and smaller, the ensemble of surviving chains approaches the ensemble for the unperturbed macrocycle [145]. This ensemble can be used to evaluate properties of the ensemble directly, or to determine how easily polydimethylsiloxane macrocycles of a given n can be threaded [146]. The unperturbed ensemble can also be edited to discard chains that attempt placement of their atoms in regions of space that are deemed to be inaccessible. This approach generates ensembles of chains that are tethered by one end to an impenetrable surface [147], or chains in a melt that contains impenetrable spherical filler particles [148]. The complete ensemble of unperturbed chains can also be perturbed by the introduction of new interactions, not considered explicitly in the RIS model, as in the re-weighting of the ensemble to investigate the properties of bolaform electrolytes (polymer with ionic groups at their ends) [149].

The $p_{\eta;i}$ and $q_{\xi\eta;i}$ can be used to cause coarse-grained chains to mimic the conformational properties of specific real chains, because these probabilities enforce the proper distribution function for $\mathbf{r}$ for the entire coarse-grained chain, as well as all of its subchains [150,151]. This feature facilitates the recovery of atomistically detailed models from equilibrated ensembles of coarse-grained chains [152]. It also causes the coarse-grained chains to be sensitive to subtleties such as the dependence of the miscibility of polypropylene chains in the melt on their stereochemical composition [153,154].

3.13.3 Applications That Depend on Properties in Addition to Z and the Geometry of the Chains

Generator matrices are easily formulated for the computation of the mean square dipole moment, $\langle\mu^2\rangle_0$, using the analogy between formulating $\mathbf{r}$ as a sum of bond vectors and

formulating $\boldsymbol{\mu}$ as a sum of bond dipole moment vectors [10,15,130]. This analogy can be extended, via the valence optical scheme, to conformation-dependent properties that depend on the anisotropy of the polarizability of a bond [10,12]. This analogy leads to generator matrices for the optical anisotropy, stress-optical coefficient, electrical birefringence, i.e., molar Kerr constant, and magnetic birefringence, i.e., molar Cotton-Mouton constant.

3.14 WHY ARE SOME CHAINS DESCRIBED WITH MORE THAN ONE RIS MODEL?

The appearance in the literature of several RIS models for a single polymer may initially be confusing, but it is not at all surprising when one considers the objectives of the RIS approach. The exact description of the physical properties of a polymer would start from the Schrödinger equation, in a manner similar to one appropriate for small molecules. That approach is not practical. Therefore we resort to practical models that contain sufficient detailed information to let us account in a satisfactory manner for the physical properties that are of interest to us. Sometimes this objective can be obtained to a similar degree of accuracy with somewhat different values for the parameters in the model. This situation is illustrated by the first two entries in Table 3.2. The two RIS models for polyethylene place the *gauche* states at slightly different displacements, $\pm(120^\circ - \Delta\phi)$, from the *trans* state. In order to maintain the proper values for C_n, a change in the geometry of the chain, produced by a change in the value of $\Delta\phi$, requires compensating changes in the weighting of the chains, which is achieved by adjustments in the values of E_σ and E_ω [14]. If the value of $\Delta\phi$ were increased from 0 to 7.5° without any other changes in the model, C_n would increase because the g states would have been moved closer to the geometry of the t state. This increase in C_n can be avoided by increasing slightly the probability for g state, and that objective is achieved by the changes in E_σ and E_ω. The literature contains many similar examples where a given chain is described by various RIS models that have the same form, but slightly different values of the parameters.

There are also numerous examples where the RIS models have more substantial differences, because they use statistical weight matrices of different dimensions. Several examples are presented in Table 3.6. An obvious origin of the differences in dimension of the **U**'s is a difference in the number of rotational isomeric states assigned to individual bonds. Thus polyethylene has been described with RIS models that assign three [14], five [14], or seven [155] states to each internal bond. An increase in ν should lead to a more accurate model, because it permits the incorporation of more detail into the calculation. Of course, it also introduces more parameters into the model, with the added burden on the user of assigning values to these parameters. The most popular RIS models for polyethylene use $\nu = 3$ because the increased accuracy accessible with a larger value of ν usually is not justified because it makes a trivial improvement in the agreement between the calculated values and experiment. The principle here is to incorporate into the RIS model as much detail as is necessary . . . but no more detail than necessary.

TABLE 3.6. *Representative polymers that have been described by RIS models with different ν's*

Polymer	ν	References
Polyethylene	3	[14]
	5	[14]
	7	[155]
Polytetrafluoroethylene	3	[24]
	4	[25]
	6	[25]
Polyisobutylene	3	[32]
	4	[34,35]
	6	[33,35]
Poly(vinylidene chloride)	3	[156]
	6	[41]
Polypropylene	3	[69,71]
	4	[155]
	5	[72,157]
	6	[70]
Poly(methyl methacrylate)	2	[92]
	3	[94]
	6	[93]
Polycarbonate	2	[117,158]
	4	[16]

The necessary amount of detail required in the RIS model may depend on the physical property that is calculated from the model. For example, the dependence of C_∞ on stereochemical composition in poly(methyl methacrylate) is described nearly as well by a relative simple three-state model [94] and by a much more complex six state model that contains many more parameters [93]. However, the six-state model is superior to its simpler relative in the description of the scattering function, $P(\mu)$, which is sensitive to the precise description of the conformations of relatively short subchains [159]. In the case of polypropylene, the stereochemical composition achieved after epimerization to stereochemical equilibrium is captured correctly by a three-state model [71], but accurate description of the behavior of C_∞ with changes in stereochemical composition is better achieved with a five-state model [72]. The stereochemical composition at stereochemical equilibration does not depend explicitly on the geometry (l, θ, ϕ) when it is calculated with the RIS model [71], but C_∞ is obviously sensitive to this geometry [72]. In particular, the manner in which C_∞ depends on the probability of a *meso* dyad, p_m, as $p_m \to 1$ can be improved by going from a three-state to a five-state model.

The dimensions of **U** change, at constant ν, if higher order interactions are incorporated in the RIS model. Thus

polyethylene has been treated using a 9×9 representation of **U**. The calculation retains $\nu = 3$, but the increase in dimensions of **U** was necessary to test the potential importance of third-order interactions [160]. In order to introduce into **U** a statistical weight that depends on a third-order interaction, the rows are indexed by the states at bonds $i - 2$ and $i - 1$, and the columns are indexed by the states at bonds $i - 1$ and i, leading to a $\nu^2 \times \nu^2$ representation for **U**. The only nonzero elements in this **U** are those where the row and column agree on the state at bond $i - 1$. For this reason, 2/3 of the elements are zero. Any nonzero element corresponds to a unique combination of rotational isomeric states at bond $i - 2$, $i - 1$, and i. Third-order interactions have also been included in **U** for polyoxyethylene, requiring an expansion in the dimension of **U**, even though $\nu = 3$ [45]. Interactions of higher than third order are sometimes important, as illustrated by the transition from a random coil to an intramolecular antiparallel sheet with tight bends [161]. Under these circumstances, each **U** becomes a sparse matrix. The sparse character of the matrix can be exploited in writing the computer code required for numerical evaluation of the model [161].

ACKNOWLEDGMENT

Over his career, much of WLM's research using the RIS model has been supported by various sources. Current financial support for this research is from NSF DMR 0098321 and from the Collaborative Center in Polymer Photonics, funded jointly by the Air Force Office of Scientific Research, Wright-Patterson Air Force Base, and The University of Akron. Some items coauthored by WLM in the reference list were supported by FAA, NIH, and other NSF grants.

REFERENCES

1. W. L. Mattice, C. A. Helfer, and A. P. Sokolov, Macromolecules **37**, 4711 (2004).
2. P. Debye, J. Chem. Phys. **14**, 636 (1946).
3. H. A. Kramers and G. H. Wannier, Phys. Rev. **60**, 252 (1941).
4. M. V. Volkenstein, Dokl. Acad. Nauk SSSR **78**, 879 (1951).
5. Yu. Ya. Gotlib, Zh. Tekhn. Fiz. **29**, 523 (1959).
6. T. M. Birshtein and O. B. Ptitsyn, Zh. Tekhn. Fiz. **29**, 1048 (1959).
7. S. Lifson, J. Chem. Phys. **30**, 964 (1959).
8. K. Nagai, J. Chem. Phys. **31**, 1169 (1959).
9. C. A. J. Hoeve, J. Chem. Phys. **32**, 888 (1960).
10. P. J. Flory, *Statistical Mechanics of Chain Molecules* (Wiley, New York, 1969). Reprinted with the same title by Hanser, München, in 1989.
11. P. J. Flory, Macromolecules **7**, 381 (1974).
12. W. L. Mattice and U. W. Suter, *Conformational Theory of Large Molecules. The Rotational Isomeric State Model in Macromolecular Systems* (Wiley, New York, 1994).
13. M. Rehahn, W. L. Mattice, and U. W. Suter, Adv. Polym. Sci. **131/132** (1997).
14. A. Abe, R. L. Jernigan, and P. J. Flory, J. Am. Chem. Soc. **88**, 631 (1966).
15. A. Abe and J. E. Mark, J. Am. Chem. Soc. **98**, 6468 (1976).
16. M. Hutnik, A. S. Argon, and U. W. Suter, Macromolecules **24**, 5956 (1991).
17. J. H. Ko and J. E. Mark, Macromolecules **8**, 869, 874 (1975).
18. P. J. Flory, V. Crescenzi, and J. E. Mark, J. Am. Chem. Soc. **86**, 146 (1964).
19. C. A. Hoeve, J. Chem. Phys. **35**, 1266 (1961).
20. W. J. Welsh, L. DeBolt, and J. E. Mark, Macromolecules **19**, 2978 (1986).
21. J. A. Semlyen, Trans. Faraday. Soc. **63**, 743 (1967).
22. J. A. Semlyen, Trans. Faraday. Soc. **64**, 1396 (1968).
23. J. W. Mark and J. G. Curro, J. Chem. Phys. **80**, 5262 (1984).
24. T. W. Bates and W. H. Stockmayer, J. Chem. Phys. **45**, 2321 (1966).
25. G. D. Smith, R. L. Jaffe, and D. Y. Yoon, Macromolecules **28**, 3166 (1994).
26. O. Borodin, G. D. Smith, and D. Bedrov, J. Phys. Chem. B **106**, 9912 (2002).
27. R. Bohmer and C. A. Angell, Phys. Rev. B: Condens. Matter & Mater. Phys. **48**, 5857 (1993).
28. P. J. Flory and J. E. Mark, Makromol. Chem. **75**, 11 (1964).
29. G. D. Smith, R. L. Jaffe, and D. Y. Yoon, J. Phys. Chem. **98**, 9078 (1994).
30. D. Chen and W. L. Mattice, Polymer **45**, 3877 (2004).
31. M. S. Beavers and J. A. Semlyen, Polymer **13**, 385 (1972).
32. G. Allegra, E. Benedetti, and C. Pedrone, Macromolecules **3**, 727 (1970).
33. R. H. Boyd and S. M. Breitling, Macromolecules **5**, 1 (1972).
34. L. C. DeBolt and U. W. Suter, Macromolecules **20**, 1424 (1987).
35. M. Vacatello and D. Y. Yoon, Macromolecules **25**, 2502 (1992).
36. L. Carballeira, A. J. Pereiras, and M. A. Rios, Macromolecules **23**, 1309 (1990).
37. O. G. Byutner and G. D. Smith, Macromolecules **32**, 8376 (1999).
38. P. R. Sundararajan, Comput. Polym. Sci. **1**, 18 (1991).
39. I. Bahar, I. Zuniga, R. Dodge, and W. L. Mattice, Macromolecules **24**, 2986 (1991).
40. J. A. Semlyen and P. J. Flory, Trans. Faraday. Soc. **62**, 2622 (1966).
41. R. H. Boyd and L. Kesner, J. Polym. Sci., Polym. Phys. Ed. **19**, 393 (1981).
42. E. Saiz, J. Polym. Sci., Polym. Phys. Ed. **25**, 1565 (1987).
43. R. D. Patil and J. E. Mark, Comput. Theor. Polym. Sci. **10**, 189 (2000).
44. J. E. Mark and P. J. Flory, J. Am. Chem. Soc. **87**, 1415 (1965).
45. G. D. Smith, D. Y. Yoon, and R. L. Jaffe, Macromolecules **26**, 5213 (1993).
46. Y. Sasanuma, H. Ohta, I, Touma, H. Matoba, Y. Hayashi, and A. Kaito, Macromolecules **35**, 3748 (2002).
47. W. G. Miller, D. A. Brant, and P. J. Flory, J. Mol. Biol. **23**, 67 (1967).
48. A. Abe, Macromolecules **13**, 546 (1980).
49. W. L. Mattice, J. Am. Chem. Soc. **102**, 2242 (1980).
50. K. Kato, A. Araki, and A. Abe, Polym. J. **13**, 1065 (1981).
51. J. E. Mark, J. Am. Chem. Soc. **88**, 4354 (1966).
52. T. Ishikawa and K. Nagai, J. Polym. Sci., Part A-2 **7**, 1123 (1969).
53. Y. Abe and P. J. Flory, Macromolecules **4**, 219 (1971).
54. G. D. Smith and W. Paul, J. Phys. Chem. A **102**, 1200 (1998).
55. J. E. Mark, J. Am. Chem. Soc. **89**, 6829 (1967).
56. T. Ishikawa and K. Nagai, Polym. J. **1**, 116 (1970).
57. Y. Abe and P. J. Flory, Macromolecules **4**, 230 (1971).
58. J. Guzmán, E. Riande, W. J. Welsh, and J. E. Mark, Makromol. Chem. **183**, 2573 (1982).
59. E. Saiz, E. Riande, J. Guzmán, and J. de Abajo, J. Chem. Phys. **73**, 958 (1980).
60. K. Inomata, N. Phataralaoha, and A. Abe, Comput. Polym. Sci. **1**, 126 (1991).
61. E. Riande, J. Guzmán, E. Saiz, and J. de Abajo, Macromolecules **14**, 608 (1981).
62. E. Riande and J. E. Mark, Macromolecules **11**, 956 (1978).
63. E. Riande, J. Guzmán, W. J. Welsh, and J. E. Mark, Makromol. Chem. **183**, 2555 (1982).
64. E. Riande and J. Guzmán, Macromolecules **12**, 952 (1979).
65. E. Riande, J. Polym. Sci., Polym. Phys. Ed. **14**, 2231 (1976).
66. M. Mutter, U. W. Suter, and P. J. Flory, J. Am. Chem. Soc. **98**, 5745 (1976).
67. P. J. Flory, J. E. Mark, and A. Abe, J. Am. Chem. Soc. **88**, 639 (1966).
68. D. Y. Yoon, P. R. Sundararajan, and P. J. Flory, Macromolecules **8**, 776 (1975).
69. Y. Abe, A. E. Tonelli, and P. J. Flory, Macromolecules **3**, 294, 303 (1970).

70. R. H. Boyd and S. M. Breitling, Macromolecules **5**, 279 (1972).
71. U. W. Suter, S. Pucci, and P. Pino, J. Am. Chem. Soc. **97**, 1018 (1975).
72. U. W. Suter and P. J. Flory, Macromolecules **8**, 765 (1975).
73. R. M. Wolf and U. W. Suter, Macromolecules **17**, 669 (1984).
74. A. E. Tonelli, Macromolecules **18**, 1086 (1985).
75. A. E. Tonelli, Macromolecules **13**, 734 (1980).
76. W. L. Mattice, Macromolecules **10**, 1171 (1977).
77. P. R. Sundararajan, Macromolecules **23**, 3178 (1990).
78. A. Abe, T. Hirano, and T. Tsurura, Macromolecules **12**, 1092 (1979).
79. Y. Sasanuma, Macromolecules **28**, 8629 (1995).
80. A. Abe, Macromolecules **10**, 34 (1977).
81. J. E. Mark, J. Chem. Phys. **56**, 451 (1972).
82. G. D. Smith, P. J. Ludovice, R. L. Jaffe, and D. Y. Yoon, J. Phys. Chem. **99**, 164 (1995).
83. U. W. Suter, J. Am. Chem. Soc. **101**, 6481 (1979).
84. A. Abe, Macromolecules **13**, 541 (1980).
85. Y. Sasanuma, Y. Hayashi, H. Matoba, I. Touma, H. Ohta, M. Sawanobori, and A. Kaito, Macromolecules **24**, 8216 (2002).
86. E. D. Akten and W. L. Mattice, Macromolecules **34**, 3389 (2001).
87. P. R. Sundararajan, Macromolecules **11**, 256 (1978).
88. P. J. Flory, J. Am. Chem. Soc. **89**, 1798 (1967).
89. D. Y. Yoon, U. W. Suter, P. R. Sundararajan, and P. J. Flory, Macromolecules **8**, 784 (1975).
90. E. A. Ovalvo, E. Saiz, R. M. Masegosa, and I. Hernández-Fuentes, Macromolecules **12**, 865 (1979).
91. J. A. Guest, K. Matsuo, W. H. Stockmayer, and U. W. Suter, Macromolecules **13**, 560 (1980).
92. P. R. Sundararajan and P. J. Flory, J. Am. Chem. Soc. **96**, 5025 (1974).
93. M. Vacatello and P. J. Flory, Macromolecules **19**, 405 (1986).
94. P. R. Sundararajan, Macromolecules **19**, 415 (1986).
95. J. E. Mark and J. H. Ko, J. Polym. Sci., Polym. Phys. Ed. **13**, 2221 (1975).
96. A. D. Williams and P. J. Flory, J. Am. Chem. Soc. **91**, 3111 (1969).
97. R. F. Rapold and U. W. Suter, Macromol. Theory Simul. **3**, 1 (1994).
98. A. E. Tonelli, Macromolecules **18**, 2579 (1985).
99. E. Saiz, E. Riande, M. P. Delgado, and J. M. Barrales-Rienda, Macromolecules **15**, 1152 (1982).
100. A. E. Tonelli, Polymer **23**, 676 (1982).
101. P. R. Sundararajan, Macromolecules **10**, 623 (1977).
102. W. J. Welsh, J. R. Damewood, Jr., and R. C. West, Macromolecules **22**, 2947 (1989).
103. P. R. Sundararajan, Macromolecules **24**, 1420 (1991).
104. J. E. Mark, J. Chem. Phys. **56**, 458 (1972).
105. J. S. Saiz, E. Riande, J. San Román, and E. L. Madruga, Macromolecules **23**, 786 (1990).
106. P. R. Sundararajan, Macromolecles **13**, 512 (1980).
107. A. Abe, H. Kobayashi, T. Kawamura, M. Date, T. Uryu, and K. Matsuzaki, Macromolecules **21**, 3414 (1988).
108. P. R. Sundararajan, Macromolecules **21**, 1256 (1988).
109. C. A. Helfer, W. L. Mattice, and D. Chen, Polymer **45**, 1297 (2004).
110. A. E. Tonelli, *NMR Spectroscopy and Polymer Microstructures. The Conformational Connection.* (VCH, New York, 1989).
111. M. Karplus, J. Chem. Phys. **30**, 11 (1959).
112. M. Karplus, J. Chem. Phys. **33**, 1842 (1960).
113. M. Karplus, J. Am. Chem. Soc. **35**, 2870 (1963).
114. F. A. Bovey, A. I. Brewster, D. J. Patel, A. E. Tonelli, and D. A. Torchia, Acct. Chem. Res. **5**, 193 (1972).
115. A. Abe, J. Am. Chem. Soc. **90**, 2205 (1968).
116. W. K. Kim and W. L. Mattice, Comput. Theor. Polym. Sci. **8**, 339 (1998).
117. A. D. Williams and P. J. Flory, J. Polym. Sci.: Part A-2 **6**, 1945 (1968).
118. A. D. Williams and P. J. Flory, J. Polym. Sci.: Part A-2 **5**, 147 (1967).
119. F. Mendicuti, E. Saiz, and W. L. Mattice, Polymer **33**, 4908 (1992).
120. G. C. Rutledge, Macromolecules **25**, 3984 (1992).
121. E. Yurtsever and B. Erman, Polymer **34**, 3887 (1993).
122. V. S. R. Rao, N. Yathindra, and P. R. Sundararajan, Biopolymers **8**, 325 (1969).
123. D. A. Brant and W. L. Dimpfl, Macromolecules **3**, 655 (1970).
124. D. A. Brant and K. D. Goebel, Macromolecules **8**, 522 (1975).
125. W. K. Olson and P. J. Flory, Biopolymers **11**, 1 (1972).
126. D. A. Brant and P. J. Flory, J. Am. Chem. Soc. **87**, 2788 (1965).
127. W. G. Miller and P. J. Flory, J. Mol. Biol. **15**, 298 (1966).
128. D. A. Brant, W. G. Miller, and P. J. Flory, J. Mol. Biol. **23**, 47 (1967).
129. D. A. Brant, A. E. Tonelli, and P. J. Flory, Macromolecules **2**, 225, 228 (1969).
130. J. E. Mark, J. Chem. Phys. **56**, 458 (1972).
131. C. A. Helfer and W. L. Mattice, Polymer **46**, 4361 (2005).
132. D. C. Poland and H. A. Scheraga, *Theory of Helix-Coil Transitions in Biopolymers; Statistical Mechanical Theory of Order–Disorder Transitions in Biological Macromolecules* (Academic, New York, 1970).
133. A. E. Tonelli and F. C. Schilling, Acct. Chem. Res. **14**, 223 (1981).
134. A. Abe, J. Am. Chem. Soc. **92**, 1136 (1970).
135. E. Saiz and M. P. Tarazona, Macromolecules **16**, 1128 (1983).
136. U. W. Suter, Macromolecules **14**, 523 (1980).
137. U. W. Suter and P. Neuenschwander, Macromolecules **14**, 528 (1980).
138. R. L. Jernigan and P. J. Flory, J. Chem. Phys. **50**, 4178 (1969).
139. H. Jacobson and W. H. Stockmayer, J. Chem. Phys. **18**, 1600 (1950).
140. R. L. Jernigan and P. J. Flory, J. Chem. Phys. **50**, 4185 (1969).
141. P. J. Flory, U. W. Suter, and M. Mutter, J. Am. Chem. Soc. **98**, 5733 (1976).
142. U. W. Suter, M. Mutter, and P. J. Flory, J. Am. Chem. Soc. **98**, 5740 (1976).
143. M. Vacatello, D. Y. Yoon, and P. J. Flory, Macromolecules **23**, 1993 (1990).
144. J. E. Mark and J. G. Curro, J. Chem. Phys. **81**, 6408 (1984).
145. W. L. Mattice, Macromolecules **13**, 506 (1980).
146. L. C. DeBolt and J. E. Mark, Macromolecules **20**, 2369 (1987).
147. R. I. Feigin and D. H. Napper, J. Colloid. Interf. Sci. **71**, 117 (1979).
148. M. A. Sharaf, A. Kloczkowski, and J. E. Mark, Comput. Polym. Sci. **4**, 29 (1994).
149. W. M. Mattice and J. Skolnick, Macromolecules **14**, 863 (1981).
150. R. F. Rapold and W. L. Mattice, Macromolecules **29**, 2457 (1996).
151. T. Haliloglu and W. L. Mattice, J. Chem. Phys. **108**, 6989 (1997).
152. P. Doruker and W. L. Mattice, Macromolecules **30**, 5520 (1997).
153. T. C. Clancy, M. Pütz, J. D. Weinhold, J. G. Curro, and W. L. Mattice, Macromolecules **33**, 9452 (2000).
154. G. Xu, T. C. Clancy, W. L. Mattice, and S. K. Kumar, Macromolecules **35**, 3309 (2002).
155. P. J. Flory, J. Polym. Sci., Polym. Phys. Ed. **11**, 621 (1973).
156. K. Matsuo and W. H. Stockmayer, Macromolecules **8**, 650 (1975).
157. F. Heatley, Polymer **13**, 218 (1972).
158. B. C. Laskowski, D. Y. Yoon, D. MacLean, and R. L. Jaffe, Macromolecules **21**, 1629 (1988).
159. M. Vacatello, D. Y. Yoon, and P. J. Flory, Macromolecules **23**, 1993 (1990).
160. W. L. Mattice, Comput. Polym. Sci. **1**, 173 (1991).
161. W. L. Mattice and H. A. Scheraga, Biopolymers **23**, 1701 (1984).

CHAPTER 4

Computational Parameters

Joel R. Fried

Department of Chemical and Materials Engineering, University of Cincinnati, Cincinnati, OH 45221-0012

This chapter discusses the form and parameterization of the potential energy terms that are used for the atomistic simulation of polymers. The sum of potential terms constitutes a molecular force field that can be used in molecular mechanics, molecular dynamics, and Monte Carlo simulations of polymeric systems. Molecular simulation methods can be used to determine such properties as PVT data, self-diffusion coefficients, modulus, phase equilibrium, x-ray and neutron diffraction spectra, small molecule solubility, and glass transition temperatures with considerable accuracy and reliability using current force fields. Included in the coverage of Chapter 4 is a review of the fundamentals of molecular mechanics and a survey of the most widely used force fields for the simulation of polymer systems. In addition, references to the use of specific force fields in the study of important polymer groups are given.

4.1 MOLECULAR MECHANICS

Traditional molecular mechanics methods developed by Allinger [1] and others view a molecule as a series of beads (i.e., the nuclei) joined together by springs (i.e., the bonds). The total potential energy, V, of the system is the sum of all bonded and nonbonded terms as

$$V(\mathbf{r}) = V^{\mathbf{B}}(\mathbf{r}) + V^{\mathrm{NB}}(\mathbf{r}). \tag{4.1}$$

The bonded terms include bond stretching, angle bending, and dihedral (i.e., torsional) contributions as

$$V^{\mathrm{B}}(\mathbf{r}) = \sum_{\text{bonds}} V^{\mathrm{bond}}(r_{ij}) + \sum_{\text{bends}} V^{\mathrm{bend}}(\theta_{ijk}) + \sum_{\text{dihedrals}} V^{\mathrm{tors}}(\phi_{ijkl}), \tag{4.2}$$

where the summations are made over all contiguous atoms constituting bonds (i.e., two-body interactions), angles (three-body interactions), and torsions (four-body interactions) in the system. Torsional contributions also may include improper torsion and out-of-plane bending terms in some force fields as discussed in Section 4.2.

Nonbonded terms typically include steric (e.g., van der Waals) and electrostatic (e.g., Coulombic) terms but may also include polarization contributions. Force field parameters for each bonded or nonbonded term are obtained by fitting potential energy terms to ab initio (e.g., HF/6-31G*) or DFT calculations of small molecules or by fitting to experimental data such as crystal structure and the heat of vaporization[1] (ΔH_{V}) for low-molecular-weight compounds. The form of specific terms used by different commercial, public domain, and customized force fields for polymer simulations are given in the sections that follow.

4.1.1 Bonded Terms

Bond Stretching

Bond-stretching terms can have several different forms including the simple harmonic function

$$V^{\mathrm{bond}}(r_{ij}) = \frac{1}{2}\sum_{\text{bonds}} k_{ij}^{\mathrm{bond}}\left(r_{ij} - r_{ij}^{0}\right)^2, \tag{4.3}$$

where k_{ij}^{bond} is the bond-stretching parameter and r_{ij}^{0} is the equilibrium bond distance (for which the potential energy contribution is zero). The summation is taken over all bonds in the system. Alternately, additional higher order (i.e.,

[1] The heat of vaporization is related to the cohesive energy density (CED), the total intermolecular energy, through the expression

$$E_{\mathrm{CED}} = \frac{\rho}{M}(\Delta H_{\mathrm{V}} - RT)$$

where M is the molecular weight and ρ is the density of the low-molecular-weight compound.

anharmonic) terms may be included as a polynomial such as the quartic expression

$$V^{\text{bond}}(r_{ij}) = \frac{1}{2}\sum_{\text{bonds}}\left[k_2\left(r_{ij}-r_{ij}^0\right)^2 + k_3\left(r_{ij}-r_{ij}^0\right)^3 + k_4\left(r_{ij}-r_{ij}^0\right)^4\right]. \quad (4.4)$$

A Morse exponential potential [2] can also be used for the bond-stretching term in the form

$$V^{\text{bond}}(r_{ij}) = \sum_{\text{bonds}} D_{ij}\left\{\exp\left[-\alpha\left(r_{ij}-r_{ij}^0\right)\right]-1\right\}^2, \quad (4.5)$$

where D_{ij} is the bond dissociation energy and

$$\alpha = \left(\frac{k_{ij}}{2D_{ij}}\right)^{1/2}. \quad (4.6)$$

The Morse function is an accurate representation of the bond-stretching potential since the exponential term in Eq. (4.5) implicitly includes anharmonic terms.

Angle Bending

The harmonic term for (valence) angle bending can be written as

$$V^{\text{bend}}(\theta_{ijk}) = \frac{1}{2}\sum_{\text{bends}} k_{ijk}^{\text{bend}}\left(\theta_{ijk}-\theta_{ijk}^0\right)^2, \quad (4.7)$$

where θ_{ijk}^0 is the equilibrium (i.e., minimum energy) valence angle. The quartic form may be written as

$$V^{\text{bend}}(\theta_{ijk}) = \frac{1}{2}\sum_{\text{bends}}\left[k_2\left(\theta_{ijk}-\theta_{ijk}^0\right)^2 + k_3\left(\theta_{ijk}-\theta_{ijk}^0\right)^3 + k_4\left(\theta_{ijk}-\theta_{ijk}^0\right)^4\right]. \quad (4.8)$$

An alternative to the harmonic expression Eq. (4.7) is the Urey–Bradley expression

$$V_{\text{UB}} = \sum_{\text{UB}} K_{\text{UB}}(S-S_0)^2. \quad (4.9)$$

where S is the Urey–Bradley 1,3 distance (i.e., the A–C distance in bond angle ABC).

Torsion

Torsional terms can have several different forms such as

$$V^{\text{tors}}(\phi_{ijkl}) = \frac{1}{2}\sum_{\text{dihedrals}}\sum_{n=1,2,\ldots} k_{ijkl}^{\text{tors}}(n)[1-\cos(n\phi_{ijkl})], \quad (4.10)$$

where n is the periodicity of the torsional motion. Another torsional form that has been used is the Ryckaert–Bellemans potential [3,4]

$$V^{\text{tors}}(\phi_{ijkl}) = \sum_{\text{dihedrals}}\sum_{n=0}^{5} a_n\cos^n\phi_{ijkl}. \quad (4.11)$$

Improper (out-of-plane bending) torsion potentials appear in some force fields. These are used to represent potential energy required to maintain the configuration of four contiguous atoms within certain geometric limits. The form of this potential term can be written as

$$V^{\text{oop}}(\omega_{ijkl}) = \frac{1}{2}\sum_{\substack{\text{improper}\\ \text{torsions}}} k_{ijkl}^{\text{oop}}\left(\omega_{ijkl}-\omega_{ijkl}^0\right)^2, \quad (4.12)$$

where ω_{ijkl}^0 represents the equilibrium (i.e., minimum energy) improper torsion angle.

Cross-Coupling Terms

Cross-coupling terms have been used in several force fields as a means to represent the effect of one type deformation on another such as the interrelationship between bond stretching and angle bending which can be expressed in a bond–bend potential term as

$$V^{\text{b,b}}(r_{ij},\theta_{ijk}) = \frac{1}{2}\sum_{\text{bonds}}\sum_{\text{bends}} k^{\text{b,b}}\left(r_{ij}-r_{ij}^0\right)^2\left(\theta_{ijk}-\theta_{ijk}^0\right)^2. \quad (4.13)$$

Other cross-coupling terms include bond–torsion and bend–bend–torsion. Cross-coupling terms are important for accurate modeling of normal mode vibrational frequencies and to better model the potential at large deformation (i.e., positions far from the potential minimum).

4.1.2 Nonbonded Terms

Nonbonded terms include intramolecular interactions between pairs of atoms separated by three or more bonds and those belonging to different molecules (i.e., intermolecular interactions). Interactions between pairs of atoms separated by one or two bonds are contained in the bonded energy terms of the bond-stretch and angle-bending terms, respectively. All interactions in a simulation system may be included (i.e., Ewald summation) or distance cutoffs, typically in the range from 8 to 12 Å, may be used.

Steric Terms

Steric interactions are typically represented by some form of a Lennard-Jones (LJ) potential such as the LJ 6–12 potential or the LJ 6–9 potential as illustrated below

$$V^{\text{LJ}} = \sum_{i\neq j}\varepsilon_{ij}\left[2\left(\frac{r_{ij}^0}{r_{ij}}\right)^9 - 3\left(\frac{r_{ij}^0}{r_{ij}}\right)^6\right]. \quad (4.14)$$

The 6th order term in the LJ expression represents dispersion (long-range) interactions while the 9th (or 12th) order term represents short-range repulsion. Sometimes an exponential potential may be used as the short-range term in combination with a 6th order dispersion term in the form

$$V^{\exp-6} = \sum_{i \neq j} \left[A_{ij} \exp(-B_{ij} r_{ij}) - \frac{C_{ij}}{r_{ij}^6} \right]. \tag{4.15}$$

The exponential form is a better representation of repulsive interactions than the LJ inverse-12 form. The combination of an exponential and a 6th order term has been called the Buckingham potential function, the exponential-6 equation, or the modified Hill equation.

The LJ parameters ε_{ij} and r_{ij}^0 appearing in Eq. (4.14) are obtained by a combination rule using individual atomic parameters. These combination rules include the Lorentz and Berthelot rule and the 6th order combination law given as [5]

$$r_{ij}^0 = \left[\frac{(r_i^0)^6 + (r_j^0)^6}{2} \right]^{1/6} \tag{4.16}$$

and

$$\varepsilon_{ij} = \frac{2(\varepsilon_i \varepsilon_j)^{1/2} (r_i^0 r_j^0)^3}{(r_i^0)^6 + (r_j^0)^6}. \tag{4.17}$$

Electrostatic Terms

The electrostatic terms include the simple Coulombic expression in the general form

$$V^{\text{es}} = \sum_{i \neq j} \frac{f q_i q_j}{r_{ij}}, \tag{4.18}$$

where q_i represents the charge on atom i of the atom pair i,j, r_{ij} is the separation between atoms i and j, and $f = 1/\pi\varepsilon_0$ where ε_0 is the dielectric constant.

Hydrogen Bonding Contributions

An additional nonbonded term sometimes appearing in force fields for biological systems (especially older force field versions) is used to model the interaction between hydrogen donor and acceptor atoms involved in hydrogen bonding. An example is the potential energy term

$$V^{\text{HB}} = \sum_{i \neq j} \left(\frac{C_{ij}}{r_{ij}^{12}} - \frac{D_{ij}}{r_{ij}^{10}} \right) \cos^4 \theta_{\text{DHA}}, \tag{4.19}$$

where θ_{DHA} is the angle between the donor (D), hydrogen (H), and acceptor (A) atoms. Current force field versions do not explicitly treat hydrogen bonding since extensive parameterization of nonbonded terms ideally should include hydrogen bonding. Incorporation of multiple nonbonded terms, including polarization terms as discussed in the next section, significantly adds to the computational time since nonbonded interactions must be calculated between thousands of atoms at each timestep, typically 1 fs.

Polarization

Some force fields also include a polarization term, V^{pol}, along with steric (i.e., LJ or Buckingham) and electrostatic terms in the nonbonded potential expression as

$$V^{\text{NB}}(\mathbf{r}) = V^{\text{steric}}(\mathbf{r}) + V^{\text{es}}(\mathbf{r}) + V^{\text{pol}}(\mathbf{r}). \tag{4.20}$$

An example of the form of a polarization term is [6]

$$V^{\text{pol}} = \frac{1}{2} \sum_i \mu_i E_i, \tag{4.21}$$

where μ_i is the dipole moment associated with atom i and E_i is the electrostatic field experienced at atom i. A detailed discussion of polarization contributions is given by Smith and Borodin [7]. Polarizable force fields allow the charge distribution to respond to the dielectric environment [8] and are particularly important in the atomistic simulation of water and the detailed simulation of biological systems in general. A problem associated with inclusion of a polarization potential term is the additional computational cost incurred by including another nonbonded term. In the case of polymers, polarizable force fields are particularly important in the treatment of polymer electrolytes including those of poly(ethylene oxide)/Li^+ as discussed by Smith and Borodin [7] and in the atomistic simulation of systems in which chemical reactions can occur as in the case of proton transfer (e.g., fuel cell applications) or the simulation of combustion events. Force fields that can treat bond formation or breaking include ReaxxFF [9] as discussed briefly in the next section.

4.2 FORCE FIELDS

Many different force fields are now available from commercial and other sources. Some force fields like the MM series[2] of force fields developed by Allinger and the Merck MM [10] have been parameterized primarily for molecular mechanics and dynamics of small molecules. Due to their limited importance for polymer simulations, they will not be covered in this section; however, they have been used to study conformational properties of model compounds for some aromatic polymers. In some cases, force fields primarily developed for biomolecules such as AMBER, CHARMM, and GROMOS have been used in the molecular simulation of polymeric systems. Force fields having particular importance for polymers include simple but versatile

[2] The most recent version is MM4.

generic Class I force fields like DREIDING [11]. At the upper end are ab initio parameterized Class II force fields such as the consistent force field (CFF) family to which the force field COMPASS[3] [12] belongs. COMPASS has been extensively parameterized using physical property data and includes anharmonic and cross-coupling contributions in the bonded interactions (Section 4.1.1). In the discussion that follows, force fields are grouped into the categories of generic force fields, biological force fields, and Class II force fields. As shown by references given in Table 4.1 that surveys the literature from 1990 to 2005, all the force fields discussed in this section have been used for the atomistic simulation of polymeric systems. Many of these articles provide information on parameterization. References prior to 1990 were included in the previous review by Roe [13].

4.2.1 Generic Force Fields

Universal. The parameters in the Universal force field (UFF) [14–16] are calculated using general rules based only upon the element, its hybridization, and its connectivity. For this reason, the UFF has broad applicability but is inherently less accurate than extensively parameterized force fields such as COMPASS. Bond-stretching terms in the UFF are either harmonic or Morse functions. The angle-bending and torsion terms are described by a small cosine Fourier expansion. For nonbonded terms, the LJ 6–12 potential and Coulombic terms are used for steric and electrostatic terms, respectively.

DREIDING. DREIDING is another general-purpose force field that uses generalized force constants and geometry parameters. Parameterization of DREIDING is biased toward the first row elements (and carbon); however, DREIDING can be custom parameterized from ab initio or semiempircal data from calculations of model compounds with very good success in the atomistic simulation of polymers as shown by Fried and Goyal [17] and others. The default form of DREIDING uses the harmonic term, Eq. (4.3), for bond stretching and a harmonic cosine form of the angle-bend term given as

$$V^{\text{bend}}(\theta_{ijk}) = \frac{1}{2}\sum_{\text{bends}} k_{ijk}^{\text{bend}}\left(\cos\theta_{ijk} - \cos\theta_{ijk}^{0}\right)^2 \qquad (4.22)$$

The torsion term has the form

$$V^{\text{tor}}(\phi_{ijk}) = \frac{1}{2}\sum_{\text{dihedrals}} k_{jk}^{\text{tor}}\left\{1 - \cos\left[n_{jk}(\phi_{\text{jk}} - \phi_{\text{jk}}^{0})\right]\right\} \qquad (4.23)$$

where ϕ is the dihedral or torsional angle between the *ijk* and *jkl* planes formed by two consecutive bonds *ij* and *kl*. In addition, DREIDING includes an inversion term that has

[3] *C*ondensed-phase *O*ptimized *M*olecular *P*otentials for *A*tomistic *S*imulation *S*tudies.

TABLE 4.1. *Literature citations (1990–2005) for force fields used in the atomistic simulations of polymers.*

Polymer	Force field	Reference
Poly(aryl ether ether ketone)	TRIPOS	[41]
	DREIDING	[42]
Polyarylates	CHARMM	[43]
Poly(2,5-benzimidazole)	TRIPOS	[44]
Polybenzoxazoles	DREIDING	[45]
trans-1,4-Polybutadiene	CHARMM	[46]
Polycarbonate	CFF93	[36]
	DREIDING	[47,48]
	TRIPOS	[49]
Polydimethylsiloxane	TRIPOS	[50]
	ReaxxFF	[9]
Polyethersulfone	DREIDING	[51]
Polyethylene	custom	[52]
	custom	[53]
	COMPASS	[54]
Poly(ethylene oxide)	CFF93	[39]
	custom	[55]
	CVFF	[56]
	PCFF	[57]
	DREIDING	[58]
Poly(ethylene terephthalate)	CFF93+	[37]
	Custom	[59]
	DREIDING	[60]
Poly(*p*-hydroxybenzoic acid)	CFF93	[37]
Polyimides	DREIDING	[61–66]
	TRIPOS	[67]
Polyisobutylene	Custom	[53]
Polyisoprene	PCFF	[68]
Polymethacrylates	AMBER	[69]
	PCFF	[70]
Poly(methyl methacrylate)	PCFF	[70,71]
Poly(naphthalic anhydride)	DREIDING	[72]
Poly(*p*-phenylene)	DREIDING	[73]
	UFF	[74]
Poly(*p*-phenylene isophthalate)	AMBER	[75]
Poly(*p*-phenylene sulfide)	Custom	[76]
Poly(*p*-phenylene terephthalate)	COMPASS	[77]
	AMBER	[75]
Polyphosphazenes	COMPASS	[40]
	AMBER	[78]
Polypropylene	CFF91	[79]
Poly(propylene oxide)	Custom	[80]
Polypyrrole	GROMOS	[81]
Polyrotaxanes	Tripos5.2	[82]
Polysilanes	CFF93	[38]
Polystyrene	CHARMM	[83,84]
	AMBER	[85]
syndiotactic-polystyrene	Custom	[86]
Poly[1-(trimethylsilyl)-1-propyne]	DREIDING	[17]
Polyurethanes	DREIDING	[87]
Poly(vinyl chloride)	custom	[88]
	CVFF, CFF91	[89]
Poly(vinyl methyl ether)	PCFF2	[90]
Poly(vinylene fluoride)	Custom	[91]

importance for atoms that are bonded to three other atoms (e.g., N in NH_3 and P in PH_3). The inversion term represents the difficulty of forcing all three bonds for atom i bonded to exactly three other atoms j, k, l, into the same plane. For nonbonded interactions, DREIDING uses a LJ 6–12 potential, a Coulombic expression for electrostatic interactions, and a term to accommodate hydrogen bonding.

where the bonded terms are all harmonic and there are no cross-terms.

CHARMM. The CHARMM[4] [19] force field includes harmonic terms for bond stretching and angle bending. Both proper and improper torsion terms are included in CHARMM as are LJ 6–12 and Coulombic nonbonded contributions.

4.2.2 Biological Force Fields

Empirical force fields for biological macromolecules have been reviewed by Mackerell [6] and by Ponder and Case [18]. These include CHARMM, AMBER, OPLS, and GROMOS. All may be classified as a Class I force field of the general form given by Eg. (4.24)

$$V(\mathbf{r}) = \frac{1}{2}\sum_{\text{bonds}} k_{ij}^{\text{bond}}(r_{ij}-r_{ij}^0)^2 + \frac{1}{2}\sum_{\text{bends}} k_{ijk}^{\text{bend}}(\theta_{ijk}-\theta_{ijk}^0)^2 + \sum_{\text{torsions}} k_\phi[1+\cos(n\phi-\delta)] + \frac{1}{2}\sum_{\substack{\text{improper}\\ \text{torsions}}} k_{ijkl}^{\text{oop}}(\omega_{ijkl}-\omega_{ijkl}^0)^2 + \sum_{i\neq j}\varepsilon_{ij}\left[2\left(\frac{r_{ij}^0}{r_{ij}}\right)^{12} - 3\left(\frac{r_{ij}^0}{r_{ij}}\right)^{6}\right] + \sum_{i\neq j}\frac{q_i q_j}{\varepsilon r_{ij}}, \tag{4.24}$$

AMBER. AMBER [20,21] has been extensively used in the simulation of proteins and nucleic acids but recently has been generalized with parameters for most organic acid and pharmaceutical molecules [22].

OPLS. The OPLS[5] force field [23–25] was introduced in the early 1980s to simulate liquid-state properties of water and more than 40 organic liquids. The form of the OPLS-AA force field is given as [25]

$$V(\mathbf{r}) = \sum_i k_{\mathrm{b},i}(r_i - r_i^0)^2 + \sum_i k_{\theta,i}(\theta_i-\theta_i^0)^2 + \sum_i \left[V_{0,i} + V_{1,i}(1+\cos\phi_i)/2 + V_{2,i}(1-\cos 2\phi_i)/2 + V_{3,i}(1+\cos 3\phi_i)/2\right] + \sum_i\sum_j \left\{(q_i q_j e^2/r_{ij}) + 4\varepsilon_{ij}\left[(\sigma_{ij}/r_{ij})^{12} - (\sigma_{ij}/r_{ij})^6\right]\right\}. \tag{4.25}$$

TRIPOS. A force parameterized for biomolecules and small organic molecules, but sometimes used for polymers, is the TRIPOS force field [26] in the Sybyl molecular modeling package. The TRIPOS 5.2 force field includes harmonic bond stretching and angle bending with a torsional function consisting of a single cosine term. Nonbonded terms include a LJ 6–12 potential and a Coulombic term with either a constant or distance dependent dielectric function.

GROMACS. Another force field originally targeted for the molecular simulations of biomolecules, but also useful for polymers, is GROMACS[6] that runs molecular dynamics in a message-passing parallel mode. GROMACS [27] is a new implementation of GROMOS[7] developed by van Gunsteren and Berendsen at the University of Groningen in the late 1980s [28,29]. Provisions are available in GROMACS for conversion between GROMACS and GROMOS formats including the GROMOS87 and GROMOS96 force fields that are provided in GROMACS. Current features of GROMACS 3.0 have been reviewed by Lindahl *et al*. [30].

For bonded terms, GROMACS uses either a two-body harmonic potential (Eq. (4.3)) or Morse function for bond stretching and a three-body harmonic potential for angle bending (Eq. (4.7)). For both bond stretching and angle bending, a constraint can be used in place of the potential term. Four-body potentials include proper torsions and improper torsion potentials in the form of Eqs. (4.11) and (4.12), respectively. GROMACS uses a LJ 6–12 potential (an exponential short-range term, Eq. (4.15), is optional) and a Coulombic term (Eq. (4.18)) for nonbonded interactions. Force fields options include GROMOS, OPLS, and AMBER. Any united atom (UA) or all-atom force fields based on the general types of potential functions implemented in the GROMOS code can be used. GROMACS also permits the use of arbitrary forms of interactions with spline-interpolated tables as well as external potential terms for position-restraining forces and external acceleration (for nonequilibrium molecular dynamics).

[4] *C*hemistry at *HAR*vard *M*acromolecular *M*echanics).
[5] Optimized Potentials for Liquid Simulations.
[6] *GRO*ningen *MA*chine for *C*hemical *S*imulation.
[7] *GRO*ningen *M*olecular *S*imulation.

CVFF. The consistent valence force field (CVFF) originally applied to biological systems [31] is a forerunner of the consistent force field (CFF) and its later derivatives (the polymer consistent force field PCFF and COMPASS) as discussed in Section 4.24. Terms in CVFF included a Morse potential for bond stretching, a harmonic term for angle bending, cosine torsional and out-of-plane torsional terms, four cross-coupling terms (bond–bond, angle–angle, bond–angle, and angle–torsion), and LJ 6–12 and Coulombic terms for nonbonded interactions. CVFF has been reported to perform less favorably than an early version of CFF (CFF91) for predicting the conformational energies of small molecules [32].

4.2.3 Specialized Force Field and MD Codes

ReaxFF. ReaxFF allows for bond breaking and bond formation in MD simulation so that thermal decomposition can be modeled as has been shown recently for polydimethylsiloxane [9]. ReaxxFF includes terms for traditional bonded potentials as well as nonbonded potentials (i.e., van der Waals and Coulombic). Bond breaking and bond formation are handled through a bond order/bond distance relationship. Parameterization is through high-level DFT calculations (B3LYP/6-311++G**).

DL_POLY. DL_POLY[8] is a parallel molecular dynamics simulation package originally developed at the Daresbury Laboratory in England. Parameters for the current DL_POLY_3 force field may be obtained from the GROMOS, AMBER, and DREIDING force fields that share functional forms.

LAMMPS. Another message-passing MD code is LAMMPS[9][33] used for high-performance parallelized molecular dynamics calculations. The current version (version 17) is compatible with both AMBER and CHARMM.

4.2.4 Class II Force Fields

Class II force fields make extensive use of both anharmonic and cross-coupling terms to adequately represent the ab initio potential energy surface (PES). These include the original consistent force field (CFF) that developed out of CVFF (Section 4.2.2) and subsequent variations, the most recent being the COMPASS force field.

CFF. The consistent force field (CCF) [34] developed by Biosym[10] is a descendent of CVFF but differs in the specific types of potential terms. The nonbonded terms of CFF include a quartic bond-stretch term (Eq. (4.4)), a quartic angle-bending term (Eq. (4.8)), a three-term Fourier expansion term for torsion (Eq. (4.10)), and an out-of-plane torsion term (Eq. (4.12)). CFF includes several different versions (CFF91, CFF93 [35], CFF95) and the polymer consistent force field (PCFF). CFF93 has been parameterized for polycarbonates [36], aromatic polyesters [37], polysilanes [38], and poly(ethylene oxide) [39].

COMPASS. COMPASS is an example of a Class II force field parameterized by using an analytic representation of the ab initio (e.g., HF/6-31G*) potential energy surface. The functional form of the COMPASS force field is the same as CFF93 and includes an out-of-plane potential term (angle χ), a LJ 6–9 potential as well as nonharmonic terms for bond stretching and angle bending, a Fourier cosine series for torsion, and a number of cross-coupled terms for the bonded interactions. The form of the COMPASS force field described in detail by Sun [12] is

$$
\begin{aligned}
V(\mathbf{r}) = {} & \sum_b \left[k_2(b-b_0)^2 + k_3(b-b_0)^3 + k_4(b-b_0)^4\right] + \\
& \sum_\theta \left[k_2(\theta-\theta_0)^2 + k_3(\theta-\theta_0)^3 + k_4(\theta-\theta_0)^4\right] + \\
& \sum_\phi \left[k_1(1-\cos\phi) + k_2(1-\cos 2\phi) + k_3(1-\cos 3\phi)\right] + \\
& \sum_\chi k_2\chi^2 + \sum_{b,b'} k(b-b_0)\left(b'-b_0^{'}\right) + \sum_{b,\theta} k(b-b_0)(\theta-\theta_0) + \\
& \sum_{b,\phi} (b-b_0)\left[k_1(1-\cos\phi) + k_2(1-\cos 2\phi) + k_3(1-\cos 3\phi)\right] + \\
& \sum_{b,\theta} k\left(\theta'-\theta_0^{'}\right)(\theta-\theta_0) + \sum_{\theta,\theta,\phi} k(\theta-\theta_0)\left(\theta'-\theta_0^{'}\right)\cos\phi + \\
& \sum_{i,j} \frac{q_i q_j}{r_{ij}} + \sum_{i,j} \varepsilon_{ij}\left[2\left(\frac{r_{ij}^0}{r_{ij}}\right)^9 - 3\left(\frac{r_{ij}^0}{r_{ij}}\right)^6\right].
\end{aligned}
\tag{4.26}
$$

The partial charge for atom i in COMPASS is the sum of all charge bond increments, δ_{ij}, as

$$q_i = \sum_j \delta_{ij}. \tag{4.27}$$

The LJ parameters are obtained from the 6th order combination law (Eqs. (4.16) and (4.17)).

The parameterization of COMPASS for bonded potential terms includes a fitting of the total energies as well their first derivatives (gradients) and second derivatives (Hessians) to ab initio (HF/6–31G*) calculations of low-molecular-weight analogs. Examples of such analogs in the parameterization of COMPASS terms for polycarbonate are diphenyl carbonate, dimethyl carbonate, and 2,2-diphenylpropane [36]. Nonbonded parameters are obtained from ab initio calculations and by parameter fitting to crystal structures. Valence parameters and charges are further scaled to fit experimental data. Full descriptions of the parameterization procedures and a tabulation of force constants for COMPASS have been given in several sources [12,40].*

[8] http://www.cse.clrc.ac.uk/msi/software/DL_POLY/.

[9] *L*arge-scale *A*tomic/*M*olecular *M*assively *P*arallel *S*imulator; http://www.cs.sandia.gov/~sjplimp/lammps.html.

[10] Biosym was merged with Molecular Simulations into the current company Accelrys.

REFERENCES

1. N. L. Allinger, in *Physical Advances in Organic Chemistry*, edited by V. Gold (Academic Press, London, 1976), Vol. 13, pp. 1–82.
2. P. M. Morse, Phys. Rev. **34**, 57 (1929).
3. J. P. Ryckaert and A. Bellemans, Faraday Discuss. Chem. Soc. **66**, 95 (1978).
4. J. P. Ryckaert and A. Bellemans, Chem. Phys. Lett. **30**, 123 (1984).
5. M. Waldman and A. T. Hagler, J. Comput. Chem. **14**, 1077 (1993).
6. A. Mackerell Jr., J. Comput. Chem. **25**, 1584 (2004).
7. G. D. Smith and O. Borodin, in *Molecular Simulation Methods for Predicting Polymer Properties*, edited by V. Galiatsatos, (Wiley-Interscience, Hoboken, 2005), pp. 47–94.
8. T. A. Halgren and W. Damm, Curr. Opin. Struct. Biol. **11**, 236 (2001).
9. K. Chenoweth, S. Cheung, A. C. T. van Duin, *et al*. J. Am. Chem. Soc. **127**, 7192 (2005).
10. T. A. Halgren, J. Comput. Chem. **17**, 490 (1996).
11. S. L. Mayo, B. D. Olafson and W. A. Goddard III, J. Phys. Chem. **94**, 8897 (1990).
12. H. Sun, J. Phys. Chem. B **102**, 7338 (1998).
13. R.-J. Roe, in *Physical Properties of Polymers Handbook*, edited by J. E. Mark, AIP Press, Woodbury, NY, 1996.
14. A. K. Rappe, C. J. Casewit, K. S. Colwell *et al*., J. Am. Chem. Soc. **114**, 10024 (1992).
15. C. J. Casewit, K. S. Colwell and A. K. Rappe, J. Am. Chem. Soc. **114**, 10047 (1992).
16. C. J. Casewit, K. S. Colwell and A. K. Rappe, J. Am. Chem. Soc. **114**, 10035 (1992).
17. J. R. Fried and D. K. Goyal, J. Polym. Sci., Part B: Polym. Phys. **36**, 519 (1998).
18. J. W. Ponder and D. A. Case, Adv. Protein Chem. **66**, 27 (2003).
19. B. R. Brooks, R. E. Bruccoleri, B. D. Olafson, *et al*., J. Comput. Chem. **4**, 187 (1983).
20. C. J. Weiner, P. A. Kollman, D. A. Case, *et al*., J. Am. Chem. Soc. **106**, 765 (1984).
21. D. A. Perlman, D. A. Case, J. W. Caldwell, *et al*., Comput. Phys. Commun. **91**, 1 (1995).
22. J. Wang, R. M. Wolf, J. W. Caldwell, *et al*., J. Comput. Chem. **25**, 1157 (2004).
23. W. L. Jorgenson and J. Tirado-Reeves, J. Am. Chem. Soc. **110**, 1657 (1988).
24. W. L. Jorgensen, D. S. Maxwell and J. Tirado-Rives, J. Am. Chem. Soc. **118**, 11225 (1996).
25. N. A. McDonald and W. L. Jorgensen, J. Phys. Chem. B **102**, 8049 (1998).
26. M. Clark, R. D. Cramer III and N. van Opdenbosch, J. Comput. Chem. **10**, 982 (1989).
27. H. J. C. Berendsen, D. van der Spoel and R. van Drunen, Comput. Phys. Commun. **91**, 43 (1995).
28. J. Hermans, H. J. C. Berendsen, W. F. van Gunsteren, *et al*., Biopolymers **23**, 1513 (1984).
29. W. R. P. Scott, P. H. Hunenberger, I. G. Tironi, *et al*., J. Phys. Chem. A **103**, 3596 (1999).
30. E. Lindahl, B. Hess and D. van der Spoel, J. Mol. Model. **7**, 306 (2001).
31. P. Dauber-Osguthorpe, V. A. Roberts, D. J. Osguthorpe, *et al*., Proteins: Struct. Funct. Genet. **4**, 31 (1988).
32. K. Gundertofte, T. Liljefors, P.-O. Norrby, *et al*., J. Comput. Chem. **17**, 429 (1996).
33. S. Plimpton and B. Hendrickson, J. Comput. Chem. **17**, 326 (1996).
34. J. R. Maple, M.-J. Hwang, T. P. Stockfisch, *et al*., J. Comput. Chem. **15**, 162 (1994).
35. M. J. Hwang, T. P. Stockfisch and A. T. Hagler, J. Am. Chem. Soc. **116**, 2515 (1994).
36. H. Sun, S. J. Mumby, J. R. Maple, *et al*., J. Am. Chem. Soc. 2978 (1994).
37. H. Sun, J. Comput. Chem. **15**, 752 (1994).
38. H. Sun, Macromolecules **28**, 701 (1995).
39. D. Rigby, H. Sun and B. E. Eichinger, Polym. Int. **44**, 331 (1997).
40. H. Sun, P. Ren and J. R. Fried, Comput. Theor. Polym. Sci. **8**, 229 (1998).
41. C. L. Chen, C. L. Lee, H. L. Chen, *et al*., Macromolecules **27**, 7872 (1994).
42. J. Kendrick, E. Robson and M. Weave, J. Chem. Soc., Faraday Trans. **91**, 2609 (1995).
43. S. G. Charati, R. Vetrivel, M. G. Kulkarni, *et al*., Macromolecules **25**, 2215 (1992).
44. J. Cho, J. Blackwell, S. N. Chvalun, *et al*., J. Polym. Sci., Part B: Polym. Phys. **42**, 2576 (2004).
45. V. J. Vasudevan and J. E. McGrath, Macromolecules **29**, 637 (1996).
46. R. Dodge and W. L. Mattice, Macromolecules **24**, 2709 (1991).
47. C. F. Fan, T. Cagin, Z. M. Chen, *et al*., Macromolecules **27**, 2383 (1994).
48. S. Kim and J. Liu, Korean Polym. J. **9**, 129 (2001).
49. J. H. Shih and C. L. Chen, Macromolecules **28**, 4509 (1995).
50. I. Bahar, I. Zuniga, R. Dodge, *et al*., Macromolecules **24**, 2986 (1991).
51. T. Shi and W. Jiang, Macromol. Theory Simul. **10**, 232 (2001).
52. D. W. Noid, B. G. Sumpter and B. Wunderlich, Macromolecules **24**, 4148 (1991).
53. P. V. K. Pant and R. H. Boyd, Macromolecules **26**, 679 (1993).
54. G. Zifferer and A. Kornherr, J. Chem. Phys. **122**, 204906 (2005).
55. G. D. Smith, R. L. Jaffe and D. Y. Yoon, J. Phys. Chem. **97**, 12752 (1993).
56. K. Tasaki, Macromolecules **29**, 8922 (1996).
57. J. Ennari, J. Hamara and F. Sundholm, Polymer **38**, 3733 (1997).
58. L. J. A. Siqueira and M. C. C. Ribeiro, J. Chem. Phys. **122**, 194911 (2005).
59. S. U. Boyd and R. H. Boyd, Macromolecules **34**, 7219 (2001).
60. D. Pavel and R. Shanks, Polymer **46**, 6135 (2005).
61. J. W. Kang, K. Choi, W. H. Jo, *et al*., Polymer **39**, 7079 (1998).
62. Y. Kitano, I. Usami, Y. Obata, *et al*., Polymer **36**, (1995).
63. M. V. Brillhart, Y. Y. Cheng, P. Nagarkart, *et al*., Polymer **38**, 3059 (1997).
64. R. Zhang and W. L. Mattice, Macromolecules **26**, 6100 (1993).
65. U. Natarajan and W. L. Mattice, Macromol. Theory Simul. **6**, 949 (1997).
66. A. Shimazu, T. Miyazaki and K. Ikeda, J. Phys.: Condens. Matter **166**, 113 (2000).
67. T.-M. Wu, S. Chvalum, J. Blackwell, *et al*., Polymer **36**, 2123 (1995).
68. F. Alvarez, A. Alegria, J. Colmenero, *et al*., Macromolecules **33**, 8077 (2000).
69. K.-Y. Jung, H.-I. Kim and J. Liu, Korean Polym. J. **8**, 59 (2000).
70. A. Soldera, Polymer **43**, 4269 (2002).
71. T. M. Nicholson and G. R. Davies, Macromolecules **30**, 5501 (1997).
72. J. Liu and P. H. Geil, J. Polym. Sci., Part B: Polym. Phys. **35**, 1575 (1997).
73. S. Hill, I. Hamerton and B. J. Howlin, Polymer **43**, 4103 (2002).
74. K. C. Park, L. R. Dodd, K. Levon, *et al*., Macromolecules **29**, 7149 (1996).
75. M. Depner and B. L. Schurmann, Polymer **33**, 398 (1992).
76. R. Napolitano, B. Pirozzi and A. Salvione, Macromolecules **32**, 7682 (1999).
77. T. Launne, I. Neelov and F. Sundholm, Macromol. Theory Simul. **10**, 1371 (2001).
78. H. R. Allcock, M. E. Napierala, D. L. Olmeijer, *et al*., Macromolecules **32**, 732 (1999).
79. B. Kuhn, M. Ehrig and R. Ahlrichs, Macromolecules **29**, 4051 (1996).
80. P. Ahlstrom, O. Borodin, G. Wahnstrom, *et al*., J. Chem. Phys. **112**, 10669 (2000).
81. J. J. L. Cascales and T. F. Otero, J. Chem. Phys. **120**, 1951 (2004).
82. J. Pozuelo, F. Mendicuti and W. L. Mattice, Macromolecules **30**, 3685 (1997).
83. R. Khare, M. E. Paulaitus and S. R. Lustig, Macromolecules **26**, 7203 (1993).
84. R. Khare and M. E. Paulaitis, Macromolecules **28**, 4495 (1995).
85. M. Mondello, H.-J. Yang, H. Furuya, *et al*., Macromolecules **27**, 3566 (1994).
86. Y. Tamai and M. Fukuda, Polymer **44**, 3279 (2003).
87. H. Yang, Z.-s. Li, Z.-y. Lu, *et al*., Polymer **45**, 6753 (2004).
88. G. D. Smith, R. L. Jaffe and D. Y. Yoon, Macromolecules **26**, 298 (1993).
89. R. J. Meier and L. C. E. Struik, Polymer **39**, 31 (1998).
90. C. Saelee, T. M. Nicholson and G. R. Davies, Macromolecules **33**, 2258 (2000).
91. N. Karasawa and W. A. Goddard III, Macromolecules **25**, 7268 (1992).

CHAPTER 5

Theoretical Models and Simulations of Polymer Chains

Andrzej Kloczkowski* and Andrzej Kolinski†

*L .H. Baker Center for Bioinformatics and Biological Statistics, Iowa State University, Ames, IA 50011, USA**; *Faculty of Chemistry, Warsaw University, Pasteura 1, 02-093 Warsaw, Poland*†

5.1 INTRODUCTION

In the first part of this article the review of various theoretical models for polymer chains is given. The models of freely jointed chains, freely rotating chains (including wormlike chains), and chains with fixed bond angles and independent rotational potentials and with interdependent potentials, including rotational isomeric state approximation, are presented.

In the second part various theories of polymer networks are presented. The affine network model, phantom network, and theories of real networks are discussed. Scattering from polymer chains is also briefly presented.

The third part of this article covers computer simulations of polymer chains. Methods of simulation of chains on lattices are presented and the equivalence between lattice chains and off-lattice chain models is discussed. The simulation of excluded volume effect is examined. The polymer chain collapse from random coil to dense globular state, and simulations of dense polymer systems are discussed.

This article describes models for linear chains of homopolymers and for unimodal, unfilled polymer networks. Theoretical models for other systems, such as star, branched, and ring polymers, random and alternating copolymers, graft and block copolymers are discussed in the book by Mattice and Suter [1]. Block copolymers are discussed in Chap. 32 of this Handbook [2]. Theories of branched and ring polymers are presented in the book by Yamakawa [3]. Liquid–crystalline polymers are discussed in the book by Grosberg and Khokhlov [4], and liquid crystalline elastomers in the recent book of Warner and Terentjev [5]. Bimodal networks are discussed by Mark and Erman [6,7]. Molecular theories of filled polymer networks are presented by Kloczkowski, Sharaf and Mark [8] and recently by Sharaf and Mark [9].

This first part of this article deals only with treatment of ''bonded'' interactions of polymer chains, appropriate only for modeling chains under Θ-point conditions. Problems connected with effects of excluded volume are presented at the end of this chapter. The excluded volume effect for chains in good solvents are also presented in Chaps. IIB [10] and IIID [11] of this handbook and in books by Freed [12], de Gennes [13], des Cloizeaux and Jannink [14], and

Forsman [15]. More information about computer modeling of polymers is provided by Binder [16,17], Baumgartner [18], Kolinski and Skolnick [19], and most recently by Kotelyanskii and Therodorou [20].

5.2 THE FREELY JOINTED CHAIN

The freely jointed chain model (known also as random flight model) was proposed for polymers by Kuhn in 1936. The chain is assumed to consist of n bonds of equal length l, jointed in linear succession, where the directions (θ, ϕ) of bond vectors may assume all values $(0 \le \theta \le \pi; 0 \le \phi \le 2\pi)$ with equal probability (see Fig. 5.1).

This means that directions of neighboring bonds are completely uncorrelated. The freely jointed chain model corresponds to a chain with fixed bond lengths and with unconstrained, free to adjust valence angles and with free torsional rotations. The mean square end-to-end vector $\langle r^2\rangle_0$ in the unperturbed state (denoted by subscript 0) for the freely jointed chain is

$$\langle r^2\rangle_0 = \langle (\sum_{i=1}^{n} \mathbf{l}_j)\cdot(\sum_{j=1}^{n}\mathbf{l}_j)\rangle_0 = nl^2 \tag{5.1}$$

because

$$\langle \mathbf{l}_i \cdot \mathbf{l}_j\rangle_0 = 0 \quad \text{for } i \neq j. \tag{5.2}$$

It is convenient to compare real polymer chains with freely jointed chain by using the concept of the characteristic ratio defined as the ratio of the mean-square end-to-end vectors of a real chain and freely jointed chain with the same number of bonds

$$C_n = \frac{\langle r^2\rangle_0}{nl^2}. \tag{5.3}$$

The characteristic ratio is a measure of chain flexibility. Flexible chains have C_n close to unity, while semiflexible and rigid polymers have usually much larger values of C_n. The mean-square radius of gyration for freely jointed chain is:

$$\langle s^2\rangle_0 \equiv \frac{\sum\limits_{0 \le i < j \le n} \langle r_{ij}^2\rangle_0}{(n+1)^2} = \frac{(n+2)nl^2}{6\ (n+1).} \tag{5.4}$$

For longer chains (in the limit $n \to \infty$) we have

$$\frac{\langle s^2\rangle_0}{\langle r^2\rangle_0} = \frac{1}{6}. \tag{5.5}$$

The freely jointed chain model has an exact analytical solution for the distribution function of the end-to-end vector. The probability that the chain of n bonds has the end-to-end vector $\mathbf{r}$ is

$$P(\mathbf{r},n) = \int \mathrm{d}\mathbf{l}_1\mathrm{d}\mathbf{l}_2\ldots\mathrm{d}\mathbf{l}_n\delta[(\sum_{i=1}^{n}\mathbf{l}_i) - \mathbf{r}]\prod_{j=1}^{n}\exp\left(\frac{-\mathrm{u}(\mathbf{l}_j)}{kT}\right), \tag{5.6}$$

where T is the absolute temperature, k is the Boltzmann constant, $u(\mathbf{l}_j)$ is the potential energy of two segments connected by the j-th bond $\mathbf{l}_j$, and δ denotes Dirac delta function. For the freely jointed chain model we have

$$\exp\left(\frac{-\mathrm{u}(\mathbf{l}_j)}{kT}\right) = \frac{1}{4\pi l^2}\delta(|\mathbf{l}_j| - \ell). \tag{5.7}$$

By using the Fourier representation of the δ function we obtain

$$\begin{aligned} P(\mathbf{r},\ n) &= \frac{1}{8\pi^3}\int \mathrm{d}\mathbf{k}\,\mathrm{e}^{-\mathrm{i}\mathbf{k}\cdot\mathbf{r}}\left[\frac{\sin(kl)}{kl}\right]^n \\ &= \frac{1}{2\pi^2 r}\int_0^\infty \sin(kr)\left[\frac{\sin(kl)}{kl}\right]^n k\mathrm{d}k. \end{aligned} \tag{5.8}$$

The solution of Eq. (5.8) is

$$P(\mathbf{r},\ n) = \frac{1}{2^{n+1}\pi l^2 r(n-2)!}\sum_{i=0}^{i\le(n-r/l)/2} (-1)^i\frac{n!}{i!(n-i)!}(n-2i-r/l)^{n-2}. \tag{5.9}$$

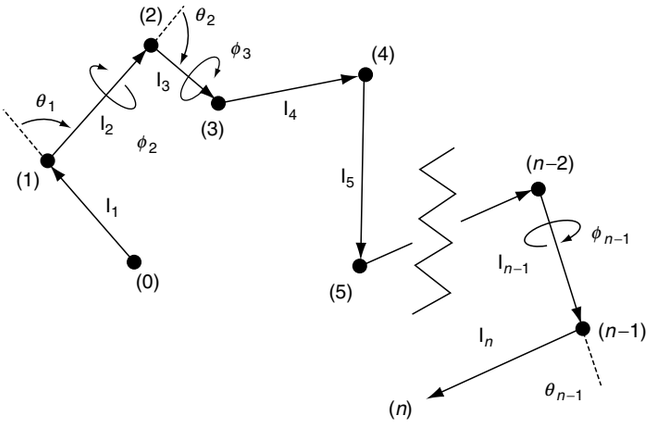

FIGURE 5.1. Polymer chain composed of n bonds. Angles θ are defined as complementary angles.

In the limit $n \to \infty$ the distribution function of the end-to-end vector for freely jointed chain asymptotically approaches a Gaussian function

$$P(\mathbf{r}, n) = \left(\frac{3}{2\pi n l^2}\right)^{3/2} \exp\left(\frac{-3r^2}{2nl^2}\right). \tag{5.10}$$

5.3 THE FREELY ROTATING CHAIN

The freely rotating chain model is a freely-jointed chain with fixed bond angles. It is assumed that all bond have equal length l and all bond angles are equal. The angle θ_i is defined as a supplementary angle of the skeletal bond angle at segment i as seen in Fig. 5.1, and therefore

$$\langle \mathbf{l}_{i+1} \cdot \mathbf{l}_j \rangle = l^2 \cos\theta. \tag{5.11}$$

Similarly for two bonds i and $i+k$ we have

$$\langle \mathbf{l}_{i+k} \cdot \mathbf{l}_i \rangle = l^2 (\cos\theta)^k. \tag{5.12}$$

This result follows from the fact that the projection of a given bond on the preceding bond is $\cos\theta$, while projections in two transverse directions averaged over free rotations are zero. This means that the projection of the $k+i$ bond on the $k+i-1$ bond is $\cos\theta$, the projection of this projection on the $k+i-2$ bond is $(\cos\theta)^2$, etc., which finally leads to the Eq. (5.12). The mean square end-to-end vector for freely rotating chain is

$$\begin{aligned}\langle r^2 \rangle &= \sum_{i=1}^{n} \langle \mathbf{l}_i \rangle^2 + 2 \sum_{i=1}^{n} \sum_{k=1}^{n-i} \langle \mathbf{l}_i \cdot \mathbf{l}_{j+k} \rangle \\ &= nl^2 \left[\frac{1+\cos\theta}{1-\cos\theta} - \frac{2\cos\theta[1-(\cos\theta)^n]}{n(1-\cos\theta)^2} \right]. \end{aligned} \tag{5.13}$$

For infinitely long chains the second term in Eq. (5.13) may be neglected and the characteristic ratio defined by Eq. (5.3) becomes:

$$C_\infty = \frac{1+\cos\theta}{1-\cos\theta}. \tag{5.14}$$

The mean square radius of gyration (defined by Eq. (5.4)) for freely rotating chain is

$$\begin{aligned}\frac{\langle s^2 \rangle_0}{nl^2} &= \frac{(n+2)(1+\cos\theta)}{6(n+1)(1-\cos\theta)} - \frac{\cos\theta}{(n+1)(1-\cos\theta)^2} \\ &\quad + \frac{2(\cos\theta)^2}{(n+1)^2(1-\cos\theta)^3} \\ &\quad - \frac{2(\cos\theta)^3[1-(\cos\theta)^n]}{n(n+1)^2(1-\cos\theta)^4}. \end{aligned} \tag{5.15}$$

For very long chains the last three terms in Eq. (5.15) become negligible and $\langle s^2 \rangle_0 = \langle r^2 \rangle_0 / 6$.

5.3.1 Worm-like Chain Model

The projection of the end-to-end vector of a chain $\mathbf{r}$ on the direction of the first bond $\mathbf{l}_1/l$ for the freely rotating chain is

$$\begin{aligned}\left\langle \frac{\mathbf{r} \cdot \mathbf{l}_1}{l} \right\rangle &= \frac{1}{l} \sum_{i=1}^{n} \langle \mathbf{l}_1 \cdot \mathbf{l}_i \rangle = l \sum_{i=0}^{n-1} (\cos\theta)^i \\ &= l \frac{1-(\cos\theta)^n}{1-\cos\theta}, \end{aligned} \tag{5.16}$$

where θ is the angle between bonds. In the limit $n \to \infty$ this converges to

$$\lim_{n\to\infty} \left\langle \frac{\mathbf{r} \cdot \mathbf{l}}{l} \right\rangle = \frac{1}{1-\cos\theta} \equiv a. \tag{5.17}$$

The quantity a is called the persistence length and is a measure of chain stiffness. The wormlike chain model (sometimes called the Porod-Kratky chain) is a special continuous curvature limit of the freely rotating chain, such that the bond length l goes to zero and the number of bonds n goes to infinity, but the contour length of the chain $L = nl$ and the persistance length a are kept constant. In this limit

$$\left\langle \frac{\mathbf{r} \cdot \mathbf{l}_1}{l} \right\rangle = a(1 - e^{-L/a}) \tag{5.18}$$

and

$$\frac{\langle r^2 \rangle_0}{L} = 2a\left[1 - \frac{a}{L}(1 - e^{-L/a})\right]. \tag{5.19}$$

When the chain length L is much larger than the persistance length a, the effect of chain stiffness becomes negligible. In the limit $L \to \infty$ we have $\langle r^2 \rangle_0 / L \to 2a$ and the wormlike chain reduces to a freely-jointed chain.

5.4 CHAINS WITH FIXED BOND ANGLES AND INDEPENDENT POTENTIALS FOR INTERNAL BOND ROTATION

The more realistic model than freely rotating chain is a chain with fixed bond angles and hindered internal rotations. For simplicity it is assumed that the total configurational energy of the chain is a sum of configurational energies of chain bonds, and the energy of a given bond is independent on the configurational states of other bonds in the chain including the neighboring bonds. We should note that this is an approximation and for real polymer chains because of the steric interactions the energy of a given bond depends on the energy of its neighbors.

We define a local Cartesian coordinate system for each of the bonds. We assume that the axis x_i is directed along the bond i, and the y_i axis lies in the plane formed by bonds i and $i-1$, while the z_i axis is directed to make the coordinate system right-handed. The components of the $(i+1)$th bond $\mathbf{l}_{i+1}$ can be expressed in the coordinate system of the preceding bond i

$$\mathbf{l}'_{i+1} = \mathbf{T}_i \mathbf{l}_{i+1}, \tag{5.20}$$

where $\mathbf{T}_i$ is the orthogonal matrix of the rotational transformation

$$\mathbf{T}_i = \begin{bmatrix} \cos\theta_i & \sin\theta_i & 0 \\ \sin\theta_i\cos\phi_i & -\cos\theta_i\cos\phi_i & \sin\phi_i \\ \sin\theta_i\sin\phi_i & -\cos\theta_i\sin\phi_i & -\cos\phi_i \end{bmatrix} \quad (5.21)$$

Here θ_i is the supplementary bond angle (see Fig. 5.1) and ϕ_i is a dihedral angle between two planes defined by two pairs of bonds: bonds $i-1$ and i, and i and $i+1$.

The scalar product of two bonds $\mathbf{l}_i \cdot \mathbf{l}_j$ written in the matrix notation is $\mathbf{l}_i^{\mathrm{T}}\mathbf{l}_j$ where $\mathbf{l}_j$ is the column vector and $\mathbf{l}_i^{\mathrm{T}}$ is the transpose of $\mathbf{l}_i$ (i.e., the row vector)

$$\mathbf{l}_j = l_j \begin{bmatrix} 1 \\ 0 \\ 0 \end{bmatrix} \quad \mathbf{l}_i^{\mathrm{T}} = \mathbf{l}_j[100], \quad (5.22)$$

where l_i and l_j are lenghts of bonds i and j ($l_i = l_j = l$ in our model but for polymers with different types of bonds in the backbone they may differ). Transforming successively over the intervening bonds the vector representation of the bond j to the coordinate system of bond i ($j > i$) we have

$$\langle \mathbf{l}_i \cdot \mathbf{l}_j \rangle = \langle \mathbf{l}_i^{\mathrm{T}} \mathbf{T}_i \mathbf{T}_{i+1} \cdots \mathbf{T}_{j-1} \mathbf{l}_j \rangle = l_i l_j \langle \mathbf{T}_i \mathbf{T}_{i+1} \cdots \mathbf{T}_j \rangle_{11}. \quad (5.23)$$

Here $\langle \mathbf{T}_i \mathbf{T}_{i+1} \ldots \mathbf{T}_{j-1} \rangle_{11}$ denotes configurational average of the (1–1) element of the matrix product $\mathbf{T}_i \mathbf{T}_{i+1} \ldots \mathbf{T}_{j-1}$. The configurational average of the product of rotational transformation matrices is generally given by

$$\langle \mathbf{T}_i \mathbf{T}_{i+1} \cdots \mathbf{T}_{j-1} \rangle = \frac{\int \cdots \int (\mathbf{T}_i \mathbf{T}_{i+1} \cdots \mathbf{T}_{j-1}) \exp\left[\frac{-E(\mathbf{l}_1, \mathbf{l}_2, \cdots, \mathbf{l}_n)}{kT}\right] \mathrm{d}\mathbf{l}_1 \mathrm{d}\mathbf{l}_2 \cdots \mathrm{d}\mathbf{l}_n}{\int \cdots \int \exp\left[\frac{-E(\mathbf{l}_1, \mathbf{l}_2, \cdots, \mathbf{l}_n)}{kT}\right] \mathrm{d}\mathbf{l}_1 \mathrm{d}\mathbf{l}_2 \cdots \mathrm{d}\mathbf{l}_n}, \quad (5.24)$$

where k is the Boltzmann constant, T is the absolute temperature and $E(\mathbf{l}_1, \mathbf{l}_2, \ldots, \mathbf{l}_n)$ is the conformational energy of the whole chain of n bonds. For a chain with fixed bond lenghts this energy depends only on the orientations of bonds described by bond angles θ_i and rotational angles ϕ_i, where $1 \le i \le n-1$, since the orientation of the last n-th bond is fully determined by the orientation of preceding bonds. For a chain with fixed bond angles the conformational energy is only a function of rotational angles ϕ_i, with $2 \le i \le n-1$, because ϕ_1 is undefined. For chains with independent potentials for internal bond rotation the conformational energy of the chain is a sum of bond energies $E_i(\phi_i)$

$$E(\phi_2, \phi_3, \cdots, \phi_{n-1}) = \sum_{i=2}^{n-1} E_i(\phi_i) \quad (5.25)$$

and

$$\langle \mathbf{T}_i \mathbf{T}_{i+1} \cdots \mathbf{T}_{j-1} \rangle = \prod_{k=1}^{j-1} \langle \mathbf{T}_k \rangle, \quad (5.26)$$

where for symmetric rotational potentials with $u_i(\phi_i) = u_i(-\phi_i)$ we have

$$\langle \mathbf{T}_k \rangle = \begin{bmatrix} \cos\theta_k & \sin\theta_k & 0 \\ \sin\theta_k\langle\cos\phi_k\rangle & -\cos\theta_k\langle\cos\phi_k\rangle & 0 \\ 0 & 0 & -\langle\cos\phi_k\rangle \end{bmatrix}. \quad (5.27)$$

Here $\langle \cos\phi_k \rangle$ is

$$\langle \cos\phi_k \rangle = \frac{\int_0^{2\pi} \cos\phi_k \exp\left[\frac{-E_k(\phi_k)}{kT}\right] \mathrm{d}\phi_k}{\int_0^{2\pi} \exp\left[\frac{-E_k(\phi_k)}{kT}\right] \mathrm{d}\phi_k}. \quad (5.28)$$

Using Eqs. (5.23) and (5.27) we may calculate the mean-square end-to-end vector for fixed bond angles and independent potentials for internal bond rotation

$$\langle r^2 \rangle_0 = nl^2 + 2l^2 \left[\sum_{i=1}^{n} \sum_{k=1}^{n-i} \langle \mathbf{T} \rangle^k \right]_{11} = nl^2 \left[\frac{\mathbf{E} + \langle \mathbf{T} \rangle}{\mathbf{E} - \langle \mathbf{T} \rangle} - 2\langle \mathbf{T} \rangle \frac{(\mathbf{E} + \langle \mathbf{T} \rangle^n)}{n(\mathbf{E} - \langle \mathbf{T} \rangle)^2} \right]_{11}, \quad (5.29)$$

where $\mathbf{E}$ is the unit matrix, and the subscript 11 denotes the (1–1) element of the matrix in square parenthesis. Equation (5.29) resembles Eq. (5.13) for freely rotating chain with $\cos\theta$ replaced by $<\mathbf{T}>$. Similarly to Eq. (5.15) the mean square radius of gyration is

$$\frac{\langle s^2 \rangle_0}{nl^2} = \left[\frac{(n+2)(\mathbf{E} + \langle \mathbf{T} \rangle)}{6(n+1)(\mathbf{E} - \langle \mathbf{T} \rangle)} - \frac{\langle \mathbf{T} \rangle}{(n+1)(\mathbf{E} - \langle \mathbf{T} \rangle)^2} + \frac{2\langle \mathbf{T} \rangle^2}{(n+1)^2(1 - \langle \mathbf{T} \rangle)^3} - \frac{2\langle \mathbf{T} \rangle^3 [1 - \langle \mathbf{T} \rangle^n]}{n(n+1)^2(1 - \langle \mathbf{T} \rangle)^4} \right]_{11}. \quad (5.30)$$

The general solution of eqs. (5.27) and (5.28) is possible by diagonaliziation of the matrix $<\mathbf{T}>$ defined by Eq. (5.27). The eigenvalues of $<\mathbf{T}>$ are

$$\lambda_{1,2} = \frac{1}{2}\left[\cos\theta(1 - \langle\cos\phi\rangle) \pm \sqrt{\cos^2\theta(1 - \langle\cos\phi\rangle)^2 + 4\langle\cos\phi\rangle} \right]. \quad \lambda_3 = -\langle\cos\phi\rangle \quad (5.31)$$

For example, the expression for $\langle r^2 \rangle_0$ in terms of eigenvalues of $<\mathbf{T}>$ is

$$\frac{\langle r^2 \rangle_0}{nl^2} = \frac{(1 + \cos\theta)(1 + \langle\cos\phi\rangle)}{(1 - \cos\theta)(1 - \langle\cos\phi\rangle)} - \frac{2\lambda_1(\cos\theta\langle\cos\phi\rangle + \lambda_1)(1 - \lambda_1^n)}{n(\lambda_1 - \lambda_2)(1 - \lambda_1)^2} + \frac{2\lambda_2(\cos\theta\langle\cos\phi\rangle + \lambda_2)(1 - \lambda_2^n)}{n(\lambda_1 - \lambda_2)(1 - \lambda_2)^2}. \quad (5.32)$$

For very long chains only first terms in Eqs. (5.29) and (5.30) are important and we have

$$C_\infty = \lim_{n\to\infty} \frac{\langle r^2 \rangle_0}{nl^2} = \left[\frac{\mathbf{E} + \langle \mathbf{T} \rangle}{\mathbf{E} - \langle \mathbf{T} \rangle} \right]_{11} = \frac{(1 + \cos\theta)(1 + \langle\cos\phi\rangle)}{(1 - \cos\theta)(1 - \langle\cos\phi\rangle)} \quad (5.33)$$

and

$$\frac{\langle s^2\rangle_0}{nl^2} = \frac{n+2}{6(n+1)} = \left[\frac{\mathbf{E}+\langle\mathbf{T}\rangle}{\mathbf{E}-\langle\mathbf{T}\rangle}\right]_{11} = \frac{(n+2)(1+\cos\theta)(1+\langle\cos\phi\rangle)}{6(n+1)(1-\cos\theta)(1-\langle\cos\phi\rangle)}. \tag{5.34}$$

5.5 CHAINS WITH INTERDEPENDENT ROTATIONAL POTENTIALS. THE ROTATIONAL ISOMERIC STATE APPROXIMATION

In real polymer chains the rotational potentials depend on the steric interactions between pendant groups of neighboring bonds, and are generally not mutually independent. In the simplest case of hydrocarbons the bond rotational potential has three minima as shown in Fig. 5.2. The global minimum at the torsional angle 0° corresponds to the *trans* two other minima with the same energies at torsional angle around $+120^\circ$ and -120° correspond to the *gauche*$^+$ and the *gauche*$^-$ states (g^+ and g^-). The energy difference between the *trans* the *gauche*$^\pm$ states for *n*-alkanes is about 500 cal/(mole). We may use the rotational isomeric state approximation that each bond in the chain occur in one of these rotational states. This assumption enables us to replace all integrals over rotational angles in the partition function and statistical averages by summations over bonds rotational states. Additionally steric interactions between pendant groups of neighboring bonds become important, e.g., the sequence $g^\pm g^\pm$ becomes energetically very unfavorable.

We may neglect the longer range interactions and assume that the configurational energy is a sum of energies of nearest-neighbor pairs

$$E(\phi_2,\phi_3,\cdots,\phi_{n-1}) = \sum_{i=2}^{n-1} E_i(\phi_{i-1},\phi_i). \tag{5.35}$$

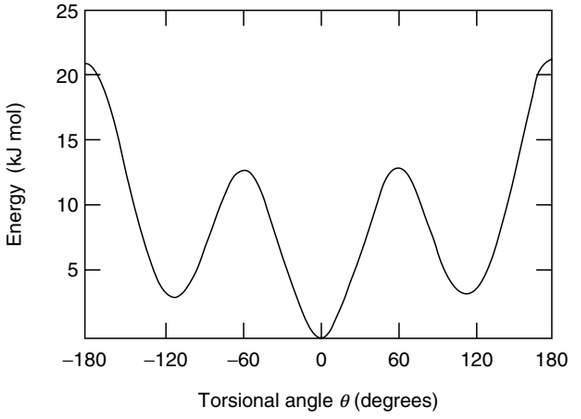

FIGURE. 5.2. The dependence of the conformational energy on the torsional angle in *n*-alkanes.

The configurational partition function becomes

$$Z = \int\cdots\int \exp\left[-\frac{1}{kT}E(\phi_2,\cdots,\phi_{n-1})\right] d\phi_2\cdots d\phi_{n-1} = \sum_{\{\phi\}}\prod_{i=2}^{n-1}\exp\left[-\frac{1}{kT}E_i(\phi_{i-1},\phi_i)\right], \tag{5.36}$$

where $\{\phi\}$ denotes the set of all available states (t,g^+,g^-) for all bonds in the chain. We define the statistical weight corresponding to bond i being in the η state while bond $i-1$ being in the ζ state (where η and ζ are sampled from the t,g^+,g^- set)

$$u_{\zeta\eta,i} = \mathbf{exp}\left(\frac{-E_{\zeta\eta,i}}{kT}\right) \tag{5.37}$$

and the statistical weight matrix

$$\mathbf{U}_i = \begin{bmatrix} u_{tt,i} & u_{tg^+,i} & u_{tg^-,i} \\ u_{g^+t,i} & u_{g^+g^+,i} & u_{g^+g^-,i} \\ u_{g^-t,i} & u_{g^-g^+,i} & u_{g^-g^-,i} \end{bmatrix}. \tag{5.38}$$

It is convenient to express the energy of a given single bond relative to the energy of the *trans* state. The energy of a pair of bonds $E_{\eta\zeta,i}$ is defined relative to the state where the bond i is in the *trans* state, and all subsequent bonds $j > i$ are also in the *trans* states. From this definition follows $E_{\eta t} = 0$ for $\zeta = t,g^+,g^-$. Additionally $E_{tg^+} = E_{tg^-} = E_{g^+g^+} = E_{g^-g^-}$ ($\approx$ 500 cal/mol for *n*-alkanes), and $\mathrm{E_{g^+g^-}} = \mathrm{E_{g^-g^+}}$ ($\approx$ 3,000 cal/mole for *n*-alkanes). This means that the statistical weight matrix may be written as

$$\mathbf{U} = \begin{bmatrix} 1 & \sigma & \sigma \\ 1 & \sigma\psi & \sigma\omega \\ 1 & \sigma\omega & \sigma\psi \end{bmatrix}, \tag{5.39}$$

where $\sigma\psi$ and $\sigma\omega$ denote $u_{g^+g^+}$ and $u_{g^+g^-}$, respectively.

By using the statistical weight matrices we may express the configuration partition function as

$$\mathbf{Z} = \sum_{\{\phi\}}\prod_{i=2}^{n-1} u_{\eta\zeta,i} = \mathbf{J}^*\left[\prod_{i=2}^{n-1}\mathbf{U_i}\right]\mathbf{J}, \tag{5.40}$$

where $\mathbf{J}^*$ and $\mathbf{J}$ are row and column vectors, respectively

$$\mathbf{J}^* = [\,1 \quad 0 \quad 0\,] \quad \mathbf{J} = \begin{bmatrix} 1 \\ 1 \\ 1 \end{bmatrix}. \tag{5.41}$$

For very long chains (in the limit $n \to \infty$) the partition function is determined by the largest eigenvalue λ_1 of the statistical weight matrix $\mathbf{U}$

$$Z \cong \lambda_1^{n-2}. \tag{5.42}$$

The largest eigenvalue of the matrix $\mathbf{U}$ defined by Eq. (5.39) is

$$\lambda_1 = \frac{1}{2}\left[1+\sigma(\psi+\omega)+\sqrt{[1-\sigma(\psi+\omega)]^2+8\sigma}\right]. \tag{5.43}$$

The probability that bonds $i-1$ and i occur in states η and ζ, respectively is

$$p_{\eta\zeta,i} = \frac{1}{Z}\mathbf{J}^*\left[\prod_{k=2}^{i-1}\mathbf{U}_k\right]\frac{\partial \mathbf{U}_i}{\partial \ln u_{\eta\zeta,i}}\left[\prod_{k=i+1}^{n-1}\mathbf{U}_k\right]\mathbf{J} \cong \frac{\partial \ln \lambda_1}{\partial \ln u_{\eta\zeta}}. \tag{5.44}$$

The probability that bond i is in the state ζ, irrespective of the state of bond $i-1$ is

$$p_{\zeta,i} = \sum_{n=t,g^+,g^-} p_{\eta\zeta,i} \cong \sum_{\eta=t,g^+,g^-}\frac{\partial \ln \lambda_1}{\partial \ln u_{\eta\zeta}}. \tag{5.45}$$

The conditional probability that bond i is in ζ state, given that bond $i-1$ is in state η is

$$q_{\eta\zeta,i} = \frac{p_{\eta\zeta,i}}{p_{\eta,i-1}}. \tag{5.46}$$

In order to calculate the mean square end-to-end vector or a radius of gyration we have to calculate averages $\langle \mathbf{T}_i\mathbf{T}_{i+1}\ldots\mathbf{T}_{j-1}\rangle$ (Eq. (5.24)). For bonds with independent rotational potentials this average is a product of averages $\langle \mathbf{T}\rangle$ for single bonds. For chains with interactions between neighboring bonds we define for each bond i the supermatrix $\| \mathbf{T}_i \|$ of the order 9×9

$$\| \mathbf{T}_i \| = \begin{bmatrix} \mathbf{T}(\phi_1) & & \\ & \mathbf{T}(\phi_2) & \\ & & \mathbf{T}(\phi_3) \end{bmatrix}_i, \tag{5.47}$$

where $\mathbf{T}$ is rotation matrix given by Eq. (5.21), and the $\phi_1 = 0^\circ, \phi_2 = 120^\circ, \phi_3 = -120^\circ$, are the torsional angles corresponding to the *trans*, *gauche*$^+$ and *gauche*$^-$ states.

We define also a direct product $\mathbf{U}_i \otimes \mathbf{E}_3$ of the statistical weight matrix $\mathbf{U}_i$ (defined by Eq. (5.38)) and the unit matrix of order three $\mathbf{E}_3$.

$$\mathbf{U}_i \otimes \mathbf{E}_3 = \begin{bmatrix} u_{tt}\mathbf{E}_3 & u_{tg^+}\mathbf{E}_3 & u_{tg^-}\mathbf{E}_3 \\ u_{g^+t}\mathbf{E}_3 & u_{g^+g^+}\mathbf{E}_3 & u_{g^+g^-}\mathbf{E}_3 \\ u_{g^-t}\mathbf{E}_3 & u_{g^-g^+}\mathbf{E}_3 & u_{g^-g}\mathbf{E}_3 \end{bmatrix}. \tag{5.48}$$

The statistical average of the product of rotation matrices may then be written as

$$\langle \mathbf{T}_i\mathbf{T}_{i+1}\ldots\mathbf{T}_{j-1}\rangle = \langle \mathbf{T}_i^{(j-i)}\rangle = \frac{1}{Z}\left[(\mathbf{J}^*\mathbf{U}_2^{(i-2)})\otimes\mathbf{E}_3\right]\times [(\mathbf{U}\otimes\mathbf{E}_3)\parallel \mathbf{T} \parallel]_i^{(j-i)}\left[(\mathbf{U}_j^{(n-j)}\mathbf{J})\otimes\mathbf{E}_3\right] \tag{5.49}$$

Then the mean-square end-to-end vector and the mean square radius of gyration are

$$\langle r^2\rangle_0 = nl^2 + 2\sum_{i=1}^{n-1}\sum_{j=i+1}^{n}\mathbf{l}_i^T\langle \mathbf{T}_i^{(j-i)}\rangle\mathbf{l}_j \tag{5.50}$$

and

$$\langle s^2\rangle_0 = \frac{1}{(n+1)^2}\sum_{0\le h\le k\le n}\sum_{i=h+1}^{k}\sum_{j=h+1}^{k}\mathbf{l}_i^T\langle \mathbf{T}^{(j-i)}\rangle\mathbf{l}_j \tag{5.51}$$

with $\langle \mathbf{T}_i^{(j-i)}\rangle$ given by Eq. (5.49). Both $\langle r^2\rangle_0$ and $\langle s^2\rangle_0$ may be written in a more compact form in terms of proper supermatrices. The details are given in Flory's monograph [21]. Additional information is given in the Handbook chapter by Honeycutt [22].

5.6 THEORIES OF POLYMER NETWORKS

5.6.1 The Affine Network

The theory of affine networks was developed by Kuhn and improved by Treloar, and is based on the assumption that the network consists of ν freely-jointed Gaussian chains and the mean-square end-to-end vector of network chains in the undeformed network is the same as of chains in the uncross-linked state. This assumption is supported by experimental data. It is also assumed that there is no change in volume on deformation and the junctions displace affinily with macroscopic deformation. The intermolecular interactions in the model are neglected, i.e., the system is similar to the ideal gas.

The elastic free energy of a chain is related to the distribution function of the end-to-end vector $P(\mathbf{r})$

$$A_{\text{el}} = c(T) - kT\ln P(\mathbf{r}) = A^*(T) + \frac{3}{2}kT\frac{\langle r^2\rangle}{\langle r^2\rangle_0} \tag{5.52}$$

for the Gaussian distribution given by Eq. (5.10). Here $c(T)$ and $A^*(T)$ are constants dependent only on the temperature T, k is a Boltzmann constant, and $\langle r^2\rangle_0$ is the average of the mean-square end-to-end vector in the undeformed state.

The elastic free energy of the network ΔA_{el} relative to the undeformed state is a sum of free energies of individual chains

$$\Delta A_{\text{el}} = \frac{3kT}{2\langle r^2\rangle_0}\sum_{\nu}(r^2 - \langle r^2\rangle_0) = \frac{3}{2}\nu kT\left(\frac{\langle r^2\rangle}{\langle r^2\rangle_0} - 1\right) \tag{5.53}$$

Here $\langle r^2\rangle$ is the end-to-end vector in the deformed state averaged over the ensemble of chains

$$\langle r^2\rangle = \langle x^2\rangle + \langle y^2\rangle + \langle z^2\rangle. \tag{5.54}$$

In the affine model of the network it is assumed all junction points are imbedded in the network, and each Cartesian component of the chain end-to-end vector transforms linearly with macroscopic deformation

$$x = \lambda_x x_0, \quad y = \lambda_y y_0, \quad z = \lambda_z z_0 \tag{5.55}$$

$$\langle x^2\rangle = \lambda_x^2\langle r^2\rangle_0, \quad \langle y^2\rangle = \lambda_y^2\langle y^2\rangle_0, \quad \langle z^2\rangle = \lambda_z^2\langle z^2\rangle_0 \tag{5.56}$$

and therefore

$$\Delta A_{\text{el}} = \frac{1}{2}\nu kT(\lambda_x^2 + \lambda_y^2 + \lambda_z^2 - 3). \tag{5.57}$$

Here, λ_x, λ_y, and λ_z are the components of the deformation tensor $\boldsymbol{\lambda}$, defined as the ratios of the final length of the

sample L_t to the initial length $L_{t,0}$ in $t = x$, y, and z direction, respectively. (The more rigorous statistical mechanical analysis by Flory [23] has shown that Eq. (5.57) should contain additional logarithmic term $-\mu kT \ln(V/V_0)$, where μ is the number of junctions, V is the volume of the network, and V_0 is volume of the network at the state of formation).

The force f under uniaxial tension in direction z is obtained from the thermodynamic expression:

$$f = \left(\frac{\partial \Delta A_{\mathrm{el}}}{\partial L}\right)_{T,V} = L_0^{-1}\left(\frac{\partial \Delta A_{\mathrm{el}}}{\partial \lambda}\right)_{T,V}, \tag{5.58}$$

where $\lambda = \lambda_z = L_z/L_{z,0}$. Because the volume of the sample is constant during deformation the x and y components of the deformation are $\lambda_x = \lambda_y = \lambda^{-1/2}$. Performing the differentiation in Eq. (5.58) leads to the elastic equation of state

$$f = \left(\frac{\nu kT}{L_0}\right)(\lambda - 1/\lambda^2). \tag{5.59}$$

5.6.2 The Phantom Network Theory

The theory of phantom network was formulated by James and Guth [24] in the forties. They assumed that chains are Gaussian with the distribution $P(\mathbf{r})$ of the end-to-end vector

$$P(\mathbf{r}) = \left(\frac{\gamma}{\pi}\right)^{3/2} \exp(-\gamma r^2), \tag{5.60}$$

where

$$\gamma = \frac{3}{2\langle r^2\rangle_0} \tag{5.61}$$

and interact only at junction points. This means that chains may pass freely through one another, i.e., are ''phantom'', the excluded volume effects and chain entanglements are neglected in the theory. They assumed also that all junctions at the surface of the network are fixed and deform affinely with macroscopic strain, while all junctions and chains inside the bulk of the network fluctuate around their mean positions. The idea of the phantom network is very similar to the concept of the ideal gas. The theory based on these simple assumptions leads to significant improvements in the understanding of the properties of networks, such as microscopic fluctuations and neutron scattering behavior.

The configurational partition function Z_N of the phantom network is the product of the configurational partition functions of its individual chains. junctions i and j:

$$Z_N = C\prod_{i<j} \exp(-3r_{ij}^2/2\langle r_{ij}^2\rangle_0) = C\prod_{i<j} \exp\left(-\frac{1}{2}\sum_i \sum_j \gamma_{ij}^* |\mathbf{R}_i - \mathbf{R}_j|^2\right). \tag{5.62}$$

Here, $\mathbf{R}_i$ and $\mathbf{R}_j$ are positions of junctions i and j, $\gamma_{\mathrm{ij}}^* = 3/2\langle r_{\mathrm{ij}}^2\rangle_0$ if junctions i and j are connected by a chain, and zero otherwise, and C is a normalization constant. The position vectors $\mathbf{R}_i$ with i ranging from 1 to μ, where μ is a number of junctions, may be arranged in column form, represented as $\{\mathbf{R}\}$. Equation (5.62) may then be written

$$Z_N = C\exp(-\{\mathbf{R}\}^T \boldsymbol{\Gamma} \{\mathbf{R}\}), \tag{5.63}$$

where the superscript T denotes the transpose. The symmetric matrix $\boldsymbol{\Gamma}$ known as the Kirchhoff valency-adjacency matrix in the graph theory describes the connectivity of the network and its elements γ_{ij} are

$$\boldsymbol{\Gamma} = \begin{cases} \gamma_{ij} = -\gamma_{ij}^*, & i \neq j \\ \gamma_{ii} = \sum_j \gamma_{ij}^* = \sum_j \gamma_{ij}^*. \end{cases} \tag{5.64}$$

James and Guth assumed that all μ junctions in the network may be divided into two sets of junctions: (i) μ_σ fixed junctions at the bounding surface of the polymer and (ii) μ_τ free junctions fluctuating about their mean positions $\{\bar{\mathbf{R}}_\tau\}$ inside the polymer. The partition function of the network due to fluctuating junctions is

$$Z_N = C\exp(-\{\Delta\mathbf{R}_\tau\}^T \boldsymbol{\Gamma}_\tau \{\Delta\mathbf{R}_\tau\}), \tag{5.65}$$

where $\{\Delta\mathbf{R}_\tau\}$ denotes fluctuations of free junctions

$$\{\Delta\mathbf{R}_\tau\} = \{\mathbf{R}_\tau\} - \{\overline{\mathbf{R}}_\tau\}. \tag{5.66}$$

The product of the fluctuations of two junctions i and j averaged over the network may be obtained from Eq. (5.65) as

$$\langle \Delta\mathbf{R}_i \cdot \Delta\mathbf{R}_j\rangle = \frac{\int \Delta\mathbf{R}_i \cdot \Delta\mathbf{R}_j \exp[-\{\Delta\mathbf{R}_\tau\}^{\mathrm{T}} \boldsymbol{\Gamma}_\tau \{\Delta\mathbf{R}_\tau\}]\mathrm{d}\{\Delta\mathbf{R}_\tau\}}{\int \exp[-\{\Delta\mathbf{R}_\tau\}^{\mathrm{T}} \boldsymbol{\Gamma}_\tau \{\Delta\mathbf{R}_\tau\}]\mathrm{d}\{\Delta\mathbf{R}_\tau\}} = -\frac{\partial \ln Z_\tau}{\partial \gamma_{ij}}, \tag{5.67}$$

where $\mathrm{d}\{\Delta\mathbf{R}_\tau\} \equiv \mathrm{d}\Delta\mathbf{R}_{1\tau}\mathrm{d}\Delta\mathbf{R}_{2\tau}\ldots\mathrm{d}\Delta\mathbf{R}_{\mu\tau}$ and

$$Z_\tau = \int \exp[-\{\Delta\mathbf{R}_\tau\}^{\mathrm{T}} \boldsymbol{\Gamma}_\tau \{\Delta\mathbf{R}_\tau]\mathrm{d}\{\Delta\mathbf{R}_\tau\} = \left(\frac{\pi^{\mu_\tau}}{\det\boldsymbol{\Gamma}_\tau}\right)^{3/2}. \tag{5.68}$$

This leads to the expression

$$\langle \Delta\mathbf{R}_i \cdot \Delta\mathbf{R}_j\rangle = \frac{3}{2}\frac{\partial}{\partial \gamma_{ij}} \ln|\det\boldsymbol{\Gamma}_\tau| = \frac{3}{2}(\boldsymbol{\Gamma}_\tau^{-1})_{ij}, \tag{5.69}$$

where $(\boldsymbol{\Gamma}_\tau^{-1})_{ij}$ denotes the $(i-j)$-th element of the inverse matrix $\boldsymbol{\Gamma}_\tau^{-1}$. Fluctuations of junctions from their mean positions in a phantom network depend on the network's functionality ϕ and are independent of macroscopic deformation.

For example for the infinitely large network with the symmetrical tree-like topology (such as shown in Fig. 5.3) the mean-square fluctuations of junctions $\langle(\Delta\mathrm{R})^2\rangle$ and

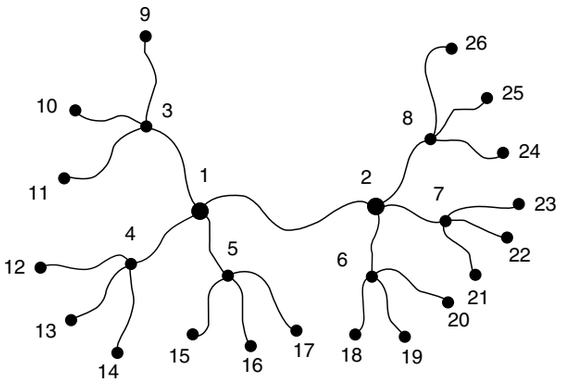

FIGURE 5.3. First three tiers of a unimodal, symmetrically grown, tetrafunctional network ($\phi = 4$) with tree-like topology.

correlations between fluctuations of two junctions i and j $\langle \Delta\mathbf{R}_i \cdot \Delta\mathbf{R}_j \rangle$ separated by m other junctions are:

$$\begin{bmatrix} \langle (\Delta \mathrm{R}_i)^2 \rangle & \langle \Delta\mathbf{R}_i \cdot \mathbf{R}_j \rangle \\ \langle \Delta\mathbf{R}_j \cdot \Delta\mathbf{R}_i \rangle & \langle (\Delta \mathrm{R}_j)^2 \rangle \end{bmatrix} = \frac{3}{2} \begin{bmatrix} (\Gamma_\tau^{-1})_{ii} & (\Gamma_\tau^{-1})_{ij} \\ (\Gamma_\tau^{-1})_{ji} & (\Gamma_\tau^{-1})_{jj} \end{bmatrix}$$

$$= \frac{3}{2\gamma} \begin{bmatrix} \frac{\phi-1}{\phi(\phi-2)} & \frac{1}{\phi(\phi-2)(\phi-1)^m} \\ \frac{1}{\phi(\phi-2)(\phi-1)^m} & \frac{\phi-1}{\phi(\phi-2)} \end{bmatrix}. \tag{5.70}$$

The mean-square fluctuations of the distance $r_{ij} = |\mathbf{R}_i - \mathbf{R}_j|$ between junctions i and j are

$$\begin{aligned} \langle (\Delta r_{ij})^2 \rangle &= \langle (\Delta\mathbf{R}_i - \Delta\mathbf{R}_i)^2 \rangle \\ &= \frac{3}{2}[(\Gamma_\tau^{-1})_{ii} + (\Gamma_\tau^{-1})_{jj} - 2(\Gamma_\tau^{-1})_{ij}] \\ &= \frac{2[(\phi-1)^{m+1} - 1]}{\phi(\phi-2)(\phi-1)^m} \langle r^2 \rangle 0. \end{aligned} \tag{5.71}$$

For a special case of mean-square fluctuations of the end-to-end vector ($m = 0$) we have

$$\langle (\Delta r)^2 \rangle = \frac{2}{\phi} \langle r^2 \rangle_0. \tag{5.72}$$

Equations (5.70) and (5.71) may be easily generalized for fluctuations of points along the chains in the network, since each point along the chain may be considered as bi-functional junction. As a consequence the valence-adjacency matrix in this generalized case contains additional elements describing the connectivity of bi-functional junctions. More details is provided in the review article by Kloczkowski, Mark, and Erman [25].

The vector $\mathbf{r}_{ij}$ between junctions i and j is

$$\boldsymbol{r}_{ij} = \bar{\boldsymbol{r}}_{ij} + \Delta\boldsymbol{r}_{ij}, \tag{5.73}$$

where $\Delta\mathbf{r}_{ij}$ is the instantaneous fluctuation of $\mathbf{r}_{ij}$ and $\bar{\mathbf{r}}_{ij}$ is the time average of $\mathbf{r}_{ij}$. Squaring both sides of the above equation and taking the ensemble average leads to

$$\langle r_{ij}^2 \rangle = \langle \bar{r}_{ij}^2 \rangle + \langle (\Delta r_{ij})^2 \rangle \tag{5.74}$$

since instantaneous fluctuations and mean values are uncorrelated. From Eqs. (5.72) and (5.74) follows:

$$\langle \bar{r}^2 \rangle = (1 - \frac{2}{\phi}) \langle r^2 \rangle_0. \tag{5.75}$$

According to the theory the mean positions of junctions transform affinely with macroscopic strain while the fluctuations are strain independent:

$$\boldsymbol{r}_{ij} = \bar{\boldsymbol{r}}_{ij} + \Delta\boldsymbol{r}_{ij} \tag{5.76}$$

i.e.,

$$\langle r^2 \rangle = \left[(1 - \frac{2}{\phi}) \frac{\lambda_x^2 + \lambda_y^2 + \lambda_z^2}{3} + \frac{2}{\phi} \right] \langle r^2 \rangle_0. \tag{5.77}$$

Using Eq. (5.53) for the elastic free energy, we obtain the following expression for the free energy of the phantom network

$$\Delta A_{\mathrm{el}} = \frac{1}{2}(1 - \frac{2}{\phi}) \nu kT (\lambda_x^2 + \lambda_y^2 + \lambda_z^2 - 3). \tag{5.78}$$

Equation (5.78) is very similar to Eq. (5.57) for the affine network. The only difference is that the so called front factor (equal $\nu/2$ for affine network model) is replaced by $\xi/2$ for the phantom network model where

$$\xi = (1 - \frac{2}{\phi}) \nu. \tag{5.79}$$

The equation for the elastic force is similar to Eq. (5.59) for the affine network with ν replaced by ξ.

5.7 STATISTICAL THEORIES OF REAL NETWORKS

In real polymer network the effects of excluded volume and chain entanglements should be taken into account. In 1977 Flory [26] formulated the constrained junction model of real networks. According to this theory fluctuations of junctions are affected by chains interpenetration, and as the result the elastic free energy is a sum of the elastic free energy of the phantom network ΔA_{ph} (given by Eq. (5.78)) and the free energy of constraints ΔA_{c}

$$\Delta A_{\mathrm{el}} = \Delta A_{\mathrm{ph}} + \Delta A_{\mathrm{c}} \tag{5.80}$$

with ΔA_{c} given by the formula

$$\Delta A_{\mathrm{c}} = \frac{1}{2} \mu kT \sum_{t=x,y,z} [B_t + D_t - \ln(1 + B_t) - \ln(1 + D_t)], \tag{5.81}$$

where

$$B_t = \frac{\kappa^2(\lambda_t^2 - 1)}{(\lambda_t^2 + \kappa^2)^2} \tag{5.82}$$

and

$$D_t = \frac{\lambda_t^2 B_t}{\kappa}. \tag{5.83}$$

Here κ is a parameter which measures the strength of the constraints. For $\kappa = 0$ we obtain the phantom network limit, and for infinitely strong constraints ($\kappa = \infty$) the affine limit is obtained. Erman and Monnerie [27] developed the constrained chain model, where constraints effect fluctuations of the centers of the mass of chains in the network. Kloczkowski, Mark, and Erman [28] proposed a diffused-constraint theory with continuous placement of constraints along the network chains.

A different statistical–mechanical approach based on so called replica formalism was developed by Edwards and coworkers [29,30]. They studied the effect of topological entanglements between chains on the elastic free energy of the network and formulated the slip-link model. The elastic energy of constraints in the slip-link theory is

$$\Delta A_{\mathrm{c}} = \frac{1}{2} N_{\mathrm{s}} kT \sum_{t=x,y,z} \left[\frac{(\lambda_t^2 - 1)}{1 + \eta\lambda_t^2} + \ln \left[\frac{1 + \eta\lambda_t^2}{1 + \eta} \right] \right], \quad (5.84)$$

where N_{s} is the number of slip-links and η is the slipage parameter. Equation (5.84) is very similar to Eq. (5.81) for the constrained junction model. Vilgis and Erman [31] showed that for small deformations both equations have the same form (except minor volume term) with $\kappa = 1/\eta$.

5.8 SCATTERING FROM POLYMER CHAINS

The scattering form factor $S(\mathbf{q})$ from a labeled chain in the network is given by the Fourier transform of the distribution function $\Omega(\mathbf{r}_{ij})$ of the vector $\mathbf{r}_{ij}$ between two scattering centers i and j averaged over all pairs of scattering centers along the chain:

$$S(\mathbf{q}) = \frac{1}{N^2} \sum_{i,j=1}^{N} \int \exp(i\mathbf{q} \cdot \mathbf{r}_{ij}) \Omega(\mathbf{r}_{ij}) \mathrm{d}\mathbf{r}_{ij}. \quad (5.85)$$

Here $\mathbf{q}$ is the scattering vector representing the difference between the incident and scattered wave vectors $\mathbf{k}_0$ and $\mathbf{k}$, respectively, and N is the total number of scattering centers along the chain.

The distribution function $\Omega(\mathbf{r}_{ij})$ of the vector $\mathbf{r}_{ij}$ between scattering centers in the undeformed state is assumed to be Gaussian. The distribution function $\Omega(\mathbf{r}_{ij})$ in the deformed state is

$$\Omega(\mathbf{r}_{ij}) = [(2\pi)^3 \langle x_{ij}^2 \rangle \langle y_{ij}^2 \rangle \langle z_{ij}^2 \rangle]^{-1/2} \exp(- x_{ij}^2/2\langle x_{ij}^2 \rangle - y_{ij}^2/2\langle y_{ij}^2 \rangle - z_{ij}^2/2\langle z_{ij}^2 \rangle), \quad (5.86)$$

where $\langle x_{ij}^2 \rangle$, $\langle y_{ij}^2 \rangle$, and $\langle z_{ij}^2 \rangle$ are the mean-square components of the vector $\mathbf{r}_{ij}$ in the deformed state. Substituting the expression for $\Omega(\mathbf{r}_{ij})$ given by Eq. (5.86) into Eq. (5.85) leads to

$$S(\mathbf{q}) = \frac{1}{N^2} \sum_{i,j=1}^{N} \exp(- q_x^2 \langle x_{ij}^2 \rangle/2 - q_y^2 \langle y_{ij}^2 \rangle/2 - q_z^2 \langle z_{ij}^2 \rangle/2), \quad (5.87)$$

where q_x, q_y, and q_z are the components of the scattering vector $\mathbf{q}$. The vector $\mathbf{r}_{ij}$ between two scattering centers may be written for a phantom network as $\mathbf{r}_{ij} = \bar{\mathbf{r}}_{ij} + \Delta\mathbf{r}_{\mathrm{ij}}$ where $\bar{\mathbf{r}}_{ij}$ is the time average of $\mathbf{r}_{ij}$, and $\Delta\mathbf{r}_{ij}$ is the instantaneous fluctuation of $\mathbf{r}_{ij}$ from its mean time-averaged value. Assuming that mean-square fluctuations are strain independent and that mean positions transform affinely with macroscopic strain and applying Eqs. (5.74)–(5.77) leads to

$$\langle x_{ij}^2 \rangle = \left[\lambda_x^2 + (1 - \lambda_x^2) \frac{\langle \Delta x_{ij}^2 \rangle_0}{\langle x_{ij}^2 \rangle_0} \right] \langle x_{ij}^2 \rangle_0, \quad (5.88)$$

where λ_x is the x component of the principal deformation gradient tensor $\boldsymbol{\lambda}$, with similar expressions for the y and z components. For a freely jointed chain

$$\langle x_{ij}^2 \rangle_0 = \langle r_{ij}^2 \rangle_0 / 3 = \eta \langle r^2 \rangle_0 / 3,$$

where $\eta = |i - j|/N$ is the fractional distance, and $\langle r^2 \rangle_0$ is the mean-square end-to-end vector for the undeformed chain. Substituting these results to Eq. (5.87) leads to

$$S(\mathbf{q}) = \frac{1}{N^2} \sum_{i,j=1}^{N} \exp\left[-\upsilon \frac{|i - j|}{N} \left(1 - (1 - \lambda^{*2}) \frac{(\phi - 2)}{\phi} \frac{|i - j|}{N} \right) \right]. \quad (5.89)$$

In this equation

$$\upsilon = q^2 \langle r^2 \rangle_0 / 6 \quad (5.90)$$

and the *vector* $\boldsymbol{\lambda}^*$ is

$$\boldsymbol{\lambda}^* = \boldsymbol{\lambda}\mathbf{q}/q. \quad (5.91)$$

For scattering parallel to the direction of extension $\lambda^* = \lambda_{\parallel}$ and for scattering perpendicular to the direction of extension $\lambda^* = \lambda_{\perp} = 1/\sqrt{\lambda_{\parallel}}$. Replacing the double summation by integration and evaluating one of the integrals leads to

$$S(\mathbf{q}) = 2 \int_0^1 \mathrm{d}\eta (1 - \eta) \exp\left[-\upsilon\eta \left[1 - \eta(1 - \lambda^{*2}) \frac{\phi - 2}{\phi} \right] \right] \quad (5.92)$$

the result obtained by Pearson [32]. As the strain goes to zero Eq. (5.92) has the limiting form

$$\lim_{\lambda \to 1} S(\mathbf{q}) = \frac{2}{\upsilon} (\mathrm{e}^{-\upsilon} + \upsilon - 1) \quad (5.93)$$

derived by Debye [33], corresponding to the scattering from an unperturbed Gaussian coil. Readers interested in scattering from labeled cross-linked paths in unimodal and bimodal networks should consult the review article by Kloczkowski, Mark, and Erman [25].

5.9 SIMULATIONS OF POLYMERS

System composed of polymers or containing polymers immersed in low molecular media are extremely complex

for many reasons. First, polymer chains (linear, branched, or cyclic) have often a huge molecular mass. Large fraction of single covalent bonds in the main chain imply at least a limited internal rotational freedom for each such bond, and consequently lead to an enormous number of available conformational isomers. Second, due to the excluded volume effect polymer chains are non-Markovian, i.e., conformational space accessible to a selected portion of the chain depends on the actual conformation of the remaining fragments. Consequently, a rigorous analytical treatment of polymer conformational statistics and dynamics is essentially impossible; although various aspects of polymer physics could be quite successfully addressed within framework of approximate theories (see the previous sections). Third, the chain connectivity imposes a complex network of topological obstacles. A moving chain cannot cross its own contour or the paths of the other chains present in the system. This has pronounced consequences for polymer dynamics in solutions and polymeric melts, where motion of polymers has to be extremely correlated and the correlation distances are several orders of magnitude larger than it is observed in typical disordered low molecular systems. The nature of these correlations could be extremely complex.

For the above reasons computer simulations are very important components of methodology of theoretical polymer physics. Properly designed computational experiments expand our understanding of these complex systems, provide excellent test of the existing theories and stimulate development of new theoretical approaches. Due to the large size, time scales involved, and complexity of polymeric systems numerous new simulation techniques have been developed to meet these extreme computational demands. This way theoretical physics of polymers had significant influence on progress in computational physics in general.

Simulations of polymers could be designed on various levels of molecular details treated in an explicit way [16–20, 34–36]. Molecular Dynamics (or Brownian Dynamics) of all-atom systems are limited to short chains or/and to studies of local and fast relaxation processes. It is rather impractical, and often nonfeasible, to do MD simulations of long polymer collapse or a self diffusion of polymer chain in a melt, to give just a couple of typical examples. Monte Carlo simulations of the all-atom systems have a bit less limitations, but still large scale rearrangements are difficult to study. For these reasons frequently reduced representations of polymer conformational space are employed. These range from united atom models, where groups of atoms are treated as single interaction units, to lattice models where entire mers (or large united atoms) are restricted to a lattice, thereby enormously reducing the number of available states and simplifying energy calculations. While simple lattice models are of very limited utility in the physics of low molecular mass system, for polymers they provided general solutions to very fundamental problems. This qualitative difference is strictly related to the difference in the correlation length scales in the two types of systems. In polymers the local details become usually irrelevant at large distances. Because of their importance for general physics of polymers and educational values we start from a discussion of simple lattice models of polymers and polymer dynamics.

5.9.1 Ideal Lattice Chains are Equivalent to Off-lattice Models

Let us consider a chain restricted to a simple cubic lattice, with the lattice spacing equal to 1. The chain is a string of vectors with the six allowed orientations belonging to the following set $\{|1,0,0|, |-1,0,0|, |0,1,0|, |0,-1,0|, 0,0,1, |0,0,-1|\}$. A chain vector could be followed by any of the vectors from the set. Thus, there is no any average orientational correlation between the chain vectors, in spite of the lattice restrictions. Note, that for this ideal model a lattice site can be occupied by more than one bead of the chain. It could be immediately seen that the Eqs. (5.1) and (5.2) written for the freely joined chain are true as well for the ideal lattice chain. The models are equivalent, and an exact analytical theory of their conformational statistics exists. Such analogy goes much further. Let us now consider a chain restricted to the diamond lattice with a constant tetrahedral value of the valence angle and three discrete values of the torsional angle corresponding to the *trans* and two *gauche* states. Again, it is easy to note that this model is equivalent (in respect to its global properties) to the ideal, freely rotating chain with the tetrahedral value of the planar angle. It is also easy to show that such chain can mimic the chain with restricted rotations and interdependent rotations, provided Boltzmann weights are assigned to the *trans* and *gauche* conformations and proper correlations between the weights are taken into account.

Equivalence of the ideal continuous and the lattice models extends also on the dynamic properties of a single chain. The Rouse model [37,38] , (or the bead and spring model) consists of a string of points (or beads) of equal mass connected by harmonic springs of equal length and equal strength of the harmonic potentials, although without any angular interactions. An exact analytical solution for the relaxation spectrum of this model is relatively easy to derive. For the ideal (without excluded volume limitations) lattice chain a simple model of dynamics, simulated by a long random sequence of small local conformational changes, could be formalized in a stochastic Master Equation of motion. It has been shown by Verdier and Stockmayer [39], that such model is equivalent to the Rouse model [37,38] in almost entire relaxation spectrum, except the fastest local oscillations involving a couple of chain segments.

5.9.2 Simulation of the Excluded Volume Effect in a Single Chain

The ideal models described in the previous sections ignored a very important fact, that a polymer has its own volume, i.e., two segments cannot occupy the same place in space. Using a series of approximations Flory has shown that the exclude volume leads to a significant increase of the average random coil dimensions and changes the number of accessible conformers. Flory, has also shown that in a thermodynamically ''poor'' solvent the proper volume of the chain segments could be balanced by their mutual attractions, leading to a pseudoideal state, very similar to the Boyle point for the real gases. Typical, however, is the situation of a ''good'' solvent, where the effect of excluded volume is large. Exact analytical solution to the excluded volume problem does not exist. It is unknown how to calculate partition function of a single chain, since the probability of a given conformation of the $(n+1)$th bond added to a chain depends on the conformation of the preceding n bonds. The process of virtual growth of a ''real'' (with excluded volume, in contrast to the ideal, lacking volume chains) chain is non-Markovian. This is exactly a situation where the data from computer simulations are needed for estimations of true (in silico) experimental properties of the model system and for subsequent evaluation of the assumptions and predictions of various approximate theories.

In the context of a simple lattice model the problem could be formulated as follows. Compute the number of non-self-intersecting random walks on the lattice and the distribution of the segment density, size, shape, etc., of the resulting random coils as a function of the chain length. The first thought is to use computer for an exact enumeration of all possible conformations of a n-segment chain. Unfortunately, the number of possible random walks grows exponentially with the chain length. Exact enumeration is possible only for n range of few tens of segments. In this range the finite length effects are still large and an extrapolation of the obtained (exact) data to higher values of n is uncertain. Another approach is to employ a stochastic sampling (Monte Carlo method) to get a ''representative'' ensemble of non-self-intersecting random walks of the assumed length n. There the result is not exact, however avoids any systematic errors. The magnitude of the statistical error could be always reduced by the increase of the sample size. The algorithm is very simple.

1. Start from the first bond.
2. Add the next bond in a randomly selected direction (the simple ''back'' step could be a priori prohibited and the resulting bias easily removed from the results).
3. Check for non-self-intersection and repeat from (2) if a double occupancy of a lattice site is not detected, otherwise erase the chain and start from (1).
4. Stop the chain growth when the requested length n is reached and add the chain to the statistical ensemble.
5. Repeat the entire process starting from (1) until the required number of chain in the sample is collected.
6. Perform statistical analysis of the collected ensemble.

The process of the MC chain growth is illustrated in Fig. 5.4.

Situations, as that schematically depicted in Fig. 5.4B happen quite frequently. Therefore, the algorithm outlined above has a huge sample attrition rate; only a small fraction of the staring chains are finally accepted in the statistical

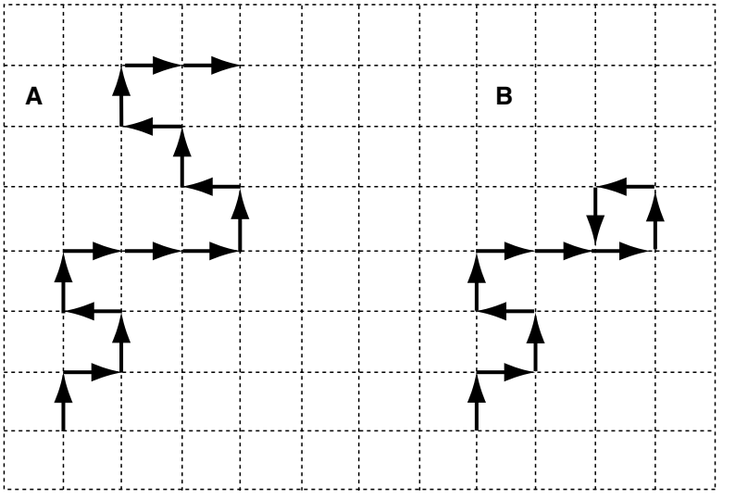

FIGURE 5.4. Two dimensional illustration of the MC growth of non-self-intersecting walks (see the text for details). On the left side (A) an example of the successful structure composed of $n = 15$ segments is shown. On the right side (B) an intersection has been detected before reaching $n = 15$, the final chain length, and the chain has to be removed from the statistical ensemble.

pool. To overcome this problem Rosenbluth and Rosenbluth [40] proposed a modified approach. The segments are selected only from the set of orientations which do not cause the intermediate chain clash. In the case shown in Fig. 5.4B the segment number 11 would be selected only from the following two possibilities; to the left, and to the top of the plane. Obviously, this introduces a bias to the sample. This bias could be easily removed with a proper weighting of the particular conformation with a factorials depending on the number of the allowed continuations at each step. The R&R method allows for generation of much longer chains. Their length is limited by the ''cull-the-sack'' effect, where the growing chain end is surrounded by the chain segments, blocking all the possibilities for the further continuation of the growth process. A number of extensions of the original R&R method have been proposed since then. In general, these methods look into possibility of a continuation in a larger perspective than just one segment ahead.

There are several qualitatively different ways of sampling the polymer conformational space. One may start from a chain of a given length and successively modify its conformation. Two examples of such types of algorithms are illustrated in Fig. 5.5. One of them is the ''pivot'' algorithm, where a single step consist of a random selection of a bond and a rotation (in two dimensional case it is reduced just to a flip; vertical or horizontal) of the selected end of the chain. Advantage of this algorithm is that in a single step a large modification of the chain conformation is attempted. However the acceptance rate for longer chain could be rather small. A number of different global rearrangements of the chain conformations were designed aiming on a more efficient sampling. An example is the ''reptation'' algorithm, where a bond (or a small number of bonds) is cut-off from one end of the chain and added in a random direction on the opposite end. The acceptance ratio for this type of global update algorithms could be quite high. Yet another example is a technique that could be viewed as a complex ''pivot-like'' algorithm, where a part of the chain on one end is erased and then re-grown in a random or semirandom fashion. Of course, the statistical sample is collected in along series of attempts (sometimes successful) to successive modifications of subsequently generated conformations. In the second type of algorithms (Fig. 5.5A) local micromodiffications of the chain conformation are randomly selected at random position of the chain. Marginally, let us note that the local move algorithm could be interpreted as a simulated Brownian motion of a polymer chain. This is a ''real'' chain version of the before mentioned Verdier–Stockmayer model [39] of polymer dynamics. Again, it should be stressed out, that an accurate analytical theory for the real chain dynamics does not exist. The local move algorithms are powerful tools for study of long-time (and large scale) polymer dynamics. There are however several problems with the models employing a limited set of local moves and low coordination number lattices. The algorithms could be nonergodic, or rather ergodic in a subset of its full conformational space. This is explained in Fig. 5.6. There is no path to- and no path from the conformation shown in the drawing. The problem may be cured using a higher coordination lattices and/or a larger set of ''less-local'' micromodiffications. An example of such larger scale move is shown in Fig. 5.6B. The backfire of such update of the local move algorithms is a less clear relation with the model of the Brownian motion. Perhaps, the ''wave-like'' move, when attempted rarely could be interpreted as a particular coincidence of a series of local moves, which somehow were able to pass the local conformational barriers. An additional flaw of the low coordination lattice models (beside the ergodicity

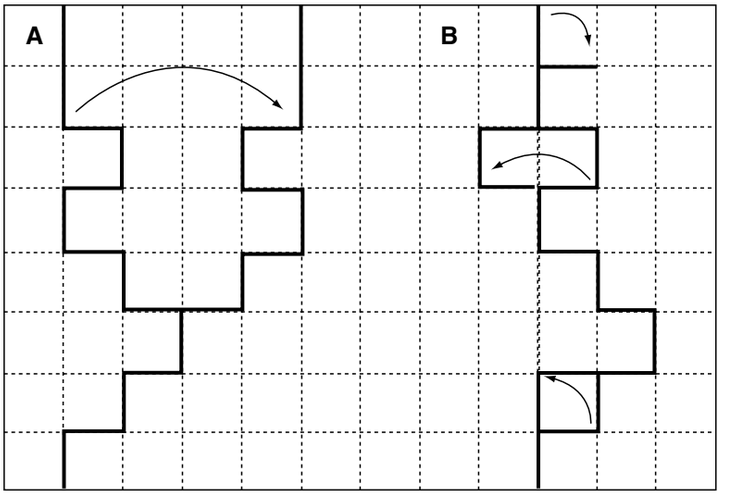

FIGURE 5.5. The idea of the pivot algorithm (A), and the local moves algorithm (B). The black contours indicate the initial structures, the lighter bonds show the accepted modifications. The local moves include (from top to the bottom of B): random chain end modification, a crankshaft move and a corner move.

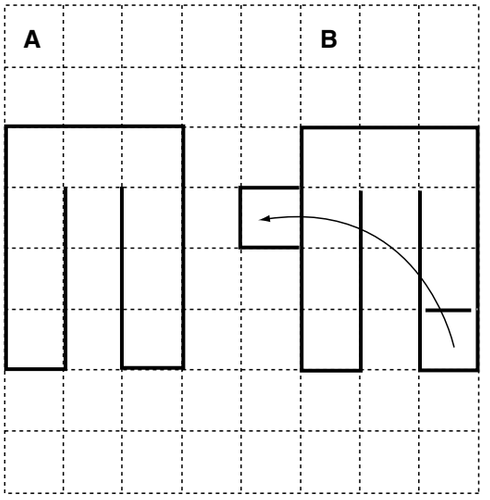

FIGURE 5.6. A trapped conformation for the algorithm with only local moves for a chain on the simple square lattice (A). A longer distance move that guarantees the ergodicity of the algorithm, where a U shaped fragment at one part of the chain is cut-off and attached somewhere else (B).

problems) of polymer dynamics is the difficulty of controlling the effects of the lattice anisotropy on the observed motion. Obviously, simple models of polymer conformations and dynamics, very similar to those described above could be design in the continuous space. Such models could be sampled using MD, MC, or via various hybrid sampling techniques based on a combination of genetic algorithms (GA) and molecular mechanics (usually MC dynamics). The results from simplified lattice and off-lattice models are essentially equivalent. For instance, the average chain dimensions of the real chain models scale as $\langle S^2 \rangle \sim n^{\gamma}$. Interestingly, the value of the universal constant for the 3-dimensional chains is close (but not identical) to the value resulting from the mean-field analytical theory of Flory. More qualitative differences are observed between the results of the "real" chain simulation of the polymer dynamics and the ideal chain theory of Rouse [37].

5.9.3 Simulations of Polymer Chain Collapse

Polymer chains in solution can undergo a collapse transition from an expanded random coil state to a dense globular state. The transition could be induced by decrease of temperature or by adding a "poor" solvent to the solution [41]. This process is difficult to describe analytically, but could be studied in details via computer simulations. Let us again consider a very simple lattice model. Representation of protein conformational state could be done using any kind of simple lattice. In such context it is easy to design a very simple potential mimicking the balance between the volume of the chain segments and their mutual attractions in the solution. The simplest form of such potential is given below:

$$E_{ij} = \begin{cases} \infty, for\ r_{ij} < 1 \\ \varepsilon, for\ r_{ij} = 1 \\ 0, for\ r_{ij} > 1. \end{cases} \quad (5.94)$$

In the formula above r_{ij} is the distance between two beads of the chain, 1 is the lattice spacing, and ε is a negative constant. With $\varepsilon = 0$ the model reduces to the model of a "real" chain in a good solvent, where mutual attractions of the chain segments could be ignored. Energy of the entire chain is a sum of the binary contributions ΣE_{ij}.

With decreasing temperature (or with increasing strength of the long-range interactions ε) the mean dimensions of the chain decrease (the solid curve in Fig. 5.7). The curves become steeper with increasing chain length; nevertheless the collapse transition remains continuous. The dashed horizontal line corresponds to the dimensions of an ideal chain of the same local geometry. The vertical dashed line denotes the collapse transition temperature. Slightly higher than ideal dimensions of the real chain at the transition midpoint are due to a bit higher prefactor – the scaling of the mean dimension with the chain length is at this point the same as for an ideal chain i.e., $\langle S^2 \rangle \sim n$. At very low temperatures, the globular state is a dense droplet with $\langle S^2 \rangle \sim n^{2/3}$. Obviously, at very high temperatures the chain behaves as the thermal "real" chain discussed in the previous section, i.e., $\langle S^2 \rangle \sim n^{\gamma}$.

Very interesting are the models where on top of the long range interactions a local stiffness of the model chain is superimposed. Let us assume that we are dealing now with a simple chain restricted to the diamond lattice (although any other lattice or off-lattice model can include the short-range interactions that simulate the polymer limited flexibility). Then let us assume that the *trans* conformation is favored energetically in respect to the two *gauche* conformations. At some critical ratio of the potential energy

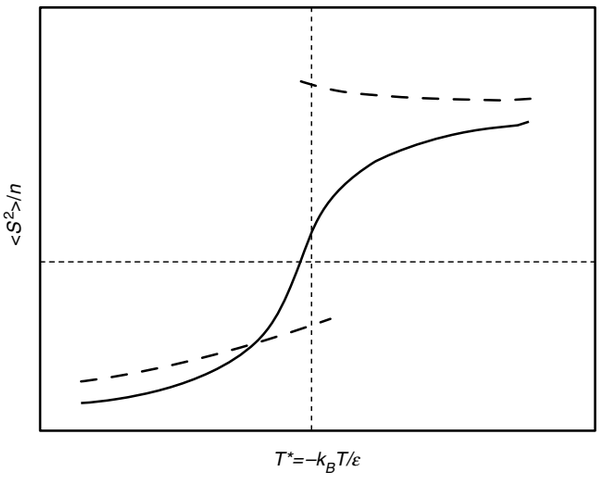

FIGURE 5.7. Collapse transition of a flexible polymer chain (solid line) and a semiflexible chain (dashed line) of a limited length (see the text for an explanation).

of these two types of local geometries the behavior of a chain of a limited length changes dramatically. In the range of high temperatures with decreasing temperature the chain dimensions increase due to increasing effect of the stiffness. Relatively long expanded segments could be seen at this range. At a critical temperature, these ''rods'' of fluctuating length coalesce due to a huge decrease of the potential energy of the long-range interactions for a small entropic expense. The transition is abrupt, highly cooperative (the average length of the expanded sequences jumps up at the transition), and has all features of the first-order phase transition, including easily detected metastable region, an ''almost'' singularity of the heat capacity and an extremely low population of the intermediate states. At the transition midpoint the simulated molecules adopt essentially only two types of conformations; swollen random coils with a short sequences of expanded states and a densely packed, highly ordered globular state, with much longer sequences of the expanded local conformations. This behavior of the semiflexible model has a number of essential properties of globular proteins. First, the collapse transition is pseudo first-order (all-or-none in the language of protein biophysics). Second, it is cooperative and the collapse induces a sudden increase of the length of the regular expanded fragments, very much as the formation of secondary structure during the protein folding transition. Third, the collapsed structure is highly ordered with relatively well defined (however not unique) number of ''secondary structure'' expanded elements. Note, that these striking similarities are observed in the homopolymer model where all polymer units are the same. This leads to the conclusion that one of the most important general aspects of protein folding is a competition between the long-range and the short-range (stiffness) interactions. In this picture, differentiation of the interactions along the polypeptide chains (sequence of amino acids) plays a ''fine-tuning'' role, selecting the structural detail of the globular state. This analogy to protein folding extends even further. As the length of the semiflexible chain increases the ordering of the globular state becomes modular – domains are formed upon the collapse. Each domain can form at slightly different temperature, within the range of the metastable states shown in Fig. 5.7. When the number of domains becomes large the collapse transition becomes continuous, as it should be for any infinitely long flexible (or semiflexible) polymer chain. Such detailed insight into the collapse transition of semiflexible polymers could be gain only from computer simulations, although a very approximate theories for a single globule collapse of semiflexible polymers were published in past.

A single polymer simulations could address also the issues of chain topology, including the effect of polymer branching and macrocycles on the thermodynamics of the collapse transition and the dynamics in a diluted media. This can be addressed on various levels of details, from a large scale conformational sampling within a framework of reduced models to a detailed molecular mechanics study of local conformational transitions. For instance, a very interesting simulation of DNA collapse has been recently performed using the bead and string model with a short range bending potential and the Brownian Dynamics as a sampling technique. These simulations led to a very plausible and nontrivial picture of the DNA collapse pathway. It is also possible to employ a multiscale sampling, where the large scale relaxations are modeled on a low resolution level and the details are studied with the all-atom representation.

Finally, it is worth to mention a very broad class of approaches to a specific problem of polymer collapse transition, the protein folding transition. This field attracts a lot of researches due to its importance for molecular biology, and biotechnology, genetics, and molecular medicine (including new drugs design in particular). In the case of the protein folding problem, the details of physics and the pathway description of the collapse transition are (at least by now) of a lesser importance. The mean goal is to predict the unique structure of protein globular state. The task is nontrivial, since the copolymers of interest are composed of twenty different mers (amino acids) and the sequence of these mers dictates a vast variety of three-dimensional globular structures, with a very specific local conformations and their well defined mutual packing in the globule. Two types of algorithms are now the most successful. The first one uses a large set of ''prefabricated'' protein fragments, extracted from a collection of known three-dimensional structures, and the sampling scheme are based on an iterative shuffling of these fragments within the simulated chain. Another approach is more in spirit of the classic polymer algorithms. It employs a local move schemes, however with a complex representation of the polypeptide conformational space and elaborated set of mean field potentials, derived either from the physical properties of the small molecules or from statistical analysis of the structural regularities seen in known structures of globular proteins. An amazing progress was achieved in this field during the last few years. The second approach is probably somewhat more general; it opens a possibility of a qualitative study of protein folding pathways and molecular mechanisms, not only the predictions of the globular structure. The predictive power of the both type of approaches are similar. Nevertheless, the second one seems to be a bit more open for a wider range of applications. These applications include the bootstrapped (resolution- and time-vise multiscale) implementations of the polypeptide representation and dynamics. Coupling of the various levels of resolution enables for a quite detailed study of protein dynamics and thermodynamics. The simulation techniques and models developed specifically for proteins are easily adaptable for more general applications in polymer computational physics. [43]

5.9.4 Simulations of Dense Polymeric Systems

Dense polymeric systems include polymer solutions, polymer networks, polymer melts, polymer liquid crystals

and solids, and many more. There is a vast body of literature on each of these subjects [42]. The modeling approaches are also of great variety, from a simple reduced models (lattice and continuous) to the detailed molecular mechanics and even a quantum mechanics. It is beyond scope of this chapter to go through the detail of various applications. Let us just outline some of problems that could be addressed in computer simulations, increasing our understanding of complex systems and providing important stimuli for theoretical studies and practical applications in material science and biotechnology.

Typical dense polymer solutions and melts are globally disordered; however the level of local ordering could be relatively high. This is a very complex phenomenon that involves long-range correlations that are the results of specific local interactions. A general insight could be gain from the low resolution models that allow for study of the large scale conformational rearrangements; although specific details could be very sensitive to the atomic structure and require extensive molecular mechanic study of carefully selected starting conformations. The same could be said about the phase transitions in bulk polymers.

The rate polymer diffusion in polymer media spans orders of magnitude. The mechanism of the process is unclear. It is very difficult to provide even a qualitative mechanistic picture how a long chain can move throughout a complex network of entanglements superimposed by the other macromolecules. The reptation theory of DeGennes [13] is probably only qualitatively true and only for very specific conditions. Simulations could be extremely helpful in at lest qualitative understanding of this process.

Another challenging (however not really macromolecular) polymeric system are biological membranes. It is known from various experiments that the spectrum of relaxation processes in membranes is extremely wide; from local cooperative motion of phospholipide chain and occasional jumping of molecules from one side of a membrane to the other one to a global flexing of the membrane and formation of vesicles. Simulations are done on various levels of generalization. There are mesoscopic model which treat the membrane as a kind of elastic network, but also a very detailed all-atom study of membrane structure and local dynamics. Bootstrapped, multiscale simulations could be a very promising way to attack this problem.

REFERENCES

1. W.L. Mattice and U.W. Suter, *Conformational Theory of Chain Molecules*, Wiley, New York, 1994.
2. M.F. Schulz and F.S. Bates, this volume, Chap. 32
3. H. Yamakawa, *Modern Theory of Polymer Solutions*, Harper & Row, New York, 1971.
4. A.Y. Grosberg and A.R. Khokhlov, *Statistical Physics of Macromolecules*, AIP, New York, 1994.
5. M. Warner and E.M. Terentjev, *Liquid Crystal Elastomers*, Oxford University Press, Oxford, 2003.
6. J.E. Mark and B. Erman, *Rubberlike Elasticity. A Molecular Primer*, Wiley, New York, 1988.
7. B. Erman and J.E. Mark, *Structures and Properties of Rubberlike Networks*, Oxford University Press, Oxford, 1997.
8. A. Kloczkowski, M.A. Sharaf and J.E. Mark, *Chem. Eng. Sci.* **49**, 2889 (1994).
9. M.A. Sharaf and J.E. Mark, *Polymer*, **45**, 3943 (2004).
10. W. Zhao and J.E. Mark, this volume, Chap. IIB.
11. J.D. Honeycutt, this volume, Chap. IIID.
12. K.F. Fried, *Renormalization Group Theory of Macromolecules*, Wiley, New York, 1987.
13. P.G. DeGennes, *Scaling Concepts in Polymer Physics*, Cornell University Press, New York, 1979.
14. J. des Cloizeaux and C. Jannink, *Polymers in Solutions: Their Modeling and Structure*, Clarendon, Oxford, 1990.
15. W.C. Forsman, Ed., *Polymers in Solution*, Plenum, New York, 1986.
16. K. Binder, Ed., *Monte Carlo Methods in Statistical Physics*, Springer-Verlag, Berlin Heidelberg New York, 1986.
17. K. Binder, *Monte Carlo and Molecular Dynamics Simulations in Polymer Sciences*, Oxford University Press, Oxford, 1995.
18. A. Baumgaertner, Simulation of polymer motion, *Ann. Rev. Phys. Chem.* **35**, 419 (1984).
19. Kolinski and J. Skolnick, *Lattice Models of Protein Folding, Dynamics and Thermodynamics*. R.G. Landes, Austin, TX, 1996.
20. M. Kotelyanskii and D.N. Therodorou, Ed., *Simulation Methods for Polymers*, Marcel Dekker, New York, 2004.
21. P.J. Flory,*Statistical Mechanics of Chain Molecules*, Interscience, New York, 1969.
22. J.D. Honeycutt, this volume, Chap. XX.
23. P.J. Flory, *Proc. Roy. Soc. London, Ser. A* **351**, 351 (1974).
24. H.M. James and E. Guth, *J. Chem. Phys.* **15**, 669 (1947).
25. A. Kloczkowski, J.E. Mark and B. Erman, *Comput. Polym. Sci.* **2**, 8 (1992).
26. P.J. Flory, *J. Chem. Phys.* **66**, 5720 (1977).
27. B. Erman and L. Monnerie, *Macromolecules*, **22**, 3342 (1989), **25**, 4456 (1992).
28. A. Kloczkowski, J.E. Mark and B. Erman, *Macromolecules*, **28**, 5089 (1995).
29. R.T. Deam and S.F. Edwards, *Phil. Trans. R. Soc, A,* **280**, 317 (1976).
30. R.C. Ball, M. Doi and S.F. Edwards, *Polymer*, **22**, 1010 (1981).
31. T. Vilgis and B. Erman, *Macromolecules*, **26**, 6657 (1993).
32. D.S. Pearson, *Macromolecules*, **10**, 696 (1977).
33. P. Debye, *J. Phys. Colloid. Chem.* **51**, 18 (1947).
34. R.H. Boyd and P.J. Philips, *The Science of Polymer Molecules*, Cambridge, New York, 1993.
35. P.R. Schleyer, Ed. *Encyclopedia of Computational Chemistry*, Wiley, New York, 1998.
36. W.F. van Gunsteren and P.K. Weiner, *Computer Simulations of Biomolecular Systems. Theoretical and Experimental Applications.* Escom, Leiden, 1989.
37. P.E. Rouse, *J. Chem. Phys.* **21**, 1272 (1953).
38. M. Doi and S.F. Edwards, *The Theory of Polymer Dynamics*, Clarendon, Oxford, 1986.
39. P.H. Verdier and W.H. Stockmayer, *J. Chem. Phys.* **36**, 227 (1962).
40. M. Rosenbluth and N. Rosenbluth, *J. Chem. Phys.* **23**, 356 (1955).
41. A. Montesi, M. Pasquali and M.C. MacKintosh, *Phys. Rev. E* **69**, 021916 (2004).
42. J.E. Mark, K. Ngai, W. Graessley, L. Mandelkern, E. Samulski, J. Koenig and G. Wignall, *Physical Properties of Polymers,* Cambridge University Press, Cambridge 2004.
43. A. Kolinski, Acta Biochim. Polonica **51**, 349 (2004).

CHAPTER 6

Scaling, Exponents, and Fractal Dimensions

Mohamed Daoud,* H. Eugene Stanley,† and Dietrich Stauffer‡

* *Laboratorie Léon Brillouin (CEA-CNRS), CE Saclay; Gif-sur-Yvette, Cedex, France*
† *Center for Polymer Studies and Department of Physics, Boston University, Boston, MA 02215*
‡ *Institute of Theoretical Physics, Cologne University, D-50923 Köln, Euroland*

6.1 LINEAR POLYMERS

Textiles, much of living matter, plastics, and many other materials consist of linear or branched polymers. Each polymer usually is a carbon chain consisting of many monomers like -CH_2-. We emphasize here the modeling of such polymers and compare the theoretical results with experiments.

First, we consider the conformation of a random linear chain, which is a model for a dilute solution of a polymer in a solvent [1–6]. Typical examples are polystyrene in benzene or polydimethylsiloxane in toluene or cyclohexane. We assume that the macromolecules are made of N statistical units which are randomly oriented with respect to each other. Because the actual monomers have to respect chemical bond angles, independent units can be regarded as made of several monomers. It is possible to define such independent units which will be used in all cases. This procedure was first presented by Kuhn, who defined the concept of local rigidity of a polymer [1]. Here, we consider the chains as completely flexible, and we do not distinguish between actual monomers and statistically independent units.

6.1.1 The Random Walk

The simplest model to describe the structure of a linear chain made of N units of length l each is the random walk. This is an ideal chain where no interactions are present between monomers. The distribution function $P(r,N)$, which is the probability that a chain made of N steps starts at the origin and ends at point r, is a Gaussian. In three-dimensional space,

$$P(r, N) = (3/2\pi N\ell^2)^{3/2} \exp\{-3r^2/2N\ell^2\}. \tag{6.1}$$

From the second moment we define the fractal dimension d_f of the walk by $\langle r^2\rangle^{d_f/2} \sim N$. For any spatial dimension d, the second moment $R_0^2 \equiv \langle r^2\rangle$ of $P(r, N)$ is

$$R_0^2 \sim N\ell^2, \tag{6.2a}$$

Thus the fractal dimension [6] is

$$d_f = 2 \tag{6.2b}$$

for any d. It is important to stress that any definition of a characteristic length for the random walk leads to this result.

What is a fractal and its dimension? A long spaghetti is one dimensional since its mass increases linearly with the length. A pizza has a mass proportional to the square of the radius, if its thickness is constant, and thus is two dimensional. A glass of red wine has a volume and mass proportional to the third power of the length, and is three dimensional. Thus an object with mass proportional to $(\text{radius})^{d_f}$ has a dimension d_f. It is called a fractal with the fractal dimension d_f if d_f differs from the Euclidean dimension (usually 3) of the space into which the object is embedded. The apple-like Mandelbrot set is perhaps the most famous deterministic fractal, whereas the random walks of Eq. (6.2a) are random fractals with mass $\propto N \propto (\text{radius})^2$. In deterministic fractals, small parts are mathematically similar to suitably chosen large parts; in random fractals this "self-similarity" (a large branch of a tree looks similar to a small twig on it) is often described but seldom defined in any precise way.

For a polymer chain, it is possible to use the mean square end-to-end distance, as we did above. It is also possible to

define the average radius of gyration. One finds that these lengths are proportional to each other if both are long, and that the fractal dimension is 2 (for a discussion, see Chapter 1 in [7]). This is the reason for using the sign $\sim$, which denotes asymptotic proportionality, and scaling laws are assumed to be valid only asymptotically. It is important that the precise way the length is defined will change the prefactor, but not the exponents. In this sense, we can say that there is only one characteristic length, and we will not be interested in the differences between the prefactors.

The fractal dimension may be observed experimentally by light or neutron scattering [8]. The scattered intensity $S(\vec{q})$ is the Fourier transform of the pair correlation function

$$S(\vec{q}) = \sum_{i,j=1}^{N} \langle \exp[i\vec{q} \cdot (\vec{r}_i - \vec{r}_j)] \rangle, \tag{6.3}$$

where the brackets $\langle \cdots \rangle$ represent an average over all configurations, and $\vec{q}$ is the momentum transfer in the scattering experiment: for a neutron with wavelength λ elastically scattered with an angle θ, we have

$$q \equiv |\vec{q}| = \frac{4\pi}{\lambda} \sin\frac{\theta}{2}. \tag{6.4}$$

Because Eq. (6.1) is valid for any pair of units in a random walk, Eq. (6.3) may be calculated exactly. This was done by Debye [1] some years ago. He found

$$S(q) = \frac{2}{X^2}(e^{-x} - 1 + X), \tag{6.5}$$

with

$$X = q^2 R_0^2/3. \tag{6.6}$$

Here, R_0 is the radius of gyration of the ideal chain. In the intermediate range, $l^{-1} \gg q \gg R_0^{-1}$, where the fractal nature of the walk appears, relation (6.5) may be approximated by

$$S(q) \sim q^{-2}. \tag{6.7}$$

This relation provides a convenient way to measure the fractal dimension of a single polymer, whenever the intermediate range may be reached experimentally. Neutron scattering is an excellent technique for this: The available wave vector range is particularly well suited for polymers; since the typical unit size is around 10*A*, and the radius of gyration is several hundred Ångströms. Linear chains behave actually as random walks in two cases: in a melt, when no solvent is present, and in a theta solvent [9]. The latter is introduced in Section 6.1.2 when we discuss the actual interactions between monomers.

6.1.2 The Self-Avoiding Walk

Random walks are ideal chains in the sense that there is no interaction between monomers. For actual polymers, there is an interaction between any two monomers. The interaction consist of an attractive part for large distances, goes through a minimum at intermediate distances, and becomes a repulsive core at short distances. Because of this ''steric'' constraint, two monomers cannot be in the same location.

At high temperatures, the repulsive core is dominant, and the local minimum may be neglected completely. This is the excluded volume effect, and corresponds to what is called a good solvent [10,11]. There exists a critical temperature called the Flory theta temperature, where the excluded volume effect and the attractive part compensate each other. Such solutions are said to be in a theta solvent [12–14]. For still lower temperatures, the attractive part of the potential becomes dominant, and although two monomers are not allowed to be in the same location, they tend to be in the vicinity of each other. As a consequence, the chain tends to collapse on itself [15–17]. Solvents in which this happens are known as poor solvents.

As mentioned above, at the theta temperature, because of the compensation between attractive and repulsive parts of the potential, the random walk model gives an adequate description of a chain in three-dimensional space [1–6]. Actually, there are still logarithmic corrections, but they may be neglected. In two dimensions, a chain at theta temperature is still not equivalent to a random walk [18]. In what follows, we will be concerned with solutions in a good solvent. It was realized by Edwards [10] that the exact shape of the potential is not important, and that it could be described by a parameter $v(T)$, where T is the temperature, called the excluded volume parameter, defined as

$$v(T) = \int \{1 - e^{V(r)/\kappa T}\} dr, \tag{6.8}$$

like the classical second virial coefficient, where $V(r)$ is the effective monomer–monomer potential. This parameter is positive in a good solvent, vanishes at the theta temperature and becomes negative in a poor solvent.

In the good solvent, steric interactions are dominant, as mentioned above, and the polymer is swollen compared to the ideal chain. This swelling corresponds to a change in the fractal dimension of the chain, which now becomes smaller than 2.

The fractal dimension was calculated by various renormalization group techniques and by computer simulations [19,20]. Here, we describe the Flory approximation which, although being wrong [1–6], gives the fractal dimension within a very good accuracy for all dimensions. In this approximation one assumes that the free energy can be written as

$$F/\kappa T = \frac{R^2}{R_0^2} + v\frac{N^2}{R^d}. \tag{6.9}$$

The first term is the elastic energy, in which one considers the chain as a spring with spring constant $1/R_0^2$, where R_0 is

the ideal radius from Eq. (6.2). The radius R is the actual radius of the chain, to be determined. The second term is the interaction energy which can be estimated as follows. In a unit volume, the number of monomers is N/R^d, the number of pair interactions scales as $(N/R^d)^2$, and the interaction energy is therefore $v(N/R^d)^2$. Thus, the total interaction energy in the volume R^d scales as $R^d v(N/R^d)^2$, which is the second term in Eq. (6.9). Minimizing F with respect to R gives the fractal dimension d_f of a linear chain in the Flory approximation,

$$N \sim R^{d_f}, \tag{6.10a}$$

$$d_f = \frac{d+2}{3}. \tag{6.10b}$$

This prediction $d_f = 5/3$ in three dimensions is close to the actual value near 1.7; $d_f = 1$ and 4/3 for $d = 1$ and 2, respectively, is even exact. Note that we recover the ideal chain dimension for $d = 4$. This is the upper critical dimension above which the excluded volume interaction becomes irrelevant, and the chain is ideal. For higher dimensions, the interaction with itself is negligible for the exponents, because space is sufficiently large that the polymer almost does not cross itself. Therefore, for $d \geq d_c$ chains with or without interactions are equivalent.

Equation (6.10) was checked directly, using polymers with different masses. It was also tested using scattering experiments, by measuring the Fourier transform $S(q)$ of the pair correlation function. As above Eq. (6.7), one can show that the scattered intensity is related to the wave vector q by the fractal dimension. In $d = 3$ one finds, using Eq. (6.10), that

$$S(q) \sim q^{-\frac{5}{3}} (\ell^{-1} \gg q \gg R_0^{-1}). \tag{6.11}$$

Relations (6.10) and (6.11) were tested experimentally by small angle neutron scattering. Let us mention that star-shaped polymers are in this same universality class: the mass dependence of their radius of gyration also follows relations (6.10). However, it also depends on the number f of branches, indicating the special geometry of the object. For more details, the reader is referred to Refs. [21–25].

6.1.3 Dilute Solutions

So far, we have considered only a single polymer chain. Actual solutions contain many chains! We expect the above results to hold as long as the various polymers are far from each other. This is the case for dilute solutions, where we expect the concentration effects to be only perturbations to the various laws that we found.

Let C be the monomer concentration. It is common to define the overlap concentration C^* where the distance between centers of masses of the chains is of the order of the radius of the macromolecules. Assuming the polymers are randomly distributed, the average distance between their centers of masses is

$$\delta \sim (C/N)^{-1/d}. \tag{6.12}$$

Equating Eq. (6.12) to the radius of gyration, and using Eq. (6.10), we get

$$C^* \sim N^{1-d/d_f} \approx N^{-4/5} \quad (d = 3). \tag{6.13}$$

Relation (6.13) exhibits the fractal character of the chains; because they are fractals, their volume grows faster than their mass. Therefore, the overlap concentration decreases as the polymers become larger.

As mentioned above, we expect two concentration regimes, with C/C^* smaller or larger than unity. Therefore, we do not expect N and C to act as independent variables for all the properties, but to appear only through the ratio C/C^*. This scaling behavior occurs in many properties, but we will consider here only the scaling behavior of the radius of gyration R and of the osmotic pressure π. In both cases, one may write a scaling relation deduced from the definition of the fractal dimension, Eq. (6.10):

$$R(N,C) \sim N^{1/d_f} f(C/C^*), \tag{6.14a}$$

and

$$\pi(N,C) = \frac{C}{N} g(C/C^*). \tag{6.14b}$$

Here the prefactor $C_p \equiv C/N$ in Eq. (6.14b) is merely the pressure of an ideal gas that is obtained for very low concentrations when the chains are very far from each other.

The unknown functions $f(x)$ and $g(x)$ may be expanded for small x in the dilute regime but have singular behavior for large x in the semidilute regime. Therefore, in the dilute concentration regime, one expects corrections both for the radius and the osmotic pressure.

In the latter case, we may write

$$\pi(N,C) = \frac{C}{N} \{1 + \alpha C/C^* + \beta (C/C^*)^2 + \dots\}, \tag{6.15a}$$

where $\alpha, \beta, \dots$ are constants. This may be identified with a virial expansion,

$$\pi(N,C) = \frac{C}{N} + A_2 C^2 + \dots \tag{6.15b}$$

Comparing Eqs. (6.15a) and (6.15b) and using Eqs. (6.13) and (6.10) leads to the following expression for the second virial coefficient:

$$A_2 \sim (NC^*)^{-1} \sim N^{3/d_f}. \tag{6.16}$$

A similar expansion can be obtained for scattering intensity $S(q,C) \propto 1/(1 + q^2R^2 + \dots)$. For very low q, in the Guinier regime $qR \ll 1$, this expansion is the basis for the so-called Zimm plots that are commonly used to determine the radius of a chain and the second virial coefficient of a solution.

6.1.4 Semidilute Solutions

When the concentration C is increased above the overlap concentration C^*, one reaches a different regime where the macromolecules interpenetrate each other, and we expect the concentration effects to become dramatic. In dilute solutions, the concentration effects are represented by corrections to the power laws. Because the chains are fractals, the volume they occupy grows much faster than their mass. As indicated by Eq. (6.13), the larger the macromolecule, the smaller is C^*. For a typical polymer of 10^5 units, C^* is of the order of $10^{-2}\mathrm{g/cm^3}$.

For infinite chains, the overlap concentration vanishes, and one is left only with the semidilute range. In this range, because the chains are flexible, they overlap each other, and we expect the simple laws we discussed above to break down. Still, the scaling laws (6.14) are valid, but one has to look for other limits. The basic idea to understand the behavior of a polymer in this regime was given in the limit of a melt by Flory [1] and was later generalized to semidilute solutions by Edwards [26].

In a melt, the average interaction should cancel, since each monomer is surrounded by other monomers, and therefore the polymer should behave as an ideal chain.

We will see below that although this argument is valid for linear chains, it turns out to be wrong for branched polymers. The reason for this is related to the interpenetration of the various chains. For linear chains, this interpenetration effect was studied by Edwards [10], who introduced the concept of a screening length ξ. The idea here is that if we consider two monomers on a given chain, their total interaction is the sum of the direct excluded volume interaction and all the contributions coming from indirect interactions between them via other monomers belonging to other chains. This is equivalent to Debye–Hückel screening in an electrolyte solution. Because of this, the notion of "blob" was introduced. It corresponds to a part of the chain, made of g units, with radius ξ. Thus one may consider a polymer in a semidilute solution as an ideal chain if the blob is chosen as a statistical unit. Inside the blob, excluded volume interactions are still present. Note that at the overlap concentration, the blob is identical to the whole chain. Using these ideas, it was shown that

$$\xi \sim C^{-3/4} \tag{6.17}$$

and

$$R \sim \left(\frac{N}{g}\right)^{1/2} \xi \sim N^{1/2} C^{-1/8}. \tag{6.18}$$

Note that as concentration increases, the sizes of the blob and of the chain decrease. In the bulk, we recover Flory's results: the interaction completely screened, the size of the blob is the step length, and the chain is ideal. Thus the present model ensures a gradual cross-over from the swollen to the ideal behaviors for increasing concentrations.

The next quantity we will consider is the osmotic pressure [27]. We may use the same arguments as above to determine its dependence on C, starting with relation (6.14b). In the semidilute regime, we do not expect the expansion (6.15) to be valid, since the variable $x = C/C^*$ is larger than unity. Instead, we assume that $g(x)$ behaves as a power law. Its exponent is determined by the following condition. In this concentration range, we expect the osmotic pressure to be given by the density of contacts between polymers. This is again a collective property of the solution that should depend only on concentration and not on the mass of the individual chains. Using this condition, we find

$$\pi \sim C^{-d/(d_f - d)} \approx C^{9/4}, \tag{6.19}$$

a relation that was found first by des Cloizeaux [28]. Equation (6.19) was tested experimentally by Noda *et al.* [29].

Many points are remarkable in Eq. (6.19). The first is that these results differ strongly from what one would expect in a mean field approach. The second, and most remarkable result is that the fractal dimension controls the thermodynamic properties of the solution. This is extremely interesting because the fractal dimension was introduced to describe the properties of a single chain, where only small concentrations and distances in the order of several hundreds of Ångströms were considered. We are now discussing thermodynamic, macroscopic, properties of a solution that is semidilute, and where the polymers strongly interact. Thus what was introduced to describe a local property of a single chain controls a solution that may be rather concentrated: even a 20% solution may be in this concentration range.

6.2 GELATION FOR BRANCHED POLYMERS

So far we have considered polymers made of bifunctional units. These may react by two ends, or functionalities. When the monomers are more than bifunctional, polymerization leads to branched structures, and eventually to a solid called a gel [48]. In this section we will consider this case. As we will see, every polymer has still a fractal behavior. In addition to this, there is a very broad distribution of molecular weights, called polydispersity. Because of this, what is observed is an effective dimension that depends also on the dimension of the distribution. This holds for many polydisperse systems, with restrictions that will be discussed below. We will first present the distribution of molecular weights that is naturally found in the reaction bath. We will turn to dilute solutions, where the fractal dimension is smaller because of swelling. We will discuss the effective dimension that is observable. Then we will turn to the semidilute solutions and to the swollen gels. Finally, we will discuss the dynamics of these systems in the reaction bath.

6.2.1 The Sol–Gel Transition

Let us consider a vessel with multifunctional monomers. Each monomer may react by one or more of its f functional groups. As time proceeds, there is a formation of dimers, trimers, ..., polymers; this is the sol. This process makes the solution more and more viscous, because of the presence of large macromolecules. The viscosity diverges, and this defines a threshold time t_c. For $t > t_c$, in addition to the sol, there is an infinite molecule, the gel. Thus, there appears an elastic modulus due to the presence of a solid-like phase.

Although there are probably other universality classes, this transition was successfully modeled by bond percolation [6]. Generally, bond percolation on a lattice has each bond (line connecting two neighboring lattice sites) present randomly with probability p and absent with probability 1–p. Clusters are groups of sites connected by present bonds. For $p > p_c$ an infinite cluster is formed. Percolation theory (in a Bethe lattice approximation) was invented by Flory (1941) to describe gelation for three-functional polymers.

Sites are the unreacted monomers, bonds are the reacted functionalities. Clusters are the polymers, and the infinite cluster is the gel. We recall very briefly some results of percolation. The main result concerns the distribution of cluster sizes. This corresponds to what we called polydispersity. The distribution is very broad. If we call p the probability that a bond is reacted, p_c is its value at the gelation threshold, the average probability $P(N, \varepsilon)$ that a randomly selected monomer belongs to a large polymer with N monomers each at a small "distance" $\varepsilon \equiv p - p_c$ from the threshold is

$$P(N,\varepsilon) \sim N^{1-\tau} f(\varepsilon N^{\sigma}), \tag{6.20}$$

where τ and σ are percolation exponents [30] to be discussed below. The moments of the distribution have several interesting properties. The first moment is normalized below p_c. The higher moments diverge with different exponents

$$N_w \equiv \frac{\int NP(N,\varepsilon)\mathrm{d}N}{\int P(N,\varepsilon)\mathrm{d}N} \sim \varepsilon^{-\gamma} \tag{6.21}$$

and

$$N_z \equiv \frac{\int N^2 P(N,\varepsilon)\mathrm{d}N}{\int NP(N,\varepsilon)\mathrm{d}N} \sim \varepsilon^{-1/\sigma}. \tag{6.22}$$

Higher order moments defined the same way as above are proportional to N_z. The number of polymers with N units each is proportional to $P(N,\varepsilon)/N$

The exponent γ is the susceptibility exponent in percolation. Similarly, one may also define a characteristic length, corresponding to the size of the typical polymers in the sol, dominating in diverging moments like N_z. This length diverges as

$$\xi \sim \varepsilon^{-\nu}. \tag{6.23}$$

Using relations (6.22) and (6.23), we find the fractal dimension d_f for percolation clusters,

$$1/d_f = \sigma\nu. \tag{6.24}$$

Let us stress that this is the fractal dimension of the polymers in the reaction bath. We assume that all polymers that constitute the sol have this same fractal dimension. This was calculated by renormalization group techniques and computer simulations [31,32,33,34]. We will give a simple Flory derivation [35] that is close to the former results for all space dimensions. The polydispersity exponent τ can be shown to be related to the fractal dimension,

$$\tau = 1 + d/d_f. \tag{6.25}$$

This hyperscaling relation is valid for space dimensions $d \leq 6$.

Equation (6.25) implies that the distribution is very special; if one considers polymers with a given mass, they are in a C^* situation, i.e., they are in a space-filling configuration. Since they are fractals, however, voids are left in the structure. These voids are filled by polymers with smaller masses, with the same requirement for every mass: each one is in a C^* situation. Therefore, if one looks at the distribution, for any size considered, one always observes polymers at C^*. In this sense, the distribution is fractal [36,37]. Note that it is possible to relate the "masses" N_z and N_w (in units of the monomer mass) defined above by eliminating ε,

$$N_z \sim N_w^{d_f/(2d_f-d}. \tag{6.26a}$$

Using relation (6.25), we get

$$N_z \sim N_w^{1/(3-\tau)}. \tag{6.26b}$$

Note that both relations (6.26a) and (6.26b) hold only if $d_f < d$, or equivalently if $\tau > 2$. If $d_f = d$, or $\tau = 2$, both masses become proportional to each other, and in our definitions, there is only one mass present in the problem. This will prove to be important in the discussion for the scattered intensity for dilute solutions below.

6.2.2 The Flory Approximation

Let us consider the large polymers, with mass N_z and radius ξ in the distribution. In the Flory approximation, one writes down a free energy made of two contributions

$$F = \frac{\xi^2}{\xi_0^2} + \frac{v}{N_w}\frac{N_z^2}{\xi^d}. \tag{6.27}$$

The first one is an entropic term where we assume that the polymer behaves like a spring with constant ξ_0^2, where ξ_0 is the radius of an ideal chain when no interactions are present. The second term is the interaction energy in which v is the excluded volume interaction, discussed for linear chains. Except for the presence of N_w, this is very similar to what we considered for chains. The presence of this factor is due

to the fact that the large polymers are penetrated by the small ones. Because of this, there is a screening of the interactions, as in the semidilute case for linear chains. The precise form for the energy was evaluated by Edwards [26] and de Gennes [38] in a Debye–Huckel approximation. The ideal chain radius ξ_0 was calculated on a Cayley tree [39] and was shown to be

$$N_z \sim \xi_0^4. \tag{6.28}$$

In the Flory approximation, all quantities, except the radius which is to be calculated, are assumed to have a mean-field behavior. Therefore there is a relation between N_z and N_w,

$$N_z \sim N_w^2. \tag{6.29}$$

Minimizing the free energy with respect to ξ and using relations (6.23) and (6.24), we get the fractal dimension d_f of the large percolation clusters,

$$d_f = \frac{1}{2}(d+2). \tag{6.30}$$

This was tested indirectly by measurements of the mass distribution and the exponent τ (6.25).

6.2.3 Dilute Solutions

Once the distribution of polymer sizes is known, it is possible to dilute the sol, and to consider dilute solutions. Let us stress that the growth of the polymers is quenched before dilution and that the distribution function is given. Because of the excluded volume interactions the polymers swell and their fractal dimension changes from d_f to d_f^a. The new fractal dimension d_f^a may be obtained within a Flory approximation by considering a free energy similar to that in Eq. (6.27). The difference between a dilute solution and the reaction bath which was considered above is in the interaction term. We expect that the excluded volume interactions are present in the dilute case whereas they are fully screened in the previous case [40]. Therefore, this contribution has the same form as in relation (6.9) for linear chains. It is straightforward to minimize the free energy with respect to the radius, which yields,

$$d_f^a = \frac{2}{5}(d+2). \tag{6.31}$$

The observation of this fractal dimension, however, is not easy, as we discuss now. Any experiment provides the average of the observed quantity over the whole distribution of masses. This averaging procedure leads to an effective dimension [41–44] that is different from the actual one. In order to see this, let us consider the scattered intensity. For a single mass, we have

$$S_1(q, N) = Ng[qR(N)]. \tag{6.32a}$$

where the function $g(x)$ behaves as a power law in the fractal range, $qR > 1$ and $qa \ll 1$, in such a way that the mass dependence disappears. For a distribution of masses, and in the dilute regime where one may neglect correlations between monomers belonging to different polymers, the total scattered intensity [45] is

$$S_{\text{total}}(q) = \sum P(N,\varepsilon) S_1(q, N). \tag{6.32b}$$

Using relations (6.32), (6.20), and (6.21), we get

$$S_{\text{total}}(q) = CN_w g(qR_z), \tag{6.32c}$$

where C is the monomer concentration and R_z is the radius of the largest polymers,

$$R_z \equiv \frac{\int NR^2(N)P(N,\varepsilon)\mathrm{d}N}{\int NP(N,\varepsilon)\mathrm{d}N}. \tag{6.33}$$

The radius R_z can be related to the largest masses N_z, Eq. (6.22), through the fractal dimension

$$R_z \sim N_z^{d_f^a} \approx N_w^{5/8} \quad (d=3). \tag{6.34}$$

This relation was tested by light scattering measurements and found to be in good agreement with experimental results. In the intermediate scattering range, $l^{-1} \gg q \gg R_z^{-1}$, the function $g(x)$ in Eq. (6.32) behaves as a power law. The exponent of $S_{\text{total}}(q)$ is determined by the requirement that we are now in the fractal regime where no explicit mass dependence should appear. Using relations of Eq. (6.26), we get

$$S_{\text{total}}(q) \sim q^{-d_f^a(3-\tau)} \approx q^{-8/5} (l^{-1} \gg q \gg R_z^{-1}) \quad (d=3). \tag{6.35}$$

Therefore, an effective fractal dimension appears, that describes the behavior of the polydisperse system. As can be seen from Eq. (6.32), this effective dimension is related to the actual one, but also to the exponent τ characterizing the distribution of masses. Note that this holds for percolation and for other distributions, as long as $\tau > 2$, as discussed above. The polydispersity effect disappears when $\tau = 2$. In this sense, we will say that such systems are not polydisperse.

This has an important implication. Measuring an exponent in a scattering experiment does not necessarily imply that one gets the fractal dimension directly. First one has to check the polydispersity by independent measurements, either with viscosity, or with second virial coefficient experiments. The latter may be calculated following the same steps as above and taking into account the interactions between the centers of masses of different polymers.

Finally, we define two more exponents related to the viscosity η and the elastic modulus G

$$\eta \sim \varepsilon^{-\kappa} G \sim \varepsilon^f \tag{6.36}$$

for which the theory is less clear [46–51]. Note that for crosslinks between very long linear chains one expects the Bethe lattice or Cayley tree exponents to be valid except in an unmeasurably small interval at the transition. We end by

noting that recently, very similar ideas were successfully applied to the diffusion of cancer cells in tissues modelled by a gel [52,53].

ACKNOWLEDGMENTS

The authors are much indebted to M. Adam, E. Bouchaud, W. Burchard, R. Colby, M. Delsanti, D. Durand, B. Farnoux, P.G. de Gennes, O. Guiselin, G. Jannink, L.T. Lee, L. Leibler, J. E. Martin, and M. Rubinstein for many discussions.

REFERENCES

1. P. J. Flory, *Principles of Polymer Chemistry* (Cornell University Press, Ithaca, 1953).
2. P. G. de Gennes, *Scaling Concepts in Polymer Physics* (Cornell University Press, Ithaca, 1979).
3. M. Doi and S. F. Edwards, *The Theory of Polymer Dynamics* (Oxford Science Publications, London, 1986).
4. J. des Cloizeaux and G. Jannink, *Les polymers en solutions* (ed. de Physique, Paris, 1987) [Engl. Transl: *Polymers in Solution*, Oxford University Press, 1990].
5. A. Yu. Grosberg and A. R. Khokhlov, *Statistical Physics of Macromolecules*, translated by Y. A. Atanov (AIP Press, New York, 1994).
6. D. Stauffer and H. E. Stanley, *From Newton to Mandelbrot: A Primer in Theoretical Physics* (Springer-Verlag, Heidelberg & New York, 1990).
7. A. Bunde and S. Havlin, eds., *Fractals and Disordered Systems* (Springer, Berlin, 1991).
8. J. Teixeira, in *On Growth and Form*, edited by H. E. Stanley and N. Ostrowsky (Martinus, Nijhoff, 1985).
9. J. P. Cotton, D. Decker, H. Benoit, B. Farnoux, J. Higgins, G. Jannink, R. Ober, C. Picot, and J. des Cloizeaux, Macromolecules **7**, 863 (1974).
10. S. F. Edwards, Proc. Phys. Soc. **65**, 613 (1965).
11. P. G. de Gennes, Phys. Lett. **38A**, 339 (1972).
12. M. J. Stephen, Phys Lett. **53A**, 363 (1975).
13. M. Daoud and G. Jannink, J. Phys. Lett. **37**, 973 (1976).
14. M. Moore, J. Phys. A **10**, 305 (1977).
15. I. M. Lifshitz, A. Grosberg, and A. Khoklov, Rev. Mod. Phys. **50**, 685 (1978).
16. M. Nierlich, J. P. Cotton, and B. Farnoux, J. Chem. Phys. **69**, 1379 (1978).
17. C. Williams, F. Brochard, and H. L. Frisch, Ann. Rev. Phys. Chem. **32**, 433 (1981).
18. B. Duplantier, Phys. Rev. Lett. **59**, 539 (1987).
19. B. Derrida, J. Phys. A **14**, L5 (1981).
20. H. J. Hilhorst, Phys. Rev. B **16**, 1253 (1977).
21. M. Daoud and J. P. Cotton, J. Phys. **43**, 531 (1982).
22. T. Birstein and E. Zhulina, Polymer **25**, 1453 (1984).
23. G. S. Grest, K. Kremer, and T. A. Witten, Macromolecules **20**, 1376 (1987).
24. J. Roovers, N. Hadjichristidis, and L. J. Fetters, Macromolecules **16**, 214 (1983).
25. A. Halperin, M. Tirrell, and T. P. Lodge, Adv. Polym. Sci. **100**, 31 (1991).
26. S. F. Edwards, Proc. Phys. Soc. **88**, 265 (1966).
27. M. Daoud, J. P. Cotton, B. Farnoux, G. Jannink, G. Sarma, H. Benoit, R. Duplessix, C. Picot, and P. G. de Gennes, Macromolecules **8**, 804 (1975).
28. J. des Cloizeaux, J. Phys. **36**, 281 (1975).
29. I. Noda, N. Kato, T. Kitano, and M. Nagasawa, Macromolecules **14**, 668 (1981).
30. H. Nakanishi and H. E. Stanley, Phys. Rev. B **22**, 2466 (1980).
31. T. C. Lubensky and J. Isaacson, Phys. Rev. Lett. **41**, 829 (1978); Phys. Rev. A **20**, 2130 (1979).
32. G. Parisi and N. Sourlas, Phys. Rev. Lett. **46**, 891 (1981).
33. P. J. Reynolds, W. Klein, and H. E. Stanley, J. Phys. C **10**, L167 (1977).
34. B. Derrida and J. Vannimenus, J. Phys. Lett. **41**, 473 (1980).
35. J. Isaacson and T. C. Lubensky, J. Phys. **42**, 175 (1981).
36. M. E. Cates, J. de Phys. Lett. **38**, 2957 (1985).
37. M. Daoud and J. E. Martin, in *The Fractal Approach to Heterogeneous Chemistry,* edited by D. Avnir (John Wiley, New York, 1990).
38. P. G. de Gennes, J. Polym. Sci. Polym., Symp. **61**, 313 (1977).
39. B. H. Zimm and W. H. Stockmayer, J. Chem. Phys. **17**, 1301 (1949).
40. M. Daoud and J. F. Joanny, J. de Phys. **42**, 1359 (1981).
41. M. Daoud, F. Family, and G. Jannink, J. de Phys. Lett. **45**, 119 (1984).
42. S. J. Candau, M. Ankrim, J. P. Munch, P. Rempp, G. Hild, and R. Osaka, in *Physical Optics of Dynamical Phenomena in Macromolecular Systems* (W. De Gruyter, Berlin, 1985), p. 145.
43. F. Schosseler and L. Leibler, J. Phys. Lett. **45**, 501 (1984).
44. F. Schosseler and L. Leibler, Macromolecules **18**, 398 (1985).
45. J. E. Martin and B. J. Ackerson, Phys. Rev. A **31**, 1180 (1985).
46. L. de Arcangelis, Comput. Sci. Eng. **5**, 78 (2004).
47. B. Ratajska-Gadomska and W. Gadomski, J. Phys. Cond. Matter 16, 9191 (2004).
48. J. P. Cohen, *Physical Properties of Polymeric Gels* (Addad, Wiley and Sons, 1996).
49. F. Prochazka, T. Nicolai and D. Durand, Macromolecules **29**, 2260 (1996).
50. T. Nicolai, H. Randrianantoandro, F. Prochazka and D. Durand, Macromolecules **30**, 5897 (1997).
51. D. Durand, and T. Nicolai, in *Encyclopaedia of Materials Science and Technology*, edited by K. H. J. Bushow, R. W. Cahn, M. C. Fleming, B. Ilschner, E. J. Kramer and S. Mahajan (Elsevier, **6**, 6116, 2001).
52. G. C. Fadda, D. Lairez, B. Arrio, J. P. Carton and V. Larreta-Garde, Biophys. **85**, 2808 (2003).
53. T. Abete, A. de Candia, D. Lairez and A. Coniglio, Phys. Rev. Lett. **93**, 228302 (2004).

CHAPTER 7

Densities, Coefficients of Thermal Expansion, and Compressibilities of Amorphous Polymers

Robert A. Orwoll

Department of Chemistry, College of William and Mary, Williamsburg, VA 23187-8795

Tables in this chapter contain published pressure-volume-temperature data for amorphous homopolymers. Measurements below the melting temperatures for semi-crystalline materials are not included because of the potentially large variance among samples with differing degrees of crystallinity. Rogers [1] and Zoller [2] have also compiled equation-of-state data for amorphous polymers.

7.1 DENSITIES AS A FUNCTION OF TEMPERATURE

The temperature dependence of polymer densities at atmospheric pressure is given in Tables 7.1 and 7.2. Table 7.1 gives densities measured above the glass transition temperature T_g and, for semi-crystalline polymers, above the melting temperature. Table 7.2 lists densities of amorphous polymers below T_g. Volumetric data are presented here in terms of the density ρ rather than the more commonly reported specific volume $\nu_{sp} = 1/\rho$ because, for most systems, ρ is a more linear function of temperature than is ν_{sp}. For most entries, the densities have been fitted to a power series

$$\rho(t) = a_0 + a_1 t + a_2 t^2 + \ldots, \tag{7.1}$$

with t representing the centigrade temperature. In the other cases, the polymer density is written as an exponential function of the centigrade temperature t

$$\rho(t) = \rho(0) e^{-\alpha_0 t}. \tag{7.2}$$

This latter form is for measurements in which the thermal expansion coefficient

$$\alpha = \frac{1}{v_{sp}} \left(\frac{\partial v_{sp}}{\partial t} \right)_P = -\frac{1}{\rho} \left(\frac{\partial \rho}{\partial t} \right)_P, \tag{7.3}$$

was found to be independent of temperature; i.e., $\alpha = \alpha_0$. Additional density data can be found in Chapter 29.

Tables 7.3 and 7.4 are compilations of densities and thermal expansion coefficients at one atmosphere tabulated at 20 °C intervals. Measurements below T_g are indicated by a g preceding the value. Some of the entries in these tables are taken directly from the published reports; consequently, there are occasional small variations between these values and those computed from the smoothing expressions in Tables 7.1 and 7.2. Densities judged to be more accurate than $\pm 0.001 \mathrm{g/cm^3}$ are recorded in Table 7.3 with an additional digit. Thermal expansion coefficients can also be determined from the power series expressions in Tables 7.1 and 7.2 using

$$\alpha = -\frac{a_1 + 2a_2 t + \ldots}{a_0 + a_1 t + a_2 t^2 + \ldots}, \tag{7.4}$$

which follows from Eqs. (7.1) and (7.3).

TABLE 7.1. *Densities, measured above T_g, as a function of temperature.*

Polymer	ρ, g/cm^3, (t in °C)	Temp. range, °C	Ref.
Natural Rubber, unvulcanized	$0.9283 - 6.10 \times 10^{-4} t$	0–25	[3]
Natural Rubber, cured	$0.9210 - 5.86 \times 10^{-4} t$	0–25	[3]
Polyamide, Nylon 6	$1.316 \exp(-4.70 \times 10^{-4} t)$	236–295	[4]
Polyamide, Nylon 6,6	$1.306 \exp(-6.60 \times 10^{-4} t)$	245–297	[4]
	$1.145 - 6.47 \times 10^{-4} t$	270–285	[5]
Poly (butene-1), isotactic	$0.876 \exp(-6.75 \times 10^{-4} t)$	133–246	[6]
Poly(*n*-butyl methacrylate)	$1.0695 - 5.82 \times 10^{-4} t - 0.98 \times 10^{-6} t^2 + 0.241 \times 10^{-8} t^3$	34–200	[7]
	$1.070 - 6.95 \times 10^{-4} t + 0.40 \times 10^{-6} t^2$	20–120	[8]
Poly(ε-caprolactone)	$1.110 - 7.81 \times 10^{-4} t + 0.519 \times 10^{-6} t^2$	101–148	[1]
Polycarbonate, (with Bisphenol *A*)	$1.254 - 6.35 \times 10^{-4} t - 0.116 \times 10^{-6} t^2$	151–340	[9]
	$1.2739 \exp(-6.21 \times 10^{-4} t)$	171–330	[38]
Poly(cyclohexyl methacrylate)	$1.1394 - 5.90 \times 10^{-4} t - 0.163 \times 10^{-6} t^2$	110–199	[7]
Poly(2,6-dimethylphenylene ether)	$1.168 - 6.95 \times 10^{-4} t - 0.070 \times 10^{-6} t^2$	203–320	[10]
Poly(dimethyl siloxane)	$0.9919 - 8.925 \times 10^{-4} t + 0.265 \times 10^{-6} t^2 - 0.0030 \times 10^{-8} t^3$	20–207	[11]
	$0.994 - 9.76 \times 10^{-4} t + 0.904 \times 10^{-6} t^2$	25–70	[12]
	$0.990 - 8.59 \times 10^{-4} t + 0.23 \times 10^{-6} t^2$	16–145	[49]
Poly(1,3-dioxepane)	$1.064 - 3.5 \times 10^{-4} t$	6–16	[43]
Poly(1,3-dioxolane)	$1.254 - 10.9 \times 10^{-4} t$	25–80	[44]
Polyetheretherketone	$1.397 \exp(-6.69 \times 10^{-4} t)$	338–400	[13]
Polyethylene, branched	$0.868 \exp(-6.73 \times 10^{-4} t)$	112–225	[14]
	$0.882 - 7.97 \times 10^{-4} t + 0.74 \times 10^{-6} t^2$	135–198	[7]
Polyethylene, linear	$0.8674 - 6.313 \times 10^{-4} t + 0.367 \times 10^{-6} t^2 - 0.055 \times 10^{-8} t^3$	130–207	[15]
	$0.863 - 4.73 \times 10^{-4} t - 0.38 \times 10^{-6} t^2$	142–200	[7]
Poly(ethylene terephthalate)	$1.390 - 7.82 \times 10^{-4} t$	274–342	[16]
Poly(ethyl methacrylate)	$1.156 - 6.59 \times 10^{-4} t$	65–95	[8]
Polyisobutylene	$0.9297 - 5.123 \times 10^{-4} t + 0.0615 \times 10^{-6} t^2$	0–150	[17]
Poly(methyl methacrylate)	$1.223 - 5.29 \times 10^{-4} t - 0.507 \times 10^{-6} t^2$	120–270	[18]
	$1.2135 - 4.64 \times 10^{-4} t - 0.648 \times 10^{-6} t^2$	114–159	[7]
	$1.228 \exp(-5.23 \times 10^{-4} t)$	115–230	[4]
	$1.211 - 5.96 \times 10^{-4} t$	105–150	[8]
	$1.229 - 7.12 \times 10^{-4} t$	110–194	[48]
Poly(methyl methacrylate), isotactic	$1.252 - 8.40 \times 10^{-4} t + 0.56 \times 10^{-6} t^2$	55–190	[19]
Poly(4-methyl pentene-1)	$0.843 - 5.11 \times 10^{-4} t$	240–319	[45]
Poly(*o*-methyl styrene)	$1.064 - 5.58 \times 10^{-4} t + 0.125 \times 10^{-6} t^2$	139–198	[20]
Polyoxybutylene	$0.985 - 6.82 \times 10^{-4} t$	30–90	[42]
Polyoxyethylene	$1.142 \exp(-7.09 \times 10^{-4} t)$	88–224	[1,21]
	$1.140 - 8.08 \times 10^{-4} t$	30–90	[42]
	$1.139 - 7.31 \times 10^{-4} t$	75–136	[47]
Polyoxymethylene	$1.336 \exp(-6.77 \times 10^{-4} t)$	183–220	[22]
Polypropylene, atactic	$0.848 - 0.19 \times 10^{-4} t - 3.05 \times 10^{-6} t^2$	80–120	[1]
Polypropylene, isotactic	$0.859 \exp(-6.60 \times 10^{-4} t)$	175–230	[4]
	$0.862 \exp(-6.70 \times 10^{-4} t)$	170–300	[6]
	$0.8414 - 3.79 \times 10^{-4} t - 0.316 \times 10^{-6} t^2$	180–300	[38]
Polystyrene	$1.0865 - 6.19 \times 10^{-4} t + 0.136 \times 10^{-6} t^2$	100–222	[23]
	$1.077 - 5.49 \times 10^{-4} t + 0.124 \times 10^{-6} t^2$	115–196	[20]
	$1.067 - 5.02 \times 10^{-4} t - 0.135 \times 10^{-6} t^2$	79–320	[10]
Polysulfone, (with Bisphenol *A*)	$1.314 - 6.49 \times 10^{-4} t - 0.018 \times 10^{-6} t^2$	185–371	[24]
Polytetrafluoroethylene	$2.340 - 24.33 \times 10^{-4} t + 0.309 \times 10^{-6} t^2$	330–372	[25]
Polytetrahydrofuran	$0.996 \exp(-6.691 \times 10^{-4} t)$	62–166	[1,21]
Poly(vinyl acetate)	$1.2124 - 8.62 \times 10^{-4} t + 0.223 \times 10^{-6} t^2$	35–100	[26]
Poly(vinyl chloride)	$1.394 - 2.03 \times 10^{-4} t - 2.19 \times 10^{-6} t^2$	100–150	[1]
Poly(vinylidene fluoride)	$1.816 - 26.77 \times 10^{-4} t + 4.75 \times 10^{-6} t^2$	180–220	[40]
Poly(vinyl methyl ether)	$1.0725 - 7.259 \times 10^{-4} t + 0.116 \times 10^{-6} t^2$	25–120	[27]

TABLE 7.2. *Densities of polymer glasses as a function of temperature.*

Glassy polymer	T_g, °C	ρ, g/cm^3, (t in °C)	Temp. range, °C	Ref.
Poly(*n*-butyl methacrylate)	20	$1.063 - 4.01 \times 10^{-4} t$	−30–20	[8]
Polycarbonate, (with Bisphenol *A*)	151	$1.204 - 3.05 \times 10^{-4} t$	30–151	[9]
	142	$1.2044 \exp(-2.21 \times 10^{-4} t)$	40–121	[38]
Poly(cyclohexyl methacrylate)	107	$1.106 - 2.69 \times 10^{-4} t$	19–85	[7]
Poly(2,6-dimethylphenylene ether)	203	$1.070 \exp(-2.09 \times 10^{-4} t)$	30–203	[10]
Poly(ethyl methacrylate)	65	$1.131 - 3.06 \times 10^{-4} t$	−35–65	[8]
Poly(methyl methacrylate)	100	$1.188 - 1.34 \times 10^{-4} t - 0.91 \times 10^{-6} t^2$	30–100	[18]
	105	$1.188 - 1.72 \times 10^{-4} t - 1.04 \times 10^{-6} t^2$	17–80	[7]
	105	$1.175 - 2.47 \times 10^{-4} t$	−30–105	[8]
	105	$1.187 - 2.35 \times 10^{-4} t - 0.67 \times 10^{-6} t^2$	20–95	[48]
Poly(methyl methacrylate), isotactic	47	$1.225 - 2.65 \times 10^{-4} t$	9–26	[19]
Poly(*o*-methyl styrene)	131	$1.027 - 2.64 \times 10^{-4} t$	29–82	[20]
Polystyrene	92	$1.048 - 1.88 \times 10^{-4} t - 0.608 \times 10^{-6} t^2$	8–75	[20]
	79	$1.052 \exp(-2.86 \times 10^{-4} t)$	30–79	[10]
Polysulfone, (with Bisphenol *A*)	186	$1.242 - 2.59 \times 10^{-4} t$	30–186	[24]
Poly(vinyl acetate)	31	$1.196 - 3.37 \times 10^{-4} t$	−30–20	[26]

7.2 DENSITIES AS A FUNCTION OF PRESSURE

Pressure-volume data have been reported for many polymers. In most cases the Tait equation

$$\rho(P,t) = \frac{\rho(0,t)}{1 - C \ln\left[1 + \dfrac{P}{B(t)}\right]}, \tag{7.5}$$

accurately represents the relationship between ρ and the pressure P. In it, the unitless parameter C is usually equated to 0.0894, while the temperature-dependent parameter $B(t)$ is written as a function of two other empirical parameters b_0 and b_1:

$$B(t) = b_0 e^{-b_1 t}. \tag{7.6}$$

As above, t is the centigrade temperature. Literature values for C, b_0, and b_1 are collected in Tables 7.5 (above T_g) and 7.6 (below T_g). The zero-pressure density ρ(0,t), which is virtually the same as the density at atmospheric pressure, can be computed from expressions in Tables 7.1 and 7.2.

Table 7.7 lists equations for the temperature dependence of thermal pressure coefficients $\gamma = (\partial p/\partial t)_v$ that have been directly determined.

Isothermal compressibilities

$$\kappa_T = -\frac{1}{v_{sp}}\left(\frac{\partial v_{sp}}{\partial P}\right)_t = \frac{1}{\rho}\left(\frac{\partial \rho}{\partial P}\right)_t, \tag{7.7}$$

at atmospheric pressure are summarized in Table 7.8. Most are derived from the Tait equation with parameters from Tables 7.5 and 7.6:

$$\kappa_T = \frac{C}{b_0} e^{b_1 t} (\text{at zero pressure}). \tag{7.8}$$

Others are obtained from thermal pressure and expansion coefficients through the relation

$$\kappa_T = \frac{\alpha}{\gamma}. \tag{7.9}$$

In most instances the latter values of κ_T have smaller uncertainties because of the greater accuracy that usually accompanies direct measurements of γ and α. Values of κ_T for glasses are preceded with a g in Table 7.8.

Related information can be found in Chapter 29.

TABLE 7.3. *Densities* (g/cm^3).

Temperature (deg C)	0	20	40	60	80	100	120	140	160	180	200	220	240	260	280	300	320	340	360	380	Ref.
Natural rubber, unvulcanized	0.9283	0.9162																			[3]
Natural rubber, cured	0.9211	0.9093																			[3]
Polyamide, Nylon 6													1.176	1.165	1.154	1.143					[4]
Polyamide, Nylon 6,6															0.963						[5]
														1.100	1.086	1.071					[4]
Poly(butene-1), isotactic								0.797	0.786	0.776	0.765	0.755	0.745								[6]
Poly(*n*-butyl methacrylate)			1.045	1.032	1.018	1.004	0.990	0.975	0.961	0.947	0.933										[7]
	*g*1.063[a]	1.057	1.043	1.030	1.017	1.005	0.993														[8]
Poly(ε-caprolactone)						1.037	1.023	1.010													[1]
Polycarbonate, (with Bisphenol *A*)			*g*1.192	*g*1.186	*g*1.180	*g*1.174	*g*1.167	*g*1.161	1.150	1.136	1.123	1.109	1.095	1.081	1.067	1.053	1.039	1.025			[9]
			*g*1.194	*g*1.188	*g*1.183	*g*1.178	*g*1.173			1.139	1.125	1.111	1.097	1.084	1.070	1.057	1.044				[38]
Poly(cyclohexyl methacrylate)		*g*1.101	*g*1.095	*g*1.090	*g*1.084		1.066	1.054	1.041	1.028	1.015										[7]
Poly (2,6-dimethylphenylene ether)			*g*1.061	*g*1.057	*g*1.052	*g*1.048	*g*1.043	*g*1.039	*g*1.035	*g*1.030	*g*1.026	1.012	0.997	0.983	0.968	0.953	0.939				[10]
Poly(dimethyl siloxane)		0.9742	0.9566	0.9393	0.9222	0.9053	0.8887	0.8722	0.8560	0.8400	0.8242										[11]
			0.9566	0.9389																	[12]
		0.974	0.956	0.939	0.922	0.905	0.889	0.873	0.857												[41]
		0.973	0.956	0.939	0.923	0.906	0.890	0.874													[49]
Poly(1,3-dioxolane)			1.210	1.188	1.167																[44]
Polyetheretherketone																		1.113	1.098	1.084	[13]
Polyethylene, branched							0.801	0.790	0.780	0.769	0.759	0.749									[14]
								0.785	0.774	0.763	0.752										[7]
Polyethylene, linear								0.7847	0.7735	0.7624	0.7514										[15]
								0.789	0.778	0.766	0.753										[7]
								0.784	0.774	0.763											[41]
Poly(ethylene terephthalate)															1.172	1.156	1.140	1.125			[16]
Poly(ethyl methacrylate)	*g*1.131	*g*1.125	*g*1.119	*g*1.113	1.103																[8]
Poly(hydroxybutyrate)		1.177																			[46]
Polyisobutylene	0.9297	0.9195	0.9093	0.8992	0.8891	0.8791	0.8691	0.8592													[17]
		0.912	0.901	0.890	0.880	0.870	0.861	0.851	0.842												[41]
Poly(methyl methacrylate)			*g*1.181	*g*1.177	*g*1.171	*g*1.166	1.153	1.139	1.126	1.112	1.097	1.082	1.067	1.052							[18]
		*g*1.184	*g*1.179	*g*1.174	*g*1.168		1.148	1.136	1.123												[7]
							1.153	1.141	1.129	1.117	1.106	1.094									[4]
	*g*1.175	*g*1.170	*g*1.165	*g*1.160	*g*1.155	*g*1.150	1.140	1.128													[8]
		*g*1.182	*g*1.177	*g*1.171	*g*1.164		1.144	1.129	1.115	1.101											[48]
Poly(methyl methacrylate), isotactic		*g*1.220		1.204	1.189	1.174	1.160	1.146	1.132	1.119											[19]
Poly(4-methyl pentene-1)													0.720	0.710	0.700	0.690	0.679				[45]
Poly(*o*-methyl styrene)			*g*1.016	*g*1.011	*g*1.006			0.9881	0.9777	0.9674	0.9571										[20]
Polyoxybutylene			0.958	0.944	0.931																[42]
					0.944	0.931	0.919	0.907	0.895												[1,21]
Polyoxyethylene					1.086	1.070	1.053	1.037	1.022	1.007	0.992										[41]
			1.107	1.091	1.075																[42]
						1.063	1.048	1.033	1.018	1.004	0.990	0.976									[1,21]
					1.081	1.066	1.051														[47]
Polyoxymethylene											1.167	1.151									[22]
Polypropylene, atactic					0.827	0.816	0.802														[1]
									0.773	0.762	0.752										[41]
Polypropylene, isotactic										0.764	0.754	0.744	0.734	0.724	0.714	0.705					[6]
										0.763	0.753	0.743	0.732	0.721	0.711	0.699					[38]
										0.763	0.753	0.743									[4]
Polystyrene						1.0260	1.0142	1.0025	0.9909	0.9795	0.9681	0.9569									[23]
		*g*1.044	*g*1.040	*g*1.035			1.0125	1.0021	0.9919	0.9818	0.9717										[20]
			*g*1.040	*g*1.034	1.026	1.016	1.005	0.994	0.984	0.973	0.961	0.950	0.939	0.928	0.916	0.905	0.893				[10]
Polysulfone, (with Bisphenol *A*)			*g*1.232	*g*1.226	*g*1.221	*g*1.216	*g*1.211	*g*1.206	*g*1.201	*g*1.195	1.183	1.170	1.157	1.144	1.130	1.117	1.104	1.091	1.078		[24]
Polytetrafluoroethylene																		1.548	1.504		[25]
Poly(vinyl acetate)	*g*1.196	*g*1.189	1.1783	1.1615	1.1449	1.1285															[26]
Poly(vinyl chloride)						1.352	1.338	1.322													[1]
Poly(vinylidene fluoride)										1.488	1.471	1.457									[40]
Poly(vinyl methyl ether)		1.0580	1.0436	1.0294	1.0152	1.0011	0.9871														[27]

[a] g = glass.

TABLE 7.4. *Thermal expansion coefficients* ($\times 10^{-4} K^{-1}$).

Temperature (deg C)	0	20	40	60	80	100	120	140	160	180	200	220	240	260	280	300	320	340	360	380	Ref.
Natural Rubber, unvulcanized	6.6	6.6																			[3]
Natural Rubber, cured	6.5	6.4																			[3]
		6.7																			[28]
Polyamide, Nylon 6													4.7	4.7	4.7						[4]
Polyamide, Nylon 6.6														6.6	6.6						[4]
															6.8						[5]
Poly(butene-1), isotactic								6.7	6.7	6.7	6.7	6.7	6.7								[6]
Poly(*n*-butyl methacrylate)			6.2	6.5	6.8	7.0	7.2	7.3	7.4	7.4	7.4										[7]
	*g*3.8[a]	6.4	6.4	6.3	6.2	6.1	6.1														[8]
Poly(ϵ-caprolactone)							6.4	6.3													[1]
Polycarbonate, (with Bisphenol *A*)			*g*2.6	*g*2.6	*g*2.6	*g*2.6	*g*2.6	*g*2.6	5.8	5.9	6.1	6.2	6.3	6.4	6.6	6.7	6.8	6.9			[9]
			*g*2.2	*g*2.2	*g*2.2	*g*2.2	*g*2.2			6.2	6.2	6.2	6.2	6.2	6.2	6.2					[38]
Poly(cyclohexyl methacrylate)		*g*2.4	*g*2.5	*g*2.5	*g*2.5		5.9	6.0	6.2	6.3	6.4										[7]
Poly(2,6-dimethylphenylene ether)			*g*2.1	*g*2.1	*g*2.1	*g*2.1	*g*2.1	*g*2.1	*g*2.1	*g*2.1	*g*2.1	7.1	7.3	7.4	7.6	7.7	7.8				[10]
Poly(dimethyl siloxane)		9.06	9.11	9.17	9.23	9.29	9.35	9.41	9.47	9.53	9.59										[11]
		9.0																			[28]
			9.4	9.2																	[12]
Poly(1,3-dioxolane)			9.0	9.2																	[44]
Polyetheretherketone							6.7	6.7	6.7	6.7	6.7	6.7						6.7	6.7	6.7	[13]
Polyethylene, branched							6.7	6.7	6.7	6.7	6.7	6.7									[14]
								7.5	7.2	6.9											[7]
									7.5	7.7	7.8	8.0									[39]
Polyethylene, linear								7.14	7.18	7.24	7.32										[15]
									7.3	7.4	7.5	7.6									[39]
										7.0	7.0										[29]
									7.6	7.9											[7]
Poly(ethylene terephthalate)															6.8	6.8	6.8	6.8			[16]
Poly(ethyl methacrylate)	*g*2.7	*g*2.7	*g*2.7	*g*2.7	6.0																[8]
Polyisobutylene	5.51	5.54	5.58	5.61	5.65	5.68	5.72	5.75													[17]
Poly(methyl methacrylate)			*g*1.8	*g*2.1	*g*2.4	*g*2.7	5.5	5.8	6.1	6.4	6.7	7.0	7.2	7.5							[18]
		*g*1.8	*g*2.2	*g*2.5	*g*2.9		5.4	5.7	6.0												[7]
							5.2	5.2	5.2	5.2	5.2	5.2									[4]
	*g*2.1	*g*2.1	*g*2.1	*g*2.1	*g*2.1	*g*2.1	5.2	5.2													[8]
			*g*2.5	*g*2.7	*g*2.9																[48]
Poly(methyl methacrylate), isotactic		*g*2.2		6.4	6.3	6.2	6.1	5.9	5.8	5.7											[19]
Poly(4-methyl pentene-1)												7.1	7.2	7.3	7.4	7.5					[45]
Poly(*o*-methyl styrene)			*g*2.6	*g*2.6	*g*2.6			5.3	5.3	5.3											[20]
Polyoxybutylene			7.1	7.2	7.3																[42]
					6.7	6.7	6.7	6.7	6.7												[1,21]
Polyoxyethylene						7.1	7.1	7.1	7.1	7.1	7.1	7.1									[1,21]
			7.3	7.4	7.5																[42]
					6.7	6.8	7.0														[47]
Polyoxymethylene										7.9											[29]
											6.8	6.8									[22]
Polypropylene, atactic					6.1	7.7	9.3														[1]
Polypropylene, isotactic										6.6	6.6	6.6									[4]
											6.9	7.1	7.3	7.5	7.7	8.0					[38]
										6.7	6.7	6.7	6.7	6.7	6.7	6.7					[6]
										6.7	6.7										[29]
Polystyrene						5.78	5.79	5.81	5.82	5.84	5.85	5.87									[23]
		*g*2.0	*g*2.3	*g*2.5			5.1	5.1	5.1	5.1	5.1										[20]
			*g*2.9	*g*2.9	5.0	5.2	5.3	5.4	5.6	5.7	5.8	5.9	6.0	6.2	6.3	6.4	6.5				[10]
Polysulfone, (with Bisphenol *A*)			*g*2.1	*g*2.1	*g*2.1	*g*2.1	*g*2.1	*g*2.1	*g*2.2	*g*2.2	5.5	5.6	5.7	5.8	5.9	6.0	6.1	6.1			[24]
Polytetrafluoroethylene																		14.4	14.7		[25]
Poly(vinyl acetate)	*g*2.8	*g*2.8	7.13	7.17	7.20	7.23															[26]
Poly(vinyl chloride)						4.7	5.5	6.2													[1]
Poly(vinylidene fluoride)											5										[40]
Poly(vinyl methyl ether)			6.87	6.92	6.96	7.01	7.06														[27]

[a] g = glass.

TABLE 7.5. *Parameters for the Tait equation, Eqs. (7.5) and (7.6), for amorphous polymers above T_g.*

Polymer	C	b_0, bar	b_1, deg C^{-1}	Temp. range, deg C	Pressure range, bar	Ref.
Natural Rubber, cured	0.0894	1916	0.00425	0–25	0–500	[3]
Natural Rubber, unvulcanized	0.0894	1937	0.00517	0–25	0–500	[3]
Polyamide, Nylon 6	0.0894	3767	0.00466	236–295	0–2000	[4]
Polyamide, Nylon 6,6	0.0894	3538	0.00376	270–285	0–600	[5]
	0.0894	3164	0.00504	245–297	0–2000	[4]
Poly(butene-1), isotactic	0.0894	1675	0.00453	133–246	0–2000	[6]
Poly(*n*-butyl methacrylate)	0.0894	2267	0.00534	34–200	0–2000	[7]
Poly(ε-caprolactone)	0.0894	1890	0.00393	100–148	0–2000	[1]
Polycarbonate, (with Bisphenol *A*)	0.0894	3100	0.00408	151–340	0–1800	[9]
	0.0894	2803	0.00387	171–330	100–2000	[38]
Poly(cyclohexyl methacrylate)	0.0894	2952	0.00522	123–200	0–2000	[7]
Poly(2,6-dimethylphenylene ether)	0.0894	2278	0.00429	203–320	0–1800	[10]
Poly(dimethyl siloxane)	0.1009	1041	0.00585	25–70	0–1000	[30]
	0.0988	960	0.00604	29–60	0–800	[31]
	0.0894	885	0.00610	25–70	0–900	[12]
	0.0894	915	0.00609	18–150	0–2200	[49]
Polyetheretherketone	0.0894	3880	0.00412	338–400	0–2000	[13]
Polyethylene, branched	0.0894	1867	0.00439	112–225	0–2000	[14]
	0.0970	1987	0.00510	140–200	0–1000	[30]
	0.0894	1771	0.00470	130–200	0–2000	[7]
	0.0894	1884	0.00488	140–203	0–2000	[32,33]
Polyethylene, linear	0.0894	1767	0.00466	142–200	0–2000	[7]
	0.0894	1683	0.00429	140–200	0–2000	[7]
Poly(ethylene terephthalate)	0.0894	3697	0.00415	274–342	0–2000	[16]
Polyisobutylene	0.0871	1907	0.00415	53–110	0–1000	[30]
Poly(methyl methacrylate)	0.0894	3000	0.00508	105–255	0–1800	[18]
	0.0894	2875	0.00415	114–160	0–2000	[7]
	0.0894	3850	0.00672	120–139	0–2000	[33,34]
	0.0894	4278	0.00369	115–230	0–2000	[4]
	0.0894	3006	0.00426	110–194	0–2000	[48]
Poly(methyl methacrylate), isotactic	0.0894	2992	0.00456	55–190	0–2000	[19]
Poly(*o*-methyl styrene)	0.0894	2619	0.00411	139–198	0–2000	[20]
Polyoxybutylene	0.0894	1786	0.00422	62–166	0–700	[1,21]
Polyoxyethylene	0.0894	2077	0.00395	88–224	0–700	[1,21]
	0.0894	2870	0.00473	75–136	0–2000	[47]
Polyoxymethylene	0.0894	3058	0.00433	183–220	0–2000	[22]
Polypropylene, atactic	0.0894	1621	0.00660	80–120	0–1000	[1]
Polypropylene, isotactic	0.0894	1491	0.00418	170–300	0–2000	[6]
	0.0894	1475	0.00413	175–230	0–2000	[4]
	0.0894	1705	0.00498	180–300	100–2000	[38]
Polystyrene	0.0894	2169	0.00332	115–196	0–2000	[20]
	0.0894	2521	0.00408	79–320	0–1800	[10]
	0.0894	2435	0.00414	115–249	0–2000	[33,34]
Polysulfone, (with Bisphenol *A*)	0.0894	3659	0.00376	186–370	0–2000	[24]
Polytetrafluoroethylene	0.0894	4252	0.00938	343–372	0–2000	[25]
Poly(vinyl acetate)	0.1046	2231	0.00343	64–120	0–1000	[30]
	0.0894	2035	0.00426	35–100	0–800	[26,35]
Poly(vinyl chloride)	0.0894	3522	0.00565	82–97	0–2000	[33,34]
	0.0894	2942	0.00532	100–150	0–2000	[1]
Poly(vinylidene fluoride)	0.0894	1066	0.00042	180–220	0–1200	[40]

TABLE 7.6. *Parameters for the Tait equation, Eqs. (7.5) and (7.6), for polymer glasses.*

Glassy polymer	C	b_0, bar	b_1,deg C^{-1}	T_g, deg C	Temp. range, deg C	Pressure range, bar	Ref.
Polycarbonate, (with Bisphenol *A*)	0.0894	3878	0.00261	151	30–151	0–1800	[9]
	0.0894	3251	0.00133	142	40–141	100–1500	[38]
Poly(cyclohexyl methacrylate)	0.0894	3762	0.00298	107	19–74	0–2000	[7]
Poly(2,6-dimethylphenylene ether)	0.0894	3314	0.00200	203	30–203	0–1800	[10]
Poly(methyl methacrylate)	0.0894	3767	0.00470	100	30–100	0–1800	[18]
	0.0894	3564	0.00323	105	17–91	0–2000	[7]
	0.0894	3717	0.00396	111	20–100	0–2000	[33]
	0.0894	4296	0.00416	105	20–95	0–2000	[48]
Poly(methyl methacrylate), isotactic	0.0894	4968	0.00670	47	9–26	0–2000	[19]
Poly(*o*-methyl styrene)	0.0894	3596	0.00355	131	29–82	0–2000	[20]
Polystyrene	0.0894	3449	0.00271	92	8–75	0–2000	[20]
	0.0894	3917	0.00431	79	30–79	0–1800	[10]
	0.0894	3337	0.00330	88	20–61	0–2000	[33,34]
Polysulfone, (with Bisphenol *A*)	0.0894	4323	0.00154	186	30–186	0–2000	[24]
Poly(vinyl acetate)	0.0894	3079	0.00097	31	−30–20	0–800	[26,35]
Poly(vinyl chloride)	0.0894	3751	0.00241	75	20–51	0–2000	[33,34]

TABLE 7.7. *Thermal pressure coefficients as a function of temperature.*

Polymer	$(\partial P/\partial t)_v$, bar/K, (t in °C)	Temp. range, °C	Ref.
Natural Rubber, cured	$13.75 - 0.0545t - 0.481 \times 10^{-4}t^2$	20–50	[28]
Poly(dimethyl siloxane)	$8.71 - 0.0474t + 0.93 \times 10^{-4}t^2$	25–162	[11]
	$9.00 - 0.0538t + 1.54 \times 10^{-4}t^2$	−20–50	[28]
Polyethylene, high density	$13.22 - 0.0558t + 0.896 \times 10^{-4}t^2$	139–192	[15]
Polyisobutylene	$12.66 - 0.0545t + 1.02 \times 10^{-4}t^2$	10–172	[17]
Polyoxyethylene	$15.79 - 0.0250t + 1.532 \times 10^{-4}t^2$	50–103	[36]
Polypropylene, isotactic	$23.19 - 0.1757t + 4.22 \times 10^{-4}t^2$	158–195	[37]
Polystyrene	$15.81 - 0.0859t + 2.70 \times 10^{-4}t^2$	27–100	[23]
Poly(vinyl methyl ether)	$13.81 - 0.0514t + 0.005 \times 10^{-4}t^2$	20–120	[27]

TABLE 7.8. *Isothermal compressibilities* ($\times 10^{-5}$ bar^{-1}) *at atmospheric pressure.*

Temperature (deg C)	0	20	40	60	80	100	120	140	160	180	200	220	240	260	280	300	320	340	360	380	Ref.
Natural Rubber, cured		5.3																			[28]
	4.6	5.0																			[3]
Natural Rubber, unvulcanized	4.6	5.0																			[3]
Polyamide, Nylon 6													7.3	8.0	8.8						[4]
Polyamide, Nylon 6,6															7.2						[5]
														10.5	11.6						[4]
Poly(butene-1), isotactic								10.1	11.0	12.1	13.2	14.5	15.8								[6]
Poly(*n*-butyl methacrylate)			4.9	5.4	6.0	6.7	7.5	8.3	9.3	10.3	11.5										[7]
Poly(ϵ-caprolactone)						7.0	7.6	8.2													[1]
Polycarbonate, (with Bisphenol *A*)			*g*2.6[a]	*g*2.7	*g*2.8	*g*3.0	*g*3.2	*g*3.3	5.5	6.0	6.5	7.1	7.7	8.3	9.0	9.8	10.6	11.5			[9]
			*g*2.9	*g*3.0	*g*3.1	*g*3.1	*g*3.2	*g*3.3		6.4	6.9	7.5	8.1	8.7	9.4	10.2	11.0				[38]
Poly(cyclohexyl methacrylate)		*g*2.5	*g*2.7	*g*2.8					6.3	7.0	7.7	8.6									[7]
Poly(2,6-dimethylphenylene ether)			*g*2.9	*g*3.0	*g*3.2	*g*3.3	*g*3.4	*g*3.6	*g*3.7	*g*3.9	*g*4.0	10.1	11.0	12.0	13.0	14.2	15.5				[10]
Poly(dimethyl siloxane)			13.1	14.8	16.7	19.0	21.4	24.1	27.0												[11]
	10.0	11.3	12.8																		[28]
			12.3	13.8																	[30]
			13.1	14.8																	[31]
			12.9	14.6																	[12]
		11.0	12.5	14.1	15.9	18.0	20.3	22.9													[49]
Polyetheretherketone																		9.4	10.2	11.0	[13]
Polyethylene, branched							8.1	8.9	9.7	10.6	11.5	12.6									[14]
								10.0	11.0	12.2	13.5										[30]
								9.7	10.7	11.8	12.9										[7]
								9.4	10.4	11.4	12.6										[32,33]
Polyethylene, linear								10.0	11.0	12.1											[15]
									10.7	11.7	12.9										[7]
								9.7	10.6	11.5	12.5										[7]
Poly(ethylene terephthalate)															7.7	8.4	9.1	9.9			[16]
Polyisobutylene		4.8	5.2	5.8	6.3	6.9	7.5	8.2													[17]
				5.9	6.4	6.9															[30]
Poly(methyl methacrylate)			*g*2.9	*g*3.1	*g*3.5	*g*3.8	5.5	6.1	6.7	7.4	8.2	9.1	10.1								[18]
		*g*2.7	*g*2.9	*g*3.0	*g*3.2		5.1	5.6	6.0												[7]
		*g*2.6	*g*2.8	*g*3.1	*g*3.3	*g*3.6	5.2	5.9													[33,34]
		*g*2.3	*g*2.5	*g*2.7	*g*2.9		5.0	5.4	5.9	6.4											[48]
Poly(methyl methacrylate), isotactic		*g*2.1		3.9	4.3	4.7	5.2	5.7	6.2	6.8											[19]
Poly(4-methyl pentene-1)													19	20	22	24	27				[45]
Poly(*o*-methyl styrene)			*g*2.9	*g*3.1	*g*3.3			6.1	6.6	7.2											[20]
Polyoxymethylene											6.9	7.6									[22]
Polyoxyethylene						6.4	6.9	7.5	8.1	8.8	9.5	10.3									[1,21]
				5.2	5.5	6.0															[36]
					4.5	5.0	5.5														[47]
Polypropylene, atactic					9.4	10.7	12.2														[1]
Polypropylene, isotactic										12.7	13.8	15.0	16.3	17.8	19.3	21.0					[6]
										12.7	13.8	15.0									[4]
									11.2	12.8											[4,6,37]
										13	14	16	17	19	21	23					[38]
Polystyrene			4.5	5.0	5.5	6.0															[23]
		*g*2.7	*g*2.9	*g*3.1			6.1	6.6	7.0	7.5											[20]
			*g*2.7	*g*3.0	4.9	5.3	5.8	6.3	6.8	7.4	8.0	8.7	9.4	10.2	11.1	12.1	13.1				[10]
		*g*2.9	*g*3.1	*g*3.3			6.0	6.6	7.1	7.7	8.4	9.1	9.9								[33,34]
Polysulfone, (with Bisphenol *A*)			*g*2.2	*g*2.3	*g*2.3	*g*2.4	*g*2.5	*g*2.6	*g*2.6	*g*2.7	5.2	5.6	6.0	6.5	7.0	7.5	8.1	8.8	9.4		[24]
Polytetrafluoroethylene																			61.6		[25]
Polytetrahydrofuran					7.0	7.6	8.3	9.0	9.8												[1,21]
Poly(vinyl acetate)					6.2	6.6	7.1														[30]
	*g*2.9	*g*3.0	5.2	5.7	6.2	6.7															[26,35]
Poly(vinyl chloride)		*g*2.5	*g*2.6		4.0	4.5															[33,34]
						5.2	5.8	6.4													[1]
Poly(vinylidene fluoride)										8.9	9.0	9.0									[40]
Poly(vinyl methyl ether)		5.3	5.8	6.4	7.2	8.1	9.2														[27]

[a] *g* = glass.

REFERENCES

1. P. A. Rogers, J. Appl. Polym. Sci. **48**, 1061 (1993).
2. P. Zoller, in *Polymer Handbook*, edited by J. Brandrup and E. H. Immergut (Wiley, New York, 1989), pp. VI/475–483.
3. L. A. Wood and G. M. Martin, J. Res. Nat. Bur. Stand. **68A**, 259 (1964).
4. Y. Z. Wang, W. J. Chia, K. H. Hsieh, *et al*. J. Appl. Polym. Sci. **44**, 1731 (1992).
5. H. W. Starkweather, Jr., P. Zoller, and G. A. Jones, J. Polym. Sci., Polym. Phys. Ed. **22**, 1615 (1984).
6. P. Zoller, J. Appl. Polym. Sci. **23**, 1057 (1979).
7. O. Olabisi and R. Simha, Macromolecules **8**, 206 (1975).
8. S. S. Rogers and L. Mandelkern, J. Phys. Chem. **61**, 985 (1957).
9. P. Zoller, J. Polym. Sci., Polym. Phys. Ed. **20**, 1453 (1982).
10. P. Zoller and H. H. Hoehn, J. Polym. Sci., Polym. Phys. Ed. **20**, 1385 (1982).
11. H. Shih and P. J. Flory, Macromolecules **5**, 758 (1972).
12. R. N. Lichtenthaler, D. D. Liu, and J. M. Prausnitz, Macromolecules **11**, 192 (1978).
13. P. Zoller, T. A. Kehl, H. W. Starkweather, Jr., *et al*. J. Polym. Sci. B. Polym. Phys. **27**, 993 (1989).
14. P. Zoller, J. Appl. Polym. Sci. **23**, 1051 (1979).
15. R. A. Orwoll and P. J. Flory, J. Am. Chem. Soc. **89**, 6814 (1967).
16. P. Zoller and P. Bolli, J. Macromol. Sci.-Phys. **B18**, 555 (1980).
17. B. E. Eichinger and P. J. Flory, Macromolecules **1**, 285 (1968).
18. C. K. Kim and D. R. Paul, Polymer **33**, 2089 (1992).
19. A. Quach, P. S. Wilson, and R. Simha, J. Macromol. Sci.-Phys. **B9**, 533 (1974).
20. A. Quach and R. Simha, J. Appl. Phys. **42**, 4592 (1971).
21. R. K. Jain and R. Simha, J. Polym. Sci., Polym. Phys. Ed. **17**, 1929 (1979).
22. H. W. Starkweather, Jr., G. A. Jones, and P. Zoller, J. Polym. Sci. B, Polym. Phys. **26**, 257 (1988).
23. H. Höcker, G. J. Blake, and P. J. Flory, Trans. Faraday Soc. **67**, 2251 (1971).
24. P. Zoller, J. Polym. Sci., Polym. Phys. Ed. **16**, 1261 (1978).
25. P. Zoller, J. Appl. Polym. Sci. **22**, 633 (1978).
26. J. E. McKinney and M. Goldstein, J. Res. Nat. Bur. Stand. **78A**, 331 (1974).
27. T. Shiomi, F. Hamada, T. Nasako, *et al*. Macromolecules **23**, 229 (1990).
28. G. Allen, G. Gee, D. Mangaraj, *et al*. Polymer **1**, 467 (1960).
29. V.-H. Karl, F. Asmussen, and K. Ueberreiter, Makromol. Chem. **178**, 2037 (1977).
30. S. Beret and J. M. Prausnitz, Macromolecules **8**, 536 (1975).
31. K. Kubota and K. Ogino, Macromolecules **11**, 514 (1978).
32. D. P. Maloney and J. M. Prausnitz, J. Appl. Polym. Sci. **18**, 2703 (1974).
33. K.-H. Hellwege, W. Knappe, and P. Lehmann, Kolloid-Z. Z. Polym. **183**, 110 (1962).
34. R. Simha, P. S. Wilson, and O. Olabisi, Kolloid-Z. Z. Polym. **251**, 402 (1973).
35. J. E. McKinney and R. Simha, Macromolecules **7**, 894 (1974).
36. G. N. Malcolm and G. L. D. Ritchie, J. Phys. Chem. **66**, 852 (1962).
37. G. C. Fortune and G. N. Malcolm, J. Phys. Chem. **71**, 876 (1967).
38. Y. Sato, Y. Yamasaki, S. Takishima, *et al*. J. Appl. Polym. Sci. **66**, 141 (1997).
39. L. Zhao, L. Capt, M. R., Kamal, *et al*., Polym. Eng. Sci. **44**, 853 (2004).
40. N. Mekhilef, J. Appl. Polym. Sci. **80**, 230 (2001).
41. R.-J. Roe, J. Phys. Chem. **72**, 2013 (1968).
42. S.-M. Mai, C. Booth, and V. M. Nace, Eur. Polym. J. **33**, 991 (1997).
43. J. Garza, C. Marco, J. G. Fatou, *et al*. Polymer **22**, 477 (1981).
44. P. Archambault and R. E. Prud'homme, J. Polym. Sci., Polym. Phys. Ed. **18**, 35 (1980).
45. P. Zoller, J. Appl. Polym Sci. **21**, 3129 (1977).
46. P. J. Barham, A. Keller, E. L. Otun, *et al*. J. Mater. Sci. **19**, 2781 (1988).
47. M. Schmidt and F. H. J. Maurer, J. Polym. Sci. B, Polym. Phys. **36**, 1061 (1998).
48. M. Schmidt and F. H. J. Maurer, Macromolecules **33**, 3879 (2000).
49. V. K. Sachdev, U. Yahsi, and R. K. Jain, J. Polym. Sci. B, Polym. Phys. **36**, 841 (1998).

CHAPTER 8

Thermodynamic Properties of Proteins

George I. Makhatadze

Department of Biochemistry and Molecular Biology Penn State University College of Medicine, Hershey, PA 17033

Proteins are heteropolymers consisting of 20 different type of amino acid residues. They all share a common backbone

$$\begin{array}{c} H_2N{-}CH{-}COOH \\ \quad\quad | \\ \quad\quad R \end{array}$$

and differ by the side chain radical, R. Amino acid residues are arranged into a polypeptide chain through formation of peptide bonds

$$H_2N{-}CH{-}\left(\begin{array}{c} HN{-}CH{-}CO \\ \quad\quad | \\ \quad\quad R_1 \end{array}\right)_{N-2} {-}HN{-}CH{-}\begin{array}{c} COOH \\ | \\ R_N \end{array}$$

The side chains, R_N, vary in size and chemical nature (Table 8.1), allowing a great variety of properties. Naturally occurring polypeptides adopt a unique three dimensional conformation in solution. The structures of many of them have been solved by X-ray crystallography and 2D-NMR.

8.1 HEAT CAPACITY

Tables 8.2 and 8.3 present molar heat capacities of solid amino acids and polyamino acids. Table 8.4 presents specific heat capacities of anhydrous and hydrated proteins. All of the measurements were done by using adiabatic absolute calorimetry and their accuracy is better than 1–2%. Heat capacity of anhydrous proteins can be predicted using empirical approach developed by Wunderlich (see e.g., [1]).

In the presence of the solvent water, the heat capacity of proteins increases. The partial molar heat capacity of proteins in the native state, $C_p^N(T)$, appears to be a linear function of temperature [2–5]. The $C_p^N(T)$ increases with the increase of temperature with a slope from 0.005 to $0.008\,J\,K^{-2}\,g^{-1}$ for small globular proteins depending on the protein [6]. The absolute value of $C_p^N(T)$ at 25 °C ranges between 1.25 and $1.80\,J\,K^{-1}\,g^{-1}$, depending on the proteins [6]. The heat capacity of the denatured state, $C_p^D(T)$, for small globular proteins is always larger than the heat capacity of the native state, and depends on temperature in a more complicated way. The temperature dependence is nonlinear at low temperatures (0–75 °C). At temperatures above 75 °C the heat capacity function appears to be almost independent of temperature. At 25 °C, $C_p^D(T)$ values for different proteins range from 1.85 to $2.20\,J\,K^{-1}\,g^{-1}$, while at 100 °C they are higher, 2.1–2.4 $J\,K^{-1}\,g^{-1}$. A nonlinear dependence of the heat capacity of denatured protein is in agreement (within 5%) with what one can expect for the heat capacity of an unfolded polypeptide chain, $C_p^U(T)$, of the same amino acid composition [7–10]. The latter can be calculated as a sum of contributions from side chains and from the peptide unit:

$$C_{p,2}^U = (N - 1) \cdot C_{p,2}(\text{—CHCONH—}) + \sum_{i=1}^{N} C_{p,2}(-R_i), \tag{8.1}$$

where $C_{p,2}$(—CHCONH—) is the heat capacity of the peptide unit, $C_{p,2}(-R_i)$ is the heat capacity contribution of the side-chain of the ith amino acid residue, and N is the number of amino acid residues in the polypeptide chain. These contributions, for the temperature range 5–125 °C are listed in Table 8.5. The agreement is observed not only in the temperature dependence of these two functions ($C_p^D(T)$ and $C_p^U(T)$) but in majority of cases in the absolute values as well [7–10]. The close correspondence between the measured

TABLE 8.1a. *Properties of 20 naturally occurring amino acids.*

Name	Three letter code	One letter code	Side Chains (–**R**) **R**–CH(NH_2)COOH	Mol Mass Da	pK_a	ΔH_{ion} kJ mol^{-1}	Volume $Å^3$	ASA_{mc} $Å^2$	ASA_{sc}^{npl} $Å^2$	ASA_{sc}^{pol} $Å^2$
Alanine	Ala	A	$-CH_3$	71.08			88.6	46	67	
Arginine	Arg	R	$-(CH_2)_3-CNH(=NH)NH_3$	156.20	12	44.9	173.4	45	89	107
Asparagine	Asn	N	$-CH_2-CONH_2$	114.11			117.7	45	44	69
Aspartic acid	Asp	D	$-CH_2-COOH$	115.09	4.5	4.6	111.1	45	48	58
Cystein	Cys	C	$-CH_2-SH$	103.14	9.1–9.5	36.0	108.5	36	35	69
Glutamine	Gln	Q	$-(CH_2)_2-CONH_2$	128.14			143.9	45	53	91
Glutamic acid	Glu	E	$-(CH_2)_2-COOH$	129.12	4.6	1.6	138.4	45	61	77
Glycine	Gly	G	–H	57.06			60.1	85		
Histidine	His	H		137.15	6.2	43.6	153.2	43	102	49
Isoleucine	Ile	I	$-CH(CH_3)-C_2H_5$	113.17			166.7	42	140	
Leucine	Leu	L	$-CH(CH_3)_2-CH_2$	113.17			166.7	43	137	
Lysine	Lys	K	$-(CH_2)_4-NH_2$	128.18	10.4	53.6	168.6	44	119	48
Methionine	Met	M	$-(CH_2)_2-S-CH_3$	131.21			162.9	44	117	43
Phenylalanine	Phe	F		147.18			189.9	43	175	
Proline	Pro	P	*	97.12			122.7	38	105	
Serine	Ser	S	$-CH_2-OH$	87.08			89.0	42	44	36
Threonine	Thr	T	$-CH_2-(CH_3)-OH$	101.11			116.1	44	74	28
Tryptophane	Trp	W		186.21			227.8	42	190	27
Tyrosine	Tyr	Y		163.18	9.7	25.1	193.6	42	144	43
Valine	Val	V	$-CH-(CH_3)_2$	99.14			140	43	117	
			α-amino		6.8–7.9					
			α-carboxyl		3.5–4.3					

*Proline is an imono acid; Enthalpies of ionization of side chains at 25 °C, ΔH_{ion}, are from [19]; van der Waals volume from [20]; ASA_{mc}, surface area of the backbone, ASA_{sc}^{npl}, nonpolar surface area of the side chains, and, ASA_{sc}^{pol}, polar surface area of the side chains are from [14].

TABLE 8.1b. *Heat capacities ($J\,K^{-1}\,mol^{-1}$) of solid amino acids.*

T/K	C_p	T/K	C_p	T/K	C_p
L-Alanine (89.1 Da) [21]					
10	0.494	90	47.87	220	96.23
15	1.674	100	52.55	230	99.58
20	3.849	110	56.94	240	102.93
25	6.724	120	61.09	250	106.32
30	10.09	130	65.10	260	111.55
35	13.75	140	68.99	270	113.05
40	17.37	150	72.72	280	116.40
45	20.91	160	76.32	290	119.66
50	24.40	170	79.83	300	122.84
55	27.78	180	83.22	310	125.98
60	31.02	190	86.53	273.15	114.10
70	37.03	200	89.79	298.15	122.26
80	42.64	210	93.01	310.15	126.02
L-Arginine·HCl (210.7 Da) [22]					
10	2.326	90	105.52	220	205.10
15	6.481	100	114.68	230	212.21
20	12.25	110	123.26	240	219.37
25	19.21	120	131.46	250	226.52
30	26.91	130	139.37	260	233.72
35	34.91	140	147.15	270	241.00
40	42.93	150	154.72	280	248.20
45	50.71	160	162.09	290	255.27
50	58.16	170	169.41	300	262.25
55	65.27	180	176.65	310	269.16
60	72.05	190	183.76	273.15	243.26
70	84.43	200	190.87	298.15	260.96
80	95.48	210	197.90	310.15	269.28
L-Aspartic acid (134.1 Da) [23]					
10	0.732	90	64.02	220	122.51
15	2.686	100	69.45	230	126.69
20	6.033	110	74.64	240	130.88
25	10.31	120	79.54	250	134.98
30	15.14	130	84.27	260	139.03
35	20.09	140	88.83	270	143.14
40	25.18	150	93.26	280	147.32
45	30.06	160	97.57	290	151.63
50	34.70	170	101.80	300	155.98
55	39.10	180	106.06	310	160.37
60	43.30	190	110.21	273.15	144.47
70	50.88	200	114.31	298.15	155.19
80	57.70	210	118.41	310.15	160.42

TABLE 8.1b. *Continued.*

T/K	C_p	T/K	C_p	T/K	C_p
L-Asparagine · H_2O (150.1 Da) [23]					
10	0.686	90	76.48	220	161.21
15	2.343	100	83.93	230	167.28
20	5.376	110	91.13	240	173.34
25	9.531	120	98.07	250	179.41
30	14.63	130	104.85	260	185.44
35	20.29	140	111.46	270	191.38
40	26.18	150	117.95	280	197.28
45	32.13	160	124.35	290	203.18
50	37.95	170	130.71	300	208.99
55	43.56	180	136.94	310	214.81
60	48.95	190	143.09	273.15	193.26
70	58.99	200	149.12	298.15	207.90
80	68.12	210	155.19	310.15	214.89
L-Cystine (240.3 Da) [24]					
10	1.644	90	102.13	220	206.98
15	5.284	100	111.13	230	214.18
20	15.25	110	120.00	240	221.33
25	18.03	120	128.66	250	228.49
30	25.49	130	137.24	260	235.60
35	33.14	140	145.52	270	242.59
40	40.63	150	153.64	280	249.53
45	47.87	160	161.59	290	256.40
50	54.85	170	169.54	300	263.17
55	61.51	180	177.23	310	269.91
60	67.91	190	184.81	273.15	244.81
70	79.87	200	192.30	298.15	261.92
80	91.21	210	199.70	310.15	269.99
L-Glutamic acid (147.1 Da) [23]					
10	0.276	90	70.17	220	137.24
15	2.782	100	76.53	230	142.01
20	6.259	110	82.34	240	146.78
25	10.86	120	87.95	250	151.54
30	16.12	130	93.22	260	156.31
35	21.69	140	98.37	270	161.17
40	27.18	150	103.39	280	166.11
45	32.59	160	108.41	290	171.08
50	37.80	170	113.39	300	175.98
55	42.68	180	118.24	310	180.79
60	47.28	190	122.93	273.15	162.72
70	55.65	200	127.70	298.15	175.06
80	63.18	210	132.47	310.15	180.87

TABLE 8.1b. *Continued.*

T/K	C_p	T/K	C_p	T/K	C_p
L-Glutamine (146.2 Da) [23]					
10	0.728	90	72.55	220	144.06
15	2.460	100	78.99	230	149.45
20	5.791	110	84.94	240	154.72
25	10.48	120	90.67	250	159.91
30	15.91	130	196.23	260	165.02
35	21.80	140	101.76	270	170.04
40	27.72	150	107.28	280	175.10
45	33.46	160	112.63	290	180.12
50	38.93	170	117.95	300	185.10
55	44.06	180	123.18	310	189.83
60	48.87	190	128.37	273.15	171.63
70	57.66	200	133.60	298.15	184.18
80	65.48	210	138.74	310.15	189.91
Glycine (75.1 Da) [21]					
10	0.255	90	39.53	220	77.49
15	0.967	100	43.26	230	80.08
20	2.393	110	46.69	240	82.84
25	4.464	120	50.00	250	85.60
30	7.037	130	53.09	260	88.45
35	9.933	140	56.07	270	91.25
40	13.00	150	58.91	280	94.06
45	16.12	160	61.67	290	96.90
50	19.25	170	64.39	300	99.75
55	22.26	180	67.03	310	102.63
60	25.15	190	69.66	273.15	92.13
70	30.49	200	72.30	298.15	99.20
80	35.26	210	74.89	310.15	102.68
Glycylglycine (132.1 Da) [25]					
10	0.707	90	67.86	220	130.12
15	2.607	100	73.85	230	134.35
20	6.071	110	79.50	240	138.62
25	10.70	120	84.89	250	142.84
30	15.87	130	89.87	260	147.19
35	21.23	140	94.81	270	151.50
40	26.56	150	99.58	280	155.85
45	31.65	160	104.27	290	160.29
50	36.58	170	108.74	300	164.81
55	41.21	180	113.09	310	169.45
60	45.61	190	117.40	273.15	152.88
70	53.81	200	121.71	298.15	163.97
80	61.21	210	125.90	310.15	169.54

TABLE 8.1b. *Continued.*

T/K	C_p	T/K	C_p	T/K	C_p
L-Histidine·HCl (191.6 Da) [22]					
10	1.711	90	102.63	220	195.39
15	5.690	100	111.09	230	202.13
20	11.93	110	119.04	240	208.91
25	19.33	120	126.57	250	215.81
30	27.29	130	133.85	260	222.80
35	35.38	140	140.96	270	229.87
40	43.26	150	147.90	280	236.90
45	50.88	160	154.81	290	243.89
50	58.12	170	161.63	300	250.79
55	64.81	180	168.36	310	257.65
60	71.17	190	175.14	273.15	232.09
70	82.80	200	181.92	298.15	249.53
80	93.22	210	188.66	310.15	257.73
L-Isoleucine (131.2 Da) [26]					
10	2.741	90	74.89	220	147.53
15	6.343	100	81.80	230	152.59
20	10.80	110	88.41	240	157.74
25	15.82	120	94.68	250	162.97
30	20.93	130	100.63	260	168.16
35	26.12	140	106.36	270	173.26
40	31.22	150	111.88	280	178.53
45	36.22	160	117.24	290	183.76
50	41.08	170	122.55	300	189.28
55	45.82	180	127.70	310	194.89
60	50.38	190	132.72	273.15	174.93
70	58.95	200	137.65	298.15	188.28
80	67.15	210	142.59	310.15	194.97
L-Leucine (131.2 Da) [26]					
10	2.452	90	75.44	220	148.91
15	6.468	100	82.22	230	154.60
20	11.50	110	88.53	240	160.46
25	16.93	120	94.64	250	166.52
30	22.53	130	100.50	260	172.93
35	28.08	140	106.15	270	179.70
40	33.32	150	111.63	280	186.77
45	38.40	160	117.03	290	194.31
50	43.26	170	122.38	300	202.51
55	47.82	180	127.70	310	211.38
60	52.17	190	132.93	273.15	181.88
70	60.42	200	138.11	298.15	200.96
80	68.20	210	143.43	310.15	211.50

TABLE 8.1b. *Continued.*

T/K	C_p	T/K	C_p	T/K	C_p
L-Lysine·HCl (182.7 Da) [22]					
10	2.460	90	97.74	220	186.61
15	6.594	100	106.36	230	192.92
20	12.23	110	114.47	240	199.33
25	18.82	120	122.22	250	205.81
30	25.89	130	129.54	260	212.42
35	33.08	140	136.40	270	219.16
40	40.11	150	143.05	280	225.94
45	46.94	160	149.58	290	232.97
50	53.64	170	155.94	300	240.25
55	60.12	180	162.09	310	247.86
60	66.32	190	168.16	273.15	221.25
70	77.70	200	174.26	298.15	238.91
80	88.12	210	180.41	310.15	247.99
L-Methionine (149.2 Da) [24]					
10	2.017	90	82.68	220	157.28
15	5.883	100	89.50	230	164.14
20	11.48	110	95.90	240	172.05
25	17.79	120	101.96	250	181.13
30	24.23	130	107.70	260	192.67
35	30.65	140	113.26	270	208.28
40	36.70	150	118.66	280	229.79
45	42.43	160	124.01	290	259.20
50	47.87	170	129.24	300	298.28
55	53.01	180	134.47	310	298.19
60	57.91	190	139.70	273.15	214.30
70	66.99	200	145.19	298.15	290.04
80	75.19	210	151.04	310.15	296.85
L-Phenylalanine (165.2 Da) [27]					
10	2.594	90	74.73	220	152.05
15	6.682	100	80.96	230	158.49
20	11.87	110	86.94	240	165.02
25	17.36	120	92.72	250	171.54
30	23.16	130	98.49	260	178.07
35	28.93	140	104.31	270	184.60
40	34.36	150	110.17	280	191.13
45	39.44	160	116.11	290	197.69
50	44.23	170	122.01	300	204.22
55	48.74	180	127.95	310	210.71
60	53.01	190	133.93	273.15	186.65
70	60.79	200	139.87	298.15	203.01
80	67.99	210	145.85	310.15	210.79

TABLE 8.1b. *Continued.*

T/K	C_p	T/K	C_p	T/K	C_p
L-Proline (115.1 Da) [27]					
10	1.301	90	59.08	220	116.06
15	4.105	100	63.60	230	120.50
20	8.314	110	67.91	240	124.93
25	13.01	120	72.17	250	129.33
30	17.85	130	76.36	260	133.85
35	22.65	140	80.63	270	138.16
40	27.17	150	84.98	280	142.67
45	31.42	160	89.45	290	147.28
50	35.38	170	93.93	300	152.09
55	39.02	180	98.41	310	156.98
60	42.43	190	102.84	273.15	141.00
70	48.62	200	107.24	298.15	151.17
80	54.10	210	111.63	310.15	157.07
L-Serine (105.1 Da) [28]					
10	0.816	90	55.90	220	107.78
15	2.703	100	61.09	230	111.25
20	5.556	110	65.73	240	114.77
25	9.063	120	70.12	250	118.28
30	13.03	130	74.35	260	121.84
35	17.21	140	78.41	270	125.39
40	21.46	150	82.34	280	128.99
45	25.63	160	86.11	290	132.59
50	29.69	170	89.83	300	136.23
55	33.59	180	93.47	310	139.91
60	37.31	190	97.11	273.15	126.52
70	44.18	200	100.67	298.15	135.56
80	50.33	210	104.22	310.15	140.00
L-Tryptophane (204.2 Da) [27]					
10	4.393	90	84.56	220	178.20
15	10.02	100	91.92	230	185.69
20	16.51	110	99.04	240	193.34
25	23.04	120	106.06	250	201.08
30	29.35	130	113.18	260	208.87
35	35.28	140	120.33	270	216.52
40	40.78	150	127.45	280	224.22
45	45.61	160	134.64	290	231.92
50	51.00	170	141.80	300	239.58
55	55.73	180	148.99	310	247.32
60	60.17	190	156.27	273.15	218.95
70	68.70	200	163.59	298.15	238.15
80	76.86	210	170.88	310.15	247.44

TABLE 8.1b. *Continued.*

T/K	C_p	T/K	C_p	T/K	C_p
L-Tyrosine (181.2 Da) [27]					
10	1.389	90	75.06	220	162.72
15	3.908	100	82.05	230	169.45
20	7.724	110	88.83	240	176.23
25	12.57	120	95.56	250	183.05
30	18.07	130	102.26	260	189.91
35	23.91	140	108.87	270	196.86
40	29.62	150	115.52	280	203.84
45	35.24	160	122.26	290	210.79
50	40.59	170	128.99	300	217.74
55	45.56	180	135.77	310	224.60
60	50.29	190	142.38	273.15	199.08
70	59.20	200	149.12	298.15	216.44
80	67.49	210	155.81	310.15	224.72
L-Valine (117.2 Da) [24]					
10	1.100	90	64.73	220	133.01
15	3.192	100	71.34	230	137.57
20	6.615	110	77.57	240	142.05
25	10.69	120	83.55	250	146.61
30	15.18	130	89.16	260	151.17
35	19.86	140	94.56	270	155.85
40	24.46	150	99.83	280	160.50
45	29.04	160	104.98	290	165.06
50	33.50	170	109.91	300	169.70
55	37.87	180	114.73	310	174.31
60	42.09	190	119.37	273.15	157.28
70	50.04	200	123.89	298.15	168.82
80	57.61	210	128.41	310.15	174.39

heat capacity of the denatured protein and the calculated one for the unfolded polypeptide chain is a strong argument that heat denatured proteins are indistinguishable thermodynamically from fully unfolded (D $\approx$ U).

8.2 PARTIAL VOLUME

The partial specific volume of proteins can be measured experimentally [11,12] or can be estimated from the amino acid composition of the protein using equation

$$V_2 = (N - 1) \cdot V_2(\text{—CHCONH—}) + \sum_{i=1}^{N} V_2(\text{—}R_i), \quad (8.2)$$

where N is number of amino acid residues in the protein sequence, V_2(—CHCONH—) is the contribution of a peptide unit, and $V_2(\text{—}R_i)$ is the contribution of the ith amino acid side chain. These contributions are listed in Table 8.6. For more details, compilation of the experimental data on the partial volume of proteins is recommended [12].

8.3 THERMODYNAMIC FUNCTIONS

Because the absolute value of the heat capacity of the native state is always larger than the heat capacity of the unfolded state, and because they have different temperature dependencies, the heat capacity change upon unfolding is positive and temperature dependent itself:

$$\Delta_{\mathrm{N}}^{\mathrm{U}} C_{\mathrm{p}}(T) = C_{\mathrm{p}}^{\mathrm{U}}(T) - C_{\mathrm{p}}^{\mathrm{N}}(T), \quad (8.3)$$

where $\Delta_{\mathrm{N}}^{\mathrm{U}} C_{\mathrm{p}}(T)$ is a nonlinear function of temperature. It has maximum at around 50 °C, decreases at high temperatures and appears to reach zero at ~140 °C). The heat capacities of proteins in the native and unfolded states and the heat capacity change upon unfolding are presented in Table 8.7.

TABLE 8.2. *Temperature dependence of the partial molar volumes ($cm^3\,mol^{-1}$) of the peptide unit and of the side chains of amino acid residues for the temperature range 5–125 °C [11].*

	Temperature (°C)					
	5	25	50	75	100	125
–CHCONH–	28.3	28.0	28.6	28.9	29.0	29.4
$-R_i$						
Ala	24.8	27.2	30.1	33.1	36.3	39.4
Arg	81.2	85.7	88.4	90.4	92.1	93.5
Asn	44.1	45.7	47.8	49.3	50.8	52.4
Asp	39.0	41.5	44.5	47.3	49.9	52.6
Cys	40.5	40.5	40.5	40.5	40.5	40.5
Gln	58.4	61.0	63.2	66.0	68.5	69.7
Glu	54.9	57.5	60.7	63.6	66.3	69.3
Gly	10.9	10.3	9.6	9.2	8.9	8.5
His	65.1	64.0	63.1	62.4	61.8	61.1
Ile	64.5	66.1	67.7	69.8	71.8	74.0
Leu	75.0	77.6	80.2	82.9	86.5	89.4
Lys	72.4	73.5	75.8	78.5	81.3	84.8
Met	73.3	72.1	70.2	69.0	67.9	66.7
Phe	82.0	86.3	92.0	97.9	102.6	107.9
Pro	36.0	35.8	34.1	33.7	33.5	33.2
Ser	27.1	27.8	28.8	29.7	30.7	32.0
Thr	44.2	44.7	45.9	47.6	50.9	54.6
Trp	110.9	110.9	110.9	110.9	110.9	110.9
Tyr	88.2	90.0	92.2	94.1	95.9	97.8
Val	60.7	63.0	65.7	68.5	71.7	74.5

The non-zero heat capacity change upon protein unfolding means that all other thermodynamic functions are also temperature dependent:

$$\Delta_{\mathrm{N}}^{\mathrm{U}}H(T) = \Delta_{\mathrm{N}}^{\mathrm{U}}H(T_0) + \int_{T_0}^{T} \Delta_{\mathrm{N}}^{\mathrm{U}}C_{\mathrm{p}}(T)\mathrm{d}T \qquad (8.4)$$

$$\Delta_{\mathrm{N}}^{\mathrm{U}}S(T) = \Delta_{\mathrm{N}}^{\mathrm{U}}S(T_0) + \int_{T_0}^{T} \Delta_{\mathrm{N}}^{\mathrm{U}}C_{\mathrm{p}}(T)\mathrm{d}\ln T \qquad (8.5)$$

$$\Delta_{\mathrm{N}}^{\mathrm{U}}G = \Delta_{\mathrm{N}}^{\mathrm{U}}H - \mathrm{T}\Delta_{\mathrm{N}}^{\mathrm{U}}\mathrm{S} \qquad (8.6)$$

These functions are presented in Table 8.7 for a selected set of 20 proteins, for which the thermodynamics of unfolding have been measured with highest accuracy.

8.4 HYDRATION EFFECTS

The contribution of solvent (water) to the observed changes of the thermodynamic parameters of proteins can be assumed to be proportional to the changes in water accessible surface area of the protein groups. The water accessible surface area can be calculated from the X-ray or NMR structure of the native protein by computing the surface formed by the center of a spherical probe rolling on the surface of the protein (see e.g., [13,14]). As was shown earlier, the hydration effects of protein groups exposed to water upon unfolding [15–18] can be expressed as follows:

$$\Delta C_{p,k}^{\mathrm{hyd}}(T) = \sum_i \Delta_{\mathrm{N}}^{\mathrm{U}}\mathrm{ASA}_{k,i} \times \Delta\hat{C}_{p,k,i}^{\mathrm{hyd}}(T) \qquad (8.7)$$

$$\Delta H_k^{\mathrm{hyd}}(T) = \sum_i \Delta_{\mathrm{N}}^{\mathrm{U}}\mathrm{ASA}_{k,i} \times \Delta\hat{H}_{k,i}^{\mathrm{hyd}}(T) \qquad (8.8)$$

$$\Delta S_k^{\mathrm{hyd}}(T) = \sum_i \Delta_{\mathrm{N}}^{\mathrm{U}}\mathrm{ASA}_{k,i} \times \Delta\hat{S}_{k,i}^{\mathrm{hyd}}(T) \qquad (8.9)$$

$$\Delta G_k^{\mathrm{hyd}}(T) = \sum_i \Delta_{\mathrm{N}}^{\mathrm{U}}\mathrm{ASA}_{k,i} \times \Delta\hat{G}_{k,i}^{\mathrm{hyd}}(T), \qquad (8.10)$$

where $\Delta_{\mathrm{N}}^{\mathrm{U}}\mathrm{ASA}_{k,i}$ is the change of water accessible surface area of protein group i of type k upon unfolding and $\Delta\hat{C}_{p,k,i}^{\mathrm{hyd}}(T)$, $\Delta\hat{S}_{k,i}^{\mathrm{hyd}}(T)$, $\Delta\hat{G}_{k,i}^{\mathrm{hyd}}(T)$, and $\Delta\hat{H}_{k,i}^{\mathrm{hyd}}(T)$ are the hydration heat capacity change, enthalpy, entropy, and Gibbs energy change of this type of group the normalized per square angstrom. These normalized hydration effects were determined by the transfer of model compounds from the gaseous phase to water and their values are listed in Table 8.8.

TABLE 8.3. *Heat capacities (J K^{-1} mol^{-1}) of solid poly (amino acids).*

Poly-L-Alanine (m.w 15,000 Da) [29]					
T / K	C_p	T / K	C_p	T / K	C_p
0.1	0.00	190	42.65	590	120.06
0.2	0.00	200	44.96	600	121.57
0.3	0.00	210	47.19	610	123.07
0.4	0.00	220	49.46	620	124.55
0.5	0.00	230	51.71	630	126.02
0.6	0.00	240	53.93	640	127.47
0.7	0.00	250	56.18	650	128.91
0.8	0.00	260	58.39	660	130.34
0.9	0.00	270	60.61	670	131.76
1.0	0.00	273.15	61.30	680	133.16
1.2	0.00	280	62.79	690	134.56
1.4	0.00	290	64.97	700	135.95
1.6	0.00	298.15	66.76	710	137.32
1.8	0.00	300	67.17	720	138.69
2	0.01	310	69.30	730	140.05
3	0.02	320	71.40	740	141.40
4	0.05	330	73.54	750	142.75
5	0.10	340	75.60	760	144.08
6	0.17	350	77.64	770	145.41
7	0.27	360	79.65	780	146.74
8	0.40	370	81.64	790	148.06
9	0.56	380	83.72	800	149.38
10	0.75	390	85.66	810	150.70
15	1.95	400	87.58	820	152.01
20	3.31	410	89.47	830	153.32
25	4.66	420	91.35	840	154.63
30	5.95	430	93.31	850	155.94
40	8.40	440	95.13	860	157.25
50	10.75	450	96.93	870	158.55
60	13.06	460	98.72	880	159.86
70	15.35	470	100.48	890	161.16
80	17.63	480	102.22	900	162.47
90	19.89	490	103.94	910	163.78
100	22.15	500	105.64	920	165.10
110	24.43	510	107.32	930	166.41
120	26.70	520	108.98	940	167.74
130	28.99	530	110.62	950	169.06
140	31.25	540	112.24	960	170.39
150	33.52	550	113.84	970	171.73
160	35.78	560	115.42	980	173.09
170	38.05	570	116.98	990	174.44
180	40.37	580	118.53	1000	175.80

TABLE 8.3. *Continued.*

Poly-L-Arginine·HCl (m.w 132,000 Da) [30]					
T / K	C_p	T / K	C_p	T / K	C_p
0.1	0.00	190	168.39	590	410.48
0.2	0.00	200	174.72	600	415.75
0.3	0.00	210	180.99	610	420.90
0.4	0.00	220	187.37	620	426.02
0.5	0.00	230	193.59	630	431.08
0.6	0.00	240	199.90	640	436.12
0.7	0.00	250	206.23	650	441.09
0.8	0.00	260	212.56	660	446.07
0.9	0.00	270	218.86	670	451.00
1.0	0.01	273.15	220.85	680	455.91
1.2	0.01	280	225.21	690	460.79
1.4	0.01	290	231.62	700	465.91
1.6	0.02	298.15	236.88	710	470.48
1.8	0.03	300	237.99	720	475.28
2	0.04	310	244.49	730	480.05
3	0.14	320	250.83	740	484.81
4	0.34	330	257.21	750	489.54
5	0.66	340	263.60	760	494.23
6	1.13	350	269.96	770	498.98
7	1.77	360	276.31	780	503.65
8	2.57	370	282.71	790	508.31
9	3.51	380	289.10	800	512.93
10	4.58	390	295.25	810	517.55
15	10.76	400	301.53	820	522.18
20	17.16	410	307.69	830	526.80
25	23.29	420	313.80	840	531.38
30	29.14	430	319.89	850	535.98
40	40.34	440	325.97	860	540.57
50	51.21	450	332.02	870	545.16
60	61.91	460	338.03	880	549.75
70	72.42	470	343.99	890	554.32
80	82.61	480	349.82	900	558.90
90	92.43	490	355.58	910	563.48
100	101.85	500	361.27	920	568.07
110	110.73	510	366.89	930	572.67
120	119.11	520	372.45	940	577.26
130	127.01	530	377.96	950	581.87
140	134.57	540	383.44	960	586.49
150	141.75	550	388.86	970	591.12
160	148.67	560	394.31	980	595.77
170	155.41	570	399.73	990	600.42
180	161.97	580	405.15	1000	605.07

TABLE 8.3. *Continued.*

Poly-L-Aspartic acid·Na (m.w 42,500 Da) [30]					
T / K	C_p	T / K	C_p	T / K	C_p
0.1	0.00	190	105.03	590	249.25
0.2	0.00	200	109.57	600	252.01
0.3	0.00	210	114.02	610	254.74
0.4	0.00	220	118.55	620	257.41
0.5	0.00	230	122.86	630	260.03
0.6	0.00	240	127.19	640	262.63
0.7	0.00	250	131.48	650	265.19
0.8	0.00	260	135.71	660	267.74
0.9	0.00	270	139.84	670	270.26
1.0	0.00	273.15	141.14	680	272.77
1.2	0.01	280	143.96	690	275.25
1.4	0.01	290	148.05	700	278.00
1.6	0.01	298.15	151.40	710	280.19
1.8	0.02	300	152.07	720	282.63
2	0.02	310	156.17	730	285.05
3	0.08	320	160.08	740	287.47
4	0.19	330	164.01	750	289.86
5	0.38	340	167.90	760	292.22
6	0.65	350	171.71	770	294.65
7	1.01	360	175.46	780	297.02
8	1.47	370	179.27	790	299.37
9	2.01	380	182.83	800	301.65
10	2.62	390	186.42	810	303.98
15	6.16	400	190.09	820	306.30
20	9.83	410	193.59	830	308.62
25	13.34	420	197.03	840	310.94
30	16.69	430	200.44	850	313.25
40	23.10	440	203.81	860	315.55
50	29.33	450	207.18	870	317.85
60	35.48	460	210.50	880	320.15
70	41.58	470	213.78	890	322.43
80	47.59	480	216.97	900	324.72
90	53.48	490	220.11	910	327.02
100	59.27	500	223.19	920	329.32
110	64.90	510	226.23	930	331.62
120	70.40	520	229.22	940	333.93
130	75.70	530	232.18	950	336.24
140	80.90	540	235.10	960	338.55
150	85.89	550	237.99	970	340.87
160	90.88	560	240.94	980	343.21
170	95.65	570	243.74	990	345.55
180	100.39	580	246.51	1000	347.89

TABLE 8.3. *Continued.*

Poly-L-Asparagine (m.w 10,400 Da) [30]					
T / K	C_p	T / K	C_p	T / K	C_p
0.1	0.00	190	97	590	235.78
0.2	0.00	200	100.96	600	238.61
0.3	0.00	210	104.88	610	241.40
0.4	0.00	220	108.90	620	244.14
0.5	0.00	230	112.73	630	246.84
0.6	0.00	240	116.63	640	249.51
0.7	0.00	250	120.52	650	252.16
0.8	0.00	260	124.40	660	254.80
0.9	0.00	270	128.19	670	257.41
1.0	0.00	273.15	129.40	680	260.00
1.2	0.01	280	132.02	690	262.58
1.4	0.01	290	135.84	700	265.41
1.6	0.01	298.15	138.99	710	267.70
1.8	0.02	300	139.62	720	270.23
2	0.03	310	143.51	730	272.75
3	0.09	320	147.23	740	275.27
4	0.22	330	150.98	750	277.77
5	0.43	340	154.71	760	280.23
6	0.74	350	158.39	770	282.77
7	1.14	360	162.02	780	285.24
8	1.64	370	165.73	790	287.71
9	2.22	380	169.20	800	290.09
10	2.85	390	172.73	810	292.54
15	6.39	400	176.35	820	294.98
20	9.92	410	179.79	830	297.41
25	13.29	420	183.19	840	299.85
30	16.50	430	186.56	850	302.27
40	22.69	440	189.91	860	304.69
50	28.72	450	193.27	870	307.11
60	34.66	460	196.59	880	309.52
70	40.49	470	199.87	890	311.93
80	46.16	480	203.07	900	314.34
90	51.66	490	206.22	910	316.76
100	56.96	500	209.32	920	319.18
110	62.02	510	212.39	930	321.61
120	66.88	520	215.42	940	324.04
130	71.54	530	218.41	950	326.47
140	76.09	540	221.37	960	328.91
150	80.41	550	224.31	970	331.36
160	84.70	560	227.30	980	333.82
170	88.84	570	230.15	990	336.28
180	92.96	580	232.98	1000	338.75

TABLE 8.3. *Continued.*

Poly-L-Glutamic Acid·Na (m.w 74,000 Da) [30]					
T / K	C_p	T / K	C_p	T / K	C_p
0.1	0.00	190	100.57	590	282.92
0.2	0.00	200	106.20	600	286.38
0.3	0.00	210	111.79	610	289.78
0.4	0.00	220	117.49	620	293.13
0.5	0.00	230	122.98	630	296.42
0.6	0.00	240	128.45	640	299.68
0.7	0.00	250	133.90	650	302.91
0.8	0.00	260	139.28	660	306.11
0.9	0.00	270	144.57	670	309.28
1.0	0.00	273.15	146.23	680	312.42
1.2	0.00	280	149.83	690	315.54
1.4	0.01	290	155.07	700	318.90
1.6	0.01	298.15	159.33	710	321.72
1.8	0.01	300	160.21	720	324.77
2	0.02	310	165.42	730	327.80
3	0.07	320	170.42	740	330.83
4	0.16	330	175.41	750	333.82
5	0.31	340	180.36	760	336.78
6	0.53	350	185.21	770	339.80
7	0.83	360	189.98	780	342.76
8	1.20	370	194.80	790	345.70
9	1.64	380	199.34	800	348.55
10	2.14	390	203.89	810	351.47
15	5.03	400	208.50	820	354.37
20	8.02	410	212.91	830	357.26
25	10.89	420	217.26	840	360.15
30	13.62	430	221.56	850	363.03
40	18.86	440	225.83	860	365.90
50	23.96	450	230.06	870	368.76
60	28.99	460	234.25	880	371.62
70	34.05	470	238.38	890	374.46
80	39.17	480	242.39	900	377.32
90	44.38	490	246.33	910	380.15
100	49.71	500	250.21	920	383.01
110	55.12	510	254.02	930	385.88
120	60.64	520	257.79	940	388.74
130	66.24	530	261.50	950	391.60
140	71.96	540	265.17	960	394.47
150	77.65	550	268.80	970	397.35
160	83.41	560	272.47	980	400.25
170	89.13	570	276.00	990	403.15
180	94.87	580	279.48	1000	406.04

TABLE 8.3. *Continued.*

Poly-Glycine II (m.w 15,000 Da) [29]					
T / K	C_p	T / K	C_p	T / K	C_p
0.1	0.00	190	64.83	590	163.11
0.2	0.00	200	67.40	600	165.32
0.3	0.00	210	69.93	610	167.40
0.4	0.00	220	72.48	620	169.46
0.5	0.00	230	75.06	630	171.51
0.6	0.00	240	77.62	640	173.53
0.7	0.00	250	80.17	650	175.55
0.8	0.00	260	82.75	660	177.56
0.9	0.00	270	85.25	670	179.55
1.0	0.00	273.15	86.07	680	181.53
1.2	0.00	280	87.91	690	183.50
1.4	0.01	290	90.45	700	185.46
1.6	0.01	298.15	92.53	710	187.40
1.8	0.02	300	93.01	720	189.34
2	0.02	310	95.58	730	191.26
3	0.07	320	98.42	740	193.17
4	0.17	330	100.85	750	195.07
5	0.34	340	103.43	760	196.97
6	0.58	350	105.99	770	198.85
7	0.88	360	108.61	780	200.73
8	1.25	370	112.07	790	202.60
9	1.67	380	113.75	800	204.47
10	2.11	390	116.28	810	206.33
15	4.52	400	118.87	820	208.18
20	6.87	410	121.42	830	210.03
25	9.09	420	123.91	840	211.88
30	11.22	430	126.39	850	213.72
40	15.34	440	128.84	860	215.57
50	19.38	450	131.26	870	217.41
60	23.38	460	133.69	880	219.26
70	27.32	470	136.15	890	221.10
80	31.17	480	138.47	900	222.93
90	34.86	490	140.93	910	224.74
100	38.46	500	143.23	920	226.58
110	41.89	510	145.51	930	228.42
120	45.16	520	147.77	940	230.26
130	48.25	530	150.01	950	232.13
140	51.22	540	152.23	960	233.99
150	54.11	550	154.43	970	235.84
160	56.91	560	156.72	980	237.71
170	59.56	570	158.86	990	239.56
180	62.21	580	161.00	1000	241.44

TABLE 8.3. *Continued.*

Poly-L-Histidine (m.w 49,000 Da) [30]					
T / K	C_p	T / K	C_p	T / K	C_p
0.1	0.00	190	113.43	590	322.88
0.2	0.00	200	119.22	600	327.05
0.3	0.00	210	124.97	610	331.18
0.4	0.00	220	131.00	620	335.25
0.5	0.00	230	136.77	630	339.26
0.6	0.00	240	142.71	640	343.24
0.7	0.00	250	148.55	650	347.16
0.8	0.00	260	154.44	660	351.08
0.9	0.00	270	160.16	670	354.96
1.0	0.00	273.15	161.98	680	358.80
1.2	0.01	280	165.99	690	362.62
1.4	0.01	290	171.78	700	366.68
1.6	0.01	298.15	176.53	710	370.18
1.8	0.02	300	177.51	720	373.92
2	0.02	310	183.37	730	377.62
3	0.08	320	188.85	740	381.32
4	0.19	330	194.70	750	385.35
5	0.38	340	200.39	760	388.63
6	0.65	350	206.06	770	392.33
7	1.01	360	211.37	780	395.95
8	1.46	370	217.02	790	399.55
9	2.00	380	222.34	800	403.07
10	2.61	390	227.64	810	406.63
15	6.13	400	233.12	820	410.19
20	9.77	410	238.35	830	413.74
25	13.26	420	243.62	840	417.29
30	16.60	430	248.73	850	420.81
40	22.98	440	253.79	860	424.33
50	29.18	450	258.82	870	427.83
60	35.30	460	263.82	880	431.33
70	41.45	470	268.78	890	434.81
80	47.55	480	273.62	900	438.34
90	53.66	490	278.34	910	441.82
100	59.79	500	282.98	920	445.31
110	65.84	510	287.56	930	448.80
120	71.95	520	292.09	940	452.29
130	77.90	530	296.63	950	455.74
140	83.91	540	301.19	960	459.24
150	89.79	550	305.55	970	462.75
160	95.72	560	309.97	980	466.26
170	101.66	570	314.36	990	469.77
180	107.57	580	318.66	1000	473.28

TABLE 8.3. *Continued.*

Poly-L-Leucine (m.w 150,000 Da) [30]					
T / K	C_p	T / K	C_p	T / K	C_p
0.1	0.00	190	116.64	590	300.37
0.2	0.00	200	121.12	600	304.48
0.3	0.00	210	125.58	610	308.56
0.4	0.00	220	130.13	620	312.57
0.5	0.00	230	134.68	630	316.52
0.6	0.00	240	139.08	640	320.46
0.7	0.00	250	143.73	650	324.36
0.8	0.00	260	148.34	660	328.25
0.9	0.00	270	152.93	670	332.10
1.0	0.00	273.15	154.40	680	335.93
1.2	0.01	280	157.73	690	339.73
1.4	0.01	290	162.40	700	343.79
1.6	0.01	298.15	166.35	710	347.30
1.8	0.02	300	167.14	720	351.05
2	0.03	310	172.11	730	354.77
3	0.10	320	176.90	740	358.49
4	0.23	330	181.86	750	362.18
5	0.45	340	186.62	760	365.84
6	0.77	350	191.58	770	369.57
7	1.20	360	196.37	780	373.22
8	1.74	370	201.29	790	376.87
9	2.39	380	206.03	800	380.43
10	3.11	390	210.82	810	384.04
15	7.31	400	215.77	820	387.65
20	11.65	410	220.55	830	391.24
25	15.81	420	225.28	840	394.84
30	19.78	430	230.00	850	398.43
40	27.39	440	234.67	860	402.00
50	34.77	450	239.32	870	405.57
60	42.05	460	243.94	880	409.14
70	49.23	470	248.57	890	412.70
80	56.23	480	253.07	900	416.26
90	63.02	490	257.58	910	419.83
100	69.61	500	262.12	920	423.39
110	75.80	510	266.50	930	426.97
120	81.73	520	270.85	940	430.55
130	87.31	530	275.16	950	434.13
140	92.66	540	279.43	960	437.72
150	97.73	550	283.68	970	441.32
160	102.69	560	287.99	980	444.93
170	107.40	570	292.15	990	448.55
180	112.07	580	296.28	1000	452.17

TABLE 8.3. *Continued.*

Poly-L-Lysine·HBr (m.w 560,000 Da) [30]					
T / K	C_p	T / K	C_p	T / K	C_p
0.1	0.00	190	145.15	590	369.70
0.2	0.00	200	150.98	600	374.53
0.3	0.00	210	156.76	610	379.32
0.4	0.00	220	162.67	620	384.05
0.5	0.00	230	168.43	630	388.73
0.6	0.00	240	174.25	640	393.34
0.7	0.00	250	180.11	650	397.95
0.8	0.00	260	185.97	660	402.53
0.9	0.00	270	191.81	670	407.07
1.0	0.00	273.15	193.66	680	411.59
1.2	0.01	280	197.69	690	416.07
1.4	0.01	290	203.67	700	420.81
1.6	0.02	298.15	208.57	710	424.99
1.8	0.03	300	209.60	720	429.41
2	0.04	310	215.67	730	433.88
3	0.12	320	221.57	740	438.27
4	0.28	330	227.54	750	442.64
5	0.55	340	233.53	760	446.93
6	0.95	350	239.48	770	451.33
7	1.47	360	245.45	780	455.65
8	2.14	370	251.45	790	459.97
9	2.93	380	257.16	800	464.20
10	3.81	390	262.98	810	468.44
15	8.97	400	268.86	820	472.72
20	14.30	410	274.58	830	476.98
25	19.40	420	280.24	840	481.25
30	24.27	430	285.88	850	485.49
40	33.60	440	291.53	860	489.73
50	42.66	450	297.16	870	493.97
60	51.59	460	302.74	880	498.20
70	60.41	470	308.28	890	502.42
80	69.03	480	313.68	900	506.65
90	77.39	490	319.02	910	510.88
100	85.48	500	324.29	920	515.12
110	93.23	510	329.49	930	519.36
120	100.61	520	334.64	940	523.61
130	107.63	530	339.75	950	527.86
140	114.40	540	344.82	960	532.12
150	120.83	550	349.88	970	536.39
160	127.20	560	354.99	980	540.68
170	133.25	570	359.90	990	544.98
180	139.25	580	364.88	1000	549.28

TABLE 8.3. *Continued.*

Poly-L-Methionine (m.w 160,000 Da) [30]					
T / K	C_p	T / K	C_p	T / K	C_p
0.1	0.00	190	108.51	590	281.22
0.2	0.00	200	113.39	600	284.80
0.3	0.00	210	118.22	610	288.35
0.4	0.00	220	123.15	620	291.84
0.5	0.00	230	127.96	630	295.28
0.6	0.00	240	132.69	640	298.70
0.7	0.00	250	137.51	650	302.09
0.8	0.00	260	142.24	660	305.45
0.9	0.00	270	146.91	670	308.80
1.0	0.00	273.15	148.39	680	312.12
1.2	0.01	280	151.59	690	315.42
1.4	0.01	290	156.30	700	318.96
1.6	0.01	298.15	160.16	710	321.96
1.8	0.02	300	160.95	720	325.21
2	0.02	310	165.71	730	328.44
3	0.08	320	170.29	740	331.66
4	0.19	330	174.90	750	334.86
5	0.38	340	179.52	760	338.03
6	0.65	350	184.14	770	341.27
7	1.02	360	188.63	780	344.44
8	1.48	370	193.22	790	347.60
9	2.02	380	197.58	800	350.67
10	2.63	390	201.95	810	353.81
15	6.19	400	206.41	820	356.94
20	9.87	410	210.69	830	360.07
25	13.39	420	214.94	840	363.19
30	16.76	430	219.15	850	366.30
40	23.20	440	223.35	860	369.41
50	29.47	450	227.55	870	372.51
60	35.63	460	231.71	880	375.61
70	41.81	470	235.82	890	378.69
80	47.91	480	239.84	900	381.79
90	53.95	490	243.80	910	384.89
100	59.95	500	247.75	920	387.99
110	65.83	510	251.60	930	391.10
120	71.58	520	255.42	940	394.21
130	77.17	530	259.20	950	397.33
140	82.68	540	262.94	960	400.45
150	87.98	550	266.66	970	403.59
160	93.28	560	270.43	980	406.73
170	98.43	570	274.06	990	409.89
180	103.53	580	277.65	1000	413.04

TABLE 8.3. *Continued.*

Poly-L-Phenylalanine (m.w 23,000 Da) [30]					
T / K	C_p	T / K	C_p	T / K	C_p
0.1	0.00	190	105.52	590	320.05
0.2	0.00	200	111.58	600	324.19
0.3	0.00	210	117.56	610	328.26
0.4	0.00	220	123.77	620	332.27
0.5	0.00	230	129.77	630	336.22
0.6	0.00	240	135.84	640	340.12
0.7	0.00	250	141.94	650	343.98
0.8	0.00	260	148.03	660	347.80
0.9	0.00	270	154.06	670	351.58
1.0	0.00	273.15	155.97	680	355.33
1.2	0.00	280	160.10	690	359.04
1.4	0.01	290	166.22	700	362.99
1.6	0.01	298.15	171.17	710	366.38
1.8	0.01	300	172.21	720	370.01
2	0.02	310	178.30	730	373.60
3	0.07	320	184.21	740	377.19
4	0.16	330	190.14	750	380.73
5	0.32	340	196.03	760	384.24
6	0.54	350	201.84	770	387.81
7	0.85	360	207.56	780	391.32
8	1.23	370	213.32	790	394.79
9	1.68	380	218.82	800	398.15
10	2.19	390	224.34	810	401.59
15	5.15	400	229.91	820	405.01
20	8.21	410	235.28	830	408.42
25	11.14	420	240.58	840	411.82
30	13.93	430	245.81	850	415.23
40	19.30	440	250.98	860	418.69
50	24.54	450	256.11	870	421.97
60	29.82	460	261.18	880	425.33
70	35.20	470	266.17	890	428.68
80	40.69	480	271.04	900	432.03
90	46.37	490	275.83	910	435.38
100	52.17	500	280.53	920	438.73
110	57.97	510	285.16	930	442.10
120	63.85	520	289.73	940	445.46
130	69.77	530	294.23	950	448.82
140	75.67	540	298.67	960	452.19
150	81.61	550	303.05	970	455.57
160	87.59	560	307.46	980	458.96
170	93.53	570	311.71	990	462.36
180	99.53	580	315.91	1000	465.75

TABLE 8.3. *Continued.*

Poly-L-Proline (m.w 44,000 Da) [30]					
T / K	C_p	T / K	C_p	T / K	C_p
0.1	0.00	190	75.68	590	224.54
0.2	0.00	200	79.12	600	227.75
0.3	0.00	210	82.65	610	230.92
0.4	0.00	220	86.17	620	234.04
0.5	0.00	230	89.84	630	237.11
0.6	0.00	240	93.57	640	240.14
0.7	0.00	250	97.35	650	243.15
0.8	0.00	260	101.24	660	246.14
0.9	0.00	270	105.05	670	249.09
1.0	0.00	273.15	106.28	680	252.02
1.2	0.00	280	108.98	690	254.93
1.4	0.01	290	112.99	700	258.08
1.6	0.01	298.15	116.23	710	260.69
1.8	0.01	300	116.90	720	263.54
2	0.02	310	120.99	730	266.37
3	0.06	320	125.05	740	269.19
4	0.14	330	129.05	750	271.98
5	0.28	340	133.07	760	274.76
6	0.48	350	137.11	770	277.52
7	0.75	360	141.16	780	280.27
8	1.08	370	145.18	790	283.00
9	1.48	380	149.17	800	285.72
10	1.93	390	153.17	810	288.43
15	4.54	400	157.15	820	291.13
20	7.25	410	160.94	830	293.81
25	9.83	420	164.77	840	296.49
30	12.30	430	168.58	850	299.16
40	17.03	440	172.40	860	301.82
50	21.63	450	176.17	870	304.48
60	26.15	460	179.91	880	307.13
70	30.64	470	183.62	890	309.78
80	35.04	480	187.24	900	312.42
90	39.31	490	190.88	910	315.06
100	43.46	500	194.46	920	317.70
110	47.45	510	197.95	930	320.34
120	51.27	520	201.40	940	322.98
130	54.95	530	204.81	950	325.63
140	58.51	540	208.19	960	328.28
150	62.00	550	211.54	970	330.93
160	65.43	560	214.84	980	333.59
170	68.84	570	218.11	990	336.26
180	72.27	580	221.35	1000	338.94

TABLE 8.3. *Continued.*

Poly-L-Serine (m.w 6,000 Da) [30]					
T / K	C_p	T / K	C_p	T / K	C_p
0.1	0.00	190	73.88	590	188.29
0.2	0.00	200	77.23	600	190.62
0.3	0.00	210	80.53	610	192.92
0.4	0.00	220	83.94	620	195.17
0.5	0.00	230	87.14	630	197.39
0.6	0.00	240	90.38	640	199.59
0.7	0.00	250	93.62	650	201.77
0.8	0.00	260	96.82	660	203.93
0.9	0.00	270	99.94	670	206.07
1.0	0.00	273.15	100.94	680	208.20
1.2	0.00	280	103.08	690	210.31
1.4	0.01	290	106.22	700	212.68
1.6	0.01	298.15	108.82	710	214.51
1.8	0.01	300	109.32	720	216.60
2	0.02	310	112.52	730	218.67
3	0.06	320	115.57	740	220.74
4	0.13	330	118.65	750	222.79
5	0.26	340	121.72	760	224.81
6	0.44	350	124.74	770	226.90
7	0.68	360	127.71	780	228.93
8	0.99	370	130.76	790	230.95
9	1.36	380	133.58	800	232.90
10	1.77	390	136.46	810	234.90
15	4.16	400	139.44	820	236.90
20	6.64	410	142.26	830	238.89
25	9.01	420	145.06	840	240.89
30	11.27	430	147.83	850	242.88
40	15.60	440	150.58	860	244.86
50	19.82	450	153.34	870	246.83
60	23.96	460	156.08	880	248.81
70	28.13	470	158.79	890	250.77
80	32.26	480	161.41	900	252.74
90	36.36	490	164.00	910	254.72
100	40.44	500	166.55	920	256.69
110	44.46	510	169.06	930	258.68
120	48.42	520	171.54	940	260.66
130	52.29	530	174.00	950	262.64
140	56.10	540	176.43	960	264.63
150	59.75	550	178.84	970	266.62
160	63.42	560	181.32	980	268.63
170	66.95	570	183.67	990	270.64
180	70.46	580	185.99	1000	272.64

TABLE 8.3. *Continued.*

Poly-L-Tryptophane (m.w 160,000 Da) [30]					
T / K	C_p	T / K	C_p	T / K	C_p
0.1	0.00	190	110.46	590	392.95
0.2	0.00	200	117.96	600	398.53
0.3	0.00	210	125.38	610	404.03
0.4	0.00	220	133.19	620	409.44
0.5	0.00	230	140.76	630	414.76
0.6	0.00	240	148.48	640	420.03
0.7	0.00	250	156.27	650	425.24
0.8	0.00	260	164.15	660	430.40
0.9	0.00	270	171.89	670	435.50
1.0	0.00	273.15	174.37	680	440.57
1.2	0.00	280	179.76	690	445.58
1.4	0.01	290	187.75	700	450.81
1.6	0.01	298.15	194.19	710	455.48
1.8	0.01	300	195.57	720	460.36
2	0.02	310	203.53	730	465.21
3	0.06	320	211.25	740	470.03
4	0.15	330	219.15	750	474.98
5	0.29	340	226.94	760	479.53
6	0.49	350	234.59	770	484.32
7	0.77	360	242.15	780	489.05
8	1.12	370	249.75	790	493.72
9	1.53	380	257.06	800	498.26
10	1.99	390	264.45	810	502.88
15	4.67	400	271.85	820	507.48
20	7.45	410	279.00	830	512.06
25	10.12	420	286.06	840	516.63
30	12.66	430	293.07	850	521.19
40	17.53	440	300.03	860	525.81
50	22.31	450	306.93	870	530.23
60	27.14	460	313.70	880	534.73
70	32.15	470	320.37	890	539.22
80	37.44	480	326.92	900	543.70
90	43.07	490	333.34	910	548.18
100	48.96	500	339.67	920	552.66
110	55.06	510	345.91	930	557.14
120	61.47	520	352.06	940	561.62
130	68.11	530	358.13	950	566.10
140	74.83	540	364.12	960	570.59
150	81.71	550	370.03	970	575.08
160	88.75	560	375.95	980	579.59
170	95.85	570	381.69	990	584.11
180	103.12	580	387.36	1000	588.62

TABLE 8.3. *Continued.*

Poly-L-Tyrosine (m.w 125,000 Da) [30]					
T / K	C_p	T / K	C_p	T / K	C_p
0.1	0.00	190	112.30	590	351.96
0.2	0.00	200	119.12	600	356.61
0.3	0.00	210	125.88	610	361.20
0.4	0.00	220	132.86	620	365.71
0.5	0.00	230	139.62	630	370.15
0.6	0.00	240	146.44	640	374.54
0.7	0.00	250	153.27	650	378.89
0.8	0.00	260	160.08	660	383.20
0.9	0.00	270	166.81	670	387.46
1.0	0.00	273.15	168.94	680	391.68
1.2	0.00	280	173.55	690	395.86
1.4	0.01	290	180.35	700	400.28
1.6	0.01	298.15	185.86	710	404.13
1.8	0.01	300	187.02	720	408.22
2	0.02	310	193.78	730	412.26
3	0.07	320	200.35	740	416.30
4	0.16	330	206.93	750	420.29
5	0.31	340	213.47	760	424.24
6	0.54	350	219.92	770	428.26
7	0.84	360	226.28	780	432.22
8	1.22	370	232.68	790	436.13
9	1.66	380	238.80	800	439.92
10	2.16	390	244.94	810	443.79
15	5.09	400	251.13	820	447.65
20	8.12	410	257.11	830	451.49
25	11.01	420	263.01	840	455.32
30	13.78	430	268.84	850	459.15
40	19.09	440	274.61	860	463.04
50	24.28	450	280.34	870	466.74
60	29.52	460	285.98	880	470.53
70	34.92	470	291.55	890	474.29
80	40.53	480	297.00	900	478.07
90	46.43	490	302.35	910	481.84
100	52.53	500	307.62	920	485.61
110	58.80	510	312.81	930	489.39
120	65.28	520	317.93	940	493.17
130	71.86	530	322.97	950	496.95
140	78.48	540	327.95	960	500.74
150	85.16	550	332.87	970	504.54
160	91.94	560	337.81	980	508.35
170	98.69	570	342.59	990	512.17
180	105.51	580	347.30	1000	515.98

TABLE 8.3. *Continued.*

Poly-L-Valine (m.w 7,230 Da) [29]					
T / K	C_p	T / K	C_p	T / K	C_p
0.1	0.00	190	100.26	590	255.89
0.2	0.00	200	104.36	600	259.29
0.3	0.00	210	108.39	610	262.65
0.4	0.00	220	112.55	620	265.96
0.5	0.00	230	116.53	630	269.23
0.6	0.00	240	120.58	640	272.47
0.7	0.00	250	124.67	650	275.70
0.8	0.00	260	128.75	660	278.90
0.9	0.00	270	132.79	670	282.06
1.0	0.00	273.15	134.07	680	285.22
1.2	0.01	280	136.83	690	288.36
1.4	0.01	290	140.90	700	291.75
1.6	0.01	298.15	144.29	710	294.60
1.8	0.02	300	144.98	720	297.70
2	0.03	310	149.19	730	300.78
3	0.09	320	153.30	740	303.85
4	0.21	330	157.63	750	306.90
5	0.41	340	161.52	760	309.92
6	0.70	350	165.61	770	313.02
7	1.09	360	169.67	780	316.04
8	1.57	370	173.83	790	319.05
9	2.13	380	177.77	800	321.99
10	2.75	390	181.78	810	324.98
15	6.26	400	185.90	820	327.97
20	9.82	410	189.87	830	330.94
25	13.20	420	193.83	840	333.93
30	16.43	430	197.71	850	336.89
40	22.65	440	201.57	860	339.86
50	28.70	450	205.43	870	342.82
60	34.68	460	209.28	880	345.77
70	40.64	470	213.09	890	348.72
80	46.51	480	216.82	900	351.67
90	52.26	490	220.56	910	354.63
100	57.88	500	224.34	920	357.59
110	63.32	510	227.95	930	360.56
120	68.54	520	231.54	940	363.52
130	73.53	530	235.10	950	366.49
140	78.37	540	238.62	960	369.47
150	82.98	550	242.13	970	372.46
160	87.52	560	245.69	980	375.46
170	91.86	570	249.12	990	378.47
180	96.11	580	252.52	1000	381.47

TABLE 8.3. *Continued.*

Poly(L-Lysine·HBr-Alanine) (molar ratio 46 / 54, m.w 37,000 Da) [31]					
T / K	C_p	T / K	C_p	T / K	C_p
0.1	0.00	190	206.38	590	506.35
0.2	0.00	200	214.69	600	512.75
0.3	0.00	210	222.88	610	518.97
0.4	0.00	220	231.18	620	525.12
0.5	0.00	230	239.30	630	531.21
0.6	0.00	240	247.45	640	537.26
0.7	0.00	250	255.56	650	543.26
0.8	0.00	260	263.67	660	549.20
0.9	0.01	270	271.64	670	555.12
1.0	0.01	273.15	274.17	680	561.01
1.2	0.01	280	279.76	690	566.87
1.4	0.02	290	287.85	700	572.96
1.6	0.03	298.15	294.45	710	578.50
1.8	0.04	300	295.86	720	584.27
2	0.06	310	304	730	590.01
3	0.20	320	312.22	740	595.73
4	0.48	330	320.06	750	601.42
5	0.93	340	328.04	760	607.07
6	1.58	350	335.95	770	612.79
7	2.45	360	343.82	780	618.42
8	3.51	370	352.64	790	624.04
9	4.73	380	359.42	800	629.57
10	6.07	390	367.07	810	635.16
15	13.49	400	374.86	820	640.74
20	20.89	410	382.42	830	646.30
25	27.91	420	389.84	840	651.87
30	34.62	430	397.23	850	657.42
40	47.57	440	404.59	860	662.97
50	60.21	450	411.91	870	668.51
60	72.70	460	419.19	880	674.07
70	85.10	470	426.46	890	679.59
80	97.26	480	433.46	900	685.14
90	109.08	490	440.54	910	690.66
100	120.58	500	447.40	920	696.22
110	131.63	510	454.17	930	701.79
120	142.27	520	460.88	940	707.36
130	152.37	530	467.53	950	712.98
140	162.12	540	474.12	960	718.58
150	171.43	550	480.65	970	724.21
160	180.55	560	487.33	980	729.85
170	189.29	570	493.72	990	735.51
180	197.91	580	500.06	1000	741.19

TABLE 8.3. *Continued.*

Poly (L-Lysine·HBr-Phenylalanine) (molar ratio 51/49, m.w 49,700 Da) [31]					
T / K	C_p	T / K	C_p	T / K	C_p
0.1	0.00	190	231.52	590	695.94
0.2	0.00	200	244.11	600	705.37
0.3	0.00	210	256.66	610	714.69
0.4	0.00	220	269.59	620	723.87
0.5	0.00	230	282.20	630	732.92
0.6	0.00	240	294.93	640	741.90
0.7	0.00	250	307.72	650	750.80
0.8	0.00	260	320.48	660	759.62
0.9	0.00	270	333.16	670	768.37
1.0	0.01	273.15	337.16	680	777.05
1.2	0.01	280	345.88	690	785.66
1.4	0.02	290	358.75	700	794.76
1.6	0.02	298.15	369.22	710	802.74
1.8	0.03	300	371.42	720	811.20
2	0.05	310	384.33	730	819.67
3	0.16	320	396.86	740	828.05
4	0.37	330	409.47	750	836.36
5	0.72	340	422.04	760	844.52
6	1.23	350	434.47	770	852.88
7	1.92	360	446.82	780	861.11
8	2.79	370	459.25	790	869.28
9	3.81	380	471.09	800	877.26
10	4.97	390	483.04	810	885.32
15	11.68	400	495.11	820	893.40
20	18.63	410	506.80	830	901.45
25	25.28	420	518.34	840	909.50
30	31.63	430	529.79	850	917.53
40	43.79	440	541.18	860	925.61
50	55.66	450	552.50	870	933.49
60	67.48	460	563.70	880	941.46
70	79.47	470	574.76	890	949.39
80	91.68	480	585.56	900	957.34
90	104.15	490	596.21	910	965.29
100	116.76	500	606.70	920	973.24
110	129.47	510	617.04	930	981.21
120	142.32	520	627.25	940	989.18
130	155.16	530	637.35	950	997.16
140	168.01	540	647.34	960	1005.15
150	180.69	550	657.26	970	1013.16
160	193.48	560	667.26	980	1021.20
170	206.10	570	676.89	990	1029.26
180	218.82	580	686.52	1000	1037.32

TABLE 8.3. *Continued.*

Poly(L-Glutamic Acid·Na-Tyrosine) (molar ratio 50/50, m.w 30,000 Da) [31]					
T / K	C_p	T / K	C_p	T / K	C_p
0.1	0.00	190	223.26	590	637.55
0.2	0.00	200	235.44	600	645.58
0.3	0.00	210	247.51	610	653.52
0.4	0.00	220	259.88	620	661.31
0.5	0.00	230	271.82	630	668.98
0.6	0.00	240	283.82	640	676.57
0.7	0.00	250	295.79	650	684.09
0.8	0.00	260	307.68	660	691.54
0.9	0.00	270	319.39	670	698.92
1.0	0.01	273.15	323.08	680	706.23
1.2	0.01	280	331.08	690	713.48
1.4	0.01	290	342.82	700	721.21
1.6	0.02	298.15	352.36	710	727.84
1.8	0.03	300	354.34	720	734.93
2	0.04	310	366.04	730	741.98
3	0.15	320	377.35	740	748.99
4	0.35	330	388.67	750	755.91
5	0.68	340	399.92	760	762.78
6	1.17	350	410.98	770	769.79
7	1.83	360	421.89	780	776.66
8	2.65	370	432.89	790	783.48
9	3.63	380	443.36	800	790.10
10	4.73	390	453.86	810	796.85
15	11.12	400	464.48	820	803.57
20	17.73	410	474.70	830	810.27
25	24.06	420	484.79	840	816.97
30	30.10	430	494.76	850	823.65
40	41.68	440	504.65	860	830.37
50	52.98	450	514.47	870	836.91
60	64.23	460	524.18	880	843.53
70	75.67	470	533.74	890	850.11
80	87.33	480	543.08	900	856.72
90	99.27	490	552.26	910	863.31
100	111.42	500	561.30	920	869.92
110	123.70	510	570.19	930	876.55
120	136.19	520	578.97	940	883.16
130	148.71	530	587.64	950	889.79
140	161.26	540	596.19	960	896.43
150	173.67	550	604.65	970	903.08
160	186.19	560	613.19	980	909.77
170	198.54	570	621.40	990	916.47
180	210.96	580	629.53	1000	923.16

TABLE 8.3. *Continued.*

Poly(L-Proline-Glycine-Proline) (molar ratio 66/34, m.w 5,300 Da) [31]					
T / K	C_p	T / K	C_p	T / K	C_p
0.1	0.00	190	194.56	590	568.71
0.2	0.00	200	203.74	600	576.61
0.3	0.00	210	213	610	584.43
0.4	0.00	220	222.29	620	592.12
0.5	0.00	230	231.85	630	599.69
0.6	0.00	240	241.51	640	607.20
0.7	0.00	250	251.27	650	614.63
0.8	0.00	260	261.23	660	621.99
0.9	0.00	270	271.04	670	629.29
1.0	0.01	273.15	274.20	680	636.53
1.2	0.01	280	281.05	690	643.71
1.4	0.02	290	291.24	700	651.36
1.6	0.03	298.15	299.50	710	657.92
1.8	0.04	300	301.22	720	664.96
2	0.05	310	311.51	730	671.95
3	0.18	320	321.71	740	678.90
4	0.43	330	331.81	750	685.80
5	0.84	340	341.90	760	692.66
6	1.44	350	351.99	770	699.48
7	2.22	360	362.07	780	706.27
8	3.19	370	372.08	790	713.02
9	4.29	380	382.11	800	719.74
10	5.50	390	392.03	810	726.43
15	12.24	400	401.90	820	733.10
20	18.95	410	411.35	830	739.74
25	25.31	420	420.84	840	746.36
30	31.40	430	430.41	850	752.96
40	43.14	440	439.84	860	759.54
50	54.63	450	449.18	870	766.11
60	65.95	460	458.42	880	772.67
70	77.21	470	467.57	890	779.22
80	88.32	480	476.53	900	785.77
90	99.14	490	485.51	910	792.31
100	109.70	500	494.35	920	798.85
110	119.99	510	502.98	930	805.39
120	129.90	520	511.52	940	811.94
130	139.55	530	519.96	950	818.49
140	148.95	540	528.32	960	825.06
150	158.18	550	536.58	970	831.64
160	167.27	560	544.75	980	838.25
170	176.34	570	552.83	990	844.87
180	185.52	580	560.81	1000	851.51

TABLE 8.4. *Heat capacities ($J\,K^{-1}\,g^{-1}$) of anhydrous and hydrated proteins.*

Anhydrous bovine zinc insulin (5,665 Da) [32]					
T / K	$C_p \times 10^2$	T / K	$C_p \times 10^2$	T / K	$C_p \times 10^2$
10	1.987	90	45.56	220	94.73
15	4.427	100	49.87	230	98.58
20	7.305	110	53.93	240	102.42
25	10.42	120	57.78	250	106.32
30	13.64	130	61.51	260	110.21
35	16.86	140	65.27	270	114.14
40	19.95	150	69.04	280	118.03
45	22.90	160	72.80	290	122.05
50	25.74	170	76.53	300	126.11
55	28.48	180	80.21	310	130.25
60	31.14	190	83.81	273.15	115.35
70	36.21	200	87.40	298.15	125.35
80	41.00	210	91.04	310.15	130.29

Hydrated (4.0% H_2O) bovine zinc insulin (5,665 Da) [32]					
T / K	$C_p \times 10^2$	T / K	$C_p \times 10^2$	T / K	$C_p \times 10^2$
10	1.933	90	46.94	220	98.95
15	4.339	100	51.25	230	103.01
20	7.284	110	55.40	240	107.07
25	10.49	120	59.41	250	111.21
30	13.89	130	63.39	260	115.44
35	17.23	140	67.32	270	119.75
40	20.46	150	71.30	280	124.10
45	23.56	160	75.23	290	128.45
50	26.55	170	79.20	300	132.84
55	29.43	180	83.14	310	137.24
60	32.20	190	87.03	273.15	121.13
70	37.46	200	90.96	298.15	132.01
80	42.38	210	94.94	310.15	137.28

Anhydrous bovine chymotrypsinogen (25,666 Da) [32]					
T / K	$C_p \times 10^2$	T / K	$C_p \times 10^2$	T / K	$C_p \times 10^2$
10	1.874	90	46.86	220	97.82
15	4.343	100	51.09	230	101.67
20	7.297	110	55.31	240	105.56
25	10.53	120	59.33	250	109.50
30	13.87	130	63.26	260	113.55
35	17.15	140	67.15	270	117.57
40	20.33	150	70.96	280	121.67
45	23.38	160	74.77	290	125.86
50	26.39	170	78.58	300	130.08
55	29.34	180	82.43	310	134.27
60	32.19	190	86.23	273.15	118.87
70	37.48	200	90.08	298.15	129.29
80	42.26	210	93.97	310.15	134.35

TABLE 8.4. *Continued.*

Hydrated (10.7% H_2O) bovine chymotrypsinogen (25,666 Da) [32]					
T / K	$C_p \times 10^2$	T / K	$C_p \times 10^2$	T / K	$C_p \times 10^2$
10	1.778	90	51.13	220	114.56
15	4.184	100	55.98	230	120.16
20	7.309	110	60.71	240	125.86
25	10.84	120	65.44	250	131.59
30	14.43	130	70.12	260	137.40
35	18.06	140	74.81	270	143.30
40	21.61	150	79.50	280	149.24
45	25.03	160	84.22	290	155.23
50	28.28	170	88.95	300	161.34
55	31.45	180	93.76	310	167.11
60	34.55	190	98.70	273.15	145.35
70	40.45	200	103.85	298.15	160.42
80	45.94	210	109.12	310.15	167.40

Anhydrous native bovine serum albumin (66,433 Da) [33]					
T / K	$C_p \times 10^2$	T / K	$C_p \times 10^2$	T / K	$C_p \times 10^2$
10	1.854	90	46.23	220	96.48
15	4.234	100	50.54	230	100.25
20	7.058	110	54.69	240	104.01
25	10.14	120	58.74	250	107.91
30	13.36	130	62.63	260	111.88
35	16.60	140	66.44	270	115.90
40	19.72	150	70.25	280	119.96
45	22.71	160	74.06	290	124.14
50	25.71	170	77.82	300	128.32
55	28.61	180	81.59	310	132.55
60	31.37	190	85.31		
70	36.62	200	89.08		
80	41.59	210	92.80		

Anhydrous denatured bovine serum albumin (66,433 Da) [33]					
T / K	$C_p \times 10^2$	T / K	$C_p \times 10^2$	T / K	$C_p \times 10^2$
10	1.866	90	46.44	220	97.15
15	4.272	100	50.79	230	101.04
20	7.176	110	54.94	240	105.02
25	10.36	120	58.99	250	109.08
30	13.62	130	62.93	260	113.22
35	16.87	140	66.78	270	117.45
40	20.00	150	70.63	280	121.71
45	23.05	160	74.43	290	126.02
50	26.08	170	78.20	300	130.37
55	29.06	180	81.92	310	134.77
60	31.92	190	85.69	273.15	118.78
70	37.10	200	89.50	298.15	129.54
80	41.88	210	93.30	310.15	134.81

TABLE 8.4. *Continued.*

Hydrated (2.14% H_2O) bovine serum albumin (66,433 Da) [33]

T / K	$C_p \times 10^2$	T / K	$C_p \times 10^2$	T / K	$C_p \times 10^2$
10	1.678	90	47.07	220	99.75
15	4.038	100	51.46	230	103.81
20	7.079	110	55.65	240	107.86
25	10.54	120	59.75	250	111.92
30	13.70	130	63.68	260	116.06
35	16.96	140	67.66	270	120.33
40	20.11	150	71.67	280	124.52
45	23.18	160	75.73	290	128.78
50	26.20	170	79.75	300	133.05
55	29.09	180	84.31	310	137.28
60	31.90	190	87.70		
70	37.29	200	91.71		
80	42.34	210	95.73		

Anhydrous bovine serosal collagen (280,950 Da) [33]

T / K	$C_p \times 10^2$	T / K	$C_p \times 10^2$	T / K	$C_p \times 10^2$
10	1.774	90	45.10	220	93.09
15	4.105	100	49.20	230	96.65
20	6.891	110	53.22	240	100.25
25	10.00	120	57.11	250	103.93
30	13.18	130	60.88	260	107.70
35	16.33	140	64.56	270	111.46
40	19.42	150	68.16	280	115.31
45	22.37	160	71.71	290	119.12
50	25.28	170	75.23	300	122.93
55	28.07	180	78.83	310	126.73
60	30.77	190	82.43	273.15	112.68
70	35.94	200	86.02	298.15	122.22
80	40.71	210	89.58	310.15	126.78

Hydrated (13.53% H_2O) bovine serosal collagen (280,950 Da) [33]

T/K	$C_p \times 10^2$	T / K	$C_p \times 10^2$	T / K	$C_p \times 10^2$
10	1.536	90	50.63	220	113.60
15	3.895	100	55.52	230	118.95
20	6.945	110	60.25	240	124.52
25	10.41	120	64.94	250	130.29
30	14.00	130	69.58	260	136.23
35	17.68	140	74.35	270	142.34
40	21.26	150	78.87	280	148.57
45	24.53	160	83.55	290	155.02
50	27.86	170	88.28	300	161.63
55	31.10	180	93.09	310	168.41
60	34.16	190	98.07	273.15	144.31
70	39.95	200	103.14	298.15	160.42
80	45.44	210	108.32	310.15	168.49

TABLE 8.4. *Continued.*

Rat tail tendon collagen at different water content, R (grams of water per gram of protein) [34]					
R (g/g)	Temperature (°C)				
	− 60	− 40	− 20	0	20
	Before denaturation				
1.44	1.582	1.778	2.343	3.033	3.117
1.01	1.548	1.849	2.469	2.816	2.908
0.93	1.598	1.891	2.510	2.812	2.900
0.79	1.582	1.862	2.594	2.669	2.812
0.65	1.556	1.841	2.803	2.481	2.586
0.527	1.577	1.883	2.761	2.339	2.435
0.468	1.498	1.799	2.803	2.259	2.335
0.428	1.494	1.757	2.469	2.176	2.247
0.376	1.381	1.715	1.925	2.000	2.155
	After denaturation				
1.44	1.674	1.904	2.929	3.293	3.548
1.02	1.686	1.946	3.347	3.138	3.439
0.93	1.695	1.950	3.766	2.966	3.314
0.79	1.715	2.029	3.347	2.862	3.264
0.651	1.715	2.050	3.347	2.715	3.130
0.524	1.766	2.121	3.347	2.607	2.853
0.468	1.674	2.033	3.347	2.552	2.778
0.428	1.582	1.941	2.510	2.481	2.653
0.375	1.464	1.799	2.929	2.393	2.569

Keratin (merino wool) [35]										
	Water content (% of weight of keratin)									
T / °C	0	2.8	7.6	10.4	16.9	20.9	24.8	28.4	30.7	33.9
− 70	0.887	0.925	1.004	1.013	1.088	1.176	1.230	1.247	1.264	1.230
− 60	0.929	0.971	1.059	1.067	1.159	1.255	1.322	1.351	1.364	1.343
− 50	0.971	1.013	1.109	1.121	1.234	1.335	1.414	1.456	1.464	1.460
− 40	1.008	1.054	1.159	1.176	1.305	1.414	1.506	1.561	1.565	1.573
− 30	1.046	1.096	1.213	1.230	1.377	1.494	1.607	1.665	1.682	1.674
− 20	1.088	1.142	1.264	1.280	1.448	1.577	1.715	–	–	–
− 10	1.125	1.184	1.318	1.335	1.519	1.657	1.787	–	–	–
0	1.167	1.226	1.368	1.393	1.590	1.745	1.883	1.992	2.063	2.079
10	1.205	1.272	1.423	1.452	1.665	1.837	1.975	2.079	2.146	2.159
20	1.243	1.314	1.473	1.523	1.745	1.933	2.067	2.167	2.230	2.234
30	1.284	1.356	1.527	1.594	1.837	2.050	2.197	2.255	2.310	2.318
40	1.322	1.402	1.582	1.665	1.933	2.142	2.255	2.330	–	2.356
50	1.364	1.443	1.636	1.732	2.025	2.201	2.310	2.372	–	2.393
60	1.402	1.494	1.695	1.803	2.105	2.255	2.356	2.402	2.460	2.439
70	1.443	1.540	1.757	1.879	2.180	2.314	2.402	2.439	2.494	2.481
80	1.481	1.590	1.820	1.962	2.238	2.360	2.448	2.494	2.540	2.519
90	1.523	1.640	1.887	2.054	2.293	2.406	2.494	2.540	–	2.556
100	1.561	1.690	1.950	2.151	2.330	2.448	2.536	2.586	–	2.602

TABLE 8.5. *Temperature dependence of the partial molar heat capacities ($J\ K^{-1}\ mol^{-1}$) of the peptide unit and of the side chains of amino acid residues for the temperature range 5–125 °C [18].*

	Temperature (°C)					
	5	25	50	75	100	125
–CHCONH–	3.7	15.2	26.2	29.8	33.7	33.7
$-R_i$						
Ala	175.7	166.7	156.2	144.7	134.6	124.1
Arg	204.6	273.4	305.8	315.1	318.7	318.5
Asn	72.9	88.8	109.8	125.2	140.5	154.2
Asp	72.8	89	106.2	124.5	140.7	154.3
Cys	225.4	237.6	250.8	260.7	268.2	276.1
Gln	168	180.2	193.4	203.3	210.8	218.7
Glu	168.3	179	192	203.7	211.4	217.8
Gly	82.3	78	71.7	66.4	59.7	53.9
His	205.7	179.6	177.2	179.6	187.1	196.8
Ile	406.8	402.3	397.1	390.8	386	380.8
Leu	385.9	381.7	377.8	372.9	369.4	365.5
Lys	215.1	249.8	266.9	274.4	278.1	274.4
Met	197.1	175.9	158.1	150.3	148.1	143.9
Phe	395.7	383	370.3	358.4	348.3	339.6
Pro	214.6	177.7	152.3	142.8	135.6	130.1
Ser	75.6	81.2	85.7	91.4	97.3	102.1
Thr	194.2	184.5	182.2	186.5	199	216.2
Trp	471.2	458.5	445.8	433.9	423.8	415.1
Tyr	310.6	301.7	295.2	294.5	300.1	304
Val	324.6	314.4	305	294.7	285.7	269.6

TABLE 8.6. *Temperature dependence of the partial molar volumes ($cm^3\ mol^{-1}$) of the peptide unit and of the side chains of amino acid residues for the temperature range 5–125 °C [11].*

	Temperature (°C)					
	5	25	50	75	100	125
–CHCONH–	28.3	28.0	28.6	28.9	29.0	29.4
$-R_i$						
Ala	24.8	27.2	30.1	33.1	36.3	39.4
Arg	81.2	85.7	88.4	90.4	92.1	93.5
Asn	44.1	45.7	47.8	49.3	50.8	52.4
Asp	39.0	41.5	44.5	47.3	49.9	52.6
Cys	40.5	40.5	40.5	40.5	40.5	40.5
Gln	58.4	61.0	63.2	66.0	68.5	69.7
Glu	54.9	57.5	60.7	63.6	66.3	69.3
Gly	10.9	10.3	9.6	9.2	8.9	8.5
His	65.1	64.0	63.1	62.4	61.8	61.1
Ile	64.5	66.1	67.7	69.8	71.8	74.0
Leu	75.0	77.6	80.2	82.9	86.5	89.4
Lys	72.4	73.5	75.8	78.5	81.3	84.8
Met	73.3	72.1	70.2	69.0	67.9	66.7
Phe	82.0	86.3	92.0	97.9	102.6	107.9
Pro	36.0	35.8	34.1	33.7	33.5	33.2
Ser	27.1	27.8	28.8	29.7	30.7	32.0
Thr	44.2	44.7	45.9	47.6	50.9	54.6
Trp	110.9	110.9	110.9	110.9	110.9	110.9
Tyr	88.2	90.0	92.2	94.1	95.9	97.8
Val	60.7	63.0	65.7	68.5	71.7	74.5

TABLE 8.7. *Thermodynamics characteristics of the proteins (partial molar heat capacity of the native, C_p^N(kJ K^{-1} mol^{-1}), and unfolded state, C_p^U(kJ K^{-1} mol^{-1}), and the heat capacity, $\Delta_N^U C_p$(kJ K^{-1} mol^{-1}), enthalpy, $\Delta_N^U H$(kJ mol^{-1}), entropy, $\Delta_N^U S$(J K^{-1} mol^{-1}), and Gibbs energy changes upon unfolding, $\Delta_N^U G$(kJ · mol^{-1}))*.*

Protein		Temperature (°C)					
		5	25	50	75	100	125
ROP[1]	C_p^N	7.9	9.0	10.4	11.7	13.1	14.4
	C_p^U	11.9	12.9	13.9	14.2	14.5	14.6
	$\Delta_N^U C_p$	7.9	7.9	7.0	5.0	2.9	0.4
	$\Delta_N^U H$	107	265	451	580	601	700
SH3 domain[2]	C_p^N	9.7	10.6	11.7	12.8	13.9	15.0
	C_p^U	14.7	15.4	16	16.4	16.6	16.6
	$\Delta_N^U C_p$	5.0	4.8	4.3	3.6	2.7	1.6
	$\Delta_N^U H$	− 32	52	146	222	274	296
	$\Delta_N^U S$	− 166	126	428	653	797	856
	$\Delta_N^U G$	14.1	14.5	7.8	− 5.2	− 23.3	− 44.7
BPTI[3]	C_p^N	8.7	9.5	10.5	11.4	12.4	13.4
	C_p^U	11.5	12.5	13.1	13.5	13.7	13.7
	$\Delta_N^U C_p$	2.8	3.0	2.6	2.1	1.3	0.3
	$\Delta_N^U H$	72	130	200	259	303	323
	$\Delta_N^U S$	87	288	514	690	809	864
	$\Delta_N^U G$	47.8	44.2	34.0	18.9	1.2	− 20.9
CI2[4]	C_p^N	12.4	13.3	14.5	15.6	16.7	17.8
	C_p^U	15.8	16.9	17.8	18.0	18.2	18.0
	$\Delta_N^U C_p$	3.4	3.6	3.3	2.4	1.5	0.2
	$\Delta_N^U H$	66	135	221	292	341	362
	$\Delta_N^U S$	119	360	636	850	986	1041
	$\Delta_N^U G$	32.9	27.7	15.6	− 3.8	− 26.8	− 52.3
Eglin-c[5]	C_p^N	11.9	12.9	14.1	15.4	16.6	17.9
	C_p^U	16.1	16.8	17.6	17.9	18.2	18.1
	$\Delta_N^U C_p$	4.2	3.9	3.5	2.5	1.6	0.2
	$\Delta_N^U H$	33	115	208	283	335	358
	$\Delta_N^U S$	− 22	262	561	786	929	989
	$\Delta_N^U G$	39.1	36.9	26.8	9.5	− 11.5	− 35.6
Protein G[6]	C_p^N	8.1	8.9	9.9	10.9	11.9	12.9
	C_p^U	11.7	12.5	13.2	13.5	13.9	13.9
	$\Delta_N^U C_p$	3.6	3.6	3.3	2.6	2.0	1.0
	$\Delta_N^U H$	− 4	67	153	227	283	320
	$\Delta_N^U S$	− 103	145	422	643	801	897
	$\Delta_N^U G$	24.6	23.8	16.7	3.2	− 15.8	− 37.0
Tendamistat[7]	C_p^N	11.4	12.1	13.0	13.9	14.8	15.7
	C_p^U	14.9	15.7	16.6	16.8	17.1	17.1
	$\Delta_N^U C_p$	3.5	3.6	3.6	2.9	2.3	1.4
	$\Delta_N^U H$	− 22	70	176	262	321	351
	$\Delta_N^U S$	− 213	109	452	711	877	955
	$\Delta_N^U G$	37.2	37.5	30.0	14.6	− 6.1	− 29.1

TABLE 8.7. *Continued.*

Protein		Temperature (°C)					
		5	25	50	75	100	125
Ubiquitin[8]	C_p^N	11.2	12.6	14.3	16.0	17.7	19.4
	C_p^U	17.0	18.3	19.4	19.8	20.2	20.2
	$\Delta_N^U C_p$	5.8	5.7	5.1	3.8	2.5	0.8
	$\Delta_N^U H$	− 88	27	162	273	351	393
	$\Delta_N^U S$	− 444	− 44	393	727	959	1068
	$\Delta_N^U G$	35.4	40.1	35.1	20.0	− 6.7	− 32.1
RNase T1[9]	C_p^N	14.6	16.1	17.8	19.7	21.9	24.3
	C_p^U	20.1	21.4	22.8	24.0	24.9	25.1
	$\Delta_N^U C_p$	5.5	5.3	5.0	4.3	3.0	0.8
	$\Delta_N^U H$	173	281	410	528	621	672
	$\Delta_N^U S$	444	817	1233	1584	1845	1976
	$\Delta_N^U G$	49.6	37.5	11.7	− 23.2	− 67.2	− 114.4
Met-J[10]	C_p^N	37.8	40.2	43.2	46.2	49.2	52.2
	C_p^U	45.8	49.2	52.1	53.2	54.3	54.3
	$\Delta_N^U C_p$	8.0	9.0	8.9	7.0	5.1	2.1
	$\Delta_N^U H$	92	270	498	692	832	902
Cytochrome c[11]	C_p^N	15.8	17.5	19.7	21.9	24.0	26.2
	C_p^U	22.7	24.3	25.8	26.3	26.8	26.8
	$\Delta_N^U C_p$	6.9	6.8	6.1	4.4	2.8	0.6
	$\Delta_N^U H$	− 53	89	268	421	532	593
	$\Delta_N^U S$	− 319	174	752	1210	1520	1681
	$\Delta_N^U G$	35.7	37.1	25.1	− 1.1	− 35.0	− 76.0
Barnase[12]	C_p^N	16.5	18.5	21.0	23.5	26.0	28.5
	C_p^U	23.6	25.4	26.9	27.4	28.0	28.1
	$\Delta_N^U C_p$	7.1	6.9	5.9	3.9	2.0	0.1
	$\Delta_N^U H$	167	307	467	590	664	690
	$\Delta_N^U S$	379	866	1384	1752	1959	2029
	$\Delta_N^U G$	61.6	48.9	20.0	− 19.7	− 66.7	− 117.5
RNase A[11]	C_p^N	19.5	20.8	22.5	24.2	25.8	27.5
	C_p^U	24.1	26.0	27.8	28.5	29.3	29.5
	$\Delta_N^U C_p$	4.6	5.2	5.3	4.3	3.5	2.0
	$\Delta_N^U H$	220	294	405	512	603	664
	$\Delta_N^U S$	641	896	1254	1574	1826	1989
	$\Delta_N^U G$	41.8	27.0	− 0.0	− 35.8	− 78.1	− 127.6
Lysozyme[11]	C_p^N	18.2	20.0	22.2	24.4	26.7	28.9
	C_p^U	26.7	29.1	31.1	31.8	32.4	32.5
	$\Delta_N^U C_p$	8.5	9.1	8.9	7.4	5.7	3.6
	$\Delta_N^U H$	111	242	408	562	683	753

TABLE 8.7. *Continued.*

Protein		Temperature (°C)					
		5	25	50	75	100	125
	$\Delta_N^U S$	164	618	1153	1615	1954	2138
	$\Delta_N^U G$	65.4	57.8	35.6	− 0.0	− 45.8	− 97.9
Interleukin 1β[13]	C_p^N	26.4	28.1	30.1	32.2	34.3	36.4
	C_p^U	33.3	35.6	37.6	38.4	39.2	39.2
	$\Delta_N^U C_p$	6.9	7.5	7.5	6.2	4.9	2.8
	$\Delta_N^U H$	7	151	330	501	640	736
	$\Delta_N^U S$	− 99	401	1006	1516	1903	2155
	$\Delta_N^U G$	34.5	31.5	5.1	− 26.6	− 69.8	− 121.7
Myoglobin[11]	C_p^N	21.8	24.2	27.3	30.3	33.4	36.5
	C_p^U	35.6	37.6	39.5	40.0	40.5	40.3
	$\Delta_N^U C_p$	14.4	14.0	12.8	10.3	7.7	4.4
	$\Delta_N^U H$	− 231	6	291	555	774	920
	$\Delta_N^U S$	− 919	− 116	805	1595	2207	2588
	$\Delta_N^U G$	24.5	40.6	31.0	− 0.1	− 49.2	− 110.0
T4-Lyz[14]	C_p^N	25.2	28.1	31.8	35.5	39.1	42.8
	C_p^U	36.2	39.1	41.5	42.2	43.1	43.0
	$\Delta_N^U C_p$	11.0	11.0	9.7	6.7	4.0	0.2
	$\Delta_N^U H$	20	240	499	671	805	856
	$\Delta_N^U S$	− 190	576	1413	1928	2302	2439
	$\Delta_N^U G$	72.8	68.4	42.6	0.1	− 53.6	− 114.7
Papain[15]	C_p^N	28.1	32.0	36.8	41.7	46.5	51.4
	C_p^U	45.0	48.0	50.5	51.3	52.1	51.9
	$\Delta_N^U C_p$	16.9	16.0	13.7	9.6	5.6	0.5
	$\Delta_N^U H$	− 166	164	535	826	1015	1091
	$\Delta_N^U S$	− 911	236	1438	2312	2840	3042
Chymotrypsin[15]	C_p^N	34.3	37.7	42.0	46.3	50.6	54.8
	C_p^U	49.2	51.8	54.3	55.1	56.0	55.8
	$\Delta_N^U C_p$	14.9	14.1	12.3	8.8	5.4	1.0
	$\Delta_N^U H$	− 21	268	598	862	1039	1119
	$\Delta_N^U S$	− 260	746	1813	2602	3099	3312
	$\Delta_N^U G$	51.3	45.7	12.4	− 43.5	− 116.9	− 199.2
Pepsinogen[15]	C_p^N	44.2	51.7	61.1	70.4	79.8	89.2
	C_p^U	78.4	82.3	86.3	87.7	89.6	89.7
	$\Delta_N^U C_p$	34.2	30.6	25.2	17.3	9.8	0.5
	$\Delta_N^U H$	− 577	72	770	1301	1639	1767
	$\Delta_N^U S$	− 2279	− 19	2242	3739	4687	5030

[1]ROP[36]; [2]SH3[37]; [3]BPTI[5]; [4]CI-2[38]; [5]Eglin-c[39]; [6]protein G[40]; [7]Tendamistat[41]; [8]Ubiquitin[42]; [9]RNase T1[43]; [10]Met-J[44]; [11]Cytochrome c, RNase A, Lysozyme, Myoglobin[45,46]; [12]Barnase[47]; [13]Interleukin-1β[48]; [14]T4-Lyz[49]; [15]Papain, Chymotrypsin, Pepsinogen[50].

*Reported entropies and Gibbs energies are for the conditions of maximal stability [17]. The entropies and Gibbs energy of unfolding for rop and met-J are not available since the unfolding represents a bimolecular two-state process.

TABLE 8.8. *Normalized values of the heat capacities ($\Delta\hat{C}_p^{hyd}$ in J K^{-1} mol^{-1} Å^{-2}), enthalpies ($\Delta\hat{H}^{hyd}$ in J mol^{-1} Å^{-2}), entropies ($\Delta\hat{S}^{hyd}$ in 10^{-3} J K^{-1} mol^{-1} Å^{-2}), and Gibbs energies ($\Delta\hat{G}_p^{hyd}$ in J K^{-1} mol^{-1} Å^{-2}) of hydration of various surfaces [17].*

		Temperature (°C)					
		5	25	50	75	100	125
				Nonpolar surfaces			
Aliphatic	$\Delta\hat{C}_p^{hyd}$	2.24	2.14	2.03	1.91	1.80	1.66
	$\Delta\hat{H}^{hyd}$	− 166	− 122	− 70	− 21	26	69
	$\Delta\hat{S}^{hyd}$	− 730	− 578	− 409	− 263	− 134	− 22
	$\Delta\hat{G}^{hyd}$	37	50	62	71	75	77
Aromatic	$\Delta\hat{C}_p^{hyd}$	1.65	1.55	1.41	1.29	1.19	1.09
	$\Delta\hat{H}^{hyd}$	− 180	− 148	− 111	− 77	− 46	− 18
	$\Delta\hat{S}^{hyd}$	− 430	− 319	− 199	− 98	− 12	62
	$\Delta\hat{G}^{hyd}$	− 61	− 53	− 47	− 43	− 42	− 43
				Polar surfaces of:			
Arg	$\Delta\hat{C}_p^{hyd}$	− 0.38	− 0.20	− 0.12	− 0.04	0.01	0.08
	$\Delta\hat{H}^{hyd}$	− 821	− 827	− 831	− 833	− 834	− 833
	$\Delta\hat{S}^{hyd}$	− 458	− 478	− 492	− 497	− 498	− 495
	$\Delta\hat{G}^{hyd}$	− 694	− 685	− 672	− 660	− 647	− 635
Asn	$\Delta\hat{C}_p^{hyd}$	− 1.27	− 1.01	− 0.67	− 0.41	− 0.16	0.09
	$\Delta\hat{H}^{hyd}$	− 871	− 894	− 915	− 928	− 936	− 936
	$\Delta\hat{S}^{hyd}$	− 575	− 654	− 723	− 763	− 783	− 785
	$\Delta\hat{G}^{hyd}$	− 711	− 699	− 681	− 663	− 643	− 623
Asp	$\Delta\hat{C}_p^{hyd}$	− 1.72	− 1.40	− 1.07	− 0.71	− 0.40	− 0.11
	$\Delta\hat{H}^{hyd}$	− 684	− 715	− 746	− 768	− 782	− 788
	$\Delta\hat{S}^{hyd}$	− 360	− 469	− 569	− 636	− 675	− 691
	$\Delta\hat{G}^{hyd}$	− 584	− 575	− 562	− 547	− 530	− 513
Cys	$\Delta\hat{C}_p^{hyd}$	1.80	2.01	2.23	2.42	2.54	2.70
	$\Delta\hat{H}^{hyd}$	− 309	− 271	− 218	− 160	− 98	− 32
	$\Delta\hat{S}^{hyd}$	− 535	− 402	− 232	− 59	113	283
	$\Delta\hat{G}^{hyd}$	− 160	− 151	− 143	− 139	− 140	− 145
Gln	$\Delta\hat{C}_p^{hyd}$	− 0.38	− 0.22	− 0.06	0.07	0.17	0.30
	$\Delta\hat{H}^{hyd}$	− 697	− 703	− 706	− 706	− 703	− 697
	$\Delta\hat{S}^{hyd}$	− 571	− 591	− 604	− 603	− 594	− 579
	$\Delta\hat{G}^{hyd}$	− 538	− 527	− 511	− 497	− 481	− 467
Glu	$\Delta\hat{C}_p^{hyd}$	− 0.71	− 0.55	− 0.35	− 0.17	− 0.05	0.09
	$\Delta\hat{H}^{hyd}$	− 549	− 562	− 573	− 580	− 583	− 582
	$\Delta\hat{S}^{hyd}$	− 392	− 436	− 473	− 492	− 500	− 498
	$\Delta\hat{G}^{hyd}$	− 440	− 432	− 420	− 409	− 396	− 383

TABLE 8.8. *Continued.*

		Temperature (°C)					
		5	25	50	75	100	125
His	$\Delta\hat{C}_p^{hyd}$	− 1.96	− 2.43	− 2.38	− 2.26	− 2.07	− 1.82
	$\Delta\hat{H}^{hyd}$	− 1,084	− 1,128	− 1,188	− 1,247	− 1,301	− 1,349
	$\Delta\hat{S}^{hyd}$	− 542	− 693	− 888	− 1060	− 1211	− 1337
	$\Delta\hat{G}^{hyd}$	− 933	− 922	− 901	− 878	− 848	− 816
Lys	$\Delta\hat{C}_p^{hyd}$	− 1.31	− 1.53	− 1.59	− 1.36	− 1.15	− 0.94
	$\Delta\hat{H}^{hyd}$	− 685	− 714	− 753	− 789	− 821	− 847
	$\Delta\hat{S}^{hyd}$	− 384	− 482	− 609	− 716	− 804	− 870
	$\Delta\hat{G}^{hyd}$	− 578	− 570	− 556	− 540	− 519	− 498
Met	$\Delta\hat{C}_p^{hyd}$	− 3.51	− 3.83	− 4.07	− 4.04	− 3.91	− 3.75
	$\Delta\hat{H}^{hyd}$	− 399	− 473	− 572	− 672	− 774	− 869
	$\Delta\hat{S}^{hyd}$	− 158	− 412	− 732	− 1031	− 1308	− 1555
	$\Delta\hat{G}^{hyd}$	− 356	− 350	− 335	− 315	− 283	− 247
Ser	$\Delta\hat{C}_p^{hyd}$	− 1.62	− 1.40	− 1.20	− 0.96	− 0.72	− 0.48
	$\Delta\hat{H}^{hyd}$	− 1015	− 1045	− 1078	− 1104	− 1126	− 1140
	$\Delta\hat{S}^{hyd}$	− 878	− 983	− 1089	− 1168	− 1227	− 1265
	$\Delta\hat{G}^{hyd}$	− 771	− 752	− 726	− 698	− 667	− 636
Thr	$\Delta\hat{C}_p^{hyd}$	− 1.09	− 1.29	− 1.22	− 0.89	− 0.29	0.55
	$\Delta\hat{H}^{hyd}$	− 1262	− 1287	− 1318	− 1343	− 1359	− 1356
	$\Delta\hat{S}^{hyd}$	− 971	− 1053	− 1156	− 1232	− 1274	− 1265
	$\Delta\hat{G}^{hyd}$	− 992	− 972	− 944	− 916	− 881	− 850
Trp	$\Delta\hat{C}_p^{hyd}$	1.05	0.96	1.07	1.08	1.03	1.05
	$\Delta\hat{H}^{hyd}$	− 1,181	− 1,161	− 1,135	− 1,110	− 1,084	− 1,055
	$\Delta\hat{S}^{hyd}$	− 766	− 693	− 615	− 534	− 460	− 392
	$\Delta\hat{G}^{hyd}$	− 968	− 954	− 936	− 924	− 912	− 899
Tyr	$\Delta\hat{C}_p^{hyd}$	− 1.46	− 1.48	− 1.36	− 1.15	− 0.86	− 0.59
	$\Delta\hat{H}^{hyd}$	− 824	− 854	− 889	− 921	− 946	− 963
	$\Delta\hat{S}^{hyd}$	− 314	− 415	− 531	− 625	− 695	− 742
	$\Delta\hat{G}^{hyd}$	− 735	− 730	− 717	− 703	− 686	− 667
CONH	$\Delta\hat{C}_p^{hyd}$	− 2.08	− 1.81	− 1.56	− 1.53	− 1.49	− 1.55
	$\Delta\hat{H}^{hyd}$	− 1662	− 1702	− 1745	− 1785	− 1823	− 1862
	$\Delta\hat{S}^{hyd}$	− 890	− 1026	− 1162	− 1278	− 1383	− 1481
	$\Delta\hat{G}^{hyd}$	− 1415	− 1396	− 1370	− 1340	− 1307	− 1272

REFERENCES

1. Zhang G, Lebedev BV, Wunderlich B, Zhang JY J. P.S.P. B-P. P. 1995; 33: 2449–2455.
2. Privalov PL, Khechinashvili NN J. Mol. Biol. 1974; 86: 665–684.
3. Privalov PL, Tiktopulo EI, Venyaminov SY, Griko YV, Makhatadze GI, Khechinashvili NN. J. Mol. Biol. 1989; 205: 737.
4. Sturtevant JM. Ann. Rev. Phys. Chem. 1987; 38: 463–488.
5. Makhatadze GI, Kim KS, Woodward C, Privalov PL. Prot. Sci. 1993; 2: 2028.
6. Makhatadze GI. Heat capacities of amino acids, peptides and proteins. Biophys. Chem. 1998; 71: 133–156.
7. Privalov PL, Makhatadze GI. J. Mol. Biol. 1990; 213: 385.
8. Privalov PL, Makhatadze GI. J. Mol. Biol. 1992; 224: 715–723.
9. Richardson JM, McMahon KW, MacDonald CC, Makhatadze GI. Biochemistry 1999; 38: 12869–12875.
10. Richardson JM, Makhatadze GI. Temperature dependence of the thermodynamics of helix-coil transition. J. Mol. Biol. 2004; 335: 1029–1037.
11. Makhatadze GI, Medvedkin VN, Privalov PL. Biopolymers 1990; 30: 1001–1010.
12. Durchschlag H. In: Hinz H-J, editor. Thermodynamic Data for Biochemistry and Biotechnology. New York: Springer-Verlag; 1986. p 45–128.
13. Lee BK, Richards FM. J. Mol. Biol. 1971; 55: 379–400.
14. Miller S, Janin J, Lesk AM, Chothia C. J. Mol. Biol. 1987; 196: 641–656.
15. Wesson L, Eisenberg D. Protein Sci. 1992; 1: 227–235.
16. Oobatake M, Ooi T. Prog. Biophys. Mol. Biol. 1993; 59: 237–284.
17. Makhatadze GI, Privalov PL. Adv. Protein Chem. 1995; 47: 307.
18. Makhatadze GI, Privalov PL. J. Mol. Biol. 1990; 213: 375.
19. Izatt RM, Christensen JJ. In: Fasman GD, editor. The CRC Handbook of Biochemistry and Molecular Biology, Physical and Chemical Data Boca Raton, FL: CRC Press 1976. p 151–269.
20. Zamyatnin AA. Prog. Biophys. Mol. Biol. 1972; 24: 107–123.
21. Hutchens JO, Cole AG, Stout JW. J. Am. Chem. Soc. 1960; 82: 4813.
22. Cole AG, Hutchens JO, Stout JW. J. Phys. Chem. 1963; 67: 2245.
23. Hutchens JO, Cole AG, Robie RA, Stout JW. J. Biol. Chem. 1963; 238: 2407.
24. Hutchens JO, Cole AG, Stout JW. J. Biol. Chem. 1964; 239: 591.
25. Hutchens JO, Cole AG, Stout JW. J. Biol. Chem. 1969; 244: 33.
26. Hutchens JO, Cole AG, Stout JW. J. Phys. Chem. 1963; 67: 1128.
27. Cole AG, Hutchens JO, Stout JW. J. Phys. Chem. 1963; 67: 1852.
28. Hutchens JO, Cole AG, Stout JW. J. Biol. Chem. 1964; 239: 4194.
29. Roles KA, Wunderlich B. Biopolymers 1991; 31: 477.
30. Roles KA, Xenopoulos A, Wunderlich B. Biopolymers 1993; 33: 753.
31. Roles KA, Wunderlich B. J. Polym. Sci. Part B Polym. Phys. 1993; 31: 279.
32. Hutchens JO, Cole AG, Stout JW. J. Biol. Chem. 1969; 244: 26.
33. Mrevlishvili GM. In: Hinz H-J, editor Thermodynamic Data for Biochemistry and Biotechnology. New York: Springer-Verlag; 1986 p 148.
34. Haly AR, Snaith JW. Biopolymers 1971;10:1681.
35. Haly AR, Snaith JW. Biopolymers 1968; 6:1355.
36. Steif C, Weber P, Hinz HJ, Flossdorf J, Cesareni G, Kikkinidis M, Biochemistry 1993; 32: 3867–3876.
37. Viguera AR, Martinez JC, Filimonov VV, Mateo PL, Serrano L, Biochemistry 1994; 33: 2142.
38. Jackson SE, Fersht AR, Biochemistry 1991; 30:10428–10435.
39. Bae SJ, Sturtevant JM, Biophys. Chem. 1995; 55: 247–252.
40. Alexander P, Fahnestock S, Lee T, Orban J, Bryan P, Biochemistry 1992; 31: 3597–3603.
41. Renner M, Hinz HJ, Scharf M, Engels JW, J. Mol. Biol. 1992; 223:769.
42. Wintrode PL, Makhatadze GI, Privalov PL, Proteins: Struct. Func. Gen. 1994;18: 246.
43. Yu Y, Makhatadze GI, Pace N, Privalov PL, Biochemistry 1994; 33: 3312.
44. Johnson CM, Cooper A, Stockley PG, Biochemistry 1992; 31: 9717–9724.
45. Makhatadze GI, Privalov PL, J. Mol. Biol. 1993; 232: 639–659.
46. Privalov PL, Makhatadze GI, J. Mol. Biol. 1993; 232: 660–679.
47. Griko YV, Makhatadze GI, Privalov PL, Hartley RW, Protein Sci. 1994; 3: 669.
48. Makhatadze GI, Clore GM, Gronenborn AM, Privalov PL, Biochemistry 1994; 33: 9327.
49. Kitamura S, Sturtevant JM, Biochemistry 1989; 28: 3788–3792.
50. Privalov PL, Gill SJ, Adv. Protein Chem. 1988; 39:191–234.

CHAPTER 9

Heat Capacities of Polymers

Jianye Wen

ALZA Corporation, 1900 Charleston Road, Mountain View, CA 94039

9.1 INTRODUCTION

The heat capacity of a substance can be defined as the amount of heat required to change its temperature by one degree. A more useful quantity is specific heat capacity, which is the amount of heat required to change the temperature of one unit mass of a material by one degree. Heat capacity is a fundamental property of any material. It is a macroscopic parameter that can be linked to molecular structure and vibrational motions at microscopic level [1].

Heat capacity under constant pressure (C_p) is defined as the heat quantity which is required to increase the temperature of the unit mass of a material by 1 K or 1°C under constant pressure. It is given by the following equation:

$$C_p = \Delta Q/m\Delta T \quad (\text{unit: J/(g K)}), \tag{9.1}$$

where ΔQ is the required heat quantity (in Joules), m is the mass of the sample (in grams or kilograms), ΔT is the temperature increase from T_1 to T_2 (in degrees Celsius or Kelvins). The molar heat capacity under constant pressure is defined as that heat quantity which is required to heat the unit mole of a material through 1 K or 1°C under constant pressure (in J/(mol K)). The experimental heat capacities are measured at constant pressure. However, in order to link heat capacity with the vibrational spectrum, C_p must first be converted to the heat capacity at constant volume.

At constant volume, heat capacity can be defined as follows;

$$C_v = \Delta Q/m\Delta T \quad (\text{unit: J/(g K)}). \tag{9.2}$$

The relationship between two heat capacities is

$$C_p - C_v = V\alpha^2 T/K_T \tag{9.3}$$

where α is the thermal expansion coefficient and K_T is the isothermal bulk modulus.

Heat capacity is a fundamental property of any material. It can be measured by adiabatic calorimetry (0–100 K), differential scanning calorimetry (DSC) (above 100 K), and some other techniques [2–4]. Theoretical interpretation of heat capacity has been carried out by various researchers through analysis based on the separation of the vibrational spectrum into group and skeletal vibrations as well as normal mode and their dispersion analysis [5–8]. The table in this chapter contains the heat capacity data in the literature for selected polymers. The heat capacity for any given polymer is a temperature-dependent quantity. Due to the space limitations, the heat capacity values at selected temperatures are listed in this table for the selected polymers. Temperatures are chosen such that at least two data points are included in both the glassy and rubbery regions. A crude extrapolation could be used to compare experimental data at other temperatures. The specific heat increment at T_g, ΔC_p, is also given for the selected polymers. Readers can find more detailed information about ΔC_p from the original references. Since heat capacity also depends on the state of the polymer, the state of the polymer is specified by the following abbreviations whenever possible:

a = amorphous; c = crystalline; s = solid;
m = melt; sc = semicrystalline; g = glassy.

The description of the theory of heat capacity and the application of heat capacity measurements have been given by Wunderlich and other researchers [2,3–17]. The most comprehensive and updated heat capacity data are collected in the ATHAS data bank (Advanced THermal AnalysiS) which has been developed over the last 25 years by Wunderlich (Chemistry Department, The University of Tennessee), and coworkers.

TABLE 9.1. *Heat capacities of selected polymers.*

Polymer	Abbreviations	Molecular[a] weight (g/mol)	T_g (K)	Temperature (K)	C_p[b] (kJ/(kg K))	C_p[b] (J/(mol K))	ΔC_p[c] (J/(mol K))	Ref.
1. Main-chain carbon polymers								
Poly(acrylics)								
Poly(*iso*-butyl acrylate)	PiBA	128.17	249	220	1.2156	155.80	36.60	[18]
				240	1.3365	171.30		
				300	1.8108	232.09		
				500	2.3388	299.77		
Poly(*n*-butyl acrylate)	PnBA	128.17	218	80	0.5598	71.75	45.40	[18]
				180	1.0632	136.27		
				300	1.8201	233.28		
				440	2.1803	279.45		
Poly(ethyl acrylate)	PEA	100.12	249	90	0.5792	57.99	45.60	[18]
				200	1.0301	103.13		
				300	1.7867	178.88		
				500	2.2189	222.16		
Poly(methyl acrylate)	PMA	86.09	279	100	0.6154	52.98	42.30	[18]
				200	0.9816	84.51		
				300	1.765	151.99		
				500	2.143	184.49		
Poly(dienes)								
1,4-Poly(butadiene)	PBD	54.09						
cis-			171	50	0.3694	19.98	29.10	[19,20]
				150	0.8967	48.50		
				300	1.960	106.00		
				350	2.214	114.90		
trans-			180	50	0.3465	18.74	28.20	[19,20]
				150	0.9057	48.99		
				300	NA	NA		
				500	2.616	141.50		
Poly(1-butene)	PB	56.11	249	100	0.6733	37.78	23.06	[19]
				200	1.2190	68.40		
				300	2.086	117.02		
				600	3.071	172.31		
Poly(1-butenylene)	PBUT	55.10						
cis-			171	30	0.2140	11.79	28.91	[3,19,20]
				130	0.7775	42.838		
				300	1.924	106.03		
				450	2.409	132.73		
trans-			190	30	0.1761	9.704	26.48	[3,19,20]
				130	0.7898	43.516		
				300	1.924	106.03		
				450	2.409	132.73		
Poly(alkenes)								
Poly(ethylene)	PE	14.03	252	100	0.674	9.45 (c)	10.1	[21]
				200	1.110	15.57		
				300	1.555	21.81 (s)		
					2.202	30.89 (m)		
				600	3.127	43.87		
Poly(1-hexene)	PHE	84.16	223	100	0.7020	59.08 (a)	25.1	[19]
				200	1.3319	112.09		
				250	1.903	160.18 (a)		
				290	2.079	174.98 (a)		

TABLE 9.1. *Continued.*

Polymer	Abbreviations	Molecular[a] weight (g/mol)	T_g (K)	Temperature (K)	C_p[b] (kJ/(kg K))	C_p[b] (J/(mol K))	ΔC_p[c] (J/(mol K))	Ref.
Poly(isobutene)	PiB	56.11	200	50	0.2440	13.69 (a)	22.29	[19]
				150	0.8660	48.59		
				300	1.962	110.09 (a)		
				380	2.311	129.66		
Poly(2-methylbutadiene)	PMBD	68.12						
cis-			200	50	0.3573	24.34	30.87 (a)	[19]
				150	0.9025	61.48		
				300	1.911	130.20		
				360	2.216	144.80		
Poly(4-methyl-1-pentene)	P4MPE	84.16	303	80	0.5610	47.21	33.7 (a)	[19]
				180	1.090	91.75		
				250	1.4449	121.60		
				300	1.728	145.40		
Poly(1-pentene)	PPE	70.14	233	200	1.253	87.90	27.03 (a)	[19]
				220	1.338	93.82		
				300	2.058	144.34		
				470	2.770	194.32		
Poly(propylene)	PP	42.08	260	100	0.6238	26.25 (c)	17.37	[22]
				200	1.132	47.63 (c)		
				300	1.622	68.24 (s)		
					2.099	88.34 (m)		
				600	3.178	133.73 (a)		
			Poly(methacrylics)					
Poly(*n*-butyl methacrylate)	PnBMA	142.20	293	80	0.5472	77.81	29.70	[18]
				200	1.1557	164.34		
				300	1.8524	263.41		
				450	2.3673	336.63		
Poly(*i*-butyl methacrylate)	PiBMA	142.20	326	230	1.2229	173.90	39.00	[18]
				300	1.5710	223.40		
				350	2.0190	287.10		
				400	2.1127	300.43		
Poly(ethyl methacrylate)	PEMA	114.15	338	80	0.5155	58.84	31.70	[18]
				300	1.4666	167.42		
				350	1.9489	222.47		
				380	2.0462	233.57		
Poly(hexyl methacrylate)	PHMA	170.25	268	270	1.8264	310.77	—	[18]
				300	1.9091	324.83		
				420	2.2396	381.06		
Poly(methacrylic acid)	PMAA	86.09	—	100	0.5248	45.18	—	[18]
				200	0.9456	81.41		
				300	1.307	112.50		
Poly(methacrylamide)	PMAM	85.11	—	100	0.5904	50.25	—	[18]
				200	1.032	87.81		
				300	1.395	118.70		
Poly(methyl methacrylate)	PMMA	100.12	378	100	0.5742	57.49	33.5	[18]
				300	1.3755	137.72		
				400	2.0766	207.91		
				550	2.4323	243.52		
			Poly(styrenes)					
Poly(styrene)	PS	104.15	373	100	0.4548	47.37 (g)	30.7 (a)	[23]
				300	1.2230	127.38		
					1.2730	132.58		[4]

TABLE 9.1. *Continued.*

Polymer	Abbreviations	Molecular[a] weight (g/mol)	T_g (K)	Temperature (K)	C_p[b] (kJ/(kg K))	C_p[b] (J/(mol K))	ΔC_p[c] (J/(mol K))	Ref.
				400	1.9322	201.24		
				600	2.4417	254.30		
—, α-methyl	PαMS	118.18	441	100	0.4712	55.69	25.3	[19]
				300	1.2752	150.70 (g)		
				460	2.1868	258.44		
				490	2.3331	275.72		
—, *p*-bromo-	PBS	183.05	410	300	0.79650	145.800	31.9	[3,24]
				350	0.92349	169.045		
				420	1.2651	231.582		
				550	1.4641	267.995		
—, *p*-chloro-	PCS	138.60	406	300	1.0229	141.780	31.1	[3,24]
				350	1.19848	166.110		
				410	1.6331	226.345		
				550	1.9134	265.195		
—, *p*-fluoro-	PFS	122.14	384	130	0.47611	58.152	33.3	[3,24]
				200	0.62048	75.786		
				300	0.93079	113.687		
				380	1.2672	154.773		
—, *p*-iodo-	PIS	230.05	424	300	0.67607	155.53	37.9	[3,24]
				400	0.89102	204.980		
				430	1.1145	256.41		
				550	1.2570	289.17		
—, *p*-methyl-	PMS	118.18	380	300	1.2743	150.600	34.6	[3,24]
				350	1.4917	176.290		
				390	1.9449	229.846		
				500	2.2766	269.05		
Poly(vinyl halides) and poly(vinyl nitriles)								
Poly(acrylonitrile)	PAN	53.06	378	100	0.5695	30.22	—	[18]
				200	0.9286	49.27		
				300	1.297	68.83		
				370	1.624	86.16		
Poly(chlorotrifluoroethylene)	PC3FE	116.47	325	80	0.2787	32.46	—	[19]
				200	0.6257	72.87		
				300	0.85945	100.10		
				320	0.90667	105.60		
Poly(tetrafluoroethylene)	PTFE	50.01	240	100	0.3873	19.37	7.82	[3,19,25]
				200	0.6893	34.47		
				300	0.9016	45.09 (s)		
					1.028	51.42 (m)		
				700	1.454	72.69		
Poly(trifluoroethylene)	P3FE	82.02	304	100	0.4049	33.21	21.00	[19]
				200	0.7128	58.46		
				300	1.078	88.40		
Poly(vinyl chloride)	PVC	62.50	354	100	0.4291	26.82 (g)	19.37 (a)	[19]
				300	0.9496	59.35 (g)		
				360	1.457	91.08		
				380	1.569	98.05		
Poly(vinylidene chloride)	PVC2	96.95	255	100	0.3745	36.31	70.26	[19]
				200	0.5932	57.51		
				250	0.7115	68.98		
				300	NA	NA		
Poly(vinylidene fluoride)	PVF2	64.03	233	100	0.4435	28.40	22.80	[19]

TABLE 9.1. *Continued.*

Polymer	Abbreviations	Molecular[a] weight (g/mol)	T_g (K)	Temperature (K)	C_p[b] (kJ/(kg K))	C_p[b] (J/(mol K))	ΔC_p[c] (J/(mol K))	Ref.
				150	0.6185	39.60		
				230	0.8918	57.10		
				250	0.7856	50.30		
				300	NA	NA		
Poly(vinyl fluoride)	PVF	46.04	314	100	0.5204	23.96	17.80 (a)	[19]
				200	0.8692	40.02		
				300	1.301	59.91		
				310	1.353	62.29		
			Others					
Poly(*p*-phenylene)	PPP	76.10	—	80	0.3708	28.22 (sc)	—	[26,27]
				150	0.58135	44.241 (sc)		
				250	0.92926	70.717 (sc)		
				300	1.117	85.040 (sc)		
Poly(vinyl acetate)	PVAc	86.09	304	80	0.3230	27.81	53.7	[19]
				300	1.183	101.86		
				320	1.8409	158.48		
				370	1.898	163.37		
Poly(vinyl alcohol)	PVA	44.05	358	60	0.2674	11.78	—	[19]
				150	0.7187	31.66		
				250	1.185	52.21		
				300	1.546	68.11		
Poly(vinyl benzoate)	PVBZ	148.16	347	190	0.71808	106.39	69.5	[19]
				300	1.1025	163.35		
				400	1.8390	272.47		
				500	2.0333	301.25		
Poly(*p*-xylylene)	PPX	104.15	286	220	0.91445	95.241 (sc)	37.6 (a)	[3,28]
				250	1.0576	110.149 (sc)		
				300	1.3022	135.622 (sc)		
				410	1.8686	194.619 (sc)		
			2. Main-chain heteroatom polymers					
			Poly(amides)					
Poly(iminoadipoy-liminododecamethylene)	Nylon 612	310.48	319	230	1.2296	381.78	214.8 (a)	[3,29,30]
				300	1.5926	494.48		
				400	2.4842	771.30		
				600	3.1596	980.986		
Poly(iminoadipoy-liminohexamethylene)	Nylon 66	226.32	323	230	1.1139	252.10	145.0 (a)	[31]
				300	1.4638	331.30		
				400	2.3794	538.50		
				600	2.793	632.1		
Poly(iminohexamethylene-iminoazelaoyl)	Nylon 69	268.40	331	230	1.1980	321.53	—	[3,29,30]
				300	1.5204	408.080		
				400	2.3840	639.874		
				600	3.0720	824.534		
Poly(iminohexamethylene-iminosebacoyl)	Nylon 610	282.43	323	230	1.2069	340.870	—	[3,29,30]
				300	1.5644	441.820		
				400	2.3975	677.125		
				600	3.1041	876.685		

TABLE 9.1. *Continued.*

Polymer	Abbreviations	Molecular[a] weight (g/mol)	T_g (K)	Temperature (K)	C_p[b] (kJ/(kg K))	C_p[b] (J/(mol K))	ΔC_p[c] (J/(mol K))	Ref.
Poly(imino-(1-oxohexamethylene))	Nylon 6	113.16	313	70	0.4400	49.78	93.6 (a)	[31]
				300	1.5023	170.00		
				400	2.5186	285.00		
				600	2.7881	315.50		
Poly(imino-1-oxododecamethylene)	Nylon 12	197.32	314	230	1.2874	254.020	—	[3,29,30]
				300	1.6952	334.49		
				400	2.4709	487.565		
				600	3.2786	646.945		
Poly(imino-1-oxoundecamethylene)	Nylon 11	183.30	316	230	1.2996	238.21	—	[3,29,30]
				300	1.7507	320.91		
				400	2.4567	450.314		
				600	3.2449	594.794		
Poly(methacrylamide)	PMAM	85.11	—	100	0.5904	50.25	—	[18]
				200	1.032	87.81		
				250	1.214	103.30		
				300	1.395	118.70		
Poly(amino acids)								
Poly(L-alanine)	PALA	71.08	—	230	1.102	78.33	—	[32]
				300	1.315	93.47		
				350	1.498	106.5		
				390	1.622	115.3		
Poly(L-asparagine)	PASN	114.10	—	230	0.958	109.3	—	[33]
				300	1.218	139.0		
				350	1.397	159.4		
				390	1.537	175.4		
Polyglycine	PGLY	57.05	—	230	0.929	53.00	—	[32]
				300	1.170	66.75		
				350	1.356	77.36		
				390	1.516	86.49		
Poly(L-methionine)	PMET	131.19	—	220	0.936	122.8	—	[33]
				300	1.347	176.7		
				350	1.595	209.3		
				390	1.768	232.0		
Poly(L-phenylalanine)	PPHE	147.18	—	220	0.830	122.1	—	[33]
				300	1.153	169.7		
				350	1.382	203.4		
				390	1.548	227.8		
Poly(L-serine)	PSER	87.08	—	220	0.959	83.50	—	[33]
				300	1.297	112.9		
				350	1.541	134.2		
				390	1.747	152.1		
Poly(L-valine)	PVAL	99.13	—	230	1.213	120.2	—	[32]
				300	1.455	144.2		
				350	1.647	163.3		
				390	1.802	178.6		
Poly(esters)								
Poly(butylene adipate)	PBAD	200.24	199	80	0.54302	108.734	140.046	[26,27]
				150	0.87449	175.107		
				300	1.9706	394.595		
				450	2.2147	443.470		

TABLE 9.1. *Continued.*

Polymer	Abbreviations	Molecular[a] weight (g/mol)	T_g (K)	Temperature (K)	C_p[b] (kJ/(kg K))	C_p[b] (J/(mol K))	ΔC_p[c] (J/(mol K))	Ref.
Poly(butylene terephthalate)	PBT	220.23	248	150	0.61075	134.505 (sc)	106.77	[3]
			320	200	0.82262	181.166	77.812	
				300	1.6134	355.311		
				400	1.8187	400.532		
				570	2.1678	477.407		
Poly(ethylene terephthalate)	PET	192.16	342	100	0.4393	84.42	77.8 (a)	[3,34,31]
				300	1.172	225.2		
				400	1.8203	349.80		
				600	2.1136	406.15		
Poly(tridecanolactone)	PTDL	212.34	237	185	0.95	202	—	[35]
				260	1.45	308		
				300	1.79	380		
				395	2.15	457		
Poly(trimethylene adipate)	PTMA	186.21	—	300	NA	NA	—	[3,36]
				310	1.8710	348.401		
				330	1.9137	356.341		
				360	1.9776	368.252		
Poly(trimethylene terephthalate)	PTT	206.2	331	180	0.73	150.53	—	[37]
				250	0.97	201.29		
				350	1.54	318.41		
				400	1.79	368.75		
Poly(trimethylene succinate)	PTMS	158.15	—	300	NA	NA	—	[3,36]
				310	1.8401	291.014		
				330	1.8721	296.074		
				360	1.9201	303.664		
Poly(γ-butyrolactone)	PBL	86.09	214	100	0.6012	51.760	57.4	[3,31,38]
				210	1.024	88.170		
				300	1.810	155.858 (m)		
				350	1.870	161.031 (m)		
Poly(ε-caprolactone)	PCL	114.15	209	100	0.62322	71.140	59.5	[3,31,38,39]
				200	1.0243	116.923		
				300	1.4229	162.42		
					1.8138	207.04 (s)		
				350	1.9415	221.62 (m)		
Poly(glycolide)	PGL	58.04	318	100	0.5250	30.470	44.4	[3,31,38,39]
				300	1.127	65.42		
				400	1.999	116.039 (m)		
				550	2.098	121.75 (m)		
Poly(β-propiolactone)	PPL	72.07	249	100	0.5568	40.130	50.4	[3,31,38,39]
				240	1.044	75.220		
				300	1.878	135.354 (m)		
				400	2.081	149.994 (m)		
Poly(ethylene oxalate)	PEOL	116.07	306	100	0.49910	57.930	56.23	[3,40,41]
				300	1.1175	129.705		
				320	1.6395	190.295 (m)		
				360	1.7012	197.456 (m)		

TABLE 9.1. *Continued.*

Polymer	Abbreviations	Molecular[a] weight (g/mol)	T_g (K)	Temperature (K)	C_p[b] (kJ/(kg K))	C_p[b] (J/(mol K))	ΔC_p[c] (J/(mol K))	Ref.
Poly(ethylene sebacate)	PES	228.29	245	120	0.66292	151.338 (s)	154.059	[3,31]
				200	0.95269	217.490 (sc)		
				300	1.9245	439.34 (m)		
				410	2.1923	500.500 (m)		
			Poly(oxides)					
Poly(oxy-2,6-dimethyl-1, 4-phenylene)	PPO	120.15	482	80	0.4418	53.08	31.9 (a)	[42]
				300	1.2459	149.70		
				500	2.1232	255.10		
				570	2.2555	271.00		
Poly(oxyethylene)	POE	44.05	206	100	0.6114	26.93 (s)	38.96	[42,43]
				200	0.9507	41.88 (s)		
				300	1.257	55.36 (s)		
					1.995	87.89 (m)		
				450	2.223	97.91		
Polyoxymethylene	POM	30.03	190	100	0.5554	16.68 (s)	27.47	[42,43]
				150	0.7266	21.82 (s)		
				300	1.283	38.52 (s)		
					1.920	57.67 (m)		
				600	2.292	68.83		
Poly(oxy-1,4-phenylene)	POPh	92.10	358	300	1.185	109.10 (s)	21.4 (a)	[42]
				350	1.367	125.90 (s)		
				400	1.694	156.00 (m)		
				600	2.003	184.50 (m)		
Poly(oxypropylene)	POPP	58.08	198	80	0.537	31.21 (s)	32.15	[42]
				180	1.014	58.89 (s)		
				300	1.915	111.23 (m)		
				370	2.105	122.27 (m)		
Poly(oxytetramethylene)	PO4M	72.11	189	80	0.5465	39.41 (s)	46.49	[42]
				180	1.033	74.52 (s)		
				300	1.985	143.15 (m)		
				340	2.081	150.04 (m)		
Poly(oxytrimethylene)	PO3M	58.08	195	80	0.5095	29.59 (s)	50.73	[42]
				180	0.9464	54.97 (s)		
				300	1.373	79.73 (s)		
					2.055	119.34 (m)		
				330	2.107	122.37		
			Others					
Poly(diethyl siloxane)	PDES	102.21	135	50	0.38820	39.678 (sc)	30.189	[3,44–47]
				100	0.73995	75.630 (sc)		
				300	1.6184	165.417 (m)		
				360	1.7525	179.125 (m)		
Poly(dimethyl itaconate)	PDMI	158.16	377	110	0.59700	94.419 (a)	54.23	[48]
				300	1.3183	208.507 (a)		
				400	1.9282	304.968 (m)		
				450	2.0009	316.463 (m)		
Poly(dimethyl siloxane)	PDMS	74.15	146	50	0.3672	27.23	27.7 (a)	[44,49,50]
				100	0.7131	52.88		
				300	1.591	118.0		
				340	1.657	122.9		
Poly(4-hydroxybenzoic acid)	PHBA	120.11	434	170	0.58914	70.762	34	[51]
				300	1.0207	122.60		
				400	1.3662	164.091		
				434	1.4686	176.399		

TABLE 9.1. *Continued.*

Polymer	Abbreviations	Molecular[a] weight (g/mol)	T_g (K)	Temperature (K)	C_p[b] (kJ/(kg K))	C_p[b] (J/(mol K))	ΔC_p[c] (J/(mol K))	Ref.
Poly(lactic acid)	PLA	72.07	332.5	200	0.97	69.75	—	[52]
				300	1.32	95.30		
				400	2.09	150.56		
				470	2.16	155.77		
Poly(4,4′-isopropylidene diphenylenecarbonate)	PC	254.27	418	100	0.43143	109.70 (s)	48.5	[44]
				300	1.207	306.8 (s)		
				450	1.9570	497.60 (m)		
				560	2.207	561.3 (m)		
Poly(oxy-1,4-phenylene-oxy-1, 4-phenylene-carbonyl-1, 4-phenylene)	PEEK	288.30	419	300	NA	NA	78.1	[53–55]
				419	1.789	515.8		
				500	1.928	555.9		
				750	2.358	679.8		
Poly(oxy-1,4-phenylene-sulphonyl-1, 4-phenylene-oxy-1,4-phenylene-(1-methylidene)-1, 4-phenylene)	PBISP	442.54	458.5	200	0.75870	335.754	102.482	[3,56,57]
				300	1.1161	493.934		
				500	1.9436	860.132		
				540	2.0251	896.19		
Poly(*p*-phenylenebenzobisoxazole)	PBO	234.21	—	10	0.01	2.69	—	[58]
				100	0.32	76.00		
				200	0.64	148.82		
				300	0.97	226.84		
Poly(1,4-phenylene sulphonyl)	PAS	140.16	492.6	150	0.597	83.7	—	[57]
				300	1.009	141.4		
				500	1.571	220.2		
				620	1.642	230.1		
Poly(1-propene sulphone)	P1PS	106.14	10	0.01580	1.677	—		[59]
				30	1.165	123.7		
Trigonal selenium	SEt	78.96	303.4	100	0.2304	18.19 (s)	13.29	[60]
				300	0.318	25.11		
				400	0.3338	26.36 (s)		
					0.4777	37.72 (m)		
				600	0.4343	34.29		

[a] This is the molecular weight of the repeat unit of the polymer.
[b] Except the data for PTDL and P1PS, C_p data reported in the unit of kJ/(kg K) were converted from the C_p data in J/(mol K) which were directly cited from the literature, using the molecular weight of the repeat unit.
[c] Specific heat increment at T_g.

REFERENCES

1. A. Einstein, Ann. Physik, **22**, 180, 800, 1907.
2. B. Wunderlich, "Thermal Analysis", Academic Press, Inc., San Diego, CA, 1990.
3. M. Varma-Nair and B. Wunderlich, J. Phys. Chem. Ref. Data, **20**, 349, 1991.
4. Y. Agari, A. Ueda, and S. Nagai, J. Polym. Sci., Polym. Phys. Ed., **33**, 33, 1995.
5. B. Wunderlich, Thermochimica, **300**, 43, 1997.
6. B. Wunderlich, Pure Appl. Chem., **67**, 1019, 1995.
7. P. Tandon, V. D. Gupta, O. Prasad, S. Rastogi, and V. P. Gupta, J. Polym. Sci.: Part B: Polym. Phys., **35**, 2281, 1997.
8. R. Pan, M. Y. Cao, and B. Wunderlich, "Polymer Handbook", 3rd ed., J. Brandrup and E. H. Immergut (eds.), Wiley-Interscience, New York, 1989, VI 371.
9. R. Agarwal, R. Misra, P. Tandon, and V. D. Gupta, Polymer, **45**, 5307, 2004.
10. B. Wunderlich, S. Z. D. Cheng, and K. Loufakis, "Encyclopedia of Polymer Science and Engineering", Vol. 16, 2nd ed., Wiley & Sons Limited, New York, 1989, p. 767.
11. W. W. Wundlandt, "Thermal Analysis", 3rd ed., Wiley & Sons, Inc., New York, 1985.
12. W. Reese, J. Macromol. Sci. Chem., **A3**, 1257, 1969.
13. H. E. Bair, "ASTM STP 1249", R. J. Seyler (ed.), American Society for Testing and Materials, Philadephia, 1994, pp. 50–74.
14. H. Baur and B. Wunderlich, Adv. Polym. Sci., **7**, 151, 1970.
15. T. Hatakeyama, H. Kanetsuna, and S. Ichihara, Thermochim. Acta, **146**, 311, 1989.
16. Y. Jin and B. Wunderlich, Thermochim. Acta, **226**, 155, 1993.
17. A. Boller, Y. Jin, and B. Wunderlich, J. Therm. Anal., **42**, 307, 1994.
18. U. Gaur, S. F. Lau, B. B. Wunderlich, and B. Wunderlich, J. Phys. Chem. Ref. Data, **11**, 1065, 1982.
19. U. Gaur, S. F. Lau, B. B. Wunderlich, and B. Wunderlich, J. Phys. Chem. Ref. Data, **12**, 29, 1983.
20. J. Grebowicz, W. Avcock, and B. Wunderlich, Polymer, **27**, 575, 1986.
21. U. Gaur and B. Wunderlich, J. Phys. Chem. Ref. Data, **10**, 119, 1981.
22. U. Gaur and B. Wunderlich, J. Phys. Chem. Ref. Data, **10**, 1051, 1981.
23. U. Gaur and B. Wunderlich, J. Phys. Chem. Ref. Data, **11**, 313, 1982.
24. L. H. Judovits, R. C. Bopp, U. Gaur, and B. Wunderlich, J. Polym. Sci., Polym. Phys. Ed., **24**, 2725, 1986.
25. S. F. Lau, H. Suzuki, and B. Wunderlich, J. Polym. Sci., Polym. Phys. Ed., **22**, 379, 1984.
26. I. B. Rabinnovich, V. P. Nistratov, A. G. Babinkov, K. G. Shvetsova, and V. N. Larina, Vysokomol. Soedin, **A26**, 743, 1984.
27. I. B. Rabinnovich, V. P. Nistratov, A. G. Babinkov, K. G. Shvetsova, and V. N. Larina, Polym. Sci., U.S.S.R., **26**, 826, 1984.
28. D. E. Kirkpatrick, L. Judovits, and B. Wunderlich, J. Polym. Sci., Polym. Phys. Ed., **24**, 45, 1986.
29. A. Xenopoulos and B. Wunderlich, Polymer, **31**, 1260, 1990.
30. A. Xenopoulos and B. Wunderlich, J. Polym. Sci., Polym. Phys. Ed., **28**, 2271, 1990.
31. U. Gaur, S. F. Lau, B. B. Wunderlich, and B. Wunderlich, J. Phys. Chem. Ref. Data, **12**, 65, 1983.
32. K. A. Roles, A. Xenopoulos, and B. Wunderlich, Biopolymers, **31**, 477, 1992.
33. K. A. Roles, A. Xenopoulos, and B. Wunderlich, Biopolymers, **31**, 753, 1992.
34. S. J. Collocot, J. Phys. Chem., Solid State Phys., **20**, 2995, 1987.
35. P. Skoglund and Å. Fransson, J. Polym. Sci., Polym. Phys. Ed., **32**, 1999, 1994.
36. R. Pan, "Heat Capacities of Linear Macromolecules", PhD Thesis, Dept. of Chem., Rensselaer Polytechnic Inst., Troy, NY, 1987.
37. M. Pyda, A. Boller, J. Grebowicz, H. Chuah, B. V. Lebedev, B. Wunderlich, J. Polym. Sci.: Part B: Polym. Phys., Vol. 36, 2499–2511, 1998.
38. B. Lebedev and A. Yevstropov, Makromol. Chem., **185**, 1235, 1984.
39. R. Pan, Master Thesis, Dept. of Chem., Rensselaer Polytechnic Inst., Troy, NY, 1986.
40. B. V. Lebedev, T. G. Kulajina, Y. B. Lyudvig, and T. N. Ovchinnkova, Vysokomol. Soedin, **A24**, 1490, 1982.
41. B. V. Lebedev, T. G. Kulajina, Y. B. Lyudvig, and T. N. Ovchinnkova, Polym. Sci. USSR, **24**, 1695, 1982
42. U. Gaur and B. Wunderlich, J. Phys. Chem. Ref. Data, **10**, 1001, 1981.
43. H. Suzuki and B. Wunderlich, J. Polym. Sci., Polym. Phys. Ed., **23**, 1671, 1985.
44. U. Gaur, S. F. Lau, and B. Wunderlich, J. Phys. Chem. Ref. Data, **12**, 91, 1983.
45. B. V. Lebedev, T. G. Kulagina, U. S. Svistunov, V. S. Papkov, and A. A. Zhdanov, Vysokomol. Soedin, **A26**, 2476, 1984.
46. B. V. Lebedev, T. G. Kulagina, U. S. Svistunov, V. S. Papkov, and A. A. Zhdanov, Polym. Sci. USSR, **26**, 2773, 1984.
47. J. P. Wesson, "Mesophase Transitions in Poly(diethyl siloxane)", PhD Thesis, Dept. of Chem., Rensselaer Polytechnic Inst., Troy, NY, 1988.
48. J. M. G. Cowie, I. J. McEwen, and B. Wunderlich, Macromolecules, **16**, 1151, 1983.
49. V. A. Lebedev, N. N. Mukhina, and T. G. Kulagina, K. Vysokomol. Soedin. Ser., **A20**, 1297, 1978.
50. V. A. Turdakin, V. V. Tarasov, and A. K. Mal'tesv, Zh. Fiz. Khim., **50**, 1980, 1976.
51. M. Y. Cao and B. Wunderlich, J. Polym. Sci., Polym. Phys. Ed., **23**, 521, 1985.
52. M. Pyda, R. C. Bopp, and B. Wunderlich, J. Chem. Thermodyn., **36**, 731, 2004.
53. D. J. Kemmish and J. N. Hay, Polymer, **26**, 905, 1985.
54. S. Z. D. Cheng, M.-Y Cao, and B. Wunderlich, Macromolecules, **19**, 1868, 1986.
55. S. Z. D. Cheng and B. Wunderlich, J. Polym. Sci., Polym. Phys. Ed., **24**, 1755, 1986.
56. N. V. Novoselova, L. Y. Tsvetkova, I. B. Rabinovich, E. M. Moseeva, and L. A. Faninskaya, J. Phys. Chem., **59**, 350, 1985.
57. M. Varma-Nair, J. Yimin, and B. Wunderlich, Polymer, **33**, 5272, 1992.
58. K. Saito, Y. Takahashi, M. Sorai, J. Polym. Sci., Part B: Polym. Phys., Vol. 38, 1584–1588, 2000.
59. F. S. Dainton, D. M. Evans, F. E. Hoare, and T. P. Melia, Polymer, **3**, 310, 1962.
60. U. Gaur and B. Wunderlich, J. Phys. Chem. Ref. Data, **10**, 89, 1981.

CHAPTER 10

Thermal Conductivity

Yong Yang

Benjamin Moore and Company, Flanders, NJ 07836

Thermal conductivity of polymers is an important thermal property for both polymer applications and processing. Polymers typically have intrinsic thermal conductivity much lower than those for metals or ceramic materials, and therefore are good thermal insulators. Further enhancement of this thermal insulating quality can be achieved by foaming polymers. In other applications which require higher thermal conductivity, such as in electronic packaging and encapsulations, satellite devices, and in areas where good heat dissipation, low thermal expansion and light weight are needed, polymers reinforced with fillers, organic or inorganic, are becoming more and more common in producing advanced polymer composites for these applications [1–8].

Most polymeric materials are processed and fabricated at elevated temperatures, often above their melting temperatures. This process may be long and expensive because of the low thermal conductivity of polymers. Subsequently, the cooling process or annealing may also be controlled by heat transport properties of polymers, which eventually affect the physical properties of the materials. One example is crystalline polymers, for which the structural and morphological features may be significantly changed with the speed of cooling. Careful consideration in designing polymer processing is vital to achieve desired properties.

Definition. For one-dimensional and rectilinear heat flow, the steady-state heat transfer in polymeric materials can be described by the Fourier's law of heat conduction:

$$q = -k\frac{\mathrm{d}T}{\mathrm{d}x}, \tag{10.1}$$

where q is the heat flux (i.e., the heat transfer rate per unit area normal to the direction of flow), x is the thickness of the material, $\mathrm{d}T/\mathrm{d}x$ is the temperature gradient per unit length, and the proportionality constant k is known as the thermal conductivity.

The units for thermal conductivity k are expressed as W/(m K) in SI units, Btu in./(ft^2 h °F) in English units, and cal/(cm s °C) in cgs units. The corresponding units for heat flux are expressed as W/(m^2), Btu/(ft^2 h), and cal/(cm^2 s), respectively. The conversion factors of units transform for k in these systems are listed in Part XI, Chapter 63.

Polymers and foamed polymers. Temperature, pressure, density of polymer, orientation of chain segments, crystal structures, degree of crystallinity, and many other factors may significantly affect thermal conductivity of polymers [9–18]. Therefore the thermal conductivity values can be varied in literatures for same polymers. In addition, discrepancies also occur for thermal conductivity values obtained using different test methods [19]. The data in the tables in this chapter may be the representative values of thermal conductivity and are not necessarily the absolute ones.

Generally, pure polymers have low thermal conductivities, ranging from 0.1 το 0.6 W/(m K), as listed in Table 10.1. Foaming polymers may further enhance this low thermal conductivity. Polymer foams with lower density have more air and thus have lower thermal conductivity. The cell size of foamed polymers may also have an effect on thermal conductivity. Smaller foam cell size tends to yield lower thermal conductivity. Most foamed polymers have thermal conductivity values in the order of 10^{-2}W/(m K), which is about 10 times less than the same polymers. Table 10.2 is the list of thermal conductivities for common commercial foamed polymers.

The effect of temperature on polymers is of practical importance because most polymers are processed at relatively high temperature and have applications in a wide temperature range. The temperature dependence of thermal conductivity of polymers has been studied from extremely low temperatures at 0.1 K to above melting point [11,13–18,20]. Generally, with increase in temperature, thermal conductivity for amorphous polymers increases gradually

TABLE 10.1. *Thermal conductivity k of polymers.*

Polymer	Temperature (K)	*k* (W/m K)	Reference
Polyamides			
Polyauryllactam (nylon-12)		0.25	[21]
		0.19	[22]
Polycaprolactam (nylon-6)			
Moldings	293	0.24	[19]
Crystalline	303	0.43	[9]
Amorphous	303	0.36	[9]
Melt	523	0.21	[9]
Poly(hexamethylene adipamide) (nylon-6,6)			
Moldings	239	0.24	[19]
Crystalline	303	0.43	[9]
Amorphous	303	0.36	[9]
Melt	523	0.15	[23]
Poly(hexamethylene dodecanediamide)(nylon-6,12)		0.22	[24]
Poly(hexamethylene sebacamide) (nylon-6,10)		0.22	[19]
Polyundecanolactam (nylon-11)		0.23	[21]
Polycarbonates, polyesters, polyethers, and polyketones			
Polyacetal		0.3	[21]
		0.23	[19,24]
Polyaryletherketone	293	0.30	[24]
Poly(butylene terephthalate) (PBT)	293	0.29	[19]
		0.16	[9]
Polycarbonate (Bisphenol A)	293	0.20	[9,19]
Temperature dependence	300–573	*a*	[13]
	150–400	*a*	[14]
Poly(dially carbonate)		0.21	[19]
Poly(2,6-dimethyl-1,4-phenylene ether)		0.12	[22]
Polyester			
Cast, rigid		0.17	[19]
Chlorinated		0.33	[19]
Polyetheresteramide	303	0.24–0.34	[25]
	353	0.20–0.26	[25]
Polyetheretherketone (PEEK)		0.25	[22]
Poly(ethylene terephthalate) (PET)	293	0.15	[19]
Temperature dependence	200–350	*a*	[26,27]
Poly(oxymethylene)	293	0.292	[23]
	293	0.44	[26]
Temperature dependence	100–400	*a*	[26]
Poly(phenylene oxide)			
Molding grade		0.23	[21]
Epoxides			
Epoxy resin			
Casting grade	293	0.19	[19]
Temperature dependence	300–500	0.19–0.34	[28]
Halogenated olefin polymers			
Polychlorotrifluoroethylene	293	0.29	[19]
	311–460	0.146–0.248	[20]
Poly(ethylene–tetrafluoroethylene) copolymer		0.238	[22]
Polytetrafluoroethylene	293	0.25	[19]
	298	0.25	[29]
	345	0.34	[29]
Low temperature dependence	5–20.8	*a*	[20]
Poly(tetrafluoroethylene–hexafluoropropylene)			

TABLE 10.1. *Continued.*

Polymer	Temperature (K)	*k* (W/m K)	Reference
Copolymer(Teflon EEP)		0.202	[23]
Poly(vinyl chloride)			
Rigid	293	0.21	[19]
Flexible	293	0.17	[19]
Chlorinated	293	0.14	[19]
Temperature dependence	103	0.129	[23]
	273	0.158	[23]
	373	0.165	[23]
Poly(vinylidene chloride)	293	0.13	[23]
Poly(vinylidene fluoride)	293	0.13	[19,21]
	298–433	0.17–0.19	[22]
Hydrocarbon polymers			
Polybutene		0.22	[22]
Polybutadiene			
Extrusion grade	293	0.22	[19]
Poly(butadiene–styrene) copolymer (SBR)			
23.5% Styrene content			
Pure gum vulcanizate		0.190–0.250	[9]
Carbon black vulcanizate		0.300	[9]
Polychloroprene (Neoprene)			
Unvulcanized	293	0.19	[9,19]
Pure gun vculcanizate		0.192	[9]
Carbon black vulcanizate		0.210	[9]
Polycyclooctene			
80% *trans* content		0.27	[4]
Poly(1,3-cyclopentylenevinylene) [poly(2-norbornene)]		0.29	[9]
Polyethylene			
Low density		0.33	[19]
Medium density		0.42	[19]
High density		0.52	[19]
Temperature dependence	20–573	*a*	[9,13,20]
Molecular weight dependence		*a*	[20]
Poly(ethylene–propylene) copolymer		0.355	[9]
Polyisobutylene		0.13	[29]
Polyisoprene (natural rubber)			
Unvulcanized		0.13	[9,19]
Pure gum vulcanizate		0.15	[9]
Carbon black vulcanizate		0.28	[9]
Poly(4-methyl-1-pentene)	293	0.167	[22]
Polypropylene	293	0.12	[19]
		0.2	[9]
Temperature dependence		*a*	[15–17]
Polystyrene	273	0.105	[9]
	373	0.128	[9]
	473	0.13	[9]
	573	0.14	[9]
	673	0.160	[22]
Poly(*p*-xylylene) (PPX)		0.12	[22]
Polyimides			
Polyetherimide		0.07	[24]
Polyimide			
Thermoplastic	293	0.11	[19,24]
Thermoset		0.23–0.50	[24]
Temperature dependence	300–500	*a*	[14]

TABLE 10.1. *Continued.*

Polymer	Temperature (K)	k (W/m K)	Reference
Phenolic resins			
Poly(phenol–formaldehyde) resin			
Casting grade		0.15	[19]
Molding grade		0.25	[19]
Poly(phenol–furfural) resin			
Molding grade	293	0.25	[19]
Polysaccharides			
Cellulose			[23]
Cotton		0.071	[23]
Rayon		0.054–0.07	[23]
Sulphite pulp, wet		0.8	[23]
Sulphite pulp, dry		0.067	[23]
Laminated Kraft Paper		0.13	[23]
Alkali cellulose		0.046–0.067	
Different papers	303–333	0.029–0.17	[23]
Cellulose acetate	293	0.20	[19]
Cellulose acetate butyrate	293	0.33	[19]
Cellulose nitriate		0.23	[24]
Cellulose propionate		0.20	[21]
Ethylcellulose		0.21	[30]
Polysiloxanes			
Poly(dimethylsiloxane)	230	0.25	[31]
	290	0.20	[31]
	340	0.20	[31]
	410	0.17	[31]
Poly(methylphenylsiloxance)			
9.5% Phenyl, $d = 1{,}110\,\mathrm{kg/m^3}$	273	0.158	[32]
	323	0.150	[32]
	373	0.144	[32]
48% Phenyl, $d = 1{,}070\,\mathrm{kg/m^3}$	273	0.143	[32]
	323	0.136	[32]
	373	0.127	[32]
62% Phenyl, $d = 1{,}110\,\mathrm{kg/m3}$	273	0.141	[32]
	323	0.137	[32]
	373	0.132	[32]
Polysulfide and polysulfones			
Polyarylsulfone		0.18	[9]
Polyethersulfone		0.18	[9]
Poly(phenylene sulfide)	293	0.29	[21]
	240–310	0.288	[9]
Poly(phenylene sulfone)		0.18	[22]
Udel polysulfone		0.26	[9]
Polyurethanes			
Polyurethane			
Casting resin	293	0.21	[19]
Elastomer	293	0.31	[19]
Vinyl polymers			
Polyacrylonitrile	293	0.26	[19,24]
Poly(acrylonitrile–butadiene) copolymer (NBR)			
35% Acrylonitrile	333	0.251	[9]
	413	0.184	[9]
Poly(acrylonitrile–butadiene–styrene) copolymer (ABS)			
Injection molding grade		0.33	[19]
Poly(acrylonitrile–styrene) copolymer	293	0.18	[9]
Poly(*i*-butyl methacrylate)			
At 0.82 atm		0.13	[18]
Pressure and temperature dependence		*a*	[18]

TABLE 10.1. *Continued.*

Polymer	Temperature (K)	*k* (W/m K)	Reference
Poly(*n*-butyl methacrylate)			
At 0.82 atm		0.45	[18]
Pressure and temperature dependence		*a*	[18]
Poly(butyl methacrylate–triethylene glycol dimethacrylate) copolymer		0.15	[29]
Poly(chloroethylene–vinyl acetate) copolymer	293	0.134	[20]
	325	0.146	[20]
	375	0.218	[20]
Poly(dially phthalate)		0.21	[19]
Poly(ethyl acrylate)	310.9	0.213	[20]
	422.1	0.230	[20]
	533.2	0.213	[20]
Poly(ethyl methacrylate)m			
At 0.82 atm	273	0.175	[18]
Pressure and temperature dependence		*a*	[18]
Poly(ethylene vinyl acetate)		0.34	[33]
Poly(methyl methacrylate)	293	0.21	[19]
Temperature dependence		*a*	[20,34–37]
Poly(methyl methacrylate–acrylonitrile) copolymer		0.18	[21]
Polymer(methyl methacrylate–styrene) copolymer		0.12–0.21	[24]
Poly(vinyl acetate)		0.159	[9]
Poly(vinyl acetate–vinyl chloride) copolymer		0.167	[30]
Poly(vinyl alcohol)		0.2	[9]
Poly(*N*-vinyl carbozole)	293	0.126	[22]
	443	0.168	[22]
Poly(vinyl fluoride)	243	0.14	[9]
	333	0.17	[9]
Poly(vinyl formal)			
Molding grade	293	0.27	[19]

[a]See references citied in column 4.

in the glassy region and decreases slowly or remains constant in the rubbery region. For crystalline polymers, thermal conductivity decreases steadily with the increase in temperature below the melting point. At temperature above the melting point, it behaves in a similar way as amorphous polymers. Some of the values of polymer thermal conductivity measured at various temperatures are listed in Table 10.1. More results on temperature dependence can be found in the references cited.

Thermal conductivity of polymers is highly dependent on polymer chain segment orientation [10,12]. This is because thermal energy transports more efficiently along the polymer chain. Crystalline polymers have highly ordered chain segments, and therefore have higher thermal conductivity than amorphous polymers. Amorphous polymers may exhibit anisotropic thermal transport properties if polymer chains are partially oriented, with thermal conductivity along the chains higher than that perpendicular to the chains.

Reinforced polymers and thermally conductive polymer composites. Polymers are often reinforced with fillers to improve their mechanical, electrical, and thermal properties. The thermal conductivity of filled polymers is primarily determined by the type and amount of fillers used. The thermal properties of the filler, the size, shape, and orientation of filler particles or fibers in polymer matrix, and the percentage of fillers are all important factors that determine the thermal conductivity of reinforced polymers. As shown in Table 10. 3, polymers reinforced with inorganic fillers usually increase their thermal conductivities from a few percent to a few times. The filler percentages listed in Table 10.3 are weight percentages, unless otherwise indicated.

Highly thermal conductive polymer composites can be obtained by using fillers with high thermal conductivity and at high percentages. Thermally conductive polymer composites find wide applications in semiconductor industry such as electronic components encapsulation, in which the heat dissipation of circuit boards becomes more and more important as silicon chips get denser and faster. Other applications of thermally conductive polymer composites

TABLE 10.2. *Thermal conductivity k of foamed polymers.*

Polymer	k (W/m K)	Reference
Poly(acrylonitrile–butadiene) copolymer		
$d = 160$–$400\,\mathrm{kg/m^3}$	0.036–0.043	[9]
Cellulose acetate		
$d = 96$–$128\,\mathrm{kg/m^3}$	0.0450–0.45	[9]
Polychloroprene (neoprene)		
$d = 112\,\mathrm{kg/m^3}$	0.040	[9]
$192\,\mathrm{kg/m^3}$	0.065	[9]
Poly(dimethylsiloxane)		
Sheet, $d = 160\,\mathrm{kg/m^3}$	0.086	[9]
Epoxy		
$d = 32$–$48\,\mathrm{kg/m^3}$	0.016–0.022	[9]
80–$128\,\mathrm{kg/m^3}$	0.035–0.040	[9]
Polyethylene		
Extruded plank		
$d = 35\,\mathrm{kg/m^3}$	0.053	[9]
$64\,\mathrm{kg/m^3}$	0.058	[9]
$96\,\mathrm{kg/m^3}$	0.058	[9]
$144\,\mathrm{kg/m^3}$	0.058	[9]
Sheet, extruded, $d = 43\,\mathrm{kg/m^3}$	0.040–0.049	[9]
Sheet, crosslinked, $d = 26$–$38\,\mathrm{kg/m^3}$	0.036–0.040	[9]
Polyisocyanurate		
$d = 24$–$56\,\mathrm{kg/m^3}$	0.012–0.02	[9]
Polyisoprene (natural rubber)		
$d = 56\,\mathrm{kg/m^3}$	0.036	[9]
$320\,\mathrm{kg/m^3}$	0.043	[9]
Phenolic resin		
$d = 32$–$64\,\mathrm{kg/m^3}$	0.029–0.032	[9]
112–$160\,\mathrm{kg/m^3}$	0.035–0.040	[9]
Polypropylene		
$d = 54$–$96\,\mathrm{kg/m^3}$	0.039	[9]
Polystyrene		
$d = 16\,\mathrm{kg/m^3}$	0.040	[19]
$32\,\mathrm{kg/m^3}$	0.036	[19]
$64\,\mathrm{kg/m^3}$	0.033	[19]
$96\,\mathrm{kg/m^3}$	0.036	[19]
$160\,\mathrm{kg/m^3}$	0.039	[19]
Poly(styrene–butadiene) copolymer (SBR)		
$d = 72\ \mathrm{kg/m^3}$	0.30	[9]
Poly(urea–formaldehyde) resin		
$d = 13$–$19\ \mathrm{kg/m^3}$	0.026–0.030	[9]
Polyurethane		
Air blown, $d = 20$–$70\,\mathrm{kg/m^3}$		
At 0°C	0.033	[38]
At 20°C	0.036	[38]
At 70°C	0.040	[38]
CO_2 blown, $d = 64\,\mathrm{kg/m^3}$, at 20°C	0.016	[19]
20% closed cells, at 20°C	0.033	[19]
90% closed cells, at 20°C	0.016	[19]
500 μm cell size, at 20°C	0.024	[19]
100 μm cell size, at 20°C	0.016	[19]
Poly(vinyl chloride)		
$d = 56\,\mathrm{kg/m^3}$	0.035	[9]
$d = 112\,\mathrm{kg/m^3}$	0.040	[9]

TABLE 10.3. *Thermal conductivity k of reinforced polymers and thermally conductive polymer composites.*

Polymer	k (W/m K)	Reference
Polyacetal		
5–20% PTFE	0.20	[24]
Poly(acrylonitrile–butadiene–styrene) copolymer (ABS)		
20% Glass fiber	0.20	[19]
Polyaryletherketone		
40% Glass fiber	0.44	[24]
Polybenzoxazine (bisphenol A/methylamine/formaldehyde		
93% Aluminum nitride	7.4	[5]
94.1% Aluminum oxide	3.4	[5]
Polybenzoxazine (bisphenol A/methylamine/formaldehyde		
50–90% Boron nitride	1.7–37.5	[5]
Polybenzoxazine (bisphenol F/methylamine/formaldehyde)		
85% Boron nitride	20.9	[5]
Polybenzoxazine (bisphenol A/aniline)		
85% Boron nitride	19.8	[5]
Polybenzoxazine (bisphenol F/aniline)		
85% Boron nitride	10.6	[5]
Poly(butylenes terephthalate) (PBT)		
30% Glass	0.29	[19]
	0.20	[9]
40–50% Glass fiber	0.42	[24]
Polycarbonate		
10% Glass fiber	0.22	[19]
30% Glass fiber	0.32	[19]
Polychloroprene (neoprene)		
33% Carbon black	0.210	[9]
Polycyclooctene		
80% *trans* content, 20% boron oxide	0.41	[4]
Poly(dially phthalate)		
Glass fiber	0.21–0.62	[22]
Epoxy		
50% Aluminum	1.7–3.4	[39]
25% Al_2O_3	0.35–0.52	[39]
50% Al_2O_3	0.52–0.69	[39]
75% Al_2O_3	1.4–1.7	[39]
30% Mica	0.24	[19]
50% Mica	0.39	[19]
Silica	0.42–0.84	[19,39]
Epoxy (cresol–novolak)		
70% Boron nitride	6.07–11.6	[6]
Polyetheretherketone (PEEK)		
30% Glass fiber	0.21	[24]
30% Carbon fiber	0.21	[24]
Polyethylene		
5–25% (vol.) Al_2O_3	1–1.6	[2]
30% Glass fiber	0.36–0.46	[24]
Poly(ethylene terephthalate) (PET)		
30% Glass fiber	0.29	[9,19]
45% Glass fiber	0.31	[9]
30% Graphite fiber	0.71	[24]
40% PAN carbon fiber	0.72	[24]
Polyimide		
Thermoplastic, 15% graphite	0.87	[39]
40% graphite	1.73	[24,39]
Thermoset, 50% glass fiber	0.41	[24]

TABLE 10.3. *Continued.*

Polymer	k (W/m K)	Reference
Polyisoprene (natural rubber)		
33% carbon black	0.28	[9]
Poly(melamine–formaldehyde) resin		
Asbestor	0.544–0.73	[9]
Cellulose fiber	0.27–0.42	[24]
Glass fiber	0.42–0.48	[24]
Macerated fabric	0.443	[9]
Wood flour/cellulose	0.17–0.48	[24]
Poly(melamine–phenolic) resin		
Cellulose fiber	0.17–0.29	[39]
Wood flour	0.17–0.29	[39]
Nylon-6 (polycaprolactam)		
30–35% Glass fiber	0.24–0.28	[24]
Nylon-6,6 [poly(hexamethylene adipamide)]		
30–33% Glass fiber	0.21–0.49	[24]
40% Glass fiber and mineral	0.46	[24]
30% Graphite or PAN carbon fiber	1.0	[24]
Nylon-6,12 [poly(hexamethylene dodecanediamide)]		
30–35% Glass fiber	0.427	[24]
Poly(phenylene oxide)		
30% Glass fiber	0.16	[24]
Poly(phenylene sulfide)		
40% Glass fiber	0.288	[9]
30% Carbon fiber	0.28–0.75	[24]
Polypropylene		
40% Talc	0.32	[19]
40% CaCO3	0.29	[19]
40% Glass fiber	0.37	[19]
Polyurethane		
49% Boron nitride,1% silicon dioxide	0.55	[40]
Polystyrene		
20% Glass fiber	0.25	[26]
Poly(styrene–acrylonitrile) copolymer		
20% Glass fiber	0.28	[24]
Poly(styrene–butadiene) copolymer (SBR)		
33% Carbon black	0.300	[9]
Polytetrafluoroethylene		
25% Glass fiber	0.33–0.41	[24]
Poly(urea–formaldehyde) resin		
33% Alpha cellulose	0.423	[9]

include communication satellite device, structural components for spacecraft, computer cases, and many others that require light weight and good thermal conduction. Fillers used in thermally conductive polymers include metal and metal oxides, boron oxide, and graphitic carbon fibers. High thermalconductive polymer composites may have thermal conductivities 10 to over a 100 times higher than those of pure polymers, equal to or higher than thermal conductivities for some metals. Table 10.3 also includes some of those high thermal conductivity polymer composites.

REFERENCES

1. M. J. Hodgin and R. H. Estes, *Proceedings of the Technical Programs, NEPCO WEST Conference*, Anaheim, CA (1999), pp. 359–366.
2. I. H. Tavman, in *Nanoengineered Nanofibrous Materials*, *NATO Science Series II, Mathematics, Physics and Chemistry*, edited by S. I. Guceri, Y. Gogotsi, and V. Kuzentsov (Kluwer Academic Book Pub., Dordrecht, Netherlands, 2004), Vol. 169, p. 449.
3. Ho-Sung Lee and S-Won Eun, in *Composites 2004 Convention and Trade Show*, (American Composites Manufacturers Association, Tampa, Florida, 2004).
4. C. Liu and T. Mather, *ANTEC 2004* (Society of Plastic Engineers, 2004), pp. 3080–3084.

5. H. Ishida and S. Heights, *Composition for Forming High Thermal Conductivity Polybenzoxazine-Based Material and Method*, US Patent 5,900,447 (1999).
6. H. R. Frank and D. S. Phillip, *Enhanced Boron Nitride Composition and Polymer Based High Thermal Conductivity Molding Compound*, EP 0 794 227 B1 (2002).
7. R. D. Hermansen, *Room-Temperature Stable, One-Component, Thermally-Conductive, Flexible Epoxy Adhesives*, EP 0 754 741 B1 (2001).
8. H. Ishida, *Surface Treated Boron Nitride for Forming A Low Viscosity High Thermal Conductivity Polymer Based on Boron Nitride Composition and Method*, US Patent, 6,160,042 (2000).
9. *Encyclopedia of Chemical Technology*, 3rd ed., edited by H. F. Mark, D. F. Othmer, C. G. Overberger, and G. T. Seaborg (Wiley-Interscience, New York, 1989).
10. K. Kurabayashi, Int. J. Thermophys. **22**(1), 277 (2001).
11. D. M. Finlayson, P. Mason, J. Phys. C: Solid State Phys. **18**, 1777 (1985).
12. K. Kurabayashi, M. Asheghi, M. Touzelbaev, and K. E. Goodson, IEEE J. Microelectromech. Syst. **8**(2), 1057 (1999).
13. S. Pattnaik and E. V. Thompson, Polym. Prepr. **22**(1), 299 (1981).
14. L. C. Choy, W. P. Leung, and Y. K. Ng, J. Polym. Sci. Polym. Phys. Ed. **25**, 1779 (1987).
15. K. Eiermann, Kolloid Z. Z. Polym. **180**, 163 (1962).
16. T. R. Fuller and A. L. Fricke, J. Polym. Sci. **15**, 1729 (1971).
17. J. C. Ramsey III, A. L. Fricke, and J. A. Caskey, J. Polym. Sci. **17**, 1597 (1973).
18. R. S. Frost, R. Y. S. Chen, and R. E. Barker, Jr., in *Thermal Conductivity 14, Proceedings of the 14th International Thermal Conference*, edited by P. G. Klemens and T. K. Chu (Plenum, New York, 1975).
19. E. V. Thompson, in *Encyclopedia of Polymer Science and Engineering*, edited by H. F. Mark, N. M. Bikales, C. G. Overberger, G. Menges, and J. I. Kroschwitz (Wiley-Interscience, New York, 1985), Vol. 16, pp. 711–737.
20. *Thermal Conductivity, Nonmetallic Solid*, Vol. 2 of *Thermophysical Properties of Matter*, edited by Y. S. Touloukian, R. W. Powell, C. Y. Ho, and P. G. Klemens (IFI/Plenum, New York, 1970).
21. *International Plastics Handbook*, 2nd ed., edited by H. Saechtling (Hanser, 1987)
22. *Encyclopedia of Polymer Science and Engineering*, edited by H. F. Mark, N. M. Bikales, C. G. Overberger, G. Menges, and J. I. Kroschwitz (Wiley-Interscience, New York, 1985), Vols. 2, 4, 9, 13, 16, and 19.
23. *Polymer Handbook*, edited by J. Brandrup and E. H. Immergut (Wiley-Interscience, New York, 1989).
24. *Handbook of Plastics, Elastomers, and Composites*, edited by C. A. Harper (McGraw-Hill, New York, 1992).
25. *Handbook of Thermoplastic Elastomers*, 2nd ed., edited by B. M. Walker and C. P. Rader (Van Nostrand Reinhold, New York, 1978).
26. F. C. Chen, Y. M. Poon, and L. L. Choy, Polymer **18**, 135 (1977).
27. K. Eiermann and K. H. Kellwege, J. Polym. Sci. **57**, 99 (1962).
28. B. C. Chern *et al*., in *Thermal Conductivity 14, Proceedings of the 14th International Thermal Conference,* edited by P. G. Klemens and T. K. Chu (Plenum, New York, 1975).
29. *Handbook of Thermoproperties of Solid Materials*, edited by A. Gold-Smith, T. E. Waterman, and J. Hirschborn (MacMillan, New York, 1961), Vol. IV.
30. *Plastic Mold Engineering Handbook*, 4th ed., edited by J. H. Bubois and W. I. Pribble (Van Nostrand Reinhold, New York, 1987).
31. A. Sugawarea and T. Takehashi, in *Thermal Conductivity 14, Proceedings of the 14th International Thermal Conference*, edited by P. G. Klemens and T. K. Chu (Plenum, New York, 1975).
32. R. T. Jamieson and J. B. Irving, in *Thermal Conductivity 14, Proceedings of the 14th International Thermal Conference*, edited by P. G. Klemens and T. K. Chu (Plenum, New York, 1975).
33. *D. A. T. A. Digest*, 11th ed., edited by J. A. Morgon (Morgan, San Diego, 1990), Vol. 1.
34. K Ueberreiter, Kolloid Z. Z. Polym. **216**, 217 (1967).
35. J. S. Fox and M. Imber, J. Appl. Polym. Sci. **12**, 571 (1968).
36. P. Lohe, Z. Z., Kolloid Polym. **203**, 115 (1965).
37. P. Anderson and B. Sundgvist, J. Polym. Sci. Polym. Phys. Ed. **13**, 243 (1975).
38. *Polyurethane Handbook*, edited by G. Oertel (Janser, New York, 1985).
39. *Handbook of Thermoset Plastics*, edited by I. Goodman and H. Sidney (Noyes, Park Ridge, NJ, 1986).
40. M. V. Huynh, *Low Dielectric Constant Polyurethane Filleting Composition*, US Patent: 5, 221, 783 (1993).

CHAPTER 11

Thermodynamic Quantities Governing Melting

L. Mandelkern* and R. G. Alamo†

*Department of Chemistry and Biochemistry, Florida State University, Tallahassee, FL 32306-3015; †Department of Chemical and Biomedical Engineering, Florida Agricultural and Mechanical University and Florida State University College of Engineering, 2525 Pottsdamer St., Tallahassee, FL 32310–6046

11.1 PREFATORY REMARKS

In this section a compilation and tabulation of the key thermodynamic parameters that govern the fusion of crystalline homopolymers is presented. The key parameters of interest are the equilibrium melting temperature, T_m^0, defined as the melting temperature of a large perfect crystal comprising infinite molecular weight chains, the enthalpy of fusion per chain repeating unit, ΔH_u, which is independent of the level of crystallinity, and the entropy of fusion, ΔS_u, which is obtained from the above quantities. The data listed in Tables 11.1–11.3 are limited to those homopolymers for which a complete set of thermodynamic parameters are available. Copolymers will not be included since this would involve specifying the sequence distribution of the comonomer. An exception will be made, however, for stereoregular polymers which, from the point of view of crystallization behavior, should be treated as copolymers [1]. Most polymers in this category are not completely stereoregular and cognizance must be taken of this fact when using the data assigned. We shall not be tabulating melting temperatures by themselves, without the auxiliary thermodynamic parameters. Before examining and using the data listed it is important to understand the theoretical and experimental foundations for the quantities that are given and the limitations that are imposed.

Although a collection of regularly structured, flexible chains will crystallize, they never do so completely. Depending on the molecular constitution, the chemical nature of the chain and the crystallization conditions the level of crystallinity attained can range from 90% to just a few percentage. In order for the crystallization of polymers from the melt to be carried out at finite rates, it must be conducted at temperatures well below the equilibrium melting temperature. Consequently, a polycrystalline, partially ordered, system is the one that actually develops. This crystalline system is well removed from equilibrium and can be considered to be in a metastable state. A structural and morphological complex system is thus developed that governs properties, including thermodynamic ones.

The kinetic restraints that are placed on the crystallization of polymers make it difficult, if not impossible to directly determine their equilibrium melting temperatures. The directly observed melting temperatures are primarily a reflection of the structure and morphology of the actual crystalline systems. The primary factors involved are the crystallite thickness, the interfacial free energy, and the influence, if any, of the noncrystalline region. There are, however, indirect methods by which to estimate the value of T_m^0. One of these is a theoretical method. The others are based on extrapolative procedures. To properly use the T_m^0 values that are tabulated, and to understand their limitations, the basic assumption involved and the problems in execution need to be recognized.

The theoretical method is based on the work of Flory and Vrij [2]. Here, the equilibrium melting temperatures of a series of oligomers (low molecular weight chains of uniform length) are analyzed. In this treatment an additional entropic term is added to the expression for the molar entropy of fusion of long-chain molecules in an ordered crystalline array. This term, which takes into account the disruption on fusion of the terminal groups of neighboring molecules, exerts an important influence in analyzing the experimental melting temperatures for *n*-paraffins and their convergence to the limit, T_m^0 for the infinite length chain. By analyzing the fusion of the *n*-alkanes, up to $C_{100}H_{202}$, the T_m^0 value for linear polyethylene was found to be 418.7 ± 1 K. This is the only polymer to

which this theoretical method has been applied. There are not enough data available for oligomers with other type repeating units to apply this method to other polymers. It is important in utilizing this method that all the molecules be of uniform chain length so that molecular crystals can be formed.

Both of the extrapolative methods are based on the Gibbs–Thomson equation for the melting of crystallites of finite size [3]. For a lamellar crystallite, whose length is very much greater than its thickness, this equation can be expressed as:

$$T_m = T_m^0\left(1 - \frac{2\sigma_{ec}}{\Delta H_u l}\right). \tag{11.1}$$

Here T_m is the experimentally observed melting temperature of a crystallite of thickness l and σ_{ec} is the interfacial free energy associated with the basal plane of the lamellar crystallite. Eq. (11.1) was developed to describe the melting of small crystals in equilibrium with the melt. Hence only two phases (or regions) are involved. The implicit assumption is made that the boundary between them is a sharp one. In general, long-chain molecules do not fulfill this condition. It is now well established, by theory and experiment, that there is a diffuse interfacial region, 10–30 Å thick, which connects the crystalline with the liquid-like region [4]. The analog to Eq. (11.1) to account for the melting of small crystallites, when equilibrium between three phases is involved, has yet to be developed.

Despite the problem described above, Eq. (11.1) has been used to determine T_m^0 by measuring the observed melting temperature, T_m, as a function of the crystallite thickness. Accordingly, a plot of T_m against $1/l$ should be linear and extrapolate to T_m^0. An example of this procedure is illustrated in Fig. 11.1 for poly(tetrafluoroethylene) [5]. A straight line clearly results in the plot of T_m against $1/l$. An extrapolated value of 335 °C is obtained for T_m^0. In this example the largest crystallite thickness that was generated was about 5,000 Å. Thus, the extrapolation was not unduly long. This method appears to be quite satisfactory for poly(tetrafluoroethylene). However, for many of the flexible chain-type polymers, such as linear polyethylene, poly(propylene), poly(hexamethylene adipamide), poly (pivalolactone), among others, the maximum thickness used in the extrapolation is usually less than 200 Å. In many cases it is less than 100 Å. Hence, most commonly there is a very long and treacherous extrapolation to $l = \infty$.

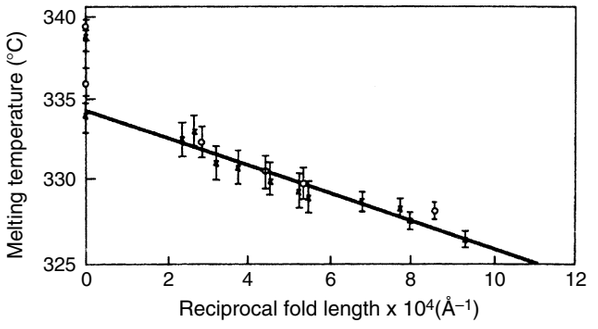

FIGURE 11.1. Melting temperature, in degrees Celsius, as a function of reciprocal crystallite thickness in Ångstroms for poly(tetrafluoroethylene) [5].

There are also other matters of concern that need to be taken into account when using this method. It is very rare to develop a uniform crystallite thickness distribution. In particular, the distribution becomes very broad after high-temperature crystallization. The question then arises as to what portion of the distribution curve corresponds to the observed melting temperature. Usually some average crystallite thickness is measured. The use of this method with polymer systems where a large proportion of the crystallinity develops during the quenching process, after isothermal crystallization, would introduce major uncertainties if the crystallite thickness (l) is measured at room temperature.

When linearly extrapolating Eq. (11.1) it is tacitly assumed that σ_{ec} is independent of the crystallite thickness. Crystallite thicknesses are usually controlled by varying the crystallization temperature. Theory has shown that, among other factors, σ_{ec} depends on the flux of chains emanating from the basal plane of the lamellar crystallite [4]. This flux will in term depend on the tilt angle of the chain, i.e., the angle between the chain axis and the normal to the basal plane [6]. For many polymers the tilt angle depends on the crystallization temperature. Consequently, a variation in σ_{ec} with crystallite thickness can be expected, for many systems. Whether using Eq. (11.1), or the appropriate equivalent equation (when available), the functionality between σ_{ec} and l is needed to properly estimate T_m^0.

Consideration should also be given to the meaning of the extrapolated value, obtained by measuring melting of folded chain crystallites, when the equilibrium state requires an almost completely extended state [7,8]. The interfacial free energies will be different in the two cases.

Small-angle x-ray scattering is one of the standard methods that are used to determine crystallite thickness. A crystalline system comprising a set of stacked lamellae gives a characteristic long period. The long period must then be corrected for the level of crystallinity to obtain the crystallite thickness. In many studies this correction has not been made. Consequently, in these cases there is an indeterminate error in the extrapolation to T_m^0.

For the reasons that have been cited above, it is not surprising that there are serious discrepancies in the T_m^0 values determined by different studies of the same polymer using this method. For example, linear polyethylene, T_m^0 values, which were obtained by this extrapolative method, vary from 411.3 to 419.0 K among different investigators [9]. Although the difference is not a large range on an absolute basis, it is crucially important in analyzing crystallization kinetics because the undercooling, $\left(T_m^0 - T_c\right)$ is involved.

The other extrapolative method that is used was also developed from the Gibbs–Thomson equation [10,11].

Here, l and σ_{ec} are related to the corresponding quantities that define a nucleus of critical size, namely, l^* and σ_{ec}. For a Gibbs type two-dimensional coherent nucleus $l^* = 2\sigma_{en}/\Delta G_u$, where $\Delta G_u = \Delta H_u \Delta T/T_m^0$ [12] and $\Delta T = T_m^0 - T_c$. The interfacial free energy σ_{en} now represents that of the critical size nucleus. If it is assumed that $l/l^* = m$ and $\beta = \sigma_{ec}/\sigma_{en}$ over the complete range of crystallization temperatures then

$$T_m = T_m^0\left(1 - \frac{\beta}{m}\right) + \frac{\beta}{m}T_c. \tag{11.2}$$

For a three-dimensional homogeneous nucleus, or for certain types of heterogeneous nuclei [13–l5], under the same assumptions

$$T_m = T_m^0\left(1 - \frac{\beta}{2m}\right) + \frac{\beta}{2m}T_c. \tag{11.3}$$

The further assumption is commonly made that $\beta = 1$. In this case Eq. (11.2) becomes

$$T_m = \frac{(m-1)}{2m}T_m^0 + \frac{T_c}{2m} \tag{11.4}$$

and Eq. (11.3) becomes

$$T_m = \frac{(2m-1)}{2m}T_m^0 + \frac{T_c}{2m}. \tag{11.5}$$

For this type of extrapolation we need not concern ourselves with which type of nucleation is controlling the crystallization since the only interest is evaluating T_m^0. In either case, assuming that m is constant over the complete interval of crystallization temperatures, there is a linear relation between T_m and T_c. Thus, a linear extrapolation to the $T_m = T_c$ straight line should in principle lead to T_m^0. The concept, as outlined above, requires low levels of crystallinity so that the mature crystallite will resemble the critical nucleus as closely as possible. However, independent experiments have made clear that the quantity m, a measure of crystallite thickening, is strongly dependent on the crystallization temperature [16,17]. It is also dependent on molecular weight. In addition it is reasonable to expect that $\sigma_{ec} > \sigma_{en}$ so that β will not be constant.

With this theoretical background we can examine some of the experimental results typical of this popular extrapolative method that is used to obtain T_m^0. In brief summary, the results depend on the nature of the polymer, the level of crystallinity that is developed, and the range of crystallization temperatures that is used. A set of $T_m - T_c$ data for poly(ethylene oxide), $M_w = 6.1 \times 10^5$, are given in Fig. 11.2 [18]. At the low levels of crystallinity the data are represented by two intersecting straight lines. The line with the steeper slope extrapolates to a T_m^0 value of 349.2 K. When the crystallinity level is increased, the observed melting points are represented by a single straight line. The extrapolated T_m^0 value of 341.2 K is now much lower. The value obtained at the lower crystallinity level is preferred by theory. However, this quantity still does not represent the highest T_m^0 value that has been deduced for this polymer (see Table 11.1). It is important to note that the data obtained at the low crystallinity level can also be represented by a continuous curve.

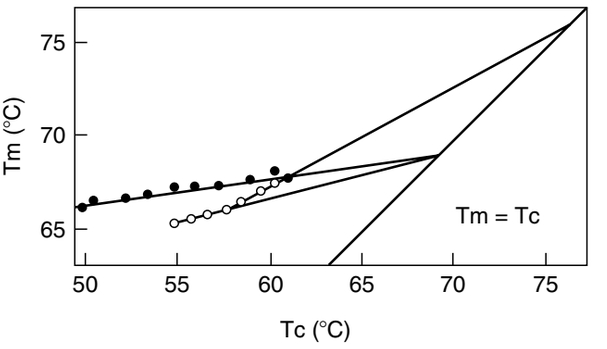

FIGURE 11.2. Plot of melting temperature against crystallization temperature for poly(ethylene oxide), (●) high crystallinity; ○ low crystallinity. Temperature in degrees Celsius [18].

The question arises as to what happens if the T_c range is extended to higher temperatures. An example is given in Fig. 11.3 for a linear polyethylene sample having a most probable molecular weight distribution, $M_w = 351,000$, that was crystallized to a crystallinity level of less than 10% [12]. For the range in crystallization temperatures shown the data are best represented by a curve. If, however, the measurements are restricted to 126 °C, or less, the data would be represented by two intersecting straight lines. Within this range the extrapolated $T_m^0 = 417\,\text{K} - 418$ is in agreement with theoretical expectations [2]. However, if the range of crystallization temperatures is increased to 131 °C (a high T_c for this polymer), then, the data points deviate from the straight line toward high values and a linear extrapolation is no longer operationally feasible. This behavior

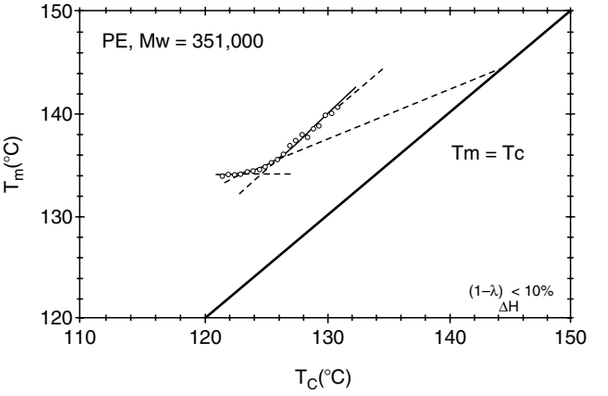

FIGURE 11.3. Plot of observed melting temperature, T_m, against crystallization temperature, T_m, for a linear polyethylene having a most probable molecular weight distribution, $M_w = 351,000$. Degree of crystallinity less than 10%. Temperature in degrees Celsius [12].

is not unique to linear polyethylene, it is also shown by many other polymers. There is, therefore, a serious dilemma in using this method. If T_c is too high then the extrapolation cannot be made. In order to carry out the extrapolation an arbitrary decision must be made as to the highest T_c value to be used. Thus the value obtained for T_m^0 will also involve an element of arbitrariness. The fact that the parameter m varies with the crystallization temperature is a major reason for the curvature that is observed. Several theoretical proposals have been made to improve the data analysis in order to obtain a more reliable extrapolated value of T_m^0 [19,20]. The validity and reliability of the proposed methods awaits further study.

There are obvious difficulties in obtaining T_m^0 by either of these extrapolative methods. Therefore, caution must be used in accepting, and using, the values so obtained. Equilibrium melting temperatures listed in Tables 11.1 and 11.3 have been obtained by one or the other of these methods, except for the theoretical value for linear polyethylene.

11.2 ENTHALPY OF FUSION PER REPEATING UNIT, ΔH_u

There are several experimental methods that allow ΔH_u to be determined. Two of these are based on direct thermodynamic methods. They do not involve knowledge of the crystallinity level of the polymer. A third method is an indirect one that does require such knowledge.

One of the thermodynamic methods involves the adaptation of the classical freezing point-composition relation to the melting of polymer-diluent mixtures. The most common situation encountered when a low molecular weight diluent is admixed with a polymer, is that the crystalline phase remains pure. Under these conditions, for polymers of high molecular weight, the melting temperature of a polymer-diluent mixture, T_m, can be expressed as [7,21]

$$\frac{1}{T_m} - \frac{1}{T_m^0} = \frac{R}{\Delta H_u}\frac{V_u}{V_1}\left[(1 - v_2) - \chi_1(1 - v_2)^2\right]. \qquad (11.6)$$

In deriving this equation, the chemical potentials in the melt of the two components are given by the Flory–Huggins theory [22]. In Eq. (11.6), V_u and V_1 are the molar volumes of the chain repeating unit and diluent, respectively; v_2 is the volume fraction of polymer in the mixture and χ_1 is the Flory–Huggins interaction parameter [22]. The implicit assumption is made in deriving Eq. (11.6) that σ_{ec} is independent of composition. The similarity of Eq. (11.6) to the classical expression for the freezing point depression is readily apparent. It has been found that, for a given polymer, the same value of ΔH_u is obtained irrespective of the diluent used, giving support to the validity of Eq. (11.6) [23]. Measurement of the melting point depression is a powerful method for determining ΔH_u. Enthalpies of fusion per repeating unit that were determined by this method are listed in Table 11.1.

The other thermodynamic method that can be used to determine ΔH_u involves the variation of the equilibrium melting temperature with applied hydrostatic pressure, p. The Clapeyron equation

$$\frac{dT_m^0}{dp} = T_m^0\frac{\Delta V_u}{\Delta H_u} \qquad (11.7)$$

has been shown to apply to polymers [24], as it does to all substances. In this equation ΔV_u is the difference between the volume, per unit, of the pure melt and of the pure crystal. It is important, therefore, that these two quantities be known as a function of both temperature and pressure in order to properly apply Eq. (11.7). The ΔH_u values that have been obtained by this method are given in Table 11.2.

The ΔH_u values, obtained by indirect methods, of polymers that, except for minor exceptions, are not included in Table 11.1 or 11.2, are listed in Table 11.3. In general, the enthalpy of fusion is measured for a given sample and the level of crystallinity of the same specimen is determined, by one of the many methods that are available. The ΔH_u value can then be calculated from these measurements. One problem associated with this procedure is that not all methods of measuring the level of crystallinity give exactly the same value. Small but significant differences are found between different techniques that reflect different sensitivities to the elements of phase structure [25]. A corollary to this procedure is to determine the enthalpy of fusion as a function of density for a sample that is crystallized in different ways. The results are then extrapolated to the density of the unit cell in order to obtain ΔH_u. The density of the unit cell needs to be well established, and a long extrapolation is usually involved.

The purpose of these prefatory remarks has been to explain the underlying theoretical basis for the data that appear in the tables that follow and the experimental difficulties that are involved. Such tabulations must always be taken cautiously and critically. However, with proper care, and understanding, the data should be very useful.

Related information can be found in Chapters 30 and 31.

TABLE 11.1. *Thermodynamic quantities determined by use of diluent equation [Eq. (11.6)].*

Polymer		T_m^0 (K)	ΔH_u (J/mol)	$\Delta H_u/M_0$ (J/g)	ΔS_u (J/K mol)	References
Ethylene $[CH_2]_n$		418.7	4,142	295.8	9.9	[26–28]
Isot.-propylene[a] $[CH_2-CH]_n$ $\vert$ CH_3	α β	485.2 465.2	8,786 8,201	208.8 194.9	18.1 17.6	[29–36]
Isot.-butene-1 $[CH_2-CH]_n$ $\vert$ CH_2 $\vert$ CH_3	(I) (II) (III)	408.7 397.2 379.7	6,318 6,276 6,485	112.5 111.9 115.6	15.5 15.8 17.1	[37–38]
4-Methyl pentene-1 $[CH-CH_2]_n$ $\vert$ CH_2 $\vert$ CH $/\ \backslash$ $CH_3\ CH_3$		523.2	5,297	63.7	10.1	[39]
1-Methyl octamer $[CH-(CH_2)_6-CH_2]_n$ $\vert$ CH_3		268.2	10,857	86.2	40.5	[40]
Isot.-styrene $-\{CH_2-CH\}_n-$ ⬡		>516.2[b]	8,682[c]	83.4	16.8	[41–44]
Synd.-styrene $-\{CH_2-CH\}_n-$ ⬡		>560.5[d]	8,577	82.4	15.3	[45–47]
Vinyl alcohol $[CH_2-CH]_n$ $\vert$ OH		523.2	6,862	156.1	13.1	[48–50]
Acrylonitrile $[CH_2-CH]_n$ $\vert$ $C\equiv N$		593.2	5,021	94.7	8.5	[51,52]
Isot.-*iso*-propyl acrylate $[CH_2-CH]_n$ $\vert$ $C(=O)-O-CH(CH_3)_2$		450.2	5,857	51.4	13.0	[53]
trans-1,4 Butadiene $[CH_2-C(H)=C(H)-CH_2]_n$	(I) (II)	369.2 421.2	13,807 4,602	255.7 85.2	37.4 10.9	[54]
cis-1,4 Butadiene $[CH_2-C(H)=C(H)-CH_2]_n$		273.2	9,205	170.4	33.7	[55]

TABLE 11.1. *Continued.*

Polymer		T_m^0 (K)	ΔH_u (J/mol)	$\Delta H_u/M_0$ (J/g)	ΔS_u (J/K mol)	References
trans-1,4 Isoprene $[CH_2-C(CH_3)=CH-CH_2]_n$	(α) (β)	360.2 354.2	12,719 10,544	187.0 155.1	35.3 29.8	[56–58]
cis-1,4 Isoprene $[CH_2-C(H_3C)=CH-CH_2]_n$		308.7	4,393	64.6	14.2	[59,60]
trans-1,4 Chloroprene $[CH_2-C(Cl)=CH-CH_2]_n$		380.2	8,368[e]	94.6	22.0	[61–63]
trans-Pentenamer $[CH=CH-CH_2-CH_2-CH_2]_n$		307.2	12,008	176.3	39.1	[64,65]
trans-Octenamer[e] $[CH=CH-(CH_2)_5-CH_2]_n$		350.2	23,765	215.7	67.9	[66]
cis-Octenamer $[CH=CH-(CH_2)_5-CH_2]_n$		311.2	21,000	190.9	67.5	[67]
trans-Decenamer[e] $[CH=CH-(CH_2)_7-CH_2]_n$		353.2	32,844	237.6	92.9	[66]
trans-Dodecenamer $[CH=CH-(CH_2)_9-CH_2]_n$		357.2	41,171	247.6	115.3	[66,68]
Methylene oxide $[CH_2-O]_n$		479.2	7,012	233.7	14.6	[69–72]
Ethylene oxide $[CH_2-CH_2-O]_n$		353.2	8,703	197.8	24.6	[73–75]
Isot.-propylene oxide $[CH_2-CH(CH_3)-O]_n$		355.2	7,531 8,368[f]	129.8	21.2	[76,77]
Trimethylene oxide $[(CH_2)_3-O]_n$		323.2	8,786	151.5	27.2	[78]
Tetramethylene oxide $[(CH_2)_4-O]_n$		330.2	15,899	220.8	48.2	[79]
Hexamethylene oxide $[(CH_2)_6-O]_n$		346.7	23,640	236.4	68.2	[80]
1,3 Dioxolane $[O-CH_2-O-(CH_2)_2]_n$		366.2	15,481	209.2	42.3	[81]
1,3 Dioxepane $[O-CH_2-O-(CH_2)_4]_n$		303.0	14,454	141.7	47.7	[82]
1,3 Dioxocane $[O-CH_2-O-(CH_2)_5]_n$		319.2	7,740	75.9	24.3	[83]
3,3 Dimethyl oxetane $[O-CH_2-C(CH_3)_2-CH_2]_n$	II III	349.2 329.2	9,205 7,448	107.0 86.6	26.3 22.6	[84]

TABLE 11.1. *Continued.*

Polymer	T_m^0 (K)	ΔH_u (J/mol)	$\Delta H_u/M_0$ (J/g)	ΔS_u (J/K mol)	References
3-Ethyl 3-methyl oxetane 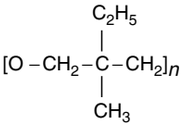	334.2	6,276	62.8	18.8	[85]
3,3 Diethyl oxetane	373.2	10,460	91.8	28.0	[86]
Monoclinic	353.2	10,042	88.1	28.4	[86]
Orthorhombic 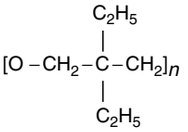					
3,3-bis Ethoxy methyl Oxetane 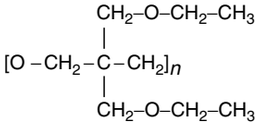	398.2	9,414	54.1	23.6	[87]
3,3-bis Azido methyl Oxetane 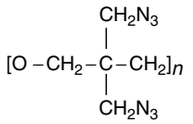	401.2	53,555	318.8	133.5	[87]
2,6 Dimethyl,1,4 phenylene oxide 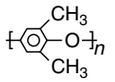	548.2	5,230	43.6	9.5	[88,89]
2,6 Dimethoxy,1,4 phenylene oxide 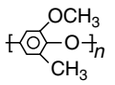	560.2	3,184	20.9	5.7	[90]
Trimethylene sulfide $[(CH_2)_3-S]_n$	363.2	10,460	141.4	28.8	[91]
Propanone-1 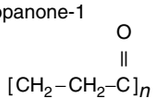	>528.2	12,600	225.0	<23.8	[92]
Ethylene azelate 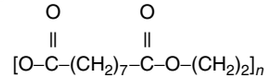	338.2	43,095	138.1	127.6	[93]
Decamethylene adipate 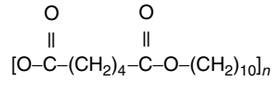	352.7	42,677	150.3	121.0	[94]

TABLE 11.1. *Continued.*

Polymer	T_m^0 (K)	ΔH_u (J/mol)	$\Delta H_u/M_0$ (J/g)	ΔS_u (J/K mol)	References
Decamethylene azelate 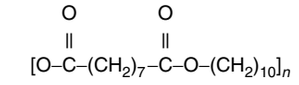	342.2	41,840	129.7	121.3	[93]
Decamethylene sebacate 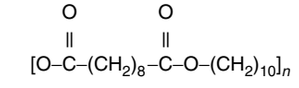	353.2	50,208	147.7	142.2	[95]
Ethylene terephthalate 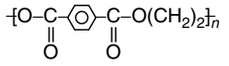	613.2	23,430	122.0	38.2	[96–98]
Tetramethylene terephthalate 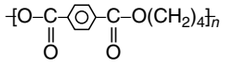	503.2	31,798	144.5	63.2	[99]
Hexamethylene terephthalate 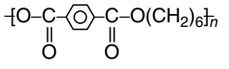	433.7	35,564	143.4	82.0	[93]
Decamethylene terephthalate 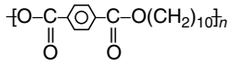	411.2	46,024	151.4	111.9	[93]
Tetramethylene isophthalate 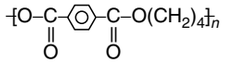	425.7	42,258	192.1	99.3	[99,100]
Diethylene glycol terephthalate 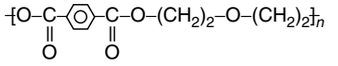	373.2	39,748	168.4	106.5	[101]
β-propiolactone 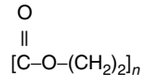	357	8,577	119.1	24.0	[102]
ε-caprolactone 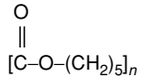	337	16,297	142.9	48.3	[102]
α,α' Dimethyl propiolactone 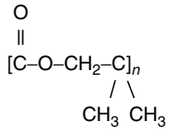	542.2	14,853	148.5	27.4	[103–105]

TABLE 11.1. *Continued.*

Polymer		T_m^0 (K)	ΔH_u (J/mol)	$\Delta H_u/M_0$ (J/g)	ΔS_u (J/K mol)	References
α,α' Dimethyl propiolactone 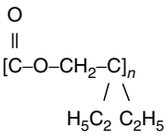		531.2	20,920	163.4	39.4	[106]
α-Methyl, α- *N* propyl, β–propiolactone 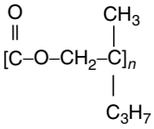		425.2	14,602	114.1	34.3	[107]
Decamethylene azelamine 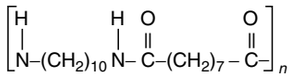		487.2	36,819	112.9	75.3	[93]
Decamethylene sebacamide 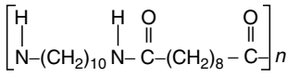		489.2	34,727	102.7	71.0	[93]
N,N' sebacoyl piperazine 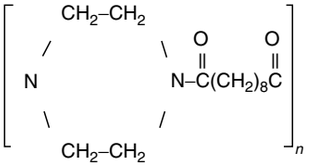		453.2	25,941	102.9	57.2	[108]
Caprolactam 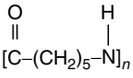	γ^g	502.2	17,949	158.8	35.7	[109]
Ester amide[h] 6-6		526	92,885	188.3	176.6	[110]
Ester amide[h] 12-2		517	102,522	194.6	198.3	[110]
Ester amide[h] 12-6		487	116,315	200.8	238.8	[110]
Ester amide[h] 12-12		470	140,164	211.3	298.2	[110]
Urethane[i]						
$n = 2$		440.2	44,267	192.5	100.6	[111]
$n = 5$		428.2	45,522	167.4	106.3	[111]
$n = 10$		427.2	61,505	179.8	144.0	[111]

TABLE 11.1. *Continued.*

Polymer		T_m^0 (K)	ΔH_u (J/mol)	$\Delta H_u/M_0$ (J/g)	ΔS_u (J/K mol)	References
Urethane[j]						
$n = 5$		462.2	54,810	154.8	118.6	[111]
$n = 10$		465.2	70,961	167.4	152.5	[111]
Vinyl fluoride 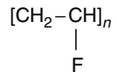		470.2	7,531	163.7	16.0	[112]
Vinylidene fluoride 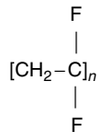	(α)	532.2	6,694	104.6	12.6	[113–115]
Chloro trifluoro ethylene 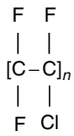		483.2	5,021	43.1	10.4	[116]
Vinylidene chloride 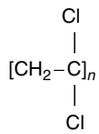		468.2	5,623	58.6	12.0	[117]
Dimethyl siloxane[k] 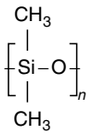		233	2,767	36.7	11.9	[118]
Tetramethyl-*p*-silphenylene siloxane 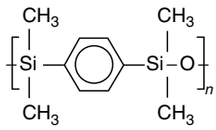		433.2	11,340	54.4	26.2	[119]
2,2'-bis 4,4'(Oxyphenyl) propane carbonate 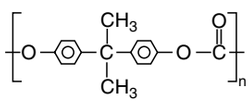		590.2	34,008	133.9	57.6	[120,121]
Cellulose tributyrate[l] 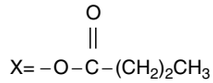		480.2	12,552	33.7	26.1	[122]

TABLE 11.1. *Continued.*

Polymer	T_m^0 (K)	ΔH_u (J/mol)	$\Delta H_u/M_0$ (J/g)	ΔS_u (J/K mol)	References
Cellulose trinitrate[l] X= –O–NO_2	>973	3,765–6,276	12.6–21.1	3.9–6.4	[123]
Cellulose (2.44) nitrate[l] Cellulose $[O-NO_2]_{2.44}$	890.2	5,648	21.5	6.3	[124]
Cellulose tricaprylate[l] X= –O–C(=O)–$(CH_2)_6CH_3$	389.2	12,970	24.0	33.3	[125]
Collagen	418.2[m]	9,414	100.4	22.5	[126]

[a]The equilibrium melting temperature of isotactic polypropylene is still debated between values ranging from 458 to 493 K. See for example refs [200, 201, 202].
[b]516.2 K is the highest T_m observed [44]. Therefore, T_m^0 should be greater.
[c]Average value of references cited.
[d]Extrapolated equilibrium melting temperatures of the α and β forms are very close to one another. Depending on the method used they are close to 545 or 573 K [203].
[e]Extrapolated to all *trans*.
[f]Obtained by direct determination of activity coefficients in polymer-diluent mixtures.
[g]That these data belong to the γ form is deduced from the reported specific volumes (V_c^γ) and the heat of fusion data of Fig. 13 of von K-H Illers et al. ref [166].
[h]Ester-amide (*n–m*)

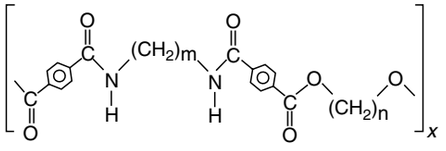

i

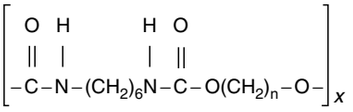

j

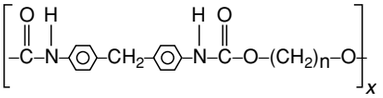

[k]The value of ΔH_u was determined with only one diluent. It was originally reported in terms of calories per mole of chain atoms and misinterpreted. The value in joules per gram was subsequently clarified by M. I. Arangurem [204].

l

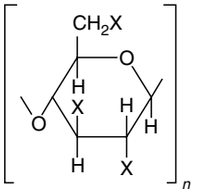

[m]Extrapolated from the melting point of glycol mixtures.

TABLE 11.2. *Thèrmodynamic quantities determined by the use of Clapeyron equation [Eq. (11.7)]*

Polymer	$T_m^{0\,a}$ (K)	ΔH_u (J/mol)	$\Delta H_u/M_0$ (J/g)	ΔS_u (J/K mol)	References
Ethylene $[CH_2]_n$	414.6	4,059	289.9	9.8	[127]
Isot.-propylene (γ) $[CH_2-CH(CH_3)]_n$	460.2	6,300[b]	150	13.7	[128]
		7,980[b]	190	17.3	[128]
Isot.-butene-1 (I) $[CH_2-CH(CH_2-CH_3)]_n$	406.2	7,782[c]	138.7	19.2	[129,130]
(II)	392.9	7,531[c]	134.2	19.2	
4-Methyl pentene-1 $[CH(CH_2-CH(CH_3)_2)-CH_2]_n$	506.2	5,205	61.9	10.3	[131]
Methylene oxide $[CH_2-O]_n$	456.2	11,673	389.1	25.6	[132]
Ethylene oxide $[CH_2-CH_2-O]_n$	339.2	9,037	205.4	26.6	[133]
Tetramethylene oxide $[(CH_2)_4-O]_n$	315.9	14,728	204.6	46.6	[133]
Glycolic acid $[C(=O)-O-(CH_2)]_n$	504.6	10,626	183.2	21.1	[134]
Ethylene adipate $[O-C(=O)-(CH_2)_4-C(=O)-O-CH_2]_n$	326.2	20,150	127.5	61.8	[135]
Ethylene pimelate $[O-C(=O)-(CH_2)_5-C(=O)-O-CH_2]_n$	309.2	27,489	159.8	88.9	[135]
Ethylene suberate $[O-C(=O)-(CH_2)_6-C(=O)-O-CH_2]_n$	336.2	24,451	131.4	72.8	[135]

TABLE 11.2. *Continued.*

Polymer	T_m^0 (K)	ΔH_u (J/mol)	$\Delta H_u/M_0$ (J/g)	ΔS_u (J/K mol)	References
Ethylene azelate 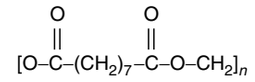	320.2	40,488	202.4	126.4	[135]
Ethylene terephthalate 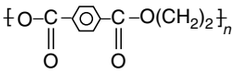	535.2	26,150	136.2	48.9	[136]
Hexamethylene Adipamide α_2 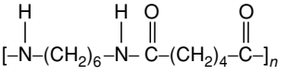	542.2	43,367	191.9	79.9	[137]
Tetrafluoro ethylene (virgin)	619.2	5,105	102.1	8.2	[138]
Tetrafluoro ethylene (melt cured) 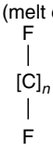	601.2	4,632	92.6	7.7	[138]
aryl-ether–ether–ketone 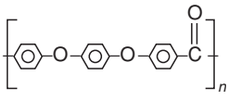	611.2	47,359	164.4	77.5	[139]
2,2'bis(4,4' Oxyphenyl) propane carbonate 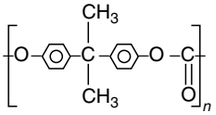	506.2	39,497	155.5	78.0	[140]

[a] Melting temperature actually used in calculation.
[b] Both values are quoted.
[c] Average values.

TABLE 11.3. *Unique values of thermodynamic parameters determined by indirect methods.*

Polymer		T_m^0 (K)	ΔH_u (J/mol)	$\Delta H_u/M_0$ (J/g)	ΔS_u (J/K mol)	Method	References
Synd.-propylene 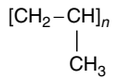		455.2[a]	8,274	196.7	18.2	DSC-x ray	[141,142]
Methyl methacrylate 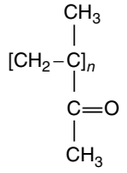	Isot. Synd.	411.2 >397.5	5,021	50.2	12.2	DSC-x ray DSC-Mn	[143] [144]
Synd.-vinyl chloride 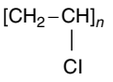		538.2[b] 658.2[c]	4,937 6,694	79.0 107.1	9.2 10.2	DSC-x ray DSC-x ray	[145]
Octamethylene oxide		356.2	32,401	253.1	91.0	DSC-density	[146]
3-Tertbutyl oxetane 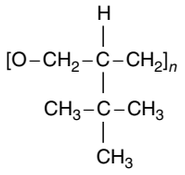		350.2	5,021	45.2	14.3	DSC-x ray	[147]
1,4 Phenylene ether 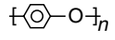		535.2	7,824	85.0	14.6	DSC-x ray	[148]
2,6 diphenyl 1,4 phenylene ether 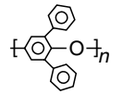		757.2	12,201	50.0	16.1	DSC-x ray	[149]
Ethylene sulfide 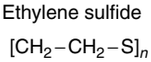		489.2	14,226	237.1	29.1	(T_m-mol. wt)[d]	[150]
3,3'-Dimethyl thietane 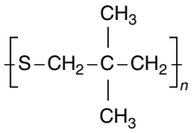		286.2	5,442	56.7	19.0	DSC-x ray	[151]
p-Phenylene sulfide 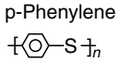		621.7	12,092	112.0	19.4	DSC-x ray	[152–154]
Ethylene sebacate 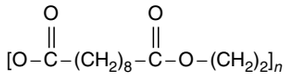		356.2	36,765	161.2	103.2	DSC-density	[155]

TABLE 11.3. *Continued.*

Polymer	T_m^0 (K)	ΔH_u (J/mol)	$\Delta H_u/M_0$ (J/g)	ΔS_u (J/K mol)	Method	References
Hexamethylene sebacate 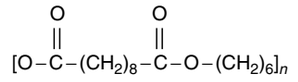	344.2	38,456	133.8	111.8	(T_m-mol. wt)[d]	[156]
3-Hydroxy butyrate 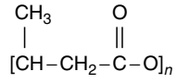	476.2[e]	13,286[f]	154.5	27.9	DSC-x ray density	[157–159]
L-Lactic acid 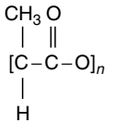	480.2 457	5,858 14,580[g]	81.2 202.5	12.2 31.9	DSC-x ray DSC-Mn	[160,161] [162]
P-Dioxanone 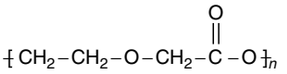	387	10,496	102.9	27.1	DSC-additive group	[163]
Tetrachloro bis phenol-A-adipate 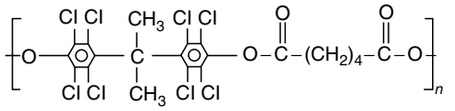	556.2	33,890	55.2	60.9	DSC-x ray	[164]
Ethylene 2,6-naphthalene dicarboxylate 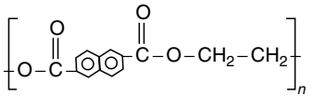	610.2	24,987	93.9	40.9	DSC-x ray density	[165]
Caprolactam (nylon 6) 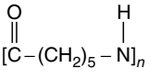	γ α	481 ± 2 551 ± 6	30,271[h]	267.9	56.8	DSC-specific volume	[166,167]
Undecane amide (nylon 11) 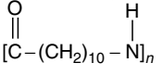	514.2	35,982	196.6	70.0	DSC-density	[168,169]
Laurolactam (nylon 12) 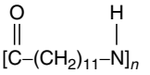	500	48,403	245.7	96.8	DSC-additive heat capacities	[170]

TABLE 11.3. *Continued.*

Polymer	T_m^0 (K)	ΔH_u (J/mol)	$\Delta H_u/M_0$ (J/g)	ΔS_u (J/K mol)	Method	References
Hexamethylene adipamide (nylon 6, 6)	545.7	42,556	188.3	78	DSC-specific volume	[171,172]
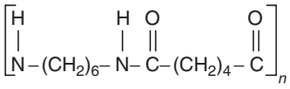						
Hexamethylene azelamide (nylon 6, 9)	500	69,010	257.5	138	DSC-additive heat capacities	[170]
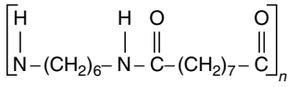						
Hexamethylene sebacamide (nylon 6, 10)	511	59,699	211.7	116.8	DSC-specific volume	[173,174]
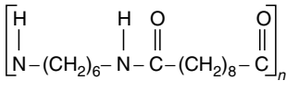						
Hexamethylene decaneamide (nylon 6, 12)	520	80,100	258.4	154	DSC-additive heat capacities	[170]
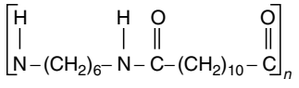						
Tetramethylene adipamide (nylon 4, 6)	623.2	41,618	210.2	66.8	DSC-x ray	[175]
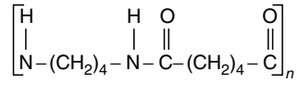						
Decamethylene sebacamide (nylon 10, 10)	487	82,472	244.0	169.3	DSC-specific volume	[176]
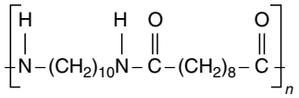						
Dodecamethylene decaneamide (nylon 12,12)	477.7	115,127	292.2	241.0	DSC-specific volume	[177]
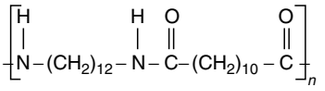						
Imide[i]						
n=1	613.2	72,467	143.8	118.2	DSC-x ray	[178]
n=2	577.2	80,165	146.3	138.9	DSC-x ray	[178]
n=3	541.2	87,956	148.6	162.5	DSC-x ray	[178]

TABLE 11.3. *Continued.*

Polymer	T_m^0 (K)	ΔH_u (J/mol)	$\Delta H_u/M_0$ (J/g)	ΔS_u (J/K mol)	Method	References
3,3' bischloro Methyl Oxacyclobutane 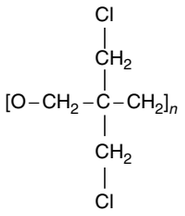	476.2	19,456	126.3	40.9	DSC-density	[179]
2-Hydroxy ethoxy benzoate 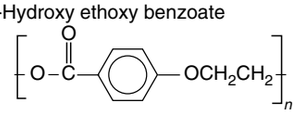	505	15,088 ± 656	92 ± 4	29.9	DSC-x ray	[180]
Ethylene terephthalate 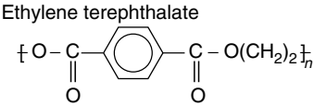	613	25,920	135	42.3	DSC-density-x-ray	[181]
Trimethylene terephthalate 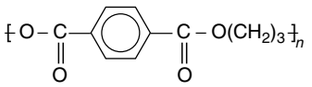	525	28,800	139.8	54.9	DSC-x ray	[182,183]
Butylene terephthalate 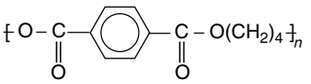	509.2	31,240	142	61.4	DSC-x ray	[184]
Pentamethylene terephthalate 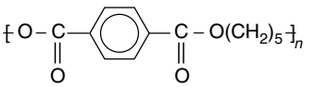	422.6	39,944	170.7	94.5	DSC-x ray	[185]
Aryl-ether–ether ketone 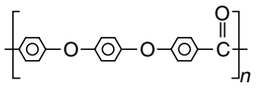	668.2	38,258	132.8	57.3	DSC-density-x ray	[181,186]
Aryl-ether–ether ketone–ketone 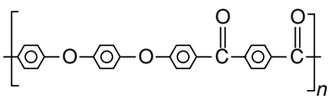	660	48,608	124	73.6	DSC-x ray	[187,188]

TABLE 11.3. *Continued.*

Polymer	T_m^0 (K)	ΔH_u (J/mol)	$\Delta H_u/M_0$ (J/g)	ΔS_u (J/K mol)	Method	References
Methyl-substituted aryl-ether–ether ketone 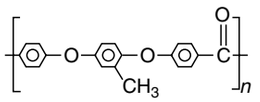	> 513.2	22,348	74.0	< 43.5	DSC-x ray	[189]
Trimethylene 2,6 naphthalate 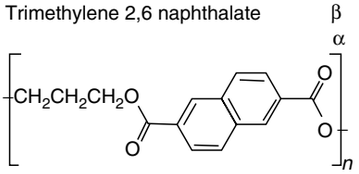	496 470	26,051	101.8	52.5	DSC-x ray	[190]
Butylene 2,6 naphthalate 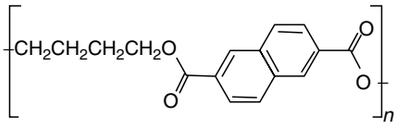	567	32,940	122	58.1	DSC-x ray	[191,192]
LARC-CPI 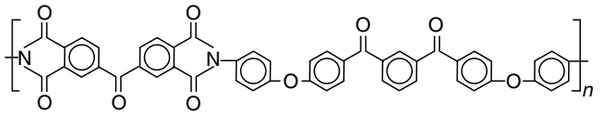	663.2	100,294	127.6	151.2	DSC-x ray	[193]
New-TPI 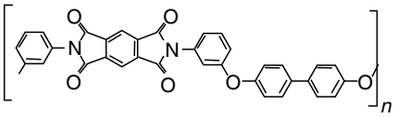	679.2	63,800	116	93.9	DSC-density	[194]
Dimethylsiloxane[j] 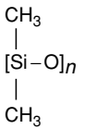	235.2	4,619[k]	62.4	19.6	Calorimetry-DSC	[195–197]
Dichlorophosphazene 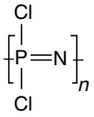	306.2	8,380	71.0	27.4	DSC-x ray	[198]
Urethane[l]						
$n = 2$	440.2	41,547	180.6	94.4	DSC-x ray	[111]
$n = 3$	434.2	41,840	171.5	96.4	DSC-x ray	[111]
$n = 4$	453.2	48,534	188.1	107.1	DSC-x ray	[111]
$n = 5$	428.2	41,463	152.4	96.8	DSC-x ray	[111]
$n = 6$	438.2	51,882	181.4	118.4	DSC-x ray	[111]
$n = 7$	419.2	58,534	161.8	115.8	DSC-x ray	[111]

TABLE 11.3. *Continued.*

Polymer	T_m^0 (K)	ΔH_u (J/mol)	$\Delta H_u/M_0$ (J/g)	ΔS_u (J/K mol)	Method	References
$n = 8$	430.2	55,229	175.9	128.4	DSC-x ray	[111]
$n = 9$	420.2	52,300	159.5	124.5	DSC-x ray	[111]
$n = 10$	427.2	56,484	165.2	132.2	DSC-x ray	[111]
Urethane[m]						
$n = 2$	510.2	48,534	155.6	95.1	DSC-x ray	[111]
$n = 3$	500.2	47,279	145.0	94.5	DSC-x ray	[111]
$n = 4$	505.2	52,718	155.1	104.4	DSC-x ray	[111]
$n = 5$	462.2	51,045	144.2	110.4	DSC-x ray	[111]
$n = 6$	470.2	51,882	141.0	110.3	DSC-x ray	[111]
$n = 7$	464.2	50,626	132.5	109.1	DSC-x ray	[111]
$n = 8$	469.2	59,413	150.0	126.6	DSC-x ray	[111]
$n = 9$	463.2	58,576	142.9	126.4	DSC-x ray	[111]
$n = 10$	465.2	69,036	162.8	148.4	DSC-x ray	[111]
Cellulose Tributyrate	465	12,851	34.5	27.6	DSC-heat capacity	[199]

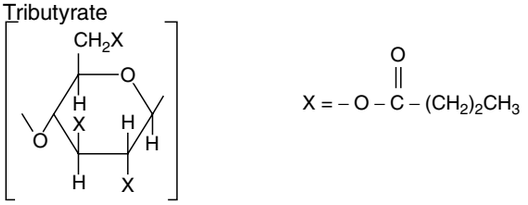

[a]For a sample 94% syndiotactic content (diads based analysis by ^{13}C NMR), $T_m = 160\ ^\circ C$, $\Delta H_u = 1920$ cal/mol. Data from S. & D. Cheng et al [205].
[b]For 64% syndiotactic polymer.
[c]Calculated in Reference 145 for 100% syndiotactic material by modifying the data of D. Koekott, [206].
[d]Samples do not have most probable molecular weight distribution.
[e]Cited R. P. Pearce and R. H. Marchessault, [207].
[f]Average of literature values.
[g]The observed heat of fusion of a highly regular poly L-lactide (>99.9%) is 98.4 J/g (see E.J. Munson et al. [208]).
[h]Taking $V_c^\alpha = 0.814$ cm^3/g from D. R. Holmes, et al. [209]. If all literature values for V_c^α are considered, ΔH_u ranges from 6215 cal/mol to 7250 cal/mol (26000 J/mol–30334 J/mol).
[i]

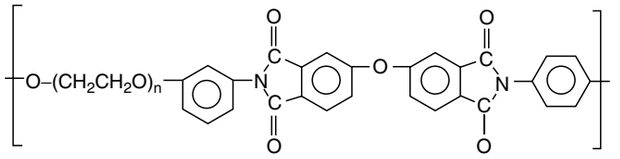

[j]Higher alkyl siloxanes are not included due to their liquid-crystal characteristics
[k]Average value.
[l]

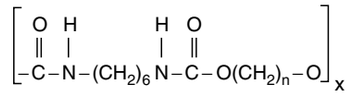

[m]

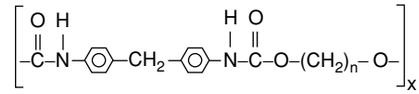

REFERENCES

1. L. Mandelkern, *Crystallization of Polymers* (Cambridge University Press, Cambridge, 2002), 2nd Ed., Vol. 1, p. 141ff.
2. P.J. Flory and A. Vrij, J. Am. Chem. Soc. **85**, 3548 (1963).
3. J.W. Gibbs, *The Scientific Work of J. Willard Gibbs*, (V. I. Longmans Green, New York, 1906); J.J. Thomson, *Applications of Dynamics*, London, 1888.
4. L. Mandelkern, Chemtracts-Macromol. Chem. **3**, 347 (1992).
5. D.C. Bassett and R. Davitt, Polymer **15**, 721 (1974).
6. S.K. Kumar and D.Y. Yoon, Macromolecules **22**, 3458 (1989).
7. P.J. Flory, J. Chem. Phys. **17**, 223 (1949).
8. T. Nakaoki, R. Kitamaru, R.G. Alamo, W.T. Huang, and L. Mandelkern, Polym. J. **32**, 876 (2000).
9. L. Mandelkern, G.M. Stack, and P.J.M. Mathieu, Anal. Calorimetr. **5**, 223 (1984).
10. J.D. Hoffman, J.J. Weeks, and J. Res. Natl Bur. Stand., Part A **66**, 13 (1962).
11. L. Mandelkern, J. Polym. Sci. **47**, 494 (1960).
12. R.G. Alamo, B.D. Viers, and L. Mandelkern, Macromolecules **28**, 3205 (1995).
13. L. Mandelkern, Fatou, and C. Howard, J. Phys. Chem. **68**, 3386 (1964).
14. M. Gopalan and L. Mandelkern, J. Phys. Chem. **71**, 3833 (1967).
15. C. Devoy and L. Mandelkern, J. Chem. Phys. **52**, 3827 (1970).
16. G.M. Stack, L. Mandelkern, and I.G. Voigt-Martin, Polym. Bull. **8**, 421 (1982).
17. G.M. Stack, Doctoral Dissertation, Florida State University, 1983.
18. D.R. Beech and C. Booth, J. Polym. Sci., Polym. Lett. Ed. **8**, 731 (1970).
19. J. Huang, A. Prasad, and H. Marand, Polymer **35**, 1896 (1994).
20. H. Marand, J. Xu, and S. Srinivas, Macromolecules **31**, 8219 (1998).
21. P.J. Flory, in *Principles of Polymer Chemistry* (Cornell Press, Ithaca, 1953), p. 563ff.
22. P.J. Flory, in *Principles of Polymer Chemistry* (Cornell Press, Ithaca, 1953), p. 495ff.
23. L. Mandelkern, *Crystallization of Polymers* (McGraw-Hill, New York, 1964), p. 38ff.
24. P. Zoller, T.A. Kehl, H.W. Starkweather, and G.A. Jones, J. Polym. Sci., Polym. Phys. Ed. **27**, 993 (1989).
25. L. Mandelkern, Acc. Chem. Res. **23**, 380 (1990).
26. P.J. Flory and A. Vrij, J. Am. Chem. Soc. **85**, 3548 (1963).
27. F.A. Quinn Jr. and L. Mandelkem, J. Am. Chem. Soc. **80**, 3178 (1958); L. Mandelkem, Rubber Chem. Tech. **32**, 1392 (1959).
28. A. Nakajima and F. Hamada, Koll. Z. Z. Polymere **205**, 55 (1965).
29. J. Xu, S. Srinivas, H. Marand, and P. Agarwal, Macromolecules **31**, 8230 (1998).
30. M. Mucha, J. Polym. Sci, Polym. Symp. **69**, 79 (1981).
31. J.G. Fatou, Eur. Polym. J. **7**, 1057 (1971).
32. B. Monasse and J.M. Haudin, Colloid Polym. Sci. **263**, 822 (1985).
33. Y. Fujiwara, Colloid Polym. Sci. **265**, 1027 (1987).
34. W.R. Krigbaum and I. Uematsu, J. Polym. Sci., Polym. Chem. Ed. **3**, 767 (1965).
35. F. Danusso and G. Gianotti, Eur. Polym. J. **4**, 165 (1968).
36. G. Shi, B. Huang, and J. Zhang, Makromol. Chem. Rapid Commun. **5**, 573 (1984).
37. F. Danusso and G. Gianotti, Makromol. Chem. **61**, 139 (1963).
38. H. Wilski and T. Grewer, J. Polym. Sci., Polym. Symp. **6**, 33 (1964).
39. G. Charlet and G. Delmas, J. Polym. Sci., Polym. Phys. Ed. **26**, 1111 (1988).
40. G. Gianotti, G. Doll'Asta, A. Valyassori, and V. Zambori, Makromol. Chem. **149**, 117 (1971).
41. M. Al-Hussein and G. Strobl, Macromolecules **35**, 1672 (2002).
42. R. Dedeurwaerder and J.F.M. Oth, J. Chim. Phys. **56**, 940 (1959).
43. F. Danusso and G. Moraglio, Rend. Accad. Naz., Lincei **27**, 381 (1959).
44. P.J. Lemstra, T. Kooistoa, and G. Challa, J. Polym. Sci., Polym. Phys. Ed. **10**, 823 (1972).
45. G. Gianotti and A. Valvassori, Polymer **31**, 473 (1990).
46. N.V. Gvozdic and D.J. Meier, Polym. Commun. **32**, 183 (1991).
47. E.M. Woo, Y.S. Sun, and C.-P. Yang, Prog. Polym. Sci. **26**, 945 (2001).
48. H. Ohgi and T. Sato, Macromolecules **26**, 559 (1993).
49. K. Fujii, J. Polym. Sci., Macromol. Rev. **5**, 431 (1971).
50. R.K. Tubbs, J. Polym. Sci., Polym. Phys. Ed. **3**, 4181 (1965).
51. W.R. Krigbaum and N. Takita, J. Polym. Sci. **43**, 467 (1960).
52. V.G. Hinrichsen, Angew. Makromol. Chem. **20**, 121 (1971).
53. R.A. Wessling, J.E. Mark, and R.E. Hughes, J. Phys. Chem. **70**, 1909 (1966).
54. G. Natta and G. Moraglio, Rubber Plast. Age **44**, 42 (1963).
55. G. Natta and G. Moraglio, Makromol. Chem. **66**, 218 (1963).
56. L. Mandelkem, F.A. Quinn Jr., and D.E. Roberts, J. Am. Chem. Soc. **78**, 926 (1956).
57. E.G. Lovering and D.C. Wooden, J. Polym. Sci., Polym. Phys. Ed. **9**, 175 (1971).
58. R.D. Flanagan and A.M. Rijke, J. Polym. Sci., Polym. Phys. Ed. **10**, 1207 (1972).
59. D.E. Roberts and L. Mandelkem, J. Am. Chem. Soc. **77**, 781 (1955).
60. E.N. Dalal, K.D. Taylor, and P.J. Phillips, Polymer **24**, 1623 (1983).
61. W.E. Mochel and J.T. Maynard, J. Polym. Sci. **13**, 235 (1954).
62. W.R. Krigbaum and J.H. O'Mara, J. Polym. Sci., Polym. Phys. Ed. **8**, 1011 (1970).
63. R.R. Garret, C.A. Hargreaves II, and D.N. Robinson, J. Macromol. Sci. Chem. **A4**(8), 1679 (1970).
64. A. Caplizzi and G. Gianotti, Makromol. Chem. **157**, 123 (1972).
65. C.E. Wilkes, M.J.P. Peklo, and R.J. Minchak, J. Polym. Sci., Polym. Symp. **43**, 97 (1973).
66. G. Gionotti and A. Capizzi, Eur. Polym. J. **6**, 743 (1970).
67. G. Gionotti, A. Capizzi, and L. DelGiucide, Rubber Chem. Technol. **49**, 170 (1976).
68. E. Martuscelli and V. Vittoria, Polymer **13**, 360 (1972).
69. M. Inoue, J. Polym. Sci. **51**, 518 (1961).
70. K.F. Wissbrun, J. Polym. Sci., Polym. Phys. Ed. **4**, 827 (1966).
71. T. Majer, Kunstoffe **52**, 535 (1963).
72. T. Korenga, F. Hamada, and A. Nakajima, Polym. J. **3**, 21 (1972).
73. R.S. Allen, Master Thesis Florida State University (1980).
74. G.C. Alfonso and T.P. Russell, Macromolecules **19**, 1143 (1986).
75. L. Mandelkem, J. Appl. Phys. **26**, 443 (1955).
76. C. Booth, C.J. Devoy, and G. Gee, Polymer **12**, 327 (1971).
77. C. Booth, C.J. Devoy, D.V. Dodgson, and I.H. Hillier, J. Polym. Sci., Polym. Phys. Ed. **8**, 519 (1970).
78. E. Perez, J.G. Fatou, and A. Bello, Eur. Polym. J. **23**, 469 (1987).
79. A. Takahashi and Y. Yamishita, in *Copolymers. Blends and Composites. Advances in Chemistry Series 142*, edited by N.A.J. Plazec (American Chemical Series, Washington, 1975).
80. C. Marco, A. Bello, and J.G. Fatou, Makromol. Chem. **179**, 1333 (1978).
81. R. Alamo, Doctoral Thesis, University of Madrid (1981).
82. J. Garza, C. Marco, J.G. Fatou, and A. Bello, Polymer **22**, 477 (1981).
83. R. Alamo, A. Bello, and J.G. Fatou, J. Polym. Sci., Polym. Phys. Ed. **28**, 907 (1990).
84. E. Perez, J.G. Fatou, and A. Bello, Eur. Polym. J. **23**, 469 (1987).
85. A. Bello, E. Perez, and J.G. Fatou, Macromolecules **19**, 2497 (1986).
86. M.A. Gomez, J.G. Fatou, and A. Bello, Eur. Polym. J. **22**, 43 (1986).
87. K.E. Hardenstine, G.V.S. Henderson Jr., L.H. Sperling, C.J. Murphy, and G.E. Mauser, J. Polym. Sci., Polym. Phys. Ed. **23**, 1597 (1985).
88. A.R. Shultz and C.R. McCullough, J. Polym. Sci., Polym. Phys. Ed. **10**, 307 (1972).
89. H. Janeczelk, H. Turska, T. Szeholy, M. Lengyel, and F. Till, Polymer **19**, 85 (1975).
90. A. Savolainen, Eur. Polym. J. **10**, 9 (1974).
91. A. Sanchez, C. Marco, J.G. Fatou, and A. Bello, Eur. Polym. J. **24**, 355 (1988).
92. J.M. Machado and J.E. Flood, Polym. Prepr. **36**, 291 (1995).
93. P.J. Flory, H.D. Bedon, and E.H. Keefer, J. Polym. Sci. **28**, 151 (1958).
94. L. Mandelkern, R.R. Garret, and P.J. Flory, J. Am. Chem. Soc. **74**, 3939 (1952).
95. R.D. Evans, H.R. Mighton, and P.J. Flory, J. Am. Chem. Soc. **72**, 2018 (1950).
96. D.J. Blundell and B.N. Osborn, Polymer **24**, 953 (1983).
97. R.C. Roberts, Polymer **10**, 113 (1969).
98. A. Wlochowicz and W. Przygock, J. Appl. Polym. Sci. **17**, 1197 (1973).
99. A. Conix and R. Van Kerpel, J. Polym. Sci. **40**, 521 (1959).
100. R.A. Phillips, J.M. McKenna, and S.L. Cooper, J. Polym. Sci., Polym. Phys. Ed. **32**, 791 (1994).

101. J. Guzman and J.G. Fatou, Eur. Polym. J. **14**, 943 (1978).
102. V. Crescenzi, G. Manzini, G. Calzalari, and C. Born, Eur. Polym. J. **8**, 449 (1972).
103. C. Borri, S. Brückner, V. Crescenzi, G. Della Fortuna, A. Mariano, and P. Scarazzato, Eur. Polym. J. **7**, 1515 (1971).
104. H. Marand and J.D. Hoffman, Macromolecules **23**, 3682 (1990).
105. J. Noah and R.E. Prud'Homme, Eur. Polym. J. **17**, 353 (1981).
106. Y. Normand, M. Aubin, and R.E. Prud'Homme, Makromol. Chem. **180**, 769 (1979).
107. D. Grenier, A. Leborgne, N. Spassky, and R.E. Prud'Homme, J. Polym. Sci., Polym. Phys. Ed. **19**, 33 (1981).
108. P.J. Flory, L. Mandelkern, and H.K. Hall, J. Am. Chem. Soc. **73**, 2532 (1951).
109. G.B. Gechele and L. Crescentini, J. Appl. Polym. Sci. **7**, 1349 (1963).
110. G. Manzini, V. Crescenzi, A. Ciana, L. Ciceri, G. Della Fortuna, and L. Zotteri, Eur. Polym. J. **9**, 941 (1973).
111. T. Kajiyama and W.J. Macknight, Polym. J. **1**, 548 (1970).
112. D.I. Sapper, J. Polym. Sci. **43**, 383 (1960).
113. A.K. Nandi and L. Mandelkern, J. Polym. Sci., Polym. Phys. Ed. **29**, 1287 (1991).
114. G.J. Welch and R.L. Miller, J. Polym. Sci., Polym. Phys. Ed. **14**, 1683 (1976).
115. K. Nakagawa and Y. Ishida, J. Polym. Sci., Polym. Phys. Ed. **11**, 2153 (1973).
116. A.M. Bueche, J. Am. Chem. Soc. **74**, 65 (1952).
117. K. Okuda, J. Polym. Sci., Polym. Chem. Ed. **2**, 1749 (1964).
118. C.L. Lee, O.K. Johanson, O.L. Flaningan, and P. Hahn, Polym. Prepr. **10**, 1311 (1969).
119. N. Okui, H.M. Li, and J.H. Magill, Polymer **19**, 411 (1978).
120. R. Legres and J.P. Mercier, J. Polym. Sci., Polym. Phys. Ed. **15**, 1283 (1977).
121. L.D. Jones and F.E. Karasz, J. Polym. Sci., Polym. Lett. **4**, 803 (1966).
122. L. Mandelkern and P.J. Flory, J. Am. Chem. Soc. **73**, 3026 (1951).
123. P.J. Flory, R.R. Garrett, S. Newman, and L. Mandelkern, J. Polym. Sci. **12**, 97 (1954).
124. S. Newman, J. Polym. Sci. **13**, 179 (1954).
125. P. Goodman, J. Polym. Sci. **24**, 307 (1957).
126. P.J. Flory and R.R. Garrett, J. Am. Chem. Soc. **80**, 4836 (1958).
127. T. Davidson and B. Wunderlich, J. Polym. Sci., Polym. Phys. Ed. **7**, 377 (1969).
128. K. Mezghani and P.J. Phillips, Polymer **39**, 3735 (1998).
129. H.W. Starkweather Jr., G.A. Jones, J. Polym. Sci., Polym. Phys. Ed. **24**, 1509 (1986).
130. U. Leute and W. Dollhopt, Colloid Polym. Sci. **261**, 299 (1983).
131. P. Zoller, H.W. Starkweather, and G.A. Jones, J. Polym. Sci., Polym. Phys. Ed. **24**, 1451 (1986).
132. H.W. Starkweather Jr., G.A. Jones, and P. Zoller, J. Polym. Sci., Polym. Phys. Ed. **26**, 257 (1988).
133. Y. Tsujita, T. Nose, and T. Hata, Polym. J. **6**, 51 (1974).
134. C. Nakafuku, H. Yoshimura, Polymer **45**, 3583 (2004).
135. K. Ueberreiter, W.H. Karl, and A. Altmeyer, Eur. Polym. J. **14**, 1045 (1978).
136. H.W. Starkweather Jr., P. Zoller, and G.A. Jones, J. Polym. Sci., Polym. Phys. Ed. **21**, 295 (1983).
137. H.W. Starkweather Jr., P. Zoller, and G.A. Jones, J. Polym. Sci., Polym. Phys. Ed. **22**, 1615 (1984).
138. H.W. Starkweather Jr., P. Zoller, G.A. Jones, and A.D. Vega, J. Polym. Sci., Polym. Phys. Ed. **20**, 751 (1982).
139. P. Zoller, T.A. Kehl, H.W. Starkweather, and G.A. Jones, J. Polym. Sci., Polym. Phys. Ed. **27**, 993 (1989).
140. L.D. Jones and F.E. Karasz, J. Polym. Sci., Polym. Lett. **4**, 803 (1966).
141. S. Haftka, K. Könnecke, J. Macromol. Sci.-Phys. **B30**, 319 (1991).
142. C. De Rosa, F. Auriemma, V. Vinti, M. Galimberti, Macromolecules **31**, 6206 (1998).
143. R.P. Kusy, J. Polym. Sci., Polym. Chem. Ed. **14**, 1527 (1976).
144. K. Ute, N. Miyatake, K. Hatada, Polymer **36**, 1415 (1995).
145. E.V. Guinlock, J. Polym. Sci., Polym. Phys. Ed. **13**, 1533 (1975).
146. C. Marco, J.G. Fatou, A. Bello, and A. Blanco, Makromol. Chem. **181**, 1357 (1980).
147. A. Bello, E. Perez, and J.G. Fatou, Makromol. Chem., Macromol. Symp. **20/21**, 159 (1988).
148. W. Wrasidlo, J. Polym. Sci., Polym. Phys. Ed. **10**, 1719 (1972).
149. W. Wrasidlo, Macromolecules **4**, 642 (1971).
150. A. Nicco, J.P. Machon, H. Fremaux, J.Ph. Pied, B. Zindy, and M. Thieny, Eur. Polym. J. **6**, 1427 (1970).
151. A. Bello, S. Lazcano, C. Marco, and J.G. Fatou, J. Polym. Sci., Polym. Chem. Ed. **22**, 1197 (1984).
152. J.D. Menczel and G.L. Collins, Polym. Eng. Sci. **32** 1264 (1992).
153. S.Z.D. Cheng, Z.Q. Wu, and B. Wunderlich, Macromolecules **20**, 2802 (1987).
154. P. Huo and P. Cebe, Colloid Polym. Sci. **270**, 840 (1992).
155. S.W. Hobbs and F.W. Billmeyer, J. Polym. Sci., Polym. Phys. Ed. **8**, 1387 (1970).
156. J.J. O'Malley and W.J. Stauffer, J. Polym. Sci., Polym. Chem. Ed. **12**, 865 (1974).
157. S.J. Organ and P.J. Barham, Polymer **34**, 2169 (1993).
158. P.J. Barham, A. Keller, E.L. Otun, and P.A. Holmes, J. Mater. Sci. **19**, 2781 (1984).
159. S. Bloembergen, D.A. Holden, T.L. Bluhm, G.K. Hamer, and R.H. Marchessault, Macromolecules **22**, 1656 (1989).
160. R. Vasanthakumari and A.J. Pennings, Polymer **24**, 175 (1983).
161. E.W. Fischer, H.J. Sterzel, and G. Wegner, Koll. Z. Z. Polymere **251**, 980 (1973).
162. K. Jamshidi, S.-H. Hyon, and Y. Itaka, Polymer **29**, 2229 (1988).
163. A.P.T. Pezzin, G.O.R. Alberda van Ekenstein, and E.A.R. Duek, Polymer **42**, 8303 (2001).
164. E. Lanza, H. Berghmann, and G. Smets, J. Polym. Sci., Polym. Phys. Ed. **1l**, 75 (1973).
165. S.Z.D. Cheng and B. Wunderlich, Macromolecules **21**, 789 (1988).
166. Von K.-H. Illers and H. Haberkorn, Makromol. Chem. **142**, 31 (1971).
167. N. Avramova and S. Fakirov, J. Polym. Sci., Polym. Lett. Ed. **20**, 635 (1982).
168. S. Fakirov, N. Avramova, P. Tidick, and H.G. Zachmann, Polym. Commun. **26**, 26 (1985).
169. S. Gogolewski, Colloid Polym. Sci. **257**, 811 (1979).
170. A. Xenopoulos and B. Wunderlich, J. Polym. Sci., Polym. Phys. Ed. **28**, 2271 (1990).
171. J.V. McLaren, Polymer **4**, 175 (1963).
172. H. Haberkorn, Von K.-H. Illers, and P. Simak, Colloid Polym. Sci. **257**, 820 (1979).
173. G.M. Wang, D.Y. Yang, and H.S. Bu, Chin. J. Polym. Sci. **16**, 243 (1998).
174. Y. Jin and D. Chen, Chin. J. Appl. Chem. **4**, 25 (1987).
175. R.J. Gaymans, D.K. Doeksen, and S. Harkema, *Integration of Fundamental Polymer. Science and Technology*, edited by L.A. Kleintjens and P.J. Lemstra (Elsevier Applied Science Publisher, New York, 1986), p. 573.
176. Z. Mo, Q. Meng, J. Feng, H. Zhang, and D. Chen, Polym. Int. **32**, 53 (1993).
177. M. Ren, Z. Mo, Q. Chen, J. Song, S. Wang, H. Zhang, and Q. Zhao, Polymer **45**, 3511 (2004).
178. S.Z.D. Cheng, D.P. Heberer, H.S. Lien, and F.W. Harris, J. Polym. Sci., Polym. Phys. Ed. **28**, 655 (1990).
179. N. Wiemers and G. Wegner, Makromol. Chem. **175**, 2743 (1974).
180. L. Finelli, V. Siracusa, A. Munari, and M. Gazzano, J. Polym. Sci., Polym. Phys. Ed. **40**, 1354 (2002).
181. D.J. Blundell and B.N. Osborn, Polymer, **24**, 953 (1983).
182. W.T. Chuang, W.J. Yeh, and P.D. Hong, J. Appl. Polym. Sci. **83**, 2426 (2002).
183. M. Pyda, A. Boller, J. Grebowicz, H. Chuah, B.V. Lebedev, and B. Wunderlich, J. Polym. Sci., Polym. Phys. Ed. **36**, 2499 (1998).
184. J. Runt, D.M. Miley, X. Xhang, K.P. Gallagher, K. McFeaters, and J. Fishburn, Macromolecules **25**, 1929 (1992).
185. P.-L. Wu and E.M. Woo, J. Polym. Sci., Polym. Phys. Ed. **42**, 1265 (2004).
186. Y. Lee and R.S. Porter, Macromolecules **20**, 1336 (1987).
187. J. Wang, J. Cao, Y. Chen, Y. Ke, Z. Wu, and Z. Mo, J. Appl. Polym. Sci. **61**, 1999 (1996).
188. H.J. Zimmermann and K. Könnecke, Polymer **32**, 3162 (1991).
189. Y.P. Handa, J. Roovers, and F. Wang, Macromolecules **27**, 551 (1994).
190. Y.G. Jeong, W.J. Jo, and S.C. Lee, Polymer **44**, 3259 (2003).
191. S.C. Lee, K.H. Yoon, and J.H. Kim, Polym. J. **29**, 1 (1997).
192. D.W. Van Krevelen, *Properties of Polymers* (Elsevier Scientific, Amsterdam, 1990), Chap. 5.
193. J.T. Muellerleile, B.G. Risch, D.E. Rodrigues, G.L. Wilkes, and D.M. Jones, Polymer **34**, 789 (1993).

194. B.S. Hsiao, B.B. Sauer, and A. Biswas, J. Polym. Sci., Polym. Phys. Ed. **32**, 737 (1994).
195. C.E. Weir, W.H. Leser, and L.A. Wood, J. Res. Natl Bur. Std. **44**, 367 (1950).
196. B.V. Lebedev, N.N. Mukhina, and T.G. Kulagina, Polym. Sci., USSR **20**, 1458 (1978).
197. V.S. Papkov, Yu.K. Godovskii, V.S. Svistunov, V.M. Litvinov, and A.A. Zhdanov, J. Polym. Sci., Polym. Chem. Ed. **22**, 3617 (1984).
198. H.R. Allcock and R.A. Arcus, Macromolecules **12**, 1130 (1979).
199. U. Piana, M. Pizzoli, and C.M. Buchanan, Polymer **36**, 373 (1995).
200. K. Yamada, M. Hikosaka, A. Todas, S. Yamazaki, and K. Tagashira, Macromolecules **36**, 4790 (2003).
201. K. Yamada, M. Hikosaka, A. Toda, S. Yamazaki, and K. Tagashira, Macromolecules **36**, 4802 (2003).
202. K. Mezghani, R.A. Campbell, and P.J. Phillips, Macromolecules **27**, 997 (1994).
203. R-M. Ho, C-P. Lin, H-Y. Tsai, and E-M. Woo, Macromolecules **33**, 6517 (2000).
204. M.I. Aranguren, Polymer, **39**, 4897 (1998).
205. J. Rodriguez-Arnold, A. Zhang, S.Z.D. Cheng, A.J. Lovinger, E.T. Hsieh, P. Chu, T.W. Johnson, K.G. Honnell, R.G. Geerts, S.J. Palackal, G.R. Hawley, and M.B. Welch, Polymer, **35**, 1884 (1994).
206. D. Kockott, Kolloid-Z.Z. Polym. **198**, 17 (1964).
207. R.P. Pearce and R.H. Marchessault, Macromolecules **27**, 3869 (1994).
208. K.A.M. Thakur, R.T. Kean, J.M. Zupfer, N.U. Buehler, M.A. Doscotch, and E.J. Munson, Macromolecules **29**, 8844 (1996).
209. D.R. Holmes, C.W. Bunn, and D.J. Smith, J. Polym. Sci. **17**, 159 (1955).

CHAPTER 12

The Glass Temperature

Donald J. Plazek* and Kia L. Ngai†

*Department of Materials Science and Engineering, University of Pittsburgh, Pittsburgh, PA 15261;
†Naval Research Laboratory, Washington, DC 20375

12.1 INTRODUCTION

The equilibrium liquid state certainly is not as well understood as the crystalline state, and glasses which are nonequilibrium liquids are less well understood, but their unusual time-dependent properties have fascinated investigators for many years. There is no intention here to completely cover all the known properties of glasses or the ground covered by the numerous exhaustive reviews [1–10] and pertinent monographs, [11–34] but an attempt will be made to direct the reader to many of the significant observations, papers, theories, monographs, and review articles dealing with many of their interesting facets.

Many of the kinetic phenomena exhibited by glasses were described in the early monograph by G. O. Jones [12]. The so-called Kauzman Paradox or "catastrophe" drew attention to the precipitous decrease of the entropy of disordered glasses toward values which were less than that of the ordered crystalline state [1]. A second order thermodynamic transition appeared to be necessary to avert the "catastrophe." Kinetic phenomena were encountered that led to decades of controversy about the nature of the glass "transition" temperature. Nearly all of the manifestations of glassy behavior have been determined to be kinetic in nature. In fact, it will be seen below that glass formation and the associated time and rate dependent changes in properties are examples of volume viscoelasticity.

Any liquid which does not crystallize upon cooling is destined to become a glass. When a liquid is cooled continuously, the rate of diffusion decreases while the viscosity increases, reflecting a diminishing molecular mobility.

The enhanced sluggishness of molecular response is due to the increasing molecular crowding and the attendant cooperativity of the molecular motions. At relatively high temperatures the mobility of the molecules of a liquid is great enough to maintain an equilibrium density, reflecting the more efficient packing that occurs during cooling. Eventually the mobility decreases to the point where the molecular rearrangements, necessary to alter the liquid structure, cannot keep up with a given fixed rate of cooling. Subsequently the liquid's specific volume becomes increasingly greater than its equilibrium value at each lower temperature. At the same time, the liquid exhibits glassy properties, an extremely high viscosity, greater than 10^{12} poise (10^{11} P sec), and a low compliance, about 10^{-10}cm^2/dyne (10^{-9}Pa^{-1}). Most significantly, at temperatures near the departure from an equilibrium density during cooling, any and all liquids are measurably, if not markedly, viscoelastic. The departure from equilibrium during cooling signals the glass temperature T_g. Note, we do not call it a glass "transition" temperature since no transition occurs in the liquid. It is still a liquid below T_g, albeit with an enormous, but measurable, viscosity. For T_g to be a material characterizing function, it must be defined in a cooling experiment, whether it be a quench or a constant rate of cooling, so that it emanates from a unique equilibrium condition. When determined from a cooling experiment, T_g is found to be a unique function of the cooling rate, q. This is because it is a manifestation of viscoelastic behavior. Viscoelastic behavior is a time-, rate-, and frequency-dependent behavior. T_g reflects a characteristic molecular mobility, virtually by the definition given above. When the rate of molecular rearrangement cannot keep up with the rate of cooling, equilibrium is lost.

While polymer glasses are of principal interest here, it must be kept in mind that qualitatively all glasses behave similarly whether they are organic, inorganic, or metallic.

The glass temperature T_g of a given polymer depends on the rate of cooling, q, the pressure, P, the number average molecular weight, M_n, and if in solution, its volume fraction, ϕ_2. In short, $T_g(q,P,M_n,\phi_2)$. For a polycrystalline polymer, changes of T_g occur with a variation of the degree of crystallinity and the nature of the morphology of the material. The effect of each of these experimental variables will be discussed below with minimal reference to model-dependent analyses. The emphasis will be on the phenomenology that has been observed. The free volume [36–38], entropy [39–42], coupling [43], and fictive temperature [44–46] models have all been used in analyzing the phenomena with conflicting results in many cases. In addition to the original presentations, the models have been outlined in the many review papers referred to above.

12.2 DEPENDENCE OF T_g ON THE RATE OF COOLING q

Although the rate dependence of T_g is constantly acknowledged, its direct observation has rarely been systematically

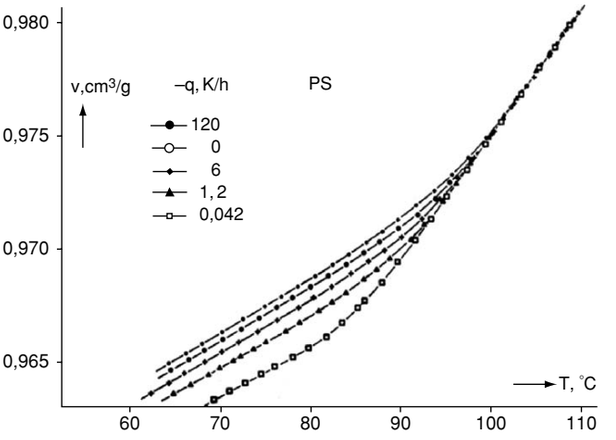

FIGURE 12.1. Volume-temperature curves of PS extending through the glass temperature under various rates of cooling, as indicated. (From Greiner and Schwarzl, by permission [5b].)

observed. Fig. 12.1 shows the dilatometric results of Greiner and Schwarzl [5b] on a polystyrene covering 3 1/2 decades of cooling rate, q. The T_g, determined from the intersection of the equilibrium line with the varying glassy lines varies from 96 °C at the highest q of 2.0 °C/min down to 86 °C at the lowest rate of cooling employed which was 7×10^{-4} °C/min. Illustrative values of the thermal contraction coefficient, α, curves calculated from the curves of Fig. 12.1 are seen in Fig. 12.2

$$\alpha = \frac{1}{v}\left(\frac{\partial v}{\partial T}\right)_P$$

A slightly lower glassy α is found with decreasing q but the temperature span between the limiting equilibrium and glassy lines is found to significantly diminish with decreas-

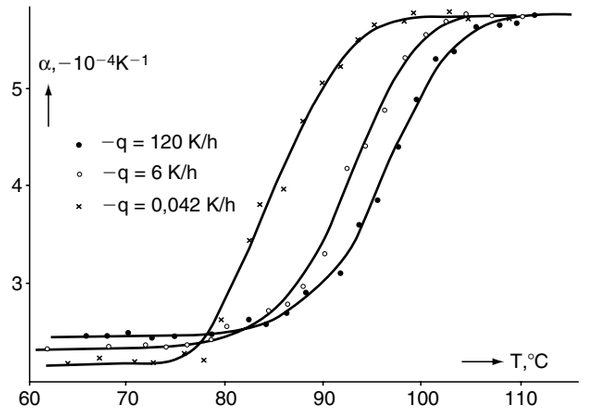

FIGURE 12.2 Thermal expansion coefficient, calculated from the data of Fig. 12.1, for PS under various rates of cooling. (From Greiner and Schwarzl, by permission [5b].)

ing q. This observation is in accord with that reported by Moynihan *et al*. [46,47] on several inorganic glasses. Using the Macedo-Litovitz hybrid equation, Rekhson and Scherer rationalized this broadening [48]. Bero and Plazek observed the same broadening on a fully cured epoxy resin which is a viscoelastic solid since it is comprised of a molecular network which precludes flow [49]. This is in contrast with the polystyrene of Greiner and Schwarzl which is a viscoelastic liquid, because it is constituted of linear molecules and it does flow. The specific volume-temperature cooling curves for the epoxy resin are shown in Fig. 12.3. The extent of the temperature range between equilibrium liquid-like and glassy contractions is shown in Fig. 12.4. The rate dependence of T_g is also presented by Greiner and Schwarzl [5b] for polymethyl-methacrylate, PMMA, polyvinylchloride, PVC, and polycarbonate, PC.

12.3 VOLUME AND ENTHALPY VARIATIONS AND THE FICTIVE TEMPERATURE T_f

With great care and effort, Richardson and Savill [50] have succeeded in measuring the T_g of polystyrene in cooling as a function of rate in a differential scanning calorimeter,

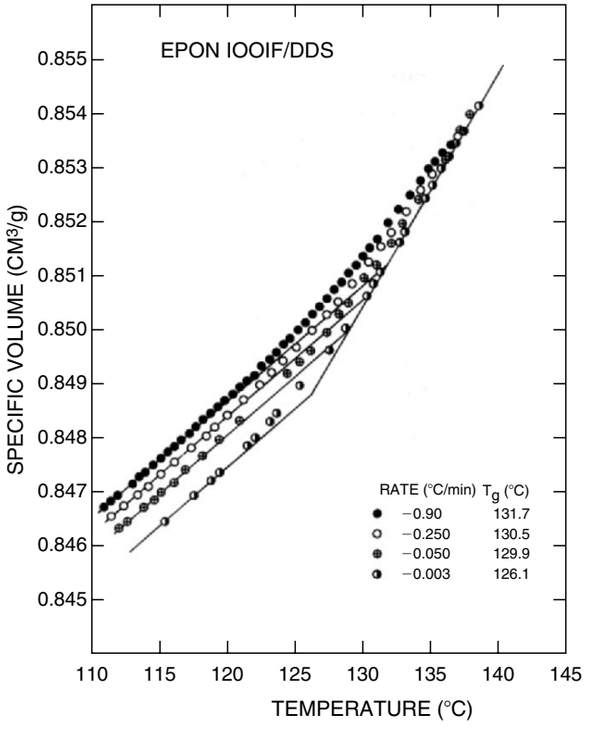

FIGURE 12.3 The specific volume $\bar{V}$(cm^3/g) of EPON 1001F fully cured with a stoichiometric amount of 4,4′–diamino diphenyl sulfone (DDS) shown as a function of temperature at four different rates of cooling 0.90, 0.25, 0.050, and 0.003 °C/min. Glass temperatures identified by the intersection point of the equilibrium and glass lines are listed.

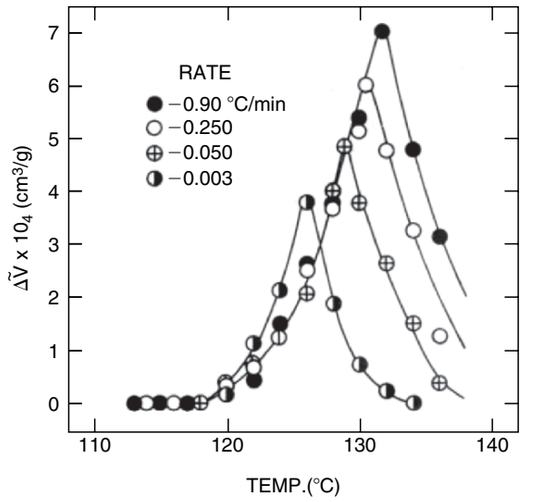

FIGURE 12.4. Deviation of measured specific volume points from the equilibrium and glass lines of Fig. 12.1 plotted as a function of temperature, showing the extent of the transformation range and its change with the rate of cooling.

DSC, and have compared the results obtained dilatometrically. Their study covered the molecular weight range from 580 up to 2.0×10^6. The checks agreed within about 1 °C. The difficulty of the study was made clear. Most investigators do not have the opportunity to exercise the effort needed to obtain accurate $T_g s$ from DSC measurements. Most DSC measurements are carried out as heating scans [51] which result in yielding something close to the fictive temperature T_f of Tool [44]. Investigators of inorganic glasses have long appreciated the distinction between T_g and T_f while polymer scientists in general are not aware of or ignore it. Figure 12.5 shows the glass temperature as the intersection point of the volume, v, or enthalpy, H, temperature lines of the equilibrium (or metastable equilibrium) liquid and the glass

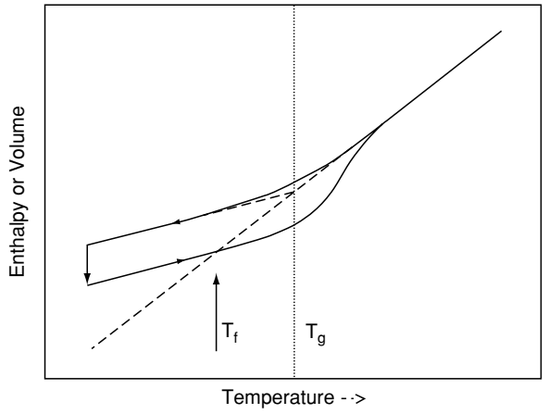

FIGURE 12.5. Schematic plot of the enthalpy or the volume as a function of temperature for glass-forming liquids. The fictive, T_f and glass, T_g, temperatures are indicated.

obtained in cooling. The intersection point is usually chosen as T_g. [3,23,34,49,50]. For a given substance this definition is a material characterizing function of the rate of cooling since it is the measure of the departure from a unique equilibrium. Figure 12.5 also shows how T_f which identifies the state of a specimen. T_f is the result of a simple geometric operation. The specific volume or enthalpy of a specimen must be known and a line having the slope of a glass line is drawn through it. The intersection of this glass line with the equilibrium line is T_f. Note that T_f is not a function of the heating rate. A fictive temperature measured by heating at the same rate as that of an immediately preceding cooling from above T_g approximates T_g and is called $T_{f,g}$.

In an actual heating curve, if it is slow enough, an appreciable spontaneous contraction or decrease in H can occur during the heating, which would yield an intersection point slightly below T_f. For equal cooling and heating rates, T_f is measurably lower than T_g. Without corrections for thermal lags, actual scans often show indicated temperatures where $T_f > T_g$. This is a clear indication of the error incurred. DSC measurements in the past have almost universally been carried out in the heating mode [51,52] because thermal lags can be corrected with melting point standards. Since freezing is a nucleated process, super cooling always occurs which prevents an accurate calibration during cooling. However, it has been observed that some liquid-crystal meso-phase transitions do not show super-cooling, thus making accurate calibrations during cooling a convenient possibility [53].

In addition, it should be noted that, while it is generally recognized that the dynamic loss tangent peaks are 15°–20 °C higher than $T_g(q = 1\ ^\circ/\text{min})$, [54,55a] the temperatures of these maxima continue to be reported as T_gs. Twenty degrees above T_g, the rate of molecular motion in many polymers is about a million times greater than that found at T_g. Therefore, predictions for rate processes based on such incorrect T_gs can be in error by six orders of magnitude. The uncertainty of many of the reported values, therefore, should not be taken lightly for practical purposes. In addition, serious differences of opinion exist concerning the molecular mobility at T_g. Such differences cannot be resolved until a better collection of T_gs is available. Even then, different analyses and models appear to lead to differing conclusions. Some discussion of these will be found below.

12.4 ISOTHERMAL CONTRACTION NEAR AND BELOW T_g

The kinetics of spontaneous time-dependent contraction of a glass following a quench from equilibrium above T_g is frequently studied. This kind of measurement is one of the experiments carried out by Kovacs [3] in his classical studies on the time-dependent variation of the specific volume of glasses. The most common study involves quenching from a fixed temperature above T_g down to different temperatures below T_g. At each chosen lower temperature, the spontaneous contraction is monitored as a function of time. The results of such quenches and annealing are illustrated in Fig. 12.6. A commercial polystyrene (Dylene 8; Arco Polymers, $M_n = 0.93 \times 10^5$, $M_w = 2.2 \times 10^5$) was studied [55b]. The fractional excess (above equilibrium) specific volume $(v(t)/v_{\text{inf}}) - 1$ is plotted as a function of the logarithmic annealing or aging time. $\bar{v}(t)$ is the time-dependent specific volume and $\bar{v}_{\text{inf}} = v(\infty)$ is the equilibrium value for the temperature at which the densification is occurring.

Measurements such as these can be used to define a T_g which would be a material-characterizing function of the time of annealing (or physical aging [31]). In spite of the acknowledged intrinsic nonlinearity of the contractions linear parallel segments of the response are observed which can be easily extrapolated to zero excess specific volume [3]. In Fig. 12.6, lines tangent at the points of inflection can be extrapolated to zero. This intersection with the logarithmic time axis yields the time-temperature relationship for this T_g. T_g would then be a function of the aging time. The advantage of this kind of T_g is the greater resolution that is possible relative to that available from a cooling curve. The intersection point of the equilibrium and glass lines yields a T_g value which is probably valid to within a degree. The rate of time-scale shifts with temperature in the quench experiments is equivalent to that of viscoelastic processes [49], which are large. An order of magnitude change in rate of transport processes near T_g requires a temperature change from 1.5° to 6 °C depending on the material.

12.5 THE CONCENTRATION DEPENDENCE OF THE GLASS TEMPERATURE, $T_g(\phi_2)$

Usually a diluent decreases the T_g of a polymer severely. Early measurements [56] indicated that solvents with lower T_gs of their own decreased the T_g of a polymer to a greater

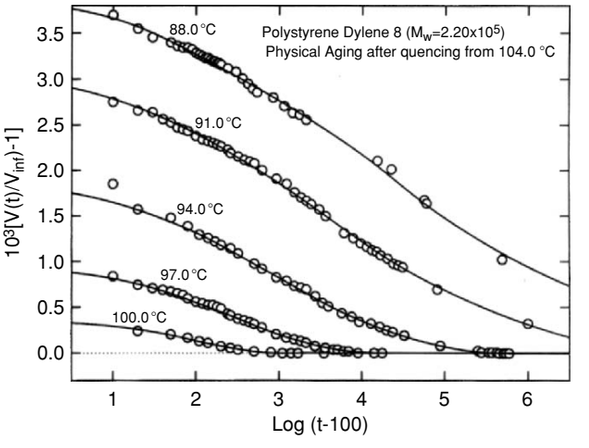

FIGURE 12.6. The fractional excess specific volume $[\bar{v}(t) - \bar{v}(\infty)]/\bar{v}(\infty)$ for a polystyrene at different temperatures shown as a function of the logarithmic time after quenching from $T = 104.0$ °C. (100 sec is subtracted as the approximate time to reach the temperature indicated.)

extent. This can be seen in Fig. 12.7 where the compositional variation of the T_g of polystyrene in a number of solvents is shown. Solutions of a polymer in solvents with T_gs higher than its own will usually have a greater value than that of the neat polymer [57].

The impression of a simple relationship given by Fig. 12.7 is misleading since a continuously decreasing negative slope is indicated. For polystyrene, PS, solutions in toluene [58] and *m*-tricresyl phosphate [59,60] this has been shown not to be the case. In 1964 Braun and Kovacs reported results on the polystyrene/toluene system which showed two descending curves which came together in a cusp [58] (see Fig. 12.8). The results were rationalized by fitting the Kelley–Bueche equation [61],

$$T_g = \frac{\phi_2\alpha_2 T_{g2} + \phi_1\alpha_1 T_{g1}}{\phi_2\alpha_2 + \phi_1\alpha_1},$$

to the data above the temperature of the cusp, T_c. This equation was derived assuming that the free volumes of the polymer and the solvent were additive and that T_g is an

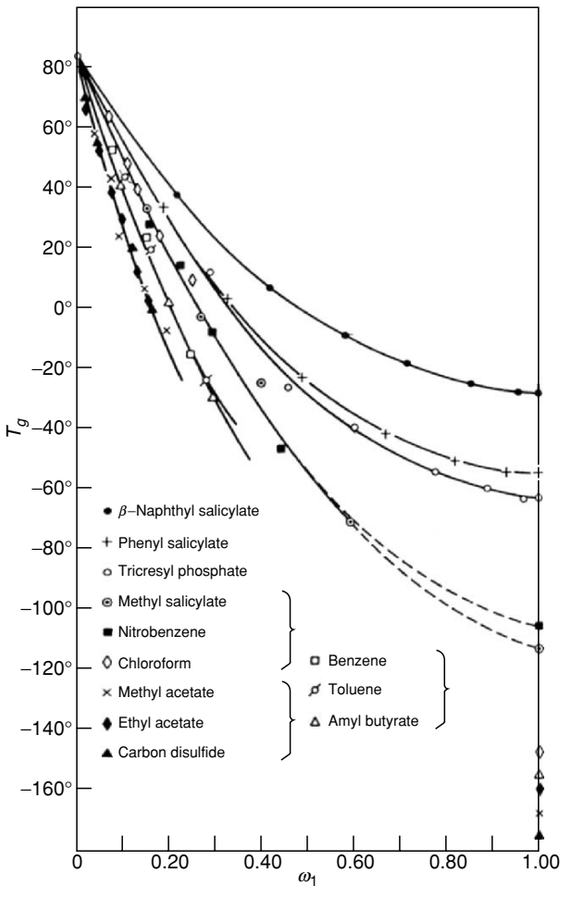

FIGURE 12.7. The compositional variation of the glass temperature T_g of polystyrene in 12 different solvents. W_1 is the weight fraction of solvent. (From Jenckel and Heusch, by permission, [56].)

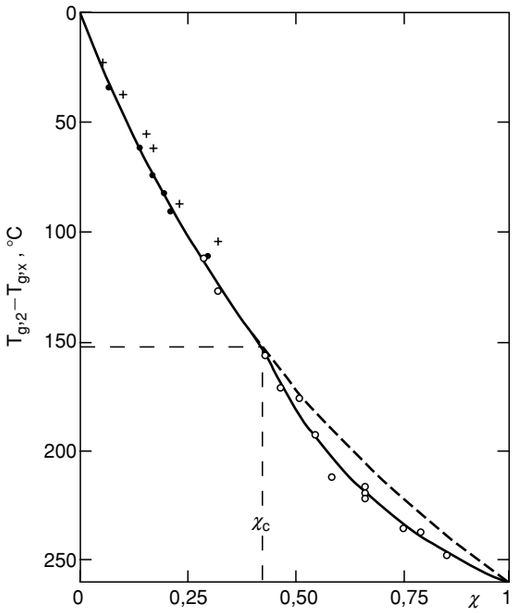

FIGURE 12.8. The depression of T_g of a polystyrene by dissolution in toluene. x is the weight fraction of toluene. Filled circles represent dilatometric determinations and unfilled circles were obtained by means of differential thermal analysis, DTA. The crosses represent the results of Jenckel and Heusch [56]. (From Braun and Kovacs by permission, [58].)

iso-free volume temperature.[a] ϕ is the volume faction; α is the cubical thermal expansion coefficient of the fractional free volume, $f = v_f/v$; subscripts 1 and 2 represent the solvent and polymer, respectively. v_f is the free volume and v the measured volume. Below T_c, Braun and Kovacs used the equation [58],

$$T_g = T_{g1} + \frac{f_{g2}}{\alpha_1}\left(\frac{\phi_2}{\phi_1}\right),$$

where f_{g2} is the fractional free volume of the polymer at its T_g.

Pezzin *et al*. found the same kind of behavior exhibited by polyvinyl chloride PVC in two different plasticizers, dibutyl phthalate, DBP, and dicyclohexylphthalate, DCHP [62,63]. The same two equations provided excellent fits to the PVC solution data (see Fig. 12.9). For polystyrene dissolved in *m*-tricresyl phosphate, TCP, additional factors were noted.

Differential thermal analysis measurements indicated double T_gs for solutions with lower polymer concentrations beyond the depicted cusp in Fig. 12.10 [59]. Creep recovery measurements on this system showed that the solvent molecules in the solutions have higher mobilities than the polymer chain segments. A lower temperature and greater crowding is therefore necessary to force the solvent molecules from an equilibrium response. Therefore, it was

[a] Other treatments are now available [137,138].

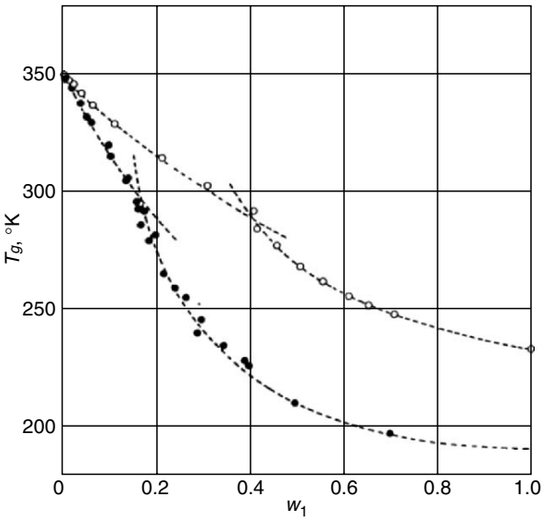

FIGURE 12.9. The T_g of a polyvinlychloride as a function of diluent concentration in two different solvents. Open circles-dicyclohexylplthate and filled circles-dibutylphthalate. W_1 is the weight fraction of diluent. (From Pezzin, Omacini, and Zilio-Grandi by permission [62].)

concluded that the higher T_gs reflected those of the polymer chain segments in a solvent-altered environment and the lower T_gs reflected the solvents mobility in the presence of the polymer chain segments [60]. For different bulk polymers, T_g local mode or short-range molecular motions are found within experimental uncertainty at the same place on the time or frequency scales of response [64–66]. For the solutions of PS in TCP, the T_gs from the lower ''altered solvent'' curve were necessary to bring the solvent contribution to the recoverable compliance into correspondence with other solutions. The higher T_gs were also needed to bring the contribution from polymer local modes into correspondence [60]. The mobility of solvent molecules and how it is influenced by the presence of polymer solute molecules has been investigated and documented by measurements of pulsed field-gradient NMR [67], oscillatory electric bire-fringence [68,69], ^{13}C NMR relaxation [70], photon correlation spectroscopy [71–73a], and dielectric dispersion [73b]. Solvent molecules generally have a decreased mobility in the presence of polymer molecules with greater T_gs.

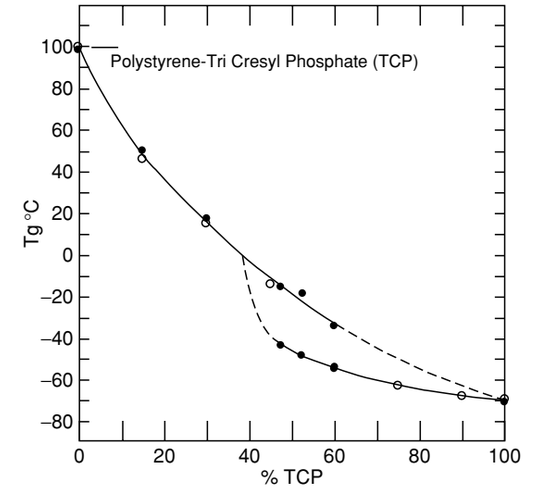

FIGURE 12.10. The T_gs of a polystyrene as a function of the weight percent of the solvent *m*-tricresyl phosphate.

In most cases, free volume concepts at least qualitatively predict the shift of solvent and polymer chain segment mobilities towards one another. The most frequently encountered case, where a polymer with a higher T_g than that of the solvent, brings to the solution a smaller contribution of free volume which decreases the solvent's mobility. At the same time the solvent, being far above its T_g, brings a large contribution of free volume to the solution which accelerates polymer segment motions. However, there are solutions where the solvent's mobility is *increased* by the presence of a polymer whose undiluted T_g is higher than that of the solvent. In this case, obviously, free volume concepts are inadequate. In these cases, the coupling model of Ngai has been able to attribute the unexpected solvent acceleration to a ''primitive'' or uncoupled relaxation time of the polymer which is smaller than that of the solvent [73].

12.6 DEPENDENCE OF T_g ON MOLECULAR WEIGHT AND CROSSLINKING

During the transformation of a monomer into a polymer, many atoms separated by van der Waals distances (~5 Å) participate in the formation of covalent bonds (1–3 Å). Therefore during polymerization, an increase in the macroscopic density ensues, while on the molecular level a decrease in free volume and entropy occurs while the cooperativity of motions increase. Concomitantly the glass temperature can increase by more than 100 °C. Several important adhesive systems are based on this increase. The cyanoacrylate ''Super Glue'' starts as a monomer with a $T_g < 0$ °C and it polymerizes to a linear soluble polymer with a T_g which is in the neighborhood of 100 °C upon application under anaerobic conditions. For linear polymers the simple equation [74]

$$T_g = T_g(\infty) - K/M_n,$$

which reflects the linear decrease in T_g with the increase in concentration of polymer chain ends does an adequate job of describing most existing data in the literature. Deviations may occur at very low molecular weight. The more elaborate Gibbs-Dimarzio theory [40,41] which concentrates on the conformational entropy can fit data to lower molecular weights.

Uncatenated cyclic polydimethylsiloxane, PDMS, shows [75] a slight increase in T_g with decreasing molecular

weight. This trend has been rationalized by Gutman and Dimarzio [76]. However, it was observed that the rate of creep at 120 °C for cyclic polystyrene, PS, with $M_w = 1.11 \times 10^4$ in the softening dispersion was the same within experimental uncertainty as a cyclic sample with a $M_w = 1.85 \times 10^5$. This indicates that the T_gs of the two samples had to be within one or two tenths of a degree of one another [77]. For their linear counterparts, the rate of creep of the lower molecular weights is about 100 times faster where the difference in T_gs is about 10 °C.

Crosslinking can increase the T_g above that of the infinite molecular weight linear polymer. This increase can be accounted for with the equation of Fox and Loshaek [74].

$$T_g \simeq T_g(\infty) - K/M_n + K_x\rho,$$

where ρ is the number of crosslinks/gram.

Epoxy resins based on the diglycidyl ether of bisphenol A, DGEBA, are the most widely produced and studied. Their chemical structure is represented by

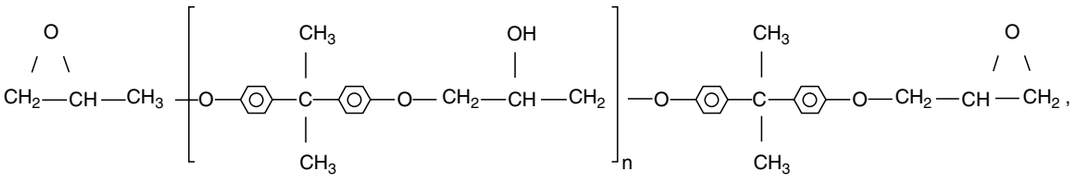

where $(n+1)$ is the average number of repeat units in the epoxy resin molecule. Diamines are most often used in curing these resins. Two examples are:

4,4′-methylene dianiline, MDA,

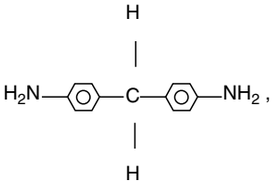

whose molecular weight is 198.3 g/mol, melting point range 90–93 °C and density, $\rho(23\ ^\circ\text{C}) = 1.16\,\text{g/cm}^3$; and 4,4′ diamino diphenyl sulfone, DDS

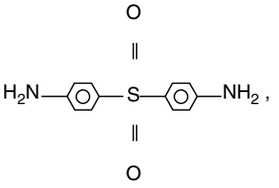

M W 248.3 g/mol, *Mp* 175–178 °C, $\rho(23\ ^\circ\text{C}) = 1.38\,\text{g/cm}^3$.

The effect of the developing network during curing on T_g and the mechanical behavior is illustrated with an epoxy resin Epon[b] 1001F ($n = 2.3$) cured with DDS [81]. The degree of network development was determined by reacting the epoxy resins stoichiometrically with varying ratios of the tetrafunctional crosslinker DDS and the chain-stopping monofunctional methyl aniline. Some properties of the resin at different stages of network development are given in Table 12.1. Fictive temperatures $T_{f,g}$ [82–84] which approximate T_g are presented along with closely related temperatures. The $T_{f,g}$ (10°/min) for the neat unreacted epoxy resin was 31 °C. The short-term ($0.1–10^2$ sec) behavior at T_g can be described by a viscoelastic recoverable compliance which appears to be the same for all amorphous materials, without secondary viscoelastic dispersions contributions in this timescale range. A recoverable creep compliance is found that can be fitted to the Andrade equation [85–87].

$$J_r(t) = J_g + \beta t^{1/3},$$

where J_g is the glassy compliance which has a value in the neighborhood of $1 \times 10^{-9}\text{Pa}^{-1}(1 \times 10^{-10}\,\text{cm}^2/\text{dyne})$; t is the time; and β is a constant which depends on the choice of $T_g(q)$. For the choice of $q = 10\ ^\circ/\text{min}$ it can be seen in Table 12.1 that $\beta(T_{f,g}) \simeq 2 \times 10^{-9}(\text{Pa sec}^{1/3})^{-1}$. The first three levels of crosslinking yielded viscoelastic liquids (gel fraction=0) that flow and exhibit steady-state recoverable compliances [18]. A material which was extremely close to the incipient point of gelation was yielded by 45% DDS, where a macroscopic molecular network just appears. At this point the recoverable compliance at long times is immeasurably high; i.e., J_e^0 is operationally infinite. At higher crosslinker ratios, the equilibrium compliance J_e of the molecular network is readily measurable. At 50% crosslinking agent $J_e \simeq 1.0 \times 10^{-4}\text{Pa}^{-1}$ (see Fig. 12.11).

T_gs of fully cured bisphenol-*A*-based epoxy resins with varying crosslink densities were measured during cooling (5°/min) in a pressurized bellows dilatometer (5 MPa). The crosslinking agent was DDS. The results are shown in Fig. 12.12. The molecular weights per crosslinked unit, M_x, were 420 for Epon 828; 910 for 1001F; 1520 for 1004F; and 2870 for 1007F. The T_gs obtained were 204°, 127°, 112°, and 101 °C, respectively. The loosest network epoxy, 1007F, has the highest specific volumes and the lowest T_g. The volume changes during the curing of Epon 1001F are shown in Figs. 12.13a and 12.13b. In Fig. 12.13a the temperature history of the cure is shown along with the volume changes due to heating, curing, and cooling as a

[b] Shell Corp. trademark.

TABLE 12.1. *Characterizing parameters.*

DDS	$T_{f,g}$[a]	$T_{0,J}$[b]	$T_{0,a}$[c]	$J_g \times 10^{10}$[d] (cm^2/dyne)	$\beta \times 10^{10}$[d]	$\rho(25\ ^\circ C)$[e] (g/cm^3)	$\log J_e$[f] (cm^2/dyne)	M_x[g]
0.25	63.0	64.1	66.3	1.13	1.46	—	−5.53	—
0.35	65.0	66.0	65.0	0.685	1.43	1.188	−4.10	—
0.40	70.6	69.9	66.4	0.65	1.95	—	−3.60	—
0.45	72.5	72.5	69.9	1.45	2.06	1.189	—	—
0.50	73.4	75.4	73.7	1.06	1.19	1.191	−5.00	2.95×10^5
0.60	80.0	84.9	82.0	1.15	2.63	1.194	−5.98	3.10×10^4
0.70	86.4	89.2	88.7	1.24	1.78	1.218	−6.43	1.12×10^4
1.0	132.0	135.6	135.5	1.36	1.95	1.205	−7.04	680

[a]Measured using DSC; all heating rates were 10 °C/min, following cooling at a rate of 10 °C/min (20 °C/min rate of cooling for 0.35 and 0.45 DDS; and 80 °C/min for 1.0 DDS).
[b]Reference temperatures that match the softening region on the creep compliance reduced time scale. Reference system was 0.45 DDS.
[c]Reference temperatures obtained from the temperature shift factor, a_T, analysis (see Fig. 12 in Ref. 81).
[d]Andrade equation parameters for $T = T_{0,J}$.
[e]Density of fully cured samples measured by flotation; followed by pycnometry.
[f]For the viscoelastic liquids J_e is the steady-state recoverable compliance and for the viscoelastic solids, beyond the gel point it is the equilibrium compliance.
[g]Average molecular weight per crosslinked unit calculated from J_e: $M_x = \rho RTJ_e$.

function of time [82]. The volume changes are presented in Fig. 12.13b as a function of temperature, where the initial fictive temperature, T_f, of the reactant mixture and the glass temperature, T_g, of the fully cured resin can be seen.

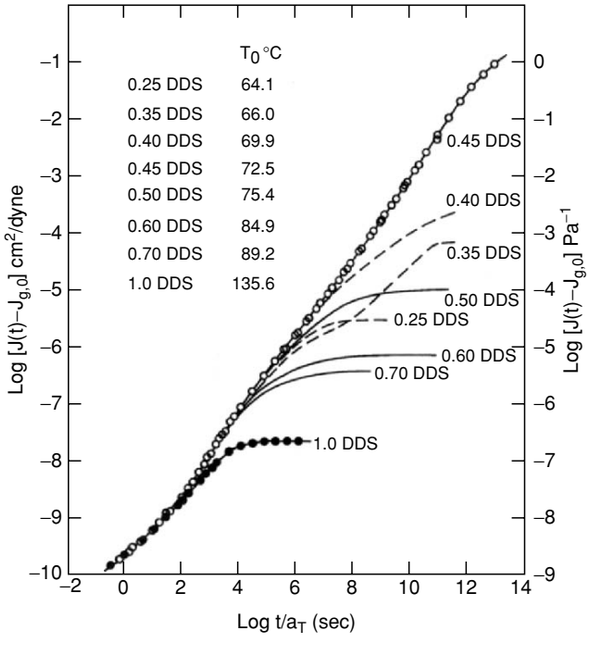

FIGURE 12.11. Comparison of all of the time-dependent reduced compliance $[J(t) - J_{g,0}]$ as logarithmic functions of $\log t/a_T$. Comparison temperatures are indicated above and in Table 12.1. $J_r(t) - J_{g,0}$ is shown for the viscoelastic liquids (dashed lines); i.e., specimens with no gel fraction.

The increase in $T_{f,g}$ during curing has been seen to track the degree of cure. This can be seen in Fig. 12.14 where five variables have been monitored during the curing of Epon 1001F at 142 °C which is about 10 °C above the T_g of the fully cured material. The degree of cure was monitored by the increase in density. The gel fraction became measurable after several hours signaling the presence of a macroscopic

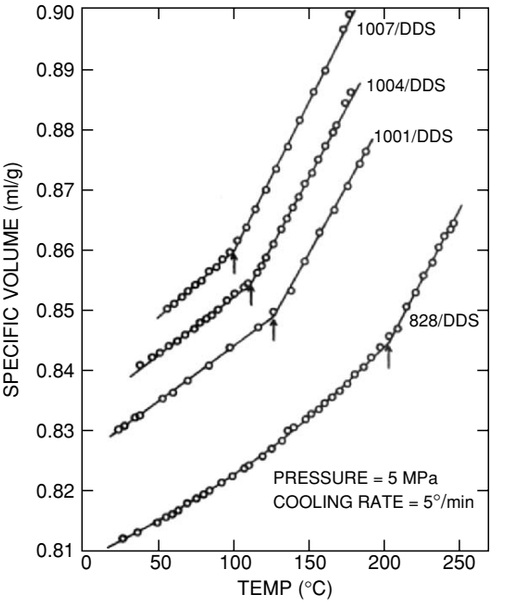

FIGURE 12.12. Specific volume - temperature curves for four epoxy resins with increasing crosslink density from 1007/DPS to 828/DPS. Measurements were made during cooling at 5°/min under a pressure of 5 MPa.

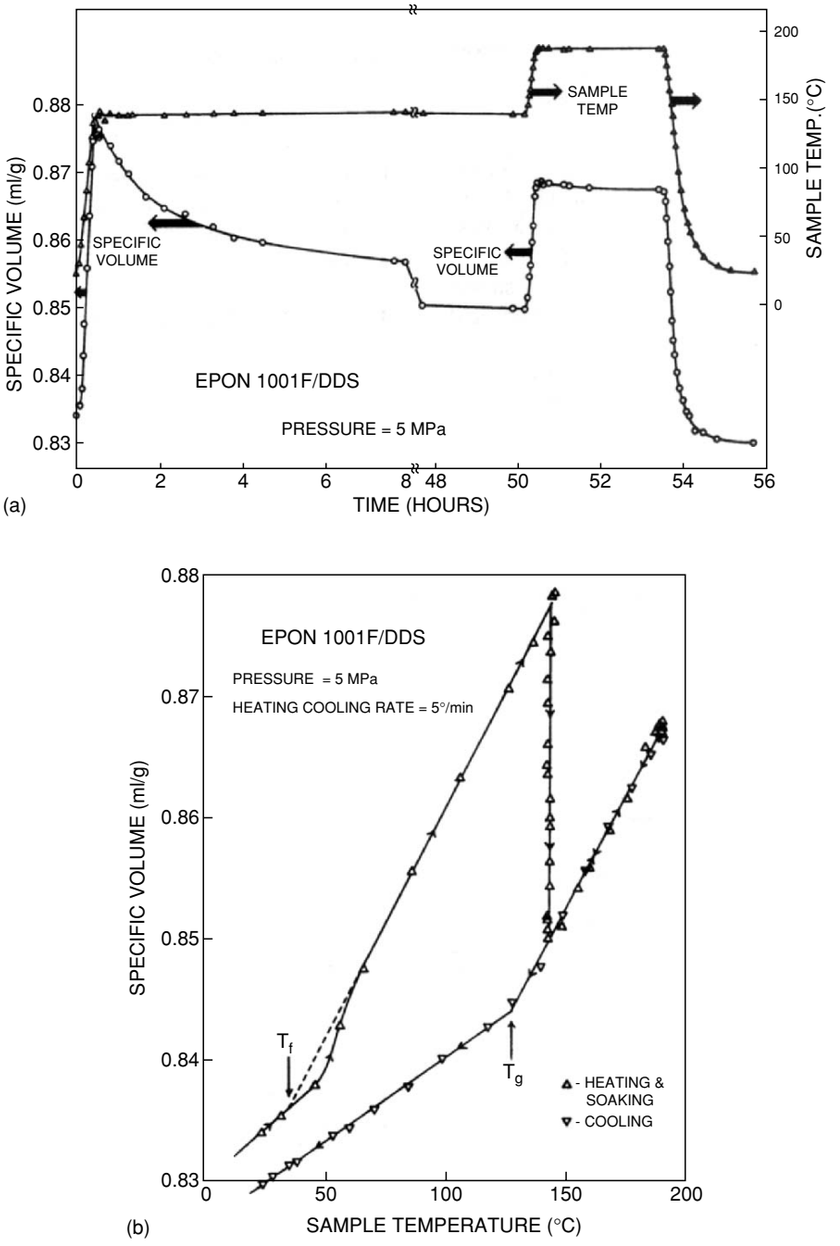

FIGURE 12.13 (a) Specific volume - temperature history of 1001F/DDS epoxy resin during curing under a pressure of 5 MPa. (b) Specific volume data from Fig. 12.13a plotted as a function of the temperature.

molecular network. Before the point of incipient gelation, the viscosity can be seen to climb toward infinity before gelation. After gelation, the precipitous drop in the equilibrium compliance of the developing network continues until a complete cure is achieved in about two days. Using the starting and final $T_{f,g}$s as limits it can be seen that they follow the degree of cure.

When an epoxy resin is cured at a temperature which is below its ultimate $T_g(\infty)$ at full cure, the $T_{f,g}$ will increase rapidly as the reaction proceeds until the T_g becomes equal and surpasses the temperature of cure T_c. The reaction then becomes diffusion-controlled and the rate of reaction and increase in $T_{f,g}$ decelerates to a much lower but still perceptible value as can be seen in Fig. 12.15 [82]. The curing reaction continues significantly even when T_c is 50 °C below T_g. Room temperature cures of epoxy resins can therefore be expected to continue for years.

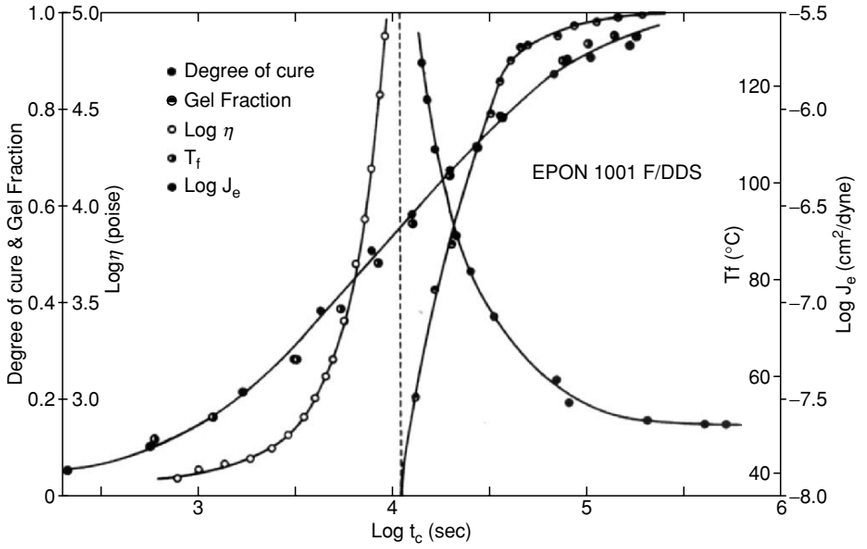

FIGURE 12.14. Comparison of changing parameters during the curing of 1001F/DDS at 142 °C. The logarithm of the viscosity $\eta(p)$ and the equilibrium compliance $J_e(\text{cm}^2/\text{dyn})$ as well as the fictive temperature T_f, the degree of cure, and the gel fraction are shown as functions of the logarithm of the time of curing $T_c(s)$.

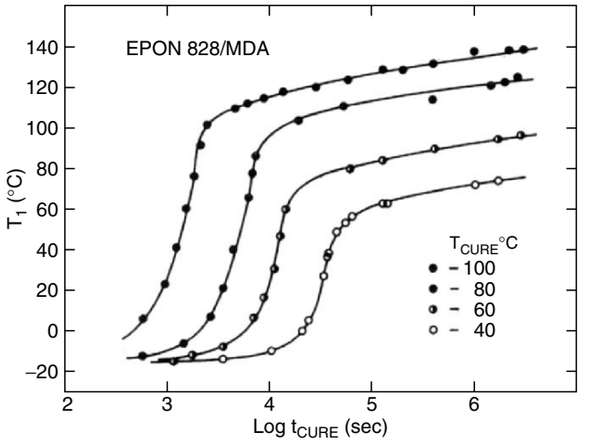

FIGURE 12.15 Fictive temperatures, T_f, observed during the curing of an epoxy resin at temperatures below the $T_g(\infty)$ of the fully cured state.

12.7 DEPENDENCE OF T_g ON THE DEGREE OF CRYSTALLINITY AND MORPHOLOGY

Nearly all crystalline polymers contain chain segments that do not reside in a crystalline lattice. Usually these noncrystalline segments can be considered to constitute an amorphous phase which therefore can become glassy. The T_g of this amorphous phase depends on the degree of crystallinity. T_g increases and decreases with the presence of crystallinity. It can increase or decrease with the degree of crystallinity depending on the relative density of the amorphous and crystalline states. Most often the more orderly crystalline state has the higher density at T_g and the noncrystalline molecular chains are constrained by being anchored to the immobile crystallites and T_g increases. On rare occasions the crystalline state has a lower density than the amorphous material [88]. In this case, less constraint on the noncrystalline chain segments increases the entropy causing T_g to decrease. T_g is not a unique function of the degree of crystallinity. At least in the usual case where the density of the crystalline state at T_g is higher than that of the amorphous state, the temperature at which the crystallites are formed plays a dominating role. At temperatures above the maximum in the crystal growth rate [89], and of course, below the melting temperature T_m, the rate of nucleation is low and therefore relatively few spherulites are formed and the tie molecules in between crystallites are relatively unconstrained. Hence the increase in T_g with increased crystallinity is relatively slight [89] as seen in Fig. 12.16. However, at temperatures below the maximum in crystal growth rate and near T_g, the rate of nucleation can be profuse. Many crystallites are formed and tie molecules are therefore shorter and more constrained. Therefore a given degree of crystallinity is more effective in raising T_g (see Fig. 12.17). The above conclusions are drawn from the mechanical results reported by Groeninckx *et al.* [89] where the onset of the steep decrease in $\log E_r(10)$ with temperature can be considered as a rough estimate of T_g. Direct confirmation with proper T_g measurements is desirable.

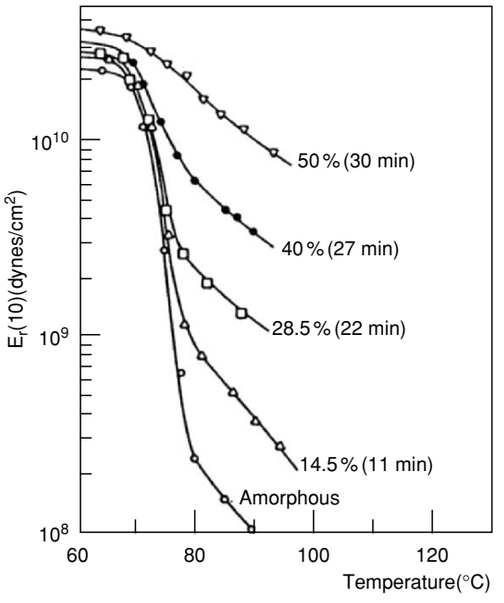

FIGURE 12.16. Ten-second stress relaxation moduli $E_r(10)$ of PET crystallized at 227°C to different degrees presented as a function of temperature. Crystallization times are also shown as well as the estimated degree of crystallinity from density measurements. (From Groeninckx, Berghmans, and Smets, by permission, [89].)

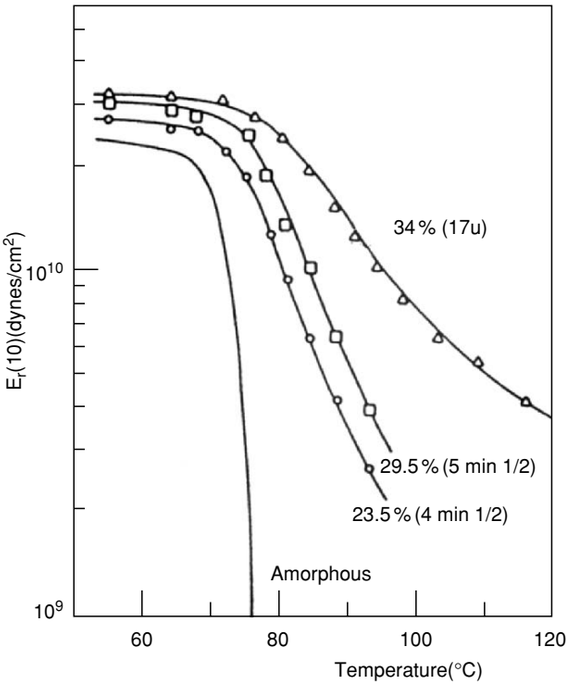

FIGURE 12.17. Ten second stress relaxation moduli $E_r(10)$ of PET crystallized at 120°C to different degrees presented as a function temperature. (From Groeninckx, Berghmans, and Smets, by permission, [89].)

12.8 DEPENDENCE OF T_g ON INTERMOLECULAR FORCES

The greater the intermolecular interaction, all other things being equal, the higher T_g will be. It has been proposed that T_g is a linear function of the cohesive energy density CED [90].

$$\text{CED} = 0.5\text{MRT}_\text{g} - 25\text{M},$$

where R is the gas constant and M is a parameter analogous to the number of degrees of freedom of a molecule. Eisenberg has shown how T_g increases dramatically in a phosphate glass with the decrease in size of incorporated anions and with increases in their charge [91]. He has also shown how in ionomers (specifically ethyl acrylate-acrylic acid copolymers neutralized with various cations) T_g is a common smoothly increasing function of $c\ q/a$ as shown in Fig. 12.18. c is the cation concentration, q is its charge, and a is the distance between centers of charge, as shown in Fig. 12.18. The onset of the observed sigmoid coincides with the domination of a wide range of properties by ionic clusters.

12.9 THE EFFECT OF PRESSURE ON T_g

An increase in pressure on an amorphous material increases molecular crowding and interactions along with decreasing the entropy. Regardless of the variable which one looks upon as significant, an increase in T_g is expected. If a rapid pressure increase is incurred, a time-dependent decrease in volume will follow if the temperature is near or below T_g. This is indeed a simple voluminal viscoelastic creep process. The resultant behavior is quite analogous to that seen following a temperature quench as discussed above. The similar response to pressure jumps has been shown by Goldbach and Rehage [92]. The expected increase in T_g with increases in pressure has been documented by McKinney and M. Goldstein [93]. Discussions in the literature are confounded by not restricting the definition of T_g to cooling from an equilibrium state.

12.10 EFFECT OF MOLECULAR STRUCTURE ON T_g

12.10.1 Internal Plasticization and Chain Stiffness

If side chains on the polymer backbone are increased in length only, it is generally observed that T_g decreases, ostensively because the linear side chains increase the fractional free volume between the chains and any structural change which increases the diameter of the side chains reverses the tendency; i.e., T_g increases. This is a reflection of the following general principle.

Any structural feature which increases the size of the jumping unit of the molecular chain will increase T_g. An

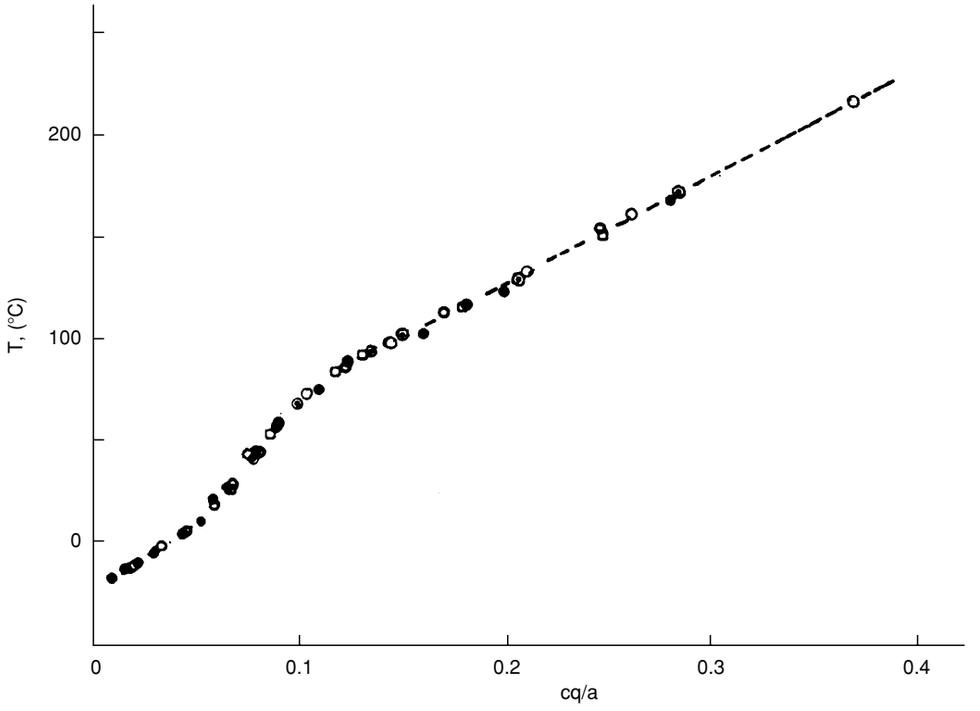

FIGURE 12.18. T_g of ethyl acrylate - acrylic acid copolymers neutralized with various cations shown as a function of cq/a, where c is the cation concentration, q is its charge, and a is the distance between centers of charge. (From Matsuura and Eisenberg, by permission, [91b].) Different symbols represent different cations.

increase in chain stiffness resulting from longer rigid units in the chain backbone or more bulky side groups which drastically increase the potential barriers to rotation, cause substantial increases in T_g. Steric barriers to rotation are raised appreciably if a second side group is introduced on alternate chain backbone atoms. The pairs, polymethylmethacrylate PMMA ($T_g \simeq 115c$)-polymethylacrylate PMA (14 °C) and poly(α-methylstyrene) ($\sim$168 °C)-polystyrene (100 °C), illustrate the effect. Introducing paraphenyl rings into a chain backbone increases T_g since a longer portion of the chain has to be involved in a molecular segmental displacement. To the contrary introducing additional methylene (—CH_2—) groups or ether oxygens into the polymer chain backbone lowers T_g because of the increased chain flexibility. With no side atoms or groups and a wide open bond angle ($> 111^\circ$) the ether oxygen is considered the premier flexibilizing unit.

12.10.2 Effect of Polarity

The stronger the interactions between neighboring polymer chain segments, the greater the thermal kinetic energy must be to create holes of sufficient size to allow a diffusive jump of a chain segment to occur. Therefore, the greater the polarity of a polymer, the higher the T_g will be. The greatest effect will be due to resultant components of dipole units which are perpendicular to the chain backbone. The greater T_g of polyacrylonitrile ($\sim$ 103 °C) relative to that of polypropylene ($-$ 14 °C) must be due to the large electron affinity of the nitrile group (—C $\equiv$ N).

Enhancing the flexibility of a polymer chain by introducing an ether oxygen into its backbone will lower T_g and the melting temperature, T_m. Increasing the polarity or the opportunity for hydrogen bonding between neighboring chain segments increases T_g and T_m. The effects of such variations are illustrated in Table 12.2 where the coupling units are varied in a family of otherwise similar polymers.

TABLE 12.2. *Effect of polarity and hydrogen bonding.*

Low T_gs and T_Ms	—R—O—R′—	polyethers
	—C(=O)—O—	polyesters
	—N(H)—C(=O)—O—	polyurethanes
	—N(H)—C(=O)—	polyamides
High T_gs and T_Ms	—N(H)—C(=O)—N(H)—	polyureas

12.10.3 Influence of Symmetry

On the basis of some of the above comments it would be expected that the T_g of polyisobutylene PIB $[CH_2—C(CH_3)_2]_n$ would be higher than that of polypropylene PP $[CH_2—C(H)CH_3]_n$. The polarity of PIB is lower than that of PP because the opposing dipoles tend to cancel one another. However, the polarity is low in both cases and would not be expected to be a dominating factor. The two side groups on alternate carbon backbone atoms of the PIB certainly should present overall higher barriers to rotation than that present in the PP. Yet the T_g of PIB at $-73\ ^\circ C$ is some $59\ ^\circ$ lower than that of PP. Likewise, the T_g of polyvinylidene chloride $[CH_2—CCl_2]_n$ at $-17\ ^\circ C$ is 63° lower than that of polyvinylchloride $[CH_2—CClH]_n$. It was discovered by Boyd and Breitling [95] that whereas there are indeed higher barriers to rotation in the vinylidene polymers, there are adjacent potential energy wells with an extremely low barrier in between them, thus allowing for very free rotation over a limited angle of about 20° which permits liquid structures to adjust far more rapidly than expected.

12.10.4 Effects of Tacticity

It is surprising that stereochemical variations in tacticity [96] have no measurable effect on the T_g of polymethylacrylate PMA and polystyrene PS, but they have a substantial effect on that of polymethylmethacrylate PMMA and poly(α-methylstyrene) PαMS [97]. The explanation appears to lie in the added steric repulsion to rotation due to the presence of the asymmetric double side groups on alternate chain backbone atoms. Extended planar zig-zag configurations of the chains are not possible and it is clear that different helical forms of highly isotactic and syndiotactic chains obtain. The stiffness of the helices are obviously significantly different. A reflection of the differences in the helical character of the chain conformation is seen in the variation of the dielectric permittivity as a function of the tacticity [98]. Highly syndiotactic samples of PMMA have a dominant β loss peak reflecting independent motion of the carbonyl dipole in the ester side group. However, as the degree of istacticity is increased, the dipole activity is shifted to the α backbone loss peak. As the limit of total isotacticity is approached, the β loss peak virtually vanishes, indicating that the carbonyl dipole motion is locked in with the chain backbone motion. A consequence of the lack of independent side chain motion (β mechanism) in iso-PMMA is a much smaller glassy compliance, J_g [99]. Secondary (sub-t_g) loss mechanisms are listed in this handbook in the chapter authored by Fried.

12.11 DIFFERENCES OF OPINION CONCERNING T_g

Qualitatively free volume concepts usually provide a rationale for observed behavior [18], but clearly they do not provide a comprehensive understanding. Interactions and coupling also play a role. Occasionally, as mentioned above, a polymer with a T_g, which is higher than that of its solvent will increase the mobility of the solvent molecules. This is contrary to what is expected according to free volume concepts. Such acceleration can be understood if the uncoupled mobility of the polymer is greater than that of the solvent [73].

In addition to the free volume [36,37] and coupling [43] models, the Gibbs–Adams–DiMarzo [39–42], (GAD), entropy model and the Tool–Narayanaswamy–Moynihan [44–47], (TNM), model are used to analyze the history and time-dependent phenomena displayed by glassy supercooled liquids. Havlicek, Ilavsky, and Hrouz have successfully applied the GAD model to fit the concentration dependence of the viscoelastic response of amorphous polymers and the normal depression of T_g by dilution [100]. They have also used the model to describe the compositional variation of the viscoelastic shift factors and T_g of random Copolymers [101]. With Vojta they have calculated the model molecular parameters for 15 different polymers [102]. They furthermore fitted the effect of pressure on kinetic processes with this thermodynamic model [103]. Scherer has also applied the GAD model to the kinetics of structural relaxation of glasses [104]. The GAD model is based on the decrease of the conformational entropy of polymeric chains with a decrease in temperature. How or why it applies to nonpolymeric systems remains a question.

The TNM model has been used to describe structural relaxation during the heating and cooling of amorphous crowded liquids by O'Reilly [8] and by Hodge [10]. A disturbing result of the application of the TNM model is that the effective relaxation time, τ, is not constant at T_g but varies almost eight orders of magnitude when comparing values for different materials [8]. This variation is in serious conflict with the nearly constant rate of creep at T_g observed on a wide variety of amorphous materials [60,64–66]. The TNM model employs the stretched time-scale of the Kohlrausch [105]-William-Watt [106] function: i.e., relaxation which is proportional to $\exp[-(t/\tau)^m]$. The Kovacs, Aklonis, Hutchinson, and Ramos, KAHR, model employs a distribution function of retardation times to describe volume memory and other viscoelastic effects. In the KAHR model it is assumed that the retardation function shifts to longer times with decreasing temperature while its shape is conserved. This requires thermorheological simplicity[c] which does not always hold near and below T_g [78,107].

[c] See the discussion on thermorheological simplicity in Chapter 26 on Viscoelastic Behavior.

The influence of rates on T_g and glass formation has recently been treated by Shi [108]. His results should be examined and tested. He predicts upper and lower bounds for T_g based on thermodynamic and kinetic factors.

12.12 SOME CORRESPONDING PROPERTIES AT T_g

In Table 12.3 a number of properties determined in the neighborhood of T_g are listed [109]. The T_gs were determined at or reduced to a rate of cooling of 0.2°/min. A wide variety of amorphous materials are represented. The first five materials tri-α-naphthylbenzene, Tri cresyl phosphate Aroclor 1248, 6 phenyl ether, and 1,2 diphenylbenzene (o-terphenyl) are nonpolymeric compounds; $Tl_2SeAs_2Te_3$ is an inorganic glass-former; selenium is a polymeric element; polystyrene, amorphous polypropylene, polyvinylacetate, and polyisobutylene are linear organic polymers; Epon 1004/DDS, Epon 1007/DDS, and Viton 10A are crosslinked organic polymers; and 20 PB/A1248 is a solution of a linear organic polymer, 1,2 polybutadiene in an organic solvent, Aroclor 1248. The T_∞ is the hypothetical temperature in the Vogel, Fulcher, Tamman, and Hesse (VFTH) equation [18] and the Williams, Landel, and Ferry (WLF) equation [18] where the viscosity becomes infinite. It is hypothetical because it is implicitly assumed that an equilibrium density persists. At an infinitely slow rate of cooling it appears by extrapolation that $T_g(q = -\infty) = T_\infty$ [49] which, in this limit, makes it a candidate for the second order thermodynamic transition of the GAD model. According to the "universal" form of the WLF equation $T_g - T_\infty \simeq 52$. In Table 12.3, the values vary from 29° to 175 °C. Logarithmic values of the glassy shear compliance $J_g(\text{cm}^2/\text{dyne})$ at T_g are given. Most values are close to $-$ 10.0 as is often observed. Values as high as -9.4 have been reported [110] and the chalcogenide glass $Tl_2SeAs_2Te_3$ is the lowest at -11.1.

Logarithmic values for the steady-state recoverable shear compliance $J_e^0(\text{cm}^2/\text{dyne})$ are also shown. For the nonpolymer J_e^0 values are 2.5 to 3.0 times larger than J_g. For the linear polymers, since J_e^0 is a function of the molecular weight up to value 5 times that of the entanglement value, M_e, and its distribution, much larger ratios are seen. Of course, the network polymers exhibit equilibrium compliances that are determined by the level of crosslinking and are not steady-state values. Steepness indices, $S_{Tg}, = -T_g[d \log a_T/dT]_{Tg}$ which indicate the temperature sensitivity of viscoelastic processes at T_g are also listed. S_{Tg} correlates with the breadth of the effective viscoelastic spectrum; i.e., the higher S_{Tg} is, the broader the viscoelastic response is. Thus, the tempera-

TABLE 12.3. *Properties of amorphous materials near and below T_g.*

	T_∞	J_g	Log$J_e^0(T_g)$	T_g	S_{T_g}	Log$\eta(T_g)$	$\beta_{T_g} \times 10^12$	$T_g^{1\ell}$	ΔT_g
Material	**°C**			**°C**		**poise**	**cm²/dyne-s$^{1/3}$**	**°C**	**°C**
Tri-α-naphthylbenzene	−73.2	−10.022	−9.548	63.8[i]	74.8	12.445	16.67	60.8	3.0
Tri-cresyl phosphate	−116.7	−10.110	−9.586	−73.0[i]	80.5	12.905	10.09	−73.0	—
Aroclor 1248[a]	−181.1	−10.372	−9.987	−50.0[i]	62.0	12.746	6.146	−47.7	−2.3
6-Phenyl ether[b]	−99.8	−10.140	−9.766	−25.0[i]	84.6	12.677	7.700	−23.9	−1.1
1,2 Diphenylbenzene	−101.3	−10.347	−9.926	−32.4[i]	87.6	12.367	9.746	−31.3	−1.1
$Tl_2SeAs_2Te_3$	−113.2	−11.102	−10.64	67.4	60.5	12.246	3.980	69.9	−2.5
Se	10.5	−10.482	−8.480	32.0	155	12.67	7.590	32.8	−0.8
Polystyrene[c]	69.0	−10.022	−4.660	97.5[i]	137.4	13.74[h]	20.88	95.7	1.8
Polypropylene[d]	−46.4	−9.934	−4.820	−14.0	135.4	13.85[h]	15.80	−15.0	1.0
Polyvinylacetate[e]	6.0	−10.046	−4.650	34.8[i]	94.2	17.05[h]	16.95	36.4	−1.6
Polyisobutylene[f]	−135	−10.460	−5.715	−76.2[i]	45.1	15.23[h]	14.62	−77.4	1.2
EPON 1004/DDS[g]	60.8	−9.879	−7.390	107.7	147.8	—	9.816	107.5	0.2
EPON 1007/DDS[g]	50.7	−9.928	−7.100	97.3	144.0	—	7.590	98.1	−0.8
Viton 10A[j]	−54.0	−9.969	−5.940	−26.1	136.3	—	14.56	−26.9	0.8
20PB/A1248[k]	−163.6	−10.495	−4.750	−50.0[i]	61.7	17.0[h]	9.900	−49.8	−0.2

[a] Aroclor 1248 is a chlorinated biphenyl.
[b] 6-Phenyl ether is an abbreviation for bis(*m*-(*m*-phenoxy phenoxy)phenyl)ether.
[c] Commercial Polystyrene ($M_w = 2.20 \times 10^5$)
[d] Amorphous Polypropylene ($M_w = 2.05 \times 10^5$)
[e] Polyvinylacetate ($M_w = 6.50 \times 10^5$)
[f] Polyisobutylene ($M_w = 7.80 \times 10^4$)
[g] EPONs are epoxy resins consisting of a diglycidyl ether of bisphenol *A* cross-linked using diaminodiphenyl sulfone(DDS) as the curing agent. They are network polymers that do not flow.
[h] Viscosities were calculated using the Vogel, Fulcher, Tamman, and Hesse (VFTH) equation.
[i] Glass temperatures were measured at a cooling rate of 0.2 °C/min otherwise they were calculated using the shift factors.
[j] Viton 10A is a fluoroelastomer.
[k] 20PB/A1248 is a 20-wt % solution of a Polybutadiene ($M_w = 1.34 \times 10^5$) in Aroclor 1248.
[l] T_g' is the temperature at which $\beta = 10 \times 10^{-12}\text{cm}^2/\text{dyne-sec}^{1/3}$.

ture dependence of dissipative processes is related to their time and frequency dependence [139].

Although the viscosities of nonpolymeric liquids have close to the same viscosity at T_g of $\sim 3 \times 10^{12}$ poise ($\sim 3 \times 10^{11}$Pa sec), this value is smaller than the classically referred to value of 1.0×10^{13} poise in spite of the fact that most common T_gs have been determined at a rate of cooling of 1°/min. At the cooling rate of 0.2°/min the T_gs reported here would be several degrees lower and thus higher viscosities would be expected. The widely accepted value for $\eta(T_g) \simeq 10^{13}$ poise does not hold at all for linear polymers, as noted above, because of the dependence of η on the molecular weight [140], and for crosslinked polymers, which do not flow. The local segmental mobility is obviously the determining factor for the packing density of amorphous polymers, whether or not chain-like molecules are entangled or crosslinked. Local molecular packing and motions are believed to be the determining factors for the liquid structure. Long range motions cannot be influential in defining the density. Molecular packing beyond several nearest neighbors in an amorphous system such as a supercooled liquid cannot be coordinated because of the absence of long-range order. Evidence for this assertion can be seen by comparing the retardation spectra obtained from volume contraction with that obtained from shear creep.

The kinetics of isothermal volume contraction and expansion of a cured epoxy resin, which is completely amorphous, below its T_g has been followed [49]. Since the free volume determines the molecular mobility, contraction following a decrease in temperature is going to be faster than the expansion following an increase to the same temperature since its starting specific volume is larger. This is the reason for the well known asymmetry of approach toward an equilibrium density. To minimize the asymmetry a series of small temperature jumps of 2.5 °C were utilized in following the contraction and expansion kinetics. Figure 12.19 shows that the asymmetry is minimal with such temperature changes.

This study of physical aging was different from conventional studies in that each temperature increment was incurred after equilibrium was achieved. The results on an epoxy resin derived from a diglycidyl ether of bisphenyl A (Epon 1001), which was fully cured with DDS (4,4′-diamino diphenyl sulphone), are shown in Fig. 12.20, where $V(t)$ is the specific volume after the temperature step, and $V(\infty)$ is the equilibrium volume at the final temperature.

Since the thermal driving force was virtually the same with each step, simple temperature reduction could be attempted with horizontal time-scale shifts. The successful reduction is presented in Fig. 12.21.

It was assumed that the results were reasonably close to linear behavior and the more extensive curve obtained from the cooling steps was analyzed to obtain a normalized retardation spectrum $L(\tau)$.

$$\int L_0(\tau) \mathrm{d}\ln\tau = 1$$

then

$$\frac{V(0^+) - V(t)}{V(0^+) - V(\infty)} = \int_{-\infty}^{+\infty} \left(L_0(\tau)(1 - \mathrm{e}^{-\frac{t}{\tau}}) \mathrm{d}\ln\tau \right).$$

The $L_0(\tau)$ that was obtained is shown in Fig. 12.22 with the retardation spectrum obtained from the shear creep compliance function, $J(t)$. The levels of the short time behavior are matched. Three features should be noted. The functionality at short times is the same within experimental uncertainty. The 1/3 slope of log $L(\tau)$ at short time indicates that the response is dominated by motions that contribute to Andrade creep. [66,85–87,141,142]

$$J_A(t) = J_A + \beta\, t^{1/3},$$

where t is the time of creep, and J_A and β are characterizing constants.

The positive curvature and the following maximum of the creep compliance $L(\tau)$ indicate the contribution of polymeric molecular modes of motion to the recoverable compliance. Since no positive curvature is seen in the volume contraction $L_0(\tau)$, no polymeric modes are present and no long range coordinated motions of any kind are detected.

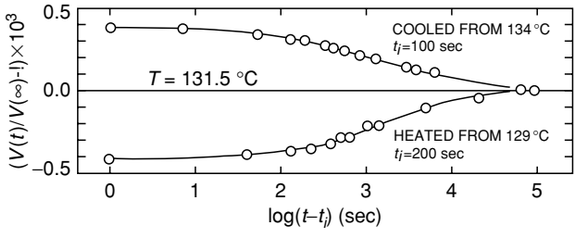

FIGURE 12.19. Fractional volume deviation from equilibrium as a function of time at 131.5 °C after cooling from 134 °C and after heating from 129 °C plotted versus the logarithm of the corrected aging time $t - t_i$ where t_i is the estimated time for the specimen to reach a uniform temperature. Reproduced from Donald J. Plazek and Craig A. Bero, Precise Glass Temperature, *J. Phys.: Condens. Matter.* **15** (2003) 5789–5802 with permission from Institute of Physics Publishing.

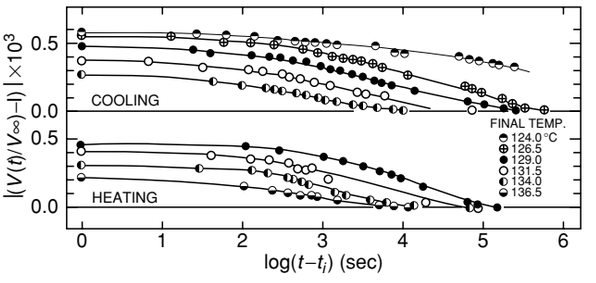

FIGURE 12.20. Absolute fractional volume deviation from equilibrium as a function of the logarithm of the corrected aging time for five temperature after cooling 2.5 °C from equilibrium and four temperatures after heating. Reproduced from Donald J. Plazek and Craig A. Bero, Precise Glass Temperature, *J. Phys.: Condens. Matter.* **15** (2003) 5789–5802 with permission from Institute of Physics Publishing.

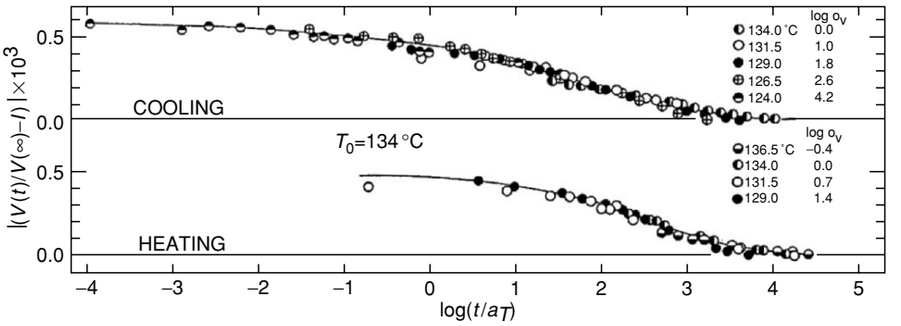

FIGURE 12.21. Volume contraction and expansion from Fig. 12.3 reduced by time-scale shifts to the chosen reference temperature $T_o = 134$ °C. The time t/a_T is the corrected reduced value. Reproduced from Donald J. Plazek and Craig A. Bero, Precise Glass Temperature, *J. Phys.: Condens. Matter*. **15** (2003) 5789–5802 with permission from Institute of Physics Publishing.

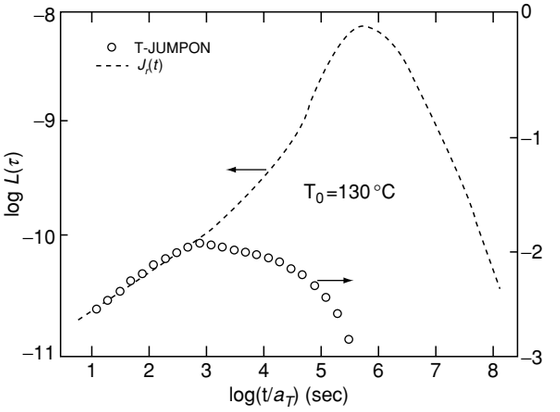

FIGURE 12.22. Comparison of retardation spectra for voluminal L_0 and shear deformation L_s. In this double logarithmic plot of the distribution functions of retardation times τ the ordinate scales have been adjusted to superpose the short-time results. τ/a_T is the reduced retardation time.Reproduced from Donald J. Plazek and Craig A. Bero, Precise Glass Temperature, *J. Phys.: Condens. Matter*. **15** (2003) 5789–5802 with permission from Institute of Physics Publishing.

Only local mode molecular motions contribute to changes in the local packing structure of a liquid and the mobility of those modes decrease rapidly with decreasing temperature. At some temperature, because of the diminishing rate of possible molecular rearrangements, the equilibrium liquid structure can no longer be maintained. Below this temperature the liquid is a glass. The average relaxation time for these motions should be same for all amorphous materials, since the local molecular rearrangement rate that is insufficient to keep up with a given rate of cooling is only a function of that rate of cooling.

12.13 VISCOELASTIC BEHAVIOR AT T_g

The viscoelastic behavior of an amorphous nonpolymeric dehydroabietic acid DHAA as seen at the glass temperature along with that of a low molecular weight unentangled polystyrene ($M = 1.64 \times 10^4$) and a high molecular weight entangled polystyrene ($M = 3.8 \times 10^6$) has been shown in the form of many of the commonly presented functions. They are shown as logarithmic functions of the reduced time t/a_T (sec) and/or frequency ωa_T (rad/sec), where a_T is the temperature shift factor [18]. The viscoelastic functions presented include:

1. The shear creep & recoverable (dashed line) compliance $J(t)$ & $J_r(t)\text{cm}^2/\text{dyne}$ or Pa^{-1};
2. The stress relaxation modulus $G(t)$, dynes/cm^2 or Pa;
3. The dynamic storage $J'(\omega)$ and loss $J''(\omega)$ compliances;
4. The dynamic storage $G'(\omega)$ and loss $G''(\omega)$ moduli;
5. The loss tangent $\tan\delta = J''(\omega)/J'(\omega) = G''(\omega)/G'(\omega)$;
6. The real component of the dynamic viscosity $\eta'(\omega)$ and the imaginary component $\eta''(\omega)$;
7. The retardation function $L(\tau)\text{cm}^2/\text{dyne}$ or Pa^{-1}; and
8. The relaxation spectrum $H(\tau)\text{dyne}/\text{cm}^2$ or Pa.

The systematic variation of the viscoelastic functions with molecular structure can clearly be seen. Because of the additivity of strains arising from different molecular mechanisms [143,144] it should be noted that the clearest picture is seen in the development of $L(\log\tau)$ with changes in molecular weight. Effects of branching and molecular weight distribution are not considered here. The simplest behavior is exhibited by the nonpolymeric DHAA (See Fig. 12.23 [115]). The logarithm of the retardation spectrum exhibits a linear increase with the logarithmic reduced time scale time scale at relatively short times up to a rather abrupt maximum value. The slope of the linear portion has a value of 1/3 within experimental uncertainty. This slope reflects the fact that the recoverable creep compliance appears to display Andrade creep with a proportionality to the cube root of time before the long-time limiting steady-state recoverable compliance is approached. Although the amorphous materials that have been examined can be fit to the Andrade $t^{1/3}$ linearity at short times near T_g there is the

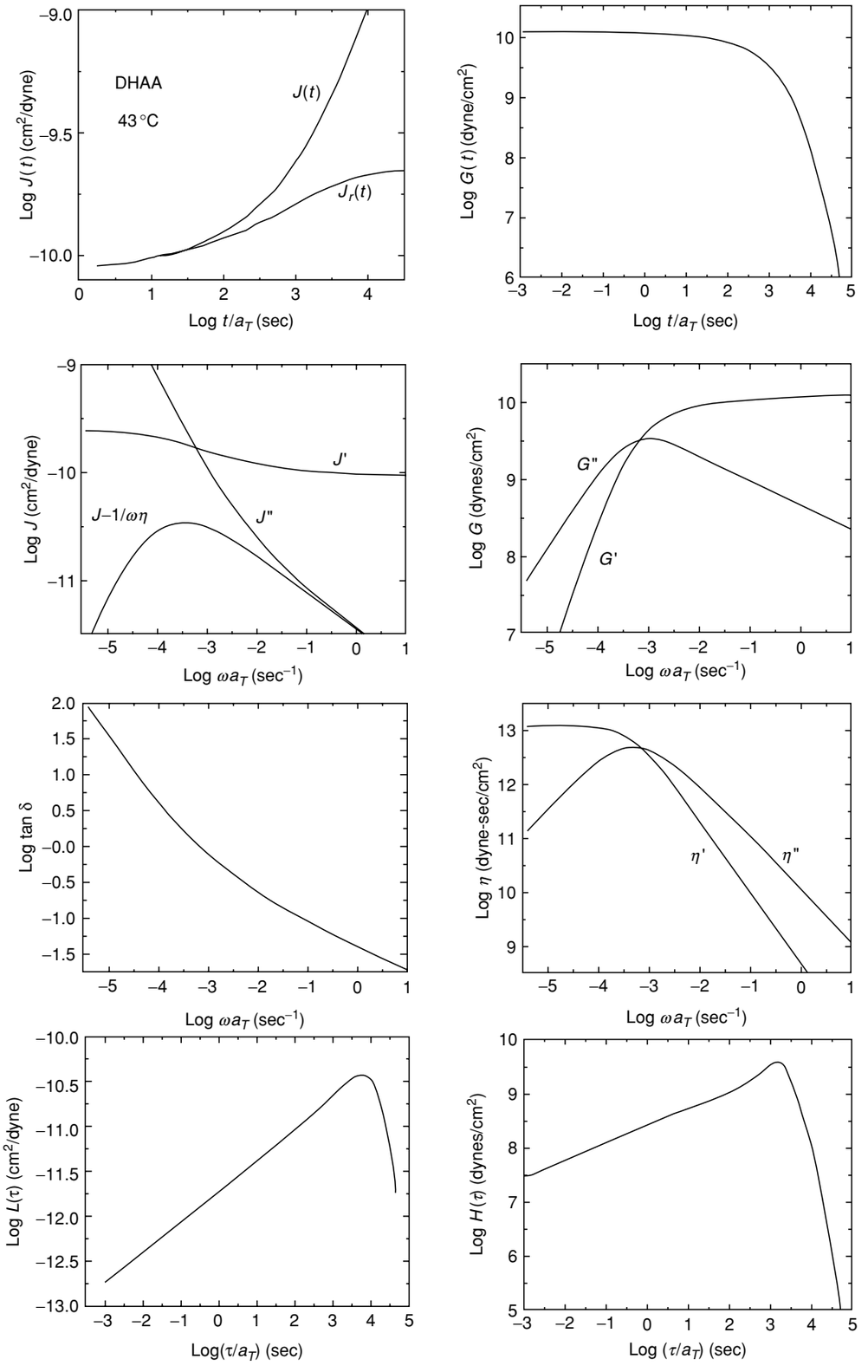

FIGURE 12.23. Viscoelastic functions of a nonpolymeric glass former (DHAA). Reproduced from Donald J. Plazek and Craig A. Bero, Precise Glass Temperature, *J. Phys.: Condens. Matter*. **15** (2003) 5789–5802 with permission from Institute of Physics Publishing.

possibility that such fits are an approximation to a functionality that varies from material to material. The functionality is the generalized Andrade creep t^{1-n} [145–155], where $(1-n)$ is the fractional exponent of the Kohlrausch relaxation function, $\exp[-(t/\tau)^{1-n}]$ [156]. The complement of the Kohlrausch exponent, n, is the coupling parameter of the Coupling Model [145–155]. To be able to utilize an operationally effective means to determine corresponding glass temperature we will assume that the Andrade creep observed is real. In any case the contributions to the recoverable deformation in this regime are identified as local mode intermolecular motions which are also seen in permittivity measurements and are referred to as the alpha mechanism.

The same behavior can be seen in low molecular weight polymers as is illustrated with the polystyrene PS A61 [3]. It's molecular weight is just below the molecular weight between entanglements, $M_e = 17{,}000$ for polystyrene. Hence there is no entanglement network. In fact the presence of entanglements is not seen until $M > M_c = 35{,}000$, for polystyrene. Above M_c the viscosity is proportional to $M^{3.4}$ and the entanglement plateau appears in the compliance and modulus functions. The additional feature seen in the $\log[L(\tau)]$ for this polystyrene in Fig. 12.24 as a function of the logarithmic reduced time is the pronounced peak seen at long-times [115]. The molecular motions contributing to the recoverable deformation at Logarithmic reduced times between 4 and 7 are believed to be the polymeric normal Rouse modes [18]. The most complicated viscoelastic response is exhibited by high molecular weight polymers with entangled linear molecular chains (Fig. 12.25 [115]). The data shown were obtained on a narrow distribution polystyrene PS F380 with a molecular weight of 3.8×10^6. At moderate long-times beyond the local mode and the Rouse normal mode motions a second Andrade $t^{1/3}$ region is seen in the entanglement rubbery region where polymeric chains with varying chain lengths are sequentially being partially oriented. At still longer times where the polymeric chains are disentangling permanent viscous flow deformation is accumulating linearly with time and the maximum orientation per unit stress is being approached, involving the molecular contortions with retardation times between $\mathrm{Log}(t/a_T) = 11$ and 14.

12.14 UNIVERSAL BEHAVIOR AT T_g

As mentioned above, if it is assumed that Andrade creep is the true functional form exhibited by amorphous materials at short times at T_g, a common behavior is operationally observed that can be used to determine corresponding T_g's for these materials. Since the mobility of the local mode motions determines the T_g, a kinetic characterizing variable, such as the Andrade coefficient β, which is determined by these motions, can be associated with T_g. If we examine the glassy Andrade regions of the retardation spectra for many amorphous materials at their respective T_g's we find that they are all close to one another as seen in Fig. 12.26. Fourteen amorphous materials including organic and inorganic polymers and nonpolymers are represented. They are identified in Table 12.3 [109].

In producing Fig. 12.26 the best T_g's that were available for a cooling rate $Q = 0.2$ °C/min were used to fix the time-scale. The variability relative to the average position is about one decade on the time-scale. Tricresyl phosphate (TCP) was chosen as the reference material; i.e., the position of it's log $L(\tau)$ was assumed to be correct for its T_g (0.2 °C/min cooling). The T_g's of the other glass-formers were adjusted to match the position of the glassy Andrade region to that of TCP. The required changes of the T_g's were about 2 °C or less. The T_g adjustments are listed in Table 12.3. Since glass temperatures are often in doubt by more than several degrees it is felt that the Andrade line seen in Fig. 12.27 represents all of the materials within experimental uncertainty and therefore the common curve can be used to determine relative T_g's with a precision that is not possible by any other means.

12.15 DETERMINATION OF T_g FROM THE COMPLIANCE FUNCTIONS

From the common line in the retardation functions shown at T_g in Fig. 12.27 the Andrade coefficient β_{Tg} can be calculated. Smith showed [157] that when Andrade creep is observed

$$L(\tau) = 0.246\beta\tau^{1/3}.$$

Therefore since at T_g, $L(\tau) = 2.24 \times 10^{-12}$ at $\tau = 1\ sec$

$$\beta_{Tg} = 9.11 \times 10^{-12}(\mathrm{cm}^2/\mathrm{dyne\ sec}^{1/3})$$

or

$$\beta_{Tg} = 9.11 \times 10^{-11}\left(\mathrm{m}^2/\mathrm{N\ sec}^{1/3}\right),$$

one simply has to determine β as a function of temperature to find out where β has this value to determine T_g. The T_g defining β_{Tg} can be obtained from dynamic mechanical properties as well as from the recoverable creep compliance $J_r(t)$, since we showed [87] that

$$J'(\omega) = J_A + 0.773\beta\omega^{-1/3}$$

and

$$J''(\omega) = 0.446\beta\omega^{-1/3}$$

when $J'(\omega)$ and $J''(\omega)$ are the storage and loss components of the complex dynamic compliance

$$J^*(\omega) = J'(\omega) - iJ''(\omega)$$

and β is the same Andrade coefficient seen in $J_r(t)$.

At present, β_{Tg} seems to be the best indicator of the mobility at T_g. Some T_gs with the experimental conditions, where available, are given in Table 12.4. They appear to be

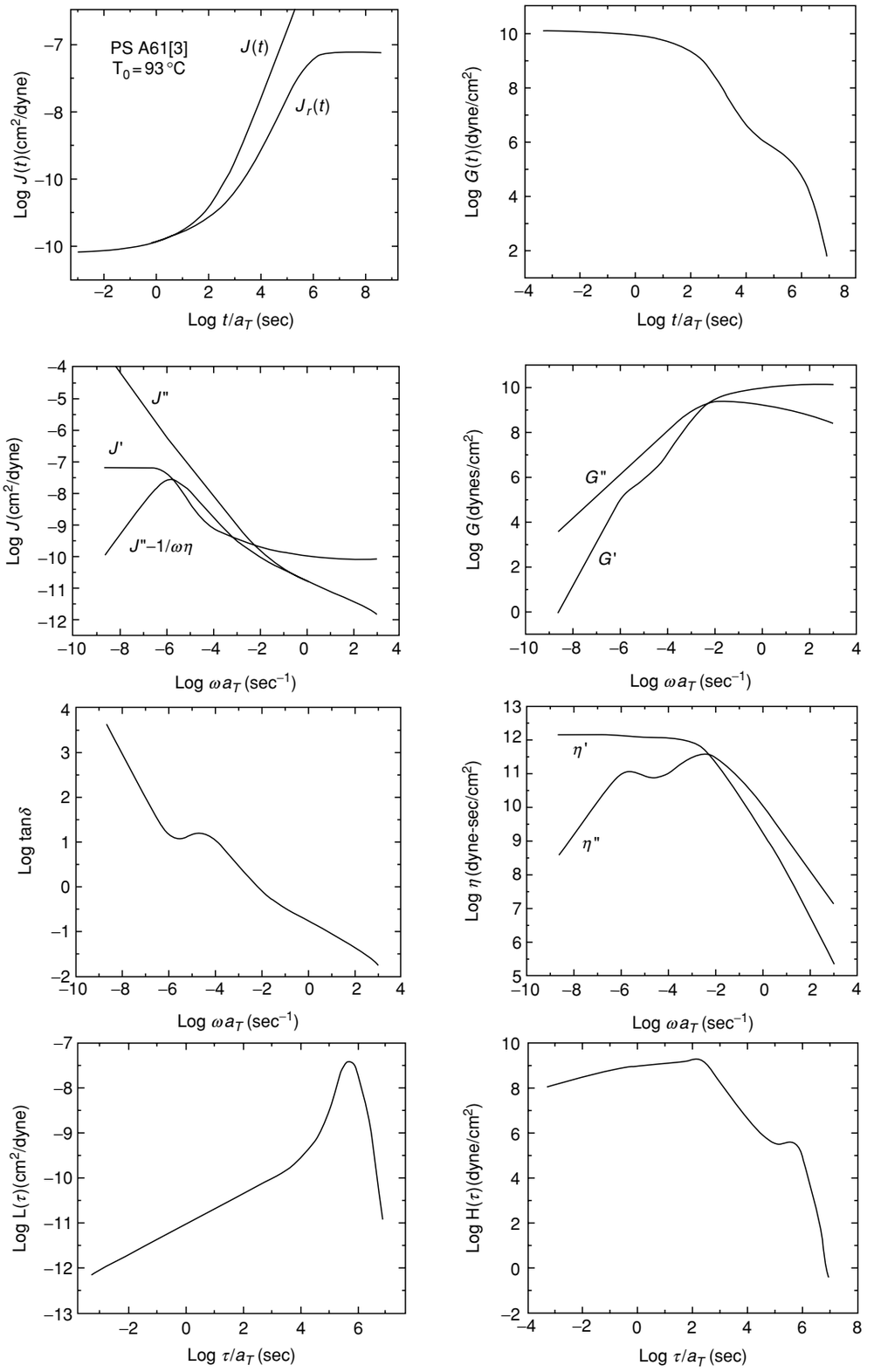

FIGURE 12.24. Viscoelastic functions of a low molecular weight polystyrene (16,400). Reproduced from Donald J. Plazek and Craig A. Bero, Precise Glass Temperature, *J. Phys.: Condens. Matter.* **15** (2003) 5789–5802 with permission from Institute of Physics Publishing.

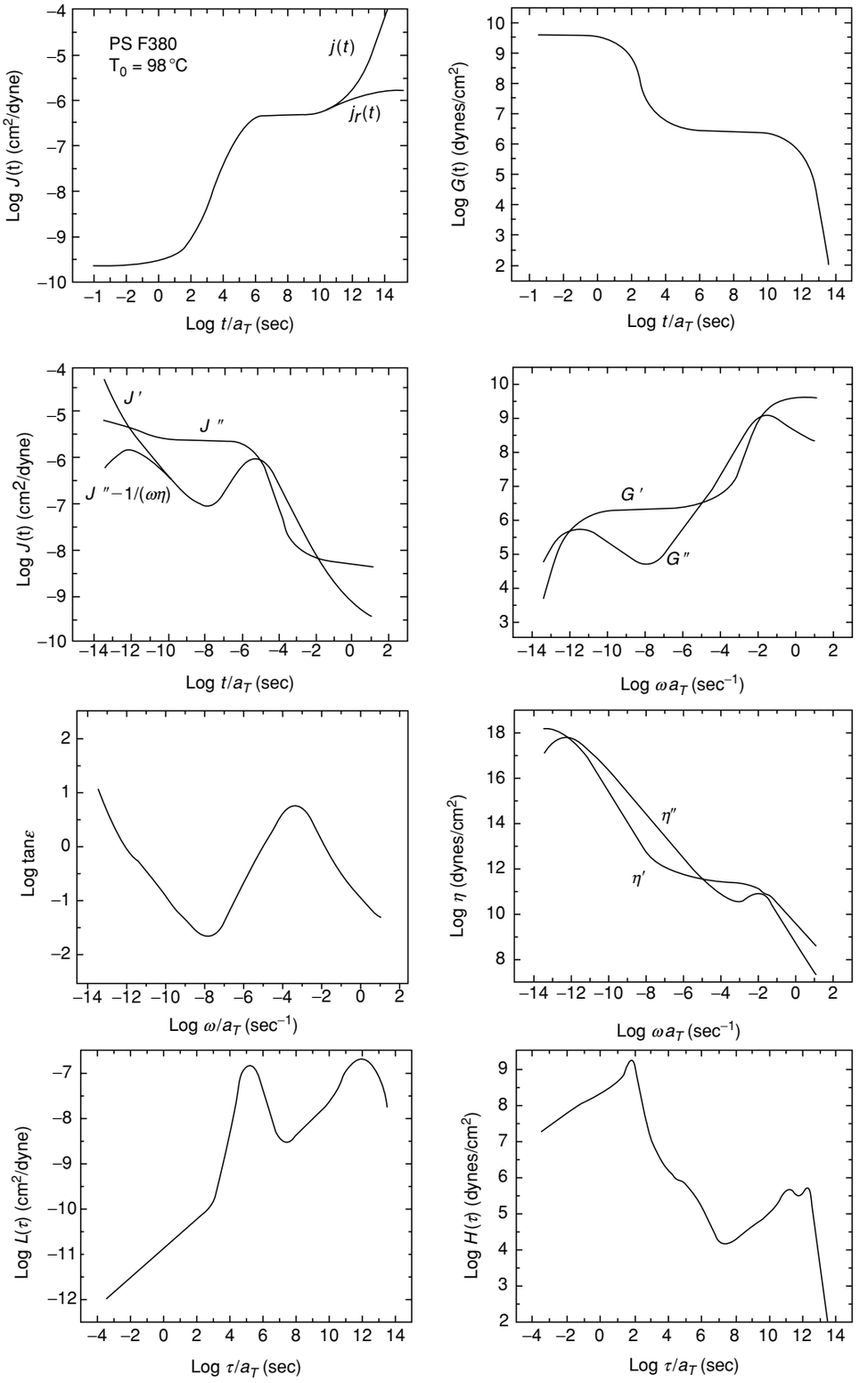

FIGURE 12.25. Viscoelastic functions of a high molecular weight polystyrene, 3.8×10^6. Reproduced from Donald J. Plazek and Craig A. Bero, Precise Glass Temperature, *J. Phys.: Condens. Matter.* **15** (2003) 5789–5802 with permission from Institute of Physics Publishing.

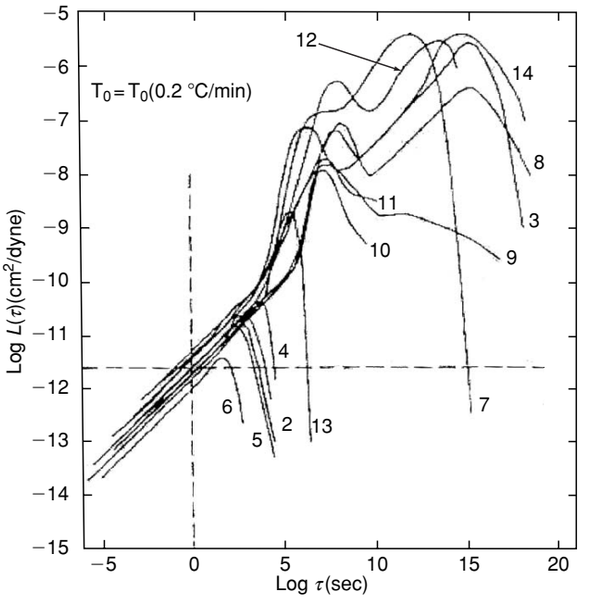

FIGURE 12.26. Comparison of the retardation spectra at $T_0 = T_g(0.2\ ^\circ\text{C/min})$ for (1) 6PE, (2) Aroclor 1248, (3) polypropylene, (4) TCP, (5) OTP, (6) $Tl_2SeAs_2Te_3$, (7) PS Dylene 8, (8) PIB, (9) Viton 10A, (10)Epon 1004/DDS, (11) Epon 1007/DDS, (12)PB/Aroclor 1248 soln., (13) Se, (14) PVAc. Reproduced from Donald J. Plazek and Craig A. Bero, Precise Glass Temperature, *J. Phys.: Condens. Matter.* **15** (2003) 5789–5802 with permission from Institute of Physics Publishing.

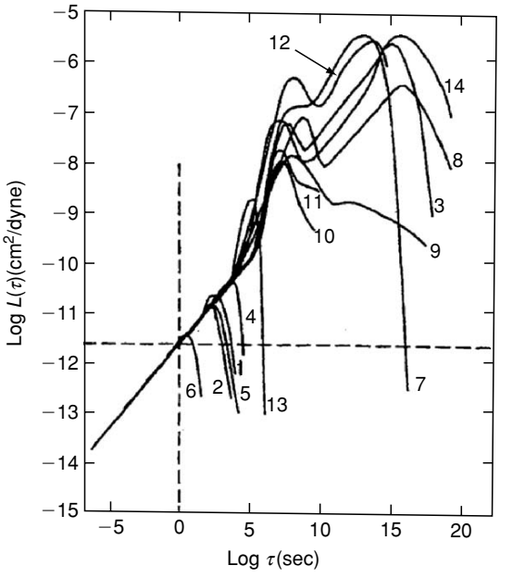

FIGURE 12.27. Superposition of the retardation spectra at short times for the glass-formers of Fig. 12.26. Reproduced from Donald J. Plazek and Craig A. Bero, Precise Glass Temperature, *J. Phys.: Condens. Matter.* **15** (2003) 5789–5802 with permission from Institute of Physics Publishing.

among the best published values. All of the above mentioned caveats should be noted when utilizing these literature values.

12.16 T_g OF POLYMER THIN FILMS AND POLYMER CONFINED IN NANOMETER SCALE DIMENSIONS

The change of the T_g of bulk polymers when reducing one or more of its dimensions to nanometer scale is of interest to workers in fundamental research as well as in applications to technology. The experimental activities in the last decade are mostly on measurements of T_g of nanoscale polymer thin films, and only in recent years some studies of polymers confined inside nanoporous host systems have been reported [158]. The results reported so far are confusing. The glass temperature of polymers subject to nanometer-scale confinement have been reported to increase, decrease, or not changed, depending on the polymer, the geometry and nature of the confinement, and the technique of measurement [159]. For example, the T_g of free-standing thin polystyrene films was reported to decrease continuously with thickness h by about 60 K when h is near 20 nm as measured by ellipsometry and Brillouin scattering [160]. On the other hand, much smaller reductions of T_g were reported for thin polymer films on substrates, and free-standing atactic poly(methyl methacrylate) thin films of comparable molecular weight and thickness as polystyrene [158]. While T_g of isotactic poly (methyl methacrylate) films on aluminum are lower than that of the bulk and decrease with film thickness, the opposite is found if the films are sandwiched between two polystyrene films [161]. The change of T_g thus depends on the nature of the interfaces of the polymer thin film. This dependence resembles that found by molecular dynamics simulations of thin films of binary Lennard-Jones particles nanoconfined by walls defined by a smooth repulsive potential or by frozen binary Lennard-Jones particles [162]. A plausible explanation of the observed dependence of change of T_g on interface was given by the Coupling Model [163]. Experimental techniques and computer simulations that probe the viscoelastic response from global chain dynamics do not find the reduction of T_g in nanometer thin films as deduced by the studies of the local segmental dynamics [164].

For studies of polymers confined inside nanoporous host systems, the most comprehensive study was reported for poly(dimethyl siloxane) and poly(methylphenyl siloxane) down to 5 nm by neutron scattering and dielectric and calorimetric measurements [165]. An increase of molecular mobility, implying a decrease of T_g, was observed on decreasing the pore size. The increment of the specific heat capacity at the glass transition normalized by the mass of confined polymers also decreases with pore size, indicating a concomitant decrease of the cooperative length scale with a decrease of T_g. An explanation has been offered [163].

Excluding some experimental results which may turn out to be artifacts, the majority of the data in the literature are real and worth consideration. The variability of the results, arising from dependence on polymer, nature and geometry of confinement, and experimental techniques, does not necessarily mean that the situation is unmanageable. It makes

TABLE 12.4. *Selected T_gs for some common polymers.*

Name	Repeat unit	M_n	$T_g(q_c)$ °C(deg/min.)	$T_{f,g}(q_c,q_h)$ °C	Method[a]	Reference
Nonaromatic hydrocarbon backbone polymers						
Polyethylene		2×10^5		−26(−,2) −120	Lin. dil. Lin. dil. Dil.	[112] [122] [135]
			−20,−130			
Polypropylene (amorphous)	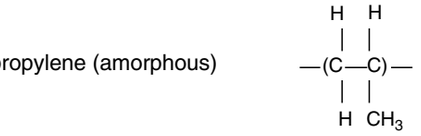	6×10^4		−10(10,10)	DSC	[113]
Polyisobutylene		4.9×10^3 6.6×10^5	−76(0.017) −76(0.2)		Dil. Dil.	[114] [115]
Cis 1,4 polyisoprene	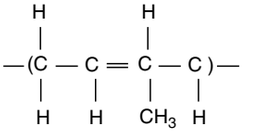			−70	Lin. dil.	[122]
Trans 1,4 polyisoprene	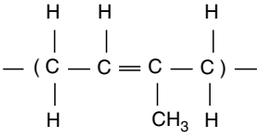		−58		Dil.	[132]
Cis 1,4 polybutadiene	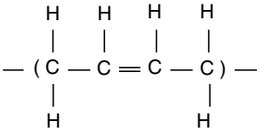		−105 −114		Dil. Dil.	[121] [129]
Trans 1,4 polybutadiene	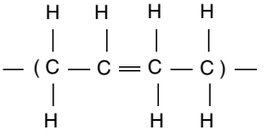		−102		Dil.	[129]
1,2 Polybutadiene	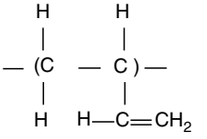		−7		Dil.	[129]

TABLE 12.4. *Continued.*

Name	Repeat unit	M_n	$T_g(q_c)$ °C(deg/min.)	$T_{f,g}(q_c,q_h)$ °C	Method[a]	Reference
Cis neoprene	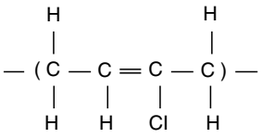		−20		DTA	[130]
Trans neoprene	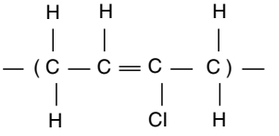	$\sim 10^5$	−45 −45 Lin. dil. −40	131	DTA Dil.	[130] [132]
Polyacrylates						
Polylacrylic acid	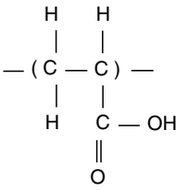		103		Lin. dil.	[127]
Polymethylacrylate	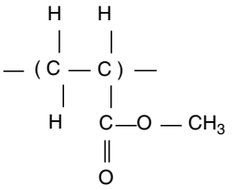	9×10^5	14(20) 8		DSC Dil.	[125] [123]
Polybutylacrylate	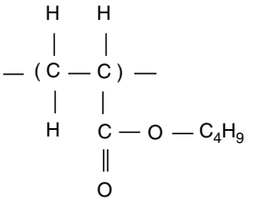			−24	Dil.	[123]
Polymethyl-methacrylate	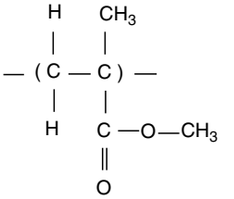	$\sim 10^{5(b)}$ $6.0 \times 10^{4(c)}$ $6.0 \times 10^{4(c)}$ $6.0 \times 10^{4(c)}$ $\sim 3 \times 10^{5b}$ $\sim 3 \times 10^{5b}$ $\sim 3 \times 10^{5b}$ $\sim 3 \times 10^{5d}$	102.8(1) 106(0.017) 117(0.017) 43(0.5)	 108(1) 110(1)[e] 120(−1) 122(−,1)[e] 	Dil. DTA DTA Dil. DTA DTA Dil. Dil.	[5b] [116] [116] [116] [116] [116] [116] [136]
Polyethyl-methacrylate	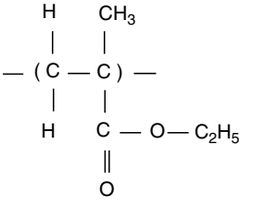	$\sim 10^5$	66 65		Dil. Dil.	[123] [126]

TABLE 12.4. *Continued.*

Name	Repeat unit	M_n	$T_g(q_c)$ °C(deg/min.)	$T_{f,g}(q_c,q_h)$ °C	Method[a]	Reference
Poly-*i*-propylmethacrylate	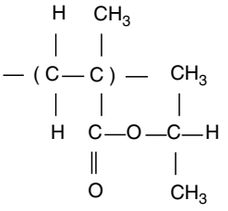	$\sim 10^5$	81 88		Dil. Dil.	[123] [126]
Poly-*n*-propylmethacrylate	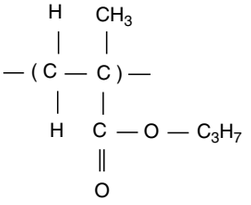	$\sim 10^5$	35 43		Dil. Dil.	[124] [126]
Poly-*n*-butylmethacrylate	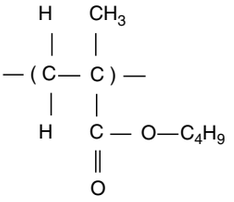	$\sim 10^5$	19 20 23		Dil. Dil. Dil.	[123] [124] [126]
Poly-*n*-hexylmethacrylate	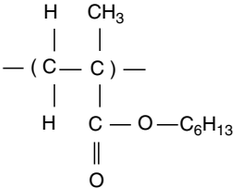		−5		Dil.	[124]
Poly-*n*-octylmethacrylate	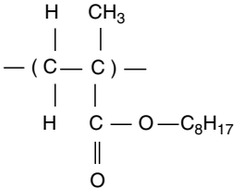		−20		Dil.	[124]
Poly-*n*-dodecylmethacrylate	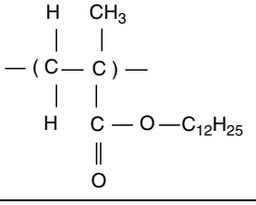		−65		Dil.	[124]

TABLE 12.4. *Continued.*

Name	Repeat unit	M_n	$T_g(q_c)$ °C(deg/ min .)	$T_{f,g}(q_c,q_h)$ °C	Method[a]	Reference
Poly-*i*-butylmethacrylate	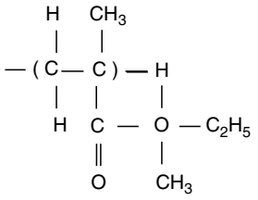		53		Dil.	[124]
Poly-cyclo-hexylmethacrylate	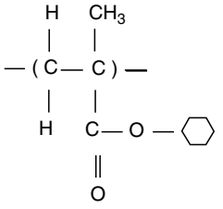	$\sim 10^5$	66 62		Dil. Dil.	[123] [126]
Vinyl polymers						
Polystyrene	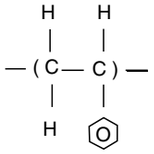	2.1×10^5 9.2×10^4	94.8(1.0) 92.1(0.1) 97.5(0.2)		Dil. Dil. Dil.	[5b] [5b] [115]
Polyvinylacetate	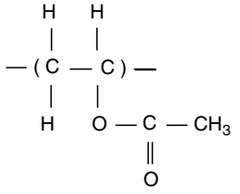	$\sim 3 \times 10^5$	34.8(0.2)		Dil.	[115]
Polyvinylchloride	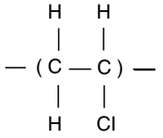	2.8×10^3	71.0(1.0)		Dil.	[5b]
Polyvinylalcohol	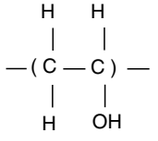			95	DTA	[128]
Heterogeneous backbone polymers						
Polydimethylsiloxane	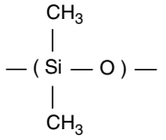		−123(0.3)		Dil.	[117]

TABLE 12.4. *Continued.*

Name	Repeat unit	M_n	$T_g(q_c)$ °C(deg/min.)	$T_{f,g}(q_c,q_h)$ °C	Method[a]	Reference
Bisphenol *A* polycarbonate	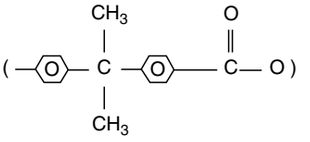		144		Lin. dil.	[118]
Polyethylene-terephthalate	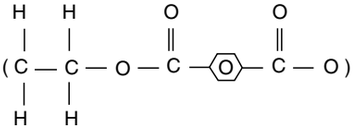			70(10,10)	DSC	[119]
Nylon 66	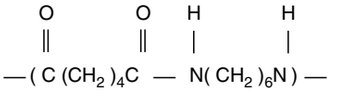	$-\,-3\times10^4$	50(−,1) 52		DTA DTA	[133] [134]
Nylon 6	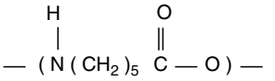		40		DTA	[134]
Polyetherimide	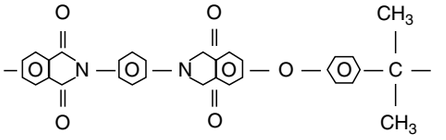			213(80,10)	DSC	[120]

[a]Dil. ≡ volume dialtometry; Lin dil. ≡linear dilatometry; DSC≡differential scanning calorimetry; DTA≡differential thermal analysis.
[b]∼75% syndiotactic.
[c]Ideally atactic.
[d]∼99% isotactic.
[e]Dried at 170 °C in vacuum for 68 h.

the problem more difficult, but more studies in the future should help to improve the understanding of the diverse experimental results.

12.17 WHEN DO VOLUME AND ENTROPY FIRST ENTER INTO DETERMINING MOLECULAR MOBILITY?

Conventional models or theories consider only the segmental relaxation of amorphous polymers and the primary relaxation of nonpolymeric glass-formers in the change of molecular mobility with temperature and pressure (and concomitant changes in free volume and/or configurational entropy) leading to vitrification. Here we wish to recognise two different kinds of secondary relaxation processes. There is one that precedes and leads *to* the primary relaxation and others that are not related such as side group motion which are independent of the chain backbone motion. The same can be said for secondary relaxations in nonpolymeric glass-formers that involve isolated intramolecular motion of a part of the basic unit. However, there are secondary relaxations which must involve the polymer backbone like polybutadiene (PB) and even polyisoprene (PI). The existence of a secondary relaxation in PB is well known [166], but in PI it was found only recently [167]. Equally intriguing is the appearance of secondary relaxations in rigid small molecule glass-formers such as toluene and chlorobenzene [168,169], where there are no internal degrees of freedom. Therefore these secondary relaxations must originate from some local intermolecular motion of the entire molecule. Such secondary relaxations are called the Johari–Goldstein (JG)

β-relaxation to honor their discovery of secondary relaxations even in totally rigid molecules. They are supposedly universal, existing in all glass-formers, and are considered to be the precursor of the primary structural relaxation. Some criteria for distinguishing JG β-relaxation from other garden variety of secondary relaxations have been established based on their properties that mimic the primary relaxation [170]. The relaxation time τ_β of JG β-relaxation has Arrhenius temperature dependence in the glassy state, but the actual temperature dependence of τ_β at temperatures above T_g is not a continuation of the Arrhenius temperature dependence below T_g. It is more like another VFTH temperature dependence that is weaker than that of τ_α [170–172]. Also τ_β is pressure dependent in the equilibrium liquid state ($T > T_g$) [170], and increases on physical aging in the glassy state [173]. Polymerization and cross-linking experiments on Epon 828 have shown that τ_β increases with the increase of covalent bonds formed during the process, which follows the trend of the primary relaxation [174–176]. In binary miscible mixtures of two glass-formers, the relation between τ_β and the primary relaxation time of a component changes systematically with the composition [177]. Although all the properties are less spectacular than that of the primary relaxation, they indicate that τ_β depends on volume and entropy. There is also good correspondence between τ_β and the primitive relaxation time τ_0 of the Coupling Model [170–171,173,178], the latter is definitely a precursor of the primary relaxation and is volume and entropy dependent.

The relaxation strength, $\Delta\varepsilon_\beta$, of the JG relaxation in all these glass-formers is found to change on heating through the glass temperature in a similar manner as the changes observed in the enthalpy H, entropy S, and volume V [179,180]. The derivative of $\Delta\varepsilon_\beta$ with respect to temperature, $d\Delta\varepsilon_\beta/dT$, increases from lower values at temperatures below T_g to higher values at temperatures above T_g, a mimicry of the same behavior of the specific heat C_p and the expansion coefficient, which are the derivatives dH/dT and dV/dT, respectively.

Thus, volume and entropy have already entered into the determination of molecular mobility of the JG β-relaxation and τ_β, at times long before the emergence of the α-relaxation and τ_α in the equilibrium liquid state. Since time is the natural variable, the dependence of molecular mobility on temperature, pressure, volume, and entropy originate in τ_β or τ_0. The stronger dependences of the primary relaxation time on the same variables are the consequence of the many-molecule (cooperative and dynamically heterogeneous) dynamics that increase the magnitude of τ_β naturally. It is the involvement of an increasing number of molecules (proportional to the cooperative length-scale and the width of the dispersion) in the primary relaxation than that involved in the local JG β-relaxation. The results suggest models and theories of vitrification that address only the α-relaxation need a new paradigm [181].

Related information can be found in Chapter 13.

REFERENCES

1. W. Kauzmann, Chem. Rev. **43**, 219 (1948).
2. P. J. Flory, J. Ric. Sci. **25A**, 636 (1955).
3. A. J. Kovacs, Adv. Polym. Sci. **3**, 394 (1963).
4. M. C. Shen and A. Eisenberg, "Glass Transitions in Polymers," in *Progress in Solid State Chemistry* vol. 3 (Pergamon Press, Oxford and New York, 1966), p. 407.
5. a. F. R. Schwarzl, "The Glass Transition of Amorphous Polymers and the Free Volume," in *Rheolgy, vol. I*, Int. Cong. Rhelogy, Naples, edited by G. Astarita, G. Marucci, and L. Niclolais. 243–262 (Plenum Pub. Corp., New York, 1980), p. 243. b. R. Greiner and F. R. Schwarzl, Rheol. Acta. **23**, 378 (1984).
6. D. J. Plazek and G. C. Berry, "Physical Aging in Polymer Glasses," in *Glass Science and Technology*, vol. 3, edited by D. R. Uhlmann and N. J. Kreidl (Academic Press, Orlando, FL, 1986), p. 363.
7. S. Rekhson, J. Non-Crystalline Solids **95 & 96**, 131 (1987).
8. J. M. O'Reilly, *Review of Structure and Mobility in Amorphous Polymers*, CRC Critical Reviews in Solid State and Materials Science **13**, 259 (1987).
9. G. B. McKenna, *Comprehensive Polymer Science, vol. 2, Polymer Properties*, edited by C. Booth and C. Price (Pergamon, Oxford, 1989), p. 311.
10. I. M. Hodge, J. Non-Crystalline Solids **169**, 211 (1994).
11. A. J. Kovacs, Ph.D. Thesis, "Contribution à l'étude de l'évolution isotherme du volume des hauts polymères," University of Paris, 1954.
12. G. O. Jones, *Glass* (Methuen & Co., Ltd., London, 1956).
13. Proc. Intern Conf. on Physics of Non-Crystalline Solids, Delft, July, 1964, edited by J. A. Prins (North-Holland Pub. Co., Amsterdam & John Wiley & Sons, Inc., New York, 1965).
14. *The Physics of Glassy Polymers*, edited by R. N. Haward (John Wiley & Sons, New York, 1973).
15. "Metallic Glasses," Materials Science Seminar, Metals Park, Ohio, held in 1976, American Society for Metals, published in 1978.
16. A. V. Tobolsky, *Properties and Structure of Polymers* (John Wiley & Sons, Inc., New York, 1960).
17. F. Bueche, *Physical Properties of Polymers* (Interscience Pub., New York, 1962).
18. J. D. Ferry, *Viscoelastic Properties of Polymers*, third ed. (John Wiley & Sons, Inc., New York, 1980).
19. L. E. Nielsen and R. F. Landel, *Mechanical Properties of Polymers and Composites*, 2nd edition (Marcel Dekher, Inc., New York, 1994).
20. G. M. Bartenev, *The Structure and Properties of Inorganic Glasses* (Wolters-Noordhoff Pub. Groningen, The Netherlands, 1970).
21. R. Zallen, *The Physics of Amorphous Solids* (John Wiley & Sons, New York, 1983).
22. S. Brawer, *Relaxation in Viscous Liquids and Glasses* (The American Ceramic Society, Inc., Columbus, OH, 1985).
23. G. W. Scherer, *Relaxation in Glass and Composites* (John Wiley & Sons Inc., New York, 1986).
24. S. R. Elliot, *Physics of Amorphous Materials*, 2nd ed. (Longman Scientific & Technical, Essex, England (copublished with John Wiley & Sons, New York, 1990).
25. *Glass Science and Technology, Vol. 1: Glass-Forming Systems*, 1983; *ibid. Vol. 3: Viscosity and Relaxation*, edited by D. R. Uhlmann and H. J. Kreidl (Academic Press, Inc., Corpus Christie, 1986).
26. M. Goldstein and R. Simha (eds.), Ann. N.Y. Acad. Sci. **279**, (1976).
27. J. M. O'Reilly and M. Goldstein (eds.), Ann. N.Y. Acad. Sci. **371**, (1981).
28. a. C. A. Angell and M. Goldstein (eds.), Ann. N.Y. Acad. Sci. **484**, (1986), b. C. A. Angell, J. Non-Crystalline Solids **131–133**, 13 (1991).
29. K. L. Ngai and G. B. Wright (eds.), *Relaxations in Complex Systems* (U.S. Government Printing Office, Washington, DC, 1984) Available from National Technical Information System Service, 2285 Port Royal Rd. Springfield, VA, 22161, USA.
30. P. H. Gaskell (ed.), *The Structure of Non-Crystalline Materials* (Taylor and Francis, London, 1977).
31. L. C. E. Struik, *Physical Aging in Amorphous Polymers and Other Materials* (Elsview, Amsterdam, 1978).
32. K. Kawasaki, M. Tokuyama, and T. Kawakatsu, (eds.) AIP Conf. Proc. 256, Slow Dynamics in Condensed Matter, Fukuoka, Japan, 1991 (AIP, New York, 1992).

33. K. L. Ngai and G. B. Wright (eds.), Proc. Intern. Disc Meeting on Relaxation in Complex System Heraklion, Crete, Greece, June 18–29, 1990, J. Non-Crystalline Solids **131–133** (1991).
34. A. Eisenberg in *Physical Properties of Polymers*, edited by J. E. Mark, 2nd ed. (American Chemical Society, Washington, DC, 1993), p. 61.
35. M. L. Williams, R. F. Landel, and J. D. Ferry, J. Am. Chem. Soc. **77**, 3701 (1955).
36. M. H. Cohen and D. Turnbull, J. Chem. Phys. **31**, 1164 (1959).
37. D. Turnbull and M. H. Cohen, J. Chem. Phys. **34**, 120 (1961).
38. A. J. Kovacs, J. J. Aklonis, J. M. Hutchinson *et al*. J. Polymer Sci., Polym. Phys. Ed. **17**, 1097 (1979).
39. J. H. Gibbs and E. A. Dimarzio, J. Chem. Phys. **28**, 373 (1958).
40. E. A. Dimarzio and J. H. Gibbs, J. Polym. Sci. **40**, 121 (1959).
41. E. A. Dimarzio, J. Res. Natl. Bur. Stand., Section A, **A68**, 611 (1964).
42. G. Adam and J. H. Gibbs, J. Chem. Phys. **43**, 139 (1965).
43. K. L. Ngai in *Non Debye Relaxation in Condensed Matter*, edited by T. V. Ramakrishna and Raj Lakshmi (World Scientific Publishing, Singapore, 1987), pp. 23–192.
44. A. Q. Tool, NBS J. Res. **34**, 199 (1945).
45. O. S. Narayanaswamy, J. Am. Cer. Soc. **54**, 491–498, (1971).
46. C. T. Moynihan, A. J. Easteal, M. A. DeBolt *et al*. J. Am. Cer. Soc. **59**, 12 (1976).
47. C. T. Moynihan, A. J. Easteal, J. Wilder *et al*., J. Phys. Chem. **78** 2673 (1974).
48. S. M. Rekhson and G. W. Scherer, J. de Phys. Colloque C9, **48**, 427 (1982).
49. C. A. Bero and D. J. Plazek, J. Polym. Sci. Part B: Polym. Phys. **29**, 39 (1991).
50. M. J. Richardson and N. G. Savill, Polymer **16**, 753 (1975).
51. P. Peyser "Glass Transition Temperatures of Polymers," in *Polymer Handbook*, 3rd ed., edited by J. Brandrup and E. H. Immergut (John Wiley & Sons, New York, 1989), pp. VI–209.
52. W. W. Wendlandt and P. K. Gallagher, *Instrumentation in Thermal Characterization of Polymeric Materials*, edited by E. A. Turi (Academic Press, New York, 1981), p. 3.
53. C. A. Angell (private communication).
54. D. J. Plazek, J. Polymer Sci.: Polym. Phys. Ed. **20**, 1533 (1982).
55. a. W. A. Lee and R. A. Rutherford "Glass Transition Temperatures of Polymers" in *Polymer Handbook*, 2nd edition, edited by J. Brandrup and E. H. Immergut (John Wiley & Sons, New York, 1975), pp. III–139. b. D. J. Plazek and L. Zhang (unpublished data).
56. E. Jenckel and R. Heusch, Kolloid Z. **130**, 19 (1953).
57. D. J. Plazek, C. Seoul, and C.A. Bero, J. Non-Crystalline Solids **131–133**, 570 (1991).
58. G. Braun and A. J. Kovacs, in Proc. Int. Conf. on Phys. Non-Crystalline Solids, Delft, July, 1964, edited by J. A. Prins (North-Holland Pub. Co. Amsterdam, 1965).
59. E. Riande, H. Markovitz, D. J. Plazek *et al*., J. Polym. Sci. Symposium No. 50, **405–430** (1975).
60. D. J. Plazek, E. Riande, H. Markovitz *et al*., J. Polym. Sci. **17**, 2189 (1979).
61. F. N. Kelley and F. Bueche, J. Polymer Sci. **50**, 549 (1961).
62. G. Pezzin, A. Omacini, and F. Zilio-Grandi, Chim. Ind. (Milan) **50**, 309 (1968).
63. G. Pezzin, Pure and Appl. Chem. **25**, 241 (1971).
64. D. J. Plazek, I.-C. Choy, F. N. Kelley, *et al*., Rubber Chem. Tech. **56**, 866 (1983).
65. D. J. Plazek, G.-F. Gu, R. G. Stacer, *et al*., J. Mat., Sci. **23**, 1289 (1988).
66. D. J. Plazek, C. A. Bero, and I.-C. Choy. J. Non-Crystalline Solids **172–174**, 181 (1994).
67. E. D. von Meerwell, S. Amelar, and T. P. Lodge, Macromolecules **22**, 295 (1989).
68. R. L. Morris, S. Amelar, and T. P. Lodge, J. Chem. Phys. **89**, 6523 (1988).
69. S. Amelar, J. R. Krahn, K. C. Hermann, *et al*., Spectrochim. Acto Rev. **14**, 379 (1991).
70. D. J. Gisser and M. D. Ediger, Macromolecules **25**, 1248 (1992).
71. G. Fytas, A. Rizos, G. Floudas *et al*., J. Chem. Phys. **93**, 5096 (1990).
72. A. Rizos, G. Fytas, T. P. Lodge *et al*., J. Chem. Phys. **95**, 2980 (1991).
73. a. A. K. Rizos, and K. L. Ngai, Phys. Rev. B **46**, 8127 (1992). b. A. K. Rizos, and K. L. Ngai, Macromolecules **27**, 7076 (1994).
74. T. G. Fox and L. Loshaek, J. Polym. Sci. **15**, 371 (1955).
75. S. J. Clarson, K. Dodgson, and J. A. Semlyen, Polym. **26**, 930 (1985).
76. C. M. Guttmann and E. A. Dimarzio, Macromolecules **20**, 1403 (1987).
77. G. B. McKenna, B. J. Hostetter, N. Hadjichristidis, Macromolecules **22**, 1834 (1989).
78. D. J. Plazek and V. M. O'Rourke, J. Polym. Sci. Part A-2, **9**, 209 (1971).
79. K. Ueberreiter and G. Kanig, J. Chem. Phys. **18**, 399 (1950).
80. S. Loshaek, J. Polym. Sci. **15**, 391 (1955).
81. D. J. Plazek and I.-C. Chay, J. Polym. Sci. Part B: Polym. Phys. **29**, 17 (1991).
82. I.-C. Choy and D. J. Plazek, J. Polym. Sci., Part B: Polym. Phys. **24**, 1303 (1986).
83. D. J. Plazek and I.-C. Choy, J. Polym. Sci., Part B: Polym. Phys. **27**, 307 (1989).
84. D. J. Plazek and Z. N. Frund, Jr., J. Polym. Sci.; Part B: Polym. Phys. **28**, 431 (1990).
85. E. N. da C. Andrade, Proc. Roy. Soc. (London) **A84**, 1 (1970); **A254**, 291 (1960).
86. D. R. Reid, British Plastics **32**, 460 (1959).
87. D. J. Plazek, J. Colloid Sci. **15**, 50 (1960).
88. B. G. Ranby, K. S. Chan, and H. Brumberger, J. Polym. Sci. **58**, 545 (1962).
89. G. Groeninckx, H. Berghmans, and G. Smets. J. Polym. Sci.: Polym. Phys. Ed. **14**, 591 (1976).
90. A. Eisenberg *et al*., in *Physical Properties of Polym.s*, 2nd edition ACS Prof. Ref. Book (American Chemical Society, Washington, DC, 1993), p. 61.
91. a. A. Eisenberg, H. Farb, and L. G. Cool, J. Polym. Sci. A-2, **9**, 2131 (1971). b. H. Matsuura and A. Eisenberg, J. Polym. Sci., Polym. Phys. Ed. **14**, 1201 (1976).
92. G. Goldbach and G. Rehage, Rheological Acta **6**, 30 (1967).
93. J. E. McKinney and M. Goldstein, R. Res. Natl. Bun. Stand. Sect. A **78A**, 331, 1974.
94. R. Hill and E. E. Walker, J. Polym. Sci. **3**, 609 (1948).
95. R. H. Boyd and S. M. Breitling, Macromolecules **5**, 1 (1972).
96. G. Natta and F. Danusso, J. Polym. Sci. **34**, 3 (1959). M. L. Huggins, G. Natta, V. Desreux, and H. Mark, J. Polym. Sci. **56**, 153 (1962).
97. F. E. Karasz and W. J. MacKnight, Macromolecules **1**, 537 (1968).
98. G. P. Mikhailov and T. I. Borisova, Polym. Sci. USSR **2**, 387 (1961).
99. D. J. Plazek, V. Tan, and V. M. O'Rourke, Rheol. Acta **13**, 367 (1974).
100. I. Havlicek, M. Ilavsky, and J. Hrouz, J. Polym. Sci. Polym. Phys. Ed. **16**, 653 (1978).
101. I. Havlicek, M. Ilavsky, and J. Hrouz: Polym. Bull. **2**, 25 (1980).
102. I. Havlicek, V. Vojta, M. Ilavsky *et al*. Macromolecules **13**, 357 (1980).
103. I. Havlicek, M. Ilavsky, and J. Hrouz, J. Macomol. Sci., Phys. **B21**, 425 (1982).
104. G. W. Scherer, J. Amer. Cer. Soc. **67**, 504 (1984); **69**, 374 (1986).
105. R. Kohlrausch, Pogg. Ann. Phys. IV-91, 56–82 and 179–214 (1854).
106. G. Williams and D. C. Watts, Trans. Faraday Soc. **66**, 800 (1971).
107. N. G. McCrum, Plastics, Rub. and Comp. Proc. and Appl. **18**, 181 (1992).
108. F. G. Shi, J. Mater. Res. **9**, 1908 (1994).
109. C. A. Bero, Ph.D. Thesis, University of Pittsburgh, 1994.
110. D. J. Plazek, C. Seoul, and C. A. Bero, J. Non-Crystalline Solids **131–133**, 570 (1991).
111. P. C. Taylor, S. G. Bishop, and D. L. Mitchell, Phys. Rev. Let. **27** (No. 7), 414 (1971).
112. J. H. Magill, S. S. Pollack, and D. P. Wyman, J. Polym. Sci.: Part A **3**, 3781 (1965).
113. D. L. Plazek and D. J. Plazek, Macromolecules **16**, 1469 (1983).
114. J. D. Ferry and G. S. Parks, J. Chem. Phys. **4**, 70 (1936).
115. D. J. Plazek and C. A. Bero, J. Phys.: Condens. Matter **15**, S789–S802 (2003).
116. D. J. Plazek, V. Tan, and V. M. O'Rourke, Rheol, Acta **13**, 367 (1974).
117. K. E. Polmanteer and M. J. Hunter, J. Appl. Polym. Sci. **1**, 3 (1959).
118. S. C. Temin, J. Appl. Polym. Sci. **9**, 471 (1965).
119. M. F. Vallat and D. J. Plazek, J. Polym. Sci.: Part B: Polym. Phys. **26**, 545 (1988).

120. Ping-Chung Su, MS thesis, University of Pittsburgh, 1994.
121. M. Takeda, K. Tanaka, and R. Nagao, J. Polym. Sci. **57**, 517 (1962).
122. M. L. Dannis, J. Appl. Polym. Sci. **1**, 121 (1959).
123. J. A. Shetter, J. Polym. Sci. B **1**, 209 (1963).
124. S. S. Rogers and L. Mandelkern, J. Phys. Chem. **61**, 985 (1957).
125. D. J. Plazek, M. J. Rosner, and D. L. Plazek, J. Polym. Sci.: Part B: Polym. Phys. **26**, 473 (1988).
126. Z. G. Gardlund and J. J. Laverty, J. Polym. Sci.: Part B: **7**, 719 (1969).
127. A. Eisenberg, T. Yokoyama, and E. Sambalido, J. Polym. Sci.: Part A-1: **7**, 1717 (1969).
128. J. E. Clark, Polym. Engr. & Sci. **7**, 137 (1967).
129. G. Krauss, W. Childers, and J. T. Gruver, J. Appl. Polym. Sci. **11**, 158 (1967).
130. C. A. Aufdermarsh and R. Pariser, J. Polym. Sci.: A **2**, 4727 (1964).
131. R. R. Garrett, C. A. Hargraves II, and D. N. Robinson, J. Macromol. Sci. **A4**, 1679 (1970).
132. R. Nagao, Polym. **9**, 517 (1968).
133. J. H. Magill (private communication).
134. G. A. Gordon, J. Polym. Sci.: Part A-2 **9**, 1693 (1971).
135. P. R. Swan, J. Polym. Sci. **42**, 525 (1960).
136. J. C. Wittmann and A. J. Kovacs, J. Polym. Sci., C **16**, 4443 (1967).
137. P. R. Couchman, Polym. Engr. Sci. **29**, 135, (1984).
138. T. S. Chow, J. Rheology **30**, 729 (1986).
139. D. J. Plazek and K. L. Ngai, Macromolecules **24**, 1222 (1991).
140. S. J. Orbon and D. J. Plazek, J. Polym. Sci., Polym. Phys. Ed. **23**, 41 (1985).
141. G. C. Berry, J. Polm. Sci. **14**, 407 (1976).
142. K. M. Bernatz, Ph D Thesis, University of Pittsburgh, PA (1999).
143. D. J. Plazek, J. Rheol. **36**, 1671 (1992).
144. D. J. Plazek and J. Echeverria, J. Rheol. **44**, 831 (2000).
145. D. J. Plazek, X. D. Zheng, and K. L. Ngai, Macromolecules **25**, 4920 (1992).
146. K. L. Ngai, D. J. Plazek, and C. Bero, Macromolecules **26**, 1065 (1993).
147. D. J. Plazek, A. Schönhals, E. Schlosser, and K. L. Ngai, J. Chem. Phys. **98**, 6488 (1993).
148. D. J. Plazek, C. Bero, S. Neumeister, G. Floudas, G. Fytas and K. L. Ngai, Colloid Polym. Sci. **272**, 1430 (1994).
149. K. L. Ngai and D. J. Plazek, Rubber Chem. Tech. Rubber Rev. **68**, 376 (1995).
150. K. L. Ngai, D. J. Plazek, and R. W. Rendell, Rheol. Acta **36**, 307 (1997).
151. K. L. Ngai, I. Echeverria, and D. J. Plazek, Macromolecules **29**, 7937 (1997).
152. K. L. Ngai, D. J. Plazek, and A. K. Rizos, J. Polym. Sci. B: Polym. Phys. **35**, 599–614 (1997).
153. K. L. Ngai, J. Non-Cryst. Solids **7**, 275 (2000).
154. K. L. Ngai and D. J. Plazek, Macromolecules **35**, 9136 (2002).
155. K. L. Ngai, G. Floudas, D. J. Plazek, and A. K. Rizos, "*Amorphous Polymers*" in *Encyclopedia of Polymer Properties*, (John Wiley & Sons, New York, 2002).
156. R. Kohlrausch, Pogg. Ann. Phys. **12**(3), 393 (1847).
157. T. L. Smith, Personal communication (1959).
158. For collection of papers, see (i) B. Frick, R. Zorn, and H. Büttner (eds.) Proceedings in International Workshop on Dynamics in Confinement, J. Phys. IV **10**, Pr7 (2000). (ii) B. Frick, M. Koza, and R. Zorn (eds.) Proceedings of 2nd International Workshop on Dynamics in Confinement, Eur. Phys. J. E **12**, 5–194 (2003). (iii) *Special issue on Properties of Thin Polymer Films* G. Reiter and J. A. Forrest (eds) Eur. Phys. J. E **8**, 101–266 (2002).
159. A summary of the confusing results can be found in G. B. McKenna, Eur. Phys. J. E **12**, 191 (2003).
160. J. A. Forrest and K. Dalnoki-Veress, Adv. Colloid Interf. Sci. **94**, 167 (2001).
161. M. R. Wübbenhorst, C. A. Murray, and J. R. Dutcher, Eur. Phys. J. E **12**: S109–S112 Suppl. (2003).
162. P. Scheidler, W. Kob, and K. Binder, Eur. Phys. J. E **12**, 5 (2003).
163. K. L. Ngai, Phil. Mag. B. **82**, 291 (2002).
164. For references to experimental works and computer simulations, see K. L. Ngai, Eur. Phys. J. E **8**, 225 (2002). A plausible explanation is given therein.
165. A. Schönhals, H. Goering, Ch. Schick, B. Frick, and R. Zorn, Eur. Phys. J. E **12**, 173 (2003), and to be published.
166. R. Casalini, K. L. Ngai, C. G. Robertson, and C. M. Roland, J. Polym. Sci. Polym. Phys. Ed. **38**, 1841 (2001).
167. C. M. Roland, M. J. Schroeder, J. J. Fontanella, and K. L. Ngai, Macromolecules **37**, 2630 (2004).
168. G. P. Johari and M. Goldstein, J. Chem. Phys. **53**, 2372 (1970).
169. G. P. Johari, Ann. N. Y. Acad. Sci. **279**, 117 (1976).
170. K. L. Ngai and M. Paluch, J. Chem. Phys. **120**, 2857 (2004).
171. M. Paluch, C. M. Roland, S. Pawlus, J. Ziolo, and K. L. Ngai, Phys. Rev. Lett. **91**, 115701 (2003).
172. See Figure 9 in S. C. Kuebler, D. J. Schaefer, C. Boeffel, U. Pawelzik, and H. W. Spiess, Macromolecules **30**, 6597 (1997). The secondary relaxation of poly(ethyl metacrylate) involves some motion of the main chain and is hence a JG relaxation according to [170].
173. D. Prevosto, S. Capaccioli, M. Lucchesi, P. A. Rolla, and K. L. Ngai, J. Chem. Phys. **120**, 4808 (2004).
174. M. G. Parthun and G. P. Johari, J. Chem. Phys. **103**, 7611 (1995); **103**, 440 (1995).
175. D. A. Wasylyshyn and G. P. Johari, J. Chem. Phys. **104**, 5683 (1996).
176. M. Beiner and K. L. Ngai, Macromolecules, **38**, 7033–7042 (2005).
177. K. L. Ngai and C. M. Roland, Rubber Chem. Tech. Rubber Rev. **77**, 579 (2004).
178. K. L. Ngai, J. Phys.: Condens. Matter **15** (2003) S1107. K. L. Ngai, in AIP Conference Proceedings, **708**, p. 515 (2004), Am. Inst. Phys. Melville NY.
179. G. P. Johari, G. Power, and J. K. Vij, J. Chem. Phys. **116**, 5908 (2002); **117**, 1714 (2002).
180. G. Power, G. P. Johari, and J. K. Vij, J. Chem. Phys. **119**, 435 (2003).
181. K. L. Ngai, J. Non-Cryst. Solids, **351**, 2635–2642 (2005).

CHAPTER 13

Sub-T_g Transitions

Joel R. Fried

Department of Chemical and Materials Engineering, University of Cincinnati, Cincinnati, OH 45221–0012

There have been a number of good general reviews of relaxation processes that occur at temperatures below the glass-transition temperature (T_g) [1–6]. Early dynamic-mechanical studies were surveyed by Woodward and Sauer [7]. Although now outdated, the seminal work reviewing both dynamic-mechanical and dielectric data is still the excellent 1967 monograph by McCrum, Read, and Williams [8]. It is not the purpose of this review to approach the comprehensive coverage provided by McCrum et al. but to summarize important results for the major polymer groups and to include more recent studies, especially for engineering thermoplastics not available prior to 1967. Where appropriate, mention is made of recent efforts at molecular modeling that aid in understanding the nature of molecular processes that operate below T_g.

A variety of techniques can be used to detect relaxational processes occurring below T_g. These include dynamic-mechanical, dielectric, NMR (e.g., ^{1}H line width and pulsed ^{13}C NMR relaxation times), and thermally stimulated discharge current (TSC) measurements. Of these, dynamic-mechanical methods [9] have been the most widely used to study secondary-relaxation processes in polymers. These include free vibration methods, principally torsional pendulum [10,11] and torsional braid [12], and forced oscillation (FO) methods utilizing mechanically driven tensile, torsional, and flexural strains provided by a number of commercial instruments. The ability to vary oscillation frequency over a wide range makes FO (ca. 0.016–160 Hz) and dielectric techniques (ca. 10–10^6 Hz) especially useful for the determination of activation energies. Early dynamic methods also included resonance electrostatic methods that provide dynamic data over a higher (acoustic) frequency range (ca. 10^3–10^4 Hz) than is possible using FO dynamic mechanical methods. Basic principles and instrumentation for resonance electrostatic and other dynamic measurements are given by Ferry [13].

In the following sections, the results of dynamic-mechanical and dielectric measurements of important amorphous and semicrystalline polymers are summarized and conclusions regarding the origin of sub-T_g molecular motions are offered. As illustrated by Fig. 13.1, temperature assignments for principal relaxations are the temperatures at the maximum of the dynamic-mechanical or dielectric tan δ or loss modulus peaks at the reported frequencies. Values determined from tan γ data are slightly higher than those determined from loss modulus values, and temperature assignments increase with increasing frequency. Typically, peak assignments for T_g are slightly higher (ca. 15–20 °C) than obtained by dilatometry at low cooling rates. Where available, data for only dry, unconditioned samples are reported in this review.

13.1 AMORPHOUS POLYMERS

The prevailing view is that the glass transition (α relaxation in amorphous polymers) is associated with the coordinated motion of 50–100 carbon atoms and associated substituent groups about the chain axis, while secondary relaxations reflect the motions of smaller numbers (e.g., 4–8) of carbon atoms about the chain axis (e.g., crankshaft-type motions) or motions of substituent groups [1]. Sub-T_g relaxations occurring in the amorphous glass are labeled in order of decreasing temperature assignment as β, γ, and δ and reflect motions of progressively smaller molecular units with correspondingly lower activation energies.

The β relaxation in amorphous glasses has been assigned to the onset of motions which are precursors to

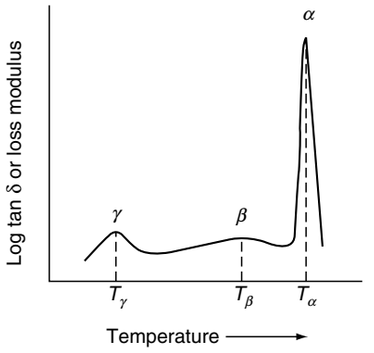

FIGURE 13.1. Idealized representation of the dynamic mechanical spectrum for an amorphous polymer illustrating temperature assignments for the $\alpha(T_g)$, β, and γ relaxations.

the long-range segmental motions occurring at T_g and, therefore, may be considered to be a general phenomenon of glassy materials, polymeric or otherwise [14–16]; however, the β relaxation is not always detectable and remains a somewhat controversial subject. In the case of a number of polymers such as polycarbonate [17], polysulfone [18,19], and polyarylates [20], the β relaxation has been attributed to defects in the glass and as such is affected by thermal treatment sometimes evident when the sample has been quenched from the melt but reduced or eliminated by annealing.

Several relationships have been proposed to relate the temperature assignment for the β transition to T_g. For example, Boyer [3] has suggested that (at 100 Hz)

$$T_\beta \approx 0.75T_g \tag{13.1}$$

for both amorphous and semicrystalline polymers, where temperature is in degrees Kelvin. Van Krevelen [21] has proposed that

$$T_\beta + T_g \approx 635 \tag{13.2}$$

for amorphous polymers and

$$T_\beta \approx 0.8T_g - 40 = 0.5T_m - 25 \tag{13.3}$$

for semicrystalline polymers, where T_m is the crystalline-melting temperature.

In general, secondary-relaxation processes are affected by sample history and the presence of diluents. For example, the method of film preparation (e.g., molding or casting), thermal history (annealed or quenched), and moisture absorption can affect the temperature range, activation energy, and magnitude of some sub-T_g transitions. The dynamic-mechanical and dielectric spectra of polyamides and related polymers such as poly(amide–imides) that are highly water absorbent are particularly sensitive to the presence of absorbed water. Thermal treatment (annealing or quenching) will affect the tail (onset) of the glass transition peak (β transition) but may have little affect on lower-temperature relaxations (i.e., γ peak) [22,23].

Secondary relaxation processes have been correlated with a number of physical and mechanical properties. For example, there is a good correlation between impact strength and the occurrence of main-chain secondary loss processes [24–26], especially for amorphous polymers [21]. There is also reasonable correlation between secondary loss processes and gas permeability [27–29].

Energies required for main-chain and side-group motions can be obtained by determining the effect of frequency on the maximum temperatures of the loss or tan δ peaks. The temperature at the peak maxima, T_{max}, increases with increasing frequency and the activation energy, E_a, of the relaxational process may be determined from the slope of a semilog plot of frequency (f) versus reciprocal peak-temperature ($1/T_{max}$) as

$$\ln f = -\left(\frac{E_a}{R}\right)\frac{1}{T_{max}} + \ln f_0, \tag{13.4}$$

where f_0 is a constant obtained from the intercept.

Typically, activation energies for low-temperature (i.e., γ) relaxations are small (ca. 10–80 kJ mol^{-1}). Heijboer [30] has suggested that for sub-T_g relaxations other than local main-chain motions

$$E_a = 0.060T_{max} \text{ (at 1 Hz)}, \tag{13.5}$$

where E_a is in kcal mol^{-1} and T_{max} is in degrees K. Activation energies are about 20% higher than given by Eq. (13.5) for main-chain motions. Corresponding activation energies for the glass transition, reflecting longer-range cooperative motions, are about an order of magnitude greater than those for sub-T_g relaxations.[†] High activation energies mean that the temperature location of the glass transition (i.e., the α relaxation in amorphous glasses) is relatively insensitive to a change in frequency compared to secondary-relaxation processes.

13.1.1 Poly(Alkyl Acrylates) and Poly(Alkyl Methacrylates)

Dynamic-mechanical and dielectric data for several poly(alkyl acrylates) including poly(methyl acrylate) (PMA) (1), poly(ethyl acrylate) (PEA) (2), poly(*n*-butyl acrylate) (PBA) (3), and poly(cyclohexyl acrylate) (PCA) (4)

[†] In the case of the glass transition, the relationship between T_m and frequency is given by the WLF equation and not the Arrhenius relationship given by Eq. (13.4). Therefore, a semilog plot of f versus $1/T_{max}$ will appear curved over a sufficiently wide frequency range. An *apparent* activation energy for the glass (α_a) transition may be calculated from use of Eq. (13.4) over a more limited frequency range as is typical for most dynamic-mechanical measurements.

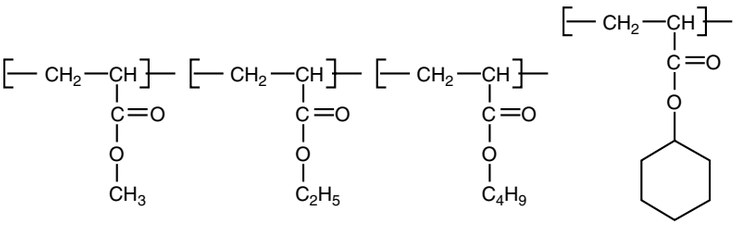

1 2 3 4

are given in Table 13.1. As shown by this data, the predominant (β) relaxation process in poly(alkyl acrylates) occurs at low temperatures (145–197 K) with an activation energy of ca. 30–60 kJ mol^{-1}. Both T_g and the β-relaxation temperature decrease with increasing length of the side chain in the case of linear alkane substitution (i.e., PMA>PEA>PBA) [31]. From ^{13}C NMR (spin-lattice relaxation time) measurements and molecular-dynamics simulations, Kikuchi et al. [32] have concluded that molecular motions in PEA and PBA consist of internal rotation or torsional oscillation of each functional group and a slower motion induced by backbone motion.

Also included in Table 13.1 are data for several poly(alkyl methacrylates) including poly(methyl methacrylate) (PMMA) (5), poly(ethyl methacrylate) (PEMA) (6), poly(2-hydroxyethyl methacrylate) (PHEMA) (7), poly(*n*-propyl methacrylate) (PnPMA) (8), poly(*n*-butyl methacrylate) (PnBMA) (9), and poly(isobutyl methacrylate) (PiBMA) (10).

The predominant sub-T_g process in poly(alkyl methacrylates) is the β relaxation (activation energy of 80–121 kJ mol^{-1}) appearing around 285–336 K and nearly independent of the length of the alkyl group (e.g., methyl, ethyl, propyl, and butyl) while T_g decreases with increasing side chain length (i.e., internal plasticization) [33]. In the case of PMMA, the intensity of the β relaxation of amorphous samples increases with increasing syndiotacticity but decreases with increasing isotacticity [34]. ^{13}C NMR studies have indicated that the nature of the β relaxation in PMMA may be a π (180°) flip of the OCO plane of the side group coupled to a random rotation (20° amplitude) of the main chain [35].

In the case of poly(methacrylates) with longer alkyl groups such as poly(isobutyl methacrylate) (PiBMA) and poly(*n*-butyl methacrylate) (PnBMA), a low-temperature (γ) relaxation is reported near 125–133 K due to side-chain motions involving the four-atom sequence —O—C—C—C or —C—C—C—C— [36]. Poly(isopropyl methacrylate) (PiPMA) which does not have this sequence does not exhibit a relaxation at 120 K but does show one at 50 K (1,000 Hz) similar to that reported for PEMA (see Table 13.1). In those two cases, the low-temperature (δ) relaxation is attributed to rotation of the isopropyl or ethyl group that is attached to the COO group [37]. Esteve-Marco et al. [38] have reported results of dielectric measurements and molecular mechanics calculations of poly(chloroethyl methacrylate) and poly(chloropropyl methacrylate).

Molecular-mechanics simulation has been used extensively to study molecular motions in poly(alkyl methacrylates). As an example, Cowie and Ferguson [33,39] have

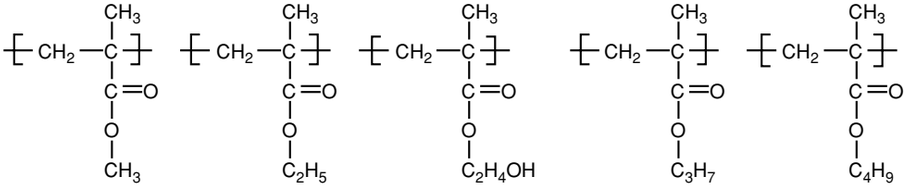

5 6 7 8 9

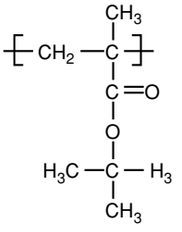

10

TABLE 13.1. *Glass-transition and secondary-relaxation temperatures of poly(alkyl acrylates) and poly(alkyl methacrylates).*

Polymer[a]	Technique[b]	f[c] Hz	T_g (K)	E_a[d] kJ mol^{-1}	T_β (K)	E_a kJ mol^{-1}	T_γ (K)	E_a kJ mol^{-1}	T_δ (K)	E_a kJ mol^{-1}	Ref.
PMA	D	1,000	307		195	43					[31]
PEA	D	1,000	278		177	50					[31]
PBA	D	1,000	250		145	29					[31]
PCA	Dilatometry		290								[118]
	FO	1			197	60					
	D	1			192						
PMMA	TP	1			299						[24]
PMMA	FO	1	386	955	281	81					[119]
a-PMMA	TBA	1.24	388		297						[34]
s-PMMA	TBA	1.25	403		300						
i-PMMA	TBA	1.4	336		285						
PMMA	D					80					[120]
i-PMMA	FO										[121]
amorph.		3			336	105					
crystal.		3			311						
PEMA	D	110							50	9	[122]
PEMA	D	10			310	80					[120]
PHEMA	D	0.02			323	121					[120]
PnPMA	VR	40–600					123				[110]
PnBMA	VR	40–600					115				[110]
PnBMA	D	30					133	23			[37]
PnBMA						80					[110]
PiBMA	D	10					125	25			[37]

[a]PMA, poly(methyl acrylate); PEA, poly(ethyl acrylate); PBA, poly(*n*-butyl acrylate); PCA, poly(cyclohexyl acrylate); PMMA, poly(methyl methacrylate); PEMA, poly(ethyl methacrylate); PHEMA, poly(2-hydroxyethyl methacrylate); PnPMA, poly(*n*-propyl methacrylate); PnBMA, poly(*n*-butyl methacrylate); PiBMA, poly(isobutyl methacrylate).
[b]ES, resonance electrostatic method; FO, forced oscillation dynamic-mechanical analysis; FV, free vibration; TP, torsion pendulum; TSC, thermally stimulated discharge current measurement; D, dielectric; VR, vibrating reed.
[c]$\omega = 2\pi f$ where ω is the angular frequency (rad s^{-1}) and f is frequency in units of Hz; 10 rad^{-1} = 1.5915 Hz.
[d]Apparent activation energy calculated from Eq. (13.4); 1 kJ mol^{-1} = 0.2387 kcal mol^{-1} = 0.0104 eV/molecule.

concluded that the β relaxation of PMMA is due to the rotation of the oxycarbonyl unit with an activation energy of 70–90 kJ mol^{-1}. Studies by Heijboer et al. [40] of (syndiotactic) PMMA indicate that the calculated barrier to alkoxycarbonyl group rotation is lower than experimentally observed for the β relaxation unless main-chain torsion angles are constrained. In the case of PnPMA, molecular-mechanics calculations suggest that the γ relaxation observed at about 90 K at 1 Hz (activation energy of 22 kJ mol^{-1}) could be attributed to hindered rotation around the O—CH_2—CH_2 bond of the propyl group; similar loss peaks have been observed in the case of poly(*n*-alkyl methacrylates) with longer alkyl groups (e.g., butyl, pentyl, and hexyl) [41]. Similar correlation of the δ relaxations of syndiotactic PEMA, PIPMA, and poly(cyclohexyl methacrylate) with limited rotations around the O-alkyl bond was made more recently by Heijboer et al. [42] through the use of molecular-mechanics calculations.

13.1.2 Polycarbonates

The most extensive studies of the dynamic-mechanical properties of polycarbonates have been reported by Yee et al. [17,43,44] and by Vardarajan and Boyer [45]. Some results of dynamic-mechanical and dielectric measurements of bisphenol-A polycarbonate (PC) and two tetrasubstituted bisphenol-A polycarbonates,

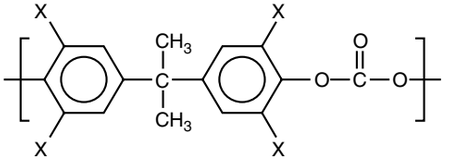

tetramethylbisphenol-A polycarbonate (TMPC, X = CH_3) and tetrachlorobisphenol-A polycarbonate (TCPC, X = Cl), are summarized in Table 13.2. Results for PC reveal a β relaxation in the range from 320 to 370 K and a γ relaxation in the range from 150 to 230 K. In addition, Varadarajan and Boyer [45] report a very low-temperature transition (δ) near 53 K. As appears to be the case of for several other thermoplastics such as poly(2,6-dimethyl-1, 4-phenylene oxide) and polysulfone, the β relaxation is affected by thermal history (i.e., observable in samples

TABLE 13.2. *Glass-transition and secondary-relaxation temperatures of polycarbonates.*

Polymer[a]	Technique[b]	f[c] Hz	T_g (K)	E_a[d] kJ mol^{-1}	T_β (K)	E_a kJ mol^{-1}	T_γ (K)	E_a kJ mol^{-1}	Ref.
PC	TP	0.5–1.2	423				164		[123]
PC	D	100	423				153		[124]
PC					373				[125]
PC	TP	1			340		183		[24]
PC	TP	1					173	36	[49]
PC	TP	1.24					165	44	[73]
PC	TSC	0.032					140	27	[46]
							219	50	
PC	FO	1	426	800			163	52	[119]
PC	D	10	423	800	>343 shoulder		173	10–45	[48]
PC	FO	1	423		353		173	54	[17]
PC	D	120	420	838			160		[47]
							220		
PC	FO	10–50			343	193	187		[45]
PC	TP	~1					173		[126]
PC	FO	1	411		343		178	59	[127]
PC	D	10^6					230	18	[128]
PC	D	100					188	48	[129]
	FO	90					222		
PC	FO	1	431		321		188		[130]
PC	FO	11					188	56	[43]
PC	FO	1	436						[131]
PC	NA						168		[106]
PC	TO	110	423		363		193		[78]
PC	FO	15.9					176	45	[132]
TMPC	FO	1	476				323	80	[133]
TMPC	FO	11					347	103	[43]
TMPC	NA						318		[106]
TCPC	TP	0.5–1.2					351		[123]

[a]Polymer abbreviations: PC, bisphenol-A polycarbonate; TMPC, tetramethylbisphenol-A polycarbonate; TCPC, tetrachlorobisphenol-A polycarbonate.
[b–d]Legend in Table 13.1.

quenched from the melt but absent in annealed samples) [46,47]. There is evidence that the γ relaxation may consist of two [46–48] and possibly three [45] overlapping relaxations. The intensity of the γ relaxation peak has been reported to increase with increasing water content [49].

The molecular basis for sub-T_g molecular relaxations in the case of PC may include segmental motion and rotations of phenyl and methyl groups. The nature of these motions have been studied in detail by ^{13}C NMR spectroscopy and explored by semiempirical molecular-orbital (MO) calculations. Results of ^{13}C NMR measurements (spin–lattice relaxation times) by Jones and Bisceglia [50] indicate that several molecular processes may be coupled or synchronous. NMR studies by Schaefer et al. [51] have shown that the dominant motion in PC may be π flips of the phenylene ring about the main chain extending over a broad frequency range and superimposed on 30° ring oscillations; chlorine substitution of the rings eliminates both ring and main-chain motions. Activation energies of 37–50 kJ mol^{-1} for phenylene group motion have been obtained from NMR measurement [52,53]. Methyl-group substitution at the orthopositions (e.g., TMPC) shifts the onset of fast ring flips by about 180 K [54]. As indicated by the dynamic-mechanical data given in Table 13.2, the low-temperature relaxation (comparable to the γ relaxation in PC) reported for TMPC and TCPC occurs at substantially higher temperatures (ca. >320 K) than for PC in agreement with the NMR results. Comparison of the dynamic mechanical spectra of bisphenol-A PC with trimethylcyclohexylbisphenol PC and spirobisindane-PC for which phenylene ring motion is greatly restricted has led Wimberger-Friedl and Schoo [55] to conclude that the γ relaxation originates from motion of the carbonate group while phenylene group motion contributes as a separate mechanism to the high-temperature side of this relaxation.

Semiempirical MO calculations of model compounds suggest that the γ relaxation of PC may result from phenylene-ring flips (calculated activation energies of about 41 kJ mol^{-1}) as well as methyl-group rotation while the δ relaxation mentioned earlier may be due to *oscillations* of the phenylene ring and the methyl group as well as rocking motions of carbonyl groups [56,57]. In agreement with results from NMR studies, semiempirical MO calculations of TMPC indicate that phenylene rotation is restricted due to

repulsion between the aromatic methyl group and the carbonyl oxygen atom [58].

13.1.3 Polyimides and other Imide Polymers

Polyimides (PIs) represent a broad class of high-T_g polymers derived from the polycondensation of an aromatic dianhydride and diamine. The most widely investigated polyimide is polypyromellitimide or poly(4,4′-oxydiphenylenepyromellitimide) (Kapton®) whose repeat unit structure is given below

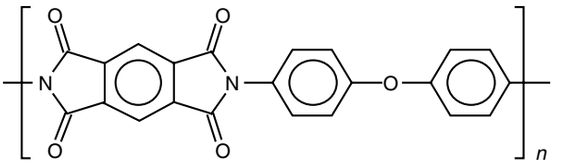

Very recently, Wang et al. [29] have reported dynamic mechanical data for a number of polyimides derived from 1,4-bis(4-aminophenoxy) 2-*tert*-butylbenzene (BATB) and 3,3′,5,5′-tetramethyl-bis[4-(4-aminophenoxy)-phenyl]sulfone (TMBPS). Temperatures for the γ relaxation (DMA, 1 Hz) ranged from 152 to 185 K for the BATB-based polyimides and 150–161 K for the TMBPS-based polyimides. In general, bulky groups in the dianhydride segment, such as the hexafluoroisopropylidene group of 6FDA, reduces polymer packing, increases fractional free volume, and consequently causes the γ relaxation to occur at lower temperature.

Other polymers that contain imide groups include polyetherimide (PEI) (e.g., Ultem®)

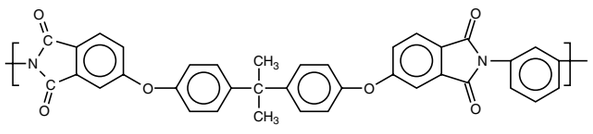

poly(amide-imide) (PAI) (e.g., Torlon®)

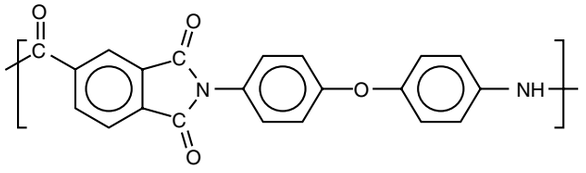

Representative dynamic-mechanical and dielectric data for Kapton PI, PEI, and PAI are given in Table 13.3. In general, an important sub-T_g relaxation for PIs is the β relaxation observed in the temperature range between 338 and 405 K and having an activation energy of about 84–117 kJ mol^{-1} [59]. In addition, PIs exhibit a γ relaxation in the range between 160 and 250 K that has been attributed to water absorption. For example, early dynamic-mechanical measurements of Kapton PI revealed two sub-T_g relaxations at 15,000 Hz—one at 400 K (β) attributed to torsional oscillations of the phenylene ring and another at 250 K identified here at the γ relaxation which was observed to increase in intensity with sorbed water [60]. Computer modeling suggests that the β relaxation is probably associated with the relatively noncooperative motion of the diamine unit which is suppressed by crystallinity or orientation [59]. Other molecular-dynamics simulations of Kapton PI reveal near out-of-phase torsional motions about the nitrogen–phenyl bonds that involve the whole chain and is not localized in one small region [61]. Molecular dynamics studies of a semicrystalline PI (PTDA–DMDA) by Natarajan and Mattice [62] suggest that π-flips of phenoxy rings in the amorphous phase covers a broad range of activation energies.

Dynamic-mechanical data for PEI given in Table 13.3 indicates a β relaxation at about 340–380 K and a γ relaxation at about 160–186 K. These relaxations are comparable to those cited above for Kapton although they occur at slightly lower temperatures. As in the case of Kapton, the γ-relaxational peak of PEI is reported to increase in intensity with sorbed water [63]. From comparison of the dielectric spectra of PEI, poly(ether sulfone) (PES) (see Section 13.1.6), and polyarylates with their corresponding low-molecular-weight compounds, Schartel and Wendorff [64] have concluded that both intrachain and interchain interactions contribute to the γ relaxation in these polymers.

Results of dynamic-mechanical measurements of a sample of PAI dried at 190°C are summarized in Table 13.3. The locations of the β- and γ-relaxational peaks at 338 and 204 K (at 1 Hz) are comparable to that of Kapton and PEI. As in the previous cases, sorbed water has been observed to increase the intensity and decrease slightly the temperature of the γ relaxation while the temperature and activation energy of the β relaxation increases with increasing water content [65].

13.1.4 Poly(phenylene oxides)

Dynamic-mechanical and dielectric properties of three poly(phenylene oxides)

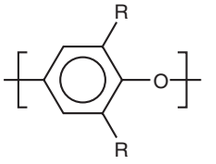

TABLE 13.3. *Glass-transition and secondary-relaxation temperatures of imide polymers.*

Polymer[a]	Technique[b]	f[c] Hz	T_g (K)	E_a[d] kJ mol^{-1}	T_β (K)	E_a Kj mol^{-1}	T_γ (K)	E_a kJ mol^{-1}	Ref.
PI	ES	15,000			400	84–105	250	66	[60]
PI	ES	14,000			405				[134]
PI	TP	1					185	44	[69]
PEI	TP	(∼1)	485		343		168		[63]
PEI	FO	1	492		355		160 (shoulder)		[130]
PEI	FO	1	501	330–1,250					[135]
	D	1,000	513						
PEI	FO	35			379		186		[136]
PEI	D							43	[64]
PAI	FO	1	549		338	117	204		[65]

[a]PI, polypyromellitimide (Kapton polyimide) or poly(4,4'-oxydiphenylenepyromellitimide); PEI, poly(ether-imide); PAI, poly(amide-imide).
[b–d]Legend given in Table 13.1.

poly(*p*-phenylene oxide) (R = H), poly(2,6-dimethyl-1,4-phenylene oxide) (R = CH_3), and poly(2,6-diphenyl-1,4-phenylene oxide) (R = C_6H_5), are summarized in Table 13.4. Dynamic measurements of poly(*p*-phenylene oxide) (H_2PPO) reveal a γ relaxation in the region of 120–160 K (1 Hz) having an activation energy of about 50 kJ mol^{-1}.

The majority of dynamic-mechanical studies for poly(2,6-dimethyl-1,4-phenylene oxide) (PPO) provide evidence for only a weak shoulder (γ relaxation) in the vicinity of 125–160 K; however, a distinct peak has been observed by dielectric measurements [66,67]. In addition, there is evidence for a broad, low-intensity β peak in the range from 240 to 370 K. Sample preparation and impurities appear to have a significant effect on the appearance of the weak sub-T_g relaxational processes in PPO [68,69]. By comparison, dynamic-mechanical data for poly(2,6-diphenyl-1,4-phenylene oxide) (P_2PPO), a semicrystalline polymer (T_m = 753 K), suggests as many as three distinct sub-T_g relaxations [68,70].

In terms of intramolecular flexibility, the poly(2,6-disubstituted-1,4-phenylene oxides) are freely rotating chains [71]; however, intermolecular steric effects may limit phenylene rotation in the solid state and perhaps account for the absence of detectable sub-T_g relaxational processes. For example, results of ^{13}C NMR measurements indicate that the phenylene rings of PPO can execute only small amplitude motions due to the relative stiffness and dense packing of the PPO chain and blockage from rings on adjacent chains.

TABLE 13.4. *Glass-transition and secondary-relaxation temperatures of poly(phenylene oxides).*

Polymer[a]	Technique[b]	f[c] Hz	T_g(K)	E_a[d] kJ mol^{-1}	T_β(K)	E_a kJ mol^{-1}	T_γ(K)	E_a kJ mol^{-1}	Ref.
H_2PPO	ES	7,000	423				121 (shoulder)		[134]
H_2PPO	TP	1					160	50	[68]
H_2PPO	FO	110	363				155		[70]
PPO	ES	7,040			370	84	140 (shoulder)		[137]
PPO	TP	1			273		158		[24]
PPO	ES	7,000			370	84	140 (shoulder)		[134]
PPO	FO	110			240				[138]
PPO	D	100	512	628			158	36	[66]
PPO	D	100	517				157		[67]
PPO	TP	1					205	44	[49]
PPO	TP	∼1.3			277	78	125 (shoulder)	40	[73]
PPO	TP	∼1			286	67	135 (shoulder)	42	[68]
PPO	ES	9,640			373		126	29–34	[69]
P_2PPO	TP	∼1			348	96	γ 238	50	[68]
							δ 83	17	
P_2PPO	FO	110	502		363		143		[70]

[a]H_2PPO, poly(*p*-phenylene oxide); PPO, poly(2,6-dimethyl-1,4-phenylene oxide); P_2PPO, poly(2,6-diphenyl-1,4-phenylene oxide).
[b–d]Legend given in Table 13.1.

13.1.5 Polystyrenes

Molecular motions in polystyrene (PS) have been extensively reviewed by Boyer [72]. Results of dynamic-mechanical studies of polystyrene, poly(4-methylstyrene) (P4MS), poly(4-chlorostyrene) (P4CS), and poly(α-methylstyrene) (PAMS) are summarized in Table 13.5. These and other studies show evidence for three transitions for PS below T_g. These include β (ca. 325 K), γ (ca. 130–180 K), and δ (ca. 30–40 K) transitions with activation energies of about 147, 42, and 8–13 kJ mol^{-1}, respectively. The δ relaxation has been associated with hindered partial rotation and wagging of the phenyl group [73]. It decreases in intensity with crystallinity in isotactic PS [74]. The origin of the γ transition is less certain and may be due to motion of end groups.

Results of molecular-dynamics simulations suggest that sub-T_g relaxations may include crankshaft-type motions of the PS backbone and librational motions of the pendant phenyl rings that depend upon the local environment [61]. NMR measurements indicate that the most prevalent molecular motion is restricted phenyl-group rotation with an average total displacement of ranging from 40° for *ortho*-substituted polystyrene to 70° for *para*-substituted polystyrenes having bulky nonpolar substituent groups [75]. Restrictions are due to intramolecular steric interactions and interchain packing (for unsubstituted PS). These conclusions are consistent with molecular mechanics studies reported by Khare and Paulaitis [76].

13.1.6 Polysulfones

Extensive studies of the dynamic-mechanical properties of a number of different polysulfones has been reported by Robeson et al. [77] and by Aitken et al. [78] Most of studies reported in the literature have focused on the two commercially important polysulfones — bisphenol-A polysulfone (PSF)

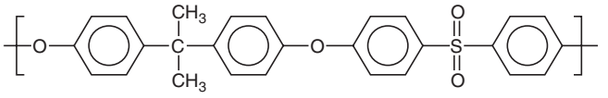

and polyethersulfone (PES)

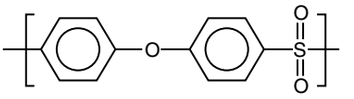

Results of dynamic-mechanical and dielectric studies of PSF and PES are summarized in Table 13.6. Results for PSF indicate a well-defined γ relaxation located near 162–229 K. There is substantial evidence that the intensity of the γ-relaxational peak increases with sorbed water content [49,77,79]. Substitutions that hinder phenylene mobility increase the temperature of the γ relaxation [78]. There is controversy concerning the existence of a β relaxation located around 330–360 K that is sensitive to thermal history as has been reported for polycarbonate [18,19,80]. The dynamic-mechanical behavior of PES, which has a slightly lower T_g, is similar to that of PSF with a prominent γ relaxation that is also water sensitive [49] and is located in the region from 163 to 265 K.

Results of semiempirical molecular orbital (CNDO/2) calculations suggest that the γ relaxation is due to phenylene-group rotation of the isopropylidene moiety with a calculated activation energy of 42 kJ mol^{-1}, rotation of the methyl groups in the isopropylene group with an activation energy of 41 kJ mol^{-1}, and possibly the diphenyl sulfone rotation with an activation energy of 42 kJ mol^{-1} while the β relaxation is attributed to diphenyl ether rotation with an activation energy of 167 kJ mol^{-1} [18,19]. Molecular simulations have shown that the rotational barriers for C—O or C—C bonds are higher than those for C–S bonds in PSF and that the mechanism for relaxation in the bulk state may be due to cooperative ring-flip motions associated with rotations about the C—S linkage [81]. NMR studies have indicated that the β-relaxation is due to π flips of the aromatic rings that are unaffected by sorbed water but decrease in frequency in the presence of antiplasticizers [82]. Dynamic mechanical studies of PES by Shi et al. [83] indicated that the low-temperature (γ) transition (ca. 193 K) is associated

TABLE 13.5. *Glass-transition and secondary-relaxation temperatures of polystyrenes.*

Polymer[a]	Technique[b]	f[c] Hz	T_α(K)	T_β(K)	T_γ(K)	T_δ(K)	E_a kJ mol^{-1}	Ref.
PS	ES	5,590			185	38	8.4	[134]
PS	FO	110	379	325	133			[138]
PS	TP	1				38		[74]
PS	D	100	394		154			[67]
PS	TP	1.7				33		[73]
P4MS	ES	9,700				92	8.8	[134]
P4CS	ES	8,330				95	9.2	[134]
PAMS	ES	7,850				126	16	[134]

[a]PS, polystyrene; P4MS, poly(4-methylstyrene); P4CS, poly(4-chlorostyrene); PAMS, poly(α-methylstyrene).
[b–d]Legend given in Table 13.1.

TABLE 13.6. *Glass-transition and secondary-relaxation temperatures of bisphenol-A polysulfone and polyethersulfone.*

Polymer[a]	Technique[b]	f[c] Hz	T_g(K)	E_a[d] kJ mol^{-1}	T_β(K)	E_a kJ mol^{-1}	T_γ(K)	E_a kJ mol^{-1}	Ref.
PSF	ES	6,088					229	50	[79]
PSF	TP	1	468				163		[139]
PSF	TP	1					206	70	[49]
	D	1,000					207		
PSF	TP	0.67					162		[73]
PSF	TP	1	448				183		[140]
PSF	FO	11			333		173		[80]
PSF	FO	1.59		920		282	173	45	[19]
PSF	FO	1	470				177		[130]
PSF	FO	110	459		358		193		[78]
PES	TP	1			273		163		[139]
PES	TP	1					226	55	[49]
PES	TP	1	476				183		[140]
PES	D	2.1×10^6					265	21	[128]
PES	TP	$\sim$1					178		[141]
PES	FO	35					170		[136]
PES							175		[106]
PES	FO	110	498				193		[78]
PES	D							45	[64]

[a]PSF, bisphenol-A polysulfone; PES, polyethersulfone.
[b–d]Legend given in Table 13.1.

with the rotation of phenylene rings. Recent quasielastic neutron scattering of PES [84] and PSF [85] have suggested that the γ and δ relaxations may be associated with π-flips and oscillations of phenyl rings, respectively.

13.1.7 Poly(vinyl chloride)

The dynamic spectrum of poly(vinyl chloride) (PVC) has been widely reported and reveals a major β relaxation located in the range from 195 to 273 K. Havriliak and Shortridge [86,87] have suggested that the molecular nature of the β relaxation in PVC is a hindered rotation of a segment about its main-chain axis. Results of dynamic-mechanical and dielectric studies of PVC are summarized in Table 13.7. PVC is weakly crystalline due to syndiotactic sequences of repeating units. Harrell and Chartoff [88] have shown that crystallinity shifts the α relaxation to slightly higher temperature, shifts the β relaxation to lower temperature, and reduces peak intensity. Kakutani et al. [89] have suggested that the β relaxation may be composed of two overlapping relaxational processes at 223 and 273 K due to motions in the amorphous and crystalline regions, respectively. Chlorination of PVC shifts the α relaxation to higher temperatures and broadens the β relaxation peak while plasticization decreases the β relaxation and shifts it to lower temperature (i.e., the high-temperature portion of the β peak is reduced) [90]. Molecular dynamics studies of torsional angles changes by Meier and Struik [91] suggest that a localized five-bond transition may result in activation energies responsible for the β relaxation and higher activation energies associated with the glass transition.

13.2 SEMICRYSTALLINE POLYMERS

Boyd has provided a detailed review of relaxational processes that occur in semicrystalline polymers [92] as well as a discussion of their molecular origins [93]. In general, the dynamic-mechanical and dielectric spectra of semicrystalline polymers are more complex than those of amorphous ones. This complexity results from the presence of additional transitions resulting from crystalline regions, varying degrees of crystallinity in different samples, and the possibility of different crystalline forms. While discussing the dynamic-mechanical and dielectric properties of semicrystalline polymers in this section, the usual convention will be used where the α peak is now associated with the crystalline–melting transition, the β peak is commonly identified with the glass-transition of the amorphous region, and sub-T_g relaxations are indicated as γ and δ [92].

13.2.1 Polyamides

Dynamic-mechanical and dielectric data have been widely reported for most aliphatic polyamides, especially poly(ε-caprolactam) (nylon-6 or PA-6; $T_g \approx 313$ K) and poly(hexamethylene adipamide) (nylon-6,6 or PA-6,6; $T_g \approx 323$ K). Results of dynamic-mechanical and dielectric measurements of PA-6 and PA-6,6 (Table 13.8) provide evidence for three relaxations (β, γ, and δ) in these polymers at temperatures below their crystalline–melting temperature T_m (487–506 K for PA-6 and 523–545 K for PA-6,6) [8]. The β relaxation (located at above 310–347 K for PA-6,6 and 357–370 K for PA-6,6) is associated with high

TABLE 13.7. *Glass-transition and secondary-relaxation temperatures of PVC.*

Technique[a]	f[b] Hz	T_g(K)	E_a[c] kJ mol^{-1}	T_β(K)	E_a kJ mol^{-1}	Ref.
D			364		63	[96]
TP	~2	358		223	63	[90]
D			524		63	[142]
TP	1			208–218	42–54	[143]
FO (D)	110			223 (β_2)	67	[89]
				273 (β_1)	45	
D					50–60	[144]
TP	~2			233		[145]
FO	3.5			239	65	[88]
FO		360	754	226	54	[119]
FO	11			235		[146]
TSC				195		[147]

[a]ES, resonance electrostatic method; FO, forced oscillation dynamic-mechanical analysis; FV, free vibration; TP, torsion pendulum; TSC, thermally stimulated discharge current measurement; D, dielectric; VR, vibrating reed.
[b]$\omega = 2\pi f$ where ω is the angular frequency (rad s^{-1}) and f is frequency in units of Hz; 10 rad^{-1} = 1.5915 Hz.
[c]Apparent activation energy calculated from Eq. (4); 1 kJ mol^{-1} = 0.2387 kcal mol^{-1} = 0.0104 eV/molecule.

TABLE 13.8. *Secondary-relaxation temperatures of polyamides.*

Polymer[a]	Technique[b]	f[c] Hz	T_β (K)	E_a[d] kJ *mol*$^{-1}$	T_γ (K)	E_a kJ *mol*$^{-1}$	T_δ (K)	E_a kJ *mol*$^{-1}$	Ref.
PA-6	D					61			[96]
PA-6	ES	~10,000	310		241		156		[97]
PA-6	TP	~1	330		203		123		[94]
PA-6	FO	1	347						[131]
PA-6	FO	1	335		220		147		[148]
PA-66	VR	40–600			249		156		[110]
PA-66	FO	11	363						[149]
PA-66	FO		357		245		186		[95]
PA-66	FO	1	370						[131]
Nomex	ES	~10,000			291 (γ)				[97]
					442 (γ^*)				
Nomex	TP	~1	550	665	352	83	120	24	[98]
Kevlar	ES	~10,000			291 (γ)	63			[97]
					417 (γ^*)	92			
Kevlar	FO	110	733	767	333	204	243	52	[99]
Kevlar	TP	~1	816	813	235 (γ)	54	115	21	[98]
					440 (γ^*)	83			

[a]Polymer abbreviations: PA-6,6, nylon-66; PA-6, nylon-6; Nomex, poly(*m*-phenylene isophthalamide); Kevlar, poly(*p*-phenylene terephthalamide).
[b–d]Legend given in Table 13.1.

activation-energy molecular motions occurring in the amorphous phase (i.e., glass transition) that are affected by the overall degree of crystallinity and crystalline morphology [94] as well as plasticization by sorbed water [95]. The γ relaxation (ca. 200–240 K for PA-6) is comparatively weak with an activation energy approximately 61 kJ mol^{-1} [96]. The γ relaxation increases in intensity with sorbed water suggesting motions involving (amide) carbonyl groups that are hydrogen bonded to water molecules. The intensity of the γ relaxation increases with the relative concentration of amide groups and shifts to lower temperatures in the presence of sorbed water [97]. The δ relaxation (activation energy of ca. 42 kJ mol^{-1} in the case of PA-6) occurs at ca. 120–160 K and is believed to be due to motions of the methylene groups [94]. Frosini and Butta [97] have suggested that the δ relaxation occurs at about the same temperature (160–180 K at $\sim 10^4$ Hz) for all aliphatic polyamides but increases in intensity with increasing number of methylene groups.

Two important aromatic polyamides (aramids) are poly(*m*-phenylene isophthalamide) (Nomex) ($T_g > 503$ K)

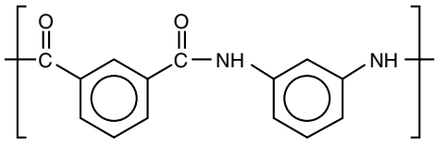

and poly(*p*-phenylene terephthalamide) (Kevlar) ($T_g \sim$ 618 K)

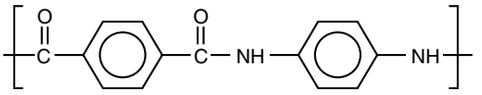

Unfortunately, the number of good dynamic mechanical and dielectric studies of well-characterized samples is limited. Some dynamic mechanical data for these two aramids are given in Table 13.8. A study by Badayev et al. [98] (Table 13.7) indicates that although the β and γ peaks of these aramids are located at temperatures higher than those for the aliphatic polyamides, their activation energies are comparable with those of the two aliphatic polyamides. Both aliphatic and aromatic polyamides display a low-temperature relaxation (δ) at ca. 115–190 K; however, a molecular mechanism other than methylene group motion suggested for aliphatic polyamides must exist for the aramids. Kunugi et al. [99] report three principle relaxations (β, γ, and δ) for Kevlar fiber where the δ relaxation was observed to be more prominent in the presence of sorbed water. The results of Kunugi et al. for annealed samples and those of several other investigations (Table 13.8) indicate that the γ peak of aramids may appear as two weak peaks – one in the region above and below room temperature (291–333 K) and one at 417–440 K (γ^*) with a slightly higher activation energy.

13.2.2 Poly(alkylene oxides)

Results of dielectric and dynamic-mechanical measurements of several poly(alkylene oxides) including poly(oxymethylene) (POM), poly(ethylene oxide) (PEO), poly(propylene oxide) (PPO), and poly(tetramethylene oxide) (PTMO) are summarized in Table 13.9. The sub-T_g γ-relaxation in PEO has been attributed to local twisting motion of main chains in both amorphous region and defective regions of the crystalline regions [100]. The γ relaxation (amorphous) has been reported to increase as the proportion of oxygen in the main chain increases (i.e., POM > PEO > PPO > PTMO).

13.2.3 Poly(aryl ether ether)

Results of dynamic-mechanical measurements of poly(aryl ether ether ketone) (PEEK) (T_m = 613–673 K)

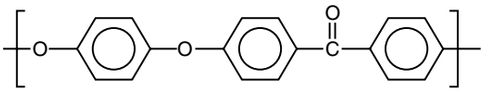

are summarized in Table 13.10. An β peak corresponding to the glass transition occurs at about 420 K and is sensitive to the crystalline morphology of the sample [101]. Candia et al. [102] report two β peaks at 423 and 488 K where the higher temperature peak represents reorganization following the crystallization process. In addition, there is evidence for a broad γ relaxation in the region between 170 and 213 K which may be due to contributions from two [103,104] or three [105] overlapping relaxations. This low-temperature sub-T_g relaxation has been attributed to localized wagging of the polar bridges within the amorphous regions while the high-temperature relaxation is attributed to a combination of wagging motions and phenylene flips and is affected by intermolecular interactions [101].

Sommer et al. [106] have looked at the effect of substituent group structure of the bisphenol groups on the T_g and the γ-relaxation temperature of the following four polyetherketones (PEKs):

TABLE 13.9. *Glass-transition and secondary-relaxation temperatures of poly(alkylene oxides).*

Polymer[a]	Technique[b]	f[c] Hz	T_β(K)	E_a[d] kJ mol^{-1}	T_γ(K)	E_a kJ mol^{-1}	Ref.
POM	TP	1			203		[24]
POM	D	2.1×10^6			247	19	[128]
PEO	TP	1	206	126–147			[150]
PEO	D	12,800	236		198	38	[100]
PEO	D	20			140	33	[151]
PPO	VR		228		164		[110]
PPO	TP	1	211				[150]
PPO	D	2,000	208	130–155	150	25–30	[152]
PTMO	VR	40–600	221		164		[110]
PTMO	D	2,000	188–198	155–163		13–21	[152]

[a]POM, polyoxymethylene; PEO, poly(ethylene oxide); PPO, poly(propylene oxide); PTMO, poly(tetramethylene oxide).
[b–d]Legend given in Table 13.1.

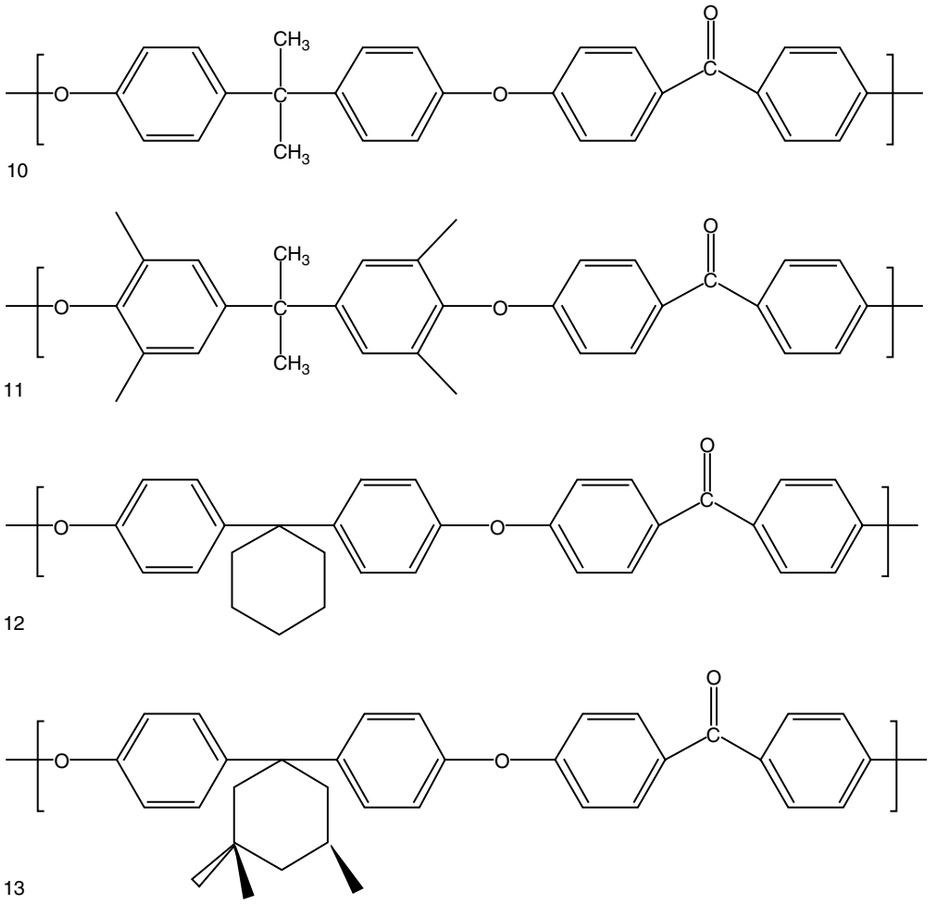

As shown by the data in Table 13.10, the temperature for the γ relaxation increases with increasing steric hindrance to rotation of the bisphenol group in the order PEK(10) $>$*TMBPA-PEK*(11) $>$ *BPZ-PEZ*(12). Methyl substitution of the cyclohexylidene ring in the case of TMC-PEK(13) lowers the γ temperature compared to PPZ-PEZ.

13.2.4 Polyesters

Dielectric and dynamic mechanical data for poly(ethylene terephthalate) (PET) ($T_m \approx 538$ K), poly(butylene terephthalate) (PBT) ($T_m \approx 493$ K), and several fully aromatic polyesters or polyarylates having the general structure shown below

TABLE 13.10. *Glass-transition and secondary-relaxation temperatures of poly(aryl ether ether).*

Polymer[a]	Technique[b]	f[c] Hz	T_β (K)	E_a[d] kJ mol^{-1}	T_γ (K)	E_a kJ mol^{-1}	Ref.
PEEK	TP	~1	423		193		[105]
	TP	~1	416		176		[63]
	TP	~1			183	30–100	[103]
	FO	35			170		[136]
	FO	5		amorph. 1,250–1,900	213	80	[104]
	FO	110	423		208	31	[102]
PEK	NA				180		[106]
TMBPA-PEK					198		[106]
BPZ-PEK					209		[106]
TMC-PEK					191		[106]

[a]PEEK, poly(aryl ether ether ketone); PEK, bisphenol-A polyetherketone; TMBPA-PEK, tetramethylbisphenol-A PEK; BPZ-PEK, PEK from cyclohexylidene; TMC-PEZ, PEK from trimethyl-cyclohexylidene PEK.
[b–d]Legend given in Table 13.1.

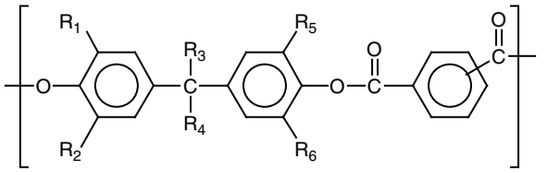

are summarized in Table 13.11. Results for both PET and PBT are comparable with a $\beta(T_g)$ relaxation observable in crystalline samples in the region from 344 to 366 K and a sub-T_g γ-relaxation in the region of 188–237 K. The β-relaxation temperature increases with crystallinity while the γ relaxation is relatively unaffected [107].

Charati et al. [20] have reported dynamic-mechanical data for a number of different polyarylates. They concluded that the γ relaxation originates from defects of the glass and is reduced through thermal annealing. A δ relaxation (water sensitive) was attributed to phenylene motion in the bisphenol moiety and is shifted to high temperatures with substitution of the bisphenol moiety. From molecular-mechanics calculation of conformational energies of three polyarylates derived from terephthalic acid, Charati et al. [108] have concluded that low-energy π phenyl-ring flips are possible through cooperative motions of both rings. From dielectric measurements of several polyarylates and related polymers, Schartel and Wendorff [64] concluded that the δ relaxation (activation energy of $\sim 46\,\text{kJ mol}^{-1}$) must involve both intrachain and interchain contributions with a correlation length of no greater than a single repeat unit.

del Campo et al. [109] have reported the dielectric spectra of a series of nematic polyesters following the form of structure 14 where R is a methylene chain of 4, 6, 8, 10, or 12 units. They attributed the β and γ relaxations to local reorganizations of the mesogenic units and the methylene units of the spacer groups, respectively. The characteristics of the molecular motions associated with the β relaxation are influenced by the conformation arrangement of chains in the nematic phase.

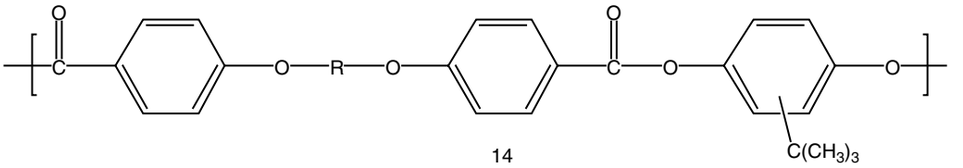

14

13.2.5 Polyolefins

The presence of a varying numbers of side branches having different lengths and varying levels of crystallinity in different grades of polyethylene (PE), including low-density (LDPE), linear low-density (LLDPE), and high-density polyethylene (HDPE), complicate the interpretation of the dynamic-mechanical spectrum of this polymer. In addition, the nonpolar nature of polyethylene makes it unsuitable for dielectric analysis in its unmodified form although electrical properties can be enhanced by irradiation in air. In general, the relaxational processes in polyethylene may be characterized as α, β, and γ in order of decreasing temperature. The α process has been associated with the melting of PE crystallites of different sizes and decreases in intensity with decreasing crystallinity as may be achieved through irradiation [110] or chlorination as examples. The α-peak temperature is higher for high-density samples. There is evidence that the overall α process may result from two and possibly three different mechanisms [111]. Alberola et al. [112] report

TABLE 13.11. *Glass-transition and secondary-relaxation temperatures of polyesters.*

Polymer[a]	Technique[b]	f[c] Hz	T_β (K)	E_a[d] kJ mol^{-1}	T_γ (K)	E_a kJ mol^{-1}	T_δ (K)	E_a kJ mol^{-1}	Ref.
PET	TP	1	292 (amorph.) 365 (cryst.)	770	208	52 (wet) 71 (dry)			[153]
PET	D								[142]
amorph.				829		63			
Crystal.				387		NA			
PET	D					50			[154]
PET	FO	1	366						[131]
PBT	D					50			[154]
PBT	D	10,000	344	281	237	55			[155]
	FV	10	334		188				
PBT	FO	1	353						[131]
PBT	D	1,600	355	483	198	27			[107]
PAR	FO	1.6	423–587	1,060–1,144	353–493	369	172–383		[20]

[a]PET, poly(ethylene terephthalate); PBT, poly(butylene terephthalate); PAR, various polyarylates.
[b–d]Legend given in Table 13.1.

TABLE 13.12. *Glass-transition and secondary-relaxation temperatures of polyolefins.*

Polymer[a]	Technique[b]	f[c] Hz	T_α (K)	E_a[d] kJ mol^{-1}	T_β (K)	E_a kJ mol^{-1}	T_γ (K)	E_a kJ mol^{-1}	Ref.
LDPE	VR	40–600			265		159		[110]
LDPE	D	1,000					153	48	[113]
							175		
HDPE	TP	1					153		[24]
HDPE	TP	1					152		[114]
LLDPE	FV	1.59	297–303		256		149		[156]
i-PP	FV	1	325–400	110–170	275	380			[115]
i-PP	TP	1	343–359		279				[116]

[a]LDPE, low-density polyethylene; HDPE, high-density polyethylene; LLDPE, linear low-density polyethylene; *i*-PP, isotactic polypropylene.
[b–d]Legend given in Table 13.1.

two high-temperature (α) processes in the temperature range from 303 to 393 K with activation energies of 80–210 kJ mol^{-1}. The weak β relaxation, particularly evident in low-density samples, is typically observed between 220 and 280 K and is sometimes identified with motions in the interlaminar region (amorphous–crystalline interphase) and is observed to decrease in intensity upon annealing [113]. The γ relaxation typically lies in the temperature range from 123 to 153 K. Willbourn [110] has suggested that this transition is characteristic of coordinated motions of a minimum of three or four methylene groups (e.g., crankshaft-type mechanism). The γ relaxation is observed to increase in intensity as sample crystallinity increases and the α peak decreases. In the case of LDPE, as many as three low-temperature (γ) relaxations have been detected by TSC measurements [113]. Both the β and γ relaxations have characteristics that may be associated with the glass transition such as high activation energy (ca. 150–200 kJ mol^{-1}) and WLF dependence [112] although the β relaxation may be associated with side chain motions involving CH_3 groups [114]. It is also noted that polyethylene can achieve structural recovery by annealing at temperatures below the γ-relaxation temperature [112].

Some representative dynamic-mechanical data for isotactic polypropylene (*i*-PP) are given in Table 13.12. It is noted that the activation energy of the α relaxation is smaller than that of the β relaxation (glass transition of amorphous fraction) suggesting a less cooperative process attributed to the diffusion of defects in the crystalline phase [115]. Jawad and Alhaj-Mohammad [116] associated the β relaxation with the glass transition and report that the intensity of the β peak decreases with drawing suggesting that β relaxation depends on mobility of chains in the amorphous regions.

13.2.6 Poly(phenylene sulfide)

Poly(*p*-phenylene sulfide) (PPS) ($T_m \approx 558$ K) exhibits only weak sub-T_g relaxational processes. Dynamic-mechanical data [68,70] suggest a low-temperature (δ) relaxation in the region of 165–233 K with an activation energy of about 46 kJ mol^{-1} [68]. There may be a higher-temperature relaxation at 313 K (γ) and one at 361 K (β) [70]. Deuterium NMR studies of deuterated amorphous PPS by Henrichs et al. [117] suggest that PPS can undergo rapid π flips with a distribution of activation energies centered about 46 kJ mol^{-1}.

ACKNOWLEDGEMENT

The author would like to acknowledge the contribution of R.-J. Roe to the version of this chapter appearing in the first edition of this handbook.

REFERENCES

1. R. F. Boyer, Polym. Eng. Sci. **8**, 161 (1968).
2. J. Heijboer, Br. Polym. J. **1**, 3 (1969).
3. R. F. Boyer, Polymer **17**, 996 (1976).
4. J. Heijboer, Intern. J. Polym. Mater. **6**, 11 (1977).
5. D. J. Meier, ed. *Molecular Basis of Transitions and Relaxations* (Gordon and Breach Science Publishers, London, 1978).
6. J. M. G. Cowie, J. Macromol. Sci. Phys. **B18**, 569 (1980).
7. A. E. Woodward and J. A. Sauer, Fortschr. Hochpolym.-Forsch. **1**, 114 (1958).
8. N. G. McCrum, B. E. Read and G. Williams, *Anelastic and Dielectric Effects in Polymeric Solids* (Wiley, New York, 1967).
9. T. Murayama, *Dynamic Mechanical Analysis of Polymeric Materials* (Elsevier, London, 1978).
10. L. E. Nielsen, SPE J. **16**, 525 (1960).
11. J. Heijboer, Polym. Eng. Sci. **19**, 664 (1979).
12. J. K. Gillham, in *Developments in Polymer Characterisation*, edited by J. V. Dawkins (Applied Science Publishers, London, 1982), Vol. 3, pp. 159–227.
13. J. D. Ferry, *Viscoelastic Properties of Polymers* (Wiley, New York, 1980).
14. M. Goldstein, J. Chem. Phys. **51**, 3728 (1969).
15. G. P. Johari and M. Goldstein, J. Chem. Phys. **53**, 2372 (1971).
16. V. A. Bershtein and V. M. Yegorov, Polym. Sci. USSR **27**, 2743 (1985).
17. A. F. Yee and S. A. Smith, Macromolecules **14**, 54 (1981).
18. J. R. Fried, A. Letton and W. J. Welsh, Polymer **31**, 1032 (1990).
19. A. Letton, J. R. Fried and W. J. Welsh, in *Order in the Amorphous "State" of Polymers*, edited by S. K. Keinath, R. L. Miller and J. K. Rieke (Plenum, New York, 1987), pp. 359–370.
20. S. G. Charati, J. P. Jog, S. S. Kulkarni, et al., J. Appl. Polym. Sci. **54**, 1093 (1994).

21. D. W. van Krevelen, *Properties of Polymers* (Elsevier, Amsterdam, 1990).
22. J. L. G. Ribelles and R. D. Calleja, Polym. Eng. Sci. **24**, 1202 (1984).
23. L. C. E. Struik, Polymer **28**, 57 (1987).
24. J. Heijboer, J. Polym. Sci., Polym. Symp. **16**, 3755 (1968).
25. P. I. Vincent, Polymer **15**, 111 (1974).
26. E. Sacher, J. Appl. Polym. Sci. **19**, 1421 (1975).
27. R. R. Light and R. W. Seymour, Polym. Eng. Sci. **22**, 857 (1982).
28. K. M. P. Kamps, H. A. Teunis, M. Wessling, et al., J. Membr. Sci. **74**, 193 (1992).
29. Y.-C. Wang, S.-H. Huang, C.-C. Hu, et al., J. Membr. Sci. **248**, 15 (2005).
30. J. Heijboer, in *Molecular Basis of Transitions and Relaxations*, edited by D. A. Meier (Gordon and Breach Science Publishers, London, 1978), Vol. 4, pp. 75–102.
31. J. L. G. Ribelles, J. M. M. Duenas and M. M. Pradas, J. Appl. Polym. Sci. **38**, 1145 (1989).
32. H. Kikuchi, H. Tokumitsu and K. Seki, Macromolecules **26**, 7326 (1993).
33. J. M. G. Cowie and R. Ferguson, Polymer **28**, 503 (1987).
34. J. K. Gillham, S. J. Stadnicki and Y. Hazony, J. Appl. Polym. Sci. **21**, 401 (1977).
35. K. Schmidt-Rohr, A. S. Kulik, H. W. Beckham, et al., Macromolecules **27**, 4733 (1994).
36. E. A. W. Hoff, D. W. Robinson and A. H. Willbourn, J. Polym. Sci. **18**, 161 (1955).
37. K. Shimizu, O. Yano and Y. Wada, J. Polym. Sci. Polym. Phys. **13**, 1959 (1975).
38. C. Esteve-Marco, M. J. Sanchis and R. Diaz-Calleja, Polymer **38**, 3805 (1997).
39. J. M. G. Cowie and R. Ferguson, Polym. Commun. **25**, 66 (1984).
40. J. Heijboer, J. M. A. Baas, B. v. d. Graaf, et al., Polymer **28**, 509 (1987).
41. J. Heijboer, J. M. A. Baas, B. v. d. Graaf, et al., Polymer **33**, 1359 (1992).
42. J. M. A. Baas and B. v. d. Graaf, Polymer **32**, 2141 (1991).
43. J. Y. Jho and A. F. Yee, Macromolecules **24**, 1905 (1991).
44. C. Xiao and A. F. Yee, Macromolecules **25**, 6800 (1992).
45. K. Vardarajan and R. F. Boyer, J. Polym. Sci. Polym. Phys. **20**, 141 (1982).
46. Y. Aoki and J. O. Brittain, J. Polym. Sci. Polym. Phys. 1297 (1976).
47. J. M. Pochan, H. W. Gibson and D. L. F. Pochan, Macromolecules **15**, 1368 (1982).
48. D. C. Watts and E. P. Perry, Polymer **19**, 248 (1978).
49. G. Allen, J. McAinsh and G. M. Jeffs, Polymer **18**, 85 (1971).
50. A. A. Jones and M. Bisceglia, Macromolecules **12**, 1136 (1979).
51. J. Schaefer, E. O. Stejskal, R. A. McKay, et al., Macromolecules **17**, 1479 (1984).
52. A. K. Roy, A. A. Jones and P. T. Inglefield, Macromolecules **19**, 1356 (1986).
53. M. Wehrle, G. P. Hellmann and H. W. Spiess, Colloid Polym. Sci. **265**, 815 (1987).
54. M. T. Hansen, C. Boeffel and H. W. Spiess, Colloid Polym. Sci. **271**, 446 (1993).
55. R. Wimberger-Friedl and H. F. M. Schoo, Macromolecules **29**, 8871 (1996).
56. J. Bicerano and H. A. Clark, Macromolecules **21**, 585 (1988).
57. J. Bicerano and H. A. Clark, Macromolecules **21**, 597 (1988).
58. Y. J. Sung, C. L. Chen and A. C. Su, Macromolecules **24**, 6123 (1991).
59. F. E. Arnold, K. R. Bruno, D. Shen, et al., Polym. Eng. Sci. **33**, 1373 (1993).
60. E. Butta, S. d. Petris and M. Pasquini, J. Appl. Polym. Sci. **13**, 1073 (1969).
61. A. R. Tiller, Macromolecules **25**, 4605 (1992).
62. U. Natarajan and W. L. Mattice, Macromol. Theory Simul. **6**, 949 (1997).
63. J. E. Harris and L. M. Robeson, J. Appl. Polym. Sci. **35**, 1877 (1988).
64. B. Schartel and J. H. Wendorff, Polymer **36**, 899 (1995).
65. G. Dallas and T. Ward, Eng. Plast. **7**, 329 (1994).
66. F. E. Karasz, W. J. MacKnight and J. Stoelting, J. Appl. Phys. **41**, 4357 (1970).
67. W. J. MacKnight, J. Stoelting and F. E. Karasz, in *Multicomponent Polymer Systems*, edited by R. F. Gould (American Chemical Society, Washington, 1971), Vol. 99, pp. 29–41.
68. A. Eisenberg and B. Cayrol, J. Polym. Sci., Polym. Symp. **35**, 129 (1971).
69. T. Lim, V. Frosini, V. Zaleckas, et al., Polym. Eng. Sci. **13**, 51 (1973).
70. M. Aguilar-Vega and D. R. Paul, J. Polym. Sci. Polym. Phys. **31**, 1577 (1993).
71. A. E. Tonelli, Macromolecules **6**, 503 (1973).
72. R. F. Boyer and S. G. Turley, in *Molecular Basis of Transitions and Relaxations*, edited by D. J. Meier (Gordon and Breach Science Publishers, London, 1978), Vol. 4, pp. 333–358.
73. C. I. Chung and J. A. Sauer, J. Polym. Sci. Polym. Phys. **9**, 1097 (1971).
74. C. D. Armeniades, E. Baer and J. K. Rieke, J. Appl. Polym. Sci. **14**, 2635 (1970).
75. J. Schaefer, M. D. Sefcik, E. O. Stejskal, et al., ACS Symp. Ser. **247**, 43 (1984).
76. R. Khare and M. E. Paulaitis, Macromolecules **28**, 4495 (1995).
77. L. M. Robeson, A. G. Farnham and J. E. McGrath, in *Molecular Basis of Transitions and Relaxations*, edited by D. J. Meier, Gordon and Breach, New York, 1978, pp. 405–425.
78. C. L. Aitken, J. S. McHattie and D. R. Paul, Macromolecules **25**, 2910 (1992).
79. M. Baccaredda, E. Butta, V. Frosini, et al., J. Polym. Sci. Polym. Phys. **5**, 1296 (1967).
80. J. R. Fried and H. Kalkanoglu, J. Polym. Sci. Polym. Lett. **20**, 381 (1982).
81. C. F. Fan and S. L. Hsu, Macromolecules **24**, 6244 (1991).
82. J. J. Dumais, A. L. Cholli, L. W. Jelinski, et al., Macromolecules **19**, 1884 (1986).
83. T. Shi, W. Jiang, L. An, et al., Mscromol. Theory Simul. **10**, 232 (2001).
84. I. Quintana, A. Arbe, J. Colmenero, et al., Macromolecules **38**, 3999 (2005).
85. S. Arrese-Igor, A. Arbe, A. Alegria, et al., J. Chem. Phys. **120**, 423 (2004).
86. S. Havriliak and T. J. Shortridge, J. Vinyl Technol. **10**, 127 (1988).
87. S. Havriliak and S. T. Shortridge, Macromolecules **23**, 648 (1990).
88. E. R. Harrell and R. P. Chartoff, Polym. Int. **14**, 362 (1974).
89. H. Kakutani and M. Asahina, J. Polym. Sci. Polym. Phys. **7**, 1473 (1969).
90. G. Pezzin, J. Appl. Polym. Sci. **11**, 2553 (1967).
91. R. J. Meier and L. C. E. Struik, Polymer **39**, 31 (1998).
92. R. H. Boyd, Polymer **26**, 323 (1985).
93. R. H. Boyd, Polymer **26**, 1123 (1985).
94. O. V. Startsev, A. L. Iordanskii and G. Y. Zaikov, Polym. Sci. USSR **30**, 1625 (1988).
95. C. Birkinshaw, M. Buggy and S. Daly, Polym. Commun. **28**, 286 (1987).
96. Y. Ishida, Kolloid Z. Z. Polym. **168**, 29 (1960).
97. V. Frosini and E. Butta, J. Polym. Sci. Polym. Lett. **9**, 253 (1971).
98. A. S. Badayev, I. I. Perepechko and Y. Y. Sorokin, Polym. Sci. USSR **30**, 892 (1988).
99. T. Kunugi, H. Watanabe and M. Hashimoto, J. Appl. Polym. Sci. **24**, 1039 (1979).
100. Y. Ishida, M. Matsuo and M. Takayanagi, J. Polym. Sci. Polym. Lett. **3**, 321 (1965).
101. A. Jones and R. Legras, Macromolecules **26**, 813 (1993).
102. F. de Candia, A. Michele and A. Renzulli, J. Macromol. Sci. Phys. **B33**, 307 (1994).
103. L. David and S. Etienne, Macromolecules **25**, 4302 (1992).
104. R. K. Krishnaswamy and D. S. Kalika, Polymer **35**, 1157 (1994).
105. T. Sasuga and M. Hagiwara, Polymer **26**, 501 (1985).
106. K. Sommer, W. Jilge, I. Morbitzer, et al., Adv. Mater. **3**, 590 (1991).
107. F. Sandrolini, A. Motori and A. Saccani, J. Appl. Polym. Sci. **44**, 765 (1992).
108. S. G. Charati, R. Vetrivel, M. G. Kulkarni, et al., Macromolecules **25**, 2215 (1992).
109. A. del Campo, T. A. Ezquerra, G. Wilbert, et al., Macromol. Chem. Phys. **203**, 2089 (2002).
110. A. H. Willbourn, Trans. Faraday Soc. **54**, 717 (1950).
111. H. Nakayasu, H. Markovitz and D. J. Plazek, Trans. Soc. Rheol. **5**, 261 (1961).

112. N. Alberola, J. Y. Cavaille and J. Perez, J. Polym. Sci. Polym. Phys. **28**, 569 (1990).
113. P. Colomer-Vilanova, S. Montserrat-Ribas, M. A. Ribes-Greus, et al., Polym.-Plast. Technol. Eng. **28**, 635–647 (1989).
114. N. Alberola, J. Y. Cavaille and J. Perez, Eur. Polym. J. **28**, 935 (1992).
115. C. Jourdan, J. Y. Cavaille and J. Perez, J. Polym. Sci. Polym. Phys. **27**, 2361 (1989).
116. S. A. Jawad and M. H. Alhaj-Mohammad, Polym. Int. **35**, 395 (1994).
117. P. M. Henrichs, V. A. Nicely and D. R. Fagerburg, Macromolecules **24**, 4033 (1991).
118. R. Diaz-Calleja, E. Riande and J. S. Roman, J. Polym. Sci. Polym. Phys. **30**, 1239 (1992).
119. W. M. Davis and C. W. Macosko, Polym. Eng. Sci. **17**, 32 (1977).
120. J. L. G. Ribelles and R. D. Calleja, J. Polym. Sci. Polym. Phys. **23**, 1297 (1985).
121. I. Katime and R. D. Calleja, Polym. Int. **35**, 281 (1994).
122. K. Shimizu, O. Yano, Y. Wada, et al., J. Polym. Sci. Polym. Phys. **11**, 1641 (1973).
123. F. P. Reding, J. A. Faucher and R. D. Whitman, J. Polym. Sci. **54**, S56 (1961).
124. S. Matsuoka and Y. Ishida, J. Polym. Sci., Polym. Symp. **14**, 247 (1966).
125. W. Frank, H. Goddar and H. A. Stuart, J. Polym. Sci. Polym. Lett. **5**, 711 (1967).
126. C. Bauwens-Crowet and J.-C. Bauwens, Polymer **24**, 921 (1983).
127. Y. P. Khanna, J. Therm. Anal. **30**, 153 (1985).
128. A. W. Aziz and K. N. Ab-el-nour, J. Appl. Polym. Sci. **31**, 2267 (1986).
129. H. W. Starkweather and P. Avakian, Macromolecules **22**, 4040 (1989).
130. J. R. Fried, H.-C. Liu and C. Zhang, J. Polym. Sci. Polym. Lett. **27**, 385 (1989).
131. I. Chung, E. Throck Morton and D. Chundury, in Annual Technical Conference (Society of Plastics Engineers, XXXVII, 1991), p. 681.
132. G. Floudas, J. S. Higgins, G. Meier, et al., Macromolecules **26**, 1676 (1993).
133. A. F. Yee and M. A. Maxwell, J. Macromol. Sci. Phys. **B17**, 543 (1980).
134. M. Baccaredda, E. Butta, V. Frosini, et al., Mater. Sci. Eng. **3**, 157 (1969).
135. F. Biddlestone, A. A. Goodwin, J. N. Hay, et al., Polymer **32**, 3119 (1991).
136. M. Pegoraro and L. D. Landro, Plast. Rubber Compos. Process. Appl. **17**, 269 (1992).
137. de Petris, V. Frosini, E. Butta, et al., Makromol. Chem. **109**, 54 (1967).
138. J. Stoelting, F. E. Karasz and W. J. MacKnight, Polym. Eng. Sci. **10**, 133 (1970).
139. J. E. Kurz, J. C. Woodbrey and M. Ohta, J. Polym. Sci. Polym. Phys. **8**, 1169 (1970).
140. R. Y. Ting and R. L. Cottington, in *Rheology*, edited by G. Astarita, G. Marrucci and L. Nicolais (Plenum, New York, 1980), Vol. 3, pp. 349–354.
141. T. Sasuga, N. Hayakawa and K. Yoshida, Polymer **28**, 236 (1987).
142. S. Saito, H. Sasabe, T. Nakajima, et al., J. Polym. Sci. Polym. Phys. **6**, 1297 (1968).
143. A. Gonze, Pure Appl. Chem. **18**, 553 (1969).
144. G. Williams and D. C. Watts, Trans. Faraday Soc. **67**, 1971 (1971).
145. G. Pezzin, G. Ajroldi, T. Casiraghi, et al., J. Appl. Polym. Sci. **16**, 1839 (1972).
146. J. Fried, S.-Y. Lai, L. W. Kleiner, et al., J. Appl. Polym. Sci. **27**, 2869 (1982).
147. del Val, A. Alegria, J. Colmenero, et al., J. Appl. Phys. **59**, 3829 (1986).
148. K. P. Pramoda and T. Liu, J. Polym. Sci., Part B: Polym. Phys. **42**, 1823 (2004).
149. T. Murayama, Polym. Eng. Sci. **22**, 788 (1982).
150. B. E. Read, Polymer **3**, 529 (1962).
151. A. Bartolotta, G. D. Marco, G. Galli, et al., Colloid Polym. Sci. **271**, 726 (1993).
152. R. E. Wetton, G. S. Fielding-Russell and K. U. Fulcher, J. Polym. Sci., Polym. Symp. **30**, 219 (1970).
153. K. H. Illers and H. Breuer, J. Colloid Sci. **18**, 1 (1963).
154. E. Ito and Y. Kobayashi, J. Appl. Polym. Sci. **25**, 2145 (1980).
155. W. P. Leung and C. L. Choy, J. Appl. Polym. Sci. **27**, 2693 (1982).
156. J. H. Daly, Eur. Polym. J. **26**, 933 (1990).

CHAPTER 14

Polymer–Solvent Interaction Parameter χ

Robert A. Orwoll* and Pamela A. Arnold†

* *Department of Chemistry, College of William and Mary, Williamsburg, VA 23187-8795*
† *Chemistry Department, Gettysburg College, Gettysburg, PA 17325*

Many thermodynamic properties of polymer solutions such as solubilities, swelling equilibria, and the colligative properties can be expressed in terms of the polymer-solvent interaction parameter χ. This unitless quantity was originally introduced by P. J. Flory [1] and M. L. Huggins [2] as an exchange interaction parameter in their lattice model of polymer solutions. In their definition, the quantity $kT\chi$ (k is the Boltzmann constant; T, the absolute temperature) is the average change in energy when a solvent molecule is transferred from pure solvent to pure, amorphous polymer. The reader is referred to Flory [3] for details. However, as explained in the following section, for this compilation χ is defined empirically, independent of the Flory–Huggins or any other model.

Values of χ have been collected in the table below for binary mixtures of homopolymers and low molecular weight liquids. Interaction parameters for systems with two polymeric components, i.e., polymer blends, can be found in Chapter 19. Other tabulations of χ are available [119,120,136].

14.1 DEFINITION

The change in the Gibbs free energy for mixing two components at constant temperature T and pressure P depends on the heat ΔH_{mix} and entropy ΔS_{mix} of mixing through the general thermodynamic relation

$$\Delta G_{\text{mix}} = \Delta H_{\text{mix}} - T\Delta S_{\text{mix}}. \tag{14.1}$$

In the case of n_2 moles of an amorphous polymer dissolving in n_1 moles of solvent, the combinatorial contribution to the entropy of mixing [1–3] is

$$\Delta S_{\text{mix}}^{(\text{comb})} = -R(n_1 \ln \phi_1 + n_2 \ln \phi_2). \tag{14.2}$$

Here, R is the gas constant and ϕ_1 and ϕ_2 are the volume fractions of solvent and polymer, respectively, in the resulting solution. The volume fraction of polymer can be expressed in terms of the weight fraction w_2 of polymer and densities ρ_1 and ρ_2 of the pure components:

$$\phi_2 = 1 - \phi_1 = \frac{w_2\rho_1}{\rho_2 + w_2(\rho_1 - \rho_2).} \tag{14.3}$$

That part of ΔG_{mix} that exceeds the contribution from the combinatorial entropy, namely,

$$\Delta G_{\text{mix}}^{\text{R}} = \Delta G_{\text{mix}} - (-T\Delta S_{\text{mix}}^{(\text{comb})}), \tag{14.4}$$

is the residual free energy [4].

Many thermodynamic properties of interest can be directly related to the change that the chemical potential of the solvent undergoes on mixing,

$$\mu_1 - \mu_1^0 = \left(\frac{\partial \Delta G_{\text{mix}}}{\partial n_1}\right)_{T,P,n_2} \tag{14.5}$$

Differentiation of Eq. (14.4) with respect to n_1 yields the residual chemical potential,

$$(\mu_1 - \mu_1^0)^R = (\mu_1 - \mu_1^0) - RT[\ln(1 - \phi_2) + \phi_2(1 - 1/x)], \tag{14.6}$$

where x is the ratio of the molar volume of polymer to that of solvent:

$$x = \frac{\rho_1 M_2}{\rho_2 M_1}. \tag{14.7}$$

M_1 and M_2 are the (number-average) molecular weights. The unitless interaction parameter χ is defined for this

compilation as a reduced residual chemical potential using Eq. (14.6):

$$\chi = \frac{(\mu_1 - \mu_1^0)^R}{\phi_2^2 RT} = \frac{(\mu_1 - \mu_1^0)}{\phi_2^2 RT} - \frac{\ln(1-\phi_2) + \phi_2(1-1/x)}{\phi_2^2}. \quad (14.8)$$

14.2 METHODS OF MEASUREMENT

Most of the entries in the table below were obtained from osmotic pressure, vapor sorption, or inverse gas chromatography measurements [5].

Osmotic pressure measurements can be used to evaluate χ at small volume fractions of polymer. The osmotic pressure Π of a solution relative to pure solvent is related to the chemical potential and, with Eq. (14.8), to χ through the thermodynamic expression

$$\mu_1 - \mu_1^0 = -\Pi V_1, \quad (14.9)$$

where V_1 is the molar volume of solvent. The interaction parameter in the limit of infinite dilution can also be determined from the second virial coefficient A_2, i.e., the slope of a plot of Π/RTc_2 versus the concentration $c_2 = \rho_2\phi_2$ (i.e., mass of polymer per volume of solution) at $c_2 = 0$:

$$\chi = \frac{1}{2} - A_2 V_1 \rho_2^2. \quad (14.10)$$

Vapor sorption studies yield values of χ for solutions at intermediate-to-high polymer concentrations. The vapor pressure P_1 of solvent above a polymer solution relative to that of pure solvent P_1^0 at the same temperature is

$$(\mu_1 - \mu_1^0) = RT \ln \frac{P_1}{P_1^0}. \quad (14.11)$$

Substitution for $(\mu_1 - \mu_1^0)$ in Eq. 14.8 from Eq. 14.11 yields χ.

Inverse gas chromatography can be used to obtain the polymer-solvent interaction parameter in the limit of $\phi_2 = 1$. Here χ is found from the retention volume of the low molecular-weight component in the vapor phase as it is eluted over the polymer which is the stationary component in a gas-phase chromatography experiment.

The Flory Θ-temperature affords another means of determining the interaction parameter. The Θ-temperature is defined [3] such that at $T = \Theta$ and $\phi_2 = 0$, $\chi = 1/2$. Θ-temperatures are tabulated in Chapter 15.

14.3 GENERAL FEATURES AND SIGNIFICANCE

For many systems, χ has been found to increase with polymer concentration and decrease with temperature with a dependence that is approximately linear with, but in general not proportional to, $1/T$. According to Eqs. 14.5 and 14.8, for a given volume fraction ϕ_2 of polymer, the smaller the value of χ, the greater the rate at which the free energy of the solution decreases with the addition of solvent. Consequently, liquids with the smallest χ's are usually the best solvents for a polymer. Negative values of χ often indicate strong polar attractions between polymer and solvent. Solutions for which χ increases with increasing temperature at constant ϕ_2 have a negative partial molar heat of mixing, $(\partial \Delta H_{\text{mix}}/\partial n_1)_{P,T,n_2} < 0$, i.e., the addition of a small quantity of solvent to a solution is exothermic. In the limit of infinite molecular-weight polymer, $\chi = 1/2$ at the critical solution temperature which occurs at $\phi_2 \to 0$ and $T = \Theta$.

The interaction parameters tabulated in Table 14.1 have been collected either directly from the sources cited or from an earlier compilation [5]. For some entries, a range of χ values is given, representing measurements made over a range of temperatures or concentrations. In these cases, the first value in the range of χ's corresponds to the first temperature or concentration in the range of temperatures or concentrations, with χ varying monotonically between the extremes. For example, in the system poly(dimethyl siloxane)+benzene at 20 °C [6], χ is reported as "0.64–0.85" for ϕ_2 between 0.4 and 1 to indicate that $\chi = 0.64$ at $\phi_2 = 0.4$ and $\chi = 0.85$ at $\phi_2 = 1$.

The polymer–solvent interaction parameter is only slightly sensitive to the molecular weight provided that the molecular weight is high. Thus, studies using only low molecular weight polymers have not been used for the table. In those cases in which measurements were made with polymers of different molecular weights, only the results for the highest molecular weight material are reported in Table 14.1.

Measurements on dilute solutions, especially osmotic pressure measurements, can yield unusually accurate values for χ. These entries are recorded to the thousandth place. At the other extreme, the experimental uncertainty in χ is large for the larger values of χ obtained, for example, in inverse gas chromatography at $\phi_2 \to 1$; these entries are written to the nearest tenth.

The values of χ found in Table 14.1 were obtained using the volume fraction ϕ_2 as the measure of polymer concentration, consistent with Eq. 14.8. However, instead of χ, many of the studies cited in the table reported χ_{wt} or χ^*, interaction parameters which are based on the weight fraction (particularly in connection with inverse gas chromatographic studies) or the segment fraction (using the model of Flory for polymer solutions [137]), respectively. Since both χ_{wt} and χ^* differ from the volume-fraction based χ, these interaction parameters have been recalculated using Eq. 14.8 for Table 14.1 to give χ. Thus, for example, in the case of inverse gas chromatography, $\chi = \chi_{\text{wt}} + \ln(\rho_1/\rho_2)$ in the limit $\phi_2 \to 1$, where ρ_1/ρ_2 is the ratio of the density of the solvent and to that of the liquid (as opposed to glassy or crystalline) polymer.

Related information can be found in Chapters 15–17, and 19.

TABLE 14.1. *Interaction parameters.*

Solvent	Temperature (°C)	Volume fraction, ϕ_2	χ	References
Cellulose acetate, 2.3 acetate groups per residue				
acetone	25 to 45	0	0.44	[7–9]
acetic acid	25 to 45	0	0.40	[9]
aniline	25 to 35	0	0.375 to 0.34	[7–9]
1,4-dioxane	25 to 45	0	0.38	[7–9]
methyl acetate	25 to 35	0	0.45	[7–9]
nitromethane	25 to 45	0	0.43	[7–9]
2-picoline	25	0	0.36	[7]
3-picoline	25	0	0.285	[7]
4-picoline	25	0	0.26	[7]
pyridine	25 to 45	0	0.28	[7–9]
Cellulose acetate, 2.5 acetate groups per residue				
acetone	30	0.2 to 0.4	0.30 to 0.51	[10]
1,4-dioxane	30	0.2 to 0.4	0.31 to 0.51	[10]
methyl acetate	30	0.2 to 0.4	0.43 to 0.59	[10]
pyridine	30	0.2 to 0.4	0.07 to 0.09	[10]
tetrahydrofuran	13	0	0.442	[11]
Cellulose acetate, 3.0 acetate groups per residue				
chloroform	25	0	0.34	[12]
	30	0.2 to 0.6	0.36 to 0.51	[13]
dichloromethane	25	0 to 0.6	0.3 to 0.49	[13]
Cellulose nitrate, 2.4 nitrate groups per residue				
acetone	25	0	0.27	[7]
	30	0 to 0.2	0.24 to 0.05	[10]
amyl acetate	25	0	0.02	[7]
2-butanone	25	0	0.21	[7]
butyl acetate	25	0	0.015	[7]
ethyl acetate	25	0	0.22	[7]
2-heptanone	25	0	0.02	[7]
2-hexanone	25	0	0.15	[7]
methyl acetate	25	0	0.30	[7]
	30	0 to 0.2	0.17 to −0.06	[10]
2-octanone	25	0	0.16	[7]
propyl acetate	25	0	0.13	[7]
Cellulose nitrate, 2.6 nitrate groups per residue				
acetone	20	0.2 to 0.8	0.14 to −1.24	[14]
acetonitrile	20	0.4 to 1	0.59 to −0.1	[14]
cyclopentanone	20	0.2 to 0.8	0.42 to −2.4	[14]
2,4-dimethyl-3-pentanone	20	0.2 to 0.6	0.62 to −1.7	[14]
1,4-dioxane	20	0.4 to 0.8	1.2 to −1.7	[14]
ethyl acetate	20	0.2 to 0.6	0.04 to −1.35	[15]
ethyl formate	20	0.2 to 0.8	−0.08 to −3.2	[15]
ethyl *n*-propyl ether	20	0.8	1.20	[14]
isoamyl acetate	20	0.2 to 0.6	−0.89 to −3.3	[15]
3-methylbutanone	20	0.2 to 0.6	−0.5 to −1.6	[14]
nitromethane	20	0.2 to 0.8	0.66 to 0.45	[14]
pinacolone	20	0.2 to 0.8	0.16 to −3.7	[14]
propyl acetate	20	0.2 to 0.8	−0.38 to −4.1	[15]
Ethyl cellulose, 2.3 ethyl groups per residue				
acetone	25	0	0.46	[7]
benzene	25	0	0.48	[7]
n-butyl acetate	25	0	0.24	[7]
carbon tetrachloride	25	0	0.46	[7]
chloroform	25	0	0.34	[7]
ethyl acetate	25	0	0.395	[7]

TABLE 14.1. *Continued.*

Solvent	Temperature (°C)	Volume fraction, ϕ_2	χ	References
2-heptanone	25	0	0.38	[7]
methyl acetate	25	0	0.41	[7]
2-pentanone	25	0	0.37	[7]
n-pentyl acetate	25	0	0.28	[7]
n-propyl acetate	25	0	0.33	[7]
toluene	25	0	0.47	[7]
Hydroxypropyl cellulose				
acetone	25	0.60 to 0.90	0.58 to 0.83	[124]
ethanol	25	0.61 to 0.90	0.57 to 0.55	[124]
tetrahyrofuran	25	0.52 to 0.90	0.34 to 0.48	[124]
water	25	0 to 0.13	0.480 to 0.52	[122]
	25	0.51 to 1	0.63 to 1.55	[123]
	40	0 to 0.13	0.499 to 0.54	[122]
Polyacrylamide				
water	3	0.10	0.51	[111]
	25	0	0.495	[104]
	25	0.06	0.53	[109]
	60	0.08	0.49	[111]
0.2N HCl	20 to 61	0	0.499 to 0.491	[105]
Polyacrylonitrile				
dimethylformamide	14	0	0.2	[16]
Poly(*N*-acryloylpyrrolidine)				
ethanol	10 to 60	0.08	0.45	[111]
water	3	0.07	0.49	[111]
	30	0.12	0.53	[111]
	60	0.35	0.66	[111]
Poly(*cis*-1,4-butadiene)				
benzene	35	0.06 to 0.10	0.28	[125]
carbon tetrachloride	23.5	0.62 to 0.85	0.11 to 0.02	[106]
chloroform	23.5	0.60 to 0.80	−0.06 to −0.20	[106]
dichloromethane	23.5	0.69 to 0.85	0.32 to 0.21	[106]
cyclohexane	23.5	0.65 to 0.83	0.46 to 0.34	[106]
n-decane	35	0.16 to 0.23	0.46	[125]
n-hexadecane	35	0.26 to 0.30	0.54	[125]
n-hexane	23.5	0.67 to 0.88	0.61 to 0.45	[106]
n-octane	*ca.* 50	0.38 to 0.42	0.31 to 0.27	[108]
Polybutadiene, 10% *cis*, 21% *trans*, 69% vinyl				
acetone	40 to 100	1	1.64 to 1.32	[126]
acetonitrile	40 to 100	1	2.86 to 2.36	[126]
benzene	40 to 100	1	0.26 to 0.19	[126]
1-butanol	40 to 100	1	2.76 to 1.64	[126]
2-butanone	40 to 100	1	1.19 to 0.97	[126]
butyl acetate	40 to 100	1	0.52 to 0.44	[126]
butyronitrile	40 to 100	1	1.90 to 1.57	[126]
carbon tetrachloride	40 to 100	1	0.10 to 0.15	[126]
chloroform	40 to 100	1	0.05 to 0.07	[126]
1-chlorobutane	40 to 100	1	0.33 to 0.25	[126]
1-chloropentane	40 to 100	1	0.37 to 0.32	[126]
1-chloropropane	40 to 100	1	0.36 to 0.30	[126]
cyclohexane	40 to 100	1	0.22 to 0.15	[126]
ethanol	40 to 100	1	3.41 to 2.30	[126]
ethyl acetate	40 to 100	1	0.86 to 0.69	[126]
ethylcyclohexane	40 to 100	1	0.08 to 0.04	[126]
ethyl ether	40 to 100	1	0.42 to 0.40	[126]
n-heptane	40 to 100	1	0.36 to 0.31	[126]
1-heptene	40 to 100	1	0.25 to 0.23	[126]
n-hexane	40 to 100	1	0.37	[126]

TABLE 14.1. *Continued.*

Solvent	Temperature (°C)	Volume fraction, ϕ_2	χ	References
1-hexene	40 to 100	1	0.32 to 0.28	[126]
methanol	40 to 100	1	3.85 to 2.70	[126]
methyl acetate	40 to 100	1	1.14 to 0.92	[126]
methylcyclohexane	40 to 100	1	0.17 to 0.13	[126]
methyl isobutyl ketone	40 to 100	1	0.95 to 0.72	[126]
n-octane	40 to 100	1	0.34 to 0.28	[126]
1-octene	40 to 100	1	0.23 to 0.21	[126]
n-pentane	40 to 100	1	0.44 to 0.36	[126]
3-pentanone	40 to 100	1	0.82 to 0.67	[126]
1-propanol	40 to 100	1	2.97 to 1.97	[126]
2-propanol	40 to 100	1	2.93 to 1.86	[126]
proprionitrile	40 to 100	1	2.25 to 1.82	[126]
n-propyl acetate	40 to 100	1	0.67 to 0.55	[126]
n-propyl ether	40 to 100	1	0.51 to 2.26	[126]
tetrahydrofuran	40 to 100	1	0.35 to 0.29	[126]
toluene	40 to 100	1	0.14 to 0.12	[126]
Poly(1-butene)				
benzene	135	1	0.49	[17]
cyclohexane	135	1	0.20	[17]
n-decane	115 to 135	1	0.30	[17]
2,5-dimethylhexane	115 to 135	1	0.36	[17]
2,4-dimethylpentane	115 to 135	1	0.40	[17]
2,3-dimethylpentane	115 to 135	1	0.35	[17]
3-ethylpentane	115 to 135	1	0.34	[17]
n-heptane	115 to 135	1	0.38	[17]
2-methylhexane	115 to 135	1	0.39	[17]
3-methylhexane	115 to 135	1	0.38	[17]
n-nonane	115 to 135	1	0.32	[17]
n-octane	115 to 135	1	0.36	[17]
toluene	135	1	0.47	[17]
2,2,4-trimethylpentane	115 to 135	1	0.35	[17]
Poly(butylene adipate)				
acetone	120	1	0.54	[18]
benzene	120	1	0.27	[18]
2-butanone	120	1	0.43	[18]
carbon tetrachloride	120	1	0.55	[18]
chloroform	120	1	−0.06	[18]
dichloromethane	120	1	0.70	[18]
ethyl acetate	120	1	0.43	[18]
n-heptane	120	1	1.5	[18]
n-hexane	120	1	1.4	[18]
n-pentane	120	1	1.3	[18]
Poly(*n*-butyl methacrylate)				
ethanol	27	0 to 1	0.492 to 1.29	[118]
	86	0 to 1	0.399 to 0.95	[118]
2-propanol	40	0 to 1	0.509 to 1.4	[118]
	80	0 to 1	0.477 to 1.0	[118]
Poly(ε-caprolactone)				
acetone	100 to 120	1	0.46 to 0.54	[18, 19]
benzene	100 to 120	1	0.06 to 0.11	[18, 19]
	70 to 140	1	−0.04 to 0.01	[114]
n-butane	100	1	1.22	[19]
1-butanol	100	1	0.59	[19]
2-butanone	100 to 120	1	0.36 to 0.45	[18, 19]
n-butyl acetate	70 to 140	1	0.21 to 0.26	[114]
	100	1	0.31	[19]

TABLE 14.1. *Continued.*

Solvent	Temperature (°C)	Volume fraction, ϕ_2	χ	References
carbon tetrachloride	100 to 120	1	0.25 to 0.37	[18, 19]
chlorobenzene	100	1	−0.08	[19]
	80 to 140	1	−0.18 to −0.06	[114]
1-chlorobutane	100	1	0.33	[19]
chloroform	100 to 120	1	−0.40 to −0.22	[18, 19]
chloromethane	100	1	0.16	[19]
1-chloropentane	100	1	0.33	[19]
cycloheptane	100	1	0.83	[19]
cyclohexane	100	1	0.88	[19]
cyclohexene	100	1	0.60	[19]
cyclooctane	100	1	0.83	[19]
cyclopentane	100	1	0.82	[19]
n-decane	100	1	1.44	[19]
1, 1-dichloroethane	100	1	−0.04	[19]
1,2-dichloroethane	100	1	−0.14	[19]
dichloromethane	100	1	−0.26	[19]
1,4-dioxane	100	1	0.13	[19]
ethanol	100	1	1.01	[19]
ethyl acetate	100 to 120	1	0.36 to 0.42	[18, 19]
	70 to 140	1	0.32 to 0.29	[114]
ethylbenzene	100	1	0.16	[19]
	70 to 140	1	0.10 to 0.14	[114]
n-heptane	100 to 120	1	1.2	[18, 19]
n-hexane	100 to 120	1	1.2	[18, 19]
methyl acetate	100	1	0.39	[19]
	70 to 140	1	0.35 to 0.32	[114]
n-nonane	100	1	1.37	[19]
n-octane	100	1	1.30	[19]
n-pentane	100 to 120	1	1.2	[18, 19]
1-pentanol	100	1	0.46	[19]
2-pentyl acetate	70 to 140	1	0.40 to 0.28	[114]
propane	100	1	1.21	[19]
1-propanol	100	1	0.72	[19]
propyl acetate	100	1	0.33	[19]
	70 to 140	1	0.29 to 0.24	[114]
n-propylbenzene	90 to 140	1	0.20 to 0.19	[114]
2-propylbenzene	80 to 140	1	0.10 to 0.13	[114]
tetrahydrofuran	100	1	0.13	[19]
toluene	100	1	0.08	[19]
	70 to 140	1	−0.01 to 0.07	[114]
1,1,1-trichloroethane	100	1	0.07	[19]
trichloroethylene	100	1	0.02	[19]
n-undecane	100	1	1.52	[19]
Polycarbonate				
benzene	179 to 253	1	0.49 to 0.39	[121]
cyclohexane	179 to 253	1	1.23 to 0.77	[121]
n-decane	179 to 253	1	1.67 to 1.52	[121]
n-dodecane	179 to 253	1	1.74 to 1.46	[121]
ethylbenzene	179 to 253	1	0.49 to 0.47	[121]
ethylcyclohexane	179 to 253	1	1.12 to 0.92	[121]
n-heptane	179 to 253	1	1.73 to 1.34	[121]
n-hexadecane	211 to 253	1	1.73 to 1.57	[121]
n-hexane	179 to 231	1	1.87 to 1.19	[121]
methylcyclohexane	179 to 253	1	1.19 to 0.82	[121]
n-nonane	179 to 253	1	1.69 to 1.43	[121]

TABLE 14.1. *Continued.*

Solvent	Temperature (°C)	Volume fraction, ϕ_2	χ	References
n-octane	179 to 253	1	1.60 to 1.45	[121]
n-tetradecane	179 to 253	1	1.82 to 1.54	[121]
toluene	179 to 253	1	0.46 to 0.37	[121]
n-undecane	179 to 253	1	1.73 to 1.53	[121]
Polychloroprene				
acetone	100	1	0.87	[19]
benzene	100	1	0.18	[19]
n-butane	100	1	0.99	[19]
1-butanol	100	1	1.61	[19]
2-butanone	100	1	0.61	[19]
butyl acetate	100	1	0.44	[19]
carbon tetrachloride	100	1	0.23	[19]
chlorobenzene	100	1	0.10	[19]
1-chlorobutane	100	1	0.39	[19]
chloroform	100	1	0.28	[19]
chloromethane	100	1	0.52	[19]
1-chloropentane	100	1	0.33	[19]
cycloheptane	100	1	0.45	[19]
cyclohexane	100	1	0.55	[19]
cyclohexene	100	1	0.38	[19]
cyclooctane	100	1	0.40	[19]
cyclopentane	100	1	0.55	[19]
n-decane	100	1	0.94	[19]
1,1-dichloroethane	100	1	0.37	[19]
1,2-dichloroethane	100	1	0.48	[19]
dichloromethane	100	1	0.43	[19]
1,4-dioxane	100	1	0.46	[19]
ethanol	100	1	2.27	[19]
ethyl acetate	100	1	0.64	[19]
ethylbenzene	100	1	0.16	[19]
n-heptane	100	1	0.88	[19]
n-hexane	100	1	0.91	[19]
methyl acetate	100	1	0.81	[19]
n-nonane	100	1	0.92	[19]
n-octane	100	1	0.90	[19]
n-pentane	100	1	0.96	[19]
1-pentanol	100	1	1.41	[19]
propane	100	1	1.36	[19]
1-propanol	100	1	1.83	[19]
propyl acetate	100	1	0.51	[19]
tetrahydrofuran	100	1	0.06	[19]
1,1,1-trichloroethane	100	1	0.21	[19]
trichloroethylene	100	1	0.24	[19]
toluene	100	1	0.14	[19]
n-undecane	100	1	0.96	[19]
Poly(*o*-chlorostyrene)				
butyl acetate	30	0	0.490	[20]
chlorobenzene	30	0	0.472	[20]
toluene	30	0	0.470	[20]
Poly(*p*-chlorostyrene)				
butyl acetate	30	0	0.448	[20]
chlorobenzene	30	0	0.465	[20]
toluene	22	0.2 to 0.6	0.55	[21]
	30	0	0.489	[20]

TABLE 14.1. *Continued.*

Solvent	Temperature (°C)	Volume fraction, ϕ_2	χ	References
Poly(*N*, *N*-diethylacrylamide)				
ethanol	10 to 60	0.08	0.47	[111]
water	3	0.07	0.50	[111]
	30	0.05	0.62	[111]
	60	0.85	1.16	[111]
Poly(*N*,*N*-dimethylacrylamide)				
ethanol	10 to 60	0.08	0.40 to 0.41	[111]
water	3	0.07	0.48	[111]
	60	0.10	0.52	[111]
Poly(dimethyl siloxane)				
acetone	100	1	1.33	[19]
benzene	20	0.4 to 1	0.64 to 0.85	[6]
	25	0.2 to 1	0.56 to 0.82	[22–25]
	30	0.08 to 0.47	0.50 to 0.36	[116]
	30	0.88 to 1	0.745 to 0.759	[135]
	25 to 70	1	0.80 to 0.74	[25,26]
	40 to 100	1	0.79 to 0.58	[19,25]
n-butane	100	1	0.25	[19]
1-butanol	100	1	1.91	[19]
2-butanone	20	0.08 to 0.30	0.52 to 0.61	[27]
	25	0	0.50	[28]
	30	0.35 to 0.66	0.44 to 0.66	[138]
	50	0.08 to 0.29	0.50 to 0.58	[27]
butyl acetate	100	1	0.68	[19]
carbon dioxide ($20 < P < 62$ bar)	35	0.78 to 0.94	0.75	[117]
carbon dioxide ($P = 300$ bar)	45	0.67	0.45	[115]
carbon tetrachloride	100	1	0.36	[19]
chlorobenzene	20	0 to 0.2	0.475 to 0.54	[29]
	60	0 to 0.2	0.455 to 0.52	[29]
	100	1	0.76	[19]
1-chlorobutane	100	1	0.49	[19]
chloroform	100	1	0.60	[19]
chloromethane	100	1	0.44	[19]
1-chloropentane	100	1	0.48	[19]
cycloheptane	25 to 70	1	0.56 to 0.53	[26]
	100	1	0.42	[19]
cyclohexane	20	0 to 0.2	0.409 to 0.44	[29]
	25	0.2 to 0.6	0.46 to 0.50	[23]
	25 to 70	1	0.48	[26]
	30	0.35 to 0.95	0.42	[22]
	100	1	0.35	[19]
cyclohexene	100	1	0.36	[19]
cyclooctane	25 to 70	1	0.66 to 0.61	[26]
	100	1	0.50	[19]
cyclopentane	25 to 70	1	0.42 to 0.46	[26]
	100	1	0.28	[19]
n-decane	100	1	0.51	[19]
1,1-dichloroethane	100	1	0.60	[19]
1,2-dichloroethane	100	1	0.96	[19]
dichloromethane	100	1	0.69	[19]
2,6-dimethyl-4-heptanone	35	0.08 to 0.22	0.45 to 0.49	[27]
1,4-dioxane	25 to 70	1	1.32 to 1.18	[26]
	100	1	1.06	[19]

TABLE 14.1. *Continued.*

Solvent	Temperature (°C)	Volume fraction, ϕ_2	χ	References
ethyl acetate	100	1	0.82	[19]
ethanol	100	1	2.6	[19]
ethylbenzene	24	0.4 to 1	0.54 to 0.77	[6]
	25 to 70	1	0.83 to 0.78	[25]
	25 to 70	1	0.77 to 0.73	[26]
	100	1	0.62	[19]
n-heptane	20	0.4 to 1	0.46	[6]
	35	0.06 to 0.19	0.42	[30]
	50	0.06 to 0.16	0.43	[30]
	25 to 70	1	0.49	[25,26]
	100	1	0.35	[19]
3-heptanone	35	0.08 to 0.29	0.48 to 0.56	[27]
	50	0.08 to 0.26	0.47 to 0.53	[27]
hexamethyldisiloxane	23	0.4 to 1	0.30 to 0.25	[6]
	25 to 70	1	0.28 to 0.34	[26]
n-hexane	20	0.03 to 0.17	0.39 to 0.37	[30]
	30	0.86 to 1	0.387 to 0.397	[135]
	50	0.06 to 0.11	0.41	[30]
	25 to 70	1	0.46	[25,26]
	100	1	0.30	[19]
mesitylene	25 to 70	1	0.95 to 0.86	[26]
methyl acetate	100	1	1.01	[19]
2-methylbutane	25	1	0.39	[25]
	100	1	1.10	[19]
2-methylheptane	25 to 70	1	0.50	[25,26]
2-methylhexane	25 to 70	1	0.45	[25,26]
3-methylhexane	25 to 70	1	0.44	[26]
2-methylpentane	25 to 70	1	0.44	[25]
4-methyl-2-pentanone	20	0.10 to 0.22	0.49 to 0.55	[27]
	35	0.09 to 0.24	0.48 to 0.53	[27]
n-nonane	20	0.07 to 0.21	0.48 to 0.49	[30]
	50	0.07 to 0.21	0.46 to 0.49	[30]
	100	1	0.45	[19]
octamethylcyclotetrasiloxane	25	0.10 to 0.17	0.31 to 0.37	[31]
octamethyltrisiloxane	23	0.4 to 1	0.22 to 0.14	[6]
n-octane	20	0.4 to 1	0.50	[6]
	20	0.05 to 0.21	0.45 to 0.46	[30]
	50	0.06 to 0.19	0.43 to 0.45	[30]
	25 to 100	1	0.56 to 0.40	[19,25]
n-pentane	20	0.4 to 1	0.43 to 0.40	[6]
	25 to 70	1	0.42	[25]
	25 to 70	1	0.45 to 0.49	[26]
	100	1	0.31	[19]
1-pentanol	100	1	1.75	[19]
propane	100	1	0.21	[19]
1-propanol	100	1	2.06	[19]
propyl acetate	100	1	0.72	[19]
tetrahydrofuran	100	1	0.48	[19]
toluene	20	0 to 1	0.445 to 0.82	[6,29]
	25 to 70	1	0.80 to 0.75	[25]
	25 to 70	1	0.75 to 0.71	[26]
	100	1	0.59	[19]
	30	0.07 to 0.45	0.47 to 0.57	[116]

TABLE 14.1. *Continued.*

Solvent	Temperature (°C)	Volume fraction, ϕ_2	χ	References
1,1,1-trichloroethane	100	1	0.37	[19]
trichloroethylene	100	1	0.53	[19]
2,2,4-trimethylpentane	25 to 70	1	0.44	[25,26]
n-undecane	100	1	0.58	[19]
m-xylene	25 to 70	1	0.82 to 0.76	[26]
o-xylene	25 to 70	1	0.86 to 0.80	[26]
p-xylene	25	0.6 to 1	0.58 to 0.78	[6]
	25 to 70	1	0.80 to 0.77	[25,26]
Poly(1,3-dioxocane)				
tetrahydrofuran	25	0	0.38	[128]
toluene	25	0	0.37	[112]
Polyepichlorohydrin				
acetone	100	1	0.28	[19]
benzene	100	1	0.25	[19]
n-butane	100	1	1.65	[19]
1-butanol	100	1	1.12	[19]
2-butanone	100	1	0.20	[19]
butyl acetate	100	1	0.36	[19]
carbon tetrachloride	100	1	0.69	[19]
chlorobenzene	100	1	0.24	[19]
1-chlorobutane	100	1	0.62	[19]
chloroform	100	1	0.25	[19]
chloromethane	100	1	0.36	[19]
1-chloropentane	100	1	0.65	[19]
cycloheptane	100	1	1.19	[19]
cyclohexane	100	1	1.25	[19]
cyclohexene	100	1	0.84	[19]
cyclooctane	100	1	1.20	[19]
cyclopentane	100	1	1.16	[19]
n-decane	100	1	2.12	[19]
1,1-dichloroethane	100	1	0.33	[19]
1,2,-dichloroethane	100	1	0.20	[19]
dichloromethane	100	1	0.18	[19]
1,4-dioxane	100	1	0.04	[19]
ethanol	100	1	1.58	[19]
ethyl acetate	100	1	0.35	[19]
ethylbenzene	100	1	0.44	[19]
n-heptane	100	1	1.79	[19]
n-hexane	100	1	1.72	[19]
methyl acetate	100	1	0.39	[19]
n-nonane	100	1	1.99	[19]
n-octane	100	1	1.89	[19]
n-pentane	100	1	1.64	[19]
1-pentanol	100	1	1.03	[19]
propane	100	1	1.71	[19]
1-propanol	100	1	1.22	[19]
propyl acetate	100	1	0.33	[19]
tetrahydrofuran	100	1	0.01	[19]
1, 1, 1-trichloroethane	100	1	0.46	[19]
trichloroethylene	100	1	0.53	[19]
toluene	100	1	0.31	[19]
n-undecane	100	1	2.24	[19]

TABLE 14.1. *Continued.*

Solvent	Temperature (°C)	Volume fraction, ϕ_2	χ	References
Poly(*N*-ethylacrylamide)				
ethanol	10 to 60	0.08	0.39 to 0.40	[111]
water	3	0.05	0.42	[111]
	30	0.06	0.46	[111]
	60	0.10	0.51	[111]
Polyethylene, low density				
benzene	125 to 135	1	0.43 to 0.36	[32,33]
1-butanol	135	1	1.38	[32]
carbon tetrachloride	135	1	0.24	[32]
chlorobenzene	135	1	0.34	[32]
1-chlorobutane	135	1	0.44	[32]
chloroform	135	1	0.41	[32]
cyclohexane	125 to 135	1	0.18	[32,33]
cyclohexanol	135	1	1.22	[32]
cis-decahydronaphthalene	120 to 145	1	0.03	[34]
trans-decahydronaphthalene	120 to 145	1	0.01	[34]
n-decane	120 to 145	1	0.25 to 0.29	[32,34]
2,4-dimethylhexane	120 to 145	1	0.33	[34]
2,5-dimethylhexane	120 to 145	1	0.35	[34]
3,4-dimethylhexane	120 to 145	1	0.25	[34]
n-dodecane	110 to 145	1	0.18	[35]
	120 to 145	1	0.24	[34]
ethylbenzene	120 to 145	1	0.33	[34]
n-heptane	109	0.2 to 0.6	0.29 to 0.34	[36]
mesitylene	120 to 145	1	0.24	[34]
3-methylheptane	120 to 145	1	0.30	[34]
3-methylhexane	120 to 145	1	0.34	[34]
n-nonane	120 to 145	1	0.28	[32,34]
n-octane	120 to 145	1	0.30	[34]
1-octene	135	1	0.31	[32]
2-pentanone	135	1	0.88	[32]
phenol	135	1	1.5	[32]
1,2,3,4-tetrahydronaphthalene	105	0	0.495	[37]
	120 to 145	1	0.28	[34]
toluene	120 to 145	1	0.34	[34]
2,2,4-trimethylhexane	120 to 145	1	0.28	[34]
2,2,4-trimethylpentane	120 to 145	1	0.34	[34]
m-xylene	120 to 145	1	0.29	[34]
p-xylene	81	0	0.45	[38]
	120 to 145	1	0.28	[34]
xylene	73 to 92	0	0.49	[39,40]
Polyethylene, high density				
cis-decahydronaphthalene	149	1	0.07	[34]
trans-decahydronapthalene	149	1	0.05	[34]
n-decane	145 to 190	1	0.18	[35]
	149	1	0.31	[34]
	185	1	0.12	[41]
2,4-dimethylhexane	149	1	0.38	[34]
2,5-dimethylhexane	149	1	0.40	[34]
3,4-dimethylhexane	149	1	0.31	[34]
n-dodecane	149	1	0.28	[34]
ethylbenzene	149	1	0.37	[34]
mesitylene	149	1	0.28	[34]
2-methylheptane	149	1	0.39	[34]
3-methylhexane	149	1	0.40	[34]
n-nonane	149	1	0.34	[34]
n-octane	149	1	0.36	[34]

TABLE 14.1. *Continued.*

Solvent	Temperature (°C)	Volume fraction, ϕ_2	χ	References
1,2,3,4-tetrahydronaphthalene	149	1	0.32	[34]
toluene	149	1	0.39	[34]
2,2,4-trimethylhexane	149	1	0.35	[34]
2,2,4-trimethylpentane	149	1	0.40	[34]
m-xylene	149	1	0.34	[34]
o-xylene	110	0	0.31	[37]
p-xylene	105	0	0.22	[37]
	149	1	0.32	[34]
xylene	85	0	0.34	[39]
Poly(ethylene adipate)				
acetone	120	1	0.53	[18]
benzene	120	1	0.58	[18]
2-butanone	120	1	0.88	[18]
carbon tetrachloride	120	1	0.88	[18]
chloroform	120	1	0.29	[18]
dichloromethane	120	1	0.96	[18]
ethyl acetate	120	1	0.55	[18]
n-heptane	120	1	2.1	[18]
n-hexane	120	1	2.0	[18]
n-pentane	120	1	1.8	[18]
Poly(ethylene oxide)				
acetone	100	1	0.47	[19]
benzene	50	0.2 to 0.6	0.18 to 0.10	[42]
	70	0.2 to 0.8	0.19 to 0.09	[42]
	100	1	0.13	[19]
n-butane	100	1	1.64	[19]
1-butanol	100	1	0.41	[19]
2-butanone	100	1	0.43	[19]
butyl acetate	100	1	0.48	[19]
carbon tetrachloride	100	1	0.38	[19]
chlorobenzene	100	1	−0.04	[19]
1-chlorobutane	100	1	0.57	[19]
chloroform	100	1	−0.55	[19]
chloromethane	100	1	0.12	[19]
1-chloropentane	100	1	0.63	[19]
cycloheptane	100	1	1.23	[19]
cyclohexane	100	1	1.23	[19]
cyclohexene	100	1	0.85	[19]
cyclooctane	100	1	1.26	[19]
cyclopentane	100	1	1.12	[19]
n-decane	100	1	2.10	[19]
1,1-dichloroethane	100	1	−0.04	[19]
1,2-dichloroethane	100	1	−0.31	[19]
dichloromethane	100	1	−0.51	[19]
1,4-dioxane	100	1	0.20	[19]
ethanol	100	1	0.70	[19]
ethyl acetate	100	1	0.39	[19]
ethylbenzene	100	1	0.40	[19]
n-heptane	100	1	1.75	[19]
n-hexane	100	1	1.70	[19]
methyl acetate	100	1	0.36	[19]
n-nonane	100	1	1.97	[19]
n-octane	100	1	1.85	[19]
n-pentane	100	1	1.66	[19]
1-pentanol	100	1	0.34	[19]
propane	100	1	2.17	[19]

TABLE 14.1. *Continued.*

Solvent	Temperature (°C)	Volume fraction, ϕ_2	χ	References
1-propanol	100	1	0.47	[19]
propyl acetate	100	1	0.43	[19]
tetrahydrofuran	100	1	0.30	[19]
1,1,1-trichloroethane	100	1	0.20	[19]
trichloroethylene	100	1	0.08	[19]
toluene	100	1	0.26	[19]
n-undecane	100	1	2.22	[19]
Poly(ethylene succinate)				
acetone	120	1	0.61	[18]
benzene	120	1	0.79	[18]
2-butanone	120	1	0.69	[18]
carbon tetrachloride	120	1	1.32	[18]
chloroform	120	1	0.49	[18]
dichloromethane	120	1	1.09	[18]
ethyl acetate	120	1	0.70	[18]
n-heptane	120	1	1.9	[18]
n-hexane	120	1	1.9	[18]
n-pentane	120	1	2.6	[18]
Poly(hexamethylene sebacate)				
acetone	120	1	0.82	[18]
benzene	120	1	0.21	[18]
2-butanone	120	1	0.58	[18]
carbon tetrachloride	120	1	0.37	[18]
chloroform	120	1	0.06	[18]
dichloromethane	120	1	0.81	[18]
ethyl acetate	120	1	0.57	[18]
n-heptane	120	1	1.0	[18]
n-hexane	120	1	1.2	[18]
n-pentane	120	1	1.1	[18]
Poly(2-hydroxyethyl methacrylate)				
di(ethylene glycol)	25	0 to 0.35	0.49 to 0.40	[43]
Poly(4-hydroxystyrene)				
acetone	170 to 190	1	0.25 to 0.58	[110]
2-butanone	170 to 190	1	0.52 to 0.62	[110]
n-butyl acetate	170 to 190	1	1.47 to 1.20	[110]
chlorobenzene	190	1	1.99	[110]
dioxane	190	1	−0.03	[110]
ethyl acetate	170 to 190	1	1.06 to 1.07	[110]
2-methyl-1-propanol	190	1	1.10	[110]
3-pentanone	170 to 190	1	1.08 to 0.76	[110]
1-propanol	190	1	1.01	[110]
2-propanol	170 to 190	1	0.96 to 0.84	[110]
n-propyl acetate	170 to 190	1	1.22 to 1.10	[110]
tetrahydrofuran	170 to 190	1	0.21 to 0.27	[110]
toluene	170 to 190	1	2.20 to 2.22	[110]
Polyisobutylene				
acetone	100	1	1.90	[44]
benzene	10	0.4 to 0.8	0.67 to 0.92	[45]
	25	0 to 1	0.498 to 1.06	[45–47]
	25 to 65	1	0.88 to 0.61	[48–51]
	27	0.6 to 1	0.73 to 1.07	[52]
	30	0	0.495	[53]
	40	0.6 to 0.8	0.70 to 0.80	[45]
	50	0 to 0.2	0.485 to 0.583	[47]
	100	1	0.70	[44]
	37 to 200	1	1.18 to 0.70	[107]
n-butane	25 to 46	1	0.66	[54]

TABLE 14.1. *Continued.*

Solvent	Temperature (°C)	Volume fraction, ϕ_2	χ	References
	100	1	0.65	[44]
1-butanol	100	1	2.45	[44]
2-butanone	100	1	1.55	[44]
butyl acetate	100	1	1.06	[44]
carbon tetrachloride	100	1	0.48	[44]
	23.5	0.76 to 0.87	0.54	[130]
chlorobenzene	100	1	0.70	[44]
1-chlorobutane	100	1	0.68	[44]
chloroform	100	1	0.78	[44]
	23.5	0.82 to 0.91	0.67	[130]
chloromethane	100	1	0.91	[44]
1-chloropentane	100	1	0.59	[44]
cycloheptane	100	1	0.29	[44]
cyclohexane	8	0.2	0.437	[47]
	25	0 to 1	0.43	[46,51,55]
	25 to 65	1	0.55 to 0.40	[48–51]
	30	0 to 0.2	0.44	[47,53]
	100	1	0.39	[44]
	23.5	0.75 to 0.86	0.38	[130]
cyclohexene	100	1	0.40	[44]
cyclooctane	100	1	0.24	[44]
cyclopentane	100	1	0.41	[44]
	23.5	0.79 to 0.86	0.32 to 0.27	[130]
n-decane	100	1	0.48	[44]
1,1-dichloroethane	100	1	0.87	[44]
1,2-dichloroethane	100	1	1.13	[44]
dichloromethane	100	1	1.00	[44]
2,2-dimethylbutane	23.5	0.71 to 0.85	0.49 to 0.46	[130]
2,2-dimethylpropane	25 to 46	1	0.82 to 0.87	[54]
	35	0.8	0.82	[54]
1,4-dioxane	100	1	1.26	[44]
ethanol	100	1	3.3	[44]
ethyl acetate	100	1	1.35	[44]
ethyl benzene	100	1	0.59	[44]
n-heptane	25 to 65	1	0.57 to 0.47	[48,49]
	100	1	0.53	[44]
	23.5	0.80 to 0.87	0.51	[130]
n-hexane	25 to 65	1	0.65 to 0.50	[48,49]
	100	1	0.56	[44]
methyl acetate	100	1	1.55	[44]
2-methylbutane	25 to 35	0.8	0.65	[54]
	35 to 46	1	0.65 to 0.68	[54]
2-methylpropane	25 to 46	1	0.78 to 0.70	[54]
n-nonane	25	1	0.49	[49]
	100	1	0.49	[44]
n-octane	25	0.2 to 0.4	0.44 to 0.48	[56]
	25 to 65	1	0.52 to 0.43	[48,49]
	100	1	0.50	[44]
n-pentane	25	0 to 1	0.48 to 0.75	[48,49,51,54,57,58]
	35	0.4 to 1	0.62	[54,57]
	40	0 to 0.4	0.49 to 0.57	[57]
	40 to 65	1	0.61 to 0.57	[48,51,54]
	55	0.6 to 0.8	0.63	[57]
	100	1	0.60	[44]
1-pentanol	100	1	2.20	[44]
propane	35	1	0.61	[54]
	100	1	0.79	[44]

TABLE 14.1. *Continued.*

Solvent	Temperature (°C)	Volume fraction, ϕ_2	χ	References
propyl acetate	100	1	1.19	[44]
tetrahydrofuran	100	1	0.68	[44]
toluene	100	1	0.60	[44]
1,1,1-trichloroethane	100	1	0.56	[44]
trichloroethylene	100	1	0.54	[44]
2,2,4-trimethylpentane	23.5	0.67 to 0.87	0.50 to 0.45	[130]
n-undecane	100	1	0.48	[44]
Poly(*cis*-isoprene)				
acetone	0	1	2.1	[59]
	25	0.8 to 1	1.27 to 1.8	[59]
benzene	10	0.6 to 0.8	0.42	[60]
	25	0 to 1	0.40 to 0.43	[60–62]
	25 to 55	1	0.46 to 0.43	[63]
	40	0.8	0.41	[60]
	23.5	0.69 to 0.86	0.33 to 0.28	[106]
2-butanone	25	0.6 to 1	0.86 to 1.43	[59]
	45	0.6 to 1	0.83 to 1.2	[59]
carbon tetrachloride	23.5	0.69 to 0.84	0.14 to 0.02	[106]
chloroform	23.5	0.66 to 0.85	0.19 to −0.01	[106]
cyclohexane	20	0 to 0.20	0.31	[113]
	23.5	0.64 to 0.84	0.29 to 0.21	[106]
dichloromethane	23.5	0.69 to 0.89	0.54 to 0.41	[106]
ethyl acetate	25	0.4 to 1	0.69 to 1.24	[59,64]
	50	0.4 to 1	0.68 to 1.0	[59,64]
ethylbenzene	25 to 55	1	0.34 to 0.30	[63]
n-heptane	25 to 55	1	0.50	[63]
	23.5	0.68 to 0.84	0.37 to 0.29	[106]
n-hexane	25 to 55	1	0.54 to 0.50	[63]
2-methylheptane	25 to 55	1	0.50 to 0.47	[63]
2-methylhexane	25 to 55	1	0.51	[63]
2-methylpentane	25 to 55	1	0.56 to 0.52	[63]
n-octane	25 to 55	1	0.49 to 0.46	[63]
n-pentane	25 to 55	1	0.61 to 0.53	[63]
toluene	25 to 55	1	0.36 to 0.32	[63]
2,2,4-trimethylpentane	25 to 55	1	0.49 to 0.46	[63]
p-xylene	25 to 55	1	0.27	[63]
Poly(*N*-isopropylacrylamide)				
ethanol	10 to 60	0.09	0.46 to 0.47	[111]
water	3	0.07	0.49	[111]
	30	0.14	0.55	[111]
	60	0.74	1.08	[111]
Poly(*DL*-lactide)				
acetone	120	1	0.56	[18]
benzene	120	1	0.52	[18]
2-butanone	120	1	0.53	[18]
carbon tetrachloride	120	1	0.89	[18]
chloroform	120	1	0.32	[18]
dichloromethane	120	1	0.99	[18]
ethyl acetate	120	1	0.46	[18]
n-heptane	120	1	2.0	[18]
n-hexane	120	1	2.0	[18]
n-pentane	120	1	1.6	[18]
Poly(methacrylamide)				
water	23 to 56	0	0.500 to 0.499	[105]

TABLE 14.1. *Continued.*

Solvent	Temperature (°C)	Volume fraction, ϕ_2	χ	References
Poly(methacrylic acid)				
0.02 N HCl	20 to 58	0	0.498 to 0.500	[105]
Poly(methyl acrylate)				
acetone	100	1	0.40	[19]
benzene	90 to 110	1	0.51 to 0.37	[19,65]
n-butane	100	1	1.86	[19]
1-butanol	100	1	0.79	[19]
2-butanone	100	1	0.40	[19]
butyl acetate	100	1	0.58	[19]
butylbenzene	90 to 110	1	1.14 to 1.05	[65]
tert-butylbenzene	90 to 110	1	1.03 to 0.95	[65]
butylcyclohexane	90 to 110	1	2.3 to 2.1	[65]
carbon tetrachloride	100	1	0.68	[19]
chlorobenzene	100	1	0.31	[19]
1-chlorobutane	100	1	0.74	[19]
chloroform	100	1	−0.10	[19]
chloromethane	100	1	0.34	[19]
1-chloropentane	100	1	0.84	[19]
cycloheptane	100	1	1.56	[19]
cyclohexane	90 to 110	1	1.7 to 1.5	[19,65]
cyclohexene	100	1	1.31	[19]
cyclooctane	100	1	1.61	[19]
cyclopentane	100	1	1.47	[19]
cis-decahydronaphthalene	90 to 110	1	2.1 to 1.8	[65]
trans-decahydronaphthalene	90 to 110	1	2.1 to 1.9	[65]
n-decane	88 to 100	1	2.7 to 2.4	[19,65]
1,1-dichloroethane	100	1	0.20	[19]
1,2-dichloroethane	100	1	0.02	[19]
dichloroethane	100	1	−0.09	[19]
1,4-dioxane	100	1	0.20	[19]
n-dodecane	90 to 110	1	3.0 to 2.7	[65]
ethanol	100	1	1.01	[19]
ethyl acetate	100	1	0.43	[19]
ethylbenzene	90 to 110	1	0.83 to 0.67	[19,65]
n-heptane	100	1	2.10	[19]
n-hexane	100	1	2.08	[19]
methyl acetate	100	1	0.38	[19]
naphthalene	100 to 110	1	0.48	[65]
n-nonane	100	1	2.4	[19]
n-octane	90 to 100	1	2.4 to 2.2	[19,65]
n-pentane	100	1	1.92	[19]
1-pentanol	100	1	0.76	[19]
propane	100	1	2.5	[19]
1-propanol	100	1	0.82	[19]
propyl acetate	100	1	0.49	[19]
n-tetradecane	90 to 110	1	3.4 to 3.1	[65]
tetrahydrofuran	100	1	0.34	[19]
1,2,3,4-tetrahydronaphthalene	90 to 110	1	1.04 to 0.95	[65]
3,3,4,4-tetramethylhexane	90 to 110	1	2.2 to 1.9	[65]
toluene	90 to 110	1	0.67 to 0.62	[65]
	100	1	0.53	[19]
1,1,1-trichloroethane	100	1	0.43	[19]
trichloroethylene	100	1	0.45	[19]
3,4,5-trimethylheptane	90 to 110	1	2.4 to 2.2	[65]
2,2,5-trimethylhexane	90 to 110	1	2.5 to 2.2	[65]

TABLE 14.1. *Continued.*

Solvent	Temperature (°C)	Volume fraction, ϕ_2	χ	References
2,2,4-trimethylpentane	90 to 110	1	2.4 to 2.1	[65]
n-undecane	100	1	2.7	[19]
Poly(methyl methacrylate)				
acetone	25 to 27	0	0.48	[66,67]
benzene	16 to 27	0	0.47 to 0.44	[16,67]
butyl acetate	2 to 60	0	0.496 to 0.487	[68]
1-chlorobutane	14 to 48	0	0.515 to 0.495	[68]
chloroform	27	0	0.44	[67]
1,4-dioxane	27	0	0.42	[67]
4-heptanone	16 to 62	0	0.515 to 0.490	[68]
isoamyl acetate	20 to 60	0	0.524 to 0.499	[68]
3-pentanone	27	0	0.49	[67]
tetrahydrofuran	25 to 27	0	0.494 to 0.46	[67,69]
toluene	27	0	0.45	[67]
m-xylene	27	0	0.50	[67]
Poly(α-methylstyrene)				
toluene	25	0.3 to 0.7	0.48 to 0.65	[70]
Polypropylene				
acetone	100	1	1.72	[44]
benezene	25	0	0.498	[71]
	100	1	0.51	[44]
butane	100	1	0.37	[44]
1-butanol	100	1	2.23	[44]
2-butanone	100	1	1.36	[44]
butyl acetate	100	1	0.84	[44]
carbon tetrachloride	100	1	0.29	[44]
chlorobenzene	100	1	0.54	[44]
1-chlorobutane	100	1	0.48	[44]
chloroform	100	1	0.61	[44]
chloromethane	100	1	0.76	[44]
1-chloropentane	100	1	0.39	[44]
cycloheptane	100	1	0.10	[44]
cyclohexane	25	0	0.42	[71]
	100	1	0.17	[44]
cyclohexene	100	1	0.22	[44]
cyclooctane	100	1	0.06	[44]
cyclopentane	100	1	0.21	[44]
1,1-dichloroethane	100	1	0.70	[44]
1,2-dichloroethane	100	1	0.97	[44]
dichloromethane	100	1	0.86	[44]
1,4-dioxane	100	1	1.15	[44]
ethanol	100	1	3.0	[44]
ethyl acetate	100	1	1.14	[44]
ethylbenzene	100	1	0.40	[44]
n-decane	100	1	0.18	[44]
n-heptane	100	1	0.24	[44]
n-hexane	80	1	0.18	[72]
	100	1	0.28	[44]
methyl acetate	100	1	1.37	[44]
n-nonane	100	1	0.20	[44]
n-octane	100	1	0.22	[44]
n-pentane	100	1	0.35	[44]
1-pentanol	100	1	1.99	[44]
propane	100	1	0.46	[44]
propyl acetate	100	1	0.96	[44]
tetrahydrofuran	100	1	0.55	[44]

TABLE 14.1. *Continued.*

Solvent	Temperature (°C)	Volume fraction, ϕ_2	χ	References
toluene	100	1	0.43	[44]
1,1,1-trichloroethane	100	1	0.37	[44]
trichloroethylene	100	1	0.39	[44]
n-undecane	100	1	0.17	[44]
Polystyrene				
acetic acid	162 to 229	1	3.0 to 2.1	[73]
acetone	25	0.6 to 1	0.81 to 1.1	[74]
	40	1	1.08	[75]
	50	0.6 to 0.8	0.80 to 0.92	[74]
	162 to 229	1	1.30 to 0.56	[73]
acetonitrile	162 to 229	1	2.02 to 0.93	[73]
aniline	162 to 229	1	1.11 to 0.68	[73]
benzaldehyde	162 to 229	1	1.22 to 0.80	[73]
benzene	15	0.3 to 0.8	0.40 to 0.26	[76]
	25 to 30	0	0.455 to 0.43	[77,78]
	30	0.3 to 0.8	0.40 to 0.26	[76]
	40	1	0.26	[75]
	45	0.3 to 0.8	0.40 to 0.26	[76]
	60	0.3 to 0.8	0.40 to 0.26	[76]
	120 to 200	1	0.32 to 0.39	[41,51]
	160 to 180	1	0.29 to 0.24	[65]
	162 to 229	1	0.66 to 0.13	[73]
	23.5	0.61 to 0.79	0.28 to 0.17	[129]
benzyl alcohol	162 to 229	1	1.42 to 0.65	[73]
1-butanol	162 to 229	1	1.47 to 0.82	[73]
2-butanone	10 to 50	0.2	0.547 to 0.542	[79]
	25	0.4 to 0.8	0.63 to 0.77	[80]
	27 to 52	0	0.490 to 0.474	[78,81–84]
	40	1	0.84	[75]
	70	0.6 to 0.8	0.63 to 0.72	[80]
	162 to 229	1	1.16 to 0.36	[73]
butyl acetate	30	0	0.466	[20]
	162 to 229	1	1.01 to 0.45	[73]
tert-butyl acetate	22 to 64	0	0.501 to 0.494	[132]
	64 to 111	0	0.494 to 0.501	[132]
	30 to 90	0.12 to 0.32	0.60 to 0.59	[133]
	143 to 183	1	0.39 to 0.1	[133]
butylbenzene	183 to 203	1	0.38 to 0.34	[65]
butylcyclohexane	160 to 180	1	0.77 to 0.71	[65]
carbon tetrachloride	40	1	0.29	[75]
	162 to 229	1	0.90 to 0.26	[73]
	23.5	0.71 to 0.81	0.22 to 0.24	[129]
chlorobenzene	30	0	0.454	[20]
	162 to 229	1	0.68 to 0.28	[73]
	137.6	1	0.30	[107]
chloroform	25	0.2 to 0.8	0.52 to 0.17	[74]
	40	1	0.13	[75]
	50	0.2 to 0.8	0.45 to 0.14	[74]
	162 to 229	1	0.43 to -0.01	[73]
	23.5	0.62 to 0.81	0.05 to -0.15	[129]
cumene	25	0	0.444	[77]
cyclohexane	15	0.5	0.77	[85]
	24	0 to 0.2	0.508 to 0.58	[86]
	30	0.3	0.62	[85]
	34	0 to 0.8	0.500 to 0.93	[86]
	35	0 to 0.3	0.50 to 0.57	[87]

TABLE 14.1. *Continued.*

Solvent	Temperature (°C)	Volume fraction, ϕ_2	χ	References
	40	1	0.64	[75]
	44	0 to 0.8	0.494 to 0.93	[86]
	45	0 to 0.3	0.49 to 0.56	[87]
	49 to 60	0	0.495 to 0.486	[84]
	50	0.1	0.51	[85]
	65	0 to 0.3	0.47 to 0.54	[87]
	160 to 180	1	0.62 to 0.53	[65]
	162 to 229	1	1.11 to 0.46	[73]
	23.5	0.78 to 0.84	0.79 to 0.81	[129]
	30 to 50	0	0.52 to 0.39	[134]
	35	0.28 to 0.94	0.61 to 1.08	[139]
	65	0.23 to 0.92	0.52 to 0.69	[139]
cyclohexanone	27 to 57	0	0.436	[81]
cyclopentane	40	1	0.64	[75]
cis-decahydronapthalene	183 to 203	1	0.47 to 0.42	[65]
trans-decahydronaphthalene	183 to 203	1	0.52 to 0.46	[65]
n-decane	183 to 203	1	1.01 to 0.94	[65]
	120 to 160	1	1.36 to 1.03	[107]
1,2-dichloroethane	162 to 229	1	0.85 to 0.22	[73]
dichloromethane	40	1	0.34	[75]
	162 to 229	1	0.62 to −0.21	[73]
	23.5	0.64 to 0.82	0.17 to 0.05	[129]
1,4-dioxane	40	1	0.43	[75]
	162 to 229	1	0.95 to 0.42	[73]
n-dodecane	183 to 203	1	1.09 to 1.00	[65]
ethanol	162 to 229	1	1.80 to 0.43	[73]
ethyl acetate	27 to 49	0	0.490	[84]
	162 to 229	1	1.14 to 0.35	[73]
ethylbenzene	10 to 60	0.2	0.44	[88]
	25	0	0.450	[77]
	120 to 185	1	0.22 to 0.14	[72]
ethylene glycol	162 to 229	1	3.8 to 2.2	[73]
ethyl ether	162 to 229	1	0.78 to 0.71	[73]
fluorobenzene	40	1	0.37	[75]
formamide	162 to 229	1	4.1 to 3.2	[73]
n-heptane	40	1	0.95	[75]
	162 to 229	1	1.33 to 0.25	[73]
n-hexane	40	1	0.97	[75]
	162 to 229	1	1.35 to −0.03	[73]
n-hexadecane	183 to 203	1	1.22 to 1.14	[65]
isopropyl ether	40	1	0.78	[75]
	162 to 229	1	1.42 to 0.41	[73]
methanol	162 to 229	1	2.19 to 0.44	[73]
methylcyclohexane	72	0 to 0.4	0.49 to 0.67	[89]
2-methyl-1-propanol	162 to 229	1	1.71 to 0.81	[73]
naphthalene	183 to 203	1	0.12	[65]
nitrobenzene	162 to 229	1	1.18 to 0.72	[73]
n-octane	40	1	0.95	[75]
	162 to 229	1	2.19 to 0.80	[73]
1-octanol	162 to 229	1	1.41 to 0.55	[73]
n-pentane	162 to 229	1	1.12 to 0.83	[73]
1-pentanol	162 to 229	1	1.75 to 0.86	[73]
1-propanol	162 to 229	1	1.71 to 0.27	[73]
2-propanol	40	1	2.6	[75]
	162 to 229	1	1.74 to −0.15	[73]

TABLE 14.1. *Continued.*

Solvent	Temperature (°C)	Volume fraction, ϕ_2	χ	References
propyl acetate	25	0.4 to 0.8	0.66	[74]
	40	1	0.52	[75]
	70	0.4 to 0.8	0.60	[74]
pyridine	162 to 229	1	1.02 to 0.23	[73]
tetrachloroethylene	40	1	0.36	[75]
n-tetradecane	183 to 203	1	1.14 to 1.08	[65]
tetrahydrofuran	162 to 229	1	0.70 to −0.16	[73]
1,2,3,4-tetrahydronaphthalene	183 to 203	1	0.20	[65]
3,3,4,4-tetramethylhexane	160 to 180	1	0.90 to 0.76	[65]
toluene	22	0.2 to 0.6	0.40	[21]
	25	0.4 to 0.8	0.42 to 0.31	[80,87]
	25	0.2 to 0.8	0.37 to 0.16	[76]
	27 to 40	0	0.437 to 0.482	[20,53,69,78,81,82,84]
	40	1	0.19	[75]
	45	0 to 0.3	0.41 to 0.37	[87]
	60	0.8	0.32	[80]
	65	0 to 0.3	0.40 to 0.37	[87]
	68	0	0.452	[81,84]
	80	0.4 to 0.6	0.40 to 0.35	[80]
	162 to 229	1	0.67 to 0.04	[73]
	23.5	0.66 to 0.83	0.34 to 0.22	[129]
	25	0.03 to 0.34	0.43 to 0.40	[127]
	25	0.07 to 0.20	0.40 to 0.39	[131]
	40	0.06 to 0.18	0.42	[131]
	137.6	1	0.32	[107]
trichloroethylene	40	1	0.19	[75]
	162 to 229	1	0.69 to 0.12	[73]
2,2,4-trimethylpentane	162 to 229	1	1.72 to 0.35	[73]
water	162 to 229	1	4.4 to 3.1	[73]
o-xylene	162 to 229	1	0.72 to 0.26	[73]
Poly(tetramethylene oxide)				
acetone	100	1	0.73	[19]
benzene	100	1	0.04	[19]
n-butane	100	1	0.76	[19]
1-butanol	100	1	0.54	[19]
2-butanone	100	1	0.53	[19]
butyl acetate	100	1	0.30	[19]
carbon tetrachloride	100	1	0.10	[19]
chlorobenzene	100	1	−0.09	[19]
1-chlorobutane	100	1	0.22	[19]
chloroform	100	1	−0.38	[19]
chloromethane	100	1	0.19	[19]
1-chloropentane	100	1	0.18	[19]
cycloheptane	100	1	0.41	[19]
cyclohexane	100	1	1.23	[19]
cyclohexene	100	1	0.28	[19]
cyclooctane	100	1	0.40	[19]
cyclopentane	100	1	0.45	[19]
n-decane	100	1	0.80	[19]
1,1-dichloroethane	100	1	0.00	[19]
1,2-dichloroethane	100	1	0.05	[19]
dichloromethane	100	1	−0.12	[19]
1,4-dioxane	100	1	0.39	[19]
ethanol	100	1	1.08	[19]
ethyl acetate	100	1	0.45	[19]
ethylbenzene	100	1	0.07	[19]

TABLE 14.1. *Continued.*

Solvent	Temperature (°C)	Volume fraction, ϕ_2	χ	References
n-heptane	100	1	0.73	[19]
n-hexane	100	1	0.74	[19]
methyl acetate	100	1	0.58	[19]
n-nonane	100	1	0.78	[19]
n-octane	100	1	0.75	[19]
n-pentane	100	1	0.76	[19]
1-pentanol	100	1	0.37	[19]
propane	100	1	0.90	[19]
1-propanol	100	1	0.71	[19]
propyl acetate	100	1	0.36	[19]
tetrahydrofuran	100	1	0.13	[19]
1,1,1-trichloroethane	100	1	−0.02	[19]
trichloroethylene	100	1	−0.06	[19]
toluene	100	1	0.04	[19]
n-undecane	100	1	0.83	[19]
Poly(ε-valerolactone)				
acetone	120	1	0.64	[18]
benzene	120	1	0.34	[18]
2-butanone	120	1	0.43	[18]
carbon tetrachloride	120	1	0.61	[18]
chloroform	120	1	−0.02	[18]
dichloromethane	120	1	0.86	[18]
ethyl acetate	120	1	0.54	[18]
n-heptane	120	1	1.6	[18]
n-hexane	120	1	1.6	[18]
n-pentane	120	1	1.5	[18]
Poly(vinyl acetate)				
acetaldehyde	125 to 140	1	0.35 to 0.32	[90]
acetone	25 to 29	0	0.40	[91–93]
	30 to 40	0.8	0.34	[94]
	30 to 50	1	0.31 to 0.39	[94]
	100 to 140	1	0.32 to 0.21	[19,90]
acetonitrile	125 to 140	1	0.54 to 0.49	[90]
allyl chloride	40	1	0.27	[94]
benzene	5	0.2	0.46	[95]
	20	0	0.42	[16]
	30	0.4 to 0.8	0.45 to 0.29	[96]
	35 to 62	0	0.51 to 0.42	[97]
	30 to 50	1	0.30 to 0.26	[94]
	80 to 140	1	0.44 to 0.25	[19,90,98]
	125 to 145	1	0.37 to 0.32	[32,99,100]
n-butane	100	1	1.97	[19]
1-butanol	100 to 135	1	0.62 to 0.38	[19,99]
2-butanol	135	1	0.31	[99]
2-butanone	10 to 45	0	0.43	[91]
	100 to 140	1	0.34 to 0.20	[19,90]
butyl acetate	100	1	0.51	[19]
butylbenzene	125 to 145	1	0.95 to 0.88	[100]
butylcyclohexane	125 to 145	1	1.90 to 1.75	[100]
carbon tetrachloride	90 to 135	1	0.85 to 0.63	[19,32,98]
chlorobenzene	100 to 135	1	0.28 to 0.33	[19,32]
1-chlorobutane	100 to 135	1	0.73 to 0.66	[19,32]
chloroform	80 to 135	1	−0.17 to −0.09	[19,32,98]
chloromethane	100	1	0.25	[19]
1-chloropentane	100	1	0.82	[19]
1-chloropropane	40	1	0.75	[94]

TABLE 14.1. *Continued.*

Solvent	Temperature (°C)	Volume fraction, ϕ_2	χ	References
cycloheptane	100	1	1.63	[19]
cyclohexane	100 to 140	1	1.65 to 1.16	[19,32,90,98,100]
cyclohexene	100	1	1.18	[19]
cyclohexanol	135	1	0.44	[32,99]
cyclooctane	100	1	1.67	[19]
cyclopentane	100	1	1.53	[19]
cis-decahydronaphthalene	125 to 145	1	1.65 to 1.50	[100]
n-decane	100 to 145	1	2.5 to 2.01	[19,32,99,100]
1-decanol	135	1	0.81	[99]
1,1-dichloroethane	100	1	0.19	[19]
1,2-dichloroethane	100 to 140	1	−0.04 to 0.00	[19,90]
dichloromethane	100	1	−0.14	[19]
dimethylphthalate	25	0	0.400	[91]
1,4-dioxane	25	0	0.407	[91]
	100 to 140	1	0.17 to 0.03	[19,90]
n-dodecane	125 to 145	1	2.48 to 2.27	[99,100]
ethanol	50	0	0.47	[97]
	100	1	0.80	[19]
ethyl acetate	20	0	0.415	[16]
	100	1	0.36	[19]
ethylbenzene	100 to 135	1	0.66 to 0.58	[19,99]
n-heptane	100 to 120	1	2.14 to 1.63	[19,90,98]
1-heptanol	135	1	0.55	[99]
n-hexadecane	135	1	2.99	[99]
n-hexane	100 to 120	1	2.06 to 1.71	[19,98]
1-hexanol	135	1	0.49	[99]
isopropylamine	40	1	0.66	[94]
methanol	125 to 140	1	0.77 to 0.73	[90]
methyl acetate	100	1	0.30	[19]
2-methyl-2-propanol	135	1	0.30	[99]
nitroethane	125 to 140	1	0.14 to 0.19	[90]
n-nonane	100 to 145	1	2.38 to 1.88	[19,32,99,100]
n-octane	90 to 120	1	2.3 to 1.94	[19,98]
1-octanol	135	1	0.65	[99]
1-octene	135	1	1.55	[32]
n-pentane	100	1	2.06	[19]
1-pentanol	100 to 135	1	0.59 to 0.41	[19,99]
2-pentanone	135	1	0.38	[32]
propane	100	1	3.2	[19]
1-propanol	30 to 50	1	1.3 to 1.0	[94]
	100 to 135	1	0.64 to 0.38	[19,99]
2-propanol	125 to 140	1	0.44 to 0.35	[90,99]
propyl acetate	100	1	0.42	[19]
propylamine	40	1	0.61	[94]
n-tetradecane	135	1	2.70	[99]
tetrahydrofuran	100 to 140	1	0.30 to 0.14	[19,90]
1,2,3,4-tetrahydronaphthalene	125 to 145	1	0.83 to 0.77	[100]
3,3,4,4-tetramethylhexane	125 to 145	1	1.72 to 1.56	[100]
toluene	80 to 140	1	0.56 to 0.40	[19,90,98,99]
1,1,1,-trichloroethane	100	1	0.49	[19]
trichloroethylene	100	1	0.40	[19]
1,2,3-trichloropropane	15 to 50	0	0.38	[91]
2,2,4-trimethylpentane	100 to 120	1	2.17 to 1.86	[98]
n-undecane	100 to 145	1	2.7 to 2.14	[19,99,100]
vinyl acetate	30	0.4 to 0.8	0.41 to 0.22	[96]
water	40	1	2.5	[101]

TABLE 14.1. *Continued.*

Solvent	Temperature (°C)	Volume fraction, ϕ_2	χ	References
Poly(vinyl alcohol)				
water	30	0	0.494	[102]
Poly(vinyl chloride)				
acetaldehyde	125 to 140	1	0.76 to 0.69	[90]
acetone	120 to 140	1	0.77 to 0.53	[18,90]
acetonitrile	125 to 140	1	0.98 to 0.92	[90]
benzene	120	1	0.75	[18]
	125 to 140	1	0.41 to 0.37	[90]
2-butanone	0 to 50	0	0.402 to 0.413	[103]
	120 to 140	1	0.72 to 0.46	[18,90]
carbon tetrachloride	120	1	1.14	[18]
chloroform	120	1	0.91	[18]
cyclohexane	125 to 140	1	1.21 to 1.09	[90]
cyclohexanone	30 to 69	0	0.240 to 0.264	[103]
1,2-dichloroethane	125 to 140	1	0.55 to 0.49	[90]
dichloromethane	120	1	1.63	[18]
1,4-dioxane	14 to 77	0	0.518 to 0.454	[103]
	125 to 140	1	0.18 to 0.13	[90]
ethyl acetate	120	1	0.94	[18]
n-heptane	120	1	2.0	[18]
	125 to 140	1	1.64 to 1.54	[90]
n-hexane	120	1	2.1	[18]
methanol	125 to 140	1	1.42 to 1.24	[90]
nitroethane	125 to 140	1	0.69 to 0.61	[90]
n-pentane	120	1	1.7	[18]
2-propanol	125 to 140	1	1.10 to 0.97	[90]
tetrahydrofuran	125 to 140	1	0.43 to 0.34	[90]
toluene	125 to 140	1	0.45 to 0.41	[90]
Poly(vinyl methyl ether)				
acetone	40	1	0.75	[75]
benzene	40	1	0.15	[75]
2-butanone	40	1	0.50	[75]
carbon tetrachloride	40	1	0.06	[75]
chloroform	40	1	−0.92	[75]
cyclohexane	40	1	1.16	[75]
cyclopentane	40	1	1.14	[75]
dichloromethane	40	1	−0.39	[75]
1,4-dioxane	40	1	0.20	[75]
ethylbenzene	25	0.06 to 0.16	0.29 to 0.27	[131]
fluorobenzene	40	1	0.00	[75]
n-heptane	40	1	1.15	[75]
n-hexane	40	1	1.16	[75]
isopropyl ether	40	1	0.76	[75]
n-octane	40	1	1.16	[75]
2-propanol	40	1	0.90	[75]
propyl acetate	40	1	0.25	[75]
tetrachloroethylene	40	1	0.34	[75]
toluene	40	1	0.14	[75]
	25	0.06 to 0.15	0.28 to 0.26	[131]
trichloroethylene	40	1	−0.26	[75]
Poly(*N*-vinyl pyrrolidone)				
water	25	0.06	0.48	[109]

REFERENCES

1. P. J. Flory, J. Chem. Phys. **9**, 660 (1941); **10**, 51 (1942).
2. M. L. Huggins, J. Chem Phys. **9**, 440 (1941); J. Phys. Chem. **46**, 151 (1942); Ann. N.Y. Acad. Sci. **41**, 1 (1942); J. Am. Chem. Soc. **64**, 1712 (1942).
3. P. J. Flory, *Principles of Polymer Chemistry* (Cornell University Press, Ithaca, 1953), Chapter XII.
4. P. J. Flory, J. Am. Chem. Soc. **87**, 1833 (1965).
5. R. A. Orwoll, Rubber Chem. Technol. **50**, 451 (1977).
6. R. S. Chahal, W. -P. Kao, and D. Patterson, J. Chem. Soc., Faraday Trans. 1 **69**, 1834 (1973).
7. W. R. Moore, J. A. Epstein, A. M. Brown, *et al*. J. Polym. Sci. **23**, 23 (1957).
8. W. R. Moore and B. M. Tidswell, J. Polym. Sci. **29**, 37 (1958).
9. W. R. Moore and B. M. Tidswell, J. Polym. Sci. **27**, 459 (1958).
10. W. R. Moore and R. Shuttleworth, J. Polym. Sci. Part A **1**, 733 (1963).
11. D. W. Tanner and G. C. Berry, J. Polym. Sci., Polym. Phys. Ed. **12**, 941 (1974).
12. P. Howard and R. S. Parikh, J. Polym. Sci., Part C **30**, 17 (1970).
13. W. R. Moore and R. Shuttleworth, J. Polym. Sci., Part A **1**. 1985 (1963).
14. E. C. Baughan, A. L. Jones, and K. Stewart, Proc. Roy. Soc. London, Ser. A **225**, 478 (1954).
15. A. L. Jones, Trans. Faraday Soc. **52**, 1408 (1956).
16. C. Masson and H. W. Melville, J. Polym. Sci. **4**, 337 (1949).
17. G. Charlet, R. Ducasse, and G. Delmas, Polymer **22**, 1190 (1981).
18. B. Riedl and R. E. Prud'homme, J. Polym. Sci., Part B. Polym. Phys. **24**, 2565 (1986).
19. P. Munk, P. Hattam, Q. Du, *et al*. J. Appl. Polym. Sci.: Appl. Polym. Symp. **45**, 289 (1990).
20. K. Kubo and K. Ogino, Bull. Chem. Soc. Japan **44**, 997 (1971).
21. R. Corneliussen, S. A. Rice, and H. Yamakawa, J. Chem. Phys. **38**, 1768 (1963).
22. R. W. Brotzman and B. E. Eichinger, Macromolecules **15**, 531 (1982).
23. P. J. Flory and H. Shih, Macromolecules **5**, 761 (1972).
24. M. J. Newing, Trans. Faraday Soc. **46**, 613 (1950).
25. W. R. Summers, Y. B. Tewari, and H. P. Schreiber, Macromolecules **5**, 12 (1972).
26. R. N. Lichtenthaler, D. D. Liu, and J. M. Prausnitz, Ber. Bunsengesell. **78**, 470 (1974).
27. T. Shiomi, Z. Izumi, F. Hamada, and A. Nakajima, Macromolecules **13**, 1149 (1980).
28. D. W. Scott, J. Am. Chem. Soc. **68**, 1877 (1946).
29. N. Kuwahara, T. Okazawa, and M. Kaneko, J. Polym. Sci., Part C **23**, 543 (1968).
30. K. Sugamiya, N. Kuwahara, and M. Kaneko, Macromolecules **7**, 66 (1974).
31. T. Shiomi, Y. Kohra, F. Hamada, and A. Nakajima, Macromolecules **13**, 1154 (1980).
32. G. DiPaola-Baranyi, J. E. Guillet, H.-E. Jeberien, and J. Klein, Makromol. Chem. **181**, 215 (1980).
33. R. D. Newman and J. M. Prausnitz, AIChE J. **19**, 704 (1973).
34. H. P. Schreiber, Y. B. Tewari, and D. Patterson, J. Polym. Sci., Polym. Phys. Ed. **11**, 15 (1973).
35. D. Patterson, Y. B. Tewari, H. P. Schreiber, *et al*. Macromolecules **4**, 356 (1971).
36. J. H. van der Waals and J. J. Hermans, Rec. Trav. Chim. Pays Bas. **69**, 971 (1950).
37. L. H. Tung, J. Polym. Sci. **24**, 333 (1957).
38. Q. A. Trementozzi, J. Polym. Sci. **23**, 887 (1957).
39. I. Harris, J. Polym. Sci. **8**, 353 (1952).
40. M. S. Muthana and H. Mark, J. Polym. Sci. **4**, 527 (1949).
41. N. F. Brockmeier, R. W. McCoy, and J. A. Meyer, Macromolecules **5**, 130 (1972).
42. C. Booth and C. J. Devoy, Polymer **12**, 309 (1971).
43. I. Bahar, H. Y. Erbil, B. M. Baysal, and B. Erman, Macromolecules **20**, 1353 (1987).
44. Q. Du, P. Hattam, and P. Munk, J. Chem. Eng. Data **35**, 367 (1990).
45. B. E. Eichinger and P. J. Flory, Trans. Faraday Soc. **64**, 2053 (1968).
46. P. J. Flory, J. Am. Chem. Soc. **65**, 372 (1943).
47. P. J. Flory and H. Daoust, J. Polym. Sci. **25**, 429 (1957).
48. Y.-K. Leung and B. E. Eichinger, Macromolecules **7**, 685 (1974).
49. Y.-K. Leung and B. E. Eichinger, J. Phys. Chem. **78**, 60 (1974).
50. R. N. Lichtenthaler, D. D. Liu, and J. M. Prausnitz, Macromolecules **7**, 565 (1974).
51. R. D. Newman and J. M. Prausnitz, J. Phys. Chem. **76**, 1492 (1972).
52. R. S. Jessup, J. Res. Nat. Bur. Stand. **60**, 47 (1958).
53. W. R. Krigbaum and P. J. Flory, J. Am. Chem. Soc. **75**, 1775 (1953).
54. S. Prager, E. Bagley, and F. A. Long, J. Am. Chem. Soc. **75**, 2742 (1953).
55. B. E. Eichinger and P. J. Flory, Trans. Faraday Soc. **64**, 2061 (1968).
56. P. J. Flory, J. L. Ellenson, and B. E. Eichinger, Macromolecules **1**, 279 (1968).
57. C. H. Baker, W. B. Brown, G. Gee, *et al*. Polymer **3**, 215 (1962).
58. B. E. Eichinger and P. J. Flory, Trans. Faraday Soc. **64**, 2066 (1968).
59. C. Booth, G. Gee, G. Holden, *et al*. Polymer **5**, 343 (1964).
60. B. E. Eichinger and P. J. Flory, Trans. Faraday Soc. **64**, 2035 (1968).
61. G. Gee, J. Chem. Soc. 280 (1947).
62. G. Gee, J. B. M. Herbert, and R. C. Roberts, Polymer **6**, 541 (1965).
63. Y. B. Tewari and H. P. Schreiber, Macromolecules **5**, 329 (1972).
64. C. Booth, G. Gee, and G. R. Williamson, J. Polym. Sci. **23**, 3 (1957).
65. G. DiPaola-Baranyi and J. E. Guillet, Macromolecules **11**, 228 (1978).
66. J. Bischoff and V. Desreux, Bull. Soc. Chim. Belg. **61**, 10 (1952).
67. G. V. Schulz and H. Doll, Z. Elektrochem. **56**, 248 (1952).
68. R. Kirste and G. V. Schulz, Z. Phys. Chem. (Frankfurt) **27**, 301 (1961).
69. G. V. Schulz, H. Baumann, and R. Darskus, J. Phys. Chem. **70**, 3647 (1966).
70. I. Noda, N. Kato, T. Kitano, *et al*. Macromolecules **14**, 668 (1981).
71. J. B. Kinsinger and R. E. Hughes, J. Phys. Chem. **63**, 2002 (1959).
72. N. F. Brockmeier, R. W. McCoy, and J. A. Meyer, Macromolecules **5**, 464 (1972).
73. G. Gündüz and S. Dinçer, Polymer **21**, 1041 (1980).
74. C. E. H. Bawn and M. A. Wajid, Trans. Faraday Soc. **52**, 1658 (1956).
75. C. S. Su and D. Patterson, Macromolecules **10**, 708 (1977).
76. I. Noda, Y. Higo, N. Ueno, *et al*. Macromolecules **17**, 1055 (1984).
77. J. Biroš, K. Šolc, and J. Pouchlý, Faserforsch. Textiltechn. **15**, 608 (1964).
78. J. W. Breitenbach and H. P. Frank, Monatsh. Chem. **79**, 531 (1948).
79. P. J. Flory and H. Höcker, Trans. Faraday Soc. **67**, 2258 (1971).
80. C. E. H. Bawn, R. F. J. Freeman, and A. R. Kamaliddin, Trans. Faraday Soc. **46**, 677 (1950).
81. P. Doty, M. Brownstein, and W. Schlener, J. Phys. Chem. **53**, 213 (1949).
82. H. P. Frank and H. Mark, J. Polym. Sci. **6**, 243 (1951).
83. A. I. Goldberg, W. P. Hohenstein, and H. Mark, J. Polym. Sci. **2**, 503 (1947).
84. M. J. Schick, P. Doty, and B. H. Zimm, J. Am. Chem. Soc. **72**, 530 (1950).
85. B. Erman and B. M. Baysal, Macromolecules **18**, 1696 (1985).
86. W. R. Krigbaum and D. O. Geymer, J. Am. Chem. Soc. **81**, 1859 (1959).
87. Th. G. Scholte, Eur. Polym. J. **6**, 1063 (1970).
88. H. Höcker and P. J. Flory, Trans. Faraday Soc. **67**, 2270 (1971).
89. K. Kamide, K. Sugamiya, T. Kawai, *et al*. Polym. J. **12**, 67 (1980).
90. W. Merk, R. N. Lichtenthaler, and J. M. Prausnitz, J. Phys. Chem. **84**, 1694 (1980).
91. G. V. Browning and J. D. Ferry, J. Chem. Phys. **17**, 1107 (1949).
92. R. E. Robertson, R. McIntosh, and W. E. Grummitt, Can. J. Res. **324**, 150 (1956).
93. R. E. Wagner, J. Polym. Sci. **2**, 27 (1947).
94. R. J. Kokes, A. R. DiPietro, and F. A. Long, J. Am. Chem. Soc. **75**, 6319 (1953).
95. T. Kawai, J. Polym. Sci. **32**, 425 (1958).
96. A. Nakajima, H. Yamakawa, and I. Sakurada, J. Polym. Sci. **35**, 489 (1959).
97. G. R. Cotton, A. F. Sirianni, and I. E. Puddington, J. Polym. Sci. **32**, 115 (1958).
98. D. D. Deshpande and O. S. Tyagi, Macromolecules **11**, 746 (1978).
99. R. C. Castells and G. D. Mazza, J. Appl. Polym. Sci. **32**, 5917 (1986).

100. G. DiPaola-Baranyi, J. E. Guillet, J. Klein, *et al*. J. Chromatography **166**, 349 (1978).
101. L. J. Thompson and F. A. Long, J. Am. Chem. Soc. **76**, 5886 (1954).
102. A. Nakajima and K. Furutachi, J. Soc. High Polym. Japan **6**, 460 (1949).
103. P. Doty and E. Mishuck, J. Am. Chem. Soc. **69**, 1631 (1947).
104. J. C. Day and I. D. Robb, Polymer **22**, 1530 (1981).
105. A. Silberberg, J. Eliassaf, and A. Katchalsky, J. Polym. Sci. **23**, 259 (1957).
106. S. Saeki, C. Holste, and D. C. Bonner, J. Polym. Sci., Polym. Phys. Ed. **20**, 793 (1982).
107. C. Etxabarren, M. Iriarte, C. Uriarte, A. Etxeberría, and J. J. Iruin, J. Chromatogr. A, **969**, 245 (2002).
108. J. J. Manikath, B. Francis, M. Jacob, R. Stephen, S. Joseph, S. Jose, and S. Thomas, J. Appl. Polym. Sci. **82**, 2404 (2001).
109. M. Şen, A. Yakar, and O. Güven, Polymer **40**, 2969 (1999).
110. E. G. Lezcano, C. Salom, R. M. Masegosa, and M. G. Prolongo, Polym. Bull. **34**, 677 (1995).
111. Y. H. Bae, T. Okano, and S. W. Kim, J. Polym. Sci., B, Polym. Phys. Ed. **28**, 923 (1990).
112. R. G. Alamo, A. Bello, J. G. Fatou, and C. Obrador, J. Polym. Sci., B, Polym. Phys. Ed. **28**, 907 (1990).
113. J.-P. Queslel and L. Monnerie, Makromol. Chem. Macromol., Symp. **30**, 145 (1989).
114. A. Sarac, D. Şakar, O. Cankurtaran, and F. Y. Karaman, Polym. Bull. **53**, 349 (2005).
115. K. J. Thurecht, D. J. T. Hill, and A. K. Whittaker, Macromolecules **38**, 3731 (2005).
116. S. K. Patel, S. Malone, C. Cohen, J. R. Gillmor, and R. H. Colby, Macromolecules **25**, 5241 (1992).
117. G. K. Fleming and W. J. Koros, Macromolecules **19**, 2219 (1986).
118. S. P. Nunes, B. A. Wolf, and H. E. Jeberien, Macromolecules **20**, 1948 (1987).
119. N. Schuld and B. A. Wolf, in *Polymer Handbook*, edited by J. Brandrup, E. H. Immergut, and E. A. Grulke (John Wiley, New York, 1999), p. VII/247.
120. A. F. M. Barton, *CRC Handbook of Polymer–Liquid Interaction Parameters and Solubility Parameters* (CRC Press, Boca Raton, Florida, 1990).
121. I. Kikic, P. Alessi, and A. Cortesi, Fluid Phase Equilib. **169**, 117 (2000).
122. R. Bergman and L.-O. Sundelöf, Eur. Polym. J. **13**, 881 (1977).
123. J. S. Aspler and D. G. Gray, Macromolecules **12**, 562 (1979).
124. J. S. Aspler and D. G. Gray, Polymer **23**, 43 (1982).
125. R. W. Brotzman and P. J. Flory, Macromolecules **20**, 351 (1987).
126. P. Alessi, A. Cortesi, P. Sacomani, and E. Vallés, Macromolecules **26**, 6175 (1993).
127. S. Kinugasa, H. Hayashi, F. Hamada, and A. Nakajima, Macromolecules **18**, 582 (1985).
128. R. Alamo, J. G. Fatou, and A. Bello, Polym. J. **15**, 491 (1983).
129. S. Saeki, J. C. Holste, and D. C. Bonner, J. Polym. Sci., Polym. Phys. Ed. **19**, 307 (1981).
130. S. Saeki, J. C. Holste, and D. C. Bonner, J. Polym. Sci., Polym. Phys. Ed. **20**, 805 (1982).
131. T. Shiomi, K. Kohno, K. Yoneda, T. Tomita, M. Miya, and K. Imai, Macromolecules **18**, 414 (1985).
132. B. A. Wolf and H.-J. Adam, J. Chem. Phys. **78**, 4121 (1981).
133. K. Schotsch, B. A. Wolf, H.-E. Jeberien, J.Klein, Makromol. Chem. **185**, 2169 (1984); K. Schotsch and B. A. Wolf, Makromol. Chem. **185**, 2161 (1984).
134. W. R. Krigbaum, J. Am. Chem. Soc. **76**, 3758 (1954).
135. A. J. Ashworth and G. J. Price, Macromolecules **19**, 358 (1986).
136. *Polymer Data Handbook*, edited by J. E. Mark (Oxford University Press, New York, 1999).
137. P. J. Flory, Disc. Faraday Soc. **49**, 7 (1970).
138. A. Muramoto, Polymer **23**, 1311 (1982).
139. H.-M. Petri and B. A. Wolf, Macromolecules **27**, 2714 (1994).

CHAPTER 15

Theta Temperatures

P. R. Sundararajan

Department of Chemistry, Carleton University, 1125 Colonel By Drive, Ottawa, ON, Canada K1S 5B6

15.1 INTRODUCTION

The statistically averaged configurations of polymers can conceptually be treated under the framework of a *freely jointed* chain, similar to that of a diffusing particle executing a random flight, with each of the skeletal bonds of the chain resembling a step in the random walk. Apart from the condition that each step size (or bond length) is fixed, there is no restriction on the spatial positions of successive steps in this model. However, the significant differences which set a real chain apart from a random flight model are that (1) the ''cross over'' of paths of any two bonds is prohibited resulting in *volume exclusion* and (2) the contiguous bonds are restricted to a narrow range of bond angles. These factors result in an expansion of the random coil compared to the ideal freely jointed chain. In addition, steric hindrance between atoms and groups limit the dihedral rotational range as well, limiting the scope of the *freely rotating* chain concept. In the latter, the bond length and bond angle are constrained but the dihedral angles may assume any value. Thus, the random coil of a real chain will be more expanded than predicted by the freely jointed or freely rotating chain models.

The concept of the excluded volume and the theta conditions have been explained eloquently by Flory [1,2]. The average configuration of a polymer chain in a dilute solution is dictated by short-range and long-range interactions. The former is determined by the geometrical constraints such as the bond length, bond angle, and the hindrance to dihedral rotations caused by steric interactions between the atoms or groups separated by a short sequence of bonds. The long-range effects are due to the interactions between units which are remote from one another in *sequence*, but close to each other in *space*. The configuration of the polymer chain must depend also on its environment. In a good solvent, the energy of interaction between a chain element and an adjacent solvent molecule would exceed the mean of the energies of interaction between the polymer-polymer and the solvent-solvent pairs. The chain will then tend to expand further, so as to reduce the frequency of contacts between pairs of polymer elements. In a poor solvent, however, where the energy of polymer-solvent interaction is unfavorable, more compact configurations, in which polymer-polymer contacts occur more often, will be preferred. If the solvent medium is sufficiently poor, i.e., the interaction energy with the polymer is sufficiently positive, the energy of interaction, at a certain temperature, may compensate exactly the influence of volume exclusion. When this condition, called the ''Theta (Θ) condition'' is achieved, the polymer chain will assume its so-called random flight configuration, its overall dimensions then being determined solely by short-range bond lengths, bond angles, and sterically favorable dihedral rotations. At this temperature an exact balance occurs between the effect of mutual volume exclusion of the segments, which tends to enlarge the molecule, and the effect of a positive energy of mixing, which encourages first neighbor contacts between polymer segments, and hence a more compact configuration for the molecule. The chain dimension will then be unperturbed by self-interaction of long range. The unperturbed dimensions thus obtained may then be interpreted in terms of the short-range features of the chain molecule.

In terms of the thermodynamics of mixing the polymer and the solvent, the Θ temperature is defined as that at which the excess chemical potential is zero. The latter ($\Delta\mu$) is given by Flory [1]

$$\Delta\mu = RT(\kappa_1 - \psi_1)(v_2)^2, \tag{15.1}$$

where κ_1 and ψ_1 are the enthalpy and entropy parameters and v_2 refers to the volume fraction of the polymer in a

volume element. R and T are the gas constant and absolute temperature, respectively. Defining an ideal temperature (Θ) by

$$\Theta = \kappa_1 T/\psi_1, \tag{15.2}$$

such that

$$\psi_1 - \kappa_1 = \psi_1(1 - \Theta/T), \tag{15.3}$$

Eq. (1) transforms to

$$\Delta\mu = -RT\psi_1(1 - \Theta/T)(\upsilon_2)^2. \tag{15.4}$$

When the temperature $T = \Theta$, the excess chemical potential due to the polymer segment-solvent interaction reduces to zero. Thus at the theta temperature, the deviation from ideality vanishes. The system in this case can be binary, consisting of the solvent and the polymer or ternary, with a mixture of two solvents and the polymer.

In terms of the phase equilibrium of the poor-solvent/polymer mixture, the Θ temperature is identified with the critical miscibility temperature in the limit of infinite molecular weight. This then leads to the possibility of a Θ_l corresponding to the lower critical solution temperature (LCST) and Θ_u for the upper critical solution temperature (UCST) (see e.g., [3]). Although in most cases the LCST is inaccessible due to the boiling point of the solvent or the polymer degradation, both Θ_l and Θ_u have been determined in a few cases [4–6]. (In polymer science, the definitions of LCST and UCST are such that the lower critical solution temperature actually corresponds to the higher temperature in the phase diagram. In the tables which follow, notice that Θ_l is higher than Θ_u. This is in contrast to the case in colloid chemistry, where the lower critical flocculation temperature in indeed a lower temperature than the upper critical flocculation temperature.)

At the theta temperature, the intrinsic viscosity [η] is related to the unperturbed dimension of the polymer and its molecular weight [1] by

$$[\eta]_\Theta = \Phi(\langle r^2\rangle_0/M)^{3/2}M^{1/2}, \tag{15.5}$$

or

$$[\eta]_\Theta = K_\Theta M^{1/2}, \tag{15.6}$$

where $\langle r^2\rangle_0$ is the unperturbed mean square end-to-end distance, Φ is the Flory universal constant and K_Θ is a constant defined by

$$(\langle r^2\rangle_0/M)_\infty = (K_\Theta/\Phi)^{2/3}. \tag{15.7}$$

Flory [2] recommended a value of 2.6×10^{21} for Φ, when r is expressed in centimeters and [η], in deciliters per gram.

The "characteristic ratio" of the unperturbed end-to-end distance of a chain with n skeletal bonds is defined by

$$C_n = \langle r^2\rangle_0/nl^2 \tag{15.8}$$

where l is the average bond length per repeat unit. The denominator, nl^2, in Eq. 15.8 corresponds to the value of the mean square end-to-end distance if no correlations exist between bond directions, i.e., that of a freely jointed chain. Thus, the characteristic ratio represents the ratio between the actual unperturbed dimension of a real chain to that of a conceptual freely jointed chain. Hence, the more rigid and extended the chain is, the higher will be the value of C_n.

In the limit of infinite molecular weight, the characteristic ratio C_∞ can be calculated from K_Θ using the relationship [2]

$$C_\infty = (K_\Theta/\Phi)^{2/3}(M_0/l^2). \tag{15.9}$$

Here, M_0 is the mean molecular weight of the repeat unit of the chain (averaged over the skeletal bonds in the repeat unit) and l is the average bond length per skeletal bonds of the repeat unit. K_Θ in Eq. (15.9) is expressed in dl.g^{-1}(g mol wt)$^{-1/2}$.

Let us illustrate the calculation of C_∞ from K_Θ, using Eq. 15.9 with two examples, one for a chain with two skeletal bonds in the repeat unit and the other with three skeletal bonds:

1. For poly(isobutylene), [—CH_2—$C(CH_3)_2$—]$_n$, $K_\Theta = 10.7 \times 10^{-4}$ [7] (see Table 15.1). Two skeletal bonds comprise the repeat unit, with a molecular weight of 56. Hence, $M_0 = 28$. With an average skeletal bond length of 1.53×10^{-8} cm,

$$M_0/l^2 = 11.96 \times 10^{16}.$$

With the value of Φ cited above, $(K_\Theta/\Phi)^{2/3} = 5.5328 \times 10^{-17}$. The value of C_∞ is then 6.6.

2. The repeat unit of poly(oxyethylene), [—O—CH_2—CH_2—]$_n$, consists of three skeletal bonds and hence $M_0 = 14.67$. With a value of 1.53×10^{-8} cm for the length of the C—C bond and 1.43×10^{-8} cm for the two C—O bonds, the average l is 1.46×10^{-8} cm. Using a value of 11×10^{-4} for K_Θ [8] (see Table 15.9), the value of C_∞ is 3.88.

Studies, experimental or theoretical, under the Θ condition allow probing of the influence of the chain structure, tacticity, nature of the side groups, and the composition of the polymers on the overall chain configuration in terms of the local interactions which are dictated by bond lengths, bond angles, and the distribution of torsion angles. This enables relating these molecular features to the ultimate functional properties of the polymers. For example, the entanglement molecular weight, distance between entanglements, and viscoelastic properties have been correlated with the characteristic ratio, C_∞, of the unperturbed end-to-end distance [9–13].

The determination of the theta temperature by several techniques, such as intrinsic viscosity, phase equilibria, osmometry, light scattering, sedimentation equilibrium, and cloud point titration has been discussed comprehensively in a number of sources [1,14–16]. The influence of

tacticities of select polymers on their theta temperatures and the unperturbed dimensions has also been reviewed [15,16]. The differences in the θ temperatures of protiated and deuterated systems have been studied [16a,b].

This chapter presents a collection of theta temperatures reported for various polymers, in Tables 15.1–15.11. In cases where a number of authors have studied the same polymer, the results are given in chronological order. This, in a sense, serves to follow the progress in this area. The solvents and the corresponding theta temperatures are grouped together from the results of a particular author(s) so that these would correspond to samples with the same characteristics in terms of M_w and its distribution.

In these tables, the polymer name is given in the first column. The tacticities of the polymer studied, if reported by the authors, are given either in terms of the diad fraction (f_m or f_r), or triad fractions (f_{mm}, f_{mr+rm}, and f_{rr}). Here the subscripts m and r refer to meso and racemic diads, respectively (see Chapter 1 on Chain Structures for these definitions). In Table 15.11, which is devoted to copolymers, the

TABLE 15.1. *Poly(alkanes).*

Polymer	$M_w \times 10^{-4}$	Dispersity (M_w/M_n)	Solvent	Theta temperature °C	$K_\theta.10^4$ [dl.g^{-1} (g mol wt)$^{-1/2}$]	Refs.
Poly(acenaphthalene)	3.3–170	1.2–1.5	ethylene dichloride	30.0	3.35	[20]
	7.3–231			35.0	4.56	[21]
Polybutene-1, isotactic	10.5–93.5	1–1.2	anisole	89.1		[22]
	12.8–94		cyclohexane/*n*-propanol (69/31)	35.0	24.7	[23]
	39–259		anisole	89.0	11.1	[24]
			phenylether	148.0	10.3	
			phenetole	64.5	11.3	
Polybutene-1, atactic	4.4–130		anisole	86.2		[22]
	11.8–290		anisole	83.0	10.8	[24,25]
			i-amylacetate	23.0	11.3	
			phenylether	141.0	10.4	
			phenetole	61.0	10.5	
			toluene	−46.0	13.3	
Polyethylene	34–149		bis (2-ethylhexyl)adipate	145 (low density) 170 (high density)		[26]
	8.2–16.5	11.3	biphenyl	125.0	-	[27]
			diphenylene oxide	118.0	-	
	and	and	dodecanol-1	138.0	31.6	
			2-ethylhexyl sebacate	150.0	-	
	31.7	1.6	2-ethylhexyl adipate	170.0	-	
	2.19–103.5		biphenyl	127.5	32.3	[28,29]
			decanol	153.3	30.2	
			diphenyl ether	161.4	29.5	
			diphenyl methane	142.2	31.5	
			dodecanol-1	137.3	30.7	
			octanol-1	180.1	28.6	
	4.5–39.3	1.65–3.34	biphenyl	125.0 (high density)	39.8	[30]
	$M_\eta = 1.4$–44.2		*p*-tert amyl phenol	199.2		[31,32]
			anisole	153.5		
			benzyl phenyl ether	191.5		
			biphenyl	127.5	33.0	
			n-decanol	153.3		
			diphenyl ether	163.9	30.9	
			diphenyl methane	142.2	32.2	
			n-lauryl alcohol	137.3		
			p-nonyl phenol	162.4		
			n-octanol	180.1		
	8.98–90.9	∼1.3	dioctyl adipate	145	23.7	[33]
	4.1–15.1		*p*-xylene/*n*-hexanol (30:70)	155,160		[34,35]

TABLE 15.1. *Continued.*

Polymer	$M_w \times 10^{-4}$	Dispersity (M_w/M_n)	Solvent	Theta temperature °C	$K_\theta.10^4$ [dl.g^{-1} (g mol wt)$^{-1/2}$]	Refs.
	0.49–44.0		*n*-pentane	80.0		[36]
			n-hexane	133.3		
			n-heptane	173.9		
			n-octane	210.0 (all LCST)		
	low density 0.87–699	low density 1.11–6.94	biphenyl	118 (low density)		[37]
	high density 5.73–27.1	high density 1.68–1.95		130 (high density)	30.2 at 130 °C	
	0.9–68.8	1.0–1.97	biphenyl	128.0	38.0	[38]
			dodecanol	143.4	32.8	
			3,5,5 trimethylhexylacetate	121.0	34.6	
Poly(hexene-1)	8.13–143		phenetole	61.3	9.57	[39]
Poly(hexene-1 sulphone)	10.9–69.5		*n*-hexyl chloride	13.0		[40]
			MEK/isopropanol (37/63)	24.0		
			MEK/isopropanol (41.5/58.5)	4.0		
	$M_n = 7$–88.6		*n*-hexyl chloride	13.0	5.3	[41]
			MEK/*n*-hexane (29.8/70.2)	8.0		
	9.2–107	1.13	dioxane/*n*-hexane (40/60)	20.5	6.5	[42]
Poly(isobutylene)	$M_\eta = 18$–188		benzene	24.0	10.7	[7,43]
	(Ref. 7) 0.5–131		ethylbenzene/phenyl ether (75/25)	26.8	10.8	
	(Ref. 43)		ethylbenzene/phenyl ether (50/50)	76.0	11.7	
			phenetole	86.0	9.1	
			anisole	105.5	9.1	
			toluene	−13.0		
			ethyl *n*-caprylate	22.0		[44]
	117.1		*n*-butanol/*n*-hexane (23.6/76.4)	25.0		[45]
			n-butanol/methylcyclohexane (29.2/70.8)			
			butanone/carbon tetrachloride (33.7/66.3)			
			butanone/cyclohexane (36.8/63.2)			
			butanone/*n*-hexane (36.6/63.4)			
			carbon tetrachloride/dioxane (63.8/36.2)			
			chlorobenzene/*n*-propanol (76/24)			
			chloroform/*n*-propanol (77.1/22.9)			
			cyclohexane/dioxane (45.1/54.9)			
			cyclohexanol/toluene (29.3/70.7)			
			n-decanol/*n*-hexane (41.1/58.9)			
			n-decanol/methylcyclohexane (47.5/52.5)			
			dioxane/*n*-hexane (48.2/51.8)			
			dioxane/methylcyclohexane (51/49)			
			n-heptanol/*n*-hexane (37.4/62.6)			
			n-heptanol/methylcylohexane (39.5/60.5)			
			n-hexane/*n*-hexanol (68.3/31.7)			
			n-hexane/3-methylbutanone (57.6/43.4)			
			n-hexane/*n*-octanol (63.7/36.3)			
			n-hexane/*n*-pentanol (71.7/28.3)			
			n-hexane/ *n*-propanol (80.3/19.7)			

TABLE 15.1. *Continued.*

Polymer	$M_w \times 10^{-4}$	Dispersity (M_w/M_n)	Solvent	Theta temperature °C	$K_\theta.10^4$ [dl.g^{-1} (g mol wt)$^{-1/2}$]	Refs.
			methylcylohexane/*n*-octanol (56/44)			
			methylcyclohexane/*n*-pentanol (65.2/34.8)			
			methylcyclohexane/*n*-propanol (74.2/25.8)			
	900	1.3	benzene	24.5		[46]
			n-pentane	θ_1:76.0		
			dibutyl ether	θ_1:204.0		
	16–470	~1.1	*i*-amyl isovalerate	22.1	11.0	[47]
	15–71		*i*-amyl isovalerate	21.0		[48]
			i-amyl benzyl ether	23.7	10.8	
			i-amyl *n*-butyrate	28.0	11.4	
			n-amyl *n*-butyrate	22.0		
			benzene	22.8	11.5	
			n-butyl *n*-butyrate	46.2		
			3-methyl 5-heptanone	55.5	10.9	
	0.01–179		benzene	25.0		[49]
			i-amyl isovalerate	25.0		
	8–160		*i*-amyl isovalerate	27.0		[50]
Poly-((S)-4-methyl hexene-1) $f_m > 0.95$	13.6–1200	2–6.8	α-chloronaphthalene	165.0	8.88	[51]
			o-dichlorobenzene	133.0	11.5	
Poly(4-methylpentene-1), isotatic			biphenyl	194.6		[52]
			diphenyl ether	210.0		
			diphenyl methane	176.6		
Poly(2-methylpentene-1 sulphone)	$M_n = 4.7$–56.3		MEK/isopropanol (39.5/60.5)	22.5	9.1	[41]
			MEK/*n*-hexane (35.4/64.6)	11.5	9.1	
Poly(octene-1)	25–400		phenetole	50.4	6.55	[53]
Poly(pentene-1), isotactic	$M_n = 10.8$		phenetole	56.0		[54]
syndiotactic	$M_n = 2.8$		phenetole	48.5		
isotactic	$M_n = 13.2$–42.7		isoamyl acetate	31.0		[55]
isotactic	6.1–306		2-pentanol	64.0	12.1	[56]
isotactic, atactic	0.2–23.1 (isotactic)		anisole	85.0	*i*:10.6;*a*:9.9	[57]
			i-butylacetate	32.5	*i*:12.0;*a*:10.0	
	0.2–55 (atactic)		diphenylmethane	121.0	*i*:9.8	
			phenetole	64.0	*i*:11.3;*a*:9.8	
Poly(1-phenyl-1-propyne)	1.5–145	1.06–1.09	phenylether	149.0	*i*:9.8;*a*:9.4	
Poly(propylene) syndiotactic	11.7		cyclohexane	36.0		[58]
Poly(propylene), isotactic			isoamyl acetate	42.0	17.2	[59]
			phenyl ether	145.4		[60]
			isoamyl acetate	~70.0		[61]
	2.8–56.4		*p*-tert-amylphenol	140.8		[62,63]
			benzyl phenyl ether	181.8		
			benzyl propionate	157.5		
			n-butanol	147.2		
			p-tert-butyl phenol	166.0		
			dibenzyl ether	183.2	10.6	
			biphenyl	125.1	15.2	
			diphenyl ether	142.8	13.7	

TABLE 15.1. *Continued.*

Polymer	$M_w \times 10^{-4}$	Dispersity (M_w/M_n)	Solvent	Theta temperature °C	$K_\theta.10^4$ [dl.g^{-1} (g mol wt)$^{-1/2}$]	Refs.
	$M_\eta = 5.0$–53.1		diphenyl	125.0	14.1	[64]
			phenylether	143.0	13.0	
Poly(propylene), atactic			phenyl ether	153.5		[60]
			1-chloronaphthalene	74.0		[65,66]
			cyclohexanone	92.0		
	$M_\eta = 4.3$–70.8		biphenyl	129.0	12.8	[64]
			diphenyl ether	146.0	12.5	
			isobutyl acetate	58.0	15.8	
			isoamylacetate	34.0	16.8	
	2.3–42.0	1.02–1.35	1-octanol	77.0	11.5	[67]
Poly(propylene), atactic [hydrogenated poly (2-methyl-1,3-pentadiene)] $f_m = 0.502$	3.91–37.1	1.04–1.12	2-octanol	37.6	13.2	[68]
Polypropylene (head-to-head)	$M_n = 0.22$–4.19		isoamylacetate	43.0	10.3	[69]
	1.64–43.3	1.0–1.07	isoamylacetate	56.8	12.6	[70]

TABLE 15.2. *Poly(alkenes).*

Polymer	$M_w \times 10^{-4}$	Dispersity (M_w/M_n)	Solvent	Theta temperature °C	$K_\theta.10^4$ [dl.g^{-1} (g mol wt)$^{-1/2}$]	Refs.
Poly(butadiene), (*cis*: 0.98)	$M_n = 5.3$–48.9		isobutyl acetate	20.5	18.5	[71]
Poly(butadiene), *cis* (*cis*: 0.95; *trans*: 0.01; 1,2: 0.04)			diethyl ketone	10.3	18.1	[72]
			methylisoamyl ketone	12.6	17.8	
			methyl *n*-propyl ketone	59.7	15.7	
			methylisoamyl ketone/ methyl *n*-propyl ketone			
			(3/1)	22.3	17.5	
			(1/1)	32.7	17.1	
			(1/3)	46.2	16.7	
			diethyl ketone/methyl *n*-propyl ketone (3/2)	30.0	17.4	
Poly(butadiene), *cis*	5.0–110		*n*-heptane/*n*-hexane (50/50)	5.0		[73]
Poly(butadiene), *cis* (*cis*: 0.93; *trans*: 0.04; 1,2: 0.03)	$M_\eta = 10.8$–69.2		diethyl ketone	θ_u:14.0 θ_i:208.0		[4]
			ethyl propyl ketone	θ_u:−22.0 θ_i:237.0		
			propylene oxide	θ_u:35.0 θ_i:141.0		
Poly(butadiene) (*cis*:0.36; *trans*: 0.57; 1,2 *vinyl*: 0.07)	1.08–57.1	≤1.1	dioxane	26.5	17.8	[74]
Poly(butadiene), *trans* (*trans*: 0.94; 1,2: 0.06)	$M_\eta = 4.7$–19.3		diethyl ketone	213.0		[4]
			ethyl propyl ketone	240.0		
			propylene oxide	146.0		
Poly(butadiene), *cis*, cyclized Deg. Cycl.			cyclohexane/dioxane		K_θ as a function of cyclization is given in Figure 6 of this ref.	[75]

TABLE 15.2. *Continued.*

Polymer	$M_w \times 10^{-4}$	Dispersity (M_w/M_n)	Solvent	Theta temperature °C	$K_\theta.10^4$ [dl.g^{-1} (g mol wt)$^{-1/2}$]	Refs.
9%	10.8–51.8		(12/88)	30.0		
31%	6.2–116		(17/83)	30.0		
46%	4.8–34.6		(21/79)	30.0		
63%	3.6–110		(30/70)	30.0		
81%	5.5–86		(39/61)	30.0		
1,4-poly(2,3-dimethyl butadiene) (>85% *trans*-1,4; 3% 1,2 *vinyl*)	$M_n = 5.01$ and 1.81		cyclohexane/*n*-propanol (81.3/18.7)	25.0	22.7	[76]
1,4-1,2-poly(dimethylbutadiene) (*trans* 1,4: 23%; *cis* 1,4: 32%; 3,4: 45%)	2.51–23.8	1.03–1.19	isoamylacetate	30.0	12.6	[70]
Poly(chloroprene)	5.6–79.4	1.22–1.5	MEK	25.0	11.6	[77]
			cyclohexane	45.5	10.7	
			cylopentane	56.3	-	
	15.1–304		MEK	25.0	11.3	[78]
	58.7–171		trans decalin	2.0		[79]
Poly(isoprene) (43% brominated)	380		cyclohexane	20.0		[80]
Poly(isoprene)			methyl isobutyl ketone	13.0		[81]
Poly(isoprene), *cis*	5–100		n-hexane/isopropanol (50/50)	21.0	16.6	[73]
Poly(isoprene), *cis* (96%)	6.9–75	1.29–1.98	dioxane	31.2	13.4	[82]
Poly(isoprene), *cis* (94%)	linear 9.4		methyl isobutyl ketone	16.5		[83]
			methyl propyl ketone	33.0		
3 branches	5.7; Br: 1.75		methyl propyl ketone	33.0		
11 branches	18; Br: 1.6		methyl propyl ketone	27.8		
22 branches	34.2; Br: 1.6		methyl propyl ketone	23.5		
			methyl isobutyl ketone	15.0		
Poly(isoprene), *trans* (96%)	$M_\eta = 9.2$–27		dioxane toluene/*n*-propanol	47.7	19.1	[82]
			(68.4/31.6)	25.0	22.2	
			(67.6/32.4)	30.0	21.9	
			(66.5/33.5)	35.0	21.7	
			(65.8/34.2)	40.0	21.4	
			(64.5/35.5)	45.0	21.3	
			(63.8/36.2)	50.0	21.1	
Poly(isoprene), *cis*: 0.70; *trans*: 0.23;						[74,84, 85]
3,4: 0.07, star linear	0.5–222.5	1.06–1.17	dioxane	34.1	11.5	
4-arm star	3.8–195	1.0–1.1	dioxane	33.4	8.9	
6-arm star	4.5–144.6	1.01–1.04	dioxane	33.5	7.2	
			methyl isobutyl ketone	12.2		
			methyl *n*-propyl ketone	25.4		
8-arm star	arm:0.51–75; star: 4.1–590		dioxane	32.8		
12-am star	arm:0.35–44.5; star: 4.1–526		dioxane	32.9		
Poly(isoprene) (1,2: 0.35; 3,4: 0.65)			benzene/isopropanol (55/45)	20.0		86
Poly(2-methyl-1,3-pentadiene) (*cis/trans*: 64/36)	4.45–37.7		2-octanol	28.9	11.2	[87]
Poly(methylbutylene) (hydrogenated 1,4 polyisoprene)	0.84–60.0	1.02–1.13	*n*-hexyl acetate	60.9	18.9	[88]
1,4 polymyrcene (1,4: 90%; 3,4: 10%)	6.66–58.3	≤1.07	2-octanol	35.9	6.28	[70]

TABLE 15.2. *Continued.*

Polymer	$M_w \times 10^{-4}$	Dispersity (M_w/M_n)	Solvent	Theta temperature °C	$K_\theta.10^4$ [dl.g^{-1} (g mol wt)$^{-1/2}$]	Refs.
Poly(pentenamer) (80% *trans*)	3.6–63.5	1.0–1.22	isoamyl acetate	38.0	23.4	[89]
Poly(vinylethylene)	1.22–52.1	1.02–1.13	2-octanol	32.8	12.0	[90]
Poly(vinylethylene) (1,2: 98%; 1,4: 2%)	1.12–48.9	≤1.07	1-hexanol	66.0	11.8	[70]

TABLE 15.3. *Poly(vinyl)s.*

Polymer	$M_w \times 10^{-4}$	Dispersity (M_w/M_n)	Solvent	Theta temperature °C	$K_\theta.10^4$ [dl.g^{-1} (g mol wt)$^{-1/2}$]	Refs.
Poly(ethylethylene)	2.66–55	1.03–1.11	2-octanol	23.5	7.4	[90]
	5.2–54.5	1.03–1.11	2-octanol	21.0	8.22	[70]
			1-octanol	53.0	7.49	
Poly(vinyl acetate)	87–346		methyl isopropyl ketone/*n*-heptane (73.2/26.8)	25.0		[91]
	2.7–126.8	∼2.0	*n*-heptane/methyl isopropyl ketone (27.3/72.7)	30.0	9.2	[92]
	4.1–83		ethyl *n*-butyl ketone	29.0	9.29	[93]
			ethyl isoamyl ketone	66.0	8.20	
	0.35–150	1.02–1.05	methanol	6.0	10.1	[94]
	3.0–32		ethyl *n*-butyl ketone	29.0	9.55	[95]
			carbon tetrachloride	46.4		
			ethanol	19.0		[83]
			3-heptanone	29.0		
	0.8–130		cetyl alcohol	123.0	5.37	[96]
Branched			ethanol	12–15		[83]
			3-heptanone	26.0		
Poly(9-vinyladenine)	$M_n = 9.4$, 13, and 51		sodium cacodylate/water (0.1 m/L)	40.0	2.92	[[97]
Poly(vinyl alcohol)	1.35, 3.44, and 7.41		water	97.0		[98]
			t-butanol/water (32/68/w/w)	25.0		[99]
			ethanol/water (41.5/58.5 w/w)	25.0		
			methanol/water (41.7/58.3 w/w)	25.0		
			i-propanol/water (39.4/60.6 w/w)	25.0		
			n-propanol/water (35.1/6.49 w/w)	25.0		
Poly(vinyl alcohol), urethanized 4.9%; 8.1% or 11.5%	DP = 770–2040		*n*-propanol/water(30/40)	30.0		[100]
			n-propanol/water(40/50)	60.0		
			toluence	37.0	7.62	[101]
Poly (vinyl carbanilate)			cyclohexanol	55		[101a]
			diethyl ketone	35		

TABLE 15.3. *Poly(vinyl)s*.

Polymer	$M_w \times 10^{-4}$	Dispersity (M_w/M_n)	Solvent	Theta temperature °C	$K_\theta.10^4$ [dl.g^{-1} (g mol wt)$^{-1/2}$]	Refs.
Poly(*N*-vinylcarbazole)	34.6–229		chlorobenzene	−36.5		[102]
	7.6–56.4	1.2–1.3	nitrobenzene	−20.4		
			chlorobenzene/methanol (85.9/14.1)	25.0	7.38	[103]
		7.2–4.9	1,3-dichlorobenzene/ methanol(85/15)	25.0	8.77	
Poly(vinyl chloride)			benzyl alcohol	155.4	15.6	[104]
	4.3–48.7		THF/water (100/11.9); (100/9.5)	30.0		[105]
			n-butanol/cyclohexanone (15.8/100)	59.0		[106]
			n-butanol/cyclohexanone (41.5/100)	72.0		
			cyclohexane/DMF (100/12.8)	40.5		
			cyclohexanone	51.0		
			DMF	36.5		
			THF/water (100/5)	17.0		
	$M_n = 1.89$–10.2		methanol/THF (42/58)	22.0		[107]
$f_r = 0.53$–0.57	6.8 and 11.8		THF/water (91/9)	25.0		[108]
Poly(3-vinylpyrene)	3.5–48.7	∼1.1	chloroform	25.0	5.2	[109]
			methanol/THF (8/92)	25.0		
Poly(2-methyl-5-vinyl pyridine)	10.4–99		isoamyl acetate	53.2	8.4 (average)	[110]
			n-amyl acetate	48.2		
			isobutyl acetate	49.0		
			n-butyl acetate	21.8		
			ethyl *n*-butyrate	50.0		
			ethyl propionate	25.4		
			methyl isobutyl ketone	37.4		
			n-propyl acetate	19.3		
			n-propyl propionate	58.0		
			propionitrile	−3.6		
			tetrahydronaphthalene	49.5		
	6.7–120		*n*-amyl acetate	48.2	8.3	[111]
			n-butyl acetate	21.8	8.4	
			methyl isobutyl ketone	37.4	8.0	
Poly(2-vinylpyridine)	42–445		*n*-heptane/*n*-propanol (59.6/40.4 w/w)	25.0	12.0	[112]
	3.5–23.3	≤1.2	benzene	15.0	7.2	[113]
Poly(*N*-vinylpyrrolidone)	1.15		acetone/water (66.8/33.2)	25.0		[114]
	$M_n = 9.9$–45.7	≤1.4	acetone/water (66.8/33.2)	25.0	7.4	[115]
			Na_2SO_4/water (0.55 m/l)	28.0	5.8	
Poly(vinyl sulfonic acid)	DP=366–3640		KBr/water (0.347M)	5.7	7.72	[116]
			KCl/water (0.349M)	5.5	7.65	
			KCl/water (0.650M)	26.0	8.91	
			KCl/water (1.001M)	44.5	9.01	
			NaBr/water (0.346M)	−0.6	10.72	
			NaBr/water (1.008M)	40.1	10.6	
			NaCl/water (1.003M)	32.4	10.78	
Poly(vinyltriazole)	197		dimethyl formamide/dioxane (76.6/23.4)	25.0		[117]

TABLE 15.4. *Poly(styrenes).*

Polymer	$M_w \times 10^{-4}$	Dispersity (M_w/M_n)	Solvent	Theta temperature °C	$K_\theta.10^4$ [dl.g^{-1} (g mol wt)$^{-1/2}$]	Refs.
Poly (*p*-tert-butylstyrene) ($f_i = 0.15$, $f_s = 0.55$, $f_h = 0.30$)	1.8–640	1.02–1.22	1-nitropropane	31.0	6.1	[118,119]
Poly (*p*-tert-butylstyrene)	2.74–45.5 and 5.1–748	≤1.11 and 1.05–1.17	3-nonanol	10.9	5.95	[120–122]
			2-octanol	32.7	5.57	
			1-hexanol	65.0	5.11	
			1-nitropropane	31.0	6.00	
Poly(*p*-chlorostyrene)	20.1–125		ethyl benzene	−14.7	6.4	[123,124]
			ethyl carbitol	27.8	6.4	
			ethyl chloroacetate	−1.8	5.9	
			methyl chloroacetate	64.6	6.4	
			i-propyl acetate	75.7	6.4	
			i-propyl benzene	59.0	6.5	
			i-propyl chloroacetate	−8.2	5.6	
	M_η =34.1–1.79.9	1.37–1.79	benzene	8.0		[125]
			benzene/methanol			
			(5.5/1)	26.7		
			(5/1)	32.4		
			(4.5/1)	41.6	5.61	
Poly(*p*-decylstyrene)	21.3–57		MEK/butylethylketone (1/1.24)	21.2		[126]
Poly(3,4-dichlorostyrene)	35–540		butyl acetate/butyl alcohol (13/1 w/w)	32.9	5.6	[127]
Poly(*p*-hexylstyrene)	60–90		MEK	30.2		[126]
Poly(*p*-isopropylstyrene)			dioxane/isopropanol (35/65)	20.0		[86]
Poly(*p*-methoxystyrene)	8–150		*t*-butyl benzene	52.2	7.4	[128]
			isoamylacetate	75.0	6.9	
			dichlorodecane	92.6		
			methyl isobutylketone	23.4	6.4	
Poly(*p*-methoxystyrene)	$M_\eta = 7.6$–63.1		benzene/methanol (73.7/26.3)	25.0		[129]
			chloroform/methanol (66.5/33.5)	25.0		
			chloroform/cyclohexane (36.1/63.9)	25.0		
			MEK/*n*-heptane (80/20)	25.0		
			MEK/*n*-propanol (80.6/16.4)	25.0		
			toluene/cyclohexanol (62.8/37.2)	25.0		
Poly(α-methyl styrene)	29.4; 30.6; and 38.0		cyclohexane	36.2		[81]
Poly(α-methyl styrene)						[130,131]
f_{mm}: 0.08; f_{mr}: 0.48; f_{rr}: 0.44	9–400		cyclohexane	37.0	7.8	
f_{mr}: 0.10; f_{rr}: 0.90	2.7–367	1.8–2.8	cyclohexane	32.5	7.39	
f_{mr}: 0.19; f_{rr}: 0.81	2.6–17.5	1.11–1.60	cyclohexane	33.3	7.52	
f_{mm}: 0.03; f_{mr}: 0.29; f_{rr}: 0.68			cyclohexane	34.5		
f_{mm}: 0.06; f_{mr}: 0.40; f_{rr}: 0.55			cyclohexane	35.6		
f_{mm}: 0.11; f_{mr}: 0.45; f_{rr}: 0.44			cyclohexane	37.0	7.89	
Poly(α-methyl styrene)	20.4–747; also two samples with $M_n = 3.93$ and 8.01		cyclohexane	34.5	7.3	[132]
			trans-decalin	9.5	6.7	
	2.01–90.3	1.01–1.12	1-chloro-*n*-hexane	10.0	6.51	[133]
			cyclohexane	34.5	6.88	
			1-chloro-*n*-octane	53.0	6.31	

TABLE 15.4. *Continued.*

Polymer	$M_w \times 10^{-4}$	Dispersity (M_w/M_n)	Solvent	Theta temperature °C	$K_\theta.10^4$ [dl.g^{-1} (g mol wt)$^{-1/2}$]	Refs.
Poly (α-methyl styrene) 53% syndio; 41% hetero; 5% iso	5.9–341	1.03–1.15	cyclohexane	36.2		[133a]
Poly (α-methyl styrene) $f_r = 0.72$	0.053–322	1.01–1.05	cyclohexane	30.5		[133b]
Poly(*p*-methylstyrene)	16.3–197		diethyl succinate	16.4	7.0	[134]
Polystyrene	$M_\eta = 7.0$–127		cyclohexane	34.0	7.9	[135]
			ethylcyclohexane	70.0	7.3	
	$M_\eta = 0.4$–697		cyclohexane	34.0	8.2	[43]
	4–146		MEK/isopropanol (6/1)	23.0	7.30	[136]
	$M_\eta = 10.2$–53.2		toluene/methanol			[137]
			(76.9/23.1)	25.0	9.2	
			(75.2/24.8)	34.0	8.9	
			(72.8/27.2)	45.0	8.8	
	$M_\eta = 1.8$–271.6		decalin (23.1% *cis*)	19.3		[138]
	8.5–395		cyclohexane	35.0	8.0	[139]
	40.6	1.05	1-chloro-*n*-undecane	32.8	7.86	[140]
			diethyl malonate	35.9	7.69	
			cyclohexane	34.8	8.66	
	17		*n*-butyl formate	−9.0		[141]
			cyclohexane	34.0		
			cyclohexanol	83.5		
			decalin	29.5		
			diethyl malonate	31.0		
			diethyl oxalate	51.5		
			hexyl-*m*-xylene	12.5		
			methylcyclohexane	68.0		
	33.5		benzene/cyclohexanol (38.4/61.6)	25.0		[142]
			benzene/*n*-hexane (34.7/65.3)	25.0		
			benzene/methanol (77.8/22.3)	25.0		
			benzene/isopropanol (64.2/35.8)	25.0		
			butanone/methanol (88.7/11.3)	25.0		
			carbontetrachloride/methanol (81.7/28.3)	25.0		
			chlorobenzene/di-isopropyl ether (32/68)	25.0		
			chloroform/methanol (75.2/24.8)	25.0		
			dioxane/methanol (71.4/28.6)	25.0		
			methanol/tetrahydrofuran (28.7/71.3)	25.0		
	40.6		1-chloro-*n*-decane	6.6		[143]
			1-chloro-*n*-undecane	32.8		
			1-chloro-*n*-dodecane	58.6		
	M_η = 1.04– 123		benzene/isopropanol (66/34)	20.0		[86]
			dioxane/isopropanol (55/45)	20.0		
	M_n = 0.054– 0.72	≤1.1	cyclohexane	34.5	8.4	[144]
			n-hexane/3-methylbutanone (48/52)	20.0		[145]
			cyclohexane	34.5	7.8	[72]
			methyl cyclohexane	70.5	7.0	
			diethyl malonate	34.2	7.2	
			diethyl oxalate cyclohexane/ methylcyclohexane	55.8	7.3	
			(2/1)	43.0	7.8	
			(1/1)	48.0	7.5	
			(1/2)	54.0	7.3	

TABLE 15.4. *Continued.*

Polymer	$M_w \times 10^{-4}$	Dispersity (M_w/M_n)	Solvent	Theta temperature °C	$K_\theta.10^4$ [dl.g^{-1} (g mol wt)$^{-1/2}$]	Refs.
			diethylmalonate/diethyl oxalate			
			(4/1)	40.0	7.1	
			(1/1)	47.4	7.1	
			(1/4)	52.6	7.1	
	5.8–200		trans decalin	23.8		[61]
			cyclohexanol	83.5		[146]
	4–440		decalin			[147]
			62% cis	15.2		
			100% cis	12.0		
	1.9–440		dioctyl phthalate	22.0		[148]
			trans decalin	23.5		[149]
	28 and 62	1.86 and 1.38	trans decalin	18.2		[150]
	220	≤1.1	benzene/*n*-butanol (58/42)	35.0		[151]
			benzene/heptane (44/56)	35.0		
			benzene/isopropanol (61/39)	35.0		
			benzene/methanol (74.7/25.3)	35.0		
			carbontetrachloride/heptane (53/47)	35.0		
			carbontetrachloride/*n*-butanol (65/35)	35.0		
			dioxane/heptane (41.5/58.5)	35.0		
			dioxane/isopropanol (51.5/48.5)	35.0		
			dioxane/methanol (66.5/33.5)	35.0		
			nitropropane/heptane (42/58)	35.0		
	7.0		cyclohexane	34.5		[152]
			methyl cyclohexane	60.0		
			d, l-terpineol	78.5	8.25 at 80 °C	
			cyclohexanol	83.5		
			3-methyl cyclohexanol	98.0		
			d, l-menthol	115.0		
	9–56	<1.2	dioxane/methanol (66.5/33.5)	35.0	8.2	[153]
	7.0; 16, and 800		benzene/methanol (78/22)	21.5, 23.5		[83]
			cyclohexane	34.5		
			decalin	14.5		
			diethyl malonate	35.6		
	2.2–137	1.19–2.8	cyclohexanol	86.0		[34,154]
	49–1340	<1.07	cyclohexane	34.5	8.77	[155]
			trans-decalin	20.4	8.05	
	3.7–270	<1.1	cyclopentane	θ_u:19.6	8.0	[156,157]
				θ_l:154.2	7.9	
	1–20;	<1.06	ethyl acetate	θ_u:−44.0		[5]
				θ_l:139.0		
	67; and 270	<1.15; and <1.1	isoamyl acetate	θ_u:−49.0		
				θ_l:220.0		
			isobutyl acetate	θ_u:−46.0		
				θ_l:172.0		
			isopropyl acetate	θ_u:−27.0		
				θ_l:107.0		
			methyl acetate	θ_u:43.0		
				θ_l:114.0		
			n-propyl acetate	θ_u:−80.0		
				θ_l:178.0		
	21.5 and 250	<1.1 and ∼2.0	dimethoxy methane/diethyl ether (330/70)	θ_u:−27.0		[6]
				θ_l:−5.0		
	11–270	1.15–1.94	1-chlorodecane	6.2	6.9	[158]
			trans decalin	22.8	6.7	

TABLE 15.4. *Continued.*

Polymer	$M_w \times 10^{-4}$	Dispersity (M_w/M_n)	Solvent	Theta temperature °C	$K_\theta.10^4$ [dl.g^{-1} (g mol wt)$^{-1/2}$]	Refs.
			1-chlorodecane/3-methyl cyclohexanol (78/22)	22.8	7.5	
			cyclohexane	35.0	8.4	
			1-chlorodecane/3-methyl cyclohexanol (75/25)	35.0	7.4	
			diethyl oxalate	59.6	7.2	
			1-chlorodecane/3-methyl cyclohexanol (50/50)	59.6	7.2	
			cyclohexanol	87.8	7.1	
			1-chlorodecane/3-methyl cyclohexanol (10/90)	87.8	7.05	
			3-methyl cyclohexanol	98.4	6.5	
	3.7–200		Tetrahydrofuran/water (92.3/7.7)	25.0		[159]
	2.2–137	1.18–1.48	cyclohexanol	79.0		[160]
	10, 39, and 60	<1.1	1-phenyl decane	28.0		[161]
	10.6–96	<1.09	cyclohexane	34.5	8.59	[162]
			diethyl malonate	36.0	7.4	[163]
	10.6–77	<1.09	toluene/methanol (77/23)	25.1	9.0	[164]
Polystyrene, atactic	3.7–95	1.03–1.19	1-chloro-*n*-decane	8.5	8.01	[165]
			cycloheptane	19.0	8.09	
			cyclooctane	20.5	8.16	
			cyclopentane	20.5	8.40	
			1-chloro-*n*-undecane	32.8	7.74	
			cyclohexane	34.5	8.37	
			diethyl malonate	34.5	7.53	
			diethyl oxalate	58.2	7.35	
			1-chloro-*n*-dodecane	58.6	7.40	
			dimethyl succinate	67.6	7.30	
			methylcyclohexane	68.0	7.82	
			ethylcyclohexane	75.0	7.80	
Polystyrene atactic	0.047–347	1.00–1.05	methyl acetate	41.5		[165a]
Polystyrene, comb	M_n (backbone): 9.5–9.7 M_n (branch): 6.5–35.8		cyclohexane	31–33		[166]
	15–850		benzene/methanol (78/22)	16–24		[83]
			cyclohexane	18–33		
			decalin	4.5		
			diethyl malonate	22		
	backbone: 15.1–86; branch: 17.8–362		cyclohexane	25–33		[167]
Polystyrene, trifunctional star	34.8		cyclohexane	34.8		[168]
Polystyrene, four-arm star	8.5–311		cyclohexane	34.5	6.6	[168a]
Polystyrene, six-arm star	5.6–320		cyclohexane	34.5	5.5	[168b]
Polystyrene, star, 9.4 br/mol	47		cyclohexane	22.0		[169]
Polystyrene (head-to-head)	8.28	2.0	cyclohexane	19.0		[170]
Polystyrene, deuterated	7.3	2.08	cyclohexane	30.0		[170]
Polystyrene, deuterated	11.5		cyclohexane	30.0		[16a]
Polystyrene, deuterated	11.5		cyclohexane-D_{12}	35, 36		[16a]
Polystyrene	13.0		cyclohexane-D_{12}	38, 40		[16a]
Polystyrene	2.5–1320	1.06–1.3	cyclohexane-D_{12}	38		[16b]

Θ_u: theta temperature corresponding to the upper critical solution temperature; Θ_l: corresponding to lower critical solution temperature (see Introduction).

TABLE 15.5. *Poly(acrylics)/ poly(methacrylics).*

Polymer	$M_w \times 10^{-4}$	Dispersity (M_w/M_n)	Solvent	Theta temperature °C	$K_\theta.10^4$ [dl.g^{-1} (g mol wt)$^{-1/2}$]	Refs.
Poly(acrylamide)	0.33–80		methanol/water (40/60)	20.0	12.7	[171]
	43–1000		methanol/water (41/59)	25.0	15.0	[172]
Poly(*N*-isopropylacrylamide)	13.8–910	1.2–1.4	water	30.6		[173]
Poly(2-acrylamido-2-methyl propane sulfonamide)	24.5–122.5		dioxane/water (18.5/81.5)	25.0	17.2	[174]
sodium poly(acrylate)	1.5–50		Aq. sodium bromide (1.504 m/L)	15.0	12.4	[175]
Poly(acrylonitrile), isotactic	M_η = 4.6–20.6		ethylene-carbonate	60.0	29.5	[176]
Poly(acrylonitrile)	113–297		ethylene carbonate/ water (85/15)	44.0	29.8	[177]
Poly(methacrylonitrile)	0.54–8.0		dimethylformamide	29.2	30.6	[178]
Poly(cetyl acrylate)	4.7–14 000	1.18–1.47	butyl acetate	15.2		[179]
Poly(decyl acrylate)			*i*-amylalcohol	−8.5		[180]
			n-butylalcohol	−24.5		
			ethylacetate	9–11		
Poly(ethyl acrylate)	M_η = 1.8–74		*n*-butanol	44.9		[181]
			ethanol	37.4		
			methanol	20.5		
			n-propanol	39.5		
	30–160	1.4	*n*-propanol	39.5	7.89	[182]
Poly(phenyl acrylate)	16–257	2.0	ethyl lactate	11.5	5.52	[183]
Poly(benzyl methacrylate)	19–170	1.4	cyclopentanol	73.2	2.8	[184]
Poly(*p*-biphenyl methacrylate)	8–108		benzene	11.0		[185]
Poly(*n*-butyl methacrylate)	30–260		isopropanol	21.5	2.95	[186]
	40–170		isopropanol	23.7	3.66	[187]
	11.7–64		isopropanol	25.0	4.2	[188]
		1.15	*n*-octane	68.9	3.81	[189]
			n-decane	84.8	4.07	
			n-dodecane	101.0	4.23	
			n-hexadecane	119.8	3.50	
			isopropanol	20.9	4.02	
			isobutanol	10.7	3.88	
Poly(tert-butyl methacrylate) (free radical, f_{mm}: 0.03; f_{mr+rm}: 0.38; f_{rr}: 0.59)	3.42–155	1.07–1.26	cyclohexane	10.0	4.89	[190]
			n-heptane	64.0	4.86	
Poly(tert-butyl methacrylate) (anionic, f_{mm}: 0.08; f_{mr+rm}: 0.47; f_{rr}: 0.45)	2.77–107	≤1.1	cyclohexane	10.0	6.08	[190,191]
Poly(4-*t*-butylcyclohexyl methacrylate)	23–110	1.4	*n*-butanol	25.0	3.1	[192]
Poly(*t*-butylcyclohexyl methacrylate)	15–193		*n*-butanol	40.0		[193]
Poly(2-*t*-butylphenyl methacrylate)	4.2–110	1.3	cyclohexane	18.4	3.5	[194]
Poly(4-*t*-butylphenyl methacrylate)	18–86	1.4	cyclohexane	25.0	4.4	[192]
Poly(*p*-*t*-butylphenyl methacrylate)	7–204	1.1–1.5	cyclohexane	25.0	4.5	[193a]
Poly(2-chloroethyl methacrylate) (f_{mm}: 0.07; f_{mr+rm}: 0.37; f_{rr}: 0.56)	3.2–54	1.2	*o*-dichlorobenzene	35.7	4.73	[194a]
Poly(cyclobutyl methacrylate) (f_{mm}: 0.03; f_{mr+rm}: 0.32; f_{rr}: 0.65)	4.83–31.1	∼1.1	*n*-butanol	37.5	4.8	[195]
Poly(cyclobutylmethyl methacrylate) (f_{mm}: 0.03; f_{mr+rm}: 0.30; f_{rr}: 0.65)	7.02–89.1	1.2–1.4	1-butanol	40.0	3.82	[196]
Poly(cyclododecyl methacrylate) (f_{mm}: 0.03; f_{mr+rm}: 0.34; f_{rr}: 0.63)	5.1–470	1.3	*n*-hexylacetate	35.0	3.3	[16,195]
Poly(cyclohexyl methacrylate) (f_{mm}: 0.13; f_{mr}: 0.36; f_{rr}: 0.51)	10–420	1.2	*n*-butanol	23.0	4.5	[197]

TABLE 15.5. *Continued.*

Polymer	$M_w \times 10^{-4}$	Dispersity (M_w/M_n)	Solvent	Theta temperature °C	$K_\theta.10^4$ [dl.g^{-1} (g mol wt)$^{-1/2}$]	Refs.
Poly(cyclohexyl methacrylate)	10–125	~1.1	*n*-butanol	22.5	4.52	[198]
			octane	83.4	4.07	[199]
			decane	93.6	4.24	
			dodecane	97.5	4.29	
			propanol	39.5	4.90	
			butanol	22.5	4.58	
			hexanol	9.2	4.39	
			octanol	17.9	4.53	
			nonanol	20.2	4.55	
			decanol	23.0	4.64	
Poly(cyclohexylmethyl methacrylate) (f_{mm}: 0.03; f_{mr+rm}: 0.30; f_{rr}: 0.65)	5.59–81.5	1.2–1.4	1-butanol	45.0	4.23	[196]
Poly(cyclopentyl methacrylate) (f_{mm}: 0.02; f_{mr+rm}: 0.32; f_{rr}: 0.66)	2.9–358		cyclohexane	36.0	4.6	[195]
Poly(cyclooctyl methacrylate) (f_{mm}: 0.03; f_{mr+rm}: 0.34; f_{rr}: 0.63)	6.6–460	1.3	2-butanol	45.0	3.7	[16]
Poly(2-decahydronaphthyl methacrylate)	7–320	1.4	dipropyl ketone	25.0	4.2	[200]
Poly(decyl methacrylate)	25–73	1.14–1.6	1-pentanol	9.6		[201]
Poly(*n*-decyl methacrylate) (f_{mm}: 0.02; f_{mr}: 0.29; f_{rr}: 0.69)	3–90	1.4	ethyl acetate	11.0	3.5	[202]
Poly(2,6-diisopropylphenyl methacrylate)	5.1–40	1.2–1.24	THF/water (90.9/9.1)	25	9.4	[203]
Poly(2,6-dimethylphenyl methacrylate)	3.4–82.3	1.05–1.27	toluene	25.0	7.7	[204]
			THF/water (90.6/9.4)	25.0		
Poly(diphenylmethyl methacrylate) (f_{mm}: 0.25; f_{mr+rm}: 0.46; f_{rr}: 0.29)	8.7–574	1.1–1.26	3-heptanone	45.0	3.31	[205]
Poly(*n*-docosyl methacrylate) (f_{mm}: 0.04; f_{mr}: 0.33; f_{rr}: 0.63)	6–140	1.4	amyl acetate	31.0	3.7	[202]
Poly(*n*-dodecyl methacrylate)	26–360		*n*-amylalcohol	29.5	3.5	[206]
Poly(dodecyl methacrylate)	15–800		*n*-amylalcohol	29.5	2.85	[207]
	26–360		isopropyl acetate	13.0	3.2	[208]
Poly(ethyl methacrylate)	20–263		MEK/isopropanol (12.5/87.5)	23.0	4.73	[209]
	22–127		isopropanol	36.9	4.8	[187]
			MEK/isopropanol (1/7)	23.0	4.7	
	59.7–191		*n*-butyl chloride	−13.3		[210]
			methyl *n*-butyl bromide	0		
			methyl *n*-propyl ketone	−0.5		
			m-xylene	−2.7		
	22.0		isopropanol	36.9	5.91	[211]
Poly(2-ethylbutyl methacrylate)	50–330	1.3	isopropanol	27.4	3.4	[212]
Poly(n-hexyl methacrylate)	64–400		isopropanol	32.6	4.3	[213]
Poly(hexyleneoxy phenylenecarboxy phenyleneoxymethylene methacrtylate) (side chain LC polymer)	16.2–128		toluene	15.5		[214]
Poly (2-hydroxyethyl methacrylate)			isopropanol	37.0	6.0	[215]
	10–500		urea/water (mol/L)			[216]
			4	10.0	2.5	
			6	27.2	4.0	
			8	52.5	4.25	
Poly (2-hydroxyethyl methacrylate) f_m>0.85	M_η:3.9–81.6		water	15.3	2.15	[217]
			ethanol	15.8	6.23	
			1-propanol	32.1	6.10	
			2-propanol	14.0	6.45	
			2-butanol	3.7	6.50	

TABLE 15.5. *Continued.*

Polymer	$M_w \times 10^{-4}$	Dispersity (M_w/M_n)	Solvent	Theta temperature °C	$K_\theta.10^4$ [dl.g^{-1} (g mol wt)$^{-1/2}$]	Refs.
Poly(*dl*-isobornyl methacrylate)	10–120	1.3	1-octanol	39.6	3.2	[218]
Poly(isobutyl methacrylate)	$M_n = 50.1$–115.9		2-hydroxy	19.5	2.65	[219]
Poly(isooctyl methacrylate)	84.7		acetone/*n*-heptane (64.1/35.9)	25.0		[220]
Poly(*n*-octyl methacrylate)	33–1300		*n*-butanol	16.8	2.7	[221]
Poly(*n*-lauryl methacrylate)	27–241		*n*-amyl alcohol	29.5	3.48	[208]
	M_n=16–122	1.63–1.69	*n*-amyl alcohol	29.5	3.48	[222]
Poly(5-*p*-methyl methacrylate) (f_m: 0.13)	13–230	1.5	methylpropyl ketone	25.0	4.4	[194]
Poly(1-{6-[4-(4-methoxyphenoxycarbonyl) phenoxy] hexyloxycarbonyl}-1-methylethylene)	8.9–107.6	1.22–1.56	toluene	17.0	2.69	[223]
Poly(methyl methacrylate)	30–284		MEK/isopropanol (50/50)	25.0	5.92	[223a]
	58–294		toluene/methanol (5/9)	26.2	5.59	[187]
	0.27–250	1.2–1.4	acetonitrile	30.0		[224]
	$M_\eta = 1$–260		acetonitrile	45.0	4.8 (average)	[225]
			diisopropyl ketone	46.0		
			2-ethyl butyraldehyde	22.0		
			4-heptanone	33.8		
			methyl neopentyl ketone	35.0		
			3-octanone	72.0		
	20, 130, and 650		*n*-butylchloride	35.0	5.3	[226]
			dioxane/*n*-hexane (59/41)	20.0		[86]
			n-hexane/3-methylbutanone (17/83)	20.0		[145]
	5.1 and	1.57 and	acetone/ethanol (47.7/52.3)	25.0	5.34	[227]
			acetone/methanol (78.1/21.9)	25.0	7.38	
	367	1.68	butanone/cyclohexane (59.5/40.5)	25.0	6.32	
			butanone/*n*-hexane (70.7/29.3)	25.0	7.61	
			butanone/isopropanol (58.2/41.8)	25.0	6.29	
			carbon tetrachloride/*n*-hexane (99.4/0.6)	25.0	7.21	
			carbon tetrachloride/methanol (53.3/46.7)	25.0	8.69	
			dioxan/cyclohexane (53.4/46.4)	25.0	7.70	
			cyclohexanol	77.6		[146]
			butanol	85.0		[181]
			propanol	83.2		
	M_η = 5– 110		cyclohexanone/isopropanol (51.6/48.4 w/w)	21–22	5.25	[228]
	3–30	<1.2	dioxane/cyclohexane (53/47)	20.0	6.4	[153]
			acetonitrile	38.0	5.25	[229]
	11–142	≤1.1	acetonitrile	32.3	4.0	[230]
			2-ethoxyethanol	37.8	5.6	
isotactic, $f_m = 0.9$	7.9–131.4		MEK/isopropanol (50/50)	30.3	9.0	[231]
			3-heptanone	40.0	8.7	
			n-propanol	75.9	7.61	
			p-cymene	152.1	5.66	
isotactic	M_η = 2.8– 52	1.0–1.5	acetonitrile	27.6	7.55	[232]
isotactic, $f_m = 0.94$	17.3		butanone/isopropanol (55/45)	25.0		[233]
			n-butyl chloride	26.5		

TABLE 15.5. *Continued.*

Polymer	$M_w \times 10^{-4}$	Dispersity (M_w/M_n)	Solvent	Theta temperature °C	$K_\theta.10^4$ [dl.g^{-1} (g mol wt)$^{-1/2}$]	Refs.
syndiotactic	16.8		butanone/isopropanol (55/45)	8.0		
			n-butyl chloride	35.0		
$f_r = 0.8$	$M_\eta = 379$		nitrobenzene/isopropanol (42.9/57.1 w/w)	18.0		[149]
			m-xylene	24.0		
syndiotactic, $f_r = 0.78$	8.57–162	1.06–1.24	3-octanone	72.0	5.52	[233a]
			4-heptanone	33.8	5.00	
syndiotactic, $f_r = 0.92$	3.4	1.17	acetonitrile	44.0		[234]
PMMA $f_r = 0.79$	0.06–158	1.00–1.09	acetonitrile	44.0		[234a]
			n-butyl chloride	40.8		
atactic, $f_m = 0.07$	6.6–171		MEK/isopropanol (50/50)	25.0	5.92	
			3-heptanone	33.7	6.31	
			n-propanol	84.4	6.79	
			p-cymene	159.7	5.75	
f_{rr}: 0.60; f_{mr+rm}: 0.34; f_{mm}: 0.06	14–274	1.3–2.8	acetonitrile	28.0	4.30	[235]
			butyl chloride	35.0	5.15	
			m-xylene	25.0	5.15	
f_{rr}:0.43; f_{mr+rm}:0.51; f_{mm}:0.06	16.9	≤1.1	acetonitrile/butanol (93/7)	25.0		[236]
			acetonitrile/methanol (90/10)	25.0		
			acetonitrile/pentyl acetate (93/7)	25.0		
			acetonitrile/*n*-propanol (93/7)	25.0		
atactic, $f_r = 0.79$	0.03–283	≤1.07	acetonitrile	44.0		[237–240]
			n-butyl chloride	40.8		
Poly(β-naphthyl methacrylate)	21–290	1.6	benzene	25.0	5.4	[200]
	5.9–275	∼1.5	tetralin	20.0	4.75	[241]
			toluene	55.0	3.9	
Poly(*n*-octadecyl methacrylate) (f_{mm}:0.02; f_{mr}:0.28; f_{rr}:0.70)	1.5–93	1.3	*n*-propyl acetate	36.0	3.7	[202]
Poly(octadecyl methacrylate)	62–320	1.7–2.2	butyl acetate	10.5		[242]
Poly(pentachlorophenyl methacrylate)	5.3–70	1.4	benzene	40.0	5.37	[243]
			ethylbenzene	25.0	5.37	
	$M_n = 1.6$, 14.4, and 23.9		benzene/toluene (10/90)	10.0		[244]
			benzene/toluene (50/50)	14.0		
			ethylbenzene	25.0		
			benzene/ethylbenzene (50/50)	30.0		
			chloroform	35.0		
			benzene	37.0		
	$M_n = 1.6$, 14.4, and 23.9		ethyl benzene	25.0		[193]
Poly(4-phenylbutyl-1-methacrylate) (f_{rr}:0.63; f_{mr+rm}:0.29; f_{mm}:0.08)	14.3–472	1.14–1.32	1-chloroundecane	23.0	3.37	[245]
Poly(2-phenylethyl-1-methacrylate) (f_{rr}:0.60; f_{mr+rm}:0.34; f_{mm}:0.06)	5.9–118	1.1–1.41	1-chloroheptane	27.5	3.67	[245]
Poly(phenylthiol methacrylate) (f_{mm}:0.16; f_{mr}:0.38; f_{rr}:0.46)	4.1–25	1.3	MEK	25.0	3.86	[246]
Poly(stearyl methacrylate) (f_{rr}:0.7; f_{mr+rm}:0.28; f_{mm}:0.02)	1.5–93.4	1.3	*n*-propyl acetate	36.0	3.71	[202]
Poly(tetrahydrofurfuryl methacrylate)	M_n = 16.9–61.3		2-hydroxymethyl tetrahydrofuran/methanol (80/20)	31.2	3.49	[247]

TABLE 15.5. *Continued.*

Polymer	$M_w \times 10^{-4}$	Dispersity (M_w/M_n)	Solvent	Theta temperature °C	$K_\theta.10^4$ [dl.g^{-1} (g mol wt)$^{-1/2}$]	Refs.
Poly(tetrahydro-4 *H*-pyranyl-2-methacrylate) ($f_{rr} = 0.5$)	4.8–84	1.2	isobutanol	30.5	3.3	[248]
Poly(4-(1,1,3,3-tetramethylbutyl)phenyl methacrylate) (f_{mm}:0.15; f_{mr}:0.4; f_{rr}:0.45)	M_n = 16–71		benzyl acetate	14.0	4.4	[249]
Poly(*n*-tridecyl methacrylate) (f_{mm}:0.02; f_{mr}:0.28; f_{rr}:0.70)	8–140	1.4	ethyl acetate	27.0	3.2	[202]

TABLE 15.6. *Other carbon chains.*

Polymer	$M_w \times 10^{-4}$	Dispersity (M_w/M_n)	Solvent	Theta temperature °C	$K_\theta.10^4$ [dl.g^{-1} (g mol wt)$^{-1/2}$]	Refs.
Poly(dibenzyl itaconate)	1.7–17	1.37	acetone	25.0	3.6	[250]
			THF/water (87.4/12.6)	25.0	5.02	
Poly (monobenzyl itaconate)	3.1–19.28		methanol	25.0		[251]
Poly(monocyclohexyl itaconate)	2.2–20.2	1.25–1.4	methanol	25.0	14.0	[251a]
Poly(monocyclopentyl itaconate)	2–21.5	1.1–1.4	methanol	25.0	12.0	[251a]
Poly(mono-methyl itaconate)	8.7–59.3	1.20–1.25	methanol	25.0	5.05	[252]
			2-ethoxyethanol	25.0	4.90	
Poly(mono-*n*-octyl itaconate)	7.8–110	1.25–1.30	2-propanol	30.0		[252a]
(di-methyl); (di-ethyl); (di-*n*-propyl); (di-*n*-butyl); (di-*n*-amyl); (di-*n*-hexyl); (di-*n*-heptyl); (di-*n*-octyl); (di-*n*-nonyl); (di-*n*-decyl); (di-*n*-undecyl) Polyitaconates	10–50		various common solvent mixtures	30.0		[253]
Poly[*N*-(*n*-octadecyl)maleimide]	$M_n = 0.12$–19		1-butanol	120.7	-	[254]
			1-decanol	39.5	18.2	
			1-hexanol	79.1	37.0	
			1-octanol	53.8	23.4	

TABLE 15.7. *Chains with silicon/oxygen/sulphur atoms.*

Polymer	$M_w \times 10^{-4}$	Dispersity (M_w/M_n)	Solvent	Theta temperature °C	$K_\theta.10^4$ [dl.g^{-1} (g mol wt)$^{-1/2}$]	Refs.
Poly(dimethylsiloxane)	55–120		MEK	20.0	7.8	[255]
			$C_8F_{18} + C_2Cl_4F_2$ (33.2/66.8)	22.5	10.6	[255]
	$M_n = 7.76$ and 10.7		benzene	−6.0		[256]
			bromobenzene	78.5		
			bromocyclohexane	28.0		
			n-butyl acetate	−38.0		
			chlorobenzene	−19.0		
			cyclohexane	−68.0		
			ethyl acetate	5.0		
			n-heptane	−173.0		
			n-hexane	−173.0		
			methylcyclohexane	−113.0		
			methylcyclopentane	−98.0		

TABLE 15.7. *Continued.*

Polymer	$M_w \times 10^{-4}$	Dispersity (M_w/M_n)	Solvent	Theta temperature °C	$K_\theta.10^4$ [dl.g^{-1} (g mol wt)$^{-1/2}$]	Refs.
			methyl ethyl ketone	20.0		
			n-nonane	−113.0		
			n-octane	−143.0		
			phenetole	89.5		
			n-propyl acetate	−28.0		
			toluene	−33.0		
			xylene	−48.0		
	$M_\eta = 1.9$–80		*o*-dichlorobenzene	87.0	8.1	[257]
	1.7–88.6		bromocyclohexane	28.0	7.9	[258]
Poly(methylphenylsiloxane)	5–150	1.05–1.12	diisobutylamine	30.4	5.15	[259]
Poly(methyl-3,3,3-trifluoropropylsiloxamer)	6–550	1.2	cyclohexyl acetate	25.0	4.10	[260]
			methyl hexanoate	72.8	4.45	
Poly(phenylsilasesquioxane)	1–900		mesitylene/toluene (30/70)	25.0		[261]
Poly(propylene sulphide) ($f_m = 0.55$)	17–74	1.1–2.38	*n*-heptane/toluene (31.5/68.5)	25.0	9.42	[262]

TABLE 15.8. *Poly(esters).*

Polymer	$M_w \times 10^{-4}$	Dispersity (M_w/M_n)	Solvent	Theta temperature °C	$K_\theta.10^4$ [dl.g^{-1} (g mol wt)$^{-1/2}$]	Refs.
Polyarylate (terephthalic/isophthalic: 50/50)	$M_\eta = 1.45$–6.84		dioxane/cyclohexane (68/32)	25.0	27.1	[263]
Poly(arylate-arylenesulphonoxide)			dioxane	23.5		[264]
Poly(ethylene terephthalate)	2.7–15.2		dichloroacetic acid/cyclohexane (60/40)	25.0	22.0	[265]
Poly(ε-caprolactone)	1.38; 9.73		benzene/*n*-hexane (85.1/14.9)	25.0		[266]
	and 42.1		chlorobenzene/*n*-hexane (70.2/29.8)	25.0		
			n-hexane/nitrobenzene (33.0/67.0)	25.0		
Polycarbonate, bisphenol-*A*	0.5–76		*n*-butyl benzyl ether	170.0	21.0	[267]
			dioxane/cyclohexane (64/36)	25.0		
	2.76–8.8	1.07–1.3	cyclohexane/dioxane (36.1/63.9 w/w)	25.0	23.4	[268]
Poly(*D*,*L*- β-methyl-β-propiolactone)	1.96–15.0		*n*-butyl chloride	13.0	10.0	[269]
Poly(octamethylene sebacate)	4.5		benzene/*n*-hexane (48.3/51.7)	25.0		[266]
			bromobenzene/*n*-hexane (45.0/55.0)	25.0		
			chlorobenzene/*n*-hexane (37.5/62.5)	25.0		
Poly[2,2-propane-*bis*(4-phenylthiocarbonate)]	0.94–19	1.2–1.4	chloroform/cyclohexane (76.5/23.5)	25.0	19.0	[267a]
Poly(tetramethylene adipate)	2.29		benzene/*n*-hexane (83.3/16.7)	25.0		[266]
			chlorobenzene/*n*-hexane (75.9/24.1)	25.0		
			n-hexane/nitrobenzene (43.3/56.7)	25.0		

TABLE 15.9. *Poly(acetals) and poly(ethers).*

Polymer	$M_w \times 10^{-4}$	Dispersity (M_w/M_n)	Solvent	Theta temperature °C	$K_\theta \cdot 10^4$ [dl.g^{-1} (g mol wt)$^{-1/2}$]	Refs.
Poly(2,6-dimethyl-1,4-phenylene oxide)	3.7	2.0	methylene chloride	69.0		[268a]
Poly(diphenylether sulfone)	6.3–14		DMF/methanol (83/17)	25.0	11.2	[269a]
			DMF/toluene (39/61)	30.0	12.4	
Poly(oxyethylene)	0.5–700		0.45M K_2SO_4/water	35	13.0	[8]
			0.39M $MgSO_4$/water	45	11.0	
	0.07–3.7		chloroform/*n*-hexane (47.4/52.6)	20.0		[114]
	0.4–3.8		acetonitrile/isopropyl ether (45/55)	20.0		[86]
			chloroform/*n*-hexane (54/46)	20.0		
			nitroethane/isopropyl ether (45/55)	20.0		
	0.16–103	1.05–1.25	methyl isobutyl ketone	50.0	12.0	[270]
			diethylene glycol diethyl ether	50.0	14.0	
	$M_n = 0.1$–0.6		water	5.0		[271]
	0.12–5.5	1.06–1.68	benzene/isooctane (100/48)	71.0		[272]
	2		water aqueous:	96.0		[273]
			2.4M NaCl	54.0	12.0	
			2.4M KCl	48.0	11.8	
			0.3M K_2CO3	56.0	14.6	
			0.3M Na_2SO_4	52.0	14.8	
			0.3M K_2SO_4	52.0	14.2	
			0.39M $MgSO_4$	43.0	17.8	
			0.45M $MgSO_4$	32.0	17.0	
			0.50$MgSO_4$	26.0	17.6	
	2	1.08	aqueous sodium acetate			[274]
			0.75M	75.0	-	
			1.50M	55.0	-	
			2.00M	45.0	-	
			3.00M	31.0	-	
			aqueous KF			
			0.30M	78.0	-	
			0.50M	66.0	-	
			0.80M	49.0	16.1	
			1.00M	38.0	-	
			aqueous $Na_2S_2O_3$			
			0.20M	74.0	-	
			0.30M	63.0	-	
			0.40M	52.0	-	
			0.50M	41.0	-	
			aqueous K_3PO_4			
			0.20M	63.0	-	
			0.30M	45.0	16.6	
			0.35M	38.0	-	
			0.40M	26.0	-	
			aqueous $ZnSO_4$			
			0.30M	54.0	16.8	
			0.35M	48.0	17.7	
			0.45M	35.0	18.7	
Poly(oxyethylethylene) (poly(1-butene oxide))	5.5–117	1.3–2.1	isopropanol	30.0	11.1	[275]
Poly(oxypropylene)	65–90		isooctane	50.0		[276]
Poly(oxytrimethylene)	$M_n = 6.5$–29.2		cyclohexane	27.0	8.89	[277]

TABLE 15.9. *Poly(acetals) and poly(ethers).*

Polymer	$M_w \times 10^{-4}$	Dispersity (M_w/M_n)	Solvent	Theta temperature °C	$K_\theta \cdot 10^4$ [dl.g^{-1} (g mol wt)$^{-1/2}$]	Refs.
Poly(tetrahydrofuran)	$M_n = 3.2$–11.8		toluene	−28.0		[278]
	3.5–110	∼1.04	ethyl acetate/*n*-hexane (22.7/77.3)	32–33		[279]
	$M_n = 3.8$–21		isopropanol	44.6	23.1	[280]
			diethyl malonate	33.5	24.3	
			ethyl acetate/*n*-hexane (22.7/77.3)	30.4	26.7	
	14		diethyl malonate	33.5		[281]

TABLE 15.10. *Poly(amides), poly(phosphates), poly(ureas), etc.*

Polymer	$M_w \times 10^{-4}$	Dispersity (M_w/M_n)	Solvent	Theta temperature °C	$K_\theta \cdot 10^4$ [dl.g^{-1} (g mol wt)$^{-1/2}$]	Refs.
Poly(*n*-*n*-hexyl isocyanate)	3.8–42.4		methanol/toluene (19.5/80.5)	25.0		[282]
			methanol/carbon tetrachloride (18.5/81.5)	25.0		
Nylon 6	15.1–19		*m*-cresol/decalin (25/75)	30.0		[281]
Nylon 66	3.2	1.88	KCl (2.3M) formic acid (90%)/water	25.0	19.2	[283, 284]
			KCl (2M)/formic acid (86.5%)/water	25.0		
	0.26–5.3		KCl (2.3M)/formic acid (90%)/water	25.0	25.3	[285]
	3.2	1.74	carbon tetra chloride/ cyclohexane/*m*-cresol (0.55/0.40/0.05)	25.0		[286]
Poly(*N*-methyldodecane lactam)	0.5–8		1,4-dioxane	30.5	21.5	[287]
Poly(trimethyl hexamethylene terephthalamide) (poly(iminoterephthaloylimino-2,2,4/2,4,4-trimethylhexamethylene)) (Trogamid T®)	1.16–27.6	1.3–2.0	aniline	142.0	14.8	[288]
			pyrroline	62.0	15.1	
Poly[ethylene methylene bis (4-phenyl carbamate)] (or poly(ethylene glycol co-4,4′-diphenylmethane diisocyanate))	0.33–4.2		acetone/dimethyl formamide (29/71)	25.0	30.0	[289]
Poly(heptamethylene urea)			dichloroacetic acid	46.0	35.4	[290]
			sulfuric acid (90%)	46.0	27.0	
Lithium polyphosphate	100		LiCl (0.4M)/water	20.0		[291]
Sodium polyphosphate	1.1–125		NaBr/water (0.415 mol/l)	25.0	4.94	[292]
Poly(diphenoxyphosphazene)	60	4.7	tetrahydrafuran	30		[292a]
Polyurethane (toluene-2,4-diisocyanate extended polypropylene glycol)	0.77–7.3		toluene/isooctane (1/1.4)	39.5	10.75	[293]

TABLE 15.11. *Copolymers.*

Polymer	$M_w \times 10^{-4}$	Dispersity (M_w/M_n)	Solvent	Theta temperature °C	$K_\theta \cdot 10^4$ [dl.g^{-1} (g mol wt)$^{-1/2}$]	Refs.
Poly(acrylonitrile-*co*-butadiene) (26/74 w/w)	5–130		cyclohexane/MEK (64/36)	20.0		[73]
(40/60 w/w)	3–80		cyclohexane/MEK (52.5/47.5)	22.0		
Poly(1-butenylene-*co*-vinylethylene) (high 1,2 polybutadiene with 1,2 = 43%; *trans:cis*=2.3:1)	0.88–22	1.01–1.1	1,4 dioxane	15.7	17.3	[88]
Poly(*p*-chlorostyrene-*co*-methyl methacrylate) (52/48)	15–120		trans-decalin/trichloro ethylene (78/22)	22.3	6.4	[294]
Poly(divinyl ether-*co*-maleic anhydride methyl ester) (1:2)	1.5–54.3		tetrahydrofuran	30.0	4.89	[295]
Poly(ethylene-*co*-butene) (40 ethyl branches/100 backbone carbons)	1.95–53.6	≤1.07	3-octanol	5.0	9.36	[70]
			2-octanol	29.0	8.92	
			1-octanol	59.0	8.37	
Poly(ethylene-*co*-isopropylethylene); *ethylene-1-butene copolymer, hydrogenated 1,2 polybutadiene*	0.92–22.8	1.01–1.09	*n*-hexyl acetate	65.0	18.8	[88]
Poly(ethylene-*alt*-propylene)	2.45–39.1	1.03–1.07	benzene	19.0	20.6	[67]
Poly(isobutyl vinyl ether-*alt*-maleic anhydride)	15.1–56		acetone	30.0	12.5	[296]
			NaCl/water (1.0 m/L)	25.0	21.0	
Poly(isopropenylethylene- *co*-1-methyl-1-vinylethylene) (high vinyl content polyisoprene with 1,2= 20–25%; 3,4 = 70–75%; 1,4<5%)	1.34–27	1.0–1.22	2-octanol	30.5	10.2	[88]
Poly(isopropylethylene-*co*-1-methyl-1-ethylethylene) (hydrogenated high vinyl polyisoprene)	1.5–27.8	1.03–1.18	2-octanol	26.2	8.3	[88]
Poly(*p*-isopropylstyrene -*co*-styrene)			dioxane/isopropanol			[86]
88/12			(37/63)	20.0		
56/44			(44/56)	20.0		
33/67			(48/52)	20.0		
Poly(*p*-methoxystyrene -*co*-styrene)						[297, 298]
26.4/73.6	6.1–66.5		isoamyl formate	30.5	9.6	
53/47	6.6–178.3		isoamyl formate	22.8	8.7	
			isoamyl propionate	18.1	8.4	
			n-esyl methyl ketone	27.0	9.5	
75.6/24.4	7.9–171.7		isoamyl formate	37.0	8.1	
			t-butyl benzene	12.5	7.5	
Poly(1-methyl-1 -butylene-*co*-isopropenylethylene) [essentially polyisoprene, with 1,4 (mostly *trans*) = 51%; 3,4 = 49%]	1.07–41.1	≤1.07	2-octanol	41.3	9.6	[88]
Poly(1-methyl-butylene -*co*-isopropylethylene) (hydrogenated polyisoprene)	1.13–42.5	1.02–1.08	2-octanol	55.3	9.1	[88]
Poly(1-(4-methylpentyl) -1-butylene-*co* -1-(1,5-dimethylhexyl)ethylene) (hydrogenated 1,4-polymyrcene)	7.1–63.2	≤1.1	2-octanol	51.0	7.14	[70]
Poly(styrene-*co*-acrylonitrile) (49/51)	27–224		ethyl acetate	43.0		[299]
Poly(styrene-*co*-butadiene) (23.9/76.1 w/w)	M_η = 15.2–86		methyl *n*-propyl ketone	21.0	22.0	[300]

TABLE 15.11. *Continued.*

Polymer	$M_w \times 10^{-4}$	Dispersity (M_w/M_n)	Solvent	Theta temperature °C	$K_\theta \cdot 10^4$ [dl.g^{-1} (g mol wt)$^{-1/2}$]	Refs.
			methyl isobutyl ketone	46.0		
Poly(styrene-*co*-butadiene) (25/75 w/w)	4–80		*n*-octane	21.0	16.2	[73]
Poly(styrene-*co*-isooctyl methacrylate) (80/20)	$M_n = 46.9$		butanone/methanol (99.4/0.6)	25.0		[220]
Poly(styrene-*co*-methylmethacrylate)						[145]
(76.3/23.7)			benzene/*n*-hexane (44/56)	20.0		
			benzene/isopropanol (57/43)	20.0		
			n-hexane/3-methyl butanone (40/60)	20.0		
(58.1/41.9)			benzene/*n*-hexane (51/49)	20.0		
			benzene/isopropanol (51/49)	20.0		
			n-hexane/3-methyl butanone (34/66)	20.0		
(42.3/57.7)			benzene/*n*-hexane (59/41)	20.0		
			benzene/isopropanol (48/52)	20.0		
			n-hexane/3-methyl butanone (29/71)	20.0		
(26.1/73.9)			benzene/*n*-hexane (62/38)	20.0		
			benzene/*n*-propanol (41/59)	20.0		
			n-hexane/3-methyl butanone (24/76)	20.0		
Poly(styrene-*co*-methyl methacrylate)						[301]
(29.3/70.7)	$M_n = 4.7$–59.2		2-ethoxy ethanol	40.0		
			cyclohexanol	68.0		
(56.2/43.8)	$M_n = 3.4$–50		2-ethoxy ethanol	58.4		
			cyclohexanol	61.3		
(70.2/29.8)	$M_n = 4.0$–43		2-ethoxy ethanol	72.8		
			cyclohexanol	63.0	8.75	
Poly(styrene-*co*-methyl methacrylate) (50/50)			cyclohexanol	68.6		[146]
Poly(trifluoro nitrosomethane-*co*-tetrafluoroethylene) (50/50)	28.3–197		trichlorotrifluoroethane (Freon 113)	35.0	3.8	[302]
Poly(arylate-*b*-arylenesulphonoxide) (50/50)			dioxane	23.5		[264]
Poly(isoprene-*b*-styrene) (80% *cis* 1,4 isoprene; 11.8–52.2% styrene)	$M_n = 10.4$–49.7	≤ 1.14	methyl ethyl ketone	44.0	11.63	[303]
Poly(styrene-*b*-methyl methacrylate) (50/50)			cyclohexanol	81.6		[146]
Poly(styrene-*b*-methyl methacrylate)						[301, 304]
(36/64)			2-ethoxy ethanol	69.5		
			cyclohexanol	80.5		
(49.6/50.4)	$M_n = 31.7$		2-ethoxy ethanol	81.0		
			cyclohexanol	81.3		
(73.2/26.8)			cyclohexanol	84.0		
(85.1/14.9)			cyclohexanol	84.0		

TABLE 15.11. *Continued.*

Polymer	$M_w \times 10^{-4}$	Dispersity (M_w/M_n)	Solvent	Theta temperature °C	$K_\theta \cdot 10^4$ [dl.g^{-1} (g mol wt)$^{-1/2}$]	Refs.
Poly(vinyl acetate-*g*-styrene)	copolymer: $M_n = 28.9$–60.3; backbone $M_n = 13.9$–29.2; vAc content 48.2–63.1%		diisobutyl ketone	136.5		[305]
			ethyl acetoacetate	108.5		

Starch and cellulose.

Polymer	$M_w \times 10^{-4}$	Dispersity (M_w/M_n)	Solvent	Theta temperature °C	$K_\theta \cdot 10^4$ [dl.g^{-1} (g mol wt)$^{-1/2}$]	Refs.
Amylose	15–220		0.5N potassium chloride	25		[306]
			0.5N potassium hydroxide	25		
Amylose tricarbanilate			cyclohexanol	120		[101a]
			diethylene glycol–diethylether	90		
Dextran	2.9–19.1 (M_n)		dimethyl sulfoxide	50.4, 54.4		[307]
			water	43.6, 44.8		[308]
			ethylene glycol	55		[309]
			methoxy ethylene glycol	60		[310]
	8.0	1.5	ethylene glycol	8		[311]
	40			15		
	200			34		
Cellulose, regenerated	8.0		8 wt% aq NaOH	40		[312]
Cellulose diacetate	5.9, 9.8, and 14.2	1.21, 1.27, 1.20	2-butanone	50		[313]
Cellulose diacetate			2-butanone	$\theta_l = 160$		[314]
				$\theta_u = 37$		
Cellulose diacetate	3.76–17.5	1.23–1.38	acetone	$\theta_l = 155$		[315]
Cellulose triacetate			benzyl alcohol	$\theta_l = 140$		[316]
				$\theta_u = 80$		
Cellulose triacetate			methylene chloride	27		[317]
Cellulose triacetate	1.4–12.6		nitromethane	47		[318]
Cellulose triacetate, hydrolyzed			epichlorohydrin	24		[319]
Hydroxypropyl cellulose	7.3 ($M_{s,D}$)	2		$\theta_l = 41$		[320]
Cellulose tributyrate	$M_n = 7.7 - 22.2$		dodecane/toluene: 75:25 (v/v)	122	8.4	[321]
Cellulose tricaproate	4.1–148	1.03–1.76	dimethyl			[322]
			formamide	41		
			dioxane/water: 100/7 (v/v)	43		
Cellulose tricaprylate	$M_n = 8.1 - 35$		dimethyl			[321]
			formamide	140	11.3	
			-phenylpropyl alcohol	48	12.9	
Cellulose tricarbanilate			anisole	94		[323]
			cyclohexanol	73		
Cellulose tricarbanilate			dibutyl ketone	45		[101a]
			diethylene glycol-dibutylether	45		
			cyclohexanol	80		
Pullulan	30	1.3–1.5	ethylene glycol	12		[311]
	51			16		
	100			24		

TABLE 15.11. *Continued.*

Effect of co-solutes.

Polymer	$M_w \times 10^{-4}$	Dispersity (M_w/M_n)	Solvent	Co-solute	Theta temperature °C	$K_\theta \cdot 10^4$ [dl.g^{-1} (g mol wt)$^{-1/2}$]	Refs.
Poly (*N*-vinyl pyrrolidone)	7.8	1.7	water	NaH_2PO_4			[324]
				0.8 m/L	77		
				1.2 m/L	35		
				KH_2PO_4			
				0.8 m/L	64		
				1.1 m/L	35		
				Na_2SO_4			
				0.35 m/L	73		
				0.5 m/L	36		
				Na_2CO_3			
				0.4 m/L	59		
				0.6 m/L	19		
				K_2CO_3			
				0.45 m/L	56		
				0.55 m/L	40		
				K_2HPO_4			
				0.4 m/L	55		
				0.5 m/L	33		
				Na_3PO_4			
				0.25 m/L	57		
				0.35 m/L	16		
				K_3PO_4			
				0.30 m/L	61		
				0.35 m/L	40		
Poly (*N*-vinyl-2-pyrrolidone)	7.8	1.7	water	benzoic acid 0.5×10^{-3}	73.8		[325]
				o-hydroxy benzoic acid 0.5×10^{-3}	72.5		
				p-hydroxy benzoic acid 0.5×10^{-3}	72		
				aniline 0.5×10^{-3}	77.8		
				o-hydroxy aniline 0.5×10^{-3}	73.4		
				p-hydroxy aniline 0.5×10^{-3}	73.2		
Poly (*N*-vinyl- 2-pyrrolidone)	7.8	1.7	water	hydroquinone			[326]
				1.0×10^{-2}M	54.5		
				1.5×10^{-2}M	35.3		
				catechol			
				1.0×10^{-2}M	66.4		
				3.0×10^{-2}M	27.3		
				phenol			
				1.0×10^{-2}M	69.5		
				2.0×10^{-2}M	55.5		
				resorcinol			
				4.0×10^{-3}	69.3		
				9.0×10^{-3}	45.4		
				phloroglucinol			
				1.5×10^{-3}	59.6		
				3.0×10^{-3}	42.4		
Cellulose I				Na Fe tartrate complex	20		[327]
Cellulose II				Na Fe tartrate complex	25		[327]

compositions of the monomers comprising the copolymer are given, where available. The range of molecular weight (M_w) of the samples used and the dispersity (M_w/M_n) are given in the second and third columns, respectively. In most of the cases, the value of M_w refers to the weight average molecular weight. In some papers, only the viscosity-average molecular weights (M_η) were specified, and in some others, only the number-average molecular weight (M_n) data have been reported. In these cases, it is so noted in the second column. In cases where the authors did not specify the molecular weight in tables or in the text, no attempt was made to read the molecular weight range from the figures in their papers. The solvent and the theta temperature are given in the fourth and fifth columns. In the case of mixed solvents, the composition is given in terms of the volume ratio (eg., v_1/v_2) of the two solvents. Occasionally, if an author had used weight fractions (w_1/w_2) of the two solvents, it is so indicated.

In addition, the values of K_Θ, corresponding to Eq. (15.6) above, are also given, if the authors had reported them. This would enable the reader to estimate the characteristic ratio C_∞ using Eq. (15.9), as shown in the examples above. It was felt that since a number of properties of polymers are being correlated to C_∞ as mentioned above, listing the values of K_Θ would be of value. Although under Θ conditions, the value of K_Θ should be the same at a given temperature irrespective of the solvent used, deviations have been discussed [15,17].

The value of K_Θ can also be deduced without resort to establishing Θ conditions, by measurements in good solvents and determining the expansion factor. Several methods have been used to this end [15,18,19]. These are dealt with in other chapters in this handbook.

ACKNOWLEDGMENTS

Support from the Natural Sciences and Engineering Research Council of Canada (NSERC) and Xerox Research Centre of Canada is gratefully acknowledged.

Related information can be found in Chapter 17.

REFERENCES

1. P. J. Flory, *Principles of Polymer Chemistry* (Cornell University Press, Ithaca, NY, 1953).
2. P. J. Flory, *Statistical Mechanics of Chain Molecules* (John Wiley, New York, 1969), Chapter II (republished by Hanser Publishers).
3. J. M. G. Cowie, *Polymers: Chemistry and Physics of Modern Materials* (Intertext Books, Buck, U.K., 1973), p. 140.
4. J. M. G. Cowie and I. J. McEwen, Polymer **16**, 933 (1975).
5. S. Saeki, S. Konno, N. Kuwahara *et al*., Macromolecules **7**, 521 (1974).
6. B. A. Wolf, H. F. Bieringer, and J. W. Breitenbach, Polymer **17**, 605 (1976).
7. T. G. Fox and P. J. Flory, J. Am. Chem. Soc. **73**, 1909 (1951).
8. F. E. Bailey and R. W. Callard, J. Appl. Polym. Sci. **1**, 56 (1959).
9. S. M. Aharoni, Macromolecules **16**, 1722 (1983).
10. T. A. Kavassalis and J. Noolandi, Macromolecules **21**, 2869 (1988).
11. T. A. Kavassalis and J. Noolandi, Macromolecules **22**, 2709 (1989).
12. R. P. Wool, Macromolecules **26**, 1564 (1993).
13. L. J. Fetters, D. J. Lohse, D. Richter, *et al*. Macromolecules **27**, 4639 (1994).
14. H. G. Elias, in *Polymer Handbook*, edited by J. Brandrup and E. H. Immergut (John Wiley, New York, 1989).
15. R. Jenkins and R. S. Porter, Adv. Polym. Sci. **36**, 1 (1980).
16. J. W. Mays and N. Hadjichristidis, J. Macromol. Sci., Rev. Macromol. Chem. Phys. **C28**, 371 (1988).

16a. C. Strazielle and H. Benoit, Macromolecules **8**, 203 (1975)

16b. A. Siporska, J. Szydlowski, and L. P. N. Rebelo, Phys. Chem. Chem. Phys. **5**, 2996 (2003)

17. A. Dondos and H. Benoit, Macromolecules **4**, 279 (1971).
18. M. Kurata and W. H. Stockmayer, Fortschr. Hochpolym. Forsch. **3**, 196 (1963).
19. J. M. G. Cowie, Polymer **7**, 487 (1966).
20. J. M. Barrales-Rienda and D. C. Pepper, Polymer **8**, 337, 351 (1967).
21. J. Moacanin, A. Rembaum, R. K. Laudenslager, *et al*. J. Macromol. Sci., Chem. **A1**, 1497 (1967).
22. W. R. Krigbaum, J. E. Kurz, and P. Smith, J. Phys. Chem. **65**, 1984 (1961).
23. K. S. Sastry and R. D. Patel, Eur. Polym. J. **5**, 79 (1969).
24. G. Moraglio, G. Gianotti, F. Zoppi, *et al*. Eur. Polym. J. **7**, 303 (1971).
25. G. Moraglio, G. Gianotti, and F. Danusso, Eur. Polym. J. **3**, 251 (1967).
26. L. D. Moore, J. Polym. Sci. **36**, 155 (1959).
27. C. J. Stacy and R. L. Arnett, J. Phys. Chem. **69**, 3109 (1965).
28. R. Chiang, J. Phys. Chem. **69**, 1645 (1965).
29. R. Chiang, J. Phys. Chem. **70**, 2348 (1966).
30. W. R. A. D. Moore and W. Millns, Br. Polym. J. **1**, 81 (1969).
31. A. Nakajima, H. Fujiwara, and F. Hamada, J. Polym. Sci., Part A-2 **4**, 507 (1966).
32. A. Nakajima, F. Hamada, and S. Hayashi, J. Polym. Sci., Part C **15**, 285 (1966).
33. T. Hama, K. Yamaguchi, and T. Suzuki, Makromol. Chem. **155**, 283 (1972).
34. A. M. Afifi-Effat, J. N. Hay, and M. Wiles, J. Polym. Sci., Polym. Letters **11**, 87 (1973).
35. J. N. Hay and M. Wiles, Br. Polym. J. **10**, 181 (1978).
36. F. Hamada, K. Fujisawa, and A. Nakajima, Polym. J. **4**, 316 (1973).
37. G. R. Williamson and A. Cervenka, Eur. Polym. J. **10**, 295 (1974).
38. H. L. Wagner and C. A. J. Hoeve, J. Polym. Sci., Polym. Symp. **54**, 327 (1976).
39. F. C. Lin, S. S. Stivala, and J. A. Biesenberger, J. Appl. Polym. Sci. **17**, 1073, 3465 (1973).
40. K. J. Ivin, H. A. Ende, and G. Meyerhoff, Polymer **3**, 129 (1962).
41. T. W. Bates, J. Biggins, and K. J. Ivin, Makromol. Chem. **87**, 180 (1965).
42. T. W. Bates and K. J. Ivin, Polymer **8**, 263 (1967).
43. W. R. Krigbaum and P. J. Flory, J. Polym. Sci. **11**, 37 (1953).
44. S. Newman, W. R. Krigbaum, C. Laugier, *et al*. J. Polym. Sci. **14**, 451 (1954).
45. H. G. Elias and F. W. Ibrahim, Makromol. Chem. **89**, 12 (1965).
46. G. Delmas and D. Patterson, Polymer **7**, 513 (1966).
47. T. Matsumoto, N. Nishioka, and H. Fujita, J. Polym. Sci., Part A-2 **10**, 23 (1972).
48. T. Tsuji and H. Fujita, Polym. J. **4**, 409 (1973).
49. F. Abe, Y. Einaga, and H. Yamakawa, Macromolecules **24**, 4423 (1991).
50. K. Akasaka, Y. Nakamura, T. Norisuye, *et al*. Polym. J. **26**, 363 (1994).
51. P. Neuenschwander and P. Pino, Makromol. Chem. **181**, 737 (1980).
52. S. Tani, F. Hamada, and A. Nakajima, Polym. J. **5**, 86 (1973).
53. J. B. Kinsinger and L. E. Ballard, J. Polym. Sci., Part A **3**, 3963 (1965).
54. W. R. Krigbaum and J. D. Woods, J. Polym. Sci., Part A **2**, 3075 (1964).
55. G. Moraglio and J. Brzezinski, J. Polym. Sci., Polym. Letters Ed. **2**, 1105 (1964).
56. J. E. Mark and P. J. Flory, J. Am. Chem. Soc. **87**, 1423 (1965).
57. G. Moraglio and G. Gianotti, Eur. Polym. J. **5**, 781 (1969).
58. T. Hirao, A. Teramoto, T. Sato, *et al*. Polym. J. **23**, 925 (1991).
59. H. Inagaki, T. Miyamoto, and S. Ohta, J. Phys. Chem. **70**, 3420 (1966).
60. J. B. Kinsinger and R. A. Wessling, J. Am. Chem. Soc. **81**, 2908 (1959).

61. H. Inagaki, H. Suzuki, M. Fujii, *et al*. J. Phys. Chem. **70**, 1718 (1966).
62. A. Nakajima and A. Saijyo, J. Polym. Sci., Part A-2 **6**, 735 (1968).
63. A. Nakajima and H. Fujiwara, J. Polym. Sci., Part A-2 **6**, 723 (1968).
64. G. Moraglio, G. Gianotti, and U. Bonicelli, Eur. Polym. J. **9**, 623 (1973).
65. J. B. Kinsinger and R. E. Hughes, J. Phys. Chem. **63**, 2002 (1959).
66. J. B. Kinsinger and R. E. Hughes, J. Phys. Chem. **67**, 1922 (1963).
67. J. W. Mays and L. J. Fetters, Macromolecules **22**, 921 (1989).
68. Z. Xu, J. W. Mays, C. Xuexin, *et al*. Macromolecules **18**, 2560 (1985).
69. S. Arichi, M. Y. Pedram, and J. M. G. Cowie, Eur. Polym. J. **15**, 113 (1979).
70. P. Hattam, S. Gauntlett, J. W. Mays, *et al*. Macromolecules **24**, 6199 (1991).
71. F. Danusso, G. Moraglio, and G. Gianotti, J. Polym. Sci. **51**, 475 (1961).
72. M. Abe and H. Fujita, J. Phys. Chem. **69**, 3263 (1965).
73. I. Ya. Poddubnyi, V. A. Grechanovskii, and A. V. Podalinskii, J. Polym. Sci., Part C **16**, 3109 (1968).
74. N. Hadjichristidis, Z. Xu, L. J. Fetters, *et al*. J. Polym. Sci., Polym. Phys. Ed. **20**, 743 (1982).
75. K. Yamamoto, N. Bessho, T. Shiibashi, *et al*. Polym. J. **13**, 555 (1981).
76. J. Ansorena, J. J. Iruin, and G. M. Guzmán, J. Polym. Sci., Polym. Phys. Ed. **18**, 173 (1980).
77. K. Hanafusa, A. Teramoto, and H. Fujita, J. Phys. Chem. **70**, 4004 (1966).
78. K. Kawahara, T. Norisuye, and H. Fujita, J. Chem. Phys. **49**, 4339 (1968).
79. T. Norisuye, K. Kawahara, A. Teramoto, *et al*. J. Chem. Phys. **49**, 4330 (1968).
80. G. V. Schulz and A. Mula, Makromol. Chem. **44**, 479 (1961).
81. C. F. Cornet and H. van Ballegooijen, Polymer **7**, 293 (1966).
82. F. J. Ansorena, L. M. Revuelta, G. M. Guzmán, *et al*. Eur. Polym. J. **18**, 19 (1982).
83. F. Candau, C. Strazielle, and H. Benoit, Makromol. Chem. **170**, 165 (1973).
84. N. Hadjichristidis and J. E. L. Roovers, J. Polym. Sci., Polym. Phys. Ed. **12**, 2521 (1974).
85. B. J. Bauer, N. Hadjichristidis, L. J. Fetters, *et al*. J. Am. Chem. Soc. **102**, 2410 (1980).
86. H. G. Elias and U. Gruber, Makromol. Chem. **78**, 72 (1964).
87. Z. Xu, J. W. Mays, C. Xuexin, *et al*. Macromolecules **18**, 2560 (1985).
88. J. W. Mays, N. Hadjichristidis, and L. J. Fetters, Macromolecules **17**, 2723 (1984).
89. G. Gianotti, U. Bonicelli, and D. Borghi, Makromol. Chem. **166**, 235 (1973).
90. Z. Xu, N. Hadjichristidis, J. M. Carella, *et al*. Macromolecules **16**, 925 (1983).
91. A. R. Shultz, J. Am. Chem. Soc. **76**, 3422 (1954).
92. M. Matsumoto and Y. Ohyanagi, J. Polym. Sci. **46**, 441 (1960).
93. M. Matsumoto and Y. Ohyanagi, J. Polym. Sci. **50**, S1 (1961).
94. M. Ueda and K. Kajitani, Makromol. Chem. **108**, 138 (1967).
95. S. Gundiah, Makromol. Chem. **104**, 196 (1967).
96. G. C. Berry, H. Nakayasu, and T. G. Fox, J. Polym. Sci., Polym. Phys. Ed. **17**, 1825 (1979).
97. H. Kaye and H. J. Chou, J. Polym. Sci., Polym. Phys. Ed. **13**, 477 (1975).
98. H. A. Dieu, J. Polym. Sci. **12**, 417 (1954).
99. E. Wolfram, Kolloid. Z., Z. Polym. **227**, 86 (1968).
100. I. Sakurada, A. Nakajima, and K. Shibatani, J. Polym. Sci., Part A **2**, 3545 (1964).
101. N. Kuwahara, S. Higashida, M. Nakata, *et al*. J. Polym. Sci., Part A-2 **7**, 285 (1969).
101a. W. Burchard, Polymer **10**, 467 (1969)
102. L. M. León, J. Galaz, L. M. Garcia, *et al*. Eur. Polym. J. **16**, 921 (1980).
103. C. González, F. Zamora, G. M. Guzmán, *et al*. Makromol. Chem. **185**, 339 (1984).
104. M. Sato, Y. Koshiishi, and M. Asahina, J. Polym. Sci., Polym. Letters **1**, 233 (1963).
105. A. Nakajima and K. Kato, Makromol. Chem. **95**, 52 (1966).
106. P. Adamski, Polym. Sci. U.S.S.R. **13**, 803 (1971).
107. W. Hayduk and H. A. Bromfield, J. Appl. Polym. Sci. **22**, 149 (1978).
108. P. Kratochvíl and D. Straková, Makromol. Chem. **154**, 325 (1972).
109. G. Sitaramaiah and D. Jacobs, Makromol. Chem. **164**, 237 (1973).
110. G. B. Gechele and L. Crescentini, J. Polym. Sci., Part A **3**, 3599 (1965).
111. C. Garbuglio, L. Crescentini, A. Mula, *et al*. Makromol. Chem. **97**, 97 (1966).
112. A. J. Hyde and R. B. Taylor, Polymer **4**, 1 (1963).
113. A. Dondos, Makromol. Chem. **135**, 181 (1970).
114. H. G. Elias, Makromol. Chem. **50**, 1 (1961).
115. R. Meza and L. Gargallo, Eur. Polym. J. **13**, 235 (1977).
116. H. Eisenberg and D. Woodside, J. Chem. Phys. **36**, 1844 (1962).
117. H. G. Elias, Makromol. Chem. **54**, 78 (1962).
118. Z. Küçüükyavuz and S. Küçuükyavuz, Eur. Polym. J. **14**, 867 (1978).
119. S. Küçuükyavuz and Z. Küçuükyavuz, Polym. Commun. **31**, 35 (1990).
120. J. W. Mays, S. Nan, and D. Whitfield, Macromolecules **24**, 315 (1991).
121. J. W. Mays, W. M. Ferry, N. Hadjichristidis, W. G. Funk, and L. J. Fetters, Polymer **27**, 129 (1986).
122. A. George, W. W. Wilson, J. S. Lindner, *et al*. Polymer **35**, 600 (1994).
123. Y. Izumi and Y. Miyake, Polym. J. **3**, 647 (1972).
124. Y. Izumi and Y. Miyake, Polym. J. **4**, 205 (1973).
125. I. Hernández-Fuentes and M. G. Prolongo, Eur. Polym. J. **15**, 571 (1979).
126. S. Ya. Magarik, A. P. Filippov, and N. V. D'yakonova, Polym. Sci. U.S.S.R. **29**, 772 (1987).
127. V. E. Eskin and L. N. Andreeva, J. Polym. Sci. **56**, S39 (Russian Abstracts) (1962).
128. M. Pizzoli, G. Stea, G. Ceccorulli, *et al*. Eur. Polym. J. **6**, 1219 (1970).
129. A. Mattiussi, E. Conti, and G. B. Gechele, Eur. Polym. J. **8**, 429 (1972).
130. J. M. G. Cowie, S. Bywater, and D. J. Worsfold, Polymer **8**, 105 (1967).
131. J. M. G. Cowie and S. Bywater, J. Polym. Sci., Part A-2 **6**, 499 (1968).
132. I. Noda, K. Mizutani, T. Kato, *et al*. Macromolecules **3**, 787 (1970).
133. J. W. Mays, N. Hadjichristidis, W. W. Graessley, *et al*. J. Polym. Sci., Polym. Phys Ed. **24**, 2553 (1986).
133a. J. Li, S. Harville, and J. W. Mays, Macromolecules **30**, 466 (1997)
133b. T. Kawaguchi, M. Osa, T. Yoshizaki, and H. Yamakawa, Macromolecules **37**, 2240 (2004)
134. G. Tanaka, S. Imai, and H. Yamakawa, J. Chem. Phys. **52**, 2639 (1970).
135. T. G. Fox and P. J. Flory, J. Amer. Chem. Soc. **73**, 1915 (1951).
136. S. N. Chinai, P. C. Scherer, C. W. Bondurant, and D. W. Levi, J. Polym. Sci. **22**, 527 (1956).
137. U. Bianchi and V. Magnasco, J. Polym. Sci. **41**, 177 (1959).
138. R. Okada, Y. Toyoshima, and H. Fujita, Makromol. Chem. **59**, 137 (1963).
139. T. Homma, K. Kawahara, H. Fujita, *et al*. Makromol. Chem. **67**, 132 (1963).
140. T. A. Orofino and J. W. Mickey, J. Chem. Phys. **38**, 2512 (1963).
141. G. V. Schulz and H. Baumann, Makromol. Chem. **60**, 120 (1963).
142. H. G. Elias and O. Etter, Makromol. Chem. **66**, 56 (1963).
143. T. A. Orofino and A. Ciferri, J. Phys. Chem. **68**, 3136 (1964).
144. T. Altares, D. P. Wyman, and V. R. Allen, J. Polym. Sci., Part A **2**, 4533 (1964).
145. U. Gruber and H. G. Elias, Makromol. Chem. **86**, 168 (1965).
146. D. Froelich and H. Benoit, Makromol. Chem. **92**, 224 (1966).
147. G. C. Berry, J. Chem. Phys. **44**, 4550 (1966).
148. G. C. Berry, J. Chem. Phys. **46**, 1338 (1967).
149. O. Quadrat and M. Bohdanecký, J. Polym. Sci., Part A-2 **5**, 1309 (1967).
150. A. Kotera, H. Matsuda, K. Konishi, *et al*. J. Polym. Sci., Part C **23**, 619 (1968).
151. J. M. G. Cowie, J. Polym. Sci., Part C **23**, 267 (1968).
152. C. Reiss and H. Benoit, J. Polym. Sci., Part C **16**, 3079 (1968).

153. A. Dondos and H. Benoit, J. Polym. Sci., Polym. Letters **7**, 335 (1969).
154. A. Afifi-Effat and J. N. Hay, Br. Polym. J. **8**, 91 (1976).
155. M. Fukuda, M. Fukutomi, Y. Kato, *et al*. J. Polym. Sci., Polym. Phys. Ed. **12**, 871 (1974).
156. S. Saeki, N. Kuwahara, S. Konno, *et al*. Macromolecules **6**, 589 (1973).
157. N. Kuwahara, S. Saeki, S. Konno, *et al*. Polymer **15**, 66 (1974).
158. A. Bazuaye and M. B. Huglin, Polymer **20**, 44 (1979).
159. T. Spychaj, D. Lath, and D. Berek, Polymer **20**, 437 (1979).
160. J. N. Hay and P. A. Fitzgerald, J. Polym. Sci., Polym. Sci., Polym. Chem. Ed. **18**, 1079 (1980).
161. H. Geerissen and B. A. Wolf, Makromol. Chem., Rapid Commun. **3**, 17 (1982).
162. A. A. Abdel-Azim and M. B. Huglin, Polymer **24**, 1429 (1983).
163. M. Bohdanecký and D. Berek, Makromol. Chem., Rapid Commun. **6**, 275 (1985).
164. A. A. Abdel-Azim, Macromol. Chem. Phys. **195**, 159 (formerly Makromol. Chem.) (1994).
165. J. W. Mays, N. Hadjichristidis, and L. J. Fetters, Macromolecules **18**, 2231 (1985).
165a. M. Yamada, T. Yoshizaki, and H. Yamakawa, Macromolecules **31**, 7728 (1998)
166. I. Noda, T. Horikawa, T. Kato, *et al*. Macromolecules **3**, 795 (1970).
167. J. Roovers, Polymer **20**, 843 (1979).
168. T. A. Orofino and F. Wenger, J. Phys. Chem. **67**, 566 (1963).
168a. M. Okumoto, K. Terao, Y. Nakamura, T. Norisuye, and A. Teramoto, Macromolecules **30**, 7493 (1997)
168b. M. Okumoto, Y. Tasaka, Y. Nakamura, and T. Norisuye, Macromolecules **32**, 7430 (1999)
169. C. Tsitsilianis, E. Pierri, and A. Dondos, J. Polym. Sci., Polym. Lett. Ed. **21**, 685 (1983).
170. C. Strazielle, H. Benoit, and O. Vogl, Eur. Polym. J. **14**, 331 (1978).
171. M. Bohdanecký, V. Petrus, and B. Sedláček, Makromol. Chem. **184**, 2061 (1983).
172. A. L. Izyumnikov, L. V. Mineyev, V. A. Maslennikov, *et al*. Polym. Sci. U.S.S.R. **30**, 1062 (1988).
173. K. Kubota, S. Fujishige, and I. Ando, Polym. J. **22**, 15 (1990).
174. S. R. Gooda and M. B. Huglin, Polymer **34**, 1913 (1993).
175. A. Takahashi and M. Nagasawa, J. Am. Chem. Soc. **86**, 543 (1964).
176. K. Kamide and T. Terakawa, Makromol. Chem. **155**, 25 (1972).
177. B. Simionescu, S. Ioan, M. Bercea, *et al*. Eur. Polym. J. **27**, 589 (1991).
178. C. G. Overberger, E. M. Pearce, and N. Mayes, J. Polym. Sci. **34**, 109 (1959).
179. V. N. Tsvetkov, L. N. Andreyeva, Ye. V. Korneyeva, *et al*. Polym. Sci. U.S.S.R. **13**, 2501 (1971).
180. V. N. Tsvetkov, L. N. Andreyeva, Ye. V. Korneyeva, *et al*. Polym. Sci. U.S.S.R. **14**, 1944 (1972).
181. J. Llopis, A. Albert, and P. Usobiaga, Eur. Polym. J. **3**, 259 (1967).
182. K. S. V. Srinivasan and M. Santappa, Polymer **14**, 5 (1973).
183. F. Hooshmand-Mozaffar, M. K. Hoseinalizadeh-Khorasani, and M. B. Huglin, Polymer **21**, 413 (1980).
184. R. W. Richards, Polymer **18**, 114 (1977).
185. N. Hadjichristidis, Polymer **16**, 848 (1975).
186. S. N. Chinai and R. A. Guzzi, J. Polym. Sci. **21**, 417 (1956).
187. S. N. Chinai and R. J. Valles, J. Polym. Sci. **39**, 363 (1959).
188. R. Van Leemput and R. Stein, J. Polym. Sci., Part A **2**, 4039 (1964).
189. D. Lath and M. Bohdanecký, J. Polym. Sci., Polym. Letters Ed. **15**, 555 (1977).
190. A. Karandinos, S. Nan, J. W. Mays, *et al*. Macromolecules **24**, 2007 (1991).
191. A. Karandinos, J. W. Mays, and N. Hadjichristidis, Polym. Bulletin **24**, 251 (1990).
192. L. Gargallo, Colloid Polym. Sci. **253**, 288 (1975).
193. D. Radić and L. Gargallo, Polymer **22**, 410 (1981).
193a. L. Gargallo, D. Radić, and I. Katime, Eur. Polym. J. **16**, 383 (1980).
194. M. Tricot, J. P. Bleus, J.-P. Riga, *et al*. Makromol. Chem. **175**, 913 (1974).
194a. J. W. Mays, W. Ferry, N. Hadjichristidis, *et al*. Macromolecules **18**, 2330 (1985).
195. E. Siakali-Kioulafa, N. Hadjichristidis, and J. W. Mays, Macromolecules **22**, 2059 (1989).
196. D. Pateropoulou, E. Siakali-Kioulafa, N. Hadjichristidis, *et al*. Macromol. Chem. Phys. **195**, 173 (1994). (Formerly Makromol. Chem.)
197. N. Hadjichristidis, M. Devaleriola, and V. Desreux, Eur. Polym. J. **8**, 1193 (1972).
198. I. A. Katime and G. Sanchez, Eur. Polym. J. **11**, 223 (1975).
199. K. Sedlak and D. Lath, Chem. Abstracts **89**, 180549e (1978).
200. N. Hadjichristidis and V. Desreux, J. Macromol. Sci., Chem. **A6**, 1227 (1972).
201. F. K. Herold and B. A. Wolf, Makromol. Chem. **184**, 2539 (1983).
202. Z. Xu, N. Hadjichristidis, and L. J. Fetters, Macromolecules **17**, 2303 (1984).
203. L. Gargallo, N. Hamidi, and D. Radić, Polym. Int. **24**, 1 (1991).
204. L. Gargallo, N. Hamidi, and D. Radić, Polymer **31**, 924 (1990).
205. J. W. Mays, N. Hadjichristidis, and J. S. Lindner, J. Polym. Sci., Polym. Phys. Ed. **28**, 1881 (1990).
206. S. N. Chinai and R. A. Guzzi, J. Polym. Sci. **41**, 475 (1959).
207. U. Moritz and G. Meyerhoff, Makromol. Chem. **139**, 23 (1970).
208. H. T. Lee and D. W. Levi, J. Polym. Sci. **47**, 449 (1960).
209. S. N. Chinai and R. J. Samuels, J. Polym. Sci. **19**, 463 (1956).
210. P. Vasudevan and M. Santappa, Makromol. Chem. **137**, 261 (1970).
211. A. Kuntman and B. M. Baysal, Polymer **34**, 3723 (1993).
212. F. E. Didot, S. N. Chinai, and D. W. Levi, J. Polym. Sci. **43**, 557 (1960).
213. S. N. Chinai, J. Polym. Sci. **25**, 413 (1957).
214. H. G. Ohm, R. G. Kirste, and R. C. Oberthür, Makromol. Chem. **189**, 1387 (1988).
215. M. Bohdanecký and Z. Tuzar, Coll. Czech. Chem. Cummun. **34**, 3318 (1969) (quoted in Ref. 16).
216. K. Dušek, M. Bohdanecký, and E. Prokopová, Eur. Polym. J. **10**, 239 (1974).
217. S. H. Oh and M. S. Jhon, J. Polym. Sci., Polym. Chem. Ed. **27**, 1731 (1989).
218. N. Hadjichristidis, J. W. Mays, W. Ferry, *et al*. J. Polym. Sci., Polym. Phys. Ed. **22**, 1745 (1984).
219. M. M. Zafar, R. Mahmood, and S. A. Wadood, Makromol. Chem. **160**, 313 (1972).
220. M. Kalfus and J. Mitus, J. Polym. Sci., Part A-1 **4**, 953 (1966).
221. S. N. Chinai, A. L. Resnick, and H. T. Lee, J. Polym. Sci. **33**, 471 (1958).
222. D. W. Levi, H. T. Lee, and R. J. Valles, J. Polym. Sci. **62**, S163 (1962).
223. L. Fritz and J. Springer, Makromol. Chem. **194**, 2047 (1993).
223a. S. N. Chinai and C. W. Bondurant J. Polym. Sci. **22**, 555 (1956).
224. E. Cohn-Ginsberg, T. G. Fox, and H. F. Mason, Polymer **3**, 97 (1962).
225. T. G. Fox, Polymer **3**, 111 (1962).
226. H. Lütje and G. Meyerhoff, Makromol. Chem. **68**, 180 (1963).
227. H. G. Elias and O. Etter, Makromol. Chem. **89**, 228 (1965).
228. O. Quadrat, M. Bohdanecký, and P. Munk, J. Polym. Sci., Part C **16**, 95 (1967).
229. K. Kamada and H. Sato, Polym. J. **2**, 593 (1971).
230. M. Guaita, O. Chiantore, and W. Burchard, Makromol. Chem. **192**, 2333 (1991).
231. I. Sakurada, A. Nakajima, O. Yoshizaki, *et al*. Kolloid-Z. **186**, 41 (1962).
232. S. Krause and E. Cohn-Ginsberg, J. Am. Chem. Soc. **67**, 1479 (1963).
233. G. V. Schulz, W. Wunderlich, and R. Kirste, Makromol. Chem. **75**, 22 (1964).
233a. J. M. Mays, S. Nan, W. Yunan, J. Li, and N. Hadjichristidis, Macromolecules **24**, 4469 (1991).
234. T. Yoshizaki, H. Hayashi, and H. Yamakawa, Macromolecules **27**, 4259 (1994).
234a. F. Abe, K. Horita, Y. Einaga, H. Yamakawa, Macromolecules **27**, 725 (1994)
235. O. Quadrat, M. Bohdanecký, and L. Mrkvičková, Makromol. Chem. **182**, 445 (1981).
236. R. M. Masegosa, M. G. Prolongo, I. Hernández-Fuentes, *et al*. Macromolecules **17**, 1181 (1984).
237. Y. Tamai, T. Konishi, Y. Einaga, *et al*. Macromolecules **23**, 4067 (1990).
238. Y. Fujii, Y. Tamai, T. Konishi, *et al*. Macromolecules **24**, 1608 (1991).

239. Y. Takaeda, T. Yoshizaki, and H. Yamakawa, Macromolecules **26**, 3742 (1993).
240. F. Abe, K. Horita, Y. Einaga, *et al*. Macromolecules **27**, 725 (1994).
241. J. Niezette, N. Hadjichristidis, and V. Desreux, Eur. Polym. J. **13**, 41 (1977).
242. M. Ricker and M. Schmidt, Makromol. Chem. **192**, 679 (1991).
243. M. Becerra, D. Radić, and L. Gargallo, Makromol. Chem. **179**, 2241 (1978).
244. D. Radić and L. Gargallo, Makromol. Chem. **180**, 1329 (1979).
245. Y-J. Chen, J. W. Mays, and N. Hadjichristidis, J. Polym. Sci., Polym. Phys. Ed. **32**, 715 (1994).
246. D. Kokkiaris, C. Touloupis, and N. Hadjichristidis, Polymer **22**, 63 (1981).
247. M. M. Zafar and R. Mahmood, Makromol. Chem. **175**, 903 (1974).
248. N. Hadjichristidis, J. W. Mays, R. D. Vargo, *et al*. J. Polym. Sci., Polym. Phys. Ed. **21**, 189 (1983).
249. T. Ojeda, D. Radić, and L. Gargallo, Makromol. Chem. **181**, 2237 (1980).
250. M. Yazdani-Pedram, L. Gargallo, and D. Radić, Eur. Polym. J. **21**, 461 (1985).
251. M. Yazdani-Pedram, and A. Horta, Eur. Polym. J. **25**, 1059 (1989).
251a. L. Gargallo and D. Radić, J. Macromol. Sci., Phys. **B33**, 75 (1994).
252. L. Gargallo and D. Radić, Makromol. Chem. **186**, 1289 (1985).
253. J. Veličković, V. Juraničovà, and J. Filipović, Angew. Makromol. Chem. **24**, 77 (1972).
254. J. M. Barrales-Rienda, C. Romero Galicia, J. J. Freire, *et al*. Macromolecules **16**, 1707 (1983).
255. V. Crescenzi and P. J. Flory, J. Am. Chem. Soc. **86**, 141 (1964).
256. N. Kuwahara and M. Kaneko, Makromol. Chem. **82**, 205 (1965).
257. J. V. Dawkins and M. Hemming, Makromol. Chem. **155**, 75 (1972).
258. J. G. Zilliox, J. E. L. Roovers, and S. Bywater, Macromolecules **8**, 573 (1975).
259. R. R. Buch, H. M. Klimisch, and O. K. Johannson, J. Polym. Sci., Part A-2 **8**, 541 (1970).
260. R. R. Buch, H. M. Klimisch, and O. K. Johannson, J. Polym. Sci., Part A-2 **7**, 563 (1969).
261. J. Kovář, L. Mrkvičková-Vaculová, and M. Bohdanecký, Makromol. Chem. **176**, 1829 (1975).
262. D. W. Nash and D. C. Pepper, Polymer **16**, 105 (1975).
263. J. I. Eguiazábal, J. Areizaga, J. J. Iruin, *et al*. Eur. Polym. J. **21**, 711 (1985).
264. I. A. Ronova, M. A. Ponomareva, L. V. Dubrovina, *et al*. Int. Polym. Sci. Tech. **13**, T90 (1986).
265. Z. Tuzar, V. Vošický, M. Bohdanecký, *et al*. Makromol. Chem. **180**, 1399 (1979).
266. R. Knecht and H. G. Elias, Makromol. Chem. **157**, 1 (1972).
267. G. C. Berry, H. Nomura, and K. G. Mayhan, J. Polym. Sci., Part A-2 **5**, 1 (1967).
267a. L. Gargallo, E. Soto, F. R. Diaz, *et al*. Eur. Polym. J. **23**, 571 (1987).
268. W. R. Moore and M. Uddin, Eur. Polym. J. **5**, 185 (1969).
268a. A. R. Shultz and C. R. McCullough, J. Polym. Sci., Part A-2 **7**, 1577 (1969).
269. T. Hirosye, Y. Einaga, and H. Fujita, Polym. J. **11**, 819 (1979).
269a. Y. H. Park and D. C. Lee, Polymer (Korea) **12**, 749 (1988).
270. D. R. Beech and C. Booth, J. Polym. Sci., Part A-2 **7**, 575 (1969).
271. B. Chew and A. Couper, J. Chem. Soc., Faraday Trans I **72**, 382 (1976).
272. J. N. Hay and A. M. Afifi-Effat, Br. Polym. J. **9**, 1 (1977).
273. E. A. Boucher and P. M. Hines, J. Polym. Sci., Polym. Phys. Ed. **16**, 501 (1978).
274. M. Ataman and E. A. Boucher, J. Polym. Sci., Polym. Phys. Ed. **20**, 1585 (1982).
275. C. Booth and R. Orme, Polymer **11**, 626 (1970).
276. G. Allen, C. Booth, and C. Price, Polymer **7**, 167 (1966).
277. D. S. Chiu, Y. Takahashi, and J. E. Mark, Polymer **17**, 670 (1976).
278. S. M. Ali and M. B. Huglin, Makromol. Chem. **84**, 117 (1965).
279. M. Kurata, H. Utiyama, and K. Kamada, Makromol. Chem. **88**, 281 (1965).
280. J. M. Evans and M. B. Huglin, Makromol. Chem. **127**, 141 (1969).
281. N. Howard, M. B. Huglin, and R. W. Richards, J. Appl. Polym. Sci. **16**, 1525 (1972).
282. M. N. Berger and B. M. Tidswell, J. Polym. Sci., Polym. Symp. **42**, 1063 (1973).
283. P. R. Saunders, J. Polym. Sci. **57**, 131 (1962).
284. P. R. Saunders, J. Polym. Sci., Part A **2**, 3765 (1964).
285. H. G. Elias and R. Schumacher, Makromol. Chem. **76**, 23 (1964).
286. J. O. Threlkeld and H. A. Ende, J. Polym. Sci., Part A-2 **4**, 663 (1966).
287. R. Puffr, Z. Tuzar, L. Mrkvičková, *et al*. Makromol. Chem. **184**, 1957 (1983).
288. J. Herold and G. Meyerhoff, Eur. Polym. J. **15**, 525 (1979).
289. H. C. Beachell and J. C. Peterson, J. Polym. Sci., Part A-1 **7**, 2021 (1969).
290. J. Feisst and H. G. Elias, Makromol. Chem. **82**, 78 (1965).
291. G. Saini and L. Trossarelli, J. Polym. Sci. **23**, 563 (1957).
292. U. P. Strauss and P. L. Wineman, J. Am. Chem. Soc. **80**, 2366 (1958).
292a. R. E. Singler, G. L. Hagnauer, N. S. Schneider, B. R. Laliberte, R. E. Sacher, and R. W. Matton, J. Polym. Sci. Polym. Chem. Ed. **12**, 433 (1974)
293. J. Moacanin, J. Appl. Polym. Sci. **1**, 272 (1959).
294. R. B. Mohite, S. Gundiah, and S. L. Kapur, Makromol. Chem. **108**, 52 (1967).
295. R. J. Samuels, Polymer **18**, 452 (1977).
296. S. Miyamoto, Y. Ishii, and H. Ohnuma, Makromol. Chem. **182**, 483 (1981).
297. M. Pizzoli, G. Ceccorulli, and G. Stea, Makromol. Chem. **164**, 273 (1973).
298. M. Pizzoli and G. Ceccorulli, Eur. Polym. J. **8**, 769 (1972).
299. P. V. Mangalam and V. Kalpagam, J. Polym. Sci., Polym. Phys. Ed. **20**, 773 (1982).
300. T. Homma, K. Kawahara, and H. Fujita, J. Appl. Polym. Sci. **8**, 2853 (1964).
301. T. Kotaka, H. Ohnuma, and Y. Murakami, J. Phys. Chem. **70**, 4099 (1966).
302. G. A. Morneau, P. I. Roth, and A. R. Shultz, J. Polym. Sci. **55**, 609 (1961).
303. J. R. Urwin and M. Girolamo, Makromol. Chem. **150**, 179 (1971).
304. T. Kotaka, H. Ohnuma, and H. Inagaki, Polymer **10**, 517 (1969).
305. F. Horii, Y. Ikada, and I. Sakurada, J. Polym. Sci., Polym. Chem. Ed. **12**, 323 (1974).
306. W. W. Everett and J. F. Foster, J. Am. Chem. Soc. **81**, 3459, 3464 (1959).
307. E. Çatiker and A. Gűner, Polym. Bull. **41**, 223 (1998).
308. A. Gűner, J. Appl. Polym. Sci. **72**, 871 (1999); A. Gűner and G. Kibarer, Eur. Polym. J. **37**, 619 (2001)
309. E. Çatiker and A. Gűner, Eur. Polym. J. **36**, 2143 (2000)
310. A. Gűner and E. Çatiker, J. Appl. Polym. Sci. **82**, 948 (2001)
311. E. Nordmeier, J. Phys. Chem. **97**, 5770 (1993)
312. K. Kamide, M. Saito, and K. Kowsaka, Polym. J. **19**, 1173 (1987)
313. H. Suzuki, Y. Muraoka, M. Saito, and K. Kamide, Eur. Polym. J. **18**, 831 (1982)
314. H. Suzuki, Y. Muraoka, M. Saitoh, and Kamide, Br. Polym. J. **14**, 23 (1982)
315. H. Suzuki, K. Kamide, and M. Saitoh, Eur. Polym. J. **18**, 123 (1982)
316. I. I. Ryskina and I. Yu. Zhiganova, Vysokomol. Soed. Ser A **36**, 503 (1994); CA 121:159559
317. I. I. Ryskina, V. P. Lozgacheva, E. D. Pokhvalenskii, and V. M. Aver' yanova, Vysokomol. Soed. Ser A **18**, 2500 (1976); CA 86:30223
318. V. M. Aver'yanova, N. I. Panina, and G. N. Timofeeva, Vysokomol. Soed Ser B **21**, 502 (1979); CA 91:142258.
319. Kh. N. Musaev, V. I. Goloborod'ko, S. A. Tashmukhamedov, and Kh. U. Usmanov, Doklady Akad. Nauk Ussr **49** (1978); CA 91:21324
320. B. Nyström and R. Bergman, Eur. Polym. J. **14**, 431 (1978); R. Bergman and L. –O. Sundelöf, Eur. Polym. J. **13**, 881 (1977).
321. L. Manderlkern and P. J. Flory, J. Am. Chem. Soc. **74**, 2517 (1952).
322. W. R. Krigbaum and L. H. Sperling, J. Phys. Chem. **64**, 99 (1960).
323. V. P. Shanbhag and J. Ohman, Arkiv foer Kemi **29**, 163 (1968); CA 69:3815.
324. A. Gűner, J. Appl. Polym. Sci. **62**, 785 (1996); U. U. Salamova, Z. M. O. Rzaev, S. Altindal, and A. A. Masimov, Polymer **37**, 2415 (1996).
325. S. Kavlak and A. Gűner, J. Appl. Polym. Sci. **78**, 507 (2000).
326. B. Kirci and A. Gűner, Eur. Polym. J. **37**, 361 (2001).
327. M. A. Ivanov and M. I. Koroleva, Koksnes Kimija 114, (1983) CA: 98:91253.

CHAPTER 16

Solubility Parameters

W. Zeng, Y. Du, Y. Xue, and H. L. Frisch

Department of Chemistry, State University of New York, Albany, NY 12222

Solubility parameters provide a simple method of correlating and predicting the cohesive and adhesive properties of materials from a knowledge of the properties of the components only. Particularly for polymers, applications include finding compatible solvents for coating resins, predicting the swelling of cured elastomers by solvents, estimating solvent pressure in devolatilization and reactor equipment [1] and predicting polymer–polymer [2], polymer–binary-solvent [3], random copolymer [4], and multi-component solvent equilibria [5–8].

16.1 COHESIVE ENERGY DENSITY AND SOLUBILITY (HILDEBRAND) PARAMETER

If U is defined as the molar internal energy (the molar potential energy of a material relative to the ideal vapor at the same temperature), then the molar cohesive energy (the energy associated with the net attractive interactions of the material) is defined as $-U$. As presented by Polak [9]:

$$-U = {}_l\Delta_g U + {}_g\Delta_\infty U, \tag{16.1}$$

where ${}_l\Delta_g U$ is the molar vaporization energy and ${}_g\Delta_\infty U$ is the energy required to expand the saturated vapor to infinite volume at constant temperature, that is, the energy necessary to completely separate the molecules.

The stabilizing or cohesive effect in condensed phases can be expressed in terms of the cohesive energy density, defined as

$$c = -U/V, \tag{16.2}$$

where V is the molar volume. Cohesive energy was the basis of the original definition by Hildebrand and Scott [10–12] of what is now generally called the solubility parameter or Hildebrand parameter:

$$\delta = c^{0.5} = (-U/V)^{0.5}. \tag{16.3}$$

This parameter was intended for nonpolar, nonassociating systems in which ${}_g\Delta_\infty U = 0$ and $-U = {}_l\Delta_g U$, but the concept has been extended to all types of systems. The dimension of δ is $(\text{cal/cm}^3)^{0.5} = 2.046 \times 10^3 (\text{J/m}^3)^{0.5} = 2.046\ \text{MPa}^{0.5}$. The solubility parameter can be considered as the ''internal pressure'' of the solvent [13–15].

Based on the pioneering work of van der Waals [16] and van Laar [17], the Hildebrand–Scatchard equation was derived on semitheoretical grounds by Scatchard [18,19] and Hildebrand [20–24] and popularized by Hildebrand, Scott, Prausnitz and others [25–37, 10–12]. For a binary mixture, the Hildebrand–Scatchard equation is expressed as

$$\Delta H_m / V_m = (\delta_1 - \delta_2)^2 \phi_1 \phi_2, \tag{16.4}$$

where ΔH_m is the enthalpy change on mixing, V_m the volume of the mixture, ϕ_i the volume fraction of i in the mixture, and δ_i the solubility parameter of the ith component. In general, $(\delta_1 - \delta_2)^2$ must be small for the components to be miscible. Equation (16.4) gives the heat of mixing of regular solutions in which (a) the components mix with no volume change on mixing at constant pressure, (b) the interaction forces act between the center of the molecules and the interaction between a pair of molecules is not influenced by the presence of other molecules, (c) the mixing is random and the distribution is temperature independent, (d) no reaction occurs between the components, and (e) there is no complex formation or special association. These assumptions are not generally valid, but they produce an

equation which has proven valuable both in its own right and as a starting point for other empirical expressions.

16.2 EXPANDED SOLUBILITY PARAMETERS

The solubility parameter describes the enthalpy change on mixing of nonpolar solvents well but does not give uniform results when extended to polar systems. Complete miscibility is expected to occur if the solubility parameters are similar and the degree of hydrogen bonding is similar between the components. Other investigators have decomposed the Hildebrand parameter into several terms, representing different contributions to the energy of mixing. van Arkel [38], Small [39], and Andersen, Prausnitz, and co-workers [12,40–45] divided the total solubility parameter into two main components, defining a nonpolar solubility (δ_λ) and a polar solubility parameter (δ_τ). Although this tends to neglect induction interactions, these may be taken care of by an additional parameter. Polar–nonpolar parameters are related to the Hildebrand parameter by

$$\delta^2 = \delta_\lambda^2 + \delta_\tau^2. \tag{16.5}$$

Here δ_λ can be identified with the dispersive term and δ_τ corresponds to the polar orientational term. This approach has been also applied to polymer solutions [41] and complex formation [46].

Hansen and co-workers [47–68] proposed a practical extension of the Hildebrand parameter method to polar and hydrogen-bonding systems, primarily for use in polymer–liquid interactions. It was assumed that dispersion, polar, and hydrogen-bonding parameters were valid simultaneously, related by Eq. (16.6), with the values of each component being determined empirically on the basis of many experimental observations:

$$\delta_t^2 = \delta_d^2 + \delta_p^2 + \delta_h^2, \tag{16.6}$$

where δ_t is Hansen's total solubility parameter, δ_d the dispersive term, δ_p the polar term, and δ_h the hydrogen-bonding term. Hansen's total solubility parameter should be equal to the Hildebrand parameter, although the two quantities may differ for materials with specific interactions when they are determined by different methods. The three component parameters were plotted on a set of three mutually perpendicular axes. The Hansen parameters give improved agreement with data but are still not completely accurate in predicting solution thermodynamics for every system.

Parameters describing and correlating the solvent abilities of liquids have been based on a great variety of chemical and physical properties. Some are measures of solvent basicity, and others are obtained from direct determinations of the solubility of a representative solute in a range of liquids. For example, the solubility of hydrogen chloride in liquids at 10 °C was used in this way by Gerrard and co-workers [69,70] and the resulting solvent basicity scale was compared with other scales by Arnett [71] and by Dack [72]. More direct measures of liquid basicity include the enthalpy of mixing with trichloromethane and with other hologenated hydrogen-bond donors in basic solvents [72,71] and the enthalpy of coordination with antimony trichloride [71,73]. Most of the other numerous scales of ''basicity'' or ''electron donating ability'' are single-valued and even more difficult to correlate with each other or with solubility parameters. Although they agree in their general trends, the detailed orders of solvent basicity depend on the system from which the scale is derived [72,74].

16.3 CALCULATION AND CORRELATIONS FOR SOLUBILITY PARAMETERS

16.3.1 Solvents

Solubility parameters can be determined by direct measurement, correlations with other physical parameters, or indirect calculations. The solubility parameters of solvents usually can be determined directly. The following methods can be used to develop correlations between solubility parameters and other physical properties of solvents.

Vaporization Enthalpy

If the enthalpy of vaporization, ΔH, has been determined calorimetrically (or from the temperature dependence of the vapor pressure) at the required temperature, and if this is well below the boiling point of the liquid, the Hildebrand parameter may be evaluated with the assumption that the vapor is ideal:

$$\delta = (\Delta H - RT)^{0.5}/V^{0.5}. \tag{16.7}$$

When the value of the vaporization enthalpy is known at one temperature (commonly at normal boiling point), it is desirable to be able to evaluate it at another temperature. In such procedures for extrapolating volumes or enthalpies, a corresponding state procedure is often used. This is frequently based on the reduced temperature T_r, reduced vapor pressure P_r, and reduced molar volume V_r, defined by

$$T_r = T/T_c,\ P_r = P/P_c,\ V_r = V/V_c, \tag{16.8}$$

where the subscript c refers to the values at the critical point. For example, ΔH may be evaluated to within about 2% over a wide range of temperatures, even within a few degrees of T_c by means of the Watson empirical relationship [75–77]:

$$\begin{aligned}\Delta H_2/\Delta H_1 &= (T_c - T_2)^{0.38}/(T_c - T_1)^{0.38} \\ &= (1 - T_{r,2})^{0.38}/(1 - T_{r,1})^{0.38}.\end{aligned} \tag{16.9}$$

Solvent molar volume are often available or can be calculated by group molar volume methods at 25 °C [76]. The molar volume for solids at 25 °C can be extrapolated from liquid-state values (if the liquid is assumed to be subcooled).

Boiling Point

A simple, convenient method of estimating the vaporization enthalpy is the application of the Hildebrand and Scott equation [12,24,35], which expresses ΔH at 25 °C (ΔH^0) in terms of the normal boiling point T_b:

$$\Delta H^0(\text{J mol}^{-1}) = -12\ 340 + 99.2[T_b(\text{K})] + 0.084[T_b(\text{K})]^2 \tag{16.10}$$

Van der Waals Gas Constant

Tables are available in many handbooks for the van der Waals correction constants to the ideal gas law, a and b. For some liquids, these values may be at hand when other data are not available. They can be used to check Hildebrand parameter values obtained from other sources:

$$\delta = 1.2\frac{a^{1/2}}{V}, \tag{16.11}$$

where a has units of 1^2 atm.

Surface Tension

Michaels [78] has shown that the surface tension can be related to the cohesive energy density

$$\frac{{}_l\Delta_g V}{V_i} = A\left(\frac{I}{V_i}\right)^{1/3}\gamma_L, \tag{16.12}$$

where γ_L is the surface tension, V_i is the molar volume of species i, and A is a constant. Koenhen and Smolders [79] correlated surface tension and two Hansen parameters:

$$\delta_d^2 + \delta_p^2 = 13.8\left(\frac{I}{V_i}\right)^{1/3}\gamma_L. \tag{16.13}$$

Equation (16.9) does not describe cyclic compounds, acetonitrile, carboxylic acids, polyfunctional alcohols, and other polar compounds as well. δ_h is probably not related to the liquid–vapor interfacial energy; these interactions do not involve breaking hydrogen bonds.

Internal Pressure

The internal pressure is defined as

$$\pi = (\partial U/\partial V)_T. \tag{16.14}$$

Bagley and co-workers [14,15,80,81] and Scigliano [82] utilized the chemical-bond-discriminating property of cohesive and internal pressures to subdivide the Hildebrand parameter in another way. One part corresponding to the physical or nonchemical effects is the volume-dependent Hildebrand parameter, defined by

$$\delta_v^2 = \pi. \tag{16.15}$$

The other component is a residual parameter, arising from chemical effects:

$$\delta_p^2 = (\Delta U - \pi V)/V, \tag{16.16}$$

$$\delta_p^2 \approx \delta_h^2,\ \delta_v^2 \approx \delta_d^2 + \delta_p^2. \tag{16.17}$$

One advantage of this approach for separation of the component parameters is that it makes use of the thermodynamic quantities π and ΔU, which are fairly readily available for most liquids, in contrast to other empirically determined component solubility parameters. The internal pressure can be measured experimentally by determining the thermal pressure coefficient or the coefficient of expansion and isothermal compressibility, it also can be calculated from other physical properties. Vavruch [83] developed and tested an expression for internal pressure in terms of critical temperature T_c,

$$\pi\ (\text{MPa}) = 63.0(1.5T_c - T)/V, \tag{16.18}$$

where V is the molar volume. The mean percentage deviation was 3.8% for 25 selected liquids (excluding alkanes, alkenes, monohydric alcohols, carboxylic acids, water, liquid metals, and probably cryogenic fluids).

Index of Refraction

The dispersive Hansen parameter δ_d can be related to the index of refraction n_D [79,84]:

$$\delta_d = 9.55n_D - 5.55. \tag{16.19}$$

The interaction energy between nonpolar molecules should depend on the molar polarizability (London dispersion forces) and therefore the index of refraction.

Dipole Moment

Hansen and Skaarup [66] related the polar Hansen parameter to the dielectric constant ε and the dipole moment μ:

$$\delta_p^2 = \frac{12\ 108}{V^2}\frac{\varepsilon - 1}{2\varepsilon + n_D^2}(n_D^2 + 2)\mu^2. \tag{16.20}$$

Beerbower and Dicky [85] proposed an empirical relationship:

$$\delta_p^2 = 9.5\mu/V_i^{1/2}. \tag{16.21}$$

16.3.2 Polymers

Measurements

For polymers, solubility parameters cannot be calculated from heat of vaporization data because of their nonvolatility. Other methods of estimation must be used.

The Internal Pressure P_i

Olabisi and Simha [86] developed one approach to calculate the solubility parameter through the internal pressure, P_i:

$$\delta^2 = P_i = \left(\frac{\partial U}{\partial V}\right)_T \approx T\alpha/\beta, \tag{16.22}$$

where α is the thermal expansion coefficient ($^\circ C^{-1}$) and β is the compressibility (cm^3/cal).

Swelling Data

A method often used for slightly cross-linked polymers [87] and applicable to partially crystalline material such as polyvinyl chloride (PVC) is based on finding the maximum swelling using a series of solvents of varying and known solubility parameters. The assumption is that the interaction and the degree of swelling will be a maximum when the solubility parameter of the polymer matches that of the solvent. This may be inaccurate for systems having opposite polarities or interacting through hydrogen bonding for which the heat of mixing is negative.

Inverse Phase Gas Chromatography

A number of investigations have been performed to measure infinite dilution weight fraction activity coefficients by applying inverse phase gas chromatography [88–97]. These coefficients can be related to solubility parameters by using a thermodynamic theory for polymer solutions, such as Flory–Huggins theory. The polymer is the stationary phase in a gas-chromatography column. Both binary and multicomponent equilibra [98,99] can be studied using this technique. Values of the enthalpy of vaporization can be determined at the experimental temperature [93]. Chromatographic methods have the advantage of measurement of thermodynamic values once the columns have been made. Both V_1 and ΔH_1^v must be known at the temperature of the column. Molar volumes for the solvents can be determined by using literature density equations or generating equations from density data.

Refractive Index

Dispersive Hansen parameters can be predicted from refractive-index measurements of polymers [79]. Wu [100] has suggested an effective cross-sectional area to relate the cohesive energy density and surface tension.

$$\delta_d^2 = A\left(\frac{n_s}{V_{i,s}}\right)^{1/3} \gamma_s^d, \tag{16.23}$$

where n_s is the number of atoms in a segment, $V_{i,s}$ is the molar volume of a segment, and γ_s^d is the dispersion contribution to the free surface energy.

Intrinsic Viscosity

Solubility parameters can also be estimated from intrinsic viscosity. Flory [101] related intrinsic viscosity to polymer molecular weight and the chain-expansion factor. The chain-expansion factor can, in turn, be related to the polymer-solvent interaction parameter using the Flory-Huggins theory. A variety of models can be used to relate the interaction parameter to solubility parameters [87,102,103]; these equations have the form

$$[\eta] = K_{\mathrm{I}} - K_{\mathrm{II}} V_i^n \Delta\delta^2, \tag{16.24}$$

where $[\eta]$ is the intrinsic viscosity, K_i are constants, and n is either 1/2 or 1 [104].

Other Methods

The dipole moment has been successfully applied to measure δ_p by Koenhen and Smolders [79]. The dipole moments of polymers are between 70% and 90% of those of the corresponding monomer units. The Hansen hydrogen-bonding parameter δ_h is given by [63]

$$\delta_h^2 = E_h/V_i. \tag{16.25}$$

The solubility parameter can also be calculated through the heat of solution directly [105,106], solution behavior [107,108], and by extrapolation [109].

Group Contribution Methods

Group contribution methods have been applied to the problem of estimating the solubility parameter without physical measurements [110–117,39,118,119]. Small [39] was one of the first to recognize the additive properties of the molar attraction constant F_i, which is defined by

$$F_i = (E_i V_i)^{1/2}, \tag{16.26}$$

where E_i and V_i are the cohesion energy and molar volume of the group being considered. Values of F_i, in units of $cal^{1/2}cm^{3/2}$, were obtained by regression analysis for various common structural groups in low-molecular-weight compounds. From the additivity of the F_i values and Eq. (16.3) one obtains:

$$\delta = \rho \frac{\sum_i F_i}{M}, \tag{16.27}$$

where ρ is the density of the polymer, M is the molar mass of the polymer, and the summation is carried over all structural features in the molecule.

The contributions of Hoy [116], Konstam and Feairlieller [120], and Van Krevelen [121] is summarized in Table 16.1. Some values of F_i, from which solubility parameters can be calculated with the aid of Eq. (16.27), are listed.

TABLE 16.1. *Group contributions to solubility parameter*[a].

Group	F_i		
	Small	van Krevelen	Hoy
–CH_3	437	420	303
=CH_2	272	280	269
=CH–	57	140	176
=C=	−190	0	65
=CH_2	388	—	259
=CH–	227	222	249
=C <	39	82	173
–CH=(aromatic)	—	—	240
–C=(aromatic)	—	—	201
–$CH(CH_3)$–	495	560	479
–$C(CH_3)_2$–	685	841	672
–CH=CH–	454	444	497
HC≡C–	583	—	—
–C≡C–	454	—	—
Cyclopentyl	—	1,380	1,300
Cyclohexyl	—	1,660	1,470
Phenyl	1,500	1,520	1,400
Phenylene	1,350	1,380	1,440
Naphthyl	2,340	—	—
–OH	—	754	462
–CO–	562	685	538
–CHO	—	—	599
–COO–	634	511	688
–COOH	—	651	998
–O–(C=O)–O–	—	767	904
–(C=O)–O–(C=O)–	—	767	1,160
–NH_2	—	—	464
–NH–	—	—	368
–N<	—	—	125
–CHCN	896	1,120	901
–CN	839	982	725
–(C=O)–NH–	—	1,290	906
–O–(C=O)–NH–	—	1,480	1,040
–N=C=O	—	—	734
–H	164–205	140	−103
–S–	460	460	428
–SH	644	—	—
–F	250	164	84
–C1(primary)	552	471	420
–Br(primary)	695	614	528
–I	870	—	—
–CF_2–	307	—	—
–CF_3	561	—	—
–O–N=O	900	—	—
–NO_2	900	—	—
–PO_4	1,020	—	—
–Si–	−77	—	—

[a]Adapted from D. W. van Krevelen, Properties of Polymers, 3rd edition (Elsevier, Amsterdam), p. 200 (1990).

16.4 POLYMER-SOLVENT INTERACTION PARAMETER

The enthalpic component of polymer–solvent interaction parameter χ_H can be related to the solubility parameters via

$$\chi_H = \frac{V_i}{RT}(\delta_i - \delta_j)^2. \tag{16.28}$$

This equation links the polymer–solvent interaction parameter with the solubility parameters of polymer and solvent. For nonpolar systems the entropic term χ_s is usually taken to be a constant between 0.3 and 0.4 ($\chi_s = 0.34$ is often used) [41,122]. Equation (16.33) can thus be rewritten as

$$\chi = 0.34 + \frac{V_i}{RT}(\delta_i - \delta_j)^2 \tag{16.29}$$

for nonpolar systems $\chi = \chi_H + \chi_s$ where Eq. (16.27) is a good description of the enthalpic portion of the interaction parameter. According to Flory [123,124] a polymer j and a solvent i are expected to be completely miscible through the entire composition range provided that

$$\chi < \frac{1}{2}\left[1 + \left(\frac{V_i}{V_j}\right)^{1/2}\right]^2. \tag{16.30}$$

There is thus a critical polymer–solvent interaction parameter value

$$\chi_c = \frac{1}{2}\left[1 + \left(\frac{V_i}{V_j}\right)^{1/2}\right]^2 \tag{16.31}$$

and for $(V_i/V_j) \to 0$,

$$\chi_c = 0.5. \tag{16.32}$$

If χ must be less than 0.5 for full polymer–solvent miscibility, and χ_s is about 0.3, it follows that χ_H must be very small to meet the miscibility criterion, and that δ_i and δ_j must have very similar values. Specific interactions (such as hydrogen bonding between molecules of type i and type j to a greater extent than i-i and j-j hydrogen bonding) can result in the lower χ_H and thus enhance the mutual solubility.

For real polymer–solvent systems the experimental χ values and their dependences on composition, temperature, and molar mass provide useful indications of the nature and extent of the polymer–solvent interaction. For a polymer to be soluble in a solvent at a particular temperature, χ must be below 0.5 at high levels of ϕ_j. If the χ value is only slightly larger than 0.5, the polymer is expected to be swollen by the solvent.

There exist a number of extensive published collections of solubility parameters for both low-molecular-weight compounds (e.g., organic solvents) and high polymers [121,125–127]. Our purpose is to give a select number of solubility parameters data in Tables 16.2–16.5 that are representatives for the solvents used in various polymer technologies and the more important representative classes of high polymers used in industry and academic investigations. For the latter we have followed the suggested classes in Billmeyers's text [128]. We have taken some pains to include more recent data not necessarily found in the more exhaustive collections.

TABLE 16.2. *Hildebrand parameters of representative solvents at 25 °C*[a].

Solvent	$\delta[(MPa)^{1/2}]$	H-bonding tendency[b]
Acetaldehyde	21.1	m
Acetic acid	20.7	s
Acetic anhydride	21.1	s
Acetone	20.3	m
Acetonitrile	24.3	p
Acetophenone	21.7	m
Acetyl chloride	19.4	m
Acetylmorpholine (*N*)	23.7	m
Acetylpiperidine (*N*)	22.9	s
Acetylpyrrolidine (*N*)	23.3	s
Acrolein	20.1	s
Acrylic acid	24.6	s
Acrylonitridle	21.5	p
Allyl acetate	18.8	m
Allyl alcohol	24.1	s
Allyl chloride	18.0	m
Ammonia	33.4	s
Amyl acetate (normal)	17.4	m
Amyl alcohol	20.5	s
Amylamine (normal)	17.8	s
Amyl bromide (normal)	15.6	m
Amyl chloride	17.0	m
Amylene	14.1	p
Amyl ether (normal, di-)	14.9	m
Amry formate (normal)	17.4	m
Amyl iodide (normal)	17.2	m
Anethole (*para*)	17.2	m
Aniline	21.1	s
Anthracene	20.3	p
Apco#18 solvent	15.3	p
Apco thinner	16.0	p
Aroclor 1248	18.0	p
Benzaldehyde	19.2	m
Benzene	18.8	p
Benzonitrile	17.2	p
Benzyl alcohol	24.8	s
Bicyclohexyl	17.4	p
Bromobenzene	20.3	p
Bromonaphthalene	21.7	p
Bromostyrene (*ortho*)	20.1	p
Butadiene-1,3	14.5	p
Butane (normal)	13.9	p
Butanediol-1,3	23.7	s
Butanediol-1,4	24.8	s
Butanediol-2,3	22.7	s
Butyl acetate (*iso*)	17.0	m
Butyl acetate (normal)	17.4	m
Butyl acylate (*iso*)	17.4	m
Butyl acylate (normal)	18.0	m
Butyl alcohol (*iso*)	21.5	s
Butyl alcohol (normal)	23.3	s
Butylamine (mono, normal)	17.8	s
Butyl bromide (normal)	17.8	m
Butyl (iso) butyrate (normal)	16.0	m
Butyl (normal) butyrate (normal)	16.6	m
Butyl chloride (*iso*)	16.6	m
Butylene-2,3 carbonate	24.8	m
Butylene (*iso*)	13.7	p
Butyl ether	16.0	m
Butyl formate (*iso*)	16.8	m
Butyl formate (normal)	18.2	m
Butyl idoide (normal)	17.6	m
Butyl lactate (normal)	19.2	m
Butyl methacrylate	16.8	m
Butyl stearate	15.3	m
Butyl propionate	18.0	m
Butyraldehyde	18.4	m
Butyric acid (*iso*)	21.1	s
Butyric acid (normal)	21.5	s
Butyrolactone	25.8	m
Butyronitrile (*iso*)	20.1	p
Butyronitrile (normal)	21.5	p
Carprolactam	26.0	m
Caprolactone	20.7	m
Capronitrile	19.2	p
Carbon disulfide	20.5	p
Carbon tetrachloride	17.6	p
Celanese solvent 601	18.8	m
Chloroacetonitrile	25.8	p
Chlorobenzene	19.4	p
Chloroethyl acetate (beta)	19.8	m
Chloroform	19.0	p
Chlorostyrene (*ortho* or *para*)	19.4	p
Chlorotoluene (*para*)	18.0	p
Cresol (*meta*)	20.9	s
Cyclobutanedione	22.5	m
Cyclohexane	16.8	p
Cyclohexanol	23.3	s
Cyclohexanone	20.3	m
Cyclopentane	17.8	p
Cyclopentanone	21.3	m
Cymene (*para*)	16.8	p
Decahydronaphthalene	18.0	p
Decane (normal)	13.5	p
Decyl acrylate (*iso*)	16.8	m
Diacetone alcohol	18.8	m
Diacetone alcohol methyl ether	16.8	m
Diacetylpiperazine (*N,N*)	28.0	m
Diamyl phthalate	18.6	m
Dibenzyl ether	19.2	m
Dibromoethane-1,2	21.3	p
Dibromoethylene-1,2	20.7	p
Dibutoxyethyl phthalate (Kronisol)	16.4	m
Dibutylamine	16.6	s
Dibutyl fumarate	18.4	m
Dibutyl maleate	18.4	m
Dibutyl phenyl phosphate	17.8	m
Dibutyl phthalate	19.0	m

TABLE 16.2. *Continued.*

Solvent	$\delta[(MPa)^{1/2}]$	H-bonding tendency[b]
Dibutyl sebacate	18.8	m
Dichloroacetic acid	22.5	s
Dichlorobenzene (*ortho*)	20.5	p
Dichlorodifluoromethane (Feon 12)	11.3	p
Dichloroethyl ether	20.1	m
Dichloroethylene, *cis*-1,2	18.6	p
Dichloroethylene, *trans*-1,2	18.4	p
Dichlorofluoromethane (Freon 21)	17.0	p
Dichloropropane-1,2	18.4	p
Dichloropropane-2,2	16.8	p
Diethylacetamide (*N,N*)	20.3	m
Diethylamine	16.4	s
Diethyl carbonate	18.0	m
Diethylene glycol	24.8	s
Diethylene glycol monobutyl ether (normal)	19.4	m
Diethylene glycol monobutyl ether	20.9	m
Diethylene glycol monobutyl ether acetate	17.4	m
Diethylene glycol monolaurate	17.8	m
Diethyl ether	15.1	m
Diethylformamide (*N,N*)	21.7	m
Diethyl ketone	18.0	m
Diethyl maleate	20.3	m
Diethyl oxalate	17.6	m
Diethyl phathalate	20.5	m
Diethyl-2,2-propanediol-1,2 (heptylene glycol)	20.3	s
Diethyl sulfone	25.4	m
Difluoro-tetrachloroethane (Freon 112)	16.0	p
Diformylpiperazine (*N,N*)	31.5	m
Dihexyl ether	16.4	m
Epichlorohydrin	22.5	s
Ethane	12.3	p
Ethylacetamide (*N*)	25.2	s
Ethyl acetate	18.6	m
Ethyl acrylate	17.6	m
Ethyl alcohol	26.0	s
Ethylamine	20.5	s
Ethyl amyl ketone	16.8	m
Ethylbenzene	18.0	p
Ethyl benzoate	16.8	m
Ethyl bromide	19.6	m
Ethyl-2-butanol-1	21.5	s
Ethyl *n*-butyrate	17.4	m
Ethyl caprylate	14.9	m
Ethyl chloride	18.8	m
Ethyl cyanoacetate	22.5	m
Ethylene bromide	19.8	p
Ethylene carbonate	30.1	m
Ethylene chlorohydrin	25.0	s
Ethylene cyanohydrin	31.1	s
Ethylenediamine	25.2	s
Ethylene dichloride	20.1	p

TABLE 16.2. *Continued.*

Solvent	$\delta[(MPa)^{1/2}]$	H-bonding tendency[b]
Ethylene glycol	29.9	s
Ethylene glycol diacetate	20.5	m
Fluorocarbons, aliphatic	12.7	p
Fluorocarbons, aromatic	15.3	p
Formamide	39.3	s
Formic acid	24.8	s
Formylmorpholine (*N*)	26.6	m
Formylpiperidine (*N*)	23.5	m
Furane	19.2	m
Furfural	22.9	m
Furfuryl alcohol	25.6	s
Glycerol	33.8	s
Heptane (normal)	15.1	p
Heptyl alcohol (normal)	21.7	s
Hexamethylphosphoramide	21.5	s
Hexane (normal)	14.9	p
Hexanediaol-2,5	21.1	s
Hexene-1	15.1	p
Hexyl alcohol (normal)	21.9	s
Hydrazine	37.3	s
Hydrogen	6.9	p
Hydrogenated terphenyl	18.4	p
Hydrogen cyanide	24.8	s
Idobenzene	20.7	p
Isophorone	18.6	m
Isoprene	15.1	p
Lauryl alcohol	16.6	s
Low odor mineral spirits	14.1	p
Maleic anhydride	27.8	s
Malononitrile	30.9	p
Mesitylene	18.0	p
Mesityl oxide	18.4	m
Methacrylic acid	22.9	s
Methane	11.0	p
Methanol	29.7	s
Methylacetamide	29.9	s
Methyl acetate	19.6	m
Methyl acrylate	18.2	m
Methylamine	22.9	s
Methyl amyl acetate	16.4	m
Methyl amyl ketone	17.4	m
Methyl benzoate	21.5	m
Methyl bromide	19.6	m
Naphthalene	20.3	p
Neopentane	12.9	p
Neopentyl glycol	22.5	s
Nitrobenzene	20.5	p
Nitroethane	22.7	p
Nitromethane	26.0	p
Nitro-*n*-octane	14.3	p
Nitro-1-propane	21.1	p
Nitro-2-propane	20.3	p
Nonyl phenol	19.2	s
Octane (normal)	15.6	p
Octyl alcohol (normal)	21.1	s

TABLE 16.2. *Continued.*

Solvent	$\delta[(MPa)^{1/2}]$	H-bonding tendency[b]
Pentachloroethane	19.2	p
Pentane (normal)	14.3	p
Pentanediol-1,5	23.5	s
Pentanediol-2,4	22.1	s
Perchloroethylene	19.0	p
Perfluoroheptane	11.9	p
Perfluoromethylcyclohexane	12.3	p
Phenathrene	20.1	p
Phenylhydrazine	25.6	s
Pine oil	17.6	p
Piperdine	17.8	s
Piperidone	27.8	s
Propane	13.1	p
Propyl formate	18.8	m
Pyridine	21.9	s
Quinoline	22.1	s
Styrene	19.0	p
Styrene oxide	21.5	m
Succinic anhydride	31.5	s
Tetrachloroethane-1,1,2,2	19.8	p
Tetrachloroethylene	19.0	p
Tetraethylene glycol	20.3	s
Tetrahydrofuran	18.6	m
Tetrahydronaphthalene	19.4	p
Tetramethylene sulfone	27.4	m
Tetramethyloxamide	23.3	m
Thiophene	20.1	m
Toluene	18.2	p

TABLE 16.2. *Continued.*

Solvent	$\delta[(MPa)^{1/2}]$	H-bonding tendency[b]
Tolylenediisocyanate	23.7	s
Tributylamine	15.8	s
Trichloroethane-1,1,2	19.6	p
Trichloroethylene	18.8	p
Trichlorofluoromethane	15.5	p
Trichlorotrifluoroethane	14.9	p
Tricresyl phosphate	17.2	m
Triethylamine	15.1	s
Triethyleneglycol	21.9	s
Triethylenetetramine	22.7	s
Trimethyl-3,5,5-hexanol	17.2	s
Triphenyl phosphate	17.6	m
Triphenyl phosphite	19.0	m
Tripropylene glycol	18.8	s
Turpentine	16.6	p
Valeric acid (normal)	20.1	s
Valeronitrile (normal)	15.6	p
Varnolene (varsol #2)	19.6	p
Vinyel acetate	18.4	m
Vinyel chloride	16.0	m
Vinyel toluene	18.6	p
V M & P naphtha	15.6	p
Water	47.9	s
Xylene	18.0	p

[a]Adapted from J. Brandrup, E. H. Immergut, and E. A. Grulke, Polymer Handbook, 4th edition, John Wiley & Sons, New York (1999).
[b]p denotes poor; m, moderate; s, strong.

TABLE 16.3. *Hansen solubility parameters of representative liquids at 25 °C[a].*

Solvent	V (cm^3/mol)	Solubility parameter $[(MPa)^{1/2}]$			
		δ_d	δ_p	δ_h	δ_t
Acetaldehyde	57.1	14.7	8.0	11.3	20.3
Acetic acid	57.1	14.5	8.0	13.5	21.3
Acetic anhydride	94.5	16.0	11.7	10.2	22.3
Acetone	74.0	15.5	10.4	7.0	20.1
Acetonitrile	52.6	15.3	18.0	6.1	24.6
Acetophenone	117.4	19.6	8.6	3.7	21.7
Acetyl chloride	71.0	15.8	10.6	3.9	19.4
Acrylonitrile	67.1	16.4	17.4	6.8	24.8
Allyl alcohol	68.4	16.2	10.8	16.8	25.8
Amyl (i) acetate	148.8	15.3	3.1	7.0	17.2
Aniline	91.5	19.4	5.1	10.2	22.5
Anisole	119.1	17.8	4.1	6.8	19.4
Benzaldehyde	101.5	19.4	7.4	5.3	21.5
Benzene	89.4	18.4	0.0	2.0	18.6
Benzenediol-1,3	87.5	18.0	8.4	21.1	28.8
Benzoic acid	100.0	18.2	7.0	9.8	21.9
Benzonitrile	102.6	17.4	9.0	3.3	19.8
Benzyl alcohol	103.6	18.4	6.3	13.7	23.7

TABLE 16.3. *Continued.*

Solvent	V (cm^3/mol)	Solubility parameter [(MPa)$^{1/2}$]			
		δ_d	δ_p	δ_h	δ_t
Biphenyl	154.1	21.5	1.0	2.0	21.7
Bis(2-chloroethyl) ether	117.6	18.8	9.0	5.7	21.7
Bis-(*m*-phenoxyphenyl) ether	373.0	19.6	3.1	5.1	20.5
Bromobenzene	105.3	20.5	5.5	4.1	21.7
Bromochloromethane	65.0	17.4	5.7	3.5	18.6
Bromoform	87.5	21.5	4.1	6.1	22.7
Bromotrifluoromethane	97.0	9.6	2.5	0.0	10.0
Butanol-1	91.5	16.0	5.7	15.8	23.1
Butanol-2	92.0	15.8	5.7	14.5	22.1
Butyl (i) acetate	133.5	15.1	3.7	6.3	16.8
Butyl (*n*) acetate	132.5	15.8	3.7	6.3	17.4
Butyl (*n*) benzyl phthalate	306.0	19.0	11.3	3.1	22.3
Butylamine-*n*	99.0	16.2	4.5	8.0	18.6
Butylchloride (*n*)	104.9	16.4	5.5	2.0	17.4
Butyl-*n* lactate	149.0	15.8	6.5	10.2	19.8
Butyraldehyde	88.5	14.7	5.3	7.0	17.2
Butyric-*n* acid	110.0	14.9	4.1	10.6	18.8
Butyronitrile	87.0	15.3	12.5	5.1	20.5
Carbon disulfide	60.0	20.5	0.0	0.6	20.5
Carbon tetrachloride	97.1	17.8	0.0	0.6	17.8
Chloro-3-propanol	84.2	17.6	5.7	14.7	23.7
Chlorobenzene	102.1	19.0	4.3	2.0	19.6
Chlorodifluoromethane	72.9	12.3	6.3	5.7	14.9
Chloroform	80.7	17.8	3.1	5.7	19.0
Cyclohexanol	106.0	17.4	4.1	13.5	22.5
Cyclohexanone	104.0	17.8	6.3	5.1	19.6
Cyclohexylamine	115.2	17.4	3.1	6.5	18.8
Decanol-1	191.8	17.6	2.7	10.0	20.5
Di-(2-chloro-*i*-propyl) ether	146.0	19.0	8.2	5.1	21.3
Di-(2-methoxyethyl) ether	142.0	15.8	6.1	9.2	19.2
Di-(*i*-butyl) ketone	177.1	16.0	3.7	4.1	16.8
Diacetone alcohol	124.2	15.8	8.2	10.8	20.9
Dibenzyl ether	192.7	17.4	3.7	7.4	19.2
Di-butyl stearate	382.0	14.5	3.7	3.5	15.3
Dichlorobenzene (o)	112.8	19.2	6.3	3.3	20.5
Dichloroethane-1,1	84.8	16.6	8.2	0.4	18.4
Dichloroethylene-1,1	79.0	17.0	6.8	4.5	18.8
Dichlorofluoromethane	75.4	15.8	3.1	5.7	17.0
Dichlorofluoromethane	92.3	12.3	2.0	0.0	12.5
Diethyl carbonate	121.0	16.6	3.1	6.1	18.0
Diethyl ether	104.8	14.5	2.9	5.1	15.8
Diethyl ketone	106.4	15.8	7.6	4.7	18.2
Diethyl phthalate	198.0	17.6	9.6	4.5	20.5
Diethyl sulfate	131.5	15.8	14.7	7.2	22.7
Diethyl sulfide	108.2	17.0	3.1	2.0	17.4
Diethylamine	103.2	14.9	2.3	6.1	16.4
Diethylbenzene (*p*)	156.9	18.0	0.0	0.6	18.0
Diethylene glycol monobutyl-*n* ether	170.6	16.0	7.0	10.6	20.5
Diethylene glycol monoethyl ether	130.9	16.2	9.2	12.3	22.3
Diethylene glycol monomethyl ether	118.0	16.2	7.8	12.7	21.9
Diethylenetriamine	108.0	16.8	13.3	14.3	25.8
Dimethyl phthalate	163.0	18.6	10.8	4.9	22.1
Dimethyl sulfone	75.0	19.0	19.4	12.3	29.9

TABLE 16.3. *Continued.*

Solvent	V (cm^3/mol)	Solubility parameter [(MPa)$^{1/2}$]			
		δ_d	δ_p	δ_h	δ_t
Dimethyl sulfoxide	71.3	18.4	16.4	10.2	26.6
Dimethyl-1,3-butanol-1	127.2	15.3	3.3	12.3	19.8
Dimethylformamide	77.0	17.4	13.7	11.3	24.8
Dimethylformamide-*N,N*	92.5	16.8	11.5	10.2	22.7
Dimethylhydrazine-1,1	76.0	15.3	5.9	11.0	19.8
Di-*n*-butyl phthalate	266.0	17.8	8.6	4.1	20.3
Di-*n*-butyl sebacate	339.0	13.9	4.5	4.1	16.2
Di-*n*-propylamine	136.9	15.3	1.4	4.1	16.0
Dioctyl phthalate	277.0	16.6	7.0	3.1	18.2
Dioxane-1,4	85.7	19.0	1.8	7.4	20.5
Epichlorhydrin	79.9	19.0	10.2	3.7	21.9
Ethanethiol	74.3	15.8	6.5	7.2	18.4
Ethanolamine	60.2	17.2	15.5	21.3	31.5
Ethanolamine	58.5	15.8	8.8	19.4	26.6
Ethoxyethyl acetate-2	136.2	16.0	4.7	10.6	19.6
Ethyl acetate	98.5	15.8	5.3	7.2	18.2
Ethyl bromide	76.9	16.6	8.0	5.1	19.0
Ethyl chloroformate	95.6	15.5	10.0	6.8	19.6
Ethyl cinnamate	166.8	18.4	8.2	4.1	20.5
Ethyl formate	80.2	15.5	8.4	8.4	19.6
Ethyl lactate	115.0	16.0	7.6	12.5	21.7
Ethyl-1-butanol-1	123.2	15.8	4.3	13.5	21.3
Ethyl-2-hexanol-1	157.0	16.0	3.3	11.9	20.1
Ethylbenzene	123.1	17.8	0.6	1.4	17.8
Ethylene carbonate	66.0	19.4	21.7	5.1	29.5
Ethylene cyanohydrin	68.3	17.2	18.8	17.6	30.9
Ethylene diamine	67.3	16.6	8.8	17.0	25.4
Ethylene dibromide	87.0	19.6	6.8	12.1	23.9
Ethylene dichloride	79.4	19.0	7.4	4.1	20.9
Ethylene glycol monobutyl-*n* ether	131.6	16.0	5.1	12.3	20.9
Ethylene glycol monoethyl ether	97.8	16.2	9.2	14.3	23.5
Ethylene glycol monomethyl ether	79.1	16.2	9.2	16.4	24.8
Formamide	39.8	17.2	26.2	19.0	36.6
Formic acid	37.8	14.3	11.9	16.6	25.0
Furan	72.5	17.8	1.8	5.3	18.6
Furfuraldehyde	83.2	18.6	14.9	5.1	24.3
Furfuryl alcohol	86.5	17.4	7.6	15.1	24.3
Hexamethyl phosphoramide	175.7	18.4	8.6	11.3	23.3
Isophorone	150.5	16.6	8.2	7.4	19.8
Mesityl oxide	115.6	16.4	7.2	6.1	18.8
Mesitylene	139.8	18.0	0.0	0.6	18.0
Methanol	40.7	15.1	12.3	22.3	29.7
Methyl acetate	79.7	15.5	7.2	7.6	18.8
Methyl chloride	55.4	15.3	6.1	3.9	17.0
Methyl ethyl ketone	90.1	16.0	9.0	5.1	19.0
Methyl *i*-amyl ketone	142.8	16.0	5.7	4.1	17.4
Methyl *i*-butyl ketone	125.8	15.3	6.1	4.1	17.0
Methyl oleate	340.0	14.5	3.9	3.7	15.5
Methyl-2-propanol-1	92.8	15.1	5.7	16.0	22.7
Methylene dichloride	63.9	18.2	6.3	6.1	20.3
Methylene diiodide	80.5	17.8	3.9	5.5	19.0
Methylnaphthalene-1	138.8	20.6	0.8	4.7	21.2
Methyl-*N*-pyrrolidone-2	96.5	18.0	12.3	7.2	22.9

TABLE 16.3. *Continued.*

Solvent	V (cm^3/mol)	Solubility parameter [(MPa)$^{1/2}$]			
		δ_d	δ_p	δ_h	δ_t
Morpholine	87.1	18.8	4.9	9.2	21.5
Naphthalene	111.5	19.2	2.0	5.9	20.0
Nitrobenzene	102.7	20.1	8.6	4.1	22.1
Nitroethane	71.5	16.0	15.5	4.5	22.7
Nitromethane	54.3	15.8	18.8	5.1	25.0
Nitropropane-2	86.9	16.2	12.1	4.1	20.7
Nonyl phonoxyl ethanol	275.0	16.8	10.2	8.4	21.3
Octanol-1	157.7	17.0	3.3	11.9	20.9
Octanol-2	159.1	16.2	4.9	11.0	20.3
Octoic-*n* acid	159.0	15.1	3.3	8.2	17.6
Oleic acid	320.0	14.3	3.1	5.5	15.8
Oleyl alcohol	316.0	14.3	2.7	8.0	16.6
Pentanol-1	109.0	16.0	4.5	13.9	21.7
Perfluorodimethylcyclohexane	217.4	12.5	0.0	0.0	12.5
Perfluoromethylcyclohexane	196.0	12.5	0.0	0.0	12.5
Perfluoro-*n*-heptane	227.3	12.1	0.0	0.0	12.1
Phenol	87.5	18.0	5.9	14.9	24.1
Propanol-1	75.2	16.0	6.8	17.4	24.6
Propanol-2	76.8	15.8	6.1	16.4	23.5
Propionitrile	70.9	15.3	14.3	5.5	21.7
Propyl (*i*) palmitate	330.0	14.3	3.9	3.7	15.3
Propyl (*n*) chloride	88.1	16.0	7.8	2.0	17.8
Propylamine-*n*	83.0	17.0	4.9	8.6	19.6
Propylene carbonate	85.0	20.1	18.0	4.1	27.2
Pyridine	80.9	19.0	8.8	5.9	21.7
Pyrrolidone-2	76.0	19.4	17.4	11.3	28.4
Quinoline	118.0	19.4	7.0	7.6	22.1
Stearic acid	326.0	16.4	3.3	5.5	17.6
Styrene	115.6	18.6	1.0	4.1	19.0
Succinic anhydride	66.8	18.6	19.2	16.6	31.5
Tetrachloroethane-1,1,2,2	105.2	18.8	5.1	9.4	21.7
Tetrachloroethylene	101.1	19.0	6.5	2.9	20.3
Tetrahydrofuran	81.7	16.8	5.7	8.0	19.4
Tetrahydronaphthalene	136.0	19.6	2.0	2.9	20.0
Tetramethylurea	120.4	16.8	8.2	11.0	21.7
Toluene	106.8	18.0	1.4	2.0	18.2
Trichlorobiphenyl	187.0	19.2	5.3	4.1	20.5
Trichloroethane-1,1,1	100.4	17.0	4.3	2.0	17.6
Trichloroethylene	90.2	18.0	3.1	5.3	19.0
Trichlorofluoromethane	92.8	15.3	2.0	0.0	15.5
Tricresyl phosphate	613.0	19.0	12.3	4.5	23.1
Tridecyl alcohol	242.0	14.3	3.1	9.0	17.2
Triethyl phosphate	171.0	16.8	11.5	9.2	22.3
Triethylene glycol mono-oleyl ether	418.5	13.3	3.1	8.4	16.0
Trimethyl phosphate	99.9	16.8	16.0	10.2	25.4
Tri-*n*-butyl phosphate	345.0	16.4	6.3	4.3	18.0
Water	18.0	15.5	16.0	42.4	47.9
Xylene (*o*)	121.2	17.8	1.0	3.1	18.0

[a]Adapted from J. Brandrup, E. H. Immergut, and E. A. Grulke, Polymer Handbook, 4th edition, John Wiley & Sons, New York (1999).

TABLE 16.4. *Solubility parameters of representative polymers.*

Polymer	δ(MPa$^{1/2}$)	T (°C)	Method	Reference
Cellulose	32.02			[129]
Cellulose diacetate	23.22		Calc.	[39]
Cellulose nitrate (11.83% N)	21.44		Calc.	[39]
Epoxy resin	22.3			[130]
Natural rubber	16.2			[131]
	17.09			[132]
Poly(4-acetoxystyrene)	22.7	25	Visc.	[133]
Poly(acrylic acid)				
—, butyl ester	18.0	35		[134]
	18.52		Swelling	[134]
—, methyl ester	20.77		Swelling	[134]
	20.7		Swelling	[135]
Poly(acrylonitrile)	26.09	25	Calc.	[39]
Poly(butadiene)	16.2	75	IPGC	[136]
	17.15		Calc.	[39]
Poly(butadiene-co-acrylonitrile)				
BUNA N (72/25)	18.93	25	Calc.	[39]
(61/39)	20.5	75	IPGC	[136]
Poly(butadiene-co-styrene)				
BUNA S (85/15)	17.41		Calc.	[137]
	17.39		Obs.	[137]
Poly(butadiene-co-vinylpyridine)				
(72/25)	19.13			[132]
Poly(chloroprene)	18.42	25		[129]
	19.19		Calc.	[39]
	17.6		Swelling	[131]
Poly(dimethyl siloxane)	14.9	30	Calc.	[138]
Poly(ethylene)	16.6		Calc.	[39]
Poly(ethylene)	16.4		Calc.	[139]
	16.2		Obs.	[140]
Poly(ethylene-co-vinyl-acetate)	18.6	25	IPGC	[93]
	17.0	75	IPGC	[136]
Poly(*tetra*-fluoroethylene)	12.7		Calc.	[39]
Poly(heptamethylene *p,p′*-bibenzoate)	19.50	25	Visc.	[141]
Poly(4-hydroxystyrene)	23.9	25	Visc.	[133]
Poly(isobutene)	16.06	35	Av.	[142]
	16.47		Swelling	[142]
	16.06	25		[129]
Poly(isobutene-co-isoprene) butyl rubber	16.47			[122]
Poly(isoprene)	15.18	25	Calc.	[112]
1,4-*cis*	16.68	25		[142]
	16.57	35		[142]
	20.46	35	Swelling	[142]
	16.6		Swelling	[134]
	16.68	25	Calc.	[39]
Poly(methacrylic acid)				
—, isobutyl ester	14.7	140	IPGC	[91]
—, ethyl ester	18.31		Swelling	[135]
—, methyl ester	18.58	25		[87]
Poly(methacrylonitrile)	21.9		Calc.	[39]
Poly(methylene)	14.3	20	Extrap.	[143]
Poly(α-methyl styrene)	18.75	30	Visc.	[144]
Poly(σ-methylstyrene-co-acrylonitrile)	16.4	180	IPGC	[145]
Poly(oxyethylene)	20.2	25	IPGC	[91]
Poly(propylene)	18.8	25		[114]
Poly(styrene)	18.72	35		[142]
Poly(styrene-co-*n*-butyl-methacrylate)	15.1	140	IPGC	[91]
Poly(thioethylene)	19.19		Swelling	[131]

TABLE 16.4. *Continued.*

Polymer	δ(MPa$^{1/2}$)	T (°C)	Method	Reference
Poly(vinyl acetate)	19.62	25	Calc.	[112]
Poly(vinyl alcohol)	25.78			[129]
Poly(vinyl chloride)	19.28		Calc.	[112]
	19.8		Obs.	[94]
Poly(vinyl chloride), chlorinated	19.0	25	Visc.	[146]
Poly(vinyl propionate)	18.01	35		[147]

TABLE 16.5. *Hansen solubility parameters of representative polymers.*

	Solubility parameter (MPa$^{1/2}$)				
Polymer (trade name, supplier)	δ_d	δ_p	δ_h	δ_t	Reference
Acrylonitrile-butadiene elastomer (Hycar 1052, BF Goodrich)	18.6	8.8	4.2	21.0	[54]
Alcohol soluble resin (Pentalyn 255, Hercules)	17.5	9.3	14.3	24.4	[54]
Alcohol soluble resin (Pentalyn 830, Hercules)	20.5	5.8	10.9	23.5	[54]
Alkyd, long oil (66% oil length, Plexal P65, Polyplex)	20.42	3.44	4.56	21.20	[54]
Alkyd, short oil (Coconut oil 34% phthalic anhydride; Plexal C34)	18.50	9.21	4.91	21.24	[54]
Blocked isocyanate (Phenol, Suprasec F5100, ICI)	20.19	13.16	13.07	27.42	[54]
Cellulose acetate (Cellidore A, Bayer)	18.60	12.73	11.01	25.08	[54]
Cellulose nitrate (1/2 s; H-23, Hagedon)	15.41	14.73	8.84	23.08	[54]
Epoxy (Epikote 1001, Shell)	20.36	12.03	11.48	26.29	[54]
Ester gum (Ester gum BL, Hercules)	19.64	4.73	7.77	21.65	[54]
Furfuryl alcohol resin (Durez 14383, Hooker Chemical)	21.16	13.56	12.81	28.21	[54]
Hexamethoxymethyl melamine (Cymel 300 American Cyanimid)	20.36	8.53	10.64	24.51	[54]
Isoprene elastomer (Cariflex IR 305, Shell)	16.57	1.41	−0.82	16.65	[54]
Methacrylonitrile/methacrylic acid copolymer	17.39	14.32	12.28	25.78	[148]
Nylon 66	18.62	5.11	12.28	22.87	[6]
Nylon 66 (Zytel, DuPont)	18.62	0.00	14.12	23.37	[54]
Petroleum hydrocarbon resin (Piceopale 110, Penn. Ind. Chem.)	17.55	11.19	3.60	17.96	[54]
Phenolic resin (Resole, Phenodur 373 U Chemische Werke Albert)	19.74	11.62	14.59	27.15	[54]
Phenolic resin, pure (Super Beckacite 1001, Reichhold)	23.26	6.55	8.35	25.57	[54]
Poly(4-acetoxy, α-acetoxy styrene)	17.80	10.23	7.37	21.89	[149]
Poly(4-acetoxystyrene)	17.80	9.00	8.39	21.69	[133]
Poly (acrylonitrile)	18.21	16.16	6.75	25.27	[6]
Polyamid, thermoplastic (Versamid 930, General Mills)	17.43	−1.92	14.89	23.02	[54]
Poly(*p*-benzamide)	18.0	11.9	7.9	23.0	[150]
cis-Poly(butadiene)elastomer (Bunahuls CB10, Chemische Werke Huels)	17.53	2.25	3.42	18.00	[54]
Poly(isobutylene) (Lutonal IC/123, BASF)	14.53	2.52	4.66	15.47	[54]
Poly(ethyl methacrylate) (Lucite 2042, DuPont)	17.60	9.66	3.97	20.46	[54]
Poly(ethylene terephthalate)	19.44	3.48	8.59	21.54	[6]
Poly(4-hydroxystyrene)	17.60	10.03	13.71	24.55	[133]
Poly(methacrylic acid)	17.39	12.48	15.96	26.80	[148]
Poly(methacrylonitrile)	18.00	15.96	7.98	25.37	[148]
Poly(methyl methacrylate)					
Poly(sulfone), Bisphenol A (Polystyrene LG, BASF)	21.28	5.75	4.30	22.47	[54]
Poly(sulfone), Bisphenol A (Udel)	19.03	0.00	6.96	20.26	[151]
Poly(vinyl acetate) (Mowilith 50, Hoechst)	20.93	11.27	9.66	25.66	[54]
Poly(vinyl butyral) (Butvar B76, Shawinigan)	18.60	4.36	13.03	23.12	[54]
Poly(vinyl chloride) (Vipla KR $K = 50$, Montecatini)	18.23	7.53	8.35	21.42	[54]
Poly(vinyl chloride)	18.72	10.03	3.07	21.46	[113]
Poly(vinyl chloride)	18.82	10.03	3.07	21.54	[6]
Saturated polyester (Desmophen 850, Bayer)	21.54	14.94	12.28	28.95	[54]

TABLE 16.5. *Continued.*

Polymer (trade name, supplier)	Solubility parameter ($MPa^{1/2}$)				Reference
	δ_d	δ_p	δ_h	δ_t	
Styrene-butadiene (SBR) raw elastomer (Polysar 5630, Polymer Corp.)	17.55	3.36	2.70	18.07	[54]
Terpene resin (Piccolyte S-1000, Penn. Ind. Chem.)	16.47	0.37	2.84	16.72	[54]
Urea-formaldehyde resin (Plastopal H, BASF)	20.81	8.29	12.71	25.74	[54]
Vinylidene cyanide/4-acetoxy, α-acetoxy styrene copolymer	21.48	11.25	7.16	21.89	[149]
Vinylidene cyanide/4-chloro-styrene copolymer (Rohm and Haas)	16.98	12.07	8.18	22.38	[149]
Poly(styrene)	18.64	10.52	7.51	22.69	[54]

ACKNOWLEDGMENT

The preparation of this chapter was supported by the National Science Foundation Grant No. DMR 9023541.

REFERENCES

1. R. F. Blanks, Polym. Plast. Technol. Eng. **8** (1), 13 (1977).
2. M. T. Shaw, J. Appl. Polym. Sci. **18**, 449 (1974).
3. S. Piccarolo and G. Titomanilo, Ind. Eng. Chem. Proc. Des. Dev. **22**, 146 (1982).
4. B. Schneier, Polym. Lett. **10**, 245 (1972).
5. P. E. Froehling and L. T. Hillegers, Polymer **22**, 261 (1981).
6. Z. Rigbi, Polymer **19**, 1229 (1978).
7. Shell Chemicals, *Solubility Parameters*, 2nd ed., Tech. Bull. International Chemical Society (X)/78/1 (1978).
8. Shell Chemicals, *Solvent Systems Design*, Tech. Bull. International Chemical Society (X)/78/2 (1987).
9. J. Polak, Collect. Czech. Chem. Commun. **31**, 1483 (1966).
10. J. H. Hildebrand and R. L. Scott, *Solubility of Non-Electrolytes*, 3rd ed. (Reinhold, New York, 1950; Dover, New York, 1964).
11. J. H. Hildebrand and R. L. Scott, *Regular Solutions* (Prentice-Hall, Englewood Cliffs, NJ, 1962).
12. J. H. Hildebrand, J. M. Prausnitz, and R. L. Scott, *Regular and Related Solutions* (Van Nostrand-Reinhold, Princeton, NJ, 1970).
13. E. Bagley *et al*., J. Paint Technol. **41**, 495 (1969).
14. E. B. Bagley, T. P. Nelson, J. W. Barlow, and S. A. Chen, Ind. Eng. Chem. Fund. **9**, 93 (1970).
15. E. Bagley *et al*., J. Paint Technol. **43**, 35 (1971).
16. J. D. van der Waals, Z. Phys. Chem. **5**, 133 (1890).
17. J. J. van Laar, *Sechs Vorträge uber das Thermodynamische Potential* (Vieweg, Braunschweig, 1906).
18. G. Scatchard, Chem. Rev. **8**, 321 (1931).
19. G. Scatchard, Chem. Rev. **44**, 7 (1949).
20. J. H. Hildebrand, J. Am. Chem. Soc. **38**, 1452 (1916).
21. J. H. Hildebrand, J. Am. Chem. Soc. **41**, 1067 (1919).
22. J. H. Hildebrand, Phys. Rev. **34**, 649 (1929).
23. J. H. Hildebrand, J. Am. Chem. Soc. **51**, 66 (1929).
24. J. H. Hildebrand, *Solubility of Non-Electrolytes*, 2nd ed. (Reinhold, New York, 1936; Russian translation: GONTI, Moscow, 1938).
25. J. H. Hildebrand, Chem. Rev. **44**, 37 (1949).
26. J. H. Hildebrand, Nature (London) **168**, 868 (1951).
27. J. H. Hildebrand, J. Phys. Chem. **58**, 671 (1954).
28. J. H. Hildebrand, Science **150**, 441 (1965).
29. J. H. Hildebrand, in *Structure–Solubility Relationships in Polymers*, Proceedings of the Symposium, 1976), edited by F. W. Harris and R. W. Seymour, (Academic, New York, 1977), p. 1.
30. J. H. Hildebrand, Ind. Eng. Chem. Fundam. **17**, 365 (1978).
31. J. H. Hildebrand, Proc. Natl. Acad. Sci. USA **76**, 6040 (1979).
32. J. H. Hildebrand and J. H. Dymond, Proc. Natl. Acad. Sci. USA **54**, 1001 (1965).
33. J. H. Hildebrand and R. H. Lamoreaux, Ind. Eng. Chem. Fundam. **13**, 110 (1974).
34. R. L. Scott, thesis, Princeton University, Princeton, NJ, 1945.
35. R. L. Scott, J. Am. Chem. Soc. **70**, 4090 (1948).
36. R. L. Scott, Disc. Faraday Soc. **15**, 44 (1953).
37. A. J. Staverman, Rec. Trav. Chim. Pays-Bas **60**, 827 (1941).
38. A. E. van Arkel, Trans. Faraday Soc. **42B**, 81 (1946).
39. P. A. Small, J. Appl. Chem. **3**, 71 (1953).
40. R. Andersen, Ph.D. thesis, Dept. of Chemical Engineering, University of California, Berkeley, 1961.
41. R. F. Blanks and J. M. Prausnitz, Ind. Eng. Chem. Fundam. **3**, 1 (1964).
42. R. Kumar and J. M. Prausnitz, in *Solutions and Solubilities*, edited by M. R. J. Dack (Wiley-Interscience, New York, 1975), Part 1, Chap. 5.
43. J. M. Prausnitz and R. Anderson, Am. Inst. Chem. Eng. J. **7**, 96 (1961).
44. R. F. Weimer and J. M. Prausnitz, Hydrocarbon Proc. Petr. Ref. **44**, 237 (1965).
45. J. M. Prausnitz and F. H. Shair, Am. Inst. Chem. Eng. J. **7**, 682 (1961).
46. H. G. Harris and J. M. Prausnitz, Ind. Eng. Chem. Fund. **8**, 180 (1969).
47. C. M. Hansen, Doctoral dissertation (Danish Technical Press, Copenhagen, 1967).
48. C. M. Hansen, J. Paint Technol. **39**, 104 (1967).
49. C. M. Hansen, J. Paint Technol. **39**, 505 (1967).
50. C. M. Hansen, Skand. Tidskr. Färg Lack **13**, 132 (1967).
51. C. M. Hansen, Skand. Tidskr. Färg Lack **14** (2), 28 (1968).
52. C. M. Hansen, Ind. Eng. Chem. Prod. Res. Dev. **8**, 2 (1969).
53. C. M. Hansen, J. Paint Technol. **42**, 660 (1970).
54. C. M. Hansen, Skand. Tidskr. Färg Lack **17**, 69 (1971).
55. C. M. Hansen, J. Paint Technol. **44**, 57 (1972).
56. C. M. Hansen, Chemtech **2**, 547 (1972).
57. C. M. Hansen, in *Solvents Theory and Practice*, Advances in Chemistry Series No. 124, edited by R. W. Tess (American Chemical Society, Washington, D.C., 1973), Chap. 4.
58. C. M. Hansen, Ind. Eng. Chem. Prod. Res. Dev. **16**, 266 (1977).
59. C. M. Hansen, Farbe Lack **83**, 595 (1977).
60. C. M. Hansen, Fed. Assoc. Tech. Ind. Peint. Vernis Emaux Encres Impr. Eur. Cont. Congr. **14**, 97 (1978).
61. C. M. Hansen, in *Macromolecular Solutions: Solvent–Polarity Relationships in Polymers*, Proceedings of the Symposium, American Chemical Society, New York, 1981, edited by R. B. Seymour and G. A. Stahl (Pergamon, New York, 1982), p. 1; Org. Coat. Plast. Chem. **45**, 227 (1981).
62. C. M. Hansen, Prog. Org. Coat. **10**, 331 (1982).
63. C. M. Hansen and A. Beerbower, in *The Kirk–Othmer Encyclopedia of Chemical Technology*, 2nd ed., edited by A. Standen (Interscience, New York, 1971), Suppl. Vol. p. 889.
64. C. M. Hansen and P. E. Pierce, Ind. Eng. Chem. Prod. Res. Dev. **13**, 218 (1974).
65. K. Skaarup, Skand. Tidskr. Färg Lack **14**, 45 (1968).
66. C. M. Hansen and K. Skaarup, J. Paint Technol. **39**, 511 (1967).
67. C. M. Hansen and K. Skaarup, Dan. Kemi **48**, 81 (1967).
68. C. M. Hansen and E. Wallström, J. Adhesion **15**, 275 (1983).
69. E. M. Arnett, Progr. Phys. Org. Chem. **1**, 223 (1963).
70. W. Gerrard, A. M. A. Mincer, and P. L. Wyvill, J. Appl. Chem. **10**, 115 (1960).
71. W. Gerrard, *Solubility of Gases and Liquids: A Graphic Approach* (Plenum, New York, 1976).

72. M. R. J. Dack, in *Solutions and Solubilities*, edited by M. R. J. Dack (Wiley-Interscience, New York, 1976), Part II, Chap. 11.
73. V. Gutmann, Rec. Chem. Progr. **30**, 169 (1969).
74. V. Gutmann, Z. Chem. **20**, 37 (1980).
75. J. Amoros, J. R. Solana, and E. Villar, Mater. Chem. Phys. **10**, 557 (1984).
76. R. F. Fedors, Jet Propul. Lab. Quart. Tech. Rev. **3**, 45 (1973); Polym. Eng. Sci. **14**, 147, (1974); **14**, 472 (1974).
77. K. M. Watson, Ind. Eng. Chem. **23**, 360 (1931); **35**, 398 (1943).
78. A. S. Michaels, ASTM Tech. Pub. **340**, 3 (1963).
79. D. M. Koenhen and C. A. Smolders, J. Appl. Polym. Sci. **19**, 1163 (1975).
80. I. A. Wiehe and E. B. Bagley, Am. Inst. Chem. Eng. J. **13**, 836 (1967).
81. E. B. Bagley and S.-A. Chen, J. Paint Technol. **41**, 494 (1969).
82. J. M. Scigliano, Ph.D. thesis, Washington University, St. Louis, MO, 1972; Diss. Abstr. B **32**, 6984 (1972).
83. I. Vavruch (personal communication).
84. J. H. Sewell, RAE Technical Report No. 66185, June, 1966.
85. A. Beerbower and J. R. Dickey, Am. Soc. Lubr. Eng. Trans. **12**, 1 (1969).
86. O. Olabisi and R. Simha, J. Appl. Polym. Sci. **21**, 149 (1977).
87. G. M. Bristow and W. F. Watson, Trans. Faraday Soc. **54**, 1731 (1958); **54**, 1742 (1958).
88. P. Alessi, I. Kikic, G. Torriano, and A. Papo, J. Coatings Technol. **51**, 62 (1979).
89. G. DiPaola-Baranayi and J. E. Guillet, Macromolecules **11**, 228 (1978).
90. G. DiPaola-Baranayi, J. E. Guillet, J. Klein, and H.-E. Jeberein, J. Chromatogr. **166**, 349 (1978).
91. G. DiPaola-Baranayi, Macromolecules **15**, 622 (1982).
92. K. Ito and J. E. Guillet, Macromolecules **12**, 1163 (1979).
93. J. E. G. Lipson and J. E. Guillet, J. Coatings Technol. **54**, 90 (1982).
94. M. Magat, J. Chem. Phys. **46**, 344 (1949).
95. D. Patterson, Macromolecules **4**, 30 (1971).
96. D. Patterson, Y. B. Tewari, H. P. Schreiber, and J. E. Guillet, Macromolecules **4**, 356 (1971).
97. C. Smidsrod and J. E. Guillet, Macromolecules **2**, 272 (1968).
98. W. A. Ruff, C. J. Glover, and A. T. Watson, Am. Inst. Chem. Eng. J. **32**, 1948 (1986).
99. W. A. Ruff, C. J. Glover, A. T. Watson, W. R. Lau, and J. C. Holste, Am. Inst. Chem. Eng. J. **32**, 1954 (1986).
100. S. Wu, J. Phys. Chem. **27**, 3332 (1968).
101. P. J. Flory, *Principles of Polymer Chemistry (Cornell University Press, Ithaca, NY*, 1953).
102. T. Matsuo, Preprints Atlantic Systems Conferences/Journal Chemical Society **20**, 895 (1979).
103. W. H. Stockmayer and M. Fixman, J. Polym. Sci. C 137 (1963).
104. J. W. Van Dyk, H. L. Frisch, and D. T. Wu, Ind. Eng. Chem. Prod. Res. Dev. **24**, 473 (1985).
105. J. E. Guillet, British Patent No. 1,331,429 (1973).
106. R. D. Newman and J. M. Prausnitz, J. Phys. Chem. **76**, 1492 (1972).
107. A. J. Manning and F. Rodriguez, J. Appl. Polym. Sci. **17**, 1651 (1973).
108. W. R. Song and D. W. Brownawell, Polym. Eng. Sci. **10**, 222 (1970).
109. B. A. Wolf, Macromol. Chem. **178**, 1869 (1977).
110. S. T. Bowden and W. J. Jones, Philos. Mag. **39**, 155 (1948).
111. C. W. Bunn, J. Polym. Sci. **16**, 323 (1955).
112. A. T. DiBenedetto, J. Polym. Sci. A **1**, 3459 (1963).
113. M. Dunkel, J. Phys. Chem. A **138**, 42 (1928).
114. R. A. Hayes, J. Appl. Polym. Sci. **5**, 318 (1961).
115. P. J. Hoftyzer and D. W. Van Krevelen, Paper No. IIIs-15, presented at the International Symposium on Macromolecules of International Union of Pure and Applied Chemistry, Lyden, 1970.
116. K. L. Hoy, J. Paint Technol. **42**, 76 (1970).
117. A. E. Rheineck and K. F. Lin, J. Paint Technol. **40**, 611 (1968).
118. D. W. Van Krevelen, Fuel **44**, 229 (1965).
119. D. W. Van Krevelen and P. J. Hoftyzer, J. Appl. Polym. Sci. **11**, 2189 (1967).
120. A. H. Konstam and W. R. Feairheller, Jr., Am. Inst. Chem. Eng. J. **16**, 837 (1960).
121. D. W. Van Krevelen, *Properties of Polymers, Correlations with Chemical Structure 2nd ed. (Elsevier Amsterdam,* 1976).
122. R. L. Scott and M. Magat, J. Polym. Sci. **4**, 555 (1949).
123. P. J. Flory, J. Chem. Phys. **10**, 51 (1942).
124. P. J. Flory and J. Rehner, Jr., J. Chem. Phys. **11**, 512 (1943).
125. A. F. M. Barton, in *Polymer Cohesion Parameters and Polymer–Liquid Interaction Parameters, Polymer Yearbook 6, edited by R. A. Pethrick, G. E. Zaikou, and T. Tsuruta, (Harwood Academic Publishers, New York,* 1990), *p.* 94.
126. J. Brandrup and E. H. Immergut, *Polymer Handbook, 3rd ed. (Wiley, New York*, 1989).
127. Allan F. M. Barton, *CRC Handbook of Solubility Parameters and Other Cohesion Parameters 2nd ed.* (*CRC, Boca Raton, FL*, 1991).
128. F. W. Billmeyer, Jr., *Textbook of Polymer Science, 2nd ed. (Wiley-Interscience, New York*, 1971).
129. A. G. Shvarts, Kolloid Zh. **18**, 755 (1956).
130. A. V. Tobolsky, *Properties and Structure of Polymers (Wiley, New York*, 1960), *pp*. 64 *and* 66.
131. G. Gee, Trans. Inst. Rubber Ind. **18**, 266 (1943).
132. H. Mark and A. V. Tobolsky, *Physical Chemistry of High Polymers (Interscience, New York*, 1950), *p*. 263.
133. S. Arichi and S. Himuro, Polymer **30**, 686 (1989).
134. D. Mangaraj, S. Patra, and S. B. Rath, Makromol. Chem. **67**, 84 (1963).
135. D. Mangaraj, S. Patra, and S. Rashid, Makromol. Chem. **65**, 39 (1963).
136. J. E. G. Lipson and J. E. Guillet, J. Polym. Sci. Polym. Phys. Ed. **19**, 1199 (1981).
137. M. Lautout and M. Magat, Z. Phys. Chem. (Frankfurt) **16**, 292 (1958).
138. M. Roth, J. Appl. Polym. Sci. B Polym. Phys. **28**, 2715 (1990).
139. F. Vocks, J. Polym. Sci. **A-2**, 5319 (1964).
140. L. Mandelkern, private communication to H. Burrell, *Polymer Handbook, 1st ed. (Interscience Publishers, New York*, 1966).
141. M. M. Marugan, E. Perez, R. Benavente, A. Bello, and J. M. Perena, Europ. Polym. J. **28**, 1159 (1992).
142. D. Mangaraj, S. K. Bhatnagar, and S. B. Rath, Makromol. Chem. **67**, 75 (1963).
143. G. Gee, G. Allen, and G. Wilson, Polymer (London) **1**, 456 (1960).
144. K. K. Chee and S. C. Ng, J. Appl. Polym. Sci. **50**, 1115 (1993).
145. K. S. Siow, S. H. Goh, and K. S. Yap, Polym. Mater. Sci. Eng. **51**, 532 (1984).
146. R. S. Tillaev, M. Khasaukhanova, S. A. Tashmukhamedov, and Kh. U. Usmanov, J. Polym. Sci. C **39**, 107 (1972).
147. D. Mangaraj, S. Patra, P. C. Roy, and S. K. Bhatnagar, Makromol. Chem. **84**, 225 (1965).
148. B. C. Ho, W. K. Chin, and Y. D. Lee, J. Appl. Polym. Sci. **42**, 99 (1991).
149. A. Belfkira and J. P. Montheard, J. Appl. Polym. Sci. **51**, 1849 (1994).
150. S. M. Aharoni, J. Appl. Polym. Sci. **45**, 813 (1992).
151. T. Matsuura, P. Blais, and S. Sourirajan, J. Appl. Polym. Sci. **20**, 1515 (1976).

CHAPTER 17

Mark–Houwink–Staudinger–Sakurada Constants

W. Zeng, Y. Du, Y. Xue, and H. L. Frisch

Department of Chemistry, State University of New York, Albany, NY 12222

17.1 INTRODUCTION

The viscosity of a dilute polymer solution depends on the nature of polymer and solvent, the concentration of the polymer, its average molecular mass and molecular mass distribution, the temperature, and the shear rate. The most important characteristic quantity in a very dilute solution, at vanishing shear rate, is the limiting viscosity number, which is defined as [1]

$$[\eta] = \lim_{c \to 0} \frac{\eta - \eta_s}{\eta_s c}, \tag{17.1}$$

where η is the viscosity of the solution, η_s that of the pure solvent, and c the polymer concentration. The importance of this number is that it is the basis of a convenient, rapid relative determination of a certain average molar mass of a polymer sample. $[\eta]$ has the dimensions of a reciprocal concentration or a reciprocal density, for which ml/g is used here. The concentration is expressed in grams of solute per milliliter of solution, or more frequently, in grams of solute per 100 milliliters of solution. The quantity $[\eta]$ of a polymer solution is connected with the dimension of the isolated polymer molecule. Within a given series of polymer homologs, $[\eta]$ increases with the molar mass M; hence it is a measure of M. The limiting viscosity number $[\eta]$ for a series of homologous polymers under a fixed solvent condition (solvent species and temperature) follows the Mark–Houwink–Staudinger–Sakurada (MHSS) relation [2]:

$$[\eta] = K\overline{M}_v^{\,a} \tag{17.2}$$

over an extended range of molar masses. Here K is the MHSS "constant," and a the MHSS "exponent"; $\overline{M}_v$ is called viscosity average molar mass, which is defined as

$$\overline{M}_v(a) = (\Sigma M_i^a w(M_i))^{1/a}, \tag{17.3}$$

where $w(M_i)$ is the weight fraction of molecules of molar mass M_i. In a sample consisting of N_i molecules of molar mass M_i, the weight fraction $w(M_i) = M_i N_i / \Sigma M_i N_i$. Mathematically it follows that

$$\Sigma w(M_i) = 1, \tag{17.4}$$

$$\overline{M}_v(a_1) > \overline{M}_v(a_2),\ a_1 > a_2. \tag{17.5}$$

In the MHSS equation both the exponent a and the coefficient K depend on the polymer solvent pair and the temperature. Empirically the value of the exponent a is roughly characterized by the difference of the solubility parameters of polymer (δ_p) and solvent (δ_s) [3].

The parameters K and a are evaluated from the intercept and slope, respectively, of the double-logarithmic plots of $[\eta]$ against M_v determined for a series of samples that differ only in their molar mass. The main experimental facts that have to be explained theoretically are as follows [4]:

1. When $[\eta]$ of a sharp (i.e., essentially monodisperse) polymer fraction of molar mass M is plotted against M on a log–log graph paper, it gives a straight line over a wide range of M.
2. The slope a of the line for linear flexible polymers in non-θ solvents is in the range $0.5 < a < 0.8$; polymers having an a larger than 0.8 are suspected to be semiflexible.
3. In general, a is larger for a better solvent.
4. Under θ conditions (unperturbed random coil), for linear, flexible polymers, Eq. (17.2) becomes

$$[\eta]_\theta = K_\theta \overline{M}_v^{1/2}, \tag{17.6}$$

and for a given polymer K_θ is nearly independent of the solvent species.

The ratio of $[\eta]/[\eta]_\theta$ is called the viscosity expansion factor α^3. The viscosity-averaged molar mass (M_v) obtained from the MHSS equation may also be used to get information about the degree of molar mass dispersion from the comparison of the $\overline{M}_v$ values of a polymer sample in two different solvents [5,6].

The prefactor K in Eq. (17.6) can be expressed in terms of the hydrodynamic factors Φ_θ, ρ_θ, and P_θ, which are defined as follows:

$$\Phi_\theta = [\eta]_\theta M/(6\langle s^2\rangle_\theta)^{1.5}, \tag{17.7}$$

$$\rho_\theta = \langle s^2\rangle_\theta^{0.5}/R_{H\theta}, \tag{17.8}$$

$$P_\theta = k_B\Theta/[(6\langle s^2\rangle_\theta)^{0.5}\eta_s D_0], \tag{17.9}$$

where Θ denotes the theta temperature in degrees Kelvin, $\langle s^2\rangle^{0.5}$ is the root-mean-square radius of gyration, k_B is Boltzmann's constant, η_s is the viscosity coefficient of the solvent, and R_H is the Stokes radius, the hydrodynamic size of the polymer coil. Θ_θ, ρ_θ, and P_θ are independent of molecular weight M; they were first introduced by Flory, Fox, and Mandelkern [7,8].

In the nondraining limit,

$$K_\theta = N_A(\pi/6)^{1.5}a^3m^{-1.5}\Gamma, \tag{17.10}$$

$$\Phi_\theta = N_A(\pi/6)^{1.5}\Gamma, \tag{17.11}$$

$$\rho_\theta = 6^{0.5}\pi\Gamma', \tag{17.12}$$

where N_A is Avogadro's constant, a is the spring length defined by Eq. (17.17), m is the molar mass of one bead in the spring–bead polymer chain, and Γ and Γ' are dimensionless constants whose values depend on what theory is employed. According to the Krikwood–Riseman theory, we have $\Gamma = 1.259$ and $\Gamma' = 0.192$ [9], which yield $\Phi_\theta = 2.87 \times 10^{23}\,\text{mol}^{-1}$ and $\rho_\theta = 1.48$.

Experimental values of Φ_θ and ρ_θ are considerably influenced by the polydispersity of polymer samples used; however, both Φ_θ and ρ_θ are universal to a first approximation, the former being mostly found to be in the range $(2.0 - 2.7) \times 10^{23}\text{mol}^{-1}$ and the latter in the range 1.25–1.35 (6.15–5.70 for P_θ). Recently, Oono and Kohmoto [10,11] applied renormalization-group theory to the polymer hydrodynamics of the Krikwood–Riseman scheme and computed the values of $\Phi_\theta = 2.36 \times 10^{23}\text{mol}^{-1}$ and $P_\theta = 6.20$, which compares rather favorably with experimental values.

After the Krikwood–Riseman theory [12], there are many theories that have been developed by other researchers, such as the dependence of intrinsic viscosity on molecular weight by Flory and Fox [13,7], and by Yu and Stockmayer [14], and others [15,16]; the effect of rate of shear by Kuhn [17], Cerf [18], and others [19–23]; Ham–Zimm theory of branched polymers [24,25]; Crothers and Zimm theory of wormlike chains [26]; theories for rigid rod molecules [17,27–30]; theories for rigid sphere molecules [28,31–33]; and theories for flexible ring molecules by Fukatusu and Kurata [34] and by Bloomfield and Zimm [35], etc. We will not go into details here.

The abbreviations of the methods for determining the molar mass of polymer samples are as follows:

1. Methods for the number-average molecular weight, M_n: CR, cryoscopy; EB, ebullioscopy; EG, end-group titration; OS, osmotic pressure; VOS, vapor pressure osmometry.
2. Methods for the weight-average molecular weight, M_w: LS, light scattering; SA, approach to the sedimentation equilibrium (Archibald's method).
3. Empirical or semiempirical methods: GPC, gel permeation chromatography; LV, limiting viscosity-number–molecular-weight relationship; SD, sedimentation diffusion.

Practically, the MHSS constants are obtained for the $[\eta]$–M relationships expressed in terms of number-average molar mass $\overline{M}_n$ or weight-average molar mass $\overline{M}_w$ determined by the above methods, i.e.,

$$[\eta] = K_n\overline{M}_n^a \tag{17.13}$$

or

$$[\eta] = K_w\overline{M}_w^a. \tag{17.14}$$

The values of K_n and K_w are influenced by the polydispersity of molar mass of the polymer samples. For the exponential polydispersity of molar mass,

$$K_n = K\Gamma(a + h + 1)/h^a\Gamma(h + 1), \tag{17.15}$$

$$K_w = K\Gamma(a + h + 1)/(h + 1)^a\Gamma(h + 1), \tag{17.16}$$

where h is a constant and Γ is the gamma function. For the log-normal polydispersity of molar mass,

$$K_n = K(\overline{M}_w/\overline{M}_n)^{0.5a(a+1)}, \tag{17.17}$$

$$K_w = K(\overline{M}_w/\overline{M}_n)^{0.5a(a-1)}. \tag{17.18}$$

Therefore, K_n is more sensitive to the polydispersity of molar mass.

Extensive tables of K and a values exist [36,37]. In Tables 17.1 and 17.2 we provide two tables of MHSS constants of commonly used polymer–solvent systems with original references.

TABLE 17.1. *Martk-Houwink constant-K values.*

Polymer	Solvent	Temperature (°C)	$K\times10^3$ (ml/g)	Range $M\times10^{-4}$	Method	Reference
Amylose	(aq)KCl (0.33M)	25	112	16–230	LS	[38]
Cellulose tricarbanilate	Anisole	94	130	31–220	LS	[39]
Cellolose trioctanoate	Dimethylformamide	140	113	10–32	OS	[40]
Poly(butadiene)						
98%-*cis*, 2%-1,2	Benzene	30	33.7	5–50	OS	[41]
	Toulene	20.5	185	5–50	OS	[41]
95%-*cis*, 1%-*trans*, 4%-1,2	Benzene	30	8.5	15–50	LS	[42]
	Toulene	30	33.9	10–65	OS	[43]
94%-*cis*, 4%-*trans*, 2%-1,2	Benzene	25	41.4	9–120	OS	[44]
	Dioxane	20.2	205	9–120	OS	[44]
92%-*cis*, 3%-*trans*, 6%-1,2	Benzene	32	10	10–160	LS	[45]
51%-*cis*, 43%-*trans*, 6%-1,2	Toluene	30	39	11–25	OS	[46]
Poly(butadiene-*co*-acrylonitrile)						
Buna-*N* rubber	Acetone	25	50	2.5–10	OS	[47]
	Benzene	25	13	2.5–10	OS	[47]
	Toulene	25	49	2.5–40	OS	[47]
Poly(butadiene-*co*-styrene)						
Buna-S, GR-S, or SBR rubber	Benzene	25	52.5	1–160	OS	[48]
	Toulene	25	52.5	2.5–50	OS	[47]
Poly(2-*tert*-butylbutadiene)	Benezene	21	4.2	6–90	SD	[49]
	Octane	21	4.2	6–35	SD	[49]
Poly(chloroprene)						
Neoprene CG	Benzene	25	2.02	6–150	OS	[50]
Neoprene GN	Benzene	25	14.6	2–96	OS	[51]
Neoprene W	Benzene	25	15.5	5–100	OS	[52]
Poly(isoprene)						
Natural rubber	Benzene	30	18.5	8–28	OS	[53]
	Toulene	25	50.2	7–100	OS	[54]
Synthetic *cis*	hexane	20	68.4	5–80	SD	[55]
	Toulene	30	8.51	20–100	LS	[56]
Synthetic *trans*	Benzene	32	43.7	8–140	LS	[57]
Poly(1,2-trichlorobutadiene)	Benzene	25	31.6	25–130	LS	[58]
Poly(alkene) C_{10}–C_{18}	Toluene	25	12.7	2–18	LS	[59]
Poly(alkene) C_{12}–C_{18}	Cetane	38	21	4–700	LS	[60]
Poly(1-butene)						
Atactic	Benzene	30	22.4	0.03–0.5	EG	[61]
Isotactic	Heptane	35	4.73	4.5–90	LS	[62]
Poly(ethylene)						
Low pressure	Bibhenyl	127.5	323	2–30	LV	[63]
	Octanol	180.1	286	2–105	LV	[63]
High pressure	Decalin	70	38.73	0.2–3.5	OS	[64]
Poly(isobutene)						
	Benzene	24	107	18–188	LV	[65]
	Carbon tetrachloride	30	29	0.05–126	OS, CR	[66]
	Toluene	0	40	1–146	LV	[66]
Poly(isobutene-*co*-isoprene), butyl rubber	Benzene	22.8	115	15–72	LS	[67]
	Toluene	25	66	15–30	OS	[68]
Poly(3-methyl-1-butene)	Diisobutylene	20	42	1–20	LS	[69]
Poly(4-methyl-1-butene)	Biphenpl	194.6	152	6–30	OS	[70]
Poly(1-octene)	Bromobenzene	25	2.9	25–400	LS	[71]
	Cyclohexane	30	5.75	25–400	LS	[71]
Poly(pentenamer)						
80 ∼ 85%*trans*, 19 ∼ 12%-*cis*	Cyclohexane	30	56.9	3.6–63	LS	[72]
	Toluene	30	52.1	3.6–63	LS	[72]

TABLE 17.1. *Continued.*

Polymer	Solvent	Temperature (°C)	$K\times10^3$ (ml/g)	Range $M\times10^{-4}$	Method	Reference
Poly(propylene)						
Atactic	Benzene	25	27	6–31	OS	[73]
	Toluene	30	21.8	2–34	OS	[74]
Isotactic	Biphenyl	125.1	152	5–42	LV	[75]
Syndiotactic	Heptane	30	31.2	9–45	LS	[76]
Poly(acrylamide)	Water	30	6.31	2–50	SD	[77]
Poly(butyl arylate)	Acetone	25	6.85	5–27	LS	[78]
Poly(*tert*-butyl arylate)	Acetone	25	4.7	7–31	LS	[79]
	Hexane	24.2	49	7–31	LS	[79]
	Methanol	25	16	7–31	LS	[79]
Poly(1, 1-dihydroperfluorobutyl acrylate)	Benzofluoride	26.6	13	20–200	LS	[80]
Poly(*N, N*-dimethylamide)	Methonal	25	17.5	5–122	LS	[81]
	Water	25	23.2	5–122	LS	[81]
Poly(ethyl scrylate)	Acetone	25	51	35–450	LS	[82]
	Benzene	30	27.7	5–67	OS	[83]
	Chloroform	30	31.4	9–54	OS	[83]
Poly(2-ferrocenylethyl acrylate)	Benzene	25	4.68	1.4–2.7	VOS, GPC	[84]
Poly(ferrocenylethly acrylate)	Benzene	25	6.84	0.7–2	VOS, GPC	[85]
Poly(hexadecyl acrylate)	Methanol	30	48.7	6–70	OS	[83]
	Heptane	20	1.74	1–10	LS	[86]
Poly(isopropyl acrylate)	Acetone	30	13	6–30	LS	[87]
	Benzene	25	14.9	7–70	OS	[88]
	Chloroform	30	14.1	7–30	LS	[89]
Poly(methyl acrylate)	Acetone	20	7.4	7–32	OS	[90]
	Benzene	25	2.58	20–130	OS	[91]
	Toluene	30	7.79	25–190	LS	[92]
Polt(1-methylphenyl acrylate)	Butyl acetate	25	14.7	2–110	SD	[93]
Poly(morpholinocarbonylethylene)	Dimethylformamide	25	18	?	LS	[94]
Poly(piperidinocarbonylethylene)	Dimethylformamide	25	32	?	LS	[94]
Poly(propyl acrylate)	Butanone	30	15	71–181	LS	[95]
Poly(benzyl methacrylate)	Benzene	30	1.03	17–120	LS	[96]
Poly(butyl methacrylate)	Acetone	25	18.4	100–600	LS	[97]
	Benzene	30	(4.0)	8–300	LS	[98]
	Butanone	23	1.56	25–260	LS	[99]
	Chloroform	20	0.78	4–800	LS	[100]
Poly(*tert*-butyl methacrylate)	Butyl acetate	25	22	46–870	LS	[101]
Poly(2-*tert*-butylphenyl methacrylate)	Benzene	25	7.8	4–113	LS	[102]
	Butanone	25	9.0	4–113	LS	[102]
	Cyclohexane	18.4	35.5	4–113	LS	[102]
Poly(4-*tert*-butylphenyl methacrylate)	Acetone	20	5.75	6–350	LS	[103]
	Bromobenzene	20	4.1	15–2,500	LS	[104]
	Chloroform	20	2.4	6–300	LS	[105]
	Cyclohexane	25	47	11–204	LS	[106]
	Tetrahydrofuran	25	9.4	7–88	LS	[106]
Poly(cyclohexyl methacrylate)	Benzene	30	8.4	80–200	LS	[107]
	Butanol	23	33.7	57–445	LS	[108]
	Cyclohexane	25	8.8	10–419	LS	[109]
Poly(cyclohexyl thiolmethacrylate)	Cyclohexane	25	8.65	4–60	LS	[110]
	Tetrahydrofuran	35	4.07	4–60	LS	[110]
Poly(dodecyl methacrylate)	Butyl acetate	23	8.64	26–360	LS	[111]
Poly(2-ethylbutyl methacrylate)	Butanone	25	2.21	48–332	LS	[112]
	2-propanol	27.4	33.7	48–332	LS	[112]
Poly(ethyl methacrylate)	Butanone	23	2.83	20–263	LS	[113]
	Ethyl acetate	35	8.6	65–1,200	LS	[114]
Poly(2-ferrocenylethyl methacrylate)	Benzene	N/A	3.12	2–9	VOS,GPC	[84]
Poly(ferrocenylmethyl methacrylate)	Benzene	25	27.8	0.6–3.6		[85]
Poly(hexadecyl methacrylate)	Benzene	21	5.9	130–440	SD	[115]
	Heptane	21	3.92	130–440	SD	[115]

TABLE 17.1. *Continued.*

Polymer	Solvent	Temperature (°C)	$K\times10^3$ (ml/g)	Range $M\times10^{-4}$	Method	Reference
Poly[4-(4- hexadecyloxy-benzoyloxy)-phenyl methacrylate]	Carbon tetrachloride	N/A	33.1	10–2,000	SD	[116]
Poly(hexyl methacrylate)	Butanone	23	2.12	6–41	LS	[117]
	2-propanol	32.6	43	6–41	LS	[117]
Poly(2-hydroxyethyl methacrylate)	Dimethylformamide	30	10.6	4–52	LS	[118]
	Methanol	30	52.4	4–52	LS	[118]
Poly(isobutyl methacrylate)	Acetone	25	0.199	300–1,100	LS	[119]
	Benzene	25	7.03	50–116	OS	[120]
	Butanone	20	5.56	300–1,100	LS	[119]
Poly(5-*p*-menthyl methacrylate)	Benzene	25	9.6	12–230	LS	[102]
	Cyclohexane	25	11.5	12–230	LS	[102]
	Tetrahydrofuran	25	11.5	12–230	LS	[102]
Poly(methacrolein)	Dimethylformamide	20	2.8	0.5–2	OS,CR	[121]
Poly(methacrylic acid)	Methanol	26	242	4–20	OS	[122]
Poly(methacrylonitrile)	Acetone	20	95.5	35–100	OS	[123]
	Dimethylformamide	29.2	306	0.6–8	LV	[124]
Poly(2-methoxyethyl methacrylate)	Butanone	25	7.34	4–220	LS	[125]
	Tetrahydrofuran	25	7.57	4–220	LS	[125]
Poly(methyl butacrylate)	Butanol	13	57	6–60	LS	[126]
	Butanone	30	5.43	7–430	LS	[126]
Poly(methyl *a*-chloroacrylate)	Chloroform	30	3.08	20–780	LS	[127]
Poly(methyl ethacrylate)	Benzene	30	2.35	16–110	LS	[126]
	Butanone	30	4.29	4–200	LS	[126]
Poly(methyl methacrylate)	Acetone	20	5.5	7–700	SD	[128]
	Acetonitrile	30	39.3	10–86	LV	[129]
	Benzene	20	8.35	7–700	SD	[128]
	Butanone	25	6.8	8–137	LS	[130]
Poly(octadecyl methacrylate)	Tetrahydrofuran	30	2.5	20–170	LS	[131]
Poly(octyl methacrylate)	Butanol	16.8	26.8	33–1,250	LS	[132]
	Butanone	23	4.47	33–1,250	LS	[132]
Poly(*N*-phenyl methacrylamide)	Acetone	20	28.2	10–320	LS	[133]
Poly(stearyl methacrylate)	Tetrahydrofuran	30	9	1.5–94	LS	[134,135]
Poly(tetrahydrofurfuryl methacrylate)	Acetone	30	24	16–62	OS	[136]
Poly[(hexadecyloxy)ethylene]	Heptane	21	70.8	0.5–3	SD	[137]
Poly(methoxyethylene)	Benzene	30	76	1–45	LS	[138]
	Butanone	30	137	1–45	LS	[138]
Poly[(octadecyloxy)ethylene]	Benzene	25	170	0.1–1.5	LS	[131]
	Tetrahydrofuran	30	224	9.4–11	LS	[131]
Poly(chlorotrifluoroethylene)	2,5-dichlorobenzotrifluoride	130	6.15	7–51	OS	[139]
Poly(vinyl alcohol)	Water	25	20	0.6–2.1	OS	[140]
Poly(vinyl bromide)	Cyclohexane	25	32.8	2–10	LS	[141]
	Tetrahydrofuran	25	15.9	2–10	LS	[141]
Poly(vinyl chloride)	Benzyl alcohol	155.4	156	4–35	LS	[142]
	Chlorobenzene	30	71.2	3–19	SA	[143]
	Cyclohexanone	20	11.6	2–10	OS	[144]
	Tetrahydrofuran	20	3.63	2–17	OS	[145]
Poly(vinyl flouride)	Dimethylformamide	90	6.42	14–66	SV	[146]
Poly(vinylidene chloride)	Hexamethylphosphoramide	25	25.8	0.8–12	LS	[147]
Poly(allyl acetate)	Benzene	27	66	0.1–0.3	CR	[148]
Poly(vinyl acetate)	Benzene	30	22	34–102	LS	[149]
	Butanone	25	13.4	25–346	LS	[150]
	Chlorobenzene	25	110	0.15–7	OS	[151]
	Chloroform	20	15.8	7–68	OS	[152]
	Dioxane	25	11.4	4–34	OS	[153]
	Ethanol	56.9	90	4–150	OS,LS	[154]
	Methanol	6	101	0.3–150	OS,LS, VOS	[154,155]
	Toluene	25	108	4–15	OS	[153]

TABLE 17.1. *Continued.*

Polymer	Solvent	Temperature (°C)	$K\times10^3$ (ml/g)	Range $M\times10^{-4}$	Method	Reference
Poly(vinyl benzoate)	Xylene	32.5	62	10–24	OS	[156]
Poly(vinyl butyrate)	Benzene	30	11.15	3–15	OS	[157]
Poly(vinyl caproate)	Benzene	30	15.47	3–126	OS	[157]
Poly(vinyl 4-chlorobenzoate)	Water	30	64	6–35	LV	[158]
Poly(vinyl formate)	Acetone	30	29.3	3–41	LV	[159]
	Acetonitrile	30	14.1	3–41	LV	[159]
	Dioxane	30	20.7	3–41	LV	[159]
	Methyl acetate	30	37.6	3–24	LV	[159]
Poly(vinyl isobutyrate)	Benzene	30	11.05	5–20	OS	[157]
Poly(vinyl isocaproate)	Benzene	30	51	3–17	OS	[157]
Poly(vinyl pivalate)	Acetone	25	2.88	40–217	LS	[160]
Poly(4-bromostyrene)	Benzene	20	95.5	3–30	OS	[161]
	Chlorobenzene	30	7.43	59–400	LS	[162]
	Toluene	30	18.2	63–400	LS	[163]
Poly(p-*tert*-butylstyrene)	Benzene	35	7.1	1.8–640	LS	[164]
	Cyclohexane	35	9.9	1.8–640	LS	[164]
	1-nitropropane	31	61	1.8–640	LS	[164]
Poly(2-chlorostyrene)	Toulene	25	11.5	14–101	LS	[165]
Poly(4-chlorostyrene)	Benzene	30	30.6	10–200	LS	[166]
	Butanone	25	29	3–140	LS	[167]
	Chloroform	30	14.8	10–200	LS	[166]
	Dioxane	30	17.6	10–200	LS	[166]
	Toluene	20	24.1	2–40	LS	[168]
Poly(4-cyclohexylstyrene)	Heptane	30	32.3	4–30	OS	[169]
	Toluene	30	10.6	2–30	OS	[169]
Poly(2,5-dichlorostyrene)	Toluene	21	12.6	7–66	LS	[170]
Poly(3,4-dichlorostyrene)	Chlorobenzene	30	4.39	8–51	OS	[169]
Poly(2,4-dimethylstyrene)	Benzene	20	3.8	3–22	LS	[171]
	Butyl acetate	20	10.2	3–22	LS	[171]
	Cyclohexane	20	14.8	3–22	LS	[171]
	Toluene	30	9.52	5–12	LS	[172]
Poly(3-fluorostyrene)	Benzene	25	15.3	N/A	LS	[173]
	Butanone	25	13.8	N/A	LS	[173]
	Chloroform	25	12.8	1–15	LS	[173]
Poly(4-fluorostyrene)	Benzene	25	40.8	N/A	LS	[173]
	Butanone	25	11.1	N/A	LS	[173]
	Chloroform	25	16.1	0.2–13	LS	[173]
Poly(4-iodostyrene)	Dioxane	20	33	10–118	LV	[174]
Poly(*p*-isopropylstyrene)	Toluene	25	12.3	14–75	LS	[175]
Poly(*o*-methoxystyrene)	Toluene	30	6.4	13–35	LS	[176]
Poly(*p*-methoxystyrene)	Butanone	30	3.75	13–75	LS	[176]
	Pentyl acetate	25	55	22–220	LS	[177]
	Toluene	25	10.5	22–220	LS	[177]
Poly(*m*-methylstyrene)	Benzene	30	7.36	8–115	OS	[178]
	Cyclohexane	30	11.76	15–83	OS	[178]
	Ethyl acetate	30	17.72	15–83	OS	[178]
Poly(*p*-methylstyrene)	Diethyl succinate	16.4	70	16–200	LS	[179]
	Toluene	30	8.86	19–180	LS	[179]
Poly[(2,3,4,5,6-pentafluorostyrene)]	4-methyl-2-pentanone	20	4.37	10–260	OS	[180]
Poly(styrene)						
Atactic	Benzene	30	6.3	1–300	SD	[181]
	Butanone	25	39	1–180	LS	[182]
	Butyl chloride	40.8	15.1	29–106	LS	[183]
	Chlorobenzene	25.7	7.4	62–424	LS	[183]
	Chloroform	25	7.16	12–280	LS	[184]
	Cyclohexane	28	108	0.6–69	OS	[185]
	Dichloroethane	25	21	1–180	LS	[182]

TABLE 17.1. *Continued.*

Polymer	Solvent	Temperature (°C)	$K\times10^3$ (ml/g)	Range $M\times10^{-4}$	Method	Reference
	Dimethylformamide	35	31.8	0.4–87	LS	[186]
	Dioxane	34	15	8–80	DV	[187]
	Ethylbenzene	25	17.6	7–150	OS	[188]
	Tetrahydrofuran	25	11	1–100	GPC	[189]
	Toluene	20	4.16	4–137	LS	[183]
Atactic, anionic	Benzene	25	100	0.04–1	VOS,EB	[190]
	Cyclohexane	34	74.5	N/A	LS	[191]
	Cyclohexene	25	16.3	20–107	LS	[192]
	Toluene	20	10.69	3–4,000	LS,OS,SD	[193]
Isotactic	Benzene	30	9.5	4–75	OS	[194]
	Chloroform	30	25.9	9–32	OS	[195]
	Toluene	30	11	3–37	OS	[196]
Poly(styrenesulfonic acid)	Aqueous HCl (0.52 M)	25	0.344	18–46	LV	[197]
	Aqueous HaCl (0.52 M)	25	0.312	18–46	LV	[197]
Poly[(biphenyl-4-yl)-ethylene]	Benzene	20	21.4	7–170	LS	[198]
Poly(*tert*-butyl crotonate)	Toluene	25	7.7	0.6–35	OS,GPC	[199]
Poly(vinyl carbanilate)	Dioxane	20	13.7	6–200	LS	[200]
Poly(dibutyl itaconate)	Toluene	25	5.7	20–105	LS	[201]
Poly(dicyclohexyl itaconate)	Toluene	25	13.1	5–56	LS	[202]
Poly(didecyl itaconate)	Toluene	25	8.01	13–82	LS	[201]
Poly(diethyl itaconate)	Toluene	25	1.48	5–61	LS	[201]
Poly(dihexyl itaconate)	Toluene	25	3.71	12–122	LS	[201]
Poly(dimethyl itaconate)	Benzene	25	5.18	4–120	LS	[201]
Poly(dioctyl itaconate)	Toluene	25	3.67	11–163	LS	[201]
Poly(dipropyl itaconate)	Toluene	25	1.62	13–109	LS	[201]
Poly(dipropylcyclohexyl itaconate)	Pentyl acetate	25	14	16–91	LS	[203]
	Toluene	25	2.23	16–91	LS	[203]
Poly(diundecyl itaconate)	Toluene	25	10.01	9–250	LS	[201]
Poly(vinylcarbazole)	Benzene	25	30.5	0.7–45	LS	[204]
	Bromobenzene	25	5.14	7–49	GPC	[205]
	Chlorobenzene	30	5.23	7–57	GPC	[206]
	Chloroform	25	5.93	7–49	GPC	[205]
	Cyclohexanone	25	20	2–45	LS	[204]
	1,2-dichlorobenzene	25	11	4–44	GPC	[207]
	1,3-dichlorobenzene	25	5.6	7–49	GPC	[207]
	Nitrobenzene	25	9.25	7–49	GPC	[205]
	Tetrachloroethane	25	12.9	2–45	LS	[204]
	Tetrahydrofuran	25	14.4	1–45	LS	[204]
	Toluene	37	76.2	4–107	OS	[208]
Poly(1-vinylimidazol)	Aqueous NaCl(0.1 M)	25	122	9–90	LS	[209]
	Aqueous NaCl(0.5 M)	25	121	9–90	LS	[209]
Poly(5-vinyl-2-methylpyridine)	Butanone	25	13.9	13–88	LS	[210]
	Dimethylformamide	25	13	4–40	OS	[211]
	Methanol	25	18	4–40	OS	[211]
Poly(1-vinynaphthalene)	Benzene	20	2.2	4–17	LS	[198]
Poly(2-vinynaphthalene)	Benzene	17	1.7	10–100	LS	[212]
Poly(3-vinylpyrene)	Chloroform	25	51	3–50	LS	[213]
	1,2-dichlorobenzene	25	11.7	3–50	LS	[213]
	Tetrahydrofuran	25	31.8	3–50	LS	[213]
Poly(2-vinylpyridine)	Benzene	25	6.6	3–11	LS	[214]
	Butanone	25	97.2	3–93	LS	[215]
	Dimethylformamide	25	14.7	3–93	LS	[216]
	Dioxane	25	30.9	3–93	LS	[216]
	Methonal	25	11.3	3–93	LS	[216]
	Pyridine	25	13.8	3–93	LS	[215]
Poly(4-vinylpyridine)	Ethanol	25	1.51	1–4	SD	[217]
	Water	25	22	10–185	LS	[218]

TABLE 17.1. *Continued.*

Polymer	Solvent	Temperature (°C)	$K\times10^3$ (ml/g)	Range $M\times10^{-4}$	Method	Reference
Poly(vinylpyrrolidone)	Chloroform	25	19.4	2–23	LS	[219]
	Methanol	30	23	2–23	LS	[219]
	Water	20	64	1–9	SD	[220]
Poly(vinyltrimethylsilane)	Cyclohexane	25	8.2	59–213	LS	[221]
Poly(acrylonitrile-*co*-styrene)						
38.3/61.7 mol. Azeotropic	Butanone	30	36	15–120	LS	[222]
	Tetrahydrofuran	25	21.5	10–78	LS	[223]
62.7/37.4 mol., random	Butanone	30	53	19–56	LS	[224]
	Dimethylformamide	30	12	19–56	LS	[224]
Poly(acrylonitrile-stat-styrene)						
27.4/72.6 mol	Dimethylformamide	30	12	14–58	LS	[225]
38.5/61.5 mol	Dimethylformamide	30	16.2	22–106	LS	[225]
47.5/52.5 mol	Dimethylformamide	30	17.2	14–78	LS	[225]
Poly(dimethyl itaconate-*co*-styrene)						
75/25 wt	Toulene	25	6.6	6–22	LS	[226]
67/33 wt	Toulene	25	9	4–19	LS	[226]
27/73 wt	Toulene	25	10.9	6–40	LS	[226]
0/100 wt	Toulene	25	11.45	3–58	LS	[226]

TABLE 17.2. *Mark–Houwink constants K and a values.*

Polymer	Solvent	T (°C)	$K\times10^2$(ml/g)	a	Range $M\times10^{-5}$	Method	Reference
Amylose	Dimethyl sulfoxide	20	0.397	0.82	0.2–21.7	LS	[227]
	Ethylenediamine	25	1.55	0.70	3.1–31.0	LS	[228]
	Water	20	1.32	0.68	3.6–21.7	LS	[227]
Cellulosetricarbanilate	Acetone	25	0.143	0.91	3.1–22.0	LS	[229]
	Dioxane	25	0.0813	0.97	3.1–22.0	LS	[229]
	Pyridine	20	0.346	0.86	0.7–27.0	LS	[230]
Cellulosetrioctanoate	Toluene	30	1.73	0.70	0.8–3.5	OS	[40]
Ethyl cellulose	Acetone	20	0.151	1.05	0.11–0.8	SD	[231]
	Benzene	25	2.92	0.81	0.4–1.4	OS	[232]
	Methanol	25	5.23	0.65	1.0–4.1	LS	[233]
Poly(acrylamide)	Water	30	0.631	0.80	0.2–5.0	SD	[234]
		30	0.65	0.82	0.4–12.7	OS	[235]
Poly(acrylic acid)							
—, sodium salt	(aq)NaBr (0.5 M)	15	5.27	0.62	0.1–5.0	LV	[236]
	(aq)NaOH (2 M)	25	4.22	0.64	0.4–5.0	OS	[237]
Poly(acrylonitrile-co-styrene) 38.3/61.7 mol, azeotropic	tetrahydrofuran	25	2.15	0.68	1.0–7.8	LS	[238]
Poly(butadiene)							
98% *cis*, 2% 1,2	Benzene	30	3.37	0.715	0.5–5.0	OS	[239]
	Toluene	30	3.05	0.725	0.5–5.0	OS	[240]
95% *cis*, 1% *trans*, 4%, 1,2	Cyclohexane	30	1.12	0.75	1.5–5.0	LS	[241]
ca. 100% *cis*	Benzene	32	1.45	0.76	0.8–1.8	LS	[242]
	Heptane/hexane (50/50 vol)	20	13.8	0.53	0.5–	SD	[243]
97% *trans*, 3% 1,2	Cyclohexane	40	2.82	0.70	0.4–1.7	LS	[244]
	Toluene	30	2.94	0.753	0.5–1.6	OS	[245]
Poly(butadiene-co-acrylonitrile)							
Buna-N rubber	Acetone	25	5.0	0.64	0.25–1.0	OS	[246]
	Benzene	25	1.3	0.55	0.25–1.0	OS	[246]
	Chloroform	25	5.4	0.68	0.25–1.0	OS	[246]

TABLE 17.2. *Continued.*

Polymer	Solvent	T (°C)	$K \times 10^2$ (ml/g)	a	Range $M \times 10^{-5}$	Method	Reference
Poly(butadiene-co-styrene)							
Buna-S, GR-S, or SBR rubber	Benzene	25	5.25	0.66	0.1–16.0	OS	[247]
	Cyclohexane	30	3.16	0.70	0.5–2.5	OS	[248]
	Toluene	25	5.25	0.667	0.25–5.0	OS	[246]
Poly(1-butene)							
Atactic	Benzene	30	2.24	0.72	0.003–0.05	EG	[249]
	Ethylcyclohexane	70	0.734	0.80	0.4–13.0	LS	[250]
Isotactic	Decalin	115	0.949	0.73	0.45–9.0	LS	[251]
	Ethylcyclohexane	70	0.734	0.80	0.8–9.4	LS	[250]
	1,2,4-trichlorobenzene	135	1.18	0.729		GPC	[252]
Poly(*tert*-butylacrylate)	Acetone	25	0.47	0.75	0.7–3.1	LS	[253]
	Methanol	25	1.60	0.61	0.7–3.1	LS	[253]
Poly(*N*-*n*-butylitaconimide)	Benzene	30	3.99	0.707	1.2–15.4	LS	[254]
	Tetrahydrofuran	30	2.57	0.790	1.2–15.4	LS	[254]
	Toluene	30	12.7	0.570	1.2–15.4	LS	[254]
Poly(chloroprene)							
Neoprene W	Benzene	25	1.55	0.72	0.5–8.0	LS	[255]
	Carbontetrachloride	25	2.21	0.69	1.5–30.0	LS	[256]
Poly(dihexoxyphosphazene)	Benzene	25	2.01	0.79	0.26–22.8	LS	[257]
Poly(ethylene)							
Low pressure	Decalin	135	6.2	0.70	0.2–10.5	LS	[258,259]
	1,2,4-trichlorobenzene	135	9.54	0.64	0.3–4.5	LS	[260]
		135	5.1	0.706	0.08–12.3	GPC,LS	[261]
		135	5.16	0.691		GPC	[252]
	p-Xylene	105	5.1	0.725	0.04–5.0	LV	[262]
High pressure	Decalin	70	3.873	0.738	0.02–0.4	OS	[263]
	p-Xylene	75	13.5	0.63	0.02–0.8	OS	[264]
Poly(ethyl acrylate)	Acetone	25	5.1	0.59	3.5–45.0	LS	[265]
	Benzene	30	2.77	0.67	0.5–6.7	OS	[266]
Poly(ethylmethacrylate)	Butanone	23	0.283	0.79	2.0–26.3	LS	[267]
	Ethyl acetate	35	0.86	0.71	6.5–120.0	LS	[268]
Poly(3-hexylthiophene)	Terahydrofuran	25	0.12	0.58	0.15–5.0	GPC,OS	[269]
	Toluene	25	1.312	0.77	0.4–2.2	GPC,LS	[270]
Poly(imionoadipoylimino-hexamethylene) (nylon 66)	*m*-cresol	25	24.0	0.61	0.14–0.5	LS,EG	[271]
	(aq)HCOOH (90 vol %)/ HCOOHa (0.1 *M*)	25	3.28	0.74	0.1–0.5	EG	[272]
Poly(isoprene)							
Natural rubber	Benzene	30	1.85	0.74	0.8–2.8	OS	[273]
	Cyclohexane	27	3.0	0.70	18.5–	LS,OS	[274]
	Toluene	25	5.02	0.667	0.7–10.0	OS	[275]
Synthetic *cis*	Hexane	20	6.84	0.58	0.5–8.0	SD	[276]
	Toluene	30	0.851	0.77	2.0–10.0	LS	[277]
Synthetic *cis*							
84% *cis*, 14% *trans*, 2%-1,2	Benzene	25	1.33	0.78	0.2–8.0	OS	[278]
		25	1.12	0.78	0.2–6.0	OS	[278]
Synthetic *trans*	Benzene	32	4.37	0.65	0.8–14.0	LS	[242]
Synthetic *trans* (98%)	Benzene	30	1.81	0.722	1.4–7.7	LS	[279]
	Cyclohexane	30	1.62	0.736	1.4–7.7	LS	[279]
Poly(methylacrylate)	Acetone	25	0.55	0.77	2.8–16.0	LS	[280]
	Benzene	25	0.258	0.85	2.0–13.0	OS	[281]
	Ethyl acetate	35	1.1	0.69	2.4–14.8	LS	[282]
Poly(methyl methacrylate)							
Atactic	Acetone	25	0.53	0.73	0.2–78.0	LS	[283]
	Benzene	25	0.55	0.76	0.2–74.0	LS	[283]
	Butanone	25	0.68	0.72	0.8–13.7	LS	[284]

TABLE 17.2. *Continued.*

Polymer	Solvent	T (°C)	$K \times 10^2$ (ml/g)	a	Range $M \times 10^{-5}$	Method	Reference
Isotactic	Acetone	30	2.30	0.63	0.5–12.8	LS	[285]
	Benzene	30	0.52	0.76	0.5–12.8	LS	[285]
	Acetonitrile	20	13.0	0.448	0.3–1.9	LV	[286]
Poly(methyl methacrylate)-block-poly(styrene), A_k–B_n, k/n, 54/46 wt.	Toluene	30	0.73	0.73	0.58–9.3	LS	[287]
Poly(oxy-2,6-dimethyl-1,4-phenylene)	Benzene	25	2.6	0.69	0.3–1.7	LS	[288]
Poly[oxy(dimethyl-silylene)]	Benzene	20	1.2	0.68	0.55–1.2	LV	[289]
	Toluene	20	2.0	0.66	0.03–2.0	LS,OS	[290]
	Cyclohexane	35	1.02	0.735	0.7–9.0	LS	[291]
Poly(oxy-1-oxo-3-methyltrimethylene) *D,L*	Chloroform	30	1.66	0.76	0.2–1.5	LS	[292]
D-Poly(propylene)	Trifluoro ethanol	25	2.22	0.76	0.2–1.5	LS	[292]
Atactic	Benzene	25	2.7	0.71	0.6–3.1	OS	[293]
	Cyclohexane	25	1.6	0.80	0.6–3.1	OS	[293]
	Toluene	30	2.18	0.725	0.2–3.4	OS	[294]
Isotactic	Decalin	135	1.10	0.80	0.2–6.2	LS	[293]
		135	1.00	0.80	1.0–10.0	LS	[295]
	p-Xylene	85	9.6	0.63		OS	[294]
Head to head 94% *trans*, 6% 1,2	Cyclohexane	30	0.416	0.86	0.21–0.4 1	VOS,OS	[296]
Syndiotactic	Heptane	30	3.12	0.71	0.9–4.5	LS	[297]
Poly(styrene)							
Atactic	Benzene	20	1.23	0.72	0.06–52.0	SD	[298]
	Butanone	25	3.9	0.58	0.1–18.0	LS	[299]
	Chloroform	25	0.716	0.76	1.2–28.0	LS	[300]
		25	1.12	0.73	0.7–15.0	OS	[301]
	Dichloroethane	25	2.10	0.66	0.1–18.0	LS	[299]
	N-methylpyrrolidone	30	4.92	0.577	0.3–4.0	GPC	[302]
	Tetrahydrofuran	25	1.10	0.725	0.1–10.0	GPC	[303]
	Toluene	25	1.05	0.73	1.6–10.0	LS	[304]
Atactic, anionic	Benzene	25	0.78	0.75	4.0–600.0	LS	[305]
	Toluene	25	0.977	0.73	0.1–10.4	SD	[306]
Isotactic	Benzene	30	1.06	0.735	0.4–3.7	OS	[307]
	Chloroform	30	2.59	0.734	0.9–3.2	OS	[308]
	o-Dichlorobenzene	25	1.79	0.677	0.2–10.0	LV	[309]
	Toluene	30	1.10	0.725	0.3–3.7	OS	[308]
Poly[sulfonyl-(butylethylene)]	Benzene	25	0.89	0.70	0.9–10.7	OS	[310]
	Chloroform	25	0.58	0.75	0.7–5.4	OS	[311]
	Dioxane	25	0.62	0.76	0.9–10.7	OS	[310]
Poly(vinyl acetate)	Acetone	25	2.14	0.68	0.4–3.4	OS	[312]
		25	1.46	0.72	0.07–0.13	EG	[313]
		25	1.08	0.72	0.09–0.25	EG	[313]
	Benzene	30	2.2	0.75	3.4–10.2	LS	[314]
		30	5.63	0.62	0.3–8.6	OS	[315]
		30	5.63	0.62	0.7–5.4	LS	[316]
	Chloroform	25	2.03	0.72	0.4–3.4	OS	[317]
	Methanol	25	3.80	0.59	0.4–2.2	OS	[312]
Poly(vinyl alcohol)	Water	30	4.53	0.64	0.1–8.0	LS	[318]
	Water	80	9.4	0.56	1.0–4.6	LS	[319]
Poly(vinyl chloride)	Chlorobenzene	30	7.12	0.59	0.3–1.9	SA	[320]
	Cyclohexane	25	1.38	0.78	0.1–1.2	OS	[321]
	Tetrahydrofuran	25	1.63	0.776	0.2–3.0	LS	[322]

ACKNOWLEDGMENT

This work was supported by the National Science Foundation Grant No. DMR 9023541.

Related information can be found in Chapter 15.

REFERENCES

1. E. O. Kraemer, Ind. Eng. Chem. **30**, 1200 (1938).
2. H. Mark, in *Der feste Körper*, edited by R. Sänger (Hirzel, Leipzig, 1938); R. Houwink, J. Prakt. Chem. **15**, 157 (1940); H. Staudinger and W. Heuer, Berton's New Brunswick Report **63**, 222 (1930); M. Bohdanecky, and J. Kovár, *Viscosity of Polymer Solutions* (Elsevier Scientific, New York, 1982), p. 87.
3. D. W. Van Krevelen, *Properties of Polymers* (Elsevier, New York, 1990), p. 253.
4. Hiroshi Fujita, *Polymer Solutions* (Elsevier Science, New York, 1990).
5. H. L. Frisch and J. L. Lundberg, J. Polym. Sci. **37**, 123 (1959).
6. P. F. Onyon, J. Polym. Sci. **183**, 1670 (1959).
7. P. J. Flory and T. G. Fox, Jr., J. Am. Chem. Soc. **73**, 1904 (1951).
8. L. Mandelkern and P. J. Flory, J. Chem. Phys. **20**, 212 (1952).
9. H. Yamakawa, *Modern Theory of Polymer Solutions* (Harper and Row, New York, 1971).
10. Y. Oono, Adv. Chem. Phys. **61**, 301 (1985).
11. Y. Oono and M. Kohmoto, J. Chem. Phys. **78**, 520 (1983).
12. J. G. Kirkwood and J. Riseman, J. Chem. Phys. **16**, 565 (1948).
13. P. J. Flory, *Principles of Polymer Chemistry* (Cornell University Press, Ithaca, New York, 1953), Chap. XIV.
14. H. Yu and W. H. Stockmayer, J. Chem. Phys. **47**, 1369 (1967).
15. Yu. E. Eizner and O. B. Ptitsyn, Vysokomolekul. Soedin. **4**, 1725 (1962).
16. O. B. Ptitsyn and Yu. E. Eizner, Dokl. Acad. Nauk SSSR **142**, 134 (1962).
17. W. Kuhn and H. Kuhn, Helv. Chim. Acta **28**, 97 (1945); **28**, 1533 (1945); **29**, 72 (1946).
18. R. Cerf, J. Polym. Sci. **23**, 125 (1957); Fortschr. Hochpolymer. Forsch. **1**, 382 (1959).
19. A. Peterlin and M. Copic, J. Appl. Phys. **27**, 434 (1956); M. Copic, J. Chim. Phys. **53**, 440 (1956).
20. Y. Ikeda, J. Phys. Soc. Jpn. **12**, 378 (1957).
21. A. Peterlin, J. Chem. Phys. **33**, 1799 (1960).
22. B. H. Zimm, Ann. N. Y. Acad. Sci. **89**, 670 (1961).
23. M. Fixman, J. Chem. Phys. **45**, 793 (1966).
24. J. S. Ham, J. Chem. Phys. **26**, 625 (1957).
25. B. H. Zimm and R. W. Kilb, J. Polym. Sci. **37**, 19 (1959).
26. D. M. Crothers and B. H. Zimm, J. Mol. Biol. **12**, 525 (1965).
27. R. Simha, J. Phys. Chem. **44**, 22 (1940).
28. M. L. Huggins, J. Phys. Chem. **42**, 911 (1938); **43**, 439 (1939); J. Appl. Phys. **10**, 700 (1939).
29. J. G. Kirkwood and P. L. Auer, J. Chem. Phys. **19**, 281 (1951).
30. J. Riseman and J. G. Kirkwood, J. Chem. Phys. **18**, 512 (1950).
31. J. J. Hermans, Rec. Trav. Chim. **63**, 219 (1944).
32. H. A. Kramers, J. Chem. Phys. **14**, 415 (1946).
33. P. Debye, J. Chem. Phys. **14**, 636 (1946).
34. M. Fukatsu and M. Kurata, J. Chem. Phys. **44**, 4539 (1966).
35. V. A. Bloomfield and B. H. Zimm, J. Chem. Phys. **44**, 315 (1966).
36. J. D. Ferry, C. G. Overbenger, G. V. Schulz, A. J. Staverman, and H. A. Stuart, *Advances in Polymer Science* (Springer, Berlin, 1961).
37. J. Brandrup and E. H. Immergut, *Polymer Handbook*, 3rd ed. (Wiley, New York, 1989).
38. W. Banks and C. T. Greenwood, Eur. Polym. J. **5**, 649 (1969).
39. V. P. Shanbhag and J. Oehman, Arkiv Kemi **29**, 163 (1968).
40. L. Mandelkern and P. J. Flory, J. Am. Chem. Soc. **74**, 2517 (1952).
41. F. Danusso, G. Moraglio, and G. Gianott, J. Polym. Sci. **51,** 475 (1961).
42. H. Fujita, N. Takeguchi, K. Kawahara, M. Abe, H. Utiyama, and M. Kurata, Paper given at 12th Polymer Symposium, Nagoya, Japan (Nov. 1963).
43. R. Endo, Nippon Gomu Kyokaishi (J. Rubber Ind. Japan), **34,** 522 (1961). See also, M. Takeda, and R. Endo, Rept. Progr. Polym. Phys. Jpn. **6,** 37 (1963).
44. I. Ya. Poddubnyi, Ye. G. Erenberg, and M. A. Yeremina, Vysokomol. Soedin. Ser. A, **10,** 1381 (1968).
45. W. G. Cooper, G. Vaughan, D. E. Eaves, and R. W. Madden, J. Polym. Sci. **50,** 159 (1961).
46. R. Endo, Nippon Gomu Kyokaishi (J. Rubber Ind. Jpn.), **35,** 658 (1962).
47. R. L. Scott, W. C. Carter, and M. Magat, J. Am. Chem. Soc. **71,** 220 (1949).
48. H. C. Tingey, R. H. Ewart, and G. E. Hulse, unpublished work; cited in Ref. 28. See also, D. M. French, R. H. Ewart, Anal. Chem. **19,** 165 (1947).
49. V. S. Skazka, M. Kozhokaru, G. A. Fomin, and L. F. Roguleva, Vysokomol. Soedin. Ser. A, **9,** 177 (1967).
50. W. E. Mochel, and J. B. Nichols, J. Am. Chem. Soc. **7,** 3435 (1949).
51. W. E. Mochel, J. B. Nichols, and C. J. Mighton, J. Am. Chem. Soc. **70,** 2185 (1948).
52. W. E. Mochel, and J. B. Nichols, Ind. Eng. Chem. **43,** 154 (1951).
53. H. L. Wagner, and P. J. Flory, J. Am. Chem. Soc. **74,** 195 (1952).
54. W. C. Carter, R. L. Scott, and M. Magat, J. Am. Chem. Soc. **68,** 1480 (1946).
55. I. Ya. Poddubnyi, V. A. Grechanovskii, and A. V. Podalinskii, Vysokomol. Soedin. **5,** 1588 (1964).
56. M. Abe, M. Iwama, and T. Homma, Kogyo Kagaku Zasshi (J. Chem. Soc. Jpn. Ind. Chem. Sec.), **72,** 2313 (1969).
57. W. Cooper, D. E. Eaves, and G. Vaughan, J. Polym. Sci. **59,** 241 (1962).
58. S. A. Pavlova, and T. A. Soboleva, Vysokomol. Soedin. **6**, 122 (1964).
59. J. L. Jungnickel, and F. T. Weiss, J. Polym. Sci. **49,** 437 (1961).
60. D. L. Flowers, W. A. Hewett, and R. D. Mullineaux, J. Polym. Sci. A **2,** 2305 (1964).
61. R. Endo, K. Iimura, and M. Takeda, Bull. Chem. Soc. Jpn. **37,** 950 (1964).
62. S. S. Stivala, R. J. Valles, and D. W. Levi, J. Appl. Polym. Sci. **7,** 97 (1963).
63. R. Chiang, J. Phys. Chem. **70,** 2348 (1966).
64. K. Ueberreiter, H. J. Orthman, and S. Sorge, Makromol. Chem. **8,** 21 (1952).
65. T. G. Fox, and P. J. Flory, J. Am. Chem, Soc. **73,** 1909 (1951).
66. T. G. Fox, and P. J. Flory, J. Phys. Colloid Chem. Soc. **53,** 197 (1949).
67. T. Tsuji, and H. Fujita, Polym. J. **4,** 409 (1973).
68. N. M. Tret'yakova, L. V. Kosmodem'yanskii, R. G. Romanova, and E. G. Lazaryants, Vysokomol. Soedin. Ser. A, **12,** 2754 (1970).
69. I. H. Billick, and J. P. Kennedy, Polymer, **6,** 175 (1965).
70. S. Tani, F. Hamada, and A. Cervanka, Eur. Polym. J. **5,** 86 (1973).
71. J. B. Kinsinger, and L. E. Ballard, J. Polym. Sci. A, **3,** 3963 (1965).
72. G. Gianotti, U. Bonicelli, and D. Borghi, Makromol. Chem. 166, 235 (1973).
73. J. B. Kinsinger, and R. E. Hughes, J. Phys. Chem. **63,** 2002 (1959).
74. F. Danusso and G. Moraglio, Rend. Acad. Naz. Lincei, **25,** 509 (1958).
75. A. Nalajima, and A. Saijo, J. Polym. Sci. A-2, **6,** 735 (1968).
76. H. Inagaki, T. Miyamoto, and S. Ohta, J. Phys. Chem. **70,** 3420 (1966).
77. W. Scholtan, Makromol. Chem. **14,** 169 (1954).
78. G. Saini, and L. Trossarelli, Atti Accad. Sci. Torino, Classe Sci. Fis., Mat. Nat. **90,** 410 (1955–56). cf. Ref. 10.
79. R. Jerome, and V. Desreux, Eur. Polym. J. **17,** 607 (1985).
80. G. B. Rathmann, and F. A. Bovey, J. Polym. Sci. **15,** 544 (1955).
81. L. Trossarelli, and M. Meirone, J. Polym. Sci. **57,** 445 (1962).
82. M. Giurgea, C. Ghita, I. Baltog, and A. Lupu, J. Polym. Sci. A-2, **4,** 529 (1966).
83. H. Sumitomo, Y. Hachihama, and Kobunshi Kagaku (Chem. High Polym. (Tokyo)). **12,** 479 (1955). See also Y. Hachihama, and H. Sumitomo, Technol. Rept. Osaka University **5,** 485 (1956).
84. C.U. Pittman, Jr., R. L. Voges, Macromolecules, **4,** 291 (1971).
85. C.U. Pittman, Jr., J. C. Lai, D. P. Vanderpool, M. Good, and R. Prado, Macromolecules, **3,** 746 (1970).
86. I. G. Soboleav, N. V. Makletsova, and S. S. Medvedev, Dokl. Akad. Nauk. SSSR, **94,** 289 (1954).
87. E. S. Cohn, T. A. Orofino, and I. L. Scogna, unpublished work; cited in Ref. 10.

88. J. E. Mark, R. A. Wessling, and R. E. Hughes, J. Phys. Chem. **70,** 1895 (1966).
89. S. Krause, unpublished work; cited in Ref. 10.
90. H. Staudinger, and H. Warth, Z. Prakt. Chem. **155,** 261 (1940).
91. G. M. Guzman, Anales Real Soc. Espan. Fis. Quim. (Madrid) Ser. B, **52,** 377 (1956); cited in Ref. 10.
92. H. Matsuda, K. Yamano, and H. Inagaki, J. Polym. Sci. A-2, **7,** 609 (1969).
93. V. N. Tsvetkov, V. S. Shazka, N. A. Nikitin, and I. B. Steparenko, Vysokomol. Seodin. **6,** 69 (1964).
94. J. Parrod, and J. Elles, J. Polym. Sci. **29,** 411 (1958).
95. D. Mangaraj, and S. K. Patra, Makromol. Chem. **107,** 230 (1967).
96. E. S. Cohn, unpublished work, cited in Ref. 10.
97. R. van Leemput, and R. Stein, J. Polym. Sci. A-1, 985 (1963).
98. Rohm and Hass, old data; reported in Ref. 10.
99. S. N. Nair, and M. S. Muthana, Makromol. Chem. **47,** 114 (1961).
100. V. N. Tsvetkov, and S. I. Klemin, Zh. Tekhn. Fiz. **29,** 1393 (1959).
101. M. Kozhokaryu, V. S. Skazka, and K. G. Berdnikova, Vysokomol. Soedin. **8,** 1063(1967).
102. M. Tricot, J. Bleus, J. P. Riga, and V. Desreux, Makromol. Chem. **175,** 913 (1974).
103. V. N. Tsvetkov, and O. V. Kalisov, Zh. Fiz. Khim. **33,** 710 (1959).
104. O. V. Kalisov, and I. N. Shtennikova, Vysokomol. Soedin. **1,** 842 (1959).
105. V. N. Tsvetkov, and S. I. Klenin, J. Polym. Sci. **30,** 187 (1958).
106. L. Gargallo, D. Radic, and I. Katime, Eur. Ploym. J. **16,** 383 (1980).
107. E. S. Cohn, I. L. Scogna, and T. A. Orofino, unpublished work; cited in Ref. 10.
108. J. Hakozaki, and Hippon Kagaku Zasshi (J. Chem. Soc. Jpn. Pure Chem. Sec.). **82,** 158 (1961).
109. N. Hadjichristidis, M. Devaleriola, and V. Desreux, Eur. Ploym. J. **8,** 1193 (1972).
110. N. Hadjichristidis, C. Touloupis, and L. J. Fetters, Macromolecules, **14,** 128 (1981).
111. S. N. Chinai, and R. J. Guzzi, J. Polym. Sci. **41,** 475 (1959).
112. F. E. Didot, S. N. Chinai, and D. W. Levi, J. Polym. Sci. **43,** 557 (1960).
113. S. N. Chinai, and R. J. Samuels, J. Polym. Sci. **19,** 463 (1956).
114. K. Karunakarn, and M. Santappa, Makromol. Chem. **111,** 20 (1968).
115. V. N. Tsvetkov, D. Khardi, I. N. Shtennikova. Ye. V. Komeyeva, G. F. Pirogova, and K. Nitrai, Vysokomol. Soedin. Ser. A. 11, 349 (1969).
116. V. N. Tsvetkov, E.I. Riumtsev, I. N. Shtennikova, E. V. Korneeva, B. A. Krenstel, and Yu. B. Amerik, Eur. Polym. J. **9,** 481 (1973).
117. S. N. Chinai, J. Polym. Sci. **25,** 413 (1957).
118. R. J. Fort, and T. M. Polyzoidis, Eur. Polym. J. **12,** 685 (1976).
119. R. J. Valles, J. Polym. Sci. A, **3,** 3853 (1965); See also R. J. Valles, and E. C. Schramm. ibid., **3,** 3664 (1965); and Ref. 167.
120. M. M. Zafar, R. Mahmood, and S. A. Wadood, Makromol. Chem. **160,** 313 (1972).
121. R. C. Schulz, S. Suzuki, H. Cherdron. and W. Kern, Makromol, Chem. **53,** 145 (1962).
122. N. M. Weiderhorn, and A. R. Brown, J. Polym. Sci. **8,** 651 (1952).
123. N. Fuhrman, and R. B. Mesrobian, J. Am. Chem. Soc. **76,** 3281 (1954).
124. C. G. Overberger, E. M. Pearce, and N. Mayes, J. Polym. Sci. **34,** 109 (1959).
125. J. Stejskal, J. Janca, and P. Kratochvil, Polym. J. **8,** 549 (1976).
126. M. Iwama, H. Utiyama, and M. Kurata, J. Makromol. Chem. **1,** 701 (1966).
127. J. N. Helbert, C.-Y. Chen, C. U. Pittman, Jr., and G. L. Hagnauer, Macromolecules, **11,** 1104 (1978).
128. G. Meyerhoff, and G. V. Schulz, Makrimol. Chem. **1,** 701 (1966).
129. E. Cohn-Ginsberg, T. G. Fox, and H. F. Mason, Polymer, **3,** 97 (1962).
130. J. Bischoff, and V. Desreux, Bull Soc. Chim. Belges, **61,** 10 (1952).
131. J. G. Fee. W. S. Port, and L. P. Whitnauer, J. Polym. Sci. **33,** 95 (1958).
132. S. N. Chinai, A. L. Resnick, and H. T. Lee, J. Polym. Sci. **33,** 471 (1958).
133. V. N. Tsvetkov, and V. G. Aldoshin, Zh. Fiz. Khim. **33,** 2767 (1959).
134. X. Zhongde, S. Mingshi, N. Hadjichristidis, and L. J. Fetters, Marcomolecules, **14,** 1591 (1981).
135. Z. Xu, N. Hadjichistidis, and L. J. Fetters, cited in Ref. 733.
136. M. M. Zafar, and R. Mahmood, Markomol. Chem. **175,** 903 (1974).
137. Ye. V. Korneyeva, V. N. Tsvetko, and P. N. Lavrenko, Vysokomol. Soedin. Ser. A, **12,** 1369 (1970).
138. J. A. Manson, and G. J. Arquette, Makromol. Chem. **37,** 187 (1960).
139. E. K. Walsh, and H. S. Kaufman, J. Polym. Sci. **26,** 1 (1957).
140. P. J. Flory, and F. Lentner, J. Polym. Sci. **3,** 880 (1948).
141. A. C. Ciferri, M. Kryszewski, and G. Weil, J. Polym. Sci. **27,** 167 (1958).
142. M. Sato, Y. Koshiishi, and M. Asahina, J. Polym. Sci. B **1,** 233 (1963).
143. H. Inagaki, and J. Nakazawa, Private communication.
144. J. W. Breitenbach, E. L. Forster, and A. J. Renner, Kolloidz, **127,** 1 (1952).
145. H. Batzer, and A. Nisch, Makromol. Chem. **22,** 131 (1957).
146. M. L. Wallach, and M. A. Kabayama, J. Polym. Sci. A-1, **4,** 2667 (1966).
147. K. Matsuo, and W. H. Stockmayer, Macromolecules, **8,** 660 (1975).
148. M. Litt, and F. R. Eirich, J. Polym. Sci. **45,** 379 (1960).
149. M. R. Rao, and V. Kalpagam, J. Polym. Sci. **49,** S 14 (1961).
150. A. R. Schulz, J. Am. Chem. Soc. **76,** 3423 (1954). See also R. O. Howard, Thesis, Mass. Inst. Tech., Cambridge, Mass. USA 1952.
151. E. Patrone, and E, Bianchi, Makromol. Chem. **94,** 52 (1966).
152. K. Z. Fattakhov, E. S. Pisarenko, and L. N. Verkotina, Kolloidn. Zh. **18,** 101 (1956).
153. W. R. Moore, and M. Murphy, J. Polym. Sci. **56,** 519 (1962).
154. M. Ueda, and K. Kajitani, Makromol. Chem. **108,** 138 (1967): and private communication.
155. R. Natio, and Kobunshi Kagaku (Chem. High Polym. (Tokyo)), **16,** 7 (1959).
156. I. Sakurada, Y. Sakaguchi, S. Kokuryo, and Kobunshi Kagaku (Chem. High Polym. (Tokyo)), **17,** 227 (1960).
157. C. J. Kurian, and M. S. Muthana, Makromol. Chem. **29,** 1 (1959).
158. Y. Sakaguchi, J. Nishino, K. Tsugawa, and Kobunshi Kagaku (Chem. High Polym. (Tokyo)), **20,** 661 (1963).
159. K. Fujii, S. Imoto, J. Ukida, M. Matsumoto, and Kobunshi Kagaku (Chem. High Polym. (Tokyo)), **19,** 581 (1962).
160. H. Hopff, and J. Dohany, Makromol. Chem. **69,** 131 (1963).
161. W. Kern, and D. Brawn, Makromol. Chem. **27,** 23 (1958).
162. K. Takashima, G. Tanaka, and H. Yamakawa, Polym. J. **2,** 245 (1971).
163. Y. Noguchi, A. Aoki, G. Tanaka, and H. Yamakawa, J. Chem. Phys. **52,** 2651 (1970).
164. Z. Kucukyavuz, and S. Kucukyavuz, Eur. Polym. J. **14,** 867 (1978).
165. K. Matsumura, Polym. J. **1,** 332 (1970).
166. R. B. Mohite, S. Gundish, and S. L. Kapur, Makromol. Chem. **116,** 280 (1968).
167. A. Kotera, T. Satio, H. Matsuda, and R. Kamata, Rept. Progr. Polym. Phys. Jpn. **3,** 51 (1960).
168. G. Greber, J. Tolle, and W. Burchard, Makromol. Chem. **71,** 47 (1964).
169. N. Kuwahara, K. Ogino, M. Konuma, N. Iida, and M. Kaneko, J. Polym. Sci. A-2, **4,** 173 (1966).
170. E. F. Frisman, and L. F. Shalaeva, Dokl. Akad. Nauk. SSSR, **101,** 970 (1955).
171. V. E. Eskin, and T. N. Nekrasova, U. Juraev. Polym. J. **11,** 341 (1975).
172. C. S. H. Chen, and R. F. Stamm, J. Polym. Sci. **58,** 369 (1962).
173. M. Matsuo, and W. H. Stockmayer, J. Polym. Sci., Polym. Phys. Ed. **11,** 43 (1973).
174. D. Braun, T.-O. Ahn, and W. Kern, Makromol. Chem. **53,** 154 (1962).
175. F. S. Holahan, S. S. Stivala, and D. W. Levi, J. Polym. Sci. A, **3,** 3987 (1955).
176. Y. Imanishi, T. Higashimura, S. Okamura, and Kobunshi Kagaku (Chem. High Polym., Jpn. Toyko) **22,** 241 (1965).
177. G. Ceccorulli, M. Pizzoli, and G. Stea, Makromol. Chem. **142,** 153 (1971).
178. A. K. Chaudhuri, D. K. Sarkar, and S. Palit, Makromol. Chem. **111,** 36 (1968).
179. Tanaka, S. Imai, and H. Yamakawa, J. Chem. Phys. **52,** 2639 (1970).
180. W. A. Pryor, and T.-L. Huang, Macromolecules **2,** 70 (1969).
181. M. Cantow, G. Meyerhoff, and G. V. Schulz, Makromol. Chem. **49,** 1 (1961).
182. P. Outer, C. I. Carr, and B. H. Zimm, J. Chem. Phys. **18,** 830 (1950).
183. H. Utiyama, Thesis, Kyoto University, Kyoto, Japan 1962.

184. J. Oth, and V. Desreux, Bull. Soc. Chim. Belges, **63,** 285 (1954).
185. L. Utracki, and R. Simha, J. Phys. Chem. **67,** 1052 (1963).
186. C. W. Tsimpris, B. Suryanrayanan, and K. G. Mayhan, J. Polym. Sci. A-2, **10,** 1837 (1972).
187. U. Bianchi, V. Magnasso, and C. Rossi, Chim. Ind. (Milan), **40,** 263 (1958); See also, Ref. 276.
188. C. E. H. Bawn, C. Freeman, and A. Kamaliddin, Trans. Faraday Soc. **46,** 1107 (1950).
189. A. L. Spatorico, and B. Coulter, J. Polym. Sci., Polym. Phys. Ed. **11,** 1139 (1973).
190. T. Altares, D. P. Wyman, and V. R. Allen, J. Polym. Sci. A, **2,** 4533 (1964).
191. M. Morton, T. E. Helminiak, S. D. Gadkary, and F. Bueche, J. Polym. Sci. **57,** 471 (1962).
192. J. M. G. Cowie, and E. L. Cussler, J. Chem. Phys. **46,** 4886 (1967).
193. G. Meyerhoff, and B. Appelt, Macromolecules, **12,** 968 (1979), **13,** 657 (1980).
194. R. Endo, and M. Takeda, J. Polym. Sci. **56,** 28 (1962). The tabulated constants are calculated from the original figure.
195. F. Ang, J. Polym. Sci. **25,** 126 (1957).
196. G. Natta, F. Danusso, and G. Moraglio, Makromol. Chem. **20,** 37 (1956). See also Ref. 300.
197. M. Kato, T. Nakagawa, and H. Akamatsu, Bull. Chem. Soc. Jpn. **33,** 322 (1960).
198. L. A. Utracki, and R. Simha, Makromol. Chem. **117,** 94 (1968). See also, L. A. Utracki, R. Simha, and N. Eliezer, Polmer, **10,** 43 (1969).
199. I. Noda, Y. Yamamoto, T. Kitano, and M. Nagasawa, Macromolecules, **14,** 1306 (1981).
200. W. Burchard, and M. Nosseir, Makromol. Chem. **82,** 109 (1964).
201. J. Velickovic, and S. Vasovic, Makromol. Chem. **153,** 207 (1972).
202. J. Velickovic, S. Coseva, and R. J. Fort, Eur. Polym. J. **11,** 377 (1975).
203. J. Velickovic, J. Filipovic, and S. Coseva, Eur. Polym. J. **15,** 521 (1979).
204. G. Sitaramaiah, and D. Jacobs, Polymer, **11,** 165 (1970).
205. L. M. Leon, I. Katime, M. Gonzalez, and J. Figueruelo, Eur. Polym. J. **14,** 671 (1978).
206. L. M. Leon, J. Galaz, L. M. Garcia, and M. S. Anasagasti, Eur. Polym. J. **16,** 921 (1980).
207. L. M. Leon, I. Katime, and M. Rodriguez, Eur. Ploym. J. **15,** 29 (1979).
208. N. Kuwahara, S. Higashide, M. Nakata, and M. Kaneko, J. Polym. Sci. A-2, **7,** 285 (1985).
209. J. S. Tan, and A. R. Sochor, Macromolecules, **14,** 1700 (1981).
210. M. Miura, Y. Kubota, and T. Masuzukawa, Bull. Chem. Soc. Jpn. **38,** 316 (1965).
211. H. Sato, T. Yamamoto, and Nippon Kagaku Zasshi (J. Chem. Soc. Jpn. Pure Chem. Sec.), **80,** 1393 (1959).
212. V. E. Eskin, and O. Z. Korokina, Vysokomol. Soedin. **1,** 1580 (1959).
213. G. Sitaramaiah, and D. Jacobs, Makromol. Chem. **164,** 237 (1973).
214. G. Fourche, and C. Tourenne, Eur. Polym. J. **12,** 663 (1976).
215. S. Arichi, J. Sci. Hiroshima Univ. Ser. A-II, **29,** 97 (1965).
216. S. Arichi, Bull. Chem. Soc. Jpn. **39,** 439 (1966).
217. D. O. Jorden, A. R. Mathieson, and M. R. Porter, J. Polym. Sci. **21,** 473 (1956).
218. J. B. Berkowitz, M. Yamin, and R. M. Fuoss, J. Polym. Sci. **28,** 69 (1958).
219. G. B. Levy, and H. P. Frank, J. Polym. Sci. **17,** 247 (1955); See also Ref. 380.
220. K. Dialer, and K. Vogler, Makromol. Chem. **6,** 191 (1951).
221. A. B. Duchkova, N. S. Nametkin, V. S. Khotimskii, L. Ye. Gusel'nikov, and S. G. Durgar'yan, Vysokomol. Soedin. **8,** 1814 (1966).
222. Y. Shimura, I. Mita, and H. Kambe, J. Polym. Sci. B, **2,** 403 (1964).
223. H. Gerrens, H. Ohlinger, and R. Fricker, Makromol. Chem. **87,** 209 (1965).
224. Y. Shimura, J. Polym. Sci. A-2, **4,** 423 (1966).
225. C. R. Reddy, and V. Kalpagam, J. Polym. Sci., Polym. Phys. Ed. **14,** 749 (1976).
226. J. Velickovic, D. Jovanovic, and J. Vukajlovic, Makromol. Chem. **129,** 203 (1969).
227. W. Burchard, Makromo. Chem. **64**, 110 (1963).
228. J. M. G. Cowie, Makromol. Chem. **42**, 230 (1961).
229. V. P. Shanbhag, Arkiv Kemi. **29**, 1 (1968).
230. W. Burchard, and E. Husemann, Makromol. Chem. **44–46**, 358 (1961).
231. G. Meyerhoff, and N. Suetterlin, Makromol. Chem. **87**, 258 (1965).
232. W. R. Moore, and A. M. Brown, J. Colloid Sci. **14**, 343 (1959).
233. V. N. Tsvetkov, and S. Ya. Kotlyar, Zh. Fiz. Khim. **30**, 1100 (1956).
234. W. Scholtan, Makromol. Chem. **14**, 169 (1954).
235. G. S. Misra, and S. H. Bhattacharya, Eur. Polym. J. **15**, 125 (1979).
236. A. Takahashi, N. Nagasawa, J. Am. Chem. Soc. **86**, 543 (1964).
237. A. Takahashi, N. Hayashi, and I. Kagawa, Kogyo Kagaku Zasshi, J. Chem. Soc. Jpn. Ind. Chem. Sec. **60**, 1059 (1957).
238. H. Gerrens, H. Ohlinger, and R. Fricker, Makromol. Chem. **87**, 209 (1965).
239. I. Ya. Poddubnyi, Ye. G. Erenberg, and M. A. Yeremina, Vysokomol. Soedin. Ser. A, **10**, 1381 (1968).
240. F. Danusso, G. Moraglio, and G. Gianott, J. Polym. Sci. **51**, 475 (1961).
241. H. Fujita, N. Takeguchi, K. Kawahara, M. Abe, H. Utiyama, and M. Kurata, paper given at the 12th Polymer Symposium, Nagoya, Japan, November (1963).
242. W. Cooper, D. E. Eaves, and G. Vaughan, J. Polym. Sci. **59**, 241 (1962).
243. I. Ya. Poddubnyi, and V. A. Grechanovskii, Vysokomol. Soedin. **6**, 64 (1964).
244. M. Kurata, H. Utiyama, K. Kajitani, T. Koyama, and H. Fujita, paper given at the 12th Polymer Symposium, Nagoya, Japan, November (1963).
245. R. Endo, Nippon Gomu Kyokaishi (J. Rubber Ind. Jpn), **34**, 527 (1961).
246. R. L. Scott, W. C. Cater, and M. Magat, J. Am. Chem. Soc. **71**, 220 (1949).
247. D. M. French, and R. H. Ewart, Anal. Chem. **19**, 165 (1947).
248. T. Altares, D. P. Wyman, and V. R. Allen, J. Polym. Sci. A, **2**, 4533 (1964).
249. R. Endo, K. Iimura, and M. Takeda, Bull. Chem. Soc. Jpn. **37**, 950 (1964).
250. W. R. Krigbaum, J. E. Kurz, and P. Smith, J. Phys. Chem. **65**, 1984 (1961).
251. S. S. Stivala, R. J. Valles, and D. W. Levi, J. Appl. Polym. Sci. **7**, 97 (1963).
252. D. Constantin, Eur. Polym. J. **13**, 907 (1977).
253. R. Jerome, and V. Desreux, Eur. Polym. J. **6**, 411 (1970).
254. A. Matsumoto, S. Umehara, H. Watanabe, and T. Otsu, J. Polym. Sci. Part B, **31**, 527 (1993).
255. K. Hanafusa, A. Teramoto, and H. Fujita, J. Phys. Chem. **70**, 4004 (1966).
256. K. Kawahara, T. Norisuye, and H. Fujita, J. Chem. Phys. **49**, 4339 (1968).
257. J. Bravo, M. P. Tarazona, and E. Saiz, Polymer **33**, 3312 (1992).
258. R. Chiang, J. Phys. Chem. **69**, 1645 (1965).
259. R. Chiang, J. Polym. Sci. **36**, 91 (1959).
260. G. R. Williamson, and A. Cervenka, Eur. Polym. J. **8**, 1009 (1972).
261. E. P. Otocka, R. J. Roe, M. Y. Hellman, and P. M. Muglia, Macromolecules, **4**, 507 (1971).
262. R. A. Mendelsenm, and E. E. Drott, J. Polym. Sci. B, **11**, 795 (1968).
263. K. Ueberreiter, H. J. Orthman, and S. Sorge, Makromol. Chem. **8**, 21 (1952).
264. I. Harris, J. polym. Sci. **8**, 353 (1952).
265. M. Giurgea, C. Ghita, I. Baltog, and A. Lopu, J. Polym. Sci. A-2, **4**, 529 (1966).
266. H. Sumitomo, and Y. Hachihama, Kobunshi Kagaku [Chem. High polym. (Toyko)], **12**, 479 (1955).
267. S. N. Chinai, and R. J. Samuels, J. Polym. Sci. **19**, 463 (1956).
268. K. Karunakaran, and M. Santappa, Makromol. Chem. **111**, 20 (1968).
269. G. W. Heffner, and D. S. Pearson, Macromolecules, **24**, 6295 (1991).
270. X. P. Bi, Q. C. Ying, and R. Y. Qian, Makromol. Chem. Macro. Chem. Phys. **193**, 2905 (1992).
271. J. J. Burke, and T. A. Orfino, J. Polym. Sci. A-2, **7**, 1 (1969).
272. G. J. Howard, J. Polym. Sci. **37**, 310 (1959).
273. H. L. Wagner, and P. J. Flory, J. Am. Chem. Soc. **74**, 195 (1952).
274. K. Altgelt, and G. V. Schulz, Makromol. Chem. **36**, 209 (1960).
275. W. C. Carter, R. L. Scott, and M. Magat, J. Am. Chem. Soc. **68**, 1480 (1946).
276. I. Ya. Poddubnyi, V. A. Grechanovski, and A. V. Podalinskii, Vysokomol. Soedin. **5**, 1588 (1964).
277. M. Abe, M. Iwama, and T. Homma, Kogyo Kagaku Zasshi (J. Chem. Soc. Jpn. Ind. Chem. Sec.) **72**, 2313 (1969).

278. I. Y. Poddubnyi, and E. G. Ehrenberg, J. Polym. Sci. **57**, 545 (1962).
279. P. N. Chatuevedi, and C. K. Patel, J. Polym. Sci., Polym. Phys. Ed. **23**, 1255 (1985).
280. L. Trossareli, and G. Saini, Atti Accad. Sci. Torino, Classe Sci. Fis. Mat. Nat. **90**, 419 (1955–1956).
281. G. M. Guzman, Anales Real Soc. Espan. Fis. Quim. (Madrid) Ser. B, **52**, 377 (1956).
282. K. Karunakaran, and M. Santappa, J. Polym. Sci. A-2, **6**, 713 (1968).
283. H. J. Cantow, and G. V. Schulz, Z. Phys. Chem. (Frankfurt) **2**, 117 (1954).
284. J. Bischoff, and V. Desreux, Bull. Soc. Chim. Belg. **61**, 10 (1952).
285. S. Krause, and E. Cohn-Ginsberg, Polymer. **3**, 565 (1962).
286. S. Krause, and E. Cohn-Ginsberg, J. Phys. Chem. **67**, 1479 (1963).
287. T. Tanaka, T. Kotaka, K. Ban, M. Hattori, and H. Inagaki, Macromolecules, **10**, 960 (1977).
288. P. J. Akers, G. Allen, and M. J. Bethell, Polymer, **9**, 575 (1968).
289. V. Crescenzi, and P. J. Flory, J. Am. Chem. Soc. **86**, 141 (1964).
290. A. J. Barry, J. Appl. Phys. **17**, 1020 (1946).
291. J. G. Zilliox, J. E. L. Roovers, and S. Bywater, Macromolecules, **8**, 573 (1975).
292. T. Hirose, Y. Einaga, and H. Fujita, Polym. J. **11**, 819 (1979).
293. J. B. Kinsinger, and R. E. Hughes, J. Phys. Chem. **63**, 2002 (1959).
294. F. Danusso, and G. Moraglio, Rend. Acad. Naz. Lincei. **25**, 509 (1958).
295. R. Chiang, J. Polym. Sci. **38**, 235 (1958).
296. S. Arichi, M. Y. Pedram, and J. M. G. Cowie, Eur. Polym. J. **15**, 113 (1979).
297. H. Inagaki, T. Miyamoto, and S. Ohta, J. Phys. Chem. **70**, 3420 (1966).
298. G. Meyerhoff, Z. Phys. Chem. (Frankfurt), **4**, 335 (1955).
299. P. Outer, C. I. Carr, and B.H. Zimm, J. Chem. Phys. **18**, 830 (1950).
300. J. Oth and V. Desreux, Bull. Soc. Chim. Belg. **63**, 285 (1954).
301. C. E. H. Bawn, C. Freeman, and A. kamaliddin, Trans. Faraday Sci. **46**, 1107 (1950).
302. M. Konas, and A. R. Shulta, Collece. Czech. Chem. Commun. **58**, 2400 (1993).
303. A. L. Spatorico, and B. Coulter, J. Polym. Sci. polym. Phys. Ed. **11**, 1139 (1973).
304. J. W. Breitenbach, H. Gabler, and O. F. Olaj, Makromol. Chem. **81**, 32 (1964).
305. Y. Einaga, Y. Miyaki, and H. Fujita, J. Polym. Sci. Polym. Phys. Ed. **17**, 2103 (1979).
306. H. W. McCormick, J. Polym. Sci. **36**, 341 (1959).
307. G. Natta, F. Danusso, and G. Moraglio, Makromol. Chem. **20**, 37 (1956).
308. R. Endo, and M. Takeda, J. Polym. Sci. **56**, 28 (1962).
309. W. R. Krigbaum, D. K. Carpenter, and S. Newman, J. Phys. Chem. **62**, 1586 (1958).
310. T. W. Bates, and K. J. Ivin, Polymer, **8**, 263 (1967).
311. T. W. Bates, J. Biggins, and K. J. Ivin, Makromol. Chem. **87**, 180 (1965).
312. W. R. Moore, and M. Murphy, J. Polym. Sci. **56**, 519 (1962).
313. G. S. Misra, and V. P. Gupta, Makromol. Chem. **71**, 110 (1964).
314. M. R. Rao, and V. Kalpagam, J. Polym. Sci. **49**, s 14 (1961).
315. A. Nakajima, and K. Kagaku, Chem. High Polym. Yokyo, **11**, 142 (1954).
316. V.V. Varadiah, J. Polym. Sci. **19**, 477 (1956).
317. M. Ueda, and K. Kajitani, Makromol. Chem. **108**, 138 (1967).
318. M. Matsumoto, and Y. Ohyanagi, Kobunshi Kagaku [Chem. High Polym. (Tokyo)] **17**, 191 (1960).
319. T. Matsuom, and H. Inagaki, Makromol. Chem. **55**, 151 (1962).
320. H. Inagaki, and J. Nakazawa (unpublished).
321. G. Ciampa, and H. Schwindt, Makromol. Chem. **21**, 169 (1954).
322. M. Freeman, and P.P. Manning, J. Polym. Sci. A-2, 2017 (1964).

CHAPTER 18

Polymers and Supercritical Fluids

Annette D. Shine

Department of Chemical Engineering University of Delaware Newark, DE 19716

Mixtures of polymers and supercritical fluids (SCFs) have many features in common with mixtures of polymers and conventional incompressible liquids. As a result, a variety of operations, such as polymerization, dissolution and precipitation, swelling, fractionation, plasticization, impregnation, and extraction, can be carried out on polymers using SCFs. Several monographs and review articles address these and other applications [1–13]. A supercritical fluid is a substance at conditions above its critical temperature (T_c) and critical pressure (P_c). Such compounds used with polymers are often gaseous at ambient or near-ambient conditions, and have critical temperatures which are low enough to prevent excessive thermal degradation of the polymer. When temperature or pressure conditions are below the critical point, the compound is not a true SCF, but such compressible fluids are also included here under the abbreviation SCF. Table 18.1 below lists the properties of some representative SCF compounds, most of which have been used with polymers. The low normal boiling points (T_b) of many of these materials insure that little or none of the SCF remains to contaminate the polymer after a mixture has been depressurized to atmospheric conditions.

Two significant features distinguish SCFs from conventional liquid solvents:

1. The SCF is compressible, so pressure can be adjusted as an independent variable. In liquid solvent systems, only temperature can be varied, and
2. SCFs often have lower density (or, equivalently, higher specific volume) than liquids. Hence, they can be more effective than liquids at increasing the polymer free volume and enhancing transport properties.

Additionally, pure SCFs have no interfacial tension (since no vapor–liquid interface exists), so penetration into and removal from solid porous structures is facilitated. Note, however, that an SCF-swollen polymeric fluid will exhibit an interfacial tension with an SCF phase.

Of these features, the pressure-dependence of SCF properties dominates or influences virtually every process conducted on polymers. Pressure governs such properties as density, solubility parameter, and dielectric constant; changes of more than an order of magnitude are common when pressure is sufficiently increased to transform a gas into a supercritical fluid. This chapter primarily compiles experimental data on the pressure dependence of physical properties of fluid phase polymer-SCF mixtures. Phase equilibria are addressed, including the solubility of polymers in SCFs, the solubility of SCFs in liquid polymers, and the three-phase solid–fluid–fluid equilibria of crystalline polymers saturated with SCFs. Additional thermodynamic properties include glass transition temperature depressions of polymers, and interfacial tension between SCF-swollen polymers and the SCF. The viscosity of fluid phase polymer-SCF mixtures is also treated.

TABLE 18.1. *Critical properties of some compounds.*

SCF	T_c(°C)	P_c(MPa)	T_b(°C)
Ethylene	9.3	5.06	−103.7
Fluoroform	26.0	4.82	−82
Chlorotrifluoromethane	28.9	3.92	−81.1
Carbon dioxide	31.0	7.38	−78.8[a]
Ethane	32.2	4.88	−88.6
Nitrous oxide	36.5	7.26	−88.5
Propylene	91.9	4.62	−47.4
Chlorodifluoromethane	96	4.91	−40.8
Propane	96.7	4.25	−42.1
1,1,1,2-tetrafluoroethane	101	4.06	−26.2
Dimethyl ether	127	5.33	−24.8
Ammonia	132.5	11.28	−33.35
1-chloro-1,1-difluoroethane	137	4.05	−10
n-Butane	152	3.80	−0.5
Dichlorofluoromethane	178.5	5.17	9
Dichlorotrifluoroethane	183	3.68	27.6
Ethylene oxide	195.6	7.19	10.6
n-Pentane	196.6	3.37	36.1
Trichlorofluoromethane	198.1	4.41	23.7
Trifluoroethanol	225.4	4.825	75
Acetone	235	4.8	56.2
Isopropanol	235.2	4.76	82.3
Methanol	240	7.95	64.6
Ethanol	243	6.38	78.5
Ethyl acetate	257	3.88	77
Chloroform	263	5.47	61.7
Isooctane	270.7	2.57	99.2
Cyclohexane	280.3	4.07	80.7
Benzene	318.6	4.90	80.0
Toluene	320.8	4.10	110.6
p-Xylene	343.1	3.52	138.4
Water	374.2	22.05	100.0

[a]Sublimation temperature.

18.1 SOLUBILITY OF POLYMERS IN SCFS

The heuristic rule for solubility in liquid solvents, ''like dissolves like,'' applies similarly to polymers dissolving in SCFs. Thus, hydrocarbon polymers such as polyethylene are soluble in hydrocarbon SCFs such as the alkenes and *n*-alkanes, while polar polymers such as poly(methyl methacrylate) are soluble in polar SCFs such as chlorodifluoromethane. Carbon dioxide is generally a poor solvent for most high molecular weight polymers [14], but notable exceptions exist, such as siloxane polymers and fluorinated polymers. Solubility in CO_2 is also enhanced when CO_2-philic moieties are located in accessible side chains rather than in the less accessible main chain [15].

The solubility parameter for a compressible fluid increases from the gaseous state with increasing pressure (or density). Since solubility parameters for polymers, especially polar polymers, are relatively high, increasing pressure (or density) at constant temperature facilitates dissolution of polymers in SCFs. Conversely, decreasing the pressure at constant temperature causes the polymer to be rejected from solution.

The effect of temperature on polymer solubility in SCF solutions is more varied than the effect of pressure. Polymer solutions exhibit two different types of phase behavior: upper consolute solution temperature (UCST) or lower consolute solution temperature (LCST). In UCST behavior, two equilibrium liquid phases are converted to a single phase as the temperature is increased at constant pressure. In LCST behavior, a single liquid phase separates into two phases as the temperature is increased. U-L-CST behavior, where a two-phase solution becomes a single phase with increasing temperature, and, upon a further increase in temperature separates again into two phases, is also possible, but rarer. In conventional liquid solvents, LCST behavior is attributed to the difference in thermal expansion coefficients between the solvent and polymer, and to entropic effects as the solvent ''condenses'' around the polymer in order to solvate it. In polymer/SCF solutions, the mismatch in thermal expansion coefficients can be quite pronounced, since the solvent is highly compressible while the polymer is not. Also, ''clustering'' of SCF molecules around solute molecules is well-known in SCF solutions with low molecular weight solutes [16], so LCST phase behavior is common in polymer/SCF solutions.

Since both pressure and temperature are independent variables for controlling polymer/SCF phase behavior, it is informative to plot phase behavior in a P–T diagram, as shown schematically in Fig. 18.1. Coexistence curves separate regions where a single-phase solution exists from regions where two or more phases exist. If the coexistence curve exhibits a positive slope with temperature, the solution shows LCST behavior, while a negative slope is indicative of UCST behavior. Although curves for both types of behavior are shown in Fig. 18.1, for a given polymer/solvent system it may not be possible to see both branches, as solvent freezing or polymer degradation may occur at low and high temperatures, respectively. Increasing polymer molecular weight shifts the coexistence curves to higher pressures (i.e., decreased solubility), while improving the solubility parameter match (through changes in solvent type or composition, or changes in copolymer composition), shifts the P–T curves to lower pressures.

Polymer concentration also influences the location of the coexistence curves for polymer/SCF mixtures. Figure 18.2 shows a pressure-composition diagram for polycaprolactone ($M_w/M_n = 1.6$) in chlorodifluoromethane; this system exhibits LCST phase behavior. The curve shape is typical of that seen for most other polymer/SCF systems, including highly monodisperse polymers. The cloud point pressure increases steeply with increasing polymer concentration in very dilute solutions, reaches a somewhat broad maximum at intermediate concentrations ranging from about 2 to 10 wt %, and then decreases again in highly concentrated solutions. Increasing polymer molecular weight increases

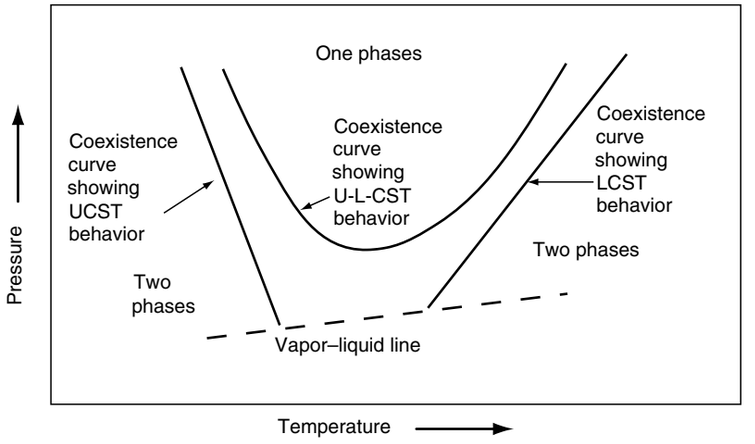

FIGURE 18.1. Schematic P–T diagram of polymer/SCF solutions.

the cloud point pressure, except at high polymer concentrations where molecular weight has little effect on the phase equilibrium.

The phase behavior of polymer/SCF mixtures can be described using versions of the lattice fluid (LF) model such as that developed by Sanchez and Lacombe [17]. The LF equation of state is relatively simple, and has been successfully used to describe either polymers dissolved in SCFs, or SCFs dissolved in polymers [18,19], including phenomena such as retrograde vitrification. The statistical associating fluid theory (SAFT) [20] can also describe the phase behavior of polymers dissolved in SCFs. The SAFT model, while somewhat more cumbersome to implement than the LF model, is especially well-suited for polymers with varying backbone architecture, such as branched polymers or copolymers. Both the Sanchez–Lacombe and SAFT models have been incorporated into commercially available modeling software [21].

Table 18.2 below lists polymer/SCF solutions which have been experimentally characterized for phase behavior.

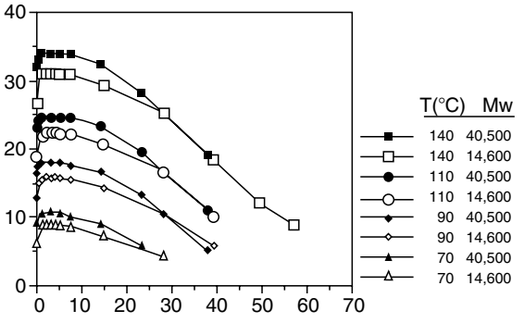

FIGURE 18.2. Phase behavior of polycaprolactone/$CHClF_2$ solutions.

Experimental techniques generally fall into one of two categories: optical measurements or sampling procedures. Optical techniques include qualitative visual observation of the cloud point, or quantitative determination of turbidity changes as pressure is lowered. Solution pressure may be lowered either by increasing the solution volume, usually by a movable piston, or else by venting off solution from a constant volume cell. Visual cloud points are difficult to distinguish accurately at extremely low or high concentrations, so much optical data center on the intermediate concentration regime where the P–x curve is flat. Sampling procedures involve analysis of the compositions of the two fluid phases in equilibrium with each other. These measurements are also difficult at extremely high concentrations because of the high viscosity of the polymer-rich phase. Alternately, only the solvent-rich phase may be sampled in a flow-through cell, provided that mass transfer does not limit the polymer concentration. Unless otherwise noted, the phase behavior results in Table 18.2 were acquired by visual observation of cloud points in a variable volume view cell. Equation of state models used to fit the experimental data are also noted in Table 18.2.

18.2 SOLUBILITY OF SCFS IN POLYMERS

Supercritical carbon dioxide is of special interest as an SCF for use with polymers, owing to its low critical point and nontoxic, nonflammable nature. However, as Table 18.2 demonstrates, the number of high molecular weight (>10 kDa) polymers which dissolve in supercritical CO_2 is relatively small. However, CO_2 and other SCFs are readily sorbed into a wide variety of polymers at elevated pressures. When the polymer in which the SCF dissolves is in the liquid or rubbery state, the sorption of SCF into the polymer generally follows Henry's law [77],

TABLE 18.2. *Solubility of polymers in supercritical fluids.*

Polymer	Mw (kDa)	Solvent	Temp. (°C)	Pressure (MPa)	Polym. Conc. (wt%)	Phase Behavior	Ref.	Technique	Modeling
Polyethylene									
Linear	4–118	Ethylene	130–170	155–190	2–24	UCST	[22]	Visual cloud point (CP)[a]	
Linear	13–120	Propane	110–135	40–70	.25–24	Flat[b]	[23]		
Linear	2–420	*n*-Butane	100–200	5–30	1–10	LCST	[24]		
	420	*n*-Butane/ 0–33% CO_2	100–200	25–80	5	Changes with % CO_2	[24]		
Linear	121	Cyclohexane/ 35–52% CO_2	160–210	27–55	3–20	LCST or Flat (high%CO_2)	[25]		
		Toluene/41–65% CO_2	160–210	38–70	3–12	UCST, ULCST	[25]		
		n-Pentane/ 30–40% CO_2	160–210	10–70	3–9	UCST, ULCST	[25]		
Linear	NR	CCl_3F	150–200	1.7–13.6	0.5–20	LCST	[26]		
Branched	315	Ethylene	105–140	140–200	0.33–30	UCST	[27]	Visual CP	
Branched	108	Ethane	95–130	120–130	5	Flat	[28]		SL[c] with temperature-dependent mixing parameters
		Propane	100–130	55–60	5	Flat			
		Ethylene	115–135	160–180	5	UCST			
		Propylene	90–140	60	5	Flat			
Branched	65–113	Dimethyl ether	110–165	50–140	5	UCST	[29]		SAFT[d]
Branched	NR	Ethylene	100–270	119–175	0.7–30	UCST	[30]	Visual CP with sampling	
Branched	46–108	Ethane	115–152	100–128	5.5	UCST	[31]		
	46–108	Propane	105–152	45–58	5.5	Flat	[31]		
Branched	17–246	Propane	110–150	40–60	0.15–29	Flat	[32]	Visual CP, constant vol.[e]	
	246	Ethane	120–150	115–120	5	UCST	[32]		
	246	*n*-Butane			5	Flat	[32]		
	246	*n*-Pentane	90–160	0.5–11	5	LCST	[32]		
Branched	28[d]	Ethylene	130	130–190	5–45	UCST	[33]	Visual CP	
Low density	45.3	Ethylene	130–248	120–164	5	UCST	[34]		PC-SAFT[f]
Linear low density	52	Ethylene	122–167	140–175	0.5–18	UCST	[35]	1.08 PDI	SL
Polyethylene	121	*n*-pentane	97–167	8–50	5	LCST	[36]	Transmitted intensity	
Branched polyethylene	32–2,000	ethylene	117–172	90–200	0.2–20	UCST	[37]		
Polyethylene	0.5–5	ethylene	140–240	53–62	0.3–3.2 (mol%)	UCST	[38]		PRSV[2] with Wong–Sandler mixing rule

TABLE 18.2. *Continued.*

Polymer	Mw (kDa)	Solvent	Temp. (°C)	Pressure (MPa)	Polym. Conc. (wt%)	Phase Behavior	Ref.	Technique	Modeling
Ethylene copolymers									
Ethylene-*co*-propylene	0.8–96	Propylene	−10–200	30–46	15	ULCST, LCST	[39]		
						LCST	[39]		
	Butene/ Ethylene	−25–200	1.5–40	15		LCST	[39]		
	Hexene/ Ethylene	−25–200	1–27	15		UCST, LCST	[39]		
	0.8–96	Propylene	100, 150	18–42	0.8–33	LCST	[40]		SAFT
		Ethylene	20–200	57–172	3.8, 16	ULCST	[40]		SAFT
	5.9	Propylene	100, 150	18–30	1.8–33	LCST	[41]		
Ethylene-*co*-methyl acrylate	69–279	*n*-Butane	135–210	60–250	5	UCST	[29]		
Ethylene-*co*- methyl acrylate	75–99	Ethane	160–175	230–260	5	UCST	[28]		SL with temperature-dependent mixing parameters
		Propane	45–170	100–280	5	UCST			
		Ethylene	25–130	120–260	5	UCST			
		Propylene	25–135	40–140	5	UCST			
	99	*n*-Hexane Propane other	145–155	80–260	5	UCST	[42]		
		Propane	70–160	150–220	5	UCST	[42]		
		Propane / 10 %alcohol	70–160	80–240	5	UCST	[42]		
Ethylene-*co*-methyl acrylate	110–128	Ethylene	100–220	118–211	5	UCST	[34]		PC-SAFT
Ethylene-*co*-methyl acrylate	34–59	Propane	65–160	60–200	5	UCST	[43]		SL
		Propane / 0–9% Ethanol	65–160	45–200	5	UCST, Flat			
		Propane / 0–41% Acetone	40–140	25–175	5	UCST, Flat			SL
		$CHClF_2$	65–150	6–30	5	LCST			
		$CHClF_2$ / 0–39% Ethanol	65–150	3–20	5	LCST			
		$CHClF_2$ / 0–39% Acetone	65–150	3–25	5	LCST			
Ethylene-*co*-methyl acrylate	75–185	Ethylene	30–240	125–270	5	UCST	[44]		
Ethylene-*co*-ethyl acrylate	117–157	Ethylene	80–260	98–163	5	UCST	[34]		PC-SAFT
Ethylene-*co*-propyl acrylate	112–147	Ethylene	80–260	98–153	5	UCST	[34]		PC-SAFT
Ethylene-*co*-butyl acrylate	35–297	Ethylene	50–245	75–180	5	UCST	[44]		SAFT
Ethylene-*co*-acrylic acid	24–247	1-Butene	120–220	50–250	5	UCST	[29]		
Ethylene-*co*-methyl methacrylate	20–84	Ethylene	80–255	104–186	5	UCST	[34]		PC-SAFT

TABLE 18.2. *Continued.*

Polymer	Mw (kDa)	Solvent	Temp. (°C)	Pressure (MPa)	Polym. Conc. (wt%)	Phase Behavior	Ref.	Technique	Modeling
Polystyrene									
Polystyrene	20	Diethyl ether	−70–170	5–200	15.4	LCST	[45]	Turbidity	
Polystyrene	110	Diethyl ether/ Acetone	−100–200	0–31	10	UCST, LCST	[45]		
Polystyrene	4,9	*n*-Butane	120–200	4–65	0.5–80	LCST(high, low polymer concn) USCT(inter-mediate concn)	[46]	Laser turbidity CP, variable vol.	
	9	*n*-Pentane	130–220	4–35	5–80	LCST(high, low polymer concn) USCT(inter-mediate concn)	[46]		
	0.4–3	Ethane	40–60	8.5–34	0.001–20	LCST	[47]	Sampling	
	0.4–1.1	CO_2	40	25	0.01–1	NR	[47]	Sampling	
	0.4–1.6	Ethane / 13% Propane	40	25	1–10	NR	[47]	Sampling	
	1,9	Propane	50–180	25–67	0.2–4	UCST	[48]		
	114, 929	Dichloro-trifluoro-ethane	75–145	3–35	0.03–7.3	LCST	[49]		
Polystyrene	270	*trans*-decahydro-naphthalene	1–16	10–90	4.2–21.6 (vol%)	UCST	[50]	Light Scattering	SL
Isotactic	22	*n*-Butane	155–201	9–13	13–26	LCST	[51]	Visual CP, constant vol.	
Other hydrocarbon polymers									
Polypropylene		CO_2	163–208	45–95	6.7–38	UCST	[52]	Laser CP, constant, vol.	
Atactic polypropylene	6 (M_v)	CO_2	25, 32	13.5	0.15–0.25	LCST	[53]		
Poly(1-butene)		*n*-Butane	167–190	12–17	5.5–21	LCST	[52]		
		CO_2	132–146	30–90	6.3–38	UCST	[52]		
Poly(1-butene) (atactic)	0.4–1.3 (M_v)	CO_2	30–33	17.9–23.4	0.6–1		[53]		
Polybutadiene	5(M_v)	CO_2	25	19.3	0.27		[53]		
Polyisobutylene	0.5(M_v)	CO_2	25	20.3	0.44	NR	[53]		
Polyisobutylene	50	*n*-Butane	155–200	7–10	18.8–31.4	LCST	[51]	Visual CP constant vol.	
Polyisobutylene (telechelic)	1–11	Propane	25–150	25–45	7	LCST, ULCST	[54]	Visual CP constant vol.	SAFT
	1–11	Dimethyl ether	75–150	45–65	5	ULCST, LCST	[54]		SAFT
	0.2–11	Ethane	25–150	2–120	9–43	LCST, UCST (high MW)	[54]		SAFT
	0.2–1	CO_2	50–180	4–200	5–52		[54]		SAFT
Polyisobutylene	1.25	Propane	90–113	4–7	27.1	LCST	[55]	Sampling	

TABLE 18.2. *Continued.*

Polymer	Mw (kDa)	Solvent	Temp. (°C)	Pressure (MPa)	Polym. Conc. (wt%)	Phase Behavior	Ref.	Technique	Modeling
Acrylate or Methacrylate Polymers									
Poly(methyl methacrylate)	10.6	$CHClF_2$/Acetone	65–155	2.5–25	5	LCST	[43]	Visual CP, variable vol.	
Poly(methyl methacrylate)	50	$CHClF_2$	75–150	3–30	0.08–0.26	LCST	[56]	Visual CP, variable vol.	
Poly(methyl methacrylate)	74	$CHClF_2$	65–140	3–29	0.03–15	LCST	[57]	Visual CP, variable vol.	SL-HB[h]
Poly(methyl methacrylate)	104.7	Propylene	154–259	108–270	5	UCST	[34]		PC-SAFT
Poly(ethyl methacrylate)	280	$CHClF_2$	75–140	3–25	0.08	LCST	[56]		
Poly(butyl methacrylate)	65.5	Ethylene	100–235	103–138	5	UCST	[34]		PC-SAFT
Poly(decyl methacrylate)	250–730	Isooctane	230–320	1.5–7.5	5–30	LCST	[58]		
Polystyrene-*b*-poly(methyl methacrylate)	70	$CHClF_2$	110	21	0.08		[56]		
Poly(methyl acrylate)	2.03	CO_2	25	22–54	1–6		[15]		
	2.85	CO_2	25–50	67–102	1–10	LCST	[15]		
Poly(methyl acrylate)	30.7	$CHClF_2$	64–136	2.5–22.5	5	LCST	[43]		
Poly(methyl acrylate)	186.9	Propylene	200–258	140–275	5	UCST	[34]		PC-SAFT
Poly(ethyl acrylate)	153.7	Ethylene	81–260	101–161	5	UCST	[34]		PC-SAFT
Poly(propyl acrylate)	108.3	Ethylene	80–258	87–109	5	UCST	[34]		PC-SAFT
Poly(*n*-butyl acrylate)	30–940	Nitrous oxide	75	10.3–51.7	0.006–0.03		[59]		
Aliphatic Polyesters									
Poly(ε-caprolactone)	14.6, 40.5	$CHClF_2$	55–145	3–35	0.03–19	LCST	[57]		SL-HB
Poly(L-lactic acid)	50	$CHClF_2$	55–150	3–28	0.08	LCST	[56]	Constant vol.	
Poly(L-lactic acid)	1–10	CO_2/10–40% $CHClF_2$	55–65	7–20	0.001–0.05	LCST	[60]	Flow cell sampling	
Poly(L-lactic acid)	1–2.1	CO_2/0–1% Acetone	55–65	7–20	0.001–0.05	LCST	[61]	Flow cell sampling	
Poly(L-lactic acid)	1–2.1	$CClF_3$	55	11–12	<0.5	NR[i]	[61]	Flow cell sampling	
Poly(D,L-lactic acid)	0.9	CO_2	55	20	<0.5	NR	[61]		
Poly(glycolic acid)	NR	CO_2	55	18–20	<0.5	NR	[61]		
Poly(lactic-*co*-glycolic acid)	70–149	CO_2	33–97	131–300	5	Nearly athermal	[62]		
Poly(lactic-*co*-glycolic acid)	128–130	CHF_3	27–81	54–147	5	LCST	[62]		
Poly(lactic-*co*-glycolic acid)	70–130	$CHClF_2$	36–72	1.5–24	5	LCST	[62]		
Poly(γ-hydroxybutyrate)	800	CO_2	35–75	12–35	0.05–1	LCST	[63]	Extraction	
Polyethers									
Polyethylene glycol	0.4–0.6	CO_2	40	20	0.25–1.25	NR	[64]		SL
Poly(ethylene glycol)	0.2–0.6	CO_2	40	20	0.05–4	NR	[65]	Sampling	
Poly(propylene glycol) (Low polydispersity)	0.45–2.16	Ethane	20–100	5–30	0.5–4	ULCST	[66]		SL-HB
Poly(propylene oxide)	3.5	CO_2	50–70	98–135	5	UCST	[15]		
PEG/nonylphenylether	2.5	CO_2	45;60	12–30	0.005–0.07	LCST	[67]	extraction	

TABLE 18.2. *Continued.*

Polymer	Mw (kDa)	Solvent	Temp. (°C)	Pressure (MPa)	Polym. Conc. (wt%)	Phase Behavior	Ref.	Technique	Modeling
Siloxane Polymers									
Poly(dimethyl siloxane)	135	CO_2	25, 52	19.3	0.3, 1	UCST	[53]		
Poly(dimethyl siloxane)	13	CO_2	22	25–32	1–10		[68]	Visual CP, constant vol.	
Poly(dimethyl siloxane-co-methylhydrosiloxan-g-propyl acetate); other side chains also reported	Degree of polymerization = 25	CO_2	22	12–35	0.4–5.5	NR	[69]	Transmitted light intensity	
Fluorinated Polymers									
Poly(hexafluoro-propylene oxide)	13.6	CO_2	22	6–15	1–10		[68]	Visual CP, constant vol.	
Poly(tetrahydroperfluoro-decylacrylate)		CO_2	10–70	5–25	0.087–7.32	LCST	[70]	Visual CP, variable vol.	
Poly(vinylidene fluoride)	180; 275	$CHClF_2$	120–180	71–73	5	UCST	[71]		
		$CHClF_2$	129–207	72–76	5				
Poly(vinylidene fluoride)	180; 275	CO_2	140–200	159–165; 158–170	5	UCST	[71]	Visual CP, variable vol.	
			125–220						
Poly(vinylidene fluoride)	180; 275	CHF_3	170–225	180–230	5	UCST	[71]		
Poly(vinylidene fluoride)		Dimethyl ether				LCST	[71]		
Poly(1,1-dihydroperfluorooctylacrylate)	1,400	CO_2	30–90	10–200	0.09–16	LCST	[72]		SAFT
Poly(tetrafluoroethylene-*co*-vinyl acetate)	140–180	CO_2	25; 75–128	50–56	1–10		[73]	Visual CP, variable vol.	
				74–90	5	LCST			
Methacrylate, perfluorinated propylene oxide graft copolymers	6.2–11	CO_2	40	16–42	1–28		[74]		
Other Polymers									
Cellulose triacetate	145.7	Ethyl acetate	185–235	3.5–8.5	0.5–5	LCST	[75]	Visual CP, variable vol.	
Poly(vinyl acetate)		CO_2	25	63–66	3–6	NR	[73]	Visual CP, variable vol.	
Poly(vinyl acetate)	0.98–585	CO_2	25	13.6–67.6	1–12	NR	[15]		
Poly(vinyl acetate)	585	CO_2	17–207	67–125	5	LCST	[15]		
Poly(ε-caprolactam)		Trifluoroethanol / 0–48% CO_2	25–100	13–35	3–14		[76]		SAFT, SL
Poly(ε-caprolactam)		CO_2	233–241	40–50	13.8–16.5	UCST	[52]		

[a]Cloud point determined by eye.
[b]Phase boundary nearly independent of temperature.
[c]Sanchez–Lacombe equation of state.
[d]Statistical associating fluid theory equation of state.
[d]Viscosity average molecular weight.
[e]Constant volume view cell.
[f]Perturbed chain SAFT model.
[g]Peng-Robinson-Stryjek-Vera equation of state.
[h]Sanchez–Lacombe hydrogen bond model.
[i]Not reported.

shown in Eq. (18.1), where the mass fraction of sorbed SCF (w_{SCF}) is proportional to the partial pressure of the SCF, P_{SCF}.

$$w_{SCF} = k_H P_{SCF}. \tag{18.1}$$

The Henry's law constant, k_H, is independent of molecular weight except at extremely low molecular weight (< 1kDa), but is often a strong function of temperature, typically showing an Arrhenius-like dependence. The slope of the Arrhenius plot can be correlated with the enthalpy of dissolution of the SCF in the polymer [78]. An alternate correlation based on corresponding states suggests that k_H should scale with $(T_c/T)^2$, rather than with $1/T$ [79]. However, the proportionality constant for $(T_c/T)^2$ scaling is not a universal constant. Over the temperature range common for SCF-polymer mixtures, little difference is detectable between $1/T$ scaling and $1/T^2$ scaling, so data are presented here with the $1/T$ scaling. The solubility of the SCF in the polymer may either increase with temperature (for polymer-SCF pairs exhibiting UCST phase behavior), or solubility may decrease with increasing temperature (for polymer-SCF pairs exhibiting LCST phase behavior.) Hence, the Arrhenius coefficient for k_H may be either positive or negative. Table 18.3 lists Henry's law constants for rubbery and molten polymers. The temperature dependence of the Henry's law constants are correlated with absolute temperature via the Arrhenius expression:

$$\ln(k_H) = \frac{A}{T} + B, \tag{18.2}$$

where k_H (from Eq. (18.1)) has units of mass fraction per MPa, and T has units of degrees Kelvin.

Care should always be exercised when using solubility data for glassy or crystalline polymers (not included here), because SCF sorption occurs preferentially in the amorphous phase, which may additionally experience swelling-related stress. Solubility data for CO_2 in solid polymers is compiled in [5]. Often, the pressure dependence of SCF sorption in glassy polymers follows a dual-mode sorption model, with substantial deviations from Henry's law.

Solubility of SCFs in polymers is determined experimentally by one of several general techniques. Gravimetric techniques monitor the in situ weight gain of a polymer sample exposed to a surrounding high pressure SCF. These techniques require the application of a buoyancy correction term to the raw data, since the polymer swells upon exposure to the SCF. The swollen volume may be measured experimentally, or it may be estimated using an equation of state, typically the Sanchez–Lacombe model. Another experimental technique measures mass gain of a polymer exposed to an SCF by monitoring the change in resonant frequency of an oscillating sensor, typically a quartz crystal. The amount of SCF sorbed in a polymer may also be determined by recording the pressure decay in a reservoir of SCF in contact with the polymer.

18.3 MELTING POINT DEPRESSIONS OF POLYMERS IN THE PRESENCE OF SCFS

The melting temperature (T_m) of a semicrystalline polymer is usually lower in the presence of a soluble SCF than it is in the pure polymer at ambient pressure. When a polymer crystallizes from an SCF-saturated solution, the resulting three-phase (S–L–G), two-component equilibrium is univariant, according to the phase rule, so T_m is only a function of pressure under these conditions. Experimental measurements of the polymer melting point in the presence of an excess of CO_2 typically exhibit the pressure dependence shown in Fig. 18.3. The melting temperature decreases approximately linearly with increasing pressure above ambient conditions, then it abruptly levels off to a near constant value. Occasionally, some deviations from this behavior are seen: (1) a small (1–2°C) increase is T_m is sometimes recorded at low pressure, before the linearly decreasing region occurs. This is attributed to annealing of small crystallites; (2) at very high pressure, following the plateau zone, T_m sometimes begins to increase with increasing pressure; and (3) the plateau zone where T_m is constant is sometimes missing, so that a region of linearly decreasing T_m is followed immediately by a region of linearly increasing T_m. The qualitative features of the SCF-saturated melting point curves are similar for polymers and for sparingly soluble low molecular weight crystalline compounds such as naphthalene and biphenyl [100].

The melting point of a polymer saturated with an SCF is determined experimentally either visually, or else by high pressure calorimetry, although the pressure range for the latter is often limited by instrument constraints to a few MPa. Table 18.4 presents values of dT_m/dP in the linear region (low pressure) for polymers saturated with an SCF. In cases where an increase in T_m occurred at very low pressure, as in Fig. 18.3, the lowest pressure points were not included in the linear least squares line fitting. When the experimental pressures were high enough so that the second (plateau) region could be seen, this has been noted in the Comments.

18.4 SCF-INDUCED T_g DEPRESSION

Sorption of an SCF in a polymer can lower its glass transition temperature (T_g) significantly below that seen at atmospheric pressure. For a given polymer, the glass transition temperature depression is found to increase as the amount of SCF sorbed increases [105]. Because CO_2 solubility usually decreases with increasing temperature, it is possible for a polymer/CO_2 mixture at elevated pressure to undergo a liquid-to-glass transition as the temperature is raised. This phenomenon, referred to as ''retrograde vitrification'' [18], has been observed for poly(methyl methacrylate) [105,106]. Table 18.5 reports the pressure dependence of T_g observed for polymers which have been exposed to a high pressure SCF. T_g depression curves look similar to

TABLE 18.3. *Henry's law constants of SCFs in Polymers.*

Polymer	Diluent	Temp. Range (C)	Pressure (MPa)	k_H (mass fraction/MPa)	A (Eq. (18.2))	B (Eq. (18.2))	Ref.	Technique	Comments
Polyethylene	CO_2	185–227	0.7–2.0		171	−4.87	[77] [80]	Pressure decay	
Polyethylene, branched	CO_2	125–250	NR		546	−6.235	[81]	Gas–liquid chromatography	
Polystyrene	CO_2	65–129	4–44				[82]	MSB[a] and pressure decay	
Polystyrene	CO_2	100–200	2–20		1080	−8.081	[83]	MSB	SL[b]
Polystyrene	*n*-Butane	75–200	0.1–3		2034	−8.231	[84]	Volumetric	Only mass fraction <0.05 used in fitting
Polystyrene	Isobutane	75–200	0.1–3		1846	−8.094	[84]	Volumetric	Only mass fraction <0.05 used in fitting
Polystyrene	HCF_2Cl	85	0–2.5	0.0539			[85]	QCM[c]	
Polypropylene	CO_2	160–200	5.4–17.5		760	−6.637	[86]	Pressure decay	SL used for swelling correction
Polypropylene	*n*-Butane	165–210	0.3–3.1		2366	−8.144	[84]	Volumetric	
Polypropylene	Isobutane	165–210	0.3–3		2025	−7.637	[84]	Volumetric	
Poly(methyl methacrylate)	HCF_2Cl	70	0–1	0.153			[85]	QCM	
Poly(ε-caprolactone)	CO_2	70–85	0.2–6.5		1131	−7.524	[87]	Quartz spring microbalance	SL
Poly(butylene succinate)	CO_2	50–180	1–20		1038	−7.528	[88]	MSB	SL used for swelling correction
Poly(lactic-*co*-glycolic acid) (48L/52G)	CO_2	40	1–3	0.0152			[89]	Gravimetric	
Poly(lactic-*co*-glycolic acid) (53L/47G)	CO_2	40	1–3	0.0162, 0.0164			[89]	Gravimetric	
Poly(lactic-*co*-glycolic acid) (54L/46G)	CO_2	40	1–3	0.0195			[89]	Gravimetric	
Polyethylene glycol	CO_2	65–100	4–14		1687	−8.807	[90]	Sampling	SAFT[d] modeling
Polyethylene glycol	CO_2	40	5–11	0.0198			[91]	NIR[e]	
Polypropylene glycol	CO_2	25	2–6	0.0294			[91]	NIR	
Polypropylene glycol	CO_2	35	2–6	0.0200			[91]	NIR	
Poly(phenylene oxide)	CO_2	150	2–20	0.00524			[92]	MSB	SL used for swelling correction
Poly(phenylene oxide)	CO_2	200	2–20	0.00405			[92]	MSB	SL used for swelling correction
Poly(vinyl acetate)	CO_2	40–100	0.2–17.4		1882	−9.344	[83]	MSB	SL used for swelling correction

[a]Magnetic suspension balance.
[b]Sanchez–Lacombe equation of state used.
[c]Quartz crystal microbalance.
[d]Statistical associating fluid theory.
[e]Near infrared spectroscopy.

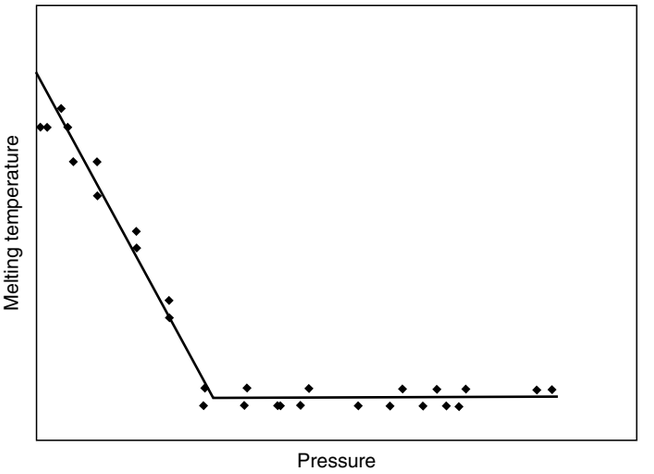

FIGURE 18.3. Representative plot of melting point depression of polymer exposed to CO_2. Lines are added as a guide to the eye.

melting point depression curves – a near linear decrease of T_g with increasing pressure is seen at low pressures. However, the typical magnitude of the slope of the T_g vs. P curve is considerably higher (about 5–10 times) than the typical magnitude of the T_m vs. P curve (e.g., from Table 18.4). An equation of state can be used to predict SCF-induced T_g depression, using either an isofree volume condition or the isoconfigurational entropy condition of the Gibbs-DiMarzio criterion.

18.5 INTERFACIAL TENSION BETWEEN SCF AND SCF-SWOLLEN POLYMER

The interfacial tension (IFT) between an SCF-swollen polymer and the saturating SCF decreases with pressure, as the solubility of the SCF in the polymer increases. For polymers which exhibit complete miscibility with the SCF at an experimentally achievable pressure, the IFT will vanish as the pressure approaches the apex of the P–x curve. Several comprehensive studies of the IFT of polymers swollen with CO_2 have been conducted; these are summarized in Table 18.6. These studies indicate that the molecular weight of the polymer does not influence IFT, probably because SCF solubility in the polymer is independent of molecular weight. For mixtures exhibiting LCST phase behavior, temperature has a minor effect on IFT, because the decrease in IFT associated with increasing temperature in pure polymers is largely offset by an increase in IFT due to decreased solubility of the SCF in the polymer. Plots of IFT vs. CO_2 pressure typically show a steep decreasing slope at lower pressure, followed by a more gradual decrease at higher pressure. The values of IFT in Table 18.6 were measured by analyzing the shape of a pendant drop.

18.6 VISCOSITY OF POLYMER/SCF MIXTURES

Because SCFs typically have lower density and higher compressibility than a pure polymer melt, dissolution of the SCF into the polymer melt results in swelling of the polymer. This in turn leads to an increase in free volume of the mixture, so transport properties such as viscosity and diffusion coefficient can be significantly enhanced. The semi-empirical Doolittle equation [128,129] predicts that the zero-shear rate viscosity, η_0, of a polymer is exponentially related to the fractional free volume, f, via:

$$\eta_0 = A \exp\left[B\left(\frac{1}{f} - 1\right)\right]. \tag{18.3}$$

A viscoelastic shift factor, a_S, can be found from the ratio of the experimentally measured zero shear rate viscosity (at test conditions of P, T, and SCF concentration), to the experimentally measured zero shear rate viscosity (at some reference conditions of P_{ref}, T_{ref}, and reference SCF concentration). Once a_S is determined experimentally, a master curve can be constructed by plotting η/a_S vs. $a_S\dot{\gamma}$ where η is the measured viscosity and $\dot{\gamma}$ is the measured shear rate. If the fractional free volume, f, is estimated from an equation of state as $f = 1 - \rho/\rho^*$, where ρ is the mixture density and ρ^* is the mixture close-packed density, then the shift factor due to the presence of the SCF can be calculated from Eq. (18.3), provided the constant B is known. Experimentally, B for SCF-swollen polymers has been found to be near unity [130,131], in agreement the universal constants of the WLF equation [132] for the temperature dependence of pure polymers.

TABLE 18.4. *Melting point depressions of semicrystalline polymers saturated with* CO_2.

Polymer	M_w (kDa)	T_{m0} (°C)	$-dT_m/dP$ (°C/MPa)	Pressure range (MPa)	Minimum T_m (°C)	Ref.	Comments
Low density polyethylene		105.4	0.5	0.1–10.4	NS[a]	[93]	Monitored temperature of high pressure melt cooling.
Low density polyethylene		112	5	0.1–30	85.6	[94]	No region of $dT_m/dP = 0$. Slope changes sign abruptly
Syndiotactic polystyrene		277	1.71	0.1–7	NS	[95]	HP-DSC[b]
Isotactic polypropylene		147–154	1.24	0.1–4.5	NS	[96]	HP-DSC
Isotactic polypropylene	85	165	1.0	0.1–3	NS	[97,98]	HP-DSC
Isotactic polypropylene	133	180	1.18	0.1–10	NS	[98,99]	HP-DSC
Isotactic polypropylene		154,164	1.24	0.1–4.5	NS	[96]	HP-DSC
Poly(ε-caprolactone)	4	63	2.41	0.1–28	36	[100]	
Poly(butylene succinate)	140	118	1.14	0.1–20	102	[100]	
Poly(L-lactide)	180	160	2.2	0.5–2	NS	[98]	HP-DSC
Poly(ethylene terephthalate)	180	257	0.67	0.1–8.5	NS	[95]	HP-DSC
Poly(ethylene terephthalate)	50.7	253	0.42	1–3	NS	[101]	HP-DSC
Polyethylene glycol	1.5	45	2.6	0.1–30	29	[102]	
Polyethylene glycol	4	57	2.14	0.1–30	42	[102,103]	
Polyethylene glycol	12	62	1.55	0.1–31	47	[103]	
Polyethylene glycol	35	61	1.55	0.1–30	47	[102]	
Poly(vinylidene fluoride)	530	158	0.48	0.1–68	135	[104]	Dilation
Other Solvents							
Low density polyethylene/$CHClF_2$		105.4	1.38	0.1–6.9	NS	[93]	

[a]Not seen in the experimental pressure range.
[b]High pressure differential scanning calorimetry.

TABLE 18.5. *Glass transition temperature depressions of polymers in the presence of SCFs.*

Polymer	Diluent	T_{g0}(°C)	$-dTg/dP$ (°C/MPa)	Wt%CO_2	P (MPa)	$T_{g,P}$ (°C)	Ref.	Technique
Polystyrene	CO_2	100			2.03	78	[107]	DSC[a]
Polystyrene	CO_2	100			6.08	35	[105]	CC[b]
Polystyrene	CO_2	100			8.0	40	[108]	High pressure partition chromatograpy
Polystyrene	CO_2	104	8.1		5.33	61	[109]	HP-DSC
Polystyrene	1,1,1,2-tetrafluoroethane	104	8.5		3.28	76	[109]	HP-DSC
Poly(4-methyl-1-pentene)	CO_2	40			1.5	20	[110]	Soprtion
Poly(methyl methacrylate)	CO_2	105			3.95	32.7	[105]	CC
Poly(methyl methacrylate)	CO_2	105			8.0	40	[108]	High pressure partition chromatograpy
Poly(methyl methacrylate)	CO_2	105			10.0	36	[108]	High pressure partition chromatograpy
Poly(methyl methacrylate)	CO_2	92	8.9		4.7	50	[111]	Molecular probe chromatography
Poly(methyl methacrylate)	CO_2	90.7	10.6		3.77	50.8	[112]	High pressure calorimetry
Poly(methyl methacrylate)	Methane	90.7			22	73.5	[112]	High pressure calorimetry
Poly(methyl methacrylate)	Ethylene	90.7			5.52	57.3	[112]	High pressure calorimetry
Poly(methyl methacrylate)	CO_2	105			3.95	58.5	[105]	CC
Poly(methyl methacrylate)	CO_2	105			3.95(rv)[c]	32.7(rv)	[105]	CC
Poly(methyl methacrylate)	CO_2	105			4.05	42	[105]	CC
Poly(methyl methacrylate)	CO_2	105			3.75	75	[106]	CC
Poly(methyl methacrylate)	CO_2				3.75(rv)	5(rv)	[106]	CC
Poly(methyl methacrylate)	CO_2				6.08	45	[106]	CC
Poly(ethyl methacrylate)	CO_2	61			2.13	24	[113]	Sorption
Poly(ethyl methacrylate)	CO_2	61			1.62	24	[113]	Dilation
Acrylonitrile/methyl acrylate terpolymer (Barex)	CO_2	85		6.7		54	[114]	Ambient pressure DSC
Poly(acrylic acid)	CO_2	100			8.0	48	[115]	IGC[d]
Poly(L-lactide)	CO_2	NR	3.5		2		[98]	
Poly(ethylene terephthalate)	CO_2	74			2.03	52	[107]	DSC
Poly(ethylene terephthalate)	CO_2	74			2.03	52	[107]	DSC
Poly(ethylene terephthalate)	CO_2	74			2.03	52	[107]	DSC
Poly(phenylene oxide)	CO_2	210			1.4	25	[116]	Sorption isotherm
Poly(phenylene oxide)	CO_2	216			6.20	184.4	[117]	DSC
Poly(phenylene oxide)	CO_2	219			4.46	55	[118]	DSC
Poly(phenylene oxide)	CO_2	209			8.0	156 101 (rv)	[115]	IGC
					10.0	126		
Polycarbonate	CO_2	148			2.03	97	[107]	DSC
Polycarbonate	CO_2	150			8.0	75	[108]	High pressure partition chromatograpy
Polycarbonate	CO_2	145	9.0		9.3	60	[109]	HP-DSC
Polycarbonate	CO_2	151			3.1	25	[116]	Sorption isotherm

TABLE 18.5. *Continued*

Polymer	Diluent	T_{g0}(°C)	$-dTg/dP$ (°C/MPa)	Wt%CO_2	P (MPa)	$T_{g,P}$ (°C)	Ref.	Technique
Polycarbonate	CO_2	156			1.11	138	[119]	HP-DSC
					3.4(rv)	0(rv)	[111]	
Polycarbonate	CO_2	148			2.03	97	[107]	DSC
Polycarbonate	CO_2	148			6.08	55	[118]	DSC
Tetramethyl polycarbonate	CO_2	195	6.6		5.62	160	[120]	High pressure scanning calorimetry
Polycarbonate	CO_2	150	7.1		5.62	109	[120]	High pressure scanning calorimetry
Tetrachloro polycarbonate	CO_2	233	4.74		5.62	206	[120]	High pressure scanning calorimetry
Tetrabromo polycarbonate	CO_2	267	3.65		5.62	247	[120]	High pressure scanning calorimetry
Poly(vinyl chloride)	CO_2	75			2.03	57	[107]	DSC
Poly(vinyl chloride)	CO_2	77	13.4		4.26	16	[109]	HP-DSC
Poly(vinyl pyrrolidone)	CO_2	165			8	120, 71(rv)	[115]	IGC
					10	106, 96(rv)	[115]	IGC
Poly(vinyl pyrrolidone)	CO_2	161			8	100.5, 81(rv)	[115]	IGC
Poly(vinyl pyrrolidone-co-vinyl acetate)	CO_2	96			8	36	[115]	IGC
Polysulfone	CO_2	182			3.4	23	[116]	Sorption isotherm
Poly(ether sulfone)	CO_2	222			2.7	21	[116]	Sorption isotherm
Poly(ether imide)	CO_2	199			2.8	21	[116]	Sorption isotherm
Cellulose acetate	CO_2	187			1.1	27	[116]	Sorption isotherm
Cellulose triacetate	CO_2	185			1.0	24	[116]	Sorption isotherm
Poly(vinylidene fluoride)	CO_2	105			2.53	60	[107]	DSC
Poly(amic acid)	CO_2	156			6.08	−8	[118]	DSC
Polyimide	CO_2	227			6.08	0	[118]	DSC
Poly(*p*-phenylene sulfide)	CO_2	85.5			2.03	75	[121]	Sorption isotherm
Poly(vinyl benzoate)	CO_2	65.5			3.39	25	[122]	Dilation
Poly(vinyl butyral)	CO_2	51			2.63	25	[122]	Dilation

[a]Differential scanning calorimetry.
[b]Creep compliance.
[c]Retrograde vitrification.
[d]Inverse gas chromatography.

TABLE 18.6. *Interfacial tension between polymers and carbon dioxide.*

Polymer	M_w (kDa)	Temp. (°C)	Pressure (MPa)	IFT (mN/m)	Ref.
Polystyrene	158	90	10	15.02	[123]
			25.4	9.38	
		140	3.9	37.61	
			20.2	12.41	
		160	5	24.54	
			17	13.91	
Polystyrene	309	100	8.2	20	[124]
			29	7.4	
		150	6.9	29	
			30	9.9	
Polystyrene	120	200	0.1	27.5	[125]
			10	17	
	NR	210–230	0.1	24	
			7	14	
Polypropylene	985	160–180	10.6	17	[124]
			25	7.3	
Poly(methyl methacrylate)	89.2	90	10	13	[124]
			33	4.5	
Poly(ethylene glycol)	0.6	45	8	10.5	[126]
			13	5	
			30	3.1	
Poly(ethylene glycol) nonylphenyl ether	2.5	50	9.9	22	[127]
			14.9	16	
			25.4	10	
		70	9.9	18	[127]
			14.9	11	
			25.4	9	
Poly(dimethyl siloxane)	*100 Pa s	40	1.7	16.4	[123]
			30.7	0.08	
	*1,000 Pa s	40	4.75	11.4	
			30	0.09	
	*15,000 Pa s	40	5.2	8.9	
			30.24	0.23	

*Viscosity at 25°C.

Table 18.7 lists viscosity reductions measured due to the presence of an SCF in the polymer. Because few researchers have reported the zero shear rate viscosity for both the pure polymer melt and the SCF-swollen melt, an experimental shift factor cannot usually be estimated from the data. Instead, Table 18.7 lists the ratio of viscosity measured in the presence of SCF diluent (η_{Dil}) to the viscosity measured in the absence of diluent (η), at some reference conditions. Unless otherwise specified, the reference state has no SCF, and has the same temperature as the experimental state. The pressure for the reference state, and dynamic characterization conditions (e.g., constant stress, σ, or constant $\dot{\gamma}$) are also specified in Table 18.7.

Experimental techniques for the characterization of SCF-diluted polymer viscosity generally fall into one of two categories – pressure-driven or drag-driven flow. Pressure-driven techniques include capillary flow and slit die extrusion, with viscosity calculated from the pressure drop vs. flow rate relation. Because viscosity is a function of pressure in these systems, the viscosity measured by pressure-driven techniques is an average quantity for the pressure range used in the experiment. Vibrating sensor surfaces or translating spheres are examples of drag-driven viscosity measurement devices. These avoid the difficulty of pressure variations, but usually lack the dynamic range of pressure-driven devices, i.e., are restricted to a limited range of $\dot{\gamma}$.

TABLE 18.7. *Viscosity reduction of polymer/SCF mixtures.*

Polymer	Diluent	Temp (°C)	Reference viscosity (Pa-s)	Reference Pressure (MPa)	Matching condition	η_{Dil}/η_{Ref}	*P* (MPa)	SCF Concn (wt%)	Ref.	Technique
High density polyethylene	CH_3CF_2Cl	200	NR	NR	$\sigma = 50\,kPa$	0.604	NR	8.96	[133]	Pressure-driven slit die rheometer
Low density polyethylene	CO_2	150	602	1.4	$\dot{\gamma} = 45\,s^{-1}$	0.71	4.7	7.8	[131]	Capillary rheometer
Low density polyethylene	CO_2	200	1.5×10^4	NR	$\dot{\gamma} = 10\,s^{-1}$	0.53	NR	4.0	[134]	Extrusion slit die
Low density polyethylene	CO_2	195	1,230	19.2	$\dot{\gamma} = 16\,s^{-1}$	0.759	19.2	7	[135]	Extrusion wedge die
Linear low density polyethylene	CH_3CF_2Cl	135	NR	NR	$\sigma = 50\,kPa$	0.475	NR	10.97	[133]	Pressure-driven slit die rheometer
Polystyrene	CO_2	195	3,900	19.2	$\dot{\gamma} = 13\,s^{-1}$	0.405	19.2	4	[135]	Extrusion wedge die
Polystyrene	CO_2	200	4,800	11.2	$\dot{\gamma} = 25\,s^{-1}$	0.389	9.3	4	[136]	Extrusion slit die
Polystyrene	CO_2	150	9,900	0.1	$\dot{\gamma} = 10\,s^{-1}$	0.187	12.18	5.2	[137]	Capillary
Polystyrene	CH_3CHF_2	150	5,600	0.1	$\dot{\gamma} = 21\,s^{-1}$	0.052	16.41	10.4	[137]	Capillary
Polypropylene	CH_3CF_2Cl	175	NR	NR	$\sigma = 50\,kPa$	0.438	NR	10	[133]	Pressure-driven slit die rheometer, constant stress
Polypropylene	*n*-pentane	200	2,200	NR	$\sigma = 50\,kPa$	0.413	NR	5.14	[133]	Pressure-driven slit die rheometer
Polypropylene	CO_2	175	NR	NR	$\sigma = 50\,kPa$	0.282	NR	4.9	[133]	Pressure-driven slit die rheometer
Polypropylene	CO_2	190	9,200	NR	$\dot{\gamma} = 10\,s^{-1}$	0.576	NR	6.0	[134]	Extrusion slit die
Poly(methyl methacrylate)	CO_2	210	1.1×10^4	6.89	$\dot{\gamma} = 10\,s^{-1}$	0.29	7.72	6.0	[134]	Extrusion slit die
Acrylonitrile/methyl acrylate terpolymer (Barex)	CO_2	180	10^5	NR	$\dot{\gamma} = 15\,s^{-1}$	0.395	17.2	6.7 Sat	[114]	Capillary rheometer
Poly(butylenes succinate)	CO_2	180	4,000	29.6	$\dot{\gamma} = 10\,s^{-1}$	0.625	31	6	[138]	Extrusion slit die
Poly(ethylene glycol)	CO_2	40	0.044	0.1		0.112	20	Sat	[139]	Vibrating Wire
Poly(ethylene glycol) 6,000	CO_2	80	0.83	0.1	$\dot{\gamma} = 10^5\,s^{-1}$	0.204	32.4	Sat	[103]	High frequency oscillatory shear
Poly(ethylene glycol) 6,000	CO_2	100	0.57	0.1	$\dot{\gamma} = 10^5\,s^{-1}$	0.309	29.8	Sat	[103]	High frequency oscillatory shear
Poly(ethylene glycol) 6,000	CO_2	120	0.39	0.1	$\dot{\gamma} = 10^5\,s^{-1}$	0.479	30.3	Sat	[103]	High frequency oscillatory shear
Poly(ethylene glycol) 20,000	CO_2	80	3.48	0.1	$\dot{\gamma} = 10^5\,s^{-1}$	0.358	31.9	Sat	[103]	High frequency oscillatory shear
Poly(ethylene glycol) 20,000	CO_2	100	3.10	0.1	$\dot{\gamma} = 10^5\,s^{-1}$	0.454	32.1	Sat	[103]	High frequency oscillatory shear
Poly(ethylene glycol) 20,000	CO_2	120	3.19	0.1	$\dot{\gamma} = 10^5\,s^{-1}$	0.476	33.6	Sat	[103]	High frequency oscillatory shear
Poly(propylene glycol) 2,700	CO_2	25	0.56	0.1	NR	0.111	4.0	20.7 Sat	[140]	Vane torque rheometer
Poly(propylene glycol) 2,700	CO_2	35	0.34	0.1	NR	0.186	4.0	17.3 Sat	[140]	Vane torque rheometer
Poly(ethylene glycol) nonylphenyl ether	CO_2	50	NR	NR	Bubble size	0.79 Pa s	10	Sat	[127]	Bubble rise
						0.56 Pa s	20	Sat		
Poly(dimethyl siloxane)	CO_2	30	65	0.1	Zero shear rate	0.036	20.7	29.32	[141]	Levitated sphere
Poly(dimethyl siloxane)	CO_2	50,80	248	NR	$\dot{\gamma} = 100\,s^{-1}$	0.366	9.1	20.7Sat	[142]	Capillary
		80	214			0.617	8.7	8.8 Sat		
Poly(vinylidene fluoride)	CO_2	210	10^4	NR	$\dot{\gamma} = 10\,s^{-1}$	0.5	NR	3.0	[134]	Extrusion slit die
Polyamide 11	CO_2	225	40	NR	$\dot{\gamma} = 100\,s^{-1}$	0.75	NR	3.0	[143]	Slit die rheometer

REFERENCES

1. McHugh, M.A. and V.J. Krukonis, *Supercritical fluid extraction: principles and practice*. 2nd ed. 1994, Boston: Butterworth-Heinemann. 512.
2. Bungert, B., G. Sadowski, and W. Arlt, *Separations and material processing in solutions with dense gases*. Industrial & Engineering Chemistry Research, 1998. **37**(8): p. 3208–3220.
3. Cooper, A.I., *Porous materials and supercritical fluids*. Advanced Materials, 2003. **15**(13): p. 1049–1059.
4. Kazarian, S.G., *Polymers and supercritical fluids: Opportunities for vibrational spectroscopy*. Macromolecular Symposia, 2002. **184**: p. 215–228.
5. Tomasko, D.L., et al., *A review of CO2 applications in the processing of polymers*. Industrial & Engineering Chemistry Research, 2003. **42**(25): p. 6431–6456.
6. Weidner, E., M. Petermann, and Z. Knez, *Multifunctional composites by high-pressure spray processes*. Current Opinion in Solid State & Materials Science, 2003. **7**(4,5): p. 385–390.
7. Kikic, I. and F. Vecchione, *Supercritical impregnation of polymers*. Current Opinion in Solid State & Materials Science, 2003. **7**(4,5): p. 399–405.
8. Kendall, J.L., et al., *Polymerizations in supercritical carbon dioxide*. Chemical Reviews, 1999. **99**(2): p. 543–563.
9. Woods, H.M., et al., *Materials processing in supercritical carbon dioxide: surfactants, polymers and biomaterials*. Journal of Materials Chemistry, 2004. **14**(11): p. 1663–1678.
10. Reverchon, E., M.C. Volpe, and G. Caputo, *Supercritical fluid processing of polymers: composite particles and porous materials elaboration*. Current Opinion in Solid State & Materials Science, 2003. **7**(4,5): p. 391–397.
11. Beckman, E.J., *Supercritical and near-critical CO2 in green chemical synthesis and processing*. Journal of Supercritical Fluids, 2004. **28**(2,3): p. 121–191.
12. Cooper, A.I., *Polymer synthesis and processing using supercritical carbon dioxide*. Journal of Materials Chemistry, 2000. **10**(2): p. 207–234.
13. Jung, J. and M. Perrut, *Particle design using supercritical fluids: Literature and patent survey*. Journal of Supercritical Fluids, 2001. **20**(3): p. 179–219.
14. Rindfleisch, F., T.P. DiNoia, and M.A. McHugh, *Solubility of polymers and copolymers in supercritical CO2*. Journal of Physical Chemistry, 1996. **100**(38): p. 15581–15587.
15. Shen, Z., et al., *CO2-solubility of oligomers and polymers that contain the carbonyl group*. Polymer, 2003. **44**(5): p. 1491–1498.
16. Debenedetti, P.G., I.B. Petsche, and R.S. Mohamed, *Clustering in supercritical mixtures - theory, applications and simulations*. Fluid Phase Equilibria, 1989. **52**: p. 347–356.
17. Sanchez, I.C. and R.H. Lacombe, *Statistical thermodynamics of polymer-solutions*. Macromolecules, 1978. **11**(6): p. 1145–1156.
18. Condo, P.D., et al., *Glass-transition behavior including retrograde vitrification of polymers with compressed fluid diluents*. Macromolecules, 1992. **25**(23): p. 6119–6127.
19. Kalospiros, N.S. and M.E. Paulaitis, *Molecular thermodynamic model for solvent-induced glass transitions in polymer supercritical-fluid systems*. Chemical Engineering Science, 1994. **49**(5): p. 659–668.
20. Chapman, W.G., et al., *New reference equation of state for associating liquids*. Industrial & Engineering Chemistry Research, 1990. **29**(8): p. 1709–1721.
21. Orbey, H., C.P. Bokis, and C.C. Chen, *Equation of state modeling of phase equilibrium in the low-density polyethylene process: The Sanchez-Lacombe, statistical associating fluid theory, and polymer-Soave-Redlich-Kwong equations of state*. Industrial & Engineering Chemistry Research, 1998. **37**(11): p. 4481–4491.
22. Deloos, T.W., W. Poot, and G.A.M. Diepen, *Fluid phase-equilibria in the system polyethylene + ethylene .1. systems of linear polyethylene + ethylene at high-pressure*. Macromolecules, 1983. **16**(1): p. 111–117.
23. Condo, P.D., E.J. Colman, and P. Ehrlich, *Phase-equilibria of linear polyethylene with supercritical propane*. Macromolecules, 1992. **25**(2): p. 750–753.
24. Xiong, Y. and E. Kiran, *High-pressure phase-behavior in polyethylene N-butane binary and polyethylene N-butane Co2 ternary-systems*. Journal of Applied Polymer Science, 1994. **53**(9): p. 1179–1190.
25. Kiran, E., W.H. Zhuang, and Y.L. Sen, *Solubility and demixing of polyethylene in supercritical binary fluid mixtures - carbon-dioxide cyclohexane, carbon-dioxide toluene, carbon-dioxide pentane*. Journal of Applied Polymer Science, 1993. **47**(5): p. 895–909.
26. Anderson, R.D. and J.E. Ramano, *Process and apparatus for flash spinning of fibrillated flexifilamentary material*. 1966.
27. Swelheim, T., J.D.S. Arons, and G.A.M. Diepen, *Fluid Phase Equilibria in System Polyethene-Ethene*. Recueil Des Travaux Chimiques Des Pays-Bas, 1965. **84**(2): p. 261.
28. Hasch, B.M., et al., *High-pressure phase-behavior of mixtures of poly(ethylene-co-methyl Acrylate) with low-molecular-weight hydrocarbons*. Journal of Polymer Science Part B-Polymer Physics, 1992. **30**(12): p. 1365–1373.
29. Lee, S.H., M.A. Lostracco, and M.A. McHugh, *High-pressure, molecular weight-dependent behavior of (co)polymer-solvent mixtures - experiments and modeling*. Macromolecules, 1994. **27**(17): p. 4652–4658.
30. Steiner, R. and K. Horle, *Phase behavior of ethylene polyethylene mixtures under high-pressure*. Chemie Ingenieur Technik, 1972. **44**(17): p. 1010.
31. Hasch, B.M., et al., *The effect of backbone structure on the cloud point behavior of polyethylene ethane and polyethylene propane mixtures*. Polymer, 1993. **34**(12): p. 2554–2558.
32. Ehrlich, P. and J.J. Kurpen, *Phase equilibria of polymer-solvent systems at high pressures near their critical loci - polyethylene with N-alkanes*. Journal of Polymer Science Part A-General Papers, 1963. **1**(10): p. 3217.
33. Ehrlich, P., *Phase equilibria of polymer-solvent systems at high pressures near their critical loci. 2. polyethylene-ethylene*. Journal of Polymer Science Part A-General Papers, 1965. **3**(1PA): p. 131.
34. Becker, F., et al., *Cloud-point curves of ethylene-(meth)acrylate copolymers in fluid ethene up to high pressures and temperatures - experimental study and PC-SAFT modeling*. Fluid Phase Equilibria, 2004. **215**(2): p. 263–282.
35. Trumpi, H., et al., *High pressure phase equilibria in the system linear low density polyethylene+ethylene: experimental results and modelling*. Journal of Supercritical Fluids, 2003. **27**(2): p. 205–214.
36. Zhang, W., et al., *Phase behavior, density, and crystallization of polyethylene in n-pentane and in n-pentane/CO2 pressures*. Journal of Applied Polymer Science, 2003. **89**(8): p. 2201–2209.
37. deLoos, T.W., W. Poot, and R.N. Lichtenthaler, *The influence of branching on high-pressure vapor-liquid equilibria in systems of ethylene and polyethylene*. Journal of Supercritical Fluids, 1995. **8**(4): p. 282–286.
38. Heukelbach, D. and G. Luft, *Critical points of mixtures of ethylene and polyethylene wax under high pressure*. Fluid Phase Equilibria, 1998. **146**(1,2): p. 187–195.
39. Chen, S.J., I.G. Economou, and M. Radosz, *Density-tuned polyolefin phase-equilibria .2. multicomponent solutions of alternating poly (ethylene propylene) in subcritical and supercritical olefins - experiment and saft model*. Macromolecules, 1992. **25**(19): p. 4987–4995.
40. Gregg, C.J., et al., *Phase-behavior of binary ethylene-propylene copolymer solutions in subcritical and supercritical ethylene and propylene*. Fluid Phase Equilibria, 1993. **83**: p. 375–382.
41. Gregg, C.J., et al., *A variable-volume optical pressure-volume-temperature cell for high-pressure cloud points, densities, and infrared-spectra, applicable to supercritical-fluid solutions of polymers up to 2 Kbar*. Journal of Chemical and Engineering Data, 1994. **39**(2): p. 219–224.
42. Lostracco, M.A., S.H. Lee, and M.A. McHugh, *Comparison of the effect of density and hydrogen-bonding on the cloud-point behavior of poly(ethylene-co-methyl acrylate) propane-cosolvent mixtures*. Polymer, 1994. **35**(15): p. 3272–3277.
43. Hasch, B.M., et al., *Cosolvency effects on copolymer solutions at high-pressure*. Journal of Polymer Science Part B-Polymer Physics, 1993. **31**(4): p. 429–439.
44. Byun, H.S., et al., *Poly(ethylene-co-butyl acrylate). Phase behavior in ethylene compared to the poly(ethylene-co-methyl acrylate)-ethylene system and aspects of copolymerization kinetics at high pressures*. Macromolecules, 1996. **29**(5): p. 1625–1632.

45. Wolf, B.A. and G. Blaum, *Pressure influence on true cosolvency - measured and calculated solubility limits of polystyrene in mixtures of acetone and diethylether*. Makromolekulare Chemie-Macromolecular Chemistry and Physics, 1976. **177**(4): p. 1073–1088.
46. Saraf, V.P. and E. Kiran, *Supercritical fluid polymer interactions - phase-equilibrium data for solutions of polystyrenes in normal-butane and normal-pentane*. Polymer, 1988. **29**(11): p. 2061–2065.
47. Kumar, S.K., et al., *Solubility of polystyrene in supercritical fluids*. Macromolecules, 1987. **20**(10): p. 2550–2557.
48. Pradhan, D., C. Chen, and M. Radosz, *Fractionation of polystyrene with supercritical propane and ethane - characterization, semibatch solubility experiments, and saft simulations*. Industrial & Engineering Chemistry Research, 1994. **33**(8): p. 1984–1988.
49. Haschets, C.W., T.A. Blackwood, and A.D. Shine, *Phase-behavior of polymer-Hcfc compressed solvent solutions*. Abstracts of Papers of the American Chemical Society, 1993. **205**: p. 28.
50. Jiang, S.C., et al., *Pressure effects on the thermodynamics of trans-decahydronaphthalene/polystyrene polymer solutions: Application of the Sanchez-Lacombe lattice fluid theory*. Macromolecular Chemistry and Physics, 2003. **204**(4): p. 692–703.
51. Ali, S., *Thermodynamic properties of polymer-solutions in compressed gases*. Zeitschrift Fur Physikalische Chemie-Wiesbaden, 1983. **137**(1): p. 13–21.
52. Bangert, L.H., et al., *Advanced technology applications in garment processing*, in *NSF/RA-770428*, N.T. Report, Editor. 1977.
53. Heller, J.P., et al., *Direct thickeners for mobility control of CO2 floods*. SPE J., 1983. **Paper 11789**: p. 173.
54. Gregg, C.J., F.P. Stein, and M. Radosz, *Phase-behavior of telechelic polyisobutylene (Pib) in subcritical and supercritical fluids .1. inter-association and intra-association effects for blank, monohydroxy, and dihydroxy pib(1k) in ethane, propane, dimethyl ether, carbon-dioxide, and chlorodifluoromethane*. Macromolecules, 1994. **27**(18): p. 4972–4980.
55. Chen, S.J., et al., *Mass-spectrometer composition probe for batch cell studies of supercritical fluid phase-equilibria*. Journal of Chemical and Engineering Data, 1993. **38**(2): p. 211–216.
56. Lele, A.K. and A.D. Shine, *Effect of ress dynamics on polymer morphology*. Industrial & Engineering Chemistry Research, 1994. **33**(6): p. 1476–1485.
57. Haschets, C.W. and A.D. Shine, *Phases behavior of polymer supercritical chlorodifluoromethane solutions*. Macromolecules, 1993. **26**(19): p. 5052–5060.
58. Maderek, E., G.V. Schulz, and B.A. Wolf, *High-temperature demixing of poly(decyl methacrylate) solutions in isooctane and its pressure-dependence*. Makromolekulare Chemie-Macromolecular Chemistry and Physics, 1983. **184**(6): p. 1303–1309.
59. Scholsky, K.M. and L.W. Morgan, *Fractionation of synthetic-polymers using supercritical nitrous-oxide*. Journal of Polymer Science Part C-Polymer Letters, 1988. **26**(4): p. 181–184.
60. Tom, J.W., P.G. Debenedetti, and R. Jerome, *Precipitation of poly (L-lactic acid) and composite poly(L-lactic acid) - pyrene particles by rapid expansion of supercritical solutions*. Journal of Supercritical Fluids, 1994. **7**(1): p. 9–29.
61. Tom, J.W. and P.G. Debenedetti, *Formation of bioerodible polymeric microspheres and microparticles by rapid expansion of supercritical solutions*. Biotechnology Progress, 1991. **7**(5): p. 403–411.
62. Conway, S.E., et al., *Poly(lactide-co-glycolide) solution behavior in supercritical CO2, CHF3, and CHClF2*. Journal of Applied Polymer Science, 2001. **80**(8): p. 1155–1161.
63. Khosravi-Darani, K., et al., *Solubility of poly(beta-hydroxybutyrate) in supercritical carbon dioxide*. Journal of Chemical and Engineering Data, 2003. **48**(4): p. 860–863.
64. Daneshvar, M., S. Kim, and E. Gulari, *High-pressure phase-equilibria of poly(ethylene glycol) carbon-dioxide systems*. Journal of Physical Chemistry, 1990. **94**(5): p. 2124–2128.
65. Lopes, J.A., et al., *On the effect of polymer fractionation on phase equilibrium in CO2 + poly(ethylene glycol)s systems*. Journal of Supercritical Fluids, 2000. **16**(3): p. 261–267.
66. Martin, T.M., R.B. Gupta, and C.B. Roberts, *Measurements and modeling of cloud point behavior for poly(propylene glycol) in ethane and in ethane plus cosolvent mixtures at high pressure*. Industrial & Engineering Chemistry Research, 2000. **39**(1): p. 185–194.
67. Dimitrov, K., et al., *Solubility of poly(ethylene glycol)nonylphenyl ether in supercritical carbon dioxide*. Journal of Supercritical Fluids, 1998. **14**(1): p. 41–47.
68. Hoefling, T., et al., *The incorporation of a fluorinated ether functionality into a polymer or surfactant to enhance Co2-solubility*. Journal of Supercritical Fluids, 1992. **5**(4): p. 237–241.
69. Kilic, S., et al., *Effect of grafted Lewis base groups on the phase behavior of model poly(dimethyl siloxanes) in CO2*. Industrial & Engineering Chemistry Research, 2003. **42**(25): p. 6415–6424.
70. Mawson, S., et al., *Formation of poly(1,1,2,2-tetrahydroperfluorodecyl acrylate) submicron fibers and particles from supercritical carbon dioxide solutions*. Macromolecules, 1995. **28**(9): p. 3182–3191.
71. Byun, H.S. and Y.H. Yoo, *Thermodynamic phase behavior of fluoropolymer mixtures with supercritical fluid solvents*. Korean Journal of Chemical Engineering, 2004. **21**(6): p. 1193–1198.
72. Luna-Barcenas, G., et al., *Phase behavior of poly(1,1-dihydroperfluorooctylacrylate) in supercritical carbon dioxide*. Fluid Phase Equilibria, 1998. **146**(1,2): p. 325–337.
73. Baradie, B., et al., *Synthesis and solubility of linear poly(tetrafluoroethylene-co-vinyl acetate) in dense CO2: Experimental and molecular modeling results*. Macromolecules, 2004. **37**(20): p. 7799–7807.
74. Lepilleur, C., et al., *Effect of molecular architecture on the phase behavior of fluoroether-functional graft copolymers in supercritical CO_2*. Fluid Phase Equilibria, 1997. **134**(1,2): p. 285–305.
75. Blasig, A. and M.C. Thies, *Rapid expansion of cellulose triacetate from ethyl acetate solutions*. Journal of Applied Polymer Science, 2005. **95**(2): p. 290–299.
76. Suresh, S.J., R.M. Enick, and E.J. Beckman, *Phase-behavior of nylon 6/trifluoroethanol/carbon dioxide mixtures*. Macromolecules, 1994. **27**(2): p. 348–356.
77. Durrill, P.L. and R.G. Griskey, *Diffusion and solution of gases in thermally softened or molten polymers .I. development of technique and determination of data*. Aiche Journal, 1966. **12**(6): p. 1147.
78. Sherwood, A.E. and J.M. Prausnitz, *The heat of solution of gases at high pressure*. Aiche Journal, 1962. **8**(4): p. 519–521.
79. Stern, S.A., J.T. Mullhaupt, and P.J. Gareis, *The effect of pressure on the permeation of gases and vapors through polyethylene. Usefulness of the corresponding states principle*. Aiche Journal, 1969. **15**(1): p. 64–73.
80. Durrill, P.L. and R.G. Griskey, *Diffusion and solution of gases into thermally softened or molten polymers .2. Relation of diffusivities and solubilities with temperature pressure and structural characteristics*. Aiche Journal, 1969. **15**(1): p. 106.
81. Liu, D.D. and J.M. Prausnitz, *Solubilities of gases and volatile liquids in polyethylene and in ethylene-vinyl acetate copolymers in region 125–225degreesc*. Industrial & Engineering Chemistry Fundamentals, 1976. **15**(4): p. 330–335.
82. Hilic, S., et al., *Simultaneous measurement of the solubility of nitrogen and carbon dioxide in polystyrene and of the associated polymer swelling*. Journal of Polymer Science Part B-Polymer Physics, 2001. **39**(17): p. 2063–2070.
83. Sato, Y., et al., *Solubilities and diffusion coefficients of carbon dioxide in poly(vinyl acetate) and polystyrene*. Journal of Supercritical Fluids, 2001. **19**(2): p. 187–198.
84. Sato, Y., et al., *Solubility of butane and isobutane in molten polypropylene and polystyrene*. Polymer Engineering and Science, 2004. **44**(11): p. 2083–2089.
85. Boudouris, D., et al., *Measurement of HCFC-22 and HFC-152a sorption by polymers using a quartz crystal microbalance*. Industrial & Engineering Chemistry Research, 2001. **40**(2): p. 604–611.
86. Sato, Y., et al., *Solubilities and diffusion coefficients of carbon dioxide and nitrogen in polypropylene, high-density polyethylene, and polystyrene under high pressures and temperatures*. Fluid Phase Equilibria, 1999. **162**(1,2): p. 261–276.
87. Cotugno, S., et al., *Sorption thermodynamics and mutual diffusivity of carbon dioxide in molten polycaprolactone*. Industrial & Engineering Chemistry Research, 2003. **42**(19): p. 4398–4405.
88. Sato, Y., et al., *Solubility and diffusion coefficient of carbon dioxide in biodegradable polymers*. Industrial & Engineering Chemistry Research, 2000. **39**(12): p. 4813–4819.
89. Elvassore, N., K. Vezzu, and A. Bertucco, *Measurement and modeling of CO2 absorption in poly (lactic-co-glycolic acid)*. Journal of Supercritical Fluids, 2005. **33**(1): p. 1–5.
90. Wiesmet, V., et al., *Measurement and modelling of high-pressure phase equilibria in the systems polyethyleneglycol (PEG)-propane,*

PEG-nitrogen and PEG-carbon dioxide. Journal of Supercritical Fluids, 2000. **17**(1): p. 1–12.
91. Guadagno, T. and S.G. Kazarian, *High-pressure CO2-expanded solvents: Simultaneous measurement of CO2 sorption and swelling of liquid polymers with in-situ near-IR spectroscopy*. Journal of Physical Chemistry B, 2004. **108**(37): p. 13995–13999.
92. Sato, Y., et al., *Solubility of carbon dioxide in PPO and PPO/PS blends*. Fluid Phase Equilibria, 2002. **194**: p. 847–858.
93. Dey, S.K., C. Jacob, and J.A. Biesenberger. *Effect of physical blowing agents on crystallization temperature of polymer melts*. in *ANTEC 94 Plastics: gateway to the future*. 1994. San Francisco: Society of Plastics Engineers.
94. Fukne-Kokot, K., et al., *Comparison of different methods for determination of the S-L-G equilibrium curve of a solid component in the presence of a compressed gas*. Fluid Phase Equilibria, 2000. **173**(2): p. 297–310.
95. Zhang, Z.Y. and Y.P. Handa, *CO2-assisted melting of semicrystalline polymers*. Macromolecules, 1997. **30**(26): p. 8505–8507.
96. Varma-Nair, M., et al., *Effect of compressed CO2 on crystallization and melting behavior of isotactic polypropylene*. Thermochimica Acta, 2003. **396**(1,2): p. 57–65.
97. Takada, M., M. Tanigaki, and M. Ohshima, *Effects of CO2 on crystallization kinetics of polypropylene*. Polymer Engineering and Science, 2001. **41**(11): p. 1938–1946.
98. Takada, M., S. Hasegawa, and M. Ohshima, *Crystallization kinetics of poly(L-lactide) in contact with pressurized CO2*. Polymer Engineering and Science, 2004. **44**(1): p. 186–196.
99. Kishimoto, Y. and R. Ishii, *Differential scanning calorimetry of isotactic polypropene at high CO2 pressures*. Polymer, 2000. **41**(9): p. 3483–3485.
100. Lian, Z., S.A. Epstein, C.W. Blenk, and A.D. Shine, *Carbon dioxide-induced melting point depression of biodegradable polymers*. Journal of Supercritical Fluids, 2006, DOI:10.1016/j.supflu.2006.02.001.
101. Takada, M. and M. Ohshima, *Effect of CO2 on crystallization kinetics of poly(ethylene terephthalate)*. Polymer Engineering and Science, 2003. **43**(2): p. 479–489.
102. Weidner, E., et al., *Phase equilibrium (solid-liquid-gas) in polyethyleneglycol-carbon dioxide systems*. Journal of Supercritical Fluids, 1997. **10**(3): p. 139–147.
103. Kukova, E., M. Petermann, and E. Weidner, *Phase behavior (S-L-G) and transport properties of binary systems consisting of highly viscous polyethylene glycols and compressed carbon dioxide*. Chemie Ingenieur Technik, 2004. **76**(3): p. 280–284.
104. Shenoy, S.L., T. Fujiwara, and K.J. Wynne, *Quantifying plasticization and melting behavior of poly(vinylidene fluoride) in supercritical CO2 utilizing a linear variable differential transformer*. Macromolecules, 2003. **36**(9): p. 3380–3385.
105. Wissinger, R.G. and M.E. Paulaitis, *Glass Transitions in Polymer Co2 Mixtures at Elevated Pressures*. Journal of Polymer Science Part B-Polymer Physics, 1991. **29**(5): p. 631–633.
106. Condo, P.D. and K.P. Johnston, *Retrograde vitrification of polymers with compressed fluid diluents - experimental confirmation*. Macromolecules, 1992. **25**(24): p. 6730–6732.
107. Chiou, J.S., J.W. Barlow, and D.R. Paul, *Plasticization of glassy-polymers by Co2*. Journal of Applied Polymer Science, 1985. **30**(6): p. 2633–2642.
108. Alessi, P., et al., *Plasticization of polymers with supercritical carbon dioxide: Experimental determination of glass-transition temperatures*. Journal of Applied Polymer Science, 2003. **88**(9): p. 2189–2193.
109. Zhang, Z.Y. and Y.P. Handa, *An in situ study of plasticization of polymers by high-pressure gases*. Journal of Polymer Science Part B-Polymer Physics, 1998. **36**(6): p. 977–982.
110. Kumazawa, H., et al., *Gas-transport in polymer membrane at temperatures above and below glass-transition point*. Journal of Applied Polymer Science, 1994. **51**(6): p. 1015–1020.
111. Edwards, R.R., et al., *Chromatographic investigation of the effect of dissolved carbon dioxide on the glass transition temperature of a polymer and the solubility of a third component (additive)*. Journal of Polymer Science Part B-Polymer Physics, 1998. **36**(14): p. 2537–2549.
112. Handa, Y.P., P. Kruus, and M. Oneill, *High-pressure calorimetric study of plasticization of poly(methyl methacrylate) by methane, ethylene, and carbon dioxide*. Journal of Polymer Science Part B-Polymer Physics, 1996. **34**(15): p. 2635–2639.
113. Kamiya, Y., et al., *Sorption and dilation in poly(ethyl methacrylate) carbon-dioxide system*. Journal of Polymer Science Part B-Polymer Physics, 1989. **27**(4): p. 879–892.
114. Bortner, M.J. and D.G. Baird, *Absorption of CO2 and subsequent viscosity reduction of an acrylonitrile copolymer*. Polymer, 2004. **45**(10): p. 3399–3412.
115. Kikic, I., et al., *Polymer plasticization using supercritical carbon dioxide: Experiment and modeling*. Industrial & Engineering Chemistry Research, 2003. **42**(13): p. 3022–3029.
116. Bos, A., et al., *CO2-induced plasticization phenomena in glassy polymers*. Journal of Membrane Science, 1999. **155**(1): p. 67–78.
117. Handa, Y.P., S. Lampron, and M.L. Oneill, *On the Plasticization of Poly(2,6-Dimethyl Phenylene Oxide) by Co2*. Journal of Polymer Science Part B-Polymer Physics, 1994. **32**(15): p. 2549–2553.
118. Hachisuka, H., et al., *Glass-transition temperature of glassy-polymers plasticized by Co2 gas*. Polymer Journal, 1990. **22**(1): p. 77–79.
119. Mi, Y.L. and S.X. Zheng, *A new study of glass transition of polymers by high pressure DSC*. Polymer, 1998. **39**(16): p. 3709–3712.
120. Banerjee, T. and G.C. Lipscomb, *Direct measurement of the carbon dioxide-induced glass transition depression in a family of substituted polycarbonates*. Journal of Applied Polymer Science, 1998. **68**(9): p. 1441–1449.
121. Bourbon, D., Y. Kamiya, and K. Mizoguchi, *Sorption and dilation properties of poly(para-phenylene sulfide) under high-pressure carbon-dioxide*. Journal of Polymer Science Part B-Polymer Physics, 1990. **28**(11): p. 2057–2069.
122. Kamiya, Y., et al., *Sorptive dilation of polyvinyl benzoate) and polyvinyl butyral) by carbon-dioxide*. Journal of Polymer Science Part B-Polymer Physics, 1988. **26**(7): p. 1409–1424.
123. Jaeger, P.T., R. Eggers, and H. Baumgartl, *Interfacial properties of high viscous liquids in a supercritical carbon dioxide atmosphere*. Journal of Supercritical Fluids, 2002. **24**(3): p. 203–217.
124. Otake, K., et al., *Surface activity of myristic acid in the poly(methyl methacrylate)/supercritical carbon dioxide system*. Langmuir, 2004. **20**(15): p. 6182–6186.
125. Li, H.B., L.J. Lee, and D.L. Tomasko, *Effect of carbon dioxide on the interfacial tension of polymer melts*. Industrial & Engineering Chemistry Research, 2004. **43**(2): p. 509–514.
126. Harrison, K.L., K.P. Johnston, and I.C. Sanchez, *Effect of surfactants on the interfacial tension between supercritical carbon dioxide and polyethylene glycol*. Langmuir, 1996. **12**(11): p. 2637–2644.
127. Dimitrov, K., L. Boyadzhiev, and R. Tufeu, *Properties of supercritical CO2 saturated poly(ethylene glycol) nonylphenyl ether*. Macromolecular Chemistry and Physics, 1999. **200**(7): p. 1626–1629.
128. Doolittle, A.K., *Studies in newtonian flow .2. The dependence of the viscosity of liquids on free-space*. Journal of Applied Physics, 1951. **22**(12): p. 1471–1475.
129. Doolittle, A.K., *Studies in newtonian flow .3. The dependence of the viscosity of liquids on molecular weight and free space (in homologous series)*. Journal of Applied Physics, 1952. **23**(2): p. 236–239.
130. Gerhardt, L.J., et al., *Concentration-dependent viscoelastic scaling models for polydimethysiloxane melts with dissolved carbon dioxide*. Journal of Polymer Science Part B-Polymer Physics, 1998. **36**(11): p. 1911–1918.
131. Areerat, S., T. Nagata, and M. Ohshima, *Measurement and prediction of LDPE/CO2 solution viscosity*. Polymer Engineering and Science, 2002. **42**(11): p. 2234–2245.
132. Williams, M.L., R.F. Landel, and J.D. Ferry, *Mechanical properties of substances of high molecular weight .19. The temperature dependence of relaxation mechanisms in amorphous polymers and other glass-forming liquids*. Journal of the American Chemical Society, 1955. **77**(14): p. 3701–3707.
133. Gendron, R. and M.F. Champagne, *Effect of physical foaming agents on the viscosity of various polyolefin resins*. Journal of Cellular Plastics, 2004. **40**(2): p. 131–143.
134. Royer, J.R., J.M. DeSimone, and S.A. Khan, *High-pressure rheology and viscoelastic scaling predictions of polymer melts containing liquid and supercritical carbon dioxide*. Journal of Polymer Science Part B-Polymer Physics, 2001. **39**(23): p. 3055–3066.
135. Lee, M., C. Tzoganakis, and C.B. Park, *Effects of supercritical CO2 on the viscosity and morphology of polymer blends*. Advances in Polymer Technology, 2000. **19**(4): p. 300–311.

136. Royer, J.R., et al., *High-pressure rheology of polystyrene melts plasticized with CO2: Experimental measurement and predictive scaling relationships.* Journal of Polymer Science Part B—Polymer Physics, 2000. **38**(23): p. 3168–3180.
137. Kwag, C., C.W. Manke, and E. Gulari, *Rheology of molten polystyrene with dissolved supercritical and near-critical cases*. Journal of Polymer Science Part B-Polymer Physics, 1999. **37**(19): p. 2771–2781.
138. Ladin, D., et al., *Study of shear and extensional viscosities of biodegradable PBS/CO2 solutions*. Journal of Cellular Plastics, 2001. **37**(2): p. 109–148.
139. Gourgouillon, D., et al., *Simultaneous viscosity and density measurement of supercritical CO2-saturated PEG 400*. Journal of Supercritical Fluids, 1998. **13**(1–3): p. 177–185.
140. Flichy, N.M.B., C.J. Lawrence, and S.G. Kazarian, *Rheology of poly(propylene glycol) and suspensions of fumed silica in poly(propylene glycol) under high-pressure CO2*. Industrial & Engineering Chemistry Research, 2003. **42**(25): p. 6310–6319.
141. Royer, J.R., et al., *Polymer melt rheology with high-pressure CO2 using a novel magnetically levitated sphere rheometer*. Polymer, 2002. **43**(8): p. 2375–2383.
142. Gerhardt, L.J., C.W. Manke, and E. Gulari, *Rheology of polydimethylsiloxane swollen with supercritical carbon dioxide*. Journal of Polymer Science Part B-Polymer Physics, 1997. **35**(3): p. 523–534.
143. Martinache, J.D., et al., *Processing of polyamide 11 with supercritical carbon dioxide*. Industrial & Engineering Chemistry Research, 2001. **40**(23): p. 5570–5577.

CHAPTER 19

Thermodynamics of Polymer Blends

Hany B. Eitouni[*,†] and Nitash P. Balsara[*,†,‡]

[*]*Department of Chemical Engineering, University of California, Berkeley, CA 94720*
[†]*Materials Sciences Division, Lawrence Berkeley National Laboratory, Berkeley, CA 94720*
[‡]*Energy and Environmental Technologies Division, Lawrence Berkeley National Laboratory, Berkeley, CA 94720*

19.1 INTRODUCTION

Polymer blends have found widespread uses in phase-separated as well as homogeneous states [1–4]. In some cases such as high impact polystyrene, a dispersed polymeric phase is introduced to improve the mechanical properties of the matrix. In other cases blends are created inadvertently due to side-reactions during polymerization. Low-density polyethylene, which is a mixture of several different kinds of linear and branched chains, is an example of such a blend. The physical properties of polymer blends depend crucially on morphology. The mechanical and optical properties of phase separated blends, for instance, are fundamentally different from those of homogeneous mixtures. The range of accessible morphologies is, to a large extent, determined by thermodynamic interactions.

There is considerable interest in organizing polymer domains on the nanometer length scale. Block copolymers comprising covalently bonded immiscible chains offer one avenue for creating such structures. These molecules are amphiphilic and thus organize into microphases that are similar to those found in systems containing surfactants. The main purpose of this paper is to provide a listing of the properties that enable the determination of the phase behavior of homopolymer blends as well as more complex periodic phases formed in the presence of block copolymers.

Current understanding of thermodynamic interactions and their effect on the phase behavior of polymer mixtures rests on three theoretical developments: (1) The derivation of an expression for the free energy of mixing in polymer systems by Huggins and Flory [5–7]. (2) The development of the random phase approximation (RPA) for characterizing concentration fluctuations in homogeneous polymer mixtures by de Gennes, Leibler, and others [8–12]. (3) The development of self-consistent field theory (SCFT) for characterizing microphase separated systems by Helfand and Edwards [13–15]. In the Flory–Huggins theory (FHT), the thermodynamics of mixing is dependent on a parameter, χ, which must be determined experimentally. The RPA was originally proposed by de Gennes to relate the scattering functions of single-phase homopolymer blends to the χ parameter and statistical segment lengths of the chains, l. In subsequent work the RPA has been extended to predict the scattering from homogeneous block copolymer melts [9] and complex multicomponent mixtures [11,12]. Experimentally measured scattering curves from homogeneous mixtures can thus be used to determine χ and l parameters. The properties of microphase separated mixtures can be

predicted by SCFT if χ and l are known. The thermodynamic properties of systems that cannot exhibit macrophase separation such as diblock copolymer melts can be entirely described by a combination of RPA and SCFT. More complex mixtures of homopolymers and block copolymers can, however, exhibit both microphase and/or macrophase separation. In such cases, all three thermodynamic frameworks (RPA, SCFT, and FHT) are required for making predictions.

This chapter summarizes the available data (χ and l parameters) for polymer–polymer interactions in the melt state. The equations that are necessary to convert χ parameters into binary homopolymer blend phase diagrams are also provided. We also summarize methods for predicting the properties of nanostructures with interfaces that are stabilized by the presence of block copolymers.

19.2 DEFINITIONS AND THERMODYNAMIC THEORIES

The Flory–Huggins theory provides an expression for the free energy density of mixing of two homopolymers labeled A and B [5–7].

$$\frac{\Delta G_m}{kT} = \frac{\phi_A \ln \phi_A}{v_A \hat{N}_A} + \frac{(1-\phi_A)\ln(1-\phi_A)}{\nu_B \hat{N}_B} + \frac{\chi \phi_A (1-\phi_A)}{v}. \tag{19.1}$$

$\hat{N}_i$ is the number of monomers in chain i, and ν_i is the volume of each monomer on chain i, ϕ_A is the volume fraction of component A in the mixture, v is an arbitrary reference volume, χ is the Flory–Huggins interaction parameter, ΔG_m is the free energy change on mixing per unit volume, k is the Boltzmann constant, and T is the absolute temperature. In this work the reference volume, v, is equal to $0.1\,\text{nm}^3$.

The first two terms in the right hand side (RHS) of Eq. (19.1) represent the combinatorial contribution to ΔG_m which arises due to an increase in the number of possible chain configurations in the mixture relative to the pure components. The third term in the RHS of Eq. (19.1) represents noncombinatorial contributions to ΔG_m. If we assume that this contribution arises from random, pair-wise contact between monomers, then it is proportional to $\phi_A(1-\phi_A)$ and the χ parameter is a measure of its strength. In this case χ would depend only on T and would be independent of $\hat{N}_i$ and ϕ_A. However, additional constraints due to monomer architecture and connectivity, specific interactions, and finite compressibility can also give rise to noncombinatorial contributions. If the χ parameter contains contributions from such effects then it may be a complicated function of $\hat{N}_i$, ϕ_A, and T. The expression for the combinatorial contribution was derived on the basis of several simplifications, and inadequacies of this expression are also lumped into χ.

It is convenient to rewrite Eq. (19.1) as

$$\frac{\Delta G_m v}{kT} = \frac{\phi_A \ln \phi_A}{N_A} + \frac{(1-\phi_A)\ln(1-\phi_A)}{N_B} + \chi \phi_A (1-\phi_A), \tag{19.2}$$

where

$$N_i = \frac{\hat{N}_i \nu_i}{\nu}, \tag{19.3}$$

N_i, the number of monomers of volume v in a chain of type i, is a more convenient measure of chain length than $\hat{N}_i$. However, it is important to note that N_i depends weakly on temperature (because ν_i depends on temperature) while $\hat{N}_i$ does not.

Classical thermodynamics can be used to predict phase diagrams in polymer blends on the basis of Eq. (19.2). We present the governing equations assuming that χ is only a function of T. The spinodal curve, i.e., the curve enclosing the region within which a homogeneous mixture is thermodynamically unstable, is given by

$$\chi(T) = \frac{1}{2}\left[\frac{1}{N_A \phi_A} + \frac{1}{N_B \phi_B}\right]. \tag{19.4}$$

The binodal curve, i.e., the locus of compositions of the two phases in thermodynamic equilibrium with each other, can be obtained by solving two simultaneous equations:

$$\ln\left[\frac{\phi_A^I}{\phi_A^{II}}\right] + (\phi_A^{II} - \phi_A^I)(1 - N_A/N_B) + \chi(T) N_A \left[(1-\phi_A^I)^2 - (1-\phi_A^{II})^2\right] = 0, \tag{19.5a}$$

$$\ln\left[\frac{1-\phi_A^I}{1-\phi_A^{II}}\right] + (\phi_A^I - \phi_A^{II})(1 - N_B/N_A) + \chi(T) N_B \left[(\phi_A^I)^2 - (\phi_A^{II})^2\right] = 0, \tag{19.5b}$$

where ϕ_A^I and ϕ_A^{II} are the volume fractions of polymer A in the coexisting phases.

The binodal and spinodal curves meet at the critical point. The volume fraction of component A at the critical point is given by

$$\phi_{A,c} = \frac{1}{1 + (N_A/N_B)^{1/2}} \tag{19.6}$$

and the value of χ at the critical point is given by

$$\chi_{A,c} = \frac{1}{2}\left[\frac{1}{N_A^{1/2}} + \frac{1}{N_B^{1/2}}\right]^2 = \frac{1}{2N_{ave}}, \tag{19.7}$$

where

$$N_{ave} = \left[\frac{1}{N_A^{1/2}} + \frac{1}{N_B^{1/2}}\right]^{-2}. \tag{19.8}$$

While the spinodal curve and the critical points can easily be calculated for polymer mixtures with arbitrary N_i, ϕ, and ν_i the calculation of the binodal curve requires numerical

methods [16]. However, for blends consisting of polymers with equal molecular volumes ($N = N_A = N_B$), the equations simplify considerably. The spinodal curve is given by

$$\chi(T) = \frac{1}{2N\phi_A(1-\phi_A)}, \tag{19.9}$$

the binodal curve is given by an analytical expression,

$$\chi(T) = \frac{1}{N(1-2\phi_A)} \ln\left[\frac{1-\phi_A}{\phi_A}\right] \tag{19.10}$$

and critical point is located at

$$\phi_{A,c} = 1/2 \quad \text{and} \quad \chi_c = 2/N. \tag{19.11}$$

The phase diagram of a polymer blend in $T - \phi$ space can thus be determined from Eqs. (19.1–19.11) if the temperature dependence of χ is known.

The χ parameters obtained from polymer blends are often linear functions of $1/T$.

$$\chi(T) = A + B/T. \tag{19.12}$$

However, in some cases a distinct nonlinearity is observed when χ is plotted versus $1/T$. In such cases the data can be fit to a quadratic function in $1/T$.

$$\chi(T) = A + B/T + C/T^2. \tag{19.13}$$

Predicting the phase behavior of a block copolymer composed of N_A monomers of type A and N_B monomers of type B requires knowledge of the size of the chains in addition to χ and N_i. The unperturbed radius of gyration of a polymer chain, $R_{g,i}$ is given by

$$R_{g,i}^2 = \frac{1}{6}\hat{N}_i\hat{l}_i^2 = \frac{1}{6}\left[\frac{\hat{N}_i v_i}{v}\right] l_i^2 = \frac{1}{6}N_i l_i^2, \tag{19.14}$$

where $\hat{l}_i$ and l_i are statistical segment lengths of chains of type i based on monomer volumes v_i and v, respectively. Note that the value of l_i depends explicitly on our definition of v. To a good approximation $R_{g,i}$ is independent of temperature [17], which implies that $\hat{l}_i$ is independent of temperature. The temperature dependence of l_i arises due to the temperature dependence of v_i.

When polymers self-assemble to give periodic ordered phases, only a fraction of chain configurations that are available in homogeneous phases are permissible. SCFT provides a convenient framework for computing the reduction in entropy due to this effect. In this theory, individual chains are assumed to be affected by the presence of a spatially varying external field $w_m(z)$. For convenience, we restrict our attention to one-dimensional phases. The partition function of a chain of s monomers of type i constrained so that the sth monomer is held fixed at z, q_i, is given by

$$\frac{\partial q_i(z,s)}{\partial s} = \frac{l_i^2}{6}\frac{d^2 q_i(z,s)}{dz^2} - w_m(z) q_i(z,s). \tag{19.15}$$

The field $w_m(z)$ depends on the composition profiles, $\phi_i(z)$, and χ_{ij} between the different chains in the system. We use subscripts i and j for χ to acknowledge the fact that in many systems we will have more than two types of monomers. Since the composition of component i at z is proportional to the number of chain configurations reaching that point, there is a relationship between $\phi_i(z)$ and $q_i(z,s)$,

$$\phi_i(z) = C_i \int_{s=0}^{N_i} ds\, q_i(z,s) q_i^*(z,s), \tag{19.16}$$

where C_i is a normalizing constant, and $q^*(z,s)$ obeys Eq. (19.15) with a minus sign in front of the right hand side. $q(z,s)$ and $q^*(z,s)$ are partition functions of subchains from 0 to s and from s to N, respectively.

To compute the composition profiles at equilibrium, one assumes a set of composition profiles, computes q_i using Eq. (19.15) and then computes new composition profiles using Eq. (19.16). This iterative procedure is repeated until the computed composition profiles converge. A more detailed description of SCFT is given in [15]. Details regarding SCFT computations used by our group are given in [17,18].

The simplest application of RPA and SCFT is for a symmetric diblock copolymer with $N = N_A = N_B$. The theoretically predicted order-to-disorder occurs when [9,15,19]

$$\chi(T)N = 5.268 - 0.134(l_B/l_A) + 0.114(l_B/l_A)^2, \tag{19.17}$$

where we have assumed that $1 \le l_B/l_A \le 2$, which covers the range of l values in this chapter. If the two statistical segment lengths are assumed to be equal, $l = l_A = l_B$, then Eq. (19.17) reduces to the more familiar result that $\chi N = 5.248$ at the order-disorder transition, and the repeat distance of the lamellar phase that forms when $\chi > 5.248/N$, $d = 1.865N^{1/2}l$. In the disordered state when $\chi < 5.248/N$, concentration fluctuations with length scale $= d$ form spontaneously and grow in amplitude as the order–disorder transition temperature is approached. This results in a scattering peak that can be detected by either SAXS or SANS, at scattering vector $q = 2\pi/d$. The scattering profiles obtained from weakly ordered block copolymers and disordered block copolymers are thus not very different.

It is important to recognize that Eqs. (19.1–19.17) can only be used if χ_{ij}, l_i, and ν_i, are known. For convenience, all three quantities are tabulated in this chapter.

19.3 EXPERIMENTAL METHODS FOR DETERMINING χ AND l

Most of the data presented in this chapter were obtained by applying RPA to small angle neutron scattering profiles from homogeneous homopolymer blends. This approach was pioneered by Herkt-Maetzky and Schelten, Murray *et al.*, and Hadziioannou and Stein [20–22]. The composition and molecular weight dependence of χ thus obtained has been studied in some systems. While χ is generally

found to be independent of N_i, linear and quadratic dependences on ϕ_A have been reported in some cases [23,24]. Since relatively little is known about the ϕ_A dependence of χ at this stage, we do not consider such refinements. In this chapter we use values of χ obtained from $\phi_A \approx 1/2$ mixtures and ignore its dependence on ϕ_A and N_i. Statistical segment lengths of polymer chains are usually determined from SANS experiments on binary hydrogenous and deuterated versions of the same homopolymer. l_i has been found to vary by as much as 20% from sample to sample [25].

Experiments of Roe *et al*. [26] and Hashimoto *et al*. [27] demonstrated that scattering experiments on disordered block copolymers may also be used to determine χ and l parameters, using the RPA theory of Leibler [9]. In a subsequent paper, Fredrickson and Helfand showed that fluctuation corrections to the RPA are important in block copolymer melts [28]. When available, χ parameters obtained from block copolymer melts are reported after fluctuation corrections have been incorporated. l_i values obtained from block copolymers are often [29,30] but not always [31] larger than those obtained in homopolymer blends.

Aside from RPA based techniques, χ can also be estimated from experimentally determined binodal and spinodal curves, using Eqs. (19.4) and (19.5). Methods to obtain binodal and spinodal curves are summarized in [2].

19.4 OBSERVED TEMPERATURE DEPENDENCES OF χ AND BINARY PHASE DIAGRAMS

A variety of phase behaviors have been observed in binary homopolymer blends. Some blends phase separate on heating while others phase separate on cooling. This depends on whether χ increases or decreases with temperature. Blends in which χ changes nonmonotonically with temperature exhibit more complex phase diagrams. The temperature dependence of χ for 83 polymer blends is summarized in Table 19.1. The nomenclature is defined in a section just above Table 19.1 and chemical structures of the polymers are given in Table 19.2. Blends are classified into six types, based on the temperature dependence of χ. The properties of each blend type are illustrated with the help of an example extracted from Table 19.1. Binodal and spinodal curves (T versus ϕ_A) for a particular blend were calculated using Eqs. (19.9) and (19.10), respectively. The example calculations are restricted to blends with $N_1 = N_2$.

19.4.1 Type I. χ is Positive and Increases Linearly with $1/T$ ($B > 0$, $C = 0$)

The χ parameters of a large number of polymer blends exhibit this kind of temperature dependence. An example of this is the SPB(88)/*d*SPB(78) blend [system 27a], and the temperature dependence of χ is shown in Fig. 19.1(a). Increasing temperature in such blends leads to increased miscibility. This behavior is often referred to as upper critical solution temperature (UCST) behavior. A typical phase diagram obtained from such systems is shown in Fig. 19.1(b). The spinodal and binodal curves were calculated for a SPB(88)/*d*SPB(78) blend with $N = 2,000$. A 50/50 mixture of these polymers is predicted to be two phase at room temperature but single phase at temperatures above 105 °C. The qualitative features of the phase diagrams obtained from all type I blends will be similar to Fig. 19.1(b). Of course the locations of the phase boundaries will depend on A, B, and N.

19.4.2 Type II. χ is Negative and Decreases Linearly with $1/T$ ($B < 0$, $C = 0$)

These systems exhibit linear χ versus $1/T$ plots but with negative slopes. The role of temperature is thus reversed in

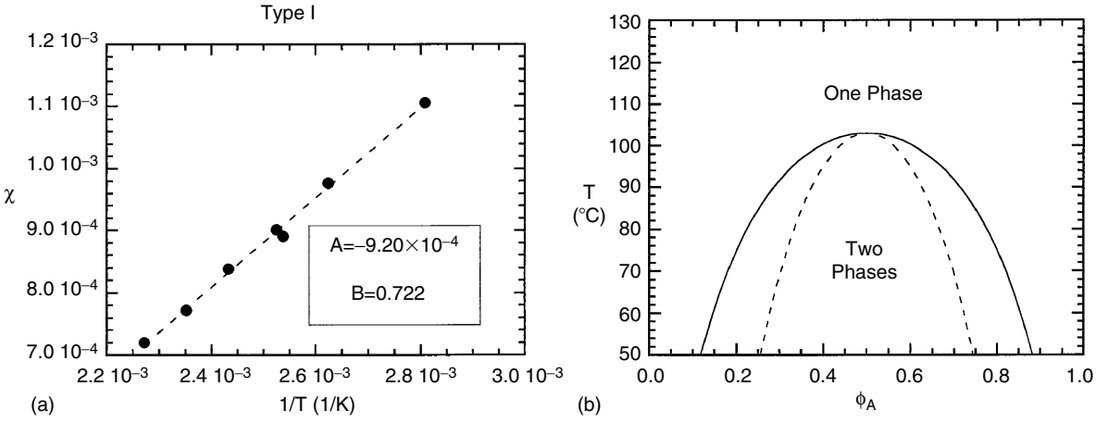

FIGURE 19.1. Example of a Type I blend [system 27a]. (a) A plot of χ versus $1/T$ for a SPB(88)/*d*SPB(78) blend. Symbols represent experimental data and the dashed line represents a least squares fit, using criteria described in Section 19.10. (b) Predicted binodal (solid curve) and spinodal (dashed curve) of a SPB(88)/*d*SPB(78) blend with $N = 2,000$.

such blends, relative to its role in type I blends. Increasing temperature leads to an increase in χ and hence, lower miscibility. Such behavior is referred to as lower critical solution temperature or LCST behavior. The PIB/*d*HHPP blend [system 62] is a typical example, and the temperature dependence of χ is shown in Fig. 19.2(a). The χ parameter is negative over most of the observable temperature window. Note that B is an order of magnitude larger than that obtained in the SPB(88)/*d*SPB(78) system (a typical type I blend). Several type II blends such as PS/PVME and PS/PXE exhibit similarly large B values. As a consequence, phase transition temperatures are remarkably insensitive to composition and component molecular weights. The phase diagram for a PIB/*d*HHPP blend with $N = 6{,}000$ is shown in Fig. 19.2(b). Note that the transition from single phase to two phase occurs at 170 ± 5 °C regardless of composition. If the molecular weight of the components is decreased by a factor of two, the resulting change in the critical temperature is only 7 °C—from 166 to 173 °C. In contrast, the phase diagram of most type I blends would be altered dramatically if N were decreased by a factor of two.

19.4.3 Type III. χ is Positive and Increases Nonlinearly with $1/T$ ($C \neq 0$, $d\chi/dT \neq 0$)

These systems are qualitatively similar to type I in that χ decreases with increasing temperature, and thus they also exhibit UCST behavior. The only difference is that the χ versus $1/T$ plots are nonlinear. An example of such behavior is PEB/*d*SPI(7) [system 41b], and the temperature dependence of χ is shown in Fig. 19.3(a). The calculated phase diagram for this blend with $N = 2{,}900$ is shown in Fig. 19.3(b). This phase diagram is qualitatively different

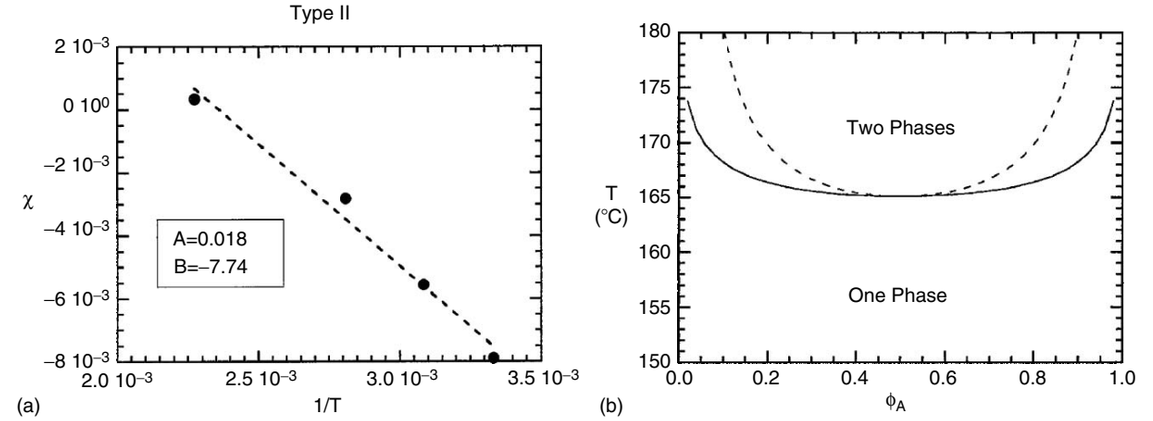

FIGURE 19.2. Example of a Type II blend [system 62]. (a) A plot of χ versus $1/T$ for a PIB/*d*HHPP blend. Symbols represent experimental data and the dashed line represents a least squares fit, using criteria described in Section 19.10. (b) Predicted binodal (solid curve) and spinodal (dashed curve) of a PIB/*d*HHPP blend with $N = 6{,}000$.

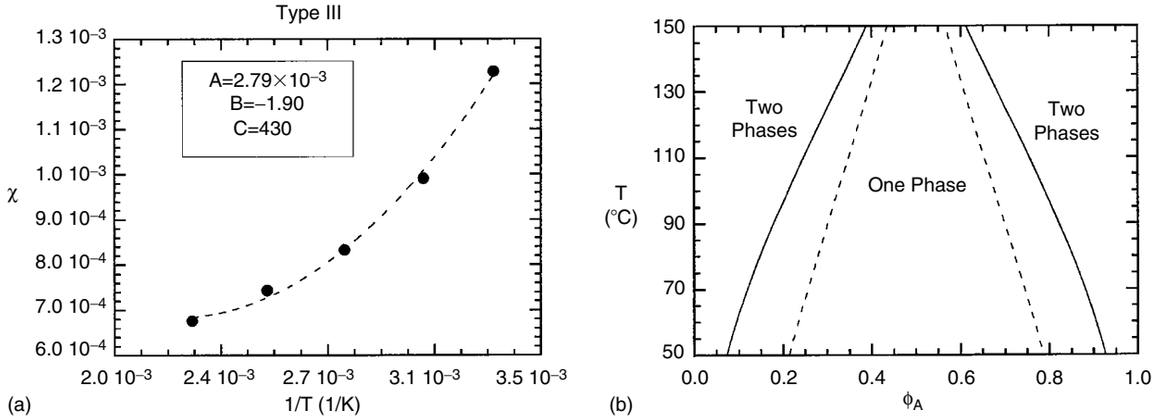

FIGURE 19.3. Example of a Type III blend [system 41b]. (a) A plot of χ versus $1/T$ for a PEB/*d*SPI(7) blend. Symbols represent experimental data and the dashed curve represents a least squares fit, using criteria described in Section 19.10. (b) Predicted binodal (solid curve) and spinodal (dashed curve) of a PEB/*d*SPI(7) blend with $N = 2{,}700$.

from type I because of the appearance of a "neck" at elevated temperatures. This is due to the fact that the gradient of the χ versus $1/T$ plot decreases with increasing temperature, i.e., C is positive. In other words, increasing temperature results in relatively little increase in miscibility at high temperatures. For blends that have positive C values, the phase diagram would abruptly "flatten out" at elevated temperatures instead of "necking". Unlike type I blends, the qualitative features of the type III phase diagrams are affected by component molecular weights. For example, the calculated phase diagram of a PEB/*d*SPI(7) blend with $N = 2{,}700$ does not show a neck, and is qualitatively similar to Fig. 19.1(b), i.e., a type I blend. This is due to the fact that the critical temperature of this blend is 100 °C, and over the limited temperature range between 27 and 100 °C, the nonlinearity of χ versus $1/T$ is relatively unimportant.

19.4.4 Type IV. χ is Positive and Nonmonotonic with Temperature, and $C > 0$

The χ parameter in these systems is also parabolic in $1/T$ and thus these systems are in many respects like type III blends. The difference is that the bottom of the parabola occurs at an experimentally accessible temperature. An example of such a system is HHPP/*d*SPI(7) [system 51] and the dependence of χ on $1/T$ is presented in Fig. 19.4(a). For a given ϕ_A, such behavior can lead to multiple solutions to Eqs. (19.9) and (19.10) that lie within the accessible temperature window. These systems can thus exhibit both LCST and UCST behavior. A HHPP/*d*SPI(7) blend with $N = 5{,}700$ is predicted to exhibit such behavior, and the calculated phase diagram is shown in Fig. 19.4(b). Single phase behavior is observed at intermediate temperatures and phase separation is observed toward the outer edges of the available temperature window. LCST behavior is predicted at high temperatures and UCST behavior is predicted at low temperatures.

19.4.5 Type V. χ is Positive and Nonmonotonic with Temperature, and $C < 0$

The χ versus $1/T$ plots from these systems also show an extremum as was the case with type IV blends; however the sign of the curvature (C) is negative. The SPI(7)/*d*PP [system 47b] blend exhibits such behavior as can be seen in Fig. 19.5(a). Like type IV blends, these systems can thus exhibit both LCST and UCST behavior. The difference is that UCST behavior is predicted at high temperatures and LCST behavior is predicted at low temperatures. The binodal and spinodal curves for such systems thus form closed loops and the two-phase region is restricted to the middle of the phase diagram. The calculated phase diagram for a SPI(7)/*d*PP blend with $N = 580$ has these characteristics and is shown in Fig. 19.5(b).

19.4.6 Type VI. Athermal Mixing, χ is Independent of T ($B = 0$ and $C = 0$)

In a few cases χ is, within experimental error, independent of temperature. Examples of such systems are SPI(7)/SPB(66) blend [system 39] and SPI(50)/SPB(78) blends [system 54]. The temperature dependence of χ for the SPB(66)/*d*SPI(7) blend is shown in Fig. 19.6(a). If A is finite, $B \equiv 0$, and $C \equiv 0$ then the phase diagram is composed of vertical lines. Blends that are single phase at room temperature will remain single phase at all temperatures, while blends that are phase separated at room temperature will remain phase separated at all temperatures. Figure 19.6(b) shows the predicted phase diagram for a SPB(66)/*d*SPI(7) blend with $N = 3{,}000$. The phase boundaries are not exactly vertical because the experimentally determined B is not identically zero.

It is obvious that measured values of B and C can never be identically equal to zero. Thus precise measurements on

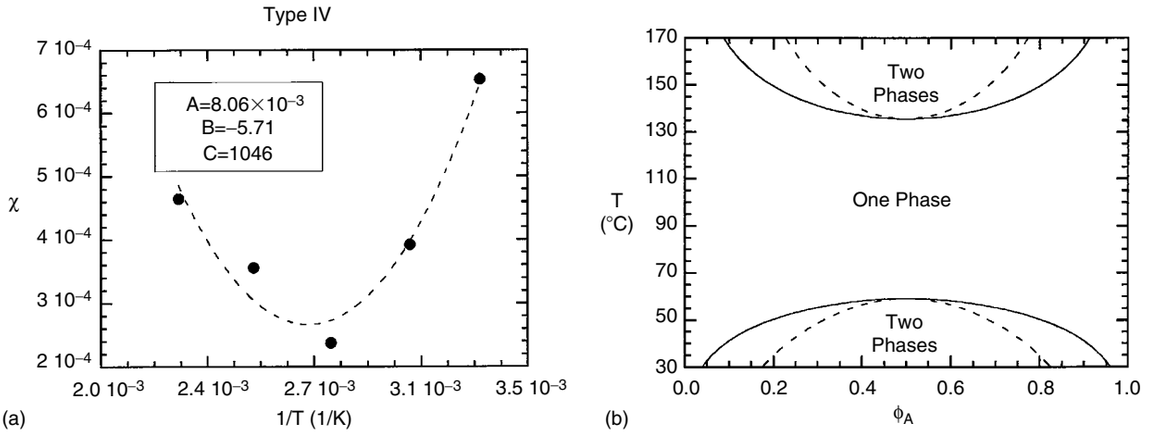

FIGURE 19.4. Example of a Type IV blend [system 51]. (a) A plot of χ versus $1/T$ for a HHPP/*d*SPI(7) blend. Symbols represent experimental data and the dashed curve represents a least squares fit, using criteria described in Section 19.10. (b) Predicted binodal (solid curves) and spinodal (dashed curves) of a HHPP/*d*SPI(7) blend with $N = 5{,}700$.

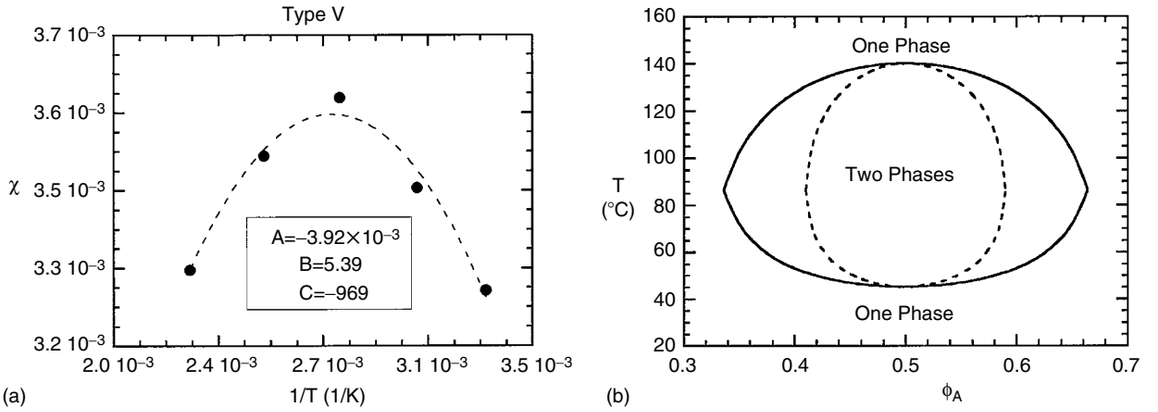

FIGURE 19.5. Example of a Type V blend [system 47b]. (a) A plot of χ versus $1/T$ for a SPI(7)/*d*PP blend. Symbols represent experimental data and the dashed curve represents a least squares fit, using criteria described in Section 19.10. (b) Predicted binodal (solid curves) and spinodal (dashed curves) of a SPI(7)/*d*PP blend with $N = 580$.

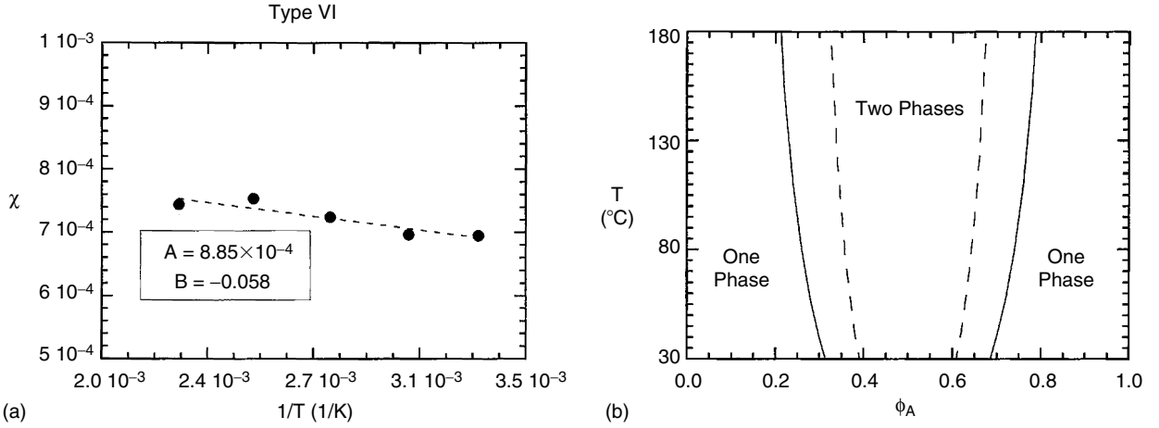

FIGURE 19.6. Example of a Type VI blend [system 39b]. (a) A plot of χ versus $1/T$ for a SPB(66)/*d*SPI(7) blend. Symbols represent experimental data and the dashed curve represents a least squares fit, using criteria described in Section 19.10. (b) Predicted binodal (solid curves) and spinodal (dashed curves) of a SPB(66)/*d*SPI(7) blend with $N = 3{,}000$.

Type VI systems will eventually lead to a reclassification. In fact, systems in this category have the potential to display extremely rich thermodynamics because χ could, in principle oscillate about a constant value. System 10 is an example of such behavior. In [32] it is shown that χ is an oscillatory function of T. In this case, the temperature dependence of χ cannot be described by Eq. (19.13). The parameters given for system 10 are thus valid over a restricted temperature window.

The smallest value of $|\chi|$ reported thus far in the polymer blend literature is obtained from the SPI(50)/SPB(78) system [system 54]. The χ parameter is nearly zero over the entire temperature window. Such a blend is unique because it is predicted to be single phase regardless of composition and temperature. The phase diagram of this system is predicted to be blank, regardless of component molecular weights.

19.5 SIMPLIFICATIONS

The phase diagrams presented above were calculated assuming that χ is independent of composition. Also, small changes in N with temperature were ignored. It may be of interest to note that all the examples chosen to illustrate the various types of blends were mixtures of polyolefins. The calculated binodal and spinodal curves represent extrapolations of χ parameters determined in the single-phase region. The composition dependence of χ in polyolefin blends is relatively weak in the mid-range of compositions $1/4 < \phi_A < 3/4$ [24,25]. Thus calculated phase boundaries in the examples are expected to be in agreement with experimental measurements. Direct measurements of the binodal and spinodal curves in some polyolefin blends were found to be consistent with χ parameters derived from SANS [33,34]. For other systems such as the PS/PVME

system, χ exhibits a more pronounced composition dependence [23]. If $\chi(\phi_A)$ is known then the phase diagrams can be predicted using classical thermodynamics as demonstrated in [23]. In such cases, the experimentally determined phase diagram may differ significantly from predictions based on the χ parameters reported in this work.

The classification of blends into different types is based on current knowledge and may not be permanent. It is possible that future experiments on these mixtures may unravel new features in the temperature dependence of χ, due to widening of the temperature window, more detailed measurements, or better instrumentation. For instance, type II behavior cannot persist at arbitrarily high temperature because all blends must be single phase in the limit $T \to \infty$. Hence, the two-phase region must close to form a loop at higher temperatures. Type II blends may thus be considered to be type V blends which have only been explored over a limited temperature range. On the other hand, practical limitations such as chain degradation may prevent all type II blends from showing type V behavior.

19.6 PREDICTIONS OF THE χ PARAMETER

The solubility parameter formalism, introduced by Hildebrand and Scott [35], may be used to predict χ parameters. In this approach, χ parameters are estimated from differences in solubility parameters of the pure components, δ_i, which in turn are related to their cohesive energy densities.

$$\chi = \frac{\nu_{\text{ref}}}{kT}(\delta_2 - \delta_1)^2 \tag{19.17}$$

Graessley, Lohse, and coworkers have found that the data from several polyolefin blends were consistent with the solubility parameter approach [36]. They were thus able to estimate δ from χ parameters measured by SANS. Group contribution methods have been developed by Small [37], Hoy [38], and van Krevelen [39] for predicting cohesive energy densities. None of these methods are based on data obtained from polymer mixtures [40] and usually lead to large errors when applied to polymer blends.

19.7 EFFECT OF DEUTERIUM SUBSTITUTION ON χ

Most of the data given in Table 19.1 were obtained from mixtures in which one of the polymers was labeled with deuterium. Of course, the objective of these experiments is to obtain χ between undeuterated polymers because deuterated polymers are seldom used in practical applications. The effect of deuterium labeling on thermodynamics of chemically dissimilar polymers was studied by Rhee and Crist [41], and Graessley, Lohse, and coworkers [42]. It was found that χ in polyolefin blends could either increase or decrease depending upon which species was labeled. They also found that χ between unlabeled polymers was equal to the average of the χs obtained from the two labeled blends. Values of A, B, and C for unlabeled polyolefin mixtures in Table 19.1 were calculated on this basis. However, this rule is not universal and has only been verified in a few polyolefin blends [41,42]. Other systems such as PMMA/PS [system 1] do not obey this rule.

In the early years (prior to 1980), the effect of deuterium substitution on polymer blend thermodynamics was assumed to be negligible. In a pioneering publication, Buckingham and Hentschel [43] estimated χ between protonated and deuterated polymers that are otherwise identical (isotopic blends) to be about 10^{-3}. They thus came to the surprising conclusion that isotopic blends should be phase separated at modest molecular weights ($N \sim 10^3$). Elegant experimental proof for this effect was provided by Bates and coworkers [44].

19.8 COMPLEX PHASE BEHAVIOR IN MULTICOMPONENT MIXTURES

The Flory–Huggins theory, RPA, and SCFT, along with the information in Tables 19.1 and 19.2 enable prediction of the structure and phase behavior of complex polymer mixtures in the mean-field limit. We discuss two illustrative examples of such predictions. More details regarding these examples can be found in the original references [18,45,46].

19.8.1 Interfacial Adsorption in a Multicomponent Type I System

A–B diblock copolymers adsorb spontaneously at the interface between two immiscible A and B homopolymers. Our objective here is to make quantitative predictions of the nature of the adsorbed layer. In this case, the phase behavior depends on only one χ parameter, that between the A and B homopolymers, and the statistical segment lengths of the A and B chains. The specific example that we will study is the adsorption of a SPB(89)–SPB(63) diblock copolymer at the interface between SPB(89) and SPB(63) homopolymers at room temperature [A = SPB(89) and B = SPB(63)]. For this system, $\chi = 0.0064$ (system 33 in Table 19.1), $l_A = 0.49\,\text{nm}$, and $l_B = 0.75\,\text{nm}$. We consider the interface between SPB(89) and SPB(63) homopolymers with $N_A = 4,230$ and $N_B = 3,600$. It is straightforward to show that the two homopolymers are highly immiscible because $\chi N_{\text{ave}} = 6.2$ which is much greater than 2 (see Eq. (19.8) for definition of N_{ave}). We consider the adsorption of a SPB(89)-SPB(63) diblock copolymer with $N_{Ab} = 790$ and $N_{Bb} = 730$ where the subscript "b" refers to the chains comprising the block copolymer. We consider two flat homopolymer-rich phases with the diblock copolymer adsorbed at the interface. The z-axis of our coordinate frame is perpendicular to the interface. The results of SCFT predictions for $\phi_{AB}(z)$, the volume fraction of the A–B diblock copolymer across an interface between the

homopolymers located at $z = 190$ nm, is shown by the curve in Fig. 19.7(a). The average volume fraction of the diblock copolymer in the system was 0.07. The peak value of ϕ_{AB} is 0.43 which is substantially larger than 0.07. This indicates a strong tendency for the block copolymer to accumulate at the interface. The symbols in Fig. 19.7(a) are experimentally measured values of $\phi_{AB}(z)$ for the same system. While some discrepancies are evident, especially in predicting ϕ_{AB} far away from the interface, it is clear that our SCFT predictions of the nature of the adsorbed block copolymer layer are in excellent agreement with the measurements. The two quantities of importance in an adsorption experiment are Γ, the interfacial excess of diblock copolymer, and σ, the thickness of the adsorbed layer. The data in Fig. 19.7(a) are replotted on a linear scale in Fig. 19.7(b). The shaded region in Fig. 19.7(b) is Γ while the width of the peak is σ. In Fig. 19.7(c) we plot Γ as a function of $\phi_{AB,A}$, the concentration of the block copolymer in the A-rich phase. The

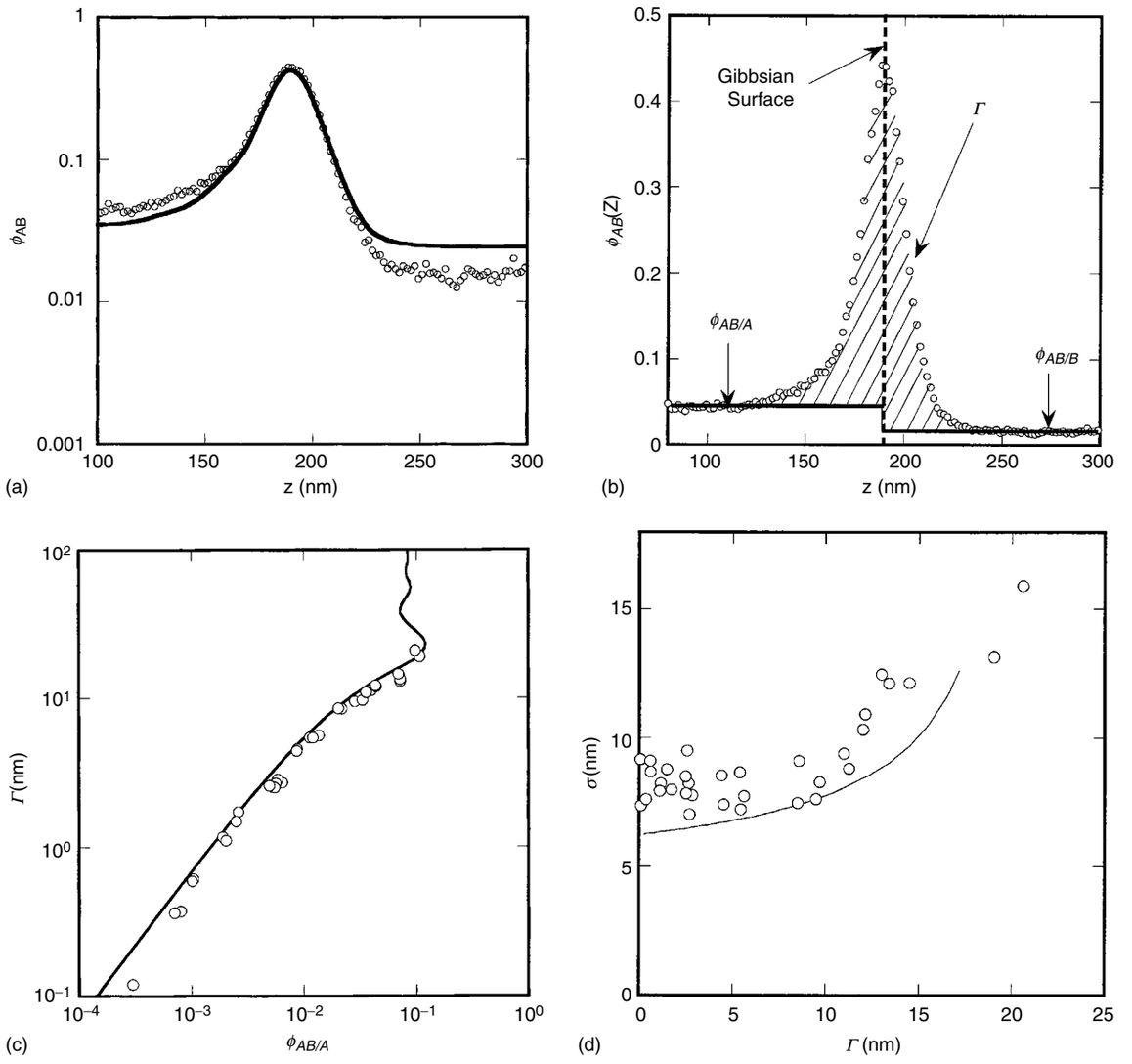

FIGURE 19.7. Interfacial activity in a Type I blend of an A–B diblock copolymer added to a blend of A and B homopolymers [A = SPB(89) and B = SPB(63)]. $N_A = 4{,}230$ and $N_B = 3{,}600$ for the homopolymers, while $N_{Ab} = 790$ and $N_{Bb} = 730$ for the block copolymer. Symbols show experimental measurements using secondary-ion mass spectrometry (SIMS), and curves show SCFT predictions using χ and l values from Tables 19.1 and 19.2. (a) Volume fraction profile in loglinear format of the diblock copolymer for a sample with 0.07 volume% block copolymer with an A/B interface at $z = 190$ nm. (b) Volume fraction profile in linear-linear format of the diblock copolymer for a sample with 0.07 volume% block copolymer with an A/B interface at $z = 190$ nm. The cross-hatched area represents the adsorbed amount, Γ. (c) Adsorption isotherm: the dependence of the adsorbed amount, Γ, on the copolymer volume fraction in the A-rich phase $\phi_{AB/A}$. (d) The thickness of the adsorbed layer (standard deviation of the volume fraction profile near the peak), σ, plotted versus the amount adsorbed, Γ.

symbols in Fig. 19.7(c) represent experimental measurements while the curve is the SCFT prediction. We find that the dependence of Γ on copolymer loading is also accurately captured by SCFT. In Fig. 19.7(d) we compare measurements of σ versus Γ with SCFT predictions. The increase in σ at high values of Γ indicates stretching of the copolymer brush due to molecular crowding at the interface. Both the value of Γ, where stretching is first observed, and the magnitude of chain stretching can be predicted entirely on the basis of unperturbed chain dimensions and the binary χ parameter.

19.8.2 Multicomponent Mixtures with Different Interaction Types

We now consider the behavior of multicomponent mixtures where we add an A–C copolymer to a blend of A and B homopolymers. Our objective was to study the effect of attractive interactions between B and C monomers (i.e., $\chi < 0$) on interfacial properties and microphase separation. The complexity in these mixtures is the fact that their phase behavior is governed by three χ parameters χ_{AB}, χ_{AC}, and χ_{BC} and three statistical segment lengths, l_A, l_B, and l_C. We consider the case where A = SPB(89), B = PIB, and C = SPB(63). The temperature dependence of χ_{AB} (system 61), χ_{AC} (system 33), and χ_{BC} (system 59) are shown in Fig. 19.8(a). Note that the three systems have very different temperature dependencies. χ_{AB} is a Type VI system, χ_{AC} is a Type I system, and χ_{BC} is a Type II system. Multicomponent A/B/A–C mixtures can thus exhibit unusual phase behavior. This is illustrated in a mixture with $N_A = 464$, $N_B = 437$, $N_{Ab} = 1{,}510$, and $N_{Cb} = 1{,}263$. In Fig. 19.8(b) we show the results of scattering studies on an A/B/A–C mixture with 25% A, 25% B, and 50% A–C by volume. This sample is microphase separated between room temperature and 140 °C, homogeneous at temperatures between 140 and 190 °C and phase separated at temperatures above 190 °C. It is not surprising that some systems macrophase separate upon heating. In fact, this is a characteristic of Type II systems. It is, however, unusual for a microphase separated system to become homogeneous at intermediate temperatures before exhibiting macrophase separation. In Fig. 19.8(b), we compare the characteristics of our A/B/A–C mixture measured by SANS (symbols) with theoretical predictions (curves). Between room temperature and 140 °C, the domain spacing of the microphase separated state d decreases with increasing temperature. The experimental data in this regime is in quantitative agreement with SCFT predictions (dashed curve). The SCFT analysis shows that the observed change in d is entirely due to the temperature dependence of the three χ_{ij} parameters and not a change in the size of the chains because $\hat{l}_i$ is constant. As the temperature approaches 140 °C, SCFT calculations, where we assume the presence of one-dimensional periodic concentration profiles, fail to converge. This implies that some other kind of phase is stable at temperatures ≥140 °C. RPA and FHT calculations indicate that the homogeneous phase is stable at temperatures between 140 and 190 °C. In this regime, the scattering profiles contain peaks due to the presence of concentration fluctuations with a well-defined length scale, and their length scale increases with increasing temperature. This trend is also captured

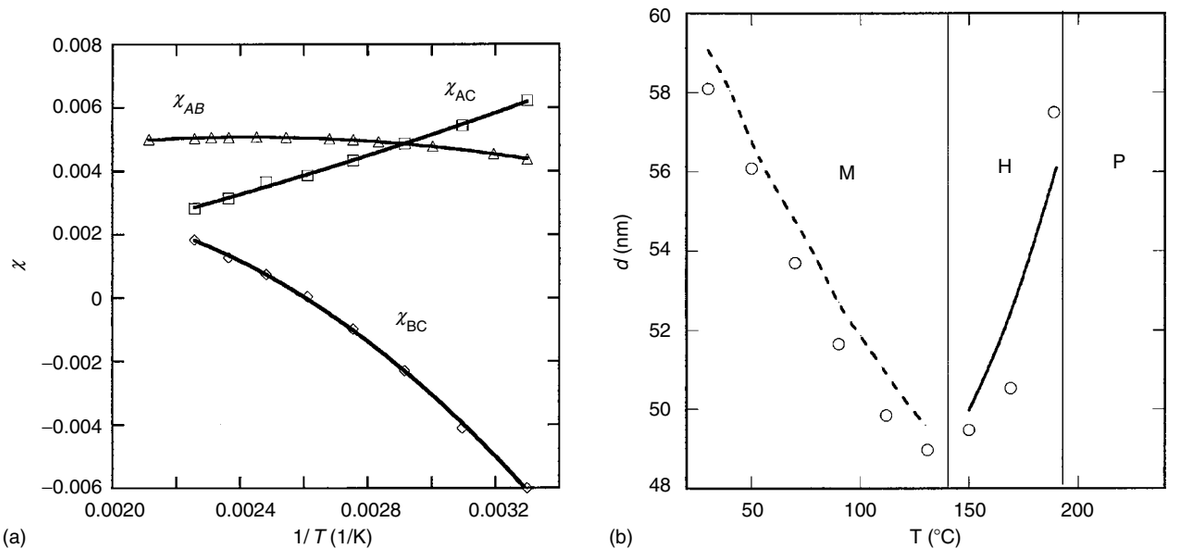

FIGURE 19.8. Phase behavior of a mixture of two homopolymers A and B in the presence of an A–C block copolymer [A = SPB(89), B = PIB, and C = SPB(63)]. (a) The temperature dependence of χ_{AB} (system 61, Type VI), χ_{AC} (system 33, Type I), and χ_{BC} (system 59, Type II). (b) The structure and phase behavior of a mixture containing 25% A, 25% B, and 50% A–C by volume. $N_A = 464$ and $N_B = 437$ for the homopolymers, while $N_{Ab} = 1{,}510$, and $N_{Cb} = 1{,}263$ for the block copolymer. Circles indicate the variation of domain spacing d with temperature measured by SANS. The dashed curve shows SCFT predictions while the solid curve shows RPA predictions. M≡microphase separation, H≡homogeneous, and P≡macrophase separation.

quantitatively by RPA (solid curve). Above 190 °C, the sample phase separates on macroscopic length scales (the SANS peak is lost and the sample turns cloudy). The theoretically predicted macrophase separation temperature, 205 °C, is in reasonable agreement with experiments.

19.9 ACKNOWLEDGMENT

This chapter is an expanded version of a chapter with the same name published in the first version of this handbook published by AIP Press. That effort was supported by the National Science Foundation Young Investigator Award (DMR-9457950). The present effort was also supported by the National Science Foundation (DMR-0514422 and CTS-0305711). NPB thanks Bill Graessley, Ramanan Krishnamoorti, Dave Lohse, and Ben Reynolds for introducing him to the subject matter discussed here, and Hyun Sik Jeon, Chenchy Lin, Joon Lee, Amy Lefebvre, Amish Patel, Tim Rappl, and Megan Ruegg for continued education in polymer blends.

19.10 ORGANIZATION OF TABLES AND NOMENCLATURE

1. Table 19.1 gives values of A, B, and C for a given polymer pair. These parameters can be used to estimate χ parameters within the specified temperature range. In cases where χ was approximately a linear function of $1/T$, the parameters A and B represent best linear fits through the data and C was set to zero. The parameter C was only used in cases where the nonlinearity was evident. In border-line cases where the nonlinearity was not as pronounced, the results of both linear and nonlinear fits are tabulated. Only one set of A, B, and C values are reported for each system. Systems such as polystyrene/polyisoprene and polystyrene/poly(vinyl methyl ether) have been examined by several groups. In many instances, the values obtained were consistent with each other. In cases where inconsistencies were found, some personal judgment was exercised.
2. In Table 19.1 and in the text, polymers are referred to by their abbreviated names. The full names and chemical structures of the polymers are given in Table 19.2. Monomer volumes and statistical segment lengths, necessary for obtaining phase diagrams from χ, are also listed in Table 19.2.
3. The letter "*d*" in front of the polymer name indicates that it was labeled with deuterium. The number of H atoms substituted by D per monomer is indicated for each system within curly brackets—{*d*3} implies that 3 of the H atoms in the monomer (defined in Table 19.2) were replaced by D. If deuteration levels are not specified it indicates that the polymer was fully deuterated.
4. The letter "S" in front of a name indicates that the polymer was obtained by saturating the double bonds of a polymeric precursor. For example, SPS is the polymer obtained by saturating polystyrene (PS) and is often referred to in the literature as poly(vinyl cyclohexane).
5. Dienes such as butadiene (isoprene) usually polymerize by 1,4- or 1,2- (3,4-) addition. The number in parentheses at the end of a name refers to the percentage of 1,2- units in the polybutadiene chains and the percentage of 3,4- units in the polyisoprene chains.

These materials are, to a good approximation, random copolymers of 1,4- and 1,2- (or 3,4-) units.

TABLE 19.1. *The dependence of χ on temperature.* $\chi = A + B/T + C/T^2$.

	System	A^a	B (K)^a	C(K^2)^a	T Range (°C)	Type	Refs.
1a	PMMA/*d*PS	1.74×10^{-2}	2.39	—	120–180	I	[47]
1b	PS/*d*PMMA	1.80×10^{-2}	1.96	—	170–210	I	[47]
1c	PS/PMMA	1.29×10^{-2}	1.96	—	100–200	I	[48]
1d	*d*PS/*d*PMMA	1.54×10^{-2}	1.96	—	130–210	I	[47]
2a	PVME/*d*PS	9.73×10^{-2}	−41.6	—	60–150	II	[16,49]
2b	PS/PVME	1.03×10^{-1}	−43.0	—	60–150	II	[49]
3a	PS/*d*PXE	5.8×10^{-2}	−37.7	—	100–280	II	[50]
3b	PXE/*d*PS	5.9×10^{-2}	−32.5	—	180–330	II	[51]
4	PS/PI(7)	7.85×10^{-3}	17.6	—	100–180	I	[52]
5	PS/PB(95)	-1.57×10^{-2}	18.7	—	50–180	I	[53]
6	PS/SPB(95)	4.11×10^{-3}	15.2	—	50–180	I	[53]
7	TMPC/*d*PS	1.57×10^{-1}	−81.3	—	190–250	II	[54]
8	PCHA/*d*PS	6.7×10^{-2}	−35	—	120–155	II	[55]
9	PS/P2VP	-1.8×10^{-2}	35	—	155–230	I	[56]
10	PPMA/*d*PS	5.15×10^{-2}	−27.2	5,127	80–130	IV	[57]
11	PBMA/*d*PS	1.07×10^{-1}	−60.4	9,807	20–130	III	[58]
12	PB(7)/PαMS	-5.5×10^{-2}	38	—	130–190	I	[59]
13	PS/PαMS	-1.17×10^{-3}	1.9	—	170–200	VI	[59]
14	PMMA/PαMS	3.14×10^{-2}	−2.53	—	170–210	II	[60]

TABLE 19.1. *Continued.*

	System	A^a	B (K)^a	C(K^2)^a	T Range (°C)	Type	Refs.
15	P4MS/PαMS	2.3×10^{-2}	−1.30	—	140–170	VI	[61]
16	P4MS/PS	-4.6×10^{-3}	3.2	—	160–230	I	[62]
17	PI(7)/*d*PB(12)	4.20×10^{-3}	−0.906	—	20–130	II	[63]
18	PI(7)/*d*PB(97)	7.42×10^{-3}	−3.22	—	30–110	II	[64]
19	PB(68)/*d*PB(63)	-1.30×10^{-3}	0.411	—	20–180	I	[65]
20	PB(7)/*d*PB(63)	-5.64×10^{-4}	0.825	—	20–180	I	[65]
21	PB(97)/*d*PB(11)	6.79×10^{-3}	0.561	—	(−7)–90	I	[66]
22	SPS/SPI(7)	1.47×10^{-2}	7.48	—	30–180	I	[67]
23	SPS/SPI(5)	-3.1×10^{-3}	13.3	—	140–250	I	[68]
24	SPS/SPB(7)	-1.47×10^{-2}	24.9	—	160–280	I	[68]
25	SPS/SPB(90)	-7.4×10^{-3}	9.5	—	180–330	I	[68]
26a	SPB(97)/*d*SPB(88) {d3}	-6.26×10^{-4}	0.543	—	30–170	I	[24,25,36,69–73]
26b	SPB(88)/*d*SPB(97) {d3}	-8.70×10^{-4}	0.650	—	30–170	I	[24,25,36,69–73]
26c	SPB(97)/SPB(88)	-7.48×10^{-4}	0.597	—	30–170	I	[24,25,36,69–73]
27a	SPB(88)/*d*SPB(78) {d2}	-9.20×10^{-4}	0.722	—	30–170	I	[24,25,36,69–73]
27b	SPB(78)/*d*SPB(88) {d3}	-1.07×10^{-3}	0.889	—	30–170	I	[24,25,36,69–73]
27c	SPB(88)/SPB(78)	-9.95×10^{-4}	0.806	—	30–170	I	[24,25,36,69–73]
28a	SPB(78)/*d*SPB(66) {d3}	-6.67×10^{-4}	0.607	—	80–170	I	[24,25,36,69–73]
28b	SPB(66)/*d*SPB(78) {d3}	-6.51×10^{-4}	0.647	—	110–170	I	[24,25,36,69–73]
28c	SPB(78)/SPB(66)	-6.59×10^{-4}	0.627	—	110–170	I	[24,25,36,69–73]
29a	SPB(66)/*d*SPB(52) {d3}	-7.81×10^{-4}	0.653	—	110–170	I	[24,25,36,69–73]
29c	SPB(52)/*d*SPB(66) {d3}	-6.26×10^{-4}	0.751	—	140–170	I	[24,25,36,69–73]
29c	SPB(66)/SPB(52)	-7.04×10^{-4}	0.702	—	140–170	I	[24,25,36,69–73]
30a	SPB(52)/*d*SPB(38) {d3}	-9.65×10^{-4}	0.598	—	50–170	I,III	[24,25,36,69–73]
		(1.95×10^{-3})	(−1.607)	(412)	50–170		
30b	SPB(38)/*d*SPB(52) {d3}	-9.74×10^{-4}	0.707	—	110–170	I	[24,25,36,69–73]
30c	SPB(52)/SPB(38)	-9.70×10^{-4}	0.653	—	110–170	I	[24,25,36,69–73]
31a	SPB(38)/*d*SPB(32) {d3}	-4.26×10^{-4}	0.232	—	80–170	I	[24,25,36,69–73]
31b	SPB(32)/*d*SPB(38) {d3}	-5.90×10^{-4}	0.396	—	80–170	I	[24,25,36,69–73]
31c	SPB(38)/SPB(32)	-5.08×10^{-4}	0.314	—	80–170	I	[24,25,36,69–73]
32a	SPB(25)/*d*SPB(8) {d3}	-2.02×10^{-3}	1.10	—	120–170	I	[24,25,36,69–73]
32b	SPB(8)/*d*SPB(25) {d4}	-3.14×10^{-3}	1.68	—	120–170	I	[24,25,36,69–73]
32c	SPB(25)/SPB(8)	-2.58×10^{-3}	1.39	—	120–170	I	[24,25,36,69–73]
33	SPB(89)/*d*SPB(63) {d3}	-1.47×10^{-3}	1.32	300	30–250	III	[74]
34	SPB(7)/SPB(90)	-3.8×10^{-3}	10.2	—	110–280	I	[68]
35	PE/*d*SPB(32) {d3}	-3.46×10^{-3}	2.59	—	140–200	I	[24,25,36,69–73]
36	PE/*d*SPB(25) {d4}	-3.23×10^{-3}	2.09	—	140–200	I	[24,25,36,69–73]
37a	PEB/*d*SPB(78) {d2}	-2.53×10^{-3}	2.50	−383	30–170	III	[24,25,36,69–73]
37b	SPB(78)/*d*PEB {d3}	-2.17×10^{-3}	2.24	−382	30–170	III	[24,25,36,69–73]
37c	PEB/SPB(78)	-2.35×10^{-3}	2.37	−383	30–170	III	[24,25,36,69–73]
38a	PEB/*d*SPB(66) {d3}	1.41×10^{-3}	−1.17	291	30–170	III	[24,25,36,69–73]
38b	SPB(66)/*d*PEB {d3}	2.40×10^{-3}	−1.87	405	30–170	III	[24,25,36,69–73]
38c	PEB/SPB(66)	1.91×10^{-3}	−1.52	348	30–170	III	[24,25,36,69–73]
39a	SPI(7)/*d*SPB(66) {d3}	6.90×10^{-4}	0.119	—	30–170	I,VI	[24,25,36,69–73]
39b	SPB(66)/*d*SPI(7) {d5}	8.85×10^{-4}	−0.058	—	30–170	VI	[24,25,36,69–73]
39c	SPI(7)/SPB(66)	7.88×10^{-4}	0.03	—	30–170	VI	[24,25,36,69–73]
40a	SPI(7)/*d*SPB(52) {d3}	3.66×10^{-3}	−3.22	676	30–170	III	[24,25,36,69–73]
40b	SPB(52)/*d*SPI(7) {d5}	2.43×10^{-3}	−2.03	443	30–170	III	[24,25,36,69–73]
40c	SPI(7)/SPB(52)	3.05×10^{-3}	−2.63	560	30–170	III	[24,25,36,69–73]
41a	SPI(7)/*d*PEB {d3}	2.71×10^{-3}	−1.85	420	30–170	III	[24,25,36,69–73]
41b	PEB/*d*SPI(7) {d5}	2.79×10^{-3}	−1.90	430	30–170	III	[24,25,36,69–73]
41c	PEB/SPI(7)	2.75×10^{-3}	−1.88	425	30–170	III	[24,25,36,69–73]
42a	SPI(7)/*d*SPB(38) {d3}	-2.01×10^{-3}	0.940	—	110–170	I	[24,25,36,69–73]
42b	SPB(38)/*d*SPI(7) {d5}	-2.93×10^{-3}	1.56	—	110–170	I	[24,25,36,69–73]
42c	SPI(7)/SPB(38)	-2.47×10^{-3}	1.25	—	110–170	I	[24,25,36,69–73]
43	SPI(5)/SPB(90)	-4×10^{-4}	4.2	—	130–310	I	[68]
44	SPI(5)/SPB(7)	-1.37×10^{-2}	7.5	—	110–170	I	[68]
45a	PP/*d*SPB(97) {d3}	4.54×10^{-3}	−4.71	1,364	30–130	III	[24,25,36,69–73]
45b	SPB(97)/*d*PP {d4}	2.44×10^{-3}	−3.27	1,051	30–130	III	[24,25,36,69–73]

TABLE 19.1. *Continued.*

	System	A^a	B (K)^a	C(K^2)^a	T Range (°C)	Type	Refs.
45c	PP/SPB(97)	3.49×10^{-3}	−3.99	1,208	30–130	III	[24,25,36,69–73]
46a	PP/*d*SPB(78) {d3}	7.47×10^{-3}	−6.38	1,426	50–170	III	[24,25,36,69–73]
46b	SPB(78)/*d*PP {d4}	3.81×10^{-3}	−3.50	895	50–170	III	[24,25,36,69–73]
46c	PP/SPB(78)	5.64×10^{-3}	−4.94	1,161	50–170	III	[24,25,36,69–73]
47a	PP/*d*SPI(7) {d5}	-3.02×10^{-3}	4.59	−944	30–170	III	[24,25,36,69–73]
47b	SPI(7)/*d*PP {d4}	-3.92×10^{-3}	5.39	−969	30–170	V	[24,25,36,69–73]
47c	PP/SPI(7)	-3.47×10^{-3}	4.99	−957	30–170	V	[24,25,36,69–73]
48a	HHPP/*d*SPB(78) {d2}	-1.53×10^{-3}	1.24	—	110–170	I	[24,25,36,69–73]
48b	SPB(78)/*d*HHPP {d4}	-2.20×10^{-3}	1.40	—	30–170	I	[24,25,36,69–73]
48c	HHPP/SPB(78)	-1.87×10^{-3}	1.32	—	110–170	I	[24,25,36,69–73]
49a	HHPP/*d*SPB(66) {d3}	7.16×10^{-3}	−6.17	1,338	30–170	III	[24,25,36,69–73]
49b	SPB(66)/*d*HHPP {d4}	6.75×10^{-3}	−5.84	1,280	30–170	III	[24,25,36,69–73]
49c	HHPP/SPB(66)	6.96×10^{-3}	−6.01	1,309	30–170	III	[24,25,36,69–73]
50a	HHPP/*d*PEB {d3}	1.27×10^{-3}	−0.96	282	30–170	III	[24,25,36,69–73]
50b	PEB/*d*HHPP {d4}	2.43×10^{-3}	−1.86	457	30–170	III	[24,25,36,69–73]
50c	HHPP/PEB	1.85×10^{-3}	−1.41	370	30–170	III	[24,25,36,69–73]
51	HHPP/*d*SPI(7) {d5}	8.06×10^{-3}	−5.71	1,046	30–170	IV	[24,25,36,69–73]
52a	HHPP/*d*PP {d4}	-4.27×10^{-3}	2.13	—	30–130	I	[24,25,36,69–73]
52b	PP/*d*HHPP {d4}	-3.01×10^{-3}	1.54	—	30–130	I	[24,25,36,69–73]
52c	HHPP/PP	-3.64×10^{-3}	1.84	—	30–130	I	[24,25,36,69–73]
53a	SPI(50)/*d*HHPP {d4}	-2.20×10^{-3}	1.24	—	30–170	I,III	[24,25,36,69–73]
		(1.11×10^{-3})	(−1.17)	(430)	30–170		[24,25,36,69–73]
53b	HHPP/*d*SPI(50) {d5}	-1.74×10^{-3}	1.29	—	50–170	I	[24,25,36,69–73]
53c	SPI(50)/HHPP	-1.97×10^{-3}	1.27	—	50–170	I	[24,25,36,69–73]
54a	SPI(50)/*d*SPB(78) {d2}	-1.62×10^{-4}	−0.04	—	50–170	VI	[24,25,36,69–73]
54b	SPB(78)/*d*SPI(50) {d5}	-1.63×10^{-4}	+0.02	—	30–170	VI	[24,25,36,69–73]
54c	SPI(50)/SPB(78)	-1.63×10^{-4}	−0.01	—	50–170	VI	[24,25,36,69–73]
55a	SPI-3,4/*d*SPB(97) {d3}	-2.85×10^{-4}	0.297	—	30–170	I	[24,25,36,69–73]
55b	SPB(97)/*d*SPI-3,4 {d5}	-2.40×10^{-4}	0.298	—	30–140	I	[24,25,36,69–73]
55c	SPI-3,4/SPB(97)	-2.63×10^{-4}	0.298	—	30–140	I	[24,25,36,69–73]
56	PI-3,4/*d*PTMSS	1.40×10^{-2}	−4.9	—	140–200	II	[75]
57	PI-3,4/PαMS	3.3×10^{-2}	6.07	—	190–200	I	[76]
58	PIB/*d*SPB(66) {d3}	2.20×10^{-2}	−7.92	—	30–110	II	[77]
59	PIB/*d*SPB(63) {d3}	-5.27×10^{-3}	10.3	−3,168	30–250	II	[74]
60	PIB/*d*SPB(78) {d3}	1.30×10^{-2}	−4.37	—	30–110	II	[77]
61	PIB/*d*SPB(89) {d3}	-4.43×10^{-4}	4.52	−927	30–250	VI	[74]
62	PIB/*d*HHPP {d4}	1.80×10^{-2}	−7.74	—	30–170	II	[77]
63	SPI(7)/*d*SPB(97)	4.01×10^{-4}	3.79	—	130–190	I	[78]
64	PI(6)/SPB(99)	-2.13×10^{-2}	8.61	—	50–125	I	[79]
65	PI(7)/*d*SPI(7)	-2.38×10^{-2}	17.2	—	40–210	I	[80]
66	PB(7)/*d*PB(7)	-2.15×10^{-4}	0.305	—	(−23)–90	I	[81]
67	PB(97)/*d*PB(97)	1.04×10^{-4}	0.158	—	40–100	I	[82]
68	PS/*d*PS	-1.73×10^{-4}	0.117	—	150–220	I	[81]
69	SPB(97)/*d*SPB(97)	-0.37×10^{-4}	0.261	—	30–100	I	[82]
70	PEO/*d*PMMA	-2.1×10^{-3}	0	—	80–160	VI	[83]
71	PEO/PS	-1.73×10^{-2}	23.7	—	210–230	I	[84]
72	PEO/PI(7)	1.38×10^{-1}	72	—	80–130	I	[85]
73	PEO/PBO	-8.2×10^{-2}	74.5	—	60–300	I	[86]
74	PI(6)/PFDMS	2.5×10^{-2}	4.83	—	170–200	I	[87]
75	PS/PFDMS	2.3×10^{-2}	3.11	—	160–210	I	[88]
76	PS/PFI	-9.4×10^{-2}	92	—	130–180	I	[89]
77	PS/PFB	7.8×10^{-2}	192	—	120–195	I	[90]
78	PB(99)/PFB	1.7×10^{-1}	89	—	120–195	I	[90]
79	SPB(99)/PFI	-1.83×10^{-1}	231	—	50–125	I	[79]
80	PI(6)/PFI	7.77×10^{-2}	83.7	—	50–125	I	[79]
81	PDMS/PEMS	1.93×10^{-3}	2.15	—	60–150	I	[91]
82	PDMS/PS	3.1×10^{-2}	58	—	165–225	I	[92]
83	PDMS/PI(7)	-8.5×10^{-3}	25.3	—	165–225	I	[92]

[a]Parameters χ, A, B, and C are based on a reference volume, $v = 0.1\,\text{nm}^3$.

TABLE 19.2. *Nomenclature, definitions, and monomer volumes.*

Polymer	Chain composition and definition of monomer[a]	Monomer volume[b] v_i(nm^3)	Statistical segment length[c] l_i (nm)	Temperature (°C)	Refs.
PS polystyrene	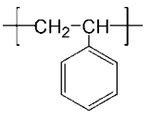	0.179	0.50	140	[30]
PαMS poly(α-methyl styrene)	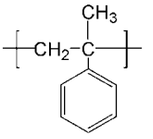	0.185	0.53	140	[30,93]
P4MS poly(4-methyl styrene)	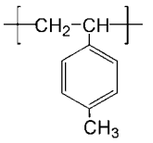	0.189	0.50	23	[62,94]
P2VP poly(2-vinyl pyridine)	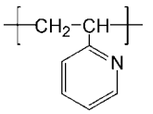	0.179	0.50	140	[95]
SPS saturated polystyrene	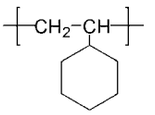	0.199	0.42	140	[30]
PTMSS poly(4-trimethylsilyl styrene)	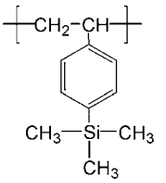	0.305	0.42	25	[75]
PI(x) polyisoprene	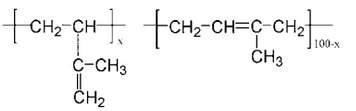	0.136	0.56 ($x = 5$)	140	[30]
PI-3,4 3,4-polyisoprene	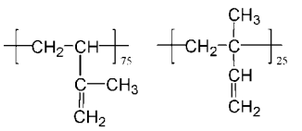	0.127	0.55	25	[30]
PB(x) polybutadiene	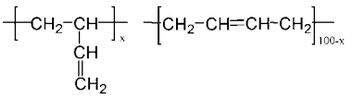	0.111	0.66 ($x = 10$)	140	[30]

TABLE 19.2. *Continued.*

Polymer	Chain composition and definition of monomer[a]	Monomer volume[b] v_i(nm^3)	Statistical segment length[c] l_i (nm)	Temperature (°C)	Refs.
SPI(x) saturated polyisoprene	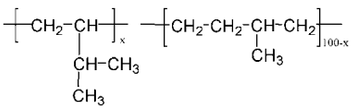	0.147	0.63 ($x = 5$)	140	[30]
SPI-3,4 saturated 3,4-polyisoprene	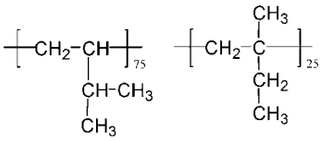	0.144	0.51	140	[30]
SPB(x) saturated polybutadiene	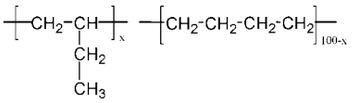	0.117	0.47 ($x = 89$) 0.72 ($x = 63$)	140	[74]
PEB poly(ethyl butylene)	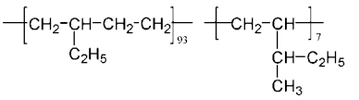	0.174	0.62	140	[30]
HHPP head-to-head polypropylene	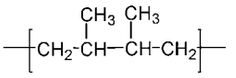 + 3% other isomers	0.172	0.58	140	[30]
PP polypropylene	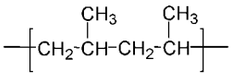 + 3% other isomers	0.176	0.57	140	[30]
PE polyethylene	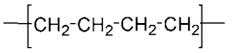	0.119	0.77	140	[30]
PIB polyisobutylene	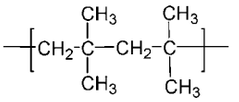	0.218	0.58	140	[74]
PEO poly(ethylene oxide)	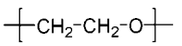	0.069	0.72	140	[30]
PBO poly(butylene oxide)	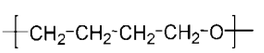	0.134	0.57	140	[30,86]
PVME poly(vinyl methylether)	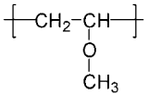	0.094	0.62	140	[93,96]
PXE poly(2,6-dimethyl-1, 4-phenylene oxide)	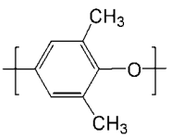	0.204	0.88	173	[94]

TABLE 19.2. *Continued.*

Polymer	Chain composition and definition of monomer[a]	Monomer volume[b] v_i(nm^3)	Statistical segment length[c] l_i (nm)	Temperature (°C)	Refs.
TMPC tetramethyl-bisphenol-A polycarbonate	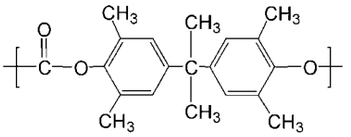	0.470	0.48	140	[97]
PMMA poly(methyl methacrylate)	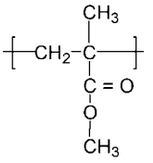	0.149	0.54	140	[30]
PBMA poly(*n*-butyl methacrylate)	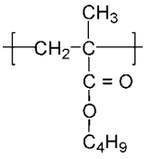	0.220	0.49	25	[58,98]
PPMA poly(*n*-pentyl methacrylate)	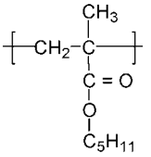	0.252	0.45	25	[98]
PCHA poly(cyclohexyl acrylate)	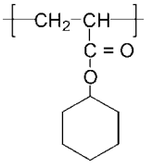	0.237	N.A.	20	[55]
PDMS poly(dimethyl siloxane)	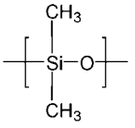	0.138	0.50	140	[92]
PEMS poly(ethylmethyl siloxane)	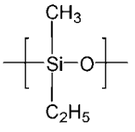	0.150	0.52	25	[91]
PFDMS Poly(ferrocenyl dimethylsilane)	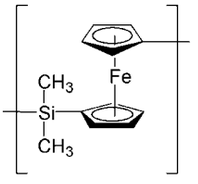	0.340	0.82	140	[87,88]

TABLE 19.2. *Continued.*

Polymer	Chain composition and definition of monomer[a]	Monomer volume[b] v_i(nm^3)	Statistical segment length[c] l_i (nm)	Temperature (°C)	Refs.
PFI fluorinated polyisoprene	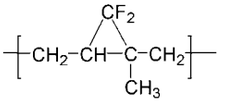	0.156	0.58	25	[89]
PFB fluorinated polybutadiene	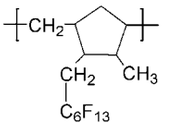	N.A.	N.A.	N.A.	[90]

[a]For random copolymers consisting of two kinds of repeat units, monomers are defined as either of the structures shown.
[b]Monomer volume (nm^3) $= 1.66 \times 10^{-3} \times$ [molar mass of monomer (g/mol)]/density(g/cm^3)]. To obtain monomer volumes at other temperatures, the expansion coefficient d ln v_i/dT must be known. For many polymers the expansion coefficient is about $(7 \pm 1) \times 10^{-4}$(1/K).
[c]Statistical segment lengths are based on a reference volume of 0.1 nm^3 at the temperatures listed. Statistical segment lengths can be computed at other temperatures based on the assumption that Rg is independent of temperature. N.A. implies data not available. A useful summary of polymer properties is given by Fetters *et al.* [99].

REFERENCES

1. D. R. Paul, S. Newman, eds., "*Polymer Blends*", vols. 1 and 2, Academic Press, San Diego (1978).
2. O. Olabisi, L. M. Robeson, M. T. Shaw, "*Polymer–Polymer Miscibility*", Academic Press, New York (1979).
3. D. R. Paul, J. W. Barlow, H. Keskkula, *Encyclopedia of Polymer Science and Engineering*, 2nd ed., H. F. Mark, C. G. Overberger, G. Menges, eds., Wiley Interscience, New York, **12**, 399 (1988).
4. S. Krause, J. Macromol. Sci. Rev. Macromol. Chem. **C7**, 251 (1972).
5. M. L Huggins, J. Chem. Phys. **9**, 440 (1941).
6. P. J. Flory, J. Chem. Phys. **9**, 660 (1941).
7. The Flory–Huggins theory, originally developed for polymer/solvent systems, was extended to polymer blends and other multicomponent mixtures by R. L. Scott, J. Polym. Sci. **9**, 423 (1952).
8. P. G. de Gennes, "*Scaling Concepts in Polymer Physics*", Cornell University Press, Ithaca, NY (1979).
9. L. Leibler, Macromolecules **13**, 1602 (1980).
10. L. Leibler, Macromolecules **15**,1283 (1982).
11. H. Benoit, M. Benmouna, W. L Wu, Macromolecules **23**, 1511 (1990).
12. A. Z. Akcasu, M. Tombakoglu, Macromolecules **23**, 607 (1990).
13. A. K. Dolan, S. F. Edwards, Proc. R. Soc. Lond. A **337**, 509 (1974).
14. E. Helfand, J. Chem. Phys. **62**, 999 (1975).
15. M. W. Matsen, J. Phys.: Condens. Matter **14**, R21 (2002).
16. C. C. Hsu, J. M. Prausnitz, Macromolecules **7**, 320 (1974).
17. B. J. Reynolds, M. L. Ruegg, N. P. Balsara, C. J. Radke, T. D. Shaffer, M. Y. Lin, K. R. Shull, D. J. Lohse, Macromolecules **37**, 7401 (2004).
18. B. J. Reynolds, M. L. Ruegg, T. E. Mates, C. J. Radke, N. P. Balsara, Macromolecules **38**, 3872 (2005).
19. J. H. Lee, N. P. Balsara, A. K. Chakraborty, R. Krishnamoorti, B. Hammouda, Macromolecules **35**, 7748 (2002).
20. C. Herkt-Maetzky and J. Schelten, Phys. Rev. Lett. **51**, 896 (1983).
21. C. T. Murray, J. W. Gilmore, and R. S. Stein, Macromolecules **18**, 996 (1985).
22. G. Hadziioannou and R. S. Stein, Macromolecules **17**, 567 (1984).
23. C. C. Han, B. J. Bauer, J. C. Clark, Y. Muroga, Y. Matsushita, M. Okada, Q. Tran-cong, T. Chang, I. C. Sanchez, Polymer **29**, 2002 (1988).
24. R. Krishnamoorti, W. W. Graessley, N. P. Balsara, D. J. Lohse, J. Chem. Phys. **100**, 3894 (1994).
25. N. P. Balsara, D. J. Lohse, L. J. Fetters, N. Hadjichristidis, C. C. Han, W. W. Graessley, R. Krishnamoorti, Macromolecules **25**, 6317 (1992).
26. R. J. Roe, M. Fishkis, J. C. Chang, Macromolecules **14**, 1091 (1981).
27. T. Hashimoto, M. Shibayama, H. Kawai, Macromolecules **16**, 1093 (1983).
28. G. H. Fredrickson, E. Helfand, J. Chem. Phys. **87**, 697 (1987).
29. Compare l obtained for polystyrene in N. P. Balsara, C. C. Lin, H. J. Dai, R. Krishnamoorti, Macromolecules **27**, 1216 (1994) with that given in ref. 30.
30. J. E. Mark, ed., "*Physical Properties of Polymers Handbook*", Chapter 24 Chain Dimensions and Entanglement Spacings, AIP Press, Woodbury, NY (1996).
31. H. S. Jeon, J. H. Lee, N. P. Balsara, M. C. Newstein, Macromolecules **31**, 3340 (1998).
32. D. Y. Ryu, U. Jeong, D. H. Lee, J. Kim, H. S. Youn, J. K. Kim, Macromolecules **36**, 2894 (2003).
33. F. Scheffold, E. Eiser, A. Budkowski, U. Steiner, J. Klein, L. J. Fetters, J. Chem. Phys. **106**, 8786 (1996).
34. A. A. Lefebvre, N. P. Balsara, J. H. Lee, C. Vaidyanathan, Macromolecules, **35**, 7758 (2002).
35. J. H. Hildebrand, R. L. Scott, "*The Solubility of Non-Electrolytes*", Dover, New York (1964).
36. R. Krishnamoorti, W. W. Graessley, N. P. Balsara, D. J. Lohse, Macromolecules **27**, 3073 (1994).
37. P. A. Small, J. Appl. Chem. **3**, 71 (1953).
38. K. L. Hoy, J. Paint Technol. **42**, 76 (1970).
39. D. W. van Krevelen "*Properties of Polymers*", Elsevier, Amsterdam (1972).
40. Small's values were derived from heats of vaporization [37]. Hoy's values were derived from vapor pressures [38]. van Krevelen's values were based on dilute solution properties of polymers [39].
41. J. Rhee, B. Crist, J. Chem. Phys. **98**, 4174 (1993).
42. W. W. Graessley, R. Krishnamoorti, N. P. Balsara, L. J. Fetters, D. J. Lohse, D. N. Schulz, J. A. Sissano, Macromolecules **26**, 1137 (1993).
43. A. D. Buckingham, H. G. E. Hentschel, J. Polym. Sci., Polym. Phys. Ed. **18**, 853 (1980).
44. F. S. Bates, G. D. Wignall, W. C. Koehler, Phys. Rev. Lett. **55**, 2425 (1985).
45. M. L. Ruegg, B. J. Beynolds, M. Y. Lin, D. J. Lohse, N. P. Balsara, Macromolecules, **39**, 1125 (2006).
46. The calculations presented in this paper are based on the χ, l_i, and v_i values given in Tables 19.1 and 19.2. These values differ slightly from those used in ref. 45.
47. T. P. Russell, Macromolecules **26**, 5819 (1993).
48. T. A. Callaghan, D. K. Paul, Macromolecules **26**, 2439 (1993).

49. B. Hammouda, R. M. Briber, B. J. Bauer, Polym. Commun. **33** 1785 (1992).
50. A. Mocannachie, R. P. Kambour, D. M. White, S. Rostami, D. J. Walsh, Macromolecules **17**, 2645 (1984).
51. R. J. Composto, E. J. Kramer, D. M. White, Macromolecules **21**, 2580 (1988).
52. C. C. Lin, S. V. Jonnalagadda, P. K. Kesani, H. J. Dai, N. P. Balsara, Macromolecules **27**, 7769 (1994).
53. J. N. Owens, I. S. Gancarz, J. T. Koberstein, T. P. Russell, Macromolecules **22**, 3380 (1989).
54. E. Kim, E. J. Kramer, J. O. Osby, D. J. Walsh, J. Polym. Sci., Polym. Phys. Ed. **33**, 467 (1995).
55. D. W. Schubert, V. Abetz, M. Stamm, T. Hack, W. Siol, Macromolecules **28**, 2519 (1995).
56. K. H. Dai, E. J. Kramer, Polymer **35**, 157 (1994).
57. D. Y. Ryu, M. S. Park, S. H. Chae, J. Jang, J. K. Kim, T. P. Russell, Macromolecules **35**, 8676 (2002).
58. B. Bauer, B. Hammouda, T. P. Russell, Macromolecules **27**, 2357 (1994).
59. J.-L. Lin, R.-J. Roe, Macromolecules **20**, 2168 (1987).
60. T. A. Callaghan, D. R. Paul, Macromolecules **26**, 2439 (1993).
61. L. L. Chang, E. M. Woo, Macromolecules **33**, 6892 (2000).
62. J. D. Londono, G. D. Wignall, Macromolecules **30**, 3821 (1997).
63. H. Hasegawa, S. Sakurai, M. Takenaka, T. Hashimoto, C. C. Han, Macromolecules **24**, 1813 (1991).
64. D. W. Tomlin, C. M. Roland, Macromolecules **25**, 2994 (1992).
65. S. Sakurai, H. Hasegawa, T. Hashimoto, I. G. Hargis, S. L. Aggarwal, C. C. Han, Macromolecules **23**, 451 (1990).
66. F. S. Bates, M. A. Hartney, Macromolecules **18**, 2478 (1985).
67. N. P. Balsara, C. C. Lin, H. J. Dai, R. Krishnamoorti, Macromolecules **27**, 1216 (1994).
68. E. W. Cochran, F. S. Bates, Macromolecules **35**, 7368 (2002).
69. N. P. Balsara, D. J. Lohse, W. W. Graessley, R. Krishnamoorti, J. Chem. Phys. **100**, 3905 (1994).
70. W. W. Graessley, R. Krishnamoorti, N. P. Balsara, L. J. Fetters, D. J. Lohse, D. N. Schulz, J. A. Sissano, Macromolecules **27**, 2574 (1994).
71. W. W. Graessley, R. Krishnamoorti, N. P. Balsara, B. Butera, L. J. Fetters, D. J. Lohse, D. N. Schulz, J. A. Sissano, Macromolecules **27**, 3896 (1994).
72. W. W. Graessley, R. Krishnamoorti, G. C. Reichart, N. P. Balsara, L. J. Fetters, D. J. Lohse, Macromolecules **28**, 1260 (1995).
73. R. Krishnamoorti, PhD Thesis, Princeton University (1994).
74. B. J. Reynolds, M. L. Ruegg, N. P. Balsara, C. J. Radke, T. D. Shaffer, M. Y. Lin, K. R. Shull, D. J. Lohse, Macromolecules **37**, 7401 (2004).
75. M. Harada, T. Suzuki, M. Ohya, D. Kawaguchi, A. Takano, Y. Matsushita, Macromolecules **38**, 1868 (2005).
76. D. A. Durkee, PhD Thesis, University of California, Berkeley, in preperation.
77. R. Krishnamoorti, W. W. Graessley, L. J. Fetters, R. T. Garner, D. J. Lohse, Macromolecules **28**, 1252 (1995).
78. F. S. Bates, J. H. Rosedale, P. Stepanek, T. P. Lodge, P. Wiltzius, G. H. Fredrickson, R. P. Hjelm, Phys. Rev. Lett. **65**, 1893 (1990).
79. D. A. Davidock, M. A. Hillmyer, T. P. Lodge, Macromolecules **37**, 397 (2004).
80. F. S. Bates, J. H. Rosedale, G. H. Fredrickson, J. Chem. Phys. **92**, 6255 (1990).
81. F. S. Bates, G. D. Wignall, Phys. Rev. Lett. **57**, 1429 (1986).
82. F. S. Bates, L. J. Fetters, G. D. Wignall, Macromolecules **21**,1086 (1988).
83. H. Ito, T. P. Russell, G. D. Wignall, Macromolecules **20**, 2213 (1987).
84. L. Zhu, S. Z. D. Cheng, B. H. Calhoun, Q. Ge, R. P. Quirk, E. L. Thomas, B. S. Hsiao, F. Yeh, B. Lotz, Polymer **42**, 5829 (2001).
85. G. Floudas, R. Ulrich, U. Wiesner, J. Chem. Phys. **110**, 652 (1999).
86. S.-M. Mai, J. P. Fairclough, I. W. Hamley, M. W. Matsen, R. C. Denny, B.-X. Liao, C. Booth, A. J. Ryan, Macromolecules **29**, 6212 (1996).
87. H. B. Eitouni, N. P. Balsara, J. Am. Chem. Soc. **126**, 7446 (2004).
88. H. B. Eitouni, N. P. Balsara, H. Hahn, J. A. Pople, M. A. Hempenius, Macromolecules **35**, 7765 (2002).
89. Y. Ren, T. P. Lodge, M. A. Hillmyer, Macromolecules **33**, 868 (2000).
90. Y. Ren, T. P. Lodge, M. A. Hillmyer, Macromolecules **35**, 3889 (2002).
91. G. Meier, B. Momper, E. W. Fischer, J. Chem. Phys. **97**, 5884 (1992).
92. E. W. Cochran, D. C. Morse, F. S. Bates, Macromolecules **36**, 782 (2003).
93. J. K. Kim, H. H. Lee, H. W. Son, C. D. Han, Macromolecules **31**, 8566 (1998).
94. A. Maconnachie, J. R. Fried, P. E. Tomlins, Macromolecules **22**, 4606 (1989).
95. C. E. Eastman, T. P. Lodge, Macromolecules **27**, 5591 (1994).
96. M. Shibayama, H. Yang, R. S. Stein, C. C. Han, Macromolecules **18**, 2179 (1985).
97. E. Kim, G. Krausch, E. J. Kramer, J. O. Osby, Macromolecules **27**, 5927 (1994).
98. J. Scherble, B. Stark, B. Stuhn, J. Kressler, H. Budde, S. Horing, D. W. Schubert, P. Simon, M. Stamm, Macromolecules **32**, 1859 (1999).
99. L. J. Fetters, D. J. Lohse, D. Richter, T. A. Witten, A. Zirkel, Macromolecules **27**, 4639 (1994).

CHAPTER 20

NMR Spectroscopy of Polymers

Alan E. Tonelli* and Jeffery L. White†

*Fiber & Polymer Science Program, North Carolina State University, Raleigh, NC 27695
†Department of Chemistry, Oklahoma State University

20.1 INTRODUCTION

Nuclei of all atoms possess charge and mass, and fortunately some have angular momentum and a magnetic moment. Nuclei with odd mass numbers have spin angular momentum quantum numbers I that are odd-integral multiples of 1/2. Nuclei with even mass numbers and odd nuclear charges have integral spin I, while those with even nuclear charge are spinless.

A nucleus with spin I has an angular momentum $I(h/2\pi)$, where h is Planck's constant. If $I \neq 0$, the nucleus will possess a magnetic moment μ, which is taken parallel to the angular momentum vector. A set of magnetic quantum numbers, m, given by the series

$$m = I, I-1, I-2, \ldots -I, \tag{20.1}$$

describes the values of the magnetic moment vector which are permitted along any chosen axis. For spin 1/2 nuclei (^{1}H,^{13}C,^{15}N,^{19}F,^{29}Si,^{31}P), $I = 1/2$ and $m = +1/2$ and $-1/2$. In general there are $2I + 1$ possible orientations of μ, or magnetic states of the nucleus. The ratio of the magnetic moment to the angular momentum is called the gyromagnetic ratio, γ,

$$\gamma = 2\pi\mu/hI \tag{20.2}$$

and is characteristic for a given nucleus (see Table 20.1).

With the exception of ^{2}H, the nuclei common to the NMR studies of polymers usually have spin $I = 1/2$, and are characterized by $2I + 1 = 2$ magnetic states, $m = +1/2$ and $-1/2$. In the absence of an applied magnetic field, both nuclear magnetic states have the same energy, but they correspond to states of different potential energy upon application of a uniform magnetic field B_0. The magnetic moment is either aligned along ($m = +1/2$) or against ($m = -1/2$) the applied field B_0, with the antiparallel state ($m = -1/2$) corresponding to a higher energy. The nuclear magnetic resonance (NMR) phenomenon makes it possible to detect transitions of the magnetic nuclei between these spin states.

TABLE 20.1. *Nuclei of major interest to the NMR spectroscopy of polymers [1].*

Isotope	Abundance (%)	Nuclear charge (z)	Spin	μ^a	$\gamma \times 10^b$	Relative^c *sensitivity*	ν_0 at 1 T (MHz)
^{1}H	99.9844	1	1/2	2.7927	2.6752	1.000	42.577
^{2}H	0.0156	1	1	0.8574	0.4107	0.00964	6.536
^{13}C	1.108	6	1/2	0.7022	0.6726	0.0159	10.705
^{15}N	0.365	7	1/2	−0.2830	−0.2711	0.00104	4.315
^{19}F	100	9	1/2	2.6273	2.5167	0.834	40.055
^{29}Si	4.70	14	1/2	−0.5548	−0.5316	0.0785	8.460
^{31}P	100	15	1/2	1.1305	1.0829	0.0664	17.235

[a]Magnetic moment in units of the nuclear magneton, $eh/(4\mu M_p c)$.
[b]Magnetogyric ratio in SI units.
[c]For equal numbers of nuclei at constant field.

20.2 RESONANCE

In Fig. 20.1 we have schematically drawn a nuclear magnetic moment μ in the presence of an applied field B_0 acting along the z-direction. The angle θ between μ and B_0 does not change, because the torque,

$$L = \mu \times B_0 \tag{20.3}$$

tending to tip μ toward B_0 is exactly balanced by the spinning of the magnetic moment, resulting in a nuclear precession about the z-axis. Attempting to force the alignment of μ along the z-axis by increasing B_0 only results in faster precession. A spinning top experiencing the earth's gravitational field is a good analogy to nuclear precession in a magnetic field. The precessional or Larmor frequency, v, of the spinning nucleus is given by

$$v = (\gamma/2\pi)B_0, \tag{20.4}$$

and is independent of θ. The energy of the system does, however, depend on the angle between μ and B_0:

$$E = -\mu \cdot B_0 = -\mu B_0 \cos\theta. \tag{20.5}$$

By application of a small rotating magnetic field B_1 orthogonal to B_0 (see Fig. 20.1), the orientation θ between μ and B_0 may be altered. μ will now experience the combined effects of B_1 and B_0 if the angular frequency of B_1 coincides with v, the precessional frequency of the nuclear spin. In this situation, the nucleus absorbs energy from B_1 and the orientation between μ and B_0 changes; otherwise B_1 and μ would not remain in phase and no energy would be transferred between them.

If the rotation rate of B_1 is varied through the Larmor frequency of the nucleus, a resonance condition is achieved (NMR), and a transfer of energy from B_1 to the spinning nucleus occurs producing an oscillation of the angle θ between μ and B_0. At $B_0 = 1$T (1 T = 1 Tesla = 10 kilogauss) the resonant frequencies (v_0) of the nuclei commonly observed in polymers are listed in Table 20.1.

20.3 NUCLEAR SPIN INTERACTIONS AND RELAXATION

Figure 20.2 illustrates the magnetic energy levels for a spin-1/2 nucleus in a magnetic field B_0. The energy separation between spin states is

$$\Delta E = 2\mu B_0, \tag{20.6}$$

and the relative populations of the upper (+) and lower (−) energy states is given by the Boltzmann expression

$$N_+/N_- = \exp(-\Delta E/kT) = \exp(-2\mu B_0/kT). \tag{20.7}$$

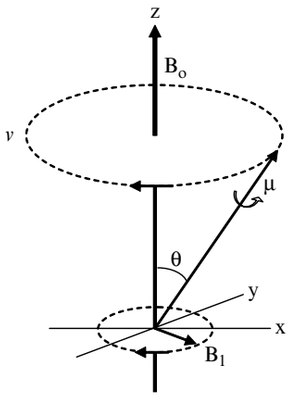

FIGURE 20.1. Nuclear magnetic moment μ in a magnetic field B_0.

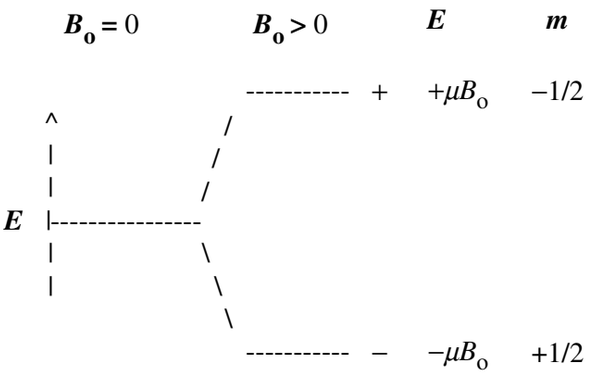

FIGURE 20.2. Energy levels for a spin 1/2 nucleus in a magnetic field B_0.

If we make the approximation $e^{-x} = 1 - x$ for small x, then the excess population of the lower energy spin state (−) is

$$(N_- - N_+)/N_- = 2\mu B_0/kT. \tag{20.8}$$

At a field strength of $B_0 = 2.34$T, $\nu_0 = 100$ MHz for ^{1}H nuclei, the separation between magnetic energy levels for proton nuclei is ca. 10^{-2} cal, which results in an excess population of ca. 2×10^{-5} spins of lower energy aligned parallel with B_0. This small spin population difference leads for an assemblage of nuclei to a correspondingly small macroscopic magnetic moment directed along B_0. (NMR spectroscopy is a relatively low sensitivity technique for this reason, and usually requires extensive signal averaging.) Because the magnetic energy levels are degenerate in the absence of B_0, removal of the applied field results in a loss of the macroscopically observable net magnetic moment.

What mechanisms are responsible for establishing the Boltzmann distribution of spin states following application of B_0, and how long does it take? Such a relaxation is possible because each spin is not completely isolated or decoupled from the rest of the molecules in the sample, referred to as the lattice. Molecular motions of the neighboring nuclei, which constitute the lattice, provide the mechanism for transferring thermal energy between the spins and their surroundings. The relative motion of neighboring nuclei generates fluctuating magnetic fields which are felt by the observed nucleus as it precesses about the direction of the applied field B_0. A broad range of frequencies will be associated with the fluctuating fields produced by the lattice motions, because, relative to the observed nucleus, these motions are nearly random. Components of the fluctuating magnetic fields generated by the lattice motions which lie along B_0 (see Fig. 20.1) and have frequency ν_0 will, like B_1, induce transitions between the magnetic energy levels of the observed nuclei. Therefore, the rates of spin–lattice relaxation must be directly connected to the rates of molecular motions in the lattice.

T_1, the spin–lattice relaxation time, is the time required for the difference between excess and equilibrium spin populations to be relaxed by a factor of e. In liquids, T_1 usually ranges from 10^{-2} to 10^2s, while T_1 may be as long as hours in rigid solid samples. Spin–lattice relaxation produces a change in energy by redistributing magnetic moments with components along the applied field B_0.

Consequently, T_1 is often called the longitudinal relaxation time and is associated with a decay of the macroscopic nuclear moment along the direction (longitudinal or z-axis direction) of the applied field B_0.

A second mode by which nuclear magnetic moments may interact is illustrated in Fig. 20.3. Here a pair of nuclear moments precess about the B_0-axis and each is decomposed into a static component along B_0 (a) and a component rotating in the xy-plane (b) transverse to B_0. If the rotating component precesses at the Larmor frequency ν_0, then a neighboring nucleus may be induced to undergo a spin transition, or flip, *via* a spin exchange, i.e., from $\uparrow\downarrow$ to $\downarrow\uparrow$ for example. Though no net change in the total energy of the system or in the net macroscopic magnetization is produced by the exchange of neighboring nuclear spins, clearly the lifetimes of the interacting spins are affected. Exchange, or flipping, of neighboring nuclear spins is called spin–spin relaxation and is characterized by T_2, the spin–spin relaxation time. Because T_2 is concerned with the rate of change of magnetization in the xy-plane, transverse to B_0, it is also called the transverse relaxation time.

In general spin–lattice relaxation (T_1), through molecular motions, effects NMR signal intensities, while spin–spin relaxation (T_2), is reflected in the broadening of NMR signals.

20.4 NMR FREQUENCIES AND CHEMICAL SHIFTS

By application of a rotating magnetic field B_1 transverse to the static field B_0, about which a spinning nuclear magnetic moment is precessing at $\nu_0 = (\gamma/2\pi)B_0$, we can flip the nuclear spin by rotating B_1 at ν_0. However, if all nuclei of the same type, e.g., all protons, were to flip or resonate at the same field strength B_0, then NMR would not be a spectroscopic tool useful for the study of molecular structure or for observing the relative mobilities of different portions (micro- and/or macroscopic) of a sample.

Fortunately, the resonant frequency of a nucleus depends on its chemical and/or structural environment in addition to its nuclear characteristics (γ).

When placed in a magnetic field B_0, the cloud of electrons about each nucleus produces orbital currents which are accompanied by small local magnetic fields proportional to B_0 but in the opposite direction (diamagnetic), thereby effectively shielding the nucleus from B_0. A slightly higher value of B_0 is needed to achieve resonance, because the actual local magnetic field B_{loc} experienced by a nucleus is expressed as

$$B_{loc} = B_0(1 - \sigma), \tag{20.9}$$

where σ is the electronic screening constant. (Subsequently we will point out that σ is not strictly a constant, but actually is a vector due to the anisotropic distribution of electrons that shield nuclei.) σ is highly sensitive to molecular structure, but is independent of B_0. The resonant Larmor frequency becomes

$$\nu_0 = \mu B_{loc}/hI = \mu B_0(1 - \sigma)/hI, \tag{20.10}$$

and the separation between nuclear spin energy levels is reduced to (see Eq. (20.6))

$$\Delta E = 2\mu B_{log} = 2\mu B_0(1 - \sigma). \tag{20.11}$$

Clearly, nuclear screening decreases the spacing of nuclear magnetic energy levels. An increase in magnetic shielding

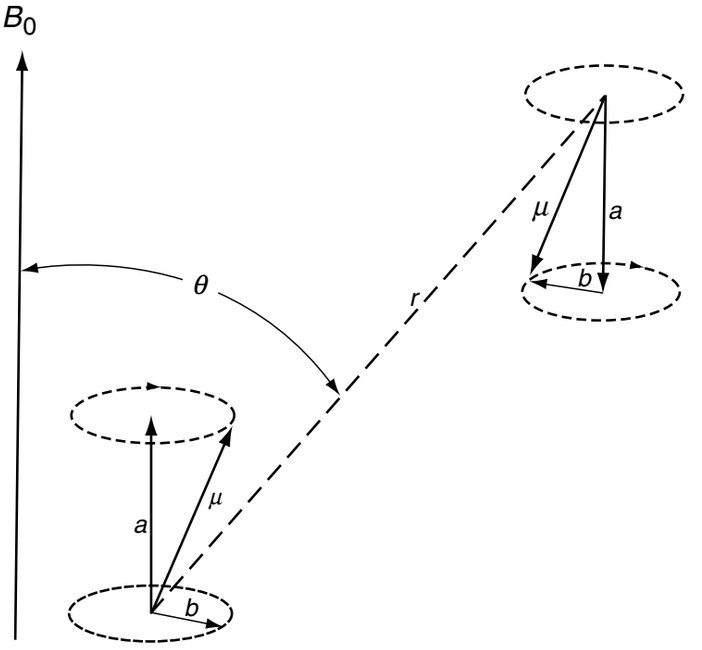

FIGURE 20.3. A pair of precessing nuclear moments with static (a) and rotating (b) components.

(σ) requires an increase in B_0 at constant v_0 or a decrease in v_0 at constant field strength B_0 to achieve resonance.

The numbers and types of atoms and groups of atoms attached to or near the observed nucleus influence nuclear shielding. It is this dependence of σ upon molecular structure that lies at the heart of NMR's utility as a probe of molecular structure and permits the observation of the spin relaxation behavior and therefore the mobility of each nucleus with a distinct resonance frequency. We can see from Eq. (20.10) that the resolution of NMR spectra can be improved by maximizing the static applied field B_0. Increasing B_0 also increases the sensitivity of the NMR experiment (see Chapter 2 of [1], for example). Consequently, the manufacture of superconducting, high-field strength magnets ($B \geq 20$ T) continues.

There is no natural fundamental scale unit in NMR spectroscopy. Both the energies of transition between spin quantum levels and the nuclear shielding produced by the screening constant σ are proportional to the applied field B_0. In addition, there is no absolute zero ''reference point'' in NMR. These difficulties are avoided by expressing the resonant frequencies of nuclei in parts-per-million (ppm, or relative changes in B_0), and referring the observed changes or displacements in resonance frequencies, called chemical shifts, to the ppm relative change in the resonant frequency of an arbitrary reference substance added to the sample. In ^{1}H and ^{13}C NMR spectroscopy, for example, it is customary to use tetramethylsilane (TMS) as the reference compound, where the chemical shifts δ of both ^{1}H and ^{13}C nuclei of TMS are taken as $\delta = 0$ ppm. TMS is selected because both its protons and ^{13}C nuclei are more shielded (resonate at higher magnetic fields) than the nuclei of nearly all other organic molecules.

20.5 SPIN–SPIN COUPLING

Nuclei with magnetic moments may be coupled to each other either directly through space (dipolar coupling) or indirectly through their intervening chemical bonds (scalar coupling). As mentioned previously, two nuclei will feel, in addition to B_0, a local magnetic field B_{loc} produced by each other. B_{loc} is given by

$$B_{loc} = \pm\mu r^{-3}(3\cos^2\theta - 1), \qquad (20.12)$$

where r is the distance between the nuclei and θ is the angle between B_0 and the line joining them (see Fig. 20.3).

Note that B_{loc} in Eq. (20.12) is distinct from the B_{loc} in Eq. (20.9), where nuclear shielding is produced by the motion of the surrounding cloud of electrons. The θ angles in Figs. 20.1 and 20.3 are distinct, because in Fig. 20.1 θ describes the angle of precession between the nuclear magnetic moment μ and the applied magnetic field B_0. The fact that B_{loc} may add to or subtract from B_0 depending upon whether the neighboring magnetic dipole is aligned with or against B_0 is reflected in the $\pm$ sign in Eq. (20.12). This form of spin–spin coupling is called dipolar coupling and can act to broaden the resonance line of a specific nucleus.

There are two important circumstances where dipolar coupling does not contribute to the broadening of resonances.

The first is when all nuclei are rigidly oriented to each other at the magical angle of $\theta = 54.7°$, because then $\cos^2\theta = 1/3$, and $3\cos^2\theta - 1$ and $B_{\text{loc}} = 0$ (see Eq. (20.12)). If the relative orientations of neighboring nuclear spins vary rapidly with respect to the time a nucleus spends in a given spin state (along or opposed to B_0), then B_{loc} is given by its space-average

$$B_{\text{loc}} = \mu r^{-3} \int_0^{\pi} (3\cos^2\theta - 1)\sin\theta \, d\theta, \qquad (20.13)$$

which also vanishes. Both of these circumstances are important for observing high-resolution NMR spectra of polymers and will be discussed further.

Nuclear spins may also be coupled by orbital motions of their valence electrons or polarization of their spins occurring indirectly through their intervening chemical bonds. Unlike direct dipolar coupling of nuclear spins, this indirect or scalar coupling is not affected by molecular tumbling and is also independent of B_0. Two spin-1/2 nuclei so coupled will each split the other's resonance into a doublet, because in a large collection of such nuclear pairs, the probabilities of finding each other's spin with $(+1/2)$ or against $(-1/2)\,B_0$ are nearly equal (see Eqs. (20.7) and (20.8)). If one nucleus of this pair is further coupled to a second group of two identical nuclei with $++$, $+-(-+)$, and $--$ spin orientations, then the resonance of the first nucleus will appear as a 1:2:1 triplet, while the resonances of the identical pair will be a doublet. A single nucleus scalar-coupled to three equivalent neighboring spins with $+++$; $++-$, $+-+$, $-++$ $(--+, -+-, +--)$; and $---$ orientations would exhibit a 1:3:3:1 quartet of resonances. A spin-1/2 nucleus with n equivalently coupled neighbors also each of spin-1/2 will have its resonance split into $n + 1$ peaks.

Typically, in the NMR spectra of polymers, only ^{1}H–^{1}H, ^{13}C–^{1}H, ^{13}C–^{19}F, ^{15}N–^1H, ^{19}F–^{19}F, ^{19}F–^1H, ^{29}Si–^1H, and ^{31}P–^{1}H scalar couplings are important. The magnitude and sign of the scalar coupling of two magnetic nuclei depend on their local substituents and geometries. The strength of the coupling in Hz is designated ^xJ, where the superscript x denotes the number of intervening chemical bonds between the coupled nuclei. A particularly useful relation is based on the observed geometry; conformation-dependent vicinal ^{1}H–^{1}H couplings ^3J, which are observed to be large ($\sim$ 12 Hz) when vicinal protons are *trans*, exhibit markedly smaller ($\sim$ 2 Hz) values in their *gauche* conformation.

20.6 EXPERIMENTAL OBSERVATION OF NMR

A drawing of a superconducting magnet used in modern high-field NMR spectrometers is presented in Fig. 20.4. The magnet is bathed in liquid helium to maintain its superconductivity, thereby alleviating the exorbitant electrical power operating requirements of electromagnets producing these same high magnetic fields. The radio frequency coil provides the rf energy appropriate to excite the nuclei in the sample to resonance. The degeneracy of the nuclear magnetic spin energy levels is removed by the static magnetic field B_0. Application of the rotating magnetic, or electromagnetic, field B_1 excites transitions between these energy

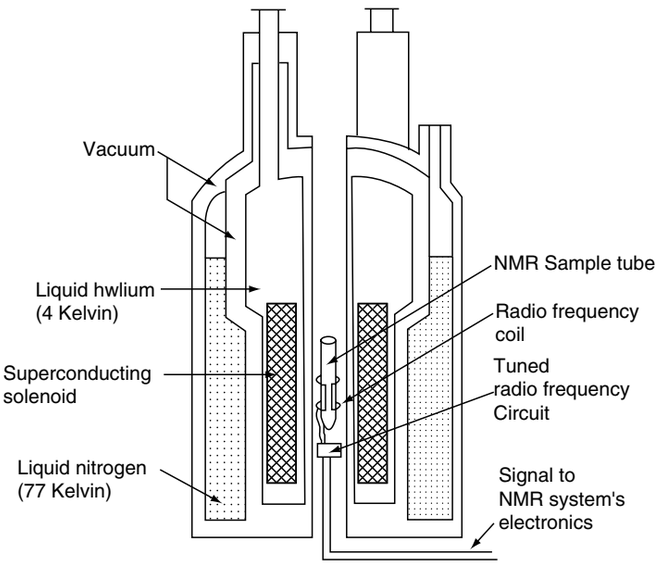

FIGURE 20.4. Cross-section of a superconducting NMR magnet (adapted from Bovey and Jelinski [2]). Magnet assembly has a diameter of 70 cm, while the sample tude is 1 cm in diameter. B_0 and B_1 lie along the horizontal and vertical directions, respectively, in this diagram.

levels. When the frequency of the B_1 field (radio frequency, or rf, in megahertz) is equal to the Larmor frequency of the observed nucleus, the resonance condition occurs, i.e., when

$$B_1 = \nu_0 = \gamma(B_{\text{loc}}/\pi). \tag{20.14}$$

Most samples will have nuclei with multiple Larmor frequencies, because most molecules have more than a single magnetically equivalent group (CH, CH_2, CH_3, for example), leading to several resonance frequencies or chemical shifts.

The method used to excite the nuclei and achieve resonance must clearly be capable of covering all of the Larmor frequencies in the sample. This is achieved in the Fourier transform (FT) method by simultaneously exciting all the Larmor frequencies by application of a pulse (short burst) of rf signal (B_1) at or near all ν_0s, which results in the equalization of the populations of the nuclear spin energy levels. Equilibrium spin populations are reestablished in a free-induction-decay (FID) process following the rf pulse. The vector diagram in Fig. 20.5 can be used to visualize the effect of the rf pulse (B_1) on the nuclear spins and their subsequent FID to equilibrium.

In general terms, T_2 influences the line widths and T_1 influences the relative intensities of signals observed in a NMR spectrum. T_2 is the decay time constant of the FID, and the inverse relationship between time and frequency leads to

$$\Delta\nu \text{ (Hz)} = 1/(\pi T_2), \tag{20.15}$$

where $\Delta\nu$ is the line-width-at-half-height.

Figure 20.6 gives a pulse sequence representation of the vector diagram in Fig. 20.5. The detected signal, or FID, is obtained as a voltage in the time domain. The rf pulse is repeated many times to improve signal-to-noise ratio, and the delay time between pulses must be long enough for T_1 processes to be complete. Fourier transformation of the time-domain signal results in the usual frequency-domain spectrum. The FT method of acquiring NMR signals saves time by collecting data (all ν_0s) simultaneously, and is well suited to signal averaging by collecting multiple FIDs from weak signals before Fourier transformation.

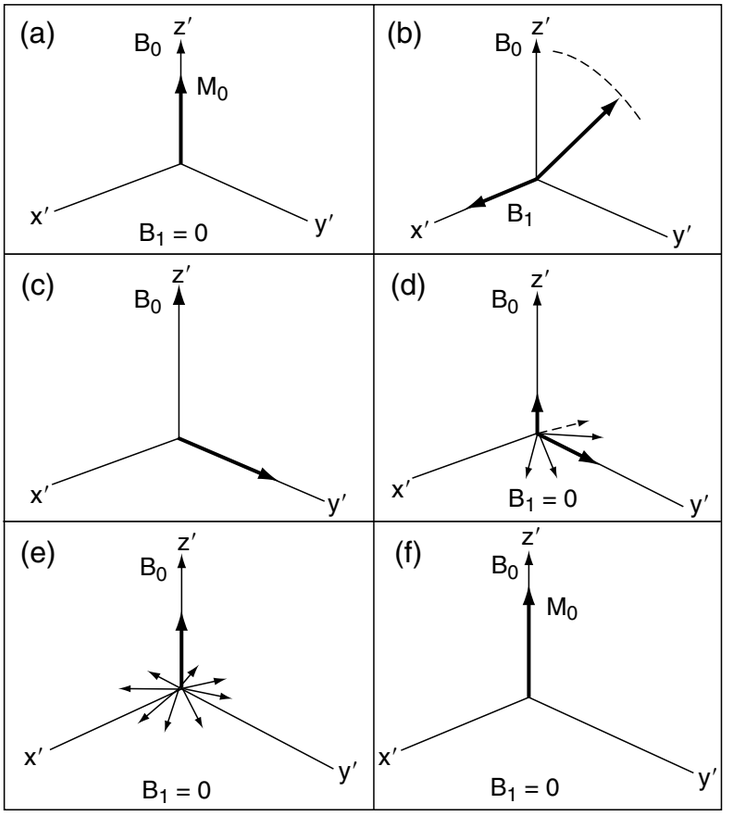

FIGURE 20.5. Rotating frame diagrams describing the pulsed NMR experiment. (The "primed" axes are used to indicate a coordinate system that is rotating at the Larmor frequency.) (a) The net equilibrium nuclear magnetization M_0 is aligned along the direction of the static magnetic field B_0. (b) and (c) An rf field B_1 is applied perpendicular to B_0. The duration of B_1 is sufficient to tip the net magnetization by 90°. (d) and (e) The spins begin to relax in the x', y' plane by spin–spin (T_2) processes and in the observable z′ direction by spin–lattice (T_1) processes. (f) The equilibrium magnetization M_0 is reestablished along B_0.

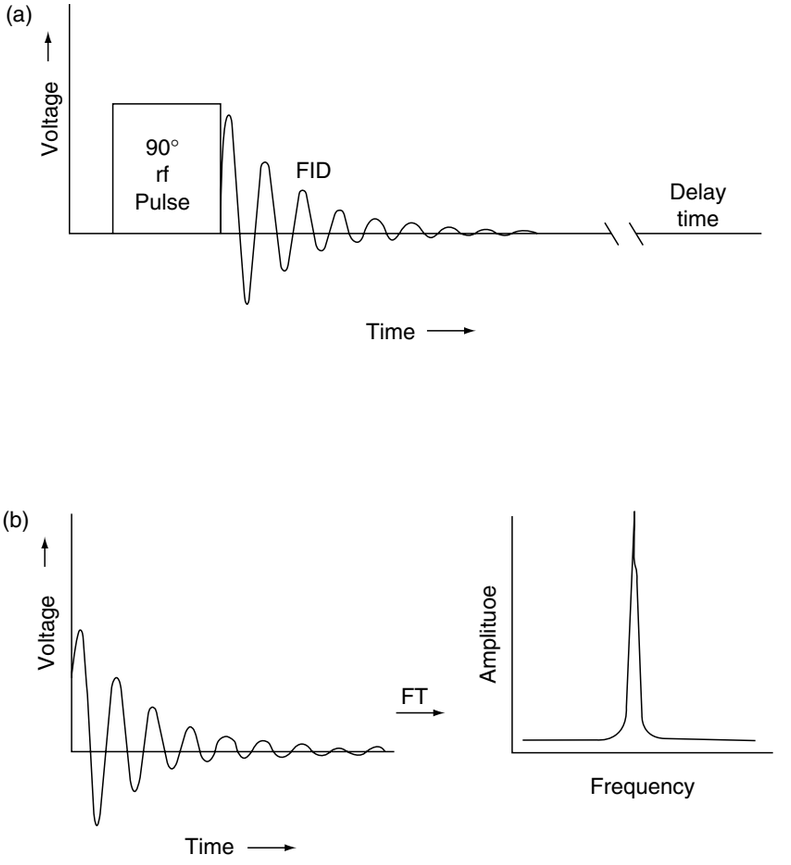

FIGURE 20.6. (a) Representation of a 90° rf pulse (B_1) and the ensuing Free-induction-decay (FID). (b) Fourier transformation of the time-domain FID into the frequency-domain signal.

20.7 HIGH RESOLUTION NMR OF POLYMERS

Unlike small molecules, the volumes pervaded and influenced by dissolved and randomly coiled macromolecules are much larger (ca. 100 times) than the sum of their hard-sphere molecular volumes. This leads to entrapment of surrounding solvent molecules and polymer–polymer entanglements, resulting in solutions with very high viscosities. However, both the frequency at which a magnetic nucleus resonates and the width or resolution of the resulting resonance peak depend on the local polymer microstructure and its motional dynamics in the immediate vicinity of the observed nucleus. The local segmental motions of dissolved polymers are usually rapid (nano- to picosecond range), so NMR serves as a local microscopic probe of polymer microstructures and their motions. As a consequence, NMR can even provide highly resolved spectra for dissolved polymers whose overall motion may be sluggish (high solution viscosities), but whose local segmental motions are rapid.

20.8 ^{1}H NMR

The 500 MHz proton NMR spectra recorded with a superconducting magnet (11.7 T) for two samples of poly (methyl methacrylate) (PMMA) as 10% solutions in chlorobenzene-d_5 at 100 °C are presented in Fig. 20.7 [3]. A free radical initiator was used in the polymerization of the syndiotactic sample (s-PMMA) in (a), while the isotactic sample (i-PMMA) in (b) was obtained with an anionic initiator [4]. It is apparent from the methylene proton portions of both spectra that free radical and anionic initiated polymerization of methyl methacrylate results in PMMA samples with very different microstructures.

The methylene protons in the *racemic* (*r*) diad drawn in Fig. 20.7(a) are magnetically equivalent because of the twofold axis of symmetry present in an *r*-diad. They resonate at the same frequency, leading to a singlet, despite the strong two-bond geminal ^2J coupling between them. In the *meso* (*m*) diad of Fig. 7(b), which lacks a symmetry axis, the methylene protons are magnetically nonequivalent and

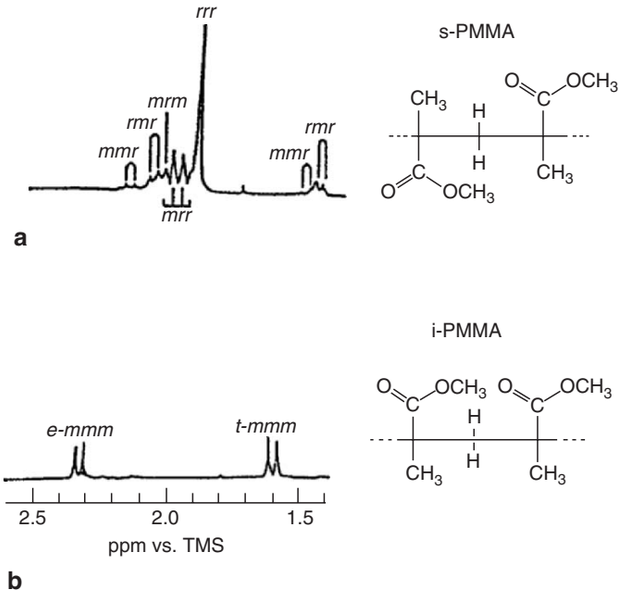

FIGURE 20.7. 500 MHz ^{1}H NMR spectra of (a) s-PMMA and (b) i-PMMA. Only the methylene proton regions are shown. (Adapted from Schilling *et al.* [3].) *e*, *t* methylene protons lie on the same side of the planar, zigzag backbone as the $-\overset{\overset{O}{\|}}{C}-O-CH_3$, $-CH_3$ side chains.

therefore appear as a pair of doublets, each with a spacing of ~15 Hz produced by their ^2J geminal coupling.

The PMMA sample produced by anionic initiation does show (b) almost exclusively a pair of doublets, indicating that nearly all of its diads are *m*, so this sample of PMMA is very highly isotactic. The principal methylene proton resonance observed for the free radical PMMA is a singlet at 1.9 ppm (a), meaning that most of its diads are *r* and that this sample is predominantly syndiotactic, though more stereochemically irregular than the anionically initiated sample. It is clear from this example that ^{1}H NMR can provide information about the absolute stereoregularity of a vinyl polymer (isotactic versus syndiotactic), which is often impossible to obtain by other methods (including x-ray diffraction from crystalline polymer samples).

The 220-MHz ^{1}H NMR spectra of three polypropylene (PP) samples are presented in Fig. 20.8 [5–7]. Note the apparent greater resolution of the spectra in (a) and (c) recorded for the stereoregular samples (isotactic and syndiotactic) than for atactic PP in (b). The impression of degraded resolution in the spectrum for atactic PP is a consequence of the overlapping of many slightly different resonance frequencies or chemical shifts corresponding to the various triad and tetrad stereosequences present in the atactic sample. Only the *rr* (*rrr*) and *mm* (*mmm*) triads (tetrads) are present in the stereoregular syndiotactic and isotactic samples, respectively.

In addition to the geminal coupling (^2J) of methylene protons in meso diads, the methine and methyl and the methylene and methine protons show significant vicinal, three-bond scalar couplings (^3J) in nearly all stereosequences. By application of ^{1}H–^{1}H homonuclear decoupling or double resonance, some of these couplings can be removed. The scalar, or *J*, coupling between magnetically nonequivalent nuclei A, B can be removed by irradiating B with a strong transverse rf field B_2 tuned to its resonance frequency, while observing A with the weaker B_1 field. B_2 causes a rapid oscillation of nucleus B between its spin states such that it no longer couples to nucleus A. Unfortunately, in PP the methine protons are coupled to both methylene and methyl protons, requiring a triple resonance experiment to simultaneously remove all vicinal couplings. Because the methylene protons in *m*-diads resonate at widely separated frequencies, which in turn are also distinct from the resonance frequency of methylene protons in *r*-diads (see Fig. 20.8), complete removal of the vicinal couplings observed in the ^{1}H NMR spectra of PPs is very unlikely.

20.9 ^{13}C NMR

The ^{13}C nucleus occurs at a natural abundance of only 1.1% and has a small magnetic moment, about one-fourth that of the proton. Both factors tend to mitigate the observation of high resolution ^{13}C NMR spectra (see Table 20.1). However, employing a greater number of spectral accumulations during the FT recording of spectra can compensate for the decrease in the sensitivity of the ^{13}C nucleus. Suitable signal-to-noise ratios can also be achieved in ^{13}C NMR

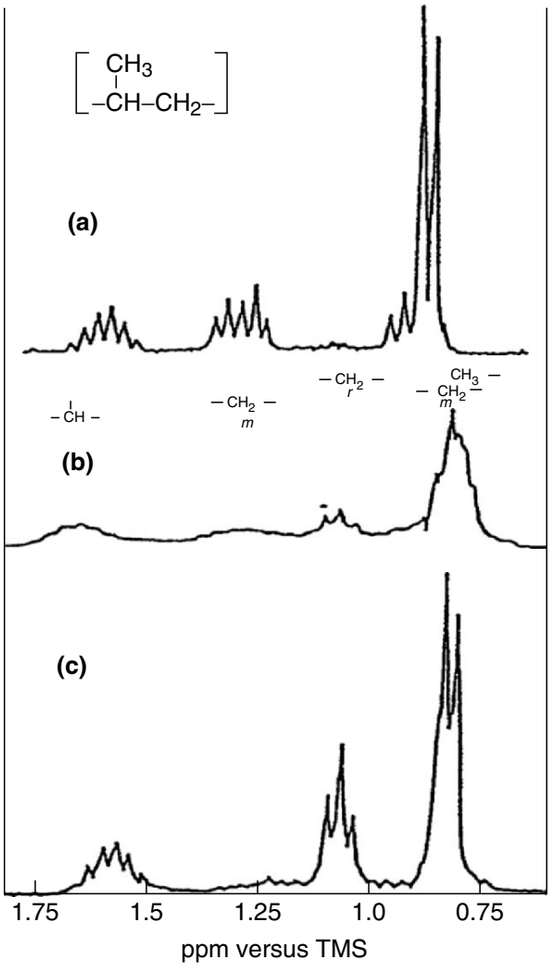

FIGURE 20.8. 200 MHz ^{1}H NMR spectra of (a) isotactic, (b) atactic, and (c) syndiotactic polypropylenes [5–7].

spectra, but at the expense of considerably longer observation times due to this necessary signal averaging.

Further increase in signal intensity is obtained by removing the heteronuclear spin coupling between ^{13}C nuclei and their directly bonded protons, as well as the resulting nuclear Overhauser enhancement (NOE) [8]. Removal of the strong (125–250 Hz) ^{13}C–^{1}H heteronuclear coupling, through application of a second transverse rf field at the proton resonance frequencies, results in the collapse of ^{13}C multiplets and an improved signal-to-noise ratio. Saturation of nearby protons produces a nonequilibrium polarization of the ^{13}C nuclei, which exceeds their thermal value, and increases the observed signal strength. It has been demonstrated [9] that the dipolar coupling mechanism dominates for the ^{13}C isotope, and a maximum NOE factor of 3 for the ^{13}C intensity is provided by a directly bonded proton.

An additional means of increasing the sensitivity of ^{13}C NMR spectroscopy can be realized by transferring the polarization of a sensitive nucleus, such as ^{1}H (large γ) to the insensitive ^{13}C (small γ) nucleus. This is achieved by the technique of selective population transfer (SPT) [10] and can enhance the ^{13}C signal intensity by a factor of $\gamma H/\gamma C = 4$. In practice, this is achieved in modern NMR via two-dimensional heteronuclear correlation and polarization transfer experiments (*vide infra*).

Though requiring the application of several additional observational techniques to overcome the inherent insensitivity of the ^{13}C nucleus, ^{13}C NMR spectroscopy can be, and is, used to greater advantage for probing the molecular structures of organic molecules, including polymers. The reason is the much greater sensitivity of ^{13}C nuclear shielding to molecular structure, in the 200 ppm range for neutral organics compared with 10–12 ppm for ^{1}H shielding. The increased sensitivity of ^{13}C resonance frequencies/chemical shifts to local microstructural environments has generally made ^{13}C NMR spectroscopy the method of choice for investigating molecular structure.

The ^{13}C NMR spectra presented in Fig. 20.9 [11] for the same PP samples whose ^{1}H NMR spectra appear in Fig. 20.8 make the superior microstructural sensitivity of ^{13}C NMR plainly evident. While ^{13}C resonances are spread over an $\sim$30 ppm range, all ^{1}H resonances observed for PPs are within $<$ 1 ppm of each other. In addition, the absence of homonuclear (^{13}C–^{13}C) and the easy removal of heteronuclear (^{13}C–^{1}H) scalar couplings further simplify the ^{13}C spectra. Both of these advantages result in the kind of microstructural sensitivity seen in the methyl carbon region of the PP spectra; note that in atactic PP sample all ten possible pentad stereosequences (*mmmm*, *rrrr*, *mmrm*, etc.) are distinctly observed. (Also see in Fig. 20.10 an expansion of the methyl region of the atactic PP spectrum observed at a higher magnetic field, which we will subsequently discuss.)

^{13}C NMR solution spectra of polymers are often recorded at high temperatures for reasons of solubility (especially for crystalline polymers) and segmental mobility (reduction of dipolar line-broadening). At high temperatures a solvent of low volatility (e.g., tetrachloroethene or trichlorobenzene) and with carbon atoms that resonate in spectral regions distinct from the polymer are most advantageous. Since TMS evaporates at high temperatures, an alternative NMR chemical shift reference material, hexamethyldisiloxane (HMDS), is often used.

To insure acquisition of quantitative ^{13}C NMR spectra, the rf B_1 field pulses must be sufficiently separated by delay times that insure spin relaxation is realized for all carbon nuclei in the sample (see Fig. 20.5). If the repetition rate of the rf pulses approaches the T_1s of some of the ^{13}C nuclei in the sample, then incorrect relative intensities will be recorded. As a practical rule [12], the delay between rf pulses should be five times the T_1 of the slowest relaxing carbon nucleus in the sample.

20.10 ^{13}C NMR SPECTRAL ASSIGNMENTS

Of the nuclei, ^{1}H and ^{13}C, which both possess nuclear spin and are common to synthetic polymers, ^{13}C is by far the more sensitive spin probe for polymer NMR studies. ^{13}C NMR spectra suffer neither from a narrow dispersion of chemical shifts (see Figs. 20.8 and 20.9) nor from extensive homonuclear spin–spin (scalar) coupling, both of which complicate the analyses of ^{1}H NMR spectra. (See below how two-dimensional observations increase the sensitivity of ^{1}H NMR to molecular microstructures.) It is the sensitivity of ^{13}C resonance frequencies or chemical shifts, $\delta^{13}C$, to the microstructures of polymers which makes ^{13}C NMR so useful as a structural probe. We noted in Fig. 20.9 that the methyl carbon resonances observed in the 25 MHz ^{13}C

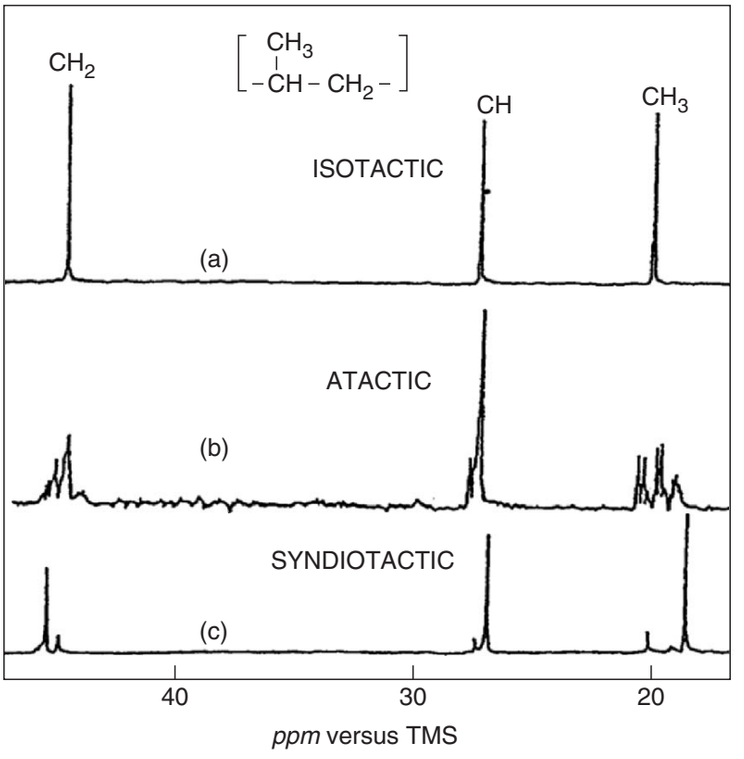

FIGURE 20.9. 25 MHz ^{13}C NMR spectra of the same (a) isotactic, (b) atactic, and (c) syndiotactic PPs [11], whose ^{1}H NMR spectra are also presented in Fig. 20.8.

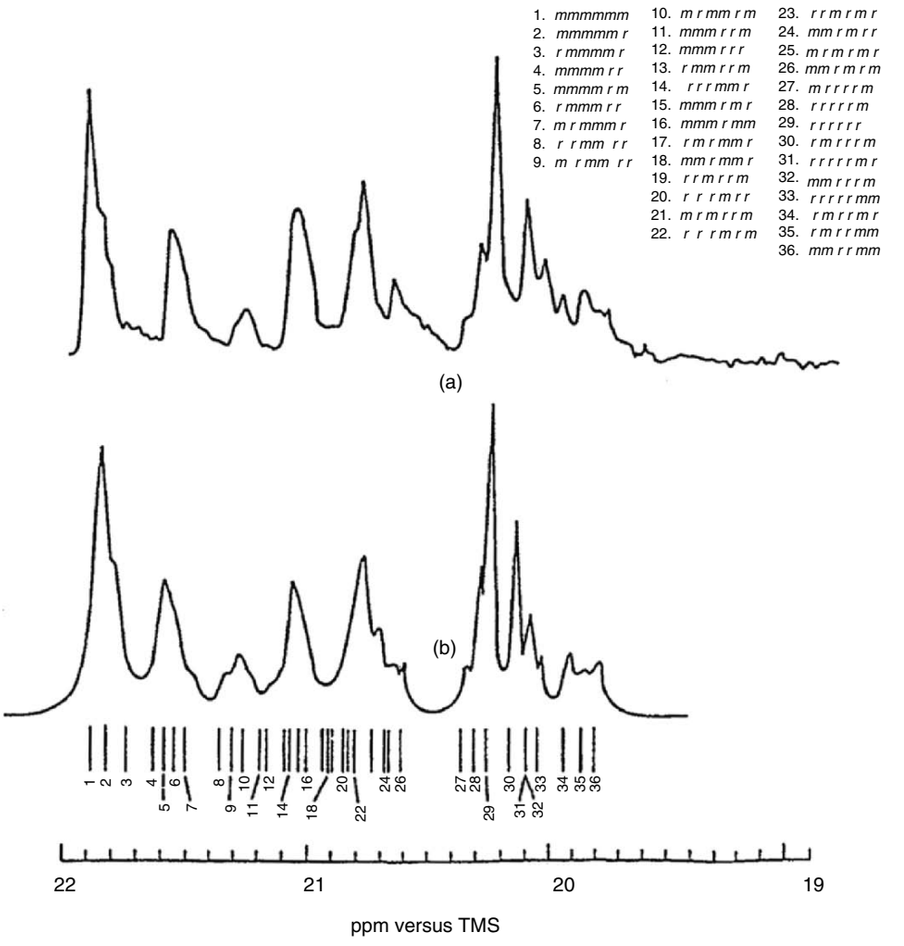

FIGURE 20.10. (a) Methyl carbon region of the ^{13}C NMR spectrum of the same atactic PP shown in Figs. 20.8 and 20.9 recorded at 90 MHz in *n*-heptane at 67°C. (b) Simulated methyl carbon spectrum obtained from chemical shifts calculated using the γ-*gauche* effect method, as represented by the line spectrum below, and assuming Lorentzian peaks of < 0.1 ppm width at half-height [11].

NMR spectrum of atactic PP were sensitive to pentad stereosequences. At 90.5 MHz (see Fig. 20.10), the methyl carbon resonances show sensitivity to heptad stereosequences (*mmmmmm*, *rrrrrr*, *mrmmrr*, etc.) [13]. The ^{13}C NMR spectra of PPs are sensitive to stereosequences extending over 4 (pentads) and 6 (heptads) bonds in both directions along the PP backbone. This long-range sensitivity to microstructural detail makes ^{13}C NMR a valuable tool in the determination of polymer structures.

To realize the full potential of ^{13}C NMR in microstructural studies of polymers, the connections between constituent microstructural features and their corresponding effects on chemical shifts must be established. Traditionally synthesis and NMR spectroscopic analysis of model compounds and polymers with known microstructures have provided the means for assigning the NMR spectra of polymers to their underlying microstructural features. These laborious approaches to the assignment of the NMR spectra of polymers could be eliminated if it were possible to predict the ^{13}C NMR chemical shifts expected for each type of carbon nucleus residing in all potential structural environments.

We have seen that the magnetic field B_i required to obtain the resonance condition for nucleus i at a particular irradiating rf field (B_1) is not equal to the applied static field B_0, but is instead $B_i = B_0(1 - \sigma)$ [see Eq. (20.9)], where the nuclear screening constant, σ, depends on the chemical structural environment of nucleus i. The local electron density in the vicinity of the nucleus shields it from the applied field B_0 by producing small local magnetic fields (diamagnetic currents). Any structural feature that alters the electronic environment of a nucleus will affect its screening constant σ and lead to an alteration in its resonance frequency or chemical shift δ_i.

To date it has not been possible to make sufficiently accurate predictions of ^{13}C NMR chemical shifts

even when applying the most sophisticated ab initio quantum mechanical methods [14,15, and especially 16]. Instead, the effects of substituents and local conformation have been used to correlate the ^{13}C chemical shifts and the microstructures of molecules, including polymers [17,18].

^{13}C NMR studies of paraffinic hydrocarbons [19–23] have led to the following substituent effect rules. Carbon substituents attached at α, β, and γ positions to an observed carbon produce a deshielding of ca. 9 ppm, a deshielding of ca. 9 ppm, and a shielding of ca. -2 ppm, respectively, compared with an observed carbon that is unsubstituted. In PP, for example, the CH_3 carbons possess 1α, 2β, and 2γ carbon substituents; the CH carbons possess 3α, 2β, and 4γ carbon substituents; and CH_2 carbons 2α, 4β, and 2γ carbon substituents. Based on $\alpha = \beta = 9$ ppm and $\gamma = -2$ ppm, we would expect the CH_2 carbons to resonate down-field from the CH carbons by $-1\alpha + 2\beta - 2\gamma = -9 + 18 + 4 = 13$ ppm, while the CH carbons should resonate $2\alpha + 2\gamma = 18 - 4 = 14$ ppm downfield from the CH_3 carbons. This pattern of ^{13}C resonances expected on the basis of these substituent effects is indeed observed (see Fig. 20.9).

The extensive, though smaller, splitting of resonances belonging to the same carbon type (CH, CH_2, or CH_3) observed in the ^{13}C NMR spectra of atactic PP (see Figs. 20.9 and 20.10), must be produced by the presence of different stereosequences, because the numbers of α, β, and γ substituents possessed by each carbon type are independent of stereosequence. On the other hand, it is well known that the local conformations in vinyl polymers like atactic PP are sensitive to stereosequence [24]. The local magnetic field B_i experienced by a carbon nucleus i must be dependent upon the local conformation in its vicinity, Thus,

$$\text{Microstructure} \rightarrow \text{Conformation} \rightarrow B_i \rightarrow \delta^{13}C_i$$

To make the connection between polymer microstructures and $\delta^{13}C_i$s, we need to know the dependence of the local magnetic field B_i on the local conformation. The γ-substituent effect, which shields an observed carbon nucleus, is the source of the dependence of the local magnetic field B_i on the local conformation. Because the observed carbon C^o and its γ-substituent C^γ are separated by three intervening bonds ($-C^o-C-\overset{\phi}{\frown}-C-C^\gamma-$), their mutual distance and orientation are variable, depending on the conformation (ϕ) of the central bond. Note that the distance between C^o and C^γ is reduced from 4 to 3 Å on changing their arrangement from *trans* ($\phi = 0°$) to *gauche* $^{\pm}$ ($\phi = \pm 120°$).

Grant and Cheney [25] first suggested the conformational origin of the γ-substituent effects on $\delta^{13}Cs$. In their model it is the polarization of the C^o–H and C^γ–H bonds, resulting from their compression caused by proton–proton (o–γ) repulsion, that leads to a shielding of both carbons. More recently Li and Chestnut [26] presented evidence that correlate shielding γ-effects with attractive van der Waals forces and not repulsive steric interactions, though their results still suggest that their gauche arrangement is required for shielding. Using both semiempirical and ab initio quantum mechanical calculations Seidman and Maciel [27] concluded that the γ-substituent effect is conformational in origin, but cannot be attributed solely to the proximity of the interacting C^o and C^γ carbons. Thus it seems apparent that the γ-substituent effect on δ^{13} Cs has a conformational origin and is, as we will shortly demonstrate, useful in characterizing both the local microstructures and conformations of polymers.

For a γ-substituent to shield a carbon nucleus, we have suggested that they must be in a *gauche* arrangement. The methyl carbons in butane and higher *n*-alkanes have a single γ-substituent, while the methyl carbons in propane have none, but the same number and kinds of α- and β-substituents. The methyl carbons in liquid butane and higher *n*-alkanes resonate at $\sim$13 ppm, while in liquid propane the methyls resonate at $\sim$15 ppm [8]. In their solids the *n*-alkanes crystallize in the fully extended all *trans* conformation, and so here the methyl carbons of butane and the higher *n*-alkanes are not *gauche* to their γ-methyl or methylene carbon substituents. Thus we would expect that $\delta CH_3(\text{solid}C_nH_{2n+2}, n \geq 4) = \delta CH_3(\text{liquid propane})$. Vander-Hart [28] has observed the methyl carbons in the solid *n*-alkanes with $n = 19$, 20, 23, and 32 to resonate at $\sim$15 ppm just like the methyls in liquid propane which have no γ-substituents.

If we know how much *gauche* character (P_g = fractional population of $\Phi = \pm 120°$ conformations (See J. D. Honeycutt in this volume who describes the methodology used to calculate the bond conformational populations), then we can estimate the γ-*gauche* shielding (γ_{C-C}) produced at the methyl carbons in butane, for example. When the observed shielding $\Delta\delta CH_3 = \delta CH_3(\text{butane}) - \delta CH_3(\text{propane}) = 13.2 - 15.6 = -2.4$ ppm is divided by the *gauche* character of the intervening bond ($P_g = 0.46$), $\gamma_{C-C} = \Delta\delta CH_3/P_g = -2.4/0.46 = -5.2$ ppm. When this procedure is applied to *n*-butane, 1-propanol, and 1-chloropropane, the following γ-*gauche* shielding effects are derived: $\gamma_{C-C} = -5.2$ ppm, $\gamma_{C-O} = -7.2$ ppm, and $\gamma_{C-Cl} = -6.8$ ppm [18]. Thus, the shielding produced at a carbon nucleus by a γ-substituent in a *gauche* arrangement can be comparable in magnitude (-5 to -7 ppm) to the $+9$ ppm deshielding produced by the more proximal α- and β-substituents. More important, however, is the conformational dependence of the γ-substituent effect on ^{13}C NMR chemical shifts. Any microstructural variation in a molecule which effects its local conformation can be expected to be reflected in its $\delta^{13}Cs$ *via* the γ-*gauche*-effect.

The conformationally sensitive γ-*gauche*-effect permits us to draw the connection between a polymer's microstructure and its ^{13}C NMR spectrum:

$$\text{Microstructure} \rightarrow \text{Conformation} \rightarrow B_i \rightarrow \delta^{13}C_i.$$

By means of the methods described in sections A and B of this handbook, it is possible to establish the connection between the microstructures and the conformations of polymers. The γ-*gauche*-effect establishes the connection between the local polymer conformation and the local magnetic field experienced by a ^{13}C nucleus, so finally

$$\text{Microstructure} \xrightarrow[\text{Effect}]{\gamma\text{-gauche}} \delta^{13}\text{Cs} \qquad [18].$$

To predict the ^{13}C chemical shifts observed for the methyl carbons in a-PP (see Fig. 20.10), which show sensitivity to heptad stereosequences, we simply have to calculate the *trans* and *gauche* probabilities for the backbone bonds in each of the 36 heptad stereosequences. When this is carried out with the Suter–Flory rotational isomeric state (RIS) conformational model for PP [29] and the resultant probabilities of finding CH_3 in a *gauche* arrangement with its γ-substituents (CHs) are multiplied by $\gamma_{CH_3-CH} = -5.2$ ppm, we obtain the δCH_3s shown as the stick spectrum in Fig. 20.10.

Because the γ-*gauche*-effect method of calculating δ^{13}Cs only leads to relative stereosequence-dependent chemical shifts, we are free to translate the calculated shifts as a group to achieve the best agreement with the observed δ^{13}Cs. This has been done in Fig. 20.10, where the agreement between observed and calculated $\delta^{13}CH_3$s has been used to make the stereosequence assignments indicated there. The γ-*gauche*-effect method of assigning resonances in the methyl carbon region of the ^{13}C NMR spectrum of a-PP to heptad stereosequences has been achieved without recourse to the syntheses and study of PP model compounds or stereoregular PPs and without assuming a particular statistical model to describe the expected frequencies of stereosequences produced during polymerization.

Having assigned all heptad stereosequence dependent ^{13}C NMR resonances in a-PP [11,13], integration of the resonances provides us with a detailed accounting of how much of each stereosequence is present. Such information is needed to test various statistical models of PP polymerization [18]. Furthermore, the close agreement between observed and calculated chemical shifts provides strong confirmation of the Suter–Flory rotational isomeric state (RIS) conformational model for PP [29].

20.11 TWO-DIMENSIONAL NMR

If, instead of transforming (FT) the free-induction decay (FID) immediately after the 90° rf pulse in the usual way (see Fig. 20.6), we allow a time interval for the nuclear spins to precess in the transverse x', y'-plane (see Fig. 20.5) and for the evolution of interactions between them, then it is possible to obtain important information concerning the nuclear spin system. We may divide such an NMR experiment into three time domains as indicated in Fig. 20.11. The nuclear spins are permitted to equilibrate with their surroundings *via* spin–lattice relaxation during the preparation period. Following the $90^\circ_{x'}$ pulse, the x',y', and z' components of the nuclear spins (see Fig. 20.5) evolve under all the forces acting upon them, including their direct through-space, dipole–dipole and through-bonds, scalar (J) couplings. This time domain, t_1, is termed the evolution period and defines, along with the acquisition or detection time t_2 common to all pulse experiments, the two-dimensional (2D) character of this experimental approach.

Systematic incrementation of the evolution time t_1 (see Fig. 20.11) provides the second time dependence. After each t_1 period a second $90^\circ_{x'}$ pulse is applied, and the exchange of nuclear spin magnetization may occur. The FID is acquired during t_2 and transformed.

The pulse sequence illustrated in Fig. 20.11 is appropriate for observation of a chemical shift correlated or COSY spectrum, where the correlating influence between nuclear spins is their scalar J-coupling. In a typical experiment we might utilize 1 k, or 1,024, t_1-increments, with $t_1 = 0.5$–500 ms. The FID following each t_1 is different because the interacting spins modulate each other's response.

Each FID detected in t_2 is transformed, producing a series of 1,024 matrix rows, one for each t_1-value. Each row may consist of 1,024 points (square data matrix) representing the frequency-domain spectrum for a particular value of t_1, while the columns provide information about how the FIDs were modulated as a function of t_1.

1024 new FIDs are constructed by looking down the columns of the data matrix in an operation called the ''transpose'' in Fig. 20.11. (Note that at this stage the spectrum is represented for simplicity as a single resonance.) A second Fourier transformation is performed on the newly transposed FIDs, leading to a 2D data matrix which is actually a surface in three-dimensional space. The surface may be represented as either a stacked plot or a contour plot. The contour plot is usually preferred, because recording of the stacked plot is time intensive and it does not clearly demonstrate the complex relationships between the interacting nuclear spins.

Nuclei which do not exchange magnetization have the same frequencies, F_1 and F_2, respectively, during t_1 and t_2 (i.e. $F_1 = F_2$) and yield the normal 1D spectrum along the diagonal of the contour plot. Scalar-coupled nuclei exchange their magnetization and have a final frequency different from the initial frequency, i.e. $F_1 \neq F_2$. These coupled nuclei give rise to the off-diagonal or cross peaks shown in Fig. 20.11. The 2D COSY spectrum provides a diagram of all the J-coupled connectivities in a molecule, and is consequently a very useful technique for assigning the resonances of complex molecules.

A closely related 2D NMR technique, termed NOESY, permits the establishment of through-space connectivities. This technique relies on the through-space dipolar coupling of nuclear spins and uses a 2D version of the nuclear

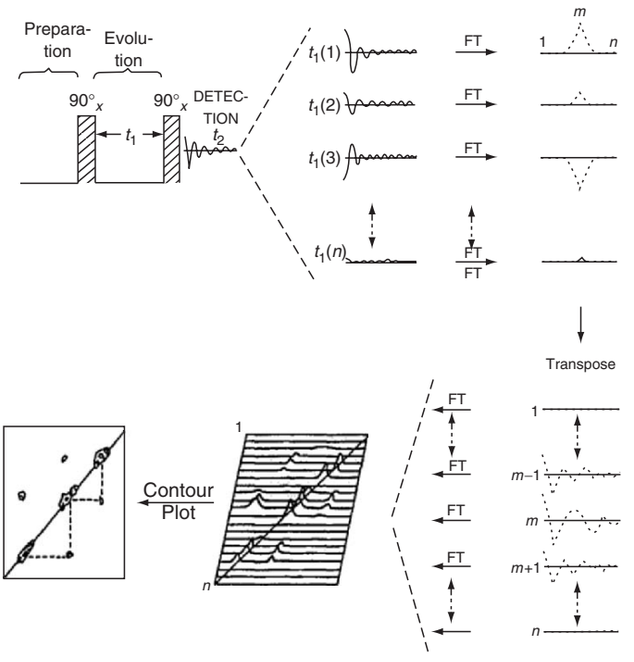

FIGURE 20.11. Schematic repesentation of a two-dimensional (2D) correlated (COSY) NMR experiment and spectrum after Jelinski [30].

Overhauser effect (NOE, see Section 20.9) to map, in effect all intra- and internuclear distances (usually protons) less than ~4 Å.

The advent of these and related multidimensional NMR techniques [31] has resulted in a rebirth of ^{1}H NMR as a means to study molecular structure. Extensive homonuclear J-coupling of protons, which unduly complicate 1D ^{1}H NMR spectra, are used to advantage in 2D ^{1}H NMR to map the atomic connectivities of molecules. Furthermore, the significantly improved resolution observed in 2D ^{1}H NMR spectra somewhat ameliorates the narrow dispersion of ^{1}H chemical shifts.

20.12 NMR OF SOLID POLYMERS

There exist two interactions between nuclear spins and their neighbors or with the applied magnetic field that result in severe broadening of their solid-state NMR spectra when recorded under conditions that produce high-resolution NMR spectra for their solutions. Both of these nuclear interactions, the direct through-space dipolar coupling and the anisotropic electronic shielding of nuclei from the applied magnetic field, are also present in the liquid. They do not lead to resonance line-broadening there because they are averaged to zero (see Eqs. (20.12) and (20.13)) by the rapid and essentially isotropic motions occurring in the liquid. In rigid solid samples like glassy or crystalline polymers, the motional averaging of these nuclear interactions are incomplete and produce spectra like the one shown in Fig. 20.12(a).

^{13}C nuclei observed at natural abundance are dipolar coupled to the usually abundant and nearby ^{1}H nuclei. (see Fig. 20.13) resulting in the splitting (D) of ^{13}C resonances given (in Hz) by

$$D = [h\gamma_C\gamma_H/2\pi r^3](3\cos^2\theta - 1). \qquad (20.16)$$

This splitting is illustrated in Fig. 20.13(b) and corresponds to the dipolar coupling of a ^{13}C nucleus with the two spin states (up and down) of a ^{1}H nucleus located at a distance r and orientation θ (to B_0). The magnitude of this splitting is ca. 10 kHz [34]. In a rigid glassy or crystalline solid polymer powder, the ^{13}C nuclei and their nearby protons are randomly arranged and their C–H vectors assume all possible angles with respect to the external applied magnetic field. This results in a Pake pattern [35] of ^{13}C resonances, as depicted in Fig. 20.13(c), assuming all C–H vectors are of the same magnitude, distance r. Because the ^{13}C nuclei in rigid, solid polymers are dipolar-coupled to protons located at more than a single internuclear distance r, when their dipolar interaction (Eq. (20.16) is averaged over both the distances (r) and orientations (θ) of all the C–H vectors present in the sample, the broad Gaussian lineshape presented in Fig. 20.13(d) is produced.

As a result of their dipolar interactions with nearby abundant protons, the ^{13}C resonance linewidths observed in rigid organic polymers are typically tens of kHz. Since the range of ^{13}C NMR resonance frequencies, or chemical shifts, observed in a given polymer is usually less than 200 ppm, which at an applied field strength of 4.7 T (50 MHz for ^{13}C)

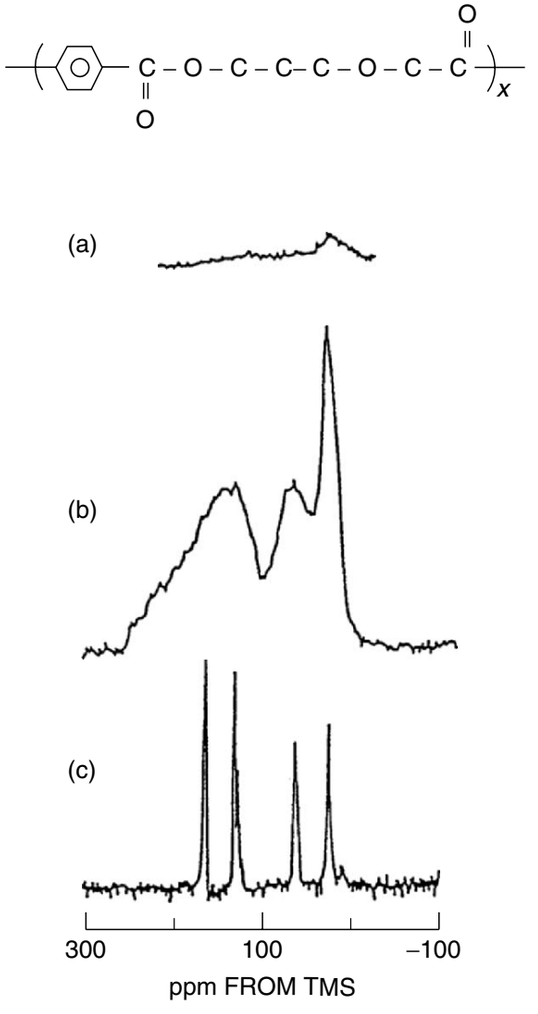

FIGURE 20.12. ^{13}C NMR spectra of bulk poly(butylene terephthalate) (PBT) obtained with low-power dipolar decoupling (a), high-power dipolar decoupling (b), and high-power dipolar decoupling with rapid sample spinning at the magic angle (c) [32].

corresponds to a frequency range of 10 kHz, ^{13}C NMR spectra of solids whose lines are broadened by ^{1}H dipolar coupling (ca. 20 kHz) cannot resolve their chemically shifted, resonance frequencies. Without removing this ^{13}C–^{1}H coupling, ^{13}C NMR spectra of solid polymers, like poly-(butylene terephthalate) (PBT) in Fig. 20.12, cannot provide useable structural information.

If the proton spins could be driven to flip at a rate that is rapid compared to the static ^{13}C–^{1}H dipolar interaction, which occurs naturally in mobile polymer solutions, then the resonance lines observed in solid-state ^{13}C NMR spectra would likewise no longer be broadened by these heteronuclear, spin–dipolar interactions. The ^{13}C NMR spectrum of PBT shown in Fig. 20.12(b) was recorded by applying an rf field B_1 at the resonance frequency of protons, with a field strength of 50 kHz, in a direction perpendicular to the applied field B_0 (analogous to the broadband ^{1}H scalar-J decoupling of ^{13}C NMR solution spectra). Note the substantial increase in spectral resolution [compare (a) and (b) in Fig. 20.12] produced by high-power ^{1}H dipolar decoupling (DD), though falling far short of the resolution observed in spectra recorded in solution. The remaining line broadening in solid-state spectra is due primarily to chemical shift anisotropy (CSA).

CSA reflects the anisotropy inherent in the distribution of electronic currents about nuclei which screen (σ) them from the applied magnetic field B_0. The local magnetic field experienced by a nucleus is anisotropic and therefore three dimensional, so the nuclear screening constant σ is in fact a tensor and may be described [1,32] by

$$\sigma = \sigma_{11}\lambda_{11}^2 + \sigma_{22}\lambda_{22}^2 + \sigma_{33}\lambda_{33}^2. \tag{20.17}$$

The principal values of the chemical shift tensor (σ_{11}, σ_{22}, σ_{33}) give the magnitudes of nuclear shielding in

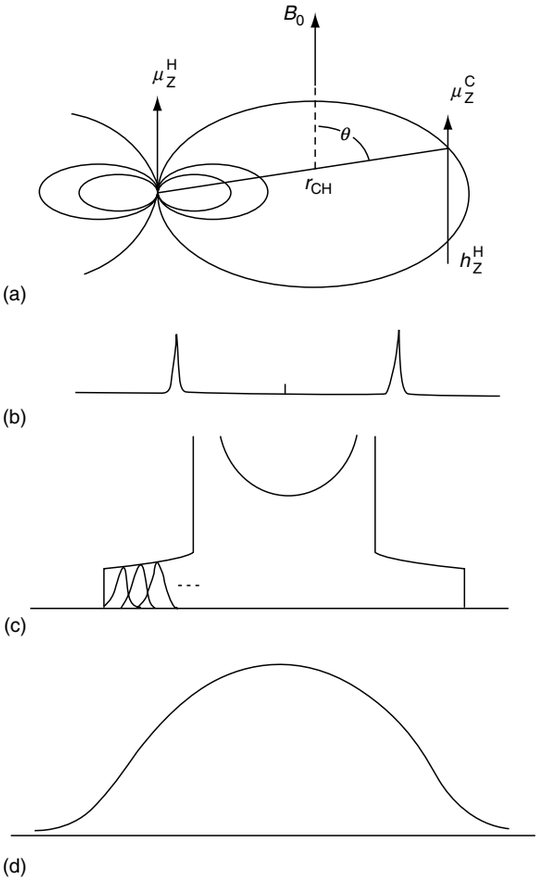

FIGURE 20.13. (a) The through-space dipolar interaction between a ^{13}C and a ^{1}H nuclear spin. The μ_z are the z components of the magnetic moments and h is the z component of the proton dipolar field at the ^{13}C nucleus. (b) Dipolar splitting of isolated C–H pairs at one angle θ relative to the applied magnetic field. (c) Pake pattern expected for isolated C–H pairs distributed at all angles as in polycrystalline or glassy materials. Several components are schematically illustrated. (d) Approximate Gaussian lineshape observed for nonisolated C–H pairs, where all dipolar interactions are operating [33].

three mutually perpendicular directions (Cartesian coordinates), and the λ_s are direction cosines specifying the orientation of the molecular coordinate system with respect to the applied field B_0. Rapid molecular motion experienced by polymer segments in solution results in the observation of isotropic chemical shifts, σ_i, because averaging σ over all orientations yields

$$\sigma_i = 1/3(\sigma_{11} + \sigma_{22} + \sigma_{33}) = 1/3 \text{ trace}(\sigma). \qquad (20.18)$$

It is apparent from Eq. (20.17) that in a rigid, solid sample the chemical shift will depend on its orientation with respect to the applied field. A sample having all like carbon nuclei with the same orientations—as in a single crystal—will exhibit chemical shifts that vary as the crystal is rotated in the applied magnetic field. In a powdered sample, all possible crystalline orientations are present, so the NMR spectrum will consist of the chemical shift tensor powder pattern.

Two theoretical [36] chemical shift tensor powder patterns are illustrated in Fig. 20.14. Principal values σ_{11}, σ_{22}, σ_{33} are indicated, and their isotropic averages, σ_i, are given as dotted lines. In the axially symmetric case (b), $\sigma_{\|}$ and $\sigma_{\perp}$ are the resonance frequencies observed when the principal molecular-axis system is aligned $\|$ and $\perp$ to the applied field. Molecular motion will narrow the chemical shift tensor, by partial averaging, and the resultant powder pattern will then contain information concerning both the axis and angular range of the motion. However, the chemical shift powder pattern contributes to significant broadening of solid-state NMR spectra [see Fig. 20.12(b)] and often obscures the structural information available from the isotropic chemical shifts as observed in solution. This broadening can, however, be removed by high-speed sample spinning at the magic angle.

If a solid powder sample is rotated rapidly about an axis making an angle β with respect to the applied field B_0 [see Fig. 20.14 (c)], the direction cosines (λ_{11}, λ_{22}, λ_{33}) in

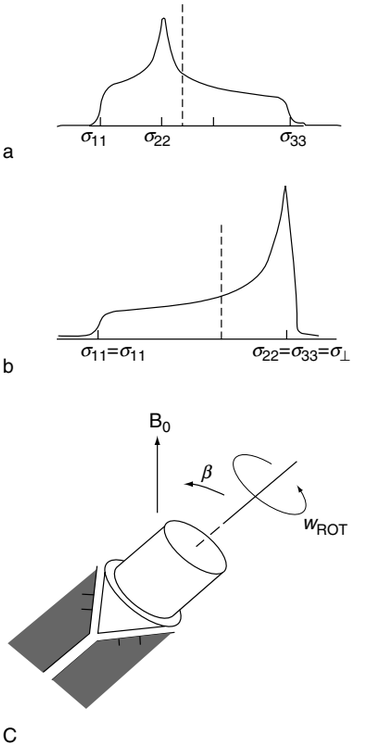

FIGURE 20.14. Schematic CSA tensor powder pattern for an axially asymmetric (a) and axially symmetric (b) tensor. Isotropic chemical shifts (σ_i) are indicated by dashed lines. (c) Typical Andrews [37] sample holder (rotor) rotating on air bearings within a stator (shaded).

Eq. (20.17) vary during each rotation period. For rapid sample rotation, the time average of Eq. (20.17) becomes

$$\sigma = 1/2\sin^2\beta(\sigma_{11}+\sigma_{22}+\sigma_{33}) + 1/2(3\cos^2\beta - 1)$$
$$\times(\text{functions of the direction cosines}). \qquad (20.19)$$

When the angle β between the sample rotation axis and the applied magnetic field is 54.7° (the magic angle), $\sin^2\beta = 2/3$, $3\cos^2\beta - 1 = 0$, and thus $\sigma = \sigma_i$, the isotropic chemical shift.

Rapid magic-angle spinning (MAS) reduces the anisotropic chemical shift tensor powder patterns [see Fig. 20.12(b) and (c)] to their isotropic averages. Chemical shift anisotropies (CSA) of ^{13}C nuclei in different structural environments vary from $\sim$30 ppm for CH_2 carbons to $\sim$200 ppm for aromatic carbons. MAS spinning at a few kHz reduces the CSAs of the aromatic and carbonyl carbons in PBT to their isotropic averages, leading to the ''high resolution'' spectrum seen in Fig. 20.12(c).

Application of high-power ^{1}H-DD and rapid MAS techniques to record the ^{13}C-NMR spectra of solid polymers can produce high-resolution spectra. However, to practically achieve signally averaged, pulsed FT spectra, the rate at which signal averaging can be repeated or the pulse repetition rate is dictated by the spin–lattice relaxation times, T_1, of the ^{13}C nuclei. Because most solids exhibit little motion in the MHz frequency range, which is required for coupling of the ^{13}C spins to their surrounding nuclei or to the lattice, ^{13}C T_1s are long for solids, typically minutes or longer. Rare nuclei, such as ^{13}C (1.1% natural abundance), require extensive signal averaging and the repetition rate of rf pulses becomes an important consideration in their observation by NMR.

The long signal accumulation times required by the low repetition rate for ^{13}C nuclei with long T_1s in solids can be circumvented by transferring polarization from abundant ^{1}H nuclear spins with short T_1s to the ^{13}C nuclei. The repetition rates for signal averaging are now determined by the shorter ^{1}HT_1s (ms–s), because energy is transferred from the proton to the carbon nuclei, a process termed cross-polarization (CP) [38].

Hartmann and Hahn [39] showed that CP can be achieved when two rf fields B_{1H} and $B_{1C} = 4B_{1H}$ are simultaneously applied. $\gamma_H/\gamma_C = 4$, so, when $B_{1C} = 4B_{1H}$ energy is transferred between them, or they are cross-polarized, because $\gamma_C B_{1C} = \gamma_H B_{1H}$ (which is called the Hartmann–Hahn match of heteronuclear rotating-frame frequencies). In the CP experiment ^{13}C nuclei obtain their spin polarization from ^{1}H nuclei, so, not only do the shorter proton spin–lattice relaxation times determine the repetition rate of

the experiment, but their signals also show enhancement by a factor as large as $\gamma_H/\gamma_C = 4$. The CP experiment results in both a time savings and an improvement in the signal-to-noise ratio in the ^{13}C NMR spectroscopy of solid samples.

The initial truly high-resolution ^{13}C NMR spectra of solid polymers were reported by Schaefer and Stejskal [40]. They combined for the first time the three previously developed techniques of high-power proton dipolar decoupling (DD), rapid magic-angle sample spinning (MAS), and cross-polarization (CP), or (CPMAS/DD), to obtain these spectra, which can be utilized to probe the conformations, packing, and motions of solid polymer samples.

20.13 SOLID-STATE NMR APPLICATIONS IN POLYMER SCIENCE

The applications of solid state NMR to polymer science range from simple solution-like experiments, in which the chemical shifts for specific nuclei are observed following the application of a single pulse of radio frequency energy, to complex multidimensional experiments involving hundreds of pulses, which detect both the temporal and spatial relationship of multiple interactions among many dissimilar nuclear spins in a polymer sample. In this brief review, we will make quick mention of well-established methods, with a greater focus on more recent developments that have increased the range of polymer science questions addressable by NMR. The spatial arrangement of polymer chains in bulk crystalline, semicrystalline, or amorphous macromolecules is controlled both by intramolecular energies, e.g., conformational barriers based on the structure of the monomer units, and intermolecular contributions, such as attractive chemical forces between specific chemical moieties. Solid-state NMR can address many of these structural variables, with length scales ranging from monomeric dimensions up to hundreds of nanometers. We summarize recent contributions in the literature that describe the use of solid-state NMR to elucidate chain structure, conformation and stereochemistry, local versus long-range chain dynamics and structural or temporal heterogeneities, and the organization of polymer chains in pure polymers, blends, and composite materials. Recognizing that only an extremely small fraction of recent work may be mentioned here, the more specialized NMR reader may wish to examine Refs. [41–44] for additional details about specific NMR experiments, as well as an extensive source of reference topics.

Why should the polymer scientist consider solid-state NMR as a critical component in the search for new materials or structure–property insights? In almost all cases, polymeric materials are used as solids. Increasingly, these materials are complex mixtures of both crystalline and amorphous components, thereby limiting the efficacy of traditional diffraction techniques. Solid-state NMR is equally adept at interrogating local structure and dynamics in crystalline, amorphous, or mixed physical states composed of both organic and inorganic constituents (i.e., polymer nanocomposites). In addition to this flexibility in the type of sample amenable to analysis, the shear magnitude of possible types of experiments probing local structure, morphology, and dynamics (subhertz to gigahertz frequency ranges) makes solid-state NMR an indispensably powerful tool for polymer science. In particular, the reader will note the large number of references in this review dealing with multicomponent systems, reflecting both the growing importance of blends, copolymers, and composites in polymer material science and the increased selectivity afforded by modern solids NMR techniques.

20.13.1 Conformation and Extended Chain Structure

Syndiotactic polystyrene, s-PS, is a highly stereoregular, semicrystalline vinyl polymer that normally melts at $\sim 270\ ^{\circ}C$ [45,46]. S-PS shows a large number of crystalline polymorphs [47–50] obtained by melt crystallization and solvent-exposure techniques. However, s-PS assumes only two distinct crystalline conformations [all *trans*, planar zigzag (. . . *ttttttt* . . .) and 2_1-helical (. . . *ttggttgg* . . .); $t = trans$ and $g = gauche$], which are characterized by fiber repeats of 5.1 and 7.5 Å, respectively.

Figure 20.15 presents the high resolution CPMAS/DD ^{13}C NMR spectra of two s-PS crystalline polymorphs [51], one with s-PS chains adopting the . . . *tttt-tttt* . . . conformation (a) and the other the . . . *ttggttgg* . . . conformation. We note in spectrum (b) that two CH_2 carbon resonances appear at 38 and 49 ppm, while in spectrum (a) only a single CH_2 carbon resonance at 49 ppm is evident. In the . . . *ttggttgg* . . . polymorph half of the CH_2 carbons are *gauche* to both of their γ-substituent CH carbons, while the other half are *trans* to both γ-CH carbons. We expect, as was also observed for s-PP crystallized in the 2_1-helical . . . *ttggttgg* . . . conformation [52], two CH_2 resonances separated by $\sim 2\times 5.2$ ppm ~ 10 ppm in agreement with spectrum (b). Also the single CH_2 resonance observed for the . . . *ttttttt* . . . polymorph in (a) comes at nearly the same frequency ($\sim$49 ppm) as the most downfield CH_2 resonance observed for the . . . *ttggttgg* . . . polymorph in spectrum (b). These and other observations [18] confirm the validity of the conformationally sensitive γ-*gauche* substituent effects on ^{13}C chemical shifts, with extension of their applicability to solid polymer samples. This strongly implies that the ^{13}C chemical shifts observed for solid polymers are in general primarily influenced by the conformations adopted by their rigid backbones and only to a very minor extent by the crystalline packing of their chains.

Though all of the crystalline polymorphs of s-PS exhibit distinct x-ray diffraction patterns, they exhibit only one or the other of the two $^{13}CPMAS/DD^{13}C$ NMR spectra seen in Fig. 20.15, which correspond to their distinct . . . *ttttttt*

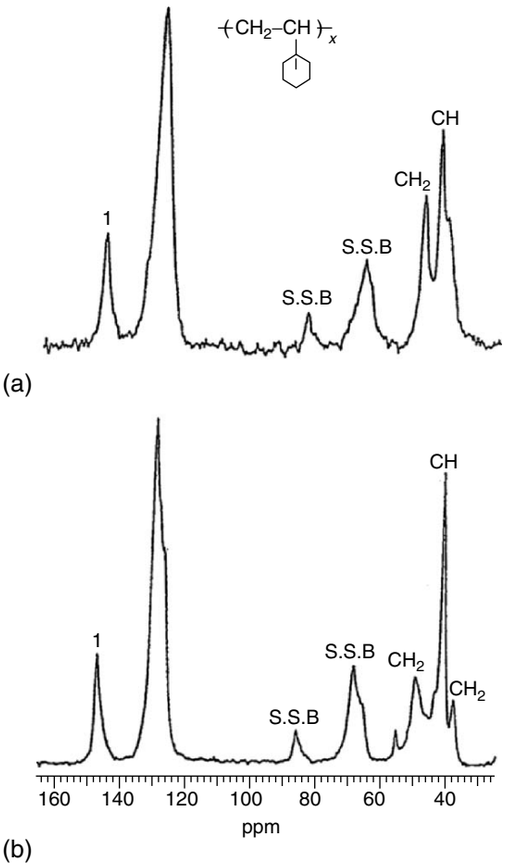

FIGURE 20.15. CPMAS/DD ^{13}C NMR spectra of form I (...*ttttttt*...) (a) and form II (...*ttggttgg*...) (b) s-PS crystalline polymorphs [51].

...and...*ttggttgg*...conformations with fiber repeats of 5.1 and 7.5 Å, respectively. As a consequence, we can conclude that among all the crystalline polymorphs observed for s-PS only two chain conformations are represented. Apparently differences in packing of s-PS chains in these two crystalline conformations result in the variety of crystalline polymorphs observed for s-PS [47–50].

However, CPMAS/DD ^{13}C NMR can still be utilized to distinguish among these many crystalline polymorphs. In Table 20.2 the ^{13}C spin–lattice relaxation times (T_1s) observed at room temperature [51] for several of these polymorphs are presented. Samples S_a, $S_{\alpha 1}$ and $S_{\alpha 2}$, and S_0 and $S_{\delta 1}$ represent amorphous,...*ttttttt*...crystalline, and...*ttggttgg*...crystalline s-PSs, respectively. Clearly the...*ttttttt*...polymorphs have longer T_1s (2–10 times longer) than the...*ttggttgg*...polymorphs. Even amorphous s-PS has longer T_1s than the...*ttggttgg*...polymorphs. When the T_1 results are coupled with the observation of small solvent peaks in the CPMAS/DD and MAS/DD spectra of the S_0 *and* $S_{\delta 1}$ samples (not presented here [51]), we can conclude that small quantities of the solvents used to induce crystalinity in these s-PS samples are retained in both their crystalline and amorphous glassy regions. Solvent incorporated in the crystalline regions of the...*ttggttgg*...polymorphs may act as defects causing the crystalline chains to be at least as mobile as those in the completely disordered, glassy portions of these samples.

While straightforward one-dimensional spectra are extremely useful in the analysis of solid polymer chain conformations, recent two-dimensional techniques applied to s-PS and PET (polyethylene terephthalate) demonstrate that correlation of specific spin interactions can provide extremely detailed quantitative information regarding conformer population distributions [53,54].

Polymer Morphology, Organization, and Phase Behavior

Spin-Diffusion Techniques

Spin-diffusion NMR techniques, typically involving abundant homonuclei like ^1H and ^{19}F, are an important and powerful avenue for interrogating heterogeneous systems. Excellent reviews of this area have recently been published [55,56]. While the general use of spin-diffusion to probe length scales of mixing in polymer blends, or to

TABLE 20.2. ^{13}C *spin–lattice relaxation times,* T_1*(s), for the crystalline carbons in s-PS polymorphs [51].*

Sample	C_1	C_{2-6}	CH_2 (~49 ppm),	CH	CH_2 (~38 ppm),
S_a	78	60	83	65	
$S_{\alpha 1}$	400	120	400	200	
$S_{\alpha 2}$	140	134		280	
S_0	74	54	58	59	55
$S_{\delta 1}$	32	24	30	28	30

determine crystallite dimensions in semicrystalline polymers, is not new, recent improvements in spin-diffusion experiments that address some long-standing limitations warrant mention. In general, spin-diffusion techniques require that specific polarization originating from only one component or phase of the sample be generated, or selected, as an initial condition, subsequent redistribution of that magnetization gradient throughout the entire sample during a controlled mixing time, and a final spectroscopic detection step in which the extent of polarization redistribution is quantified as a function of the mixing time. Based on analogies with physical or thermal diffusion models, rate equations describing the diffusion process, along with spin-diffusion coefficient values, may be used to determine approximate length scales (or domain sizes) associated with the diffusion process in a heterogeneous polymer system. Typical dimensions accessible by this static dipole–dipole method range from 1 to 200 nm. While dipolar spin-diffusion between rare nuclei does occur, this review will be limited to ^1H–^1H examples due to their more general interest and applicability.

Following publication of the aforementioned reviews, two limiting problems have been addressed which increase the applicability of this already successful experimental strategy to a wider range of materials. First, insufficient contrast (either spectroscopic chemical shift contrast or dynamic relaxation-based contrast) between many different types of polymers often precludes generation of a polarization gradient and/or detection of its redistribution. In practice, ^{13}C detection of the spin-diffusion process is most amenable to polymeric systems, given the extremely small chemical shift range and large dipolar couplings between abundant ^1H spins. While polymers or blends containing both rigid and mobile regions can easily be interrogated using ^{13}C-detected Goldman-Shen or dipolar filter methods [57], polymer systems with similar molecular dynamics and similar ^1H chemical shifts are difficult to interrogate. Building on a previous 2D ^{13}C exchange experiment employing ^1H spin-diffusion by Spiess and coworkers [58], Schmidt-Rohr and coworkers recently described a triple cross-polarization experiment that correlates individual ^{13}C resonances with one another *via* ^1H spin-diffusion [59]. Figure 20.16 shows the resulting correlation spectra for a blend of polystyrene (PS) and poly(2,6-dimethylphenyleneoxide) (PXE), in which the quantitative extent of spin-diffusion is assessed *via* extraction of specific rows or columns from the 2D contour plot. The method is attractive since no isotopic labeling is required, and the high-resolution characteristic of ^{13}C spectra is preserved in each dimension. Although sensitivity is improved relative to previous multiple cross-polarization experiments by a factor of 4, the overall efficiency is still quite low. In addition, the technique requires long values of $T_{1\rho H}$ (>5 ms), which potentially excludes many polymer systems of interest.

A second problem that has hindered the application of spin-diffusion methods to a broader range of polymeric materials involves the variation in values of spin diffusion coefficients (D) that have been reported in the literature, and the difficulty with experimentally determining D for any sample of interest. Until recently, the strategy for determination of spin-diffusion coefficients in amorphous polymers involved comparisons of static ^1H linewidths (for rigid polymers) or $^1HT_2$ values (for low T_g polymers) to those obtained for well-characterized, model block copolymers [60]. The model block copolymers have either lamellar, cylindrical, or spherical morphologies, as measured by SAXS or electron microscopy. By ratioing the measured values of linewidth or T_2 obtained for the sample of interest to similar parameters in the literature for these standards, appropriately scaled values of the spin-diffusion coefficient may be estimated for the sample. While this approach is viable, and provides accurate values for D in some cases, an alternative strategy in which direct measurement of spin-diffusion rates in the polymers of interest, and calculations of D based on that measurement, would be attractive. Such an approach would be particularly important for polymer systems in which scattering and microscopy contrast is poor or nonexistent, e.g., blends of amorphous polymers with similar chemical structures, or for which well-characterized block copolymers of similar structure and molecular dynamics were not available.

White and coworkers have recently described an experimental approach in which intramonomer spin-diffusion is used to quantitatively define upper limits on the value of spin-diffusion coefficients D in mobile and rigid homopolymers, as well as in copolymers and blends [61–63]. The independent determination of the diffusion coefficient using only NMR data would be possible if a unique, invariant reference volume or distance existed in the polymer sample that could be used to quantitatively define the diffusive length scale. In other words, an internal distance calibration on the sample itself would eliminate the need for independent

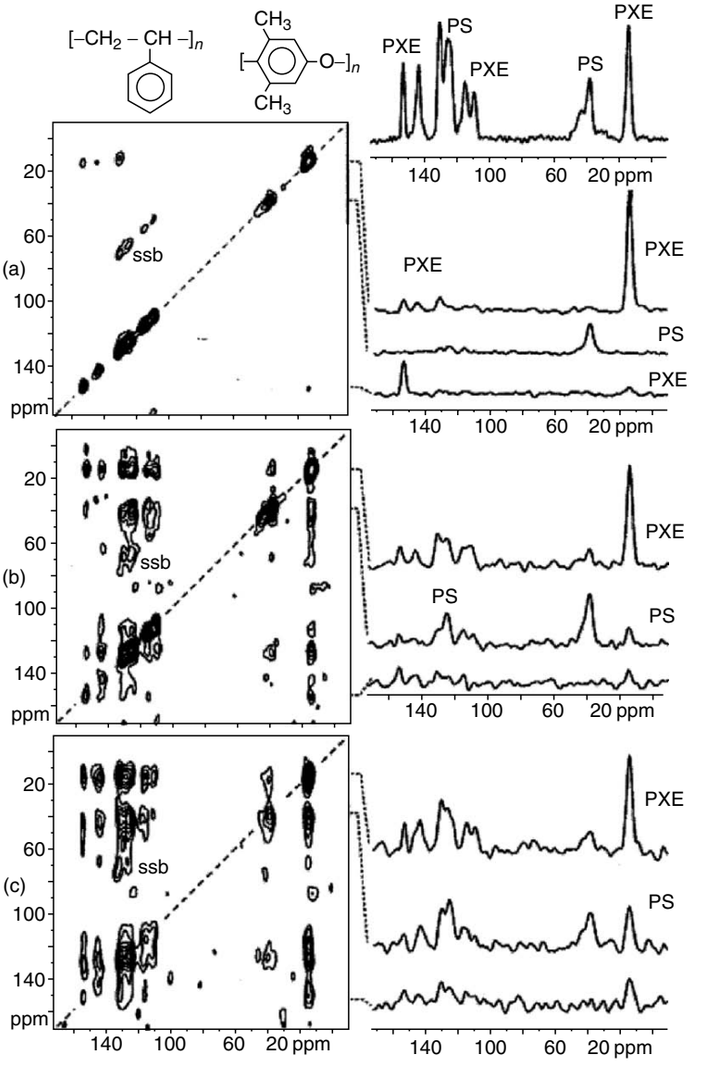

FIGURE 20.16. Series of 2D MAD $^{13}C(HH)^{13}C$ spectra and ^{13}C slices of PS/PXE blends as a function of spin-diffusion mixing time equal to (a) 0.01, (b) 0.5, and (c) 2 ms). [Adapted from Ref. [59] with permission.]

validation of the mixing length scale by scattering or microscopy experiments. White and coworkers reported that the dimensions of the cylinder inscribing a monomer unit in a chain-extended polymer serves as this reference distance, thereby resulting in calculation of an accurate spin-diffusion coefficient in cases where a polarization gradient may be prepared within the monomer itself. While there are several strategies available for generating an initial ^1H polarization gradient in a monomer, particular attention is devoted to using 2D solid-state heteronuclear correlation (Hetcor) methods for measuring intramonomer spin-diffusion in rigid polymers. The main advantage of this experiment is that naturally occurring ^1H magnetization gradients are exploited. In other words, no special manipulation of the proton spin reservoir is required to generate an initial polarization gradient; all local ^1H magnetization is preserved prior to the spin-diffusion period and therefore one can be confident that the sampled spin-response is representative of the bulk. The benefit of the Hetcor spin-diffusion experiment relative to direct ^1H-observe methods is much greater resolution in the ^1H dimension due to ^{13}C chemical shift separation, allowing different polarization-transfer processes (occurring over different length scales) to be detected simultaneously as might occur in blends or block polymers. Figure 20.17 shows example results for a pure glassy homopolymer and amorphous polymer blends.

The two preceding types of experiments directly measure spin-diffusion, i.e., employ a specific mixing time during which spin-diffusion occurs. Several groups have recently employed direct measurement of ^1H spin-diffusion to probe domain sizes in blends containing either polar or nonpolar polymers, inclusion compounds, and composites [64–70].

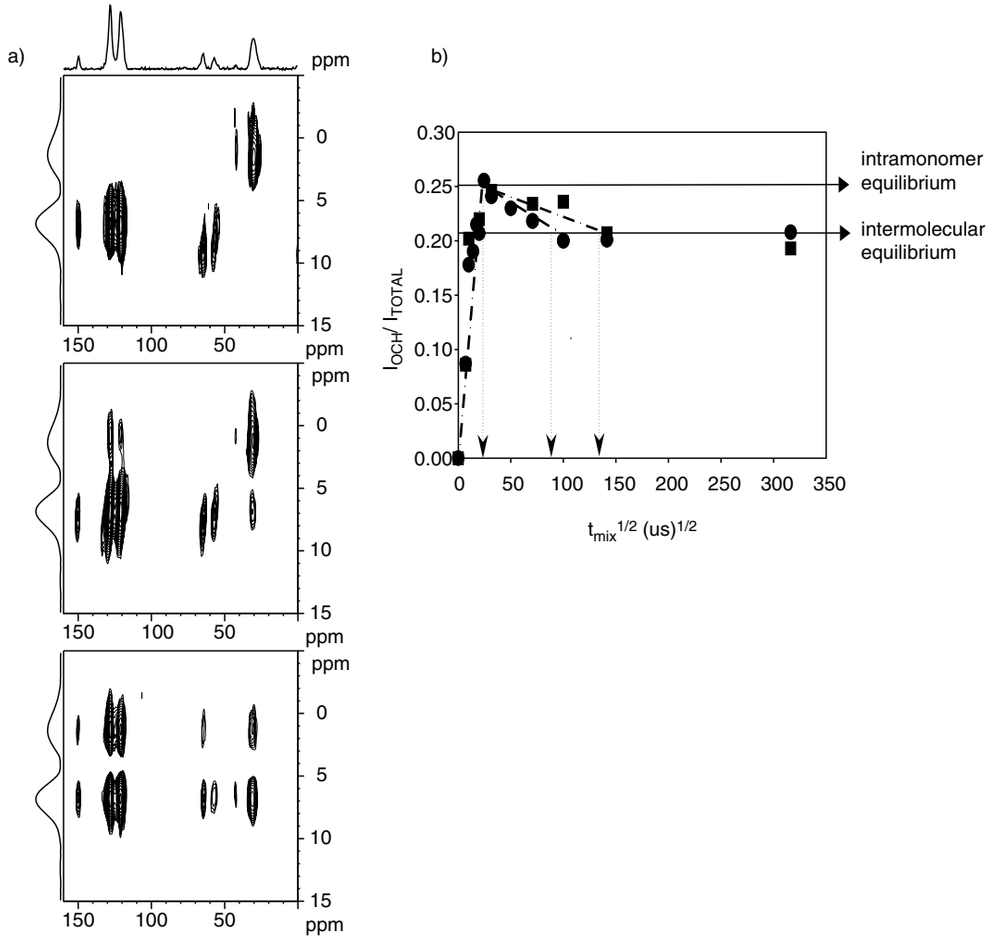

FIGURE 20.17. (a) Series of ^{1}H–^{13}C spin-diffusion Hetcor data for polycarbonate at mixing times of (top) 0 ms, (middle) 0.1 ms, and (bottom) 2.0 ms. (b) Representative spin-diffusion curves extracted from Hector spin-diffusion data, like that in (a), for two different poly(ε-caprolactone)/poly-(L-lactic acid) blends. Note the clear distinction between intramolecular and interchain/interdomain equilibration, the latter occurring at longer times for one blend versus the other. [Adapted with permission from Refs. [62] and [63].

As shown above, ^{1}H spin-diffusion may be detected *via* ^{13}C observation; ^{19}F has also been used to follow ^{1}H spin-diffusion in fluoropolymers [71]. An interesting case of homonuclear spin-diffusion between ^{13}P nuclei has been reported for domain size determination in phosphazene polymers [72]. In general, most researchers still use traditional $^{1}HT_{1\rho}$ and T_1 measurements to indirectly access the limits of spin-diffusion in an approximate fashion, as reported in many recent applications of these methods to a variety of semicrystalline polymers, blends, and composites [73–78].

Chain Packing

As an example of recent developments in the use of solid-state NMR to probe interchain packing relationships, the independent works of Schaefer and Suter deserve mention [79–84]. Polycarbonate (PC) is an industrially important polymer, and its excellent impact properties have been attributed to low-frequency molecular motions which serve as a mechanism for energy dissipation. Using a variety of dipolar recoupling/magic-angle spinning-based techniques, Schaefer and coworkers have found strong evidence for local ordering, or "bundles," in amorphous PC. These bundles are composed of ordered chain pairs over short distances (<10 Å), but the bundles themselves are irregularly spaced/oriented, consistent with the overall glassy structure [79–81]. In contrast, Suter and coworkers used static or slow magic-angle spinning 2D solids NMR to obtain homonuclear dipolar coupling data consistent with a "melt-like" structure with little or no order unless the polymer is mechanically deformed [82–84]. In all cases, direct dipolar couplings were measured between specifically labeled nuclear spins (e.g., ^{13}C, ^{2}H, ^{19}F), and computational structure simulations were used in conjunction with the solid-state NMR data in each approach (Fig. 20.18).

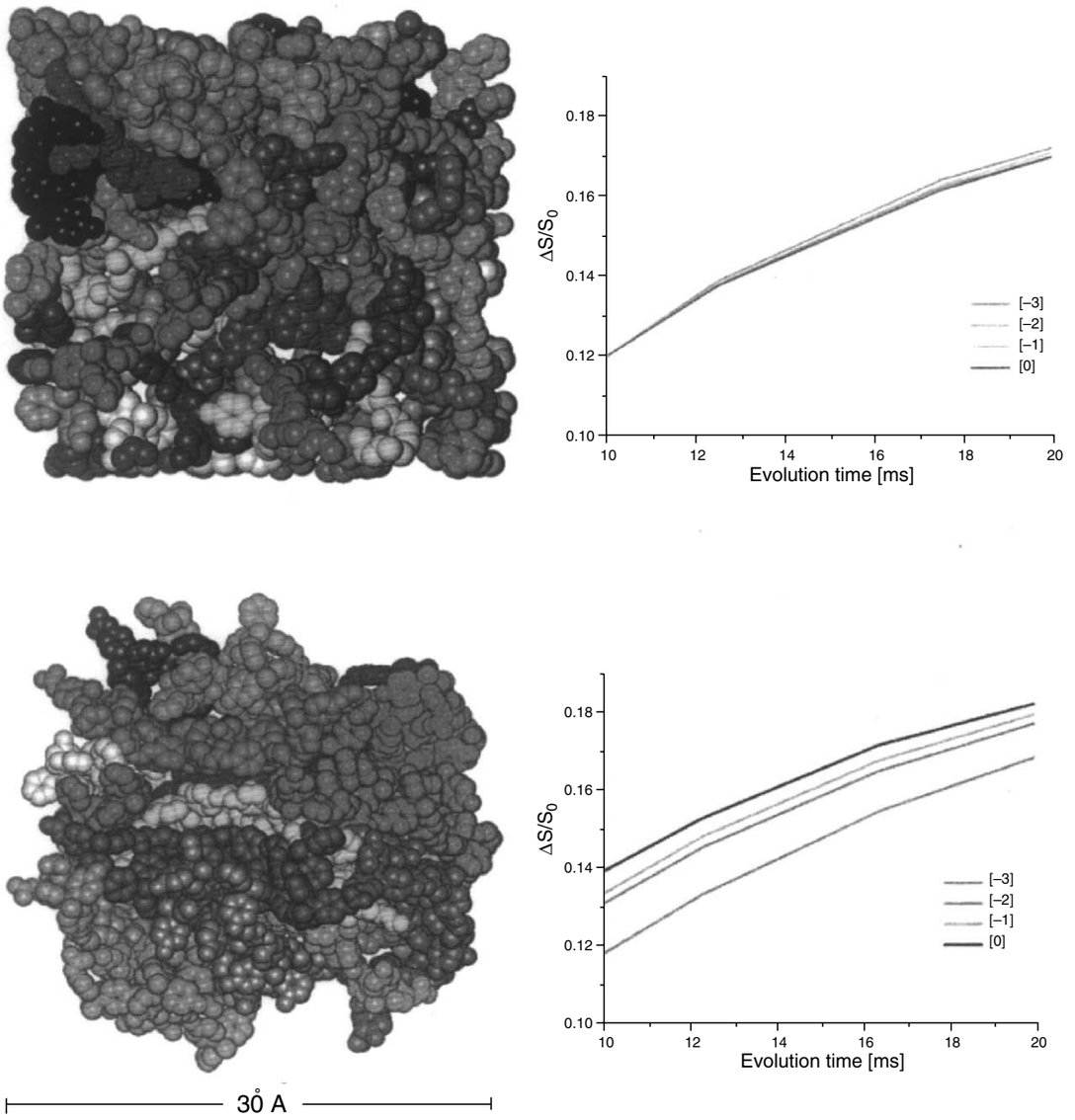

FIGURE 20.18. Comparison of molecular simulations of random (top row) and paired segment (bottom row) chain packing in phenol-substituted polycarbonate, extracted from orientation-dependent REDOR data. [Adapted from Ref. [81] with permission.]

Polymer Dynamics in the Solid State

An excellent review text has recently been published by Tycko outlining various experimental NMR approaches to molecular dynamics, both in small and macromolecules [85]. In terms of the application of these various methods to polymers, one can generally categorize the techniques as direct (e.g., 2D exchange, ^{2}H labeling and lineshape analysis) or indirect (e.g., relaxation, cross-relaxation) probes of molecular dynamics, and additionally, rank them in terms of whether they probe a specific, local type of motion or longer range, correlated chain dynamics. Finally, solid-state NMR experiments can probe an extremely wide range of characteristic timescales for the molecular or chain motion, ranging from nanosecond to many seconds. For example, isolated CH_3 group motion, typically in the form of a tunneling or rotation about the C_3 axis, occurs in essentially all rigid solids, including polymers. As a result, several authors have used methyl groups as ''motional labels'' to interrogate local structure in polymers and blends *via* dipolar or deuterium quadrupolar interactions [86–90]. While the relaxation or cross-relaxation methods measure very fast dynamic events, 2D solid-state exchange techniques are among the most useful for direct inspection of slower events, i.e., on

the order of milliseconds to seconds, which are believed to be most relevant to mechanical properties [91]. Typically, conformational interchange between adjacent segments of the polymer chain, or local substituent reorientations, is accessible by the 2D solid-state exchange technique. References [41–43] contain many examples of ^{13}C, ^{2}H, and ^{31}P 2D exchange data, demonstrating that exchange may be followed between resolved isotropic peaks, similar to traditional solution exchange data, or also within an anisotropically broadened lineshape. Here, we mention only a few more recent examples. Solid-state ^{2}H exchange was used to interrogate the molecular contributions to differential mechanical relaxations in polyacrylates [92], while Horii and coworkers used ^{13}C exchange experiments to determine the activation energy for backbone dynamics in a phenoxy resin [93]. These methods are also useful for interrogation of blend miscibility, as has been recently demonstrated for the case of polyolefin blends [94]. In addition to homonuclear exchange methods, heteronuclear 2D correlation methods, also known as wideline separation (WISE) allow indirect detection of differential chain or side-group dynamics *via* resolved line-shape analysis combined with spin diffusion [95,96].

Two-dimensional exchange techniques offer many advantages for direct detection and analysis of polymer dynamics. However, they often suffer from long acquisition times or insufficient spectral resolution between the polymer chain sites one wishes to interrogate. Several high-resolution one-dimensional methods offer alternatives. Subtle variations in polycarbonate chain dynamics with changes in ring functionalization have recently been reported by Wu *et al*. using heteronuclear dipolar recoupling experiments [97 and references therein]. Hu and coworkers determined that large amplitude chain flips occur in polyethylene crystallites using homonuclear ^{13}C dipolar coupling techniques, in agreement with earlier 2D exchange data [98,99]. These examples illustrate the complimentary information accessible by a variety of dynamic solid-state NMR techniques.

REFERENCES

1. F. A. Bovey, *Nuclear Magnetic Resonance Spectroscopy,* second ed., Academic Press, San Diego, CA, 1988, p. 3.
2. F. A. Bovey and L. W. Jelinski, *Nuclear Magnetic Resonance*, Encyclopedia of Polymer Science, vol. 10, Wiley, New York, 1987, p. 254.
3. F. C. Schilling, F. A. Bovey, M. D. Bruch, and S. H. Kozlowski, *Macromolecules* 1985, *18*, 1418.
4. See Chapter on "Chain Structures" by P. R. Sundararajan in this Handbook.
5. R. C. Ferguson, *ACS Polym. Preprs*. 1967, *8*, 1026.
6. R. C. Ferguson, *Trans. N.Y. Acad. Sci*. 1967, *29*, 495.
7. F. Heatley and A. Zambelli, *Macromolecules* 1969, *2*, 618.
8. J. B. Stothers, *C-13 NMR Spectroscopy,* Academic Press, New York, 1972.
9. K. F. Kuhlman and D. M. Grant, *J. Am. Chem. Soc*. 1968, *90*, 7355.
10. A. E. Derome, *Modern NMR Techniques for Chemistry Research*, Pergamon, New York, 1987.
11. A. E. Tonelli and F. C. Schilling, *Acc. Chem. Res*., 1981, *14*, 233.
12. T. C. Farrar and E. D. Becker, *Pulse and Fourier Transform NMR*, Academic Press, New York, 1987.
13. F. C. Schilling and A. E. Tonelli, *Macromolecules*, 1980, *13*, 270.
14. R. Ditchfield, *Nucl. Magn, Reson*., 1976, *5*, 1.
15. P. V. Schastnev and A. A. Cheremisin, *J. Struct. Chem*., 1982, *23*, 440.
16. J. R. Cheeseman, G. W. Trucks, T. A. Keith, and M. J. Frisch, *J. Chem. Phys*., 1996, *104*, 5497.
17. H. Duddeck, in *Topics in Stereochemistry,* vol. 16, E. I. Eliel, S. H. Wilen, and N. L. Allinger, eds., Wiley-Intersceince, New York, 1986, p. 219.
18. A. E. Tonelli, *NMR Spectroscopy and Polymer Microstructure: The Conformational Connection*, Wiley-Interscience, New York, 1989.
19. H. Spiesecke and W. G. Schneider, *J. Chem. Phys*., 1961, *35*, 722.
20. D. M. Grant and E. G. Paul, *J. Am. Chem. Soc*. 1964, *86*, 2984.
21. L. P. Lindeman and J. Q. Adama, *Anal. Chem*., 1971, *43*, 1245.
22. D. E. Dorman, R. E. Carhart, and J. D. Roberts, in *Proceedings of the International Symposium on Macromolecules, Rio de Janerio, July 26–31, 1974*, E. B. Mano, ed., Elsevier, New York, 1974.
23. F. A. Bovey in *Proceedings of the International Symposium on Macromolecules, Rio de Janerio, July 26–31, 1974*, E. B. Mano, ed., Elsevier, New York, 1974, p. 169.
24. P. J. Flory, *Statistical Mechanics of Chain Molecules*, Wiley-Interscience, New York, 1969.
25. D. M Grant and V. B. Cheney, *J. Am. Chem. Soc*., 1967, *89*, 5315.
26. S. Li and D. B. Chesnut, *Magn. Reson. Chem*., 1985, *23* 625.
27. K. Seidman and G. E. Maciel, *J. Am. Chem. Soc*., 1977, *99*, 659.
28. D. L. VanderHart, *J. Magn. Reson*., 1981, *44*, 117.
29. U. W. Suter and P. J. Flory, *Macromolecules*, 1975, *8*, 765.
30. L. W. Jelinski, *Chem. Eng. News, Nov*, 1984, p. 26.
31. A. Bax, *Two-Dimensional Nuclear Magnetic Resonance in Liquids*, D. Reidel Pub. Co., Hingham, MA, 1982.
32. L. W. Jelinski, in *Chain Structure and Conformation of Macromolecules*, F. A. Bovey, ed., Academic Press, New York, 1982.
33. A. E. Tonelli, *NMR Spectroscopy of Polymers,* R. N. Ibbett, ed., Blackie, Glasgow, 1993.
34. T. M. Duncan and C. R. Dybowski, *Surf. Sci. Repts*., 1981, *1*, 57.
35. G. E. Pake, *J. Chem. Phys*., 1948, *16*, 327.
36. M. Mehring, *High Resolution NMR in Solids*, second ed., Springer-Verlag, Berlin, 1983.
37. E. R Andrews, A. Bradbury, and R. G. Eades, *Nature*, 1959, *183*, 1802.
38. A. Pines, M. G. Gibby, and J. S. Waugh, *J. Chem. Phys*., 1972, *56*, 1776; *Chem. Phys. Lett*., 1972, *15*, 373.
39. Hartman and Hahn, *Phys. Revs*., 1962, *128*, 2042.
40. J. Schaefer and E. O. Stejskal, *J. Am. Chem. Soc*., 1976, *98*, 1031.
41. K. Schmidt-Rohr and H. W. Spiess, *Multidimensional Solid-State NMR and Polymers*, Academic Press, New York, 1994.
42. I. Ando and T. Asakura, *Solid State NMR of Polymers*, Elsevier, Tokyo, 1998.
43. F. A. Bovey and P. A. Mirau, *NMR of Polymers*, Academic Press, New York, 1996.
44. S. P. Brown and H. W. Spiess, *Chem. Rev*, 2001, *101*, 4125.
45. N. Ishihara, T. Seimiya, N. Kuramoto, and M. Uoi, *Macromolecules*, 1986, *19*, 2462.
46. C. Pellecchia, P. Longo, A. Grassi *et al*., *Makromol. Chem. Rapid Commun*., 1987, *8*, 277.
47. A. Immirizi, F. deCandia, P. Ianelli *et al*., *Makromol. Chem. Rapid Commun*., 1988, *9*, 761.
48. O. Greis, Y. Xu, T. Arsano, and J. Peterman, *Polymer*, 1989, *30*, 590.
49. R. A. Nyquist, *Appl. Spectrosc*., 1989, *43*, 440.
50. N. M. Reynolds, J. D. Savage, and S. L. Hsu, *Macromolecules*, 1989, *22*, 2867.
51. M. A. Gomez and A. E. Tonelli, *Macromolecules*, 1990, *23*, 3385.
52. A. Bunn, E. A. Cudby, R. K. Harris *et al*., *J. Chem. Soc*., 1981, *15*.
53. M. G. Dunbar, D. Sandstrom, and K. Schmidt-Rohr, *Macromolecules*, 2000, *33*, 6017.
54. K. Schmidt-Rohr, W. Hu, and N. Zumbulyadis, *Science*, 1998, *280*, 714.
55. D. L. VanderHart and G. M. McFadden, *Solid State NMR*, 1996, *7*, 45.
56. J. Clauss, K. Schmidt-Rohr, and H. W. Spiess *Acta Polym*., 1993, *44*, 1.
57. N. Egger, K. S. Schmidt-Rohr, B. Blumich, W. D. Domke and B. Stapp, *J. Appl. Polym. Sci*., 1992, *44, 289*.
58. M. Wilhelm, H. Feng, U. Tracht, and H. W. Spiess, *J. Magn. Reson*., 1998, *134*, 255.

59. S. S. Hou, Q. Chen, and K. Schmidt-Rohr, *Macromolecules*, 2004, *37*, 1999.
60. F. Mellinger, M. Wilhelm, and H. W. Spiess, *Macromolecules*, 1999, *32*, 4686.
61. X. Wang and J. L. White *Macromolecules*, 2002, *35*, 3795.
62. X. Jia, J. Wolak, X. Wang, and J. L. White, *Macromolecules*, 2003, *36*, 712.
63. X. Jia, X. Wang, A. E. Tonelli, and J. L. White, *Macromolecules*, 2005, 38, 2775.
64. K. Beshah and L. K. Molnar, *Macromolecules*, 2000, *33*, 1036.
65. T. M. Werkhoven, F. M. Mulder, C. Zune, R. Jerome, and H. J. M. de Groot, *Macromol. Chem. Phys*., 2003, *204*, 46.
66. W. G. Hu and K. Schmidt-Rohr, *Polymer*, 2000, *41*, 2979.
67. K. Landfester, V. L. Dimonie, and M. S. El-Aasser, *Macromol. Chem. Phys*., 2002, *203*, 1772.
68. P. A. Mirau, S. A. Heffner, and M. Schilling, *Solid State NMR*, 2000, *16*, 47.
69. A. Buda, D. E. Demco, M. Bertmer, B. Blumich, B. Reining, H. Keul, and H. Hocker, *Solid State NMR*, 2003, *24*, 39.
70. W. Heinen and H. J. M. deGroot, *Macromolecules*, 1998, *31*, 7404.
71. P. Holstein, G. A. Monti, and R. K. Harris, *Phys. Chem. Chem. Phys*., 1999, *1*, 3549.
72. S. Taylor, J. L. White, R. Crosby, G. C. Campbell, N. Elbaum, J. F. Haw, and G. Hatfield, *Macromolecules*, 1992, *25*, 3369.
73. C. Neagu, J. E. Puskas, M. A. Singh, and A. Natansohn, *Macromolecules*, 2000, *33*, 5976.
74. J. Z. Yi and S. H. Goh, *Polymer*, 2003, *44*, 1973.
75. P. J. M. Serrano, J. P. M. van Duynhoven, R. J. Gaymans, and R. Hulst, *Macromolecules*, 2002, *35*, 8013.
76. A. E. Tonelli, *J. Mol. Struct*., 1995, *355*, 105.
77. M. I. B. Tavares, *J. Appl. Polym. Sci*., 2003, *87*, 473.
78. N. J. Clayden, *J. Appl. Polym. Sci*., 1994, *32*, 2321.
79. C. A. Klug, W. Zhu, K. Tasaki, and J. Schaefer, *Macromolecules*, 1997, *30*, 1734.
80. J. M. Goetz, J. Wu, A. F. Yee, and J. Schaefer, *Macromolecules*, 1998, *31*, 3016.
81. R. D. O'Conner, B. Poliks, D. H. Bolton, J. M. Goetz, J. A. Byers, K. L. Wooley, and J. Schaefer, *Macromolecules*, 2002, *35*, 2608.
82. P. Robyr, Z. Gan, and U. W. Suter, *Macromolecules*, 1998, *31*, 6199.
83. M. Utz, A. S. Atallah, P. Robyr, A. H. Widmann, R. R. Ernst, and U. W. Suter, *Macromolecules*, 1999, *32*, 6191.
84. M. Utz, P. Robyr, and U. W. Suter, *Macromolecules*, 2000, *33*, 6808.
85. R. Tycko, *Nuclear Magnetic Resonance Probes of Molecular Dynamics*, Kluwer Academic Press, The Netherlands, 1994.
86. J. L. White and P. A. Mirau, *Macromolecules*, 1993, *26*, 3049.
87. K. Saalwachter, *Chem. Phys. Lett*., 2002, *362*, 331.
88. M. Wachowicz, J. Wolak, H. Gracz, E. O. Stejskal, S. Jurga, and J. L. White, *Macromolecules*, 2004, *37*, 4573–4579.
89. W. Lin and F. D. Blum, *J. Am. Chem. Soc*., 2001, *123*, 2032.
90. K. Schmidt-Rohr, A. S. Kulik, H. W. Beckham, A. Ohlemacher, and H. W. Spiess, *Macromolecules*, 1994, *27*, 4733.
91. X. Qiu and M. D. Ediger, *J. Polym. Sci. B: Polym. Phys*., 2000, *38*, 2634.
92. S. C. Kubler, D. J. Schaefer, C. Boeffel, U. Pawelzik, and H. W. Spiess, *Macromolecules*, 1997, *30*, 6597.
93. H. Kaji, T. Tai, and F. Horii, *Macromolecules*, 2001, *34*, 6318.
94. J. E. Wolak, X. Jia, and J. L. White, *J. Am. Chem. Soc*., 2003, *125*, 13660.
95. K. Schmidt-Rohr, J. Clauss, and H. W. Spiess, *Macromolecules*, 1992, *25*, 3273.
96. X. Qiu and P. A. Mirau, *J. Magn. Reson*, 2000, *142*, 183.
97. J. Wu, C. Xiao, A. F. Yee, J. M. Goetz, and J. Schaefer, *Macromolecules*, 2000, *33*, 6849.
98. W. G. Hu, C. Boeffel, and K. Schmidt-Rohr, *Macromolecules*, 1999, *32*, 1611.
99. K. Schmidt-Rohr and H. W. Spiess, *Macromolecules*, 1991, *24*, 5288.

CHAPTER 21

Broadband Dielectric Spectroscopy to Study the Molecular Dynamics of Polymers Having Different Molecular Architectures

F. Kremer

Universität Leipzig, Germany

21.1 INTRODUCTION

Broadband dielectric spectroscopy (BDS) is a versatile experimental tool to study the dynamics of polymeric systems. In its modern form it covers the extraordinary frequency range from 10^{-3} Hz to 10^{9} Hz with the option to extend both limits to lower and higher values, respectively. This enables one to analyse the molecular dynamics on a large time scale especially if the temperature of the sample is varied as well. In the present review article examples will be discussed for polymers of widely varying molecular architectures (linear and cyclic chains, star-branched systems, and liquid crystalline polymers).

21.2 BROADBAND DIELECTRIC SPECTROSCOPY (BDS)

In principle in a dielectric experiment [1a,b] an electric field is applied to a material under study and the resulting polarisation current is measured (Fig. 21.1). It is composed out of two contributions, the induced (time constant $\cong 10^{-12}$s) and the orientational polarisation (time constant $> 10^{-12}$s). Modern broadband dielectric measurements are carried out in the frequency domain. The sample geometry has to be adapted to the spectral range in which the measurements are carried out (Fig. 21.2).

Dielectric spectra are usually fitted by the empirical relaxation function suggested by Havriliak and Negami:

$$\varepsilon^*(\omega) = \varepsilon_\infty + \frac{\Delta\omega}{\left(1 + (i\omega\tau_{\mathrm{HN}})^{\beta}\right)^{\gamma}} \qquad (21.1)$$

in which $\Delta\varepsilon$ is the relaxational strength, τ_{HN} the mean relaxation time and ε_∞ the value of the real part of the dielectric function in the limit $\omega \gg \frac{1}{\tau_{\mathrm{HN}}}$. The parameters β and γ describe the symmetric and asymmetric broadening of the relaxation time distribution function. Details are discussed in Chapter 3 of [1a].

21.3 THE DYNAMICS OF POLYMERS HAVING DIFFERENT MOLECULAR ARCHITECTURES

21.3.1 Linear and Cyclic Chains of Poly(methylphenylsiloxane)

The fact that poly(methylphenylsiloxane) (PMPS) has a dielectrically active relaxation process originates from the dipole moment of the Si–O bond [2]. Due to the chemical structure of PMPS (Fig. 21.3) the dipole components in the main axis of the polymer cancel each other, while they add up in the perpendicular direction.

Thus, one has to expect *one* dielectric relaxation process, assigned to a local motion of the Si–O bond. It corresponds to the dynamic glass transition (α-relaxation) of the bulk polymer. Measured from temperatures between -25 °C to 33 °C this relaxation process shifts from about 1 Hz to about 10^{8} Hz (Fig. 21.4).

On the low-frequency side the measurement is limited by a conductivity contribution, on the high frequency side by

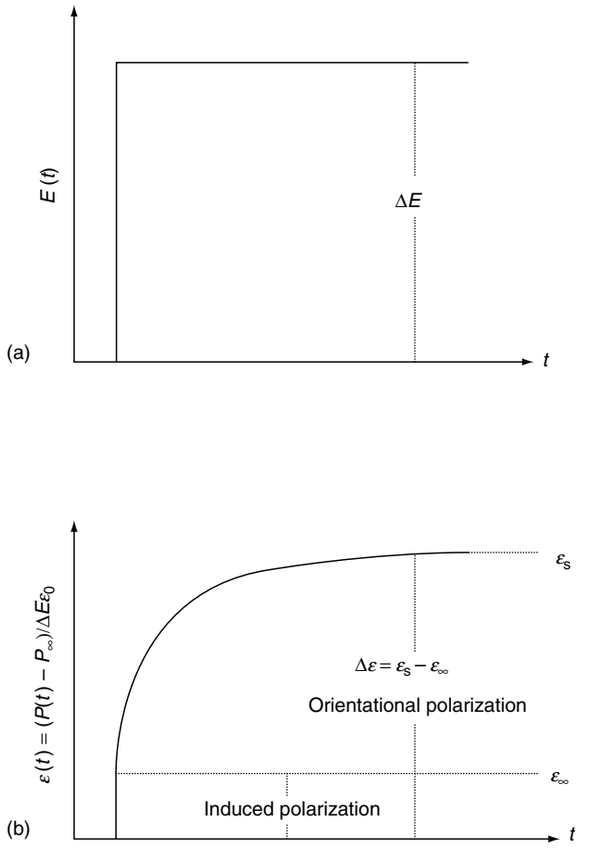

FIGURE 21.1. Scheme of time dependence of the electric field $E(t)$ and the resulting polarisation being composed out of the induced and the orientational contribution.

resonance effects of the sample cell. In order to deduce the mean relaxation rate and the shape parameter of the relaxation time distribution from the measured data the ansatz of Havriliak-Negami in Eq. (21.1) is used. The experimental data can be described by this fit-function within experimental accuracy—over the entire frequency range (Fig. 21.5) leading to the fit parameters listed in Table 21.1. The latter shows a pronounced temperature dependence proving that time-temperature superposition is *not* fulfilled for this system.

The temperature dependence of the mean relaxation time τ_{HN} can be described by the empirical function according to Williams, Landel and Ferry (WLF):

$$\log a_{\mathrm{T}} = \frac{C_1(T - T_0)}{C_2 + T - T_0}. \qquad (21.2)$$

Here a_{T} is a shift factor ($a_\tau = \tau_{\mathrm{HN}}/\tau_{\mathrm{reference}}$). If for $1/\tau_{\mathrm{reference}}$ the relaxation rate at the glass transition temperature is chosen $C_1 = 11.8\,\mathrm{K}$ and $C_2 = 67.9\,\mathrm{K}$ is obtained. The WLF dependence is typical for the dynamic glass transition (Fig. 21.6). It covers nearly 10 decades in the relaxation rate and scales with the calorimetric glass transition temperature as $\tau(T_{\mathrm{g}}) \simeq 10^{-2}\,\mathrm{Hz}$. The dynamic glass transition

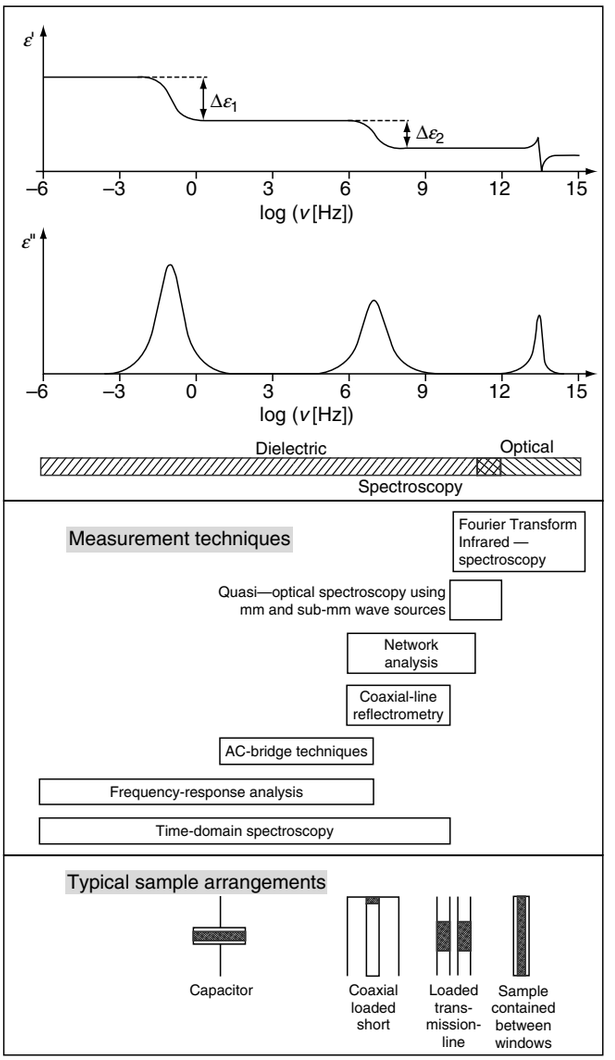

FIGURE 21.2. Survey of measurement techniques used in the frequency range from 10^{-6} Hz–10^{15} Hz. Taken from [1a] with permission.

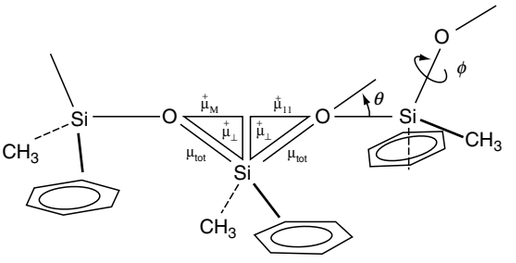

FIGURE 21.3. Chemical structure of poly(methylphenylsiloxane). Taken from [2] with permission.

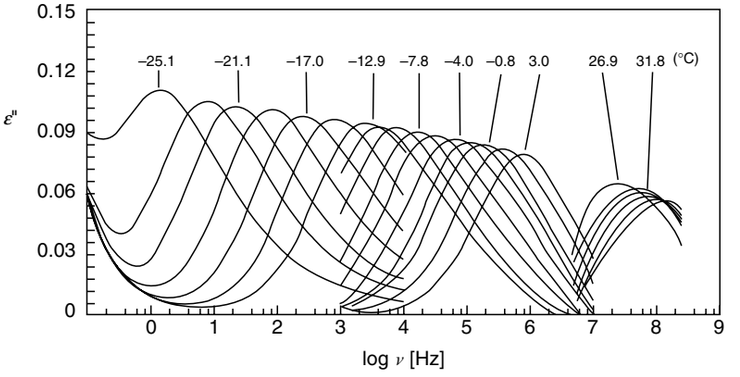

FIGURE 21.4. Dielectric loss $\varepsilon''(\nu)$ versus frequency for PMPS ($M_n = 28500$ with $T_g = -26$ °C) at different temperatures as indicated. The accuracy of the measurement of the dielectric loss is $\pm$ 5% in the low frequency region; above 1 MHz the measurement accuracy is $\pm$ 10%. Taken from [2] with permission.

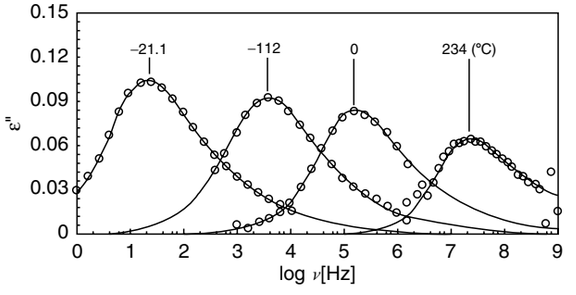

FIGURE 21.5. Data from Fig. 21.4 as fitted (solid line) using the Havriliak-Negami equation [Eq. (21.1)]. The fit parameters are shown in Table 21.1. Taken from [2] with permission.

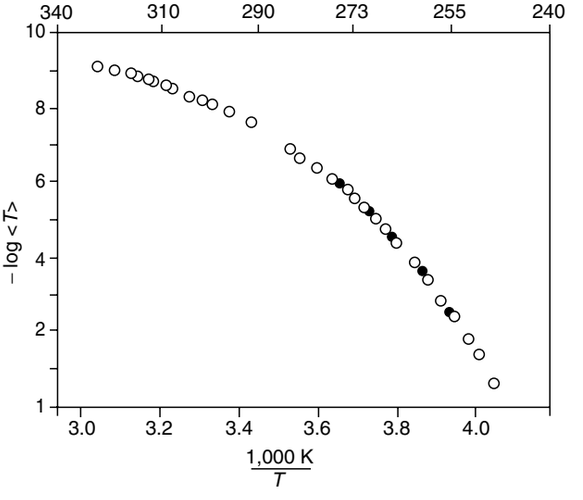

FIGURE 21.6. Plot of the logarithm of the mean relaxation times vs. the reciprocal temperature. The open symbols (○) denote the dielectric data, the solid symbols (●) are the results obtained by quasielastic light scattering. Taken from [2] with permission.

TABLE 21.1. *Temperature dependence of the HN-fit parameters (s. Eq. (21.1)) for the segmental relaxation of poly(methylphenylsiloxane) having a molecular weight of* $M_n = 28{,}500$.

T [C]	$\Delta\varepsilon_{HN}$	β	γ	τ_{HN} [s]
−22.8	0.42	0.76	0.56	4.7×10^{-2}
−21.1	0.41	0.80	0.46	1.7×10^{-2}
−19.1	0.40	0.82	0.43	5.1×10^{-3}
−17.0	0.40	0.84	0.39	1.7×10^{-3}
−11.2	0.35	0.76	0.56	7.6×10^{-5}
−9.7	0.35	0.77	0.55	4.1×10^{-5}
−7.8	0.34	0.83	0.46	2.3×10^{-5}
−6.0	0.34	0.85	0.43	1.3×10^{-5}
−4.0	0.34	0.89	0.36	7.1×10^{-6}
0	0.31	0.85	0.46	2.1×10^{-6}
23.4	0.25	0.96	0.34	1.7×10^{-8}
28.7	0.25	0.99	0.29	1.1×10^{-8}

is assigned to fluctuations of an ensemble of 2–3 segments between structural substates.

The temperature at a relaxation rate of 1 Hz shows a pronounced dependence on the molecular weight M_n and the molecular architecture (Fig. 21.7). While linear polymers follow the Fox–Flory equation this is not the case for cyclic systems.

21.3.2 Linear and Star-Branched Chains of Poly(*cis*-1,4-isoprene)

Poly(*cis*-1,4-isoprene) has due to the lack of symmetry in its chemical structure (Fig. 21.8) non-zero components of

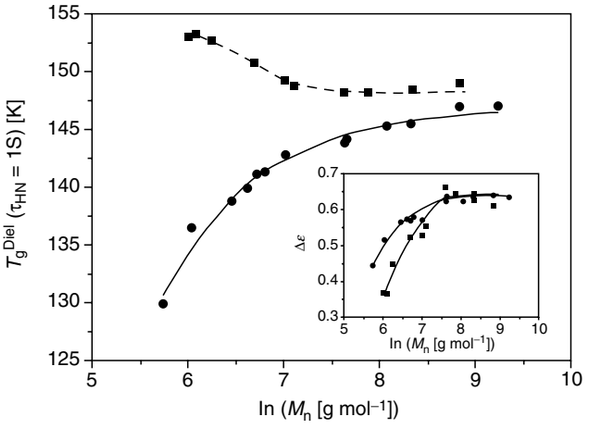

FIGURE 21.7. T ($\tau_{HN} = 1$ s) versus molecular weight: ●, linear chains; ■, rings; the solid line is a fit of Fox/Flory equation to the data ($T_{g,\infty} = 147$ K,K = 5057 K mol g^{-1}), the dashed line is a guide for the eyes. The inset shows $\Delta\varepsilon$ versus molecular weight at T = 298 K: ●, linear chains; ■, rings, lines are guides for the eyes. All data are taken from [4].

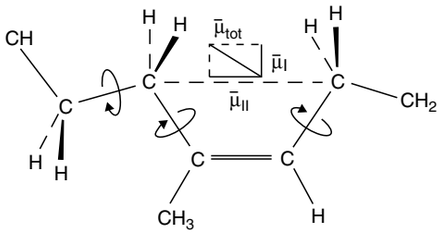

FIGURE 21.8. Chemical structure and dipole moment of poly(*cis*-1,4-isoprene).

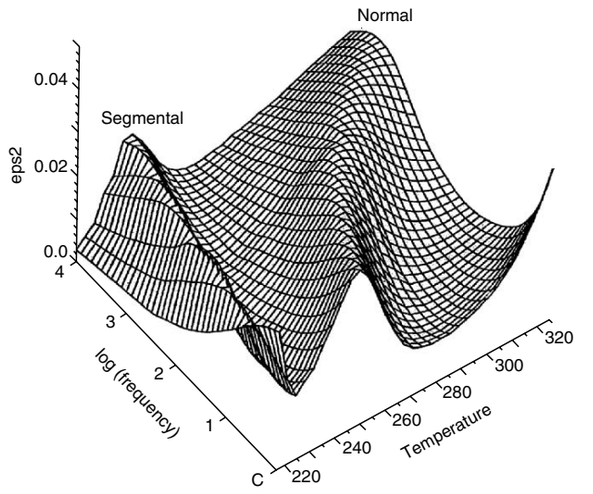

FIGURE 21.9. 3D representation of the frequency and temperature dependence of the dielectric loss ε'' for *cis*-1,4-polyisoprene PIP-12. Taken from [5b] with permission.

the dipole moment both perpendicular and parallel to the chain axis.

Thus *two* dielectric relaxation processes, a segmental and a normal mode process, are present [5]; they are well-separated on the frequency and temperature scale (Fig. 21.9). The relaxation process around 220 K originates from a local segmental motion perpendicular to the main axis, while the second relaxation process at higher temperatures is assigned to fluctuations of the dipole components parallel to the chain contour (normal mode).

It is to expect that the segmental mode does not depend on the molecular weight of the chain (Fig. 21.10). In contrast

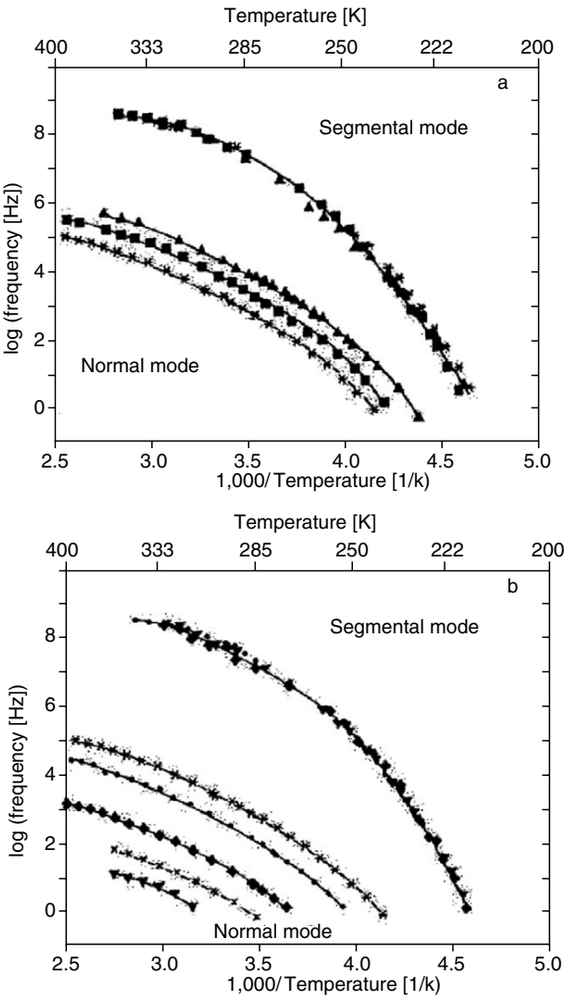

FIGURE 21.10. (a) Activation plot for the segmental mode and the normal mode of *cis*-1,4-polyisoprene samples with molecular weights of $M_w < M_c$: ▲, PIP-05; ■, PIP-08; **x**, PIP-12. The solid lines represent the WLF fit with the fit parameters given in Table 21.3. (b) Activation plot for the segmental mode and the normal mode of *cis*-1,4-polyisoprene samples with molecular weights of $M_w > M_c$: *, PIP-12; ●, PIP-17; ◆, PIP-38; ★, PIP-65; ▼, PIP-97. The solid lines represent the WLF fit with the fit parameters given in Table 21.3. Taken from [5a] with permission.

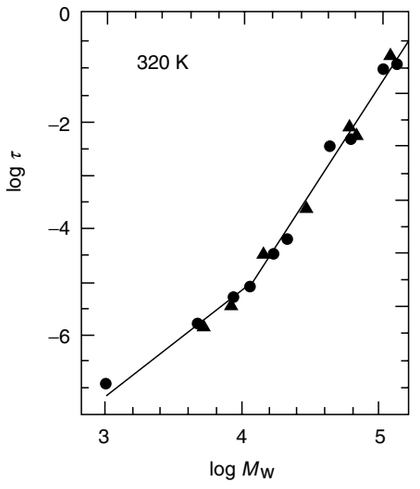

FIGURE 21.11. Dependence of the mean dielectric relaxation time, $\tau = (2\pi\nu_{max})^{-1}$, on molecular weight, M_w, for the normal mode process of *cis*-1,4-polyisoprene (▲) at 320 K; data are reported by Adachi and Kotaka (●) in [5a]. Taken from [5b] with permission.

TABLE 21.2. *Temperature dependence of the HN-fit parameters (s. Eq. (21.1)) for the segmental and normal mode of linear poly(cis-1,4-isoprene) having a molecular weight of* 17,000 gmol^{-1} *[5a].*

T [K]	$\Delta\varepsilon_{HN}$	β	γ	τ_{HN} [s]
			Segmental Mode	
222.3	0.117	0.70	0.50	2.2×10^{-2}
224.3	0.115	0.68	0.51	8.7×10^{-3}
226.4	0.114	0.65	0.55	3.0×10^{-3}
229.5	0.111	0.65	0.56	8.8×10^{-4}
240.4	0.097	0.64	0.59	2.2×10^{-5}
244.4	0.097	0.64	0.68	8.5×10^{-6}
253.9	0.091	0.62	0.66	9.0×10^{-7}
			Normal Mode	
263.9	0.127	1.0	0.38	4.6×10^{-2}
272.5	0.118	1.0	0.40	1.2×10^{-2}
283.7	0.105	1.0	0.42	3.5×10^{-3}
297.7	0.096	1.0	0.44	9.4×10^{-4}
324.4	0.085	1.0	0.45	1.3×10^{-4}
341.7	0.082	1.0	0.45	6.1×10^{-5}
359.4	0.078	1.0	0.44	3.2×10^{-5}
376.6	0.077	1.0	0.44	2.0×10^{-5}

the normal mode must depend sensitively on the molecular weight M_W: The critical molecular weight M_c where Rouse-like fluctuations change into a reptation-like dynamics has for PI a value of 10^4. Thus one finds

$$\begin{matrix} \langle\tau\rangle \infty M^{2.0} \text{ for } M_w < M_c \\ \langle\tau\rangle \infty M^{3.7\pm0.1} \text{ for } M_w \geq M_c \end{matrix} . \qquad (21.3)$$

These molecular weight dependencies are explained by the Rouse theory and by the reptation theory in its recent modifications.

As for PMPS the data can be fitted within the limits of experimental accuracy by the empirical HN-function. The fit parameters (Table 21.2) for the normal and segmental mode of PI having a molecular weight of 17,000 g mol^{-1} show that the distribution parameters β and γ are strongly temperature dependent. This means that again the conjecture of time-temperature superposition is *not* fulfilled.

Both, the segmental and the normal mode can be described in its temperature dependence by the WLF-equation (Eq. (21.2)). While the former is only weakly dependent on temperature, the normal mode shows especially for the parameter C_2 a strong effect (Tab. 21.3). Star-branched polymers of PI have in principle similar dynamics as linear chains: Two relaxation processes are observed being assigned to the segmental and normal mode. Linear chains have free ends in

TABLE 21.3. *WLF-fit parameters of the segmental and the normal mode of linear PI having molecular weight varying between* $M_w = 1{,}000$ *(PI-01) to* $M_w = 130{,}000$ *(PI-130) [5a].*

	Segmental mode $T_0 = 250$ K			Normal mode $T_0 = 300$ K		
Code	C_1	C_2 [K]	$10^{-5}\nu_0$ [Hz]	C_1	C_2 [K]	ν_0 [Hz]
PIP-01				4.0	151.6	2.0×10^6
PIP-05	5.7	80.0	1.2	4.0	133.9	3.1×10^4
PIP-08	5.7	70.0	2.1	4.3	136.2	7.4×10^3
PIP-12	5.8	76.0	2.5	4.2	132.3	2.0×10^3
PIP-13	5.8	74.3	2.2	4.2	128.8	1.3×10^3
PIP-14	6.0	69.7	1.5	4.4	130.5	8.1×10^2
PIP-17	6.1	70.9	1.4	4.4	129.5	3.9×10^2
PIP-38	6.0	71.2	1.6	4.2	119.9	2.2×10^1
PIP-65	6.1	73.4	1.7	3.6	97.5	3.1
PIP-97	6.1	70.9	1.4	0.9	57.9	0.02
PIP-130	6.1	72.5	1.6			

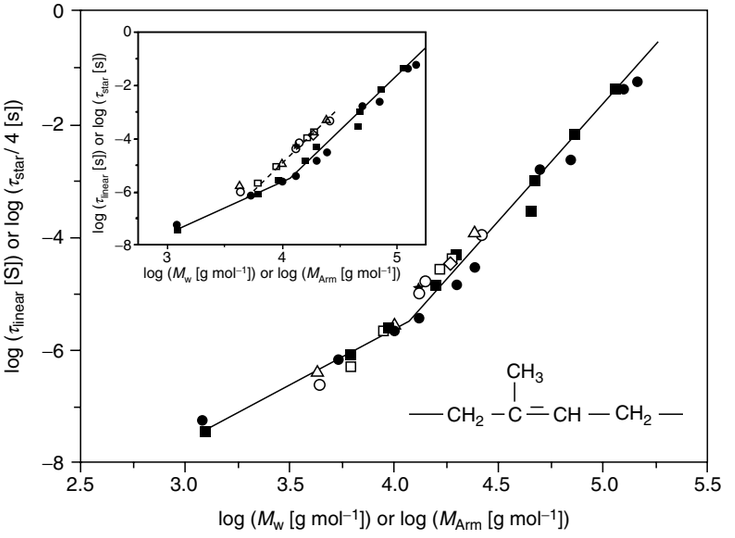

FIGURE 21.12. τ_{Linear} and $\tau_{Star}/4$ versus molecular weight of the chain or the arm of different linear and star-like poly(*cis*-1,4-isoprene)s at $T = 320$ K. The inset shows τ_{Linear} and τ_{Star} versus molecular weight of the chain or the arm. ●, linear chains [5a]; ■, linear chains [5b]; ○, 18-arm star; Δ, 12-arm star; □, 8-arm star; ◇, 4-arm star, *, 3-arm star. The solid lines are linear fits for $M < M_C$ (Slope 2.0, Rouse regime) and $M > M_C$ (Slope 3.7, reptation regime). The dashed line is a parallel shift of the line obtained for the reptation regime for the data of the stars polymers. Taken from [1a] with permission.

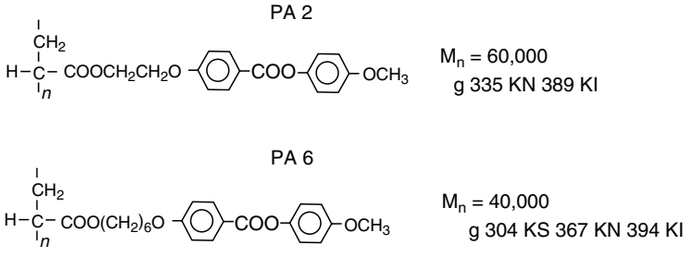

FIGURE 21.13. Scheme of the side group liquid crystalline polymer.

contrast to star-branched polymers where an arm of the system has to be comprehended as a tethered chain, which is fixed at one end. This leads to special boundary conditions for the normal mode relaxation resulting in a scaling factor of 1/4 for the relaxation rate (Fig. 21.12).

21.3.3 Liquid Crystalline Polymers

Mesogenic groups can be incorporated into polymeric systems [7]. This results in materials of novel features like main chain systems of extraordinary impact strength, side-chain systems with mesogens which can be switched in their orientation by external electric fields or—if chiral groups are attached to the mesogenic units—ferroelectric liquid crystalline polymers and elastomers. The dynamics of such systems depends in detail on its molecular architecture, i.e. especially the main chain polymer and its stiffness, the spacer molecules and their length and the mesogenic unit broadband dielectric spectroscopy enables one to unravel in detail the molecular and—for chiral systems—as well the collective fluctuations.

In side chain liquid crystalline polymers the mesogenic unit is connected to the main chain by a flexible spacer. The molecular fluctuations of the rigid mesogenic core are characterised by two librational modes, one corresponding to fluctuations around the long molecular axis (“β-relaxation”) and a libration around the short molecular axis (“δ-relaxation”). Additionally the mesogens might have an attached polar group causing a further secondary process (“γ-relaxation”). Usually the main chain has a dynamic glass transition corresponding to fluctuations of chain segments between structural substates (“α-relaxation”).

For a side chain liquid crystalline polymer [8] with a poly(acrylate) main chain and a 2- or 6-fold aliphatic spacer (Fig. 21.13) one finds three relaxation processes: The β-relaxation, the δ-relaxation, and the dynamic glass

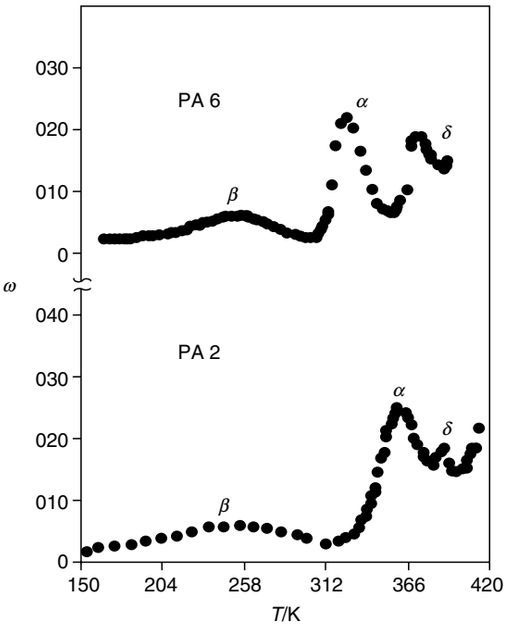

FIGURE 21.14. Dielectric loss versus temperature at 10 kHz. Sample: PA2 and PA6 (both unaligned). The error bars in this and the following figures are not larger than the size of the symbols. Taken from [8] with permission.

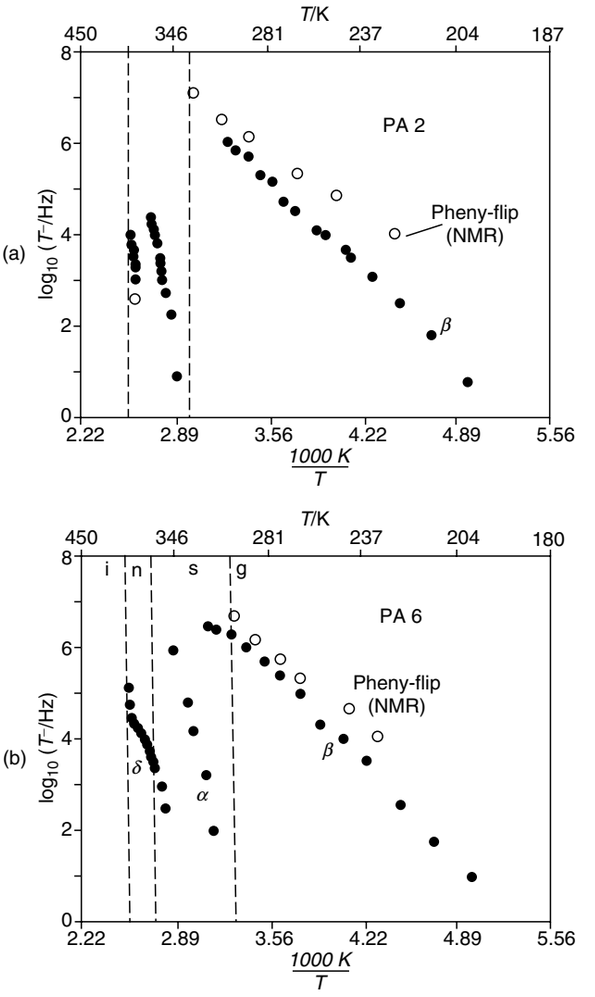

FIGURE 21.15. (a) Activation plot (relaxation rates versus inverse temperature) for unaligned PA2. ●, dielectric measurements; ○, NMR measurement for 180° phenyl-flip. (b) Activation plot (relaxation rate versus inverse temperature) for unaligned PA6. ●, dielectric measurements; ○, NMR data for the 180° phenyl-flip. Taken from [8] with permission.

transition (“α-relaxation”) (Fig. 21.14). The temperature dependence of these fluctuations is summarised in activation plots (Fig. 21.15). It is remarkable that the change from a two-fold (PA2) to a six-fold (PA6) spacer has such a strong influence on the dynamics. The δ-relaxation shows at the phase transition into the isotropic state a pretransitional change of its temperature dependence. The fluctuations in this side chain system are schematically sketched in Fig. 21.16.

For a combined main chain side group liquid crystalline polymer (Fig. 21.17) two librational β-relaxations are observed [9] originating from the two different mesogenic units (Fig. 21.18).

A δ-relaxation is not found, presumably due to the high viscosity of the system and an underlying conductivity contribution. If the sample with a chiral group in the side chain mesogen is oriented in the bookshelf geometry a completely novel dynamics takes place due to the ferroelectric order of the mesogenes [10]. One observes two collective processes a soft-mode and a Goldstone-mode corresponding to fluctuations of the phase and the amplitude of the helical superstructure (Fig. 21.19). Additionally one finds in the frequency range between 10^6 and 10^9 Hz a secondary β-relaxation being assigned to librations around the long molecular axis. This refined dynamic interplay is schematically summarised in Fig. 21.20.

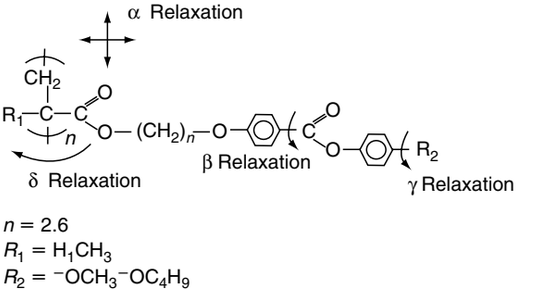

FIGURE 21.16. Scheme of the liquid–crystalline side group polymers and the fluctuations which were observed in the measurements (indicated by arrows). Taken from [8] with permission.

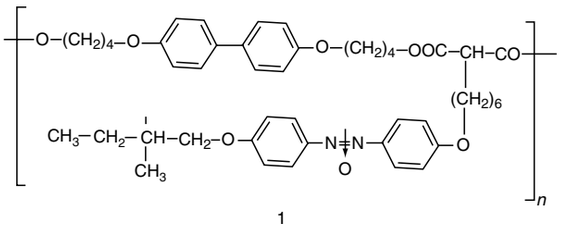

1

FIGURE 21.17. Scheme of combined main chain/side group liquid crystalline polymer. Molar mass $M = 23{,}000\, g/mol^{-1}$. Phase transition temperatures in K: S_j^* 350 S_c^* 391 S_A^* 404I.

21.3.4 Conclusions

Broadband dielectric spectroscopy enables one to analyse the dynamics of polar groups in polymeric systems. Due to its broad frequency range of more than 10 decades a manifold of different molecular fluctuations can be studied from the dynamic glass transition (spanning already more than 10 decades in times) to secondary relaxations. Additionally one finds in chiral liquid crystals cooperative processes like soft- and Goldstone modes.

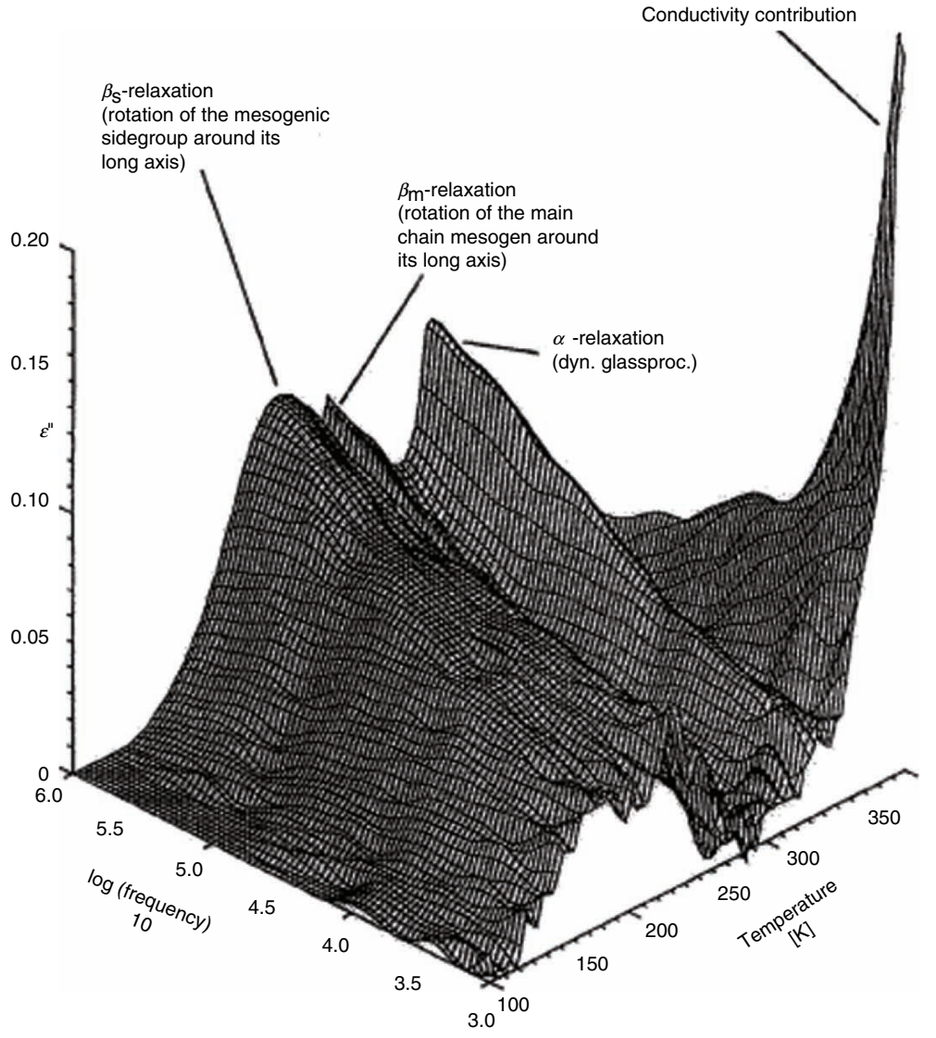

FIGURE 21.18. Dielectric loss ε'' versus temperature and logarithm of frequency using an *unaligned* (200 μm thick) sample (Fig. 21.17) (only dielectric relaxation processes are observable). Taken from [9] with permission.

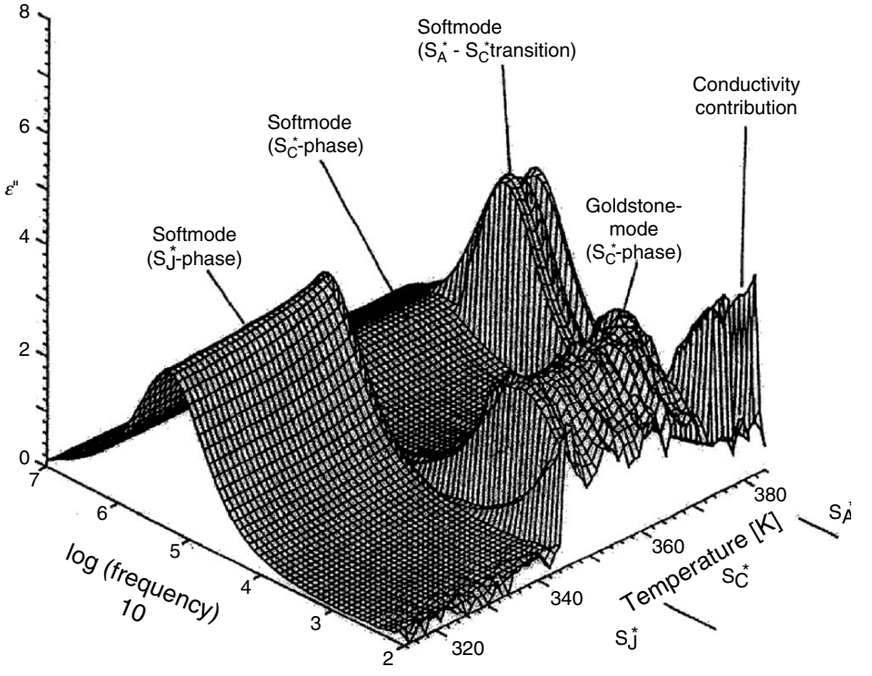

FIGURE 21.19. Dielectric loss ε'' versus temperature and logarithm of frequency using a thin (10 μm) *aligned* sample (ferroelectric modes are observable). Note the different ε''-scale as compared with Fig. 21.18. Taken from [10] with permission.

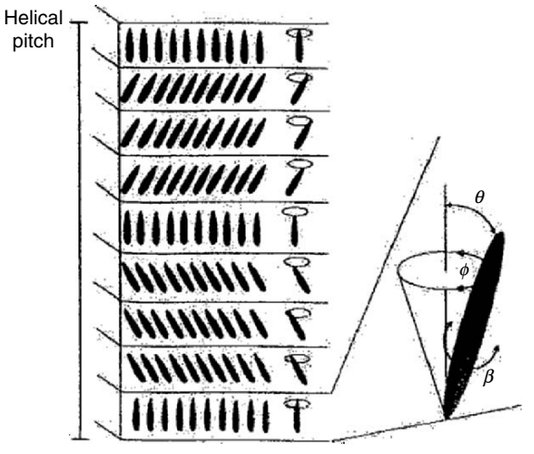

FIGURE 21.20. Scheme of the collective and molecular dynamics in FLC: The Goldstone-mode corresponds to fluctuations of the phase Φ (phason) and the soft-mode of the amplitude θ (amplitudon) of the helical superstructure. The high frequency β-relaxation is assigned to librations of the mesogen around its long molecular axis.

REFERENCES

1a. Kremer F, Schönhals A (Eds) (2002) In: Broadband Dielectric Spectroscopy. Springer, Berlin, Heidelberg, New York
1b. McCrum NG, Read BE, Williams G (1967) In: Anelastic and Dielectric Effects in Polymeric Solids. Dover Publications, New York
2. Boese D, Momper B, Meier G, Kremer F, Hagenah JU, Fischer EW (1989) Macromolecules 22: 4416
3. Kremer F, Boese D, Meier G, Fischer EW (1989) Prog. Colloid Polym. Sci. 80: 129
4. Kirst U, Kremer F, Pakula T, Hollingshurst J (1994) J. Colloid Polym. Sci. 272: 1420
5a. Adachi K, Kotaka T (1985) Macromolecules 18: 466
5b. Boese D, Kremer F (1990) Macromolecules 23: 829
6a. Boese D, Kremer F, Fetters LJ (1990) Macromolecules 23: 1826
6b. Boese D, Kremer F, Fetters LJ (1990) Polymer 31: 1831
7. Spiess HW, Vill V (1998) In: Handbook of Liquid Crystals. Demus D, Groby J, Webray G (Eds) Wiley-VCH, Vol. 3
8. Vallerien SU, Kremer F, Boeffel C (1989) Liquid Cryst. 4: 79
9. Kremer F, Vallerien SU, Zentel R, Kapitza H (1989) Macromolecules 22: 4040
10. Vallerien SU, Zentel R, Kremer F, Kapitza H, Fischer EW (1989) Makromol. Chem. Rapid. Commun. 10: 333

CHAPTER 22

Group Frequency Assignments for Major Infrared Bands Observed in Common Synthetic Polymers

I. Noda*, A. E. Dowrey†, J. L. Haynes*, and C. Marcott†

*The Procter & Gamble Company, Beckett Ridge Technical Center, 8611 Beckett Road, West Chester, OH 45069
†The Procter & Gamble Company, Miami Valley Innovation Center, 11810 E. Miami River Rd., Cincinnati, OH 45252

22.1 INFRARED SPECTROSCOPY OF POLYMERS

Infrared (IR) spectroscopy plays a very important role in the physical characterization of polymers. IR absorption bands are well known for their marked specificity to individual chemical functionalities. Furthermore, the unique sensitivity toward the configuration, conformation, and other local sub- and supramolecular environments (e.g., different phases of semicrystalline polymers, moieties participating in specific interactions of miscible blends, and block polymer segments undergoing different stages of relaxation processes) makes IR spectroscopy a very powerful probing tool for numerous scientific investigations in polymer physics.

One of the limitations of IR spectroscopy often cited by polymer physicists has been the lack of unambiguous band assignments of chemical moieties for IR spectra of different polymers. The assignment of IR absorption bands for specific modes of molecular vibrations in polymers is not always straightforward. While, it is true there have been numerous published IR spectroscopic studies of polymeric materials, relatively little is provided for the useful and practical tabulation of specific group-frequency band assignments for typical synthetic polymers commonly studied by polymer physicists.

In this section, mode assignments of IR absorption bands for 24 selected solid polymers most often encountered by polymer physicists are compiled. Only frequencies of relatively well-assignable bands actually observed at room temperature are listed. No attempts were made to include information on intensity or band shape. IR bands can be strongly affected by various physical factors such as phase, morphology, sample history, and IR sampling techniques. Tables 22.1–22.24 are intended for physicists interested in

TABLE 22.1. *Polyethylene, linear [1–9].*

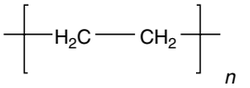

Frequency (cm^{-1})	Phase	Transition moment orientation[a]	Assignment
720	Crystalline	∥ *b*-axis	Out-of-phase CH_2 rock of the two chains in the unit cell
	Amorphous	⊥ *b*-axis	CH_2 rock $(tttt)_n$ $n > 4$
731	Crystalline	∥ *a*-axis	In-phase CH_2 rock of the two chains in the unit cell
888	Amorphous	∥	CH_2 rock
1,050	Crystalline	∥	CH_2 twist
1,078	Amorphous	⊥	Skeletal C–C stretch (*g* and *t* confirmation)
1,176	Crystalline	∥	CH_2 wag

TABLE 22.1. *Continued.*

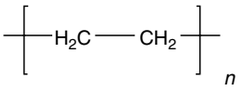

Frequency (cm^{-1})	Phase	Transition moment orientation[a]	Assignment
1,303	Amorphous	∥	CH_2 wag (*gtg* conformation)
1,353	Amorphous	∥	CH_2 wag (*gtg* conformation)
1,368	Amorphous	∥	CH_2 wag (*gtg* conformation)
1,463	Crystalline	∥ *b*-axis	CH_2 bend
	Amorphous		CH_2 bend
1,473	Crystalline	∥ *a*-axis	CH_2 bend
1,820	Crystalline	∥	Combination of 1,100 or 1,130 + 720, 730 (weak)
1,894	Crystalline	⊥	Combination of CH_2 rock, 1,168 + 720, 730 (weak)
2,016	Both	∥	Combination of 1,294 + 720, 730 (weak)
2,150	Both	⊥	Combination of CH_2 1,440 + 720, 730 (weak) or 1,100 + 1,050
2,850			CH_2 symmetric stretch
2,918			CH_2 symmetric stretch

[a]With respect to uniaxial stretch.

TABLE 22.2. *Polyethylene, linear low density [23].*

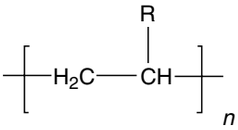

$R = CH_3$ (methyl)
$R = CH_2CH_3$ (ethyl)
$R = CH_2CH_2CH_2CH_3$ (*n*-butyl)
$R = CH_2CH_2CH_2CH_2CH_3$ (*n*-hexyl)
$R = CH_2CH_2CH_2CH(CH_3)CH_3$ (Isobutyl)

Frequency (cm^{-1})	Assignment
720/730	CH_2 deformation (rock) split when PE is crystalline
937	CH_3 rock
890	*n*-hexyl rock
894	*n*-butyl rock
920/952	Isobutyl rock
1,365.5	Isobutyl symmetrical
1,375	CH_3 symmetric deformation
1,377	Methyl symmetrical
1,378.1	*n*-butyl symmetrical
1,377.9	*n*-hexyl symmetrical
1,379	Ethyl symmetrical
1,383.6	Isobutyl symmetrical
1,475/1,462	CH_2 deformation (scissors) split when PE is crystalline
2,850	CH_2 symmetric C–H stretch
2,916	CH_2 asymmetric C–H stretch

TABLE 22.3. *Polypropylene, isotactic [1–3,7,10].*

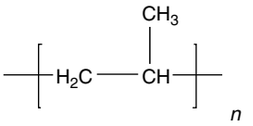

Frequency (cm^{-1})	Species[a]	Phase	Polarization[b]	Assignment
809	*E*	Crystalline	⊥	CH_2 rock + C–C chain stretch + C–CH stretch
841	*A*	Crystalline	∥	CH_2 rock + C– CH_3 stretch
899	*E*	Crystalline	⊥	CH_3 rock + CH_3 rock + CH bend
941	*E*	Crystalline	⊥	CH_3 rock + C–C chain stretch
973	*A*	Amorphous	∥	CH_3 rock + C–C chain stretch
998	*A*	Crystalline	∥	CH_3 rock + CH_3 wag + CH bend
1,045	*A*	Crystalline	∥	C– CH_3 stretch C–C chain stretch + CH bend
1,104	*E*	Crystalline	⊥	C–C chain stretch + CH_3 rock + CH_2 wag + CH twist + CH bend
1,168	*A*	Crystalline	∥	C–C chain stretch + CH_3 rock + CH bend
1,220	*E*	Crystalline	⊥	CH_2 twist + CH bend + C–C chain stretch
1,256	*A*	Both	∥	CH bend + CH_2 twist + CH_3 rock
1,377	*E*	Both	⊥	CH_3 symmetric bend + CH_2 wag
1,458				CH_2 scissors
2,837				CH_2 symmetric stretch
2,868				CH_3 symmetric stretch
2,919				CH_2 asymmetric stretch
2,951				CH_3 asymmetric stretch

[a] *A* species are vibrating in phase and *E* species have a phase difference $2p/3$ between adjacent monomer unit.
[b] With respect to helix.

TABLE 22.4. *Poly(tetrafluoroethylene) [2,9,10].*

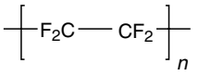

Frequency (cm^{-1})	Assignment
516	C–C–F bend
553	CF_2 bend
636	C–C–F bend
1,150	CF_2 stretch + CF_2 bend (?)
1,210	CF_2 symmetric stretch
1,240	CF_2 asymmetric stretch
2,450	Combination of CF_2 stretch

TABLE 22.5. *Polybutadiene [1,2].*

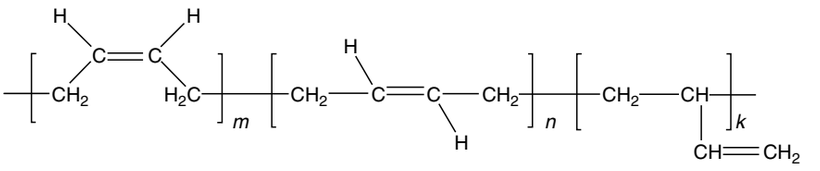

Frequency (cm^{-1})	Repeating unit type	Assignment
730	*cis*-1,4	In-phase out-of-plane CH wag
910	1,2	In-phase out-of-plane CH_2 wag

TABLE 22.5. *Continued.*

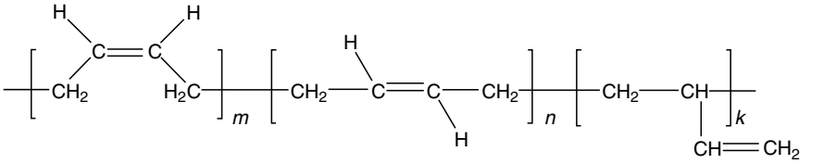

Frequency (cm^{-1})	Repeating unit type	Assignment
967	*trans*-1,4	In-phase out-of-plane CH wag
990	1,2	In-phase out-of-plane CH wag
1,230	*trans*-1,4	CH_2 wag
1,310	*cis*-1,4	CH_2 wag
1,437	*trans*-1,4	CH_2 bend
1,451	*cis*-1,4	CH_2 bend
1,640	1,2	C=C stretch
1,655	*cis*-1,4	C=C stretch
1,820	1,2	Overtone of CH_2 wag
2,840		Backbone CH_2 symmetric stretch
2,916		Backbone CH_2 asymmetric stretch
2,965	1,2	Vinyl CH_2 symmetric stretch
3,000		Olefinic CH stretch
3,065	1,2	Vinyl CH_2 asymmetric stretch

TABLE 22.6. *Polyisoprene, cis [1–3,15,19].*

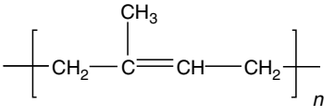

Frequency (cm^{-1})	Assignment
836	Trisubstituted olefin out-of-plane CH wag[a]
1,129	CH_3 rock
1,300	CH_2 wag
1,376	CH_3 symmetric (umbrella) deformation
1,450	CH_2 symmetric (scissors) + CH_3 asymmetric deformation
1,664	C=C stretch
2,720	Overtone of CH_2 umbrella
~ 2,850	CH_2 and CH_3 symmetric stretch
2,920	CH_2 asymmetric stretch
2,962	CH_3 asymmetric stretch
3,030	Olefin CH stretch

[a]Intensity increases with crystallinity.

TABLE 22.7. *Poly(dimethyl siloxane) [1,2].*

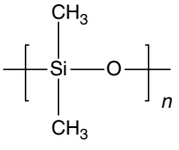

Frequency (cm^{-1})	Assignment
800	CH_3 rock
1,000–1,150	Si–O–Si stretch
1,260	CH_3 symmetric (umbrella) deformation
2,905	CH_3 symmetric stretch
2,960	CH_3 asymmetric stretch

TABLE 22.8. *Poly(ethylene terephthalate) [1,3,10–13].*

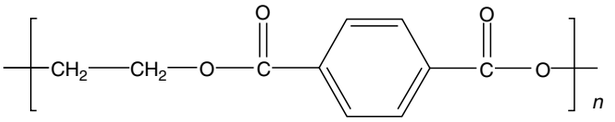

Frequency (cm^{-1})	Phase	Polarization	Assignment
730		⊥	Aromatic in-phase CH wag
795		⊥	C═O rock + –C–O deformation
875	Crystalline	⊥	Aromatic out-of-plane CH wag
896	Amorphous	∥	Gauche configuration CH_2 rock
975	Both	∥	Trans configuration C–O stretch
1,019		∥	Aromatic ring in-plane CH bend
1,102–1,127			C–O stretch + others
1,260			C–O stretch
1,343	Crystalline	∥	CH_2 wag
1,410			Ring semicircle stretch
1,504			Ring semicircle stretch
1,725		⊥	C═O stretch
2,969			CH_2 asymmetric stretch

TABLE 22.9. *Poly(lactic acid) [24].*

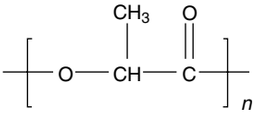

Frequency (cm^{-1})	Assignment
716	Skeletal vibration
755	Skeletal vibration
812	C–C–O stretch
870	O–H deformation
1,048	Symmetric C–O stretch (ether)
1,092	Asymmetric C–O stretch (ether)
1,132	Symmetric C–O stretch (ester)
1,184	Asymmetric C–O stretch (ester)
1,268	O–H deformation w/C–O stretch
1,364	CH_3 symmetric deformation
1,384	CH_3 symmetric deformation
1,456	CH_3 asymmetric deformation
1,759	C═O stretch
2,881	CH_3 symmetric stretch
2,948	CH_3 asymmetric stretch
2,997	CH_3 asymmetric stretch
3,506	O–H stretch (acid terminator)

TABLE 22.10. *Poly(vinyl chloride) [1–3,14,15].*

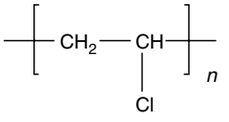

Frequency (cm^{-1})	Phase	Polarization	Assignment
603	Crystalline	∥ (⊥)[a]	C–Cl stretch
610	Amorphous	⊥	C–Cl stretch, syndiotactic segment . . . *ttt* . . .

TABLE 22.10. *Continued.*

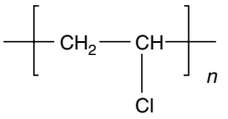

Frequency (cm^{-1})	Phase	Polarization	Assignment
620	Amorphous	⊥	C–Cl stretch, isotactic segment (*tg*)*tt*(*gt*)
685	Amorphous	⊥	C–Cl stretch, isotactic segment (*tg*)*tg*(*tg*)
693	Amorphous	∥	C–Cl stretch, syndiotactic segment (*tt*)*gg*(*tt*)
957	Crystalline	∥ (⊥)[a]	CH_2 rock
970	Amorphous	⊥	CH_2 rock
1,243	Amorphous	⊥	CH bend
1,254	Crystalline	∥ (⊥)[a]	CH bend
1,333	Crystalline	⊥	CH bend
1,354	Crystalline	∥ (⊥)[a]	CH_2 wag
1,424	Crystalline	⊥	
1,431	Amorphous	⊥	CH_2 symmetric (scissors) deformation
2,837			CH_2 symmetric stretch
2,904			CH_2 asymmetric stretch
2,965			CH stretch next to Cl (?)

[a](⊥) Dichroism observed at high draw ratios.

TABLE 22.11. *Poly(vinyl alcohol) [24].*

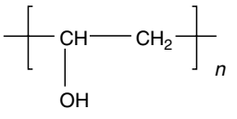

Frequency (cm^{-1})	Assignment
851	C–C–O stretch (alcohol)
945	C–C–O stretch (acetate)
1,026	CH_3 rock
1,096	C–O stretch
1,138	CH_2 deformation (twist or wag)
1,255	C–O stretch (acetate)
1,324	CH deformation (wag)
1,375	CH_3 symmetric deformation (acetate)
1,433	CH_2 deformation (scissors) coupled with O–H deformation (alcohol)
1,734	C=O stretch (acetate)
2,940	CH_2 asymmetric stretch (C–H stretch)
3,360	O–H stretch (alcohol)

TABLE 22.12. *Polyacrylonitrile [3].*

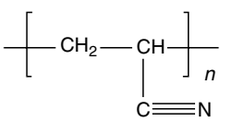

Frequency (cm^{-1})	Polarization	Assignment
1,247		CH bend
1,358		CH_2 asymmetric bend
1,452	⊥	CH_2 bend
2,241	⊥	C ≡ N stretch

TABLE 22.12. *Continued.*

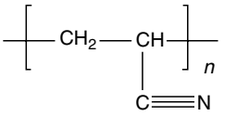

Frequency (cm^{-1})	Polarization	Assignment
2,243		C ≡ N stretch
2,870	⊥	CH_2 symmetric stretch
2,940	⊥	CH_2 asymmetric stretch

TABLE 22.13. *Poly(vinyl acetate) [1,2].*

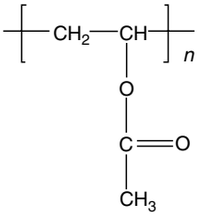

Frequency (cm^{-1})	Assignment
1,022	C–O stretch
1,239	C–O stretch
1,373	CH_3 symmetric (umbrella) deformation
1,432	CH_2 symmetric (scissors) deformation
1,737	C=O stretch
2,850	CH_2 symmetric stretch
2,920	CH_2 asymmetric stretch
2,970	CH_3 asymmetric

TABLE 22.14. *Poly(methyl methacrylate) [1,2,9,16].*

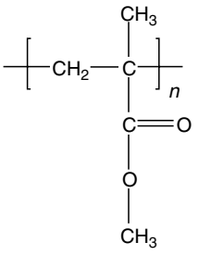

Frequency (cm^{-1})	Assignment
753	Skeletal $+CH_2$ rock
841, 964	Skeletal
988	C–O–C stretch
1,150, 1,195	C–O stretch
1,241, 1,277	C–O stretch
1,387	CH_3 symmetric (umbrella) deformation
1,448	CH_2 symmetric (scissors) deformation, O–CH_3 deformation
1,485	CH_3 (α-methyl) asymmetric deformation
1,732	C=O
2,850	Overtone of ester CH_3 deformation
2,950	CH_3 (ester methyl) stretch
2,998	CH_3 (α-methyl) stretch

TABLE 22.15. *Polystyrene, atactic [1,2,9,17].*

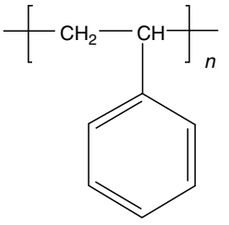

Frequency (cm^{-1})	Assignment
540	Out-of-plane ring bend
697	Mono-substituted ring out-of-plane bend
758	Mono-substituted ring in-phase H wag
1,029	Ring in-phase CH bend
1,220	Ring in-phase CH bend
1,454	Ring semicircle stretch + CH_2 symmetric (scissors) deformation
1,494	Ring semicircle stretch
1,601	Ring quadrant stretch
2,850	CH_2 symmetric stretch
2,924	CH_2 asymmetric stretch
3,000 ~ 3,100	Aromatic CH stretch

TABLE 22.16. *Polysulfone [1,22].*

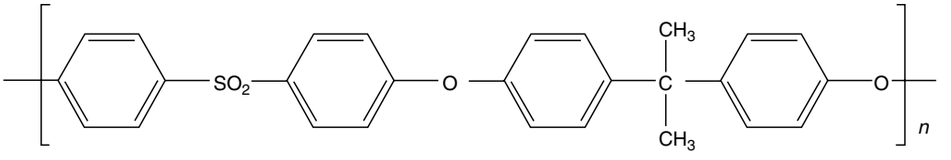

Frequency (cm^{-1})	Assignment
560	SO_2 scissors deformation
690	Aromatic ring bend
834	*Para* out-of-plane aromatic CH wag, two adjacent Hs
1,014	*Para* in-plane aromatic CH bend
1,105	*Para* in-plane aromatic CH bend
1,151	SO_2 symmetric stretch
1,175	SO_2 symmetric stretch
1,244	Aryl-*O*-aryl C–O stretch
1,294	SO_2 asymmetric stretch
1,325	SO_2 asymmetric stretch
1,365	CH_3 symmetric (umbrella) deformation
1,410	*Para* aromatic ring semicircle stretch
1,490	*Para* aromatic ring semicircle stretch
1,505	*Para* aromatic ring semicircle stretch
1,585	*Para* aromatic ring quadrant stretch
2,875	CH_3 symmetric stretch
2,970	CH_3 asymmetric stretch
3,000–3,200	Aromatic CH stretches

TABLE 22.17. *Polycarbonate [1,22].*

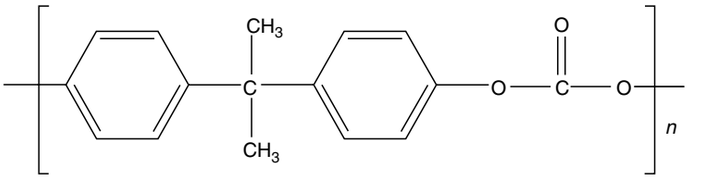

Frequency (cm^{-1})	Assignment
830	*Para* out-of-plane aromatic CH wag, two adjacent Hs
1,015	*Para* in-plane aromatic CH bend
1,080	$(CH_3)_2$ rock/ C–C stretch
1,160	Carbonate C–O stretch
1,193	Carbonate C–O stretch
1,230	Carbonate aryl-*O*-aryl C–O stretch
1,362	CH_3 symmetric (umbrella) deformation
1,405	*Para* aromatic ring semicircle stretch
1,505	*Para* aromatic ring semicircle stretch
1,600	*Para* aromatic ring quadrant stretch
1,775	Carbonate C=O stretch
2,875	CH_3 symmetric stretch
2,970	CH_3 asymmetric stretch
3,000–3,200	Aromatic CH stretches

TABLE 22.18. *Poly(vinyl methyl ether) [1,18].*

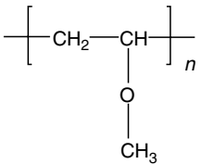

Frequency (cm^{-1})	Assignment
785	CH_2 rock
950	C–O–C symmetric stretch
1,090	C–O–C asymmetric stretch (ether)
1,189	CH_3 rock
1,381	CH_3 deformation
1,460	CH_2 symmetric (scissors) deformation
2,830	O–CH_3 symmetric stretch
2,934	CH_2 asymmetric stretch
2,970	CH_3 asymmetric stretch

TABLE 22.19. *Poly(ethylene oxide) [1,2,20,21].*

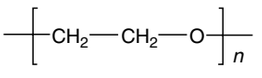

Frequency (cm^{-1})	Assignment
840	C–O–C symmetric stretch, CH_2 rock
947	CH_2 rock
963	CH_2 rock
1,102	C–O–C asymmetric stretch
1,345	CH_2 wag
1,467	CH_2 symmetric (scissors) deformation
2,883	CH_2 asymmetric stretch

TABLE 22.20. *Polyvinylpyrrolidone [1,22].*

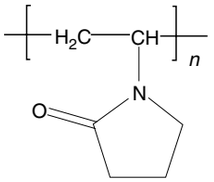

Frequency (cm^{-1})	Assignment
750	CH_2 rock
1,285	C–N stretch
1,420	CH_2 symmetric scissors deformation (CH_2 next to C=O)
1,460	CH_2 symmetric scissors deformation
1,490	CH_2 symmetric scissors deformation (CH_2 next to N)
1,680	Cyclic amide C=O stretch
2,880	CH_2 symmetric stretch
2,920	CH_2 asymmetric stretch
2,951	Cyclic CH_2 asymmetric stretch

TABLE 22.21. *Cellulose acetate [1,22].*

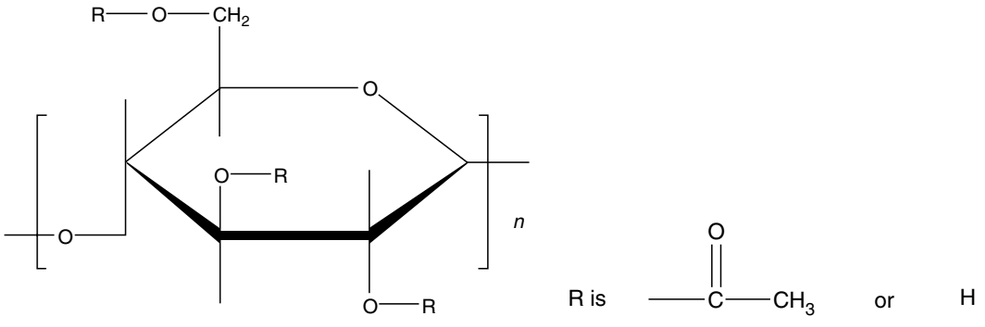

Frequency (cm^{-1})	Assignment
1,050	C–O stretch
1,235	Acetate C–C–O stretch
1,370	CH_3 symmetric (umbrella) deformation
1,432	CH_3 asymmetric deformation
1,750	C=O stretch
2,860	CH_3 symmetric stretch
2,950	CH_3 asymmetric stretch
3,300	OH stretch
3,500	2 × C=O stretch (1,750) overtone

TABLE 22.22. *Nylon 6 [1,22].*

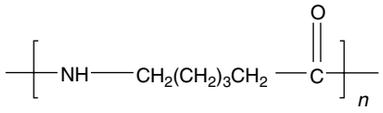

Frequency (cm^{-1})	Assignment
700	NH wag (broad)
722	CH_2 rock
1,170	N–C=O/skeletal vibration
1,200	N–C=O/skeletal vibration
1,370	CH_2 wag

TABLE 22.22. *Continued.*

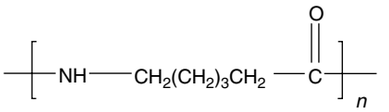

Frequency (cm^{-1})	Assignment
1,420	CH_2 symmetric scissors deformation (CH_2 next to C=O)
1,440	CH_2 symmetric scissors deformation (CH_2 next to N)
1,460	CH_2 symmetric scissors deformation
1,540	NH bend/C–N stretch
1,640	Amide C=O stretch
2,860	CH_2 symmetric stretch
2,920	CH_2 asymmetric stretch
3,100	2 × NH bend (1,540) overtone
3,300	NH stretch

TABLE 22.23. *Polyurethane (polyester based) [1,22].*

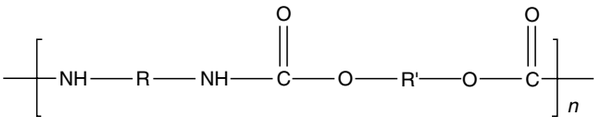

Frequency (cm^{-1})	Assignment
1,060	C–O stretch
1,215	N–C–O stretch
1,460	CH_2 symmetric (scissors) deformation
1,540	C–N stretch
1,590	N–H bend
1,690	C=O stretch (amide)
1,735	C=O stretch (ester)
2,860	CH_2 symmetric stretch
2,925	CH_2 asymmetric stretch
3,320	NH stretch

TABLE 22.24. *Poly(hydroxy butyrate), PHB [1,25].*

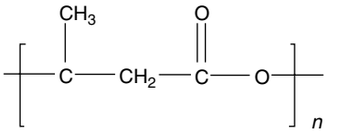

Frequency (cm^{-1})	Assignment
1,050	C–O stretch, ether
1,096	C–O stretch, ether
1,128	C–O stretch, ester
1,180	C–O stretch, ester
1,228	C–O–C stretching mode, crystalline
1,259	C–O–C stretching mode, amorphous
1,263	C–O–C stretching mode, crystalline
1,278	C–O–C stretching mode, crystalline
1,289	C–O–C stretching mode, crystalline
1,302	C–O–C stretching mode, amorphous
1,378	CH_3 symmetric deformation

TABLE 22.24. *Continued.*

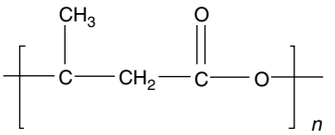

Frequency (cm^{-1})	Assignment
1,449	CH_3 asymmetric deformation
1,458	CH_2 deformation
1,723	C=O stretch, crystalline
1,740	C=O stretch, amorphous
2,875	CH_2,CH_3 symmetric stretch
2,933	CH_2 asymmetric stretch
2,967	CH_3 asymmetric stretch, crystalline
2,974	CH_3 asymmetric stretch, crystalline
2,983	CH_3 asymmetric stretch, amorphous
2,995	CH_3 asymmetric stretch, crystalline
3,009	CH_3 asymmetric stretch, crystalline
3,436	1st overtone, C=O stretch, crystalline

using the information for spectroscopic studies of known polymers. Some assignments are not absolutely conclusive. For analytical identification, entire reference spectra must be used instead. To further guide those who need more in-depth information on this subject, a set of general references is also provided.

REFERENCES

1. N. B. Colthup, L. H. Daly, and S. E. Wiberley, *Introduction to Infrared and Raman Spectroscopy*, 2nd ed. (Academic, New York, 1975).
2. *The Infrared Spectra Atlas of Monomers and Polymers* (Sadtler Res. Labs., Philadelphia, 1980).
3. B. Jasse and J. L. Koenig, J. Makromol. Sci.-Rev. Macromol. Chem. **C17**, 61 (1979).
4. R. G. Snyder and J. H. Schachtschneider, Spectrochim. Acta **20**, 853 (1964).
5. R. S. Stein, J. Chem. Phys. **23**, 734 (1955).
6. J. R. Nielsen and R. F. Holland, J. Mol. Spectrosc. **6**, 394 (1961).
7. G. Zerbi and L. Piseri, J. Chem. Phys. **49**, 3840 (1968).
8. R. G. Snyder and J. H. Schachtschneider, Spectrochim. Acta **21**, 1527 (1965).
9. P. C. Painter, M. M. Coleman, and J. L. Koenig, *The Theory of Vibrational Spectroscopy and Its Applications to Polymeric Materials* (Wiley, New York, 1982).
10. L. J. Bellamy, *The Infra-red Spectra of Complex Molecules*, Vol. 1 (Chapman and Hall, London, 1975).
11. S. Krimm, Fortschr. Hochpolym. Forsch. **2**, 51 (1960).
12. A. Miyake, J. Polym. Sci. **38**, 479 (1959).
13. I. V. Yannas and A. C. Lunn, J. Polym. Sci., Part B **9**, 611 (1971).
14. S. Krimm, L. F. Folt, J. J. Shipman, and A. R. Berens, J. Polym. Sci., Part A **1**, 2621 (1963).
15. Y. Shindo, B. E. Read, and R. S. Stein, Makromol. Chem. **118**, 272 (1968).
16. I. Lipschitz, Polym. Plast. Technol. Eng. **19**, 53 (1982).
17. C. Y. Liang and S. Krimm, J. Polym. Sci. **27**, 241 (1958).
18. M. M. Satkowski, J. T. Grothaus, S. D. Smith, A. Ashraf, C. Marcott, A. E. Dowrey, and I. Noda, in *Polymer Solutions, Blends, and Interfaces*, edited by I. Noda and D. N. Rubingh, (Elsevier, New York, 1992), p. 89.
19. R. Gotoh, T. Takenaka, and N. Hayama, Kolloid Z. **205**, 18 (1965).
20. C. Y. Liang, in *Newer Methods of Polymer Characterization*, edited by B. Ke (Wiley, New York, 1964).
21. H. Matsuura and K. Fukuhara, J. Polym. Sci., Part B: Polym. Phys. **24**, 1383 (1986).
22. C. J. Pouchert, *The Aldrich Library of FT-IR Spectra* (Aldrich Chemical, Mikwaukee, 1985).
23. T. Usami and S. Takayama, Polym. J. **16**(10), 733 (1984)
24. *The Infrared Spectra Atlas of Monomers and Polymers* (Sadtler Res. Labs., Philadelphia, 1980).
25. H. Sato, R. Murakami, A. Padermshoke, F. Hirose, K. Senda, I. Noda and Y. Ozaki, Macromolecules, **37**, 7203 (2004).

GENERAL REFERENCES ON POLYMER IR SPECTROSCOPY

D. I. Bauer and W. F. Maddams, *The Vibrational Spectroscopy of* Polymers (Cambridge University, New York, 1989).

L. J. Bellamy, *The Infra-red Spectra of Complex Molecules*, Vols. 1 and 2 (Chapman and Hall, London, 1975 and 1980).

N. B. Colthup, L. H. Daly, and S. E. Wiberley, *Introduction to Infrared and Raman Spectroscopy*, 2nd ed. (Academic, New York, 1975).

A. Elliot, *Infrared Spectra and Structure of Organic Long-Chain Polymers* (Arnold, London, 1969).

D. O. Hummel, Ed., *Polymer Spectroscopy* (Verlag Chemie, Weinheim, 1974).

J. L. Koenig, *Chemical Microstructure of Polymer Chains* (Wiley, New York, 1980).

J. L. Koenig, *Spectroscopy of Polymers* (ACS, Washington, 1992).

P. C. Painter, M. M. Coleman and J. L. Koenig, *The Theory of Vibrational Spectroscopy and Its Applications to Polymeric Materials* (Wiley, New York, 1982).

CHAPTER 23

Small Angle Neutron and X-Ray Scattering

George D. Wignall

Neutron Scattering Sciences Division, Oak Ridge National Laboratory, Oak Ridge, Tennessee TN 37831-6393

23.1 INTRODUCTION

Scattering in the context of this article means the deflection of a beam of radiation (neutrons/x-rays/light, etc.) from its original direction by interaction with the nuclei or electrons of polymer/solvent molecules in a sample. The angular distribution of the intensity reflects the structure of the sample and such techniques have been employed since the beginnings of polymer science to provide information on the spatial arrangements of macromolecules [1]. The first measurements were made in the 1920s using x-rays to determine crystal structures via the Bragg law

$$n\lambda = 2D \sin\theta, \tag{23.1}$$

where D is the distance between crystallographic planes, λ is the wavelength of the radiation used, 2θ is the angle of scatter, and n is the (integer) order of reflection. The intensity is conventionally measured as a function of the momentum transfer, Q, which is related to 2θ via

$$Q = 4\pi\lambda^{-1} \sin\theta \tag{23.2}$$

although several different symbols have been used to denote this parameter in the literature for the different types of radiation used (e.g., Q, K, h, k, s, q, μ etc.). Combining Eqs. (23.1) and (23.2) gives

$$D = 2\pi/Q \tag{23.3}$$

which indicates the distance scale probed by a measurement at a given value of Q. Experiments in the range $0.6 < Q < 15$ Å^{-1} contain most of the information relevant for the determination of unit cell dimensions and are conventionally referred to as wide-angle scattering, which probe a distance scale $\sim 0.4 < D < 10$ Å. Wide-angle x-ray scattering (WAXS), with a wavelength ~ 1 Å, has been the principal technique for the determination of polymer crystal structures [2]. Unit cell dimensions [3], along with details of the WAXS technique [4] are given in standard reference works [2–4]. Subsequently, neutron diffraction or wide-angle neutron scattering (WANS) has supplemented these measurements of crystal structures [5,6].

In the amorphous state, the intermolecular correlations are more diffuse, and the information available from wide-angle scattering is less precise. A Fourier transform of the data gives a radial distribution function (RDF) which is a weighted sum of interatomic pair correlation functions $g_{ij}(r)$, which express the probability of finding atomic species i and j separated by a distance r. In the crystalline regions of polymers the $g_{ij}(r)$ reduce to a series of delta-functions defining the interatomic distances in the unit cell. For amorphous materials, the RDFs are generally featureless for $r > 10$ Å, indicating the absence of long range order between neighboring chains [7].

Although Bragg's law does not apply to amorphous materials, the Fourier or inverse relationship between the structure in real-space (r) and the scattering in Q-space, means that Eq. (23.3) may be applied to first order for all types of scattering. Thus, data at lower Q-values probe longer length scales, and x-ray methods have been widely used to determine chain dimensions in dilute solution, lamellar spacings in crystalline polymers, etc. These measurements are conventionally referred to as small-angle x-ray scattering (SAXS), though it is the Q-range (typically $10^{-3} < \mathrm{Q} < 10^{-1}$ Å^{-1}) which determines the size of objects studied and radiation with other wavelengths (e.g., light, neutrons) can

provide similar information in different angular ranges. For example, light scattering (LS), with $\lambda \sim 2$–6,000 Å, probes a much smaller Q-range ($\sim 2 \times 10^{-6} < Q < 2 \times 10^{-3}$ Å^{-1}) than SAXS, even though the angular range can be quite large (up to $2\theta \sim 160°$). Hence, the measurements probe distance scales, via Eq. (23.3), up to $\sim 10\,\mu$m and the technique has been used extensively since the 1940s, to determine the molecular weight and global dimensions of polymer molecules, for example in dilute solution.

For over two decades, small-angle neutron scattering (SANS), with a wavelength $\lambda \sim 5$–20 Å, has proven to be extremely useful for the evaluation of polymer chain conformation. Due to a combination of high bulk penetrating power, the ability to manipulate scattering amplitudes through isotopic labeling (e.g., deuteration), or an appropriate choice of solvent (contrast variation), SANS has developed into a powerful tool for the study of polymers, particularly in systems inaccessible to SAXS or LS (e.g., bulk polymers, concentrated solutions etc.).

For most applications in polymer science, neutron, x-ray, and light scattering are examples of predominantly elastic scattering, where the incident and scattered radiation have the same energy or wavelength. Such experiments give information on the time-averaged structure and conformation of polymer molecules and form the bulk of the work undertaken on polymers. There has been less work involving inelastic processes, where there is a change of energy on scattering, and the incident and scattered radiation have different wavelengths. This technique gives valuable information on polymer dynamics, though this methodology is beyond the scope of this article [8–10]. Also, due to space limitations, is not possible to survey all contributions to the understanding of polymer structure by all types of radiation (neutrons, x-rays, light, electrons etc.) in different Q-ranges (small-angle, wide-angle, etc.). Similarly, it is not possible to derive the scattering theory, which will be quoted from existing reviews of neutron [8,11–13], x-ray [14,15], and light scattering techniques [12,16]. Most of the work on polymers has been undertaken at small Q-values to probe the longer length scales associated with these materials. The article will illustrate the type of information provided by SANS and SAXS, along with analogies and differences between neutron and photon scattering.

The treatment will emphasize the importance of placing data on an absolute scale, typically in the form of a differential scattering cross section $d\Sigma/d\Omega(Q)$, per unit sample volume (in units of cm^{-1}) for SAXS and SANS. The equivalent quantity for LS is the Rayleigh ratio, which is directly analogous to $d\Sigma/d\Omega$ [8,17,18]. The use of absolute units is not essential for the measurement of spatial dimensions (e.g., the determination of the radius of gyration of polymer molecules). However, it forms a valuable diagnostic tool for the detection of artifacts, to which scattering techniques are particularly vulnerable.

Because the cross-section varies as the sixth power of the dimensions [14], it is a very sensitive indicator of whether an appropriate structural model has been chosen. Thus, absolute SANS measurements of melt-crystallized blends of normal (hydrogenous) and deuterium-labeled polyethylenes showed that the scattering could exceed the expected intensity for randomly mixed molecules by three orders of magnitude. This indicated that some kind of previously unsuspected aggregation or clustering phenomenon was taking place [19]. Similarly, scattering studies of colloidal micellar solutions may be modeled by calculation of the interparticle correlations between spherical micelles as a function of a set of parameters describing the particle structure (inner/outer radius, degree of ionization etc.). On an arbitrary intensity scale, it is possible to produce excellent fits of the particle shape, which may be in error by as much as 3–4 orders of magnitude in intensity [20]. Thus, absolute calibration allows such artifacts to be recognized, and the model parameters may be restricted to those which reproduce the observed cross section. Because the literature often contains general formulae, as opposed to practical examples of how such calculations are actually accomplished, this article will illustrate such comparisons via a range of examples on different polymeric systems.

Figure 23.1 illustrates the relationship between the neutron energy and wavelength. The kinetic energy of a neutron of particle velocity ~ 750 m/sec (wavelength $\lambda = 5.3$ Å) is ~ 3 meV or 4.7×10^{-15} ergs [8]. Such energies are of the same order as the vibrational and diffusional energies of molecular systems and much lower than x-ray photons (~ 10 keV). For LS, the scattering patterns are very dependent on the polarization directions, though because of the much higher energies of x-rays, chemical bonding has little effect on SAXS and there is negligible influence of the differences between the directions of radiation polarization and molecular orientation [21]. Hence polarization effects,

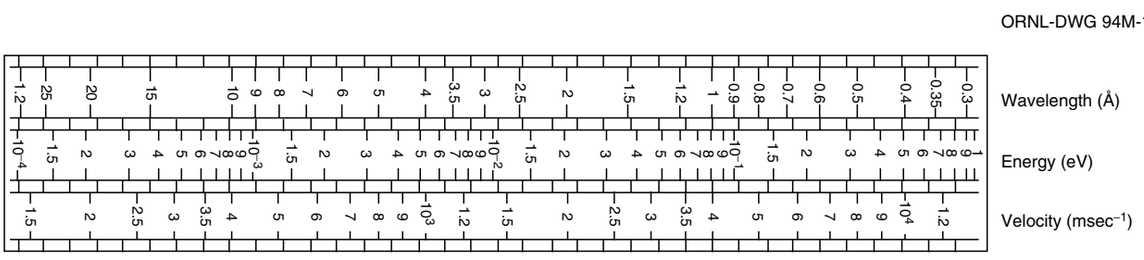

FIGURE 23.1. Conversion chart for neutron wavelength, energy, and velocity.

which are important for LS, can be neglected in SAXS and also for SANS experiments on polymers[1].

SANS, SAXS, and LS all involve interference phenomena between the wavelets scattered by different elements in the system. When a plane wave, described by a wave function of unit density [8] interacts with a single nucleus, the scattered wave is given by

$$\Psi_1 = -\frac{b}{r}\exp(ikr). \tag{23.4}$$

The quantity b has the dimensions of length and is called the scattering length, which may be regarded as a real (known) constant for a given nucleus (isotope). The scattered single atom cross section is given [8,22,23] by

$$\sigma = 4\pi b^2. \tag{23.5}$$

It can be seen from Eq. (23.5) that σ has the dimensions of area. The magnitude of b is typically of the order of 10^{-12}cm, and this gives rise to the usual unit for a cross section which is called a barn (10^{-24}cm^2).

Neutrons are scattered isotropically from individual nuclei, whereas for LS and SAXS, the scattering originates in the electron cloud, so the atomic form factors are in principle Q-dependent. However, the variation is very small in practice ($< 1\%$ for $Q < 0.1\,\text{Å}^{-1}$) for SAXS and LS, and is usually neglected [4]. The Thompson scattering amplitude of a classical electron is $r_T = 0.282 \times 10^{-12}$cm [24], so the x-ray scattering length of an atom, f, is proportional to the atomic number ($f = r_T Z$) and increases with the number of electrons per atom. For neutrons, there is no general trend throughout the periodic table in the values of b, which vary from isotope to isotope. If the nucleus has nonzero spin, it can interact with the neutron spin, and the total cross section (σ_{coh}) splits into coherent and incoherent components defined by

$$\sigma_{coh} = 4\pi < b >^2, \tag{23.6}$$

$$\sigma_{inc} = \sigma_{tot} - \sigma_{coh} = 4\pi[< b^2 > - < b >^2], \tag{23.7}$$

where the brackets $<>$ represent a thermal average over the spin state population.

If the isotope has no spin, then $< b^2 > = < b >^2$ as $< b > = b$ and there is no incoherent scattering for neutrons. Only coherent scattering contains information on the structure of the sample. The incoherent cross section contains no information on interference effects and forms an isotropic (flat) background which must be subtracted off in SANS structural investigations. While most of the atoms encountered in neutron scattering from polymers are mainly coherent scatterers (e.g., carbon, oxygen, deuterium), there is one important exception [8,22,23]. In the case of hydrogen (H^1)

$$\sigma_{coh} = 1.76 \times 10^{-24}\text{cm}^2, \tag{23.8}$$

$$\sigma_{inc} = 79.7 \times 10^{-24}\text{cm}^2. \tag{23.9}$$

For photons, there is no strict analog of incoherent scattering of neutrons due to nonzero spin in the scattering nucleus. Compton scattering which occurs for x-rays is similar in that it contains no information on interference effects, i.e., the structure of the sample, and forms a background to the coherent signal. However, to a good first approximation this background goes to zero in the limit $Q \to 0$ and is usually neglected in SAXS and LS studies.

Table 23.1 gives the cross sections and scattering lengths for atoms commonly encountered in synthetic and natural polymers. These cross sections refer to bound protons and neglect inelastic effects arising from interchange of energy with the neutron. For coherent scattering which is a collective effect arising from the interference of scattered waves over a large correlation volume, this approximation is reasonable [8]. However, for incoherent scattering, inelastic effects become increasingly important for long wavelength neutrons with the result that the H^1 incoherent cross section, and hence the sample transmission, is a function of both the

TABLE 23.1. *Bound atom scattering lengths and cross sections for typical elements in synthetic and natural polymers.*

Atom	Nucleus	$b_{coh}(10^{-12}\text{cm})$	$\sigma_{coh} = 4\pi b_{coh}^2(10^{-24}\text{cm}^2)$	$\sigma_{inc}(10^{-24}\text{cm}^2)$	$\sigma_{abs}(10^{-24}\text{cm}^2)$	$f_{x\text{-ray}}(10^{-12}\text{cm})$
Hydrogen	^{1}H	−0.374	1.76	79.7	0.33**	0.28
Deuterium	^{2}H(D)	0.667	5.59	2.01	0	0.28
Carbon	^{12}C	0.665	5.56	0	0	1.69
Nitrogen	^{14}N	0.930	11.1	0	1.88**	1.97
Oxygen	^{16}O	0.580	4.23	0	0	2.25
Fluorine	^{19}F	0.556	4.03	0	0	2.53
Silicon	^{28}Si	0.415	2.16	0	0.17**	3.94
Chlorine	Cl*	0.958	11.53	5. 9	33.6**	4.74

*Values are for the naturally occuring element and are an average over the mixture of isotopes; $f_{x\text{-ray}}$ is given for $\Theta = 0$, though the angular dependence is small (<1%) for $Q < 0.1\,\text{Å}^{-1}$.

**Values of the absorption cross section (σ_{abs}) are a function of wavelength (λ) and are given at $\lambda = 1.8$Å. As $\sigma_{abs} \sim \lambda$, values at other wavelengths may be estimated by scaling via the ratio $\lambda/1.8$.

[1] Except in the hypothetical case of a material containing elements with unpaired spins (e.g., Fe, Mn, rare earths etc.), where polarization effects can theoretically occur, due to the interaction with the neutron spin. In practice, polymers do not contain such elements, so polarization effects can also be neglected in SANS.

incident neutron energy and sample temperature [25]. In addition, because of inelastic effects due to torsion, rotation, and vibration, the effective incoherent cross section is a function of the particular chemical group (methyl, hydroxyl etc.) in which the proton is situated [26]. This is illustrated in Table 23.2, which shows the total hydrogen atom cross section (σ_{tot}) in various liquids and polymers. σ_{tot} is dominated by the incoherent component (σ_{inc}), and hence is also a strong function of λ and only approaches $\sim$ 80 barns at $\lambda \sim 4.5$ Å. Thus, the cross sections given in Table 23.1 cannot be used to calculate the incoherent background because although $\sigma_{inc} = 79.7 \times 10^{-24}\text{cm}^2$ is widely quoted in the literature, this value almost never applies to real polymer systems.

It may be seen from Table 23.1 that there is a large difference in the coherent scattering length between deuterium and hydrogen and that the latter value is actually negative. This arises from a change of phase of the scattered wave and results in a marked difference in scattering power (contrast) between molecules synthesized with deuterated or protonated monomer units.

The majority of neutron scattering experiments undertaken on polymers fall into the category of SANS from a fraction of deuterated chains in a matrix of normal (protonated) polymer and such experiments are examples of predominantly coherent elastic scattering, which gives information on the time-averaged structure (e.g., chain configuration or orientation in the bulk, polymer compatibility, segregation etc.). Similarly, for x-ray scattering, the energy changes are much less than the incident energy, so SAXS and WAXS are effectively elastic processes, which give complementary information (e.g., lamellar spacings, chain configuration in solution, crystal structures etc.).

As LS probes longer length scales, the most commonly observed pattern for unoriented samples is due to spherulites, which may be interpreted in terms of the scattering of anisotropic spheres to investigate the spherulite size as a function of the crystallization conditions [21]. For liquids, it is well known that LS is particularly sensitive to contaminants (dirt, dust etc.), and that samples must be carefully filtered. This has meant that LS methods have been largely restricted to dilute solutions, though SANS is much less sensitive to this artifact. Accordingly, SANS has been the preferred technique to investigate concentrated solutions [27,28] and bulk polymers [8,13,21,29].

For such experiments, we can define a coherent scattering length of the repeat monomer unit (segment) by

$$a_H = \Sigma_k b_k, \tag{23.10}$$

where the summation runs over all the atoms in an unlabeled monomer unit and a similar equation may be written for the coherent scattering length of a labeled monomer unit a_D. If the two polymers, with polymerization index (N) and segment (monomer) volume (V) are blended together so that the volume fraction of H- and D-labeled components are φ_H and φ_D, respectively, the coherent cross section is given [8] by

$$\frac{d\Sigma}{d\Omega}(Q) = V^{-1}N\varphi_H\varphi_D(a_H - a_D)^2P(Q) \tag{23.11}$$

after subtracting off the incoherent signal (principally due to H^1 atoms) and the coherent background due to heterogeneities (voids, catalyst residues) or density fluctuations (crystal–

TABLE 23.2. *Experimental (total) hydrogen atom cross sections (σ_{tot}) in various liquids and polymers at room temperature.*

Compound	Formula	Cross section per H^1 atom $\sigma_{tot}(10^{-24}\text{cm}^2)$ $\lambda = 9.0$ Å	$\lambda = 4.75$ Å
Methanol	CH_3OH	137	
Ethanol	CH_3CH_2OH	124	
Isopropanol	$CH_3CHOHCH_3$	123	
n-Butanol	$CH_3CH_2CH_2CH_2OH$	117	
n-Propanol	$CH_3CH_2CH_2OH$	113	
Ethanediol	$HOCH_2CH_2OH$	108	
Propanetriol	$HOCH_2CHOHCH_2OH$	100	
Polyvinylalcohol	$-(CH_2CHOH)_n-$	97	
Polymethylmethacrylate	CH_3 | $-(CH - CH_2)_n-$ | $-CO_2CH_3-$	115	92[a]
Polyethylene	$-(CH_2CH_2)_n-$	113	89[b]
Water ($T = 23$ °C)	H_2O	114	89[c]

Values of σ at $\lambda = 9.0$ Å are taken[2] from reference [26].
[a]Reference [68].
[b]Reference [69].
[c]Reference [66].

[2] By permission of Butterworth-Heinemann Ltd.©

amorphous boundaries, thermal vibrations). The coherent scattering is governed by the single chain form factor, $P(Q)$, which originates from monomer pairs belonging to the same chain [$P(0) = 1$].$d\Sigma/d\Omega(Q)$ is directly analogous to the Rayleigh ratio, used in light scattering [18] and contains information on the single chain (intramolecular) scattering function, $P(Q)$. The mole fraction of each component modulates the coherent cross section and $P(Q)$ may be obtained from the measured intensity at labeling levels up to 50%, though this result was not appreciated in the earliest SANS studies of bulk polymers and concentrated solutions. These experiments relied on analogies with LS where the limit of zero concentration was required to eliminate interchain interference. It may be seen that for $\varphi_D \ll 1$, $\varphi_H \sim 1$ and the cross section is proportional to the concentration [14,32], as assumed in the Guinier [14] and Zimm [30] approximations.

23.2 CONTRAST

The quantity $(a_D - a_H)^2$ is related to the difference in scattering power between labeled and unlabeled chains and is called the contrast factor. In general, radiation incident on a medium whose scattering power is independent of position is scattered only into the forward direction ($\theta = 0$), and all scattering cancels unless the scattering power fluctuates from point-to-point in the sample. X-rays and light photons interact with electrons in the sample and hence are scattered by fluctuations in the electron density (ρ_e). Neutrons on the other hand, have no interaction with electrons, so the contrast arises from fluctuations in scattering length density (ρ_n). Because each nucleus has a different scattering amplitude (Table 23.1), the scattering length density (SLD) is defined as the sum of coherent scattering lengths over all atoms lying in a given volume ΔV, divided by ΔV [31]. For example, in bulk polymers, the SLD is given by the coherent neutron scattering length [Eq. (23.10)] divided by the monomer volume. The coherent cross sections of a system of uniform scattering length density is zero, though fluctuations may be introduced by means of isotopic substitution, thus giving rise to a finite cross section which is proportional to $(a_H - a_D)^2$. Table (23.3) shows values of the SLDs of some H- and D-labeled polymers and solvents.

The parameter used to describe the overall size of a polymer chain is the radius of gyration (R_g), the root mean square distance of all scattering elements from the center of gravity

$$R_g^2 = \frac{\Sigma f_k \, r_k^2}{\Sigma f_k}. \tag{23.12}$$

The summation runs over all scattering elements (k), which are the electrons in the case of SAXS or LS. For SANS, the summation runs over all nuclei, and is weighted by the scattering length of each atom. Thus in principle, the R_g may be different when measured via different techniques. However, in practice each monomer has the same scattering power for a given incident radiation, so for large polymerization indices the differences between SANS, SAXS, and LS radii are negligible. R_g may be derived by expanding $P(Q)$ [Eq. (23.11)] in a power series for low Q ($Q < R_g^{-1}$) and plotting $d\Sigma^{-1}(Q)/d\Omega$ versus Q^2 (30). Alternatively, these parameters may be obtained by plotting ln $[d\Sigma(Q)/d\Omega]$ versus Q^2 at low Q [14]. These types of plots are conventionally referred to as Zimm and Guinier plots, respectively, and the former is generally used for investigating polymer configurations as it has been found to be linear over a wider Q-range. As mentioned earlier, the first measurements in bulk amorphous polymers and concentrated solutions were generally performed in the limit of low relative labeling ($\varphi_D \ll 1$), and extrapolated to zero concentration. In this range, Eq. (23.11) may be expanded to give

$$\frac{d\Sigma^{-1}}{d\Omega}(Q) = \frac{V}{(a_H - a_D)^2 N \varphi_D}\left[1 + \frac{Q^2 R_g^2}{3} + \ldots\right]. \tag{23.13}$$

TABLE 23.3. *Comparison of the scattering length densities of various polymers and solvents.*

Polymer or solvent	Density[3], ρ (at $T \simeq 23$ °C unless otherwise stated) (gm cm^{-3})	Scattering length density, ρ_n (10^{10}cm^{-2})
Carbon disulfide	1.63	1.24
Water	1.0	−0.56
D_2O		6.4
Xylene	0.880	0.79
Xylene-d_{10}		6.04
Toluene	0.867	0.94
Toluene-d_8		5.66
Benzene	0.8765	1.18
Benzene-d_6		5.4
Polybutadiene	0.89	0.41
Polyethylene	0.78 ($T = 145$ °C)	−0.28
Polyethylene-d_4		6.71
Polymethylmethacrylate	1.2	1.06
PMMA-d_8		7.09
Polystyrene	1.05	1.41
Polystyrene-d_8		6.47

23.3 EXAMPLES OF THE APPLICATION OF SANS AND SAXS TO POLYMERS

23.3.1 SANS from Amorphous Polystyrene

Figure (23.2) shows a Zimm plot for 5.0 wt% ($\varphi_D = 0.047$) deuterated polystyrene (PSD) in a matrix of hydrogenous (normal) polymer (PSH). The coherent

[3] The values of SLD are calculated at the indicated densities, which may vary slightly with temperature, tacticity (e.g., for PMMA), degree of crystallinity (e.g., for polyethylene) etc. For different densities, the SLD is proportional to ρ and may be scaled from the values shown. For deuterated materials, it is assumed that the number of monomers per unit volume is independent of deuteration.

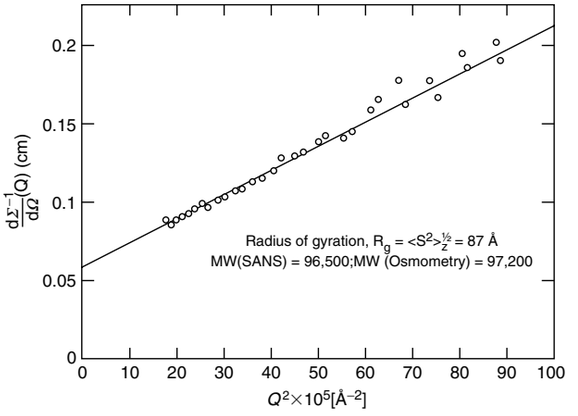

FIGURE 23.2. $\frac{d\Sigma^{-1}}{d\Omega}(Q)$ VS Q^2 for sample containing 5 wt % labeled PSD molecules in polystyrene (PSH).

scattering lengths of the labeled (C_8D_8) and unlabeled (C_8H_8) are 2.328×10^{-12}cm and 10.66×10^{-12}cm, respectively, [via Eq. (23.10) and Table 23.1]. Given a density, $\rho \simeq 1.05$ gm cm^{-3}, the segment volume is 164.5×10^{-24}cm^3 and the extrapolated cross section $[d\Sigma/d\Omega(0) = 17.4 \pm 0.5\,\text{cm}^{-1}]$, leads to a polymerization index of the labeled chains of $N_D = 928 \pm 30$ or a molecular weight of $(96.5 \pm 3) \times 10^3$, in reasonable agreement with independent determinations via osmometry [32]. The radius of gyration is close to that measured in ideal Θ-solvents [8,21] and this supports the unperturbed Gaussian coil as a good approximation to the molecular configuration in amorphous polymers [8,13,32].

23.3.2 SANS and SAXS from Melt-Crystallized Polyethylene

Figure 23.3 shows a Zimm plot of the SANS differential scattering cross section for 6.0 wt% ($\varphi_D = 0.053$) of deuterated polyethylene (PED) in a matrix of unlabeled PEH after rapidly quenching from the melt. The coherent scattering lengths of C_2H_4 and C_2D_4 are -0.166×10^{-12} and 4.00×10^{-12}cm^{-1}, respectively, [via Eq. (23.10) and Table 23.1], and based on an average density of $\rho \simeq 0.94$ gm cm^{-3}, the segment volume is 49.5×10^{-24}cm^3. Thus the extrapolated

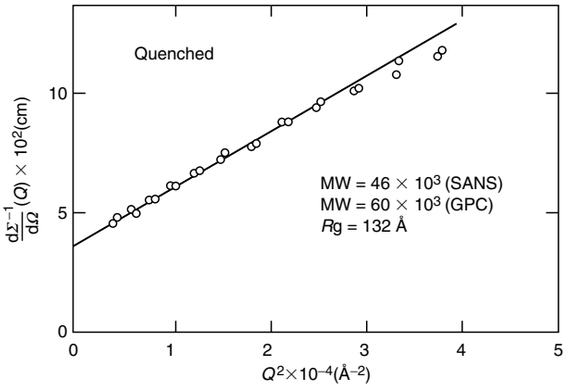

FIGURE 23.3. Typical Zimm plot for 6 WT % PED molecules in PEH matrix quenched from the melt.

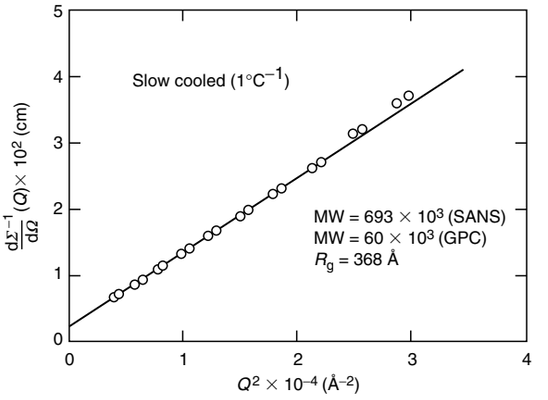

FIGURE 23.4. Typical Zimm plot for 6 wt% PED molecules in PEH matrix slow cooled (1°C^{-1}) from the melt.

cross section $[d\Sigma/d\Omega(0) = 28.0 \pm 2\,\text{cm}^{-1}]$ leads to a polymerization index (N) of 1,600, which is of the same order as the value from gel permeation chromatography [33]. However, when the same sample is slow cooled from the melt [Fig. 23.4], the extrapolated cross section increases by over an order of magnitude. It is clear that these data do not originate in the scattering from single molecules, and it has been shown that the excess intensity is caused by aggregation or clustering of the labeled molecules [19], though this would not be apparent if the data were in arbitrary units. This behavior illustrates the point referred to above that the intensity is extremely sensitive to the particle or molecular dimensions and even an approximate ($\pm 25\%$) absolute calibration is sufficient to reveal the presence of such artifacts.

Figure 23.5 shows SAXS data from the polyethylene sample described above. Because PED and PEH have the same electron density, there is no contrast between the different isotopes and PEH, PED and partially labeled

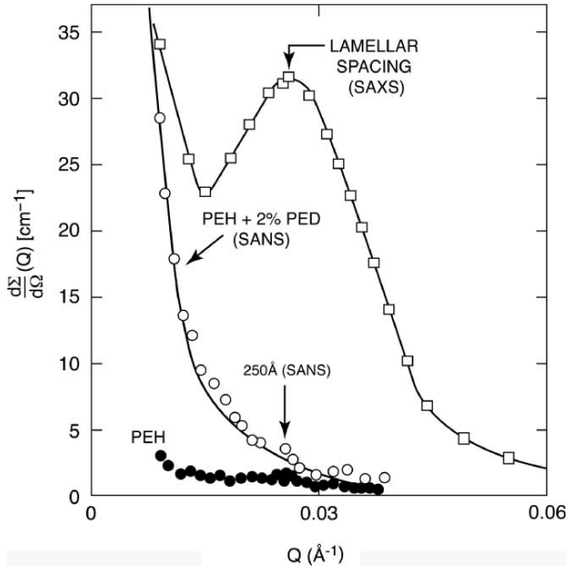

FIGURE 23.5. $\frac{d\Sigma}{d\Omega}(Q)$ vs Q for SAXS and SANS data from melt crystallized polyethylenes.

samples all have the same SAXS profile. The background due to Compton scattering is virtually zero in this Q-range [4] and the signal arises from density fluctuations [13]. The interlamellar peak at $Q \sim 0.025\,\text{Å}^{-1}$ is proportional to the square of electron density difference between the amorphous and crystalline regions (lamellae). The upturn as $Q \to 0$ probably arises from voids and other large scale structures such as spherulites. Figure 23.5 also shows the SANS data for PEH (solid circles), where the coherent signal is superimposed on a flat (incoherent) background $\sim 1\,\text{cm}^{-1}$. The open circles show the extra (coherent) cross section produced by adding 2% deuterated molecules (PED), which is proportional to the contrast difference $(a_H - a_D)^2$ between deuterated and protonated segments.

Departures from the flat incoherent background of the PEH sample (solid circles) are caused by density fluctuations in the sample and it is just possible to see the peak at $Q \sim 0.025\,\text{Å}-1$, due to the periodic stacking of crystalline lamellae alternating with amorphous regions. The SANS coherent signal in PEH is very weak, however, due to the cancellation between the scattering lengths of carbon and hydrogen (Table 23.1), which makes the SLD very small for PEH (Table 23.3).

In the case of PED, there is no cancellation between the coherent scattering lengths of carbon and deuterium (Table 23.1), and the incoherent background is very much smaller than for PEH. Thus, PED should have virtually identical SAXS and SANS cross sections apart from a scale factor. Figure 23.6 shows absolute SAXS and SANS data for the same sample of PED, which should scale as the ratio of the electron density to the scattering length density. As the number of segments per unit volume is the same for SAXS and SANS, this term cancels and the ratio (R) reduces to

$$R = \frac{(0.282 \times 10^{-12} \times 16)^2}{(4.00 \times 10^{-12})^2} = 1.27, \qquad (23.14)$$

where $r_T = 0.282 \times 10^{-12}$cm is the Thompson scattering factor of one electron, and 4.00×10^{-12}cm is the neutron scattering length of a C_2D_4 monomer, which contains 16 electrons. Thus the measured (1.31 ± 0.1) and theoretical ratios are in good agreement [34].

23.3.3 Application of Contrast Variation Methods to Core–Shell Latex Structures

Contrast variation methods can sometimes be used to remove a component of the scattering by matching its scattering power with that of the medium in which it is dispersed. This principle can be used in SANS experiments via isotopic solvent mixtures (e.g. H_2O/D_2O) to adjust the scattering power of the medium, as for example in studies of polymer latexes. Grancio and Williams [35] postulated a polymer-rich spherical core surrounded by a monomer-rich shell which serves as the major locus of polymerization, thus giving rise to core–shell morphology. Thus, the first formed polymer constitutes the core and the second formed polymer makes up the shell, and neutron scattering has been used to test this hypothesis by isotopically labeling chains generated at specific points in the polymerization process [36–40].

For a homogeneous particle, suspended in a solvent, the neutron scattering cross section is given by

$$\frac{d\Sigma}{d\Omega}(Q) = (\rho_{np} - \rho_{ns})^2 N_p V_p^2 P(Q), \qquad (23.15)$$

where ρ_{np} and ρ_{ns} are the neutron scattering length densities of the particle and solvent, respectively, N_p is the number of particles per unit volume, V_p is the particle volume, and $P(Q)$ is the particle form factor [$P(0) = 1$]. According to Grancio and Williams [35], polymerization takes place in a surface shell and thus if the monomer feed is changed from protonated to deuterated material, this will result in a predominantly D-labeled shell. When examined by SANS in an H_2O–D_2O mixture which matches the scattering length density of the protonated core, the scattering will arise from a hollow sphere with a particle form factor [41] given by

$$P(Q) = 9\frac{[\sin(QR) - \sin(QR1) - QR\cos(QR) + QR1\cos(QR1)]^2}{Q^6R^6(1-l)^6}, \qquad (23.16)$$

where R and a are the outer and inner radii, respectively, ($l = a/R$).

Figure 23.7 shows SANS data from a 4.6 vol% latexes with a fully deuterated PMMA-D shell, (thickness 30 Å) polymerized on a PMMA-H core (radius, $a = 498$ Å), after desmearing corrections for the finite instrumental resolution [37,42]. The absolute intensity at zero scattering angle is given by Eq. (23.15) with $P(0) = 1$ and Vp equal to the volume of the D-labeled polymer in the shell with SLD[4], $\rho_{np} = 6.97 \times 10^{10}\text{cm}^{-2}$. The SLD of the solvent is close to that of the PMMA-H core ($\rho_{ns} = 1.06 \times 10^{10}\text{cm}^2$) and thus

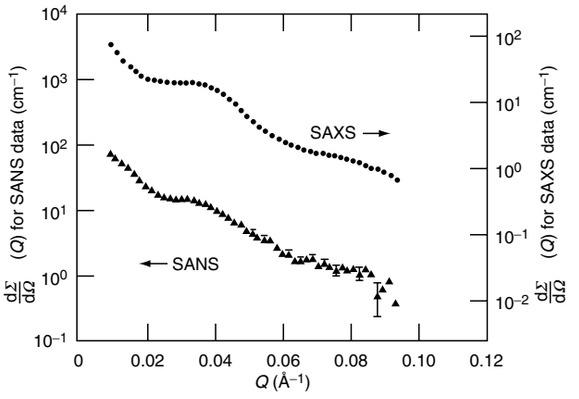

FIGURE 23.6. $\frac{d\Sigma}{d\Omega}(Q)$ vs Q for deuterated polyethylene sample after subtraction of incoherent background.

[4] This value is slightly different to that quoted in Table 23.3, based on a density of 1.2 gm cm^{-3}, which is an average over the atactic, isotactic and syndiotactic homopolymers. For atactic PMMA, $\rho \simeq 1.18$ gm cm^{-3}.

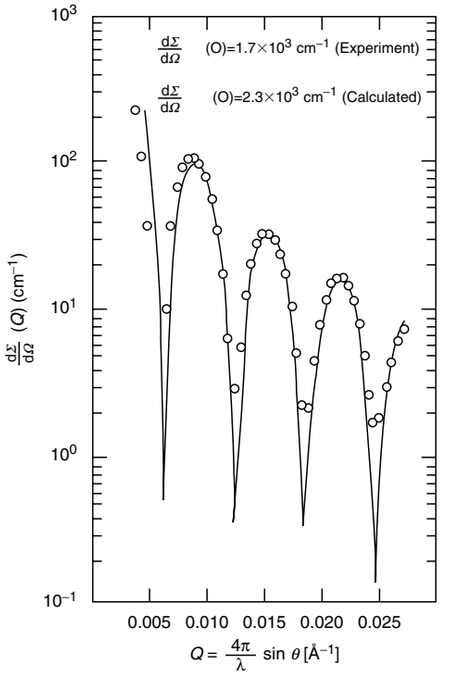

FIGURE 23.7. Desmeared SANS data (O) for PMMA Latex CI (4.6 vol%) with 30 Å D-DMMA shell on surface (core contrast matched) compared with theoretical hollow shell scattering. Reprinted from the Journal of Colloid and Interface Science, **123**, L. W. Fisher, S. Melpolder, J. M. O'reilly, V. Ramakrishnan, and G. D. Wignall, "Neutron Scattering from Interfacially polymerized Latexes", 29–33, Copyright (1988) with permission of Elsevier.

the core contrast is negligible compared to the PMMA-D shell. The extrapolated cross section, $d\Sigma/d\Omega(0) = 1.7 \times 10^3 cm^{-1}$, is in good agreement with the calculated value of $(2.3 \times 10^3 cm^{-1})$, in view of the extreme sensitivity of the calculations to slight variations in shell thickness, mismatches in SLD, surface roughness etc. [37,42]. Similarly the particle dimensions from SANS are in excellent agreement with independent techniques (e.g., LS).

23.3.4 SAXS and SANS from 2-Phase Systems

Blends of High- and Low-Density Polyethylenes

SANS experiments have indicated that blends of high density (linear) and long-chain branched low density polyethylenes (HDPE/LDPE) are homogeneous in the melt, though the components may separate on slow cooling due to the difference in crystallization mechanisms [43]. The semicrystalline blends form effectively two-phase systems in the solid state, and it was shown [43, 44] that the Debye–Bueche (DB) [45,46] model was appropriate to describe the morphology, with a SANS cross section of the form

$$\frac{d\Sigma}{d\Omega}(Q) = \frac{8\pi a^3 \varphi_1 \varphi_2 [\rho_{n1} - \rho_{n2}]^2}{(1 + Q^2 a_1^2)^2}, \qquad (23.17)$$

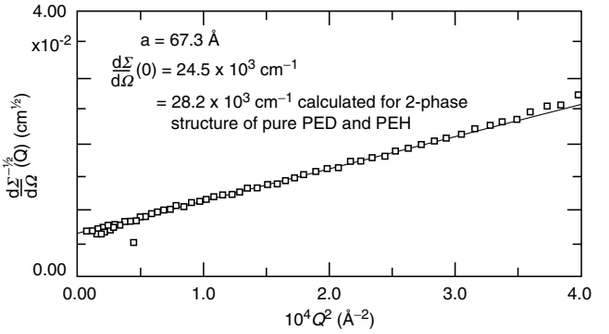

FIGURE 23.8. Debye–Bueche plot for phase separated blend of deuterated HDPE and protonated LDPE slow cooled from the melt AT 0.75 °C^{-1}. Reprinted with permission from R. G. Alamo, J. D. Londono, L. Mandelkern, F. C. Stehling and G. D. Wignall, Macromolecules, **27**, 411 (1994). Copyright (1994) American Chemical Society.

where a_1 is a length characterizing the structure, φ_1 and φ_2 are the volume fractions, and ρ_{n1} and ρ_{n2} are the neutron scattering length densities of the two phases [43,44]. Figure 23.8 shows a DB plot $[d\Sigma/d\Omega(Q)^{-1/2} \text{vs} Q^2]$ of the data for a 50/50 blend after cooling from the melt at 0.75°C min^{-1}. The extrapolated cross section $[d\Sigma/d\Omega(0) = 24.5 \times 10^3 cm^{-1}]$ is well over an order of magnitude higher than in the melt, indicating that the components have phase-separated on cooling. The plot is reasonably linear and the $(Q = 0)$ cross section is given by Eq. (23.17) where the correlation length (a) is derived from the ratio of slope/intercept of the DB plot [44–47]. Assuming complete separation of the H- and D-labeled components, the SLDs in the solid state can be scaled (via the density) from the melt values shown in Table 23.3, to give a calculated cross section of $28.2 \times 10^3 cm^{-1}$. In view of the fact that the experiments are independently calibrated with no arbitrary fitting factors in the intensity scale, the agreement with the absolute cross sections calculated from the DB theory is excellent.

Interpenetrating Polymer Networks

Figure 23.9 shows DB plots of SANS data from polystyrene–polybutadiene interpenetrating polymer networks [47].

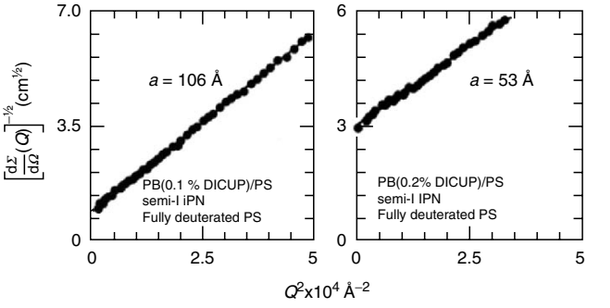

FIGURE 23.9. $\left[\frac{d\Sigma}{d\Omega}(Q)\right]^{-1/2}$ vs. Q^2 for two PB/PS semi-I-IPN systems with different amounts of cross-linker (DICUP).

Assuming complete segregation of the components, $d\Sigma/d\Omega(0)$ may be calculated from Eq. (23.17), via the measured correlation lengths (Fig. 23.9) and the SLDs given in Table 23.3. For the data from the two samples shown in Fig. 23.9, this leads to calculated values of $17.2 \times 10^3 cm^{-1}$ and $2.7 \times 10^3 cm^{-1}$, compared to experimental determinations of $21.6 \times 10^3 cm^{-1}$ and $2.0 \times 10^3 cm^{-1}$. The discrepancies are not unreasonable in view of the strong dependence of the cross section on the domain dimensions, which is a general feature of absolute intensity comparisons. However, this illustrates the point made earlier that even an approximate ($\pm$ 25%) absolute calibration is sufficient to test the assumption of complete phase separation of the blend components.

In the limit $Qa \gg 1$, Eq. (23.17) reduces to $d\Sigma/d\Omega \sim PQ^{-4}$

$$P = 2\Pi(\rho_{n1} - \rho_{n2})^2 S/V, \tag{23.18}$$

where P is the Porod constant, which contains information on the specific surface of the material, i.e., the total interphase surface (S) area per unit volume (V). By comparison of Eqs. (23.17) and (23.18)

$$S/V = 4\varphi_1\varphi_2/a. \tag{23.19}$$

For the data shown in Fig. 23.9, this leads to specific surface values in the range $(58–150) \times 10^4 cm^{-1}$ or $(58–150) m^2 gm^{-1} (\rho \simeq 1.0\, gm\ cm^{-3})$.

Void Content of Hompolymers via SAXS Invariant Analysis

Figure 23.10 shows a Kratky plot [$(Q^2 d\Sigma/d\Omega(Q)$ vs Q] for a polyimide sample made from the condensation of pyromellitic-dianhydride and oxydianiline (PMDA-ODA). The integrated area under this curve is the invariant which for a 2-phase system is given by

$$\mathbf{Q_0} = \int_0^\infty Q^2 d\Sigma/d\Omega(Q) dQ = 2\pi^2 \varphi_1\varphi_2 r_T^2 [\rho_{e1} - \rho_{e2}]^2, \tag{23.20}$$

where φ_1, φ_2, and ρ_{e1}, ρ_{e2} are the volume fractions and electron densities of the two phases, respectively. PMDA-ODA may be regarded as a 2-phase system consisting of polymer and voids [48], with $\varphi_1 \ll 1$ and $(1 - \varphi_1) \simeq 1$. The polymer has a density of $1.4\, gm\ cm^{-3}$ and the repeat unit (mass 382) contains 196 electrons, so $\rho_{e2} = 0.43 \times 10^{24}$ electrons cm^{-3} and $\rho_{e1} = 0$. From Fig. 23.10 the invariant, $\mathbf{Q_0} = 0.25 \times 10^{-4} cm^{-1} Å^{-3}$, or $0.25 \times 10^{20} cm^{-4}$, giving a void fraction, $\varphi_1 \simeq 8.7 \times 10^{-5}$, which is typical for such materials [48].

An alternative estimate for φ may be obtained via Guinier analysis if the voids are reasonably monodisperse, as indicated in Fig. 23.11. Assuming that the voids are spherical, the radius (R) may be obtained from the measured R_g via $R = (5/3)^{0.5} R_g \simeq 348$ Å. The extrapolated cross section $d\Sigma/d\Omega(0) \simeq 142\, cm^{-1}$ is given by

$$\frac{d\Sigma}{d\Omega}(0) = N_P V^2 r_T^2 \varphi_1\varphi_2 [\rho_{e1} - \rho_{e2}]^2, \tag{23.21}$$

where $V = 4/3\pi R^3 = 176 \times 10^6$ Å^3 (or $176 \times 10^{-18} cm^3$) is the particle (void) volume and N_p is the number of particles per unit volume. For $\varphi_1 \ll 1$, $N_p V \simeq \varphi_1$ and Eq. (23.21) gives $\varphi_1 \simeq 5.6 \times 10^{-5}$. The two estimates from the invariant and Guinier analysis are of the same order, and the difference probably results from the Guinier assumption of a relatively monodisperse void distribution. Departures from nonlinearity in the Guinier plot observed at the higher Q-values in Fig. 23.11 may reflect polydispersity effects, and thus the estimate via invariant analysis (which is independent of such assumptions) is probably more accurate.

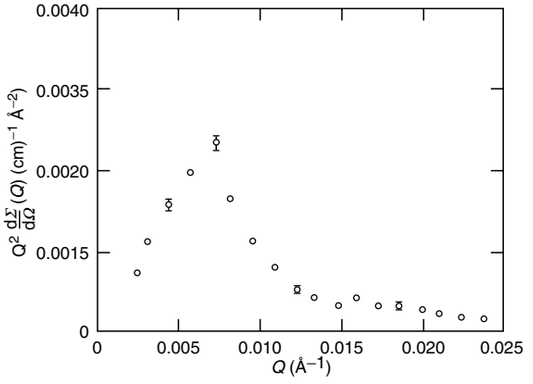

FIGURE 23.10. Integrated scattering curve for PMDA–ODA imidized at 350 °C.

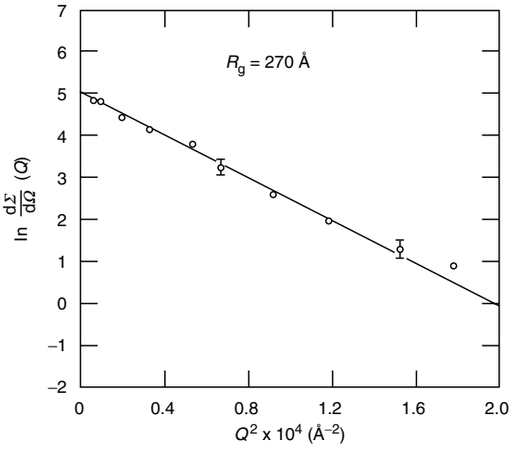

FIGURE 23.11. SAXS Guinier plot for PMDA–ODA Imidized at 350 °C.

23.3.5 Characterization of Multiphase Systems by SANS and SAXS

Blends of High-Density and Linear Low-Density Polyethylenes

Equations (23.17)–(23.20) are strictly valid only for two-phase morphologies, and for multiphase systems, an extension of the SAXS invariant analysis may be employed by generalizing Eq. (23.20) and summing over the number of phases involved

$$\mathbf{Q_0} = 2\pi^2 \sum_{i \neq j} r_T^2 \varphi_i \varphi_j [\rho_{e1} - \rho_{e2}]^2. \tag{23.22}$$

Such an analysis has been applied to semicrystalline blends of polycaprolactone and polycarbonate via SAXS [49] and complementary SANS experiments [50] have employed the DB analysis described above [see Sections ''Blends of High-and Low-Density Polyethylene'' and ''Interpenetrating Polymer Networks'']. For semicrystalline blends of high density and short-chain branched linear low density polyethylenes (LLDPE), complementary DSC and TEM techniques indicate that the compositions of the various crystals and surrounding amorphous regions are such that the system cannot be described by a two-phase model [51]. The ($Q = 0$) cross section [$d\Sigma/d\Omega(0)$] cannot be calculated for multiphase systems, though it may be estimated via a ''pseudo two-phase'' model to a good approximation. For example, with deuterated HDPE-D and protonated LLDPE-H (to provide SANS contrast), the SLD of the HDPE-D crystal is $8.57 \times 10^{10}\text{cm}^{-2}$, whereas the SLDs of the mixed (HDPE-D/LLDPE-H) crystals and amorphous are 0.44 and 0.46 ($\times 10^{10}\text{cm}^{-2}$). Thus, the SANS cross section [$d\Sigma/d\Omega(0)$] can be calculated to a good approximation by grouping the mixed phases into an average background ($\rho_{av} = 0.45 \times 10^{10}\text{cm}^{-2}$) surrounding pure HDPE-D crystal in a pseudo two-phase model. The SANS invariant may be calculated for a multiphase morphology [Eq. (23.22)] by substituting the neutron scattering length densities (ρ_n) for the x-ray scattering length density ($r_T\rho_{e1}$) and summing over the various phases [51]. The ($Q = 0$) cross section may be estimated via Eq. (23.17) for the pseudo two phase model. For series of HDPE-D/LDPE-H samples isothermally crystallized from the met at 117 °C, the experimental data are compared with calculations for two possible morphologies suggested by DSC and TEM analysis:

A. A fraction of the HDPE-D component segregates during isothermal crystallization and the remainder co-crystallizes with LLDPE-H on cooling.

B. HDPE-D partially segregates from the LLDPE-H during isothermal crystallization and the remainder also segregates on cooling. A compositionally mixed homogeneous amorphous phase was assumed to surround the crystals in both cases.

The experimental and calculated Q_0 values are listed in Table 23.4, and for the 18/82 (vol%) blend the calculated Q_0 and the experimental data are identical for morphology type A. Similarly, the value of $d\Sigma/d\Omega(0)$ calculated from the pseudo two-phase model and Eq. (23.1) is $41.4 \times 10^3\text{cm}^{-1}$ for morphology type A, which agrees closely with the experimental value of $39.3 \times 10^3\,\text{cm}^{-1}$. When morphology type B is assumed, the calculated values do not agree with the experimental data for this blend. Thus, SANS supports the idea that predominantly LLDPE-rich blends crystallize isothermally with morphology A, where a fraction of the HDPE-D component segregates during isothermal crystallization and the remainder co-crystallizes with the LLDPE-H on cooling.

For the linear-rich, 78/22 blend the agreement between the experimental and calculated Q_0 and $d\Sigma/d\Omega$ (0) values is closer for morphology type B. SANS indicates that for this blend the intensity and invariant conforms a more segregated morphology of the linear and branched components than for the LLDPE-rich blend. For 50/50 blends, the measured and calculated values of Q_0 and $d\Sigma/d\Omega(0)$ indicate an intermediate between the A and B types, where part of the HDPE component that crystallizes on cooling is co-crystallized with the branched LLDPE and part crystallizes as pure HDPE [51].

In view of the fact that the experiments are independently calibrated with no arbitrary fitting factors in the intensity scale and that the crystal/amorphous compositions are obtained from DSC, the general agreement with the SANS data is excellent. Thus, the two-phase approximation is able to reproduce not only the SANS invariant, but also the ($Q = 0$) cross section with good accuracy.

TABLE 23.4. *Measured and calculated cross sections and invariants for HDPE-D/LDPE-H blends isothermally crystallized at 117 °C.*

Composition (% volume) HDPE-D/LLDPE-H	$d\Sigma/d\Omega(Q=0)$ $\times 10^{-3}(\text{cm}^{-1})$ expt.	Q_0 $\text{cm}^{-1}\text{Å}^{-3}$ expt.	Proposed morphology	$d\Sigma/d\Omega(Q=0)$ $\times 10^{-3}(\text{cm}^{-1})$ calc.	Q_0 $\text{cm}^{-1}\text{Å}^{-3}$ calc.
18/82	41.4	0.009	A	39.2	0.009
			B	58.1	0.013
78/22	36.1	0.0158	A	18.4	0.007
			B	33.1	0.013

Carbon-filled polyethylenes

Other multiphase systems involving polymers include composite materials produced by mixing with filler particles to modify their mechanical properties or conductivity. For example, carbon black has been extensively used as a reinforcing filler in a number of applications such as automotive tires and can also be blended with insulators such as semicrystalline polyethylene (PE) to produce conductive composites used in electrical products. When the concentration of carbon black at room temperature is above the percolation threshold, the composite is conducting. However, at higher current loading, the system heats and expands the polyethylene (PE) matrix, and when this approaches the percolation threshold it becomes highly resistive [52]. This results in a lower current and the device cools to its original state, so a mixture of carbon black and polyethylene acts as a resettable fuse [53].

For materials with particle sizes in the range $\sim$ 10–1,000 Å, both SANS and SAXS may be used to explore the morphology and a combination of these techniques can provide greater insight than either technique in isolation. For example, combined SAXS/SANS studies of carbon-PE composites [52] suggested the presence of a third phase (voids) and subsequent experiments using the contrast options available from deuterium-labeling of the PE-matrix were designed to quantify the void fraction and its variation with temperature [53]. Figure 23.12 illustrates schematically the contrast options available from the combination of SAXS/SANS and deuterium labeling in the study of the three-phase system (polymer, carbon black, and voids), and makes it clear that one cannot resolve void morphology solely with SAXS. However, if one examines a normal composite (with protonated or H-labeled polymer) via SANS, the sample is essentially two-phase because the neutron scattering length densities of polyethylene and voids are virtually identical (see Table 23.5). For such a two-phase system, it has been shown that the morphology may be described by an extension of the DB theory [45,46] and Eq. (23.17) is modified to

$$\frac{d\Sigma}{d\Omega}(Q) = \frac{8\pi a_1^3 \varphi_1 \varphi_2 f[\rho_{n1} - \rho_{n2}]^2}{(1 + Q^2 a_1^2)^2} + \pi^{3/2} a_2^3 \varphi_1 \varphi_2 (1 - f)[\rho_{n1} - \rho_{n2}]^2 \exp\frac{-Q^2 a_2^2}{4}, \tag{23.23}$$

where a_2 is a second correlation length characterizing long range structural features. $(1 - f)$ and f are the fractional contribution of long ranged ($a_2 \sim$ 500–860 Å) and short ranged ($a_1 \sim$ 130–290 Å) components of the structural model, respectively, [46,52,53]. As before, φ_1 and φ_2 are the volume fractions and ρ_{n1} and ρ_{n2} are the neutron scattering length densities of the effectively two-phase system of carbon (SLD $= 6.4 \times 10^{10}$cm^{-2}) and polyethylene/voids (SLD ~ 0); see Table 23.5. Typically f is in the range $0.82 < f < 0.97$ for $0.27 < \varphi < 45.5$ vol% and for $f = 1$, Eq. (23.23) reduces to Eq. (23.17). Thus, a "pseudo two-phase model" may be again applied to this three-phase composite material, as in section "Blends of High-Density and Linear Low-Density Polyethylenes", and it was shown [52] that Eq. (23.23) gives excellent fits to the SANS data over a wide range of carbon black compositions. Table 23.6 compares the measured and calculated cross sections at $(Q = 0)$ and it may be seen that the discrepancies for any given concentration are in the range $\pm$ 25%. Such fluctuations are not unexpected in view of the extreme sensitivity of the cross section to the fitted correlation lengths, both of which are cubed to calculate $d\Sigma/d\Omega(0)$. However, the overall agreement is excellent, as there is no systematic distortion and the deviations are both positive and negative in virtually equal proportions.

If one blends carbon black with deuterated polyethylene, it may be seen from Fig. 23.12, that presence of voids is highlighted within the carbon black/*d*-polyethylene matrix. Through a combination of SAXS/SANS experiments, one can extract information about void size and quantity [53] using the theoretical formalism developed by Wu [54] to model microvoids in composite materials. Typical void concentrations $\sim$ 2 vol%, 400–500 Å in size were measured at room temperature in composite materials containing 30–40 vol% carbon. These voids decrease significantly in concentration during the melt transition however, dropping by an order of magnitude to $\sim$ 0.2 vol%. This decrease might be expected and suggests that the polyethylene domains

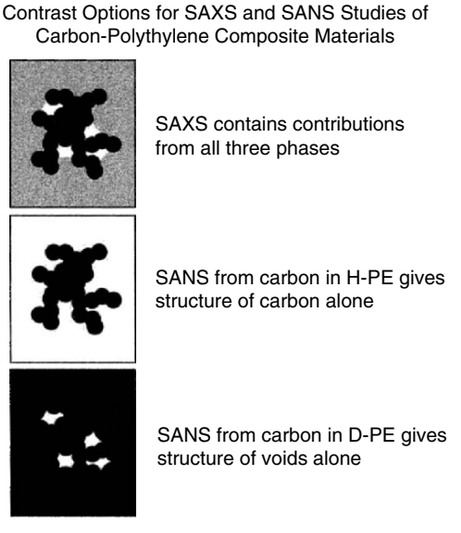

FIGURE 23.12. Contrast options for SAXS and SANS studies of carbon–polyethylene composite materials.

TABLE 23.5. *Neutron (ρ_n) and X-ray ($\rho_x = r_T\rho_{e1}$) scattering length densities of components of carbon-polyethylene composite materials.*

Species	Density, ρ(gm cm^{-3})	X-Ray scattering length density, $\rho_x(10^{10}\text{cm}^{-2})$	Neutron scattering length density, $\rho_n(10^{10}\text{cm}^{-2})$
Carbon black	1.92	16.2	6.4
Voids	0.0	0.0	0.0
Polyethylene	0.95	9.12	−0.34
Polyethylene-d_4	1.08	9.12	8.13

grow at the expense of the voids as the temperature is brought above the melting point.

23.3.6 Isotope Effects in SANS

SANS studies of deuterium labeled polymers were based initially on the assumptions that the molecular configurations and interactions are independent of deuteration, and the interaction parameter between D-labeled and unlabeled segments of the same species χ_{HD} is zero. Nevertheless, there have been several experimental observations which suggested that isotopic substitution does influence polymer thermodynamics and Buckingham and Hentschell [55] suggested that this might arise from a finite interaction parameter ($\chi_{HD} \sim 10^{-4} - 10^{-3}$) between H- and D-labeled segments. Subsequently, SANS was used to measure χ_{HD} for a range of isotopic mixtures [56–58], to delineate the circumstances under which demixing can occur.

For a blend of two polymer species (A and S), one of which (A) is deuterium labeled, the coherent cross section (after subtracting the incoherent background) is given [8,13] by

$$\frac{d\Sigma}{d\Omega}(Q) = V^{-1}(a_H - a_D)^2 S(Q), \tag{23.24}$$

where $S(Q)$ is the structure factor, which contains information regarding both molecular architecture and thermodynamic interactions. In the mean field random phase approximation [59], $S(Q)$ is given by

$$S^{-1}(Q) = [\varphi_A N_A P_A(QR_{gA})]^{-1} + [(1-\varphi_A)N_S P_S(QR_{gS})]^{-1} - 2\chi, \tag{23.25}$$

where $\varphi_A = \varphi_D$ is the volume fraction of the A species and R_{gA}, R_{gS}, N_A and N_S are the radii of gyration and polymerization indices of the two species. The intra-chain functions $P_A(Q)$ and $P_S(Q)$ are represented by Debye functions [60], based on the assumption of a Gaussian distribution of chain elements.

$$P(Q) = 2[R_g^2\, Q^2 + \exp(-R_g^2\, Q^2) - 1]/(R_g^4 Q^4). \tag{23.26}$$

By regarding the H- and D- molecules as different species with volume fractions φ_H and φ_D, the random phase approximation [Eq. (23.19)] may be fitted to the data with χ_{HD} as the only adjustable parameter [56–58]. Complementary experiments on polystyrene [61] and poly (dimethyl siloxane) [62] confirm the existence of a universal isotope effect, arising from the small differences in volume and polarizability between C–H and C–D bonds [63]. Table (23.7) lists typical values of the isotopic interaction parameter for various polymers in the concentration range $0.2 < \varphi_D < 0.8$,

TABLE 23.6. *Comparison of measured and calculated values of the absolute SANS cross section at $Q = 0$ for carbon–polyethylene composite materials.*

Vol % carbon black	$d\Sigma/d\Omega(Q=0)$ $\times 10^{-3}(\text{cm}^{-1})$ measured	$d\Sigma/d\Omega(Q=0)$ $\times 10^{-3}(\text{cm}^{-1})$ calculated
44.5	98	77
39.5	159	118
34.8	177	166
26.3	237	200
16.5	317	380
12.4	247	345
5.6	178	182
1.08	49	50
0.53	32	24
0.27	8	11

TABLE 23.7. *Isotopic interaction parameter for various polymers.*

Polymer	φ_D	T °C	$10^4\chi_{HD}$
Polystyrene	0.5	160	1.8[a] 2.3[b]
1,4 Polybutadiene	0.31	50	7.2[c]
1,2 polybutadiene (polyvinyl ethylene)	0.5	47	6.8[d]
1,2 Polybutene (Polyethyl ethylene)	0.5	47	8.8[d]
Polydimethylsiloxane		∼296	17[e]
Polyethylene	0.5	160	4.0[f]

[a] Reference [56].
[b] Reference [61].
[c] Reference [56].
[d] Reference [58].
[e] Reference [62].
[f] Reference [65].

where χ_{HD} has been shown to be relatively independent of concentration [58,61].

The above results raise the important question of how SANS studies are influenced by isotope effects. As explained earlier, initial SANS experiments on polymers relied on analogies with LS, where the limit of zero concentration was required to eliminate inter-chain scattering. Under such conditions, the isotope effect contributes almost insignificantly to the intensity, and this may be illustrated by calculating $d\Sigma/d\Omega(0)$ via Eqs. (23.24) and (23.25) for the sample of 5.0 wt% PSD in PSH as in Section 23.3.1. The inclusion of an isotopic interaction parameter $\chi_{HD} = 1.8 \times 10^{-4}$ changes $d\Sigma/d\Omega(0)$ to $17.5\,cm^{-1}$ compared to $17.4\,cm^{-1}$ calculated from Eq. (23.11) in the absence of isotope effects. Upon recognizing that information on chain statistics could equally well be obtained from concentrated isotopic mixtures, many experiments were conducted under such conditions in order to enhance the intensity. It is under these conditions that isotope-induced segregation effects are manifested.

In the bulk state many of the systems studied are solids at room temperature and have been exposed for only a limited time in the liquid state, as for example during melt pressing. For polybutadiene, with a glass transition temperature below $-90\,^{\circ}C$, isotopic blends are liquid at room temperature, and this facilitates the attainment of equilibrium. Hence, isotope effects can be particularly dramatic in this system and Fig. (23.13) shows the scattering cross section of mixtures of deuterated ($N_D = 4{,}600$) and protonated ($N_H = 960$) as a function of temperature. It can be seen that the extrapolated zero-Q cross section exceeds by large factors the value it would have ($\sim 100\,cm^{-1}$) if the H–D interactions were negligible. For sufficiently high molecular weight, this system will even phase separate [64], as will other isotopic mixtures (e.g., polyethylene [65]). Thus, it is prudent to evaluate future experiments, based on measured values of χ_{HD} (Table 23.7), and to check for excess scattering. This is best accomplished by calibrating data on an absolute scale and comparing the measured and theoretical intensities [66].

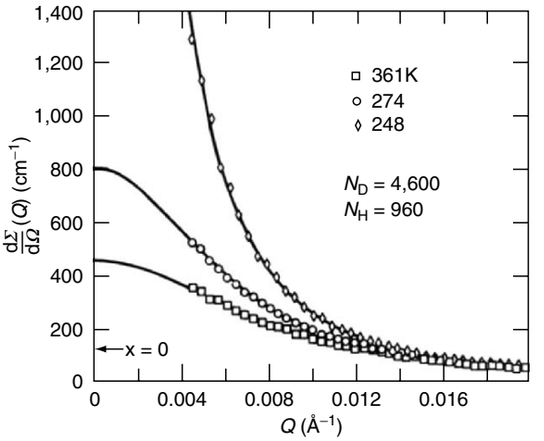

FIGURE 23.13. $\frac{d\Sigma}{d\Omega}(Q)$ VS Q for blend of 69 vol% protonated and 31% deuterated 1, 4-Polybutadiene at the critical composition. The curves were obtained from the homogeneous mixture scattering function by adjusting χ_{HD} (one adjustable parameter). Reprinted with permission from F. S. Bates, G. D. Wignall and W. C. Koehler, Phys Rev. Lett., **55**, 2425 (1985). Copyright (1985) American Physical Society.

Table 23.8 summarizes the formulae for the scattering parameters defined in the above examples. Scattering techniques have been one of the main sources of structural information since the beginnings of polymer science. Over the past two decades, SANS has been extensively applied to complement existing scattering methods (SAXS, WAXS, LS etc.) and the above examples illustrate the new information which it has provided. The complementary aspects of neutron, light, and X-ray scattering, as applied to polymers and colloids, have been surveyed in a current volume edited by Lindner and Zemb [12]. A wide range of applications of neutron scattering to study polymer structure have been described by Higgins and Benoit [29], and Gabrys [67].

TABLE 23.8. *Scattering parameters and formulae.*

Scattering parameter	Particular assumptions of Model[a]	Formula	Equation
Forward ($Q = 0$) cross section, $d\Sigma/d\Omega(0)$	Guinier model (relatively monodisperse particles)	$\frac{d\Sigma}{d\Omega}(0) = N_p V_p^2 (\rho_{n1} - \rho_{n2})^2$ (SANS[b])	(23.15)
Forward ($Q = 0$) cross section, $d\Sigma/d\Omega(0)$	Debye–Bueche model (randomly intermixed phases)	$\frac{d\Sigma}{d\Omega}(0) = 8\pi a^3 \varphi_1 \varphi_2 (\rho_{n1} - \rho_{n2})^2$ (SANS[b])	(23.17)
Invariant, $\mathbf{Q}_0 \int_0^\infty Q^2 d\Sigma/d\Omega(Q) dQ$		$\mathbf{Q}_0 = 2\pi^2 \varphi_1 \varphi_2 r_T^2 [\rho_{e1} - \rho_{e2}]^2$ (SAXS[b])	(23.20)
Porod constant $P = Q^4 d\Sigma/d\Omega(Q)$		$P = 2\pi(\rho_{n1} - \rho_{n2})^2 S/V$ (SANS[b])	(23.18)

[a] The Guinier, Debye–Bueche, Invariant and Porod analyses are all based on the assumption of well defined phases with sharp interfacial boundaries. In addition, the Guinier approach is based on the assumption that the length distribution function (23.15), or probability $P_{00}(r)$ that a randomly placed rod (length, r) can have both ends in the same scattering particle (phase) is zero beyond a well defined limit. For example, for monodisperse spheres, diameter D, $P_{00} = 0$, for $r > D$. In the Debye–Bueche model, P_{00} has no cut off and approaches zero via an exponential correlation function only in the limit $r \to \infty$ [45,46].

[b] For SAXS, the neutron scattering length density (ρ_n) is replaced by the product of the electron density (ρ_e) and the Thompson scattering length ($r_T = 0.282 \times 10^{-12}$ cm), and vice-versa.

ACKNOWLEDGMENTS

The author wishes to thank W. L. Wu and P. A. Egelstaff for permission to include Table 23.2 and Fig. 23.1, respectively. This research was supported by the Division Materials Science, US Department of Energy under contract DE-AC05-00OR22725 with the Oak Ridge National Laboratory, managed by UT-Battelle, LLC.

REFERENCES

1. P. J. Flory, Principles of Polymer Chemistry, Cornell Press, Ithaca, New York p. 22 (1953).
2. L. E. Alexander, X-Ray Diffraction Methods in Polymer Science, Krieger Publishing Co. Inc., London (1969).
3. Chapter IV, Polymer Handbook, ed. J. Brandrup and E. H. Immergut, Wiley Interscience, New York (1975).
4. Chapter 3, International Tables for X-ray Crystallography, ed. C. H. Macgillavry and G. D. Rieck, Kynoch Press, Birmingham (1968).
5. A. Avitabile, R. Napolitano, B. Pirrozzi, K. D. Rouse, M. W. Thomas and B. T. M. Willis, J. Polym. Sci., Polym. Lett. Ed., **13**, 351 (1975).
6. M. Stamm, J. Polym. Sci., Polym. Phys. Ed., **20**, 235 (1982); M. Stamm, E. W. Fischer, M. Dettenmaier, and P. Convert, Discuss. Faraday Soc. **68**, 263 (1979).
7. G. D. Wignall, Chapter 4 in Applied Fiber Science ed. F. W. Happey, Academic Press, London (1978).
8. G. D. Wignall, Encyclopedia of Polymer Science and Engineering, ed. M. Grayson and J. Kroschwitz, Wiley and Sons, New York, 10, 112 (1978).
9. G. Allen and J. S. Higgins, Rep. Prog. Phys. **36**, 1073 (1973).
10. K. Nicholson, Contemp. Phys. **22**, 451 (1981).
11. J. S. Higgins and A. Maconnachie, Chapter 22 in Neutron Scattering, eds. K. Skold and D. L. Price, Academic Press, New York, p. 287 (1987).
12. Neutron, X-Ray and Light Scattering, ed. P. Lindner and T. Zemb, North-Holland Delta Series, Elsevier Publishers, New York, (1991).
13. G. D. Wignall, Chapter 7, p. 313 in The Physical Properties of Polymers, ed. J. E. Mark, ACS Books (1993).
14. A. Guinier and G. Fournèt, Small-Angle Scattering of X-Rays, John Wiley, New York (1955).
15. O. Glatter and O. Kratky, Small-Angle X-Ray Scattering, Academic Press, London (1982).
16. M. G. Huglin, Light Scattering from Polymer Solutions, Academic Press, London (1982).
17. G. Hadziioannou and R. S. Stein, Macromolecules, **17**, 567 (1984); Macromolecules, **17**, 1059 (1984).
18. R. G. Kirste, W. A. Kruse and K. Ibel, Polymer, **16**, 120 (1975).
19. J. Schelten, G. D. Wignall, D. G. H. Ballard and G. W. Longman, Polymer, **18**, 1111 (1977).
20. J. B. Hayter and J. Penfold, Colloid Polym. Sci. **261**, 1022 (1983).
21. J. S. Higgins and R. S. Stein, J. Appl. Cryst. **11**, 346 (1978).
22. V. E. Turchin, Slow Neutrons, Israel Program for Scientific Translations, Jerusalem (1965).
23. G. E. Bacon, Neutron Diffraction, Clarendon Press, Oxford, England (1971).
24. R. W. James, The Optical Principles of the Diffraction of X-rays, Bell, London (1958).
25. A. Maconnachie, Polymer, **25**, 1068 (1984).
26. L. D. Coyne and W. Wu, Polym. Commun. **30**, 312 (1989).
27. J. P. Cotton, B. Farnoux, G. Jannink, J. Mons and C. Picot, C. R. Acad. Sci. (Paris), 275, 3C, 175 (1972).
28. J. S. King, W. Boyer, G. D. Wignall and R. Ullman, Macromolecules, **18**, 709 (1985).
29. J. S. Higgins and H. Benoit, Neutron Scattering from Polymers, Clarendon Press, Oxford (1994).
30. B. H. Zimm, J. Chem. Phys. **16**, 157 (1948).
31. J. B. Hayter in V. Degiorgio and M. Corti, eds. Proceedings of Enrico Fermi School of Physics Course XC, North Holland, Amsterdam (1985), p. 59.
32. G. D. Wignall, D.G.H. Ballard and J. Schelten, Eur. Polym. J., **10**, 861 (1974).
33. J. Schelten, D.G.H. Ballard, G. D. Wignall, G. Longman, and W. Schmatz, Polymer, **27**, 751 (1976).
34. T. P. Russell, J. S. Lin, S. Spooner and G. D. Wignall, J. Appl. Cryst. **21**, 629 (1988).
35. M. P. Grancio and D. J. Williams, J. Polym. Sci. (Al), **8**, 2617 (1970).
36. M. P. Wai, R. A. Gelman, M. G. Fatica, R. H. Hoerl and G. D. Wignall, Polymer, **28**, 918 (1987).
37. L. W. Fisher, S. M. Melpolder, J. M. O'Reilly, V. R. Ramakrishnan and G. D. Wignall, J. Colloid Interface Sci. **123**, 24 (1988).
38. J. W. Goodwin, R. H. Ottewill, N. M. Harris and J. Tabony, J. Colloid and Polym. Sci. **78**, 253 (1980); J. Colloid Interface Sci. **78**, 253 (1980).
39. K. Alexander, D. J. Cebula, J. W. Goodwin, R. H. Ottewill and A. Parentich, Colloids Surf. **7**, 233 (1983).
40. D. J. Cebula, J. W. Goodwin, R. H. Ottewill, G. Jenkin and J. Tabony, Colloid and Polym. Sci. **261**, 555 (1983); Discuss. Faraday Soc. **76**, 37 (1983).
41. Lord Rayleigh, Proc. R. Soc. London A. **84**, 24 (1911).
42. G. D. Wignall, V. R. Ramakrishnan, M. A. Linne, A. Klein, L. H. Sperling, M. P. Wai, R. A. Gelman, M. G. Fatica, R. H. Hoerl, L. W. Fisher, S. M. Melpolder and J. M. O'Reilly, Mol. Cryst. Liq. Cryst. **180A**, 25 (1990).
43. R. G. Alamo, J. D. Londono, L. Mandelkern, F. C. Stehling and G. D. Wignall, Macromolecules, **27**, 411 (1994).
44. G. D. Wignall, J. D. Londono, J. S. Lin, R. G. Alamo and L. Mandelkern, Macromolecules, **28**, 3156 (1995).
45. P. Debye and A. M. Bueche, J. Appl. Phys. **20**, 518 (1949).
46. P. Debye, H. R. Anderson and H. Brumberger, J. Appl. Phys. **28**, 679 (1957).
47. A. M. Fernandez, L. H. Sperling, and G. D. Wignall, Multicomponent Polymer Materials, ACS Advances in Chemistry Series 211 (1985).
48. T. P. Russell, Polym. Eng. Sci. **24**, 345 (1984).
49. Y. W. Cheung, R. S. Stein, J. S. Lin and G. D. Wignall, Macromolecules, **27**, 2520 (1994).
50. Y. W. Cheung, R. S. Stein, G. D. Wignall and H. E. Yang, Macromolecules, **26**, 5365 (1993).
51. G. D. Wignall, R. G. Alamo, J. D. Londono, J. S. Lin, L. Mandelkern, M. H. Kim and G. M. Brown, Macromolecules, **33**, 551–561 (2000).
52. G. D. Wignall, N. R. Farrar, and S. Morris, J. Mater. Sci. **25**, 69–77 (1990).
53. D. W. Marr *et al*., Macromolecules, **30**, 2120–2130 (1997).
54. W.-L. Wu, Polymer, **23**, 1907–1912 (1982).
55. A. B. Buckingham and H. G. E. Hentschel, J. Polym. Sci. Polym. Phys. Ed. **18**, 853 (1984).
56. F. S. Bates, G. D. Wignall and W. C. Koehler, Phys. Rev. Lett. **55**, 2425 (1985).
57. F. S. Bates and G. D. Wignall, Macromolecules **19**, 932 (1986).
58. F. S. Bates, M. Muthukumar, G. D. Wignall and L. J. Fetters, Macromolecules, **89**, 535 (1988); Macromolecules, **21**, 1086 (1988).
59. P. G. deGennes, Chapter 5 in Scaling Concepts in Polymer Physics, Cornell University Press, Ithaca (1979).
60. P. Debye, J. Appl. Phys. **15**, 338 (1944).
61. D. Schwahn, K. Hahn, J. Streib and T. Springer, J. Chem Phys. **93**, 8383 (1989).
62. A. Lapp, C. Picot and H. Benoit, Macromolecules, **18**, 2437 (1985).
63. F. S. Bates and G. D. Wignall, Phys. Rev. Lett. **57**, 1429 (1986).
64. F. S. Bates, S. B. Dierker and G. D. Wignall, Macromolecules, **19**, 1938 (1986).
65. J. D. Londono, A. H. Narten, G. D. Wignall, K. G. Honnell, E. T. Hsieh, T. W. Johnson and F. S. Bates, Macromolecules, **27**, 2864 (1994).
66. G. D. Wignall and F. S. Bates, J. Appl. Cryst. **20**, 28 (1987).
67. Applications of Neutron Scattering to Soft Condensed Matter (Edited by Barbara J. Gabrys), Gordon and Breach Science Publishers (2000).
68. J. M. O'Reilly, D. M. Teegarden and G. D. Wignall, Macromolecules **18**, 2747 (1985).
69. B. Crist and G. D. Wignall, J. Appl. Cryst. **21**, 701 (1988).

CHAPTER 24

Mechanical Properties

Witold Brostow

Department of Materials Science and Engineering and Department of Physics, University of North Texas, POBox 305310, Denton, TX 76203-5310, USA; http://www.unt.edu/LAPOM/; brostow@unt.edu

24.1 RELAXATIONAL AND DESTRUCTIVE PROCESSES

24.1.1 Introduction; Service Performance and Reliability

Service performance and reliability constitute the bottom line of the entire polymer science and engineering. Since this statement might appear an exaggeration, let me immediately explain why. Synthesis of macromolecules is of interest primarily to synthetic chemists; polymer rheology is of interest to polymer rheologists; rotational injection molding is of interest to rotational injection molders; and so on. There is, however, an exception: reliability of polymeric materials and components is of interest to everybody—polymer scientists, polymer engineers, and all laymen including those who do not even know what the word ''polymer'' means. A very good example provides a little girl playing with a plastic doll. If the doll will break into pieces, the girl will certainly cry first. Somewhat later, however, some captains of industry might cry also.

Given this situation, let us formulate two highly pertinent and often asked questions:

1. Will a given polymeric material or component serve for a reasonable amount of time, or will it fail prematurely?
2. Can we get a material or component with better properties?

While both questions are often asked simultaneously, the second question deals with development of new materials and will not be considered per se in this Chapter; some answers are provided in Chapter 41 on polymer liquid crystals. The first question shows that failure is related to prediction of performance under given service conditions, and this is the way we are going to tackle this problem. More specifically, we need prediction of long-term performance from short-term tests, and this will be one of the leitmotivs of the present chapter.

The subject of this chapter is a vast one. There exist entire books devoted to it, including classical books by Ferry [1] and Aklonis and McKnight [2] as well as more recent ones [3,4].

24.1.2 The Chain Relaxation Capability (CRC)

Polymeric materials are all viscoelastic. The ''face'' each polymer shows to the observer—elastic, viscous flow, a combination of both—depends on the rate and duration of force application as well as on the nature of the material and external conditions including the temperature T. We discuss the nature of viscoelasticity below and additionally in Section 5. In general, properties of viscoelastics depend on *time*, in contrast to metals and ceramics.

To get a clear picture of the problem we are about to tackle, let us return to the girl with her plastic doll. Playing with the doll, the girl applies forces with various duration, direction(s) and application rate(s). For instance, the girl applied a tensile force to the head and both legs of the doll. The doll is a physical system which thus received energy U_0 from outside. Important for the girl—and for us—is the question number 1 formulated above. Will the energy U_0 be spent on destruction and eventual fracture of the doll, or will it get somehow dissipated and the doll will ''live long''? We can write a general equation [5–7]

$$U = U_0 - U_b - U_r, \tag{24.1}$$

here U is the energy furnished from outside which at a given time has not yet been spent one way or the other; U_b (b for bond breaking) at the same time has been spent on destructive processes (such as crack formation or propagation); U_r at the given time has been dissipated, that is spent on nondestructive processes. Dissipation in a viscoelastic material is largely related to relaxational processes; the subscript r stands for relaxation. The quantities in Eq. (24.1) may refer to the material as a whole, but it is usually convenient to take them per unit weight of the polymer such as 1 g. U_r is quite important. It will be related soon to the chain relaxation capability (CRC) which has been defined [5–7] as follows:

CRC is the amount of external energy dissipated by relaxation in a unit of time per unit weight of polymer. In the following we shall use the abbreviation CRC for the concept and the symbol U_{CRC} for the, respective, amount of energy. Thus, at a given time t

$$U_r = \int_0^t U_{CRC} dt. \tag{24.2}$$

The main reason why the concept of CRC is so useful is the following fact: it takes approximately 1,000 times more energy to break a primary chemical bond such as a carbon–carbon bond in a carbonic chain (what contributes to U_b and to crack propagation) than to execute a conformational rearrangement around the same bond. This is the basis of the following key statement [5–7]:

Relaxational processes have priority in the utilization of external energy. The excess energy which cannot be dissipated by such processes goes into destructive processes.

Nature is very kind to us! A viscoelastic material will relax rather than fracture—as long as it can go on relaxing. Unless there is a high concentration of external energy at a particular location, and as a consequence a number of primary bonds will break starting a crack, that energy will be dissipated. In contrast to nonchain materials, when we pull at a polymeric chain we gradually engage all segments of it; this by itself lowers the probability of local concentration of external energy and of destruction. Of course, there exist local energy concentrators and we shall discuss them below. There exist a number of constituents of CRC; we have just named one of them, but let us list them together:

1. Transmission of energy across the chain producing intensified vibrations of the segments.
2. Transmission—mainly by entanglements but also by segment motions—of energy from the chain to its neighbors.
3. Conformational rearrangements (such as *cis* into *trans* in carbonic macromolecules) executed by the chains.
4. Elastic energy storage resulting from bond stretching and angle changes.
5. Phase transformation toughening first observed by Kim and Robertson [8] and also studied by Karger-Kocsis [9].

Incidentally, fairly often the penultimate factor is excluded—with bad consequences for models based on such an assumption.

24.1.3 Correspondence Principles

Given the conclusions from the previous section, we naturally ask: when will a given polymeric material or component have high CRC—so that we can expect a reasonable service time? We need to answer this question before dealing with specific properties and specific classes of materials.

Paul Flory has shown how free volume v^f is important for thermophysical properties of materials—and not only polymeric ones [10,11]; see also a chapter by Orwoll in this Handbook [12]. There are also seminal papers by Litt and Tobolsky [13] and Tschoegl [14–16] showing importance of v^f for mechanical properties of viscoelastic materials. Consider now our CRC from this point of view. It is easy to envisage that the larger v^f is, the larger is the maneuvering ability of the chains—what means the higher is CRC. Using specific quantities (typically per 1 g), we write

$$v = v^* + v^f. \tag{24.3}$$

Here v is the total specific volume and v^* is the characteristic (hard-core, incompressible) volume. The last two names are based on the concept of ''squeezing out'' the whole free volume by applying a very high pressure so that only v^* remains. Instead of free volume, some people work with the reduced volume

$$\tilde{v} = v/v^* = 1 + v^f/v^*. \tag{24.4}$$

Equations such as (3) or (4) are not usable until a specific equation of state of the general form $\tilde{v} = \tilde{v}(\tilde{P}, \tilde{T})$ or $\tilde{P} = \tilde{P}(\tilde{v}, \tilde{T})$ is assumed. Here P is the pressure and we need two more reduced quantities:

$$\tilde{P} = P/P^* \text{ and } \tilde{T} = T/T^*. \tag{24.5}$$

The idea of reduced quantities goes all the way back to Johannes D. van der Waals in the eighteenth century. Thus, an equation of state requires three reducing quantities, v^*,P^*, and T^*. We have found repetitively good results using the Hartmann equation of state [17–19]

$$\tilde{P}\tilde{v}^5 = \tilde{T}^{3/2} - \ln \tilde{v}. \tag{24.6}$$

Since experiments are often conducted at the atmospheric pressure $P \approx 0.1\,\mathrm{J\ cm^{-3}}$, then the term containing $\tilde{P}$ in Eq. (24.6) is negligible, and we have simply

$$\tilde{v} = \exp[\tilde{T}^{3/2}]. \tag{24.7}$$

The pressure unit of $\mathrm{J\ cm^{-3}}$ has been used for instance by Flory [11] and in contrast to Pa saves our time in calculations. Fortunately $1\,\mathrm{J\ cm^{-3}} = 1\,\mathrm{MPa} = 1\,\mathrm{MN\ m^{-2}} = 10^7$ erg $\mathrm{cm^{-3}} = 10^7$ dyne $\mathrm{cm^{-2}} = 10$ bar $= 145.04$ psi $=$ 9.86923 atm.; the last number depends on the geographic location.

Given Eqs. (24.6) and (24.7), we need to evaluate the characteristic parameters v^*, T^* and if we deal not only with the atmospheric pressure also P^*. One can use the *thermomechanical analysis* (TMA) in the expansion mode to determine at the atmospheric pressure the dependence of specific volume v on temperature T. By fitting the experimental results to Eq. (24.7) one obtains the characteristic parameters v^* and T^*. Zoller and coworkers have long ago developed a so-called Gnomix apparatus which performs full *P–V–T* determination [20]. There are several machines around the world based on the Zoller invention. We have used a Gnomix to advantage for organic polymers [21,22] as well as for inorganic ones [23]. One then represents experimental results by Eq. (24.6) and one calculates by a least-squares procedure the parameters P^*, v^*, and T^*.

To connect free volume to mechanical properties, we now need the classical Doolittle equation

$$\ln \eta = A' + Bv^*/v^{\mathrm{f}}, \tag{24.8}$$

where η is the viscosity. The connection can be made through *correspondence principles* which now we are going to discuss. Consider first a conformational rearrangement in a polymeric chain so fast that one cannot record it at room temperature. Clearly the total volume decreases when the temperature decreases, and along with it the free volume becomes smaller too. Thus, we can reach a temperature low enough to ''catch'' the process under investigation. This idea works also in the opposite direction. Instead of conducting experiments for 100 years at the ambient temperature, we can go to a higher temperature, thus produce higher free volume v^{f} in the material, and ''catch'' within, say, 10 hours the same series of events. This is the basis for the *time–temperature correspondence*. Clearly we now have what we have been looking for: the capability to predict long-term behavior from short term tests. One performs experiments at a series of temperatures. There exists a temperature of particular interest, for instance 20 °C. There is also at least one parameter of particular interest, such as the tensile compliance $D(t)$. In elastic materials we simply have $D(t) = \varepsilon(t)/\sigma = 1/E$, where E is the tensile modulus. However, our strain depends on time t; at constant T and σ we have generally

$$D(t) = \varepsilon(t)/\sigma = 1/E(t). \tag{24.9}$$

We now create a large diagram of $D = D(t)$ (or more often of $\log D = \log d(\log t)$. We begin with results for 20 °C and also include isothermal results for all other temperatures. Then, without moving the curve for 20 °C, we shift results for all other temperatures so that they would form a single curve. We shall show below examples of such diagrams, often called master curves, an approach advocated for a long time by Ferry and his coworkers [27,1]. Each $D(t)$ isotherm is moved left or right by a distance a_T called the shift factor; clearly a_T is different for each temperature. The whole procedure is also known as the method of reduced variables and means that

$$D(t, T;\ \sigma = \text{const.}) = D(t/a_T,\ T_{\mathrm{ref}};\ \sigma = \text{const.}). \tag{24.10}$$

Here T_{ref} (often also denoted by T_0) is the temperature to which the master curve pertains. Thus, in our case $T_{\mathrm{ref}} = 20\,^{\circ}\mathrm{C}$ while in general $a_{\mathrm{T}}(T_{\mathrm{ref}}) = 1$.

Changing the temperature is not the only option. By varying stress we can also change the free volume. *Time–stress correspondence* has been demonstrated experimentally already in 1948 by O'Shaughnessy [24]. Little attention has been paid to it, except for work in Latvia summarized by Goldman [25]. Only in 2000 an equation which makes possible quantitative predictions has been developed [26].

We can also apply an oscillating (typically sinusoidal) force to a polymeric component. If the frequency ν of the oscillations is low, the chains will be able to adjust better to the externally imposed field, just as they do at higher temperatures. The inverse is true as well: high frequencies will give little opportunity for such rearrangements—as if the free volume and the temperature were low. Thus, we have time–frequency correspondence. We can write a series of approximate proportionalities [7]

$$\mathrm{CRC} \sim v^{\mathrm{f}} \sim T - \nu \sim \rho^{-1} \tag{24.11}$$

Here $\rho = \nu^{-1}$ is the mass density.

The correspondence principles allow us to achieve our goal: prediction of long-term mechanical properties—and thus performance and reliability—from short-term tests. It is possible to predict behavior for, say, 16 decades of time from experiments each of which was made over four decades only; examples will be given below. It is easy to see that, when using the time–temperature correspondence, essential is the capability to predict the temperature shift factor $a_T(T)$. Similarly, when using the time–stress correspondence one needs the stress shift factor $a_\sigma(\sigma)$. Starting from the Doolittle equation (24.8), it was possible to obtain a general equation [26]

$$\begin{aligned}\ln a_{T,\sigma} = {} & A_{T,\sigma} + \ln T_{\mathrm{ref}}/T + \ln[v(T, \sigma)/v_{\mathrm{ref}}] \\ & + B/(\tilde{v} - 1) + C(\sigma - \sigma_{\mathrm{ref}}).\end{aligned} \tag{24.12}$$

Here v_{ref} pertains to the stress level of interest and is thus similar to T_{ref}. If we assume a constant stress level, we obtain an equation which allows us to apply the time–temperature correspondence:

$$\ln a_T = A_T + B/(\tilde{v} - 1). \tag{24.13}$$

Similarly, if we assume a constant temperature and perform experiments at several stress levels, from Eq. (24.12) we obtain

$$\ln a_s = A_s + \ln T_{\text{ref}}/T + \ln [v(\sigma)/v_{\text{ref}}] + B/(\tilde{v} - 1) + C(\sigma - \sigma_{\text{ref}}). \tag{24.14}$$

Later in this Chapter we shall show applications of these concepts. Before doing so, however, we need to deal with the essential concepts of fracture mechanics.

24.2 FRACTURE MECHANICS FOR POLYMERIC MATERIALS

24.2.1 Stress Concentrators and Stress Concentration Factor

As noted in the beginning of this Chapter, fracture is the bottom line of polymer science and engineering, and indeed of the entire materials science and engineering. As a result of the processing procedures used, plus handling in transport, etc., polymeric materials and components exhibit structure imperfections at various levels. Thus, there exist knit lines: areas in injection-molded parts of thermoplastics in which separate polymer melt flows arise, meet, and then to some extent—but not quite—combine together during manufacturing. Consequences of the presence of knit lines on mechanical properties are discussed by Criens and Moslé [28]. Due to the presence of crazes, scratches, cracks and other imperfections, mechanical properties of real polymeric materials are not as good as they theoretically could be. In this section we shall deal particularly with stress concentrators such as *cracks* (which appear although we did not want them) and *notches* (which are well-defined cracks introduced deliberately).

The deteriorating effects of cracks and notches on material properties are represented by *the stress concentration factor*

$$K_t = 1 + 2(h/r)^{1/2}. \tag{24.15}$$

Here h is the depth (length) of the crack or notch, or one-half of the length of the major axis in an elliptical hole; r is the radius of curvature at the tip of the notch, or at each end of the major axis of an elliptical crack. The name stress concentration factor is very appropriate. Consider again a tensile test with the stress σ applied to the ends of the specimen (for details see below Section 3). The lines of force applied to these ends cannot go through the air; they must go through the material, and thus around the crack. As a consequence, when the lines meet (or separate, depending on the direction) at the crack tip, that tip is subjected not to the stress σ, but to the stress $\sigma \times K_t$. The phenomenon is well known to anybody who wanted to make two smaller sheets from a plastic sheet and found that his or her own hands are not strong enough for this operation. However, a small incision with a pair of scissors on one side of the sheet led to success. The incision was in fact a notch—and created stress concentration defined by Eq. (24.15).

Equation (24.15) corresponds to our intuitive notions about the deterioration produced by a crack. The deeper the crack is (h larger) the more "evil" it can produce. The more blunt the crack is (less sharp, larger r), the more "benign" it will turn out to be when external forces "attack" the component.

24.2.2 Stress Intensity Factor

To account for differences on the loading modes (tensile, shear or tearing), a somewhat different measure of the "evil" produced by a crack or notch called the *stress intensity factor* is used

$$K_{\text{I}} = \alpha^* \pi^{1/2} \sigma h^{1/2}. \tag{24.16}$$

K_{I} characterizes the stress distribution field near the crack tip; the subscript Roman one, I, refers to the opening or tensile mode of crack extension; α^* is a geometric factor appropriate to a particular crack and component shape; the remaining symbols are the same as in Eq. (24.15). Unfortunately, K_t and K_{I} have similar symbols, similar names, and are expressed in terms of the same quantities. However, our effort to change this situation would largely be wasted.

For an infinite plate in plane stress, the geometric factor $\alpha^* = 1$. Plane stress means that the stress s_z along the z axis perpendicular to the plane surface is equal to zero; in practice this is not exactly true, but represents a reasonable approximation. For other geometries there exist tabulations of α^* values [29].

24.2.3 Griffith's Theory of Fracture

Entire books have been written on fracture of polymers, so here we shall quote the most important results. We go back to the story of the girl with her plastic doll. Griffith [30,31] considered for elastic bodies the question: when will a crack propagate? His answer was: this will happen if the crack growth will lower the overall energy. He considered three contributions: (1) the potential energy of the external forces which are doing work on the body deforming it, (2) the stored elastic strain energy, and (3) the work done against the cohesive forces as new crack surfaces are formed. He thus derived an equation which we can write as

$$\sigma_{\text{cr}} = (2\Gamma E/\pi h)^{1/2}. \tag{24.17}$$

Here σ_{cr} is the stress level at and above which the crack will propagate; Γ is the surface energy per unit area (corresponds to the last of the three factors): E is the elastic modulus (also often called the Young modulus); h is the same as before. Thus, if the actual stress imposed is $\sigma < \sigma_{\text{cr}}$, the material will sustain the stress without the crack growing. The

equation is the same for both constant load and constant displacement conditions, hence it should work also for any intermediate conditions.

Equation (24.17) has been the inspiration for much further work—some pertinent and some just rewriting it introducing new symbols and new names. One of these reformulations is

$$G_r = \pi h \sigma^2 / E, \tag{24.18}$$

where G_r is known as the *elastic energy release rate*. Another such quantity is

$$R = 2\Gamma \tag{24.19}$$

Which is called the *crack resistance*. Substituting into Eq. (24.19) the value of 2Γ from Eq. (24.17), we get

$$R = \pi h \sigma_{cr} / E, \tag{24.20}$$

where the right hand sides of Eqs. (24.18) and (24.20) are similar. This leads to a new concept of

$$G_{cr} = \pi h \sigma_{cr}^2 / E, \tag{24.21}$$

where G_{cr} is called the *critical energy release rate*. This is followed by a statement such as: when the elastic energy release rate G_r given by Eq. (24.18) becomes equal to the crack resistance R, then G_r acquires the critical value G_{cr} and a crack will propagate. It is amazing how many people are investing their efforts into rewording knowledge created by others! The whole story from Eq. (24.18) to (24.21) is nothing new beyond what we have learned already from the Griffith Eq. (24.17). We are mentioning this only because quantities such as the energy release rate are in use. For the same reason we still need to mention connections resulting from Eqs. (24.18), and (24.21) and the definition (16) of K_1. Making pairwise comparisons, we immediately find

$$K_1 = \alpha^* (G_r E)^{1/2} \tag{24.22}$$

and

$$K_{1c} = \alpha^* (G_{cr} E)^{1/2}, \tag{24.23}$$

where, as expected, K_{1c} is called the *critical stress intensity factor*; it is also known as *fracture toughness*. Important, however, is the following generalization of Eq. (24.17):

$$\sigma_{cr} = [2[\Gamma + \Gamma_p)E / \pi h]^{1/2}. \tag{24.24}$$

Recall that the whole theory of Griffith has been developed for elastic bodies—what applies to metals within a certain range of imposed stresses. Thus, Eqs. (24.17)–(24.23) form the essence of linear elastic fracture mechanics (LEFM). In Eq. (24.24) a "plastic" term Γ_p has been added to the elastic term Γ; metals exhibit also plasticity, hence the improvement displayed in Eq. (24.24). If we make a further step and assume that Γ_p includes all nonelastic contributions, we shall have an equation usable also for viscoelastic materials. We, therefore, have to use Eq. (24.24) instead of (24.17) while in Eqs. (24.18)–(24.23) we need to put $\Gamma + \Gamma_p$ instead of just Γ. Values of K_{1c} for a number of polymers are listed in Table 24.1. The impact strength values listed at the end of this chapter are also pertinent since they represent a different measure of fracture toughness.

TABLE 24.1. *Fracture toughness K_{1c} values for selected polymers.*

Polymer	K_{1c}/(J cm^{-3} m$^{1/2}$)
Epoxy	0.6
Polyester thermoset	0.6
Polystyrenes	0.7–1.1
high-impact polystyrenes	1–2
Poly(methyl methacrylate)s	0.7–1.6
Poly(ether sulfone)	1.2
Acrylonitrile-butadiene-styrene	2.0
Polycarbonate	2.2
Poly(vinyl chloride)s	2–4
Polyamide (nylon 6,6)	2.5–3
Polyethylenes	1–6
Polypropylenes	3–4.5
Polyoxymethylene	4
Poly(ethylene terephthalate)	5

Note: J cm^{-3} m$^{1/2}$ = MPa m$^{1/2}$ = 0.9100 ksi in.$^{1/2}$

24.2.4 Crazes and Shear Yielding

We need to consider the problem of the origin of the cracks. Crazes constitute one source of cracks. They are observed in glassy thermoplastics. Originally, crazes were thought to be just tiny cracks, but this turned out not to be true. We now recognize three kinds of these structures: surface crazes, internal crazes, and crazes at the crack tip. All three kinds consist of elongated voids and fibrils. The fibrils consist of highly oriented chains while each fibril is oriented at approximately 90° to the craze axis. The fibrils span the craze top-to-bottom, resulting in an internal sponge-like structure. Extensive studies of crazes and their behavior under loads have been conducted by Kramer and his school [32–42] and have been reviewed by Donald [43]. We know from their work that there are two unique regions within a craze: (1) the craze/bulk interface, a thin (10–25 nm) strain-softened polymer layer in in which the fibrillation (and thus craze widening) takes place; and (2) the craze midrib, a somewhat thicker (50–100 nm wide) layer in the craze center which forms immediately behind the advancing craze. The relative position of the midrib does not change as the craze widens. By contrast, as the phase boundaries advance, new locally strain-softened regions are continuously generated, while strain-hardened craze fibrils are left behind.

We already know that cracks are more dangerous than crazes. The latter are capable of bearing significant loads thanks to the fibrils. Therefore, we need to know under what conditions can crazes transform into cracks? Kramer,

Donald, and coworkers have established that the craze fibril stability depends on the average number of effectively entangled strands n_e that survive the formation of fibril surfaces. Equations for calculating the original number of strands n_0 as well as the number n_e have been developed by Kramer and Berger [38]. It turns out that polymers with $n_e > 11.0 \times 10^{25}$ strands m^{-3} and concomitantly a short entanglement length l_e are ductile and deform by shear yielding. Such materials exhibit engineering strains up to $\varepsilon = 0.25$ or even more prior to macroscopic fracture. Polymers with $n_e < 11.0 \times 10^{25}$ strands m^{-3} and thus with large l_e are brittle and deform by crazing only. For polymers with intermediate values of n_e and l_e there is a competition between shear deformation and crazing.

In Fig. 24.1 we show a part of a craze. The parameter D is the (mean) craze fibril diameter while D_0 is the craze fibril spacing. Both D and D_0 increase somewhat with increasing n_e. Berger [42] traced the craze fibril breakdowns to the formation of small pear-shaped voids at the craze/bulk interface. The results in [42] confirm the microscopic model of Kramer and Berger [38] which we see in Fig. 24.1.

In general, providing from outside energy in excess of CRC may result in crazing, shear yielding, or cracking. In *shear yielding* oriented regions are formed at 45° angles to the stress. The shear bands are birefringent; in contrast to crazes, no void spaces are produced. Thus, crazing—created by tensile fields—is accompanied by volume dilation while shear yielding—created by compressive fields—is not. Combined fields result in mixed responses.

The presence of liquids or vapors in the environment of a polymeric component affects the response to external mechanical forces. Thus, for instance polyarylate (Par) under uniaxial extension exhibits exclusively shear yielding without crazing. However, exposure to organic vapor (methylethyl ketone) results in crystallization, embrittlement, and conversion of the response to deformation from shear yielding to crazing [42].

Finally, let us mention that *crack healing* is possible. This phenomenon has been investigated by Kausch and also by Wool and reviewed by these authors [44,45].

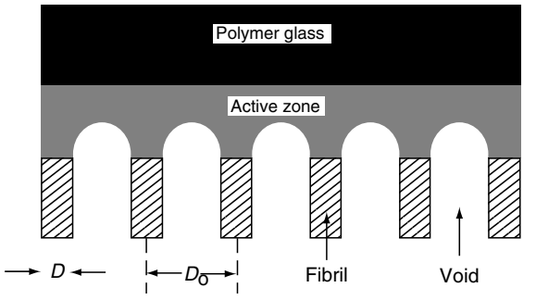

FIGURE 24.1. A schematic of a fraction of one side of a craze.

24.2.5 Rapid Crack Propagation and Its Prevention

The general definition of CRC in Subsection 24.1.2 does not specify a quantitative measure. Such a measure has to be defined for each specific problem. As an example, we shall now consider rapid crack propagation (RCP). RCP is a dangerous process. Velocities of 100–400 m s^{-1} (that is 300–1,400 feet s^{-1}) have been observed in polyethylene (PE) pipes. Since such pipes are being used for fuel gas distribution within localities; RCP might be accompanied by an explosion of the gas pressurized inside.

Given the importance of the problem, studies were made with the objective of connecting the crack length L with a variety of parameters: fuel pressure inside, pipe fatigue, tensile behavior of the piping material, and so on. L was determined by a standard procedure of Greig and Smith [46] such that a knife is pushed through a pressurized pipe by falling weight; given the rate at which RCP takes place, the length L is achieved almost instantaneously. However, no such connections were found—until Gaube and Müller [47] found a correspondence between the notch impact energy U_1 (see Section 24.4.2) and L. An analysis of the problem [48] led to the following equation:

$$L = L_0 + L_1/U_1, \tag{24.25}$$

where L_0 is a material constant with the dimensions of length, L_1 is another constant with the dimensions of length and energy, and U_1 is the notch impact energy. What is required here is a criterion showing when RCP will *not* occur. Since the notch impact energy U_1 is the independent variable in Eq. (24.25), it constitutes the appropriate measure of CRC for the problem under consideration. U_1 can be determined by an independent and fairly widely available experimental procedure. L can be measured in an outdoor 14 m long stand at Hoechst AG in Frankfurt-on-the-Main (although such facilities are not widely available). Therefore, CRC will be represented here by a limiting impact energy $U_{1\text{-lim}}$ defined as

$$L(U_1 > U_{1\text{-lim}}) = 0. \tag{24.26}$$

Now we simply substitute the definition of $U_{1\text{-lim}}$ from Eq. (24.26) into Eq. (24.25), with the result

$$U_{1\text{-lim}} = -L_1/L_0. \tag{24.27}$$

An example of the application of the criterion just defined is shown in Fig. 24.2. The coordinates are L and U_1, as defined by Eq. (24.25). The criterion applies to all classes of materials; if all plastic pipes were identical, we would have only one point on the diagram, so here again differences in processing, handling, transport etc. appear. Each pipe is slightly different, and there is a certain scatter due to the limited accuracy of the two kinds of experiments, but it is clear that Eq. (24.25) is obeyed. Therefore, the criterion Eq. (24.27) derived from (24.25) is valid. For the data shown in Fig. 24.2 we have $L_0 = -896\,mm$, $L_1 = 269$ J mm,

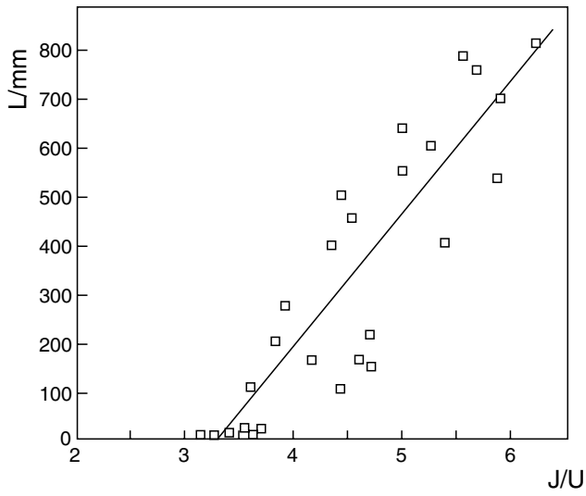

FIGURE 24.2. Length L/mm of the cracks in PE pipes determined by the Greig-Smith test 50 vs. the reciprocal Charpy impact energy $(U/J)^{-1}$; after [48].

therefore $U_{\text{l-lim}} = 0.300\,\text{J}$. If the impact energy determined in the Charpy test (see the section on impact behavior) is higher than this value, rapid crack propagation will not occur. Since the criterion is defined for a class of polyethylenes, a safety factor somewhat larger than unity may be introduced.

24.2.6 Slow Crack Propagation and Its Prediction

The slow crack propagation (SCP) is vastly different from RCP, not at all spectacular but in fact "quiet" and insidious. The crack propagation rate dh/dt might be only, say, 1 mm per month; an observation for instance two weeks after installing a polymeric component might reveal nothing. Experimentalists customarily present the dh/dt rates as a function of the logarithmic stress intensity factor K_1 as defined by Eq. (24.16); we now use h as the crack length (as we did before) to differentiate it from the length L which pertained to RCP. The problem clearly consisted in relating dh/dt to K_1. It was solved [49] by using the CRC approach in conjunction with the Eq. (24.17) of fracture mechanics. The problem was different than that of Griffith. He needed the critical stress σ_{cr} above which crack propagation occurs for a given crack length h. In our problem we need to know whether the crack length is below a certain value, call it h_{cr}, so that the crack will not propagate [49]. We therefore reformulate the Griffith Eq. (24.17) as

$$h_{\text{cr}} = 2\Gamma E/\pi\sigma^3. \tag{24.28}$$

By definition, the crack will propagate only when $h > h_{\text{cr}}$. This is not only a consequence of the CRC concept but also supported by the molecular dynamics computer simulations [50,51] showing that a crossover exists from the force field region dominated by chain relaxation to one in which crack propagation occurs.

Since notches with $h < h_{\text{cr}}$ do not cause crack propagation, it was only natural to assume

$$\frac{dh}{dt} = \beta(h - h_{\text{cr}}) \text{ for } h \geq h_{\text{cr}}, \tag{24.29}$$

where β is a time-independent proportionality factor characteristic for the material since it depends on CRC. We do not have space here to provide details of the derivation; the final result [49] is

$$\log K_1 = (1/2)\log(\alpha^{*2}2\Gamma E) + (1/2)\log[1 + (1/\beta h_{\text{cr}})]dh/dt. \tag{24.30}$$

Equation (24.30) provides the desired connection between K_1 and dh/dt. In the derivation both the stress level σ and the original crack length h_0 were used but both canceled out, with the unexpected result that the crack propagation rate is independent of both! The experimental results support Eq. (24.30) as shown for instance in Fig. 24.3 for Hoechst PEs studied under uniaxial tension in water medium at 60 °C. Each symbol pertains to a different stress level and a different original notch length. It is clear that all polyethylenes with the molecular mass M_A form a common curve, and the same is true for the other molecular masses. Moreover, we see that a higher M results in a lower crack propagation rate; this result is related to the constituents of CRC listed at the end of Section 24.1.3, particularly the first two of them.

In the beginning we have called SCP "insidious". The lowest experimental crack propagation rate value in Fig. 24.3 is $dh/dt = 10^{-8}\,cm\,s^{-1}$; this is only 0.315 cm per year, but the crack does grow. This fact gives us an idea on the utility of Eq. (24.30).

24.3 QUASISTATIC TESTING AND TRANSIENT TESTING

24.3.1 Types of Testing Procedures

We have already referred to various kinds of data on mechanical behavior of polymers. We are now going to consider methods of acquisition of such information. The most frequently used are the so-called *quasistatic* methods which involve relatively slow loading. *Tension, compression, and flexure* belong here. The quasistatic methods have to be distinguished from so-called *transient tests* which include *stress relaxation* and *creep*. There are also impact tests and dynamic mechanical procedures which will be defined later.

Specimens for testing may be produced by processing operations such as injection molding, compression molding, or machining from sheets. Machined surfaces have to be smoothed in their long axis direction with abrasive paper. Any flash on molded specimens shall be removed; the cross-sectional area has to be uniform along the whole length subjected to testing. Consequences of any nonuniformity would show up as stress concentrators discussed above.

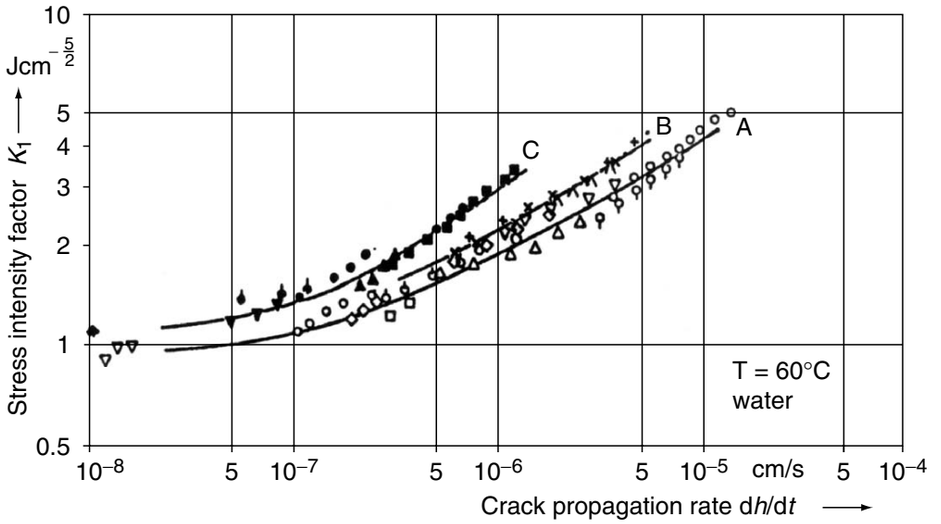

FIGURE 24.3. Crack propagation rate vs. the stress intensity factor for Hoechst polyethylenes. Each PE class such as A has the same molecular mass, with $M_A < M_B < M_C$; after [49].

The recommended number of tests on each sample is at least five, 10 or more are preferred. If producing design data for a particular application is the objective, the samples must be prepared by the same method as the part in question.

Testing of materials is governed by standards. We shall often refer below to those of the American Society for Testing and Materials (ASTM), West Conshohocken, PA. However, as national economies become more and more connected into a global economy, the use of standards defined by the International Standards Organization (ISO) is on the increase. In Table 24.2 we list several ISO and ASTM tests.

24.3.2 Tensile Properties

Tensile testing is the most frequently used method to characterize the material strength. The machine used is presented schematically in Fig. 24.4. It should be of the constant-rate-of-crosshead-movement type, consisting of one fixed and one movable member, both carrying self-aligning grips. The movable member shall move with a uniform, controlled velocity with respect to the stationary one. An extensometer is used to determine the distance between two designated points within the gage length of the test specimen as this is stretched. Speed of testing is defined as the relative rate of motion of the grips or test fixtures. It is specified for different types of specimens, varying typically from 1 to 500 mm/min (0.2–20 in. min^{-1}). The lowest speed that produces rupture in the time range 0.5–5 min for the specimen geometry used is to be selected.

One tests dumbbell-shaped or straight-sided specimens under defined conditions of pretreatment, temperature, humidity, and deformation rate. The former specimens are shown in Fig. 24.5.

There are two essential properties determined each time. The first is the *engineering stress*

$$\sigma = F/A_0, \tag{24.31}$$

where F is the applied force and A_0 is the initial cross-sectional area. Determination of the *true stress* based on the actual cross-sectional area A which changes during the

TABLE 24.2. *ISO and ASTM tests for important mechanical properties.*

Property	ISO standard	ASTM standard
Tensile modulus	527-1 & 2	D 638
Yield stress	527-1 & 2	D 638
Yield strain	527-1 & 2	D 638
Nominal strain at break	527-1 & 2	—
Elongation at break	527	D 638
Stress at 50% strain	527-1 & 2	—
Stress at break	527-1 & 2	D 638
Strain at break	527-1 & 2	D 638
Flexural modulus	178	D 790
Flexural strength	178	D 790
Charpy impact strength at −30 °C	179	D 256
Charpy impact strength at +23 °C	179	D 256
Charpy notched impact strength at −30 °C	179	D 256
Tensile impact	8256	D 1822
Izod impact strength at −30 °C	180	D 4812
Izod impact strength at +23 °C	180	D 4812
Izod notched impact strength at −30 °C	180	D 256
Izod notched impact strength at +23 °C	180	D 256

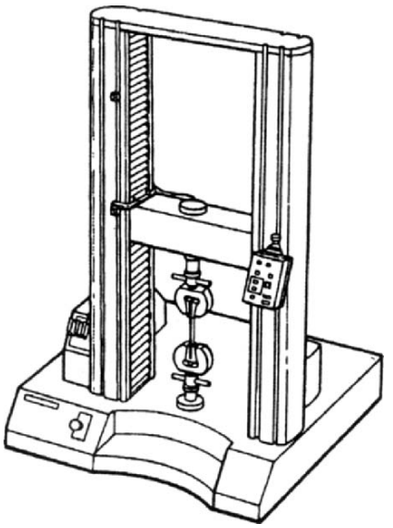

FIGURE 24.4. The machine for quasistatic testing—including tension, compression, 3-point bending and/or 4-point bending.

experiment is possible but more difficult. The other key property is the *engineering strain* (also known as the nominal tensile strain)

$$\varepsilon = (l - l_0)/l_0 = \Delta l/l_0. \tag{24.32}$$

Here l is the current length of the specimen while l_0 is the original length.

The quantities obtained most often from tensile testing are:

Tensile strength: The maximum load divided by A_0.

Percent elongation: If the specimen gives a yield load larger than the load at break, calculate *percent elongation at yield*. Otherwise, *percent elongation at break* is reported.

Modulus of elasticity: It is the proportionality factor E appearing in *Hooke's law*:

$$\sigma = E\varepsilon \tag{24.33}$$

and is also often called *Young's modulus*. It is calculated from the initial linear portion of the load vs. extension curve giving us the stress vs. strain curve. For materials where there is no clear linearity of the initial portion of the stress–strain curve, the modulus is calculated by dividing the nominal (= engineering) stress value by the corresponding designated strain (secant modulus).

In Fig. 24.6 we show several types of behavior seen in tensile testing of polymers. For performing a specific test, consult one of the standards listed in Table 24.2.

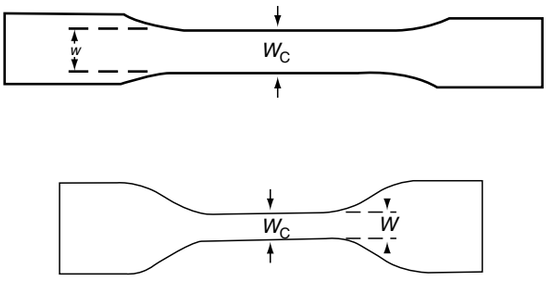

FIGURE 24.5. The dumbbell ("dogbone") specimens for tensile testing.

24.3.3 Compressive Properties

Of course, in compressive testing the strain defined by Eq. (24.32) is negative, but the definitions (31)–(33) are applicable. Basically two different testing methods are available here. In the first one the sample is deformed at a constant rate under simultaneous recording of the stress and deformation. This method, in essence a mirror image of the tensile test, is defined in ASTM D 695M. According to the second method, a constant load is applied to the specimen, the deformation of which is recorded after a given period of time with additional reading of the recovery of the specimen following unloading. This method, basically a compressive creep recovery test, is the subject of ASTM D 621.

Compression is an important mode of load application. An example of compressive loading is assemblies of conductors and insulators held together by suitable fastening devices. However, the compressive strength as such has a rather limited design value, since this type of loading apart from exceptions, such as collapsing foams or shatter of brittle plastics, seldom results in failure.

Testing of flexible materials, like rubbers, may involve complications due to their deformability. For instance, one finds that compressive stiffness is markedly dependent on contact surface constraints and specimen shape.

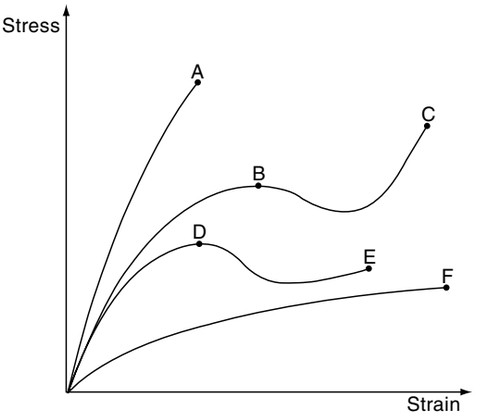

FIGURE 24.6. Typical engineering tensile stress vs. engineering strain curves. Points A, C, E, and F correspond to the tensile strength and elongation at break, D and B at yield. The curve ending at A represents a brittle material, those with C and E tough materials each with a yield point, while the curve ending at F shows a tough material without a yield point.

24.3.4 Flexure and Bending

We already mentioned that the machine shown in Fig. 24.4 serves also for bending. Most popular are two kinds, 3 point and 4 point, shown in Fig. 24.7, and described in standards D 790, D 790 M (=metric) and ISO 178. There are also less used but more specific standards: ASTM D 747 for apparent bending modulus of plastics by means of a cantilever beam and D 648 for deflection temperature of plastics under flexural load.

For brittle materials, flexure testing is believed to yield more reliable strength, modulus, and other data than the tensile method, this primarily by reducing the pronounced effects of misalignment in tension. For sheet materials (except laminated thermosets, high-strength reinforced composites) the dimensions of the specimens depend on whether tested flatwise or edgewise; the thickness of the sheet is the depth, or width, respectively. The depth shall not exceed the width in the latter case. ASTM standards specify also that, for sheets less than 1.5 mm in thickness, a specimen 50 mm long by 10 mm wide shall be tested flatwise on a 25 mm support span. Molding materials shall be 80 by 10 by 4 mm tested flatwise on a 64 mm support span. Special rules apply to laminated thermosets and highly anisotropic composites, which shall be tested with a larger span-to-thickness ratio (up to 60:1). Anisotropic materials require four different specimens, tested edgewise and flatwise, and cut in lengthwise and crosswise directions.

24.3.5 Stress Relaxation

Stress relaxation is typically determined in the uniaxial mode in a specimen or part kept at constant deformation. This pertains to parts in service such as fasteners, seals, or screws. An example of results of such a test are shown in Fig. 24.8. The relaxing stress could conceivably fall to zero (curve a in the bottom part of Fig. 24.8) but in practice the behavior displayed as curve b is observed, so that a certain level of *internal stress* σ_i is established.

The concept of internal stress is very useful for bringing out common features of stress relaxation behavior of different kinds of materials. Instead of plotting stress vs. time t, let us plot $(\sigma - \sigma_i)/(\sigma_0 - \sigma_i) = \sigma_i^*/\sigma_0^*$ vs. t. Here σ_0 pertains to the time of strain imposition. Such a plot was proposed by Kubát already in 1965 [52]. An example is shown in Fig. 24.9. We see that curves for ostensibly very different materials have similar shapes. A large central part of each curve has almost the same slope s as the other curves, so that

$$s = (-\mathrm{d}\sigma/\mathrm{d}\ln t)_{\max} = (0.1 \pm 0.01)(\sigma_0 - \sigma_i). \quad (24.34)$$

To explain the situation displayed in Fig. 24.8, Kubát has proposed a cooperative theory of stress relaxation [53,54]. He assumed that single units (metal atoms, polymer chain segments) do not relax individually but clusters of such units relax together. Thus, the Kubát theory is quite general an explains the observed behavior of metals and polymers alike. Molecular dynamics computer simulations have confirmed that indeed cluster relaxations prevail over individual relaxation, and this both for metals [55] and for polymers [56,57].

In Section 24.1.3 we have discussed among others the time–temperature correspondence principle. An example of application of that principle is shown in Fig. 24.10. The results pertain to high density polyethylene (HDPE) subjected to different levels of predrawing [58]. The draw ratio is defined as

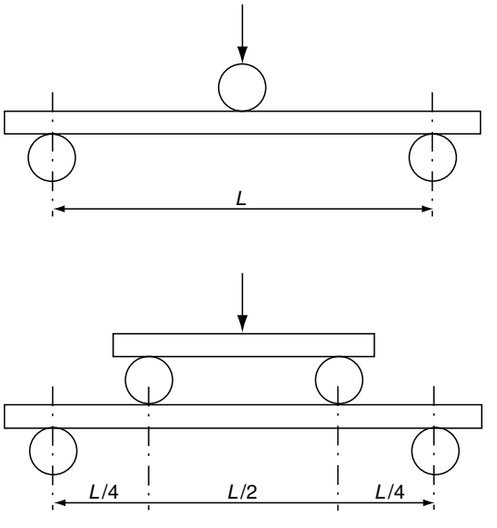

FIGURE 24.7. 3-point and 4-point loading modes in bending.

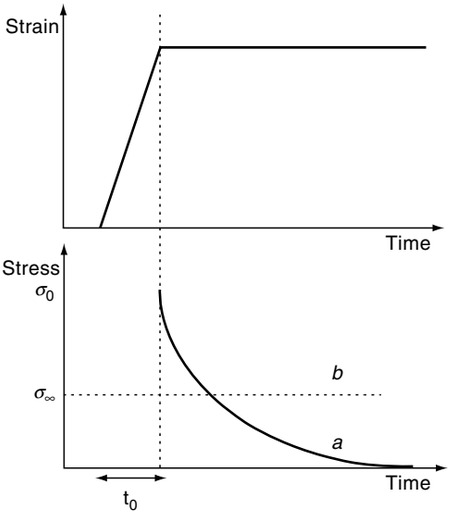

FIGURE 24.8. Stress relaxation represented by strain vs. time and stress vs. time curves. Explanation in text.

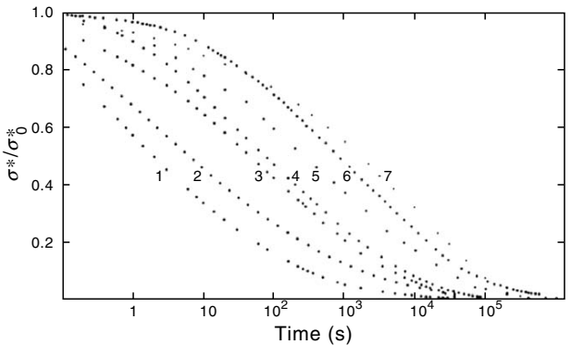

FIGURE 24.9. Stress relaxation curves—as explained in the text—for polyisoprene (natural rubber, 1), oriented low density polyethylene (LDPE) with the draw ratio $\lambda = 1.8$ (curve 2), indium (3), unoriented LDPE (4), cadmium (5), polyisobutylene (6), and lead (7).

$$\lambda = \varepsilon + 1, \tag{24.35}$$

where ε is the engineering strain defined by Eq. (24.32). The curves in Fig. 24.10 have the same shape as those in Fig. 24.9. The final horizontal parts are fairly long in Fig. 24.10, a consequence of prediction over 16 decades of time. The necessary shift factor values have been calculated from

$$\ln a_T = 1/(a + c\lambda) + B/(\tilde{v} - 1). \tag{24.36}$$

Equation (24.36) reduces to Eq. (24.13) for $\lambda = 1$. Equation (24.7) has been also used along with a representation of T^* as a quadratic function of λ. We see that indeed predict of long-term behavior from short-term tests can be accomplished.

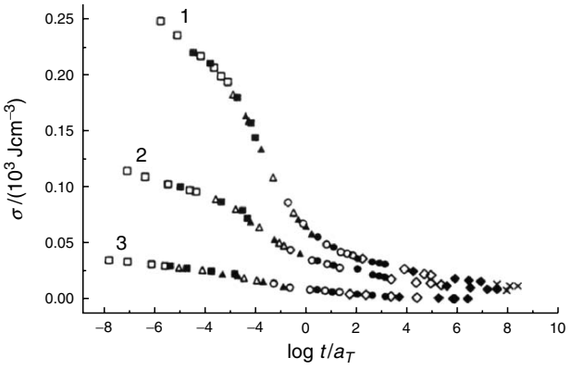

FIGURE 24.10. Master stress relaxation curves for HDPE at the reference temperature $T = 313.2$ K (= 40 °C), the constant tensile strain $\varepsilon = 0.025$ and at different values of the draw ratio: $\lambda = 12.2$ in the top (1) curve; $\lambda = 5.5$ in the middle (2) curve; and the material without predeformation ($\lambda = 1$) in the bottom (3) curve. The symbols pertaining to the experiment temperatures are the same in all three curves: □ for −50 °C; ■ for − 30 °C; △ for − 10 °C; ▲ for 0 °C; ○ for + 20 °C; ● for + 40 °C; ◇ for + 60 °C; ◆ for + 80 °C; and × for + 100 °C. The vertical coordinate is the tensile stress σ, the horizontal is log t/a_T; after [58].

24.3.6 Creep

Creep denotes the time-dependent elongation of a specimen or part subjected to a constant stress. Normally, the deformation range is relatively limited; the stress provided by a dead-weight can thus be considered as fairly constant and the change in the cross-section during the process neglected. Such a loading mode emulates the loading situations normally encountered in engineering practice. The pertinent standards include ASTM D 2990.

Figure 24.11 shows a schematic picture of a creep curve plotted as strain vs. time. There is an initial elastic deformation which at higher stress levels may also include a plastic component. This is followed by the primary creep stage characterized by a decreasing creep rate—stabilizing at a level corresponding to the secondary or stationary creep stage. In the end phase of the process, called tertiary creep, the rate becomes higher again, eventually resulting in creep rupture. It is to be noted that *long-term failure may occur at significantly lower stresses than those determined in normal tensile testing*. The logarithm of the time to rupture is often found to decrease linearly with the applied load.

Primary (transient) creep can be considered as a consolidation process during which the structure of the material adjusts itself to the following steady-state creep stage. In some instances, like in cross-linked elastomers at low stresses, the steady state is absent, with the creep rate decreasing to zero, and the total creep strain remaining constant. In this case, primary creep is a delayed response of the material to the applied stress. At higher stress levels, chain scission, oxidation effects etc. may influence this simple behavior.

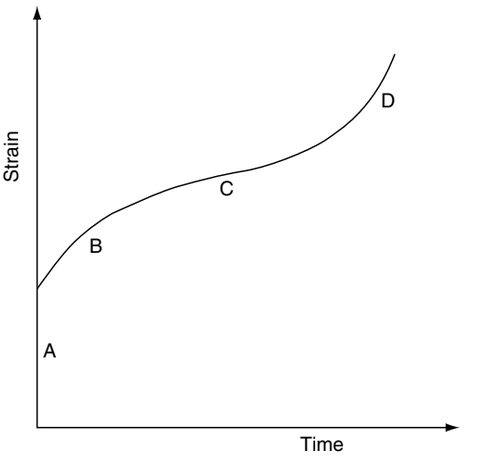

FIGURE 24.11. A schematic of a creep curve. A = instantaneous initial deformation which may contain a plastic component; B = primary, C = secondary and D = tertiary creep stage.

During the steady-state stage the material flows in a viscous (plastic) manner. In some instances, this stage may not be clearly discernible, constituting only a transition between the primary and tertiary portions of the creep curve. It may be noted that the acceleration of the creep rate in the latter part is not due entirely to a decrease in the cross-section of the specimen and thus to an increase in the stress level in tests where the specimen is loaded with a dead-weight.

We have already mentioned *creep recovery*. An example including the recovery stage is shown in Fig. 24.12.

We observe that the recovery curve is almost a mirror image of the primary creep stage.

In Section 24.1 we have defined ways of prediction of long-term behavior from short-term tests. Let us now provide more examples of application of these concepts. Creep and stress relaxation have been determined for PET/0.6PHB, where PET is the poly(ethylene terephthalate), PHB, the p-hydroxybenzoic acid, and 0.6 is the mole fraction of the latter in the copolymer [58]. PET/0.6PHB is a polymer liquid crystal, see chapter 41 on PLCs in this Handbook. In temperature ranges of interest it forms 4 coexisting phases [60]. Conventional wisdom said that prediction methods work only for so-called rheologically simple materials, practically for one-phase polymers. Therefore, we have decided to apply as severe a test as possible to our prediction methods and a multiphase PLC is a good choice.

In Fig. 24.13 we show several isotherms of tensile creep compliance (see Eq. (24.9)) for PET/0.6PHB [58]. In Fig. 24.14 we show a master curve for $T_{\text{ref}} = 62\ ^{\circ}\text{C}$ (the glass transition temperature of PET, the nonliquid crystalline component of the PLC) based on the curves from Fig. 24.13. We see a successful prediction over 16 decades of time.

Important here of course is whether the shift factor a_T values calculated from Eq. (24.13) agree with the experimental ones. These results are displayed in Fig. 24.15. The continuous line is calculated from our Eq. (24.13). The dotted line is from an equation proposed in 1955 by Williams, Landel, and Ferry (WLF) [27], a pioneering $a_T(T)$ formula at that time. We see that the WLF equation works well in a certain temperature range—this seems the reason it is still in use—but fails miserably outside of that range. Nobody else but Ferry [1] stated that range of application of WLF amounts to 50 K or so, not more. If one makes a primitive and unfounded assumption in our Eq. (24.13), one gets from it the WLF equation as a special case [6]. The problem is when people use the WLF equation blindly in wide temperature ranges, obtain bad results, and draw a false conclusion that the time—temperature correspondence principle does not work.

As already mentioned, stress relaxation was also determined for PET/0.6PHB [59]. We do not present the results here, although also in this case one obtains a master curve which covers 16 decades of time. Important, however, is the comparison of $a_T(T)$ values from creep and stress relaxation. This is made in Fig. 24.16. The continuous line is again obtained from Eq. (24.13). We see that the a_T values obtained from these two kinds of experiments practically coincide. Thus, Eq. (24.13) serves to predict a true material property rather than a property related to just one kinds of experiments.

The time—stress correspondence principle as embodied by Eq. (24.14) has also been used successfully [61]. We do not include such results for brevity. One could argue that the use of equations discussed in Section 24.1 requires fairly large amounts of experimentation. This impression might be

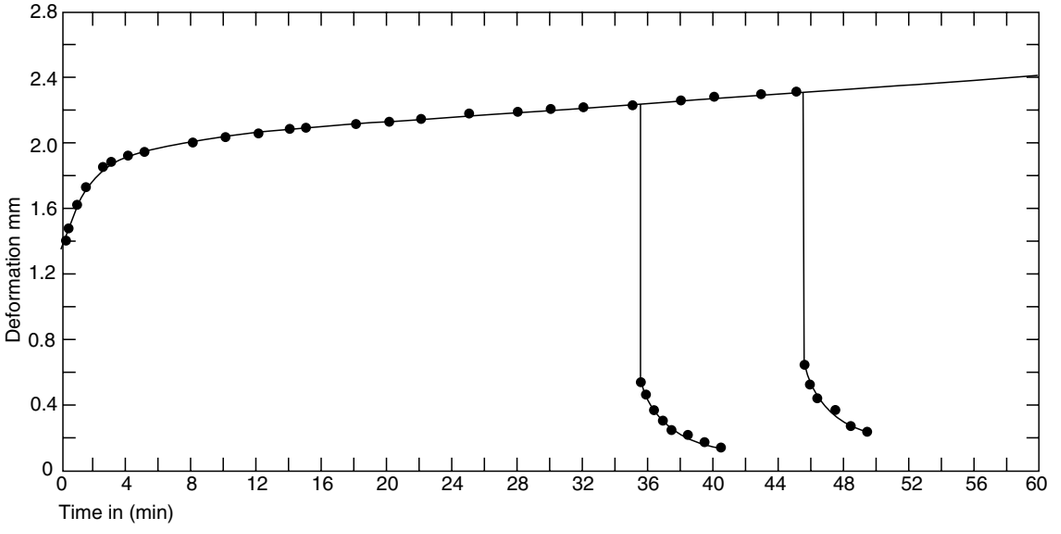

FIGURE 24.12. Creep and creep recovery of an oriented polypropylene monofilament with 0.35 mm in radius at 60.7 °C and stress level $\sigma = 36\,\text{J cm}^{-3}$ unloaded at 35.5 and 45.5 min. Deformation in mm relates to a specimen length $l_0 = 100\,\text{mm}$.

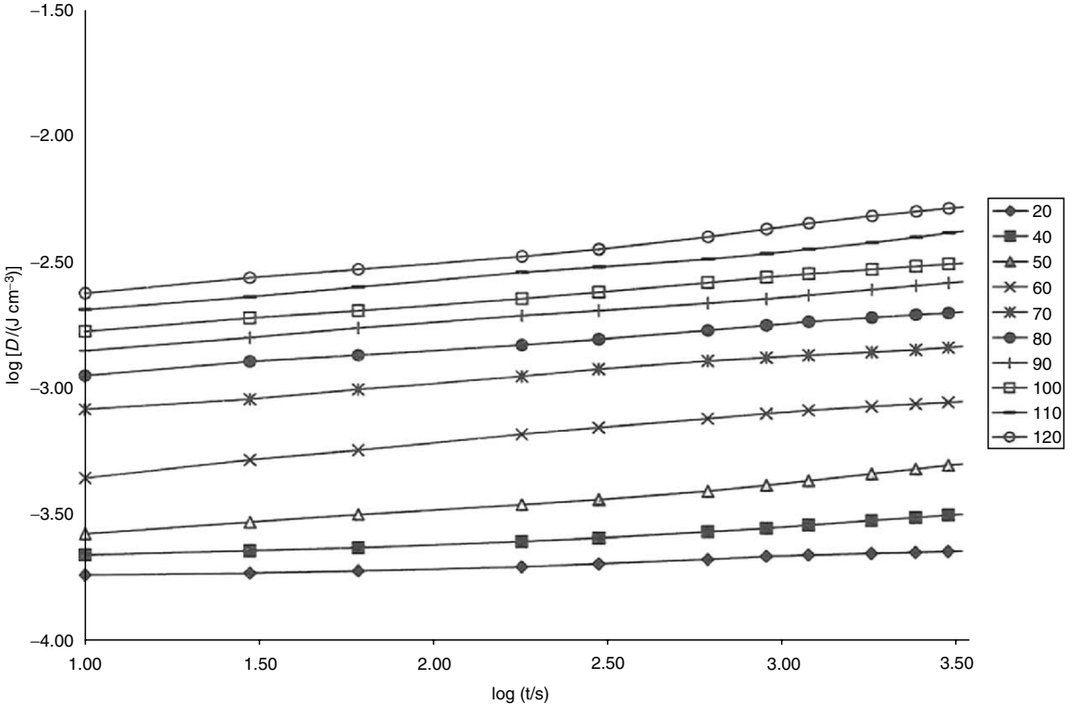

FIGURE 24.13. Experimental tensile creep compliance for PET/0.6PHB in logarithmic coordinates at 20 °C (the bottom curve) and other temperatures indicated in the insert; after [59].

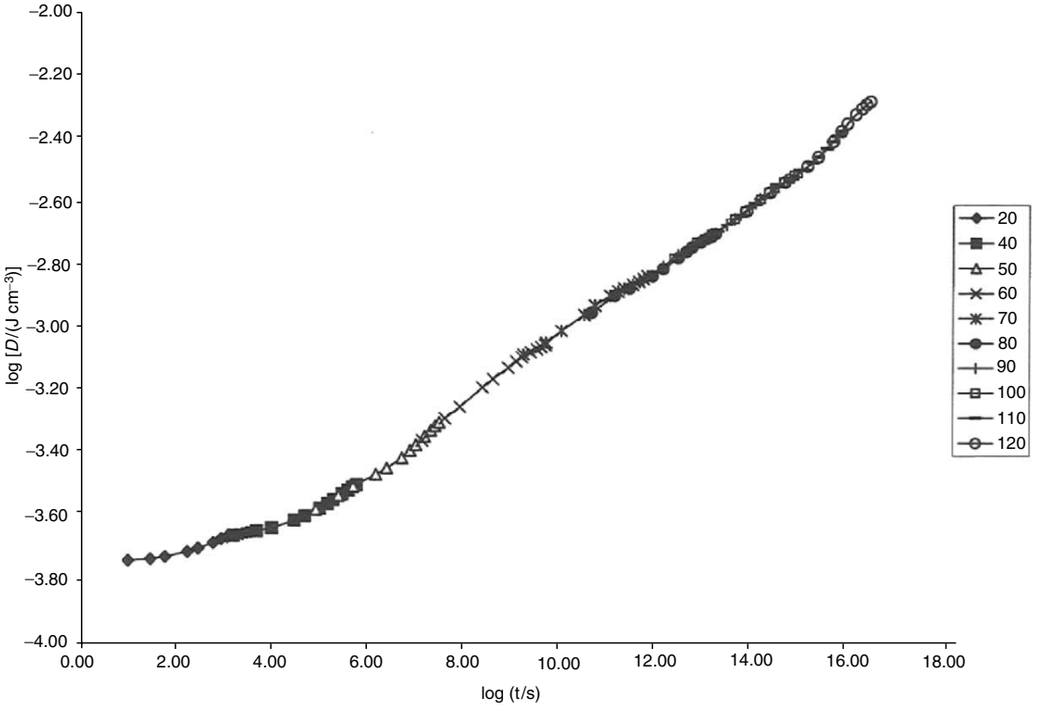

FIGURE 24.14. Tensile creep compliance for PET/0.6PHB in logarithmic coordinates as the master curve for 62 °C; after [59].

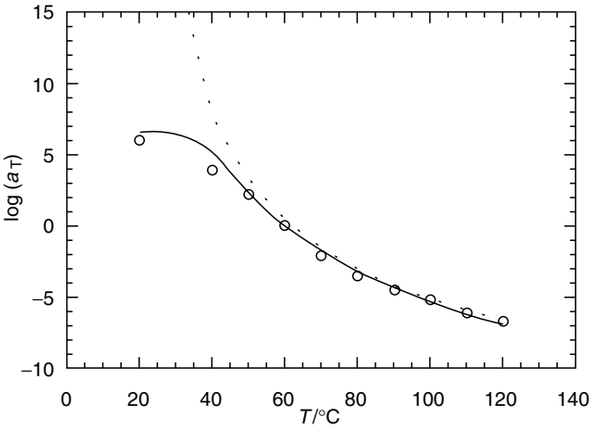

FIGURE 24.15. The temperature shift factor $a_T(T)$ for PET/0.6PHB for 62 °C. Circles are experimental values, the dotted line from the WLF equation and the continuous line from Eq. (24.13) in conjunction with Eq. (24.7); after [59].

confirmed for instance by our Fig. 24.13 which contains 10 isotherms. Therefore, methods of prediction of long-term behavior from short-term tests based on our Eqs. (24.12)–(24.14) have been developed [62, 63] such that one uses two or three experimental isotherms or results for two or three stress levels. Again, we are not going to discuss these results here for brevity.

24.4 IMPACT BEHAVIOR

24.4.1 Rates of Force Application

We have noted in Subsection 24.2.5 that a measure of CRC has to be defined for each specific problem. Imagine a slow-loading process, such as a part (an early stage) of quasistatic loading by compression. Then U_{CRC} featured in Eq. (24.2) might be relatively low; as a consequence U_r will be low too, but still $U_r > U_0$, and the material or component will "survive an attack". However, if the loading occurs at a fast rate, the same external energy U_0 will exceed U_r because relaxational processes take time, and fracture will occur. We shall now consider impact testing with this situation in mind.

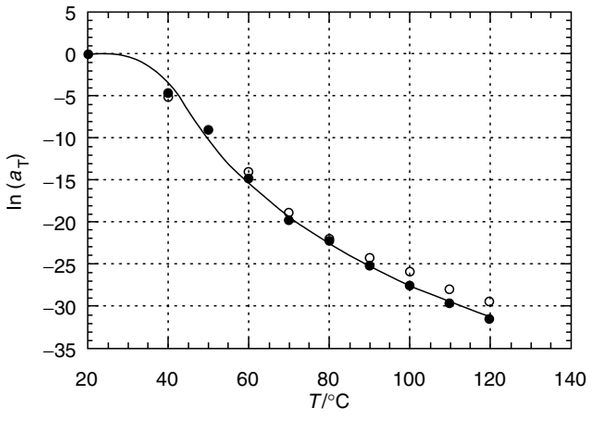

FIGURE 24.16. Experimental shift factors $a_T(T)$ from creep (full circles) and from stress relaxation (empty circles). The continuous line is from Eq. (24.13) in conjunction with Eq. (24.7); after [59].

24.4.2 Impact Testing

The most frequently applied impact tests are shown in Fig. 24.17 A and B. A pendulum (shown as a filled arrow) falls from a certain height; the loss in the potential energy of the pendulum is assumed equal (with a correction for losses such as friction) to the energy U_0 absorbed by the specimen; see Eq. (24.1). The Charpy test is described by the ASTM D 256 standard method B, the lzod test by the same standard method A. We see (Fig. 24.17 A) that in the Charpy test there is a symmetry with respect to the center of the specimen. By contrast, in the lzod test (Fig. 24.17 B) the bottom half of the specimen remains "untouched" while the top part is broken off. We—and more and more laboratories around the world—perform now both tests with a sensor installed on the pendulum and connected to a computer. Thus, not only a single value of the energy but a whole curve is obtained. For convenience single values of impact strength (IS) for a number of polymers are listed in Tables at the end of this chapter.

There is also a combination of tension with impact shown schematically in Fig. 24.17 C. This test is also symmetric with respect to the center, just as the Charpy procedure.

24.4.3 Impact Transition Temperature: Determination and Prediction

Traditionally—and that started with metals—one distinguishes two types of mechanical behavior of polymers: brittle and ductile. It will be clear to us after discussion of the free volume concept in Subsection 24.1.3 that brittle behavior will dominate at low temperatures when the free

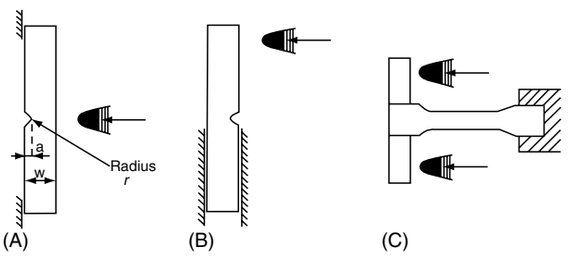

FIGURE 24.17. Schematics of impact tests showing geometry, loading mechanisms, and clamping modes.

volume is low. Therefore, there is a transition temperature T_1 above which the material will be ductile. We shall discuss the CRC connections and a way to predict T_1 in the next Subsection. Now we shall define a procedure of experimental determination of T_1. It should be noted immediately that the index I refers to impact; determination of brittle-to-ductile transition by loading at a rate slower than impact will result in finding not a single temperature, but a temperature range; the range might be as large as 10 K [64].

In view of this, we define T_1 as the temperature at which the response of the material changes from brittle to ductile under high-impact conditions. The Charpy test described above can be used to achieve those conditions [6]. As discussed in Subsection 24.2.5, two specimens are hardly ever identical. At T_1 we have, therefore, 50% failing in the brittle way and the other half in the ductile way.

The difference between the two kinds of failure are easily visible when one compares fracture surfaces, macroscopically as well as in micrographs obtained by scanning electron microscopy (SEM). Macroscopically, the fracture surface of a brittle failure appears smooth. SEM micrographs show in this case a "flaky" surface. By contrast, ductile failure is characterized by "hills and valleys" with deformed strands coming out from the surface, as well as holes in the surface left by strands which at break time have "joined" the other surface. Examples of the two types of micrographs are shown, respectively, in Figs. 24.18 and 24.19. There is a whole book by Michler [65] on polymer micromechanics which contains many instructive SEM micrographs of fracture surfaces as well as crazes, shear yielding, and also combinations such as crazes crossing shear bands.

Using the concepts discussed in Sections 24.1 and 24.2, the following equation [6] was derived:

$$K_t = F \times \mathrm{e}^{-B/(v_1 - 1)} \tag{24.37}$$

here K_t is the stress concentration factor as defined by Eq. (24.15); B is the Doolittle constant from Eq. (24.8); and the reduced volume $\tilde{v}_1$ is that at the impact-transition temperature T_1. Thus, we have an implicit formula for T_1 which can be related to $\tilde{v}_1$ by an equation of state such as Eq. (24.6) or (24.7); there is a T_1 value corresponding to each stress concentration factor.

Equation (24.37) was tested for LDPE for which sufficient data were available. The results are shown in Fig. 24.20. We see that the equation is obeyed within the limits of the experimental accuracy. Thus, two pairs of T_1 and K_t values are sufficient for the calculation of the parameters F and B and for subsequent prediction of the entire diagram.

24.4.4 Prediction of Volumetric Properties from Impact Data

We have used above free volume to explain mechanical properties. Since we have at our disposal quantitative relationships which work well, it was tempting to see whether the relationships can be used also in the opposite direction: going from mechanical properties toward volumetric ones. Thus, Eq. (24.37) was used in this opposite direction [66]:

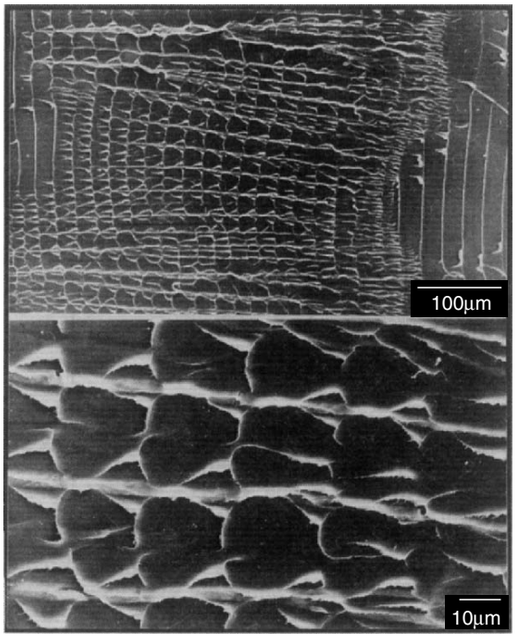

FIGURE 24.18. SEMicrograph of a brittle fracture surface; after [65].

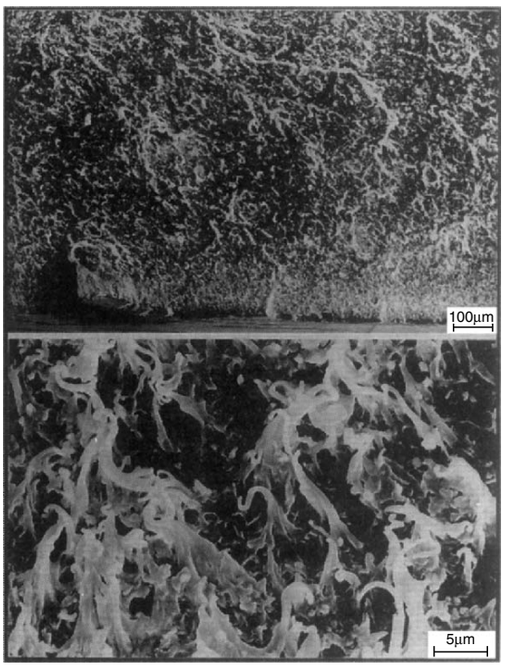

FIGURE 24.19. SEMicrograph of a ductile fracture surface; after [65].

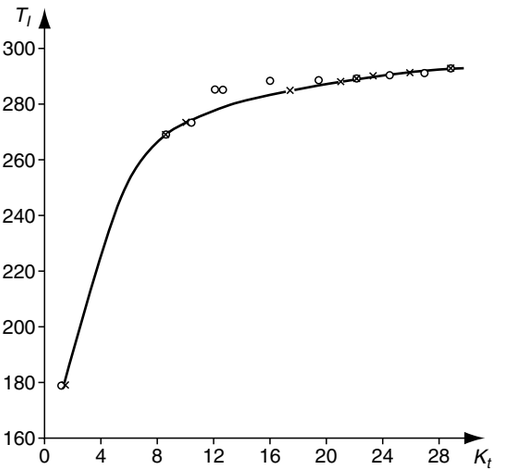

FIGURE 24.20. Relation between the stress concentration factor K_t and the impact transition temperature T_I in K for LDPE. Circles represent experimental values obtained by the Charpy method and crosses those calculated from Eq. (24.37).

specific volume v was obtained for the first time from mechanical parameters—the impact transition data—via an equation of state. The result was prediction of v over a temperature range of 100 K. The average difference between calculated and experimental specific volume values was only 0.092%. This constitutes one more confirmation—and of a different type—of the physical significance of the CRC concept and of the relations based on that concept.

24.5 VISCOELASTICITY AND DYNAMIC MECHANICAL TESTING

24.5.1 Objectives and Definitions

As noted in Subsection 24.1.2, viscoelasticity of polymers represents a combination of elastic and viscous flow material responses. Dynamic mechanical analysis (DMA, also called dynamic mechanical thermal analysis, DMTA) enables simultaneous study of both elastic (symbol $'$) and viscous flow (symbol $''$) types of behavior. One determines the response of a specimen to periodic deformations or stresses. Normally, the specimen is loaded in a sinusoidal fashion in shear, tension, flexion, or torsion. If, say, the experiment is performed in tension, one determines the elastic tensile modulus E' called *storage modulus* and the corresponding viscous flow quantity E'' called the *loss modulus*.

Diagrams showing the temperature or frequency dependence of storage and loss modulae can be used to locate the thermal transition regions such as the glass transition—although other methods such as differential scanning calorimetry (DSC) can be used for that purpose as well. At the same time, the dynamic mechanical methods constitute the primary technique for the study of dissipation mechanisms, and thus of CRC. Clearly DMA data are of importance in designing products to be used in, for instance, vibration isolation, where the mechanical damping properties are used to convert mechanical vibrations into heat. Methods of this type are also highly useful in studies of phase separation in multicomponent systems, effects of fillers and other additives, different processing variables, degree of crystallinity, molecular orientation, internal stresses, etc.

Consider a material subjected to an oscillating load of small amplitude that is in the linear viscoelastic range. The angular frequency of the sinusoidal oscillation is ω. A sinusoidal stress σ will produce a sinusoidal strain ε, and vice versa. However, because of the viscous component of the deformation, there will be a phase shift between stress and strain. The pertinent quantities can be represented as follows:

$$\varepsilon = \varepsilon_0 \sin \omega t \tag{24.38}$$

$$\begin{aligned}\sigma &= \sigma_0 \sin(\omega t + \delta) \\ &= \sigma_0 \sin \omega t \cos \delta + \sigma_0 \cos \omega t \sin \delta.\end{aligned} \tag{24.39}$$

Here σ_0 and ε_0 denote, respectively, the amplitudes of stress and strain, t the time, and δ the phase shift between stress and strain. An illustration is provided in Fig. 24.21.

As already mentioned, the description of the response of a viscoelastic material to a sinusoidal tensile strain requires the introduction of two modulae; they are defined as

$$E' = \frac{\sigma_0}{\varepsilon_0} \cos \delta = E_{\mathrm{d}} \cos \delta \tag{24.40}$$

$$E'' = \frac{\sigma_0}{\varepsilon_0} \sin \delta = E_{\mathrm{d}} \sin \delta, \tag{24.41}$$

E_{d} is named the absolute value of the dynamic modulus. Obviously,

$$E_{\mathrm{d}} = [(E')^2 + (E'')^2]^{1/2}. \tag{24.42}$$

The introduction of E' and E'' enables us to write Eq. (24.39) as

$$\sigma = \varepsilon_0 E' \sin \omega t + \varepsilon_0 E'' \cos \omega t. \tag{24.43}$$

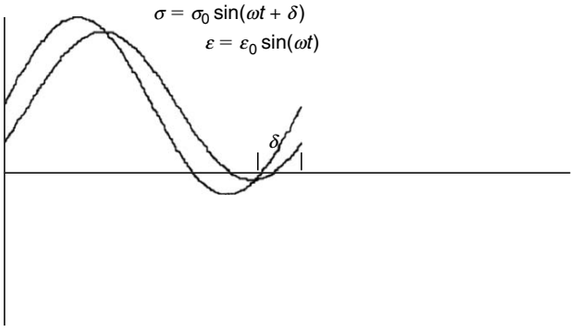

FIGURE 24.21. The phase lag of the strain ε resulting from an applied sinusoidal stress σ.

The ratio

$$\frac{E''}{E'} = \tan\delta \tag{24.44}$$

is the mechanical loss factor. It is a measure of the energy dissipated during a loading cycle relative the energy stored elastically in the material. Sometimes the term internal friction is used instead.

Another way of describing this type of response is to use the similarity between Eq. (24.42) and the decomposition of a number in the complex plane into its real and imaginary components. We can thus define a complex dynamic modulus E^* in the following way

$$E^* = E' + iE'' = E_d e^{i\delta}, \tag{24.45}$$

where E_d is the absolute value of the dynamic modulus introduced in Eqs. (24.40) and (24.41) and equal to σ_0/ε_0.

Figure 24.22 illustrates the decomposition of E^* into its components according to Eq. (24.45). As can be seen, the complex representation is equivalent to that introduced above; see Eqs. (24.40) and (24.41). The modulae relating to dynamic shear and hydrostatic compression, that is G and K, respectively, are defined in the same way as E in the above equations.

In some cases, the inverse values of the complex modulae named compliances are used; these are similar to the transient modulae and compliances such as seen in Eq. (24.9). The complex tensile compliance D^* is thus defined as

$$D^* = \frac{1}{E^*}, \tag{24.46}$$

and the complex shear compliance J^* as

$$J^* = \frac{1}{G^*}. \tag{24.47}$$

The following equations relate the components of D and E:

$$E' = \frac{D'}{D_d^2},\ E'' = \frac{D''}{D_d^2}, \tag{24.48}$$

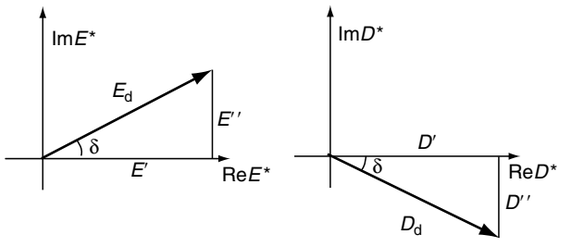

FIGURE 24.22. Graphical representation of the storage and loss moduli E' and E'' as components of a vector E_d in the complex plane. E_d is the absolute value of the dynamic modulus. The corresponding compliances are shown in the right hand part of the figure.

$$D' = \frac{E'}{E_d^2},\ D' = \frac{E'}{E_d^2}, \tag{24.49}$$

where D_d is given by $D_d E_d = 1$. Similar relations apply to the other moduli and the corresponding compliances. The graphical visualization of the compliance components using the complex plane is shown also in Fig. 24.22.

It should be remembered that the moduli and compliances under discussion are functions of frequency. The quantities E', D' etc. should thus be written $E'(\omega)$, $D'(\omega)$, and so forth. The frequency dependence of these quantities is governed by the same distribution of relaxation or retardation times as is stress relaxation, creep or other time-dependent mechanical phenomena. Single relaxation or retardation times cannot depict the frequency dependence of the dynamic mechanical behavior of polymers.

There is just one book in the world literature on the subject of dynamic mechanical analysis (DMA) which discusses the quantities briefly defined above, namely by Menard [67]. A summary is provided also by Menard in a book chapter [68].

24.5.2 Experimental Procedures

Dynamic mechanical testing allows the use of a variety of instrument types and a wide range of experimental conditions. The temperature may range from practically obtainable subambient up to levels where thermal degradation occurs, the frequencies typically from 0.01 to 1,000 Hz. The results should be examined for possible self-resonances. The elastic modulus of the material to be examined may range from $0.1\,\mathrm{J\,cm^{-3}}$ to $100\,\mathrm{J\,cm^{-3}}$ depending on type of polymer, temperature, and frequency.

The different techniques available for the determination of dynamic mechanical properties include several modes of load application and a number of dependent variables (temperature, frequency, and time). ASTM D 4092 provides a collection of definitions and terms, the most important of them described in Section 24.5.1. ASTM D 4065 describes standard practice in determining dynamic mechanical properties according to a variety of experimental methods; see Fig. 24.23.

24.5.3 Fatigue Determination

Plastics parts subjected to repeated loading may undergo failure by so-called dynamic fatigue. The term dynamic intends to distinguish this type of failure from that mentioned in static loading—as for instance in creep where the term static fatigue is sometimes used; see Section 24.3.6. The stress levels leading to failure are in both cases lower than those recorded in short-term tests. In dynamic fatigue, it is often observed that no failure occurs when the stress amplitude is lower than a certain value, the so-called fatigue or endurance limit, often characteristic of the material being studied.

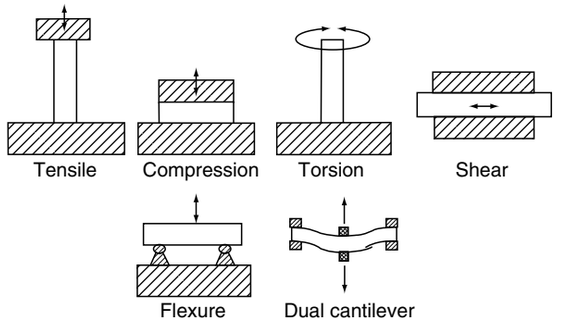

FIGURE 24.23. Schematic picture of various loading modes used in dynamic mechanical testing.

Fatigue testing of polymers cannot be accelerated by simply increasing the loading frequency. The reason is the relatively high level of mechanical damping (internal friction) in common polymers which would produce an excessive heating of the specimen.

Fatigue tests provide data on the number of loading cycles producing certain types of deterioration of the material (crack initiation and propagation, fatigue failure, softening due to energy dissipation). The ASTM test D 671, based on a constant force amplitude, allows these effects to be studied at varying stress levels and environmental conditions. When used for design purposes, the testing and end-use conditions are to be similar. Differences in the fatigue behavior may also be noted when employing testing equipment different from that described in the standard.

There exists a related but different German Standard DIN 53 442 which uses dumb-bell-shaped specimens differing from those used for tensile testing by a rounded middle section. Another difference in comparison with the above ASTM method is the use of constant deformation amplitude of the vibrations. This results in a stress amplitude decreasing with time due to stress relaxation. Apart from this, the stress amplitude diminishes also due to the heating of the specimen. The results are reported in a similar manner as required by the ASTM standard with the stress amplitude relating to the first cycle.

24.5.4 Application of Time–Frequency Correspondence Principle

We have explained the correspondence principles in Section 24.1.3, including the time—frequency correspondence. We were not able to apply this particular principle before becoming familiar with dynamic mechanical experiments. We need to provide at least an example of the application of the correspondence in the frequency domain. In Fig. 24.24 we show results from [58] pertaining to HDPE. The shift factors used to obtain that diagram have been calculated from equations in Section 24.1.3. More examples can be found for instance in the same paper [58].

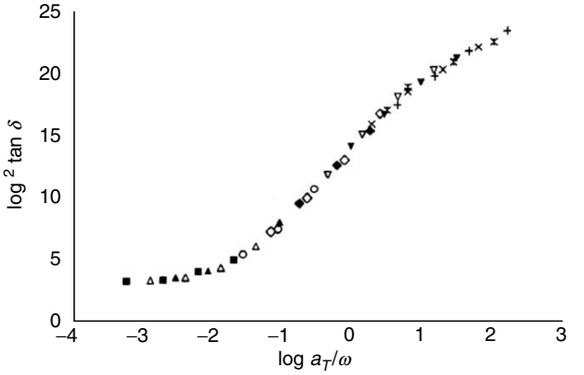

FIGURE 24.24. The master curve for HDPE of tan δ vs. log a_T/ω for 40°C and $\lambda = 1$; after [58].

24.6 ELASTOMERS

24.6.1 Mechanical Behavior as a Function of Temperature

The most amazing thing about elastomeric polymers is the fact that they can be stretched by several hundreds of percent and still behave elastically; that is the engineering stress σ (Eq. (24.31) will still be directly proportional to the engineering strain ε (Eq. (24.32)). This in contrast to other polymers, and in an even sharper contrast to metals and ceramics in which the elastic region ends at one percent elongation or even less. As a result, the elastic tensile modulus E (see Eq. (24.33)) is $1.1 \times 10^5 \mathrm{J\,cm^{-3}}$ for copper, $7.2 \times 10^4 \mathrm{J\,cm^{-3}}$ for clear fused quartz, $2 \times 10^3 \mathrm{J\,cm^{-3}}$ for nylon (that is a nonelastomeric polymer) and only about $1 \mathrm{J\,cm^{-3}}$ for gum rubber.

The explanation of the behavior which is ordinarily called rubbery lies in the huge number of possible conformations in elastomeric chains. When a copper wire is drawn, we soon come to weakening and eventual destruction of primary chemical bonds between Cu atoms. When a rubber band is drawn, rotations and other changes results in new conformations, but the primary bonds are preserved. This can be described as *unkinking* and *straightening out* of kinked and "mixed up spaghetti-like" elastomeric chains.

It is essential to note that elastomers do *not* always behave in the manner known from stretching a rubber band at room temperature. Some of us might have seen an experiment when such a rubber band was put into liquid nitrogen, became brittle, and when stretching was attempted the band broke into little fragments. Thus, in general the type of behavior of an elastomer depends on the *temperature*. This is shown in Fig. 24.25: the elastic modulus E (for a certain fixed time after the imposition of a force) as a function of temperature T. At low temperatures we have the brittle behavior—as the rubber band in liquid nitrogen;

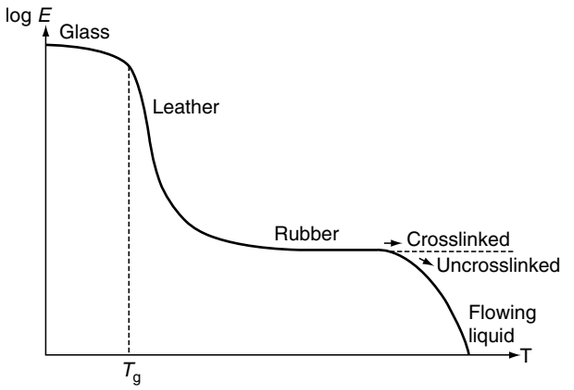

FIGURE 24.25. Dependence of the tensile modulus E (for a fixed time t since the imposition of a force) on temperature T for an elastomer.

the modulus E is relatively high. Then from the glass transition temperature T_g up to approximately $T_g + 30\,K$ we have the *leathery* state—with *retarded* high elasticity. Then comes the *rubbery* behavior known to us from stretching the elastomeric band at room temperature: *instantaneous* high elasticity. Finally, if the elastomer is not cross-linked, we have melting and liquid flow. If the elastomer is cross-linked, the rubbery plateau persists. We conclude that an elastomer might exhibit glassy, leathery, rubbery, or liquid flow behavior.

24.6.2 Thermodynamic and Molecular Behavior

We have already referred to the fact that the explanation for the instantaneous high elasticity lies at the molecular level. This is a vast area of active research, and we do not have space to discuss details, but we can recommend to the reader a book by Mark and Erman [69] which covers precisely that field.

Here we shall mention only two facts. First, the behavior at the molecular level can be related to the macroscopic *thermodynamic* description. For the simple uniaxial tension we have

$$\mathrm{d}U = T\mathrm{d}S - P\mathrm{d}V + F\mathrm{d}l \tag{24.50}$$

$$\mathrm{d}A = -S\mathrm{d}T - P\mathrm{d}V + F\mathrm{d}l, \tag{24.51}$$

where the symbols have the same meaning as before: U is energy; S, entropy; F, force; and l is the length while A is the Helmholtz function. Second, Eqs. (24.50) and (24.51) can be used in conjunction with the analysis of a *memoryless* system (also known as the story of the drunkard walk) to obtain the following relation:

$$F = kTl/Nh^2, \tag{24.52}$$

where N is a constant proportional to the degree of polymerization, k is the Boltzmann constant while h is the length of one segment. We can easily verify that the last result is true: when we put a stretched piece of rubber between our lips, under given tension the specimen shrinks when warmed. In other words, since F, N, and h^2 are all constant, an increase in T must produce a decrease in l. Other cases such as biaxial extension and shear are treated in the already quoted book of Mark and Erman [69].

24.6.3 Swelling of Networks

Some polymeric materials are water-repellent and thus used for instance as impregnation of overcoats, but some elastomeric and other networks absorb liquid penetrants avidly and swell—until an equilibrium degree of swelling is reached. Since this is only one chapter in the Handbook, of limited length, again we shall take the same short-cut as in the preceding Subsection: we recommend to the reader the book by Mark and Erman [69]. Since the behavior of elastomers is characterized in terms of energy and Helmholtz function, as in our Eqs. (24.50) and (24.51), we need a relation for the calculation of change of A caused by swelling [70]:

$$\Delta A_{\mathrm{swelling}} = \Delta A_{\mathrm{el}} + \Delta A_{\mathrm{mix}}. \tag{24.53}$$

That is, the change in the Helmholtz function on swelling consists of an elastic (''mechanical'') contribution ΔA_{el} resulting from the change of dimensions of the network caused by the solvent penetration and also from the ''thermodynamic'' contribution ΔA_{mix} caused by polymer + solvent interactions upon mixing. The latter can be calculated for the swelling process by similar procedures as for polymer + polymer or liquid + liquid systems. Equation (24.53) is thus the starting point for dealing with mechanical, thermodynamic, and molecular behavior of swollen networks. The assumption that there is no mixed term, that is mechanical effects do not affect thermodynamic ones nor vice versa, has been supported by results for several systems [70].

24.6.4 Filled Elastomers

Natural rubber crystallizes on elongation—a phenomenon called *strain-induced crystallization*—what enhances mechanical properties. However, a filler in the form of carbon black is typically added to natural rubber to additionally modify the mechanical properties. Elastomers which cannot undergo strain-induced crystallization contain even more fillers. Carbon black is used in such cases also, but silicone rubbers are filled with silica.

Automotive tires constitute the classic example of carbon-black reinforced elastomers. The elastomer can be either natural rubber—as typically is the case of truck and aircraft tires, or else a synthetic rubber—as is typical for automobile tires. However, reinforcing fillers constitute only one of many additives. There are also antioxidants, light stabilizers,

plasticizers, antiplasticizers, impact modifiers, processing aids, colorants, flame retardants, crosslinking agents etc. There exists a thorough collective book edited by Zweifel [71] on polymer additives, which discusses filers and reinforcements in some detail.

24.7 OTHER ISSUES

24.7.1 Brittleness and Aging

There is still a number of topics related to mechanical properties of polymers which we did not cover. One of them is *aging* in the glassy state: tending toward equilibrium, the material increases its density, and thus lowers its free volume. We do not have space for it, but aging is understandable in terms of CRC as explained in Section 24.1, and is discussed in some detail by Robertson and Kim [72].

An important result of aging *is brittleness*. Of course, there are also materials which are brittle even without aging. Brittleness is not a simple inverse of ductility (for which there is more than one definition) nor of toughness. Brittleness has been defined [73] as

$$B = 1/(\varepsilon_b \cdot E') \tag{24.54}$$

where ε_b is the elongation at break in tensile testing (along with the stress at break σ_b and other quantities, see Tables below) while E′ is known to us From Section 24.5.1. Thus, the first term in the denominator comes from quasi-static tensile testing and the second from DMA. Application of Eq. (24.54) shows that polystyrene is highly brittle, what explains odd behavior of PS in a variety of circumstances [73].

24.7.2 Nanoindentation

Nanoindentation is a technique gaining increasing popularity [74–76]. Actually, the technique is sometimes abused by attempts to calculate the elastic modulus E on the basis of a model valid for fully elastic materials only [74]. While such attempts fail, a connection has been found by Fujisawa and Swain between E and the unloading strain rate [75]. As shown by Tweedie and Van Vliet [76], spherical indentation provides lower contact strains and more reliable results than conical indentation. A modification providing repetitive indenter hits perpendicular to the specimen surface at the same spot and thus nanoindentation fatigue testing (NIFT) exists also [77].

24.7.3 Tribology

Another important area is *tribology* which includes friction, scratch resistance, wear and design of interactive surfaces in relative motion [78]. Rabinowicz [78] describes vividly huge annual losses to industry caused by wear. Some tribologists claim that their discipline is not a part of mechanics but independent and comparable to mechanics in its importance. A review of polymer tribology which includes fundamental definitions is available [79]. Similarly as mechanical properties, tribological properties of polymers can be varied by using additives; thus, carbon black can be used for the purpose [80]. By contrast, using external liquid lubricants—which work so well for metal surfaces—is in many cases dangerous because of swelling described above. Another option is application of magnetic fields which cause polymer orientation and thus can improve scratch resistance [81].

24.8 TABLES OF SELECTED MECHANICAL DATA

Following are selected data for the most often used polymers. They have been divided (partly arbitrarily, because of the overlap in definitions) into four tables, numbered from 24.3 to 24.6 respectively, for general purpose polymers, engineering polymers, thermosets, and elastomers. The third column in each of these tables shows the values of density, the fourth of the tensile modulus, the fifth the stress at break, the sixth the elongation at break; IS denotes the Izod impact strength for notched specimens. The letters *A* and *C* in the last column in Tables 24.3 and 24.4 pertain respectively to amorphous and crystalline thermoplastic polymers.

ACKNOWLEDGMENTS

Professor Josef Kubát of the Chalmers University of Technology in Gothenburg and Dr. Michael J. Kubát of the Royal Institute of Technology in Stockholm have participated in writing this chapter for the first Handbook edition. Thanks are due to Professor G.H. Michler of the Institute of Materials Science of the Martin Luther University in Merseburg for providing us with the micrographs used in Section 24.4. I appreciate discussions with: Professor Michael Bratychak, Lvivska Politechnika National University; Dr. Georg Broza, Technical University of Hamburg; Dr. Rimantas Levinskas, Lithuanian Energy Institute, Kaunas; Professor Robert Maksimov, Institute of Polymer Mechanics, the Latvian National University, Riga; Professor Moshe Narkis, Technion, Haifa, Dr. Dorota Pietkiewicz, LAPOM, University of North Texas, Denton; and Professor Anuvat Sirivat, Chulalongkorn University, Bangkok.

TABLE 24.3. *Mechanical properties of thermoplastics: commodity (general purpose) plastics.*

Polymer	Grade	$\rho/(g/cm^3)$	E/(GPa)	σ_b/(MPa)	ε_b/(%)	IS/(J/m)	Structure
PE LD, LDPE Polyethylene, low density		0.915–0.93	0.14–0.3	7–17	200–900	NB	C
PE HD, HDPE Polyethylene, high density		0.94–0.97	0.7–1.4	20–40	100–1000	30–200	C
PE UHMW, UHMW PE Polyethylene, ultra-high molecular weight		0.93–0.94	0.1–0.7	20–40	200–500	NB	C
PP polypropylene	Homopolymer	0.90–0.91	1.1–2	30–40	100–600	20–75	C
PP polypropylene	−40% glass fiber filled	1.22–1.23	6.8–7.2	60–110	1.5–4	75–110	
PP	Copolymer	0.89–0.905	0.9–1.2	28–40	200–500	60–750	C
PVC Poly(vinyl chloride)	Rigid (RPVC)	1.32–1.58	1–3.5	40–75	30–80	20–1000	A
PVC	Flexible (FPVC, plasticized)	1.16–1.70	0.05–0.15	6–25	150–400	—	A
PS Polystyrene		1.04–1.05	2.4–3.2	30–60	1–4	13–25	A
SB Styrene-butadiene	Rubber-modified PS High-impact PS, HIPS	0.98–1.10	1.5–2.5	15–40	15–60	50–400	A
ABS Acrylonitrile-butadiene-styrene	Medium IS	1.03–1.06	2–2.8	30–50	15–30	130–320	A
ABS Acrylonitrile-butadiene-styrene	High IS	1.01–1.04	1.6–2.5	30–40	5–70	350–600	A
SAN Styrene-acrylonitrile		1.07–1.09	3.4–3.7	55–75	2–5	15–30	A
ASA Acrylate-styrene-acrylonitrile		1.05–1.07	2.2–2.4	30–50	20–40	450–600	A

TABLE 24.4. *Mechanical properties of thermoplastics: engineering plastics.*

Polymer	Grade	$\rho/(g/cm^3)$	E/(GPa)	σ_b/(MPa)	ε_b/(%)	IS/(J/m)	Structure
PA 6 Polyamide 6 (Polycaprolactam)	[a]	1.13	3	80	50–120	30–120	C
PA 6 Polyamide 6 (Polycaprolactam)	[b]		1.5	50	160–200	160	
PA 6 Polyamide 6 (Polycaprolactam)	[a] 30–35% glass fiber	1.35–1.42	8–10	170–180	2–4	50	C
PA 6 Polyamide 6 (Polycaprolactam)	[b] 30–35% glass fiber		5.5	110		95	
PA 66 Polyamide 66 [Poly(hexamethyleneadipamide)]	[a]	1.14	3.4	75–90	20	30–55	C
PA 66 Polyamide 66 [Poly(hexamethyleneadipamide)]	[b]		17–2	50	80	50–110	C
PA 11 Polyamide 11 [Poly(11-aminoundecanoic acid)]	[a]	1.04	1.5	45–50	400–500	100–NB	C
POM Polyacetal Polyoxymethylene	Homopolymer	1.42	3.1	65–70	25–75	60–120	C
POM Polyacetal Polyoxymethylene	Copolymer	1.41	2.8	65–72??	40–75	50–80	C
PET Poly(ethylene terephthalate)		1.29–1.40	3	50	50–300	12–40	C
PBT Poly(butylene terephthalate)		1.31	2.3–2.5	50–60	120–200	40–55	C
PBT Poly(butylene terephthalate)	+ 30% glass fiber	1.52	10	100–140	2–4	80–130	
PC Polycarbonate		1.2	2.1–2.4	70–90	100–120	650–1000[c]	A
CA Cellulose acetate		1.27–1.32	1.5–2.5	25–45	10–70	100–450	A
CAB Cellulose acetate butyrate		1.18	1.4–1.8	30–35	30–100	50–500	A
PMMA Poly(methyl methacrylate)		1.17–1.20	2.5–3.3	55–75	3–5	10–20	A
PTFE Polytetrafluoroethylene		2.15–2.20	0.41	7–30	200–400	150	C
PSU (PSO) Polysulfone		1.25	2.5–2.6	70	50–100	65–70	A
PES Polyethersulfone		1.37	2.5	80–90	40–80	75–120	A
PPS Poly(phenylene sulfide)		1.35	3.6	65–75	1–2	70	C
PPO (PPE) Poly(phenylene oxide) or -ether	Modified with PS	1.06–1.08	2.2–2.7	50–60	200–350	200–370	A
PEEK Polytetheretherketone		1.32	3.6	90–200	50	80	C
PEEK Polyetheretherketone	30% glass fiber	1.49	10	100	2	100	C

[a] dry as molded.
[b] at 50% relative humidity.
[c] thickness 3.2 mm.

TABLE 24.5. *Mechanical properties: thermosets.*

Polymer	Grade	ρ/(g/cm^3)	*E*/(GPa)	σ_b/(MPa)	ε_b/(%)	IS/(J/m)
PF Phenol-formaldehyde resin	Wood-flour (ca. 50%) filled molding compound	1.37–1.46	5.5–12	30–60	0.4–0.8	10–30
PF Phenol-formaldehyde resin	Impact modified, cellulose filled (ca. 50%)	1.38–1.42		25–45	1–2	20–60
MF Melamine-formaldehyde resin	Cellulose filled (ca. 50%)	1.47–1.52	8–10	35–100	0.5–1	10–20
UF Urea-formaldehyde resin	Cellulose filled (ca. 50%)	1.46–1.48	7–9	40–60	0.4–0.8	10–20
Polyester thermosetting resin	Cast, rigid	1.04–1.46	2–4.5	30–40	1.5–2.5	10–20
Polyester thermosetting resin	Premix, chopped glass	1.65–2.30	7–17	20–60	1	80–320
Polyester thermosetting resin	Woven glass cloth	1.5–2.1	10–30	200–350	1–2	300–1600
Epoxy resin	Unfilled	1.2–1.3	3–5	30–90	1–2	10–50
SMC Sheet molding compound	Glass fiber reinforced SMC	1.6–2	15–30	140–250	0.5–2	1600–2100

TABLE 24.6. *Mechanical properties: elastomers.*

Polymer	Grade	ρ/(g/cm^3)	*E*/(MPa)	σ_b/(MPa)	ε_b
NR (Natural rubber) *Cis*-polyisoprene	Unfilled vulcanisate	0.93	1–2	17–30	650–900
	50 pph CB, vulc.[a]		3.5–6	14–28	450–600
SBR Styrene-butadiene rubber	Unfilled, vulc. (23–25% styrene)	0.93–1.0	1–2	1.4–2.8	450–600
	50 pph CB, vulc.[a]		14–19	14–27	400–650
IIR (Butyl rubber) Isobutylene-isoprene rubber	Unfilled, vulc.	0.91–0.98	—	17–21	750–950
	50 pph CB, vulc.[a]		4–10	9–21	300–700
NBR (Nitrile rubber) Acrylonitrile-butadiene rubber	Unfilled, vulc. (AN content 26–27%)	0.92	—	4–7	350–800
	50 pph CB, vulc.[a]		8–18	10–30	350–800
CR (Chloroprene rubber) Poly(2-chloro-1,3-butadiene)	Unfilled, vulc.	1.2–1.25	1–3	13–22	800–1000
	50 pph CB, vulc.[a]		3–5	23–25	200–450
EPDM Ethylene-propylene rubber	Unfilled, vulc.	0.85–0.87	—	1.2	400
	50 pph CB, vulc.[a]		5–10	10–16	250–750

[a]pph=parts per hundred; CB=carbon black.

REFERENCES

1. J.D. Ferry, *Viscoelastic Properties of Polymers*, 3rd edition (Wiley, New York 1980).
2. J.J. Aklonis and W.J. MacKnight, *Introduction to Polymer Viscoelasticity*, 2nd edition (Wiley, New York 1983).
3. *Failure of Plastics*, edited by W. Brostow and R.D. Corneliussen (Hanser, Munich, Vienna, New York 1986, 1989, 1992).
4. *Performance of Plastics*, edited by W. Brostow (Hanser, Munich, Cincinnati 2000).
5. W. Brostow, *Mater. Chem. Phys.* **13,** 47 (1985).
6. W. Brostow, Chapter 10 in Ref. 3.
7. W. Brostow, Chapter 5 in Ref. 4.
8. J. Kim and R.E. Robertson, *J. Mater. Sci.* **27,** 300 (1992).
9. J. Karger-Kocsis, *Polym. Eng. Sci.* **36,** 203 (1996).
10. P.J. Flory, *Statistical Mechanics of Chain Molecules* (Wiley, New York 1969).
11. P.J. Flory, *Faraday Soc. Disc.* **49,** 7 (1970).
12. R.A. Orwoll, Chapter 7 in this Handbook.
13. M.H. Litt and A.V. Tobolsky, *J. Macromol. Sci. Phys.* **1,** 433 (1967).
14. D.G. Fesko and N.W. Tschoegl, *J. Polymer Sci. C* **35,** 51 (1971).
15. R.W. Fillers and N.W. Tschoegl, *Trans. Soc. Rheol.* **21,** 51 (1977).
16. W.K. Moonan and N.W. Tschoegl, *Internat. J. Polym. Mater.* **10,** 199 (1984).
17. B. Hartmann, *Proc. Can. High Polym. Forum* **22,** 20 (1983).
18. B. Hartmann and M.A. Haque, *J. Appl. Phys.* **58,** 2831 (1985).
19. B. Hartmann and M.A. Haque, *J. Appl. Polym. Sci.* **30,** 1553 (1985).
20. P. Zoller, P. Bolli, V. Pahud and H. Ackermann, *Rev. Sci. Instrum.* **47,** 948 (1976).
21. J.M. Berry, W. Brostow, M. Hess and E.G. Jacobs, *Polymer* **39,** 4081 (1998).
22. W. Brostow, V.M. Castaño, G. Martinez-Barrera and D. Pietkiewicz, *Physica B* **344,** 206 (2004).
23. W. Brostow, V.M. Castaño, G. Martinez-Barrera and D. J.-M. Saiter, *Physica B* **334,** 436 (2003).
24. M.T. O'Shaughnessy, *Textile Res. J.* **18,** 263 (1948).
25. A.Y. Goldman, Prediction of Deformation Properties of Polymeric and Composite Materials (American Chemical Society, Washington, DC 1994).
26. W. Brostow, *Mater. Res. Innovat.* **3,** 347 (2000).
27. M.L. Williams, R.F. Landel and J.D. Ferry, *J. Am. Chem. Soc.* **77,** 3701 (1955).
28. R.M. Criens and H.-G. Moslé, Chapter 21 in Ref. 3.
29. J.E. Shigley and C.R. Mischke, *Mechanical Engineering Design* (McGrawHill, New York 1989).
30. A.A. Griffith, *Phil. Trans. R. Soc.* **A211,** 163 (1921).
31. A.A. Griffith, *Proc. 1st Int. Congress Appl. Mech.* p. 55 (Delft 1924).
32. A.M. Donald and E.J. Kramer, *J. Mater. Sci.* **17,** 1871 (1982).
33. E.J. Kramer, *Adv. Polym. Sci.* **52/53,** 1 (1983).
34. E.J. Kramer, *Polym. Eng. Sci.* **24,** 761 (1984).

35. C.S. Henkee and E.J. Kramer, *J. Mater. Sci.* **21,** 1398 (1986).
36. L.L. Berger and E.J. Kramer, *J. Mater. Sci.* **22,** 2739 (1987).
37. L.L. Berger and E.J. Kramer, *J. Mater. Sci.* **23,** 3536 (1988).
38. E.J. Kramer and L.L. Berger, *Adv. Polym. Sci.* **91/92,** 1 (1990).
39. L.L. Berger, *Macromolecules* **22,** 3162 (1989).
40. L.L. Berger, *Macromolecules* **23,** 2926 (1990).
41. C.J.G. Plummer and A.M. Donald, *Polymer* **32,** 409 (1991).
42. L.L. Berger, *J. Polym. Sci. Phys.* **27,** 1629 (1989).
43. A.M. Donald, Chapter 13 in Ref. 4.
44. H.H. Kausch, Chapter 5 in Ref. 3.
45. R.P. Wool, Chapter 15 in Ref. 4.
46. J.M. Greig and T.R. Smith, *Paper 3 at the Conference on Designing to Avoid Mechanical Failure*, Plastics Institute of London, Cranfield Institute of Technology, 8–10 January 1973.
47. E. Gaube and W.F. Müller, *Kunststoffe* **70,** 72 (1980).
48. W. Brostow and W.F. Müller, *Polymer* **27,** 76 (1986).
49. W. Brostow, M. Fleissner and W.F. Müller, *Polymer* **32,** 419 (1991).
50. R. Simoes, A.M. Cunha and W. Brostow, e-Polymers 2004, no. 067.
51. R. Simoes, A.M. Cunha and W. Brostow, *Model. & Simul. Mater. Sci. & Eng.* **14,** 157 (2006); R. Simoes, A.M. Cunha and W. Brostow, *Comput. Mater. Sci.* **36,** 319 (2006).
52. J. Kubát, *Nature* **204,** 378 (1965).
53. J. Kubát, *Phys. Status Solidi B* **111,** 599 (1982).
54. J. Kubát and M. Rigdahl, Chapter 4 in Ref. 3.
55. W. Brostow and J. Kubát, *Phys. Rev. B* **47,** 7659 (1993).
56. W. Brostow, J. Kubát and M.J. Kubát, *Mater. Res. Soc. Symp.* **321,** 99 (1994).
57. S. Blonski, W. Brostow and J. Kubát, *Phys. Rev. B* **49,** 6494 (1994).
58. Yu. M. Boyko, W. Brostow, A. Ya. Goldman and A.C. Ramamurthy, *Polymer* **36,** 1383 (1995).
59. W. Brostow, N.A. D'Souza, J. Kubát and R. Maksimov, *J. Chem. Phys.* **110,** 9706 (1999).
60. W. Brostow, M. Hess and B.L. López, *Macromolecules* **27,** 2262 (1994).
61. A.E. Akinay, W. Brostow and R. Maksimov, *Polym. Eng. Sci.* **41,** 977 (2001).
62. A.E. Akinay and W. Brostow, *Polymer* **42,** 4527 (2001).
63. A.E. Akinay, W. Brostow, V.M. Castaño, R. Maksimov and P. Olszynski, *Polymer* **43,** 3593 (2002).
64. E.H. Andrews, *Fracture in Polymers* (American Elsevier, New York 1968).
65. G.H. Michler, *Kunststoff-Mikromechanik* (Carl Hanser Verlag, München, Wien 1992).
66. W. Brostow and M.A. Macip, *Macromolecules* **22,** 2761 (1989).
67. K.P. Menard, *Dynamic Mechanical Analysis – An Introduction* (CRC Press, Boca Raton – London, 1999).
68. K.P. Menard, Chapter 8 in Ref. 4.
69. J.E. Mark and B. Erman, *Rubberlike Elasticity - A Molecular Primer* 2nd edn. (Cambridge University Press, 2000).
70. W. Brostow, *Macromolecules* **4,** 742 (1971).
71. *Plastics Additives Handbook*, edited by H. Zweifel (Hanser, Munich, Cincinnati 2000).
72. R.E. Robertson and J.-H. Kim, Chapter 14 in Ref. 4.
73. W. Brostow, H.E. Hagg Lobland and M. Narkis, *J. Mater. Res.* **21,** 2422 (2006).
74. W.C. Oliver and G.M. Pharr, *J. Mater. Res.* **7,** 1564 (1992); W.C. Oliver and G.M. Pharr, *J. Mater. Res.* **19,** 3 (2004).
75. N. Fujisawa and M.V. Swain, *J. Mater. Res.* **21,** 708 (2006).
76. C.A. Tweedie and K.J. Van Vliet, *J. Mater. Res.* **21,** 1576 (2006).
77. B.D. Beake, B. Bilyeu, W. Brostow and W. Chonkaew, *Polymer Internat.* 56 (2007) to be published.
78. E. Rabinowicz, *Friction and Wear of Materials*, 2nd edn. (Wiley, New York, 1995).
79. W. Brostow, J.-L. Deborde, M. Jaklewicz and P. Olszynski, *J. Mater. Ed.* **24,** 119 (2003).
80. W. Brostow, M. Keselman, I. Mironi-Harpaz, M. Narkis and R. Peirce, *Polymer* **46,** 5058 (2005).
81. W. Brostow and M. Jaklewicz, *J. Mater. Res.* **19,** 1038 (2004).

CHAPTER 25

Chain Dimensions and Entanglement Spacings

L. J. Fetters*, D. J. Lohse†, and R. H. Colby‡

*Chemical and Biomedical Engineering, Cornell University, Ithaca, NY 14853-5201; †ExxonMobil Research and Engineering Company, Annandale, NJ 08801-0998; ‡Materials Science and Engineering, Penn State University, University Park, PA 16802

This chapter summarizes data on chain dimensions and entanglement spacings for a number of linear flexible polymers. The polymers are listed in the Appendix along with their abbreviations used in the Tables. The equations relating various important parameters are from the literature [1–3]. While polymer chain entanglement is far from being understood [4–6], one natural idea based on overlap [7] appears useful for thinking about entanglement effects in polymer melts. This concept leads to the entanglement criterion: *a fixed number of entanglement strands (P_e) share a volume equal to the cube of the tube diameter (a^3)* [8–12]. One of the main purposes of this chapter is to test this criterion using literature data on flexible polymer melts and evaluate this universal number. Empirical relations useful for estimating the plateau modulus and entanglement molar mass of polymer melts emerge from this analysis. Chain entanglement is important, not merely for melt rheology, but also for mechanical properties of glassy [13] and semicrystalline polymers [14]. This chapter first discusses chain dimensions of polymers and then discusses chain entanglement and the tube diameter. The critical molar mass for entanglement effects in melt viscosity is then discussed, followed by the temperature dependence of chain dimensions.

25.1 CHAIN DIMENSIONS

In either the melt state or in a θ-solvent solution, linear flexible polymers adopt Gaussian statistics, and their average conformation is described as a random walk. Consequently, the ratio of their unperturbed mean-square end-to-end distance $<R^2>_0$ and their molar mass M is a constant, for large M, that characterizes their chain dimensions. In practice, the ratio $<R^2>_0/M$ depends weakly on temperature in the melt and the specific choice of θ-solvent, imparting a weak temperature dependence to various quantities calculated from that ratio.

The Kuhn length b of a polymer is the ratio of the mean-square end-to-end distance $<R^2>_0$ and the fully extended size R_{max}

$$b \equiv \frac{\langle R^2\rangle_0}{R_{max}}. \tag{25.1}$$

Aliphatic backbone polymers have n backbone bonds, with a well-defined average backbone bond length l, and known backbone bond angle θ, making $R_{max} = nl\cos(\theta/2)$ in the all-*trans* conformation. Flory defined [15] the characteristic ratio C_∞ as the ratio of the actual unperturbed mean-square end-to-end distance $<R^2>_0$ and that of a freely jointed chain nl^2, which is a polymer-specific constant at large M

$$C_\infty \equiv \frac{\langle R^2\rangle_0}{nl^2} = \frac{m_b\langle R^2\rangle_0}{l^2 M}. \tag{25.2}$$

The second equality uses the equation $n = M/m_b$, where m_b is the average molar mass per backbone bond. Using this definition of C_∞, the Kuhn length can be rewritten as:

$$b = \frac{C_\infty nl^2}{nl\cos(\theta/2)} = \frac{C_\infty l}{\cos(\theta/2)}. \tag{25.3}$$

It is common to assume the fully extended conformation is a linear chain (ignoring bond angles) and hence $R'_{max} = nl$, and $b' = C_\infty l$. Since the bond angle of a polyethylene chain

is $\theta = 68°$, $b'/b = \cos(\theta/2) = 0.83$. In principle, either convention may be utilized; here we use Eq. (25.3) to calculate the Kuhn length.

The Kuhn length is the effective monomer size for the equivalent freely jointed chain (N Kuhn monomers of length b instead of n backbone bonds of length l)

$$\langle R^2\rangle_0 = C_\infty nl^2 = Nb^2, \quad R_{\max} = Nb. \tag{25.4}$$

The molar mass of a Kuhn monomer is $M_0 = M/N$ and the volume occupied by the Kuhn monomer is $\nu_0 = M_0/\rho N_{\mathrm{Av}}$, where ρ is the density and N_{Av} is Avogadro's number. This description of chain dimensions can be used to calculate many quantities. For example, combining Eqs. (25.3) and (25.4) yields the number of main chain bonds in a Kuhn monomer $n/N = C_\infty/\cos^2(\theta/2)$.

Witten *et al*. [16] define the packing length p as the ratio of the occupied volume of a chain $M/\rho N_{\mathrm{Av}}$ and the mean-square end-to-end distance

$$p \equiv \frac{M}{\langle R^2\rangle_0\ \rho N_{\mathrm{Av}}} = \frac{M_0}{b^2\rho N_{\mathrm{Av}}} = \frac{\nu_0}{b^2}. \tag{25.5}$$

25.2 CHAIN ENTANGLEMENT AND TUBE DIAMETER

The plateau modulus G_{e} defines the entanglement spacing of a polymer melt, and the entanglement molar mass M_{e}[17]

$$M_{\mathrm{e}} \equiv \frac{\rho RT}{G_{\mathrm{e}}} = V_{\mathrm{e}}\rho N_{\mathrm{Av}}, \tag{25.6}$$

where $R = kN_{\mathrm{Av}}$ is the ideal gas constant (k is the Boltzmann constant), T is the absolute temperature, and $V_{\mathrm{e}} \equiv kT/G_{\mathrm{e}} = M_{\mathrm{e}}/(\rho N_{\mathrm{Av}})$ is the entanglement volume. The length scale associated with the entanglement spacing is the tube diameter a [3]. Since a chain in the melt is Gaussian on all scales larger than the Kuhn length, and for flexible chains $a \gg b$, the tube diameter is related to the entanglement molar mass through the chain dimensions

$$a = \sqrt{\frac{\langle R^2\rangle_0\ M_{\mathrm{e}}}{M}} = b\sqrt{N_{\mathrm{e}}}, \tag{25.7}$$

where N_{e} is the number of Kuhn monomers in an entanglement strand (of molar mass M_{e}). The occupied volume of an entanglement strand is V_{e}

$$V_{\mathrm{e}} = \nu_0 N_{\mathrm{e}} = \nu_0\left(\frac{a}{b}\right)^2 = a^2 p. \tag{25.8}$$

In analogy to polymer networks (where the equilibrium modulus is kT per network strand) the plateau modulus is kT per entanglement strand

$$G_{\mathrm{e}} = \frac{kT}{V_{\mathrm{e}}} = \frac{b^2 kT}{\nu_0 a^2} = \frac{kT}{a^2 p}. \tag{25.9}$$

The number of entanglement strands P_{e} within the confinement volume a^3 is determined as the ratio of confinement volume and entanglement strand volume (an overlap parameter [3] for entanglement)

$$P_{\mathrm{e}} \equiv \frac{a^3}{V_{\mathrm{e}}} = \frac{a}{p}. \tag{25.10}$$

This number appears to be constant for flexible polymers, with the average value $P_{\mathrm{e}} = 20.6(\pm 8\%)$. Table 25.1 shows data for polyolefin melts listing density ρ, plateau modulus G_{e}, melt chain dimensions from SANS $<R^2>_0/M$, entanglement molar mass M_{e} calculated from Eq. (25.6), Kuhn length b, packing length p, tube diameter a, and the overlap parameter for entanglement P_{e}, all at temperature T.

Since P_{e} is apparently a polymer-independent constant, Eq. (25.10) suggests that the tube diameter and packing length are proportional, and the constant of proportionality thus has the empirical temperature dependence [1,2]:

$$a = 14.0\exp(T/1270)\ p. \tag{25.11}$$

Using Eqs. (25.6), and (25.9)–(25.11), we can obtain useful empirical equations [2] for the entanglement molar mass and the plateau modulus

$$M_{\mathrm{e}} = P_{\mathrm{e}}^2 p^3 \rho N_{\mathrm{Av}} = 200\exp(T/635)\ \rho p^3 N_{\mathrm{Av}}, \tag{25.12}$$

$$G_{\mathrm{e}} = \frac{\exp(-T/635)}{200}\frac{kT}{p^3}. \tag{25.13}$$

Table 25.1 lists these quantities for polyolefins. Table 25.2 lists these quantities for polydienes while polyacrylics and polymethacrylics are listed in Table 25.3. Table 25.4 lists these quantities for various other flexible linear polymers.

25.3 CRITICAL MOLECULAR WEIGHT

The critical molar mass (M_{c}) parameter [18,19] denotes the transition in the melt viscosity/molar mass relation as the exponents change from ~1 to ~3.4. Table 25.5 presents the polymers for which the M_{c} values are known while Table 25.6 lists the polymers for which, seemingly, $M_{\mathrm{c}}/M_{\mathrm{e}}$ is one. The ratio of $M_{\mathrm{c}}/M_{\mathrm{e}}$ was long taken to be ~2 [18] and thus to be species independent. However, a recent empirical compilation [19] has shown that the ratio is p dependent and varies from ~3.5 (PE; $p = 1.69$) to ~1.4 (a-PCHE; $p = 5.59$). Based upon the data of Table 25.5 this ratio is empirically expressed as:

$$\frac{M_{\mathrm{c}}}{M_{\mathrm{e}}} = 3.42p^{-0.534} = \left[\frac{p^*}{p}\right]^{0.534}. \tag{25.14}$$

M_{c} hence follows the empirical expression:

$$M_{\mathrm{c}} = M_{\mathrm{e}}\left[\frac{p^*}{p}\right]^{0.534}, \tag{25.15}$$

where $M_{\mathrm{c}} = M_{\mathrm{e}}$ at $p = p^* \approx 10$ Å. With M_{c} expressed in this fashion, M_{e} overtakes M_{c} as p approaches p^* in the 10 Å range. At least four polymers exist with $p \cong 10$ Å (see Table

TABLE 25.1. *Molecular characteristics of olefinic polymers and copolymers.*

Polymer	T (K)	ρ (g cm^{-3})	G_e (MPa)	$<R^2>_o/M$ (Å^2)	C_∞	b (Å)	ν_o (Å^3)	M_o	p (Å)	M_e	a (Å)	N_e	P_e
PE	298	0.851	3.5	1.40	8.26	15.4	329	168.3	1.39	602	29.0	3.58	20.8
PE	413	0.785	2.6	1.25	7.38	13.7	318	150.4	1.69	1,040	36.0	6.89	21.3
PEB-2	389	0.802	2.5	1.25	7.70	14.3	339	163.5	1.66	1,040	36.0	6.34	21.7
PEB-2	413	0.785	2.2	1.22	7.51	14.0	338	159.5	1.73	1,220	38.7	7.68	22.3
PEB-5	413	0.788	1.90	1.15	7.47	13.9	353	167.3	1.83	1,420	40.5	8.51	22.1
PEB-7	413	0.789	1.55	1.05	7.08	13.2	347	164.9	1.90	1,750	42.8	10.6	23.0
PEB-10	413	0.791	1.35	1.05	7.53	14.0	391	186.2	2.00	2,010	46.0	10.8	23.0
PEB-12	298	0.860	1.50	1.04	7.72	14.3	382	197.6	1.86	1,420	38.4	7.18	20.7
PEB-12	413	0.793	1.20	0.952	7.06	13.1	379	180.9	2.20	2,270	46.5	12.5	21.1
alt-PEP	298	0.856	1.10	0.924	7.21	13.4	376	194.0	2.10	1,930	42.2	9.93	20.1
alt-PEP	373	0.812	1.03	0.871	6.80	12.6	374	182.9	2.35	2,440	46.1	13.4	19.6
alt-PEP	413	0.790	0.97	0.834	6.51	12.1	368	175.1	2.52	2,790	48.3	16.0	19.2
PEB-18	298	0.860	1.12	0.926	7.42	13.8	396	205.1	2.09	1,900	42.0	9.27	20.1
PEB-18	413	0.797	0.90	0.913	7.31	13.6	421	202.2	2.28	3,040	52.7	15.0	23.1
HPI-16	373	0.812	0.88	0.813	6.51	12.1	368	180.1	2.52	2,860	48.2	15.9	19.2
HPI-20	373	0.812	0.79	0.788	6.45	12.0	372	181.9	2.60	3,190	50.1	17.5	19.3
PEB-25	298	0.864	0.69	0.800	7.08	13.2	416	216.4	2.40	3,100	49.8	14.3	20.7
PEB-25	413	0.799	0.67	0.799	7.07	13.1	449	216.2	2.60	4,090	57.2	18.9	22.0
a-PP	298	0.852	0.48	0.678	6.00	11.2	358	183.4	2.88	4,390	54.6	23.9	19.0
a-PP	348	0.825	0.48	0.678	6.00	11.2	369	183.4	2.97	4,970	58.1	27.1	19.5
a-PP	413	0.791	0.47	0.678	6.00	11.2	385	183.4	3.10	5,780	62.6	31.5	20.2
a-PP	463	0.765	0.42	0.678	6.00	11.2	398	183.4	3.20	7,010	68.9	38.2	21.5
i-PP	463	0.766	0.43	0.694	6.15	11.4	407	187.8	3.12	6,850	69.0	36.5	22.1
s-PP	463	0.766	1.35	1.03	9.12	16.9	604	278.7	2.10	2,180	47.4	7.83	22.5
HHPP	298	0.878	0.52	0.691	6.12	11.4	353	187.0	2.74	4,180	53.8	22.4	19.6
HHPP	413	0.810	0.52	0.691	6.12	11.4	383	187.0	2.97	5,350	60.8	28.6	20.5
HPI-34	373	0.812	0.50	0.703	6.25	11.6	392	192.0	2.91	5,030	59.5	26.2	20.4
alt-PEB	298	0.861	0.58	0.725	6.88	12.8	434	225.2	2.66	3,680	51.6	16.3	19.4
alt-PEB	413	0.800	0.52	0.692	6.57	12.2	446	214.9	3.00	5,280	60.4	24.6	20.1
PEB-32	298	0.863	0.44	0.641	6.22	11.5	400	208.0	3.00	4,860	55.8	23.3	18.6
PEB-32	413	0.802	0.43	0.692	6.71	12.5	465	224.6	2.99	6,400	66.6	28.5	22.2
HPI-50	373	0.812	0.35	0.632	6.21	11.5	430	210.5	3.24	7,190	67.4	34.2	20.8
PEB-40	298	0.864	0.24	0.570	6.06	11.3	427	222.1	3.37	8,910	71.3	40.1	21.1
PEB-40	413	0.805	0.30	0.595	6.32	11.7	478	231.8	3.47	9,210	74.0	39.7	21.3
PIB	298	0.918	0.34	0.570	6.73	12.5	496	274.2	3.18	6,690	61.7	24.4	19.4
PIB	413	0.849	0.30	0.557	6.58	12.2	524	267.9	3.51	9,710	73.6	36.3	20.9
a-PEE	298	0.866	0.18	0.480	5.67	10.5	443	230.9	4.00	11,900	75.6	51.6	18.9
a-PEE	413	0.807	0.20	0.508	6.00	11.1	503	244.3	4.05	13,800	83.9	56.7	20.7
HPI-75	300	0.855	0.12	0.452	6.67	12.4	660	339.7	4.30	17,800	89.6	52.3	20.8
HPMYRC	324	0.832	0.12	0.434	6.73	12.5	720	360.6	4.60	18,700	90.0	51.8	19.6
a-PHEX	273	0.871	0.14	0.542	9.60	17.8	1119	586.6	3.52	14,100	87.5	24.1	24.9
HPMYRC-64	308	0.871	0.10	0.409	7.36	13.7	895	457.5	4.78	21,700	94.3	47.5	19.7
a-PCHE	433	0.920	0.068	0.323	7.49	13.9	1082	599.4	5.59	48,700	125.4	81.2	22.4

TABLE 25.2. *Molecular characteristics of polydiene polymers and copolymers.*

Polymer	T (K)	ρ (g cm^{-3})	G_e (MPa)	$<R^2>_o/M$ (Å^2)	C_∞	b (Å)	ν_o (Å^3)	M_o	p (Å)	M_e	a (Å)	N_e	P_e
cis-PI	298	0.910	0.58	0.679	5.20	9.34	235	128.6	2.69	3,890	51.4	30.2	19.1
PI-7	298	0.900	0.35	0.596	4.70	8.44	221	119.6	3.10	6,370	61.6	53.2	19.9
PI-16	298	0.899	0.35	0.593	4.88	8.82	243	131.2	3.12	6,360	61.4	48.5	19.8
PI-20	298	0.898	0.35	0.591	4.96	8.98	253	136.5	3.13	6,350	61.3	46.5	19.6
PI-29	298	0.896	0.35	0.587	5.20	9.39	279	150.3	3.16	6,340	61.0	42.2	19.3

TABLE 25.2. *Continued.*

Polymer	T (K)	ρ (g cm^{-3})	G_e (MPa)	$<R^2>_o/M$ (Å^2)	C_∞	b (Å)	ν_o (Å^3)	M_o	p (Å)	M_e	a (Å)	N_e	P_e
PI-34	298	0.895	0.35	0.585	5.26	9.58	291	156.9	3.17	6,330	60.9	40.4	19.2
PI-50	298	0.893	0.41	0.528	4.80	8.80	273	146.6	3.52	5,390	53.4	36.8	15.1*
PI-75	298	0.890	0.37	0.563	8.07	15.0	745	399.3	3.32	5,960	57.9	14.9	17.5
cis-PBd	298	0.900	0.76	0.758	4.61	8.28	167	90.5	2.44	2,930	47.1	32.4	19.4
PBd-7	298	0.895	1.15	0.876	5.52	9.93	209	112.5	2.12	1,930	41.1	17.1	19.4
PBd-15	298	0.896	1.10	0.854	5.54	10.0	218	117.7	2.17	2,020	41.5	17.1	19.1
PBd-18	298	0.895	1.05	0.846	5.56	10.1	222	119.8	2.19	2,110	42.3	17.6	19.3
PBd-20	298	0.895	1.07	0.841	5.61	10.1	227	122.4	2.21	2,070	41.7	16.9	18.9
PBd-23	298	0.895	1.05	0.832	5.66	10.2	234	125.9	2.23	2,110	41.9	16.8	18.8
PBd-26	298	0.895	1.00	0.824	5.68	10.3	238	128.0	2.25	2,220	42.7	17.3	19.0
PBd-30	298	0.894	0.98	0.813	5.67	10.3	244	131.2	2.28	2,260	42.9	17.2	18.8
PBd-62	298	0.890	0.81	0.727	6.17	11.3	328	175.9	2.57	2,720	44.5	15.5	17.4
PBd-98	300	0.890	0.57	0.661	7.39	13.7	532	284.8	2.82	3,890	50.7	13.7	18.0
SBR**	298	0.913	0.78	0.818	6.41	11.9	316	173.6	2.22	2,900	48.7	16.7	22.0
PEBd	298	0.891	0.29	0.543	4.85	9.02	279	149.7	3.43	7,610	64.3	50.8	18.7
55-DMBD	348	0.861	0.33	0.640	7.31	13.6	556	288.4	3.01	7,550	69.5	26.2	23.1
PMYRC-0	298	0.892	0.10	0.398	5.30	9.85	454	243.8	4.68	22,100	93.8	90.6	20.0
PMYRC-64	298	0.891	0.071	0.374	5.87	10.9	592	317.5	4.98	31,100	107.8	97.9	21.7

*The low value of P_e likely indicates the real plateau modulus is lower.
**Styrene content 25 wt%.

TABLE 25.3. *Molecular characteristics of poly(acrylics) and poly(methacrylics).*

Polymer	T (K)	ρ (g cm^{-3})	G_e (MPa)	$<R^2>_o/M$ (Å^2)	C_∞	b (Å)	ν_o (Å^3)	M_o	p (Å)	M_e	a (Å)	N_e	P_e
a-PMA	298	1.11	0.25	0.436	7.91	14.7	740	494.6	3.43	11,000	69.2	22.2	20.2
a-PEA	298	1.13	0.36	0.463	9.76	18.1	1,040	710.1	3.17	7,770	60.0	10.9	18.9
a-POA	298	0.98	0.16	0.442	17.1	31.9	3,890	2,295	3.83	15,200	81.9	6.61	21.4
a-PMMA	413	1.13	0.31	0.390	8.22	15.3	880	598	3.77	12,500	69.9	20.9	18.5
a-PEBMA	373	0.988	0.15	0.315	11.3	21.0	2,350	1,396	5.34	20,400	80.2	14.6	15.0*
a-PHMA	373	0.960	0.090	0.366	13.1	24.4	2,800	1,622	4.73	33,100	110.0	20.4	23.3
a-POMA	373	0.923	0.033	0.272	11.4	21.1	2,950	1,635	6.61	86,700	153.6	53.0	23.2
a-PDDMA	298	0.929	0.016	0.254	13.6	25.3	4,500	2,513	7.04	144,000	191.1	57.2	27.1*
a-PAPHMA	393	1.00	0.012	0.167	14.5	26.9	7,220	4,348	9.95	272,000	213.2	62.6	21.4
a-PBPHMA	393	1.00	0.0092	0.154	15.2	28.2	8,600	5,173	10.8	355,000	233.8	68.6	21.7

*These two samples yield P_e values at odds with the value of ~21. This indicates the potential presence of pronounced errors in the chain dimension and/or plateau modulus values. From the trend shown in the chain dimension column the primary error seems to exist with this parameter.

TABLE 25.4. *Molecular characteristics of miscellaneous polymers.*

Polymer	T (K)	ρ(g cm^{-3})	G_e(MPa)	$<R^2>_o/M$ (Å^2)	p (Å)	M_e	a (Å)	P_e
a-PαMS	473	1.04	0.32	0.442	3.61	12,800	75.1	20.8
a-PS	413	0.969	0.20	0.437	3.92	16,600	85.2	21.7
i-PS	413	0.969	0.19	0.420	4.08	17,500	85.7	21.0
a-PtBS	473	0.957	0.10	0.361	4.81	37,600	116.5	24.2
a-PVA	333	1.08	0.35	0.490	3.14	8,540	64.7	20.6
a-PVME	303	1.05	0.41	0.580	2.73	6,450	61.2	22.4
m-AEK	473	1.20	2.2	0.775	1.79	2,140	40.8	22.8
Me-PEEK	463	1.16	3.3	0.834	1.72	1,350	33.6	19.6
PC	473	1.14	2.7	0.864	1.69	1,660	37.9	22.5

TABLE 25.4. *Continued.*

Polymer	T (K)	ρ(g cm^{-3})	G_e(MPa)	$<R^2>_o/M$ (Å^2)	p (Å)	M_e	a (Å)	P_e
PDMS	298	0.970	0.20	0.422	4.06	12,000	71.2	17.5
PET	548	0.989	3.1	0.845	1.99	1,450	35.0	17.6
PN6	543	0.985	1.8	0.853	1.98	2,470	45.9	23.2
PEO	353	1.06	1.8	0.805	1.95	1,730	37.3	19.2
POM	473	1.14	1.7	0.763	1.91	2,640	44.8	23.5
PPO	505	0.998	1.2	0.741	2.24	3,500	50.9	22.7
PSF	523	1.15	2.1	0.756	1.91	2,380	42.4	22.2
PTFE	653	1.46	1.7	0.598	1.90	4,660	52.8	27.7
RADEL-R	555	1.22	3.6	0.821	1.66	1,560	35.8	21.6

TABLE 25.5. *Entanglement and critical molecular weights of miscellaneous polymers.*

Polymer	T (K)	ρ(g cm^{-3})	$<R^2>_o/M$ (Å^2)	p (Å)	M_e	M_c	M_c/M_e
PE	443	0.768	1.21	1.79	980**	3,480	3.5
PBd-7	298	0.895	0.876	2.12	2,000	6,380	3.2
PI-7	243	0.919	0.618	2.92	3,250*	10,000	3.0
PEO	353	1.081	0.805	1.91	2,000	5,870	2.9
SBR	298	0.930	0.708	2.52	2,960	8,210	2.8
a-PVA	428	1.08	0.490	3.14	9,100	24,500	2.7
alt-PEP	373	0.812	0.871	2.40	3,100	8,100	2.6
PI-7	298	0.900	0.625	2.95	6,025	13,100	2.2
a-PMMA	490	1.09	0.425	3.58	13,600	29,500	2.2
PBd-98	300	0.889	0.720	2.59	3,850	8,200	2.1
a-PαMS	459	1.04	0.460	3.47	13,300	28,000	2.1
PDMS	298	0.970	0.422	4.06	12,000	24,500	2.0
PIB	298	0.918	0.570	3.17	6,900	13,100	1.9
a-PS	490	0.959	0.434	3.39	18,100	31,200	1.7
PIB	490	0.817	0.570	3.57	10,500	17,000	1.6
a-PCHE	453	0.920	0.323	5.59	48,750	80,000	1.6

*Calculated value is 6,000.
**Measured value at 413 K. The calculated value (via Eq. (25.12)) at 443 K is 1,150.

TABLE 25.6. *Polymers with large packing lengths.*

Polymer	T (K)	ρ(g cm^{-3})	$<R^2>_o/M$ (Å^2)	p (Å)	M_e	$[M_c/M_e]$
a-PHDEC	418	0.796	0.213	9.79	173,000*	1.01**
a-PAPHMA	393	1.0	0.167	9.94	268,000	1.00
a-PBPHMA	393	1.0	0.154	10.8	355,000	0.96
PMA-CH3	363	1.17	0.123	11.5	485,000*	0.93

*Via Eq. (25.12).
**Via Eq. (25.15).

25.6). Since it seems improbable that $M_e > M_c$ for any polymer, we expect the limiting value for M_c/M_e of 1, independent of p for $p \geq 10$ Å. An unexplained facet of these empirical observations is that as p increases, fewer entanglement events are seemingly required to reach the regime where the melt viscosity becomes proportional to the 3.4 power of molar mass. This is displayed in Table 25.5 where the M_e and M_c data for various flexible polymers are listed. Note that while the relation between M_e and packing length is understood [1], the corresponding state of play between p and M_c remains purely empirical [19].

25.4 TEMPERATURE DEPENDENCE OF CHAIN DIMENSIONS

A feature of chain dimensions is their temperature dependence that is expressed in terms of

$$\kappa \equiv \frac{\mathrm{d}\ \ln \langle R^2 \rangle_0}{\mathrm{d}T} = \frac{f_e/f}{T} \tag{25.16}$$

where f_e/f denotes the energetic fraction of the temperature-dependent force in a polymer network at constant volume.

TABLE 25.7. *Melt state values of* $\kappa = d\ln\langle R^2\rangle_0/dT$.

Polymer samples	$\kappa \times 10^3(K^{-1})$	
	From SANS	From f_e/f
alt-PEP (PEP)*	−1.1 [25]	−1.5 [26,27]
HPI-50	−0.2 [21]	—
a-PCHE	∼0 [21]	—
a-PEE	+0.40 [28,29]	+0.30 [30]
a-PMMA	+0.10 [31]	−0.10 [24]
a-PP	−0.1 [32]	—
a-PS	∼0 [31]	+0.17 [33,34]
a-PPEN	—	+0.33 [30]
alt-PEB	0 [21]	—
HHPP	0 [21]	—
i-PP	∼0 [35]	—
PBd-7	—	+0.16 [36]
PDMS	—	+0.78 [37]
PEB-2(PE)	−1.2 [38]	−1.2 [39]
PEB-5	−1.3 [29]	—
PEB-7	−0.65 [29]	—
PEB-10	−0.44 [29]	—
PEB-12	−0.44 [29]	—
PEB-18	−0.1 [29]	—
PEB-25	0 [29]	—
PEB-32	+0.63 [29]	—
PEB-40	+0.55 [29]	—
PEO	−0.30 [40]	+0.03 [41]
PIB	—	−0.28 [42]
HPI-75	+1.2 [21]	—
PI-7 (*cis*-PI)	+0.40 [21]	+0.41 [43]

*Ethylene–propylene random copolymer.

The empirical sign of κ can be +, 0, or – (see Table 25.7). The modes of measurement have included theta condition measurements utilizing a family of theta solvents or melt state measurements. The latter include thermoelastic measurements on networks [22] and small angle neutron scattering (SANS) measurements on labeled chains in a polymer melt [23]. Generally, the theta condition approach (multiple theta solvents over a wide temperature range) is recognized to be unreliable [21,24]. An example of this [21] is *a*-PEE, where extensive theta condition work (over the temperature range of ∼200 K) led to a negative value of $\kappa = -1.2 \times 10^{-3}\ K^{-1}$, as opposed to the two positive values found for the melt state by SANS and thermoelastic measurements; see Table 25.7. The role of κ on the packing length, plateau modulus and entanglement volume can be significant, particularly for cases where the melt rheology is studied over a wide temperature range. A 200 K range is common for amorphous polymers having low glass transition temperatures.

The packing length has two sources of temperature dependence ($\langle R^2\rangle_0$ and ρ, see Eq. (25.5)). For typical temperatures (350 K) the change in density for polymer liquids as a function of temperature is $d\ln\rho/dT \approx -6 \times 10^{-4}\ K^{-1}$. $\langle R^2\rangle_0$ is the more interesting parameter, in that it can increase, decrease, or remain constant as temperature is changed.

APPENDIX *Alphabetical Listing of Polymers.*

Name	References	Description
alt-PEB	[44,45]	essentially alternating poly(ethylene-*co*-1-butene); hydrogenated PEBd
alt-PEP	[25,46,47]	essentially alternating poly(ethylene-*co*-propylene); hydrogenated PI-7
a-PαMS	[1,17,18,48,49]	atactic poly(α-methyl styrene)
a-PAPHMA	[50,51]	atactic poly[6-{4(anisyloxycarbonyl)phenoxy}-hexyl methacrylate]
a-PBPHMA	[50,51]	atactic poly[6-{4(butoxycarbonyl)phenoxy}-hexyl methacrylate]
a-PCHE	[1,19,21,52]	atactic poly(cyclohexyl)ethylene or poly(vinyl cyclohexane)
a-PDDMA	[53,54]	atactic poly(dodecyl)methacrylate
a-PEA	[53,55]	atactic poly(ethyl)acrylate
a-PEBMA	[17,53,56]	atactic poly(ethyl butyl)methacrylate
a-PEE	[28,57]	atactic poly(ethyl ethylene); also called poly(butene-1);may be made via the hydrogenation of poly(vinyl ethylene)
a-PHDEC	[58]	atactic poly(hexadecene-1)
a-PHEX	[59,60]	atactic poly(hexene-1)
a-PHMA	[53,61]	atactic poly(hexyl)methacrylate
a-PMA	[55,62]	atactic poly(methyl)acrylate
a-PMMA	[17,18,21,31,63]	atactic poly(methyl)methacrylate
a-POA	[55,59]	atactic poly(octyl)acrylate
a-POMA	[17,53,54,64]	atactic poly(octylmethyl)methacrylate
a-PP	[32,65,66]	atactic polypropylene; hydrogenated poly(2-methyl 1,3-pentadiene)
a-PPEN	[59]	atactic poly(pentene-1)
a-PS	[17–19,31,67]	atactic polystyrene
a-PtBS	[1,68]	atactic poly(*t*-butyl styrene)

APPENDIX *Continued.*

Name	References	Description
a-PVA	[17,18,54]	atactic poly(vinyl acetate)
a-PVME	[69,70]	atactic poly(vinyl-methylether)
cis-PBd	[17,71]	1,4-polybutadiene ~ 96% *cis* content.
cis-PI	[17,72,73]	1,4-polyisoprene ~ 100% *cis* content; natural rubber
55-DMBD	[1]	poly-2,3(dimethyl butadiene) 55% 1,4; 45% 3,4 content.
HHPP	[1,21,45]	hydrogenated poly(2,3 dimethyl)butadiene:head-to-head polypropylene (alternating copolymer of ethylene and butene-2).
HPI-*x*	[1,26,74]	hydrogenated polyisoprene where $x = 3,4$ content of parent polyisoprene
HPMYRC-*x*	[1,45]	hydrogenated poly(myrcene) with *x*% 3,4
i-PMMA	[54,63]	isotactic-poly(methylmethacrylate)
i-PP	[35,66]	isotactic polypropylene
i-PS	[54,75]	isotactic polystyrene
m-AEK	[76]	poly(*m*-arylene–ether–ketone)
Me-PEEK	[77,78]	methyl-poly(aryl–ether–ether–ketone); prepared from methyl hydroquinone and 4,4′-difluorobenzophenone.
PBd-*x*	[57,79–82]	polybutadiene, $x =$ vinyl percent; for 100% vinyl content the material is identified as poly(vinyl ethylene) or 1,2-polybutadiene.
PC	[1,54,76,83,84]	polycarbonate of bisphenol A(4, 4'-isopropylidenediphenol)
PDMS	[17,85–87]	poly(dimethylsiloxane)
PE	[17,19,38,88–90]	polyethylene
PEBd	[1,44]	poly(ethyl butadiene) ~ 75/20/5 *cis*/*trans*/3,4
PEB-*x*	[29,57]	poly(ethylene–butene) random copolymer; *x* denotes number of ethyl branches per 100 backbone carbons
PEO	[18,19,40]	poly(ethylene oxide)
PET	[54,91,92]	poly(ethylene terephthalate)
PIB	[17,18,93–95]	polyisobutylene
PI-*x*	[21,47,96–98]	1,4-polyisoprene where $x = 3,4$ content; PI-75 is 75% 3,4, and 25% 1,2 (with essentially no 1,4 addition)
PMA-CH3	[99]	main-chain liquid crystal polyester
PMYRC-*x*	[1,44,45]	poly(myrcene) with *x*% 3,4 [myrcene = 1,6-octadiene-7-methyl-3-methylene]
PN6	[54,100,101]	polycaprolactam-nylon 6
POM	[28,54]	poly(oxymethylene)
PPO	[76,102]	poly(phenylene oxide)
PSF	[76,103]	alternating copolymer of bisphenol A and dichlorodiphenyl sulfone (UDEL)
PTFE	[104,105]	poly(tetrafluoro)ethylene
RADEL-R	[76,103]	alternating copolymer of 4,4′-biphenol and dichlorodiphenyl sulfone
SBR	[17,106]	solution prepared copolymer (anionic polymerization) styrene–butadiene (34% vinyl; 19% *cis* and 47% *trans*) 25 wt% styrene
s-PP	[66,107,108]	syndiotactic polypropylene

REFERENCES

1. Fetters, L. J.; Lohse, D. J.; Richter, D.; Witten, T. A.; Zirkel, A. *Macromolecules* 1994, **27**, 4639.
2. Fetters, L. J.; Lohse, D. J.; Colby, R. H. Ch. 24 of *Physical Properties of Polymers Handbook* (J. E. Mark, editor) AIP Press, Woodbury, NY (1996).
3. Rubinstein, M.; Colby, R. H. *Polymer Physics*, Oxford University Press, Oxford (2003).
4. Graessley, W. W.; Edwards, S. F. *Polymer* 1981, **22**, 1329.
5. Edwards, S. F. *Proc. R. Soc. London A* 1988, **419**, 221.
6. Colby, R. H.; Rubinstein, M.; Viovy, J. L. *Macromolecules* 1992, **25**, 996.
7. de Gennes, P. G. *Scaling Concepts in Polymer Physics*, Cornell University Press, Ithaca, New York (1979).
8. Ronca, G. *J. Chem. Phys.* 1983, **79**, 1031.
9. Lin, Y.-H. *Macromolecules* 1987, **20**, 3080.
10. Kavassalis, T. A.; Noolandi, J. *Phys. Rev. Lett.* 1987, **59**, 2674.
11. Kavassalis, T. A.; Noolandi, J. *Macromolecules* 1988, **21**, 2869.
12. Kavassalis, T. A.; Noolandi, J. *Macromolecules* 1989, **22**, 2709.
13. Ho, J.; Govaert, L.; Utz, M. *Macromolecules* 2003, **36**, 7398.
14. Hiss, R.; Hobeika, S.; Lynn, C.; Strobl, G. *Macromolecules* 1999, **32**, 4390.
15. Flory, P. J. *Statistical Mechanics of Chain Molecules*, Wiley, New York (1969), Chap. II; see Tables 1 and 2.
16. Witten, T. A.; Milner, S. T.; Wang, Z.-G. in *Multiphase Macromolecular Systems* (B. M. Culbertson, editor) Plenum Press New York (1989).
17. Ferry, J. D. *Viscoelastic Properties of Polymers*, 3rd Ed., Wiley, New York (1980); Table 13–1.
18. Berry, G. C.; Fox, T. G *Adv. Polym. Sci.* 1968, **5**, 261.
19. Fetters, L. J.; Lohse, D. J.; Milner, S. T.; Graessley, W. W. *Macromolecules* 1999, **32**, 6847.

20. Graessley, W. W.; Fetters, L. J. *Macromolecules* 2001, **34**, 7147.
21. Krishnamoorti, R.; Graessley, W. W.; Zirkel, A.; Richter, D.; Hadjichristidis, N.; Fetters, L. J.; Lohse, D. J. *J. Polym. Sci., Part B: Polym. Phys.* 2002, **40**, 1768.
22. Price, C. *Proc. R. Soc. London* 1976, **351**, 331.
23. Higgins, J. S.; Benoit. H. C. *Polymers and Neutron Scattering*, Oxford University Press, Oxford (1994).
24. Ciferri, A. *J. Polym. Sci. Part-A* 1964, **2**, 3089.
25. Zirkel, A.; Richter, D.; Pyckhout-Hintzen, W.; Fetters, L. J. *Macromolecules* 1992, **25**, 954.
26. Mark, J. E. *J. Chem. Phys.* 1972, **57**, 2541.
27. Mark, J. E. *J. Polym. Sci., Part B: Polym. Phys.* 1974, **12**, 1207.
28. Zirkel, A.; Richter, D.; Fetters, L. J.; Schneider, D.; Graciano, V.; Hadjichristidis, N. *Macromolecules* 1995, **28**, 5262.
29. Fetters, L. J.; Graessley, W. W.; Krishnamoorti, R.; Lohse, D. J. *Macromolecules* 1997, **30**, 4973.
30. Mark, J. E.; Flory, P. J. *J. Am. Chem. Soc.* 1965, **87**, 1423.
31. Boothroyd, A. T.; Rennie, A. R.; Wignall, G. D. *J. Chem. Phys.* 1993, **99**, 9135.
32. Zirkel, A.; Urban, V.; Richter, D.; Fetters, L. J.; Huang, J. S.; Kampmann, R.; Hadjichristidis, N. *Macromolecules* 1992, **25**, 6148.
33. Orofino, T. A.; Ciferri, A. *J. Phys. Chem.* 1964, **68**, 3136.
34. Dusek, K. *Collect. Czech. Chem. Commun.* 1966, **31**, 1893.
35. Ballard, D. G. H.; Cheshire, P.; Longman, G. W.; Schelten, J. *Polymer* 1978, **19**, 379.
36. Mark, J. E.; Llorente, M. A. *Polym. J.* 1981, **13**, 543.
37. Price, C., Padget, J.; Kirkham, M. C.; Allen, G. *Polymer* 1969, **10**, 573.
38. Boothroyd, A. T.; Rennie, A. R.; Boothroyd, C. B. *Europhys. Lett.* 1991, **15**, 715.
39. Ciferri, A.; Hoeve, C. A. J.; Flory, P. J. *J. Am. Chem. Soc.* 1961, **83**, 1015.
40. Smith, G. D.; Yoon, D. Y.; Jaffe, R. L.; Colby, R. H.; Krishnamoorti, R.; Fetters, L. J. *Macromolecules* 1996, **29**, 3462.
41. Mark, J. E.; Flory, P. J. *J. Am. Chem. Soc.* 1965, **87**, 1415.
42. Allen, G.; Gee, G.; Kirkham, M. C.; Price, C.; Padget, J. *J. Polym. Sci., Part C* 1968, **23** 201.
43. Flory, P. J. *Trans. Faraday Soc.* 1961, **57**, 829.
44. Hattam, P.; Gauntlett, S.; Mays, J. W.; Hadjichristidis, N.; Young, R. N.; Fetters, L. J. *Macromolecules* 1991, **24**, 6199.
45. Fetters, L. J.; Kiss, A. D.; Mays, J. W. unpublished results.
46. Richter, D.; Butera, R.; Fetters, L. J.; Huang, J. S.; Farago, B.; Ewen, B. *Macromolecules* 1992, **25**, 6156.
47. Gotro, J. T.; Graessley, W. W. *Macromolecules* 1984, **17**, 2767.
48. Mays, J. W.; Hadjichristidis, N.; Graessley, W. W.; Fetters, L. J. *J. Polym. Sci., Part B: Polym. Phys.* 1986, **24**, 2553.
49. Fujimoto, T.; Ozaki, N.; Nagasawa, M. *J. Polym. Sci. A-2* 1968, **6**, 129.
50. Kirste, R. G.; Ohm, H. G. *Makromol. Chemie - Rapid Commun.* 1985, **6**, 179.
51. Rubin, S. F.; Kannan, R. M.; Kornfield, J. A.; Boeffel, C. *Macromolecules* 1995, **28**, 3521.
52. Abdel-Goad, M.; Pyckhout-Hintzen, W.; Fetters, L. J. unpublished results.
53. Mays, J. W.; H adjichristidis, N. *J. Macromol. Sci.: Rev. Macromol. Chem. Phys.* 1988, **C28**, 371.
54. Wu, S. *J. Polym. Sci., Polym. Phys. Ed.* 1989, **27**, 723.
55. Janáček, L.; Hrouz, J. *J. Polym. Sci., Polym. Symp.* 1975, **53**, 283.
56. Yin, T. P.; Ferry, J. D. *J. Colloid Sci.* 1961, **16**, 166.
57. Carella, J. M.; Graessley, W. W.; Fetters, L. J. *Macromolecules* 1984, **17**, 2775
58. Pena, B.; Aroca, M.; Perez, E.; Bello, A.; Riande, E.; Benavente, R.; *Macromol. Chem. Phys.* 1997, **198**, 1691.
59. Sundararajan, P. R. in *Physical Properties of Polymers Handbook* (J. E. Mark, Ed.) AIP Press, Woodbury, NY (1996) p. 197.
60. Fetters, L. J.; Lohse, D. J.; Garcia-Franco, C. A.; Brant, P.; Richter, D.; *Macromolecules* 2002, **35**, 10096.
61. Child, Jr., W. C.; Ferry, J. D. *J. Colloid Sci.* 1957, **12**, 389.
62. Fujino, K.; Senshu, K.; Kawai, H. *J. Colloid Sci.* 1961, **16**, 262.
63. Fuchs, K.; Friedrich, C.; Weese, J. *Macromolecules* 1996, **29**, 5893.
64. Dannhauser, W.; Child, Jr., W. C.; Ferry, J. D. *J. Colloid Sci.* 1958, **13**, 103.
65. Xu, Z.; Mays, J. W.; Chen, X.; Hadjichristidis, N.; Schilling, F. C.; Bair, H. E.; Pearson, D. S.; Fetters, L. J. *Macromolecules* 1985, **18**, 2560.
66. Eckstein, A.; Suhm, J.; Friedrich, C.; Maier, R.-D.; Sassmannshausen, J.; Bochmann, M.; Mülhaupt, R. *Macromolecules* 1998, **31**, 1335.
67. Onogi, S.; Masuda, T.; Kitagawa, K. *Macromolecules* 1970, **3**, 109.
68. Mays, J. W.; Ferry, W. M.; Hadjichristidis, N.; Funk, W. G.; Fetters, L. J. *Polymer* 1986, **27**, 129.
69. Kannan, R. M.; Lodge, T. P. *Macromolecules* 1997, **30**, 3694.
70. Choi, S.; Liu, X.; Briber, R. M. *J. Polym. Sci., Part B: Polym. Phys.* 1998, **36**, 1.
71. Brandrup, J.; Immergut, E. H., Eds. *Polymer Handbook*, 3rd Ed., Wiley, New York (1989).
72. Ansorena, F. J.; Revuelta, L. M.; Guzmán, G. M.; Iruin, J. J. *Eur. Polym. J.* 1982, **18**, 19.
73. Sanders, J. F.; Ferry, J. D.; Valentine, R. H. *J. Polym. Sci. A-2* 1968, **6**, 967.
74. Mays, J. W.; Hadjichristidis, N.; Fetters, L. J. *Macromolecules* 1984, **17**, 2723.
75. Guenet, J. M.; Picot, P.; Benoit, H. *Macromolecules* 1979, **12**, 86.
76. Roovers, J. Toporowski, P. M.; Ethier, R. *High Perform. Polym.* 1990, **2**, 165.
77. Hermann-Schönherr, O.; Schneller, A.; Seifert, A. M.; Soliman, M.; Wendorff, J. H. *Makromol. Chem.* 1992, **193**, 1955.
78. Wang, F.; Roovers, J.; Toporowski, P. M. *Macromolecules* 1993, **26**, 3826.
79. Fetters, L. J.; Lohse, D. J.; Graessley, W. W. *J. Polym. Sci., Part B: Polym. Phys.* 1999, **37**, 1023.
80. Roovers, J. *Polym. J.* 1986, **18**, 153.
81. Roovers, J.; Toporowski, P. M. *Rubber Chem. Tech.* 1990, **63**, 734.
82. Colby, R. H.; Fetters, L. J.; Graessley, W. W. *Macromolecules* 1987, **20**, 2226.
83. Hutnik, M.; Argon, A. S.; Suter, U. W. *Macromolecules* 1991, **24**, 5956.
84. Aloisio, C. J.; Boehm, V. W. in *Rheology* Vol.2 (G. Astarita and G. Marrucci, L. Nicholais, Eds.) Plenum Press, New York (1980), p. 513.
85. Kirste, R. G.; Lehnen, B. R. *Makromol. Chem.* 1976, **177**, 1137.
86. Beltzung, M.; Picot, C.; Rempp, P.; Herz, J. *Macromolecules* 1982, **15**, 1594.
87. Plazek, D. J.; Dannhauser, W.; Ferry, J. D. *J. Colloid Sci.* 1961, **16**, 101.
88. Lieser, G.; Fischer, E. W.; Ibel, K. *J. Polym. Sci., Polym. Lett. Ed.*, 1975, **13**, 39.
89. Pearson, D. S.; Fetters, L. J.; Graessley, W. W.; Ver Strate, G.; von Meerwall, E. *Macromolecules* 1994, **27**, 711.
90. Han, J.; Jaffe, R. L.; Yoon, D. Y. *Macromolecules* 1997, **30**, 7245.
91. McAlea, K. P.; Schultz, J. M.; Gardner, K. H.; Wignall, G. D. *Macromolecules* 1985, **18**, 447.
92. Wallach, M. L. *Makromol. Chem.* 1967, **103**, 19.
93. Hayashi, H.; Flory, P. J.; Wignall, G. D. *Macromolecules* 1983, **16**, 1328.
94. Fetters, L. J.; Graessley, W. W.; Kiss, A. D. *Macromolecules* 1991, **24**, 3136.
95. Pyckhout-Hinzen, W.; Fetters, L. J. unpublished data (PIB at 298K).
96. Nemoto, N.; Moriwaki, M.; Odani, H.; Kurata, M. *Macromolecules* 1971, **4**, 215.
97. Nemoto, N.; Odani, H.; Kurata, M. *Macromolecules* 1972, **5**, 531.
98. Abdel-Goad, M.; Pyckhout-Hintzen, W.; Kahle, S.; Allgaier, J.; Richter, D.; Fetters, L. J. *Macromolecules* 2004, **37**, 8135.
99. Fourmaux-Demange, V.; Boué, F.; Brulet, A.; Keller, P.; Cotton, J. P. *Macromolecules* 1998, **31**, 801.
100. Mattiussi, A.; Gechele, G. B.; Francesconi, R. *J. Polym. Sci.* A 1969, **7**, 411.
101. Flory, P. J.; Williams, A. D. *J. Polym. Sci. A-2* 1967, **5**, 399.
102. Cai, H.; Ait-Kadi, A.; Brisson, J. *Polymer* 2003, **44**, 1481.
103. Roovers, J.; Toporowski, P. M.; Ethier, R. *High Perform. Polym.* 1990, **2**, 151.
104. Tuminello, W. H.; Treat, T. A.; English, A. D. *Macromolecules* 1988, **21**, 2606.
105. Chu, B.; Wu, C. *Macromolecules* 1987, **20**, 93.
106. Kraus, G. in *The Stereo Rubbers* (Saltman, W. M. Ed.) Wiley, New York, (1977); p. 613.
107. Wheat, W. R. *ANTEC Proc.* 1995, p. 2275.
108. Jones, T. D.; Chaffin, K. A.; Bates, F. S.; Annis, B. K.; Hagaman, E. W.; Kim, M.-H.; Wignall, G. D.; Fan, W.; Waymouth, R. *Macromolecules* 2002, **35**, 5061.

CHAPTER 26

Temperature Dependences of the Viscoelastic Response of Polymer Systems

K. L. Ngai* and D. J. Plazek†

*Naval Research Laboratory, Washington, D.C. 20375-5320; †Department of Materials Science and Engineering, University of Pittsburgh, Pittsburgh, PA 15216

26.1 THE WLF EQUATION

The most successful temperature dependence for the viscous flow [1,2], viscoelastic response [1], dielectric dispersion [3–5], nuclear magnetic resonance response [6–8] and dynamic light scattering [9–10] of polymers and supercooled liquids with various chemical structures is the Williams, Landel, and Ferry (WLF) equation [11,12]

$$\log \frac{J_s^0(T)\eta(T)}{J_s^0(T_0)\eta(T_0)} \approx \log \frac{\tau(T)}{\tau(T_0)} = \log a_T = -\frac{C_1(T-T_0)}{C_2+T-T_0}, \tag{26.1}$$

where J_s^0 is the steady state recoverable compliance; η is the shear viscosity; τ is a retardation or relaxation time; a_T is the time-scale shift factor; T_0 is the chosen reference temperature; and C_1 and C_2 are characterizing constants. $J_s^0(T)$ is a very weak function of the temperature. In fact in the temperature range where T/T_g varies from 1.2 to 2.0, J_s^0 has been found to be independent of temperature [13]. Therefore its variation is often ignored. It will be ignored in this chapter. Some authors identify magnitude variations with temperature which are reported as $b_T = J_s^0(T)/J_s^0(T_0)$.

Williams, Landel, and Ferry [12] reported that such an expression is valid for polymers over the temperature range $T_g < T < T_g + 100°$. When T_g is chosen as the reference temperature, i.e., when the response curves measured at different temperatures are shifted primarily along the time or frequency scales to superimpose upon the response curve measured at T_g, it was initially noted that the constants C_1^g and C_2^g assume values close to 17.44° and 51.6°, respectively, for 17 polymers [12]. Individual treatment of the data on a wide range of polymers indicates that C_1^g may take values between 15° and 26° and C_2^g between 20° and 130°. The fit extends to temperatures below T_g if the polymer is at its equilibrium density.

The WLF expression has been shown [12] to be related to the Vogel–Fulcher–Tammann–Hesse equation [14–16],

$$\log \tau_i = \log A + \frac{(C/2.303)}{T-T_\infty}, \tag{26.2}$$

for η or τ where A, C and T_∞ are empirical constants. It follows that

$$\log a_T = \frac{C/2.303}{T-T_0} - \frac{C/2.303}{T_0-T_\infty}. \tag{26.3}$$

This is identical to the WLF expression provided the Vogel parameters and the WLF parameters are related as

$$C = 2.303 C_1 C_2 \tag{26.4}$$

and

$$T_0 - T_\infty = C_2. \tag{26.5}$$

26.2 RELATION OF WLF EQUATION TO FREE VOLUME

The WLF equation for a_T has been rationalized in terms of Doolittle's free volume theory [17]. According to this theory

that portion of the volume which is accessible to the kinetic process of interest is considered to be the free volume $v_f = v - v_0$, where v is the measured volume and the inaccessible volume v_0 is called the occupied volume. The Doolittle equation states that the viscosity is an exponential function of the reciprocal of the relative free volume $\phi \equiv v_f/v_0$.

$$\eta = Ae^{b/\phi}, \tag{26.6}$$

where A and b are characterizing constants.

Williams, Landel, and Ferry chose to use the fractional free volume $f = v_f/v$ in place of ϕ. This substitution made no difference in their derivation of the equation for the temperature shift factor a_T

$$\log a_T = \frac{b}{2.303}\left[\frac{1}{f} - \frac{1}{f_g}\right], \tag{26.7}$$

since $[1/f - 1/f_g] = [1/\phi - 1/\phi_g]$.

With the assumption that the fractional free volume is a linear function of temperature

$$f = f_0 + \alpha_f(T - T_0). \tag{26.8}$$

Substituting of Eq. 26.8 in Eq. 26.7 yields

$$\log a_T = -\frac{(B/2.303f_0)(T - T_0)}{f_0/\alpha_f + T - T_0} \tag{26.9}$$

which is identical in form with the WLF equation.

26.3 THERMORHEOLOGICAL COMPLEXITIES

In the frame work of the free volume theory, the molecular mobility at any temperature is assumed to depend primarily on the free volume remaining. It is generally further assumed in this approach that this molecular mobility determines the temperature dependence of the shift factors of *all* different kinds of molecular motions involving various length scales in the polymer melt. Hence free volume approach usually purports that the temperature shift factors of *different* viscoelastic mechanisms are the *same*. This result coming from the free volume theory of molecular mobility is perhaps the justification of the practice of obtaining *the* (meaning that there is only one) shift factor curve, a_T, which is usually derived by superposing curves of viscoelastic functions measured at different temperatures within the time or frequency range of the instrumentation. So long as the curve of the stress relaxation modulus, the creep and recoverable compliance, dynamic moduli or compliance do not change their shape in logarithmic plots, unique reduced curves with extended time or frequency range can be obtained. This will be the case, principally, if all of the molecular mechanisms contributing to the time- and frequency-dependent modulus and compliance functions, have the same temperature dependence. When this is so, the polymer is identified as being thermorheologically simple [18]. This appears to be true, in general, for closely related mechanisms, i.e., those within a group contributing to a single-loss tangent maximum; however mechanisms contributing to different loss peaks inevitably have different temperature dependences. This is widely recognized for the sub-T_g loss peaks, identified by the Greek letters β, γ, and δ. However, it is not as widely recognized that the so-called α mechanism, which is normally seen above T_g involves contributions from possibly three groups of molecular mechanisms with specifically different sensitivities to the variation of temperature [19–21]. In spite of the fact that a single loss peak is generally observed, a growing body of knowledge shows that local mode, sub-Rouse, and Rouse normal modes of chain backbone motions have different temperature dependences [19–24] which are most often different from that of the mechanisms of the terminal zone [19,25–32] which leads to steady-state behavior. Consequently, the temperature dependence of the viscosity is usually different from that of the glass to rubber-softening dispersion.

Therefore, it is important to know from which region or viscoelastic zone the WLF constants C_1 and C_2 were determined. Table 26.1 presents WLF constants and contains such information, when possible.

It should be noted that the shift factors that can be fitted to the WLF equation show positive curvature when plotted logarithmically against the temperature. Quite often, $\log a_T$ values obtained near and below T_g show negative curvature at low temperatures simply is an indication that the lower temperature measurements were made before the density of the material reached its equilibrium value.

26.4 TEMPERATURE DEPENDENCES UNDER PRESSURE

The loss of molecular mobility on approaching the glassy state by decreasing temperature may be due to increased molecular crowding (decrease in free volume) as well as a decrease in thermal energy (decrease in entropy). The relative importance of these two factors, volume (or free volume) and thermal energy (or entropy) has been a controversial issue for many years. It cannot be resolved by temperature variations alone in experimental studies, since the volume, entropy, and thermal energy all depend on temperature. The introduction of pressure, P, as an additional experimental variable makes a difference, because the specific volume, V, can be altered while maintaining temperature, T, constant. By combining the dielectric or light scattering results for polymeric and nonpolymeric glass-formers with the corresponding equation of state (PVT data), the volume and temperature dependence of the primary (local segmental for polymers) relaxation times τ_α can be obtained [181–185]. The results indicate that in general neither T (or entropy) nor V is exclusively the appropriate thermodynamic variable for describing the dynamics of glass formers, but rather τ_α is a function of the product variable, $T^{-1}V^{-\gamma}$, where γ is material-dependent, reflecting the nature of the intermolecular potential. Number polymers have been studied thus far, yielding the following

TABLE 26.1. *WLF parameters characterizing temperature dependencies of shift factors for relaxation and retardation times in various polymer systems.*

Polymer	T_0 °K	C_1 °K	C_2 °K	T_g °K	Ref.	Comments
Nonaromatic hydrocarbon backbone polymers						
Poly(acetaldehyde)	243	14.5	24	243	[33]	• $a_{T,\alpha}$ of local segmental motion from dielectric relaxation data.
Polyethylene (solution chlorinated) *Cl content = 56.6 w/w, amorphous*	312.3	12.7	63.3	317	[180]	• $a_{T,\alpha}$ of local segmental motion from a combination of dielectric relaxation and dynamic mechanical relaxation data for log $\tau_\alpha = -12.7 + 804/(T - 249\,\text{K})$.
Poly(hexene-1)	218	17.4	51.6	218	[34]	• The shift factors, $a_{T,S}$, of the softening dispersion with G' ranging from about $10^6 < G' < 10^{9.2}$ dyne/cm^2 and temperature T from -27.5 °C to 70 °C.
Polyisobutylene PIB *(the NBS sample with $M = 1.3 \times 10^6$ distributed by R.S. Marvin [35–37] on which the most comprehensive studies of viscoelastic properties were carried out in many laboratories)*	298	8.61	200.4	201	[38,39]	• $a_{T,S}$ of the entire softening dispersion, from dynamic mechanical measurement of $J^*(f)$, $10<f<6000$ Hz and $228.4<T<373$°K. Its T-dependence is much weaker than that of $a_{T,G(t)}$ given below.
	197	6.14	56	201	[40–42], [19–20], [43]	• $a_{T,E(t)}$ of the entire viscoelastic spectrum, from glassy state to the terminal zone, from stress relaxation, $E(t)$, between -83 and 25 °C in the time region of about $10^{0.6} < t < 10^{2.6}$ s. Its T-dependence is in agreement with the shift factor obtained from creep data, $J_r(t)$, (to be given below) throughout the softening region.
	228.5	13.18	130.9	201	[20,43]	• $a_{T,\text{Rouse}}$ of Rouse modes in the softening dispersion located in the compliance range $J_N > J_r(t) > 10^{-8}$ cm^2/ *dyne*, where J_N is the plateau compliance, and resolved as a tan δ peak by a combination of isothermal (i.e., shift factor in this case not obtained from time-temperature superpositioning of viscoelastic curves as commonly done) creep and dynamic mechanical measurements in the wide real time range of $10^6 > t > 3 \times 10^{-4}$ s from -74.2 to -35.8 °C. τ_{Rouse} (-66.9 °C) $= 2.74$.
	245.3	21.24	147.7		[43,20]	• $a_{T,\alpha}$ of local segmental mode from $G(t)$ and $J_r(t)$ data in the softening dispersion for viscoelastic response with $J_r(t) < J_{e\alpha}$ (where $J_{e\alpha}$ is the relaxed compliance of the local segmental motion and has the value of approximately 5 times the glassy compliance J_g) and combined with data from the resolved local segmental motion obtained by photon correlation spectroscopy. Log $\tau_\alpha(T = -66.9\text{C}) = -0.5$.
	215.3	20.36	117.7		[43,20]	• $a_{T,\text{sub-Rouse}}$ the sub-Rouse modes in the softening dispersion located in the compliance range of $J_{e\alpha} < J_r(t) < 10^{-8}$ cm^2 dyne and resolved as a tan δ peak situated at a higher frequency than the Rouse tan δ peak by a combination of isothermal creep and dynamic mechanical measurements in the real time range of $10^6 < t < 3 \times 10^{-4}$ s from -74.2 to -35.8 °C. log $\tau_{\text{sub-Rouse}}$ (-66.9 °C) $= 1.63$.

TABLE 26.1. *Continued.*

Polymer	T_0 °K	C_1 °K	C_2 °K	T_g °K	Ref.	Comments
PIB	205	14.3	72.5	201	[44]	• $a_{T,\text{Rouse}}$ resolved by a combination of stress relaxation and dynamic birefringence measurements in the range $10^{0.2} < t < 10^{3.8}$ s. Log τ_{Rouse} (-66.9 °C) = 2.13. This result is in fair though not perfect agreement with that obtained by the tan δ peak (see above).
	205	13.7	64.8	201	[44]	• $a_{T,G}$ of the "stress that relaxes through monomer rotation around the chain axis" resolved by a combination of stress relaxation and dynamic birefringence measurements in the range $10^{0.2} < t < 10^{3.8}$ s. Log $\tau_G(-66.9°\text{C}) = 0.1$. This technique has not resolved the sub-Rouse modes possibly because time temperature superposition was used. Hence the result is a compromise between the local segmental mode and the sub-Rouse modes. Log $\tau_G(-68.2°\text{C}) = 0.77$ which is close to the average between τ_α and $\tau_{\text{sub-Rouse}}$ at -66.9 °C obtained from isothermal mechanical data taken over 9 decades of real time (see above).
PIB (*E*-19) $M = 78\,500$	198	15.99	62.99	200.4	[45]	• $a_{T,J(t)}$ of the entire viscoelastic spectrum from $J_r(t)$. Its T-dependence is similar to that of viscous flow, η.
PIB	202	16.96	80	202	[47]	• $a_{T,\eta}$ of viscosity η. When extrapolated down to lower temperatures, its temperature dependence remarkably (in the sense that this does not happen in most other polymers) is nearly the same as that of $a_{T,G(t)}$ discussed above [Tobolsky and coworkers, Refs. 40–42].
PIB $2.7 \times 10^4 < M_w < 7 \times 10^5$	298.2	7.49	192	205	[48]	• $a_{T,\eta}$ of the terminal dispersion measured from 243 to 473 K.
PIB ($M = 4900$)	298.2	7.60	184		[49]	• $a_{T,\eta}$ of viscosity from -50 to 170 °C. Its temperature dependence similar to that given above.
Polypropylene PP (*atactic*)	298	7.53	85	262	[29]	• $a_{T,\eta}$ of viscosity measured up to $10^{12.6}$ poise at 266 K. It has a weaker temperature dependence than that of $a_{T,S}$ of the softening dispersion in the temperature range where the viscoelastic response has $J_r(t)$ principally less than $10^{-8}\text{cm}^2/\text{dyne}$.
	298	6.86	65	262	[29]	• $a_{T,S}$ of the softening dispersion from $J_r(t)$. It has a stronger temperature dependence than that of $a_{T,\eta}$.
Same sample as above	267.74	12.9	34.74	262	[50]	• $a_{T,\phi}$ of local segmental motion from correlation functions measured by photon correlation spectroscopy (PCS) carried out in the temperature range of $268 < T < 280$ K. The correlation times determined lie within the range: $10^{-5} < \tau < 10^0$ s.
Same sample as above	262.65	13.14	21.7	262	[51]	• $a_{T,\alpha}$ of local segmental motion from dynamical mechanical data taken in the frequency range of 0.01 to 100 Hz. Its T-dependence is in good agreement with that ($a_{T,\phi}$) obtained from PCS and that ($a_{T,S}$) obtained from creep measurement.
PP (*atactic*)	253	18.2	47.6		[7a]	• $a_{T,\tau(\text{NMR})}$ of local segmental motion from 2D exchange NMR and spin-lattice relaxation data which determined the NMR correlation time in the range $10^{-10} < \tau_{\text{NMR}} < 12$, s. The T-dependence of $\alpha_{T,\tau(\text{NMR})}$ is significantly w3eaker than that of $a_{T,S}$ from creep or $a_{T,\phi}$ from photon correlation spectroscopy, but comparable to that of $a_{T,\eta}$ from creep. The sample may not be totally atactic.
	258	14.5	30	258	[7b]	• $a_{T,\tau(\text{NMR})}$ of local segmental motion in different poly(-propylene) samples, $10^{-10} < \tau_{\text{NMR}} < 10^3$ s. $\tau_{\text{NMR}}(T_g) = 10^2$ s.

TABLE 26.1. *Continued.*

Polymer	T_0 °K	C_1 °K	C_2 °K	T_g °K	Ref.	Comments
PP (*atactic prepared by polymerization of 2-methyl-1,3-pentadiene followed by saturation with hydrogen)*	348.2	4.73	123.9	268.5	[52]	• $a_{T,\eta}$ of the terminal relaxation from dynamic mechanical, $G^*(\omega)$, data taken from 25 °C to above 75 °C. Its temperature dependence is slightly stronger than that found by Plazek (see $a_{T,\eta}$ in above) consistent with the sample having a higher T_g by about 6 °C.
Vinyl polymers						
Polystyrene PS	428.9	13.46	28.9	371	[25]	• Shift factors $a_{T,S}$ given here were obtained from recoverable compliance, $J_r(t)$, with the terminal zone excluded from the consideration. Data from samples with molecular weights that range from 1.1×10^3 to 8.0×10^5 were included. Thus the T_g listed here applies to the high molecular weight samples only. At lower temperatures near T_g where the $a_{T,S}$s are for the local segmental motion, the temperature dependence of $a_{T,S}$ is significantly stronger than that of the viscosity η, $a_{T,\eta}$, to be given in the next entry below.
	371	14.63	60	371	[25]	• Shift factor, $a_{T,\eta}J_e$, for the product of the viscosity η and the equilibrium recoverable compliance J_e and samples with molecular weights ranging from 1.1×10^3 to 6×10^5. Thus the T_g listed here applies to the high molecular weight sample only. Also for the high molecular weight samples, J_e is almost temperature independent and the shift factor given here is the same as that for the viscosity, $a_{T,\eta}$. Its temperature dependence is weaker than that of $a_{T,S}$ (see comment in entry immediately above).
PS	373	16.35	52.5	373	[8]	• Shift factor, $a_{T,\tau(\mathrm{NMR})}$ for the local segmental motion from 375<T<443°K obtained by 2D exchange NMR combined with ^{2}H- spin-lattice measurements covering the correlation time range $10^{-6} < \tau_{\mathrm{NMR}} < 10^3$ s. Temperature dependence of $a_{T,\tau(\mathrm{NMR})}$ agrees closely with that of the $a_{T,S}$ in the low temperature range near T_R where $a_{T,S}$ comes from local segmental motion. Beyond this temperature range $a_{T,\tau(\mathrm{NMR})}$ has a stronger temperature dependence than that of $a_{T,S}$, indicating that the local segmental motion probed by NMR has a more sensitive temperature dependence than the Rouse modes. Reported spectrum of local segmental motion from 2D exchange NMR narrows dramatically with increasing temperature.
PS (*high mol. wt*)	375	12.0	49.9	375	[53]	• $a_{T,\mathrm{Rouse}}$ of the Rouse modes in the softening dispersion resolved by a combination of stress relaxation and dynamic birefringence measurements. $\tau_{\mathrm{Rouse}}(T_g) = 10^{1.4}$ s.
	375	12.0	41.6	375	[53]	• $a_{T,G}$ of the G component in the softening dispersion, which represents the stress that relaxes through monomer rotation around the chain axis, resolved by a combination of stress relaxation and dynamic birefringence measurements. $\tau_G(T_g) = 10^{0.1}$ s.
PS(*A-25*)	373	12.7	49.8	370	[54,55]	• This shift factor, $a_{T,\eta}$, is for viscous flow in a monodisperse sample *(A-25)* with $(M_v)_{av} = 4.7 \times 10^4$ as reported by Ferry in Table 11-II of his book [1]. The shift factor for the softening dispersion, $a_{T,S}$, not reported in Table 11-II has a stronger temperature dependence and is given in the next line.

TABLE 26.1. *Continued.*

Polymer	T_0 °K	C_1 °K	C_2 °K	T_g °K	Ref.	Comments
PS(*A*-25)	373	10.7	29.9	370	[55]	• $a_{T,S}$ from creep in the softening dispersion (see remarks immediately above).
	371	12.95	60	371	[25]	• $a_{T,\eta}$ for viscosity from Berry and Fox [2]. It has even a weaker temperature dependence than that of any of the $a_{T,\eta}$ s determined from creep data described in the above.
PS *(Commercial sample: Hostyrene N-7000, mol. wt. not given.)*	378	9.4	39	363.5 *(from dilatometry at a cooling rate of 3K/h)*	[56]	• $a_{T,S}$ of the entire softening dispersion from creep, $J_r(t)$, data with $10^{-1.8} < t < 10^{3.2}$ s and temperature ranging from −90 to 130 °C. Its temperature dependence is considerably weaker than that of $a_{T,S}$ found by Plazek and O'Rourke [25] by recoverable creep compliance, $J_r(t)$, data with $10^{-0.5} < t < 10^{5.5}$ s. If the difference in T_g of about 7.5° is accounted for (Schwarzl's sample has a lower T_g) then there is reasonable agreement between the the two sets of data.
PS	373	13.7	50.0	373	[57]	
PS (2.5×10^5)					[58]	• Polymer J. **1**, 485 (1970).
PS *M>29 000*	433	7.14	112.1	373	[59]	• $a_{T,\eta}$ of the terminal dispersion measured in the temperature range of 393 to 493 K. Its *T*-dependence is slightly stronger than that of the terminal dispersion determined by Plazek [25,54,55].
Poly(α-methyl styrene)	445	13.7	49.3	445	[60]	
PαMS	441	16.8	53.5	441	[61]	
Poly(4-chloro styrene) P4CS	411.5	11.4	58.0		[62]	• $a_{T,\alpha}$ for local segmental motion from dielectric relaxation data.
Poly(vinyl acetal)	344.1	16.1	77.38		[63–66]	• $a_{T,\alpha}$ of local segmental motion from dielectric relaxation: $10^{-6} < \tau_\alpha < 10^{-3}$ s, $\tau_\alpha(T_0) = 1$ s.
Poly(vinyl acetate) PVAc	349	8.86	101.6	305	[67,68]	• $a_{T,S}$ of the entire softening dispersion from dynamic mechanical $J^*(f)$ with $10<f<6000$ Hz. Sample in equilibrium with ambient moisture and the water absorbed lower the sample's T_g. Its *T*-dependence is considerably weaker than either of the shift factors obtained from creep compliance in dried samples given immediately below.
	310.2	12.0	31.1	310	[27,28]	• $a_{T,S}$ of the softening dispersion obtained from creep compliance $J_r(t)$ data. It has a stronger temperature dependence than that of the shift factor of the terminal dispersion, $a_{T,\eta}$, given immediately below.
	311.1	15.57	60.0	310	[27,28]	• $a_{T,\eta}$ of viscous flow or the terminal dispersion from data of $J_r(t)$.
	373	7.43	125	310	[28]	• a_T of the entire viscoelastic spectrum including the softening and the terminal dispersions obtained when all data ($J_r(t)$, dynamic mechanical, dielectric) are combined together.
PVAc $M_\eta = 8.2 \times 10^4$	316.37	12.67	71.07	308	[4]	• $a_{T,\varepsilon}$ of the local segmental motion from 26.85 to 84.77 °C resolved by dielectric relaxation measurement of $\varepsilon^*(f)$ on dried samples in the range: $10^{-6} < f < 10^6$ Hz. $\tau(34.95\ ^\circ\text{C}) = 10^{1.4}$ s. Its *T*-dependence is considerably weaker than that of the local segmental motion, which is $a_{T,S}$ at temperatures close to T_g, as determined from recoverable compliance, $J_r(t)$, data (see above).

TABLE 26.1. *Continued.*

Polymer	T_0 °K	C_1 °K	C_2 °K	T_g °K	Ref.	Comments
PVAc ($M_\eta = 15\,000$)	307.4	14.19	69.40	290.2	[69]	• $a_{T,\alpha}$ of the local segmental motion obtained by PCS data. Its temperature dependence is similar to that found by McKinney and Belcher [174] from dynamic compressibility on another sample with approximately the same T_g.
Poly(vinyl butyral)	336.4	17.24	85.18		[64,66] [70,71]	• $a_{T,\alpha}$ of local segmental motion from dielectric relaxation: $10^{-6} < \tau_\alpha < 10^{-3}$ s, $\tau_\alpha(T_0) = 1$ s.
Poly(vinyl chloroacetate) PVCAc	346	8.86	101.6	296	[72,80]	
Poly(vinyl chloride) PVC	352	19.84	43.89	353	[73]	• $a_{T,\alpha}$ of local segmental motion from tensile stress relaxation (10^{-1} s $< t <$ 1 day) and dynamic mechanical data in the frequency range $10^{-5} < f < 10^4$ Hz from 63 to 123 °C.
PVC	358.7	13.42	28.7	358	[74]	• $a_{T,\alpha}$ of local segmental motion from $365 < T < 410$ K obtained by dielectric relaxation. The relaxation times lie within the range: $10^{-7} < \tau_\alpha < 1$ s. Log $\tau_\alpha(380\,\text{K}) = -4.64$.
PVC (*commercial sample: Solvay & Cie, type Solvic 229)*	346.5	11.2	34.6	338.7 (*from dilatometry at a cooling rate of 3K/h)*	[56]	• $a_{T,S}$ of the softening dispersion from creep, $J(t)$, data. It has a much weaker temperature dependence compared with $a_{T,\alpha}$ from dynamic mechanical and dielectric relaxation given above. This discrepancy between the shift factors of the mechanical data of Schwarzl with the other sets of data may be due to the much lower T_g of the sample used.
Poly(vinyl formal)	381.3	10.33	26.76		[63,64]	• $a_{T,\alpha}$ of local segmental motion from dielectric relaxation data determining the relaxation time in the range: $10^{-7} < \tau_\alpha < 10^{-3}$s. $\tau_\alpha(T_0) = 1$ s.
Poly(vinyl hexanal)	312.6	16.0	85.62		[75]	• $a_{T,\alpha}$ of local segmental motion from dielectric relaxation data determining the relaxation time in the range: $10^{-6} < \tau_\alpha < 10^{-3}$s. $\tau_\alpha(T_0) = 1$ s.
Poly(vinyl methyl ether) PVME	244	14	42	250	[76]	• $a_{T,\alpha}$ of local segmental motion from dielectric relaxation in the range: $10^{-0.5} > \tau_\alpha > 10^{-7}$ s.
PVME	246.5	15.25	47.23		[77,78]	• $a_{T,\alpha}$ from dielectric data of Zetsche *et al.* [78]. Similar to that given above.
Acrylates and methacrylate polymers						
Poly(methyl acrylate) PMA	324	8.86	101.6	276 (*value seems too low*)	[79,80]	• This shift factor was obtained by combining the dynamic mechanical data of the entire softening dispersion ($25 < T < 90$ °C and $30 < f < 3000$ Hz) and early dielectric relaxation data of Mead and Fuoss [79] in a comparable frequency range. Its temperature dependence is weaker than that of the shift factors $a_{T,S}$ and $a_{T,\varepsilon}$ to be described below.
	287.4	11.08	27.9	287	[24]	• $a_{T,S}$ of the entire softening dispersion from $J_r(t)$.
	287.72	12.8	38.2		[5]	• $a_{T,\varepsilon}$ of the local segmental motion from 293 to 373 K by dielectric measurement ($10^{-1} < f < 10^{10}$ Hz). Temperature dependence of $a_{T,\varepsilon}$ is in good agreement with that of $a_{T,S}$ for viscoelastic response principally in the compliance range $J_g > J(t) < 10^{-8}\,\text{cm}^2/\text{dyne}$. Dielectric and creep data are in good agreement.
	326	8.86	101.6		[81]	• a_T of the entire viscoelastic response from relaxation modulus in extension, $E(t)$.

TABLE 26.1. *Continued.*

Polymer	T_0 °K	C_1 °K	C_2 °K	T_g °K	Ref.	Comments
	276	16.67	60	276 (*value seems too low*)	[2]	• $a_{T,\eta}$ of viscosity. It has a weaker temperature dependence than $a_{T,S}$ and $a_{T,\varepsilon}$.
Poly(methyl methacrylate) PMMA (*atactic*)	381	34	80	381	[2]	• $a_{T,\eta}$ for viscosity. Its T-dependence similar to that of conventional PMMA given below. If extrapolated down to the temperature regime of $a_{T,S}$ (see next entry) it has a different T-dependence than that of $a_{T,S}$.
PMMA (*atactic*)	382.55	9.34	32.5	381	[82]	• $a_{T,S}$ for the softening dispersion determined by $J_r(t)$ from 376 to 404 K. The T-dependence of $a_{T,S}$ is stronger than that of the viscoelastic mechanism above the rubbery plateau.
PMMA (*isotactic*)	326.5	9.34	32.5	323	[82–84]	• $a_{T,S}$ for the softening dispersion determined from 29.2 to 159.3 °C.
PMMA (*conventional*)*I*	388	32.2	80	390	[2]	• $a_{T,\eta}$ for viscosity determined in the high temperature range. If extrapolated down to the temperature regime of $a_{T,S}$ (to be given below) it has a different T-dependence than that of $a_{T,S}$.
PMMA (*conventional*)	493	7.0	173	378	[85]	• $a_{T,\eta}$ of viscosity. It has a considerably weaker T-dependence than that given by Berry and Fox [2].
PMMA (*conventional*)	393.5	9.34	32.5	390	[82]	• $a_{T,S}$ of the softening dispersion obtained by $J_r(t)$ in the range from 387 to 462 K. In good agreement with the T-dependence of the shift factors obtained from stress relaxation $E(t)$ data of McLoughlin and Tobolsky [175] in a similar temperature range.
PMMA (*conventional*)	390.5	14.27	63.1		[81]	• $a_{T,S}$ of the softening dispersion. However, the T-dependence as reported is weaker than that given in the entry above. The reason for this discrepancy is not clear. We recommended the WLF parameters given in the entry above because they are corroborated by two different experimental measurements.
PMMA (*conventional*)	393.1	12.21	70.1	390	[82]	• $a_{T,\text{plateau}}$ of the viscoelastic mechanism with compliance above the rubbery plateau determined in the same temperature range as $a_{T,S}$, but has weaker T-dependence than that of the latter.
PMMA (*commercial, Röhm Plexiglas 240/218*)	396.5	8.0	36.0	380.2 (*from dilatometry at a cooling rate of 3 K/h*)	[56]	• $a_{T,S}$ for the entire softening dispersion from 100 to 145 °C. Its temperature dependence is weaker than that of $a_{T,S}$ obtained by Plazek *et al.* [82–84]. It is possible the discrepancy is caused by the sample studied by Schwarzl *et al.* has a lower T_g. A correction of the difference in T_g of about 3 degrees will bring the two sets of shift factors into agreement.
Poly(ethyl methacrylate) PEMA	373	11.18	103.5	335	[86]	• $a_{T,S}$ of the softening dispersion from dynamic shear compliance $J^*(\omega)$ from 352.7 to 428°K.
Poly(*n*-butyl methacrylate) Pn-BMA	373 300	9.7 17.0	169.6 96.6	300 300	[87]	• $a_{T,S}$ of the softening dispersion from dynamic shear compliance $J^*(\omega)$ from 316.7 to 403.1 K.
Pn-BMA	373	8.5	185	300	[88]	• $a_{T,\alpha}$ of local segmental motion from dielectric relaxation: $10^0 < f < 10^7$ Hz and $313 < T < 403$ K. Its T-dependence is comparable but slightly weaker than that of $a_{T,S}$ given in the entry above.
Pn-BMA *($M = 250000$)*	300	18.2	96.6	300	[89]	• $a_{T,\alpha}$ of local segmental motion from PCS measurement from 35.8 °C to 70.6 °C and $\log\langle\tau\rangle$ from 10 to 10^{-4} s. Its T-dependence is similar to that of $a_{T,S}$ from dynamic mechanical data.

TABLE 26.1. *Continued.*

Polymer	T_0 °K	C_1 °K	C_2 °K	T_g °K	Ref.	Comments
Poly(*n*-hexyl methacrylate)						
Pn-HMA	373	9.8	234.4	268	[90]	• $a_{T,S}$ of the softening dispersion from dynamic shear compliance $J^*(\omega)$ from 277.7 to 398 K.
Pn-HMA	268.1	10.95	67.12	268	[91]	• $a_{T,\alpha}$ of local segmental motion from dielectric relaxation: $10^0 < f < 10^6$ Hz and $275 < T < 333$°K. Its T-dependence is nearly the same as that of $a_{T,S}$ (see above) within this temperature range.
Poly(*n*-octal methacrylate) Pn-OMA	373	7.6	227.3	253	[92–95]	• $a_{T,S}$ of the softening dispersion from dynamic shear compliance $J^*(\omega)$ from 258.7 to 402.5 K.
Poly(2-ethyl hexyl)	373	11.58	208.9	284	[96]	• $a_{T,S}$ of the softening dispersion from dynamic shear compliance $J^*(\omega)$.
Poly(*n*-lauryl methacrylate)						
Pn-LMA	298.2	8.52	139.2	208?	[97]	• $a_{T,S}$ of the softening dispersion from dynamic shear compliance $J^*(\omega)$ from 232.6 to 318.3 K.
Pn-LMA $M_w = 1.1 \times 10^5$ g/mol	233.8	9.06	62.3	225	[98]	• $a_{T,\alpha}$ of the local segmental motion determined from dielectric relaxation and PCS for the range $10^0 > \tau_\alpha > 10^{-5/2}$ s. It has a weaker T-dependence than that of $a_{T,S}$.
Poly(cyclohexyl methacrylate) PCHMA $M_w = 2 \times 10^5$	359.7	14.8	75.67	374	[99]	• $a_{T,\alpha}$ of local segmental motion from data of local density fluctuation observed by PCS, mechanical relaxation and dielectric relaxation. When referenced to the respective T_gs (i.e. plotting $\log(a_{T,\alpha})$ against $(T-T_g)$ the shift factor of PCHMA has a considerably stronger temperature dependence than that of Pn-HMA.
Heterogeneous backbone polymers						
bisphenol A Polycarbonate BPA-PC	418	22.88	78.64		[100]	• $a_{T,S}$ of the entire softening dispersion from dynamic mechanical measurements obtained in the range $405 < T < 426$ K.
BPA-PC	425.7	10.4	52.2	423.6	[101]	• $a_{T,\eta}$ of viscosity from 478 to 597°K obtained on Lexan (General Electric Co.) with $M_w = 72\,600$ and $M_n = 28\,100$.
BPA-PC (*branched*)	425.7	9.61	120.7	425.7	[102]	• $a_{T,\eta}$ from terminal relaxation $G^*(\omega)$ data measured over the temperature range from 473 to 573 K. Its T-dependence is nearly the same as that for Lexan given above and is much weaker than that of $a_{T,S}$ for linear BPA-PC given above when the latter is extrapolated to high temperatures and compared at 473 K, the lowest temperature of measurement of $a_{T,\eta}$.
BPA-PC	427.7	12.18	51.97	423	[103]	• $a_{T,E}$ obtained from stress relaxation measurements $(10 < \pm < 10^4$ s) and $(140.5 < T < 172.5$ C) from the glass to the terminal zone.
Poly(dimethyl siloxane)						
PDMS	303	1.90	222	150	[104]	• $a_{T,\eta}$ of viscous flow determined at temperatures significantly higher than T_g. Do not extrapolate down to low temperatures near and above T_g because it shows a T-dependence unrealistically much weaker than that of $a_{T,\alpha}$ of the local segmental motion (given below).
PDMS	150	5.08	120	150	[105]	• $a_{T,\eta}$ of viscous flow from creep (remarks given immediately above apply here).

TABLE 26.1. *Continued.*

Polymer	T_0 °K	C_1 °K	C_2 °K	T_g °K	Ref.	Comments
PDMS ($M_n = 10\,370$)	147	10.4	14.24	149.5	[106]	• $a_{T,\varepsilon}$ of local segmental motion from dielectric relaxation in the frequency range $10^{-2} < f < 10^{7}$ Hz and temperature range $T_g < T < T_g + 20°$ K. If this is extrapolated to higher temperatures, the extrapolated values turns out to agree with $a_{T,\eta}$ throughout the temperature range in which the latter was determined, e.g., $-233 < T < 300$ K.
PDMS ($M_n = 3230$)	145.3	14.12	23.06	148.8	[106]	• Same as above.
PDMS ($M_n = 420$)	136.5	11.46	14.01	135.9	[106]	• Same as above.
PDMS *cyclic* ($M_n = 6920$)	149	11.48	15	150.3	[106]	• Same as above.
PDMS *cyclic* ($M_n = 2120$)	148.2	14.03	23.86	151.6	[106]	• Same as above.
PDMS *cyclic* ($M_n = 410$)	153	13.53	18.05		[106]	• Same as above.
Poly(aryl ether ether ketone) $M_w = 90\,000$; $M_n = 45\,000$ *(450 G.ICI)*	412.9	29.96	53.74	417	[178]	• $a_{T,\alpha}$ of local segmental motion obtained by $G^*(\omega)$ from dynamic mechanical measurements from 1 to 10^{-4} Hz in the temperature range of 412 to 423 K and τ_α ranging from $10^{-0.24}$ to 10^{5} s.
methyl-substituted Poly(aryl ether ether ketone) (Me)PEEK	514.1	3.24	132.1	424.1	[107]	• $a_{T,\eta}$ of terminal dispersion measured by $G^*(\omega)$ on a sample with $M_w = 33\,800$. The author has given the shift factor originally as the VFTH form of $\log a_T = B/(T - T_\infty)$ with B=428 $\pm$ 30 K and $T_\infty = T_g - 42°$C for samples with different molecular weights.
Poly(oxy-1,4-phenylene sulfoneyl-1,4-phenylene), *also called poly(aryl ether sulfone)* PES	485.2	70.98	241.2	497	[178]	• $a_{T,\alpha}$ of local segmental motion from dynamic mechanical measurement of $G^*(\omega)$ from 1 to 10^{-4} Hz in the temperature range from 485 to 516 K and τ_α ranging from $10^{-2.4}$ to $10^{5.6}$ s.
Poly(ethylene terephthalate) PET (*amorphous*)	352.8	9.04	25.5	346.6	[108]	• $a_{T,\alpha}$ of local segmental motion from dielectric relaxation.
PET (*amorphous*)	346.6	17.7	42.63	346.6	[5]	• $a_{T,\alpha}$ of local segmental motion from dielectric relaxation.
Poly(2-hydroxypropyl ether Bisphenol A) PH	356.6	14.21	31.6	359	[76]	• $a_{T,\alpha}$ of local segmental motion from dielectric relaxation in the range: $10^{-1} > \tau_\alpha > 10^{-8}$ s.
Poly(methyl phenyl siloxane) PMPS (*M = 5000)*	181.2	20.4	56.76	223.3	[30]	• $a_{T,S}$ of the softening dispersion from $J_r(t)$ from 23.4 to -50 °C.
PMPS (*M = 2500)*	207	18.1	39.8		[109, 110]	• $a_{T,\alpha}$ of the local segmental motion from local density fluctuation in PCS. It has a stronger T-dependence than that of chain diffusion (given below).

TABLE 26.1. *Continued.*

Polymer	T_0 °K	C_1 °K	C_2 °K	T_g °K	Ref.	Comments
PMPS ($M = 2500$)	207	5.6	56.76		[109, 110]	• shift factor of chain diffusion from concentration fluctuation in PCS.
PMPS ($M = 12\,000$)	237.4	23.96	48.8	237.4	[111, 112]	• $a_{T,\alpha}$ of local segmental motion from dynamic mechanical measurement of $G^*(f)$ in the range: $10^{-1.5} < f < 10^{1.5}$ Hz.
	258.4	7.32	32.5	237.4	[111, 112]	• $a_{T,\alpha}$ from dielectric measurement in the range: $10^2 < f < 10^6$ Hz. • Good correspondence to $a_{T,\alpha}$ from mechanical data.
PMPS ($M = 130\,000$)	243.2	17.69	34.71	243.2	[111, 112]	• $a_{T,\alpha}$ from dynamic mechanical (see above).
	261.8	7.47	36.1	243.2	[111, 112]	• $a_{T,\alpha}$ from dielectric relaxation (see above).
PMPS ($M = 28\,500$)	273.2	14.8	66.4	247.2	[113]	• $a_{T,\alpha}$ from PCS.
	248.2	14.8	55.9	248.2		
	273.2	11.8	67.9	247.2	[113]	• $a_{T,\alpha}$ from dielectric relaxation.
	248.2	15.2	49.2	248.2		
	248.2	16.1	53.2	248.2	[177]	• $a_{T,\eta}$ of shear viscosity from -25° to 100 °C and $1 < \eta < 10^{7.7}$ Pa.s.
Poly(methyl-*p*-tolyl siloxane) PMpTS ($M_w = 18\,400$)	262.2	12.9	55.1	262.2	[177]	• a_T of entire viscoelastic response from the glass level to the terminal zone obtained from $G^*(\omega)$.
	259.1	15	45	262.2	[179]	• $a_{T,\alpha}$ of local segmental motion from photon correlation measurement in the range $10^{-6} < \tau_\alpha < 10^1$s and $260 < T < 290$K.Log$[\tau_\alpha(T = 270\text{K})/\text{s}] = -2.9$.
	258.1	12.8	37.8	262.2	[179]	• $a_{T,\alpha}$ of local segmental motion from dielectric relaxation measurement in the range $10^{-9.8} < \tau_\alpha < 10^2$ s and $252 < T < 370$ K. Log $[\tau_\alpha(T = 270\,\text{K})/\text{s}] = -3.06$.
Poly(propylene oxide) PPO	198	16.2	24	198	[114]	• $a_{T,\alpha}$ of the local segmental motion from dielectric relaxation measurements in the frequency range $10^{-4} < f < 10^6$ Hz.
Poly(propylene glycol) PPG (4000, 2000, 1000)	198.8	16.8	48.8		[115]	• $a_{T,\alpha}$ of local segmental motion from dielectric relaxation measurements in the frequency range: $10^6 < f < 10^{-4}$ Hz. It has stronger temperature dependence than that of $a_{T,n}$, the shift factor of the normal modes.
PPG (4000)	216.66	10.1	63.66		[115]	• $a_{T,n}$ of the normal modes from dielectric relaxation measurements (see remarks immediately above).
PPG (40 000)	216.66	8.85	50		[116]	• $a_{T,\eta}$ of the shear viscosity. Its temperature dependence is close to that of $a_{T,n}$, the shift factor of the normal mode from dielectric data.
PPG *linear*, $M_n = 3100$	205.9	9.24	22.93		[117]	• $a_{T,\phi}$ of the local segmental motion from PCS from -49° to -66.7 °C. $\tau_\alpha(-60.7^\circ\text{C}) = 1.00 \times 10^{-2}$s.
Poly(thio-1,4-phenylene), *also called poly(phenylene sulfur) PPS* ($M_w = 37\,000$) *T1. Solvay*	355.3	22.21	49.63	362	[178]	• $a_{T,\alpha}$ of local segmental motion from dynamic mechanical measurement of $G^*(\omega)$ from 1 to 10^{-4} Hz in the temperature range from 355 to 371 K.
Polysulfone PSF	459	15.1	49	459	[118]	• $a_{T,\text{Rouse}}$ of the resolved Rouse modes by the combination of stress relaxation and dynamic birefringence. $\tau_{\text{Rouse}}(T_g) = 10^{0.7}$s.

TABLE 26.1. *Continued.*

Polymer	T_0 °K	C_1 °K	C_2 °K	T_g °K	Ref.	Comments
	459	15.8	43.7	459	[118]	• $a_{T,G}$ of the resolved *G*-component of the softening dispersion which represents the stress that relaxes through monomer rotation around the chain axis. $\tau_G(T_g) = 1$ s.
Tetra methyl polycarbonate TMPC	456.4	8.9	29.0	456.4	[119]	• $a_{T,\alpha}$ of local segmental motion from dielectric relaxation.
Zinc phosphinate polymer	373	6.94	66.6	324	[120]	
Rubbers						
Butyl rubber (*lightly vulcanized with sulfur*)	298	9.03	201.6	205	[121]	• $a_{T,S}$ of the softening dispersion from dynamic shear measurements.
Ethylene-propylene copolymer *(ethylene:propylene = 16:84 by mole)*	298	5.52	96.7	242	[122]	• $a_{T,S}$ of the softening dispersion from dynamic shear measurements.
(ethylene:propylene = 56:44 by mole)	298	4.35	122.7	216	[122]	• $a_{T,S}$ of the softening dispersion from dynamic shear measurements.
Hypalon-20 *(chloro-sulfonated polyethylene)*	248.5	17.44	51.6	248.5	[123]	• $a_{T,S}$ of the softening dispersion from dynamic shear modulus, $G^*(\omega)$, data in the frequency range of 25 to 2500 Hz from 264.6 to 341.4 °K. Values of G' range from 2×10^9 to 7×10^6 dyne/cm^2 in the glass–rubber region.
Hevea brasiliensis Natural Rubber	248	8.86	101.6	200	[124]	• From dynamic mechanical $G^*(\omega)$ data taken from $10^{-2.2} < \omega < 10^{1.2}$ rad/s in the temperature range of -73 °C to 60 °C. Shift factors are mostly for the entire softening dispersion. G' is about 10^7 dyne/cm^2 in the neighborhood of -30 °C.
	298	5.94	151.6		[125]	• Similar *T*-dependent as found by Payne and given above.
	211	11.4	37.8		[56]	• $a_{T,S}$ of the entire softening dispersion from creep, $J(t)$, data from 193 to 253 °K. Its *T*-dependence is similar to that of Payne.
	209	13.5	17.2		[126, 127]	• $a_{T,\alpha}$ of local segmental motion from dynamic mechanical $G^*(\omega)$ data from 203 to 217 °K. It has a much stronger *T*-dependence than that found by Payne [124] and by Dickie and Ferry [125] in the same temperature range. This large discrepancy may come from different samples being used. The sample studied in this work is of exceptional high grade and substantially masticated.
	210.4	12.26	38.6		[127]	• $a_{T,\alpha}$ of local segmental motion from dielectric relaxation data from 207 to 249 °K in the frequency range of $10^{-2} < f < 10^6$ Hz on the same sample as that used in $G^*(\omega)$ measurement. Its *T*-dependence is almost the same as, though slightly weaker than, that of $a_{T,\alpha}$ from $G^*(\omega)$ data.
Poly(isoprene) PI *linear 75.7% cis-1,4;18.1% trans-1,4;6.2% vinyl-3,4.* $M_w = 97\,000$	250	6.1	70.9	213.2	[128]	• $a_{T,\alpha}$ from dielectric relaxation data in the range of $10^{-1} < f < 10^9$ Hz.
	300	0.9	57.9	213.2	[128]	• $a_{T,n}$ of the dielectric normal mode which correspond to the terminal relaxation. These WLF parameters for this high mol. wt. sample is probably not reliable because of limited data.

TABLE 26.1. *Continued.*

Polymer	T_0 °K	C_1 °K	C_2 °K	T_g °K	Ref.	Comments
PI *linear* *77.9% cis-1,4* *18.1% tran-1,4* *4% vinyl-3,4* $M_w = 13\,000$	250	5.8	74.3	211.5	[128]	• $a_{T,\alpha}$ from dielectric relaxation data in the range of $10^{-1} < f < 10^9$ Hz.
	300	4.2	128.8	211.5	[128]	• $a_{T,n}$ of the dielectric normal mode which correspond to the terminal relaxation. Its T-dependence is in excellent agreement with that of the viscosity, $a_{T,\eta}$, determined from dynamic mechanical data [Gotro *et al.* Ref. 133] (see below).
PI *linear* *78.8% cis-1,4;* *17.9% trans-1,4* *3.3% vinyl-3,4* $M_w = 5100$	250	5.7	80	207.1	[128]	• $a_{T,\alpha}$ from dielectric relaxation data in the range of $10^{-1} < f < 10^9$ Hz.
	300	4.0	133.9	207.1	[128]	• $a_{T,n}$ of the dielectric normal mode which correspond to the terminal relaxation.
PI *cis-1,4; $M_w = 2350$*	211.4	12.3	40.4	206	[129]	• $a_{T,\alpha}$ of the local segmental motion from a combination of PCS and dielectric relaxation data. $\tau(T_0) = 1$ s.
PI *cis-1,4; $M_w = 35\,000$*	209.4	12.3	37.4	213	[130]	• $a_{T,\alpha}$ of the local segmental motion from $-56 < T < -47$ °C obtained by PCS. $\tau(T_0) = 1$ s.
	210.9	12.85	49.6	210.9	[131]	• $a_{T,\alpha}$ of local segmental motion from 2D deuteron exchange NMR data. Its temperature dependence is in good agreement with that determined from dielectric data.
PI *18 arms star* *76.5% cis-1,4* *17.9% trans-1,4* *5.6% vinyl-3,4* $M_w = 384\,000$	250	6.2	75.0	213.0	[128]	• $a_{T,\alpha}$ from dielectric relaxation data in the range of $10^{-1} < f < 10^9$ Hz.
	300	3.4	100.4	213.0	[128]	• $a_{T,n}$ of the dielectric normal mode which correspond to the terminal relaxation.
PI *4 arms star* *77.6% cis-1,4* *16.8% trans-1,4* *5.6% vinyl-3,4* $M_w = 380\,000$	250	6.2	78.7	212.2	[128]	• $a_{T,\alpha}$ from dielectric relaxation data in the range of $10^{-1} < f < 10^9$ Hz.
	300	2.3	40	212.2	[128]	• $a_{T,n}$ of the dielectric normal mode which correspond to the terminal relaxation.
PI *cis-1,4* $M_w = 2350$	211.38	12.3	40.4	206	[128]	• $a_{T,\alpha}$ of local segmental motion determined by combining PCS and dielectric relaxation data over the frequency range of $10 < f < 10^5$ Hz.
PI *7% vinyl, 84.5% cis-1,4* $1.6 \times 10^5 < M_w < 1.1 \times 10^6$	243.2	8.2	89.5		[132]	• a_T of viscoelastic response in the compliance range of $10^{-9.6} < J_p(t)$ including the terminal relaxation from -70 to 42 °C for $M_w = 6.2 \times 10^5$.
PI *8% 3,4* *high mol. wt.*	298	4.1	122	205	[133]	• $a_{T,\eta}$ of the terminal relaxation determined by dynamic modulus. Its T-dependence is in excellent agreement with that of $a_{T,n}$ obtained from dielectric normal mode data (see above for the 13 000 mol. wt. PI dielectric data). The C_1 and C_2 parameters given here apply also for the other PI microstructures if T_0 is adjusted for the change in T_g: $T_0 = 25 + \Delta T_g$, where ΔT_g is the difference in T_g from 206°K, the value for the 8% 3,4 microstructure.

TABLE 26.1. *Continued.*

Polymer	T_0 °K	C_1 °K	C_2 °K	T_g °K	Ref.	Comments
PI *(70% cis, 23% trans, 7%, 3,4; $M_w = 63\,400$)*	211.6	12.2	53.7	211.6	[134]	• $a_{T,\eta}$ of terminal dispersion from dynamic mechanical, $G^*(\omega)$, data.
PI *(70% cis, 23% trans, 7%, 3,4; $M_w = 103\,000$)*	212	11.7	52.9	212	[134]	• $a_{T,\eta}$ of terminal dispersion from dynamic mechanical, $G^*(\omega)$, data.
Hydrogenated polyisoprene						
HPI $4 \times 10^4 < M_w < 3 \times 10^5$						• $a_{T,\eta}$ of terminal dispersion from dynamic mechanical data for T-T_g from ~90 to ~250 °C.
8% 3,4	373	3.91	227	211	[133]	
16% 3,4	376	3.91	227	214	[133]	
20%, 3,4	379	3.91	227	217	[133]	
29% 3,4	386	3.91	227	224	[133]	
34%, 3,4	393	3.91	227	231	[133]	
Poly(vinyl ethylene)						
PVE *97% 1,2*	270.9	14.54	47.39	272.5	[135]	• $a_{T,\alpha}$ of local segmental motion from dielectric relaxation data from 268 to 305°K and $10^{1.2} > \tau_\alpha > 10^{-6}$ s.
	268.2	11.66	23.89	272.5	[136]	• $a_{T,S}$ of the softening dispersion from recoverable creep compliance, $J_r(t)$, data obtained on the same sample as above from −12.6 to 30.1 °C. Same sample as above.
	264.4	13.33	24.33	272.5	[135]	• $a_{T,\alpha}$ of local segmental motion from dynamic mechanical $G^*(\omega)$ data. Same sample as above. Its temperature dependence is in excellent agreement with that for dielectric relaxation data given above.
cross-linked with 0.056 wt % dicumyl peroxide cross-linker	270.0	12.77	24.33		[137]	• $a_{T,\alpha}$ of local segmental motion from dielectric relaxation data from $10^{1.2} > \tau_\alpha > 10^{-6}$ s.
cross-linked with 0.111 wt %dicumyl peroxide cross-linker	277.4	12.1	32.8		[137]	• Same as above
cross-linked with 0.222 wt % dicumyl peroxide cross-linker	276.5	13.36	23.55		[137]	• Same as above.
cross-linked with 0.444 wt % dicumyl peroxide cross-linker	277.6	22.2	52.0		[137]	• Same as above.
cross-linked with 0666 wt % dicumyl peroxide cross-linker	282.9	10.8	13.9		[137]	• Same as above.
PVE *94% 1,2*	271.2	12.3	48.6	271.2	[131]	• $a_{T,\alpha}$ of local segmental motion from 2D deuteron exchange NMR data obtained from 273 to 286°K. Its T-dependence is similar to that determined by dielectric and dynamic mechanical data (see above).
	265.18	13.66	44.72	273	[138]	• $a_{T,S}$ of the terminal relaxation from dynamic stress-optical measurements made in the temperature range from 295 to 353°K.
PVE *(91.5% vinyl)*	298	6.23	72.5	261	[139]	• $a_{T,S}$ Its T-dependence is weaker than the corresponding shift factors obtained in other PVE samples with higher vinyl content and higher T_gs.
PVE (> 99%,1,2; $M_w = 84\,400$)	279	11.4_5	56.0	279	[134]	• $a_{T,\eta}$ of terminal dispersion from dynamic mechanical, $G^*(\omega)$ data.
PVE (> 99%1,2; $M_w = 204\,000$)	279.5	11.3	59.2	279.5	[134]	• $a_{T,\eta}$ of terminal dispersion from dynamic mechanical, $G^*(\omega)$ data.

TABLE 26.1. *Continued.*

Polymer	T_0 °K	C_1 °K	C_2 °K	T_g °K	Ref.	Comments
PVE (95% 1,2; $M_w = 19\,000$)	272.2	11.34	28.6	272	[140]	• a_T for the entire viscoelastic response from softening to terminal. This is a compromise of two different temperature dependences of shift factors for the segmental, $a_{T,\alpha}$ and for the terminal motion, $a_{T,\eta}$, found by Zorn *et al.* in PVE, similar to what Plazek and coworkers have seen in PS, a-PP, PVAc, PMPS and etc. [25–32]. However the two shift factors obtained by Zorn *et al.* were determined in two *non*-overlapping temperature regions ($T \leq -0.2$°C for $a_{T,\alpha}$ and $T \geq 40.4$°C for $a_{T,\eta}$), while Plazek and coworkers, using the Leaderman's trick [176] of measuring creep during recovery at a lower temperature, managed to measure both $a_{T,\alpha}$ and $a_{T,\eta}$ over a common temperature range and found them to be different.
Polybutadiene PB						
96% cis, 2% trans, 2% vinyl	298	3.44	196.6	161	[141]	• Softening $a_{T,S}$.
43% cis, 50% trans, 7% vinyl	298	3.64	186.5	172	[142]	• Softening $a_{T,S}$.
27% cis, 37% trans, 36% vinyl	263	5.97	123.2	205	[143]	• Softening $a_{T,S}$.
7% cis, 1.5% trans, 91.5% vinyl PB	298	6.23	72.5	261	[139]	• Softening $a_{T,S}$.
20% vinyl-1,2	173.3	10.2	11.32	173.3	[126]	• $a_{T,\alpha}$ of local segmental motion by dynamic mechanical, $E^*(\omega)$, data in the frequency range of 0.01 to 100 Hz and temperatures near but above T_g. The sample is lightly cross-linked to attain dimensional stability for uniaxial extension measurement.
50% vinyl-1,2	200	27.15	64.17	200	[126]	• Same as above.
71% vinyl-1,2	225.5	14.4	25.5	225.5	[126]	• Same as above.
83% vinyl-1,2	249	20.7	42.1	249	[126]	• Same as above.
97% vinyl-1,2 PB	271.5	14.6	24.5	271.5	[126]	• Same as above.
7% vinyl-1,2, 52% trans-1,4, 41% cis-1,4	177.9	18.0	37.6	178	[140]	• $a_{T,\alpha}$ of local segmental motion by dynamic mechanical, $G^*(\omega)$, data in the frequency range of 0.01 to 100 rads/s and temperatures near but above T_g. The sample is not cross-linked.
52% vinyl-1,2, 29% trans-1,4, 19% cis-1,4	215.6	15.1	38.0	216	[140]	• Same as above.
68% vinyl-1,2, 20% trans-1,4, 12% cis-1,4	238	11.8	38.8	238	[140]	• Same as above.
86% vinyl-1,2, 8% trans-1,4, 6% cis-1,4	249.7	16.6	31.3	250	[140]	• Same as above.
95% vinyl-1,2 PB	272.2	14.9	37.5	272	[140]	• Same as above.
99% vinyl-1,2	323	5.78	94.8	268	[144]	• $a_{T,\eta}$ of the terminal relaxation from dynamic mechanical, $G^*(\omega)$, data in the T-range of 50 to 150°K above T_g.
x% vinyl-1,2 0.145<x<0.99	$55 + T_g(x)$	5.78	94.8	$T_g(x)$	[144]	• $a_{T,\eta}$ of the terminal relaxation from dynamical mechanical, $G^*(\omega)$, data in the T-range of 50–150°K above T_g for the high-vinyl compositions and of 100–200°K above T_g for the low-vinyl compositions. Results similar to that found by Kraus and Gruver [145].
PB						
35% cis, 54% trans, 10% vinyl $M = 1.30\checkmark \sim 10^5$	298	3.48	163	175	[146]	• a_T of the entire viscoelastic spectrum from dynamic mechanical, $G(\omega)$, data in the T-range of 182 to 398°K.

TABLE 26.1. *Continued.*

Polymer	T_0 °K	C_1 °K	C_2 °K	T_g °K	Ref.	Comments
35% cis, 56% trans, 8% vinyl $M = 6.29 \times 10^3$	298	3.22	160	173.7	[146]	• a_T of the entire viscoelastic spectrum from dynamic mechanical, $G^*(\omega)$, data.
PB *39% cis, 53% trans, 8% vinyl* $2 \times 10^4 < M_w < 2 \times 10^5$	301.2	4.17	196.8	182.2	[147]	• $a_{T,\eta}$ of mainly the terminal relaxation from dynamical mechanical, $G^*(\omega)$, data.
PB *cyclic* *7% cis, 30% trans, 63% vinyl* $3.8 \times 10^4 < M_w < 6.0 \times 10^4$	299.2	5.36	121.2	233	[148]	• $a_{T,\eta}$ of the terminal relaxation from dynamic mechanical, $G^*(\omega)$, data in the T-range of 248 to 361°K.
Polybutadiene crosslinked with dicumyl peroxide						
PB, 40% cis, 50% trans, 10% vinyl *(0.25% DiCup)*	273.2	3.0	120	180.2	[154]	• $a_{T,S}$ of the softening dispersion from creep measurement.
PB, 36% cis, 54% trans, 10% vinyl *(0.80% DiCup)*	273.2	2.95	125	175.2	[154]	• $a_{T,S}$ of the softening dispersion from creep measurement.
Hydrogenated polybutadiene HPB						
99% vinyl-1,2	323	6.35	146	246	[144]	• $a_{T,\eta}$ of the terminal relaxation from dynamic mechanical, $G^*(\omega)$, data in the T-range of 300 to 486°K.
x% vinyl-1,2 *0.145<x<0.99*	77 $+T_g(x)$	6.35	146	$T_g(x)$	[144]	• $a_{T,\eta}$ of the terminal relaxation from dynamic mechanical, $G^*(\omega)$, data in the T-range of about 180–300 °K above T_g for the low-vinyl compositions. Results similar to that found earlier by Arnett and Thomas.
Poly(1,3-dimethyl-1-butenylene) PDMB	348.2	4.88	1119.5	275.4	[150]	• $a_{T,\eta}$ of the terminal relaxation from dynamic mechanical, $G^*(\omega)$, data from 25 °C to 190 °C. Its T-dependence is similar to that of *a- PP* which can be obtained from PDMB by hydrogenation.
Polyurethane PU *(cross-linked)*	283	8.86	101.6	238	[151]	• $a_{T,S}$ of the softening dispersion from rubber to glass from dynamic mechanical data taken over the frequency range of 45–6000 Hz and the T-range of −16–39 °C. The loss tangent exhibits a broad maximum resembling the behavior of PIB.
PU *(network)*	251.1	14.46	33.1		[152]	• $a_{T,\alpha}$ of the local segmental motion from PCS, Brillouin scattering and dielectric relaxation data in the T-range of −14 °C to 105 °C.
PU *(cross-linked)*	228.2	12.5	42.5		[56]	• $a_{T,S}$ of the softening dispersion from creep compliance data.
Styrene-butadiene copolymer *(styrene: butadiene = 23.5:76.5, random, by weight)*	298	4.57	113.6	210	[153]	• $a_{T,S}$
Hydroxy terminated polybutadiene (20% cis, 60% trans, 20% vinyl)						

TABLE 26.1. *Continued.*

Polymer	T_0 °K	C_1 °K	C_2 °K	T_g °K	Ref.	Comments
HTPB-1 *(Mol. wt. per crosslinked unit, $M_x = 1760$)*	273.2	36.79	273.2 *(Arrhenius)*	194.2	[154]	• $a_{T,S}$ of the softening dispersion from creep measurement.
HTPB-2 ($M_x = 2370$)	273.2	41.59	273.2 *(Arrhenius)*	194.2	[154]	• $a_{T,S}$ of the softening dispersion from creep measurement.
HTPB-3 ($M_x = 5930$)	273.2	33.59	273.2 (*Arrhenius*)	194.2	[154]	• $a_{T,S}$ of the softening dispersion from creep measurement.
Hydroxy terminated styrene butadiene rubber						
HTSBR ($M_x = 2980$)	273.2	41.59	273.2 (*Arrhenius*)	194.2	[154]	• $a_{T,S}$ of the softening dispersion from creep measurement.
Fluorinated hydrocarbon elastomers						
Viton 11A(Air) (*Mol. wt. per crosslinked unit, $M_x = 7220$*)	253.2	11.62	37	249	[155]	• $a_{T,S}$ of the softening dispersion from creep measurement.
Viton 10A(Vac) ($M_x = 5220$)	256.2	11.62	37	250.5	[155]	• $a_{T,S}$ of the softening dispersion from creep measurement.
Viton 10B(Air) ($M_x = 3070$)	260.2	11.62	37	253.6	[155]	• $a_{T,S}$ of the softening dispersion from creep measurement.
Viton 10B(Vac) ($M_x = 3070$)	262.0	11.62	37		[155]	• $a_{T,S}$ of the softening dispersion from creep measurement.
Bisphenol A based epoxy resins/4,4′ diamino diphenyl sulfone (DDS) 828/DDS ($M_x = 419$)	478.2	144.4	478.2 (*Arrhenius*)	477.2	[156]	• $a_{T,S}$ of the softening dispersion from creep measurement.
1001/DDS ($M_x = 908$)	403.2	19.26	50.0	400.2	[156]	• $a_{T,S}$ of the softening dispersion from creep measurement.
1004/DDS ($M_x = 1520$)	384.0	21.02	50.0	385.2	[156]	• $a_{T,S}$ of the softening dispersion from creep measurement.
1007/DDS ($M_x = 2870$)	373.9	20.50	50.0	374.2	[156]	• $a_{T,S}$ of the softening dispersion from creep measurement.
Epoxy model networks *from a diepoxy prepolymer, DGEBA, and three different diamines or mixtures of a monoamine and a diamine.*						
DDM *(4,4′ diamino diphenyl methane*) network	457.2	10.9	34.8	457.2 (at 1 Hz)	[149]	• $a_{T,S}$ of the softening dispersion from dynamic mechanical, $E^*(\omega)$.
DDM/Aniline network	394.2	9.5	25.6	394.2 (at 1 Hz)	[149]	• $a_{T,S}$ of the softening dispersion from dynamic mechanical, $E^*(\omega)$.
Hexamethylene diamine *(HMDA)*	391.2	11.0	41.5	391.2 (1 Hz)	[149]	• $a_{T,S}$ of the softening dispersion from dynamic mechanical, $E^*(\omega)$.
HMDA/Hexylamine	336.7	9.9	34.4	336.7 (at 1 Hz)	[149]	• $a_{T,S}$ of the softening dispersion from dynamic mechanical, $E^*(\omega)$.
IPD *(isophorone diamine*)	442.2	12.5	52.9	442.2 (at 1 Hz)	[149]	• $a_{T,S}$ of the softening dispersion from dynamic mechanical, $E^*(\omega)$.
IPD/Trimethylcylcohexy lamine	382.2	9.2	41.9	382.2 (at 1 Hz)	[149]	• $a_{T,S}$ of the softening dispersion from dynamic mechanical, $E^*(\omega)$.

TABLE 26.1. *Continued.*

Polymer	T_0 °K	C_1 °K	C_2 °K	T_g °K	Ref.	Comments
Miscible Blends and Copolymers						
Styrene-*n*-hexyl methacrylate copolymers S-nHMA copolymer *(0.26:0.74)*	373	7.11	192.6	277	[157]	
S-nHMA copolymer *(0.41:0.59p)*	373	6.56	156.4	287	[157]	
Polyisoprene-polyvinylethylene blends (1–*x*)PI-xPVE blends, Resolved component dynamics						
x=0%, PI	210.4	12.26	38.59		[127]	• $a_{T,\alpha}$ of local segmental motion of PI from dielectric relaxation.
x=20%, PVE component	223.9	15.0	85.82		[127]	• $a_{T,\alpha}$ of local segmental motion of the PVE component resolved in the dielectric relaxation spectra which are not thermorheologically simple.
x=25%, PI component	216.7	12.2	38.66		[127]	• $a_{T,\alpha}$ of local segmental motion of the PI component resolved in the dielectric relaxation spectra (not thermorheologically simple).
x=25%, PVE component	255.47	12.2	125.4		[127]	• $a_{T,\alpha}$ of local segmental motion of the PVE component resolved in the dielectric relaxation spectra (not thermorheologically simple).
x=50%, PVE component	235.85	11.64	52.65		[127]	• $a_{T,\alpha}$ of local segmental motion of the PVE component resolved in the dielectric relaxation spectra (not thermorheologically simple).
x=75%, PVE component	255.47	12.2	125.4		[127]	• $a_{T,\alpha}$ of local segmental motion of the PVE component resolved in the dielectric relaxation spectra (not thermorheologically simple).
x=100%, PVE	271.3	12.0	36.8		[127]	• $a_{T,\alpha}$ of local segmental motion of PVE from dielectric relaxation.
(1–*x*)PI-*x*PVE blends, Resolved component dynamics						
x=0%, PI	215.7	10.16	54.14		[131]	• $a_{T,\alpha}$ of local segmental motion of PI from 2D deuteron exchange NMR (2D DE NMR).
x=25%, PI component	218.2	13.0	50.0		[131]	• $a_{T,\alpha}$ of local segmental motion of the PI component resolved by 2D DE NMR.
x=25%, PVE component	227.3	13.32	84.24		[131]	• $a_{T,\alpha}$ of local segmental motion of the PVE component resolved by 2D DE NMR.
x=50%, PI component	226.2	14.43	64.86		[131]	• $a_{T,\alpha}$ of local segmental motion of the PI component resolved by 2D DE NMR.
x=50%, PVE component	236.7	13.83	88.27		[131]	• $a_{T,\alpha}$ of local segmental motion of the PVE component resolved by 2D DE NMR.
x=75%, PI component	236.6	15.15	69.78		[131]	• $a_{T,\alpha}$ of local segmental motion of the PI component resolved by 2D DE NMR.
x=75%, PVE component	253.5	14.1	80.01		[131]	• $a_{T,\alpha}$ of local segmental motion of the PVE component resolved by 2D DE NMR.
x=100%, PVE	273.5	12.3	50.50		[131]	• $a_{T,\alpha}$ of local segmental motion of PVE by 2D DE NMR.
Poly(vinylmethylether)-polystyrene blends 50% PVME/ 50%PS blend: the PVME *component*	255.9	14.79	44.35		[77, 78]	• $a_{T,\alpha}$ of the local segmental motion of the PVME component in the blend from dielectric spectra, which are not thermorheologically simple. Its *T*-dependence is stronger than that of pure PVME.

TABLE 26.1. *Continued.*

Polymer	T_0 °K	C_1 °K	C_2 °K	T_g °K	Ref.	Comments
Diluted Systems						
Cellulose tributyrate in dimethyl phthalate						
(21%)	247	8.86	101.6	188	[158, 159]	• $a_{T,S}$ from creep and dynamic mechanical measurements.
(43%)	251	8.86	101.6	193	[158, 159]	• $a_{T,S}$ from creep and dynamic mechanical measurements.
Cellulose nitrate in diethyl phthalate *(23%)*	298	8.84	165.5	166		• $a_{T,S}$ from creep and dynamic mechanical measurements.
Polyethylene (solution chlorinated) *Cl content = 56.6 w/w, amorphous, in bis(2-ethylhexyl)phthalate*						
(88 polymer)	295.5	11.4	56.5	295	[180]	• $a_{T,\alpha}$ of local segmental motion from dielectric relaxation data for $\log \tau_\alpha = -11.4 + 644/\ (T\text{-}239\,\text{K})$.
(74% polymer)	292.6	12.5	61.6	279	[180]	• $a_{T,\alpha}$ of local segmental motion from dielectric relaxation data for $\log \tau_\alpha = -12.5 + 770/\ (T\text{-}231\,\text{K})$.
(59% polymer)	262.3	12.8	74.3	245	[180]	• $a_{T,\alpha}$ of local segmental motion from dielectric relaxation data for $\log \tau_\alpha = -12.8 + 951/\ (T\text{-}188\,\text{K})$.
Polyisoprene ($M_w = 395\ 000$) in Aroclor: *polymer concentration, c.*						
($c = 0.92$ g/ml, 100% PI)	258	7.02	104.5		[161]	• a_T for $J_p(t) > 10^{-8}\,\text{cm}^2/\text{dyne}$ including viscous flow.
($c = 0.849$ g/ml)	258	7.69	107.3		[161]	• a_T of the terminal dispersion. Its T-dependence becomes stronger with addition of Aroclor.
($c = 0.60$ g/ml)	258	10.7	124.6		[161]	• a_T of the terminal dispersion. Its T-dependence becomes stronger with addition of Aroclor.
($c = 0.449$ g/ml)	258	13.1	138.7		[161]	• a_T of the terminal dispersion. Its T-dependence becomes stronger with addition of Aroclor.
($c = 0.30$ g/ml)	258	24.2	197.2		[161]	• a_T of the terminal dispersion. Its T-dependence becomes stronger with addition of Aroclor.
($c = 0.20$ g/ml)	258	21.0	164.6		[161]	• a_T of the terminal dispersion. Its T-dependence becomes stronger with addition of Aroclor.
($c = 0.10$ g/ml)	258	10.3	59.4		[161]	• a_T of the terminal dispersion. Its T-dependence becomes stronger with addition of Aroclor.
PMPS in 1,1-bis(*p*-methoxyphenyl) cyclohexane 90% *(PMPS $M = 130\ 000$)*	242.5	12.47	23.23	242.5	[111, 112]	• $a_{T,\alpha}$ of local segmental motion from dynamical mechanical, $G^*(\omega)$, data obtained in the frequency range $10^{-2} < f < 10^2$ Hz. $\tau_\alpha(T_0) = 10^2$ s.
Polystyrene in Decalin 62%	291	8.86	101.6		[162, 163]	• $a_{T,S}$
Polystyrene/Tricresyl phosphate (PS/TCP)						
100% PS	373.2	14.24	66.0	371	[164]	• $a_{T,\eta}$ of the terminal dispersion which has a weaker T-dependence than that of the softening dispersion, $a_{T,S}$ to be given below.
100% PS	373.2	12.09	32.87	371	[164]	• $a_{T,S}$ of the softening dispersion which has a stronger temperature dependence than that of $a_{T,\eta}$.
85% PS	326.2	13.50	38.0		[164]	• $a_{T,S}$ of the softening dispersion.
70% PS	293.2	15.13	60.0		[164]	• $a_{T,\eta}$ of the terminal dispersion which still has a weaker T-dependence than that of the softening dispersion, $a_{T,S}$ to be given below. However, the difference decreases with increasing TCP.
70% PS	293.2	14.96	45.05		[164]	• $a_{T,S}$ of the softening dispersion.
55% PS	268.2	13.8	65.0		[164]	• $a_{T,\eta}$ of the terminal dispersion which has an almost the same though still slightly weaker T-dependence than that of the softening dispersion, $a_{T,S}$ to be given below.

TABLE 26.1. *Continued.*

Polymer	T_0 °K	C_1 °K	C_2 °K	T_g °K	Ref.	Comments
55% PS	268.2	14.75	60.0		[164]	• $a_{T,S}$ of the softening dispersion.
25% PS	212.2	24.46	69.0		[164]	• $a_{T,S}$ of the softening dispersion.
PS in DOP *(70%)*	277	14.43	56.0		[165]	• $a_{T,\alpha}$ of the local segmental motion of PS in the concentrated solution obtained by PCS. $\tau_\alpha(T_0) = 10^2$ s.
PCHMA/di(2-ethylhexyl phthalate (PCHMA/DOP)						
100% PCHMA	359.7	15.5	87.74		[166]	• $a_{T,\alpha}$ of the local segmental motion from PCS data.
95% PCHMA	356.7	15.5	87.74			• $a_{T,\alpha}$ of the local segmental motion from PCS data.
90% PCHMA	342.7	15.5	87.74			• $a_{T,\alpha}$ of the local segmental motion from PCS data.
85% PCHMA	329.7	15.5	87.74			• $a_{T,\alpha}$ of the local segmental motion from PCS data.
PMMA/DOP						
PMMA *plasticized by DOP,* $C_{PMMA} = 0.9\,g/mL$	316.6	15.9	47.6	313 (T_g *of bulk polymer is 351 K*)	[167]	• $a_{T,\alpha}$ of local segmental motion from photon correlation spectroscopy in the range: $10^{-5} < \tau_\alpha < 10^0$ s.
PMMA *plasticized by DOP,* $C_{PMMA} = 0.8\,g/mL$	295	16.9	98	313 (T_g of bulk polymer is 351 K)	[167]	• $a_{T,\alpha}$ of local segmental motion from photon correlation spectroscopy in the range: $10^{-5} < \tau_\alpha < 10^0$ s.
PMMA/toluene						
PMMA $M = 5.4 \times 10^5$, *isotactic rich* 67% PMMA	202.3	11.2	52.7	230	[168]	• $a_{T,\alpha}$ of local segmental motion from dielectric relaxation data from $256<T<345$ K and $10^0 < f < 10^{7.5}$ Hz.
30% PMMA	161.6	11.2	53.6	163	[168]	• $a_{T,\alpha}$ of local segmental motion from dielectric relaxation data from $178<T<294$ K and $10^0 < f < 10^{7.5}$ Hz.
30% PMMA in Diethyl phthalate	298	7.11	130.1	211	[169]	• $a_{T,S}$ from dynamic mechanical measurement.
Pn-BMA in diethyl phthalate						
(50%)	273	9.98	153.1	206	[170]	• $a_{T,S}$ from dynamic mechanical measurement.
(60%)	273	12.8	157.3	227	[170]	• $a_{T,S}$ from dynamic mechanical measurement.
PVAc in tricresyl phosphate *(50%)*	293	8.86	101.6		[163, 171]	• $a_{T,S}$ from dynamic mechanical measurement.
PVC/tetrahydrofuran (PVC/THF) 100% PVC	355.3	12.4	45.25	344	[172]	• $a_{T,\alpha}$ for the local segmental motion from dielectric relaxation in the frequency range $10^2 < f < 10^6$ Hz. $\tau_\alpha(T_0) = 1$ s.
84% PVC	282.1	11.0	36.1	275		• Same as above.
59% PVC	209.9	11.8	50.85	201		• Same as above.
51% PVC	200.9	10.8	37.87	193		• Same as above.
38% PVC	173.5	11.1	46.5	162		• Same as above.
PMA/toluene 100% PMA	292.4	13.8	48.55	286	[173]	• $a_{T,\alpha}$ for the local segmental motion from dielectric relaxation in the frequency range $10^2 < f < 10^6$ Hz. $\tau_\alpha(T_0) = 1$ s.
75% PMA	235.4	13.8	43.56	225		• Same as above.
60% PMA	209.5	15.9	57.0	201		• Same as above.

results. $\gamma = 1.9$ for poly(vinyl ethylene) with 88% vinyl and $M_w = 3$ kg/mol; $\gamma = 3.0$ for 1, 4-polyisoprene with $M_w = 11$ kg/mol; $\gamma = 2.55$ for poly(vinyl methyl ether) with $M_w = 99$ kg/mol; $\gamma = 2.6$ for poly(vinyl acetate) with $M_w = 170$ kg/mol; $\gamma = 2.5$ for poly(propylene glycol) with $M_w = 4$ kg/mol; $\gamma = 5.6$ for poly(methyl phenyl siloxane) with $M_w = 23$ kg/mol; and $\gamma = 5.0$ for poly(methyl tolyl siloxane) with $M_w = 35$ kg/mol. For some low molecular weight glass-formers, the results are $\gamma = 3.3$ for poly[(*o*-cresyl glycidyl ether)-*co*-formaldehyde] with $M_w = 0.87$ kg/mol; $\gamma = 2.8$ for diglycidyl ether of bisphenol *A* with $M_w = 1.8$ kg/mol; and $\gamma = 8.5$ for poly(phenyl glycidyl ether)-*co*-formaldehyde with $M_w = 0.35$ kg/mol. The parameter γ is claimed to be a measure of the relative importance of V as opposed to T. If the local segmental dynamics were strictly thermally activated and volume does not enter, then γ would be exactly equal to zero. Although $\log(\tau_\alpha)$ is a monotonic increasing function of $T^{-1}V^{-\gamma}$, in general the dependence is not linear. Instead the slope increases with increasing $T^{-1}V^{-\gamma}$, a behavior like the VFTH or the WLF temperature dependence of the τ_α data taken at constant pressure. Thus, a VFTH equation based the variable TV^γ instead of the usual T can be constructed to describe the data.

Recently the analysis was extended to the polymer chain dynamics (i.e., the dielectric normal mode) for polymers that have dipole moment parallel as well as normal to the backbone. They are polypropylene glycol (PPG), 1,4-polyisoprene (PI) [186] , and polyoxybutylene (POB) [187]. The normal mode relaxation times (strictly speaking, the longest normal mode relaxation times, τ_n) taken at various combinations of temperature and pressure superpose to a single master curve when plotted against $T^{-1}V^{-\gamma}$, using the same value of γ as for the segmental relaxation times, τ_α. It is paradoxical that τ_n and τ_α are functions of the *same* quantity, $T^{-1}V^{-\gamma}$, yet they have *different* $T^{-1}V^{-\gamma}$-dependences.The dependence of τ_α on $T^{-1}V^{-\gamma}$ is stronger than that of τ_n, similar to the relation between their temperature dependences at ambient pressure [19,25,30,46,115,188–191] or their pressure dependences at constant temperature [192]. The explanation of τ_n and τ_α are functions of the same $T^{-1}V^{-\gamma}$ and yet the dependence of τ_α is stronger than τ_n was given [193] by an application of the Coupling Model [194–197] in the same manner as the explanation given previously for their different T-dependences at constant P or P-dependences at constant T [30,46,115,189–191]. These scaling analyses do not constitute a test of the free volume theory stemming from the Doolittle and WLF equations, since these depend on the relative or fractional free volume and not the total volume.

26.5 SOME IMPORTANT SECONDARY RELAXATIONS

Secondary relaxations are commonly found in glass-formers including polymers. Some secondary relaxations involve intramolecular degrees of freedom and have no relation to the α-relaxation such as the motion of a side group of a polymer isolated from the chain backbone. However some secondary β-relaxations are more intriguing. For example, the secondary relaxation found in totally rigid molecules such as chlorobenzene [198–200], and in polymers which have no side groups such as 1,4 polybutadiene [201] and polyisoprene [202] (excluding the very fast rotation of the methyl group). Even in polymers that have side groups such as poly(*n*-ethyl methacrylate) (PEMA), multidimensional ^{13}C solid-state NMR study of the carboxyl moiety [203] found that the β-relaxation involves a π-flip of the side group coupled to a rocking motion around the local chain axis with a $\pm 20^\circ$ amplitude in the glassy state. The rocking amplitude increases upon raising the temperature above T_g and is as large as $\pm 50^\circ$ at $T_g + 27$ K. The temperature dependence of the secondary relaxation time, τ_β, of PEMA above T_g is stronger than the Arrhenius dependence extrapolated from the glassy state. In fact, the temperature dependence of τ_β above T_g could be regarded as having another VFTH dependence albeit weaker than that of the α-relaxation. In the research community of nonpolymeric glass-formers, the secondary relaxations which have properties mimicking the α-relaxations are sometimes called the Johari–Goldstein relaxations for the purpose of distinguishing them from secondary relaxations of lesser importance [204]. The properties of these secondary relaxations that bear similarity to that of the α-relaxation include the VFTH temperature dependence and pressure dependence of τ_β in the equilibrium liquid state [203,204]. These secondary relaxations are potentially the originator of the α-relaxation, which is certainly the case of the primitive relaxation of the Coupling Model [194–197]. A remarkable finding is that the primitive relaxation time τ_0 calculated entirely from the parameters of the α-relaxation turns out to be approximately the same as the most probable relaxation time, τ_β, of these secondary relaxation in many polymeric glass-formers, including polybutadiene, polyisoprene, polyvinylacetate, PEMA, and others, as well as many nonpolymeric glass-formers [201,202,205–211]. There is also microscopic experimental evidence for a close connection between the secondary relaxation or the primitive relaxation processes to the α-relaxation. Multidimensional NMR [212,213] experiments have shown that the dynamically heterogeneous molecular reorientations of the α-relaxation (i.e., the primitive relaxation in the coupling model) occurs by relatively small jump angles having an exponential time dependence. Furthermore, from one and two-dimensional 2H NMR studies [214], the secondary relaxations in toluene and polybutadiene are seen to also involve angular jumps of similar magnitude for temperatures above T_g. This similarity in size of the jump angles supports the relation between the secondary and the primitive relaxations, and their role as the origin of the α-relaxation.

Related information can be found in Chapters 23 and 24.

REFERENCES

1. D. J. Ferry, *Viscoelastic Properties of Polymers, 3rd ed*. (John Wiley & Sons, New York, 1980), pp. 277–279.
2. G. C. Berry and T. G. Fox, Adv. Polymer Sci. **5**, 261 (1968).
3. N. G. McCrum, B. E. Read, and G. Williams, *Anelastic and Dielectric Effects in Polymeric Solids* (John Wiley & Sons, London, 1967).
4. R. Nozaki and S. Mashimo, J. Chem. Phys. **84**, 3575 (1986).
5. A. Hoffmann, K. Kremer, E. W. Fischer, *et al*. in *Disorder Effects on Relaxational Processes*, edited by R. Richert and A. Blumen (Springer-Verlag, Berlin and Heidelberg, 1994), p. 309.
6. H. W. Spiess, J. Non-Cryst. Solids **131–133**, 766 (1991).
7. a. D. Schaefer, H. W. Spiess, U. W. Suter, *et al*. Macromolecules **23**, 3431 (1990); U. Pschorn, E. Rössler, H. Sillescu, *et al*. Macromolecules **24**, 398 (1991); (b) K. Zemke, K. Schmidt-Rohr, and H. W. Speiss, Acta Polymer **45**, 148 (1994).
8. S. Kaufmann, S. Wefing, D. Schaeffer, *et al*. J. Chem. Phys. **93**, 197 (1990).
9. G. D. Patterson, in *Dynamic Light Scattering*, edited by R. Pecora, Academic, New York (1986), p. 260.
10. G. Fytas and G. Meier in *Dynamic Light Scattering, the Method and Some Applications*, edited by W. Brown (Clarendon Press, Oxford, 1993), p. 427.
11. M. L. Williams, J. Phys. Chem. **59**, 95 (1955).
12. M. L. Williams, R. F. Landel, and D. J. Ferry, J. Am. Chem. Soc. **77**, 3701 (1955).
13. D. J. Plazek and A. J. Chelko, Jr., Polymer **18**, 15 (1977).
14. H. Vogel, Phys. Z. **22**, 645 (1921).
15. G. S. Fulcher, J. Am. Chem. Soc. **8**, 339, 789 (1925).
16. G. Tamman and W. H. Hesse, Z. Anorg. Allg. Chem. **156**, 245 (1926).
17. A. K. Doolittle, J. Appl. Phys. **22**, 1471 (1951); **23**, 236 (1952).
18. F. Schwarzl and A. J. Staverman, J. Appl. Phys. **23**, 838 (1952).
19. K. L. Ngai and D. J. Plazek, in Rubber Chem. Tech., Rubber Review, **68**, 376 (1995).
20. D. J. Plazek, I.-C. Chay, K. L. Ngai and C. M. Roland, Macromolecules **28**, 6423 (1995).
21. A. K. Rizos, T. Jian, and K. L. Ngai, Macromolecules **28**, 517 (1995).
22. D. J. Plazek, J. Polym. Sci.: Part A-2 **6**, 621 (1968).
23. J. Y. Cavaille, C. Jordan, J. Perez, *et al*. J. Polym. Sci.: Part B: Polymer Phys. **25**, 1235 (1987).
24. D. J. Plazek, M. J. Rosner and D. L. Plazek, J. Polym. Sci.: Part B: Polymer Phys. **26**, 473 (1988).
25. D. J. Plazek and M. V. O'Rourke, J. Polym. Sci. A-2 **9**, 209 (1971).
26. D. J. Plazek, J. Phys. Chem. **69**, 3480 (1965).
27. D. J. Plazek, Polym. J. **12**, 43 (1980).
28. D. J. Plazek, J. Polym. Sci.: Polymer Physics Edition **20**, 729 (1982).
29. D. J. Plazek and D. L. Plazek, Macromolecules **16**, 1469 (1983).
30. D. J. Plazek, C. Bero, S. Neumeister, *et al*. J. Colloid Polymer Sci. **272**, 1430 (1994).
31. D. J. Plazek, J. Non-Cryst. Solids **131–133**, 836 (1991).
32. K. L. Ngai in *Disorder Effects on Relaxational Processes*, edited by R. Richert and A. Blumen (Springer-Verlag, Berlin and Heidelberg, 1994), p. 89.
33. G. Wiliams, Tran. Faraday Soc. **59**, 1397 (1963)
34. S. F. Kurath, E. Passaglia, and R. Pariser, J. Appl. Phys. **28**, 499 (1957).
35. R. S. Marvin and H. Oser, J. Res. Nat. Bur. Stand. **B66**, 171 (1962).
36. R. S. Marvin, *Proceedings of the Second International Congress on Rheology*, edited by V. G. W. Harrison (Butlerworths, London, 1954), p. 156.
37. R. S. Marvin and H. Oser, J. Res. Nat. Bur. Stand. **B66**, 171 (1962)
38. E. R. Fitzgerald, L. D. Grandine, and J. D. Ferry, J. Appl. Phys. **24**, 65 (1953).
39. J. D. Ferry, L. D. Grandine, Jr., and E. R. Fitzgerald, J. Appl. Phys. **24**, 911 (1953).
40. E. Catsiff and A. V. Tobolsky, J. Colloid Sci. **10**, 375 (1955).
41. A. V. Tobolsky and E. Catsiff, J. Polym. Sci. **19**, 111 (1955).
42. A. V. Tobolsky, *Properties and Structure of Polymers* (John Wiley and Sons, New York, 1960), pp. 157–159.
43. K. L. Ngai, D. J. Plazek, and A. K. Rizos (1995), submitted to Macromolecules.
44. H. Okamoto, T. Inoue, K. Osaki, J. Polym. Sci. Phys. Ed. **33**, 417 (1995).
45. D. J. Plazek, X. D. Zheng, and K. L. Ngai, Macromolecules **25**, 4920 (1992).
46. K. L. Ngai, D. J. Plazek, and C. Bero, Macromolecules **26**, 1065 (1993).
47. G. C. Berry and T. G. Fox, Fortschr. Hochpolym. Forsch. (Adv. Polymer Sci.), **5**, 261 (1968).
48. L. J. Fetters, W. W. Graessley, and A. D. Kiss, Macromolecules **24**, 3136 (1991).
49. J. D. Ferry and G. S. Parks, Physics **6**, 356 (1935).
50. G. Fytas and K. L. Ngai, Macromolecules **21**, 804 (1988).
51. P. Santangelo and C. M. Roland, unpublished.
52. D. S. Pearson, L. J. Fetters, L. B. Younghouse, *et al*. Macromolecules **21**, 478 (1988).
53. T. Inoue, H. Hayashihara, H. Okamoto, and K. Osaki, J. Polym. Sci. Part B: Polym. Phys. **30**, 409 (1992).
54. D. J. Ferry, *Viscoelastic Properties of Polymers*, 3rd ed. (John Wiley & Sons, New York), p. 277.
55. D. J. Plazek, J. Phys. Chem. **69**, 3480 (1965)
56. F. R. Schwarzl and F. Zahradnik, Rheol. Acta **19**, 137 (1980).
57. A. J. Barlow, A. Erginsay, and J. Lamb, Proc. R. Soc. **A298**, 481 (1967).
58. N. Nemoto, Polym. J. **1**, 485 (1970).
59. S. Onogi, T. Masuda, and K. Kitagawa, Macromolecules **3**, 110 (1970).
60. H. Endo, T. Fujimoto, and M. Nagasawa, J. Polym. Sci. **7**, 1669 (1960).
61. H. Odani, N. Nemoto, S. Kitimura, M. Kuratas, and M. Tamura, Polym. J. **1**, 356 (1970).
62. K, Yoshimori and R. Work, J. Chem. Phys. **72**, 5909 (1980).
63. B. L. Funt and T. H. Sutherland, Can. J. Chem. **30**, 940 (1952).
64. P. F. Veselovskii, Ber. Tomsk. Polytech. Inst., USSR **91**, 399 (1956).
65. S. P. Kabin, Vysokomol. Soed. **2**, 1324 (1960).
66. G. P. Mikhailov, Usp. Khim. **24**, 875 (1955).
67. J. D. Ferry and R. F. Landel, Kolloid-Z. **148**, 1 (1956).
68. M. L. Williams and J. D. Ferry, J. Colloid Sci. **9**, 479 (1954).
69. G. Fytas, C. H. Wang, G. Meier, and E. W. Fischer, Macromolecules **18**, 1492 (1985); C. H. Wang, G. Fytas, and E. W. Fischer, J. Chem. Phys. **82**, 4332 (1985).
70. B. L. Funt, Can. J. Chem. **30**, 84 (1952).
71. Y. Takahashi, J. Appl. Polym. Sci. **5**, 468 (1961); J. Phys. Soc. Japan **16**, 1024 (1961).
72. J. D. Ferry, M. L. Williams, and E. R. Fitzgerald, J. Phys. Chem. **59**, 403 (1955).
73. W. Sommer, Koll.-Z. **167**, 97 (1959)
74. J. Colmenero, A. Arbe, and A. Alegria, J. Non-Cryst. Solids **172–174**, 126 (1994).
75. T. H. Sutherland and B. L. Funt, J. Polym. Sci. **11**, 177 (1953).
76. A. Alegria, E. Macho, and J. Colmenero, Macromolecules **24**, 5196 (1991); J. Non-Cryst. Solids **131–133**, 860 (1991).
77. C. M. Roland and K. L. Ngai, Macromolecules **25**, 363 (1992).
78. A. Zetsche, F. Kremer, W. Jung *et al*. Polymer **31**, 1883 (1990)
79. M. L. Williams and J. D. Ferry, J. Colloid Sci. **10**, 474 (1955).
80. J. D. Ferry and R. F. Landel, Kolloid-Z. **148**, 1 (1956).
81. K. Fujino, K. Senshu, and H. Kawai, J. Colloid Sci. **16**, 262 (1961).
82. D. J. Plazek, V. Tan, and V. M. O'Rourke, Rheol. Acta **13**, 367 (1974).
83. D. J. Plazek and N. Raghupathi, Polymer Preprints **15**, 53 (1974).
84. D. J. Plazek, in *Relaxations in Complex Systems*, edited by K. L. Ngai and G. B. Wright, Government Printing House, Naval Research Laboratory, Washington, D. C. (1984).
85. T. Masuda, N. Toda, Y. Aoto and S. Onogi, Polym. J. **3**, 315 (1972).
86. J. D. Ferry, W. C. Child, and R. Zand, J. Colloid Sci. **12**, 53 (1957).
87. W. C. Child and J. D. Ferry, J. Colloid Sci. **12**, 327 (1957)
88. G. P. Mikhailov, T. I. Borisova, and A. S. Nigmankhodzhayev, Vysokomol. Soyed. **8**, 969 (1966).
89. G. Meier, G. Fytas, and T. Dorfmüller, Macromolecules **17**, 957 (1984).
90. W. C. Child and J. D. Ferry, J. Colloid Sci. **12**, 389 (1957)
91. G. Meier, F. Kremer, G. Fytas, and A. K. Rizos, J. Polym. Sci., Polym. Phys. Ed. (in press); L. Giebel, G. Meier, G. Fytas, and E. W. Fischer, J. Polym. Sci., Polym. Phys. Ed. **30**, 129 (1992).
92. W. Dannhauser, W. C. Child, and J. D. Ferry, J. Colloid Sci. **13**, 103 (1958).

93. J. W. Berge, P. R. Saunders, and J. D. Ferry, J. Colloid Sci. **14**, 135 (1959).
94. D. M. Stern, J. W. Berge, S. F. Kurath, C. Sakoonkim, and J. D. Ferry, J. Colloid Sci. **17**, 409 (1962)
95. T. E. Newlin, S. E. Lovell, P. R. Saunders, and J. D. Ferry, J. Colloid Sci. **17**, 10 (1962).
96. T. P. Yin and J. D. Ferry, J. Colloid Sci. **16**, 166 (1961).
97. S. F. Kurath, T. P. Yin, J. W. Berge, and J. D. Ferry, J. Colloid Sci. **14**, 147 (1959)
98. G. Floudas, P. Placke, P. Štěpánek, W. Brown, G. Fytas, and K. L. Ngai, Macromolecules **28**, 6799 (1995).
99. G. Fytas, Macromolecules **22**, 211 (1989).
100. W. J. Sichina, American Laboratories, **1**, 42 (1988).
101. D. K. Yoshimura and W. D. Richards, 89CRD211, General Electric Polymer Materials Laboratory Technical Information Series (1989).
102. R. H. Colby, M. G. Hansen, and A. R. Schultz, General Electric Company Corporate REsearch and Development Memo Report MOR-81-069 (1981).
103. J. P. Mercier and G. Groenincks, Rheol. Acta. **8**, 516 (1969).
104. A. J. Barlow, G. Harrison, and J. Lamb, Proc. Royal Soc. **282**, 228 (1964).
105. D. J. Plazek (unpublished).
106. K. U. Kirst, F. Kremer, T. Pakula, and J. Hollingshurst, Colloid Polym. Sci. **272**, 1420 (1994).
107. F. Wang, J. Roovers, and P. Toporowski, Macromolecules **26**, 3826 (1993).
108. J. C. Coburn and R. H. Boyd, Macromolecules **19**, 2238 (1986).
109. G. Fytas, T. Dorfmuller, and B. Chu, J. Polym. Sci., Polym. Phys. Ed. **22**, 1471 (1984).
110. K. L. Ngai and G. Fytas, J. Polym. Sci.: Part B: Polymer Physics **24**, 1683 (1986).
111. C. M. Roland, P. G. Santangelo, K. L. Ngai, and G. Meier, Macromolecules **26**, 6164 (1993).
112. P. G. Santangelo, C. M. Roland, K. L. Ngai, A. K. Rizos, and H. Katerinopoulos, J. Non-Cryst. Solids **172–174**, 1084 (1994).
113. D. Boesse, B. Momper, G. Meier, F. Kramer, and E. W. Fischer, Macromolecules **22**, 4416 (1989).
114. G. Williams, Trans. Faraday Soc. **61**, 1564 (1965).
115. K. L. Ngai, A. Schönhals, and E. Schlosser, Macromolecules **25**, 4915 (1992).
116. J. Cochrane, G. Harrison, J. Lamb, *et al*. Polymer **21**, 837
117. C. H. Wang, G. Fytas, and T. Dorfmüller, Macromolecules **16**, 68 (1983).
118. E. J. Hwang, T. Inoue, and K. Osaki, Polym. Eng. Sci. **34**, 135 (1994)
119. K. L. Ngai, C. M. Roland, J. M. O'Reilley, and J. S. Sedita, Macromolecules **25**, 3906 (1992)
120. J. D. Ferry, L. D. Grandine, Jr., and E. R. Fitzgerald, J. Appl. Phys. **24**, 911 (1953).
121. J. F. Sanders and J. D. Ferry, Macromolecules **7**, 681 (1974).
122. J. R. Richards, R. G. Mancke, and J. D. Ferry, Polym. Lett. **2**, 197 (1964).
123. S. F. Kurath, E. Passaglia, and R. Pariser, J. Appl. Polym. Sci. **1**, 150 (1959).
124. A. R. Payne, in *Rheology of Elastomers*, edited by P. Mason and N. Wookey (Pergamon, London, 1958), p. 86.
125. R. A. Dickie and J. D. Ferry, J. Phys. Chem. **70**, 2594 (1966).
126. C. M. Roland and K. L. Ngai, Macromolecules **24**, 5315 (1992); C. M. Roland, Macromolecules **25**, 7031 (1992); C. M. Roland and K. L. Ngai, Macromolecules **26**, 2688 (1993).
127. A. Allegria, J. Colmenero, K. L. Ngai, and C. M. Roland, Macromolecules **27**, 4486 (1994).
128. D. Boesse, F. Kremers, and L. J. Fetters, Macromolecules **23**, 1826 (1990); J. Non-Cryst. Solids **131–133**, 728 (1991); D. Boesse and F. Kremer, Macromolecules **23**, 829 (1990).
129. J. Kanetakis, G. Fytas, F. Kremer, *et al*. Macromolecules **25**, 3484 (1992).
130. A. K. Rizos (unpublished data).
131. G.-C. Chung, J. A. Kornfield, and S. D. Smith, Macromolecules **27**, 964 (1994).
132. N. Nemoto, M. Moriwaki, H. Odani, and S. Onogi, Macromolecules **4**, 215 (1971).
133. W. Gotro and W. W. Graessley, Macromolecules **17**, 2767 (1984).
134. J. Roovers and P. M. Toporowski, Macromolecules **25**, 3454 (1992).
135. J. Colmenero, A. Alegria, P. G. Santangelo, K. L. Ngai, and C. M. Roland, Macromolecules **27**, 407 (1994).
136. C. Bero and D. J. Plazek, 1994 (unpublished).
137. C. M. Roland, Macromolecules, **27**, 4242 (1994).
138. B. H. Arendt, R. M. Kannan, M. Zewail, and J. Kornfield, Rheol. Acta. **33**, 322 (1994)
139. J. F. Sanders, R. H. Valentine, and J. D. Ferry, J. Polym. Sci. A2 **6**, 967 (1968).
140. R. Zorn, G. B. McKenna, L. Wilner, and D. Richter, Macromolecules **28** (in press) (1995).
141. J. F. Sanders, Ph.D. thesis, University of Wisconsin, 1968.
142. E. Maekawa, R. G. Mancke, and J. D. Ferry, J. Phys. Chem. **69**, 2811 (1965).
143. C. R. Taylor, as referenced by J. D. Ferry (Reference 1, page 320).
144. J. M. Carella, W. W. Graessly, and L. Fetters, Macromolecules **17**, 177 (1984).
145. G. Kraus and J. T. Gruver, J. Appl. Polym. Sci. **9**, 739 (1965).
146. R. H. Colby and W. W. Graessley, Macromolecules **20**, 2226 (1987).
147. M. Baumgaertel, M. E. De Rosa, J. Machado, and H. Winter, Rheol. Acta **31**, 75 (1992).
148. J. Roovers, Macromolecules **21**, 1517 (1988).
149. J. F. Gerard, J. Galy, J. P. Pascault, *et al*. Polym. Eng. Sci. **31**, 615 (1991).
150. D. S. Pearson, L. J. Fetters, L. B. Younghouse, *et al*. Macromolecules **21**, 478 (1988).
151. R. F. Landel, J. Colloid Sci. **12**, 308 (1957)
152. A. K. Rizos, G. Fytas, R. J. Ma, *et al*. Macromolecules **26**, 1869 (1993).
153. R. G. Mancke and J. D. Ferry, Trans. Soc. Rheol. **12**, 335 (1968).
154. D. J. Plazek, G.-F. Gu, R. G. Stacer, *et al*. J. Mat. Sci. **23**, 1289 (1988).
155. D. J. Plazek, I.-C. Choy, F. N. Kelley, *et al*. Rubber. Chem. Tech. **56**, 866 (1983).
156. D. J. Plazek and I.-C. Choy, J. Polym. Sci.: Part B: Polym. Phys. **27**, 307 (1989).
157. A. S. Nigmankhodjaev, L.-K. Bi, C.-P. Wong, J. L. Schrag, and J. D. Ferry, J. Polym. Sci. A-2 **8**, 1927 (1970).
158. R. F. Landel and J. D. Ferry, J. Phys. Chem. **60**, 294 (1956).
159. D. J. Plazek, J. Colloid Sci. **15**, 50 (1960).
160. M. N. Vrancken and J. D. Ferry, J. Polym. Sci. **24**, 27 (1957).
161. N. Nemoto, T. Ogawa, H. Odani, and S. Onogi, Macromolecules **5**, 641 (1972).
162. L. D. Grandine and J. D. Ferry, J. Appl. Phys. **24**, 679 (1953).
163. J. D. Ferry and R. F. Landel, Kolloid-Z. **148**, 1 (1956).
164. D. J. Plazek, E. Riande, H. Markovitz, *et al*. J. Plym. Sci.: Polym. Phys. Edition **17**, 2189 (1979).
165. A. K. Rizos, R. M. Johnsen, W. Brown, and K. L. Ngai, Macromolecules **28**, 5450 (1995).
166. G. Floudas, G. Fytas, and K. L. Ngai, Macromolecules **24**, 1955 (1991).
167. G. Floudas, A. Rizos, W. Brown, and K. L. Ngai, Macromolecules **27**, 2719 (1994).
168. K. Adachi and T. Kotaka, Polymer J. **13**, 687 (1981).
169. D. M. Stern, J. W. Berges, S. F. Kurath, and J. D. Ferry, J. Colloid Sci. **17**, 409 (1962).
170. P. R. Saunders, D. M. Stern, S. F. Kurath, and J. D. Ferry, J. Colloid Sci. **14**, 222 (1959).
171. M. L. Williams and J. D. Ferry, J. Colloid Sci. **10**, 1 (1955)
172. K. Adachi and Y. Ishida, J. Polym. Sci.: Polymer Physics edition **14**, 2219 (1975).
173. K. Adachi and Y. Ishida, Polym. J. **3**, 233 (1972).
174. J. E. McKinney and H. V. Belcher, Res. Natl. Bur. Stand., Section A **67A**, 43 (1963).
175. J. R. McLoughlin and A. V. Tobolshy, J. Colloid Sci. **7**, 555 (1952).
176. H. Leaderman, R. G. Smith, and R. W. Jones, J. Polym. Sci. **14**, 47 (1954).
177. B. Momper, Doctoral Dissertation, Chemistry Department, Johannes Gutenberg Universität Mainz, Germany (1989).
178. L. David, A. Sekkat, and S. Etienne, J. Non-Cryst. Solids **172–174**, 214 (1994).
179. T. Kanaya, A. Patkowski, E. W. Fischer, J. Seils, H. Gläser, and K. Kaji, Macromolecules (1995), in press.
180. G. Floudas, J. S. Higgins, F. Kremer, and E. W. Fischer, Macromolecules **25**, 4955 (1992).

181. R. Casalini and C.M. Roland, Colloid Polym. Sci. **283**, 107 (2004).
182. R. Casalini and C.M. Roland, Phys. Rev. E **69**, 062501 (2004).
183. C. Alba-Simionesco, A. Cailliaux, A. Alegria A, and G. Tarjus Europhys. Lett. **68**, 58 (2004).
184. C. Dreyfuss, A. Aouadi, J. Gapinski, M. Matos-Lopes, W. Steffen, A. Patkowski, and R.M. Pick, Phys. Rev. E **68**, 011204 (2003).
185. C. Dreyfus, A. Le Grand, J. Gapinski, W. Steffen, and A. Patkowski, Europhys. J. B **42**, 309 (2004).
186. C.M. Roland, R. Casalini, M. Paluch, J. Polym. Sci. Polym. Phys. Ed. **42**, 4313 (2004).
187. R. Casalini and C.M. Roland, Macromolecules, **38**, 1779 (2005).
188. A. Schönhals, Macromolecules **26,** 1309 (1993).
189. C.M. Roland, K.L. Ngai, P.G. Santangelo, X.H. Qiu, M.D. Ediger, and D.J. Plazek, Macromolecules, **34**, 6159 (2001).
190. C.M. Roland, K.L. Ngai, and D.J. Plazek, Macromolecules, **37**, 7051 (2004).
191. K.L. Ngai, Chapter 2 in *Physical Properties of Polymers*; 3rd edition, (Cambridge University Press, Cambridge, England, 2004).
192. G. Floudas and T. Reisinger, J. Chem. Phys. **111**, 5201 (1999).
193. K.L. Ngai, R. Casalini, and C.M. Roland, Macromoelcules, **38**, 4363 (2005).
194. K.L. Ngai, D.J. Plazek and R.W. Rendell. Rheol. Acta, **36**, 307 (1997).
195. K.L. Ngai and K. Y. Tsang, Phys. Rev. E **60,** 4511 (1999).
196. K.L. Ngai and R.W. Rendell, in *Supercooled Liquids, Advances and Novel Applications*, edited by J.T. Fourkas, D. Kivelson, U. Mohanty, K. Nelson, ACS Symposium Series Vol. 676; American Chemical Society: Washington, DC (1997); Chapter 4, p 45.
197. K. L. Ngai, IEEE Trans. Dielectr. Electr. Insul. **8,** 329 (2001).
198. G. P. Johari and M. Goldstein, J. Chem. Phys. **53**, 2372 (1970).
199. G. P. Johari, J. Chem. Phys. **58**, 1766 (1973).
200. G. P. Johari, Ann. N.Y. Acad. Sci. **279,** 117 (1976).
201. K. L. Ngai, J. Phys.: Condens. Matter **15,** S1107 (2003).
202. C.M., Roland, M.J. Schroeder, J.J. Fontanella, and K.L. Ngai, Macromolecules, **37**, 2630 (2004).
203. A. S. Kulik, H. W. Beckham, K. Schmidt-Rohr, D. Radloff, U. Pawelzik, C. Boeffel, and H. W. Spiess, Macromolecules **27**, 4746 (1994).
204. K. L. Ngai and M. Paluch, J. Chem. Phys. **120,** 857 (2004).
205. K. L. Ngai and C.M. Roland, Polymer **43,** 567 (2002).
206. K. L. Ngai, J. Chem. Phys. **109,** 6982 (1998).
207. K.L. Ngai, Macromolecules, **32,** 7140 (1999).
208. D. Prevosto, S. Capaccioli, M. Lucchesi, P. A. Rolla, and K. L. Ngai, J. Chem. Phys. **120**, 4808 (2004).
209. K.L. Ngai and M. Beiner, Macromolecules, **37**, 8123 (2004).
210. K.L. Ngai, in AIP Conference Procedings Vol. 708, p. 515 (2004), Amer. Inst. Phys, Melville, NY.
211. K.L. Ngai and S. Capaccioli, Phys. Rev. E **69,** 031501 (2004).
212. R. Böhmer, G. Diezemann, G. Hinze, and E. Rössler, Prog. Nucl. Magn. Res. Spectrosc. **39**, 191 (2001).
213. H. Sillescu, R. Böhmer, G. Diezemann, and G. Hinze, J. Non-Cryst. Solids **307–310**, 16 (2002).
214. M. Vogel, C. Tschirwitz, G. Schneider, C. Koplin, and P. Medick, J. Non-Cryst. Solids **307–310**, 326 (2002).

CHAPTER 27

Adhesives

Alphonsus V. Pocius

3M Corporate Research Materials Laboratory, St. Paul, MN 55144–1000

The term ''adhesive'' applies to a wide range of materials that are used to join other materials together by means of surface attachment. Thus, an ''adhesive'' joins ''adherends'' together to generate an ''adhesive joint'' or an ''adhesively bonded assembly.'' Adhesive technology is a joining technology in much the same sense that rivets, screws, nuts and bolts, welding and brazing are joining technologies. Most materials that we recognize as adhesives are based upon organic materials that are either polymers or react to form polymers. There are also inorganic adhesives, such as Portland cement and solder, which will not be discussed in this chapter.

27.1 ADHESION AND POLYMERS

Adhesives are joining systems based upon surface attachment, i.e., adhesion. Adhesion is the physical attraction of the surface of one material for the surface of another. These physical attractions are the same physical attractions that one normally associates with descriptions of the states of matter, i.e., van der Waals forces and electrostatic forces. In general, van der Waals forces play a significant role in the adhesion processes of polymeric materials. In addition, adhesives can be synthesized such that they can chemically interact with a surface through the formation of donor–acceptor bonds, hydrogen bonds, and covalent bonds.

The science of polymeric adhesion is concerned with the description of two distinct steps: the formation of the adhesive bond (''adhesive bond making'') and the physical strength of the adhesive bond (''adhesive bond breaking''). The bulk of this chapter is associated with the latter topic, that is, the strength of joints made with adhesives. For this first section, we deal primarily with the former topic.

Polymeric materials are ''van der Waals solids.'' That is, the forces of attraction between chains can be described, for most polymeric materials, by van der Waals attractions. Thus, the cohesive energy density of a polymer and, hence, the surface energy of a polymer, is low relative to most inorganic materials where other intermolecular forces may dominate. The room temperature surface energy of polymers varies from about $12\,mJ/m^2$ to about $70\,mJ/m^2$. By comparison, the surface energy of aluminum oxide is $638\,mJ/m^2$.

In order to obtain maximum adhesion, one needs to have intimate contact between the adhesive and the adherend. The attainment of intimate contact is termed ''complete wetting.'' In the 1950s, Zisman and coworkers codified this concept using contact angle measurements and the definition of a parameter related to the surface energy of a polymer, the ''critical wetting tension [1].'' Table 27.1 provides a list of critical wetting tensions of a number of polymers. The Zisman wetting criterion states that the surface energy of an adhesive must be less than the critical wetting tension of the adherend in order for the adhesive to exhibit complete wetting of an adherend. For the most part, polymeric materials are lower in surface energy than most clean inorganic surfaces and would be expected to wet most of them completely. The situation becomes more complicated when discussing adhesion between polymers. In that case, whether or not the polymer is the adhesive or the adherend becomes very important.

In the case of polymer-polymer adhesion, one can have another basis for providing a strong joint between two materials. This is the phenomenon of interdiffusion. In general, it is difficult for two high polymeric materials to interdiffuse because of poor entropy gain. Entropic effects are overcome in the case when the two polymers interact

TABLE 27.1. *Critical wetting tension of some common polymeric materials [1].*

Polymer	Critical wetting tension (mJ/m^2)
Poly(tetrafluoroethylene)	18
Poly(dimethylsiloxane)	21
Poly(propylene)	28
Poly(ethylene)	31
Poly(vinyl chloride)	38
Cured epoxy resin	43
Poly(ethylene terephthalate)	45

exothermically or in the case when the two polymers have very similar or identical solubility parameters. One can also describe this situation in terms of the χ-parameter.

The work of adhesion is defined by the following equation:

$$W_A = \gamma_1 + \gamma_2 - \gamma_{12} \tag{1}$$

where W_A is the thermodynamic work of adhesion, the γ_1 are the surface energies of materials 1 and 2 γ_{12} and is the interfacial energy between them. Realizing that interfacial energies are usually less than surface energies, one can easily see that the work of adhesion is a relatively small number, usually on the order of a few hundreds of mJ/m^2. In the case of applying a polymer to an inorganic surface or in the case of an incompatible polymeric adherend, one can obtain higher adhesion by means of chemical interactions at surfaces. These chemical interactions include acid-base interactions (which include donor-accepter, Bronsted-Lowrey acid-base, and hydrogen-bonding interactions) and covalent bonding. Providing covalent bonding at an interface can lead to levels of interfacial interaction that are in the tens of J/m^2.

The energy necessary to break a polymer-based adhesive joint is almost always much higher than the energy of interaction at an interface. A natural rubber-based pressure sensitive adhesive (*vide infra*) has only van der Waals interactions available to it for adhering to a surface. Despite that, the energy to break an adhesive joint made with such an adhesive at room temperature and a rate of about 2.54 cm/min is on the order of 100 J/m^2. The discrepancy between interfacial energetics and the energy necessary to break a joint is due to dissipative processes in the materials making up the joint.

The ability to dissipate mechanical energy is the key to the ability of polymers to perform as adhesives. One can imagine the following scenario. A polymer is tethered to a surface by one or more attachments each having an energy of interaction with the surface on the order of a van der Waals energy. That same polymer is also entangled with and associated with segments of itself or other polymers in the adhesive. As long as the energy of interaction of the polymer with the surface is higher than the energy of interaction between polymer segments, the polymer will tend to disentangle and dissipate mechanical energy as heat, rather than separate from the surface. If the energy of interaction between the polymer and the surface is less than the energy necessary to disentangle, the polymer will likely separate from the surface. Also, if the polymer has no mobility (such as in the case of a glassy material) the energy of interaction with the surface must be significant. Examples of efforts to model adhesives by molecular dynamics can be found in the work of Baljon [2] and Robbins [3].

If the energy of interaction with the surface cannot be made to exceed the segment–segment interaction energy then other means can be used to improve the interaction with the surface. In general, this means that the adherend surface has to be made mechanically rough by some type of surface preparation. If the adhesive has the correct viscosity, it will wet into the nooks and crannies of such a surface. When the adhesive hardens, it will be mechanically interlocked with the adherend. Now the energy required to remove the adhesive becomes equal to the plastic deformation energy of either the adherend or the adhesive. In this way, even stiff polymers such as thermoset epoxy adhesives can be used as adhesives, providing an energy to fail a joint in excess of $1{,}000\,J/m^2$.

27.2 PHYSICAL PROPERTY TESTING

Adhesive test methods and their test results are related to but are not the same as other polymer property tests described in this handbook. In general, adhesive property tests are ultimate properties measured at the failure load of an adhesive joint. Adhesive joint properties are certainly related to adhesion (vide supra) but are primarily due to the physical properties of the adhesive and the physical properties of the adherends. In addition, the design of the adhesive joint has a major effect on the measured strength. Indeed, a properly designed adhesive joint will always lead to failure of the adherend. In addition, adhesive joint properties are as temperature- and rate-dependent as the properties of the polymers used to make the adhesive. Unfortunately, in many cases in the literature, the rate of test is not described. In this chapter, the type of adherend or backing will be described, if at all possible.

A primary method used to characterize adhesives is the lap shear test. A diagram of the test is shown in Fig. 27.1 and is described in Standard Test Method ASTM D1002 [4]. The specimen is usually 1 in. (2.54 cm) wide. The lap shear test places the adhesive in normal as well as shear stress [5]. This type of test is used for many types of adhesives, with the exception of pressure-sensitive adhesives (PSAs, defined below). In the tables presented later, lap shear strength is presented in units of mega Pascal (MPa) and pounds per square inch (psi). The latter is shown in parenthesis. The temperature of the test will always be room temperature.

FIGURE 27.1. Diagram of an ASTM D1002 lap shear specimen. The adherends are usually 2.54 cm wide and 10.16 cm long. The thickness of the adherend depends upon the adherend material. If the adherend is aluminum, that thickness is usually 0.16 cm thick.

A T-peel test is shown in Fig. 27.2. The specimen is usually 1 in. (2.54 cm) wide and is described in Standard Test Method ASTM D1876 [6]. This specimen is symmetrical (both adherends are the same thickness). Other peel test specimens are not symmetrical, such as the floating roller peel test [7] or the climbing drum peel test [8]. The test measures the fracture resistance of an adhesive under conditions in which the adherends may plastically deform. In the tables presented later, the peel strength is given in Newtons per centimeter of width (N/cm) and in units of pounds per inch width (piw). The latter is shown in parenthesis. In some cases, the peel strength is derived from climbing drum peel measurements in which the results are presented in torque, in. lb/in. For pressure sensitive adhesives, the testing procedures are somewhat different and this is described below. Rubber-based adhesives are often evaluated using a modification of the PSA-type peel tests in which a piece of canvas is used as the flexible adherend.

The last important test for evaluating adhesive properties is a cleavage or fracture test. Figure 27.3 shows an example of such a test, the double cantilever beam test. The adherends are usually 1 in. (2.54 cm) wide and the thickness depends on the adherend modulus. Described in Standard Practice ASTM D3433 [9], the test is meant to measure fracture resistance (strain energy release rate) under conditions in which the adherends do not plastically deform. The units of fracture resistance (strain energy release rate) are joules per square meter and this quantity is given the symbol $\mathcal{G}_{IC}$.

FIGURE 27.2. Diagram of an ASTM D1876 T-peel specimen.

FIGURE 27.3. Diagram of an ASTM D3433 double cantilever beam specimen. The load is usually applied by attaching a fixture to holes located near the front of the specimen. In general, the initial portion of the specimen is not bonded in order to provide an initial crack.

27.3 TYPES OF ADHESIVES AND THEIR PHYSICAL PROPERTIES

Adhesives can be classified in a number of ways. Thy can be classified according to chemistry (e.g., epoxy versus neoprene), according to application method (e.g., hot melt versus spray applied), or according to strength. It is important to note that, in adhesive technology, high strength is not necessarily related to ''best.'' Rather, having the correct strength along with the most appropriate and economical application conditions is usually equated with ''best.'' The choice of adhesive for a particular end use is based upon criteria of modulus, ultimate strength, fracture resistance, compatibility with the adherend, resistance to adverse environments, and considerations of economy. The adhesives described in the following paragraphs are presented in order of decreasing strength.

27.3.1 Structural Adhesives

Structural adhesives are a class of adhesives, usually thermosets, that can bond high strength materials such as metals and composites and sustain a high load (often defined as being in excess of 1,000 psi) for long periods of time. Another definition includes the criterion that the adhesive must sustain a significant load without measurable creep. Materials ranging from naturally occurring proteins to epoxy resins to acrylic resins have been used as structural adhesives. The properties of a structural adhesive depend not only upon the properties of the base resin but also on the type of cross-linker and the kinds of modifiers that are added to enhance performance. Especially important are the elastomeric modifiers that have been added to increase the fracture resistance of otherwise brittle thermoset resins. Table 27.2 provides a representative listing of room tem-

TABLE 27.2. *Representative physical properties of adhesive bonds made with structural adhesives.*

Adhesive	Adherend	Lap shear strength, MPa (psi)	Peel stength, N/cm (piw)	$\mathcal{G}_{IC}$, J/m^2
Methyl cyanoacrylate	Aluminum	22 (3,190) [10]		
Ethyl cyanoacrylate	Aluminum	17 (2,465) [10]		
300 series surface-activated acrylic	Steel	15 (2,175) [10]		
	Aluminum		12 (7) [10]	
Modern two-part acrylic adhesive	Steel	29.6 (4,300) [11]	51 (29) [11]	
Toughened two-part acrylic	Aluminum	32.6 (4,727) [12]	78 (45) [12]	3,600 [12]
Two-part acrylic adhesive for low surface energy plastics	Polyethylene	5.5 (799) [13][a]		
	Polypropylene	6.9 (993) [13][a]		
FM73 (rubber modified 120 °C curing film adhesive)	Etched aluminum			2,107 [14]
EA946 two-part epoxy	Steel			1,150 [15]
EA913NA two-part epoxy	Steel			375 [15]
FM1000 (nylon epoxy film adhesive)	Aluminum	48.9 (7,090) [16]	175 in. lb/in. [16][b]	
Diglycidyl ether of bisphenol-A cured with dicyandiamide	Aluminum	13.8 (2,000) [17]	19 (11) [17]	
Thermoplastic polyimide	Titanium	41.4 (6,000) [18]		
LARC-13 (polyimide adhesive)	Titanium		2.3 (1.3) [19]	70 [19]
LARC-13 modified with aromatic amine terminated acrylonitrile–butadiene copolymer	Titanium	25.2 (3,650) [19]	9.6 (5.5) [19]	371 [19]
Bis-maleimide-based adhesive	Aluminum	20 (2,900) [20]		
Bis-maleimide-based adhesive mdofied with carboxy terminated acrylonitrile–butadiene copolymer	Steel	24 (3,480) [21]		776 [22]
X-PQ (crosslinkable poly(phenyl quinoxaline)	Titanium	26.6 (3,650) [23]	11.7 in. lb/in [23][b]	
Poly(vinyl formal)-phenolic	Aluminum	27.6–34.5 (4,000–5,000) [16]	14–18 in. lb/in [16][b]	
Nitrile-phenolic	Aluminum	24.1 (3,500) [16]	20 in. lb/in. [16][b]	1,000–1,500 [14]
Phenol/formaldehyde/resorcinol	Wood	6.9 (1,000) [24]		
EC-3549 B/A (two-part polyurethane adhesive)	Aluminum	13.8 (2,000) [25]	43 (25) [25]	

[a]Adherends yielded and elongated, bond did not fail, adherend yield strength is quoted.
[b]Climbing drum peel results are given in values of torque (in. lb/in).

perature lap shear, peel strengths, and strain energy release rates for a number of structural adhesives. Trade names for several structural adhesives are also listed in Table 27.2 and the generic chemistry for that product is also given in parenthesis following the trade name.

Table 27.2 lists a wide range of chemistries including phenolics, epoxies, bis-maleimides, and polyimides. Most of these adhesives are considered to be heat curing although epoxies and phenolics can be made to be room temperature curing. Urethanes and acrylics are often formulated to be two-part, room temperature-curing adhesives. Cyanoacrylates cure at room temperature as a one-part system. Of the chemistries used to formulate structural adhesives, the epoxies offer the widest range of formulation possibilities and resultant performance. For example, epoxy curing conditions can be tuned for almost any temperature between room temperature and 200+ °C. Lap shear strengths from 10 to 48 MPa are available as are peel strengths from about 9 to 175 N/cm. Cross-linked epoxies are brittle. A cross-linking system is chosen such that the cured epoxy resin "matrix" has some level of ductility (low enough yield strength). In addition, an elastomeric modifier is added in order to provide internal stress concentrators to yield the matrix, thus providing a means for internal energy absorption. Cross-linking agents are usually polyamines (such as dicyandiamide) although other reactive ingredients such as phenolics, anhydrides, and imidazoles have been used. An elastomeric modifier that is widely referenced in the literature is the butadiene–acrylonitrile copolymer, in particular, telechelic, epoxy reactive, low molecular weight butadiene–acrylonitrile copolymers. Epoxy adhesives are used in a wide range of applications, too great to list. Of particular interest is their use in the aircraft construction industry as well as in electronic components and assemblies.

Epoxy adhesives are limited to about 171 °C long-term service conditions. Phenolic adhesives, bis-maleimides, and polyimides exceed epoxies in terms of heat resistance. Phenolic resins are either self-curing (resoles) or they require a curing agent (novolacs). A standard heat-curing agent for a novolac phenolic is hexamethylene tetraamine ("hexa"). Cured, unmodified phenolic resins are brittle and would be very poor adhesives. As with epoxy resins, elastomeric modifiers have been used to improve the fracture resistance of phenolics. High molecular weight butadiene–acrylonitrile rubbers and poly(vinyl acetal)s have been used to modify phenolics. These adhesives are used in a number of demanding applications such as friction surface bonders in automobile brake and clutch assemblies.

Table 27.2 lists a variety of very-high-temperature-resistant structural adhesives such as the bis-maleimides, polyimides, and polyphenyl quinoxolines. These adhesives can give reasonable lap shear performance at temperatures as high as 220 °C. These materials are also brittle when cured. Despite many attempts to improve their performance by the addition of various modifiers, their use is limited to their lack of fracture resistance. LARC-13 is given as an example of this situation in Table 27.2. It is thought that the reason for the lack of ability to obtain fracture resistance in these adhesives is the high yield strength (low ductility) of the cured matrix.

Room temperature-curing structural adhesives include epoxies, acrylics, and urethanes. Acrylic systems offer very rapid cure but in much the same manner as described above, they are brittle after cure. Chlorosulfonated polyethylene has been used as a modifier for acrylic adhesives to achieve fracture resistance. Acrylic adhesives can be two-part systems in which the free-radical generating species are kept separate from each other. Typical free-radical initiator systems include cumene hydroperoxide plus saccharin and *N*,*N*′- dimethyl-*p*-toluidine. An example of a new technology in this area is a two-part acrylic adhesive that bonds to polyolefins without surface preparation of the adherend. In light of the section on wetting on adhesion, acrylic adhesives with surface energies in excess of $35\,\mathrm{mJ/m^2}$ should not be able to wet and adhere to polyethylene (critical wetting tension of $31\,\mathrm{mJ/m^2}$). The new technology adhesives adhere so well to unprepared polyolefins that the adherend breaks before the bond does. Tables 27.2 provides an example of that adhesive. Acrylics are also used in so-called anaerobic cures in which adhesive polymerization is inhibited by the presence of oxygen but the polymerization is promoted in its absence. Thread-locking adhesives are an example of this type of acrylic structural adhesive. Cyanoacrylates cure by the action of ambient moisture. Even though these materials appear to cure, the resultant material is a thermoplastic unless cross-linking agents are added. Polyurethanes are typically used as two-part adhesives in which the isocyanate and polyol are kept in separate containers. Cure is effected upon mixing. Polyurethane performance is dependent upon the type of isocyanate, polyol, and catalyst. Organotin compounds are often used to catalyze these reactions. Polyurethane performance is typified by high peel strength but relatively low shear strength.

27.3.2 Hot-Melt Adhesives

Hot-melt adhesives are materials that are applied from the melt state and are capable of producing moderate strength bonds upon cooling. The properties of hot-melt adhesives are heavily dependent upon the primary polymeric formulation material, which is generally based upon a polyolefin or a poly(vinyl acetate-*co*-ethylene) copolymer. Properties are optimized by formulation with materials such as crystalline waxes and tackifiers. Crystalline waxes are used to decrease the melt viscosity and the surface tension of the molten adhesive. Properly formulated, the wax might also increase the strength of the solidified adhesive. Tackifiers are unique low-molecular weight materials that are typically high glass temperature solids. They have the interesting property of conferring increased compliance at low rates of strain application but increasing stiffness at high rates of strain

application. That is, tackifiers decrease the plateau modulus but increase the glass temperature of a formulation. Hot-melt adhesives also include an antioxidant in the formulation, as the adhesive may have to sit for long periods of time at high temperature in an applicator. Melt temperatures are often in excess of 120 °C. Much of hot-melt adhesive performance is dependent upon the melt-flow index (inversely proportional to molecular weight) of the primary polymer as well as the surface energy of the molten adhesive. Thus, high melt-flow index adhesives, while having easy application, will have poor properties due to the low molecular weight (sometimes below or only approaching the entanglement molecular weight of the polymer). Low melt-flow index adhesives will have better performance due to the higher molecular weight but are often difficult to apply. Base polymers with high vinyl acetate content will have higher cohesive strength (and higher surface energy) but will wet poorly on low surface energy adherends. The formulator must balance these properties by having appropriate melt-flow index, and the appropriate content of vinyl acetate, tackifier, and wax.

A distinct set of hot-melt adhesives are designed through synthetic rather than formulation means. Thus, polyesters and polyamides are synthesized with appropriate monomers to provide the desired performance. The polyester chemistry used to make these hot-melt adhesives is the same as that used to make polyester film and fiber but the molecular weight is usually lower and the mixtures of diols and diesters are chosen to control crystallinity and flexibility. One class of monomers used to make polyamide amide hot melts is based on dimer acids that are made from natural products.

Representative physical properties of some hot-melt adhesives are shown in Table 27.3. Note that some of the synthetic hot-melt adhesives are almost structural in strength but, because they are thermoplastic, they would likely creep under load. Hot-melt adhesives are increasing in usage due to the lack of volatile emissions during application. They are used in packaging, bookbinding, furniture manufacture, and other applications.

27.3.3 Elastomer-Based Adhesives

Rubber-Based Adhesives

Rubber-based adhesives are moderate strength materials whose primary formulation ingredient is a rubber. Neoprene (chloroprene) is widely used in these adhesives. Other elastomers used in the formulation of rubber-based cements are natural rubber, styrene–butadiene rubber, and nitrile rubber. Rubber-based adhesive formulations may include phenolic resins, tackifiers, and, sometimes, cross-linking agents. When neoprene is used, the formulation must also contain an acid acceptor such as ZnO or MgO in order to guard against dehydrohalogenation. Formulations are optimized to obtain a balance between shear and peel properties. These adhesives are most often tacky when applied but are not tacky after solvents and carriers evaporate. This makes these materials distinct from pressure-sensitive adhesives (vide infra), which must remain aggressively and permanently tacky. A particular form of rubber-based adhesive, known as a ''contact cement,'' must remain tacky during the bonding operation. This control of tack is known as the ''open time'' between application of the adhesive and closing of the bond. The choice of elastomer, tackifier and, in particular, the solvent, controls the ''open time.'' Rubber-based adhesives have been sold in a solvent vehicle for decades. Recent regulations controlling levels of solvent emissions have forced the industry to provide water-thinned rubber-based adhesives or, alternatively, have forced users to switch to hot-melt adhesives.

Rubber based adhesives are used in a myriad of applications which are familiar to the consumer. Tile and paneling adhesives are examples of these adhesives used in home construction. The largest use of rubber-based adhesives is in laminated furniture manufacture. Representative physical properties of rubber-based adhesives are shown in Table 27.4. The adhesives are characterized as having low to moderate shear strength and high peel strength.

TABLE 27.3. *Representative physical properties of adhesive bonds made with hot-melt adhesives.*

Adhesive	Adherend	Lap shear strength, MPa (psi)	Peel strength, N/cm (piw)
Co-polyetheramide from polyetherdiamine and dimer acid	Aluminum	11 (1,600) [26]	16 (9) [26]
Low-melt-flow index dimer acid-based polyamide (Versamide)	Aluminum	1.4–6.8 (200–1,000) [27]	
Low-melt-flow index dimer acid-based polyamide (Milvex)	Aluminum	25.2 (3,660) [27]	61 (35) [27]
Ethylene–vinyl acetate copolymer modified with tackifier and microwax	Wood	2.8 (400) [28]	
	ABS	1.7 (245) [28]	
Co-polyester	Aluminum	24.5 (3,550) [29]	
Crystallizable co-polyester-amide	Reinforced plastic	16.7 (2,421) [30]	1.5 (0.9) [30]
Co-polyester modified with 2,2′-bis [4′-(β-hydroxyethoxy)phenyl]propane	Unspecified metal	16.9 (2,450) [31]	2–3 (1–2) [31]
Poly(vinyl acetate) (unmodified)	Aluminum	3.9 (570) [32]	1.9 (1.1) [32]

TABLE 27.4. *Representative properties of adhesive bonds made with rubber-based adhesives.*

Adhesive	Adherends	Lap shear strength, MPa (psi)	Peel strength, N/cm (piw)
Acrylic/styrene latex formulated with plasticizers, to provide a solvent-free mastic adhesive	Mahogony to mahogany	1.2 (172) [33]	
Polyurethane elastomer construction adhesive (EC-5230)	Douglas fir to Douglas fir	1.6 (236) [34][a]	
Acrylic latex/phenolic dispersion (2/1)	Canvas to cold rolled steel		35 (20) [35]
Neoprene latex/phenolic dispersion (2/1)	Canvas to cold rolled steel		3.5 (2) [35]
Neoprene latex/butylated phenolic resin/MgO	Canvas to painted steel	0.34 (50) [36]	52.5 (30) [36][b]
Solvent-based neoprene, Fastbond™ 5	Canvas to steel		33 (19) [25]
	Birch to Birch	3.3 (482) [25]	
Solvent-based neoprene contact bond adhesive, EC-1357	Canvas to steel		40.3 (23) [25]
	Birch to birch	3.7 (536) [25]	
Solvent-based nitrile EC-1099	Aluminum to aluminum	9 (1306) [25]	
	Canvas to steel		53 (30) [25]

[a]Block shear according to ASTM D143.
[b]Canvas to canvas peel at 140 °F after 2 weeks of aging.

Pressure-Sensitive Adhesives

Pressure-sensitive adhesives (PSAs) are a class of elastomer-based materials that have the following characteristics: they are aggressively and permanently tacky, they adhere without the need of more than finger pressure, they require no heat or activation, they adhere ''well,'' and they can be removed without leaving a visible residue. PSAs are considered low strength materials. The shear strength values are on the order of a few to ten pounds per square inch and the peel strengths are on the order of a few ounces to ten pounds per inch width. PSAs are usually sold on a backing as a tape and are very familiar to the consumer as Scotch™ Brand tape. The properties of the tape are dependent not only on

Table 27.5. *Representative physical properties of pressure-sensitive adhesives and bonds made with them.*

Adhesive chemistry	Backing	Adherend	Peel strength, N/cm (piw)	Shear holding power (min)	Tack (g/cm^2)
Emulsion polymerized copolymer of butyl acrylate, styrene, acrylic acid, and acrylamide	Polyester	Stainless steel	42 (24) [39][a]	190 [39][b]	370 [39][c]
Kraton 107 block copolymer tackified with Wingtack 95	Polyester	Aluminum	24 (13) [40]		1,500 [40][c]
Acrylic latex tackified with Staybelite ester 10 (50/50 blend)	?	?	5.4 (3.1) [41]	>6,000 [41]	830 [41]
Carboxylated styrene–butadiene rubber	Polyester	Stainless steel	0.4 (0.24) [42][a]	60 [42][b]	248 [42][c]
Carboxylated styrene (46%)–butadiene rubber tackified with Foral 85 (50/50 blend)	Polyester	Stainless steel	5.9 (3.4) [42][a]	10,000 [42][b]	492 [42][c]
Waterborne acrylic PSA for box sealing tape	Poly(propylene)	Stainless steel	2.8–3.3 (1.6–1.9) [43][a]	6,000 [43][b]	
Acrylic hot-melt	Polyester	Stainless steel	2.6 (1.5) [43][a]	190 [43][b]	
Natural rubber tackified with Piccolyte 85 (50/50 blend), aqueous	Polyester	Stainless steel	4.4 (2.5) [44][a]	>6,000 [44][b]	1,200 [44][c]
Poly(*iso*-butylene)-based PSA (6×10^5 Daltons)	?	Stainless steel	2.6–4.4 (1.5–2.5) [45]	1,100 [45][d]	100–300 [45][c]
Acrylic foam tape "VHB 4929"	Aluminum foil	Stainless steel	35 (20) [46][e]	10,000 [46][f]	

[a]180° peel, Pressure Sensitive Tape Council Method 1.
[b]1 kg weight for a 0.5 $in.^2$ lap, Pressure Sensitive Tape Council Method 7.
[c]Polyken Probe Tack Test, ASTM D2979.
[d]500 g weight for a 0.5 $in.^2$ lap otherwise similar to Pressure Sensitive Tape Council Test Method 7.
[e]90° Peel.
[f]1.5 kg weight for a 0.5 $in.^2$ lap, Pressure Sensitive Tape Council Method 7.

the adhesive but the backing as well. PSAs are usually formulated by using an elastomeric material such as natural rubber in combination with a tackifier resin such as a rosin ester. The balance of peel and shear properties is obtained by the rubber to resin ratio. Other elastomer chemistries important to PSA technology are acrylics, nitriles, styrene–isoprene block copolymers, silicones, vinyl ethers, and butyl rubber. Of these, all have to be externally tackified with the exception of the acrylics. Tackifiers include the rosin esters (mentioned above), terpene resins, the so-called C-5 and C-9 resins, which are low molecular weight polymers formed from petroleum streams. Silicone PSAs are made tacky by the addition of unique silicate resins known as ''MQ.'' MQ resin is material of unspecified structure made by the reaction of monofunctional trimethyl silane (''M'') with quadrafunctional silicon tetrachloride (''Q'').

Instead of the normal lap shear strengths that we have described for other adhesives, PSAs are evaluated for their ''shear holding power [37].'' In this test, a piece of tape is applied to a clean surface and a known weight is attached to the end of the tape. The time to failure is determined. As shown in Table 27.5, this value is given in minutes. Shear holding power is determined not only by the choice of elastomer, tackifier, and their ratio but also by the level of cross-linking. When styrene–isoprene block copolymers are used as the PSA elastomer, the system does not need to be cross-linked. The unique structure of these elastomers induces phase separation of the styrene blocks. The phase-separated segments act as virtual cross-links. There are also special tapes having an acrylic foam core which provide properties having exceptional peel and shear holding power that approach that of rubber-based adhesives.

For peel testing of PSAs, the usual configuration differs from that shown in Fig. 27.2. That is, one adherend is usually rigid while the other is the backing for the tape. The peel test can be conducted in such a fashion that the tape is peeled at 90° or 180° with respect to the rigid adherend.

Another important property of PSAs is their tack or response to light pressure. Bringing a probe of known composition in contact with the adhesive with a specified force for a specified time and then measuring the amount of force necessary to remove the probe from the adhesive at a specified rate measures tack [38]. Peel strength and tack are dependent upon the rubber to resin ratio and are inversely dependent upon the cross-link density. Representative physical propertied of PSA tapes are provided in Table 27.5.

REFERENCES

1. W. A. Zisman, Ind. Eng. Chem., **55**(10), 19 (1963).
2. A. R. C. Baljon, J. Vorselaars and T. R. Depuy, Macromolecules, **37**, 5800 (2004).
3. A. R. C. Baljon, and M. O. Robbins, Science, **271**, 482 (1996).
4. ASTM D1002, American Society for Testing and Materials, Philadelphia, PA.
5. M. Goland and E. Reissner, J. Appl. Mech. Trans. Am. Soc. Eng., **66**, A17 (1944).
6. ASTM D1876, American Society for Testing and Materials, Philadelphia, PA.
7. ASTM D3176, American Society for Testing and Materials, Philadelphia, PA.
8. ASTM D1781, American Society for Testing and Materials, Philadelphia, PA.
9. ASTM D3433, American Society for Testing and Materials, Philadelphia, PA.
10. F. R. Martin, in *Developments in Adhesives-1*, edited by W. C. Wake (Applied Science, London, 1977), Ch. 6.
11. P. C. Briggs, U. S. Patent 4,536,546, assigned to Illinois Tool Works, Aug 20, 1985.
12. C. Burrows, N. Sammes, G. Stables, M. H. Stone and C. Tempest, in *Adhesion-8*, edited by K. W. Allen (Applied Science, Essex, England,1984), Ch. 7.
13. A. V. Pocius and E. J. Deviney, U.S. Patent 5,935,711, Assigned to 3M Company, Issued Aug. 10, 1999.
14. R. Y. Ting and R. L. Cottington, Adhes. Age, **24**(6), 35 (1981).
15. G. L. Anderson, J. Adhes., **41**, 129 (1993).
16. L. T. Eby and H. P. Brown, in *Treatise on Adhesion and Adhesives*, edited by R. L. Patrick, (Marcel Dekker, New York, 1969), vol. 2, pp. 77–171.
17. Y. Lee, S. Wang and W. Chin, J. Appl. Polym. Sci., **32**, 6317 (1986).
18. A. K. St. Clair and T. L. St. Clair, NASA Technical Memorandum No. 84516, June 1982.
19. A. K. St. Clair and T. L. St. Clair, U. S. Patent 4,497,935, assigned to the United Staes Government, issued February 5, 1985.
20. S. J. Shaw, Mater. Sci. Technol., **3**, 589 (1987).
21. S. J. Shaw and A. J. Kinloch, in *Proceedings of the International Adhesion Conference, 1984* (The Plastics and Rubber Institute, London, 1984), pp. 3.1–3.4.
22. H. Stenzenberger, in *Structural Adhesives: Developments in Resins and Primers*, edited by A. J. Kinloch (Elsevier Applied Science, London and New York, 1986), Ch. 4.
23. C. L. Hendicks, S. G. Hill and J. N. Hale, NASA Contractor Report No. 177936, October, 1985, p. 33.
24. R. T. Hood and R. L. Bender, U. A. Patent 4,608,408, assigned to Koppers Company, issued Aug. 26, 1986.
25. 3M Product Literature, Industrial Adhesives and Tapes, St. Paul MN and www.3M.com
26. A. T. Hu, R. Tsai and Y. Lee, J. Appl. Polym. Sci., **37**, 1863 (1989).
27. R. D. Dexheimer and L. R. Vertnik, Adhes. Age, **15**(8), 39 (1972).
28. P. R. Lakshmanian and B. J. Monachino, Adhes. Age, **24**(9), 27 (1981).
29. F. Eichhorn, Schweissen Schneiden, **35**, 116 (1983).
30. D. D. Donermeyer, J. G. Martins,J. C. Martins, U. S. Patent 4,581,410, assigned to Monsanto Company, issued April 8, 1986.
31. L. Buxbaum and R. Hugl, British Patent 2,000,790, assigned to Ciba-Geigy AG, issued January 17, 1979.
32. Y. Hatano, B. Tomita and H. Mizumachi, Holzforschung, **40**, 255 (1986).
33. J. Bax, Adhes. Age, **24**(10) 22 (1981).
34. R. J. Hoyle, Adhes. Age, **24**(7), 43 (1981).
35. R. G. Azrak, B. L. Joesten and W. F. Hale, in *Adhesion Science and Technology*, edited by L-H. Lee (Plenum, New York, 1975), pp. 233–248.
36. J. Keramedjian, Adhes. Age, **5**(6), 34 (1962).
37. PSTC-7, Pressure Sensitive Tape Council, Chicago, IL.
38. ASTM D2979, American Society for Testing and Materials, Philadelphia, PA.
39. M. J. Skoglund, PCT WO 91/18739, applied for by Ashland Chemical Co., published December 12, 1991.
40. N. Nakajima, R. Babrowicz and E. R. Harrell, J. Appl. Polym. Sci., **44**, 1437 (1992).
41. K. F. Foley and S. G. Chu, Adhes. Age, **29**(10), 24 (1986).
42. A. Midgley, Adhes. Age, **29**(10), 14 (1986).
43. W. J. Sparks, Adhes. Age, **25**(3), 38 (1982).
44. S. G. Chu, in *Adhesive Bonding*, edited by L-H. Lee (Plenum press, New York, 1991), pp. 97–138.
45. M. A. Krenceski and J. F. Johnson, Polym. Eng. Sci., **29**, 36 (1989).
46. 3M Data Sheet ''VHB Double Coated Acrylic Foam'', April 2001.

CHAPTER 28

Some Mechanical Properties of Typical Polymer-Based Composites

Jianye Wen

ALZA Corporation, 1900 Charleston Rd., Mountain View, CA 94039

28.1 INTRODUCTION

Composite materials have a variety of definitions and there is no universally accepted one. The definition in the literature differ widely [1–6]. In the broadest definition, any material composed of two or more distinct components is a composite, but this definition is too broad to be useful. To be more inclusive, the level of definition, the forms and composition of constituents have to be considered together. For many of the materials now commonly considered composites, a working definition can be given as follows:

A composite is a multiphase material brought about by combining materials which differ in composition or form on a macroscale in order to obtain specific characteristics and properties. The constituents retain their identities and properties such that they exhibit an interface between one another and act in concert to achieve improved synergistic properties not obtainable by any of the components acting alone.

Even this definition needs to be classified [7, 8]. To some researchers it is still too broad because it includes many materials that are not usually thought of as composites such as concrete, copolymers and blends, reinforced plastics, and carbon-black-filled rubber. On the other hand, some of the more recent composites are excluded from the category of composites if this definition is strictly applied. For example, many particulate-type composites such as dispersion-hardened alloys and cermets have composite structures that are microscopic rather than macroscopic [2,8]. In some cases, the composite structures are nanoscopic, with the physical constraint of several nanometers as the minimum size of the components [9–16]. The terms 'microcomposite', ''nanocomposite'', or 'molecular composite'' are suggested instead. They differ from traditional composites in the smaller sizes of the component phases and exhibit unique behaviors due to the smaller size effect, the large interface effect, and the quantum confining effect.

Composite structures open up a whole new dimension of design freedom which is not available with traditional homogeneous materials. Composite can be designed to provide us with an almost unlimited selection of properties to meet the demands of different environments as well as any other specific needs. The behavior and properties of composites are determined by three factors: the intrinsic properties of constituents, the form and structural arrangement of the constituents, and the interaction between the constituents. The properties of constituents determine the general order or range of the properties of composite. The form (shape and size), the structural arrangement, and the composition and distribution of constituents give composites their versatility and contribute to the overall performance. The interaction between the constituents also plays a critical role in improving the mechanical properties of composites.

The constituents of a composite are generally arranged in such a way so that one or more discontinuous phases are embedded in a continuous phase. The continuous phase is the matrix. The discontinuous phase are called reinforcement and generally much stronger and stiffer than the matrix although exception dose exist (such as the use of rubber particles). The matrix of composite could be polymer, ceramics, or metal. The main thrust of this chapter will be directed at polymeric matrix composites. These materials usually have exceptional mechanical properties and often termed high performance composites. They can be classified

on the basis of the form of their structural components: (1) fibrous (composed of fibers in a matrix), (2) laminar (layers of materials), (3) particulates (composed of particles, skeletal, or flakes in a matrix), (4) hybrid (combination of any of the above). In general, the reinforcing agents can be either fibers, particles, laminae, whiskers, or flakes and either an organic, metallic, inorganic, or ceramic material. They are structural constituents. They determine the internal structure of composite and provide the high strength and modulus. Composite strength is directly proportional to the basic reinforcing agent and can be improved at the expense of stiffness. The polymeric matrices can be either thermoplastics (capable of being repeatedly hardened and softened by increasing and decreasing temperature) or thermoset (changing into an infusible and insoluble material after cured by applying heat or by chemical means). Although the properties of the matrix are not directly related to the composite strength, the matrix does play an important role. They are the body constituents and serve to enclose the composite and give them their bulk forms, spread the load as well as offering resistance to weathering and corrosion. Typical thermoplastic resins include ABS, polyethylene, polypropylene, polycarbonate, nylon, polysulfone, and polyetheretherketone (PEEK). The most used thermosetting resins include epoxy, polyester, phenolic, vinyl ester, polyimide, and silicone. At present, the use of fibrous reinforcing agent combined with thermosetting resins predominates [2]. In this chapter, the mechanical and some physical properties of most used reinforcing agents, thermoplastic and thermosetting resins used as composite matrix, and high performance polymeric matrix composites were summarized in Tables 28.1–28.4.

28.2 TERMINOLOGY

(1) Elastic modulus (ASTM-D638, D759, D-1708)

It is the ratio of nominal tensile stress to corresponding strain below the proportional limit of a material.

Units: psi; kgf cm^{-2}; Nm^{-2}

(2) Tensile strength (ASTM-D638, D759, D-1708)

At break: maximum tensile stress sustained by the specimen at break.

At yield: maximum tensile stress sustained by the specimen at the yield point.

Units: psi; kgf cm^{-2}; Nm^{-2}

(3) Elongation (ASTM-638)

The elongation of a specimen at break expressed as a percentage of the original length.

Units: %

(4) Impact strength (ASTM D-256, ASTM D-758, ISO R 180, BS 2782)

In pendulum-impact methods: energy expended by a standard pendulum-impact tester to break a test specimen

TABLE 28.1. *Physical properties of reinforcing agents—fiber, particulate.*

Material	Elastic modulus GPa	Tensile strength MPa	Density g cm^{-3}	Specific stiffness MJ kg^{-1}	specific strength MJ kg^{-1}	Reference
Synthetic inorganic						
E-glass fiber	72.4	3450	2.54	28.5	1.36	[2,17,18]
S-glass fiber	85.5	4820	2.49	34.3	1.94	[2,17,18]
M-glass fiber	110	3500	—	—	—	[19,20]
Boron fiber	441	3450	2.30	192	1.50	[17,18]
Carbon	200	2760	1.76	114	1.57	[17]
Graphite fiber						
high-strength	253	4500	1.8	140	2.5	[2,18]
high-modulus	520	2400	1.85	281	1.3	[2,18]
intermediate	186	2482	1.74	107	1.43	[18]
Alumimum oxide	323	689	3.97	81.4	0.174	[17]
Aluminum silicate	100	4130	3.90	25.6	1.06	[17]
Beryllium oxide	352	517	3.03	116	0.171	[17]
Quartz (fuses silica)	70	—	2.2	31.8		[17]
Tungsten	414	4200	—	—	—	[19,20]
Natural inorganic						
Asbestos	172	1380	2.50	68.8	0.552	[17]
Synthetic organic						
Aramid fiber*						
Kevlar 29	59	3500	1.44	41.0	2.43	[2,18]
Kevlar 49	124	3600	1.44	86.11	2.50	[2,18]

*Chemical structure: 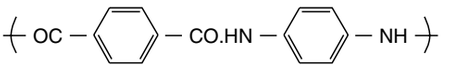

TABLE 28.2. *Physical properties of most used unreinforced thermosets and thermoplastics.*

Material	Property	Elastic modulus	Tensile strength	Elongation	Impact strength Izod, notched	Specific gravity (Density)	Specific stiffness	Specific strength	Reference
	Units	GPa	MPa	%	J m^{-1}	g cm^{-3}	MJ kg^{-1}	MJ kg^{-1}	
	Methods of determination	D638	D638	D638	D256	D792			
Polyester		4.1	689	1.40	2.93	0.492			[17]
Polyamide		2.8	827	1.14	2.46	0.725			[17]
Polyacrylonitrile		200–390	2,100–3,400	—	—	—			[19,20]
Thermoplastics									
Acetal		2.83	60.28	40.0	50	1.41	2.01	0.043	[7,21]
ABS		2.07	41.10	5.0	270	1.03	2.01	0.040	[7,21]
Nylon 6		2.62	80.83	30.0	30	1.12	2.34	0.072	[7,21,22]
Nylon 66		2.76	78.78	60.0	40	1.13	2.44	0.069	[7,21,23]
Polycarbonate		2.34	65.08	110.0	850	1.20	1.95	0.054	[7,21]
Polyester (PBT)		1.93	56.17	50.0	40	1.31	1.47	0.042	[7,21]
Polyester (PET)		2.76	58.23	50.0	10–30	1.34	2.06	0.044	[7,21]
Polyetheretherketone (PEEK)		3.6	92	50	—	1.32	2.73	0.070	[24, 25]
Polyetherketoneketone (PEEK)		4.5	102	4	—	—	—	—	[26,27]
Polyethylene									
LDPE		—	20	350	—	0.925	—	0.022	[28]
HDPE		—	27	100	133	0.95	—	0.028	[28]
Polyphenylene oxide (PPO)		2.62	53.43	50.0	270	1.080	2.43	0.050	[7,21]
Polyphenylene sulfide		0.31	65.08	1.0	<30	1.30	2.55	0.050	[7,21]
Polypropylene		0.69	34.25	200.0	100–1,010	0.89	0.775	0.039	[7,21]
Polystyrene acrylonitrile (SAN)		2.76	65.08	0.5	20	1.05	2.63	0.065	[7,21]
Polyurethanes		–	42.76	480	—	1.23	—	0.035	[29]
Polyvinyl Chloride		—	34.48–62.07	1–25	—	1.33–1.45	—	0.03–0.062	[30]
Thermosets									
Unsaturated polyester resins									
rigid		2–4.4	40–90	<5.0	16–32	1.10–1.46	1.83–3.01	0.036–0.062	[31]
flexible		—	3.4–21	40–310	370	1.01–1.20	—	0.003–0.018	[31]
Vinyl ester resins*									
MW = 500		3.3	80.7	4.5	—	—	—	—	[32]
MW = 900		3.2	79.9	5.0	—	—	—	—	[32]
MW = 1200		3.0	78.6	5.5	—	—	—	—	[32]
Vinyl ester resins**									
phenolic novolac		0.4	75.8	3.5	—	—	—	—	[32]
tetrabromo bisphenol A		—	73.1	4.0	—	—	—	—	[32]
bisphenol A		3.4	84.1	5.0	—	—	—	—	[32]
Polybutadiene resins		—	235	600	—	0.86–0.90	—	—	[33,34]
Epoxy resins		2.8–4.2	55–130	—	5.3–53	1.2–1.3	2.33–3.23	0.046–0.10	[2,35]
Polyimides		3.2	55.8	—	—	1.43	2.24	0.039	[2]

*Bisphenol A epoxy-based vinyl ester resins containing 50 wt% styrene.
**Vinyl ester resins containing 40 wt% styrene.

TABLE 28.3. *Physical properties of most used reinforced thermosets and thermoplastics.*

Material	Property	Elastic modulus	Tensile strength	Elongation	Flexural Strength	Flexural Modulus	Impact strength Izod notched	Specific gravity (Density)	Specific stiffness	Specific strength	Reference
	Unit	GPa	MPa	%	MPa	GPa	J m^{-1}	g cm^{-3}	MJ kg^{-1}	MJ kg^{-1}	
	Methods of determination	D638	D638	D638	D790	D790	D256	D792			
Reinforced Thermoplastics											
ABS											
glass fiber											
10 wt%		4.6	65	3.0	102	4.5	64	1.10	4.18	0.0591	[7]
20 wt%		5.1	76	2.0	107	4.9	59	1.22	4.18	0.0623	[7]
30 wt%		6.3	90	1.4	116	6.4	53	1.28	4.92	0.0703	[7]
asbestos fiber											
30 wt%		—	96	—	—	7.8	—	—	—	—	[36]
carbon fiber											
16.6 wt%		—	42	—	—	5.8	—	—	—	—	[36]
Acetal											
glassfiber											
10 wt%		6.6	72	2.4	107	6.1	53	1.54	4.29	0.0468	[7]
30 wt%		7.7	83	2.0	114	7.2	43	1.63	4.72	0.0509	[7]
Ethylene tetrafluoroethylene (ETFE)											
graphite fiber											
30 wt%		—	103	2–3	138	1.65	213–267	1.73	—	0.0509	[37]
Nylon 6											
glass fiber											
15 wt%		5.9	104	4.0	159	5.4	80	1.25	4.72	0.0832	[7]
30 wt%		7.2	166	3.0	200	6.9	117	1.37	5.26	0.121	[7]
30 wt%		—	159	3–4	234	8.3	123	1.37	—	0.116	[22]
Nylon 6/6											
glass fiber											
13 wt%		6.2	97	4.0	173	4.5	53	1.23	5.041	0.0789	[7]
30 wt%		9.0	173	3.0	235	9.0	107	1.37	6.569	0.126	[7]
aluminum flake											
30 wt%		—	69	2–3	121	7.6	54	1.38	—	0.050	[38]
35 wt%		—	69	2–3	121	7.6	54	1.43	—	0.048	[38]
Nylon 6/12											
glass fiber											
30 wt%		8.3	135	4.0	193	7.6	117	1.30	6.39	0.104	[7]
kevlar											
20 vol%		8.55	151.7	2.8	—	—	—	—	—	—	[39]

TABLE 28.3. *Continued*

Material	Property	Elastic modulus	Tensile strength	Elongation	Flexural Strength	Flexural Modulus	Impact strength Izod notched	Specific gravity (Density)	Specific stiffness	Specific strength	Reference
	Unit	GPa	MPa	%	MPa	GPa	J m^{-1}	g cm^{-3}	MJ kg^{-1}	MJ kg^{-1}	
	Methods of determination	D638	D638	D638	D790	D790	D256	D792			
Polycarbonate											
glass fiber											
10 wt%		5.2	83	9.0	110	4.1	107	1.26	4.13	0.0659	[7]
30 wt%		8.6	121	2.0	141	6.9	128	1.43	6.01	0.0846	[7]
kevlar 49											
20 vol%		9.8	163.4	2.1	—	—	—	—	—	—	[40]
graphite		12.6	176.5	1.7	—	—	—	—	—	—	[41]
aluminum flake											
30 wt%		—	46	2–3	93	4.8	80	1.44	—	0.0032	[38]
40 wt%		—	44	2	86	6.6	70	1.54	—	0.0029	[38]
Polyethertherketone (PEEK)											
63 Vf% AS4*		140	2,040	1.4	2,280	135	—	—	—	—	[26]
Polyetherketoneketone (PEKK)											
58 Vf% AS4*		129.6	1,675	—	1,620	—	—	—	—	—	[42]
Polyetherketonesetherketoneketone (PEKEKK)											
60 Vf% AS4*		130	1,724	—	1,759	112	—	—	—	—	[26]
Thermoplastic polyester											
PBT											
glass fiber											
30 wt%		8.3	131	3.0	193	7.9	80	1.52	5.46	0.0862	[7]
PET											
glass fiber											
30 wt%		9.0	144	2.0	221	8.6	60	1.56	5.77	0.0923	[7]
Polyethylene											
glass fiber											
10 wt%		2.5	36	4.0	46	2.5	75	1.04	2.40	0.0346	[7]
30 wt%		5.0	59	3.0	89	4.9	91	1.18	4.24	0.0496	[7]
kevlar 49		10.6	131.7	2.3	—	—	—	—	—	—	[39]
graphite		19.3	110.3	0.7	—	—	—	—	—	—	[39]
Poly(methyl methacrylate)											
kevlar 49											
20 Vol%		11.1	207.5	2.0	—	—	—	—	—	—	[39]

TABLE 28.3. *Continued*

Material	Property	Elastic modulus	Tensile strength	Elongation	Flexural Strength	Flexural Modulus	Impact strength Izod notched	Specific gravity (Density)	Specific stiffness	Specific strength	Reference
	Unit	GPa	MPa	%	MPa	GPa	J m^{-1}	g cm^{-3}	MJ kg^{-1}	MJ kg^{-1}	
	Methods of determination	D638	D638	D638	D790	D790	D256	D792			
Poly(phenylene oxide), modified											
glass fiber											
20 wt%		6.4	100	5.0	128	5.2	96	1.21	5.29	0.0826	[7]
Poly(phenylene sulfide)											
glass fiber											
40 wt%		14.1	152	3.0	255	13.0	80	1.64	8.60	0.0927	[7]
Polypropylene											
glass fiber											
10 wt%		2.5	43	4.0	54	2.4	43	0.98	2.55	0.0439	[7]
20 wt%		3.7	45	3.0	57	3.6	59	1.04	3.56	0.0433	[7]
30 wt%		4.4	47	2.0	63	4.3	69	1.12	3.93	0.0420	[7]
talc**											
20 wt%		—	40***	4.1****	—	2.7	22	—	—	—	[41]
40 wt%		—	37***	3.1****	—	4.1	15	—	—	—	[41]
50 wt%		—	34***	2.4****	—	4.8	37	—	—	—	[41]
Polysulfone											
glass fiber											
20 wt%		6.0	97	2.5	138	5.9	64	1.38	4.35	0.0703	[7]
40 wt%		11.6	124	1.5	173	10.7	80	1.55	7.484	0.080	[7]
Thermoplastic Polyurethane											
glass fiber											
10 wt%		0.7	33	48.0	43	0.6	747	1.22	0.574	0.027	[7]
PVC											
glass fiber											
20 wt%		0.8	97	3.0	145	6.9	80	1.58	0.506	0.0614	[7]
SAN											
glass fiber											
20 wt%		8.6	100	1.8	131	7.6	64	1.22	7.05	0.082	[7]
35 wt%		10.4	110	1.4	155	9.3	53	1.35	7.70	0.0815	[7]
Reinforced Thermosets											
Epoxy											
E-glass fiber		45	1,100	—	—	—	—	(2.1)	21.4	0.52	[2]
S-glass fiber		55	2,000	—	—	—	—	(2.0)	27.5	1.0	[2]

TABLE 28.3. *Continued*

Material	Property	Elastic modulus	Tensile strength	Elongation	Flexural Strength	Flexural Modulus	Impact strength Izod notched	Specific gravity (Density)	Specific stiffness	Specific strength	Reference
	Unit	GPa	MPa	%	MPa	GPa	J m^{-1}	g cm^{-3}	MJ kg^{-1}	MJ kg^{-1}	
	Methods of determination	D638	D638	D638	D790	D790	D256	D792			
glassfiber*****											
80 wt%		28	548	1.6	690	1.33	34.5	(1.91)	14.4	0.289	[7,21]
boron fiber		207	1,600	—	—	—	—	(2.1)	99	0.76	[2]
graphite fiber											
–high strength		145	2,300	—	—	—	—	(1.6)	90.6	1.42	[2]
–high modulus		290	1,000	—	—	—	—	(1.63)	178	0.61	[2]
aramid fiber											
(Kevlar)		80	2,000	—	—	—	—	(1.38)	58	1.45	[2]
Kevlar 49											
50 vol%		31	517	1.7	345	27.6	—	1.33	23.3	0.39	[39]
Unsaturated polyester											
woven cloth		10.3–31.0	206–344	0.5–2.0	276–550	172–344	267–1,600	1.5–2.1	6.9–14.8	0.14–0.16	[31]
chopped roving		5.5–13.8	103–206	0.5–5.0	69–276	103–206	107–1,070	1.35–2.3	4.1–6	0.08–0.08	[31]
Corezyn polyester											
Kevlar 49											
40 vol%		24	414	—	207	20	—	1.30	18.5	0.32	[39]
Polyester SMC											
glass fiber											
20 wt%		11.72	36.31	0.4	110.32	9.65	430	(1.772)	6.61	0.021	[7,21]
30 wt%		11.72	82.20	<1.0	179.27	11.03	850	(1.827)	6.41	0.045	[7,21]
50 wt%		15.65	157.55	1.7	310.28	13.79	1030	(2.000)	7.83	0.080	[7,21]
Polyurethane											
glass fiber											
13 wt%		—	19.18	140.0	—	0.26–0.27	—	(1.052)	—	0.018	[7,21]
23 wt%		—	30.21	38.9	—	1.03	110	(1.163)	—	0.026	[7,21]

*Continuous carbon fibres from Hercules
**Talc is a fine-ground product consisting of thin platelets, preferably white in color.
***Tensile strength at yield.
****Tensile elongation at yield.
*****Filament wound.

TABLE 28.4. *Mechanical properties of glass fiber unidirectional lamina.*

Composite	Property / Unit	Elastic moduli E_L GPa	E_T GPa	G_{LT} GPa	Strengths F_L GPa	F_T GPa	F'_L GPa	F'_T GPa	F_LT GPa	Reference
Epoxy										
E-glass fiber		45	12	5.5	1,100	40	620	140	70	[2]
S-glass fiber		55	16	7.6	1,600–2,000	40	690	140	80	[2]
graphite fiber										
–high strength		145	10	4.8	1,240–2,300	41	1,200	170	80	[2]
–high modulus		220–290	6.2–6.9	4.8	900–1,200	21	620	170	60–70	[2]
Kevlar 49		80	5.5	2.1	2,000	20	280	140	40	[2]

(plain or notched) under stipulated conditions of specimen mounting, notching, and pendulum velocity at impact. There are two pendulum methods in common use: Izod method and Charpy method.

In falling-weight methods: the minimum value of the product of fall height and mass to cause fracture of a test specimen.

Units: J/m, ft lb, cm kgf

(5) Specific gravity (ASTM D-792)

The ratio of the mass in air of a unit volume of the material at 23 °C to the mass (determined in identical conditions) of an equal volume of gas-free distilled water.

Units: gcm^{-3}, $lbft^{-3}$

(6) Flexural strength (ASTM D-790, ISO R 178, BS 2782, DIN 53 452)

At break: maximum stress in the outer fiber of the specimen at the moment of break in bending.

At yield: stress at yield (calculated from formulae appropriate to the test method).

Units: psi; $kgfcm^{-2}$; $N\ m^{-2}$

(7) Flexural modulus (ASTM D-790, ISO R 178, BS 2782, DIN 53 452)

The ratio of stress to corresponding strain in bending within the elastic limit, calculated by the appropriate theory.

Units: psi; $kgf\ cm^{-2}$; $N\ m^{-2}$

(8) Specific stiffness

The ratio of elastic modulus to density or specific gravity.

Units: $MJ\ kg^{-1}$

(9) Specific strength

The ratio of tensile strength to density or specific gravity.

Units: $MJ\ kg^{-1}$

(10) Lamina

The simplest representative form of high performance composites which consists of fibers oriented in a single direction and bonded together by a resin.

(11) Thermoplastics

A material that can be melted by heating and then resolidified by cooling.

(12) Thermoset

A material which hardens or sets by heat, chemical, or radiation cross-linking techniques and which, once set, cannot be resoftened by heating.

4. REFERENCES

1. G. Lubin, Handbook of Fiberglas and Advanced Composites, Van Nostrand Reinhold, New York, 1982.
2. Frank P. Gerstle, Jr., Encyclopedia of Polymer Science and Technology, John Wiley & Sons, New York, 1985, Volume 3, pp. 776–820.
3. Reference Book for Composites Technology, Ed. by Stuart M. Lee, Technomic Publishing Company, Inc., Lancaster, PA, 1989.
4. G. H. Staab, Laminar Composites, Elservier Science Ltd, Amsterdam 1999.
5. S. T. Peter, Handbook of composites (2nd edition), Kluwer Academic Publishers, London, 1998.
6. D. D. L. Chang, Carbon Fiber Composites, Elsevier Science Ltd, Amsterdam 1994.
7. D. V. Rosato, International Encyclopedia of Composites, Ed. by Stuart M. Lee, VCH Publishers, New York, 1990, pp. 148–180.
8. Mel M. Schwartz, Composite Materials Handbook, McGraw-Hill, Inc., New York, 1992.
9. H. Schmidt and H. Wolter, *J. Non-Cryst. Solids*, 121, 428, 1990.
10. G. L. Wilkes, H. H. Huang, R. H. Glaser, American Chemical Society, Washington DC, 1990, p. 207.
11. E. J. A. Pope, M. Asami, J. D. Mackenzie, *J. Mater. Rev.* 4, 1018, 1989.
12. J. Wen and J. E. Mark, *Polym. Prepr.* 34, 362, 1993.
13. J. Li, "Nanocomposites" in Handbook of Nanophase and Nanostructured Materials, 4, 69, 2003.
14. J. Wen and G. L. Wilkes, *Chem. Mater.* 8, 1667, 1996.
15. G. l. Wilkes and J. Wen, The Polymeric Encyclopedia: Synthesis, Properties and Applications, CRC Press, FL, USA 1996, Vol. 6, p. 4782.

16. J. Wen, Encyclopedia of Materials: Science & Technology, Elsevier Science Ltd, Amsterdam 2001, p. 7610.
17. Dominick V. Rosato, Handbook of Composites, Ed. by George Lubin, Van Nostrand Reinhold, New York, 1982, Chapt. 1, p. 1.
18. Dusan C. Prevorsek, Reference Book for Composites Technology, Ed. by Stuart M. Lee, Technomic Publishing Company, Inc., Lancaster, PA, 1989, Chapt. 9, p. 168.
19. C. C. Evans, Whiskers, Mills & Boon Limited, London, 1972.
20. B. D. Agarwal and L. J. Broutman, Analysis and Performance of Fiber Composites, John Wiley & Sons, New York, 1980.
21. Fiberglas Plus Design: A Comparison of Materials & Process for fiber Glass Composites, Owens-Corning Fiberglas Corporation, Grandville, OH, 1987.
22. W. V. Titow and B. J. Lanham, Reinforced Thermoplastics, John Wiley & Sons, New York, 1975, p. 55.
23. W. V. Titow and B. J. Lanham, Reinforced Thermoplastics, John Wiley & Sons, New York, 1975, p. 54.
24. L. S. Penn and J. D. Muzzy, Handbook of Composites, Ed. by George Lubin, Van Nostrand Reinhold, New York, 1982, Chapt. 5, p. 57.
25. Raymond B. Seymour, Polymeric Composites, VSP BV, The Netherland, 1990, p. 146.
26. A. S. Wood, "Unmatched Performance Sparks a Buildup in Ketone Resins", Modern Plastics, pp. 46–48, April 1987.
27. I. Y. Chang and J. K. Lee, J. Thermoplastic Composite Materials, Vol. 1, pp. 277–296, July 1988.
28. Raymond B. Seymour, Polymeric Composites, VSP BV, The Netherland, 1990, pp. 126–127.
29. W. V. Titow and B. J. Lanham, Reinforced Thermoplastics, John Wiley & Sons, New York, 1975, p. 69.
30. W. V. Titow and B. J. Lanham, Reinforced Thermoplastics, John Wiley & Sons, New York, 1975, p. 68.
31. H. Updegraff, Handbook of Composites, Ed. by George Lubin, Van Nostrand Reinhold, New York, 1982, Chapt. 2, p. 19.
32. M. B. Launikitis, Handbook of Composites, Ed. by George Lubin, Van Nostrand Reinhold, New York, 1982, Chapt. 3, p. 38.
33. Raymond B. Seymour, Polymeric Composites, VSP BV, The Netherland, 1990, p. 112.
34. M. Stander, Handbook of Composites, Ed. by George Lubin, Van Nostrand Reinhold, New York, 1982, Chapt. 4, p. 50.
35. L. S. Penn and J. D. Muzzy, Handbook of Composites, Ed. by George Lubin, Van Nostrand Reinhold, New York, 1982, Chapt. 5, p. 57.
36. W. V. Titow and B. J. Lanham, Reinforced Thermoplastics, John Wiley & Sons, New York, 1975, p. 55.
37. D. M. Riggs, R. J. Shuford, R. W, Lewis, Handbook of Composites, Ed. by George Lubin, Van Nostrand Reinhold, New York, 1982, Chapt. 11, p. 196.
38. Vincent Sussman, Handbook of Fillers for Plastics, Ed. by Harry S. Katz and John V. Milewski, Van Nostrand Reinhols Company, New Yowk, 1987, Chapt. 13, p. 262.
39. C. C. Chiao and T. T. Chiao, Handbook of Composites, Ed. by George Lubin, Van Nostrand Reinhold, New York, 1982, Chapt. 12, p. 272.
40. C. Wittman and G. D. Shock, Handbook of Composites, Ed. by George Lubin, Van Nostrand Reinhold, New York, 1982, Chapt. 13, p. 321.
41. J. A. Radosta and N. C. Trivedi, Handbook of Fillers for Plastics, Ed. by Harry S. Katz and John V. Milewski, Van Nostrand Reinhols Company, New York, 1987, Chapt. 11, pp. 224–228.
42. Y. Chang, "PEKK as a New Thermoplastic Matrix for High Performance Composites", SAMPE Quarterly, pp. 29–34, July 1988.

CHAPTER 29

Polymer Networks and Gels

Ferenc Horkay* and Gregory B. McKenna†

*National Institutes of Health, National Institute of Child Health and Human Development, Laboratory of Integrative and Medical Biophysics, Section on Tissue Biophysics and Biomimetics, Bethesda, MD 20892
†Department of Chemical Engineering, Texas Tech University, Lubbock, TX 79409-3121

Abstract: When long polymer molecules are chemically linked together to form a three-dimensional network, the resulting material exhibits a unique set of properties that have come to be referred to as ''rubberlike.'' Among these are large deformation elasticity which has important consequences for mechanical behavior and resistance to solvent attack. As for the latter, when solvent molecules penetrate into the polymer it undergoes swelling rather than dissolution, and the diluted network is referred to as a chemically crosslinked gel. A survey of the thermodynamics and mechanics of crosslinked gels is presented. Subjects include the phenomenological description of crosslinked networks within the framework of finite elasticity theory and continuum thermodynamics. Particular emphasis is placed on the Valanis–Landel form of the strain energy density function. Several statistical mechanical models of rubber elasticity are also presented. Of particular usefulness are the affine and phantom network models, which are commonly used to derive information about the molecular parameters of the gel from swelling or mechanical measurements. Techniques for using these models and the more modern Flory–Erman constrained junction model and its most recent modifications are described. The application of Scaling Theory to polymer gels is also considered.

Key Words: Crosslinked Rubber, Flory–Rehner Hypothesis, Gels, Networks, Polymer, Rubber Elasticity, Scaling Theory, Solution Thermodynamics, Swelling, Valanis–Landel Function.

29.1 INTRODUCTION

Polymer networks and gels have a wide range of technical and biological applications. Crosslinked polymers are the building blocks of systems as different as rubber tires and scaffolds for tissue engineering. Morphology, molecular and supermolecular structures play important roles, especially when considering processing and final properties. While such materials have been the subjects of experimental and theoretical investigations for more than six decades, their understanding still presents a challenge. Gels exhibit both solid-like and liquid-like properties. The three-dimensional network structure obtained by joining long flexible polymer strands at junction points is the most important molecular characteristic required to achieve ''rubberlike'' behavior. Numerous models have been proposed to develop a rigorous molecular description of polymer gels. Statistical mechanical theories along these lines encounter serious mathematical difficulties. Rubber elasticity theories, therefore, omit a detailed description of the conformation of polymer chains. Earlier models focus on the effects of topological constraints on the crosslinks. Modern theories are made more realistic by applying the constraints to other parts of the chains. As a result, it is of great interest and importance to understand the structure–property relationships that determine network and gel behaviors.

To begin, when long polymer molecules are chemically linked together to form a three-dimensional network, the resulting material exhibits a unique set of properties that

have come to be referred to as rubberlike. Among these are large deformation elasticity which has important consequences for mechanical behavior and resistance to solvent attack. As for the latter, when solvent molecules penetrate into the polymer it undergoes swelling rather than dissolution, and the diluted network is referred to as a chemically crosslinked gel. While there are several structures that exhibit gellike behavior, e.g., (1) covalent networks of large chain molecules, (2) physical networks formed by aggregation of polymer chains (gelatin, agarose), (3) lamellar, fibrillar, or reticular systems exhibiting partially ordered structures (clays, surfactants, etc.), the focus of this work is solely on elastomeric polymer networks containing a three-dimensional permanent structure of high molecular weight chain molecules swollen in a low molecular weight diluent as depicted in Fig. 29.1.

The covalent network, composed of long flexible chains capable of adopting large conformational changes (chain deformations), extends throughout the sample providing the ability to undergo large and reversible (elastic) deformations and a corresponding ability to swell rather than dissolve. Though the molecular origins of rubber elasticity were recognized as early as the 1930s and 1940s [1–5], a complete theoretical description of the swelling behavior of rubberlike polymers has yet to be achieved. The result is that, while there is a general understanding of the behavior of crosslinked materials within the framework of some "classical" models of rubber elasticity, there are still several unresolved problems. For example, even the fundamental assumption, originally put forth by Frenkel [5], Flory and Rehner [2,4] that the free energy of mixing of a solvent and rubber network can be separated into an elastic term for the network and a mixing term for the solvent and polymer has been a subject for much research and discussion over the years [6–32].

There is a diversity of theroetical models used to elucidate the relationships between the molecular parameters of the network and the various experimental results [33–57]. Hence, the resulting deduction of the molecular structure of the network can depend on the model chosen for data analysis. Additionally, the structure of the networks at the supermolecular level is a function of the preparation conditions (temperature, concentration at crosslinking, chemical nature of the crosslinker, etc.). During network formation imperfections in the structure may also develop. In many cases the crosslinking process leads to fixation of otherwise nonequilibrium states. A wide variety of molecular superstructures may be produced within networks prepared from the same starting materials. This makes comparisons of experimental results from different literature sources extremely complicated. Consequently, a simple tabulation of previously published data is not particularly useful.

The present work is intended to survey briefly the basic thermodynamic considerations of rubber elasticity and

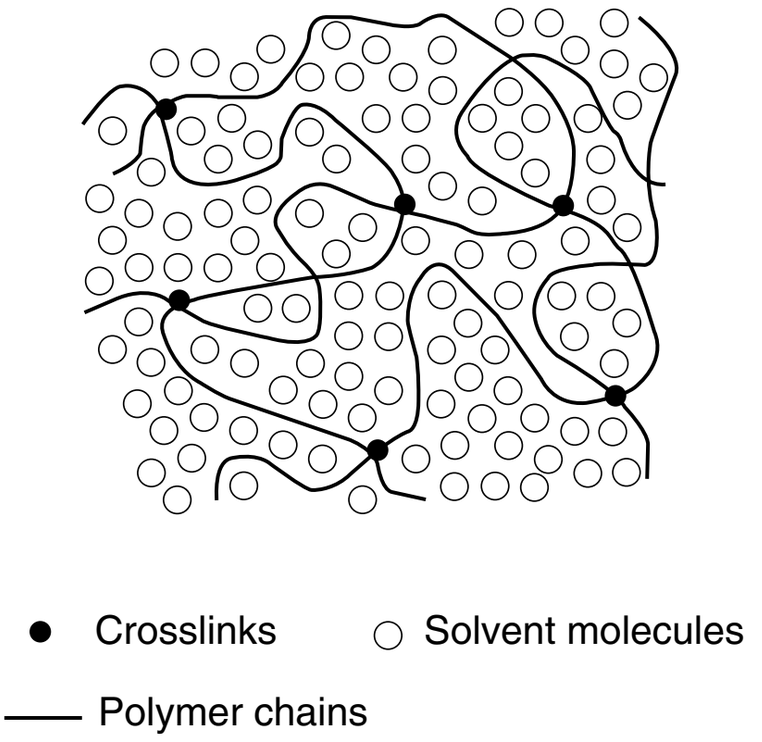

FIGURE 29.1. Schematic representation of a chemically crosslinked polymer network swollen by a low molecular weight solvent.

swelling from both a continuum point of view and with regard to existing network models. Our goal is to illustrate the range of applicability and the limitations of the different approaches for the description of experimental data. The main emphasis is to discuss the structure–property relationships of amorphous polymer networks and gels. We briefly summarize what we believe are the most important ideas of the theories, and compare them with experimental observations made on well-defined networks. For details of each model the reader is referred to the original literature. We focus exclusively on the equilibrium properties of model networks in the dry and swollen states, and the relationships between macroscopically measurable physical quantities. We do not deal with the consequences of the morphology and supermolecular architecture of the polymer network, which can be revealed by scattering measurements. Certain fundamental topics (e.g., effect of charged groups, finite chain extensibility, contribution of filler particles, dynamic properties such as relaxation behavior) are not discussed here.

Additionally, this work should provide the reader with the ability to use the models to obtain estimates of the molecular structure of the gel through analysis and interpretation of typical sets of experimental data. Conversely, the swelling and mechanical responses of new networks should be able to be estimated from a chemist's knowledge of the molecular parameters of the network.

29.2 THEORETICAL BACKGROUND

29.2.1 General Considerations

In thinking about the behavior of rubber networks and gels, there are two features of behavior that we will consider in the following. First, the fundamental nature of the elastomeric network itself in the undiluted state needs to be weighed. This will be done using both the phenomenological theories of rubber elasticity and the molecular (statistical mechanical) models. Both approaches result in forms of the free energy function (Helmholtz) of the network and ultimately need to give the same descriptions of the phenomenological behavior of the dry network. Second, we will consider the specific behavior of the swollen network or gel from similar considerations. In the latter case the formulation of a mixing free energy as a function of the swelling ratio is also required in addition to the elastic free energy. We also remark that the mere presence of the crosslink sites may alter the expressions for the free energy of mixing.

Laboratory measurements, for the most part, record the macroscopic behavior of the material. Depending on the purposes of the experimenter, the link between the molecular models and the phenomenological models provides a basis for either deducing molecular parameters from the measurements or for predicting future measurements from known molecular structures. The latter is primarily important to estimate the physical properties of a given gel whose molecular structure is known. The background provided in what follows should permit one to do both within the limitations of current knowledge.

29.2.2 The Strain Energy Density Function—The Mechanical Contribution to the Helmholtz Free Energy

Continuum Description

There is an extensive body of literature describing the stress–strain response of rubberlike materials that is based upon the concepts of Finite Elasticity Theory which was originally developed by Rivlin and others [58,59]. The reader is referred to this literature for further details of the relevant developments. For the purposes of this paper, we will discuss the developments of the so-called Valanis–Landel strain energy density function, [60] because it is of the form that most commonly results from the statistical mechanical models of rubber networks and has been very successful in describing the mechanical response of crosslinked rubber. It is resultingly very useful in understanding the behavior of swollen networks.

Here we begin with a sample of rubber having initial dimensions l_1, l_2, l_3. We deform it by an amount $\Delta l_1, \Delta l_2, \Delta l_3$ and define the stretch (ratio) in each direction as $\lambda_i = (l_i + \Delta l_i)/l_i = l/l_i$. The purpose of Finite Elasticity Theory has been to relate the deformations of the material to the stresses needed to obtain the deformation. This is done through the strain energy density function, which we will describe using the Valanis–Landel formalism as $W(\lambda_1, \lambda_2, \lambda_3)$. Importantly, as we will see later, this is the mechanical contribution to the Helmholtz free energy. Valanis and Landel assumed [60] that the strain energy density function is a separable function of the stretches λ_i:

$$W(\lambda_1, \lambda_2, \lambda_3) = w(\lambda_1) + w(\lambda_2) + w(\lambda_3) + a \ln(\lambda_1\, \lambda_2\, \lambda_3). \tag{29.1}$$

While the term $a\ \ln(\lambda_1\lambda_2\lambda_3)$ is not important in the mechanical response, because of the incompressibility assumption, it may be important in swelling [61]. We also note that some of the molecular models include this logarithmic term. Then, the principal stresses σ_{ii} in any deformation can be related through the strain energy function and deformations as follows:

$$\sigma_{ii} - \sigma_{jj} = \lambda_i\ w'(\lambda_i) - \lambda_j\ w'(\lambda_j), \tag{29.2}$$

where $w'(\lambda) = \mathrm{d}w(\lambda)/\mathrm{d}\lambda$ is the derivative of the VL function $w(\lambda)$. We note that the stresses are the true stresses in that they are referred to the deformed sample geometry. In the dry, unswollen rubber, the material is generally assumed to be incompressible, meaning that the distortional or shape changing deformations are much more easily made than are the volume changing ones, so the latter are

negligible. Hence Eq. (29.2) is written in terms of the principal stress differences. In the case of a uniaxial deformation $\lambda = \lambda_1$ in the 1 direction Eq. (29.2) becomes:

$$\sigma_{11} - \sigma_{22} = \lambda_1\ w'(\lambda_1) - \lambda_2\ w'(\lambda_2) \tag{29.3}$$

and because of the incompressibility condition that $\lambda_1\lambda_2\lambda_3 = 1$ we find that $\lambda_2 = \lambda_1^{-1/2}$ and Eq. (29.3) becomes:

$$\sigma_{11} - \sigma_{22} = \lambda\ w'(\lambda) - \lambda^{-1/2} w'(\lambda^{-1/2}), \tag{29.4}$$

where $\lambda = \lambda_1$. For uniaxial extension $\lambda > 1$ while for uniaxial compression $\lambda < 1$.

From a practical viewpoint, Eq. (29.4) can be used to describe the stress–strain relation of a material if $w'(\lambda)$ is known. $w'(\lambda)$ can be obtained in the laboratory in various ways, such as pure shear experiments as described by Valanis and Landel [60], by torsional measurements as described by Kearsley and Zapas [62] and by a combination of tension and compression experiments as also described by Kearsley and Zapas [62]. Treloar and co-workers [63] have also shown that the VL function description of the mechanical response of rubber is a very good one. The reader is referred to the original literature for these methods.

Another point to keep in mind here is that, in most models, the description of rubber elasticity given from statistical mechanical models results in a Valanis–Landel form of strain energy density function. This will be important in the following developments. We now look at some common representations of the strain energy density function used to describe the stress–strain behavior of crosslinked rubber.

There are two common phenomenological strain energy functions that have been used to describe the stress–strain response of rubber [58,59,64]. These are referred to as the Neo-Hookean form and the Mooney–Rivlin form and both can be written as Valanis–Landel forms, although they represent truncated forms of more general strain energy density functions. The Neo-Hookean form is a special form of the Mooney–Rivlin form, so we will begin with the latter. For a Mooney–Rivlin material the strain energy density function is written as:

$$W(\lambda_1,\lambda_2,\lambda_3) = C_1(\lambda_1^2 + \lambda_2^2 + \lambda_3^2 - 3) + C_2(\lambda_1^{-2} + \lambda_2^{-2} + \lambda_3^{-2} - 3) \tag{29.5}$$

and we see that the VL function for this is of the form $w(\lambda_i) = C_1\lambda_i^2 + C_2\lambda_i^{-2}$ and the VL derivative is given as:

$$w'(\lambda_i) = 2C_1\lambda_i - 2C_2\lambda_i^{-3}, \tag{29.6}$$

where C_1 and C_2 are material constants, often referred to as the Mooney–Rivlin Coefficients.

For uniaxial deformations of magnitude λ one then writes Eq. (29.4) for the Mooney–Rivlin stress–strain response as:

$$\sigma_{11} - \sigma_{22} = (\lambda^2 - 1/\lambda)\{2C_1 + 2C_2/\lambda\}. \tag{29.7}$$

Equation (29.7) makes obvious the reasons for the representation of experimental data in the so-called Mooney–Rivlin plot. If the material has a Mooney–Rivlin strain energy density function then a plot of $(\sigma_{11} - \sigma_{22})/(\lambda^2 - 1/\lambda)$ vs.$1/\lambda$ results in a straight line with the slope and intercept at $\lambda = 1$ determining $2C_2$ and $(2C_1 + 2C_2)$, respectively.

For the Neo-Hookean material, the strain energy density function is the same as the Mooney–Rivlin material but with $C_2 = 0$:

$$W(\lambda_1,\lambda_2,\lambda_3) = C_1(\lambda_1^2 + \lambda_2^2 + \lambda_3^2 - 3). \tag{29.8}$$

The VL derivative is:

$$w'(\lambda_i) = 2C_1\lambda_i. \tag{29.9}$$

The corresponding reduced stress σ_R is:

$$\sigma_R = (\sigma_{11} - \sigma_{22})/(\lambda^2 - 1/\lambda) = 2C_1. \tag{29.10}$$

Hence, in the Mooney–Rivlin plot, the stress–strain data are reduced to a line of slope zero.

A point worth noting here is that several of the molecular models that will be described in the subsequent sections are Neo-Hookean in form. Normally, dry rubbers do not exhibit Neo-Hookean behavior. As for the Mooney–Rivlin form of strain energy density function, rubbers may follow such behavior in extension, yet they do not behave as Mooney–Rivlin materials in compression. In Fig. 29.2, we depict typical experimental data for a polydimethylsiloxane network [39] and compare the response to Mooney–Rivlin and Neo-Hookean behaviors. The horizontal lines represent the affine and the phantom limits (see "Network Models" in Section 29.2.2). The straight line in the range $\lambda^{-1} < 1$ shows the fit of the Mooney–Rivlin equation to the experimental data points.

Statistical Theories

Structural Characteristics of Polymer Networks

In this section we discuss the most important structural parameters characteristic of an ideal polymer network. The structure of a real network always displays deviation from that of an ideal network. Network defects, such as unreacted functionalities, cyclic structures and entanglements, arise from the statistics of the crosslinking process. The crosslinking reaction, in general, results in a length distribution for the network chains. In addition to the molecular imperfections, real networks always contain inhomogeneities, i.e., regions in which the polymer concentration is permanently higher than the average concentration. The topological structure of any real network can be very complex and treatment of the topology is beyond the scope of the present work. (The reader is referred to [56,66–69] for discussions of this topic.) It is worthwhile, however, to define the structural parameters for a perfect network because it allows us to treat any real network by reference to these parameters.

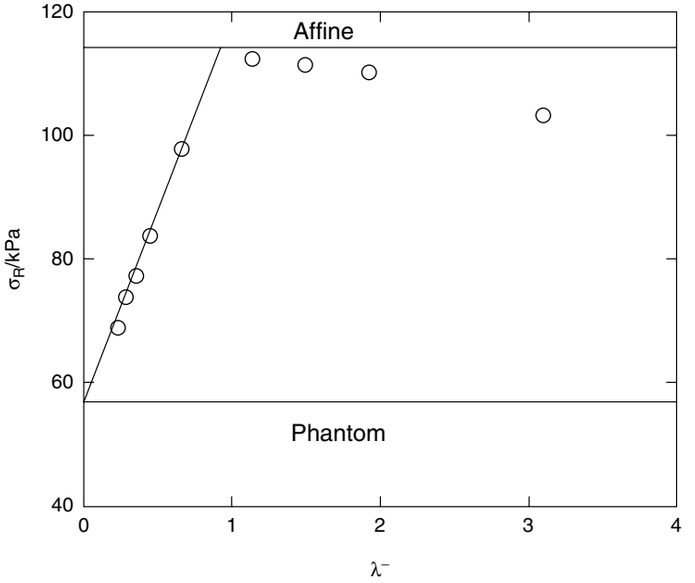

FIGURE 29.2. Comparison of typical stress–strain data for PDMS rubber [39] in a "Mooney–Rivlin" plot with "Neo-Hookean" and "Mooney–Rivlin" strain energy function descriptions. (See text for discussion).

Statistical models yield explicit expressions for the relation between the molecular structure of the network and the elastic properties.

The most important molecular parameter characteristic of a polymer network is the concentration of the elastic chains or that of the crosslinks connecting the macromolecules. An active junction is joined by at least three paths to the polymer network and an active chain is defined as one terminated by active junctions at both ends. There are several ways to express the extent of crosslinking: (1) the concentration of the elastically active chains, ν_{el}/V_0, where ν_{el} is the number of chains connecting two elastically active junctions and V_0 is the volume of the dry network, (2) the molecular weight of the polymer chains between the junctions

$$M_c = \rho(V_0 N_A/\nu_{el}), \tag{29.11}$$

where ρ is the density of the polymer and N_A is Avogadro's number, (3) the crosslink density, μ_{el}/V_0, where μ_{el} is the number of the crosslinks and (4) the cycle rank density, ξ/V_0, where ξ is the cycle rank, i.e., the number of the independent circuits in the system. Naturally, these quantities are not independent. The relationship between ν_{el}, μ_{el}, and ξ for a perfect network is given by [35]

$$\xi = \nu_{el} - \mu_{el} + 1. \tag{29.12}$$

In Fig. 29.3 a network structure is shown with $\xi = 4$, $\nu_{el} = 12$, and $\mu_{el} = 9$.

Another important parameter is the crosslink functionality, f, which is the number of chains emanating from a network junction. Only junctions with functionality higher than 2 are elastically active. For perfect networks, i.e., crosslinked polymers containing no defects, ν_{el} and μ_{el} are connected by the functionality of the crosslinks [70]

$$\mu_{el} = (2/f)\nu_{el}. \tag{29.13}$$

Real networks always contain molecular imperfections, such as pendant chains bound to the network at one end only, intramolecular loops formed by linking of two units of the same chain, and intermolecular entanglements. For an imperfect tetrafunctional network Flory [4,65] proposed a simple formula for correction for pendant chains

$$\nu_{el} = \nu_0(1 - 2M_c/M_n), \tag{29.14}$$

where ν_0 is the total number of chains in the network and M_n is the number average molecular weight of the primary molecules.

The extent to which entanglements contribute to network elasticity is not yet fully resolved. In the model of Langley[45], Dossin and Graessley [46–49] a contribution to the equilibrium modulus is associated with the plateau modulus of viscoelasticity. On the other hand, Flory [36] and Erman [38–40] assume that interpenetration of chains is solely reflected by suppression of the fluctuations of junctions.

Another type of network defect occurs due to the presence of inhomogeneities. Clustering of chains or network junctions causes permanent departures from the homogeneous distribution of the polymer throughout the gel. Regions of higher polymer concentration build up that appear as permanent departures from uniformity. They are specific to the given system and dependent upon the condition of crosslinking. The effects of inhomogeneities on the elastic and swelling behavior of the networks has not been considered

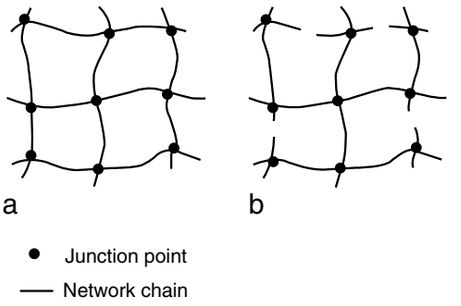

FIGURE 29.3. Schematic representation of a network structure with $\nu_{el} = 12$, $\mu_{el} = 9$, and $\xi = 4$ (a). Note that the cycle rank is the number of cuts needed to reduce the network to a tree (b).

quantitatively in any theoretical models of rubber elasticity. The reader is referred to several relevant papers in references [71–74].

Network Models

The primary goal of a general statistical theory is to derive an equation of state for the elastomeric molecular network which will hold for any deformation including swelling. Since the major contribution to the elasticity is entropic the molecular interpretation depends on how the stress affects the conformational distribution of an assembly of chains. The successful statistical model will provide predictive relationships between the molecular structure and topology of the network and its macroscopic behavior, e.g., mechanical and swelling responses.

The classical theories of rubber elasticity rest on two basic assumptions [4]:

1. The elastic free energy of the network is the sum of the elastic free energies of the network chains, i.e., the interactions between the constituent chains are independent of the state of deformation, and do not make any contribution to the elastic free energy; and
2. The end-to-end distribution of the network chains is Gaussian, i.e., the excluded volume interactions are ignored.

The affine and the phantom models derive the behavior of the network from the statistical properties of the individual molecules (single chain models). In the more advanced constrained junction fluctuation model the properties of these two classical models are bridged and interchain interactions are taken into account. We remark for completeness that other molecular models for rubber networks have been proposed [32,57,75–87], however, these are not nearly as widely used and remain the subject of much debate. Here we briefly summarize the basic concepts of the affine, phantom, constrained junction fluctuation, diffused constraint, tube and slip-tube models.

The Affine Model. In the early version of this model it was assumed that the components of length at all scales are deformed affinely [88,89], i.e., local deformations are the same as the macroscopically imposed deformation. Later this view was revised to treat only the displacement of the mean positions of the junctions and the end-to-end vectors of the chains as transforming affinely [6]. Fluctuations of the network junctions are completely suppressed by intermolecular entangling with neighboring coils sharing the same region of space. The elastic free energy of the affine network is given by [35,88–90]

$$\Delta F_{el}^{aff}/kT = (\nu_{el}/2V_0)(\lambda_1^2 + \lambda_2^2 + \lambda_3^2 - 3) - (\mu_{el}/V_0)\ln(\lambda_1\lambda_2\lambda_3), \tag{29.15}$$

where ν_{el} and μ_{el} are the number of elastic chains and junctions in the network, respectively. λ_1, λ_2, and λ_3 are the principal deformation ratios, k is the Boltzmann constant and T is absolute temperature. Here we note that the affine model is of the Neo-Hookean form with $C_1 = \nu_{el}/2V_0$, if there is no volume change upon deformation. Note also the presence of a logarithmic term in the free energy expression.

The Phantom Model. In this model polymer chains are allowed to move freely through one another and the network junctions fluctuate around their mean positions [3,91–93]. The conformation of each chain depends only on the position of its ends and is independent of the conformations of the surrounding chains with which they share the same region of space. The junctions in the network are free to fluctuate around their mean positions and the magnitude of the fluctuations is strain invariant. The positions of the junctions and of the domains of fluctuations deform affinely with macroscopic strain. The result is that the deformation of the mean positions of the end-to-end vectors is not affine in the strain. This is because it is the convolution of the distribution of the mean positions (which is affine) with the distribution of the fluctuations (which is strain invariant, i.e., nonaffine). The elastic free energy of deformation is given by

$$\Delta F_{el}^{ph}/kT = (\xi/2V_0)(\lambda_1^2 + \lambda_2^2 + \lambda_3^2 - 3) \tag{29.16}$$

and again the free energy function is of the Neo-Hookean form, with $C_1 = \xi/2V_0$.

The Constrained Junction Fluctuation Model. The affine and phantom models are two limiting cases on the network properties and real network behavior is not perfectly described by them (recall Fig. 29.2). Intermolecular entanglements and other steric constraints on the fluctuations of junctions have been postulated as contributing to the elastic free energy. One widely used model proposed to explain deviations from ideal elastic behavior is that of Ronca and Allegra [34] and Flory [36]. They introduced the assumption of constrained fluctuations and of affine deformation of fluctuation domains.

In the constrained junction fluctuation model [36,38–40] developed by Flory and Erman the spatial fluctuations of junctions are inhibited from the large values allowed in the phantom network by restrictions due to neighboring chains. The effect of conformational constraints is assumed to be imposed solely on the network junctions. The situation is illustrated by Fig. 29.4. The mean position of the network junction is located at point A. In a phantom network (Fig. 29.4(a)) the radius of the circle shows the average root-mean-square fluctuation $\langle(\Delta R)^2\rangle_{\text{ph}}^{1/2}$ around the mean position. The domain of constraints due to intermolecular interactions with neighboring chains and to steric requirements is represented by the smaller circle in Fig. 29.4(b). This latter is centered at point B. Because of the effect of constraints, the mean position of the junction (i.e., the equilibrium position in the unstrained network) is removed from point A to point C. The instantaneous position of the junction may differ significantly, however, from the equilibrium position because the junction fluctuates around its mean position. Thus, in addition to the phantom network contribution to the free energy, an important new parameter in this model is the measure of the severity of the constraints relative to those imposed by a phantom network $\kappa = <\Delta R^2>_{\text{ph}}/<\Delta s^2>_0$ where $<\Delta R^2>_{\text{ph}}$ is the mean-squared fluctuation in the positions of junctions from their mean locations in the phantom model, and $<\Delta s^2>_0$ is the mean-squared fluctuation of junctions from their mean positions under the action of constraints. The range of κ therefore is from 0 (phantom limit) to ∞ (affine limit). The size of the domains of constraints is assumed to decrease with increasing strain so that the junction fluctuations become larger. If the network is deformed the fluctuations become anisotropic in the stretching direction because the constraints become smaller.

The elastic free energy is given by

$$\Delta F_{\text{el}} = \Delta F_{\text{el}}^{\text{ph}} + \Delta F_{\text{el}}^{\text{c}} \tag{29.17}$$

where $\Delta F_{\text{el}}^{\text{c}}$ is the contribution to the elastic free energy arising from entanglement constraints relative to those in the phantom network $\Delta F_{\text{el}}^{\text{ph}}$ (see Eq. 29.16). This term can be written

$$\frac{\Delta F_{\text{el}}^{\text{c}}}{kT} = \frac{\mu_{\text{el}}}{2V_0}\sum_{t=1}^{3}[(1+g_t)B_t - \ln((B_t+1)(g_tB_t+1))] \tag{29.18a}$$

with

$$B_t = (\lambda_t - 1)(1 + \lambda_t - \zeta\lambda_t^2)(1+g_t)^{-2}, \tag{29.18b}$$

$$g_t = \lambda_t^2[\kappa^{-1} + \zeta(\lambda_t - 1)], \tag{29.18c}$$

where the parameter ζ characterizes the nonaffine transformation of the domains of constraint with deformation.

Importantly, the model spans the behavior between the phantom and affine models. When $\kappa = \infty$ and $\zeta = 0$ we recover the affine network behavior. In this case the junction fluctuations are completely suppressed, i.e., $<\Delta s^2>_0 = 0$. When $\kappa = 0$, i.e., the junctions are free to fluctuate, we recover the phantom network model.

The constrained junction fluctuation theory was modified by Erman and Monnerie [94]. The fundamental difference between the modified and the original models is the adoption of the assumption that constraints affect the centers of mass of the chains rather than the junction points only. They considered two different cases: (1) the fluctuations of all points along the chains in the phantom network are independent of macroscopic strain (constrained chain scheme, CC) and (2) the fluctuations of the points in the phantom network are dependent on the macroscopic strain, only the junctions are invariant to strain (modified constrained chain

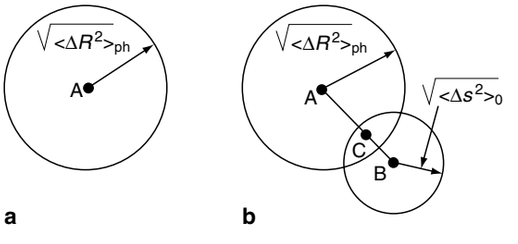

FIGURE 29.4. Effect of constraints on the fluctuations of network junctions. (a) Phantom model and (b) constrained junction fluctuation model. Note that the domain boundaries (circles in the figures) are diffuse rather than rigid. The action of domain constraint is assumed to be a Gaussian function of the distance of the junction from B similar to the action of the phantom network being a Gaussian function of ΔR from the mean position A.

scheme, MCC). The important consequence is that κ of the constrained junction fluctuation theory has been replaced by the function [94]

$$h(\lambda_x) = \kappa_G[1 + (\lambda_x^2 - 1)\Phi]^{-1}, \tag{29.19a}$$

where κ_G is a parameter corresponding to κ, and

$$\Phi = (1 - 2/f)^2/3 \quad \text{(CCmodel)}, \tag{29.19b}$$

$$\Phi = (1 - 2/f)^2 \quad \text{(MCCmodel)}. \tag{29.19c}$$

Both constrained chain models predict that the elastic modulus exceeds the value obtained from the phantom model, and according to the MCC scheme it exhibits a more sensitive dependence upon elongation or swelling than given by the original Flory–Erman theory. The effect of constraints is represented by a single parameter κ_G instead of the two parameters κ and ζ in the previous model, which makes the new theory more straightforward for the interpretation of the experimental stress–strain-swelling data.

We note that the free energy function in the Flory–Erman model is a specific form of the Valanis–Landel strain energy density function. McKenna and Hinkley [61] determined the Valanis–Landel function for the junction constraint model

$$w'(\lambda_t) = \xi kT\lambda_t + (\mu_{el}kT/2)\{B_t^*(1 + g_t) + g_t^* B_t - B_t^*(B_t + 1)^{-1} - (g_t B_t^* + B_t g_t^*)(g_t B_t + 1)^{-1}\}, \tag{29.20}$$

where

$$B_t^* = B_t\{[2\lambda_t(\lambda_t - 1)] - 1 + (1 - 2\zeta\lambda_t)[2\lambda_t(1 + \lambda_t - \zeta\lambda_t^2)]^{-1} + 2g_t^*(1 + g_t)^{-1}\} \tag{29.21}$$

and

$$g_t^* = \kappa^{-1} - \zeta(1 - 3\lambda_t/2). \tag{29.22}$$

We will come back to these models subsequently.

Diffused Constraint Model of Polymer Networks. This model, which is an extension of the Erman–Monnerie model, is more realistic in that the constraints are assumed to act continuously along the chains, instead of allowing the constraints to affect only the fluctuations of the junctions or the centers of mass of the network chains. Because the constraints affect fluctuations of all points along the macromolecule, the elastic energy of constraints must be averaged over all segments of the chain. Following a similar argument used by Flory [36] in the original constrained-junction theory, Kloczkowski, Mark, and Erman [95] derived the elastic free energy of the constraints

$$\Delta F_{el^c} = \frac{1}{2}\nu kT \sum_{t=1}^{3} \int_0^1 W(\theta)[B_t(\theta) + D_t(\theta) - \ln[B_t(\theta) + 1] - \ln[D_t(\theta) + 1]]d\theta \tag{29.23}$$

with

$$B_t(\theta) = \frac{\kappa^2(\theta)(\lambda_t^2 - 1)}{[\lambda_t^2 + \kappa(\theta)]^2} \tag{29.23a}$$

and

$$D_t(\theta) = \frac{B_t(\theta)\lambda_t^2}{\kappa(\theta)}. \tag{29.23b}$$

In Eq. (29.23) $W(\theta)$ is the distribution of constraints among different points along the network chain and $\theta = i/n$ is the position of the ith segment of the chain as a fraction of the contour length between two crosslinks. If the distribution is uniform, then $W(\theta) = 1$ inside the integrand of Eq. (29.23). In the case when constraints are assumed to affect only fluctuations of junctions (as in the constrained-junction theory), θ is limited to $\theta = 0$ or $\theta = 1$ only. [95] It is important to note that this theory does not reduce identically to the constrained-chain theory, because the latter characterizes the deformation-dependent fluctuations of the centers of mass of the chains and not the deformation-independent fluctuations of the midpoints [95].

In summary, the common feature of all constrained chain models is that they impose only limited constraints on chain fluctuations. [101] The constrained-junction fluctuation model restricts fluctuations of junctions and of the center of mass of network chains. The diffused constraint model restricts fluctuations of a single randomly chosen monomer for each network strand. Consequently, all these models can only represent the crossover between the phantom and affine limits. [101] The phantom limit corresponds to a weak constraining case, while the affine limit corresponds to a very strong constraining potential.

Tube Models. Several versions of the tube models have been developed. These models take into account the fact that constraints act along the whole chain and restrict the fluctuations of all monomers of the chain. The tube models consider that each network strand is confined within a configurational tube with a harmonic potential modeling topological constraints of entanglements. [101,120] The field is described as an uncrossable tube of constraints the centerline of which is the primitive path of the strand. The constraining field of force penalizes excursions of a strand [126] from its primitive path, i.e., a random-walk trajectory running from one network junction to the other. [126] The free energy penalty increases with excursion amplitude. The elastic free energy is given by the sum of two terms. One has the Gaussian form due to chain connectivity, while the other represents the loss of the degrees of freedom of the chains due to their spatial localization originating from entanglements. [120]

In the Edwards tube model [80] the topological potential is applied to every monomer of the chain restricting its fluctuations to a confining tube with the diameter $a \approx bN_e^{1/2}$ where N_e is the degree of polymerization between network entanglements. [101] In the model this

potential is independent of the network deformation and the tube diameter changes affinely with the macroscopic deformation of the network, $a \sim \lambda$. However, this assumption is unrealistic and disagrees with the experimental observations. [97,101]

In the Gaylord–Douglas model [57,81] the chains are localized in a tube defined by the interactions with neighboring chains. The first term of the elastic free energy is the same as that of a phantom network model, while the second term accounts for the loss of degrees of freedom of the chains due to chain localization. In the dry network the cross-sectional dimension of the tube is of the order of the hard-core cross-sectional radius of the polymer chain, and the volume of the tube is comparable with the chain molecular volume. The tube volume is considered to be invariant with macroscopic strain, since the molecular volume of the chains is independent of the deformation. The elastic free energy is given by

$$\Delta F_{\mathrm{el}} = (G_{\mathrm{net}}/2)(\lambda_1^2 + \lambda_2^2 + \lambda_3^2 - 3) + G_{\mathrm{e}}(\lambda_1 + \lambda_2 + \lambda_3 - 3), \tag{29.24}$$

where

$$G_{\mathrm{net}} = \nu_{\mathrm{el}} kT/(2V_0) \tag{29.24a}$$

and

$$G_{\mathrm{e}} = \gamma G_{\mathrm{net}} + G_{\mathrm{N}}. \tag{29.24b}$$

G_{N} is the plateau modulus of the polymer melt, V_0 is the volume of the dry network, and γ is a constant. In the absence of localization interactions, $G_{\mathrm{e}} = 0$, and Eq. (29.24) reduces to the result obtained for the phantom model. Since the constraining effect of the surrounding network chains diminishes upon swelling, G_{e} is predicted to depend on swelling as well as the conditions under which the network was formed [32,96]. The concentration dependence of G_{e} is especially large for lightly crosslinked gels (roughly linear in the concentration), however, the concentration dependence for highly crosslinked networks is relatively weak (comparable to that of the phantom model).

A challenging problem in the theory of rubber elasticity is to determine how the macroscopic deformation of the network affects the conformation of the polymer chains. At macroscopic length scales polymer networks behave as elastic solids, while at microscopic length scales the network chains move relatively freely. The elasticity is mainly entropic and is governed by deformations occurring on short length scales. Therefore, it is important to distinguish between affine and nonaffine length scales. [97] The affine length is the shortest length scale at which the network deformation is the same as that of the macroscopic deformation of the sample. At smaller length scales the deformation of the network chains is nonaffine. [97]

The nonaffine tube model developed by Rubinstein and Panyukov [97] captures the basic features of the phantom and affine models. In this model the amplitude of fluctuations that defines the tube diameter changes proportionally with the deformation of the network. The network deforms affinely on length scales larger than the affine length, R_{aff}. However, on length scales smaller than R_{aff} the confining potential has little effect on the conformation of the individual chains. The most important feature of this model is that the tube diameter a changes nonaffinely with network deformation $a \sim \lambda^{1/2}$. The prediction for the elastic free energy and the reduced force of the nonaffine tube model is [97]

$$\Delta F^{\mathrm{el}} = \Delta F^{\mathrm{el}}_{\mathrm{ph}} + \frac{ckT}{2N_{\mathrm{e}}} \sum_{\alpha} \left(\lambda_\alpha + \frac{1}{\lambda_\alpha} \right), \tag{29.25}$$

$$f^*(\lambda^{-1}) = G_{\mathrm{ph}} + \frac{G_{\mathrm{e}}}{\lambda - \lambda^{1/2} + 1}, \tag{29.26}$$

where c is the monomer concentration, G_{ph} is the phantom modulus, G_{e} is the entanglement contribution to the modulus, and N_{e} is the number of monomers between entanglements.

A more advanced version of this model combines the ideas of slip-link [98] and tube models. The ''slip-tube'' model allows slippage of the network chains and redistribution of the monomers between different sections of the tube [101]. The idea of slippage of the chain along the contour of the tube was originally proposed by de Gennes [105] in the reptation model of polymer melts, and the analysis of the redistribution of stored length was made by Doi [100]. The basic concept of the slip-link models is that permanent entanglements act as slip-links connecting neighboring chains. The slip-links are allowed to pass through each other, but each of them can slide along the chain only up to a limited distance. [101] If this distance is equal to the chain length, the slip-link model reduces to the phantom network model. In the opposite limit, when the sliding distance of the slip-links is small compared to the average distance between neighboring slip-links, the model is reduced to the affine model.

In the slip-tube model [101] the topological constraints imposed by the neighboring network chains are represented by virtual chains attached to the elastic nonfluctuating background at one end and ending with slip-links at the other. The network chains pass through these slip-links but they are not allowed to pass through each other. [101] The amplitude of the slip-link fluctuations depends on the density of the slip-links. At high density the slip-links are located at every monomer and the fluctuations are completely suppressed. In this limit the slip-tube model reduces to the nonaffine tube model. If slippage along the tube is allowed the network chains redistribute their lengths along the contour of their confining tubes. [101] In the anisotropically deformed network the number of monomers in a given direction α will be changed due to the slippage.

The elastic free energy of the network is given as [101]

$$\Delta F^{\mathrm{el}} = \Delta F^{\mathrm{el}}_{\mathrm{ph}} + \frac{kT\nu L}{2}\sum_{\alpha}\left(\frac{\lambda_\alpha}{g_\alpha^{1/2}} + \frac{g_\alpha^{1/2}}{\lambda_\alpha}\right) - \nu TS\{g_\alpha\}, \tag{29.27}$$

where L is the number of slip-links per network chain and g_α is the "redistribution parameter" that depends on the number of monomers along the axis α in the deformed network relative to that in the undeformed network. The function $S\{g_\alpha\}$ is related to the entropy of the degrees of freedom corresponding to different positions of slip-links along the chains.

Numerical solution of the slip-tube model yields for the reduced stress [101]

$$f^*(\lambda^{-1}) = G_{\mathrm{ph}} + \frac{G_{\mathrm{e}}}{0.74\lambda + 0.61\lambda^{1/2} - 0.35}. \tag{29.28}$$

In this equation the deformation ratio λ appears only in the entanglement contribution. Thus, the experimental data can be analyzed in the form of a universal plot. Moreover, Eq. (29.28) allows one to separate the phantom and entanglement contributions to the elasticity of the network.

The Mixing Contribution to the Free Energy

So far we have discussed the behavior of networks in the dry state. In the case of a swollen network additional effects must be taken into account. The thermodynamics of mixing is governed by the interaction between the polymer and the solvent molecules. As we have seen in "Network Models" in Section 29.2.2 in gels the fluctuations of the network junctions are significantly altered by the presence of crosslinks. The formulation of a mixing free energy for the swollen network would require the detailed knowledge of the effect of osmotic forces on the size and shape of the fluctuation domains. This is beyond the scope of the existing molecular theories.

Because of the lack of an explicit molecular theory which accounts for the effect of crosslinking on the structure of a polymer solution, it is generally assumed that the functional dependence of the free energy of mixing in the swollen network is the same as in a polymer solution. Although this is a strong approximation, the application of the theoretical free energy functions derived for polymer solutions provides a simple and straightforward way to interpret the results of mechanical and swelling measurements performed on swollen polymer networks. There are two essentially different ways to describe the thermodynamics of polymer solutions: classical (mean field) theories [4] including recent renormalized models [102,103] and asymptotic scaling theories [104,105] based on the analogy found between critical phenomena and polymer chain statistics.

Flory–Huggins Theory of Polymer Solutions

The classical treatment of polymer solution thermodynamics due to Flory and Huggins [4] is based on a lattice model which assumes a uniform polymer segment concentration throughout the entire system. The free energy of mixing of a polymer solution is given by

$$\Delta F_{\mathrm{mix}} = RT[n_1 \ln(1-\varphi) + n_2 \ln\varphi + \chi n_1 \varphi)], \tag{29.29}$$

where φ is the volume fraction of the polymer, χ is the Flory–Huggins interaction parameter, and n_1 and n_2 are the numbers of moles of solvent and polymer, respectively. The chemical potential of the solvent is defined as the derivative of the free energy of mixing with respect to amount of solvent

$$(\Delta\mu_1)_{\mathrm{mix}} = (\partial\Delta F_{\mathrm{mix}}/\partial n_1) = RT[\ln(1-\varphi) + (1-\mathrm{N}^{-1})\varphi + \chi\varphi^2], \tag{29.30}$$

where N is the degree of polymerization. For a crosslinked polymer $N = \infty$. In general, χ depends on the polymer concentration [106], i.e.,

$$\chi = \chi_0 + \chi_1\varphi + \ldots, \tag{29.30a}$$

where χ_0 and χ_1 are constants.

Scaling Theory

In the 1970s a new theory of polymers, taking account of correlations between monomers, was developed based on the analogy found between polymer statistics and critical phenomena [105]. For the chemical potential of mixing in the semidilute region scaling theory yields

$$(\Delta\mu_1)_{\mathrm{mix}} = ART\varphi^n \quad (\varphi^* < \varphi \ll 1), \tag{29.31}$$

where the prefactor A is characteristic of the polymer/solvent system and the value of the exponent n depends on the thermodynamic quality of the solvent. In a good solvent $n \approx 2.31$, and in the theta condition $n=3$. φ^* is the polymer volume fraction above which the domains of the coils start to overlap, i.e., the volume fraction of the polymer inside a separate coil

$$\varphi^* \propto N/R^3 \propto N^{1-3\nu}, \tag{29.32}$$

where ν is the excluded volume exponent, the value of which is $\nu \approx 3/5$ (good solvent condition) or $\nu = 1/2$ (theta condition).

De Gennes proposed a description of the properties of swollen polymer networks based on the analogy found between the swollen network and semidilute polymer solutions (φ^* theorem) [105]. The fully swollen gel is expected to maintain a polymer volume fraction, φ_{e}, which is proportional to the overlap concentration. In good solvent condition

$$\varphi_{\mathrm{e}} = z(f)\varphi^* \propto z(f)(1/2-\chi)^{-3/5}N^{-4/5}, \tag{29.33}$$

where $z(f)$ is a constant factor of the order of unity and f is the crosslink functionality.

Many attempts to explain the results of osmotic and mechanical measurements on swollen polymer networks have invoked analogies with semidilute polymer solutions. Scaling forms for different physical quantities have been derived from the φ^* theorem.

For example, the elastic (shear) modulus of a gel is given by [99,105]

$$G = B(\varphi_e/N_c), \tag{29.34}$$

where φ_e is the volume fraction of the polymer in the fully swollen gel, N_c is the degree of polymerization between crosslink points and B is a constant which depends on the polymer/solvent system. From Eqs. (29.32) and (29.34) it follows that

$$G = B\varphi_e^n, \tag{29.35}$$

where $n = 3\nu/(3\nu - 1)$. Equation (29.35) predicts that the concentration dependence of the elastic moduli of gel homologues (chemically similar gels having different crosslinking densities) follows a simple power law behavior. The value of n depends on the thermodynamic quality of the solvent: in good solvent condition $n \approx 2.31$, in theta condition n=3.

Here we note that in the simple scaling theory used earlier, the polymer is considered as an infinitely thin chain possessing length but not volume. At higher polymer concentration, however, the finite volume of the structural elements may no longer be neglected. Advanced scaling theories [102,103] using the Flory–Huggins lattice model as a starting point are able to incorporate the polymer volume into their formalism.

Swelling of Polymer Networks—The Frenkel–Flory–Rehner Hypothesis

A crosslinked polymer exposed to a thermodynamically compatible diluent absorbs solvent molecules. The driving force of the mixing process is mainly entropic. As the volume increases the network chains are deformed and an elastic retractive force develops. The chain deformation causes a decrease in the entropy, because the extended configuration of the chains is less probable. Equilibrium is achieved when these opposing forces are balanced.

The basic assumption in the Frenkel–Flory–Rehner theory describing the swelling of a crosslinked polymer is that the elastic (ΔF_{el}) and mixing (ΔF_{mix}) contributions in the free energy that accompanies the swelling of the dry network are separable and additive [2,4,5]

$$\Delta F = \Delta F_{el} + \Delta F_{mix}, \tag{29.36}$$

where ΔF is the total free energy of the polymer–solvent system. At equilibrium with the pure solvent (at constant temperature and pressure) the free energy is at minimum with respect to any changes in composition, i.e.,

$$\begin{aligned}(\partial \Delta F/\partial n_1) &= \mu_1 - \mu_1^0 = 0 \\ &= (\mu_1 - \mu_1^0)_{mix} + (\mu_1 - \mu_1^0)_{el},\end{aligned} \tag{29.37}$$

where n_1 is the number of moles of solvent, μ_1 is the chemical potential of solvent in the gel and μ_1^0 is the chemical potential of the pure solvent. The subscripts mix and el refer to the mixing and elastic contributions to the chemical potential, respectively. How the Frankel–Flory–Rehner model can be used to relate macroscopic swelling observations to the molecular structure of the network is developed subsequently.

Experimental Characterization of Swollen Polymer Networks

Molecular theories of rubber elasticity (see ''Network Models'' in Section 29.2.2) allow the interpretation of the experimental data obtained for elastomeric materials in terms of structural characteristics of the network. The most frequently used experimental techniques are stress–strain measurements and swelling measurements.

Stress–Strain Isotherms

Uniaxial stress–strain measurements are often used to characterize polymer networks both in the dry state and in equilibrium with a diluent. The analysis of the stress–strain isotherms is usually performed in terms of the reduced force

$$[f^*] = f^*\varphi^{1/3}/(\alpha - \alpha^{-2}), \tag{29.38}$$

where f^* is the force per unit unstrained cross-section of the unswollen network and α is the deformation ratio relative to the undeformed swollen state of volume V. The relationship between α and λ is given by

$$\lambda_1 = \alpha(V/V_0)^{1/3} \tag{29.39a}$$

and

$$\lambda_2 = \lambda_3 = \alpha^{-1/2}(V/V_0)^{1/3}. \tag{29.39b}$$

In both the phantom and affine models the reduced force is identified with the elastic modulus. In the affine limit the shear modulus is expressed as

$$G_{aff} = [f^*]_{aff} = kT(\nu_{el}/V_0), \tag{29.40}$$

while in the phantom limit

$$G_{ph} = [f^*]_{ph} = kT(\xi/V_0). \tag{29.41}$$

In general, experimental stress–strain isotherms differ from the predictions of the simple statistical theories.

The constrained junction fluctuation theory provides a description of the network behavior which lies between the

affine and phantom limits [36,38–40]. According to this theory the elastic force, f, is the sum of two contributions

$$f = f_{ph} + f_c, \tag{29.42}$$

where f_{ph} is the phantom network contribution and f_c arises from the entanglement constraints. The reduced stress $[f^*]$ is given by

$$[f^*] = kT(\xi/V_0)(1 + f_c/f_{ph}) \tag{29.43}$$

and the expression for f_c/f_{ph} in uniaxial deformations is

$$f_c/f_{ph} = (\mu/\xi)[\alpha K(\lambda_x^2) - \alpha^{-2}K(\lambda_y^2)](\alpha - \alpha^{-2})^{-1}, \tag{29.44}$$

where $\lambda_1 = \lambda$ and $\lambda_2 = \lambda^{-1/2}$. The function K is defined by

$$K(\lambda_t^2) = B_t[B_t^*(B_t + 1)^{-1} + g_t(g_t B_t^* + g_t^* B_t)(g_t B_t + 1)^{-1}], \tag{29.45}$$

where B_t,B_t^* and g_t are the same as in Eqs. (29.18), (29.21) and (29.22).

The ratio f_c/f_{ph} is expected to decrease with increasing deformation, and at $\alpha^{-1} = 0$ the modulus approaches the phantom limit.

The Flory theory considers topological interactions among junctions and chains only in that they restrict junction fluctuations. Ferry [107], Langley [45], Dossin [46] and Graessley [49] assume that these interactions are also present in the small-strain limit. Their argument is based on the existence of a rubbery plateau modulus, G_N^0, which is observed in the viscoelastic properties of high molecular weight linear polymers. The plateau modulus is assumed to be a measure of the entanglement interactions between the chains. In a permanent network the interchain entanglements are fixed due to the presence of the chemical bonds. Dossin and Graessley [46] proposed that

$$G = \nu kT(1 - 2h/f)(V/V_0)^{2/3}/V + T_e G_e^{max}, \tag{29.46}$$

where G is the small-strain modulus, T_e is the fraction of the maximum concentration of topological interactions which are permanently trapped by the network, G_e^{max} is the maximum possible contribution of entangled chains to the modulus, and h is an empirical constant, the value of which is between 0 and 1, depending on the extent to which the junction fluctuations are impeded in the network (h=0 in the affine limit and h=1 in the phantom limit). Thus Eq. (29.46) predicts a small-strain modulus greater than that predicted by the Flory–Erman theory and greater than that of the affine model.

The apparent discrepancy between the Flory theory and the entanglement concept of Dossin and Graessley has been addressed by Gottlieb and Macosco [55]. They pointed out that the two parameters h and κ, both measuring the severity of constraints are related. For the case of a perfect, incompressible, unswollen network the analytical relationship is given by

$$h = 1 - (\kappa^2 + 1)(\kappa + 1 - p/2)^2(\kappa + 1)^{-4}, \tag{29.47}$$

where p is a constant. For the case of the Flory theory p=2. Importantly the Flory–Erman theory has been developed for finite (large) deformations, which is not true of the trapped entanglement model, which resultingly limits the latter's usefulness in terms of making quantitative estimates of experimental results, particularly in large deformation experiments, including swelling.

Swelling Measurements

In addition to mechanical measurements, swelling measurements are frequently used to characterize rubber networks. Of particular interest is the relationship between the molecular weight between crosslinks and the degree of swelling. Unfortunately, the numerical values of the molecular parameters obtained by elastic and swelling measurements strongly depend upon the particular theoretical model used to evaluate the experiments. The model behaviors are described in the following paragraphs. The swelling equation for a phantom network is given as [44,108]:

$$\ln(1 - \varphi_e) + \varphi_e + \chi\varphi_e^2 = -(\xi/N_A V_0)V_1\varphi_e^{1/3}, \tag{29.48}$$

while for an affine network

$$\ln(1 - \varphi_e) + \varphi_e + \chi\varphi_e^2 = -(\xi/N_A V_0)V_1\varphi_e^{1/3}[1 + (\mu/\xi)(1 - \varphi_e^{2/3})], \tag{29.49}$$

where N_A is Avogadro's number and the complexity in Eq. (29.49) arises due to the logarithmic contribution to the free energy in the affine network model (see Eqs. (29.1) and (29.15)).

The corresponding equation according to the Flory–Erman constrained junction fluctuation model is

$$\ln(1 - \varphi_e) + \varphi_e + \chi\varphi_e^2 = -(\xi/N_A V_0)V_1\varphi_e^{1/3}[1 + K(\lambda^2)], \tag{29.50}$$

where $K(\lambda^2)$ was defined previously (see Eq. (29.45)). Queslel *et al*. [108] made a comparison between the values of the molecular network parameters calculated through Eqs. (29.48)–(29.50). The highest value of M_c (chain molecular weight) is obtained by the affine model. The phantom model yields lower M_c than the affine model, because in the former junction fluctuations decrease the impact of chain entropy changes. Using Eq. (29.49) the same elastic contribution as that of an affine network is thus achieved if ξ is higher (or correspondingly M_c is smaller). The value of M_c determined from the Flory–Erman model lies between these limiting values. It is worth mentioning that Eqs. (29.48) and (29.49) enable one to estimate a range for M_c without any prior knowledge of the network structure.

Both the affine and the phantom network models predict that the reduced stress, [f*], measured in uniaxial deformation is independent of the deformation ratio. However, it

became clear from early studies of rubber elasticity that real networks, in general, exhibit significant departures from this prediction: the reduced stress decreases with elongation and also with increasing swelling. It was recognized that the limiting value of the reduced stress at high elongation or swelling ratio is a characteristic quantity of the network.

The detailed calculations according to the constrained junction fluctuation model and other advanced models can only be performed numerically. The fitting of the stress–strain (or swelling) data to the Flory–Erman model, in principle, requires three parameters: $[f^*]_{ph}$, κ and ζ. Here we briefly outline the steps of the fitting procedure [113,114]:

1. In many cases it is reasonable to take the initial value of $[f^*]_{ph} = 2C_1$, where $2C_1$ is the first Mooney–Rivlin constant. An alternative possibility is to estimate $[f^*]_{ph}$ from the stoichiometry of the chemical reaction using Eqs. (29.12)–(29.14) and (29.41).

2. The initial value of κ can be obtained from the Flory–Erman theory on the basis of the following argument [109]. Since κ is assumed to be proportional to the number of chains sharing the volume occupied by one chain, it is the measure of the degree of interpenetration of the network chains, i.e.,

$$\kappa = I<r^2>_0^{3/2}(\nu/V_0), \tag{29.51}$$

where $<r^2>_0$ is the unperturbed dimension of a chain and I is a proportionality constant. Expressing Eq. (29.51) in terms of measurable quantities one gets [109]

$$\kappa = A(2C_1)^{-1/2}\varphi_c^{(4/3)+m}, \tag{29.52}$$

where φ_c is the volume fraction of the polymer at crosslinking and

$A = I(<r^2>_{0/M})^{3/2}(1 - 2/f)N_A^{3/2}\rho^{3/2}/(kT)^{1/2}$, where N_A is Avogadro's number, ρ is the density of the polymer and f is the crosslink functionality. The experimental value of A is the order of unity (for PDMS networks Erman and Mark [110] reported A=1.29 and m=0.385).

3. In a first approximation the parameter ζ can be assumed to be zero.

4. Using these initial values the differences between theory and experiment should be minimized. In order to achieve this the value of κ obtained in step (2) is used to calculate $[f^*]_{ph}$ from Eqs. (29.43) and (29.44). Then $2C_1$ in Eq. (29.52) is replaced by $[f^*]_{ph}$ to obtain a new value of κ. These steps are iterated until κ converges. Using the new values of $[f^*]_{ph}$ and κ the function $[f^*]$ vs. α^{-1} is calculated from Eq. (29.43).

5. The procedure described in 4 is repeated for a new value of m (and A), and the values of $[f^*]_{ph}$ and κ are recalculated. The calculation is continued until the error between the experimental and the calculated data reaches a minimum.

6. If the agreement between calculated data and experiment is still not satisfactory, the value of ζ can be varied to match theory and experiment. The values of ζ giving the best agreement with experiments are usually close to zero.

29.3 ANALYSIS OF EXPERIMENTAL RESULTS

29.3.1 General Comments

The primary goal of the molecular theories is to derive the structure–property relationships for polymeric networks. A quantitative understanding of the dependence of the physical properties upon the network structure is essential to deduce molecular parameters (e.g., molecular weight between crosslinks) from measurements. This is also required to synthesize new polymer networks having desired physical properties.

To test the validity of different network theories is particularly difficult because the structure of the network, at the molecular level, is unknown. Usually crosslinks are introduced in a less perfectly controlled manner than desired. The extent of imperfections depends on the mechanism of the crosslinking process, e.g., clustering of chains or junctions may lead to deviations from the complete randomness assumed in the theories. In many cases, the distribution of the network chains and junctions is not uniform throughout the sample.

Analysis of the experimental data obtained for model networks having known structure provides a straightforward way of understanding the structure–property relationships. Such model networks can be synthesized by specific chemical reactions, e.g., by end-linking of well-characterized polymer chains through a controlled chemical reaction. The characteristics of the chains, prior to crosslinking, can be determined using the usual solution characterization techniques (gel chromatography, viscometry, etc.). In this way the average molecular weight between crosslinks (M_c) and the distribution of M_c can be varied in a controlled manner. The crosslink functionality (f) is known from the chemistry of the crosslinking reaction. Since ν_{el} and f are known. $\xi = \nu_{el} - \mu_{el} + 1$ is also known. Assuming that the chemical reaction between the endgroups of the chains and the crosslinking agent is stoichiometric, and that the effects of entanglements and network imperfections (cycles, pendent chains) are negligible, the elastic properties of the gel can be predicted. Equations (29.40) and (29.41) allow the elastic modulus both in the phantom and the affine limits to be calculated. The decrease of the modulus with λ depends on the values of κ and ζ in the Flory–Erman theory. Unfortunately, this theory does not make an a priori prediction for these parameters. Since no independent information is available about the actual size of fluctuation domains of junctions and about the anisotropy of these domains, the values of κ and ζ can only be determined empirically using a fitting procedure such as that described in "Swelling Measurements" in Section 29.2.2

The testing of the network models with regard to the prediction of the equilibrium swelling degree of the crosslinked polymer as a function of the thermodynamic activity of the diluent requires further assumptions concerning the mixing free energy contribution. This term is supposed, firstly, to be separable from the total change in the free energy (see Eq. 29.36) and, secondly, to be identical for the gel and for the solution of the uncrosslinked polymer of infinite molecular weight. The latter assumption presumes that the polymer solvent interaction parameter is unaffected by the presence of crosslinks. Thus, the only difference between the swollen network and the polymer solution is the existence of a permanent elastic modulus and the theoretical dependence of the equilibrium volume fraction upon the molecular parameters is predicted by Eqs. (29.48)–(29.50).

The structure of any real network exhibits departures from that of the ideal (model) network. A comparison between the experimental and theoretical values of the network parameters provides quantitative information on the deviation from the behavior of the hypothetical model system, and allows one to treat real networks by reference to the structural parameters of a perfect network.

In the following sections typical experimental results obtained for different network systems and analyzed using several of the theoretical approaches are briefly reviewed. For a more extensive discussion, we refer the reader to a work by Han, Horkay, and McKenna [111] where a critical evaluation of many of the modern theories of molecular rubber elasticity was performed. Based on an analysis of carefully selected data sets reported in the literature, these authors concluded that, of the tested models, the Flory–Erman theory and its modified versions provided the best agreement with the stress–strain data in both the dry and the swollen states for polymer networks.

29.3.2 Determination of the Model Parameters from Stress–Strain Measurements

A large amount of experimental work has been reported on the stress–strain behavior of swollen polymeric networks. Fitting of stress–strain data measured at different degrees of dilution to Eqs. (29.43)–(29.45) enables one to determine ξ,κ, and ζ.

Erman and Flory [39] reanalyzed the data of Allen *et al.* [112] on swollen natural rubber samples crosslinked with dicumyl peroxide. It was found that the shape of the $[f^*]$ vs. α^{-1} curves in a wide range of dilution in *n*-decane ($0.24<\varphi<1$) can be well reproduced using a single set of parameters $[f^*]_{ph} = 0.166\,\mathrm{Nmm^2}$, $\kappa = 8$, and $\zeta = 0.12$. Similar analysis of the data of Flory and Tatara [33] for radiation crosslinked PDMS samples swollen in benzene yields the values $[f^*]_{ph} = 0.136\,\mathrm{MPa}$, $\kappa = 6$, and $\zeta = 0.12$. For poly(ethyl acrylate) networks [37] having different crosslink densities swollen in bis(2-ethoxyethyl)ether κ varied in the range 1.8–16.0, and ζ varied between 0.0 and 0.1. It was also found that the stress–strain isotherms for the same networks in the unswollen state and in swelling equilibrium with a diluent are consistently described by the same set of parameters, κ and ζ. Typical $[f^*]$ vs. α^{-1} data set along with the fit of the Flory–Erman theory is shown in Fig. 29.5.

Swelling equilibrium measurements provide an independent route to determine $[f^*]_{ph}$. At swelling equilibrium the sum of the contributions to the chemical potential from

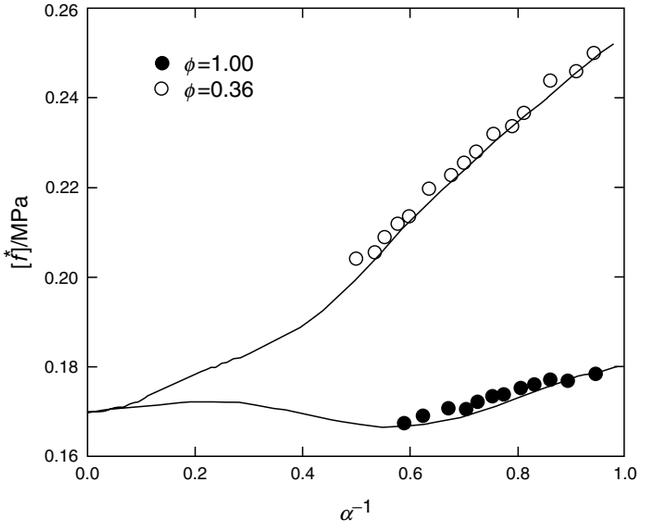

FIGURE 29.5. "Mooney–Rivlin" reduced stress plot showing comparison of experimental data with modified constrained chain model (MCC) predictions for dry (○) and swollen (●) natural rubber networks [112, 117]. Swelling agent: *n*-Decane. continuous lines are theoretical curves calculated with paremeters $\xi kT/V_0 = 0.17\,\mathrm{MPa}$ and $\kappa_G = 2.0$.

mixing and from the elastic deformation of the network should be zero (see Eq. 29.37). Thus

$$0 = \ln(1-\varphi) + \varphi + \chi\varphi^2 + (V_1\xi/N_A V_0)\lambda^{-1} [1 + K(\lambda^2)], \quad (29.53)$$

where N_A is the Avogadro number. Substitution for ξ/V_0 according to Eq. (29.41) yields

$$[f^*]_{ph} = -(RT/V_1)[\ln(1-\varphi) + \varphi + \chi\varphi^2]\lambda / [1 + K(\lambda^2)], \quad (29.54)$$

where $K(\lambda^2)$ is defined by Eq. (29.45).

Using Eq. (29.54) Erman and Flory [39] analyzed the results of Mark and Sullivan [113] on end-linked PDMS networks swollen in benzene as well as the data from Erman, Wagner, and Flory [37] on poly(ethyl acrylate). They compared the values of $[f^*]_{ph}$ obtained from stress–strain isotherms and swelling measurements with data calculated from the chemistry of crosslinking. The $[f^*]_{ph}$ values derived from elasticity measurements were slightly higher than those calculated from the known molecular weights of the primary chains on the basis of stoichiometry. The deviation was attributed to possible departures from equilibrium in the force measurements. The most pronounced departure was observed for networks of low degrees of crosslinking in which the approach of equilibrium is protracted. No such deviation was detected for $[f^*]_{ph}$ obtained from swelling measurements. The satisfactory agreement between the experimental and the calculated values of $[f^*]_{ph}$ led the authors to the conclusion that trapped entanglements do not have a significant contribution to the elastic response of the network. If the effective degree of interlinking is enhanced by discrete entanglements, the values of $[f^*]_{ph}$ deduced from elastic or swelling measurements should exceed the chemical values of $kT\xi/V_0$ calculated from the chemistry of crosslinking.

Gottlieb *et al*. [54] reached the opposite conclusion by the analysis of data on PDMS from different sources, including the same data set of Mark and Sullivan [113]. They argue that trapped entanglements contribute substantially to the stress. Erman and Flory [39] criticized this interpretation on several grounds. Their main criticism was that Gottlieb *et al*. [54] confined their attention to stresses at small strains and did not deduct the contribution to the reduced stress from restraints on junction fluctuations. In the analysis of Gottlieb *et al*. such fluctuations are assumed to be totally suppressed at small strains, as if $\kappa = \infty$ for all networks, and the contribution arising from the constraints is treated as a constant fraction of the reduced stress. This procedure may enhance the reduced forces by factors that increase with decreasing crosslink density, and lead to a finite value of $[f^*]_{ph}$ at $\xi = 0$. According to Flory and Erman [39] the large entanglement contribution in the analysis conducted by Gottlieb *et al*. [54] is largely a fiction of their data treatment.

A comprehensive analysis of previously reported stress–strain data for five different elastomers both in the swollen and unswollen states was performed on the basis of the Flory–Erman theory by Brotzman and Mark [114] (Table 29.1). They found that, in most cases, as the polymer volume fraction decreases, the value of κ required to describe the experimental data also decreases. The analysis also revealed that when ζ is set to zero the high-extension intercept of the $[f^*]_{ph}$ vs. α^{-1} curves is practically independent of the degree of swelling. In Table 29.2 the values of $2C_1$ and $2C_1 + 2C_2$ obtained for the same networks by using the linear Mooney–Rivlin equation of the reduced force, $[f^*] = 2C_1 + 2C_2\alpha^{-1}$, are listed. The $2C_1$ values are in reasonable agreement with the $[f^*]_{ph}$ data given in Table 29.1, indicating that the Mooney–Rivlin treatment can yield similar estimates of the cycle rank of the network as does the more detailed theoretical approach. Poorer agreement was found between $[f^*]_{ph}$ and $2C_1$ by Sharaf and Mark [115]. These authors re-examined the small-strain modulus data reported for unswollen PDMS model networks (Table 29.3). The values $[f^*]_{ph}$ were found two- or threefold lower than the corresponding values of $2C_1$. For comparison in Table 29.4 the characteristic quantities of the same PDMS model networks are given in terms of the entanglement model (see Eq. (29.46)).

Fontaine *et al*. [116,117] compared the prediction of the constrained chain models with the results of elongation measurements performed on dry and swollen natural rubber, poly(ethylene oxide), polybutadiene, poly(dimethylsiloxane) and *cis*-1,4-polyisoprene networks. In Table 29.5 the parameters obtained by analysis of the same network systems using both the CC and the MCC models are listed. It was found that the strong dependence of the reduced force on extension and swelling, observed in all the experiments, can be satisfactorily described by the constrained chain models. The value of the parameter, κ_G, varies between 0.9 and 6.0 for all five network systems investigated. (The other parameter, $\xi kT/V_0$, required to describe the strain and swelling dependence of the data is obtained directly from the experimental stress–strain isotherms at $\alpha^{-1} = 0$.) In the framework of the Flory–Erman model quantitative agreement between the theory and the data for the polybutadiene and poly(ethylene oxide) networks has been achieved only when both κ and the phantom modulus $\xi kT/V_0$ were allowed to be dependent on φ. The formulation according to the constrained chain models, however, does not require φ dependent values of $\xi kT/V_0$ and κ_G.

Kloczkowski, Mark, and Erman [95] compared the prediction of the diffused constraint model with the results of the Flory constrained-junction fluctuation theory [36] and the Erman–Monnerie constrained chain theory [94]. They found that the shapes of the [*f**] vs. α^{-1} curves for all three theories were very similar. Rubinstein and Panyukov [101] reanalyzed the data of Pak and Flory [118] obtained for uniaxially deformed crosslinked PDMS samples. They concluded that the fit of the experimental data by the diffused

TABLE 29.1. *Parameters of the stress–strain isotherms calculated from the fit of the Flory–Erman model for different networks systems [114].*

Polymer[a]	Diluent	f	Crosslinker	T (°C)	φ	$[f^*]_{ph}$ (MPa)	κ	ζ
PDMS [134]	Lin. PDMS	4	γ-Irradiation	30	1.00	0.0325	7.66	0.00
					0.80	0.0317	4.79	0.00
					0.60	0.0317	4.10	0.00
					0.40	0.0318	3.96	0.00
					1.00	0.0355	6.75	0.05
					0.80	0.0334	4.91	0.05
					0.60	0.0330	5.02	0.05
					0.40	0.0333	4.69	0.05
					1.00	0.0366	6.94	0.10
					0.80	0.0341	6.09	0.10
					0.60	0.0335	7.72	0.10
					0.40	0.0343	9.96	0.10
PDMS [134]	Lin. PDMS	4	γ-Irradiation	30	1.00	0.0245	14.3	0.00
					0.80	0.0238	4.74	0.00
					0.60	0.0232	4.63	0.00
					0.40	0.0221	4.35	0.00
PDMS [134]	Lin. PDMS	4	γ-Irradiation	30	1.00	0.0146	15.3	0.00
					0.80	0.0139	8.23	0.00
					0.60	0.0129	10.8	0.00
					0.40	0.0130	4.77	0.00
PBD-S [135]	1,2,4-Trichlorobenzene	4	1% Sulfur	25	1.00	0.222	7.93	0.00
					0.80	0.213	6.43	0.00
					0.60	0.204	6.74	0.00
					0.40	0.192	8.07	0.00
					0.20	0.212	5.21	0.00
					1.00	0.245	6.83	0.05
					0.80	0.232	6.04	0.05
					0.60	0.227	5.47	0.05
					0.40	0.219	7.68	0.05
					0.20	0.231	12.0	0.05
					1.00	0.250	10.3	0.10
					0.80	0.237	7.77	0.10
					0.60	0.232	8.12	0.10
					0.40	0.229	25.0	0.10
					0.20	0.240	4.81	0.10
PBD-G [135]	1,2,4-Trichlorobenzene	4	γ-Irradiation	10	1.00	0.107	20.2	0.00
					0.80	0.097	16.4	0.00
					0.60	0.98	9.77	0.00
					0.40	0.93	8.11	0.00
					0.20	0.93	6.78	0.00
		24		10	1.00	0.162	24	0.00
					0.80	0.135	20	0.00
					0.60	0.127	22.8	0.00
					0.40	0.111	27.2	0.00
					0.20	0.101	29.7	0.00
PBDG-P [135]	1,2,4-Trichlorobenzene	4	1% BPO	10	1.00	0.147	2.96	0.00
					0.80	0.143	2.16	0.00
					0.60	0.142	1.42	0.00
					0.40	0.142	0.84	0.00
					0.20	0.140	1.07	0.00
		24		10	1.00	0.164	18.2	0.00
					0.80	0.153	16.1	0.00
					0.60	0.143	17.7	0.00
					0.40	0.138	25.4	0.00
					0.20	0.136	23.0	0.00

TABLE 29.1. *Continued.*

Polymer[a]	Diluent	f	Crosslinker	T (°C)	φ	$[f^*]_{ph}$ (MPa)	κ	ζ
PIB [136]	1,2,4-Trichlorobenzene	4	Disulfide	30	1.00	0.082	10.0	0.00
					0.80	0.083	2.44	0.00
					0.60	0.073	3.98	0.00
					0.40	0.070	2.65	0.00
				20	1.00	0.166	3.22	0.00
					0.80	0.104	3.74	0.00
					0.60	0.104	2.75	0.00
					0.40	0.095	3.14	0.00
				15	1.00	0.131	3.95	0.00
					0.80	0.123	4.11	0.00
					0.60	0.119	2.16	0.00
					0.40	0.107	1.21	0.00
POE [137]	Phenylacetate	3	Triisocyanate	25	1.00	0.721	1.14	0.00
					0.597	0.637	1.58	0.00
					0.565	0.549	2.26	0.00
					0.488	0.337	14.8	0.00
					0.390	0.608	1.58	0.00
POE [137]	Phenylacetate	3	Triisocyanate	25	0.429	0.608	1.56	0.00
					0.325	0.240	2.52	0.00
					0.220	0.259	0.960	0.00
POE [137]	Phenylacetate	3	Triisocyanate	25	0.457	0.314	1.29	0.00
					0.341	0.345	1.19	0.00
					0.291	0.314	1.29	0.00
					0.488	0.337	14.8	0.00
					0.390	0.608	1.58	0.00
POP [138]	Benzene		Tris(*p*-phenylisocyanate)	60	0.216	0.285	2.0	0.00
					0.216	0.315	2.2	0.00
			$M_c = 3{,}000$		0.286	0.400	1.5	0.00
			$M_c = 2{,}000$		0.286	0.417	1.7	0.00
					0.273	0.376	1.7	0.00
			$M_c = 1{,}025$		0.406	0.805	0.5	0.00
					0.421	0.773	0.5	0.00
			$M_c = 725$		0.464	0.750	0.5	0.00
					0.456	0.769	0.5	0.00
			$M_c = 730$		0.473	0.725	0.4	0.00
					0.477	0.758	0.4	0.00
					0.440	0.755	0.4	0.00
			$M_c = 740$		0.522	0.695	0.5	0.00
					0.519	0.645	0.4	0.00
			$M_c = 725$		0.480	0.850	0.5	0.00
					0.510	0.829	0.4	0.00

[a]PDMS: poly(dimethylsiloxane); PDB: *cis*-1,4-polybutadiene; PIB: polyisobutylene; POE: poly(oxyethylene); POP: poly(oxypropylene).

constraint model was significantly better than by the Mooney–Rivlin expression or by the nonaffine tube model [97].

Urayama *et al*. [119–121] tested the diffused constraint model using both uniaxial compression and equibiaxial elongation data for end-linked PDMS networks in which trapped entanglements were dominant in number relative to chemical crosslinks. The parameter κ was used as an empirical fitting parameter, and the best-fit procedure yielded $\kappa = 2.9$. The structural parameters (ν, ξ, μ, f) were estimated from the stoichiometry using the Miller–Macosko model [56] in conjunction with the measured sol fraction. They concluded that the diffused constraint model successfully reproduced the reduced stress–strain data over a wide range of deformations, but the model underestimated the modulus, G, because it did not consider trapped entanglements as additional crosslinks contributing to G. The theoretical value of G calculated using $\kappa = 2.9$ was approximately one order of magnitude smaller (G=5.22 kPa) than the experimental value (G=64.9 kPa).

TABLE 29.2 *Mooney–Rivlin parameters of the stress–strain isotherms for different networks systems [114].*

Polymer	Diluent	f	Crosslinker	T (°C)	φ	$2C_1$ (MPa)	$2C_1 + 2C_2$ (MPa)
PDMS	Lin. PDMS	4	γ-Irradiation	30	1.00	0.0304	0.0571
					0.80	0.0298	0.0476
					0.60	0.0299	0.0433
					0.40	0.0305	0.0398
PDMS	Lin. PDMS	4	γ-Irradiation	30	1.00	0.0218	0.0533
					0.80	0.0220	0.0365
					0.60	0.0218	0.0324
					0.40	0.0208	0.0290
PDMS	Lin. PDMS	4	γ-Irradiation	30	1.00	0.0118	0.0364
					0.80	0.0121	0.0255
					0.60	0.0117	0.0230
					0.40	0.0126	0.0168
PBD-S[a]	1,2,4-Trichlorobenzene	4	1% Sulfur	25	1.00	0.203	0.406
					0.80	0.202	0.343
					0.60	0.202	0.302
					0.40	0.196	0.272
					0.20	0.204	0.254
PBD-G	1,2,4-Trichlorobenzene	4	γ-Irradiation	10	1.00	0.0904	0.280
					0.80	0.0864	0.210
					0.60	0.0915	0.167
					0.40	0.0933	0.135
					0.20	0.0878	0.117
		24		10	1.00	0.0904	0.28
					0.80	0.0868	0.210
					0.60	0.0915	0.167
					0.40	0.0933	0.135
					0.20	0.0878	0.117
PBDG-P	1,2,4-Trichlorobenzene	4	1% BPO	10	1.00	0.142	0.228
					0.80	0.140	0.178
					0.60	0.138	0.160
					0.40	0.138	0.150
					0.20	0.142	0.144
		24		10	1.00	0.164	0.168
					0.80	0.140	0.178
					0.60	0.138	0.160
					0.40	0.138	0.150
					0.20	0.135	0.144
PIB	1,2,4-Trichlorobenzene	4	Disulfide	30	1.00	0.072	0.159
					0.80	0.083	0.103
					0.60	0.074	0.0953
					0.40	0.073	0.0777
				20	1.00	0.113	0.165
					0.80	0.0976	0.148
					0.60	0.104	0.131
					0.40	0.0905	0.115
				15	1.00	0.128	0.194
					0.80	0.123	0.170
					0.60	0.114	0.145
					0.40	0.108	0.114
POE	Phenylacetate	3	Triisocyanate	25	1.00	0.744	0.934
					0.597	0.660	0.795
					0.565	0.613	0.722
					0.488	0.575	0.732
					0.390	0.593	0.715
POE	Phenylacetate	3	Triisocyanate	25	0.429	0.251	0.320
					0.325	0.231	0.296
					0.220	0.263	0.266

TABLE 29.2 *Continued*

Polymer	Diluent	f	Crosslinker	T (°C)	φ	$2C_1$ (MPa)	$2C_1 + 2C_2$ (MPa)
POE	Phenylacetate	3	Triisocyanate	25	0.457	0.280	0.390
					0.341	0.329	0.402
					0.291	0.310	0.348
POP	Benzene		Tris(*p*-phenylisocyanate)	60	0.216	0.322	0.423
					0.216	0.328	0.477
			$M_c = 3{,}000$		0.286	0.450	0.546
			$M_c = 2{,}000$		0.286	0.448	0.594
					0.273	0.398	0.537
			$M_c = 1{,}025$		0.406	0.839	0.899
					0.421	0.839	0.859
			$M_c = 725$		0.464	0.810	0.835
					0.456	0.847	0.851
			$M_c = 730$		0.473	0.779	0.785
					0.477	0.796	0.832
					0.440	0.814	0.817
			$M_c = 740$		0.522	0.723	0.776
					0.519	0.647	0.713
			$M_c = 725$		0.480	0.861	0.959
					0.510	0.891	0.904

It should be noted that the effect of G is cancelled when reduced stress–strain data are analyzed. This explains the success of this model in describing the shape of the experimental curves. On the basis of the diffused constraint theory a detailed comparison between theory and experiment on swollen polymer networks has not yet been made.

TABLE 29.3. *Parameters of the stress–strain isotherms calculated from the Flory–Erman model for unswollen PDMS model networks[115].*

M_n(g mol^{-1})	f	$[f^*]_{ph}$(MPa)	κ	$2C_1$(MPa)	$2C_2$(MPa)
32,900	3	0.013	19.4	0.033	0.034
25,600	3	0.014	18.2	0.043	0.052
18,500	3	0.021	15.0	0.066	0.061
9,500	3	0.053	9.5	0.093	0.057
4,700	3	0.075	7.9	0.148	0.011
4,000	3	0.101	6.8	0.192	0.015
45,000	4	0.008	22.3	0.038	0.030
32,900	4	0.015	16.4	0.058	0.042
25,600	4	0.028	11.9	0.084	0.055
18,500	4	0.023	13.3	0.089	0.040
9,500	4	0.062	8.0	0.167	0.050
4,700	4	0.119	5.8	0.353	0.031
4,000	4	0.195	4.5	0.395	0.021
18,500	4	0.020	14.3	0.096	0.043
18,500	4	0.020	14.3	0.089	0.043
18,500	4	0.020	14.3	0.089	0.040
11,300	4	0.082	7.0	0.196	0.083
11,300	4	0.079	7.1	0.169	0.115
11,300	4	0.084	6.9	0.199	0.076
11,300	4	0.064	7.9	0.188	0.092
11,300	4	0.060	8.2	0.178	0.098
11,300	4	0.062	8.1	0.165	0.120
21,500	4	0.038	10.3	0.142	0.098
11,100	4	0.086	6.8	0.207	0.087
8,800	4	0.104	6.2	0.244	0.084

TABLE 29.4. *Parameters of the stress–strain isotherms for PDMS model networks calculated from the entanglement model (Eq. (29.46)) [54].*

M_n(g mol^{-1})	f	T (K)	$10^{-5}G$(Pa)	$10^{-5}(\nu RT)$(Pa)	T_e
32,900	3	298	0.699	0.286	0.467
25,600	3		0.947	0.377	0.474
18,500	3		1.27	0.508	0.467
9,500	3		1.50	1.41	0.641
4,700	3		1.59	2.00	0.467
4,000	3		2.07	2.66	0.536
45,000	4	298	0.68	0.185	0.278
32,900	4		1.00	0.335	0.38
25,600	4		1.40	0.618	0.571
18,500	4	298	1.29	0.517	0.324
9,500	4		2.17	1.38	0.466
4,700	4		3.84	2.63	0.439
4,000	4		4.16	4.185	0.625
18,500	4		1.35	0.45	0.278
11,300	4	298	2.79	1.72	0.744
11,300	4		2.84	1.68	0.723
11,300	4		2.75	1.77	0.769
11,300	4		2.75	1.50	0.804
11,300	4		2.76	1.41	0.752
11,300	4		2.85	1.44	0.771
21,600	4	298	2.40	0.871	0.774
11,100	4		2.94	1.87	0.866
8,800	4		3.28	2.28	0.783

29.3.3 Determination of the Model Parameters from Swelling Measurements

Swelling of elastomers in a solvent is a relatively simple technique for the characterization of polymer networks. Empirical information, such as the degree of swelling and the elastic modulus, can be obtained by direct measurements. Equilibrium swelling measurements and stress–strain measurements are the most frequently used methods for determining the relative degree of crosslinking. A quantitative analysis of the swelling data, however, requires further considerations.

According to the Frenkel–Flory–Rehner hypothesis the elastic and mixing contributions to the free energy are additive, and the mixing free energy for the network is the same as that of the corresponding uncrosslinked polymer. It follows from these assumptions that the thermodynamic activity of the solvent in the network contains two separable contributions, $a_{1,c}$ and $a_{1,u}$, representing the diluent activities in the crosslinked and the uncrosslinked polymers, respectively, and the ratio $a_{1,c}/a_{1,u}$ at identical concentrations yields the elastic component of the solvent activity. Experimental tests of this prediction have been performed by differential sorption measurements first conducted by

TABLE 29.5. *Network parameters calculated by the constrained chain (CC) and modified constrained chain (MCC) models [116,117].*

System	Crosslinker[a]	φ	$\xi kT/V_0$ (MPa)		κ_G	
			CC	MCC	CC	MCC
cis 1,4-	DCP 1.3%	0.197	0.312	0.325	1.1	0.9
Isoprene/	DCP 0.75%	0.165	0.215	0.220	1.6	1.6
benzene	DCP 0.30%	0.133	0.115	0.125	3.0	2.5
T=25 °C	DCP 0.20%	0.112	0.083	0.092	3.8	3.0
	DCP 0.10%	0.081	0.043	0.045	5.0	6.0
NR/*n*-decane	DCP	0.24–1.0	0.150	0.170	3.0	2.0
PEO/phenylac.	isocyanate	0.22–1.0	0.260	0.275	1.5	1.6
PBD/chl.benz.	sulfur	0.2–1.0	0.235	0.235	2.0	2.6
PDMS/benzene	el.radiation	0.32–1.0	0.125	0.135	2.5	2.0

[a]DCP: dicumyl peroxide.

Gee *et al*. [122]. In this experiment on natural rubber/benzene system the vapor pressure of the solvent and the amount of solvent absorbed by the crosslinked and uncrosslinked rubbers were determined simultaneously by using a sensitive microbalance housed in a vacuum system. Similar experiments were performed by Yen and Eichinger [6], Brotzman and Eichinger [7–9], Neuburger and Eichinger [10], Zhao and Eichinger [11] and McKenna *et al*. [13–16]. Conventionally the results of these measurements are given in term of the dimensionless swelling activity parameter [15] (or dilation modulus [6–11])

$$S = \lambda \ln (a_{1,c}/a_{1,u}). \tag{29.55}$$

Typical theoretical and experimental S vs. $\varphi^{-1/3}(=\lambda)$ curves are shown in Fig. 29.6. The phantom network theory predicts constancy while the affine network model predicts a monotonic increase of S with increasing $\varphi^{-1/3}$. Many of the experimental S vs. $\varphi^{-1/3}$ curves, including that of Gee *et al*. [122] exhibit a maximum. This behavior is consistent with the Flory–Erman theory, although the experimental peak is, in general, much sharper and of significantly greater magnitude than that predicted by the model. Neuburger and Eichinger [10] determined the swelling activity parameter for poly(dimethylsiloxane) networks in benzene and cyclohexane at 20 and 30 °C. They found that the benzene data at 20 °C can be reasonably well described by the Flory–Erman model with the parameters: $\xi/(N_A V_0) = 4.09\times 10^{-4}$ mol/cm^3, $\kappa = 1.0$, and $\zeta = 90$ (this value of ζ is much bigger than that required to fit the stress strain data). The value of the molecular weight between crosslinks, M_c, calculated from the equation $\xi/(N_A V_0) = \rho/2M_c$ was $M_c = 1{,}190$ g/mol. It is significantly smaller than the actual $M_c = 26{,}000$ g/mol. Even larger discrepancies were found between the calculated and the actual values of M_c for the PDMS/cyclohexane system. In this case the best fit was obtained using the phantom network model with $\xi/(N_A V_0) = 0.0012$ mol/cm^3 corresponding to $M_c = 406$ g/mol. The authors concluded that the deviation is the consequence of the breakdown of the Frenkel–Flory–Rehner theory, namely the hypothesis that the elastic and mixing free energies are separable.

McKenna *et al*. [13–16] performed similar investigations on natural rubber networks swollen in different diluents. They assumed that the elastic free energy contribution is adequately described by the phenomenological Valanis–Landel function (see Eq. (29.1)) and for the measured degree of swelling they calculated it from the values of $w'(\lambda_s)$ determined in the unswollen state. Comparing these data with the mixing contribution obtained by using Eq. (29.24) they came to the conclusion that the value of the interaction parameter for the crosslinked polymer, χ_c, exceeds that of the solution of the uncrosslinked polymer, χ_u. This conclusion has been supported by lattice model calculations of Freed and Pesci [123], who pointed out that the effective interaction parameter depends on the crosslink density.

McKenna *et al*. [13–16] use the following relation for the swelling activity parameter:

$$S = \lambda \ln (a_{1,c}/a_{1,u}) = (\chi_c - \chi_u)\lambda^{-5} + V_1 w'(\lambda)/RT\lambda. \tag{29.56}$$

The important point to note from this equation is the assumption that $\chi_c = \chi_u$ often found in the use of the Frenkel–Flory–Rehner hypothesis, has been suppressed. Hence the first term on the right hand side of Eq. (29.56) provides insight into the thermodynamics of swelling and in particular is in accord with the experimental observation that $S \neq 0$ as $\lambda \to 1$, i.e., no swelling. A typical value for $\chi_c - \chi_u$ of

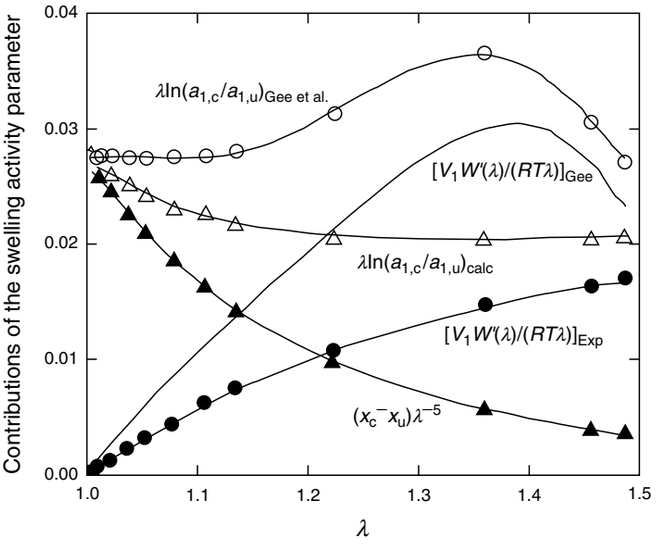

FIGURE 29.6. Thermodynamic parameters that contribute to the swelling activity parameter S vs. the swelling deformation $\lambda_s = \varphi^{-1/3}$. (After Ref. 15 see text for discussion).

0.027 can be obtained by examining the curve labeled $\lambda \ln (a_{1,c}/a_{1,u})_{\text{Gee et al.}}$ of Fig. 29.6 and taking the value at $\lambda = 1$.

In Fig. 29.6 we show the thermodynamic parameters from Eq. (29.56) and a comparison with the swelling data of Gee *et al* [122]. The curve labeled $\lambda \ln (a_{1,c}/a_{1,u})_{\text{Gee et al.}}$ refers to the data obtained by Gee *et al*. for S. The curve labeled $\lambda \ln (a_{1,c}/a_{1,u})_{\text{calc}}$ refers to a calculation of S from Eq. (29.56) using the values of $(\chi_c - \chi_u)\lambda^{-5}$ depicted in the plot on the curve so labeled summed with the values of $[V_1 w'(\lambda)/RT\lambda]_{\text{Exp}}$ determined experimentally by measurements on a rubber similar to that used by Gee *et al*. [122] and depicted with solid circles. The solid line without points labeled $[V_1 w'(\lambda)/RT\lambda]_{\text{Gee}}$ represents the value of the elastic contribution that would have been needed to have in order to agree with the Gee *et al*. [122] results for S, i.e., when added to the measured values of $(\chi_c - \chi_u)\lambda^{-5}$. The deviation between the measured and calculated curves is significant, i.e., the crosslink dependence of the interaction parameter does not provide an adequate explanation for the anomalous behavior of the swelling activity parameter. The reader is referred to McKenna *et al*. [13–16] for further discussion.

McKenna and Crissman [16] also investigated the effect of temperature on the shape of the S vs. $\varphi^{-2/3}(= \lambda^2)$ curves. In the polyisoprene/benzene system they did not observe a maximum in S at 30 and 40 °C, rather a rapid decrease occurred which was followed by a plateau region above $\lambda^2 = 1.2$. At 50 °C, however, a pronounced maximum was found at $\lambda^2 = 1.13$. Neuburger and Eichinger [10] reported similar changes in the swelling behavior for the PDMS/benzene system in the temperature range between 20 and 30 °C. Similar results were reported for changing solvent quality by Zhao and Eichinger [11]. Such abrupt changes in behavior imply significant changes in the free energy of the network over a narrow range of temperatures (or solvent qualities). None of the existing network theories predicts such a possibility.

Sivasailam and Cohen [124] studied the effect of swelling on the elastic modulus of end-linked polydimethyl siloxane networks synthesized at the theta condition from a series of molecular weight precursors ($9{,}900 < M < 101{,}700$) at polymer concentrations from 100% to 40%. These networks exhibited a minimal number of defects as they were prepared from low polydispersity chains at an optimal ratio of crosslinks to precursor chains. The optimum ratio was chosen as the one that produced the network with the highest elastic modulus, the minimum equilibrium swelling, and the minimum soluble fraction. The wide range of precursor molecular weights allowed the investigation of the effect of trapped entanglements as a function of the molecular weight. Equilibrium swelling concentrations were determined in PDMS oligomer ($M_n = 3{,}900$ g/mol), and the elastic modulus was measured at three different states: in swelling equilibrium (fully swollen state), at the concentration at which the network was formed (reference state), and in the unswollen (dry) state (Table 29.6 and Table 29.7). The dependence of the modulus after cure, the dry modulus

TABLE 29.6. *Elastic modulus of end-linked PDMS networks made at different precursor concentrations [124,126].*

Molecular weight (g/mol)	Diluent	Volume fraction φ_{ref}	*Sol fraction w%	G_{ref} (kPa)
101,700		1.00	2.60	111
	PDMS	0.89	2.50	95
	oligomer	0.79	1.28	72
		0.74	2.10	62
		0.67	2.99	50
71,500		1.00	0.28	176
	PDMS	0.89	−1.41	143
	oligomer	0.78	−0.75	98
		0.49	−1.84	48
		0.40	−1.67	27
30,200		1.00	0.26	210
	PDMS	0.89	0.12	168
	oligomer	0.78	0.13	150
		0.70	−0.05	106
		0.59	−0.96	85
		0.50	−2.50	61
		0.40	−4.90	39
9,900		1.00	0.25	343
	PDMS	0.89	−0.07	277
	oligomer	0.80	−0.05	251
		0.69	−0.98	193
		0.57	−3.04	147
		0.51	−6.90	123

*The negative value indicates that solvent is expelled from the swollen network by syneresis. In these gels the amount of uncrosslinked polymer is practically negligible.

TABLE 29.7. *Experimental and calculated values of the elastic modulus of end-linked PDMS networks swollen in PDMS oligomer (M=3,900 g/mol, theta solvent) and in the dry state [124,126].*

Molecular weight (g/mol)	Polymer volume fraction		G_{sw} (kPa)		G_{dry} (kPa)	
	φ_{ref}	φ_θ	Exp.	Calc.	Exp.	Calc.
101,700	1.00	0.38	59	37	111	111
	0.89	0.37	62	32	105	87
	0.79	0.34	45	27	82	68
	0.74	0.32	36	23	71	60
	0.67	0.23	16	16	57	49
71,500	1.00	0.48	129	84	175	191
	0.89	0.44	110	70	148	150
	0.78	0.37	61	52	105	116
	0.50	0.30	36	29	77	51
30,200	1.00	0.51	153	121	210	229
	0.89	0.47	130	101	172	185
	0.78	0.45	109	87	159	148
	0.59	0.37	67	59	98	95
	0.50	0.33	48	48	72	74
9,900	1.00	0.62	280	258	342	363
	0.89	0.59	240	228	286	310
	0.80	0.56	212	203	263	270
	0.69	0.52	161	175	208	226
	0.57	0.47	133	141	172	182

after solvent extraction, and the degree of equilibrium swelling on precursor concentration during cure were compared to scaling predictions. The experimental scaling exponents were found to be strong functions of the molecular weight of the precursor chains and for high molecular weight precursors their values approached the theoretical prediction by Obukhov *et al*. [125] for entanglement-dominated networks. The authors concluded that for networks made of high molecular weight chains a major contribution to the modulus is from trapped entanglements. They also pointed out that at molecular weights below the entanglement molecular weight the modulus of the network is affected by the mutual interpenetration of interspersed chains.

The data of Sivasailam and Cohen were reanalyzed by Graessley [126] in terms of the entanglement model. According to this model the shear modulus at the reference state G_{ref} is the sum of crosslink and entanglement contributions

$$G_{ref} = \nu_{ref} kT + T_0 G_N^0 \varphi_{ref}^{2.3}, \tag{29.57}$$

where G_N^0 is the plateau modulus of the polymer melt (for PDMS $G_N^0 = 0.2\,MPa$), T_0 is the entanglement trapping factor, and φ_{ref} is the volume fraction of the polymer at crosslinking. Assuming that the first term (crosslink contribution) in Eq. (29.57) varies with the concentration as in the phantom network, and the second term (entanglement contribution) varies like the Mooney–Rivlin term C_2, the following equations can be derived

$$G_{ref} = G_0 \varphi_{ref} + T_0 G_N^0 \varphi_{ref}^{2.3}, \tag{29.58a}$$

$$G_{swollen} = G_0 \varphi_{ref}^{2/3} \varphi^{1/3} + T_0 G_N^0 \varphi_{ref} \varphi^{1.3}, \tag{29.58b}$$

$$G_{dry} = G_0 \varphi_{ref}^{2/3} + T_0 G_N^0 \varphi_{ref}^{2.3}, \tag{29.58c}$$

where $G_0 (= \nu kT)$ is the crosslink contribution in the dry state (this excludes trapped entanglement effects). Using Eqs. (29.58a–c) in conjunction with empirically obtained data for T_0 and the sol fraction, the elastic moduli of these gels were calculated (Table 29.7). No systematic deviation can be observed between the predicted and measured moduli.

Urayama *et al*. [127,128] made similar investigations on end-linked PDMS networks cross-linked in solution. The elastic moduli of gels made from M=29,400g/mol and M=4,400 g/mol precursor chains were measured in the fully swollen state in toluene (good solvent), and in the reference state (Table 29.8). The sol fraction of these gels was less than 10%. The same analysis described above indicates that at high polymer volume fractions the calculated and experimental values agree fairly well, while at high swelling ratios the deviation is pronounced [126]. The discrepancy may be the consequence of structural and chemical changes accompanied by the crosslinking process.

In general, the reasonable agreement between the predicted and measured values of the elastic modulus suggests that the effect of swelling on the elastic properties can be approximated as a sum of two distinct contributions: one due to the chemical crosslinks and the other due to the entanglements. The latter in polymer melts is independent of chain lengths and represent an entanglement contribution

TABLE 29.8. *Elastic modulus and polymer volume fraction of end-linked PDMS networks at the preparation state and in the fully swollen state in toluene (good solvent) [127,128].*

Molecular weight (g/mol)	Diluent	Polymer volume fraction		G_{ref} (kPa)	G_{sw} (kPa)
		φ_{ref}	φ_{sw}		
29,400	toluene	1.0	0.187	113	33
		0.852	0.155	93	27
		0.709	0.126	63	17
		0.544	0.093	30	73
		0.411	0.078	19	47
		0.281	0.055	9	2.3
		0.179	0.038	3	0.9
4,400	toluene	1.0	0.275	680	251
		0.777	0.216	423	149
		0.654	0.208	330	137
		0.601	0.194	297	119
		0.584	0.195	301	113
		0.504	0.180	241	100
		0.381	0.140	150	53
		0.298	0.109	61	29

when the network is formed. [126] Chemical crosslinks trap a fraction of this contribution into the structure that governs the elastic response of the network.

29.3.4 Analysis of the Experimental Results on the Basis of the Scaling Theory

The validity of scaling laws has been tested on several swollen network systems (Table 29.9). Munch *et al*. [99] studied the concentration dependence of the shear modulus for polystyrene model networks synthesized by copolymerization of styrene and divinylbenzene and swollen to equilibrium in benzene (good solvent for polystyrene). It was found that the modulus obeys a scaling law with equilibrium concentration, similar to that obtained for semidilute polymer solutions. The best fit to the equation $G = B\varphi_e^n$ yields B=4,200 kPa and n=2.28. Hild *et al*. [129] compared the concentration dependence of the shear moduli of poly(ethylene oxide) networks crosslinked by aliphatic pluriisocyanate in two diluents: dioxane and water. The corresponding scaling laws were found: $G = 8{,}430\varphi_e^{2.30}$ kPa (in 1,4-dioxane) and $G = 10{,}400\varphi_e^{2.51}$ kPa (in water). The exponent obtained in 1,4-dioxane is in excellent agreement with the prediction of the scaling theory. However, for the same networks swollen in water a significantly higher exponent, n=2.51, was obtained. They assumed that the deviation from the theoretical exponent is due to the insolubility of the urethane linkages in water, which may induce inhomogeneities in the gels at the molecular level. Hecht and Geissler [130] investigated the elastic properties of polyacryamide gel homologs in a theta solvent (water–methanol mixture, 3:1 by volume). They found that in the concentration range $0.07<\varphi<0.3$ the longitudinal elastic modulus, E_L, obtained

TABLE 29.9. *Power law exponents for the concentration dependence of the elastic modulus in swollen network homologs.*

System	T (°C)	φ	A (kPa)	n	r	Ref.
NR/*n*-decane	20	0.06–0.40	4,500	2.06	0.992	[139, 140]
PS/benzene	20	0.05–0.20	4,200	2.28	0.955	[99]
PS/benzene	25	0.05–0.50	4,140	2.35	0.993	[99]
PS/cyclohexane	37	0.12–0.28	1,750	3.14	0.980	[28]
PEO/dioxane	25	0.03–0.35	8,430	2.30	0.984	[129]
PEO/water	25	0.03–0.30	10,401	2.51	0.992	[129]
PHPMA	25	0.08–0.35	2,590	2.59	0.995	[129]
PDMS/toluene	25	0.10–0.40	2,650	2.20	0.988	[23]
PVAC/toluene	25	0.06–0.30	2,430	2.27	0.990	[22]
PVAC/acetone	25	0.05–0.25	4,420	2.25	0.992	[22]
PVAC/isopropanol	70	0.10–0.60	3,388	2.31	0.977	[132]
PAA/water	25	0.03–0.30	4,880	2.23	0.991	[141]
PVA/water	25	0.03–0.30	3,500	2.11	0.993	[139]

NR: natural rubber; PS: polystyrene; PEO: poly(ethylene oxide); PHPMA: poly(hydroxi-ethyl-methacrylate); PDMS: polydimethylsiloxane; PVAC: poly(vinyl acetate); PAA: poly(acryamide); PVA: poly(vinyl alcohol); r: correlation coefficient.

from light scattering observations, obeys a scaling law $E_L = 8.090\varphi_e^{3.07}$ kPa in reasonable agreement with the theoretical prediction. Richards and Davidson [131] determined the shear moduli of randomly crosslinked polystyrene networks swollen in cyclohexane at the theta (Θ) temperature and also in toluene (good solvent condition). The power law exponent, n=3.7, reported for the theta system exceeds that of the theoretical value. In good solvent condition (toluene, 20 °C) they found the value n=2.25. A comprehensive study of the dependence of the elastic (shear) modulus on the polymer concentration was performed by Zrínyi and Horkay [132] on poly(vinyl acetate) gels swollen to equilibrium in isopropylalcohol. The thermodynamic quality of the solvent was varied by changing the temperature in the range from 30 °C to 70 °C. Isopropylalcohol is a theta solvent for poly(vinyl acetate) at 52°C and a good solvent at 70 °C. It was found that G vs. φ exhibits a simple power law behavior at each temperature. The exponent n varies between the values of 2.32 (good solvent condition, 70 °C) and 14.1 (poor solvent condition, 30 °C) [133]. At the theta temperature (52 °C) the best fit to the experimental data yields n=3.10.

The osmotic response of swollen polymeric networks was studied on the basis of the scaling theory by Horkay *et al.* [17–19,22,23,133]. They measured both the swelling pressure, ω, and the shear modulus of gels, G, at different stages of dilution. The swelling pressure vs. polymer volume fraction data were analyzed according to the equation [22]

$$\omega = \Pi - G = A\varphi^n - G_v{}^e(\varphi/\varphi_e)^m, \tag{29.59}$$

where Π is the ''osmotic'' pressure of the swollen network and G_v^e is the value of the volume elastic modulus at equilibrium with the pure solvent ($\omega = 0$) and the constant A depends on the polymer/solvent system. The exponents n and m were iteratively adjusted to minimize the variance of ω for each set of data points. The resulting values of A, n, m, and G_v^e for poly(vinyl acetate) gels are displayed in Table 29.10. The n values are consistent with the scaling prediction for the mixing term. Also displayed in Table 29.10 are the values of the shear modulus, G_s^e, measured at the swelling equilibrium condition. The agreement between the numerical values of the shear and the volume elastic moduli provides experimental evidence that in highly swollen networks the separability of the elastic and mixing terms is a reasonable approximation.

29.4 SUMMARY

A survey of the thermodynamics and mechanics of crosslinked gels has been presented. Subjects include the phenomenological description of crosslinked networks within the framework of finite elasticity theory and continuum thermodynamics. Particular emphasis is placed on the Valanis–Landel form of the strain energy density function. Several statistical mechanical models of rubber elasticity are also presented. Of particular usefulness are the affine and phantom network models, which are commonly used to derive information about the molecular parameters of the gel from swelling or mechanical measurements. Techniques for using these models and the more modern Flory–Erman constrained junction model and its most recent modifications are described. Experimental data from the literature are presented and used to deduce molecular parameters for the networks using the different models. The application of Scaling Theory to polymer gels is also considered.

ACKNOWLEDGMENTS

FH acknowledges the support of the Intramural Research Program of the NIH, NICHD. GBM would like to acknowledge the support of the National Science Foundation for partial support of this work under grant DMR-0307084. We also thank J. Wang for help with the figures.

TABLE 29.10. *Swelling pressure and shear modulus parameters of PVAc networks in toluene and acetone [22].*

Sample	φ_e	A	n	m	G_v^e(kPa)	G_s^e(kPa)
Toluene 25 °C						
3/50	0.089	2171	2.28	0.342	8.6	8.9
6/50	0.146	2613	2.29	0.331	31.6	32.4
6/200	0.078	2072	2.22	0.340	7.2	6.9
9/50	0.208	2481	2.27	0.355	70.8	70.3
9/100	0.141	2350	2.25	0.336	28.6	28.3
9/200	0.112	2374	2.27	0.326	16.6	16.7
9/400	0.074	2273	2.27	0.315	6.16	6.26
12/50	0.229	3100	2.35	0.383	95.7	99.8
12/200	0.133	2425	2.26	0.335	25.5	25.2
Acetone 25 °C						
9/100	0.103	4264	2.24	0.321	24.9	25.9
9/200	0.078	4731	2.26	0.346	14.9	14.8
9/400	0.051	4262	2.24	0.369	5.44	5.24

REFERENCES

1. Guth, E. and Mark, H. *Monatshefte*, **65**, 93 (1934).
2. Flory, P.J. and Rehner, J. *J. Chem. Phys.*, **11**, 521 (1943).
3. James, H.M. and Guth, E. *J. Chem. Phys.*, **15**, 651 (1947).
4. Flory, P.J. *Principles of Polymer Chemistry*; Cornell University. Press, Ithaca, NY, 1953.
5. Frenkel, J. *Rubber Chem. Technol.*, **13**, 264 (1940).
6. Yen, L.Y. and Eichinger, B.E. *J. Polym. Sci. Polym. Phys. Ed.* **16**, 121 (1978).
7. Brotzman, R.W and Eichinger, B.E. *Macromolecules* **14**, 1445 (1981).
8. Brotzman, R.W. and Eichinger, B.E. *Macromolecules* **15**, 531 (1982).
9. Brotzman, R.W. and Eichinger, B.E. *Macromolecules* **16**, 1131 (1983).
10. Neuburger, N.A. and Eichinger, B.E. *Macromolecules* **21**, 3060 (1988).
11. Zhao, Y. and Eichinger, B.E. *Macromolecules* **25**, 6988 (1992).
12. Gottlieb, M. and Gaylord, R.J. *Macromolecules* **17**, 2024 (1984).
13. McKenna, G.B., Flynn, K.M. and Chen, Y. *Polym. Commun.* **29**, 272 (1988).
14. McKenna, G.B., Flynn, K.M. and Chen, Y. *Macromolecules* **22**, 4507 (1989).
15. McKenna, G.B., Flynn, K.M. and Chen, Y. *Polymer* **31**, 1937 (1990).
16. McKenna, G.B. and Crissmann, J.M. *J. Polym. Sci B. Polym. Phys.* 35, 817 (1997).
17. Horkay, F. and Zrinyi, M. *Macromolecules*, **15**, 1306 (1982).
18. Horkay, F. and Zrinyi, M. *J. Macromol. Sci. Phys.* **B25**, 307 (1986).
19. Horkay, F., Geissler, E., Hecht, A.M. and Zrinyi, M. *Macromolecules*, **21**, 2589 (1988).
20. Geissler, E., Horkay, F., Hecht, A.M. and Zrinyi, M. *J. Chem. Phys.* **90**, 1924 (1989).
21. Horkay, F., Hecht, A.M. and Geissler, E. *Macromolecules*, **22**, 2007 (1989).
22. Horkay, F., Hecht, A.M. and Geissler, E. *J. Chem. Phys.* **91**, 2706 (1989).
23. Horkay, F., Zrinyi, M., Geissler, E., Hecht, A.M. and Pruvost, P. *Polymer*, **32**, 835 (1991).
24. Horkay, F., Hecht, A.M., Mallam, S., Geissler, E. and Rennie, A.R. *Macromolecules*, **24**, 2896 (1991).
25. Hecht, A.M., Horkay, F., Geissler, E. and Benoit, J.P. *Macromolecules*, **24**, 4183 (1991).
26. Geissler, E., Horkay, F. and Hecht, A.M. *Macromolecules*, **24**, 6006 (1991).
27. Hecht, A.M., Guillermo, A., Horkay, F., Mallam, S., Legrand, J.F. and Geissler, E. *Macromolecules*, **25**, 3677 (1992).
28. Hecht, A.M., Horkay, F., Mallam, S. and Geissler, E. *Macromolecules*, **25**, 6915 (1992).
29. Horkay, F., Burchard, W., Geissler, E. and Hecht, A.M. *Macromolecules*, **26**, 1296 (1993).
30. Horkay, F., Burchard, W., Hecht, A.M. and Geissler, E. *Macromolecules*, **26**, 3375 (1993).
31. Geissler, E., Horkay, F. and Hecht, A.M. *Phys.Rev.Lett.* **71**, 645 (1993).
32. Douglas, J.F. and McKenna, G.B. *Macromolecules*, **26**, 3282 (1993).
33. Flory, P.J. and Tatara, Y. *J. Polym. Sci., Polym. Phys. Ed.*, **13**, 683 (1975).
34. Ronca, G. and Allegra, G. *J. Chem. Phys.*, **63**, 4990 (1975).
35. Flory, P.J. *Proc. R. Soc. Lond.* **A351**, 351 (1976).
36. Flory, P.J. *J. Chem. Phys.*, **66**, 5720 (1977).
37. Erman, B. Wagner, W. and Flory, P.J. *Macromolecules* **13**, 1554 (1980).
38. Flory, P.J. and Erman, B. *Macromolecules* **15**, 800 (1982).
39. Erman, B. and Flory, P.J. *Macromolecules* **15**, 806 (1982).
40. Erman, B. and Flory, P.J. *Macromolecules* **16**, 1600 (1983).
41. Mark, J.E. *Adv. Polym. Sci.*, **44**, 1 (1982).
42. Queslel, J.P. and Mark, J.E. *J. Polym. Sci., Polym. Phys. Ed.* 22, 49 (1984).
43. Queslel, J.P. and Mark, J.E. *Adv. Polym. Sci.*, **65**, 135 (1984).
44. Queslel, J.P. and Mark, J.E. *Adv. Polym. Sci.* **71**, 229 (1985).
45. Langley, N.R. *Macromolecules* **1**, 348 (1968).
46. Dossin, L.M. and Graessley, W.W. *Macromolecules* **12**, 123 (1979).
47. Pearson, D.S. and Graessley, W.W. *Macromolecules* **11**, 528 (1978).
48. Pearson, D.S. and Graessley, W.W. *Macromolecules* **13**, 1001 (1980).
49. Graessley, W.W. *Adv. Polym. Sci.*, **47**, 67 (1982).
50. Marucci, G. *Rheol. Acta* **18**, 193 (1979).
51. Marucci, G. *Macromolecules* **14**, 434 (1981).
52. Gottlieb, M. and Gaylord, R.J. *Polymer* **24**, 1644 (1983).
53. Gottlieb, M., Macosco, C.W. and Lepsch, T.C. *J. Polym. Sci., Polym. Phys. Ed.* **19**, 1603 (1981).
54. Gottlieb, M., Macosco, C.W., Benjamin, G.S., Meyers, K.O. and Merrill, E.W. *Macromolecules* **14**, 1039 (1981).
55. Gottlieb, M. and Macosco, C.W. *Macromolecules* **15**, 535 (1982).
56. Miller, D.R. and Macosco, C.W. *Macromolecules* **9**, 206 (1976).
57. Gaylord, R.J. and Douglas, J.F. *Polym. Bull.* **23**, 529 (1990).
58. Rivlin, R.S. *Philos. Trans. R. Soc.* **A241**, 379 (1948).
59. Treloar, L.R.G. *The Physics of Rubber Elasticity*, Clarendon, Oxford, 1975.
60. Valanis, K.C. and Landel, R.F. *J. Appl. Phys.*, **38**, 2997 (1967).
61. McKenna, G.B. and Hinkley, J.A. *Polymer* **27**, 1368 (1986).
62. Kearsley, E.A. and Zapas, L.J. *J.Rheol.* **24**, 483 (1980).
63. Jones, D.F. and Treloar, L.R.G. *J. Phys. D. (Appl. Phys.)* **8**, 1285 (1975).
64. Mooney, M. *J. Appl. Phys.*, **11**, 582 (1940).
65. Flory, P.J. *Chem. Rev.* 35, 51 (1944).
66. Vega, D.A., Villar, M.A., Alessandrini, J.L. and Valles, E.M. *Macromolecules*, **34**, 4591 (2001).
67. Edwards, S.F. and Muller-Nedebock, K.K. *J. Phys. A—Math. Gen.*, **32**, 3301 (1999).
68. Sommer, J.U., Vilgis, T.A. and Heinrich, G. *J. Chem. Phys.*, **100**, 9181 (1999).
69. Ryzmski, W.M. and Walska, B. *Polimery*, **48**, 246 (2003).
70. Graessley, W.W. *Macromolecules* **8**, 186 (1975).
71. Horkay, F., McKenna, G.B., Deschamps, P. and Geissler, E. *Macromolecules*, **33**, 5215 (2000).
72. Jackson, C.L. and McKenna, G.B. *Rubber Chem. Technol.*, **64**, 760 (1991).
73. Madkour, T. and Mark, J.E. *Polym. Bull.*, **31**, 615 (1993).
74. Saalwachter, K., Kleinschmidt, F. and Sommer, J.U. *Macromolecules*, **37**, 8556 (2004).
75. Ball, R.C., Edwards, S.F. and Warner, M. *Polymer* **22**, 1010 (1981).
76. Ball, R.C. and Edwards, S.F. *Macromolecules* **13**, 748 (1980).
77. DiMarzio, E.A. *J. Chem. Phys.*, **36**, 1563 (1962).
78. DiMarzio, E.A. *Polymer* **35**, 1819 (1994).
79. Deam, R.T. and Edwards, S.F. *Philos. Trans. R. Soc. Lond., A*, **280**, 378 (1978).
80. Edwards, S.F. *Proc. Phys. Soc.*, **92**, 9 (1967).
81. Gaylord, R.J. and Douglas, J.F. *Polym. Bull.*, **18**, 347 (1987).
82. Edwards, S.F. and Vilgis, Th. *Polymer* **27**, 483 (1986).
83. Kilian, H.G. *Polymer* **22**, 209 (1982).
84. Enderle, H.F. and Kilian, H.G. *Prog. Colloid Polym. Sci.*, **75**, 55 (1987).
85. Gao, J. and Weiner, J.H. *Macromolecules* **20**, 2520 (1987).
86. Gao, J. and Weiner, J.H. *Macromolecules* **22**, 979 (1989).
87. Deloche, B. and Samulski, E.T. *Macromolecules* **21**, 3107 (1988).
88. Wall, F.T. *J. Chem. Phys.*, **11**, 527 (1943).
89. Flory, P.J. and Wall, F.T. *J. Chem. Phys.*, **19**, 1435 (1951).
90. Hermans, J.J. *Trans. Faraday Soc.* **43**, 591 (1947).
91. James, H.M. and Guth, E. *J. Chem. Phys.*, **15**, 669 (1947).
92. James, H.M. and Guth, E. *J. Chem. Phys.*, **21**, 1039 (1953).
93. Guth, E. *J. Polym. Sci., Pt. C*, **12**, 89 (1966).
94. Erman, B. and Monnerie, L. *Macromolecules* **22**, 3342 (1989).
95. Kloczkowski, A., Mark, J.E. and Erman, B. *Macromolecules* **28**, 5089 (1995).
96. Douglas, J.F. and McKenna, G.B. in *Elastomeric Polymer Networks*, edited by J.E. Mark and E. Burak, Prentice Hall, Englewood Cliffs, NJ, 1993.
97. Rubinstein, M. and Panyukov, S. *Macromolecules* **30**, 8036 (1997).
98. Doi, M. and Edwards, S.F. *The Theory of Polymer Dynamics*, Clarendon Press, Oxford, England, 1986.
99. Munch, J.P., Candau, S., Herz, J. and Hild, G. *J. Phys.*, **38**, 971 (1977).
100. Doi, M. *J. Polym. Sci., Polym. Phys. Ed.* **21**, 667 (1983).
101. Rubinstein, M. and Panyukov, S. *Macromolecules* **35**, 6670 (2002).
102. Muthukumar, M. and Edwards, S.F. *J. Chem. Phys.*, **76**, 2720 (1982).
103. Muthukumar, M. *J. Chem. Phys.*, **85**, 4722 (1986).
104. des Cloiseaux, J. *J. Phys. (Les Ulis)* **36**, 281 (1973).

105. de Gennes, P.G. *Scaling Concepts in Polymer Physics*, Cornell, Ithaca, NY, 1979.
106. Flory, P.J. *Discuss Faraday. Soc*., **49**, 7 (1970).
107. Ferry, J.D. *Viscoelastic Properties of Polymers*, Wiley, New York, 1970.
108. Queslel, J.P., Fontaine, F. and Monnerie, L. *Polymer* **29**, 1086 (1988).
109. Erman, B. and Mark, J.E. *Macromolecules* **20**, 2892 (1987).
110. Erman, B. and Mark, J.E. *Macromolecules* **25**, 1919 (1992).
111. Han, W.H., Horkay, F. and McKenna, G.B. *Math. Mech. Solids*, **4**, 139 (1999).
112. Allen, G., Kirkham, M.J., Padget, J. and Price, C. *Trans. Faraday Soc*., **67**, 1228 (1971).
113. Mark, J.E. and Sullivan, J.L. *J. Chem. Phys*., **66**, 1006 (1977).
114. Brotzman, R.W. and Mark, J.E. *Macromolecules* **19**, 667 (1986).
115. Sharaf, M.A. and Mark, J.E. *Polymer* **35**, 740 (1994).
116. Fontaine, F., Morland, C., Noel, C., Monnerie, L. and Erman, B. *Macromolecules* **22**, 3348 (1989).
117. Fontaine, F., Noel, C., Monnerie, L. and Erman, B. *Macromolecules* **22**, 3352 (1989).
118. Pak, H. and Flory, P.J. *J. Polym. Phys.,* **17**, 1845 (1979).
119. Kawamura, T., Urayama, K. and Kohjiya, S. *Macromolecules*, **34**, 8252 (2001).
120. Urayama, K., Kawamura, T. and Kohjiya, S. *Macromolecules*, **34**, 8261 (2001).
121. Urayama, K., Kawamura, T. and Kohjiya, S. *J. Chem. Phys*., **118**, 5658 (2003).
122. Gee, G., Herbert, J.B.M. and Roberts, R.C. *Polymer* **6**, 541 (1965).
123. Freed, K.F. and Pesci, A.I. *Macromolecules* **22**, 4048 (1989).
124. Sivasailam, K. and Cohen, C. *J. Rheol*., **44**, 897 (2000).
125. Obukhov, S.P., Rubinstein, M. and Colby, R.H. *Macromolecules,* **27**, 3191 (1994).
126. Graessley, W.W. *Polymeric Liquids and Networks: Structure and Properties*, Garland Science, New York, 2004.
127. Urayama, K. and Kohjiya, S. *J. Chem. Phys*., **104**, 3352 (1996).
128. Urayama, K., Kawamura, T. and Kohjiya, S. *J. Chem. Phys*., **105**, 4833 (1996).
129. Hild, G., Okasha, R., Macret, M. and Gnanou, Y. *Makromol. Chem.* **187**, 2271 (1986).
130. Hecht, A.M. and Geissler, E. *J. Phys*. **39**, 631 (1978).
131. Richards, R.W. and Davidson, N.S. *Macromolecules* **19**, 1381 (1986).
132. Zrinyi, M. and Horkay, F. *Macromolecules* **17**, 2805 (1986).
133. Horkay, F. and Zrinyi, M. *Macromolecules* **21**, 3260 (1988).
134. Chiu, D.S. and Mark, J.E. *Colloid Polym. Sci.* **255**, 644 (1977).
135. Chiu, D.S., Su, T.K. and Mark, J.E. *Macromolecules* **10**, 1110 (1977).
136. Rahalkar, R.R. and Mark, J.E. *Polym. J. (Tokyo)* **12**, 835 (1980).
137. Sung, P.H. and Mark, J.E. *J. Polym. Sci. Polym. Phys. Ed*. **19**, 507 (1981).
138. Andrady, A.L. and Llorente, M.A. *J. Polym. Sci. Polym. Phys. Ed*. **25**, 507 (1987).
139. Horkay, F. and Zrinyi, M. *Polym. Bull*. **4**, 21, 361 (1981).
140. Bristow, G.M. *J. Appl. Polym. Sci*. **9**, 1571 (1965).
141. Geissler, E., Hecht, A.M., Horkay, F. and Zrinyi, M. *Macromolecules* **21**, 2594(1988).

CHAPTER 30

Force Spectroscopy of Polymers: Beyond Single Chain Mechanics

Xi Zhang, Chuanjun Liu, and Weiqing Shi

Department of Chemistry, Tsinghua University, Beijing 100084, P. R. China

Abbreviations

AFM	atomic force microscopy
SMFS	single molecule force spectroscopy
Force curve	force-extension curve
FJC	freely jointed chain
WLC	worm-like chain
PDDA	poly(diallyldimethylammonium chloride)
PFDMS	poly(ferrocenyldimethylsilane)
THF	tetrahydrofuran
M-FJC	modified freely jointed chain
l_k	Kuhn length
L_c	contour length
k_B	Boltzmann constant
l_p	persistence length
CM-amylose	carboxymethyl amylose
CM-cellulose	carboxymethyl cellulose
PFS	poly(ferrocenylsilane)
PDMA	poly(dimethylacrylamide)
PDEA	poly(diethylacrylamide)
FTIR	the Fourier transform infrared spectrum
PEG	poly(ethylene glycol)
PVA	poly(vinyl alcohol)
PS	polystyrene
PNIPAM	poly(*N*-isopropylacrylamide)
PNIPAM-*seg*-PS	poly(*N*-isopropylacrylamide-*seg*-styrene)
F_{MPD}	the most probable desorption force
$V_{stretch}$	stretching velocity
pN	piconewton
PAMPS	poly(2-acrylamido-2-methylpropane-sulfonic acid)

The mechanical property of polymer materials is a classical topic in polymer science, however it is very difficult to be studied at a single chain level. To study and manipulate single polymer chain become possible because of the appearance of AFM [1]. Actually, AFM is not only a tool for the imaging of surfaces with high resolution, but also a high sensitive force sensor. SMFS, a new technique based on AFM, has become a platform for studying the minute force in polymers as well as in supramolecular systems [2–5]. The force signals versus extension curves can provide new insight into traditional aspects of polymer science, and moreover, some new information which is not accessible by conventional methods.

Besides AFM based SMFS, there are several other nanotechnologies which have also been used to measure the minute force in molecular scale, including magnetic beads [6], optical tweezers [7], glass microneedles [8], and biomembrane force probe [9]. These different methods can offer force signals with different timescale and sensitivity. The AFM based SMFS becomes popularized in single polymer chain experiment, because it is relatively easy to be handled. Till now, many elegant experiments have been

done, such as the force–extension relationship of a normal random coil [10–21], for which force curves are fitted well by using the FJC or WLC model; the unfolding force of the titin Ig-domain [22–34], seen as a zigzag-like force curve; the chair-to-boat conformational transition of individual glucopyranose rings [35–43], which may be identified by a plateau in the force curves; the splitting or unwinding force of helical structure [10,11,37,38,44–47], for which a plateau or a kink has been observed in the force curve; and the detachment of single polymer chains from the substrate [48–57], for which a saw-tooth pattern or a long plateau has been achieved; based on the force fingerprint of amylose, the rupture force of silicon–carbon and sulfur–gold bonds has been measured [58].

Here we attempt to briefly introduce the principle of the AFM based SMFS and then focus on using SMFS to address three main questions: force induced conformation transition, interaction between small molecules and polymers, and the interfacial conformation and adhesive energy of polymers.

30.1 THE BASIC PRINCIPLE OF AFM BASED SMFS

30.1.1 The SMFS Methodology

The experiment of SMFS can be described as follows and the schematic drawing is shown in Scheme 30.1. In brief, the polymer chains are physisorbed or chemisorbed onto a solid substrate from their solutions. Then the sample is mounted onto the instrument. A drop of liquid, acting as the buffer, is injected between the substrate and the cantilever holder, and both the substrate and the cantilever are immersed in the buffer. By the movement of the piezo tube, the sample approaches the AFM tip. During this process, when there are no strong long-range interactions, the cantilever stays in its relaxed state, as shown in step 1, so only a base line, part a in graph A, is recorded. When the sample is brought into contact with the AFM tip, there exist a strong repulsion force between the tip and the solid substrate. As a result, the cantilever bends against the substrate, as shown in step 2. This repulsive signal is recorded and converted in the b region, which is perpendicular to the base line. The curve in graph A is called an approaching force curve. During step 2, polymer chains adsorb onto the AFM tip to form bridge structure between the AFM tip and substrate. That bridge structure will be stretched when the tip and substrate separate, resulting in the bending of cantilever toward the substrate, as shown in step 3. This process is traced and shown in region c in graph B. When the bridge structure is stretched further, the weakest part in it will break. At the same time the bent cantilever will go back to its relaxed state rapidly, resulting in a sudden drop of the force, seeing region d. The deflection of the cantilever and the displacement of the piezo tube are recorded at the same time. Then the deflection is converted into force signal, and the relationship between the force and the extension is obtained. More attention is paid to the retracting force curve, since it contains more information about the polymer chain being stretched.

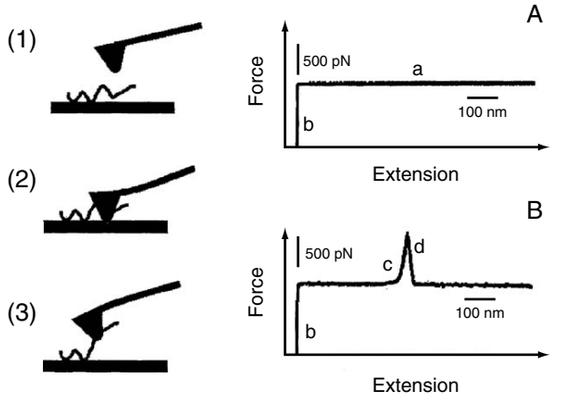

SCHEME 30.1. Schematic drawing of the principle of AFM based SMFS.

One of the key issues of the AFM based SMFS is to build a polymer bridge between the AFM tip and the substrate. The polymer chain can be immobilized onto the substrate by physical or chemical adsorption. In the physical adsorption, the polymer chains are simply adsorbed onto the substrate from their dilute solution. The physical adsorption is not that weak as expected, and actually the multipoint interaction between the polymers and the tip or substrate is strong enough to form a polymer bridge [4,5]. To obtain the single chain stretching, it is important to use a dilute polymer solution during the sample preparation. So the density of molecules at the solid–liquid interface will be low enough to suppress intermolecular entanglement and knotting, simplifying the explanation of the experimental data. However, the paucity of polymers on the substrate creates difficulty in obtaining a force signal. The optimal concentration of the polymer solution for the sample preparation varies for different polymer systems [5,16].

In the chemical adsorption, polymers bearing reactive groups react with the substrate or AFM tip, forming covalent bonds, as shown in Scheme 30.2. Two chemical modification methods are utilized frequently for the covalent bonding based anchoring of molecules on the solid substrate or AFM tip, including gold–thiol [14,58,59] and silanization chemistry [51,58]. When a chemical modification method is adopted during the immobilization process, one can decrease the surface density of polymers by incorporating ''dilute molecules'', such as short alkyl or hydroxy-silane, into the film [14]. The specific interaction, such as ligand–receptor interaction, can also be used in the immobilization of the polymer chains onto the substrate [35]. Recently, a new method is proposed to isolate polymer chains individually at the quartz surface by utilizing the defects in the self-assembled monolayers of organosilane. This method makes it possible to measure the desorption force of a single PDDA chain from a substrate directly [53].

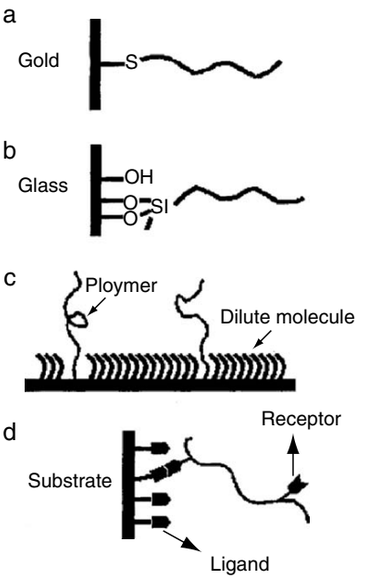

SCHEME 30.2. Schematic drawing of the immobilization of polymers on the solid support: (a) the gold–thiol chemistry; (b) silanization; (c) incorporating the dilute molecules; (d) ligand–receptor interaction.

30.1.2 Evidence on Single Chain Elongation

How can we confirm that the force extension curves are from the single polymer chains? We take single chain elongation of PFDMS as an example. The force curves of PFDMS in THF contain one force signal in each curve, as shown in Fig. 30.1, indicating that it is likely a single polymer chain elongation [21]. The contour length of the polymer chain is varied because the molecular weight of polymers is polydisperse, and the anchor points that attach to the tip or the surface is stochastic. To scale the contour length, the force curves of PFDMS are divided by the relative extension under the same force value, which is called normalizing process. The force signals from individual polymer chain should superimpose after the normalization, since the measured stretching force is linearly proportion with the relative extension [4]. The inset of Fig. 30.1 shows that the normalized force curves of PFDMS in THF superimpose well, which indicates the single chain stretching in the experiment. Moreover, if the stretching force can be controlled well below the rupture force, the PFDMS polymer chain can be stretched and relaxed repeatedly. There is no hysteresis between the stretching and relaxing force curves, as shown in Fig. 30.2, which suggests that the elongation of PFDMS polymer chain is in equilibrium condition and the elongation is reversible [21]. Fitting the force curves with the theoretical models, e.g., FJC and WLC models, is another way to check whether the force curves show the properties of the individual polymer chains. The details of the two models are described as follows. If all the force curves can be fitted well with similar parameters, it provides a further evidence of single chain experiment. Only after the above analysis we can conclude whether the force signals represent single chain characteristics or not.

30.1.3 M-FJC and WLC Models

The M-FJC is used to describe the extension of the polymer and the entropic restoring force generated. The M-FJC model treats a macromolecule as a chain of statistically independent segments of Kuhn lengths l_k, and the segment can be deformed under stress, as shown in Scheme 30.3a. The relationship between the extension and external force acting on the polymer chain is based on the extended Langevin function [13,60]:

$$x(\mathrm{F}) = \{\coth[(Fl_k)/(k_BT)] - (k_BT)/(Fl_k)\} \\ (L_c + nF/K_s). \tag{30.1}$$

In Eq. (30.1), F is the external force, x is the extension of polymer under external force (end to end distance), L_c is the

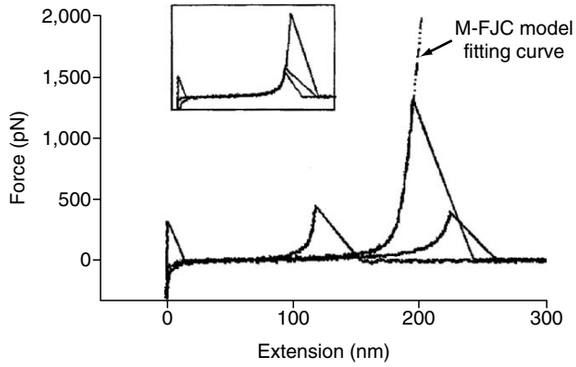

FIGURE 30.1. Several typical force curves of PFDMS in THF buffer. One of the force curves is fitted by the M-FJC model curve, shown in the dashed line. Inset: superposition of the normalized force curves. Reproduced from Macromolecules (2004) with permission from American Chemical Society [21].

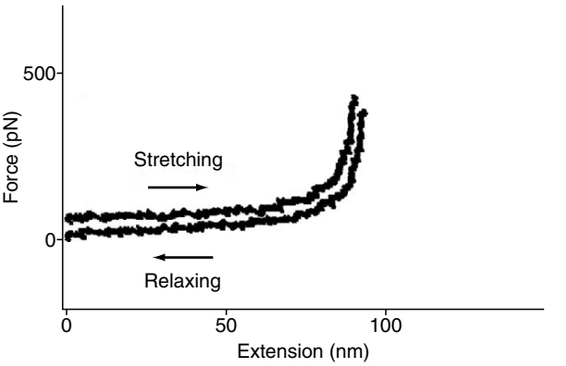

FIGURE 30.2. Successive manipulation of a PFDMS single chain, suggesting that the elongation of the polymer chain in the experiment is reversible. The stretching force curve is shifted. Reproduced from Macromolecules (2004) with permission from American Chemical Society [21].

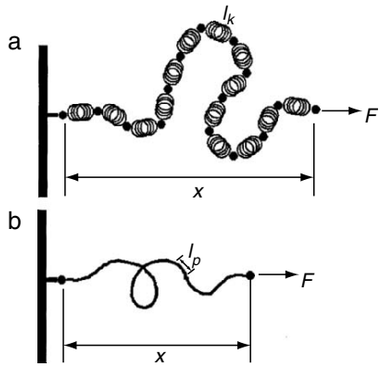

SCHEME 30.3. Schematic drawing of M-FJC and WLC models: (a) M-FJC model; (b) WLC model.

contour length of the polymer chain, n is the number of segments being stretched, k_B is the Boltzmann constant, and T is the temperature. The deformability of segments is characterized by a specific parameter, the segment elasticity, K_s. The elasticity of an M-FJC is dominated by the entropic contribution at low force region, and at high force region the elasticity is dominated by enthalpy as well as entropy.

Another model frequently used to describe the polymer chain is WLC. In WLC model, a polymer is treated as a homogenous string of constant bending elasticity. Both entropic and enthalpic contributions are combined in this model [6,61]. Scheme 30.3b shows the WLC model and the relationship between force and the extension of a WLC is shown as follows:

$$F(x) = [(1 - x/L_c)^{-2}/4 - 1/4 + x/L_c]k_BT/l_p. \quad (30.2)$$

In Eq. (30.2), l_p is the persistence length.

Although the M-FJC and WLC models fit many systems investigated so far, it needs to be pointed out that the two models fail to describe the elastic behavior of polymers containing complex structures [12,13,16].

30.2 FORCE INDUCED CONFORMATION TRANSITION

Synthetic and natural polymers may undertake conformation transition upon external force. Different spectroscopic methods, e.g., FTIR and Raman spectroscopy, can be used to monitor their conformation transition the process, and with these methods the structure change can be revealed. However, it is rather difficult to manipulate a single polymer chain, and to determine the energy barrier that is needed to induce the conformation transition by conventional methods.

30.2.1 Fingerprinting Property of Polysaccharides

Polysaccharides are essential components of all living organisms and are the most abundant classes of biological polymers. Under an external force, the chair conformation, the most stable conformation of the glucopyranose ring, transforms into a boat conformation after passing over an energy barrier. A set of polysaccharides have been investigated by SMFS focusing on the unique transition has been reported [35–43]. For example, Rief *et al*. have studied the single chain elongation of dextran and observed that there are shoulder-like plateaus at 700–850 pN in the force curves, caused by a flip of the C5–C6 bond in the pyranose ring [35].

The various linkages of the glucose residues, such as α-(1,4) and β-(1,3)-linked, can influence the transitional energy during the elongation of the polysaccharides. CM-amylose and CM-cellulose are two isomers, and their primary structures only differ in the linkage of the glucose residues: CM-amylose is linked by α-D-(1,4)-glucosidic bonds, while CM-cellulose is β-(1,4)-linked. Li *et al*. and Marszalek *et al*. have independently found that the small difference in the primary structure induces a great difference in their chain elongation properties [36,39]. For CM-amylose, a marked shoulder-like plateau on the force curves is observed at about 300 pN. The plateau shows a 0.08 nm elongation of each glucose residue and the estimated energy to induce this conformational transition is about 7.3 kT per glucose residue [39]. For CM-cellulose, the force curves of the single chain elongation only show a sharp increase in force with the extension, and no plateau is present, as shown in Fig. 30.3. The different linkage influences the mechanical property of the polysaccharide chain greatly: each successive β-(1,4)-linked glucose residue can easily flip 180° to a extended conformation under external force; however, α-(1,4)-linked residues can easily adopt a chair–boat transition to achieve a extended conformation during the elongation. Hence the force induced conformational transition is a unique property of CM-amylose. Similar shoulder-like plateau is also observed in the force curves of heparin, which is another type of the familiar polysaccharides with the α-(1,4)-linkage [39]. This finding further confirms the fingerprint of the α-(1,4)-linked residues. In order to understand the physical nature of the force induced conformation transition, molecular dynamic simulation is needed to provide the molecular details: a chair–boat transition of the pyranose ring in CM-amylose will happen under external force; elongation of the β-(1,4)-linked pyranose ring induces only slight rotations which do not notably affect its elastic properties [62].

The force induced conformational transition of the pyranose ring will not arise if an oxygen bridge is introduced over the ring, as predicted by theory [63]. This interesting speculation can be confirmed by the experiments of single-chain force spectroscopy. Zhang and his coworkers have done the control experiment using a set of carrageenans bearing oxygen bridges or not and clearly found the influence of the oxygen bridge during the conformational transition [42]. As shown in Fig. 30.4, the primary structure of λ-, κ-, and ι-carrageenan are identical in one part of the repeating unit,

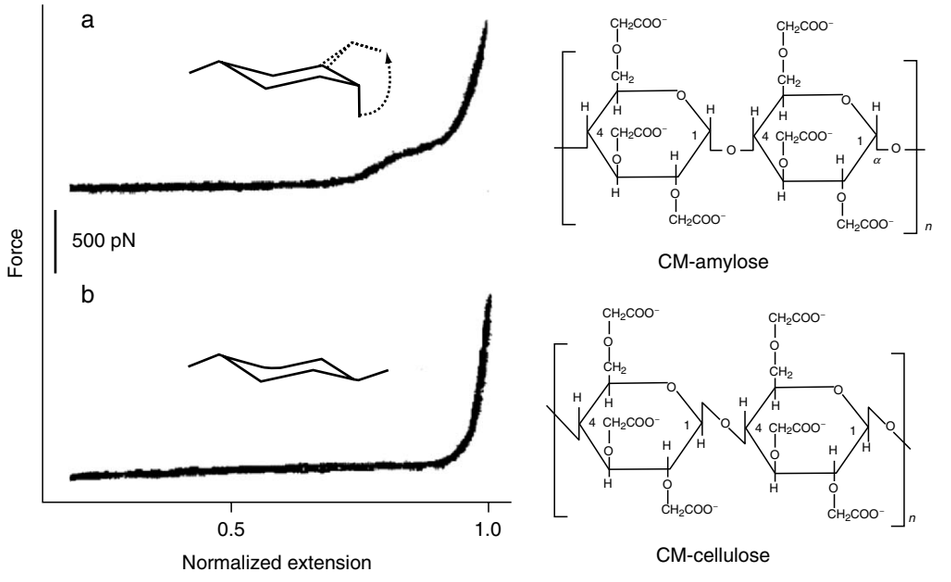

FIGURE 30.3. Comparison of normalized force curves of CM-amylose and CM-cellulose.

the 1,3-linked β-D-pyranose ring; however, there is an oxygen bridge over the 1-4-linked α-D-galactopyranose ring in the other part of the repeating unit of κ- and ι-carrageenan. The typical shoulder-like plateau about 300 ± 50 pN high appears in the force curves of λ-carrageenan, as shown in Fig. 30.4. This shoulder-like plateau indicates that force induced conformational transition can still take place in the elongation of the λ-carrageenan single chain if there are no oxygen bridges. But for κ- and ι-carrageenan, the shoulder-like plateaus disappear in the force curves and the M-FJC model can fit the force curves of κ- and ι-carrageenan well. These results suggest that the conformational transition of the galactopyranose rings is inhibited efficiently due to the additional barrier of the oxygen bridges.

30.2.2 Single-Molecule Optomechanical Cycle

SMFS has also proven to be a useful tool in the investigation of "molecular machine," whose working principle is based on the energy conversion cycle of stimuli-responsive

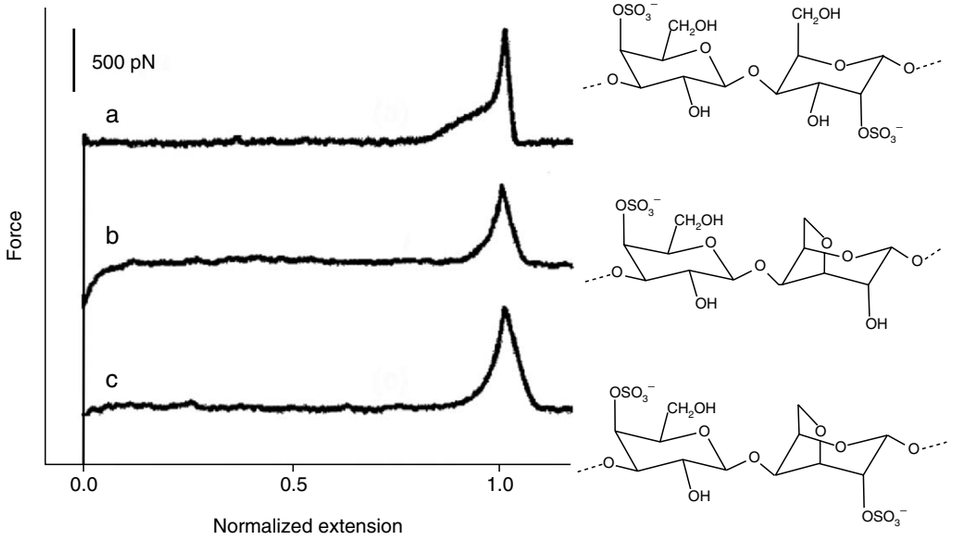

FIGURE 30.4. Primary structures of λ,κ,ι-carrageenan and the typical normalized force curves obtained on (a) λ-, (b) κ-, and (c) ι-carrageenan.

polymers. Gaub and his coworkers firstly demonstrate an example of the optomechanical energy conversion at single molecule level [64,65]. They utilize a stimuli-responsive polymer of synthetic polypeptide with multiple photoactive azobenzene groups incorporated into the backbone. The contour length of the polymer could be selectively lengthened or shortened by switching between the *trans*- and *cis*-azo configurations with 420 and 365 nm wavelength lights, respectively. In their experiment, the polymer end groups were covalently coupled to both the AFM tip and a supporting glass slide by heterobifunctional chemistry. As Fig. 30.5 shows, an individual azopolymer is first lengthened by five pulses with $\lambda = 420\,\text{nm}$ at a force of 80 pN (I) and then expanded mechanically to a restoring force of 200 pN (II). Then five pulses at $\lambda = 365\,\text{nm}$ are applied, resulting in a contraction of the polymer against the external force (III). Then the force on the polymer is reduced to 85 pN (IV). Finally, the cycle is completed by applying five pulses at $\lambda = 420\,\text{nm}$, resulting in an optical expansion of the molecule to its original length. From which, a new cycle can be started by switching the shortened configuration to the extended state.

Besides the optomechanical energy conversion, PFS can be used as a model system for the realization of an electrochemically powered molecular motor as proposed by Vancso *et al*. [66]. Surface immobilized PFS macromolecules are reversibly oxidized and reduced in situ by applying an electrochemical potential or chemically oxidized by addition of tetracyanoethylene. The entropic elasticity of the neutral PFS chains is found to be larger compared to the oxidized PFS in the lower force region, whereas the segment elasticity can be reversibly controlled in situ by adjusting the applied potential in electrochemical SMFS experiments. For a defined single PFS molecule operating cycle, a work of about 3.4×10^{-19} J is estimated based on the single chain experimental data. The efficiency is estimated as 5%, and it could be improved further if reducing the input energy [67].

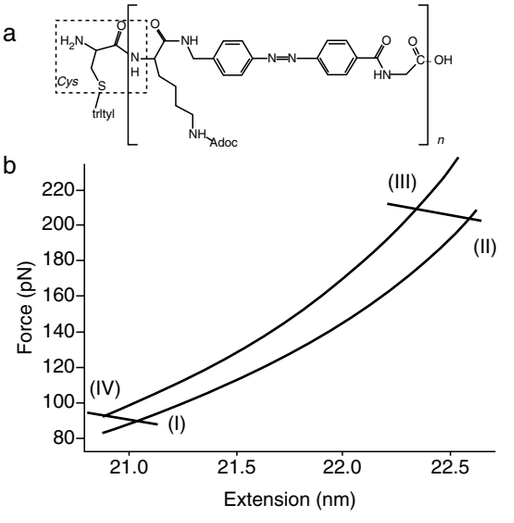

FIGURE 30.5. The scheme of the experimental realization of the single molecule operating cycle with polyazopeptides.

30.3 INTERACTION BETWEEN SMALL MOLECULES AND POLYMERS

Since the SMFS experiments are carried out at a solid–liquid interface in a liquid cell, it allows for studying the interaction between small molecules and polymers by easily changing buffers. The difference of the single chain elasticity before and after the addition of small molecules can indicate whether there exists interaction between the polymer and small molecules or not. Zhang *et al*. have employed PDMA and PDEA for studying their interaction with urea molecules [17]. It is well understandable that the single polymer chain of PDEA is stiffer than that of PDMA in deionized water because of the different substitutes, as shown in Fig. 30.6. The elasticity of the two polymers increases when using urea aqueous solution instead of the deionized water. In order to understand how the urea molecules affect the elasticity of the polymer, FTIR is used to identify the interaction between PDMA and urea molecules. The band at approximately $1{,}639\,\text{cm}^{-1}$ is attributed to the carbonyl stretching mode in the FTIR spectrum of PDMA film, while there is a shoulder at approximately $1{,}610\,\text{cm}^{-1}$ region in the spectrum of PDMA and urea mixture. These experimental data suggest the formation of hydrogen bonds between urea molecules and carbonyl groups of PDMA. Due to the formation of hydrogen bonds, urea can enlarge the enthalpic elasticity of the polymer backbone by binding to the side groups directly. In addition, the elasticity of PDMA chain is dependent on the concentration of urea, as shown in Fig. 30.7. The urea molecules have a similar influence on the elasticity of PDEA chain.

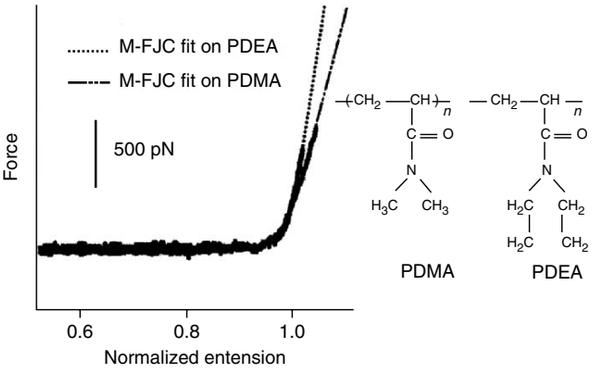

FIGURE 30.6. Primary structures of PDMA and PDEA, and a comparison of the normalized curve of PDMA and PDEA in water. The two dotted lines are the modified FJC fitting curves. Reproduced from Nano Letters (2002) with permission from American Chemical Society [17].

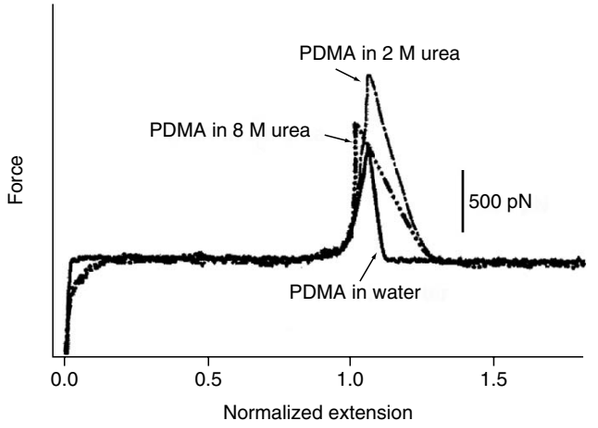

FIGURE 30.7. Comparison of normalized force curves of PDMA in water, 2 and 8 M urea aqueous solutions. Reproduced from Nano Letters (2002) with permission from American Chemical Society [17].

Of interest is that the effects of urea molecules on the elasticity of single PDMA and PDEA chains depend on the urea concentration. When comparing the elasticity between PDMA and PDEA in the 2 M urea buffer solution, the elasticity of PDEA is still greater than that of PDMA, similar to the situation in water. The discrepancy in the high force region may also be attributed to the effects of different side groups. However, in the 8 M urea buffer solutions, as shown in Fig. 30.8, no discrepancy is seen. This result indicates that when the concentration of urea solution is sufficiently high to become the dominating factor in determining the elasticity of a single polymer chain, the discrepancy in the elasticity between PDMA and PDEA is shielded completely.

There exists hydrogen bonding governed elasticity in many water-soluble polymers, such as PEG, and PVA [11–13]. The single chain elongation of PEG is like the behavior of an ideal entropic string in hexadecane, and can be described well with M-FJC model. However, in aqueous solution an evident deviation in the middle force region of the force curves is observed, indicating the deformation of a suprastructure within the polymer. The binding free energy is estimated as 3.0 ± 0.3 kT [13]. Further analysis of the force curves based on the Markovian two-level systems, agreeing well with the ab initio calculations, identifies the nonplanar suprastructure, water bridges, between the PEG chain and the water molecules.

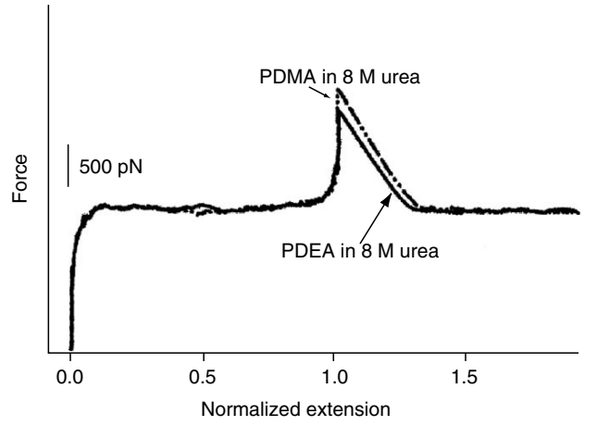

FIGURE 30.8. Comparison of normalized force curves of PDMA and PDEA in 8 M urea aqueous solution. Reproduced from Nano Letters (2002) with permission from American Chemical Society [17].

30.4 INTERFACIAL CONFORMATION AND ADHESIVE ENERGY OF POLYMERS

Polymers generally interact strongly with surfaces. Even if the gain of energy per monomer is weak, once a monomer is adsorbed, there is a strong probability that other monomers will also be adsorbed [68]. This energy gain must be compared to the entropy loss of the chain in order to predict its conformation [69]. So both enthalpy and entropy can drive the adsorption process. It has been generally known that the conformation of a long polymer chain adsorbed on a surface is in the form of a ''train'', ''loop'', or ''tail'', though lack of direct experimental evidence [70]. Let's take a few model systems to discuss the possibility by using AFM based SMFS to reveal the macromolecular conformation and the adhesive energy.

30.4.1 Saw-Tooth Pattern and The Loop Structure

For a homopolymer or statistically random copolymer chain, the adsorption normally results in a mixture of trains, loops, and tails on a surface. Therefore, one has no control over the number of monomer units adsorbed on each site. One can only measure the average interaction strength per chain, not per monomer unit, adsorbed on the substrate. To bridge the gap between force profile and interfacial conformation, Zhang and Wu have used a segment copolymer as a model system, in which short hydrophobic PS segments are more uniformly inserted into a linear PNIPAM chain backbone [71]. The structure and composition of such a copolymer chain are schematically shown in Scheme 30.4a. As this segment copolymer chains adsorb onto the PS substrate in water, it is reasonable to expect that the adsorption of insoluble short PS segments onto the PS substrate results in many PNIPAM loops, as shown in Scheme 30.4b. Therefore, the typical force curves of the segment copolymer on PS substrate exhibit a similar characteristic, saw-tooth pattern, as shown in Fig. 30.9. The analysis of the distance between each two adjacent peaks in the force curves, as shown in Fig. 30.10a, shows an average distance of about 114 nm. This value is very similar to the average length of the ''repeat unit'', i.e., one long PNIPAM segment plus one short PS segment, in the copolymer chain. These results suggest that the copolymer chain does form loops with a similar size on

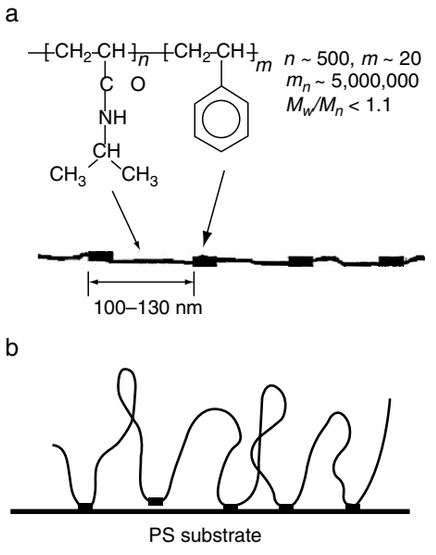

SCHEME 30.4. (a) Schematic of a linear segment PNIPAM-*seg*-PS prepared by micelle copolymerization, in which short PS segments are relatively evenly distributed on the chain backbone. (b) A possible adsorption conformation of a linear PNIPAM-*seg*-PS chain on a hydrophobic PS substrate in water. Reproduced from Macromolecules (2003) with permission from American Chemical Society [50].

the PS substrate. Therefore, the saw-tooth pattern corresponds to the detachment of the adsorbed segments in a single chain from the substrate. Moreover, the force curves obtained on a quartz substrate have single peak force signals, which is similar to PNIPAM [16]. This result is reasonable since short hydrophobic PS segments cannot adsorb onto the hydrophilic quartz substrate. This finding further confirms that the weak rupture force obtained on the PS substrate corresponds to the desorption of short PS segments from the PS substrate [50].

The most probable desorption force at a given stretching velocity, which is obtained from the histogram of desorption force, is about 41 pN, as shown in Fig. 30.10b. Such a distribution varies with the stretching velocity. The linear dependence of the most probable desorption force on the logarithm of the stretching velocity experimentally reveals that the adsorption and desorption of the PS segments on the PS substrate is a dynamic process [50]. Since it is known that each PS segment contains 20 monomer units on average, the desorption force for per PS monomer unit from the PS substrate in water is estimated in the range 1.3–2.1 pN, depending on the imposed stretching velocity.

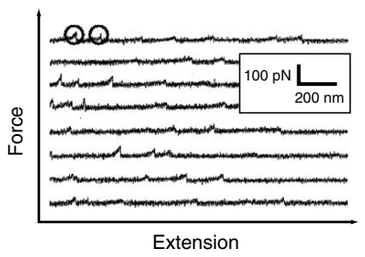

FIGURE 30.9. Measured force curves of linear segment PNIPAM-*seg*-PS chains adsorbed on a hydrophobic polystyrene substrate in water. Reproduced from Macromolecules (2003) with permission from American Chemical Society [50].

Besides the physical adsorption, the stable covalent attachment of a single or a small number of polymer molecules to AFM cantilever tip is a most important prerequisite in order to employ individual polymer molecules as interfacial, analytical probes for the identification and measurement of various types of polymer-surface interactions [54]. Recently, Haschke *et al*. have covalently attached polyacryamide molecule to the AFM cantilever tip. By approaching and retracting the tip with the molecule to the surface of interest, they have obtained force curves with multipeaks [72]. The covalent attachment of the chain to the tip ensures that any detachment measured in the force spectroscopy experiment is the force between the molecule and the sample surface. Therefore, the multipeaks of force curves correspond to detachment of multiple loops that are formed by the physisorption of polyacryamide at interface, as shown in Fig. 30.11.

30.4.2 Long Plateau Versus Train-like Structure

Provided that the polymer forms a train-like conformation at interface, the desorption force should be similar when detaching each adsorption point during the polymer chain elongation. As a result, the force curves should show a characteristic plateau. Seitz and his coworkers have used chemisorption to immobilize polyvinylamine polymer chain and studied the elasticity of the single polymer chain as a function of polymer's charge density and electrolyte concentration [51]. Their results indicate that, in addition to electrostatic interaction between polyvinylamine and negatively charged silica substrate which depends linearly on the Debye screening length and the polymer's line charge density, a constant nonelectrostatic interaction plays an important role in the desorption process [51].

PAMPS and its random copolymer containing 18-crown-6 (PAMPS-*co*-crown), are used to further study the nonelectrostatic contribution to desorption force [56]. The primary structures of polymers are shown in Scheme 30.5. As shown in Fig. 30.12, the typical force curves of PAMPS with a plateau are obtained from amino-modified quartz in the buffer of water. The long plateau suggests that the desorption process of the PAMPS chain from the substrate is smooth and that it adopts a train-like conformation at the interface and the desorption force remains about 120 pN. The desorption–adsorption process is in equilibrium in the experimental time scale, which is confirmed by the constant desorption force when changing the stretching velocity. The desorption force of PAMPS from the amino-modified quartz has been

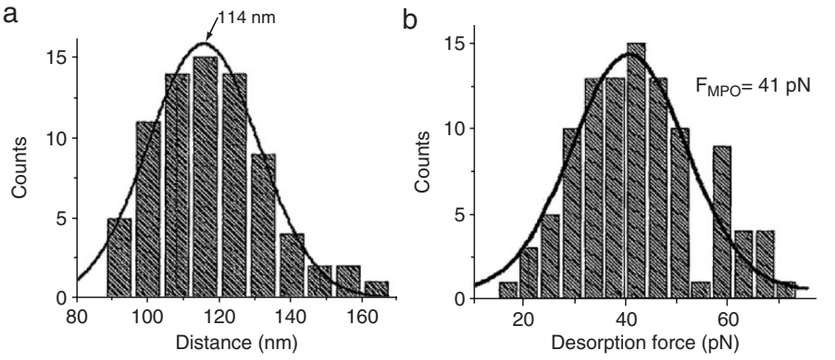

FIGURE 30.10. (a) Statistics of the distance between two adjacent peaks in the measured force curves. (b) Distribution of the measured desorption force for linear PNIPAM-*seg*-PS chains adsorbed on hydrophobic polystyrene substrate, where the stretching velocity is kept at 4,600 nm/s. Reproduced from Macromolecules (2003) with permission from American Chemical Society [50].

studied using different concentration of electrolyte as buffer. A series of experiments show that the external salt does not influence the desorption force of PAMPS.

In experiments, when the sample is immersed in the salt solution, the ion screening effect would influence largely on the electrostatic interaction but little on the nonelectrostatic interaction between the polyelectrolyte and the substrate [4,51]. It is possible for both the hydrophobic backbone and the charged groups of PAMPS to adsorb onto the substrate, since the static contact angle of amino-modified substrate is about 67°. It is reported that there is a ''zero charge contribution'' by about 38 pN in the ionic strength sensitive desorption force for the polyelectrolyte without spacer [51,54]. In the case of PAMPS, the introduced spacer between the charged groups and the backbone effectively enhances the nonelectrostatic contribution to the interfacial interaction, making the interfacial interaction insensitive to the ionic strength. These results together reveal the nonelectrostatic origin for the adsorption of the polyelectrolytes [56].

The force curves of PAMPS-*co*-crown obtained from amino-modified substrate are resembled to the curves shown in Fig. 30.12, which also show a long plateau with a height of about 120 pN. The long plateau indicates that PAMPS-*co*-crown chains also assume a train-like conformation at the interface. Similar to PAMPS, the desorption force of PAMPS-*co*-crown is independent of the concentration of electrolyte and the stretching velocity. The result indicates that the 20% content of crown ether side groups in the copolymer chain does not influence the desorption force. In other words, the interaction between PAMPS-*co*-crown chain and the substrate could be mainly dominated by the hydrophobic interaction. Based on the above discussion, SMFS allows to measure adhesive forces on the single molecule level and to gain new insight into the fundamental interactions in polymer adsorption.

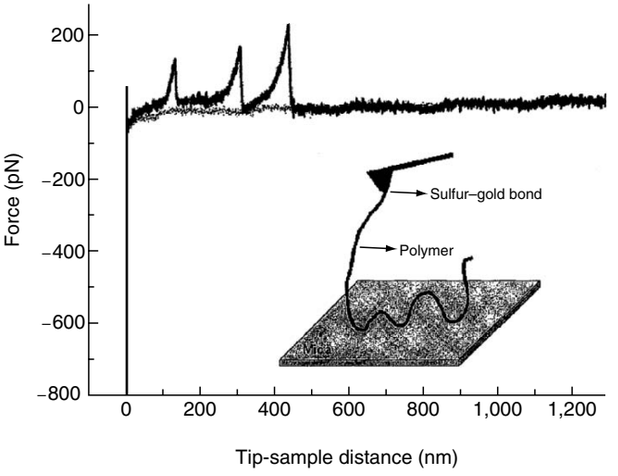

FIGURE 30.11. Force curve with a polyacrylamide molecule end-grafted to a gold-coated cantilever tip obtained on mica in water. Reproduced from Macromolecules (2004) with permission from American Chemical Society [72].

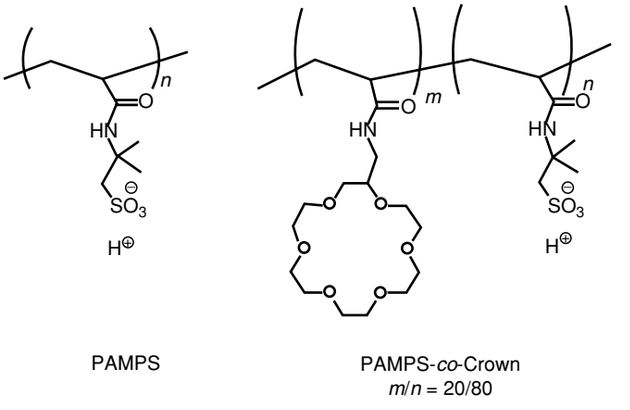

SCHEME 30.5. Primary structures of PAMPS and PAMPS-*co*-crown.

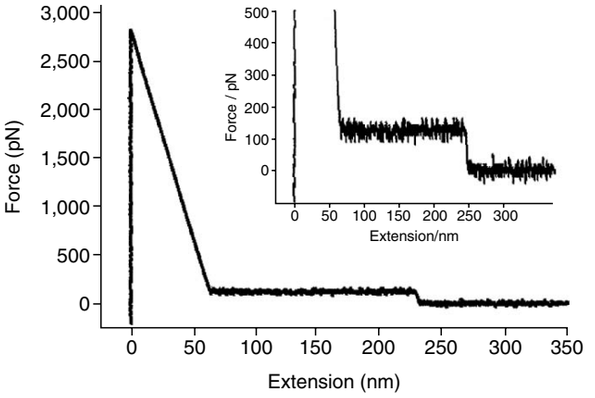

FIGURE 30.12. Typical force curve of PAMPS in water that shows a long plateau with a height of about 120 pN. Reproduced from Macromolecules (2004) with permission from American Chemical Society [56].

30.5 OUTLOOK

AFM based SMFS is a powerful tool in studying the intermolecular and intramolecular interaction in polymer systems, leading to opening a new field of nanomechanics of polymers. Although many elegant experiments have been performed, it must be point out that SMFS is still in the nascent stage. The technique itself can be improved and introduce new functions. For example, introduction of force clamp mode allow for following the dynamic process of the folding or unfolding probability of proteins [73]. It will be necessary to combine SMFS with other spectroscopic methods in order to link the force signal with structure change. In addition, theoreticians and experimenters need collaborate to realize the full potential of SMFS. After accumulating enough data in her information storeroom and in combination with other detection methods, SMFS will provide us new insight into the basic problems in polymer science and life science.

ACKNOWLEDGMENTS

This research was supported by the Major State Basic Research Development Program (G2000078102), National Natural Science Foundation of China (20474035), and Ministry of Education.

REFERENCES

1. Binnig G, Quate CF, Gerber C (1986) Phys. Rev. Lett. 56:930
2. Weisenhorn AL, Hansma PK, Albrecht TR, Quate CF (1989) Appl. Phys. Lett. 54:2651
3. Janshoff A, Neitzert M, Oberdorfer Y, Fuchs H (2000) Angew. Chem., Int. Ed. 39:3212
4. Hugel T, Seitz M (2001) Macromol. Rapid Commun. 22:989
5. Zhang WK, Zhang X (2003) Prog. Polym. Sci. 28:1271
6. Smith SB, Finzi L, Bustamante C (1992) Science (Washington, DC, US) 258:1122
7. Ashkin A, Schütze K, Dziedzic JM, Euteneuer U, Schliwa M (1990) Nature (London, UK) 348:346
8. Kishino A, Yanagida T (1988) Nature (London, UK) 334:74
9. Evans E, Ritchie K, Merkel R (1995) Biophys. J. 68:2580
10. Li HB, Liu BB, Zhang X, Gao CX, Shen JC, Zou GT (1999) Langmuir 15:2120
11. Li HB, Zhang WK, Zhang X, Shen JC, Liu BB, Gao CX, Zou GT (1998) Macromol. Rapid Commun. 19:609
12. Li HB, Zhang WK, Xu WQ, Zhang X (2000) Macromolecules 33:465
13. Oesterhelt F, Rief M, Gaub HE (1999) New J. Phys. 1:6.1
14. Ortiz C, Hadziioannou G (1999) Macromolecules 32:780
15. Bemis JE, Akhremitchev BB, Walker GC (1999) Langmuir 15:2799
16. Zhang WK, Zou S, Wang C, Zhang X (2000) J. Phys. Chem. B 104:10258
17. Wang C, Shi WQ, Zhang WK, Zhang X, Katsumoto Y, Ozaki Y (2002) Nano Lett. 2:1169
18. Zhang WK (2002) PhD Thesis, Jilin University
19. Zhang WK, Xu QB, Zou S, Li HB, Xu WQ, Zhang X, Shao ZZ, Kudera M, Gaub HE (2000) Langmuir 16:4305
20. Yamamoto S, Tsujii Y, Fukuda T (2000) Macromolecules 33:5995
21. Shi WQ, Cui SX, Wang C, Wang LY, Zhang X, Wang XJ, Wang L (2004) Macromolecules 37:1839
22. Rief M, Gautel M, Oesterhelt F, Fernandez JM, Gaub HE (1997) Science (Washington, DC, US) 276:1109
23. Rief M, Gautel M, Schemmel A, Gaub HE (1998) Biophys. J. 75:3008
24. Tskhovrebova L, Trinick J, Sleep JA, Simmons RM (1997) Nature (London, UK) 387:308
25. Oberhauser AF, Marszalek PE, Erickson HP, Fernandez JM (1998) Nature (London, UK) 393:181
26. Marszalek PE, Lu H, Li HB, Carrion-Vazquez M, Oberhauser AF, Schulten K, Fernandez JM (1999) Nature (London, UK) 402:100
27. Oberhauser AF, Marszalek PE, Carrion-Vazquez M, Fernandez JM (1999) Nat. Struct. Biol. 6:1025
28. Carrion-Vazquez M, Marszalek PE, Oberhauser AF, Fernandez JM (1999) Proc. Natl. Acad. Sci. USA. 96:11288
29. Carrion-Vazquez M, Oberhauser AF, Fowler SB, Marszalek PE, Broedel SE, Clarke J, Fernandez JM (1999) Proc. Natl Acad. Sci. USA. 96:3694
30. Li HB, Oberhauser AF, Fowler SB, Clarke J, Fernandez JM (2000) Proc. Natl Acad. Sci. USA. 97:6527
31. Carrion-Vazquez M, Oberhauser AF, Fisher TE, Marszalek PE, Li HB, Fernandez JM (2000) Prog. Biophys. Mol. Biol. 74:63
32. Yang GL, Cecconi C, Baase WA, Vetter IR, Breyer WA, Haack JA, Matthews BW, Dahlquist FW, Bustamante C (2000) Proc. Natl Acad. Sci. USA. 97:139
33. Li HB, Linke WA, Oberhauser AF, Carrion-Vazquez M, Kerkviliet JG, Lu H, Marszalek PE, Fernandez JM (2002) Nature (London, UK) 418:998
34. Linke WA, Kulke M, Li HB, Fujita-Becker S, Neagoe C, Manstein DJ, Gautel M, Fernandez JM (2002) J. Struct. Biol. 137:194
35. Rief M, Oesterhelt F, Heymann B, Gaub HE (1997) Science (Washington, DC, US) 275:1295
36. Marszalek PE, Oberhauser AF, Pang YP, Fernandez JM (1998) Nature (London, UK) 396:661
37. Li HB, Rief M, Oesterhelt F, Gaub HE (1998) Adv. Mater. (Weinheim, Germany) 10:316
38. Li HB, Rief M, Oesterhelt F, Gaub HE (1999) Appl. Phys. A 68:407
39. Li HB, Rief M, Oesterhelt F, Gaub HE, Zhang X, Shen JC (1999) Chem. Phys. Lett. 305:197
40. Marszalek PE, Pang YP, Li HB, Yazal JE, Oberhauser AF, Fernandez JM (1999) Proc. Natl Acad. Sci. USA. 96:7894
41. Marszalek PE, Li HB, Fernandez JM (2001) Nat. Biotechnol. 19:258
42. Xu QB, Zhang WK, Zhang X (2002) Macromolecules 35:871
43. Marszalek PE, Li HB, Oberhauser AF, Fernandez JM (2002) Proc. Natl Acad. Sci. USA. 99:4278
44. Rief M, Calusen-Schaumann H, Gaub HE (1999) Nat. Struct. Biol. 6:346
45. Clausen-Schaumann H, Rief M, Tolksdorf C, Gaub HE (2000) Biophys. J. 78:1997
46. Xu QB, Zou S, Zhang WK, Zhang X (2001) Macromol. Rapid Commun. 22:1163
47. Krautbauer R, Rief M, Gaub HE (2003) Nano Lett. 3:493

48. Zhang WK, Cui SX, Fu Y, Zhang X (2002) J. Phys. Chem. B 106:12705
49. Haupt BJ, Ennis J, Sevick EM (1999) Langmuir 15:3886
50. Cui SX, Liu CJ, Zhang WK, Zhang X, Wu C (2003) Macromolecules 36:3779
51. Hugel T, Grosholz M, Clausen-Schaumann H, Pfau A, Gaub HE, Seitz M (2001) Macromolecules 34:1039
52. Chatellier X, Senden TJ, Joanny JF, di Meglio JM (1998) Europhys. Lett. 41:303
53. Cui SX, Liu CJ, Zhang X (2003) Nano Lett. 3:245
54. Seitz M, Friedsam C, Jostal W, Hugel T, Gaub HE (2003) Chem. Phys. Chem. 4:986
55. Friedsam C, del Campo BA, Jonas U, Seitz M, Gaub HE (2004) New J. Phys. 6:9
56. Cui SX, Liu CJ, Wang ZQ, Zhang X, Strandman S, Tenhu H (2004) Macromolecules 37:946
57. Friedsam C, del Campo BA, Jonas U, Gaub HE, Seitz M (2004) Chem. Phys. Chem. 5:388
58. Grandbois M, Beyer M, Rief M, Clausen-Schaumann H, Gaub HE (1999) Science (Washington, DC, US) 283:1727
59. Oesterhelt F, Oesterhelt D, Pfeiffer M, Engel A, Gaub HE, Muller DJ (2000) Science (Washington, DC, US) 288:143
60. Smith SB, Cui YJ, Bustamante C (1996) Science (Washington, DC, US) 271:795
61. Senden TJ, di Meglio JM, Auroy P (1998) Eur. Phys. J. B 3:211
62. Heymann B, Grubmüller H (1999) Chem. Phys. Lett. 305:202
63. Eliel E, Allinger NL, (1974) Topics in Stereochemistry, Interscience: New York, Vol.8 p. 159
64. Hugel T, Holland NB, Cattani A, Moroder L, Seitz M, Gaub HE (2002) Science (Washington, DC, US) 296:1103
65. Holland NB, Hugel T, Neuert G, Cattani-Scholz A, Renner C, Oesterhelt D, Moroder L, Seitz M, Gaub HE (2003) Macromolecules 36:2015
66. Zou S, Ma YJ, Hempenius MA, Schonherr H, Vancso GJ (2004) Langmuir 20:6278
67. Zou S (2005) PhD Thesis, University of Twente
68. Levy R, Maaloum M (2004) J. Phys.: Condens Matter 16:7199
69. de Gennes PG (1979) Scaling concepts in polymer physics, Cornell University Press, New York
70. Conti M, Bustanji Y, Falini G, Ferruti P, Stefoni S, Samor B (2001) Chem. Phys. Chem. 2:610
71. Zhang GZ, Winnik FM, and Wu C (2003) Phys. Rev. Lett. 90: 035506
72. Haschke H, Miles MJ, Koutsos V (2004) Macromolecules 37:3799
73. Fernandez JM, Li HB (2004) Science (Washington, DC, US) 303: 1674

CHAPTER 31

Carbon Black

Manfred Klüppel*, Andreas Schröder†, and Gert Heinrich‡

*Deutsches Institut für Kautschuktechnologie eV, Eupener Str. 33, D-30519 Hannover, Germany
†Rheinchemie Rheinan GmbH, Düsseldorfer str. 23–27, D-68219 Mannheim, Germany
‡Leibniz Institut für Polymerforschung Dresden eV, Hohe Str. 6, D-01069 Dresden, Germany

31.1 INTRODUCTION

Carbon black (c.b.) plays an important role in the improvement of the mechanical and/or electrical properties of high performance rubber materials. The reinforcing potential is mainly attributed to two effects: (i) the formation of a physically bonded flexible filler network and (ii) strong polymer filler couplings. Both of these effects refer to a high surface activity and specific surface of the filler particles [1–3].

So far, the formation and structure of the c.b. network and the mechanical response is not fully understood. Considerable progress has been obtained in the past in relating the pronounced drop of the elasticity modulus with increasing dynamical strain (Payne effect) to a cyclic breakdown and reagglomeration of filler–filler bonds [3–6]. Thereby, different geometrical arrangements of particles in a particular filler network structures, resulting e.g., from percolation [6] or kinetic cluster–cluster aggregation [7–9], have been considered. Nevertheless, a full micromechanical description of energy storage and -dissipation in reinforced rubbers is still outstanding. Reviews of the different attempts are given in [10,11] (see also Chapter ''Reinforcement Theories'' of this book).

Useful hints concerning the structure and properties of conducting c.b. networks in elastomers can be obtained from examinations of the electrical percolation threshold and the dielectric properties in a broad frequency range [8,11–13]. In particular, the percolation threshold decreases with increasing specific surface and/or structure of the c.b. particles and decreasing compatibility between polymer and filler. This emphasizes the role of the mean particle distance or gap size between particles or particle clusters. It refers to a thermally activated hopping of charge carriers across the gaps that governs the conductivity of c.b. filled polymers above the percolation threshold [11–13].

The dielectric properties are closely related to the hopping conductivity mechanism, as well. At low frequencies a delayed charge carrier motion across the gaps that may also be combined with a polarization of dead ends of the c.b. network leads to extraordinary high values of the relative dielectric constant (permittivity) $\varepsilon' \cong 10^3$–10^4. With increasing frequencies a polarization transition takes place and the permittivity falls off drastically [14]. At high frequencies the permittivity approaches a low plateau value and the conductivity σ' increases according to a power law. The conductivity exponent in the high frequency regime can be related to the anomalous diffusion exponent on fractal c.b. clusters [11–13].

For a deeper understanding of the mechanical and electrical properties of c.b. filled rubbers it is necessary to consider the morphology of the c.b. particles (primary aggregates) more closely. Due to the disordered nature of c.b. formation during processing in a furnace reactor, the morphology of furnace blacks is well described by referring to a fractal analysis. Recent investigations of the surface roughness of c.b. by static gas adsorption point out that all furnace

blacks exhibit a pronounced surface roughness with an almost unique surface fractal dimension $D_s \approx 2.6$ on atomic length scales below 6 nm [15]. This universality can be related to a particular random deposition mechanism of carbon nuclei on the particles that governs the surface growth of the particles during processing [16]. It will be considered more closely in the following two sections. According to the universal surface roughness of furnace blacks independent of grade number one can expect that the reinforcing potential and electrical effects owing to the surface roughness of c.b. are similar.

Specific effects of the different grades of furnace blacks on the mechanical and electrical properties result mainly from differences in the specific surface and/or structure of the primary aggregates. The specific surface depends strongly on the size of the primary particles and differs from about $10\,m^2/g$ up to almost $200\,m^2/g$. The structure of the primary aggregates describes the amount of void volume and is measured e.g., by oil (DBP) absorption. It typically varies between $0.3\,cm^3/g$ and $1.7\,cm^3/g$ for furnace blacks [1]. The typical shape of c.b. aggregates is illustrated in Fig. 31.1, where transmission electron micrographs (TEM) of three different grades of furnace blacks (N220, N330, N550) are shown. The various sizes of the primary particles, increasing from top to bottom, become apparent. It implies a decline of the specific surface from $113\,m^2/g$ for N220, $83\,m^2/g$ for N330 up to $39\,m^2/g$ for N550. The structure or amount of specific voids of the three grades is almost the same and differs between $1\,cm^3/g$ and $1.2\,cm^3/g$, only [8]. Since the specific weight of c.b. is almost twice of that for DBP, this corresponds to a factor two for the void volume as compared to the solid volume of the aggregates. It means that about 2/3 of the aggregate volume is empty space, i.e., the solid fraction $\phi_{A,1}$ of the primary aggregates is relative small ($\phi_{A,1} \approx 0.33$). It is shown in [8,11] that $\phi_{A,1}$ fulfills a scaling relation which involves the size and mass fractal dimension of the primary aggregates. Due to the significant deviation of the solid fraction $\phi_{A,1}$ from one, the filler volume fraction ϕ has to be treated as an effective one in most applications, i.e., $\phi_{eff} = \phi/\phi_{A,1}$.

The fractal nature of the primary c.b. aggregates and flocculated clusters can be quantified by TEM-techniques [1] or dielectric measurements [8,11]. A further technique that gives information about the morphological arrangement of filler particles in elastomers is small angle X-ray scattering (SAXS). Figure 31.2 shows results of scattering investigations obtained for natural rubber (NR) samples filled with different c.b. grades of varying specific surface. The concentration of c.b. is kept constant (46 phr). The double logarithmic plot in Fig. 31.2 demonstrates that in all cases two scaling regimes are obtained. For small values of the scattering vector q the slope is larger than -3, indicating that the scattering is initiated by mass fractals. The mass fractal dimension D_f equals the negative value of the slope β ($D_f = -\beta$). It is found to vary between $D_f \approx 2.1$–2.4. This is in fair agreement with TEM-estimates for the primary aggregates [1,8]. The lower cut off length L_c is obtained from the cross-over points of Fig. 31.2 and increases some what with decreasing specific surface ($50\,nm < L_c < 80\,nm$). Its value is of the order of the primary particle diameters, which appears reasonable since the primary particles represent the smallest units of the primary aggregates.

For large values of q the slope β in Fig. 31.2 is almost constant and smaller than -3. This refers to a surface scattering by the filler particles. Accordingly, the surface fractal dimension $D_s = 6 + \beta$ is found to be almost independent of specific surface ($D_s \approx 2.5$). This is evaluated in the length scale regime between 60 nm and 20 nm, roughly.

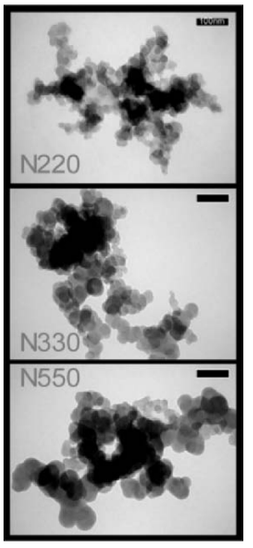

FIGURE 31.1. Transmission electron micrographs (TEM) of three different grades of furnace blacks (N220, N330, N550). The bar indicates a size of 100 nm. Reprinted from [11] with kind permission of Springer Science + Business Media.

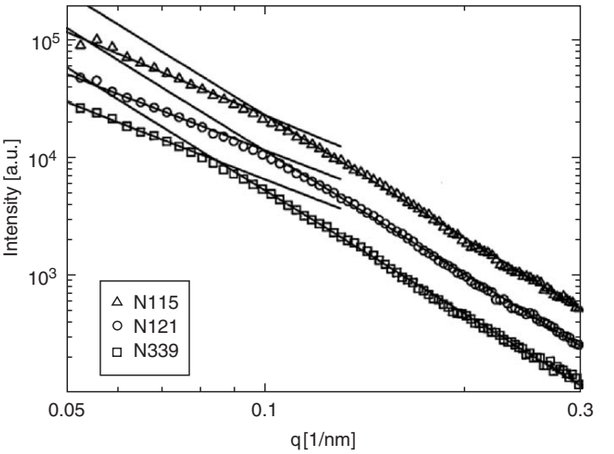

FIGURE 31.2. SAXS-data for the carbon black grades N115, N121, and N339.

It compares to scattering results investigated in [17]. Note however, that for smaller length scales at about 6 nm one observes again a cross-over of the scattering intensity. Hence, the surface fractal dimension $D_s \approx 2.5$ is related to the surface roughness on a mesoscopic length scale regime and doesn't reflect the surface roughness on atomic length scales, as obtained, e.g., by gas adsorption technique [15].

31.2 SURFACE ROUGHNESS FROM STATIC GAS ADSORPTION

In this section we will demonstrate in some detail, how the surface roughness of c.b. aggregates can be estimated by gas adsorption techniques in the mono- and multilayer regime. For this purpose, a classical volumetric adsorption apparatus equipped with absolute capacitance pressure transducers has been used for the estimation of adsorption isotherms in the pressure range $10^{-3}\,\text{mbar} < p < 10^{3}\,\text{mbar}$. Before adsorption measurements the c.b. samples were extracted with toluene and water/methanol (1:1) and after drying degassed at 300°C at a pressure below 10^{-4} mbar overnight. The time allowed for equilibrium of each point of the isotherm was between five and ninety minutes depending on the sample and the adsorbed amount.

For the morphological surface characterization in the monolayer regime we refer to a variation of the estimated BET-surface area with the size of adsorbed probe molecules (yardstick method). On smooth flat surfaces the BET-area is independent of the adsorbed probe size or applied yardstick, while on rough surfaces it decreases with increasing probe (yardstick) size due to the inability of the large molecules to explore smaller cavities. This behavior is shown schematically in Fig. 31.3. A closer analysis shows that in the case of c.b. a power law behavior of the BET-surface area with varying yardstick size is observed, indicating a self-similar structure of the c.b. surface. Double logarithmic ''yardstick-plots'' of the BET-monolayer amount N_m vs. cross-section σ of the probe molecules are shown in Fig. 31.4 for the original furnace black N220 and a graphitized (T = 2,500 °C) sample N220g. It demonstrates that the roughness exponent or surface fractal dimension D_s differs for the two c.b. samples. By using the relation introduced by Mandelbrot [18]:

$$N_m \sim \sigma^{-\frac{D_s}{2}} \tag{31.1}$$

one obtains from the slopes of the two regression lines of Fig. 31.4 a surface fractal dimension $D_s \approx 2.56$ for the N220-sample and $D_s \approx 2.32$ for the graphitized N220g sample. An extrapolation of both regression lines yields an intersection at an ultimate cross-section that corresponds to a yardstick length of about 1 nm, indicating that graphitization reduces the roughness of c.b. on small length scales below 1 nm, only. Figure 31.4 also demonstrates that the reduction of BET-surface area due to graphitization is length scale (yardstick) dependent, proving that it is related to a change of surface morphology and not e.g., a result of reduced energetic surface activity.

An important point in the above evaluation of c.b. surface morphology is the correct estimation of the cross-section σ of the applied probe molecules. This is done by referring to the mass density ρ of the probe molecules in the bulk liquid state that are considered as spheres in a hexagonal close packing:

$$\sigma = 1.091\left(\frac{M}{N_A \rho}\right)^{2/3}. \tag{31.2}$$

Here, M is the molar mass of the probe molecules and N_A is the Avogadro number. Note that any other close packing of

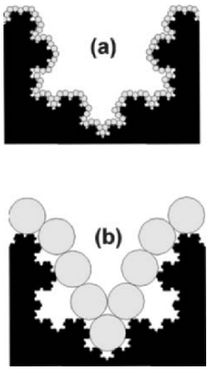

FIGURE 31.3. Schematic presentation of a fractal surface covered with monolayers of (a) small and (b) large gas molecules, demonstrating the impact of the yardstick on the estimated surface area. Reprinted from [11] with kind permission of Springer Science + Business Media.

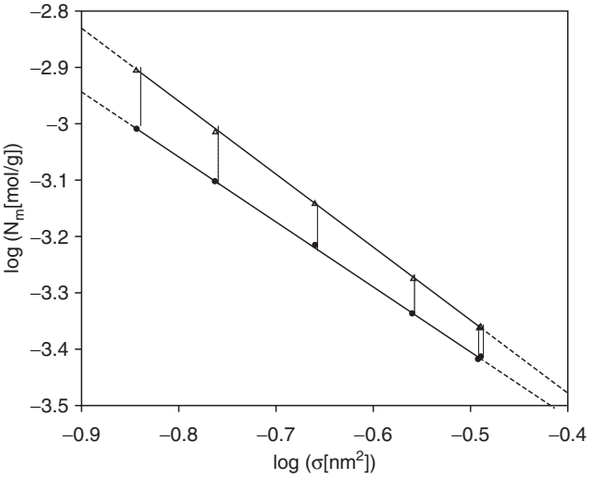

FIGURE 31.4. Yardstick-plot of N220 (△) and a graphitized N220g (●) with adsorption cross section σ determined from the bulk liquid density ρ according to Equ. (31.2); Applied gasses are: 1 argon, 2 methane, 3 ethane, 4 propane, 5 isobutane, 6 *n*-butane; The slopes yield for N220: $D_s = 2.56 \pm 0.04$, for N220g: $D_s = 2.32 \pm 0.03$. Reprinted from [11] with kind permission of Springer Science + Business Business Media.

probe molecules can be used since it doesn't alter the scaling exponent 2/3 of Eqn. (31.2). The crucial point is the temperature dependence of ρ that differ for the different probe molecules, mainly due to variations in the characteristic temperatures, e.g., the evaporation points.

It was found [15] that Eq. (31.2) can be applied without further corrections and high correlation coefficients of the "yardstick-plots" in Figs. 31.4 and 31.5 are obtained, only if: (i) the temperature during the adsorption experiments is chosen according to the theory of corresponding states and (ii) a series of chemically similar gases is used. Fig. 31.5 shows that for the same c.b. (N220g) a different scaling factor is obtained for the "yardstick-plots", if the adsorption temperatures are chosen with respect to different reference pressures, i.e., the evaporation temperatures at $p_0 = 10^3$ mbar and $p_0 = 10^4$ mbar, respectively. A different scaling factor is also observed in Fig. 31.5 for the two homological series of gases, i.e., the alkanes and alkenes, respectively. However, the scaling exponent and hence the surface fractal dimension $D_s \approx 2.3$ is unaffected by the choice of the reference pressure or applied series of adsorption gases.

An alternative approach to the characterization of surface morphology of c.b. is the consideration of film formation of adsorbed molecules in the multilayer regime. In this case, the surface roughness is evaluated with respect to a fractal extension of the classical Frenkel-, Halsey-, Hill (FHH)-theory, where beside the van der Waals surface potential the vapor–liquid surface tension has to be taken into account [19,20]. Then the Helmholtz free energy of the adsorbed film is given as the sum of the van der Waals attraction potential of all molecules in the film with all atoms in the adsorbent, the vapor–liquid surface free energy and the free energy of all molecules in the bulk liquid film. This leads to

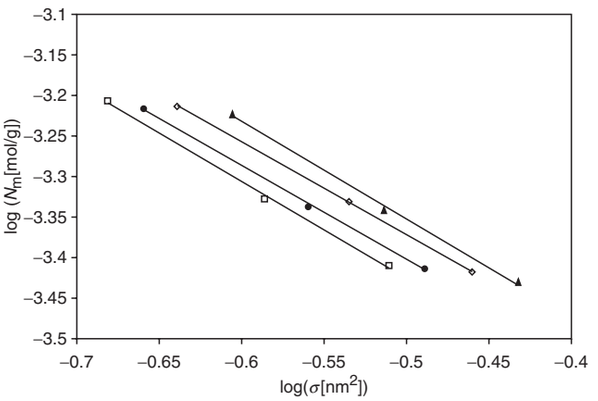

FIGURE 31.5. Yardstick-plots of the graphitized black N220g obtained with alkenes (ethylene, propylene, isobutylene) (hollow symbols) and alkanes (ethane, propane, isobutane) (filled symbols); Adsorption temperatures are chosen as evaporation points at vapor pressures $p_0 \approx 1{,}000$ mbar (lower curves) and $p_0 \approx 1{,}000$ mbar (upper curves) of the condensed gases, respectively. Reprinted from [11] with kind permission of Springer Science + Business Media.

the following relation between the adsorbed amount N and the relative pressure p/p_0 [19,20]:

$$N \sim \left(ln\frac{p_0}{p}\right)^{-\vartheta}$$

with:

$$\vartheta = \frac{3 - D_s}{3} \quad \text{FHH-regime} \tag{31.3a}$$

$$\vartheta = 3 - D_s. \quad \text{CC-regime} \tag{31.3b}$$

The different exponents for the FHH- and capillary condensation (CC)-regime consider the two cases where adsorption is dominated by the van der Waals potential and the vapor–liquid surface tension, respectively. Note that in the CC-regime a flat vapor–liquid surface is obtained due to a minimization of curvature by the surface tension. In the FHH-regime the vapor–liquid surface is curved, since it is located on equipotential lines of the van der Waals potential with constant distance to the adsorbent surface.

At low relative pressures p/p_0 or thin adsorbate films, adsorption is expected to be dominated by the van der Waals attraction of the adsorbed molecules due to the solid potential that falls off with the third power of the distance to the surface (FHH-regime, Eq. (31.3a)). At higher relative pressures p/p_0 or thick adsorbate films the adsorbed amount N is expected to be determined by the surface tension γ of the adsorbate vapor interface (CC-regime, Eq. (31.3b)), because the corresponding surface potential falls off less rapidly with the first power of the distance to the surface, only. The cross-over length $z_{\text{crit.}}$ between both regimes depends on the number density n, the surface tension γ, the van der Waals interaction parameter α as well as on the surface fractal dimension D_s [19,20]:

$$z_{\text{crit.}} = \sqrt{\frac{\alpha n}{(D_s - 2)\gamma}}. \tag{31.4}$$

Note, that the cross-over length $z_{\text{crit.}}$ decreases with increasing surface fractal dimension D_s, implying that the FHH-regime may not be observed on very rough surfaces, i.e., the film formation may be governed by the surface tension γ on all length scales $z > a$ (compare Fig. 31.7).

The film thickness z is related to the surface relative coverage N/N_m and the mean thickness $a \approx 0.35$ nm of one layer of nitrogen molecules [21] according to the scaling law [18]:

$$\frac{N}{N_m} = \left(\frac{z}{a}\right)^{3-D_s} \tag{31.5}$$

The monolayer amount N_m can be estimated from a classical BET-plot and hence the film thickness z can be obtained directly from the adsorbed amount N if the surface fractal dimension D_s is known.

So called FHH-plots of the nitrogen adsorption isotherms at 77 K of two graphitized furnace blacks are shown in Fig. 31.6. The graphitized furnace blacks have three linear

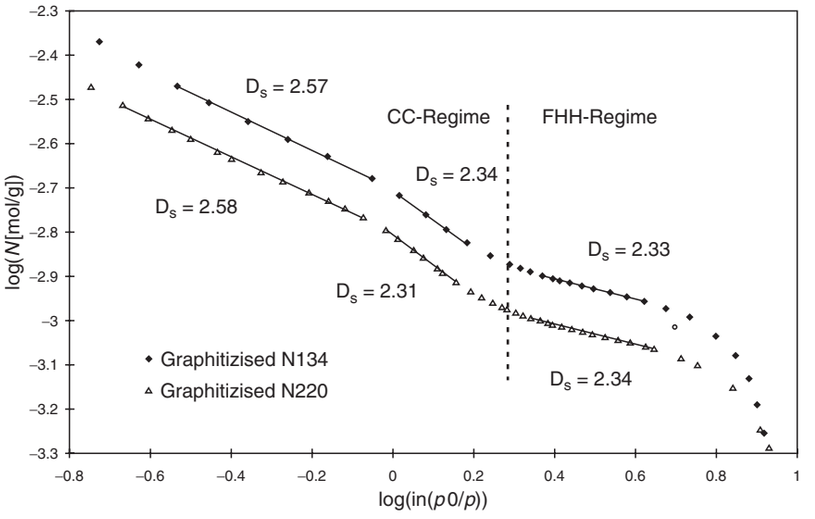

FIGURE 31.6. FHH-plot of nitrogen adsorption isotherms at 77 K for the two graphitized blacks N134g and N220g.

ranges. Starting from low pressures the first linear range is fitted by Eq. (31.3a), because the film is not very thick and the van der Waals attraction of the molecules by the solid governs the adsorption process (FHH-regime). With rising pressure, at a critical film thickness of about $z_{\text{crit.}} \approx 0.5$ nm, the vapor–liquid surface tension γ becomes dominant and a second linear range appears that is fitted according to Eq. (31.3b). The fractal FHH-theory claims almost identical fractal dimensions of $D_s \approx 2.3$ for both linear regimes up to a length scale of $z \approx 1$ nm. At this length scale a geometrical cut-off appears and the surface becomes rougher. In the final linear regime ($z > 1$ nm) the fractal dimension takes the value $D_s \approx 2.6$ (CC-regime). This linear range has an upper cut off length of approximately $z \approx 6$ nm.

Figure 31.7 shows that, contrary to the graphitized blacks, the untreated furnace blacks have only one linear range with a fractal dimension of $D_s \approx 2.6$ (CC-regime, Eq. (31.3b)). Obviously the van der Waals attraction can be neglected and the surface tension γ controls the adsorption process on all length scales. This is due to the larger surface fractal dimension D_s as compared to the graphitized furnace blacks that shifts the cross-over length $z_{\text{crit.}}$ to smaller values (Eq. (31.4)). Assuming that the number density n, the surface tension γ of the adsorbate and the van der Waals interaction parameter α are approximately the same for a nitrogen adsorbate film on graphitized and untreated furnace blacks, a cross-over length of $z_{\text{crit.}} \approx 0.35$ nm can be estimated from Eq. (31.4) with the experimental values of the fractal

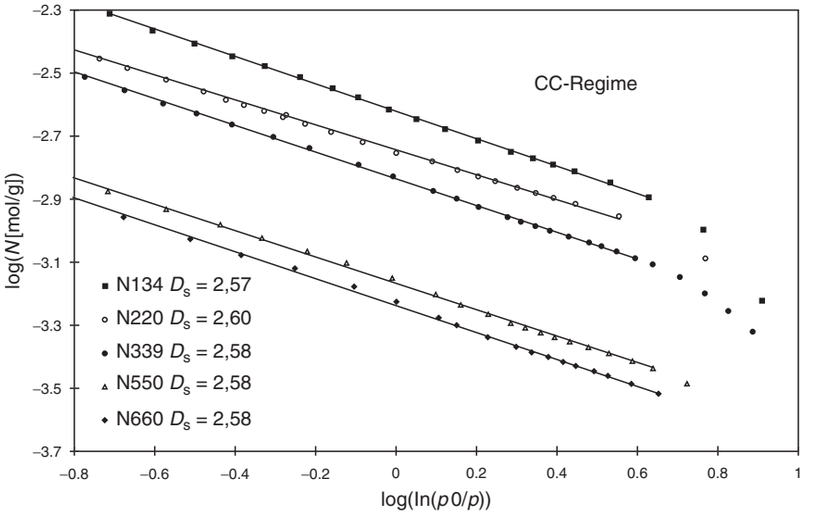

FIGURE 31.7. FHH-plot of nitrogen adsorption isotherms at 77 K for several furnace blacks. Reprinted from [11] with kind permission of Springer Science + Business Media.

dimensions and the crossover length $z_{\text{crit.}} \approx 0.5\,\text{nm}$ on a graphitized c.b. The value $z_{\text{crit.}} \approx 0.35\,\text{nm}$ is already in the range of the detection limit given by the layer thickness $a \approx 0.35$ nm. Hence, the nitrogen adsorption on furnace c.b.s is dominated by the vapor–liquid surface tension on all length scales and a cross over between the FHH- and the CC-regime does not appear. More details of these investigations are found in [15,22,23].

It must be noted that these results obtained by a rigorous gas adsorption analysis are not contradictory to recent small angle X-ray scattering results [17,24,25] that indicate a nonuniversal surface roughness of furnace blacks with significantly smaller values for D_s. The scattering results were obtained in a complementary length scale regime for scattering vectors $q < 1\,\text{nm}^{-1}$. This corresponds to length scales larger than about 6 nm. Below this length scale the scattering data show a cross-over to a different scaling behavior indicative for sheet like structures consistent with graphitic layers [24]. Obviously, on atomic length scales smaller than 6 nm the scattering from the surface is shielded by that of the graphitic crystallite structures.

In the following we present a hypothetical mechanism of c.b. formation that explains the universal value $D_s \approx 2.6$ of c.b. surface topography on atomic length scales. The model is based on physical concepts of disordered surface growth, which were recently applied in many different fields in nature.

31.3 SURFACE GROWTH DURING CARBON BLACK FORMATION

The morphology of c.b. is closely related to the conditions of surface and primary aggregate growth during c.b. processing, which is now discussed in some detail. Figure 31.8 shows a schematic representation of c.b. formation in a furnace reactor, where a jet of gas and oil is combusted and quenched, afterwards. Beside the aggregate growth, resulting from the collision of neighboring aggregates, surface growth due to the deposition of carbon nuclei on the aggregates takes place during the formation of primary c.b. aggregates. Due to the high temperature in the reactor, aggregate as well as surface growth take place under ballistic conditions, i.e., the mean free path length of both growth mechanisms is large compared to the characteristic size of the resulting structures [11,32]. Then the trajectories of colliding aggregates (or nuclei) can be considered to be linear. Numerical simulations of ballistic cluster-cluster aggregation yield a mass fractal dimension $D_f \approx 1.9$–1.95 [37]. This prediction is somewhat smaller than the SAXS-result shown in Fig.31.2. However, the assumption of ballistic cluster–cluster aggregation during c.b. processing should hold only in the asymptotic limit of large aggregates and for the relatively fine blacks. For the more coarse blacks, with a typically small primary particle number, finite size effects can lead to a more compact morphology that differs from the scaling prediction of ballistic cluster aggregation. A further deviation can result from electrostatic repulsion effects due to the application of processing agents (alkali metal ions) for designing the coarse blacks.

It is a challenging problem to model chemical and physical phenomena that take place in a few milliseconds of the c.b. formation process. These processes go so quickly from a hydrocarbon with a few carbon atoms to an aggregate made of several millions of carbon atoms. This is a kind of gaseous–solid phase transition where the solid phase exhibits no unique chemical and physical structure. The c.b.

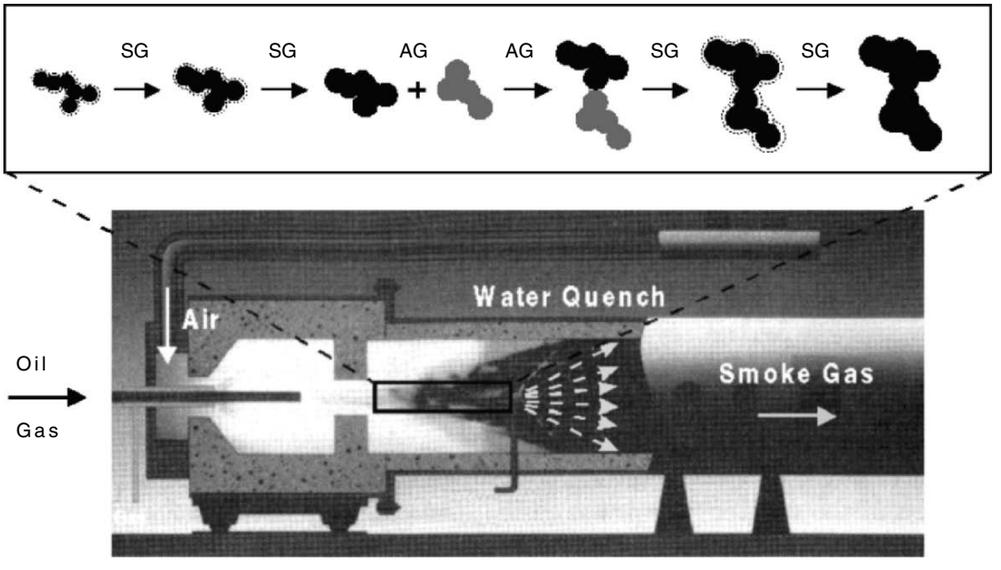

FIGURE 31.8. Schematic view of c.b. processing in a furnace reactor. Primary aggregates are built by two simultaneous growth processes: (i) surface growth (SG) and (ii) aggregate growth (AG). Reprinted from [11] with kind permission of Springer Science + Business Media.

or soot formation[1] mechanism generally described can be summarized by the following steps [26–30]: inception (nucleation), growth (by picking up growth components from the gas phase through c.b. inelastic collision and deposition), and oxidation. It is believed that either fullerenes or fullerene precursors could play an important role in c.b. black formation, especially in the inception step [29,30]. Note that recent studies on the formation of c.b. have even resulted in finding of fullerene (C60) in trace quantities in the toluene extractable materials [31]. High-resolution transmission electron microscopy experiments indicate the molecule may be functioning as a nucleation site in the formation of primary particles of c.b. [31]. The inception of c.b. particles is a key process in c.b. formation. The hydrocarbon fuel in premixed flames is degraded during oxidation into small hydrocarbon radicals from which, under fuel-rich conditions, small hydrocarbon molecules, particular acetylene are formed. The latter adds hydrocarbon radicals for growth and the growing unsaturated (radicalic) hydrocarbons form aromatic rings when containing a sufficiently large number of carbon atoms. The formation of larger aromatic rings occurs mainly via the addition of acetylene. All these processes occur within molecular length scales.

However, only ~5–10% of the c.b. mass is produced during the inception step. The remaining ~90–95% of the total yield is due to surface growth rather than soot inception, i.e., the deposition of carbonaceous species on c.b. particles that have already been formed [26,27]. Mostly it is assumed that particle growth is similar to formation of Polycyclic Aromatic Hydrocarbons (PAH), i.e., addition of acetylene and, probably, aromatics. The problem in this connection is that surface growth is not a gas-phase reaction of small molecules, but a heterogeneous process, where adsorption and desorption processes at the surface have to be considered as well [32]. Some phenomenological approaches are found in the literature (see, for example [32], Section 18.4); However, the corresponding growth rate parameters are empirical fits, and their simple structure does not reveal the underlying mechanisms. Especially, for interpretations of the ''deactivation'' of the soot surface a really convincing physical explanation is not yet available [32]. We note here, that in the physical well founded ballistic deposition model, that we propose here, ''deactivation'' can be easily explained as a kind of surface relaxation which will be explained later.

By using phase-contrast electron microscopy, it appears that surface growth occurs on both individual particles and on the aggregates formed by collision of the individual particles [26]. From this reason, the surface growth is also responsible for the stability of the primary aggregates, since it proceeds in the contact range of the collided aggregates implying a strong bonding by sinter bridges (compare Fig. 31.8). Accordingly, the bonds between neighboring particles of a primary c.b. aggregate are not stabilized by weak short-range forces, but by a continuous carbon network. Surface growth contributes to the major part to the final c.b. concentration in soothing flames while coagulation – switching the length scales to particle dimension – determines the final size of the c.b. particles.

A comparison with deposit models and simulation results of disordered growth processes that might appear during c.b. processing can provide a deeper physical background for an explanation of the universal value $D_s \approx 2.6$ of c.b. surface topography [33]. The models are based on physical concepts of surface growth, which were recently applied in many different fields in nature. Deposition models are classified, for example, in [34–37]. The simplest are ''random deposition'', ''random deposition with surface diffusion'', and ''ballistic deposition''. In all these cases, rough surfaces are generated by growth processes. It seems to be a general feature that randomness is essential in the development of the self-affine character of the surfaces.

Random deposition (RD) is the simplest (but most unrealistic) deposition model for surface growth. The particles fall vertically at a constant rate independently of one another and stick when they reach the top of a column of deposited particles. As there is no horizontal correlation between the neighboring columns, the surface is extremely rough and the surface structure is compact, i.e., $D_s = d = 3$ for the case of three dimensional simulations [34–37].

In the case of ballistic deposition (BD) a particle is released from a randomly chosen position above the surface located at a distance larger than the maximum height of the interface. The particle follows a straight vertical trajectory until it reaches the surface, where upon it sticks. Contrary to the RD model, the particle can stick also to neighboring columns and typically overhangs appear in the interface structure. One important property of the BD growth process is that, due to the ability to stick at neighboring columns, correlation develops along the surface, which imply that the different sites of the surface are not completely independent, but depend on the heights of the neighboring sites. This is different to the RD model where the interface is uncorrelated and the columns grow independently, as there is no mechanism that can generate correlation along the interface. Numerical calculations of the BD model in $d = 2$ give $D_s \approx 1.5$ [35,37]. In particular, numerical simulation of the BD model with restricted step height yield $D_s \approx 1.5$ in two dimensions ($d = 2$) and for $d = 3$ one obtains $D_s = 2.6$–2.64, dependent on the details of simulations [35,37].

A similar realistic model for surface growth during c.b. processing is random deposition with surface ''diffusion'' [35,38]. There a particle reaches the surface as in the random deposition model, but then is allowed to ''diffuse'' on the surface. The diffusion continues until the particle finds the column of minimum height inside a domain of finite size around the initial contact. A schematic view of the model and an example of the resulting interface for $d = 2$ is shown in Fig. 31.9. The surface diffusion generates a nontrivial

[1] We note that soot and carbon black have the similar mechanism of inception and growth.

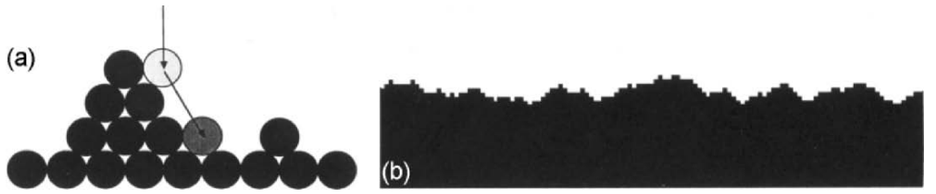

FIGURE 31.9. Random deposition model with surface diffusion. (a) Schematic view of the model in a triangular lattice. (b) Simulation result for a square lattice. Reprinted from [16] with kind permission of Springer Science + Business Media.

correlation between the heights of the columns. Therefore, the roughness of the surface scales with an exponent different from the random deposition model.

The simplest continuum equation describing kinetic roughening is based on a Langevin equation approach and has been introduced by Edwards and Wilkinson (EW) [39]:

$$\frac{\partial h(r,t)}{\partial t} = \nu \cdot \nabla^2 h(r,t) + \eta(r,t). \tag{31.6}$$

The first term on the right side comes from a kind of surface tension and tends to smooth the surface, while the second term is a Gaussian fluctuating white noise satisfying the fluctuation dissipation theorem. Equation (31.6) leads for $d = 2$ to $D_s = 1.5$. Also numerically, this result is well verified for random deposition with surface diffusion [34–38]. For $d = 3$, we find from Eq. (31.6) $D_s = 3$. In this case the correlation decays logarithmically. The discrete growth model, random deposition with surface diffusion, and the continuous EW equation define a universality class, different from random deposition. The construction of the EW equation provides a general procedure that will be useful where more complicated growth models and processes are discussed [34].

The first extension of the EW equation to include nonlinear terms was proposed by Kardar, Parisi, and Zhang (KPZ),

$$\frac{\partial h(r,t)}{\partial t} = \nu \cdot \nabla^2 h(r,t) + \frac{\lambda}{2}(\nabla h)^2 + \eta(r,t), \tag{31.7}$$

where $\lambda/2$ is the coupling of the nonlinear term [40]. Again, the noise η is assumed to be uncorrelated and white and to have a Gaussian distribution. A nonlinear coupling $\lambda \neq 0$ is generated whenever the growth velocity depends on the tilt of the surface [34]. For $d = 2$ the roughness exponent of the interface is $D_s = 1.5$ [34]. Comparing with the numerically-obtained exponents for the BD model ($D_s \approx 1.5$), we find remarkable agreement, suggesting that indeed the KPZ equation and the BD model belong to the same universality class. Kardar, Parisi, and Zhang [40] conjectured that the $d = 2$ result might be superuniversal (independent of d) but this is evidently not correct [36]. At present, no rigorous results are available from Eq. (31.7) for $d > 2$.

A further model of interest for surface growth during c.b. processing is obtained if anisotropy effects are considered in the KPZ equation. The presence of anisotropy is expected to lead to surface tension and nonlinear terms that are different in the two directions. This has been incorporated in the growth equation by considering two different coefficients ν and λ:

$$\frac{\partial h(r,t)}{\partial t} = \nu_x \cdot \partial_x^2 h + \nu_y \cdot \partial_y^2 h + \frac{\lambda_x}{2}(\partial_x h)^2 + \frac{\lambda_y}{2}(\partial_y h)^2 + \eta(r,t). \tag{31.8}$$

Equation (31.8) is called the anisotropic KPZ (AKPZ) equation (see [34] and references therein). If $\nu_x = \nu_y$ and $\lambda_x = \lambda_y$, Eq. (31.8) reduces to the KPZ equation (31.7).

The nontrivial effect of the anisotropy can be observed in the case of stepped surfaces [41,42] or in the three-dimensional discrete Toom model [34,43–45] that is described by the AKPZ equation. The original two-dimensional Toom model has attracted much attention since its nonergodicity in the presence of small perturbations has been proved [45], leading to the possibility that the model is "generic" for a variety of physical systems, including c.b. growth. In this model, spins with values $S = \pm 1$ are simultaneously updated at every time step with the following rule: S becomes equal 1 with probability p, -1 with probability q, and becomes aligned with the majority of itself and a specified set $\{S\}$ of neighboring spins with probability $1-p-q$. When $p = q = 0$, the Toom model is deterministic. For small enough p and q, the model for any dimension has two stable phases: one phase has most spins aligned up $(+1)$ and the other phase has most spins aligned down (-1).

The origin of the surface anisotropy is the anisotropy of the set $\{S\}$ in the updating rule: the x and y directions are not equivalent. Numerical simulations indicate that the interface is described by the AKPZ equation in the strong-coupling or KPZ limit, the scaling exponent in $d = 3$ being $D_s = 2.57 \pm 0.04$ [43]. The mechanisms and results of the $3d$ Toom model can be mapped to surface growth in the case of c.b. formation. Already in the two-dimensional case, where the Toom interface is formed by a rule of simple probabilistic cellular automation [46], this model leads to a $(1+1)$-dimensional solid-on-solid type (SOS) model. Therein, the dynamics of spin flips may be regarded as a "deposition-evaporation" process of particles which occurs in an avalanche fashion [44]. This physics has been generalized in [44], where the spin dynamics in three dimensions is mapped into particle dynamics via the deposition and evaporation process with an avalanche on a checkerboard

lattice. For the biased case the interface is described by the AKPZ equation.

31.4 SURFACE ENERGY DISTRIBUTION FROM STATIC GAS ADSORPTION

The systematic study of c.b. particle surface properties and organization underlines the role of surface morphology in rubber compound properties [47]. In addition to well investigated reinforcing effects caused by the fractal nature of particulate filler aggregates and networks in the rubber matrix [1,8–13,48], the surface activity of fillers plays a key role in reinforcement by controlling the polymer-filler phase bonding and the filler–filler interaction. The surface activity includes: (i) the surface roughness on atomic length scales and (ii) the site energy distribution in relation to the primary particle microstructure and the specific reactivity of adsorption sites with the polymer matrix under consideration. In the previous sections it was demonstrated by equilibrium gas-adsorption measurements on c. b. that the surface roughness, characterized by its surface fractal dimension, is similarly graded for all furnace blacks irrespective of their specific surface area and DBP-number [15]. These results confirm previous findings that all furnace blacks adsorb the same amount (or number) of polymer chains per unit surface area [49]. This would leads to the conclusion that polymer chains of similar chemical nature behave similar concerning their conformational entropy during adsorption on the c.b. surface. Therefore the contribution of the surface roughness cannot explain specific reinforcing effects observed in c.b. filled rubbers.

Early investigations performed by equilibrium gas adsorption have established qualitative differences in the adsorption heat above a surface coverage of 5–10% for original and graphitized c. b. [50]. Nonequilibrium inverse gas-chromatography investigations [51,52] indicate a relationship between the dispersive surface energy contributions and the primary particle size and deliver hints for a heterogeneous surface energy distribution.

In this section we will demonstrate how the site energy distribution, obtained by equilibrium gas-adsorption measurements of ethene on different c.b. grades, can explain the characteristic differences in reinforcement [22,53]. In a typical gas-adsorption experiment the amount N of adsorbed molecules is measured in dependence of the equilibrium pressure p at a constant temperature T. N_m is the maximum number of adsorption sites for a monolayer coverage. The surface coverage Θ is the quotient N/N_m. At low pressures mostly sites with high energies Q are occupied by the gas molecules. With rising pressure more and more molecules adsorb on sites with lower energies Q. At very high pressures p near the vapor pressures p_0 of the pure condensed gas at T the molecules become adsorbed in multilayers. Therefore the isotherms are determined by the energetic surface structure for a given adsorbent. The overall isotherm $\Theta(p,T)$ can be considered as the sum of local isotherms $\theta(p,T,Q)$ of sites with a given energy Q. The local isotherms $\theta(p,T,Q)$ are weighted by the site energy distribution function $f(Q)$. For a continuous distribution function the overall isotherm is given by:

$$\Theta(p,T) = \int_0^\infty \theta(pT,Q) \cdot f(Q)\mathrm{d}Q. \qquad (31.9)$$

The site energy distribution function $f(Q)$ can be calculated by using the experimentally observed overall isotherm $\Theta(p,T)$ and a theoretical local isotherm function $\theta(p,T,Q)$. Here a Langmuir type model equation $\theta(p,T,Q)$ with corrections for multilayer adsorption and lateral interactions between the adsorbed molecules is chosen [54–56]. Then the integral equation can be solved by an analytical iterative method based on numerical integration [57]. More details about this procedure are found in [22,53].

For a precise estimation of the site energy distribution function it is necessary to measure adsorption isotherms down to very low pressures from about 0.001 up to one full monolayer. For this purpose a volumetric gas adsorption apparatus equipped with three capacitance manometers (MKS Instruments Baratron; pressure range: 0.0001–1400 mbar) was used. The temperature T of the c.b. samples was regulated with a cryostat (Huber, $-80\ ^\circ\mathrm{C} - 20\ ^\circ\mathrm{C}$, $\pm$ 0.1 K). Prior to each adsorption measurement, the samples were all subjected to purification extraction treatment (methanol/water (1:1) and toluene each for 48 h) and dried at 40 °C in vacuum. Out-gassing of the samples was carried out at 200 °C in high vacuum for at least 24 h. Ethene (Messer Griesheim, purity $> 99.95\%$) was taken as measurement gas. The investigated c.b. samples with similar aggregate structures (DBP-numbers) and varying mean particle sizes (nitrogen surface area) are shown in Table 31.1. In addition a graphitized N220g was examined as a reference system. The graphitization was performed at 2,500 °C under nitrogen atmosphere.

Figure 31.10 shows the adsorption isotherms of ethene at $T = 223$ K for the examined c.b. samples. As the pressure rises the amount N of adsorbed molecules increases (submonolayer regime) until the isotherms reach a plateau which signifies the monolayer capacity N_m. It can be seen that N115 with the smallest mean particle size has the highest monolayer capacity N_m, whereas N550 with the highest mean particle size has the lowest monolayer capacity N_m. For $p/p_0 \rightarrow 1$ the isotherms increases steeply, because the

TABLE 31.1. *Specific nitrogen surface area (*N_2-SA*) and DBP-number of the investigated c.b. samples.*

	N115	N220	N220g	N550
N_2-SA[m^2/g]	143	118	88	44
DBP [ml/100g]	113	114	–	122

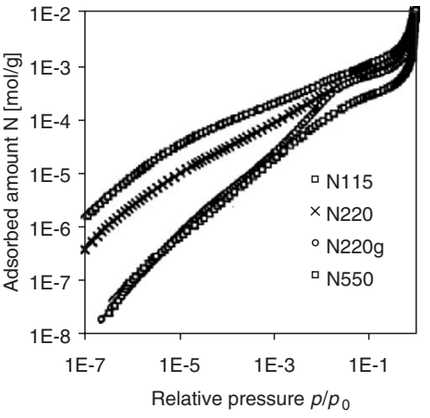

FIGURE 31.10. Adsorption isotherms $N(p,T)$ of ethene on four c.b. samples at $T = 223$ K. Reprinted from [11] with kind permission of Springer Science + Business Media.

gas molecules are adsorbed in multilayers. This regime was extrapolated according to the BET-theory [55]. The symbols in Fig. 31.10 denote the experimental points. The solid lines are the calculated isotherms. Obviously the correlation between the experimental and the fitted isotherms is very good.

The corresponding energy distribution functions $f(Q)$ of ethene calculated from the isotherms are shown in Fig. 31.11. For the original c.b. samples multimodal site energy distribution functions $f(Q)$ are found. The result of an energetic heterogeneous surface structure for N220 has been confirmed by thermodynamic values for isosteric heats of adsorption and infrared spectra of the furnace black N220 in a flow of ethene [22]. The sum curves of the distribution functions $f(Q)$ can be deconvoluted to four gaussian peaks, as shown in Fig. 31.12 for N220. This result demonstrates the existence of discrete energetic surface sites I – IV with

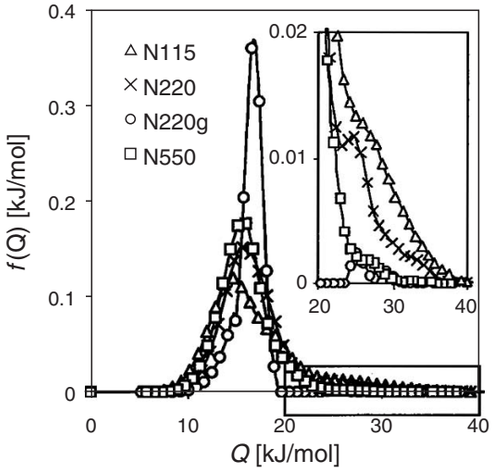

FIGURE 31.11. Site energy distribution function $f(Q)$ for ethene on the c.b. samples shown in Fig. 31.10. Reprinted from [11] with kind permission of Springer Science + Business Media.

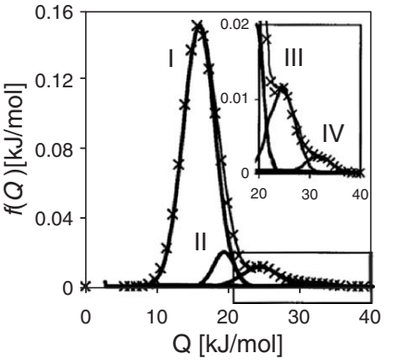

FIGURE 31.12. Deconvolution of the site energy distribution function of N220 to four Gaussian peaks (I–IV). Reprinted from [11] with kind permission of Springer Science + Business Business Media.

energies of $Q(\mathrm{I}) \approx 16$ kJ/mol, $Q(\mathrm{II}) \approx 20$ kJ/mol, $Q(\mathrm{III}) \approx 25$ kJ/mol, and $Q(\mathrm{IV}) \approx 30$ kJ/mol. These sites can be attributed to the microstructure of the spherical primary particles from a comparison of the distribution functions $f(Q)$ of untreated N220 with graphitized N220g (Fig. 31.13).

Contrary to untreated N220, the surface of N220g is energetically more homogeneous (Fig. 31.11). It consists of more than 99% of sites of type I. Sites II are missing and sites III and IV can only be found in traces. It is well known [1] that graphitization increases the degree of crystallization of c. b. with the graphitic planes oriented parallel to the particle surface. So energetic sites I have to be attributed to adsorption sites on graphitic planes and energetic sites II – IV to defect structures which have normally higher interaction energies Q. Possible defect structures are amorphous carbon II with sp^3-hybridization, crystallite edges III or cavities IV between to crystallites. Upon graphitization all amorphous carbon is transformed to carbon incorporated in graphitic planes as revealed by Raman spectroscopy [58] and no energetic sites II are left on the surface (Fig. 31.11). On the other hand side, crystallite edges and cavities should always be present on the surface, because the microcrystallites have to form spherical particles. Compared

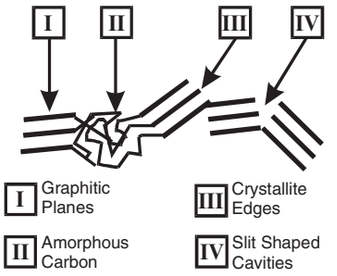

FIGURE 31.13. Proposed attribution for the energetic sites I–IV to the surface microstructure, obtained from the deconvolution of the energy distribution function in Fig. 31.12. Reprinted from [11] with kind permission of Springer Science + Business Media.

to the crystallite edges the cavities IV should have higher energies Q, because an adsorbed gas molecule interacts with the surface from several directions. In a slit shaped cavity the interaction energy Q was calculated to be enhanced by a factor of 1.6 at maximum [59] which can explain interaction energies as high as 40 kJ/mol.

The results of the deconvolution with four gaussian peaks are given in Table 31.2. The percentages at surface of adsorption sites I- IV calculated from the areas of the Gaussian peaks vary significantly: The percentage of high energetic sites III and IV increases with decreasing particle size or increasing specific nitrogen surface area. Accordingly, the percentage of the low energy sites I increases with increasing particle size.

31.5 SUMMARY AND CONCLUSIONS

In conclusion it has been shown that the presented gas adsorption technique gives equal estimates for the surface roughness independent of adsorption temperature or pressure, which is clearly not the case if other evaluation procedures for the cross section that are proposed in the literature are applied. Based on the consideration of film formation of adsorbed molecules in the multilayer regime, it was demonstrated that all examined c. b.s have a unique surface roughness on atomic length scales with a surface fractal dimension $D_s \approx 2.6$ (Fig. 31.7). Thereby, capillary condensation was demonstrated to be the relevant mechanism of film formation of adsorbed probe molecules. This result was confirmed by investigations in the monolayer regime (Fig. 31.4), where the same relatively high value of the surface fractal dimension for the untreated furnace black N220 was found.

We point out that experimental investigations of c. b. surface roughness by two different gas adsorption techniques indicate a universal surface morphology for all furnace blacks. We have presented numerical and theoretical attempts to explain c. b. formation within the today well founded statistical physics of surface growth mechanisms. The universal and scaling properties of the discussed growth models explain the universal topography of c. b. particle surface, independent of c. b. grade. This property can be seen in the universal value of the surface fractal dimension $D_s \approx 2.6$. These universal features can now be understood and traced back to the deeper physical origin of correlation between neighboring sites during the growth process.

The results concerning the energy distribution functions $f(Q)$ of ethene, calculated from the isotherms on a broad pressure range, lead to the conclusion that the examined furnace blacks have an energetic heterogeneous surface structure. With increasing particle size the amount of high energetic sites per gram of filler decreases dramatically showing the very different surface activities to polymers, respectively, the different reinforcement potentials of the fillers. The percentage of high energetic sites is not constant for the grades with different mean particle size. Therefore the value of the specific nitrogen surface area is not sufficient to describe the surface activity of the filler. Upon graphitization the surface becomes nearly energetically homogeneous.

TABLE 31.2. *Estimated fractions [%] of adsorption sites I–IV at the surfaces of the four examined c.b. samples*

	N115	N220	N220g	N550
I ($Q \approx 16$ kJ/mol)	69	84	99	93
II ($Q \approx 20$ kJ/mol)	13	7	–	6
III($Q \approx 25$ kJ/mol)	15	7	< 1	1
IV ($Q \approx 30$ kJ/mol)	3	2	< 1	< 1

ACKNOWLEDGMENTS

The authors are indebted to Professor R. H. Schuster (DIK), Dr. M. Gerspacher and Professor T. A. Vilgis (MPI Mainz) for helpful discussions and to the Deutsche Kautschukgesellschaft (DKG) for financial support.

REFERENCES

1. J. B. Donnet, R. C. Bansal, M. J. Wang (eds), Carbon Black: Science and Technology. Marcel Decker, New York Hongkong (1993)
2. G. Kraus (ed), Reinforcement of Elastomers. Interscience Publisher, New York London Sydney (1965)
3. R. Payne, J. Appl. Polym. Sci. **6**, 57 (1962); ibid. **7**, 873 (1963); ibid. **8**, 2661 (1965); ibid. **9**, 2273, 3245 (1965)
4. G. Kraus, J. Appl. Polym. Sci., Appl. Polym. Symp. **39**, 75 (1984)
5. A. van de Walle, G. Tricot, M. Gerspacher, Kautsch. Gummi Kunstst. **49**, 173 (1996)
6. C. R. Lin, Y. D. Lee, Macromol. Theory Simul. **5**, 1075 (1996); ibid. **6**, 102 (1997)
7. T. A. Witten, M. Rubinstein, R. H. Colby, J. Phys. II (France) **3**, 367 (1993)
8. M. Klüppel, G. Heinrich, Rubber Chem. Technol. **68**, 623 (1995)
9. G. Heinrich, M. Klüppel, T.A. Vilgis, Curr. Opin. Solid State Mater. Sci. **6**, 195 (2002)
10. G. Heinrich, M. Klüppel, Adv. Polym. Sci. **160**, 1 (2002)
11. M. Klüppel, Adv. Polym. Sci. **164**, 1 (2003)
12. A. I. Medalia, Rubber Chem. Technol. **59**, 432 (1986)
13. M. Klüppel, R. H. Schuster, G. Heinrich, Rubber Chem. Technol. **70**, 243 (1997)
14. S. Havriliak, S. Negami, Polymer **8**, 161 (1967)
15. A. Schröder, M. Klüppel, R. H. Schuster, Kautsch. Gummi Kunstst. **52**, 814 (1999), ibid. **53**, 257 (2000)
16. A. Bunde, S. Havlin (eds), Fractals and Disordered Systems, Chap. 7, Springer Verlag, Berlin Heidelberg New York (1991)
17. J. Fröhlich, S. Kreitmeier, D. Göritz, Kautsch. Gummi Kunstst. **51**, 370 (1998)
18. B. Mandelbrot, "The Fractal Geometry of Nature", Freeman, New York, (1977)
19. P. Pfeifer, M. Obert, M. W. Cole, Proc. R. Soc. London, **A 423**, 169, (1989)
20. P. Pfeifer, M. W. Cole, New J. Chem. **14**, 221, (1990)
21. B. C. Lippens, B. G. Linsen, J. H. De Boer; J. Catalysis, **3**, 32, (1964)
22. A. Schröder, PhD-Thesis, University of Hannover (2000)
23. M. Klüppel, A. Schröder, R. H. Schuster, J. Schramm, "The Disordered Morphological Structure of Carbon Black", Paper No. XLI, 157th ACS Rubber Division Meeting, Dallas Texas, 4–6 April (2000)

24. T. P. Rieker, S. Misono, F. Ehrbourger-Dolle, Langmuir **15**, 914 (1999)
25. T. P. Rieker, M. Hindermann-Bischoff, F. Ehrbourger-Dolle, Langmuir **1**6, 5588 (2000)
26. R. C. Bansal, J-B. Donnet, "Mechanism of Carbon Black Formation", in Carbon Black. Sci. Technol. (Eds. J-B. Donnet, R. C. Bansal, M-J. Wang), Marcel Dekker, New York, Basel, Hong Kong (1993)
27. J. Lahaye, F. Ehrburger-Dolle, 'Mechanism of Carbon Black Formation. 'Correlation with the Morphology of Aggregates', in Proceedings 2nd Int. Conf. on Carbon Black, Mulhouse (F), 27–30. September 1993, pp. 11–23
28. H. Bockhorn, "A Short Introduction to the Problem", in H. Bockhorn (Ed.), Soot Formation in Combustion, Mechanisms and Models, Springer-Verlag, Berlin Heidelberg New York, pp. 3–7
29. J. B. Donnet, T.-K. Wang, C. C. Wang, M. Monthioux, M. P. Johnson, D. T. Norman, R. W. Wansborough, P. Bertrand, Kautschuk, Gummi, Kunststoffe **52**, 340 (1999)
30. F. Cataldo, Fullerene Sci. Technol. **8**, 105 (2000)
31. M. P. Johnson, R. W. Locke, J. B. Donnet, T. K. Wang, C. Wang, P. Bertrand, Paper No. 179, "Carbon Black and Fullerenes: New Discoveries in Early Formation Mechanisms and Nucleation", 156th ACS Rubber Division Meeting, Orlando, FL. September 1999
32. J. Warnatz, U. Maas, R. W. Dibble, "Combustion", Springer-Verlag, Berlin Heidelberg New York (1999)
33. G. Heinrich, M. Klüppel, Kautsch. Gummi Kunstst. **54**, 159 (2001)
34. A.-L. Barabási, H. E. Stanley, Fractal Concepts in Surface Growth, Cambridge University Press, Cambridge (1996)
35. J.-F. Gouyet, M. Rosso, B. Sapoval, "Fractal Surfaces and Interfaces", in A. Bunde, S. Havlin (Eds.), "Fractals and Disordered Systems", Springer-Verlag, Berlin Heidelberg New York (1991)
36. J. Kertész, T. Vicsek, "Self-Affine Interfaces", in A. Bunde, S. Havlin (Eds.), "Fractals in Science", Springer-Verlag, Berlin Heidelberg New York (1994)
37. P. Meakin, "Fractal Structures", Progr. Solid St. Chem. **20**, 135–233 (1990)
38. F. Family, J. Phys. **A 19**, L441 (1986)
39. S. F. Edwards, D. R. Wilkinson, Proc. R. Soc. London A 381, 17 (1982)
40. M. Kardar, G. Parisi, Y. C. Zhang, Phys. Rev. Lett. **56**, 889 (1986)
41. K. Moser, D. E. Wolf, "Kinetic roughening of vicinal surfaces", in "Surface Disordering: Growth, Roughening and Phase Transitions", in R. Jullien, J. Kertész, P. Meakin and D. E. Wolf (Eds.), Nova Science, New York (1992), pp. 21–30
42. D. E. Wolf, Phys. Rev. Lett. **67**, 1783 (1991)
43. A.-L. Barabási, M. Araujo, H. E. Stanley, Phys. Rev. Lett. **68**, 3729 (1992)
44. H. Jeong, B. Kahng, D. Kim, Phys. Rev. Lett. **71**, 747 (1993)
45. A. L. Toom, in 'Multicomponent Random Systems', (Eds.: R. L. Dobrushin, Ya. G. Sinai), Dekker, New York (1980)
46. B. Derrida, J. L. Lebowitz, E. R. Speer, H. Spohn, Phys. Rev. Lett. **67**, 165 (1991)
47. J. B. Donnet, Rubber Chem. Technol. **71**, 323 (1998)
48. M. Gerspacher, C. P. O'Farrell, L. Nikiel, H. H. Yang; F. LeMehauté, Rubber Chem. Technol. **69**, 789 (1996)
49. D. Bussmann, Ph. D. Thesis, Universität Hannvoer (1992)
50. R. A. Beebe, J. Biscoe, W.R. Smith, C.B. Wendell, J. Am. Chem. Soc. **69**, 2294 (1947)
51. J.-B. Donnet, Carbon **32**, 1305 (1994)
52. M.-J. Wang, S. Wolff, Rubber Chem. Technol. **65**, 715 (1992)
53. A. Schröder, M. Klüppel, R. H. Schuster, J. Heidberg, Kautsch. Gummi Kunstst. **54**, 260 (2001), ibid. Carbon 40, 207 (2002)
54. I. Langmuir, J. Am. Chem. Soc. **40**, 1361 (1918)
55. S. Brunauer, P. H. Emmett, E. J. Teller, J. Am. Chem. Soc. **60**, 309 (1938)
56. R. H. Fowler, E. A. Guggenheim, "Statistical Thermodynamics", Cambridge University Press, Cambridge (1952)
57. A. W. Adamson, I. Ling, Adv. Chem. **33**, 51 (1961)
58. T. W. Zerda, W. Xu, H. Yang, M. Gerspacher, Rubber Chem. Technol. **71**, 26 (1998)
59. D. H. Everett, J. C. Powl, J. Chem. Soc. Faraday Trans. I **72**, 619 (1976)

CHAPTER 32

Properties of Polymers Reinforced With Silica

Chandima Kumudinie Jayasuriya* and Jagath K. Premachandra†

*Department of Chemistry, University of Kelaniya, Dalugama, Kelaniya, Sri Lanka
†Department of Chemical and Process Engineering, University of Moratuwa, Katubedda, Moratuwa, Sri Lanka

32.1 INTRODUCTION

The elastomers which cannot undergo strain-induced crystallization are generally reinforced with permanent reinforcing fillers [1–5]. The incorporation of fillers into polymers has the advantage of increased tensile strength, tear strength, abrasion resistance, resilience, and extensibility. However, the incorporation of fillers into a polymer has several disadvantages including increases in hysterisis and thus heat build-up resulting permanent deformation [1–5]. Two of the most important examples for the use of reinforcing fillers are the incorporation of carbon black fillers into natural rubber and to some other elastomers [6–8] and the incorporation of silica fillers into siloxane polymers [5,9]. Other polymers that have been reinforced using fillers include acrylates [10–13], polyamides [13], polyimides [15], polybenzoxazoles [16,17], and polybenzothiazoles [16,17]. Fillers such as titania, zirconia, mixed fillers of silica–titania and silica–zirconia, clays, metallic particles, and even glassy polymers have been used to achieve reinforcement.

The focus of this review is the properties of polymers reinforced with silica, however, the synthetic approaches of incorporating silica into polymers will also be briefly discussed.

32.2 IN SITU GENERATION OF SILICA

Experimental evidences indicate that the extent of the reinforcement depends strongly on the particle size. The maximum reinforcement is obtained for particles with diameters ranging from 10 to 100 nm. Although polymers filled with such nanoscaled silica fillers, i.e., polymer–silica nanocomposites can be prepared by a variety of approaches, the majority of such composites are prepared through the sol–gel technique. Sol–gel reaction of a silicon alkoxide is a method for preparing inorganic silicon oxides under mild conditions [18]. It involves simultaneous hydrolysis and condensation of silicon alkoxide to form a three-dimensional silica network.

The sol–gel reaction has been used to in situ precipitate very small, well-dispersed silica particles into a polymeric material [19,20]. Silica particles thus produced give good reinforcement to a variety of elastomers. This technique avoids the difficult, time-consuming and energy extensive process of blending agglomerated filler into high molecular-weight polymers, especially when this is applied to elastomers. Insitu precipitation of silica using sol–gel technique can be done after, during or before crosslinking [20]. In situ filled elastomer is then extracted with a good solvent to achieve reinforcement. Various polymeric phases such as elastomers, glassy polymers, semicrystalline polymers and high-temperature polymers have been reinforced with silica in situ generated by the sol–gel technique [21,22].

Among elastomers, poly(dimethyl siloxane) (PDMS) has been the most extensively studied polymer with in situ generated filler. PDMS has frequently been chosen since it is compatible with silica or any other organometallic material used to generate ceramic phases. In addition, being a low-strength material, PDMS requires a considerable reinforcement from fillers before it is useful in many industrial applications [5,6]. A large number of other elastomeric phases including poly(phenyl methyl siloxane) [20,21], polybutadiene [21,23], and polyisobutylene [21,24] have been reinforced with silica using the sol–gel approach. Examples of glassy polymers [21] reinforced with in situ

generated silica include polyacrylates [12], poly(vinyl acetate) [25–27], and polyanilines [28]. Semicrystalline phases treated by the sol–gel technique include poly(tetra methylene oxide) [29,30], poly(ethylene oxide) [31,32], and poly(vinyl alcohol) [21,22]. Although it is difficult to treat high-temperature polymers in the usual sol–gel technique, few studies on aromatic polyamides [33,34], polyimides [35–40], polybenzobisoxazoles [16,17], and polybenzobisthiazoles [16,17] have been reported. High-temperature, high-performance polymers are generally unreactive which cause poor bonding between the polymeric and ceramic phases. This problem can be minimized by functionalizing the polymer or by adding a bonding agent [16,17,21,41].

32.3 CHARACTERIZATION TECHNIQUES

Polymer–silica nanocomposites thus prepared are characterized by electron microscopy, scattering techniques, nuclear magnetic resonance spectroscopy, etc. to determine the structural features. In addition, properties such as mechanical, thermal, optical, and other important physical properties are generally determined.

32.3.1 Structural Features

Electron Microscopy

Both transmission electron microscopy (TEM) and scanning electron microscopy (SEM) have been used to determine structural features of various polymer–silica systems. Electron microscopic techniques generally provides information on the nature of the filler, average particle size, or the distribution of particle sizes, smoothness of the interfaces, and the degree of agglomeration of particles.

Transmission electron micrographs obtained for silica-filled PDMS elastomers in base (ethyl amine) catalyzed hydrolysis of tetraethoxysilane (TEOS) and acid (acetic) catalyzed hydrolysis of TEOS are given in Figs. 32.1 and 32.2, respectively [2,3]. Figure 32.1 shows that the particles in this silica-filled PDMS network have an average diameter of approximately 80 Å which is a very much desirable size with regard to reinforcement. Figure 32.1 also indicates that the filler particles have a relatively narrow size distribution, very little agglomeration, and well-defined surfaces. On the other hand, acidic catalysts yield poorly defined, agglomerated particles (Fig. 32.2) [2,3].

Electron microscopic results on networks filled in situ by the sol–gel approach have shown that the filler particles typically have a narrow distribution of sizes, with most diameters in the range 200–250 Å. TEM studies on the distribution of silica in situ generated within PDMS have shown that well-distributed particles can be obtained by using basic catalysts, thin samples, and long hydrolysis times, while the silica was found to precipitate mainly in the sample periphery in the case of acidic conditions, bulky

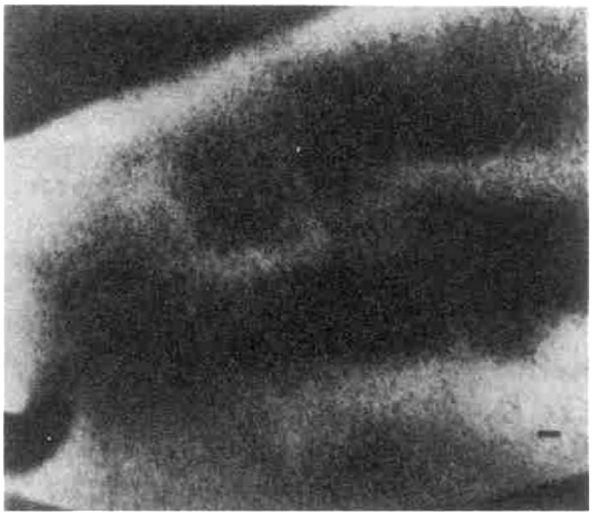

FIGURE 32.1. Transmission electron micrograph for PDMS filled with silica using basic catalysts. From [2] 1988 © John Wiley and Sons.

samples, and short hydrolysis times [42]. TEM was also used for characterizing PDMS networks filled with silica–titania and silica–zirconia mixed oxides [48–50]. The distributions of particle sizes in such systems were relatively narrow with average particle diameter approximately 200–250 Å which increased to 300–350 Å when the molecular weight of the PDMS chains increase from 18,000 g/mol to 26,000 g/mol presumably due to the confining effect of the network pores. The silica–zirconia mixed oxide fillers were found to have particle sizes and distributions very similar to those of the silica–titania ones [48–50].

TEM studies performed on silica filled poly(tetramethylene oxide) by the sol–gel process showed an increase in the

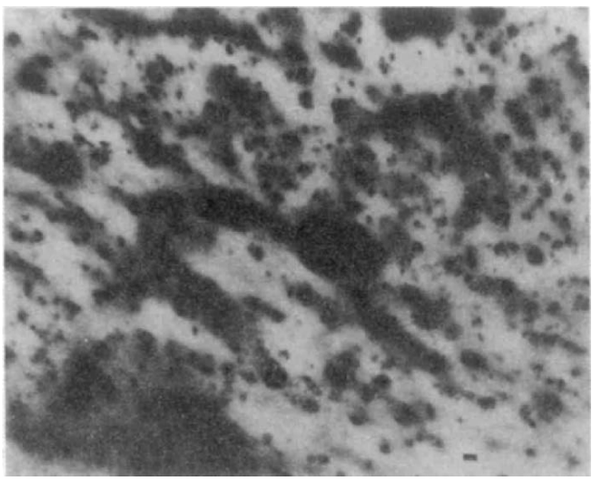

FIGURE 32.2. Transmission electron micrograph for PDMS filled with silica using acid catalysts. From [2] 1988 © John Wiley and Sons.

particle size as the TEOS concentration was increased [43]. This is due to the fact that the phase separation between the metal oxide and oligomeric phases is greater when the metal alkoxide content is increased. Similar results have been obtained for poly(phenylene terephthalamide)–silica ceramers with interface bonding achieved by the use of aminopropyltriethoxysilane [34].

Electron microscopy results for composites prepared using TEOS and tetramethylorthosilicate (TMOS) in trialkoxysilane-functionalized and unfunctionalized polyacrylates indicated phase separation behavior in the composites of methacrylate polymers when the methyl groups are substituted with butyl groups, due to the absence of hydrogen bonding between the silicate and the polymer [44]. Electron microscopy has also been used to demonstrate the particle distribution in a study of the effects of dispersion and aggregation of silica in poly(methyl methcrylate) [45]. In addition, SEM results on nanocomposites prepared using mesoporous silica particles in a methacrylate polymer indicated spherical silica particles ranging from 1 to 10 μm in diameter [46]. The composites showed a certain degree of chain orientation. SEM results also suggested that the composites were composed of polymer that threaded through the mesoporous silica particles and the polymer formed among these filler particles. Compared with conventional particle/polymer composites prepared using dense particles as fillers, it was suggested that these porous fillers may serve as pseudo crosslinking points with the nanocomposites [46].

SEM results on polyimide–silica composites also showed dispersed silica particles of diameter of 3–7 μm [15]. The particle size increased with the silica content as already mentioned for other composite systems [43]. When a bonding agent, (aminophenyl)trimethoxy silane (APTMOS) was incorporated to provide bonding sites between the polymer and the silica like phase, the particles were much smaller and more uniform. This could be explained by the fact that aminophenyl group on the substituted silicon trialkoxide reacted with the polymer chains, possibly improving the compatibility of silica with the polymer. It also has the tendency to prevent the formation of high molecular weight silicate, thus reducing the size of clusters [38,47]. In a similar study, polyimide–silica hybrid materials prepared by the incorporation of small amounts of γ-glycidyloxypropyltrimethoxysilane exhibited finely-dispersed co-continuous phase morphology [39]. Similar observations were made for other composites such as polybenzoxazole–silica and polybenzobisthiazole–silica prepared with interfacial bonding achieved by the use of bonding agents [16,17]. In another study, partial replacement of TEOS with a nonpolar network modifier, dimethylethoxysilane, in polyimide–silica composites caused precipitation of fine silica-rich particles [39]. On the other hand, SEM results obtained for composites prepared using ''site isolation'' method by trapping SiO_2 in polyimide matrices indicated the presence of oxide nanoclusters of size 1–1.5 nm up to 32% silica content and when it was increased to 42% the particles were 1 μm in size [36].

A comparison of properties of composites of poly(vinyl acetate) (PVAc) and silica prepared by the sol–gel process and those prepared by the melt milling or solution casting with fumed silica indicated that both types of films were transparent, however, TEM pictures for two types showed a microscopic heterogeneity [26]. Qualitative differences were apparent with respect to the primary particle size, the size of phase heterogeneity and the sharpness of the polymer–filler interface. TEM pictures obtained for both melt-milling and solution casting indicated that the aggregates are evenly dispersed. Figure 32.3 shows a TEM picture for PVAC–silica composites with 20 wt% silica prepared using solution casting from THF.[26]. The absence of larger micron-sized clusters are also supported by the fact that the films are optically transparent. The micrograph for PVAc film filled in situ with silica by the sol–gel process also showed a two-phase morphology, however, with a much finer texture indicating a more intimate mixture of the two phases (Fig. 32.4)

Scattering Techniques

Analyses of structural features using small angle, light, X-ray, and neutron scattering (SALS, SAXS, SANS) have been carried out for a number of polymer–silica systems [26,43,44,51,52]. In general, scattering data provides estimates of average particle size and the particle size distribution. In addition, the terminal slopes give an indication of the nature of the interfaces, with −3 corresponding to rough interfaces and −4 to smooth. Some typical SAXS results are shown in Fig. 32.5 [2].

Beaucage and coworkers analyzed the structural features of PDMS–silica composites and interrelated those features over a wide range of length scales using the unified approach

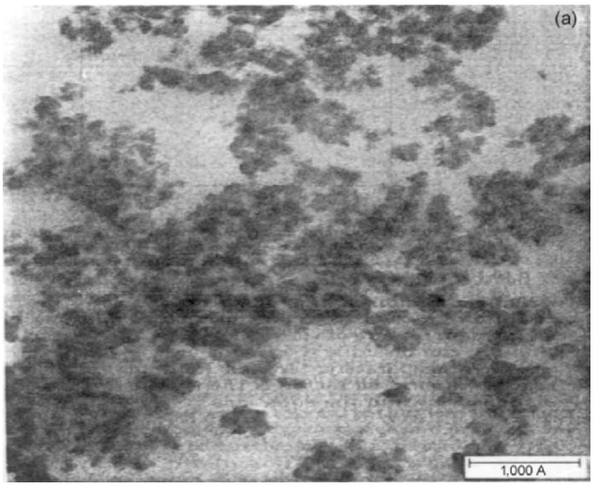

FIGURE 32.3. Transmission electron micrograph for PVAC–silica composites with 20 wt% silica prepared using solution casting from THF. From [26] 1993 © American Chemical Society.

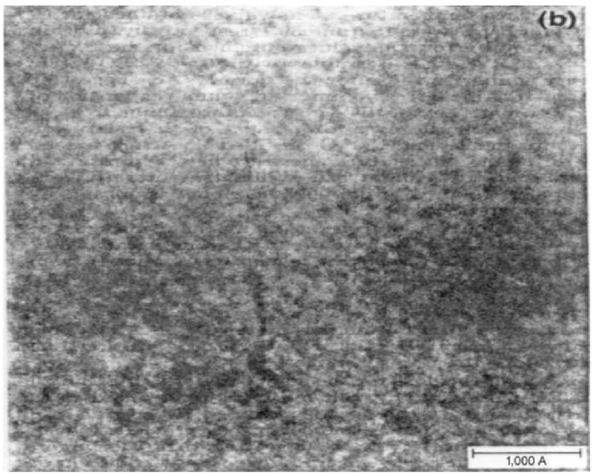

FIGURE 32.4. Transmission electron micrograph for PVAC–silica composites with 16 wt% silica prepared using the sol–gel process. From [26] 1993 © American Chemical Society.

[51]. Analysis of rubber filled with conventional filler and an in situ filled siloxane sample displayed three levels of structure in the size-range observed [51]. In another study, growth mechanism and structures of siloxane composites containing silica, and silica–titania were studied by Breiner *et al*. using SAXS. Both systems were found to yield dense particles.

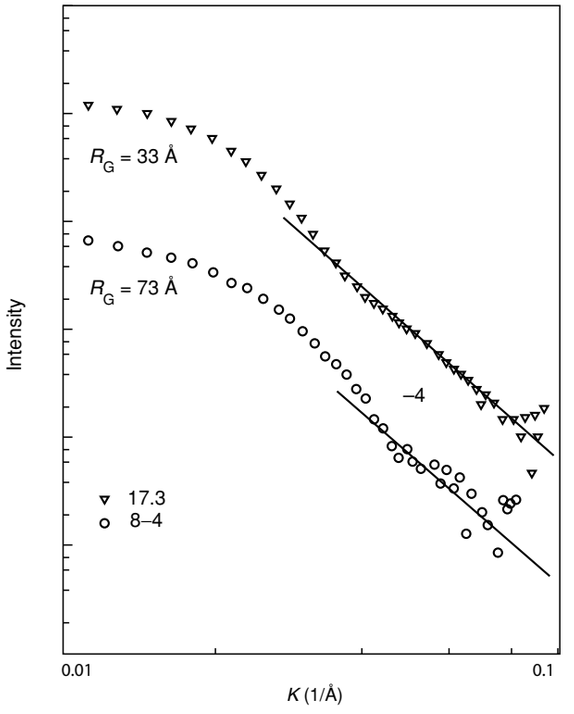

FIGURE 32.5. Intensity of small angle x-ray scattering as a function of the scattering vector for PDMS networks containing 17.3 wt% (▽) and 8.4 wt% (O) silica. From [2] © John Wiley and Sons.

The scattering results suggested that the corresponding growth processes in the mixed oxides proceeds by the formation of relatively uniform titania particles, followed by the formation of significantly larger silica particles [52].

A morphological model for PTMO–metal oxide ceramers was proposed by Rodriguez *et al*. and validity of the model was tested under a variety of variables such as temperature, metal alkoxide content, oligomer spacer length, and the solvent. All three types of ceramers investigated, PTMO–silica, PTMO–titania, and PTMO–zirconia displayed very similar SAXS profiles each showing a single interference peak suggesting the existence of a microphase-separated morphology in accordance with the proposed model [43]. Among the three metal alkoxides employed, the scattering intensity was the lowest for TEOS and the highest for zircornium propoxide. This could be explained by the fact that as the atomic number of the inorganic component increases, so does the mean square electron density difference between the inorganic and the oligomeric components which in turn causes an increase in the scattering intensity. The peaks in the scattering profiles were determined to be due to interparticle interference. Thus, by increasing the length of the organic matrix spacer between the particles, the interdomain spacing as measured from SAXS profiles also increased as expected [43].

In another study, composites made using in situ polymerization of TEOS and TMOS in the presence of tri alkoxy functionalized and unfunctionalized polyacrylates were characterized using SAXS [44]. Slight differences in the local morphology were observed by SAXS, however, macroscopic phase separation was controlled to a large degree by the ability of the backbone to interact with the growing silica network [44].

SAXS studies have also been performed for PVAc–silica composites prepared by solution casting or melt-milling techniques or by in situ [26]. SAXS profiles of PVAc–silica composites containing 20 wt% silica prepared by solution casting and melt-milling were found to be identical suggesting that the local structure of the silica aggregates is the same whether the composites were prepared by solution casting or melt-milling. The final power law slope of −4 at the highest scattering vectors indicates that the surface of primary silica particles is smooth and a sharp interface exists between the organic and inorganic phases. SAXS profiles for several compositions of in situ prepared PVAc–silica composites all approached a limiting slope of −2.45, indicating that the structures are mass fractals [26].

Nuclear Magnetic Resonance Spectroscopy

Nuclear Magnetic Resonance Spectroscopy (NMR) is a useful technique in characterizing the structures being formed and in determining the extent to which chemical reactions are occurring [21,53–57]. For example, ^{29}Si NMR spectrum of polyimide–silica composites consisted of nonhydroxy, monohydroxy, and dihydroxy siloxane

structures, suggesting that the formation of developed silica–oxygen network structure was incomplete.

In addition, NMR imaging utilizing ^{1}H and ^{29}Si magic-angle spinning, with two-dimensional Fourier transform spin echo technique has been an extremely useful nondestructive technique in determining inhomogeneities in in situ filled networks [3,21]. For example, PDMS networks reinforced by in situ precipitated silica were characterized by measuring bulk-spin lattice (T_1) and spin–spin (T_2) relaxation times [58,59]. PDMS–silica composites were intentionally made inhomogeneous by using bulky samples and carrying out the precipitation reaction for a short period of time. Thus, T_1 and T_2 maps showed significant variations of NMR signal intensity throughout the sample due to nonuniform hydrolysis of TEOS in the specimens [58,59].

Infrared Spectroscopy

Infrared spectroscopy (IR) is also a very useful technique for characterizing structure. IR spectroscopy can be used for identification purposes as well as for monitoring the progress of a chemical reaction. Comparisons of the positions of absorptions in the IR spectrum of a sample with the characteristic absorption regions, leads to identification of the bonds and functional groups present in the sample. For example, the chemical structures of polyimide–silica hybrid films were confirmed by IR spectroscopy by the appearance of two absorptions at 1,100 and 830 cm^{-1} indicating the formation of the Si–O bonds.

32.3.2 Densities

Density measurements of polymer–silica composites provide very useful information on the filler particles. In general, density of polymer–silica composites increases with increasing amount of silica because of the high density of silica compared to the polymer. Densities of the filled networks, unfilled network, and silica are used to estimate the weight% silica in the composite which could then be compared with the values obtained directly from weight increases. Such comparisons in PDMS–silica systems have shown that the densities obtained by density measurements were smaller than those determined by weight increases, suggesting possible voids or incomplete hydrolysis of TEOS. In another approach by Morikawa *et al*., the density of silica estimated by extrapolation of the density versus percent silica curve was smaller than that of the usual silica glass suggesting incompletion of polycondensation to form silica structure. This result was consistent with those obtained for NMR studies.

32.3.3 Water Absorption

The knowledge of the relative rate of water absorption is important, since water can influence many physical properties such as electrical insulating ability, dielectric loss, dimensional stability, and appearance. The relative rate of water absorption measured for several polyamide–silica [34,41], polybenzoxazole–silica [16,17] and polybenzobisthiazole–silica [16,17] systems showed a considerable decrease in water absorption in the films containing 5–10 wt% silica with a slight additional decrease for higher silica contents. The decreased hydrophilicity could be explained by the fact that silica hindered the access of water to the polar, hydrogen-bonding regions of the composites.

32.3.4 Transparency

Transparency in some polymer–silica composites make them qualify for various optical applications. One example is PDMS–silica composites which show excellent transparency [60]. On the other hand, polyimide–silica hybrid films containing very low amounts of silica were transparent even after the films were heated to 270 °C where as the films containing more than 10 wt% silica were opaque and were phase separated upon drying [15]. This is due to the fact that increase in amount of silica increases the size of particles, increasing the magnitude of scattering, resulting opaque films. Another example involves polyamide–silica composites which were transparent up to 20 wt% silica content [33,34]. The films containing 25 wt% silica was only semi-transparent and partial phase separation was found to occur during the drying process with the films containing higher silica contents. When a bonding agent was used, the films with up to 25 wt% silica content were completely transparent indicating that the bonding agent has chemically bonded the two phases suppressing the phase separation [33,34]. In addition, transparent polymer–silica composites were prepared using other high temperature polymers such as polybenzoxazoles and polybenzothiazoles with interfacial bonding achieved through the use of bonding agents [16,17].

32.3.5 Thermal Properties

Thermogravimetric Analysis

Thermogravimetric analysis (TGA) which records the weight of the sample against the temperature is a useful technique in determining how the sample is deteriorated at various temperatures. Thus, it can be used not only to study thermal decomposition and stability of materials but also to give important structural information.

Thermogravimetric analyses of various polymer–silica composites including PDMS–silica [61], polyamide–silica [33,34], polyimide–silica [15,38,47], polybenzoxazole–silica [16,17], polybenzobisthiazole–silica [16,17] and PDMS–silica–titania [62] have been reported, in all cases indicating that the incorporation of silica raises the temperature of thermo oxidative degradation of the polymer. A possible mechanism for the improvements in degradation temperature could be due to silica inactivating the terminal OH groups

which participate in the degradation process [3]. In addition, weight residues at elevated temperatures, for example at 800 °C, were found to increase with the increase in amount of silica in the composites which could also be attributed to the same reasoning indicated above [15,17,33,34,38,47].

A comparative study of thermal stabilities involving PDMS–silica composites showed that commercial fume silica caused more severe degradation problem than did in situ precipitated silica [61]. This improvement in the case of in situ precipitated silica could be due to the increased capability of silica introduced in situ to tie up hydroxyl chain ends [3,61].

Differential Scanning Calorimetry

The basis of differential scanning calorimetry (DSC) is the change in specific heat of the polymer as it passes through the glass transition, upon the change of temperature. DSC is one of the most convenient methods of determining glass transition temperature. A study of low temperature properties of unfilled and filled PDMS networks in the unstretched state [63] using DSC showed that the filler reduces both the extent of crystallization and the rate of crystallization, in contrast to the results obtained for PDMS networks in the stretched state [3,64]. Influence of silica content on T_g was determined for various polymer–silica composites including PDMS–silica [63], PMMA–silica [12,45,65], and PVAc–silica [12] using DSC. Results indicated that the T_g of a composite can increase, decrease or stay unchanged depending on the specific polymer-filler system.

Thermal Expansivity

Polymers, in general, show high expansivities than most metals and ceramics. Therefore, changes in composition can produce significant changes in thermal expansivities [66]. Thus, preparing composites by incorporating inorganic and metallic fillers into polymers can result materials with reduced thermal expansivities. For example, thermal expansivities of polyimide–silica composites were found to decrease with increase in silica content [15]. Such composites prepared with a compatibilizer resulted a larger reduction in thermal expansivities possibly due to the co-continuous phase morphology achieved by compatibilization [39]. However, in applications in which large temperature changes must be tolerated, a compromise between modulus and expansivity to minimize thermal stress is required.

32.3.6 Mechanical Properties

Uniaxial Extension

There have been numerous experiments carried out on various polymer networks in situ filled with silica in uniaxial extension [3,14,15,17,19–21,67,68]. In fact, the uniaxial extension is the mostly studied deformation to characterize the effects of particles produced in situ on the mechanical properties of filled elastomers. Only few studies are available on other deformations such as biaxial extension, shear, and torsion because of the difficulties of imposing such deformations. In general, the results for uniaxial extension are represented as stress–strain isotherms. Such isotherms represented as the dependence of nominal stress on elongation for silica-filled PDMS by simultaneous curing and filling is given in Fig. 32.6 [68]. In this representation, the area under each curve corresponds to the energy required for network rupture.

Same set of isotherms in Fig. 32.6, when represented as reduced stress as a function of reciprocal elongation is given in Fig. 32.7. Upturns in [f^*] observed at high elongations clearly demonstrate the reinforcing effect.

Studies of uniaxial extension on noncrystallizable elastomer, poly(phenyl methyl siloxane) showed results which are consistent and comparable with those obtained for PDMS, suggesting that the crystallization is not important for this type of reinforcement [20]. Other examples for reinforcement effects achieved with the addition of silica fillers include polyisobutylene [24], poly(ethyl acrylate) [3], poly (tetra methylene oxide) [29,30], and some high-temperature polymers such as aromatic polyamides [14,33,34], polyimides [15,38,39], polybenzoxazoles [16,17], and polybenzobisthiazoles [16,17]. Results indicated that the modulus increases with increase in silica content while the tensile

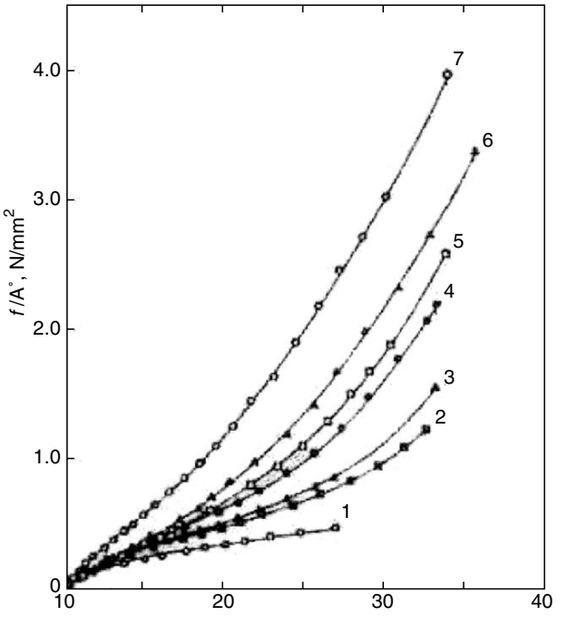

FIGURE 32.6. Nominal stress as a function of elongation for PDMS networks filled with silica by simultaneous curing and filling: 1—unfilled, 2—1.80 wt%, 3—1.96 wt%, 4—5.12 wt%, 5—5.59 wt%, 6—5.74 wt%, and 7—8.61 wt% silica determined by density measurements. From [68] 1984 © American Chemical Society.

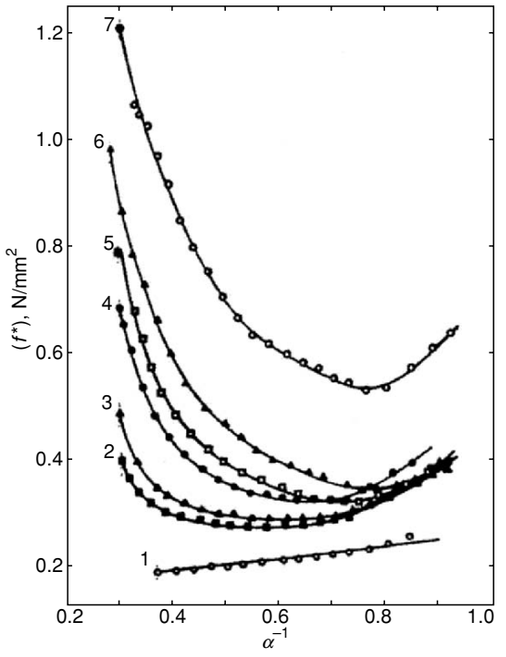

FIGURE 32.7. Same set of isotherms in Fig. 32.6, when represented as reduced stress as a function of reciprocal elongation. From [68] 1984 © American Chemical Society.

strength and the elongation at break decreases. This could be explained by the incorporation of large silica particles. However, by incorporating small amounts of bonding agents to provide better bonding between the two phases, both the modulus and the tensile strength were increased [14,17,38,39]. The improvements thus obtained could be explained by both reductions in particle size which increases the interfacial area and by the introduction of bonding between the polymer chain and silica. The reinforcement achieve will depend on the structure of the polymer involved. For example, a study of linear and nonlinear polyamide–silica chemically bonded systems showed that the latter had low strength relative to the former due to the irregularity of the polyamide structure [14].

In one study with polyamide–silica composites compatibilised with γ-glycidyloxypropyltrimethoxysilane, the increase in tensile strength up to about 25 wt% silica was explained by more stress transfer mechanism between the two components due to the co-continuous phase morphology developed with the addition of the coupling agent [39]. The same study indicated that the elongation at break decreased equally in both cases with or without coupling agent with increasing silica content, confirming that failure is controlled mainly by events within the polymer phase [39].

Biaxial Extension

Only a few studies on elastomers filled with silica in biaxial extension are available simply because of the difficulty in imposing such deformation [69–71]. The state of deformation for biaxial extension can be described using equations similar to those used for uniaxial extension [2,3]. A state of biaxial extension is achieved by stretching a thin sheet of elastomer in two directions in its own plane. The most convenient way of producing equibiaxial extension is inflation of a circular sheet, clamped around its circumference, into the form of a part of a spherical balloon [69–71]. Since biaxial extension is equivalent to uniaxial compression, both biaxial and uniaxial deformation data can be combined in the same plot. In this way, a full spectrum of stress–strain data for both elongation and compression can be viewed, and the behavior of networks in the deformation regions can be compared directly [69]. Results obtained for a PDMS network filled with in situ generated silica for both elongation ($\alpha^{-1} < 1$) and compression ($\alpha^{-1} > 1$) are therefore depicted in Fig. 32.8 where modulus is plotted against α^{-1}. It is obvious that very strong reinforcing effects from the precipitated silica occur for biaxial extension as well as for elongation. This is evident from both the large upward shifts of isotherms as a whole and from pronounced upturns at both high elongations($\alpha^{-1} < 1$) and at high compressions ($\alpha^{-1} > 1$). As can be seen from the figure 32.8, such reinforcing effects do not exist in the unfilled PDMS sample.

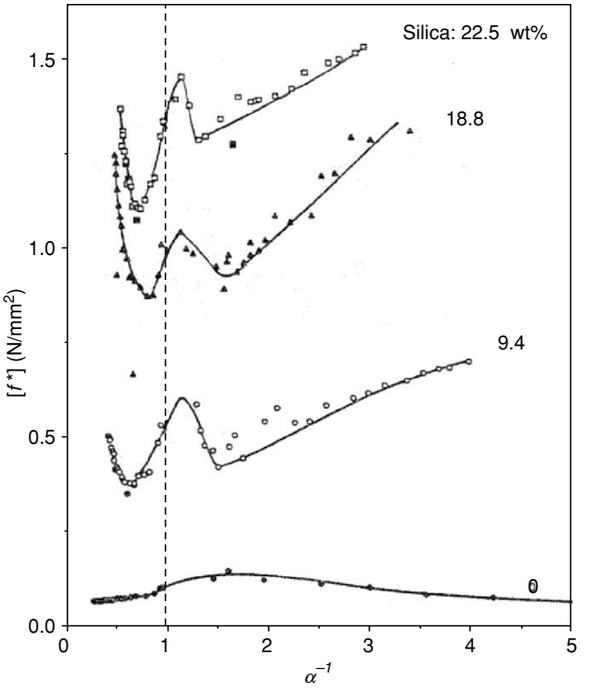

FIGURE 32.8. Stress–strain isotherms for PDMS networks filled with in situ generated silica for both elongation ($\alpha^{-1} < 1$) and compression ($\alpha^{-1} > 1$). The filled points represent the data used to test for reversibility. From [69] 1991 © American Chemical Society.

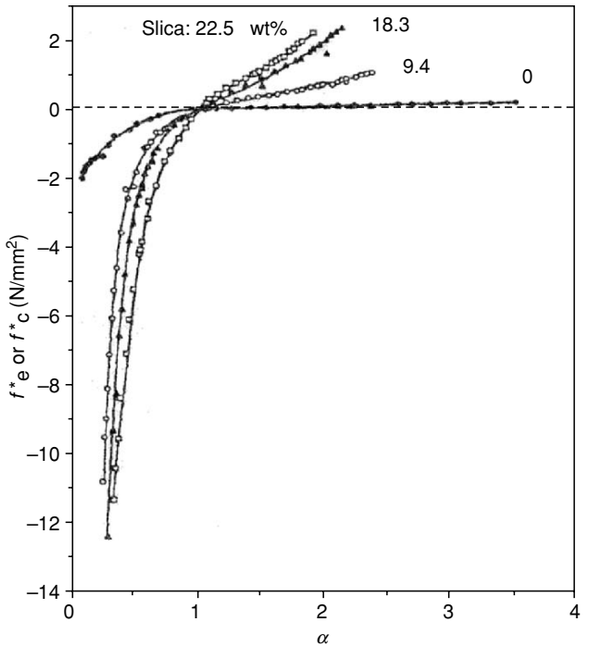

FIGURE 32.9. The same set of isotherms shown in Fig. 32.8, now represented as the dependence of the nominal stress on deformation for both elongation (e) and compression (c). In this representation, tensile stress (f^*_e) is positive and the compressive stress (f^*_c) is negative. From [69] 1991 © American Chemical Society.

The same results are represented in Fig. 32.9 where nominal stress is plotted as a function of deformation. The tensile stress is positive while the compressive stress is negative and a single continuous curve represents both elongation and compression without any discontinuity in passing through the point (1,0) characterizing the undeformed state. Compared to the unfilled sample, the silica-filled samples showed large reinforcing effects. Specifically their values of the modulus, ultimate strength, and rupture energy were increased significantly. The reinforcing effects thus produced, as gauged by the magnitude of the upturns, is approximately the same in uniaxial and in biaxial extension. However, the range of deformation over which it occurs seems to be larger in the case of biaxial extension. Results also indicate that the increase in filler content decreases the deformation at rupture.

Shear

Only a very few studies have been carried out to characterize the reinforcement of in situ precipitated silica in elastomers in shear [3,69,72,73]. There are two types of shear: simple shear and pure shear. Simple shear is a type of strain obtained by sliding a plane which is parallel to a given plane, through a distance which is proportional to the distance from the given plane [3,69]. The lateral faces of a cube are transformed by simple shear into parallelograms, and the amount of shear is measured by the tangent of the angle ϕ through which a vertical edge is tilted [3,69]. Pure shear involves extension in three perpendicular directions without rotation of the principal axis of the strain. The stress–strain isotherms obtained for both unfilled and filled PDMS networks, represented in terms of the shear modulus G and principal extension ratio α, is shown in Fig. 32.10. The results in simple shear, in terms of shear strain were essentially identical [72]. For filled networks, there is an initial decrease in the modulus with increase in deformation. Also, the larger the amount of filler present, the more pronounced the decrease. This may be due to strain-induced rear arrangements of the chains in the vicinity of the filler particles. Also of possible relevance is the fact that an increase in amount of filler decreases the number of load-bearing chains passing through the unit cross-sectional area and changes the distribution of their end-to-end distances [69]. In an alternative representation, the pure shear nominal stress f^* is plotted against the extension ratio α, as shown in Fig. 32.11. Results showed that the filled samples have much higher shear moduli than the corresponding unfilled sample. Also, at high deformation, pronounced upturns in the reduced stress or modulus appear in the case of filled samples which indicate good reinforcement. The extension

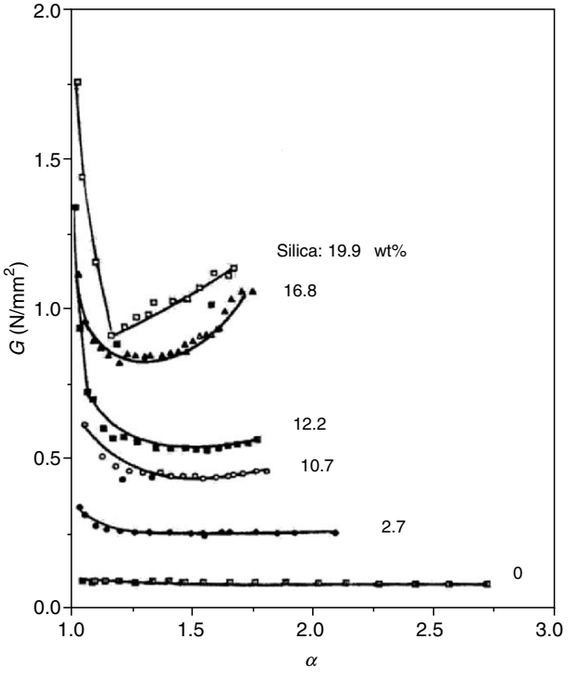

FIGURE 32.10. Stress–strain isotherms represented in terms of the shear modulus G and principal extension ratio α, for both unfilled and filled PDMS networks in pure shear. The filled points represent the data used to test for reversibility. From [69] 1991 © American Chemical Society.

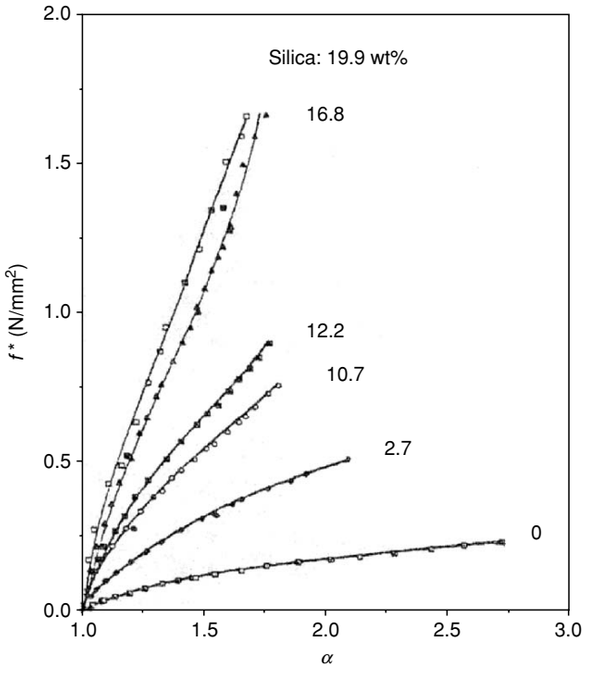

FIGURE 32.11. The stress–strain data shown in Fig. 32.10, now represented in terms of the nominal stress against the extension ratio α. From [69] 1991 © American Chemical Society.

ratio or shear strain γ at which the upturn appears is seen to decrease with increase in weight% filler and as expected the maximum deformability was decreased. The behavior observed for shear is very similar to those observed for uniaxial and biaxial extension. However, shear moduli calculated using torsion measurements for PDMS–silica networks were significantly different from those for other types of deformation in that there is little evidence for upturns in the modulus at high deformation [72,73]. Shear modulus experiments have indicated that the presence of PDMS can dramatically shorten the incipient gelation time in PDMS–silica composites [62].

Impact Strength

The impact strength of a material is its ability to withstand the application of a sudden load which results in fracture. Impact strength of some PDMS–silica composites have been determined by the Charpy pendulum impact test and by the falling weight impact test. The composites thus tested had PDMS contents sufficiently low to produce composites with the brittleness required in impact strength testing. The higher the molecular weight or the larger the amount of PDMS introduced, the higher the impact strength. This can be explained by the fact that PDMS component can behave as an elastomeric phase because its glass transition temperature is well below the room temperature and when the material is subjected to an impact test, the PDMS component can absorb a great deal of energy delaying the growth of cracks and fracture. Increasing the amount of PDMS would increase the number of the phase-separated domains helping to absorb the impact energy. Impact strength values obtained using dart impact tests and energy of rupture obtained from the area under the curve of nominal stress versus elongation had a good correlation as measures of impact resistance [74,75].

Dynamic Mechanical Properties

Dynamic mechanical tests provide useful information on transition occurring in polymers including polymer–silica composites. Such results document the effect of filler on the glass transition temperature and on the melting point of the systems. For example, glass transition temperature determined by the peak temperature of the loss modulus curves for polyimide–silica composites indicated low T_g values compared to that of the original poyimide films for low silica contents up to 8 wt% followed by an increase of T_g with increase in silica content [15]. This could be explained by the fact that at low TEOS concentration, TEOS was polymerized incomplete in the polymer giving rise to low molecular weight silica which is more compatible with polyimide and as the TEOS concentration is increased further, high molecular weight silica is formed and the compatibility between silica phase and polyimide decreased giving rise to increase in T_g [15].

Tear Strength

Tear strength of a material is defined as the energy required to propagate a crack per unit area torn through. It has been shown that the tear strength is independent of the particular test method or the form of the test piece, thus it is an intrinsic property of the material under the given test conditions [76,77]. Tear strength measurements have shown that filled systems generally show a rather complicated tear behavior compared to that of unfilled systems [78,79]. Tear strength measurements conducted on PDMS–silica composites showed steady tearing at low rates of tearing similar to that observed for unfilled networks. However, at higher rates of tearing, somewhat unstable tearing behaviour was observed and it could be explained by the deviation of the tear path from the straight-ahead direction by curving around and stopping when it encounters a filler particle, followed by a possible new tear which then tend to repeat the same process [80]. As the amount of silica incorporated was increased, the tear strength increased as expected in agreement with the results for tensile measurements in which both the energy of rupture and ultimate strength were increased upon increase in the amount of silica.

REFERENCES

1. J. E. Mark, A. Eisenberg, W. W. Graessley, L. Mandelkern, E. T. Samulski, J. L. Koenig and G. D. Wignall, Physical Properties of Polymers, Second Edition, American Chemical Society, Washington, DC, 1993, pp. 48–53.
2. J. E. Mark and B. Erman, Rubberlike Elasticity: A Molecular Primer, John Wiley & Sons, NY, 1988, pp. 145–153.
3. B. Erman, and J. E. Mark, Structures and Properties of Rubberlike Networks, Oxford University, NY, 1997, pp. 265–306.
4. A. I. Medalia and G. Kraus, In Science and Technology of Rubber, J. E. Mark, B. Erman, and F. R. Eirich, Eds., Second Edition, Academic Press, NY, 1994, p. 387.
5. E. L. Warrick, O. R. Pierce, K. E. Polmanteer and J. C. Saam, Rubber Chem. Technol., **52**, 437 (1979).
6. B. B. Boonstra, Polymer, **20**, 691 (1979).
7. Z. Rigbi, Adv. Polym. Sci., **21**, 36 (1980).
8. L. Karasek and M. sumita, J. Mater. Sci., **31**, 281 (1996).
9. E. P. Giannelis, In Biomimetic Materials Chemistry, S. Mann, Ed., VCH Publishers, NY, 1996, p. 337
10. E. J. A. Pope and J. D. Mackenzie, J. Mater. Res., **4**, 1017 (1989).
11. C. J. T. Landry and B. K. Coltrain, Polym. Prepr., **32(3)**, 514 (1991).
12. C. J. T. Landry, B. K. Coltrain, J. A. Wesson, N. Zumbulyadis and J. L. Lippert, Polymer, **33**, 1496 (1992).
13. Y. Wei, D. Jin, G. Wei, D. Yang and J. Xu, J. Appl. Polym. Sci., **70**, 1989 (1998).
14. Z. Ahmad, M. I. Sarwar and J. E. Mark, **7(2)**, 259 (1997).
15. A. Morikawa, Y. Iyoku, M. Kakimoto and Y. Imai, Polym. J., **24**, 107 (1992).
16. J. E. Mark, J. K. Premachandra, C. Kumudinie, W. Zhao, T. D. Dang, J. P. Chen and F. E. Arnold, in Better Ceramics Through Chemistry VII: Organic/Inorganic Hybrid Materials, B. K. Coltrain, C. Sanchez, D. W. Schaefer, and G. L. Wilkes, Eds., Materials Research Society, Pittsburgh, PA 1996, vol. 435, p. 93.
17. J. Premachandra, C. Kumudinie, W. Zhao, J. E. Mark, T. D. Dang, J. P. Chen and F. E. Arnold, J. Sol–Gel Sci., **7**, 163 (1996)
18. C. J. Brinker and G. W. Scherer, Sol–Gel Science; The Physics and Chemistry of Sol–Gel Processing, Academic Press, NY, 1990
19. J. E. Mark and S. J. Pan, Makromol. Chem., Rapid Commun., **3**, 681 (1982).
20. S. J. Clarsn and J. E. Mark, Polym. Commun., **28**, 249 (1987).
21. J. E. Mark, Heterogeneous Chem. Rev., **3(4)**, 307 (1996).
22. J. E. Mark, Polym. Eng. Sci., **36(24)**, 2905 (1996).
23. H. Kaddami, F. Surivet, J. F. Gerald, T. M. Lam and J. P. Pascault, J. Inorg. Organomet. Polym., **4**, 183 (1984).
24. C.-C. Sun and J. E. Mark, J. Polym. Sci., Polym. Phys. Ed., **25**, 1561 (1987).
25. J. J. Fitzgerald, C. J. T. Landry and J. M. Pochan, Macromolecules, **25**, 3715 (1992).
26. C. J. T. Landry, B. K. Coltrain, M. R. Landry, J. J. Fitzgerald and V. K. Long, Macromolecules, **26**, 3702 (1993).
27. C. J. T. Landry and B. K. Coltrain, J. Macromol. Sci., Pure Appl. Chem., **31**, 1965 (1994).
28. Y. Wei, J.-M. Yeh, D. Jin, X. Jia and J. Wang, Chem. Mater., **7**, 969 (1995).
29. H.-H. Huang, G. L. Wilkes and J. G. Carlson, Polymer, **30**, 2001 (1989).
30. H. H. Huang, R. H. Glaser and G. L. Wilkes, In Inorganic and Organometallic Polymers, M. Zeldin, K. J. Wynne and H. R. Allcock, Eds, American Chemical Society, Washington, DC, 1994, vol. 360, p. 354.
31. D. Ravaine, A. Seminel, Y. Charbouillot and M. Vincens, J. Non-Cryst. Solids, **82**, 210 (1986).
32. T. Kyprianidou-Leodidou, W. Caseri and U. W. Suter, J. Phys. Chem., **98**, 8992 (1994).
33. S. Wang. Z. Ahmad and J. E. Mark, Polym. Bull., **31**, 323 (1993).
34. S. Wang. Z. Ahmad and J. E. Mark, in Better Ceramics Through Chemistry VI, A. K. Cheetham, C. J. Brinker, M. L. Mecartney, and C. Sanchez, Eds., Materials Research Society, Pittsburgh, 1994, vol. 346, p. 127.
35. M. Spinu, A. Brennan, J. Rancourt, G. L. Wilkes and J. E. McGrath, in Multi-functional Materials, D. R. Ulrich, F. E. Karasz, A. J. Buckley and G. Gallagher-Daggit, Eds., Materials Research Society, Pittsburgh, 1990, vol. 175, p. 179.
36. M. Nandi, J. A. Conklin, J. L. Salvati and A. Sen, Chem. Mater., **3**, 201 (1991).
37. A. Morikawa, Y. Iyoku, M. Kakimoto and Y. Imai, J. Mater. Chem., **2**, 679 (1992).
38. S. Wang. Z. Ahmad and J. E. Mark, Chem. Mater., **6**, 943 (1994).
39. L. Mascia and A. Kioul, Polymer, **36**, 3649 (1995).
40. L. Mascia and A. Kioul, J. Mat. Sci. Lett., **13**, 641 (1994).
41. Z. Ahmad, S. Wang and J. E. Mark, In Hybrid Organic Inorganic Composites, J. E. Mark, C. Y-C. Lee and P. A. Bianconi, Eds., 1995, American Chemical Society, Washington, DC, p. 291.
42. S. Wang and J. E. Mark, Macromolecular Reports, **A31 (Suppls. 3 & 4)**, 253 (1994).
43. D. E. Rodrigues, A. B. Brennan, C. Betrabet, B. Wang and G. L. Wilkes, Chem. Mater., **4**, 1437 (1992).
44. B. K. Coltrain, C. J. T. Landry, J. M. O'Reilly, A. M. Chamberlain, G. A. Rakes, J. S. Sedita, L. W. Kelts, M. R. Landry and V. K. Long, Chem. Mater., **5**, 1445 (1993).
45. Z. Pu, J. E. Mark, J. M. Jethmalani and W. T. Ford, Chem. Mater., **9**, 2442 (1997).
46. X. Ji, J. E. Hampsey, Q. Hu, J. He, Z. Yang and Y. Lu, Chem. Mater., **15**, 3656 (2003).
47. S. Wang, Z. Ahmad and J. E. Mark, Macromolecular Reports, **A31(Suppls. 3 & 4)**, 411 (1994).
48. J. Wen and J. E. Mark, J. Appl. Polym. Sci., **58**, 1135 (1995).
49. J. Wen and J. E. Mark, Rubber Chem. Technol., **67**, 806 (1994).
50. T. A. Ulibarri, G. Beaucage, D. W. Schafer, B. J. Oliver and R. A. Assink, Mat. Res. Symp. Proc., 274 (1992).
51. G. Beaucage, T. A. Ulibarri, E. P. Black and D. W. Schafer, In Hybrid Organic-Inorganic Composites, J. E. Mark, C. Y.-C. Lee and P. A. Bianconi, Eds., American Chemical Society, Washington, DC, 1995, p. 97.
52. J. M. Breiner and J. E. Mark, Polymer, **39**, 5483 (1998).
53. G. M. Jamison, D. A. Loy, R. A. Assnk and K. J. Shea, In Better Ceramics Through Chemistry VI, A. K. Cheetham, C. J. Brinker, M. L. Mecartney and C. Sanchez, Eds., Materials Research Society, Pittsburgh, 1994, vol. 346, p. 487.
54. D. A. Loy, R. J. Buss, R. A. Assink, K. J. Shea and H. Oviatt, In Better Ceramics Through Chemistry VI, A. K. Cheetham, C. J. Brinker, M. L. Mecartney and C. Sanchez, Eds., Materials Research Society, Pittsburgh, 1994, vol. 346, p. 825.
55. R. A. Assink and B. D. Kay, In Better Ceramics Through Chemistry, C. J. Brinker, D. E. Clark and D. R. Ulrich, Eds., Materials Research Society, New York, 1984, vol. 32, p. 301.
56. F. Surivet, T. M. Lam, J.-P. Pascautt and Q. T. Pham, Macromolecules, **25**, 4309 (1992).
57. M. Spinu and J. E. McGrath, J. Inorg. Organomet. Polym., **2**, 103 (1992).
58. L. Garrido, J. L. Ackerman and J. E. Mark, Mat. Res. Soc. Symp. Proc., **65**, 171 (1990).
59. L. Garrido, J. E. Mark, C. C. Sun, J. L. Ackerman and C. Chang, Macromolecules, **24**, 4067 (1991).
60. H.-H. Huang, B. Orler and G. L. Wilkes, Polym. Bull., **14**, 557 (1985).
61. G. B. Sohoni and J. E. Mark, J. Appl. Polym. Sci., **45**, 1763 (1992).
62. J. Wen and J. E. Mark, Polym. J., **27**, 492 (1995).
63. S. J. Clarson, J. E. Mark and K. Dodgson, Poly. Commun., **29**, 208 (1988).
64. V. Y. Levin, G. L. Solonimski, K. A. Andrianov, A. A. Zhdanov, Y. A. Godovski, V. S. Papkov and A. Y. Lyubavskaya, Polym. Sci., USSR, **15**, 256 (1963).
65. C. J. T. Landry, B. K. Coltrain, J. A. Wesson, N. Zumbulyadis and J. L. Lippert, Polymer, **33**, 1486 (1992).
66. C. Hall, Polymer Materials, An Introduction for Technologists and Scientists, 2nd edition, MacMillan Education Ltd., 1989, p. 96.
67. J. E. Mark, J. Appl. Polym. Sci., **50**, 273 (1992).
68. J. E. Mark, C. Y. Jiang and M. Y. Tang, Macromolecules, **17**, 2614 (1984).
69. S. Wang, P. Xu and J. E. Mark, Rubber Chem. Technol., **64**, 746 (1991).
70. P. Xu and J. E. Mark, Rubber Chem. Technol., **63**, 276 (1990).
71. P. Xu and J. E. Mark, J. Polym Sci., Polym. Phys. Ed., **29**, 355 (1991).
72. S. Wang, Ph.D. in Chemistry, University of Cincinnati, OH, 1991.
73. J. Wen and J. E. Mark, Polym. J., **26**, 151 (1994).
74. M.-Y. Tang, A. Letton and J. E. Mark, Colloid and Polym. Sci., **262**, 990 (1984).
75. J. E. Mark and Y.-P. Ning, Polym. Bull., **12**, 413 (1984).
76. R. S. Rivlin and A. G. Thomas, J. Polym. Sci., **10**, 291 (1953).
77. A. G. Thomas, J. Appl. Polym. Sci., **3**, 168 (1960).
78. L. C. Yanyo and F. N. Kelley, Rubber Chem. Technol., **60**, 78 (1987).
79. T. L. Smith, B. Haidar and J. L. Hedrick, Rubber Chem. Technol., **60**, 98 (1987).
80. C. Kumudinie and J. E. Mark, Mat. Sci. Eng., **C11**, 61 (2000).

CHAPTER 33

Physical Properties of Polymer/Clay Nanocomposites

Clois E. Powell and Gary W. Beall

Center for Nanophase Research, Texas State University, San Marcos, TX 78666

Polymer/clay nanocomposites have been reported since the 1960s and early 1970s [1–4]. However, when workers at the Toyota Central Research Laboratories reported a Nylon 6/clay nanocomposite that was utilized in a timing belt cover on the Toyota Camry [5–9], an expansion of activity with a wide range of polymer types was soon evident in the literature and conferences. The nylon 6/clay nanocomposites exhibited some very substantial enhancements of the physical properties of the composite relative to the pure nylon 6 polymer. These physical property improvements include substantial increases in tensile strength, modulus, and heat distortion temperature without loss of impact strength. The maintenance of the impact strength in these composites with substantial increases in strength and stiffness are surprising. Also, the decrease of water uptake and gas barrier improvements of the nanocomposites were substantially improved when compared to pure nylon. This series of papers initiated a huge research effort throughout the world on polymer/clay nanocomposites.

The ultimate clay nanocomposite is formed when individual clay plates are completely dispersed into a polymer matrix. This type of composite yields the maximum improvement in properties. This complete dispersion is normally referred to as full exfoliation. In many cases the composites reported in the literature are intercalated or partially exfoliated. Intercalated systems are characterized by insertion of polymer between plates of clay with retention of well-defined spacing distance between the plates. This spacing is called the gallery spacing and is determined from wide angle x-ray diffraction (WAXS). The x-ray diffraction pattern in many cases has been misleading in determining the level of intercalation/exfoliation. Disordered systems with a distribution of spacings mimic the pattern that an exfoliated system would yield. The only reliable technique for establishing the extent of exfoliation in nanocomposites is transmission electron microscopy.

The clays utilized in these composites belong to the smectite family of clays. These clays are characterized by a 2:1 structure built of a central layer of octahedrally coordinated metal, normally Al^{3+} or Mg^{2+}, sandwiched between two tetrahedral coordinated layers of silicon. Figure 33.1 is a model of this structure viewed from the edge of the plate. The morphology of these platy materials is characterized by a thickness of 1 nm. The two other dimensions are in the range of 100–1,500 nm. When dispersed as individual plates these materials exhibit surface areas of greater than $750\,m^2/g$. This large surface area and aspect ratio dominate the interaction of these materials with polymers. Complete separation of the plates is important to realize their full benefit. One must modify this surface to render the clay compatible with the polymer of interest. In clays of this type isomorphous substitution is quite common. The octahedral metal layer contains Al^{3+} which is replaced by Mg^{2+} or Fe^{2+} and Mg^{2+} is replaced by Li^{+}. Substitution can occur in the tetrahedral layer by exchanging Al^{3+} for Si^{4+}. Isomorphous substitution results in a charge imbalance in the structure. This is compensated by exchangeable cations on the surface of the clay plate shown in Fig. 33.1 as atoms

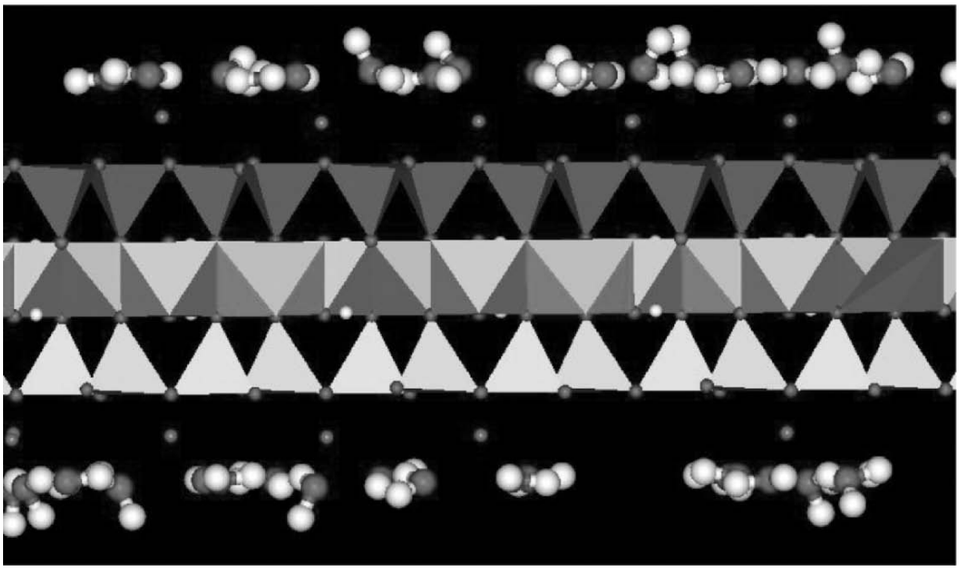

FIGURE 33.1. Representation of the two to one structure of montmorillonite showing the central octahedrally coordinated Aluminums sandwiched between two tetrahedrally coordinated silicons. Atoms above and below the layer are exchangeable cations and their associated waters of hydration.

slightly above and below the clay plate. The exchangeable cation is normally sodium, potassium, calcium, or magnesium. Sodium is preferred due to the ease of exchange reactions. The clay in its cation form is very hydrophilic and will disperse into aqueous solutions forming thixotropic gels. Figure 33.1 shows waters of hydration that normally surround the exchangeable cation. This hydrophilic character makes them suitable for polymer systems that are water soluble or dispersable such as polyvinylalcohol, polyethylene oxides, latex, and polyvinylpyrrolidone. In order to render these clays to be more compatible with more hydrophobic polymers ion exchange reactions utilizing organic onium ions are employed. The most common onium ions are quaternary ammonium ions. They are commercially available due to their use in the detergent industry. Most of these materials derived from natural fats and oils are hydrophobic. The surface of the clay can also be modified with organic molecules that contain appreciable dipole moments. These molecules do not ion exchange but form ion–dipole bonds to the exchangeable cation on the surface.

In most commercially available clay the average exchange capacity is in the range of 95 meq./100 g of clay. When this type of clay is exchanged fully with quaternary ammonium ions there is an appreciable amount of clay silicate surface still available for interaction with polymers. It has been reported that small amounts of selected polymers can be mixed with the quaternary amine prior to treating the clay with the resulting surface modified clay being more hydrophobic. The polymer apparently covers the silicate surface where exchange sites do not exist.

A fourth type of treatment is edge treatment with coupling agents. The edges of the plates are terminated in metal and silica hydroxides. These hydroxides act as a barrier to hydrophobic polymer entering the clay gallery for exfoliation. Silane coupling agents can react with these hydroxides via condensation reactions. Silane coupling agents are available with a variety of functional organic groups. This allows the edges of the plates to be tailored to the polymer of interest. The edge treatment appears to effect the kinetics of intercalation but not the ultimate formation of and characteristics of the final nanocomposite.

The use of surface modified clays to form polymer nanocomposites in a large variety of polymers has been thoroughly reviewed recently by Ray *et al*. [10]. In this chapter we will not attempt to cover in detail all of these nanocomposites but will describe the general physical properties observed for nanocomposites as a whole. The method of formation of these composites will also not be covered in detail. The majority of the examples will fall into two categories concerning the method of formation. The methods include in situ polymerization and melt compounding. In the case of in situ polymerization the polymer is being produced in the presence of the clay and in most cases is actually tethered to the clay surface. The melt compounding approach is normally accomplished by addition of the surface modified clay to a melt of the polymer in an extruder. The discussion will attempt to cover the engineering, barrier, and flame retardancy characteristics of polymer/clay nanocomposites and will be divided broadly into thermoplastics, thermosets, and rubbers.

33.1 ENGINEERING PROPERTIES OF THERMOPLASTIC/CLAY NANOCOMPOSITES

The engineering properties of polymer/clay nanocomposites in general exhibit substantial improvement in tensile strength, tensile modulus, flexural strength and modulus, heat distortion temperature, and in ideal cases no loss in impact strength. In some cases the improvements in strength and stiffness are also accompanied by improvements in elongation at break. These observed characteristics do not fit conventional polymer physics where increases in strength and stiffness are normally accompanied by loss in impact and elongation at break.

The thermoplastic that has been most extensively studied is nylon 6. This will serve as a basis for comparison of other polymer groups. Table 33.1 contains a compilation of data for Nylon 6 /clay nanocomposites from a number of sources. The first data is from Okada *et al*. [11] describing in situ produced nylon 6/ montmorillonite. The surface treatment was 12-aminolauric acid. The nylon 6 chains predominately grow from the surface of the clay. The tensile strength increases by 55% and the tensile modulus by 91%, and the heat distortion temperature increased by 134%. The impact strength showed no statistical change. The transmission electron micrographs (TEM) of this nanocomposite shows that the clay is almost totally exfoliated. The work reported by Fornes *et al*. [12] on melt compounding of organoclays into various molecular weight nylon 6 polymers can be compared to this data. Interpolation of the data to match the clay content of the in situ nylon 6 indicates that the tensile strength would show a 26% increase and the tensile modulus a 59% increase. These numbers are lower than the in situ polymerized composite. Detailed TEM analysis of these compounded samples showed that a large portion of the plates were exfoliated but that there was a significant number of aggregates containing two and three plates and infrequently ones with larger numbers of plates. The impact strength was retained as seen in the in situ material. The elongation at break dropped drastically in the compounded material. Melt compounding work by Hasegawa *et al*. [13] reported a tensile strength increase of 48% and tensile modulus increase of 71%. These numbers are extrapolated to match the 4.2% clay content of the in situ composite. These numbers are closer to those seen in the in situ material. TEM analysis showed almost complete exfoliation with some two and three layer agglomerates. The HDT increases by 80% uncorrected for clay content. In both in situ derived and melt compounded nanocomposites, substantial improvements in strength and modulus are realized. The increases seen in the in situ material yield the greatest increases possibly due to greater exfoliation. In order to predict modulus and HDT the theories of reinforcement in composites, Halpin–Tsai and Mori–Tanaka, has been applied to nylon 6 nanocomposites by Fornes [14]. The theoretical modulus (Mori–Tanaka) increase predicted in this paper for 4.2% clay loading is 56%. This is in very good agreement with the 59% observed for the melt processed nylon 6/montmorillonite nanocomposite [12]. The effect on modulus due to agglomerates was also calculated as a reinforcing factor (RF). The RF for fully exfoliated plates using Mori–Tanaka is 34.8 and for agglomerates containing two plates it is 23.8. This could be a viable explanation for the lower modulus seen in melt compounded material. The nylon 6 studied in the in situ composite had an inherently lower modulus [11]. When this lower value is utilized to predict a modulus for the in situ produced nanocomposite, a value of 2.0 GPa is predicted for a 4.2% clay containing nanocomposite. This is in excellent agreement with the measured 2.1 GPa. This would indicate that the differences

TABLE 33.1. *Physical properties of selected nylon 6 nanocomposites.*

Sample description	Clay (wt%)	Tensile strength (Mpa)	Tensile modulus (Gpa)	Impact strength (J/m)	HDT (°C)	Elongation at break (%)	Reference
Nylon 6	0	69	1.1	6.2*	65		
NCH-5	4.2	107	2.1	6.1*	152		[11]
Nylon 6LMW	0	69.1	2.82	36		232	[12]
NCH-LMW3	3.2	78.9	3.65	32.3		12	
NCH-LMW5	6.4	83.6	4.92	32		2.4	
Nylon 6 MMW	0	70.2	2.71	39.3		269	
NCH-MMW3	3.1	85.6	3.66	38.3		81	
NCH-MMW5	7.1	95.2	5.61	39.3		2.5	
Nylon 6 HMW	0	69.7	2.75	43.9		129	
NCH-HMW3	3.2	84.9	3.92	44.7		27	
NCH-HMW5	7.2	97.6	5.7	46.2		6.1	
Nylon 6	0	68	1.08	50	75		[13]
NCH-OC	1.8	82	1.41	42	135		
NCH-Slurry	1.6	82	1.38	44	102		

*Charpy impact kJ/m^2.

seen between in situ and melt compounded material is largely due to the differences in the moduli of the starting material and not slight differences in the level of exfoliation. The Halpin–Tsai theory was utilized successfully to predict the HDT of the nylon 6 nanocomposites [14]. This indicates that both melt compounded and in situ derived nanocomposites fits closely the composite theory of Mori–Tanaka. The Halpin–Tsai theory over estimated the modulus in all the clay nanocomposites but was very good at predicting the HDT increases. The theory predicts that polymer with lower the modulus will provide a greater increase in modulus in a fully exfoliated nanocomposite. Prediction of the lack of change in impact resistance in nylon 6 nanocomposites lies outside of the scope of the theory. This phenomena awaits further study to understand the mechanism.

The effect of larger increases in modulus for low modulus materials can be seen in dynamic mechanical analysis curves. The typical modulus increase seen in these curves below the T_g, on a percentage of starting modulus, is substantially lower than that seen above the T_g. This observation makes the large increases in HTD observed in nylon quite easy to rationalize.

Another polyamide that has been studied extensively is nylon 66. Table 33.2 contains a compilation of data on selected nylon 66/clay nanocomposites. In the case of nylon 66 all successful nanocomposites have been produced utilizing melt compounding. The average tensile strength increase, for the three selected composites at 5% clay loading, is 21% and tensile modulus of 46%. These increases are somewhat lower than that observed for nylon 6 nanocomposites. Chavarria and Paul [16] have applied the same modeling techniques that were used on nylon 6 to successfully predict the modulus of nylon 66. The Mori–Tanaka theory predicted the modulus of nylon 66 over a wider range than the Halpin–Tsai theory. Two of the studies reported an increase in impact strength [15,17]. As in the case of nylon 6 it appears that conventional composite reinforcing models do a reasonable job of predicting increases in modulus. As in nylon 6 the impact changes observed seem to go counter to experience with macroscale composites.

Lew *et al*. [18] has reported the production of a nylon 12 nanocomposite via melt compounding with synthetic fluoromica at 4% by weight loading. They reported an increase of 27% in tensile strength, 39% in tensile modulus, and a loss of only 9% in impact resistance. The magnitude of these changes seems to be in line with other polyamides. When one considers the very low modulus of the neat nylon 12, theory predicts a much greater change in modulus. The x-ray data indicates a high degree of intercalated structure as opposed to exfoliation. The most striking effect seen in this composite was an almost threefold increase in elongation at break. Fornes and Paul [19] have reported data on nanocomposites of nylon 11 and 12. At 4% by weight clay, the increase in tensile strength was 18% and 17% and tensile modulus was 56% and 51% for nylon 11 and 12, respectively. Comparisons with nylon 6 nanocomposites indicated that the level of exfoliation was much lower in nylon 11 and 12 than nylon 6. They did not observe the increase in elongation at break reported by Lew [18]. Impact strength decreased rapidly with increased clay loading. The data suggest that optimum increase in physical properties requires almost complete exfoliation.

For most polyamides, when close to full exfoliation exist, conventional composite theories do a very good job of predicting increases in strength, modulus, and HDT. The impact resistance, however, appears not to be explicable by these theories.

The physical properties of a number of other polymer nanocomposites made with clays have been measured. Table 33.3 contains a selection of reported values for some of the most common polymers. Poly(ethylene terephthalate) (PET) and Poly(butylene terephthalate) (PBT) are the most common commercial engineering polymers. The average increase in tensile modulus for most of the PET nanocomposites [21,22,24] is in the range of 35%. This is well below the prediction of a 95% increase for a 5% by weight nanocomposite utilizing Halpin–Tsai theory . The only exception was PET produced by in situ polymerization and tested as fibers [20]. In each one of these references it was acknowledged that full exfoliation had not been reached in the composite. It is reasonable to expect that substantial improvement in properties could be seen if full exfoliation were achieved. The reported increase in tensile modulus for PBT nanocomposites is only in the 36% range [23,24].

TABLE 33.2. *Physical properties of selected nylon 66 nanocomposites.*

Sample description	Clay (wt%)	Tensile strength (Mpa)	Tensile modulus (Gpa)	Impact strength (J/m)	HDT (°C)	Elongation at break (%)	Reference
Nylon 66	0	77	3	98	75		[15]
NCH66-5	5	97	4.75	145	140		
NCH66-10	10	107	5.25	140	168		
Nylon 66	0	72.6	2.91			211	[16]
NCH66-3	2.9	80.4	3.92			10	
NCH66-4	4.4	na	4.24			4	
Nylon 6	0	79	2.5	145		35	[17]
NCH66-6	4.4	90	3.1	208		10	

TABLE 33.3. *Physical properties of selected polyester and polyolefin nanocomposites.*

Sample description	Clay (wt%)	Tensile strength (Mpa)	Tensile modulus (Gpa)	Impact strength (J/m)	HDT °C	Elongation at break (%)	Reference
Polyesters							
PET	0	46	2.21			3	[20]
PETNC-3	3	71	4.1			3	
PET	0	32	2.55			370	[21]
PETNC-5	3.5	47	3.35			<5%	
PET	0	49	1.3				
PETNC-2	2	64	1.7				[22]
PBT	0	41	1.37				
PBTNC-3	3	60	1.76				[23]
PBTNC-5	5	49	1.86				
PBT	0		1.16				[24]
PBTNC-3	3		1.25				
PBTNC-5	5		1.35				
PBTSO3	0		1.08				
PBTSO3-5	5		1.48				
Polyolefins							
PP	0		1.5				[25]
PPNC-5	5		2.4				
PP	0	31	1.5(flex)	2	120		[26]
PPNC-3	3	39	2.1(flex)	3.4	130		
PP	0	37.9				1350	[27]
PPNC-2	2	39.4				36	
PE	0		0.183				[28]
PENC-3	3.5		0.258				
PE	0	28.9	0.26	66(dart)		945	[29]
PENC-1.5	1.5	30.2	0.31	57(dart)		860	
PE	0	26.1	0.8				[30]
PENC-5	5.4	33.1	1.67				
PE	0		0.19			>400	[31]
PENC-5	4.6		0.48			>400	
PE	0	21.1	0.649			773	[32]
PENC-6V	6	27.4	0.753			168	

Based upon Halpin–Tsai theory, a 5% loading of clay in PBT should increase the tensile modulus above 100%. Chisholm [24] claims that the PBT composite made with sulfated PBT was fully exfoliated. Therefore, the degree of exfoliation cannot be the reason for the low increase in modulus.

The results for polypropylene are worse than that observed for polyesters. All the nanocomposite work that is reported [25–27] acknowledges that the composites have very little exfoliation. The reported modulus increases are in the 50% range which are well below the 150% increase expected from composite theory.

Hotta and Paul [31] reported studies on melt compounding of many different organoclays into linear low density polyethylene and found that in some cases a 5% clay loading resulted in a 153% increase in modulus. The TEM images confirmed that the clay was largely exfoliated.

In general the most critical factor that governs the ultimate improvement in engineering properties in polymer/clay nanocomposites is the level of exfoliation. As full exfoliation is achieved in a composite, the modulus increase can be predicted using Halpin–Tsai or Mori–Tanaka theories. The prediction of impact strength and elongation at break of nanocomposites needs further study.

33.2 FLAME RETARDANCY OF POLYMER/CLAY NANOCOMPOSITES

The flammability of polymers in many applications is of critical importance. In the past, brominated flame retardant additives dominated this market. Concern over halogen containing compounds has resulted in the gain in popularity of various char forming phosphates. Recently clay nanocomposites were found to impart a substantial level of flame retardancy. The flame retardancy effect appears to originate from the clay's ability to contribute to char formation. This char layer forms an insulative layer to slow down heat transfer and retards movement of gases to feed the flame. Gilman [33] has recently reviewed this area. Figure 33.2

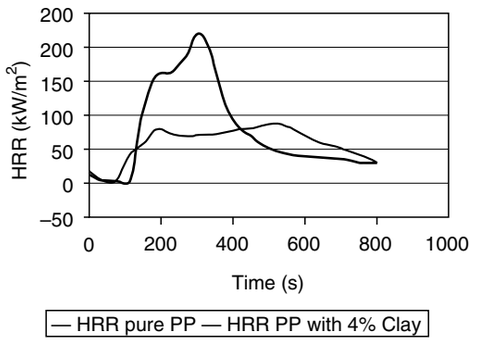

FIGURE 33.2. A plot of heat release rate (HRR) for pure polypropylene compared with a 4% loaded polypropylene/clay nanocomposite.

contains a typical cone calorimeter curve for a pure polymer compared to a nanocomposite of that polymer. In this figure several characteristics of polymer/clay nanocomposites can be seen in these type curves. The first is the reduction in both peak heat release rate (PHRR) and mean heat release rate (MHRR). It can also generally be seen that the time to ignition is also slightly lowered. Table 33.4 contains a compilation of selected cone calorimeter data for a number of polymer/clay nanocomposites compared to the pure polymer. The table contains several parameters of importance. The first is char yield, which obviously relates to char formation. The amount of char correlates directly to the amount of clay in the nanocomposite. Two other parameters of importance are the specific extinction area (SEA) and mean carbon monoxide yield. SEA relates to the amount of smoke produced when the sample burns. SEA data contained in the table has very mixed results. Gilman [33] shows an increase in smoke production; Song *et al*. [34] and Tidjani [35] report a reduction in smoke by the nanocomposites. The same mixed results is seen in carbon monoxide yield. Song *et al*. [34] also reports the synergistic effect of combining nanoclays and phosphate flame retardants. The table illustrates that intercalated systems seem to be similar to exfoliated composites. This is in marked contrast to parameters such as modulus discussed previously.

Based upon the many studies conducted on the flame retardancy of polymer/clay nanocomposites it appears that clay addition to a polymer system will improve its flame retardancy substantially. It also would appear that the flame retardancy can further be improved by combination with other flame retardants.

TABLE 33.4. *Flame retardancy data for selected polymer/clay nanocomposites.*

Sample	Residue yield (%)	Peak HRR (Δ%) (kW/m^2)	Mean HRR (Δ%) (kW/m^2)	Mean Hc (MJ/kg)	Mean SEA (m^2/kg)	Mean CO yield (kg/kg)	Reference
Nylon 6	1	1,010	603	27	197	0.01	[33]
Nylon 6 NC 2%	3	686 (32%)	390 (35%)	27	271	0.01	
Nylon 6 NC 5%	6	378 (63%)	304 (50%)	27	296	0.02	
Nylon-12	0	1,710	846	40	387	0.02	
Nylon-12NC 2%	2	1,060 (38%)	719 (15%)	40	435	0.02	
Polystyrene	0	1,120	703	29	1460	0.09	
PSNC-3%intercal. PS w/ DBDPO/	4	567 (48%)	444 (38%)	27	1730	0.08	
Sb_2O_3 30%	3	491 (56%)	318 (54%)	11	2580	0.14	
Polypropylene	0	1,525	536	39	704	0.02	
PPNC-2%intercal.	5	450 (70%)	322 (40%)	44	1028	0.02	
Polyurethane	0	923			1399	2.33	[34]
PU NC 5%	5.23	472			473	0.37	
PU+6%							
Melamine							
Polyphosphate	3.71	563			488	2.33	
PU NC 5%+6%							
Melamine							
Polyph.	9.47	243			415	0.33	
PP-MA	0	732		40.2	449	0.22	[35]
PP-MA-OD3M-5%	21	245 (66%)	40	389	0.025		
SAN		500					[36]
SAN NC 2%		450					
SAN NC 4%		420					
SAN NC 6%		340					
SAN NC 8%		320					

33.3 BARRIER PROPERTIES OF POLYMER/CLAY NANOCOMPOSITES

In many applications the gas barrier properties of polymers is critical. This is especially true in the food packaging industry. In many food packages the oxygen ingress determines the shelf life of the food in the package. In carbonated drinks the egress of carbon dioxide is the issue. It was recognized early in nanocomposite development that the high aspect ratios of clays could impart barrier to the composite. Nielsen [37] proposed a very simple model for the effect of platy materials on relative barrier performance. This model is commonly referred to as the tortuous path model. Figure 33.3 exhibits the effect of aspect ratio and clay loading on relative gas permeability of a composite utilizing this model. It can be seen that relatively low clay loadings can change the gas permeability greatly. There are a number of nanocomposites that come close to fitting the predictions of this simple model. Table 33.5 contains a listing of such composites. There are, however, a number of effects on permeability of nanocomposites that cannot be explained by this simple model and observed permeabilities that far exceed the predicted relative permeabilities. Lan *et al*. [41] observed in polyimide nanocomposites that the relative permeability for O_2, CO_2, and H_2O fit the tortuous path model reasonably well but measurements on ethyl acetate exhibited a very large dependence on relative humidity. The relative permeability of ethyl acetate at 0% RH was 0.19 and at 50% RH it was 0.09. In contrast the pure polyimides more than double its permeability going from 0 to 50% RH. Chaiko and Leyva [42] reported that in a polypropylene wax composite that they observed 62-fold decrease in oxygen permeability at 5% weight loading of clay. Beall [43] suggested a more complex model for gas permeability that attempts to take into account the change in properties of the polymer that interacts with the clay surface to form a constrained polymer region. This model was utilized to show that much of the data in the literature could be explained by the combination of tortuousity and constrained polymer regions. The theory awaits further experimental verification of the size and character of the constrained polymer region.

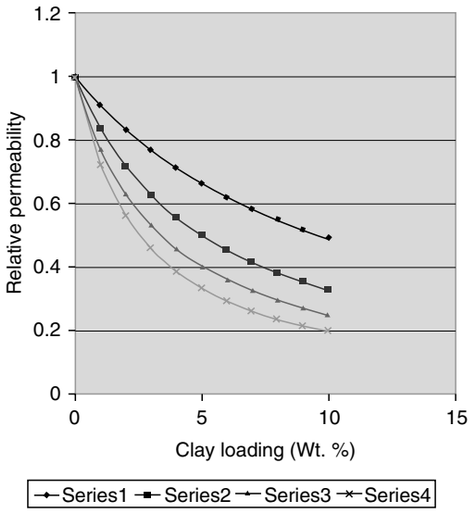

FIGURE 33.3. Relative gas permeabilty versus clay loading for polymer/clay nanocomposites per the model be Nielsen. The different curves represent aspect ratios of 50,100, 150, and 200 for series 1 to 4, respectively.

As a first approximation the simple model of Nielsen can be utilized to predict at least the minimum change in barrier properties one would expect from a polymer nanocomposite. One must use caution, however, since a substantial number of papers in the literature have observed performance far surpassing that predicted by the simple model.

33.4 THERMOSETS

There has been a considerable amount of work conducted on thermoset resin/clay nanocomposites. The overall trends seen in thermoplastics concerning engineering, flammability, and barrier properties are also seen in thermosets. Table 33.6

TABLE 33.5. *Gas permeability data for selected polymer/clay nanocomposites.*

		Permeant (Rel. Perm.)			
Sample	Clay %	Oxygen	Water	Hydrogen	Reference
Nylon 6	2	0.56	0.7	0.63	[5,9]
HDPE	3	0.65			[38]
PUU/Urea	2.5		0.7		[39]
	5		0.43		
	10		0.3		
	15		0.2		
Polylactic acid	4	0.35			[40]
	7	0.27			
	10	0.175			

TABLE 33.6. *Physical properties of selected thermoset nanocomposites.*

Sample description	Clay (wt%)	Tensile strength (MPa)	Tensile modulus (GPa)	Impact strength (kJ/m^2)	HDT (°C)	Elongation at break (%)	Reference
Epoxy 44	0	69	1.1	2.3	65		[5]
Epoxy 44 intercal.	5	61	1	2.2	89		
Epoxy 44 exfoliat.	4.2	107	2.1	2.8	145		
Epoxya 45	0	36	2.1				[44]
Epoxya 45 NC2.5	2.5	38	2.4				
Epoxya 45 NC5	5	24	2.73				
Epoxya 45 NC10	10	20	3.95				
Epoxyb 45	0		3.2				
Epoxyb 45 NC5	5		3.95				
PU 46	0	29	0.98			255	[45]
PU 46 NC1	1	33	1.26			200	
PU 46 NC3	3	34	1.3			190	
PU 46 NC%	5	35	1.5			190	

contains selected physical data on several epoxies [5,44] and one polyurethane [45]. The magnitude of change in modulus and HDT are certainly in line with values seen for thermoplastics. The greatest complication in thermosets, however, is the control of crosslink density in the pure systems as compared to the nanocomposites. As an example Fig. 33.4 contains the DMA of a flexible epoxy and its corresponding nanocomposite. As is the case with thermoplastics there is an increase in modulus below the T_g and a relatively larger percentage increase above the T_g. In contrast to thermoplastics there is a substantial shift in T_g between the pure epoxy and the nanocomposite. It would be reasonable to attribute this to a change in crosslink density since large T_g shifts have not been observed in thermoplastics. This complicates greatly any attempt at theoretically predicting changes that will occur in nanocompositing of thermosets. Uhl *et al.* [45] has measured the effect of clay on crosslink density in a polyurethane nanocomposite. The control polyurethane had a crosslink density of 6.4 (10^{-3}mol/cm^3) while the composites

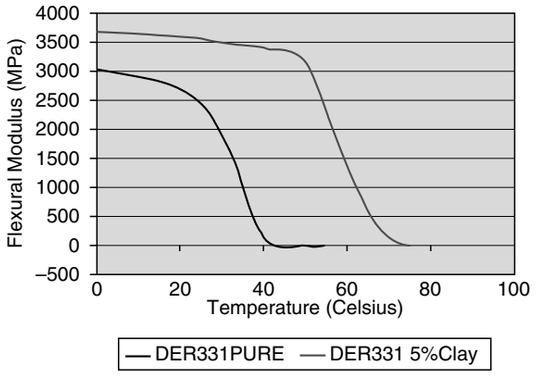

FIGURE 33.4. Comparison of flexural modulus between a pure epoxy and a 5% loaded epoxy/clay nanocomposite utilizing dynamic mechanical analysis.

containing 5% clay gave an average of 8.1. This is a 26% increase which is very close to the average increase in modulus of 28%. It appears that the clay either promotes the crosslinking reaction or acts as a crosslinker.

33.5 RUBBER NANOCOMPOSITE

Rubber is an important worldwide commodity. The worldwide consumption of rubber in 2003 was about 18.97 million metric tones. This consumption can be divided into two major categories, natural and synthetic. The synthetic rubber category is about 58.6% of the total. Of the diverse markets that utilize rubber, approximately 50% of the total rubber consumption goes into tire production.

The benefits identified earlier that relate to nanocomposite reinforcement also applies to rubber as well as increased barrier properties. One of the unique parameters for rubber that is of great importance is hysteresis. Decreased hysteresis at high temperature relates directly to lower rolling resistance for tires. A car, for example, will expend 5–15% of total fuel energy to overcome the rolling resistance of its tires. Heavy trucks will use 15–30% of their fuel to overcome tire rolling resistance. An increase in hysteresis at lower temperature provides for increased tire adhesion to icy and snow covered roads. A combination of lower rolling resistance at higher temperatures and increased adhesion at lower temperature will add value to all weather tires, for example.

Carbon black as a reinforcing additive has been employed in rubber manufacture for many years. One may argue that carbon black provides nanoparticle reinforcement for rubber. There are many reviews available on carbon black use in rubber.[46] We will focus on recent advancements in nanoparticle reinforcement. These advancements do not include carbon black. Most of the recent advancements in nanoparticle reinforcement in rubber have focused on montmorillonite clay.There are several reviews on rubber

nanocomposites found in the open literature in other languages the only one in English, however, is by Karger-Kocsis [47].

This chapter will divide the advancements in rubber nanocomposites as a function of polymer type. One should be aware that polymer blending is very prevalent in commercial applications of rubber. For example, a tire can contain eight different polymer types.

33.5.1 Styrene–Butadiene Nanocomposites

Styrene–butadiene copolymers are extremely important to the rubber industry. They are particularly important in tire manufacture. Styrene–butadiene polymer is produced by emulsion polymerization and solution polymerization. Most of the volume is by emulsion polymerization. This affords the opportunity to prepare polymer nanocomposites by several avenues. One can blend an aqueous dispersion of the nanoparticles with the styrene–butadiene latex before flocculation to produce the rubber crumb, disperse an organically treated nanoparticle in the styrene–butadiene solution polymer before the solvent is stripped from the polymer, disperse the organically treated nanoparticles into the monomers, or prepare the rubber nanocomposite in the traditional compounding approach. One finds all of these approaches in the literature. One also finds functional modifications of the styrene–butadiene polymer in the literature designed to improve the efficiency of the dispersion and interaction of the nanoparticles with the polymer.

Manoj Ajbani *et al*. [48] describes the value of amine functional block copolymers of styrene–butadiene with montmorillonite clay to prepare rubber nanocomposites. Light weight composites were evaluated with pure montmorillonite, Cloisite NA, and montmorillonite exchanged with tallow, bis(2-hydroxyethyl) methyl quaternary ammonium chloride. The focus of the work is to improve traction, tread wear, and rolling resistance of tires with a reduction of the weight of the tire. The two areas of the tire where these rubber–clay nanocomposites are applicable are the tread for lower rolling resistance and increased traction and the tire side-walls for increased flexibility with enhanced tensile strength. Cloisite 30B demonstrated a significant increase in performance at 5 phr. Transmission electron microscopy (TEM) indicated partial exfoliation of the clay into the polymer.

Parker *et al*. [49] altered the stabilization mechanism for styrene–butadiene latex prepared by emulsion polymerization from anionic to cationic so that they could get a spontaneous flocculation with aqueous montmorillonite slurry and the latex. Evaluation of the rubber nanocomposite prepared in this manner gave dramatic increases in modulus, strength, percent elongation, and decrease in hysteresis.

Sarashi [50] intercalates montmorillonite with styrene and butadiene monomer before polymerization. After the clay–monomer dispersion is polymerized to form the styrene–butadiene nanocomposite, the rubber nanocomposite is compounded with natural rubber to provide a composite with good break strength and bending fatigue resistance.

Only limited success has been achieved in compounding organomontmorillonites with styrene–butadiene rubber to prepare rubber nanocomposites [51]. Knudson *et al*. [51] discovered that flocculation of the aqueous blend of styrene–butadiene latex and montmorillonite gives an exfoliated clay–rubber nanocomposite. The approach offers the most convenient and effective method for the preparation of clay–styrene–butadiene rubber nanocomposites.

To confirm the relationship of exfoliation of montmorillonite in styrene–butadiene rubber to mechanical properties, Sadhu *et al*. [53], dissolved styrene–butadiene rubber into toluene and dispersed organically treated montmorillonite and untreated montmorillonite into the polymer solution at 4% concentration based on polymer. The organoclay was prepared by the exchange of octadecyl amine. The toluene was removed by evaporation. The degree of exfoliation of the polymer nanocomposites was measured by wide angle x-ray diffraction WAXS. The untreated clay was intercalated with polymer; the organically treated clay was fully exfoliated. The exfoliated rubber nanocomposite has significantly improved tensile strength, elongation at break, energy to break, and modulus at 50% elongation when compared to the intercalated rubber nanocomposite. Both rubber composites had superior mechanical performance when compared to the pure rubber. In a previous publication by Mousa *et al*. [54], the same organoclay that was utilized in the above publication by S. Sadhu was compounded with styrene–butadiene up to 10 phr and cured. The rheology of the polymer nanocomposite demonstrated shear rate thinning behavior. This is common with montmorillonite dispersed systems. The mechanical properties were as predicted except for the increase in percent elongation to failure as a function of clay loading. The percent elongation to failure increased along with modulus and tensile strength. This is not expected or predicted by standard reinforcing theories. For example, carbon black loaded polymer does not behave in this manner. The crosslink density was measured by swelling the composite and utilizing the Flory–Rehner equation. The crosslink density increase with organoclay loading indicated that the amine could be participating in the cure. The authors speculate that two distinct polymer morphologies develop. A higher crosslinked polymer morphology is associated with the clay particles and a lower crosslinked density polymer is associated with the bulk of the rubber composite. Ganter *et al*. [55], prepared organoclay–styrene–butadiene rubber nanocomposites in a similar fashion to Sahdu by dispersing the rubber and organoclay in toluene and evaporating the solvent to prepare the rubber nanocomposite. In addition, they utilized a sulfur functional silane(bis(triethoxysilylpropyl)-tetrasulfan to further enhance the crosslinking during cure. Transmission electron microscopy indicated intercalated and partially exfoliated montmorillonite in the rubber. They saw increased

hysteresis with clay loading. WAXS indicated that the montmorillonite was changing orientation, i.e., sliding past one another, during cyclic tensile testing. Sadhu *et al*. [56], examined the role of the chain length of the amine exchanged on montmorillonite with respect to exfoliation and mechanical properties when dispersed in styrene–butadiene. Amines with longer chain length exfoliated to a greater extent and resulted in improved mechanical performance of the rubber nanocomposite. Subsequent work by Sadhu *et al*. [57], with octadecyl amine exchanged montmorillonite exfoliated into styrene–butadiene indicated that the styrene content of the polymer was a significant variable with respect to mechanical properties. The styrene–butadiene polymer with the greatest styrene content, i.e., 40%, demonstrated a much greater increase in strength, i.e., 53%, as a rubber nanocomposite than the polymers with 23% styrene, 38% increase in strength, and 15% styrene, 13% increase in strength. An extension of the work [58] evaluated the significance of the cure system to the development of mechanical properties and found little effect of the type of cure system but longer cure time provided for improved mechanical properties. Bala *et al*. [59] evaluated dodecylamine exchanged montmorillonite compounded into styrene–butadiene. The WAXS indicated less that perfect exfoliation into the rubber. However, the tensile strength, modulus, and elongation at break increased significantly at 4% loading of the organoclay when compared to the unfilled rubber. Crosslink density increased in the rubber composite as a function of organoclay concentration.

Wang *et al*. [60] utilized positron annihilation lifetime spectroscopy to measure the polymer free volume in montmorillonite–styrene–butadiene rubber nanocomposites. There was an apparent reduction of the free volume of the polymer in the nanocomposite. The authors speculated that the reduction was primarily at the clay surface. This information is consistent with the crosslink density results reported above.

Molesa *et al*. [61] compared compounded styrene–butadiene nanocomposites with polymer nanocomposites that were prepared by blending the latex with an aqueous dispersion of the montmorillonite. The loading of the dispersed phase was at 10 phr. The initial results are consistent with the information found above. The flocculated rubber nanocomposite from the aqueous blend has superior strength properties when vulcanized and compared with the rubber nanocomposite prepared by compounding. Montmorillonite that was organically treated demonstrated superior tensile strength when compared with rubber compounded with silica.

Ganter *et al*. [62], utilized a synthetic layered fluorohectorite silicate and organomontmorillonite to evaluate the role of functional rubber exchanged onto the synthetic clay in the preparation of styrene–butadiene rubber nanocomposites. The functional rubber that was exchanged onto the fluorohectorite was amino-terminated polybutadiene. The styrene–butadiene was dispersed in solvent and then dispersed with the organoclays. Break strength, tensile strength, and hysteresis correlated with transmission electron microscopy determination of particle morphology. The particles were intercalated with polymer or partially exfoliated. Orientation of these highly anisotropic clay particles correlated with the mechanical properties of the rubber nanocomposites.

Zhang *et al*. [63] prepared styrene–butadiene nanocomposites by dispersing an aqueous dispersion of montmorillonite and latex and flocculating the dispersion with acid. The performance of the rubber nanocomposites were compared with clay, carbon black, and silica rubber composites prepared by standard compounding methods. The montmorillonite loadings for the rubber nanocomposite were up to 60 phr. The morphology of the rubber nanocomposites by transmission electron microscopy appears to indicate intercalated structures. The mechanical properties of the rubber nanocomposites were superior to all of the other additives up to about 30 phr. However, rebound resistance was inferior to all of the additives except silica. The state of cure was not evaluated.

33.5.2 Butyl Rubber Nanocomposites

Butyl rubber is the most expensive polymer utilized in tire manufacture. The primary use for butyl rubber is for the inner liner of a tire. The inner liner of the tire maintains air pressure in the tire for an extended period of time. Oxygen diffusing into the carcass of the tire from the inside will degrade the tire just as oxygen from the outside of the tire degrades the sidewalls of the tire. Butyl rubber has low mechanical durability and a relatively high specific gravity. There is a clear need for a butyl rubber nanocomposite with increased toughness and barrier resistance. Lower butyl rubber content through the use of a nanocomposite will make the tire more cost effective and increase operation efficiency without a compromise in safety and durability.

Butyl rubber is exclusively made by a solution polymerization process. Hence, nanoparticles can only be introduced as a dispersion with the butyl polymer before the solvent is removed, with the monomer, or in a standard compounding protocol. Butyl rubber is prepared from isobutylene. There are no double bonds available for cure after polymerization. A small amount of isoprene is added to the polymerization process to provide for the double bonds necessary for cure. Bromination of the polymer is also done to provide crosslinking sites.

A patent application by Maruyama *et al*. [64], teaches that anhydride modification of the butyl rubber improves the exfoliation of amine exchanged clays. This combination produces exfoliated clay–butyl rubber nanocomposites. These nanocomposites have excellent barrier performance.

Hagiwara *et al*. [65], prepares the butyl rubber nanocomposite from the polymer solution. The polymer is prepared

by solution polymerization in toluene. The polymer solution is then emulsified in water with the aid of anionic surfactants and alcohol coupling solvents. The solvent and coupling solvent is removed by reduced pressure. The aqueous dispersion of butyl rubber is blended with an aqueous dispersion of clay. The water is then removed by reduced pressure. The resultant clay–butyl rubber nanocomposite demonstrated good barrier resistance.

Work done by Gong *et al*. [66] is similar to the work by Maruyama *et al*., above. They functionalize butyl rubber with succinic anhydride to improve the compatibility of butyl rubber with an organoclay. Barrier performance of the rubber nanocomposite increases with the amount of succinic anhydride modification. In a companion publication [67], butyl rubber is functionalized by grafting maleic anhydride onto the polymer chain with peroxide. The same organoclay is utilized in this work as well to form the rubber nanocomposite. Barrier performance of the butyl rubber is significantly enhanced.

Ishida *et al*. [68], determined that organoclay compounded into halogenated butyl rubber, e.g., brominated copolymer of isobutylene and methyl styrene, provides a rubber nanocomposite with a lower air permeability index, i.e., 85, than the pure brominated butyl rubber. Yagi *et al*. [69] found that the addition of epoxidized natural rubber to the formula with halogenated butyl rubber provided for the successful utilization of clay and mica to form a butyl rubber nanocomposite with reduced air permeability, i.e., $9 \times 10{-}11$ cc cm/cm^2 s cmHg. Maiti *et al*. [70] evaluated montmorillonite exchanged with amines in brominated butyl rubber. TEM and WAXS indicated good exfoliation of the organoclay in the polymer. Tensile strength, elongation to break, and modulus were significantly greater for the rubber nanocomposites when compared to the pure rubber. Mruyama *et al*. [71] teaches that montmorillonite exchanged with long chained amino acids disperses well in brominated butyl rubber to produce rubber nanocomposites that provide good barrier to air. Tsou *et al*. [72] discovered that the addition of nylon or nylon–organoclay nanocomposites to the bromobutyl rubber–organoclay nanocomposite also enhances barrier properties.

33.5.3 Natural Rubber Nanocomposites

Natural rubber composition is polymerized *cis*-1,4-polyisoprene. However, synthetic attempts of duplicating natural rubber have been largely unsuccessful. Natural rubber is the largest polymer component of a tire. The preparation of natural rubber nanocomposites will add value to a very large segment of the rubber industry. Because natural rubber can be obtained as an aqueous dispersion from the rubber tree and as a dried solid phase, one can disperse an aqueous dispersion of nanoparticles into the latex before drying or compound the organic modified nanoparticles into the solid phase to obtain the rubber nanocomposite.

Larson [73] teaches that one can successfully compound organoclays into natural rubber. One obtains a homogeneous distribution of intercalated and exfoliated clay particles. The benefits of the rubber nanocomposite are high storage modulus with a small increase in hysteresis. Ajbani *et al*. [74] used maleic anhydride functional polybutadiene as a compatibilizer for clay incorporation into natural rubber. The organoclays were predispersed with maleic anhydride functional polybutadiene before compounding with natural rubber. The mechanical properties were excellent. The fatigue to failure cycles with the Monsanto FTF tester were especially high.

Jeon *et al*. [75] employed rheology to identify structure–property relationships of clay–natural rubber nanocomposites. The rubber nanocomposites were prepared by dispersing the rubber and organoclay in toluene. Upon evaporation of the solvent, x-ray, small and wide angle, and TEM indicate good exfoliation of the clay in the rubber. Weight concentrations of the clay varied between 1 and 9.2%. Dynamic viscosity, storage modulus, and loss modulus were determined. In the range of 3–4 wt% loading of clay, one apparently sees an interaction between the clay and the rubber that suggests chain entanglement with the clay. Above this concentration, the rubber composite seems to behave as a ''pseudosolid,'' i.e., a frequency independent, storage modulus.

Yaakub *et al*. [76], prepared natural rubber–clay nanocomposites by blending an aqueous dispersion of the clay with an aqueous dispersion of the rubber and flocculating the dispersion with other additives for cure. Hectorite and montmorillonite were evaluated. Mechanical properties improved as well as an increase in coefficient of friction and abrasion resistance.

Kgawa *et al*. [77], found that a dispersion of organoclay and epoxy functional rubber compounded into natural rubber resulted in an increase of modulus and tensile strength.

Lopez-Manchado *et al*. [78] prepared natural rubber nanocomposites with organoclay prepared from saponite. The polymer and organoclay were dispersed in organic solvent. The solvent was evaporated to yield the rubber nanocomposite with intercalated clay nanoparticles. A silane coupling agent was also evaluated with the rubber nanocomposite. The loading level of clay in the rubber was about 10 phr. Mechanical properties improved significantly. Further improvement in mechanical properties was observed when the silane coupling agent was present.

Varghese *et al*. [79,80], observed that pure, synthetic sodium fluorohectorite does not disperse well into natural rubber. However, when polyurethane rubber was dispersed with the clay and natural rubber, excellent mechanical properties were observed when the clay was present at 10 wt%. The clay preferred to be associated with the urethane dispersed phase.

Varghese *et al*. [81–84] evaluated pure montmorillonite, kaolin, and synthetic fluorohectorite by mixing an aqueous dispersion of clay, an aqueous dispersion of natural latex,

and curative additives and then drying the mixture to prepare the rubber nanocomposite. Fluorohectorite rubber nanocomposite demonstrated the best dispersion of the clay and best mechanical properties. Epoxidized natural rubber was evaluated with pure clays and several organoclays. Standard compounding methods were used to prepare 10% clay loaded rubber nanocomposites. Octadecylamine exchanged montmorillonite demonstrated the best tensile strength, modulus, and tear strength. WAXS and TEM indicated that the octadecylamine exchanged montmorillonite probably had the best dispersion in the rubber.

Magaraphan *et al*. [85] evaluated organoclays prepared from amines and quats with carbon chain lengths that varied from 12 to 18 with natural rubber. The rubber and organoclays were dispersed in toluene and then the solvent was evaporated. Based on WAXS and TEM, exfoliation of the clay in the polymer was observed up to 10 wt%. Above that concentration, the organoclays seemed to be intercalated. The amine exchanged clays with the longer hydrocarbon chains provided rubber nanocomposites that had superior mechanical performance when compared to the rubber nanocomposites prepared with the quat exchanged clays with the same hydrocarbon chain.

Vu *et al*. [86], reports similar work to that of Varghese above with montmorillonite, natural rubber, and epoxidized natural rubber. The rubber nanocomposites were prepared by compounding the clay with the rubber or dissolving the rubber in toluene or methyl, ethyl ketone, dispersing the clay in the solution, and evaporating the solvent to produce the rubber nanocomposite. Pure montmorillonite and organically modified montmorillonite were evaluated. Natural rubber and natural rubber epoxidized with 25 or 50% mole percent epoxide were evaluated. Mechanical properties are similar to those reported by Varghese above and correlate with the x-ray diffraction results. Organic modification of the montmorillonite results in improved intercalation and exfoliation in the rubber. Greater intercalation and exfoliation of the clay resulted in improved mechanical performance.

Joly *et al*. [87], prepared natural rubber nanocomposites by compounding organoclays at 10 wt% loading. The rubber nanocomposites were characterized by small angle x-ray scattering, scanning, and TEM, mechanical properties, birefringence, infrared dichroism, and crosslink density by swelling in toluene. The clay in the rubber was intercalated and exfoliated. The organoclays were very efficient in reinforcing the rubber. The clay also appears to increase the crosslink density of the rubber.

33.5.4 Acrylonitrile-Butadiene (NBR) and Hydrogenated Acrylonitrile (HNBR) Rubber Nanocomposites

Because of the thermal stability and chemical resistance of NBR and HNBR rubber, their application areas include power transmission, i.e., belts, etc., blow out preventors, packer seals, stators, fuel hoses, engine seals, and gaskets. HNBR has improved thermal stability and exterior durability but sacrifices low temperature flexibility when compared to NBR.

Akelah *et al*. [88], prepared a NBR nanocomposite by blending an aqueous dispersion of montmorillonite with a dioxane solution of amine terminated NBR. The solvent was evaporated to product the rubber nanocomposite. WAXS and TEM indicated intercalated clay morphology in the rubber. No mechanical properties were reported. Okada *et al*. [89], also prepared NBR by blending an aqueous dispersion of montmorillonite with an *N*,*N*-dimethyl sulfoxide–ethanol solution of amine terminated NBR. The solvent was evaporated away to produce the rubber nanocomposite. This nanocomposite was compounded into NBR to produce NBR–clay nanocomposites at 5 and 10 phr clay. TEM indicates an intercalated morphology for the clay in the rubber. When compared to carbon black loaded NBR at 20 and 40 phr, the Mooney viscosity of the rubber nanocomposites decreases with increased clay loading; carbon black loaded rubber always results in increasing viscosity with increased loading. Mechanical properties indicated that the clay was about four times more efficient at reinforcing NBR when compared to carbon black. The moisture and hydrogen permeability of these NBR nanocomposites were reported in a subsequent puplication [90]. Barrier properties of the clay–NBR nanocomposites are significantly superior to the carbon black filled NBR. The anisotropic-plate structure of the clay provides for this enhanced barrier.

Pazur [91] found that compounding carboxyl functional HNBR (HXNBR) with HNBR, carbon black, and 5 phr. Organoclay in a standard rubber formula provided a rubber nanocomposite with superior mechanical, barrier, and cure performance when compared to HNBR alone. A variety of organoclays and pure montmorillonite were evaluated with a 75/25 ratio of HNBR/HXNBR and 70 phr carbon black.

Previously mentioned work by Sadhu and Bhowmick evaluated NBR nanocomposites as a function of acrylonitrile content and organoclay loading. The rubber was dispersed into chloroform; the organoclay were dispersed into ethanol. The dispersions were blended and dicumyl peroxide was added for cure. The solvent was evaporated to produce the rubber nanocomposite. The acrylonitrile content of the rubber was 19, 34, and 50%. The organoclay content was evaluated at 2, 4, 6, and 8%. TEM and WAXS confirmed intercalated structure of the clay in the rubber. The general trend was the rubber with the highest acrylonitrile content provided the best mechanical performance. The tensile strength increased as a function organoclay concentration. Interestingly, for the 50% acrylonitrile containing rubber, the elongation to failure also seemed to increase as a function of organoclay content. Kim *et al*. [92] also evaluated octadecyl amine exchanged montmorillonite in NBR. The rubber nanocomposites were prepared by compounding. The role of 3-(mercaptopropyl)trimethoxysilane

coupling agent was also evaluated in the formula. The rate of cure and barrier to water vapor increased as a function of increasing clay and coupling agent content. Nah *et al*. [93] found similar mechanical properties with NBR with various organoclays. The rubber nanocomposites were prepared by compounding. The structure of the montmorillonite in the rubber was intercalated.

33.5.5 Ethylene–Propylene–Dimer Rubber Nanocomposites

Ethylene–propylene–dimer (EPDM) rubber has a good balance of toughness, durability, chemical resistance, and barrier performance that makes this rubber suitable for the manufacture of parts for power transmission, i.e., belts, etc., gaskets, and hoses. EPDM also has utility as a dispersed phase to toughen thermoplastics.

Gatos *et al*. [94], evaluated compounding processing variables, the role of functionality on the EPDM, and cure additives in relation to mechanical performance and the degree of dispersion of the clay in the rubber nanocomposite. Clay loading for the study was 10 phr. Superior tensile strength and modulus was achieved with a 1% maleic anhydride grafted EPDM with an internal mixer at elevated temperature, i.e., 100 °C. Better mechanical properties were obtained with the rubber nanocomposite when the zinc oxide and stearic acid was added to compounding on an open mill rather than added to the internal mixer. The accelerator, zinc diethyldithiocarbamate, provided the best mechanical performance in the formula. WAXS and TEM indicated that functionalized EPDM with maleic anhydride and glycidyl methacrylate increases the compatibility of the organoclay with the rubber. The morphology appears to be intercalation with the possibility of some exfoliation. Usuki *et al*. [95], also evaluated EPDM with octadecylamine exchanged montmorillonite. The rubber nanocomposite was prepared by compounding 7 phr of the organoclay into the rubber. The nature of the accelerator was found to be a significant variable in regard to the degree of dispersion of the organoclay in the rubber. Exfoliation of the organoclay appears to occur in the EPDM when the accelerators were zinc dimethyldithiocarbamate and tetramethylthiuram monosulfide based on the WAXS and TEM. The exfoliated rubber nanocomposites were significantly superior in mechanical properties and barrier performance when compared to the intercalated rubber composites. The exfoliated rubber nanocomposites demonstrated approximately two times the tensile strength, percent elongation to failure, and modulus when compared to the unfilled, cured rubber. The barrier performance based on nitrogen permeability was improved approximately 30% when compared to the unfilled, cured rubber. A series of publications by Zhueng *et al*. [96–105] focus on evaluating the role of quat surface treatment of montmorillonite in the dispersion of organoclays in EPDM. Montmorillonite exchanged with alkyl hydroxyl functional quats exfoliate in EPDM by standard compounding procedures. The other quat treatments on montmorillonite result in intercalated structures in the EPDM. The mechanical properties of the organoclay–EPDM nanocomposites significantly increased when compared to the cured rubber without reinforcing additives. Exfoliated structures demonstrated superior mechanical performance compared to intercalated morphologies. Loading levels up to 15 phr. were evaluated. At that loading level, exfoliated rubber nanocomposites demonstrated a factor of 3–4 times improvement in mechanical performance compared to the cured rubber without reinforcement. They also found that maleic anhydride grafted EPDM of at least 5.2 wt% improved the exfoliation efficiency of the organoclays and subsequent mechanical properties of the rubber nanocomposites. Comparisons of sulfur cure with peroxide cure, i.e., 2,5,-dimethyl-2, 5-di- *tert*-butylperoxyhexane, with the organoclay–EPDM nanocomposites indicated that sulfur cure produced exfoliated structures and peroxide cure of the same nanocomposite produced intercalated structures. The sulfur cured nanocomposites had lower crosslink density than the peroxide cured nanocomposites. Improved barrier performance of oxygen by the rubber nanocomposites was also determined.

REFERENCES

1. Friedlander, H. Z., *ACS Div. Polym. Chem. Reprints* (1963), **4**, 300–306.
2. Soloman, D. H., Luft, B. C., *J. Appl. Polym. Sci*. (1968), **12**, 1253–1262.
3. Blumstein, A., Blumstein, R., Vanderspurt, T. H., *J. Colloid Intef. Sci*. (1969), **31**, 236–247.
4. Blumstein, A., Parikh, K. K., Malhotra, S. L., *J. Polym. Sci*. (1971), **A2**, 1681–1691.
5. Kojima, Y., Usuki, A., Kawasumi, M., Okada, A., Fukushima, Y., Kurauchi, T., Kamigaito, O., *J. Mater. Res*. (1993), **8**, 1185–1189.
6. Kojima, Y., Usuki, A., Kawasumi, M., Okada, A., Kurauchi, T., Kamigaito, O., *J. Appl. Polym. Sci*. (1993), **49**, 1259–1264.
7. Kojima, Y., Fukumori, K., Usuki, A., Okada, A., Kurauchi, T., *J. Mater. Sci. Lett*. (1993), **12**, 889–890.
8. Usuki, A., Kawasumi, M., Kojima, Y., Okada, A., *J. Mater. Res*. (1993), **8**, 1174–1178.
9. Usuki, A., Kojima, Y., Kawasumi, M., Okada, A., Fukushima, Y., Kurauchi, T., Kamigaito, O., J. Mater. Res. (1993), **8**, 1179–1184.
10. Ray, S. S., Okamoto, M., *Prog. Polym. Sci*. (2003), **38**, 1539–1641.
11. Okada, A., Usuki, A., *Mater. Sci. Eng*. (1995), **C3**, 109–115.
12. Fornes, T. D., Yoon, P. J., Heskkula, H., Paul, D. R., *Polymer* (2001), **42**, 9929–9940.
13. Hasegawa, N., Okamoto, H., Kato, M., Usuki, A., Sato, N., *Polymer* (2003), **44**, 2933–2937.
14. Fornes, T. D., Paul, D. R., *Polymer* (2003), **44**, 4993–5013.
15. Liu, X., Wu, Q., *Macromol. Mater. Eng*. (2002), **287**, 180–186.
16. Chavarria, F., Paul, D. R., *Polymer* (2004), **45**, 8501–8515.
17. Han, B., Ji. G., Wu, S., Shen, J., *Eur. Polym. J*. (2003), **39**, 1641–1646.
18. Lew, C. Y., Murphy, W. R., McNally, G. M., Yanai, S., Abe, K., ANTEC 2003, 178–182.
19. Fornes, T. D., Paul, D. R., *Macromolecules* (2004), **37**, 7698–7709.
20. Chang, J-H., Kim, S. J., Joo, Y. L., Im, S., *Polymer* (2004), **45**, 919–926.
21. Pegoretti, A., Kolarik, J., Peroni, C., Migliaresi, C., *Polymer* (2004), **45**, 2751–2759.

22. Sanchez-Solis, A., Garcia-Rejon, A. Manero, O., *Macromol. Symp.* (2003), **192**, 281–292.
23. Chang, J.-H., An, Y. U., Ryu, S. C., Giannelis, E. P., *Polym. Bull.* (2003), **51**, 69–75.
24. Chisholm, B. J., Moore, R. B., Barber, G., Khouri, F., Hempstead, A., Larsen, M., Olson, E., Kelley, J., Balch, G., Caraher, J., *Macromolecules* (2002), **35**, 5508–5516.
25. Zhang, Q., Wang, K., Men, Y., Fu, Q., Chin. *J. Polym. Sci*. (2003), **21**, 359–367.
26. Oya, A., Kurokawa, Y., Yasuda, H., *J. Mat. Sci*. (2000), **35**, 1045–1050.
27. Wang, D., Wilkie, C., *Polym. Degrad. Stab.* (2003), **80**, 171–182.
28. Gopakumar, T. G., Lee, J. A., Kontopoulou, M., Parent, J. S., *Polymer* (2002), **41**, 5483–5491.
29. Wang, K. H., Koo, C. M., Chung, I. J., *J. Appl. Polym. Sci*. (2003), **89**, 2131–2136.
30. Wei, L., Tang, T., Huang, B., *J. Polym. Sci.*: Part A (2004), **42**, 941–949.
31. Hotta, S., Paul, D. R., *Polymer* (2004), **45**, 7639–7654.
32. Tjong, S. C., Meng, Y. Z., *J. Polym. Sci.*: Part B: *Polym. Phys*., (2003), **41** (13), 1476–1484.
33. Gilman, J. W., *Appl. Clay Sci*. (1999), **15**, 31–49.
34. Song, L., Hu, Y., Tang, Y., Zhang, R., Chen, Z., Fan, W., *Polym. Degrad. Stab.* (2005), **87**, 111–116.
35. Tidjani, A., 2005, *Polym. Degrad. Stab*. (2005), **87**, 43–49
36. Bourbigot, S., Vanderhart, D. L., Gilman, J. W., Bellayer, S., Stretz, H., Paul, D. R., *Polymer* (2004), **45**, 7627–7638.
37. Nielsen, L. E., *J. Mocromol. Sci*. (1967), **A1**, 929–942.
38. Osman, M., Atallah, A., *Macromol. Rapid Commun*. (2004), **25**, 1540–1544
39. Xu, R., Manias, E., Synder, A. J., Runt, J., *Macromolecules*, (2001), **34**, 337–339.
40. Ray, S. S., Yamada, K., Okamoto, M., Ogami, A. Ueda, K., *Chem. Mater*. (2002), **15**, 1456–1465.
41. Lan, T., Kaviratna, P. D., Pinnavaia, T. J., *Chem. Mater*. (1994), **6**, 573–575.
42. Chaiko, D. J., Leyva, A. A., *Chem. Mater*. (2005), **17**, 13–19.
43. Beall, G. W., Polymer–Clay Nanocomposites, edited by Pinnavaia, T. J. and Beall, G. W., John Wiley & Sons, Chichester, UK, (2001), 267–268.
44. Daniel, I. M., Miyagawa, H., Gdoutos, E. E., Luo, J. J., *Exp. Mech.* (2003), **43** (3), 348–354.
45. Uhl, F. M., Davuluri, S. P., Wong, S-C., Webster, D. C., *Polymer* (2004), **45**, 6175–6187.
46. Donnet, J. B., Compos. Sci. Technol. (2003), **63**, 1085.
47. Karger-Kocsis, J., Polym. Eng. Sci. (2004), **44**(6), 1083–1093.
48. Ajbani, M., Hsu, W., Halasa, A. F., Lee, G., Castner, E. S., US Pat. 6, 727, 311 (2004).
49. Parker, D. K.; Larson, B. K., Yang, X., US Pat. Appl. 2004/0054049 B1 (2004).
50. Sarashi, H., Jap. Pat. JP 2003327751 (2003).
51. Knudson, M. L., Powell, C., PCT Int. Pat. WO 02/070589 A2 (2002).
52. Heinrich, G., Herrmann, W., Kendziorra, N., Pietag, T., Recker, C., US Pat. 6, 818, 693 (2004).
53. Sadhu, S., Bhowmick, A. K., J. Polym. Sci.:Part B:Polym. Phys. (2004), **42**, 1573–1585.
54. Mousa, A., Karger-Kocsis, J., Macromol. Mater. Eng. (2001), **286**(4), 260–266.
55. Ganter, M., Gronski, W., Riechert, P., Mulhaupt, R., Rubber Chem. Technol. (2001), **74**(2), 221–235.
56. Sadhu, S., Bhowmick, A. K., Rubber Chem. Technol. (2003), **76**(4), 860–875.
57. Sadhu, S., Bhowmick, A. K., Adv. Eng. Mat. (2004), **6**(9), 738–742.
58. Sadhu, S., Bhowmick, A. K., J. Appl. Polym Sci. (2004), **92**(2), 698–709.
59. Bala, P., Samantaray, B. K., Srivastava, S. K., Nando, G. B., J. Appl. Polym. Sci. (2004), **92**, 3583–3592.
60. Wang, Y., Wu, Y., Ahang, H., Zhang, L., Wang, B., Wang, Z., *Macromol. Rapid Commu.* (2004), **25** (23), 1973–1978.
61. Malesa, M., Parasiewicz, W., Slusarski, L, Pysklo, L., Debek, C, *Materialy Konferencji, 7th* (2004), 108–111; Pub: Osrodek Badawczo-Rozwojowy Kauczukow I Tworzyw Winylowych, Oswiecim, Poland.
62. Ganter, M., Gronski, W., Semke, H., Zilg, T., Thomann, C., Muhlhaupt, R., Kautschuk Gummi Kunststoffe (2001), **54**(4), 166–171.
63. Zhang, L., Wang, Y., Wang, Y., Sui, Y., Yu, D., J. Appl. Polym. Sci. (2000), **78**(11), 1873–1878.
64. Maruyama, T., Ishikawa, K, Amino, N., Ikawa, M., US Pat. Appl. 2003/0191224 (2003).
65. Hagiwara, I., Kadota, K., Mashimo, S., Jap. Pat. JP 2003321551 (2003).
66. Gong, C., Dias, A. J., Tsou, A. H., Poole, B. J., Karp, K. R., PCT Int. Pat. WO 2004005387 A1 (2004).
67. Gong, C., Dias, A. J., Tsou, A. H., Poole, B. J., Karp, K. R., PCT Int. Pat. WO 2004005388 A1 (2004).
68. Ishida, K, Masaki, K., Jap. Pat. JP 2004224809. A2 (2004).
69. Yagi, N., Muraoka. K, Minagawa, Y., Nishioka, K., US Pat. Appl. 2004/0226643 (2004).
70. Maiti, M., Sadhu, S., Bhowmick, A. K., J. Polym. Sci., Part B: Polym. Phys. (2004), **42**(24), 4489–4502.
71. Mruyama, T., Ishikawa, K., Jap. Pat. JP 2004155912 A2 (2004).
72. Tsou, A. H., Dias, A. J., PCT Int. Pat. WO 02/100923 A2 (2002).
73. Larson, B. K., US Pat. 6598645 (2003).
74. Ajbani, M., Geiser, J. F., Parker, D. K., US Pat. Appl. 20030144401 A1 (2003).
75. Jeon, H. S., Rameshwaram, J. K., Kim, G., J. Polym. Sci., Part B: Polym. Phys. (2004), **42**(6), 1000–1009.
76. Yaakub, A., Kuen, C. P., Keane, N., Ross, M., US Pat. Appl. 20040147661 A1 (2004).
77. Kgawa, K, Maruyama, T., Ishikawa, K., Jap. Pat. JP 2004250473 A2 (2004).
78. Lopez-Manchado, M. A., Herrero, B., Arroyo, M., Polym. Int. (2004), **53**(11), 1766–1772.
79. Varghese, S., *Latex 2004, Two-Day Conference on Synthetic Emulsions, Natural Latex and Latex Based Products,* 3rd, (2004) 179–190, Rapra Technology Ltd., Shrewsbury, UK.
80. Varghese, S., Gatos, K.G., Apostolov, A. A., Karger-Kocsis, J., J. Appl. Polym. Sci. (2004), **92**(1), 543–551.
81. Varghese, S., Karger-Kocsis, J., Pannikottu, A., *Tech. Papers-American Chemical Society, Rubber Div. 164*th, (2003) 2148–2172, American Chemical Society, Rubber Div., Akron, Ohio.
82. Varghese, S., Karger-Kocsis, J., *Polymer* (2003), **44**(17), 4921–4927.
83. Varghese, S., Karger-Kocsis, J., J. Appl. Polym. Sci. (2004), **91**(2), 813–819.
84. Varghese, S., Karger-Kociss, J, Pannikottu, A., Rubber World (2004), **230**(1), 32–38.
85. Magaraphan, R., Thaijaroen, W., Lim-Ochakum, R., Rubber Chem. Technol. (2003), **76**(2), 406–418.
86. Vu, Y. T., Mark, J. E., Pham, L. H., Engelhardt, M., J. Appl. Polym. Sci. (2001), **82**(6), 1391–1403.
87. Joly, S., Garnaud, G., Ollitrault, R., Bokobza, L, Mark, J. E., Chem. Mater. (2002), **14**(10), 4202–4208.
88. Akelah, A., El-Deen, N. S., Hiltner, A., Baer, E., Moet, A., Mater. Lett. (1995), **22**, 97–102.
89. Okada, A., Fukumori, K., Usulki, A., Kojima, Y., Sato, N., Kurauchi, T., Kamigaito, O., Polym. Prepr. Am. Chem. Soc. Div. Polym. Chem. (1991), **32**, 540–541.
90. Kojima, Y., Fukumori, K., Usuki, A., Okada, A., Kurauchi, T., J. Mater. Sci. Lett. (1993), **12**, 889–890.
91. Pazur, R., Eur. Pat. Appl. EP 1475405 A1 (2004).
92. Kim, J., Oh, T., Lee, D., Polym. Int. (2004), **53**(4), 406–411.
93. Nah, C., Ryu, H.J., Kim, W. K., Chang, Y., Polym. Int. (2003), **52**(8), 1359–1364.
94. Gatos, K. G., Thomann, R., Karger-Kocsis, J., Polym. Int. (2004), **53**, 1191–1197.
95. Usuki, A., Tukigase, A., Kato, M, Polymer (2002), **43**(8), 2185–2189.
96. Zheng, H., Peng, A., Zhang, Y., Zhang, Y., Hecheng Xiangjiao Gongye (2002), **25**(5), 317.
97. Zheng, H., Zhang, Y., Zhang, Y., Peng, Z., Hecheng Xiangjiao Gongye (2003), **26**(2), 115.
98. Zheng, H., Peng, Z., Zhang, Y., Zhang, Y., Lin, H., Tanxingti (2002), **12**(6), 14–18.
99. Zheng, H., Zhang, Y., Peng, A., Zhang, Y., Lin, H., Hecheng Xiangjiao Gongye (2003), **26**(4), 226–229.

100. Zheng, H., Zhang, Y., Peng, A., Zhang, Y., Polym. Test. (2004), **23**(2), 217–223.
101. Zheng, H., Zhang, Y., Peng, Z., Zhang, Y., Li, P., Tanxingti (2003), **13**(4), 1–5.
102. Zheng, H., Zhang, Y., Peng, Z., Zhang, Y., J. Appl. Polym. Sci. (2004), **92**(1), 638–646.
103. Zheng, H., Zhang, Y., Peng, Z., Zhang, Y., Polym. Polym. Compos. (2004), **12**(3), 197–206.
104. Zheng, H., Zhang, Y., Peng, Z., Zhang, Y., Lin, H., Gaofenzi Xuebao (2004), (2), 160–164.
105. Zheng, H., Zhang, Y., Cheng, G., Li, P., Hecheng Xiangjiao Gongye (2004), **27**(3), 157–160.

CHAPTER 34

Polyhedral Oligomeric Silsesquioxane (POSS)

Guirong Pan

Department of Chemical and Materials Engineering, The University of Cincinnati, Cincinnati, OH 45221-0012

34.1 DEFINITION, HISTORY AND SYNTHESIS

The Polyhedral Oligomeric Silsesquioxanes (POSS) are an interesting class of three-dimensional inorganic/organic hybrids with the generic formula of $(RSiO_{3/2})_n$, as shown in Fig. 34.1 [1–4]. These molecules contain an inner inorganic framework covered by inert and/or reactive organic substituents. POSS molecules with well-defined shapes and sizes ranging from 1–3 nm have been described as the smallest version of colloidal silica. The R's can be inert organic groups used to enhance miscibility with polymeric host materials [5,6]. Making one or more of the R groups reactive permits bonding of the cages to polymers by copolymerization [7] or grafting [8] onto backbone chain. Incorporating such POSS cages into polymeric materials has already provided useful property enhancements, such as increased glass transition temperature, decomposition temperature, and mechanical strength. Because of the tailorability of POSS molecules, they can also be designed to probe the molecular basis of reinforcement, and to establish structure–property relationships that can then be exploited to optimize properties for particular applications. These POSS reagents have a number of desirable physical properties. For example, they are soluble in common organic solvents such as tetrahydrofuran (THF), toluene, chloroform, and hexane [9,10].

POSS was discovered in 1946 by Scott [11]. After 1990 the field developed rapidly due to the work of two groups: the Feher group at the University of California-Irvine and the Lichtenhan group at the Air Force Research Laboratory. The Feher group devised many methods for synthesizing and chemically modifying structurally well-defined Si/O frameworks [3,4,12–29]. The Lichtenhan group, on the other hand, pioneered the use of discrete POSS in polymer-related applications [7,9,30–32].

The synthesis of fully condensed POSS frameworks starts with the controlled hydrolysis and condensation of trifunctional organosilicon monomers (i.e., $RSiX_3$, R = c-C_6H_{11}, Cy or c-C_5H_9, *C*p) [13,16,33]. The functionalization of the POSS framework is then easily accomplished by corner capping of the POSS-trisilanols with silane coupling agents containing organic groups suitable for polymerization [1,13,16]. This methodology provides access to a family of cycloalkyl-substituted POSS monomers, each containing one polymerizable group, as shown in Fig. 34.2 [1]. In cases where the appropriate functionality is not directly available by the corner capping sequence, subsequent functional group transformation of the reactive group on a unique silicon atom is possible [1]. Multifunctional POSS derivatives can be made by the condensation of $R'Si(OEt)_3$, as described above, where R′ is a reactive group [2,34]. Another approach involves functionalizing POSS cages that have been formed [35–37].

The detailed methods of POSS synthesis have been reviewed by Voronkov *et al*. in 1982 [2] and Feher and co-workers in 2000 [28]. It is now possible to prepare range of useful Si/O frameworks from relatively inexpensive feedstocks. A variety of POSS reagents with one or more covalently bonded reactive functionalities has become commercially available from the Hybrid Plastics Company (http://www.hybridplastics.com).

34.2 NANOREINFORCED POSS-BASED POLYMER AND COPOLYMERS

Because of its chemical nature, POSS is easily incorporated into common plastics via copolymerization or blending, requiring little or no alteration to existing manufacturing processes. Incorporation of POSS reagents into

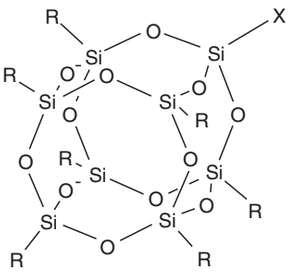

FIGURE 34.1. Schematic structure of POSS(R = c-C_6H_{11} (Cy), c-C_5H_9(Cp); X = reactive group).

linear thermoplastics or thermoset networks can be used to modify composition, local structure, and chain mobility. These modifications can ultimately affect the thermal, oxidative, and dimensional stability of many polymeric resins, resulting in improvements in properties, including increased glass-transition temperature, decomposition temperature and modulus, reduced flammability, and increased gas permeability. Depending on the number of POSS functional groups, different architectures of POSS/polymer composite can be obtained, as shown in Fig. 34.3.

A variety of POSS-containing polymer and copolymers have been synthesized based on radical [7], conventional [7,30], and atom-transfer [38], condensation [9,39] and ring-opening metathesis polymerization (ROMP) [40,41] techniques. Copolymers obtained in this manner with POSS units attached as dangling blocks to the polymer backbone include copolymers of polysiloxane [9,42], poly(methyl methacrylate) [30,32,38], poly(4-methylstyrene) [7,43–45], epoxy [39,46], polynorbornene [47–49], and polyurethane [50,51], *et al*. Monofunctional and difunctional POSS is commonly used in this case. The resulting materials represent a new category of polymers characterized by the presence of bulky POSS nanoparticles. There are some very useful review papers available on this subject [52,53].

Here, we will use POSS-styrene system as paradigm to explain the synthesis and properties of POSS-containing polymers and copolymers. Other systems are listed in Table 34.1, along with references. POSS-styrene polymers and copolymers with 4-methylstyrene have been extensively studied by Haddad *et al*. [7,44]. The reaction scheme is shown in Fig. 34.4.

The glass transition temperature T_g of poly(*co*-POSS-4-methylstyrene) varies linearly with mole percent POSS in the copolymer, from 116 °C for pure poly(4-methylstyrene) to approximately 400 °C for pure polyPOSS-substituted styrene. The decomposition temperature of the styryl backbone dramatically increases, presumably because the large pendant POSS groups reduce chain mobility. POSS modification also effects dynamical mechanical properties [43]. By varying the R groups on the POSS cages, the DMTA spectra show an increase in tan δ with R = Cy>Cp (Cy:cyclohexyl, Cp:cyclopentyl) and a plasticization effect when R = *i*-Bu. This result supports the conclusion that R groups on the POSS cages result in significant changes of bulk mechanical properties [48]. Coughlin *et al*. are studying hemi-telechelic POSS-polystyrene and are investigating

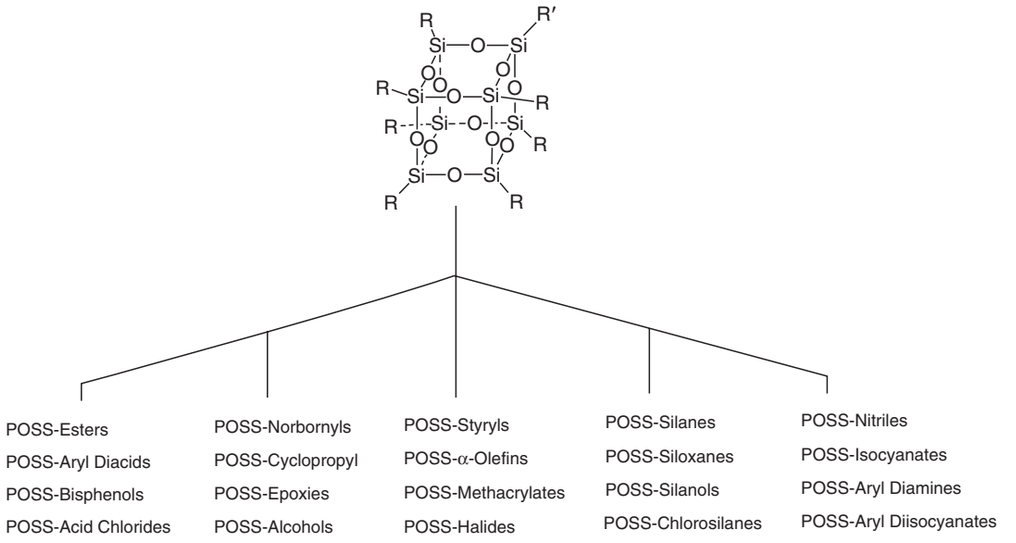

FIGURE 34.2. Some of the functionalities that can be prepared from POSS–trisilanol precursors [1]. (Applied Organometallic Chemistry, 12, Schwab, J. J. and Lichtenhan, J. D., "Polyhedral Oligomeric Silsesquioxane (POSS)-based Polymers," pp. 707–713, Copyright (1998), John Wiley and Sons Ltd., New York. Reproduced with permission.)

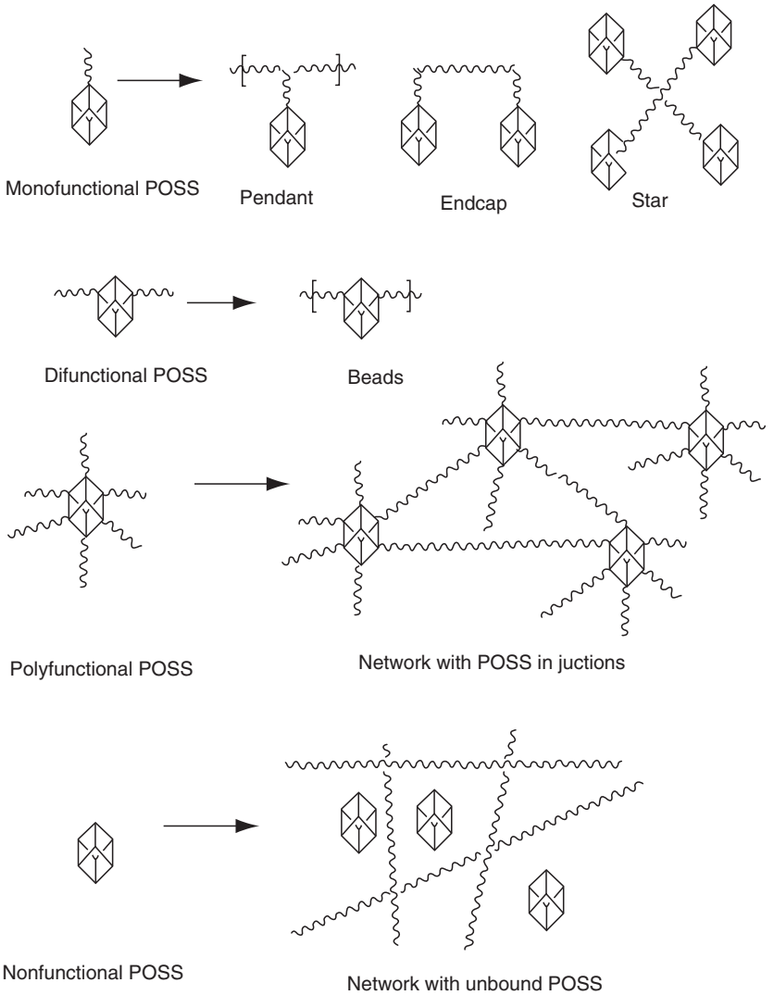

FIGURE 34.3. POSS/polymer architectures.

whether POSS moieties within a polymer matrix organize into lamellae, cylinders, or other hierarchical structures. Their visualization matches their TEM data, displaying the ''raft-like'' or lamellae structure of POSS within the polymer matrix (Fig. 34.5) [54,55].

Incorporation of multifunctional POSS into polymer systems has been investigated with different polymers [6,62–66]. In these cases, single-phase polymer networks with POSS molecularly dispersed are often formed. POSS acts as a polyhedral cross-link. But no definite effect of POSS on network properties has been established. Both a decrease [64,65] and no change in T_g [6] were reported. The rubbery modulus increases due to a high crosslink density, and thermal stability increases with POSS content.

A more convenient method of incorporating POSS into organic polymers is physical blending. Since each POSS molecule has a Si_8O_{12} core covered with alterable organic side groups, it is believed that better dispersion may result from increased interaction of compatible side groups and polymer [67–69]. Blanski *et al*. [69] studied the dispersion of POSS in polystyrene. They found that by altering the organic side groups to more compatible phenethyl groups, POSS molecules can be fully dispersed into high molecular weight polystyrene. The surface hardness of the styrenyl POSS/polystyrene film increased 30%. Molecularly dispersed POSS behave as a weak cross-linker in polymer melts and accelerate the crystallization rate of the host polymer [70]. Matejka *et al*. [64,65] studied the effect of POSS with various topological locations in a network on its structure and properties. These authors incorporated monofunctional, multifunctional, and nonfunctional POSS into epoxy networks and observe that that POSS pendant on a network chain showed a strong tendency toward aggregation and crystallization. The crystalline domains thus act as physical cross-links, leading to very strong reinforcement. The mechanical

TABLE 34.1. *POSS-contained polymer and copolymer systems.*

System	Components	Architecture	Property	References
POSS–Polystyrene	Styryl-POSS-*co*-4-methylstyrene	Pendants	T_g increases; T_d increases	[7,43–45]
POSS–Polynorbornene	Norbornyl-POSS; norbornene	Pendants	T_g increase; no effect on T_d; shape memory behavior	[47–49]
POSS–Epoxy	Epoxy–POSS; diglycidyl ether of bisphenol A	Pendants	T_g increases and broadens; the shape of viscoelastic spectrum not affected; slowing down of the chain relaxation in the glassy state	[39,46]
Siloxane–POSS	Hybrid–POSS; vinyl substituted dichlorosilanes	Beads, pendants	Thermal stability increased	[9,42]
POSS–Polyethelene	Vinyl–POSS; ethylene	Pendants	T_m decreases; thermostability increases; oxidative resistance increases	[57]
	Norbornyl–POSS	Pendants	Oxidative resistance increases; lamellae structure of POSS in polymer	[40,54,55,58,59]
Polyurethane–POSS	Hydrido–POSS; polytetramethylene glycol(PTMG); 4,4′-methyle nebis(phenylisocyanate) (MDI)	Pendants	Formation of POSS crystals	[50,51]
Acrylate–POSS	Methacrylate–POSS; *n*-butyl acrylate	Pendants, star, endcap	Effect of R on solubility; thermostability increase; T_d, T_g increase; oxygen permeability increases	[30,32,38]
Polyimide–POSS	Diamine–POSS with pyromellitic dianhydride	Pendants	Self assembly; lower dielectric constant	[60,61]

properties are affected mainly by POSS–POSS interactions while the POSS-network chain interactions are of minor importance.

34.3 POSS AS BUILDING BLOCKS FOR CONTROLLED STRUCTURED MATERIALS

Since a POSS molecule has both defined structure and specific functional groups, it provides the possibility of preparing nanocomposites with controlled structures. There has been considerable effort using POSS cages as building blocks to make controlled structure materials.

Laine *et al*. [35–37,71–78] have developed several routes to link POSS cubes by chemical reactions that lead to organic tethers (spacers) between the cages or cubes with the objective of determining whether well-defined composite nanostructure and periodically placed organic/inorganic components will offer novel and predictable properties. To date, macromonomers based on cubes functionalized with methacrylate [35,36], epoxide [76,77], alcohol [79], and aliphatic amine [78] groups have been generated and nanocomposites have been made from these octafunctional POSS molecules. Figure 34.6 illustrates the formation of nanocomposites from octafunctional POSS. Studies based on these materials suggested that nanocomposite with essentially completely defined inorganic and organic phase can be produced.

A large amount of work involves cages with vinyl and Si–H groups as links by hydrosilylation reactions [36,72,74,80–83]. Catalytic hydrosilylation is a well-studied method of forming Si–C linkages by adding Si–H moieties to C–C multiple bonds. The commonly used monomers are ${}^{R}T_8$ cages (R:H or Vinyl; T: $RSiO_{3/2}$) or ${}^{R}M_8Q_8$ (R:H or Vinyl; M: $R_3SiO_{1/2}$; Q: $SiO_{4/2}$). The chemical structures of those cages are shown in Fig. 34.7. Network structure as shown in Fig. 34.8 is formed from reactions combing these cages.

The Hoebbel and Hasegawa [80,82] research groups find that more than 60% and more commonly above 80% of the functionality Si–H and Si–Vinyl were consumed to make

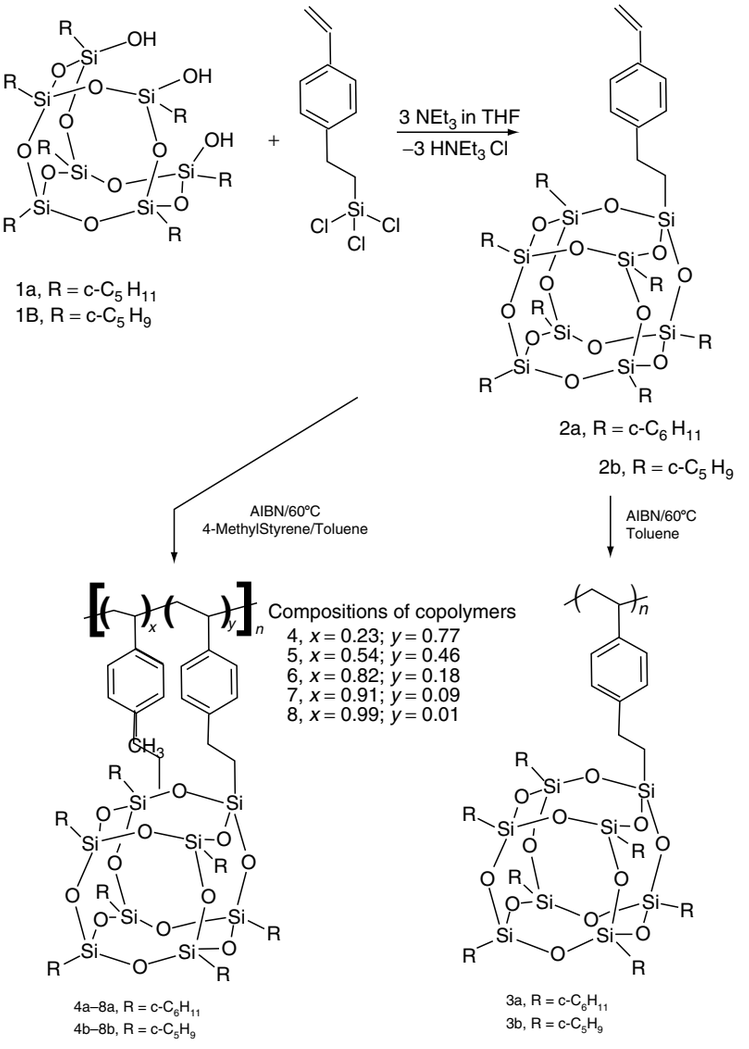

FIGURE 34.4. Styryl-POSS macromonomer synthesis and its polymerization and copolymerization [7]. Reprinted with permission from Macromolecules, 29(22), 7302–7304. Copyright (1996) American Chemical Society.

silethylene linkages by the hydrosilylation. With this type of conversion efficiency it is not surprising that none of the materials are soluble, since nearly all of the precursors are octafunctional.

Laine *et al*. [36,72,74] published a study that described both the synthesis and characterization of gels made by combining the ^{H}M8Q8, ^{V}iM8Q8, ^{H}T8, and^{Vi}T8. All of the materials were found to be a combination of micro- and mesoporous with specific surface areas between 380 and 530 m^2/g. Intercube pore size and size distribution are dominated by tether length and defects (missing cubes).

Some approaches have also been developed to make soluble controlled structure materials with T8 and M8Q8 cages by changing the stoichiometry of the reaction and limiting the extent of crosslinking [81,84,85].

Epoxy-based POSS nanocomposites have also been studied thoroughly by various groups [6,76–78,86]. In these systems, either POSS with an octaglycidyl group was connected by diaminodiphenyl methane (DDM), or POSS with an octaamino group is connected by diglycidyl ether of bisphenol A(DGEBA). The nanoarchitecture was tailored by changing the ratio between amine group and the epoxy group. Results suggest that the structure and rigidity of the organic tethers connecting the cubes strongly mediated thermal stabilities, glass transition temperatures, and consequently global mechanical properties. Aromatic tether structure and short lengths increased the char yields and decomposition temperature.

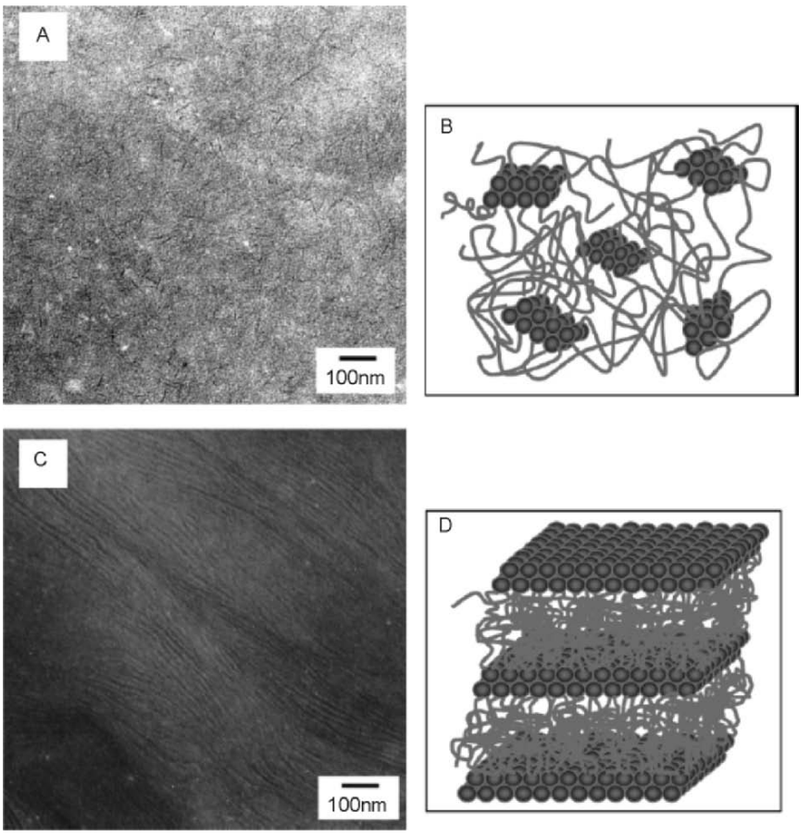

FIGURE 34.5. (A) TEM of PBD-POSS-1(10% POSS). The copolymers of low POSS concentration aggregate into short randomly oriented lamellae with lateral dimensions of approximately 50 nm. (B) Schematic drawing of PBD-POSS assembly at low POSS concentration. (C) TEM of PBD-POSS-4 (40% POSS). The copolymers of high POSS concentration form continuous lamellar morphologies with lateral lengths on the order of microns. (D) Schematic drawing of PBD-POSS assembly at high POSS concentration [56]. Reprinted with permission from Macromolecules 2004, 37(23), 8606–8611. Copyright 2004, American Chemical Society.

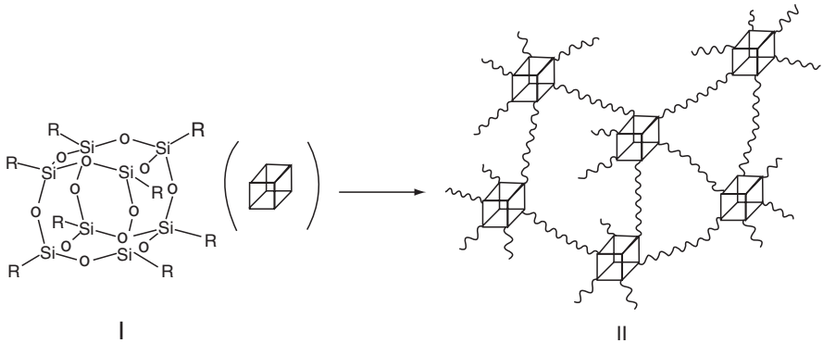

FIGURE 34.6. Nanocomposite formation (II) from octafunctional POSS (I) Via cross-linking of functional groups R [78]. Reprinted with permission from Macromolecules 2004, 37(1): 99–109. Copyright 2004, American Chemical Society.

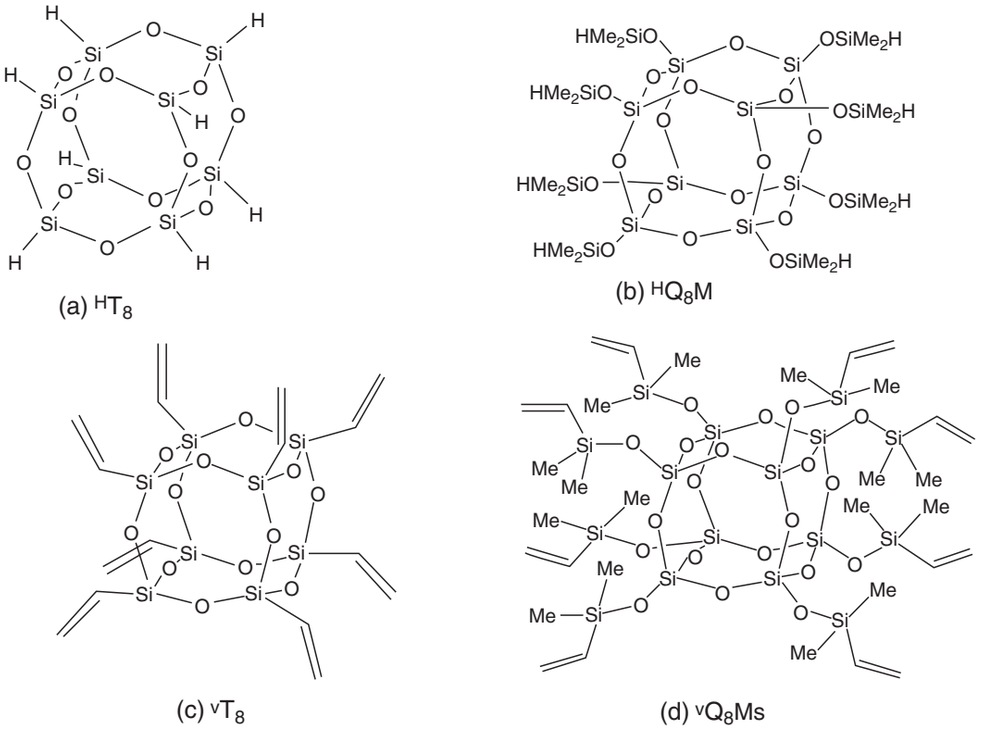

FIGURE 34.7. Hydrido (a–b) and vinyl cubes (c–d).

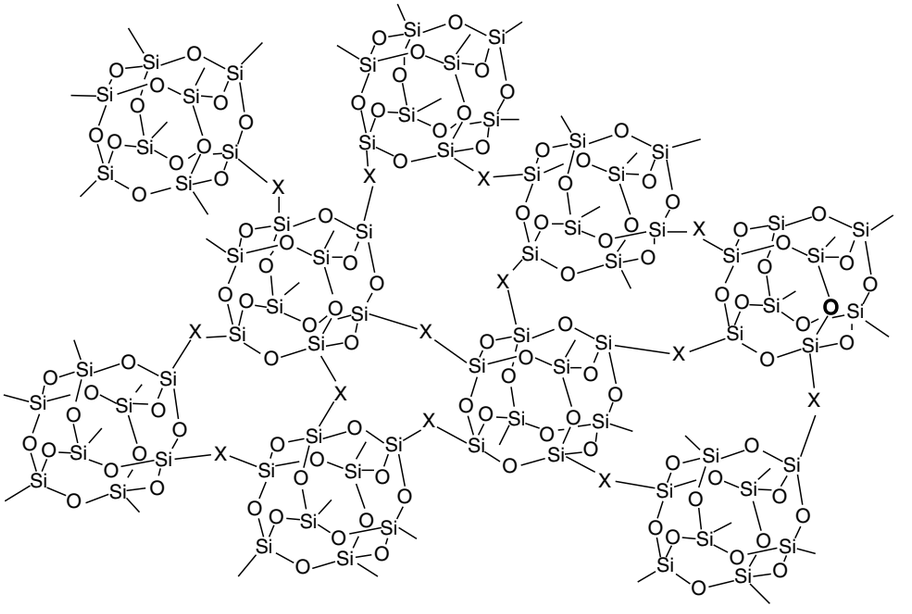

X = $–CH_2–CH_2$ (a+c);

$–O–Si(CH_3)_2–CH_2–CH_2$ (a+b or c+d);

$–O–Si(CH_3)_2–CH_2–CH_2–Si(CH_3)_2–O$ (b+d)

FIGURE 34.8. Network structures formed by combining hydrido (a–b) and vinyl cubes (c–d) [72]. Reprinted with permission from Journal of the American Chemical Society 1998, 120(33): 8380–8391. Copyright 1998, American Chemical Society.

REFERENCES

1. Schwab, J. J.; Lichtenhan, J. D. *Appl. Organometal. Chem.* **1998**, *12*, 707.
2. Voronkov, M. G.; Lavrent'ev, V. *Top. Curr. Chem.* **1982**, *102*, 199–236.
3. Feher, F. J.; Budzichowski, T. A. *J. Organometal. Chem.* **1989**, *379*, 33–40.
4. Feher, F. J.; Budzichowski, T. A. *J. Organometal. Chem.* **1989**, *373*, 153–163.
5. Lichtenhan, J. D.; Noel, C. J.; Bolf, A. G.; Ruth, P. N. In *Mat. Res. Soc. Symp. Proc.*, **1996**; *435*, 3.
6. Li, G. Z.; Wang, L. C.; Toghiani, H.; Daulton, T. L.; Koyama, K.; Pittman, C. U. *Macromolecules* **2001**, *34*, 8686–8693.
7. Haddad, T. S.; Lichtenhan, J. D. *Macromolecules* **1996**, *29*, 7302.
8. Chun, S. B.; Mather, P. T. In *Mat. Res. Soc. Symp. Proc.*, 2001; Vol. 661, p KK10.18.11.
9. Lichtenhan, J. D.; Vu, N. Q.; Carter, J. A. *Macromolecules* **1993**, *26*, 2141.
10. Schwab, J. J.; Reinerth Sr., W. A.; Lichtenhan, J. D. *Polymer Preprints* **2001**, *42*, 48.
11. Scott, D. W. *J. Am. Chem. Soc.* **1946**, *68*, 356.
12. Feher, F. J.; Budzichowski, T. A.; Weller, K. J. *J. Am. Chem. Soc.* **1989**, *111*, 7288–7289.
13. Feher, F. J.; Newman, D. A.; Walzer, J. F. *J. Am. Chem. Soc.* **1989**, *111*, 1741–1748.
14. Feher, F. J.; Blanski, R. L. *J. Chem. Soc.-Chem. Commun.* **1990**, 1614–1616.
15. Feher, F. J.; Newman, D. A. *J. Am. Chem. Soc.* **1990**, *112*, 1931–1936.
16. Feher, F. J.; Budzichowski, T. A.; Blanski, R. L.; Weller, K. J. *Organometallics* **1991**, *10*, 2526.
17. Feher, F. J.; Phillips, S. H.; Ziller, J. W. *J. Am. Chem. Soc.* **1997**, *119*, 3397–3398.
18. Feher, F. J.; Wyndham, K. D.; Knauer, D. J. *Chem. Commun.* **1998**, 2393–2394.
19. Feher, F. J.; Soulivong, D.; Nguyen, F.; Ziller, J. W. *Angew. Chem.-Int. Edit.* **1998**, *37*, 2663–2666.
20. Feher, F. J.; Wyndham, K. D.; Scialdone, M. A.; Hamuro, Y. *Chem. Commun.* **1998**, 1469–1470.
21. Feher, F. J.; Soulivong, D.; Nguyen, F. *Chem. Commun.* **1998**, 1279–1280.
22. Feher, F. J.; Wyndham, K. D. *Chem. Commun.* **1998**, 323–324.
23. Feher, F. J.; Soulivong, D.; Eklund, A. G. *Chem. Commun.* **1998**, 399–400.
24. Feher, F. J.; Terroba, R.; Ziller, J. W. *Chem. Commun.* **1999**, 2309–2310.
25. Feher, F. J.; Terroba, R.; Ziller, J. W. *Chem. Commun.* **1999**, 2153–2154.
26. Feher, F. J.; Nguyen, F.; Soulivong, D.; Ziller, J. W. *Chem. Commun.* **1999**, 1705–1706.
27. Feher, F. J.; Wyndham, K. D.; Soulivong, D.; Nguyen, F. *J. Chem. Soc.-Dalton Trans.* **1999**, 1491–1497.
28. Feher, F. J.; Terroba, R.; Jin, R.; Wyndham, K. D.; Lucke, S. *Polym. Mater. Sci. Eng.* **2000**, *82*, 301.
29. Bakhtiar, R.; Feher, F. J. *Rapid Commun. Mass Spectrom.* **1999**, *13*, 687–694.
30. Lichtenhan, J. D.; Otonari, Y. A.; Carr, M. J. *Macromolecules* **1995**, *28*, 8435.
31. Lichtenhan, J. D. *Comments Inorg. Chem.* **1995**, *17*, 115.
32. Lichtenhan, J. D.; Noel, C. J.; Bolf, A. G.; Ruth, P. N. *Mat. Res. Soc. Symp. Proc.* **1996**, *435*, 3.
33. Brown, J. F.; Vogt, L. H. *J. Am. Chem. Soc.* **1965**, *87*, 4313.
34. Frye, C. L.; Collins, W. T. *J. Am. Chem. Soc.* **1970**, *92*, 5586.
35. Sellinger, A.; Laine, R. M. *Chem. Mater.* **1996**, *8*, 1592.
36. Sellinger, A.; Laine, R. M. *Macromolecules* **1996**, *29*, 2327.
37. Zhang, C.; Laine, R. M. *J. Am. Chem. Soc.* **2000**, *122*, 6979.
38. Pyun, J.; Matyjaszewski, K. *Macromolecules* **2000**, *33*, 217.
39. Lee, A.; Lichtenhan, J. D. *Macromolecules* **1998**, *31*, 4970–4974.
40. Zheng, L.; Farris, R. J.; Coughlin, E. B. *J. Polym. Sci. Pt. B-Polym. Phys.* **2001**, *39*, 2920.
41. Haddad, T. S.; Mather, P. T.; Jeon, H. G.; Chun, S. B.; Phillips, S. H. In *Mat. Res. Soc. Symp. Proc.*, 2000; Vol. 628.
42. Manze, R. A.; Jones, P. F.; Chaffee, K. P.; Lichtenhan, J. D. *Chem. Mater.* **1996**, *8*, 1250.
43. Haddad, T. S.; Viers, B. D.; Phillips, S. H. *J Inorg Organomet Polym* **2002**, *11*, 155.
44. Romo-Uribe, A.; Mather, P. T.; Haddad, T. S.; Lichtenhan, J. D. *J. Polym. Sci. Pt. B-Polym. Phys.* **1998**, *36*, 1857–1872.
45. Xu, H. Y.; Kuo, S. W.; Lee, J. S.; Chang, F. C. *Macromolecules* **2002**, *35*, 8788–8793.
46. Lee, A.; Lichtenhan, J. D.; Reinerth Sr., W. A. *Polym. Mater. Sci. Eng.* **2000**, *82*, 235.
47. Mather, P. T.; Jeon, H. G.; Romo-Uribe, A.; Haddad, T. S.; Lichtenhan, J. D. *Macromolecules* **1999**, *32*, 1194–1203.
48. Jeon, H. G.; Mather, P. T.; Haddad, T. S. *Polym. Inter.* **2000**, *49*, 453.
49. Bharadwaj, B. K.; Berry, R. J.; Farmer, B. L. *Polymer* **2000**, *41*, 7209.
50. Fu, B. X.; Hsiao, B. S.; White, H. *Polym. Inter.* **2000**, *49*, 437.
51. Fu, B. X.; Hsiao, B.; Pagola, S.; Stephens, P. *Polymer* **2001**, *42*, 599.
52. Li, G. Z.; Wang, L. C.; Ni, H.; Pittman Jr., C. U. *J. Inorg. Organometal. Polym.* **2001**, *11*, 123.
53. Phillips, S. H.; Haddad, T. S.; Tomczak, S. J. *Curr. Opin. Solid State Mater. Sci.* **2004**, *8*, 21.
54. Zheng, L.; Hong, S.; Cardoen, G.; Burgaz, E.; Gido, S. P.; Coughlin, E. B. *Macromolecules* **2004**, *37*, 8606–8611.
55. Zheng, L.; Waddon, A. J.; Farris, R. J.; Coughlin, E. B. *Macromolecules* **2002**, *35*, 2375–2379.
56. Zhang, H. J.; Kulkarni, S.; Wunder, S. *Abstr. Pap. Am. Chem. Soc.* **2004**, *228*, 281.
57. Tsuchida, A.; Bolln, C.; Sernetz, F. G.; Frey, H. *Macromolecules* **1997**, *30*, 2818.
58. Zheng, L.; Farris, R. J.; Coughlin, E. B. *Polym. Prepr.* **2000**, *41*, 1929.
59. Zheng, L.; Farris, R. J.; Coughlin, E. B. *Macromolecules* **2001**, *34*, 8034–8039.
60. Leu, C. M.; Chang, Y. T.; Wei, K. H. *Chem. Mater.* **2003**, *15*, 3721.
61. Leu, C. M.; Chang, Y. T.; Wei, K. H. *Macromolecules* **2003**, *36*, 9122–9127.
62. Li, G. Z.; Wang, L.; Toghiani, H.; Pittman Jr., C. U. *Polymer* **2002**, *43*, 4167.
63. Li, G. Z.; Cho, H.; Wang, L. C.; Toghiani, H.; Pittman, C. U. *J. Polym. Sci. Pol. Chem.* **2005**, *43*, 355–372.
64. Matejka, L.; Strachota, A.; Plestil, J.; Whelan, P.; Steinhart, M.; Slouf, M. *Macromolecules* **2004**, *37*, 9449–9456.
65. Strachota, A.; Kroutilova, I.; Kovarova, J.; Matejka, L. *Macromolecules* **2004**, *37*, 9457–9464.
66. Lee, Y. J.; Huang, J. M.; Kuo, S. W.; Lu, J. S.; Chang, F. C. *Polymer* **2005**, *46*, 173–181.
67. Kim, K. M.; Adachi, K.; Chujo, Y. *Polymer* **2002**, *43*, 1171.
68. Yoon, K. H.; Polk, M. B.; Park, J. H.; Min, B. G.; Schiraldi, D. A. *Polym. Inter.* **2005**, *54*, 47.
69. Blanski, R. L.; Phillips, S. H.; Chaffee, K.; Lichtenhan, J. D. In *Mat. Res. Soc. Sym. Proc.*, 2000; Vol. 628.
70. Fu, B. X.; Yang, L.; Somani, R. H.; Zong, S. X.; Hsiao, B. *J. Polym. Sci. Pt. B-Polym. Phys.* **2001**, *39*, 2727.
71. Zhang, C.; Laine, R. M. *J. Organomet. Chem.* **1996**, *521*, 199.
72. Zhang, C. X.; Babonneau, F.; Bonhomme, C.; Laine, R. M. *J. Am. Chem. Soc.* **1998**, *120*, 8380.
73. Tamaki, R.; Tanaka, Y.; Asuncion, M. Z.; Choi, J. W.; Laine, R. M. *J. Am. Chem. Soc.* **2001**, *123*, 12416–12417.
74. Laine, R. M.; Zhang, C.; Sellinger, A.; Viculis, L. *Appl. Organomet. Chem.* **1998**, *12*, 715.
75. Laine, R. M.; Choi, J.; Lee, I. *Adv. Mater.* **2001**, *13*, 800.
76. Choi, J.; Harcup, J.; Yee, A. F.; Zhu, Q.; Laine, R. M. *J. Am. Chem. Soc.* **2001**, *123*, 11420–11430.
77. Choi, J.; Yee, A. F.; Laine, R. M. *Macromolecules* **2003**, *36*, 5666–5682.
78. Choi, J.; Kim, S. G.; Laine, R. M. *Macromolecules* **2004**, *37*, 99–109.
79. Costa, R. O. R.; Vasconcelos, W. L.; Tamaki, R.; Laine, R. M. *Macromolecules* **2001**, *34*, 5398–5407.
80. Hoebbel, D.; Endres, K.; Reinert, T.; Pitsch, I. *J. Non-Cryst. Solids* **1994**, *176*, 179.
81. Auner, N.; Bats, J. W.; Katsoulis, D. E.; Suto, M. *Chem. Mater.* **2000**, *12*, 3402.
82. Hasegawa, I. *J. Sol-Gel Sci. Technol.* **1995**, *5*, 93–100.
83. Pan, G.; Mark, J. E.; Schaefer, D. W. *J. Polym. Sci. Pt. B-Polym. Phys.* **2002**, *41*, 3314.
84. Hoebbel, D.; Pitsch, I.; Heldemann, D.; Jancke, H. *Z. Anorg. Allg. Chem.* **1990**, *583*, 133.
85. Tebeneva, N. G.; Rebrov, E. A.; Muzafarov, A. M. *Polym. Prepr.* **1998**, *39*, 503.
86. Kim, G. M.; Qin, H.; Fang, X.; Sun, F. C.; Mather, P. T. *J. Polym. Sci. Pt. B-Polym. Phys.* **2003**, *41*, 3299–3313.

CHAPTER 35

Carbon Nanotube Polymer Composites: Recent Developments in Mechanical Properties

M.C. Weisenberger, R. Andrews, and T. Rantell

University of Kentucky Center for Applied Energy Research
2540 Research Park Dr. Lexington, KY 40511

35.1 INTRODUCTION

Over the last decade, carbon nanotubes [1] have been the subject of intense investigation in both fundamental and applied sciences [2]. With single crystal graphite and fullerenes as a starting point, great strides have been made in understanding the properties of these materials at the nanoscale:the nature by which they transport electrons [3,4], and heat [5,6], and how they respond to applied forces and fields [7,8]. Results of these computations and experiments have demonstrated their truly remarkable properties, and have placed carbon nanotubes (CNTs) at the forefront of nanotechnology development. It is their unique and desirable properties at the nanoscale that serve as the basis and motivation for endeavors to create new advanced materials based on carbon nanotubes. For example, the use of CNTs as nanoscale reinforcing fibers in polymer matrices is an idea that is profoundly motivated by their mechanical properties. In concept, this is the nanoscale analogue to conventional carbon fiber composites, offering exciting possibilities for materials design given that CNTs have been measured to be more than 15 times stronger than the best available carbon fiber, have elastic moduli of single crystal graphite, and yet remain extremely flexible with aspect ratios of greater than 1,000 (Table 35.1). However, realizing the unique mechanical properties of CNTs in macroscale composites has proven to be a more complex issue. It is a multifaceted problem in which a number of competing factors must be considered, including: CNT diameter, length, crystalline defects, orientation, concentration, and dispersion; interfacial adhesion; composite processing method; matrix material; as well as their inter-relationships, in order to begin to optimize the final composite properties. The purpose of this paper is to discuss these issues within the scope of the recent literature, and to highlight advances and understanding in this emerging field.

35.1.1 Carbon Nanotubes:Properties and Types

The structure and properties of CNTs can be approached in many ways. Chemists and physicists may prefer to think of CNTs as linearly extended fullerenes. In fact, the most ideal carbon nanotube, a perfect, isolated single wall carbon nanotube (SWNT) is exactly that. But CNTs, in general, are not so simple, and tend to form in a range of morphologies from bundles of SWNTs [9], mats of multiwall nanotubes (MWNT) [10], to nonfullerene morphologies approaching vapor grown carbon fibers [11]. To those interested in composites, CNTs are essentially ultrafine carbon fibers capable of elastically withstanding unprecedented stresses and strains. Concurrently, they present new challenges in translating these properties to a practical length scale in a composite. Many technical hurdles exist; not the least of which is

TABLE 35.1. *On-axis mechanical properties of CNTs and graphitic materials.*

Material type	Young's modulus (GPa)		Break stress (GPa)		Strain to failure (%)	
SWNT	1,250 $\pm$ 400	[18]	$\sim$100	[20]	10–15	[21]
	$\sim$1,000	[19]				
SWNT Bundle	1,250	[22]	$>45 \pm 7$	[22]	1–6	[22]
MWNT	1,800 $\pm$ 900	[23]	11–63	[13]	5–12	[13,24,25]
	270–950	[13]	150	[24]		
	910	[24]				
Carbon Nanofiber	$\sim$100	[26]	2.7	[27]	$\sim$ 1	[27]
	400	[27]				
Graphite Whisker	700–1,000	[28]	19.6	[28]	$\sim$2	[28]
High strength Carbon fiber	220–580	[29,30]	4.3–6.4	[29,30]	1.5–2.2	[29,30]
High modulus Carbon fiber	520–827	[11]	1.9–3.3	[11]	0.3–0.6	[11]

The high strain to failure of nanotubes allows for very high break strengths.
Selected experimental mechanical testing methods reported for CNTs:[23] In situ TEM imaging of thermal vibrations of cantilevered MWNTs, [18] In situ TEM imaging of thermal vibrations of cantilevered SWNTs, [24] In situ TEM tensile testing of MWNTs, [13] In situ SEM tensile testing of MWNTs.

separating or dispersing the CNTs such that they can be individually loaded in a composite. SWNTs tend to form into bundles or ropes due to van der Waals forces, making them difficult to individually disperse into matrices [12]. Multiwall carbon nanotubes, or concentrically nested SWNTs, can be easier to disperse, but tensile stress transfer to inner walls is thought to be inefficient due to weak intershell bonding [13,14]. However it has been shown that some stress can transfer to the inner shells via fusion, or bond reforming, of a fractured outer shell to an adjacent inner shell [15].

CNTs are synthesized by various methods including electric arc discharge [1], laser ablation [16], and chemical vapor deposition [1,7,10,17], each yielding nanotubes with various characteristics such as diameter, defect density, entanglement and length. Just as using different carbon fibers yields different composite properties, using different CNT types results in varying CNT composite properties. Recent experiments have investigated the effect of the CNT type in composites for mechanical reinforcement (the results of which will be highlighted in the properties section). Typical mechanical properties of various CNT types are listed in Table 35.1. It must be acknowledged that CNTs, like oriented graphite, are very anisotropic materials. Their large strengths and elastic moduli relate only to the direction parallel to the axis of the nanotube.

35.2 NANOTUBE-POLYMER COMPOSITE PROCESSING

35.2.1 Dispersing Carbon Nanotubes

The most commonly studied matrices for CNT-reinforced composites are polymers. Fabricating composites of CNTs in polymer matrices almost invariably involves a dispersion process in which the nanotubes are incorporated into the polymer. Although the small size of CNTs precludes some conventional fiber composite fabrication techniques such as filament winding or hand lay-up, it does enable techniques such as composite fiber spinning, (discussed later). The goal of dispersion is to homogeneously distribute individual CNTs throughout the matrix material such that the applied load can be uniformly distributed among the nanotube population. For thermoplastic polymers, melt mixing the CNTs via high shear fields is often utilized [31]. In practice, this can be achieved by passing a nanotube/polymer blend though an extruder fitted with mixing screws in order to arrive at the desired level of dispersion [32]. Other methods of melt mixing invariably utilize the shearing forces generated during the mixing of molten polymer to disperse the nanotubes [33]. Nanotubes, however, are known to increase the viscosity of fluids due to their large aspect ratio, high stiffness, and ability to form entangled networks [34–36]. Therefore, achieving high loadings of CNTs in polymer melts is difficult even at high temperatures ($\sim$10–20 wt.% is a common upper limit to uniform dispersion attained with melt mixing [37]). Another method, sonication, uses high frequency sound waves to induce cavitation in low viscosity solvents in the presence of CNT agglomerates. The energy released upon cavity collapse breaks up CNT agglomerates dispersing the nanotubes into the solvent [38,39]. Matrix polymer can then be dissolved into the CNT/solvent dispersion rendering a solvent-processable dispersion. Alternatively, matrix polymer can be introduced by in situ polymerization of miscible liquid monomer in the presence of the CNT dispersion [15]. The viscosity of the final dispersion can be adjusted with both heat and solvent addition/evaporation making higher concentrations of CNTs in the final, solidified polymer possible. Loadings of up to 60 wt.% CNTs have been reported in PVA composite fibers using this method of dispersion [40]. In either case, it has

been shown that the quality of CNT dispersions has a profound impact on the resulting composite properties. Initial property enhancements at low loadings, ~1 wt.% CNTs, often do not continue or are reduced at higher loadings [32,41]. Agglomerates of CNTs can act as a stress concentrating points and reduce the mechanical properties of the matrix [42]. However, once dispersed in polymer melts or solutions, dispersions of CNTs can then be processed into composite parts via conventional polymer processing techniques such as injection molding, film casting, or fiber spinning, from which test specimens can be fashioned, and the composite properties determined.

35.2.2 Factors Influencing CNT Dispersion

The homogeneity of CNT dispersions, either via shear mixing or sonication, is not only a critical factor affecting composite properties, but an important parameter in the quality and stability of composite processing as well. The three most influential factors affecting the quality of the dispersion are the amount of dispersive energy input into system, the degree of entanglement of the bulk CNT material, and the interaction of the CNT surface with the continuous phase. The first factor was investigated by Andrews *et al*. [10] regarding melt mixing MWNTs into various thermoplastics. Dispersion quality was assessed via optical microscopy of relatively large areas of the composites (100 × 100 μm), and the observed homogeneity was correlated to the amount of mechanical energy input by the high shear melt mixer. A minimum value of approximately 1,000 J/ml, was found to effectively disperse a range of MWNT concentrations up to 5.0 vol.%. Higher loadings required higher amounts of mixing energy. A corresponding reduction in MWNT length was found to accompany shear mixing, but CNT aspect ratios of 200+ remained. CNT shortening is an unavoidable result in all dispersive processes, including sonication, given the forces that the CNTs are subjected to, and may in fact serve to enhance the dispersability of the CNTs themselves as their ability to entangle is dependent on their aspect ratio. However, excessive reduction of the CNT length may negatively impact its reinforcing capacity. Kearns and Shambaugh [43] report an optimum sonication time of 2 hr for a nanotube loading of 1wt.%; a compromise between achieving sufficient dispersion and minimizing CNT damage. The use of ultrasonic induced cavitation to disperse CNTs into low viscosity fluids is somewhat dependent on the frequency used. Ultrasonic instruments using a frequency of ~20 kHz have been shown to disperse MWNT mats very well [38]. Higher frequency sonication instruments, such as ultrasonic cleaning baths at ~40 kHz, have also shown to be effective [43]. The efficiency of ultrasonic dispersion depends upon an inverse relationship between frequency and particle size. Thus, it may be advantageous to employ a program of progressively increasing frequency to sequentially reduce bulk agglomerates of CNTs into individual tubes [44]. The degree of CNT entanglement prior to dispersing has been shown to severely limit the homogeneity of dispersion [45]. ''Bird's nest'', or highly entangled CNTs produced from floating catalyst CVD processes or bundles of SWNTs are very difficult to individually disperse by shear or sonication alone. MWNTs grown on substrates in aligned arrays with virtually no entanglement have been shown to be more easily dispersed [45].

35.2.3 Surface Treatment of CNTs

The ability to produce a homogeneous dispersion of CNTs in a polymer matrix or solution can be enhanced by chemically altering the nanotube surface to augment the solvent–nanotube or polymer–nanotube interaction. This may be accomplished by a variety of methods including the use of surfactants, chemical functionalization, and in situ polymerization. Treatment of SWNTs with a nonionic surfactant was shown to enhance the dispersion and resulting mechanical properties of epoxy-matrix composites relative to untreated SWNTs [46]. Other examples of CNT dispersions benefiting from the use of surfactants have been reported [40,47,48]. Oxidative treatments of CNTs have been widely reported as a means to improve dispersion [34,35], including the use of strong oxidizing agents such as nitric/sulfuric acids, $KMnO_4$ [49] and H_2O_2 [50], and by subjection to oxygen plasmas [51]. One of the most popular methods is the sonication of CNTs in a 3:1 solution of sulfuric:nitric acid [34,35,52,53]. Refluxing the acid/CNTs is also employed. The resulting oxygenated groups on the CNT surface, including hydroxyl and carboxylic groups counteract the van der Waals attractive forces between CNTs and enhance interaction with the matrix phase thus improving dispersion. Kim *et al*. [52] report that sonicating MWNTs for 8 hrs in 3:1 sulfuric:nitric acid, resulted in the addition of carboxylic groups at a concentration of approximately 1.3×10^{-3} mol/g. Tethering and wrapping of polymer chains to CNT surfaces by polymerizing monomers in situ with the CNTs has been shown to be effective in improving both dispersion quality and composite properties [15,49,54]. Eitan *et al*. [54] demonstrated evidence of epoxide functionalization of oxidized MWNTs, which can be used to covalently crosslink CNTs into epoxy matrices. Similarly, Valentini *et al*. [55] reported amine functionalized CNTs for crosslinking epoxy matrices. In another report, uniform dispersion and significantly enhanced moduli were observed using PMMA-grafted MWNTs in PMMA matrix composites [15]. Other methods of chemically functionalizing CNTs include the use of diazonium salts [56], radical species [57], photochemistry [58] and others [59,60] to derivitize a wide variety of organo-CNTs.

35.2.4 Processing CNT-Polymer Composite Films

CNT-polymer composites are commonly produced in the form of films for mechanical property analysis. The thicknesses of these films range from a few millimeters to

electron-transparent TEM samples. Once a suitable level of CNT dispersion is achieved in the matrix, films are easily processed by pressing CNT-polymer melts, casting CNT-polymer solutions/thermosets into molds and drying/curing, or spin casting from CNT-polymer solutions. Test specimens of precise dimensions can be cut or machined from these composite films for mechanical testing. Pressing CNT-thermoplastic films is well described in the literature and is a simple method of producing composite specimens [10,42,50,61–63]. Polymer containing dispersed CNTs is typically crushed or pelletized, placed between heated platens, and pressed at a pressure in the range of 10–30 MPa [61,62] such that molten CNT composite polymer flows outward constrained to some predetermined thickness by shims or a mold [10]. Upon solidification, test specimens are then cut from the film. For CNT-polymer solutions and CNT-thermoset matrices, composite films are typically processed utilizing a casting technique. Well-dispersed CNT-polymer fluids are transferred to molds and heated to evaporate the solvent or cure the thermoset [15,20,64–67]. In a similar method, dispersed CNTs in PVA-water solutions are allowed to settle followed by decanting the PVA solution containing well dispersed CNTs. These suspensions are then deposited dropwise onto substrates, and the solvent is evaporated. This process is repeated to build up to the desired thickness of film [12,68–71]. Very thin CNT-polymer composite films (thickness = 200 nm) [72] can be produced by means of spin casting in which suspensions of CNTs in low viscosity polymer solutions are deposited dropwise to the center of a rotating substrate. Spinning for 20–30 sec at 3,000 rpm has been reported to produce electron-transparent films [73]. The centrifugal forces induce radial flow of the drop resulting in thin films with some preferred orientation of the embedded CNTs along the direction of flow. Fabrication of continuous CNT-polymer composite films has been demonstrated by extrusion of CNT composite thermoplastic through a slit die followed by take-up onto a chilled roller [74]. Other techniques include resin infiltration into dry CNT preforms [25,75,76], polymer intercalation of aligned MWNT mats [77,78] and SWNT ''buckypaper'' [79], and complete in situ polymerization of thermoplastic matrices [49,80].

The orientation of the embedded CNTs relative to the loading conditions, as in all fiber composites, has an effect on the properties that are measured. The process of shear-mixing or sonication results in random orientation of the CNTs throughout the polymer matrix, which can be preserved throughout processing given the absence of strong uni-directional shear or elongational flow. For most CNT-polymer film processing, the CNT orientations are randomly arranged relative to the principal axes of the film. Exceptions occur when any degree of stretching or drawing of the film is implemented, which forces embedded CNTs into alignment with the direction of flow [50,64,67,74,81]. This is observed for CNT-polymer melt extrusions through slit dies [74], and injection moldings of carbon nanofiber-polymer composites [76]. Achieving the highest degrees of CNT alignment within a polymer matrix is achieved by spinning dispersions of CNTs in polymer fluids into fibers.

35.2.5 Processing CNT-Polymer Composite Fibers

Homogeneous dispersions of CNTs in viscoelastic polymer fluids can be spun into composite fibers. Melt spun, solution spun, and electro-spun CNT composite fibers have been produced. These methods have been shown to be very effective in aligning the CNTs with the direction of flow, i.e., the fiber axis. This class of oriented CNT composites is of particular interest since direct axial loading of the CNTs is possible. It is in this fashion that high-strength, lightweight CNT composites are envisioned. However, the ability to sustain stable CNT-polymer composite fiber spinning is largely dependent on the homogeneity of the dispersion. CNT agglomerates can disrupt the flow as fiber attenuation is applied leading to breakage during processing, or in the case of large agglomerates, complete blockage of the small diameter orifices through which the fibers are extruded. Achieving large attenuations or draw ratios, which serve to orient both the CNTs and the polymer chains with the fiber axis resulting in increased fiber properties, is primarily dependent on the quality of the initial CNT dispersion.

Melt spinning CNT/thermoplastic composite fibers has been investigated for numerous polymers including poly (methyl methacrylate) [32,33,50], polypropylene [43,82,83], polystyrene [10], polyamide [45], and engineering thermoplastics such as polyimide [31], and poly(ether ether ketone) [26]. In a typical process, the CNTs are dispersed in the molten polymer using a high shear mixer followed by extrusion through a cylindrical die orifice or spinneret. Before the composite fiber cools and solidifies, attenuation is accomplished by continuous collection on a rotating drum. Mechanical testing of the fibers can then be performed using a variety of techniques including single filament tensile testing. CNT composite fibers spun from polymer solutions involve a coagulation process to solidify the fibers in which the solvent is replaced by a second miscible solvent, often water, which acts as a nonsolvent to the polymer causing it to solidify. Complete removal of residual solvent in the fiber is done via a drying process. Reported solution spun CNT composite fibers include poly(vinly alcohol) [40,84,85], poly(acrylonitrile) [38,86] (an important precursor to commercially produced carbon fiber), and poly(*p*-phenylene benzobisoxazole) [87] (PBO). Electro-spun fibers are produced by generating a high voltage between a negatively charged spinning solution and a conductive collector. The advantage of this technique is the production of ultrafine fibers (<100 nm) as very fine jets of polymer are accelerated toward the collector, but unlike melt or solution spinning, the production of continuous filament is difficult. Fibers have been electrospun from dispersions of CNTs in poly(vinly alcohol) [88], poly (acrylonitrile) [89], and poly(vinylidene fluoride) [90].

35.2.6 CNT Orientation in Films and Fibers

The orientation of anisotropic reinforcing fibers relative to the loading conditions has a major impact on the measured properties. Composites containing fibers oriented in the direction of loading will display the highest properties. Tensor transformations can be used to predict the efficiency of the reinforcement for composites with fibers oriented at any arbitrary angle to the load [91]. An off-axis misalignment of 10° reduces the modulus of graphite from 1,020 GPa to 120 GPa [32]. The degree of CNT alignment within a composite structure is largely determined by the processing method used to fabricate the material. Pressed films demonstrate random alignment while drawn fibers and films exhibit some preferred alignment. Measurement of the degree of orientation of embedded CNTs with a principal axis of the composite is therefore an important consideration. The use of azimuthal or phi scanning x-ray diffraction and polarized micro-Raman spectroscopy have been shown to be effective in quantifying the CNT alignment within composite structures. The x-ray technique, analyzes the two symmetrically diffracted arcs produced by the CNTs about the azimuthal angle (Fig. 35.1). The integrated intensity of these diffracted arcs as a function of the azimuthal angle results in peaks. The breadth of a peak at half its maximum (FWHM) is inversely proportional to the degree of CNT alignment. That is, very sharp peaks correspond to a very high degree of CNT alignment. Whereas, random alignment, results in no discernable peaks as the diffracted x-rays intersect the detector in a ring of uniform intensity. This process is described by Lucas and Vigolo [92] regarding the degree of orientation of SWNTs in solution spun PVA composite fibers. It was also utilized by Kumar [86,87] to evaluate CNT alignment in PAN and PBO composite fibers, by Shaffer [26,45] in polyamide and PEEK composite fibers and by Zhou [93] in drawn poly(hydroxyaminoether) films.

Similarly, determination of CNT orientation by polarized micro-Raman spectroscopy was demonstrated by analysis of the intensity of the Raman peaks at 202 and 1,590 cm^{-1} as a function of the angle between the focused beam and the composite fiber axis [31,50]. Higher intensity peaks along the fiber axis correspond to a large degree of CNT alignment. Another technique of micro-Raman spectroscopy utilizes the principle of peak shifting as a function of the induced strain in the CNTs. Not only is this technique useful for elucidating the amount of stress transfer to the CNTs themselves [66,94,95], but the rate at which with peak shifts with respect to the applied strain correlates to the orientation of the CNTs to the load and thus their alignment [96]. Other techniques include light scattering microscopy to probe induced alignment of CNTs in shear fields [97,98]. In practice, limitations to perfecting uniaxial orientation of CNTs, even in highly drawn fiber matrices have been observed, and attributed to intrinsic ''waviness'' or graphitic misalignment within the CNT structures themselves [45].

35.3 NANOTUBE-POLYMER COMPOSITE PROPERTIES

35.3.1 CNT-Reinforced Polymers: Experimental Results

It is ultimately the properties demonstrated in the CNT composites that will determine the material's utility, while its proliferation will be determined by cost. The promise of a new class of high-performance composite materials, given the magnitude of CNT mechanical properties, remains. Selected experimental results can be used to highlight CNT-polymer composite properties, their relation to processing (dispersion, concentration, orientation), CNT type, and various matrix polymers.

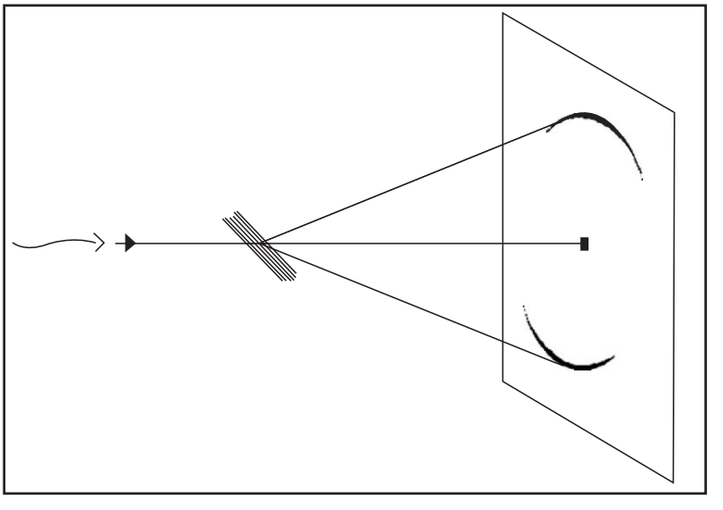

FIGURE 35.1. 2-D x-ray diffraction of aligned MWNTs.

35.3.2 Increases in Toughness

The work of Qian *et al*. [99] using in situ TEM straining of MWNT/polystyrene films demonstrated that nanotubes function to bridge crack opening by spanning the separating surfaces in the crack wake. Wagner *et al*. [100] report similar findings. At crack separations of ~800 nm, the MWNTs were observed to pull out of the crack face, especially those aligned perpendicular to the separating faces, indicative of nanotube/matrix interfacial failure [99]. Tube fracture was observed to occur for defective tubes, such as at catalyst inclusions, or for tubes aligned parallel to the crack. The mechanism of CNT crack bridging has been credited with enhancing the toughness of polymers primarily by increasing the strain to break of the material. This effect was shown by Lozano *et al*. [61]. Increases of 220% in elongation translated into a 290% increase in toughness, which was attributed to the embedded carbon nanofibers (CNFs) in HDPE arresting crack propagation from coalesced voids. Gorga and Cohen [33] report a similar result augmented by the presence of aligned MWNTs in PMMA fiber matrices. Increases in the toughness of 800% were reported in composite fiber containing 1 and 3 wt.% MWNTs, and attributed to the nanotubes bridging crazes and subsequent cracks in the matrix under uniaxial tension. They further elaborate that CNT pull-out provides energy dissipation by frictional slipping thus benefiting material toughness. Therefore aligned CNT systems, in agreement with Qian's observed pull-out of orthogonally oriented tubes, may provide for significantly enhanced toughnesses. In another report by Ruan *et al*. [66], the mechanism of toughness increase for aligned MWNTs in drawn UHMWPE films was attributed to an enhancement of chain mobility in the presence of the MWNTs. Indeed many other researchers have reported significant increases in toughness of aligned CNT composites [31,38,40,87,101], which may prove useful especially for enhancing the performance of impact resistant materials.

35.3.3 Increases in Elastic Modulus and Break Strength

Enhancement of the modulus of a polymer reflects the transfer of stress from the polymer matrix to the high-modulus embedded CNTs. Thus strong interfacial adhesion between the polymer and CNT is preferred for stiffening the composite. Enhancement in break strength also reflects strong interaction between the CNT and polymer, but strength is also profoundly affected by the presence of defects such as voids or agglomerate inclusions, which serve to initiate failure by stress concentration. Therefore, processing can have a major impact on the measured strength. Namely, poor CNT dispersion can be detrimental to strength, which may explain why increases in CNT composite strength are less often observed compared with increases in modulus. Typical increases in the elastic modulus and break strength of CNT-polymer composites are outlined in Table 35.2 for various polymer matrices. Other reported effects in CNT-polymer composites include increases in the matrix polymer glass transition temperature, and increases

TABLE 35.2. *Mechanical property enhancements of nano-composite materials.*

Matrix	Fiber	Loading wt.%	Form	E_c GPa	σ_c MPa	T_c J/g	Ref.
PEEK	CNFs	10	Fibers	+20%	+20%		[26]
PVA	SWNT	60	Fibers		1,800*	600*	[101]
	MWNT	< 1	Films	+370%	+430%	+170%	[69]
Cl-PP	MWNT	< 1	Films	+310%	+390%	+440%	[69]
PAN	SWNT	10	Fibers	+100%			[86]
	MWNT	3	Fibers	+36%	+31%	+80%	[38]
PP	SWNT	1	Fibers		+45%		[82]
	SWNT	1		+55%	+40%		[43]
	CNFs	5		+50%	+100%		[83]
	CNFs	15	Films	+90%			[42]
PBO	SWNT	10	Fibers		+50%		[87]
PMMA	MWNT	30	Films	+140%			[62]
		20		+1,100%			[15]
PMEA	MWNT	1	Films	+200%			[47]
PS	MWNT	5	Films	+10%			[74]
			Drawn Films	+49%			
		20	Films	+50%	+0%		[10]
UHMWPE	MWNT	1	Drawn Films	+25%	+48%	+150%	[66]
HDPE	CNFs	8	Films	+60%			[61]
PC	SWNT	0.06	Films	+29%			[104]

E_c = composite modulus; σ_c = composite break strength; T_c = composite toughness
* These are absolute values not increases compared to neat polymer.

in composite fatigue life. Kumar *et al*. [86] report that the T_g of PAN composite fibers increased from 103 °C to 143 °C with the inclusion of 10 wt.% SWNT into the matrix. Increases in T_g are often attributed to a restriction of interchain mobility by the presence of the CNTs [32]. Marrs *et al*. [102] reported significant increases in the fatigue life of MWNT/PMMA-based bone cement composites, an important consideration for the lifetime of joint replacements. Others compared the fatigue properties of aligned SWNT ropes in epoxy to carbon fiber/epoxy composite, and concluded the SWNT/epoxy allowed for much higher fatigue stresses while maintaining similar fatigue life as the carbon fiber/epoxy [103].

35.3.4 Factors Influencing CNT-Polymer Composite Mechanical Properties

Shaffer *et al*. [105] investigated the effect of the type of CNT reinforcement in polyamide fibers and concluded that the use of aligned substrate-grown MWNTs resulted in the best composite properties. An identical result was reached by Gorga *et al*. [33] for MWNTs in PMMA. The fact that the bulk MWNTs were not initially entangled provided for better dispersion. Other researchers reported that longer nanotubes, resulting in higher aspect ratios, improved composite properties [33,99]. A recurring inter-relation between processing and properties is dispersion. Many researchers have reported diminishing properties of their CNT composites as the concentration exceeds 1 wt.% [82], and others exceeding 5–10 wt.% [32,33]. The continuous increase in composite properties predicted by theory does not occur, and is likely due to a lack of homogeneous dispersion. The orientation of the CNTs relative to the load has also been shown to have an effect on the composite properties. Thostenson *et al*. [74] found a 50% improvement in the tensile modulus of aligned MWNT/PS composites compared to a 10% improvement for randomly oriented MWNT/PS composites. Others have shown that the strength of the interfacial bonding and other interfacial effects in CNT-polymer composites has a profound effect on the composite properties [69] (discussed later).

35.3.5 CNT-Reinforced Polymers: Theoretical Modeling of Experimental Results

The use of theoretical models to predict the properties of CNT composites has been useful in dealing with certain aspects of these nanocomposites. In particular, Brinson *et al*. [41,106] addressed the issue of CNT waviness or curvature and its effects on composite properties. TEM observations of embedded CNTs have shown that they are not rectilinear but have some degree of waviness [99], which may be due to their crystalline defects and elastic flexibility. A reduction in the modulus of wavy CNTs can be expected due to CNT anisotropy. Finite element analysis was used to calculate what the effective reinforcing modulus would be of a wavy CNT of wavelength, λ, relative to a straight CNT [41]. A second micromechanical model used this result to predict the properties of a bulk CNT composite considering a distribution of embedded CNT waviness, or amplitude of curvature to wavelength ratio. The results predicted significant reductions in effective modulus for wavy CNTs. For a waviness of 0.1, or a CNT that is 90% straight, a 40–50% reduction in modulus was predicted. This method, applied to experimental results of MWNT/PS composite films, provided a more accurate model than predicted with straight CNTs. This work and others [107,108] underscore the importance of CNT waviness to composite properties.

The issue of CNT diameter and its effects on composite properties has been modeled by Thostenson *et al*. [109]. For embedded MWNTs, the dilemma lies in the degree to which tensile stress is transferred from the outermost wall to the inner walls of the MWNT. They considered that although the MWNT acts as a solid fiber in a composite, tensile stress is only carried by the outermost tube wall due to weak interwall Van der Waals bonding. Therefore, accurately modeling the load bearing capacity of the MWNT must be calculated by averaging the stress in the outer wall over the complete cross-section of the MWNT. Thus larger diameter MWNTs containing many concentric shells, will have significantly lower effective reinforcing moduli. Experimental verification of this idea was tested by fabricating drawn films of MWNTs in polystyrene to align the MWNTs. Electron microscopy was used to measure the distribution of MWNT diameters, which was modeled in the composite by parallel partitioning of the MWNT volume fraction into discrete diameter ranges. A Halpin-Tsai based model was applied in which the effective moduli of the embedded MWNT diameter distribution was used to yield an overall composite modulus. The embedded lengths of the MWNTs were also considered, but did not play an important role considering large aspect ratios were maintained. The model was compared to experimental data for composite films with MWNT concentrations of 5 and 10 wt.% with very good agreement. Larger diameter MWNTs occupy a larger volume fraction of the composite, display lower effective moduli, and thus make a significantly reduced contribution to the composite properties.

Perhaps the most important issue in CNT-polymer composites is a good understanding of interfacial bonding between the embedded CNTs and the polymer matrix. Frankland *et al*. [110] used molecular dynamics simulations to study the interfacial forces involved with pulling a SWNT through a polyethylene matrix. Assuming a noncovalently bound interface, it was calculated that a force of 0.1 nN was required to initiate SWNT slippage. Higher forces resulted in a periodically increasing velocity of the SWNT relative to the matrix, indicative of atomistic interactions of the SWNT surface with the crystalline PE matrix. Averaging the increase in velocity and relating it to the frictional interfacial shearing stress led to an effective viscosity of 0.2 mPa s, about that of pentane at room temperature. Another molecular mechanics simulation of the pull-out of CNTs from a

polystyrene matrix resulted in quite high interfacial shear strength of 160 MPa for a noncovalently bound system, and concluded that the high strength was likely to be due to the intimate contact between the small diameter CNT and the PS chains [111]. The bonding between the CNTs and the polymer matrix is an important consideration, and could be considerably enhanced in covalently bonded systems through the use of functionalized CNTs to promote high interfacial shear strength. Sinnot *et al.* [112,113] have shown via molecular dynamics simulations that functionalization of CNT surfaces does not significantly decrease the mechanical properties of CNTs. Experimental determination of the interfacial shear strength of CNT-polymer composites has recently been demonstrated [114].

35.4 NANOTUBE–POLYMER INTERFACIAL EFFECTS

35.4.1 CNT–Polymer Interfacial Adhesion

Obviously the strength of the interfacial bonding between the CNTs and the polymer matrix will have a major impact upon their ability to reinforce the composite. Wagner *et al.* [114] studied this issue by conducting experiments in which a MWNT, attached to an AFM tip, was embedded in a polymer and pulled out. The force versus pull-out length was recorded for a poly(ethylene-butene) matrix resulting in an interfacial shear strength of 47 MPa. This value is consistent with other measurements where estimates of $\sim$50 MPa for various nanotube types were recorded [12].

35.4.2 Rule of Mixtures Inapplicability

The region of highest importance in any composite material is the interface between the reinforcing filler and the matrix material. Under an applied load, strains develop throughout the material, which can be envisioned, for the case of tension, as an overall increase in the displacement between two parallel planes of material orthogonal to the load. In the interphase region between the bulk matrix and the embedded, discontinuous fibers, these strains translate into shear stresses as the fibers are typically less compliant than the matrix, thus straining less. This scenario is applicable to CNTs in a polymer matrix. These interfacial shear stresses build along the length of the fibers acting in opposite directions from the fiber midpoint, and serve to transfer the applied load from the surrounding matrix to the embedded fibers. If the interface is strong and the volume fraction of fibers is sufficiently high, then the matrix is prevented from complying with the load and the tensile stress increases. The matrix is reinforced by the fibers. If the interface remains strong, and/or the embedded fibers are very long, the accumulated shear stresses can translate into tensile fracture of the embedded fibers representing the most efficient reinforcement possible for that composite system. This view of traditional composite micromechanics, underlies the widely accepted rule-of-mixtures approach to modeling fiber reinforced composite materials. It states that the modulus of the composite is a linear combination of the moduli of the materials from which it is composed, and weights each modulus with the volume fraction of that component. Its basis lies in continuity of parallel strain between the fibers and matrix provided a linearly elastic response of the composite occurs for small strains.

$$E_c = E_f V_f + E_m(1 - V_f),$$

where E_f is the fiber tensile modulus, E_m, the matrix modulus, and V_f is the volume fraction of fiber. This conclusion is based on some important assumptions. Some of which render it inapplicable to most CNT-polymer composites.

(1) ***The CNT-Matrix Interface is Strong (Continuity of Strain)***

This means that no slippage of the CNTs through the matrix occurs. In polymer–CNT composites, significant nanotube pull-out has been verified even at low strain indicating interfacial failure [38].

(2) ***The CNTs are all Aligned Parallel with the Direction of Load***

The fiber modulus, E_f, refers to the modulus of the fiber when loaded in pure tension. Embedded CNTs typically show some measure of curvature [115], waviness [41], and misalignment with any given material direction even for highly drawn matrices [50,64,86,105].

(3) ***The Length of CNTs is Sufficient for Maximum Interfacial Shear–Stress Build-up***

This implies that the average length of the embedded CNTs is long relative to the load transfer length (length required for complete interfacial shear–stress build-up). Embedded lengths of CNTs post sonication were measured to be primarily in the 1–10 μm range [116]. Pull-out of these CNTs was confirmed via TEM straining [38].

(4) ***The CNTs are Homogeneously Dispersed and Homogeneously Loaded***

This implies that each individual CNT is loaded homogeneously by stress transfer from the surrounding matrix. (No CNT–CNT interactions). Achieving homogeneous dispersion of CNTs, especially at concentrations $>$ 10 wt.% has been shown to be difficult [101].

(5) ***The Composite Modulus is Linearly Related to the Moduli of its Component Phases***

This implies that the modulus of each phase is independent and unchanged by the presence of the others. Nanotubes have been shown to induce polymer matrix crystallization near their surfaces thus altering the matrix [70]. In other words, the interfacial matrix potentially has different properties from the neat matrix.

More refined models of macroscale composite stiffness have been developed (such as the Halpin-Tsai equations [91]) that take into account some of the assumptions made above, e.g., fiber length, orientation, and inefficiencies in

stress transfer. These assumptions are often dealt with by giving the fiber an ''effective modulus'', which is lower than its ideal modulus, and have been applied to CNT–polymer composites with some success. Another example is the Krenchel rule of mixtures [105].

$$E_C = \eta_0 \eta_1 V_f E_f + (1 - V_f) E_m, \tag{35.1}$$

where η_0 is the CNT orientation factor [91]; η_1 is the CNT length factor [117]; and $E_f \eta_0 \eta_1$ is the CNT effective modulus. However, numerous publications citing observations of CNT-induced crystallinity in various semicrystalline polymer matrices have prompted the need to reconsider the validity of assumption (5) above [12,26,69,70,82,105].

35.4.3 CNT-Induced Polymer Crystallization

Within the past few years, many investigators have observed an increase in the degree of crystallinity or crystallite size of semicrystalline polymer–CNT composites due to the addition of CNTs. Differential scanning calorimetry (DSC) melting endotherms have been frequently employed to demonstrate this effect (Table 35.3). Recently, Coleman *et al.* [69] investigated this induced crystallization effect, and related it to the mechanical properties of the composite. The results highlight a fundamental difference between CNT–polymer composites and carbon fiber–polymer composites: with CNT composites the interface dominates all other effects due to the vast surface area/volume ratio that CNTs have relative to carbon fibers (Fig. 35.2).

Linear increases in crystallinity with increasing MWNT concentration of a MWNT/poly(vinyl alcohol) (PVA) composite were observed in DSC melting endotherms. This suggested that each CNT had a discrete crystalline polymer layer associated with it, which was supported by evidence from SEM imaging [69]. Indeed, others have observed polymer sheathing of CNTs protruding from fracture surfaces [39]. An equation for the composite crystallinity was deduced [69]:

TABLE 35.3. *Evidence of CNT-nucleated crystallinity in semicrystalline polymer matrices.*

Polymer matrix	Analytical method	Ref.
Polyamide-12	DSC	[105]
PEEK	DSC, XRD	[26]
PVA	DSC	[12,69]
PmPV	DSC, PL	[70]
PP	Density nonlinearity, DSC, XRD	[73,82]
UHMWPE	SEM	[66]

$$\chi = \frac{V_0 + N[\pi(R+b)^2 l_{NT} - \pi R^2 l_{NT}]}{V} \tag{35.2}$$

and given

$$V_{NT} = \frac{N \pi R^2 l_{NT}}{V}. \tag{35.3}$$

Substituting Eq. (35.3) into (35.2) and simplifying gives:

$$\chi = V_{NT}\left[\frac{b^2}{R^2} + 2\frac{b}{R}\right] + \frac{V_0}{V}. \tag{35.4}$$

This equation fit the DSC experimental data quite well resulting in a crystalline polymer interfacial layer thickness, b, of 21 ± 7 nm ($R = 7.5 \pm 2.5$ nm) (Figure 35.3). SEM measurement of MWNTs protruding from fractured surfaces agreed well with the DSC results indicating that $b = 25 \pm 10$ nm. It was also noted that the mean length of MWNTs protruding from the fracture surface was approximately $1.72 \pm 0.7\,\mu m \approx l_{NT}/4$. Mechanical testing of these MWNT/PVA composites yielded impressive mechanical property improvements, +370% in modulus and + 430% in strength at a loading of only 0.6 vol.% MWNTs.

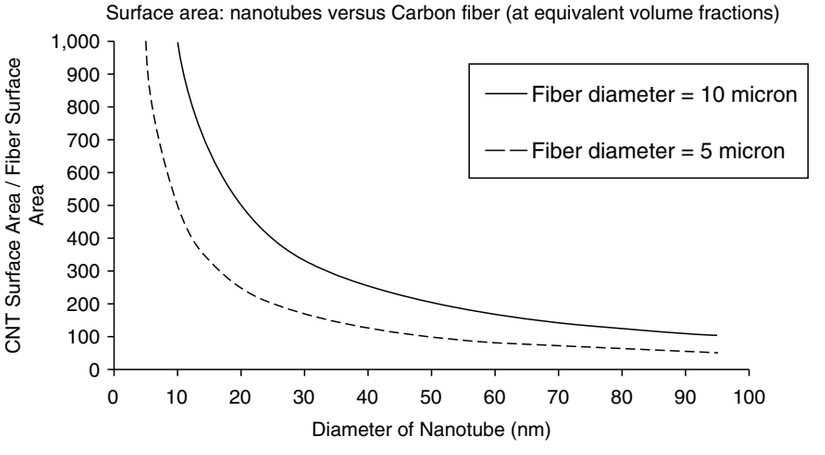

FIGURE 35.2. Increases in the ratio of CNT surface area to carbon fiber surface area as a function of the CNT diameter. Two typical carbon fiber diameters are compared.

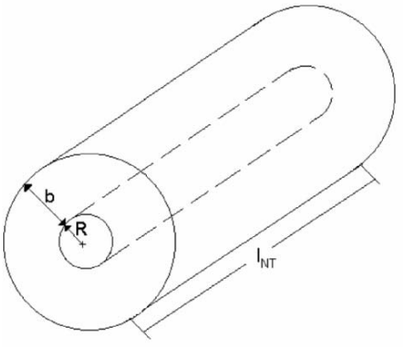

R = MWNT radius
b = crystalline polymer layer thickness
l_{NT} = MWNT length
χ = Total volume fraction polymer crystallinity
V_0 = Initial volume of neat polymer crystallinity
V_{NT} = MWNT volume fraction
N = Number of MWNTs
V = Total volume of composite

FIGURE 35.3. Crystalline Polymer Sheathing of carbon nanotube.

Inspection of the fracture surfaces of these and other composites [39,69] supports the contention that failure occurs at the interface between a crystalline polymer layer bound to the nanotube surface and the bulk polymer. This implies that the MWNTs are not being strained to failure, and that the nanotube interface with the matrix is strong enough to stay intact (i.e., the MWNT + crystalline polymer sheath are acting as a single unit). As a first approximation, short fiber composite theory has been used to model this effect since it generally applies to composites containing short fibers that cannot be strained to failure by stress transfer from the matrix. Composite strength can then be represented by:

$$\sigma_C = \left(\frac{l_{NT}\tau}{2R} - \sigma_P\right)V_{NT} + \sigma_P, \tag{35.5}$$

where τ is the interfacial shear strength between the fiber surface and the matrix.

Applying this model to MWNT/PVA composites resulted in a predicted interfacial shear strength, τ, of 348 $\pm$ 231 MPa, about an order of magnitude higher than expected. Thus, Eq. (35.5) was modified to allow for the observed interfacial failure at the boundary between the bulk polymer and the crystalline polymer layer (thickness = b) adhering to the MWNT surface.

The argument from Coleman *et al*. [69] proceeded as follows. The stress required to break the MWNT/PVA composite is the sum of the stress required to fracture the matrix and the shear stress required to fail the bulk polymer–crystalline polymer layer interface.

$$\sigma_C A = \sigma_{poly}A_{bulk} + \sigma_{shear}A_{Interface}. \tag{35.6}$$

To determine the cross-sectional areas A_{bulk} and $A_{Interface}$, the number of nanotubes, n, in a given cross-section of the composite was calculated assuming all of the MWNTs were oriented perpendicular to the fracture surface, and that each had a cylindrical volume of matrix associated with it (diameter = $2a$) such that $n(\pi a^2) = A$, the total cross-sectional area. To determine a, characterizing ideal aerial dispersion of the nanotubes, the volume fraction of nanotubes in the composite, V_{NT}, was related to the volume of matrix per nanotube, $V_{matrix/NT}$:

$$V_{matrix/NT} = \frac{V}{N} \text{ with } V_{NT} = \frac{N\pi R^2 l_{NT}}{V} \tag{35.7}$$

$$V_{matrix/NT} = \frac{\pi R^2 l_{NT}}{V_{NT}} = \pi a^2 l_{NT} \; a = \frac{R}{\sqrt{V_{NT}}} \tag{35.8}$$

and

$$A = \frac{n\pi R^2}{V_{NT}}. \tag{35.9}$$

The area of the interface and the bulk area were then calculated:

$$A_{Interface} = n2\pi(R+b)1_{pullout} \tag{35.10}$$

and

$$A_{bulk} = A - n\pi(R+b)^2. \tag{35.11}$$

Substituting Eqs. (35.9), (35.10), and (35.11) into Eq. (35.6), and allowing $l_{pullout} = l_{NT}/4$ (consistent with SEM observations) produces an expression for the composite strength:

$$\sigma_C = \sigma_{poly} + V_{NT}\left[\frac{\sigma_{shear}l_{NT}}{2R} - \sigma_{poly}\left(1+\frac{b}{R}\right)\right]\left(1+\frac{b}{R}\right). \tag{35.12}$$

This expression reduces to Eq. (35.5) for $b = 0$ and $\sigma_{shear} = \tau$, validating the form. Fitting experimental data to Eq. (35.12), yields a value for the interfacial polymer-bulk polymer shear strength, σ_{shear}, of 95 $\pm$ 64 MPa. This is consistent with the crystalline polymer layer remaining intact with the MWNT surface. It is worth noting that as b gets large relative to the nanotube radius, then $A_{bulk} \rightarrow 0$. This implies that the matrix can become all interfacial polymer at some volume fraction of nanotubes, V^*_{NT}, less than one.

$$V^*_{NT} = \frac{1}{\left(1+\frac{b}{R}\right)^2}. \tag{35.13}$$

Clearly, the key issue is that for nanotube–polymer composites in which an increase in crystallinity is observed, fundamental changes in the way traditional micromechanical composite theory is applied may be necessary.

Consideration must be given to the formation of crystalline polymer coatings, which strongly adhere to the nanotubes. Promoting the growth of this layer, perhaps by using smaller diameter nanotubes capable of seeding thick crystalline coatings, may optimize reinforcement for particular polymer matrices [69]. Small diameter, easily dispersed multiwall carbon nanotubes grown in aligned arrays have been cited numerous times as being efficient at mechanical reinforcement, and may thus fill this role [12,33,68,105].

Changes in the elastic modulus of polymers initiated by the introduction of dispersed CNTs can be equally revealing about the mechanism of material reinforcement in which they participate. These are again related to the fundamental importance of increased surface area/volume ratio of CNTs [12]. Composites of PVA containing various types of carbon nanotubes were produced, and the increase in tensile modulus of each were analyzed. Neither a rule-of-mixture nor Halpin-Tsai approach to modeling the data worked well. However, it was recognized that the rate at which the composite modulus increased with increasing nanotube volume fraction was related to the mean diameter of the nanotubes used. This rate decreased as the diameter increased. A log–log plot of the rate of modulus increase versus nanotube diameter resulted in a straight line with a slope of -1, suggesting that the efficiency of reinforcement of the PVA is inversely proportional to the nanotube diameter, or directly proportional to the ratio of the surface area to volume of the nanotubes.

$$\frac{E_C - E_m}{E_m} = k\frac{N}{V}(2\pi R l_{NT}). \tag{35.14}$$

Plotting E_C/E_m versus the nanotube surface area per total volume, $(N/V)(2\pi R l_{NT})$ did indeed result in almost all of the data falling on one master straight line of slope k. (SWNT bundles did not follow the trend due to difficulty in dispersing individual SWNTs [12])

Using Eq. (35.7) in (35.14) yields,

$$\frac{E_C}{E_m} = \frac{2kV_{NT}}{R} + 1, \tag{35.15}$$

where k is the constant of proportionality relating the increase in CNT surface area per unit volume to the increase in composite modulus. The relationship between the composite modulus and the CNT surface area was shown to be linked to crystallization of the matrix polymer at the CNT surface, independent of the CNT type or concentration of lattice defects. From DSC results a differentiated form of Eq. (35.4) was shown to predict the composite crystallinity. Another group reported that the inclusion of Carbon nanofibres (CNFs) in PEEK only nucleated crystal growth when aligned in a drawn fiber matrix, and proposed that the induced strains and changes in polymer orientation due to the presence of the CNFs led to the development of crystallinity, not simply surface heteronucluation [26]. They furthermore report that the PEEK crystallinity is not enhanced by doubling the CNF concentration from 5 to 10 wt.%, a consequence alluded to, in part, by Eq. (35.13).

35.5 CONCLUSIONS

CNT-polymer composites are an emerging new class of composite materials with unique and promising mechanical properties. Considering the problems of CNT dispersion, orientation and processing, significant progress has been made in realizing their potential to enhance the properties of matrices to which they are added. The dependence of the CNT–polymer composite properties on these issues, as well as others such as CNT diameter, length, and interfacial matrix crystallization, has been recognized and used to develop models to predict and optimize the variables for maximum composite performance. The results presented by Coleman *et al.* [69] represent the most efficient enhancements in matrix mechanical properties published to date. An effective modulus of the embedded MWNTs in PVA films of 1984 ± 239 GPa was observed resulting in enhancement of the composite by 370% in modulus, 430% in strength, and 170% in toughness at only 0.6 vol.% loading of small diameter (15 ± 5 nm) MWNTs. These enhancements represent the level of performance researchers have hoped to see since the inception of CNT composites. It remains to be seen if similar effects can be demonstrated in other, perhaps more useful, polymer matrices. However, given the mechanical properties of CNTs, realization of the full potential of CNT-reinforced polymers has yet to be achieved. Further advances in this field, especially when coupled with other properties such as enhanced thermal and electrical conductivity, have promise to result in wide application of truly multifunctional materials. This ultimately represents the greatest potential of CNT–polymer composites; allowing for the possibility of reinforced polymers that can operate at high heat loads, conduct electricity, and shield EMI radiation simultaneously. CNT–polymer composites enabling these applications, while offering lighter weights and increased manufacturability over current materials, will undoubtedly advance the engineering capabilities of polymer composites.

ABBREVIATIONS

CNT	Carbon nanotube
MWNT	Multiwall carbon nanotube (diameter $\sim$ 10–100 nm)
SWNT	Singlewall carbon nanotube (diameter $\sim$ 1 nm)
CNF	Carbon nanofiber (diameter $\sim$ 200 nm)
PAN	poly(acrylonitrile)
PE	poly(ethylene)
HDPE	high density poly(ethylene)
UHMWPE	ultra-high molecular weight poly(ethylene)
PS	poly(styrene)
PMMA	poly(methyl methacrylate)
PMEA	poly(methyl ethyl methacrylate)
PVA	poly(vinylalcohol)
PEEK	poly(ether ether ketone)
PP	poly(propylene)

cl-PP	chlorinated poly(propylene)
PBO	poly(*p*- phenylene benzobisoxazole)
PC	poly(carbonate)
PmPV	poly(*m*-phenylenevinylene-*co*-2,5-dioctyloxy-*p*-phenylenevinylene)
FWHM	full peak width at half-maximum

REFERENCES

1. Iijima, S. Helical Microtubules of Graphitic Carbon. *Nature* **354**, 56–58 (1991).
2. Sinnott, S. B. & Andrews, R. Carbon Nanotubes: Synthesis, Properties, and Applications. *Crit. Rev. Solid State Mater. Sci.* **26**, 145–249 (2001).
3. Lambin, P. Electronic structure of carbon nanotubes. *Comptes Rendus Physique* **4**, 1009–1019 (2003).
4. Kaneto, K., Tsuruta, M., Sakai, G., Cho, W. Y. & Ando, Y. Electrical conductivities of multi-wall carbon nano tubes. *Synth. Metals* **103**, 2543–2546 (1999).
5. Berber, S., Kwon, Y. K. & Tomanek, D. Unusually high thermal conductivities of carbon nanotubes. *Phys. Rev. Lett.* **84**, 4613–4616 (2000).
6. Kim, P., Shi, L., Majamdar, A. & McEuen, P. L. Thermal transport measurments of individual multiwalled nanotubes. *Phys. Rev. Lett.* **87**, 215502–1 (2001).
7. Saito, R., Dresselhaus, G. & Dresselhaus, M. S. *Physical Properties of Carbon Nanotubes* (Imperial College Press, London, 1998).
8. Salvetat-Delmotte, J.-P. & Rubio, A. Mechanical properties of carbon nanotubes: a fiber digest for beginners. *Carbon* **40**, 1729–1734 (2001).
9. Thess, A. *et al*. Crystalline ropes of metallic carbon nanotubes. *Science* **273**, 483–487 (1996).
10. Andrews, R., Jacques, D., Qian, D. & Rantell, T. Multiwall carbon nanotubes: synthesis and application. *Acc. Chem. Res.* **35**, 1008–1017 (2002).
11. Donnet, J.-B., Wang, T. K., Peng, J. C. M. & Rebouillat, S. (eds.) *Carbon Fibers Third Edition, Revised and Expanded* (Marcel Dekker Inc., New York, 1998).
12. Cadek, M. *et al*. Reinforcement of polymers with carbon nanotubes: The role of nanotube surface area. *Nano Lett.* **4**, 353–356 (2004).
13. Yu, M.-F. *et al*. Strength and breaking mechanism of multiwalled carbon nanotubes under tensile load. *Science* **287**, 637–640 (2000).
14. Yu, M.-F., Yakobson, B. I. & Ruoff, R. Controlled sliding and pullout of nested shells in individual multiwalled carbon nanotubes. *J. Phys. Chem.* **104**, 8764–8767 (2000).
15. Hwang, G. L., Shieh, Y.-T. & Hwang, K. C. Efficient load transfer to polymer-grafted multiwalled carbon nanotubes in polymer composites. *Adv. Funct. Mater.* **14**, 487–491 (2004).
16. Zhang, Y., Gu, H. & Lijima, S. Single-wall carbon nanotubes synthesized by laser ablation in a nitrogen atmosphere. *Appl. Phys. Lett.* **73**, 3827–3829 (1998).
17. Andrews, R. *et al*. Continuous production of aligned carbon nanotubes: a step closer to commercial realization. *Chem. Phys. Lett.* **303**, 467–474 (1999).
18. Krishnan, A., Dujardin, E., Ebbesen, T. W., Yianilos, P. N. & Treacy, M. M. J. Young's modulus of single-walled nanotubes. *Phys. Rev. B* **58**, 14013–14019 (1998).
19. Lier, G. V., Alsenoy, C. V., Doren, V. V. & Geerlings, P. Ab initio study of the elastic properties of single-walled carbon nanotubes and graphene. *Chem. Phys. Lett.* **326**, 181–185 (2000).
20. Schadler, L. S., Giannaris, S. C. & Ajayan, P. M. Load transfer in carbon nanotube epoxy composites. *Appl. Phys. Lett.* **73**, 3842–3844 (1998).
21. Nardelli, M. B., Yakobson, B. I. & Bernholc, J. Brittle and ductile behavior in carbon nanotubes. *Phys. Rev. Lett.* **81**, 4656–4659 (1998).
22. Walters, D. A. *et al*. Elastic strain of freely suspended single-wall carbon nanotube ropes. *Appl. Phys. Lett.* **74**, 3803–3805 (1999).
23. Treacy, M. M. J., Ebbesen, T. W. & Gibson, J. M. Exceptionally high Young's modulus observed for individual carbon nanotubes. *Nature* **381**, 678–680 (1996).
24. Demczyk, B. G. *et al*. Direct mechanical measurement of the tensile strength and elastic modulus of multiwalled carbon nanotubes. *Mater. Sci. Eng.* **A334**, 173–178 (2002).
25. Wagner, H. D., Lourie, O., Feldman, Y. & Tenne, R. Stress-induced fragmentation of multiwall carbon nanotubes in a polymer matrix. *Appl. Phys. Lett.* **72**, 188–190 (1998).
26. Sandler, J. *et al*. Carbon-nanofibre-reinforced poly(ether ether ketone) fibres. *J. Mater. Science* **38**, 2135–2141 (2003).
27. Applied Sciences (2005). Properties of Pyrograf I, http://www.apsci.com/ngm-pyro1.html
28. Bacon, R. Growth, structure, and properties of graphitic whiskers. *J. Appl. Phys.* **31**, 283–290 (1960).
29. Hexcel. (2005). Continuous carbon fiber data, http://www.hexcelfibers.com/ Markets/Products/Continuous/ _Productlist.htm
30. Toray (2005). Carbon fiber data, http://www.torayca.com/index2.html
31. Siochi, E. J. *et al*. Melt processing of SWCNT-polyimide nanocomposite fibers. *Compos. Part B: Eng.* **35**, 439–446 (2004).
32. Zeng, J., Saltysiak, B., Johnson, W. S., Schiraldi, D. A. & Kumar, S. Processing and properties of poly(methyl methacrylate)/carbon nano fiber composites. *Compos. Part B: Eng.* **35**, 173–178 (2004).
33. Gorga, R. E. & Cohen, R. E. Toughness enhancements in poly(methyl methacrylate) by addition of oriented multiwall carbon nanotubes. *J. Polym. Sci.: Part B: Polym. Phys.* **42**, 2690–2702 (2004).
34. Advani, S. G. & Fan, Z. in *Materials Processing and Design: Modeling, Simulation, and Applications, NUMIFORM 2004* (eds. Ghosh, S., Castro, J. C. & Lee, J. K.) 1619–1623 (American Institute of Physics, 2004).
35. Shaffer, M. S. P., Fan, X. & Windle, A. H. Dispersion and packing of carbon nanotubes. *Carbon* **36**, 1603–1612 (1998).
36. Shaffer, M. S. P. & Windle, A. H. Analogies between polymer solutions and carbon nanotube dispersions. *Macromolecules* **32**, 6864–6866 (1999).
37. Zeng, J., Saltysiak, B., Johnson, W. S., Schiraldi, D. A. & Kumar, S. Processing and properties of poly(methyl methacrylate)/carbon nano fiber composites. *Compos. Part B: Eng.* **35**, 173–178 (2004).
38. Weisenberger, M. C., Grulke, E. A., Jacques, D., Rantell, T. & Andrews, R. Enhanced mechanical properties of polyacrylonitrile/multiwall carbon nanotube composite fibers. *J. Nanosci. Nanotechnol.* **3**, 535–539 (2003).
39. Ding, W. *et al*. Direct observation of polymer sheathing in carbon nanotube-polycarbonate composites. *Nano Lett.* **3**, 1593–1597 (2003).
40. Dalton, A. B. *et al*. Super-tough carbon-nanotube fibres. *Nature* **423**, 703 (2003).
41. Fisher, F. T., Bradshaw, R. D. & Brinson, L. C. Fiber waviness in nanotube-reinforced polymer composites-I: Modulus predictions using effective nanotube properties. *Compos. Sci. Technol.* **63**, 1689–1703 (2003).
42. Hammel, E. *et al*. Carbon nanofibres for composite applications. *Carbon* **42**, 1153–1158 (2004).
43. Kearns, J. C. & Shambaugh, R. L. Polypropylene fibers reinforced with carbon nanotubes. *J. Appl. Polym. Sci.* **86**, 2079–2084 (2002).
44. Fuchs, F. J. In *45th Annual Technical Conference of Society of Vacuum Coaters* ISSN 0737–5921, 64–67 (2002).
45. Sandler, J. K. W. *et al*. A comparative study of melt spun polyamide-12 fibres reinforced with carbon nanotubes and nanofibres. *Polymer* **45**, 2001–2015 (2004).
46. Gong, X., Liu, J., Baskaran, S., Voise, R. D. & Young, J. S. Surfactant-assisted processing of carbon nanotube/polymer composites. *Chem. Mater.* **12**, 1049–1052 (2000).
47. Velasco-Santos, C., Martinez-Hernandex, A. L., Fisher, F. T., Ruoff, R. S. & Castano, V. M. Dynamical-mechanical and thermal analysis of carbon nanotube-methyl-ethyl methacrylate nanocomposites. *J. Phys. D: Appl. Phys.* **36**, 1423–1428 (2003).
48. Poulin, P., Vigolo, B. & Launois, P. Films and fibers of oriented single wall nanotubes. *Carbon* **40**, 1741–1749 (2002).
49. Velasco-Santos, C., Martinez-Hernandez, A. L., Fisher, F. T., Ruoff, R. S. & Castano, V. M. Improvement of thermal and mechanical properties of carbon nanotube composites through chemical functionalization. *Chem. Mater.* **15**, 4470–4475 (2003).
50. Haggenmueller, R., Gommans, H. H., Rinzler, A. G., Fischer, J. E. & Winey, K. I. Aligned single-wall carbon nanotubes in composites by melt processing methods. *Chem. Phys. Lett.* **330**, 219–225 (2000).

51. Bubert, H. *et al*. Characterization of the uppermost layer of plasma-treated carbon nanotubes. *Diamond Related Mater*. **12**, 811–815 (2003).
52. Kim, B. & Sigmund, W. M. Functionalized multiwall carbon nanotube/gold nanoparticle composites. *Langmuir* **20**, 8239–8242 (2004).
53. Esumi, K., Ishigami, A., Nakajima, A., Sawadi, K. & Honda, H. *Carbon* **34**, 279 (1996).
54. Eitan, A., Jiang, K., Dukes, D., Andrews, R. & Schadler, L. S. Surface modification of multiwalled carbon nanotubes: toward the tailoring of the interface in polymer composites. *Chem. Mater*. **15**, 3195–3201 (2003).
55. Valentini, L., Armentano, I., Puglia, D. & Kenny, J. M. Dynamics of amine functionalized nanotubes/epoxy composites by dielectric relaxation spectroscopy. *Carbon* **42**, 323–329 (2004).
56. Kyke, C. A., Stewart, M. P., Maya, F. & Tour, J. M. Diazonium-based functionalization of carbon nanotubes: XPS and GC–MS analysis and mechanistic implications. *Synlett* **1**, 155–160 (2004).
57. Holzinger, M. *et al*. Sidewall functionalization of carbon nanotubes. *Angew. Chem. Int., Ed.* **40**, 4002–4005 (2001).
58. Moghaddam, M. J. *et al*. Highly efficient binding of DNA on the sidewalls and tips of carbon nanotubes using photochemistry. *Nano Lett*. **4**, 89–93 (2004).
59. Pantarotto, D. *et al*. Synthesis, structural characterization and immunological properties of carbon nanotubes functionalized with peptides. *J. Am. Chem. Soc*. **125**, 6160–6164 (2003).
60. Dyke, C. A. & Tour, J. M. Solvent-free functionalization of carbon nanotubes. *J. Am. Chem. Soc*. **125**, 1156–1157 (2003).
61. Lozano, K., Yang, S. & Jones, R. E. Nanofiber toughened polyethylene composites. *Carbon* **42**, 2329–2331 (2004).
62. Jin, Z., Pramoda, K. P., Xu, G. & Goh, S. H. Dynamic mechanical behavior of melt-processed multi-walled carbon nanotube/poly (methyl methacrylate) composites. *Chem. Phys. Lett*. **337**, 43–47 (2001).
63. Kashiwagi, T. *et al*. Thermal degradation and flammability properties of poly(propylene)/carbon nanotube composites. *Macromol. Rapid Commun*. **23**, 761–765 (2002).
64. Jin, L., Bower, C. & Zhou, O. Alignment of carbon nanotubes in a polymer matrix by mechanical stretching. *Appl. Phys. Lett*. **73**, 1197–1199 (1998).
65. Shaffer, M. S. P. & Windle, A. H. Fabrication and characterization of carbon nanotube/poly(vinyl alcohol) composites. *Adv. Mater*. **11**, 937–941 (1999).
66. Ruan, S. L., Gao, P., Yang, X. G. & Yu, T. X. Toughening high performance ultrahigh molecular weight polyethylene using multiwalled carbon nanotubes. *Polymer* **44**, 5643–5654 (2003).
67. Ajayan, P. M., Stephan, O., Colliex, C. & Traught, D. Aligned carbon nanotube arrays formed by cutting a polymer resin–nanotube composite. *Science* **265**, 1212–1214 (1994).
68. Cadek, M. *et al.* in *Molecular Nanostructures: XVII Int'l. Winterschool/Euroconference on Electronic Properties of Novel Materials* (eds. Kuzmany, H., Fink, J., Mehring, M. & Roth, S.) 269–272 (American Institute of Physics, 2003).
69. Coleman, J. N. *et al*. High-performance nanotube-reinforced plastics: understanding the mechanism of strength increase. *Adv. Funct. Mater*. **14**, 791–798 (2004).
70. Ryan, K. P. *et al*. Carbon-nanotube nucleated crystallinity in a conjugated polymer based composite. *Chem. Phys. Lett*. **391**, 329–333 (2004).
71. Cadek, M., Coleman, J. N., Barron, V., Hedicke, K. & Blau, W. J. Morphological and mechanical properties of carbon-nanotube-reinforced semicrystalline and amorphous polymer composites. *Appl. Phys. Lett*. **81**, 5123–5125 (2002).
72. Stephan, C. *et al*. Characterization of singlewalled carbon nanotubes–PMMA composites. *Synth. Metals* **108**, 139–149 (2000).
73. Assouline, E. *et al*. Nucleation ability of multiwall carbon nanotubes in polypropylene composites. *J. Polym. Sci.: Part B: Polym. Phys*. **41**, 520–527 (2003).
74. Thostenson, E. T. & Chou, T.-W. Aligned multi-walled carbon nanotube-reinforced composites: processing and mechanical characterization. *J. Phys. D: Appl. Phys*. **35**, L77–L80 (2002).
75. Lourie, O., Cox, D. M. & Wagner, H. D. Buckling and collapse of embedded carbon nanotubes. *Phys. Rev. Lett*. **81**, 1638–1641 (1998).
76. Tibbetts, G. & McHugh, J. J. Mechanical properties of vapor-grown carbon fiber composites with thermoplastic matrices. *J. Mater. Res*. **14**, 2871–2880 (1999).
77. Koratkar, N., Wei, B. & Ajayan, P. Carbon nanotube films for damping applications. *Adv. Mater*. **14**, 997–1000 (2002).
78. Koratkar, N. A., Wei, B. & Ajayan, P. M. Multifunctional structural reinforcement featuring carbon nanotube films. *Compos. Sci. Technol*. **63**, 1525–1531 (2003).
79. Coleman, J. N. *et al*. Improving the mechanical properties of single-walled carbon nanotube sheets by intercalation of polymeric adhesives. *Appl. Phys. Lett*. **82**, 1682–1684 (2003).
80. Wang, Z. J. Z. *et al*. Study on poly(methyl methacrylate)/carbon nanotube composites. *Mater. Sci. Eng*. **A271**, 395–400 (1999).
81. Ajayan, P. M. Aligned carbon nanotubes in a thin polymer film. *Adv. Mater*. **7**, 489–491 (1995).
82. Moore, E. M., Ortiz, D. L., Marla, V. T., Shambaugh, R. L. & Grady, B. P. Enhancing the strength of polypropylene fibers with carbon nanotubes. *J. Appl. Polym. Sci*. **93**, 2926–2933 (2004).
83. Kumar, S., Doshi, H., Srinivasarao, M., Park, J. O. & Schiraldi, D. A. Fibers from polypropylene/nano carbon fiber composites. *Polymer* **43**, 1701–1703 (2002).
84. Vigolo, B., Poulin, P., Lucas, M., Luanois, P. & Bernier, P. *Appl. Phys. Lett*. **81**, 1210–1212 (2002).
85. Barisci, J. N. *et al*. Properties of carbon nanotube fibers spun from DNA-stabilized dispersions. *Adv. Funct. Mater*. **12**, 133–138 (2004).
86. Sreekumar, T. V. *et al*. Polyacrylonitrile single-walled carbon nanotube composite fibers. *Adv. Mater*. **16**, 58–61 (2004).
87. Kumar, S. *et al*. Synthesis, structure, and properties of PBO/SWNT composites. *Macromolecules* **35**, 9039–9043 (2002).
88. Ding, B., Kim, H. Y., Lee, S. C., Lee, D. R. & Choi, K. J. Preparation and characterization of nanoscaled poly(vinyl alcohol) fibers via electrospinning. *Fibers Polym*. **3**, 73–79 (2002).
89. Ko, F. *et al.* Electrospinning of continuous carbon nanotube-filled nanofiber yarns. *Adv. Mater*. **15**, 1161–1165 (2003).
90. Seoul, C., Kim, Y.-T. & Berk, C.-K. Electrospinning of poly(vinylidence fluoride)/dimethylformamide solutions with carbon nanotubes. *J. Polym. Sci.: Part B: Polym. Chem*. **41**, 1572–1577 (2003).
91. Mallick, P. K. *Fiber Reinforced Composites: Materials, Manufacturing, and Design* (Marcel Dekker, Inc., New York, 1993).
92. Lucas, M. *et al*. in *Structural and Electronic Properties of Molecular Nanostructures* (ed. Kuzmany, H.) 579–582 (American Institute of Physics, 2002).
93. Bower, C., Rosen, R., Jin, L., Han, J. & Zhou, O. Deformation of carbon nanotubes in nanotube–polymer composites. *Appl. Phys. Lett*. **74**, 3317–3319 (1999).
94. Ajayan, P. M., Schadler, L. S., Giannaris, C. & Rubio, A. Single-walled carbon nanotube–polymer composites: strength and weakness. *Adv. Mater*. **12**, 750–753 (2000).
95. Cooper, C. A., Young, R. J. & Halsall, M. Investigation into the deformation of carbon nanotubes and their composites through the use of Raman spectroscopy. *Compos. Part A: Appl. Sci. Manufact*. **32**, 401–411 (2001).
96. Wood, J. R., Zhao, Q. & Wagner, H. D. Orientation of carbon nanotubes in polymers and its detection by Raman spectroscopy. *Compos. Part A: Appl. Sci. Manufact*. **32**, 391–399 (2001).
97. Hobbie, E. K., Wang, H., Kim, H., Lin-Gibson, S. & Grulke, E. A. Orientation of carbon nanotubes in a sheared polymer melt. *Phys. Fluids* **15**, 1196–1202 (2003).
98. Lin-Gibson, S., Pathak, J. A., Grulke, E. A., Wang, H. & Hobbie, E. K. Elastic flow instability in nanotube suspensions. *Phys. Rev. Lett*. **92**, 0483021–0483024 (2004).
99. Qian, D., Dickey, C., Andrews, R. & Rantell, T. Load transfer and deformation mechanisms in carbon nanotube–polystyrene composites. *Appl. Phys. Lett*. **76**, 1–4 (2000).
100. Lourie, O. & Wagner, H. D. Transmission electron microscopy observations of fracture of single-wall carbon nanotubes under axial tension. *Appl. Phys. Lett*. **73**, 3527–3529 (1998).
101. Dalton, A. B. *et al*. Continuous carbon nanotube composite fibers: properties, potential applications, and problems. *J. Mater. Chem*. **14**, 1–3 (2004).
102. Marrs, B., Andrews, R., Pienkowski, D. & Rantell, T. in *Orthopaedic Research Society* (San Francisco, 2004).

103. Ren, Y., Li, F., Cheng, H.-M. & Liao, K. Tension–tension fatigue behavior of unidirectional single-walled carbon nanotube reinforced epoxy composite. *Carbon* **41**, 2159–2179 (2003).
104. Singh, S., Pei, Y., Miller, R. & Sundararajan, P. R. Long-range, entangled carbon nanotube networks in polycarbonate. *Adv. Funct. Mater.* **13**, 868–872 (2003).
105. Sandler, J. K. W. *et al*. A comparative study of melt spun polyamide-12 fibres reinforced with carbon nanotubes and nanofibres. *Polymer* **45**, 2001–2015 (2004).
106. Bradshaw, R. D., Fisher, F. T. & Brinson, L. C. Fiber waviness in nanotube-reinforced polymer composites. II. Modeling via numerical approximation of the dilute strain concentration tensor. *Compos. Sci. Technol.* **63**, 1705–1722 (2003).
107. Berhan, L., Li, Y. B. & Sastry, A. M. Effect of nanorope waviness on the effective moduli of nanotube sheets. *J. Appl. Phys.* **95**, 5027–5034 (2004).
108. Yi, Y. B., Berhan, L. & Sastry, A. M. Statistical geometry of random fibrous networks, revisited: waviness, dimensionality, and percolation. *J. Appl. Phys.* **96**, 1318–1327 (2004).
109. Thostenson, E. T. & Chou, T.-W. On the elastic properties of carbon nanotube-based composites: modelling and characterization. *J. Phys. D: Appl. Phys.* **36**, 573–582 (2003).
110. Frankland, S. J. V. & Harik, V. M. Analysis of carbon nanotube pull-out from a polymer matrix. *Surf. Sci.* **525**, L103–L108 (2003).
111. Liao, K. & Li, S. Interfacial characteristics of a carbon nanotube–polystyrene composite system. *Appl. Phys. Lett.* **79**, 4225–4227 (2001).
112. Garg, A. & Sinnott, S. B. Effect of chemical functionalization on the mechanical properties of carbon nanotubes. *Chem. Phys. Lett.* **295**, 273–278 (1998).
113. Namilae, S., Chandra, N. & Shet, C. Mechanical behavior of functionalized nanotubes. *Chem. Phys. Lett.* **387**, 247–252 (2004).
114. Barber, A. H., Cohen, S. R. & Wagner, H. D. Measurement of carbon nanotube–polymer interfacial strength. *Appl. Phys. Lett.* **82**, 4140–4142 (2003).
115. Narh, K. A. & Zhu, L. Numerical simulation of the effect of nanotube orientation on tensile modulus of carbon-nanotube-reinforced polymer composites. *Polym. Int.* **53**, 1461–1466 (2004).
116. Hilding, J., Grulke, E. A., Zhang, Z. G. & Lockwood, F. Dispersion of carbon nanotubes in liquids. *J. Dispers. Sci. Technol.* **24**, 1–41 (2003).
117. Cox, H. L. The elasticity and strength of paper and other fibrous materials. *Br. J. Appl. Phys.* **3**, 72–79 (1952).

CHAPTER 36

Reinforcement Theories

Gert Heinrich*, Manfred Klüppel†, and Thomas Vilgis‡

*Leibniz-Institut für Polymerforschung Dresden eV, Hohe Str. 6, D-01069 Dresden, Germany;
†Deutsches Institut für Kautschuktechnologie eV, Eupener Str. 33, D-30519 Hannover, Germany;
‡Max-Planck-Institut für Polymerforschung Postfach 3148, D-55021 Mainz, Germany

36.1 INTRODUCTION

The use of fillers—especially, carbon black or precipitated silica—, together with accelerated sulfur vulcanization, has remained the fundamental technique for achieving the incredible range of mechanical properties required for a great variety of modern rubber products. Increased reinforcement of the rubber material has been defined as increased stiffness, modulus, rupture energy, tear strength, tensile strength, cracking resistance, fatigue resistance, and abrasion resistance. Accordingly, a practical definition of reinforcement is the improvement in the service life of rubber articles that fail in a variety of ways, one of the most important being rupture failure accelerated by fatigue processes, such as occurs during the wear of a tire tread.

The main intention of the present contribution is to gain further inside into the relationship between disordered filler structures and the reinforcement of elastomers which is discussed mainly for the static and dynamic (shear or tensile) modulus. We will recognize that the classical approaches to (filled) rubber elasticity are not sufficient to describe the physics of such disordered systems. Instead, different theoretical methods have to be employed to deal with the various interactions and, consequently, reinforcing mechanisms on different length scales (see [1] and references therein).

36.2 HYDRODYNAMIC REINFORCEMENT AND THE ROLE OF POLYMER–FILLER INTERFACE

In the case of a dilute suspension of spherical inclusions the increase of the shear modulus G of filled rubbers is:

$$f = \frac{G}{G_0} = 1 - \frac{15(1-\nu_m)\left(1-\frac{G_i}{G_0}\right)\Phi}{7-5\nu_m+2(4-5\nu_m)\frac{G_i}{G_0}}, \qquad (36.1)$$

where ϕ is the volume fraction of the inclusions, ν_m is the Poisson ratio of the matrix, and the subscripts i and *0* refer to the inclusions and the matrix, respectively. With the assumption of perfectly rigid inclusions ($G_i \gg G_0$) and an incompressible matrix, $\nu_m = 1/2$, Eq. (36.1) becomes the Einstein-Smallwood equation:

$$f = 1 + \frac{5}{2}\Phi. \qquad (36.2)$$

Guth and Gold extended relationship in Eq. (36.2) to higher concentrations taking inter-particle disturbances into account. They found:

$$f = 1 + \frac{5}{2}\Phi + 14.1\Phi^2. \qquad (36.3)$$

However, for typical loadings of fillers up to volume fraction $\Phi \approx 0.35$, a Padé approximation of the expansion of f up to second order in the volume fraction,

$$f \approx 1 + \frac{5}{2}\Phi + 5.0\Phi^2 + \cdots \approx 1 + \frac{2.5\Phi}{1 - 2\Phi} \qquad (36.4)$$

turned out to be a suitable and theoretically founded expression for f. If the hypothesis of spherical particles is released, Eqs. (36.3), (36.4) do not have anymore a univocal formulation. For active fillers, however, f no longer depends on the simple filler volume fraction Φ but on some effective volume fraction Φ_{eff}. Medalia [2] added ''occluded rubber'' volume to the actual carbon black filler volume to obtain the ''effective'' volume of the rigid phase. ''Occluded rubber'' was defined as the rubber part of the elastomeric matrix which penetrated the void space of the individual carbon aggregates, partially shielding it from deformation. Mullins and Tobin [3] have recommended the use of the same strain amplification factor of the modulus, f, to relate the external strain ε_μ of the sample in spatial direction μ to the internal strain ratio λ_μ of the filled rubber matrix

$$\lambda_\mu = 1 + f\varepsilon_\mu \quad \text{for } \mu = 1,2,3. \qquad (36.5)$$

Very recently, Westermann *et al*. gave the first direct microscopic insights into the mechanisms of strain enhancement in reinforced networks [4]. They investigated the matrix chain deformation by small-angle neutron scattering (SANS) using a special designed filler-matrix system, a triblock copolymer of the type PI-PS-PI with a polystyrene middle block of $\Phi_{\text{PS}} = 0.18$ and two symmetric polyisoprene wings. Due to the repulsive interaction between the PS and PI blocks, this block copolymer undergoes a thermodynamically driven microphase separation; i.e., for this composition spherical PS domains are formed that can be considered as model fillers. The degree of the in situ filling was adjusted by blending the PI-PS-PI starlike micelles with a PI homopolymer matrix as the soft rubbery phase.

Extrapolation of the SANS data in [4] to the isotropic state confirms, indirectly, the presence of a diffuse PS–PI transition layer between filler and rubbery matrix with thickness $\Delta \sim 0.5$ nm around the PS domain with a mean filler radius of about 84 Å. Excellent agreement between measured reinforcing factor and corresponding model predictions could be realized within a very recent approach of Huber and Vilgis [5] for the hydrodynamic reinforcement of rubbers filled with spherical fillers of core-shell structures [6].

These ideas provide some insight, though we assume that the particles are freely dispersed, but have themselves elastic properties, which is different from the matrix. Examples for such filler particles are elastic microgels. The general result for the effective shear modulus Eq. (36.1) can be written as:

$$\frac{G}{G_0} = 1 + \frac{[\mu]\Phi}{1 - \frac{2}{5}[\mu]\Phi}, \qquad (36.1')$$

where $[\mu]$ is the intrinsic modulus of the filled matrix, i.e.,

$$[\mu] \equiv \lim_{\Phi \to o} \frac{1}{\Phi}\left[\frac{G - G_0}{G_0}\right].$$

Hence this equation is a natural generalization of the Einstein-Smallwood reinforcement law. For rigid and spherical filler particles at low volume fraction, the Einstein-Smallwood formula is recovered, since in this case the intrinsic modulus $[\mu] = 5/2$ (the intrinsic modulus $[\mu]$ follows from the solution of a single-particle problem). Exact analytical results can be obtained for the most relevant cases, such as uniform soft spheres, which describe the softening of the material in a proper way, as well as in the case of soft cores and hard shells [5].

For the reinforcement the case of hard core/soft shell filler particles appears more relevant. To some extend this case can be even viewed as the simplest model of filler particles (hard core with large modulus) coated with a soft layer (bound rubber with a slightly larger modulus compared to the matrix). For this case the intrinsic modulus can be calculated exactly as well and the resulting reinforcement can be computed. Figures 36.1 and 36.2 show the effective modulus for the filled system. Most interesting is the strong increase in reinforcement even for small bound rubber thickness. The curves have quite realistic features. Unfortunately, for comparison with experimental data still values for the effective bound rubber thickness and strength are lacking.

Vieweg *et al*. [7] estimated an interface thickness of $\Delta \sim 1.5$ nm for polymeric fillers (microgels) consisting of cured polybutadiene with a glass transition temperature (shear loss factor maximum at frequency 1 Hz) of about 100°C. The filler particles diameters were in between ~24 and 75 nm; and the sample matrices were commercial statistical styrene–butadiene emulsion copolymers vulcanized with dicumylperoxide. The method they used in [7] was to

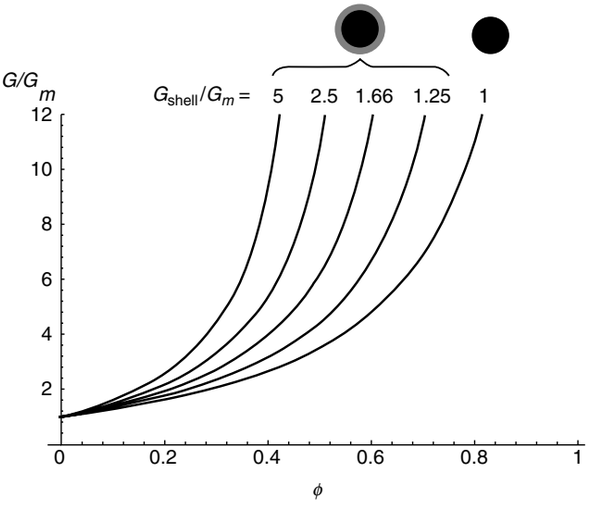

FIGURE 36.1. Filler particles with hard core: relative increase of the elastic modulus as a function of filler volume fraction for different values of the ratio shell modulus to matrix modulus The ratio between shell (total) and core radius is taken as 4/3.

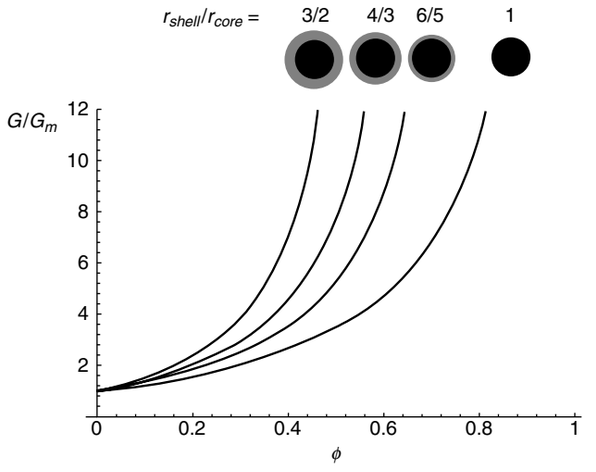

FIGURE 36.2. Filler particles with hard core: relative increase of the elastic modulus as a function of filler volume fraction for different values of the ratio between shell and core radius. The ratio shell modulus to matrix modulus of the individual particle is taken to be fixed as 2.

find the lengths of immobilized interfacial modes from optimum collapsing of (dynamic shear) data points in a scaling procedure; i.e., reinforcement in the dynamical experiments is explained by loss of mobility for longer polymer modes caused by too short lengths available. The glassy layer idea was recently improved in introducing the concept that there is a gradient of glass-transition temperature around each filler particle. This was suggested in [11] and quantified, on model filled elastomers, using both NMR and mechanical data [12–14]. Further theoretical explanations were proposed recently [15].

So far we reported some experimental determinations of the overstrain factor and filler–matrix interfaces for spherical model fillers. As already noted, active fillers like carbon black or silica are of special interest in rubber industry. First direct results of SANS measurements of the form factor of matrix chains in a cross-linked, silica filled elastomers in the isotropic state were reported, very recently, by Botti et al. [8]. Preliminary results show the influence of reinforcing agent, Si 69 in this case, on the reinforcing factor [9]. Si 69 is a bifunctional polysulfidic organosilane for the rubber industry defined chemically as *bis*(3-triethoxysilylpropyl)-tetrasulfane. It is used to improve the reinforcing capacity of fillers with silanol groups on their surface. Using this technology of precipitated silica and reinforcing agent, together with special solution polymerized statistically styrene–butadiene copolymers (S-SBR) as hydrocarbon polymer matrix, the *green tire tread* could be developed. The green tire technology dramatically improves fuel economy (rolling resistance) and overall performance (especially, antibraking-system supported wet skid behavior) over conventional tires [10].

36.3 FILLER NETWORKING AND REINFORCEMENT AT SMALL STRAIN

Filler networking in elastomer composites can be analyzed by applying TEM-flocculation- and dielectric investigations. This provides information on the fractal nature of filler networks as well as the morphology of filler–filler bonds. From the two dimensional graph in Fig. 36.3 it becomes obvious that TEM analysis gives a limited microscopic picture of the filler network morphology. This is mainly due to the spatial interpenetration of neighboring flocculated filler clusters.

Flocculation studies, considering the small strain mechanical response of the uncross-linked composites during heat treatment (annealing), demonstrate that a relative movement of the particles takes place that depends on particle size, molar mass of the polymer as well as polymer–filler and filler–filler interaction (Fig. 36.4). This provides strong experimental evidence for a kinetic cluster–cluster aggregation (CCA) mechanism of filler particles in the rubber matrix to form a filler network.

The ac-conductivity in the high frequency regime is related to an anomalous diffusion mechanism of charge carriers on fractal carbon black clusters, implying a power law behavior of the conductivity with frequency. This scaling behavior of the conductivity is observed in many carbon black filled elastomer systems. It confirms the fractal nature of filler networks in elastomers below a certain length scale, though it gives no definite information on the particular network structure [16–18]. From the dielectric investigations it becomes obvious that charge transport above the percolation threshold is limited by a hopping or tunneling mechanism of charge carriers over small gaps of order 1 nm between adjacent carbon black particles. From this finding

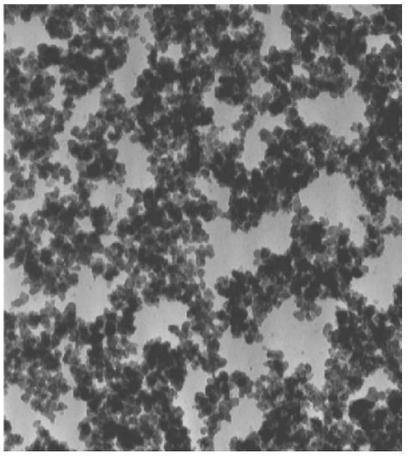

FIGURE 36.3. TEM micrograph of a carbon black network obtained from an ultrathin cut of a filled rubber sample. Reproduced from M. Klüppel and G. Heinrich, *Kautschuk, Gummi, Kunstsoffe* **58**, 217–224 (2005) with permission from Hüthig.

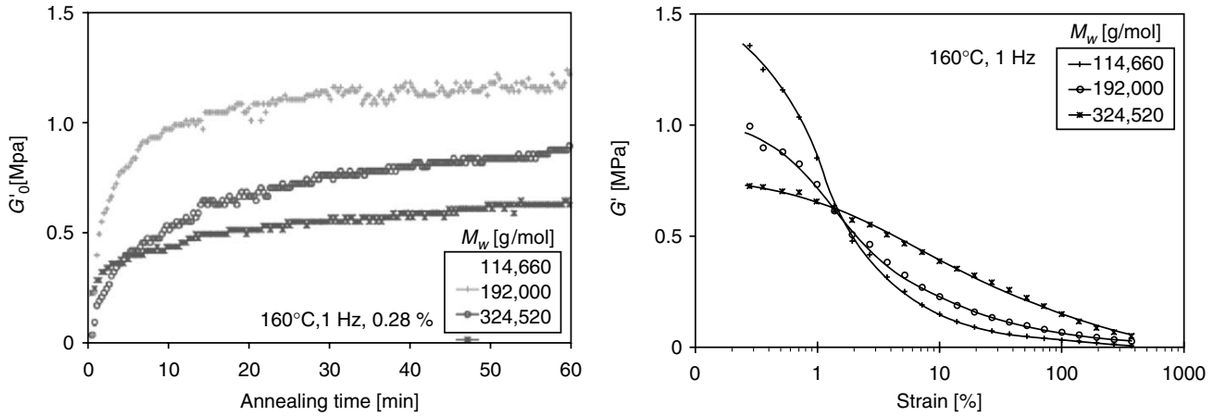

FIGURE 36.4. Flocculation behavior of the small strain modulus at 160°C of uncross-linked S-SBR-composites of various molar mass with 50 phr N234, as indicated (left) and strain dependence of the annealed samples after 60 min (right). Reproduced from M. Klüppel and G. Heinrich, *Kautschuk, Gummi, Kunstsoffe* **58**, 217–224 (2005) with permission from Hüthig.

and the observed dependency of the flocculation dynamics on the molar mass or the amount of bound rubber (Fig. 36.4), a model of filler–filler bonds in elastomers has been developed [16]. The morphological details of this model are shown schematically in Fig. 36.5.

In the framework of this approach, the mechanical stiffness of filler–filler bonds can be related to the remaining gap size between the filler particles that decreases during annealing (cross-linking) of filled rubbers. Consequently, stress between adjacent filler particles in a filler cluster is transmitted by nanoscopic, flexible bridges of glassy polymer, implying that a high flexibility and strength of filler clusters in elastomers is reached. This picture of filler–filler bonds allows for a qualitative explanation of the observed flocculation effects in Fig. 36.4 by referring to the amount of bound rubber and it is impact on the stiffness and strength of filler–filler bonds [16].

The flocculation results give strong evidence that kinetically aggregated filler clusters or networks are formed in elastomer composites, as shown schematically in Fig. 36.6. Accordingly, the model of rubber reinforcement by flexible filler clusters refers to the kinetic cluster–cluster aggregation (CCA) approach of filler networking in elastomers, which represents a reasonable theoretical basis for understanding the linear viscoelastic properties of reinforced rubbers. The CCA-model assumes that filler networks consists of a space-filling configuration of CCA-clusters with characteristic mass fractal dimension $d_f \approx 1.8$ and backbone dimension $d_{f,B} \approx 1.3$. A schematic view of this structure is shown on the right hand side of Fig. 36.6 ($\Phi > \Phi^*$). The mechanical response of this kind of filler networks depends mainly on the fractal connectivity of the CCA-clusters. It can be evaluated by referring to the Kantor-Webman model of flexible chain aggregates [19]. For the small strain modulus a power law behavior with filler concentration is predicted. The evaluated exponent $3 + d_{f,B}/(3 - d_f) \approx 3.5$ is in good agreement with the experimental data of Payne [20] for carbon black filled butyl rubber (Fig. 36.7). The predicted universal power-law behavior of the small strain modulus of filler reinforced rubbers is confirmed by a variety of experimental data, including carbon black and silica filled rubbers as well as composites with microgels (Fig. 36.8).

For a deeper understanding of the strongly nonlinear viscoelastic behavior of filler reinforced elastomers it is

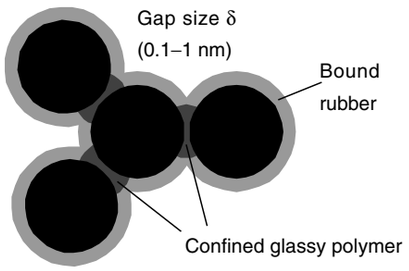

FIGURE 36.5. Schematic view of a small filler cluster in elastomers with stabilizing bound rubber and nanoscopic bridges of confined glassy polymer, implying the flexible properties of filler–filler bonds in a bulk rubber matrix. Reproduced from M. Klüppel and G. Heinrich, *Kautschuk, Gummi, Kunstsoffe* **58**, 217–224 (2005) with permission from Hüthig.

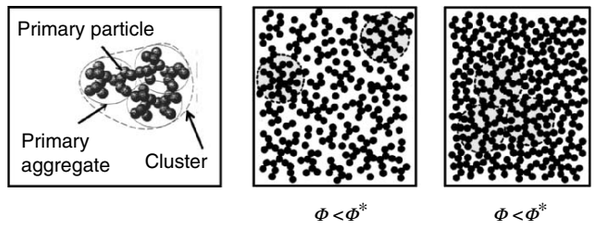

FIGURE 36.6. Schematic view of kinetically aggregated filler clusters in elastomers below and above the gel point Φ^*. The left side characterizes the local structure of carbon black clusters, build by primary particles and primary aggregates. (Every black disc in the center figure ($\Phi < \Phi^*$) and on the right hand side ($\Phi > \Phi^*$) represents a primary aggregate.) Reproduced from M. Klüppel and G. Heinrich, *Kautschuk, Gummi, Kunstsoffe* **58**, 217–224 (2005) with permission from Hüthig.

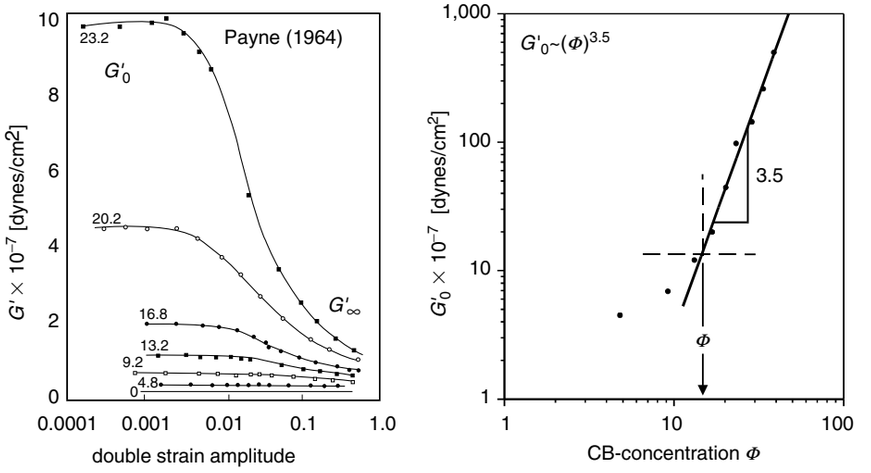

FIGURE 36.7. Payne effect of butyl composites with various amounts Φ of N330, as indicated (left) [19]. Scaling behavior of the small strain modulus of the same composites (right). Reproduced from M. Klüppel and G. Heinrich, *Kautschuk, Gummi, Kunstsoffe* **58**, 217–224 (2005) with permission from Hüthig.

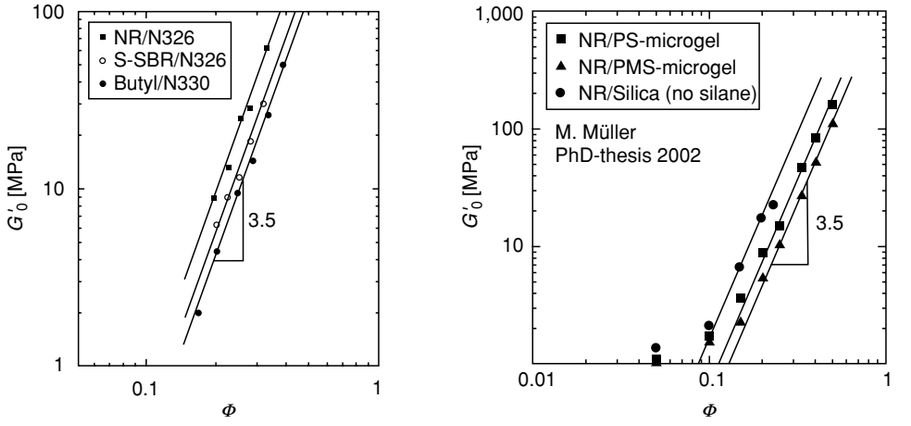

FIGURE 36.8. Scaling behavior of the small strain modulus of carbon black composites (left) and microgel or silica composites (right). In all cases an exponent close to 3.5 is found, indicating the universal character of the cluster–cluster aggregation model. Reproduced from M. Klüppel and G. Heinrich, *Kautschuk, Gummi, Kunstsoffe* **58**, 217–224 (2005) with permission from Hüthig.

necessary to consider the combined effect of immobilized polymer close to the filler interface (glassy layer) and the spatial arrangement of filler particles in the rubber matrix to form clusters [16]. A schematic view of the increased solid volume of a filler cluster due to an immobilized rubber layer is shown schematically in Fig. 36.9. The effect of a hard, glassy layer of immobilized polymer on the elastic modulus of CCA-clusters leads to the following power law dependency of the elastic storage shear modulus G′ on filler concentration Φ, particle size d, and layer thickness Δ [9]:

$$G' \cong G_p \left(\frac{(d+2\Delta)^3 - 6d\Delta^2}{d^3} \Phi \right)^{\frac{3+d_{f,B}}{3-d_f}}, \qquad (36.6)$$

where G_P is the averaged elastic bending–twisting modulus of different kinds of angular deformations of the cluster units, i.e., filler particles or bonds between filler particles. The exponent in Eq. (36.6) contains the fractal dimension d_f

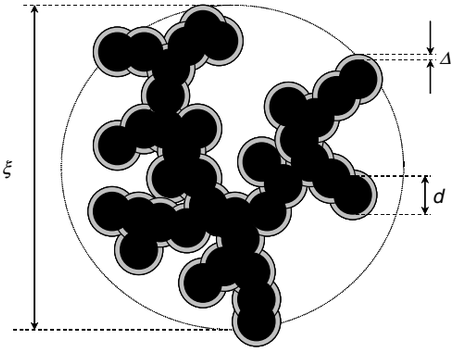

FIGURE 36.9. Schematic view of a filler cluster of size ξ in elastomers, consisting of particles (primary aggregates) of size d. The glassy layer of immobilized polymer attached to the filler surface with characteristic thickness Δ is indicated. Reproduced from G. Heinrich, M. Klüppel and T. A. Vilgis, Current Opinion in Solid State and Materials Science **6** 195–203 (2002) with permission from ELSEVIER.

of the filler cluster and the fractal dimension of its backbone $d_{f,B}$, respectively. This equation predicts a strong impact of the layer thickness Δ on the elastic modulus G′. Furthermore, the influence of particle size d becomes apparent. Using Eq. (36.6), a master procedure was applied for the small strain modulus of E-SBR samples with spherical microgel fillers of different size, yielding a layer thickness of $\Delta \sim 2$ nm [9].

Obviously, the value of G′ increases significantly if d becomes smaller, i.e., if the specific surface of the filler increases. Equation (36.6) describes the modulus G′ of the clusters as a local elastic bending–twisting term G_P times a scaling function that involves the size and geometrical structure of the clusters. Consequently, the temperature-or frequency dependency of G′ is controlled by the front factor G_P. As already pointed out, this local elastic constant is governed by the immobilized, glassy polymer between adjacent filler particles, implying that the temperature- or frequency dependence of G′ is given by that of the glassy polymer.

The model of glassy polymer bridges between adjacent filler particles of the filler network yields a physical understanding of the temperature dependence of Payne effect, i.e., the decrease of storage modulus with increasing strain amplitude. It is generally known that the amplitude of Payne effect, $G'_0 - G'_\infty$, decreases with increasing temperature. The low-strain modulus, G'_0, gradually decreases with the temperature whereas the high-strain modulus, G'_∞, remains roughly constant [9]. Hereby, two distinct mechanisms with different activation energies can be observed [21]. The low temperature one arises from the α-relaxation of the polymer which is confirmed by very large apparent activation energies, in agreement with the apparent activation energies associated to a glass transition. The high temperature one—well above the bulk glass transition temperature of the polymer system—gives activation energies in the order of ∼10 kJ/mol, which is within the range of physical (van der Waals) interactions.

In the following, we expect an Arrhenius-like temperature behavior for highly filled rubbers that is typically found for polymers in the glassy state. Therefore, we measure—far above the polymer bulk glass transition temperature—the modulus G′ for small deformation amplitudes (0.2% in our case). This is depicted schematically in Fig. 36.10. One obtains a straight line of slope E_A/R by plotting log G′(T) (or in the tensile mode log E′(T)) vs. 1/T well above the bulk glass–rubber transition region (i.e., in the range ∼20–100 °C) of the filled rubber sample. The quantity R being the gas constant.

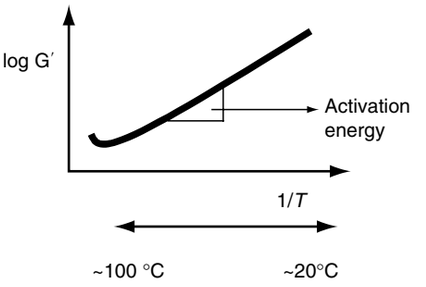

FIGURE 36.10. Schematic representation of the Arrhenius-like temperature dependency of G' and evaluation of the activation energy.

The estimation of the activation energy according to the described procedure was realized for a set of four differently filled rubber samples according to the design that is roughly sketched in Table 36.1. We note that the order of magnitude of activation energies in our systems are close to that generally presented in the literature [21].

Shore A hardness of all vulcanized samples was adjusted to approximately 70. Compounding, accelerated sulfur vulcanization and rubber physical testing was done according to standard procedures and will be described in a separate paper. As rubbers, we used standard emulsion polymerized styrene–butadiene copolymer (E-SBR 1500) and a solution polymerized styrene–butadiene copolymer (S-SBR) with a different amount of styrene and vinyl groups in comparison to the E-SBR. The used carbon black was N121 according ASTM classification. The used silica from Degussa AG was VN3 together with the coupling agent Si 69. All compounds contain a certain amount of an aromatic oil for reasons of processing. The temperature sweeps were performed with a dynamical testing device RDA from Rheometrics at frequency $f = 1$ Hz and at dynamical deformation of 0.2% in the shearing mode. The slope of the linear relation between log G' and the inverse temperature (corresponding to a temperature range T ∼ 20–80 °C) gives an estimate of the activation energy (Table 36.1). In both cases of polymers we find a lower value of the silica filled systems in comparison to the corresponding carbon black systems. Recently it was

TABLE 36.1. *Results on the variation of activation energy with filler- and polymer type, e.g., carbon black and silica filled E-SBR- and S-SBR-composites.*

Compound	E-SBR (phr)	S-SBR (phr)	Carbon black (phr)	Silica (phr)	E_A (kJ/mol)
1	100		80		13.3
2	100			80	10.2
3		100	80		12.5
4		100		80	9.3

found that the energies for silica systems were remarkably unrelated to the nature, amount and even presence of an interface agent [21].

36.4 THE DYNAMIC FLOCCULATION MODEL: STRESS SOFTENING AND FILLER INDUCED HYSTERESIS

The consideration of flexible chains of filler particles, approximating the elastically effective backbone of the filler clusters, allows for a micromechanical description of the elastic properties of tender CCA-clusters in elastomers. The main contribution of the elastically stored energy in the strained filler clusters results from the bending–twisting deformation of filler–filler bonds, which is taken into account by the elastic constant $\bar{G} = d^3 G_p$. For a consideration of filler network break-down with increasing strain, the failure properties of filler–filler bonds and filler clusters have to be evaluated in dependence of cluster size. This allows for a micromechanical description of tender but fragile filler clusters in the stress field of a strained rubber matrix [16]. A schematic view of the mechanical equivalence between a CCA-filler cluster and a series of soft and hard springs is presented in Fig. 36.11. The two springs with force constants k_s and k_b correspond to bending–twisting- and tension deformations of the filler–filler bonds with elastic constants $\bar{G}$ and Q, respectively.

The dynamic flocculation model of stress softening and filler induced hysteresis assumes that the breakdown of filler clusters during the first deformation of the virgin samples is totally reversible, though the initial virgin state of filler–filler bonds is not recovered. This implies that, on the one side, the fraction of rigid filler clusters decreases with increasing prestrain, leading to the pronounced stress softening after the first deformation cycle. On the other side, the fraction of already damaged, fragile filler clusters increases with increasing prestrain, which impacts the filler-induced hysteresis [16]. A schematic representation of the decomposition of filler clusters in rigid and fragile units for preconditioned samples is shown in Fig. 36.12.

By assuming a specific cluster size distribution $\phi(\xi_\mu)$ in reinforced rubbers, a constitutive material model of filler reinforced rubbers can be derived. As considered more closely in [16] or [22], this model is based on a nonaffine tube model of rubber elasticity, including hydrodynamic amplification of the rubber matrix by a fraction of rigid filler clusters with filler–filler bonds in the unbroken, virgin state. The filler-induced hysteresis is described by an anisotropic free energy density, considering the cyclic breakdown and reaggregation of the residual fraction of more soft, fragile filler clusters with already broken (damaged) filler–filler bonds. Accordingly, the free energy density of filler reinforced rubber consists of two contributions:

$$W(\varepsilon_\mu) = (1 - \Phi_{\text{eff}}) W_R(\varepsilon_\mu) + \Phi_{\text{eff}} W_A(\varepsilon_\mu). \tag{36.7}$$

The first addend is the equilibrium energy density stored in the extensively strained rubber matrix, including hydrodynamic reinforcement by a fraction of rigid filler clusters. The second addend considers the energy stored in the strained filler clusters (see below). The free energy density of the nonaffine tube model of rubber elasticity reads

$$W_R(\varepsilon_\mu) = \frac{G_c}{2}\left\{\frac{\left(\sum_{\mu=1}^{3}\lambda_\mu^2 - 3\right)\left(1 - \frac{T_e}{n_e}\right)}{1 - \frac{T_e}{n_e}\left(\sum_{\mu=1}^{3}\lambda_\mu^2 - 3\right)} + \ln\left[1 - \frac{T_e}{n_e}\left(\sum_{\mu=1}^{3}\lambda_\mu^2 - 3\right)\right]\right\} + 2G_e\left(\sum_{\mu=1}^{3}\lambda_\mu^{-1} - 3\right). \tag{36.8}$$

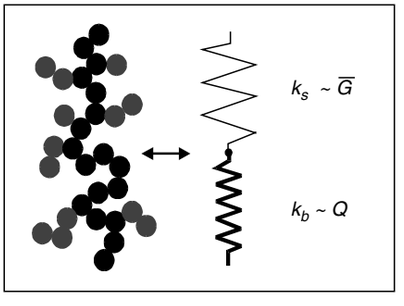

FIGURE 36.11. Schematic view demonstrating the mechanical equivalence between a filler cluster and a series of soft and stiff molecular springs, representing bending-twisting-, and tension deformation of filler–filler bonds, respectively.

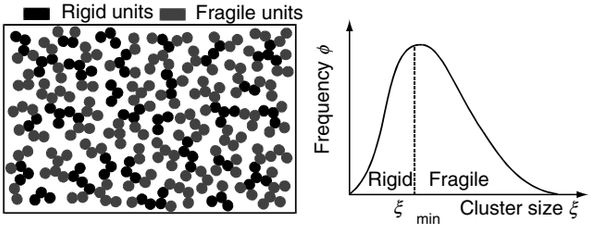

FIGURE 36.12. Schematic view of the decomposition of filler clusters in rigid and fragile units for preconditioned samples. The right side shows the cluster size distribution with the prestrain dependent boundary size ξ_{min}.

Here, n_e is the number of statistical chain segments between two successive entanglements and T_e is the trapping factor ($0 < T_e < 1$), characterizing the portion of elastically active entanglements. The first bracket term of Eq. (36.8) considers the constraints due to interchain junctions, with an elastic modulus G_c proportional to the density of network junctions. The second addend is the result of tube constraints, whereby G_e is proportional to the entanglement density of the rubber. The parenthetical expression in the first addend considers the finite chain extensibility of polymer networks by referring to a proposal of Edwards and Vilgis [23]. For the limiting case $n_e/T_e = \Sigma\lambda_\mu^2 - 3$, a singularity is obtained for the free energy W_R, indicating the maximum strain of the network, which is reached when the chains between successive trapped entanglements are fully stretched out. In the limit $n_e \to \infty$ the original Gaussian formulation of the nonaffine tube model, derived by Heinrich et al. [24] for infinite long chains, is recovered.

The presence of rigid filler clusters, with bonds in the virgin, unbroken state of the sample, give rise to hydrodynamic reinforcement of the rubber matrix. This is specified by the strain amplification factor f, which relates the external strain ε_μ of the sample to the internal strain ratio λ_μ of the rubber matrix (Eq. (36.5)). In the case of a preconditioned sample and for strains smaller than the previous straining ($\varepsilon_\mu < \varepsilon_{\mu,\max}$), the strain amplification factor f is independent of strain and determined by $\varepsilon_{\mu,\max}(f = f(\varepsilon_{\mu,\max}))$. For the first deformation of virgin samples it depends on the external strain ($f = f(\varepsilon_\mu)$). By applying a relation derived by Huber and Vilgis [25,26] for the amplification factor of overlapping fractal clusters, $f(\varepsilon_{\mu,\max})$ or $f(\varepsilon_\mu)$ can be evaluated by averaging over the size distribution of rigid clusters in all space directions. In the case of preconditioned samples this yields

$$f(\varepsilon_{\mu,\max}) = 1 + c\Phi_{\text{eff}}^{\frac{2}{3-d_f}} \sum_{\mu=1}^{3} \frac{1}{d} \left\{ \int_0^{\xi_{\mu,\min}} \left(\frac{\xi'_\mu}{d}\right)^{d_w - d_f} \phi(\xi'_\mu)\mathrm{d}\xi'_\mu + \int_{\xi_{\mu,\min}}^{\infty} \phi(\xi'_\mu)\mathrm{d}\xi'_\mu \right\}, \tag{36.9}$$

where c is a constant of order one and Φ_{eff} is the effective filler volume fraction of the structured filler particles, i.e., primary aggregates of carbon black or silica. ξ_μ is the cluster size, d is the particle size, $\phi(\xi_\mu)$ is the normalized size distribution, $d_f \approx 1.8$ is the mass fractal dimension and $d_w \approx 3.1$ is the anomalous diffusion exponent on fractal CCA-clusters [18].

The second addend in Eq. (36.7) considers the energy stored in the substantially strained fragile filler clusters

$$W_A(\varepsilon_\mu) = \sum_{\mu}^{\varepsilon_\mu/\partial t>0} \frac{1}{2d} \int_{\xi_{\mu,\min}}^{\xi_\mu(\varepsilon_\mu)} G_A(\xi'_\mu)\varepsilon_{A,\mu}^2(\xi'_\mu,\varepsilon_\mu)\phi(\xi'_\mu)\mathrm{d}\xi'_\mu, \tag{36.10}$$

where G_A is the elastic modulus and $\varepsilon_{A,\mu}$ is the strain of the fragile filler clusters in spatial direction μ. The dependency of these quantities on cluster size ξ and external strain ε_μ can be derived from basic micromechanical considerations about elasticity and fracture mechanics of tender filler clusters imbedded into a strained rubber matrix. This also allows for a specification of the strain dependent integral boundaries $\xi_\mu = \xi_\mu(\varepsilon_\mu)$ and $\xi_{\mu,\min} = \xi_\mu(\varepsilon_{\mu,\max})$. A detailed presentation of the morphological and mechanical properties of filler clusters in elastomers is found in [16].

It is demonstrated in Fig. 36.13 that the quasistatic stress–strain data (up-cycles) at different prestrains of silica filled rubbers can be well described in the scope of the above dynamic flocculation model of stress softening and filler-induced hysteresis up to large strain. Thereby, the size distribution $\phi(\xi_\mu)$ has been chosen as an isotropic logarithmic normal distribution ($\phi(\xi_1) = \phi(\xi_2) = \phi(\xi_3)$)

$$\phi(x_\mu) = \frac{\exp\left(-\frac{\ln(x_\mu/x_0)^2}{2b^2}\right)}{\sqrt{\pi/2}bx_\mu} \quad \mu = 1,2,3 \tag{36.11}$$

with the mean cluster size $x_0 \equiv \xi_0/d$ and distribution width b. A similar good agreement between experimental data and simulation as shown in Fig. 36.13 can be obtained for carbon black filled elastomers and for biaxial tension data [16]. The obtained microscopic material parameter appear reasonable, providing information on the mean cluster size ξ_0 and distribution width b, the tensile strength of filler–filler bonds Q_{ε_b}/d^3 and the polymer network chain density $\nu_c(\nu_c \sim G_c)$.

Beside the characteristic stress softening up to large strains (Mullins effect) as shown in Fig. 36.13, the model also considers the hysteresis behavior of reinforced rubbers (Payne effect). Obviously, since the sum in Eq. (36.10) is taken over stretching directions with $\partial\varepsilon/\partial t > 0$, only, up- and down cycles are described differently. An example considering a fit of the hysteresis cycles of silica filled EPDM rubber in the medium strain regime up to 50% is shown in Fig. 36.14. For these adaptations an alternative form of the cluster size distribution has been assumed, which allows for an analytical solution of the integrals in Eqs. (36.9) and (36.10):

$$\phi(x_\mu) = \frac{4x_\mu}{x_0} \exp\left(-\frac{2x_\mu}{x_0}\right) \quad \mu = 1,2,3. \tag{36.11'}$$

It must be noted that the topological constraint modulus G_e has been considered as a fixed parameter in the simulations shown in Figs. 36.11 and 36.12 and was not used as a fitting parameter. The chosen values $G_e = 0.2$ MPa and $G_e = 0.6$ MPa correspond to the known entanglement densities of the

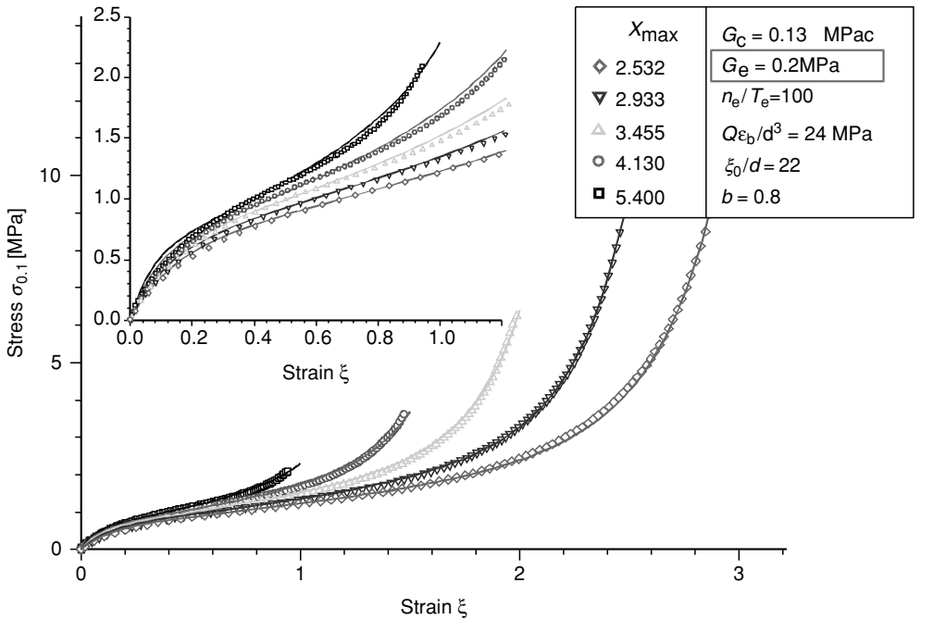

FIGURE 36.13. Uniaxial stress–strain data of S-SBR samples with 60 phr silica at different prestrains $\varepsilon_{max} = 100$, 150, 200, 250, and 300% (symbols) and fittings (lines) with the stress softening model Eqs. (36.7)–(36.11). The fitting parameters are indicated. The insert shows a magnification of the small strain data.

S-SBR- and EPDM rubber matrix, respectively, which is about three times larger in the case of EPDM.

In particular it can be shown that the dynamic flocculation model of stress softening and hysteresis fulfils a ''plausibility criterion'', important e.g., for finite element (FE) applications. Accordingly, any deformation mode can be predicted based solely on uniaxial stress–strain measurements, which can be carried out relatively easily. From the simulations of stress–strain cycles at medium and large strain it can be concluded that the model of cluster breakdown and reaggregation for prestrained samples represents a fundamental micromechanical basis for the description of nonlinear viscoelasticity of filler reinforced rubbers. Thereby, the mechanisms of energy storage and dissipation are traced back to the elastic response of tender but fragile filler clusters [16].

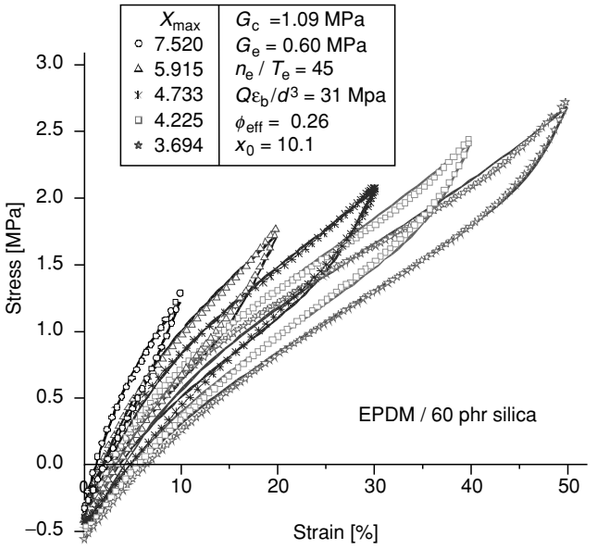

FIGURE 36.14. Uniaxial stress–strain cycles of EPDM samples with 60 phr silica at different prestrains $\varepsilon_{max} = 10$, 20, 30, 40, and 50% (symbols) and fittings (lines) with the stress softening model Eqs. (36.7)–(36.10). Here, the cluster size distribution Eq. (36.11) has been used. The obtained fitting parameters are listed in the insert.

36.5 SUMMARY AND CONCLUSIONS

During dynamic-mechanical deformation at certain (high) frequencies the silica systems are dynamically softer. This is related to ''dynamically softer'' hinge-like filler–filler interactions via the partially immobilized rubbery interfacial layers between neighboring silica aggregates within the agglomerates or the (infinite) filler network, respectively. Figure 36.3 demonstrates the structure of filler–filler bonds in a bulk rubber matrix. The gap size of neighboring filler particles with confined glassy polymer and the bound rubber layer, governing the stiffness and strength of filler–filler bonds are indicated. In general, the black discs represent primary carbon black aggregates. The finding that the silica systems are dynamically softer might explain an improved (dynamical) interlocking between

sliding tire tread rubber materials and rough road surfaces during ABS-braking on wet road surfaces where the braking process leads to a high frequency (kHz–MHz range) dynamic-mechanical deformation of the tread rubber material [10]. As a practical result, an improved wet skid performance of passenger car tires is expected with the silica technology [10].

A deeper understanding of molecular mechanisms of filler flocculation and reinforcement by active fillers like carbon black or silica represent a fundamental tool for problem solving in engineering praxis. In particular, the implementation of micromechanical models into FE-codes will open a new way for more precise simulations of the dynamic deformation and damping behavior of rubber goods, including stress softening effects and filler induced hysteresis. Even investigations and simulations of the filler cluster kinetics are of increasing interest [27,28]. This might be useful for a better understanding and prediction of complex time-dependent rubber deformations like, for example, tire tread deformations under combined driving and cornering conditions.

ACKNOWLEDGMENTS

The authors are indebted to Dr J. Meier (DIK) and Dr J. Schramm (Continental AG) for the fruitful cooperation and to the DFG (FOR 492) for financial support.

REFERENCES

1. G. Heinrich, M. Klüppel, T. A. Vilgis, Curr. Opin. Solid State Mater. Sci. **6**, 195 (2002).
2. A. Medalia, Rubber Chem. Technol. **51**, 437 (1978).
3. L. Mullins, N. R. Tobin, Rubber Chem. Technol. **39**, 799 (1966).
4. S. Westermann, M. Kreitschmann, W. Pyckhout-Hintzen, D. Richter, E. Straube, B. Farago, G. Goerigk, Macromolecules **32**, 5793 (1999).
5. G. Huber, T. A. Vilgis, Macromolecules **35**, 9204 (2002).
6. S. Westermann, W. Pyckhout-Hintzen, M. Kreitschmann, D. Richter, E. Straube, "Microscopic Deformations in Filled Polymer Networks", Proceedings Kautschuk-Herbst-Kolloquium 2002, Hannover (FRG), 99–107, 30 October–1 November 2002.
7. S. Vieweg, R. Unger, E. Hempel, E. Donth, J. Non-Cryst. Solids **235/237**, 470 (1998).
8. A. Botti, W. Pyckhout-Hintzen, D. Richter, E. Straube, V. Urban, J. Kohlbrecher, Physica B **276–278** (2000), 371; A. Botti, W. Pyckhout-Hintzen, D. Richter, E. Straube, Physica A **304**, 230 (2002); A. Botti, Microscopic deformations in filled networks. PhD thesis, University Muenster, Germany, 2001.
9. G. Heinrich, M. Klüppel, Adv. Polym. Sci. **160**, 1 (2002).
10. G. Heinrich, J. Schramm, A. Müller, M. Klüppel, N. Kendziorra, S. Kelbch, "Zum Einfluss der Straßenoberflächen auf das Bremsverhalten von Pkw-Reifen beim ABS-nass und ABS-trocken Bremsvorgang", Fortschritt-Berichte VDI, Reihe 12 (Verkehrstechnik/Fahrzeugtechnik), 69–86, 2002, Nr. 511.
11. M. J. Wang, Rubber Chem. Technol. **71**, 520 (1998).
12. H. Montes, F. Lequeux, J. Berriot, Macromolecules **36**, 8107 (2003).
13. J. Berriot, F. Lequeux, L. Monnerie, H. Montes, D. Long, P. Sotta, J. Non-Cryst. Solids **310**, 719 (2002).
14. J. Berriot, H. Montes, F. Lequeux, D. Long, P. Sotta, Macromolecules **35**, 9756 (2002); ibid. Europhys. Lett. **64**, 50 (2003).
15. G. Migliorini, V.G. Rostiashivili, T.A. Vilgis, Eur. Phys. J. **B33**, 61 (2003).
16. M. Klüppel, Adv. Polym. Sci. **164**, 1–86 (2003).
17. M. Klüppel and G. Heinrich, Rubber Chem. Technol. **68**, 623 (1995).
18. M. Klüppel, R.H. Schuster and G. Heinrich, Rubber Chem. Technol. **70**, 243 (1997).
19. Y. Kantor and I. Webman, Phys. Rev. Lett. **52**, 1891 (1984).
20. A.R. Payne, J. Appl. Polym. Sci. **8**, 2661 (1964).
21. L. Ladouce, Y. Bomal, L. Flandin, D. Labarre, "Dynamic mechanical properties of precipitated silica filled rubber: Influence of morphology and coupling agent", Paper No. 33, 157th meeting of the Rubber Division, American Chemical Society, Dallas, Texas, April 4–6, 2000.
22. M. Klüppel and J. Schramm, Macromol. Theory Simul. **9**, 742 (2000).
23. S.F. Edwards and T.A. Vilgis, Rep. Prog. Phys. **51**, 243 (1988); Polymer **27**, 483 (1986).
24. G. Heinrich, E. Straube, G. Helmis, Adv. Polym. Sci. **85**, 33 (1988).
25. G. Huber, PhD-Thesis, University Mainz, Germany (1997).
26. G. Huber and T.A. Vilgis, Euro. Phys. J. **B3**, 217 (1998); ibid. Kautschuk Gummi Kunstst. **52**, 102 (1999).
27. G. Heinrich, V. Härtel, J. Tschimmel, M. Klüppel, "Kinetics of filler structures in reinforced polymer networks", in Michler, G.H. (Hrsg.): Polymeric Materials 2004 (Halle/Saale, 29.09. – 01.10.2004), A17.
28. G. Heinrich, F.R. Costa, M. Abdel-Goad, U.Wagenknecht, B. Lauke, V. Härtel, J. Tschimmel, M. Klüppel, and A.L. Svistkov, Kautschuk, Gummi, Kunstst. **58**, 163 (2005)

CHAPTER 37

Densities of Amorphous and Crystalline Polymers

Vladyslav Kholodovych and William J. Welsh

Department of Pharmacology, University of Medicine & Dentistry of New Jersey (UMDNJ) – Robert Wood Johnson Medical School (RWJMS) and the UMDNJ Informatics Institute, Piscataway, NJ 08854

37.1 DEFINITIONS

The density ρ (or mass density) of a material is defined as its mass m per unit volume V: $\rho = m/V$. The specific volume v is the inverse of ρ: $v = 1/\rho$. The density of polymers is commonly specified in cgs units of g/cm^3, although the SI unit is kg/m^3 ($1\,g/cm^3 = 10^3 kg/m^3$) and the British engineering unit is $slugs/ft^3$ ($1\,g/cm^3 = 1.95 slugs/ft^3$). For some applications, it is more convenient to define a quantity called weight density D (or specific weight) as the weight w per unit volume V of the material: $D = w/V = (mg)/V = \rho g$, where g is the acceleration due to gravity. The corresponding units for D are lb/ft^3 in the British system and N/m^3 in SI.

The specific gravity (or relative density) ρ_{rel} of a material is the ratio of its density ρ to the density ρ_w of pure water at 4 °C (39.2°F): $\rho_{rel} = \rho/\rho_w = D/D_w$, where D_w is the weight density of water. From this definition, it is apparent that specific gravity is a dimensionless quantity. Whereas the numerical value of density will vary from one system of units to another, the specific gravity has the same value in all systems of units. Since the density of water in the cgs system is $1\,g/cm^3$, densities in that system are numerically equal to the specific gravity: $\rho(\text{in } g/cm^3) = \rho_{rel}$.

37.2 GENERAL TRENDS

Starting from the lowest members of a homologous series, the density first increases gradually then appears to approach an asymptotic limit. This behavior is illustrated in Fig. 37.1 by plots of ρ versus the number of repeated units n for the homologous series of alkanes $H[CH_2]_nH$ and the cycloalkanes $[CH_2]_n$ [1]. As n becomes larger, the difference in density between adjacent members of the series becomes relatively smaller since the changes in molecular structure are less marked.

Since synthetic polymers are formed mostly from light elements (carbon, hydrogen, oxygen, and nitrogen), the densities of solid polymers lie broadly in the range 0.8–1.8 g/cm^3. This range is considerably lower than that for inorganic materials (2.2–4.0 g/cm^3) and metals (2.7–11.5 g/cm^3). Polymers containing heavier elements such as fluorine, chlorine, and bromine, exhibit significantly higher densities: polytetrafluoroethylene (2.28 g/cm^3), poly(vinylidene fluoride) (1.77 g/cm^3), and poly(vinylidene chloride) (1.65–1.87 g/cm^3). Hydrocarbon polymers with relatively open-packed structures dominate the low end of the density scale: polypropylene (0.90 g/cm^3), ethylene–propylene copolymer elastomer (0.86 g/cm^3), and the thermoplastic polybutylene (0.60 g/cm^3) with the lowest density of all commercial polymers [2–4].

In general, the density of a polymer varies inversely with temperature but is much less sensitive to pressure. The introduction of fillers and plasticizers can alter the density and cause variations in density across a sample due to nonuniform distribution. Nevertheless, the average density is nearly invariant to small amounts of plasticizers.

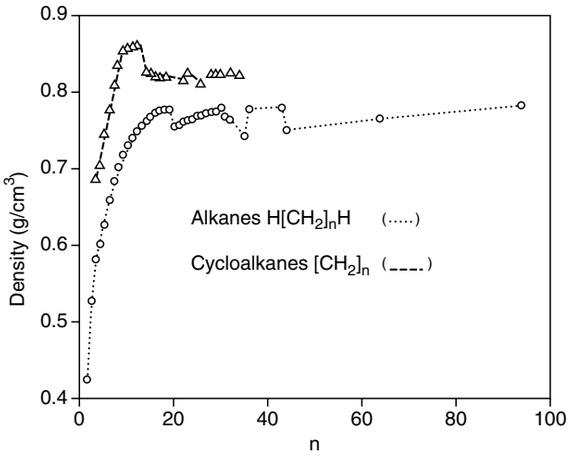

FIGURE 37.1. Density as a function of repeat unit *n* for the homologous series of alkanes (○) and cycloalkanes (Δ). Reproduced from [1].

37.3 AMORPHOUS AND CRYSTALLINE POLYMERS

Polymers can be divided into two groups morphologically: amorphous polymers and crystalline polymers. Amorphous polymers lack sufficient regularity in packing of the chains to produce the sharp x-ray diffraction pattern characteristic of highly crystalline polymers. The term crystalline polymer is actually a misnomer since no polymer is 100% crystalline, containing both crystalline domains and amorphous domains. Therefore, a more correct yet seldom used designation is ''semicrystalline'' polymer.

The polymer chains are packed together more efficiently and tightly in the crystalline region than in the amorphous region, consequently the density of the crystalline region ρ_c will typically be larger than that of the corresponding amorphous region ρ_a. For this reason, the density of a polymer increases with its degree of crystallinity x_c. The ratio ρ_c/ρ_a can vary considerably from polymer to polymer from the average value of 1.13 g/cm [3,5]. In typical cases, the ρ_c and ρ_a of a polymer will generally differ up to 15% [4]. Polymers with unsubstituted monomeric units, such as poly(ethylene) and nylon-6,6, show the largest difference between ρ_c and ρ_a. These chains crystallize in an *all-trans* conformation with particularly tight packing of the chains. In contrast, helix-forming polymers with large substituents, such as isotactic poly(styrene), pack less efficiently in the crystalline state thus $\rho_c - \rho_a$ is correspondingly smaller. For semicrystalline polymers, van Krevelen [5] gives the approximate relationship $\rho_{sc}/\rho_a = 1 + 0.13x_c$, where ρ_{sc} is the density of the (semi-) crystalline polymer.

The bulk density ρ of polymer solids is influenced strongly by the elemental composition and, to a certain degree, by the packing arrangement of chains and side groups. A polymer chain must exhibit an ordered, regular structure to allow efficient packing into the crystal lattice. Consequently, a stereoregular polymer is more likely to be crystalline and possess a higher density than the corresponding stereoirregular polymer [2–4]. Polymer chains possessing bulky, protruding side groups will pack inefficiently and are rarely crystalline. Accordingly, their densities tend to be lower than average. On the other hand, polymers capable of forming strong interchain hydrogen bonds or dipole–dipole interactions induce crystallinity and typically possess above-average densities.

Amorphous polymers generally exist as hard, rigid, glassy plastics below their glass-transition temperature T_g and as soft, flexible, rubbery materials above their T_g. Comparison of the densities of the glassy state (ρ_g) and the rubbery state (ρ_r) for various amorphous polymers indicates that $\rho_g > \rho_r$ [5].

Density is often the single parameter that is most clearly related to the physical and mechanical properties of polymers. For many polymers, properties dependent on crystallinity (e.g., stiffness, tear strength, hardness, chemical resistance, softening temperature, yield point) tend to increase with increasing density. Other properties (e.g., permeability to gases and liquids, toughness, flex life) tend to decrease with increasing density [6].

37.4 DENSITY AND CRYSTALLINITY

From the preceding discussion, it is apparent that density is a convenient measure of the degree of crystallinity. Thus ''low density'' (0.910–0.925 g/cm^3) polyethylene is about 60% crystalline, while ''high density'' (0.94–0.97 g/cm^3) polyethylene is about 95% crystalline. These differences in density arise primarily from differences in the degree of branching. The branch points sterically preclude packing into a crystal lattice in their immediate vicinity and thus lower the degree of crystallinity x_c [2–6].

The relationship between the degree of crystallinity and the observed polymer density can be derived from two slightly different perspectives, depending on whether one assumes additivity of the crystalline and amorphous regions with respect to volume ($V = V_c + V_a$) or to mass ($M = M_c + M_a$). For the former case, one obtains the relation

$$\nu = x_m \nu_c + (1 - x_m)\nu_a, \tag{37.1}$$

where $x_m = M_c/M$ is the mass crystallinity (i.e., the mass fraction that is crystalline) and ν, ν_c, and ν_a are the bulk, crystalline, and amorphous specific volumes, respectively. Solving for x_m, Eq. (37.1) yields

$$x_m = (\nu - \nu_a)/(\nu_c - \nu_a). \tag{37.2}$$

Assuming instead additivity with respect to mass, one obtains the relation

$$\rho = x_v\rho_c + (1-x_v)\rho_a. \tag{37.3}$$

Analogous to Eq. (37.1), where $x_v = V_c/V$ is the volume crystallinity (i.e., the volume fraction that is crystalline) and ρ, ρ_c, and ρ_a are the bulk, crystalline, and amorphous densities, respectively. Solving Eq. (37.3) for x_v, one obtains

$$x_v = (\rho - \rho_a)/(\rho_c - \rho_a). \tag{37.4}$$

The mass crystallinity x_m and volume crystallinity x_v thus defined are interrelated by the equation $x_m = (\nu/\nu_c)x_v = (\rho_c/\rho)x_v$. Unfortunately, it is easy to inadvertently use x_m and x_v interchangeably even though they may differ up to a few percent. In Eq. (37.5) below taken from Tadokoro [8], his "x_c" is equivalent to the x_m in Eq. (37.1) and (37.2).

$$1/\rho = x_c/\rho_c + (1 - x_c)/\rho_a. \tag{37.5}$$

37.5 EXPERIMENTAL DETERMINATION OF DENSITY

In (semi-)crystalline polymers, the measured density of a sample provides a simple way to estimate the degree of crystallinity. For example, the density of polyethylene shows a strong linear correlation with percent crystallinity [9]. The density of the crystalline region may be calculated from the dimensions of the unit cell, while the density of the amorphous region can be estimated by extrapolations from the melt density aided with a knowledge of the polymer's coefficient of thermal expansion α_T.

For a unit cell of Z monomeric units, the density ρ_c of the crystalline region is given by

$$\rho_c(\text{in g/cm}^3) = ZM/N_AV = 1.66ZM/V(\text{Å}^3), \tag{37.6}$$

where N_A is Avogadro's number (6.022×10^{23}), V is the volume of the unit cell, and M is the molecular weight of the monomeric unit [8]. The presence of any foreign matter (e.g., dirt, catalyst, solvent, additives, fillers) in the polymer sample will affect the measured density and likely reduce the degree of crystallinity. The presence of even a small number of voids can lead to more serious inaccuracies.

The bulk density ρ of even small samples may be readily determined using a density-gradient tube or by immersion in salt solutions of known density. The latter method is well adapted for rapid work in routine analyses. The density-gradient method is currently the standard method employed by numerous workers [10]. A density-gradient column contains a liquid whose density increases continuously from the meniscus down to the base [11]. Such liquids can consist, for example, of mixtures of organic solvents or of salt solutions selected to wet but not swell or dissolve the polymer sample. With the appropriate mechanical apparatus, it is possible to form density gradients in which the variation of the density with column height is linear, concave, convex, etc. The polymer sample then remains suspended at a particular height of the gradient column whose density matches the sample's density. Another, presumably more accurate, technique for measuring density is with a dilatometer [11]. Other methods for measuring density are discussed elsewhere [12].

The bulk density ρ can also be determined from straightforward measurements of the polymer's mass and volume [13]. The mass of the sample is determined by weighing it on a suitable balance. If the weighing is done in air, this apparent density should be adjusted for the buoyant effect of the air on the sample to obtain the true polymer density. The density of air under normal ambient conditions is about $0.0012\,\text{g/cm}^3$ ($0.075\,\text{lb/ft}^3$). The volume of the sample can be determined accurately using a procedure known as hydrostatic weighing based on Archimedes' Principle. The sample is weighed both in air and while submerged in a liquid of known density. The volume of the sample is then equal to its loss of weight in the liquid divided by the density of the liquid. All density measurements of solids are subject to error due to the presence of inhomogeneities such as surface imperfections, trapped air bubbles, presence of monomer, etc.

Finally, the appreciable variation in published density measurements from different workers is due in part to differences in the thermal, mechanical, and chemical history of the individual polymer samples, to differences in the laboratory skills and techniques of the worker, and to variations in the types and quality of methods employed to measure the density.

37.6 EXPERIMENTAL VALUES OF DENSITY

Tables 37.1 and 37.2 provide a compilation of representative values of macroscopic (bulk) density ρ for many of the more common polymers. For easy reference, the data are listed alphabetically by the name of the polymer. Table 37.1 contains polymers designated by their familiar or trade names (e.g., nylon, rubber), while Table 37.2 lists polymers designated by their chemical names using the prefix "poly." These are alphabetized by the letter following this prefix. For example, poly(ethylene) and poly(vinylacetate) are listed under "*e*" and "*v*", respectively. In many cases, the density of a given polymer is represented by a range of values (e.g., $0.87–0.93\,\text{g/cm}^3$) to reflect variations obtained from different sources of the data.

TABLE 37.1. *Values of density for some polymers designated by their common or trade name.*

Common or trade name	$\rho(g/cm^3)$	Reference
Acetate rayon	1.32	[6]
Acrylic	1.16	[6]
Acrylonitrile–styrene copolymer	1.075–1.10	[11a]
Acrylonitrile–styrene–butadiene copolymer (ABS)	1.04–1.07	[3]
Aniline-formaldehyde	1.22–1.25	[11a]
Ardel D-100, Arylef, U-100	1.21	[17]
Arnitel	1.17–1.27	[17]
Aramides (nomex, durette, conex, kevlar, twerlon)	1.34–1.47	[17]
Benzylcellulose	1.22	[11a]
Bisphenol-A polycarbonate (BPAPC)	1.2	[11a]
Butyl rubber	0.92	[11a]
Cellulose I	1.582–1.630	[1,14]
Cellulose II	1.583–1.62	[1,14]
Cellulose III	1.61	[14]
Cellulose IV	1.61	[1,14]
Cellulose acetate	1.28–1.32	[11a]
Cellulose acetate-butyrate	1.14–1.22	[11a]
Cellulose formate fiber	1.45	[11a]
Cellulose nitrate	1.35–1.40	[11a]
Cellulose propionate	1.18–1.24	[11a]
Cellulose triacetate	1.28–1.33	[11a,14]
Cellulose tributyrate	1.16	[14]
Chlorinated polyether	1.4	[11a]
Cotton	1.50–1.54	[1,6,11a]
Cotton, acetylated	1.43	[11a]
CXA and plexar resins (ethylene copolymers)	0.935–1.00	[17]
Durel, D-400	1.20	[17]
Ethylcellulose	1.09–1.17	[11a]
Ethylene–propylene copolymer (EPM)	0.86	[3]
Glass	3.54	[11a]
Glass and asbestos	2.5	[11a]
Hytrel	1.17–1.22	[17]
Keldax	1.67–1.83	[17]
Keltan	0.89	[17]
Kevlar	1.44	[6]
KL 1–9300/1–9310 (Bayer)	1.21–1.44	[17]
Lignocellulose	1.45	[11a]
Levasint	0.97	[17]
Levaflex	0.89–1.04	[17]
Maleic anhydride–styrene copolymer	1.286	[11a]
Melamine-formaldehyde	1.16	[11a]
Methyl polyvinyl ketone	1.12	[11a]
Methylcellulose	1.362	[11a]
Nomex	1.38	[6]
Noryl	1.06–1.2	[17]
Nylon 6	1.12–1.24	[1,3]
Nylon 66	1.13–1.15, 1.22–1.25	[1,3]
Nylon-610	1.156	[1]
Nylon-12	1.02–1.034	[1,3]
Rubber, butyl	0.92	[3]
Rubber (unvulcanized)	0.91	[1,3]
Rubber (hard) (Ebonite)	1.11–1.17	[1,11a]
Rubber, chlorinated (Neoprene) (CR), unvulcanized	1.23	[1,11a]
Rubber, chlorinated (Neoprene) (CR), vulcanized	1.32–1.42	[1]
Rubber, fluorinated silicone	1	[11a]
Rubber, silicone	0.8	[11a]
Rubber, silicone (vulcanized)	1.3–2.3	[11a]

TABLE 37.1. *Continued.*

Common or trade name	$\rho(g/cm^3)$	Reference
Rubber, styrene–butadiene (SBR), (unvulcanized)	0.93–0.94	[3,11a]
Rubber, styrene–butadiene (SBR), (vulcanized)	0.961	[11a]
Silk	1.25–1.35	[6,11a]
Santoprene	0.95–0.98	[17]
Tafmer	0.88	[17]
Toluene-sulfonamide-formaldehyde	1.21 –1.35	[11a]
Urea-formaldehyde	1.16	[11a]
Urea-thiourea-formaldehyde	1. 477	[11a]
Viscose Rayon	1.5	[6]
Vestopren	0.90–1.10	[17]
Wool	1.28–1.33	[6,11a]

TABLE 37.2. *Values of density for some polymers designated by their chemical name.*

Chemical name	$\rho(g/cm^3)$	Reference
Poly-		
acetylaldehyde	1.07	[5]
acrolein	1.322	[11a]
acrylic acid	1.22	[11a]
acrylonitrile (PAN)	1.01–1.17, 1.20	[3,11a]
acrylonitrile-vinyl acetate	1.14	[11a]
amide-6 (PA-6)	1.12–1.24	[1.3]
amide-66 (PA-66)	1.13–1.15, 1.22–1.25	[1,3]
amide-610(PA-610)	1.156	[1]
amide-12(PA-12)	1.02–1.034	[1.3]
aryl ether ketone (PEEK)	1.2, 1.3	[16,17]
arylate	1.21	[3]
benzimidazole (PBI)	1.43	[17]
bisphenol carbonate (BPAPC)	1.2	[5]
butadiene-1,2, isotactic	0.96	[1,11a]
butadiene-1,2, syndiotactic	0.96	[1,11a]
butadiene-1,4-*cis*	1.01	[1]
butadiene-1,4-*trans*	0.93– 0.97,1.01	[1,11a]
1-butene	0.85	[5]
butene	0.91–0.92	[3]
butyl acrylate	1.08	[5]
sec.-butyl acrylate	1.05	[5]
butylene	0.6	[3]
tert.-butyl methacrylate	1.03	[5]
-*n*-butyl methacrylate	1.055	[11a]
sec.-butyl methacrylate	1.04	[5]
tert.-butylstyrene	0.957	[16]
caprolactam, nylon	0.985	[16]
carbonate (PC)	1.14–1.2	[3,16]
chlorobutadiene	1.25	[11a]
chloroprene (Neoprene rubber) (CR), unvulcanized	1.23	[1,3]
chloroprene (Neoprene rubber) (CR), vulcanized	1.32–1.42	[1]
chlorotrifluoroethylene	2.03	[5]
dichlorostyrene	1.38	[11a]
2,2-dimethylpropyl acrylate	1.04	[5]
dimethylsiloxane	0.97	[16]
dodecyl methacrylate	0.93	[5]
1-ethylpropyl acrylate	1.04	[5]
etheretherketone (PEEK)	1.27	[3]

TABLE 37.2. *Continued.*

Chemical name	$\rho(g/cm^3)$	Reference
ethersulfone	1.4	[17]
ethyl acrylate	1.095, 1.12	[5,11a]
ethyl methacrylate	1.11, 1.12	[5,11a]
ethylbutadiene	0.891	[10c,16]
ethylene	0.870, 0.910–0.965	[1,6,10c,11a]
ethylene (amorphous)	0.85	[1,11a,14]
ethylene (crystalline)	0.99	[1,11a]
ethylene (high density:HDPE)	0.941–0.965	[1,3,6,15,17]
ethylene (linear low density: LLDPE)	0.918–0.935	[3,6,17]
ethylene (low density: LDPE)	0.910–0.925	[1,3,6,15,17]
ethylene (medium density: MDPE/IDPE)	0.926–0.940	[1,3,17]
ethylene (very low density: VLDPE)	0.900	[17]
ethylene glycol	1.0951	[11a]
ethylene glycol fumarate	1.385	[11a]
ethylene glycol isophthalate, cryst.	1.358	[11a]
ethylene glycol phthalate	1.352	[11a]
ethylene glycol waxes	1.15–1.20	[11a]
ethylene isophthalate	1.34	[5]
ethylene phthalate	1.34	[5]
ethylene terephthalate (PET)	1.33–1.42	[1,3,5,6]
formaldehyde	1.425	[11a]
-*n*-hexyl methacrylate	1.01	[11a]
imide	1.43	[3,6]
isobutene	0.917	[14]
isobutyl methacrylate	1.02–1.04	[5,11a]
isobutylene	0.87–0.93	[5,11a,16]
isoprene (1,4-)	0.900–0.913	[16]
-*N*-isopropylacrylamide	1.070–1.118	[11a]
isopropyl acrylate	1.08	[5]
isopropyl methacrylate	1.04	[5]
methacrylonitrile	1.1	[11a]
methyl acrylate	1.07–1.223	[5,11a,16]
methyl methacrylate (PMMA)	1.16–1.20	[1,5,11a,14]
-*p*-methylstyrene (PMA)	1.01	[17]
4-methyl-1-pentene	0.84	[5]
myrcene	0.895	[10c]
trans-octenamer (TOR)	0.91	[17]
olefin-*co*-vinyl alcohol (GL/EVAL)	0.97–1.52	[17]
oxymethylene (POM)	1.41–1.435	[1,3]
-*p*-phenylene (H resins)	1.145–1.35	[17]
phenylene oxide	1.00–1.06	[3,16]
phenylene-1,3,4-oxadiazole (POD)	1.40	[17]
polysulfide (Thiokol A)	1.6	[11a]
polysulfide (Thiokol B)	1.65	[11a]
propyl methacrylate	1.06–1.08	[5,11a]
propylene (PP)	0.85–0.92	[3,6,5,10c]
propylene, amorphous	0.87	[11a]
propylene, head-to-head	0.878	[10c]
propylene, isotactic	0.90–0.92	[1,11a]
propylene, isotactic (crystalline)	0.92–0.939	[1,11a]
propylene, syndiotactic (crystalline)	0.93	[1]
propylene oxide	1	[16]
styrene (PS)	1.04–1.09	[1,3,5,6,11a,14,17]
styrene, crystalline	1.08–1.111	[1,11a]
styrene–butadiene thermoplastic elastomer	0.93–1.10	[6]
sulfone	1.20–1.24	[3,6,17]

TABLE 37.2. *Continued.*

Chemical name	$\rho(g/cm^3)$	Reference
tetrafluoroethylene (PTFE)	2.28–2.344,2.17	[1], [17]
thiodiethanol	1.35	[17]
trifluorochloroethylene	2.11–2.13	[11a]
vinyl acetate (PVAC)	1.08–1.25	[1,3,5,11a]
vinyl alcohol (PVA)	1.21–1.31	[11a]
vinyl butyral	1.07–1.20	[11a]
vinylcarbazole	1.2	[11a]
vinyl chloride (PVC)	1.37–1.44	[1,3,5,11a,17]
vinyl chloride-*co*-methyl acrylate	1.34	[11a]
vinyl chloride, flexible	1.25–1.35	[11a]
vinyl chloride, rigid	1.35–1.55	[11a]
vinyl chloride acrylonitrile (60/40)	1.28	[11a]
vinylidene chloride (PVDC)	1.65–1.875	[3,5,6,11a]
vinylethylene	0.889	[10c,16]
vinyl formal	1.2–1.4	[11a]
-*p*-vinylphenol	1.2	[17]
-*p*-vinylphenol, brominated	1.9	[17]
vinyl pyrrolidone (PVP)	1.25	[11a]
vinyl-vinylidene chloride	1.7	[1,11a]
vinylidene fluoride (PVDF)	1.75–1.78	[1]
vinylisobutyl ether	0.91–0.92	[11a]
-*m*-xylene adipamide	1.22	[11a]

REFERENCES

1. *Physical Properties of Polymers Handbook*, Ed. James E. Mark, (AIP Press, Woodbury, New York 1996).
2. C. Hall, *Polymer Material, An Introduction for Technologists and Scientists*, second edition (Halsted Press, John Wiley & Sons, New York, 1989), p.243.
3. S. L. Rosen, *Fundamental Principles of Polymeric Materials*, second edition, (Wiley-Interscience, John Wiley & Sons, New York, 1993), pp.448.
4. H.-G. Elias, *Macromolecules*, second edition, (Plenum Press, New York, 1984), p.564.
5. D. W. van Krevelen, *Properties of Polymers: Their Correlation with Chemical Structure: Their Numerical Estimation and Prediction from Additive Group Contributions*, third edition, (Elsevier Scientific, Amsterdam, 1997), p.875.
6. F. W. Billmeyer, Jr., *Textbook of Polymer Science*, third edition (Wiley-Interscience, John Wiley & Sons, New York, 1990), p.578.
7. R. L. Miller, in *Encyclopedia of Polymer Science*, vol. 4 (John Wiley & Sons, New York, 1966), pp. 449–529.
8. H. Tadokoro, *Structure of Crystalline Polymers* (Krieger Publishing Company, Melbourne, Florida, 1990), p.486.
9. C. Tanford, *Physical Chemistry of Macromolecules* (John Wiley & Sons, New York, 1961), Chap. 2, p.710.
10. See, for example: (a) M. A. Kennedy, A. J. Peacock, and L. Mandelkern, Macromolecules **27**, 5297 (1994); (b) J. M. Carella, W. W. Graessley, and L. J. Fetters. *ibid.* **17**, 2775 (1984); (c) P. Hattam, S. Gauntlett, J. W. Mays *et al*. *ibid.* **24**, 6199 (1991).
11. (a) G. M. Brauer and E. Horowitz, in *Analytical Chemistry of Polymers*, part III, edited by G. M. Kline Interscience, (John Wiley & Sons, New York, 1962), pp. 34–45; (b) Polymer. Part B: Crystal Structure and Morphology, vol. 16, edited by R. A. Fava, in *Methods of Experimental Physics* (Editors-in Chief: L. Manor, and C. Marton) (Academic Press, New York, 1980, Chap. 10
12. (a) N. Bauer and S. Z. Lewin, "Physical Methods of Organic Chemistry", in *Technique of Organic Chemistry*, vol. 1. edited by A. Weissberger, third edition, Part I (Interscience. New York, 1959) pp. 131–190; (b) F. Schneider, *Qualitative Organic Microanalisis* (Elsevier Science & Technology Books, Amsterdam, 1964; (c) R. L. Shriner, C. Hermann, T. C. Morrill, D. Y. Curtin and R. C. Fuson. *The Systematic Identification of Organic Compounds*. 8th edition, (Wiley-Interscience, John Wiley & Sons, New York, 2003), p.723.
13. D. W. Kupke, in *McGraw-Hill Encyclopedia of Science & Technology*, edited by S. P. Parker, eighth edition (McGraw-Hill, Inc., New York, 1997), p.1510.
14. L. H. Sperling, *Introduction to Physical Polymer Science*, third edition (Wiley-Interscience, John Wiley & Sons, New York, 2001), Chaps. 4–5, p.720.
15. R. B. Seymour and C. E. Carraher, Jr., *Structure-Property Relationships in Polymers* (Kluwer Academic Publishers 1984), Chap. 12, p.246.
16. L. J. Fetters, D. J. Lohse, D. Richter *et al*., Macromolecules **27**, 4639 (1994).
17. H.-G. Elias, F. Vohwinkel, *New Commercial Polymers 2*, English edition (Gordon and Breach Science publishers, New York, 1986) p.508.

CHAPTER 38

Unit Cell Information on Some Important Polymers

Edward S. Clark

Department of Materials Science and Engineering, The University of Tennessee, Knoxville, TN 37996

In this chapter, drawings are presented for the principal crystallographic forms of several important commercial polymers using CSC Chem3D Plus® (Cambridge Scientific). X ray data are presented for polymorphs where available. The crystallographic axis most nearly parallel to the continuity of the covalent bonds (fiber axis) is indicated by †. References are given for the papers used in obtaining the data. Where available, intensity data are given for the main reflections. However, it must be strongly emphasized that observed intensities are very much a function of the crystallinity and molecular orientation in the sample as well as the experimental technique used. The usual designations of *s*, *m*, *w* (strong medium and weak) are used. See Figures 38.1–38.23 and Tables 38.1–38.14. A review of unit cells of many different polymers is given in Chapter 7 of Tadokoro [1].

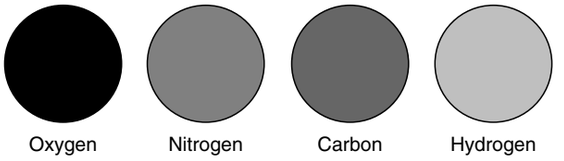

FIGURE 38.1. Key to shading of atoms.

38.1 POLYETHYLENE [—$(CH_2)_2$—]

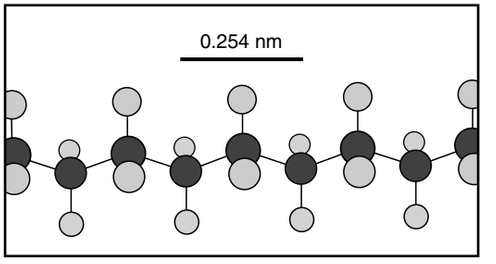

FIGURE 38.2. Polyethylene.

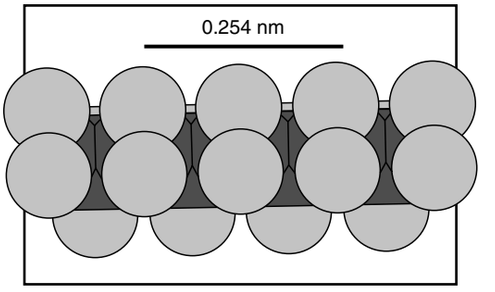

FIGURE 38.3. Polyethylene.

TABLE 38.1. *Polyethylene (orthorhombic 25 °C) [-$(CH_2)_2$-].*[a]

hkl	*d*-value (nm)	2θ (deg) ($\lambda = 0.1542$ nm)	Relative intensity
110	0.4115	21.59	vvs
200	0.3703	24.03	s
020	0.2475	36.30	m
310	0.2209	40.84	m
220	0.2058	44.01	m
011	0.2268	39.75	m
111	0.2168	41.65	m
201	0.2101	43.05	s
211	0.1934	46.98	m

[a]Space group Pnam [D_{2h}^{16}], $N = 4(CH_2)$. $a = 0.74069$ nm; $b = 0.49491$ nm; and $c = 0.25511$ nm†. Cell volume $= 0.09352$ nm^3. Density $= 996.2$ kg/m^3. (From Refs. 2 and 3.) See also Ref. 4.

TABLE 38.2. *Polyethylene high pressure (>3 kbar, near melting point) [-$(CH_2)_2$-].*[a]

hkl	*d*-value (nm)	2θ (deg) ($\lambda = 0.1542$ nm)	Relative intensity
110 (ortho)	4.227	21.02	s

[a]Space group (Hexagonal, ortho); $N = 4(CH_2)$. $a = 0.846$ nm; $b = 0.488$ nm; and $c = 0.245$ nm†. Cell volume $= 0.101$ nm^3 (approx.). Density $= 920$ kg/m^3 (approx.). (From Refs. 5 and 6.)

TABLE 38.3. *Polyethylene (metastable monoclinic 25 °C) [-$(CH_2)_2$-].*[a]

hkl	*d*-value (nm)	2θ (deg) ($\lambda = 0.1542$ nm)	Relative intensity
001	0.4558	19.47	s
200	0.3849	23.11	s
$\bar{2}01$	0.3523	25.28	s
201	0.2576	34.82	w
$\bar{4}01$	0.2008	45.15	m
400	0.1925	47.23	m
$11\bar{1}$	0.2216	40.72	m
111	0.2047	44.26	m
$11\bar{2}$[b]	0.1739	52.62	s

[a]Space group C2/m [C_{2h}^3]; $N = 4(CH_2)$. $a = 0.809$ nm; $b = 0.253$ nm†; and $c = 0.479$ nm. Cell volume $= 0.09329$ nm^3. Density=998 kg/m^3.
[b]Overlap with orthorthombic phase. (From Ref. 4.)

38.2 POLYPROPYLENE [—CH_2—CH(CH_3)—]

Polypropylene isotactic beta form. Space group $P3_121[D_4^3]$ or $P3_221[D_6^3]$. $N = 9$. $a = 1.103$ nm; $b = 1.103$ nm; $c = 0.649$ nm and $\gamma = 120°$. Cell volume $= 0.672$ nm^3. Density $= 936$ kg/m^3. (From Ref. 14.)

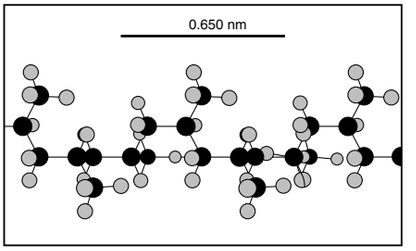

FIGURE 38.4. Polypropylene (Alpha form).

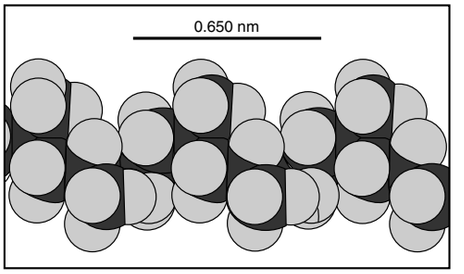

FIGURE 38.5. Polypropylene (Alpha form).

TABLE 38.4. *Polypropylene [-CH_2-CH(CH_3)-], isotactic alpha form. Space group C2/c [C_{2h}^6] or Cc [C_s^4].*[a]

hkl	*d*-value (nm)	2θ (deg) ($\lambda = 0.1542$ nm)	Relative intensity
110	0.626	14.14	vs
040	0.524	16.92	vs
130	0.478	18.55	s
111	0.417	21.31	s
$13\bar{1}$,041	0.406	21.86	s
150,060	0.351	25.35	s
200	0.328	27.18	m
220	0.313	28.51	m

[a]$N = 12$. $a = 0.665$ nm; $b = 2.096$ nm; $c = 0.650$ nm†; and $\beta = 99.33°$. Cell volume $= 0.894$ nm^3. Density $= 938$ kg/m^3. (From Ref. 8.)

TABLE 38.5. *Polypropylene [-CH_2-CH(CH_3)-], isotactic-gamma form. Space group Fddd [D_{2h}^{24}].*[a]

hkl	*d*-value (nm)	2θ (deg) ($\lambda = 0.1542$ nm)	Relative intensity
111	0.6391	13.86	m
113	0.5863	15.11	w
008	0.5210	17.02	s
115	0.5110	17.35	w
117	0.4380	20.27	m
202	0.4169	21.31	s
026	0.4045	21.97	s
206	0.3628	24.53	w
0012	0.3473	25.65	m
224	0.3088	28.91	m

[a]$N = 48$. a=0.851 nm; $b = 0.995$ nm; and $c = 4.168$ nm†. Cell volume $= 3.529$ nm^3. Density $= 0.950$ kg/m^3. (From Refs. 15 and 16.)

TABLE 38.6. *Polypropylene [-CH_2-$CH(CH_3)$-] syndiotactic monoclinic — Form 1. Space group $P2_1$ [C_{2h}^5].*[a]

hkl	*d*-value (nm)	2θ (deg) ($\lambda = 0.1542$ nm)	Relative intensity
200	7.16	12.4	s
020	5.57	15.9	m
−211	4.70	18.9	m
220	4.39	20.2	w
121	4.26	20.8	m
002	3.75	23.7	w
400	3.58	24.9	w
−321	3.27	27.2	w

[a]N = 16; $a = 14.31$ nm; $b = 11.15$ nm; $c = 7.5$ nm†; and $\gamma = 90.3^\circ$. Cell volume = 1.196 mn^3. Density = 934 kg/m^3. (From Ref. 12.)

TABLE 38.7. *Poly (ethylene terephthalate) [-(C=O)-(C_6H_4)-(C=O)-CH_2-CH_2-]; Space group $P\bar{1}$ [C_i^1].*[a]

hkl	*d*-value (nm)	2θ (deg) ($\lambda = 0.1542$ nm)	Relative intensity
$0\bar{1}1$	0.5417	16.36	s
010	0.5014	17.69	s
$\bar{1}11$	0.4092	21.72	m
$1\bar{1}0$	0.3880	22.92	s
100	0.3435	25.94	vs
$1\bar{1}1$	0.3164	28.20	w
101	0.2699	33.20	w

[a]$N = 1$. $a = 0.4509$ nm; $b = 0.5882$ nm; $c = 1.0787$ nm†; $\alpha = 100.01^\circ$; $\beta = 118.36^\circ$; and $\gamma = 110.56^b$. Cell volume = 0.2146 nm^3. Density = 1485 kg/m^3. (From Refs. 8,9,10.)

38.3 POLY (ETHYLENE TEREPHTHALATE) [—(C=O)—(C_6H_4)—(C=O)—CH_2—CH_2—]

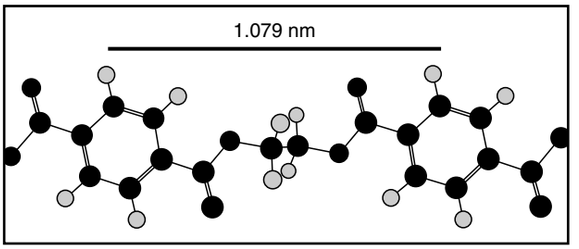

FIGURE 38.6. Poly (ethylene terephthalate).

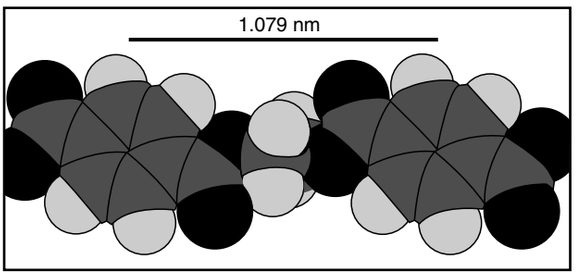

FIGURE 38.7. Poly (ethylene terephthalate).

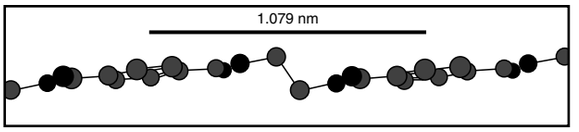

FIGURE 38.8. Poly (ethylene terephthalate).

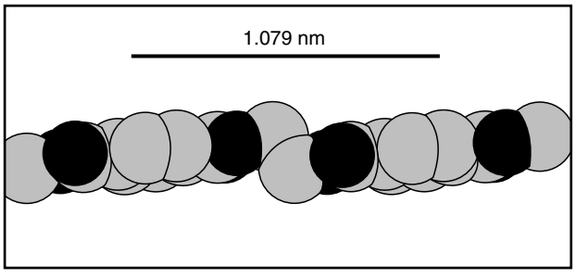

FIGURE 38.9. Poly (ethylene terephthalate).

38.4 POLYCAPROLACTAM (PA6) [—NH—(CH_2)$_5$—(C=O)—]

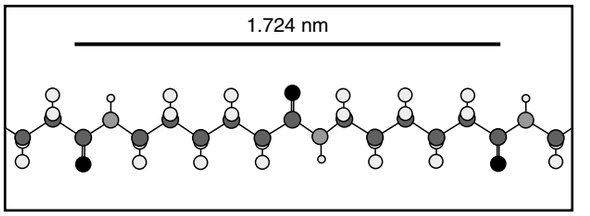

FIGURE 38.10. Polycaprolactam.

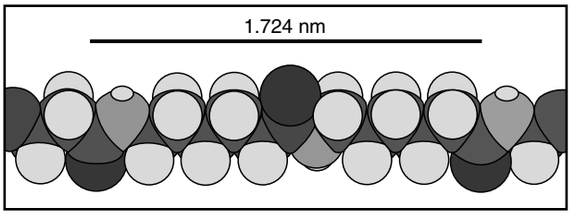

FIGURE 38.11. Polycaprolactam.

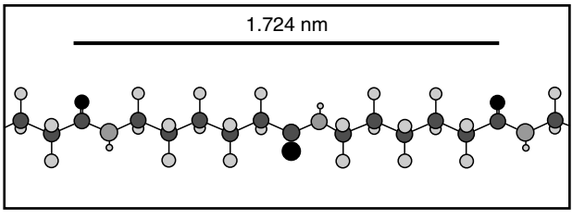

FIGURE 38.12. Polycaprolactam.

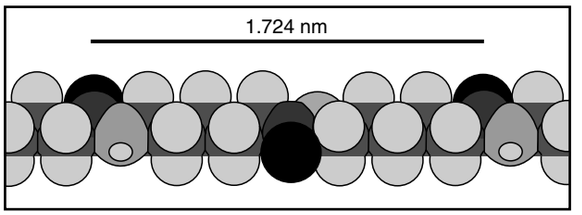

FIGURE 38.13. Polycaprolactam.

TABLE 38.8. *Polycaprolactam (PA6) alpha form [-NH-$(CH_2)_5$-(C=O)-]; Space group $P2_1/m$ [C_{2h}^2].*[a]

hkl	*d*-value (nm)	2θ (deg) ($\lambda = 0.1542$ nm)	Relative intensity
200	0.4416	20.11	vs
211,210	0.4387	20.26	w
002,202	0.3646	24.42	vvs
$\bar{2}$02,402	0.2373	37.93	m
204	0.2001	45.32	w
004,404	0.1823	50.04	w
$\bar{1}$71,271	0.2186	41.30	m
$\bar{2}$71,371	0.1959	46.35	m

[a] $N = 8$. $a = 0.956$ nm; $b = 1.724^{\dagger}$ nm; $c = 0.801$ nm; and $\beta = 67.5^{\circ}$. Cell volume $= 0.1220\,\text{nm}^3$. Density $= 1232\,\text{kg/m}^3$. (From Refs. 16 and 17.) See also Ref. 18.

Polycaprolactam (PA6) gamma form. Space group $P2_1/a$ [C_{2h}^5]. $N = 4$; $a = 0.933$ nm; $b = 1.688^{\dagger}$ nm; $c = 0.478$ nm; and $\beta = 121^{\circ}$. Cell volume $= 0.645\,\text{nm}^3$. Density $= 1160\,\text{kg/m}^3$. (From Ref. 19.)

38.5 POLY (HEXAMETHYLENE ADIPAMIDE) (PA66) [—NH—$(CH_2)_6$—NH—(C=O)—$(CH_2)_4$—(C=O)—]

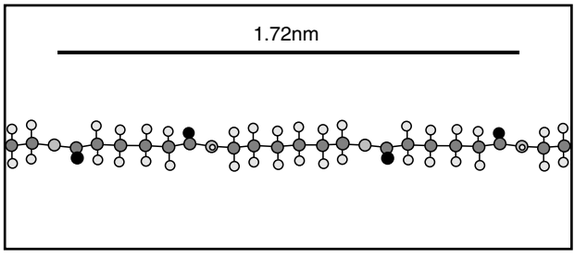

FIGURE 38.14. Poly (hexamethylene adipamide).

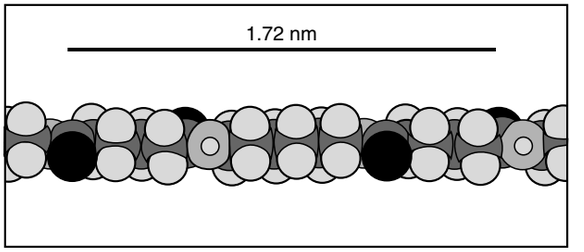

FIGURE 38.15. Poly (hexamethylene adipamide).

TABLE 38.9. *Poly (hexamethylene adipamide) (PA66) alpha form [-NH-$(CH_2)_6$-NH-(C=O)-$(CH_2)_4$-(C=O)-]. Space group $P\bar{1}$[C_i^1].*[a]

hkl	*d*-value (nm)	2θ (deg) ($\lambda = 0.1542$ nm)	Relative intensity
002	0.641	13.83	w
100,010,110	0.390	22.96	vvs
015	0.335	26.65	w
$\bar{1}$10,210	0.236	38.12	s
017,127	0.233	38.69	w
$\bar{1}$17,027	0.218	41.37	w
$\bar{1}$17,227	0.194	46.71	w
020,220	0.183	49.70	s

[a] $N = 1$. $a = 0.49$ nm; $b = 0.54$ nm; $c = 1.72^{\dagger}$ nm; $\alpha = 48.5^{\circ}$; $\beta = 77.0^{\circ}$; and $\gamma = 63.5^{\circ}$. Cellvolume $= 0.303\,\text{nm}^3$. Density $= 1238\,\text{kg/m}^3$. (From Ref. 20.)

Poly(hexamethylene adipamide) (PA 66) beta form. Space group $P\bar{1}$[C_i^1]. $N = 2$. $a = 0.49$ nm; $b = 0.08$ nm; $c = 1.72^{\dagger}$ nm; $\alpha = 90^{\circ}$; $\beta = 77.0^{\circ}$; and $\gamma = 67^{\circ}$. Cell volume $= 0.602\,\text{nm}^3$. Density $= 1220\,\text{kg/m}^3$. (From Ref. 20.)

38.6 POLYOXYMETHYLENE [—CH_2—O—]

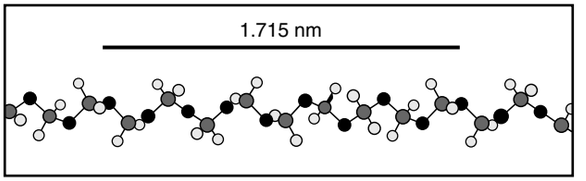

FIGURE 38.16. Polyoxymethylene.

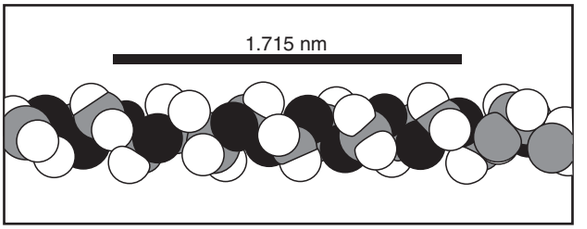

FIGURE 38.17. Polyoxymethylene.

TABLE 38.10. *Polyoxymethylene [-CH_2-O-] trigonal. Space group $P3_1$ or $P3_2$ [C_3^2 or C_3^3]; $Z = 9[19]$*[a].

hkl	*d*-value (nm)	2θ (deg) ($\lambda = 0.1542$ nm)	Relative intensity
100	0.3872	22.97	vvs
105	0.2587	34.67	s
110	0.2236	40.34	s
113	0.2086	43.38	m
108	0.1895	48.00	m
115	0.1881	48.40	s
109	0.1729	52.96	m
205	0.1692	54.22	s
118	0.1558	59.29	m
208	0.1446	64.45	m

[a] $a = 0.4471$ nm and $c = 1.739$ nm†. The repeat unit is close to $29/16 = 1.81$ units/turn; $9/5 = 1.80$ giving $c = 1.739$ nm which is approximate. Cellvolume $= 0.3011$ nm^3. Density $= 1491$ kg/m^3.
[b] Based on 9/5 helix (From Refs. 21–23).

TABLE 38.11. *Polyoxymethylene [-CH_2-O-] (othorhombic). Space group $P2_12_12_1[D_4^2]$*[a].

hkl	*d*-value (nm)	2θ (deg) ($\lambda = 0.1542$ nm)	Relative intensity
020	0.3825	23.25	vs
111	0.2673	33.52	s
021	0.2606	34.41	s
201	0.1981	45.79	m
131	0.1901	47.84	m
331	0.1759	51.97	w
041	0.1685	54.46	w
132	0.1396	67.06	w
222	0.1337	70.45	w

[a] $N = 4$[-CH_2-O-]. $a = 0.477$ nm; $b = 0.765$ nm; and $c = 0.356$ nm†. Cellvolume $= 1300$ nm^3. Density $= 1540$ kg/m^3. (From Ref. 24.)

38.7 POLYTETRAFLUOROETHYLENE [—(CF_2)—]

Polytetrafluoroethylene [-(CF_2)-] Form I (above 30 °C). Space group (hexagonal packing of helical chains of variable twist). Hexagonal approximation $a = 0.567$ nm (35 °C) to 0.574 nm (218 °C). c=0.1300 nm per CF_2 group†. Cell volume $= 0.0362 - 0.0371$ nm^3 per CF_2 group. Density $= 2290 - 2240$ kg/m^3. Diffuse pattern with sharp $hk0$ reflections (hexagonal). (From Ref. 25.)

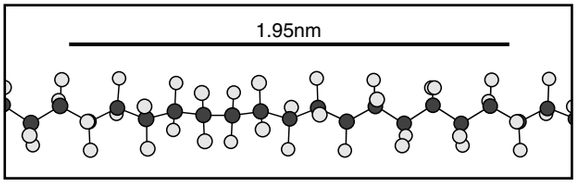

FIGURE 38.18. Polytetrafluoroethylene (From IV).

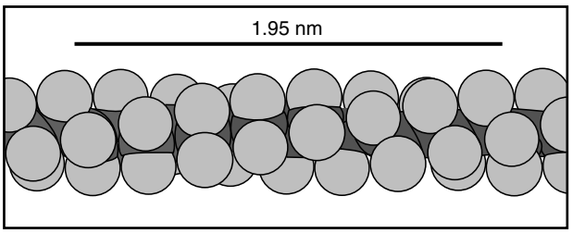

FIGURE 38.19. Polytetrafluorethylene (Form IV).

TABLE 38.12. *Polytetrafluoroethylene [-(CF_2)-] Form II (below 19 °C). Observed hk0 reflections*[a].

d-value (nm)	2θ (deg) ($\lambda = 0.1542$ nm)	Relative intensity
0.4866	18.23	vvs
0.2823	31.69	vs
0.2447	36.73	s
0.2414	37.24	m
0.1850	49.26	m
0.1828	49.88	m
0.1627	56.58	m

[a] Space group (approximate) P1 [C_1^1] (Complex structure with a regular helix of 2.1598 CF_2 units per turn). Orthogonal approximation; $a = 0.9649$ nm; $b = 0.5648$; and $c = 0.1300$ nm per CF_2 group†. Cell volume $= 0.03542$ nm^3 per CF_2 group. Density $= 2340$ kg/m^3. (From Ref. 9.)

Polytetrafluoroethylene [-(CF_2)-] Form III (high pressure) Space group Pnam [D_{2h}^{16}]. a=0.75 nm; b=0.56 nm; and c=0.26 nm†. Cell volume $= 0.1092$ nm^3. Density $= 3040$ kg/m^3. Peaks attributed to a monoclinic phase are also observed. (From Ref. 27.)

TABLE 38.13. *Polytetrafluoroethylene [-(CF_2)-] Form IV (19–30 °C)*[a].

hkl	*d*-value (nm)	2θ (deg) ($\lambda = 0.1542$ nm)	Relative intensity
100	0.4902	18.10	vvs
110	0.2830	31.61	s
200	0.2451	36.67	s
210	0.1853	49.18	m
300	0.1634	56.30	m
220	0.1415	66.02	m
310	0.1359	69.09	m
107	0.2422	37.12	vs
108	0.2183	41.37	vs
117	0.1985	45.70	w
118	0.1847	49.34	w

[a] Space group (presumed) $P3_1$ or $P3_2$ [C_3^2 or C_3^3]; Rotational disorder of helical chains. $Z = 15(CF_2)$. a=0.566 nm and $c = 1.95$ nm†. Cell volume $= 0.0541$ nm^3. Density $= 2302$ kg/m^3. (From Refs. 25, 26, 28 and 29).

38.8 POLY(P-PHENYLENE TEREPHTHALAMIDE) (PTTA) [—(C=O)—(C_6H_4)—(C=O)—NH—(C_6H_4)—(NH)—]

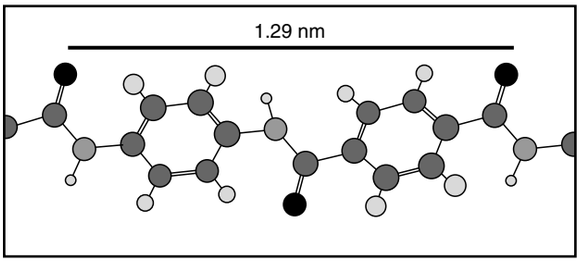

FIGURE 38.20. Poly(*p*-phenylene terephthalamide).

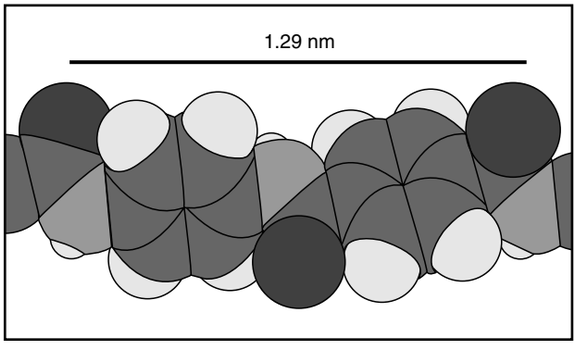

FIGURE 38.21. Poly (*p*-phenylene terephthalamide).

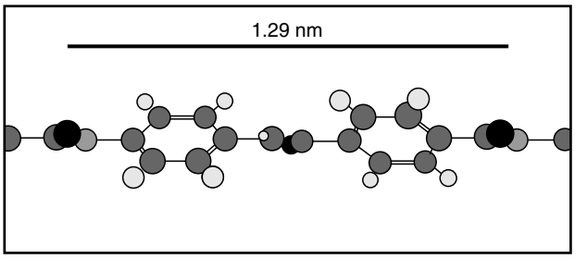

FIGURE 38.22. Poly (*p*-phenylene terephthalamide).

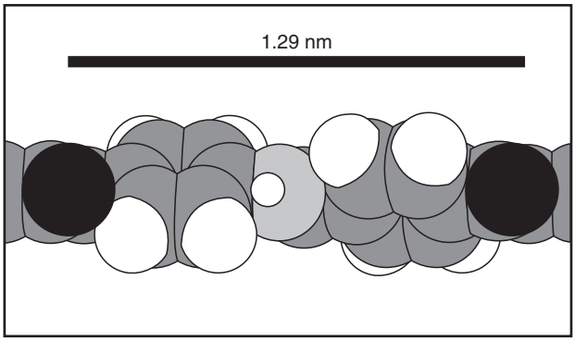

FIGURE 38.23. Poly (*p*-Phenylene terephthalamide).

TABLE 38.14. *Poly (p-phenylene terephthalamide) (PPTA) [-(C=O)-(C_6H_4)-(C=O)-(NH)-(C_6H_4)-(NH)-]; Space group $P2_1/n[C^5_{2h}]$, Monoclinic (pseudo-orthohombic)*[a].

hkl	*d*-value (nm)	2θ (deg) ($\lambda = 0.1542$ nm)	Relative intensity
110	0.4327	20.53	vs
200	0.3935	22.60	vs
020	0.2590	34.63	vw
310	0.2340	38.46	m
220	0.2163	41.75	w
011	0.4807	18.46	vw
111	0.4102	21.66	ms
211	0.3045	29.33	s
021	0.2539	35.35	w
121	0.2417	37.20	vw
311	0.2303	39.12	vw

[a] $N = 2$. $a = 0.787$ nm; $b = 0.518$ nm; and $c = 1.29$ nm†. ($\gamma = 90°$) Cell volume = 0.5259 nm^3. Density = 1504 kg/m^3. (From Ref. 30.) (See also Ref. 31).

REFERENCES

1. H. Tadokoro, in *Structure of Crystalline Polymers* (John Wiley & Sons, New York, 1979).
2. W. R. Busing, Macromolecules **23**, 4608 (1990).
3. C. W. Bunn, Faraday Soc. **35**, 482 (1939).
4. M. Lorenzen and M. Hanfland, Macromolecules **36**, 6059 (2003).
5. D. C. Bassett, S. Block, and J. Piermarini, J. Appl. Phys. **45**, 4146 (1974).
6. M. Yasuniwa, R. Enoshita, and T. Takemura, Jpn. J. Appl. Phys. **15**, 1421 (1976).
7. T. Seto, T. Hara, and K. Tanaka, Jpn. J. Appl. Phys. **7**, 31 (1968).
8. G. Natta and P. Corradini, Nuovo Cimento, Supplement **15**, 40–51 (1960).
9. S. V. Meille, D. R. Ferro, S. Brückner, *et al*. Macromolecules **27**, 2615 (1994).
10. S. V. Meille, S. Brückner, and W. Porzio, Macromolecules **23**, 4114 (1990).
11. B. Lotz, S. Graf, and J. C. Whitmann, J. Polym. Sci. **B24**, 2017 (1986).
12. D. C. De Rosa, F. Auriemma, and P. Corradini, Macromolecules **29**, 7452 (1996).
13. R. de P. Daubeny,. C. W. Bunn, and C. J. Brown, Proc. R. Soc. London **226A**, 531 (1954).
14. H. G. Killian, H. Halboth, and E. Jenkel, Kolloid-Zeitschrift **172**, 166 (1960).
15. Y. Fu, W. R. Busing, Y. Jin, *et al*. Macromolecules **26**, 2187 (1993).
16. D. R. Holmes, C.W. Bunn, and D. J. Smith, J. Polym. Sci. **27**, 159 (1955).
17. P. Simon and Gy. Argay, J. Polym. Sci. Polym. Phys. Ed. **16**, 935 (1978).
18. C. J. Parker and P. H. Lindenmeyer, J. Appl. Polym. Sci. **21**, 821 (1977).
19. H. Arimoto, J. Polym. Sci. **A2**, 2283 (1964).
20. C. W. Bunn and E. V. Garner, Proc. R. Soc. **A189**, 39 (1947).
21. Y. Takahashi and H. Tadokoro, J. Polym. Sci., Polym. Phys. **17**, 537 (1979).
22. G. A. Carazzolo, J. Polym. Sci. **A1**, 1573 (1963).
23. R. Aich and P. C. Hägele, Prog. Colloid Polym. Sci. **71**, 86 (1985).
24. G. A. Carazzolo and M. Mammi, J. Polym. Sci. **A1**, 965 (1963).
25. E. S. Clark and L.T. Muus, Z. Kristallogr. **117**, 2/3 119 (1962).
26. J. J. Weeks, E. S. Clark, and R. K. Eby, Polymer **22** 1480 (1981).
27. R. K. Eby, E. S. Clark, B. L. Farmer, *et al*. Polymer **31**, 2227 (1990).
28. E. S. Clark, J. Macromol. Sci. Phys. **B1**, 795 (1967).
29. M. Kimmig, G. Strobl, and B. Stühn, Macromolecules **27**, 2481 (1994).
30. M. G. Northolt, Eur. Polym. J. **10**, 799 (1974).
31. M. G. Northolt and H. A. Stuut, J. Polym. Sci., Polym. Phys., **16**, 939 (1978).

CHAPTER 39

Crystallization Kinetics of Polymers

Rahul Patki*, Khaled Mezghani†, and Paul J. Phillips*

*Department of Chemical and Materials Engineering, University of Cincinnati, Cincinnati, OH 45221-0012
†Department of Mechanical Engineering, King Fahd University of Petroleum and Minerals, Dhahran 31261, Saudi Arabia

39.1 INTRODUCTION

39.1.1 Crystallization Studies and Analyses

There are several methods for studying crystallization kinetics of polymers, which fall into two general categories: bulk or volumetric analysis, and crystal growth analysis. The simplest experimental study is the bulk growth, but it is the most difficult to analyze in detail. However, it can be analyzed partially using the Avrami equation [1,2].

The Avrami equation was derived from prior work by Poisson based on expanding waves created by raindrops on a pond and results in the general equation:

$$1 - v_c(t) = \exp(-Kt^n), \tag{39.1}$$

where n is known as the Avrami index and $v_c(t)$ is the crystalline volume fraction of the polymer. In general, n and K characterize the nucleation type and the crystal growth geometry. Theoretically, the Avrami index, n, can be derived as an integer which varies between 1 and 6 (Table 39.1), but due to the crystallization complexity, n is usually a decimal number. For better interpretation of the Avrami index, one needs good information about nucleation, morphology, and the mechanism of polymer crystallization.

There are several methods available for the study of bulk crystallization, including dilatometry, differential scanning calorimetry, and x-ray diffraction. Optical microscopy is the most versatile method for the study of crystallization since the use of a trinocular permits the simultaneous measurement of bulk crystallization (using transmitted light intensity) and of crystal growth kinetics using direct observation.

Depolarized light microscopy, DLM, can be used to measure light intensity (I) as a function of time (t) and permits Avrami type analyses. From this type of experiment the volume fraction, $v_c(t)$, is not directly available; therefore, a relationship between the light intensity, I, and $v_c(t)$ is needed. If it is assumed that complete crystallization is reached at the maximum level of the plot (I versus t) then $v_c(t)$ is related to I as follows:

$$v_c(t) = I(t) = \frac{I - I_{\min}}{I_{\max} - I_{\min}}, \tag{39.2}$$

where $I(t)$ is the relative intensity at time t, and $I_{\min}$ and $I_{\max}$ are the minimum and maximum intensities, respectively. Equation (39.1) can be written in a logarithmic form as:

$$1n[-1n(1 - I(t))] = 1n(K) + n1n(t). \tag{39.3}$$

The values of n and K can be determined from the plot of $1n[-1n(1 - I(t))]$ versus $1n(t)$; n is the slope, and $1n(K)$ is the intercept.

In reality, polymer crystallization is too complex to be described by a simple expression such as the Avrami equation. For example, the assumption in Avrami's expression that the volume does not change is inaccurate because the specimen tends to shrink during crystallization. In addition, secondary crystallization and crystal perfecting processes are not taken into account.

There have been many attempts to develop theories to explain the important aspects of crystallization [3,4]. The most widely accepted approach to the analysis of the linear crystal growth rates is the kinetic description due to Lauritzen and Hoffman [3]. There are alternative approaches which will not be considered here since this is not meant to be a comprehensive review chapter of theoretical approaches.

TABLE 39.1. *Theoretical values of n and K for different morphologies and nucleation mechanisms.*

Crystal growth shape	Nucleation mode	Avrami exponent (n)	Avrami constant (K)[a]
Rod	Heterogeneous[b]	1	NGA
	Homogeneous[c]	2	$\dot{N}$ GA/2
Disc	Heterogeneous	2	πNG^2D
	Homogeneous	3	$(\pi/3)\dot{N}G^2D$
Sphere	Heterogeneous	3	$(4\pi/3)NG^3$
	Homogeneous	4	$(\pi/3)\dot{N}G^3$
Sheaf	Heterogeneous	5	—
	Homogeneous	6	—

[a] A is cross-sectional area of the rod; D is thickness of the disc; G is linear growth rate; N is nucleation density; and $\dot{N}$ is nucleation rate.
[b] Heterogeneous means that the nucleation density is constant.
[c] Homogeneous, also named sporadic, means that the rate of nucleation is constant.

The general expression of crystal growth as described by Lauritzen and Hoffman is:

$$G = G_0 \exp\left(-\frac{U^*}{R(T_c - T_\infty)}\right) \exp\left(-\frac{K_g}{T_c \Delta T f}\right), \quad (39.4)$$

where G is the growth rate, G_0 is the growth rate constant; U^* is the activation energy for polymer diffusion; R is the gas constant; T_c is the crystallization temperature (K); $T_\infty = T_g - 30$ (K); $\Delta T =$ supercooling, $(T^0_m - T_c)$; f=correction factor, $2T_c/T_c + T^0_m$; K_g is the nucleation rate constant given by

$$K_g = \frac{j b_0 \sigma \sigma_e T^0_m}{k \Delta h_f}, \quad (39.5)$$

where b_0 is the width of the chain, σ is the lateral surface free energy, σ_e is the fold surface free energy, T^0_m is the equilibrium melting temperature (K), k=Boltzmann constant, and Δh_f is the heat of fusion. The parameter j is determined by the operating regime (see below) and is equal to 4 for regime I and III, and equal to 2 for regime II.

The Lauritzen–Hoffman theory analyzes the growth data according to competition between the rate of deposition of secondary nuclei (i) and the rate of lateral surface spreading (g), resulting in three different regimes (Fig. 39.1). Regime I occurs when $i << g$ and may be found at very low supercoolings; in regime II i is the order of g and occurs at moderate supercoolings; in regime III $i > g$ and is found at very high supercoolings. Regime behavior varies from polymer to polymer. For example *cis*-polyisoprene shows all regimes [5]. Until recently it was belived that polyethylene

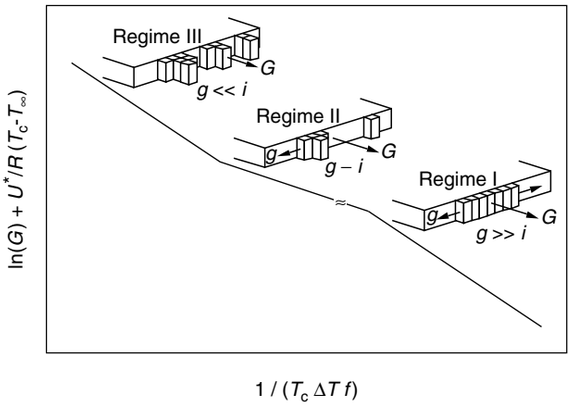

FIGURE 39.1. Schematic of regime analyses.

when crystallized shows regime I and II [6,7], whereas polypropylene shows regime II and III [7–10]. Also the regimes depend on the conditions of crystallization, for example at atmospheric pressure high molecular weight polypropylene shows regime II and III; whereas the same material shows all regimes at 150 MPa [7]. An evaluation of data in terms of regime assignment for many common polymers was published by Lovinger *et al*. [11].

It has been known for many years that an increase in molecular weight results in a decrease in growth rate for unfractionated polymers [12–15]; however, definitive data is available for few commercially significant polymers. A thorough understanding of molecular weight effects requires a detailed evaluation of fractions. Few such studies are available.

The effects of molecular weight and fractionation on the growth of polymers have been analyzed and discussed in terms of the molecular reptation concept by Hoffman and Miller [16]. In their studies of different molecular weights of polyethylene, they determined the dependence of the crystal growth rate on molecular weight at constant supercooling. The concept of reptation, which was first proposed by De Gennes [17], states that the overall friction coefficient of a linear polymer chain in the melt is proportional to its length.

In the analysis of 11 polyethylene samples (M varies from 23,000 to 203,000), high molecular weight fractions exhibit lower growth rates in both regimes I and II. According to Hoffman and Miller, this observation is solely due to molecular friction being proportional to its length.

More recent studies using newer techniques for attaining high degrees of supercooling have demonstrated that all three regimes can be observed in linear polyethylene [18, 19], both an NBS standard and an unfractionated linear polymer (see Fig. 39.2).

Similarly, in the case of polypropylene, Cheng *et al*. [10] showed that the growth rate of low molecular weight isotactic polypropylene ($M_w = 15{,}000$) is higher than that of a high molecular fraction ($M_w = 300{,}000$) at the same super cooling.

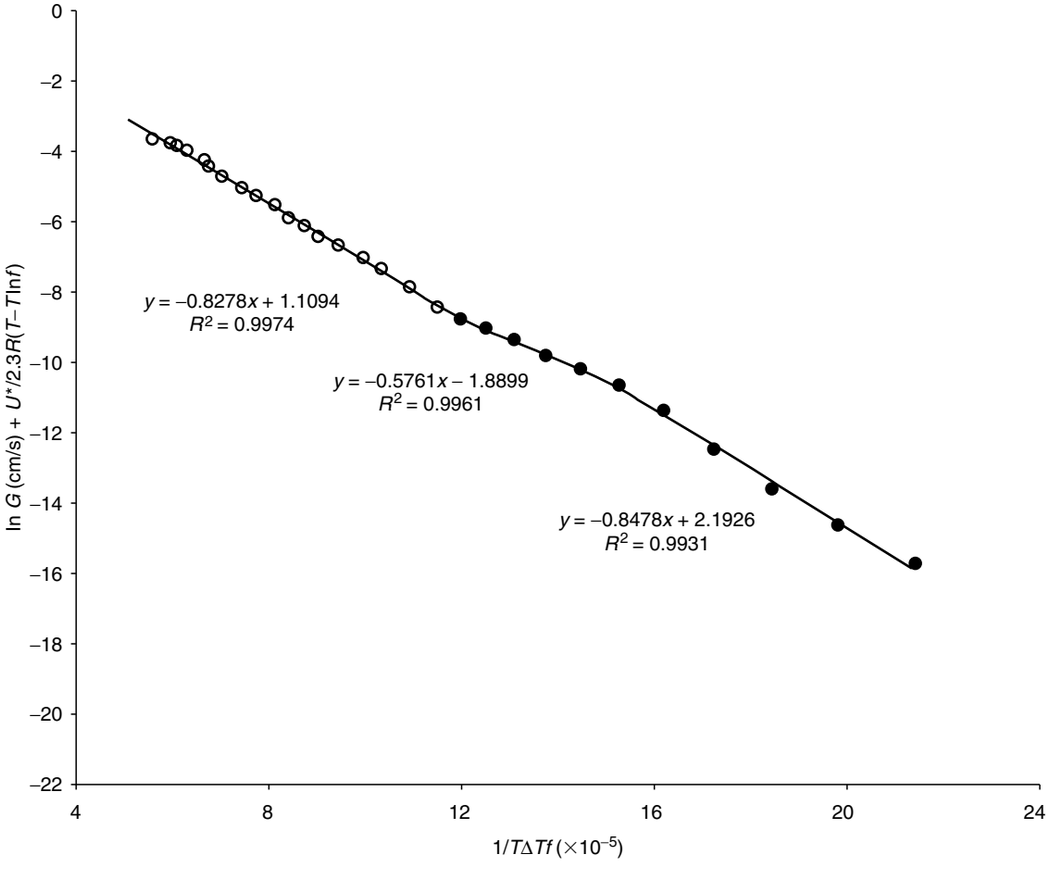

FIGURE 39.2. Secondary nucleation plot for linear polyethylene (isothermal data-filled symbols; rapid cooling data-open symbols). Reproduced from [Polymer] (2001) [19] with permission from Elsevier.

However, the reptation model is not applicable in the cases of crystallization from dilute or concentrated solutions, because in these cases considerable lateral molecular motion is possible. Nevertheless, it should be noted that regime changes have been detected in the growth of single crystals from solution [20]. Similarly, the crystallization of a polymer fraction with a large amount of noncrystallizable low molecular weight material, which is rejected at the growth front, acts like the one from concentrated solution rather than from a fully interentangled melt [21–23].

When copolymers are considered, the situation becomes very complex and depends on whether or not the comonomer units are rejected, partially or fully, from the crystal [7,24–26]. The dependences observed are controlled not only by the degree of rejection, but also by the sequence length distribution of crystallizable units. For most systems studied so far, rejection of comonomer units tends to be prevalent resulting in a decrease in growth rate. This decrease is regarded as caused primarily by the probability of formation of a critical nucleus. Systems that have been thoroughly studied so far show an inverse logarithmic dependence of growth rate on the mole fraction of impurity units [25,26]. It is also recognized that comonomer content and molecular weight interact in the determination of the behavior of any particular system. Because of the complex, and often ill-defined, dependences found in copolymers, data are not presented in the tabulations, except for a couple of cases chosen as examples of more general principles.

The subject of the crystallization of copolymers can be quite complex, dependent on the comonomer. It should also be recognized that the effects of variations in tacticity are very similar to the effects of comonomer inclusion, since both are effectively the insertion of defects into the polymer chain. The earliest treatment [26] recognized this fact, and is applicable to any defect, whether tactic, head-to-head link or comonomer, when measured as a defect content. This approach makes the assumption that all defects are excluded from the crystal. On this basis the probability of forming a critical secondary nucleus is dependent on the distribution of the defects throughout the polymer chain. The formulation of the probabilities leads to the logarithm of the rate of linear growth of a spherulite being dependent on the defect concentration. In practice, the behavior of most copolymers

follows this prediction fairly well, the rate dropping by orders of magnitude for inclusion of a few percent defects.

Data are presented for a series of copolymers of ethylene and octene, in which the evidence suggests that defect exclusion dominates the behavior (see Fig. 39.3). Note the orders of magnitude drop in crystal growth rates with increasing defect content. An unusual observation, currently not understood fully, is that the growth rates at very high supercoolings for the linear polymer and the copolymers merge, indicating a lack of selectivity at cooling rates consistent with industrial operations [19].

For isotactic polymers and copolymers the behavior is complex and depends on the method of synthesis and the types of defects that result. For instance, isotactic polypropylene synthesized using Zeigler–Natta catalysts has a quite different defect content from the same polymer synthesized using single site catalysts. In the ZN case the defects are primarily syndiotactic units, but in the SSC case they are predominantly head-to-head links. The latter result in methylene diads. Syndiotactic defects are excluded from the crystal in the normal manner. When ethylene is copolymerized into propylene the methylene sequence is lengthened, but ethylene can be incorporated into the crystal. So the situation becomes quite complex and it becomes necessary to carry out a thorough chemical analysis of the copolymer. This has rarely been done in the literature. The subject has been explored thoroughly by Alamo and coworkers [27–30], but without studies of linear growth rates. Some data is presented of recent work of DiMeska and Phillips [31], which does contain linear growth rate regime analyses. One of the major complications of polypropylene is that the defect content encourages the formation of the

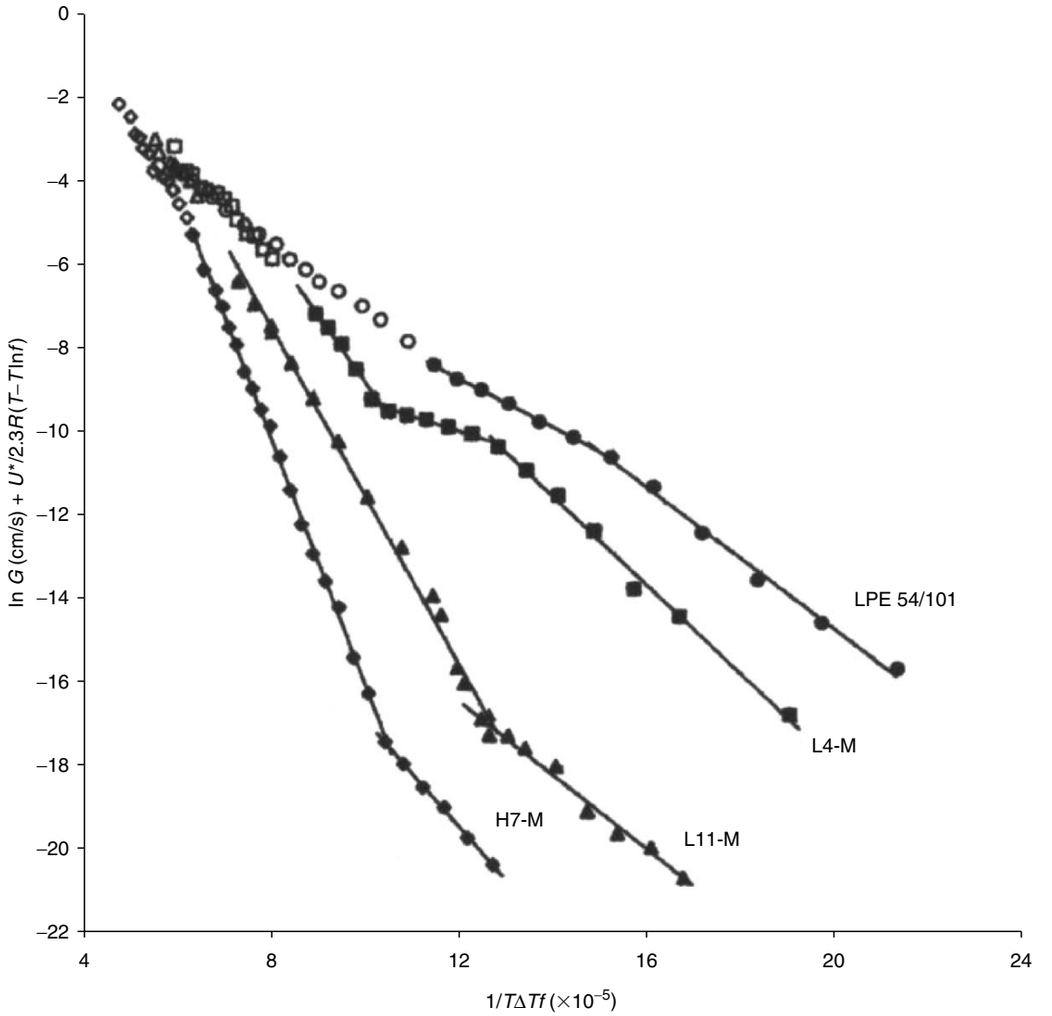

FIGURE 39.3. Secondary nucleation plot for linear polyethylene (LPE) and ethylene–octene copolymers (isothermal data-filled symbols; rapid cooling data-open symbols). For copolymers, L and H indicated low and high MW, respectively, and the number following the letters represents the number of hexyl side chains per 1,000 carbon atoms. Reproduced from [Polymer] (2001) [19] with permission from Elsevier.

γ-phase, at the expense of the commonly encountered α-phase.

For further information on current thinking and theoretical approaches to crystallization, the reader is referred to recent reviews by Phillips [32,33].

39.1.2 Case Study Using Isotactic Polypropylene

Figure 39.4 shows several chart recorded bulk crystallization traces as a function of temperatures for isotactic polypropylene (iPP, $M_w = 257{,}000$). Avrami's analysis takes the lower values of each plot; i.e., before impingement. The half-time is the point where half of the intensity is reached. Figure 39.5 presents Avrami's analysis for different crystallization temperatures, where it can be seen that all plots have similar slope, n, and different intercepts, k, in this case.

Examples of the change in spherulite radius with time for selected temperatures are shown in Fig. 39.6, where it can be seen that linear growth rates result. Plots of growth rate versus temperature for iPP can be seen in Fig. 39.7. When the data are analyzed using the Hoffman–Lauritzen equation, Fig. 39.8, it is seen that iPP shows the Regime II–Regime III transition, previously identified by several groups of workers [7–10]. In these analyses the values of T_m^0 and U^* were 186.1 °C and 1,500 cal/mol, respectively.

The effects of different values of the thermodynamic variables on the analyses and on the regime transition temperature have been explored. Variation in T_m^0 has the greatest effect on the shape of the secondary nucleation plot, but does not significantly alter the regime transition temperature. A small change of the values of U^* and T_g simply causes the curve to move up or down without changing its shape.

The Regime II–III transition is envisioned as the point at which the rate of surface spreading becomes less than the rate of secondary nucleation. Surface spreading, for an adjacent reentry system, is essentially a reeling-in process dependent on the reptational ability of the polymer chain.

The slopes of the secondary nucleation plots can be used to estimate the fold surface free energies of the two polymers. In order for these calculations to be carried out it is necessary to have estimates of the parameters which appear within Eq. 39.5. The equilibrium melting point has to be determined in separate experimentation (see Chapter 11).

The values of $\sigma\sigma_e$ can be determined from the slope of the lines. Regime II and regime III give $\sigma\sigma_e = 562$ and $678\ \mathrm{erg^2/cm^4}$, respectively. In order to proceed further it is necessary to estimate σ independently. One way to do this is to use the Hoffman modification of the Thomas–Stavely relation [24].

$$\sigma = 0.1\Delta h_f \sqrt{a_0 b_0}. \tag{39.6}$$

Values of σ have been calculated as $11.5\ \mathrm{erg/cm^2}$ for iPP. Substitution of these values into the determined values of

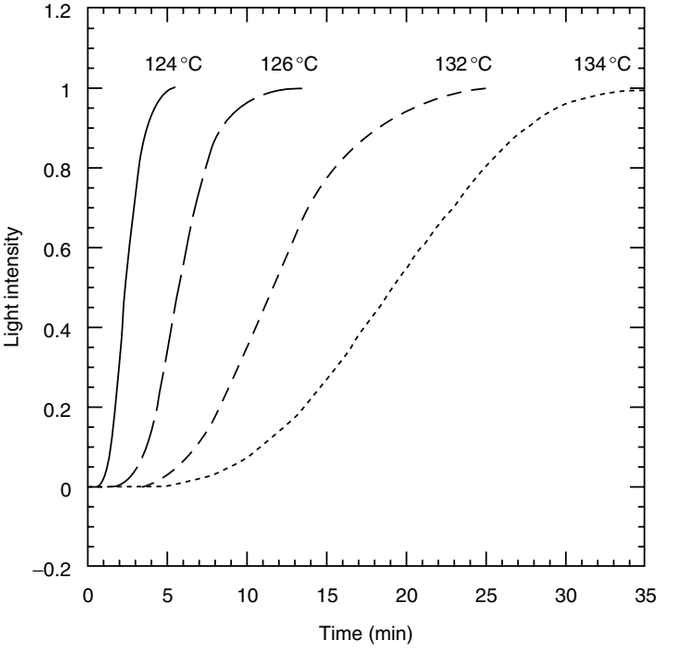

FIGURE 39.4. Isothermal bulk crystallization traces as a function of temperature.

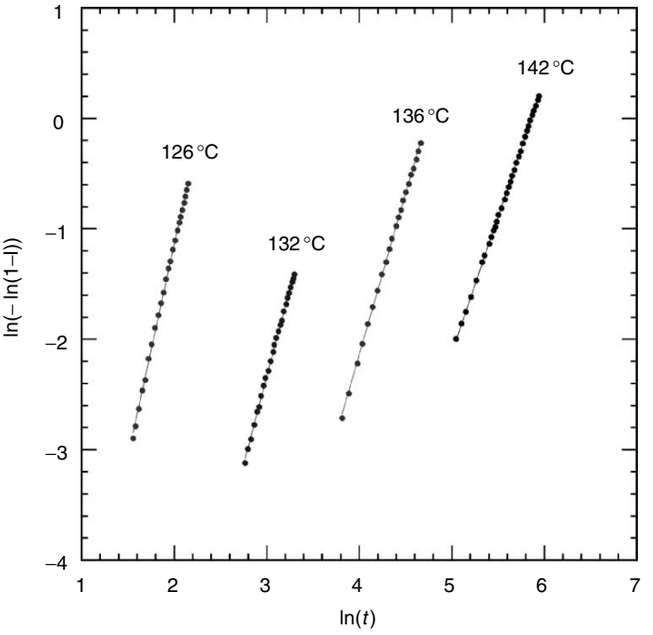

FIGURE 39.5. Avrami analyses for different crystallization temperatures.

$\sigma\sigma_e$ results in values of σ_e for regime II and regime III of 48.9 and 59.0 erg/cm^2, respectively.

The work done by the chain (q) to form a fold can be easily calculated from the following equation, when the fold surface energy is known.

$$q = 2a_0 b_0 \sigma_e \tag{39.7}$$

39.1.3 Tabulation of Data

In the tabulation, data are presented mainly for common homopolymers. When available, molecular weights are also given, but no major attempt has been made to present molecular weight dependencies. Additionally, a few illustrations of specific copolymers have been included as examples of copolymer behavior.

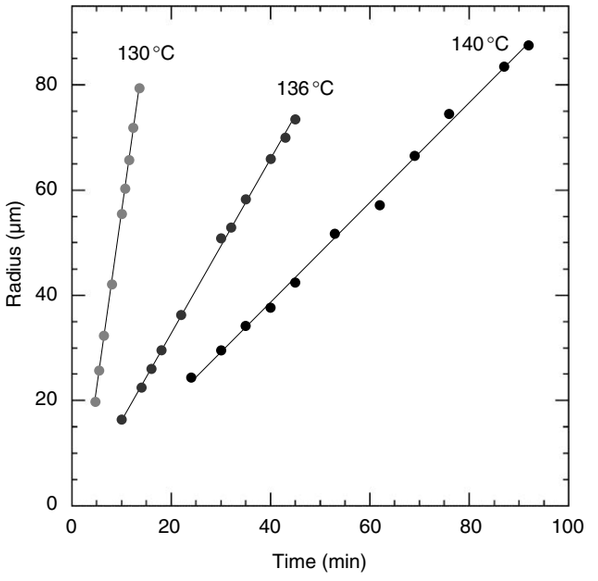

FIGURE 39.6. Spherulitic growth of iPP as a function of time for different isothermal crystallization temperatures.

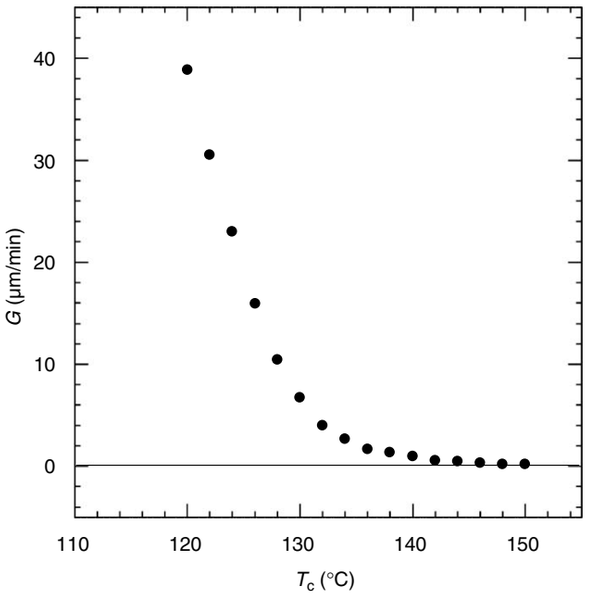

FIGURE 39.7. Growth rates of iPP versus crystallization temperature.

It should be recognized that Avrami data can vary greatly with the presence of additives, especially nucleating agents.

In Table 39.2 data are presented from bulk crystallization studies of common polymers.

In Table 39.3 data are presented from linear growth rate studies of polymers that are commonly encountered in significant basic studies or that are of commercial significance. In addition to the values of the characteristic parameters obtained from the analyses, we have added the value of other constants such as equilibrium melting points and heats of fusion which are essential to the analyses.

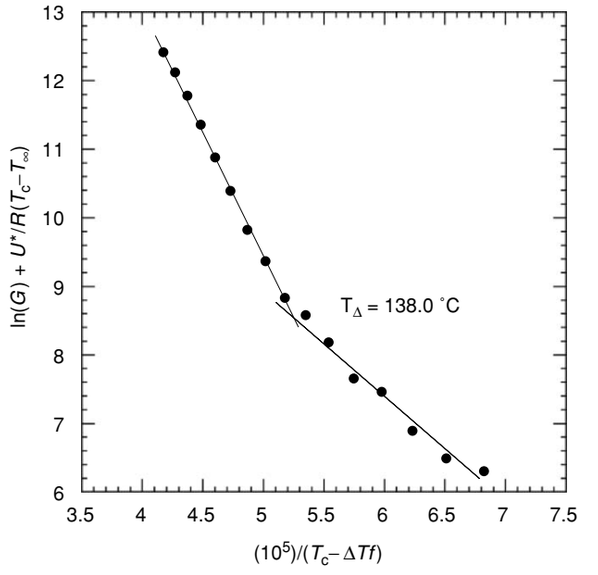

FIGURE 39.8. Secondary nucleation analyses of iPP using T^0_m of 186.1 °C.

TABLE 39.2. *Avrami coefficients.*

Polymer		M_n (kg/mol)	M_w (kg/mol)	T_c (°C)	$t_{1/2}$ (s)	n	k (s^{-n})	Remarks	Ref.
Poly (amide)	Nylon 6	16.0	29.0	194.8	43	2.5		DSC	[34]
				197.4	75	2.9			
				200.4	110	3.6			
				202.6	200	4.0			
				205.5	350	4.8			
		24.7		140	10	3		DLM	[35]
				160	15	3			
				180	70	3			
				200	950	3			
	Nylon 10 12						(min^{-n})	DSC	[36]
				165	46.2	2.21	1.34×10^{-4}		
				167	68.4	1.97	1.54×10^{-4}		
				169	144.6	1.91	5.37×10^{-5}		
				171	241.8	1.91	1.90×10^{-5}		
				173	450	2.08	1.86×10^{-6}		
	Nylon 11						(min^{-n})	DSC	[37]
				164	10.3	1.6	1.23×10^{1}		
				166	16.5	2.1	1.0×10^{1}		
				168	23.1	2.4	6.92		
				170	43.8	2.7	1.62		
				172	85.8	3.2	2.2×10^{-1}		
	Nylon 12 12						(min^{-n})	DSC	[38]
				160	34.8	2.03	2.12		
				164	63.6	1.67	6.2×10^{-1}		
				168	119.4	1.68	2.2×10^{-1}		
				170	231.6	1.64	8.0×10^{-2}		
Poly (butene-1)	PB-1	73	750	70	60			DLM	[39]
				80	96				
				90	456				
				95	1572				
Poly (ε-caprolactone)	PCL	43.6	48	40	4.5	3.46		DSC	[40]
				45	17.9	3.35			
				47	45.8	2.48			
				49	97.6	2.66			
Poly (chlorotrifluoroethylene)	PCTFE			180	180	3		Dilatometry	[41]
				186	480	3			
				191	1500	3			
				196	4200	3			
Polyethylene	HDPE			124	165	2.35		DSC	[42]
				125	338	2.29			
				126	750	2.05			
				127	1920	2.24			
		12.7	42.3	117	0.24	3.1		DLM	[43]
				119	0.67	2.9			
				121	4.00	3.0			
				123	20.00	2.7			
Polyethylene	XLPE cross-link 255 avg CH_2 units	4.5	8.7	119	3.5	2.7			[43]
				120	1.25	2.2			
				123		3.5			
				124		3.6			

TABLE 39.2. *Continued.*

Polymer		M_n (kg/mol)	M_w (kg/mol)	T_c (°C)	$t_{1/2}$ (s)	n	k (s^{-n})	Remarks	Ref.
Poly (aryl-ether–ether–ketone)	PEEK			175.2 182.3 188.8		4.7 5.7 5.1	1.6×10^{-8} 4.7×10^{-10} 1.8×10^{-7}	DSC	[44]
Poly (ethylene-terephthalate)	PET	19	40	180 190 200 210		2.36 2.30 2.43 2.37	(min^{-n}) 1.02×10^{-2} 7.43×10^{-3} 2.04×10^{-3} 2.63×10^{-4}	DSC	[45]
				190 195 200 210	63 86 133 190	1.83 1.76 1.77 1.76		DSC	[46]
Poly (propylene-terephthalate)	PPT	36.3	78.4	185 190 195 200	150 250 500 1,000	2.61 2.59 2.61 2.48	1.52×10^{-6} 4.03×10^{-7} 6.51×10^{-8} 2.42×10^{-8}	DSC	[47]
Poly (butylene-terephthalate)	PBT	36.6	77.4	180 185 190 195	50 75 150 340	2.47 2.49 2.48 2.55	5.61×10^{-5} 1.65×10^{-5} 2.74×10^{-6} 2.79×10^{-7}	DSC	[47]
Poly (trimethylene ter-ephthalate)	PTT	43		170 180 190 200 210		2.3 2.6 3.0 2.9 3.2	(min^{-n}) 7.9 3.67 0.43 9.96×10^{-3} 5.75×10^{-6}	DSC	[48]
		21.05	46.3	202 206 210	174 279 592	2.81 2.72 2.84	(min^{-n}) 33.7×10^{-3} 10.8×10^{-3} 1.0×10^{-3}	DSC	[49]
Poly (isoprene)	*cis*-PIP			−38 −33 −22 −16 −11 −5	23,400 1,440 9,000 12,000 19,800 55,200				[50] [51] [52]
	trans-PIP			35 40 45 51 57	768 1,260 6,780 31,800 2,91,000				
Poly (oxyethylene)	POE	9.0	9.6	40.1 43.4 48.4 49.6		1.9 2.0 2.3 2.1	0.18×10^{1} 6.8×10^{-1} 2.6×10^{-2} 8.3×10^{-4}	DSC	[53]
			20	55 56 57 58 59	612 1,200 1,476 4,884 6,900	1.8 1.9 2.0 2.1 2.5		DSC	[54]

TABLE 39.2. *Continued.*

Polymer		M_n (kg/mol)	M_w (kg/mol)	T_c (°C)	$t_{1/2}$ (s)	n	k (s^{-n})	Remarks	Ref.
Poly (oxypropylene)	POP		300	40.3 42.8 45.5 47.5 49.7	1,650 2,520 3,540 8,580 12,600	3.0 3.1 3.3 3.0 3.1		DLM	[55]
Poly (phenylene sulfide)	PPS			230 235 240 245	160 195 370 580	1.84 2.14 2.12 2.08		DSC	[56]
Polypropylene	iPP	58.0	151	130 132 136 142	430 650 3,200 13,500	3.11 2.61 2.84 2.91	1.29×10^{-3} 7.59×10^{-4} 1.41×10^{-4} 1.15×10^{-5}	DLM	[57]
			447	130 133 134 137	780 2,220 2,820 6,600	3.1 2.9 2.9 2.9		DLM	[58]
Polypropylene	sPP	76.2	165	60 70 80 90 95	100 118 210 684 1,698	2.68 2.68 3.07 2.96 2.41	1.06×10^{1} 6.66 8.82×10^{-1} 3.11×10^{-2} 1.33×10^{-2}	DSC	[59]
		52.3	195	75 80 90 95	56 100 439 1,294	2.44 2.33 2.40 2.32	4.72×10^{1} 1.24×10^{1} 3.43×10^{-1} 3.40×10^{-2}	DSC	[59]
Selenium				80 100 120 140 160	32,400 3,600 720 280 105	2.01 1.68 3.28 3.68 4.00	1.05×10^{-2} 0.61×10^{1} 1.20×10^{2} 3.60×10^{4} 2.60×10^{6}	dynamic density	[60]
Poly (oxymethylene)	POM			148 149 150 151	163.2 316.2 607.8 1,141.2	2.67 2.59 2.36 2.98	4.16×10^{-2} 9.48×10^{-2} 3.17×10^{-3} 1.08×10^{-4}	DSC	[61]
Poly (tetrafluoro-ethylene)	PTFE			296 304 312 315	0.057 0.116 0.332 0.301	0.96 1.01 1.006 0.87	1.21×10^{1} 5.97 2.09 1.97	DSC	[62]
Polystyrene	sPS	91.6	220	236 239 242 244	16.73 50.21 96.33 135.14	1.9 1.4 1.3 1.1	4.76×10^{2} 5.29×10^{1} 2.26×10^{1} 1.60×10^{1}	DSC	[63]
Poly (arylene-ether–ether–phenylsulfide)		34		192 200 211 218 226	2,400 4,800 30,000 60,000 600,000	2.73 2.8 2.8 2.73 2.73	(min^{-n}) 3.05×10^{-7} 4.13×10^{-8} 9.23×10^{-9} 2.27×10^{-9} 1.69×10^{-10}	DSC	[64]

TABLE 39.2. *Continued.*

Polymer		M_n (kg/mol)	M_w (kg/mol)	T_c (°C)	$t_{1/2}$ (s)	n	k (s^{-n})	Remarks	Ref.
							(min^{-n})		
Poly (arylene-ether–ether–biphenylsulfide)		19.1		279	5,400	1.7	2.75×10^{-5}		
				285	30,000	1.7	1.01×10^{-5}	DSC	[64]
				290	48,000	1.9	1.37×10^{-6}		
Poly (ester–amide)				110	19.2	2.52	6.25×10^{-4}		
				120	91.8	3.06	0.8×10^{-6}		
				130	2,124	2.71	7.4×10^{-10}	DSC	[65]
				135	3,180	2.20	1.31×10^{-8}		
Poly (butylene adipate)	PBA	7.3		29	18	3.1	8.9×10^{-5}		
				35	42	2.6	4.2×10^{-5}		
				40	180	3.0	1.2×10^{-7}	DSC	[66]
				43	486	3.1	3.3×10^{-9}		
				45	1,156	3.1	45×10^{-10}		
Poly (butylene isophthalate)	PBIP	13		70.2	1272	2.9	6.9×10^{-10}		
				80.2	630	2.9	5.3×10^{-9}		
				90.2	498	2.8	1.9×10^{-8}	DSC	[66]
				100.2	456	3.0	7.3×10^{-9}		
				109.7	672	3.0	2.3×10^{-9}		
				118.7	1,068	3.1	2.8×10^{-10}		
				123.7	1,590	2.9	3.6×10^{-10}		
							(min^{-n})		
Poly (ethylene naphthalate)	PEN			180	408	2.4	7.1×10^{-3}		
				190	270	2.9	8.6×10^{-3}	(DSC)	[67]
				200	174	2.7	3.8×10^{-2}		
				210	186	3.2	2.0×10^{-2}		
				220	204	3.1	1.6×10^{-2}		
				230	384	2.3	9.2×10^{-3}		
Polyimide*				240	1,507	2.39			
				260	600	2.37		(DSC)	[68]
				280	444	2.3			
				300	600	2.32			
				320	1,197				
							(min^{-n})		
Poly (vinylidene fluoride)	PVDF	170		147	192	2.9	1.88×10^{-2}		
				151	720	2.9	3.12×10^{-4}	(DSC)	[69]
				153	960	3.1	1.28×10^{-4}		
				155	1,800	2.9	1.83×10^{-5}		
							(min^{-n})		
1, 2-Syndiotactic Polybutadiene	1, 2-sPB			176	97.8	3.2	1.45×10^{-1}		
				177	126	2.8	8.68×10^{-2}	(DSC)	[70]
				178	169.2	3.0	3.09×10^{-2}		
				179	223.8	2.8	1.74×10^{-2}		
				180	358.2	2.9	3.9×10^{-3}		

*Polyimide synthesized from 3, 3′, 4, 4′-benzophenonetetracarboxylic dianhydride (BTDA) and 2, 2-dimethyl-1, 3-(4-amino-phenoxy) propane (DMDA).

TABLE 39.3. *Growth kinetics coefficients.*

Polymer		M_n (kg/mol)	M_w *kg/mol*	T_g (°C)	T_m° (°C)	ΔH_f (J/g)	Growth face	a_0 (Å)	b_0 (Å)	U^* (cal/mol)	Regime	T_{rt} (°C)	G_0 (cm/s)	$K_g/10^5$ (K^2)	σ (erg/cm^2)	σ_e (erg/cm^2)	q (kcal/mol)	Ref.
Poly(amide)	Nylon 6			30	232.0			4.78	3.70	1,430			0.65×10^1	1.74		118	6.0	[71]
		24.7		−10	230	10.8 (kcal/mol)		4.78	3.70	1,840			1.05×10^5	6.70	8.0	65		[72]
	Nylon 66			45.0	272	200.8		4.76	3.70	167			1.55×10^3	1.02	8.0	40		[72]
	Nylon 11			41.96	202.8	217.9 (J/cm^3)	(100)	5.4	4.44	1,500	II			1.66	10.6	110.6	7.61	[37]
Poly(butene-1)	PB-1			−54.2	127.8					1,500			0.25×10^1	0.79				[71]
Poly(ε-caprolactone)	PCL	26	40	−60	70.3	163 (J/cm^3)	(110)	4.52	4.12	1,500				0.80	6.7	94.7	5.06	[73]
		43.6	48	−63	74	148 (J/cm^3)	(110)	4.50	4.10	1,500			6.03×10^1	0.91	6.1	106		[40]
Poly(chlorotrifluoro ethylene)	PCTFE			52.0	224.0			6.50	5.60	4,000			6.50×10^4	1.72		53	5.6	[71]
		400		52	224	91.1 (J/cm^3)		6.50	5.60				0.17×10^5	0.17	5.2	36	3.8	[74]
Polyethylene	PE single crystals	30	63	−42	114	280 (J/cm^3)	(110)	4.15	4.55	1,500	I			2.11	13.7	93.4	5.1	[3]
	PE		30.6	−42.2	144.6	280 (J/cm^3)		4.55	4.15	1,500	I		4.40×10^9	2.16	14.1	90.4	5.0	[71]
				−20	141	280 (J/cm^3)	(110)	4.45	4.11		II	127	2.24×10^3 16.00×10^5	1.15 1.24	14.1 12.2	97.8 49	2.6	[74]
	HDPE	13.0	18.1	−40.0	144.5	288.7				1,500	I II	 125.3	1.45×10^{13} 1.91×10^7		11.8 11.8	105.6 111.8		[32] [75]
	HDPE-NBS standard, fractionated	66.4	74.4		144.7		(110)			5,736	I II III	 128.9 120.9	1.4×10^{10} 1.02×10^3 1.65×10^7	1.98 0.94 1.85	11.8	90		[18]
	HDPE, un-fractionated	53.9	101.3	−83	142.7		(110)			1,500	I II III	 125.6 120.8						[19]
	4 branches/ 1,000 CH_2	16.1	23.6	−40.0	143.7	256.3				1,500	I II	 124.1	3.63×10^{11} 8.91×10^7		11.8 11.8	88.3 122.0		[25]
	22 branches/ 1,000 CH_2	15.2	17.5	−40.0	139.2	212.5				1,500	I II	 123.1	6.45×10^{15} 8.51×10^6		11.8 11.8	86.0 79.0		[25]
Poly (3-hydroxybutyrate)	PHB	133	358	2	197	146	(100)			2,450	II III	 130		4.99 2.47		38		[76]
		14.1	38.6	143.0	395.0		(200) & (110)	4.86	4.68	3,980		165.0			12.1	25.1		[77] [78] [79]

Polymer		M_n (kg/mol)	M_w *kg/mol*	T_g (°C)	T_m° (°C)	ΔH_f (J/g)	Growth face	a_0 (Å)	b_0 (Å)	U^* (cal/mol)	Regime	T_{rt} (°C)	G_0 (cm/s)	$K_g/10^5$ (K^2)	σ (erg/cm^2)	σ_e (erg/cm^2)	q (kcal/mol)	Ref.
Poly(aryl-ether–ether-ketone)	PEEK	60.2	79.5	150.6	404.0	130			4.68	4,140				18.20	38.0	101		[80]
		30.9	39.2	148.6	401.2	130			4.68	4,560				12.60	38.0	65		[80]
		14.5	18.0	145.3	395.0	130			4.68	4,560				9.8	38.0	45		[80]
				144.0	395.0	130	(110)		4.68	2,000					38.0	49.0		[78]
Poly(ethylene-naphthalate 2, 6 dicarboxylate)	PEN		48		300	190		6.51	5.66							60		[81]
Poly(ethylene-terephthalate)	PET	19.0	37.0	70	280	140	(100)	4.56	5.53	2,000					10.2	190	13.1	[82]
				80	343	135	(010)		5.07	2,000					36	93		[78]
		21.0		80	278	1.8 (J/cm^3)	(100)	4.56	5.53	3,050	II III	 165		 12.8	10.5 10.5	255 301		[83]
Poly(trimethylene-terephthalate)	PTT	19–39		67	300					1,544				9.42				[12]
		43		45	252	28.8 (kJ/mol)	(010)	4.637	5.71	2,500	I II III	 215 195		7.3 3.5 8.4	 19.2	84.9 81.3 98.8	6.5 6.2 7.5	[48]
Poly(isoprene)	*cis*-PIP	262	351	−72	35.5					1,500	I II III			2.63 1.50 2.80	14.0 14.0 14.0	21.6 24.6 22.9		[84]
		344	543	−72	35.5					1,500	II III			1.28 2.46	14.0 14.0	21.0 20.1		[84]
		512	897	−72	35.5					1,500	III			2.47	14.0	20.3		[84]
	cis-PIP α-form						(100)		6.23						9.16	23.9	2.13	[85]
	cis-PIP β-form						(120)		4.19						5.99	50.3	3.45	[85]
	trans-PIP		170	−62.2	87.0			5.87	3.95	1,500			1.10×10^3	2.17		109	7.3	[71]
		165	390	−59	74	3,040 (cal/mol)									285 (cal/mol)	1,175 (cal/mol)	27.2	[86]
Poly(oxyethylene)	POE	12.0	9.97		66.2	230 (J/cm^3)	(100)		4.6						3.4	65		[87]
			150	−67.2	75.2			4.67	4.65	1,500			1.15×10^5	0.81		37	2.3	[71]
	POE from solution	307	325	−67.2	69.0	231 (J/cm^3)		4.67	4.65	2,000	I II	 53.0	15.00×10^5	1.18 0.60	10 10	64.33 65.59		[88]
Poly(oxymethylene)	POM			−60.2	186.0			4.53	3.86	1,500			1.28×10^1	1.27		61	3.0	[71]
					211	221 (J/cm^3)			4.46						14.3	150		[89]
Poly(oxypropylene)	POP			−73.2	75.0			4.67	5.20	1,320			0.296×10^1	0.785		43	3	[71]
Poly(pivalolactone)	PPVL			−3	269	183 (J/cm^3)	(1$\bar{2}$0)	7.8	5.7	1,500	II III	 203	1.50×10^2 4.30×10^8	4.32 8.59	30 30	58.1 58.4		[90]
Poly(*p*-phenylene sulphide)	PPS	34	51	92	315	80	(020)	4.33	5.61	1,400	II III	 208	5.43 3.86×10^4	8.84 18.35	16.9 16.9	125 130	8.9	[26]

TABLE 39.3. *Continued.*

Polymer		M_n (kg/mol)	M_w kg/mol	T_g (°C)	T_m° (°C)	ΔH_f (J/g)	Growth face	a_0 (Å)	b_0 (Å)	U^* (cal/mol)	Regime	T_{rt} (°C)	G_0 (cm/s)	$K_g/10^5$ (K^2)	σ (erg/cm^2)	σ_e (erg/cm^2)	q (kcal/mol)	Ref.
Polypropylene	iPP		350	−12	186.1	209	(110) (040)	5.49 6.56	6.26 5.24	1,500	II III	138	3.40×10^{-1} 3.98×10^{3}		11.5	62.3		[91]
		72	257	−12	186.1	165	(110)	5.49	6.26	1,500	II III	138.0	3.45×10^{-1} 3.03×10^{4}	1.365 3.659	11.5 11.5	48.1 59.0		[92]
		300	600	−3.4	185.0	8.3 (kJ/mol)	(110)	5.49	6.26	1,500	II III	137		1.250 2.554	11.5 11.5	51.3 52.3	5.07 5.19	[93]
		15	25.5	−6.0	170.0	8.3 (kJ/mol)	(110)	5.49	6.26	1,500	I II III	133 122		2.996 1.607 3.196	11.5 11.5 11.5	63.5 68.2 67.7	6.28 6.74 6.69	[93]
	sPP	76.2	165	−6.1	168.7	177 (J/cm^3)	(010) (200)	7.25 5.60	5.60 7.25	1,500	III	110	9.07×10^{4}	5.69	11.28 11.28	124.5 96.2	14.6 11.2	[59]
							(020) (200)	7.25 5.60	5.60 7.25	1,500	II		7.52	1.61	11.27 11.28	70.7 54.6	8.3 6.4	[94]
Polystyrene	iPS			90.5	242.0	91.1 (J/cm^3)		12.8	5.5	1,560	II			1.20	7.64	34.8	7.1	[3]
						9.1 (J/cm^3)	(110)	12.8	5.5				1.31×10^{1}		5.3	28.8		[95]
	sPS	91.6	220	100	278.8	57.5 (J/cm^3)	(040)	4.41	7.2	1,500	II III	239		1.58 3.67	3.24 3.24	48.15 56.5	4.11 4.87	[63]
Poly(tetramethyl-*p*- silphenylene)-siloxane	PPSS or TMPS		56	−24.0	153.8			6.43	6.41	990			2.16×10^{-1}	1.14		34	4.0	[71]
		286	372	−24.0	152	20.8			6.41	1,230			1.03×10^{-1}		3.5	36.3		[13–15]
Selenium				26.8	219.2			4.36	3.78	2,180			0.458×10^{1}	2.53		190	9.0	[71]
Poly(tetrafluor oethylene)	PTFE			184.6	331	47.4				1,500				0.154				[62]
Poly(arylene-ether-ether-sulfide)		34		100	292					1,500	II III	205						[64]
Poly(ester-amide)				21	170					2,800	II III			1.63 3.15				[65]
Poly(vinylidene fluoride)	PVDF	170			178	201 (J/cm^3)			4.83						9.7	38		[69]
1, 2-Syndiotactic polybutadiene	1,2-sPB			18	208					1,500	II					48		[70]
Ethylene-octene copolymers (random, metallocene)	L − 04[a]	27.3	59.9		139.3					1.500	I II III	119.5 113.5						[19]
	H − 07[a]	43.6	94		134.1					1,500	II III	115.1						
	L − 11[a]	21.2	43.7		134.9					1,500	II III	114.2						

TABLE 39.3. *Continued.*

Polymer		M_n (kg/mol)	M_w kg/mol	T_g (°C)	T_m° (°C)	ΔH_f (J/g)	Growth face	a_0 (Å)	b_0 (Å)	U^* (cal/mol)	Regime	T_{rt} (°C)	G_0 (cm/s)	$K_g/10^5$ (K^2)	σ (erg/cm^2)	σ_e (erg/cm^2)	q (kcal/mol)	Ref.
Propylene-ethylene copolymers (random, fractionated, ziegler-Natta)	iPP – 2.62PE[b]		120.6	252.2	172.6	209	(110)			1,500	I			2.808	11.5	59.6	5.89	[31]
											II	119.6		1.883		79.9	7.90	
											III	114.6		4.115		87.3	8.62	
						150	(001)				I			2.478	8.2	62.5	6.16	
											II	121.6		1.702		85.8	8.47	
											III	116.6		3.758		94.8	9.36	
	iPP – 4.38PE[b]	145.1	287.1		165.7	209	(110)			1,500	I			3.024	11.5	64.8	6.40	
											II	112.7		2.113		90.6	8.95	
						150					III	101.7		4.211		90.2	8.93	
							(001)				I			2.96	8.2	75.1	7.40	
											II	112.7		2.091		106.1	10.46	
											III	103.7		4.138		105	10.36	
	iPP – 10.45PE[b]		36.14	86.19	159.5	209	(110)			1,500	I			2.621	11.5	57	5.63	
											II	106.5		1.595		69.3	6.85	
											III	101.5		3.935		85.6	8.45	
					157.6	150	(001)				I			2.406	8.2	62.1	6.13	
											II	107.6		1.474		76.1	7.49	
											III	100.6		3.683		95.1	9.38	
	iPP – 15.57PE[b]		31.85	74.94	149.3	209	(110)			1,500	II			2.353	11.5	104.8	10.36	
											III	74.3		4.205		93.6	9.26	
					147.8	150	(001)				II			2.081		109.9	10.84	
											III	76.8		3.79	8.2	100.1	9.28	

[a] L and H represent low and high MW, respectively. The numbers following the letters represent the number of hexyl side chains per 1,000 carbon atoms.
[b] The numbers represent mole percent ethylene in the copolymers.

REFERENCES

1. M. J. Avrami, Chem. Phys. **7**, 1103 (1939).
2. M. J. Avrami, Chem. Phys. **8**, 212 (1940).
3. J. I. Lauritzen Jr. and J. D. Hoffman, J. Appl. Phys. **44**, 4340 (1973).
4. D. M. Sadler and G. H. Gilmer, Polymer **25**, 1446 (1984).
5. P. J. Phillips and N. Vatansever, Macromolecules **20**, 2138 (1987).
6. J. J. Point and M. Dosière, Polymer **30**, 2292 (1989).
7. P. J. Phillips, in Crystallization of Polymers, edited by M. Dosière (Kluwer, The Netherlands, 1993).
8. E. J. Clark and J. D. Hoffman, Macromolecules **17**, 878 (1984).
9. B. Monnasse and J. M. Handin, Colloid Polym. Sci. **263**, 822 (1985).
10. S. Z. D. Cheng, J. J. Janimak, and A. Zhang, Macromolecules **23**, 298 (1990).
11. A. Lovinger, D. D. Davis, and F. J. Padden, Polymer **26**, 1595 (1985).
12. F. Van Antwerpen and D.W. Van Krevelen, J. Polym. Sci., Polym. Phys. Ed. **10**, 2423 (1972).
13. J. H. Magill, J. Polym. Sci. **A27**, 1184 (1969).
14. J. H. Magill, J. Polym. Sci. **A25**, 89 (1967).
15. J. H. Magill, J. Appl. Phys. **35**, 3249 (1964).
16. J. D. Hoffman and R. L. Miller, Macromolecules **21**, 3038 (1988).
17. P. G. De Gennes, J. Chem. Phys. **55**, 672 (1971).
18. J. P. Armistead and J. D. Hoffman, Macromolecules **35**, 3895 (2002).
19. J. Wagner and P. J. Phillips, Polymer **42**, 8999 (2001).
20. A. Toda, in Crystallization of Polymers, edited by M. Dosière (Kluwer, The Netherlands, 1993) p. 141.
21. H. D. Keith and F. J. Padden, J. Appl. Phys. **34**, 2409 (1963).
22. H. D. Keith and F. J. Padden, J. Appi. Phys. **35**, 1270 (1964).
23. H. D. Keith and F. J. Padden, J. Appl. Phys. **35**, 1286 (1964).
24. J. D. Hoffman, Faraday Discuss. Chem. Soc. **68**, 378 (1979).
25. W. S. Lambert and P. J. Phillips, Macromolecules **27**, 3537 (1994).
26. E. H. Andrews, P. J. Owen, and A. Singh, Proc. R. Soc. Lond. **A324**, 79 (1971).
27. R. G. Alamo, D. L. Vanderhart, *et al*., Macromolecules **33**, 6094 (2000).
28. M. R. Nyden, D. L. Vanderhart, and R. G. Alamo, Comput. Theor. Polym. Sci. **11**, 175 (2001).
29. I. L. Hosier, R. G. Alamo *et al*., Macromolecules **36**, 5623 (2003).
30. I. L. Hosier, R. G. Alamo, and J. S. Lin, Polymer **45**, 3441 (2004).
31. A. Dimeska, Ph.D. Dissertation, The University of Tennessee, Knoxville, 2004.
32. P. J. Phillips, Rep. Prog. Phys. **53**, 549 (1990).
33. P. J. Phillips, in Handbook of Crystal Growth, edited by D.T.J. Hurle, vol. 2 (Amsterdam, Elsevier Science, 1994), p. 1168.
34. B. G. Risch, G. L. Wilkes, and J. M. Warakomski, Polymer **34**, 2330 (1993).
35. J. H. Magill, Polymer **3**, 655 (1962).
36. Y. Li, X. Zhu, and D. Yan, Polym. Eng. Sci. **40**, 1989 (2000).
37. S. Liu, Y. Yu *et al*., J. Appl. Polym. Sci. **70**, 2371 (1998).
38. M. Liu, Q. Zhao *et al*., Polymer **44**, 2537 (2003).
39. R. D. Icenogle, J. Polym. Sci. (Polym. Phys. Ed.) **23**, 1369 (1985).
40. L. Goulet and R. E. Prud'homme, J. Polym. Sci. Part B, Polym. Phys. **28**, 2329 (1990).
41. F. Rybnikar, Collect. Czech. Chem. Commun. **27**, 2307 (1962).
42. D. M. Hoffman and B. M. McKinley, Polym. Eng. Sci. **25**, 567 (1985).
43. P. J. Phillips and W. S. Lambert, Macromolecules **23**, 2075 (1990).
44. P. Cebe, Am. Chem. Soc., Polym. **27**, 449 (1986).
45. S. P. Kim and S. C. Kim, Polym. Eng. Sci. **31**, 110 (1991).
46. K. Ravindranath and J. P. Jog, J. Appl. Polym. Sci. **49**, 1395 (1993).
47. B. J. Chisholm and J. G. Zimmer, J. Appl. Polym. Sci. **76**, 1296 (2000).
48. P. D. Hong, W. T. Chung, and C. F. Hsu, Polymer **43**, 3335 (2002).
49. J. M. Huang and F. C. Chang, J. Polym. Sci. B: Polym. Phys. **38**, 934 (2000).
50. L. A. Wood and N. Bekkdahl, J. Res. Natl Bur. Std. **36**, 487 (1946).
51. L. Mandelkem, F. A. Quinn, and D. E. Roberts, Jr., J. Am. Chem. Soc. **78**, 926 (1956).
52. W. Cooper and G. Vaughan, Polymer **4**, 329 (1963).
53. S. Z. D. Cheng and B. Wunderlich, J. Polym. Sci. B: Polym. Phys. **24**, 595 (1986).
54. Yu K. Godovsky, G. L. Slonimsky, *et al*., J. Polym. Sci., C. **38**, 1 (1972).
55. Yu K. Godovsky and G. L. Slonimsky, J. Polym. Sci. B: Polym. Phys. **12**, 1053 (1974).
56. J. M. Kenny and A. Maffezzoli, Polym. Eng. Sci. **31**, 607 (1991).
57. R. A. Campbell, Ph.D. Dissertation, The University of Tennessee, Knoxville, 1991.
58. Yu K. Godovsky and G. L. Slonimsky, J. Polym. Sci.: Polym. Phys. Ed. **12**, 1053 (1974).
59. P. Supaphol and J. E. Spruiell, J. Appl. Polym. Sci. **75**, 44 (2000).
60. R. G. Crystal, J. Polym. Sd. A-2 **8**, 2153 (1970).
61. W. Xu and P. He, J. Appl. Polym. Sci. **80**, 304 (2001).
62. X. Q. Wang *et al*., J. Appl. Polym. Sci. **83**, 990 (2002).
63. Q. Chen *et al*., J. Appl. Polym. Sci. **83**, 2528 (2002).
64. S. Srinivas *et al*., Polym. Eng. Sci. **37**, 497 (1997).
65. E. Botines *et al*., J. Polym. Sci. B: Polym. Phys. **41**, 903 (2003).
66. M. C. Righetti *et al*., Macromol. Chem. Phys. **199**, 2063 (1998).
67. Y. S. Hu *et al*., J. Appl. Polym. Sci. **86**, 98 (2002).
68. S. Z. D. Cheng *et al*., Polym. Int. **29**, 201 (1992).
69. Y. S. Yadav, P. C. Jain, and V. S. Nanda, Thermochim. Acta **80**, 231 (1984).
70. F. Bertini, M. Canetti, and G. Ricci, J. Appl. Polym. Sci. **92**, 1680 (2004).
71. J. D. Hoffman, G. T. Davis, and J. I. Lauritzen, Jr., in Treatise on Solid State Chemistry, edited by N. B. Hannay (1976), p. 497.
72. J. H. Magill, Polymer 367 (1965).
73. P. J. Phillips, G. J. Rensch, and K. D. Taylor, J. Polym. Sci.: Polym. Phys. **25**, 1725 (1987).
74. J. D. Hoffman and J. J. Weeks, J. Chem. Phys. **37**, 1723 (1962).
75. J. D. Hoffman, L. J. Frolen, G. S. Ross *et al*., J. Res. Natl. Bur, Std. **79A**, 671 (1975).
76. P. J, Barham, A. Keller, E. L. Otun *et al*., J. Mater. Sci. **19**, 2781 (1984),
77. F. J. Iy and P. J. Phillips, Polym. Eng. Sci. **30**, 860 (1990)
78. D. J. Blundell and B. N. Osborn, Polymer **24**, 953 (1983).
79. Y. Lee and R. S. Porter, Polym. Eng. Sci. **26**, 633 (1986).
80. Y. Deslandes, F.-N. Sabir, and J. Roovers, Polymer **32**, 1267 (1991).
81. S. Buchner, D. Wiswe, and H. G. Zachmann, Polymer **30**, 480 (1989).
82. L. H. Palys and P. J. Phillips, J. Polym. Sci.: Polym. Phys. **18**, 829 (1980).
83. P. J. Phillips and H. T. Tseng, Macromolecules **22**, 1649 (1989).
84. P. J. Phillips and N. Vatansever, Macromolecules **20**, 2138 (1987).
85. B. C. Edwards, J. Polym. Sci.: Poly. Sci. Ed. **13**, 1387 (1975).
86. E. G. Lovering, J. Polym. Sci. **C30**, 329 (1970).
87. A. J. Kovacs and A. Gonthier, Kolloid-Z.Z. Polym. **250**, 530 (1972).
88. Ni Ding and E. J. Amis, Macromolecules **24**, 3906 (1991).
89. D. R. Carter and E. Baer, J. Appl. Phys. **37**, 4060 (1966).
90. D. B. Roitman, H. Marand, and R. L. Miller, J. Phys. Chem. **93**, 6919 (1989).
91. E. J. Clark and J. D. Hoffman, Macromolecules **17**, 878 (1984).
92. K. Mezghani and P. J. Phillips, Polymer **36**, 2407 (1995).
93. S. Z. D. Cheng, J. J. Janimak, and A. Zhang, Macromolecules **23**, 298 (1990).
94. P. Supaphol and J. E. Spruiell, Polymer **41**, 1205 (2000).
95. B. C. Edwards and P. J. Phillips, Polymer **15**, 351 (1974).

CHAPTER 40

Block Copolymer Melts

V. Castelletto and I. W. Hamley

Department of Chemistry, University of Reading, Reading RG6 6AD, UK

The interest in the phase behaviour of block copolymer melts stems from microphase separation of polymers that leads to nanoscale ordered morphologies. This subject has been reviewed extensively [1–4]. The identification of the structure of bicontinuous phases has only recently been confirmed, and this together with major advances in the theoretical understanding of block copolymers, means that the most up-to-date reviews should be consulted [1,3]. The dynamics of block copolymer melts, in particular rheological behaviour and studies of chain diffusion via light scattering and NMR techniques have also been the focus of several reviews [1,5,6].

The phase behaviour of block copolymer melts is, to a first approximation, represented in a morphology diagram in terms of χN and f [1]. Here f is the volume fraction of one block and χ is the Flory-Huggins interaction parameter, which is inversely proportional to temperature, that reflects the interaction energy between different segments. The configurational entropy contribution to the Gibbs energy is proportional to N, the degree of polymerization. Figure 40.1 presents a morphology diagram computed using self-consistent field theory [7,8]. It has been shown to describe qualitatively (at least in terms of the relative sequence of phases and overall topology of the phase diagram) the behaviour of real systems [1,9], and so is used as a roadmap here. When the product χN exceeds a critical value, $(\chi N)_{\mathrm{ODT}}$ (ODT: order–disorder transition) the block copolymer microphase separates into a periodically ordered structure, with a lengthscale ~5–500 nm. The structure that is formed depends on the copolymer architecture and composition [1]. For diblock copolymers, a lamellar (lam) phase is observed for symmetric diblocks ($f = 0.5$), whereas more asymmetric diblocks form hexagonal-packed cylinder (hex) or body centred cubic (BCC) spherical structures. A complex bicontinuous cubic gyroid (gyr) (spacegroup $Ia\,\bar{3}d$) phase has also been identified [10,11] for block copolymers between the lam and hex phases near the ODT, and a hexagonal-perforated layer (HPL) phase has been found to be metastable in this region [12–14]. Table 40.1 provides a compilation of the morphology of two component (A–B or A–B–A) block copolymers of various chemistries, and Table 40.2 lists studies on A–B–C triblocks.

The main techniques for investigating block copolymer microstructures are transmission electron microscopy (TEM) and small-angle x-ray or neutron scattering. TEM provides direct visual images of the structure, albeit over a small area of the sample. Usually samples are stained using the vapours from a solution of a heavy metal acid (OsO_4 or RuO_4) to increase the contrast for electrons between domains [15]. Small-angle scattering probes the structure over the whole sample volume, giving a diffraction pattern. The positions of the reflections in the diffraction pattern can be indexed to identify the symmetry of the phase [1,2]. The preparation method can have a dramatic influence on the apparent morphology, for example whether solvent casting or melt processing is performed. Numerous cases of mistaken identification of "equilibrium phases" have appeared in the literature, when the phase was simply an artifact. For instance, Lipic et al. [16] obtained different morphologies by varying the preparation conditions for a polyolefin diblock examined by them. In other cases, phases such as HPL have been observed [12] which although reproducible, have turned out to be only long-lived metastable phases, ultimately transforming to the equilibrium gyroid phase [13,14]. The ODT in block copolymers can be located via a number of methods—from discontinuities in the dynamic shear modulus [17–19] or small-angle scattering peak shape [20,21] or from calorimetry measurements [22].

To establish relationships between different block copolymer phase diagrams and also to facilitate comparison with theory, it is necessary to specify parameters in addition to χN and f. First, asymmetry of the conformation

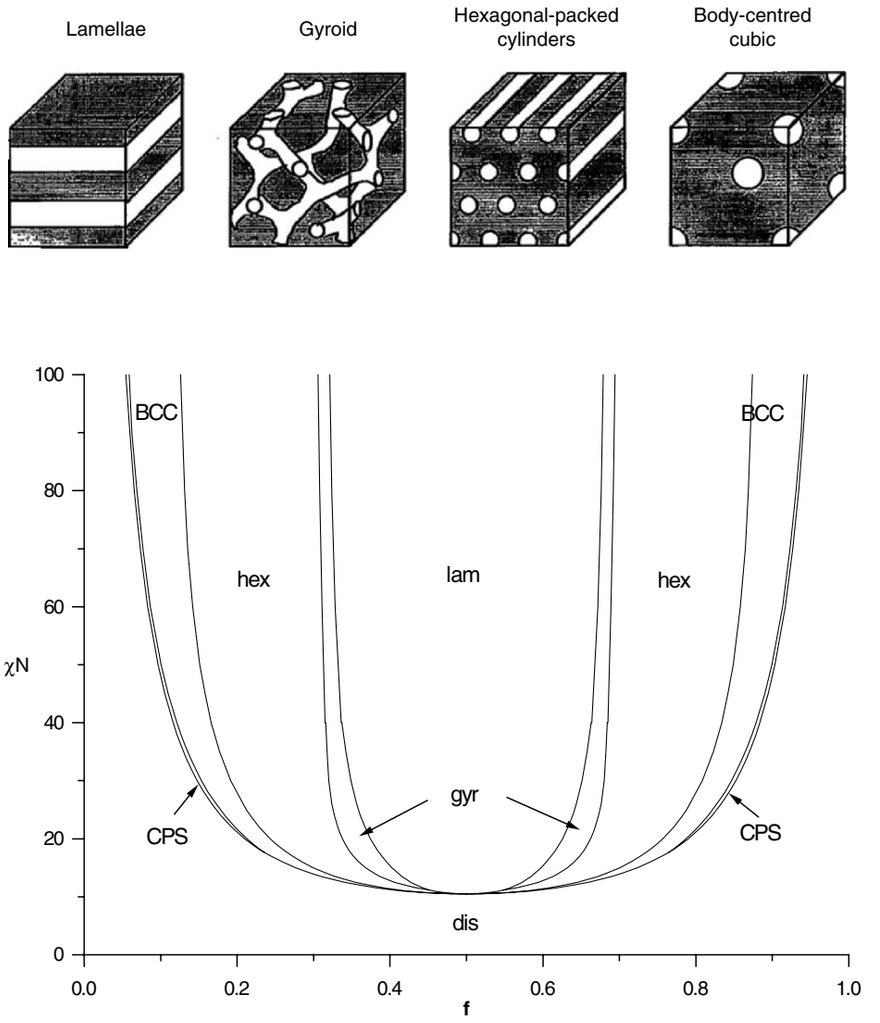

FIGURE 40.1. Phase diagram for a conformationally symmetric diblock copolymer, calculated using self-consistent mean field theory [7,8,199], along with illustrations of the equilibrium morphologies. In the phase diagram, regions of stability of disordered (dis), lamellar (lam), gyroid (gyr), hexagonal (hex), body-centred cubic (BCC) and close-packed sphere (CPS) phases are indicated.

of the copolymer breaks the symmetry of the phase diagram about $f = 0.5$. For A–B diblocks, conformational asymmetry is quantified using the ''asymmetry parameter'' $\varepsilon = (b_A^2/v_A)/(b_B^2/v_B)$ [23,24], where b_J is the segment length for block J and v_J is the segment volume. Composition fluctuations also modify the phase diagram, and this has been accounted for theoretically via the Ginzburg parameter $\bar{N} = Nb^6\rho^2$, where ρ is the number density of chains [25,26]. The extent of segregation of block copolymers depends on the magnitude of χN. For small χN, close to the order–disorder transition (up to $\chi N = 12$ for symmetric diblocks for which $\chi N_{ODT} = 10.495$), the composition profile (density of either component) is approximately sinusoidal. This is termed the weak segregation limit. At much larger values of $\chi N (\chi N >\sim 100)$, the components are strongly segregated and each domain is almost pure, with a narrow interphase between them. This is the strong segregation limit.

The first theories for block copolymers were introduced for the strong segregation limit (SSL) and the essential physical principles underlying phase behaviour in the SSL were established in the early 1970s [1]. Most notably, Helfand and coworkers [27–29] developed the self-consistent field (SCF) theory, this permitting the calculation of free energies, composition profiles and chain conformations. In the SCF theory, the external mean fields acting on a polymer chain are calculated self-consistently with the composition

TABLE 40.1. *Studies on the morphology of A–B and A–B–A block copolymers.*

System	Microstructure	Architecture	Comments	References
PB–PDMS	Cylinders	A–B		[47]
	Spheres	A–B		[47]
PE–PEE	Spheres	A–B		[48]
	Lamellae	A–B		[48–51]
	Cylinders	A–B		[48,49]
	HML	A–B		[49,50]
	HPL	A–B		[48–50]
	Bicontinous $Ia\bar{3}d$ (gyroid)	A–B		[48,49]
PE–PEP	Lamellae	A–B		[50–52]
	Cylinders	A–B		[49]
	Spheres	A–B		[49]
	HML	A–B		[50]
	HPL	A–B		[50]
PE–PVCH	Lamellae	A–B		[50,53]
PEE–PVCH	Lamellae	A–B		[53]
	HML	A–B		[50]
PEO–PtBMA	Lamellae	A–B		[54]
PE–PtBMA	Cylinders	A–B		[55]
PEP–PEE	Lamellae	A–B		[12,17,41,42,49–51,56–58]
		A–B–A		[57]
	Cylinders	A–B		[12,49,50,59–61]
	Spheres	A–B		[49,60,62]
	HML	A–B		[12,49,50]
	HPL	A–B		[12,49,50]
	Bicontinuous $Ia\bar{3}d$ (gyroid)	A–B		[49]
PEP–PVCH	Lamellae	A–B		[53]
PMTD–PxNB	Lamellae	A–B	x contains Sn or Pb or Zn	[63,64]
			x contains Pd or Pt	[65]
	Cylinders	A–B	x contains Pd or Pt	[65]
	Spheres	A–B	x contains Pd or Pt	[65]
			x contains Zn	[64]
PNB–PA	Lamellae	A–B		[66]
PxNB–PA		A–B	x contains Sn	[63,67]
	Cylinders	A–B		[66]
		A–B	x contains Sn	[67]
	Spheres	A–B	x contains Sn	[67]
PNORPHOS–PMTD	Lamellae	A–B	Complexed with Ag or Au	[68]
	Cylinders	A–B	Complexed with Ag or Au	[68]
	Spheres	A–B	Complexed with Ag or Au	[68]
PS–PB	Lamellae	A–B		[69–73]
		A–B–A		[74–78]
		$(A\text{–}B\text{–})_n\text{–}$	$n \geq 3$	[74]
	PL	A–B		[73]
	Cylinders	A–B		[69,70,79]
		A–B–A		[74,77,78,80–83]
	Spheres	$(A\text{–}B\text{–})_n\text{–}$	$n \geq 3$	[74]
		A–B		[84,85]
		A–B–A		[74]
PS–PnBMA	Lamellae	A–B		[86]
	Cylinders	A–B		[87,88]
	Spheres	A–B		[87]
PS–PChEMA	Cylinders	A–B	Tetragonal packing	[88]
		A–B–A	Tetragonal packing	[88]
PS–PDMS	Lamellae	A–B		[89]
	Cylinders	A–B		[89]
	Spheres	A–B		[72]

TABLE 40.1. *Continued.*

System	Microstructure	Architecture	Comments	References
PS–PEB	Lamellae	A–B		[90]
	Cylinders	A–B		[90]
	Spheres	A–B		[72]
PS–PEP	Lamellae	A–B		[91,92]
	Cylinders	A–B		[91]
	Spheres	A–B		[91,93]
PS–PI	Lamellae	A–B		[10,11,49,69,70,94–114]
		A–B–A		[110,112,115]
		$(A–B–)_n–$	$n \geq 3$	[116,117]
		$(A–B–)_n–$	$n \geq 2$	[118,119]
		Miktoarm star $(A)_nB$	$n = 2$	[120]
	PL	A–B		[11,49,94,114]
	Bicontinuous $Ia\bar{3}d$ (gyroid)	A–B		[10,11,49,94,111,114]
		$(A–B–)_n–$	$n \geq 3$	[121]
		A–B–A		[122]
	Bicontinuous $Pn\bar{3}m$ (OBDD)	A–B		[73,98,102,103,111,123]
		$(A–B–)_n–$	$n \geq 3$	[121,124–127]
	Cylinders	A–B		[11,49,69,70,94,98,102,109–111, 113,123,128,129]
		A–B–A		[110,126,130,131]
		$(A–B–)_n–$	$n \geq 3$	[117,125–127]
		Miktoarm star $A(B)_n$	$n = 2$	[132]
		Miktoarm star $(A)_nB$	$n = 2$	[120]
	Spheres	A–B		[11,94,102,106,109–111,113,123, 128,129,133]
		A–B–A		[110,126,130,131]
		$(A–B–)_n–$	$n \geq 3$	[116,117,126,127]
		A–B/star		[134]
PI–PS	Cylinders	Miktoarm star $(A)_nB$	$n = 2,3$	[120]
	Bicontinuous cubic	Miktoarm star $(A)_nB$	$n = 2$	[120]
	Lamellae	Miktoarm star $(A)_nB$	$n = 3,5$	[120,135]
		Miktoarm star $(A)_n(B)_n$	$n = 8$	[136]
PEO–PEE	Lamellae	A–B		[114]
	PL	A–B		[114]
	Bicontinuous $Ia\bar{3}d$ (gyroid)	A–B		[114]
PS–PMMA	Lamellae	A–B		[137,138]
PS–P2VP	Lamellae	A–B		[105,106,139–142]
	Spheres	A–B		[106,143,144]
PS–P2VP	Lamellae	A–B		[145]
	Bicontinuous $Ia\bar{3}d$ (gyroid)	A–B		[145]
	Cylinders	A–B		[145]
	Spheres	A–B		[145]
PS–P4VP	Lamellae	A–B		[146,147]
	Spheres	A–B		[146,147]
PEP–PDMS	Lamellae	A–B		[14,114,148]
	Spheres	A–B		[149]
	Cylinders	A–B		[14]
	Bicontinuous $Ia\bar{3}d$ (gyroid)	A–B		[14,114,148]
PI–PDMS	Lamellae	A–B		[148]
	Bicontinuous $Ia\bar{3}d$ (gyroid)	A–B		[148]
PEO–PI	Spheres	A–B		[150]
	PL	A–B		[150]
P2VP–PCMA	Lamellae	A–B		[142]
PS–P2MP	Lamellae	Miktoarm star $A(B)_n$	$n = 3$	[151]
	Spheres	A–B		[151]
		Miktoarm star $A(B)_n$	$n = 2$	[151]

TABLE 40.1. *Continued.*

System	Microstructure	Architecture	Comments	References
	Cylinders	A–B		[151]
		Miktoarm star $A(B)_2$		[151]
	Double gyroid	Miktoarm star $A(B)_3$		[151]
PIB–PPVL	Lamellae	A–B		[152]
	Spheres	A–B		[152]
PS–PnPMA	Lamellae	A–B		[153]
	Cylinders	A–B		[153]
	Spheres	A–B		[153]
PI–PLA	Lamellae	A–B		[154]
PEP–PLA	Lamellae	A–B		[155]
	Cylinders	A–B		[155]
	Spheres	A–B		[155]
	Bicontinuous $Ia\bar{3}d$ (gyroid)	A–B		[155]

TABLE. 40.2. *Studies on the morphology of A–B–C block copolymers.*

System	Microstructure	Architecture	References
PI–PS–P2VP	Lamellae	A–B–C	[156–159]
	Cylinders	A–B–C	[156,158,159]
	Spheres	A–B–C	[156,159]
	Ordered tricontinuous double diamond (OTDD)		
	Other	A–B–C	[156–158]
PS–PB–P4VP	Lamellae	A–B–C	[160,161]
	Other	A–B–C	[160]
PS–PEB–PMMA	Lamellae	A–B–C	[162]
	Cylinders	A–B–C	[162]
	Other	A–B–C	[162]
PS–PI–P2VP	Lamellae	A–B–C	[163]
	Cylinders	A–B–C	[163]
		miktoarm star A–B–C	[164]
	Others	A–B–C	[163]
PS–PEB–PMMA	lc	A–B–C	[162,165,166]
	hel	A–B–C	[165,167]
	s(o)c	A–B–C	[165,167]
	c(a)c	A–B–C	[165,167]
	u-c(i)c	A–B–C	[165,167]
	s(o)s	A–B–C	[168]
	Knitting pattern	A–B–C	[169]
PS–PEB–PMMA(upon hydrogenation of the central PEB block)	Knitting pattern		[166,170]
PS–PB–PMMA	ll	A–B–C	[171,172]
	hel	A–B–C	[167,171–173]
	s(o)c	A–B–C	[167,171–173]
	c(a)c	A–B–C	[167,171–173]
	u-c(i)c	A–B–C	[167,171–173]
	ml	A–B–C	[172]
	c(i)c	A–B–C	[172]
	s(o)s	A–B–C	[168,172]
	lc	A–B–C	[165,172]
	ls	A–B–C	[165,172,174,175]
	dl	A–B–C	[172]

TABLE 40.2. *Continued.*

System	Microstructure	Architecture	References
PS–PB–P2VP	Lamellae	A–B–C	[176,177]
	Cylinders	A–B–C	[176,177]
	Bicontinuous double Gyroid	A–B–C	[177,178]
PB–PS–P2VP	Lamellae	A–B–C	[177]
PS–PI–PMMA	lc	A–B–C	[179]
	ll	A–B–C	[180]
	Cylinders	A–B–C	[181]
PS–PI–PMMA	Cylinders	miktoarm star A–B–C	[182]
PS–PI–PB	Cylinders	miktoarm star A–B–C	[132]
PS–PDMS–PtBMA	Tricontinuous microdomain structure	Star A–B–C	[183]
PEP–PEB–PS	Spheres	A–B–C	[184]
	Cylinders	A–B–C	[184]
	Continuous morphology	A–B–C	[184]
PI–PB–PS	Spheres	A–B–C	[184,185]
	Cylinders	A–B–C	[184,185]
PB–PS–PI	Lamellae	A–B–C	[186]
	Cylinders	A–B–C	[186]
PS–PB–PI	Lamellae	A–B–C	[186]
PCE–PEE–PE	Tricontinuous (10, 3)c network (orthorhombic symmetry)	A–B–C	[187]
PI–PS–PEO	Tricontinuous (10, 3)c network (orthorhombic symmetry)	A–B–C	[188,189]
	Lamellae	A–B–C	[188,190]
	c(i)c	A–B–C	[190]
	Pentacontinuous Gyroid $Ia\bar{3}d$	A–B–C	[190,191]
PS–PI–PDMS	Cylinders	miktoarm star A–B–C	[192]
PS–zw–PI	Lamellae	A–B–C	[193]
PPVL–PIB–PPVL	Lamellae	A–B–A	[152]
	Spheres	A–B–A	[152]
PI–PS–PI	Spheres	super-H star A_3BA_3	[194]
	Cylinders	super-H star A_3BA_3	[194]
PLA–PI–PLA	Lamellae	A–B–A	[195]
	Spheres	A–B–A	[195]
	Cylinders	A–B–A	[195]
PI–PPMDSS–PI	Tricontinuous Gyroid $Ia\bar{3}d$	A–B–A	[196]
PPMDSS–PI–PPMDSS	Spheres	A–B–A	[196]

profile. The theory of Leibler [30] describes block copolymers in the weak segregation limit. It employs a Landau-Ginzburg approach to analyse the free energy, which is expanded with reference to the average composition profile. The free energy coefficients are computed within the random phase approximation. Weak segregation limit theory can be extended to allow for thermal composition fluctuations. This changes the mean field prediction of a second-order phase transition for a symmetric diblock copolymer to a first-order transition. Fredrickson and Helfand [25] studied this effect for block copolymers and showed that composition fluctuations, incorporated via the renormalization method of Brazovskii, lead to a ''finite size effect'', where the phase diagram depends on the degree of polymerization, $\bar{N}$. A powerful new method to solve the self-consistent field equations for block copolymers has been applied by Matsen and coworkers to analyse the ordering of many types of block copolymer in bulk and in thin films [7–9,31]. The strong and weak segregation limits are spanned, as well as the intermediate regime where the other methods do not apply. This implementation of SCF theory predicts phase diagrams, and other quantities such as domain spacings, in good agreement with experiment and represents an impressive state-of-the-art for modelling the ordering of soft materials. Accurate liquid state theories have also been used to model block copolymer melts [32,33], although they are hard to implement and consequently the method is often regrettably overlooked [1]. Recently, a method has been developed to directly simulate field theories for polymers without introducing approximations such as mean field approaches, perturbation expansions, etc. [34]. This technique holds much promise for examining the thermodynamics of

block copolymers in the limit of low molecular weight where approximate methods such as mean field theory or renormalization techniques break down.

The phase behaviour of A–B–C triblocks is much richer [3] than two-component diblocks or triblocks, as expected because multiple interaction parameters (χ_{AB}, χ_{AC} and χ_{BC}) result from the presence of a distinct third block. Summaries of work on A–B–C triblock morphologies have appeared [1,35] and Table 40.2 contains a listing of relevant studies. Figure 40.2 illustrates representative morphologies that have been observed. Because of the large number of possible morphologies, theorists are presently working to predict the phase behaviour of these copolymers using methods that do not require *a priori* knowledge of the space group symmetries of trial structures [36,37]. Some systems, such as the *poly* (styrene–butadiene–methylmethacrylate) (PS–PB–PMMA) triblock copolymers, exhibit a particularly rich complexity in phase behaviour (Figure 40.3), forming multiple ordered

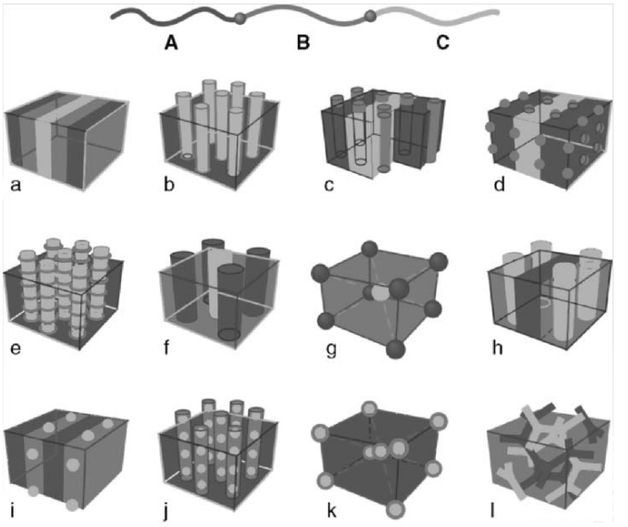

FIGURE 40.2. Schematic of several morphologies observed for ABC triblock copolymer melts [3].

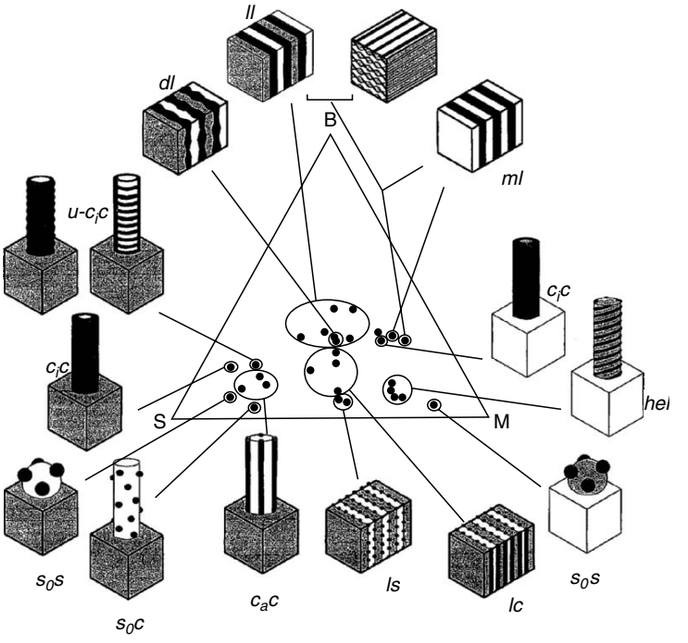

FIGURE 40.3. Morphology diagram for PS–PB–PMMA triblocks [197].

phases as listed in Table 2. Other systems form several network phases, as shown in Fig. 40.4 and listed in Table 2 for the *poly*(isoprene–styrene–ethylene oxide) (PI–PS–PEO) triblock copolymer. However, the list of phases in Table 2 is not exhaustive—many more are still to be discovered. Elucidating which are in equilibrium will be a particular challenge for these systems which often have high molecular weight and contain strongly incompatible blocks.

During processing block copolymers are subjected to flow. For example thermoplastic elastomers formed by *poly*(styrene–butadiene–styrene) (PS–PB–PS) triblock copolymers, are moulded by extrusion. This leads to alignment of microphase-separated structures. This was investigated in the early 1970s by Keller and coworkers [2,38] who obtained transmission electron micrographs from highly oriented specimens of Kraton PS–PB–PS copolymers following extrusion.

Work on the effect of flow on block copolymer melts has been reviewed [1,5,39,40]. Due to the convenience and well defined nature of the shear geometry most model studies have exploited this type of flow. The application of shear leads to orientation of block copolymer microstructures at sufficiently high shear rates and/or strain amplitudes (in the case of oscillatory shear). Depending on shear conditions

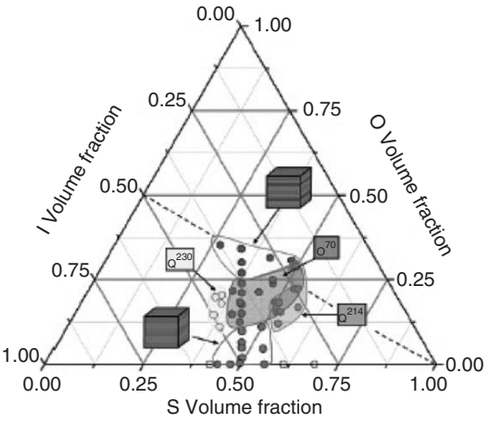

(a)

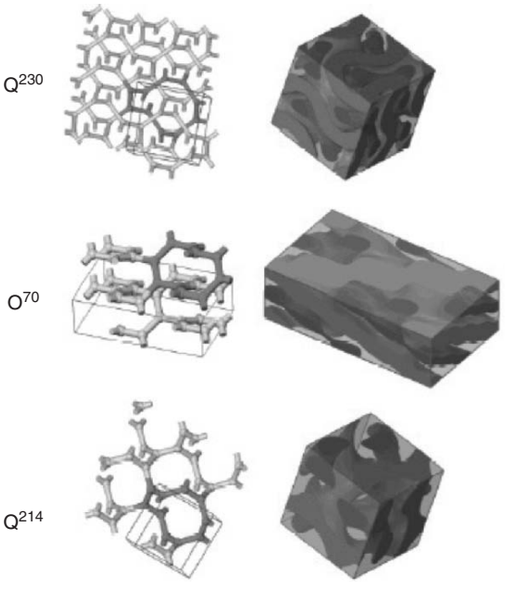

(b)

FIGURE 40.4. (**a**) Phase diagram for a PI–PS–PEO triblock showing regions of network phases, illustrated in part (**b**) (structures are identified by space group number) [189,198].

and temperature, different orientations of a morphology with respect to the shear plane can be accessed. This has been particularly well studied for the lamellar phase where so-called ''parallel'' (lamellar normal along shear gradient direction) and ''perpendicular'' (lamellar normal along the neutral direction) orientations have been observed [41]. Distinct orientation states of hex and cubic phases have also been investigated, details being provided elsewhere [40]. The ability to generate distinct macroscopic orientation states of block copolymers by shear is important in future applications of block copolymers where alignment will be important (reinforced composites, optoelectronic materials and separation media). Shear also influences thermodynamics, since the order–disorder transition shifts upwards on increasing shear rate because the ordered phase is stabilized under shear [42,43].

The phase behaviour of rod–coil block copolymers is already known to be much richer than that of coil–coil block copolymers, because the rod block can orient into liquid crystal structures [1]. The rod block may be analogous to a biomacromolecule, for example *poly*(benzyl glutamates) [44,45] and *poly*(peptides) [46] forming helical rod-like blocks have been incorporated in block copolymers. Possible applications of these materials arising from their biocompatibility are evident.

GLOSSARY

Compound names abbreviations used in Table 40.1 and Table 40.2

PLA	:	*poly*(lactide)
PA	:	*poly*(acetylene)
PB	:	*poly*(butadiene)
PnBMA	:	*poly*(*n*-butylmethacrylate)
PtBMA	:	*poly*(*tert*-butylmethacrylate)
PChEMA	:	*poly*(2-(3-cholesteryl-oxycarbonyloxy)ethylmethacrylate)
PE	:	*poly*(ethylene)
PEB	:	*poly*(ethylenebutene)
PEE	:	*poly*(ethylethylene)
PEP	:	*poly*(ethylenepropylene)
PEO	:	*poly*(ethyleneoxide)
PI	:	*poly*(isoprene)
PIB	:	*poly*(isobutylene)
PMMA	:	*poly*(methylmethacrylate)
PCMA	:	*poly*(cyclohexylmethacrylate)
PCE	:	*poly*(cyclohexylethylene)
PMDT	:	*poly*(methyltetracyclododecene)
PNB	:	*poly*(norbornene)
PxNB	:	organometallic derivative of *poly*(norbornene)
PNORPHOS	:	*poly*(2-*exo*-3-*endo* -*bis*(diphenylphosphophino)bicyclo[2,2,1] heptene)
PS	:	*poly*(styrene)
PVCH	:	*poly*(vinylcyclohexane)
P2VP	:	*poly*(2-vinylpyridine)
P4VP	:	*poly*(4-vinylpyridine)
PDMS	:	*poly*(dimethylsiloxane)
P2MP	:	*poly*(2-methyl-1,3-pentadiene)
zw	:	zwitterionic group
PPVL	:	*poly*(pivalolactone)
PnPMA	:	*poly*(*n*-pentyl methacrylate)
PPMDSS	:	*Poly*(pentamethyldisilylstyrene)

Phase morphology abbreviations used in Table 40.1 and Table 40.2

HML	:	Hexagonal modulated layers
HPL	:	Hexagonal perforated layers
PL	:	Perforated layers
s(o)s	:	spheres on spheres, according to the nomenclature shown in Fig. 40.3.

hel, c(a)c, uc(i)c, u-c(i)c, c(i)c and s(o)c are cylindrical phases named according to the nomenclature shown in Fig. 40.3.

lc, ls, ll, dl and ml are lamellar phases named according to the nomenclature shown in Fig. 40.3.

REFERENCES

1. Hamley, I. W. *The Physics of Block Copolymers*; Oxford University Press:Oxford, 1998.
2. Folkes, M. J.; Keller, A. In *The Physics of Glassy Polymers*; Haward, R. N., Ed.; Applied Science:London, 1973; pp 548–603.
3. Bates, F. S.; Fredrickson, G. H. *Phys. Today* 1999, *52 (February issue)*, 32.
4. Bates, F. S.; Fredrickson, G. H. *Ann. Rev. Phys. Chem.* 1990, *41*, 525–557.
5. Fredrickson, G. H.; Bates, F. S. *Annu. Rev. Mater. Sci.* 1996, *26*, 501–550.
6. Colby, R. H. *Curr. Opin. Colloid Interface Sci.* 1996, *1*, 454–465.
7. Matsen, M. W.; Schick, M. *Phys. Rev. Lett.* 1994, *72*, 2660–2663.
8. Matsen, M. W.; Bates, F. S. *Macromolecules* 1996, *29*, 1091–1098.
9. Matsen, M. W. *J. Phys. Condens. Matter* 2001, *14*, R21–R47.
10. Hajduk, D. A.; Harper, P. E.; Gruner, S. M.; Honeker, C. C. Kim, G.; Thomas, E. L.; Fetters, L. J. *Macromolecules* 1994, *27*, 4063–4075.
11. Förster, S.; Khandpur, A. K.; Zhao, J.; Bates, F. S.; Hamley, I. W.; Ryan, A. J.; Bras, W. *Macromolecules* 1994, *27*, 6922–6935.
12. Hamley, I. W.; Koppi, K. A.; Rosedale, J. H.; Bates, F. S.; Almdal, K.; Mortensen, K. *Macromolecules* 1993, *26*, 5959–5970.
13. Hajduk, D. A.; Takenouchi, H.; Hillmyer, M. A.; Bates, F. S.; Vigild, M. E.; Almdal, K. *Macromolecules* 1997, *30*, 3788–3795.
14. Vigild, M. E.; Almdal, K.; Mortensen, K.; Hamley, I. W.; Fairclough, J. P. A.; Ryan, A. J. *Macromolecules* 1998, *31*, 5702–5716.
15. Kato, K. *J. Electron Microsc. (Jpn.)* 1965, *14*, 220.
16. Lipic, P. M.; Bates, F. S.; Matsen, M. W. *J. Polym. Sci. B:Polym. Phys.* 2001, *37*, 2229–2238.
17. Bates, F. S.; Rosedale, J. H.; Fredrickson, G. H. *J. Chem. Phys.* 1990, *92*, 6255–6270.
18. Rosedale, J. H.; Bates, F. S. *Macromolecules* 1990, *23*, 2329–2338.
19. Han, C. D.; Baek, D. M.; Kim, J. K.; Ogawa, T.; Sakamoto, N.; Hashimoto, T. *Macromolecules* 1995, *28*, 5043–5062.
20. Mai, S. M.; Fairclough, J. P. A.; Hamley, I. W.; Denny, R. C.; Liao, B.; Booth, C.; Ryan, A. J. *Macromolecules* 1996, *29*, 6212–6221.
21. Sakamoto, N.; Hashimoto, T. *Macromolecules* 1995, *28*, 6825–6834.
22. Voronov, V. P.; Buleiko, V. M.; Podneks, V. E.; Hamley, I. W.; Fairclough, J. P. A.; Ryan, A. J.; Mai, S.-M.; Liao, B.-X.; Booth, C. *Macromolecules* 1997, *30*, 6674–6676.

23. Helfand, E.; Sapse, A. M. *J. Chem. Phys*. 1975, *62*, 1327–1331.
24. Bates, F. S.; Fredrickson, G. H. *Macromolecules* 1994, *27*, 1065–1067.
25. Fredrickson, G. H.; Helfand, E. *J. Chem. Phys.* 1987, *87*, 697–705.
26. Fredrickson, G. H.; Binder, K. *J. Chem. Phys*. 1989, *91*, 7265–7275.
27. Helfand, E. *Macromolecules* 1975, *8*, 552–556.
28. Helfand, E.; Wasserman, Z. R. *Macromolecules* 1976, *9*, 879–888.
29. Helfand, E.; Wasserman, Z. R. In *Developments in Block Copolymers 1*; Goodman, I., Ed.; Applied Science:London, 1982; pp 99–125.
30. Leibler, L. *Macromolecules* 1980, *13*, 1602–1617.
31. Matsen, M. W.; Schick, M. *Curr. Opin. Colloid Interface Sci*. 1996, *1*, 329–336.
32. David, E. F.; Schweizer, K. S. *J. Chem. Phys.* 1994, *100*, 7767–7783.
33. David, E. F.; Schweizer, K. S. *J. Chem. Phys.* 1994, *100*, 7784–7795.
34. Ganesan, V.; Fredrickson, G. H. *Europhys. Lett*. 2001, *55*, 814–820.
35. Ryan, A. J.; Hamley, I. W. In *The Physics of Glassy Polymers*; Haward, R. N.; Young, R. J., Eds.; Chapman and Hall:London, 1997.
36. Drolet, F.; Fredrickson, G. H. *Phys. Rev. Lett*. 1999, *83*, 4317–4320.
37. Bohbot-Raviv, Y.; Wang, Z.-G. *Phys. Rev. Lett*. 2000, *85*, 3428–3431.
38. Keller, A.; Pedemonte, E.; Willmouth, F. M. *Nature* 1970, *225*, 538.
39. Honeker, C. C.; Thomas, E. L. *Chem. Mater*. 1996, *8*, 1702–1714.
40. Hamley, I. W. *J. Phys. Condens. Matter*, 2001, *13*, R643–R671.
41. Koppi, K. A.; Tirrell, M.; Bates, F. S.; Almdal, K.; Colby, R. H. *J. Phys. France II*, 1992, *2*, 1941–1959.
42. Koppi, K. A.; Tirrell, M.; Bates, F. S. *Phys. Rev. Lett*. 1993, *70*, 1449–1452.
43. Almdal, K.; Mortensen, K.; Koppi, K. A.; Tirrell, M.; Bates, F. S. *J. Phys. France II*, 1996, *6*, 617–637.
44. Nakajima, A.; Hayashi, T.; Kugo, K.; Shinoda, K. *Macromolecules* 1979, *12*, 840–843.
45. Nakajima, A.; Kugo, K.; Hayashi, T. *Macromolecules* 1979, *12*, 844–848.
46. Cornelissen, J. J. L. M.; Fischer, M.; Sommerdijk, N. A. J. M.; Nolte, R. J. M. *Science* 1998, *280*, 1427–1430.
47. Li, W.; Huang, J. *J. Polym. Sci.:Part B:Polym. Phys.* 1992, *30*, 727–732.
48. Zhao, J.; Majumdar, B.; Schulz, M. F.; Bates, F. S.; Almdal, K.; Mortensen, K.; Hajduk, D. A.; Gruner, S. M. *Macromolecules* 1996, *29*, 1204–1215.
49. Bates, F. S.; Schulz, M. F.; Khanpur, A. K.; Forster, S.; Rosedale, J. H.; Almdal, K.; Mortensen, K. *Faraday Discuss.* 1994, *98*, 7–18.
50. Hamley, I. W.; Gehlsen, M. D.; Khandpur, A. K.; Koppi, K. A.; Rosedale, J. H.; Schulz, M. F.; Bates, F. S.; Almdal, K.; Mortensen, K. *J. Phys. France II*, 1994, *4*, 2161–2186.
51. Rosedale, J. H.; Bates, F. S.; Almdal, K.; Mortensen, K.; Wignall, G. D. *Macromolecules* 1995, *28*, 1429–1443.
52. Kofinas, P.; Cohen, R. E. *Macromolecules* 1994, *27*, 3002–3008.
53. Gehlsen, M. D.; Bates, F. S. *Macromolecules* 1994, *27*, 3611–3618.
54. Unger, R.; Beyer, D.; Donth, E. *Polymer* 1991, *32*, 3305–3312.
55. Schipper, F. J. M.; Floudas, G.; Pispas, S.; Hadjichristidis, N.; Pakula, T. *Macromolecules* 2002, *35*, 8860–8868.
56. Almdal, K.; Rosedale, J. H.; Bates, F. S.; Wignall, G. D.; Fredrickson, G. H. *Phys. Rev. Lett*. 1990, *65*, 1112–1115.
57. Gehlsen, M. D.; Almdal, K.; Bates, F. S. *Macromolecules* 1992, *25*, 939–943.
58. Almdal, K.; Rosedale, J. H.; Bates, F. S. *Macromolecules* 1990, *23*, 4336–4338.
59. Almdal, K.; Bates, F. S.; Mortensen, K. *J. Chem. Phys.* 1992, *96*, 9122–9132.
60. Koppi, K. A.; Tirrell, M.; Bates, F. S.; Almdal, K.; Mortensen, K. *J. Rheol.* 1994, *38*, 999–1027.
61. Karim, A.; Singh, N.; Sikka, M.; Bates, F. S.; Dozier, W. D.; Felcher, G. P. *J. Chem. Phys.* 1994, *100*, 1620–1629.
62. Almdal, K.; Koppi, K.; Bates, F. S. *Macromolecules* 1993, *26*, 4058–4060.
63. Cummins, C. C.; Beachy, M. D.; Schrock, R. R.; Vale, M. G.; Sankaran, V.; Cohen, R. E. *Chem. Mater.* 1991, *3*, 1153–1163.
64. Sankaran, V.; Yue, J.; Cohen, R. E.; Schrock, R. R.; Silbey, R. J. *Chem. Mater*. 1993, *5*, 1133–1142.
65. Chan, Y. N. C.; Craig, G. S. W.; Schrock, R. R.; Cohen, R. E. *Chem. Mater*. 1992, *4*, 885–894.
66. Saunders, R. S.; Cohen, R. E.; Schrock, R. R. *Macromolecules* 1991, *24*, 5599–5605.
67. Sankaran, V.; Cohen, R. E.; Cummins, C. C.; Schrock, R. R. *Macromolecules* 1991, *24*, 6664–6669.
68. Chan, Y. N. C.; Schrock, R. R.; Cohen, R. E. *Chem. Mater*. 1992, *4*, 24–27.
69. Winey, K. I.; Thomas, E. L.; Fetters, E. L. *Macromolecules* 1992, *25*, 2645–2650.
70. Winey, K. I.; Thomas, E. L.; Fetters, L. J. *Macromolecules* 1992, *25*, 422–428.
71. Disko, M. M.; Liang, K. S.; Behal, S. K.; Roe, R. J.; Jeon, K. J. *Macromolecules* 1993, *26*, 2983–2986.
72. Cohen, R. E.; Cheng, P.-L.; Douzinas, K.; Kofinas, P.; Berney, C. V. *Macromolecules* 1990, *23*, 324–327.
73. Thomas, E. L.; Anderson, D. M.; Henkee, C. S. *Nature* 1988, *334*, 598.
74. Aggarwal, S. L. *Polymer* 1976, *17*, 938–956.
75. Morrison, F. A.; Mays, J. W.; Muthukumar, M.; Nakatani, A. I.; Han, C. C. *Macromolecules* 1993, *26*, 5271–5273.
76. Yamaoka, I.; Kimura, M. *Polymer* 1993, *34*, 4339.
77. Sakurai, S.; Momii, T.; Taie, K.; Shibayama, M.; Nomura, S.; Hashimoto, T. *Macromolecules* 1993, *26*, 485–491.
78. Han, C. D.; Baek, D. M.; Kim, J.; Kimishima, K.; Hashimoto, T. *Macromolecules* 1992, *25*, 3052–3067.
79. Smith, D. R.; Meier, D. J. *Polymer* 1992, *33*, 3777–3782.
80. Scott, D. B.; Waddon, A. J.; Lin, Y. G.; Karasz, F. E.; Winter, H. H. *Macromolecules* 1992, *25*, 4175–4181.
81. Spontak, R. J.; Williams, M. C.; Agard, D. A. *Polymer* 1988, *29*, 387–395.
82. Albalak, R. J.; Thomas, E. L. *J. Polym. Sci. Part B:Polym. Phys.* 1994, *32*, 341–350.
83. Pakula, T.; Saijo, K.; Kawai, H.; Hashimoto, T. *Macromolecules* 1985, *18*, 1294–1302.
84. Bates, F. S.; Berney, C. V.; Cohen, R. E. *Macromolecules* 1983, *16*, 1101–1108.
85. Bates, F. S.; Cohen, R. E.; Berney, C. V. *Macromolecules* 1982, *15*, 589–592.
86. Russell, T. P.; Karis, T. E.; Gallot, Y. *Nature* 1994, *368*, 729.
87. Cohen, R. E.; Bates, F. S. *J. Polym. Sci.:Part B:Polym. Phys.* 1980, *18*, 2143–2148.
88. Fischer, H. *Polymer* 1994, *35*, 3786–3788.
89. Chu, J. H.; Rangarajan, P.; Adams, J. L.; Register, R. A. *Polymer* 1995, *36*, 1569–1575.
90. Hajduk, D. A.; Gruner, S. M.; Rangarajan, P.; Register, R. A.; Fetters, L. J.; Honeker, C.; Albalak, R. J.; Thomas, E. L. *Macromolecules* 1994, *27*, 490–501.
91. Hashimoto, T.; Kawamura, T.; Harada, M.; Tanaka, H. *Macromolecules* 1994, *27*, 3063–3072.
92. Sakurai, S.; Okamoto, S.; Kawamura, T.; Hashimoto, T. *J. Appl. Cryst*. 1991, *24*, 679–684.
93. Okamoto, S.; Saijo, K.; Hashimoto, T. *Macromolecules* 1994, *27*, 3753–3758.
94. Khandpur, A. K.; Förster, S.; Bates, F. S.; Hamley, I. W.; Ryan, A. J.; Bras, W.; Almdal, K.; Mortensen, K. *Macromolecules* 1995, *28*, 8796–8806.
95. Winey, K. I.; Thomas, E. L.; Fetters, L. J. *J. Chem. Phys.* 1991, *95*, 9367–9375.
96. Winey, K. I.; Patel, S. S.; Larson, R. G.; Watanabe, H. *Macromolecules* 1993, *26*, 2542–2549.
97. Winey, K. I.; Patel, S. S.; Larson, R. G.; Watanabe, H. *Macromolecules* 1993, *26*, 4373–4375.
98. Winey, K. I.; Gobran, D. A.; Xu, Z. D.; Fetters, L. J.; Thomas, E. L. *Macromolecules* 1994, *27*, 2392–2397.
99. Hashimoto, T.; Shibayama, M.; Kawai, H. *Macromolecules* 1980, *13*, 1237–1247.
100. Hasegawa, H.; Hashimoto, T.; Kawai, H.; Lodge, T. P.; Amis, E. J.; Glinka, C. J.; Han, C. C. *Macromolecules* 1985, *18*, 67–78.
101. Hashimoto, T.; Hideaki, T.; Hasegawa, H. *Macromolecules* 1990, *23*, 4378–4386.
102. Mori, K.; Hasegawa, H.; Hashimoto, T. *Polymer* 1990, *31*, 2368–2376.
103. Hashimoto, T.; Yamasaki, K.; Koizumi, S.; Hasegawa, H. *Macromolecules* 1993, *26*, 2895–2904.
104. Hashimoto, T.; Koizumi, S.; Hasegawa, H. *Macromolecules* 1994, *27*, 1562–1570.
105. Ishizu, K.; Yamada, Y.; Fukutomi, T. *Polymer* 1990, *31*, 2047–2052.
106. Ishizu, K.; Omote, A.; Fukutomi, T. *Polymer* 1990, *31*, 2135–2140.

107. Spontak, R. J.; Smith, S. D.; Ashraf, A. *Macromolecules* 1993, *26*, 956–962.
108. Spontak, R. J.; Smith, S. D.; Ashraf, A. *Polymer* 1993, *34*, 2233–2236.
109. Richards, R. W.; Thomason, J. L. *Polymer* 1981, *22*, 581–589.
110. Richards, R. W.; Thomason, J. L. *Macromolecules* 1983, *16*, 982–992.
111. Thomas, E. L.; Lescanec, R. L. *Phil. Trans. R. Soc. London* 1994, *348*, 149–166.
112. Hadziioannou, G.; Skoulios, A. *Macromolecules* 1982, *15*, 267–271.
113. Koizumi, S.; Hasegawa, H.; Hashimoto, T. *Macromolecules* 1994, *27*, 4371–4381.
114. Hajduk, D. A.; Ho, R.-M.; Hillmyer, M. A.; Bates, F. S.; Almdal, K. *J. Chem. Phys. B* 1998, *102*, 1356–1363.
115. Widmaier, J. M.; Meyer, G. C. *J. Polym. Sci. Part B:Polym. Phys.* 1980, *18*, 2217–2225.
116. Herman, D. S.; Kinning, D. J.; Thomas, E. L. *Macromolecules* 1987, *20*, 2940–2942.
117. Matsushita, Y.; Taskasu, T.; Yagi, K. *Polymer* 1994, *35*, 2862–2866.
118. Spontak, R. J.; Smith, S. D.; Ashraf, A. *Macromolecules* 1993, *26*, 5118–5124.
119. Matsushita, Y.; Mogi, Y.; Mukai, H.; Watanabe, J.; Noda, I. *Polymer* 1994, *35*, 246–249.
120. Tselikas, Y.; Iatrou, H.; Hadjichristidis, N.; Liang, K. S.; Mohanty, K.; Lohse, D. J. *J. Chem. Phys.* 1996, *105*, 2456–2462.
121. Hajduk, D. A.; Harper, P. E.; Gruner, S. M.; Honeker, C. C.; Thomas, E. L.; Fetters, L. J. *Macromolecules* 1995, *28*, 2570–2573.
122. Avgeropoulos, A.; Dair, B. J.; Hadjichristidis, N.; Thomas, E. L. *Macromolecules* 1997, *30*, 5634–5642.
123. Hasegawa, H.; Tanaka, H.; Yamasaki, K.; Hashimoto, T. *Macromolecules* 1987, *20*, 1651–1662.
124. Thomas, E. L.; Alward, D. B.; Kinning, D. J.; Martin, D. C.; Handlin, D. L.; Fetters, L. J. *Macromolecules* 1986, *19*, 2197–2202.
125. Herman, D. S.; Kinning, D. J.; Thomas, E. L.; Fetters, L. J. *Macromolecules* 1987, *20*, 2940–2942.
126. Alward, D. B.; Kinning, D. J.; Thomnas, E. L.; Fetters, L. J. *Macromolecules* 1986, *19*, 215–224.
127. Kinning, D. J.; Thomas, E. L.; Alward, D. B.; Fetters, L. J.; Handlin, D. L. *Macromolecules* 1986, *19*, 1288–1290.
128. Sakurai, S.; Kawada, H.; Hashimoto, T.; Fetters, L. J. *Macromolecules* 1993, *26*, 5796–5802.
129. Sakurai, S.; Kawada, H.; Hashimoto, T.; Fetters, L. J. *Proc. Jpn. Acad.* 1993, *69*, 13.
130. Morrison, F. A.; Winter, H. H.; Gronski, W.; Barnes, J. D. *Macromolecules* 1990, *23*, 4200–4205.
131. Winter, H. H.; Scott, D. B.; Gronski, W.; Okamoto, S.; Hashimoto, T. *Macromolecules* 1993, *26*, 7236–7244.
132. Floudas, G.; Hadjichristidis, N.; Iatrou, H.; Pakula, T. *Macromolecules* 1996, *29*, 3139–3146.
133. Hashimoto, T.; Fujimura, M.; Kawai, H. *Macromolecules* 1980, *13*, 1660–1669.
134. Floudas, G.; Pispas, S.; Hadjichristidis, N.; Pakula, T.; Erukhimovich, I. *Macromolecules* 1996, *29*, 4142–4154.
135. Yang, L.; Hong, S.; Gido, S. P.; Velis, G.; Hadjichristidis, N. *Macromolecules* 2001, *34*, 9069–9073.
136. Beyer, F. L.; Gido, S. P.; Poulos, Y.; Avgeropoulos, A.; Hadjichristidis, N. *Macromolecules* 1997, *30*.
137. Löwenhaupt, B.; Hellmann, G. P. *Polymer* 1991, *32*, 1065–1076.
138. Akiyama, M.; Jamieson, A. M. *Polymer* 1992, *33*, 3582–3592.
139. Schulz, M. F.; Bates, F. S.; Almdal, K.; Mortensen, K. *Phys. Rev. Lett.* 1994, *73*, 86–89.
140. Matsushita, Y.; Mori, K.; Saguchi, R.; Nakao, Y.; Noda, I.; Nagasawa, M. *Macromolecules* 1990, *23*, 4313–4316.
141. Matsushita, Y.; Mori, K.; Saguchi, R.; Noda, I.; Nagasawa, M.; Chang, T.; Glinka, C. J.; Han, C. C. *Macromolecules* 1990, *23*, 4317–4321.
142. Jiang, S.; Gopfert, A.; Abetz, V. *Macromol. Rapid Commun.* 2003, *24*, 932–937.
143. Saito, R.; Kawachi, N.; Ishizu, K. *Polymer* 1994, *35*, 866–871.
144. Saito, R.; Kotsubo, H.; Ishizu, K. *Polymer* 1994, *35*, 1747–1753.
145. Schulz, M. F.; Khandpur, A. K.; Bates, F. S.; Almdal, K.; Mortensen, K.; Hajduk, D. A.; Gruner, S. *Macromolecules* 1996, *29*, 2857–2867.
146. Ishizu, K.; Inagaki, K.; Bessho, K. *Makromol. Chem.* 1984, *185*, 1169.
147. Saito, R.; Kotsubo, H.; Ishizu, K. *Polymer* 1994, *35*, 1580–1585.
148. Almdal, K.; Mortensen, K.; Ryan, A. J.; Bates, F. S. *Macromolecules* 1996, *29*, 5940–5947.
149. Papadakis, C. M.; Almdal, K.; Mortensen, K.; Vigild, M. E.; Stepanek, M. *J. Chem. Phys.* 1999, *111*, 4319–4326.
150. Floudas, G.; Vazaiou, B.; Schipper, F.; Ulrich, R.; Wiesner, U.; Iatrou, H.; Hadjichristidis, N. *Macromolecules* 2001, *34*, 2947–2957.
151. Mavroudis, A.; Avgeropoulos, A.; Hadjichristidis, N.; Thomas, E. L.; Lohse, D. J. *Chem. Mater.* 2003, *15*, 1976–1983.
152. Known, Y.; Faust, R.; Chen, C. X.; Thomas, E. L. *Macromolecules* 2002, *35*, 3348–3357.
153. Ryu, C. Y.; Lee, D. H.; Jeong, U.; Yun, S.-H.; Park, S.; Kwon, K.; Sohn, B.-H.; Chang, T.; Kim, J. K. *Macromolecules* 2004, *37*, 3717–3724.
154. Schmidt, S. G.; Hillmyer, M. A. *Macromolecules* 1999, *32*, 4794–4801.
155. Schmidt, C. S.; Hillmyer, M. A. *J. Poly. Sci. Part B: Polym. Phys.* 2002, *40*, 2364–2376.
156. Mogi, Y.; Kotsuji, H.; Kaneko, Y.; Mori, K.; Matsushita, Y.; Noda, I. *Macromolecules* 1992, *25*, 5408–5411.
157. Mogi, Y.; Mori, K.; Matsushita, Y.; Noda, I. *Macromolecules* 1992, *25*, 5412–5415.
158. Matsushita, Y.; Tamura, M.; Noda, I. *Macromolecules* 1994, *27*, 3680–3682.
159. Mogi, Y.; Nomura, M.; Kotsuji, H.; Ohnishi, K.; Matsushita, Y.; Noda, I. *Macromolecules* 1994, *27*, 6755–6760.
160. Arai, K.; Kotaka, T.; Kitano, Y.; Yoshimura, K. *Macromolecules* 1980, *13*, 1670–1678.
161. Liang, L.; Ying, S. *J. Polym. Sci. Part B:Polym. Phys.* 1993, *31*, 1075–1081.
162. Auschra, C.; Stadler, R. *Macromolecules* 1993, *26*, 2171–2174.
163. Gido, S. P.; Schwark, D. W.; Thomas, E. L.; Gonçalves, M. C. *Macromolecules* 1993, *26*, 2636–2640.
164. Zioga, A.; Sioula, S.; Hadjichristidis, N. *Macromol. Symp.* 2000, *157*, 239–249.
165. Stadler, R.; Auschra, C.; Beckmann, J.; Krappe, U.; Voigt-Martin, I.; Leibler, L. *Macromolecules* 1995, *28*, 3080–3097.
166. Breiner, U.; Krappe, U.; Thomas, E. L.; Stabler, R. *Macromolecules* 1998, *31*, 135–141.
167. Breiner, U.; Krappe, U.; Abetz, V.; Stadler, R. *Macromol. Chem. Phys.* 1997, *198*, 1051–1083.
168. Breiner, U.; Krappe, U.; Jakob, T.; Abetz, V.; Stadler, R. *Polym. Bull.* 1998, *40*, 219.
169. Ott, H.; Abetz, R.; Altstadt, V. *Macromolecules* 2001, *34*, 2121–2128.
170. Breiner, U.; Krappe, U.; Stadler, R. *Macromol. Rapid Commun.* 1996, *17*, 567–757.
171. Brinkmann, S.; Stadler, R.; Thomas, E. L. *Macromolecules* 1998, *31*, 6566–6572.
172. Brinkmann, S. Doctoral Thesis, Mainz, 1998.
173. Krappe, U.; Stadler, R.; Voigt-Martin, I. *Macromolecules* 1995, *28*, 4558–4561.
174. Beckmann, J.; Auschra, C.; Stadler, R. *Macromol. Rapid Commun.* 1994, *15*, 67.
175. Stocker, W.; Beckmann, J.; Stadler, R.; Rabe, J. *Macromolecules* 1996, *29*, 7502–7507.
176. Huckstadt, H.; Gopfert, A.; Abetz, V. *Macromol. Chem. Phys.* 2000, *201*, 296–307.
177. Huckstadt, H.; Gopfert, A.; Abetz, V. *Polymer* 2000, *41*, 9089–9094.
178. Huckstadt, H.; Goldacker, T.; Gopfert, A.; Abetz, V. *Macromolecules* 2000, *33*, 3757–3761.
179. Stangler, S.; Abetz, V. *Rheol. Acta* 2003, *42*, 569–577.
180. Schmalz, H.; Muller, A. J.; Abetz, V. *Macromol. Chem. Phys.* 2003, *204*, 111–124.
181. Jung, K.; Abetz, R.; Stadler, R. *Macromolecules* 1996, *29*, 1076–1078.
182. Sioula, S.; Hadjichristidis, N.; Thomas, E. L. *Macromolecules* 1998, *31*, 5272–5277.
183. Okamoto, S.; Hasegawa, H.; Hashimoto, T.; Fujimoto, T.; Zhang, H.; Kazama, T.; Takano, A.; Isono, Y. *Polymer* 1997, *38*, 5275–5281.
184. Neumann, C.; Loveday, D. R.; Abetz, V.; Stadler, R. *Macromolecules* 1998, *31*, 2493–2500.
185. Neumann, C.; Abetz, V.; Stadler, R. *Colloid Polym. Sci.* 1998, *276*, 19.

186. Avgeropoulos, A.; Paraskeva, S.; Hadjichristidis, N.; Thomas, E. L. *Macromolecules* 2002, *35*, 4030–4035.
187. Cochran, E.; Bates, F. S. *Phys. Rev. Lett.* 2004, *93*, 8702.
188. Bailey, T. S.; Hardy, C. M.; Eps III, T. H.; Bates, F. S. *Macromolecules* 2002, *35*, 7007–7017.
189. Eps III, T. H.; Cochran, E.; Bailey, T. S.; Waletzko, S.; Hardy, C. M.; Bates, F. S. *Macromolecules* 2004, *37*, 8325–8341.
190. Bailey, T. S.; Pham, H. D.; Bates, F. S. *Macromolecules* 2001, *34*, 6994–7008.
191. Shefelbine, T. A.; Vigild, M. E.; Matsen, M. W.; Hajduk, D. A.; Hillmyer, M. A. *J. Am. Chem. Soc.* 1999, *121*, 8457–8465.
192. Yamauchi, K.; Takahashi, K.; Hasegawa, H.; Iatrou, H.; Hadjichristidis, N.; Kaneko, T.; Nishikawa, Y.; Jinnai, H.; Matsui, T.; Nishioka, H.; Shimizu, M.; Furukawa, H. *Macromolecules* 2003, *36*, 6962–6966.
193. Pispas, S.; Floudas, G.; Hadjichristidis, N. *Macromolecules* 1999, *32*, 9074–9077.
194. Floudas, G.; Hadjichristidis, N.; Iatrou, H.; Avgeropoulos, A.; Pakula, T. *Macromolecules* 1998, *31*, 6943–6950.
195. Frick, E. M.; Zalusky, A. S.; Hillmyer, M. A. *Biomacromolecules* 2003, *4*, 216–223.
196. Avgeropoulos, A.; Chan, V. Z.-H.; Lee, V. Y.; Ngo, D.; Miller, R. D.; Hadjichristidis, N.; Thomas, E. L. *Chem. Mater.* 1998, *10*, 2109–2115.
197. Abetz, V.; Goldacker, T. *Macromol. Rapid Commun.* 2000, *21*, 16–34.
198. Eps III, T. H.; Cochran, E.; Hardy, C. M.; Bailey, T. S.; Waletzko, R. S.; Bates, F. S. *Macromolecules* 2004, *37*, 7085–7088.
199. Cochran, E. W.; Garcia-Cervera, C. J.; Fredrickson, G. H. *Macromolecules* 2006, *39*, 2449–2451; erratum 4864.

CHAPTER 41

Polymer Liquid Crystals and Their Blends

Witold Brostow

LAPOM, Department of Materials Science and Engineering and Department of Physics, University of North Texas, P.O. Box 305310, Denton, TX 76203-5310 http://www.unt.edu/LAPOM/; brostow@unt.edu

41.1 INTRODUCTION

41.1.1 Liquid crystals, plastic crystals and condis crystals

We already know much about flexible polymers, particularly because massively produced engineering polymers (EPs) are typically flexible. More complicated, and therefore more challenging, are systems involving polymer liquid crystals (PLCs)—which are copolymers containing simultaneously relatively rigid and flexible sequences. PLCs have much better properties than EPs, and also than fiber-reinforced composites and other classes of polymer-based materials; see Section 41.1.4. However, the use of these other classes of polymers is by no means in jeopardy, and will continue to grow, since PLCs are expensive. There is a way out: blend PLCs with EPs in such proportions that the good properties of PLCs ''show up,'' while at the same time there is in each case enough of an EP to keep the costs at bay. This can be done, but it is not exactly easy; so often polymers—PLCs including—''do not like each other''; their miscibility or at least compatibility is a problem. In this chapter we shall define what PLCs are, what molecular and phase structures they have, what properties do they have, and what are current and potential applications. The problem of blending is clearly related to extending the application range.

To begin with, and contrary to a still widely held belief, the words ''liquid-crystalline'' and ''mesomorphic'' are *not* synonymous. The term *mesomorphic phases* was introduced by Friedel in 1922 [1]; it is now often abbreviated to *mesophases*. He defined them as phases with microscopic structures between solids and ordinary isotropic liquids. Not much happened in this area until 1955 when Kast [2] tried to characterize such phases in terms of lateral, longitudinal, and steric disorder. The next step occurred in 1984 when Wunderlich and Grebowicz [3] defined condis crystals for the first time. Following them [3,4] we now distinguish three kinds of mesophases: liquid crystals, plastic crystals, and condis crystals.

To see the distinctions between these three kinds of phases, we need to define first positional, orientational, and conformational ordering; this can be done easily using an example. When methane melts, various relative positions of its quasi-spherical molecules become possible—since *positional disordering* occurs. When we move to the next homolog in the *n*-alkane series, ethane, its melting is accompanied also by positional disordering; intermolecular distances become less uniform. However, melting of ethane involves at the same time *orientational disordering* since

two molecules can now be perpendicular to each other, or parallel as they largely were before, or anything in between. A longer paraffin hydrocarbon molecule such as *n*-decane also undergoes positional and orientational disordering, but *conformational disordering* dominates here: the segments acquire freedom to execute rotations about single bonds. Wunderlich and Grebowicz [3] provide an instructive example: the camphor molecule contains 10 carbon atoms, as does *n*-decane. However, the former is nearly spherical and rigid, hence there are no orientational or conformational effects on melting. Therefore, the entropy of fusion of camphor is much lower than that of *n*-decane.

With the information on the three types of disordering processes, we can now define three kinds of mesophases:

- liquid crystals exhibit positional disordering;
- plastic crystals show orientational disordering; and
- condis crystals exhibit conformational disordering.

All three kinds of mesophases show some degree of long-range order—similarly as ''decent'' crystals. Similarly to isotropic liquids, however, these three kinds of phases exhibit also some degree of mobility other than segment vibrations known in ordinary crystals.

41.1.2 Monomer liquid crystals (MLCs) and polymer liquid crystals (PLCs)

Before going any further, let us adopt the terminology introduced by Samulski [5]. We have already used above the abbreviation PLCs. Samulski contrasted PLCs to MLCs, and defined the latter as low molecular mass LCs—irrespective of the fact whether they *can or cannot* polymerize. His terminology is unequivocal and succinct. People unfamiliar with it use long and not necessarily well-defined terms, such as ''liquid-crystalline substances with low molecular weights''—when they presumably mean MLCs. Other names such as liquid crystalline polymers (LCPs) for PLCs or LMMLCs for MLCs are also in use. The abbreviation SRPs for self-reinforcing polymers and the name in situ—composites [6] are used as well. Moreover, PLCs are sometimes also called *molecular composites*.

PLC phases which appear in certain temperature intervals are called *thermotropic* ; this chapter is devoted to them almost exclusively. There are also materials called *lyotropic* in which LC properties are induced by the presence of a solvent. Basic properties of such PLCs have been reviewed by Hall and Tiddy and by Northolt and Sikkema [7]. Hsiao, Shaw, and Samulski [8] have shown that liquid crystallinity can also be brought about by pressure elevation; by analogy, such materials have been called *barotropic* [9].

It is important to note that both MLCs and PLCs can adopt the same *phase structures*—such as nematic or smectic B. The phase structures of LC systems will be discussed in Section 41.3.1.

Let us also note that there exist oligomers intermediate between MLCs and PLCs, as studied by Abe and coworkers [10] as well as by Henderson and Imrie [11]. They are trimers or tetramers from the point of view of liquid crystallinity with flexible spacers in-between, and serve as models for longitudinal PLCs (see Section 41.2.1),

41.1.3 A brief history of MLCs and PLCs

Contrary to another widely held opinion, LCs have not been first synthesized by humans. *Silkworms* have been at it for quite a while. Li and Yu [12] in 1989 have found that the middle gland of silk fibroin is liquid crystalline—nematic to be more accurate. More results on this subject were reported for instance by Kerkam and coworkers [13].

The discovery of liquid crystals by humans is due to the Austrian botanist Friedrich Reinitzer [14]; what he observed in 1888 were cholesteric MLCs (see Section 41.3.1). Some people did not believe Reinitzer that such strange structures are possible. However, a German scientist named Otto Lehmann asked Reinitzer for some samples, conducted similar experiments, and reported virtually identical results a year later [15]. Given the popular disbelief, Lehmann's results were not exactly trivial. Lehmann also coined the name ''liquid crystals''—over objections of Reinitzer, who said the name is wrong and constitutes a contradiction. As you can easily imagine, there were centennnial celebrations in Austria in 1988 and in Germany in 1989.

Some people believe that ''serious'' research on liquid crystals started only fairly recently. In fact, there is one city in the world where such work has been going on continuously for more than a century: Halle on the Saale. In 1900 or so Vorländer started at the University of Halle-Wittenberg a research group working on LCs; already in 1908 he published a book about them [16].

In 1923 Vorländer, having worked on MLCs for more than 20 years, realized that PLCs must exist as well. He asked [17]: ''What happens to the molecules when one makes them longer and longer? Will the liquid-crystalline state disappear ? From my experience, there is no limit to that state from chain elongation . . . '' (my translation—W.B.). Even more importantly, Vorländer obtained from Hermann Fischer some polymers prepared by Emil Fischer, father of Hermann. It turned out that these polymers—synthesized in the XIXth century—were liquid crystalline [17]. Thus, not only studies of MLCs but also studies of PLCs started more than a century ago—although Emil Fischer did not quite realize this at the time. The Vorländer school founded so long ago is alive and well, continued later by Horst Sackmann, Dietrich Demus, Frank Kuschel, today also by Alfred Saupe, Gerhard Pelzl, Wolfgang Weissflog, Jürgen Lindau, and others, now at the Martin Luther University of Halle-Wittenberg as well as at the Max Planck Institute for Polymer Research in Halle.

41.1.4 PLCs Among Other Classes of Polymeric Materials

For many centuries the market place—and consequently large parts of science and technology—were dominated by proprietors of *raw materials*. However, in the last quarter of the XXth century this situation has changed. As pointed out in [18], a new generation of *end-users* says: ''I need this and this, I don't care whether it has been invented yet.'' Therefore, instead of the traditional question: ''What applications can be found for the material I am now working with ?'', with an increasing frequency one asks: ''What options do I have? What kinds of materials are or might be available?''. Preparing for a meeting on polymeric materials back in December 1990, I was surprised to find that nobody before applied the last question to them. Therefore, I prepared an answer. The answer has been modified by later developments and now we need to distinguish at least the following classes of polymer-based materials:

Flexible polymers—polyethylene (PE) and other EPs (see the first sentence of this Chapter) belong here, along with for instance polysiloxanes, poly(vinyl ether) and polyphosphazenes. Their properties are typically well known, processing conditions optimized, and many are available in large quantities and at low cost per unit weight. Their mechanical strength is for certain applications insufficient—which is the reason why other classes of polymeric materials are of interest.

Semiflexible polymers—including regular AB type copolymers in which A is rigid while B flexible. Cellulose derivatives belong here, as well as poly(*p*-hydroxybenzoic acid) (PHB), and for instance poly(*p*-phenylene terephthalamide). They are of course stronger than flexible polymers, but their processing is more difficult.

Rigid polymers—which include polyphenyl, α-helical peptides, and poly(*p*-phenylenebenzobis thiazole) (PPT). Problem with processing are here somewhat similar to those with the preceding class, but more acute. These materials typically require ''exotic'' and highly corrosive solvents.

Heterogeneous composites (HCs)—we have coined this name in 1988 [19] to distinguish them from molecular composites (see the last item) and from PLCs and PLC blends. HCs consist of a flexible matrix with a heterogeneous reinforcement such as glass fibers, carbon fibers, or glass spheres. The reinforcement can be polymeric (polymer fibers) or else ceramic or even metal. In the last two cases we have *hybrids* that is materials which include inorganic as well as organic constituents. We know from textbooks of materials science and engineering (see for instance Chapter 10 in [18]) that the components in fiber composites perform different functions: rigid fibers carry load while a matrix distributes load. However, given the disparity in the nature of fibers and the matrix, sufficient adhesion between these two types of constituents is often a problem. Cases of fiber pullout and delamination are well known. Problems of creep, fracture initiation, and failure in fiber composites have been discussed by Piggott [20] and by Jansson and Sundström [21]. A thorough review of fiber-reinforced HCs has been provided by Pisanova and Zhandarov [22].

Polymer based nanohybrids—as in HCs, the matrix is polymeric. In contrast to HCs, however, the size of the minority component units (often powders) is on the scale of nanometers [23,24].

Molecular composites (MCs)—which are *polymer liquid crystals* and *PLC blends*. As in HCs, there is a rigid reinforcement. However, the reinforcement is at the molecular level—what applies to pure PLCs as well as to PLC-containing blends. Now, against the background just provided, and before going into details, let us compare PLCs with the most widely used type of polymers, that is EPs. Such comparisons have been made before [9,25,26,27]; one can summarize them by saying that PLCs

- show clear superiority over EPs with regard to *chemical stability*;
- show on the average *lower flammability* than EPs;
- have better *overall mechanical properties* than other classes listed above;
- have quite low *thermal expansivity*—sometimes even zero or negative;
- can be used at *higher temperatures* than EPs;
- thermotropic PLCs are often *easily processable* with conventional processing equipment for thermoplastics—this in contrast to rigid polymers and HCs;
- have high *stability* under *ultraviolet* (uv) and *visible light*;
- are *easily oriented* in shearing, electric and magnetic fields;
- exhibit *high stability under vacuum*.

41.2 MOLECULAR STRUCTURES

41.2.1 Classification of PLCs

The sequences in PLC chains which cause the LC character can be of different shapes: elongated (represented in the following by rectangles), approximately spherical (which will be represented by discs), or stars. The LC sequences can be placed in the main chain, or in side chains, or in both. To survey existing and possible structures, a comprehensive classification of PLCs based on their molecular structures was developed [25] and subsequently amplified [9,27]; a recent version is shown in Table 41.1.

Before the classification in [25] was proposed, one talked about main-chain and side-chain PLCs. It is clear from looking at classes such as α, β, γ, and ζ that the name ''main-chain'' is far from sufficient, since it includes

TABLE 41.1. *Classification of PLCs on the basis of molecular structures [9,25,27].*

Class	Structure	Name	
		English	German
α		longitudinal	longitudinal
β		orthogonal	orthogonal
γ		star (cross)	Stern (Kreuz)
ζS		soft disc	biegsamer Diskus
ζR		rigid disc	steifer Diskus
ζM		multiple disc	Multidiskus
εO		one-comb	Einzelkamm
εP		polisode-comb	Palisadenkomm
εD		double comb	Doppelkamm
φ		disc comb	Kammdiskus
κ		inverse comb	invertierter Kamm
$\theta 1$		parallel	parallel
$\theta 2$		biparallel	biparallel
$\lambda 1$		mixed	gemischt
$\lambda 2$			
$\lambda 3$			
$\psi 1$		double	doppelt
$\psi 2$			
σ		network	Netzwerk
ω		conic	kegelförmig

classes with vastly different structures; the same is true for "side-chain PLCs." Incidentally, since the original classification was published in *Kunststoffe*, German names for the classes were coined at the same time as the English ones, and both series of names are listed in the Table. A couple of names (cross, network) were already in existence earlier, but most names were created while building up the classification. Examples of specific PLCs belonging to each class are given in [9,25] and [27]; we do not have enough space in this Chapter for examples.

41.2.2 Molecular Structure–Property Connection

As mentioned above, the initial objective of the classification was just to survey the structures. However, already while constructing the present Table 41.1, a much better reason was found: properties of PLCs depend strongly on the molecular structures of the chains. In other words, PLC materials such that each material consists of chains from a different class have different properties. Two years after the original classification [25], Ebert and coworkers [28] reached a similar conclusion: "in most liquid-crystalline systems it is predominantly the molecular shape which determines which kind of liquid-crystalline phase is formed." Needless to say, the phase structure formed has important consequences for the properties. Similarly, Gasparoux and his colleagues [29] say that "... the riches of chemistry of polymer liquid crystals make possible, via molecular engineering, to impart structural and functional properties to a polymeric mesomorphic material aimed at new applications" (my translation—W.B.). Thus, for instance mesogenic groups can be introduced at external surfaces of dendrimers [30] leading to PLC formation. Hydrogen-bonded supramolecular complexes also can lead to PLC materials [31].

The molecular structure—macroscopic property connection is a vast subject; we shall provide an example. Consider simple or one-row combs, subclass εO. Transition from a LC state such as nematic into isotropic liquid, accomplished by a temperature increase, results in lowering the viscosity [32]—as usual and as expected. However, for longitudinal polymers, class α, similar isotropization results in a viscosity *increase*: the rigid LC sequences were aligned in the LC state, but in the isotropic state all directions are equiprobable, and the flow is more difficult.

Since molecular structures affect also packing of LC chains in the solid phases, let us provide at least one example of this. In the subclass ζR we have single discs in the main chain but with rigid spacers; see again Table 41.1. Wendorff, Ringsdorf, and collaborators who have obtained and studied such PLCs [33,34] have proposed a *sanidic* (from the Greek for board-like) structure for their packing which is shown in Fig. 41.1. Disks can form columnar structures [27]. Self-assembly of disks into structures such as columnar has been reported [35].

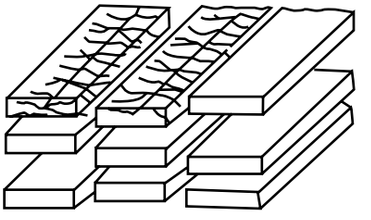

FIGURE 41.1. Sanidic packing of GR subclass PLCs; after [33,34].

41.3 HIERARCHICAL STRUCTURES, LC PHASES AND THERMOPHYSICAL PROPERTIES

41.3.1 Kinds of LC Phases

As noted before, MLCs and PLCs share essentially the same kinds of phases; these are: nematic, cholesteric, and a variety of smectic phases. These three names have been proposed by Friedel [1] in 1922 who imagined that such phases should exist—long before his concepts were confirmed by diffractometric experiments. In all these phases the entire molecules (in MLCs) or the LC sequences in the chains (in PLCs) are oriented approximately—but not quite—perpendicularly to a preferred axis in space called *director*. The degree of alignment is characterized by the order parameter (also called the anisotropy factor) defined in 1946 by Hermans [36] as

$$s = (3\langle\cos^2\theta\rangle - 1)/2, \qquad (41.1)$$

where θ is the angle between the molecular axis and the director, and the braces $\langle\rangle$ denote an average for the material (or a layer). We see from Eq. (41.1) that in a completely isotropic system $s = 0$ while a system perfectly aligned along the director would have $s = 1$.

The simplest among LC phases are *nematic*, in which the orientation along the director is the only kind of long-range order present; see Fig. 41.2(a).

A *cholesteric* phase is formed by a pile of nematic phases with the director changing from one layer to another; see Fig. 41.2(b).

Smectic phases have also layers, but each layer has at least one more element of long-range order in addition to the director. There are several such phases, distinguished by capital Latin letters. Thus, in each smectic A phase the centers of molecules (in MLCs) or of LC sequences (in PLCs) lie on equidistant planes perpendicular to the director. In smectic B phases there are also such planes, but there is additionally a two-dimensional hexagonal lattice within each plane. There is no hexagonal structure in smectic C phases, while the director is tilted with respect to the plane normal (otherwise we would have another smectic A phase); an example is shown in Fig. 41.2(c). For a more detailed discussion of LC phases see for instance Chapter 6 in [18]. Phase transitions in MLCs are listed in books by Demus, Demus, and Zaschke [37,38]. *Textures* in LC phases which are sometimes colorful or even spectacular in polarized light are illustrated in a book by Demus and Richter [39].

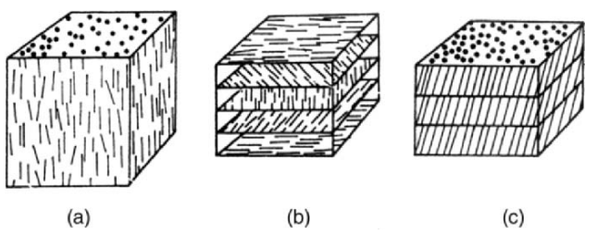

FIGURE 41.2. An example of a nematic (a), cholesteric (b) and smectic C (c) phase.

41.3.2 Hierarchical Structures

It cannot be stressed enough that in PLCs the flexible and the LC sequences form separate phases. Since these two types of sequences are typically connected by primary chemical bonds, then each predominantly flexible phase contains a certain number of LC sequences; such a phase is called a *LC-poor phase* or simply a flexible matrix. Each predominantly liquid crystalline phase, called a LC-rich phase or an *island* [19] contains necessarily a certain number of flexible sequences. Thus, even a pure PLC—not a blend—typically contains at least two phases. This fact was discussed already in 1980 by Menczel and Wunderlich [40] who using differential scanning calorimetry (DSC) observed two glass transition temperatures, one for the flexible and one for the LC-rich phase; their subsequent more extensive studies confirmed this conclusion [41].

PLCs form hierarchical structures, and a hierarchical model of PLC morphology was proposed by Sawyer and Jaffe [42] and further refined by Sawyer and her colleagues [43,44]. They point out the differences between synthetic materials and biological systems, and conclude [45] that "... an increased understanding of biology will not increase our understanding of the origin of hierarchical morphologies. ... " They refer to the fact that biological structures also are hierarchical. Not only their argument makes sense, but I believe that the inverse might work: since synthetic systems are simpler, an increased understanding of hierarchies in synthetic materials will help the biologists to deal with their systems.

Since the islands constitute the primary mechanical reinforcement regions, we need to know more about them. Using a combination of scanning electron microscopy (SEM) and wide-angle x-ray diffractometry (WAXD) we have found that the islands have a hierarchical structure [45]; see Fig. 41.3. The islands in the scanning electron micrograph have the sizes between 1.0 and 1.4 μm. In turn, an individual crystallite has the average linear dimension of 12 nm—that is two orders of magnitude less—as found by WAXD.

As seen in Fig. 41.3, hierarchical arrangements occur within individual molecules as well as in phases built by the molecules. Using the concept of *homeomorphism*, we have formulated five rules governing ascension and descension in the hierarchies as well as characterizing structures at a given hierarchical level [45]. Two sets, X and Y, are homeomorphic if f is a one-to-one mapping of X onto Y (therefore: $f^c: Y - X$) and both f and f^c are continuous. Our approach is based on the fact that each PLC molecule contains at least two kinds of building blocks which are *not* homeomorphic with respect to each other. Starting from this observation, the following rules for hierarchical structures have been formulated [45]:

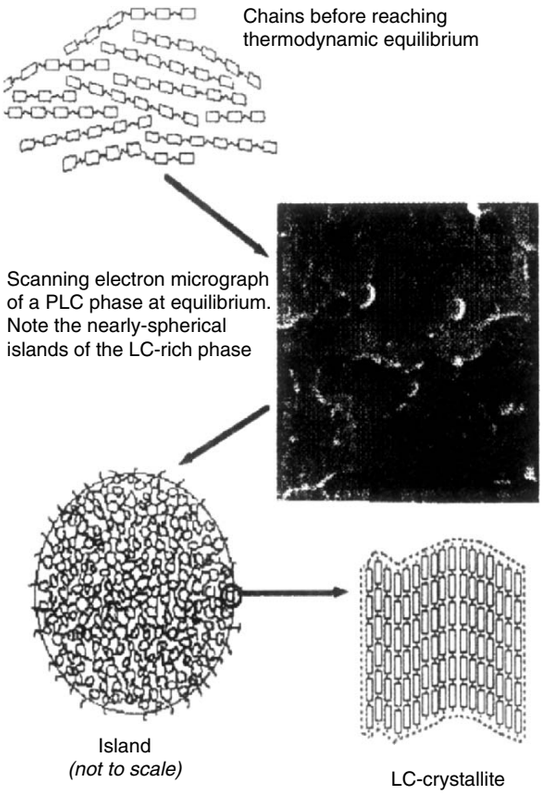

FIGURE 41.3. A hierarchical structure of LC-rich islands in a LC-poor matrix; after [45].

Rule 1. The complexity of hierarchical structures goes symbiotically with the number of building block types which are *not* homeomorphic with respect to one another.

Rule 2. Each level of hierarchy is defined by the constituting (nonhomeomorphic) types of entities, and by relations between the types. In materials the relations include (but are not limited to) connectedness by primary chemical bonds, hydrogen bridges, dispersion interactions, and interactions between phases such as adhesion forces.

Rule 3. Ascension in the hierarchy consists in defining relations such that the entities at the h level are divided into subsets, an entity at the $h + 1$ level corresponds to each subset, while each subset can consist of elements of one or more homeomorphic types. As a corollary, descent involves a relation between each h level entity and a subset of entities at the $h - 1$ level.

Rule 4. The structure of a *smaller* entity (such as the size and shape of a single molecule) determines the size, shape and structure of a *larger* entity (such as a LC phase). Since macroscopic properties are determined through *ascension* in the hierarchy, they are dependent on entities and their interactions at lower levels.

Rule 5. Assembling entities in a specified way can achieve properties which a system of unassembled entities does not have.

Let us provide at least one example of application of these rules. Sawyer and her colleagues [42–44] have defined the hierarchical fibrical structure of LC materials after processing. Macrofibrils, fibrils, and microfibrils they consider constitute the key entities at three different levels—as defined in Rule 3.

A comment on Rule 2 also seems needed, since even some researchers working on LC materials believe that LC phase formation requires structures involving primary chemical bonds—while that Rule involves a more general concept of relations. Kato and Fréchet [46] and also Bazuin and her collaborators [47,48] have found that hydrogen bonds or ionic interactions are sufficient for the formation of LC phases. Somewhat similarly, Zhao and Lei [49] have obtained ionomers which form simple one-row combs, that is class εO PLCs. Recall also the already mentioned work by Felekis and coworkers [31]. In other words, covalent bonds do *not* constitute a necessary condition for the formation of LC phases in polymers.

41.3.3 Phase Diagrams

The existence of a number of LC phases defined in Section 41.3.1 and of hierarchical structures of LC materials just discussed above has a number of consequences, including the following: phase diagrams of LC-containing systems are quite complicated.

Even if we do not have blends but only pure LC materials, multiphasicity appears a rule rather than an exception. Thus, the phase diagram of copolymers with the formula PET/*x*PHB was determined [50]; PET is poly(ethylene terephthalate), PHB is *p*-hydroxybenzoic acid; x is the mole fraction of the LC component (here PHB) in the copolymers and constitutes the horizontal variable. The diagram contains 12 phase regions. Long-living nonequilibrium phases—typical in LC systems—*are included*, and thus each region contains up to four phases, such as: PET crystals, PHB-rich islands, isotropic PET-rich glass, and PHB-rich glass.

A new phase called *quasiliquid* (q1) was defined in the course of work on phase diagrams [50,51]. It originates from the amorphous state which existed below the glass transition temperature T_g, but q1 appears between T_g and the melting transition T_m. The q1 phase has the following characteristic features:

q1 is uncrosslinked and yet it does *not* exhibit the ordinary liquid mobility. The presence of another (liquid-crystalline) component below its glass transition and/or of crystallites prevents this phase from flowing like a liquid does. The hindrance to the flow is caused by the LC sequences, which in this respect act somewhat similarly to the junctions in polymer networks. This situation

is in contrast to nonLC polymers between T_g and T_m, in which the formerly amorphous phase flows around the crystalline regions, and the liquid viscosity depends on the temperature only. The viscosity of q1 depends also on the *concentration* of LC sequences. Pertinent here are the deuteron nuclear magnetic resonance (2H-NMR) results of Zachmann and collaborators [52]: they have found in PET/*x*PHB copolymers that the PHB sequences decrease considerably the mobility of PET sequences.

A liquid upon heating can only undergo vaporization or, if it is an isotropic polymer melt, no further phase transition at all. By contrast, q1 has to undergo at least two more transitions: melting and isotropization at the *clearing point*. If more than one LC phase is formed, then there will be even more transitions; for instance, PET/*x*PHB forms a smectic E and a smectic B phase.

The cold crystallization occurs in the q1 phase.

q1 shows an analogy with the leathery state in the elastomers. Both types of systems are immediately above their glass transition regions, and both exhibit *retarded* responses to application of external forces.

So far we have discussed pure PLCs, where the only variable was the concentration of the LC sequences in the copolymers. One can easily imagine that blends have even more complicated phase diagrams, as found for blends of PET/0.6PHB with EPs, for instance with polycarbonate [51]. An important reason for the study of phase diagrams is using them as a basis of processing optimization. In other words, in contrast to the usual establishment of processing parameters by trial and error, the knowledge of a phase diagram makes possible *intelligent processing*.

41.3.4 Isobaric Thermal Expansivity

Let us first define the quantity we are going to discuss:

$$\alpha = V^{-1}(\partial V/\partial T)_P, \tag{41.2}$$

which is called *isobaric expansivity*. The names "thermal expansivity" and particularly often "coefficient of thermal expansion" (abbreviated to CTE) are also in use. However, over a century ago Lord Kelvin [53] said that the use of the word "coefficient" when talking about viscosity, elasticity, compressibility, conductivity, and the like is "illogical," "vicious," and also "a mystery of circumlocution." I admit to having used the phrase "coefficient of thermal expansion" myself, but after reading Lord Kelvin's admonition I am not going to do it again. Incidentally, members of the Commission for Symbols, Units, and Nomenclature of the International Union of Pure and Applied Physics (IUPAC) have not read Lord Kelvin either, since they recommend [54] the name "cubic expansion coefficient"; the fact that this is a quantity pertaining to constant pressure is not included in their name either. However, there is something rational in their name, because *linear isobaric expansivity* exists also:

$$\alpha_L = L^{-1}(\partial L/\partial T)_P, \tag{41.3}$$

where L is the specimen length. If a material is isotropic, then the two quantities in question can be related by simple algebra [55]

$$\alpha = (1 + \alpha_L)^3 - 1. \tag{41.4}$$

If a material is anisotropic, that is oriented during melt flow as PLCs are, we have the linear expansivity parallel to the flow α_{II} and linear expansivity $\alpha_\perp$ perpendicular to the flow. The respective relation then is [56]

$$\alpha = (1 + \alpha_{11})(1 + \alpha_\perp)^2 - 1. \tag{41.5}$$

Clearly Eq. (41.5) reduces to Eq. (41.4) for the isotropic case as it should.

There is in this Handbook a whole Chapter 7 by Robert Orwoll on equation-of-state P–V–T properties of polymers. Briefly, confining our attention to what is pertinent for PLCs, there are basically two experimental procedures for α determination. One can measure α_L in a thermomechanical analysis (TMA) apparatus and then calculate α from Eqs. (41.4) or (41.5) [57,58]. Or, one can use an apparatus which produces full P–V–T data, that is specific volume v as a function of temperature T, $v(T)$, plus $\alpha(T)$ plus also isothermal compressibility $\kappa_T(T)$, where

$$\kappa_T = V^{-1}(\partial V/\partial P)_T. \tag{41.6}$$

Such an apparatus for polymer solids and melts called Gnomix has been developed decades ago [59] and it is being used with good results for polymers [60,61] and not only [62].

Industry needs more and more materials with low isobaric expansivity. PLC sequences are typically relatively rigid, and it is well known that rigid constituents exhibit low expansivity. A simple comparison of two numbers provides a good picture of the situation. The expansivity of polyethylene $\alpha(\text{PE, } 140\ ^\circ\text{C}) = 7.20 \times 10^{-4}\text{K}^{-1}$. At the same temperature we have $\alpha(\text{PET/0.6PHB, } 140\ ^\circ\text{C}) = 1.97 \times 10^{-4}K^{-1}$. Clearly, low isobaric expansivity constitutes another reason why PLCs are going to be used more and more.

Finally, let us note that the specific volume is an important parameter characterizing the glass transition and can be connected to other quantities pertaining to that transition. A scaling relationship along these lines has been proposed by Tölle [63] and developed further by Casalini and Roland [64,65].

41.4 MECHANICAL PROPERTIES

41.4.1 Areas of Application of PLCs

As briefly noted in Section 41.1.4, PLCs provide mechanical strength without the problems of easy separation of the reinforcement from the flexible matrix (fiber pullout)

characteristic for HCs. Thermotropic PLCs do not exhibit the difficulties in processing inherent to rigid polymers, HCs, and MCs.

Given the advantages of PLCs listed at the end of the Section 41.1.4, the number of applications of these materials is already considerable, and will increase along with further progress in synthesis, characterization, mechanical testing, phase diagram determination, and intelligent processing. Areas of application of PLCs have been reviewed by Jansson [66]. Following him, let us make a brief list of typical applications:

- connectors, surface-mount components, relay bobbins, capacitor housings, potentiometers, and switches in electronic and electrical industries;
- strength members, couplers, and connectors for fiber optics;
- fuel system components and electrical systems for automotive industry;
- motor components, lamp housings, conveyor belt components, and gears for industrial plants;
- tower packings, pump housings, pump shafts, and valves for chemical industry;
- compact disc components, microwav equipment, and turntables for domestic use; and
- other applications including medical components, watch components, safety equipment, chemical analysis equipment, and leisure goods.

Jansson [66] discusses also PLC rods, oriented sheets, films, and fibers. PLC fibers can be obtained by several procedures including melt spinning and dry-jet wet spinning. He also covers in some detail reasons for the applications of PLC fibers in ballistic vests, protective gloves and clothing, tarpaulins, conveyor belts, inflatable boats, sails, ropes, cables (for oil rig mooring), filament-wound pressure vessels, sails, sewing threads, radial tires, space and aircraft applications, boats, canoes and kayaks, military helmets, sporting goods, as cement reinforcements, in building materials and pipes, and in friction uses, and/or as asbestos replacements in brake linings, clutch, facings, and gasket packing.

Even with the space limitations we have, we need to mention also applications of PLCs in *coatings*, in particular as binders for higher solid bake coatings. This subject was also reviewed by Jansson [66].

41.4.1 Strengthening of PLC Materials

As we have seen in Section 41.3.1, LC sequences or molecules are oriented approximately parallel to the director. This is related to packing and caused by thermodynamic reasons (the usual tendency to lower the Gibbs function). Then we have a second stage of improved orientation—caused by processing procedures such as extrusion or injection molding. However, we can improve the orientation still further by cold working operations. Given the natural orientation from the start, the effects here are more significant than in cold working of metals.

We shall provide an example of the effects of cold drawing as reported in [19]: specimens of PET/0.3PHB (note a relatively low concentration of the LC constituent) were drawn at 25 °C up to the elongation of 300 % and then the tensile properties determined (for a discussion of tensile testing see Section 3 in Chapter 24). The elastic modulus as a function of elongation is shown in Fig. 41.4. It is clear that drawing has resulted in a fourfold increase of the modulus. The tensile strength changes similarly; see Fig. 41.5.

Instead of cold working, we have also the option of varying the concentration of LC sequences during synthesis. In Fig. 41.6 we show the modulus as a function of x in PET/xPHB copolymers [19] in the direction parallel to flow. First

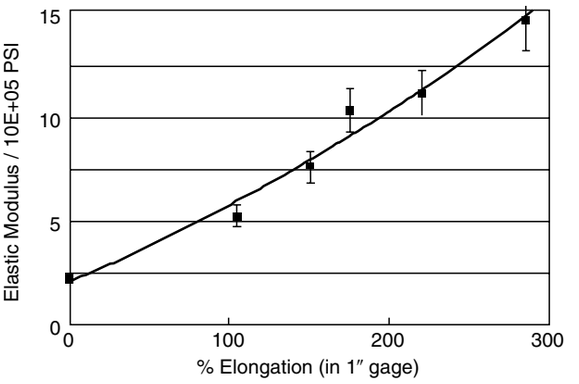

FIGURE 41.4. Elastic modulus changes at 25 °C resulting from cold drawing specimens of PET/0.3PHB. Filled squares represent each an average from five determinations; after [46].

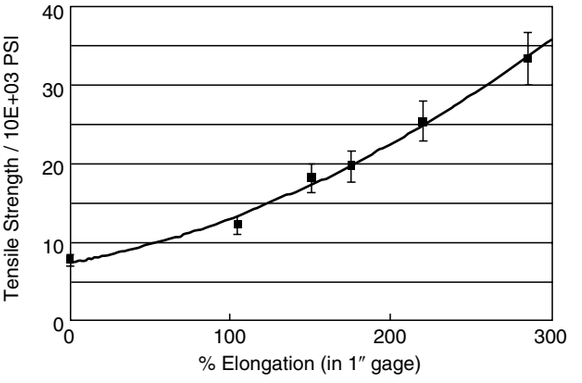

FIGURE 41.5. Tensile strength changes at 25 °C resulting from cold drawing specimens of PET/0.3PHB. Filled squares represent each an average from five determinations; after [50].

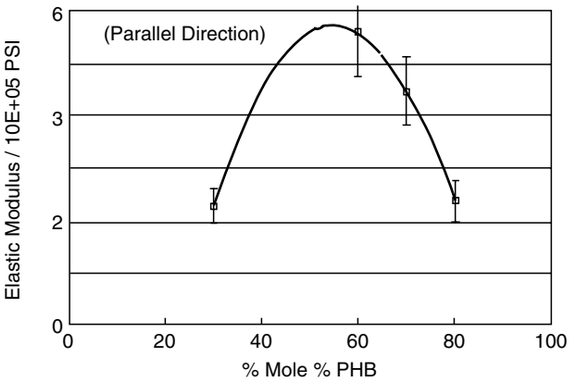

FIGURE 41.6. Elastic modulus at 25 °C of PET/*x*PHB copolymers as a function of *x* in the direction parallel to the flow during processing; after [50].

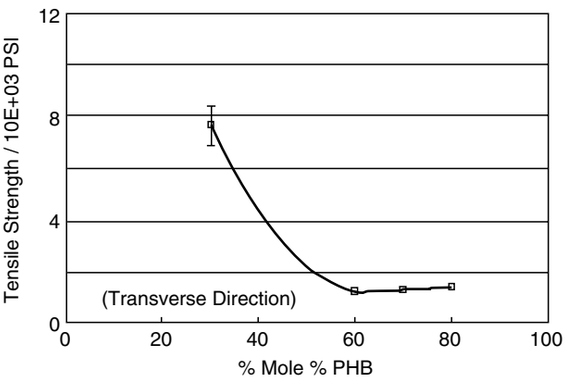

FIGURE 41.8. Elastic modulus at 25 °C of PET/*x*PHB copolymers as a function of *x* in the direction transverse to the flow during processing; after [50].

an increase in the concentration of the LC sequences *x* enhances the modulus. However, after reaching a maximum the modulus begins to decrease; we explain this by the fact that an increase in *x* also increases the brittleness of the material. The tensile strength behaves in a similar way; see Fig. 41.7. However, the story is different in the directions perpendicular (transverse) to the flow. Here increasing *x* leads to decreases in both modulus and the tensile strength; see, respectively, Figs. 41.8 and 41.9.

It should be kept in mind that the behavior just described pertains to longitudinal polymers, class α. We have noted in Section 41.2.2 connections between belonging of a PLC to a specific class and the properties. To acquire a better picture, consider now briefly networks, class σ. Küpfer and Finkelmann [67] have developed a two-step procedure for creating such networks, subsequently amplified by Küpfer, Nishikawa, and Finkelmann [68]. They first align mechanically a weakly crosslinked σ PLC; then a second crosslinking reaction of remaining free reactive groups freezes that alignment, creating materials which these authors call liquid single crystal elastomers (LSCEs). This second stage can be performed at different temperatures, resulting in different degrees of the alignment. As expected, the alignment is higher if the second stage is performed in a LC state, and lower if it is performed above the isotropization (clearing) temperature. On the other hand Ambrogi and her colleagues [69] say that liquid crystal elastomers (LCEs) are lightly crosslinked, apparently stopping at the first stage of the procedure of Finkelmann and coworkers.

41.5 TRIBOLOGICAL PROPERTIES

41.5.1 Basic Concepts

Tribology is considered by some as a part of Mechanics, and by others as a discipline within Materials Science and Engineering (MSE) at the same level as Mechanics. Our own work seems to support the latter point of view. Tribological characterization of materials deals with *friction*,

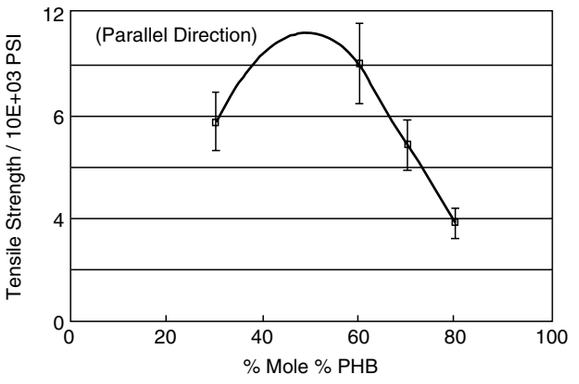

FIGURE 41.7. Tensile strength at 25 °C of PET/*x*PHB copolymers as a function of *x* in the direction parallel to the flow during processing; after [50].

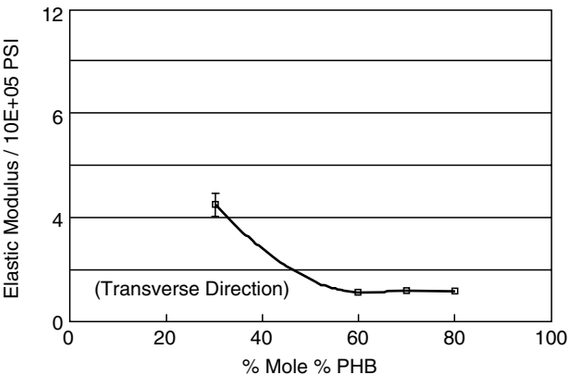

FIGURE 41.9. Tensile strength at 25 °C of PET/*x*PHB copolymers as a function of *x* in the direction transverse to the flow during processing; after [50].

wear, *scratch resistanc*e and d*esign of interactive surfaces in relative motion* [70,71]. Tribology is very well developed for metals [70] but it is quite difficult for polymers. For metals external lubricants work nicely, lowering friction and wear. Application of external lubricants to polymers in most cases results in lubricant absorption and polymer swelling. However, there is some recent progress in polymer tribology and one review of this subject [71].

Before we talk about tribological properties of PLCs, let us define some basic concepts [70, 71]. *Friction* can be defined as the tangential force of resistance to a relative motion of two contacting surfaces. In a stationary specimen we have *the static friction*, namely the force required to create motion divided by the force pressing mating surfaces together. This quantity is often called the static coefficient of friction. In Section 41.3.4 we have quoted Lord Kelvin [53]; the word ''coefficient'' conveys no information. For a specimen in motion we have *the dynamic friction* (also called *kinematic friction*), that is the force required to sustain motion at a specified surface velocity divided by the force pressing mating surfaces together. Similarly here, the term dynamic coefficient of friction is still used.

A *scratch test* method involves scratching the surface of samples and measuring the depth of the groove while the scratch is being made. This can be done under either a constant load, or a progressively increasing load, or else under a stepwise increasing load. The instantaneous depth values are called the *penetration depths* and we represent them by the symbol R_p [72]. Since polymers are viscoelastic materials, they should recover or heal after the scratch, with the bottom of the groove going up and settling at a final level called the *residual depth* R_h. Multiple scratching along the same groove is possible and serves to determine the sliding wear [73].

41.5.2 Friction and Scratch Resistance

In Section 41.7.2 we shall talk more about the fact that different force fields can produce effects on the PLC orientation. Already mentioned before PET/0.6PHB was subjected to magnetic fields and its tribological properties determined [74]. In Fig. 41.10 we display static and dynamic friction for three types of samples: unoriented, oriented along the field, and perpendicularly to the field. We know from Fig. 41.3 that the LC-rich regions form islands in a LC-poor matrix. Imposition of a magnetic field results in growth of the islands [74]. Apparently the feathery or fibrous surfaces of the islands cause higher friction. The effect is larger for the orientation along the field, smaller perpendicularly to the field, but the island growth results in both cases in higher friction than for unoriented samples. The island resistance to movement also causes *higher* dynamic than static friction, while for most polymer surfaces the reverse is true.

Since higher friction is desirable in rare cases only, one can ask what is the advantage of imposing magnetic fields on PLCs. An answer can be seen in Fig. 41.11: penetration depth of different samples, here also unoriented one, oriented along the magnetic field, and perpendicularly to the field. We see that the field-imposed orientation and island growth enhance the scratch resistance. The depth values are lower for oriented samples. It is easy to understand why the effect is larger along the orientation direction.

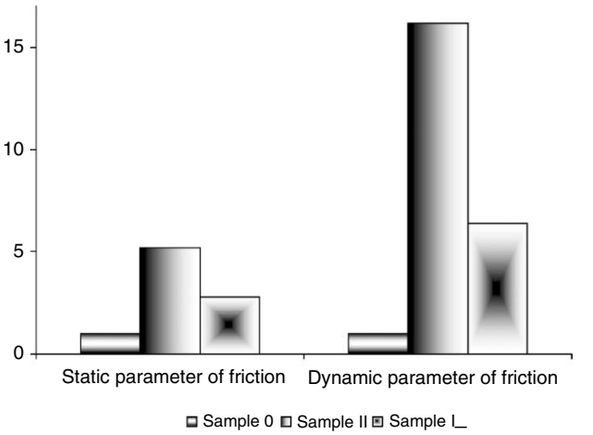

FIGURE 41.10. Static and dynamic friction at 25 °C of PET/0.6PHB as a function of orientation imposed by a magnetic field; after [74].

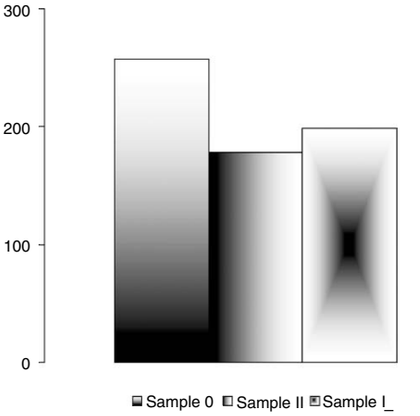

FIGURE 41.11. Penetration depth in scratching at 25 °C of PET/0.6PHB as a function of orientation imposed by a magnetic field; after [74].

41.6 BLENDING AND RHEOLOGICAL PROPERTIES

41.6.1 Rheology of Pure PLCs and of EP + PLC Blends

We discuss blending and rheology ''in one breath''—that is in one section—because PLCs are often used as rheology modifiers for EPs.

To see what the presence of a PLC can do to the viscosity of an EP, consider two examples. In Fig. 41.12 we show

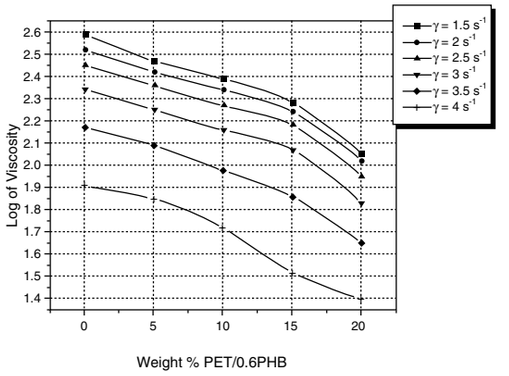

FIGURE 41.12. Logarithmic viscosity log *h* of polycarbonate + PET/0.6PHB blends at 290 °C as a function of the wt% of the PLC; shear rates defined in an insert; after [76].

logarithmic viscosity, log η, of bisphenol-A polycarbonate (PCarb) to which up to 20 wt% of PET/0.6PHB is being added [76]; curves for several shear rates are shown. We see that the effects of addition of the PLC are smaller up to 10 or 15%, and then more pronounced at higher PLC concentrations. However, this is not a general phenomenon. Analogous curves where the same PLC is added to polypropylene (PP) are different [76]; see Fig. 41.13. Already the addition of only 5% of PET/0.6PHB to PP causes a pronounced log η lowering, while further addition of the PLC has little effect. The differences between these two kinds of behavior can be explained in terms of miscibilities of the respective pairs: PET/0.6PHB exhibits more affinity to PCarb than to PP [51].

The common feature of Figs. 41.12 and 41.13 is the fact that the presence of LC sequences in a flexible matrix lowers viscosity to a certain degree—much or little. However, even this assumption is not universally valid. Jackson and Kuhfuss [77] determined viscosity of PET/*x*PHB copolymers as a function of x at 275 °C. They found that,

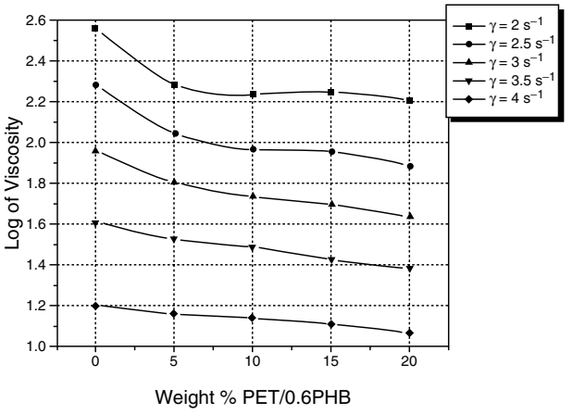

FIGURE 41.13. Logarithmic viscosity log *h* of polypropylene + PET/0.6PHB blends at 230 °C as a function of the wt% of the PLC; shear rates defined in an insert; after [76].

starting from pure PET (x =0), log η first increases, goes through a maximum, falls, goes through a minimum, and then for $x > 0.7$ increases rapidly. One has to agree with Roetting and Hinrichsen [78] that PLC rheology "is a rather complex subject." The findings of Jackson and Kuhfuss reflect a combination of effects of molecular structure (see Section 41.2), hierarchical structures (Section 41.3.2) and results of varying composition.

In spite of the complexity of the situation, there have been attempts to create theories of rheological behavior of PLCs. Wissbrun [79] represents a PLC material as a space-filling system of domains. At rest, the minimum energy arrangement is achieved when the directors in the planes of contact are parallel. Under shear, the domains slide over each other. The model predicts shear sensitiveness, a phenomenon observed experimentally: the curves of viscosity as a function of the shear rate are horizontal for low shear rates and then go down. In fact, for instance the results for PCarb + PET/0.6PHB blends—if we employ such coordinates rather than those in Fig. 41.12—exhibit shear sensitiveness [76].

It is instructive to compare rheological behavior of isotropic molten polymer phases to the simplest LC phases, that is nematic ones. In an isotropic phase molecular orientations are completely random; the flow process can only introduce some order. In a nematic PLC a certain degree of order (as measured by the parameter s, see Section 41.3.1) already exists. Therefore, a flow process can *either enhance or reduce* the existing order. This problem has been analyzed by Marrucci and Maffettone [80]. If instead of the order parameter we consider viscosity, then—as defined for MLCs already in 1946 by Miesowicz [81]—one has to distinguish three viscosities dependent on the direction: parallel to the flow direction; parallel to the gradient of viscosity; and perpendicular to both directions just named.

A very important feature of PLCs has been already mentioned in Section 41.1.4: thermotropic PLCs are often processable with conventional processing equipment for thermoplastics—in fact, given the orientation of LC sequences, more easily than thermoplastics. It is this ease of orientation which is the reason for one more name for PLCs, already mentioned above, namely self-reinforcing plastics.

Readers who want to know more about PLC rheology will find extensive literature on it. Fortunately, there is a whole book on this subject [82].

41.6.2 Properties of Blends

Here is another vast subject with which we can deal only briefly, but reviews are available [27]. Instructive here is to know a rule formulated already in 1960 by Arnold and Sackmann [83,84] for MLC + MLC pairs: complete miscibility always involves isomorphism. That is, if a nematic phase is miscible with a second LC phase, that second phase is also nematic. However, isomorphism is a necessary but not a sufficient condition. Several decades after the original

work, Sackmann [85] reviewed investigations pertaining to this rule—which all confirmed it.

As for EP + PLC blends, the main reason for using them was defined in the beginning of this Chapter; sometimes fillers (and/or other additives) are used as well. Needless to say, blends are more complicated than pure PLCs. For instance, cold crystallization of a constitutent depends on the relative proportions and chemical nature of other constituents present [50,51]. Given the problems with polymer + polymer miscibility, the trial-and-error procedures (''We shall mix a PLC with an EP, and hopefully get good properties . . . '') are *even less* usable here than for EP + EP blends.

While in a previous section we have shown elastic modulus and tensile strength of *copolymers*, *blends* exhibit typically similar behavior: an increase in the concentration of the LC component enhances the mechanical properties along the orientation direction first, but a further increase worsens these properties because of higher brittleness. The elongation at break depends strongly on the brittleness, and decreases already at PLC concentrations of only a few percent. For other mechanical properties, Figs. 41.7–41.10 qualitatively *represent blends as well*; there is little point in providing numerical values for any specific blends. The existence of the maxima is advantageous for keeping the costs reasonable. The location of a maximum depends on the particular EP + PLC pair. At very low concentrations such as 5% there is not enough of the LC component to form the reinforcing islands (or fibrils if strongly elongated), hence the reinforcing effect is absent. However, similarly as in the viscosity curves shown in Figs. 41.12 and 41.13, sometimes less than 20 wt% PLC might be sufficient for a considerable improvement of mechanical properties [50]. There is thus a clear parallelism between rheological and mechanical behavior.

One more similarity between pure PLC copolymers and PLC-containing blends shows in results of cold working. In Figs. 41.4 and 41.5 we have seen the effects of drawing on a PLC. Similar effects are observed when subjecting to drawing EP + PLC blends.

Experimental results show that the reinforcement depends primarily on the EP + PLC miscibility, PLC concentration, and sizes and shapes of the islands. A method of miscibility improvement was developed by Schleeh, Kossmehl, and Hinrichsen [86–88] who synthesized poly(*p*-phenylene terephthalates) with pentoxy groups as flexible side chains. Needless to say, such side chains mix well with EPs.

As for the islands, there is a problem of their optimization for the best mechanical properties. Too many too small islands do not do the job, because the lines of force apparently go around the islands. For a given LC sequence concentration, too large islands leave between them too large purely flexible unprotected regions. Since it is difficult to create experimentally islands of arbitrary size and shape, the problem of optimization can be solved best by computer simulations; see Section 41.8.

41.7 ELECTRICAL AND MAGNETIC PROPERTIES

41.7.1 Effects of Electric Fields

Before focusing on PLCs, let us quote the basic definitions [89]. The relative dielectric permittivity ε is the ratio of the capacities of a parallel plate condenser measured with and without (in vacuum) the dielectric material placed between the plates. If ε is independent of the field strength, it is called *dielectric constant*. Polymers are typically dielectric, so that—in contrast to electric conductors—there is a certain reversal of the relative positions of the electric charges after the removal of the field. If no permanent dipoles are present in the material, then the following Maxwell relation is valid:

$$\varepsilon = n^2, \tag{41.7}$$

where n is the refractive index. Thus, there is a connection to optical properties to be discussed in the next section. Clear deviations from Eq. (41.7) might be caused by semiconductor behavior, but more frequently by the presence of permanent dipoles in the material.

Anisotropy of structure is reflected also in the dielectric constant. Similarly as for isobaric expansivity discussed in Section 41.3.4, one distinguishes here the parameter in the along-the-flow (parallel to the director) direction $\varepsilon_{\parallel}$ from the perpendicular quantity $\varepsilon_{\perp}$. The anisotropy of the dielectric constant is usually expressed as

$$\Delta\varepsilon = \varepsilon_{\parallel} - \varepsilon_{\perp} \tag{41.8}$$

and is typically larger in smectic than in nematic phases. For MLCs both positive and negative values of $\Delta\varepsilon$ are known [90].

When an electric field is imposed upon a material, charged particles move in various ways: Electrons move with respect to the nuclei, creating induced dipole moments and electronic polarization; atoms and groups of atoms move similarly, causing atomic polarization; free ions if present move over long distances, usually to surfaces, what leads to interfacial polarization; permanent dipole moments align along the field, thus increasing in LC materials the order parameter *s*. In *dielectric relaxation spectroscopy* (DRS) sinusoidal electric fields are imposed upon the sample. This resembles sinusoidal mechanical fields discussed in Chapter 24.

Since various motions mentioned occur on various time scales, it is worthwhile to cover a wide range of frequencies. An important advantage of DRS over other spectroscopic techniques is the capability to explore a range of timescales from as slow as 10^4 s to as fast as 10^{-11} s. Therefore, this single technique allows to study a broad spectrum of motions as a function of temperature, pressure, or composition. Decomposition of DRS spectra into constituents corresponding to various processes is needed. A procedure for doing this which handles also the temperature dependencies of relaxational processes has been devised by Schlosser and his colleagues [91].

DRS results for PLCs have been reviewed by Moscicki [92]. We shall name here two findings. First, in simple one-row combs (see again Table 41.1) there are different rates of reorientation of different polar groups in side chains. This phenomenon was observed even in MLCs [93], but is apparently stronger in PLCs. Second, also in analogy to MLCs, in PLCs we observe *slow* relaxational processes along the director, and noticeably faster perpendicularly to it.

Table 41.1 shows us also a way to vary the numbers of both permanent and induced dipoles. This gives us the capability to *manipulate* dielectric properties of PLC materials over quite wide ranges.

41.7.2 Effects of Magnetic Fields and NMR Spectroscopy

It cannot be stressed enough that electric, magnetic, and mechanical (shear fields) produce in fact *similar effects of enhancing orientation*, thus increasing the order parameter s, and also affecting mechanical and other properties in ways already discussed above. There exist even favorite methods of achieving orientation for certain classes of materials. Thus, magnetic fields are typically used to orient polyacrylates, while polysiloxanes are routinely oriented by imposition of ac electric fields.

Since effects of magnetic field imposition are already known to us, we shall now discuss a method of studying the chain dynamics in PLCs at the molecular level involving such fields: nuclear magnetic resonance (NMR) spectroscopy.

A good review of NMR spectroscopy of PLCs has been written by Lauprêtre [94]. Therefore, in this Chapter we shall describe only a specific aspect of the problem. Because PLC chains typically contain both flexible and LC sequences, *orientational ordering of flexible sequences between LC sequences* is of interest. Similar behavior appears in PLC + EP blends, and also in solutions of LCs in low-molecular-mass flexible molecules. Photinos, Samulski, and Toriumi (PST) developed a theory of orientational ordering [95–97]. They regard flexible molecules as sets of rigid submolecular segments that can take different relative positions according to conformations, and formulate the potential of mean torque of the entire molecules in a modularly additive fashion. Samulski and his colleagues considered various choices of submolecular units in neat nematic LCs as well as in flexible alkane solute + nematic systems, and compared predictions of their theory with NMR data. The results indicate that in carbonlike chains a relatively simple choice of subunits (slightly biaxial atom-blocks) and a segment-wise additive potential provide an explicit and accurate representation of anisotropy of molecular shapes present simultaneously with molecular flexibility. The main reason for the success of the PST approach is fairly clear: the alignment of LC sequences is determined by the *cords* (or blocks) and not by the bonds. This is why previous treatments in terms of independent bonds did not provide satisfactory results. Moreover, a chain of $N + 1$ segments contains N bonds, $N + 1$ blocks and $N + 1$ cords, so the alternative representations are of the same complexity. When switching from the bond to the chord representation, the number of parameters in the interaction potential necessary to obtain meaningful results does not increase either. Terms beyond second neighbors are too small to be visible in NMR spectra studied by PST.

While in this section we do not deal with thermophysical properties, they are connected to those now under discussion as well. Roth and Krücke [98] have shown that the glass transition temperatures of comb PLCs can be evaluated from the line shape of the wide line NMR signals.

41.8 OPTICAL PROPERTIES

41.8.1 Nonlinear Optical (NLO) Effects

We have already noted in Section 41.6.1 the connection between electrical and optical properties. The effects of light propagation through a material can be described in terms of the polarization

$$P = P_0 + \chi_1 \cdot \mathbf{E} + \chi_2 \cdot \mathbf{E} \cdot \mathbf{E} + \chi_3 \cdot \mathbf{E} \cdot \mathbf{E} \cdot \mathbf{E} + \ldots, \quad (41.9)$$

where P_0 is the spontaneous polarization of the material, $\mathbf{E}$ is the tensor of field strength of the electrical component of the optical field, while each c_i is the optical susceptibility of the ith order of the material. In linear optical materials the propagation of light is characterized by the independence of refraction on light intensity and also for instance on the absence of any changes in frequency of the light.

The establishment of presence of nonlinear optical (NLO) effects requires very strong optical fields, typically created by laser pulses. We talk about second-order NLO materials if the term with χ_2 in Eq. (41.9) dominates, third if the χ_3-containing term is dominant, etc. The third-order optical materials are also called Kerr media. Returning once again to Table 41.1 with its variety of possible structures, we note that the NLO character of certain—even numerous—constituting units of a PLC is not enough for the whole material to exhibit NLO properties. If centers of symmetry are present, the induced dipoles largely cancel out, and χ_2 properties of the polymer are negligible.

One can base polymer design for NLO applications on the expression for the dipole moment μ in the effective electric field $\mathbf{F}$ while $\mathbf{E}$ is now a perturbing (such as oscillating) electric field:

$$\mu(\mathbf{F}, \mathbf{E}) = \mu_0(\mathbf{F}) + \alpha_0(\mathbf{F})\mathbf{E} + \beta_0(\mathbf{F})\mathbf{E} \cdot \mathbf{E}/2! + \gamma_0(\mathbf{F})\mathbf{E} \cdot \mathbf{E} \cdot \mathbf{E}/3! + \ldots \quad (41.10)$$

Here μ_0 is the intrinsic dipole moment, α_0 is the linear polarizability, β_0 the hyperpolarizability, γ_0 the second hyperpolarizability, etc. Equation (41.10) is a molecular level analog of Eq. (41.9) for the macroscopic polarization. Thus, we are for instance interested in the second harmonic

generation (SHG), that is in doubling the frequency of the incident laser light. Equation (41.10) tells us that we need a second-order NLO material (= a χ_2 material) the dipole moment of which has a substantial hyperpolarizability contribution.

Marder and coworkers [99] have stressed the fact—almost universally disregarded or not even noticed before—that α_0, β_0,γ_0, etc. are derivatives with respect to **F** of their next order polarization or polarizability; thus, β_0 is the derivative of α_0, and so on. Before them, some groups were for instance trying to optimize γ_0 in an NLO material by optimizing β_0—not knowing that the β_0 optimization will automatically result in $\gamma_0 = 0$. The work of Marder and his colleagues has useful consequences. Certain chemical changes can affect the electron density similarly as applying an electric field to the molecule. Such changes include putting donor and acceptor groups on the polyene chain (alternating singe and double carbon–carbon bonds), incorporating groups that gain aromaticity on polarization, or placing the molecule in a solvent that will stabilize charge separation.

41.8.2 PLCs for NLO Applications

Discussing optical applications of polymers, it is worth noting first of all that research objectives here go in two diametrically opposite directions. In some cases one wants to minimize the interactions with the light. This is the case with polymer optical fibers, and with all attempts to reduce the noise for optical recording and information storage on optical discs. In other cases the main objective is to maximize the polymer + light interactions, as in photonic devices when one wants to augment the light-intensity dependent change of the refractive index. Polymeric materials for optical applications have significant advantages in comparison with inorganic materials: low weights of optical components, good mechanical properties, and the ease of manufacturing parts even with complex geometries.

We have already mentioned before SHG materials; doubling of the light frequency enables a laser to encode four times as much information on a compact disc. NLO effects have significant technological implications for optical signal processing, generation of variable-frequency laser light, tunable filters, and optical data storage. The g_0 parameter is important for functions such as optical switching: a light beam alters the path of a second beam by changing the refractive index.

Optical data storage is an alternative to magnetic storage. There are several variations here: ROMs or read-only memories, DRAWs (= direct read after write) for writing once but reading many times, and erasable memories. The last technique can be realized by using comb PLCs. Such a PLC in its LC state (say one of the smectic states) is frozen below its glass transition temperature T_g, and then locally distorted by the heat absorbed from a laser pulse. Such a distortion is readable, since it scatters light. Aging of the material in the glassy state (see the section on aging in Chapter 24 on mechanical properties) can be assumed slow enough for the time period during which the information is needed. That information can be erased by simply heating the material above T_g, but below its isotropization (clearing) temperature.

MLCs also have their place in optical applications, mainly as so-called polymer-dispersed LCs (PDLCs). A PDLC constitutes a microemulsion of an MLC in a film of a conventional (nonPLC) polymer. In the "switched off" state the MLC and the polymer have different refractive indices, dispersed MLC droplets (not unlike to the islands in PLCs) scatter light quite effectively, and the film is opaque. Then an external electric field is applied, for instance across a capacitor-like metal coating on both sides of the film. The director in all MLC droplets becomes the same. One can choose the MLC + polymer pair so that the refractive index along the director is the same as that of the host polymer. In that case the film in the electric field becomes transparent. Switching the field off and on, one has a light valve with a fairly large area.

Let us mention a few more capabilities created in this growing field. Laser-induced reorientation of the optical axis is possible in PLC combs; optically induced *trans–cis* isomerization occurs. Erasable holograms can be created in PLC materials—as discussed by Eich and Wendorff [100] and pursued since by many. The rubbing of a polymer leads to an anisotropic surface morphology, since the LC molecules become aligned [101]. Scanning force microscopy can be used to create in a controlled way areas with a similar anisotropy and with a desired refractive index patterns.

A combination of approaches serves well achieving specific objectives. We have discussed above the fact that hydrogen bonds can also serve to create liquid crystallinity. Thus, cholesteric liquid crystal phases can be made by hydrogen bonding [102a,b]. Among interesting properties is the capability described by Shibaev e.a. [102b] of changing color of cholesteric PLC films by addition of certain aminoacids. In self-organized helical structures light is reflected when the wavelength matches the pitch (twice the periodicity). Cholesteric LCs are not only colored filters, but also reflectors and polarizers. Mitov and Dessaud [102c] show how MLCs converted into PLCs by curing provide reflectance exceeding 50 %.

Before going into the last section on theory and computer simulations, let us stop and ponder what various properties of PLCs briefly described above signify. It becomes clear that PLCs have current and potential applications in electrical, electronic, chemical, aircraft, aerospace, automobile, petroleum as well as other industries.

41.9 THEORY AND COMPUTER SIMULATIONS

41.9.1 Theory

One can distinguish at least four major theories of LC systems. Already in 1949 Onsager [103] formulated a dens-

ity expansion of the Helmholtz function A of anisometric particles—what made possible a prediction of the nematic-to-isotropic (N–I) transition. Flory [104] developed in 1956 a lattice model which after a period of inactivity led to significant further developments characterized below. Between 1958 and 1960 Maier and Saupe [105–107] created a theory in terms of a potential of mean torque experienced by LC or solute molecules in nematic phases. Their work became a ''standard'' in the sense of asking the question: is any new theory, first of all, able to reproduce the results of Maier and Saupe? Finally, Landau developed a molecular field theory [108] adapted by de Gennes [109] to LC systems, and is based on expanding the Helmholtz function A (or the Gibbs function G) as a power series of the order parameter s.

The framework of the Flory theory [104,105–117] can be summarized as follows. A chain segment has the length equal to its diameter, what makes possible placement at a given lattice site of either a segment or a solvent molecule. The objective is the formulation of the partition function Z. One makes the standard approximation

$$Z = Z_{\text{comb}} Z_{\text{orient}} \tag{4.11}$$

where Z_{comb} is the combinatorial (steric) contribution while Z_{orient} arises from the various orientations of the rigid sequences as well as the anisotropic interactions between their segments. Evaluation of Z_{comb} requires taking into account various possible orientations of LC sequences with respect to the director. Flory developed an ingenious method of representing such orientations on a lattice—shown in Fig. 41.14. Without going into details (which are provided for instance in [112]) let us note that for every sequence (there are four of them in the Figure) there is a parameter y which is equal to unity if that sequence is parallel to the director, and increases along with the deviation of the direction of the sequence from the LC director.

In earlier version of the theory, only fully rigid chains were treated. However, Matheson and Flory [113] extended the theory to the cases when $\theta < 1$, where θ is the average concentration of LC segments in PLC chains. A subsequent amplification [115] of the Matheson–Flory model includes the orientational distribution function of Flory and Ronca [112]. The amplified theory predicts a drastic change in the slope of s vs. η when going from $\theta = 0.1$ to 0.2, indicating a large increase in the chain alignment; here η is the average length of rigid sequences. Moreover, the liquid-crystalline-to-isotropic transition temperature TLC-i as a function of η shows a minimum for all θ values [115].

The quality of any theory can best be evaluated by comparing its predictions with the experiment. Ternary systems of the type PLC + flexible polymer + solvent were treated as well [116]. Ternary miscibility gaps were predicted; it turned out that the tie lines usually are not parallel to the PLC + flexible polymer basis of the Gibbs triangle, and the critical point is not at the top of the gap. Experimental data for such a system exist, namely PET/0.27PHB + poly(bisphenol-A-carbonate) + $CHCl_3$ [117]. As can be seen in Fig. 41.15, the predicted miscibility gap is in good agreement with the gap determined by extinction cloud point measurements [116].

One more result obtained following the Flory approach was that the concentration of hard rods q is much more important for the LC phase formation than the system temperature [115]. To pursue this issue further, the Maier–Saupe theory of MLCs was extended to PLCs taking particularly into account the system temperature [118–122]. This approach makes possible inclusion of external deformations via the system volume and also via the end-to-end distance vectors of the chains. The affine deformation developed by Flory [123] and well explained by Mark [124] was incorporated in to the model—applicable strictly to the longitudinal PLCs. Among other things, it turns out that the behavior of rigid (= LC) sequences is largely governed by orienting interactions while for the flexible sequences short-range interactions (dependent mainly on chemical structures) are

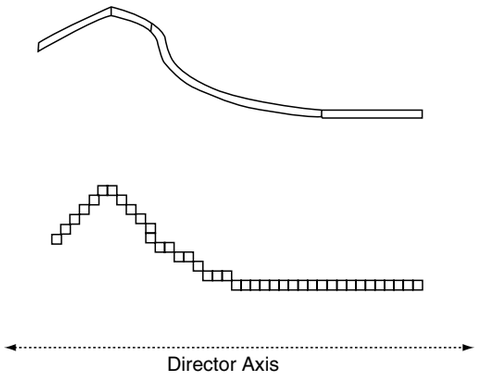

FIGURE 41.14. A four-sequence part of a chain (top) and its lattice representation (bottom). The third sequence from the left is flexible; the remaining ones are liquid-crystalline; after [115].

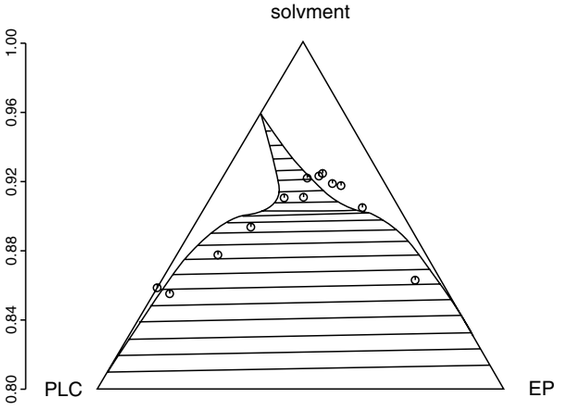

FIGURE 41.15. Comparison of experimental (circle points from [117]) and predicted (continuous lines) phase diagram. Lines calculated for the degrees of polymerization $r_{\text{PLC}} = 600$ and $r_{\text{EP}} = 1{,}200$ and for the temperature $T = 295\,\text{K}$; after [116].

the most important. The results include evaluation of orientation vs. deformation and stress vs. strain relations [122].

41.9.2 Advantages of Computer Simulations of Polymers

Getting answers from experiments is often difficult, time consuming, and the results hardly unequivocal. So-called hidden variables which exist in nature do not manifest themselves in simulations. Moreover, changing only one parameter at a time is easy in simulations, but not in real materials. One example should suffice here: to lower the density in an experiment one increases the temperature of the material. However, then the energetics changes too, heating has pumped more energy into the material. There is hardly a procedure for the separation of the two effects.

Starting with a theory, one has an advantage, particularly in multicomponent systems such as PLC + EP + solvent: it is easy to define the concentration of a flexible polymer (EP) and the average concentration q of LC sequences in PLC chains. The average concentration of flexible sequences in PLC molecules is of course $1 - \theta$, and other model parameters such as in the Flory theory can be defined as well. Somewhat similarly, it is easy in molecular dynamics (MD) simulations to set up certain chains with $\theta > 0$ and other chains with $\theta = 0$.

41.9.3 Molecular Dynamics Simulations of PLCs

We shall briefly summarize MD simulations of systems of PLC chains. First, the chains systems have to be constructed. There are various ways of generating them, and the mechanical behavior is little if at all influenced by the generation procedure. It is influenced, however, by the vacancies, or the amount of free volume v^f, as predicted by the chain relaxation capability (CRC) theory [125]. The problem is to create a realistic bulk polymer system. A procedure originally developed by Mom [126] has been modified to achieve a more realistic representation of polymeric chains [127–129].

The interaction potentials used take into account the relative rigidity of the LC sequences, possibility of *trans*-to-*gauche* conversions in flexible sequences (accomplished by using a double-well potential), and make possible bond scission (a Morse-like potential for large extensions). The simulations are typically performed at a constant temperature, multiplying the particle velocities in every time step by a factor related to the actual kinetic energy and to a reference energy [130]. The Newton differential equations of motion are transformed into difference equations employing a finite time step. The positions after a successive time step are computed using a so-called leap-frog algorithm [130]. Since the forces acting on a given particle depend on its neighbors, a list of nearest neighbors is renewed after every time step.

Fully flexible chains are of course simulated for comparison, so as to see the effects of liquid crystallinity. In our simulations we subject the materials to a tensile force (applied to top and bottom in two-dimensional specimens). As expected, under application of that force, chain conformation changes (from *gauche* to *trans*) are observed. Bond scission followed by crack propagation are observed as well. See Fig. 41.16, and note that the cracks do not propagate straight along the lines of application of the force, since the LC reinforcing units are "doing their job" [131]. In each case (that is for a given θ and LC sequence configuration) a stress level is observed at which the fraction of broken bonds increases dramatically—clearly when CRC was exceeded. Thus, simulations provide a direct confirmation of the CRC approach—discussed more in detail in this Handbook in Chapter 24 on mechanical properties of polymers.

In tensile experiments one determined always the engineering stress but determination of the true stress is much more difficult. A simulation method has been developed which allows calculation of the true stress based on cutting the specimen into sections [129,132,133]. There are significant differences between the two kinds of stresses; see Fig. 41.17.

Other issues concerning PLCs are also such that simulations provide answers to questions to which experiments cannot. For instance, what is the skin-core effect on properties? In processing of real materials always a skin which is

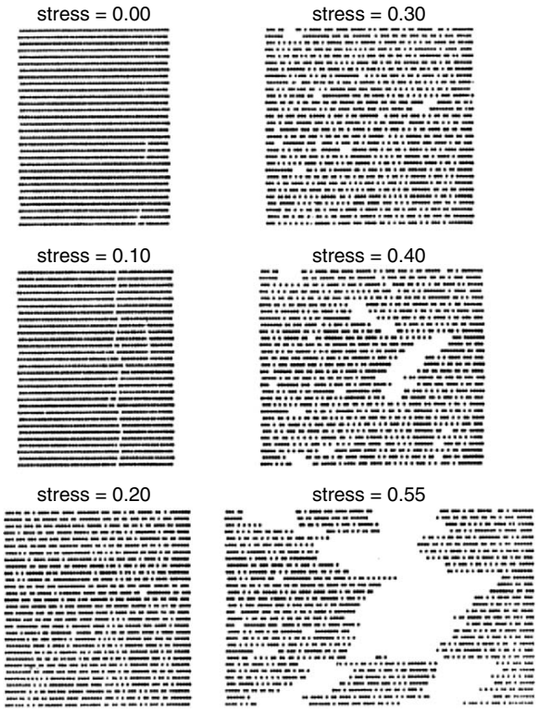

FIGURE 41.16. MD simulations of a random PLC with $\theta = 0.5$ under tensile deformations applied vertically with various stress levels (stress in reduced units); after [131].

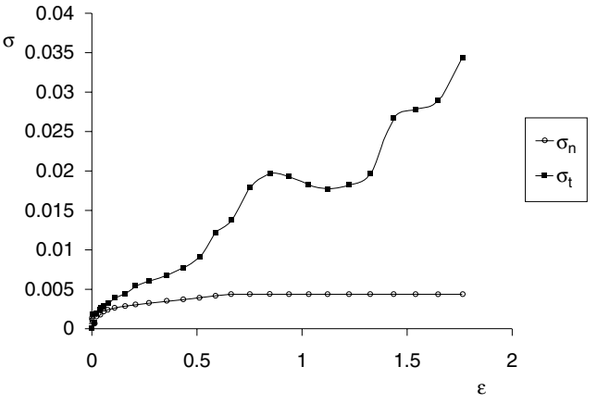

FIGURE 41.17. Engineering or nominal stress (index *n*) and true stress (index *t*) as a function of engineering strain *e* for a PLC simulated by molecular dynamics; after [132].

more oriented appears—but it is in simulations that we can create materials with arbitrary thickness of the skin, thickness of the core, and also create layers with intermediate properties. Another question is the crack propagation in PLCs. Do cracks propagate preferentially through the LC-rich islands since the islands are rigid and thus brittle, or rather through the LC-poor matrix since the matrix is mechanically weak? The answer is: cracks propagate near the island surfaces on the matrix side [127].

ACKNOWLEDGMENTS

I have learned what LCs are and which of their features are important from the late Professors Paul J. Flory, Stanford, and Horst Sackmann, Halle. This Chapter has been influenced by discussions with many colleagues and collaborators, including Antonio M. Cunha, Henryk Galina, Michael Hess, Georg Hinrichsen, Hans R. Kricheldorf, Betty L. López, Robert Maksimov, Gerhard Pelzl, Monika Plass, Edward T. Samulski, Alfred Saupe, Jukka V. Seppälä, Valery P. Shibaev, Ricardo Simoes, Jürgen Springer, Tomasz Sterzynski, Franciska Sundholm, and Janusz Walasek. Our own research referred to herein was supported by the NATO, Brussels; National Science Foundation, Washington, DC; and the Robert A. Welch Foundation (Grant B-1203), Houston.

REFERENCES

1. M.G. Friedel, *Ann. Phys.* **18**, 273 (1922).
2. W. Kast, *Angew. Chem.* **67**, 592 (1955).
3. B. Wunderlich and J. Grebowicz, *Adv. Polym. Sci.* **60/61**, 1 (1984).
4. B. Wunderlich, M. Möller, J. Grebowicz, and H. Baur, *Adv. Polym. Sci.* **87**, 1 (1988).
5. E.T. Samulski, *Faraday Discuss.* **79**, 7 (1985).
6. G. Kiss, *Polym. Eng. Sci.* **27**, 410 (1987).
7. P.J. Hall and G.J.T. Tiddy, in *Liquid Crystalline Polymers: From Structures to Applications*, edited by A.A. Collyer (Elsevier, New York 1992), Chapter 5; M.G. Northolt and D.J. Sikkema, in *Liquid Crystalline Polymers: From Structures to Applications*, edited by A.A. Collyer (Elsevier, New York 1992), Chapter 6.
8. B.S. Hsiao, M.T. Shaw, and E.T. Samulski, *Macromolecules* **21**, 543 (1988).
9. W. Brostow, *Polymer* **31**, 979 (1990).
10. A. Abe, T. Hiejima, T. Takeda, and C. Nakufuku, *Polymer* **44**, 3117 (2003).
11. P.A. Henderson and C.T. Imrie, *Macromolecules* **38**, 3307 (2005).
12. G. Li and T. Yu, *Makromol. Chem. Rapid Commun.* **10**, 387 (1989).
13. K. Kerkam, C. Viney, D. Kaplan, and S. Lombardi, *Nature* **349**, 596 (1991).
14. F. Reinitzer, *Monatsh. Chem.* **9**, 421 (1888).
15. O. Lehmann, *Z. Phys. Chem.* **4**, 462 (1889).
16. D. Vorländer, *Kristallinisch-flüssige Substanzen*, (Enke-Verlag, Stuttgart 1908).
17. D. Vorländer, *Z. Phys. Chem.* **105**, 211 (1923).
18. W. Brostow, *Science of Materials* (Wiley, New York 1979; Robert E. Krieger Publ. Co., Malabar, FL 1985); W. Brostow, *Introducción a la ciencia de los materiales* (Editorial Limusa, México, D.F. 1981); W. Brostow, *Einstieg in die moderne Werkstoffwissenschaft* (Carl Hanser Verlag, München 1985; Deutscher Verlag für Grundstoffindustrie, Leipzig 1985); updated Ukrainian edition to be published by Lvivska Politechnika.
19. W. Brostow, T.S. Dziemianowicz, J. Romanski, and W. Werber, *Polym. Eng. Sci.* **28**, 785 (1988).
20. M.R. Piggott, in *Failure of Plastics*, edited by W. Brostow and R.D. Corneliussen (Hanser, Munich 1986), Chapter 23.
21. J.-F. Jansson and H. Sundström, in *Failure of Plastics*, edited by W. Brostow and R.D. Corneliussen (Hanser, Munich 1986), Chapter 24.
22. E. Pisanova and S. Zhandarov, in *Performance of Plastics*, edited by W. Brostow (Hanser, Munich 2000), Chapter 19.
23. W. Brostow, V.M. Castaño, A. Huanosta, M. de Icaza, M.E. Nicho, and J.M. Saniger, *Mater. Res. Innovat.* **3**, 85 (1999).
24. V.M. Castaño and R. Rodriguez, in *Performance of Plastics*, edited by W. Brostow (Hanser, Munich 2000), Chapter 24.
25. W. Brostow, *Kunststoffe* **78**, 411 (1988).
26. W. Witt, *Kunststoffe* **78**, 795 (1988).
27. M. Hess, in *Performance of Plastics*, edited by W. Brostow (Hanser, Munich 2000), Chapter 21.
28. M. Ebert, R. Kleppinger, M. Soliman, M. Wolf, J.H. Wendorff, G. Latterman, and G. Staufer, *Liq. Cryst.* **7**, 553 (1990).
29. H. Gasparoux, F. Hardoin, C. Destrade, and H.T. Nguyen, *New J. Chem.* **16**, 295 (1992).
30. J.M. Fréchet and A. Tomalia, *Dendrimers and Other Dendritic Polymers* (Wiley, New York 2002).
31. T. Felekis, L. Tziveleka, D. Tsiourvas, and C.M. Paleos, *Macromolecules* **38**, 1705 (2005).
32. R. Zentel and J. Wu, *Makromol. Chem.* **187**, 1727 (1986).
33. O. Hermann-Schönherr, J.H. Wendorff, H. Ringsdorf, and P. Tschirner, *Makromol. Chem. Rapid Commun.* **7**, 791 (1986).
34. H. Ringsdorf, P. Tschirner, O. Herrmann-Schönherr, and J.H. Wendorff, *Makromol. Chem.* **188**, 1431 (1987).
35. L. Cui, J. Miao, L. Zhu, I. Sics and B.H. Siao, *Macromolecules* **38**, 3386 (2005).
36. P.H. Hermans, *Contributions to the Physics of Cellulosic Fibres* (Elsevier, Amsterdam 1946), p. 133.
37. D. Demus, H. Demus, and H. Zaschke, *Flüssige Kristalle in Tabellen*, 2nd ed. (Deutscher Verlag für Grundstoffindustrie, Leipzig 1974).
38. D. Demus, and H. Zaschke, *Flüssige Kristalle in Tabellen II*, 2nd ed. (Deutscher Verlag für Grundstoffindustrie, Leipzig 1984).
39. D. Demus and L. Richter, *Textures of Liquid Crystals* (Verlag Chemie, Weinheim 1978).
40. J. Menczel and B. Wunderlich, *J. Polym. Sci. Phys.* **18**, 1433 (1980).
41. W. Meerisi, J. Menczel, U. Gaur, and B. Wunderlich, *J. Polym. Sci. Phys.* **20**, 719 (1982).
42. L.C. Sawyer and M. Jaffe, *J. Mater. Sci.* **21**, 1897 (1986).
43. L.C. Sawyer, R.T. Chen, M.G. Jamieson, I.H. Musselman, and P.E. Russell, *J. Mater. Sci. Lett.* **11**, 69 (1992).
44. L.C. Sawyer and M. Jaffe, *Mater. Res. Soc. Symp.* **255**, 75 (1992).
45. W. Brostow and M. Hess, *Mater. Res. Soc. Symp.* **255**, 57 (1992).
46. T. Kato and J.M.J. Fréchet, *Macromolecules* **22**, 3819 (1989).

47. C.G. Bazuin and F.A. Brandys, *Chem. Mater.* **4**, 970 (1992).
48. C.G. Bazuin, F.A. Brandys, T.G. Eve, and M. Plante, *Macromol. Symp.* **84**, 183 (1994).
49. Y. Zhao and H. Lei, *Macromolecules* **27**, 4525 (1994).
50. W. Brostow, M. Hess, and B.L. López, *Macromolecules* **27**, 2262 (1994).
51. W. Brostow, M. Hess, B.L. López, and T. Sterzynski, *Polymer* **37**, 1551 (1996).
52. S. Buchner, D. Chen, R. Gehrke, and H.G. Zachmann, *Mol. Cryst. Liq. Cryst.* **155**, 357 (1988).
53. Lord Kelvin, *Math. Phys. Papers* **3**, 437 (1890).
54. IUPAC Commission for Symbols, Units and Nomenclature, *Physica A* **93**, 1 (1978).
55. W. Brostow, J.V. Duffy, G.F. Lee, and K. Madejczyk, *Macromolecules* **24**, 479 (1991).
56. W. Brostow, N.A. D'Souza, M. Hess, and E.G. Jacobs, *Polymer* **39**, 4081 (1998).
57. K.P. Menard, *Dynamic Mechanical Analysis—An Introduction* (CRC Press, Boca Raton 1999).
58. K.P. Menard, in *Performance of Plastics*, edited by W. Brostow (Hanser, Munich 2000), Chapter 8.
59. P. Zoller, P. Bolli, V. Pahud, and H. Ackermann, *Rev. Sci. Instrum.* **47**, 948 (1976).
60. W. Brostow, V.M. Castaño, G. Martinez-Barrera, and D. Pietkiewicz, *Physica B* **344**, 206 (2004).
61. G. Broza, V.M. Castaño, G. Martinez-Barrera, K.P. Menard, and C. Simoes, *Physica B* **357**, 500 (2005).
62. W. Brostow, V.M. Castaño, G. Martinez-Barrera, and J.-M. Saiter, *Physica B* **334**, 436 (2003).
63. A. Tölle, *Rep. Prog. Phys.* 64, 1473 (2001).
64. R. Casalini and C.M. Roland, *Phys. Rev. E* **69**, 62501 (2004).
65. R. Casalini and C.M. Roland, *Colloid Polym. Sci.* **283**, 107 (2004).
66. J.-F. Jansson, in *Liquid Crystalline Polymers: From Structures to Applications*, edited by A.A. Collyer (Elsevier, New York 1992), Chapter 9.
67. J. Küpfer and H. Finkelmann, *Makromol. Chem. Rapid Commun.* **12**, 717 (1991).
68. J. Küpfer, E. Nishikawa, and H. Finkelmann, *Polym. Adv. Technol.* **5**, 110 (1994).
69. V. Ambrogi, M. Giamberini, P. Cernuti, P. Pucci, N. Menna, R. Mascolo, and C. Carfagna, *Polymer* **46**, 2105 (2005).
70. E. Rabinowicz, *Friction and Wear of Materials*, 2nd ed. (Wiley, New York 1995).
71. W. Brostow, J.-L. Deborde, M. Jaklewicz, and P. Olszynski, *J. Mater. Ed.* 24, 119 (2003).
72. W. Brostow, B. Bujard, P.E. Cassidy, H.E. Hagg, and P.E. Montemartini, *Mater. Res. Innovat.* **6**, 7 (2002).
73. W. Brostow, G. Damarla, J. Howe, and D. Pietkiewicz, e-Polymers no. 025 (2004); http://www.e-polymers.org/
74. W. Brostow and M. Jaklewicz, *J. Mater. Res.* **19**, 1038 (2004).
75. W. Brostow, editor, *Mechanical and Thermophysical Properties of Polymer Liquid Crystals* (Chapman & Hall, London 1998).
76. W. Brostow, T. Sterzynski, and S. Triouleyre, *Polymer* **37**, 1561 (1996).
77. W.J. Jackson, Jr. and H.F. Kuhfuss, *J. Polym. Sci. Phys.* **14**, 2043 (1976).
78. O. Roetting and G. Hinrichsen, *Adv. Polym. Technol.* **13**, 57 (1994).
79. K.R. Wissbrun, *Faraday Discuss.* **79**, 161 (1985).
80. G. Marrucci and P.L. Maffettone, *Macromolecules* **22**, 4076 (1989).
81. M. Miesowicz, *Nature* **158**, 27 (1946).
82. D. Acierno and A.A. Collyer, editors, *Polymer Liquid Crystals Vol. 2—Rheology* (Chapman & Hall, London, 1996).
83. H. Arnold and H. Sackmann, *Z. Phys. Chem.* **213**, 137 (1960).
84. H. Arnold and H. Sackmann, *Z. Phys. Chem.* **213**, 145 (1960).
85. H. Sackmann, *Prog. Colloid Polym. Sci.* **69**, 73 (1984).
86. T. Schleeh, G. Kossmehl, and G. Hinrichsen, *Makromol. Chem.* **191**, 1075 (1990).
87. T. Schleeh, G. Hinrichsen, and G. Kossmehl, *Colloid Polym. Sci.* **270**, 207 (1992).
88. T. Schleeh, O. Roetting, D. Bettge, G. Hinrichsen, and G. Kossmehl, *Makromol. Chem.* **194**, 791 (1993).
89. D.W. van Krevelen, *Properties of Polymers*, 3rd ed. (Elsevier, Amsterdam 1990).
90. D. Demus, *Z. Chemie* **15**, 1 (1975).
91. E. Schlosser, A. Schönhals, H.-E. Carius, and H. Goering, *Macromolecules* **26**, 6027 (1993).
92. J.K. Moscicki, in *Liquid Crystalline Polymers: From Structures to Applications*, edited by A.A. Collyer (Elsevier, New York 1992), Chapter 4.
93. V.P. Shibaev and N.A. Platé, *Polym. Sci. USSR A* **19**, 1065 (1978).
94. F. Lauprêtre, in *Liquid Crystalline Polymers: From Structures to Applications*, edited by A.A. Collyer (Elsevier, New York 1992), Chapter 3.
95. D.J. Photinos, E.T. Samulski, and H. Toriumi, *J. Phys. Chem.* **94**, 4688, 4694 (1990).
96. D.J. Photinos, E.T. Samulski, and H. Toriumi, *J. Chem. Phys.* **94**, 2758 (1991).
97. D.J. Photinos, E.T. Samulski, and H. Toriumi, *Mol. Cryst. Liq. Cryst.* **204**, 61 (1991).
98. H. Roth and B. Krücke, *Makromol. Chem.* **187**, 2655 (1986).
99. S.R. Marder, C.B. Gorman, F. Meyers, J.W. Perry, G. Bourhill, J.-L. Brédas, and B.M. Pierce, *Science* **265**, 632 (1994).
100. M. Eich and J. H. Wendorff, *Makromol. Chem. Rapid Commun.* **8**, 467 (1987).
101. M. Rüetschi, P. Grütter, J. Fünfschilling, and H.-J. Güntherodt, *Science* **265**, 512 (1994).
102. a) A.V. Medvedev, E.B. Barnatov, A.S. Medvedev, V.P. Shibaev, S.A. Ivanov, M. Kozlovsky, and J. Stumpe, *Macromolecules* **38,** 2223 (2005); b) P.V. Shibaev, D. Chiappetta, R.L. Sanford, P. Palffy-Muhoray, M. Moreira, W. Cao, and M.W. Green, *Macromolecules* **39,** 3986 (2006); c) M. Mitov and N. Dessaud, *Nature Materials* **5,** 361 (2006).
103. L. Onsager, *Ann. NY Acad. Sci.* **51**, 627 (1949).
104. P.J. Flory, *Proc. R. Soc. A* **234**, 60, 73 (1956).
105. W. Maier and A. Saupe, *Z. Naturforsch. A* **13**, 564 (1958).
106. W. Maier and A. Saupe, *Z. Naturforsch. A* **14**, 1909 (1959).
107. W. Maier and A. Saupe, *Z. Naturforsch. A* **15**, 282 (1960).
108. L.D. Landau, *Collected Papers*, edited by D. ter Haar (Gordon & Breach, New York 1965), p. 193.
109. P.G. de Gennes, *The Physics of Liquid Crystals* (Oxford University Press, Oxford 1979).
110. P.J. Flory and A. Abe, *Macromolecules* **11**, 1119 (1978).
111. A. Abe and P.J. Flory, *Macromolecules* **11**, 1122 (1978).
112. P.J. Flory and G. Ronca, *Mol. Cryst. Liq. Cryst.* **54**, 289, 311 (1979).
113. R.R. Matheson, Jr. and P.J. Flory, *Macromolecules* **14**, 954 (1981).
114. R.R. Matheson, Jr., *Macromolecules* **19**, 1286 (1986).
115. D.A. Jonah, W. Brostow, and M. Hess, *Macromolecules* **26**, 76 (1993).
116. S. Blonski, W. Brostow, D.A. Jonah, and M. Hess, *Macromolecules* **26**, 84 (1993).
117. F. Schubert, K. Friedrich, M. Hess, and R. Kosfeld, *Mol. Cryst. Liq. Cryst.* **155**, 477 (1988).
118. W. Brostow and J. Walasek, *J. Chem. Phys.* **105**, 4367 (1996).
119. W. Brostow, K. Hibner, and J. Walasek, *J. Chem. Phys.* **108**, 6484 (1998).
120. W. Brostow and J. Walasek, *J. Chem. Phys.* **114**, 2466 (2001).
121. W. Brostow and J. Walasek, *J. Chem. Phys.* **115**, 8692 (2001).
122. W. Brostow and J. Walasek, *J. Chem. Phys.* **121**, 3272 (2004).
123. P.J. Flory, *Selected Works*, Vol. III. (Stanford University Press, Stanford, CA 1985).
124. J.E. Mark and B. Erman, *Rubberlike Elasticity—A Molecular Primer* (Wiley, New York 1988).
125. W. Brostow, in *Performance of Plastics*, edited by W. Brostow (Hanser, Munich 2000), Chapter 5.
126. V. Mom, *J. Comput. Chem.* **2**, 446 (1981).
127. W. Brostow, M. Donahue III, C.E. Karashin, and R. Simoes, *Mater. Res. Innovat.* **4**, 75 (2001).
128. W. Brostow, A.M. Cunha, and R. Simoes, *Mater. Res. Innovat.* **7**, 19 (2003).
129. R. Simoes, A.M. Cunha, and W. Brostow, *Polymer* **45**, 7767 (2004).
130. W.F. van Gunsteren, in *Mathematical Frontiers in Computational Chemical Physics*, edited by D.G. Truhlar (Springer, New York 1988).
131. S. Blonski and W. Brostow, *J. Chem. Phys.* **95**, 2890 (1991).
132. R. Simoes, A.M. Cunha, and W. Brostow, *Model. & Simul. Mater. Sci. & Eng.* **14,** 157 (2006).
133. R. Simoes, A.M. Cunha, and W. Brostow, *Comput. Mater. Sci.* **36,** 319 (2006).

CHAPTER 42

The Emergence of a New Macromolecular Architecture: ''The Dendritic State''

Donald A. Tomalia

Dendritic Nanotechnologies, Inc., 2625 Denison Drive, Mount Pleasant, MI 48858; Central Michigan University, Mount Pleasant, MI 48859

42.1 INTRODUCTION

The seminal ''macromolecular hypothesis'' proposed by H. Staudinger nearly 85 years ago both inspired and initiated one of the most significant technology revolutions experienced during the 20th century, namely; *the polymer(plastics) revolution* [1]. In an abstract way, Staudinger's concept, which involved chemically linking (n) multiples of monomeric building blocks into a myriad of macromolecular complexity [2], may be viewed as an elegant continuation of J. Dalton's hypothesis (i.e., ''New System of Chemical Philosophy (1808)) for chemically connecting (n') multiples of atomic modules (Fig. 42.1).

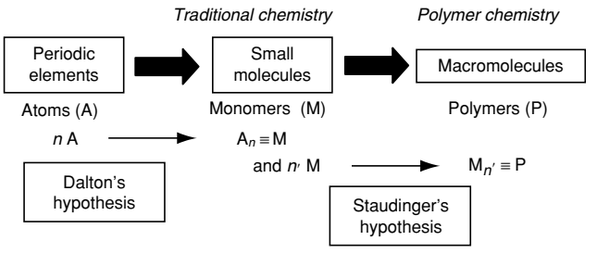

FIGURE 42.1. Historical overview of major technology revolutions "traditional chemistry" and "polymer chemistry" and associated pioneers.

This earlier concept produced the endless array of small molecules that are now recognized as our 200 year old ''traditional chemistry'' science. Although the intrinsic features of atoms or monomers as well as the rules for defining the values of (n') and (n) are most assuredly different, the enormous role that each of these technologies has played, both in the improvement of the ''human condition'' and enhancement of the world economy, is indisputable. These benefits were largely derived from unique and extraordinary ''new properties'' that emerged in each of these areas, as the technologies advanced to higher levels of complexity. A pervasive pattern that has become obvious in each of these scientific fields is the significant role that ''*architecture*'' plays in the determination of these new properties. More specifically, the importance of new macromolecular architectures has been amply recognized by a preponderance of Nobel awards associated with the discovery of such architectural features and their consequential unique properties (Fig. 42.2).

History has shown that each time a major new architecture has been discovered it has been accompanied by the emergence of a plethora of new properties, concepts, applications, products, and activities, all of which have led to enhanced new commercial markets, quality of life, and prosperity. Since the mid 1930s, four major macromolecular architectures have evolved leading to well-known classes of

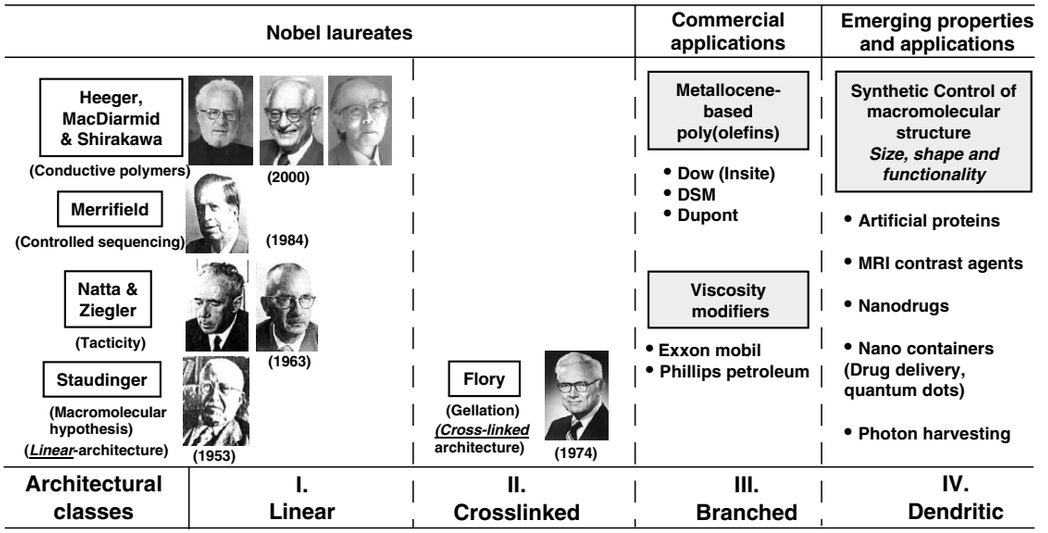

FIGURE 42.2. Nobel recognition, commercial applications/emerging properties for the four major macromolecular architectures.

thermoplastic or *thermoset* polymers, beginning with: (I) *linear*, (II) *cross-linked*, (III) *branched* and now (IV) *dendritic topologies*, as illustrated in Fig. 42.3.

42.2 HISTORICAL

42.2.1 Overview

Over the past 85 years, Staudinger's macromolecular synthesis strategy has evolved based on the catenation of reactive small molecular modules (monomers). Broadly speaking, these catenations involve the use of reactive (AB-type monomers) that may be engaged to produce large molecules with polydispersed masses. Such multiple bond formation may be driven by (a) *chain growth*, (b) *ring opening*, (c) *step-growth condensation* or (d) *enzyme catalyzed processes*. Staudinger first introduced this paradigm in the 1920s [1,3–6] by demonstrating that reactive monomers could be used to produce a statistical distribution of one-dimensional (linear) molecules with very high molecular weights (i.e., $> 10^6$ Da). As many as 10,000 or more covalent bonds may be formed in a single chain reaction of monomers. Although these macro/megamolecules may possess nanoscale dimensions, structure control of critical macromolecular design parameters, such as *size, molecular shape, spatial positioning of atoms, or covalent connectivity*—other than those affording linear or cross-linked topologies—is difficult. However, recently progress has been made using "living polymerization" techniques that afford better control over molecular weight and certain structural elements as described by Matyjaszewski and others [7,8].

$$n[\mathrm{AB}](\text{monomers}) \rightarrow [\mathrm{AB}]_n$$

Traditional polymerizations usually involve AB-type monomers based on substituted ethylenes or strained small ring compounds using chain reactions that may be initiated by free radical, anionic or cationic initiators [9]. Alternatively, AB-type monomers may be used in polycondensation reactions [9].

Multiple covalent bonds are formed to produce each macromolecule, generally giving statistical, polydispersed structures. In the case of controlled vinyl polymerizations, the average length of the macromolecule is determined by monomer to initiator ratios. If one visualizes these polymerizations as extraordinarily long sequences of individual reaction steps, the average number of covalent bonds formed/chain may be described as shown in Scheme 42.1.

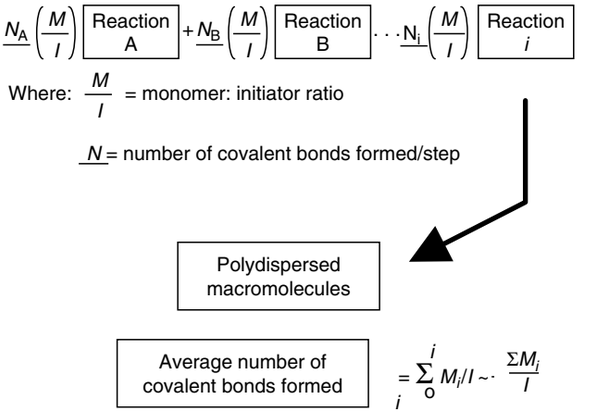

SCHEME 42.1.

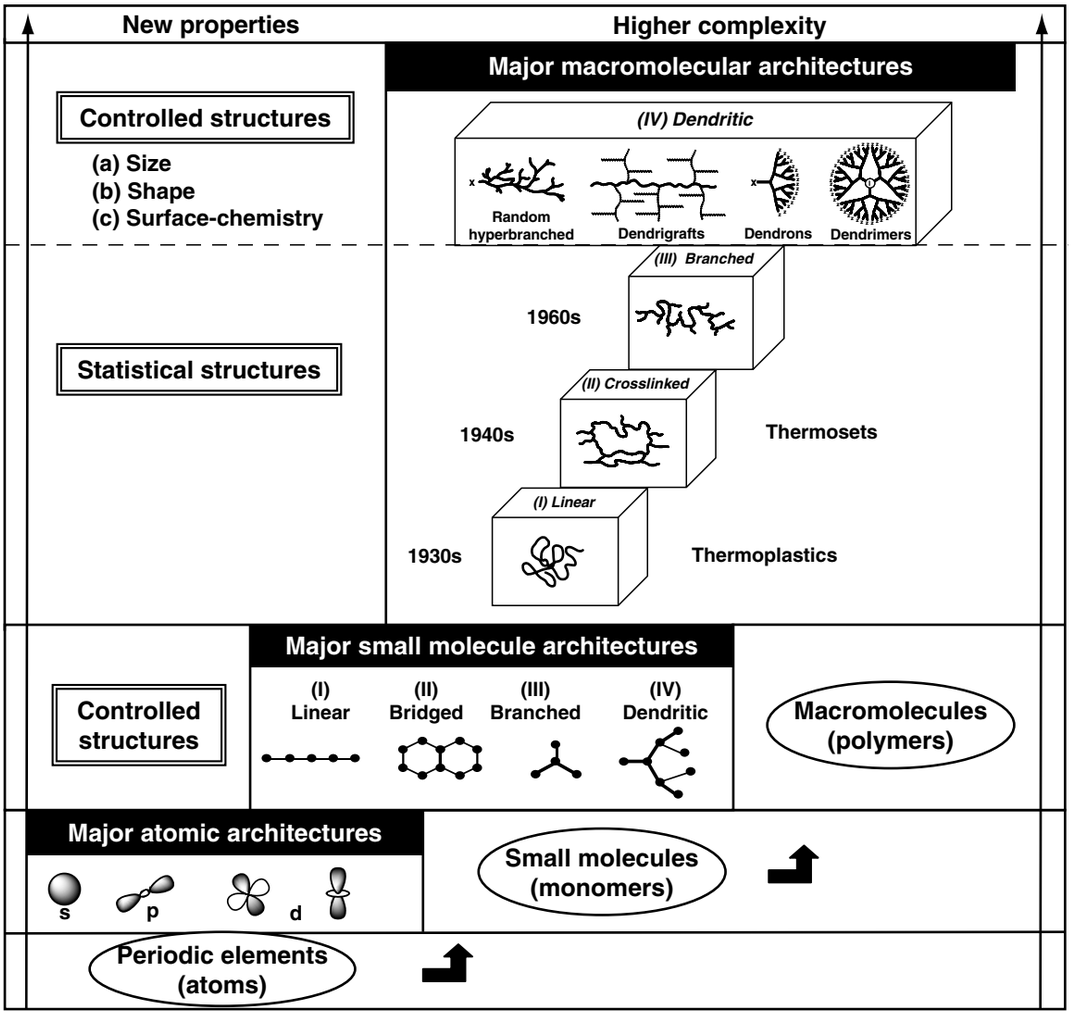

FIGURE 42.3. A comparison of major architecture for the elements (atoms), small molecules, and macromolecules (polymers) as a function of new properties and complexity.

The first traditional polymerization strategies generally produced linear architectures, however, it was soon found that branched topologies may be formed either by chain-transfer processes, or intentionally introduced by grafting techniques. In any case, the linear and branched architectural classes have traditionally defined the broad area of *thermoplastics*. Of equal importance is the major architectural class that is formed by the introduction of covalent (bridging) bonds between linear or branched polymeric topologies. These cross-linked (bridged) topologies were studied by Flory in the early 1940s and constitute the second major area of traditional polymer chemistry—namely, *thermosets*. These two broad areas of polymer science—thermoplastics and thermosets—account for billions of dollars of commerce and constitute a vast array of familiar macromolecular compositions and applications as shown in Fig. 42.4.

Historically, even 50 years after Staudinger's introduction of the ''macromolecular hypothesis,'' the entire field of polymer science was viewed to consist of only the two major architectural classes: (i) ''linear topologies'' as found in *thermoplastics* and (ii) ''cross-linked architectures'' as found in *thermosets*. The major focus of polymer science during the time frame spanning the period of the 1920s to the 1970s was on the unique architecturally driven properties manifested by either linear or cross-linked topologies. Based on the new properties exhibited by these topologies, many natural polymers critical to the World War II effort were replaced with synthetic polymers for which the combination of availability and properties were of utmost strategic importance [2]. During the 1960s and 1970s, pioneering investigation into long chain branching (LCB) involving polyolefins and other related branched systems began to emerge [10,11]. More recently, intense commercial

Thermoplastics				Thermosets			
Class I (linear)				**Class II (cross-Linked)**			
•Polymer types	Discovery	Production	Main applications	Polymer types	Discovery	Production	Main applications
•Poly(methyl methacrylate)	1880	1928	Plastics (Plexiglass®)	Phenolic resins	1907	1910	Thermosets (electrical insulators)
Poly(vinyl acetate)	1912	1930	Adhesive, poly(vinyl alcohol)	Methyl rubbers	1912	1915	Elastomers
Poly(styrene)	1839	1930	Thermoplastics, foams	Alkyl resins	1847	1926	Thermosets (coatings)
Poly(vinyl chloride)	1838	1931	Thermoplastics (synthetic fiber)	Amino resins	1915	1928	Thermosets
Poly(ethylene oxide)	—	1931	Thickeners, sizes	Poly(butadiene)	1911	1929	Elastomers (number Bunas)
Poly(vinyl ethers)	1928	1936	Adhesives, plasticizers	Poly(chloroprene)	1925	1932	Elastomers
Poly(hexamethylene adipamide)	1934	1938	Fibers, thermoplastics	Unsaturated polyesters	1930	1936	Thermosets
Poly(vinylidene chloride)	1838	1939	Thermoplastics (packing films)	Poly(isobutylene)	—	1937	Elastomers
Poly(*N*-vinyl pyrrolidone)	—	1939	Blood plasma expander, binders	Styrene–butadiene rubbers	1926	1937	Elastomers (letter Bunas)
•Poly(ethylene), low density	1933	1939	Thermoplastics				
Poly(ε-caprolactam)	1938	1939	Fibers, thermoplastics	Silicone	1901	1942	Fluids, resins, elastomers
Polyurethanes	1937	1940	Fibers, plastics, elastomers, foams	Epoxy resins	1938	1946	Adhesives
•Poly(acrylonitrile)	1940	1941	Fibers	Poly(butadiene), *cis*, 1,4	—	1956	Elastomers
Poly(tetrafluorethylene)	1939	1950	Plastics, fibers				
Poly(ethylene terephthalate)	1941	1953	Fibers, bottles				
Bisphenol A polycarbonate	1898	1953	Thermoplastics				
Poly(ethylene), high density	1953	1955	Thermoplastics, foams				
Poly(propylene), isotactic	1954	1957	Thermoplastics, fibers				
Poly(formaldehyde)	1839	1959	Thermoplastics				
Aromatic polyamides	—	1961	High modulus fibers				
Styrene–butadiene–styrene block copolymers		1965	Thermoplastic elastomers				
Class III (branched)							
Poly(olefins), long chain branching	1980s	1990s	Elastomers, plastomers				

FIGURE 42.4. Historical discovered and production dates of commercial thermoplastic and thermoset polymers organized according to their architectural class.

interest has been focused on new polyolefin architectures based on ''random long branched'' and ''dendritic topologies'' [12,13]. These architectures are reportedly produced by ''metallocene'' and ''Brookhart-type'' catalysts. By the end of the 1970s, three major architectural polymer classes and commercial commodities associated with these topologies were as described chronologically in Fig. 42.5.

42.2.2 A Comparison of Traditional Polymer Science with Dendritic Macromolecular Science

Covalent synthesis in traditional polymer science has evolved around the use of reactive modules (AB-type monomer) or ABR-type branch reagents that may be engaged in multiple covalent bond formation to produce large one-dimensional molecules of various lengths. Such multiple bond formation may be driven either by chain reactions, ring opening reactions, or polycondensation schemes. These propagation schemes and products are recognized as Class I: *Linear* or Class III: *Branched* architectures. Alternatively, using combinations and permutations of divalent A–B type monomers and/or A–B_n, A_n–B polyvalent, branch cell-type monomers produces Class II, *Cross-linked (bridged)* architectures.

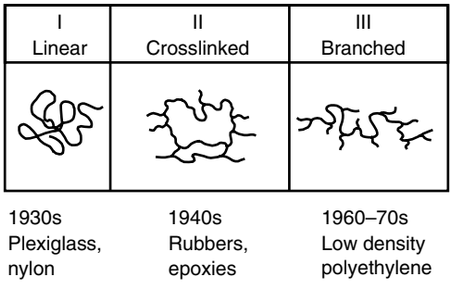

FIGURE 42.5. Traditional macromolecular architectures organized chronologically according to their commercial introduction.

A comparison of the covalent connectivity associated with each of these architecture classes (Fig. 42.6) reveals that the number of covalent bonds formed per step for linear and branched topology is a multiple (n = degree of polymerization) related to the monomer/initiator ratios. In contrast, ideal dendritic (Class IV) propagation involves the formation of an exponential number of covalent bonds per reaction step (also termed G = generation), as well as amplification of both mass (i.e., number of branch cells/G) and terminal groups, (Z) per generation (G).

Mathematically, the number of covalent bonds formed per generation (reaction step) in an ideal dendron or dendrimer synthesis varies according to a power function of the reaction steps, as illustrated below (Scheme 42.2). It is clear that covalent bond amplification occurs in all dendritic synthesis strategies. In addition to new architectural consequences, this feature clearly differentiates dendritic growth processes from covalent bond synthesis found in traditional polymer chemistry [14].

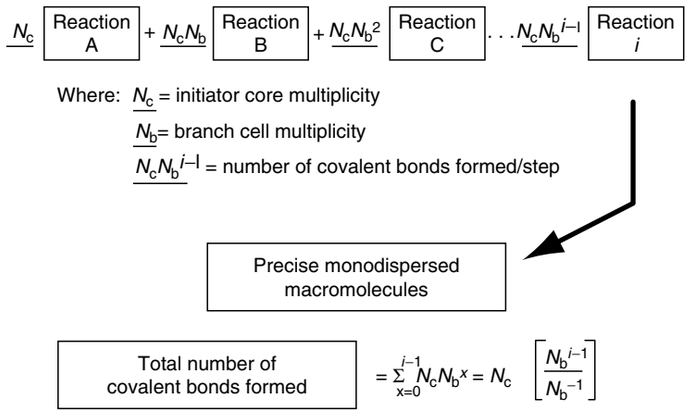

SCHEME 42.2.

It should be quite apparent that, although all major architectural polymer classes are derived from common or related repeat units, the covalent connectivity is truly discrete and different. Furthermore, mathematical analysis of the respective propagation strategies clearly illustrates the dramatic differences in structure development as a function of covalent bond formation. It should be noted that linear, branched, and dendritic topologies differ substantially both in their covalent connectivity, as well as their terminal group to initiator site ratios. In spite of these differences, these open, unlooped macromolecular assemblies clearly manifest thermoplastic polymer type behavior in contrast to the looped, bridged connectivity associated with cross-linked, thermoset systems. In fact, it is now apparent that these three ''open assembly-topologies'' (i.e., (I) linear, (III) branched, (IV) dendritic) represent a graduated continuum of architectural intermediacy between thermoplastic and thermoset behavior, as will be described later.

In summary, classical polymer science offers facile access to a vast variety of polydispersed nanoscale structures, with some control over topology, composition, flexibility, or rigidity. In the case of living polymerization strategies , increasingly better but still imperfect control over product size and mass distribution is becoming accessible. In contrast, dendritic macromolecular chemistry provides many of the required features for unparalleled control over topology, composition, size, mass, shape, and functional group placement. These are properties that truly distinguish many successful, nanostructures found in nature [15] and are of keen interest to nanoscientists [15,16].

Architectural polymer class	Polymer type	Repeat units	Covalent connectivity
(I.) *Linear*	Thermoplastic	Divalent monomers A–B	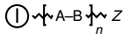
(III.) *Branched*	Thermoplastic	Divalent branch cell monomers 	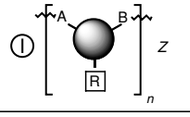
(IV.) *Dendritic*	Thermoplastic	Polyvalent branch cell monomers	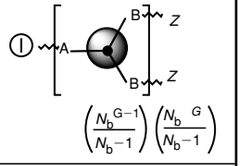
(II.) *Crosslinked (Bridged)*	Thermoset	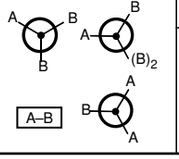	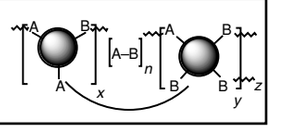

FIGURE 42.6. Examples of architectural polymer classes (I–IV) polymer type, repeat units, and covalent connectivity associated with architectural classes. (Reproduced from [88] with permission of J. Wiley & Sons.)

42.3 THE DENDRITIC STATE

42.3.1 Historical

The origins of the present three-dimensional, dendritic branching concepts can be traced back to the initial introduction of infinite network theory by Flory [17–20] and Stockmayer [21–23]. In 1943, Flory introduced the term *network cell*, which he defined as the most fundamental unit in a molecular network structure [24]. To paraphrase the original definition, *it is the recurring branch juncture in a network system as well as the excluded volume associated with this branch juncture*. Graessley [25,26] took the notion one step further by describing ensembles of these network cells as micronetworks. Extending the concept of Flory's statistical treatment of Gaussian-coil networks, analogous species that are part of an open, branched/dendritic organization are known as *branch cells* and *dendritic assemblies*.

Statistical modeling by Gordon *et al*. [27,28], Dusek [29], Burchard [30] and others reduced such branched species to graph theory designed to mimic the morphological branching of trees. These dendritic models were combined with "cascade theory" [31,32] mathematics to give a reasonable statistical treatment for network-forming events at that time.

The growth of branched and dendritic macromolecules in the sol phase of a traditional cross-linking process may be thought of as geometric aggregations of various branch cells or dendritic/ network assemblies as described above. Beginning as molecular species, they advance through the dimensional complexity hierarchy to oligomeric, macromolecular, megamolecular, and ultimately to infinite network macroscale systems. The intermediacy of dendritic architecture in this continuum will be discussed later. Traditional network-forming systems (e.g., epoxy resins, urethanes, polyesters) progress through this growth process in a statistical, random fashion. The resulting infinite networks may be visualized as a collection of unequally segmented, Gaussian chains between *f*-functional branch junctures, cross-links (loops), and dangling terminal groups.

More recently, nontraditional polymerization strategies have evolved to produce a fourth new major polymer architectural class, now referred to as *dendritic polymers*. This new architectural polymer class consists of four major subsets, namely: (a) *random hyperbranched*, (b) *dendrigrafts*, (c) *dendrons*, and (d) *dendrimers*. Dendrimers, the most extensively studied subset, were discovered by the Tomalia group while at The Dow Chemical Company laboratories (1979). They represent the first example of synthetic, macromolecular dendritic architecture [33,34]. First use of the term "dendrimer" appeared in preprints for the 1st SPSJ International Polymer Conference held in Kyoto, Japan (1984). The following year, a full article (*Polymer Journal*, Vol. 17, No. 1, pp. 117–132 (1985)) (see article abstract, Fig. 42.7) described the first preparation of a complete family of

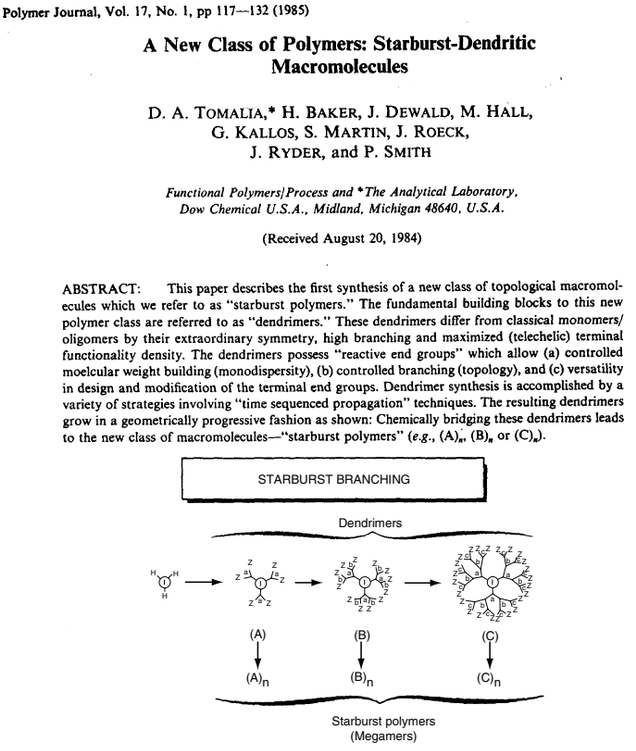

Polymer Journal, Vol. 17, No. 1, pp 117—132 (1985)

A New Class of Polymers: Starburst-Dendritic Macromolecules

D. A. TOMALIA,* H. BAKER, J. DEWALD, M. HALL,
G. KALLOS, S. MARTIN, J. ROECK,
J. RYDER, and P. SMITH

*Functional Polymers/Process and *The Analytical Laboratory, Dow Chemical U.S.A., Midland, Michigan 48640, U.S.A.*

(Received August 20, 1984)

ABSTRACT: This paper describes the first synthesis of a new class of topological macromolecules which we refer to as "starburst polymers." The fundamental building blocks to this new polymer class are referred to as "dendrimers." These dendrimers differ from classical monomers/oligomers by their extraordinary symmetry, high branching and maximized (telechelic) terminal functionality density. The dendrimers possess "reactive end groups" which allow (a) controlled moelcular weight building (monodispersity), (b) controlled branching (topology), and (c) versatility in design and modification of the terminal end groups. Dendrimer synthesis is accomplished by a variety of strategies involving "time sequenced propagation" techniques. The resulting dendrimers grow in a geometrically progressive fashion as shown: Chemically bridging these dendrimers leads to the new class of macromolecules—"starburst polymers" (*e.g.*, $(A)_n$, $(B)_n$ or $(C)_n$).

FIGURE 42.7. Abstract of the first full article describing the synthesis of a complete family of Tomalia-type PAMAM dendrimers.

Tomalia-type poly(amidoamine) (PAMAM) dendrimers and their use as precise, fundamental building blocks to form poly(dendrimers) or so-called ''starburst polymers.'' These poly(dendrimers) are now referred to as *megamers* [35,36] and are described in more detail later. Other pioneers in the ''dendritic polymer'' field include Vogtle, Newkome, Frechet, and others. These historical contributions have been reviewed recently [33].

This article will overview the ''dendritic architectural state,'' its unique architecturally driven properties, its role relative to traditional polymer science as well as describe the many enabling features that dendrimers are expected to offer to the emerging nanotechnology revolution.

42.3.2 A Fourth Major New Architectural Polymer Class

Dendritic topology has now been recognized as a fourth major class of macromolecular architecture [33,37–39]. The signature for such a distinction is the unique repertoire of new properties manifested by this class of polymers [40–45]. Numerous synthetic strategies have been reported for the preparation of these materials, and have led to a broad range of dendritic structures. Presently, this architectural class consists of four dendritic subclasses; namely, (IVa) *random hyperbranched polymers*, (IVb) *dendrigraft polymers* and (IVc) *dendrons/dendrimers* (Fig. 42.8). The order of this subset, from a to c, reflects the relative degree of structural control present in each of these dendritic architectures.

All dendritic polymers are open covalent assemblies of branch cells. They may be organized as very symmetrical, monodispersed arrays, as is the case for dendrimers, or as irregular polydispersed assemblies that typically define random hyperbranched polymers. As such, the respective subclasses and the level of structure control are defined by the propagation methodology used to produce these assemblies, as well as by the branch-cell (BC) construction parameters. The BC parameters are determined by the composition of the BC monomers, as well as the nature of the ''excluded volume'' defined by the BC. The excluded volume of the BC is determined by the length of the arms, the symmetry, rigidity/flexibility, as well as the branching and rotation angles involved within each of the branch-cell domains. As shown in Fig. 42.8 these dendritic arrays of branch cells usually manifest covalent connectivity relative to some molecular reference marker (I) or core. As such,

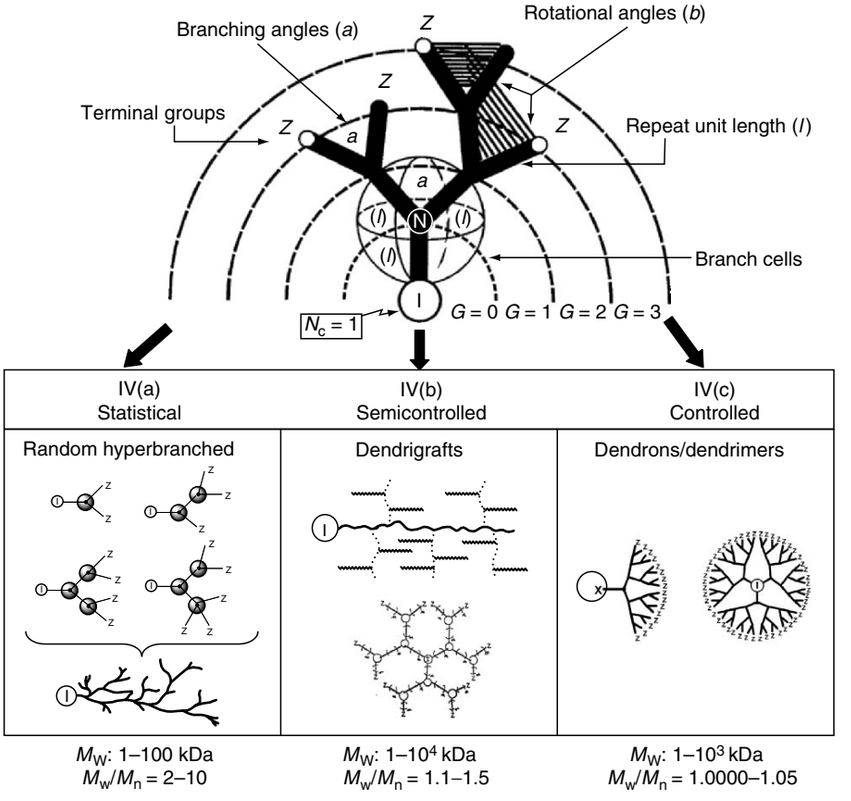

FIGURE 42.8. Branch cell structural parameters (*a*) branching angles, (*b*) rotation angles, (*l*) repeat unit lengths, (*Z*) terminal groups, and dendritic subclasses derived from branches (IVa) random hyperbranched, (IVb) dendrigrafts, and (IVc) dendrons/dendrimers.

these branch-cell arrays may be very nonideal and polydispersed (e.g., $M_w/M_n \cong 2–10$), as observed for random hyperbranched polymers (IVa), or very ideally organized into highly controlled core–shell type structures as noted for dendrons/dendrimers (IVc): $M_w/M_n \cong 1.01–1.0001$ and less. Dendrigraft (arborescent) polymers reside between these two extremes of structure control, frequently manifesting rather narrow polydispersities of $M_w/M_n \cong 1.1–1.5$, depending on their mode of preparation.

42.3.3 Dendritic Polymer Subclasses

Random Hyperbranched Polymers

Flory first hypothesized dendritic polymer concepts [18,20], which are now recognized to apply to statistical, or random hyperbranched polymers. However, the first experimental confirmation of dendritic topologies did not produce random hyperbranched polymers but rather the more precise, structure-controlled, dendrimer architecture [33,34,46,47]. This work was initiated nearly a decade before the first examples of random hyperbranched polymers were confirmed independently by Gunatillake *et al*. [48] and by Kim and Webster [49,50] in 1988. At that time, Kim and Webster coined the popular term ''hyperbranched polymers'' that has been widely used to describe this subclass of dendritic macromolecules. Hyperbranched polymers are typically prepared by polymerization of AB_x monomers. When x is 2 or more, polymerization of such monomers gives highly branched polymers (Figs. 42.3 and 42.8), as long as A reacts only with B from another molecule. Reactions between A and B from the same molecule result in termination of polymerization by cyclization. This approach produces hyperbranched polymers with a degree of polymerization n, possessing one unreacted A functional group and $[(x-1)_n + 1]$ unreacted B terminal groups. In a similar fashion, copolymerization of A_2 and B_3 or other such polyvalent monomers can give hyperbranched polymers [51,52], if the polymerization is maintained below the gel point by manipulating monomer stoichiometry or limiting polymer conversion. Random hyperbranched polymers are generally produced by the one-pot polymerization of AB_x-type monomers or macromonomers involving polycondensation, ring opening, or polyaddition reactions. Hence, the products usually have broad, statistical molecular-weight distributions, much as is observed for traditional polymers. Over the past decade, literally dozens of new AB_2-type monomers have been reported leading to an enormously diverse array of hyperbranched structures. Some general types include poly(phenylenes) obtained by the Suzuki coupling [49,50]; poly(phenylacetylenes) prepared by the Heck reaction [53]; polycarbosilanes, polycarbosiloxanes [54], and poly(siloxysilanes) by hydrosilylation [55]; poly(ether ketones) by nucleophilic aromatic substitution [56]; and polyesters [57] or polyethers [58] by polycondensations or by ring-opening polymerization [59].

New advances beyond the traditional AB_2 Flory-type, branch-cell monomers have been reported by Fréchet and coworkers [60,61]. They have introduced the concept of latent AB_2 monomers, referred to as self-condensing vinyl polymerizations (SCVP). These monomers, which possess both initiation and propagation properties, may follow two modes of polymerization; namely, polymerization of the double bond (i.e., chain growth) and condensation of the initiating group with the double bond (i.e., step growth). Recent progress involving the derivative process of self-condensing, ring-opening polymerizations (SCROP) has been reviewed by Sunder *et al*. [62] In addition, the use of enhanced processing techniques, such as pseudochain growth by slow monomer addition [63], allow somewhat better control of hyperbranched structures [62].

Dendrigraft Polymers

Dendrigraft polymers are the most recently discovered and currently the least understood subset of dendritic polymers. The first examples were reported in 1991 independently by Tomalia *et al*. [64] and Gauthier and Möller [65]. Whereas, traditional monomers are generally employed in constructing dendrimers, reactive oligomers or polymers are used in protect–deprotect or activation schemes to produce dendrigrafts. Consequently, dendrigraft polymers are generally larger structures than dendrimers, grow much faster, and amplify surface groups more dramatically as a function of generational development. Both hydrophilic (e.g., poly(oxazolines) and poly(ethyleneimines)) and hydrophobic dendrigrafts (e.g., polystyrenes) were reported in these early works. These first methodologies involved the iterative grafting of oligomeric reagents derived from living polymerization processes in various iterative *graft-on-graft* strategies. By analogy to dendrimers, each iterative grafting step is referred to as a generation. An important feature of this approach is that branch densities, as well as the size of the grafted branches can be varied independently for each generation. Furthermore, by initiating these iterative grafting steps from a point-like core versus a linear core it is possible to produce spheroidal and cylindrical dendrigrafts, respectively. Depending on the graft densities and molecular weights of the grafted branches, ultrahigh molecular-weight dendrigrafts (e.g., $M_w > 104\,\text{kDa}$) can be obtained at very low generation levels (e.g., $G = 3$). Dramatic molecular-weight enhancements vis-à-vis other dendrimer propagation methodologies are possible using dendrigraft techniques [66]. Further elaboration of these dendrigraft principles allowed the synthesis of a variety of core–shell-type dendrigrafts, in which elemental composition as well as the hydrophobic or hydrophilic character of the core were controlled independently [65].

In general, the above methodologies have involved convergent-type grafting principles, wherein preformed, reactive oligomers are grafted onto successive branched precursors to produce semicontrolled structures. Compared to dendrimers, dendrigraft structures are less controlled since grafting may occur along the entire length of each generational branch, and the exact branching densities are somewhat arbitrary and difficult to control. More recently, both Gnanou [67,68] and Hedrick [69,70] have developed approaches to dendrigrafts that mimic dendrimer topologies by confining the graft sites to the branch termini for each generation. These methods involve so-called *graft* from techniques, and allow better control of branching topologies and densities as a function of generation. Topologies produced by these methods are reminiscent of the dendrimer architecture. Since the branch-cell arms are derived from oligomeric segments, they are referred to as polymeric dendrimers [10,69,70]. These more flexible and extended structures exhibit unique and different properties as compared to the more compact traditional dendrimers. Fréchet, Hawker, and coworkers [71] have utilized the techniques of living polymerization and a staged polymerization process—in which latent polymerization sites are incorporated within growing chains—to produce dendrigrafts of mixed composition and narrow polydispersity.

Another exciting development has been the emerging role that dendritic architecture is playing in the production of commodity polymers. A recent report by Guan *et al*. [12] has shown that ethylene polymerizes to *dendrigraft*-poly ethylene at low pressures in contrast to high-pressure conditions, which produce only branched topologies. This occurs when using late-transition metal or Brookhart catalysts. Furthermore, these authors also state that small amounts of *dendrigraft*-poly(ethylene) architecture may be expected from analogous early-transition-metal metallocene catalysts.

Dendrons and Dendrimers

Dendrons and dendrimers are the most intensely investigated subset of dendritic polymers. In the past decade, over 6,000 literature references have appeared dealing with this unique class of structure-controlled polymers. The word dendrimer is derived from the Greek words *dendri-* (tree branch-like) and *meros* (part of), and was coined by Tomalia *et al*. about 20 years ago in the first full paper on poly (amidoamine) (PAMAM) dendrimers [47,72]. Since this early disclosure, over 100 dendrimer compositions (families) and 1,000 dendrimer surface modifications have been reported. The two most widely studied dendrimer families are the Fréchet-type polyether compositions and the Tomalia-type PAMAM dendrimers. PAMAM dendrimers constitute the first dendrimer family to be commercialized, and represent the most extensively characterized and best-understood series at this time [46].

In view of the vast amount of literature in this field, the remaining overview will focus on PAMAM dendrimers. Its scope will be limited to a discussion of their critical properties and unique quantized nanomodule features that make these materials very suitable for nanoscale synthesis and manipulations.

Dendrimer Synthesis: Divergent and Convergent Methods

In contrast to traditional polymers, dendrimers are unique core–shell structures possessing three basic architectural components: a core (I), an interior of shells (generations) consisting of repeating branch-cell units (II), and terminal functional groups (the outer shell or periphery) (III). In general, dendrimer synthesis involves divergent or convergent hierarchical assembly strategies that require the construction components shown in Scheme 42.3. Within each of these major approaches there may be variations in methodology for branch-cell construction or dendron construction. Many of these issues, together with experimental laboratory procedures, have been reviewed elsewhere [73–75].

PAMAM dendrimers are synthesized by the divergent approach. This methodology involves in situ branch-cell construction in stepwise, iterative stages around a desired core to produce mathematically defined core–shell structures. Typically, ethylenediamine [core multiplicity (N_c) = 4], ammonia ($N_c = 3$), or cystamine ($N_c = 4$) may be used as cores and allowed to undergo reiterative, two-step reaction sequences. These sequences consist of: (a) an exhaustive alkylation of primary amines (Michael addition) with methyl acrylate and (b) amidation of amplified ester groups with a large excess of ethylenediamine to produce primary amine terminal groups (Scheme 42.4). This first reaction sequence on the exposed core creates $G = 0$ (i.e., the core branch cell), wherein the number of arms (i.e., dendrons) anchored to the core is determined by N_c. Iteration of the alkylation–amidation sequence produces an amplification of terminal groups from 1 to 2 with the in situ creation of a branch cell at the anchoring site of the dendron that constitutes $G = 1$. Repeating these iterative sequences (Scheme 42.4) produces additional shells (generations) of branch cells that amplify mass and terminal groups according to the mathematical expressions described in the box (Fig. 42.9). It is apparent that both the core multiplicity (N_c) and branch-cell multiplicity (N_b) determine the precise number of terminal groups (Z) and mass amplification as a function of generation (G). One may view those generation sequences as quantized polymerization events. The assembly of reactive monomers [34,76], branch cells [42,46,77] or dendrons [46,78,79] around atomic or molecular cores, to produce dendrimers according to divergent or convergent dendritic branching principles, has been well demonstrated. Such systematic filling of molecular space around cores with branch cells as a function of generational growth stages (branch-cell shells)—to

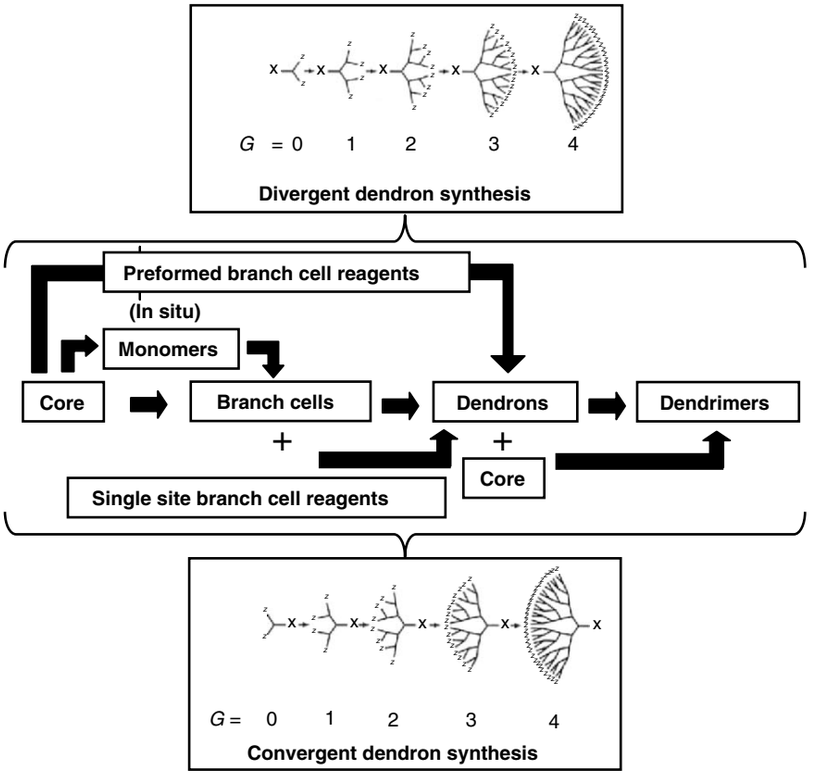

SCHEME 42.3. Hierarchical assemble scheme illustrating the options for constructing dendrimers by either divergent or convergent synthetic strategies.

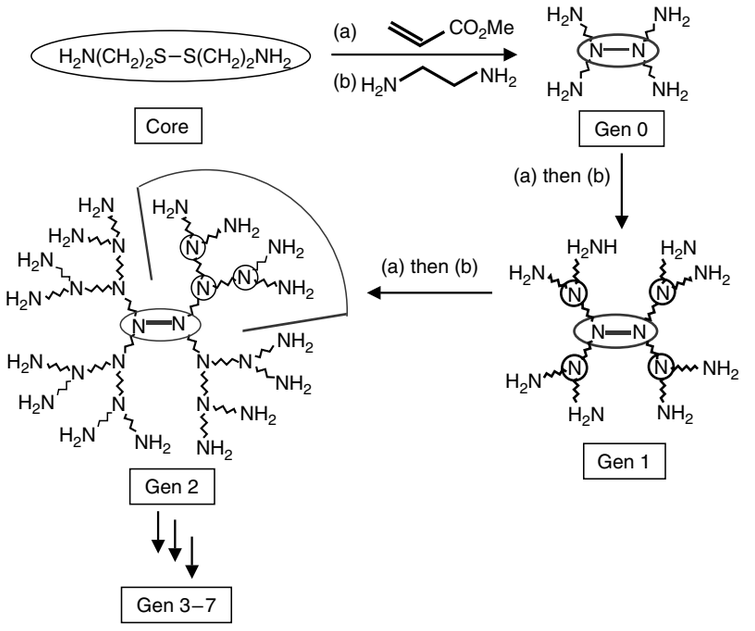

SCHEME 42.4. Divergent synthesis of [cystamine] *dendri*-PAMAM dendrimers utilizing the iterative sequence: (a) alkylation with methyl acrylate, followed by (b) amidation with excess ethylenediamine to produce generations 3–7.

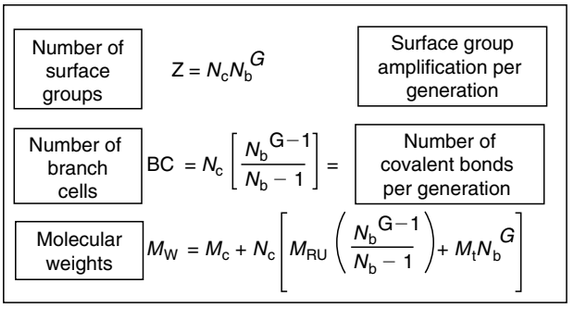

FIGURE 42.9. Mathematical expressions for calculating the theoretical number of surface groups (Z), branch cells (BC) and molecular weights (MW) as a function of generation, N_c = core multiplicities and N_b = branch cell multiplicity.

give discrete, quantized bundles of nanoscale mass—has been shown to be mathematically predictable [14,80,81]. Predicted molecular weights have been confirmed by mass spectrometry [82–85] and other analytical methods [42,78,86,87]. Predicted numbers of branch cells, terminal groups (Z), and molecular weights as a function of generation for a cystamine-core ($N_c = 4$) PAMAM dendrimer are shown in Fig. 42.10. It should be noted that the molecular weights approximately double as one progresses from one generation to the next. The surface groups (Z) and branch cells (BC) amplify mathematically according to a power function, thus producing discrete, monodispersed structures with precise molecular weights and a nanoscale diameter enhancement as described in Fig. 42.10. These predicted values are routinely verified by mass spectrometry for the earlier generations (i.e., $G = 4$–5); however, with divergent dendrimers, minor mass defects are often observed for higher generations as congestion-induced *de Gennes dense packing* begins to take effect [42,88].

Dendrimer Features of Interest to Nanoscientists

Dendrimers may be thought of as unique nanoscale devices [16,89]. Each architectural component manifests a specific function while at the same time defining properties for these nanostructures as they are grown generation by generation. For example, the *core* may be thought of as the molecular information center from which *size*, *shape*, *directionality, and multiplicity* are expressed *via* the covalent connectivity to the outer shells. Within the *interior*, one finds the *branch-cell amplification region*, which defines the type and amount of interior void space that may be enclosed by the terminal groups as the dendrimer is grown. Branch-cell multiplicity (N_b) determines the density and degree of amplification as an exponential function of generation (G). The interior composition and amount of solvent filled void space determines the extent and nature of guest–host (endoreceptor) properties that are possible with a particular dendrimer family and generation. Finally, the surface consists of reactive or passive terminal groups that may perform several functions. With appropriate function, they serve as a *template polymerization region* as each generation is amplified and covalently attached to the precursor generation. Secondly, the surface groups may function as passive or reactive gates controlling control entry or departure of guest molecules from the dendrimer interior. These three architectural components essentially determine the physicochemical properties, as well as the overall sizes, shapes, and flexibility of dendrimers. It is important to note that dendrimer diameters increase linearly as a function of shells or generations added; whereas, the terminal functional groups increase exponentially as a function of generation. This dilemma enhances ''tethered congestion'' of the anchored dendrons, as a function of generation, due to the steric crowding of the end groups. As a consequence, lower generations are generally open, floppy structures; whereas, higher generations become robust, less deformable spheroids, ellipsoids or cylinders depending on the shape and directionality of the core (Fig. 42.11).

Dendrimer Shape Changes

As illustrated in Fig. 42.12, dendrimers undergo ''congestion induced'' molecular shape changes from flat, floppy conformations to robust spheroids as first predicted by Goddard *et al*. [76]. Shape change transitions were subsequently confirmed by extensive photophysical measurements, pioneered by Turro *et al*. [90–93] and solvatochromic measurements by Hawker, Wooley, and Fréchet [94]. Depending upon the accumulative core and branch-cell multiplicities of the dendrimer family under consideration, these transitions were found to occur between $G = 3$ and $G = 5$. Ammonia core, PAMAM dendrimers ($N_c = 3$, $N_b = 2$) exhibited a molecular morphogenesis break at $G = 4.5$; whereas, the ethylenediamine (EDA) PAMAM dendrimer family ($N_c = 4$, $N_b = 2$) manifested a shape change break around $G = 3$–4 [76] and the Fréchet-type convergent dendrons ($N_b = 2$) around $G = 4$ [94]. It is readily apparent that increasing the core multiplicity to $N_c = 4$ accelerates congestion and forces a shape change at least one generation earlier. Beyond these generational transitions, one can visualize these dendrimeric shapes as nearly spheroidal or slightly ellipsoidal *core–shell type architecture*.

Gen	No. of NH_2 surface groups	Molecular formula	MW	Hydrodynamic diameter (nm)
0	4	$C_{24}H_{52}N_{10}O_4S_2$	609	1.5
1	8	$C_{64}H_{132}N_{26}O_{12}S_2$	1,522	2.2
2	16	$C_{144}H_{292}N_{58}O_{28}S_2$	3,348	2.9
3	32	$C_{304}H_{612}N_{122}O_{60}S_2$	7,001	3.6
4	64	$C_{624}H_{1252}N_{250}O_{124}S_2$	14,307	4.5
5	128	$C_{1264}H_{2532}N_{506}O_{252}S_2$	28,918	5.4
6	256	$C_{2544}H_{5092}N_{1018}O_{508}S_2$	58,140	6.7
7	512	$C_{5104}H_{10212}N_{2042}O_{1020}S_2$	116,585	8.1

Z = monomer-shell-saturation level, N_c = core (cystamine) multiplicity, N_b = branch-cell (BC) multiplicity, G = generation.

FIGURE 42.10. Approximate hydrodynamic diameters (Gen $= 0-7$) based on gel electrophoretic comparison with the corresponding [ethylenediamine core]-PAMAM dendrimers.

De Gennes Dense Packing

As a consequence of the excluded volume associated with the core, interior, and surface branch cells, steric congestion is expected to occur due to tethered connectivity to the core. Furthermore, the number of dendrimer surface groups, Z, amplifies with each subsequent generation (G). This occurs according to geometric *branching laws*, which are related to core multiplicity, (N_c) and branch-cell multiplicity (N_b). These values are defined by the following equation:

$$Z = N_c N_b^G.$$

Since the radii of the dendrimers increase in a linear manner as a function of G, whereas, the surface cells amplify according to $N_c N_b^G$, it is implicit from this equation that generational reiteration of branch cells ultimately will lead to a so-called ''dense-packed state.''

As early as 1983, de Gennes and Hervet [95] proposed a simple equation derived from fundamental principles, to predict the dense-packed generation, for Tomalia-type PAMAM dendrimers. It was predicted that at this generation ideal branching can no longer occur since available surface space becomes too limited for the mathematically predicted number of surface cells to occupy. This produces a ''closed geometric structure.'' The surface is ''crowded'' with exterior groups, which although potentially chemically reactive, are sterically prohibited from participating in ideal dendrimer growth.

This ''critical packing state'' does not preclude further dendrimer growth beyond this point in the genealogical history of the dendrimer preparation. On the contrary, although continuation of dendrimer step-growth beyond the dense-packed state cannot yield structurally ideal, next generation dendrimer, it can nevertheless occur, as indicated by further increases in the molecular weight of the resulting products. Predictions by de Gennes [95] suggested that the Tomalia-type PAMAM dendrimer series should reach a critical packing state at generations 9–10. Experimentally, we observed a moderate molecular weight deviation from predicted ideal values beginning at generation 4–7. This digression became very significant at generation 7–8 as dendrimer growth was continued to generations 12 [96]. The products thus obtained are of ''imperfect'' structure because of the inability of all surface groups to undergo further reaction. Presumably a fraction of these surface groups remain trapped under the surface of the newly formed dendrimer

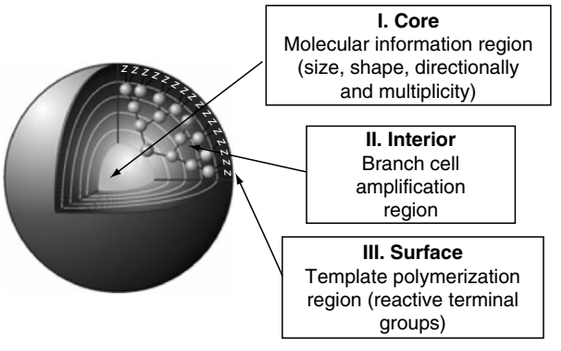

FIGURE 42.11. Three-dimensional projection of dendrimer core-shell architecture for $G = 4.5$ poly(amidoamine) (PAMAM) dendrimer with principal architectural components (I) core, (II) interior and (III) surface.

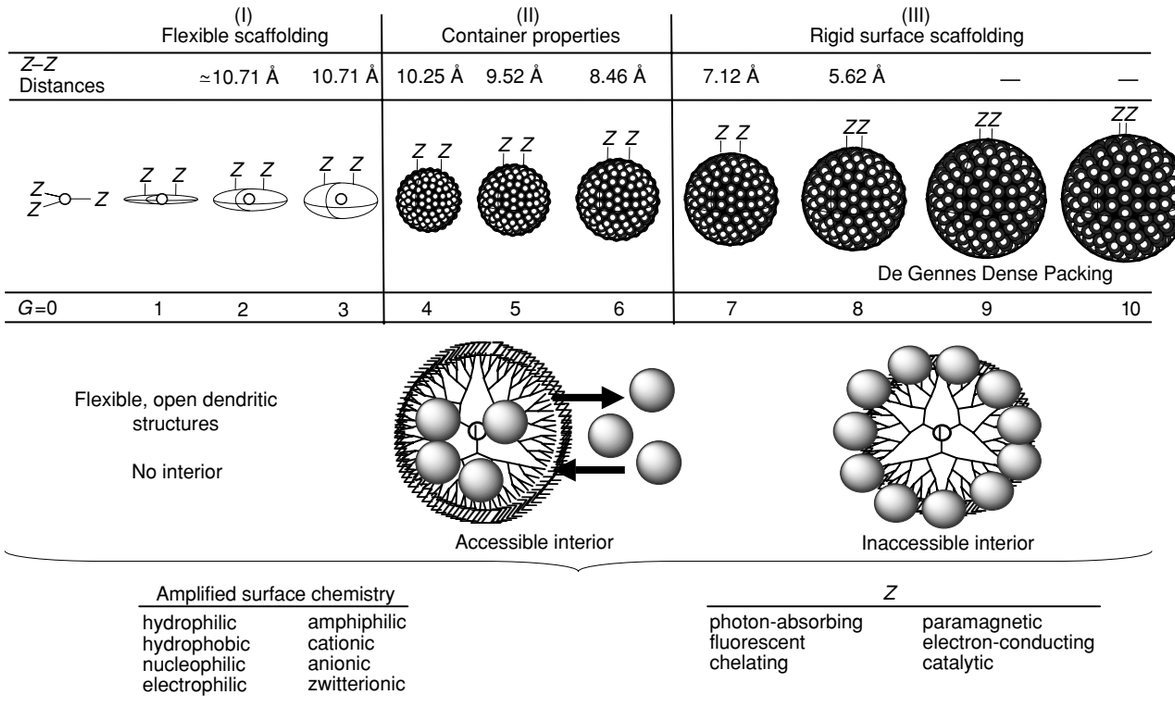

FIGURE 42.12. Periodic properties of PAMAM dendrimers as a function of generation. Various chemophysical dendrimer surfaces amplified according to $Z = N_c N_b^G$, where N_c = core multiplicity, N_b = branch-cell multiplicity and G = generation. (Reproduced from [88] with permission of J. Wiley & Sons.)

shell, yielding a unique architecture possessing two types of terminal groups. This new surface group population will consist of both those that are accessible to subsequent reiteration reagents and those that will be sterically screened. The total number of these groups will not, however, correspond to the predictions of the mathematical branching law, but will fall between that value, which was mathematically predicted for the next generations (i.e., $G + 1$), and that expected for the precursor generation (G). Thus, a mass defective dendrimer ''generation'' is formed.

Dendrimer surface congestion can be appraised mathematically as a function of generation, from the following simple relationship:

$$A_z = \frac{A_D}{N_Z} \alpha \frac{r^2}{N_c N_b^G}$$

where A_z is the surface area per terminal group Z, A_D the dendrimer surface area, and N_z the number of surface groups Z per generation. This relationship predicts that at higher generations G, the surface area per Z group becomes increasingly smaller and experimentally approaches the cross-sectional area or van der Waals dimension of the surface groups Z. The generation G thus reached is referred to as the ''*de Gennes'' dense-packed generation*. Ideal dendritic growth without branch defects is possible only for those generations preceding this dense-packed state. This critical dendrimer property gives rise to self-limiting dendrimer dimensions, which are a function of the branch-cell segment length (l), the core multiplicity N_c, the branch-cell juncture multiplicity N_b, and the steric dimensions of the terminal group Z. Whereas, the dendrimer radius r in the above expression is dependent on the branch-cell segment lengths l, large l values delay this congestion. On the other hand, larger N_c, N_b values and larger Z dimensions dramatically hasten it.

Additional physical evidence supporting the anticipated development of congestion as a function of generation is shown in the composite comparison in Fig. 42.13. Plots of intrinsic viscosity [η], density z, surface area per Z group (A_z), and refractive index n as a function of generation clearly show maxima or minima at generations = 3–5, paralleling computer-assisted molecular-simulation predictions [76] as well as extensive photochemical probe experiments reported by Turro *et al*. [90–93].

The intrinsic viscosities [η] is expected to increase in a very classical fashion as a function of molar mass (generation) but should decline beyond a certain generation because of a change from an extended to a globular shape [42]. In effect, once this critical generation is reached, the dendrimer begins to act more like an Einstein spheroid. The intrinsic viscosity is a physical property that is expressed in dL/g—the ratio of a volume to a mass. As the generation

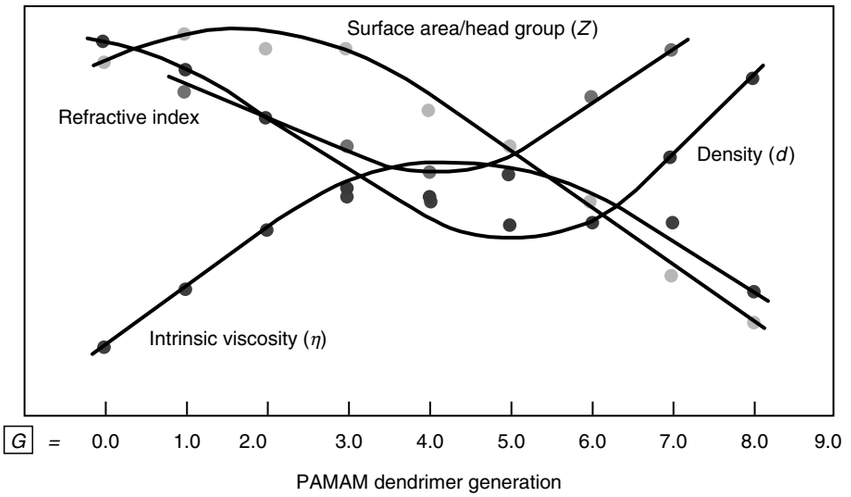

FIGURE 42.13. Comparison of surface area/head group (Z), refractive index, density (d) and intrinsic viscosity (η) as a function of generation: $G = 1-9$. (Reproduced from [88] with permission of J. Wiley & Sons.)

number increases and transition to a spherical shape takes place, the volume of the spherical dendrimer roughly increases in cubic fashion while its mass increases exponentially, hence the value of $[\eta]$ must decrease once a certain generation is reached. This prediction has now been confirmed experimentally [97].

The dendrimer density z (atomic mass units per unit volume) clearly minimizes between generations 4 and 5, then begins to increase as a function of generation due to the increasingly larger, exponential accumulation of surface groups. Since refractive indices are directly related to density parameters, their values minimize and parallel the above density relationship.

Clearly, this de Gennes dense packed congestion would be expected to contribute to (a) sterically inhibited reaction rates and (b) sterically induced stoichiometry [42]. Each of these effects was observed experimentally at higher generations. The latter would be expected to induce dendrimer mass defects at higher generations which we have used as a diagnostic signature for appraising the ''de Gennes dense packing'' effect. These issues have been reviewed extensively elsewhere [36,46].

42.3.4 New Properties Driven by the Dendritic State

Throughout much of the early growth and evolution of polymer science, the quest for new properties was focused primarily on the two traditional architectures that defined thermoplastic (linear) and thermoset (cross-linked polymers). Within each of these areas, there was intense activity to evaluate and optimize certain critical parameters. These parameters included various macromolecular chemical compositions, copolymer compositions, molecular weight effects, molecular weight distributions, and cross-link densities, just to mention a few. Relatively little attention was given to the influence of architecture until the 1970s and 1980s. During that time, the first stirring of interest began concerning the influence of long chain branching on polymer properties [10]. Significant activity ensued thereafter, as it became apparent that single site metallocene/Brookhart catalysts were producing unique poly(olefin) families with completely new, commercially valuable properties [12,13]. It is now recognized that both branched and dendritic architecture, in addition to molecular weight control, are key parameters influencing these new properties. These successful commercial developments, together with the rapid evolution of many new synthetic strategies to branched and dendritic architectures, have intensified the interest that macromolecular architecture may offer for the discovery of new properties.

Comparison of Traditional Linear Polymer and Dendritic Polymer Properties

The affect of architecture on small molecular properties has been recognized since the historical Berzelius (1832) discovery that defined the following premise: *substances of identical compositions but different architectures—''skeletal isomers''—will differ in one or more properties* [98]. These effects are very apparent when comparing the fuel combustion benefits of certain isomeric octanes or the dramatic property differences observed in the three architectural isomers of carbon; namely: graphite, diamond, and buckminsterfullerene (Fig. 42.3).

Similar patterns of property differentiation are clearly recognized at the macromolecular level. For example, dramatic changes in physical and chemical properties are observed by simply converting a linear topology of common

composition to a cross-linked architecture. In traditional macromolecular science, these issues were considered apparent and obvious. However, as novel architectures emerged, new architecture–property relationships have not been so clearly articulated and exploited. Prompted by the synthetic accessibility of many new polymeric architectures based on common compositional monomers (i.e., branch-cell monomers), this perspective was more clearly defined as early as 1994 in experiments by Fréchet and coworkers aimed at determining the influence of shape on the reactivity and physical properties of a series of comparable macromolecules including a dendrimer, a random hyperbranched polymer, and a linear aromatic polyesters all obtained from analogous building blocks [99]. This work clearly demonstrated the very significant shape-related changes in chemical reactivity as well as solubility that exist for polymers possessing the same average molecular weight and composition but differ only in their architecture and polydispersity. Following this report Tomalia introduced in 1996 the concept of ''macromolecular (architectural) isomerism.'' Simply stated—''macromolecular substances derived in the same proportions from the same monomer compositions, but in different architectural (configurations) will be expected to manifest different chemo/physical properties'' [100,101]. This hypothesis proposed a unique strategy for obtaining new polymeric properties by simply converting cost-effective traditional monomers into new macromolecular topologies (architectures). In 1997 Hawker *et al*. [102] provided the ultimate validation of this concept by preparing exact, size monodisperse, linear, and dendritic polyethers analogs with the same composition. Their study revealed significant physical property differences between the two ''architectural isomers'' confirming the earlier work of Fréchet and coworkers [99]. Most notable were substantially smaller hydrodynamic volumes (i.e., 40% smaller), as well as amorphous character (i.e., significantly more solvent soluble) for the dendritic isomers compared to the linear analog.

Parallel studies on Tomalia type PAMAM dendrimers, the Fréchet type poly(ether)dendrons, and other dendrimer families have generated an extensive list of unique properties driven by the ''dendritic state.'' Figure 42.14 compares several significant physical property differences between the linear and dendritic topologies related to conformations, crystallinity, solubilities, intrinsic viscosities, entanglement, diffusion/mobility, and electronic conductivity.

In contrast to linear polymers, that obey the Mark–Houwink–Sakurada equation, the intrinsic viscosities of dendrimers do not increase continuously with molecular weight, but reach a maximum at a certain dendrimer generation. These maxima were predicted by Tomalia *et al*. for poly(amidoamine) dendrimers [42] and later measured for poly(arylethers) [97], as well as for poly(propyleneimine) dendrimers [103], thus indicating they were not composition dependent. This property is presumably due to the fact that the dendrimer structure becomes spherical at a specific generation level due to tethered congestion , hence its volume grows by a first approximation as n^3, whereas, mass grows as 2^n (where $n =$ generation number). Since the intrinsic viscosity $[\eta]$ is expressed in volume per mass, the quotient of the foregoing volumes and mass functions is indeed expected to display a maximum. A study of the melt viscosity of convergently grown Fréchet-type polyether dendrimers [61] also demonstrated this unique behavior, quite unlike that of comparable linear polymers. It is clear that the lack of entanglement of globular dendrimers—another attribute of the dendritic state—is largely responsible for the most unusual dendritic melt viscosity behavior [61,104,105].

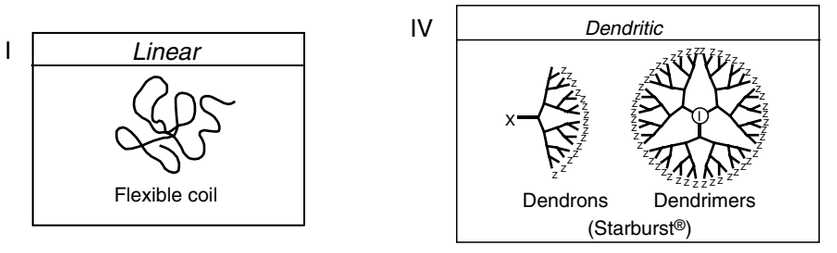

Linear

1. Random coil configurations
2. Semicrystalline/crystalline materials
   -higher glass temperatures
3. Lower solubility
   -decreases with Mwt.
4. Intrinsic viscosity follows logarithmic
   -increase with Mwt.
5. Entanglement directed rheological properties
   -shear sensitivity
6. Mobility by reptation
   -segmental and molecular mobility
7. Anisotropic electronic conductivity

Dendritic

1. Predictable shape changes as a function of Mwt. and core (I)
   -robust spheroids; breathing deformability
2. Non-crystalline, amorphous materials
   -lower glass temperatures
3. Increased solubility
   -increases with Mwt.
4. Exhibits viscosity maximum and minimum plateau with Mwt.
   -low viscosities
5. Newtonian-type rheology
   -no shear sensitivity, considerably lower viscosity
6. Mobility involving whole dendrimer as the kinetic flow unit
   -virtually no reptation
7. Isotropic electronic conductivity

FIGURE 42.14. Comparison of properties for (I) linear and (IV) dendritic architecture. (Reproduced from [88] with permission of J. Wiley & Sons.)

Fréchet [43,106] was the first to compare viscosity parameters for (A) linear topologies, as well as (B) random hyperbranched polymers and (C) dendrimers. More recently, we reported such parameters for (D) dendrigraft polymers [105] as shown in Fig. 42.15. It is clear that all three dendritic topologies behave differently than the linear architecture. There is, however, a continuum of behavior; wherein, random hyperbranched polymers behave most nearly like the linear systems. Dendrigrafts exhibit intermediary behavior; whereas, dendrimers show a completely different relationship as a function of molecular weight.

Important physical property subtleties were noted within the dendrimer subset. For example, dendrimers possessing asymmetrical branch cells (i.e., Denkewalter type) exhibit a constant density versus generation relationship (Fig. 42.20). This is in sharp contrast to symmetrical branch-cell dendrimers (Tomalia-type PAMAM) that exhibit a minimum in density between $G = 4$ and $G = 7$ (NH_3 core) [42,76]. This is a transition pattern that is consistent with the observed development of ''container properties'' described in Fig. 42.16.

Finally, other unique features offered by the ''dendritic state,'' that appear to have no equivalency in the linear topologies, and are found almost exclusively in the dendron/dendrimer subset include the following; (a) *nearly complete monodispersity*, *(b) the ability to control unimolecular nanoscale container/scaffolding properties*, *(c) exponential amplification of terminal functional groups, and (d) persistent nanoscale dimensions/shape* as a function of molecular weight (generation). These features are captured to some degree with dendrigraft polymers, but are either absent or present to a minor extent in random hyperbranched polymers.

Monodispersity

The monodispersed nature of dendrimers has been verified extensively by mass spectroscopy, size exclusion chromatography, gel electrophoresis, and electron microscopy (TEM). As is always the case, the level of monodispersity is determined by the skill of the synthetic chemist, as well as the isolation/purification methods utilized.

In general, convergent methods produce the most nearly isomolecular dendrimers. This is because the convergent growth process allows purification at each step of the synthesis and therefore no cumulative effects of failed couplings are found. Appropriately purified convergent dendrimers are probably the most precise synthetic macromolecules that exist today.

As discussed earlier, mass spectroscopy has shown that PAMAM dendrimers produced by the ''divergent method'' are very monodisperse and have masses consistent with predicted values for the earlier generations (i.e., $G = 0$–5). Even at higher generations, as one enters the de Gennes dense packed region, the molecular weight distributions remain very narrow (i.e., 1.05) and consistent in spite of the fact that experimental masses deviate substantially form predicted theoretical values. Presumably, de Gennes dense packing produces a very regular and dependable effect that is manifested in the narrow molecular weight distribution.

Unimolecular Nanoscale Container/ Scaffolding Properties

Unimolecular container/scaffolding behavior appears to be a periodic property that is specific to each dendrimer family or series. These properties will be determined by the size, shape, and multiplicity of the construction components that are used for the core, interior, and surface of the dendrimer. Higher multiplicity components and those that contribute to ''tethered congestion'' will hasten the development of ''container properties'' or rigid surface scaffolding as a function of generation. Within the PAMAM dendrimer family, these periodic properties are generally manifested in three phases as shown in Fig. 42.12.

The earlier generations (i.e., $G = 0$–3) exhibit no well-defined interior characteristics; whereas, interior development related to geometric closure is observed for the intermediate generations (i.e., $G = 4$–7). Accessibility and departure form the interior is determined by the ''size and

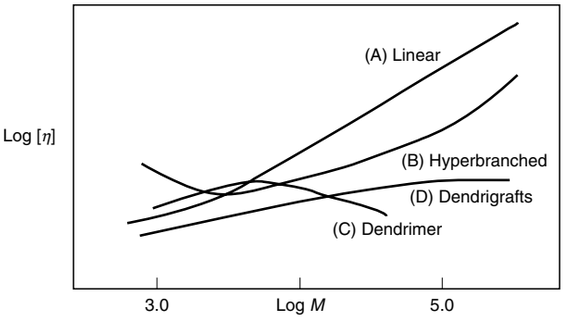

FIGURE 42.15. Comparison of intrinsic viscosities (log (η)) versus molecular weight (log M) for (A) linear, (B) random hyperbranched, (C) dendrimers, and (D) dendrigraft topologies. (Reproduced from [88] with permission of J. Wiley & Sons.)

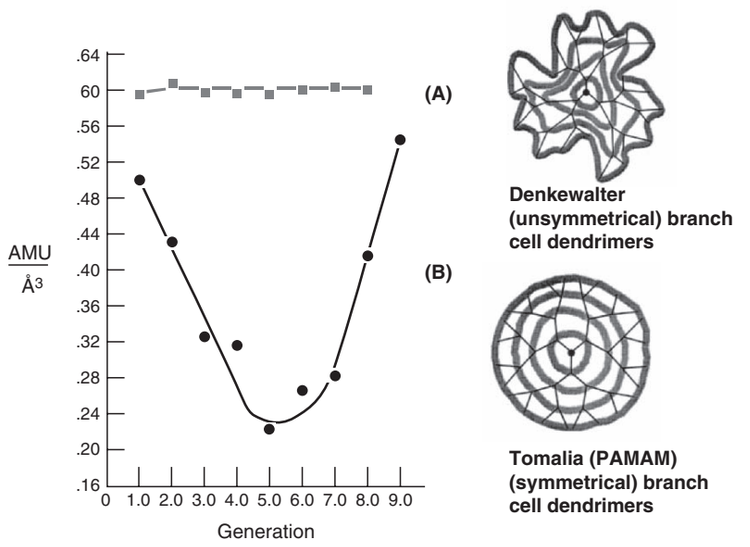

FIGURE 42.16. Comparison of densities as a function of generation for (A) assymetrical branch cell in Denkewalter-type dendrimers, (B) symmetrical branch cell in Tomalia-type dendrimers ([densities calculated from experimental hydrodrynamic diameters and theoretical, D.A. Tomalia, M. Hall, D.M. Hedstrand, *J. Am. Chem. Soc.*, **109**, 1601 (1987)]. (Reproduced from [88] with permission of J. Wiley & Sons.)

gating properties'' of the surface groups. At higher generations (i.e., $G => 7$) where de Gennes dense packing is severe, rigid scaffolding properties are observed, allowing relatively little access to the interior except for very small guest molecules. The site-isolation and encapsulation properties of dendrimers have been reviewed recently by Hecht and Fréchet [41].

Amplification of Terminal Surface Groups

Dendrimers within a generational series can be expected to present their terminal groups in at least three different modes, namely: *flexible, semiflexible*, or *rigid functionalized scaffolding*. Based on mathematically defined dendritic branching rules (i.e., $Z = N_c N_b^G$) the various surface presentations are expected to become more congested and rigid as a function of generation level. It is implicit that this surface amplification can be designed to control gating properties associated with unimolecular container development. Furthermore, dendrimers may be viewed as versatile, nanosized objects that can be surface functionalized with a vast array of features (Fig. 42.17). The ability to control and engineer these parameters provides an endless list of possibilities for utilizing dendrimers as modules for the design of nanodevices [81,107]. Recent publications have begun to focus on this area [41,108–113].

Persistent Nanoscale Shapes and Dimensions

In view of the extraordinary structure control and nanoscale dimensions observed for dendrimers, it is not surprising to find extensive interest in their use as globular protein mimics. Based on their systematic, dimensional length scaling properties (Fig. 20.18) and electrophoretic/hydrodynamic behavior [86], they are sometimes referred to as *artificial proteins*. These fundamental properties have in fact led to their commercial use as globular protein replacements for gene therapy [114] and immunodiagnostics [115–118]. Substantial effort has been focused recently on the use of dendrimers for ''site isolation'' mimicry of proteins [41], enzyme-like catalysis [119], as well as other biomimetic applications [79,120].

42.4 DENDRITIC STRUCTURES AS INTERMEDIARY ARCHITECTURES BETWEEN THERMOPLASTICS AND THERMOSETS

The first two major domains defined in polymer science were associated with certain distinguishing properties and architecture. One domain included linear, random coil thermoplastic polymers such as poly(styrenes) or poly(acrylates). These architectures were characterized as one-dimensional chains possessing two terminal groups per molecule, specific molecular weight distributions, reasonable solvent solubility, melt flow characteristics, chain entanglements consisting of inter- and intramolecular knots and loops, mobility *via* snakelike reptation, and they exhibited expanded, large molecular volumes when immersed in ''good solvents.'' The second domain of ''thermoset polymers'' included cross-linked architectures such as vulcanized rubber, epoxies, and melamine resins all of which

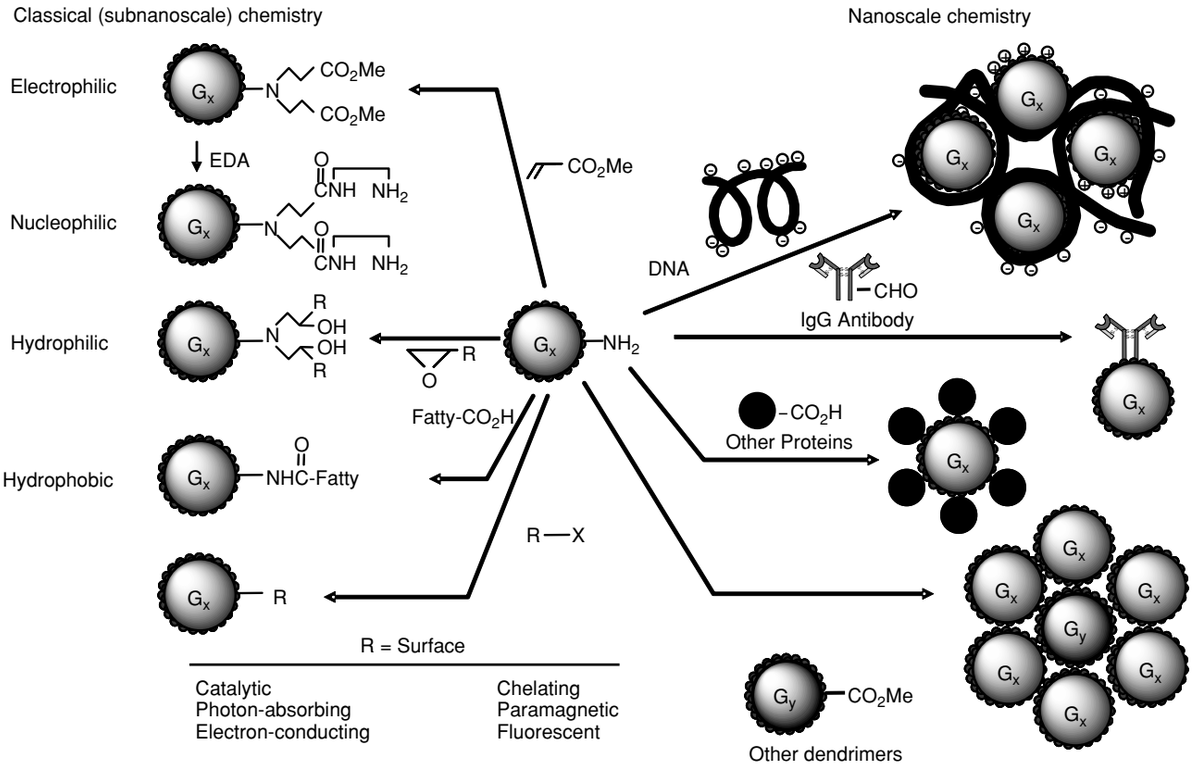

FIGURE 42.17. Options for modifying amine terminated dendrimers utilizing classical subnanoscale and nanoscale reagents. (Reproduced from [129] with permission of Aldrichimica Acta.)

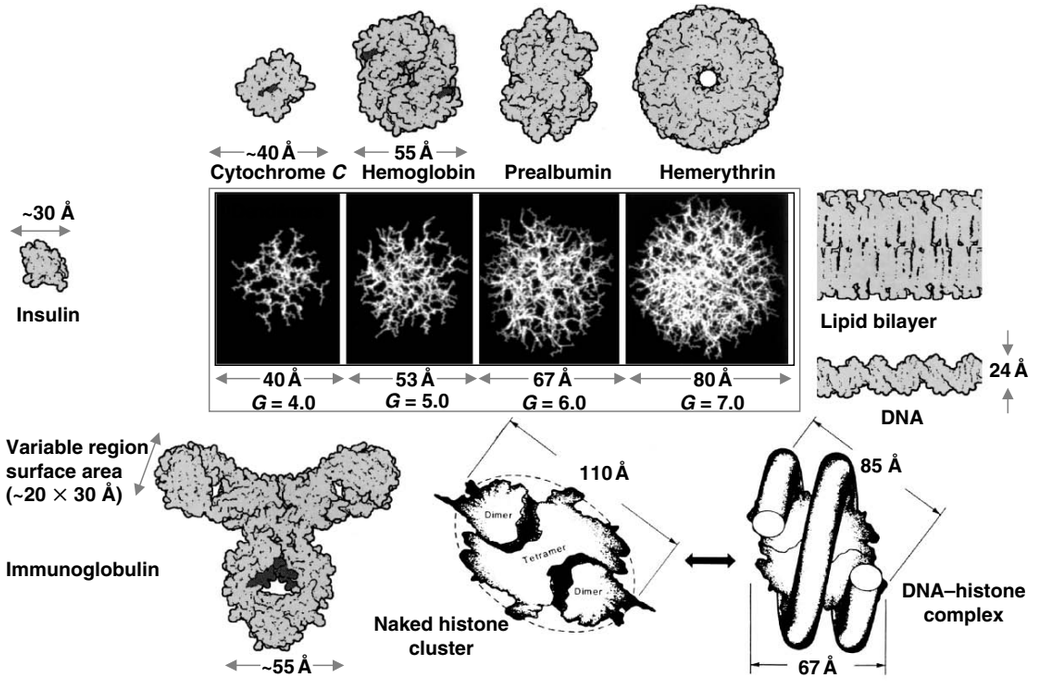

FIGURE 42.18. A comparison of dimensional length scales (A) for PAMAM dendrimers $N_c = 3$, $N_b = 2$ (NH_3 core) and various biological entities (e.g., proteins, DNA and lipid bilayers). (Reproduced from [88] with permission of J. Wiley & Sons.)

were recognized as insoluble macromolecules. They exhibited rubber-like elasticity, and no melt flow features, yet they were semipermeable and susceptible to diffusion and pronounced swelling in certain solvents.

It is now recognized that a continuum of architecture and properties, beginning with the classical branched polymers, resides between these two classes. Typical branched structures such as starch or high pressures polyethylene are characterized by more than two terminal groups per molecule, possessing substantially smaller hydrodynamic volumes and different intrinsic viscosities compared to linear polymers, yet they often exhibit unexpected segmental expansion near the ''theta state.''

Completing this continuum, we may now focus on the intermediary role that (Class IV) dendritic polymers play both in architecture and properties as penultimate thermosplastic precursors to (Class II), cross-linked thermoset systems. Within the realm of traditional architectures, branched (Class III) and random hyperbranched structures Class (IVa) may be viewed as penultimate statistical precursors residing between thermoplastic structures and thermoset architectures as illustrated in Fig. 42.19 [121,122]. The dendritic state may be visualized as advancement from a lower order (i.e., Class I–III) to a somewhat higher level of structural complexity [123]. Recent developments now demonstrate that certain dendritic subsets are manifestations of higher level structural control. In contrast to random hyperbranched polymers, the dendrimer subset, and to a lesser extent, the dendrigraft subset, represent a unique combination of high complexity with extraordinary structure control. As such, covalent bridging or crosslinking of these preformed modules would be expected to give rise to a completely new class (V) of more ordered complexity. Examples of this new architecture have been synthesized and these new topologies are referred to as ''megamers.''

42.4.1 Megamers—A New Class of Regio-Specifically Cross-linked Dendrimers

In the first full paper published on dendritic polymers [47], dendrimers were defined as ''reactive, structure-controlled macromolecular building blocks.'' It was proposed that they could be used as repeat units for the construction of a new class of topological macromolecules referred to as ''starburst polymers.'' Although there is intense activity in the field of dendrimer science, there are relatively few references focused on this specific concept [34,80,81,96]. Meanwhile, the term ''starburst'' has been claimed as a registered trademark of the Dow Chemical Company and recently assigned to Dendritic NanoTechnologies, Inc. In view of these events, the generic term, ''megamer'' has been proposed to describe those new architectures that are derived from the combination of two or more dendrimer molecules (see Figs. 42.19 and 42.20) [96,124].

Examples of both statistical, as well as structure-controlled megamer assemblies have been reported and reviewed recently [96,124]. Covalent oligomeric assemblies of dendrimers (i.e., dimers, trimers, etc.) are well-documented examples of low molecular-weight megamers. Statistical megamer assemblies have been reported as both *supramacromolecular* [109,110] and *supermacromolecular* (covalent) topologies. Many reports on the supramacromolecular self-assembly of these structures leading to dendrimeric clusters and monolayers are prime examples of

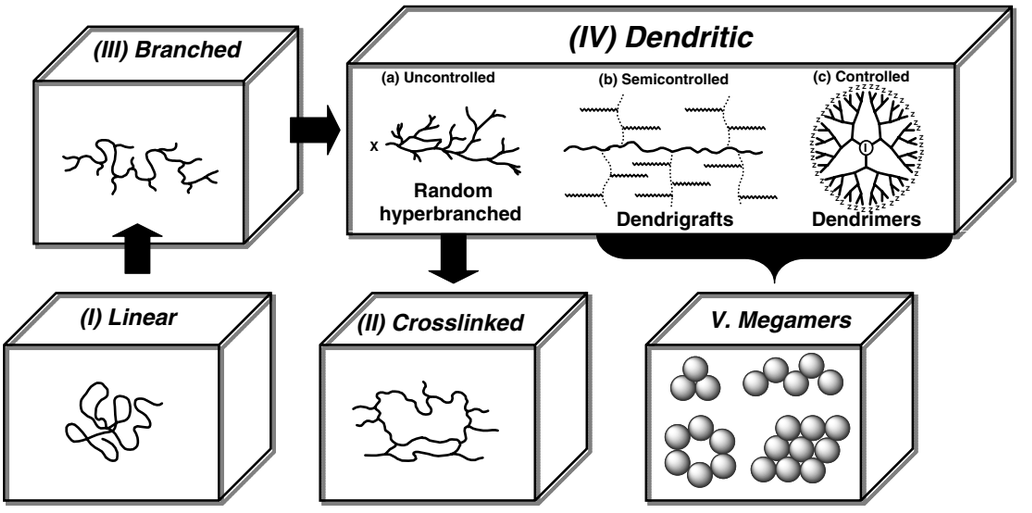

FIGURE 42.19. Examples of architectural polymer classes (I–IV) polymer type, repeat units, and covalent connectivity associated with architectural classes.

supramacromolecular megamers. Simple, low DP covalent dendrimeric oligomers such as "$[\text{dendrimer}]_n$" where $n = 2–10$, and dendrimeric gels for which $n > 10$ represent a continuum of statistical covalent megamers that are possible.

Both randomly assembled megamers [124], as well as structure-controlled megamers [124–126] have been demonstrated. Recently, new mathematically defined megamers (dendrimer clusters) or core–shell tecto(dendrimers) have been reported [35,125–127]. The principles of these structure-controlled megamer syntheses mimic those used for the core–shell construction of dendrimers. First, a megamer core reagent (usually a spheroid) is selected. Next, a limited amount of this reactive core reagent is combined with an excess of a megamer shell reagent. The objective is to completely saturate the target spheroid core surface with covalently bonded spheroidal shell reagent. Since the diameters of the megamer core and shell reagents are very well defined, it is possible to predict mathematically the number of megamer shell molecules required to saturate a targeted core dendrimer [89,128,129].

It appears that *structure-controlled complexity beyond dendrimers* is now possible. The demonstrated structure control within the dendrimer modules, and now the ability to mathematically predict and synthesize precise assemblies of these modules, provide a broad concept for the systematic construction of nanostructures with dimensions that could span the entire nanoscale region (Fig. 42.20) [16,89].

42.5 CONCLUSIONS

Dendritic polymers are expected to play a key role as enabling building blocks for nanotechnology during the 21st century, just as the first three traditional architectural classes of synthetic polymers have so successfully fulfilled critical material and functional needs in the plastics age during the past half century. The controlled shape, size,

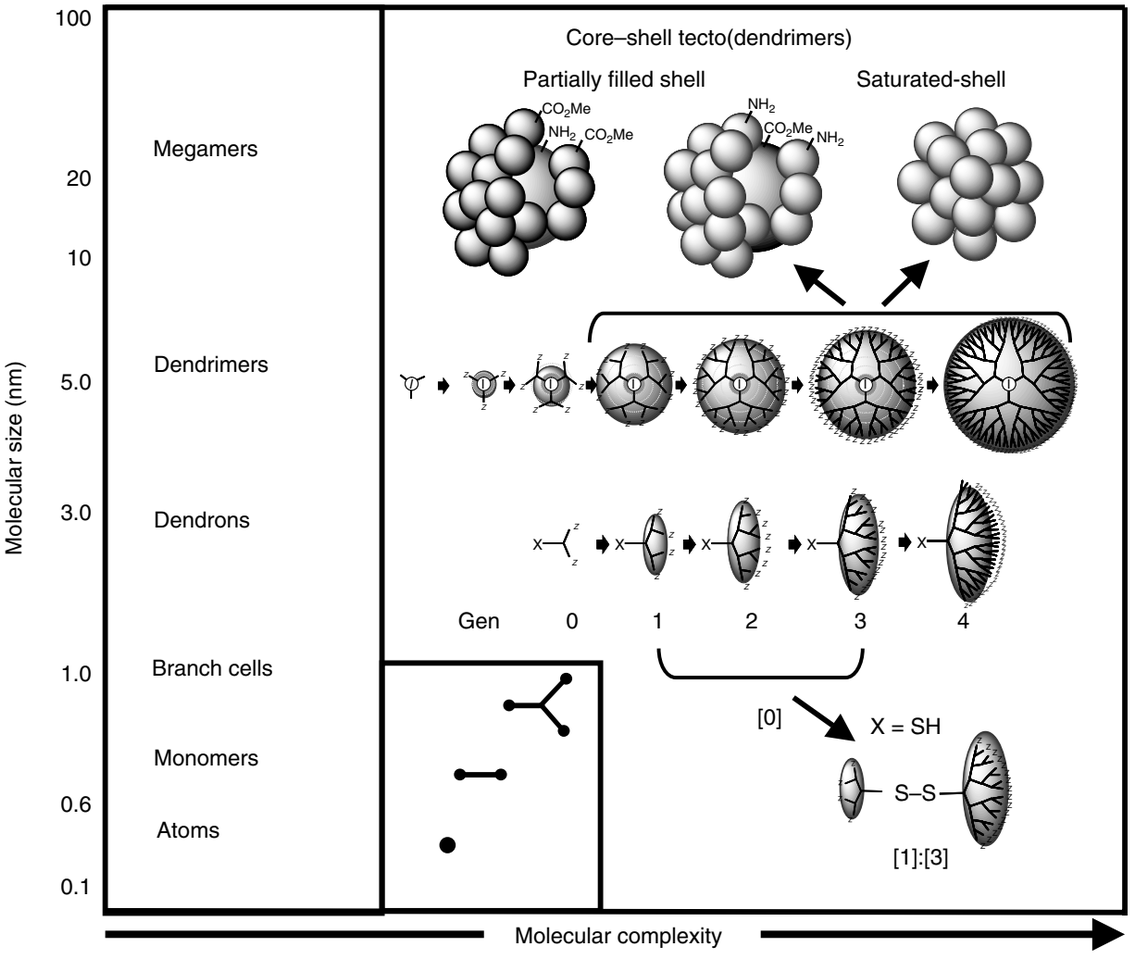

FIGURE 42.20. Approximate nanoscale dimensions as a function of atoms, monomers, branch cells, dendrimers, and megamers. (Reproduced from [129] with permission of Aldrichimica Acta.)

and differentiated functionality of dendrimers; their ability to provide both isotropic and anisotropic assemblies; their compatibility with many other nanoscale building blocks such as DNA, metal nanocrystals, and nanotubes; their potential for ordered self-assembly; their ability to combine both organic and inorganic components; and their propensity to either encapsulate or be engineered into unimolecular functional devices make dendrimers uniquely versatile amongst existing nanoscale building blocks and materials. Dendritic polymers, especially dendrons and dendrimers, are expected to fulfill an important role as fundamental modules for nanoscale synthesis. It is from this perspective that it is appropriate to be optimistic about the future of this new major polymer class, the *dendritic state* [16,130].

ACKNOWLEDGMENTS

This work was funded by the Army Research Laboratory (ARL), Dendritic Polymer Center of Excellence (Contract DAAL-01-1996-02-044). I would like to express my sincere appreciation to Ms L. S. Nixon for preparing the manuscript.

REFERENCES

1. H. Staudinger, *From Organic Chemistry to Macromolecules* (Wiley-Interscience, New York, 1970).
2. H. Morawetz, *Polymers. The Origin and Growth of a Science* (J. Wiley, New York, 1985).
3. H. Staudinger, Schweiz. Chem. Z., **105**, 28–33, 60–64 (1919).
4. H. Staudinger, Ber. Deut. Chem. Ges. **53**, 1073 (1920).
5. H. Staudinger, *From Organic Chemistry to Macromolecules, A Scientific Autobiography* (Wiley, New York, 1961).
6. L. K. James, in *Nobel Laureates in Chemistry 1901–1992*, edited by L. K. James (History of Modern Chemical Science Series, American Chemical Society, Washington, DC, 1994), pp. 359–367.
7. *Handbook of Radical Polymerization*, edited by K. Matyjaszewski and T. Davis (John Wiley & Sons, New Jersey, 2002).
8. K. Matyjaszewski and J. Spanswick, Mater. Today, 26–33 (March 2005).
9. H.-G. Elias, *Mega Molecules* (Springer-Verlag, Berlin, 1987).
10. *Advances in Polymer Science, Branched Polymers I*; *Vol. 142*, edited by J. Roovers (Springer-Verlag, Berlin, 1999).
11. *Advances in Polymer Science, Branched Polymers II*; *Vol. 143*, edited by J. Roovers (Springer-Verlag, Berlin, 2000).
12. Z. Guan, P. M. Cotts, E. F. McCord, and S. J. McLain, Science **283**, 2059–2062 (1999).
13. *Metallocene-Based Polyolefins, Vols. 1 and 2* (J. Wiley & Sons Ltd., Brisbane, 2000).
14. M. K. Lothian-Tomalia, D. M. Hedstrand, and D. A. Tomalia, Tetrahedron **53**, 15495–15513 (1997).
15. D. S. Goodsell, Am. Sci. **88**, 230–237 (2000).
16. D. A. Tomalia, Mater. Today, 34–46 (March 2005).
17. P. J. Flory, J. Am. Chem. Soc. **63**, 3083, 3091, 3096 (1941).
18. P. J. Flory, J. Am. Chem. Soc. **74**, 2718 (1952).
19. P. J. Flory, Ann. N.Y. Acad. Sci. **57**, 327 (1953).
20. P. J. Flory, *Principles of Polymer Chemistry* (Cornell University Press, Ithaca, NY, 1953).
21. W. H. Stockmayer, J. Chem. Phys. **11**, 45 (1944).
22. W. H. Stockmayer, J. Chem. Phys. **12**, 125 (1944).
23. B. Zimm and W. H. Stockmayer, J. Chem. Phys. **17**, 1301 (1949).
24. P. J. Flory and J. Rehner, J. Chem. Phys. **11**, 512 (1943).
25. W. W. Graessley, Macromolecules **8**, 185 (1975).
26. W. W. Graessley, Macromolecules **8**, 865 (1975).
27. M. Gordon and G. R. Dobson, J. Chem. Phys. **43**, 35 (1975).
28. M. Gordon and G. N. Malcolm, Proc. R. Soc. (London) **A295**, 29 (1966).
29. K. Dusek, Makromol. Chem. Suppl. **2**, 35 (1979).
30. W. Burchard, Adv. Polym. Sci. **48**, 1 (1988).
31. I. J. Good, Proc. Cambridge Phil. Soc. **45**, 360 (1948).
32. I. J. Good, Proc. R. Soc. (London) **A263**, 54 (1963).
33. D. A. Tomalia and J. M. J. Fréchet, J. of Polym. Sci: Part A: Polym. Chem. **40**, 2719–2728 (2002).
34. D. A. Tomalia, Sci. Am. **272**, 42–46 (1995).
35. D. A. Tomalia and D. R. Swanson, in *Dendrimers and Other Dendritic Polymers*, edited by J. M. J. Fréchet and D. A. Tomalia (Wiley, Chichester, 2001), pp. 617–629.
36. D. A. Tomalia, H. M. Brothers II, L. T. Piehler, H. D. Durst, and D. R. Swanson, Proc. Natl Acad. Sci. USA **99**(8), 5081–5087 (2002).
37. D. A. Tomalia, H. M. Brothers II, L. T. Piehler, and Y. Hsu, Polym. Mater. Sci. Eng. **73**, 75 (1995).
38. D. A. Tomalia, Macromol. Symp. **101**, 243–255 (1996).
39. A. K. Naj, in *The Wall Street Journal* (New York, 1996), p. B1.
40. D. A. Tomalia and R. Esfand, Chem. Ind. **11**, 416–420 (1997).
41. S. Hecht and J. M. J. Fréchet, Angew. Chem. Int. Ed. **40**(1), 74–91 (2001).
42. D. A. Tomalia, A. M. Naylor, and W. A. Goddard III, Angew. Chem. Int. Ed. Engl. **29**, 138–175 (1990).
43. J. M. J. Fréchet, C. J. Hawker, I. Gitsov, and J. W. Leon, J.M.S.—Pure Appl. Chem. **A33**, 1399 (1999).
44. F. Vögtle and M. Fischer, Angew. Chem. Int. Ed. **38**, 884–905 (1999).
45. B. I. Voit, Acta Polym. **46**, 87–99 (1995).
46. J. M. J. Fréchet and D. A. Tomalia, *Dendrimers and Other Dendritic Polymers* (Wiley, Chichester, 2001).
47. D. A. Tomalia, H. Baker, J. Dewald, M. Hall, G. Kallos, S. Martin, J. Roeck, J. Ryder, and P. Smith, Polym. J. (Tokyo) **17**, 117–132 (1985).
48. P. A. Gunatillake, G. Odian, and D. A. Tomalia, Macromolecules **21**, 1556–1562 (1988).
49. Y. H. Kim and O. W. Webster, Polym. Prepr. **29**, 310 (1988).
50. Y. H. Kim and O. W. Webster, J. Am. Chem. Soc. **112**, 4592 (1990).
51. T. Emrick, H. T. Chang, and J. M. J. Frèchet, J. Polym. Sci. A **38**, 4850 (2000).
52. T. Emrick and J. M. J. Fréchet, Curr. Opin. Colloid Interf. Sci. **4**, 15–23 (1999).
53. P. Bharati and J. S. Moore, J. Am. Chem. Soc. **119**, 3391 (1997).
54. A. M. Muzafarov, E. A. Rebrov, O. B. Gorbatsevich, M. Golly, H. Gankema, and M. Moller, Macromol. Symp. **102**, 35 (1996).
55. J. F. Miravet and J. M. J. Frèchet, Macromolecules **31**, 3461 (1998).
56. F. Chu and C. J. Hawker, Polym. Bull. **30**, 265 (1993).
57. C. J. Hawker, R. Lee, and J. M. J. Frechet, J. Am. Chem. Soc. **113**, 4583 (1991).
58. K. E. Uhrich, C. J. Hawker, J. M. J. Frèchet, and S. R. Turner, Macromolecules **25**, 4583 (1992).
59. M. Liu, N. Vladimirov, and J. M. J. Frèchet, Macromolecules **32**, 6881–6884 (1999).
60. J. M. J. Fréchet, M. Henni, I. Gitsov, S. Aoshima, M. R. Leduc, and R. B. Grubbs, Science **269**, 1080 (1995).
61. C. J. Hawker, P. J. Farrington, M. E. Mackay, K. L. Wooley, and J. M. J. Frèchet, J. Am. Chem. Soc. **117**, 4409 (1995).
62. A. Sunder, J. Heinemann, and H. Frey, Chem. Eur. J. **6**, 2499 (2000).
63. C. Gong, J. Miravet, and J. M. J. Frèchet, J. Polym. Sci. A. **37**, 3193 (1999).
64. D. A. Tomalia, D. M. Hedstrand, and M. S. Ferrito, Macromolecules **24**, 1435–1438 (1991).
65. M. Gauthier, J. Li, and J. Dockendorff, Macromolecules **36**, 2642–2648 (2003).
66. R. A. Kee, M. Gauthier, and D. A. Tomalia, in *Dendrimers and Other Dendritic Polymers*, edited by J. M. J. Frechet and D. A. Tomalia (John Wiley & Sons, West Sussex, 2001), pp. 209–235.
67. J.-L. Six and Y. Gnanou, Macromol. Symp. **95**, 137 (1995).
68. D. Taton, E. Cloutet, and Y. Gnanou, Macromol. Chem. Phys. **199**, 2501 (1998).
69. M. Trollsas and J. L. Hedrick, J. Am. Chem. Soc. **120**, 4644–4651 (1998).
70. M. Trollsas and J. L. Hedrick, Macromolecules **31**, 4390–4395 (1998).

71. R. B. Grubbs, C. J. Hawker, J. Dao, and J. M. J. Frèchet, Angew. Chem. Int. Ed. Engl. **36**, 270 (1997).
72. D. A. Tomalia, J. R. Dewald, M. J. Hall, S. J. Martin, and P. B. Smith, First SPSJ International Polymer Conference, Kyoto, Japan, August 1984, p. 65.
73. A. W. Kleij, A. Ford, J. T. B. H. Jastrzebski, and G. Van Koten, in *Dendrimers and Other Dendritic Polymers*, edited by J. M. J. Fréchet and D. A. Tomalia (Wiley, Chichester, 2001), pp. 485–514.
74. J. M. J. Fréchet, H. Ihre, and M. Davey, in *Dendrimers and Other Dendritic Polymers*, edited by J. M. J. Fréchet and D. A. Tomalia (Wiley, Chichester, 2001), pp. 569–586.
75. M. H. P. Van Genderen, M. H. A. Mak, D. B.-V. D. Berg, and E. W. Meijer, in *Dendrimers and Other Dendritic Polymers*, edited by J. M. J. Fréchet and D. A. Tomalia (Wiley, Chichester, 2001), pp. 605–616.
76. A. M. Naylor, W. A. Goddard III, G. E. Keifer, and D. A. Tomalia, J. Am. Chem. Soc. **111**, 2339–2341 (1989).
77. G. R. Newkome, C. N. Moorfield, and F. Vögtle, *Dendritic Molecules* (VCH, Weinheim, 1996).
78. C. J. Hawker and J. M. J. Fréchet, J. Am. Chem. Soc. **112**, 7638–7647 (1990).
79. F. Zeng and S. C. Zimmerman, Chem. Rev. **97**, 1681–1712 (1997).
80. D. A. Tomalia, Aldrichim. Acta **26(4)**, 91–101 (1993).
81. D. A. Tomalia, Adv. Mater. **6**, 529–539 (1994).
82. G. J. Kallos, D. A. Tomalia, D. M. Hedstrand, S. Lewis, and J. Zhou, Rapid Commun. Mass Spectrom. **5**, 383–386 (1991).
83. P. R. Dvornic and D. A. Tomalia, Macromol. Symp. **98**, 403–428 (1995).
84. J. C. Hummelen, J. L. J. van Dongen, and E. W. Meijer, Chem. Eur. J. **3**, 1489–1493 (1997).
85. J. Peterson, V. Allikmaa, J. Subbi, T. Pehk, and M. Lopp, Eur. Polym. J. **39**, 33–42 (2003).
86. H. M. Brothers II, L. T. Piehler, and D. A. Tomalia, J. Chromatogr. A **814**, 233–246 (1998).
87. C. Zhang and D. A. Tomalia, in *Dendrimers and Other Dendritic Polymers*, edited by J. M. J. Fréchet and D. A. Tomalia (Wiley, Chichester, 2001), pp. 239–252.
88. D. A. Tomalia and J. M. J. Fréchet, in *Dendrimers and Other Dendritic Polymers*, edited by J. M. J. Frechet and D. A. Tomalia (Wiley, Chichester, 2001), pp. 3–44.
89. D. A. Tomalia, Prog. Polym. Sci. **30**, 294–324 (2005).
90. N. J. Turro, J. K. Barton, and D. A. Tomalia, Acc. Chem. Res. **24(11)**, 332–340 (1991).
91. K. R. Gopidas, A. R. Leheny, G. Caminati, N. J. Turro, and D. A. Tomalia, J. Am. Chem. Soc. **113**, 7335–7342 (1991).
92. M. F. Ottaviani, N. J. Turro, S. Jockusch, and D. A. Tomalia, J. Phys. Chem. **100**, 13675–13686 (1996).
93. J. Jockusch, J. Ramirez, K. Sanghvi, R. Nociti, N. J. Turro, and D. A. Tomalia, Macromolecules **32**, 4419–4423 (1999).
94. C. J. Hawker, K. L. Wooley, and J. M. J. Frèchet, J. Am. Chem. Soc. **115**, 4375 (1993).
95. P. G. de Gennes and H. J. Hervet, J. Physique-Lett. (Paris) **44**, 351–360 (1983).
96. D. A. Tomalia, R. Esfand, L. T. Piehler, D. R. Swanson, and S. Uppuluri, High Perform. Polym. **13**, S1–S10 (2001).
97. T. H. Mourey, S. R. Turner, M. Rubinstein, J. M. J. Frechet, C. J. Hawer, and K. L. Wooley, Macromolecules **25**, 2401–2406 (1992).
98. J. Berzelius, J. Fortsch. Phys. Wissensch. **11**, 44 (1832).
99. K. L. Wooley, J. M. J. Frèchet, and C. J. Hawker, Polymer **35**, 4489 (1994).
100. P. R. Dvornic and D. A. Tomalia, Sci. Spectra **5**, 36–41 (1996).
101. D. A. Tomalia, P. R. Dvornic, S. Uppuluri, D. R. Swanson, and L. Balogh, Polym. Mater. Sci. Eng. **77**, 95–96 (1997).
102. C. J. Hawker, E. E. Malmstrom, C. W. Frank, and J. P. J. Kampf, J. Am. Chem. Soc. **119**, 9903–9904 (1997).
103. E. M. M. de Brabander-van den Berg and E. W. Meijer, Angew. Chem. Int. Ed. Engl. **32**, 1308–1311 (1993).
104. P. J. Farrington, C. J. Hawker, J. M. J. Frèchet, and M. E. Mackay, Macromolecules **31**, 5043 (1998).
105. D. Qin, R. Yin, J. Li, L. Piehler, D. A. Tomalia, H. D. Durst, and G. Hagnauer, Polym. Prepr. (ACS Div. Polym. Chem.) **40**, 171–172 (1999).
106. J. M. J. Fréchet, Science **263**, 1710–1715 (1994).
107. G. J. de A.A. Soler-Illia, L. Rozes, M. K. Boggiano, C. Sanchez, C. O. Turrin, A.-M. Caminade, and J.-P. Majoral, Angew. Chem. Int. Ed. **39**, 4250 (2000).
108. D. A. Tomalia and H. D. Durst, in *Supramolecular Chemistry I—Directed Synthesis and Molecular Recognition*, edited by E. W. Weber (Springer-Verlag, Berlin Heidelberg, 1993), pp. 193–313.
109. D. A. Tomalia and I. Majoros, in *Supramolecular Polymers*, *Chapter 9*, edited by A. Ciferri (Marcel Deker, New York, 2000), pp. 359–434.
110. D. A. Tomalia and I. Majoros, J. Macromol. Sci. **C43**, 411–477 (2003).
111. L. Balogh, D. A. Tomalia, and G. L. Hagnauer, Chem. Innov. **30**, 19–26 (2000).
112. R. M. Crooks, B. Lemon III, L. Sun, L. K. Yeung, and M. Zhao, in *Topics in Current Chemistry, Vol. 212* (Springer-Verlag, Berlin Heidelberg, 2001).
113. A. W. Freeman, S. C. Koene, P. R. L. Malenfant, M. E. Thompson, and J. M. J. Frechet, J. Am. Chem. Soc. **122**, 12385–12386 (2000).
114. J. F. Kukowska-Latallo, A. U. Bielinska, J. Johnson, R. Spindler, D. A. Tomalia, and J. R. Baker Jr., Proc. Natl Acad. Sci. USA **93**, 4897–4902 (1996).
115. P. Singh, Bioconjugate Chem. **9**, 54–63 (1998).
116. P. Singh, in *Dendrimers and Dendritic Polymers*, edited by J. M. J. Fréchet and D. A. Tomalia (Wiley, Chichester, 2001), pp. 463–484.
117. P. Singh, F. Moll III, S. H. Lin, and C. Ferzli, Clin. Chem. **42(9)**, 1567–1569 (1996).
118. P. Singh, F. Moll III, S. H. Lin, C. Ferzli, K. S. Yu, K. Koski, and R. G. Saul, Clin. Chem. **40(9)**, 1845–1849 (1994).
119. M. E. Piotti, F. Rivera, R. Bond, C. J. Hawker, and J. M. J. Frèchet, J. Am. Chem. Soc. **121**, 9471 (1999).
120. C. Bieniarz, in *Encyclopedia of Pharmaceutical Technology*; *Vol. 18* (Marcel Dekker, New York, 1998), pp. 55–89.
121. K. Dusek, TRIP **5(8)**, 268–274 (1997).
122. K. Dusek and M. Duskova-Smrckova, in *Dendrimers and Dendritic Polymers* (J. Wiley & Sons, Ltd., West Sussex, 2001), pp. 111–145.
123. D. A. Tomalia, D. M. Hedstrand, and L. R. Wilson, in *Encyclopedia of Polymer Science and Engineering*, *Index Volume, Second Edition* (John Wiley & Sons, New York, 1990), pp. 46–92.
124. D. A. Tomalia, S. Uppuluri, D. R. Swanson, and J. Li, Pure Appl. Chem. **72**, 2343–2358 (2000).
125. J. Li, D. R. Swanson, D. Qin, H. M. Brothers II, L. T. Piehler, D. A. Tomalia, and D. J. Meier, Langmuir **15**, 7347–7350 (1999).
126. S. Uppuluri, L. T. Piehler, J. Li, D. R. Swanson, G. L. Hagnauer, and D. A. Tomalia, Adv. Mater. **12(11)**, 796–800 (2000).
127. M. Freemantle, Chem. Eng. News **77(44)**, 27–35 (1999).
128. M. L. Mansfield, L. Rakesh, and D. A. Tomalia, J. Chem. Phys. **105**, 3245–3249 (1996).
129. D. A. Tomalia, *Aldrichimica Acta*, **37(2)**, 39–57 (2004).
130. S. Svenson and D. A. Tomalia, Advanced Drug Delivery Reviews, **57**, 2106–2129 (2005).

CHAPTER 43

Polyrotaxanes

Feihe Huang, Adam M.-P. Pederson, and Harry W. Gibson

Department of Chemistry, Virginia Polytechnic & State University, Blacksburg, VA 24061, fhuang@chem.utah.edu
Department of Chemistry, Virginia Polytechnic & State University, Blacksburg, VA 24061, adamp@vt.edu
Department of Chemistry, Virginia Polytechnic & State University, Blacksburg, VA 24061, hwgibson@vt.edu

ACRONYM, ALTERNATIVE NAME: Inclusion complex, molecular necklace (MN), string of pearls, rotaxane-type polymer, polymeric rotaxane.

CLASS: Mechanically-linked, threaded polymers.

STRUCTURES: Varied, see specific examples below.

MAJOR APPLICATIONS: Curing of polymers, viscosity control, increase of crosslinking density, drug delivery, metal complexation, biodegradable materials, nanoelectronic devices.

PROPERTIES OF SPECIAL INTEREST: Stable under ambient conditions; controlled variation of physical properties compared with the reference polymer.

A variety of polyrotaxane structures can be envisioned, as shown in Scheme 1 [1–3]. True rotaxanes polymers possess bulky groups at the ends of the linear species or along the backbone to prevent diffusive loss of the ring component. However, it has been shown that main chain polypseudorotaxanes dethread extremely slowly due to random coiling of the backbones [4,5], so that the distinction between pseudorotaxane and rotaxane polymers of the main chain type is somewhat blurred for these systems. Main chain polyrotaxanes are the most common type, although all of the other types shown in Fig. 43.1 have been synthesized.

A main chain polyrotaxane, a mechanically interlocked structure that can be considered as a string of pearls, in which the strand is the polymer backbone and the pearls are the cyclic species threaded onto the strand. The backbone polymer can be a polyester, polyamide, poly(ethylene oxide), or virtually any linear polymer. The cyclic species are typically crown ethers, cyclodextrins (CDs), cucurbiturils, and calixarenes. Polyrotaxanes can be made by two different methods: statistical threading or via the template approach (enthalpically driven). The statistical approach utilizes le Chatelier's principle with an excess macrocycle during the polymerization. The template approach is driven by attractive interactions of the macrocyclic species with either the monomer or the polymer, depending on whether threading takes place during polymerization or starting with a preformed polymer; both approaches have been successfully applied.

Because of the formation of the mechanically interlocked structure, polyrotaxanes have different physical properties, such as solubility, thermostability, photoelectronic properties, viscosity, and phase behavior, compared with simple reference (nonpolyrotaxanated) polymers.

Usually the solubilities of polyrotaxanes are very different from their components. Because of the hydrophilic, high polarity nature of the exterior of the CDs, many CD-based polypseudorotaxanes and polyrotaxanes are soluble in water and some polar solvents though their parent polymers are hydrophobic or nonpolar [6–9]. The solubility of crown ether-based polyrotaxanes in methanol and/or water was improved because of the hydrogen bonding between the crown ethers and solvents [5,10,11] or the hydrogen bonding between the crown ethers and the polymer backbone [4]. Even if there are strong attractive forces between their components, dethreading still can happen in some polypseudorotaxanes when a salt or competitive solvent is added or the temperature increases [1–3].

Yui's group found the thermal stability of their biodegradable polyrotaxane was better than that of the separate components, poly(ε-lysine) and α-cyclodextrin [12,13]. In some crown ether based systems, as shown below, thermal stability decreases because of the lability of the cyclic components.

A series of polyrotaxanes as light-harvesting antennae models was constructed by Ueno and coworkers [14]. These polyrotaxanes consist of various ratios of α-CD and naphthalene-appended α-CD threaded by a PEG chain bearing anthracene moieties at each end. Here naphthalene and anthracene moieties act as energy donor and energy acceptor, respectively. It was found that the antenna effect becomes more marked with increasing number of naphtha-

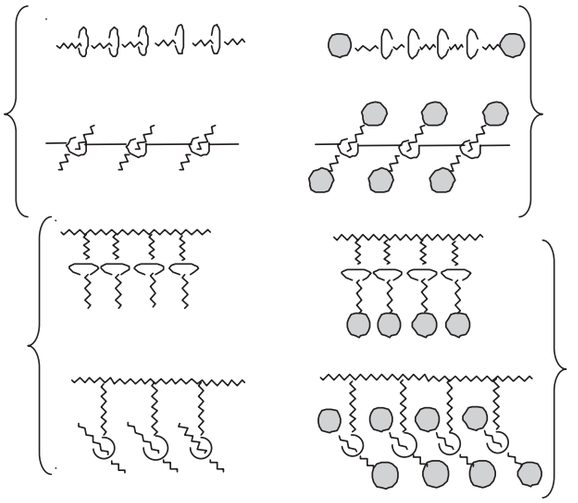

SCHEME 43.1. Cartoon representations of main chain (top) and side chain (bottom) polypseudorotaxanes (left) and polyrotaxanes (right).

lene-appended α-CD units in the polyrotaxanes, but energy transfer efficiency decreased.

The threading of cyclic components onto the polymer backbone has an important influence on the solution viscosity and melt viscosity. Up to now it has been found that this influence depends on the nature of the cyclic components and the polymer backbone, the value of mole ratio of cyclic species per repeat unit (m/n), and the types of solvents [5,15–19].

A glass transition temperature (T_g) is the temperature at which a polymer undergoes a conversion from a glassy amorphous state to a rubbery state. A melting point (T_m) is the temperature at which the physical state of a crystalline solid changes to the liquid state. Both T_g and T_m changes result from the threading of cyclic species onto the polymer backbone; the extent and direction of change depends on the properties of the cyclic species and the polymer backbone and their miscibility [1–3,5,11,16,19,21–29]. For example, Yamamoto's group found that polyurea-based polyrotaxanes have higher T_g than the corresponding CD-free polymers [20]. This increase is a result of the decrease of flexibility of the polymer chain because of the inclusion of rigid α-CDs onto the polyalkylene part of the backbone. In contrast, Shen *et al*. reported decreases in T_g of polyurethane rotaxanes with increased crown ether content due to the flexible nature of the cyclic components (see Table 43.1) [4]; moreover, the Fox equation was obeyed [30] (see below) because of the miscibility of the components through hydrogen bonding [31].

Presently, there are over 500 literature citations on polyrotaxanes, each with its own polymer and cyclic species. It is impossible to summarize the whole field here due to space limitations; therefore, as examples of the types of property changes that can be brought about and controlled by rotaxane formation, two polyrotaxane systems from our labs are presented here: polyurethane-based polyrotaxanes [4,30–33] (**1**) (Table 43.1) and polyester-based polyrotaxanes [5,34,35] (**2**) (Table 43.2). Polyurethane-based polyrotaxanes were investigated because polyurethanes are

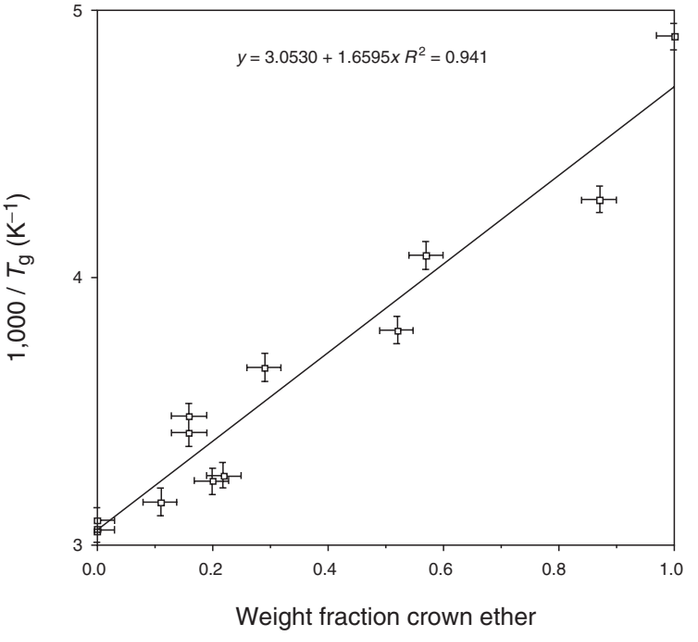

FIGURE 43.1. Fox plot: inverse glass transition temperature vs. weight fraction crown ether in polyurethane rotaxanes (data from Table 43.1) [32,33].

TABLE 43.1. *Polyurethane-based rotaxanes.*

Polymer	Cyclic species[a]	M_n (kg/mol)	M_w (kg/mol)	m/n[b]	Weight fraction crown ether	$[\eta]$ (dL/g) in NMP[c]	$[\eta]$ (dL/g) in THF[d]	T_g (K)[e]	Decomp. T (K)[f]	T_m (K)[g]	Ref.
1	None	12.1[h]/14.8[i]	27.0[h]/32.4[i]	0	0	–	–	324	543	–	[4,32]
1a	"36C12"	7.24[h]/11.3[i]	10.8[h]/16.6[i]	0.16	0.16	–	–	292	448	–	[4,32]
None	"60C20"	–	–	–	1	–	–	205	–	331.5	[32]
1	None	5.58[h]	11.1[h]	0	0	0.26	–	324	–	–	[4]
1	None	8.65[h]	26.9[h]	0	0	0.30	–	–	–	–	[4]
1	None	12.1[h]	27.0[h]	0	0	0.40	–	–	–	–	[4]
1a	"36C12"	7.24[h]	10.8[h]	0.16	0.16	0.24	–	287	–	–	[4]
1b	"42C14"	19.3[h]/29.6[i]	37.5[h]/59.7[i]	0.29	0.29	0.45	–	273	–	–	[4]
1c	"48C16"	7.01[h]/13.9[i]	10.6[h]/19.5[i]	0.52	0.45	0.24	–	263	–	–	[4]
1d	"60C20"	8.03[h]/16.5[i]	13.3[h]/21.3[i]	0.87	0.63	0.27	–	233	–	320	[4]
1	None	16.6[i]	58.7[i]	0	0	–	0.299	327	–	–	[33]
1b	"42C14"	–	–	0.092	0.113	–	0.351	316	–	–	[33]
1b	"42C14"	–	–	0.178	0.198	–	0.361	309	–	–	[33]
1b	"42C14"	–	–	0.201	0.218	–	0.369	307	–	–	[33]

[a] These cyclic species were all mixtures of aliphatic crown ethers; the average ring sizes were larger than these target values.
[b] m/n: mole ratio of cyclic species per repeat unit determined by ^{1}H NMR analyses.
[c] Measured in a Cannon-Ubbelohde semimicro dilute solution viscometer at 298.8 K.
[d] Measured in Cannon L12 50 viscometers at 298 K.
[e] Taken as the midpoint of the change in heat capacity by DSC at 10 °C/min. The crown ethers all have $T_g = 205$ K.
[f] Taken as the temperature of 5% weight loss by TGA at 10 °C/min.
[g] Taken as the maximum in the endotherm by DSC at 10 °C/min.
[h] From GPC analysis with polystyrene standards in THF.
[i] From GPC analysis with universal calibration using a viscosity detector in 6 mM LiBr/NMP.

TABLE 43.2. *Polyester-based rotaxanes.*

Polymer	Cyclic species[a]	M_n (kg/mol)	M_w (kg/mol)	m/n[b]	Wt Fr Crown ether	$[\eta]$[c] (dL/g) in THF/THF:MeOH (10:1)	η^* (Pa s)[d] 90 °C/150 °C	T_g[e] (K)	T_m[f] (K)	Ref.
2	None	5.2[g]/5.0[h]	7.1[g]/7.3[h]	0	0	0.141/0.147	–	–	–	[5]
2	None	8.9[g]	15.2[g]	0	0	—/0.160	–	–	–	[5]
2	None	17.1[h]	32.8[h]	0	0	0.543/0.549	–	–	350	[5]
2	None	4.3[h]	7.0[h]	0	0	–	3/0.9	–	–	[5]
2a	30C10	32.8[i]	58.9[i]	0.012	0.015	–	–	–	353	[5]
2b	“36C12”	14.3[i]	22.5[i]	0.22	0.25	–	–	219	315, 342, 344	[5]
2c	“42C14”	8.3[j]	14.0[j]	0.29	0.34	0.331/0.248	–	217	315, 343, 347	[5]
2c	“42C14”	10.4[h]	17.1[h]	0.13	0.19	–	3/0.8	–	–	[5]
2d	“48C16”	11.4[i]	19.[h]	0.34	0.41	–	–	215	316, 344, 348	[5]
2e	“60C20”	10.7[i]	20.7[i]	0.36	0.48	–	–	215	317, 336, 343	[5]

[a] The cyclic species specified by quotation marks (“”) were mixtures of aliphatic crown ethers; the average ring sizes were larger than these target values. 30-Crown-10 was a pure compound.
[b] m/n: mole ratio of cyclic species per repeat unit determined by ^{1}H NMR analyses.
[c] Measured in a Cannon-Fenske type viscometer at 298 K.
[d] Melt rheology was examined in a Rheometrics dynamic analyzer with a 25 mm parallel plate attachment in an oscillatory mode at 1 Hz from 90–150 °C.
[e] Taken as the midpoint of the change in heat capacity by DSC at 10 °C/min.
[f] Taken as the maximum in the endotherm by DSC at 10 °C/min. The endotherms at 336–353 K are for the polyester. Those at 315–317 K are for the crown ether crystalline phases.
[g] From GPC analysis with polystyrene standards in chloroform.
[h] From GPC analysis with universal calibration using a viscosity detector in chloroform.
[i] From GPC analysis with polystyrene standards in THF.
[j] From GPC analysis with polystyrene standards in toluene.

glassy polymers and incorporation of crystalline crown ethers allows for crystalline domains to form from the crown ethers upon annealing [32], similar to the block copolymers derived from glassy and crystalline components. Polyesters are highly crystalline and typically do not exhibit glass transitions; however, polyester-based polyrotaxanes show T_g's, dual melting transitions due to two crystalline phases, the polyester and the crown ether, and reduced melt viscosities when compared to control polyesters of similar molecular weights [5,34,35].

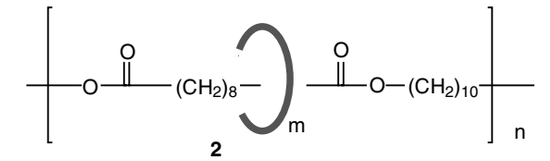

2

a. = 30C10 **b.** = "36C12" **c.** = "42C14"

d. = "48C16" **e.** = "60C20"

A noteworthy feature of the polyurethanes of Table 43.1 is that the model polymer, the first entry, is insoluble in water, dichloromethane and acetone, whereas both the polyrotaxanes derived from ''36-crown-12'' and ''60-crown-20'', **1a** and **1d**, respectively, are soluble in these three solvents [32]. The glass transition temperatures of the polyurethane rotaxanes of Table 43.1 obey the Fox equation (see Fig. 43.1); this is due to the miscibility of the components through hydrogen bonding [31].

The last four entries of Table 43.1 represent a preformed polyurethane and polyrotaxanes derived by threading crown ethers onto it in the melt. Since the backbone molecular weight is constant, this series allows us to discern the effect of ''rotaxanation'' on the intrinsic viscosity. As can be seen in Fig. 43.2, in fact, the intrinsic viscosity increases linearly

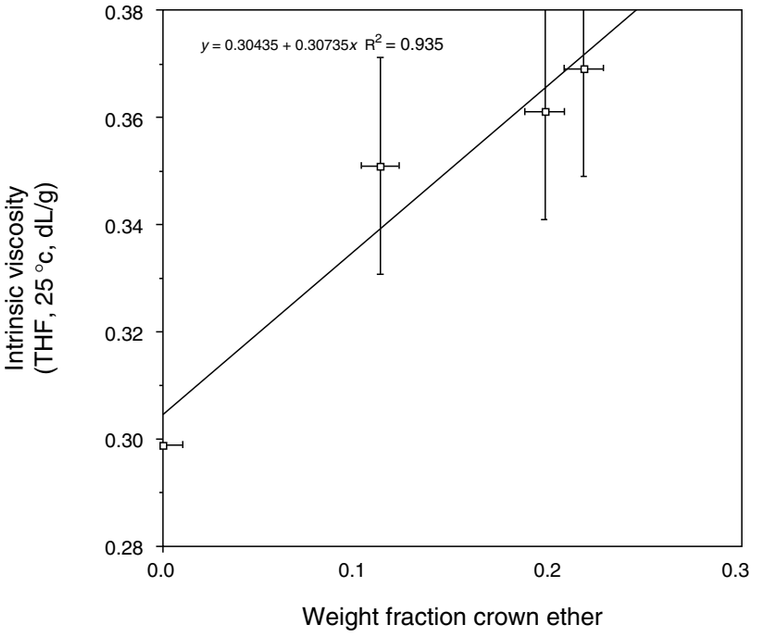

FIGURE 43.2. Plot of intrinsic viscosity vs. weight fraction of crown ether for polyurethane rotaxanes made by threading of a polymer (M_n 16.6 kDa and M_w 58.7 kDa by universal calibration and viscosity detector in NMP at 60 °C) with "42-crown-14" in the melt at 80 °C (last four entries of Table 43.1) [33].

with the crown ether content. This is expected, since the incorporation of the cyclic species increases the hydrodynamic volume of the resultant polyrotaxane relative to the parent polymer.

REFERENCES

1. *Molecular Catenanes, Rotaxanes and Knots,* edited by J. -P. Sauvage and C. O. Dietrich-Buchecker. Wiley-VCH, Weinheim, 1999; Raymo, F. M., and J. F. Stoddart. *Chem. Rev*. 99 (1999): 1, 643.
2. Mahan, E., and H. W. Gibson. In *Cyclic Polymers,* 2d ed., edited by J. A. Semlyen. Kluwer Publishers, Dordrecht, 2000, p. 415, and the references therein; Huang, F., and H. W. Gibson. *Progr. Polym. Sci.* 30 (2005): 982.
3. Panova, I. G., and I. N. Topchieva. *Russ. Chem. Rev*. 70 (2001): 23.
4. Shen, Y. X., D. Xie, and H. W. Gibson. *J. Am. Chem. Soc*. 116 (1994): 537.
5. Gibson, H. W., S. Liu, C. Gong, Q. Ji, and E. Joseph. *Macromolecules* 30 (1997): 3711.
6. Yui, N., T. Ooya, and T. Kumano. *Bioconj. Chem*. 9 (1998): 118.
7. Ooya, T., and N. Yui. *Macromol. Chem. Phys*. 199 (1998): 2311.
8. Watanabe, J., T. Ooya, and N. Yui. *J. Biomater. Sci. Polym. Ed.* 10 (1999): 1275.
9. Watanabe, J., T. Ooya, and N. Yui. *Chem. Lett*. (1998): 1031.
10. Gibson, H. W., and P. T. Engen. *New J. Chem*. 17 (1993): 723.
11. Gibson, H. W., and S. Liu. *Macromol. Symp*. 102 (1996): 55.
12. Huh, K. M., T. Ooya, S. Sasaki, and N. Yui. *Macromolecules* 34 (2001): 2402.
13. Choi, H. S., K. M. Huh, T. Ooya, and N. Yui. *J. Am. Chem. Soc*. 125 (2003): 6, 50.
14. Tamura, M., D. Gao, and A. Ueno. *Chemistry* 7 (2001): 1390.
15. Wenz, G., and B. Keller. *Angew. Chem. Int. Ed. Engl*. 31 (1992): 197.
16. Gong, C., P. B. Balanda, and H. W. Gibson. *Macromolecules* 31 (1998): 5278.
17. Born, M., and H. Ritter. *Makromol. Chem. Rapid Commun.* 12 (1991): 471.
18. Gibson, H. W., C. Gong, S. Liu, and D. S. Nagvekar. *Macromol. Symp*. 128 (1998): 89.
19. Shen, Y. X., C. Lim, and H. W. Gibson. *Polym. Prepr. (Am. Chem. Soc. Div. Polym. Chem.)* 32(1) (1991): 166.
20. Yamaguchi, I., K. Miya, K. Osakada, and T. Yamamoto. *Polym. Bull.* 44 (2000): 247.
21. Gong, C., T. E. Glass, and H. W. Gibson. *Macromolecules* 31 (1998): 308.
22. Gibson, H. W., P. T. Engen, and S.-H. Lee. *Polymer* 40 (1999): 1823.
23. Gong, C., and H. W. Gibson. *J. Am. Chem. Soc*. 119 (1997): 5862.
24. Gong, C., and H. W. Gibson. *J. Am. Chem. Soc*. 119 (1997): 8585.
25. Nagapudi, K., J. Hunt, C. Shepherd, J. Baker, and H. W. Beckham. *Macromol. Chem. Phys*. 200 (1999): 2541.
26. Noll, O., and H. Ritter. *Macromol. Chem. Phys.* 199 (1998): 791.
27. Born, M., T. Koch, and H. Ritter. *Acta Polym.* 45 (1994): 68.
28. Born, M., T. Koch, and H. Ritter. *Macromol. Chem. Phys*. 196 (1995): 1761.
29. Born, M., and H. Ritter. *Angew. Chem. Int. Ed. Engl*. 34 (1995): 309.
30. Gibson, H. W., C. Wu, Y. X. Shen, M. Bheda, A. Prasad, H. Marand, E. Marand, and D. Keith. *Polym. Prepr. (Am. Chem. Soc. Div. Polym. Chem.)* 33(1) (1992): 235.
31. Marand, E., Q. Hu, H. W. Gibson, and B. Veytsman. *Macromolecules* 29 (1996): 2555. Gong, C., and H. W. Gibson. *Angew. Chem. Int. Ed. Engl.* 36 (1997): 2331.
32. Shen, Y. X., and H. W. Gibson. *Macromolecules* 25 (1992): 2058.
33. Gong, C., Q. Ji, C. Subramaniam, and H. W. Gibson. *Macromolecules* 31 (1998): 1814.
34. Gibson, H. W., S. Liu, P. Lecavalier, C. Wu, and Y. X. Shen. *J. Am. Chem. Soc*. 117 (1995): 852.
35. Marand, H., A. Prasad, C. Wu, M. Bheda, and H. W. Gibson. *Polym. Prepr. (Am. Chem. Soc. Div. Polym. Chem.)* 32(3) (1991): 639.

CHAPTER 44

Foldamers: Nanoscale Shape Control at the Interface Between Small Molecules and High Polymers

Morris M. Slutsky, Richard A. Blatchly, and Gregory N. Tew

Contributions from the Chemistry Department at Keene State College and the Polymer Science and Engineering Department at the University of Massachusetts-Amherst

44.1 OVERVIEW

Taking inspiration from biopolymers such as proteins and RNA, foldamer chemists craft such pale imitations as they can, yet these are very complex molecules by our current laboratory standards. What inspires us to imitate certain aspects of biopolymers is that they have behaviors derived from a simple set of organizing principles: sequence derived properties, folding that depends on specific interactions with solvent, the cooperativity in folding that comes from long-chain molecules and the ability to make large structures from intermediate domains that are often of one structural type. To this end, recent attention has focused on creating new molecular backbones, called foldamers, that also fold into well-defined structures like helices and sheets [1–13]. The ability to mimic those aspects of natural systems while using a fundamentally different backbone continues to provide a wonderful challenge.

It is well known that nature folds macromolecules like proteins, RNA, and DNA into defined structures with specific shape and that these shapes are intimately related to their function [14–18]. Tremendous research effort has provided some understanding of how this folding occurs in proteins. In fact, it is now possible to design, from scratch, with great success an unnatural protein sequence which will fold into the predicted secondary structure [19]. However, many of the fundamental questions of biopolymer folding are not yet solved. Careful study of foldamers, which can be designed with more variation than natural biopolymers, can provide an important perspective on this vital problem.

The more complicated design of tertiary and quaternary structure in proteins has been attained in some cases. However, the ability to form hierarchically ordered structures, or self-assemble folded structural units into well-defined higher order assemblies, from any non-natural backbone remains an important unsolved problem. A few preliminary reports, including work on β-peptides and peptoids, with structure beyond the helix were reported recently [20–22]. These two backbones represent the more well studied sequences of foldamers and so initial reports toward structures beyond secondary elements can be expected. However, given more than a decade of foldamer research, little work toward these higher order structures has been reported.

One of the long-standing goals of foldamer research has been to mimic the function of biopolymers. While the focus has been on establishing the principles of folding, there have been some successes in designing shape-dependent function. For example, it was recently shown that β-peptides, peptoids, and simple polymers could capture the antimicrobial activity and selectivity of the natural host defense peptides [23–27]. As foldamer researchers develop more sophisticated structures, we expect many more examples.

Much of the foundation for foldamer research has been generated by the physical organic community and has focused on discrete oligomers. However, progress in fields like protein structure, enzymology, organic chemistry,

biophysics, and polymer science all requires a common knowledge of the structure and function of complex macromolecules. As a result, there is much synergy to be gained through interactions with these various disciplines in which traditional analytical tools from different fields are applied to nontraditional problems. In fact, the application of ''foldamer principles'' to synthetic high polymers is beginning to occur as discussed in the section below entitled ''From Oligomers to High Polymers''. Therefore, one of the goals of this chapter is to introduce foldamers to a wider audience. In addition, an attempt will be made to illustrate the current state of the art with specific focus on the chemical backbone, the use of high polymers, and the dynamics encountered in the folding process.

Since a comprehensive review [28] was completed in 2001, every effort will be made not to duplicate this tome. Additionally, β-peptides have been the subject of several reviews and will be mentioned more briefly than they warrant. Other recent reviews have covered oligoarylamides [29], a brief review of foldamers in general [30], and an article [31] focusing on the secondary structure aspect of foldamers. We will not include polymers like polyphenyl acetylene derivatives, polyisocyanides, and poly(trityl methacrylates) in which the conformations are dominated by nearest neighbor steric interactions, although these macromolecules represent very interesting systems that seem to adopt a limited number of the available conformations in solution [32–35].

44.1.1 Definition

In principle, a foldamer can be any oligomer or polymer which can reproducibly adopt a specific conformation in solution, leading to a single overall 3D shape. Currently there are certain restrictions that have been applied to the concept so that the synthesis and analysis of foldamers is tractable. Effectively, this means that foldamers are monodisperse oligomers of modest length (4–24 monomer units, more or less), with a single backbone chemistry and limited sequence variation making them quite distinct from polymers [36]. Foldamers are also traditionally designed to have some form of secondary structure such as a helix or extended, strand-like conformation.

To describe larger molecules in which a collection of secondary structural units pack into a larger definite structure, Moore suggested that the term ''tyligomer'' be used in place of foldamer. By analogy to protein structure, a tyligomer would contain tertiary (or possibly quaternary) conformations, while the word foldamer would be used for secondary structure components. According to this definition, tyligomers could describe either the assembly of secondary units within a single, larger MW molecule or the assembly of multiple chains into nonbonded complexes, giving rise to quaternary structure. This leads to a point of potential confusion. When used to describe proteins, the term tertiary refers to the association of secondary structural elements within the same molecular backbone while quaternary is used to describe the association of more than one molecular backbone. Most proteins are large molecular weight species and typically fold with both secondary and tertiary structure. In fact, it is rare to find natural proteins with only secondary elements that assemble into quaternary structure (although myosin is one example). In contrast, many foldamers and even de novo peptide designs are created from relatively small molecular weight molecules which only contain secondary structure and, as a result, the issue of how to describe accurately their self-assembly into higher order structures, for example helical bundles, should be addressed. It appears that this has been described as tertiary structure in the literature [22]. Although this intuitively makes sense because it is the next level of order, that is to say that secondary structural elements like helices have associated to make helical bundles, this will be confusing to other researchers coming from the traditional study of biomacromolecular structure.

For the current chapter, we will attempt to avoid the use of these terms but it would be worthwhile for the field as a whole to adopt a consistent nomenclature since the pursuit of higher ordered assemblies is a major on-going effort. One possibility is to use the term tertiary-like structure when describing the associate of secondary elements. Alternatively, if tyligomer is confined to the collection of folded elements within a single larger MW molecule then it could be a very useful term for this next level of order. Then two or more tyligomers could assemble into nonbonded complexes, resulting in what is traditionally quaternary structure.

44.1.2 Goals of Foldamer Research

The table below illustrates a small sample of the potential outcomes from the study of foldamers. This list is meant only to be representative and not inclusive or limiting. Specifically, the table attempts to integrate two classical areas, which are medicinal and materials chemistry. At the same time, much of the study is motivated by fundamental interest in learning how molecules fold and the discovery of geometrically defined shapes.

Foldamer Characteristic	Medicine	Materials	Molecular folding Properties
Sequence-dependent properties	Antibiotics	Information storage	Insight into the nature of protein folding
Designed 3D shape	Gene therapy	Molecular recognition	New elements of secondary structure
Abiotic linker chemistry	Protease resistance	Catalysis	Alternative conformational profiles

44.1.3 Classification

Several helpful attempts to classify this diverse collection of molecules have been made. Moore [28] divides foldamers into classes based primarily on whether they are single stranded or multistranded. These categories were further divided into biotic (or closely related) and abiotic. Such classifications land β-peptides and oligoureas in single-stranded peptidomimetics, while aromatic amides and phenylene ethynylenes are classified as single stranded and abiotic. Nowick's β-strands, Gong's hydrogen bond donor–acceptors, and oligopyridine–metal ion complexes are all multistranded. The β-strands are an excellent example of the difficulty of classification since they are partly biotic and partly abiotic. Both the review of β-peptides by Cheng, Gellman, and DeGrado [13] and the review of foldamers by Cubberley and Iverson [5] categorized the β-peptides according to secondary structure formed. This is helpful if the secondary structure is known rigorously, but not applicable to foldamers in the process of design. In a review of oligoaramides [29], the categories focused more on backbone design than on classification. Although we do not wish to create yet another classification of foldamers due to the likelihood for confusion, we do think it is valuable to consider them from another perspective.

We suggest that a fundamental division be made based on the degree of backbone flexibility. By assigning a degree of freedom score and a linkage type to the foldamer repeat unit, we can focus the primary distinctions on ''backbone space'' as mentioned by Cheng, Gellman, and DeGrado [13]. We have arbitrarily divided foldamers into ''semi-flexible'' foldamers, which includes those that contain two or fewer degrees of conformational freedom per monomer unit and ''flexible'' foldamers with more than two degrees of conformational freedom. Within the torsional freedom assignment, the types of interactions which are primarily responsible for maintaining the folded state were considered. This type of organization is important if true molecular understanding involved in folding is going to emerge.

When determining the degree of freedom score some assumptions, or guidelines, were followed. The ring pucker in oligopyrrolinone backbone units, due to limited flexibility, was not considered here to be a degree of freedom. Although α-aminoxy acids and azatides apparently possess more than two degrees of freedom, they are considered to only have two degrees of freedom per monomer unit due to rotational barriers around the N–O and N–N bonds. The other foldamers in Table 44.1 were relatively straightforward to assign. Although the usual categorizations of foldamers [5, 13, 28, 29] rarely place them together, this type of assignment places α-peptides and aromatic oligopyridines and phenylene ethynylenes (PEs) into the same category.

β-peptides were placed into Table 44.2, although the flexibility of these monomers is often reduced by steric effects associated with the side chain groups and may in practice not always be much more flexible than α-peptides. Due to alkylation of the peptoid amide nitrogen, *cis* conformations are accessible and add a degree of freedom to these monomers. Through this type of classification Table 44.2 finds β-peptides, peptoids, PNAs, and aedamers together. As a whole, it is interesting to note the mixture of biomimetic and nonbiomimetic foldamers found in each category.

44.2 DESIGN

44.2.1 General Issues

Linker Chemistry

Productive foldamer research requires foldamers with certain backbone characteristics. The backbone must be stable, easily synthesized and have some degree of flexibility. It is also helpful to have a well-characterized conformational profile, known intermolecular interactions (such as H-bonding), and good handling characteristics, such as solubility. As shown in Tables 44.1 and 44.2, a wide variety of bond forming reactions have been used to build foldamers. The most popular, by far, is the amide bond; however, other chemistry highlights include ureas, phosphate esters, ethers, aryl ethynylenes, biphenyls, and pyridines.

Body

One could describe the structure connecting one linker functional group to the next as the body of the monomer. The body helps define the flexibility of the monomer unit, the angle between linkers, as well as the number and relationship of the side chains. The chemical nature of the body, in contrast to the sidechains, will often determine the behavior in solvent (see below). A very large group of foldamers has been made with aromatic bodies (both hydrocarbon and heterocyclic), due to well-developed synthesis, rigidity, and chemical resistance. An equally diverse group has been made from aliphatic bodies, such as those in the β-, δ-, and γ-peptides. More rare are bodies based on sugar or phosphodiester groups. Simple geometry determines the angle(s) of attachment, although this can be tuned somewhat by intramonomer hydrogen bonding, for example.

Side Chain

In principle, the chemistry in sidechains can be used to make oligomers more generally soluble, to add solubility contrast (see the solvent section below), to add the ability to pack structures together, to add the ability to bind ions, to name but a few capabilities. Chiral sidechains can add a chiral bias to a system, inducing an enantiomeric excess in an overall chiral shape. The side chain can significantly influence the overall conformational space as observed in β-peptides.

TABLE 44.1. *Semi-flexible monomer units.*

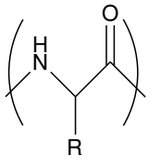	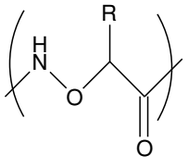	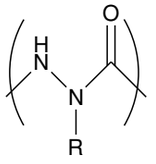	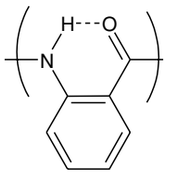
α-peptides	α-aminoxy acids	azatides	oligoanthranilamides (also may incorporate pyridinedicarboxamide units)
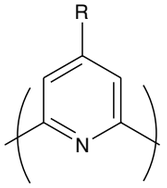	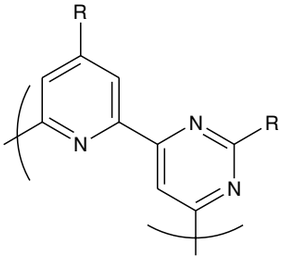	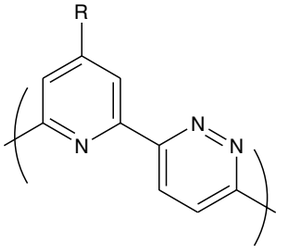	
oligopyridines	pyridine–bypyridines	pyridine–pyrimazines	
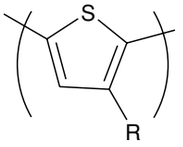	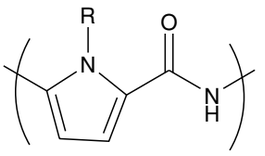	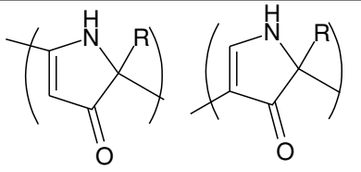	
oligothiophenes	lexitropsins	oligopyrrolinones, 2'-5' and 3'-5' linked	
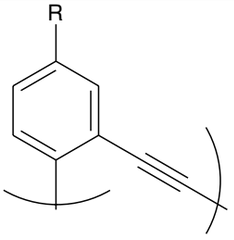	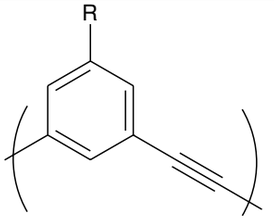	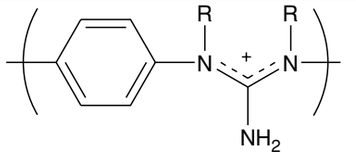	
oligo *ortho*-phenylene ethynylenes	oligo *meta*-phenylene ethynylenes	oligoguanidiniums	

Beyond these general principles, the design of functional sidechains is relatively poorly understood, largely due to their flexibility. While flexibility is probably required for function, it hampers analysis by spectroscopy or crystallography, and makes theoretical analysis more difficult. As more subunit-to-subunit interactions are designed, this will become a vital problem to solve at a more fundamental level.

From Oligomers to High Polymers

As mentioned previously, reports on oligomeric foldamers dominate the current literature (including many excellent reviews). The study of foldamers has captured the attention of macromolecular scientist for more than a decade; however, very little work on truly polymeric samples has been reported, due in large part to the complexity caused

TABLE 44.2. *Flexible monomer units.*

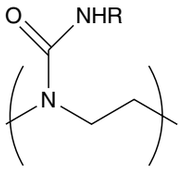	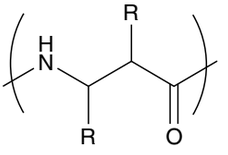	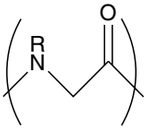	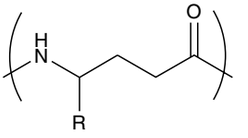
N,N-linked oligoureas	β-peptides	peptoids	γ-peptides
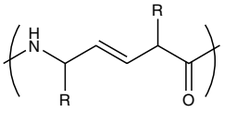	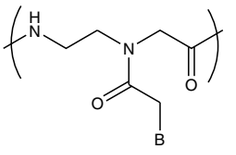	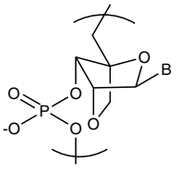	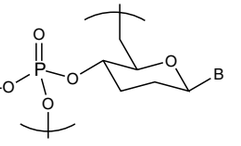
alkene-derived δ-peptides	peptide nucleic acids	bicyclo(3.2.1)-DNA	homo-DNA
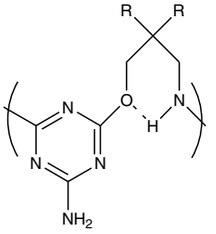	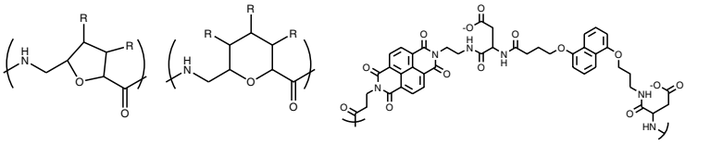		
triazene-based oligomers	carbopeptoids, furanose, and pyranose-derived		an aedamer

by high polymer dispersity (molecular weight, sequence, stereochemistry, etc.). Over the last several years, this situation has begun to change with the number of "foldamer" investigations on polydisperse systems increasing.

One of the earliest reports was the study of cationic poly (*meta*-PE) which exhibited UV and emission profiles similar to Moore's discrete foldamers. The polydisperse samples did not demonstrate cooperative folding transitions apparently due to their relatively small MW and broad MWD [38]. Hecht and coworkers reported Tg functionalized poly(*meta*-PEs) which appeared to fold cooperatively [39]. In their case, the system appeared so stable that the molecules did not completely unfold (the UV and emission curves did not flatten out at high chloroform concentration) preventing a determination of the free energy of folding. Cleverly, a reactive double bond was included within the molecular design so that the folded structure could be covalently captured to eliminate the folding dynamics. TEM images of these captured molecules remain to be reported but should allow individual molecules to be studied. In addition, the self-organization of these molecular objects should be quite unique.

In mid-2004, Schanze reported anionic poly(*meta*-PEs) that show solution photophysical properties in MeOH–water mixtures that are consistent with folding [40]. Principal component analysis allowed the spectra to be deconvoluted into two pure component spectra, which were interpreted as the folded and unfolded states. Calculating the components of free energy gave $\Delta H = -10.8\,\text{kcal mol}^{-1}$ and $\Delta S = -31.5\,\text{cal mol}^{-1}\text{K}^{-1}$ for a $\Delta G_{\text{rt}} = -1.4\,\text{kcal mol}^{-1}$. The negative entropy of folding was attributed to loss of conformational freedom of the backbone.

Chiral polymeric helices based on ureidophthalimide monomers were reported by Meijer and coworkers [41]. Figure 44.1 shows the chemical structure of the repeating monomer for this system as well as two other recently reported polymeric foldamers. Inouye and coworkers reported a series of oligomers and one polydisperse sample based on pyridine containing poly(*meta*-PEs) that folded in the presence of hydrogen bond donating saccharides [42]. Because the paper reported defined-length oligomers as well as high polymers, it represents an excellent bridge between these two categories. More recently, Ghosh and

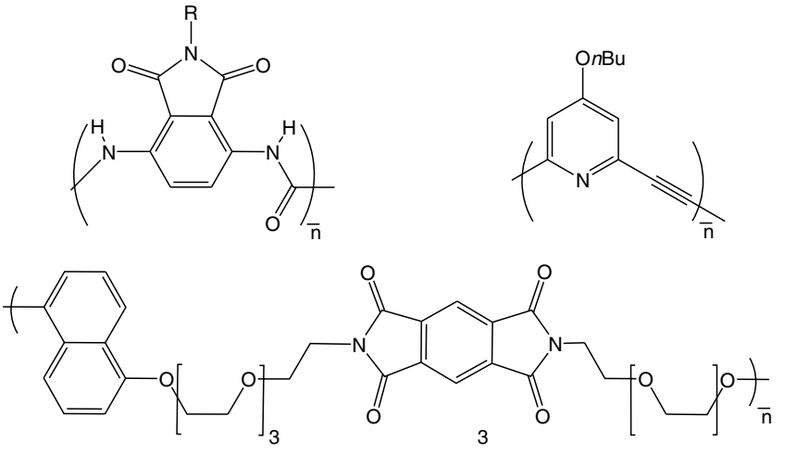

FIGURE 44.1. The chemical structure of three polymeric foldamers. These structures along with PE analogs have been studied as high polymers.

Ramakrishnan reported donor–acceptor polymers that contain three folding elements: alternating aromatic donors and acceptors, linked by oligo(oxyethylene) groups [43]. Folding was driven by the solvophobic effect, or by alkali–metal ion complexation, and characterized by the upfield shift of the NMR signals of aromatic protons shifts or by substantial changes in the UV-Vis spectra.

These early explorations into polymeric foldamers highlight some of the difficulties that will be encountered during this work but also clearly illustrate the promising future of these investigations. It is already quite clear, at this early stage, that the transfer of knowledge from discrete oligomers to high polymers will yield success as well as interesting and unexpectedly novel materials.

Solvent Interactions

Changing solvent conditions can have a tremendous impact on the folding reaction. The well-known denaturing effect of some solvents on proteins was extended to foldamers by Moore, who showed that chloroform leads to a random coil conformation in mPE oligomers while acetonitrile promotes a compact, folded, helical state.

In general, there are two levels at which to address the solvent issue. From a practical and general viewpoint, the observations associated with solvent effects can be understood. A simple principle of solubility contrast between the backbone, which is buried on folding, and the sidechains, which are exposed in both the folded and unfolded states, can explain the general behavior of foldamers quite well. This idea was highlighted by Moore when describing his oligo(mPE)s containing polar Tg units which contrast with the nonpolar aromatic backbone. This architecture was suggested to allow helix formation as the solvent was changed. The concept has similarity to native protein structures which typically have hydrophobic interiors and hydrophilic exteriors. Further, this principle of ''solubility contrast'' between backbone and side chains can, in principle, be any contrasting pairs. What has proved most frequently employed is a polar side chain set with a water-insoluble (nonpolar) backbone. It is also possible to contrast aliphatic sidechains with aromatic backbones, ionic sidechains with nonpolar backbones, or fluorinated sidechains and nonfluorinated backbones. Of course, in all of these systems the sidechain, backbone, and solvent could be inverted. An interesting inversion was also produced by using a basic backbone and sequentially protonating it, causing a reversible unfolding of oligoaramides [44]. Hence, in general, the folding reaction of a system with sufficient contrast between the backbone and the sidechains should be controlled by manipulation of the solvent.

The driving force for this control was termed ''the solvophobic effect.'' This specifically refers to Flory type interactions [45,46]. In general, solvent–polymer interactions are often dominated by enthalpic contributions related to contacts between solvent–solvent, solvent–monomer, and monomer–monomer. However, entropic contributions can also be important. Flory described the problem in great detail establishing the Flory-Huggins polymer–solvent interaction parameter, χ, which is inversely proportional to temperature and thus solely enthalpic [46]. Experiments showing that χ always has an entropic component led to empirical modifications to the theory to correct for entropy. Favorable entropic contributions usually stem from the solvent, as in the hydrophobic effect [47]. The traditional term ''hydrophobic effect'' relates to the special properties of water in which a large entropic penalty is encountered when nonpolar solutes are placed into water. This leads to the hydrophobic interaction in which hydrocarbon elements interact more favorably in water when compared to free space. As a result of these issues, and especially considering the similarity between ''solvophobic'' and ''hydrophobic,''

the term ''solvophobic'' (Flory type of enthalpic interaction of good, theta, and poor solvent) deserves more discussion [48].

The influence of solvent on the folding equilibrium has been explored only in a few cases of foldamers. In β-peptides, several solvents have been studied including TFE, MeOH, and water [13]. Similarly, a study of solvent was performed on oligo(mPE)s which concluded that chlorohydrocarbon solvents like $CHCl_3$, CH_2Cl_2, and 1,2 dichloroethane promoted complete denaturation of the helix but both non-polar solvents like CCl_4 and 1,1,1 trichloroethane (TCE) and very polar solvents like CH_3CN lead to moderate or high degrees of the folded conformation [49]. For this system, the largest contrast between solvents was found between chloroform and acetonitrile, which have been used very productively to study the equilibrium in subsequent work on variously substituted oligo(mPE)s.

Iverson performed a detailed study on a series of aedemer compounds [8] and found a relationship between folding ability and polarity. He concluded that in polar solvents the energies are dominated by hydrophobic interactions (particularly for the protic solvents, which behaved differently from the aprotic ones); however, the geometry and electrostatic complementarity of the aromatic units were able to modulate the magnitude of these interactions as well as the geometry of the association.

Examining the details involved in solvent interactions reveals a story which is particularly complicated by the interplay between enthalpic and entropic components. This is apparent even in Flory's treatment of traditional polymers, where the solutions often apply generally, but not specifically. While Moores' study of solvents showed a general trend toward better folding of his hydrophobic mPE foldamers in more polar solvents [49]; treatment of the data required rejection of chlorinated solvents, and did not include aromatics, apart from the anecdotal evidence that they did not unfold the aromatic backbone. This is a strongly interacting system which will require much more work to understand at a fundamental level.

The difficulties in grappling with the effect solvent has on folding may be more thoroughly understood by examining the set of equilibria in Fig. 44.2. The effect of solvent on the folding equilibrium can be conceptualized by considering the solvation equilibria of the unfolded vs. the folded forms (equilibria **3** and **4**). Each requires the formation of a ''hole'' in the solvent (generally larger in the case of the unfolded than the folded form), and provides different opportunities for specific solvent–solute interactions. Thus, the loss of entropy on formation of the solvent void may be balanced against the favorable enthalpic interactions between the solvent and solute in ways that are particular to each solvent class.

Clarification of the relationships will require consideration of three important factors. First, the role of system entropy should not be underestimated. For the oligo(mPE) series, it was proposed that the chlorohydrocarbon solvents formed favorable dipole CH–π interactions with the aromatic backbone, stabilizing the unfolded form enthalpically. In this case specific interactions with the unfolded form apparently overcome the entropic penalties associated with solvent ordering. However, other solvents capable of strong interactions with the unfolded forms (such as alcohols capable of OH–π interactions) cause folding. Whether this is due to favorable solvent–solvent enthalpic interactions lost in the unfolded form or the loss of solvent entropy in making the larger void for the unfolded form is unknown at this point. Further complicating this problem is the expectation that the structure and stability of the folded form probably changes on solvation. Likewise, the ensemble of unfolded forms may be strongly affected by solvent, leading to both entropic and enthalpic effects.

Secondly, the topology of the folded and unfolded forms may have an impact on the interaction with solvent. Structures with substantial central cavities (like mPE) will likely behave differently from those without the central cavity (such as oPE), as included solvent may have both different composition and different lifetimes compared to bulk. This can complicate comparisons between different structural series.

Thirdly, the repeating nature of foldamers means that polar or hydrophobic substituents on the backbone are brought into close contact in the folded form, while they are usually relatively distant in the unfolded form. The role of solvent in stabilizing or destabilizing this interaction is unknown, and may be significant. The issues of a defined topology and close, specific interactions between sidechain linkers illustrate two very significant differences that result from foldamer architectures when compared with traditional polymers.

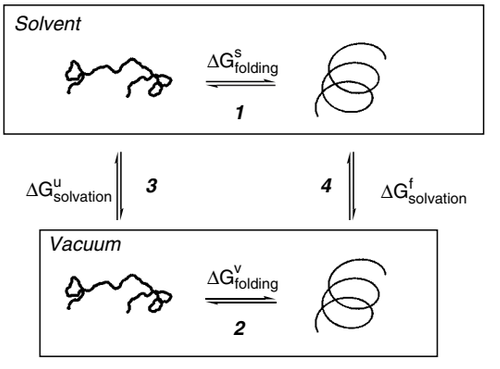

FIGURE 44.2. The equilibria for conceptualizing folding in solvent (1) include the folding reaction in vacuum (2) and the energy involved in solvating each of the separate species (3: unfolded and 4: folded, assuming a two-state model). The effect of solvation is generally different on the folded and unfolded forms, due to the different surface area and types of functionality exposed. Both entropic and enthalpic factors play an important role in understanding solvation. The solvent effect can be defined as:
$\Delta G^{f}_{\text{solvation}} - \Delta G^{u}_{\text{solvation}} = \Delta G^{s}_{\text{folding}} - \Delta G^{v}_{\text{folding}}$

Such notions allow new insight into the design elements for creating foldamer systems while at the same time illustrate the delicate balance between solvent and backbone which should be considered. It is likely that solvent effects will continue to be determined empirically in new backbones for the near future. Nonetheless, the ability to craft structures with a variety of shapes and substituents provides a powerful tool for exploring the solvent effect on folding, an issue of vital importance for understanding and predicting protein folding. It also appears that the chemical diversity and rather simple structures of foldamers make them ideal candidates for addressing these important fundamental questions.

Molecular Modeling

Computational methods have evolved rapidly over the last decade into a powerful tool to guide synthetic and design efforts of complex systems [50–53]. In fact, these tools are now used routinely in the pharmaceutical industry for lead optimization of small molecules and by scientists for protein structures but little effort has focused on their use in abiotic oligomers and their self-organization [23]. Molecular modeling can be useful in choosing reasonable synthetic targets, analyzing kinetic and thermodynamic data, and predicting such aspects of function as small-molecule binding. From the synthetic scientists' viewpoint, extensive amounts of time are spent designing molecules from the essentially unlimited number of combinations and, often, even more effort is involved in synthesizing them. As a result, predictive guidance for backbone and side chain selection would be particularly powerful.

Due to the size of the molecules studied, most work has used molecular mechanics algorithms to carry out the calculations. Modern molecular mechanics is sophisticated enough to answer most questions about predicted molecular structure. For example, a thorough theoretical study of molecular folding in *meta*-phenylene ethynylenes [54] was carried out and validated against both kinetic and thermodynamic measurements in those systems. A theoretical study of *ortho*- and *meta*-phenylene ethynylenes [55] shows that molecular mechanics compares well with both experiment and ab initio calculations [62,62b,62c] for predicting folding energies. This study also pointed out the importance of dipole interactions for foldamer stabilization, which, while they have been examined in protein structure [56–61], have not in the case of non-natural foldamers [3].

Beyond using computation to guide the choice of foldamer backbone and sequence, a few studies have recently investigated the dynamics of the folded conformation. Pande and coworkers examined the folding reaction in an all-atom simulation of an oligo(mPE) dodecamer [54]. They found that the backbone folds via on-pathway intermediate states that can get trapped in misfolded states, much like what one finds in simple models for proteins. This adds dimension to the admittedly simplistic two-state picture of the helix–coil transition. Quantitative characterization of the folding simulations found a marked deviation from exponential kinetics which agreed with experimental findings. Saven and coworkers [62] studied the dynamics of the folded structure of an oligo(mPE) octadecamer and found that the turns of the helix remained in close contact throughout the simulation although the structure exhibited large fluctuations in both the radius of the interior cavity and the effective dihedral angle between monomers. The simulation also showed clearly the presence of water molecules within the hydrophobic cavity. At the same time, the folded helical state was found to be quite flexible which is interesting to consider since the backbone represents a large six-ring aromatic surface.

In principle, information about the unfolded state should be available from molecular modeling. In practice, it is very difficult to obtain, due to the larger ensemble of unfolded molecules, and the difficulty in providing an experimental system for verification. An interesting study by Glattli and van Gurnsturn [63] compared molecular mechanics in the presence of explicit solvent to in vacuo calculations for β-peptide NMR structure calculations leaving the strong conclusion that explicit solvent calculations are superior. While they believed the ensemble of structures to be well-represented, the authors left a cautionary note that 2D-NMR data may often be consistent with more than one solution.

As work continues to represent the backbone correctly, less focus has been placed on the side chains connected to the backbone. This is predominantly related to the difficulty in precisely determining their conformation, although general solutions are relatively easy to predict. However, these interactions can be quite important in the overall energy landscape. Investigations on β-peptides showed that substitutions at positions 2 and 3 favor *gauche* conformations of the monomer, ultimately leading to helix formation [13]. Addition of alkali metal ions to Ramakrishnan's polymeric foldamers helped reduce the entropy of these flexible linkers and promoted folding [43]. No theoretical tools for packing have been developed for nonpeptide foldamers, as they have been for peptides. On the other hand, with improvements in the capabilities of molecular dynamics, one can approach the problem with a general solution. Continued advances in computational methods will surely provide much needed insight into the dynamics of side chains.

44.2.2 Helices

Nomenclature

Difficult nomenclature rapidly increases the barrier for outsiders to become familiar with the field. Table 44.3 shows several of the popular nomenclature styles associated only with β-peptide helices. In accordance with the philosophy adopted by Cheng, Gellman, and DeGrado, we prefer to use the helical nomenclature which provides information on

TABLE 44.3. Nomenclatures for β-peptide helices [13].

Applequist[a]	Subirana[b]	Gellman[c]	Seebach[d]	Helix nomenclature[e]
R_{+2}	2R	14	(P) 3_1	3_{14}
L_{+2}	2L	14	(M) 3_1	3_{14}
L_{-3}		12	(M) 2.5_1	2.5_{12}

[a] The nomenclature describing the helix handedness and hydrogen-bonding patterns between hydrogen-bond donor and acceptor atoms; $R_{\pm n}$ denotes a right-handed helix in which NH_i is hydrogen bonded to $CO_{i\pm n}$, and $L_{\pm n}$ denotes a left-handed helix with the same hydrogen-bonding pattern.
[b] The nomenclature describing the hydrogen-bonding patterns; R and L designate right- and left-handed helical topologies, respectively.
[c] A nomenclature describing the number of atoms comprising the hydrogen-bonded ring formed between donor and acceptor atoms.
[d] Seebach's nomenclature describes the helical symmetry; P and M refer to right- and left-handed helical topologies, respectively.
[e] The nomenclature provides the number of residues contained in one helical turn; the subscript denotes the number of atoms comprising the hydrogen-bonded ring formed between donor and acceptor atoms.

the number of residues contained in one turn (Roman number) and the number of atoms comprising the hydrogen-bonded ring formed between donor and acceptor atoms (subscript). This nomenclature is transferable to other helical structures if the rule for hydrogen bonding is relaxed to include other interactions like π–π stacking. For example, the oligo(mPE) helix is a 6_{30}, assuming a 6 ring repeat and 30 atoms along the interior of the backbone to complete a full turn (Fig. 44.3). Correspondingly, oPE gives a 3_{12} helix, *ortho*phenylene is 3_6, and the aromatic delta peptides are 2.5_{16}. Figure 44.4 shows the x-ray structure for an *ortho*-phenylene oligomer.

Curved Backbone Leads to a Helix

Design for "low flexibility" foldamers is simplified by the ready access to modeling and the predictability of helices or flat forms that can be made. To design a helix, one contemplates a flexible structure with a curved backbone that requires a long sequence to eventually overlap if planar. Classical geometry will predict how many subunits can be added before they begin to overlap. This straight forward principle has been expanded in a recent review [64].

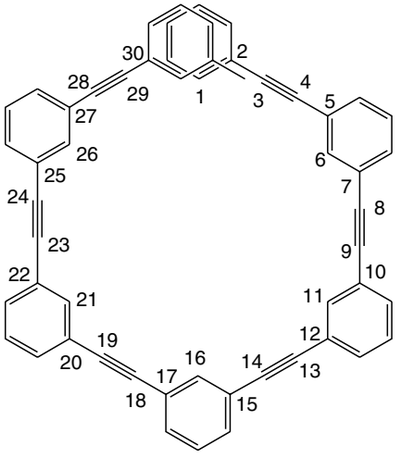

FIGURE 44.3. Repeat of the 6_{30} helix formed by mPE foldamers.

In practice, the larger the size, the more small variations in bond angle will affect the final structure, so these should be considered starting geometries. MD simulations showed the mPE helix to be quite flexible [62]. Gong installed hydrogen bonds around the perimeter of the mPE backbone and showed a helical structure in $CHCl_3$ suggesting a conformationally more confined structure [65]. A comparative MD study of this system would prove insightful.

In addition to the stiffness of the helical structure, the topology of abiotic systems can be quite different. The phenylene ethynylenes provide good examples of the concept of aspect ratio. The helical structure of a *meta* 18-mer, one of the longest sequence prepared, more closely resembles a puck as opposed to a tall cylinder due to the large helical repeat of the *meta* series. The aspect ratio of a *meta* 12-mer is 0.25 vs. 1.33 for the *ortho* as shown in Fig. 44.5. The *meta* systems include an interior cavity that can be used to bind molecules but, at the same time, creates additional surface area and potentially free volume. In fact, when these helical structures were first studied in the solid state, they

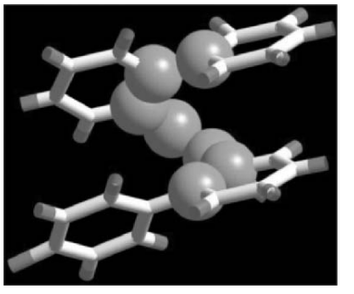

FIGURE 44.4. Crystal structure of *ortho*phenylene oligomer. The seven atoms (six plus the first atom of the next repeat) involved in the helical repeat are shown as spheres.

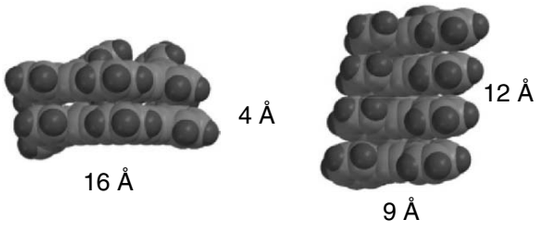

FIGURE 44.5. 12 aromatic ring helix of (left) *meta* and (right) *ortho* PE oligomers (without side chains). *Meta* is wide and short (puck-like) while ortho is tall (rod-like). This illustrates that *o*-PE derivatives will give taller helices than *meta* for the same number of rings.

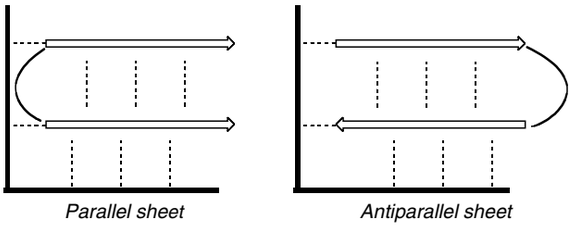

FIGURE 44.6. Schematic representation of sheet structures illustrating the effect of directionality (parallel vs. antiparallel), dashed lines highlight the interstrand interactions, and the potential interactions with adjunct sheet-stabilizing group.

unfolded into extended chain molecules to avoid pore formation. Filling this cavity with methyl groups produced stable helical structures in the solid state [45,66,67].

Manipulation of aspect ratio allows helices to be tuned for purpose: helical bundles require tall cylinder-like objects, while channels may require a low aspect ratio or at least considerable width. High aspect cylinders will also minimize end-to-end contacts, and maximize lateral contacts between helices. Varying the aspect ratio and diameter allows creation of capsules [68].

44.2.3 Sheets

The design of sheets follows fundamentally different principles from the design of helices. Just as it is difficult to produce extended, isolated single sheet structures in peptides, the production of foldamer sheets poses special problems. Nonetheless, it is vital to understand the structures conducive to sheet formation so that complex structures can be designed. This importance is emphasized by the consistency with which progress in the understanding of artificial sheet structures has been reviewed. Nowick's review [69] of models for β-sheets predates the widespread use of the term foldamer. Most progress in models for β-sheets describes work with either α- or β-amino acids teamed up with a β-sheet directing adjunct [5].

General Structural Issues

As illustrated in Fig. 44.6 the traditional sheet structures are relatively linear segments attached by a flexible loop, and held together by some intermolecular forces. In peptide sheets, these forces are complementary hydrogen bonds. For strands with directionality, such as that provided by the peptide bond, ester linkages, or asymetric monomer structures, the strands can be assembled in a parallel, antiparallel, or mixed fashion. Strands containing symmetrical structures such as ureas, guanadines, or alkynes will be called nondirectional.

Within this general description is a much broader allowance for structural variation than has been probed at this point. Since traditional sheets have been assembled with the strongest noncovalent interactions, most models have used the same strong forces to assemble the models. Sheets using synthetic adjunct groups and α-amino acids or β-amino acids dominate the recent work.

For example, Nowick's classic work involved the production of an aminobenzoic acid hydrazide as a β-sheet initiator [70], and coupled the system to a triurea template to make a three-stranded sheet (see Fig. 44.7) [71]. Bartlett's group proposes the @-group, as shown in Fig. 44.8, as a β-strand promoter and has produced a two-stranded structure by mixing α-amino acids with one @-group [72]. These two examples use various monomers, in which the conformation is controlled by specifically designed interstrand interactions.

An interesting example of a conformational switch from helical to sheet structure is given by Zimmerman's work shown in Fig. 44.9 [74]. He synthesized heterocyclic aromatic ureas which were able to hydrogen bond intramolecularly to form a helix, or intermolecularly to form sheet structures. He reported two-strand structures with as many

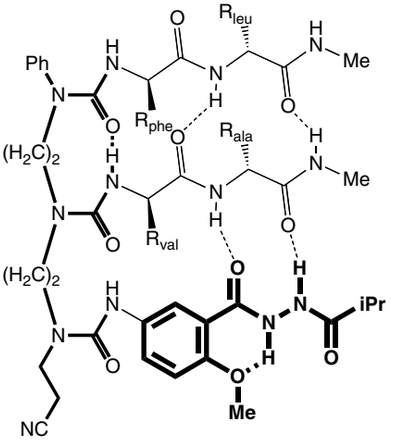

FIGURE 44.7. An example of Nowick's multistranded sheet [71] illustrating the design criteria described above. One axis of alignment, as illustrated in Fig. 44.6, is shown in the thickest lines at bottom. The structure shown aligns peptides from the edge to favor a sheet structure. The other is shown in the thinner bold lines on the left. This polyurea structure tends to orient strands from the ends.

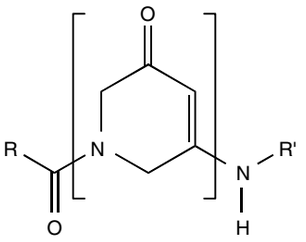

FIGURE 44.8. Bartlett's "@" structure, an extended vinylogous amide which retains planarity, hence stabilizing the sheet form. This "amino acid" can be added by normal peptide coupling methods on solid phase [73].

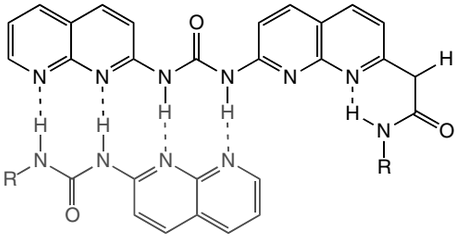

FIGURE 44.9. Zimmerman's hydrogen-bonding system showing the type of hydrogen bonding available to the sheet form on the left with four interstrand H-bonds and the type of intramolecular hydrogen-bonding that leads to the helical structure on the right. This image is meant to represent the possibilities for H-bonding, and was not observed by the authors.

as six intermolecular hydrogen bonds, and a correspondingly strong association constant. It is interesting to note that all of these sheet structures are assembled with quite inflexible unnatural monomers.

Traditionally, the aspect ratio of sheet structures is imagined as substantially larger than 1 as illustrated in Fig. 44.10. There are two exceptions to this rule which should be considered for their potential to mimic sheet structures. The first is Iverson's pleated aromatic structures, which are held together by π-stacking. Made from subunits that are overall quite flexible, they have been extended to many more ''strands'' than hydrogen-bonded sheets. These structures have a different aspect ratio (Fig. 44.10) than the peptide-inspired sheets. As such, they appear to solve one of the problems with isolated sheets by burying more of their surface area in the folded form, thus controlling the problem of nonspecific aggregation and allowing them to be susceptible to solvent control.

While not a completed model of a single-strand sheet, Tew's extended sheet-like structures [75,76] lack only connections between individual strands to fit the definition. In this case, structures were assembled at an air–water interface, and controlled by amphiphilic patterning as well as π-stacking. X-ray studies confirmed an organized sheet-like structure in aqueous solution indicating that the patterning of polar and non-polar functionality is a path to sheet formation [76b]. These strand-like structures were shown to have biological activity similar to many sheet folded peptides [26].

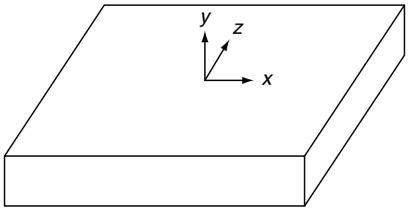

FIGURE 44.10. A sheet structure, propagated in the *z* direction by extending the foldamer chain, will have an aspect ratio of *x*/*y*. Traditionally, this is imagined as substantially larger than 1.

44.2.4 Higher Order Structures

Two independent efforts toward the assembly of helical β-peptides have recently been reported. DeGrado used large hydrophobic groups to fill voids created between two associating helices, which resulted in the stabilization of this fold [36]. Gellman patterned β-peptides with one cationic polar (P) and two nonpolar (NP) side chains and investigated their self-association in aqueous solution by ultracentrifugation, CD, and NMR [37]. They observed sedimentation equilibrium consistent with a monomer–hexamer mixture in which 30–40% of the peptide is hexameric at 1.7 mM. A combinatorial approach to screen amphiphilic structures for assembly in peptoids was also reported [35]. However, given more than a decade of foldamer research, little work toward these higher order, or tertiary-like structures (i.e., beyond secondary elements) has been reported. This next step in complexity is the center of activity for many research groups.

44.2.5 Chimeras

To illustrate the incredible diversity that chimeras (mixed sequences involving different monomer chemistry) can bring to the field, one can examine the work of Li, who designed a molecule mixing the π-stacking ability (and not coincidentally, the UV and fluorescent environmental reporting qualities) of perylene with the hydrogen bonding properties of DNA [77]. This made a rosette with DNA hairpins extending from a perylene core. This rosette could be unfolded by adding single-stranded DNA complementary to the sequence used in the foldamer. To add further intrigue, they found that the structure was actually more strongly folded at higher temperature, due to an endothermic folding (interestingly, this requires that the entropy also be positive). An organic soluble version lacked the DNA sections, and showed more normal temperature behavior with both a negative ΔS and a negative ΔH.

44.3 SYNTHESIS

44.3.1 Oligomer Synthesis

As classical polymer synthesis techniques do not provide sequence specificity, foldamers are commonly synthesized

by linking individual monomers, or small sets of monomers, either by classical organic chemistry or by solid phase synthesis. Many foldamers are linked together by backbone amide bonds, and therefore standard solid-phase peptide synthesis techniques such as Fmoc or Boc chemistry are often used for the synthesis of such foldamers as β-peptides, amide-linked aedamers [10], and peptide nucleic acids [78]. Oligoureas have been synthesized on standard Rink amide resin using Fmoc-protected β-amino acid O-succinimidyl carbamate monomers [79]. Peptoids appear particularly suitable for solid phase methods. Novel solid-phase techniques have been developed by various workers for the purpose of foldamer synthesis as well. Moore and coworkers developed a solid phase protocol [80] to synthesize oligo mPE using a resin-linked triazene and coupling of aromatic *meta* trimethylsilylacetylene iodides by Sonogashira reaction, followed by removal of the TMS group with fluoride. The product is released from the resin by treatment with iodomethane. Spivey *et al*. have designed a germanium-based linker and resin system allowing for solid phase synthesis of oligothiophenes [81]. The initial α-TBDMS-protected thiophene monomers are coupled to the resin as α-organolithium reagents, and the TBDMS group is removed by reaction with fluoride. Subsequent monomers are coupled as α-TBDMS-blocked boronic esters using Suzuki conditions, deprotected with fluoride, and α-iodinated with diiodoethane. The product is released from the resin by treatment with TFA.

Solid phase reaction allows rapid synthesis of long oligomers. Purification of resin-bound intermediates can be accomplished simply by washing the resin. Reaction conditions may be automated for greater productivity. However, there are also drawbacks to solid phase foldamer synthesis. Substantial excesses of monomer are generally required at each step of solid phase synthesis to ensure nearly complete reaction, and recovery of unreacted monomer may be difficult or impossible. Unlike the amino acid derivatives used for solid phase peptide synthesis, foldamer monomers often are not commercially available and therefore are not necessarily available in large quantities and may well be too valuable to waste. Purification at the final stage is always another issue that must be considered with solid phase approaches.

As foldamers are constructed from discrete monomer units, combinatorial methods are applicable to their synthesis. Much research has involved combinatorial construction of libraries of biomimetic foldamers [82]. Combinatorial methods have been used to study nonbiotic foldamers as well. For example, libraries of thiophenes have been studied [83], as have equilibrium mixtures of imine-linked phenylene ethynylenes [84].

Convergent synthesis strategies allow production of longer oligomers than are practically obtainable with stepwise synthesis. These strategies may be employed in conjunction with either solid-phase or solution synthesis. Phenylene ethynylene foldamers have been synthesized by convergent addition of oligomer units to form longer compounds [85,86]. Similar convergent procedures have been used for synthesis of other foldamers, such as oligo PE thiopheneethynylenes [87] and oligopyridines [88]. One potential complication present with PE oligomers, PE thiopheneethynylenes, and other foldamers formed by Sonogashira reactions is dimerization of free acetylene groups, which can complicate purification where oligomers of equal length are coupled, due to similarities in molecular weight between the product and by product. Many of the same techniques used for the purification and characterization of biological oligomers are applicable to foldamers including methods such as FPLC, HPLC, and gel filtration. Following isolation and purification, traditional techniques like NMR, mass spectrometry, UV, and elemental analysis are used to ensure the appropriate foldamer sequence has been generated.

44.4 MEASUREMENT OF FOLDING

44.4.1 General Issues

Because foldamers are designed to have a dynamic structure, testing this feature poses challenges beyond structural characterization. By analogy to peptides, the characterization described in the previous section would produce the primary structure, or sequence. Measurements described here help describe the secondary structure, folding process, and, in a few cases, the higher order assembly. In addition, care must be taken to rule out other processes that could mimic aspects of a folded structure. Systems with random aggregation, or specific dimerization, create the proximity of subunits often observed in folded forms and can be caused by similar changes in solvent or temperature.

The importance of solving this problem, and the difficulty of doing it correctly, is largely responsible for the current use of specific oligomers instead of polymers in these studies. Moderate-length oligomers still yield to high resolution NMR description, and have characteristic responses to changes in environment. In fact, the possession of a series of oligomers of increasing length is vital to solving behavior questions in new or poorly understood systems. Once systems are more thoroughly understood, we may be able to transfer that understanding to an intentional use of larger polymeric systems that may have some synthetic advantages.

As foldamers grow more capable, we will see more studies adding to the few measuring a functional role for the foldamer, such as a small-molecule receptor, ion channel, water channel, and antibacterial activity.

44.4.2 Measuring the Folding Reaction

Considerable success has been achieved with the simplifying assumption that experimental data can be modeled by

the ''two-state'' system [66]. While the unfolded form is a stochastic mixture of conformations, it can be treated as a single entity in most cases. Thus the experimental problem is reduced to the not insignificant task of finding a difference between folded and unfolded forms to mark the relative concentrations of the two. Ideally, this difference should be visible at low concentrations to avoid intermolecular association. These differences are often associated with either a chain-length dependence, or a solvent or temperature dependence, or some combination of the three.

Chain Length Dependence

For the formation of helices which represent the majority of available foldamer studies, the folding reaction should express a clear chain-length dependence. With lengths below the degree of polymerization needed for helix formation (4 monomer units in a 3_{12} helix like the oPE series or 9 monomers in a 6_{30} helix like the mPE series) there should obviously be no signal of helix formation. As lengths grow beyond that threshold, the helix form should be increasingly favored under similar conditions, due to the cooperativity of folding and the diminution of the negative entropic effect of organizing the first few monomer units [28].

Solvent vs. Temperature

Given that the entropy of folding to a single conformation must be negative [3], the most obvious way to control folding is with temperature. In the several cases in which temperature has been used to control folding, the expected melting with an increase in temperature is seen [45,89]. This melting should be relatively sharp as a result of the cooperativity of the folding reaction [66].

Because solvent affects the equilibrium between the folded and unfolded forms, the equilibrium constant can also be obtained through a solvent titration at a fixed temperature [90,91]. The use of this method for systems in which temperatures of unfolding are inconvenient or destructive has gained widespread use since Moore and coworkers pioneered its use in the study of folding in *meta* PE [45]. When the mPE oligomers are dissolved in $CHCl_3$, a good solvent for both the hydrocarbon backbone and ethylene glycol segments, a random conformation is observed. However, when the solvent quality for the backbone is reduced by addition of very polar solvent, like acetonitrile, the backbone collapses to exclude backbone–solvent interactions, leading to helix formation. Using the assumption that the ΔG depends linearly on the solvent content, one can extract ΔG values from the solvent dependence [66].

Whether the temperature or solvent titration method is used, the formation of helices should be accompanied with a chain–length dependent cooperativity, a hallmark of helix formation from a random conformation.

UV and Fluorescence

For monomers with inherent absorption and emission properties, UV-Vis [92–97] and fluorescence spectroscopy [93,96,98–101] make a well-suited pair of techniques, due in part to the low concentrations typically used, which helps avoid aggregation. If the spectra can be rigorously related to folding, these techniques are arguably the most efficient for measuring folding reaction.

UV spectra show a variety of changes on folding, induced by interactions between aromatic chromophores brought into proximity by folding. Shape changes, often an increase in absorbance in the long-wavelength side of the main absorbance band, can be seen. In addition, aromatic chromophores in particular can show hypochromicity (decrease in extinction coefficient per subunit) due to π-stacking, or shape changes in the emission spectra [102].

Two features seen in most aromatic helix forming foldamers are the quenching of fluorescence on folding, and the emergence of a new emission at longer wavelength, which, despite a number of descriptions, is not well-understood. It most likely signals some association between the aromatic units, as it is correlated with folding. To date, fluorescence work has been restricted almost exclusively to steady-state spectra.

Kohmoto's recent article [103] describes both solution and solid-state fluorescence spectra of rigid naphthylimide foldamers. While their molecules were apparently too stable in the folded form to allow measurement of the equilibrium, they did demonstrate quite clearly the red-shift in absorbance and emission.

NMR

The use of NMR is so ubiquitous in foldamer chemistry that we will limit ourselves to those studies directly related to the folding reaction. In addition to establishing structural identity, NMR can be used to measure the rate and equilibrium of the folding reaction, to establish limits for the proximity of specific portions of the foldamer, and to demonstrate the presence of chiral structures.

Chemical shift changes commonly arise from a change in hydrogen bonding, or a change in long-range effects such as the presence or absence of an anisotropic group (aromatic ring, carbonyl, etc.) [65,71,74,103]. These changes should correlate with the oligomer length and solvent effects described above. The use of nuclear Overhauser effect experiments is common for establishing the proximity of folded portions of the molecule across the foldamer spectrum [44,65]. It is common to include a dilution experiment to establish the absence of aggregation. In at least one case, the dilution experiment was used to measure dimerization equilibria [74].

Dynamic NMR can be used to quantify the rates of helix inversion or dimerization if the process occurs at a rate

within the NMR timescale [104,105]. The use of proton lifetimes is illustrated by the recent work of Gong [106]. In an interesting twist, the use of chiral shift reagents can establish the presence of chiral structures (such as helices) in the absence of enantiomeric excess [104,107].

Infrared

The use of infrared to probe the details of interactions (especially in hydrogen-bonded systems) was demonstrated nicely by Keiderling's group [108]. Coupling the use of specific isotopic labeling with the aid of ab initio calculations for the analysis, they were able to establish the pattern of cross-strand coupling in a β-hairpin peptide.

44.4.3 Chirality

While helices are inherently chiral, they form a racemic mixture unless a chiral bias is provided. In such cases where a bias is present, circular dichroism (CD) provides detailed information for proving the presence, but rarely the magnitude, of an enantiomeric excess [109]. While it should also be possible to determine the absolute configuration of the enantiomer in excess, this is considerably more difficult, and has not yet been reported. X-ray crystallographic analysis (next section) can also address the chirality of a helix, but does not directly address the species in solution. The use of fluorescence CD should prove useful for emissive chiral foldamers. One should be careful not to discount the contribution from unfolded forms, a problem which can afflict any system [110].

One factor in favor of the induction of observable chirality is the effect of chiral amplification [111,112]. This is also known as the "sergeants and soldiers" effect [111]. These effects can be either intramolecular or intermolecular [113], and is often the result of complex equilibria [114]. The article by Masu *et al*. reflects the problem of chiral induction. They found that the *S*-phenylethyl group was not sufficient to induce a measurable population difference between the two helix forms, while the *S*-napthylethyl group was [103]. Many experiments have been reported including the addition of chiral side chains which allows CD spectroscopy to be used, seclusion of chiral hosts into the cavity created by helix formation, chiral salts around the helix, EPR, and solid state x-ray studies [3,67,115,116]. A direct comparison between intermolecular and intramolecular chiral induction was possible in the case of a pyridinecarboxamide system where the intramolecular induction was considerably more effective [113].

44.4.4 X-Ray

Because of the ability to locate atoms precisely, single-crystal x-ray structure determination is a vital tool for foldamer scientists. However, whether it is used to measure folded forms [104,107,117] or unfolded ones [118], the additional step of proving a relationship between the solution structure and the crystal structure [93,107] must be taken.

44.4.5 Binding of Foldamers to Small Molecules

While the study of small-molecule binding has not been unimportant, there have been few reports aside from Moore's rod-like substrate [119], and related articles [94] which focus on that function. Exceptions include the oligopyridine ethynylenes [42] and the work of Li on the association of oligohydrazide foldamers with saccharides [98]. These oligomers made helices with large (ca. 10 Å) cavities that, with hydrogen bonding groups inside the cavity, created a system that bound saccharides. This was studied by induced CD (presumably the saccharide binds preferentially to one handedness of the helix, perturbing the equilbrium), change in the inherent fluorescence of the oligomer on binding, and by NMR chemical shift changes. No crystal structure of the complex has been achieved, but a combination of NMR NOESY experiments and molecular modeling provides a very plausible structure for the complex.

44.4.6 Other Techniques

A long list of other techniques has been employed for selected studies and includes EPR, ultracentrifugation, EM, VPO, and calorimetry. A nitroxide spin-label was used to establish helix repeat patterns in mPE oligomers [120].

44.5 FUTURE

As we look out into the 21st century, foldamers have a rich and promising future. As many arms of science push interdisciplinary science, foldamers provide an immense landscape to develop a common language, employ a host of diverse tools, and expand our knowledge of fundamental principles that apply broadly across disciplines. Advances in macromolecular chemistry and analytical tools will continue to spur more elaborate primary structures and their resulting complex folded conformations. Beyond structure, endowing foldamers with biological and material functions remain a formidable challenge but critically important research goal. The successes in these areas are just emerging. A look back at the short, but relatively prolific, history of foldamers demonstrates their value and convinces one that the future will be at least equally enjoyable.

REFERENCES

1. K. D. Stigers, M. J. Soth and J. S. Nowick, Curr. Opin. Struct. Biol. **3**, 714 (1999).
2. A. E. Barron and R. N. Zuckermann, Curr. Opin. Chem. Biol. **3**, 681 (1999).

3. D. J. Hill, M. J. Mio, R. B. Prince, T. S. Hughes and J. S. Moore, Chem. Rev. **101**, 3893 (2001).
4. H. Q. Zeng, X. W. Yang, R. A. Flowers and B. Gong, J. Am. Chem. Soc. **124**, 2903 (2002).
5. M. S. Cubberley and B. L. Iverson, Curr. Opin. Chem. Bio. **5**, 650 (2001).
6. B. Gong, Chem. Eur. J. **7**, 4336 (2001).
7. R. D. Parra, H. Q. Zeng, J. Zhu, C. Zheng, X. C. Zeng and B. Gong, Chem. Eur. J. **7**, 4352 (2001).
8. M. S. Cubberley and B. L. Iverson, J. Am. Chem. Soc. **123**, 7560 (2001).
9. H. Q. Zeng, H. Ickes, R. A. Flowers and B. Gong, J. Org. Chem. **66**, 3574 (2001).
10. A. J. Zych and B. L. Iverson, J. Am. Chem. Soc. **122**, 8898 (2000).
11. J. Q. Nguyen and B. L. Iverson, J. Am. Chem. Soc. **121**, 2639 (1999).
12. S. H. Gellman, Acc. Chem. Res. **31**, 173 (1998).
13. R. P. Cheng, S. H. Gellman and W. F. DeGrado, Chem. Rev. **101**, 3219 (2001).
14. W. F. Degrado, Z. R. Wasserman and J. D. Lear, Science **243**, 622 (1989).
15. L. Z. Song, M. R. Hobaugh, C. Shustak, S. Cheley, H. Bayley and J. E. Gouaux, Science **274**, 1859 (1996).
16. D. Fass, R. A. Davey, C. A. Hamson, P. S. Kim, J. M. Cunningham and J. M. Berger, Science **277**, 1662 (1997).
17. N. Ban, P. Nissen, J. Hansen, P. B. Moore and T. A. Steitz, Science **289**, 905 (2000).
18. W. F. DeGrado, Chem. Rev. **101**, 3025 (2001).
19. L. Baltzer, H. Nilsson and J. Nilsson, Chem. Rev. **101**, 3153 (2001).
20. T. S. Burkoth, E. Beausoleil, S. Kaur, D. Z. Tang, F. E. Cohen and R. N. Zuckermann, Chem. Biol. **9**, 647 (2002).
21. R. P. Cheng and W. F. DeGrado, J. Am. Chem. Soc. **2002**, 11564 (2002).
22. T. L. Raguse, J. R. Lai, P. R. LePlae and S. H. Gellman, Org. Lett. **3**, 3963 (2001).
23. G. N. Tew, D. H. Liu, B. Chen, R. J. Doerksen, J. Kaplan, P. J. Carroll, M. L. Klein and W. F. DeGrado, Proc. Natl Acad. Sci. USA **99**, 5110 (2002).
24. E. A. Porter, X. F. Wang, H. S. Lee, B. Weisblum and S. H. Gellman, Nature **404**, 565 (2000).
25. Y. Hamuro, J. P. Schneider and W. F. DeGrado, J. Am. Chem. Soc. **121**, 12200 (1999).
26. L. Arnt, K. Nusslein and G. N. Tew, J. Polym. Sci., Polym. Chem. **42**, 3860 (2004).
27. J. A. Patch and A. E. Barron, J. Am. Chem. Soc. **125**, 12092 (2003).
28. D. J. Hill, M. J. Mio, R. B. Prince, T. S. Hughes and J. S. Moore, Chem. Rev. **101**, 3893 (2001).
29. I. Huc, Eur. J. Org. Chem. 17 (2004).
30. R. P. Cheng, Curr. Opin. Struct. Biol. **14**, 512 (2004).
31. A. R. Sanford, K. Yamato, X. Yang, L. Yuan, Y. Han and B. Gong, Eur. J. Biochem. **271**, 1416 (2004).
32. M. M. Green, J. W. Park, T. Sato, A. Teramoto, S. Lifson, R. L. B. Selinger and S. J. V. Angew. Chem., Int. Ed. **38**, 3138 (1999).
33. T. Nakano and Y. Okamoto, Chem. Rev. **101**, 4013 (2001).
34. K. Maeda, S. Okada, E. Yashima and Y. Okamoto, J. Polym. Sci.; Polym. Chem. **39**, 3180 (2001).
35. R. Nomura, H. Nakako and T. Masuda, J. Mol. Catal. A Chem. **190**, 197 (2002).
36. In this chapter, the term oligomer is reserved specifically to mean a single MW sequence while polymer will be used only for samples with MW distributions. These polymers may or may not be composed of molecules with exactly identical sequences which characterize oligomers..
37. T. L. Raguse, J. R. Lai, P. R. LePlae and S. H. Gellman, Org. Lett. **3**, 3963 (2001).
38. L. Arnt and G. N. Tew, Macromolecules **37**, 1283 (2004).
39. S. Hecht and A. Khan, Angew. Chem. Int. Ed. **42**, 6021 (2003).
40. C. Y. Tan, M. R. Pinto, M. E. Kose, I. Ghiviriga and K. S. Schanze, Adv. Mater. **6**, 1208 (2004).
41. J. J. van Gorp, J. A. J. M. Vekemans and E. W. Meijer, Chem. Commun. **1**, 60 (2004).
42. M. Inouye, M. Waki and H. Abe, J. Am. Chem. Soc. **126**, 2022 (2004).
43. S. Ghosh and S. Ramakrishnan, Macromolecules **38**, 676 (2005).
44. C. Dolain, V. Maurizot and I. Huc, Angew. Chem., Int. Ed. **42**, 2738 (2003).
45. J. C. Nelson, J. G. Saven, J. S. Moore and P. G. Wolynes, Science **277**, 1793 (1997).
46. P. J. Flory, Principles of Polymer Chemistry, Cornell University Press, Ithaca, New York, (1953).
47. J. N. Israelachvili, Intermolecular and Surface Forces, Academic Press, New York, (1985).
48. C. Reichardt, Solvents and Solvent Effects in Organic Chemistry, 3rd, Wiley-VCH, Weinheim, (2003).
49. D. J. Hill and J. S. Moore, Proc. Natl Acad. Sci. USA **99**, 5053 (2002).
50. M. A. Willis, B. Bishop, L. Regan and A. T. Brunger, Structure **8**, 1319 (2000).
51. C. M. Summa, A. Lombardi, M. Lewis and W. F. DeGrado, Curr. Opin. Struct. Biol. **9**, 500 (1999).
52. A. Sikorski, A. Kolinski and J. Skolnick, Biophys. J. **75**, 92 (1998).
53. P. B. Harbury, J. J. Plecs, B. Tidor, T. Alber and P. S. Kim, Science **282**, 1462 (1998).
54. S. P. Elmer and V. S. Pande, J. Chem. Phys. **121**, 12760 (2004).
55. R. A. Blatchly and G. N. Tew, J. Org. Chem. **68**, 8780 (2003).
56. S. Popa, Z. Simon and L. Kurunczi, Rev. Roum. Chim. **45**, 83 (2000).
57. R. L. Baldwin, J. Biol. Chem. **278**, 17581 (2003).
58. K. C. Chou and C. Zheng, Biophys. J. **63**, 682 (1992).
59. S. M. Butterfield, P. R. Patel and M. L. Waters, J. Am. Chem. Soc. **124**, 9751 (2002).
60. C. D. Tatko and M. L. Waters, J. Am. Chem. Soc. **124**, 9372 (2002).
61. S. E. Kiehna and M. L. Waters, Protein Sci. **12**, 2657 (2003).
62. O. S. Lee and J. G. Saven, J. Phys. Chem. B **108**, 11988 (2004).

62b. B. Adisa, D. A. Bruce, J. Phys. Chem. B. **109**, 19952 (2005).

62c. B. Adisa, D. A. Bruce, J. Phys. Chem. B. **109**, 7548 (2005).

63. A. Glattli and W. F. van Gunsteren, Angew. Chem., Int. Ed. **43**, 6312 (2004).
64. C. Schmuck, Angew. Chem., Int. Ed. **42**, 2448 (2003).
65. X. W. Yang, L. H. Yuan, K. Yamamoto, A. L. Brown, W. Feng, M. Furukawa, X. C. Zeng and B. Gong, J. Am. Chem. Soc. **126**, 3148 (2004).
66. R. B. Prince, J. G. Saven, P. G. Wolynes and J. S. Moore, J. Am. Chem. Soc. **121**, 3114 (1999).
67. M. J. Mio, R. B. Prince, J. S. Moore, C. Kuebel and D. C. Martin, J. Am. Chem. Soc. **122**, 6134 (2000).
68. J. Garric, J.-M. Leger and I. Huc, Angew Chem., Int Ed. ACIEE, **44**, 1954 (2005).
69. J. S. Nowick, Acc. Chem. Res. **32** 287 (1999).
70. J. S. Nowick, K. S. Lam, T. V. Khasanova, W. E. Kemnitzer, S. Maitra, H. T. Mee and R. Liu, J. Am. Chem. Soc. **124**, 4972 (2002).
71. J. S. Nowick, E. M. Smith, J. W. Ziller and A. J. Shaka, Tetrahedron Lett. **381**, 727 (2002).
72. S. T. Phillips, L. K. Blasdel and P. A. Bartlett, J. Org. Chem. **70**, 1865 (2005).
73. S. T. Phillips, M. Rezac, U. Abel, M. Kossenjans and P. A. Bartlett, J. Am. Chem. Soc. **124**, 58 (2002).
74. P. S. Corbin, S. C. Zimmerman, P. A. Thiessen, N. A. Hawryluk and T. J. Murray, J. Am. Chem. Soc. **123**, 10475 (2001).
75. L. Arnt and G. N. Tew, J. Am. Chem. Soc. **124**, 7664 (2002).
76. L. Arnt and G. N. Tew, Langmuir **19**, 2404 (2003).

76b. T. Kim, L. Arnt, E. Atkins, G. N. Tew, Chem. Eur. J. **12**, 2423 (2006).

77. W. Wang, W. Wan, H. H. Zhou, S. Niu and A. D. Li, J. Am. Chem. Soc. **125**, 5248 (2003).
78. R. Hamzavi, T. Happ, K. Weitershaus and N. Metzler-Nolte, J. Organomet. Chem. **689**, 4745 (2004).
79. A. Violette, M. C. Averlant-Petit, V. Semetey, C. Hemmerlin, R. Casimir, R. Graff, M. Marraud, J. P. Briand, D. Rognan and G. Guichard, J. Am. Chem. Soc. **127**, 2156 (2005).
80. J. S. Moore, J. C. Nelson and J. K. Young, J. Org. Chem. **61**, 8160 (1996).
81. A. C. Spivey, D. J. Turner, M. L. Turner and S. Yeates, Synlett **1**, 111 (2004).
82. M. J. Soth and J. S. Nowick, Curr. Opin. Chem. Biol. **1**, 120 (1997).
83. C. A. Briehn and P. Bäuerle, J. Comb. Chem. **4**, 457 (2002).
84. K. Oh, K. S. Jeong and J. S. Moore, J. Org. Chem. **68**, 8397 (2003).
85. M. T. Stone and J. S. Moore, Org. Lett. **6**, 469 (2004).
86. T. V. Jones, M. M. Slutsky, R. Laos, T. F. A. d. Greef, G. N. Tew, J. Am. Chem. Soc. **127**, 17235 (2005).
87. G. R. Li, X. H. Wang, J. Li, X. J. Zhao and F. S. Wang, Synth. Commun. **35**, 115 (2005).

88. J. Uenishi, T. Ueno, S. Hata, K. Nishiwaki, T. Tanaka, S. Wakabayashi, O. Yonemitsu and S. Oae, Heterocycles **50**, 341 (1999).
89. T. V. Jones, R. A. Blatchly and G. N. Tew, Org. Lett. **5**, 3297 (2003).
90. C. N. Pace, Methods Enzymol. **131**, 266 (1986).
91. A. Jasanoff and A. R. Fersht, Biochemistry **33**, 2129 (1994).
92. X. Yang, L. Yuan, K. Yamato, A. L. Brown, W. Feng, M. Furukawa, X. C. Zeng and B. Gong, J. Am. Chem. Soc. **126**, 3148 (2004).
93. J. L. Hou, M. X. Jia, X. K. Jiang, Z. T. Li and G. J. Chen, J. Org. Chem. **69**, 6228 (2004).
94. M. T. Stone and J. S. Moore, Org. Lett. **6**, 469 (2004).
95. G. J. Gabriel, S. Sorey, and B. L. Iverson, J. Am. Chem. Soc. **127**, 2637 (2005).
96. X. Zhao, M. X. Jia, X. K. Jiang, L. Z. Wu, Z. T. Li and G. J. Chen, J. Org. Chem. **69**, 270 (2004).
97. M. T. Stone, J. M. Fox and J. S. Moore, Org. Lett. **6**, 3317 (2004)..
98. J. L. Hou, X. B. Shao, G. J. Chen, Y. X. Zhou, X. K. Jiang and Z. T. Li, J. Am. Chem. Soc. **126**, 12386 (2004).
99. J. T. Ernst, J. Becerril, H. S. Park, H. Yin and A. D. Hamilton, Angew. Chem. Int. Ed. **42**, 535 (2003).
100. C. Tan, M. R. Pinto and K. S. Schanze, Chem. Commun. 446 (2002).
101. L. Brunsveld, J. A. Vekemans, J. H. Hirschberg, R. P. Sijbesma and E. W. Meijer, Proc. Natl. Acad. Sci. USA **99**, 4977 (2002).
102. W. Y. Yang, R. B. Prince, J. Sabelko, J. S. Moore and M. Gruebele, J. Am. Chem. Soc. **122**, 3248 (2000).
103. H. Masu, M. Sakai, K. Kishikawa, M. Yamamoto, K. Yamaguchi and S. Kohmoto, J. Org. Chem. **70**, 1423 (2005).
104. H. Jiang, J. M. Leger and I. Huc, J. Am. Chem. Soc. **125**, 3448 (2003).
105. I. Huc, V. Maurizot, H. Gornitzka and J. M. Leger, Chem. Commun. 578 (2002).
106. L. Yuan, H. Zeng, K. Yamato, A. R. Sanford, W. Feng, H. S. Atreya, D. K. Sukumaran, T. Szyperski and B. Gong, J. Am. Chem. Soc. **126**, 16528 (2004).
107. H. Jiang, J. M. Leger, C. Dolain, P. Guionneau and I. Huc, Tetrahedron **59**, 8365 (2003).
108. V. Setnika, R. Huang, C. L. Thomas, M. A. Etienne, J. Kubelka, R. P. Hammer and T. A. Keiderling, J. Am. Chem. Soc. **127**, 4992 (2005).
109. N. Berova and K. N. Nakanishi, Exciton Chirality Method: Principles and Applications.
110. A. Glattli, X. Daura, D. Seebach and W. F. van Gunsteren, J. Am. Chem. Soc. **124**, 12972 (2002).
111. M. M. Green, J. W. Park, T. Sato, A. Teramoto, S. Lifson, R. L. Selinger and J. V. Selinger, Angew. Chem., Int. Ed. **38**, 3138, (1999)..
112. E. Yashima, K. Maeda and T. Nishimura, Chem. Eur. J. **10**, 43 (2004).
113. V. Maurizot, C. Dolain and I. Huc, Chemistry, Eur. J. Org. Chem. 1293 (2005).
114. H. Jiang, C. Dolain, J. M. Leger, H. Gornitzka and I. Huc, J. Am. Chem. Soc. **126**, 1034 (2004).
115. R. B. Prince, J. S. Moore, L. Brunsveld and E. W. Meijer, Chem. Eur. J. **7**, 4150 (2001).
116. L. Brunsveld, E. W. Meijer, R. B. Prince and J. S. Moore, J. Am. Chem. Soc. **123**, 7978 (2001).
117. V. Maurizot, C. Dolain, Y. Leydet, J. M. Leger, P. Guionneau and I. Huc, J. Am. Chem. Soc. **126**, 10049 (2004).
118. S. Shotwell, P. M. Windscheif, M. D. Smith and U. H. Bunz, Org. Lett. **6**, 4151 (2004).
119. A. Tanatani, T. S. Hughes and J. S. Moore, Angew. Chem. Int. Ed. **41**, 325 (2002).
120. K. Matsuda, M. T. Stone and J. S. Moore, J. Am. Chem. Soc. **124**, 11836 (2002).

CHAPTER 45

Recent Advances in Supramolecular Polymers

Varun Gauba and Jeffrey D. Hartgerink

Department of Chemistry and Bioengineering 6100 Main Street, Rice University, Houston, TX 77005

Typically polymers are defined as a long string of ''mers'' arranged linearly or in a variety of branched configurations and connected by strong covalent bonds. These materials are produced by the ton and account for billions of dollars annually. Clearly these materials have extremely important properties and price/performance ratio. Despite their amazing success there are some properties which are difficult or impossible to obtain from traditional polymers. These include the ability to form and disassemble under specific environmental conditions, the ability to accurately control molecular and nanostructure at multiple level of size hierarchy and generally to be ''smart'', responsive materials. One approach to achieve there desirable properties is to make polymer whose mers are held together by multiple weak noncovalent bonds that can be formed and broken in a predictable, controllable and reversible fashion.

These supramolecular polymers are stabilized by noncovalent forces like hydrogen bonding, pi–pi interactions, metal complexation, and the hydrophobic effect. They have unique properties of reversibility and stabilization by additive directional forces, which although not so strong on their own, give rise to stable systems by summation of all the forces. Natural systems like the DNA double helix and protein folding are a result of the ''bottom-up'' self-assembly of small biomolecules like DNA bases, amino acids in a specific fashion and orientation. Protein structure is maintained by interplay of supramolecular interactions like hydrogen bonding and hydrophobic effect. Fibrillin, main component of microfibrils, is stretchy because of the presence of folded beta-sheet domains, which fold in relaxed state and unfold when they are stretched [1]. These natural systems, with their complex architecture and diverse functions, have always fascinated and inspired people to prepare materials with novel properties. Design of structures trying to mimic self-assembly of protein units in TMV is one such example. Supramolecular forces play an important role in defining the properties of covalent systems too. For example, the presence of hydrogen bonding in covalent polymers like nylons greatly improves their material properties.

Unlike conventional polymers in which the ''mers'' are bound together by string covalent bonds, the supramolecular polymers are assembled together by the process of self-assembly, thereby leading to the formation of a multicomponent aggregate spontaneously and in accordance with the thermodynamic requirements. A homoaggregate, comprising of monomers of same kind or a heteroaggregate, comprising of monomers of different kinds can be formed. As the self-assembly is taking place by co-operative interactions of many weak supramolecular forces, the aggregate formed has the property of reversibility, thereby making the aggregate self-correcting so that it reaches the most stable thermodynamic state and also responsive to external stimuli like pH change, temperature change, stress, and so on. Monomer components associate with each other specifically, followed by hierarchical organization of the associated monomers in complex architectures with an appropriate termination to give rise to systems with the desired properties and applications. Each step from monomer association, hierarchical organization to guided termination is crucial for the generation of materials with unique and novel properties.

Recently several good review on this subject have appeared [2–5] and therefore we limit the scope of this review to only those advances published from 2002 to the present.

Zubarev and coworkers have prepared a branched amphiphile system based on polybutadiene (PB) and poly (ethylene oxide) (PEO) which can assemble into cylindrical or spherical micelles depending on the geometry of the mer, solvent composition and the temperature [6].

The monomer studied is a 12 arm star-shaped molecule with alternate PB and PEO chains connected to a rigid aromatic core, made up of aryl esters. The monomer has a rigid biphenyl chain which connects the aromatic core to PB or PEO chain. It is synthesized from a V-shaped molecule,

six of which get connected by ester bond to the hydroxyl groups on the aromatic core. In aqueous medium at room temperature, V-shaped amphiphiles form spherical micelles of approximately 18 nm diameter, whereas star-shaped amphiphiles form one dimensional cylindrical structure of about 20 nm diameter and up to 300 nm length (Fig. 45.1). Theoretically, both V- and star-shaped molecules should form spherical micelles, as PEO (which is hydrophilic) has same volume fraction in both. But the presence of rigid aromatic core in the case of star-shaped amphiphiles hinders the close association of PEO and PB chains, making PB arms interact unfavorably with water and thereby forcing the amphiphiles to aggregate with each other and form a cylinder. Also, the presence of biphenyl groups plays a role in preventing the close association of the arms, thereby furthering the formation of cylindrical but not a spherical structure. PB forms the core and PEO forms the corona in the aqueous solution.

In hexane, the assembly is reversed and PEO forms the core and PB the corona. TEM studies reveal the formation of discrete structures of diameter of around 2 μm, which do not form any further assembly. On increasing the magnification, it can se seen that these spherical structures are composed of threads with a diameter of about 20 nm, which is the cylindrical assembly of the amphiphiles. This is a named ''cotton ball'' structure, owing to the similarities with a cotton ball. Two hierarchical levels of self-organization have been observed: the formation of the cylinders and the subsequent formation of spherical structures.

The formation of these microscale spherical structures is observed to be thermo-reversible. These structures are formed by heating the solution of star-shaped amphiphiles in hexane to about 60°C and then cooling it to room temperature followed by aging for several hours. No structure is observed in the hot solution in hexane. Decreasing solubility of PB at room temperature or a partial crystallization of PEO is responsible for the formation of the spheres.

Thus, the transition from a V-shaped to star-shaped amphiphiles greatly affects the type of self-assembled structures that are formed. As the arms are not able to associate

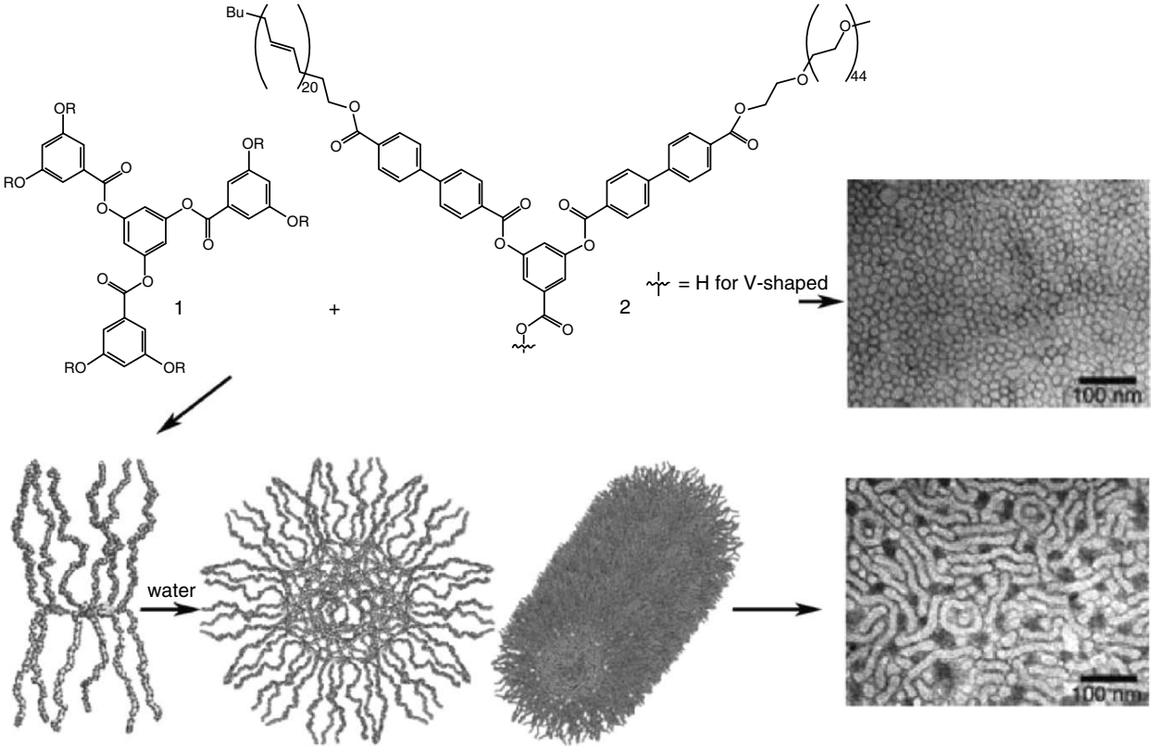

FIGURE 45.1. Illustration of self-assembly of star-shaped amphiphile (formed from 1 and 2) into a cylindrical micelle of around 20 nm diameter, 300 nm length and the assembly of V-shaped into spherical micelles of 18 nm diameter. Reprinted by permission from Angewandte Chemie International Edition (Xu et al. 2004). Copyright 2004 John Wiley & Sons, Inc.

closely, it affects the crystallization process and thus leads to the formation of noncrystalline PEO core in hexane, verified by the observation of winding cylindrical structures in high-resolution TEM. Interestingly, both regular (in water) and reverse (in hexane) structures are observed in case of branched amphiphiles, whereas only regular structures have been reported in case of linear amphiphiles, which is suggestive of the ability of branched amphiphiles to form complex and new morphologies.

Recently, Stupp and coworkers designed self-assembling peptide-amphiphile molecules, which form one-dimensional cylinders in aqueous solution having diameter of approximately 7 nm and micron scale lengths [7].

The monomeric unit of peptide-amphiphile (PA) is shown in Fig. 45.2. These PA have a long hydrophobic alkyl chain and a hydrophilic head group made of a sequence of various amino acids. Hydrophilic group is a bit bulkier than the hydrophobic group, thereby leading to the formation of cylindrical micelles. The four consecutive cysteine residues take part in the covalent capture of the self-assemble structure. Three glycine residues provide the head group flexibility, followed by the presence of a phosphorylated serine residue which binds with metal ions and further helps in the assembly. At the C-terminal end, there is a sequence which is known to help in cell adhesion [8].

These monomeric units self assemble under the appropriate conditions (length of the hydrophobic tail, pH of the solution, cross-linking region) to give rise to cylindrical micelles. The self-assembly is mainly because of the hydrophobic effect, but is complimented by the formation of a β-sheet like hydrogen bonding network oriented down the length of the self-assembled fiber. A self-supporting gel is formed on lowering the pH or adding divalent cations. This makes the molecule neutral so that it can undergo self-assembly. At neutral pH, the negative charges on the PA prevent it from self-assembling thereby hindering the formation of supramolecular structures. Formation of the disulfide bonds after the self-assembly help in the covalent capture of the formed fiber.

The strategy of using a relatively small, derivatized peptide to form a fiber and display a particular chemical functionality has the advantage that multiple chemical functionality can be mixed together to possible synergistic effects simply by mixed two different solutions of peptide amphiphile [9,10]. The system is also flexible enough to allow branched peptide systems and incorporation of a variety of unnatural amino acids [11].

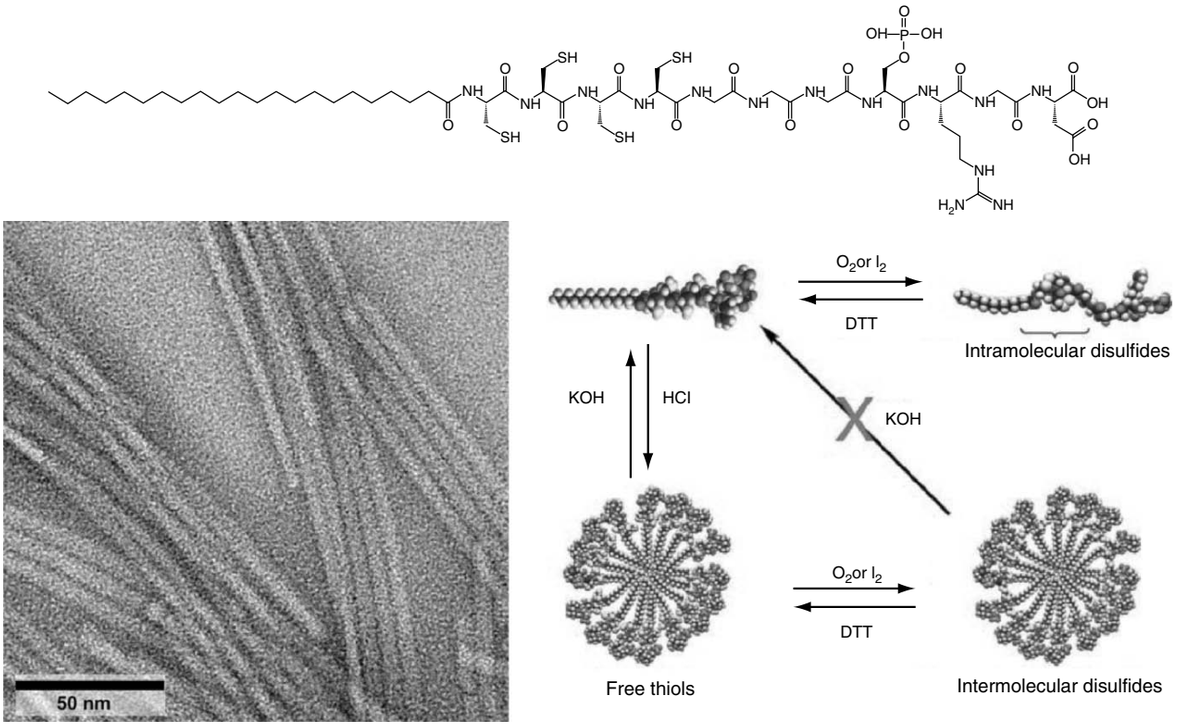

FIGURE 45.2. Illustration of self-assembly of PA's on the basis of oxidation state and pH. Self-assembly is observed at acidic pH, which is reversible at basic pH in the reduced form and irreversible in oxidized form. TEM shows the fibers formed from the PA molecule. Reprinted by permission from Proceedings of the National Academy of Sciences (Hartgerink et al. 2002). Copyright 2002 National Academy of Sciences, U.S.A.

The self-assembled structure formed by this method has very interesting properties. The versatility of the C-terminal of the peptide makes it a good scaffolding material for the formation of crystals or the adhesion to particular cells. This portion of the peptide can be further modified to incorporate properties like catalysis and bioactivity.

Using ''Orthogonal'' supramolecular interactions is a novel way of tuning self-organizing polymers by various external stimuli. Schubert and coworkers used this property of metal co-ordination and hydrogen-bonding to synthesize a novel polymer precursor which has a metal co-ordination site on one end and a hydrogen-bonding site on the other [12].

The monomeric unit used in the studies in shown in Fig. 45.3. It is based on poly(ε-caprolactone) with a terpyridine ligand (for metal complexation) at one end and an ureidopyrimidone group (for hydrogen bonding) on the other end. The polymeric spacer is used to control the solubility in various solvents, in such a way that both hydrogen-bonding and metal-complexation can take place simultaneously. This unit shows a good solubility in chloroform.

The ureidopyrimidone motif is hydrogen bonded in chloroform. On addition of $FeCl_2$ and $(CH_3COO)_2Zn$, iron(II) complexes, and zinc(II) complexes are obtained, respectively, with both of them soluble in chloroform. On addition of ammonium hexafluorophosphate (counterion exchange), the polymer is precipitated. The polymer is film-forming and is transparent at lower film thickness.

Capillary viscosimetry experiments on iron and zinc complexes showed a very high relative viscosity as compared to the starting precursor, supporting the formation of high molecular weight polymers. Viscosity is also temperature dependent, with a sudden viscosity decrease observed around 60–66°C and also around 90–120°C. The first range is because of the melting of the poly(ε-caprolactone) backbone, and the second steep fall can be attributed to the weakening of the co-ordinate bonds in the metal complex.

The complex formation is highly reversible, as verified by the experimental results. HEEDTA (hydroxyethyl ethylenediaminetriacetic acid) acts as a very strong chelating agent for transition-metal ions. Addition of HEEDTA with $CHCl_3$/MeOH decolorized the purple colored solution of iron complex, caused by the uncomplexation of the terpyridine motifs. Addition of $FeCl_2$ resulted in immediate recoloring to purple color, indicating the reformation of metal-complex.

These polymers show interesting photophysical and electrochemical properties, thereby making them of potential interest for use in devices with solar cells and light emitting diodes. With the variation of the length and type of polymeric spacers, these properties can be modified to have tailored properties.

Percec and coworkers have described the self-assembly of the fluorinated tapered dendrons, which can then lead to the formation of the supramolecular liquid crystals with interesting electronic and optoelectronic properties [13].

Semifluorinated tapered dendron, which are functionalized with electron donor (like D1) and electron acceptor (like A1) groups, self-assemble to give rise to columns 2 nm in diameter, with a core made of electron donor–acceptor (EDA) complexes (Fig. 45.4). Both donor and acceptor can be attached to the apex of the dendrons or one of them can be attached to the dendron and the other one to a polymer chain (like AP1 and DP1), which leads to the insertion of the polymer chain in the core. Carbazole derivative is used as a donor and 4,5,7-trinitrofluorenone-2-carboxylic acid (TNF) is used as an acceptor. Diethylene glycol or tetraethylene glycol spacers are used between the D and A groups and the dendrons. The column is stabilized by the pi–pi stacking of the phenyl group in fluorenones and dendrons.

The columns formed further self-organize into homeotropic liquid crystal domains, having various morphologies ranging from hexagonal columnar to centered and simple rectangular columnar. Self-assembly is driven by the fact that there is an increase in contact surface area upon cooperative packing, thereby leading to an added stabilization.

Three types of organizations are observed: self-assembly, co-assembly, and assembly with the polymer chain. Dendrons of the same type (D or A) can come together to form

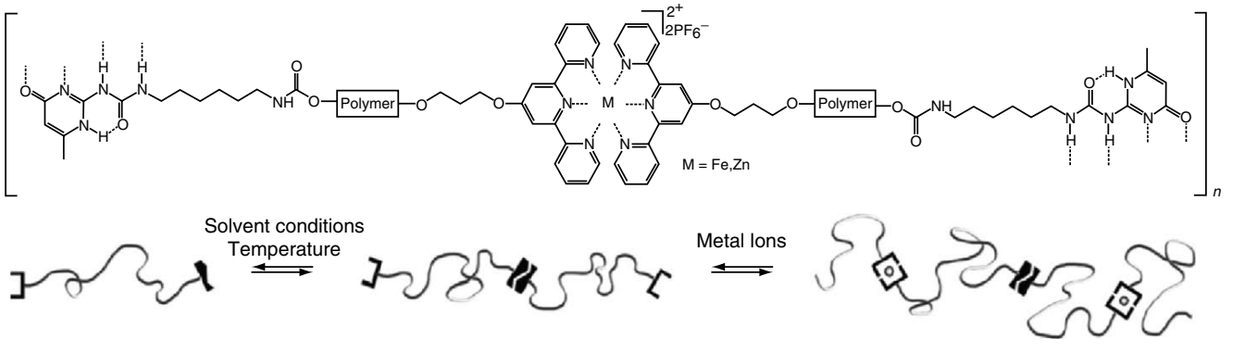

FIGURE 45.3. Illustration of the supramolecular polymer with orthogonal hydrogen bonding and metal complexation interactions. The metal complex formation is highly reversible, with the presence of HEEDTA breaking the complexes and addition of ferrous chloride reforming them. Reprinted with permission from Journal of American Chemical Society (Hofmeier et al. 2005). Copyright 2005 American Chemical Society.

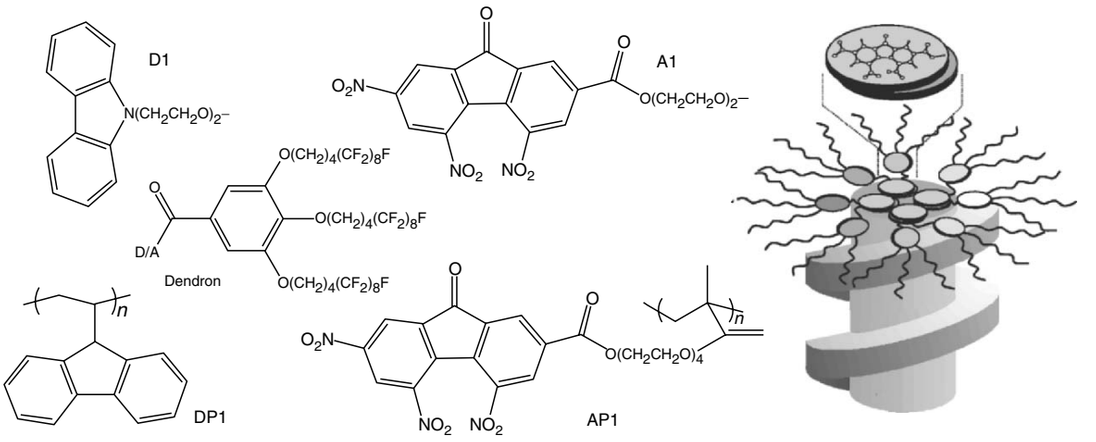

FIGURE 45.4. Illustration of the structure of semifluorinated dendron functionalized with different donors (D1, DP1) and acceptor groups (A1, AP1). Supramolecular columns with fluorenone stacks sandwiched in center are depicted. Reprinted by permission from Nature (Percec et al. 2002) Copyright 2002 Macmillan Publishers Ltd.

columns which give rise to centered–rectangular columnar (for A) or hexagonal columnar (for D). This is self-assembly. Dendron type D can co-assemble with dendron type A to form an EDA complex in the centre of the column. Also, disordered polymers having A and D side groups can form EDA complexes when type A polymer is mixed with type D dendron and vice versa.

From XRD and NMR data, it is proposed that the column adopts a supramolecular structure where the fluorenone sandwiches are stacked in the center of the column, and surrounded by dendrons with phenyl groups arranged in a helical fashion.

Liquid crystals incorporate the advantages of organic single crystals in having excellent mobilities, but they are generally hard to process. Percec and coworkers have devised a simple way to form supramolecular liquid crystals, with or without the incorporation of amorphous polymer chain in the core of the columns. The electron and hole mobilities of liquid crystals of D type dendrons, A type dendrons, and EDA polymer complexes (10–4 to 10–3 cm2V-1s-1) are 2–5 orders of magnitude higher than the corresponding values in the amorphous state (10–8 to 10–5 cm2V-1s-1). The mobility values of D type dendrons are similar to complex discotic liquid crystals. These properties make these materials highly suitable for applications in the field of electronics and optoelectronics.

Block co-polymer which use reversible supramolecular interactions like hydrogen bonding can form materials with interesting properties. As the interactions are reversible, more control can be exercised and the properties can be minutely controlled. Meijer and coworkers have designed an ureidotriazine (UTr) based systems, which on combination with poly (ethylene/butylenes) give rise to rod-coil systems [14].

The monomers used in this study are shown in Fig. 45.5. 1 has two hydrogen bonding motifs with trialkoxyphenyl substituents which are linked by a small six carbon linker. It forms the rigid-rod-like portion of the supramolecular polymer. 2 and 3 have poly (ethylene/butylenes) chains which are connected to one or two UTr units, respectively. These form the random coil portion of the supramolecular polymers.

In alkane solvents, formation of helical columns for 1 is observed, owing to solvophobic effect and hydrogen bonding interactions. 2 form copolymers with 1, as it evident from the decrease in viscosity of the solution of 1 in alkane solvent (dodecane) and also by the CD studies on achiral 1 and chiral 2. 2 works as chain-stopper by substituting 1 and thus stops the further growth of the column. Instead, 3 forms copolymers which can continue growing on both the sides, as it contains hydrogen bonding motifs on both the ends.

Atomic force microscopy (AFM) studies indicate the formation of supramolecular copolymers of 1 with 2 and 3 even in bulk. Aggregates resembling fibers, with a thickness of around 42 nm (in case of 1 and 3 blend), were observed in 1:1 (weight percent) blend of 1 with 2 and 3, as shown in the Fig. 45.5. A phase separation is observed in bulk when the sample is annealed at 60°C for 1 hour, resulting in the separation between domains of 1 and 3, thereby leading to the formation of clusters of around 90 nm in thickness.

The interesting thing about systems where there are self-complementary monomers is that there is no limit on the size of the block to be formed and its length can be controlled by varying the conditions according to the specific requirements, thereby making the system more tunable. Also, the ability to phase separate along with the reversibility of hydrogen bonding interactions makes these copolymer a very good model on basis of which new materials with better properties can be designed.

There have been a lot of efforts to mimic the naturally occurring assemblies. Lehn and coworkers have designed a synthetic helical subunit which winds around a cationic strand in the same way as protein subunits in tobacco mosaic

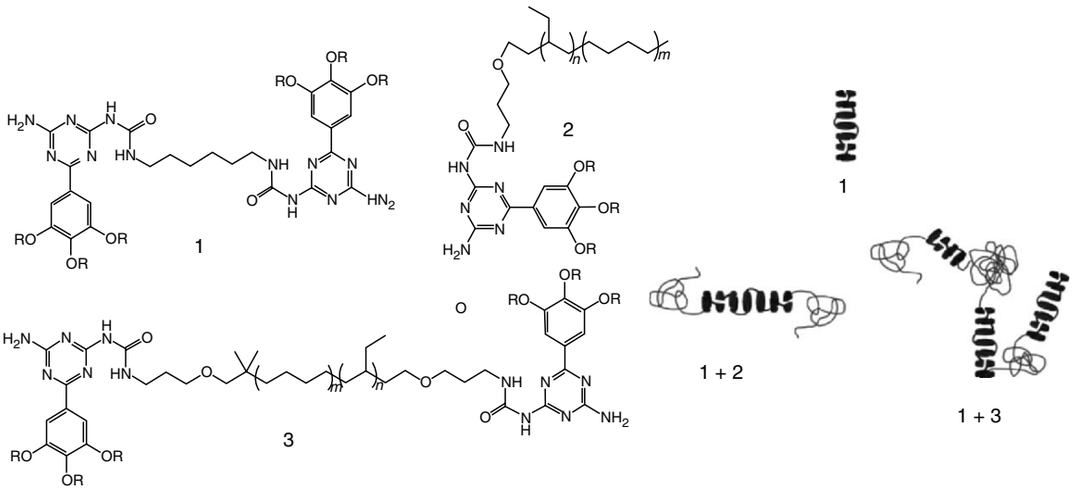

FIGURE 45.5. Illustration of organization of 1 in helical columns with itself and in block copolymers with 2 and 3. Randon coils shown in the figure are formed by poly(ethylene/butylene) which is functionalized with one or two ureidotriazine units. Reprinted with permission from Macromolecules (Hirschberg et al. 2003). Copyright 2003 American Chemical Society.

virus (TMV) self-assemble around viral RNA [15]. The length of the supramolecular tower is controlled by the length of the cationic strand, similar to the control exercised by the viral RNA.

A naphthalene based oligomer, (Fig. 45.6) is the precursor for the formation of such a supramolecular tower. Ortho-linked azaheterocycles, in their transoid conformation, pre-organize the oligomer into a helix. The inside of this helix is suited for complexation with cationic guests, which interact via van der Waal interactions and ion–dipole interactions, leading to the formation of polymolecular assemblies of the oligomer. These assemblies compare well with the pH-based and salt-induced assemblies of TMV in aqueous solutions.

The cationic strand used has several secondary amine groups separated by methylene groups with naphthyl groups on both the sides. On mixing the oligomer with these cationic strands, an assembly is observed which is confirmed by the presence of the corresponding peaks in ESMS spectrum. The efficiency of stacking depends greatly on the length of the methylene spacer between two amine groups. For molecule **1** (Fig. 45.6), the unsaturated complex is observed as a major product and the saturated complex is present as minor product. This selection is reversed when the cationic strand is molecule **2**. Thus, increasing the length of the spacer by one C greatly affects the binding of the oligomer to the strand. This can be explained by considering the space requirement of the stacking of the oligomers. The helical units need to have a spacing of more than 3.5 Å between them to take care of the van der Waal steric interactions, which is possible only in case of molecule **2** (with separation of two amine sites by 5 Å) and not in case of molecule **1** (with separation of only about 3.8 Å, in anti conformation). It is also observed that the fully saturated complex for **2** is formed specifically when the oligomer is mixed with different types of strands, in spite of the fact that this assembly has a very high entropic cost.

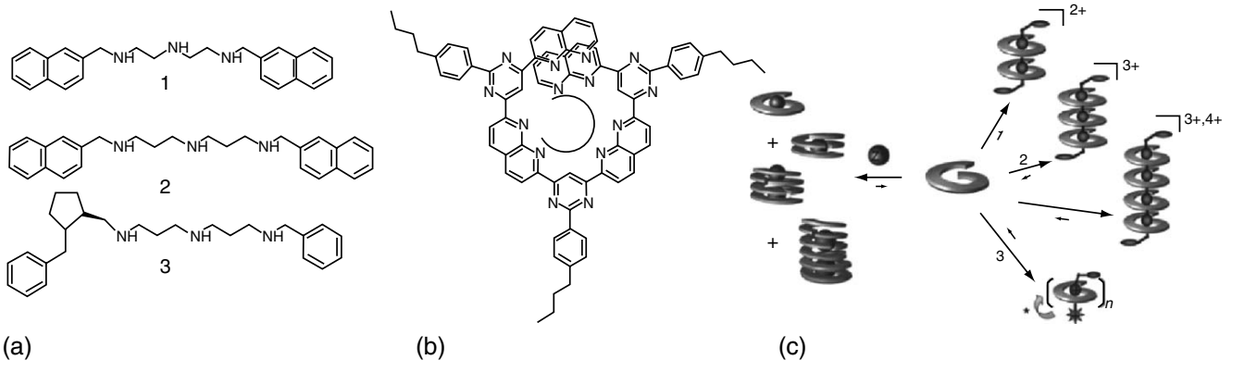

FIGURE 45.6. Illustration of the achiral (1 and 2) and chiral (3) cationic strands, naphthalene based oligomer (b) and supramolecular organization of the cationic strands. Reprinted by permission from Angewandte Chemie International Edition (Patitjean et al. 2004). Copyright 2004 John Wiley & Sons, Inc.

Also, on increasing the number of amine groups, it becomes possible to associate a unit of oligomer on even an uncharged nitrogen site, showing that the van der Waal and ion–dipole forces between the oligomers units stacked on one another are enough to keep the oligomer in place. Use of chiral cationic strands (molecule **3**, Fig. 45.6) lead to the induction of chirality in the self-assembly, which was confirmed by CD studies.

Mimicking natural systems like proteins, peptides and DNA to form supramolecular materials, although difficult is a well paying approach. Woolfson and coworkers have designed assemblies based on peptides; especially one's based on alpha-helical coiled coil systems. Polar, linear, microscale fibers of approximately 45 nm thickness are observed [16].

They used two complementary peptides in the study, which on self-assembly form sticky ends. Each peptide consists of N-terminal half (positively charged, basic), C-terminal half (negatively charged, acidic), and an asparagines residue, as depicted in Fig. 45.7.

The dimers assemble by the interaction of the asparagines residues and by specific coiled–coil interactions, leading to the formation of a longitudinally growing double-stranded coiled coil. After a certain length is reached, these formed fibrils can assemble laterally to give rise to fiber bundles stabilized by electrostatic interaction between adjacent positive and negative ends. It acts as polar substituents for the further addition of any one type of peptide. CD spectroscopy, X-ray fiber diffraction, and FTIR spectroscopy confirmed the formation of linear, microscale fibers of thickness of 45 nm, 20 times the expected thickness of a coiled coil.

Fiber bundle formation can be observed by using fluorescein and rhodamine labeled peptides and analyzing by confocal fluorescence microscopy. It was also confirmed that the bundles assemble in a polar way, by adding fluorescein and rhodamine labeled peptides one after another and observing the correct order of the colored (red followed by green) fibers.

The polarity of the assembly can be attributed to the fact that the starting peptide itself is polar, with a marked separation of charges between the N-terminal (positively charged) and C-terminal (negatively charged). Thus, the heterodimer and the subsequent assembly will be polar too, thereby leading to the addition of the peptide only from one direction.

Microtubules, actin filiments, and intermediate filaments also show such a polar assembly in natural systems. A simple system like this, designed from complementary peptides, can give a lot of information about self-assembly process occurring in natural systems. Also, the ability of the fiber to grow specifically in one direction can be controlled to give rise to fibers of microscale dimensions, paving a way for the generation of biomaterials useful in the field of nanobiotechnology.

The supramolecular polymers offer many advantages compared to conventional polymers. The foremost of them is the property of reversibility, which is altogether missing in the conventional polymers. Because of the presence of multiple co-operative forces in the supramolecular polymers, novel and unique properties are observed in the materials. Self-correcting behavior, ability to form complex architectures with relative ease as compared to the conventional polymers are some of those properties. The synthesis of supramolecular polymers which have the attractive properties of traditional polymers, along with the unique properties of supramolecular systems can go a long way in the generation of complex materials with a whole new range of properties, with applications as of yet unforeseen. Although supramolecular polymers are better than traditional polymers in some of the aspects, they lack in some too. As supramolecular polymers are based on the weak interactions as compared to the covalent bonds in traditional polymers, they are useful only under the conditions which allow the interplay of these different kinds of interactions. Extreme temperature and stress conditions typically destabilize the supramolecular interactions thereby rendering them ineffective.

Collectively these examples give a general overview of Supramolecular Polymers, ranging from those stabilized by only one type of supramolecular interaction to those which require more than one kind of interactions to give stabilized systems. Some of the systems are quite complex, but they are yet to reach the level of complexity in their biological counterparts. One of the greatest problems lies in the synthesis of the building blocks. The long-term goal should be to design systems which are synthetically more viable, and are technologically pertinent.

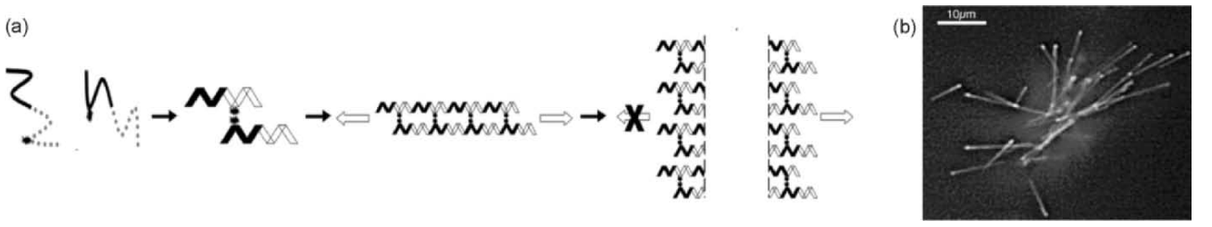

FIGURE 45.7. Illustration of a peptide with basic N-terminal half (solid lines), acidic C-terminal half (broken lines) and a single asparagines residue (starred), leading to assembly of a sticky-ended heterodimer (step 1). The heterodimer first assembles longitudinally (step 2) followed by lateral assembly (step 3). Reprinted by permission from Angewandte Chemie International Edition (Smith et al. 2005). Copyright 2005 John Wiley & Sons, Inc.

REFERENCES

1. Baldock, C.; Koster, A. J.; Ziese, U.; Rock, M. J.; Sherratt, M. J.; Kadler, K. E.; Shuttleworth, C. A.; Kielty, C. M., "The supramolecular organization of fibrillin-rich microfibrils". *J. Cell Biol*. **2001,** 152, 1045–1056.
2. Moore, J. S., "Supramolecular polymers". *Curr. Opin. Colloid Interface Sci*. **1999,** 4, 108–116.
3. Brunsveld, L.; Folmer, B. J. B.; Meijer, E. W.; Sijbesma, R. P., "Supramolecular polymers". *Chem. Rev*. **2001,** 101, 4071–4097.
4. Hartgerink, J. D.; Zubarev, E. R.; Stupp, S. I., "Supramolecular one-dimensional objects". *Curr. Opin. Solid State Mater. Sci*. **2001,** 5, 355–361.
5. Schmuck, C.; Wienand, W., "Self-complementary quadruple hydrogen-bonding motifs as a functional principle: From dimeric supramolecules to supramolecular polymers". *Angew. Chem. Int. Ed*. **2001,** 40, (23), 4363–4369.
6. Xu, J.; Zubarev, E. R., "Supramolecular assemblies of starlike and V-shaped PB-PEO amphiphiles". *Angew. Chem. Int. Ed.* **2004,** 43, 5491–5496.
7. Hartgerink, J. D.; Beniash, E.; Stupp, S. I., "Peptide-amphiphile nanofibres: A versatile scaffold for the preparation of self-assembling materials". *Proc. Natl. Acad. Sci. USA* **2002,** 99, (8), 5133–5138.
8. Silva, G. A.; Czeisler, C.; Niece, K. L.; Beniash, E.; Harrington, D. A.; Kessler, J. A.; Stupp, S. I., "Selective differentiation of neural progenitor cells by high-epitope density nanofibers". *Science* **2004,** 303, (5662), 1352–1355.
9. Niece, K. L.; Hartgerink, J. D.; Donners, J. J. J. M.; Stupp, S. I., "Self-assembly combining two bioactive peptide-amphiphile molecules into nanofibers by electrostatic attraction". *J. Am. Chem. Soc*. **2003,** 125, (24), 7146–7147.
10. Behanna, H. A.; Donners, J. J. J. M.; Gordon, A. C.; Stupp, S. I., "Coassembly of amphiphiles with opposite peptide polarities into nanofibers". *J. Am. Chem. Soc*. **2005,** 127, (4), 1193–1200.
11. Guler, M. O.; Soukasene, S.; Hulvat, J. F.; Stupp, S. I., "Presentation and recognition of biotin on nanofibers formed by branched peptide amphiphiles". *Nano Lett*. **2005,** 5, (2), 249–252.
12. Hofmeier, H.; Hoogenboom, R.; Wouters, M. E. L.; Schubert, U. S., "High molecular weight supramolecular polymers containing both terpyridine metal complexes and ureidopyrimidinone quadruple hydrogen-bonding units in the main chain". *J. Am. Chem. Soc*. **2005,** 127, (9), 2913–2921.
13. Percec, V.; Glodde, M.; Bera, T. K.; Miura, Y.; Shiyanovskaya, L.; Singer, K. D.; Balagurusamy, V. S. K.; Heiney, P. A.; Schnell, I.; Rapp, A.; Spiess, H. W.; Hudson, S. D.; Duan, H., "Self-organization of supramolecular helical dendrimers into complex electronic materials." *Nature* **2002,** 419, 384–387.
14. Hirschberg, J. H. K. K.; Ramzi, A.; Sijbesma, R. P.; Meijer, E. W., "Ureidotriazine-based supramolecular copolymers". *Macromolecules* **2003,** 36, 1429–1432.
15. Patitjean, A.; Nierengarten, H.; Dorsselaer, A. v.; Lehn, J.-M., "Self-organization of oligomeric helical stacks controlled by substrate binding in a tobacco mosaic virus like self-assembly process". *Angew. Chem. Int. Ed*. **2004,** 43, 3695–3699.
16. Smith, A. M.; Acquah, S. F. A.; Bone, N.; Kroto, H. W.; Ryadnov, M. G.; Stevens, M. S. P.; Walton, D. R. M.; Woolfson, D. N., "Polar assembly in a designed protein fiber." *Angew. Chem. Int. Ed*. **2005,** 44, 325–328.

CHAPTER 46

Conducting Polymers: Electrical Conductivity

Arthur J. Epstein

Department of Physics and Department of Chemistry, The Ohio State University, Columbus, OH 43210–1117

46.1 INTRODUCTION

For the past 50 years, conventional insulating polymer systems have been increasingly used as substitutes for structural materials such as wood, ceramics, and metals because of their high strength, light weight, ease of chemical modification/customization, and processibility at low temperatures [1]. In 1977, the first electrically conducting organic polymer, doped polyacetylene, was reported [2], spurring interest in "conducting polymers [3]." The common electronic feature of pristine (undoped) conducting polymers is the π-conjugated system which is formed by the overlap of carbon p_z orbitals and alternating carbon–carbon bond lengths [4–6], shown schematically in Fig. 46.1. (In some systems, notably polyaniline, nitrogen p_z orbitals and C_6 rings also are part of the conjugation path.) Figure 46.2 shows the chemical repeat units of pristine forms of several families of conducting polymers, i.e., *trans*- and *cis*-polyacetylene [$(CH)_x$], poly (1,6-heptadiyne), the leucoemeraldine base (LEB), emeraldine base (EB), and pernigraniline base (PNB) forms of polyaniline (PAN), polypyrrole (PPy), polythiophene (PT), poly (*p*-phenylene) (PPP), poly(*p*-phenylene vinylene) (PPV), polypyridine (PPyr), and poly (*p*-pyridyl vinylene) (PPyV). The electronic ground states of these systems are varied. Undoped *trans*-$(CH)_x$ has a twofold degenerate insulating ground state stabilized by the electron–phonon interaction (Peierls instability) [7] and contributions due to Coulomb repulsion [8–12]. Poly(1,6-heptadiyne) [13] and the pernigraniline oxidation state of PAN [14–16] and their derivatives also have degenerate ground states; that is, single and double bonds (benzenoid and quinoid rings for pernigraniline base polymer) can be interchanged without affecting the ground state energy. The remaining polymers illustrated in Fig. 46.2 and their derivatives have nondegenerate ground states; that is, interchange of single and double bonds leads to electronic structures of different energy [7].

The conductivities of the pristine polymers are transformed from insulating to metallic through the process of doping, with the conductivity increasing as the doping level increases. Both n-type (electron donating) and p-type (electron accepting) dopants have been utilized to induce an insulator–metal transition in electronic polymers [2–7]. The

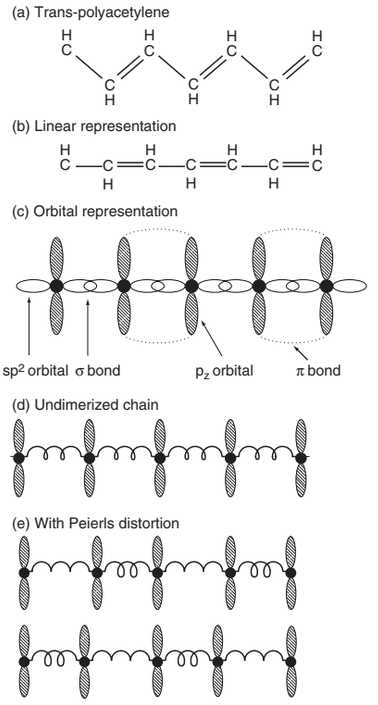

FIGURE 46.1. (a) Chemical structure of *trans*-polyacetylene [$(CH)_2$]. (b) Linear representation. (c) Orbital diagram of the carbon backbone with the sp^2 orbitals of adjacent carbons overlapping to from σ-bonds. The p_z orbitals form π-bonds between alternating pairs of atoms to create a conjugation path that allows electrons to exist in delocalized states over the chain. (d) Chain idealization in which the σ-bonds are represented as springs that exert a restoring force on the atoms. Here the chain is drawn in the ground state neglecting the effects of Peierls instability. (e) Peierls distortion due to electron-phonon coupling causes the chain to become dimerized with two degenerate ground state phases. © (1986) from [4]. Reproduced by permission of Routledge/Taylor & Francis Group, LLC.

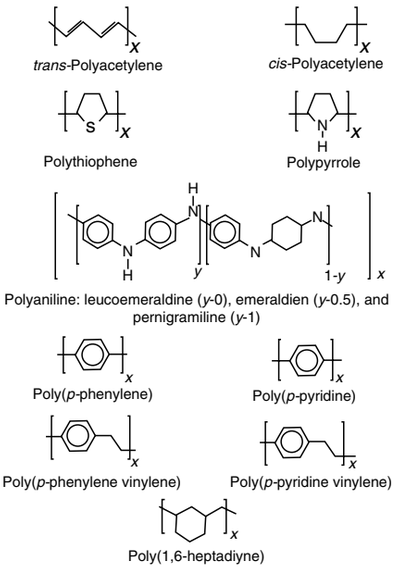

FIGURE 46.2. Repeat units of several electronic polymers.

doping procedures differ from conventional ion implantation used for three-dimensional semiconductors. The doping process for polymers is carried out electrochemically or by exposing the films to vapors or solutions of the dopant [4]. Unlike substitutional doping, as occurs for conventional semiconductors, in electronic polymers the dopant atoms are positioned interstitially between chains, and donate charge to or accept charge from the polymer backbone [2,4,17]. The polymer backbone and dopant ions form new three-dimensional structures. There is a rich variety in these structures, with differing structures occurring for different dopant levels, different structures for different processing routes, and varying degrees of local order [18–20].

The negative or positive charges initially added to the polymer chain upon doping do not simply begin to fill the rigid conduction or valence bands, immediately causing metallic behavior. The strong coupling between electrons and phonons causes lattice distortions around the doped charge [7]. For the degenerate ground states, charges added to the backbone through doping or photoexcitation are stored in soliton and polaron states [5–7,21–24]. For nondegenerate systems, the charges introduced by low doping or photoexcitation are stored as polarons or bipolarons (PT [25–30], PPy [26,31–34], PPV [35–37], PPP [38–40], and polyaniline [41,42]). Photoexcitation also leads to generation of neutral solitons [43,44] and neutral excitons [44–51]. At heavy doping of *trans*-polyacetylene, a soliton lattice that essentially overlaps the valence and conduction band is proposed to form [52,53]. For nondegenerate polymers, heavier doping to the metallic state results in polarons interacting to form a "polaron lattice" or partly filled energy band [54–56]. Some models suggest equilibrium between polarons and bipolarons [33,37,40].

In contrast to the n- and p-type doping processes applied to polyacetylene, polypyrrole, polythiophene, leucoemeraldine base, etc. for polyaniline emeraldine base (EB) form, the conductivity varies with proton (H^+ ion) doping level. In the protonation process, there is no addition or removal of electrons to form the conducting state [54]. Figure 46.3 schematically demonstrates the equivalence of protonic acid doping of emeraldine base and p-doping of leucoemeraldine base to form the conducting emeraldine salt. Similar electronic behavior has been observed for protonic acid doped PAN [54,55,57–60] as for the other nondegenerate ground state systems. Polarons are important at low doping, and, for doping into the metallic state, a polaron lattice forms [54,55,61]. Bipolarons are formed in less ordered regions [62].

Doped polyacetylene has been the prototype system since the initial report of the achievement of a conductivity of $\sigma \sim 100\,\mathrm{S/cm}[100\ (\Omega \cdot \mathrm{cm})^{-1}]$ upon doping with iodine and other donors and acceptors [2]. Subsequently, $(CH)_x$ was synthesized by alternate routes [63–69] that yielded higher conductivities upon doping. The room temperature

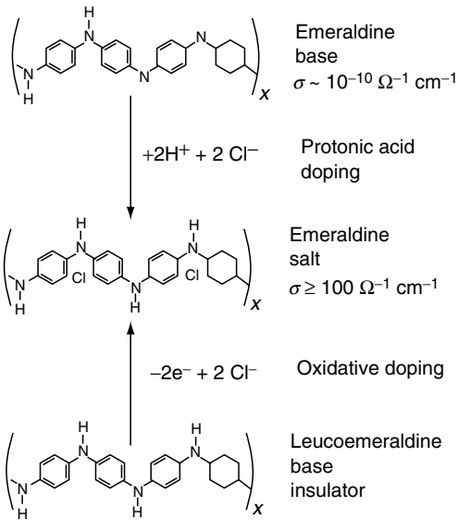

FIGURE 46.3. Illustration of the oxidative doping (p-doping) of leucoemeraldine base and protonic acid doping of emeraldine base, leading to the same final product, emeraldine salt (After Ref. [54]).

dc conductivity (σ_{DC}) for doped films of some of these new materials has been reported to be as high as $\sim 10^5$ S/cm [63,64], rivaling that of traditional metals ($\sigma_{DC} \sim 10^4 - 6 \times 10^5$ S/cm). Recent advances in the processing of other conducting polymer systems has led to improvements in their σ_{DC}, to the range of $\sim 10^3$–10^4 S/cm [3,63–65,70–72], renewing interest in the properties of the polymer metallic state. It is noted that the absolute value of the highest conductivities achieved remains controversial. With theses improvements in σ_{DC}, many traditional signatures of an intrinsic metallic nature have become apparent, including negative dielectric constants, a Drude metallic response [73–75], temperature independent Pauli susceptibility [61,62,75–79], and a linear dependence of thermoelectric power on temperature [80,81]. However, the conductivities of even new highly conducting polymers, though comparable to traditional metals at room temperature, generally decrease as the temperature is lowered. Some of the most highly conducting samples remain highly conducting though, even in the millikelvin range [70,82].

Since there is still a great diversity in the properties of materials synthesized by even the same synthetic routes, in presenting properties of these polymers, correlated structural, transport, magnetic, and optical studies of the same materials are emphasized. In this chapter, the intrinsic properties of the metallic state of a broad class of conducting polymers will be reviewed with emphasis on the universality in the observed behaviors. Throughout the article, the correlation of x-ray, dc and ac transport, optical, and magnetic measurements will be stressed to demonstrate the relationships where such correlated data is available. On those systems where the correlated results are not available, the available data will be summarized.

The outline for the chapter is as follows. A brief overview of conductivities of various conducting polymers is presented in Section 46.2. This section summarizes models for the insulator–metal transition, localization, and metallic conductivity. In Section 46.3, the structural results of x-ray diffraction studies are introduced. Section 46.4 surveys the metallic density of states of highly conducting polymers. The results of temperature-dependent dc conductivity, thermoelectric power, and microwave dielectric constant are reviewed in Sections 46.5, 46.6, and 46.7, respectively. In Section 46.8, the optical properties of the highly conducting state are presented. A discussion of the ultimate conductivity of conducting polymers including resonance quantum transport in doped conducting polymers is given in Section 46.9. Section 46.11 introduces new morphologies of conducting polymers such as fibers. Applications of conducting polymers including an electric field effect are introduced in Section 46.10. The last two sections are a summary and a glossary of frequently used terms in the chapter.

46.2 CONDUCTIVITY

46.2.1 Overview of Conductivity of Conducting Polymers

Figure 46.4 presents representative values of the room temperature conductivities reported [17,63–65,71–73,83–98] for the most widely studied doped conducting polymers. Also indicated is the dopant utilized for each value shown. The conductivities of each of these systems increase by more than ten orders of magnitude upon doping the pristine polymer. Further studies of the room temperature conductivities of these polymers and their derivatives and copolymers yield values of the dc conductivities within the ranges shown in Fig. 46.4.

46.2.2 Models of Insulator–Metal Transition

Many efforts have been made to account for the insulator–metal transition that occurs with an increasing doping level in conducting polymers. The richest area of theoretical work concerning the insulator–metal transition is for polyacetylene, which has been studied for the longest time. One of the simplest approaches is to include only the nearest neighbor overlap (leading to a one-dimensional energy band) and the electron–phonon interaction in the starting Hamiltonian [7,21–23]. Within this model, a metallic state is not stable for an isolated one-dimensional chain due to the formation of a Peierls distortion [99] yielding an energy gap at the Fermi level. Negative (n-type) or positive (p-type) doping leads to formation of negatively or positively charged solitons that form completely filled or empty bands [7]. The Su–Schrieffer–Heeger (SSH) Hamiltonian frequently has been used as the starting point for adding additional interactions. Mele and Rice suggested [100] the

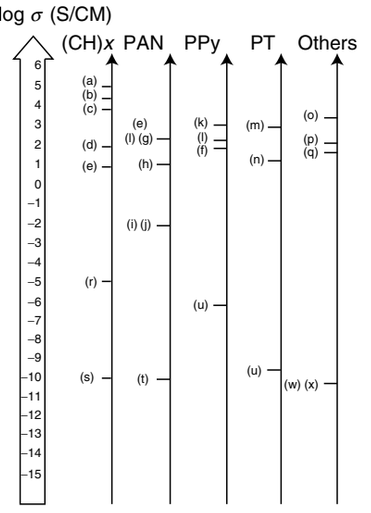

FIGURE 46.4. Overview of conductivity of conducting polymers at room temperature. (a) stretched $[CH(I_3)]_x$ (from Ref. [63]), (b) stretched $[CH(I_3)]_x$ (from Ref. [64]), (c) $[CH(I_3)]_x$ (from Ref. [65]), (d) $[CH(I_3)]_x$ (from Ref. [17]), (d') $[CH(I_3)]_x$ (from Ref. [83]), (e) stretched PAN–HCl (from Ref. [71]), (f) PAN–CSA from *m*-cresol (from Ref. [84]), (g) PAN–CSA from *m*-cresol (from Ref. [73]), (h) PAN derivative: poly(*o*-toluidine) POT-CSA fiber from *m*-cresol (from Ref. [85]), (i) POT-HCl (from Ref. [86]), (j) sulfonated PAN (from Ref. [87]), (k) stretched $PPy(PF_6)$ (from Ref. [88]), (l) $PPy(PF_6)$ and (l') PPy(TsO) (from Refs. [74,89]), (m) iodine doped poly(dodecylthiophene) (from Ref. [72]), (n) $FeCl_4$ doped PT (from Ref. [90]), (o) $PPV(H_2SO_4)$ (from Ref. [91]), (p) $PPP(AsF_5)$ (from Ref. [92]), (q) $^{84}Kr^+$ implanted (polyphenylenebenzobisoxazole) (from Ref. [93]), (r) undoped *trans*-$(CH)_x$ (from Ref. [94]), (s) undoped *cis*-$(CH)_x$ (from Ref. [95]), (t) undoped PAN (EB) (from Ref. [96]), (u) undoped PPy (from Ref. [97]), (v) undoped PT (from Ref. [90]), (w) undoped PPV (from Ref. [98]), (x) undoped PPP (from Ref. [92]). The conductivity reported from undoped polymers should be considered an upper limit due to the possibility of impurities.

commensurate charge density wave (CDW) to incommensurate CDW transition model. This model introduced a wide soliton band between the conduction and valence bands as the doping level is increased. In this model, disorder plays an important role to close the incommensurate Peierls gap and convert the system into a conductor. As the most highly conducting doped polymers are the most ordered, this mechanism is unlikely. Kivelson and Heeger later proposed that for polyacetylene there is a first-order transition from the soliton lattice to the polaron lattice with increased doping [101]. Though a charged polaron band would be a half-filled band and thus metallic (in the absence of a further Peierls transition), later studies suggested that the infrared data was inconsistent with this model [102–104].

Conwell and others have proposed that when long-range Coulomb interactions and screening are taken into account, the soliton band in *trans*-$(CH)_x$ overlaps the valence and conduction bands, giving a metallic state [52,53]. In contrast, Kivelson and Salkola have focused on the interchain interaction, which they show can lead to a simple metallic system with no residual Peierls interaction [105]. Baeriswyl and others, have shown that in some limits the Coulomb interaction is sufficient to close the Peierls gap, giving a metallic state as well [8]. Epstein *et al*. proposed that a disordered conducting state (not the metallic state) is stabilized in the presence of three-dimensional disorder [83]. Other more exotic schemes for the transition to the metallic state also have been proposed [106–109]. For the nondegenerate ground state conducting polymers, more emphasis has been placed on an empty (p-doped) or filled (n-doped) bipolaron energy band overlapping the valence or conduction band, respectively, giving rise to the metallic behavior [56]. Alternatively, a partially filled polaron (band) lattice metallic state [26,31,54–56,61,110,111] has been proposed for some materials. The role of resonant quantum tunneling is discussed in Section 46.9.2.

46.2.3 Models for Localization and Metallic Conductivity

Much work has also focused on the nature of the carriers in the highly doped metallic state. Even though there are a high density of conduction electrons at the Fermi level for the highly doped state, the carriers may be spatially localized so they cannot participate in transport except through hopping. The prime source of localization which has been studied is structural disorder in the polymers [18]. X-ray studies of these systems show that they are generally of modest crystallinity, with regions of the material that are more ordered while other regions are more disordered. Also, the fibrillar nature of many of the conducting polymers may lead to localization by reducing the effective dimensionality of the electrons delocalized in a bundle of polymer chains [112].

In a perfect crystal with periodic potentials, electron wave functions form delocalized Bloch waves [113]. Impurities and lattice defects in disordered systems introduce backward scattering. Anderson studied this phenomenon in terms of a localization effect and the disorder induced metal–insulator transition [114]. It is well known that the electronic structure of the system strongly depends on the degree of disorder. The energy fluctuation in the random potentials broadens the bandwidth and creates smooth ''band tails.'' Due to these band tails, the original band gap between the conduction and the valence bands of a semiconductor may be closed. The ramifications, a finite density of states $N(E_F)$ produced at the Fermi level E_F between mobility edges, were discussed by Mott [115]. When the Fermi level lies in the localized region, the conductivity at zero temperature is zero even for a system with a finite density of states. The Mott variable range hopping (VRH) model is applicable to systems with strong disorder such that ΔV (disorder energy) $\gg B$ (band width) [115]. The general form of the temperature dependent conductivity of Mott's variable range hopping model is described as

$$\sigma = \sigma_0 \exp\left[-\left(\frac{T_0}{T}\right)^{1/d+1}\right], \tag{46.1}$$

where d is the dimensionality and, for three-dimensional systems, $T_0 = c/k_B N(E_F)L^3$ (c is the proportionality constant, k_B the Boltzmann constant, and L the localization length). It is noted that for use of Eq. (46.1) for $d = 1$ refers to quasi-one-dimensional variable range hopping. In this case the charge carriers may hop to a near neighbor chain allowing avoidance of particularly high barriers due to disorder or chain ends. If the charges may hop only along the one-dimensional disordered chain then Eq. (46.1) is replaced by

$$\sigma = \sigma_0 \exp\left[-\left(\frac{T_1}{T}\right)\right],$$

where T_1 represents the highest energy barrier encountered by the charge hopping along the isolated chain.

If the Fermi level is at an energy such that the electronic states are extended, then finite conductivity at zero temperature is expected. This model assumes that substantial disorder is homogeneous throughout the isotropic three-dimensional sample. For three-dimensional materials near the insulator–metal transition, the Ioffe–Regel condition, $k_F l \sim 1$ where k_F is the Fermi wavevector and l is the mean free path, is satisfied, implying a very short localization length and a very short scattering time. Other external parameters such as magnetic field or pressure can affect the localization/delocalization transition and the localization lengths. This model has received much experimental attention for doped [83,116–118] and ion implanted polymers [93].

In Mott's model, electron correlations are neglected as for the classical Fermi liquid. Efros and Shklovskii pointed out that the interactions between localized electrons and holes play an important role in the hopping transport, especially at low temperature [119], changing the expected temperature dependence of the conductivity to

$$\sigma = \sigma_0 \exp\left[-\left(\frac{T_0'}{T}\right)^{1/2}\right], \tag{46.2}$$

where $T_0' = e^2/\varepsilon L$ (e is the electron charge and ε is the dielectric constant).

It is well known for a one-dimensional metallic chain that the localization of charge carriers arises for even weak disorder because of quantum interference of static backscattering [115]. In contrast, strong disorder (the mean free path is comparable with the Fermi wavelength) is required for localization in three-dimensional systems. This consequently requires a short transport time, and hence low σ_{DC} at room temperature. Anderson localization therefore is unlikely for the partially crystalline chain structured doped conducting polymers. The localization effects in the inhomogeneously disordered (partially crystalline) conducting polymers may originate from the one-dimensional localization in the disordered regions [73,120].

Prigodin and Efetov studied the insulator–metal transition of conducting polymers using a random metallic network (RMN) model [112] to represent weakly connected, fibrous bundles of metallic chains. In this zero temperature model, the phase transition is a function of the cross-sectional capture between fibers (α), and the product ($\rho = pR_{loc}$) of the localization radius (R_{loc}) and the concentration of crosslinks between fibers (p). The metallic state can be induced by strengthening the interchain (or interfibril) interaction (increasing α), increasing the density of crosslinks between fibers (increasing p), or increasing the localization length (increasing R_{loc}). This model, developed for contacts between fibers comprised of parallel polymer chains, can be generalized to the three-dimensional delocalization transition that occurs in inhomogeneously disordered (partially crystalline) nonfibrillar polymers: as the strength of connection between ordered or crystalline regions (α) is increased, the density of interconnections between ordered or crystalline regions (p) increases, and the localization length within the disordered regions (R_{loc}) increases.

The inhomogeneous disorder model was expanded [120] to account for the temperature dependence of the conductivity. Within this model, conduction electrons are three-dimensionally delocalized in the "crystalline" ordered regions (though the effects of paracrystalline disorder may limit delocalization within these regions [121]). In order to transit between ordered regions, the conduction electrons must diffuse along electronically isolated chains through the disordered regions where the electrons readily become localized. Phonon-induced delocalization increases the conductivity with increasing temperature. This model accounts for localized behavior at low temperature despite conductivities at room temperature in excess of the Mott minimum conductivity. Three-dimensional crystalline order facilitates delocalization. It has been shown [122] that nematic-like order can also increase delocalization, though less effectively.

For conventional metals, the electrical transport properties can be described by the Drude model [123,124] within which electrons are treated as free particles in a gas with a single scattering time τ. Despite its simplified assumptions, the Drude model explains high and frequency independent conductivity from dc to the microwave ($\sim 10^{10}$ Hz) frequency range, and a real part of the dielectric constant (ε_r) which is negative below the screened plasma frequency ($\omega_p^2 = 4\pi n e^2/m^*\varepsilon_b$; n is the density of carriers, m^* is the carrier effective mass, and ε_b is the background dielectric constant) [124]. Within the Drude model the real (ε_r) and imaginary part (ε_i) of the dielectric function are

$$\varepsilon_r = \varepsilon_b - \frac{\omega_p^2 \tau^2}{1 + \omega^2 \tau^2}, \tag{46.3}$$

$$\varepsilon_i = \frac{\omega_p^2 \tau}{\omega(1 + \omega^2 \tau^2)}, \tag{46.4}$$

where ω is the external frequency.

In low frequency limit ($\omega\tau \ll 1$), the Drude response can be deduced as

$$\varepsilon_r \cong \omega_p^2 \tau^2, \tag{46.5}$$

$$\varepsilon_i \cong \frac{\omega_p^2 \tau}{\omega}. \tag{46.6}$$

46.3 STRUCTURAL ORDER

Each of the conducting polymer systems exhibits different local structures and a wide range of local orders depending upon the synthesis and processing routes used [18]. The typical fraction of crystallinity and the crystalline coherence lengths for typical samples of three of the most intensively studied highly conducting polymer systems are given in Tables 46.1 and 46.2. The synthetic route, processing procedure, and dopant counterion also will affect the crystal structure as well as the percent crystallinity. For both p and n doping of polyacetylene, the polymer forms a number of different structures (stages) as a function of doping level [19,20,125]. Similar results are found for doped PPV [126]. There is less evidence for intermediate stages at various dopant/polymer stoichiometries for the other conducting polymers. Instead, data support formation of inhomogeneous regions of fully doped polymer which increase in number with increasing doping. Doped polyacetylene can be as much as 80–90% crystalline.

Polyaniline forms a rich set of structures dependent upon the processing sequence and dopant [18,62,127–132]. Generally, doped polyaniline obtained from solution in the doped (conducting salt) form exhibits a local crystalline order of type emeraldine salt-I, ES-I. In contrast, polyaniline obtained by doping powder or films cast as the base form from solution are of the ES-II types [62,122,131–133]. Both preparation methods lead to between a few percent and about 50% crystallinity dependent upon details of the processing route. In addition, there are significant differences in the type of local order to exist in the disordered regions between the crystalline ordered regions, varying from coil-like, to expanded coil-like, to more rod-like [133–135]. For undoped and doped polyaniline, short-range local order in the disordered regions resembles that in the ordered regions [18,133]. Table 46.1 summarizes the fraction of crystallinity and the x-ray coherence lengths of the various doped polyaniline systems, while Table 46.2 compares the fraction of crystallinity and x-ray coherence lengths for selected doped polyacetylene, polypyrrole, and polyaniline samples.

Similarly, the degree of local order varies for polypyrrole dependent upon the preparation method, with the degree of crystallinity varying from nearly completely disordered up to ~50% crystalline [18,136]. In contrast to polyaniline, the local order in the disordered regions of polypyrrole does not resemble that in the ordered regions [18].

The percent crystallinity for doped polyacetylene is usually larger than that of doped polyaniline or doped polypyrrole [18,137]. For each of these systems, the coherence length within the doped crystallographic regions generally is no more than 50–75 Å along the chain direction with smaller values in the perpendicular direction. It has been proposed that these coherent crystalline regions form metallic islands and the disordered weak links between more ordered regions are areas where conduction electrons are subject to localization, as expected for charges moving through isolated one-dimensional chains. That is, for each very highly conducting polymer system studied, there are regions of one-dimensional electronic character through which conduction electrons must pass [75]. The charge transport mechanism between the islands may be via phonon controlled hopping (resulting in insulating (i.e., dielectric) behavior at low temperatures) or direct or resonant quantum tunneling (resulting in a ''metallic'' behavior even to the millikelvin range).

TABLE 46.1. *Typical percent crystallinity and crystalline coherence lengths (ξ (Å)) of various polyaniline materials obtained from x-ray diffraction experiments.*

Materials	Crystallinity (%)	$\xi_{\parallel}$ (Å)	$\xi_{\perp}^{b}$ (Å)	$\xi_{\perp}^{a}$ (Å)
[i]XPAN-ES[a] (3.5×) [73,132]	~45	73	57	29
[h]XPAN-ES[a] (3.5×) [73,132]	~40	64	47	23
[h]XPAN-ES[b] (5.5×) [73,132]	~35	57	45	21
PAN-ES[b] (4×) [73,132]	~30	52	42	23
[n]XPAN-ES[b] (1×) [73,132]	<15		15	

[a]High molecular weight samples. XPAN-ES represents the "physically crosslinked" polyaniline emeraldine salt. Note that *i*, *h*, and *n* refer to intermediate, high, and noncrosslinked samples, respectively. The stretch ratio (l/l_0) is given in parentheses (e.g., 3.5×). Note that $\xi_{\perp}^{a}$, $\xi_{\perp}^{b}$, and $\xi_{\parallel}$ are obtained from full width at half maximums of (200), (010), and (002) ES-II reflections, respectively.
[b]Low molecular weight samples.

TABLE 46.2. *Typical percent crystallinity and crystallographic coherence lengths (ξ (Å)) for highly conducting polymer systems.*[a]

Highly conducting polymer	Crystallinity (%)	$\xi_{\parallel}^{a}$(Å)	$\xi_{\perp}^{a}$(Å)
T-$(CH(I_3)_y)_x$ [18,137][b]	~80	50	35
PPy-PF6 [18,136][c]	~50	20	20
PAN–CSA (*m*-cresol) [18][d]	~50	50	30

[a]The terms ∥ and ⊥ refer to parallel and perpendicular to the chain direction, respectively.
[b]*T*-$(CH(I_3)_y)_x$ is the heavily iodine doped Tsukamoto polyacetylene.
[c]PPy-PF6 is the hexafluorophosphate doped polypyrrole.
[d]PAN–CSA (*m*-cresol) is the camphor sulfonic acid doped polyaniline cast from *m*-cresol solvent.

46.4 DENSITY OF STATES

Magnetic susceptibility studies identify the charge storage mechanism at low doping levels, as well as the density of states at the Fermi level and the density of localized ''Curie'' spins at higher dopant levels. For $(CH)_x$, spinless solitons dominate at low doping levels [76,78]. In contrast, spin 1/2 polarons and spinless bipolarons are present in nondegenerate systems at low doping levels [7,33,138]. At high doping levels, the highest conducting doped polyacetylene, polypyrrole, polyaniline, polythiphene, and polyparaphenylenes are reported to have finite densities of states at the Fermi level [$N(E_F)$]. Typical literature values of $N(E_F)$ [27,61,62,71,74–76,78,79,138–148] for each of these systems are presented in Table 46.3. Having the Fermi level in a partially filled conduction band results in Pauli susceptibility ($\chi_{Pauli} = 2\mu_B^2 N(E_F)$) and enables metallic conduction. The magnitude of χ_{Pauli} depends on the structural order and morphology of the polymers as this affects the uniformity of the doping. It is noted that the values of $N(E_F)$ in Table 46.3 have not been scaled to the percent crystallinity. Hence the intrinsic density of states in each of the ordered polymers may be larger than indicated.

For the earliest studied iodine doped Shirakawa [76,78,139] and Naarmann [140] $(CH)_x$, Fig. 46.5, $N(E_F) \sim 0.1$ states/eV-C for doping levels above ~4–6% doping level. With the recently studied Tsukamoto [75,142] $(CH)_x$, which has a more compact morphology, a higher doping level was attained resulting in $N(E_F) \sim 0.2$–0.3 states/eV-C, Fig. 46.5, indicating that the doping was more homogeneous.

For PAN, $N(E_F)$ is finite and has been shown to increase with the level of protonic acid doping and the volume fraction of crystalline material for both the ES-I, Fig. 46.6, and ES-II, Fig. 46.7, structure [61,62]. The $N(E_F)$ differ for ES-I HCl and ES-II HCl, being 0.26 states/eV-(C+N), and 0.083 states/eV-(C+N), respectively [143]. For highly conducting PAN–CSA (*m*-cresol) [79], $N(E_F) \sim 0.07$ states/eV-(C+N). Recently, a differently prepared stretched PAN doped with HCl was reported to have a much higher $N(E_F)$, ~ 1.4 states/eV-(C+N) [71]. Some solutions of PAN–CSA have been reported to have a Pauli-like susceptibility [144].

Highly conducting doped polypyrrole has a large χ_{Pauli} [74]. The samples initially studied typically had conductivities in the range of ~ 1–10 S/cm with little crystallinity; for these materials, $N(E_F) \leq 0.01$ states/eV-C [145]. Later studies on BF_4 doped PPy [138,146] indicated $N(E_F) \sim 0.045$ states/eV-C, however, these films were not structurally characterized. A coordinated study of PPy doped with hexafluorophosphate [PPy(PF_6)] and toluene sulfonate [PPy(TsO)] [74] shows that for the more highly crystalline (50%), higher conductivity ($\sigma_{DC} \sim 300\,S/cm$)PPy($PF_6$), $N(E_F) \sim 0.2$ states/eV-C, similar to what was found for highly conducting iodine doped Tsukamoto $(CH)_x$. For less crystalline (25%), lower conductivity ($\sigma_{DC} \sim 120$ S/cm) PPy(TsO), $N(E_F) \sim 0.05$ states/eV-C. Figure 46.8 contrasts the density of states [$N(E_F) = \chi_{Pauli}/2\mu_B^2$] and number of localized Curie-like spins measured for the PPy-PF_6 and PPy-TsO compounds [74]. The more metallic PPy-PF_6 clearly has the larger χ_{Pauli} and the smaller number of localized Curie spins (independent polarons).

For doped polythiophene, there is variation of the doping level attained with different dopants. For BF_4 doped PT [146], $N(E_F) \sim 0.05$ states/eV-C at the 4–8% dopant level. For PT(AsF_6) [27], the doping is inhomogeneous until 26 mol% where $N(E_F) \sim 0.23$ states/eV-C.

For PPP, a metallic density of sates of $N(E_F) \sim 0.05$ states/eV-C has been reported for doping with AsF_6 [147].

TABLE 46.3. *Typical χ_{Pauli} and $N(E_F)$ for highly conducting polymer systems.*

Material	χ_{Pauli}	$N(E_F)$
$[CH(I_3)_y]_x$ [75,142,160]	1.1×10^{-5} emu/mol-C	0.33 states/eV-C
$[CH(I_3)_y]_x$ [76,139,140]	2.9×10^{-6} emu/mol-C	0.09 states/eV-C
$[CH(ClO_4)_y]_x$ [141]	3.3×10^{-6} emu/mol-C	0.11 states/eV-C
$[CH(ClO_4)_y]_x$ [139]	2.3×10^{-6} emu/mol-C	0.08 states/eV-C
$[CH(Na)_y]_x$ [139]	2.0×10^{-5} emu/mol-C	0.07 states/eV-C
PAN(HCl) ES-I [61,143]	7.9×10^{-6} emu/mol-(C + N)	0.26 states/eV-(C+N)
PAN(HCl) ES-II [62,143]	2.5×10^{-6} emu/mol-(C + N)	0.083 states/eV-(C+N)
PAN(HCl) [71]	4.0×10^{-5} emu/mol-(C + N)	1.4 states/eV-(C+N)
PAN(CSA) [79]	2.1×10^{-6} emu/mol-(C + N)	0.07 states/eV-(C+N)
PAN(SO_3) (“SPAN”) [87]	1.7×10^{-6} emu/mol-(C + N)	0.06 states/eV-(C+N)
POT(HCl) [121]	3.9×10^{-6} emu/mol-(C + N)	0.13 states/eV-(C+N)
PPy(PF_6) [74]	7.0×10^{-6} emu/mol-C	0.20 states/eV-C
PPy(TsO) [74]	1.8×10^{-6} emu/mol-C	0.05 states/eV-C
PPy(BF_4) [146]	1.7×10^{-6} emu/mol-C	0.05 states/eV-C
PT(AsF_g) [27]	7.5×10^{-6} emu/mol-C	0.23 states/eV-C
PT(BF_4) [146]	1.5×10^{-6} emu/mol-C	0.05 states/eV-C
PPP(AsF_6) [147]	1.5×10^{-6} emu/mol-C	0.05 states/eV-C
C_2H_5O-PPV(BF_4) [148]	$\leq 1 \times 10^{-6}$ emu/mol-C	0.03 states/eV-C

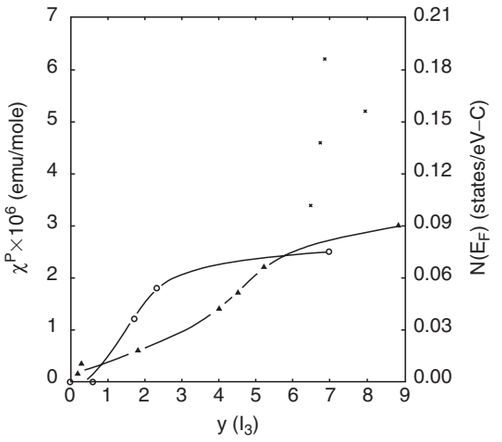

FIGURE 46.5. Pauli susceptibility and density of states as a function of I_3 doping level for an oriented ($l/l_0 \sim 6$) Naarmann polyacetylene (triangles) (N-$(CH)_x$) (from Ref. [135]), unoriented Shirakawa polyacetylene (circles) (S-$(CH)_x$) (from Ref. [140]), and Tsukamoto polyacetylene (x) (T-$(CH)_x$) (from Refs. [75,160]).

There are no reports in the literature concerning the temperature dependence of the susceptibility of doped PPV. However, if the reported room temperature magnetic susceptibility measured of BF_4 doped poly(2,5-diethoxy-*p*-phenylene–vinylene) [C_2H_5O-PPV(BF_4)] [143] is entirely due to a Pauli contribution, an upper estimate of $N(E_F)$ is 0.03 states/eV-C.

In sum, for each of these systems the metallic density of states at the Fermi level varies substantially. Where data are

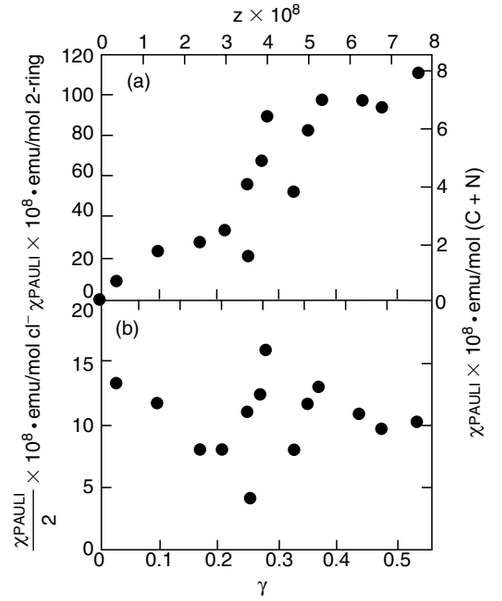

FIGURE 46.6. $N(E_F)$ versus doping level for PAN–HCl, ES-I structure. The lower curve presents χ_{Pauli} normalized to the doping level (from Ref. [61]).

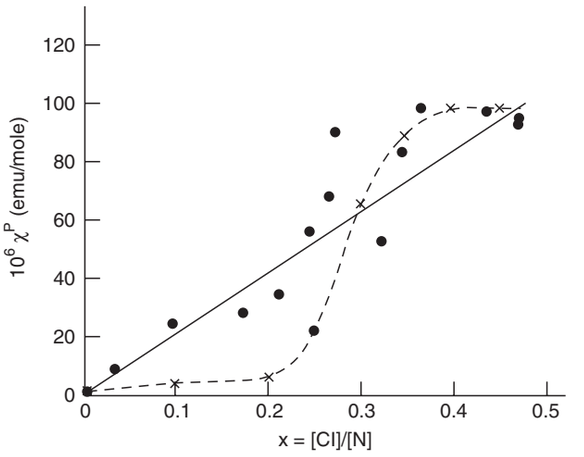

FIGURE 46.7. $N(E_F)$ versus doping level for PAN–HCl, ES-II structure (dashed line). The closed circles are for HCl doping of the ES-I structure (from Ref. [62]).

present, the Pauli susceptibility increases with increasing three-dimensional or nematic order.

46.5 TEMPERATURE DEPENDENT CONDUCTIVITY AND MAGNETORESISTANCE

46.5.1 Conductivity

The temperature dependent dc conductivity, σ_{DC} (T), provides a direct probe of the macroscopic charge conduction through the less conducting regions. Recent advances in chemical processing have resulted in higher crystallinity and conductivity for conducting polymers.

Ishiguro *et al*. reported the temperature dependent resistivity [ρ (T)] of heavily iodine doped $(CH)_x$ and hexafluorophosphate (PF_6) doped PPy down to mK range as function of aging (disorder), Figs. 46.9 and 46.10, respectively [70].

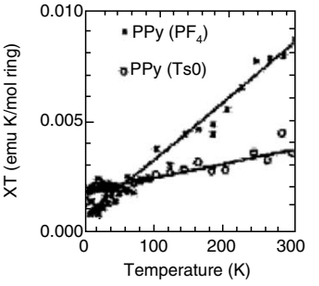

FIGURE 46.8. χ^T versus T for PPy-PF_6 and PPy-TsO (from Ref. [74]). Note that assuming $\chi = (\chi_{Pauli} + \chi_{curie})$ and that χ_{Pauli} is T independent while $\chi_{Curie} \propto T^{-1}$,PPy-$PF_6$ has the larger regions of metallic density of states while the PPy-TsO system has a great density if localized (independent polaron) spins.

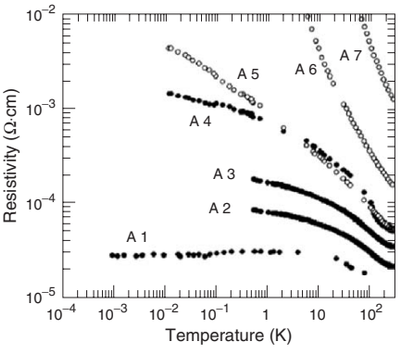

FIGURE 46.9. Temperature dependence of the resistivity for various heavily iodine doped poly-acetylenes represented in a log ρ versus log T scheme (from Ref. [70]).

The highest σ_{DC} at room temperature reported in this study is $\sim 5 \times 10^4$ S/cm for I_3 doped T-$(CH)_x$ and $\sim 10^3$ S/cm for the highest conducting PPy(PF_6). For both of these materials, the conductivity decreases with decreasing temperature to a minimum at $T_{m\sim 10\,K}$. Below T_m, σ increases by $\sim$20% and then is constant to 1 mK. Some highly conducting preparations of PAN–CSA show similar behavior [82].

Hydrochloric acid as well as camphor sulfonic acid doped polyaniline prepared in chloroform often have log σ proportional to $T^{-1/2}$ as expected for quasi-one-dimensional variable range hopping (VRH), Fig. 46.11, [73,121,143]:

$$\sigma = \sigma_0 \exp[-(T_0/T)^{1/2}], \tag{46.7}$$

where $T_0 = 16/[k_B N(E_F) L_z]$. Here L is the one-dimensional localization length and z the number of nearest neighbor chains. Generally, the higher conductivity samples have a weaker temperature dependence at low temperatures ($T_0 \sim$ 700–1,000 K for $T < 80$ K), and lower conductivity

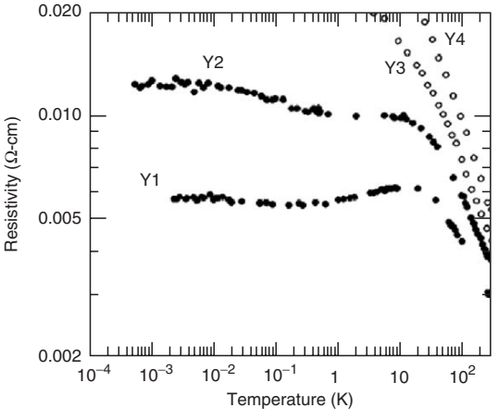

FIGURE 46.10. Temperature dependence of the resistivity for PF_6 and BF_6 doped polypyrroles represented in a log ρ versus log T scheme (from Ref. [70]).

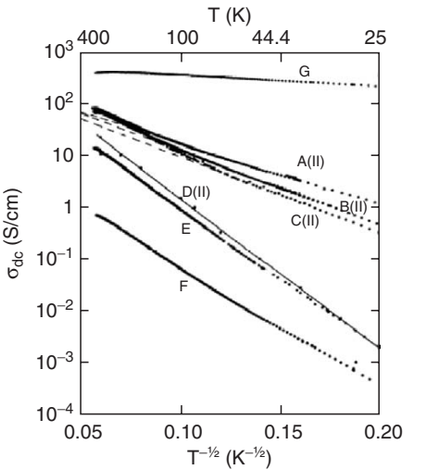

FIGURE 46.11. σ_{DC} (T) for "crosslinked" PAN-ES, PAN–CSA ($CHCl_3$), and PAN–CSA (*m*-cresol) samples (from Ref. [73]). The dashed lines are based upon the quasi-1D VRH model. Note here "crosslinks" refers to physical crosslinks (microcrystalline regions) not chemical crosslinks (covalent bonds).

samples a stronger temperature dependence ($T_0 \sim$ 4,000 K). The smaller T_0 for the more highly conducting samples has been associated with weaker localization due to improved intrachain and interchain order.

Higher conducting polyaniline films that were prepared from solutions of PAN and HCSA in *m*-cresol have an intrinsic metal-like temperature dependence at room temperature to $\sim$200 K, below which the conductivity decreases slowly, Fig. 46.12. It was shown that this metal-like behavior

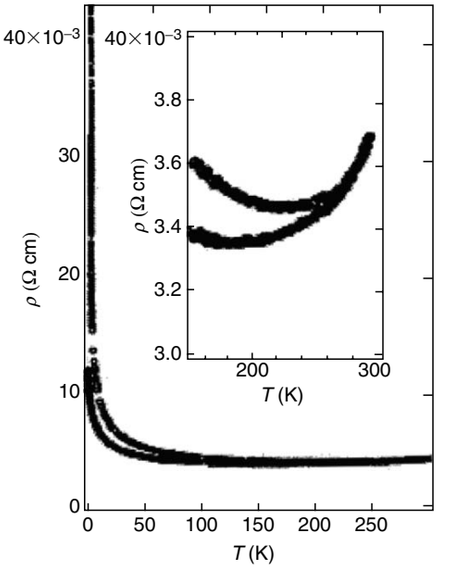

FIGURE 46.12. Resistivity versus temperature for PAN–CSA (*m*-cresol). The inset shows the resistivity minima on an expanded scale (from Ref. [116]).

for $T > 200$ K can occur in the presence of one-dimensional localization when the phonon backscattering rate becomes larger than the impurity scattering rate [120]. A similar temperature dependence for conductivity has been reported for $FeCl_3$ doped polyacetylene [149].

For PAN–CSA [116,120], PPy(PF_6) [74,118], and iodine doped $(CH)_x$ [150], the proximity of the material to the insulator–metal transition can be gauged by the resistivity ratio $\rho(1.4\,\mathrm{K})/\rho(300\,\mathrm{K})$ and a plot of the reduced activation energy: $W = -T\mathrm{d}\ln(\rho(t))/\mathrm{d}T$ [151]. For a conductor close to the insulator–metal transition, the resistivity follows a power law behavior with T [152]; for a critical regime sample, the plot of log W versus log T approaches $T = 0$ K at a constant value. The plot of log W versus log T for a critical sample provides a dividing line between the plot of log W versus log T for insulator hopping behavior which increases with decreasing T (i.e., the slope of log W versus log T is equal to γ if $\sigma \propto \exp(T_0/T)^{\gamma}$) and the plot of log W versus log T for metallic samples which decrease with decreasing T. The W plots for selected PAN–CSA materials are shown in Fig. 46.13.

46.5.2 Magnetoresistance

The charge transport can be changed in the presence of an external magnetic field because of the destruction of time-reversal symmetry, i.e., a total phase difference between two paths is created by the magnetic field [153]. The magnetoresistance is more easily detected at low temperature because of large localization effects. The fractional change of resistivity in the presence of a magnetic field, $\Delta\rho/\rho$, can be either positive or negative. A negative magnetoresistance can originate from localization effects caused by magnetic field-related dephasing. A field-dependent cutoff length $L_H = \sqrt{\hbar c/eH}$, where c is the speed of light, is important at high magnetic fields [153]. A positive magnetoresistance is detected when the mobility edge E_c is shifted by the external magnetic field [154]. For an impurity conduction mechanism, the wave functions of the impurity electrons are compressed in the transverse direction by the magnetic field, leading to an enhancement of localization effects, which also induces a positive magnetoresistance [153].

Figures 46.14–46.16 show examples [116,118,155] of the magnetoresistance of doped polyacetylene, polypyrrole, and polyaniline samples at low temperatures. A wide range of behaviors is observed. The variation in magnetoresistance for conducting polymers is closely related to the magnitude and temperature dependence of the conductivity in the absence of a magnetic field. For highly conducting doped $(CH)_x$, a negative magnetoresistance is reported [81,155] for both the parallel and perpendicular directions (Fig. 46.14). This was attributed to quantum interference though the magnitude of the magnetoresistance in the parallel direction is relatively insensitive to the magnetic field. For highly conducting PPy(PF_6) and PAN–CSA materials, the magnetoresistance is usually positive, (Figs. 46.15 and 46.16), which was interpreted as a shift of the mobility edge in the presence of a magnetic field.

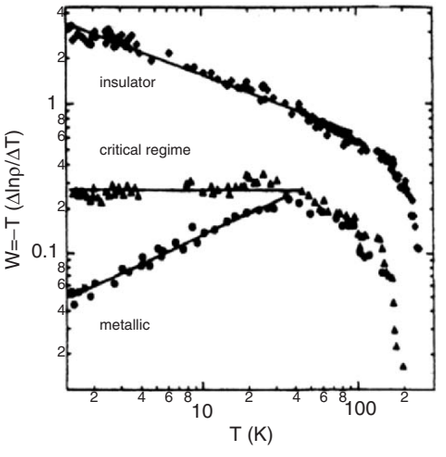

FIGURE 46.13. *W* plot for PAN–CSA (*m*-cresol) for samples in the insulating, critical, and metallic regime (from Ref. [116]).

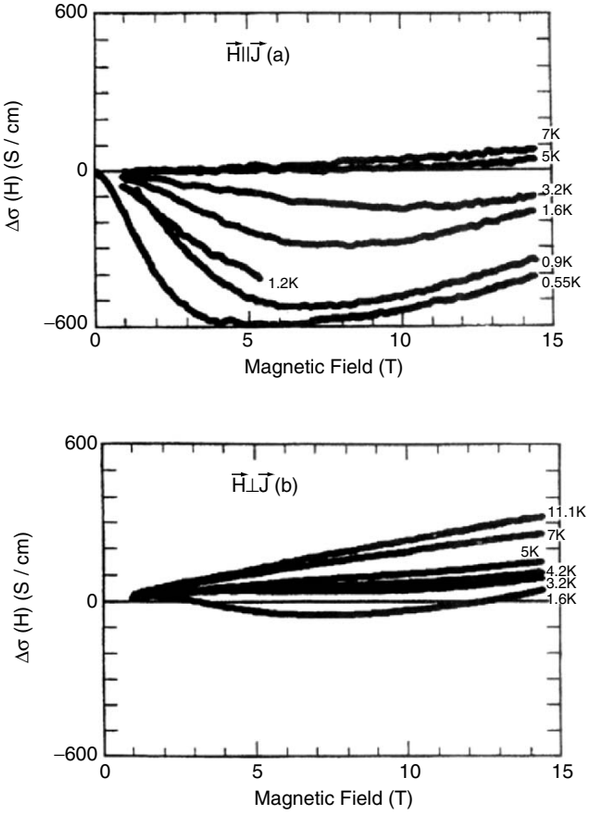

FIGURE 46.14. Magnetic field dependence of the conductivity increment $\Delta\sigma$ (H) at various temperatures for heavily iodine doped T-$(CH)_x$ (from Ref. [155]).

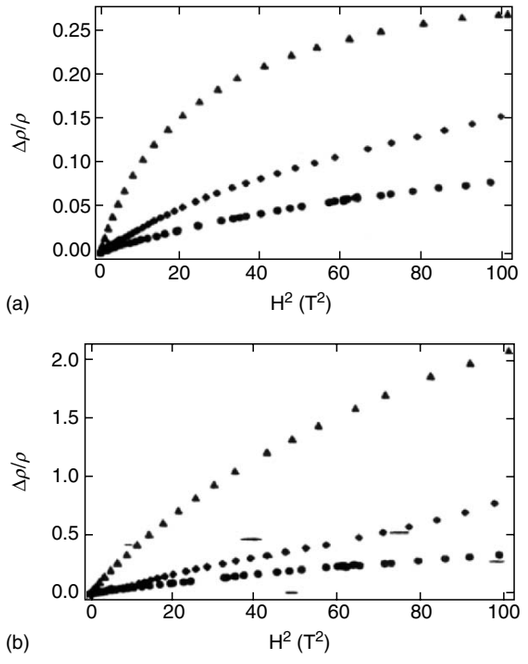

FIGURE 46.15. $\Delta\rho/\rho$ versus H^2 for PAN–CSA (*m*-cresol): (a) In the critical regimes; [$\rho(T) \propto T^{-0.26}$, 4.2 K (solid circles), 2.5 K (solid diamonds), and 1.4 K (solid triangles); (b) in the insulating regime (follows three-dimensional VRH model), 4.2 K (solid circles), 2.5 K (solid diamonds), and 1.4 K (solid triangles)] (from Ref. [116]).

46.6 THERMOELECTRIC POWER

The results of the thermoelectric power experiments determine the sign of the conducting charge, either electron-like (for a negative thermoelectric power) or hole-like (for a positive thermoelectric power). In terms of band theory, the positive or negative thermoelectric power implies p-type or n-type doping of a system, respectively. For inhomogeneous conducting polymers, there are several different contributions to the total thermoelectric power [156,157].

When the conductivity is determined by the motion of charge carriers near the Fermi level, where states are metallic (delocalized), the thermoelectric power is [115]

$$S(T) = \frac{2\pi^2}{3}\frac{k_B^2 T}{e}\left.\frac{\mathrm{d}\ln N(E)}{\mathrm{d}E}\right|_{E=E_F}. \qquad (46.8)$$

Assuming a weak energy dependence of the density of states $N(E_F)$, the thermoelectric power increases linearly as the temperature increases.

When the conduction is determined by three-dimensional VRH, $S(T) \propto \sqrt{T}$ [115]. For a quasi-one-dimensional VRH case, the thermoelectric power due to the interchain motion is constant [143] while that due to intrachain hopping is $\propto 1/T$, similar to that of doped semiconductors [115].

Park *et al*. [80] and Javadi *et al*. [81] reported metallic thermoelectric power [$S(T) \propto T$] for heavily doped highly conducting polyacetylene (Figs. 46.17 and 46.18) though VRH-type $S(T) \propto \sqrt{T}$ had been reported earlier for poorly conducting polyacetylene [83]. Similarly, highly conducting forms of polyaniline and polypyrrole have $S(T) \propto T$, Figs. 46.19 [117,158] and 46.20 [154], while more disordered materials show nonlinear temperature dependent

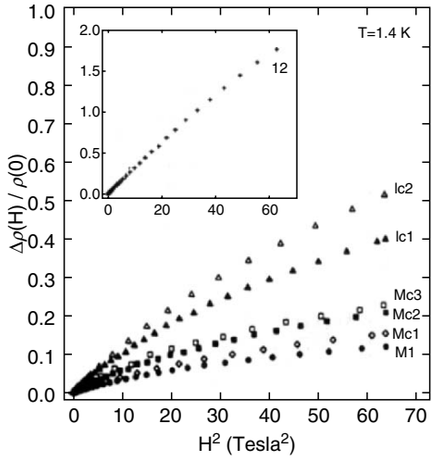

FIGURE 46.16. Magnetoresistance of doped polypyrroles (from Ref. [70, 224]). The inset shows the magnetoresistance for a less highly conducting doped PPy than in the main figure.

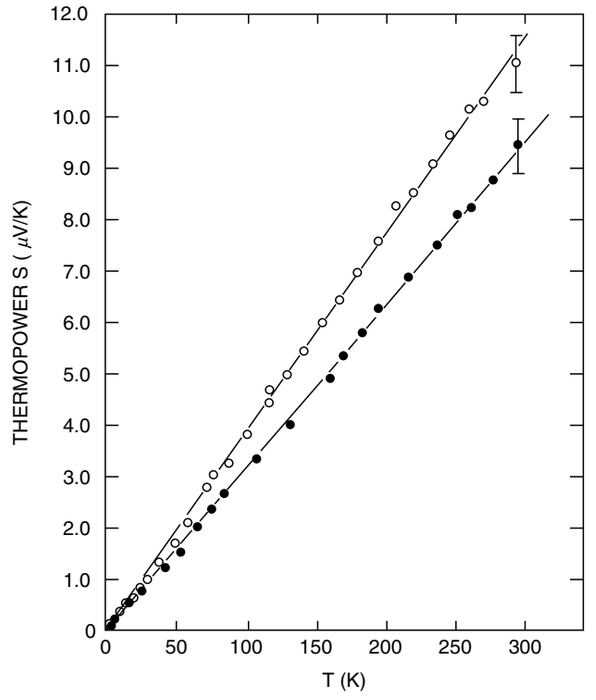

FIGURE 46.17. Temperature dependence of the thermoelectric power in unstretched (solid circles) heavily AsF_5 doped polyacetylene and stretched ($l/l_0 \sim 3.2$, open circles) ones (from Ref. [80(b)]).

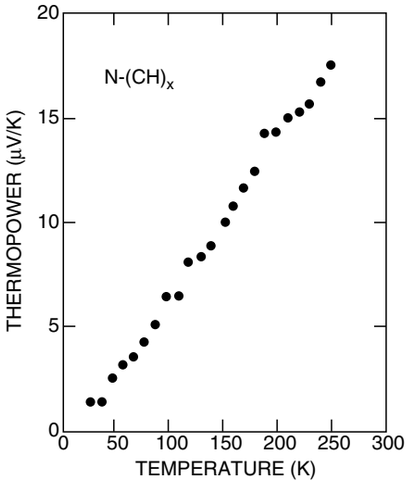

FIGURE 46.18. Thermoelectric power of stretched heavily iodine doped N-$(CH)_x$ film versus temperature measured parallel to the stretched axis (from Ref. [81]).

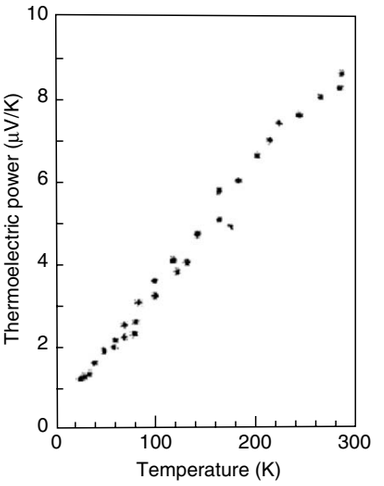

FIGURE 46.20. Temperature dependence of thermoelectric power of PF_6 doped polypyrrole (from Ref. [159]).

behavior, which might include the three-dimensional or quasi-one-dimensional VRH contributions. Figure 46.21 [143] shows the nonlinear $S(T)$ of some hydrochloride doped polyaniline materials.

46.7 MICROWAVE DIELECTRIC CONSTANT

The microwave frequency dielectric constant provides a measure of the charge delocalization in individual samples.

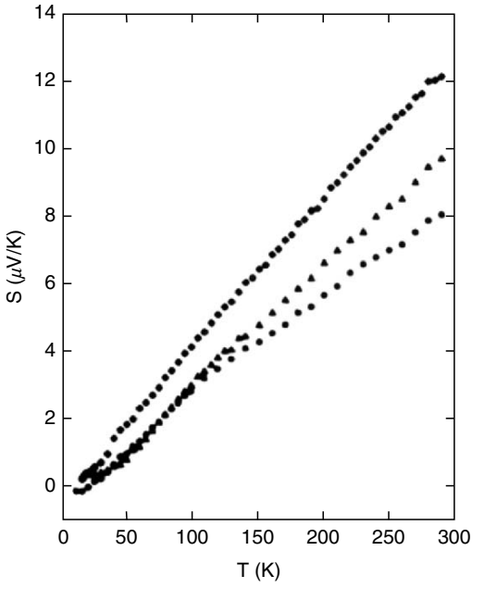

FIGURE 46.19. Temperature dependence of thermoelectric power of PAN–CSA (*m*-cresol) samples: different symbols refer to materials prepared in different casting conditions (from Ref. [117]).

Figure 46.22 presents [73] the low temperature dielectric constant ε_{mw}, for a series of emeraldine hydrochloride samples plotted against the square of the crystalline coherence length, ξ (as measured by x-ray diffraction). For low temperatures, ε_{mw} is proportional to ξ^{-} independent of the direction of orientation of the sample with regard to the microwave frequency electric field. This demonstrates that the charge is delocalized three-dimensionally within the crystalline regions of these samples. Using a simple metallic box model [73,143],

$$\varepsilon = \varepsilon_{\infty} + (2^{9/2}/\pi^3)e^2N(E_F)L^2, \tag{46.9}$$

and taking for the low temperature localization length the x-ray crystalline correlation length determined by x-ray diffraction, $N(E_F) \simeq 1.23$ state/(eV 2-rings) (0.088 state/eV-

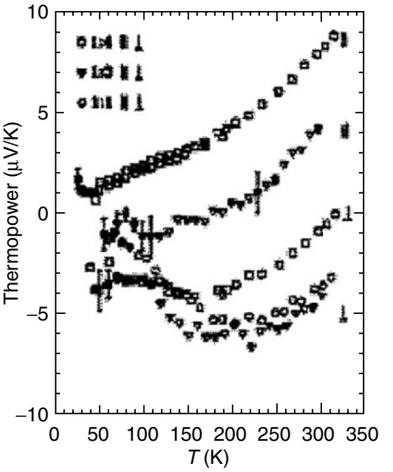

FIGURE 46.21. Comparison of temperature dependence of thermoelectric power of HCl doped PAN-ES samples (from Ref. [143]).

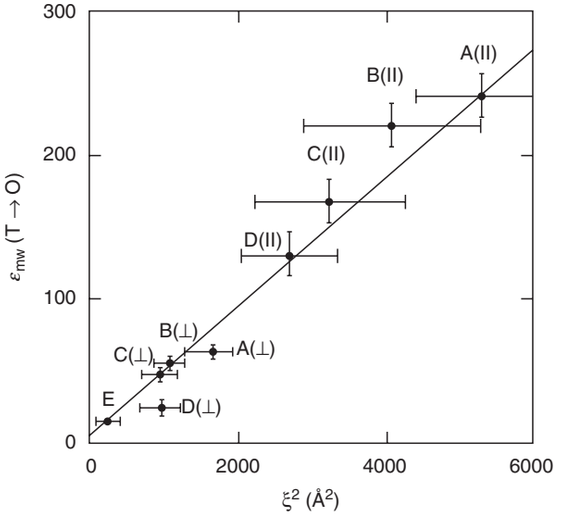

FIGURE 46.22. $\varepsilon_{mw}(6.5 \times 10^9\,\text{Hz}, T \to 0)$ versus ξ^2 for HCl doped PAN-ES ($\xi^2 = \xi_{\perp,\,a} \times \xi_{\perp,\,b}$) (from Ref. [73]).

(C+N)) for PAN–HCl. This compares very favorably with the value obtained from magnetic susceptibility experiments [61].

A positive microwave frequency dielectric constant is also found for modestly conducting iodine doped unstretched and modestly stretched Tsukamoto polyacetylene [75] and for unstretched PPy-TsO [74], Fig. 46.23(a) and (b). Using Eq. (46.9), the size of the low temperature metallic box, L, can be determined. Table 46.4 summarizes the low temperature microwave dielectric constant for typical modestly conducting doped polymers and the corresponding metallic box size calculated using Eq. (46.9). In each case L is approximately the size expected from x-ray diffraction studies of the structural coherence length, ξ.

An independent measure of the temperature dependence of the conduction electron localization length is obtained through study of the temperature dependence of the dielectric constant. For HCl doped PAN-ES samples with weaker localization in the disordered regions, $\varepsilon_{mw}(T)$ increases rapidly with increasing temperature to values in excess of 10^4 at room temperature, Fig. 46.23(c). In contrast, more localized samples have a weaker temperature dependence to the dielectric constant with $\varepsilon_{mw}(295\,\text{K}) < 2 \times 10^3$. Using Eq. (46.9) the room temperature localization length (L_{RT}) is estimated as ~1,000 Å and ~350 Å parallel and perpendicular to the chain direction, respectively, for these highly conducting materials [73]. This distance encompasses of order seven or more structurally coherent regions (''crystalline islands'') in the parallel direction and four or more in the perpendicular direction. Such materials were described [73] as having mesoscopic metallic states at room temperature. In contrast, for modestly conducting materials, L_{RT} is less than or of order twice the distance between crystalline regions implying nearly isolated ''metallic'' islands.

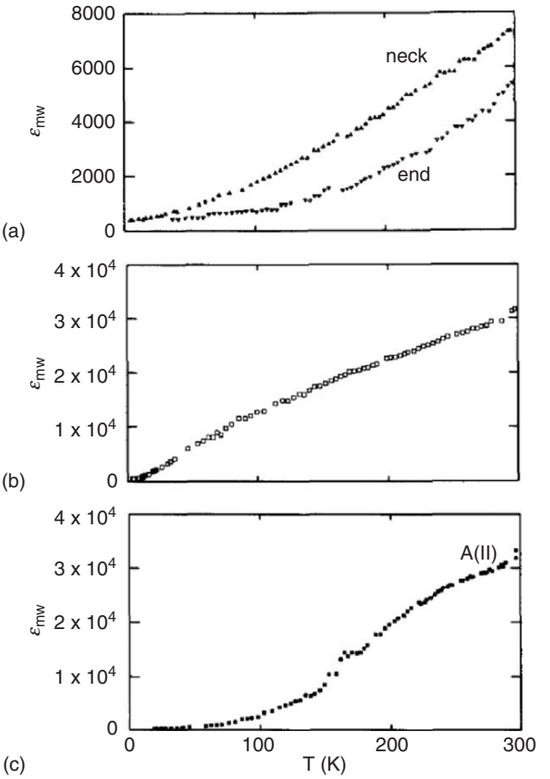

FIGURE 46.23. $\varepsilon_{mw}(6.5 \times 10^9\,\text{Hz})$ versus temperature for modestly conducting doped polymers. (a) I_3 doped Tsukamoto polyacetylene (unstretched end and modestly stretched neck portions of sample) (from Refs. [75,160]), (b) unstretched PPy-TsO (from Ref. [74]), and (c) intermediate "crosslinked" 3.5 times stretched HCl doped PAN-ES (from Ref. [73]).

The sign, magnitude, and temperature dependence of the 6.5×10^9 Hz dielectric constant for very highly conducting T-$[CH(I_3)_y]_x$ [75,160], PPy-PF_6 [74], and *m*-cresol prepared PAN–CSA [73] are quite striking, Fig 46.24. For example, PAN–CSA (*m*-cresol) has a metallic negative dielectric constant and features a maximum in microwave frequency conductivity at ~180 K [73]. A similar large and negative value of ε_{mw} and temperature dependence of ε_{mw} were determined for heavily iodine doped stretched Tsukamoto

TABLE 46.4. *Low temperature dielectric constant, $\varepsilon_{mw}(T \to 0)$ and derived metallic box size, $L(T \to 0)$, compared to the x-ray diffraction determined coherence length, ξ, for typical modestly conducting polymers.*

Modestly conducting polymer systems	ε_{mw} $(T \to 0)$	$L(T \to 0)$ (Å)	ξ(Å)
T-$(CH(I_3)_y)_x$ [75]	~400	~170	Not measured
PPy-TsO [74]	~20	~25	~15
PAN–CSA ($CHCl_3$) [73,75]	~30	~24	$\xi_{\parallel}$~35,$\xi_{\perp}$~25

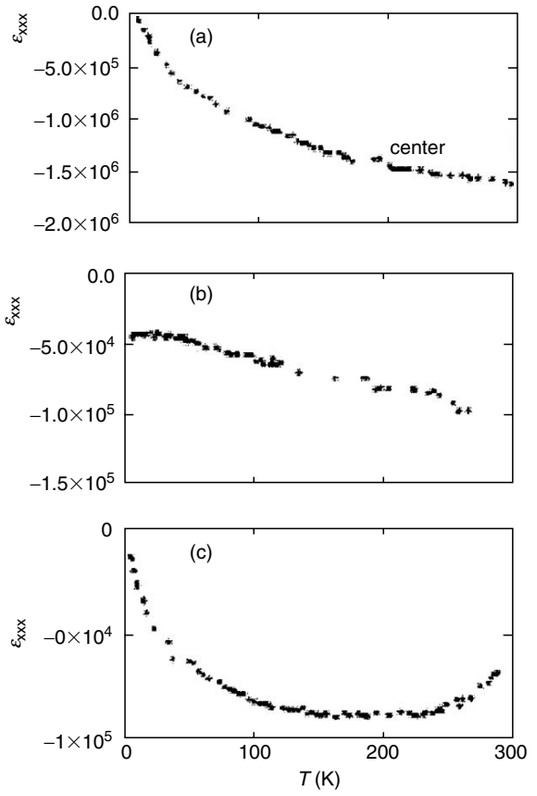

FIGURE 46.24. $\varepsilon_{mw}(6.5 \times 10^9\,\text{Hz})$ versus temperature for highly conducting doped polymers. (a) I_3 doped Tsukamoto polyacetylene (stretched central portion of sample) (from Ref. [160]), (b) unstretched PPy-PF_6 (from Ref. [74]), and (c) PAN–CSA (*m*-cresol) (from Ref. [73]). Note the large negative values of these dielectric constants.

polyacetylene [75,160] and PF_6 doped polypyrrole [74]. Using the Drude model [123,124] for low frequencies ($\omega\tau \ll 1$), a plasma frequency of $\omega_p = 0.015\,\text{eV}(120\,\text{cm}^{-1})$ and a room temperature scattering time of $\tau = 1.2 \times 10^{-11}\,\text{s}$ were calculated [73] for the PAN–CSA (*m*-cresol) system, though the exact values correlate with the sample preparation. Similar values are obtained for heavily iodine doped stretched Tsukamoto polyacetylene and PF_6 doped polypyrrole (Table 46.5). These values of ω_p are much smaller than one expects from the usual Drude model. The small values of ω_p suggest that only a small fraction of the conduction band electrons participate in this low frequency plasma response. Similarly, the value of τ is two orders of magnitude larger than usual for an alkali, noble, or transition metal [124]. The origin of the anomalously large scattering time was suggested [120] to be the ineffectiveness of forward scattering of conduction electrons in the metallic state and the need for backward scattering (i.e., the Fermi surfaces of metallic polyaniline, polyacetylene, and polypyrrole are "open" as expected for highly anisotropic materials and backward scattering from k_F to $-k_F$ may be necessary for momentum relaxation).

TABLE 46.5. *Typical low frequency plasma frequency and relaxation time obtained from microwave frequency measurements of very highly conducting polymers.*

Highly conducting polymer	$\omega_{p(cm^{-1})}$	τ (s)
T-$(CH(I_3)_y)_x$ (295 K) [75,160]	∼200	$\sim 3.3 \times 10^{-11}$
PPy-PF_6 (265 K) [74]	∼100	$\sim 3.0 \times 10^{-11}$
PAN–CSA (*m*-cresol) (295 K) [73,75,120]	∼120	$\sim 1.2 \times 10^{-11}$

The behavior of ε_{mw} for PAN–CSA of moderate conductivity (∼200 S/cm) demonstrates [120] strikingly the effect of disorder (Fig. 46.25). A metal–insulator transition as a function of temperature is reflected in $\varepsilon_{mw}.\varepsilon_{mw}$ crosses from huge and negative (Drude-type band transport) at room temperature to large and positive (insulating or "dielectric" behavior) at ∼20 K. This behavior is ascribed [120] to phonon controlled delocalization. When the phonon scattering rate is larger than the impurity scattering rate, phonon scattering destroys the localization caused by impurity scattering. The presence of this effect is suggested to arise from the key role of one-dimensional chains electronically linking three-dimensional metallic regions in the polymer.

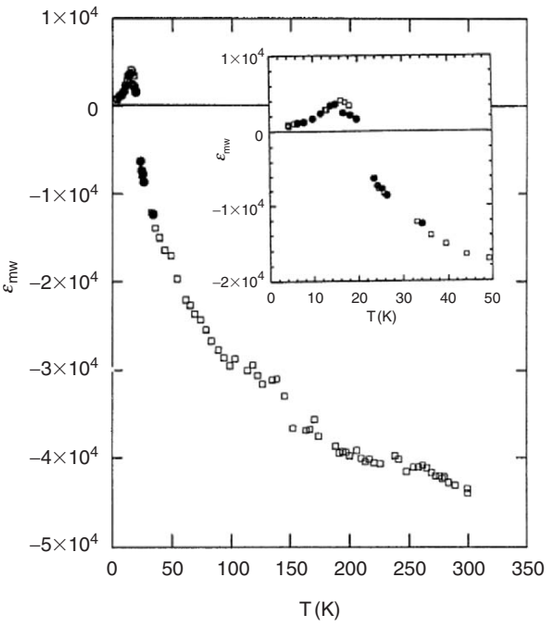

FIGURE 46.25. $\varepsilon_{mw}(6.5 \times 10^9\,\text{Hz})$ versus temperature for a sample of PAN–CSA (*m*-cresol) of moderate conductivity (∼200 S/cm), demonstrating a metal–insulator transition as a function of temperature (from Ref. [120]).

46.8 OPTICAL ABSORPTION, TRANSMISSION, AND REFLECTION

The apparent semiconducting or insulating bandgaps for the undoped forms of each of the principal conducting polymers as obtained by visible/UV spectroscopy are listed in Table 46.6 [91,161–181], though for many of the nondegenerate polymers, the lower energy optical absorption may actually represent formation of excitons [49–52,181–184]. Upon low level doping, there is a systematic change in the optical properties depending on whether the ground state is degenerate or nondegenerate, with prominent signatures for solitons, polarons, and bipolarons. However, for the most highly doped ordered states, the conducting polymers show ''metallic'' absorption and reflection behavior.

Because the metallic state is so highly reflecting, it is often studied via reflectance from films. From such data, a Kramers–Kronig analysis provides all the optical constants of interest including the absorption coefficient, dielectric functions, and conductivity [185]. The real part of the dielectric function (ε_1) and the optical conductivity (σ_1) give insight into the localized or delocalized behavior of the conduction electrons. The measured frequency response can be compared with the Drude model for free electrons and other models for localized (bound) electrons [185]. Again, the universality of the electronic behavior of the systems with improving structural order, morphology, and doping is stressed. For the materials with the highest σ_{DC}, an increased fraction of the total oscillator strength (from conduction electrons) demonstrates free electron Drude response.

46.8.1 Optical Dielectric Function

For the conducting forms of doped polyacetylene and other conducting polymers, there are zero, two, three, or one zero crossings of the real part of the dielectric function (ε_1) as the frequency is decreased. For the least conducting materials, ε_1 remains positive for the entire optical frequency range (50–50,000 cm^{-1}), reaching values of several hundred at microwave frequencies. For higher conductivity materials, ε_1 crosses zero between 1 and 3 eV (the all-conduction-electron plasma response) and then becomes positive again below $\sim 1{,}000\,cm^{-1}$, reaching values in excess of 10^4 at microwave frequencies. For the most metallic samples, two behaviors have been reported dependent upon the system. For doped PAN and PPy with modest $\sigma_{DC} \sim 400\,S/cm$, ε_1 demonstrates the previous two zero crossings, and a third zero crossing occurs to negative values at a ''delocalized conduction electron plasma frequency'' of several hundred wavenumbers. For the most highly conducting doped polyacetylene, ε_1 crosses zero at the all conduction electron plasma frequency and remains negative to the lowest measured optical frequencies.

The optical response of iodine [83,106,162,186,187] and perchlorate (ClO_4) [106,188,189] doped $(CH)_x$ and PF_6 doped poly(methylthiophene) [190] have been well characterized, as have polyaniline samples (PAN–HCl [55,191,192] and PAN–CSA prepared in *m*-cresol [75,146,193–196] and in solutions of *m*-cresol and chloroform [193,197]) and polypyrrole films (doped with PF_6 [74,89,198,199], TsO [74,89,198], ClO_4 [166], and some sulfonated poly(β-hydroxyethers) [46,192].

Figure 46.26 shows ε_1 at room temperature for selected PAN samples. PAN–CSA (*m*-cresol) ($\sigma_{DC} \sim 400\,S/cm$) has three zero crossings for ε_1 which correspond to two different plasma frequencies [193]. The higher energy zero crossing was assigned [75] to the plasma response of the whole conduction band, as the density of carriers (n) determined from the plasma frequency ($\omega_p^2 = 4\pi ne^2/m^*$; assuming m^*, the effective mass, is approximately the free electron mass) is in the range of the dopant density. There is a Lorentzian frequency dispersion at this ω_p indicating that the majority

TABLE 46.6. *Typical apparent "bandgap" values for the undoped conducting polymers. Both the absorption onset and peak are given.*

Material	Absorption onset (eV)	Absorption peak (eV)
$(CH)_x$ (*trans*) [161,162]	1.4	1.8
$(CH)_x$ (*cis*) [163]	~1.9	2.3
PAN (LEB) [164]	3.2	3.6
PAN (EB) [164]	1.6(3.0)	2.0(3.8)
PAN (PNB) [165]	1.8	2.3
PPy [166,167]	2.5	3.2
PT [168–171]	2.0	2.3–2.7
PPP [91,172–174]	3.1	3.43–3.7
PPV (old) [175–178]	2.4	2.9
PPV (new) [179]	2.25	2.46
PPyr [180]	2.9	3.3
PPyV [181]	2.5	3.0

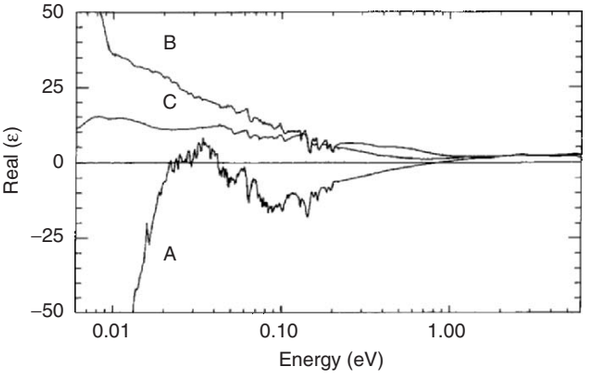

FIGURE 46.26. Real part of the room temperature dielectric response versus frequency for PAN–CSA(*m*-cresol) (A), PAN–CSA(chloroform/*m*-cresol) (B), and PAN–HCl IXL (C) (from Refs. [192,193]).

of the conduction electrons are localized or bound spatially, and require a finite amount of energy to be excited. At a lower frequency dispersion, ε_1 begins to become positive at $\sim 330\,\mathrm{cm}^{-1}$ ($\sim$0.04 eV); this is a characteristic of the Lorentzian (localized) behavior. However, at $\sim 200\,\mathrm{cm}^{-1}$ ($\sim$0.02 eV), ε_1 again crosses to negative values and grows increasingly negative with decreasing wavenumber. This plasma frequency shows Drude behavior with decreasing wavenumber and in fact appears approximately at the frequency predicted by the microwave estimates [73,74]. Similar zero crossings are reported for PPy(PF_6) ($\sigma_{DC} \sim 300\,\mathrm{S/cm}$) [74,198,199] (Fig. 46.27).

Comparison of the plasma frequencies for the Drude electrons with the plasma frequencies for the whole conduction band for these polymers, assuming that the effective mass m^* is the same as that for the whole conduction band response, yields a ratio of the density of electrons contributing to the free response compared to the localized response of $\sim 10^{-3}$. Assuming even a tenfold increase in m^* for the lower frequency ω_p (as the delocalized electrons must traverse the disordered regions with presumably narrowed energy bands), only a small fraction ($\sim 10^{-2}$) of the conduction electrons are delocalized enough to show Drude behavior in PAN–CSA (*m*-cresol).

The frequency response of ε_1 for PAN–CSA prepared from chloroform and subsequently briefly exposed to *m*-cresol vapor ($\sigma_{DC} \sim 20\,\mathrm{S/cm}$) [193] (Fig. 46.26) is characteristic of localized electrons. ε_1 is positive at all optical frequencies; the scattering due to disorder in these materials has broadened and washed out the dielectric zero crossings. Lorentzian dispersion due to a "localized polaron" [146] is evident in ε_1 around $12{,}000\,\mathrm{cm}^{-1}$ (1.5 eV) and ε_1 for this material increases positively with decreasing wavenumber in the far IR, characteristic of a material with a small residual band gap or localized carriers. Lower conductivity PAN–HCl [193] ($\sigma_{DC} \sim 10\,\mathrm{S/cm}$) materials show even less dispersion with wavenumber. ε_1 for these materials is also positive over the whole range and shows only a modest increase in the IR, becoming nearly wavelength independent in the far IR.

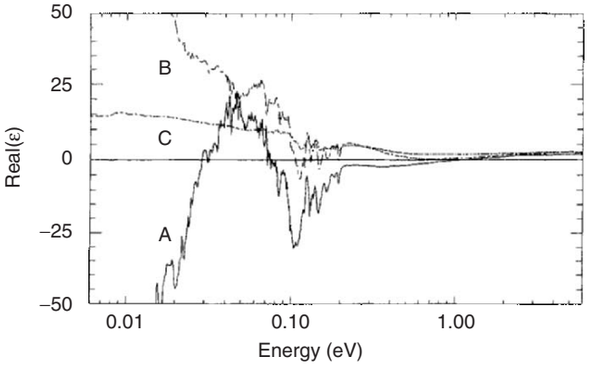

FIGURE 46.27. Real part of the room temperature dielectric response (ε_1) versus frequency for PPY(PF_6) (A), PPY(TsO) (B), and PPY(S-PHE) (C) (from Refs. [74] and [192]).

Polarized optical measurements of the dielectric response of HCl doped stretched PAN samples are shown in Fig. 46.28. The dielectric response perpendicular to the stretch direction is characteristic of insulating behavior. Along the stretch direction, a strong plasma-like response is observed [191], indicating that the scattering times along the chain are much longer than those perpendicular to the chain. This indicates that on-chain partial delocalization develops first in these systems.

Doped polypyrrole demonstrates behavior similar to polyaniline for samples with lower conductivity and structural order. In Fig. 46.27, the more disordered PPy(TsO) ($\sigma_{DC} \sim 120\,\mathrm{S/cm}$) [74,198] shows a more localized behavior than PPy(PF_6) as ε_1 remains positive throughout the optical frequency range. The carriers are weakly localized though as ε_1 increases rapidly in the far IR. For PPy(S-PHE) ($\sigma_{DC} \sim 10\,\mathrm{S/cm}$) [46,192], there is very little dispersion in ε_1; it remains positive and small in the entire optical range, becoming nearly wavelength independent in the far IR.

ε_1 for the most highly conducting iodine and perchlorate doped polyacetylene samples remains negative but small for frequencies less than its all-conduction-electron plasma frequency of $\sim$3 eV through the far IR for light polarized both parallel and perpendicular to the stretched chain direction [187,188] (Fig 46.29) again supporting the three-dimensional nature of the metallic state in conducting polymer systems. Below $\sim$0.05 eV, ε_1 becomes increasingly negative, suggesting a Drude plasma frequency for the most delocalized electrons.

Summarizing, there is an evolution of the dielectric response with increasing order. For the most disordered, lowest conducting samples, ε_1 remains positive and shows very weak dispersion. As the order and conductivity of the materials increase, ε_1 first shows more dispersion at the plasma edge of the whole conduction band as the scattering time increases, possibly turning negative in that range, but returns positive in the far IR. This behavior was seen in stretched PAN–HCl samples parallel to the stretch direction [191]. For the best current materials, ε either returns negative or remains negative in the far IR, indicative of a small density of macroscopically delocalized electrons.

46.8.2 Optical Conductivity

For materials near the insulator–metal (localization–delocalization) transition the optical conductivity is suppressed at low frequencies relative to the usual Drude conductivity [115]. The suppression is usually strong for frequencies up to a critical-frequency $\omega_c \sim D/L^2$ where D is the diffusion coefficient and L is the localization length for the electron. This conductivity suppression occurs because the carriers would diffuse a distance greater than the localization length within the period of the AC wave for

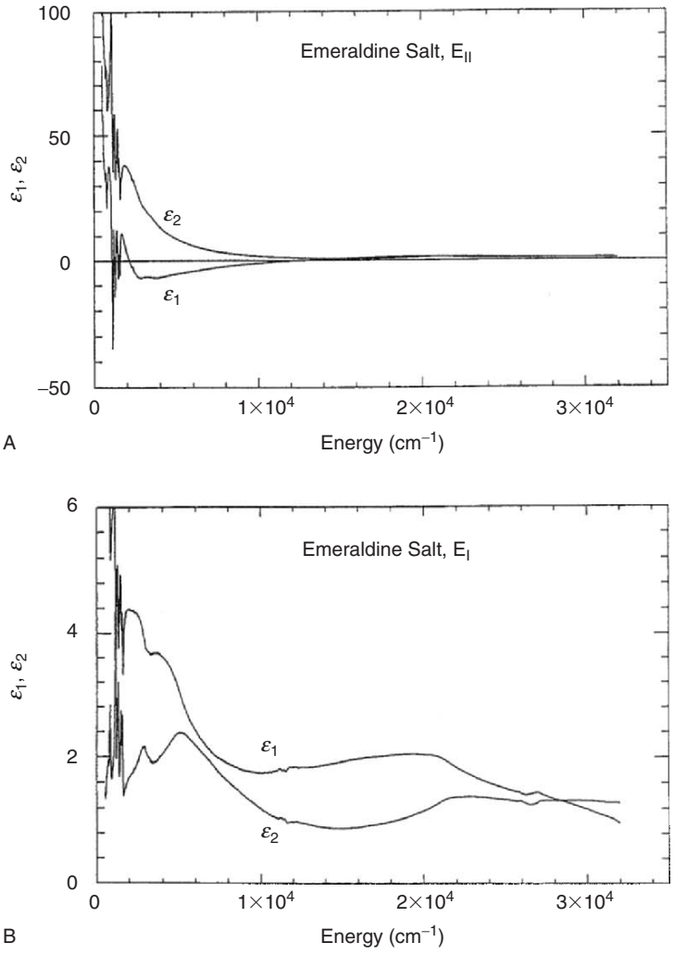

FIGURE 46.28. Real part of the dielectric constant versus frequency for light polarized (A) parallel and (B) perpendicular to the stretch direction in PAN doped with HCl (from Ref. [191]). The chain alignment is improved by stretching. ε_1 is negative in the mid IR for the parallel direction but not for the perpendicular direction, implying that the delocalization is much greater along the chain.

$\omega < \omega_c$. For frequencies greater than ω_c, the optical conductivity shows the normal Drude decrease with increasing frequency. For three-dimensional materials, localization corrections to the frequency dependent conductivity [115,194,200–202] yield

$$\sigma(\omega) = \sigma_{\text{Drude}}\left[1 - \frac{C}{(k_F v_F \tau)^2} + \frac{C(3\omega)^{1/2}}{(k_F v_F)^2 \tau^{3/2}}\right], \qquad (46.10)$$

where C is an undetermined universal constant, k_F is the Fermi wavevector, v_F is the Fermi velocity, τ is the scattering time, and σ_{Drude} is the regular Drude conductivity given by

$$\sigma_{\text{Drude}} = \frac{\Omega_p^2 \tau}{4\pi(1 + \omega^2\tau^2)}, \qquad (46.11)$$

where Ω_p is the plasma frequency of the free electrons. Notice that as $k_F l$ (i.e., $k_F v_F \tau$) becomes large for more ordered higher σ materials, the corrections to the Drude formula should become negligible and the three-dimensional conductor should obey the Drude formula.

The experimental optical conductivity of the doped polymers evolves from localized semiconducting behavior to metallic behavior with improved order. For $(CH)_x$ doped with perchlorate (ClO_4) [106,188,189], (Fig 46.30) or iodine [106,162,186] with different stretch ratios, the optical conductivity shows soliton features at midgap and a Drude plasma edge which develops with stretch alignment at $\sim 200\,\text{cm}^{-1}$ (0.02 eV) where the optical conductivity rises rapidly to its dc value with a very long scattering time. The full conduction electron plasma frequency for doped $(CH)_x$ is $\sim$3 eV; therefore, the plasma edge at 0.02 eV is associated with only a small fraction of the conduction electrons [75]. Because a small fraction of the conduction electrons appear macroscopically delocalized with a long scattering time while the majority of conduction electrons are more

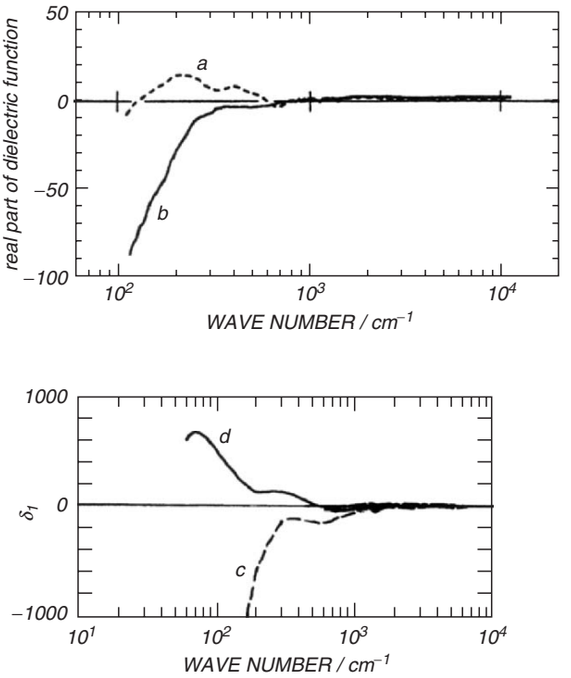

FIGURE 46.29. Top: real part of the dielectric constant versus frequency for light polarized perpendicular to the stretch direction in $(CH)_x$ doped with ClO_4 (from Ref. [188]). For sample (b), the chain alignment is improved over the sample (a) by stretching. ε_1 is negative at low frequencies indicating a three-dimensional metallic state. Bottom: real part of the dielectric constant vs. frequency for light polarized parallel to the stretch direction (from Ref. [187]). Samples (c) and (d) are both doped to the same level with iodine, but sample (c) was stretched before doping, resulting in greater ordering and a more metallic response.

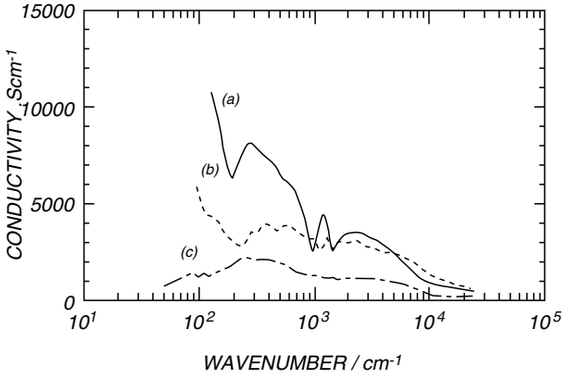

FIGURE 46.30. Optical conductivity versus frequency for $(CH)_x$ of different stretched ratios (a: stretched 8×; b: stretched 4×; c: unstretched) doped with perchlorate (ClO_4) (from Ref. [188]). There is a growth of a free carrier band (Drude response) around $\sim 200\,\mathrm{cm}^{-1}$ with increased stretch ratio.

strongly localized, with a short scattering time, the localization modified Drude model [115,194,200–202] does not simultaneously fit well the frequency dependent dielectric function and conductivity of highly conducting $(CH)_x$. Models which take into account the inhomogeneous disorder of the systems provide a better representation as they allow for composite behavior (metallic islands which percolate in a semiconducting matrix).

Typical optical conductivity spectra for PAN and PPy films are shown in Figs. 46.31 and 46.32, respectively. For highly conducting PAN–CSA (*m*-cresol) [$\sigma_{DC} \sim 120\,\mathrm{S/cm}$] [193], σ_1 begins to increase with decreasing wavenumber at $\sim 10{,}000\,\mathrm{cm}^{-1}$ ($\sim$1.2 eV) to values as high as $\sim$750 S/cm at $\sim$0.1 eV and then decreases consistent with localization behavior. However, at $\sim$0.02 eV, σ_1 begins to increase, qualitatively similar to the behavior of doped $(CH)_x$ though the increase in the far IR is not as rapid as for doped $(CH)_x$ as the dc conductivity is much lower for this PAN–CSA material. This type of frequency behavior for σ_1 is qualitatively similar to the composite behavior of metallic particles (islands) in a semiconducting matrix after percolation of the metallic particles [203]. PPy(PF_6) [74,198] [$\sigma_{DC} \approx 300$ S/cm] has similar behavior, though σ begins to increase with decreasing wavenumber at a higher all-conduction-electron "plasma edge" of $\sim 17{,}000\,\mathrm{cm}^{-1}$ ($\sim$2.1 eV).

In contrast to this behavior, σ for other doped PAN and PPy materials show more localized behavior. For example, the optical conductivity of PAN–CSA cast from a solution of chloroform and exposed to *m*-cresol [$\sigma_{DC} = 20\,\mathrm{S/cm}$] [192], PAN–HCL ("intermediate cross linked (crystallinity)" IXL) [$\sigma_{DC} \sim 10\,\mathrm{S/cm}$] [193], PPy(TsO) [74.198] [$\sigma_{DC} \approx 100\,S/cm$], and PPy(S-PHE) [$\sigma_{DC} \approx 10\,\mathrm{S/cm}$] [46,192] have maxima (in addition to phonon features) at higher energies in the IR than more highly conducting PAN and PPy. In the far IR, σ decreases with decreasing frequency more rapidly for these samples with increased disorder as expected for localized electrons. Similar behavior has been reported for perchlorate (ClO_4) doped PPy [166,187] and PF_6 doped poly(3-methylthiophene) [190] (Fig. 46.33). For the lower conductivity doped polymers, the localization modified Drude model [115,200–202] has the same frequency dependence as the experimental spectra. The low frequency conductivity peak shifts to lower energy with increasing dc conductivity in both PAN [197] (Fig. 46.31) and PPy [74] (Fig. 46.32) and likely results from the decrease of the critical frequency ω_c as the samples become more ordered. For the low conductivity PAN samples, most of the oscillator strength is shifted [146] into a peak at $\sim$1.5 eV associated [54,146] with localized polarons. Thus with decreasing order the oscillator strength shifts to higher wavenumber and thus higher binding energies.

Qualitatively, the PAN and PPy materials with $\sigma_{DC} < 200\,\mathrm{S/cm}$ show the behavior expected for both the good conductor/poor conductor composites as well as for the three-dimensional localization modified Drude model. The optical conductivity of highly conducting stretched

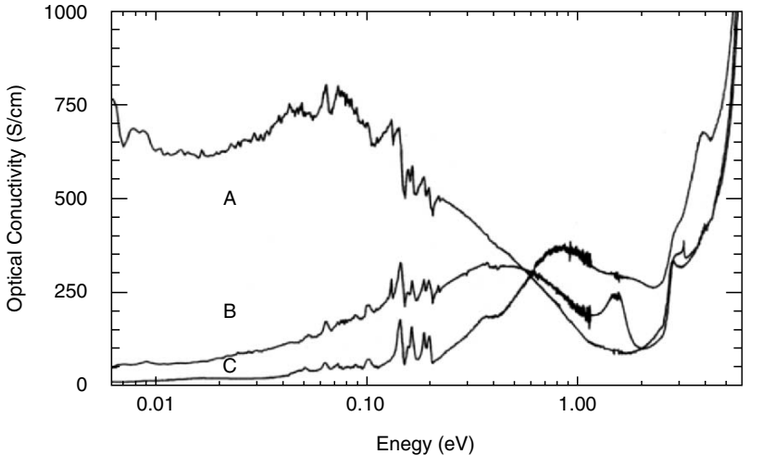

FIGURE 46.31. Room temperature optical conductivity vs. frequency for PAN–CSA(*m*-cresol) (A) PAN–CSA (chloroform/*m*-cresol) (B), and PAN–HCl IXL (C) (from Refs. [192, 193, and 224]).

polyacetylene and doped PAN and PPy with $\sigma_{DC} > 200\,S/cm$ show Drude behavior for a small fraction of the conduction electrons which essentially percolate through the film while the remaining conduction electrons are more localized.

46.9 ULTIMATE CONDUCTIVITY

46.9.1 Drude Model Analysis

The intrinsic conductivity of conducting polymers is of interest for fundamental science and future materials applications. Though the materials currently have σ_{DC} less than common metals, the conducting polymers are not fully crystalline. Past progress suggests that as the synthesis, doping routes, and processing are improved, further advances in materials properties can be expected. Estimates of the ultimate conductivity [122] of the quasi-one-dimensional polymer systems assuming the primary momentum relaxations are from $2k_F$ phonons which have modest population at room temperature suggests the ultimate conductivity for $(CH)_x$ is $\sim 2 \times 10^6\,S/cm$ (compared to $5.5 \times 10^5\,S/cm$ for copper).

From the experimental data which exist for current systems, estimates of the intrinsic conductivity also can be made [197]. The intrinsic Drude nature of metallic carriers has been identified using both microwave and optical techniques. Both of these techniques have identified the presence of a group of carriers which demonstrate Drude behavior with a long scattering time ($\tau \sim 10^{-11}\,s$). The Drude conductivity for traditional metals is given by

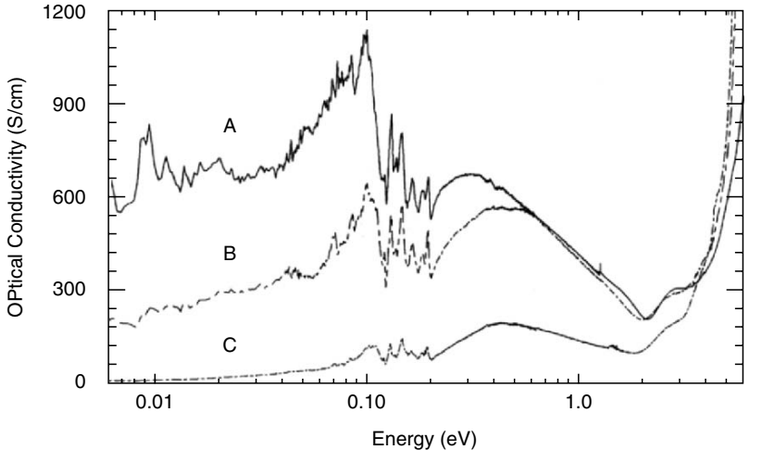

FIGURE 46.32. Room temperature optical conductivity versus frequency for PPy(PF_6) (A), PPy(TsO) (B), and PPy(S-PHE) (C) (from Refs. [74, 192, and 224]).

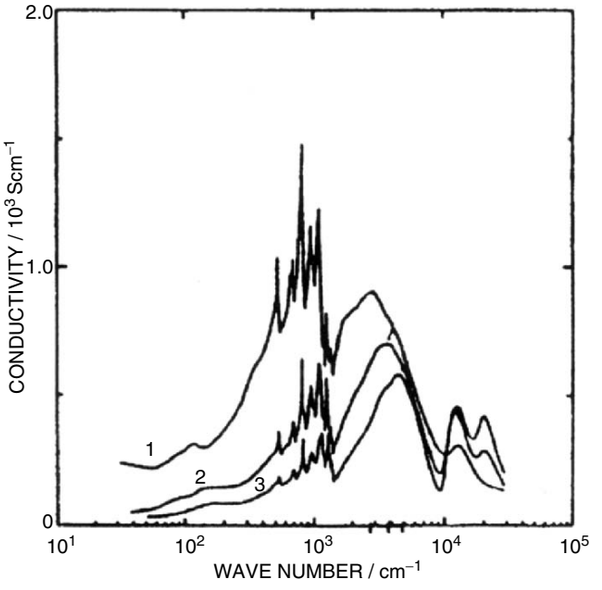

FIGURE 46.33. Optical conductivity versus frequency for poly-(methylthiophene) (PMT) doped with PF_6 as a function of doping level (from Ref. [190]). The spectra are for different doping levels [with (1) being highest and (3) the lowest doping level].

$\sigma = ne^2\tau/m^*$. In the present systems, only a small fraction ($\sim$0.1%) of the conduction electrons show this Drude behavior. If all of the conduction electrons (determined by doping percentage) have a scattering time equivalent to $\tau \sim 10^{-11}$ s, then $\sigma_{\text{ultimate}} \sim 10^7$ S/cm.

46.9.2 Resonance Quantum Transport in Doped Conducting Polymers

Metallic doped polymers (polyaniline and polypyrrole) have an electromagnetic response that, when analyzed within the standard theory of metals, is provided by an extremely small fraction of the total number of available electrons $\sim$ 0.1% (in contrast to $\sim$100% for common metals) but with anomalous long scattering time $\tau \geq 10^{-13}$ s (more then 100 times longer than for common metals). Prigodin and Epstein have shown [220] that a network of metallic grains (polymer's crystalline domains) connected by resonance quantum tunneling through localized states in surrounding disordered medium produces this behavior. The small fraction of electrons is assigned to the low density of resonance states and the long scattering time is related to the narrow width of energy levels in resonance. This differs from the general consensus [221–224] that the difference in doped conducting polymers between metal and insulator at low temperatures is caused by disorder driven localization of the conduction electrons (Anderson insulator–metal transition (IMT)) [153].

Figure 46.34 reviews the two conventional single particle transport mechanisms. For band transport (Drude theory) electrons behave as "free particles". They are accelerated by the applied electric field and loose their momentum through scattering by impurities and phonons. As a result, an electron's motion may be described as quantum diffusion. At low temperature the phonon scattering becomes weak and the conductivity increases with decreasing temperature to its residual value. For hopping the zero temperature electrical conductivity is zero because the charge carriers are localized. At finite temperatures electrons hop from one localized state to another by absorbing or emitting phonons. In contrast to band transport, hopping conductivity increases with temperature because of increased availability of phonons (see Fig. 46.34).

The dielectric constant ε can be used to identify the mechanism of charge transport [222,224]. For band transport, ε is negative because of inertia of "free electrons"; for hopping ε is positive and proportional to the square of the size of the localized state. Hopping often is expected to be the basic mechanism of transport for polymers because of their irregular structure and because even weak disorder localizes electrons in single isolated chains. This type of conductivity is observed in the dielectric polymers (doped polymers that become insulators at low temperatures) and their behavior qualitatively follows the above dependencies. However, the behavior of metallic polymers can be understood within neither the above hopping model nor the model of conventional metal with band electrons. The metallic conductivity of doped polymers decreases with decreasing temperature and a finite residual conductivity is within a decade of the room temperature value.

Though the decrease of the dc conductivity for metallic polymers with decreasing temperature can be accounted for within the band model by effects of localization caused by disorder, the experimental optical and low frequency conductivity and dielectric constant in the metallic state of doped polymers in principle cannot be accounted for by band models with homogeneous disorder. Experiments [221–224] show that the high frequency ($\geq$ 0.1 eV) conductivity and dielectric constant generally follows a Drude law with the number of electrons $\sim 10^{21}$ cm^{-3} corresponding to the total density of conduction electrons and conventional scattering time $\sim 10^{-15}$ s in both the metallic and dielectric phases (Figs. 46.26–46.28). At decreasing frequency the polymers in the dielectric phase progressively display insulator properties and ε becomes positive for frequency $\leq$ 0.1 eV signaling that charge carriers are now localized. Microwave frequency ($\sim$ 6.6 GHz) ε experiments [222] yield localization lengths $\sim$ 5 nm, depending on sample.

A surprising and remarkable feature of the metallic phase in polymers is that $\varepsilon(\omega)$ is similar to that of dielectric samples in magnitude and sign with decreasing frequency, also changing sign from negative to positive at approximately the same frequency $\sim$ 0.1 eV. However, for metallic

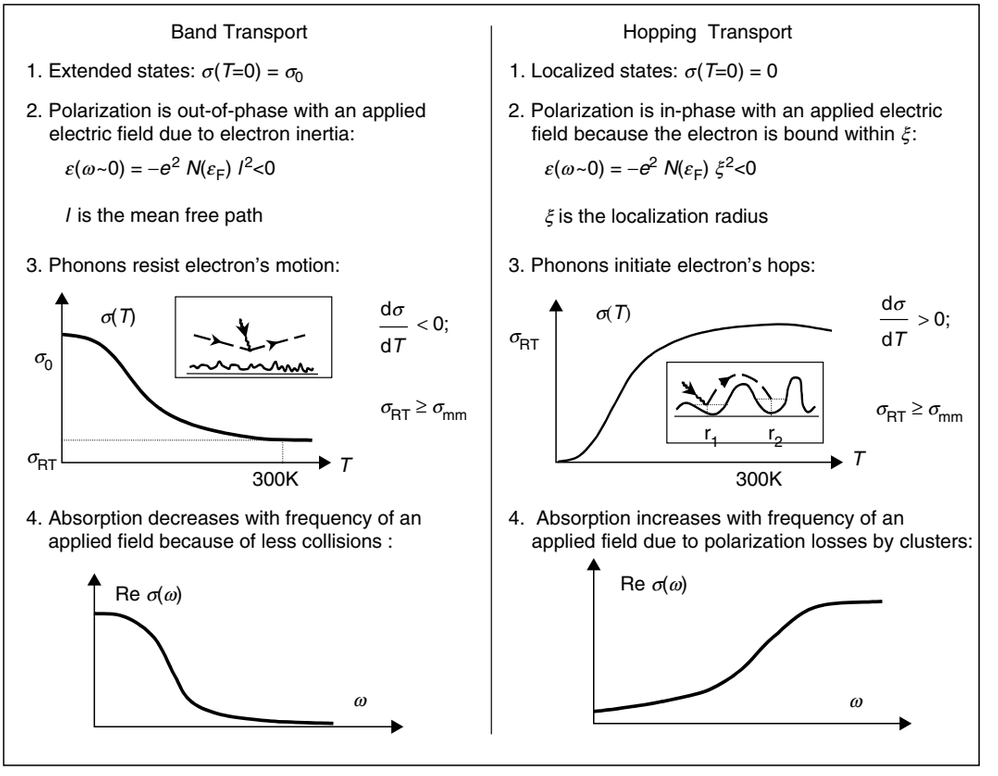

FIGURE 46.34. Comparison of band and hopping mechanisms of transport (after Ref. [220]).

samples ε changes again to negative at yet lower frequencies ≤ 0.01 eV indicating that "free electronic" motion is present, Fig. 46.35. The parameters of this low frequency coherent phase are quite anomalous. From the Drude model, the relaxation time is very long $\geq 10^{-13}$ s; also, the new plasma frequency below which ε is again negative is very small ~ 0.01 eV [3,5]. This second zero crossing of the dielectric constant at low frequency and the conclusion about a long relaxation time and a small plasma frequency were confirmed with radio frequency conductivity studies [225].

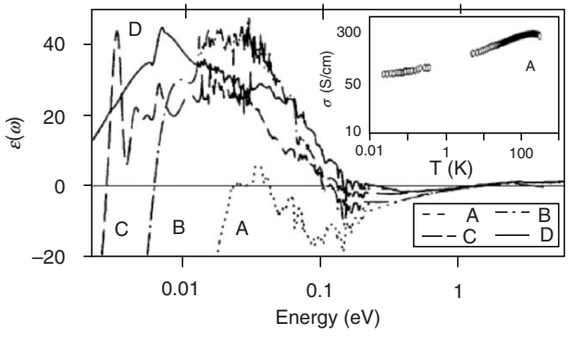

FIGURE 46.35. $\varepsilon(\omega)$ for camphor sulfonic acid doped polyaniline samples with room conductivities in the order of $\sigma_A > \sigma_B > \sigma_C > \sigma_D$ (Inset, σ_{DC} (T)). (after Ref. [222]).

These experimental data contrast with the Anderson IMT [153] in which electronic behavior is controlled by homogeneous disorder. In the dielectric phase electrons are bound by fluctuations of the random potential. On the metallic side of the transition, free carriers have short scattering times. In the metallic phase near the transition, ε is positive because the disorder causes dynamic polarization due to slowing diffusion by localization effects. When approaching the IMT the localization effects increase and ε diverges ("dielectric catastrophe" [200]).

The small plasma frequency and very long τ of the metallic state in doped polymers can be explained [222, 224,225] assuming that the conductivity is provided by a small fraction $\sim 0.1\%$ of the total carriers with long scattering time $> 10^{-13}$ s. However, it is difficult to reconcile this conclusion with the behavior for high frequencies which supports that the scattering time is usual $\sim 10^{-15}$ s and all available electrons participate in conduction. To account for these anomalies the possible presence of a collective mode, as in a charge density wave conductor, or superconductor, was suggested [199].

Prigodin and Epstein proposed [220] that in highly conducting polymers there is a new mechanism of charge transport, resonance quantum tunneling among metallic domains. These materials are strongly inhomogeneous [18,62,127,133] with "crystalline" regions within which polymer chains are well ordered (Fig. 46.36). Electrons are

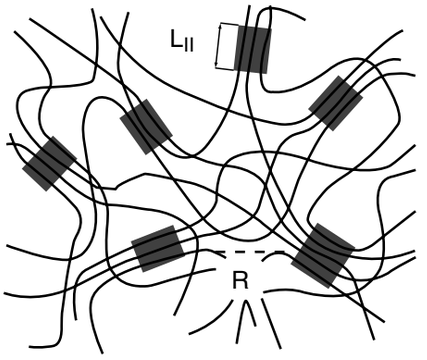

FIGURE 46.36. Schematic view of the structure of polyaniline and polypyrrole. The lines represent polymer chains. The dashed squares represent regions where polymer chains have crystalline order.

considered to be three-dimensionally delocalized over grains due to good overlap between chains within the grains. At least, when the IMT is approached, an electron's delocalization first occurs inside these regions. Outside the crystalline regions the chain order is poor and the electronic wave functions are strongly localized within single chains. Therefore, the crystalline domains can be considered as nanoscale metallic dots embedded in a disordered poorly conducting medium. The metallic grains remain always spatially separated by disordered regions, and, therefore, direct tunneling between grains is exponentially suppressed. The intergrain tunneling is possible through intermediate localized states in the disordered portion with strong contribution from resonance states whose energy is close to the Fermi level (Fig. 46.37). The dynamics of resonance tunneling can account for the frequency-dependent anomalies in the conductivity and dielectric constant of the metallic phase of these doped polymers. Reference [220] provides a detailed description and quantitative analysis of this model.

Within the Prigodin and Epstein model each grain is coupled to other grains by $2N_\perp$ independent chains. For simplicity one may assume that the two nearest grains are electrically connected by $\sim N_\perp/z$ chains, where z is the number of nearest neighboring grains. In the metallic phase the intergrain coupling leads to broadening of quantized levels in the grains, $\delta E = 2N_\perp g\Delta E$, where g is the transmission coefficient between grains through a single chain. The IMT occurs when $\delta E \sim \Delta E$ and the critical chain-link coupling g_c satisfies

$$2N_\perp g_c = 1. \tag{46.12}$$

For PAN(HCl) and similar PAN(CSA) this yields $g_c \sim 10^{-2}$.

If $g < g_c$ the system is a dielectric and the behavior (46.4) is retained for all $\omega\tau_T \ll 1$. However, on the metallic side ($g > g_c$) electrons are delocalized and their low-frequency motion is a random walk among the grains. Introducing the mean transition rate, W, for hopping between the grains and the mean distance between the centers of neighboring grains, $R(b \sim (L_\parallel/R)^3)$, the corresponding diffusion coefficient D_3 and the macroscopic conductivity are

$$D_3 = R^2W,\ \sigma(\omega \sim 0) = be^2N(\varepsilon_F)D_3. \tag{46.13}$$

When approaching the IMT from the metallic side W tends to 0 as [12]: $W = (\Delta E/(2z))\exp[-2\pi(g_c/(g-g_c))^{1/2}]$. In the metallic phase the hopping frequency W is related to the above model parameters as

$$W = \delta E/(2z) = (N_\perp/z)g\Delta E, \tag{46.14}$$

and the whole system can be represented as a network of random conductors. The nodes represent the grains where randomization of electronic motion happens. Further details of analysis and its application to specific polymers are in Ref. [220].

A principal difference between direct and resonance tunneling is the time for tunneling. Direct tunneling that occurs in a conventional granular metal is an almost instantaneous process, i.e., its characteristic time is the scattering time τ. Resonance tunneling that is anticipated to be in the metallic polymers shows a delay determined by the level width γ.

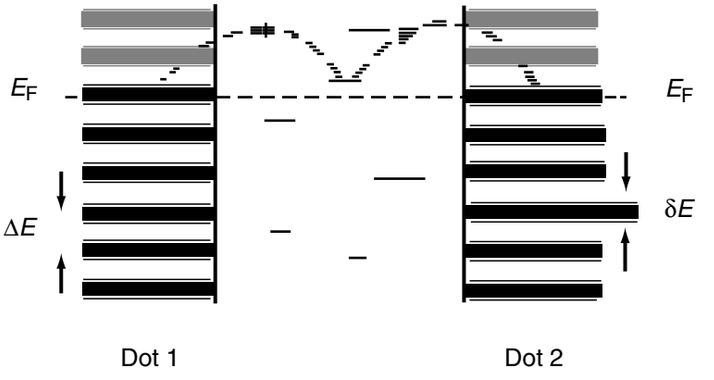

FIGURE 46.37. Schematic illustration of the electrical coupling of the metallic grains being provided by resonance tunneling of between the quantized states of the metallic grains through localized states in the amorphous region.

The temperature dependence of the dc conductivity in the metallic phase follows from that expected for resonant tunneling through the strongly localized states in the amorphous regions of the metallic polymer. With increasing temperature phonons increase the localization length of the states in the disordered regions thereby increasing the resonant transmission rate between grains and increasing the conductivity. As a result the low-frequency part of electromagnetic response is shifted with increasing temperature to a range of higher frequencies as it experimentally is observed [222].

46.10 APPLICATIONS

Intrinsically conducting polymers (ICPs) also are of interest for a wide range of applications [204]. The ICPs have been proposed for use as conducting wires, in batteries [205], as electromagnetic interference (EMI) shielding materials [206–209], joining (welding) of plastic materials [210], light emitting diodes (LEDs) [211], sensors [212], anticorrosive coatings [213], etc.

In LED studies, doped polyaniline and its blends have been used for the hole injecting layer [214], and undoped poly(*p*-phenylene vinylene) and other materials have been utilized for the light emitting layer [211]. More recently, a symmetrically configured alternating voltage light emitting (SCALE) device based on electronic polymers has been demonstrated [215,225,226,227]. The advantages of ICPs for light emitting devices include flexibility, mechanical strength, and relatively easy control of the color of light emission. Transparent conducting polymers may be incorporated as electrodes in efficient LEDs [216].

The use of plastics and their composites is rapidly increasing in numerous areas. However, the final assembly of products is often limited by the capability of existing joining techniques. The ability of ICPs, especially polyanilines, to absorb electromagnetic radiation and convert it into heat introduces another application in the welding of thermoplastics and thermosets [210].

With the rapid advances and broad implementation of computer and telecommunication technologies there is an increased need to shield EMI, especially in the radio and microwave frequency ranges. Intrinsically conducting polymers are promising materials for shielding of EMI because of their relatively high conductivity and dielectric constant and the ease of control of their conductivity and dielectric constant through chemical processing [207]. Also, they are relatively lightweight compared to standard metals, flexible, and do not corrode as common metals. The microwave conductivity and dielectric constant of polyanilines are controllable through chemical processing (e.g., stretch ratio, molecular weight, doping level, counter ion, solvent, etc.). Figure 46.38 compares the total shielding efficiency of PAN–CSA (*m*-cresol) materials with that of copper on the base of mass/area, while Fig. 46.39 compares the shielding efficiency of several different conducting polymer systems.

The ability to disperse conducting polymers into insulating hosts such as poly(3-octylthiophene) in polyethylene [217] and PAN–CSA in polymethylmethacrylate [218], or nylon [219], and achieve percolation at less than 1%, increases opportunities for applications.

Active electronic devices fabricated from semiconducting organic and polymer materials have become of increasing interest. In particularly, regioregular poly(3-hexylthiophene) (P3-HT) has been of interest because its relative

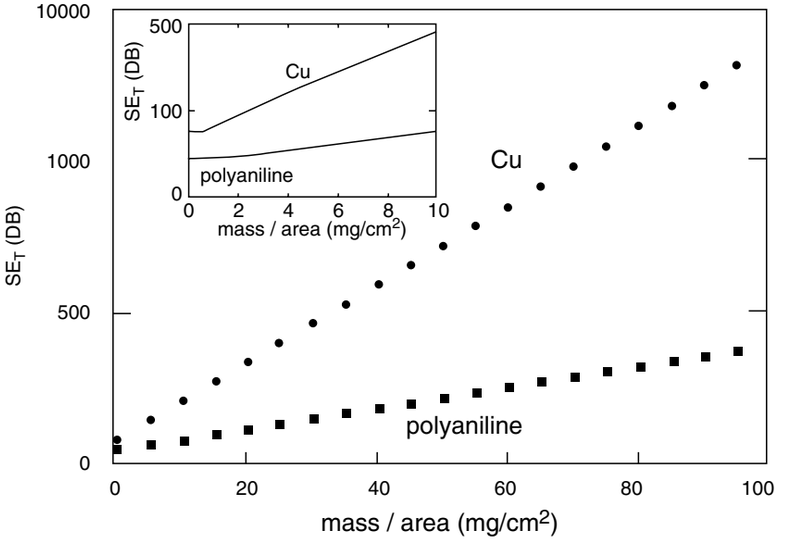

FIGURE 46.38. Comparison of total shielding efficiency (SE_T) of PAN–CSA (*m*-cresol) samples and copper (Cu) as a function of mass/area. Inset: magnification below 10 mg/cm^2 (from Ref. [207]).

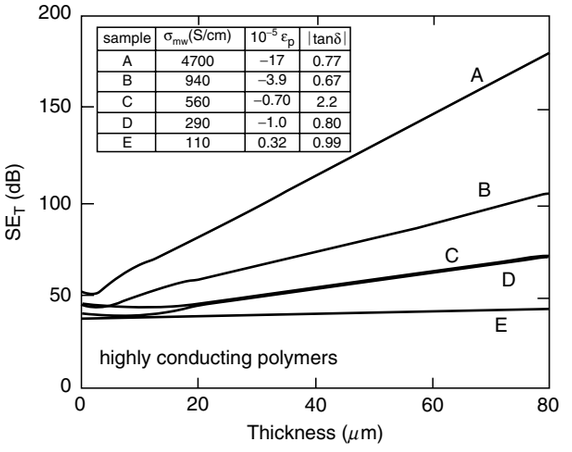

FIGURE 46.39. Comparison of total shielding efficiency (SE_T) of highly conducting polymers versus sample thickness. Sample A: stretched heavily iodine doped Tsukamoto polyacetylene; sample B: unstretched heavily iodine doped Tsukamoto polyacetylene; sample C: PAN–CSA (*m*-cresol); sample D: PPy(PF_6); sample E: PPy(TsO) (from Ref. [207]). The inset shows the microwave transport parameters σ_{mw}, ε_τ, and $\tan\delta$ for each of the materials.

structural order leads to a high mobility, in the range of $0.2\,cm^2/(Vs)$ [228–231].

Recently a new interesting phenomenon, an electric field effect, was reported for the doped highly conducting polymers [232–235]. Figure 46.40 shows I–V characteristics of such a transistor [236] in which conducting polymer PEDOT:PSS [poly(ethylene dioxythiophene): poly(styrenesulfonic acid)] with $\sigma_{RT} \sim 30\,S/cm$ is used as active electronic element and PVP [poly(vinylphenol)] is used as a dielectric separating the gate and source–drain channel. As it is shown on Fig. 46.40 the I_D current decreases with gate voltage V_G similarly to that normally observed for conventional semiconductors. The ratio I_{ON}/I_{OFF} reaches up to 10^4 in some devices [232–236].

Epstein *et al*. suggest [232,235] that the observed field effect in conducting polymers based ''transistor'' is closely related to the mesoscopic inhomogeneity of conducting polymers. They emphasize that the field effect cannot be observed if the conducting polymer is a conventional conductor. For conducting polymers with conductivity of ∼30 S/cm, the screening radius for an electric field produced by the FET gate electrode is expected to be less then 2 nm [232].

Epstein *et al*. propose that the field effect in conducting polymers is due to the ionic component of their charge conductivity. The inhomogeneous structure leaves enough free space for mobile ions. The ions inside the polymers produce the additional screening of the external field, but the crucial feature of ions is the ability of ions to migrate between the conducting polymer film and external dielectric layer interface. As a result the concentration of ions inside of the polymer is controlled by the gate potential. Due to electroneutrality the internal ionic density determines the concentration of primary charge carriers in the polymer and therefore it is anticipated that the polymer conductivity is governed by the gate potential. The critical concentration of ions for disrupting the conductivity along the polymer chains within the disordered regions was estimated within the following simple picture. If 50% crystallinity and size grain ∼10 nm were assumed, then intergrain hopping includes ∼ten intermediate sites along the chain linking two ordered regions. To interrupt this connection it is enough to introduce only one ion, i.e., approximately 5% ''dedoping'' would produce an appreciable effect. Figure 46.41 schematically illustrates the ability of a small concentration of excess ions to control the electrical conductivity of a doped polymers.

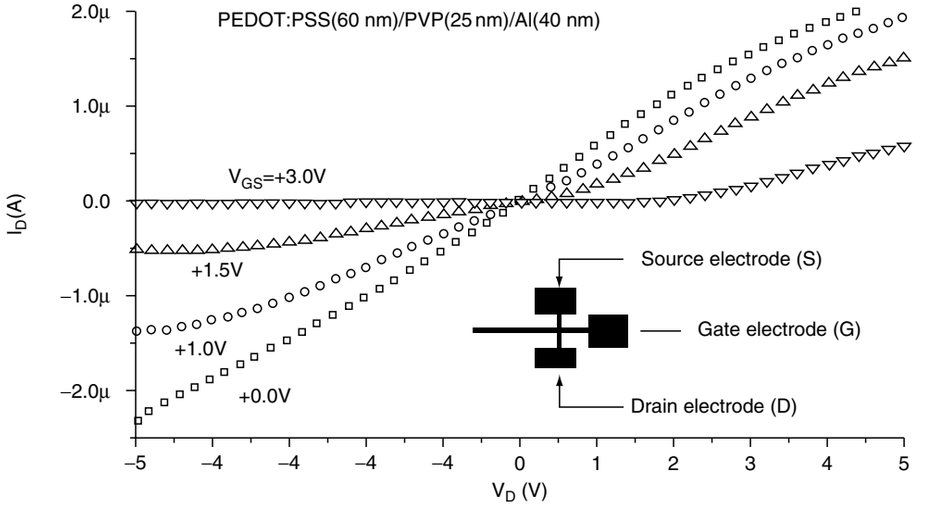

FIGURE 46.40. The drain–source current as the function of drain voltage of a thin PEDOT:PSS/PVP film. The insert shows the polymer-based transistor configuration (after Park *et al.* [236]).

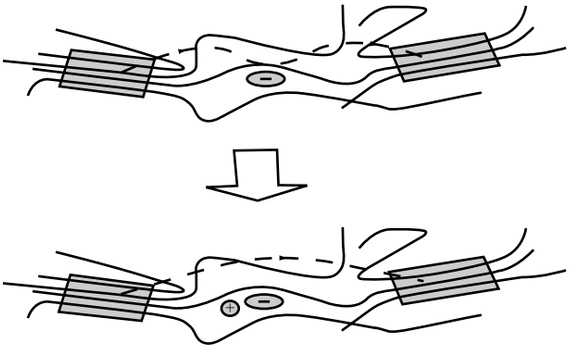

FIGURE 46.41. Schematic illustration of ionic suppression of intergrain hopping. Compensation by cations of charge of acceptors removes the nearby localized states on the polymer backbone that provide for holes easy hopping of electrons between grains. Reprinted from Ref. [235] © (2005) with permission from Elsevier.

46.11 NANOSTRUCTURING OF CONDUCTING POLYMERS

The conventional chemical polymerization of polyaniline only produces nonfibrous or irregular shaped morphologies [237,238]. In the past several years, a variety of chemical methods were reported that yield polyaniline nanofibers, such as use of hard templates [239,240], soft templates [241], electrospinning [242], interfacial polymerization [237], and seeding polymerization [238]. Recently, Chiou and Epstein discovered that polyaniline nanofibers can be directly synthesized in dilute chemical polymerization without aid of specific templates or techniques [243] (Fig. 46.42).

The nanofibrous structures prepared from dilute polymerization have no significant change when dedoped and redoped multiple times by base and acid solutions, respectively. The dispersion in deionized water of nanofibers is stable for several minutes without aggregation and precipitation [239]. Furthermore, a highly porous film of nanofibers is obtained as the dispersion is cast and dried on the glass or silicon wafer substrates. The UV/vis absorption patterns of polyaniline nanofibers obtained are consistent with previously reported results for conventionally synthesized polyaniline.

46.12 SUMMARY

The electrical transport properties of conducting polymers span the behaviors associated with semiconductors through to metals. Their properties depend critically upon the history of chemical synthesis, processing, and resulting structural order. Highly conducting doped polyacetylene, doped polypyrrole, and protonated polyaniline have similar dielectric responses, though on somewhat different scales. For each of these systems a positive dielectric constant is recorded at microwave frequencies for less conducting samples. A complex ''metallic Drude response,'' involving both an all conduction band electron response and a delocalized electron response, is detected for well-processed, highly conducting samples. The ability to engineer the electrical and dielectric properties using chemistry opens the opportunity for a wide range of applications from electrostatic dissipation to sensors and field effect transistors.

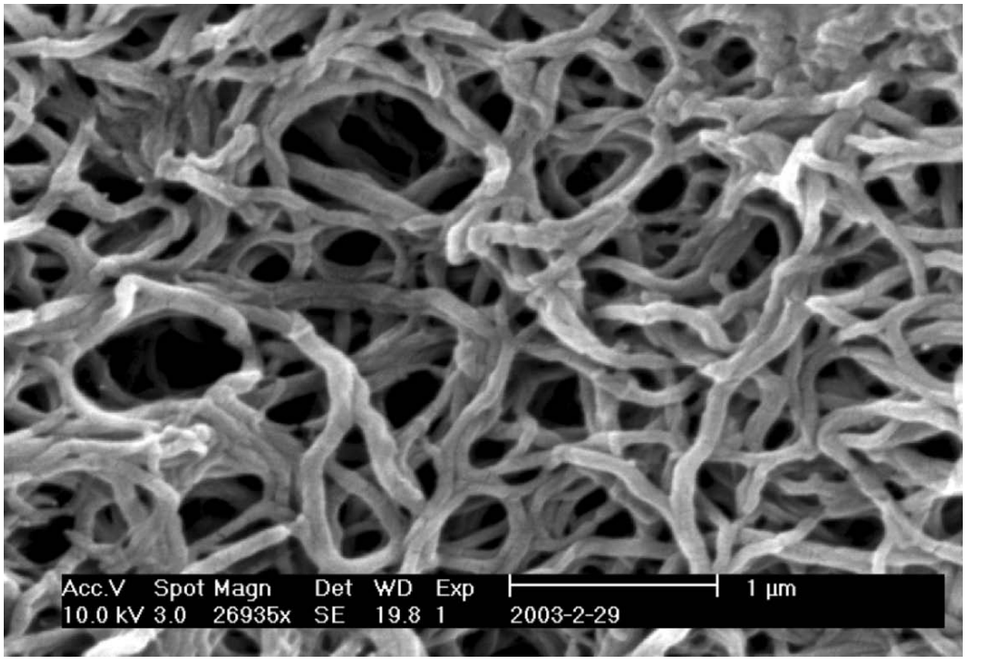

FIGURE 46.42. Nanofiber network of polyaniline prepared by dilute polymerization. Reprinted from [243] © (2005) with permission from Wiley-VCH.

Development of nanofibers and other morphologies will lead to new fundamental science and new opportunities for applications.

ACKNOWLEDGMENTS

This work was supported in part by the Office of Naval Research and National Science Foundation. The author thanks R. Kohlman, J. Joo, Vladimir Prigodin, Fang-Chi Hsu, June Hyoung Park, and Nan-Rong Chiou for discussions.

GLOSSARY OF TERMS

Anderson Localization: spatial localization of electronic wavefunctions due to randomness of the electronic potential which causes a metal–insulator transition in sufficiently disordered materials.

Antisoliton: solitons are present in materials with two degenerate phases A and B. If a soliton is a kink between A and B phase, then an antisoliton is a kink between B and A phase.

Bipolaron: a bipolaron is similar to a polaron except that it is doubly charged, spinless, and both of its energy states in the band gap are totally filled or empty.

Bloch Waves: delocalized electronic wavefunctions which have the form $\psi_k(\vec{r}) = u_k(\vec{r}) \exp(i\vec{k} \cdot \vec{r})$, where $u_k(\vec{r})$ is a function with the periodicity of the lattice unit cell and $\exp(i\vec{k} \cdot \vec{r})$ is a wave of wavelength $\lambda = 2\pi/k$.

Commensurate Charge Density Wave: a static modulation of the charge density in the system with a periodicity equal to a rational number multiplied by the underlying periodicity of the lattice. Due to the charge density wave, a gap is opened at the Fermi level which lowers the total energy of the system.

Crosslinked Polymers: polymers with greater interaction between chains either through regions of greater crystallinity (physical crosslinks between the polymer chains), or through chemical bonding between chains.

Crystalline Coherence Length: a length which characterizes the spatial correlations for the polymer chain, indicating the length over which the local order randomizes. This length is determined from the width of x-ray scattering peaks from the Scherrer formula.

Curie Susceptibility: Paramagnetic susceptibility due to uncoupled spins free to align in a magnetic field and subject only to thermal fluctuations. The Curie susceptibility is given by $\chi_{\text{Curie}} = C/T$, where C is the Curie constant (0.375 emu K/mol) and T is the temperature.

Degenerate Ground State: for a degenerate ground state, the conjugation path is such that reversal of the single and double bonds results in a phase of the system with an equivalent energy.

Doping: a process whereby charges are removed or added to the polymer chain, altering the electronic structure and response.

Drüde Model: this model of the electrons in a conductor treats the electrons as free, subject only to dissipative, inertial, and electromagnetic forces. In this model, the conductivity $\sigma(\omega)$ and the dielectric function $\varepsilon(\omega)$ are given as $\sigma(\omega) = (\Omega_p^2\tau/4\pi)/(1 - i\omega\tau)$ and $\varepsilon(\omega) = \varepsilon_B - \Omega_p^2/(\omega(\omega + i/\tau))$, where Ω_p is the plasma frequency and τ is the mean scattering for transport.

Electron–Electron Interactions: a broad term referring to the electromagnetic interaction between electrons as well as some of the effects of the Pauli exclusion principle.

Exciton: an electron–hole pair bound by Coulombic forces capable of transferring energy but not charge because it is electrically neutral.

Hole: a vacant orbital in an energy band which acts as a positive charge in an applied electric or magnetic field.

Hopping Transport: a form of charge transport which involves electron motion from one spatially localized state to another accompanied by the absorption or emission of a phonon.

Incommensurate Charge Density Wave: similar to a commensurate charge density wave except that the periodicity of the charge density modulation does not equal a rational number multiplied by the periodicity of the underlying lattice.

Inhomogeneous Disorder: Structural configuration for a polymer solid which consists of a mixture of ordered (crystalline) and disordered regions of the polymer.

Kramers–Kronig Analysis: a set of mathematical relations due to causality which relate the real (dispersive) and imaginary (absorptive) parts of a physical quantity. These relations can be used to determine the imaginary part of a quantity given information about the real part and vice versa.

Localization Modified Drude Model: a model for conduction electrons which includes suppression of the Drude conductivity at low frequencies due to finite localization lengths for the electrons.

Localized States: electronic states which are not extended over the entire solid as Bloch waves are localized states. The spatial dependence of the wavefunctions of a localized state is usually assumed to vary as $|\psi(\vec{r})| \sim \exp(-|\vec{r} - \vec{r}_0|/\xi)$, decaying exponentially in a characteristic length ξ, the localization length, away from $\vec{r}_0$. Charge transport by electrons in these states is due to hopping.

Lorentz Model: this model treats electrons as bound strongly to an atom, subject to dissipative, inertial, electromagnetic, as well as restoring forces. In this model, the dielectric function $\varepsilon(\omega)$ is given by $\varepsilon(\omega) = \varepsilon_B + \Omega_p^2/(\omega_0^2 - \omega^2 - i\omega/\tau)$, where ε_B is the background dielectric function due to everything else, Ω_p is the plasma frequency, ω_0 is the binding energy, and τ is the mean scattering time.

Mesoscopic Metallic State: a metallic state in an inhomogeneous system in which conduction electrons are delocalized over a number of crystalline regions (with disordered polymer regions between them). The size of the localization length is $\sim 10^2$–10^3 A, smaller than macroscopic dimensions (10^4 A or greater).

Mobility Edge: the critical energy which separates electronic states which are spatially localized due to disorder and thus have zero contribution to the electrical conductivity at very low temperature from those which are delocalized and therefore have nonzero contribution to the electrical conductivity at low temperature.

Mott Variable Range Hopping: a form of hopping transport which results when the electron may hop to a distant site instead of just a neighboring site if the energy difference between its current site and the distant site is smaller than the difference between its current site and the neighboring sites. Mott variable range conductivity has a form given by $\sigma(T) \cong \sigma_0 \exp[-(T_0/T)^{1/(d+1)}]$, where d is the dimensionality of the hops and T_0 is a reduced activation energy.

Nondegenerate Ground State: for a nondegenerate ground state, the conjugation path is such that reversal of the single and double bonds results in a distinctly different energy.

One-Dimensional Chain: a linear system for which the interactions along the chain direction are much stronger than the interactions perpendicular to the chain.

p_z Orbitals: electron wavefunctions with atomic principal quantum number p character which have a node in the x–y plane (the x–y plane is usually taken as the plane of the polymer sp^2 bonds.) Electrons in these orbitals usually pair to form double bonds and provide the conjugation responsible for the interesting electronic properties of conducting polymers.

π Conjugation: alternating single and double bonds in a single plane due to the overlap of atomic p_z orbitals along the polymer backbone. π conjugation leads to the electronic bands responsible for the interesting electronic properties of conducting polymers.

Pauli Susceptibility: paramagnetic, approximately temperature independent magnetic susceptibility due to conduction electrons. The Pauli susceptibility, $\chi_{\text{Pauli}} = 2\mu_B^2 N(E_F)$, where μ_B is a Bohr magneton and $N(E_F)$ is the density of states at the Fermi level.

Peierls Instability: an instability prominent in quasi-one-dimensional systems with strong electron–phonon interactions due to which the lattice spontaneously distorts with a $2k_F$ (k_F is the Fermi wavevector) periodicity, forming a gap at the Fermi level which lowers the total energy of the system.

Percolation: in a solid made up of more than one component (a composite system), the volume fraction of the different components can be varied. Percolation refers to the transitions which occur when the volume fraction of a component is such that there are connected paths of that component across the material. For example, in a composite of a metal and an insulator, the metal particles percolate when they form a connected path across the material and finite dc conductivity becomes possible.

Phonon: a quantum of lattice vibrational energy which reflects the normal vibrational modes of the lattice allowed by symmetry.

Phonon Induced Delocalization: in disordered solids, localization can result when a wavefunction interferes with itself due to elastic scattering and forms a standing wave. Phonon scattering can destroy this interference effect and cause the wavefunctions to be more extended.

Photoexcitation: the use of light (photons) to cause transitions of electrons from the ground state to excited states of the system.

Plasma Frequency: defined as $\Omega_p = 4\pi ne^2/m^*$, where n is the volume density of conduction electrons, e is the charge of an electron, and m^* is the effective mass renormalized from the free electron mass by lattice and interaction effects.

Plasma Response: an excitation of a solid for which the negative charge in the solid is displaced uniformly with respect to the ions. Plasma oscillations occur when the dielectric function is equal to zero.

Polaron: most generally a localized electronic state accompanied by a surrounding lattice distortion. In conduction polymers, it has been discussed as a bound state of a soliton and an antisoliton. This excitation can occur in degenerate and nondegenerate ground state polymers. A polaron possesses a single charge with normal spin–charge relations (i.e., with a single charge, it also has spin 1/2) and usually two states in the bandgap of the neutral polymer, one of which is half filled.

Polaron Lattice: a uniform periodic array of ''polarons'' assumed stabilized against a Peierls distortion by interchain interaction. The band structure for a polaron lattice is metallic.

Screened Plasma Frequency: the plasma frequency normalized or screened by a background dielectric constant. The screened plasma frequency, $\omega_p = \Omega_p/\sqrt{\varepsilon_B}$, where Ω_p is the plasma frequency and ε_B is the background dielectric constant due to all excitations except the conduction electrons.

Soliton: a low energy excitation of the electronic system which is localized in space and maintains its identity in the presence of other excitations. In conducting polymers, a soliton takes the form of a kink or misfit between two distinct energetically equivalent phases (in degenerate ground state systems). Its properties include a reversed spin–charge relation (i.e., when it is charge neutral, it has spin 1/2), the introduction of a single energy level within the band gap of the polymer, and a lattice distortion surrounding the soliton.

Time Reversal Symmetry: a symmetry of a system characterized by replacing t (time) with $-t$ without changing the physics of the system.

REFERENCES

For a more complete set of annotated references, see J. W. Blatchford and A. J. Epstein, Am. J. Phys. **64**, 120–135 (1996); for a compilation of original papers, see Yu Lu, *Solitons and Polarons in Conducting Polymers* (World Scientific, New Jersey, 1988).

1. See Chapters 47, 48, and 49 of this Handbook.
2. C. K. Chiang, C. R. Fincher, Jr., Y. W. Park, A. J. Heeger, H. Shirakawa, E. J. Louis, S. C. Gau, and A. G. MacDiarmid, Phys. Rev. Lett. **39**, 1098 (1977).
3. Proc. Int. Confs. on Science and Technology of Synthetic Metals. ICSM-'04, Wollongong, Australia, in Synth. Met. **152–154** (2005); ICSM-'02, Shanghai, P.R. China, in Synth. Met. **133–137** (2003); ICSM-'00, Gastein, Austria, in Synth. Met. **119–121** (2001); ICSM-'98, Montpellier, France, in Synth. Met. **101–103** (1999); ICSM-'96, Snowbird, UT, in Synth. Met. **84–86** (1997); ICSM-'94, Seoul, Korea, July 21–29, 1994, in Synth. Met. **69–71** (1995); ICSM '92, Goteborg, Sweden, Aug. 12–18, 1992, in Synth. Met. **55–57** (1993); ICSM '90, Tubingen, FRG, Sept. 2–9, 1990, in Synth. Met. **41–43** (1991); and ICSM '88, Sante Fe, NM, June 26–July 2, 1988, in Synth. Met. **27–29** (1988).
4. *Handbook of Conducting Polymers,* edited by T. A. Skotheim (Marcel Dekker, New York, 1986).
5. D. Baeriswyl, D. K. Campbell, and S. Mazumdar, in *Conjugated Conducting Polymers,* edited by H. G. Keiss (Springer-Verlag, Berlin, 1992), p. 7.
6. E. M. Conwell, IEEE Trans. Electri. Insul. **EI-22**, 591 (1987).
7. A. J. Heeger, S. A. Kivelson, J. R. Schrieffer, and W. P. Su, Rev. Mod. Phys. **60**, 781 (1988).
8. E. Jeckelmann and D. Baeriswyl, Synth. Met. **65**, 211 (1994).
9. J. E. Hirsch, Phys. Rev. Lett. **51**, 296 (1983).
10. S. N. Dixit and S. Mazumdar, Phys. Rev. B **29**, 1824 (1984).
11. W. K. Wu and S. Kivelson, Phys. Rev. B **33**, 8546 (1986).
12. C. Wu, X. Sun, and K. Nasu, Phys. Rev. Lett. **59** 831 (1987).
13. H. W. Gibson, F. C. Bailey, A. J. Epstein, H. Rommelmann, S. Kaplan, J. Harbour, X. -Q. Yang, D. B. Tanner, and J. M. Pochan, J. Am. Chem. Soc. **105**, 4417 (1983); K. Pakbaz, R. Wu, F. Wudl, and A. J. Heeger, J. Chem. Phys. **99**, 590 (1993).
14. M. C. dos Santos and J. L. Brédas, Phys. Rev. Lett. **62**, 2499 (1989).
15. J. M. Ginder and A. J. Epstein, Phys. Rev. Lett. **64**, 1184 (1990).
16. W. P. Su and A. J. Epstein, Phys. Rev. Lett. **70**, 1497 (1993).
17. J. C. Chiang and A. G. MacDiarmid, Synth. Met. **13**, 193 (1986).
18. J. P. Pouget, Z. Oblakowski, Y. Nogami, P. A. Albouy, M. Laridjani, E. J. Oh, Y. Min, A. G. MacDiarmid, J. Tsukamuto, T. Ishiguro, and A. J. Epstein, Synth. Met. **65**, 131 (1994).
19. M. Winokur, Y. B. Moon, A. J. Heeger, J. Barker, D. C. Bott, and H. Shirakawa, Phys. Rev. Lett. **58** 2329 (1987); R. H. Baughmann, S. L. Hsu, G. P. Pez, and A. J. Signorelli, J. Chem. Phys. **68**, 5405 (1978).
20. N. S. Murthy, G. G. Miller, and R. H. Baughmann, J. Chem. Phys. **89**, 2523 (1988).
21. W. P. Su, J. R. Schrieffer, and A. J. Heeger, Phys. Rev. Lett. **42,** 1698 (1979).
22. S. A. Brazovskii, Sov. Phys. JETP. Lett. **28**, 606 (1978).
23. M. J. Rice, Phys. Lett. **71A**, 152 (1979).
24. D. K. Campbell and A. R. Bishop, Phys. Rev. B **24**, 4859 (1981).
25. C. R. Wu, J. O. Nilsson, O. Inganäs, W. R. Salaneck, J. -E. Österholm, and J. L. Brédas, Synth. Met. **21**, 197 (1988).
26. C. X. Cui and M. Kertesz, Phys. Rev. B **40**, 9661 (1989).
27. F. Moraes, D. Davidov, M. Kobayashi, T. C. Chung, J. Chen, A. J. Heeger, and F. Wudl, Synth. Met. **10**, 169 (1985).
28. G. Harbeke, E. Meier, W. Kobel, M. Egli, H. Kiess, and E. Tosatti, Solid State Commun. **55**, 419 (1985).
29. G. S. Kanner, X. Wei, B. C. Hess, L. R. Chen, and Z. V. Vardeny, Phys. Rev. Lett. **69**, 538 (1992).
30. K. Kaneto, S. Hayashi, S. Ura, and K. Yoshino, J. Phys. Soc. Jpn **54** 1146 (1985).
31. J. L. Brédas, J. C. Scott, K. Yakushi, and G. B. Street, Phys. Rev. B **30**, 1023 (1984).
32. G. Zotti and G. Schiavon, Synth. Met. **41–43**, 445 (1991).
33. F. Genoud, M. Guglielmi, M. Nechtschein, E. Genies, and M. Salmon, Phys. Rev. Lett. **55**, 118 (1985).
34. O. Chauvet, S. Paschen, L. Forro, L. Zuppiroli, P. Bujard, K. Kai, and W. Wernet, Synth. Met. **63**, 115 (1994).
35. P. Gomes da Costa, R. G. Dandrea, and E. M. Conwell, Phys. Rev. B **47**, 1800 (1993).
36. M. Onoda, Y. Manda, T. Iwasa, H. Nakayama, K. Amakawa, and K. Yoshino, Phys. Rev. B **42**, 11826 (1990).
37. A. Sakamoto, Y. Furukawa, and M. Tasumi, J. Phys. Chem. **96**, 1490 (1992); A. Sakamoto, Y. Furukawa, and M. Tasumi, J. Phys. Chem. **96**, 3870 (1992); A. Sakamoto, Y. Furukawa, and M. Tasumi, Synth. Met. **55–57**, 593 (1993).
38. J. L. Brédas, R. R. Chance, and R. Sibley, Phys. Rev. B **26**, 5843 (1982).
39. G. Froyer, Y. Pelous, A. Siove, F. Genoud, M. Nechtschein, and B. Villeret, Synth. Met. **33**, 381 (1989).
40. Y. Furukawa, H. Ohtsuka, and M. Tasumi, Synth. Met. **55–57**, 516 (1993).
41. J. Libert, J. L. Brédas, and A. J. Epstein, Phys. Rev. B **51**, 5711 (1995).
42. J. M. Ginder and A. J. Epstein, Phys. Rev. B **41**, 10674 (1990).
43. S. Kivelson and W. K. Wu, Phys. Rev B. **34**, 5423 (1986).
44. X. Wei, B. C. Hess, Z. V. Vardeny, and F. Wudl, Phys. Rev. Lett. **68**, 666 (1992).
45. S. Abe, J. Yu, and W. P. Su, Phys. Rev. B **45**, 8264 (1992).
46. H. A. Mizes and E. M. Conwell, Phys. Rev. B **50**, 11243 (1994).
47. M. Chandross, S. Mazumdar, S. Jeglinski, X. Wei, and Z. V. Vardeny, Phys. Rev. B **50**, 14702 (1994).
48. M. J. Rice and Y. N. Gartstein, Phys. Rev. Lett. **73**, 2504 (1994).
49. N. F. Colaneri, D. D. C. Bradley, R. H. Friend, P. L. Burn, A. B. Holmes, and C. W. Spangler, Phys. Rev. B **42**, 11670 (1990).
50. M. Yan, L. J. Rothberg, F. Papadimitrakoupoulos, M. E. Galvin, and T. M. Miller, Phys. Rev. Lett. **72**, 1104 (1994).
51. J. M. Leng, S. Jeglinski, X. Wei, R. E. Benner, Z. V. Vardeny, F. Guo, and S. Mazumdar, Phys. Rev. Lett. **72**, 156 (1994).
52. E. M. Conwell, H. A. Mizes, and S. Javadez, Phys. Rev. B **40**, 1630 (1989).
53. S. Stafstrom, Phys. Rev. B **43**, 12437 (1993)
54. A. J. Epstein, J. M. Ginder, F. Zuo, R. W. Bigelow, H. -S. Woo, D. B. Tanner, A. F. Richtner, W.-S. Huang, and A. G. MacDiarmid, Synth. Met. **18**, 303 (1987).
55. S. Stafstrom, J. L. Brédas, A. J. Epstein, H. S. Woo, D. B. Tanner, W. S. Huang, and A. G. MacDiarmid, Phys. Rev. Lett. **59**, 1464 (1987).
56. J. L. Brédas, B. Thémans, J. G. Fripiat, J. M. André, and R. R. Chance, Phys. Rev. B **29**, 6761 (1984).
57. T. Ohsawa, O. Kimura, M. Onoda, and K. Yoshino, Synth. Met. **47**, 151 (1992).
58. M. Bartonek and H. Kuzmany, Synth. Met. **41–43**, 607 (1991).
59. K. Mizoguchi, T. Obana, S. Ueno, and K. Kume, Synth. Met. **55–57**, 601 (1993).
60. F. Genoud, M. Nechtschein, and C. Santier, Synth. Met. **55–57**, 642 (1993).
61. J. M. Ginder, A. F. Richter, A. G. MacDiarmid, and A. J. Epstein, Solid State Commun. **63**, 97 (1987).
62. M. E. Jozefowicz, R. Laversanne, H. H. S. Javadi, A. J. Epstein, J. P. Pouget, X. Tang, and A. G. MacDiarmid, Phys. Rev. B **39**, 12958 (1989).
63. J. Tsukamoto, Adv. Phys. **41**, 509 (1992); J. Tsukamoto, A. Takahashi, and K. Kawasaki, Jpn., J. Appl. Phys. **29**, 125 (1990).
64. H. Naarmann and N. Theophilou, Synth. Met. **22**, 1 (1987).
65. H. Shirakawa, Y. -X. Zhang, T. Okuda, K. Sakamaki, and K. Akagi, Synth. Met. **65**, 93 (1994).
66. T. Ito, H. Shirakawas, and S. Ikeda, J. Polym. Sci. Polym. Chem. Ed. **12**, 11 (1974).
67. K. Ito, Y. Tanabe, K. Akagi, and H. Shirakawa, Phys. Rev. B **45**, 1246 (1992).
68. J. H. Edwards and W. J. Feast, Polym. Commun. **21**, 595 (1980).
69. J. C. W. Chien, in *Polyacetylene: Chemistry, Physics, and Material Science* (Academic, New York, 1984), p. 24.
70. T. Ishiguro, H. Kaneko, Y. Nogami, H. Nishiyama, J. Tsukamoto, A. Takahashi, M. Yamaura, and J. Sato, Phys. Rev. Lett. **69**, 660 (1992); H. Kaneko, T. Ishiguro, J. Tsukamoto, and A. Takahashi, Solid State Commun. **90**, 83 (1994).
71. P. N. Adams, P. Laughlin, A. P. Monkman, and N. Bernhoeft, Solid State Commun. **91**, 895 (1994); the value of conductivity reported in Fig. 46.4 is for samples kindly provided by Monkman and coworkers, and measured at The Ohio State University.
72. R. D. McCullough, S. P Williams, S. Tristran-Nagle, M. Jayaraman, P. C. Ewbank, and L. Miller, Synth. Met. **69**, 279 (1995).

73. J. Joo, Z. Oblakowski, G. Du, J. P. Pouget, E. J. Oh, J. M. Weisinger, Y. Min, A. G. MacDiarmid, and A. J. Epstein, Phys. Rev. B **49**, 2977 (1994).
74. R. S. Kohlman, J. Joo, Y. Z. Wang, J. P. Pouget, H. Kaneko, T. Ishiguro, and A. J. Epstein, Phys. Rev. Lett. **74,** 773 (1995).
75. A. J. Epstein, J. Joo, R. S. Kohlman, G. Du, A. G. MacDiarmid, E. J. Oh, Y. Min, J. Tsukamoto, H. Kaneko, and J. P. Pouget, Synth. Met. **65**, 149 (1994).
76. A. J. Epstein, H. Rommelmann, M. A. Druy, A. J. Heeger, and A. G. MacDiarmid, Solid State Commun. **38**, 683 (1981).
77. P. K. Kahol, H. Guan, and B. J. McCormick, Phys. Rev. B **44**, 10393 (1991).
78. S. Ikehata, J. Kaufer, T. Woerner, A. Pron, M. A. Druy, A. Sivak, A. J. Heeger, and A. G. MacDiarmid, Phys. Rev. Lett. **45**, 1123 (1980).
79. N. S. Saricifti, A. J. Heeger, and Y. Cao, Phys. Rev. B **49**, 5988 (1994).
80. (a) Y. W. Park, Synth. Met. **45**, 173 (1991); (b) Y. W. Park, A. J. Heeger, M. A. Druy, and A. G. MacDiarmid, J. Chem. Phys. **73**, 946 (1980).
81. H. H. S. Javadi, A. Chakraborty, C. Li, N. Theophilou, D. B. Swanson, A. G. MacDiarmid, and A. J. Epstein, Phys. Rev. B **43**, 2183 (1991).
82. J. C. Clark, G. G. Ihas, A. J. Rafanello, M. W. Meisel, M. Reghu, C. O. Yoon, Y. Cao, and A. J. Heeger, Synth. Met. **69**, 215 (1995); R. S. Kohlman, A. J. Epstein, G. G. Ihas, and A. G. MacDiarmid, to be published.
83. A. J. Epstein, H. Rommelmann, R. Bigelow, H. W. Gibson, D. M. Hoffman, and D. B. Tanner, Phys. Rev. Lett. **50**, 1866 (1983).
84. Y. Cao, P. Smith, and A. J. Heeger, Synth. Met. **48**, 91 (1992).
85. Y. Z. Wang, J. Joo, C. -H. Hsu, J. P. Pouget, and A. J. Epstein, Phys. Rev. B **50**, 16811 (1994).
86. Z. H. Wang, H. H. S. Javadi, A. Ray, A. G. MacDiarmid, and A. J. Epstein, Phys. Rev. B **42**, 5411 (1990).
87. J. Yue, Z. H. Wang, K. R. Cromack, A. J. Epstein, and A. G. MacDiarmid, J. Am. Chem. Soc. **113**, 2655 (1991).
88. M. Yamaura, T. Hagiwara, and K. Iwata, Synth. Met. **26**, 209 (1988).
89. K. Sato, M. Yamaura, T. Hagiwara, K. Murata, and M. Tokumoto, Synth. Met. **40**, 35 (1991).
90. J. -E. Österholm, P. Passiniemi, H. Isotalo, and H. Stubb, Synth. Met. **18,** 213 (1987).
91. T. Ohnishi, T. Noguchi, T. Nakano, M. Hirooka, and I. Murase, Synth. Met. **41–43**, 309 (1991).
92. L. W Shacklette, R. R. Chance, D. M. Ivory, G. G. Miller, and R. H. Baughman, Synth. Met. **1**, 307 (1979).
93. G. Du, V. N. Prigodin, A. Burns, J. Joo, C. S. Wang, and A. J. Epstein, Phys. Rev. B **58**, 4485 (1998).
94. A. J. Epstein, H. Rommelmann, M. Abkowitz, and H. W. Gibson, Phys. Rev. Lett. **47**, 1549 (1981).
95. A. J. Epstein, H. Rommelmann, and H. W. Gibson, Phys. Rev. B **31**, 2502 (1985).
96. F. Zuo, M. Angelopoulos, A. G. MacDiarmid, and A. J. Epstein, Phys. Rev. B **39**, 3570 (1989).
97. J. C. Scott, P. Pfluger, M. T. Krounbi, and G. B. Street, Phys. Rev. B **28**, 2140 (1983).
98. G. E. Wnek, J. C. Chien, F. E. Karasz, and C. P Lillya, Polymer **20**, 1441 (1979).
99. R. E. Peierls, in *Quantum Theory of Solid* (Clarendon, Oxford, 1955), p. 108.
100. E. J. Mele and M. J. Rice, Phys. Rev. B **23**, 5397 (1981).
101. S. A. Kivelson and A. J. Heeger, Phys. Rev. Lett. **55**, 308 (1985).
102. H. -Y. Choi and E. J. Mele, Phys. Rev. B **34**, 8750 (1986).
103. D. B. Tanner, G. L. Doll, A. M. Rao, P. C. Eklund, G. A. Arbuckle, and A. G. MacDiarmid, Synth. Met. **28**, D141 (1989).
104. Y. H. Kim and A. J. Heeger, Phys. Rev. B **40**, 8393 (1989).
105. M. I. Salkola and S. A. Kivelson, Phys. Rev. B **50**, 13962 (1994); S. A. Kivelson and M. I. Salkola, Synth. Met. **44**, 281 (1991).
106. J. Tanaka, C. Tanaka, T. Miyamae, M. Shimizu, S. Hasegawa, K. Kamiya, and K. Seki, Synth. Met. **65**, 173 (1994).
107. A. Yamashiro, A. Ikawa, and H. Fukutome, Synth. Met. **65**, 233 (1994).
108. H. L. Wu and P. Phillips, Phys. Rev. Lett. **66**, 1366 (1991); P. Phillips and H. L. Wu, Science **252**, 1805 (1991).
109. F. C. Lavarda, M. C. dos Santos, D. S. Galvao, and B. Laks, Phys. Rev. Lett. **73**, 1267 (1994).
110. S. Stafstrom and J. L. Brédas, Phys. Rev. B **38**, 4180 (1988).
111. D. S. Galvao, D. A. dos Santos, B. Laks, C. P. de Melo, and M. J. Caldas, Phys. Rev. Lett. **63**, 786 (1989).
112. V. N. Prigodin and K. B. Efetov, Phys. Rev. Lett. **70**, 2932 (1993).
113. C. Kittel, in *Introduction to Solid State Physics* (John Wiley & Sons, Inc., New York, 1986), p. 157.
114. P. W Anderson, Phys. Rev. **109**, 1492 (1958).
115. N. F. Mott and E. Davis, in *Electronic Processes in Non-Crystalline Materials* (Clarendon Press, Oxford, 1979), p. 6.
116. M. Reghu, C. O. Yoon, D. Moses, A. J. Heeger, and Y. Cao, Phys. Rev. B **48**, 17685 (1993); M. Reghu, Y. Cao, D. Moses, and A. J. Heeger, Phys. Rev. B **47**, 1758 (1993).
117. C. O. Yoon, M. Reghu, D. Moses, A. J. Heeger, and Y. Cao, Phys. Rev. B **48**, 14080 (1993).
118. C. O. Yoon, M. Reghu, D. Moses, and A. J. Heeger, Phys. Rev. B **49**, 10851 (1994).
119. A. L. Efros and B. I. Shklovski, J. Phys. **C8**, L49 (1975); B. I. Shklovski and A. L. Efros, in *Electronic Properties of Doped Semiconductors* (Springer-Verlag, Heidelberg, 1984).
120. J. Joo, V. N. Prigodin, Y. G. Min, A. G. MacDiarmid, and A. J. Epstein, Phys. Rev. B **50**, 12226 (1994).
121. Z. H. Wang, A. Ray, A. G. MacDiarmid, and A. J. Epstein, Phys. Rev. B **43**, 4373 (1991).
122. S. Kivelson and A. J. Heeger, Synth. Met. **22**, 371 (1988).
123. P. Drüde, Ann. Phys. **1**, 566 (1900); **3**, 369 (1900).
124. G. Burns, in *Solid State Physics* (Academic, New York, 1985), p. 187.
125. R. H. Baughman, N. S. Murthy, and G. G. Miller, J. Chem. Phys. **79**, 515 (1983).
126. D. Chen, M. J. Winokur, M. A. Masse, and F. E. Karasz, Phys. Rev. B **41**, 6759 (1990).
127. J. P. Pouget, M. E. Jozefowicz, A. J. Epstein, X. Tang, and A. G. MacDiarmid, Macromolecules **24**, 779 (1991).
128. J. P. Pouget, C. -H. Hsu, A. G. MacDiarmid, and A. J. Epstein, Synth. Met. **69**, 119 (1995).
129. W. Fosong, T. Jinsong, W. Lixiang, Z. Hongfang, and M. Zhishen, Mol. Cryst. Liq. Cryst. **160**, 175 (1988).
130. Y. B. Moon, Y. Cao, P. Smith, and A. J. Heeger, Polym. Commun. **30**, 196 (1989).
131. M. E. Jozefowicz, A. J. Epstein, J. P. Pouget, J. G. Masters, A. Ray, and A. G. MacDiarmid, Macromolecules **25**, 5863 (1991).
132. J. Joo, Ph.D. Thesis, *Charge Localization and Delocalization Phenomena in Conducting Polymers,* The Ohio State University (1994); J. Joo, S. M. Long, J. P. Pouget, E. J. Oh, A. G. MacDiarmid, and A. J. Epstein, Phys. Rev. B **57**, 9567–9580 (1998).
133. M. Laridjani, J. P. Pouget, E. M. Scherr, A. G. MacDiarmid, M. E. Jozefowicz, and A. J. Epstein, Macromolecules **25**, 4106 (1992).
134. A. G. MacDiarmid and A. J. Epstein, Synth. Met. **65**, 103 (1994).
135. A. G. MacDiarmid, J. M. Weisinger, and A. J. Epstein, Bull. Am. Phys. Soc. **38**, 311 (1993); A. G. MacDiarmid and A. J. Epstein, Trans. 2nd Congresso Brazileiro de Polimeros, Sao Paulo, Brazil, Oct. 5–8,1993, p. 544; Y. Min, A. G. MacDiarmid, and A. J. Epstein, Polym. Prepr. **35**, 231 (1994).
136. Y. Nagomi, J. P. Pouget, and T. Ishiguro, Synth. Met. **62**, 257 (1994).
137. P. A. Albouy, J. P. Pouget, J. Halim, V Enkelmann, and G. Wegner, Makromol. Chem. **193**, 853 (1992); P. Robin, J. P. Pouget, R. Comes, H. W. Gibson, and A. J. Epstein, Polymer **24**, 1558 (1983).
138. P. Pfluger, M. T. Krounbi, and G. B. Street, Phys. Rev. B **28**, 2140 (1983).
139. J. Chen and A. J. Heeger, Synth. Met. **24**, 311 (1988).
140. N. Theophilou, D. B. Swanson, A. G. MacDiarmid, A. Chakraborty, H. H. S. Javadi, R. P McCall, S. P. Treat, F. Zuo, and A. J. Epstein, Synth. Met. **28**, 35 (1988).
141. X. Q. Yang, D. B. Tanner, M. J. Rice, H. W Gibson, A. Feldblum, and A. J. Epstein, Solid State Commun. **61**, 335 (1987).
142. Y. Nogami, H. Kaneko, T. Ishiguro, A. Fakahashi, J. Tsukamoto, and N. Hosoito, Solid State Commun. **76**, 583 (1990).
143. Z. H. Wang, C. Li, E. M. Scherr, A. G. MacDiarmid, and A. J. Epstein, Phys. Rev. Lett. **66**, 1749 (1991); Z. H. Wang, E. M. Scherr, A. G. MacDiarmid, and A. J. Epstein, Phys. Rev. B **45**, 4190 (1992).
144. Y. Cao and A. J. Heeger, Synth. Met. **52**, 193 (1992).
145. P. Pfluger, U. M. Gubler, and G. B. Street, Solid State Commun. **49**, 911 (1984).
146. K. Mizoguchi, K. Misoo, K. Kume, K. Kaneto, T. Shiraishi, and K. Yoshino, Synth. Met. **18**, 195 (1987).

147. K. Kume, K. Mizuno, K. Mizoguchi, K. Nomura, Y Maniwa, J. Tanaka, M. Tanaka, and A. Watanabe, Mol. Cryst. Liq. Cryst. **83**, 285 (1982).
148. M. Onoda, Y Manda, T. Iwasa, S. Morita, T. Kawai, and K. Yoshino, Synth. Met. **41–43**, 1469 (1991).
149. H. Kaneko and T. Ishiguro, Synth. Met. **65**, 141 (1994).
150. M. Reghu, K. Vakiparta, Y. Cao, and D. Moses, Phys. Rev. B **49**, 16162 (1994).
151. A. G. Zabrodskii and K. N. Zeninova, Zh. Eksp. Teor. Fiz. **86**, 727 (1984) [Sov. Phys. JETP **59**, 425 (1984)].
152. A. I. Larkin and D. E. Khmelnitskii, Zh. Eskp. Teor. Fiz. **83**, 1140 (1982) [Sov. Phys. JETP **56**, 647 (1982)].
153. P. Lee and T. V. Ramakrishnan, Rev. Mod. Phys. **57**, 287 (1985); H. Fukuyama, in *Electron-Electron Interactions in Disordered Systems,* edited by A. L. Efros and M. Pollak (Elsevier Science Publishers, New York, 1985), p. 155.
154. D. E. Khmelnitskii and A. I. Larkin, Solid State Commun. **39**, 1069 (1981).
155. Y. Nogami, H. Kaneko, H. Ito, T. Ishiguro, T. Sasaki, N. Toyota, A. Takahashi, and J. Tsukamoto, Phys. Rev. B. **43**, 11829 (1991).
156. F. Zuo, M. Angelopoulos, A. G. MacDiarmid, and A. J. Epstein, Phys. Rev. B **36**, 3475 (1987).
157. A. B. Kaiser, C. K. Subramaniam, P. W. Gilberd, and B. Wessling, Synth. Met. **69**, 197 (1985); R. Pelster, G. Nimtz, and B. Wessling, Phys. Rev. B **49**, 12718 (1994).
158. J. Joo, S. M. Long, J. P. Pouget, E. J. Oh, A. G. MacDiarmid, and A. J. Epstein, Phys. Rev. B **57**, 9567 (1998).
159. H. Kaneko, T. Ishiguro, K. Sato, T. Hagiwara, M. Yamaura, H. Nishiyama, and H. Ishimoto, Synth. Met. **55–57**, 1102 (1993).
160. J. Joo, G. Du, A. J. Epstein, V. N. Prigodin, and J. Tsukamoto, Phys. Rev. B **52**, 8060 (1995).
161. C. R. Fincher, M. Ozaki, M. Tanaka, D. Peebles, L. Lauchlin, A. J. Heeger, and A. G. MacDiarmid, Phys. Rev. B **20**, 1589 (1979).
162. G. Leising, Phys. Rev. B **38**, 10313 (1988).
163. J. Tanaka and M. Tanaka, in *Handbook of Conducting Polymers,* edited by T. A. Skotheim (Marcel Dekkar, New York, 1986), p. 1269.
164. R. P. McCall, J. M. Ginder, J. M. Leng, H. J. Ye, S. K. Manohar, J. G. Masters, G. E. Asturias, A. G. MacDiarmid, and A. J. Epstein, Phys. Rev. B **41**, 5202 (1990).
165. J. M. Leng, R. P. McCall, K. R. Kromack, Y. Sun, S. K. Manohar, A. G. MacDiarmid, and A. J. Epstein, Phys. Rev. B **48**, 15719 (1993).
166. K. Yakushi, L. J. Lauchlan, T. C. Clarke, and G. B. Street, J. Chem. Phys. **79**, 4774 (1983).
167. G. B. Street, T. C. Clarke, M. Krounbi, K. K. Kanazawa, V. Y. Lee, P. Pfluger, J. C. Scott, and G. Weiser, Mol. Cryst. Liq. Cryst. **83**, 253 (1982); G. B. Street, T. C. Clarke, R. H. Geiss, V. Y. Lee, A. Nazzal, P. Pfluger, J. C. Scott, and G. Weiser, J. Phys. (Paris) **44**, C3-599 (1983).
168. S. Hotta, S. D. D. V Rughooputh, A. J. Heeger, and F. Wudl, Macromolecules **20**, 212 (1987).
169. M. Kobayashi, J. Chen, T. C. Chung, F. Moraes, A. J. Heeger, and F. Wudl, Synth. Met. **9**, 77 (1984).
170. K. Kaneto, K. Yoshino, and Y. Inuishi, Solid State Commun. **46**, 389 (1983).
171. T. -C. Chung, J. H. Kaufman, A. J. Heeger, and F. Wudl, Phys. Rev. B. **30**, 702 (1984).
172. M. Satoh, M. Tabata, F. Uesugi, K. Kaneto, and K. Yoshino, Synth. Met. **17**, 595 (1987).
173. D. L. Gin, J. K. Avlyanov, and A. G. MacDiarmid, Synth. Met. **66**, 169 (1994).
174. L. M. Goldenberg and P. C. Lacaze, Synth. Met. **58**, 271 (1993).
175. N. F. Colaneri, D. D. C. Bradley, R. H. Friend, P. L. Burn, A. B. Holmes, and C. W. Spangler, Phys. Rev. B **42**, 11670 (1990).
176. J. D. Stenger Smith, R. W. Lenz, and G. Wegner, Polymer **30**, 1048 (1989).
177. R. H. Friend, D. D. C. Bradley, and P. Townsend, J. Phys. D: Appl. Phys. **20**, 1367 (1987).
178. D. D. C. Bradley, A. R. Brown, P L. Burn, J. H. Burroughes, R. H. Friend, A. B. Holmes, K. D. Mackay, and R. N. Marks, Synth. Met. **41–43**, 3135 (1991).
179. K. Pichler, D. A. Halliday, D. D. C. Bradley, P. L. Burn, R. H. Friend, and A. B. Holmes, J. Phys. Condens. Matter **5**, 7155 (1993).
180. D. D. Gebler, Y. Z. Wang, J. W. Blatchford, S. W. Jessen, L. B. Lin, T. L. Gustafson, H. L. Wang, T. M. Swager, A. G. MacDiarmid, and A. J. Epstein, J. Appl. Phys. **78**, 4264 (1995).
181. S. W. Jessen, D. D. Gebler, Y. Z. Wang, J. W. Blatchford, L. B. Lin, T. L. Gustafson, H. L. Wang, T. M. Swager, A. G. MacDiarmid, and A. J. Epstein, Polym. Mater. Sci. Eng. **72**, 573 (1995).
182. M. Furukawa, K. Mizuno, A. Matsui, S. D. D. V. Rughooputh, and W. C. Walker, J. Phys. Soc. Jpn **58**, 2976 (1989).
183. U. Rauscher, H. Bassler, D. D. C. Bradley, and M. Hennecke, Phys. Rev. B **42**, 9830 (1990).
184. K. Pakbaz, C. H. Lee, A. J. Heeger, T. W. Hagler, and D. McBranch, Synth. Met. **64**, 295 (1994).
185. F. Wooten, in *Optical Properties of Solids* (Academic, New York, 1972), p. 173.
186. H. S. Woo, D. B. Tanner, N. Theophilou, and A. G. MacDiarmid, Synth. Met. **41–43**, 159 (1991).
187. S. Hasegawa, K. Kamiya, J. Tanaka, and M. Tanaka, Synth. Met. **14**, 97 (1986); J. Tanaka, S. Hasegawa, T. Miyamae, and M. Shimizu, Synth. Met. **41–43**, 1199 (1991).
188. T. Miyamae, M. Shimizu, and J. Tanaka, Bull. Chem. Soc. Jpn **67**, 40253 (1994).
189. X. Q. Yang, D. B. Tanner, A. Feldblum, H. W. Gibson, M. J. Rice, and A. J. Epstein, Mol. Cryst. Liq. Cryst. **117**, 267 (1985).
190. S. Hasegawa, K. Kamiya, J. Tanaka, and M. Tanaka, Synth. Met. **18**, 225 (1987).
191. R. P. McCall, E. M. Scherr, A. G. MacDiarmid, and A. J. Epstein, Phys. Rev. B **50**, 5094 (1994).
192. R. S. Kohlman, Ph.D. Thesis, *Optical Studies of the Metalie in Conducting Polymers*, The Ohio State University (1996).
193. R. S. Kohlman, J. Joo, Y. G. Min, A. G. MacDiarmid, and A. J. Epstein, Phys. Rev. Lett. **77**, 2766 (1996).
194. K. Lee, A. J. Heeger, and Y. Cao, Phys. Rev. B **48**, 14884 (1993).
195. Y. Xia, A. G. MacDiarmid, and A. J. Epstein, Macromolecules **27**, 7212 (1994).
196. Y. Xia, J. M. Weisinger, A. G. MacDiarmid, and A. J. Epstein, Chem. Mater. **7**, 443 (1995).
197. R. S. Kohlman, Y. Min, A. G. MacDiarmid, and A. J. Epstein, Synth. Met. **69**, 211 (1995).
198. R. S. Kohlman, T. Ishiguro, H. Kaneko, and A. J. Epstein, Synth. Met. **69**, 325 (1995).
199. K. Lee, M. Reghu, E. L. Yuh, N. S. Saricifti, and A. J. Heeger, Synth. Met. **68**, 287 (1995).
200. N. F. Mott and M. Kaveh, Adv. Phys. **34**, 329 (1985).
201. N. F. Mott, in *Localization and Interaction in Disordered Metals and Doped Semiconductors,* edited by D. M. Finlayson, Proceedings of the Thirty-First Scottish Universities Summer School in Physics of 1986 (Scottish Universities Summer School in Physics, 1986).
202. N. F. Mott, in *Localization 1990,* edited by K. A. Benedict and J. T. Chalker (Inst. of Phys. Conf. Ser. No. 108, Institute of Physics, Bristol, Philadelphia, New York, 1990). Paper presented at the Localization 1990 Conference held at the Imperial College, London.
203. D. J. Bergman and D. Stroud, in *Solid State Physics,* edited by H. Ehrenreich and D. Turnbull (Academic, New York, 1992), vol. 46, p. 148.
204. *Intrinsically Conducting Polymers: An Emerging Technology,* edited by M. Aldissi (Kluwer Academic Publishers, Boston, 1993); *Science and Applications of Conducting Polymers,* edited by W. R. Salaneck and D. T. Clark (IOP Publishing, Lofthus, Norway, 1990).
205. A. G. MacDiarmid and R. B. Kaner, *in Handbook of Conducting Polymers,* edited by T. A. Skotheim (New York, Marcel Dekker, 1986), vol. 1, p. 687; D. Naegele and R. Bittihn, Solid State Ionics **28–30**, 983 (1988); M. Maxfield, T. R. Jow, M. G. Sewchok, and L. W. Shacklette, J. Power Sources **26**, 93 (1989).
206. N. F. Colaneri and L. W. Shacklette, IEEE Trans. Instrum. Meas. **IM-41**, 291 (1992); T. Taka, Synth. Met. **41–43**, 1177 (1991).
207. J. Joo and A. J. Epstein, Appl. Phys. Lett. **65**, 2278 (1994).
208. T. Taka, Synth. Met. **41–43**, 1177 (1991).
209. J. Joo, A. G. MacDiarmid, and A. J. Epstein, Proc. Annual Technical Conf. of Plastic Engineers **2**, 1672 (1995).
210. A. J. Epstein, J. Joo, C. Y. Wu, A. Benatar, C. F. Faisst, Jr., J. Zegarski, and A. G. MacDiarmid, in *Intrinsically Conducting Polymers: An Emerging Technology,* edited by M. Aldissi (Kluwer Academic Publishers, Dordrecht, 1993), p. 165.
211. J. H. Burroughes, D. D. C. Bradley, A. R. Brown, R. N. Marks, K. Mackay, R. H. Friend, P. L. Burns, and A. B. Holmes, Nature **347**, 539 (1990); D. Braun and A. J. Heeger, Appl. Phys. Lett. **58**, 1982 (1991); P. L. Burns, A. B. Holmes, A. Kraft, D. D. C. Bradley,

A. R. Brown, R. H. Friend, and R. W. Gymer, Nature **357**, 47 (1992); D. D. C. Bradley, Synth. Met. **54**, 401 (1993); I. D. Parker, J. Appl. Phys. **75**, 1656 (1994).
212. J. Yue and A. J. Epstein, J. Chem. Soc., Chem. Commun. **21**, 1540 (1992); F. Selampinar, L. Toppare, U. Akbulut, T. Yalcin, and S. Suzer, Synth. Met. **68**, 109 (1995); and references therein.
213. S. Jasty and A. J. Epstein, Polym. Mater. Sci. Eng. **72**, 565 (1995); D. W. DeBerry, J. Electrochem. Soc. **132**, 1022 (1985); N. Ahmad and A. G. MacDiarmid, Bull. Am. Phys. Soc. **32**, 548 (1987); B. Wessling, Adv. Mater. **6**, 226 (1994); W. K. Lu, R. L. Elsenbaumer, and B. Wessling, Synth. Met. **71**, 2163 (1995).
214. G. Gustafsson, Y. Cao, G. M. Treacy, F. Klavetter, N. Colaneri, and A. J. Heeger, Nature **357**, 477 (1992).
215. Y. Z. Wang, D. D. Gebler, L. B. Lin, J. W Blatchford, S. W. Jessen, H. L. Wang, and A. J. Epstein, Appl. Phys. Lett. **68**, 894 (1996);
216. Y. Yang and A. J. Heeger, Appl. Phys. Lett. **64**, 1245 (1994); Y. Cao, G. M. Treacy, P. Smith, and A. J. Heeger, Appl. Phys. Lett. **60**, 2711 (1992).
217. A. Fizazi, J. Moulton, K. Pakbaz, S. D. D. V. Rughooputh, P. Smith, and A. J. Heeger, Phys. Rev. Lett. **64**, 2180 (1990).
218. C. O. Yoon, M. Reghu, D. Moses, A. J. Heeger, and Y. Cao, Synth. Met. **63**, 47 (1994).
219. G. Du, J. Avlyanov, C. Y. Wu, K. G. Reimer, A. Benatar, A. G. MacDiarmid, and A. J. Epstein, Synth. Met. **85**, 1339 (1997).
220. V. N. Prigodin and A. J. Epstein, Phys. B: Phys. Condens. Matter **338,** 310 (2003).
221. T. Ishiguro, H. Kaneko, Y. Nogami, H. Ishimoto, H. Nishiyama, A. Tsukamoto, A. Takahashi, M. Yamaura, T. Hagiwara, and K. Sato, Phys. Rev. Lett. **69**, 660 (1992).
222. R. S. Kohlman, A. Zibold, D. B. Tanner, G. G. Ihas, T. Ishuguro, Y. G. Min, A. G. MacDiarmid, and A. J. Epstein, Phys. Rev. Lett. **78**, 3915 (1997).
223. T. Menon, C. O. Yoon, D. Moses, and A. J. Heeger, in *Handbook of Conducting Polymers*, T. Skotheim, R. Elsenbaumer, and J. Reynolds (Eds.) (Marcel Dekker, New York, 2nd ed.) 1998, p. 27.
224. R. S. Kohlman and A. J. Epstein, in *Handbook of Conducting Polymers*, T. Skotheim, R. Elsenbaumer, and J. Reynolds (Eds.) (Marcel Dekker, New York, 2nd ed.) 1998, p. 85.
225. (a) H. H. S. Javadi, A. Chakraborty, C. Li, N. Theophilou, D. B. Swanson, A. G. MacDiarmid, and A. J. Epstein, Phys. Rev. B **43**, 2183 (1991); (b) J. Joo, Z. Oblakowski, G. Du, J. P. Pouget, E. J. Oh, J. M. Wiesinger, Y. Min, A. G. MacDiarmid, and A. J. Epstein, Phys. Rev. B **49**, 2977 (1994); (c) H. C. F. Martens, J. A. Reedijk, H. B. Brom, D. M. de Leuw, and R. Menon, Phys. Rev. B **63**, 073203 (2001).
226. Y. Z. Wang, D. D. Gebler, D. K. Fu, T. M. Swager, and A. J. Epstein, Appl. Phys. Lett. **70**, 3215 (1997).
227. Y. Z. Wang, R. G. Sun, D. K. Wang, T. M. Swager, and A. J. Epstein, Appl. Phys. Lett. **74**, 2593 (1999).
228. Z. Bao, A. Dodabalapur, and A. J. Lovinger, Appl. Phys. Lett. **69**, 4108 (1996).
229. H. E. Katz and Z. Bao, J. Phys. Chem. B **104**, 671 (2000).
230. S. Hoshino, M. Yoshida, S. Uemura, T. Kodzasa, N. Takada, T. Kamata, and K. Yase, J. Appl. Phys. **95**, 5088 (1994).
231. G. Wang, T. Hirasa, D. Moses, and A. J. Heeger, Synth. Met. **146**, 127 (2004).
232. J. Liu, N. J. Pinto, and A. G. MacDiarmid, J. Appl. Phys. **92**, 6033 (2002).
233. A. J. Epstein, F. -C. Hsu, N. -R. Chiou, and V. N. Prigodin, Curr. Appl. Phys. **2**, 339 (2002).
234. H. Okuzaki, M. Ishihara, and S. Ashizawa, Synth. Met. **137**, 947 (2003).
235. V. N. Prigodin, F. C. Hsu, Y. M. Kim, J. H. Park, O. Waldmann, and A. J. Epstein, Synth. Met. **153**, 157 (2005).
236. F. C. Hsu, V. N. Prigodin, and A. J. Epstein, Phys. Rev. B **74** (15 Nov. 2006).
237. J. Huang and R. B. Kaner, J. Am. Chem. Soc. **126**, 851 (2004).
238. X. Zhang, W. J. Goux, and S. K. Manohar, J. Am. Chem. Soc. **126**, 4502 (2004).
239. C. G. Wu and T. Bein, Science **264**, 1757 (1994).
240. C. R. Martin, Science **266**, 1961 (1994).
241. H. Qiu, M. Wan, B. Matthews, L. Dai, Macromolecules **34**, 675 (2001).
242. I. D. Norris, M. M. Shaker, F. -K. Ko, A. G. MacDiarmid, Synth. Met. **114**, 109 (2000).
243. N. R. Chiou and A. J. Epstein, Adv. Mater. **17**, 1679 (2005).

CHAPTER 47

Electroluminescent Polymer Systems

Leni Akcelrud

Departamento de Quimica, Centro Politecnico da UFPR, Universidade Federal do Parana, CP 19081, CEP 81531-990 Curitiba, Parana, Brazil

47.1 INTRODUCTION

Organic polymers that emit light on the imposition of an electric field have commanded increasing attention in the last decade both for their scientific interest and as potential materials for electrooptical and optoelectronic applications. A number of reviews on electroluminescent polymers focusing the basic physics [1–5], synthesis and properties [6,7], device operation and materials [8–11], design and synthesis [12] blue emitting structures [13] have been published. Some books are also out on the subject [14–18].

Apart from intrinsic electronic features, the color emitted by small organic molecules depends on microenvironment characteristics, such as their location in the device and medium polarity. When attached to a polymer chain, the mobility of the chromophore is restricted in all directions, and the emission becomes dependent on the structural features of the macromolecule (including the molecule's architecture, such as regioregularity, location and distribution of chromophores, etc.). This restriction opened a new avenue in the development of electroluminescent polymers: color tuning could be achieved by introducing variations in the polymeric structure, since in doing so the energy gap of the π–π^* transition responsible for the color emitted is changed, and a broad range of colors can be achieved with one polymer. It may be noted that both low and high molecular weight organic EL materials are now under wide study. The perceived advantages of the former include the possibility of a definitive chemical structure, chemical purification at high purity levels by sublimation, and facile manufacture of complex 3D architectures, while polymers are favored for their mechanical properties, principally the ready formation of robust films and their processibility using easily accessible technology for simple device architectures. The two classes of materials are not infrequently used together in multicomponent chromophoric layers. A typical design of a polymer LED is shown in Fig. 47.1. More elaborate architectures may vary from this basic scheme, and may involve the use of a multicomponent chromophore and one or more transport layers (see below). Recent advances include microfabrication of diode-pixel arrays [19], patterned light emission with sizes of the order of 0.8 mm [20], polarized EL based on stretch or, rub aligned Langmuir-Blodgett deposited polymers, or specifically synthesized liquid crystal polymers [21–27]. The application of ultrathin and selfassembling films is an important development in LED technology. In this case the film in the device is not cast using a traditional processing technique such as spin coating, but using electrostatic layer-by-

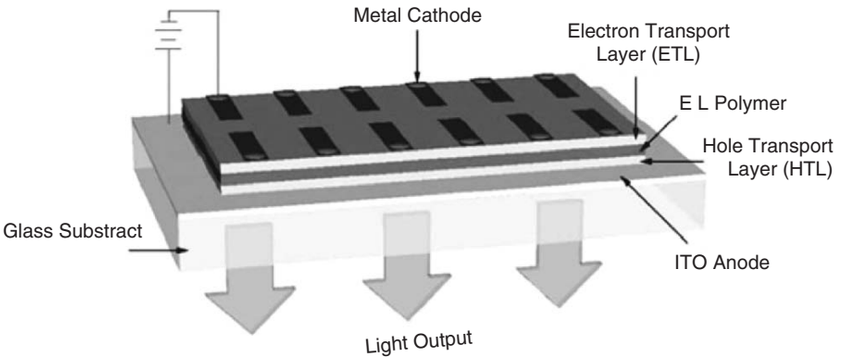

FIGURE 47.1. Design of a polymer LED showing optional HTL and ETL.

layer selfassembly methodologies [28–31]. This means that recent advances in the molecular level processing of conducting polymers have made it possible to fabricate thin film multilayer heterostructures with a high degree of control over the structural features and thickness of the deposited layers. As the dimensions of the individual layers approach molecular scales it may be possible to approach quantum effects in these multilayer contacts. Further progress is represented by the development of surface light-emitting devices (SLEDS), in which both anode and cathode lay underneath the electroluminescent layer, so that no transparent materials are required in the LED construction. These SLEDS were microfabricated using conventional silicon processing [32]. The patterning of light-emitting layers is the most important step in the manufacturing of multicolor organic electroluminescent devices, and should combine large area coatings with device patterning. One very promising methodology employs an ink jet patterning process [33–35]. Light emission of poly [3-(2-benzotriazolo)ethylthiophene] has been investigated by the cathodoluminescence (CL) spectroscopy. An electron beam was used to inject directly electrons and holes in the polymer. The introduction of benzotriazole, an electron-withdrawing moiety, to the thiophene was done to enhance electronic affinity [36].

47.2 LIGHT EMITTING DEVICES AND MECHANISM FOR LIGHT EMISSION

Light-emitting devices as shown in Fig. 47.1 can be operated in a continuous DC or AC mode. They behave like a rectifier, the forward bias corresponding to a positive voltage on the ITO electrode and are also called light-emitting diodes in analogy to p–n junction devices. Light emission is transmitted from the transparent side normal to the plane of the device. The polymer layer is usually deposited by spin coating, but dipping techniques can also be used. The cathode injects electrons in the conduction band of the polymer (π^* state), which corresponds to the lowest unoccupied molecular orbital (LUMO), and the anode injects holes in the valence band (π state), which corresponds to the highest occupied molecular orbital (HOMO). The injected charges (polarons) can travel from one electrode to the other, be annihilated by any specific process such as multiphonon emission, Auger processes, or surface recombination. These concepts have been extensively studied in inorganic systems and may also apply to polymer systems. A simplified description involves the formation of a neutral species, called an exciton, through the combination of electrons and holes. The exciton can be in the singlet or triplet state according to spin statistics. Because only singlets can decay radiatively, and there is only one singlet for each three triplet states, the maximum quantum efficiency (photons emitted per electron injected) attainable with fluorescent polymers is theoretically 25%. This limit can be overcome by using phosphorescent materials that can generate emission from both singlet and triplet excitons [37]. As a result, the internal quantum efficiency can reach 100%. Forrest *et al.* [38] reported highly efficient phosphorescent LEDs by doping an organic matrix with heavy atoms containing phosphorus. Polymer devices were also fabricated by using polyfluorene [39] or poly(vinyl carbazole) [40] as the host for the phosphorescent dye. The singlet exciton decay time is typically in the ns timescale, whereas the triplet survives for up to 1 ms at low temperatures [41]. A major fact determining the internal quantum yield for luminescence (ratio of radiative to nonradiative processes) is the competition between radiative and nonradiative decays of the electron–hole pairs created within the polymer layer. These pairs can migrate along the chains and are therefore susceptible to trapping at quenching sites where nonradiative processes may occur. The sequence of charge processes leading to exciton formation is charge injection, transport, and recombination. These processes are difficult to separate on the basis of the device electrical characteristics, and the transport mechanism affects the other two. Two modes of injection mechanisms have been discussed for the operation of LEDs: thermoionic emission over a Schottky-like contact, and tunneling into the transport bands. Theoretical modeling of charge injection has been attempted by several approaches [42–48].

47.2.1 Interchain Excitons

In LEDs the polymers are thin films, leading to the possibility of electronic interactions between neighboring

chains and the creation of new excited state species. This topic has been the subject of many recent investigations [49–52] mainly related to PPV [53,54], PPV derivatives such as poly(2-methoxy-1,4-PPV), MEH-PPV [55–60], CN-PPV [51,55,61], poly(*p*-pyridyl vinylene) [59,62], acetoxy PPV [63], and other light-emitting polymers [49,64–68], showing good evidence to suggest that interchain excitations play a significant role. The importance of these interchain excitations continues to be one of debate: if they are nonemissive, then they are detrimental to device operation, but if they are emissive, they can be used effectively [69]. The final morphology has a direct effect on the performance of MEH-PPV based LEDs. Higher degrees of interchain interactions enhance the mobility of charge carriers at the expense of lower quantum efficiencies for EL. The reduction in efficiency in well-packed regions is attributed to rapid formation of nonemissive interchain species without the involvement of ground state dimers or aggregates [60,70].

47.2.2 Transport Layers

Single layer device architecture is typically employed and is appropriate for evaluation of new polymer chromophores and for measurements of their EL and PL spectra. In the simplest cases the two spectra are quantitatively identical, although in numerous cases their noncoincidence reveals a more complicated exciton formation and decay related to the differing modes of energy input. In devices which are intended to maximize photonic output and efficiency, however, it is established practice to employ additional layers of organic material (polymeric or low molecular weight) interspersed between chromophore film and the electrodes using materials chosen for their functional ability to facilitate charge transport and block (localize) carriers, avoiding their crossing the device without recombination. Usually the carriers do not form junctions with identical (or zero) barrier heights and therefore one carrier will be preferentially injected. If the two junction barriers are not identical, higher electric fields would be required near the junction with the greater barrier energy in order to equalize the injected current density from each contact [71]. The LED efficiency is also reduced if the excitons are formed at the interface of the polymer and the electrode, lowering the carrier injection. This location is also where the greatest number of defects is expected and can act as quenching sites [72,73]. The transport layer also decreases exciton quenching near the metal electrode by acting as spacer separating the metallic contact from the active luminescent layer. To confine holes in the emissive layer an electron-conducting-hole blocking layer should be used (electron transport layer, ETL). Its valence band should be lower in energy than the EL layer and its electron affinity should be equal to or greater than the EL layer. In this way holes are confined between the emissive layer and the ETL, and the space charge formed provides a higher electric field across the interface with a more uniform distribution of charge, thus improving the balance between carriers. The same reasoning is valid for the use of hole transport layers (HTL). The use of transport materials represents an improvement in device stability since it makes it possible in certain cases to change from a lower work function ϕ_w metal electrode as calcium ($\phi_w = 2.9$ eV) which is unstable in atmospheric conditions to a higher work function material as aluminum ($\phi_w = 4.3$ eV), and adds it directly to the emitting polymer. Materials for ETL are electron deficient and the most used are oxadiazole compounds in the ''free'' form as PBD or grafted to a polymer main chain. Apart from PPV, a variety of electron-accepting polymers such as poly(vinyl carbazole) (PVK) [74,75], poly(pyridine-2,5-diyl), poly(1,10-phenanthroline-3-diyl), or poly(4,40-disubstituted-2,20-bithiazole-5,50-diyl) have been used as HTL materials. The incorporation of the transport/blocking material can also be made directly by blending them with the emissive material [76], as in the case of the green emitter poly(2-cholestanoxy-5-hexyldimethylsylyl-1,4-phenylene vinylene) (CCSPPV). With the combination of PVK as HTL and PBD as ETL it was possible to achieve internal quantum efficiency in excess of 4%. Several p-doped conjugated polymers have been used as hole injecting electrodes, like polypyrrole, polythiophene derivatives, and polyaniline [77–82], which have high work functions, providing low barriers for hole injection. There are reports of stable operation over long times for devices using polymeric dopants, which are expected to be relatively immobile. These include polystyrenesulfonic acid used to dope poly(dioxyethylene thienylene) (PEDOT) [3].

47.3 PPV AND PPV-TYPE STRUCTURES

47.3.1 Precursor Routes

47.3.1.1 The Wessling method

Like most highly conjugated materials, semiconducting polymers show poor solubility in organic solvents. Structural changes have been made to overcome this difficulty. The first highly structured electroluminescent polymer, PPV, a green-yellow emitter, was prepared via a precursor route because its insolubility in poly reactions resulted in only oligomeric materials. The precursor route involves the preparation of a soluble polymer intermediate that is cast in the appropriate substrate and after thermal treatment is converted to the final product *in situ*. This involves producing a polymer in which the arylene units are connected by ethylene units. The saturated units in the precursor contain a group which not only solubilizes the macromolecule and allows for processing, but also acts as a leaving group, thus affording the unsaturated vinylene units of a fully conjugated polymer. One of the most important soluble precursor routes to PPV was developed by Wessling and co-workers in the 1960s [83,84] based upon aqueous solvent synthesis

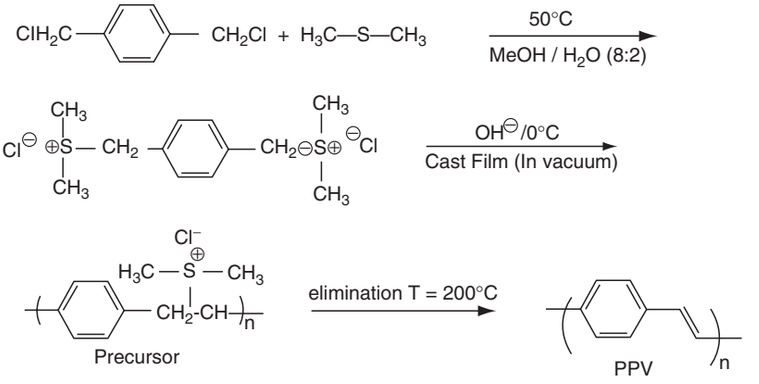

FIGURE 47.2. The sulfonium precursor route (Wessling) to PPV.

of poly(*p*-xylylene-a-dialkylsulfonium halides) from α-α′-bis(dialkylsulfonium salts), followed by thermolytic formation of the final conjugated polymer, as shown in Fig. 47.2. The charged sulfonium groups solubilize the polymer and are removed during the conversion step. The mechanism is believed to proceed according to a chain growth polymerization via the *in situ* generation of the monomer, a *p*-quinomethane-like intermediate [85,86], based on the facts that high molecular weight is formed very quickly, within the first minutes of the reaction and also that various radical inhibitors limit or prevent formation of long polyelectrolyte chains. However, the initiation process was not unequivocally identified [87–91]. Figure 47.3 depicts the radical chain mechanism for PPV synthesis [92]. A modified Wessling route where the solubilizing and leaving group is an alkoxy group has been developed and gives methoxyprecursor polymers, which are soluble in polar aprotic solvents such as chloroform, dichloromethane, and tetrahydrofurane [93,94]. The generation of precursor copolymers containing randomly placed methoxy and acetate groups (which are expected to be more labile to elimination) was an approach used to prepare poly(2,5-dimethoxy-*p*-phenylene vinylene) (DMPPV) of controlled conjugation length [95,96]. A soluble PPV derivative which could be used directly without a second step treatment was a natural development since it would simplify device fabrication and at the same time allow for less imperfections in the final structure since the conversion process inevitably introduces defects (chemical, morphological, etc.) into the chain with the result that there is a distribution of effective conjugation lengths and these are far shorter than the nominal degree of polymerization. In fact, the different precursor polymers discussed above all give PPV, but the structural and hence electronic properties can vary quite dramatically depending on which precursor polymer was utilized [97]. Derivatization of PPV with long alkyl and/or alkoxy ramifications (RPPV, ROPPV) was the first approach for the obtainment of soluble electroluminescent polymers. The solubility by derivatization is due to the lowering of the interchain interactions, which should not in principle change the rigid rod-like character of the main chains. A variety of PPV derivatives can be obtained from *p*-xylylenes by analogous routes used to obtain PPV. A wide

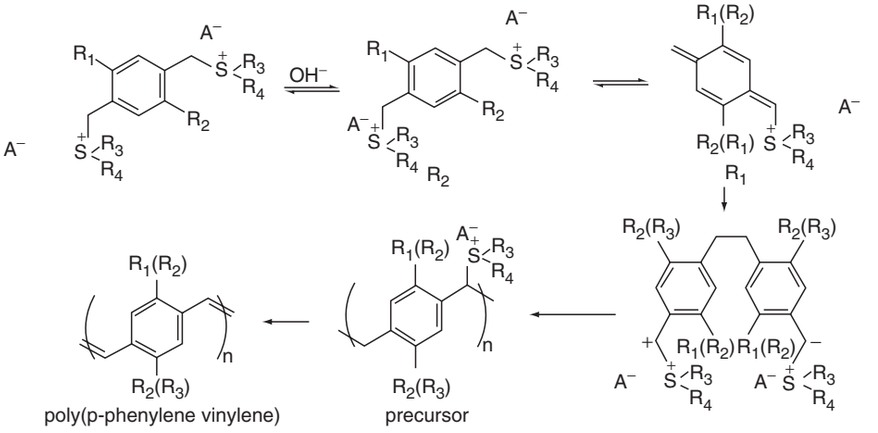

FIGURE 47.3. Mechanistic processes for the sulfonium precursor synthesis of poly(phenylene vinylene)s, showing the ylide, the xylylene, and the poly(*p*-xylylene-a-dialkylsulfonium halide) (PXD). Substituents X and Y can be alkyl, alkoxy, and aryl groups. Reprinted with permission from Synthesis, properties of poly(phenylene vinylene)s, related poly (arylene vinylene)s. 1998. p. 61. chapter 3. © 1998 Marcel Dekker, Inc.

variety of substituents are tolerated by the soluble sulfonium precursor route affording alkoxy [98–102], alkyl [103,104], alkyl and aryl [105] substituted PPVs. Attachment of alkoxy side chains to the polymer backbone lowers the optical bandgap of most polymers, thereby playing an important role in the color tuning of the polymeric materials. The solid-state properties (color, absorption, emission, fluorescence quantum yield, photoconductivity, etc.) of these polymers were found to be greatly dependent on the number, length position, and geometry of the grafted alkoxy side chains [106].

Substituted PPVs are soluble in organic solvents, which is a very useful feature in the preparation of polymer LEDs. One of the first PPV soluble derivatives, prepared by the Santa Barbara group in California via the precursor route, was methoxy-ethylhexyloxy PPV (MEH-PPV), which emitted a red-orange color [107,108]. Subsequently another PPV derivative with the bulky cholestanoxy group was prepared, namely the poly [2,5-bis(3a-5b cholestanoxy)-1,4-phenylene vinylene] (BCHAPPV). A blue shift was observed in relation to MEH-PPV; BCHA-PPV emitted in the yellow region [109,110].

47.3.1.2. The chlorine precursor route

An important soluble precursor route for PPV and related polymers involves the polymerization of 1,4-bis(chloromethyl or bromomethyl) arenes by treatment with potassium-*t*-butoxide in nonhydroxylic solvents like tetrahydrofuran. This methodology was first used by Gilch and Wheelright [111] as one of the most successful early PPV synthesis. Hoerhold and co-workers elaborated fairly extensively on this method and recently applied it to synthesis of PPVs with large solubilizing groups on the aryl ring such as cholestanoxy (Fig. 47.4(a)), high molecular weight, highly phenylated PPVs [112–118] such as the diphenyl-4-biphenyl ring substituted PPV which showed green EL [119], poly(2,3-diphenyl-1,4-phenylene vinylene) (DP-PPV) [115, 120–122] (Fig. 47.4(b)). Without the presence of solubilizing side chains on the arene ring, premature precipitation can occur, but otherwise the method has the advantage of producing a precursor that is soluble in organic nonhydroxylic solvents, and therefore useful for electronic applications that require processing. The chlorine precursor route has been also applied to the synthesis of the extensively explored poly(2-methoxy 5-(2-ethyl hexyloxy polyphenylene vinylene) (MEH-PPV). A plausible source of defects in the precursor routes resides in the remaining saturated linkages between aromatic links, which can lead to localized traps via hydrogen abstraction, causing premature device decay. The regiochemical randomness associated with the Wessling based routes [123–126] is an important point, since it affects the solid-state morphology and electronic states connected with molecular architecture. In another variation of the Wessling route, nonionic sulfinyl groups in the ethylene moiety are the leaving groups [127,128]. In addition to the substituted aryl rings that can be incorporated in PPVs by the soluble precursor routes, it is also possible to use other aryl rings, like condensed ones, as long as they are derivable from *p*-xylylenes or their monocyclic analogs. The obtainment of PPVs with aryl or alkyl substituents at the phenylene or vinylene group of PPV can also be accomplished by the

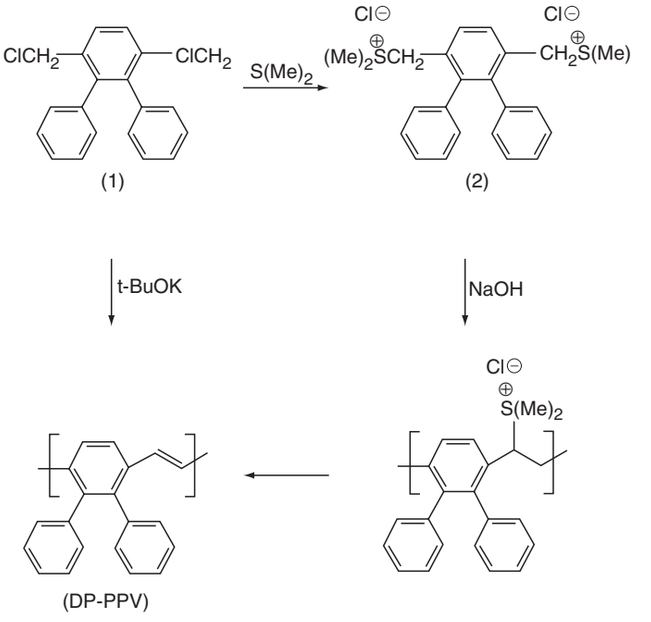

FIGURE 47.4. The dehydrohalogenation route to PPV derivatives illustrated in the synthesis of poly(2,3-diphenyl-1,4-phenylene vinylene) (DP-PPV) poly(1-methoxy-4-(2-ethylhexyloxy)-*p*-phenylene vinylene) (MEH-PPV).

palladium catalyzed coupling of dihalogenoarenes and ethylene [129]. It is a general trend that when electron donating alkoxy groups are attached to phenylene rings of PPV the bandgap is reduced and the wavelength of the emitted light shifts to red from the green region [104,107,110,130,131]. RO-PPVs where the alkoxy RO– length varied from C5 to C12 showed increasing EL intensity with increasing side chain length. This was attributed to the reductions of nonradiative decay processes due to preventing migration of excitons to traps. Apart from electronic effects, intermacromolecular packing is a major factor in determining emission color and photoluminescence efficiency (PLeff). Since this quantity is a key factor in LED efficiency (along with balanced charge injection and carrier mobility as seen above), steric effects are important in the design of EL polymers. Figure 47.5 shows the influence of side groups on the emission characteristics of some important PPV derivatives [132]. As a general trend close packing as in BEH-PPV (due to its lateral symmetry) results in reduced PLeff, whereas polymers bearing bulky side groups show increased PLeff, as BCHA-PPV, despite the symmetry which gives higher order in the polymer films. Devices using poly(2,3-diphenyl-1,4-phenylenevinylene) derivatives containing long branched alkoxy chains or fluorenyl substituents with the configuration of ITO/PEDOT/polymer /Ca/Al exhibited a low turn-on voltage (4.0 V), a very high external quantum efficiency (3.39 cd/A), and the highest brightness found in this survey (16,910 cd/m^2) [133].

Recently, a new synthetic route toward PPV and its derivatives has been reported in which the monomer is polymerized toward a dithiocarbamate precursor polymer by the addition of a strong base. The corresponding conjugated polymer is obtained via a heart treatment of the precursor polymer. This dithiocarbamate precursor route represents a compromise between several straightforward but sometimes troublesome precursor routes and the more complex sulfinyl precursor route [134].

A natural development was the introduction of hole and/or electron transporting groups in EL polymers aiming the improvement of injection/transporting properties as in the case of the incorporation of triphenyl amine and cyano groups in MEH-PPV [135,136]. Recent advances in PPV-related structures include soluble PPV derivatives containing pyrene [137] or perylene [138] dyes in the main and C60 grafted units [139].

Energy migration from a large bandgap polymer to another with lower bandgap is possible when the absorption of the latter overlaps with the emission of the former to a certain

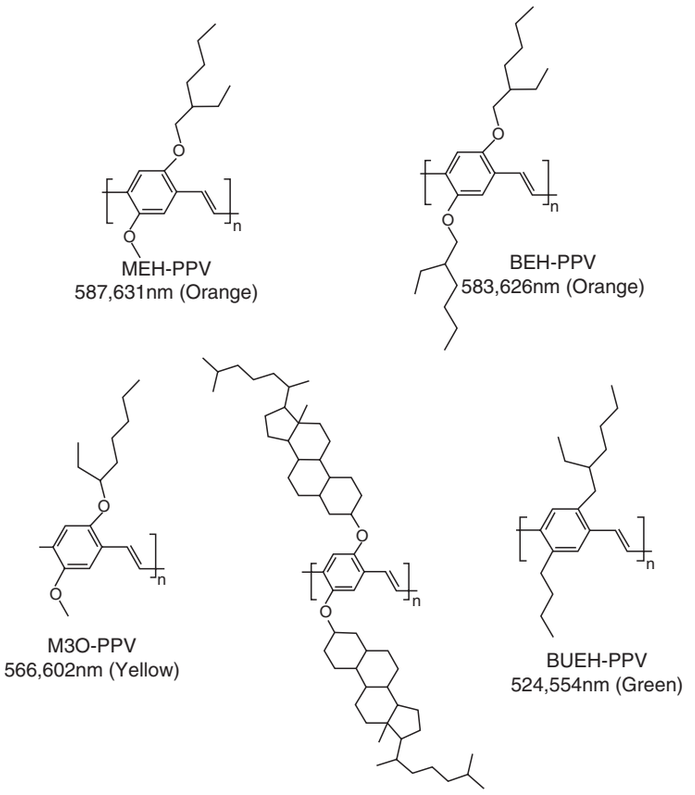

FIGURE 47.5. Influence of side groups on the emission properties of some important PPV derivatives. Reprinted with permission from Synth Met 1997;85(1–3):1275. © 1997 Elsevier Science.

extent, and the result is an enhancement of the lower bandgap emission. The dynamics of the excitation transfer process, measured in the ps timescale using an ultrafast Ti/sapphire laser, indicate that the energy transfer was completed in 10 ps when *m*-EHOP-PPV (poly [2-(*m*-2′-ethylhexoxyphenyl)-1,4-phenylene vinylene]) was used as the host with BCHA-PPV (poly[2,5-bis(cholestanoxy)-1,4-phenylene vinylene]) and BEH-PPV (poly[2,5-bis(2′-phenylene vinylene]) as the guests [140]. Mixtures of poly(2-methoxy-5-(2-ethylhexyloxy-1,4-phenylenevinylene) (MEH-PPV) which emits at 600 nm (yellow-orange) with poly [1,3-propanedioxy-1,4-phenylene-1,2-ethenylene(2,5-bis(bimethylsylyl)-1,4-phenylene) -1,2-ethenylene-1,4-phenylene]) a conjugated–nonconjugated block copolymer, DSiPV) which emits at 450 nm (blue), yielded only the large wavelength emission. By varying the ratio DSiPV/MEH-PPV from 9:1 to 1:15 the relative quantum efficiency increased by a factor of 500. This was attributed not only to energy migration of the excitons from DSiPV to MEH-PPV but also to a dilution factor. As the EL active MEH-PPV is diluted by DSiPV, the intermolecular nonradiative decay is diminished by blocking of the charge carriers [141].

47.4 CONJUGATION CONFINEMENT

47.4.1 Conjugated–Nonconjugated Block Copolymers

So far we have seen that introducing substituents in the PPV molecule leads to various EL polymers, emitting in various regions of the visible spectrum according to their chemical structures. A theoretical study of the effects of derivatization can be found in reference [142]. From the red shift of the peaks in PL found with increasing chain length, the effective conjugation length for long chain precursor route samples of PPV are theoretically estimated to be 10–17 repeat units [143]. However, experimental work with oligomeric models led to the conclusion that the effective conjugation length of the solid polymer is not larger than 7–10 units [144]. Thus fully conjugated polymers may have chromophores with different energy gaps because the effective length of conjugation is statistically distributed. However, in the mixture, the chromophores with lower energy gaps will be the emitting species because of energy transfer. To solve this problem several approaches have been developed. The confinement of the conjugation into a well-defined length of the chain is one of the most successful strategies developed so far. Illustrative examples of EL structures exploring the concept of conjugation confinement are shown in Fig. 47.6 [145–147]. Copolymers in which a well-defined emitting unit is intercalated with nonemitting blocks have demonstrated that the emitted color was not affected by the length of the inert spacers but the EL efficiency of the single layer LEDs fabricated with the copolymers was a function of the length of the nonconjugated blocks; copolymers with longer spacers yielded higher efficiency devices [148]. Those conjugated–nonconjugated copolymers (CNCPs) are soluble, homogeneous in terms of conjugation length, and can be designed to emit in any of the visible spectrum [148–151]. In such structures energy transfer from high bandgap to lower bandgap sequences in which excitons may be partially confined will provide higher luminescence efficiency when compared to similar structures of uniform conjugation [152]. In soluble poly(dialkoxy-*p*-phenylene vinylene)s, the systematic variation on the degree of conjugation showed that PL and EL increased with the fraction of nonconjugated units. At the same time, confinement of the effective conjugation has proved to be an efficient means for blue shifting the spectrum because the conjugated emitters can allow charge carriers to form but not to diffuse along the chain, thus limiting the transport to quenching sites [153,154]. This electronic localization results in a large $\pi-\pi^*$ bandgap which decreases with conjugation length [155]. A widely used route to CNCPs involves the Wittig type coupling of dialdehydes with bis(phosphoranylidene)s [156,157]. A series of CNCPs was prepared, varying the $-O(CH2)_nO-$ spacer length, and chromophore's structure (PPV type) and length allowing to correlate conjugation length with emission color and device efficiency [148–151]. Changing the aromatic ring from a *p*-phenylene to a *p*-thienylene residue caused bandgap shifts in which the emission changed from blue to yellow [150,158, 159]. The introduction of nonconjugated segments not only confines the π electrons in the conjugated part but also imparts solubility and improves the homogeneity of the films. The Wittig route (as with other condensation routes) does not lead to high molecular weight polymers because these become insoluble after a certain degree of polymerization is reached. In CNCPs the solubility provided by the spacer permits the obtainment of high molecular weight materials. Conjugation confinement can also be achieved by tailoring the polymer structure in other ways, like inserting kink (*ortho* and *meta*) linkages or imposing steric distortions. Alkoxy substituted PPVs usually carry the alkoxy groups at the 2,5-positions in the ring and are red shifted in relation to unsubstituted PPV. By placing these substituents at the 2,3-positions and the ring in a *meta*-configuration it was possible to obtain blue emitting alkoxy PPVs [160]. Efficient blue-green polymer light-emitting diodes were prepared with block copolymers composed of the fluorescent segments, 1,4-di[2-(1-naphthyl)vinyl] benzene or 2,5-dimethyloxy-1,4-di[2-(1-naphthyl)vinyl] benzene and the flexible segments, tri(ethylene oxide) [161]. A new type of cyclolinear polymer, poly(phenylene vinylene-*alt*-cyclotriphosphazene), was synthesized through Heck-type coupling reaction. Apart from controlling the conjugation length and solubility, the nonemitting cyclophosphazene rings were capable of accommodating a wide variety of substituents with minimal effect on the electronic properties [162].

47.4.2 Chromophores as Side Groups

An extension of the concept of CNCPs is the attachment of the fluorofore as a pendant group to a nonemitting

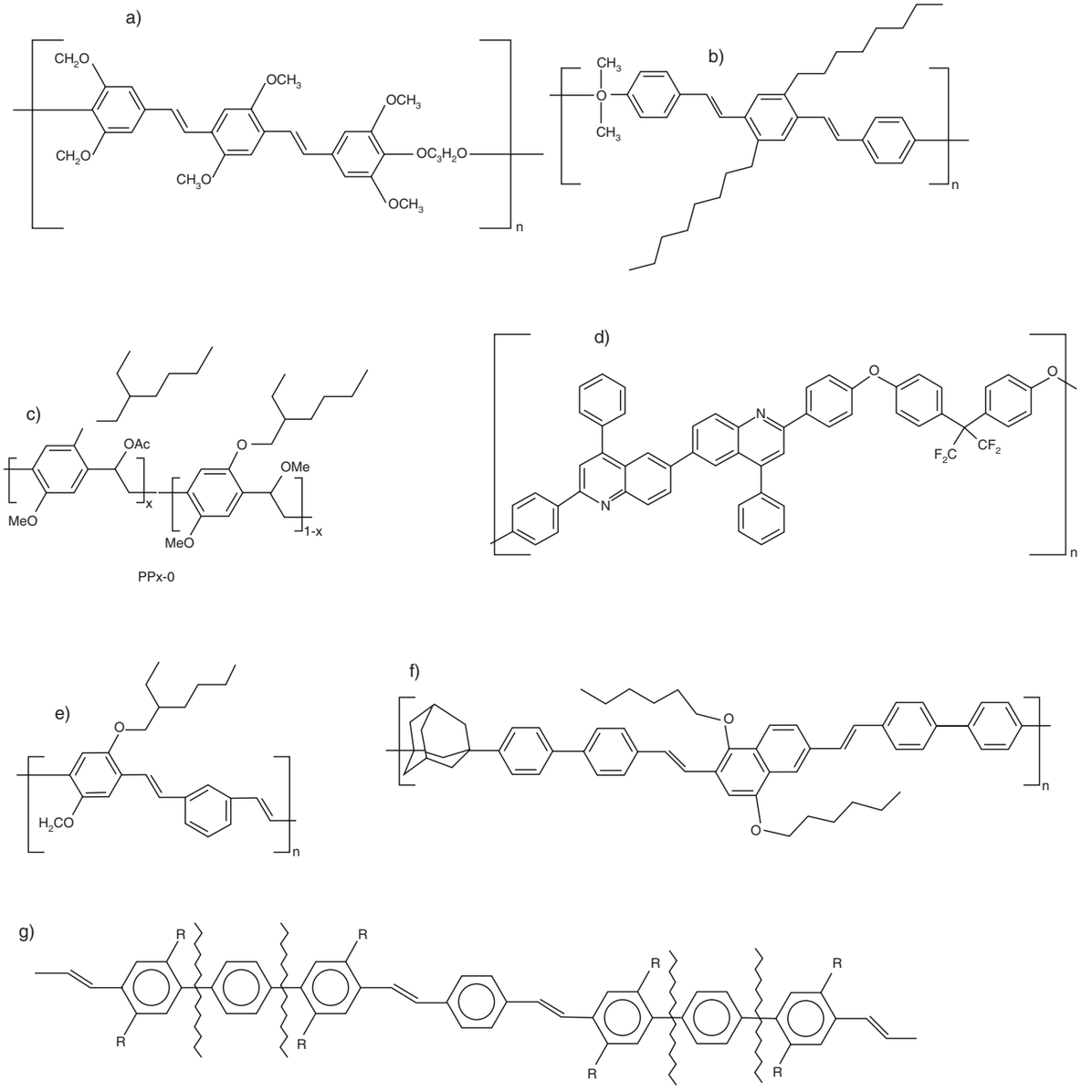

FIGURE 47.6. Examples of EL polymers exploring the concept of conjugation confinement. (a) An aliphatic spacer separating PPV type blocks; (b) dimethylsilane groups separating PPV type blocks; (c) partially eliminated MEH-PPV; (d) hexafluoroisopropylidene nonconjugated segment separating polyquinoline emitting units; (e) kink (*meta*-) linkages in MEH-PPV; (f) adamantane moiety as spacer; (g) the planarity is interrupted by the twisted *p*-phenylene groups, schematically illustrated with the wiggled lines.

random coil polymer. This idea should in principle present several advantages: the synthetic route would be simpler than that used for main-chain polymers, the solubility would be dominated by the nature of the backbone, the emission wavelength would be predetermined, and crystallization of the chromophore with concomitant degradation of the diode (in comparison with small molecular weight sublimable systems) would be prevented. In addition, an electroluminescent group could be placed on every repeat unit or in a controlled frequency along the backbone. Some representative EL structures with emitting pendant groups are shown in Fig. 47.7. Using polystyrene as the main chain, stilbene groups were attached to every repeat unit, in every other repeating unit, or in every third repeat unit (Fig. 47.7(a)) [64,163,164], resulting in blue emitting polymers. Grafting anthracene derivatives (2,3,7,8-tetramethoxy-9,10-dibutyl anthracene) (Fig. 47.7(b)) and *N*-methyl naphthalimide (Fig. 47.7(c)) gave blue and green PMMA based light emitting materials. Charge transfer and emission from associated forms (ground state dimers or excimers) are common

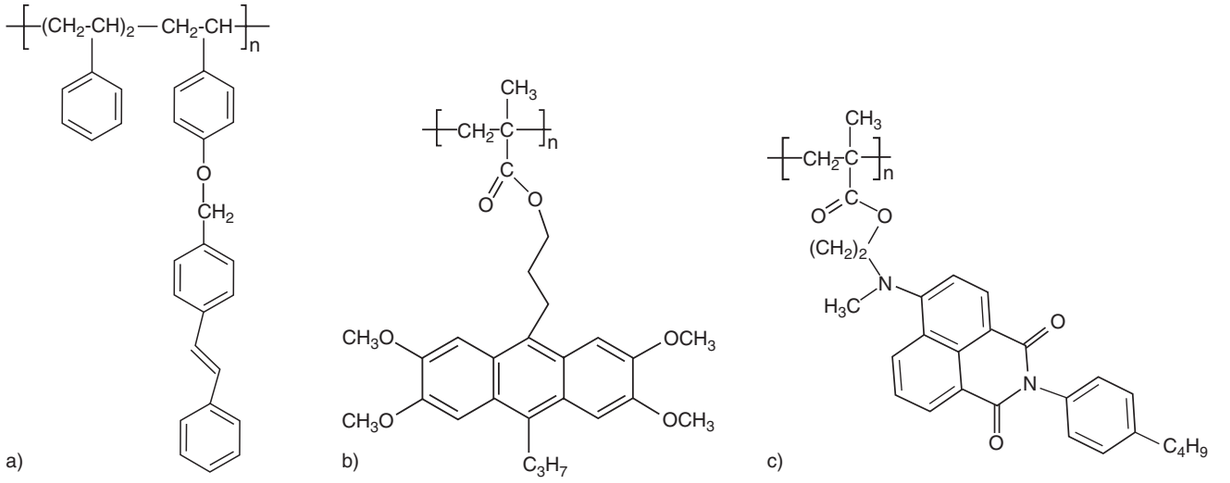

FIGURE 47.7. Examples of EL polymers with emitting pendant groups. (a) Stilbene chromophores linked to a polystyrene backbone; (b) anthracene derivatives linked to a poly(methyl methacrylate) backbone; (c) naphthalimide based chromophore as side chain in poly(methyl methacrylate).

events in pendant chromophore structures. Examples include the pyrene excimer emission only of polysiloxanes bearing a pyrene group in each mer and the suppression of carbazole emission of copolymers containing carbazole and pyrene attached to a polysiloxane backbone or carbazole and fluoranthene attached to a PMMA main chain [165]. PPV has also been used as a backbone for grafting of lumophores, giving rise to a structure with more than one simultaneously emitting center, like PPV containing the electron accepting trifluoromethyl stilbene moiety. This group emits in the violet, but the substituted PPV showed only the PPV characteristic emission, due to energy transfer [166]. The concept of pendant chromophores has been also explored to afford better transport properties, by covalently attaching charge transport groups to the emitting polymer. The hole transporting carbazole and the electron transporting 2-(4-biphenyl)-5-(4-*t*-butylphenyl)-1,3,4-oxadiazole) (PBD) were placed as side groups in each mer of PPV. A slight interaction between the π-electrons of the PPV backbone and those of the pendant groups was detected. Also, blue-shifted absorptions indicated that steric effects partially disrupted the conjugation in PPV; the copolymers showed overlapped emissions of the main chain and the side groups. The direct PBD attachment to PPV improved the EL efficiency to a great extent, but the carbazole insertion resulted in an increased imbalance in carrier transport, since PPV itself accepts and transports holes more readily than electrons [167,168]. Apart from designing a molecule capable of emitting light in a defined region of the visible spectrum, a very interesting approach is to design structures that can emit light over a broad spectral range so that the color emitted is white or close to it. With this objective polymers carrying more than one chromophore were prepared like a ring anthracenyl substituted PPV [169]. An interesting blend was prepared using a side chain copolymer with pendant perylene groups and carrier transporting copolymers, in which hole and electron transporting units were incorporated in the same chain [170].

47.5 POLYTHIOPHENES

Among various polymers for LED fabrication poly(3-alkylthiophene) (PAT) [171] has stimulated much interest because it was the first soluble and even fusible conducting polymer, and it demonstrated novel characteristics such thermochromism [172] and solvatochromism [173]. EL in these materials was first reported by Ohmori [174,175] and it is now possible to tune the emission of substituted polythiophenes from ultraviolet to IR by changing the substituent [176]. LEDs made with PAT emitted a red orange color [177] peaking at 640 nm. For the series in which the side chain is an aliphatic branch of 12, 18, or 22 carbons the EL intensity increased linearly, the latter (22 carbons) being five times brighter than the former (12 carbons). This was explained in terms of confinement of carriers on the main chain where longer substitutions accounted for greater interchain distance decreasing the probability for quenching [165,178]. The emission intensity of PAT-based LEDs increases with increasing temperature (20–80°C) contrary to inorganic GaAs and InGaP semiconductor diodes [179]. This was explained in terms of changes in effective conjugation length with temperature due to changes in the main chain conformation which decreased the nonradiative recombination probability. Some representative polythiophene structures are shown in Fig. 47.8. Polythiophene and substituted polythiophenes can be prepared by chemical or electrochemical routes [180]. The eletrochemical method

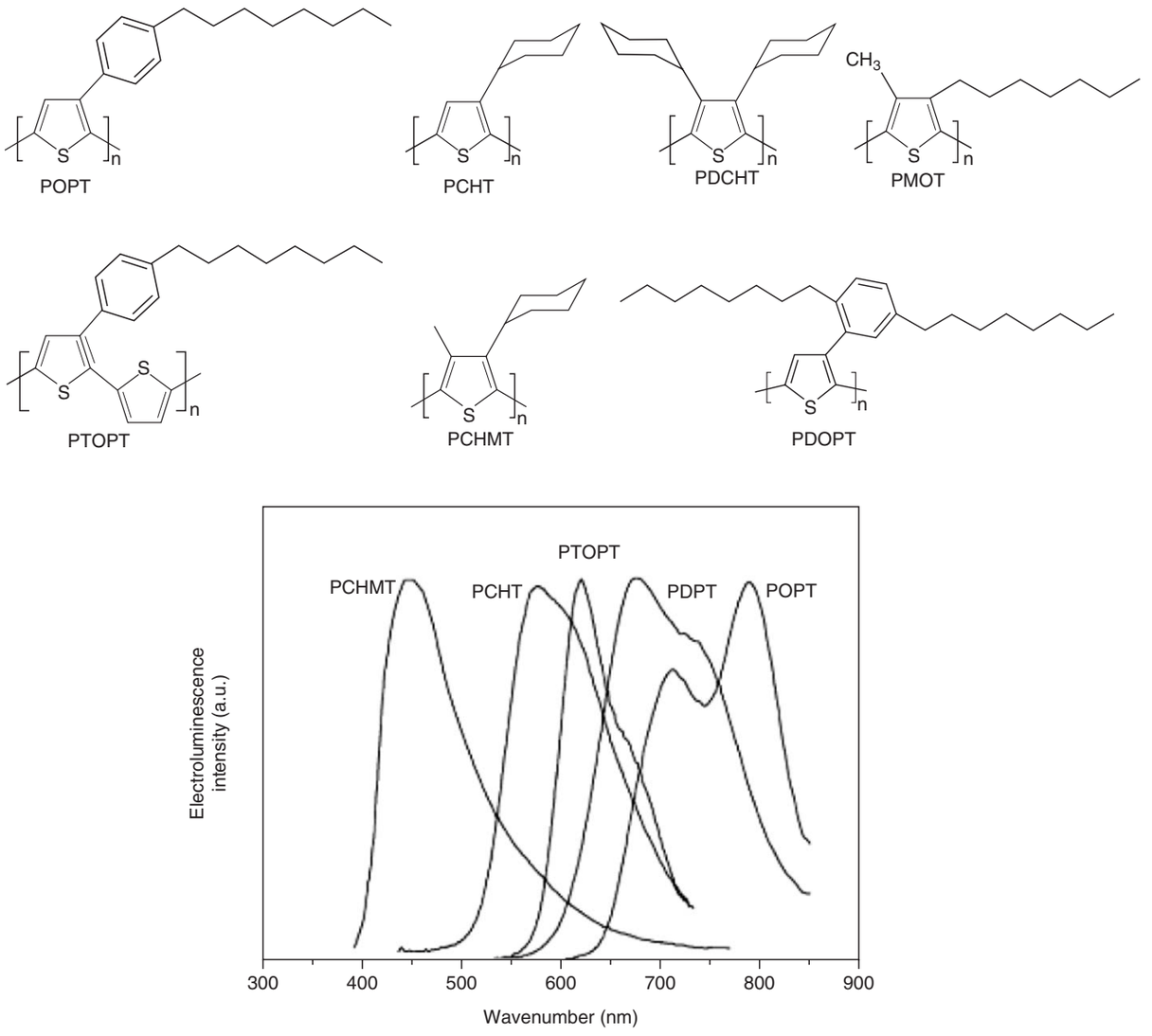

FIGURE 47.8. Effect of substitution on the emitting properties of polythiophenes. POPT* and POPT** are different forms of the same polymer, due to thermal treatment.

gives crosslinked materials, and chemical synthesis is most straightforward, in the iron chloride oxidative polymerization route. A particular point in this aspect is that of obtaining regioregular polymers, since regioregularity strongly influences the optical and transport properties of polythiophenes [181]. The dihedral angle and thus the p-orbital overlap between adjacent thiophene rings along the polymer backbone determine the conjugation length along the polymer chain. Short conjugation gives a blue-shifted emission and long conjugation gives a red-shifted emission. Three main strategies have been used for controlling the conjugation length and bandgap in polythiophenes. In the first the conjugation length is modified by adding different substituents on the repeating unit, imposing continuous steric torsions of the main chain [182]. In Fig. 47.8 polythiophenes bearing substituents at positions 3 and 4 in the ring are shown and illustrate the shifts in emission resulting from different degrees of torsion. The larger substituents give a large dihedral angle between the rings, and short conjugation along the polymer backbone is achieved, resulting in blue-shifted emission. This way emission from the blue (PCHMT), green (PCHT), orange (PTOPT) to red (and NIR) (POPT) were observed [32,183]. With mixtures of these polymers it was also possible to obtain voltage controlled EL and white light emitters. For poly(3-(2,5-octyldiphenyl)thiophene) (PDOPT) the bulky side chains efficiently separate the backbones giving the polymer a high PL yield (0.37 in. solution and 0.24 in. film). PTOPT

has a lower density of side chains, and the PL yield reduces from 0.27 to 0.05 going from solution to thin film. PMOT is twisted out of planarity by sterical hindrance and shows blue-shifted absorption and emission [184]. Substituted polythiophene-containing electron transporting groups such as benzotriazole, chlorobenzotriazole, and fluorene have also been reported [185,186]. Poly(3-octyl thiophene), which can be obtained as a 95% regioregular material, offers an example of how super structure can affect the electronic properties of an emissive polymer. Changing from poly(3-hexylthiophene) to poly(3-dodecylthiophene) increased the maximum efficiency from 0.05 to 0.2% with calcium electrodes [187]. The phase structure in blends of one or more polythiophenes with a PMMA matrix allowed the fabrication of nano-LEDs giving white light emission. The thiophene backbone has been functionalized with a wide variety of organic moieties including alkyl, fluoroalkyl, alkylthio, alkoxy, alcohol/thiol, amino, cyano, ester, carboxylic acid, and sulfonate side chains. Nitrogen-derivatized polythiophenes permit further modification of the polymers [188].

Other approaches to tune the emission color of polythiophene LEDs are the preparation of completely coplanar systems with controlled inclusion of head-to-tail dyads or the preparation of alternating block copolymer. The insertion of *p*-phenylene ring to head-to-head thiophene dyad linked [189], with different substituents on both thiophene and phenylene enhanced by 29% the PL efficiency, in comparison with other polythiophenes, and by changing the substitution on both the phenylene and thiophene rings, the electronic spectrum of the polymers could be tuned, emitting blue to green light. Photophysical and electrooptical properties of regioregular polythiophenes functionalized with tetrahydropyran moieties tethered to the main chain by alkyl spacers were prepared to access structure–property relationships of regioregular THP-bearing poly(3-alkylthiophene)s. In particular, aggregation phenomena were addressed by investigating the influence of the alkyl chain length with respect to their photophysical and electrooptical properties [190].

The emission of a series of p–n diblock copolymers with good electron transporting properties where oligothiophenes were linked with oxadiazolyl-dialkoxybenzene units could be tuned from blue to green to orange by increasing the number of thiophene rings from 1 to 3 [191,192]. In a recent study [193] of the transport properties of a polythiophene derivative, poly(3-(2′-methoxy-5′-octylphenyl)thiophene) (POMeOPT) the current–voltage characteristics of single layer devices were measured in two regimes: contact limited current and bulk-limited current. The passage from one regime to another was done upon insertion of a conducting polymer poly(3,4 ethylenedioxythiophene) doped with poly(4-styrenesulfonate) (PEDOT-PSS) between the metallic electrode and the POMeOPT. The measured mobility was seven times higher than that for MEH-PPV in the same conditions, illustrating the good transport properties and high mobility that can be attained with regioregular substituted polythiophenes. An interesting property of polthiophenes is phosphorescence emission which can be obtained by doping the polymer with a phosphorescent heavy metal as iridium, platinum, and others as in the case of poly(3-methyl-4-octylthiophene) as host and the phosphorescent compounds bis(2-phenylbenzothiazole) iridium acetylacetonate (BTIr) or platinum(II) 2,8,12,17-tetraethyl-3,7,13,18-tramethyl porphyrin as guest [194,195].

Introduction of the electron withdrawing groups as bithithiophene, pyridinyl, dipyridyl, and phenanthroline can modify their optical and electrical properties. These structures are low bandgap conjugated polymers with higher conductivity (carrier mobility), and may be transparent in visible light. Therefore, they have a great potential application in transistor, transparent conductor, nonlinear optical devices, and smart windows [196,197].

An alternating structure in which an unsubstituted thiophene ring was linked to a 3-alkyl-substituted thiophene, the two repeating units being alternated and a bulky group in the side chain showed an interesting peculiarity of combining high conjugation length with large interchain distances. Differently from the regioregular PATs, the copolymer showed high PL efficiency both in the solid form and in partially aggregated solutions [198].

47.6 CYANO POLYMERS

Most of the electroluminescent polymers are suitable as hole-injecting and transporting materials. To set an adequate balance in the injection flows coming from each side of the device it has been necessary to use electron transporting layers and/or low work function metals at the cathode, like calcium, which are unstable at atmospheric conditions. The synthesis of polymers with high electron affinity as the solution processable poly(cyanoterephthalydene)s which are derivatives of PPV with cyano groups attached to the vinylic carbons has provided the material necessary to complement the existing hole transport PPVs [57,142,199–205]. Poly(arylene vinylene)s bearing electron withdrawing groups are not easily available by application of the Wessling and related procedures and thus these cyano derivatives of PPV were synthesized via a Knoevenagel condensation route between an aromatic diacetonitrile and the corresponding aromatic dialdehyde [206–208] as exemplified in Fig. 47.9(a) or by copolymerization of dibromoarenes in basic medium. This approach permits adjustment of the bandgap by varying the proportion of the two comonomers [209]. The synthesis of fully conjugated PPV type structures containing cyano groups attached to the ring afforded a more perfect structure when a Wittig type condensation was followed, as in Fig. 47.9(b) in relation to the Knoevenagel route, emitting orange light (3000 cd/m^2 at 20 V) in a double layer device with PPV as HTL [210]. A variety of monomers with different substituents in the ring as alkyl or alkoxy solubilizing groups (as hexyloxy or

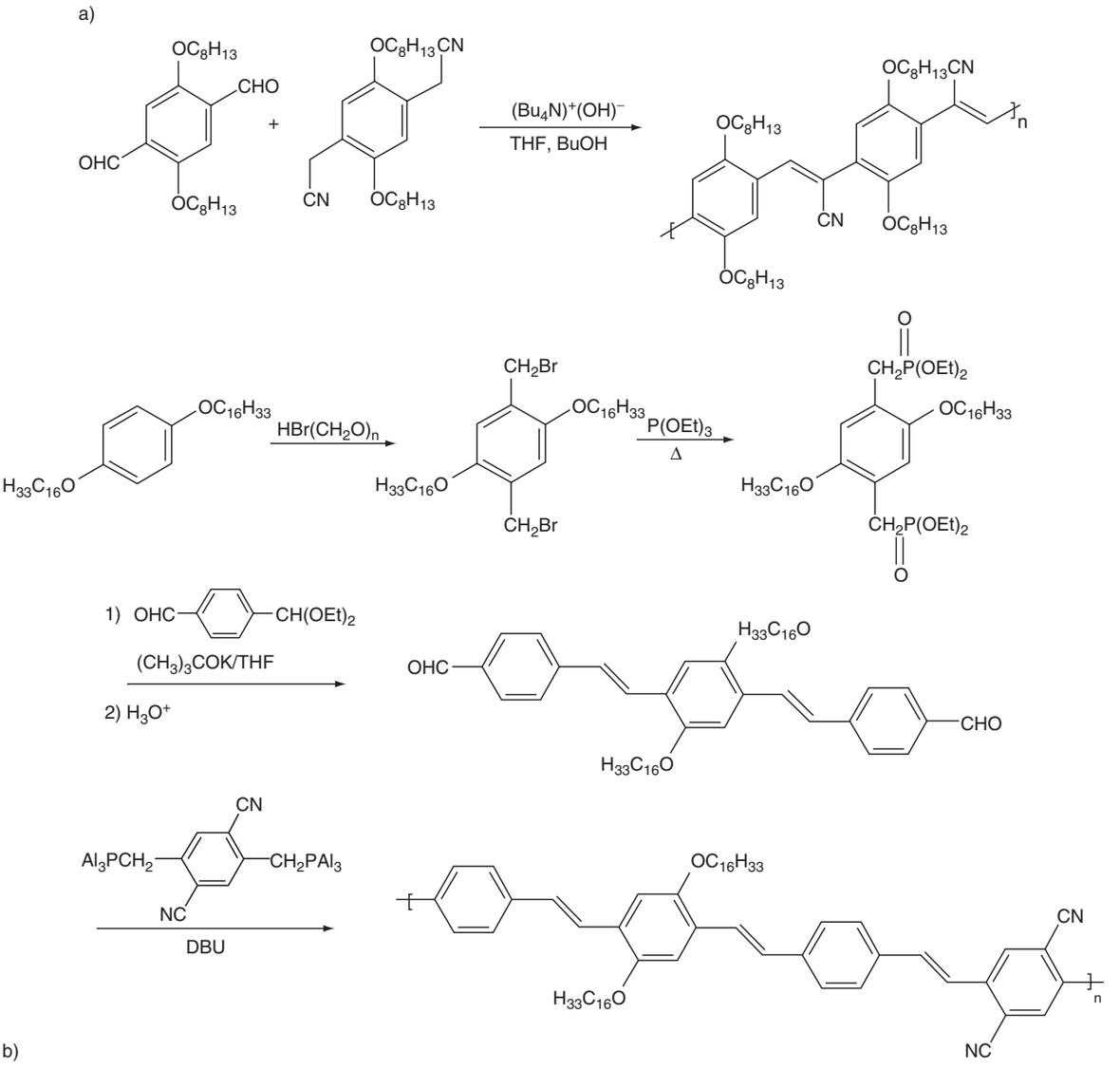

FIGURE 47.9. Synthetic routes to CN-substituted EL polymers. (a) Knoevenagel route leading to CN placement in the double bond; (b) Wittig route used to place the CN group in the aromatic ring in a conjugated–nonconjugated block copolymer.

methoxy-ethyl-hexyoxy as in MEH-PPV) were used to prepare cyano PPV like polymers emitting in the full-visible spectrum.

The inclusion of thiophene units in the main chain lowers the bandgap and shifts the emission to the infrared [211]. Examples EL polymers bearing cyano groups are given in Fig. 47.10. The electron withdrawing effect of the cyano group is calculated to increase the binding energies of both occupied π and unoccupied $\pi-\pi^*$ states, while at the same time keeping a similar $\pi-\pi^*$ gap [212]. The photophysical behavior of these polymers indicated that aggregates or excimers were probably the emitting associated form [213–216].

47.7 POLY(*P*-PHENYLENE)S (PPP) AND POLYFLUORENES

47.7.1 Polyphenylenes

Poly(*p*-phenylene) (PPP) is an interesting material for electrooptical applications as its bandgap is in the blue region of the visible spectrum and its thermal stability is combined with high PL. However, it is insoluble and infusible making it difficult to fabricate thin films. In the early stages of the search for PPP synthesis the limitations were related to the difficulties in the preparation of polymers possessing a defined architecture. Since only a few ''classical''

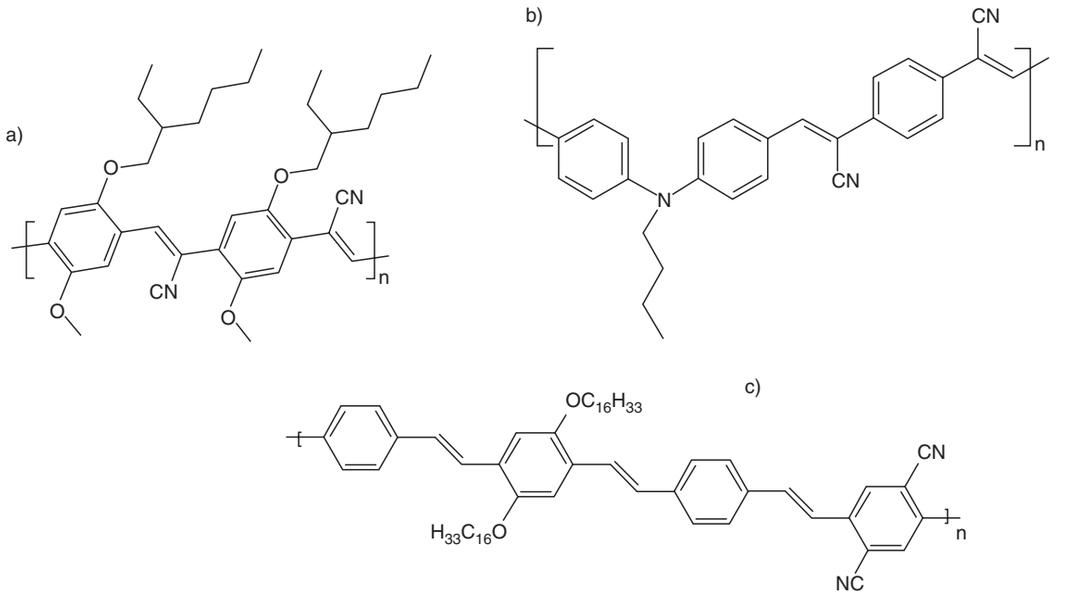

FIGURE 47.10. Examples of various EL polymers bearing the CN group in the double bond or in the aromatic ring.

organic reactions are known to generate a direct link between aromatic units, metal-catalyzed coupling reactions are commonly used for this purpose. The most successful routes are the Yamamoto route and the Suzuki crosscoupling reactions (SCC). The Yamamoto route involves the Ni mediated coupling of arenes by the reaction of the correspondent dibromo-substituted compounds [217]; the SCC involves the palladium-catalyzed crosscoupling reaction between organoboron compounds and organic halides. When applied to polymer synthesis, it proved to be a powerful tool to prepare poly(arylene)s and related polymers. In this case, SCC is a step-growth polymerization (Suzuki crosscoupling polymerization, SCP) of bifunctional aromatic monomers. The general method has been reviewed [218] and a wide variety of polymer structures prepared through this method [219]. In Fig. 47.11, a schematic representation of the step growth SCP is shown. Alkylated, soluble PPPs prepared via coupling reactions using the Yamamoto [219] or Suzuki [220] routes yielded significant torsion angles. The interring twisting significantly changes the electronic structure as well as the conjugation length [221].

Copolymers consisting of oligo *p*-phenylene sequences linked by ethylene, vinylene, or units have been reported. By the combination of different AA/BB type monomers in various concentrations in a Suzuki coupling as polymerization route, a variety of well-defined structures were prepared with high quantum yields in solution [222] as shown in Fig. 47.12. Matrix-assisted laser desorption ionization time of flight mass spectrometry (MALDI-TOF-MS) and HPLC analyses of monodisperse-substituted PPP fractions indicated that the effective conjugation length was around 11 phenylene units [223]. One way of obtaining a planar conjugated backbone was to incorporate the phenyl rings into a ladder-type structure where four C-atoms of each phenyl

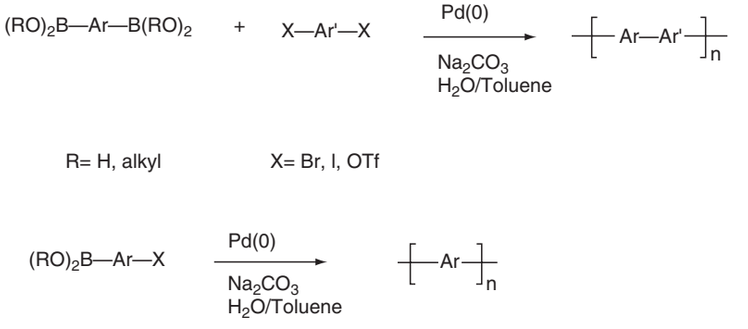

FIGURE 47.11. Schematic representation of the SCP —Ar— represent aromatic units, typically benzene derivatives.

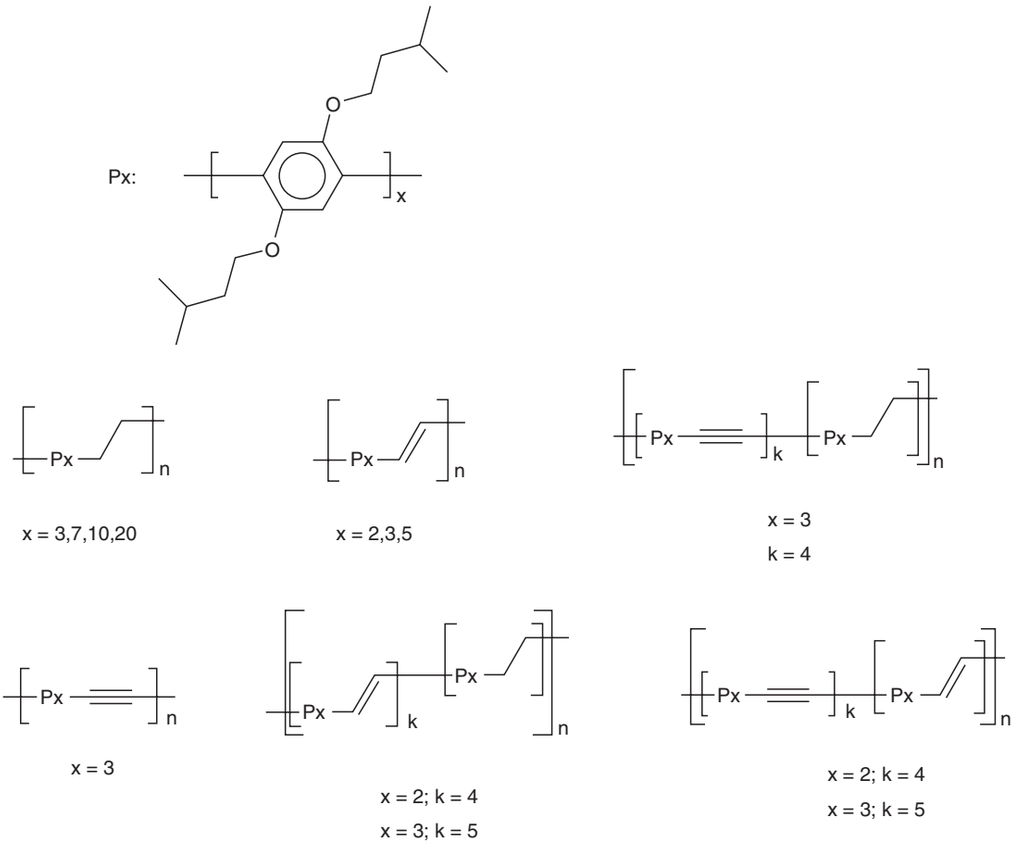

FIGURE 47.12. Polymers containing oligo-*p*-phenylene sequences linked by ethylene (E), vinylene (V) or ethynylene (A). The numbers correspond to the degree of polymerization of the phenylene sequences. The monomers were connected through the Suzuki coupling method.

ring are connected with neighboring rings (LPPP) in combination with an additional attachment of solubilizing side groups, thus creating a solution processable structure [224–229]. The forced planarity of the molecule led to a high degree of intrachain order, with a conjugation length of about eight phenyl rings [230,231]. The EL spectrum of the structures showed two emissions: a blue (461 nm) and a yellow (600 nm) which was attributed to the formation of excimers. A blue emitting PPP copolymer was reported in which tri-(*p*-phenylene) (LPP) and oligo(phenylene vinylene) segments were linked in an orthogonal arrangement to decrease quenching processes. Analogous structures with oligo (*p*-phenylene) units orthogonally and periodically tethered to a polyalkylene main chain have been prepared by the polymerization of oligomeric fluoreneacenes via an SN2 type of mechanism [232] Another class of PPP-type polymer is exemplified by the poly(benzoyl-1,4-phenylene) in a head-to-tail configuration [233]. The introduction of the carbazole unit in the ladder type tetraphenylene, blue emitting polymers brought about a slight bathochromic shift of the emission. The polymers exhibited good EL properties in initial PLED tests with high luminance values typically over 700–900 cd/m^2 at a bias of 10 but a definitive suppression of the excimer was not demonstrated [234].

47.7.2 Polyfluorenes

Recently, polyfluorenes were introduced as a prospective emitting layer for polymer LEDs. These materials are thermally stable and display high PL efficiencies both in solution and in solid films [235–239] with emission wavelengths primarily in the blue spectral region. Their photostability and thermal stability are also found to be better than those of the poly(phenylene vinylene)s. Polyfluorenes contain a rigidly planarized biphenyl structure in the fluorene repeating unit, while the remote substitution at C-9 produces less steric interaction in the conjugated backbone itself than in comparison with PPP, in which this interaction can lead to significant twisting of the main chain since the substituents used to control solubility are *ortho* to the aryl chain linkage, as is the case for the monocyclic monomers [240,241] discussed in Section 47.7.1. In this regard polyfluorenes can be considered as another version of PPP with pairs of phenylene

rings locked into a coplanar arrangement by the presence of the C-9 atom. Liquid crystallinity was observed in poly (dioctyl fluorene), which is important for the obtainment of polarized EL [26,242]. A representative number of polyfluorenes and related structures are shown in Fig. 47.13. The nickel-mediated coupling of arylene dihalides, the Yamamoto route, has been used to prepare a variety of fluorene and substituted fluorene homo- and copolymers [235–244]. As with PPPs, the SCP has been recently applied to the synthesis of a wide number of polyfluorenes and related structures. In the case of alternating copolymers obtained by SCP the optical and electronic properties of the polymers were tailored through selective incorporation of different aromatic units into the system. A variety of chromophores intercalated with fluorene has been reported, such as phenylene, naphthalene, anthracene, stilbene, cyanovinylene, thiophene, bithiophene [245] pyrazoline, quinoxaline, 1,2-cyanostilbene, pyridine, and carbazole [220, 246, 247].

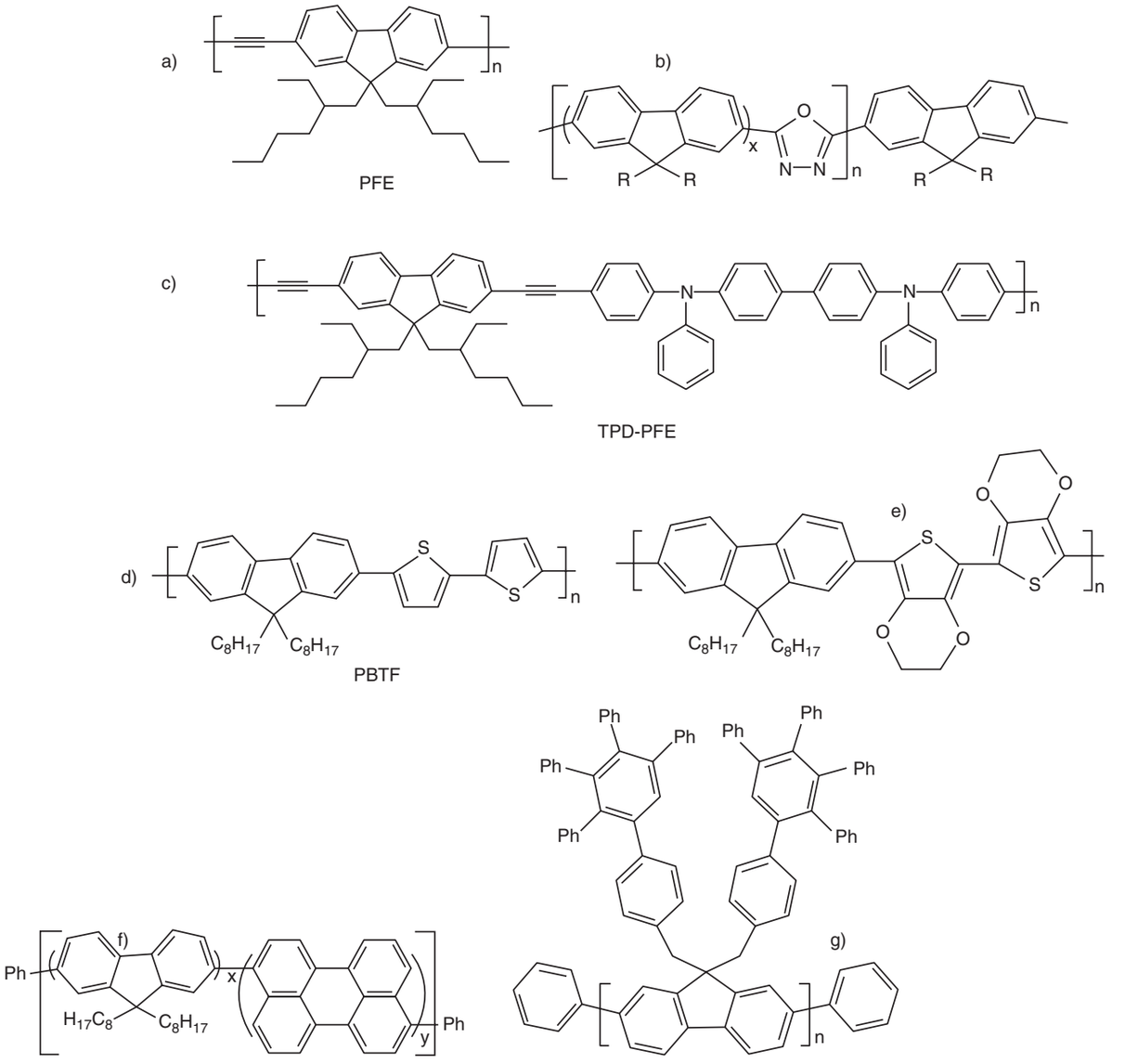

FIGURE 47.13. Examples of various fluorene based polymers. (a) Fluorene copolymer with triple bonds, poly(2,7-9,9-di-2-ethylhexylfluorenylene ethynylene); (b) alternating copolymers of 9,9-dioctylfluorene and oxadiazole; (c) copolymer containing the electron-accepting moiety 2,7-diethynylfluorene and the electron-donating moiety tetraphenyl diaminobiphenyl (TPD); (d) poly[2,20-(5,50-bithienylene)-2,7-(9,9-dioctylfluorene)] (PBTF); (e) poly[2,20-(5,50-di(3,4-ethylenedioxythienylene))-2,7-(9,9-dioctylfluorene)] (PdiEDOTF); (f) polyfluorenes with perylene groups in the main chain; (g) a dendronized polyfluorene.

Figures 47.14 and 15 show the Yamamoto and the SCP routes to synthesize fluorene-based copolymers, respectively. Well-defined monodisperse oligomers were prepared via SCP to access the effect of conjugation length on photoluminescent properties of polyfluorenes [248]. The Yamamoto route was also used to prepare 9-di-hexyl substituted oligofluorenes, containing 3–10 repeating units. The effective conjugation length was estimated to be 12 bonded fluorene units, by extrapolation of spectral data [249]. Substituted oligofluorenes in which the fluorene units alternate with triple bonds, namely oligo(9,9-dihexyl-2,7-fluorene ethynylene)s, demonstrated strong EL, and their effective conjugation length was calculated to be around 10 fluorene units (Fig. 47.13(a)) [250]. Devices with fluorene polymers appear to have electrons as the majority carriers and their performance is notably improved when modified with an appropriate HTL. Hole transporting moieties such as tertiary amines and TPD [251] have been incorporated to polyfluorenes in attempts to optimize LED performance. The HOMO levels of fluorene-based poly(iminoarylene)s (∼−5.1 eV) were close to the work function of ITO, and their use as buffer layers has been suggested (buffer layers are inserted

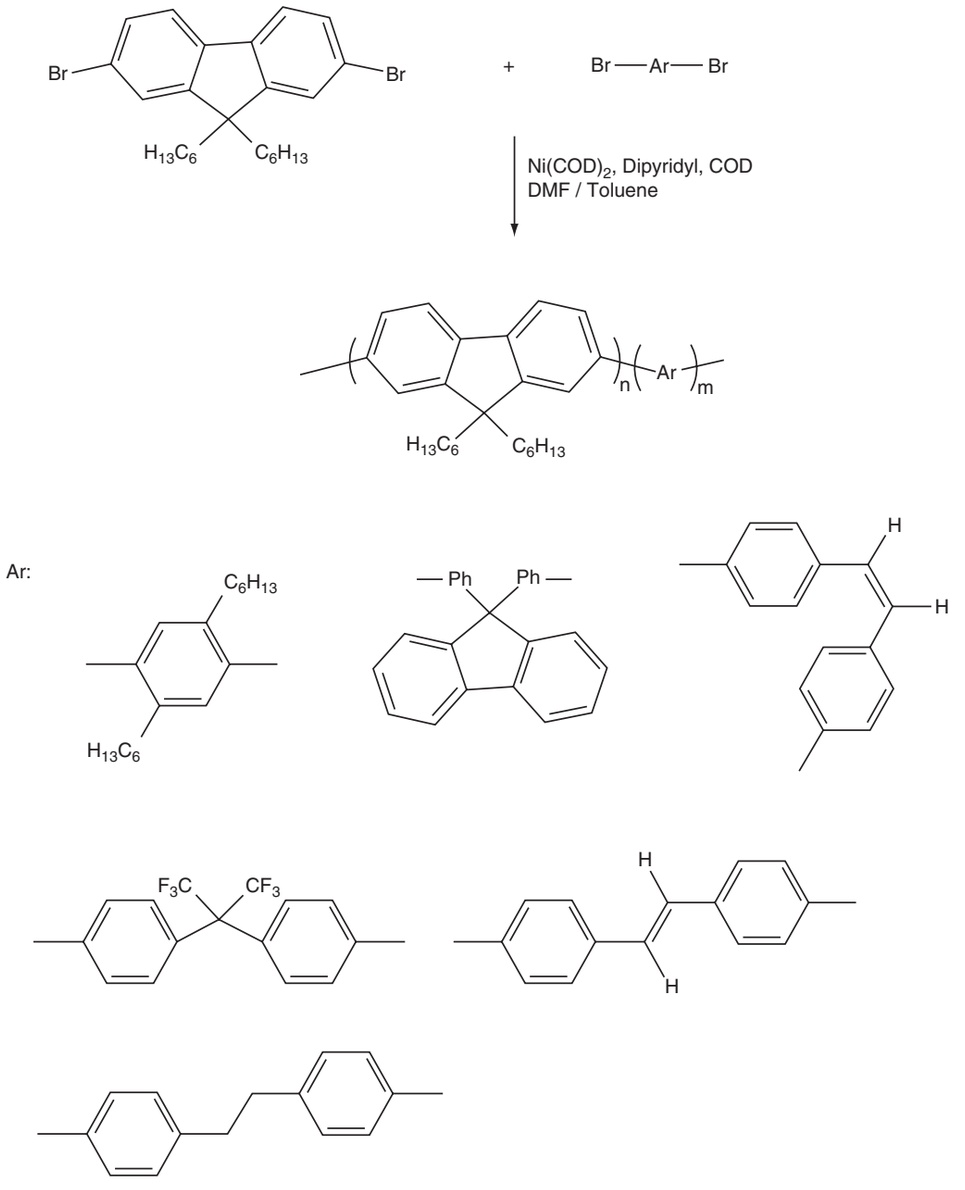

FIGURE 47.14. The Yamamoto route to polyfluorene based copolymers: nickel mediated coupling of 2,7-dibromo-9,9-dialkyl fluorene and various dibromoarenes.

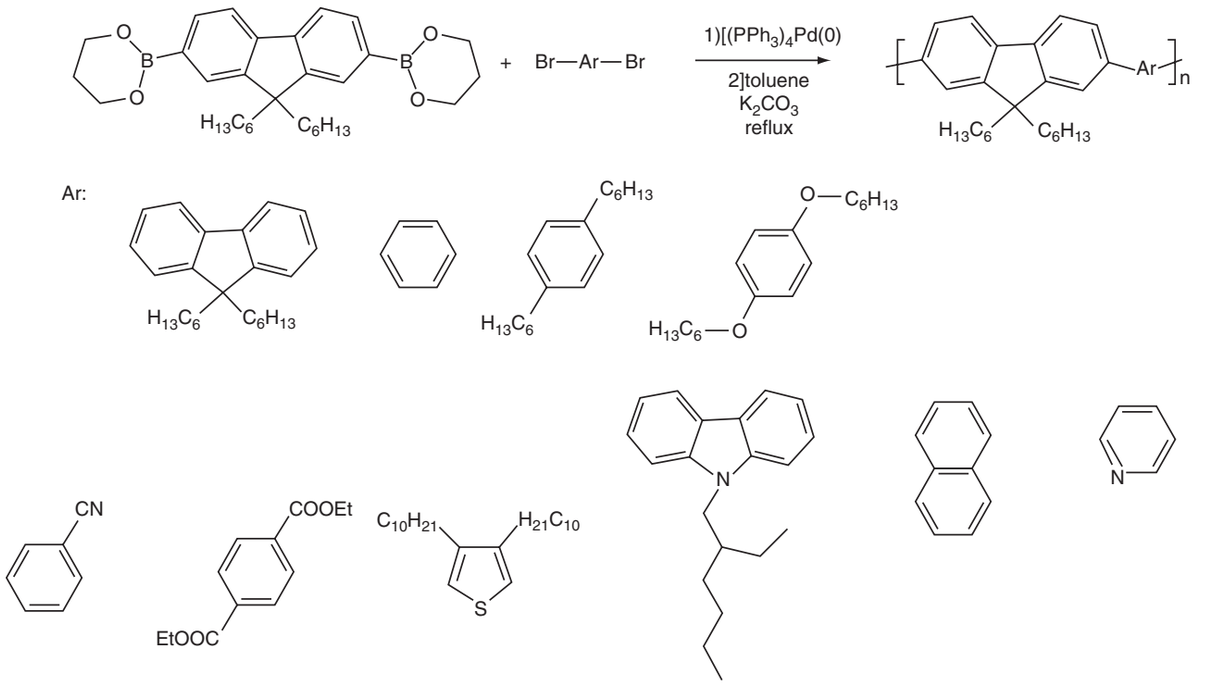

FIGURE 47.15. The SCP route to fluorene-based alternating copolymers: tetrakis(triphenylphosphine)palladium mediated condensation 9,9-dialkylfluorene-2,7-bis(trimethylene boronate) and various dibromoarenes.

between ITO anode and HTLs, as TPD). On the other hand, the incorporation of the electron withdrawing 1,3,4-oxadiazole units brought the electron affinity of the copolymers close to the work functions of Ca. These structures, shown in Fig. 47.13(b), prepared via the SCP, contained the oxadiazole evenly dispersed in the main chain, at every one, three, or four 9,9-dioctyl fluorene mers. All copolymers fluoresced in the blue range with quantum yields of about 70% in solution [252]. The combination of donor and accepting moieties in fluorene-based structures has been accomplished by alternating TPD (electron donating) with 2,7-diethylhexyl fluorene or diethynylfluorene units (electron donors), as shown in Fig. 47.13(c). A fluorinated copolymer formed by alternating mers of [2,3,5,6 tetrafluoro-1,4 phenylene] and [9,9′-dihexyl-2,7 fluorene] emitting blue light with low turn on voltages, showed a superior performance to that of the nonfluorinated analog copolymer and of the corresponding poly(9,9′dihexyl-2,7 polyfluorene) homopolymer [253]. An alternating polyfluorene with low bandgap segments has been designed and synthesized aiming to tune the emission. The low bandgap segment consists of an electron acceptor (thiophene, A), fenced by electron donors (benzodiathyazole, D). This D–A–D configuration lead to a partial charge transfer in the polymer backbone, and thereby a low bandgap (1.3 eV) [254]. The same approach was used by incorporating an analog of the red emitting dye DCM [(4-phenylamino)vinyl) pyran-4-ylidene-malononitrile] as a comonomer into the polyfluorene backbone. The emission was in the range 573–620 nm (greenish-yellow to red). DCM dye has an electron-deficient 2-pyran-4-ylidene malononitrile (PM) group and an electron-rich aromatic amine group, so both the absorption and emission show a red region because of the effect of charge transfer from triphenylene (TPA) to the PM group [255].

Another fluorene copolymer containing the luminescent dye [4-dicyanomethylene-2-methyl-6-4*H*-pyran (DCM) as acceptor compound was irradiatiated with UV light in the presence of gaseous trialkylsilanes. This reagent selectively saturates the C = C bonds in the DCM comonomer units while leaving the fluorene units essentially unaffected. As a result of the photochemical process, the red electroluminescence of the acceptor compound vanishes, and the blue-green electroluminescence from the polyfluorene units is recovered. Compared with previous processes based on polymer blends, this copolymer approach avoids problems associated with phase-separation phenomena in the active layer of OLEDs [256].

Orange-red emission was also seen in single layer devices of a series of conjugated copolymers of fluorene and 2- [2, 6-bis(2-arylvinyl)pyridine-4-ylidene]-malononitrile [257]. Another kind of red-emitting polyfluorenes with high electron affinity was reported, namely 9,9-dihexylfluorene and diketopyrrolopyrrole [258]. The Foerster-type energy transfer was efficiently used to tune the solid-state emission color of fluorene based copolymers bearing perylene dyes as end groups or side chains, as shown in Fig. 47.13(f). The emission coming almost exclusively from the perylene dyes could be tuned from yellow-green (558 nm) to red (675 nm)

[259]. Color tuning to the deep-red and NIR region was achieved by incorporating a selen-containing heterocycle, benzoselenadiazole, a selenium analog of benzothiadiazole in different compositions, resulting in a significant red shift in comparison with its sulfur analogue [260]. The abundant literature in polyfluorene and derivatives show that nowadays it is possible to tune the emission of polyfluorene derivatives from bluish-violet to deep red and near infrared [261].

One problem with polyfluorenes is the occurrence of an undesired low-energy band at 500–600 nm in the photo- and electroluminescence spectra of the pristine polymer or after annealing or the passage of current. The low-energy green band limits the emission efficiency and damages the blue color purity and stability as well. Two opposite points of view on the origin of this green emission have been reported. According to the first, the green emission is attributable to the interchain aggregates and/or excimers. Consequently, dendronization, introduction of spiro- or crosslinks, substitution with bulky side groups such as tetraphenylthiophene, blending, and the introduction of disorder units such as carbazole, pyridine, and thiophene have been applied to suppress intermolecular interaction [262]. The second point of view states that the green emission band is caused by keto defects of polyfluorenes, which are generated during the handling of the materials in air, or by a reaction with residual oxygen over the course of photophysical experimentation. Certain authors have proposed that the origin of the green-emission band stands on the fluorenone moiety and contradicted experimentally the assumption that intermolecular aggregates or excimers are involved. A series of well-defined 9,9′-dihexylfluorene-*co*-fluorenone copolymers with various fluorenone contents and a set of monodisperse oligofluorenes in the chain center have been prepared to elucidate the exact origin of the low-energy emission in polyfluorenes. On the basis of the steady-state photoluminescence (PL) and PL decay dynamics of the fluorenone-containing oligomers and copolymers both in dilute solutions and in thin films, the origin of the controversial low-energy emission band was attributed to the interaction between intrachain fluorenone moieties instead of the intermolecular aggregates or excimers. It was also proposed that a fluorene pentamer with a central fluorenone unit would be more appropriate to represent the actual chromophore responsible for the green emission in the copolymers [263]. Nevertheless the question remains still controversial. The introduction of 9-hexylcarbazole and 9-dimethylaminopropylcarbazole moieties into polyfluorene chain was claimed to effectively prevent excimer formation in the polymers [264], With the same idea 9,9-dihexylfluorenyl was inserted as a pendant group in a chain of poly(biphenylene vinylene). The insertion brought about steric interactions between adjacent rings, reducing conjugation length, but at the same time inhibited the formation of excimers. The polymer showed bright and stable blue emission [265].

Miller and co-workers at IBM have managed to overcome the low-energy emission by incorporating anthracene units which show stable blue emission even after annealing at 200°C for 3 days [266]. Mullen *et al*. [267] at the Max-Planck Institute in Germany produced nonaggregating polyfluorenes by the insertion of dendron side chains, as shown in Fig. 47.13(g) [268], giving a polymer with pure blue emission, as the bulky side chains do not cause distortion between the fluorene units. Recently, dendritic structures were attached to polyfluorenes with further addition of a low percentage of surface-modified semiconductor nanoparticles [269]. Starlike materials tethered to polyfluorene derivatives emitting blue, green, or red light were developed. Polyhedral oligomeric silsesquioxanes were incorporated into the center core of the derivatives to enhance thermal stability and reduce linear aggregation [270]. The optical properties of a series of light-emitting hyperbranched polyfluorenes through 1,3,5-substituted benzene crosspoints were investigated. With increase in crosspoint density, the emission color of the PEDOT-containing LEDs shift from green to violet and showed higher EL efficiency due to the effective exciton confinement and the reduction of intrachain or interchain exciton annihilation [271].

A series of electron-deficient, oxadiazole-, quinoline-, quinoxaline- and phenylenecyanovinylene-containing copolymers bearing ethyl hexyl in the fluorene unit was developed. These materials possess low-lying LUMO energy levels (−3.01 to −3.37 eV) and low-lying HOMO energy levels (−6.13 to −6.38 eV), with sharp blue emission, and may be promising candidates for electron transport-hole-blocking materials in LED fabrication. The film emissions were only 7–11 nm red shifted in comparison with the solution emissions, indicating that excimer formation was suppressed. This was explained in terms of the prevention of molecular stacking by the presence of sterically demanding ethyl-hexyl substitutions at the fluorene unit [272]. The formation of a network is a useful strategy in the obtainment of various performance improvements in polyfluorenes. For example, the attachment of styryl end groups, via reaction of the bromo-terminated polymer with bromostyrene in a Yamamoto coupling, allowed the deposition of a crosslinkable layer through the thermal polymerization of the terminal styrene groups. Apart from the added advantage of further casting other layers, the immobilization of the chains leads to suppression of intermolecular excited state interactions, hampering the ability to π stack [273,274]. Another kind of fluorene-containing structure consisted of conjugated polyfluorene/poly(*p*-phenylenevinylene) copolymer containing the pendant bis(4-alkoxyphenyl) groups in the C-9 position of every alternating fluorene unit. The main advantage of the use of an extended 9,9-bis(4-hydroxyphenyl)fluorenyl core in the polymerization reaction is that the insertion of a rigid phenylene spacer between the large side chain and the polymer backbone may lead to a more efficient shielding effect on the polyfluorene main chain, which would suppress the formation of aggregates/excimers while

not blocking the reaction sites of the macromonomer from the palladium catalyzed polymerization reaction. The chain stacking, however, was not completely avoided, and a green electroluminescence was observed [275].

Energy migration has been explored in polyfluorenes to enhance emission intensity. For example, devices of poly (9,9-dioctylfluorene) mixed with the amine-substituted *co*-polyfluorene poly(9,9-dioctyl-fluorene-*co*-bis-*N*,*N*′-phenyl-1,4-phenylenediamine), showed a blue emission with a luminance of 1550 cd/m^2 and a maximum external quantum efficiency of 0.4%, much larger than the original homopolymer. White-light-emitting devices have been demonstrated with new single-component fluorene-acceptor copolymers with three emitting units: blue-emitting 9,9-dihexyl-fluorene, green emitting quinoxaline (or yellow-emitting 2,1,3-benzothiadiazole), and red-emitting (thieno [3,4-b]-pyrazine) units in the same chain. The energy-transfer between the emitting moieties suggests the white-light emission could be obtained by a relatively small fraction of the acceptor moieties. The EL devices typically had a luminance of 1,870 cd/m^2 at 10 V. The CIE coordinates of this device are (0.33, 0.34), which are almost identical to the standard white emission, and they exhibit insignificant changes in driving voltages. The results suggest that very bright and highly stable white-emission devices could be achieved by single-component fluorene-acceptor copolymers with three emitting moieties as an emissive layer [276].

A recent aspect of the research in polyfluorenes is related to supramolecular ordering of these conjugated polymers by making rod-coil block copolymers. The rod-like conjugated polyfluorene was end capped on one or both ends with polyethylene oxide, forming di- or triblock copolymers. The solid-state fluorescence spectra of these materials had better resolution than the homopolymer, indicating an enhanced number of well-ordered rods in the films and an additional increase in long wave emission. Multilayer fluorene-based LEDs were reported by a Japanese group [277] where a three layer device having the structure ITO/*N*,*N*′-bis (2,5-ditertbutylphenyl)-3,4,9,10-perylene dicarboxamide (BPPC)/*N*,*N*′-diphenyl-*N*,*N*′-(3-methylphenyl)-1,10-biphenyl-4,40-diamine (TPD)/poly(9,9-dihexylfluorene) (PDHF) was able to emit either red or blue by changing the polarity of the applied voltage. TPD is a material mainly used for hole transport, BPPC is a red emitter, and the polymer emits in the blue region. The particular set of gap conditions in this system allowed the emission of blue light under positive bias conditions (ITO anode, AI cathode) and emission of red light under negative conditions. Furthermore, the device can be driven with an AC field and the emission color can be gradually modulated by changing the frequency of the applied AC field. Placing a small amount of surface-tailored CdS nanoparticles into the dendritic structure of copolyfluorene substantially improves the efficiency of the polymer's light emission, as well as the purity of the emitted light. One possible explanation for the enhancements in PL and EL may be the reduction in the concentration of interpolymer excimers, i.e., the CdS nanoparticles caused an increase in the interpolymer chain distance.

An intermediate structure between PPP and polyfluorene has been developed, the poly(2,8-indenofluorene). This blue emitting polymer is stable up to 380°C, and shows thermotropic LC behavior at high temperatures (250–300°C) making it a good candidate as the active material in polarized LEDs [278].

Models of spin statistics predict that the electron–hole recombination event should produce three times as many triplets as singlets, and this has been confirmed experimentally for electroluminescent devices. Considerable effort has been devoted nowadays to attach phosphors covalently to a conjugated polymer backbone so as to allow efficient energy transfer between polymer and phosphor. Electrofosforencesce seems to be the new trend to maximize LED performance. One exemple is the red Electrofosforescent Light Emiiting Diode based on iridium complexes with the [lr(btp)2(acac)] fragment (where btp is 2-(2′-benzo [*b*]thienyl)pyridinato and acac is acetylacetonate). The fragment was attached directly or through a $-(CH2)_8-$spacer chain at the 9-position of a 9-octylfluorene host. The dibromofunctionalized spacerless or octamethylene-tethered fluorene monomers were chain extended by Suzuki polycondensations using the bis(boronate)-terminated fluorene macromonomers in the presence of end-capping chlorobenzene solvent to produce the statistical spacerless and octamethylene-tethered copolymers containing an even dispersion of the pendant phosphorescent fragments [279].

47.8 SILICON-CONTAINING POLYMERS

The interest in silicon-based polymers resides in the delocalization of the σ electrons over a Si backbone providing electronically analogous properties to the π-conjugated polymers. Polysilanes are σ-conjugated polymers with a one-dimensional (1D) Si chain backbone and organic side chain substituents. Progress in understanding their electronic structure derived from both theoretical and experimental studies has revealed that they are quasi-1D semiconductors with a direct and wide bandgap (∼4 eV), and that the σ-conjugated electronic structure typically observed in silane high polymers appears in Si chains with more than 20–25 Si units [280]. Polysilanes exhibit photoconductivity, intense near-UV absorption, and strong PL of small Stokes shift and high hole mobility (on the order of $10^{-4}cm^{-2}\ s^{-1}$) [281]. Near-UV or UV emitting LEDs of diaryl, dialkyl, monoalkyl-aryl polysilanes have been reported [282–285], and the bandgap energies tend to shift to lower values based on the size of substituents with aromatic side groups [286]. The emissions in polysilanes have been attributed to the $\sigma-\sigma^*$ transitions of 1D excitons in the Si backbone. Nevertheless, PL studies of poly(methylphenylsilane) demonstrated the existence of another emission due to a charge transfer state from the intrachain σ to pendant π^* groups which appear in

larger wavelengths (400–500 nm) [287]. Being typical p-type semiconductors, polysilanes cannot transport electrons, and for this reason the incorporation of electron transporting groups with emitting properties seemed to be an interesting way of combining good properties [288].

Polymethyl phenyl silane (PMPS), poly [bis(*p*-*n*-butyl-phenylphenyl)silane] (PBPS), and poly(2-naphthyl phenyl silane (PNPS) are examples of polysilanes, shown in Fig. 47.16(a). A blue emission (480 nm) with a PL of 87% was achieved with a poly(methylphenylsilane) containing anthracene units in the polymer backbone [289].

Silicon-containing PPV derivatives have been developed in which the silicon unit acts a spacer to improve solubility, film forming characteristics, and confine conjugation, in analogy of the conjugated–nonconjugated block copolymers with an aliphatic spacer. While the aliphatic segments as spacers can act as a barrier to injection and mobility of the charge carriers, resulting in higher threshold voltages, the silicon units with an aromatic or flexible group are able to produce the same spacer effects with low operating voltages [290]. It has been argued that the participation of the d-orbital of the Si atom could be assisting to increase the

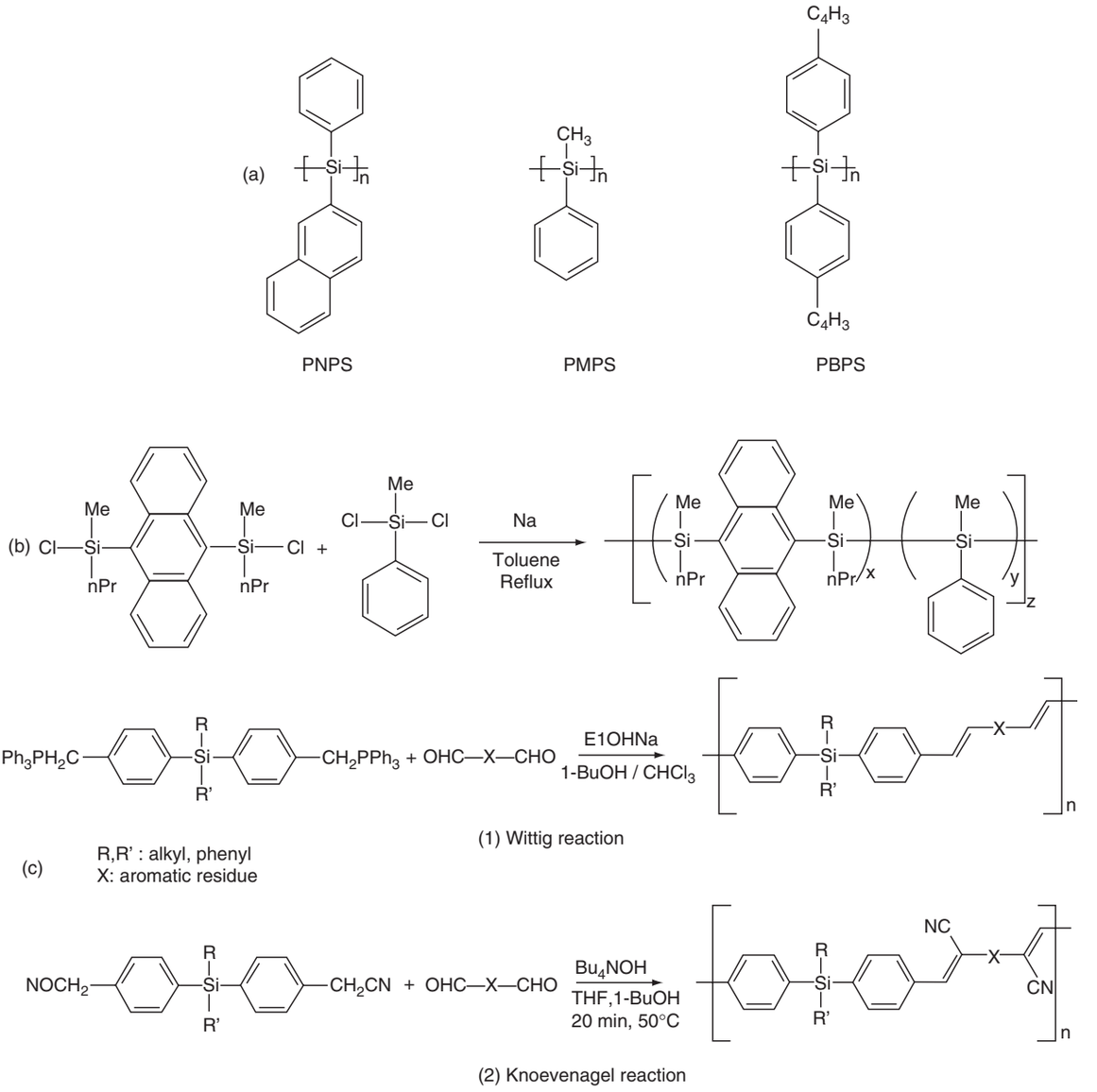

FIGURE 47.16. Examples of (a) polysilanes, where the main chain is made up of Si–Si bonds: poly(phenyl methyl silane) (PMPS), poly(naphthylmethyl silane) (PNPS), poly[bis(*p*-*n*-butylphenyl)silane] (PBPS); (b) synthetic route to poly(methyl phenyl silane) containing anthracene units; (c) copolymers with Si inserted between *p*-conjugated blocks: Wittig (top) and Knoevenagel (bottom) routes.

effective conjugation length, thus facilitating charge mobility [291], although previous theoretical work has demonstrated that Si bonds break effectively the π-conjugation [292]. A variety of PPV-related structures such as copolymers of diphenyl/dibutylsilane [293], dibutyl, butyl/methyl, diphenyl silanes [294] with PPV and alkoxy PPV [295] have been reported, in which the organosilicon groups are used as spacers [296]. Some representative examples are shown in Fig. 47.16(b). The EL spectrum of the diphenyl-substituted copolymer (SiPhPPV) gave the highest peak (450 nm) when the operating voltage of 9 V was applied. With 12 V applied bias a strong white color was emitted due to additional emissive bands. This threshold voltage was further decreased to 7 V by the introduction of a CN group into the double bond of PPV (Fig. 47.16(c)) [291]. Similar results were obtained in alternating copolymers of silane and carbazolyl or fluorenyl derivatives, peaking around 440–476 nm with operating voltages of 6–12 [297]V. In contrast to alkoxy groups, the lack of electron donor capacity (and consequent red shifting of the emission) of alkylsilicon groups has suggested the introduction of these groups as ramifications in EL polymers, improving processing characteristics [298,299].

One of the unique properties of polysilanes is the SiSi bond scission of the backbone chain under UV radiation. In the presence of oxygen it is accompanied by a SiOSi bond formation that leads to the conversion into an insulator, with no hole transport ability. Using this property, a patterning-image-display electroluminescent device was built. Before turning on the voltage, the anthracene-containing polysilane LED was irradiated in order to pattern an image onto the emission area, from the glass substrate side. Blue patterned light was obtained, corresponding to the negative photomask used [289,300].

47.9 NITROGEN-CONTAINING CONJUGATED POLYMERS

47.9.1 Pyridine-Containing Conjugated Polymers

Due to their strong electron-acceptor character, nitrogen-containing groups of various kinds have been incorporated to conjugated polymeric structures. The most extensively studied structures carry the pyridine moiety, in homopolymers (poly(2,5-pyridine), poly(3,5 pyridine)) [301,302], in PPV-type structures (poly(*p*-pyridylene vinylene))s [302,303], in copolymers with PPV (poly(phenylene vinylene pyridylene vinylene)s) or in p-phenylene derivatives [304,305]. Alternating pyridine-based backbone copolymers with substituted phenylene and fluorene units have been reported for tunability of electronic properties with enhanced stability [306].

As compared to phenylene-based analogues, one of the most important features of pyridine-based polymers is the higher electronic affinity. As a consequence, the polymer is more resistant to oxidation and shows better electron transport properties. The higher electron affinity enables the use of relatively stable metals such as Al, Cu or Au, or doped polyaniline as electrodes [302,307]. The pyridine-containing conjugated polymers are highly luminescent, especially the copolymers with phenylene vinylene. The solubility of polypyridines in organic solvents represents another advantage as compared to PPV for device fabrication. The ability to protonate and quaternize the nitrogen makes it possible to manipulate the electronic structure and thereby the emission wavelength [305,308]. The synthesis of poly(2,5-pyridine) and poly(3,5-pyridine) is straightforward: one step coupling polymerization of the 2,5 (or 3,5) dibromopyridine using a metal catalyst [309]. It was proposed that two blue electroluminescent devices emitting at 420 and 520 nm can be constructed by varying the degree of protonation. Another example illustrating the possibility of tuning spectroscopic properties by protonation of the lone pair of electrons of the pyridine ring is the red shift observed in the fluorescence and EL emission of poly(2,5-pyridylene-*co*-1,4-(2,5-bis(ethylhexyloxy)phenylene)[310]. Excitation profiles show that emission arises from both protonated and non-protonated sites in the polymer chain. Protonation is also accompanied by intramolecular hydrogen bonding to the oxygen of the adjacent solubilizing alkoxy group, providing a new mechanism for driving the polymer into a near planar conformation, extending the conjugation and tuning the emission profiles. The PL and EL spectra of copolymers of 1,4-phenylene vinylene and 2,6-pyridylene vinylene(*co*(2,6-PyV–PV)) could be tuned, respectively, in function of the excitation wavelength of the light and the external voltage applied in LED devices. The incorporation of the pyridine moiety increased the EL efficiency of the devices by a factor of 5 in relation to PPV [302,308,311]. A series of poly(2,5-dialkoxy-1,4-phenylene-alt-2,5-pyridine)s in which the [alkoxy phenylenepyridyilene] structural unit acts as donor–acceptor pair was synthesized via a SCP [304]. The electron affinity of these polymers is ca. 2.5 eV, comparable to that of copolymers containing oxadiazole moieties. The electron-withdrawing pyridinylene groups were able to lower the LUMO energy in such a way that these polymers may have similar electron injection properties as typical oxadiazole-containing electron transport polymers, when they are used as active materials in LEDs. The Wittig and Wittig–Horner reactions have been employed to prepare copolymers containing bipyridine and silicon units. The organosilicon moiety improves the solubility and limits the conjugation length [312]. Recently, the bipyridine moiety linked to metals as iridium was used to fabricate blue phosphorescent LEDs with high emission intensity [313].

47.9.2 Oxadiazole-Containing Conjugated Polymers

One of the best electron transport structures is the oxadiazole group, as noted above. The covalent attachment of the PBD moiety to an emitting polymer (Fig. 47.4(b)), was a natural development in LED technology, avoiding the

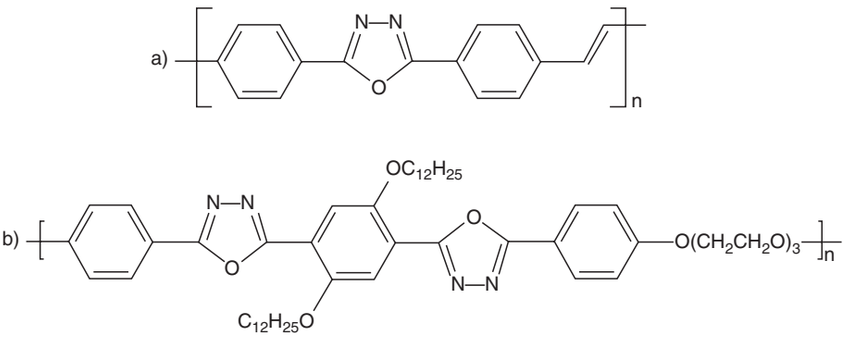

FIGURE 47.17. Oxadiazole-containing EL polymers. (a) Poly(2,5-diphenylene-1,3,4-oxadiazole)-4,40-vinylene; (b) alternating oxadiazole-*alt*-alkoxyphenylene and a aliphatic spacer.

problems with the deposition of an additional layer in diode construction and the anticipated phase separation after film preparation or under operating conditions. Some examples of oxadiazole-containing EL polymers are given in Fig. 47.17. Among the various examples found in the literature one can cite the use of oxadiazole incorporated in the main chain [168,314–316] or as a pendant group [168,214,317–320].

In the first case the oxadiazole moiety was used as a comonomer in chromophoric imides [168,321], copolymers containing thiophene sequences [322], or in a PPV type main chain [168,267,323]. Synthetic approaches for the oxadiazole-containing polymers were the Heck reaction or via the formation of a polyhydrazide precursor [324]. Oxadiazole moieties linked to PPV [168,325], alkyl-PPV, and polythiophene chains as pendant groups with improved EL efficiencies due to higher electron affinity, better injection, and transport properties have also been reported [326]. The insertion of electron-transporting groups in p-type polymers brings about bipolar carrier transport ability. The combination of donor–acceptor groups in the same chain in attempts to achieve balanced electron–hole injection and transport avoiding the use of intermediate transport layers has been widely explored, such as the combination in the same chain. Due to their strong electron-acceptor character, oxadiazole and PPV [158,326] or oxadiazole and oligothiophenes [327] have been reported, for example for PPV type chains [169,326,328] or other chromophores like naphthalimide [329], fluorene [330], anthracene, triphenyl amine.

47.9.3 Polyquinolines and Polyquinoxalines

Polyquinolines and polyquinoxalines are n-type (electron transporting) polymers and therefore offer alternative EL device engineering in conjunction with the extensively studied p-type (hole transporting) polymers such as poly(*p*-phenylene vinylene)s, polyphenylenes, and polythiophenes. A variety of polyquinolines [331,332] and polyquinoxalines [333] has been reported in the literature, acting as the active emitting layer [331,334,335] or as the transport layer [336–338] in LEDs. Figure 47.18 shows some representative examples of these emitting and electron-transporting polymers. The increased electron deficiency of the quinoxaline ring due to additional imine nitrogen, compared to the quinoline ring, enhances the electron-accepting ability of conjugated polyquinoxalines, thus improving electron transport protonated by means of acidic solvents, intense blue emission was observed at 450 nm. When the positive charge on the nitrogen atom of the quinolines reached a critical value, intermolecular electrostatic repulsion prevented the aggregation, and the emission spectra were those of the isolated chain. The nonprotonated forms formed LC structures, which formed excimers with emissions in the 550–600 nm range. pH-Tunable PL was also demonstrated in poly(vinyl diphenylquinoline) with emission maxima varying from 486 to 529 nm (blue to green). Intramolecular excimer emission was observed in acidic solutions but not in neutral solutions or thin films of the polymer. The polymer, which was obtained from a modification of polystyrene, was introduced as a prospective high T_g, electron transporting counterpart of the hole transporting side chain PVK. The electron transporting properties of copolymers bearing fluorene and quinoline units with conjugation confinement varied with the chain rigidity and conjugation length and proved to be useful in double and triple layer devices [339]. A series of polyquinolines containing 9,9′-spirobifluorene was recently reported. The two fluorene rings were orthogonally arranged and were connected via a common tetracoordinated carbon. The incorporation of the piro moiety provided good solubility due to a decrease in the degree of molecular packing and crystallinity while imparting a significant increase in both Tg and thermal stability, by restricting segmental mobility. Polymers incorporating bis(phenylquinoline) and regioregular dialkylbithiophene in the backbone showed substantial enhancement in device performance under ambient air conditions (1.4% external quantum efficiency, 2,170 cd/m^2) in bilayer MEH-PPV LEDs [340] properties [334,335]. Polyquinolines are

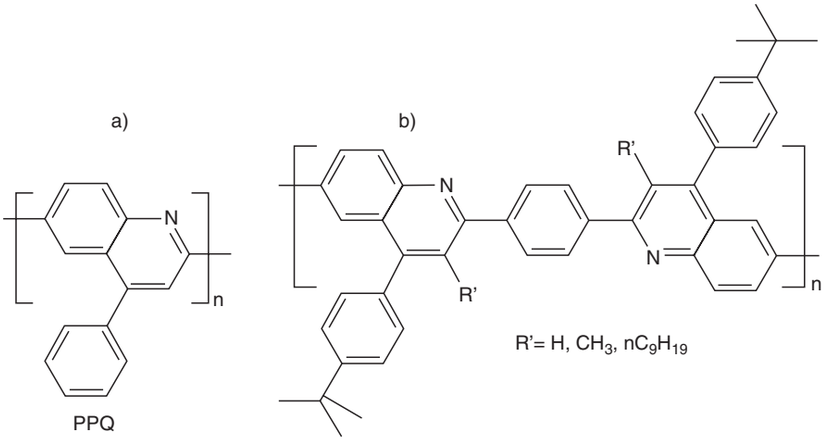

FIGURE 47.18. Examples of EL polyquinolines.

usually prepared by the acid-catalyzed Friedlandler condensation of bis(*o*-aminoketone)s and bis(ketomethylene) monomers, have good mechanical properties and high thermal stability, and can be processed into high quality thin films. A new synthetic route to organic solvent-soluble conjugated polyquinolines incorporating bis(4-alkylquinoline) units through a new A–A monomer was used to prepare 3,3′-dinonanoylbenzidine copolymers, poly(2,2¢-arylene-4,4′-bis(4-alkylquinoline)) [341].

Variations in the polyquinoline backbone linkage (R) and pendant side groups provided a means to regulate the intramolecular and supramolecular structures which in turn enabled tuning of the light emission from blue to red.

Studies of supramolecular photophysics of selfassembled block copolymers bearing styrene–polyquinoline sequences demonstrated evidence of J-aggregation in well-defined, ordered structures such as micelles and vesicles. The polymers represent a novel class of functional luminescent materials [342]. In a recent contribution, Jenekhe reported a detailed study on voltage-tunable multicolor emission-bilayer LEDs combining PPV (as typical p-type layer) with a series of polyquinolines, polyanthrazolines, polybenzothiazoles, and a poly(benzimidazobenzophenanthroline) ladder, addressing the influence of the polymer–polymer interface in the diode efficiency and luminance and showing that its electronic structure plays a more important role than the injection barrier at the cathode/polymer interface [343].

47.9.4 Carbazole-Containing Conjugated Polymers

Due to its electro- and photoproperties, the carbazole molecule has been used in various technological applications [344,345]. Polymers based on this compound have been used to enhance LED emission and also for color tuning. In Partridge's study of EL of dye doped PVK systems [346–348], the hole transport properties of this polymer were demonstrated. Devices in which the emitting layer was formed by PVK blended with other polymeric systems have shown remarkable increases in luminescence efficiency, as compared to those in which PVK was not incorporated. As an example, the blue emitting device with the ITO/polymer blend/Ca configuration made of poly(*p*-phenyl phenylene vinylene) (PPPV) blended with PVK showed a quantum efficiency of 0.16% which is a good result for a blue emitter [349]. As in all cases of PVK blends, it was observed that there is an optimum molar ratio between the emitting polymer and PVK for the increase in EL intensity. If the diode is doped excessively with PVK the conductivity can be reduced, when the other polymer is more conductive than PVK itself. Apart from the homopolymer, the carbazole moiety can be incorporated in polymer chains as part of the main chain, like poly(2,5-dihexylphenylene-*alt*-*N*-ethyl-3,6-carbazolevinylene), which was combined with an electron transporting oxadiazole-containing structure [350]. Alternating structures containing units of 2,5-bis-trimethylsilyl-*p*-phenylene vinylene, or 2-methoxy-5-(2-ethylhexyloxy)-*p*-phenylene vinylene with *N*-ethyl hexyl-3,6-carbazolevinylene or 9,9-*n*-hexyl fluorenevinylene were prepared via Wittig polycondensation. Among the four combinations the silyl-substituted carbazole copolymers presented the most interesting properties, for example, its EL quantum efficiency was 32 times higher than the MEH-PPV analog (film quantum efficiency was 0.81, one of the highest reported). The participation of the silyl group in the PL enhancement and also to the blue shift observed was attributed to its sterical hindrance and lack of electron donating ability as compared to alkoxy substituents [350]. Well defined carbazol-3,9-diyl based oligomer homologues were prepared by the Ullmann condensation and used for multilayer LEDs [351].

The hole conduction of the carbazole unit was studied by comparing polydiphenylacetylene derivatives without and with a carrier transport moiety as poly[1-(*p*-*n*-butylphenyl)2-phenylacetylene] and poly[1(*p*-*n*-carbazolylphenyl)-2-phenylacetylene], respectively. It was shown that hole mobility enhancement by the attachment of the carbazolyl side groups brings about a remarkable improvement in the EL devices. Recently carbazole-imide moieties combined with fluorene were used to prepare LEDs with a brightness of 14,228 cd/m^2, maximum luminous efficiency of 4.53 cd/A and maximum power efficiency of 1.57 lm/W [352]. A write-once read-many-times (WORM) memory device based on an acrylate polymer containing electron donating carbazole pendant groups, or poly(2-(9H-carbazol-9-yl)ethyl methacrylate) (PCz), was demonstrated [353]. Carbazole–pyrene-based compounds when blended to PVK afforded EL devices with green emission with luminance up to 1,000 cd/m^2 [354]. Semiladder poly(*p*-phenylene)s containing carbazole and fluorene moieties exhibited maximum luminescence of 5,500 cd/m^2 and maximum luminance efficiency of 0.556 cd/A in single-layer light emitting devices with pure-blue emission (λ_{max} 447 nm) [355].

A new type of electron-transporting polymer was reported as the first stereoregular polymerization of (*N*-*n*-octyl-3-carbazoyl)acetylene, initiated with a Rh norbornadiene catalyst. The resulting polymers were composed of amorphous *cis*-transoid isomers, called a columnar, with wide range of emitting colors [356].

Light-emitting alternating copolymers of 9,9-dialkylfluorene and *N*-hexylcarbazole with conjugated and δ-Si interrupted structures have been synthesized as an approach or the synthesis of nonaggregating optoelectronic polymers [357].

47.9.5 Other Nitrogen-Containing Conjugated Polymers

Other electron affinity enhancer nitrogen-containing heterocyclic groups include the triazole [358], bithiazole [359] and nonconjugated amino groups as substituents, such as =N(CH3,C6H13) attached to the ring in (poly(2,5-bis(*N*-methyl-*N*-alkylamino)phenylene vinylenes) [360]. In this case the nitrogen atom does not participate in the conjugation system, and its electron donor character provides a stronger donor effect to the amino substituent than the corresponding alkoxy substituents. As mentioned earlier (under transport layers), triamines have been used as hole transport materials. In a recent report, this class of compounds have shown emissive capacity as well, when inserted as pendant groups in conjugated backbones. Single layer devices fabricated from these copolymers can emit light ranging from yellow to bright red, depending on the aromatic units incorporated [361]. The attachment of carbazolyl groups as pendant groups grafted to a backbone as PMMA, which was blended with MEH-PPV, enhanced the emission four times when compared to that of the pure polymer [362]. Apart from hole transport ability, PVK can interact with low molecular weight compounds or polymers to form new emitting species as exciplexes [363], and consequently bring about a shift in the emission wavelength. In the case of PPPV/PVK [364] mentioned above, where PVK was used both as matrix and hole transport material, the EL spectra of the system tended to blue shift as compared to the respective pure PPP. It was speculated that this was caused by a change in molecular conformation or aggregation of the PPP in the PVK matrix. In blends of the conjugated–nonconjugated multiblock copolymer PPV derivative (CNMBC) with PVK, the EL blue shifted according to PVK increments in the blend. The new emission was attributed to an exciplex formed by the two polymers. As the composition of the blend changed from a PVK-poor to a PVK-rich ratio the emitted light changed from green to blue. Further blends of composition 97/3 (wt%) PVK/block copolymer yielded an EL spectrum with a single emission peak in the blue region different in location from either single component, whereas for a certain range of composition the new peak coexisted with those of the pure components. An exciplex where an excited PVK combines with ground state copolymer was proposed.

47.10 POLYACETYLENES AND POLYMERS WITH TRIPLE BONDS IN THE MAIN CHAIN

47.10.1 Polyacetylenes

Polyacetylene is the first conjugated polymer to exhibit a metallic conductivity. However, polyacetylene shows a very low PL efficiency [365]. Recently, in contrast, a number of good light emitting polyacetylene derivatives have been produced, covering the visible spectrum. The poor solubility of these rod-like structures with concomitant color tuning was addressed in three ways: by substituting the hydrogen atoms with alkyl or aryl groups as done in PPV, by means of copolymerization, or by a combination of both methods. In the first approach many of substituents were tried [366,367]. Monosubstituted polyacetylenes were often referred to as nonluminescent polymers, but the insertion of mesogenic pendants afforded intense blue emitting materials [368] as shown in Fig. 47.19(a). The emission observed from a series of alkyl and phenyl disubstituted polyacetylenes changed from blue-green to pure blue and the luminescence intensity was enhanced when the length of the alkyl side chain increased [369]. This effect was also observed in poly(3-alkylthiophene) and in PPV derivatives [370], indicating that the $\pi-\pi^*$ interband transition increases with the length of the side chain, and at the same time the diffusion rate of the excitons to quenching sites is reduced by the longer interchain distances. Examples of EL disubstituted polyace-

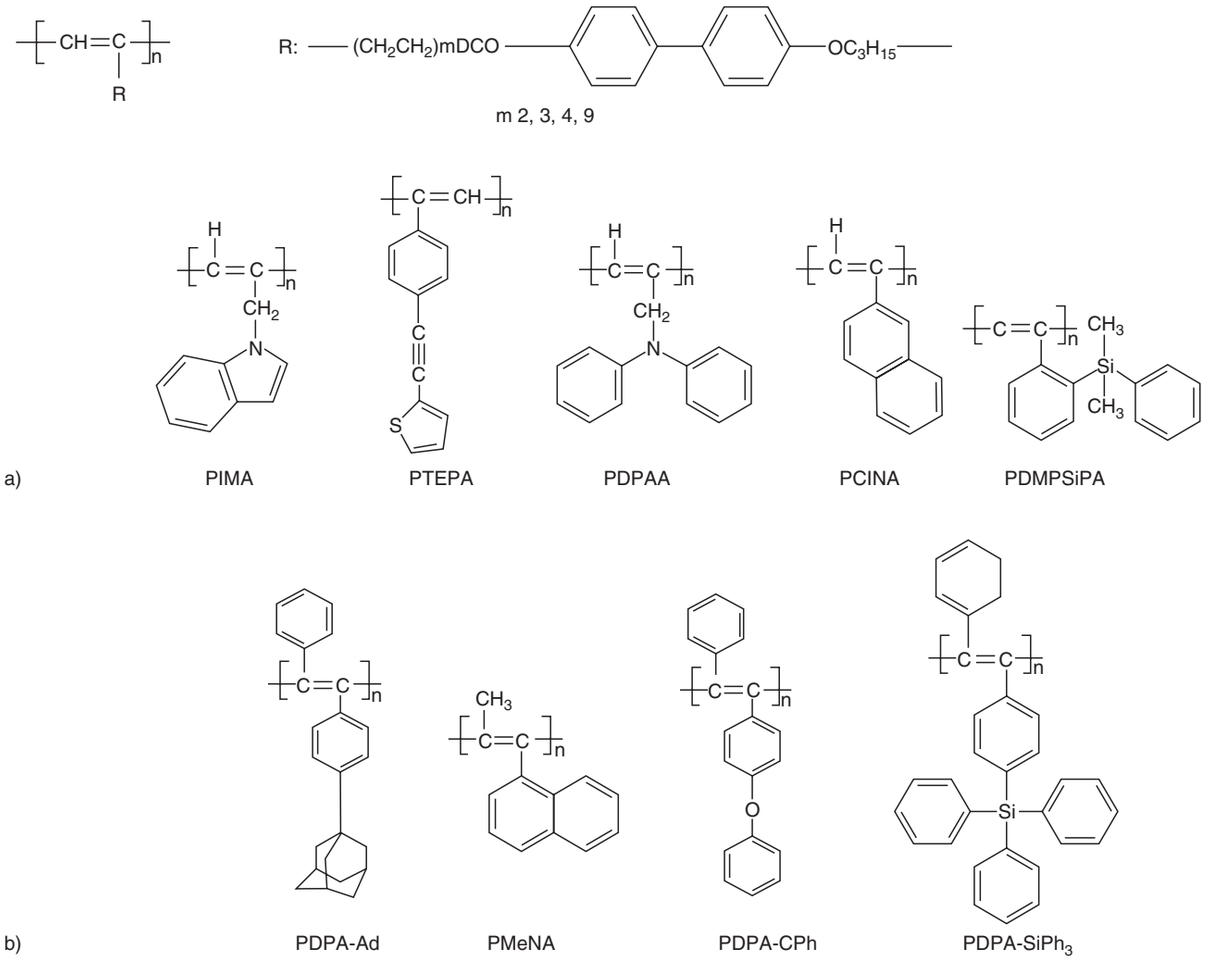

FIGURE 47.19. Examples of EL polyacetylenes. (a) Monosubstituted; (b) disubstituted. Reprinted with permission from Synth Met 1997;91:283. © 1997 Elsevier Science.

tylenes are given in Fig. 47.19(b). Aryl-substituted polyacetylenes were stable to 200°C in either air or nitrogen, according to thermogravimetric analysis. With the interest in combining the electrooptical properties of PPA and PCz in a CPN film, we have synthesized a series of substituted poly(phenylacetylene)s containing carbazole unit as side groups, which subsequently through. Electropolymerization or chemical oxidation resulted in a conjugated polymer network having both *inter*- and *intra*molecular crosslinkages between the pendant monomer units [371].

47.10.2 Poly(phenylene ethynylene)s

The HOMO–LUMO energy gap of some alkoxy substituted poly(phenylene ethynylene)s (ROPPE) is higher than that of the corresponding ROPPVs, indicating that introducing triple bonds in the main chain shortens the effective conjugation length. For example, poly(3,4-dialkyl-1,6-phenylene ethynylene) has a bandgap of 3.1 eV [372]. Poly(*p*-phenylene ethynylene)s showed a lower energy barrier for electron injection than for hole injection, in contrast with the PPV analogs. This is an important feature for cathode stability, since more stable metals can be used [373]. A high quantum efficiency was obtained with poly(2,5 dialkoxy-1,4-phenylene ethynylene) (ROPPE) in which the triple bond is equivalent to the double bond in poly(2,5-dialkoxy-1,4-phenylene vinylene) (ROPPV) [374]. Bright blue-green EL was observed from an LED made with the copolymer ROPPE and pyridine (Py) with AI/ROPPE–Py/ITO. In comparison with PPV it was suggested that the triple bonds in the chain were responsible for the blue shift and enhancement of the EL, due to the shortening of the effective conjugation length and effective confinement of the

excitons. However, the effects of the triple bonds were suppressed by the introduction of electron-rich moieties in the chain, such as in poly(2,5-dialkoxy-1,4-phenylene-diethylene-*co*-9,10-anthracenylene) (ROPPE–An). In this case the insertion of the 9,10-anthracenyl group caused a delocalization of the π-electrons and enhancement of interchain interactions [372,375].

Linear copolymers containing phenylene ethynylene linkages have been synthesized using precursor routes [376], inserting *m*-linkages [377] or aliphatic spacers [378,379]. In the precursor route, regular building blocks of *p*-phenylene, norbonadiene, and diethynyl benzene made up the soluble precursor, which was converted to a polymer with enyne units upon the release of cyclopentadiene through a retro-Diels–Alder pathway. The copolymer with phenylene with *m*-linkages made through a Heck-type route, using Pd as catalyst, displayed a PL four times stronger than that of the corresponding *p*-substituted analog. This synthetic method is very often employed in a general way in poly(arylene ethynylene)s chemistry [380]. PPE analogs obtained by copolymerization with di(2-octyldecyl)anthracene yielded stable blue and green emission without chain stacking [381].

REFERENCES

1. Bradley DDC. Synth Met 1993;54(1–3):401–15.
2. Kalinowski J. Electronic processes in organic electroluminescence. In: Miyata S, Nalwa S, editors. Organic Electroluminescent Materials and Devices. Japan: Gordon & Breach; 1997. p. 1.
3. Friend RH, Gymer RW, Holmes AB, Burroughes JH, Marks RN, Taliani C, Bradley DDC, dos Santos DA, Brë das JL, Lö glund M, Salaneck WR. Nature 1999;397:121–8.
4. Cacialli F. Phil Trans R Soc Lond Ser A— Math Phys Eng Sci 2000; 358(1765):173–92.
5. Cacialli F. Curr Opin Colloid Interf Sci 1999;4(2):159–64.
6. Segura JL. Acta Polym 1998;49(7):319–44.
7. Kraft A, Grimsdale A, Holmes AB. Angew Chem Int 1998;37(4):402–28.
8. Mori Y. Single layer organic electroluminescent devices. In: Miyata S, Nalwa S, editors. Organic Electroluminescent Materials and Devices. Japan: Gordon & Breach; 1997. p. 391.
9. Leventis N, Huang L-Y. Polym News 1995;20(10):307–13.
10. Rothberg LJ, Lovinger AJ. J Mater Res 1996;11(12):3174–87.
11. Sheats JR, Chang YL, Roitman DB, Socking A. Acc Chem Res 1999;32(3):193–200.
12. Greiner A. Polym Adv Technol 1998;9(7):371–89.
13. Kim DY, Cho HN, Kim CY. Prog Polym Sci 2000;25(8):1089–139.
14. Conwell EM, Stolka M, Miller MR. Electroluminescent materials, devices and large- screen displays. International Society for Optical Engineering (SPIE) Proceedings, San Jose, CA, 1993.
15. Miyata S, Nalwa HS. Organic Electroluminescent Materials and Devices. Amsterdam: Gordon & Breach; 1997.
16. Hsieh BR, Wei Y. Semiconducting polymers: properties and synthesis. ACS Symp Series 735, American Chemical Society; 1999.
17. Kippelen B, Bradley D. Polymer photonic devices. IV. International Society for Optical Engineering (SPIE) Proceedings, *vol*. 3281, San Jose, CA, 1998.
18. Akcelrud L. Prog Polym Sci 2003;28:875–962.
19. Faraggi EZ, Davidov D, Cohen G, Noah S, Golosovsky M, Avny Y, Neumann R, Lewis A. Synth Met 1997;85(1–3):1187–90.
20. Rogers JA, Bao Z, Dhar L. Appl Phys Lett 1998;73(3):294–6.
21. Li AK, Yang SS, Jean WY, Hsu CS, Hsieh BR. Chem Mater 2000;12(9):2741–4.
22. Clauswitz KUW, Geffarth F, Greiner A, Lüssen G, Wendorff JH. Synth Met 2000;111/ 112:169–71.
23. Miteva T, Meisel A, Grell M, Nothofer HG, Lupo D, Yasuda A, Knoll W, Kloppenburg L, Bunz UHF, Sherf U, Neher D. Synth Met 2000;111/ 112:173–6.
24. Jandke M, Strohriegl P, Gmeiner J, Brütting W, Schwoerer M. Synth Met 2000;111/ 112:177–80.
25. Contoret AEA, Farrar SR, Jackson PO, Khan SM, May L, O' Neill M, Nicholls JES, Kelly M. Richards G. Adv Mater 2000;12(13):971–4.
26. Grell M, Bradley DDC, Inbasekaran M, Woo EP. Adv Mater 1997;9(10):798.
27. Peeters E, Christiaans MPT, Janssen RAJ, Scoo HFM, Dekkers HP JM, Meijer EW. J Am Chem Soc 1997;119(41):9909–10.
28. Das S, Pal AJ. Langmuir 2002;18:458–61.
29. Tsukruk VV, Bliznyuk VN, Visser D, Campbell AL, Bunning TJ, Visser WW. Macromolecules 1997;30:6615–25.
30. Yang SY, Rubner MF. J Am Chem Soc 2002;124(10):2100–1.
31. Tang J, Li WJ, Wang Y, Wang B, Sun J, Yang B. J Photochem Photobiol A: Chem 2001;141:179–82.
32. Kaminorz Y, Smela E, Johansson T, Brehmer L, Anderson MR, Inganä s O. Synth Met 2000;113(1/ 2):103–14.
33. Speakman SP, Rozenberg GG, Clay KJ, Milne WI, Ille A, Gardner IA, Bresler E, Steinke JHG. Org Electron 2001;2:65–73.
34. Kobayashi H, Kanbe S, Seki S, Kigchi H, Kimura M, Yudasaka I, Miyashita S, Shimoda T, Towns CR, Burroughes JH, Friend RH. Synth Met 2000;111/ 112:125–8.
35. Pede D, Serra G, Rossi DD. Mater Sci Eng 1998;C5:289–91.
36. Panin GN, Kang TW, Lee H. Physica E 2004;21:1074–8.
37. Dreuth H, Heiden C. Mater Sci Eng 1998;C5:227–31.
38. Adachi C, Kwong R, Forrest SR. Org Electron 2001;2:37–43.
39. Guo TF, Chang SC, Yang Y, Kwong RC, Thompson ME. Org Electron 2000;1:15–20.
40. Lee CL, Lee KB, Kim JJ. Mater Sci Eng 2001;B85:228–31.
41. Samuel IDW, Crystall B, Rumbles G, Burn PL, Holmes AB, Friend RH. Chem Phys Lett 1993;213(5/ 6):472–8.
42. Malliaras GG, Scott JC. J Appl Phys 1998;83(10):5399–403.
43. Vestweber H, Pohmerehne J, Sander R, Mahrt RF, Greiner A, Heitz W, Bä ssler H. Synth Met 1995;68(3):263–8.
44. Blom PWM, Jong MJM. IEEE J Sel Top Quant Electron 988; 4(1):105–12.
45. Barth S, Bassler H, Hertel D, Nikitenko VI, Wolf U. Pure Appl Chem 1999;71(11):2067–77.
46. Davids PS, Kogn SM, Parker ID, Smith DL. Appl Phys Lett 1996;69(15):2270–2.
47. Conwell EM, Wu MW. Appl Phys Lett 1997;70(14):1867–9.
48. Bassler H. Polym Adv Technol 1998;9(7):402–18.
49. Jenekhe AS, Osaheni JA. Science 1994;265(5173):765–8.
50. Conwell E. Trends Polym Sci 1997;5(7):218–22.
51. Conwell E. Phys Rev B 1998;57(22):14200–2.
52. Beljonne D, Shuai Z, Cornil J, Calbert JP, Bré das JL. J Photochem Photobiol A: Chem 2001;144:57–62.
53. Hsu JWP, Yan M, Jedju TM, Rothberg LJ, Hsieh BR. Phys Rev B 1994;49(1):712–5.
54. Rothberg LJ, Yan M, Papadimitrakopoulos F, Galvin ME, Kwock EW, Miller TM. Synth Met 1996;80(1):41–58.
55. Wu MW, Conwell E. Phys Rev B 1997;56(16):R10060–2.
56. Yan M, Rothberg LJ, Kwock EW, Miller M. Phys Rev Lett 1995;75(10):1992–5.
57. Samuel ID, Rumbles G, Collison CJ, Friend RH, Moratti SC, Holmes AB. Synth Met 1997;84(1):497–500.
58. Shi Y, Liu J, Yang Y. J Appl Phys 2000;87(9):4254–63.
59. Jakubiak R, Rothberg LJ, Wan W, Hsieh BR. Synth Met 1999;101(1):230–3.
60. Nguyen TQ, Martini IB, Liu J, Schwartz BJ. J Phys Chem B 2000;104(2):237–55.
61. Samuel ID, Rumbles G, Collison CJ. Phys Rev B 1995;52(16): R11573–6.
62. Blatchford JW, Gustafson TL, Epstein AJ, Vandenbout D, Kerimo A, Higgins DA, Barbara PF, Fu DK, Swager TM, MacDiarmid AG. Phys Rev B 1996;54(6):R3683–6.
63. Aguiar M, Fugihara MC, Hummelgen IA, Peres LO, Garcia JR, Gruber J, Akcelrud L. J Lumin 2002;96:219–25.

64. Aguiar M, Karasz FE, Akcelrud L. Macromolecules 1995;28(13):4598–602.
65. Aguiar M, Hu B, Karasz FE, Akcelrud L. Macromolecules 1996;29(9):3161–6.
66. Aguiar M, Hu B, Karasz FE, Akcelrud L. Macromol Chem Phys 1998;199(7):1255–61.
67. Gruner JF, Friend RH, Scherf U, Huber J, Holmes AB. Adv Mater 1994;6(10):748–52.
68. Martin SJ, Cadby AJ, Lane PA, Bradley DDC. Synth Met 1999;101(1):665–6.
69. Rumbles G, Samuel IDW, Collison CJ, Miller PF, Moratti SC, Holmes AB. Synth Met 1997;101(1–3):158–61.
70. Collison CJ, Rothberg LJ, Treemaneekarn V, Li Y. Macromolecules 2001;34(7):2346–52.
71. Brown AR, Bradley DDC, Burroughs JH, Friend RH, Greenham NC, Burn PL, Holmes AB, Kraft A. Appl Phys Lett 1992;61(23):2793–5.
72. Bradley DDC, Friend RH. J Phys Condens Matter 1989; 1(23): 3671–8.
73. Ziemelis KE, Hussain AT, Bradley DDC, Friend RH, Ruhe J, Wegner G. Phys Rev Lett 1991;66(17):2231–4.
74. Romero DB, Schaer M, Leclerc M, Ad' es D, Siove A, Zuppiroli L. Synth Met 1996;80(3):271–7.
75. Kido J, Shinoya H, Nagai K. Appl Phys Lett 1995;67(16):2281–3.
76. Yamamoto T, Suganuma H, Saitoh Y, Maruyama T, Inoue T. Jpn J Appl Phys, Part 2: Lett 1996;35(9A):L1142–4.
77. Cao Y, Treacy GM, Smith P, Heeger AJ. Appl Phys Lett 1992;60(22):2711–3.
78. Yang Y, Heeger AJ. Appl Phys Lett 1994;64(10):1245–7.
79. Scott JC, Carter SA, Karg S, Angelopoulos M. Synth Met 1997;85(1–3):1197–200.
80. Yang Y, Westerweele E, Zhang C, Smith P, Heeger AJ. J Appl Phys 1995;77(2):694–8.
81. Yan M, Rothberg LJ, Papadimitrakopoulos F, Galvin ME, Miller TM. Phys Rev Lett 1994;72(7):1104–7.
82. Hayashi S, Etoh H, Saito S. Jpn J Appl Phys, Part 2: Lett 1986; 25(9):L773–5.
83. Wessling RA. J Polym Sci, Polym Symp 1985; 72:55–66.
84. Wessling RA, Zimmerman RG. US Patent 3,401, 152; 1968.
85. Machado JM, Karasz FE, Kovar RF, Burnett JM, Druy MA. New Polym Mater 1989; 1(3):189–207.
86. Karasz FE, Capistran JD, Gagnon DR, Lenz RW. Mol Cryst Liq Cryst 1985; 118(1–4):327–32.
87. Denton FR, Lahti PM, Karasz FE. J Polym Sci, Part A: Polym Chem 1992;30(10):2223–31.
88. Montaudo G, Vitalini D, Lenz RW. Polymer 1987; 28(5):837–42.
89. Murase I, Ohnishi T, Noguchi T, Hirooka M. Polym Commun 1984; 25(11):327–9.
90. Capistran JD, Gagnon DR, Antoun S, Lenz RW, Karasz FE. ACS Polym Prepr 1984; 25(2):282–3.
91. Gagnon DR, Capistran JD, Karasz FE, Lenz RW. Polym Bull 1984; 12(4):293–8.
92. Denton FR, Lahti PM. Synthesis and properties of poly (phenylene vinylene)s and related poly(arylene vinylene)s. In: Wise DL, Wneck GE, Trantolo DJ, Cooper TM, Gresser JD, editors. Photonic Polymer Systems: Fundamentals, Methods and Applications; 1998, p. 61–102, chapter 3; see also page 9.
93. Tokito S, Momii T, Murata H, Tetsui T, Saito S. Polymer 1990; 31(6):1137–41.
94. Burn PL, Bradley DDC, Brown AR, Friend RH, Holmes AB. Synth Met 1991;41(1/ 2):261–4.
95. Gowri R, Padmanaban G, Ramakrishnan S. Synth Met 1999;101:166.
96. Padmanaban G, Ramakrishnan S. J Am Chem Soc 2000;122(10): 2244–51.
97. Colaneri NF, Bradley DDC, Friend RH, Burn PL, Holmes AB, Spangler CW. Phys Rev B: Condens Matter 1990; 42(18): 11670–81.
98. Askari SH, Rughooputh SD, Wudl F. Polym Mater Sci Eng Proc 988; 59:1068–70.
99. Patil AO, Rughooputh SD, Heeger AJ, Wudl F. ACS Polym Mater Sci Eng Proc 1988; 59:1071–3.
100. Machado JM, Denton FR, Shlenoff JB, Karasz FE, Lahti PM. J Polym Sci, Phys Ed 989; 27(1):199–203.
101. Burn PL, Bradley DDC, Friend RH, Halliday DA, Holmes AB, Jackson RW, Kraft A. J Chem Soc, Perkin Trans 1992;23:3225–31.
102. Rughooputh HSD, Wudl F, Heeger AJ. ACS Polym Prepr 1989; 30(1):157–60.
103. Sonoda Y, Kaeriyama K. Bull Chem Soc Jpn 1992;65(3):853–7.
104. Doi S, Kuwabara M, Noguchi T, Ohnishi T. Synth Met 1993;57(1):4174–9.
105. Paulvannan K, Feld WA. ACS Polym Prepr 1991;32(1):192–3.
106. Egbe DAM, Ulbricht C, Orgis T, Carbonnier B, Kietzke T, Peip M, Metzner M, Gericke M, Birckner E, Pakula T, Neher D, Grummt U-W. Chem Mater 2005;17:6022–32.
107. Braun D, Heeger AJ. Visible Appl Phys Lett 1991;58(18):1982–4.
108. Braun D, Heeger AJ, Kroemer H. J Eletron Mater 1991;20:945.
109. Aratani S, Zhang C, Pakbaz K, Hoger S, Wudl F, Heeger AJ. Electron Mater 1993;22(7):745–9.
110. Wudl F, Hoger S, Zhang C, Pabkaz K. ACS Polym Prepr 1993;34(1):197–8.
111. Gilch HG, Wheelright WL. J Polym Sci, Part A 1996;4:1337.
112. Hoerhold HH, Raabe D. Acta Polym 1979; 30(2):86–92.
113. Hoerhold HH, Ozegowski JH, J Prakt Chem 1977; 319(4):622–6.
114. Swatos WJ, Gordon B. ACS Polym Prepr 1990; 31(1):505–6.
115. Hsieh BR, Feld WA. ACS Polym Prepr 1993;34(2):410–1.
116. Hsieh BR, Razafitrimo H, Gao Y, Nijakowski TR, Feld WA. ACS Polym Prepr 1995;36(2):85–6.
117. Wan WC, Gao Y, Goodwin TE, Gonzalez SA, Feld WA, Hsieh BR. Macromol Symp 1997;125:205.
118. Hsieh BR, Yu Y, Forsythe EW, Schaaf GM, Feld WA. J Am Chem Soc 1998;120(1):231–2.
119. Wan WC, Cao Y, Salomone JC. Polymeric Materials Encyclopedia. Boca Raton, FL: CRC Press, Inc.; 1996, chapter 6; p. 6537.
120. Hsieh BR, Antoniadis H, Bland DC, Feld WA. Adv Mater 1995;7(1):36–8.
121. Westveber H, Greiner A, Lemmer U, Richert R, Heitz W, Bassler H. Adv Mater 1992;4(2):661–2.
122. Johansson DM, Srdanov G, Yu G, Theander M, Inganäs O, Andersson M. Macromolecules 2000;33(7):2525–9.
123. Gurge RM, Sarker A, Lahti PM, Hu B, Karasz FE. Macromolecules 1996;29(12):4287–92.
124. Kim JJ, Kang SW, Hwang DH, Shim HK. Synth Met 1993;57(1):4024–8.
125. Sarker A, Lahti PM, Garay RO, Lenz RW, Karasz FE. Polymer 1994;35(6):1312–6.
126. Höger S, McNamara JJ, Schricker S, Wudl F. Chem Mater 1994;6(2):171–3.
127. Vanderzande DJ, Isaaris AC, Van der Borght MJ, Van Breemen A, Kokk M, Gelan JM. Macromol Symp 1997;125:189–203.
128. Van der Borght M, Adriaensens P, Vanderzande D, Gelan J. Polymer 2000;41(8):2743–53.
129. Martelock H, Greiner A, Heitz W. Makromol Chem 1991;192(4):967–79.
130. Bradley DDC. Adv Mater 1992;4(11):756–9.
131. Greenham NC, Samuel LDW, Hayes GR, Phillips RT, Kessener YARR, Moratti SC, Holmes AB, Friend RH. Chem Phys Lett 1995;241(1/2):89–96.
132. Anderson MR, Yu G, Heeger AJ. Synth Met 1997;85(1–3):1275–6.
133. Chen K-B, Li H-C, Chen C-K, Yang S-H, Hsieh BR, Hsu C-S. Macromolecules 2005;38:861724.
134. Henckens A, Duyssens I, Lutsen L, Vanderzande D, Cleij TJ. Polymer 2006;47:123–31.
135. Liang F, Pu Y- J, Kurata T, Kido J, Nishide H. Polymer 2005;46:3767–75.
136. Zhang Q, Yang M, Wu P, Ye H, Liu X. Mater Sci Eng, B 2004;113:130–35.
137. Mikroyannidis JA. Synth Met 2005;155:125–29.
138. Hu J, Meng F, Li J, Ding F, Fan X, Tian H. Eur Polym J 2006; 42:2686–2694.
139. Chen Y, Midorikawa T, Bai J, Liu Y, Araki Y, Itob O. Polymer 2005;46:9803–9.
140. Gupta R, Stevenson M, Dogariu A, McGehee MD, Park JY, Srdanov V, Heeger AJ. Appl Phys Lett 1998;73(24):3492–4.
141. Kang IN, Hwang DH, Shim HK, Zyung T, Kim JJ. Macromolecules 1996;29:165–9.
142. Cornil J, Beljonne D, Santos DA, Bredas JL. Synth Met 1996;76(1–3):101–4.
143. Woo HS, Lhost O, Graham SC, Brédas JL, Schenk R, Mullen K. Synth Met 1993;59(1):13–28.

144. Tian B, Zerbi G, Schenk R, Mullen K. J Chem Phys 1991;95(5):3191–207.
145. Ohnishi T, Doi S, Tsuchida Y, Noguchi T. IEEE Trans Electron Devices 1997;44(8):1253–7.
146. von Seggern H, Wnkel PS, Zhang C, Schimdt HW. Macromol J Chem Phys 1994;195(1–3):2023–37.
147. Zheng S, Shi J, Mateu R. Chem Mater 2000;12(7):1814–7.
148. Yang Z, Hu B, Karasz FE. J Macromol Sci, Pure Appl Chem 1998;A35(2):233–47.
149. Hu B, Yang Z, Karasz FE. J Appl Phys 1994;76(4):2419–22.
150. Sokolik I, Yang Z, Morton DC, Karasz FE. J Appl Phys 1993;74(5):3584–6.
151. Hu B, Morton DC, Sokolik I, Yang Z, Karasz FE. J Lumin 1994;60/61:919–22.
152. Zhang C, Braun D, Heeger AJ. J Appl Phys 1993;73(10):5177–80.
153. Sun RG, Wang YZ, Wang DK, Zheng QB, Kyllo EM, Gustafson TL, Wang F, Epstein AJ. Synth Met 2000;111/112(1):595–602.
154. Kyllo EM, Gustafson TL, Wang DK, Sun RG, Epstein AJ. Synth Met 2001;116(1–3):189–92.
155. Burn PL, Holmes AB, Kraft A, Bradley DDC, Brown AR, Friend RH, Gymer RW. Nature 1992;356(6364):47–9.
156. Hay M, Klavetter FL. J Am Chem Soc 1995;117(27):7112–8.
157. Ahn T, Jang MS, Shim H- K, Hwang D- H, Zyung T. Macromolecules 1999;32(10):3279–85.
158. Yang Z, Sokolik I, Karasz FE. Macromolecules 1993;26(5):1188–90.
159. Hu B, Karasz FE. Synth Met 1998;92(2):157–60.
160. Cacialli F, Chuah BS, Friend RH, Moratti SC, Holmes AB. Synth Met 2000;111/ 112(1):155–8.
161. Wang H, Li QSY, Li X. Thin Solid Films 2003;426:40–46.
162. Stone DA, Chang YK, Allcock HR. J Polym Sci, Part A: Polym Chem 2006;44(1):69–76.
163. Aguiar M, Karasz FE, Hu B, Akcelrud L. Macromol Chem Phys 1998;199(7):1255–61.
164. Aguiar M, Karasz FE, Hu B, Akcelrud L. Synth Met 1995;71(1–3):2189–90.
165. Bisberg J, Cumming WJ, Gaudiana RA, Hutchison KD, Ingwall RT, Kolb ES, Mehta PG, Minns RA, Petersen CP. Macromolecules 1995;28:386–9.
166. Yoon CB, Shim HK. Synth Met 2000;111/ 112:469.
167. Chung SJ, Kwon KY, Lee SK, Jin J- II, Lee CH, Lee CE, Park Y. Adv Mater 1998;10(14):1112–6.
168. Jang JW, Oh DK, Lee CH, Lee CE, Lee DW, Jin J- II. J Appl Phys 2000;87(6):3183–5.
169. Chung SJ, Jin J, Kim KK. Adv Mater 1997;9(7):551–4.
170. Lee CH, Ryyu SH, Jang HD, Oha SY. Mater Sci Eng, C 2004;24:87–90.
171. Garten F, Vrijmoeth J, Schatmann AR, Gill RE, Klapwijk TM, Hadziiiannou G. Synth Met 1996;76(1–3):85–9.
172. Yoshino K, Nakajima S, Park DH, Sugimoto R. Jpn J Appl Phys: Part 2 1988; 27(4):L716–8.
173. Yoshino K, Love P, Onoda M, Sujimoto R. Jpn J Appl Phys: Part 2 1988; 27(12):L2388–91.
174. Ohmori Y, Uchida M, Muro K, Yoshino K. Jpn J Appl Phys 1991;30:L1938.
175. Ohmori Y, Uchida M, Muro K, Yoshino K. Solid State Commun 1991;80:605.
176. Granströ m M, Inganä s O. Appl Phys Lett 1996;68(2):147–9.
177. Braun D, Gustafsson G, McBranch D, Heeger AJ. J Appl Phys 1992;72(2):564–8.
178. Uchida M, Ohmori Y, Morishima C, Yoshino K. Synth Met 1993;55–57:4168.
179. Ohmori Y, Morishima C, Uchida M, Yoshino K. Jpn J Appl Phys 1992;31(Pt 2(5A)):L568.
180. Inganäs O. Making polymer light emitting diodes with polythiophenes. In: Miyata S, Nalwa HS, editors. Organic Electroluminescent Materials and Devices. Amsterdam: Gordon & Breach; 1997.
181. McCullough RD, Tritsram-Nagle S, Williams SP, Lowe RD, Jayaraman M. J Am Chem Soc 1993;115(11):4910–1.
182. Anderson MR, Beggren M, Inganas O, Gustafsson G. Macromolecules 1995;28(22):7525–9.
183. Berggren M, Inganäs O, Gustaffson G, Anderson MR, Hjertberg T, Wennerström O. Synth Met 1995;71:2185.
184. Theander M, Anderson MR, Inganä s O. Synth Met 1999;101:331.
185. Ahn SH, Czae MZ, Kim ER, Lee H, Han SH, Noh J, Hara M. Macromolecules 2000;34:2522.
186. Skabara PJ, Serebryakov I, Perepichka IF, Sariciftci NS, Neugebauer H, Cravino A. Macromolecules 2001;34:2232.
187. Greenham NC, Brown AR, Bradley DDC, Friend RH. Synth Met 1993;55–57:4134.
188. Ogawa K, Sttaford JA, Rothstein SD, Tallman DE, Rassmunsen S. Synth Met 2005;152:137–40.
189. Pei J, Yu W-L, Huang W, Heeger AJ. Macromolecules 2000; 33:2462.
190. Vamvounis G, Yu J, Holdcroft S. Eur Polym J 2004;40:2659–64.
191. Huang W, Yu WL, Meng H, Pei J, Li SFY. Chem Mater 1998;10:3340.
192. Huang W, Meng H, Yu WL, Pei J, Chen ZK, Lai YH. Macromolecules 1999;32:118.
193. Roman LS, Inganäs O. Synth Met 2002;125:419–22.
194. Wanga X, Anderssn MR, Thompson ME, Inganäs O. Thin Solid Films 2004;468:226–33.
195. Wang XJ, Andersson MR, Thompson ME, Ingana O. Synth Met 2003;137:1019–20.
196. Wu C-G, Hsieh C-W, Chen D-C, Chang S-J, Chen K-Y. Synth Met 2005;155:618–22.
197. Wu C-G, Lin Y-C, Wu C-E, Huang P-H. Polymer 2005;46:3748–57.
198. Bolognesi A, Schieroni AG, Botta C, Marinelli M, Mendichi R, Rolandi R, Relini A, Inganäs O, Theandher M. Synth Met 2003;139:303–10.
199. Greenham NC, Moratti SC, Bradley DDC, Friend RH, Holmes HB. Nature 1993;365(6447):628–30.
200. Holoch M, Segura JL, Dottinger SE, Hohnholz D, Steinhuber E, Spreitzersand H, Hanack M. Synth Met 1997;84:319.
201. Staring EGL, Demandt RCJE, Braun D, Rikken GLJ, Kessener YARR, Ven Huizen AHJ, Van Knippenberg MMF, Bowmans M. Synth Met 1995;71:2179.
202. Baigent DR, Holmes AB, Moratti SC, Friend RH. Synth Met 1996;80:119.
203. Grem G, Leditzky G, Ulrich B, Leising G. Adv Mater 1992;4(1):36–7.
204. Moratti SC, Bradley DDC, Friend RH, Greenham NC, Holmes AB. Mater Res Soc Symp Proc 1994;328:371–6.
205. Moratti SC, Bradley DDC, Friend RH, Greenham NC, Holmes AB, Cervini R. Proc SPIE 1994;2144:108–14.
206. Ryu H, Subramanian LR, Hanack M. Tetrahedron 2006;62:6236–47.
207. Moratti SC, Bradley DDC, Friend RH, Greenham NC, Holmes AB. Polym Prepr ACS 1994;35:214.
208. Peng ZH, Galvin ME. Chem Mater 1998;10(7):1785–8.
209. Xiao Y, Yu WL, Pei J, Chen Z, Huang W, Heeger AJ. Synth Met 1999;106:165.
210. Pinto MR, Hu B, Karasz FE, Akcelrud L. Polymer 2000;41:8095–102.
211. Moratti SC, Cervini R, Holmes AB, Baigent DR, Friend RH, Greenham NC, Gruner J, Hamer PL. Synth Met 1995;71:2117.
212. Brë das JL, Heeger AJ. Chem Phys Lett 1994;217(6/ 5):507–12.
213. Pucci A, Biver T, Ruggeri G, Meza LI, Pang Y. Polymer 2005;46:11198–205.
214. Miller PF, de Souza MM, Moratti SC, Holmes AB, Samuel IDW, Rumbles G. Polym Int 2006;55(7):784–92.
215. Chasteen SV, Carter SA, Rumbles G. J Chem Phys 2006;124:214704–5.
216. Kim Y-H, Shin D-C, Kwon S-K. Polymer 2005;46:4647–53.
217. Yamamoto T, Morita A, Muyazaki Y, Maruyama T, Wakayama H, Zhou Z-H, Nakamura Y, Kanbara T, Sasaki S, Kubota K. Macromolecules 1992;25(4):1214–23.
218. Suzuki A. J Organomet Chem 1999;576(1/ 2):147–68.
219. Schlüter AD. J Polym Sci, Part A: Polym Sci 2001;39(10):1533–56.
220. Liu C, Yu WL, Lai YH, Huang W. Chem Mater 2001;13(6):1984–91.
221. Lögdlund M, Salaneck WR, Meyers F, Brédas JL, Arbuckle GA, Friend RH, Holmes AB, Froyer G. Macromolecules 1993;26(15):3815–20.
222. Remmers M, Schulze M, Wegner G. Macromol Rapid Commun 1996;17:239–52.
223. Remmers M, Müller B, Martin K, Räder HJ, Köhler W. Macromolecules 1999;23(4):1073–9.
224. Scherf U, Mullen K. ACS Symposium 1997, chapter 4; p. 358.

225. Grem G, Leditzky G, Ulrich B, Leising G. Synth Met 1992;51 (1–3):383–9.
226. Chmil K, Scherf U. Makromol Chem Rapid Commun 1993;14(4):217–22.
227. Fahnenstich U, Koch KH, Pollmann M, Scherf U, Wagner M, Wegener S, Mullen K. Makromol Chem Makromol Symp 1992;54/ 55:465–76.
228. Scherf U, Mullen K. Makromol Chem Rapid Commun 1991;12:489–97.
229. Stampfl J, Graupner W, Leising G, Scherf U. J Lumin 1995;63:117–23.
230. Graupner W, Mauri M, Stampfl J, Leising G, Scherf U, Mullen K. Solid State Commun 1994;91(1):7–12.
231. Grem G, Leising G. Synth Met 1993;57(1):4105–10.
232. Xia C, Advincula R. Macromolecules 2001;34:6922.
233. Edwards A, Blumstengel S, Sokolik I, Yun H, Okamoto Y, Dornsinville R. Synth Met 1997;84:639.
234. Mishra AK, Graf M, Grasse F, Jacob J, List EJW, Müllen K. Chem Mater 2006;18:2879–85.
235. Yang Y, Pei Q. Appl Phys Lett 1997;81(7):3294–8.
236. Klaerner G, Miller RD. Macromolecules 1998;31(6):2007–9.
237. Kreyenschimdt M, Klaerner G, Fuhrer T, Ashenhurst J, Karg S, Chen W, Lee VY, Scott JC, Miller RD. Macromolecules 1998;31(4): 1099–103.
238. Klärner G, Davey MH, Chen WD, Scott JC, Miller RD. Adv Mater 1998;10(13):993–7.
239. Bliznyuk VN, Carter SA, Scott JC, Klärner G, Miller RD. Macromolecules 1999;32(2):361–9.
240. Rehahn M, Schlüter AD, Wegner G. Macromol Chem 1990; 191(9):1991–2003.
241. Rehahn M, Schlüter AD, Wegner G, Feast WJ. Polymer 1989; 30(6):1054–9.
242. Bradley DDC, Grell M, Grice A, Tajbakhsh AR, O' Brien DF, Bleyer A. Opt Mater 1998;9:1–11.
243. Inbasekaran M, Wu W, Woo EP. US Patent 5,777,070 to Dow Company; 1998.
244. Inbasekaran M, Shiang WR, Woo EP, Roof GR. US Patent 5,962,631 to Dow Company; 1999.
245. Lin H-C, Sung H- H, Tsai C-M, Li K-C. Polymer 2005;46:9810–20.
246. Inbasekaran M, Woo EP, Wu W, Bernius M, Wujkowski L. Synth Met 2000;111/ 112:397.
247. Wong W-Y, Liu L, Cui D, Leung LM, Kwong C-F, Lee T-H, Ng H-F. Macromolecules 2005;38:4970–6.
248. Wang ZJ, Yang XH, Chen XH, Xu Z, Xu XR. Thin Solid Films 2000;363(1/ 2):94–7
249. Meng H, Huang W. J Organomet Chem 2000;65(13):3894–901.
250. Lee SH, Nakamura T, Tsutsui T. Org Lett 2001;3(13):2005–7.
251. Zhan X, Liu Y, Zhu D, Huang W, Gong Q. Chem Mater 2001;13:1540–4.
252. Ding J, Day M, Robertson G, Roovers Macromolecules 2002;35:3474–83.
253. Assaka AM, Rodrigues PC, de Oliveira ARM, Ding L, Hu B, Karasz FE, Akcelrud L. Polymer 2004;45:7071–81.
254. Perzon E, Wang X, Admassie S, Inganäs O, Andersson MR. Polymer 2006;47:4261–68.
255. Kim JH, You N-H, Lee H. J Polym Sci Part A: Polym Chem 2006;44:3729–37.
256. Buchgraber C, Pogantsch A, Kappaun S, Spanring J, Kern W. J Polym Sci, Part A: Polym Chem 2006;44:4317–27.
257. Peng Q, Kang ET, Neoh KG, Xiaob D, Zou D. J Mater Chem 2006;16:376–83
258. Cao DD, Liu Q, Zeng W, Han S, Peng J, Liu S. J Polym Sci, Part A: Polym Chem 2006;44:2395–405.
259. Yang G- Z, Wu M, Lu S, Wang M, Liu T, Huan W. Polymer 2006;47:4816–23.
260. Yang R, Tian R, Yan J, Zhang Y, Yang J, Hou Q, Yang W, Zhang C, Cao Y. Deep- Red Macromolecules 2005;38:244–53.
261. Cho NS, Hwang D-H, Jung B-J, Lim E, Lee J, Shim H-K. Macromolecules 2004;37:5265–73.
262. Mikroyannidis JA. J Polym Sci, Part A: Polym Chem 2006;44: 4015–26.
263. Zhou X- H, Zhang Y, Xie Y- Q, Cao Y, Pei J. Macromolecules 2006;39:3830–40.
264. Liu C- H, Chen S- H, Chen Y. J Polym Sci, Part A: Polym Chem 2006;44:3882–95.
265. An BK, Kim YH, Shin DC, Park SY, Yu HS, Kwon SK. Macromolecules 2001;34:3993–7.
266. Song SY, Jang MS, Shim HK, Song IS, Kim WH. Synth Met 1999;102:1116.
267. Becker S, Ego C, Grimsdale AC, List EJW, Marsitzky D, Pogantsch A, Setayesh S, Leising G, Mullen K. Synth Met 2002;125:73–80.
268. Setayesh S, Grimsdale AC, Weil T, Enkelmann V, Müllen K, Meghdadi F, List EJW, Leising G. J Am Chem Soc 2001;123: 946–53.
269. Chou C- H, Wang H- S, Wei K- H, Huang JY. Adv Funct Mater 2006;16:909–16.
270. Chen K- B, Chen H- Y, Yang S- H, Hsu C- S. J Polym Res 2006;13:237–45
271. Ding L, Bo Z, Chu Q, Li J, Dai L, Pang Y, Karasz FE, Durstock MF. Macromol Chem Phys 2006;207:870–78.
272. Zhan X, Liu Y, Wu X, Wang S, Zhu D. Macromolecules 2002;35:2529–37.
273. Klaerner G, Lee JI, Lee VY, Chan E, Chen JP, Nelson A, Markiewicz D, Siemens R, Scott JC, Miller RD. Chem Mater 1999;11:1800–5.
274. Chen JP, Klaerner G, Lee JI, Markiewicz D, Lee VY, Miller RD, Scott JC. Synth Met 1999;107:129–35.
275. Chen Y, Araki Y, Doyle J, Strevens A, Ito O, Blau WJ. Chem Mater 2005;17:1661–6.
276. Wu W- C, Lee W- Y, Chen W- C. Macromol Chem Phys 2006;207:1131–38.
277. Yoshida M, Fujii A, Ohmori Y, Yoshino K. J Appl Phys Lett 1996;69(6):734–6.
278. Setayesh S, Marsitzky D, Müllen K. 2000;33:2016–20.
279. Sandee AJ, Williams CK, Evans NR, Davies JE, Boothby CE, Köhler A, Friend RH, Holmes AB. J Am Chem Soc 2004;126:7041–8.
280. Hoshino S, Furukawa K, Ebata K, Yuan C- H, Suzuki H. J Appl Phys 2000;88(5):2892–7.
281. Stolka M, Yuh HJ, McGrane K, Pai DM. J Polym Sci: Part A 1987; 25(3):823–7.
282. Xu YH, Fujino T, Naito H, Oka K, Dohmaru T. Chem Phys Lett 1998;4:299–300.
283. Suzuki H, Hoshino S, Yuan CH, Fujiki M, Toyoda S. IEEE J Sel Top Quant Electron 1998;4(1):129–36.
284. Suzuki H, Hoshino S, Yuan CH, Fujiki M, Toyoda S, Thin Solid Films 1998;331(1/ 2):64–70.
285. Kamata N, Aihara S, Umeda M, Kanezaki S, Nagumo K, Terunuma D, Yamada JK. Luminescence 2000;87(9):1186–8.
286. Fujii A, Yoshida M, Yoshimoto K, Ohmori Y, Yoshino K, Ueno H, Kakimoto M, Kojima H. Synth Met 1997;85:1261.
287. Ito O, Terzima M, Azumi T, Matsumoto N, Takeda K, Fujino M. Macromolecules 1989; 22(4):1718–22.
288. Tonzola CJ, Alam MM, Jenekhe SA. Opt Mater 2002;21:135–142.
289. Satoh S, Suzuki H, Kimata Y, Kuriyama A. Synth Met 1996;79:97.
290. Paik KL, Baek NS, Kim HK, Lee J- H, Lee Y. Opt Mater 2002:21135–42.
291. Park JS, Kim KD, Jung SH, Kim HK, Jeoung SC, Kim YH, Kim D. Synth Met 1999;102:106.
292. Pohl A, Bredas JL. Int J Quant Chem 1997;63(2):437–40.
293. Gill RE, Malliaras GG, Wilderman J, Hadziioanou G. Adv Mater 1994;6:132–6.
294. Kim HK, Ryu MK, Cho SW, Park JW. Macromolecules 1998;31:1114.
295. Garten F, Hilberer A, Cacialli F, Essenlink FJ, Van Dam Y, Schlatmann AR, Friend RW, Klapwijk TM, Hadziioannou G. Synth Met 1997;85:1253–4.
296. Ryu MK, Lee JH, Lee SM, Zyung T, Kim HK. ACS Polym Mater Sci Eng Proc 1996;75(2):408–12.
297. Jung SH, Kim HK. J Lumin 2000;87(9):51–5.
298. Rost H, Chuah BS, Hwang DH, Moratti SC, Holmes AB, Wilson J, Morgado J, Halls JJM, DeMello JC, Friend RH. Synth Met 1999;102:937–42.
299. Zhang Q, Yanga M, Wu P, Ye H, Liu X. Mat Sci Eng, B 2004;113:130–5.
300. Lee T, Jung II, Song KH, Lee H, Choi J, Lee K, Lee BJ, Pak JY, Lee C, Kang SO, Ko J. Organometallics 2004;23:5280–5.
301. Wang YZ, Epstein AJ. Acc Chem Res 1999;32:217–24.
302. Fua YJ, Wonga TKS, Wangb GM, Hub X, Zhang HX. J Lumin 2003;10135–43.
303. Wang YZ, Gebler DD, Fu DK, Swager TM, Mac Diarmid AG, Epstein AJ. Synth Met 1997;85:1179–82.

304. Ng SC, Lu HF, Chan HSO, Fujii A, Laga T, Yoshino K. Macromolecules 2001;34:6895–903
305. Monkman AP, Palsson LO, Higgins RWT, Wang C, Bryce MR, Batsanov AS, Howard JAK. J Am Chem Soc 2002;124(21):6049–55.
306. Yang W, Huang J, Liu C, Niu Y, Hou Q, Yang R, Cao Y. Polymer 2004;45:865–72.
307. Balasubramaniam E, Tao YT, Danel A, Tomasik P. Chem Mater 2000;12:2788–93.
308. Hong H, Sfez R, Vaganova E, Yitzchaik S, Davidov D. Thin Solid Films 2000;366:260–4.
309. Yun H, Kwei TK, Okamoto Y. Macromolecules 1997;30:4633–8.
310. Meghdali F, Leising G, Wang YZ, Gebler DD, Swager TM, Epstein AJ. Synth Met 1999;102:1085.
311. Koga T, Takase A, Yasuda S, Yamashita S, Gorohmaru H, Thiemann T, Mataka S, Takahashi K. Chem Phys Lett 2002;354:173–8.
312. Yu SY, Chen ZK, Hang LH, Kang ET, Chua SJ, Huang W. Synth Met 2000;114:101.
313. Zhang X, Jiang C, Mo Y, Xu Y, Shi H, Caoa Y. Appl Phys Lett 2006;88–99.
314. Wu F- I, Reddy DS, Shu C- F. Chem Mater 2003;15:269–74.
315. Pösch P, Thelakkat M, Schmidt HW. Synth Met 1999;102:1110–2.
316. Zhu W, Hu Y, Tian H. Synth Met 2000;111/ 112:477–9.
317. Bao Z, Rogers JA, Dodabalapur A, Lovinger AJ, Katz HE, Raju VR, Peng Z, Galvin ME. Opt Mater 1999;12(2/ 3):177–82.
318. Jin S- H, Kim M- Y, Kim JY, Lee K, Gal Y- S. J Am Chem Soc 2004;126:2474–80.
319. Sung H- H, Lin H- C. Macromolecules 2004;37:7945–54.
320. Mochizuki H, Hasui T, Kawamoto M, Ikeda T, Adachi C, Taniguchi Y, Shirota Y. Macromolecules 2003;36:3457–64.
321. Peng ZH, Bao ZN, Galvin ME. Chem Mater 1998;10:2086–99.
322. Pei Q, Yang Y. Adv Mater 1995;7(6):559–61.
323. Yang X, Hua Y, Yin S, Wang Z, Hou Y, Xu Z, Xu X, Peng J, Li W. Synth Met 2000;111/ 112:455–7.
324. Zhu W, Hu Y, Tian H. Synth Met 2000;111/ 112:477–9.
325. Chung SJ, Kwon KY, Lee SW, Jin JI, Lee CH, Lee CE, Park Y. Adv Mater 1998;10(14):1112–6.
326. Yu WL, Meng H, Pei J, Huang W. J Am Chem Soc 1980; 120:1108–9.
327. Kim JL, Kim JK, Cho HN, Kim DY, Hong SI. Macromolecules 2000;33(16):5880–5.
328. Jiang X, Register RA, Killen KA, Thompson M, Pschenitza F, Sturm JC. Chem Mater 2000;12:2542–47.
329. Peng ZH, Bao ZN, Galvin ME. Chem Mater 1998;10:2086–92.
330. Yang Y, Westerweele E, Zhang C, Smith P, Heeger AJ. J Appl Phys 1995;77(2):694–8.
331. Lee JI, Klaerner G, Miller RD. Chem Mater 1999;11:1083–8.
332. Cui Y, Zhang X, Jenekhe SA. Macromolecules 1999;32:3824–6.
333. Zhang X, Kale DM, Jenekhe SA. Macromolecules 2002;35:382–93.
334. Yamamoto T, Sugiyama K, Kushida T, Inoue T, Kanbara T. J Am Chem Soc 1996;118:3930–7.
335. Zhang X, Shetty AS, Jenekhe SA. Macromolecules 1999;32:7422–9.
336. Dai Y, Katz TJ. J Organomet Chem 1997;62:1274–85.
337. Jenekhe SA, Chen XL. J Phys Chem B 2000;104(27):6332–5.
338. Lu L, Jenekhe SA. Macromolecules 2001;34:6249–354.
339. Chiang CL, Shu CF. Chem Mater 2002;14:682–7.
340. Tonzola CJ, Alam MM, Bean BA, Jenekhe SA. Macromolecules 2004;37:3554–63.
341. Tonzola CJ, Alam MM, Bean BA, Jenekhe SA. Macromolecules 2005;38:9539–47.
342. Huang WY, Yun H, Lin HS, Kwei TK, Okamoto Y. Macromolecules 1999;32:8089–93.
343. Zhang X, Jenekhe SA. Macromolecules 2000;33:2069.
344. Nespurek S. Synth Met 1993;61(1/ 2):55–60.
345. Zhang C, Von Seggern H, Kraabel B, Schimdt WH, Heeger AJ. Synth Met 1995;72:185–8.
346. Partridge RH. Polymer 1983; 24(6):739–47.
347. Partridge RH. Polymer 1983; 24(6):748–54.
348. Partridge RH. Polymer 1983; 24(6):755–62.
349. Zhang A, Von Seggern H, Pakbaz K, Kraabel B, Schmidt KHW, Heeger AJ. Synth Met 1994;62:35–40.
350. Ajn T, Song SY, Ku H. Macromolecules 2000;33:6764.
351. Grigalevicius S, Tsai M- H, Grazulevicius JV, Wu C- C. J Photochem Photobiol A: Chem 2005;174:125–9.
352. Mei C, Tu G, Zhou Q, Cheng Y, Xie Z, Ma D, Geng Y, Wang L. Polymer 2006;47:4976–84.
353. Teo EYH, Ling QD, Song Y, Tan YP, Wang W, Kang ET, Chan DSH, Zhu C. Org Electron 2006;7:173–80.
354. Xing Y, Xu X, Zhang P, Tian W, Yu G, Lu P, Liu Y, Zhu D. Chem Phys Lett 2005;408:169–73.
355. Qiu S, Liu L, Wang B, Shen F, Zhang W, Li M, Ma Y. Macromolecules 2005;38:6782–8.
356. Tabata M, Fukushima T, Sadahiro Y. Macromolecules 2004;37:4342–50.
357. Liu X- M, Xu J, Lu X, He C. Macromolecules 2006;39:1397–1402.
358. Long X, Grell M, Malinovski A, Bradley DDC, Inbasekaran M, Woo EP. Opt Mater 1998;9:70–6.
359. Politis JK, Curtis MD, Gonzalez L, Martin DC, He Y, Kanicki J. Chem Mater 1998;10(6):1713–9.
360. Stenger-Smith JD, Zarras P, Merwin LH. Macromolecules 1998;31(21):7566–9.
361. Shi J, Zheng S. Macromolecules 2001;34:6571–7.
362. Shim HK, Kim HJ, Ahn T, Kang IN, Zyung T. Synth Met 1997;91:289–99.
363. Chung SJ, Jin J, Kim KK. Adv Mater 1997;9(7):551–4.
364. Zhang A, Von Seggern H, Pakbaz K, Kraabel B, Schmidt KHW, Heeger AJ. Synth Met 1994;62:35–40.
365. Yoshino K, Hirohata M, Hidayat R, Kim DW, Tada K, Ozaki M, Teraguchi M, Matsuda T. Synth Met 1999;102:1159.
366. Yoshino K, Hirohata M, Hidayat R, Tada K, Ozaki M, Teraguchi M, Matsuda T, Sada T, Frolov SV, Shkunov M, Vardeny ZV, Hamaguchi M. Synth Met 1997;91:283–8.
367. Sun R, Masuda T, Kobayashi T. Synth Met 1997;91:301–7.
368. Yuang YM, Ge W, Lam JWY, Tang BZ. Appl Phys Lett 1999;75(26):4094–6.
369. Sun R, Masuda T, Kobayashi T. Jpn J Appl Phys: Part 2 1996;35(12B):L1673–5.
370. Chuah BS, Cacialli F, Santos DA, Feeder N, Davies JE, Moratti SC, Homes AB, Friend RH, Brédas JL. Synth Met 1999;102(1–3):935–6.
371. Fulghum T, Karim SMA, Baba A, Taranekar P, Nakai T, Masuda T, Advincula RC. Macromolecules 2006;39:1467–73.
372. Montali A, Smith P, Weder C. Synth Met 1998;97:123–8.
373. Yoshino K, Tada K, Onoda M. Jpn J Appl Phys 1994;33(12B):L1785–8.
374. Tada K, Onoda M, Hirohata M, Kawai T, Yoshino K. Jpn J Appl Phys: Part A 1996;35(2B):L251–3.
375. Choi CK, Tomita I, Endo T. Macromolecules 2000;33:1487–92.
376. Pang Y, Li J, Hu B, Karasz FE. Macromolecules 1998;31:6730–8.
377. Dellsperger S, Dotz F, Smith P, Weder C. Macromol Chem Phys 2000;201(2):192–8.
378. Yamamoto T, Honda K. J Polym Sci: Part A 1998;36(1B):2201–7.
379. Lucht BL, Mao SSH, Tilley TD. J Am Chem Soc 1998;120:4354.
380. Chen Y, Dujardin R, Elschner A, Jonas F, Quintens D, Wehrmann R. ACS Polym Prepr Proc San Francisco Meet 1997;38:345.
381. Yang C, Jacob J, Müllen K. Macromol Chem Phys 2006;207: 1107–15.

CHAPTER 48

Magnetic, Piezoelectric, Pyroelectric, and Ferroelectric Properties of Synthetic and Biological Polymers

Andrzej Kloczkowski* and Taner Z. Sen*,†

*L .H. Baker Center for Bioinformatics and Biological Statistics, Iowa State University, Ames, IA 50011, USA;
†Department of Biochemistry, Biophysics, and Molecular Biology, Iowa State University, Ames, IA 50011, USA

48.1 MAGNETIC POLYMERS

Depending on the behavior in the presence of the external magnetic field all materials may be classified as diamagnetic, paramagnetic, ferromagnetic (or antiferromagnetic).

Diamagnetism is exhibited by materials with a negative magnetic susceptibility, i.e., they magnetize in a direction opposite to the direction of the applied magnetic field, and are repelled by a magnet. All materials with zero net electronic orbital moment and zero net spin magnetic moment are diamagnetics. Most of the organic molecules and polymers have a closed shell electronic structure with a singlet ground state with all electron spins paired, and therefore have diamagnetic properties. The diamagnetism follows from the Lenz's law, that the induced field opposes the applied magnetic field. All substances including paramagnets (or ferromagnets) have diamagnetic susceptibility components, but these components are very small, usually much smaller in comparison to paramagnetic susceptibilities. Substances with nonzero net electronic orbital moments or with unpaired electron spins are paramagnetics. Paramagnetic materials have open-shell electronic structure, with some unpaired electrons. Organic molecules with one unpaired electron in doublet ground state show paramagnetic properties and are called free radicals. The magnetic moments of molecules of paramagnetic substances are randomly distributed throughout the volume of the material, and the total magnetic moment of the material is zero. Paramagnetics magnetize parallel to the direction of the external magnetic field, the magnetization of the paramagnetic material vanishes when the external magnetic field is switched off.

Ferromagnetism is a property exhibited by compounds of certain metals: iron group or rare-earth elements. The atomic magnetic moments of these materials, below the so called Currie temperature, orient in one direction. The resulting magnetic susceptibility is very high and shows a saturation effect. The large magnetization of the material is preserved when the external field is switched off, i.e., ferromagnetics may have spontaneous magnetization below the Curie point. Above the Curie temperature ferromagnetics behave as ordinary paramagnetics. Ferromagnetic materials are composed of small, spontaneously magnetized regions, so called domains. The directions of magnetization of different domains do not coincide and the net magnetic moment of the substance in the absence of the external magnetic field may be zero. The application of even weak external magnetic field aligns magnetic moments of domains of the ferromagnet and gives rise to the high magnetic moment of the sample. Antiferromagnetism is a property of certain crystals containing transition elements which show spontaneous antiparallel magnetic ordering below Néel temperature. Above the Néel temperature the antiferromagnetic

ordering vanishes. The quantum theory of ferromagnetism was developed by Heisenberg. According to the Heisenberg theory there is an effective interaction between the electron spins, which arises from to the interplay between electrostatic Coulomb forces and the effect of the Pauli exclusion principle. The exchange energy of this interaction is

$$E_{ij} = -2J_{ij}\boldsymbol{\sigma}_i \cdot \boldsymbol{\sigma}_j, \tag{48.1}$$

where σ_i and σ_j are spin angular momenta for electrons i and j, and the coupling constant J_{ij} is called the exchange integral. If the coupling constant J is positive and large enough the ferromagnetic ordering in the system is favorable. For large negative values of J the antiparallel antiferromagnetic alignment of spins is favored. If the exchange integral is small, the ferromagnetic (or antiferromagnetic) state is not possible.

Ferromagnetism of the transition and rare-earth metal salts and complexes is due to high-spin states of those atoms. The electronic structure of these metal atoms is open-shell, with d-orbitals and f-orbitals containing several unpaired electrons [1–3].

Until recently the only known ferromagnetic polymers were metallo-polymers containing transition metals or rare-earth elements. The presence of the metal, particularly Fe, Ni, Co may lead to ferromagnetic behavior due to the formation of extrinsic separate magnetic phase of the metal. Another possible mechanism of ferromagnetism in metallo-polymers, of the intrinsic nature, is the strong coupling of the spins of metal ions with organic polymeric ligand. The problem if the ferromagnetic behavior of the metallo-polymer has intrinsic or extrinsic origin is very complicated [4]. There are several known polymers containing iron atoms which show ferromagnetic properties. An example is complex of the PPH polymer with $FeSO_4 \cdot 7H_2O$ shown below, containing each iron ion surrounded by six nitrogen atoms

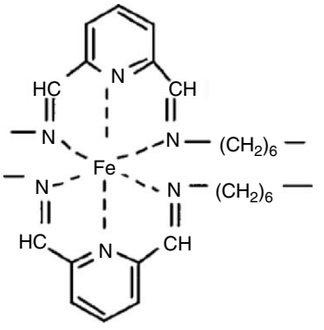

The observed ferromagnetic behavior of this polymer was first attributed to the intrinsic mechanism, but later studies have shown that the ferromagnetism is of the extrinsic nature, due to the formation of the ferromagnetic phase containing Fe_2O_3 [4].

Discoveries of purely-organic ferromagnetic materials, i.e., materials which do not contain transition metals or rare-earth elements, have been reported. The possibility of existence of organic ferromagnetic compounds has been theoretically postulated in 1963 by McConnell for high spin charge transfer complexes [5]. The proposed systems contained alternating linear sequences of donor–acceptor pairs in triplet and singlet ground states. A parallel ordering of all spins in those systems was predicted [6]. In 1968 Mataga proposed theoretically several magnetic polymer structures containing high spin blocks, as shown below with dots above carbon atoms denoting free radicals [7].

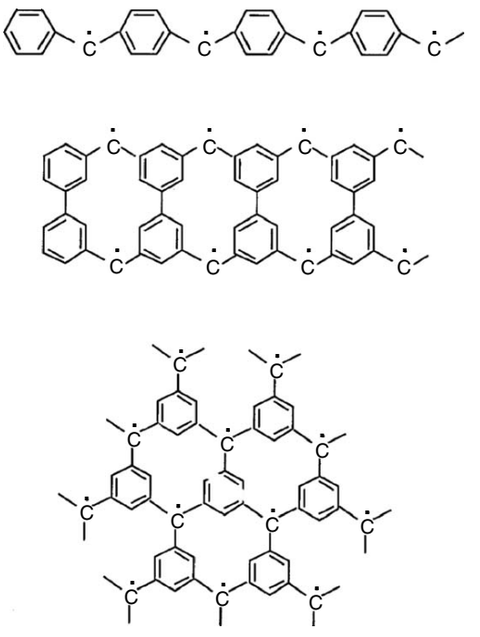

Mataga predicted that according to Hund's rule unpaired electrons in these polymers may have parallel spins, leading to ferromagnetic behavior.

In 1987 Ovchinnikov *et al*. announced the discovery of the first ferromagnetic organic polymer based on polydiacetylene chain with dangling nitroxyl radicals [8,9]. The compound was obtained by bulk polymerization of stable paramagnetic biradical BIPO initiated by light. The chemical structure of this compound is shown below.

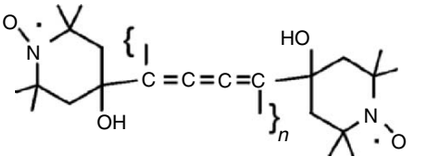

The saturation magnetization of this material was very low (0.1% of the theoretical prediction), and the fraction of crystallites showing ferromagnetic properties was also extremely small. The Curie temperature was reported to be 440 ± 20 K. Those results, however, were unverified by other laboratories. Also Torrance reported the synthesis of

an organic ferromagnet by iodine oxidation of 1,3,5-triaminobenzene [10]. Iwamura obtained fully characterized ferromagnetically coupled oligomers of polycarbenes [11,12]. These announcements have been followed by many other reports on discoveries of ferromagnetic polymers, by various authors [4]. However, all those results were unconvincing because of the poor characterization of those polymers and problems with reproducibility of the results. There is a growing list of well-characterized high spin polymers, mostly based on polyacetylene chain with pendant groups containing radical centers, but the only observed magnetic behavior of these compounds is a weak antiferromagnetism. Generally, the fraction of the bulk of the polymers exhibiting ferromagnetic behavior is very small, usually less than 5%. It is very probable that the reported ferromagnetic properties of organic polymers are due to such accidental factors, as ferrometalic impurities [4]. Several liquid–crystalline ferromagnets have also been reported [13].

Another approach to magnetic polymers are so-called polaronic ferromagnets, with spins introduced to the polymer molecules by doping, which form radical ions named polarons. With proper molecular topology ferromagnetic coupling among polarons may be possible [2]. The field of magnetic polymers are reviewed by Miller and Epstein [14] and by Kamachi [15].

48.2 PIEZOELECTRIC POLYMERS

Piezoelectricity is an effect of the generation of electric polarity in certain dielectric materials (i.e., electric insulators) in response to the applied mechanical pressure. The effect was discovered by Pierre and Jacques Curie in 1880. The polarization of the material is proportional to the applied stress. The piezoelectric effect has very important practical applications in transducers, i.e., devices which convert electric signals to mechanical signals, or the mechanical signals to electric signals, such as microphones, loudspeakers, gramophone needles, ultrasound generators, quartz clocks, etc [16,17].

The most known piezoelectric materials are some inorganic crystals, such as: quartz, barium titanate $BaTiO_3$, ammonium dihydrogen phosphate $NH_4H_2PO_4$, Rochelle salt (potassium sodium tartrate tetrahydrate $NaKC_4H_4O_6 \cdot 4H_2O$), or zinc blende ZnS. The electric polarization generates the electric potential between opposite surfaces of the crystal, and gives rise to the electric current if these two sides of the crystal are connected by a wire. The converse piezoelectric effect, i.e., the generation of the mechanical stress in the piezoelectric material by applying the electric voltage to opposite sides of the crystal is also observed. The generated piezoelectric strain is proportional to the applied electric field. (There is an important difference between converse piezoelectric effect and electrostriction, where the deformation is proportional to the square of the field). On the molecular level, piezoelectricity occurs when elastic deformations of the body are accompanied by unequal vectorial displacements of centers of gravity of positive and negative charges (ions) leading to the net polarization of the sample. The unequal vectorial displacements in the crystal require the lack of the crystallographic center of symmetry. There is a correlation between the symmetry of the crystal and the type of stresses which generate the piezoelectric polarization. The lower the symmetry of the crystal, the more different types of stresses produce piezoelectric polarization.

Generally, each of the three components of the polarization ΔP_i is linearly related to each of the nine components of the stress tensor σ_{jk}

$$\Delta P_i = \mathrm{d}_{ijk}\, \sigma_{jk}, \tag{48.2}$$

where d_{ijk} is the third-rank tensor having 27 components called piezoelectric coefficients. In the absence of body torques the stress tensor is symmetric, i.e., $\sigma_{jk} = \sigma_{kj}$ and has only 6 components so the maximum number of piezoelectric coefficients is 18 [18]. It is therefore convenient to represent the stress tensor as a six component vector σ_m, and the piezoelectric coefficients as a second-rank tensor d_{im}, where $m = 1$–6, so that

$$\Delta P_i = \mathrm{d}_{im}\, \sigma_m. \tag{48.3}$$

Similarly in the converse piezoelectric phenomena each of the 6 components of the strain tensor ε_m is related to each of the 3 components of the electric field

$$\varepsilon_m = \mathrm{d}^{\mathrm{c}}_{im}\, E_i, \tag{48.4}$$

where $\mathrm{d}^{\mathrm{c}}_{im}$ are converse piezoelectric coefficients.

The stress and strain tensors are related through the relations

$$\varepsilon_m = \mathrm{s}_{mn}\, \sigma_n \tag{48.5}$$

and

$$\sigma_m = \mathrm{c}_{mn}\, \varepsilon_n, \tag{48.6}$$

where s_{mn} and c_{mn} (with $m, n = 1$–6) are the elastic compliance tensor and the elastic stiffness tensor, respectively [17].

The most known polymer exhibiting piezoelectric behavior is poly(vinylidene fluoride) (PVF_2) which has the structure $(CF_2CH_2)_n$ [19]. The piezoelectric polymer sample is obtained by orienting dipole moments in the polymer by poling. The symmetry of the highly oriented poled polymer film reduces the number of possible piezoelectric coefficients from 18 to 5. Using the convention where 1 is the direction of drawing, 2 is in the direction of the film, and 3 is normal to the film surface the only nonzero piezoelectric coefficients for uniaxially oriented film are d_{31},d_{32},d_{33},d_{15}, and d_{24} [18]. For biaxially oriented films $\mathrm{d}_{31} = \mathrm{d}_{32}$ and $\mathrm{d}_{15} = \mathrm{d}_{24}$. The coefficient d_{33} is very difficult to measure, so sometimes it is calculated from the hydrostatic piezoelectric coefficient

$$\mathrm{d}_h = \mathrm{d}_{31} + \mathrm{d}_{32} + \mathrm{d}_{33}. \tag{48.7}$$

Table 48.1 shows some piezoelectric coefficients for thin PVF_2 films obtained by Kepler and Anderson from static measurements [18].

It should be noted that piezoelectric coefficients, especially d_{33} are very difficult to measure and stress-induced changes in polymer crystallinity contribute significantly to the piezoelectric coefficients [20]. Because of the viscoelastic properties of polymers the piezoelectric charge signal is not in phase with the stress or strain. Piezoelectric coefficients obtained from dynamic measurements depend on the frequency. It has been found that experimental values of the piezoelectric coefficients also depend on the method of processing of polymer films. For example, Wang found that in drawn and rolled films, d_{31} is about 25% higher than in films only drawn [21]. It has been shown that annealing has a large effect on the magnitude of the piezoelectric coefficients. For example Takase *et al*. found that annealing the stretched PVF_2 films in temperatures between 160 and 180 °C increased d_{31} from 20 to 28 pCN^{-1} [22]. Piezoelectric coefficients depend also on temperature. It has been found that piezoelectric coefficients increase with increasing temperature, especially rapidly above the glass transition temperature (−50 °C for PVF_2) [23].

Table 48.2 shows piezoelectric coefficients of PVF_2 obtained from dynamic measurements at frequencies 10 Hz and 25 Hz [20].

Other most known piezoelectric polymers are: poly(vinylchloride) (PVC), poly(vinylfluoride) (PVF), and Nylon 11. The piezoelectric coefficients of these polymers are much lower than piezoelectric coefficient of PVF_2. Table 48.4 shows piezoelectric coefficients of these polymers and compares them with those of some piezoelectric inorganic crystals.

TABLE 48.1. *Piezoelectric coefficients of thin* PVF_2 *films (in* pCN^{-1}*) [18].*

Coefficient	Biaxially oriented film	Uniaxially oriented film
d_{31}	4.34	21.4
d_{32}	4.36	2.3
d_{33}	−12.4	−31.5
d_h	−4.8	−9.6
d_{33} (calculated from d_h)	−13.5	−33.3

TABLE 48.2. *Piezoelectric coefficients of* PVF_2 *(in* pCN^{-1}*) obtained from dynamic measurements [20].*

Coefficient	Frequency 10 Hz	Frequency 25 Hz
d_{31}	28	17.5
d_{32}	4	3.2
d_{33}	−35	
d_h	−3	

48.3 PYROELECTRIC POLYMERS

Pyroelectricity is the effect of the generation of electric polarization in certain dielectrics by the change of temperature. The change of the electric polarization ΔP_i (for each component of the polarization vector) in the pyroelectric material is proportional to the change of the temperature ΔT

$$\Delta P_i = p_i \, \Delta T, \tag{48.8}$$

where p_i (with $i = 1$–3) are pyroelectric coefficients. Pyroelectricity is related to piezoelectricity, since it also occurs in crystals with crystallographic cells without a center of symmetry. Additional requirement for pyroelectric crystal is the occurrence of a polar axis, which reduces the number of possible crystal classes in comparison with piezoelectrics. Out of the total 32 possible crystallographic point groups, 20 groups fulfill requirements for piezoelectricity, but only 10 groups exhibit pyroelectricity. The most known pyroelectric crystals are: barium titanate $BaTiO_3$, cane sugar, and tourmaline. Because pyroelectric materials have polar axis they have permanent electric polarization, which is usually compensated by free charges on the surface of the material. The change in temperature alters the electric polarization, and leads to the pyroelectricity. The converse pyroelectric effect, the so called electrocalorimetric effect in pyroelectrics is also observed. The external electric field applied to a pyroelectric material changes its temperature. In order to eliminate the effect of the thermal expansion, measurements of the pyroelectric effect are often performed for mechanically constrained (e.g., by clamps) materials. We may also define two types of pyroelectricity: the primary pyroelectricity, which is measured when the dimensions of the sample are fixed (by clamps), and secondary pyroelectricity containing additional contribution to the polarization resulting from the thermal expansion. The secondary pyroelectricity coefficients p_i^s are related to piezoelectric coefficients d_{im}, elastic stiffness tensor c_{mn}, and thermal expansion coefficients α_n [18].

$$p_i^s = d_{im} \, c_{mn} \, \alpha_n. \tag{48.9}$$

The pyroelectric effect is widely used for the detection of infrared radiation, and for very precise measurements of the temperature [16,17].

The most known polymer showing the pyroelectric effect is poly(vinylidene fluoride) $(CF_2CH_2)_n(PVF_2)$ [19]. Polymer samples exhibiting pyroelectric properties are prepared by poling. Pyroelectric coefficients for polymers depend on the electric poling field. With the increasing poling field pyroelectric coefficients increase.

Table 48.3 shows primary and calculated secondary pyroelectric coefficients of PVF_2 films, together with thermal expansion coefficients, and elastic stiffness coefficients, obtained by Kepler and Anderson [18]. The corresponding piezoelectric coefficients were earlier shown in Table 48.1.

Other popular pyroelectric polymers are: poly(vinylchloride) (PVC), poly(vinylfluoride) (PVF), and Nylon 11, but their pyroelectric coefficients are smaller than pyroelectric coefficient of PVF_2. On the other hand the pyroelectric coefficient of PVF_2 is much smaller than pyroelectric coefficients of inorganic crystals. Table 48.4 shows the comparison of piezoelectric and pyroelectric coefficients of some inorganic crystals and polymers [24]. An extensive review of pyroelectric materials including single crystals, ceramics, liquid crystals, and composites has been recently published by Lang and Das-Gupta [25].

48.4 FERROELECTRIC POLYMERS

Ferroelectrics are materials with built-in spontaneous, permanent electric polarization. Similarly as ferromagnetics possess the spontaneous, permanent magnetization, ferroelectrics have spontaneous polarization, which can be reversed by applying external electric field. The most known ferroelectrics are inorganic monocrystals, such as Rochelle salt (potassium sodium tartrate tetrahydrate $NaKC_4H_4O_6 \cdot 4H_2O$), monopotassium dihydrophosphate (KH_2PO_4), or barium titanate ($BaTiO_3$). At sufficiently high temperatures ferroelectrics show normal dielectric behavior. However, below a certain critical temperature (so called, Curie temperature), even a small electric field causes a large polarization, which is preserved even if the external field is switched off. This means that below the Curie point ferroelectric materials show spontaneous polarization. The phase transition at the Curie temperature is related to the change of the lattice symmetry of the sample.

TABLE 48.3. *Pyroelectric coefficients p_i and p_i^s, thermal expansion coefficients α_n, and elastic stiffness coefficients c_{mn} of PVF_2 films [18].*

Coefficient	Biaxially ordered film	Uniaxially ordered film
$p_3(10^{-5}\,Cm^{-2}K^{-1})$	−1.25	−2.74
$p_3^s(10^{-5}\,Cm^{-2}K^{-1})$	−0.44	−1.48
$\alpha_1(10^{-4}\,K^{-1})$	1.24	0.13
$\alpha_2(10^{-4}\,K^{-1})$	1.00	1.45
$c_{11}(10^9 Pa)$	5.04	5.04
$c_{12}(10^9 Pa)$	3.25	3.25

TABLE 48.4. *Piezoelectric coeffiecients d and pyroelectric coefficients p of several inorganic crystals and several polymers with references to original papers.*

Material	d(in pCN^{-1})	Ref.	p(in10^{-5} $Cm^{-2}K^{-1}$)	Ref.
Quartz	2.3 (d_{11})	[26]		
PZT-4 (lead zirconate titanate)	289 (d_{33})	[27]	27	[28]
$BaTiO_3$	190 (d_{33})	[27]	20	[28]
Rochelle Salt	53 (d_{25})	[26]		
Triglycine sulfate	50	[29]	30	[28]
$Sr_{0.5}Ba_{0.5}Nb_2O_6$	95	[29]	60	[29]
PVC	0.7	[30]	0.1	[30]
PVF	1	[19]	1.0	[31]
Nylon 11	0.26	[30]	0.5	[28]
PVF_2	28 (d_{31})	[23]	4	[32]

The spontaneously polarized crystal is anisotropic and has lower symmetry than the nonpolarized one. Ferroelectric materials below the Curie temperature are also always piezoelectric, because the polarized sample has no center of symmetry. If the nonpolarized crystal has the center of symmetry, the piezoelectricity of the sample vanishes above the Curie temperature. All ferroelectrics below the Curie temperature also always show pyroelectric behavior.

Until the late sixties the only known ferroelectrics, piezoelectrics, and pyroelectrics were certain inorganic monocrystals, or polycrystalline ceramics like lead titanate zirconate perovskites. Other known materials with macroscopic polarization were electrets, (for example mixtures of beeswax and rosin) in which the polarization was produced by application of the electric field in the melted state and then by cooling and the solidification of the polarized material.

In 1969 Kawai discovered that the poly(vinylidene fluoride) polymer (known as PVF_2 or PVDF) is ferroelectric [19]. PVF_2 has a simple molecular structure $(CF_2CH_2)_n$ with the degree of polarization n usually greater than 10,000. PVF_2 is a crystalline polymer, with about the half of the polymer molecules in the amorphous noncrystalline state and another half in crystalline lamella state [33]. The crystallographic studies have shown that PVF_2 may form four different phases. One of the phases called the α-phase (or phase II) obtained by quenching from the melt is nonpolar, while other three phases called the β,γ, and the δ-phase (or phases I, III and IV), respectively, are ferroelectric [18]. The most important is the β-phase, in which the polymer has the all-*trans* conformation (and the largest dipole moment) and two chains in the unit cell are aligned in the same direction. The phases γ and δ have the electric polarization per unit cell smaller then the β-phase. The phase transformations between different phases of PVF_2 are possible by means of annealing, drawing, or poling. The ferroelectric phase of PVF_2 was discovered by poling PVF_2 film, i.e., by heating a film above temperature 100 °C and applying high electric field (above 50 MVm^{-1}) and then cooling the sample to the room temperature. The resulting material had very large piezoelectric coefficient (6.7 pCN^{-1}), about ten times larger than for any other polymer, and possessed also pyroelectric properties, at temperatures well above the glass transition temperature (−40 °C) of the polymer [16]. The magnitude of the piezoelectric coefficient and the induced polarization increase with the increasing

voltage and the increasing poling temperature. Poling can take place even at room temperature and below, if sufficiently high electric field is applied. The PVF_2β-phase melts in temperature range 175–180 °C and no ferroelectric phase transition below the melting temperature is observed. The ferroelectric phase transition is observed in copolymers of PVF_2 with poly(trifluoroethylene) (PF_3E) or with poly (tetrafluoroethylene) (PF_4E). For example the study of the 51%mol PVF_2 – 49%mol PF_3E copolymer shows the ferroelectric-to-paraelectric first order phase transition at the temperature 65 °C. The addition of PF_4E or PF_3E to PVF_2 increases the number of defects in the PVF_2 chains and lowers the Curie temperature of the copolymer in comparison to the pure PVF_2. The extrapolation of the plot of the Curie temperature as a function of the PVF_2 content in the copolymer to the pure PVF_2 gives the estimation of the Curie point of PVF_2 at 190 °C. This temperature is above the melting point temperature of PVF_2 and therefore the Curie point for pure PVF_2 is not observed [18].

Ferroelectric properties (much weaker than PVF_2) are shown also by other polymers like poly(vinylchloride) (PVC) or poly(vinylfluoride) (PVF). (See Table 48.3 for comparison of piezoelectric and pyroelectric coefficients of PVC and PVF with those for PVF_2 and for some ferroelectric inorganic crystals).

In the mid-seventies it was shown that because of the symmetry requirements, chiral smectic C liquid crystals are ferroelectric [34]. Liquid crystals are formed by anisotropic rod-like molecules. The most known liquid crystals are nematics, with orientational ordering of molecular axis of mesogenic molecules around the preferred direction, but no spatial ordering. The smectic A liquid crystals have (in addition to the orientational ordering) spatial alignment of molecules in layers, with the preferred direction perpendicular to the plane of the layers. In the smectic C phase the direction of orientational ordering is tilted relative to the normal to the plane of the layers. Chiral molecules have no center of symmetry, i.e., the mirror image of the molecule differs from the molecule itself. If a chiral mesogenic molecule has permanent dipole moment, then the unit cell of the smectic C phase has no center of symmetry and the material should be ferroelectric. The first ferroelectric liquid crystalline polymer synthesized by Shibaev and Plate [35] is shown below

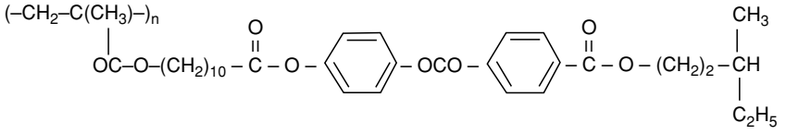

The molecule is a liquid crystalline polymer with chiral smectic C phase forming parts attached as side chains. The field required to switch the direction of polarization of the polymer is very low ($0.3\,MVm^{-1}$). There is a lot of interest in liquid crystalline ferroelectric polymers, because of their possible use for fast-switching electro-optical devices. More information about ferroelectric liquid crystals can be found in references [36,37].

Another group of ferroelectric polymers are odd nylons. The most known is Nylon 11

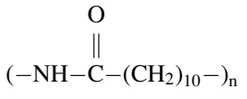

In crystal phase Nylon 11 molecules are packed in sheets with hydrogen bonds between oxygen atoms and NH groups of neighboring chains, and dipole moments of Nylon 11 chains are aligned. The piezoelectric and pyroelectric coefficients of Nylon 11 are smaller than those for PVF_2 (see Table 48.4 for comparison).

A comprehensive bibliography for ferroelectric materials (including polymers) has been recently published by Toyoda [38].

48.5 PIEZOELECTRIC, PYROELECTRIC, AND FERROELECTRIC PROPERTIES OF BIOPOLYMERS

Piezoelectricity, pyroelectricity, and ferroelectricity is hardly confined to synthetic polymers. Some biopolymers also possess these properties, and scientists study them to understand how nature exploits these properties. The earliest studies of biopolymer piezoelectricity, for example, go back to 1960s when Morris Shamos and Leroy Lavine (with Michael Morris) studied bone piezoelectricity [39] and later postulated piezoelectricity as a ''fundamental property'' of tissues of biological origins [40]. In 1968, RNA ferroelectricity was demonstrated by Stanford and Lorey [41]. However, the scientific interest in these properties of biological molecules was dwarfed by the interest in other materials. In 1999 Sidney Lang [42] indicated that compared to ''thousands'' of publications on piezoelectric, pyroelectric, and ferroelectric materials, only less than 100 of them were biologically related.

Piezoelectricity in biological molecules can be found both in soft and hard tissues as shown in Table 48.5. In this table, d_{ij} represent piezoelectric coefficient components, which

TABLE 48.5. *Piezoelectric coefficients (in* 10^{-12} m/V*) in biomaterials (taken from Lemanov [43]).*

Material	d_{14}	d_{15}	d_{31}	d_{33}
Bovine achiles tendon	−2.7	1.4	0.09	0.07
Horse femur	−0.2	0.04	0.003	0.003
Silk	−1.1	0.25	0.02	0.023

TABLE 48.6. *Pyroelectric coefficients (in* $10^{-5}Cm^{-2}K$*) in biomaterials (taken from Lemanov [43]).*

Material	Coefficient
Hoof tendon	0.00004
Insect thorax	0.35
Wheat	0.46
Plant leaves	0.015

are previously explained under piezoelectric polymers section. Pyroelectric coefficients for some biological materials are similarly given in Table 48.6. As explained under pyroelectric polymers section, pyroelectric coefficients are related to piezoelectric coefficients. Compared to those of PVF_2 films in Table 48.3, piezoelectric coefficients of biopolymers shown in Table 48.6 are very small and have positive signs.

Piezoelectricity and pyroelectricity in biopolymers originate from their building blocks: biopolymers are copolymers with 20 different monomers. These monomers are called amino acids and consist of a chiral carbon (except glycine) surrounded by an amino group, hydrogen atom, carboxyl group, and a side chain R as shown below.

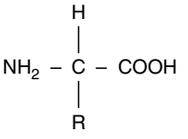

Different side chain groups determine the type of a given amino acid. These side chains can be classified as neutral, acidic, or basic; aliphatic or aromatic; hydrophobic or polar, etc. As discussed previously, the piezoelectricity and pyroelectricity requires restrictions on crystal symmetry (e.g., 20 crystallographic groups can be piezoelectric, and only 10 groups demonstrates pyroelectricity). The piezoelectric response of amino acids to the high-frequency electric pulses is shown in Table 48.7; the pyroelectric properties of amino acids were also measured, but found not significant [44].

Ferroelectricity is a requirement for some biopolymers for their biological function. Microtubules which hold the cell structurally intact are a good example. These biostructures consist of identical α and β tubulin proteins which have permanent dipole moments. Since cells utilize microtubules

TABLE 48.7. *Piezoelectricity and symmetry groups of amino acids [45] (L and D denote left-sided and right-sided enantiomers, and DL is the equimolar mixture of enantiomers).*

Amino acid	Piezoelectricity	Symmetry
α-glycene	+	C_{2h}
γ-glycene	+	C_3
L-alanine	+	D_2
L-valine	+	C_2
L-isoleucine	−	C_2,D_2
L-glutamic acid	+	C_2,D_2
L-cysteine	−	C_4,D_6
DL-alanine	+	C_{2v}
DL-valine	−	C_1
DL-serine	−	C_{2h}
DL-aspartic acid	−	C_{2h}
DL-lysine	−	D_2
DL-tyrosine	+	C_{2v}
DL-trptophan	−	C_1

in cell division and to transport motor proteins, the orientation of tubulin proteins becomes crucial for cell fitness. This orientation may be controlled by electric fields [46]. Microtubules alignment was reviewed by Cyr [47].

Another interesting biological example that shows ferroelectric properties is voltage-dependent ion channels. These channels are glycoproteins located in the cell membrane, and they are found in either open or closed conformations. In the open conformation, these proteins are ion conductors. In the closed conformation, they become non-conducting, yet they still retain their ferroelectricity, even showing liquid crystalline properties [36,48].

There is a growing interest in studying the piezoelectricity, pyroelectricity, and ferroelectricity in biological systems to understand what roles they play in cellular functions, and this interest is expected to increase in the future.

REFERENCES

1. Kahn O. Molecular magnetism, New York: VCH publishers, 1993.
2. CJ O'Connor, editor, Research frontiers in magnetochemistry, Singapore: World scientific, 1993.
3. D. Gatteschi et al., editors, Magnetic molecular materials, Dordrecht: Kluwer, 1991.
4. Miller JS. Adv. Mater. 1992; 4:298.
5. McConnell HM. J. Chem. Phys. 1963;39:1910.
6. Miller JS, Epstein AJ, Rief WM. Chem.Rev. 1988; 88:201.
7. Mataga N. Theor. Chim. Acta 1968; 10:372.
8. Korshak YV, Medvedeva TV, Ovchinnikov AA. Nature 1987;326:370.
9. Ovchinnikov AA, Spector VN. Synth. Met. 1988;27:B615.
10. Torrance JB, Oostra S, Nazzal A. Synth. Met. 1987;19:709.
11. Iwamura H. Pure Appl.Chem. 1986;58:187.
12. Iwamura H. Adv. Phys. Org. Chem. 1990;26:179.
13. Palacio F, Ramos J, Castro C. Mol. Cryst. Liq. Cryst. Technol. Sect. A 1993;232:173.
14. Miller JS, Epstein AJ. Chem. Eng. News 1995;(October 2):30.
15. Kamachi M. J. Macromol. Sci. Part C Polym. Rev. 2002;42(4):541–561.

16. Wang TT, Herbert JM, Glass AM. editors, The application of ferroelectric polymers, Glasgow: Blackie and Son, 1988.
17. Wong CP, editor, Polymers for electronic and photonic applications, San Diego: Academic Press, 1993.
18. Kepler RG, Anderson RA. J. Appl. Phys. 1978;49:4490.
19. Kawai H. Jpn. J. Appl. Phys. 1969;8:975.
20. Schewe H, McAroy BR, editors. Ultrasonics Symposium Proceedings. New York:IEEE, 1982. pp. 519.
21. Wang TT. J. Appl. Phys. 1979;50:6091.
22. Takase Y, Scheinbeim JI, Newman BA. J. Polym. Sci., Part B: Polym. Phys. 1989;27:2347.
23. Ohigashi H. J. Appl. Phys. 1976;47:949.
24. GM Sessler, editor, Electrets, 2nd. ed. Berlin: Springer-Verlag, 1987.
25. Lang SB, Das-Gupta DK. Ferroelectrics Rev. 2000;2:217–354.
26. W.G. Caddy, Piezoelectricity, New York: McGraw-Hill, 1946.
27. Berlincourt DA, Curran DR, Jaffe H. Physical Acoustics. New York: Academic Press, 1964. pp. 1.
28. Garn LE, Sharp EJ. IEEE Trans. PHP 1974;10:28.
29. Liu ST, Long D. Proc. IEEE 1978;66:14.
30. Litt MH, Hsu C, Basu P. 2005;No: 5 on Office of Naval Research Contract No. N00014–75-c-0842
31. Phelan RJ Jr., Mahler RJ, Cook AR. Appl. Phys. Lett. 1971;19:337.
32. Day GW, Hamilton RL, Phelan RJ Jr., Mullen LO. Appl. Phys. Lett. 1974;24:456.
33. Lovinger AJ. Science 1983;220:1115.
34. Meyer RB, Liebert L, Strzelecki L, Keller P. J. Phys. Lett. 1975;36:L69.
35. Shibaev V, Plate N. Pure Appl. Chem. 1985;57:1589.
36. JW Goodby et al., Ferroelectric liquid crystals: principles, properties, and applications, Philadelphia: Gordon and Breach, 1991.
37. Barny PL, Dubois JC, McArdle CB, editors. Side chain liquid crystal polymers. Glaskow:Blackie and Son, 1989.
38. Toyoda K. Ferroelectrics 2003;282:57–216.
39. Shamos MH, Shamos MI, Lavine LS. Nature 1963;197:81.
40. Shamos MH, Lavine LS. Nature 1967;213:267–269.
41. Stanford AL, Lorey RA. Nature 1968;219:1250–1251.
42. Lang SB. 10th Inter. Symp. Electrets 1999.
43. Lemanov VV. Piezo-, Pyro-, and Ferroelectricity in biological materials. In:Galassi C, Dinescu M, Uchino K, Sayer M, editors. Piezoelectric materials: advances in science, technology and applications. Kluwer, 2000.
44. Lemanov VV, Popov SN, Pankova GA. Ferroelectrics 2003;285: 581–590.
45. Lemanov VV. Ferroelectrics 2000;238:211–218.
46. White RG, Hyde GJ, Overall RL. Protoplasma 1990;158:73–85.
47. Cyr RJ. Annu. Rev. Cell Biol. 1994;10:153–180.
48. Helluin O, Beyermann M, Leuchtag HR, Duclohier H. IEEE Trans. Diec. Electr. Insul. 2001;8(4):637–643.

CHAPTER 49

Nonlinear Optical Properties of Polymers

W. M. K. P. Wijekoon, K.-S. Lee, and P. N. Prasad

The Institute for Lasers, Photonics and Biophotonics, Department of Chemistry, The State University of New York at Buffalo, Buffalo, NY 14260-3000

49.1 INTRODUCTION

Nonlinear optical (NLO) properties of organic polymers can be viewed as dielectric phenomena, and their origins can conveniently be explained by considering a planar wave propagation through a nonlinear dielectric medium [1–4]. In a dielectric medium the polarization P induced by the incident field E can be written as a power series of the field strength as follows:

$$P = \chi^{(1)} \cdot E + \chi^{(2)} \vdots EE + \chi^{(3)} \vdots EEE + \cdots, \qquad (49.1)$$

where P and E are vectors and $\chi^{(1)}$, $\chi^{(2)}$, and $\chi^{(3)}$, which relate P and E, are tensors. The linear polarizability tensor $\chi^{(1)}$ is a second-rank tensor. $\chi^{(2)}$ is the hyperpolarizability tensor and is a third-rank tensor and $\chi^{(3)}$, the second hyperpolarizability tensor, is a fourth-rank tensor. The first-order term $\chi^{(1)}$ describes linear processes such as absorption, refraction, and scattering while the higher-order terms $\chi^{(2)}$ and $\chi^{(3)}$ describe the second- and third-order NLO processes, respectively.

In general, the polarization induced in an optical medium by incident radiation can be written as [2,3]

$$P_I(\omega) = \chi^{(1)}_{IJ}(-\omega) \cdot E^{\omega}_J + \chi^{(2)}_{IJK}(-\omega;\omega_1,\omega_2) \vdots E^{\omega_1}_J E^{\omega_2}_K + \chi^{(3)}_{IJKL}(-\omega;\omega_1,\omega_2\omega_3) \vdots E^{\omega_1}_J E^{\omega_2}_K E^{\omega_3}_L + \cdots. \qquad (49.2)$$

Obviously the larger the values of $\chi^{(2)}_{IJK}$ and $\chi^{(3)}_{IJKL}$, the higher the second- and third-order polarization created in the sample, respectively. In polymeric materials, the origin of the optical nonlinearity can be traced to the molecular constituents, and therefore, one can identify polarization due to molecular units. Accordingly, the interaction of radiation with materials can be expressed in terms of the induced molecular polarization (induced dipole moment) as follows [3]:

$$p_i(\omega) = \alpha_{ij}(-\omega) \cdot F^{\omega}_j + \beta_{ijk}(-\omega;\omega_1,\omega_2) : F^{\omega_1}_j F^{\omega_2}_k + \gamma_{ijkl}(-\omega;\omega_1,\omega_2,\omega_3) \vdots F^{\omega_1}_j F^{\omega_2}_k F^{\omega_3}_l + \cdots, \qquad (49.3)$$

where the molecular susceptibilities β and γ are analogous to the bulk susceptibilities $\chi^{(2)}$ and $\chi^{(3)}$ given in Eq. (49.2)

and the local fields $F_p^{q\omega}$ take into account the difference between the actual field seen by the molecules and the applied field $E_p^{q\omega}$. There are several experimental techniques that can be employed to evaluate NLO coefficients β, γ, $\chi^{(2)}$, and $\chi^{(3)}$ of polymeric materials.

At present, polymers that exhibit large nonresonant optical nonlinearities are of considerable interest in scientific and industrial circles. Organic polymers offer significant tailoring flexibility in that their chemical structures can be modified to optimize the microscopic NLO response at the molecular level. Furthermore, at the bulk and microstructure level polymers can be processed as fibers, thin films in oriented or unoriented forms, glasses, and gels. NLO processes provide important functions of frequency conversion (for example, frequency doubling to increase the density of data storage), light controlled by electric field and even optical processes such as light controlled by light, the manifestation of which can be utilized to build photonic devices. A photonic device utilizes photons instead of electrons to acquire, process, transmit, and store information [3]. In order to be successfully applied in light-wave technology and optical circuitry a material should satisfy many criteria: easy processing, high transparency, high physical, mechanical, thermal, electrical, and chemical stability, compatibility with the other materials used for microelectronics, high optical power damage threshold, high optical nonlinearity, and reasonably low cost. Polymeric materials may be, perhaps, the first to combine most of these properties, avoiding stringent tradeoffs.

Concepts of optical computing and optical signal and image processing have been developed utilizing NLO processes to perform the functions of frequency conversions, light modulation, optical switching, optical logic, optical memory storage, and optical limiter functions. Devices performing these functions utilize two important manifestations: frequency conversion and refractive-index modulation. In the case of the second-order NLO effects refractive-index modulation is produced by application of an external electric field. Using second-order effects polymeric materials may find applications such as in second-harmonic generation, high-density data storage, and electro-optic spatial light modulation in the near future. As far as the third-order NLO effects are concerned, the refractive index is modulated by controlling the intensity of the optical field, and it provides the mechanism for optical switching and optical bistability. The main advantage of using all-optical processing is the gain of speed and gain in connectivity. Polymeric materials posses fast NLO response and also can be fabricated in the form of fibers and channel waveguides to satisfy the necessary requirements. In addition, an important third-order NLO phenomenon is two-photon absorption (TPA) in which a molecule can simultaneously absorb two photons, when irradiated by intense laser pulses. Since the availability of femtosecond (fs) laser in the 1990s, a great deal of work has been done for developing the efficient two-photon absorbing materials. Such TPA materials can be employed for various photonic applications including 3-D optical data storage, 3-D microfabrication, photodynamic therapy, and optical power limiting. In this chapter, we discuss the topics related to certain theoretical aspects, concepts of material design, and evaluation techniques for second- and third-order NLO polymers as well as for two-photon absorbing organic and polymeric materials.

49.2 MEASUREMENTS OF β OF POLYMERS

Organic polymers, being amorphous, do not exhibit any second-order NLO effect, even though the molecules themselves are acentric. Therefore, in order to observe any second-order NLO effect, the isotropy of the medium has to be perturbed. This is usually accomplished by application of a strong dc electric filed. In the liquid phase, measurements are made by the technique known as electric-field-induced second-harmonic (EFISH) generation [5]. In this technique the solution is contained in a wedge-shape fused silica cell. The cell is sandwiched between two electrodes. A large dc voltage pulse is applied to the electrodes to disturb the average molecular orientation. At the same time the probing laser beam also is incident on the cell. The emerging second-harmonic generation (SHG) signal at 2ω from the cell is recorded, as the cell is translated across the laser beam (Fig. 49.1). The NLO polarization responsible for the EFISH process can be expressed as [3]

$$P_i(2\omega) = \chi^{(3)}_{ijkl}(-2\omega;\omega,\omega,0)E^{\omega}_j E^{\omega}_k E^{0}_l. \tag{49.4}$$

As the cell is moved across the incident laser beam, the optical path inside the cell varies linearly with the translated distance, so the resulting SHG signal exhibits an oscillatory behavior. The intensity of the EFISH signal can be approximated by

$$I_{2\omega} = \left(\frac{8\pi(2\omega)^2}{n^2_{\omega}n^2_{2\omega}c^2\varepsilon^2_0}\right)\frac{\sin^2[\Delta k(l/2)]}{[\Delta k(l/2)]^2}|\chi^{(3)}|^2 l^2 I^2_{\omega}, \tag{49.5}$$

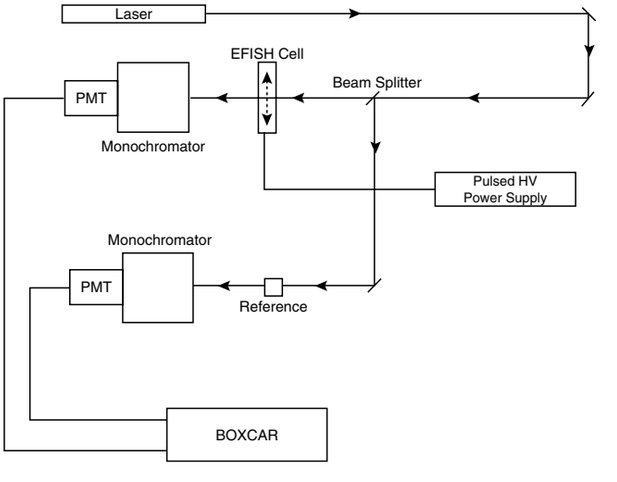

FIGURE 49.1. Schematics of experimental arrangement of electric-field-induced second-harmonic generation.

where n_i^{ω} are the refractive indices at corresponding frequencies, c is the velocity of light in vacuum, l is the thickness of the cell, ε_0 is the permittivity of free space, and Δk is the phase mismatch. Because of the dispersion of the refractive index, the fundamental and the SHG waves propagate with two different phase velocities (ω_i/K_i). Therefore, in general there exists a phase mismatch between the fundamental and the SHG waves. As shown in Eq. (49.5) when the cell is moved across the incident laser beam optical path inside the cell varies, so the emerging SHG signal generates fringes. These fringes are numerically analyzed to obtain coherence length and amplitude, which contain the necessary information to deduce β. In fact, in an EFISH experiment what one measures is an effective third-order nonlinearity $\chi^{(3)}_{\text{EFISH}}$, which can be given by

$$\chi^{(3)}_{\text{EFISH}} = f^{(0)}f^{(\omega)}f^{(\omega)}f^{(2\omega)}\sum_c N\left(\frac{\mu\beta}{5KT} + \gamma_{\text{el}}\right), \qquad (49.6)$$

where N is the number density, kT is the thermal energy, and the summation is over all components of the solution (the solute and the solvent). γ_{el} is the effective third-order hyperpolarizability for the pure four-wave mixing process ($2\omega = \omega + \omega + 0$) and it can be determined by examining the temperature behavior of $\chi^{(3)}_{\text{EFISH}}$ or can be approximated from results of a third-harmonic generation or degenerate four-wave mixing experiment. However, the magnitude of γ_{el} is generally an order of magnitude smaller than the $\mu\beta/5kT$ contribution and, therefore, can be neglected. In a centrosymmetric medium ($\mu = 0$) the EFISH signal is generated only by the third-order polarizability. The terms f describe the local field factor, which relates the applied field $E(\omega)$ to the local field $F(\omega)$.

49.3 MEASUREMENTS OF $\chi^{(2)}$ OF POLYMERS

In polymeric materials the second-order bulk susceptibility $\chi^{(2)}$ can be related to the hyperpolarizability β through the relationship [3]

$$\chi^{(2)}_{IJK}(-2\omega;\omega,\omega) = N\beta_{IJK}f_I^{2\omega}f_J^{\omega}f_K^{\omega}\langle O(\theta,\phi)\rangle, \qquad (49.7)$$

where N is the molecular number density, $f_p^{q\omega}$ is the local-field factor, and $\langle O(\theta,\phi)\rangle$ is the orientation factor that projects β_{ijk} on to macroscopic coordinates IJK. It should be noted that in the past the majority of the SHG data have been presented in terms of a d_{ijk} coefficient, which is related to $\chi^{(2)}$ by $\chi^{(2)}_{ijk} = 2d_{ijk}$. The number of nonzero components in the $\chi^{(2)}_{ijk}$ tensor depends on the point-group symmetry of the material.

There are several techniques, both absolute and relative, which can be used to evaluate $\chi^{(2)}_{ijk}$ components of a material [3]. However, in the case of polymeric materials the most useful method is Maker fringe method [6–8]. The general form of the second-order polarization created in a sample by the incoming fundamental beam can be approximated as [3]

$$P_i(2\omega) = \chi^{(2)}_{ijk}(-2\omega;\omega,\omega)E_J^{\omega}E_k^{\omega}. \qquad (49.8)$$

In the Maker fringe method the sample is rotated in a plane perpendicular to the plane of the probing laser beam (Fig. 49.2), giving rise to a fringe pattern. The magnitude of the second-order polarization created in the sample depends on a number of parameters as shown in Eq. (49.9), where $\chi^{(2)}$ is the NLO coefficient, l is the thickness of the sample, $n_{i\omega}$ is the refractive index at the relevant frequency, P_{ω} is the intensity of the fundamental beam, and Δk is the phase mismatch between the fundamental and the SHG beams:

$$P_{2\omega} \propto \left(\frac{1}{n_{\omega}^2 n_{2\omega}}\right)\frac{\sin^2[\Delta k(l/2)]}{[\Delta k(l/2)]^2}|\chi^{(2)}|^2 l^2 |p_{\omega}|^2. \qquad (49.9)$$

As shown in Eq. (49.9) the SHG polarization generated in the sample shows an oscillatory behavior as a function of the sample thickness. Therefore, if the sample is rotated the SHG intensity shows a fringe pattern as a function of the angle of rotation. These fringes under the condition $\Delta k \neq 0$ are known as Maker fringes and their period is related to the coherent length l_c. The fringes are originated due to the phase mismatch (Δk) between the forced and harmonic waves. The SHG intensity oscillates with the angle as shown in Eq. (49.10), where l is the sample thickness, $I_m(\theta)$ is the envelope function, and $l_c(\theta)$ is the coherence length. Experimentally, the coherent length is determined by fitting the Maker fringes to the appropriate theoretical expression. Once the coherent length is determined by a fitting procedure, with the proper choice of input and output polarization combinations, one can evaluate the NLO coefficients with respect to a known reference (for example, quartz) by using the simplified ($n_{\omega} \approx n_{2\omega} \approx n$) relationship given in Eq (49.11) [2]:

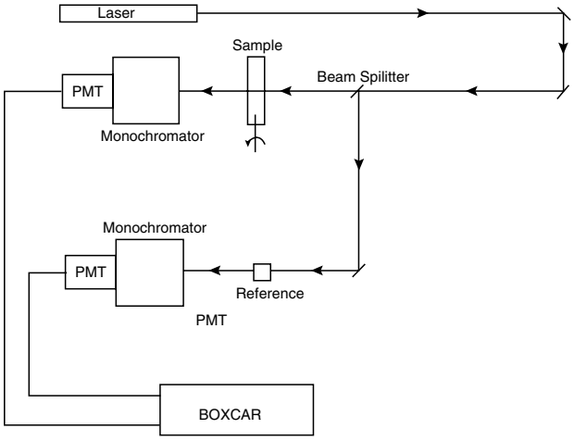

FIGURE 49.2. Schematics of experimental arrangement for measuring $\chi^{(2)}$ values of oriented polymers by the second-harmonic generation. The same arrangement can be used for the measurements ox $\chi^{(3)}$ via third-harmonic generation. In the case of the third-harmonic generation the measurement is usually carried out in a vacuum.

$$I_\omega = I_m^2(\theta)\left[\sin^2\left(\frac{\pi l}{2l_c(\theta)}\right)\right]^2, \tag{49.10}$$

$$\chi_s^{(2)} \approx \frac{\pi}{2}\left(\frac{n_s^3}{l_s^2}\right)^{1/2}\left(\frac{l_c^2}{n_r^3}\right)^{1/2}\frac{I_{2\omega,\,S}}{I_{2\omega,\,r}}\chi_r^{(2)}. \tag{49.11}$$

However, organic polymers, being amorphous, do not show second-order NLO effects. In order to employ them in second-order NLO measurements a polar order is induced by an external means such as electric field poling process or the Langmuir–Blodgett (LB) technique. Poled polymers and the majority of the LB films possess $C_{\infty v}$ symmetry. Therefore, the second-order optical susceptibility tensor for SHG has only three independent nonzero elements, namely, $\chi_{zzz}^{(2)}$, $\chi_{zxx}^{(2)}$ and $\chi_{xxz}^{(2)}$. Under Klienman symmetry [9] conjecture this reduces to two independent elements $\chi_{zzz}^{(2)}$ and $\chi_{zxx}^{(2)}$. These two elements can be evaluated by measuring the p-polarized SHG intensity emerging from the sample by incident p- and s-polarized fundamental beams, respectively.

49.4 β AND $\chi^{(2)}$ VALUES OF POLYMERS

The β and $\chi^{(2)}$ values have been measured for a large number of chromophores in solution and in polymeric films in attempts to identify efficient second-order NLO polymers. Table 49.1 shows $\mu\beta$ values that were derived from EFISH measurements of several organic polymers. All polymers in Table 49.1 have basically the same hyperpolarizability as their analogous monomers [10]. Also the copolymer and the homopolymers exhibit the same $\mu\beta$ values in solution, indicating no enhancement of NLO properties due to cooperative effects. In the case of 4-methoxy-4′-carbomethoxy-α-amino-α'-cyanostilbene polymers, again the $\mu\beta$ values are approximately the same [11]. However, in the case of NSPMA$_n$,NSV$_n$, and NBSBMA$_n$ polymers, NSPMA$_n$ has a noticeably larger hyperpolarizability which can be attributed to the electron donating strength of the amino group [10].

The early studies on electric field poling were performed mainly on the guest-host systems, for instance, DANS dissolved in thermotropic nematic liquid-crystalline polymers [12]. In this guest-host system polar order decays rapidly. The $\chi_{zzz}^{(2)}$ value was about 1 pm/V. Therefore, the later investigations on guest-host systems were focused on both increasing the temporal stability as well as the $\chi_{zzz}^{(2)}$ value.

Among guest-host systems, the most studied system is Disperse Red-doped polymethylmethacrylate (PMMA) (Fig. 49.3) [13]. The early poling experiments on this system were accomplished by using parallel-plate electrodes and different doping levels. The maximum $\chi_{zzz}^{(2)}$ value obtained with parallel-plate poling was 5 pm/V. Subsequent experiments employed corona poling, and it was possible to achieve a $\chi_{zzz}^{(2)}$ value of 13.4 pm/V in thus poled samples [14]. Table 49.2 shows $d_{33}(=0.5\chi_{zzz}^{(2)})$ values of various NLO chromophores in a PMMA polymer host [13–17].

One efficient way to increase the number density of NLO chromophores in a polymeric host, without crystallization, phase separation, and any concentration gradient, is to attach them as side chains of a polymer [15,18]. Also, the temporal stability of the poled structures of side-chain NLO polymers has been proven to be much better than that of the same guest–host system due to the higher glass transition temperature of the polymer. A number of poled side-chain NLO polymers (Fig 49.4) have employed for SHG measurements. Table 49.3 exhibits d_{33} values of some side-chain NLO polymers [16–28].

Many of the side-chain NLO polymers, both copolymers and homopolymers, have been designed using a PMMA polymer skeleton as the backbone. This includes novel methacrylate polymers which contain a molecular-ionic NLO chromophore, N-akkylpyridinium salt, in the side chain [25,26]. The corona-poled polymer films of such polymers showed a larger $\chi^{(2)}$ value of the homopolymer

TABLE 49.1. *The product ($\mu\beta$) obtained from EFISH measurements of several second-order NLO polymers.*

Polymer	$\mu\beta(10^{-48}$ esu)	$\lambda\mu$	References
NSPMA$_n$	93.1	1.9074	[9]
NSV$_n$	315	1.064	[9]
NSME-BP6-5	305	1.907	[9]
	561	1.064	
NBSBMA$_n$	93	1.907	[9]
	265	1.064	
4-Methoxy-4′-carbomethoxy-α-amino-α'-cyanostilbene: R = 4 − CH_2CH_2O−	74	1.907	[10]
4-Methoxy-4′-carbomethoxy-α-amino-α'-cyanostilbene: R = 4 − CH_2O−	61	1.907	[10]
4-Methoxy-4′-carbomethoxy-α-amino-α'-cyanostilbene: R = 4 − O−	63	1.907	[10]
4-Methoxy-4′-carbomethoxy-α-amino-α'-cyanostilbene: copolymer	79	1.907	[10]

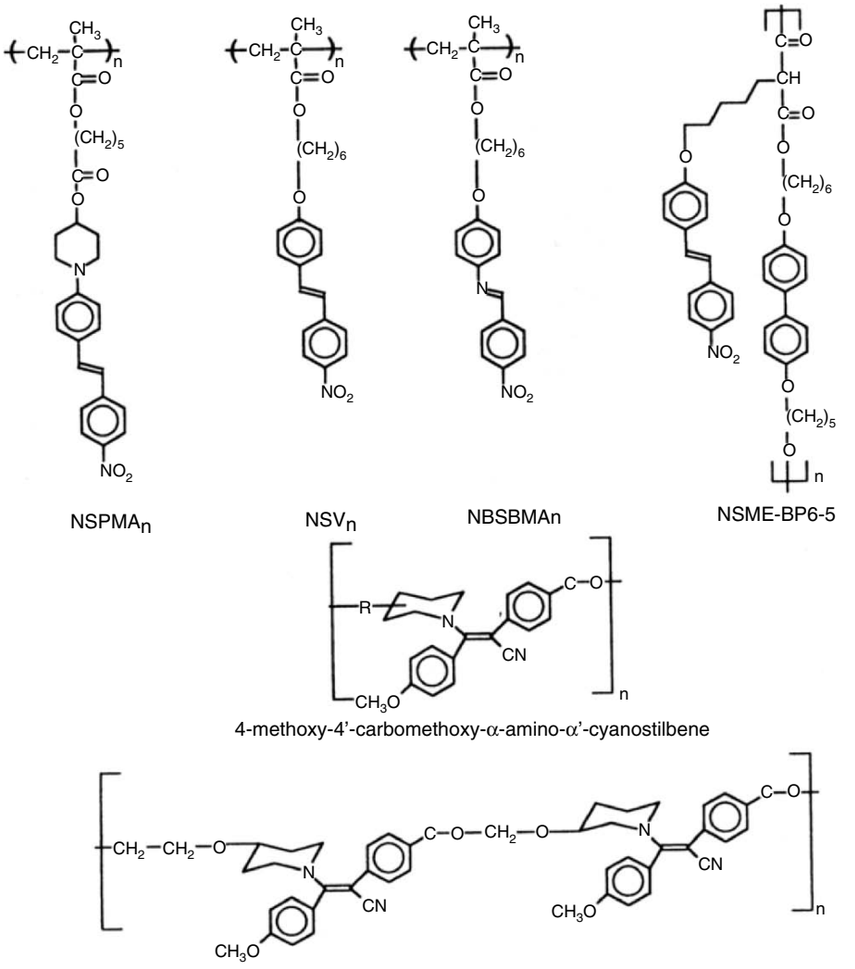

FIGURE 49.3. Molecular structures of the NLO polymers described in Table 49.1.

TABLE 49.2. *The NLO coefficient* $d_{33}(=0.5\chi^{(2)}_{333})$ *of various NLO chromophores doped in a PMMA polymer matrix. NLO chromophores have been oriented by the poling process.*

Polymer	d_{33} (pm/V)	$\lambda(\mu m)$	References
PMMA:Disperse Red (plate poling)	2.5	1.58	[12]
PMMA:Disperse Red (corona poling)	6.7	1.58	[13]
PMMA:4-(dicyanovinyl)-4-(dialkylamino) azobenzene	74	1.58	[14]
PMMA:Disperse Orange 3	5.8	1.064	[15]
PMMA:4-(tricyanovinyl)-*N*, *N*'-dimethylaniline	16	1.064	
PMMA:Disperse Red	5.8	1.064	
PMMA:3-(dicanomethylene)-5,5dimethyl-1-[[5-(dimethylamino)-2-thienyl]vinyl]cyclohexene	38	1.3	[16]
PMMA:3-(dicyanomethylene)-5,5-dimethyl-1-[*p*-(dimethylamino)styryl]cyclohexene	26	1.3	[16]
PMMA:2-[[4-[-(dimethylamino)styryl]phenyl] methylene]propanediritrile	27	1.3	[16]

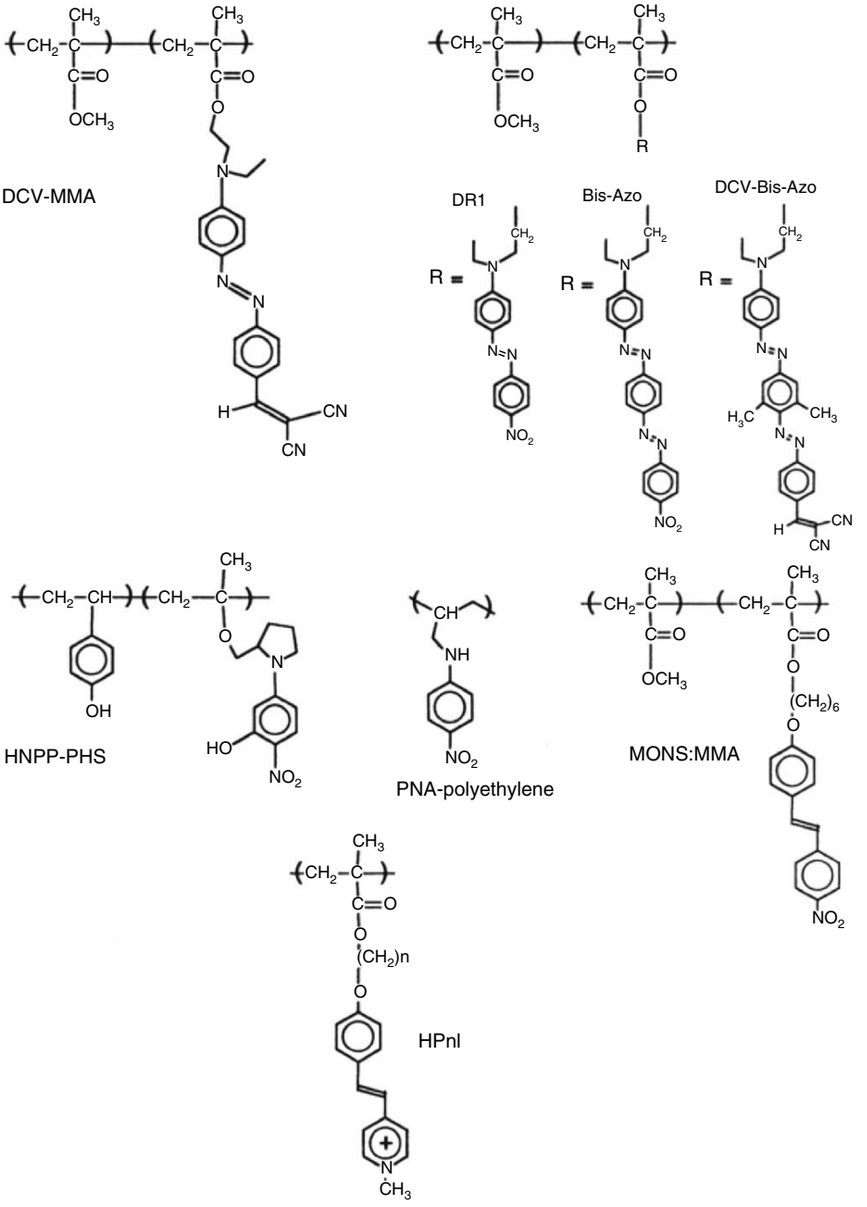

FIGURE 49.4. Molecular structures of the NLO polymers described in Table 49.3.

($\chi^{(2)}_{zzz} = 15.9\,\text{pm/V}$) compared to that of the copolymer ($\chi^{(2)}_{zzz} = 10.0\,\text{pm/V}$). The lower $\chi^{(2)}_{zzz}$ value of the homopolymer has been attributed to the lower chromophore concentration in the copolymer. The temporal stability as well as the poling-induced alignment of these side-chain molecular-ionic polymers can be largely improved by incorporation of bulky counterions. For example, the SHG intensity in a bulky counterion, tetraphenylborate, -containing polymer is about five times larger than that of the analogous iodide-containing polymer [25].

Somewhat larger d_{33} values (40 pm/V at 1.064 μm) have been obtained in several poly(styrene-co-acrylic acid esters) side-chain copolymers that were synthesized by attaching hydroxy-functionalized azobenzene, benzylidene aniline, and coumarin chromophores. The stability of the poled structures of these polymers was found to be better than that of NLO guest-loaded PMMA films [29]. Temporal stability of poled structures can be improved if NLO chromophores are attached to the polymer backbone forming a main-chain polymer (Fig. 49.5) (Table 49.4). One such example is poly(urea) [30]. This polymer can be prepared from vapor deposition polymerization. Some main-chain NLO polymers in which the dipole moment of the NLO chromophore is perpendicular to the polymer backbone

TABLE 49.3. *The NLO coefficient* $d_{33}(= 0.5\chi^{(2)}_{333})$ *of poled side-chain NLO polymers.*

Polymer	d_{33} (pm/V)	$\lambda(\mu m)$	References
DCV-MMA	>50	1.58	[15]
DR1-tethered PMMA	43	1.064	[18]
bis-Azoanalog of DR1-tethered PMMA	69	1.064	[18]
Dicyanovinyl bis-Azoanalog of DR1-tethered PMMA	150	1.064	[18]
PNA attached polyethylene	>30	1.064	[19]
HNPP-PHS	7.5	1.064	[20]
Poly(N-MNA acrylamide)	3	1.064	[21]
NPP-PPO	27	1.064	[22,23]
HPOB	15.6 (10^{-8} esu)	1.064	[24]
HP6B	36.2 (10^{-8} esu)	1.064	[24]
HP6I	7.6 (10^{-8} esu)	1.064	[24]
HP10B	21.8 (10^{-8} esu)	1.064	[24]
HPBR15	11.8	1.064	[25]
HPBR21	10.8	1.064	[25]
CP6I-HEMA	20	1.064	[25]
$NSPMA_n$	7.3 (10^{-8} esu)	1.064	[9]
$NBSBMA_n$	7.0 (10^{-8} esu)	1.064	[9]
NSME-BP6-5	1 (10^{-8} esu)	1.064	[9]
MONS:MMA	20 (10^{-8} esu)	1.064	[26]
EPO-TEK 310-2 and DANS	0.04–0.4	1.064	[27]

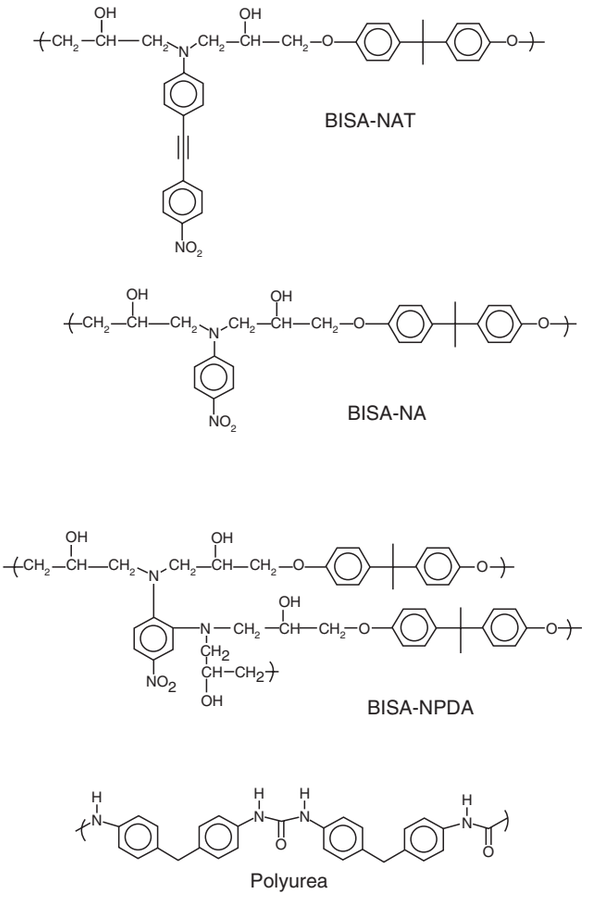

FIGURE 49.5. Molecular structures of the NLO polymers described in Table 49.4.

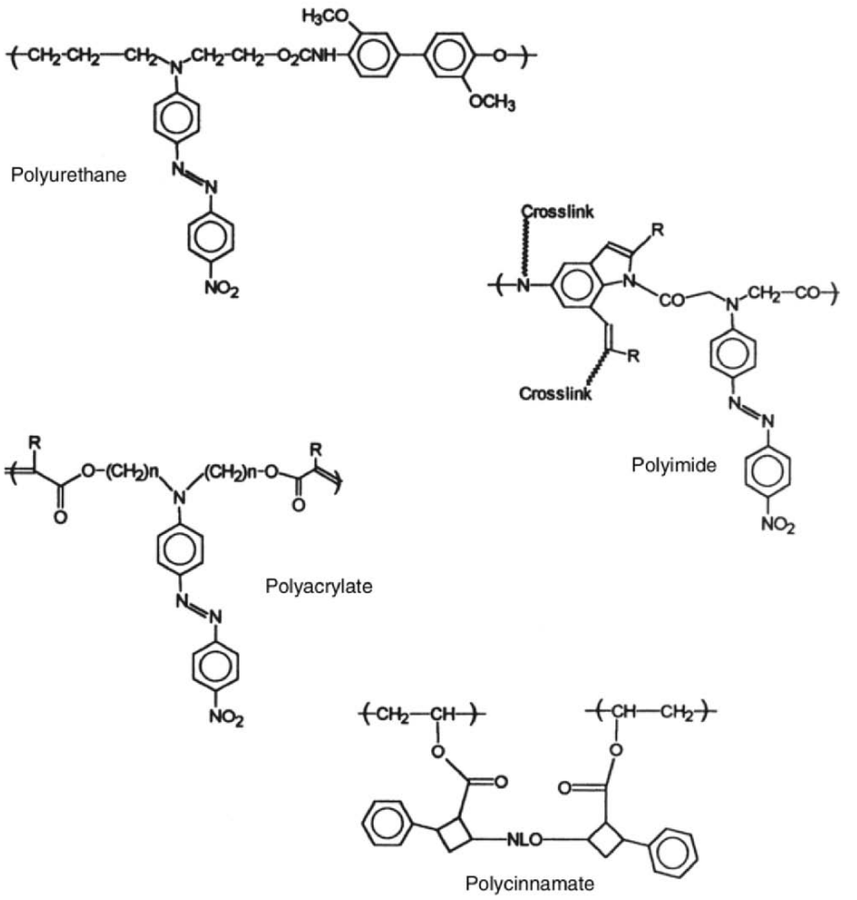

FIGURE 49.5. Continued

have also been used for NLO measurements. An example of such a polymer is bisA-ANT [31]. This type of main-chain polymer is expected to be easier to pole than the head-to-tail main-chain polymers due to their enhanced flexibility. The bulky tolane unit in bisA-ANT is supposed to improve the temporal stability of the poled films. In fact, the decay of polar order of bisA-ANT was found to be much better than that of the analogous pNA polymer.

The temporal stability of poled NLO materials is considerably improved by incorporating them in cross-linked systems (Fig. 49.6). Interesting results have also been obtained recently by Dalton and co-workers in cross-linked poly(urethanes). In their study the NLO chromophore was polymerized with bifunctional isocyanate to obtain the corresponding urethane polymer [32,33]. Both cross-linked and non-cross-linked polymers show no thermal transitions below 270°C. Although cross-linking can remarkably improve the temporal stability of poled structures, thermal and chemical cross-linking require processing of materials at elevated temperatures. These temperatures sometimes tend to degrade NLO chromophores. Therefore, an alternative cross-linking procedure such as photochemical cross-linking has been studied [34,35]. One such system is poly-

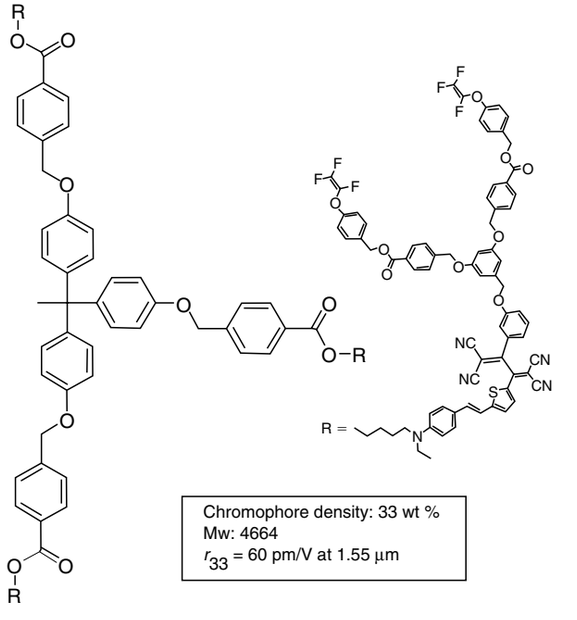

FIGURE 49.6. Chemical structure of a multiarm cross-linkable Nlo dendrimer.

(vinylcinnamate) doped with a NLO chromophore. In this guest–host system it was possible to achieve a 20% loading level of guest molecules without phase separation. Although the T_g of the system is found to be dependent on the chromophore concentration, plasticization of the chromophore was remarkably small. Absorption measurements indicate that the polar order in the poled film persists for a long period of time (many months) without any change [35]. Table 49.4 shows d_{33} values obtained from poled films of some side-chain polymers [36–43].

Also, the Langmuir–Blodgett (LB) technique has been employed to prepare oriented thin films of organic polymers for NLO investigations. An LB film containing 20 bilayers of alternating monolayer of two different polymers yield a thickness of 60 nm and a $\chi^{(2)}_{zzz}$ of 11.2×10^{-16} esu cm per bilayer at 1.047 μm [44]. Molecular nonlinearity in this LB film is supposed be arising from charge-transfer excitation in the polymer with the sulfonyl group as the acceptor and amino group as the donor. Optical waveguides capable of guiding blue light with low loss (2–6 dB cm^{-1}) over several centimeters have been fabricated from NLO polymers using the LB technique. However, it was necessary to use another NLO inactive polymer (*t*-butyl methacrylate polymer) as buffer layer in order to prevent the formation of inversion center in the film [45–48]. An LB film containing 168 bilayers (thickness $\sim 0.44\,\mu$m) showed waveguide attenuation at 457.9 nm of 5.8 dB/cm for TE polarization and 2.6 dB/cm for TM polarization. The SHG measurements on a 0.88-μm-thick LB film results in a $\chi^{(2)}_{zzz}$ value of 8×10^{-9} esu. Similar $\chi^{(2)}_{zzz}$ values ($d_{33} = 5.3 \times 10^{-9}$ esu) have been obtained for Langmuir–Schaefer films of mesogenic moieties containing polysilane copolymers [49].

Current strategies for developing highly $\chi^{(2)}$ activities of NLO polymers basically involve molecular design concepts, same as presented in the previous sections. The key steps are: (i) design of high $\mu\beta$ chromophores; (ii) improvement of temporal stability of NLO response in polymer matrices; and (iii) poling efficiency of the polymeric systems [50]. Among these, the most important factor might be to design highly efficient NLO chromophores. Therefore, to understand the structure–property relationship of chromophores with high $\chi^{(2)}$ values, quantum mechanical analysis based on a simple two-level model description and bond-order alternation principle have been investigated [51,52]. Table 49.5 shows values of $\mu\beta$ at the off-resonance wavelength of 1907 nm for some representative chromophores, with improved optical nonlinearity [53,54]. A large enhancement of optical nonlinearity can be obtained by extending the length of π-bridged chains with strong electron acceptor such as the cyano group. It was shown that very large electro-optic (E-O) coefficients could be achieved by introducing highly efficient chromophores into amorphous polymer matrix such as poly(methyl methaacrylate)(PMMA), polycarbonate, polyquinoline, etc. [55–59]. In the case of PMMA added with 17.5% of chromophore 10, the E-O coefficient was reported to be $r_{33} = 105\,\mathrm{pmV^{-1}}$ at 1.33 μm [60]. This is more than three times higher than that of lithium niobate ($LiNbO_3$; $r_{33} = 31\,\mathrm{pmV^{-1}}$), which has been used as a material for E-O modulators.

To improve the temporal and the thermal stabilities of poled NLO dipoles, polyurethanes can be considered as one of the best matrix materials, because of their extensive formation of H-bonding between the urethane linkages which would increase the rigidity of the polymer chain. Several researchers succeeded in making greatly enhanced NLO polymeric systems by using polyurethane backbone [61–68]. Also, polyimides [69–80], polyetherimides [81,82], polyamides [83–89], and polyesters [90–94] as matrix polymers can also provide an enhanced thermal stability of aligned dipoles due to high glass transition temperature (T_g) characteristics which also result in the chain stiffness. By incorporating the NLO chromophores into these polymer backbones, much improved long-term thermal stability of NLO activity were obtained.

Another promising approach for making efficient NLO systems is the employment of dendritic polymers [95–111]. Compared to common polymers, dendritic NLO polymers can provide many advantages from the viewpoint of structural variation, optimization of E-O values, thermal stability, optical loss, etc. Jen's group prepared a multiarm

TABLE 49.4. *The NLO coefficient* $d_{33}(=0.5\chi^{(2)}_{333})$ *of poled main-chain NLO polymers.*

Polymer	d_{33} (pm/V)	$\lambda(\mu m)$	References
Polyurea	6.6	1.064	[29]
BisA-NAT	90	1.064	[35]
BisA-NAT	~30	1.064	[35]
BisA-NPDA	13.5 $d_{31} = 3$	1.064	[36]
Polyurethane	40	1.064	[37]
NLO chromophore tethered	120	1.064	[38]
Polyimide (NLO chromophore tethered)	4.6–5.5	1.064	[39]
NLO-chromophore-tethered acrylate	60		[40]
Polycinnamate: photocross-linked with NLO chromophore	<11.5–21.5	1.54	[41,42]

TABLE 49.5. *The $\mu\beta$ values of NLO chromophores with the extended π-chain length and strong acceptor at the end of molecules.*

NLO Chromophores	$\mu\beta$ (10^{-48} esu)	NLO Chromophores	$\mu\beta$ (10^{-48} esu)
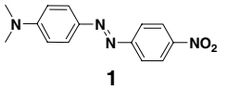 **1**	580	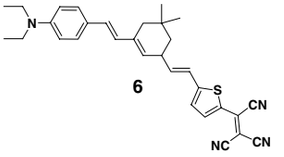 **6**	13,000
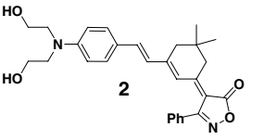 **2**	926	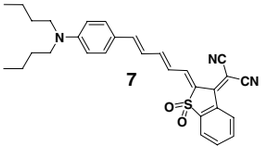 **7**	13,500
 **3**	3,300	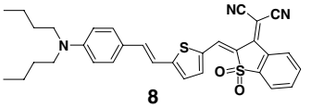 **8**	15,000
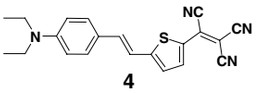 **4**	6,200	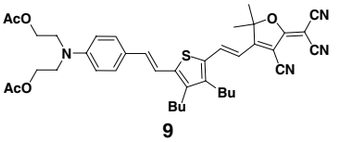 **9**	18,000
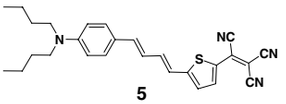 **5**	9,800	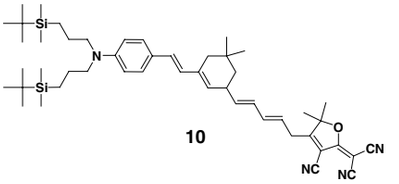 **10**	35,000

cross-linkable NLO dendrimer which consists of phenyltetracyanobutadienyl thiophene-stilbene-based NLO chromophore as the core and cross-linkable trifluorovinyl ether-containing dendrons as the exterior unit (Fig. 49.6) [99]. The maximum r_{33} value of this system was found to be 60 pmV^{-1} at 1.55 μm and long-term alignment stability was achieved for the poled dendrimer after thermal curing. It retained over 90% of its original r_{33} value at 85 °C for more than 1,000 hours.

49.5 THIRD-ORDER NLO PHENOMENA

Third-order NLO effects are described by the macroscopic term $\chi^{(3)}_{IJKL}$ in Eq. (49.2). As in the case of second-order NLO susceptibility, the third-order NLO susceptibility $\chi^{(3)}_{IJKL}$ can be related to the microscopic third-order NLO coefficient γ_{IJKL} via the following relationship [2,3]:

$$\chi^{(3)}_{IJKL} = N f_I^{\omega_1} f_J^{\omega_2} f_K^{\omega_3} f_L^{\omega_4} \gamma_{IJKL}, \tag{49.12}$$

where N is the molecular number density and f_p^{ω} is the appropriate local field factor. The γ_{IJKL} in the laboratory fixed frame can be related to the molecular frame as

$$\gamma_{IJKL} = \sum_{ijkl} a_{Ii} a_{Jj} a_{Kk} a_{Ll} \gamma_{ijkl}, \tag{49.13}$$

where a_{Ii} is the directional cosine between I and i of the laboratory and molecular frame, respectively. Being a fourth-rank tensor, $\chi^{(3)}_{IJKL}$ contains 81 elements [112]. However, the nonzero components of $\chi^{(3)}_{IJKL}$ depend on the symmetry of the molecule. Third-order NLO measurements can conveniently be made on solution or in thin films of polymers. In solution measurements an average over all directions (orientations) has to be taken into account. For example, if the solute molecules belongs to the orthorhombic point group there are 21 nonzero components in the γ_{ijkl} tensor. If one assumes Klienman symmetry [9] ($\gamma_{xxyy} = \gamma_{xyxy} = \gamma_{xyyx} = \gamma_{yyxx} = \gamma_{yxxy} = \gamma_{yxyx}$ the number of independent elements reduces to six, i.e., γ_{xxxx}, γ_{yyyy}, γ_{zzzz}, γ_{yyzz}, γ_{xxzz}, and γ_{xxyy}. What is measured in experiments is the macroscopic third-order NLO susceptibility $\chi^{(3)}_{IJKL}$. For example, in the degenerate four-wave mixing experiment, when all the beams possess the same polarization, one measures $\chi^{(3)}_{xxxx}(-\omega;\omega,\omega,-\omega)$. The third-order polarizability calculated from this measurement is an orientationally averaged quantity, $\langle\gamma\rangle$, which can be expressed as [113]

$$\langle\gamma\rangle = \frac{1}{5}(\gamma_{xxxx} + \gamma_{yyyy} + \gamma_{zzzz} + 2\gamma_{xxyy} + 2\gamma_{xxzz} + 2\gamma_{yyzz}). \quad (49.14)$$

There are several four-wave mixing techniques that can be used to evaluate $\chi^{(3)}_{IJKL}$ components of a material [3]. It should be noted that there are numerous third-order processes that are described by different $\chi^{(3)}_{IJKL}$ terms. Hence, a comparison of $\chi^{(3)}_{IJKL}$ derived from one technique with $\chi^{(3)}_{IJKL}$ evaluated with another technique should be made cautiously.

49.6 THIRD-HARMONIC GENERATION

In general, the NLO polarization responsible for third-harmonic generation (THG) can be given by [2,3]

$$P_I(3\omega) = \chi^{(3)}_{IJKL}(-3\omega;\omega,\omega,\omega)E^{\omega}_J E^{\omega}_K E^{\omega}_K. \quad (49.15)$$

THG is a coherent process and arises due to purely electronic contributions and does not depend on the population of the excited state. However, the process can be resonantly enhanced in the vicinity of one- or multiphoton absorption bands. The THG intensity created in a sample can be expressed as [2]

$$I_{3\omega} = \left(\frac{(3\omega)^2}{n_{3\omega}n^3_{\omega}c^4\varepsilon^2_0}\right)\frac{\sin^2[\Delta k(l/2)]}{[\Delta k(l/2)]^2}|\chi^{(3)}|^2 l^2 I^3_{\omega}. \quad (49.16)$$

As shown in Eq. (49.16) the THG intensity shows symmetrically damped oscillatory behavior near $\Delta k = 0$. Unlike SHG, phase matching is very difficult to achieve in THG due to dispersion of the refractive indices. In the THG experiment, the intensity of the sample is measured with respect to a standard sample under identical experimental conditions. Under the conditions $\Delta k \neq 0$, the sample is rotated around an axis perpendicular to the plane of incidence, and the THG signal is recorded as a function of the angle of rotation. The resulting THG fringes are analyzed to obtain the coherent length of the material. Then the $\chi^{(3)}_{IJKL}(-3\omega;\omega,\omega,\omega)$ of the sample is evaluated using the following relationship [3]

$$\frac{I_{3\omega,\,s}}{I_{3\omega,\,r}} = \left(\frac{\chi^{(3)}_s}{\chi^{(3)}_r}\right)^2\left(\frac{l_{c,\,r}}{l_{c,\,s}}\right)^2 \quad (49.17)$$

49.7 DEGENERATE FOUR-WAVE MIXING

In a degenerate four-wave mixing (DFWM) process, three optical beams of the same frequency interact with the material to create a fourth beam of the same frequency. The NLO polarization responsible for this process can be given by [2,3]

$$P_I(\omega) = \chi^{(3)}_{IJKL}(-\omega;\omega,\omega,-\omega)E^{\omega}_J E^{\omega}_K E^{*\omega}_L. \quad (49.18)$$

Measurements of DFWM contain both real and imaginary parts of $\chi^{(3)}_{IJKL}$. This method is convenient and versatile in measuring both electronic and dynamic nonlinearities and their response times. The experiment can be performed either in a forward (boxcar) geometry or in a backward-wave geometry. In the case of the backward-wave geometry the condition $\Delta k = 0$ is automatically satisfied. In this geometry two pump beams counterpropagate in the sample (Fig. 49.7). The probe beam is incident on the sample. The probe beam is incident on the sample at a small angle with the two pump beams. The signal beam is obtained as a phase conjugate beam (counterpropagating to the probe beam), and it corrects every distortion of the probe beam when it retraces it. The intensity of the signal beam for this process is given by

$$I_s = \left(\frac{\omega^2}{4n^2c^2}\right)|\chi^{(3)}|^2 l^2 I_f I_b I_p. \quad (49.19)$$

Both pump beams are synchronized in time with their cross-correlation, and the DFWM signal is studied as a function of the time delay of the probe beam. For nonabsorbing materials the $\chi^{(3)}$ value is calculated using the relationship [3]

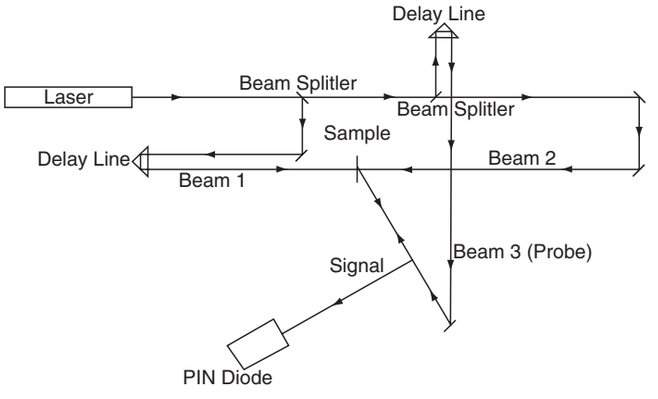

FIGURE 49.7. Schematics of experimental arrangement of the degenerate four-wave mixing (backward geometry) experiment.

$$\frac{\chi_s^{(3)}}{\chi_r^{(3)}} = \left(\frac{n_s}{n_r}\right)^2 \left(\frac{l_r}{l_s}\right) \left(\frac{I_s}{I_r}\right)^{1/2} \tag{49.20}$$

For absorbing samples a correction should be made to compensate the absorption losses; consequently, $\chi^{(3)}$ can be calculated by the following relationship [3]:

$$\frac{\chi_s^{(3)}}{\chi_r^{(3)}} = \left(\frac{n_s}{n_r}\right)^2 \left(\frac{l_r}{l_s}\right) \left(\frac{I_s}{I_r}\right)^{1/2} \frac{\alpha l_s}{e^{(-\alpha l_s/2)}(1 - e^{(-\alpha l_s)}),} \tag{49.21}$$

where α is the linear absorption coefficient. In Eqs. (49.20) and (49.21), I_s and I_r refer to intensities at zero time delay.

49.8 OPTICAL KERR GATE

The optical Kerr gate (OKG) is a process that arises due to optically induced birefringence caused by a nonlinear phase shift. The NLO polarization for the OKG can be expressed as [2,3]

$$P_I(\omega) = \chi_{IJKL}^{(3)}(-\omega;\omega,\omega,-\omega) E_J^{\omega} E_K^{\omega} E_L^{\omega}. \tag{49.22}$$

There are several different mechanisms such as electronic deformation, molecular reorientation, electrostriction, molecular redistribution, and thermal change that are responsible for the OKG process. Each of these mechanisms has its own strength and response time, which generally differ from each other. OKG measurements are usually performed by the incidence of a strong pump beam (orienting beam) on the sample. Then propagation characteristics of a weak probe beam is studied as a function of the delay time (Fig. 49.8). Initially both beams are linearly polarized. To retrieve the optical birefringence information the probe beam is passed through an analyzer.

The optical birefringence created in the sample due to penetration of strong pump beam can be expressed as

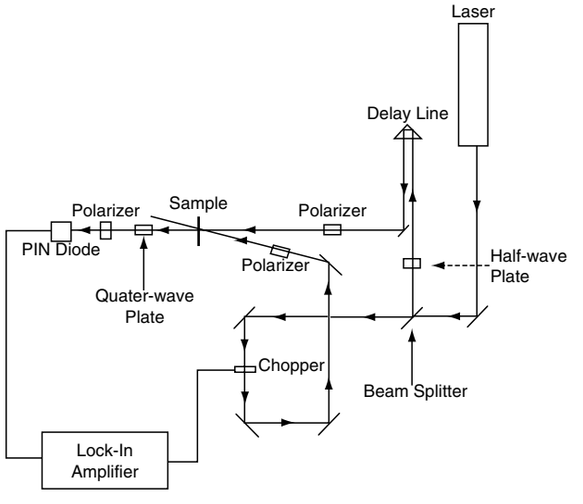

FIGURE 49.8. Schematics of experimental arrangement of the optical Kerr gate measurement.

$$\delta n = (\delta n_{\parallel} - \delta n_{\perp}) \propto \frac{\pi}{n_0}(\chi_{xxxx}^{(3)} - \chi_{xxyy}^{(3)}). \tag{49.23}$$

This birefringence is probed by the weak probe beam. By delaying the probe beam, the time evolution of the process can be studied. The intensity of the signal of the probe beam through the Kerr gate as a function of the delay time can be written as [3]

$$I_t(\tau) = \int_{-\infty}^{+\infty} \langle E_{\text{probe}}^2(t-\tau)\rangle \sin^2\left(\delta n \frac{\pi l}{2}\right) dt \tag{49.24}$$

Away from electronic resonances $\delta n = n_2 I_{\text{pump}}$. The quantity n_2 can be obtained from the measurement at $t = 0$ (peak value). Therefore, $\chi_{xxxx}^{(3)}$ can be obtained assuming that $\chi_{xxyy}^{(3)}$ is very small. However, away from resonances, in an isotropic medium a purely electronic nonlinearity leads to $\chi_{xxxx}^{(3)} = 3\chi_{xxyy}^{(3)}$. In such a situation $\chi_{xxxx}^{(3)}$ can be directly evaluated.

49.9 SELF-FOCUSING AND DEFOCUSING

Self-focusing and defocusing (SFD) also arise from the intensity dependence of the refractive index of the medium [114,115]. It is referred as self-action because the NLO polarization created by the input beam changes its own propagation characteristics. SFD does not provide any information on response time. In general the intensity-dependent refractive index responsible for SFD can be written as

$$n(\lambda) = n_0(\lambda) + n_2(\lambda) I, \tag{49.25}$$

where I is the intensity of the input beam and n_0 is the linear refractive index. The NLO refractive index n_2 is related to $\chi^{(3)}$ as shown in Eq. (49.26). The self-focusing occurs as a combined effect of a positive n_2 and spatial variation of the laser-beam intensity. If the laser-beam intensity at the center of the beam is higher than that at the beam edges, a relatively larger refractive index is resulted at the center. So the sample acts as a positive lens and focuses the beam. Similarly, self-defocusing occurs when n_2 is negative. The relationship between n_2 and $\chi^{(3)}$ is shown below:

$$n_2(\lambda) = \frac{8\pi^2}{c n_0(\lambda)} \frac{\chi^{(3)}(\lambda)}{6}. \tag{49.26}$$

There are two different $\chi^{(3)}$ measurement techniques that are based on self-action: (i) optical power limiter and (ii) the z scan. In the case of the optical power limiter the laser beam is focused in the sample with high n_2. For low input powers the transmitted beam is focused through a pinhole on the detector. As the power increases the self-focusing starts so that the focused beam is no longer focused through the pinhole and the power after pinhole decreases. Beyond a certain critical input power P_c, transmitted power levels off due to many other NLO processes. The critical power P_c is directly related to n_2 through the relation (for spatial Gaussian beam) [116]

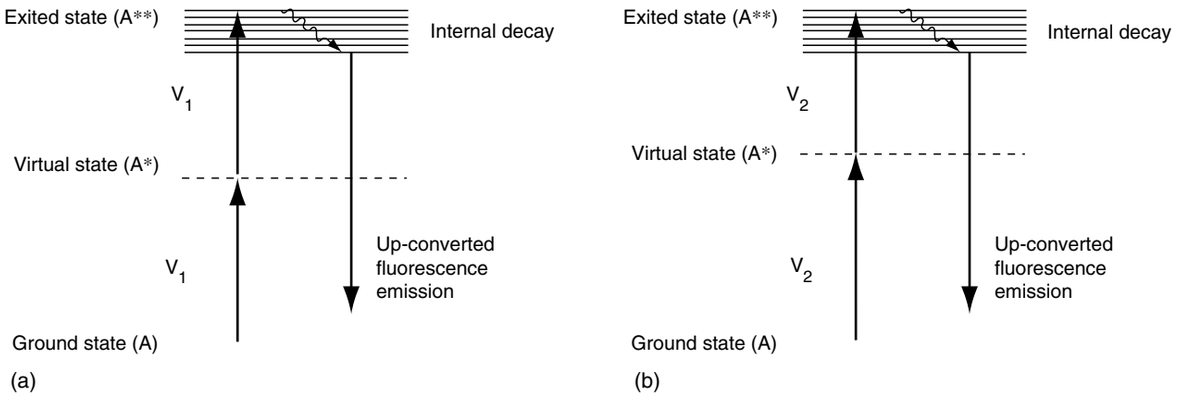

FIGURE 49.9 Two-photon absorption schemes. (a) Degenerate TPA process and (b) nondegenerate TPA process by simultaneous excitation of two-photons.

$$n_2 = \left(\frac{3.72c\lambda^2}{32\pi^2}\right)\frac{1}{P_c}. \tag{49.27}$$

Therefore, $\chi^{(3)}$ can be evaluated.

The z-scan method allows determination of both the magnitude and the sign of n_2 [117]. In this technique a gaussian beam is focused on the sample, and the transmitted power is measured with a detector after passing the beam through a pinhole kept at the far field. The sample is then moved through the focus of the beam. Near the vicinity of beam focus self-action may occur due to strong intensity. The resultant plot of the intensity of the transmitted beam through the pinhole yields a dispersionlike behavior from which n_2 can be evaluated. The z-scan method is very sensitive to the beam quality so that beam should be a pure gaussian TEM_{00}. Because of the high-power and long-interaction- length requirements, the z scan is more suitable for the $\chi^{(3)}$ measurements of polymer solutions.

49.10 TWO-PHOTON ABSORPTION

The two-photon absorption (TPA) phenomenon was proposed by Göeppert-Mayer in 1931 [118] and experimentally first observed by Kaiser and Garrett [119]. TPA is one of the important third-order NLO features. When a molecule is exposed to an intense optical field such as from a pulse laser, it can absorb two photons simultaneously by involving a virtual intermediate state. Figure 49.9 schematically represent this process. If the two photons are of the same frequency, the process is called degenerate TPA; if they are of different frequency, the process is a nondegenerate TPA [120].

For a degenerate TPA process, the transfer rate of absorbed energy can be expressed as [121]:

$$\frac{dW}{dt} = \frac{8\pi^2\omega}{n^2c^2} I^2 \chi^{(3)_{\text{imag}}}, \tag{49.28}$$

where I is the intensity of light, c is light velocity, n is refractive index, ω is optical frequency, and $\chi^{(3)}_{\text{imag}}$ is the imaginary part of $\chi^{(3)}$. Third-order NLO coefficient $\chi^{(3)}$ consists of a real part, $\chi^{(3)}_{\text{real}}$, and an imaginary part, $\chi^{(3)}_{\text{imag}}$, i.e., $\chi^{(3)} = \chi^{(3)}_{\text{real}} + \chi^{(3)}_{\text{imag}}$.

From the above equation, the following theoretical expression for TPA coefficient (center dot) can be derived because dW/dt is defined by multiplying the number of photons absorbed per unit time with the energy of light source, i.e., $dW/dt = (dn_{\text{photon}}/dt)h\nu$.

$$\sigma = \frac{8\pi^2 h\nu^2}{n^2c^2N}\chi^{(3)_{imag}} \quad \text{(unit: cm}^4\text{GW}^{-1}\text{)}, \tag{49.29}$$

where N is the number of absorbing molecules per unit volume. Also, σ can be transformed into the following equation for the use of common unit.

$$\sigma_2 = \sigma h\nu^2 \quad \text{(unit: cm}^4 \text{ sec photon}^{-1}\text{)}. \tag{49.30}$$

In addition, TPA cross-section σ_2 value is also expressed in Göeppert-Mayer (GM) unit; 1 GM is defined as 1×10^{-50} cm^4 sec photon^{-1}.

The evaluation of TPA activity of the materials can be made by various techniques such as up-converted fluorescence emission, nonlinear transmission, transient absorption, Z-scan, and four-wave mixing [122]. Among them, the up-converted fluorescence emission method is a simpler technique and the setup is shown in Fig. 49.10. In this method, the TPA cross-section value, σ_2 can be estimated according to the following equation [123]:

$$\sigma_2 = \frac{S_s\eta_r\phi_rC_r}{S_r\eta_s\phi_sC_s}\sigma_r, \tag{49.31}$$

where the subscripts s and r denote the sample and reference compounds, respectively. The intensity of the two-photon excited fluorescence emission signal collected by a PMT detector is referred as S. The η and ϕ are the overall fluorescence efficiency and the fluorescence quantum yield, respectively. The number density of the molecules in solution is denoted as C. The σ_r is the TPA cross section value of the reference. As a reference material, fluorescein or Rodamine B is generally used [124]. The observed TPA cross-sections of a large variety of organic and polymeric materials are in

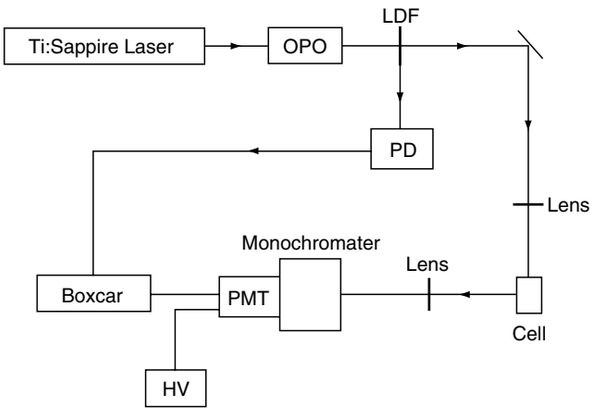

FIGURE 49.10. Schematics of experimental arrangement for measuring σ_2 values by the up-converted fluorescence emission method.

the range of several tens GM ($1\text{GM} = 1.0 \times 10^{-50}\,\text{cm}^4\,\text{sec photon}^{-1}$) to the order of $\sim 10^4$ GM. The detailed TPA cross section values of various materials are presented in Section 49.12.

By virtue of quadratic power dependence of the TPA process, a tightly focused excitation beam can be used to induce photochemical reactions such as photopolymerization and photoisomerization in three-dimensions with high spatial resolution. As a result, various photonic devices including photonic crystals [125–128], optical data storage systems [129–135], 3-D micro-waveguides [136–138], and microelectromechanical systems (MEMS) [139–142] have been fabricated. In addition to this, the two-photon approach can contribute to novel photonic and biophotonic applications like two-photon upconverted lasing [143–150], optical power limiting for the protection of human eyes and efficient sensors against intense light [151–158], two-photon fluorescence bioimaging [159–163], photodynamic therapy [164–170], etc. A detailed general description of these potential applications using TPA techniques exists in the literature [122].

49.11 γ AND $\chi^{(3)}$ VALUES OF POLYMERS

Electronic structural requirements for third-order NLO polymers are different from those for second-order polymers [3,4]. The third-order NLO properties are very sensitive to the length of the π-electron conjugation. An interesting third-order NLO polymer is polydiacetylene, which can be prepared by solid-state polymerization (Fig. 49.11). The backbone of polydiacetylene is derived from a diacetylene skeleton, $R_1C \equiv CC \equiv CR_2$, therefore, depending on the nature of substituents a variety of derivatives can

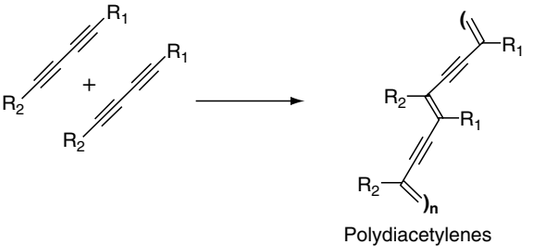

FIGURE 49.11. Molecular structures of the NLO polymers described in Table 49.5.

TABLE 49.6. *$\chi^{(3)}$ values of different forms and different derivatives of polydiacetylenes.*

R_1, R_2	$\chi^{(3)}(10^{-10}$ esu)	Method	References
R_1, $R_2 = CH_2OSO_2C_6H_4CH_3$ (single crystal)	8.5	THG	[56]
R_1, $R_2 = (CH_2)_4OCONHC_6H_5$ (single crystal)	1.6	THG	[56]
R_1, $R_2 = CH_2OSO_2C_6H_4CH_3$	90.0	DFWM	[57]
R_1, $R_2 = CH_2OSO_2C_6H_4CH_3$	2×10^5	SA	[58]
$R_1 = C_6H_3CF_3CF_3$; $R_2 = C_{13}H_{10}N$	1.1	THG	[59]
R_1, $R_2 = C_6F_4H_2(CH_2)_3CH_3$	1.2	THG	[59]
$R_1 = C_6H_3CF_3CF_3$; $R_2 = C_{13}H_{10}N$ (film)	4.3	EFISH	[60]
R_1, $R_2 = (CH_2)_3OCONHCH_2COOC_4H_9$ (film)	1.5	EFISH	[61]
R_1, $R_2 = (CH_2)_3OCONHCH_2COOC_4H_9$ (film)	0.13	DFWM	[62]
R_1, $R_2 = (CH_2)_3OCONHCH_2COOC_4H_9$ (film)	1.0	THG	[63]
R_1, $R_2 = (CH_2)_3OCONHCH_2COOC_4H_9$	2	DFWM	[64]
R_1, $R_2 = (CH_2)_3OCONHCH_2COOC_4H_9$	2.5	DFWM	[64]
R_1, $R_2 = (CH_2)_3OCONHCH_2COOC_3H_7$	9.0	DFWM	[62]
R_1, $R_2 = (CH_2)_3OCONHCH_2COOC_5H_{11}$	2.4	THG	[63]
R_1, $R_2 = C_{13}H_{10}N$ (film)	0.7	THG	[65]
R_1, $R_2 = C_{13}H_{10}N$ (oriented film)	6.0	THG	[66]
R_1, $R_2 = (CH_2)_4OCONH(CH_2)_{n-1}CH_3$	17.0	THG	[67]
R_1, $R_2 = CH_3(CH_2)_{15} - C - C = C - C(CH_2)_8COO$	0.56	THG	[68]
R_1, $R_2 = CH_3(CH_2)_{15} - C - C = C - C(CH_2)_8COO$	0.08	THG	[69]
R_1, $R_2 = C_6H_3CF_3CF_3$ (film)	0.4	THG	[59]
$R_1 = C_6H_3CF_3CF_3$;$R_2 = C_6H_4NHCH_3$ (film)	8.0	THG	[70]

be obtained. Table 49.6 shows $\chi^{(3)}$ values of a series of polydiacetylenes measured with different techniques at different wavelengths [171–185]. As seen in Table 49.6 the resonantly enhanced $\chi^{(3)}$ of polydiacetylene can be as high as 10^{-5}esu, the largest third-order nonlinearity for an organic observed to date.

Another interesting conjugated polymer is polythiophene, which has good environment stability compared to polyacetylenes (Fig. 49.12) (Table 49.7). Polythiophene has a $\chi^{(3)}$ value of 3×10^{-11} at a wavelength of 1.06 μm. The resonantly enhanced value is about 2 orders of magnitude larger than the nonresonant value. Table 49.7 shows $\chi^{(3)}$ values of a polythiophene derivatives. Polythiophenes are colored materials [186–193]. The $\chi^{(3)}$ behavior of polythiophene has been studied in several forms. Electrochemically polymerized films of polythiophene results a $\chi^{(3)}$ value of 4×10^{-10}esu as measured by DFWM at 602 nm [194]. A monolayer prepared by the LB technique (thickness $\sim$22 Å) yields a $\chi^{(3)}$ value of $\sim 10^{-9}$esu at 602 nm as measured with femtosecond DWFM technique [195].

Polyacetylene is another interesting π-conjugated one-dimensional polymer that exists in two geometrical forms: *cis* and *trans* [196]. In polyacetylene the $\chi^{(3)}$ value of the *cis* form is found to be 15–20 times smaller than that of *trans* form. The difference in $\chi^{(3)}$ for the two forms results from the fundamental difference in the polymer symmetry. Also, oriented films of polyacetylene exhibit larger $\chi^{(3)}$ values than unoriented films [197]. Polyketene, in which acetylene hydrogens are substituted with hydroxy groups, shows a $\chi^{(3)}$ value of 1.15×10^{-12}esu at 532 nm [198]. In polyphenylacetylene substitution at the phenyl ring increases $\chi^{(3)}$ significantly [199]. An *ortho*-trimethylsilyl-substituted polyphenylacetylene has a $\chi^{(3)}$ value, which is an order of magnitude larger than the $\chi^{(3)}$ value of polypphenylacetylene.

The $\chi^{(3)}$ values of polyphenylacetylene and several other polymers such as poly-*p*-phenylenevinylene (PPV), PBT, PBO, LARC-TPI, polyketene, polyaniline, polyazine, and polypyrrole are shown in Table 49.8 (Fig. 49.13). Also, included in Table 49.8 are $\chi^{(3)}$ of several heterocyclic ladder

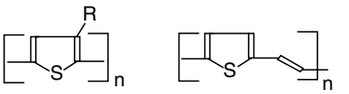

Polythiophene PTV

FIGURE 49.12. Molecular structures of the NLO polymers described in Table 49.6.

polymers. Polyazine is an NLO polymer that is isoelectronic with polyacetylene. Both polyazine and polyacetylene have a simple one-dimensional chain of alternating single and double bonds. In the case of polyazine, pairs of N are substituted for pairs of C in the backbone. Even though the optical nonlinearity of polyazine is moderate, its optical transparency and environmental stability are great advantages.

Good-optical-quality polymers of PPV and poly-*p*-thienylene vinylene (PTV) can be prepared from soluble sulfonium precursors. This feature allows one to fabricate a device structure with the precursor and then convert it to the polymer by heat treatment. Good-optical-quality, stretchoriented, free-standing films of PPV can be obtained with good mechanical strength and high optical damage thresholds. In stretched films, doping produces high electrical conductivity along the draw direction, indicating a high effective π-conjugation in polymer. Singh, Prasad, and Karasz [201] studied the anisotropy of $\chi^{(3)}$ in a stretched PPV film by measuring the DFWM signal as a function of the angle of rotation (Fig. 49.14).[7] The highest $\chi^{(3)}$ value is obtained when electric fields of all the four waves are polarized along the draw direction, while the minimum value is obtained when all the beams are polarized in a direction perpendicular to the draw direction. The ratio of $\chi^{(3)}_{\parallel}$: $\chi^{(3)}_{\perp}$ was 39 obtained by fitting the experimental data to the following expression:

$$\chi^{(3)}_{1111,L} = \chi^{(3)}_{1111,F}\cos^4\theta + \chi^{(3)}_{2222,F}\sin^4\theta + (\chi^{(3)}_{1122,F} + \chi^{(3)}_{1221,F} + \chi^{(3)}_{2122} + \chi^{(3)}_{1212,F} + \chi^{(3)}_{2211,F} + \cdots)\cos^2\theta\sin^2\theta. \quad (49.32)$$

TABLE 49.7. *$\chi^{(3)}$ values of different forms and different derivatives of polythiophenes.*

Polymer	λ(μm)	$\chi^{(3)}$(10^{-10} esu)	Method	References
Polythiophene	0.532	10	DFWM	[71]
R = H	1.907	3.52	THG	[72]
R = $C_{12}H_{25}$	0.602	0.55	DFWM	[73]
R = $C_{12}H_{25}$	0.602	5.0	DFWM	[74]
R = $C_{12}H_{25}$	0.602	5.0	DFWM	[75]
R = CH_3	1.50	0.48	THG	[76]
R = C_4H_9	1.50	0.2	THG	[77]
R = C_6H_5	1.50	0.81	THG	[76]
PTV	1.85	0.32	THG	[78]
Polythiophene (electrochemical)	0.602	0.07	DFWM	[79]
Polythiophene (LB film)	0.532	2700	DFWM	[80]

TABLE 49.8. $\chi^{(3)}$ *values of a number of third-order NLO polymers.*

Polymer	$\chi^{(3)}(10^{-12}$ esu)	$\lambda(\mu$m)	Method	References
PBT	−100.0	0.602	DFWM	[200]
	9.0			
PBO	−100.0	0.602	DFWM	[179]
PPV (stretch-oriented)	400.0	0.620	DFWM	[201]
PPV (R = H)	75	1.064	THG	[202]
PPV (R = OCH_3)	2900	1.064	THG	[203]
PPV (sol–gel)	45	0.620	DFWM	[204]
PPV (sol–gel)	6.6	0.620	OKG	[204]
MOPPV (stretch-oriented)	91	0.608	DFWM	[205]
PPV (sol–gel)	300	0.602	DFWM	[206]
MOPPV (LB film)	2900	1.064	THG	[207]
Polyphenyl acetylene	50.0	0.602	DFWM	[179]
LARC-TPI	−2	0.602	DFWM	[179]
Poly-4-BCMU, yellow	25.0	0.602	DFWM	[179]
Poly-4-BCMU, red	300.0	0.602	DFWM	[179]
Polyketene	1150	0.532	THG	[198]
Polyaniline	800	0.620	DFWM	[208]
Polypyrrole	2	0.602	DFWM	[209]
BBL	7	0.602	DFWM	[210]
	150	0.620		
BBB	4500	1.064	DFWM	[210]
Polyazomethine	2.4	0.602	DFWM	[211]
Polyquinoline	2.2	2.38	THG	[212]
Polyquinoxaline	4500	0.532	DFWM	[213]
Polyazine	8	1.5	THG	[214]

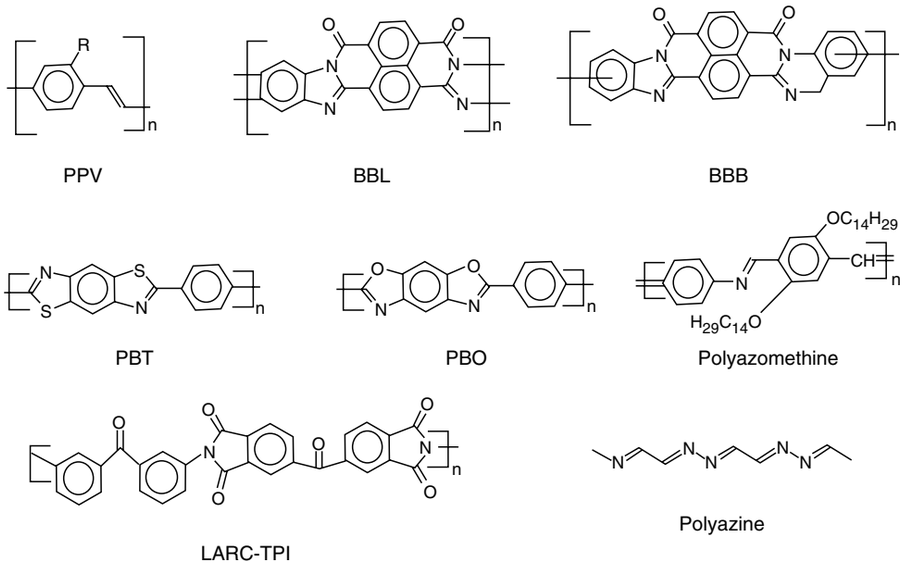

FIGURE 49.13. Molecular structures of the NLO polymers described in Table 49.8.

Similar results also has been obtained by Swiatkiewicz and co-workers [205] in stretch-oriented films of poly-(2,5-dimethoxy-*p*-phenylenevinylene) thin films. Also, oriented films of PPV have been fabricated with the LB technique [201]. The $\chi^{(3)}$ value (at $\lambda = 1.064\ \mu$m) of an LB film of poly-(2,5-dimethoxy-*p*-phenylenevinylene) is 2.9×10^{-9} and 7.5×10^{-11} esu along the orientation axis and perpendicular to the orientation axis, respectively. The above investigations show that, as in polydiacetylenes, the chain orientation is an effective way of enhancing $\chi^{(3)}$ of PPV and its derivatives.

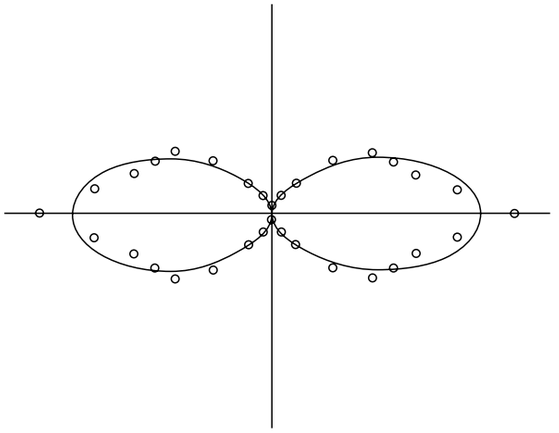

FIGURE 49.14. Polar plot (orientational anisotropy) of the square root of the DFWM signal intensity for the 10:1 stretch-oriented PPV film. Scattered are the experimental data points; continuous line is the theoretical fit [201].

Another interesting feature of PPV is that it can be incorporated into sol–gel glasses (up to 50 wt %) without phase separation. Sol–gel composites of PPV have been prepared using SiO_2 and V_2O_5 gels [206]. A light beam at 1.064 μm can be guided in a sol–gel processed PPV film (thickness $\sim 1\,\mu$m) up to 2 cm with a loss of $\sim$4 dB/cm. The refractive indices ($n_{TE} = 1.72$ and $n_{TM} = 1.60$ at 1.064 μm) indicate the presence of birefringence even in as cast film [215,216].

Another important class of photonic materials is polysilanes (Fig. 49.15) [217–222]. In polysilanes the delocalization of σ orbitals of the Si atom along the polymer backbone plays a significant role in their NLO properties. Their physical and chemical properties can be tailored by the choice of an appropriate substituent, which also determines the conformation of the polymer and its solubility. What is of more interest is their transparency in their NLO properties. $\chi^{(3)}$ values of a series of polysilanes are given in Table 49.9. Tables 49.10–49.13 contain γ and $\chi^{(3)}$ values of some other third-order materials, namely metallophthalocyanine, bismetallophthalocyanine, metallonaphthalocyanines, fullerenes, and β-carotenes. Although these molecules are not considered as polymers, they are macromolecules that have drawn a considerable amount of attention as third-order NLO materials. For example, the highly stable icosahedral-cage C_{60} molecule (fullerene) has been studied by a large number of research groups as a third-order NLO material. Fullerene is considered to be a new form of carbon in that it possesses a soccer ball structure. All the carbon atoms in fullerene are connected with sp^2 bonds and 60 π electrons are distributed in a manner giving the molecule a highly aromatic character. The interesting π conjugation in fullerenes has made it an important candidate for thirdorder NLO optics. Table 49.10 reports the NLO properties of fullerenes measured by different research groups. Other highly conjugated molecules can be considered as one-dimensional (β-carotene) and two-dimensional (phthalocyanines and naphthalocyanines) for NLO purposes.

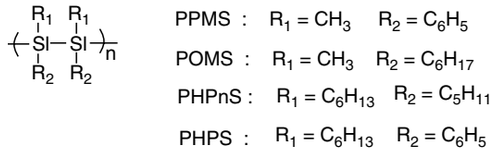

FIGURE 49.15. Molecular structures of the NLO ploymers described in Tables 49.9.

49.12 TPA CROSS-SECTION VALUES OF ORGANICS AND POLYMERS

The basic structural requirement as a TPA material is π-conjugation of the molecule, because the TPA process originates from third-order NLO activity. At the initial stage of TPA research, only commercial chromophores such as fluorescein, coumarin 307, Rodamine B, etc., were reported to exhibit TPA activities, but they all exhibited relatively low TPA cross-section σ values (< 200 GM) which is expressed in Göeppert-Mayer (GM) units ($1\text{GM} = 1 \times 10^{-50}\,\text{cm}^4$ sec photon^{-1}) [124]. To address this problem, several research groups focused attention on synthesizing materials with high TPA cross-section. This entailed an improved understanding of the structure–property relationship. In particular, there have been intense efforts to identify contributions from different structural models of a molecule on the TPA cross-section. Systems with symmetrical donors (donor–π–bridge–donor; D–π–D) and acceptors (acceptor–π–bridge–acceptor; A–π–A) as well as asymmetrical structure having both donor and acceptor (donor–π–bridge–ac-

TABLE 49.9. *$\chi^{(3)}$ values of polysilane derivatives.*

Polymer	$\chi^{(3)}$ (10^{-12}esu)	λ(μm)	Method	References
PEPS	5.3	1.064	THG	[217]
PDHS	11.3	1.064	THG	[221]
	1.3	1.907		
PDIHS	1.8	1.064	THG	[217]
PPMS	1.5	1.064	THG	[220]
	7.2	1.064	THG	[219]
	4.2	1.907	THG	[219]
POMS	2.9	0.532	THG	[218]
PtBuPS	4.9	1.064	THG	[217]
PSM-MSM	3.6	1.064	THG	[221]
PSM-*n*-HSM	3.1	1.064	THG	[221]
Polycarbosilane	0.34	1.064	THG	[221]
PHPnS	2.3	1.064	THG	[217]
PHPS	6.2	1.064	THG	[217]
PDES	3000	0.620	DFWM	[222]

TABLE 49.10. *$\chi^{(3)}$ values of fullerenes and β-carotene.*

	Method	$\chi^{(3)}(10^{-12}$ esu)	$\gamma(10^{-33}$ esu)	$\lambda(\mu$m)	References
C_{60} (solution)	DFWM	60 000	11 000	1.064	[223]
C_{60}/DEA	EFISH	...	67 000	1.064	[224]
C_{60} (solution)	*z* scan	33 200	...	0.532	[225]
C_{60} (solution)	EFISH	...	0.75	1.064	[226]
C_{60} (solution)	DFWM	0.12	...	1.064	[227]
C_{60} (film)	DFWM	200	...	0.633	[228]
C_{60} (film)	THG	200	...	1.064	[229]
C_{60} (film)	THG	20	...	1.064	[226]
C_{60} (film)	THG	30	0.43	1.32	[237]
C_{60} (film)	DFWM	7	0.3	1.064	[229]
C_{60} (solution)	DFWM	220	...	0.602	[230]
	OKG	...	$\gamma_{real} = -5$	0.620	
		...	$\gamma_{im} = 9$		
C_{70} (solution)	EFISH	...	1.3	1.064	[224]
C_{70} (solution)	*z* scan	12000	...	0.520	[225]
C_{70} (film)	DFWM	300	...	0.633	[228]
C_{70} (film)	DFWM	5.6	1200	1.064	[231]
$C_{60} + C_{70}$	DFWM	2.6	160	1.064	[232]
$C_{60} + C_{70}$	DFWM	3300	...	1.064	[232]
β-carotene	THG	...	4.8	1.89	[233]
β-carotene	DFWM	...	720	1.064	[234]
β-carotene	THG	...	11	1.908	[235]
β-carotene	OKG	...	$\gamma_{real} = -110$		[236]
			$\gamma_{im} = 160$		

ceptor; D–π–A) groups have been intensively investigated [123,247–262]. Schematics of these structures are shown in Fig. 49.16.

TABLE 49.11. *$\chi^{(3)}$ values of metallophthalocyanines and metallonaphthalocyanines.*

Compound	$\chi^{(3)}(10^{-12}$esu)	$\lambda(\mu$m)	Method	References
F-AlPc	50	1.064	THG	[238]
Cl-GaPc	25	1.064	THG	[238]
H_2Pc	3.0	1.907	THG	[239]
CoPc	7.5	1.907	THG	[239]
NiPc	2.3	1.907	THG	[239]
SnPc	40.0	1.907	THG	[239]
VOPc	93.0	1.907	THG	[239]
H_2PcCP_4	4.0	1.064	DFWM	[240]
$PbPcCP_4$	20.0	1.064	DFWM	[240]
$PtPcCP_4$	200.0	1.064	DFWM	[240]
Cl-InPc	130.0	1.907	THG	[241]
Cl-AlPc	15.0	1.907	THG	[241]
VOPc	40.0	2.1	THG	[241]
TiOPc	53.0	2.1	THG	[241]
CuPc	1.5	1.907	THG	[241]
PtPc	0.76	1.5	THG	[241]
TBH_2PC	1.9	1.907	THG	[239]
TBVOPc	6.0	1.907	THG	[239]
TBNiPc	2.0	1.907	THG	[239]
$Sb(Pc)_2$	1700.0	1.064	DFWM	[242]
SiPc (LB film)	20.0	00602	DFWM	[243]

For the π- bridges, phenylenevinylene, flourine, fused aromatics based on benzene, thiophene, or phenyleneethynylene, etc., showing high co-planarity have been used. It has been inferred that TPA activities of above-mentioned structures could be enhanced by increasing co-planarity of the π-center, donor strength, the conjugation length, and intramolecular charge redistribution. As shown in Fig. 49.17, the bis(styryl)-

TABLE 49.12. *$\chi^{(3)}$ values of several metallophthalocyanine metallonaphthalocyanine derivatives as measured by the harmonic generation technique.*

Compound	$\chi^{(3)}$ (10^{-12}esu)	λ (μm)	Method	References
$VoNc(CO_2C_5H_{11})_4$	86.0	2.1	THG	[244, 245]
$CuNc(CO_2C_5H_{11})_4$	2.0	2.1	THG	[244, 245]
$ZnNc(CO_2C_5H_{11})_4$	1.88	2.1	THG	[244, 245]
$PdNc(CO_2C_5H_{11})_4$	1.28	2.1	THG	[244, 245]
$NiNc(CO_2C_5H_{11})_4$	1.59	2.1	THG	[244, 245]
$CuPc(C_6H_{13}S)_4$	20.0	1.907	THG	[241]
$CuPc(C_7H_{15}S)_4$	12.0	2.1	THG	[241]
$CuPc(C_8H_{17}S)_4$	50.0	2.1	THG	[241]
$CuPc(C_{10}H_{21}S)_4$	26.0	2.1	THG	[241]
$CuPc(C_{12}H_{25}S)_4$	1.30	2.1	THG	[241]
$VOPc(C_6H_{13}S)_4$	31.0	2.1	THG	[241]
$ClInNc\{(CH_3)_3\}_4$	4.21	2.1	THG	[244, 245]
$IrNc\{(CH_3)_3\}_4$	1.05	2.1	THG	[244, 245]
$RuNc\{(CH_3)_3\}_4$	1.0	2.1	THG	[244, 245]
$RhNc\{(CH_3)_3\}_4$	1.16	2.1	THG	[244, 245]

TABLE 49.13. *γ values of a series of metallophthalocyanine metallonaphthalocyanine as measured by the degenerate four wave mixing technique. All measurements were made at* 1.064 μm *[131].*

Compound	$\gamma(10^{-32}$ esu)	Method
$H_2Pc(CP)_4$	0.1	DFWM
$PbPc(CP)_4$	2	DFWM
$ZnPc(CP)_4$	0.5	DFWM
$CuPc(CP)_4$	2	DFWM
$NiPc(CP)_4$	4	DFWM
$CoPc(CP)_4$	5	DFWM
$PdPc(CP)_4$	1	DFWM
$PtPc(CP)_4$	10	DFWM
bis-Phthalocyanines		
$ScPc_2$	48	DFWM
$LuPc_2$	34	DFWM
$YbPc_2$	41	DFWM
$YPPc_2$	26	DFWM
$GdPc_2$	22	DFWM
$EuPc_2$	22	DFWM
$NdPc_2$	15	DFWM

benzene derivatives with symmetrical donors (D–π–D) structures and some modified structures of donor–acceptor–donor (D–A–D) and acceptor–donor–acceptor (A–D–A) types exhibit high TPA activity [123,263]. Measurement of the

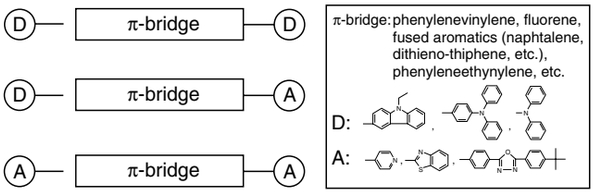

FIGURE 49.16. Various design strategies for highly efficient TPA chromophores.

TPA cross section for SM-1 give a maximum σ_2 of 210 GM at an excitation wavelength of 605 nm, which is much smaller value than that of SM-2 ($\sigma_2 = 995$ GM at 730 nm) due to the shortness of the π-conjugated chain length. The large increase in the TPA activity of SM-4, compared with SM-3, is also related to the extension of π-chain length. One of the most interesting phenomena in the TPA tendency of bis(styryl)-benzene derivatives is the role of electron acceptor in the π-center of the molecules. In the case of SM-6 with a D–A–D structure, TPA cross-section exhibits an exceptionally high value of 1,940 GM at 835 nm. This is due to the increase of the extent of charge transfer from the end of molecule to the π-center, and this indicates that symmetric charge transfer and a change in quadrupole moment greatly contribute to the enhancement of the σ_2 value. The detailed photophysical data of the above-mentioned bis(styryl)benzene derivatives are listed in Table 49.14.

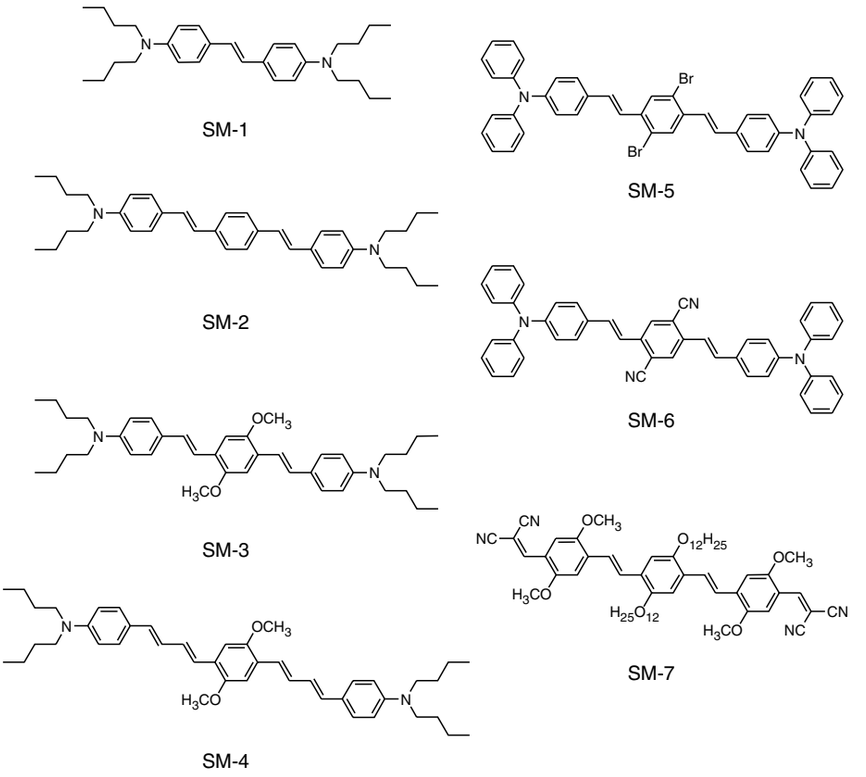

FIGURE 49.17. Molecular structures of two-photon absorbing bis(styryl)benzene derivatives.

TABLE 49.14. *The detailed photophysical date of bis(styryl)benzene derivatives depicted in Fig. 49.17.*

Chromophore	λ_{max}(UV) nm	λ_{mas}(PL) nm	λ_{max}(TPA) nm	σ_2[a] GM[b]	Φ[b]
SM-1	374	410	605 (620)	210 (100)	0.90
SM-2	408	455	730 (∼725)	995 (635)	0.88
SM-3	428	480	730 (∼725)	900 (680)	0.88
SM-4	456	509	775 (∼750)	1,250 (1,270)	0.12
SM-5	424	490	∼800 (–)	450 (–)	0.41
SM-6	472	525	835 (810)	1,940 (3,670)	0.86
SM-7	513	580	825 (815)	480 (650)	0.82

[a] σ_2 values were determined by two-photon-excited fluorescence measurements with 5-ns laser pulses. Data given in parentheses are determined with fs laser pulses.
[b] Φ is fluorescence quantum yield.

It is also helpful to understand the role of π-center in a TPA materials on its σ_2 value. Figure 49.18 shows chemical structures of TPA chromophores with four different π-center types such as fluorene [264,265], dithienothiophene (DTT) [248], phenylenevinylene (PV) [128,266,267] and phenyleneethynylene (PE) [268,269]. Among them, DTT-based molecules exhibit the highest TPA activity, considering the π-conjugated length of molecules. The maximum σ_2 of KS-3 based on DTT at the excitation wavelength of 785 nm is 1,140 GM which is a larger value compared to that of fluorene-based KS-2 ($\sigma_2 = 954$ GM at 740 nm) and PV-based KS-5 ($\sigma_2 = 470$ GM at 780 nm). This result indicates that planarity of the π-center might be a crucial molecular factor, together with the electron-donor strength at the end of molecules. Due to the longer π-conjugated length of KS-6 and KS-7, a direct comparison on PE unit with flourine, DTT, and PV as a π-bridge is difficult, but it is reasonable to surmise that PE may also be a good candidate for making efficient TPA materials (Table 49.15).

More recently, several researchers have also reported octupolar [270–272] and multibranched [273–279] type chromophores as well as dendritic molecules [280–284] showing highly efficient TPA cross-sections. Some representatives are presented in Fig. 49.19. They correlated the activity with the intramolecular charge transfer between the donor moiety and the π-center, and the increase the number density

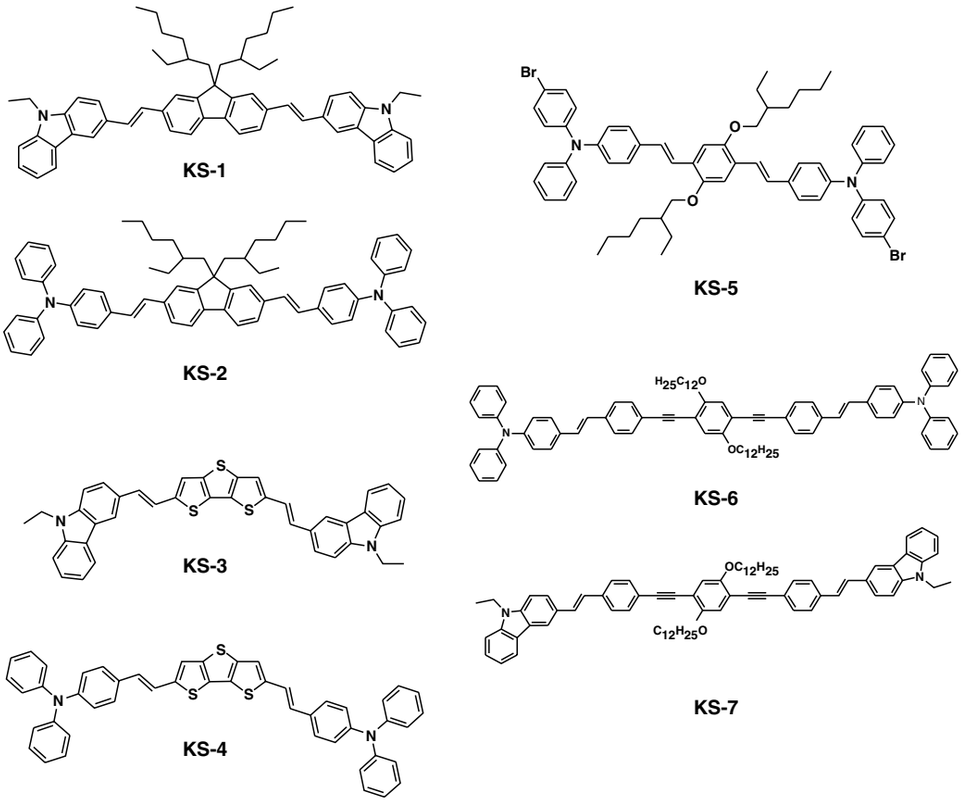

FIGURE 49.18. Molecular structures of various two-photon absorbing chromophores with different π-bridges.

TABLE 49.15. *The detailed photophysical data of various two-photon absorbing chromophores with different π-bridges depicted in Fig. 49.18.*

Chromophore	λ_{max}(UV) [a] nm	λ_{mas}(PL)[a] nm	λ_{max}(TPA) nm	σ_2 [b] GM	Φ[c]
KS-1	398	434	$\leq$ 735	290	0.80
KS-2	411	452	740	954	0.78
KS-3	441	486	740	740	0.69
KS-4	453	503	785	1,140	0.70
KS-5	424	507	780	470	0.81
KS-6	403	446	704	960	0.81
KS-7	412	464	704	1,184	0.89

[a] UV and PL data obtained in THF solution.
[b] TPA cross-section; 1 GM = 10^{-50} cm^4 sec photon^{-1} measured in two-photon fluorescence method with 80 fs pulse laser.
[c] Fluorescence quantum yield determined relative to fluorescin in 0.1 N NaOH.

of chromophore. It has been observed that the σ_2 value increases with increasing the number of octupolar units in the octupolar oligomers [271] and also with increasing the number of branches in the multibranched chromophores [273]. Moreover, the TPA activity in dendritic macromolecules can gain strong cooperative enhancement by increasing the number of constituent identical chromophore-building units [281]. As shown in Fig. 49.20, the σ_2 value increases by a factor of 2.1 and 3.8, when going from CS-2 (In the name of CS-2, 2 means the number of constituent identical chromophore unit, i.e., triphenylamine) to CS-4 and CS-6, respectively. In the case of CS-14 and CS-30, the σ_2 values were enhanced to 4,500 GM and 11,000 GM, respectively.

In addition, most TPA compounds based on π-conjugated double bond experience a reduction in TPA activities due to the quenching of fluorescence resulting from the formation of π-complex by the chromophore aggregation. This occurs both in the solid state and in solutions of high chromophore concentrations. To prevent the interaction with other chromophores in the vicinity, TPA chromophore center can be attached with dendrons (KS-9) so as to restrict a free conformation motion (Fig. 49.20). As a result, the hindered molecular twisting motion of the center TPA chromophore for a dendrimer results in about 5–16 times increase in fluorescence emission, along with increased emission lifetime [278]. For these reasons, octupolar, multibranched, and dendritic chromophores can be promising candidates for TPA science and technology.

Polymers as TPA materials provide several advantages. These are: (i) photochemical and photophysical stability against organic solvents and intense light, (ii) prevention of aggregation between chromophores, and (iii) ease of processing toward a thin film. Considering these merits, several conjugated polymers based on poly(1,4-phenyleneethynylene) (PPE), polyfluorene (PF), and poly(1,4-phenylenevinylene) (PPV) backbones have been investigated as prospective TPA materials (Fig. 49.21) [285–289].

In the case of PPE, electron-donating long alkoxy chains on each phenyleneethynylene moieties are introduced which improve its solubility and also electron density of the polymer chains. Moreover, alkoxy branches can also play an important role to restrict the π–π interaction between conjugated polymer chains which cause fluorescence quenching. The σ_2 value of PPE was 80×10^{-20} cm^{4}GW^{-1} observed by nanosecond laser pulses. Due to its high TPA activity this polymer showed efficient optical power limiting performance [286]. Also, polyfluorene was investigated for its TPA activity in chloroform (2×10^{-3} M) at wavelengths ranging from 550 to 680 nm. The TPA dispersion curve displays a peak at 625 nm with $\sigma_2 = 20{,}000$ GM, utilizing 2.6 ns pulses [288].

Poly(1,4-phenylenevinylene) derivatives also constitute another set of interesting TPA materials, and even they are well-known as third-order NLO polymers as well as efficient electroluminescence materials. According to a study of excitation dynamics and TPA properties in PPV derivatives having phenylanthracene and branched alkoxy pendants, a complete energy transfer from the pendant phenyanthracene unit to the PPV backbone in PPV-1 and PPV-2 was observed [289]. From ns and fs measurements, their TPA cross sections at around 800 nm were found to be 11.9 for PPV-1, 66.6 for PPV-2, and 44.0×10^{-20} cm^{4}GW^{-1} for PPV-3 in ns laser pulses and 0.074 for PPV-1, 0.196 for PPV-2, and 0.168×10^{-20} cm^{4}GW^{-1} for PPV-3 in fs pulses, respectively. The observation of higher TPA values obtained in ns pulses compared with that of fs pulses is due to contribution from excited-state absorption in the ns regime. PPV-2, carrying both the phenylanthracene and alkoxy branches exhibited the highest TPA performance in both of ns and fs measurements.

49.13 VARIATION IN THE $\chi^{(2)}$, $\chi^{(3)}$, AND σ_2 VALUE

It is important to note that the $\chi^{(2)}$ and $\chi^{(3)}$ values reported in this chapter has been estimated in different experimental laboratories. The main source of the error in these values is due to the inadequacy of the local-field factors. Very often the local fields are calculated from the refractive-index measurements that are made at a particular wavelength, without considering the dispersion. Also, the numerical

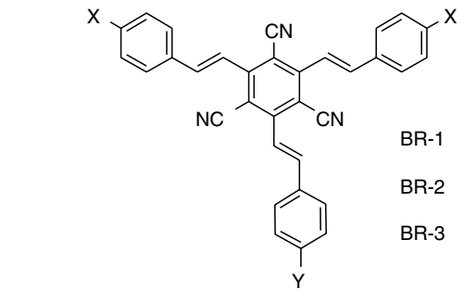

	X	Y	σ_2(180 fs)
BR-1	$NHex_2$	N(Me)EtOH	3125 GM (at 990 nm)
BR-2	N(Me)EtOH	$NHex_2$	3010 GM (at 990 nm)
BR-3	NPh_2	$NHex_2$	5395 GM (at 990 nm)

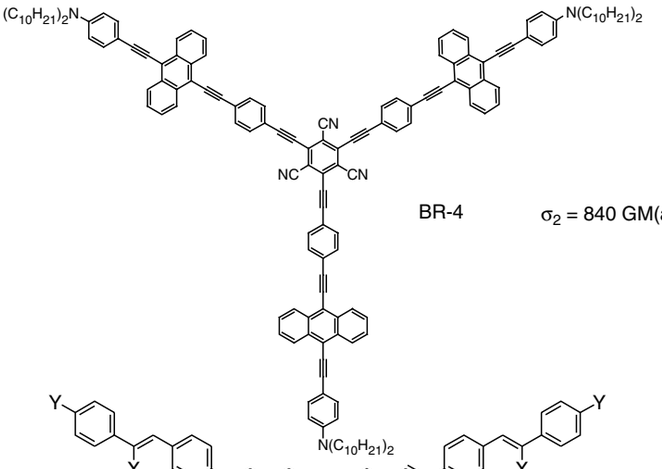

BR-4 σ_2 = 840 GM(at 780 nm; 180 fs)

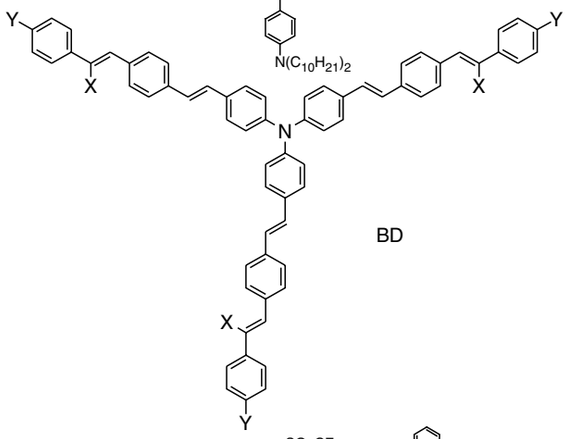

X = H (2), CN (3)

Y = 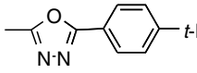 *t*-Bu (a), CN (b)

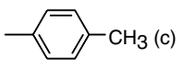 CH_3 (c)

BD

BD-2a:	950 GM at 780 nm
BD-2b:	870 GM at 780 nm
BD-3b:	740 GM at 890 nm
BD-3c:	1,360 GM at 800 nm

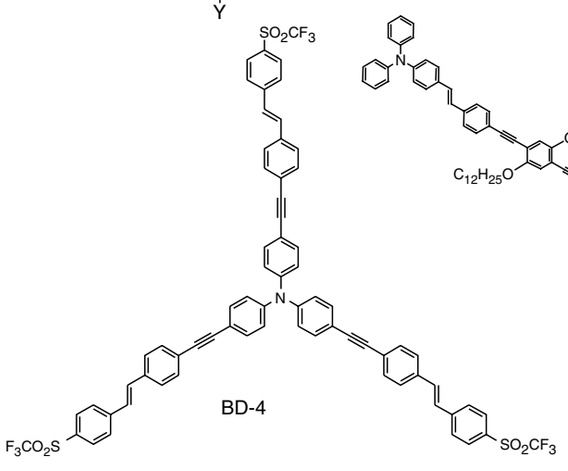

BD-4

σ_2= 1,080 GM (at 740 nm, 80 fs)

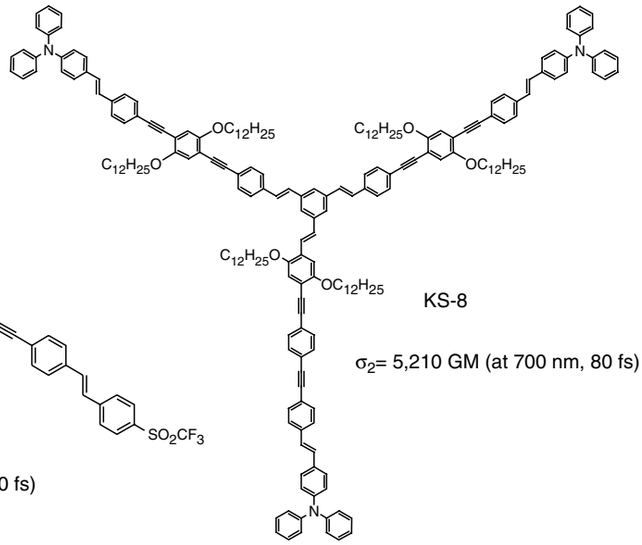

KS-8

σ_2= 5,210 GM (at 700 nm, 80 fs)

FIGURE 49.19. Chemical structures of two-photon absorbing octupolar and multibranched type chromophores.

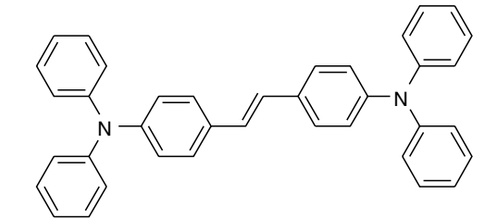

CS-2: σ_2= 320 GM (150 fs)

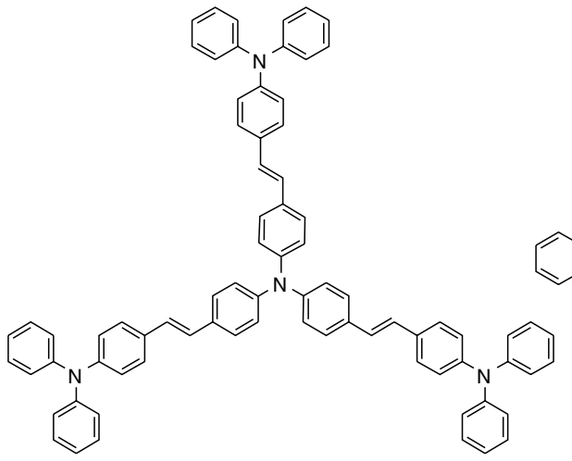

CS-4: σ_2= 1,300 GM (150 fs)

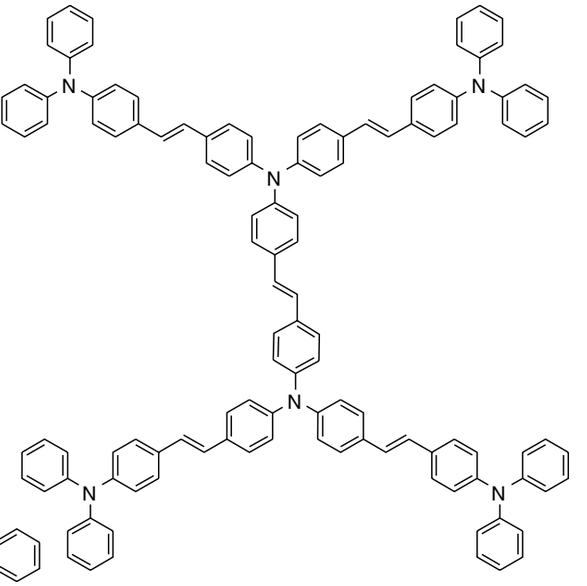

CS-6: σ_2= 2,700 GM(150 fs)

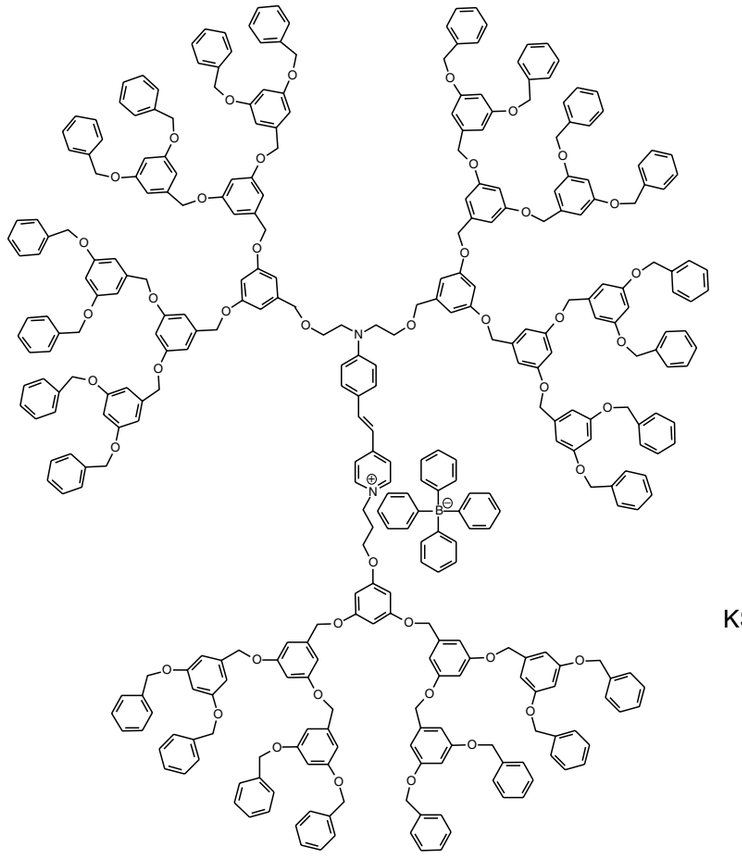

KS-9

FIGURE 49.20. Chemical structure of two-photon absorbing dendritic molecules.

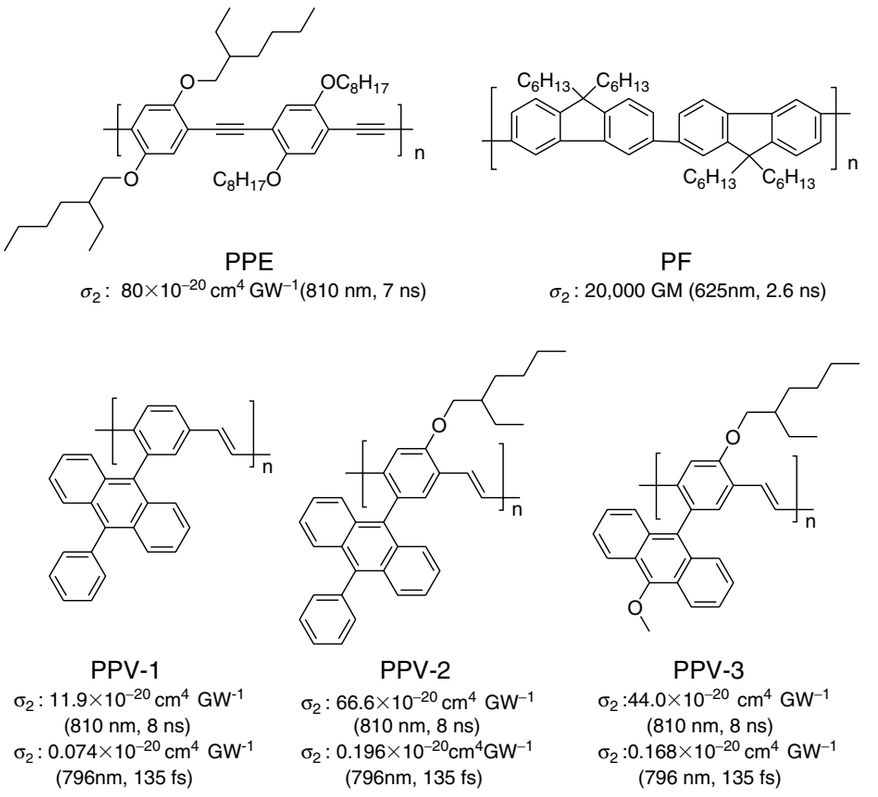

FIGURE 49.21. Molecular structure of TPA polymers.

values of $\chi^{(2)}$ and $\chi^{(3)}$ depend on the resonance contribution. The same compound may exhibit substantially different $\chi^{(2)}$ or $\chi^{(3)}$ values depending on the wavelength at which the measurement is made. Also, the variation in σ_2 values can exist, depending on experimental conditions such as pulse duration of the laser beam, the measured wavelength, laser intensity, the solvent polarity, concentration of samples in solution, and the used σ_2 values of standard materials. Therefore, a comparison of $\chi^{(2)}$, $\chi^{(3)}$, and σ_2 values should be made with caution.

Related information can be found in Chapters 34 and 35.

REFERENCES

1. N. Bloembergen, *Nonlinear Optics* (Benjamin/Cummings, New York, 1965).
2. Y. R. Shen, *Principles of Nonlinear Optics* (Wiley, New York, 1984).
3. P. N. Prasad and D. J. Williams, *Introduction to Nonlinear Optical Effects in Molecules and Polymers* (Wiley, New York, 1992).
4. *Nonlinear Optical Properties of Organic Molecules and Crystals*, edited by D. S. Chemla and J. Zyss (Academic, Orlando, FL, 1987), Vols. I and II.
5. B. F. Levine and C. G. Bethea, J. Chem. Phys. **63,** 2666 (1975).
6. P. D. Maker, R. W. Terhune, M. Nisenoff, and C. M. Savage, Phys. Rev. Lett. **8,** 21 (1962).
7. F. Zernike and J. E. Midwinter, *Applied Nonlinear Optics* (Wiley, New York, 1973).
8. J. Jerphagnon and S. K. Kurtz, J. Appl. Phys. **41**, 1667 (1970).
9. D. A. Kleinman, Phys. Rev. **126**, 1977 (1962).
10. W. M. K. P. Wijekoon, Y. Zhang, S. P. Karna, P. N. Prasad, A. C. Griffin, and A. M. Bhatti, J. Opt. Soc. Am. B **9**, 1832 (1992).
11. M. A. Mitchell, J. E. Mulvaney, H. K. Hall, Jr., C. S. Willand, H. Hampsch, and D. J. Williams, Polym. Bull. **28**, 381 (1992).
12. G. R. Meredith, J. VanDusen, and D. J. Williams, Macromolecules **15**, 1385 (1982).
13. K. D. Singer, J. Sohn, and S. Lalama, Appl. Phys. Lett. **49**, 248 (1986).
14. M. Mortazavi, A. Knoesen, S. Kowel and B. Higgins, J. Opt. Soc. Am. B **6**, 733 (1989).
15. K. D. Singer, M. Kuzyk, W. Holland, J. Sohn, S. S. Lalama, R. Comizzoli, H. Katz, and M. Schilling, Appl. Phys. Lett. **53**, 1800 (1988).
16. H. Katz, K. Singer, J. Sohn, C. Dirk, L. King, and H. Gordon, J. Am. Chem. Soc. **109**, 6561 (1987).
17. G. Gadret, F. Kajzar, and P. Raimond, Proc. SPIE **1560**, 251 (1991).
18. C. Ye, T. J. Marks, J. Yang, and J. K. Wong, Macromolecules **20**, 2322 (1987).
19. Y. Shuto, M. Amano, and T. Kaino, Jpn. J. Appl. Phys. **30**, 320 (1991).
20. M. Eich, H. Looser, D. Yoon, R. Twieg, G. Bjorklund, and G. Baumert, J. Opt. Soc. Am. B **6**, 1590 (1989).
21. C. Ye, N. Minami, T. J. Marks, J. Yang, and J. K. Wong, Macromolecules **21**, 2899 (1988).
22. L. Hayden, G. Sauter, F. Ore, P. Pasillas, J. Hoover, G. Lindsay, and R. Henry, J. Appl. Phys. **68**, 456 (1990).
23. D. Dai, T. J. Marks, J. Yang, P. Lundquist, and G. K. Wong, Macromolecules **23**, 1891 (1990).
24. D. Dai, M. A. Hubbard, J. Park, T. J. Marks, J. Wang, P. Lundquist, and G. K. Wong, Mol. Cryst. Liq. Cryst. **189**, 93 (1990).
25. D. H. Choi, W. M. K. P. Wijekoon, H. M. Kim, and P. N. Prasad, Chem. Mater. **6**, 234 (1994).
26. D. H. Choi, H. M. Kim, W. M. K. P. Wijekoon, and P. N. Prasad, Chem. Mater. **4**, 1253 (1992).

27. M. Amano, T. Kaino, F. Yamamota, and Y. Takeuchi, Mol. Cryst. Liq. Cryst. **182**, 81 (1990).
28. M. A. Hubbard, T. J. Marks, J. Yang, and G. K. Wong, Chem. Mater. **1**, 167 (1989).
29. D. M. Burland, R. D. Miller, C. A. Walsh, Chem. Rev. **94**, 31 (1994).
30. K. Kajikawa, H. Nagamori, H. Takezoe, A. Fukuda, S. Ukishima, Y. Takahashi, M. Iijima, and E. Fukuda, Jpn. J. Appl. Phys. **30**, L1737 (1991).
31. I. Teraoka, D. Jungbauer, B. Reck, D. Yoon, R. Twieg, and C. Wilson, J. Appl. Phys. **69**, 2568 (1991).
32. M. Chen, L. R. Dalton, L. P. Xu, S. Q. Shi, and W. H. Steir, Macromolecules **25**, 4032 (1992).
33. Y. Shi, W. H. Steir, M. Chen, L. Yu, and L. R. Dalton, Appl. Phys. Lett. **60**, 2577 (1992).
34. B. K. Mandal, J. Kumar, J. Huang, and S. Tripathy, Makromol. Chem. Rapid. Commun. **12**, 63 (1991).
35. B. K. Mandal, Y. M. Chen, V. Y. Lee, J. Kumar, and S. Tripathy, Appl. Phys. Lett. **58**, 2459 (1991).
36. C. P. J. Van der Vorst and S. J. Picken, J. Opt. Soc. Am. B **7**, 320 (1989).
37. M. Eich, G. Bjorklund, and G. Yoon, Polym. Adv. Technol. **1**, 189 (1990).
38. C. Xu, B. Wu, L. R. Dalton, P. Ramon, Y. Shi, and W. Steier, Macromolecules **25**, 6716 (1992).
39. M. Chen, L. R. Dalton, L. P. Xu, X. Shi, and W. Steier, Macromolecules **25**, 4032 (1992).
40. J. Lon, M. Hubbard, T. J. Marks, W. Lin, and G. K. Wong, Chem. Mater. **4**, 1148 (1992).
41. D. R. Robello, C. S. Willand, C. S. Scozzafava, A. Ulman, and D. J. Williams, in *Materials for Nonlinear Optics. Chemical Perspectives*, ACS Symposium Series No. 455, edited by S. Marder, J. Sohn, and G. Stucky (American Chemical Society, Washington, D. C. 1991), p. 279.
42. B. K. Mandal, J. Y. Lee, X. Xhu, Y. M. Chen, E. Prakienavincha, J. Kumar, and S. K. Tripathy, Syn. Met. **41–43**, 3143 (1991).
43. B. K. Mandal, Y. M. Chen, V. Lee, J. Kumar, and S. K. Tripathy, Appl. Phys. Lett. **58**, 2459 (1991).
44. H. Hsiung, Appl. Phys. Lett. **59**, 2495 (1991).
45. T. L. Penner, H. R. Motschmann, A. J. Armstrong, M. C. Ezenyilimba, and D. J. Williams, Nature **367**, 49 (1994).
46. K. Clays, N. J. Armstrong, M. C. Ezenyilimba, and T. L. Penner, Chem. Mater. **5**, 1032 (1993).
47. K. Clays, N. J. Armstrong, and T. L. Penner, J. Opt. Soc. Am. B **10**, 886 (1993).
48. H. R. Motschmann, T. L. Penner, A. J. Armstrong, and M. C. Ezenyilimba, J. Phys. Chem. **97**, 3933 (1993).
49. S. H. Ou, J. A. Mann, J. B. Lando, L. Zhou, and K. D. Singer, Appl. Phys. Lett. **61**, 2284 (1992).
50. S. R. Marder, B. Kippelen, A. K.-Y. Jen, and N. Peyghambirian, Nature **388**, 845 (1997).
51. J. L. Oudar and D. S. Chemla, J. Chem. Phys. **66**, 2664 (1977).
52. S. R. Marder, L. T. Cheng, B. G. Tiemann, A. C. Friedli, M. Blanchard-Desce, J. W. Perry, and J. Skindhøj, Science **263**, 511 (1994).
53. F. Kajzar, K.-S. Lee, and A. K.-Y. Jen, Adv. Poym. Sci. **161**, 1 (2003).
54. L. R. Dalton, Adv. Polym. Sci. **158**, 1 (2002).
55. A. K.-Y. Jen, K. Y. Wong, V. P. Rao, K. Drost, and Y. M. Cai, J. Electron. Mater. **23**, 653 (1994).
56. Y. M. Cai and A. K.-Y. Jen, Appl. Phys. Lett. **117**, 7295 (1995).
57. H. Ma, X. Wang, X. Wu, S. Liu, and A. K.-Y. Jen, Macromolecules **31**, 4049 (1998).
58. A. K.-Y. Jen, X. Wu, and H. Ma, Chem. Mater. 10, 471 (1998).
59. H. Ma, A. K.-Y. Jen, J. Wu, S. Liu, C. F. Shu, L. R. Dalton, S. R. Marder, and S. Thayumanavan, Chem. Mater. **11**, 2218 (1999).
60. L. R. Dalton, Opt. Eng. **39**, 589 (2000).
61. C.-K. Park, J. Zieba, C.-F. Zhao, B. Swedek, W. M. K. P. Wijekoon, and P. N. Prasad, Macromolecules **28**, 3713 (1995).
62. S. Jin, M. Wübbenhorst, J. Van Turnhout, and W. Mijs, Macromol. Chem. Phys. **197**, 4135 (1996).
63. K.-J. Moon, H.-K. Shim, K.-S. Lee, J. Zieba, and P. N. Prasad, Macromolecules **29**, 861 (1996).
64. K.-S. Lee, S.-W. Choi, H. Y. Woo, K.-J. Moon, H.-K. Shim, M.-Y. Jeong, and T.-K. Lim, J. Opt. Soc. Am. B **15**, 393 (1998).
65. H. Y. Woo, J.-K. Shim, and K.-S. Lee, Macromol. Chem. Phys. **199**, 1427 (1998).
66. H. Y. Woo, H.-K. Shim, and K.-S. Lee, Polym. J. **32**, 8 (2000).
67. C.-B. Yoon, B.-J. Jung, and H.-K. Shim, Synth. Met. **117**, 233 (2001).
68. T. Beltrami, M. Bösch, R. Centore, S. Concilio, P. Günter, and A. Sirigu, Polymer **42**, 4025 (2001).
69. M. Becker, L. Sapochak, L. R. Dalton, W. Steier, and A. K.-Y. Jen, Chem. Mater. **6**, 104 (1994).
70. H. Saadeh, A. Gharari, D. Yu, and L. Yu, Macromolecules **30**, 5403 (1997).
71. K. Van der Broeck, T. Verbiest, M. Van Beylen, A. Persoons, and C. Samyn, Macromol. Chem. Phys. **200**, 2629 (1999).
72. H. Y. Woo, H.-K. Shim, K.-S. Lee, M.-Y. Jeong, and T.-K. Lim, Chem. Mater. **11**, 218 (1999).
73. W. N. Leng, Y. H. Zhou, Q. H. Wu, and J. Z. Liu, Polymer **42**, 9253 (2001).
74. T.-D. Kim, K.-S. Lee, G. U. Lee, and D.-K. Kim, Polymer **41**, 5237 (2000).
75. T.-D. Kim, K.-S. Lee, Y. H. Jeong, J. H. Ju, and S. Chang, Synth. Met. **117**, 307 (2001).
76. E. Gubbelmans, T. Verbiest, M. Van Beylen, A. Persoons, and C. Samyn, Polymer **43**, 1581 (2002).
77. K. Van der Broeck, T. Verbiest, J. Degryse, M. Van Beylen, A. Persoons, and C. Samyn, Poymer **42**, 3315 (2001).
78. N. Song, L. Men, J. P. Gao, Y. Bai, A. M. R. Beaudin, G. Yu, and Z. Y. Wang, Chem. Mater. **16**, 3708 (2004)
79. J. Y. Do, S. K. Park, J.-J. Ju, S. Park, and M.-H. Lee, Opt. Mater. **26**, 223 (2004).
80. J. Y. Do, S. K. Park, J.-J. Ju, S. Park, and M.-H. Lee, Polym. Adv. Tech. **16**, 221 (2005).
81. K.-S. Lee, K.-J. Moon, H. Y. Woo, and H.-K. Shim, Adv. Mater. **9**, 978 (1997).
82. M.-H. Lee, J.-J. Ju, M.-S. Kim, J. Y. Do, S. K. Park, S. Park, and J. Kim, J. Nonlinear Opt. Phys. Mater. **13**, 391 (2004).
83. N. Nemoto, F. Miyata, Y. Nagase, J. Abe, M. Hasegawa, and Y. Shirai, Chem. Mater. **8**, 1527 (1996).
84. C. Heldann, M. Schulze, and G. Wegner, Macromolecules **29**, 4686 (1996).
85. C. Weder, B. H. Glomm, P. Neuenschwander, U. W. Suter, P. Pretre, P. Kaatz, and P. Günter, Adv. Nonlinear Opt. **4**, 63 (1997).
86. Y.-W. Kim, J.-I. Jin, M. Y. Jin, K.-Y. Choi, J.-J. Kim, and T. Zyung, Polymer **38**, 2269 (1997).
87. F. Miyata, N. Nemoto, Y. Nagase, J. Abe, M. Hasegawa, and Y. Shirai, Macromol. Chem. Phys. **199**, 1465 (1998).
88. N. Nempto, F. Miyata, T. Kamiyama, Y. Nagase, J. Abe, and Y. Shirai, Macromol. Chem. Phys. **200**, 2309 (1999).
89. B.-K. So, K.-S. Lee, S.-M. Lee, M.-K. Lee, and T. K. Lim, Opt. Mater. **21**, 87 (2002).
90. Z. Sekkat, C. S. Kang, E. F. Aust, G. Wegner, and W. Knoll, Chem. Mater. **7**, 142 (1995).
91. N. Nemoto, F. Miyata, Y. Nagase, J. Abe, M. Hasegawa, and F. Shirai, Macromolecules **29**, 2365 (1996).
92. K. Noniewicz and Z. K. Brzozowski, Reat. Funct. Polym. **33**, 343 (1997).
93. J. Luo, J. Qin, and H. Kang, Polym. Int. **49**, 1302 (2000).
94. J.-Y. Lee W.-J. Lee, C. S. Baek, and H.-B. Bang, Bull. Korean Chem. Soc. **25**, 1941 (2004).
95. S. Yokoyama, T. Nakahama, A. Otomo, and S. Mashiko, Thin Solid Films **331**, 248 (1998).
96. S. Yokoyama, T. Nakahama, A. Otomo, and S. Mashiko, J. Am. Chem. Soc. **112**, 3174 (2000).
97. J.-H. Lee and K.-S. Lee, Bull. Korean Chem. Soc. **21**, 847 (2000).
98. H. L. Bozec, T. L. Bouder, O. Maury, A. Bondon, I. Ledoux, S. Deveau, and J. Zyss, Adv. Mater. **13**, 1677 (2001).
99. H. Ma, B. Chen, T. Sassa, L. R. Dolton, and A. K.-Y. Jen, J. Am. Chem. Soc. **123**, 986 (2001).
100. H. Ma and A. K.-Y, Jen, Adv. Mater. 13, 1201 (2001).
101. P. Busson, J. Örtegren, H. Ihre, U. W. Gedde, A. Hult, G. Andersson, A. Eriksson, and M. Lindgren, Macromolecules 35, 1663 (2002).
102. M. E. Van der Boom, Angew. Chem. Int. Ed. **41**, 3363 (2002).
103. H. Ma, S. Liu, J. Luo, S. Suresh, L. Liu, S. H. Kang, M. Haller, T. Sassa, L. R. Dolton, and A. K.-Y. Jen, Adv. Funct. Mater. **12**, 565 (2002).
104. J. Luo, S. Liu, M. Haller, L. Liu, H. Ma, and A. K.-Y. Jen, Adv. Mater. **14**, 1763 (2002).

105. Y. V. Pereverzev, O. V. Prezhdo, and L. R. Dalton, Chem. Phys. Lett. **373**, 207 (2003).
106. T. L. Bouder, O. Maury, A. Bondon, K. Costuas, E. Amouyal, I. Ledoux, J. Zyss, and H. L. Bozec, J. Am. Chem. Soc. **125**, 12284 (2003).
107. O. Y.-H. Tai, C. H. Wang, H. Ma, and A. K.-Y. Jen, J. Chem. Phys. **121**, 6086 (2004).
108. J. Luo, M. Haller, H. Ma, S. Liu, T.-D. Kim, Y. Tian, B. Chen, S.-H. Jang, L. R. Dalton, and A. K.-Y. Jen, J. Phys. Chem. B **108**, 8523 (2004).
109. H. C. Jeong, M. J. Piao, S. H. Lee, M.-Y. Jeong, K. M. Kang, G. Park, S.-J. Jeon, and B. R. Cho, Adv. Funct. Mater. **14**, 64 (2004).
110. A. J. Brouwer and R. M. J. Liskamp, Eur. J. Org. Chem. 487 (2005).
111. Y. Bai, N. Song, J. P. Gao, X. Sun, X. Wang, G. Yu, and Z. Y. Wang, J. Am. Chem. Soc. **127**, 2060 (2005).
112. J. F. Nye, *Physical Properties of Crystals* (Clarendon, Oxford, 1960).
113. S. Cyvin, J. Rauch, and J. Decius, J. Chem. Phys. **43**, 4083 (1965).
114. M. J. Soileau, W. E. Williams, and E. W. Van Stryland, IEEE J. Quantum Electron. **19**, 731 (1983).
115. D. Grischkowsky, Phy. Rev. Lett. **24**, 866 (1970).
116. J. H. Marburger, in *Progress of Quantum Electronics*, edited by J. H. Sandom and S. Stenholm (Pergamon, New York, 1977), p. 35.
117. M. Sheik-Bahae, A. A. Said, and E. W. Van Stryland, Opt. Lett. **14**, 955 (1989).
118. M. Göppert-Mayer, Ann. Phys. **9**, 273 (1931).
119. W. Kaiser and C. G. B. Garret, Phys. Rev. Lett. **7**, 229 (1961).
120. R. Menzel, *Photonics; Linear and Nonlinear Interactions of Laser Light and Matter* (Springer, Berlin, 2001).
121. J. D. Bhawalkar, G. S. He, and P. N. Prasad, Rep. Prog. Phys. **59**, 1041 (1996).
122. T.-C. Lin, S.-J. Chung, K.-S. Kim, X. Wang, G. S. He, J. Swiatkiewicz, H. E. Pudavar, and P. N. Prasad, Adv. Polym. Sci. **161**, 157 (2003); Ref. therein.
123. M. Albota, D. Beljonne, J. C. Bredas, J. E. Ehrlich, J.-Y. Fu, A. A. Heikal, S. E. Hess, T. Kogej, M. D. Levin, S. R. Mader, D. McCord-Maughon, J. W. Perry, H. Rockel, M. Rumi, G. Subranmaim, W. W. Webb, X.-Y. Wu, and C. Wu, Science **281**, 1653 (1998).
124. C. Wu and W. W. Webb, J. Opt. Soc. Am. B **13**, 481 (1996).
125. H.-B. Sun, S. Matsuo, and H. Misawa, Appl. Phys. Lett. **74**, 786 (1999).
126. M. Straub and M. Gu, Opt. Lett. **27**, 1824 (2002).
127. S. Shoji, H.-B. Sun, and S. Kawata, Appl. Phys. Lett. **83**, 608 (2003).
128. H.-B. Sun, T. Suwa, K. Takada, R. P. Zaccaria, M.-S. Kim, K.-S. Lee, and S. Kawata, Appl. Phys. Lett. **85**, 3708 (2004).
129. S. Esener and P. M. Rentzepis, Proc. SPIE **1449**, 144 (1991).
130. J. H. Strickler and W. W. Webb, Opt. Lett. **16**, 1780 (1991).
131. H. J. Strickler and W. W. Webb, Adv. Mater. **5**, 479 (1993).
132. B. H. Cumpston, S. P. Ananthavel, S. Barlow, D. L. Dyer, J. E. Ehrlich, L. L. Erskine, A. A. Heikal, S. M. Kuebler, I.-Y. S. Lee, D. McCord-Maughon, J. Qin, H. Röckel. M. Rumi, X.-L. Wu, S. R. Marder, and J. W. Perry, Natuer **398**, 51 (1999).
133. S. Kawata and Y. Kawata, Chem. Rev. **100**, 1777 (2000).
134. Y. Kawata, M. Nakano, S.-C. Lee, Opt. Eng. **40**, 2247 (2001).
135. B. J. Siwick, O. Kalinina, E. Kumacheva, R. J. D. Miller, and J. Noolandi, J. Appl. Phys. **90**, 5328 (2001).
136. S. Klein, A. Barsella, H. Leblond, H. Bulou, A. Fort, C. Andraud, G. Lemercier, J. C. Mulatier, and K. Dorkenoo, Appl. Phys. Lett. **86**, 211118 (2005).
137. T. Sherwood, C. Young, J. Takayesu, K.A. Jen, L. Dalton, and A. Chen, Proc. SPIE **5724**, 356 (2005).
138. L. Luo, C. Li, S. Wang, W. Huang, C. Wu, H. Yang, H. Jiang, Q. Gong, Y. Yang, and S. Feng, J. Opt. A: Appl. Opt. **3,** 489 (2001).
139. S. Maruo and K. Ikuta, Proc. SPIE **3937**, 106 (2000).
140. H.-B. Sun, T. Kawakami, Y. Xu, J.-Y. Ye, S. Matuso, H. Misawa, M. Miwa, and R. kaneko, Opt. Lett. **25**, 1110 (2000).
141. H.-B. Sun, K. Takada, and S. Kawata, Appl. Phys. Lett. **79**, 3173 (2001).
142. S. Kawata, H.-B. Sun, T. Tanaka, and K. Takada, Nature **412**, 697 (2001).
143. A. Mukherjee, Appl. Phys. Lett. **62**, 3423 (1993).
144. G. S. He, C. F. Zhao, J. D. Bhawalkar, and P. N. Prasad, Appl. Phys. Lett. **67**, 3703 (1995).
145. G. S. He, J. D. Bhawalkar, C. F. Zhao, C.-K. Park, and P. N. Prasad, Opt. Lett. **20**, 2393 (1995).
146. A. Abbotto, L. Beverina, R. Bozio, S. Bradamante, C. Ferrante, G. A. Pagani, and R. Signorini, Adv. Mater. **12**, 1963 (2000).
147. G. Zhou, D. Wang, X. Wang, X. Xu, X. Cheng, Z. Shao, X. Zhao, Q. Fang, and M. Jiang, Opt. Laser Tech. **33**, 529 (2001).
148. A. Abbotto, L. Beverina, R. Bozio, S. Bradamante, G. A. Pagani, and R. Signorini, Synth. Met. **121**, 1755 (2001).
149. D. Wang, G. Zhou, Y. Ren, S. Yang, X. Xu, X. Zhao, Z. Shao, and M. Jiang, Opt. Eng. **41**, 1899 (2002).
150. K. Shirota, H.-B. Sun, and S. Kawata, Appl. Phys. Lett. **84**, 1632 (2004).
151. G. S. He, J. D. Bhawalker, C. F. Zhao, and P. N. Prasad, Appl. Phys. Lett. **67**, 2433 (1995).
152. G. S. He, L. Yuan, N. Cheng, J. D. Bhawalkar, P. N. Prasad, L. L. Brott, S. J. Clarson, and B. A. Reinhardt, J. Opt. Soc. Am. B **14**, 1097 (1997).
153. J. E. Ehrlich, X. L. Wu, L.-Y. Lee, Z.-Y. Hu, H. Roecker, S. R. Marder, and J. Perry, Opt. Lett. **22**, 1843 (1997).
154. C. W. Spangler, J. Mater. Chem. **9**, 2013 (1999).
155. G. S. He, T.-C. Lin, P. N. Prasad, C.-C. Cho, and L.-J. Yu, Appl. Phys. Lett. **82**, 4717 (2003).
156. M. G. Silly, L. Porrès, O. Mongin, P.-A. Chollet, and M. Blanchard-Desce, Chem. Phys. Lett. **379**, 74 (2003).
157. T.-C. Lin, G. S. He, P. N. Prasad, and L.-S. Tan, J. Mater. Chem. **14**, 982 (2004).
158. Z. Yang, Z. Wu, J. Ma, A. Xia, Q. Li, C. Liu, and Q. Gong, Appl. Phys. Lett. **86**, 061903 (2005).
159. W. Denk, J. H. Strikler, and W. W. Webb, Science **248**, 73 (1990).
160. H. Ohata, H. Yamada, T. Niioka, M. Yamamaoto, and K. Momose, J. Pharmacol. Sci. **93**, 242 (2003).
161. S. M. Dunham, H. E. Pudavar, P. N. Prasad, and M. K. Stachowiak, J. Phys. Chem. B **108**, 10540 (2004).
162. E. E. Serrano and V. B. Knight, Proc. SPIE **5705**, 225 (2005).
163. K. Baba, T. Y. Ohulchanskyy, Q. Zheng, T.-C. Lin, E. J. Bergey, and P. N. Prasad, MRS Symp. Proc. **845**, 209 (2005).
164. J. D. Bhawalkar, N. D. Kumar, C. F. Zhao, and P. N. Prasad, J. Clin. Med. Surg. **15**, 201 (1997).
165. P. K. Frederiksen, M. Jørgensen, and P. R. Ogiby, J. Am. Chem. Soc. **123**, 1215 (2001).
166. I. Roy, T. Y. Ohulchanskyy, H. E. Pudaver, E. J. Bergey, A. R. Oseroff, J. Morgan, T. J. Dougherty, and P. N. Prasad, J. Am. Chem. Soc. **125**, 7860 (2003).
167. M. Fournier, C. Pépin, D. Houde, R. Oueller, and J. E. van Lier, Photochem. Photobiol. Sci. **3**, 120 (2004).
168. M. Drobizhev, Y. Stepanenko, Y. Dzenis, A. Karotki, A. Rebane, P. N. Taylor, and H. L. Anderson, J. Phys. Chem. B **109**, 7223 (2005).
169. M. A. Oar, J. M. Serin, W. R. Dichtel, M. J. Fechet, T. Y. Ohulchanskyy, and P. N. Prasad, Chem. Mater. **17**, 2267 (2005).
170. C. W. Spangler, J. R. Starkey, F. Meng, A. Gong, M. Drobizhev, A. Rebane, and B. Moss, Proc. SPIE **5689**, 141 (2005).
171. C. Stuteret, J. P. Herman, R. Frey, F. Fradere, J. Ducuing, R. H. Daughman, and R. R. Chance, Phys. Rev. Lett. **36**, 956 (1976).
172. G. M. Carter, J. V. Hryniewicz, M. K. Thakur, Y. J. Chen, and S. E. Mayler, Appl. Phys. Lett. **49**, 998 (1986).
173. J. Bolger, T. G. Harvey, W. Ji, A. K. Kar, S. Molyneux, B. S. Wherrett, D. Bloor, and P. Norman, J. Opt. Soc. Am. B **9**, 1552 (1992).
174. M. Ohsugi, S. Takaragi, H. Matsuda, A. Okada, H. Masaki, and H. Nakanishi, Proc. SPIE **1337**, 162 (1990).
175. P. A. Chollet, F. Kazjar, and J. Messier, in *Nonlinear Optics of Organics and Semiconductors*, edited by T. Kobayashi (Springer, Berlin, 1988), p. 171.
176. P. A. Chollet, F. Kazjar, and J. Messier, Thin Solid Films **132**, 1 (1985).
177. J. M. Nunzi and F. Charra, J. Appl. Phys. **62**, 2198 (1987).
178. T. Doi, S. Okada, H. Matsuda, A. Masaki, N. Minami, H. Nakanishi, and K. Hayamizu, presented at the 52nd Meeting of the Japanese Society of Applied Physics, 1991.
179. P. N. Prasad, Proc. SPIE **1017**, 2 (1988).
180. J. Le Moigne, A. Thierry, P. A. Chollet, F. Kazjar, and J. Messier, J. Chem. Phys. **88**, 6647 (1988).
181. J. Le Moigne, A. Thierry, and F. Kazjar, Proc. SPIE **1125**, 9 (1990).
182. T. Kanetake, K. Ishikawa, T. Hesegawa, T. Koda, K. Takeda, H. Hesegawa, K. Kubodera, and H. Kobayashi, Appl. Phys. Lett. **54**, 2287 (1989).
183. F. Kazjar and J. Messier, Thin Solid Films **132**, 11 (1985).

184. F. Kazjar and J. Messier, Polym. J. **19**, 275 (1987).
185. H. Matsuda, S. Okada, and H. Nakanishi, in Proceedings of the Fifth International Conference on Photoactive Solids, Okazaki, Japan, 1991, p. 264.
186. L. Yang, R. Dorsinville, Q. Wang, W. Zou, P. Ho, N. Yang, R. Alfano, R. Zamboni, R. Danieli, G. Ruini, and C. Taliani, J. Opt. Soc. Am. B **6**, 753 (1989).
187. T. Sugiyama, T. Wada, and H. Sasabe, Synth. Met. **28**, C323 (1989).
188. Y. Pang and P. N. Prasad, J. Chem. Phys. **93**, 2201 (1990).
189. B. P. Singh, M. Samoc, H. Nalva, and P. N. Prasad, J. Chem. Phys. **92**, 2756 (1990).
190. H. Sasabe, T. Wadw, T. Sigiyama, H. Ohkawa, A. Yamada, and A. F. Garito, in *Conjugated Polymeric Materials in Electronics, Optoelectronics and Molecular Electronics*, edited by J. L. Bredas and R. R. Chance (Kluwer, London, 1990), p. 399.
191. H. Matsuda, M. Sato, S. Okada, H. Nakanishi, M. Kato, and T. Nishiyama, Polym. Prepr. Jpn. **28**, 1035 (1989).
192. F. Kazjar, J. Messier, C. Sentein, R. L. Elsenbaumer, and G. G. Miller, Proc. SPIE **1147**, 36 (1989).
193. T. Kaino, K. Kubodra, H. Kobayashi, T. Kurihara, S. Saito, T. Tsutsui, T. Takito, and H. Murata, Appl. Phys. Lett. **53**, 2002 (1988).
194. P. N. Prasad, Thin Sold Films **152**, 275 (1987).
195. P. Logsdon, J. Pfleger, and P. N. Prasad, Synth. Met. **26**, 369 (1988).
196. M. Sinlair, D. McBranch, D. Moses and A. Heeger, Synth. Met. **28**, D645 (1989).
197. E. Wintner, F. Krausz, and G. Leising, Synth. Met. **28**, D159 (1989).
198. G. A. Olah, E. Zadok, R. Edler, D. H. Adamson, W. Kasha, and G. Suryaprakash, J. Am. Chem. Soc. **111**, 9123 (1989).
199. D. Neher, A. Wolf, C. Bubeck, and G. Wegner, Chem. Phys. Lett. **163**, 116 (1989).
200. H. Vanherzeele, J. Meth, S. Jenekhe, and M. Roberts, J. Opt. Soc. Am. B **9**, 524 (1982).
201. B. P. Singh, P. N. Prasad, and F. E. Karasz, Polymer **29**, 1940 (1988).
202. D. D. Bradley and Y. Mori, Jpn. J. Appl. Phys. **28**, 174 (1989).
203. K. Kamiyama, M. Era, T. Tsutsui, and S. Saito, Jpn. J. Appl. Phys. **29**, L840 (1990).
204. Y. Pang, M. Samoc, and P. N. Prasad, J. Chem. Phys. **94**, 5282 (1991).
205. J. Swiatkiewicz, P. N. Prasad, F. E. Krausz, A. A. Druy, and P. Glatkwski, Appl. Phys. Lett. **56**, 892 (1990).
206. C. J. Wung, W. M. K. P. Wijekoon, and P. N. Prasad, Polymer **34**, 1174 (1993).
207. K. Kamiyama, M. Era, T. Tsutsui, and S. Sato, Jpn. J. Appl. Phys. **29**, L840 (1990).
208. K. Wong, S. Han, and Z. Vardeny, J. Appl. Phys. **70**, 1896 (1991).
209. S. K. Goshal, Chem. Phys. Lett. **158**, 65 (1989).
210. J. R. Lindle, F. J. Bartoli, C. A. Hoffmann, O. K. Kim, Y. S. Lee, J. S. Shirk, and Z. F. Kafafi, Appl. Phys. Lett. **65**, 712 (1990).
211. K. S. Lee and M. Samoc, Polymer **32**, 361 (1991).
212. S. A. Jenekhe, J. A. Osaheni, H. Vanherzeele, and J. Meth, Chem. Mater. **4**, 683 (1992).
213. L. Yu, D. W. Polis, M. R. McLean, and L. R. Dalton, in *Electroresponsive Molecular and Polymeric Systems*, edited by T. A. Skotheim (Dekker, New York, 1991), Vol. II, p. 113.
214. H. S. Nalva, T. Hamada, A. Kakuta, and A. Mukoh, Jpn. J. Appl. Phys. **32**, L193 (1993).
215. P. N. Prasad, Proc. SPIE **1328**, 186 (1990).
216. C. J. Wung, Ph.D. dissertation, State University of New York at Buffalo, Buffalo, 1991.
217. P. Shukla, P. M. Cotts, R. D. Miller, S. Ducharme, R. Asthana, and J. Zavislan, Mol. Cryst. Liq. Cryst. **183**, 241 (1990).
218. J. C. Baumert, G. C. Bjorklund, D. H. Dundt, M. C. Jurich, H. Looser, R. D. Miller, J. Rabolt, R. Sooriyakumaran, J. D. Swalean, and R. J. Twieg, Appl. Phys. Lett. **53**, 1147 (1988).
219. F. Kazjar, J. Messier, and C. Rosilio, J. Appl. Phys. **60**, 3040 (1986).
220. L. Yang, Q. Wang, P. Ho, R. Dorsville, R. Alfano, W. Zou, and N. Yang, Appl. Phys. Lett. **53**, 1245 (1988).
221. C. L. Callender, C. A. Carere, J. Albert, L. L. Zhou, and D. J. Worsfold, J. Opt. Soc. Am. B **9**, 518 (1992).
222. K. S. Wong, S. G. Han, Z. V. Vardeny, J. Shinar, Y. Pang, I. Maghsoodi, T. J. Barton, S. Grigoras, and B. Parbhoo, Appl. Phys. Lett. **58**, 1695 (1991).
223. W. J. Blau, H. J. Byrne, D. J. Cardin, T. J. Dennis, J. P. Hare, H. W. Kroto, R. Taylor, and D. R. Walton, Phys. Rev. Lett. **67**, 1423 (1991).
224. X. K. Wong, T. G. Zhang, W. P. Lin, S. Z. Liu, G. K. Wong, M. M. Kappes, R. P. H. Chang, and J. B. Ketterson, Appl. Phys. Lett. **60**, 810 (1992).
225. F. Henari, J. Collaghan, H. Stiel, W. Blau, and D. J. Cardin, Chem. Phys. Lett. **199**, 144 (1992).
226. J. S. Meth, H. Vanherzeele, and Y. Wang, Chem. Phys. Lett. **188**, 492 (1992).
227. Y. Wang and L. T. Chen, J. Chem. Phys. **96**, 1530 (1992).
228. M. J. Rosker, H. O. Mercy, T. Y. Chang, J. T. Khoury, K. Hansen, and R. L. Whetten, Chem. Phys. Lett. **196**, 427 (1992).
229. H. Hoshi, N. Nakamura, Y. Maruyama, T. Nakagawa, S. Suzuki, H. Shiromaru, and A. Achiba, Jpn. J. Appl. Phys. **30**, L1397 (1991).
230. G. B. Talapatra, N. Manickam, M. Samoc, M. E. Orczyk, S. P. Karna, and P. N. Prasad, J. Phys. Chem. **96**, 5206 (1992).
231. S. C. Yang, Q. Gong, Z. Xia, Y. Zou, Y. Wu, D. Qiang, Y. Sun, and Z. Gu, Appl. Phys. B **55**, 51 (1992).
232. Q. Gong, Y. Sun, Z. Xia, Z. Gu, X. Zhou, and D. Qiang, J. Appl. Phys. **71**, 3025 (1992).
233. J. P. Herman, Opt. Commun. **9**, 74 (1973).
234. C. Maloney and W. Blau, J. Opt. Soc. Am. B **4**, 1035 (1987).
235. S. H. Stevenson, D. S. Donald, and G. R. Meridith, in *Nonlinear Optical Properties of Polymers, Materials*, Research Society Symposium Proceedings Vol. 109, edited by A. J. Heeger, J. Orenstein, and D. R. Ulrich (Materials Research Society, Pittsburgh, 1988), p. 103.
236. M. E. Orczyk, J. Swiatkiewicz, N. Manickam, M. Tomoaia-Cotisel, and P. N. Prasad, Appl. Phys. Lett. **60**, 2837 (1992).
237. Z. H. Kafafi, J. R. Lidle, R. G. S. Pong, F. J. Bartoli, L. J. Lingg, and J. Milliken, Chem. Phys. Lett. **188**, 492 (1992).
238. Z. Z. Ho, C. Y. Ju, and W. M. Hetherington III, J. Appl. Phys. **62**, 716 (1987).
239. M. Hosoda, T. Wada, A. Yamada, A. F. Garito, and H. Sasabe, Nonlinear Opt. **3**, 183 (1992).
240. J. S. Shirk, J. R. Lindle, F. J. Bartoli, C. A. Hoffman, Z. H. Kafafi, and A. W. Snow, Appl. Phys. Lett. **55**, 1287 (1989).
241. H. Matsuda, S. Okada, a. Masaki, H. Nakanishi, Y. Suda, K. Shigehara, and A. Yamada, Proc. SPIE 1337, 105 (1990).
242. J. S. Shirk, J. R. Lindle, F. J. Bartoli, and M. F. Boyle, J. Phys. Chem. **96**, 5847 (1992).
243. M. Castevenss, M. Samoc, J. Pfleger, and P. N. Prasad, J. Chem. Phys. **92**, 2019 (1990).
244. H. S. Nalwa, A. Kakuta, and A. Mukoh, Chem. Phys. Lett. **203**, 109 (1993).
245. H. S. Nalwa, A. Kakuta, and A. Mukoh, J. Phys. Chem. **97**, 1097 (1993).
246. J. S. Shirk, J. R. Lindle, F. J. Bartoli, Z. H. Kafafi, A. W. Snow, and M. E. Boyle, Int. J. nonlinear Opt. Phys. **1**, 699 (1992).
247. B. A. Reinhardt, L. L. Brott, S. T. Clarson, A. G. Dillard, J. C. Bhatt, R. Kannan, L. Yuan, G. S. He, and P. N. Prasad, Chem. Mater. **10**, 1683 (1998).
248. O.-K. Kim, K.-S. Lee, H. Y. Woo, K.-S. Kim, G. S. He, J. Swiatkiewicz, and P. N. Prasad, Chem. Mater. **12**, 284 (2000).
249. B. R. Cho, K. H. Son, S. H. Lee, Y.-S. Song, Y.-K. Lee, S.-J. Jeon, J. H. Choi, H. Lee, and M. Cho, J. Am. Chem. Soc. **123**, 10039 (2001).
250. S.-J. Chung, K.-S. Kim, T.-C. Lin, G. S. He, J. Swiatkiewicz, and P. N. Prasad, J. Phys. Chem. B **103**, 10741 (1999).
251. A. Adronov, J. M. J. Frechet, G. S. He, K.-S. Kim, S.-J. Chung, J. Swiatkiewicz, and P. N. Prasad, Chem. Mater. **12**, 2838 (2000).
252. F. E. Hernandez, K. D. Belfield, and I. Cohanoschi, Chem. Phys. Lett. **391**, 22 (2004).
253. O. Mongin, L. Porrès, L. Moreaux, J. Mertz, and M. Blanchard-Dece, Org. Lett. **4**, 719 (2002).
254. L. Porres, O. Mongin, C. Katan, M. Charlot, T. Pons, J. Mertz, and M. Blanchard-Desce, Org. Lett. **6**, 47 (2004).
255. F. Meng, B. Li, S. Qian, K. Chen, and H. Tian, Chem. Lett. **33**, 470 (2004).
256. K. D. Belfield, A. R. Morales, J. M. Hales, D. J. Hagan, E. W. Van Stryland, V. M. Chapela, and J. Percino, Chem. Mater. **16**, 2267 (2004).
257. K. D. Belfield, A. R. Morales, B.-S. Kang, J. M. Hales, D. J. Hagan, E. W. Van Stryland, V. M. Chapela, and J. Percino, Chem. Mater.**16**, 4634 (2004).
258. Y. Lu, F. Hasegawa, T. Goto, S. Ohkuma, S. Fukuhara, Y. Kawazu, K. Torani, T. Yamashita, and T. Watanabe, J. Lumin. **110**, 1 (2004).

259. Y. Iwase, K. Kamada, K. Ohta, and K. Kondo, J. Mater. Chem. **13**, 1575 (2003).
260. Q. Zheng, G. S. He, and P. N. Prasad, J. Mater. Chem. **15**, 579 (2005).
261. M. Charlot, L. Porrès, C. D. Entwistle, A. Beeby, T. B. Marder, and M. Blanchard-Desce, Phys. Chem. Chem. Phys. **7**, 600 (2005).
262. S. K. Lee, W. J. Yang, J. J. Choi, C. H. Kim, S.-J. Jeon, and B. R. Cho, Org. Lett. **7**, 323 (2005).
263. M. Rumi, J. E. Ehrlich, A. A. Heikal, J. W. Perry, S. Barlow, Z. Hu, D. McCord-Maughon, T. C. Parker, H. Röckel, S. Thayumanavan, S. R. Marder, D. Beljonne, and J. L. Brédas, J. Am. Chem. Soc. **122**, 9500 (2000).
264. S. J. K. Pond, O. Tsutsumi, M. Rumi, O. Kwon, E. Zojer, J. L. Brédas, S. R. Marder, and J. W. Perry, J. Am. Chem. Soc. **126**, 9291 (2004).
265. K.-S. Lee, J.-H. Lee, K.-S. Kim, H.-Y. Woo, O.-K. Kim, H. Choi, M. Cha, G. S. He, J. Swiatkiewcz, P. N. Prasad, M.-A. Chung, and S.-D. Jung, Nonlinear Opt. **27**, 87 (2001).
266. K.-S. Lee, M.-S. Kim, H.-K. Yang, H.-B. Sun, S. Kawata, and P. Fleitz, Mol. Cryst. Liq. Cryst. **424**, 35 (2004).
267. M.-S. Kim, H.-K. Yang, R. H. Kim, K.-S. Lee, M. Cha, H. Choi, H.-B. Sun, S. Kawata. J. Nonlinear Opt. Phys. Mater. 13, 467 (2004).
268. H.-K. Yang, M.-S. Kim, S.-W. Kang, K.-S. Kim, K.-S. Lee, S. H. Park, D.-Y. Yang, H. J.Kong, H.-B. Sun, S. Kawata, and P. Fleitz, J. Photopolym. Sci. Tech. **17**, 385 (2004).
269. K.-S. Lee, S.-W. Kang, and J. Y. Kim, unpublished results.
270. W.-H. Lee, H. Lee, J.-A. Kim, J.-H. Choi, M. Cho, S.-J. Jeon, and B. R. Cho. J. Am. Chem. Soc. **123**, 10658 (2001).
271. B. R. Cho, M. J. Piao, K. H. Son, S. H. Lee, S. J. Yoon, S.-J. Jeon, and M. Cho, Chem. Eur. J. **8**, 3907 (2002).
272. W. J. Yang, C. H. Kim, M.-Y. Jeong, S. K. Lee, M. J. Piao, S.-J. Jeon, and B. R. Cho. Chem. Mater. **16**, 2783 (2004).
273. S.-J. Chung, T.-C. Lin, K.-S. Kim, G. S. He, J. Swiatkiewicz, P. N. Prasad, G. A. Baker, and F. V. Bright, Chem. Mater. **13**, 4071 (2001).
274. X. Zhou, A. M. Ren, J.-K. Feng, and X.-J. Liu, Chem. Phys. Lett. **362**, 541 (2002).
275. G. P. Bartholomew, M. Rumi, S. J. K. Pond, J. W. Perry, S. Tretiak, and G. C. Bazan, J. Am. Chem. Soc. **126**, 11529 (2004)
276. W. J. Yang, D. Y. Kim, C. H. Kim, M.-J. Jeong, S. K. Lee, S.-J. Jeon, and B. R. Cho, Org. Lett. **6**, 1389 (2004).
277. C. Li, C. Liu, Q. Li, and Q. Gong, Chem. Phys. Lett. **400**, 569 (2004).
278. S.-W. Kang, J. Y. Kim, R. H. Kim, B.-K. So, K.-S. Lee, I.-W. Hwang, D. Kim, P. Fleitz, H.-B. Sun, and S. Kawata, Proc. SPIE **5621**, 1 (2004).
279. Y.-Z. Cui, Q. Fang, G. Xue, G.-B. Xu, L. Yin, and W.-T. Yu, Chem. Lett. **34**, 644 (2005).
280. A. Adronov, J. M. J. Fréchet, G. S. He, K.-S. Kim, S.-J. Chung, J. Swiatkiewicz, and P. N. Prasad, Chem. Mater. **12**, 2838 (2000).
281. M. Drobizhev, A. Karotki, Y. Dzenis, A. Rebane, Z. Suo, and C. W. Spangler, J. Phys. Chem. B **107**, 7540 (2003).
282. M. Hara, S. Samori, X. Cai, S. Tojo, T. Arai, A. Momotake, J. Hayakawa, M. Ueda, K. Kawai, M. Endo, M. Fujitsuka, and T. Majima, J. Am. Chem. Soc. **126**, 14217 (2004).
283. M. Drobizhev, A. Rebane, Z. Suo, and C. W. Spangler, J. Lumin. **111**, 291 (2005).
284. M. A. Oar, J. M. Serin, W. R. Dichtel, M. J. Fréchet, T. Y. Ohulchanskyy, and P. N. Prasad, Chem. Mater. **17**, 2267. (2005).
285. R. K. Meyer, R. E. Benner, Z. V. Vardeny, M. Liess, M. Ozaki, K. Yoshino, Y. Ding, and T. Barton, Synth. Met. 84, 549 (1997).
286. G. S. He, C. Weder, P. Smith, and P. N. Prasad, J. Quantum Electron. **34**, 2279 (1998).
287. M. G. Harrison, G. Urbasch, R. F. Mahrt, H. Giessen, H. Bässler, and U. Scherf, Chem. Phys. Lett. **313**, 755 (1999).
288. P. Najechalski, Y. Morel, O. Stéphan, and P. L. Baldeck, Chem. Phys. Lett. **343**, 44 (2001).
289. S.-J. Chung, G. S. Maciel, H. E. Pudavar, T.-C. Lin, G. S. He, J. Swiatkiewicz, P. N. Prasad, D. W. Lee, and J.-I. Jin, J. Phys. Chem. A **106**, 7512 (2002).

CHAPTER 50

Refractive Index, Stress-Optical Coefficient, and Optical Configuration Parameter of Polymers

Vassilios Galiatsatos

*Leibniz Institute of Polymer Research, 01069 Dresden, Germany**

Refractive index is the ratio of electromagnetic radiation in vacuo to the phase velocity of electromagnetic radiation of a specified frequency in the medium (ISO definition). The definition implies that the refractive index is always greater than unity and that it is dimensionless. For anisotropic materials the state of polarization of the light and its direction must be defined relative to reference axis in the sample.

When an incident ray of light passes from vacuum into another medium, its velocity is reduced and the ray is bent (or refracted) toward the normal to the medium's surface. The angle between the incident ray and the normal is the angle of incidence (i); the angle between the refractive ray and the normal is the angle of refraction (r).

For a given medium the ratio of the sine of the angle of incidence to the sine of the angle of refraction is constant:

$$(\sin i)/(\sin r) = c/v = n. \tag{50.1}$$

The index of refraction, n, is dependent upon the wavelength of the incident light. If the incident light is not monochromatic, the constituent rays will experience varying amounts of refraction. This effect is known as dispersion. Consequently, measurements of refractive indices require the use of monochromatic incident light. All experimental values of refractive indices compiled here were measured at the Na D line, which has a wavelength of 5,893 Å.

In anisotropic crystals and fibers, the refractive index varies with the direction of (polarized) light through the structure. For example fibers have two principal values one parallel and one perpendicular with respect to the long direction of the fiber. On the other hand isotropic crystals have only one refractive index. Crystals with tetragonal and hexagonal symmetry have two principal values of refractive index. Orthorombic, monoclinic, and triclinic crystals have three principal values. The refractive index varies with frequency, temperature, and degree of polymerization.

The two measurement methods recommended by ISO489 are the Abbe refractometer technique and the Becke line technique. The latter is more useful with powdered or granulated transparent material or even with small chips of material taken from a larger sample. ASTM D542 includes only the Abbe method and it is widely used for characterization of refractive index of polymers.

An Abbe refractometer has a fixed telescope and two right-angle prisms. A thin film of the sample being measured is placed in the gap between the hypotenuses of the right-angle prisms. The monochromatic incident light is refracted through the first prism, the sample, and the second prism. The refracted beam emerges parallel to the incident beam and is viewed with the telescopic eyepiece. The prism assembly is rotated to create a field of view as seen through the telescope in which exactly one-half of the field is dark and the other half is light, with a sharp interface between the two. The refractive index of the sample is read from a graduated scale on the prism assembly. The experimental error is less than 0.01%. Imperfect alignment of the prisms can increase the error. Advances in instrument design have made measurement of refractive index an automated task.

The refractive index of a material is closely related to its polarizability (α). The two are related to each other through the molar refractivity (R_m), which is given as:

$$R_m = \frac{M}{\rho}\frac{n^2 - 1}{n^2 + 2}, \tag{50.2}$$

* Permanent address: Lyondell Chemical Co. -11530 Northlake Drive, Cincinnati, OH 45249, USA.

where M is the molar mass and ρ is the density of the material. This definition of molar refraction is due to Lorentz and Lorentz. Gladstone and Dale have also proposed a relationship between molar refraction (denoted here as $R_{m,GD}$ to distinguish it from the one given above) and refractive index:

$$n = \frac{1 + R_{m,GD}}{M/\rho,}. \tag{50.3}$$

The relationship between polarizability and molar refractivity is:

$$3\varepsilon_0 R_m = N_A \alpha(\omega) \tag{50.4}$$

where ε_0 is the dielectric constant and N_A is Avogadro's number. The (dynamic) polarizability $\alpha(\omega)$ is a function of frequency (far from an absorption band) and is given as

$$\alpha(\omega) = \frac{2}{3h} \sum_n \frac{\omega_{n0} |\langle 0|\mu|n\rangle|^2}{\omega_{n0}^2 - \omega^2}, \tag{50.5}$$

where ω is frequency, the subscript "0" denotes the ground state, the subscript "n" denotes the excited state, and μ is the electric transition dipole moment from the ground to the excited states. The correlation of optical properties of polymers to fundamental properties such as atomic polarizability is an exciting and useful field of research.

Denbigh established that the molar refraction may be considered as the sum of the bond refractions that make up the molecule. Van Krevelen has assigned chemical group refractivities that can be used to calculate refractive indices of polymers. A similar additivity approach may be used to calculate the refractive indices of semicrystalline polymers of known density, if the crystalline and amorphous densities and refractive indices are also known:

$$n = \nu_{cr} - n_{cr} + (1 - \nu_{cr}) n_{nc}, \tag{50.6}$$

$$\nu_{cr} = \frac{\rho - \rho_{nc}}{\rho_{cr} - \rho_{nc}}, \tag{50.7}$$

Refractive indices of polymers and copolymers can be found in Tables 50.1 and 50.2, respectively. In Table 50.1 footnotes have been used extensively. Footnotes containing no additional data are used to list other forms of the material which have the same refractive index according to the reference cited.

Other footnotes show additional data differing from that of the most recent reference cited. Readers are cautioned that some of the data is conflicting, and original references should be consulted when assessing the validity of such data. It should also be kept in mind that refractive indices of polymer products (films, injection molded articles, thermoformed sheets, etc.) will have optical properties that depend on the processing history of the product. Therefore one should distinguish between the fundamental refractive index of the polymer and those of the final product. The handbook makes an effort to include both types of information.

The stress-optical coefficient C is the ratio of birefringence to true stress:

$$C = \frac{\Delta n}{\tau}, \tag{50.8}$$

The stress-optical coefficient has units of mm^2/N. It is related to the optical configuration parameter, $\Delta\alpha$, a configuration-dependent property of a polymer, through

$$C = \frac{2\pi\Delta\alpha(n^2 + 2)^2}{45kTn}, \tag{50.9}$$

where T is temperature (in Kelvin) and k is the Boltzmann constant. The birefringence, or double refraction, is the difference in refractive indices along the three Cartesian coordinate axes of the polymer sample:

$$\Delta n_{xy} = n_x - n_y, \tag{50.10}$$

$$\Delta n_{xz} = n_x - n_z, \tag{50.11}$$

$$\Delta n_{yz} = n_y - n_z = \Delta n_{xz} - \Delta n_{xy}. \tag{50.12}$$

Strain-induced birefringence is measured with a rheo-optical instrument. Such an instrument may induce orientation of the polymer chains within a sample, generally via uniaxial strain, while monochromatic light passes through the sample on an axis perpendicular to that of the strain. In some other cases the orientation may be induced by an external field (such as flow) acting on the sample, or the sample may already have anisotropy already "frozen-in" as is the case of semicrystalline polymers for example. The retardation of the light passing through the sample may be measured with a Babinet compensator. Modern instruments rely on photoelastic modulators for the task. The birefringence is then calculated from the retardation, and the stress-optical coefficient is calculated from the birefringence and the stress. The experimental error in such procedures is less than 5%.

The optical configuration parameter may be calculated theoretically through the rotational isomeric state model. Its units are typically in cm^3. Stress-optical coefficient and optical configuration parameter data for polymers and copolymers can be found in Tables 50.3 and 50.4, respectively. In both tables wavelength is 6,328 Å. The data in Tables 50.1–50.4 have been compiled from more than 100 references. For consistency the polymeric material names are reported exactly as in the original references. In some cases computer databases, given the material names listed here, may be able to provide structural information about the materials.

Related information can be found in Chap. 23.

TABLE 50.1. *Refractive indices of polymers. All values reported are at a wavelength of 5,893 Å unless otherwise noted.*

Polymer	Refractive index n	Temperature (°C)	Reference
Acrylic (PMMA)	1.49		[1]
Acrylic Cont Poly Acrycal MP (see Ftn. 1)	1.49		[2]
Acrylic Cont Poly Acrycal MP CP-1000 E/E/ exc blend stock material	1.50		[2]
Acrylic Cont Poly Acrycal MP CP-1000 l/l/ best impact str transparency	1.50		[2]
Acrylic Cyro acrylite (see Ftn. 2)	1.49		[2]
Acrylic Degussa Corp. Degalan (see Ftn. 3)	1.49		[2]
Acrylic DuPont USA Lucite L super abrasion resistant exc optical	1.49		[2]
Acrylic high impact grade	1.49	23	[3,13]
Acrylic Polycast acrylic sheet clear sheet color white textured sheet	1.49		[2]
Acrylic Polysar Zylar90/l/clear impact fda exc γ ray recovery	1.52		[2]
Acrylic Polysar Zylar91/E/clear impact acrylic for extrusion	1.52		[2]
Acrylic Rohm & Haas Plexiglass (see Ftn. 4)	1.50		[2]
Acrylic sheet Aristech (see Ftn. 5)	1.49		[2]
Allyl cast resin	1.50–1.575		[4,14]
Allyl diglycol carbonate	1.50	23	[3,18]
Amber	1.538–1.548		[4,14]
Balsam (in stick form)	1.54	23	[4,14]
Balsam, Canada	1.53		[4,14]
Benzylcellulose	1.47–1.52		[4,14]
Butyl rubber (unvulcanized)	1.508		[4,5]
Butylphenol formaldehyde	1.66		[4,5]
Cellulose	1.54		[4,5]
Cellulose acetate (see Ftn. 6)	1.48–1.50		[5]
Cellulose acetate (see Ftn. 7)	1.46–1.50	23	[13,18]
Cellulose acetate butyrate (see Ftn. 8)	1.46–1.49		[5]
Cellulose acetate propionate (see Ftn. 9)	1.47–1.48		[4,14]
Cellulose acetate, highly acetyl	1.46–1.50	23	[6]
Cellulose nitrate (see Ftn. 10)	1.50–1.514		[4,5]
Cellulose propionate	1.47–1.48		[4,14]
Cellulose tripropionate	1.48–1.49		[5]
Cellulosics	1.46–1.50		[1]
Chlorinated diphenyl	1.61–1.70		[4,14]
Chlorinated rubber	1.56		[4,14]
Chlorotrifluoroethylene (CTFE)	1.42		[1]
Congo, hard amber (see Ftn. 11)	1.545 ± 0.003	20	[4,14]
Coumarone-indene resins	1.617–1.66		[4,14]
Cresylic acid-formaldehyde condensation resin	1.645 ± 0.003	20	[4,14]
Damar (see Ftn. 12)	1.535–1.538	25	[4,14]
East India gum	1.537 ± 0.003	20	[4,14]
Epoxy resins (see Ftn. 13)	1.55–1.60		[5]
Ethyl cellulose	1.479	21	[5]
Fluorinated ethylene propylene (FEP)	1.34	23	[13,18]
Glycerol-phthalate, rosin modified	1.557	25	[4,14]
Glycerol phthalate, cast resin	1.57	23	[6]
Gutta percha, α (see Ftn. 14)	1.514	21	[5]
Hexamethylene sebacamide	1.532	25	[4,14]
Hydrochlorinated rubber	1.53–1.55		[4,5]
Kapton Type H Film	1.78	23	[7,15]
Methyl cellulose (low viscosity)	1.497	25	[4,14]
Methyl methacrylate cast resin	1.485–1.50	23	[6]
Methyl methacrylate molding resin	1.49	23	[6]
Methyl rubber	1.525		[4,14]
Methyl siloxane fluids	1.375–1.403		[4,14]
Methylpentene polymer	1.465		[1]
Napthalene–formaldehyde resin	1.696		[4,14]
Natural rubber	1.519–1.52	20	[4,14]

TABLE 50.1. *Continued.*

Polymer	Refractive index *n*	Temperature (°C)	Reference
NBS casting resin (mixture of 2,5-dichlorostyrene and styrene)	1.608	25	[4,14]
Neoprene	1.5512	25	[4,14]
Nylon (see Ftn. 15)	1.566		[1]
Pentabromophenyl methacrylate	1.71		[4,14]
Phenol–formaldehyde and phenol–furfural compounds—no filler	1.58–1.66	23	[6]
Phenol–formaldehyde resins (see Ftn. 16)	1.47–1.70		[5]
Phenylene oxide (Noryl)	1.63	23	[13,18]
Phenylphenol–formaldehyde	1.47–1.7		[4,14]
Poly (2-ethoxyethyl methacrylate)	1.367		[4,14]
Poly[1,1-(1-phenylethane) bis(4-phenyl)carbonate]	1.4833	20	[5]
Poly[1,1-(2-methyl propane) bis(4-phenyl)carbonate]	1.6130	25	[8,17]
Poly[1,1-butane bis(4-phenyl)carbonate]	1.5702	25	[8,17]
Poly[1,1-cyclohexane bis(4-phenyl)carbonate]	1.5792	25	[8,17]
Poly(1,1-cyclohexane bis[4-(2,6-dichlorophenyl)]carbonate)	1.5900	25	[8,17]
Poly(1,1-cyclopentane bis(4-phenyl)carbonate)	1.5857	25	[8,17]
Poly(1,1-diethylpropyl methacrylate)	1.5993	25	[8,17]
Poly(1,1-dihydroperfluorehexyl acrylate)	1.4889	20	[5]
Poly(1,1-dihydroperfluorobutyl acrylate)	1.5937	25	[8,17]
Poly[1,1-ethane bis(4-phenyl)carbonate]	1.5000	20	[5]
Poly(1,2-butadiene)	1.5816	20	[5]
Poly(1,2-diphenylethyl methacrylate)	1.5154	25	[5]
Poly(1,3-butadiene)	1.52		[5]
Poly(1,3-butadiene) (high *cis* type)	1.5180		[5]
Poly(1,3-butadiene) (35% *cis*; 56% *trans*; 7% 1,2 content)	1.5270	20	[5]
Poly(1,3-dichloropropyl methacrylate)	1.527	20	[4,14]
Poly(1,3-dichloropropyl-2-methacrylate)	1.5160	25	[8,17]
Poly(1,4-butadiene)	1.5624	20	[5]
Poly[1-(*o*-chlorophenyl)ethyl methacrylate]	1.4730		[5]
Poly(1-decene)	1.5111	20	[4,5]
Poly(1-methycyclohexyl methacrylate)	1.4710	25	[8,17]
Poly(1-octadecene)	1.5396	20	[5]
Poly(1-phenyl-*n*-amyl methacrylate)	1.5573	20	[5]
Poly(1-phenylallyl methacrylate)	1.5645	20	[4,5]
Poly(1-phenylcyclohexyl methacrylate)	1.5487	25	[8,17]
Poly(1-phenylethyl methacrylate)	1.53		[5]
Poly(1-vinyl-2-pyrrolidone)	1.5660	25	[6,17]
Poly(2,2,2′-trimethylhexamethylene terephthalamide)	1.4185		[5]
Poly(2,2,2-trifluoro-1-methylethyl methacrylate)	1.392	25	[5]
Poly(2,2,3,4,4,4-hexafluorobutyl acrylate)	1.5783	25	[8,17]
Poly(2,2-butane bis[4-(2-methylphenyl)]carbonate)	1.5827	25	[8,17]
Poly[2,2-butane bis(4-phenyl)carbonate]	1.5745	25	[8,17]
Poly[2,2-pentane bis(4-phenyl)carbonate]	1.6056	25	[8,17]
Poly(2,2-propane bis[4-(2,6-dibromophenyl)]carbonate)	1.5739	20	[4,5]
Poly(2,2-propane bis[4-(2,6-dichlorophenyl)]carbonate)	1.5900	25	[8,17]
Poly(2,2-propane bis[4-(2-chlorophenyl)]carbonate)	1.6147	25	[8,17]
Poly(2,3-dibromopropyl methacrylate)	1.525	20	[4,5]
Poly(2,3-dimethylbutadiene) (methyl rubber)	1.6248	20	[4,5]
Poly(2,6-dichlorostyrene)	1.412	25	[5]
Poly[2-(1,1,2,2-tetrafluoroethoxy)ethyl acrylate]	1.5682		[5]
Poly[2-(phenylsulfony)ethyl methacrylate]	1.537	20	[5]
Poly(2-aminoethyl methacrylate)	1.5816	20	[4,14]
Poly(2-β-diphenylethyl methacrylate)	1.50	25	[5]
Poly(2-bromo-4-trifluoromethylstyrene)	1.5426	20	[5]
Poly(2-bromoethyl methacrylate)	1.5270	20	[5]
Poly[2-chloro-1-(chloromethyl)ethyl methacrylate]	1.5179	20	[4,5]

TABLE 50.1. *Continued.*

Polymer	Refractive index n	Temperature (°C)	Reference
Poly(2-chlorocyclohexyl methacrylate)	1.533	25	[5]
Poly(2-chloroethyl α-chloroacrylate)	1.517	20	[5]
Poly(2-chloroethyl methacrylate)	1.4899	20.5	[5]
Poly(2-decyl-1,3-butadiene)	1.4899	25	[8,17]
Poly(2-decyl-1,4-butadiene)	1.5174	20	[5]
Poly(2-diethylaminoethyl methacrylate)	1.471	25	[5]
Poly(2-ethoxyethyl acrylate)	1.4768	20	[5]
Poly(2-fluoroethyl methacrylate)	1.390	25	[5]
Poly(2-heptafluorobutoxy)ethyl acrylate)	1.500		[5]
Poly(2-heptyl-1,3-butadiene)	1.5000	25	[8,17]
Poly(2-heptyl-1,4-butadiene)	1.5119	20	[5]
Poly(2-hydroxyethyl methacrylate)	1.5028	30	[5]
Poly(2-isopropyl-1,3-butadiene)	1.5020	25	[8,17]
Poly(2-isopropyl-1,4-butadiene)	1.463	25	[5]
Poly(2-methoxyethyl acrylate)	1.5028	20	[4,5]
Poly(2-methylcyclohexyl methacrylate)	1.4868	20	[4,5]
Poly(2-nitro-2-methylpropyl methacrylate)	1.5592	20	[5]
Poly(2-phenylethyl methacrylate)	1.5060	24.6	[5]
Poly(2-*t*-butyl-1,3-butadiene)	1.5060	25	[8,17]
Poly(2-*t*-butyl-1,4-butadiene)	1.419	25	[5]
Poly(2-trifluoroethoxyethyl acrylate)	1.55	20	[5]
Poly(2-vinyltetrahydrofuran)	1.6376	20	[5]
Poly(2-vinylthiophene)	1.485	20	[4,5]
Poly(3,3,5-trimethylcyclohexyl methacrylate)	1.4580	25	[8,17]
Poly(3-butoxypropylene oxide)	1.465	25	[5]
Poly(3-ethoxypropyl acrylate)	1.4590	25	[8,17]
Poly(3-hexoxypropylene oxide)	1.471	25	[5]
Poly(3-methoxypropyl acrylate)	1.4947	20	[4,5]
Poly(3-methoxypropylene oxide)	1.6330	25	[5,17]
Poly(3-methylcyclohexyl methacrylate)	1.4630	25	[8,17]
Poly[4,4′-isopropylidene diphenoxy di(4-phenylene)sulfone]	1.6500	25	[8,17]
Poly[4,4′-sulfone diphenoxy di(4-phenylene)sulfone]	1.5602	25	[8,17]
Poly[4,4-heptane bis(4-phenyl)carbonate]	1.46		[5]
Poly(4-fluoro-2-trifluoromethylstyrene)	1.5868	20	[5]
Poly(4-methoxy-2-methylstyrene)	1.5967	20	[9]
Poly(4-methoxystyrene)	1.459–1.465		[5]
Poly(4-methyl-1-pentene) (see Ftn. 17)	1.463	20	[10]
Poly(4-methylcyclohexyl methacrylate)	1.546	25	[5]
Poly(abietic acid) (see Ftn. 18)	1.51	20	[10]
Poly(acetal)	1.61		[1]
Poly(acrolein)	1.5270	25	[5]
Poly(acrylate)	1.514	20	[10]
Poly(acrylic acid) (see Ftn. 19)	1.492		[1]
Poly(acrylonitrile) (see Ftn. 20)	1.641	20	[5]
Poly(allomer)	1.64–1.70		[4,14]
Poly(allyl methacrylate) (see Ftn. 21)	1.6411	20	[4,14]
Poly(α-methallyl methacrylate)	1.5573	20	[4,14]
Poly(α-naphthyl carbinyl methacrylate)	1.5396	20	[4,14]
Poly(α-naphthyl methacrylate (see Ftn. 22)	1.651	23	[13,18]
Poly(α-*o*-chlorophenylethyl methacrylate)	1.568	20	[4,10]
Poly(α-phenyl allyl methacrylate)	1.537	20	[4,14]
Poly(α-phenyl-*n*-amyl methacrylate)	1.5426	20	[4,14]
Poly(α-phenylethyl methacrylate)	1.533 ± 0.001	25	[4,14]
Poly(amide)	1.4833	20	[4,14]
Poly(arylsulfone)	1.508		[4,14]

TABLE 50.1. *Continued.*

Polymer	Refractive index n	Temperature (°C)	Reference
Poly(benzhydryl methacrylate)	1.511	20	[4,14]
Poly(benzyl methacrylate)	1.6298	20	[5]
Poly(β-aminoethyl methacrylate)	1.6298	20	[4,14]
Poly(β-bromoethyl methacrylate)	1.5592	20	[4,14]
Poly(β-chloroethyl chloroacrylate)	1.5682	20	[4,14]
Poly(β-ethoxyethyl methacrylate)	1.5059	20	[5]
Poly(β-methallyl methacrylate)	1.5178	20	[9,10]
Poly(β-naphthyl methacrylate) (see Ftn. 23)	1.4631	30	[5]
Poly(β-phenylethyl methacrylate)	1.50		[1]
Poly(β-phenylsulfone ethyl methacrylate)	1.5390	20	[5]
Poly(bornyl methacrylate) (see Ftn. 24)	1.586	23	[13,18]
Poly(butadiene) (see Ftn. 25)	1.6056		[4,14]
Poly(butene) (isotactic)	1.6290	25	[8,17]
Poly(butyl acetate)	1.554–1.558		[5]
Poly(butyl acrylate) (see Ftn. 26)	1.3900	25	[8,17]
Poly(butyl mercaptyl methacrylate)	1.542	25	[5]
Poly(butylene)	1.4969	20	[5]
Poly(carbonate) from 3,3′ ,5,5′ -tetrachlorodiphenyl (see Ftn. 27)	1.5570	25	[8,17]
Poly(chloro-*p*-xylylene)	1.4990		[5]
Poly(chloroprene)	1.572	20	[4,5]
Poly(chlorotrifluoroethylene) (see Ftn. 28)	1.544		[5]
Poly(cinnamyl methacrylate)	1.4035	25	[8,17]
Poly(cyclohexanediol-1,4-dimethacrylate)	1.403		[11]
Poly(cyclohexyl α-bromoacrylate)	1.395		[11]
Poly(cyclohexyl α-chloroacrylate)	1.403		[11]
Poly(cyclohexyl α-ethoxyacrylate)	1.4035		[11]
Poly(cyclohexyl bromoacrylate)	1.399		[11]
Poly(cyclohexyl methacrylate) (see Ftn. 29)	1.4031		[11]
Poly(cyclohexyl–cyclohexyl methacrylate)	1.4034		[11]
Poly(cyclohexylmethylsilane)	1.388		[11]
Poly(decamethylene glycol dimethacrylate)	1.4015		[11]
Poly(diacetin methacrylate)	1.3935		[11]
Poly(diallyl cinnamate)	1.4025		[11]
Poly[diallyl glycol carbonate (CR-39)]	1.398		[11]
Poly(diallyl phthalate) (see Ftn. 30)	1.6539	25	[8,17]
Poly(dichlorostyrene)	1.4740	20	[5]
Poly(diethylaminoethyl methacrylate)	1.5300	25	[8,17]
Poly(dihydroabietic acid)	1.60		[1]
Poly(dimethylsiloxane)	1.537–1.55	23	[6]
Poly(dimethylsiloxane) hydride terminated M.W. = 17,500	1.53–1.57	23	[6]
Poly(dimethylsiloxane) hydride terminated M.W. = 28,000	1.523–1.54		[5]
Poly(dimethylsiloxane) hydride terminated M.W. = 400	1.50–1.57	23	[13,18]
Poly(dimethylsiloxane) hydride terminated M.W. = 62,000	1.53–1.58	23	[13,18]
Poly(dimethylsiloxane) trimethylsiloxy terminated M.W.>28,000	1.658		[1]
Poly(dimethylsiloxane) trimethylsiloxy terminated M.W. = 13,650	1.4685	20	[5]
Poly(dimethylsiloxane) trimethylsiloxy terminated M.W. = 162	1.5020	25	[5]
Poly(dimethylsiloxane) trimethylsiloxy terminated M.W. = 17,250	1.4903	20	[5]
Poly(dimethylsiloxane) trimethylsiloxy terminated M.W. = 2,000	1.485	20–25	[5]
Poly(dimethylsiloxane) trimethylsiloxy terminated M.W. = 237	1.502 ± 0.001	25	[4,14]
Poly(dimethylsiloxane) trimethylsiloxy terminated M.W. = 28,000	1.555	20	[4,14]
Poly(dimethylsiloxane) trimethylsiloxy terminated M.W. = 340	1.5063	20	[5]
Poly(dimethylsiloxane) trimethylsiloxy terminated M.W. = 3,780	1.455	20	[9]
Poly(dimethylsiloxane) trimethylsiloxy terminated M.W. = 410	1.455	20	[9]
Poly(dimethylsiloxane) trimethylsiloxy terminated M.W. = 550	1.459	20	[9]
Poly(dimethylsiloxane) trimethylsiloxy terminated M.W. = 5,970	1.570 ± 0.003	20–22	[4,14]

TABLE 50.1. *Continued.*

Polymer	Refractive index n	Temperature (°C)	Reference
Poly(dimethylsiloxane) trimethylsiloxy terminated M.W. = 770	1.459	20	[10]
Poly(dimethylsiloxane) trimethylsiloxy terminated M.W. = 9,430	1.459	20	[9]
Poly(dimethylsiloxane) trimethylsiloxy terminated M.W. = 950	1.463	20	[9]
Poly[diphenylmethane bis(4-phenyl) carbonate]	1.465	20	[9]
Poly(diphenylmethyl methacrylate)	1.467	20	[9]
Poly(dodecyl methacrylate)	1.455	20	[10]
Poly(ε-caprolactam)	1.462	20	[10]
Poly(ester carbonate) (polyphthalate)	1.56–1.57		[4,14]
Poly(ester) cast resin, rigid (see Ftn. 31)	1.4840	25	[8,17]
Poly(etherimide)	1.52–1.53	20	[5]
Poly(ethersulfone)	1.545	20	[5]
Poly(ethyl acrylate)	1.54		[1]
Poly(ethyl α-chloroacrylate) (see Ftn. 32)	1.54	23	[13,18]
Poly(ethyl glycolate methacrylate)	1.51	23	[13,18]
Poly(ethyl methacrylate)	1.51	23	[13,18]
Poly(ethyl sulfide methacrylate)	1.51	23	[13,18]
Poly(ethylene chlorohydrin methacrylate)	1.54	23	[13,18]
Poly(ethylene dimethacrylate)	1.54	23	[13,18]
Poly(ethylene glycol benzoate methacrylate)	1.448	20	[9]
Poly(ethylene glycol dimethacrylate)	1.452	20	[9]
Poly(ethylene glycol fumarate)	1.451	20	[9]
Poly(ethylene glycol methyl ether) M.W. = 350	1.453	20	[9]
Poly(ethylene glycol methyl ether) M.W. = 550	1.454	20	[9]
Poly(ethylene glycol methyl ether) M.W. = 750	1.455	20	[9]
Poly(ethylene glycol monomethacrylate)	1.459	20	[9]
Poly(ethylene glycol phthalate) (see Ftn. 33)	1.5300	25	[8,17]
Poly(ethylene glycol) (see Ftn. 34)	1.547	20	[5]
Poly(ethylene glycol) (Carbowax)	1.51		[5]
Poly(cyclohexyl-α -chloroacrylate)	1.40		[11]
Poly(cyclohexyl-α -ethoxyacetate)	1.3825		[11]
Poly(ethylene glycol) M.W. = 300	1.5381		[5]
Poly(ethylene glycol) M.W. = 400	1.575 ± 0.003	20	[4,14]
Poly(ethylene glycol) methyl ester	1.4750	30	[5]
Poly(ethylene glycol) tetrahydrofurfuryl ester	1.5300	25	[8,17]
Poly(ethylene maleate)	1.481	20	[10]
Poly(ethylene oxide)	1.505–1.51		[5]
Poly(ethylene succinate)	1.477	20	[5]
Poly(ethylene terephthalate) (PET)	1.5045	20	[10]
Poly(ethylene terephthalate) grounded (PETG)	1.5050	25	[8,17]
Poly(ethylene) (see Ftn. 35)	1.521	20	[5]
Poly(ethylene) (density 0.914 g/cm^3)	1.5191	20	[9]
Poly(ethylene) (density 0.94–0.945 g/cm^3)	1.4728	20	[5]
Poly(ethylene) (density 0.965 g/cm^3)	1.645	20	[4,14]
Poly(ethylene); type 1—lower density, melt index 0.3–3.6	1.6006	20	[4,14]
Poly(ethylene); type 1—lower density, melt index 200	1.52		[5]
Poly(ethylene); type 1—lower density, melt index 6–26	1.472–1.48		[5]
Poly(ethylene); type 2—med. density, melt index 1.0–1.9	1.5672	20	[4,5]
Poly(ethylene); type 2—med. density, melt index 20	1.517	20	[5]
Poly(ethylene); type 3—higher density, melt index 0.1–12.0	1.52	20	[5]
Poly(ethylene); type 3—higher density, melt index 0.2–0.9	1.4893	23	[5]
Poly(ethylene); type 3—higher density, melt index 1.5–15	1.49	20	[9]
Poly(ethyleneglycol) 200 monononylether	1.383		[11]
Poly(ethyleneglycol) 300 monononylether	1.381		[11]
Poly(ethyleneglycol) 300 monononylether (fractionated, fraction 2)	1.382		[11]
Poly(ethyleneglycol) 300 monononylether (fractionated, fraction 4)	1.379		[11]

TABLE 50.1. *Continued.*

Polymer	Refractive index *n*	Temperature (°C)	Reference
Poly(ethyleneglycol) 300 monononylether (fractionated, fraction 5)	1.5172	20	[4,14]
Poly(ethyleneglycol) 400 monononylether (at 6,563 Å)	1.5155		[4,14]
Poly(ethyleneglycol) 600 monononylether (at 4,861 Å)	1.5248		[4,14]
Poly(ethylidene dimethacrylate) (see Ftn. 36)	1.5118	20	[4, 14]
Poly(ethylmercaptyl methacrylate)	1.451		[11]
Poly(eugenol methacrylate)	1.3979	20	[9]
Poly(fluorenyl methacrylate)	1.398	20	[10]
Poly(furfuryl methacrylate)	1.396		[11]
Poly(glycerol phthalate)	1.382		[11]
Poly(glycerol rosin–maleate)	1.397		[11]
Poly(glycol maleate)	1.443		[11]
Poly(glycol succinate)	1.445		[11]
Poly(heptafluorobutyl acrylate)	1.463		[1]
Poly(hexadecyl methacrylate)	1.455		[11]
Poly(hexamethylene adipamide)	1.43	23	[6]
Poly(hexamethylene glycol dimethacrylate) (see Ftn. 37)	1.5857	20	[5]
Poly(hexamethylene sebacamide)	1.5476	20	[4,5]
Poly(hexyl methacrylate)	1.5965	20	[4,5]
Poly(isobutene)	1.5246	20	[4,14]
Poly(isobutyl methacrylate) (see Ftn. 38)	1.4830	25	[8,17]
Poly(isobutylene) (see Ftn. 39)	1.4813	20	[4,5]
Poly(isoprene) (see Ftn. 40)	1.4840	25	[4,8]
Poly(isopropyl methacrylate) (see Ftn. 41)	1.360	25	[5]
Poly(lead dimethacrylate)	1.5823	20	[4,5]
Poly(*m*-cresyl methacrylate)	1.6040		[5]
Poly(*m*-nitrobenzyl methacrylate)	1.6098	20	[4,5]
Poly(methacrylate methyl salicylate)	1.5707	20	[5]
Poly(methacryl phenyl salicylate)	1.507	20	[4,14]
Poly(methacrylic anhydride)	1.5705	20	[4,5]
Poly(methacrylonitrile) (see Ftn. 42)	1.5932	20	[4,5]
Poly(methyl acrylate) (see Ftn. 43)	1.5750	25	[8,17]
Poly(methyl α-bromoacrylate)	1.6400	25	[8,17]
Poly(methyl α-chloroacrylate)	1.4630	25	[8,17]
Poly(methyl isospropenyl ketone)	1.4800	25	[8,17]
Poly(methyl isopropenyl ketone)	1.4900	25	[8,17]
Poly(methyl methacrylate)	1.5500	25	[8,17]
Poly(methyl methacrylate)	1.5600	25	[8,17]
Poly(methyl methacrylate)	1.4430	25	[8,17]
Poly(methyl methacrylate), beads	1.4450	25	[8,17]
Poly(methyl phenyl siloxane), trimethylsiloxy terminated	1.4510	25	[8,17]
Poly(methyl-3,3,3-trifluoropropylsiloxane), M.W. = 14,000	1.4550	25	[8,17]
Poly(methyl-3,3,3-trifluoropropylsiloxane), M.W. = 2,350	1.3830	25	[8,17]
Poly(methyl-3,3,3,-trifluoropropylisoxane), M.W. = 4,600	1.3970	25	[8,17]
Poly(methyl-3,3,3-trifluoropropylsiloxane), silanol terminated	1.465	50	[5]
Poly(methyl-α-chloroacrylate) (see Ftn. 44)	1.5671		[5]
Poly(methyl-α-methylene butyrolactone)	1.5745		[5]
Poly(methylene-α-valerolactone)	1.5602		[5]
Poly(methylhexadecylsiloxane)	1.5827		[5]
Poly(methylhydrosilane)	1.5792		[5]
Poly(methylhydrosiloxane)	1.5900		[5]
Poly(methylhydrosiloxane) trimethylsilyl terminated M.W. = 1,500	1.6539		[5]
Poly(methylhydrosiloxane) trimethylsillyl terminated M.W. = 2,270	1.5937		[5]
Poly(methylhydrosiloxane) trimethylsilyl terminated M.W. = 360–420	1.5702		[5]
Poly(methylhydrosiloxane) trimethylsilyl terminated M.W. = 4,500–5,000	1.5850		[5]
Poly(methyloctadecylsiloxane)	1.6056		[5]

TABLE 50.1. *Continued.*

Polymer	Refractive index *n*	Temperature (°C)	Reference
Poly(methyloctylsiloxane)	1.43		[5]
Poly(methylpentene)	1.4563	30	[5]
Poly(methyltetradecylsiloxane)	1.51–1.54		[5]
Poly(monochlorotrifluoroethylene)	1.555	20	[5]
Poly(monofluorethyl methacrylate)	1.4840	25	[5]
Poly[*N*(-2-methoxythyl)methacrylamide]	1.4744	25	[5]
Poly[*N*-(2-phenylethyl)methacrylate]	1.5750	20	[5]
Poly(*N*-allyl methacrylamide)	1.48	20	[5]
Poly(*N*-benzyl methacrylamide)	1.4690	25	[8,17]
Poly(*N*-β-methoxyethyl methacrylamide)	1.5840	20	[5]
Poly(*N*-β-phenylethyl methacrylamide)	1.4495		[5]
Poly(*n*-butyl methacrylate) (see Ftn. 45)	1.5559	20	[4,5]
Poly(*N*-butyl-methacrylamide)	1.5575	20	[4,5]
Poly(*n*-hexyl methacrylate)	1.6150	20	[4,5]
Poly(*N*-methyl-methacrylamide)	1.554	20	[4,5]
Poly(*n*-propyl methacrylate)	1.552	20	[4,5]
Poly(*N*-vinylphthalimide)	1.5967	20	[4,5]
Poly(nonafluoropentyl acrylate)	1.6690	25	[8,17]
Poly(*o*-chlorobenzhydryl methacrylate)	1.71	20	[5]
Poly(*o*-chlorobenzyl methacrylate)	1.608	20	[4,5]
Poly(*o*-chlorodiphenylmethyl methacrylate)	1.339	25	[5]
Poly(*o*-chlorostyrene)	1.584 ± 0.003	20	[4, 14]
Poly(*o*-cresyl methacrylate) (see Ftn. 46)	1.385	25	[5]
Poly(*o*-methoxyphenyl methacrylate)	1.612	25	[4,5]
Poly(*o*-methoxystyrene)	1.5624	20	[4,5]
Poly(*o*-methoxystyrene)	1.5706	20	[4,5]
Poly(octafluoropentyl acrylate)	1.6300	25	[8,17]
Poly(octylmethylsilane)	1.447	20	[10]
Poly[oxy(2,6-dimethyl-1,4-phenylene)]	1.4570	25	[8,17]
Poly[oxy(2,6-diphenyl-1,4-phenylene)]	1.5960	25	[8,17]
Poly[oxy(acryloxypropylmethylsilylene)]	1.49	20	[10]
Poly[oxy(dicyanopropylsilylene)]	1.49		[1]
Poly[oxy(mercaptopropylmethylsilylene)]	1.4735	20	[5]
Poly[oxy(methyl *m*-chlorophenylethylsilylene)]	1.5030	20	[5]
Poly[oxy(methyl *m*-chlorophenylsilylene)]	1.541	20	[10]
Poly[oxy(methyl *n*-hexadecylsilylene)]	1.542	25	[5]
Poly[oxy(methyl *n*-hexylsilylene)]	1.500	25	[4,5]
Poly[oxy(methyl *n*-octadecylsilylene)]	1.6568	25	[8,17]
Poly[oxy(methyl *n*-octylsilylene)]	1.59–1.592	20	[5]
Poly[oxy(methyl *n*-tetradecyl silylene)]	1.59–1.60		[4,14]
Poly[oxy(methyl-*t*-trifluoropropylsilylene)]	1.5901	25	[4,14]
Poly[oxy(methylhydrosilylene)]	1.5858		[4,14]
Poly[oxy-1-oxopentamethylene]	1.5916	20	[10]
Poly(oxy-2,6-dimethylphenylene)	1.59–1.60		[1]
Poly[oxycarbonyloxy-1,4(2,6-dichloro)phenylne-isopropylidene-1,4(2,6-dichloro)phenylene]	1.57–1.60		[1]
Poly(oxycarbonyloxy-1,4-phenylene-1,3-dimethyl-butylidene-1,4-phenylene)	1.59–1.60	23	[6]
Poly(oxycarbonyloxy-1,4-phenylene-1-methyl-butylidene-1,4-phenylene)	1.6	23	[13,18]
Poly(oxycarbonyloxy-1,4-phenylene-1-propyl-butylidene-1,4-phenylene)	1.6–1.7		[4,5]
Poly(oxycarbonyloxy-1,4-phenylene-sec-butylidene-1,4-phenylene)	1.633		[1,5]
Poly(oxycarbonyloxy-1,4-phenylenebutylidene-1,4-phenylene)	1.4638	25	[8,17]
Poly(oxycarbonyloxy-1,4-phenylenecyclohexylidene-1,4-phenylene)	1.4638	20	[10]
Poly(oxycarbonyloxy-1,4,phenylenediphenyl-methylene-1,4-phenylene)	1.4746	30	[5]
Poly(oxycarbonyloxy-1,4-phenyleneethylidene-1,4-phenylene)	1.346	25	[5]
Poly(oxycarbonyloxy-1,4-phenyleneisobutylidene-1,4-phenylene)	1.348	25	[5]
Poly(oxycarbonyloxy-1,4-phenyleneisopropylidene-1,4-phenylene)	1.360	25	[5]

TABLE 50.1. *Continued.*

Polymer	Refractive index *n*	Temperature (°C)	Reference
Poly(oxycarbonyloxybis[1,4(3,5-dichlorophenylene)])	1.35	20	[9]
Poly(oxydimethylsilylene)	1.35	23	[13,18]
Poly(oxyethylene) (see Ftn. 47)	1.35		[12]
Poly[(oxyethylene)-α-benzoate-ω-methacrylate]	1.35		[1]
Poly(oxyethyleneoxymaleoyl) [poly(ethylene maleate)]	1.46	20	[10]
Poly(oxyethyleneoxysuccinoyl) [poly(ethylene succinate)]	1.465	20	[10]
Poly(oxyethyleneoxyterephthaloyl) [poly(ethylene terephthalate)]	1.466	20	[10]
Poly(oxymethylene)	1.5096	20	[5]
Poly(oxyoctamethylene)	1.4889	20	[5]
Poly(oxypentaerythritoloxyphthaloyl)	1.43	23	[3,13]
Poly(oxypropylene)	1.407	25	[5]
Poly(*p,p′*-xylyenyl dimethacrylate)	1.437		[5]
Poly(*p*-bromophenyl methacrylate)	1.4177	20	[5]
Poly(*p*-cyclohexylphenyl methacrylate)	1.375	25	[5]
Poly(*p*-divinylbenzene)	1.356		[5]
Poly(*p*-isopropylstyrene)	1.5–1.6		[5]
Poly(*p*-methoxybenzyl methacrylate)	1.4628	30	[5]
Poly(*p*-methoxystyrene)	1.48–1.50		[5]
Poly(*p*-xylylene)	1.4665	20	[5]
Poly(pentabromophenyl methacrylate)	1.45–1.47	23	[6]
Poly(pentachlorophenyl methacrylate)	1.49–1.53		[5]
Poly(pentadecafluorooctyl acrylate)	1.49–1.53	23	[6]
Poly(pentaerythritol phthalate)	1.5775	20	[4,5]
Poly(pentaerythritol tetramethacrylate)	1.4563	20	[5]
Poly(pentafluoropropylacrylate)	1.485	20	[9,10]
Poly(pentafluorovinyl propionate)	1.47–1.49	23	[6]
Poly(phenyl α-bromoacrylate)	1.48–1.49	23	[6]
Poly(phenyl cellosolve methacrylate)	1.52–1.53	23	[6]
Poly(phenyl methacrylate)	1.54–1.55		[5]
Poly(phenylmethylsilane)	1.52–1.55		[12]
Poly(propylene glycol)	1.52		[5]
Poly(propylene oxide)	1.55		[5]
Poly(propylene sulfide)	1.54–1.55	23	[6]
Poly(propylene) (see Ftn. 48)	1.512	25	[5]
Poly(propylene) (density 0.9075 g/cm^3)	1.502	20	[5,10]
Poly(propylene), atactic (density 0.8575 g/cm^3)	1.454	20	[10]
Poly(propylene), chlorinated	1.50	23	[6]
Poly(sec-butyl α-bromoacrylate)	1.4750	20	[5]
Poly(sec-butyl α-chloroacrylate)	1.4591	30	[5]
Poly(styrene sulfide)	1.4507	30	[5]
Poly(styrene) (see Ftn. 49)	1.5129	20	[5]
Poly(sulfides) (Thiokol)	1.466	20	[10]
Poly(sulfone)	1.474	30	[5]
Poly(*t*-butyl methacrylate) (see Ftn. 50)	1.683	20	[4,5]
Poly(terpineyl methacrylate)	1.55	20	[5]
Poly(tetradecyl methacrylate)	1.60–1.63	23	[3,13]
Poly[tetrafluoro-3-(heptafluoropropoxy)propyl acrylate]	1.60–1.63	23	[6]
Poly[tetrafluoro-3(pentafluoroethoxy)propyl acrylate]	1.42	25	[5]
Poly[tetrafluoro-3(trifluoromethoxy)propyl acrylate]	1.42	23	[13,18]
Poly(tetrafluoroethylene) (PTFE) (see Ftn. 51)	1.6818	20	[5]
Poly(tetrahydrofuran) M.W. = 250	1.52		[4,14]
Poly(tetrahydrofuran) M.W. = 650	1.5196	20	[4,14]
Poly(tetrahydrofuran), with oxirane	1.54		[4,14]
Poly(tetrahydrofurfuryl methacrylate)	1.5059	20	[4,14]
Poly(triethoxyl silicol methacrylate)	1.4631	30	[4,14]

TABLE 50.1. *Continued.*

Polymer	Refractive index n	Temperature (°C)	Reference
Poly(triethylcarbinyl methacrylate) (see Ftn. 52)	1.4634	25	[4,14]
Poly(trifluorochloroethylene) (PTFCE)	1.554	20	[4,14]
Poly(trifluoroethyl acrylate)	1.39–1.43		[4,14]
Poly(trifluoroethyl methacrylate)	1.394	20	[4,14]
Poly(trifluoroisopropyl methacrylate) (see Ftn. 53)	1.5067	20	[4,14]
Poly(trifluorovinyl acetate)	1.5066	20	[4,14]
Poly(undecafluorohexyl acrylate)	1.5099	23	[4,14]
Poly(urethane), rigid (see Ftn. 54)	1.65		[1]
Poly(vinyl acetal) (see Ftn. 55)	1.4855	20	[4,14]
Poly(vinyl acetate) (at 6,563 Å) (see Ftn. 56)	1.5013	20	[4,14]
Poly(vinyl alcohol) (see Ftn. 57)	1.483–1.485	25	[4,14]
Poly(vinyl benzoate)	1.51–1.52		[4,14]
Poly(vinyl butyl ether)	1.517	20	[4,14]
Poly(vinyl butyral) (see Ftn. 58)	1.5063	20	[4,14]
Poly(vinyl chloride acetate) molding compound—rigid	1.5119	20	[4,14]
Poly(vinyl chloride) (PVC) rigid (see Ftn. 59)	1.52–1.57		[1]
Poly(vinyl chloride–acetate)	1.477	25	[4,14]
Poly(vinyl chloroacetate) (see Ftn. 60)	1.4728	20	[4,14]
Poly(vinyl cychlohexene dioxide)	1.5228	20	[4,14]
Poly(vinyl decyl ether)	1.499	20	[4,14]
Poly(vinyl dodecyl ether)	1.52		[4,14]
Poly(vinyl ethyl ether) (see Ftn. 61)	1.4725	20	[4,14]
Poly(vinyl formal) molding compound (see Ftn. 62)	1.4893	23	[4,14]
Poly(vinyl formate) (see Ftn. 63)	1.4768		[4,14]
Poly(vinyl hexyl ether)	1.5117	20	[4,14]
Poly(vinyl isobutyl ether) (see Ftn. 64)	1.514	20	[4,14]
Poly(vinyl methacrylate) (see Ftn. 65)	1.376	25	[4,14]
Poly(vinyl methyl ether) (see Ftn. 66)	1.5096	20	[4,14]
Poly(vinyl methyl ketone)	1.4177	20	[4,14]
Poly(vinyl naphthalene)	1.48–1.50		[4,14]
Poly(vinyl octyl ether)	1.47–1.49		[4,14]
Poly(vinyl pentyl ether)	1.4667	24	[4,14]
Poly(vinyl phenyl sulfide)	1.545–1.555	25	[4,14]
Poly(vinyl propionate) (see Ftn. 67)	1.51–1.55		[4,14]
Poly(vinyl sec-butyl ether) (isotactic)	1.47–1.49		[4,14]
Poly(vinyl triophene)	1.54–1.56		[4,14]
Poly(vinyl-2-ethylhexyl ether)	1.565	40	[4,14]
Poly(vinylcarbazole)	1.525–1.529	21	[4,14]
Poly(vinylfuran) (see Ftn. 68)	1.5303	20	[4,14]
Poly(vinylidene chloride) molding compound (see Ftn. 69)	1.4757	20	[4,14]
Poly(vinylidene-fluoride) (PVDF) (see Ftn. 70)	1.5129	20	[4,14]
Poly(vinylnaphthalene)	1.467	20	[4,14]
Poly(vinylpyrrolidone)	1.55	20	[4,14]
Poly(vinylsulfonic acid) (sodium salt)	1.53		[4,14]
Propylmethyl homopolymer, vinyldimethyl terminated	1.43		[11]
Pyralin Polyimide Film-PI-2540	1.78		[7,16]
Pyralin Polyimide Film-PI-2550	1.70		[7,16]
Rosin (grade M, wood)	1.525 ± 0.003	20	[4,14]
Rosin ester	1.496 ± 0.003	21–23	[4,14]
Rubber (hard, 32% S)	1.60	25	[4,5]
Rubber hydrochloride (Pilofilm)	1.540–1.550	25	[4,14]
Shellac, bleached, dry	1.534 ± 0.003	20–22	[4,14]
Shellac, orange	1.516 ± 0.003	20–22	[4,14]
Silicone, Dow-Corning 2102	1.419		[4,14]
Sulfonamide resins	1.56–1.596		[4,14]

TABLE 50.1. *Continued.*

Polymer	Refractive index *n*	Temperature (°C)	Reference
Terpene resin (Piccolyte S-10)	1.506		[4,14]
Terpene resin (Piccolyte S-40)	1.515	25	[4,14]
Toluenesulfonamide formaldehyde	1.596	25	[4,14]
Urea formaldehyde	1.54–1.56		[1,14]
Urea–thiourea formaldehyde	1.66	25	[4,14]
Footnote 1			
CP-41/l/ gen. purpose, lowest heat resistance			
CP-51/lE/ gen. purpose, medium heat resistance			
CP-61/lE/ gen. purpose, medium heat resistance			
CP-71/l/ gen. purpose, maximum heat resistance			
CP-75/l/ gen. purpose, maximum heat resistance, medium flow			
CP-80/E/ gen. purpose, unlubed			
CP-81/E/ gen. purpose, high heat resistance			
CP-82/l/ gen. purpose, maximum heat resistance			
CP-924/l/ good impact str. exc. light trans.			
CP-927/l/ better impact str. exc. surface gloss			
Footnote 2			
H-11/lE/ highest heat resistance water white			
H-12/lE/ improved flow properties water white			
H-15-011/lE/ UV absorbing automotive applications			
H-15-012/l/ UV transmitting automotive applications			
H-15/lE/ increased toughness maximum service temp. white			
L-40/lE/ improved flow easy molding water white			
M-30/lE/ improved flow easy molding water white			
Footnote 3			
6/l/ thin walled and complicated parts			
6E/El/ good flow, tough technical parts			
7/l/ good flow dimen. stability			
7E/El/ high melt viscosity			
8/l/ good surface hardness			
8E/E/ high melt viscosity, good stab.			
Footnote 4			
DR G/l/ high-impact γ radiation			
DR M/l/ high-impact, low reflectance			
DR/lE/ high-impact acrylic molding			
G-UVT// gen. purpose optical quality			
G// gen. purpose cellcast unshrunk nat.			
HFI-10/l/ high-impact high-flow pellets			
HFI-7/l/ medium-impact high-flow pellets			
II-UVA// gen. purpose preshrunk			
II-UVT// gen. purpose increases uv stab			
K// superior thermoformability			
MC// plastic sheet economical material			
MI-7/l/ medium-impact high flow			
MI-7G/lE/ medium-impact light transmission			
UF-3// ultraviolet radiation			
V-044/E/ high heat resistance			
V-045/lE/ high heat resistance			
V-052/l/ high heat resistance			
V-811/lE/ maximum heat resistance			
V-825/lE/ maximum heat resistance			
V-920/lE/ high heat resistance			
VM/lE/ medium heat resistance			
VS/l/ maximum flow lowest heat resistance			

TABLE 50.1. *Continued.*

Polymer	Refractive index n	Temperature (°C)	Reference
Footnote 5			
300// cross-linked commercial continuous cast			
Acrysteel I-GP// continuous cast impact clear			
GPA// gen purpose cast acrylic sheet clear			
Footnote 6			
Cellulose acetate (partly saponified)	1.54		[4,14]
Cellulose acetate-molding	1.46–1.50	23	[6]
Cellulose acetate-sheet	1.49–1.50	23	[6]
Footnote 7			
ASTM Grade: H2-1			
ASTM Grade: H4-1			
ASTM Grade: H6-1			
ASTM Grade: MH-1, MH-2			
ASTM Grade: MS-1, MS-2			
ASTM Grade: S2-1			
Footnote 8			
ASTM Grade: H4	1.46–1.49		[13,18]
ASTM Grade: MH	1.46–1.49		[13,18]
ASTM Grade: S2	1.46–1.49		[13,18]
Cellulose acetate butyrate	1.46–1.50		[4,14]
Cellulose acetate butyrate	1.494	21	[4,14]
Footnote 9			
Cellulose acetate propionate; ASTM Grade: 1	1.46–1.49	23	[13,18]
Footnote 10			
Cellulose nitrate	1.501	21	[4,14]
Footnote 11			
Congo copal	1.540–1.541	25	[4,14]
Congo ester	1.506 ± 0.003	20	[4,14]
Footnote 12			
Damar No. 1 (Singapore)	1.515 ± 0.003	20	[4,14]
Footnote 13			
Epoxy resins	1.57–1.61		[4,14]
Epoxy, diglycidyl ether of bisphenol A, cast flexible or molded	1.61	23	[13,18]
Footnote 14			
Gutta percha, alpha	1.514	50	[4,14]
Gutta percha, beta	1.509	50	[4,5]
Footnote 15			
Nylon 6 (Poly[imino(1-oxohenamethylene)])	1.53		[5]
Nylon 6,10 [Poly(iminoadipoyliminotetramethylene)]	1.53		[5]
Nylon 6,6 [Poly(iminoadipoylaminohexamethylene)]	1.53		[5]
Nylon molding compound	1.53–1.55		[4,14]
Nylons (polyamide) type 11	1.52		[1]
Nylons (polyamide) type 6,6	1.53		[1]
Footnote 16			
Phenol–formaldehyde	1.5–1.7		[4,14]
Footnote 17			
Poly(4-methyl-1-pentene)	1.4975	20	[4,5]
Footnote 18			
Poly(abietic acid)	1.529		[5]
Footnote 19			
Poly(acrylic acid)	1.5196	20	[5]
Footnote 20			
Poly(acrylonitrile)	1.4917	20	[4,14]
Poly(acrylonitrile)	1.63		[4,5]
Footnote 21			
Poly(allyl methacrylate)	1.5624	20	[4,14]

TABLE 50.1. *Continued.*

Polymer	Refractive index *n*	Temperature (°C)	Reference
Footnote 22			
Poly(α-naphthyl methacrylate)	1.5487	20	[4,14]
Poly(α-naphthyl methacrylate)	1.5933	20	[4,14]
Footnote 23			
Poly(β-naphthyl methacrylate)	1.466	20	[5]
Footnote 24			
Poly(bornyl methacrylate)	1.467	20	[10]
Footnote 25			
Poly(butadiene)	1.585		[4,14]
Footnote 26			
Poly(butyl acrylate)	1.5951	20	[4,14]
Poly(butyl acrylate)	1.5067	20	[5]
Footnote 27			
Poly(carbonate)	1.532 ± 0.001	25	[4,14]
Poly(carbonate) of bisphenol-A	1.4969	20	[4,14]
Poly(carbonate) of bisphenol-A	1.5857	25	[8,17]
Footnote 28			
Poly(chlorotrifluoroethylene)	1.571–1.572	20	[4,14]
Poly(chlorotrifluoroethylene)	1.62–1.64		[4,14]
Footnote 29			
Poly(cyclohexyl methacrylate)	1.375		[11]
Footnote 30			
Poly(diallyl phthalate)	1.5933	20	[5]
Footnote 31			
Poly(ester) cast resins—flexible	1.4539	20	[10]
Poly(ester) cast resins—rigid	1.4744	25	[8,17]
Poly(ester) cast, flexible	1.64		[1]
Poly(ester) cast, rigid	1.51	20	[5]
Poly(ester) resin, rigid (ca. 50% styrene)	1.567		[1]
Footnote 32			
Poly(ethyl α-chloroacrylate)	1.51	23	[6]
Footnote 33			
Poly(ethylene glycol phthalate)	1.4831	20	[5]
Footnote 34			
Poly(ethylene glycol)	1.5714	20	[4,14]
Footnote 35			
Poly(ethylene)	1.5191	20	[10]
Poly(ethylene) lonomer	1.533		[11]
Poly(ethylene) molding cmpd.	1.5705	20	[4,14]
Footnote 36			
Poly(ethylidene dimethacrylate)	1.5431	20	[4,14]
Footnote 37			
Poly(hexamethylene glycol dimethacrylate)	1.5246	20	[5]
Footnote 38			
Poly(isobutyl methacrylate)	1.5857	20	[4,14]
Footnote 39			
Poly(isobutylene)	1.4831	25	[4,14]
Footnote 40			
Poly(isoprene)	1.5398	20	[4,5]
Poly(isoprene) *cis*	1.6200	20	[4,5]
Poly(isoprene)	1.5219	20	[4,14]
Footnote 41			
Poly(isopropyl methacrylate)	1.604	20	[4,14]

TABLE 50.1. *Continued.*

Polymer	Refractive index n	Temperature (°C)	Reference
Footnote 42			
Poly(methacrylonitrile)	1.5874	20	[5]
Footnote 43			
Poly(methyl acrylate)	1.380	25	[5]
Poly(methyl acrylate)	1.4780	25	[8,17]
Footnote 44			
Poly(methyl-α-chloroacrylate)	1.575		[5]
Poly(methyl-α-chloroacrylate	1.6056		[5]
Footnote 45			
Poly(*n*-butyl methacrylate)	1.5964	20	[4,5]
Footnote 46			
Poly(*o*-cresyl methacrylate)	1.364	25	[5]
Footnote 47			
Poly(oxyethylene) (high molecular weight)	1.35	23	[6]
Footnote 48			
Poly(propylene)	1.4640	30	[5]
Poly(propylene)	1.4540	30	[5]
Footnote 49			
Poly(styrene)	1.467	20	[5,10]
Poly(styrene)	1.4700	30	[5]
Poly(styrene)	1.5000	20	[8,10]
Poly(styrene)	1.6818	20	[4,14]
Poly(styrene) (general purpose)	1.4613	30	[5]
Poly(styrene) (general purpose)	1.4665	20	[5]
Poly(styrene) (heat and chemical)	1.4581	30	[5]
Poly(styrene) modified molding compound—heat and chemical resistance type	1.57–1.60	23	[6]
Poly(styrene) molding compound—unfilled	1.6568	20	[4,5]
Footnote 50			
Poly(*t*-butyl methacrylate	1.6376		[4,14]
Poly(*t*-butyl methacrylate)	1.4626	30	[5]
Footnote 51			
Poly(tetrafluoroethylene) (PTFE)	1.389	20	[10]
Poly(tetrafluoroethylene) (PTFE)	1.356		[4,14]
Poly(tetrafluoroethylene) (PTFE)	1.4638	20	[4,14]
Poly(tetrafluoroethylene) (PTFE)	1.546	25	[4,14]
Poly(tetrafluoroethylene) (PTFE)	1.527	25	[4,14]
Poly(tetrafluoroethylene) (PTFE) molding compound	1.529		[4,14]
Footnote 52			
Poly(triethylcarbinyl methacrylate)	1.539	20	[4,14]
Footnote 53			
Poly(trifluoroisopropyl methacrylate)	1.547 ± 0.001	25	[4,14]
Footnote 54			
Poly(urethanes)	1.525	20	[4,14]
Footnote 55			
Poly(vinyl acetal)	1.5001	20	[4,14]
Footnote 56			
Poly(vinyl acetate) (at 4,861 Å)	1.5100	20	[4,14]
Poly(vinyl acetate)	1.5174	20	[4,14]
Poly(vinyl acetate) (medium acetate type)	1.4903	20	[4,14]
Poly(vinyl acetate) (low acetate type)	1.523–1.57		[4,14]
Poly(vinyl acetate) molding compound	1.4685	20	[4,14]

TABLE 50.1. *Continued.*

Polymer	Refractive index *n*	Temperature (°C)	Reference
Footnote 57			
Poly(vinyl alcohol) molding compound)	1.547	20	[4,14]
Poly(vinyl alcohol) molding compound)	1.512–1.519	25	[4,14]
Footnote 58			
Poly(vinyl butyral)	1.4563	30	[4,14]
Poly(vinyl butyral) molding compound—flexible, unfilled	1.51–1.54	25	[4,14]
Poly(vinyl butyral) molding compound—rigid	1.514	25	[4,14]
Footnote 59			
Poly(vinyl chloride) (PVC)	1.4831	20	[4,14]
Poly(vinyl chloride) (PVC)	1.5381	20	[4,14]
Poly(vinyl chloride) (PVC)	1.541	25	[4,14]
Poly(vinyl chloride) (PVC) rigid	1.484	25	[4,14]
Poly(vinyl chloride) (PVC) + 40% dioctyl phthalate	1.4744	25	[4,14]
Poly(vinyl chloride) (PVC) + 40% tricrexyl phosphate	1.5048	23	[4,14]
Poly(vinyl chloride) (PVC) molding compound—rigid	1.5066	20	[4,14]
Poly(vinyl chloride) (PVC) rigid	1.52–1.55		[1]
Footnote 60			
Poly(vinyl chloroacetate)	1.505–1.51		[4,14]
Footnote 61			
Poly(vinyl ethyl ether)	1.48	25	[4,14]
Poly(vinyl ethyl ether), low molecular weight	1.52	20	[4,14]
Footnote 62			
Poly(vinyl formal)	1.485–1.49		[4,14]
Footnote 63			
Poly(vinyl formate)	1.49	20	[4,14]
Footnote 64			
Poly(vinyl isobutyl ether)	1.49		[4,14]
Footnote 65			
Poly(vinyl methacrylate)	1.35–1.38		[4,14]
Footnote 66			
Poly(vinyl methyl ether)	1.436	20	[4,14]
Poly(vinyl methyl ether) (isotactic)	1.4889	20	[4,14]
Footnote 67			
Poly(vinyl propionate)	1.49–1.53		[4,14]
Footnote 68			
Poly(vinylfuran)	1.512	25	[4,14]
Footnote 69			
Poly(vinylidene chloride)	1.454		[4,14]
Footnote 70			
Poly(vinylidene fluoride) (PVDF)	1.452		[4,14]

TABLE 50.2. *Refractive indices of copolymers. All values reported are at a wavelength of 5,893 Å.*

Copolymer	Refractive index n	Temperature (°C)	Reference
Acrylics multipolymer	1.52		[12]
Acrylonitrile butadiene styrene copolymer (ABS), transparent	1.536		[1]
Arylef U100 (equimolar random copolymer of bisphenol-A terephthalate and bisphenol-A isophthalate)	1.61	25	[8]
Dimethyl (48–52%)–phenylmethyl siloxane (48–52%) copolymer, trimethylsiloxy terminated	1.5		[11]
Dimethyl (70%)–dodecyl (15%)–tetradecyl siloxane (15%), terpolymer	1.43		[11]
Dimethyl (70%)–methyloctadecyl siloxane (30%), copolymer	1.44		[11]
Dimethyl (79–82%)–diphenylsiloxane (18–21%) copolymer, silanol terminated	1.485		[11]
Dimethyl (79–82%)–diphenylsiloxane (18–21%) copolymer, trimethylsiloxy terminated	1.488		[11]
Dimethyl (82–88%)–diphenylsiloxane (12–18%) copolymer, silanol terminated	1.473		[11]
Dimethyl (88–92%)–phenylmethyl siloxane (18–12%) copolymer, trimethylsiloxy terminated	1.425		[11]
Dimethyl (94–96%)–diphenylsiloxane (4–6%) copolymer, trimethylsiloxy terminated	1.422		[11]
Dimethyl (97–98%)–diphenylsiloxane (2–3%) copolymer, silanol terminated	1.42		[11]
Dimethyl–tetrachlorophenyl siloxane, copolymer, branched, trimethylsiloxy terminated	1.428		[11]
Diphenyl (76.5%)–dimethyl (23.5%) copolymer, vinyl terminated, M.W. = 13, 200	1.493	22–25	[11]
Diphenyl (84%)–dimethyl (16%) copolymer, vinyl terminated, M.W. = 9,300;18,600; 18,900;19,500;35,300;54,900	1.465	22–25	[11]
Diphenyl (95%)–dimethyl (5%) copolymer, vinyl terminated, M.W. = 17,300; 49,000;80,400	1.432	22–25	[11]
Diphenyl (97%)–dimethyl (3%) copolymer, vinyl terminated, M.W. = 15,600;62,300	1.420	22–25	[11]
Diphenyl (97%)–dimethyl (3%) copolymer, vinyl terminated, M.W. = 78,000	1.421	22–25	[11]
Methyl hydro (3–4%)–cyanopropylmethylsiloxane copolymer	1.446		[11]
Methyl hydro (0.5–1.0%)–dimethylsiloxane copolymer, trimethylsilyl terminated, M.W. = 10,000,13,000	1.404		[11]
Methyl hydro (30–35%)–dimethylsiloxane copolymer, trimethylsilyl terminated, M.W. = 2,000–2,100	1.399		[11]
Methyl hydro (15–18%)–dimethylsiloxane copolymer, trimethylsilyl terminated, M.W. = 25–35	1.4		[11]
Methyl hydro (50–55%)–dimethylsiloxane copolymer, trimethylsilyl terminated, M.W. = 900–1,000	1.394		[11]
Methyl hydro (25–30%)–methyloctyl siloxane copolymer	1.44		[11]
Methyl hydro (40–60%)–methyloctyl siloxane copolymer	1.435		[11]
Methyl hydro (45–50%)–phenylmethylsiloxane copolymer, dimethylsiloxy terminated	1.5		[11]
Methyloctyl (35–40%)–vinylmethyl (3–4%)–dimethylsiloxane (56–64%), terpolymer	1.437		[11]
Methylphenyl (45–55%)–diphenylsiloxane (45–55%) copolymer, trimethylsiloxy terminated	1.582		[11]
Poly(butadiene-*co*-acrylonitrile)	1.52		[5]
Poly(butadiene-*co*-styrene) (∼30% styrene) block copolymer	1.53		[5]
Poly(butadiene-*co*-styrene) (75%–25%)	1.535		[5]
Poly(ethylene-*co*-propylene) (EPR-rubber)	1.4748–1.48		[5]
Poly(ethylene–*co*-vinyl acetate)	1.47–1.5		[5]
Poly(methyl-3,3,3-trifluoropropylsiloxane–50% dimethyl siloxane) copolymer	1.387		[11]
Poly(oxyethyleneoxymaleoyl) [poly(ethylene maleate)]	1.4840	25	[5]
Poly(oxyethyleneoxysuccinoyl) [poly(ethylene succinate)]	1.4744	25	[5]
Poly(oxyethyleneoxyterephthaloyl) [poly(ethylene terephthalate)]	1.5750	20	[5]
Poly(styrene-*co*-acrylonitrile) (75%–25%)	1.57		[5]
Poly(styrene-*co*-maleic anhydride)	1.564	21	[5]
Poly(tetrafluoroethylene-*co*-hexafluoropropylene)	1.338		[5]

TABLE 50.2. *Continued.*

Copolymer	Refractive index n	Temperature (°C)	Reference
Poly(vinyl chloride + 40% dioctyl phthalate	1.52		[5]
Poly(vinyl chloride) + 40% tricrexyl phosphate	1.55		[5]
Poly(vinyl chloride-*co*-vinyl acetate) (95/5-90/10)	1.525–1.535		[5]
Styrene acrylonitrile (SAN)	1.565–1.569	23	[3]
Styrene acrylonitrile copolymer (unfilled)	1.56–1.57		[1]
Styrene butadiene	1.571		[1]
Styrene butadiene thermoplastic elastomers	1.52–1.55		[1]
Styrene maleic anhydride (SMA)	1.6		[1]
Styrene methylmethacrylate (SMMA)	1.56		[1]

TABLE 50.3. *Optical configuration parameters ($\Delta\alpha$) and stress-optical coefficients (C) of polymers. All values reported are at a wavelength of 6,328 Å, D.S. denotes degree of substitution, and v^2 is the polymer volume fraction.*

Polymer	$\Delta\alpha$ (Å^3)	Diluent	Temp (°C)	v 2	Stress optical coefficient C (10^9 Pa^{-1})	Reference
Benzyl cellulose, D.S. = 2.5	294	Dioxane				[65]
Cellulose acetate D.S. = 2.4	0	Pyridene				[65]
Cellulose acetate D.S. = 3.0	− 34	Tetrachloroethane				[65]
Cellulose acetate D.S. = 3.0	35	Bromoform				[65]
Cellulose acetate D.S. = 3.0	61	Dioxane				[100]
Cellulose acetate D.S. = 3.0	144	Methyl ethyl ketone				[65]
Cellulose benzoate D.S. = 3.0	− 617	Dimethylformamide				[65]
Cellulose benzoate D.S. = 3.0	− 763	Chloroform				[65]
Cellulose benzoate D.S. = 3.0	− 914	Bromobenzene				[65]
Cellulose benzoate D.S. = 3.0	− 830	Dimethyl phthalate				[65]
Cellulose benzoate D.S. = 3.0	− 447	Dioxane				[100]
Cellulosedimethylphosphonocarbamate D.S. = 2.0	710	0.1 M NaCl				[101]
Cellulose dimethylphosphonocarbamate D.S. = 2.0	640	0.2 M NaCl				[101]
Cellulose diphenylacetate	1,360	Acetophenone				[102]
Cellulose diphenylacetate	1,030	Dioxane				[100]
Cellulose diphenylphosphonocarbamate D.S. = 2.0	626–640	Dioxane				[65]
Cellulose monophenylacetate D.S. = 2.8	600	Bromobenzene				[65]
Cellulose monophenylacetate D.S. = 2.8	478	Bromoform				[65]
Cellulose nitrate D.S. = 1.9	− 62	Cyclohexanone				[65]
Cellulose nitrate D.S. = 1.9	149	Dioxane				[65]
Cellulose nitrate D.S. = 2.3	− 330	Cyclohexanone				[65]
Cellulose nitrate D.S. = 2.7	− 540	Cyclohexanone				[65]
Cellulose nitrate D.S. = 2.7	− 320	Amyl acetate				[65]
Cellulose nitrate D.S. = 2.7	− 115	Acetone				[65]
Cellulose nitrate D.S. = 2.7	− 300	Butyl acetate				[65]
Cellulose nitrate D.S. = 2.7	− 140	Ethyl acetate				[65]
Cellulose nitrate D.S. = 2.8	− 820	Cyclohexanone				[65]
Cellulose phenylcarbamate	− 1,100	Acetophenone				[102]
Cellulose phenylcarbamate D.S. = 2.2	− 1,880	Dioxane				[65]
Cellulose phenylcarbamate D.S. = 3.0	− 742	Benzophenone				[103]
Cellulose phenylcarbamate D.S. = 3.0	− 572	Benzophenone				[103]
Cellulose phenylcarbamate D.S. = 3.0	− 1,830	Dioxane				[65]
Cellulose phenylcarbamate D.S. = 3.0	− 872	Dioxane				[65]
Cellulose phenylcarbamate D.S. = 3.0	− 560	Ethyl acetate				[65]

TABLE 50.3. *Continued.*

Polymer	$\Delta\alpha$ (A**3)	Diluent	Temp (°C)	v2	Stress optical coefficient C (10^9 Pa^{-1})	Reference
Cellulose stearate D.S. = 2.0	− 500	Tetrachloroethane				[104]
Cyanoethyl cellulose D.S. = 26	900	Cyclohenanone				[65]
Cyanoethylacetyl cellulose	15	Cyclohexanone				[105]
Cyanoethylacetyl cellulose	390	Acetone				[65]
Cyanoethylacetyl cellulose	90	Dimethylformamide				[65]
Cyanoethyltrityl cellulose	220	Cyclohexanone				[105]
DNA	− 30,000	Aqueous 0.2 M NaCl				[65]
Ethyl cellulose	430	Carbon tetrachloride				[106]]
Ethyl cellulose D.S. = 2.5	512	Dioxane				[65]
Poly(1,2,3-trimethyl-2,3-dihydro-1,6-indendiyl-1,4-phenylene-ethylene)	142	Bromoform				[85]
Poly(1,2,3-trimethyl-2,3-dihydro-1, 6-indenedinyl)	78	Bromoform				[85]
Poly(1-butene) atactic	33.4	Toluene				[30]
Poly(1-butene) isotactic	25.2	Toluene				[30]
Poly(1-decene) isotactic	− 82.5	Toluene				[30]
Poly(1-dodecene) isotactic	− 120	Toluene				[30]
Poly(1-heptene) isotactic	− 24.5	Toluene				[30]
Poly(1-hexadecene)	(− 205)–(− 213)	Toluene				[30]
Poly(1-hexene) atactic	12.1	Toluene				[30]
Poly(1-hexene) isotatic	− 6.5	Toluene				[30]
Poly(1-octadecene) isotactic	− 257	Toluene				[30]
Poly(1-octene) isotactic	− 39	Toluene				[30]
Poly(1-pentene) isotactic	8.0	Toluene				[30]
Poly(1-pentene) isotactic	9.3	Toluene				[30]
Poly(1-tetradecene) isotactic	− 176	Toluene				[30]
Poly(1-tetradecene) isotactic	− 171	Toluene				[30]
Poly(2.5-dichlorostyrene)	− 265	Bromoform				[67]
Poly(2.5-dimethylstyrene)	− 180	Bromoform				[67]
Poly(2-methyl-5-vinyl-*N*-butylpyridinium bromide)	− 900	0.01 M NaCl				[72]
Poly(2-methyl-5-vinyl-*N*-butypyridinium bromide)	− 270	0.1 M NaCl				[72]
Poly(2-methyl-5-vinyl-pyridine)	− 260	Bromoform				[73]
Poly(2-methyl-5-vinyl-pyridinium chloride)	− 300	0.1 M HCl				[74]
Poly[2-propenoic acid-4-(phenylazoxy)phenyl ester]	− 450	Tetrachloroethane				[65]
Poly(2-propenoic acid-4-[(4-butylphenyl) azoxy]-phenyl ester)	− 510	Tetrachloroethane				[65]
Poly(3,4-dichlorostyrene)	− 300	Tetrabromoethane				[69]
Poly(3-methyl tetrahydrofuran); isotactic, planar, *trans* config	2.473		20		1.25	[21]
Poly(3-methyl tetrahydrofuran); isotactic, planar, *trans* config	2.563		30		1.20	[21]
Poly(3-methyl tetrahydrofuran); isotactic, planar, *trans* config.	2.653		40		1.16	[21]
Poly(3-methyl tetrahydrofuran); isotactic, planar, *trans* config.	2.750		40		1.13	[21]
Poly(3-methyl tetrahydrofuran); isotactic, planar, *trans* config.	2.835		60		1.10	[21]
Poly(3-methyl-1-butene-silsesquioxane)	− 570	Benzene				[65]
Poly(3-methyl-1-butene-silsesquioxane)	− 400	Butyl acetate				[65]
Poly[4-(4-nonyloxy-benzamido) styrene]	− 2,500	Benzene				[65]

TABLE 50.3. *Continued.*

Polymer	$\Delta\alpha$ (A^{**3})	Diluent	Temp (°C)	v2	Stress optical coefficient C (10^9 Pa^{-1})	Reference
Poly(4-(hexadecyloxy)-benzoic acid-4-[(2-methyl-1-oxo-2-propenyl) oxy]phenyl ester)	− 1,000	Bromoform				[66]
Poly (4-(hexadecyloxy)-benzoic acid-4-[(2-methyl-1-oxo-2-propenyl) oxy]phenyl ester)	− 1,600	Benzene				[66]
Poly(4-(hexadecyloxy)-benzoic acid-4-[(2-methyl-1-oxo-2-propenyl) oxy]phenyl ester)	− 1,400	Chloroform				[66]
Poly(4-(hexadecyloxy)-benzoic acid-4-[(2-methyl-1-oxo-2-propenyl) oxy]phenyl ester)	− 2,700	Carbon tetrachloride				[65]
Poly(4-(hexadecyloxy)-benzoic acid-4-[(2-methyl-1-oxo-2-propenyl) oxy]phenyl ester)	− 890	Tetrahydrofuran				[66]
Poly(4-(hexadecyloxy)-benzoic acid-4-[(2-methyl-1-oxo-2-propenyl) oxy] phenyl ester)	− 4,200	Benzene/heptene, 52/48, 66/34				[67]
Poly(4-(hexadecyloxy)-benzoic acid-4-[(4-[(2-methyl-1-oxo-2-propenyl) oxy]benzoyl)oxy]phenyl ester)	− 4,900	Chloroform				[65]
Poly(4-(hexadecyloxy)-benzoic acid-4-[(4-[(2-methyl-1-oxo-2-propenyl) oxy]benzoyl)oxy]phenyl ester)	− 3,000	Benzene				[65]
Poly(4-(hexyloxy)-3-nitro-benzoic acid-4-[(2-methyl-1-oxo-2-propenyl) oxy]phenyl ester)	− 1,200	Dioxane				[65]
Poly(4-(hexyloxy)-benzoic acid-4-[(2-methyl-1-oxo-2-propenyl) oxy]phenyl ester)	− 370	Benzene				[65]
Poly(4-(nonyloxy)-benzoic acid-4-[(2-methyl-1-oxo-2-propenyl) oxy]phenyl ester)	− 600	Carbon tetrachloride				[65]
Poly(4-[(1-oxo-2-propenyl)oxy]-benzoic acid-4-butoxyphenyl ester)	− 800	Tetrachloroethane				[65]
Poly(4-[(1-oxo-2-propenyl)oxy]-benzoic acid-4-ethoxyphenyl ester)	− 630	Tetrachloroethane				[65]
Poly(4-[(1-oxo-2-propenyl)oxy]-benzoic acid-4-methoxyphenyl ester)	− 520	Tetrachloroethane				[65]
Poly(4-[(1-oxo-2-propenyl)oxy]-benzoic acid-4-propoxyphenyl ester)	− 810	Tetrachloroethane				[65]
Poly(4-[(1-oxo-2-propenyl)oxy]-benzoic acid-phenyl ester)	− 520	Tetrachloroethane				[65]
Poly(4-[(2-methyl-1-oxo-2-propenyl)oxy]-benzoic acid-4-(dodecyloxy) phenyl ester)	− 2,350	Carbon tetrachloride				[65]
Poly(4-[(2-methyl-1-oxo-2-propenyl)oxy]-benzoic acid-4-(nonyloxy)phenyl ester)	− 2,700	Carbon tetrachloride				[65]
Poly(4-[(2-methyl-1-oxo-2-propenyl) oxy]-benzoic acid-4-cyanophenyl ester)	− 240	Dimethylformamide				[65]
Poly(4-[(2-methyl-1-oxo-2-propenyl) oxy]-benzoic acid-4-methoxyphenyl ester)	− 500	Tetrachloromethane				[65]
Poly(4-[(2-methyl-1-oxo-2-propenyl) oxy]-benzoic acid-hexadecyl ester)	− 445	Carbon tetrachloride				[65]

TABLE 50.3. *Continued.*

Polymer	$\Delta\alpha$ (A^{**3})	Diluent	Temp (°C)	v2	Stress optical coefficient C (10^9 Pa^{-1})	Reference
Poly(4-[(11-[(2-methyl-1-oxo-2-propenyl)oxy]-1-oxoundecyl)oxy]-benzoic acid-4-butoxyphenyl ester)	− 90	Dioxane				[65]
Poly(4-[2-(2-methyl-1-methylene-allyloxy)-ethoxy]-benzoic acid-4-methoxy-phenyl ester]	− 117	Carbon tetrachloride				[65]
Poly(4-propoxy-benzoic acid-4-[(2-methyl-1-oxo- 2-propeny)oxy]phenyl ester)	− 320	Dimethylformamide/toluene				[65]
Poly(4-vinylpyridene)	− 240	Bromoform				[75]
Poly(4-vinylpyridinium chloride)	− 260	0.1 M HCl				[75]
Poly(4-vinylpyridinium chloride)	− 440	0.05 M HCl				[75]
Poly(acenaphthylene) helix 4/1	− 300	Bromoform				[83]
Poly(acenaphthylene) *trans*	− 300	Bromoform				[83]
Poly(acrylic acid)	− 0.5	Dioxide				[42]
Poly(acrylic acid), sodium salt	− 20	0.0012 M NaCl, pH 7				[43]
Poly(acrylic acid), sodium salt	(− 4)–(− 10)	water, pH 6.1				[43]
Poly(acrylonitrile)	− 23	Dimethylformamide				[64]
Poly(α-methylstyrene); glass					0.002	[17,68]
Poly(α-methylstyrene)	− 133	Tetrabromoethane				[70]
Poly(benzimidizole-2,6-diyl-1,4-phenylenebenzimidazol-6,2-diyl-iminoterephthaloylimino)	490	Sulfuric acid				[65]
Poly(benzimidizole-2,6-diyl-iminoterephthaloylimino-1, 4-phenylene)	5,080	Sulfuric acid				[65]
iminoterephthaloylimino-1,3-(4-hydroxyphenylene)	2,340	Sulfuric acid				[65]
Poly(benzoxazole-2,6-diyl-iminoterephthaloylimino-1, 4-(3-hydroxyphenylene)	5,940	Sulfuric acid				[65]
Poly(benzoxazole-2,6-diyl-iminoterephthaloylimino-1, 4-phenylene)	5,940	Sulfuric acid				[65]
Poly(benzyl methacrylate); glass					0.025–0.045	[17,50]
Poly(β-naphthyl methacrylate)	− 60	Tetrabromoethane				[64]
Poly(β-vinylnapthalene)	− 440	Bromoform				[83]
Poly(β-vinylnapthalene)	− 4.4	Benzene				[27]
Poly(butadiene) 1,4-cis	61.3–63	Benzene				[24]
Poly(butadiene) 1,4-cis	53.5	Carbon tetrachloride				[24]
Poly(butadiene) 1,4-*cis*	57.3	Cyclohexane				[24]
Poly(butadiene) 1,4-*cis*	72	Toluene				[24]
Poly(butadiene) 1,4-*cis*	86.9	*p*-Xylene				[24]
Poly(butadiene) 1,4-*trans*	71	Benzene				[25]
Poly(butadiene) 1,4-*trans*	61.1	Carbon tetrachloride				[24]
Poly(butadiene) 1,4-*trans*	57.3	Cyclohexane				[24]
Poly(butadiene) 1,4-*trans*	81.6	Toluene				[24]
Poly(butadiene) 1,4-*trans*	101	*p*-Xylene				[24]
Poly(butadiene); (isotactic) melt			22		3.3	[17,26]
Poly(butyl acrylate); fraction of *meso* dyads, Wm = 0.3	− 0.95		50	1.0		[20,49]
Poly(carbonate) of bisphenol-A			170–230		3.5–3.7	[17,29]
Poly(carbonate) of bisphenol-A, benzyl substituted			220		40	[17,29]
Poly(carbonate) of bisphenol-A, phenyl substituted			250		1.8–2.1	[17,29]
Poly(carbonate) of bisphenol-A; glass				0.111		[17,50]

TABLE 50.3. *Continued.*

Polymer	$\Delta\alpha$ (A^{**3})	Diluent	Temp (°C)	v2	Stress optical coefficient C (10^9 Pa^{-1})	Reference
Poly(carbonate) of bisphenol-A; melt			200	1.0	3.5	[22]
Poly(cetyl acrylate)	− 141	Decalin				[46]
Poly(cetyl acrylate)	− 164	Toluene				[45]
Poly(cetyl methacrylate)	− 160	Benzene				[56]
Poly(chloroethyl methacrylate); glass					− 0.0056	[17,57]
Poly(chlorohexyliminocarbonyl)	3,000	Carbon tetrachloride				[92]
Poly(chloroprene)	110	α-Bromonaphthalene				[27]
Poly(chloroprene)	33	Carbon tetrachloride				[27]
Poly(chloroprene)	64	Chlorobenzene				[27]
Poly(chloroprene)	39	Dichloromethane				[27]
Poly(chloroprene)	99	α-Methylnaphthalene				[27]
Poly(chloroprene)	46	Tetrachloromethane				[27]
Poly(chloroprene)	67	Toluene				[27]
Poly(chloroprene)	88	*p*-Xylene				[27]
Poly(cholestryl acrylate)	− 360	Benzene				[47]
Poly(*cis*-1,4-cyclohexane dimethanol sebacate)	9.15		40	1.0	0.352	[20,111]
Poly(*cis*-1,4-cyclohexane dimethanol sebacate)	8.76		50	1.0	0.326	[20,111]
Poly(*cis*-1,4-cyclohexane dimethanol sebacate)	8.5		60	1.0	0.306	[20,111]
Poly(*cis*-1,4-cyclohexane dimethanol sebacate)	8.37		70	1.0	0.292	[20,111]
Poly(*cis*-1,4-cyclohexane dimethanol sebacate)	8.28		80	1.0	0.280	[20,111]
Poly(*cis*-1,4-cyclohexane dimethanol sebacate)	7.5	1,3,5-Triethylbenzene	40	0.336		[20,111]
Poly(*cis/trans*-1,4-cyclohexane dimethanol-*alt*-formaldehyde) network; M_n = 4,700 g/mol; *trans* content = 10%	7.344		70		2.560	[23]
Poly(*cis/trans*-1,4-cyclohexane dimethanol-*alt*-formaldehyde) network; M_n = 4,700 g/mol; *trans* content = 10%	7.300		60		2.626	[23]
Poly(*cis/trans*-1,4-cyclohexane dimethanol-*alt*-formaldehyde) network; M_n = 4,700 g/mol; *trans* content = 10%	7.310		50		2.719	[23]
Poly(*cis/trans*-1,4-cyclohexane dimethanol-*alt*-formaldehyde) network; M_n = 4,700 g/mol; *trans* content = 10%	7.234		40		2.783	[23]
Poly(*cis/trans*-1,4-cyclohexane dimethanol-*alt*-formaldehyde) network; M_n = 4,700 g/mol; *trans* content = 10%	7.238		30		2.884	[23]
Poly(*cis/trans*-1,4-cyclohexane dimethanol-*alt*-formaldehyde) network; M_n = 4,700 g/mol; *trans* content = 10%	7.237		20		2.989	[23]
Poly(*cis/trans*-1,4-cyclohexane dimethanol-*alt*-formaldehyde) network; M_n = 4,700 g/mol; *trans* content = 10%	7.229		10		3.099	[23]
Poly(*cis/trans*-1,4-cyclohexane dimethanol-*alt*-formaldehyde) network; M_n = 6,000 g/mol; *trans* content = 70%	9.978		70		3.414	[23]
Poly(*cis/trans*-1,4-cyclohexane dimethanol-*alt*-formaldehyde) network; M_n = 6,000 g/mol; *trans* content = 70%	9.819		60		5.553	[23]
Poly(*cis/trans*-1,4-cyclohexane dimethanol-*alt*-formaldehyde) network; M_n = 6,000 g/mol; *trans* content = 70%	9.969		50		3.727	[23]
Poly(*cis/trans*-1,4-cyclohexane dimethanol-*alt*-formaldehyde) network; M_n = 6,000 g/mol; *trans* content = 70%	9.849		40		3.8.8	[23]

TABLE 50.3. *Continued.*

Polymer	$\Delta\alpha$ (A**3)	Diluent	Temp (°C)	v2	Stress optical coefficient C (10^9 Pa^{-1})	Reference
Poly(*cis/trans*-1,4-cyclohexane dimethanol-*alt*-formaldehyde) network; M_n = 6,000 g/mol; *trans* content = 70%	9.988		30		3.957	[23]
Poly(*cis/trans*-1,4-cyclohexane dimethanol-*alt*-formaldehyde) network; M_n = 6,000 g/mol; *trans* content = 70%	9.714		20		4.029	[23]
Poly(*cis/trans*-1,4-cyclohexane dimethanol-*alt*-formaldehyde) network; M_n = 6,000 g/mol; *trans* content = 70%	9.435		10		4.060	[23]
Poly(*cis/trans*-1,4-cyclohexane dimethanol-*alt*-formaldehyde); fraction of rings in *trans* configuration = 0.1	7.24		30			[20,23]
Poly(*cis/trans*-1,4-cyclohexane dimethanol-*alt*-formaldehyde); fraction of rings in *trans* configuration = 0.7	9.99		30			[20,23]
Poly(cyclohexyl methacrylate); glass					− 0.059	[17,57]
Poly(decyl acrylate)	− 74	Decalin				[45]
Poly(decyl acrylate)	− 95	Toluene				[45]
Poly(dichlorophenyl-silsesquioxane)	− 4,450	Bromoform				[65]
Poly(dichlorophenyl-silsesquioxane)	− 4,700	Tetrabromoethane				[65]
Poly(diethylene glycol terephthalate)	19.8		70	1.0		[20,111]
Poly(diethylene glycol terephthalate)	26.5	Tricresylphosphate	70	0.58		[20,111]
Poly(diethylene glycol *trans*-1,4-cyclohexane dicarboxylate)	7.4			1.0		[20,111]
Poly(dimethyl siloxane)	0.81		70	1.0		[20,32]
Poly(dimethyl siloxane)	0.68		70	1.0		[20,105]
Poly(dimethyl siloxane)	0.3–0.7		70	1.0		[20,108]
Poly(dimethyl siloxane)	0.51	Decalin	70	0.25		[20,32]
Poly(dimethyl siloxane)	0.38	Cyclohexane	70	0.16		[20,32]
Poly(dimethyl siloxane)	0.18	Carbon tetrachloride	70	0.16		[20,32]
Poly(dimethyl siloxane)	0.15–0.20	Carbon tetrachloride	70	0.35–0.71		[20,109]
Poly(dimethyl siloxane)			20–190		0.135–0.260	[17,29]
Poly(dimethyl sil-methylene)	4.27		50	1.0		[20,110]
Poly(dimethyl sil-methylene)	2.5	1,3,5-Triethylbenzene	50			[20,110]
Poly(diphenylpropylene)	80	Bromoform				[39]
Poly(epsilon, *N*-carbobenzoxy-L-lysine) helix	3,600	Dimethylformamide				[93]
Poly(ethyl acrylate)	3.0	Benzene				[48]
Poly(ethyl acrylate)	10	Bromobenzene				[48]
Poly(ethyl acrylate)	− 37	Bromoform				[48]
Poly(ethyl acrylate)	− 14	Dibromoethane				[48]
Poly(ethyl acrylate)	− 11	Dimethylformamide				[48]
Poly(ethyl acrylate); fraction of *meso* dyads, Wm = 0.3	− 0.82		50	1.0		[20,49]
Poly(ethylene)	60	Tetralin, xylene				[31]
Poly(ethylene)	30	Decalin				[31]
Poly(ethylene)	7.8		150	1.0		[20,35]
Poly(ethylene)	8.4		150	1.0		[20,34]
Poly(ethylene)	6.5	*n*-C22H$_{46}$	150	0.41		[20,32]
Poly(ethylene)	5.1	*n*-C12H$_{26}$	150	0.44		[20,32]
Poly(ethylene)	40	Decalin	150	0.33		[20,32]
Poly(ethylene)	3.9–4.0	Decalin	150	0.33		[20,33]
Poly(ethylene), cross-linked			130–180		1.5–2.2	[17,29]
Poly(ethylene), linear melt			150–190		1.8–2.4	[17,29]
Poly(gamma-benzyl-L-glutamate) coil	230	Dichloroacetic acid				[65]

TABLE 50.3. *Continued.*

Polymer	$\Delta\alpha$ (A^{**3})	Diluent	Temp (°C)	v2	Stress optical coefficient C (10^9 Pa^{-1})	Reference
Poly(gamma-benzyl-L-glutamate) helix	25,000	Dichloroethane				[65]
Poly(glycol methacrylate)	1.0	Dimethylformamide				[58]
Poly(glycol methacrylate)	− 6.0	Ethyl alcohol				[58]
Poly(glycol methacrylate)	− 6.0	Water				[58]
Poly(hexyl methacrylate)	− 40	Benzene				[59]
Poly(hexyl methacrylate)	− 9.7	Carbon tetrachloride				[59]
Poly(hydrazocarbonyl-1,4-phenylene-iminoterephthaloyl)	3,630	Dimethylsulfoxide				[65]
Poly(imino-1,3-phenyleneimino-sophthaloyl)	360	Sulfuric acid				[65]
Poly(imino-1,4-phenyleneimino-terephthaloyl)	5,250	Sulfuric acid				[65]
Poly(imino-1,4-terephthaloylimino-1, 4-phenylenediphenylmethyl-1,4-phenylene)	130	Sulfuric acid				[65]
Poly(iminocarbonyl,1,4-phenylene)	10,500	Sulfuric acid				[65]
Poly(iminocarbonyl-cyclohexylene)	390	Sulfuric acid				[65]
Poly(isobutene)	45–59	Tetrachloroethylene, *m*-Xylene				[27]
Poly(isobutene)	35	Carbon tetrachloride				[27]
Poly(isobutene)	30	Decalin				[31]
Poly(isobutene)	69	*p*-Xylene				[27]
Poly(isobutylene)	4.10		30	1.0		[20,37]
Poly(isobutylene)	3.5		30	1.0		[20,38]
Poly(isobutylene)	3.36	Carbon tetrachloride	30	0.16		[20,37]
Poly(isobutylene)	3.79	Cyclohexane	30	0.17		[20,37]
Poly(isobutylene)	2.84	Bromotrichloromethane	30	0.19		[20,37]
Poly(isobutylene) Vistanex B-100		Decalin	25	0.03	1.7	[36]
Poly(isobutylphenyl-silsesquioxane) (1:1)	− 840	Benzene				[65]
Poly(isohexylphenyl-silsesquioxane) (1:1)	− 980	Benzene				[65]
Poly(isoprene) *cis*	48	Benzene				[25]
Poly(isoprene) *cis*	53.1	Squalene				[28]
Poly(isoprene) *trans*	49	Benzene				[25]
Poly(isoprene); melt			22		1.9	[17,26]
Poly(isoprene); natural rubber (cross-linked)			20–100		1.80–2.05	[17,29]
Poly(isoprene); *trans*, gutta percha (cross-linked)			85–250		3.0	[17,29]
Poly(L-glutamic acid) coil	136	Phosphate buffer, 0.1 M, pH = 12.5				[93]
Poly(L-glutamic acid) helix	1,900	Phosphate buffer, 0.1 M, pH = 4.2				[93]
Poly(*m,p*-aromatic ester) *m*/*p* = 1/3	750	Dichloroacetic acid				[91]
Poly(*m*-chlorophenyl-silsesquioxane)	− 4,700	Carbon tetrachloride				[65]
Poly(methacrylic acid)	50	Methanol				[61]
Poly(methacrylic acid)	150	0.002 M HCl				[61]
Poly(methacrylic acid), sodium salt	150	0.012 M NaCl, pH = 7				[61]
Poly(methacrylic acid), sodium salt	400	0.0012 M NaCl, pH = 7				[61]
Poly(methacrylic acid), sodium salt	56–300	Water				[62]
Poly(methyl acrylate)	17	Benzene				[44]
Poly(methyl acrylate)	16	Toluene				[45]
Poly(methyl acrylate)	26	Toluene				[44]
Poly(methyl acrylate); fraction of *meso* dyads, Wm = 0.3	− 0.34			50	1.0	[20,49]
Poly(methyl acrylate); fraction of *meso* dyads, Wm = 0.5	− 0.84			50	1.0	[20]
Poly(methyl methacrylate) atactic	2.0	Benzene				[63]

TABLE 50.3. *Continued.*

Polymer	$\Delta\alpha$ (A^{**3})	Diluent	Temp (°C)	v2	Stress optical coefficient C (10^9 Pa^{-1})	Reference
Poly(methyl methacrylate) isotactic	25	Benzene				[63]
Poly(methyl methacrylate), glass					(− 0.0033) – (0.0045)	[17,50]
Poly(methyl phenyl siloxane); fraction of *meso* dyads, Wm = 0.5	− 12.1		25	1.000		[20,113]
Poly(methyl phenyl siloxane); fraction of *meso* dyads, Wm = 0.5	− 11.5	Decalin	25	0.673		[20,113]
Poly(methyl phenyl siloxane); fraction of *meso* dyads, Wm = 0.5	− 9.12	Decalin	25	0.488		[20,113]
Poly(methyl phenyl siloxane); fraction of *meso* dyads, Wm = 0.5	− 8.32	Decalin	25	0.350		[20,113]
Poly(methyl phenyl siloxane); fraction of *meso* dyads, Wm = 0.5	− 8.10	Decalin	25	0.211		[20,113]
Poly(methyl phenyl siloxane); fraction of *meso* dyads, Wm = 0.5	− 8.50	Decalin	25	0.204		[20,113]
Poly(*N,N*-piperazindiyl-2,5-diketo-1,3-pyrrolidindiylhexamethylene-2,5-diketo-1,3-pyrrolidindiyl)	56	Benzyl alcohol				[98]
Poly(*N,N*-piperazindiyl-2,5-diketo-1,3-pyrrolidindiylhexamethylene-2,5-diketo- 1,3-pyrrolidindiyl)	30	Bromoform/cyclohexanol, 60/40				[98]
Poly(*N*-2,4-dimethylphenylmaleimide)	− 200	Bromoform				[65]
Poly(*n*-butyl acrylate)	− 11	Benzene				[44]
Poly(*n*-butyl acrylate)	− 17.8	Decalin				[45]
Poly(*n*-butyl acrylate)	− 10.1	Toluene				[45]
Poly(*n*-butyl acrylate)	− 6.5	Toluene				[44]
Poly(*n*-butyl methacrylate) atactic	− 14	Benzene				[51]
Poly(*n*-butyl methacrylate) isotactic	− 2.0	Benzene				[52]
Poly(*n*-butyliminocarbonyl) a.k.a. poly(butyl isocyanate)	4,100	Carbon tetrachloride				[65,107]
Poly(*n*-butyliminocarbonyl) a.k.a. poly(butyl isocryanate)	800	Pentafluorophenol 0.9/0.1				[65]
Poly(*N*-isobutylmaleimide)	160	Chlorobenzene				[65]
Poly(*N*-methylcitraconimide)	150	Bromoform				[97]
Poly(*N*-phenylmathacrylamide)	− 103	*o*-Toluidine				[69]
Poly(*n*-tolyliminocarbonyl)	− 39	Bromoform				[65]
Poly(ocatdecyl acrylate)	− 190	Decalin				[45]
Poly(ocatdecyl acrylate)	− 232	Toluene				[45]
Poly(octyl acrylate)	− 57.4	Decalin				[45]
Poly(octyl acrylate)	− 47.9	Toluene				[45]
Poly(octyl acrylate; fraction of *meso* dyads, Wm = 0.3)	− 1.1		50	1.0		[20,49]
Poly(octyl methacrylate)	− 47	Benzene				[59]
Poly(octyl methacrylate)	− 12.5	Carbon tetrachloride				[59]
Poly(oxadiazole-2,5-diyl-1,4-phenylene)	1,750	Sulfuric acid				[65,112]
Poly(oxycarbonyloxy-1,4-phenylenecyclcohexylidene-1,4-phenylene)	− 114	Bromoform				[88]
Poly(oxydecamethyleneoxycarbonyl-phenyleneoxyterephthaloyloxy phenylenecarbonyl)	200	Dichloroacetic acid				[90]
Poly(oxydimethysilyene)	4.7	Petroleum ether				[94]
Poly(oxyethyleneoxyterephthaloyl)	70	Dichloroethane/phenol 1/1				[89]
Poly(oxyethyleneoxyterephthaloyl)	48.7	Dichloroacetic acid				[90]

TABLE 50.3. *Continued.*

Polymer	$\Delta\alpha$ (A^{**3})	Diluent	Temp (°C)	v2	Stress optical coefficient C (10^9 Pa^{-1})	Reference
Poly(oxyhexamethyleneoxycarbonylphenylene-oxyterephthaloyloxyphenylenecarbonyl)	250	Dichloroacetic acid				[90]
Poly(oxymethylphenylsilylene) (50–62.5)/(50–37.5)	− 36	Decalin				[95]
Poly(oxymethylphenylsilylene) 50/50	− 36	Decalin				[95]
Poly(oxymethylphenylsilylene) 75/25	− 13.6	Benzene				[96]
Poly(oxymethylphenylsilylene) 75/25 1	− 2	Decalin				[95]
Poly(oxymethylphenylsilylene) 87.5/12.5	− 10	Decalin				[95]
Poly(oxymethylphenylsilylene) 90/10	− 2.3	Petroleum ether				[94]
Poly(oxymethylphenylsilylene) atactic	− 25.5	Benzene				[96]
Poly(oxymethylphenylsilylene) atactic	− 82	Decalin, tetralin				[95]
Poly(oxymethylphenylsilylene) isotactic	− 82	Decalin, tetralin				[95]
Poly(oxyphenysilylene)	− 85	Benzene				[96]
Poly(oxypropylene)	− 18	Cyclohexane				[86]
Poly(oxypropylene); $M_c = 2{,}000$	4.66±0.04		25	1.0		[20,87]
Poly(oxypropylene); $M_c = 3{,}000$	4.33±0.09		25	1.0		[20,87]
Poly(oxypropylene); $M_c = 3{,}000$	3.05	Decalin	25			[20,87]
Poly(oxypropylene); $M_c = 3{,}000$	3.87	POP oligomers	25			[20,87]
Poly(oxytetramethyleneoxy-carbonylphenylene-oxyterephthaloylo-xyphenyleneoxycarbonyl)	280	Dichloroacetic acid				[90]
Poly(*p*-carboxyphenyl methacrylate)	180	Dioxane				[55]
Poly(*p*-carboxyphenyl methacrylate)	370	0.1 M NaCl				[55]
Poly(*p*-carbethoxy-*N*-phenylmethacrylamide)	− 230	*o*-Toluidine				[54]
Poly(*p*-chloro-*N*-phenylmethacrylamide)	− 160.0	*o*-Toluidine				[54]
Poly(*p*-chlorostyrene)	− 230	Bromoform				[67]
Poly(*p*-chlorostyrene); glass					0.024	[17,68]
Poly(*p*-methylcarboxy–phenyl methacrylate)	− 77	Dibromoethane				[55]
Poly(*p*-methylstyrene) atactic	− 147	Bromoform				[71]
Poly(*p*-methylstyrene) isotactic	− 140	Bromoform				[71]
Poly(*p*-*t*-butyl styrene); glass				0.011		[17,68]
Poly(*p*-*t*-butylphenyl methacrylate)	− 90	Bromobenzene				[53]
Poly(*p*-tolymaleiimide)	− 160	Bromoform				[99]
Poly(phenyl methacrylate)	− 10.5	Bromobenzene				[64]
Poly(phenyl methacrylate); glass					0.040	[17,57]
Poly(phenyl-silsesquioxane)	(− 1,060)–(− 1,800)	Bromoform				[65]
Poly(propylene)	0.3					[20,41]
Poly(propylene) atactic	45	Benzene, xylene				[31]
Poly(propylene) atactic	30	Carbon tetrachloride				[40]
Poly(propylene) atactic	30	Decalin				[31]
Poly(propylene) atactic	55	Toluene				[30]
Poly(propylene) isotactic	30	Carbon tetrachloride				[31]
Poly(propylene); isotactic (melt)			210		0.9	[17,29]
Poly(propylene); M.W. = 43,000–48,000			210		0.9	[19,36]
Poly(*S*-carbobenzoxymethyl-L-cystein)	22	Dichloroacetic acid				[93]
Poly(styrene)	− 1.7					[20,41]
Poly(styrene)					(− 4.1)–5.2	[17,29]
Poly(styrene) atactic	− 145	Bromoform				[67]
Poly(styrene) isotactic	− 224	Bromoform				[76]
Poly(styrene); atactic, M.W. = 9,000,000		Bromoform	25	0.01	− 6.9	[19,36]
Poly(styrene); glass					0.010	[17,50]

TABLE 50.3. *Continued.*

Polymer	$\Delta\alpha$ (A^{**3})	Diluent	Temp (°C)	v2	Stress optical coefficient C (10^9 Pa^{-1})	Reference
Poly(styrene); M.W. = 50,000–860,000			153–215	1.0	(− 4)–(− 5)	[19,36]
Poly(*t*-butyl methacrylate) atactic	2.1	Benzene				[44]
Poly(*t*-butyl methacrylate) isotactic	19.3	Benzene				[44]
Poly(triethylene glycol terephthalate)	13.3		1.0			[20,111]
Poly(vinyl acetate)	− 20	Acetone				[77]
Poly(vinyl acetate)	4.0–5.9	Benzene				[27]
Poly(vinyl acetate)	9.4	Bromobenzene				[78]
Poly(vinyl acetate)	− 20	Bromoform				[77]
Poly(vinyl acetate)	− 16	Carbon tetrachloride				[27]
Poly(vinyl acetate)	− 26	Carbon tetrachloride				[79]
Poly(vinyl acetate)	14	Chlorobenzene				[27]
Poly(vinyl acetate)	− 34.9	Chloroform				[79]
Poly(vinyl acetate)	− 24	Chloroform				[27]
Poly(vinyl acetate)	− 23	Cyclohexane				[27]
Poly(vinyl acetate)	− 36	Dichloroethane				[27]
Poly(vinyl acetate)	− 39	Dichloroethane				[27]
Poly(vinyl acetate)	− 25	Tetrabromoethane				[27]
Poly(vinyl acetate)	− 33	Tetrabromoethane				[77]
Poly(vinyl acetate)	10	Toluene				[27]
Poly(vinyl acetate)	13.5	Toluene				[44]
Poly(vinyl acetate)	19	Toluene				[79]
Poly(vinyl acetate)	2.0	*o*-Xylene				[27]
Poly(vinyl acetate)	81	Chloroform				[27]
Poly(vinyl acetate)	− 2.68		50	1.0		[20,80]
Poly(vinyl acetate)	− 1.90	1,3,5-Triethylbenzene	50	0.6		[20,80]
Poly(vinyl butyral)	173	Toluene–phenol, 79–21				[27]
Poly(vinyl butyral)	− 80	Benzene				[27]
Poly(vinyl butyrate)	− 36	Carbon tetrachloride				[27]
Poly(vinyl butyrate)	− 48	Chloroform				[27]
Poly(vinyl butyrate)	40	Tetrahydrofuran				[81]
Poly(vinyl chloride)	− 420	Bromoform				[82]
Poly(vinyl chloride)					− 0.5	[17,29]
Poly(vinyl chloride); M.W. = 14,000			210	1.0	− 0.5	[19,36]
Poly(vinyl cinnamate)	− 430	Tetrabromoethane				[64]
Poly(vinyl propionate)	− 31	Carbon tetrachloride				[27]
Poly(vinyl propionate)	− 40	Chloroform				[27]
Poly(vinyl propionate)	1.3	Toluene				[27]
Poly(vinyl stearate)	− 130	Carbon tetrachloride				[84]
Poly(vinyl toluene); glass					0.015	[17,68]
Poly(vinylpyrrolidone)	− 75	Benzyl alcohol				[64]
Poly([1,3,5,7-tetraoxo-2,3,6,7-tetrahydro-1H, 5H-benzo-(1,2-c:4,5-c′) dipyrrol- 2,6-diyl]-1,4-phenylene)	250–440	Sulfuric acid				[65]
Poly[(2,2′-diphenyl(6,6′-biquinoxaline)-3,3′-diyl)(1,1′-biphenyl)-4,4′-diyl]	175	Tetrachloroethane, chloroform				[65]
Poly[(3-β)-cholest-5-en-3-ol-2-propenoate]	− 300	Benzene				[65]
Poly[(ar,ar′-diphenyl(biquinoxaline)-ar, ar′-diyl]-1, 4-phenyleneoxy (1,1′-biphenyl)- 4,4′diyloxy-1,4-phenylene)	106	Tetrachloroethane, chloroform				[65]
Poly[(imino-4,6-dicarboxyisophthaloylimino) biphenyl-4-4′-diyl]	75	Dimethylacetamide				[65]

TABLE 50.3. *Continued.*

Polymer	$\Delta\alpha$ (A^{**3})	Diluent	Temp (°C)	v 2	Stress optical coefficient C (10^9 Pa^{-1})	Reference
Poly[(phenylquinoxalinediyl) oxy (phenylquixalinediyl)-1, 4-phenyleneoxy (1,1′-biphenyl)-4,4′-diyloxy-1,4-phenylene]	65	Tetrachloroethane, chloroform				[65]
Poly[imino(1-oxohexamethylene)] a.k.a. [Poly(epsilon-caprolactam)]	63	Sulfuric acid				[65]
Poly[imino-1,4-phenyleneimino-(4,6-dicarboxy-isophthaloylimino)–1,4, phenylene-terephthaloyl]	88	Dimethylacetamide				[65]
Sulfate cellulose, sodium salt D.S. = 0.4	634	Aqueous NaCl 0.2 M				[65]
Sulfate cellulose, sodium salt D.S. = 0.4	645	Aqueous NaCl 0.15 M				[65]
Sulfate cellulose, sodium salt D.S. = 0.4	680	Aqueous NaCl 0.10 M				[65]
Sulfate cellulose, sodium salt D.S. = 0.4	980	Aqueous NaCl 0.01 M				[65]
Sulfate cellulose, sodium salt D.S. = 0.4	1,300	Aqueous NaCl 0.005 M				[65]
Sulfate cellulose, sodium salt D.S. = 0.4	1,750	Aqueous NaCl 0.001 M				[65]

TABLE 50.4. *Optical configuration parameters of copolymers. All values reported are at a wavelength of 6,328 Å.*

Copolymer	$\Delta\alpha(A^3)$	Diluent	Reference
Poly(methyl methacrylate-*co*-*p*-*tert*-butylphenyl methacrylate) 25/75 mol %	− 44	Chlorobenzene	[5]
Poly(methyl methacrylate-*co*-*p*-*tert*-butylphenyl methacrylate) 50/50 mol %	− 30.4	Chlorobenzene	[5]
Poly(methyl methacrylate-*co*-*p*-*tert*-butylphenyl methacrylate) 80/20 mol %	− 7.4	Chlorobenzene	[5]
Poly(methyl methacrylate-*co*-*p*-*tert*-butylphenyl methacrylate) 91/9 mol %	1.5	Chlorobenzene	[5]
Poly(methyl methacrylate-*graft*-styrene) (70–90)/(30–10) mol %	100–1,100	Bromoform	[39]
Poly(methyl methacrylate-*graft*-styrene) 10/90 mol %	700–7,000	Bromoform	[114]
Poly(methyl methacrylate-*graft*-styrene) 87/13 mol %	30	Bromoform	[115]
Poly(*n*-butyl methacrylate-*graft*-styrene) 8/92 mol %	1,190	Bromoform	[115]
Poly[*p*-(4-cetoxybenzoxy)-phenyl methacrylate-*co*-cetyl methacrylate] 15/85 mol %	− 277	Carbon tetrachloride	[116]
Poly[*p*-(4-cetoxybenzoxy)-phenyl methacrylate-*co*-cetyl methacrylate] 22/78 mol %	− 400	Carbon tetrachloride	[116]
Poly[*p*-(4-cetoxybenzoxy)-phenyl methacrylate-*co*-cetyl methacrylate] 39/41 mol %	− 540	Carbon tetrachloride	[116]
Poly[*p*-(4-cetoxybenzoxy)-phenyl methacrylate-*co*-cetyl methacrylate] 4/96 mol %	− 16	Carbon tetrachloride	[116]
Poly[*p*-(4-cetoxybenzoxy)-phenyl methacrylate-*co*-cetyl methacrylate] 60/40 mol %	− 920	Carbon tetrachloride	[116]
Poly[*p*-(4-cetoxybenzoxy)-phenyl methacrylate-*co*-cetyl methacrylate] 8/92 mol %	− 180	Carbon tetrachloride	[116]
Poly[*p*-(4-cetoxybenzoxy)-phenyl methacrylate-*co*-cetyl methacrylate] 81/19 mol %	− 2,000	Carbon tetrachloride	[116]
Poly(phenylbutyl isocyanate-*co*-choral) 50/50 mol %	12	Carbon tetrachloride	[92]
Poly(propylene-*graft*-atactic styrene) 30/70 mol %	22	Chlorobenzene	[117]
Poly(styrene-*block*-propylene), atactic, 64/36 mol %	− 8	Chlorobenzene	[118]

TABLE 50.4. *Continued.*

Copolymer	$\Delta\alpha(A^3)$	Diluent	Reference
Poly(styrene-*co*-chlorostyrene) 39.5/60.5 mol %	− 226	Bromoform	[119]
Poly(styrene-*co*-chlorostyrene) 55/45 mol %	− 202	Bromoform	[119]
Poly(styrene-*co*-chlorostyrene) 68.7/31.3 mol %	− 198	Bromoform	[119]
Poly(styrene-*co*-chlorostyrene) 83.2/16.8 mol %	− 172	Bromoform	[119]
Poly(styrene-*co*-chlorostyrene) 89.7/10.3 mol %	− 165	Bromoform	[119]
Poly(styrene-*co*-methyl methacrylate) 30/70 mol %	− 34	Chlorobenzene	[120]
Poly(styrene-*co*-methyl methacrylate) 50/50 mol %	− 68	Bromobenzene	[120]
Poly(styrene-*co*-methyl methacrylate) 70/30 mol %	− 88	Bromobenzene	[120]
Poly(styrene-*co*-*N*-methylcitraconimide) 48/52 mol %	− 34	Bromoform	[97]
Poly(styrene-*co*-*N*-methylcitraconimide) 54/46 mol %	− 26	Bromoform	[97]
Poly(*tert*-butyl methacrylate-*graft*-styrene) 8/92 mol %	540	Bromoform	[121]
Poly(vinyl chloride-*graft*-styrene) 12.1/87.9 wt%	155	Benzene	[81]
Poly(vinyl chloride-*graft*-styrene) 30.7/69.3 wt%	110	Benzene	[81]
Poly(vinyl chloride-*graft*-styrene) 5.2/94.8 wt%	330	Benzene	[81]
Poly(vinyl chloride-*graft*-styrene) 5.6/94.4 wt%	180	Benzene	[81]
Poly[(imino-1,4-phenyleneimino-terephthaloyl)-*co*-(iminocarbonyl-1,4-phenylene)] (ratio 1/9)	4,380	Sulfuric acid	[65]
Poly{[(4-(hexadecyloxy)-benzoic acid-4-[(2-methyl-1-oxo-2-propenyl)oxy]phenyl ester)]-*co*-cetylmethacrylate} 50/50 mol %	− 680	Carbon tetrachloride	[65]
Poly{[(4-(hexadecyloxy)-benzoic acid-4-[(2-methyl-1-oxo-2-propenyl)oxy]phenyl ester)]-*co*-cetyl methacrylate}-70/30 mol %	− 1,050	Carbon tetrachloride	[65]

REFERENCES

1. D. V. Rosato, *Plastics Encyclopedia and Dictionary*, Hanser, New York, 1993, p. 781.
2. Nunez, Nunez, and Mann eds. *CenBASE/Materials in Print*, Wiley, New York, 1990.
3. J. F. Shackelford and W. Alexander, eds. *CRC Materials Science and Engineering Handbook*, CRC, Boca Raton, 1992, p. 776.
4. H. F. Mark, N. G. Gaylord, and N. M. Bikales, eds. *Encyclopedia of Polymer Science and Technology: Plastics, Resins, Rubbers, Fibers*, Interscience, New York, 1964.
5. J. Brandrup and E. H. Immergut, eds. *Polymer Handbook*, 3rd ed. Wiley, New York, 1989, pp. 451–461.
6. C. L. Mantell, ed. *Engineering Materials Handbook* (McGraw-Hill, New York, 1958), Sec. 33.
7. S. H. Goodman, *Handbook of Thermoset Plastics*, Noyes Park Ridge, NJ, 1986, p. 281.
8. J. Bicerano, *Prediction of Polymer Properties*, Dekker, New York, 1993, pp. 179–197.
9. *Janssen Chimica Catalog*, Janssen, Belgium, 1990.
10. *Aldrich Catalog*, Aldrich Chemical, Milwaukee, WI, 1990.
11. R. Anderson, G. L. Larson, and C. Smith, eds., *Huls Silicon Compounds Register and Review*, Huls, Piscataway, N.J., 1991.
12. C.A. Harper, ed. *Handbook of Plastics and Elastomers*, McGraw-Hill, New York, 1975.
13. C. T. Lynch, ed., *CRC Handbook of Materials Science*, CRC Press, Boca Raton, FL, 1975, Vol. 3.
14. G. M. Kline, *Analytical Chemistry of Polymers*, Interscience, New York, 1962, Part III.
15. E. I. duPont de Nemours and Co., Kapton, Summary of Property Report No. E-50533, 1982.
16. E. I. duPont de Nemours and Co., Preliminary Process Bulletin No. PC-1.
17. D. W. van Krevelen, *Properties of Polymers*, 2nd ed. Elsevier, Amsterdam, 1976.
18. *Engineering Plastics*, Vol.2 of *Engineering Materials Handbook*, ASM International, Metals Park, OH, 1988.
19. G. Allen and J. C. Bevington, *Comprehensive Polymer Science*, Pergamon, Oxford, 1989, p. 639.
20. E. Riande and E. Saiz, *Dipole Moments and Birefringence of Polymers*, Prentice-Hall, New Jersey, 1992, pp. 288–289.
21. E. Saiz, M. P. Tarazona, E. Riande, J. J. Guzman, Polym. Sci. Polym. Phys. Ed. **22**, 2165, 1984.
22. R. Wimberger-Friedl, Rheol. Acta **30**, 329, 1991.
23. E. Riande, J. Guzman, E. Saiz, and M. P. Tarazona, J. Polym. Sci., Polym. Phys. Ed., **23**, 1031, 1985.
24. M. Fukuda, G. L. Wilkes, and R. S. Stein, J. Polym. Sci. A **2**, 1417, 1971.
25. I. Ja. Poddubnyi, E. G. Erenburg, and M. A. Eryomina, Vysokomol. Soedin. **10A**, 1381, 1968.
26. G. V. Vinogradov, A. I. Isayev, D. A. Mustafaev, Y. Y. Podolosky, J. Appl. Polym. Sci. **22**, 665, 1978.
27. E. V. Frisman and A. K. Dadivanyan, J. Polym. Sci. C **16**, 1001, 1967.
28. H. Wilski, Kolloid Z. Z. Polym. **238**, 426, 1970.
29. H. Janeschitz-Kriegl, *Integration of Fundamental Polymer Science and Technology—2*, edited by P. J. Lemstra and L. A. Kleintjens Elsevier Applied Science London, 1988, pp. 405–409.
30. W. Philippoff and E. G. M. Tornqvist, J. Polym. Sci. C **N23**, 881, 1968.
31. T. I. Garmonova, Leningrad Univ. Vestnik, Ser. Fiz. Khim. **22**, 72, 1962.
32. M. H. Liberman, Y. Abe, and P. J. Flory, Macromolecules, **5**, 550, 1972.
33. A. N. Gent and V. V. Vickroy, Jr., J. Polym. Sci. A **2**, 47, 1967.
34. D. W. Saunders, D. R. Lightfoot, and D. A. Parsons, J. Polym. Sci. A **2**, 1183, 1968.
35. A. N. Gent and T. H. Kaun, J. Polym. Sci. A **2**, 927, 1971.
36. H. Janeschitz-Kriegl, *Polymer Melt Rheology and Flow Birefringence*, Springer, Berlin, 1983.
37. M. H. Liberman, L. C. DeBolt, and P. J. Flory, J. Polym. Sci. Polym. Phys. Ed. **12**, 187, 1974.
38. R. S. Stein, F. H. Holmes, and A. V. Tobolsky, J. Polym. Sci. **14**, 443, 1954.
39. P. Gramain, J. Leray, and H. Benoit, J. Polym. Sci. C **16**, 3983, 1968.

40. V. N. Tsvetkov, O. V. Kallistov, E. V. Korneeva, and I. K. Nekrasov, Vysokomol. Soedin. **5**, 1538, 1963.
41. Y. Abe, A. E. Tonelli, and P. J. Flory, Macromolecules **3**, 294, 1970.
42. V. N. Tsvetkov, S. Ya. Ljubina, and T. V. Barskaya, Vysokomol. Soedin. **6**, 806, 1964.
43. W. Kuhn, H. Oswald, and H. Kuhn, Helv. Chim. Acta **36**, 1209, 1953.
44. V. N. Tsvetkov, N. N. Boitsova, and M. G. Vitovskaja, Vysokomol. Soedin. **6**, 297, 1964.
45. V. N. Tsvetkov, L. N. Andreeva, E. V. Korneeva, and P. N. Lavrenko, Dokl. Akad. Nauk. SSSR **205**, 895, 1972.
46. V. N. Tsvetkov, L. N. Andreeva, E. V. Korneeva, P. N. Lavrenkov, N. A. Plate, V. P. Shibaev, and B. S. Petrukhin, Vysokomol. Soedin. **13A**, 2226, 1971.
47. V. N. Tsvetkov, E. V. Korneeva, I. N. Shtennikova, P. N. Lavrenko, G. F. Kolbina, D. Hardi, and K. Nitrai, Vysokomol. Soedin. **14A**, 427, 1972.
48. A. E. Grishchenko and E. P. Vorobjeva, Vysokomol. Soedin. **15A**, 895, 1973.
49. M. Ilavsky, E. Saiz, and E. Riande, J. Polym. Sci. Polym. Phys. Ed. **27**, 743, 1989.
50. A. A. Askadskii, Pure Appl. Chem. **46**, 19, 1976.
51. V. N. Tsvetkov and S. Ja. Ljubina, Vysokomol. Soedin. **1**, 577, 1959.
52. V. N. Tsvetkov, M. G. Vitovskaja, and S. Ja. Ljubina, Vysokomol. Soedin. **4**, 577, 1962.
53. V. N. Tsvetkov and I. N. Shtennikova, Zh. Tekh. Fiz. **29**, 885, 1959.
54. V. N. Tsvetkov and V. E. Bychokova, Vysokomol. Soedin. **6**, 600, 1964.
55. E. N. Zakharova, P. N. Lavrenko, G. A. Formin, and I. I. Konstantinov, Vysokomol. Soedin. **13A**, 1870, 1971.
56. V. N. Tsvetkov, D. Hardi, I. N. Shtennikova, E. V. Korneeva, G. F. Pirogova, and K. Nitral, Vysokomol. Soedin. **11A**, 329, 1969.
57. J. F. Rudd and R. A. Andrews, J. Appl. Phys. **29**, 1421, 1958; **31**, 818, 1960.
58. A. E. Grishchenko and R. I. Esrielev, Vysokomol. Soedin **14A**, 521, 1972.
59. A. E. Grishchenko, M. G. Vitovskaja, V. N. Svetkov, and L. N. Andreeva, Vysokomol. Soedin. **8**, 800, 1966.
60. V. N. Tsvetkov, S. Ya. Ljubina, and K. L. Boleskii, Vysokomol. Soedin. Sb. Karbotsepnie, Soedin. **4**, 26, 1963.
61. V. N. Tsvetkov, S. Ya. Ljubina, and K. L. Boleskii, Vysokomol. Soedin. Sb. Karbotsepnie, Soedin. **4**, 33, 1963.
62. W. Kuhn, O. Kuenzle, and A. Katchalsky, Helv. Chim. Acta **31**, 1994, 1948.
63. V. N. Tsvetkov and N. N. Boitsova, Vysokomol. Soedin. **2**, 1176, 1960.
64. V. N. Tsvetkov, V. E. Eskin, and S. Ya. Frenkel, *Structure of Macromolecules in Solutions*, Nauka, Moskow, 1964.
65. V. N. Tsvetkov, *Rigid-Chain Polymer Molecules*, Nauka, Moskow-Leningrad, 1985.
66. V. N. Tsvetkov, I. N. Shtennikova, E. I. Rjumtsev, G. F. Kolbina, I. I. Konstantinov, Ju. B. Amerik, and B. A. Krentsel, Vysokomol. Soedin. **11A**, 2528, 1969.
67. E. V. Frisman, A. M. Martsinivsky, and N. A. Domnitcheva, Vysokomol. Soedin. **2**, 1148, 1960.
68. H. Lamble and E. S. Dahmouch, Br. J. Appl. Phys. **9**, 388, 1958.
69. V. N. Tsvetkov, V. E. Bychokova, S. M. Savvon, and I. K. Nekrasov, Vysokomol. Soedin. **1**, 1407, 1959.
70. L. N. Andreeva, E. V. Beliaeva, A. A. Boikov, P. N. Lavrenko, and V. N. Tsvetkov, Vysokomol. Soedin. **25A**, 1631, 1983.
71. V. N. Tsvetkov and N. N. Boitsova, Vysokomol. Soedin. **5**, 1263, 1963.
72. V. N. Tsvetkov, S. Ya. Ljubina, V. E. Bychkova, and I. A. Strelina, Vysokomol. Soedin. **8**, 846, 1966.
73. I. N. Shtennikova, E. V. Korneeva, V. E. Bychokova, I. A. Strelina, and G. S. Sogomonyants, Vysokomol. Soedin. **14B**, 118, 1972.
74. S. Ja. Ljubina, I. A. Strelina, G. S. Sogomonyants, S. I. Dmitrieva, O. Z. Korotkina, G. V. Tarasova, V. S. Skazka, and V. M. Jamshchikov, Vysokomol. Soedin **12A**, 1560, 1970.
75. S. Ya. Lyubina, I. A. Strelina, V. S. Skazka, G. V. Tarasova, and V. M. Jamshchikov, Vysokomol. Soedin. **14A**, 1371, 1972.
76. V. N. Tsvetkov and S. Ja. Magarik, Dokl. Akad. Nauk SSSR **127**, 840, 1959.
77. E. V. Frisman and A. B. Chzu, Vysokomol. Soedin. **4**, 1564, 1962.
78. V. N. Tsvetkov, A. E. Grishchenko, L. E. De-Millo, and E. N. Rostovskii, Vysokomol. Soedin. **6**, 384, 1964.
79. E. V. Frisman and V. A. Andreichenko, Vysokomol. Soedin. **4**, 1559, 1962.
80. E. Riande, E. Saiz, and J. E. Mark, J. Polym. Sci. Polym. Phys. Ed. **22**, 863, 1984.
81. S. P. Micengendler, K. I. Sokolova, G. A. Andreeva, A. A. Korotkov, T. Kadirov, S. I. Klenin, and S. Ja. Magarik, Vysokomol. Soedin. **9A**, 1133, 1967.
82. V. N. Tsvetkov, E. N. Zakharova, G. A. Fomin, and P. N. Lavrenko, Vysokomol. Soedin. **14A**, 1956, 1972.
83. V. N. Tsvetkov, M. G. Vitovskaja, P. N. Lavrenko, E. N. Zakharova, I. F. Gavrilenko, and N. N. Stefanovskaja, Vysokomol. Soedin. **13A**, 2532, 1971.
84. V. S. Skazka, G. A. Fomin, G. V. Tarasova, I. G. Kirillova, V. M. Jamshchikov, A. E. Gryshchenko, and I. A. Alekseeva, Vysokomol. Soedin. **15A**, 2561, 1973.
85. V. N. Tsvetkov and S. Ja. Magarik, Dokl. Acad. Nauk. SSSR **115**, 911, 1957.
86. V. N. Tsvetkov, T. I. Garmonova, and R. P. Stankevitch, Vysokomol. Soedin. **8**, 980, 1966.
87. A. L. Andrady, M. A. Llorente, and E. Saiz, J. Polym. Sci. Polym. Phys. Ed. **25**, 1935, 1987.
88. T. I. Garmonova, M. G. Vitovskaja, P. N. Lavrenko, V. N. Tsvetkov, and E. V. Korovina, Vysokomol. Soedin. **13**, 884, 1971.
89. S. M. Savvon and K. K. Turoverov, Vysokomol. Soedin. **6**, 205, 1964.
90. V. N. Tsvetkov, L. N. Andreeva, P. N. Lavrenko, E. V. Baleiva, O. V. Okatova, A. Yu. Bilibin, and S. S. Skorokhodov, Eur. Polym. J. **20**, 817, 1984.
91. V. N. Tsvetkov, L. N. Andreeva, P. N. Lavrenko, O. V. Okatova, E. V. Baleiva, A. Yu. Bilibin, and S. S. Skorokhodov, Eur. Polym. J. **21**, 933, 1985.
92. V. N. Tsvetkov, I. N. Shtennikova, E. I. Rjumtsev, and Ju. P. Getmanchuk, Eur. Polym. J. **1**, 767, 1971.
93. V. N. Tsvetkov, I. N. Shtennikova, V. S. Skazka, and E. I. Rjumtsev, J. Polym. Sci. C **16**, 3205, 1968.
94. V. N. Tsvetkov, E. V. Frisman, and N. N. Boitsova, Vysokomol. Soedin. **2**, 1001, 1960.
95. V. N. Tsvetkov, K. A. Andrianov, E. L. Vinogradov, S. E. Yakushkina, and Ts. V. Vardasanidse, Vysokomol. Soedin. **9B**, 893, 1967.
96. V. N. Tsvetkov, K. A. Andrianov, E. L. Vinogradov, V. I. Pakhomov, and S. E. Yakushkina, Vysokomol. Soedin. **9A**, 1967.
97. M. G. Vitovskaja, V. N. Tsvetkov, L. I. Godunova, and T. V. Sheremeteva, Vysokomol. Soedin. **9A**, 1682, 1967.
98. T. I. Garmonova, M. G. Vitoskaja, S. V. Bushin, and T. V. Sheremeteva, Vysomokol. Soedin. **16A**, 265, 1974.
99. V. N. Tsvetkov, N. N. Kupriyanova, G. V. Tarasova, P. N. Lavrenko, and I. I. Migunova, Vysomokol. Soedin. **12A**, 1974, 1970.
100. V. N. Tsvetkov, E. I. Rjumtsev, I. N. Shtennikova, T. V. Peker, and N. V. Tsetkova, Dokl. Akad. Nauk. SSSR **207**, 1173, 1972.
101. E. N. Zakharova, L. I. Kutsenko, V. N. Tsvetkov, V. S. Skakza, G. V. Tarasova, and V. M. Jamshchikov, Leningrad Univ. Vestnik, Ser. Fiz. Khim. **N16**, 55, 1970.
102. G. I. Okhmenko, Thesis, Inst. Macromolecular Compounds Acad. Sci. SSSR, Leningrad, 1969.
103. H. Janetchitz-Kriegl and W. Burhard, Adv. Polym. Sci. **6**, 170, 1969.
104. V. N. Tsvetkov, S. Ja. Ljubina, I. A. Strelina, S. I. Klenin, and V. I. Kurljankina, Vysomokol. Soedin. **15A**, 691, 1973.
105. V. N. Tsvetkov and A. E. Grishchenko, J. Polym. Sci. C **6**, 3195, 1968.
106. V. N. Tsvetkov and I. N. Shtennikova, Vysomokol. Soedin. **2**, 808, 1960.
107. V. N. Tsvetkov and A. V. Grishchenko, Polym. Sci. USSR **7**, 902, 1965; J. Polym. Sci. C **16**, 3195, 1968.
108. N. J. Mills and D. W. Saunders, J. Macromol. Sci. B. **2**, 369, 1968.
109. N. J. Mills, Polymer **12**, 658, 1971.
110. M. A. Llorente, J. E. Mark, and E. Saiz, J. Polym. Sci. Polym. Phys. Ed. **21**, 1173, 1983.
111. E. Riande, J. Guzman, and J. G. de la Campa, Macromolecules **21**, 2128, 1988.
112. S. Ja. Magarik and V. N. Tsvetkov, Zh. Fiz. Khim. **33**, 835, 1959.
113. M. Llorente, I. Fernandez de Pierola, and E. Saiz, Macromolecules **18**, 2663, 1985.

114. V. N. Tsvetkov, S. Ja. Magarik, T. Kadirov, and G. A. Andreeva, Vysokomol. Soedin. **10A**, 943, 1968.
115. V. N. Tsvetkov, G. A. Andreeva, I. A. Branovskaja, V. E. Eskin, S. I. Klenin, and S. Ja. Magarik, J. Polym. Sci. C **6**, 239, 1967.
116. V. N. Tsvetkov, E. I. Rjumtsev, I. N. Shtennikova, E. V. Korneeva, Okhrimenko, N. A. Mikhailova, A. A. Baturin, Ju. A. Amerik, and B. A. Krentsel, Vysokomol. Soedin. **15A**, 2570, 1973.
117. V. N. Tsvetkov, E. I. Rjumtsev, I. N. Shtennikova, E. V. Korneeva, Okhrimenko, N. A. Mikhailova, A. A. Baturin, Ju. A. Amerik, and B. A. Krentsel, Vysokomol. Soedin. **15A**, 2570, 1973.
118. A. Romanov, S. Ja. Magarik, and M. Lazar, Vysokomol. Soedin. **9B**, 292, 1967.
119. T. M. Birshtein, V. P. Budtov, E. V. Frisman, and N. K. Janoskaja, Vysokomol. Soedin. **4**, 455, 1962.
120. E. V. Frisman and N. N. Boitsova, Leningrad Univ. Vestnik. **N4**, 26, 1959.
121. V. N. Tsvetkov, G. A. Andreeva, I. A. Branovskaja, V. E. Eskin, S. I. Klenin, and S. Ja. Magarik, J. Polym. Sci. C **16**, 239, 1967.

CHAPTER 51

Ultraviolet Radiation and Polymers

Anthony L. Andrady

Camille Dreyfus Laboratory, Research Triangle Institute, Research Triangle Park, NC 27709

The energies associated with near-ultraviolet radiation quanta are about 3.0–4.3 eV which correspond to 72–97 kcal/mol. Common covalent bonds encountered in polymers have bond dissociation energies which for the most part are either lower or within this energy range. Provided the ultraviolet radiation is absorbed by the polymer and suitable pathways are available for the photoexcited singlet (S) and triplet (T) species to transfer the absorbed energy to cause photochemical reactions, light-induced damage to the polymer can take place. In most systems a variety of competing photophysical processes, such as phosphorescence (from ($T_1 \rightarrow S_0$) transition) or fluorescence (from ($S_1 \rightarrow S_0$) transition), may preclude chemical reaction. When photochemical reactions of polymers do take place, they tend to involve the triplet excited states of molecules rather than the ground or singlet stage species because of the relatively longer lifetime of the former. The lowest excited triplet state, T_1, is formed by radiationless intersystem crossing from the lowest excited singlet state, S_1. Higher triplet states can form only from a triplet-triplet absorption where a molecule in the T_1 state absorbs a photon.

When photochemical pathways are available, they often involve sequences of chemical reactions with specific energy requirements. The number of photochemical degradative pathways available to polymers is quite extensive.

As the photon energy is a function of the wavelength of radiation, it is reasonable to expect the high energy, short wavelength ultraviolet radiation to be more effective than visible light in promoting a wider range of these reactions. This is found to be the case; for instance, solar UV-B range (extending from about 290 nm to 315 nm) is well known to be the most deleterious wavelengths to polymers exposed to sunlight.

Absorption of electromagnetic radiation is a necessary prerequisite for photodegradation; Table 51.1 summarizes the ultraviolet cut-off wavelength and relative stability of commodity polymers and biopolymers. Polymers such as polyolefins, which theoretically should be transparent to ultraviolet (UV) light, nevertheless do absorb UV radiation due to the presence of impurities from several sources. In most practical applications, the compounding ingredients in the formulation and the processing operation itself yield sufficient chromophores to allow these polymers to absorb UV radiation and therefore to undergo photodegradation.

Also included in Table 51.1 is data on spectral sensitivity of common polymers. Wavelength sensitivity of a given photodegradation process can be measured experimentally using either monochromatic radiation or a specific source such as a white light source. In the former technique, the change in a specific property (such as yellowness or absorbance at a selected wavelength) per unit available photon is obtained. When a specific light source is used, samples of the polymer are exposed behind a series of cut-on filters. Each cut-on filter allows only the fraction of light having a wavelength longer than the cut-on value to reach the sample. Samples exposed to the same source behind different cut-on filters therefore photodegrade at different rates and sometimes even via different mechanisms. A comparison of the changes in a selected property of the samples exposed behind different filters allows the identification of the approximate spectral region which causes the most damage. This range is both source-dependent and damage-dependent. The data in Table 51.1 pertain to white light spectrum from borosilicate-filtered xenon source radiation, which is similar to direct solar radiation at unit air mass. However, the spectral sensitivity depends on the property or mode of damage used in its determination and also on compounding

TABLE 51.1. *Absorption of UV-visible radiation by common synthetic and natural polymers.*

Polymer	Cut-off [nm][a]	Abs.max. [nm]	Stability[b]	Ref.[c]	Spectral sensitivity	
					Range [nm]	Property
Polyethylene	<180		4		260–360	Optical density
Polypropylene	<180		5		315–330	Extensibility
Polyoxymethylene	<210		4		—	
Poly(vinyl chloride)	<240		4		310–325	Yellowing
Polyamides	~240		3			
Polystyrene	~270		4		280	Chain scission
Polycarbonate	~280		4		310–340	Yellowing
Poly(phenyleneoxide)	~280		3			
Polyurethanes	~280		3			
Poly(ethylene terephthalate)	~310		2			
Poly(vinyl acetate)		240		[3]		
Poly(methylmethacrylate)	~240		1		300[e]	Chain scission
Poly(methyl vinyl ketone)		~290		[3]		
Poly(phenyl vinyl ketone)		240		[3]		
Cellulose		270[d]	4	[4]		
Lignin-softwood		280–285[d]	5	[5]	334–354	Yellowing
-hardwood		274–276[d]		[5]		
Wool		205, 280	3	[6]	340–420	Yellowing
Chitosan (acetylglucosamine)		193, 197	4	[7]		

[a]Cut-off wavelength indicated is that at which absorbance of a 10-micron film reaches 1.0.
[b]Stability is a relative, qualitative measure of the resistance of the polymer to terrestrial solar radiation.
[c]Data from [1] where not otherwise indicated. Data on spectral sensitivity are from [2]. Absorption maxima indicated in column 3, are for solution spectra.
[d]Biopolymers shown absorb very strongly at wavelengths shorter than the absorption maximum indicated.
[e]Based on quantum yield measurements.

ingredients in the polymer sample used. Therefore, the spectral sensitivity data in Table 51.1 are specific to the formulation and source used in their determination.

Irradiation of a polymer *in vacuo* or in an inert gas can lead to photolysis of the covalent bonds and sometimes subsequent rearrangement of the macroradical. However, in practical applications, UV-visible irradiation is carried out in air, and oxygen plays a key role in the photodegradation process. It is convenient to discuss the photodegradation process in terms of three stages: initiation, propagation, and termination. Initiation reactions lead to generation of free-radicals on absorption of radiation by polymers which contain a suitable chromophore (either as a part of macro-molecular structure or as an additive or impurity). The mechanism of initiation of even the common polymers, especially the relative significance of hydroperoxides, ketones, charge transfer processes, and singlet oxygen is a controversial topic. Typically, the propagation reactions take place between the polymer radical species and either oxygen or a polymer chain. The macromolecular oxy radicals formed may undergo β scission or other reactions. At a given instant during photodegradation, the polymer substrate would contain a variety of macroradicals which may terminate by bimolecular interaction or unimolecular processes.

The extent of primary photodegradation caused by the absorption of a single photon is a measure of the efficiency of the photoprocess. With most photodegradation processes, the photoproducts formed during controlled exposure of the polymer to UV radiation can be accurately determined. The chain scission and/or crosslinking in the irradiated samples can also be estimated from physical techniques (such as gel permeation chromatography, or solution viscosity). Reliable quantum yields for different products can therefore be calculated. Some typical quantum yields for photodegradative processes of common polymers are given in Table 51.2.

The photochemical initiation process is of particular interest from a mechanistic as well as a practical point of view. A better understanding of initiation allows the selection of polymers which are inherently photostable under a given exposure scenario, and also helps in the design of new light stabilizers. However, even for commodity thermoplastics, the initiation process is not fully understood. The complexity of the photoinitiation process is due to the many competing reactions involved. In polypropylene for instance, photolysis of hydroperoxides and peroxides yield radical species with a quantum yield of about 2. While this is likely to be a key initiation route, oxidation products such as carbonyles and unsaturated groups, as well as charge transfer complexes and catalyst residues, are believed to be involved in the photoinitiation process. With most common polymers, the key species contributing to the initiation

TABLE 51.2. *Quantum yields for product formation in common polymers.*

Polymer	Process	Quantum yield (mol/Einstein) In air or O_2	Quantum yield (mol/Einstein) In N_2 or Vacuo	λ [nm]	Reference
Poly(vinyl chloride)					
	HCl evolution	0.015	0.011	254–400	[1]
	Chain scission	0.003	0.003		
	Crosslinking	0.0006	0.0014		
	Carbonyl formation	0.005	—		
	HCl evolution	0.009	0.005	514.5 (laser)	[8]
Poly(vinyl acetate)					
	Acetic Acid formation	0.01	—	254	[9]
	CO_2 formation	0.0065			
	CO formation	0.0069			
	Methane formation	0.0038			
	Chain scission	0.05	0.066		[10]
	Crosslinking	0.0025	0.047		
Polystyrene					
	Oxygen absorption (600 torr)	0.027		254	[11]
	Hydroperoxide formation	0.0009			
	Acetophenone formation	0.0006			
	Ketone formation	0.0011			
	Water formation	0.0095			
	Chain scission	0.0056	0.0039	254	[12]
	Crosslinking	0.0004	0.0009		
Poly (ethyleneterephthalate)					
	CO_2 formation	0.0002		254 or 313	[13]
	CO formation	0.0006			
	Crosslinking	0.0006			

process have been reported. While some controversy exists on the relative importance of these, data are summarized in Table 51.3 for common polymers.

51.1 MECHANISMS OF PHOTODEGRADATION

Polymers irradiated in air with solar UV radiation invariably breakdown due to a combination of photodegradative as well as photo-initiated thermo-oxidative mechanisms. Both mechanisms can operate simultaneously or one can be dominant at a given stage of degradation depending on the chemical structure of the substrate polymer. With polymers such as the rigid poly(vinyl chloride) formulations used in building materials the visible damage is primarily a result of photodegradation. The photo-dehydrochlorination of the polymer results in the formation of conjugated double bonds along the chain, and leads to the characteristic

TABLE 51.3. *Techniques commonly used to measure changes in common polymers due to UV irradiation.*[a]

Changes	Property	Technique	Polymer	Reference
Surface degradation	Yellowing	Colorimetry	i) Poly(vinyl chloride)	[14]
			ii) Polycarbonate	[15]
			iii) Polystyrene foam	[16]
	Morphology	Electron microscopy	i) Poly(methyl methacrylate)	[17]
			ii) Polypropylene fiber	[18]
	Wettability	Contact angle	i) Polystyrene and Poly(methylvinylketone)	[19]
			ii) Poly(vinyl chloride) film	[20]
	Appearance	Visual evaluation	i) Chalking of Poly(vinyl chloride)	[21]
Bulk physical change	Mass	Gravimetry	i) Polyoxymethylene	[22]
			ii) Polyethylenes	[23]
	Density	Pycnometry	i) Polyethylene	[24]
	Transport	Gas permeability	i) Polyethylenes (CO_2 and H_2O)	[25]
			ii) Poly(ethyleneterephthalate)	[26]

TABLE 51.3. *Continued.*

Changes	Property	Technique	Polymer	Reference
		Water vapor permeability	i) Polyethylene films	[27]
				[25]
	Crystallinity	x ray analysis	i) (Ethylene - carbon monoxide)[b] copolymer	[28]
		ESCA (x ray photoelectron spectroscopy)		[29]
			ii) Polyethylene	[30]
			iii) Polystyrene	
Thermal properties	Transitions	Calorimetry	i) Polycarbonate, Poly(vinyl chloride), and Polystyrene	[31]
Mechanical properties		Tensile properties	i) Common polymers	[32]
			ii) Polyethylene	[33]
				[34]
			iii) Polypropylene	[35]
				[36]
			iv) Polystyrene	[37]
			v) Poly(vinyl chloride)	[38]
				[39]
			vi) Polyamides	[40]
				[41]
		Flexural properties	i) Polyamides	[42]
		Hardness	i) Polyethylene	[24]
		Tear properties	i) Wool fabric	[43]
Functional groups	Absorption of light energy	UV/Visible spectroscopy	i) Polypropylene	[44]
			ii) Poly(vinyl chloride)	[45]
				[46]
			iii) Polyamide	[44]
		FTIR spectroscopy	i) Polyethylene	[47]
				[48]
				[49]
			ii) Poly(vinyl chloride)	[50]
			iii) Poly(ethyleneterephthalate)	[51]
		Photoacoustic FTIR	i) Polyethylene	[52]
			ii) Ethylene - propylene copolymer	[53]
			iii) Poly(vinyl chloride)	[54]
		NMR spectroscopy	i) Polyethylene	[55]
			ii) Poly(vinyl chloride)	[56]
			iii) Polystyrene	[57]
			iv) Polyisoprene	[58]
		ESR spectroscopy	i) Polyethylene	[59]
			ii) Polypropylene	[60]
			iii) Polystyrene	[61]
			iv) Poly(vinyl chloride)	[62]
	Emission of light energy	Chemiluminescence	i) Polypropylene	[63]
Other properties		Dielectric properties	i) Polyethylene	[64]
			ii) Polystyrene	[65]
Macromolecular changes	Molecular weight	Gel permeation	i) Polyethylene	[49]
		Chromatography	ii) Polystyrene	[66]
	Cross linking	Sol/gel analysis	i) Polyethylene	[67]
			ii) Polystyrene	[61]

[a]Ultraviolet radiation exposure includes both solar ultraviolet exposure encountered in natural and/or accelerated weathering, as well as exposure to UV sources in the laboratory.
[b]ECO - (Ethylene - carbon monoxide ~1%) copolymer.

yellow discoloration of the material. In polyolefins, however, the only contribution of the solar UV radiation is in promoting initiation of the free radical reaction sequence. This occurs via the photolysis of the hydroperoxides and lead to an auto-oxidative reaction sequence. As hydroperoxide dissociation is catalyzed by metal compounds, the photodegradation of polyolefins is enhanced by the presence of transition metal salts.

In yet other polymers, such as with bisphenol polycarbonates both photodegradation and photo-initiated oxidative reactions take place simultaneously. The direct photoreaction is a Frie's rearrangement reaction, while the oxidative reactions result in chain scission and discoloration of the polymer. The chemical pathways involved in the latter process are not well understood.

While outdoor lifetimes of decorative and even some other building materials are limited by the rapidity with which they discolor, the more serious outcome of solar irradiation of polymers is the scission and/or crosslinking of chains that occur during exposure. Some crosslinking leading to the formation of an insoluble gel fraction as well as chain-scission leading to a low molecular weight sol fraction are generally obtained on exposure of common polymers to solar UV wavelengths. Chain scission measured by gel permeation methods or from the reduction in solution viscosity results in drastic irreversible changes in the mechanical properties of the material.

Based on the different pathways for breakdown available the photodegradation behavior can be generally classified as belonging to one of four categories:

1. Photodegradation with no significant chain scission

   Dehydrochlorination of poly(vinyl chloride) and photFrie's reaction in polycarbonates.

2. Photodegradation with significant chain scission.

   Photodegradation of ethylene–carbon monoxide copolymers by Norrish reactions.

3. Photoinitiated oxidation with significant chain scission

   Autoxidation of polyisoprene, and thermoplastic polyolefins.

4. Photoinitiated oxidation with no significant chain scission

   Hydroperoxidation of unsaturated side chains with singlet oxygen in EPDM

The above discussion pertains mostly to the pure polymer; most, polymers used in practical applications, especially those used outdoors tend to be compounded with a variety of additives. Some of these such as opacifiers, UV absorbers, and light stabilizers are intentionally added to the compound to control photodegradation and related oxidation reactions, to extend the outdoor lifetime of the material. Others such as fillers, reinforcing agents, lubricants, and flame retardants are added to improve unrelated properties of the material. These, however, can very significantly impact the photostability of the polymer. Any change in copolymer composition or the presence of a second polymer can similarly alter the photodegradability of the mix.

Blending methyl methacrylate-butadiene–styrene copolymer with poly(vinyl chloride) for instance was shown to decelerate the dehydrochlorination (leading to discoloration). The gel content, surface energy, and the spectroscopic characteristics of the blend was altered by the presence of the second polymer [158]. In ethylene–propylene–diene rubber EPDM where the third monomer is ethylene-2-norbornene (NB), the photo-oxidation rate as measured by the accumulation of typical products such as hydroperoxides, varied linearly with the NB content [159]. The same held true for peroxide-crosslinked compounds of the same EPDM except that the linear relationship was found between the relative carbonyl absorbance on photoxidation and the amount of peroxide used to crosslink the material [160]. Additives can also have a similar effect; decabromodiphenyl ether flame retardant in polypropylene was shown to enhance oxidation. Furthermore, where hindered-amine light stabilizers HALS were present in the compound, the degradation product HBr reacted with it to form the ammonium salt that has no photostabilizer effectiveness [161].

The direct and indirect effects of fillers on the photostability of polymer compositions are well known. With the recent interest in nanopowdered fillers reports of their effectiveness as photostabilizers is beginning to be reported in the literature. For instance ZnO and TiO_2 nanoparticles (primary particle size 25–70 nm) were studied in acrylic coatings. A layer that carried at least 5 weight percent of the nanoparticles was needed to shield the underlying layers from UV exposure and hence degradation [162]. Nanoscale titania was also evaluated as a stabilizer in epoxy coatings [163].

51.2 EFFECTS OF SOLAR UV INDUCED DEGRADATION

Photochemical changes in the polymer invariably affect the physical, chemical, and mechanical properties of the material. These changes are often used to quantify the photodegradation process. As the changes in different properties are brought about by different light-induced processes, the rates at which they change on exposure to radiation may differ. Understandably, most studies have concentrated on those polymer characteristics of either fundamental importance (such as changes in average molecular weights) or those of practical relevance (such as surface discoloration). The consequences of photodegradation, which are of relevance to applications of polymers, include discoloration of the surface, surface damage such as cracking or chalking, loss of integrity as evidenced by reduced

TABLE 51.4. *Initiating species in photodegradation of common polymers.*

Polymer	Potential initiating species	Reference
Polyethylene[a]	-O-O- -OOH -C=O groups C=C groups from processing or from oxidation. Pigments (titania), and metal catalyst residues. Charge transfer complexes with O_2.	[75–84]
Polypropylene[b]	Tertiary -OOH -O-O- groups from processing or from oxidation. In-chain and terminal -C=O groups. Catalyst residues. Charge-transfer complex with O_2.	[76,80,82, 85–87]
Poly(vinyl chloride)[c]	Unsaturated centers, specially $\sim CH_2$-CH=*CH-CH$_2$Cl* and $\sim$ CHCl-CH=CH-CH_2 $\sim$. $\sim$CHCl-CO=CHCl$\sim$ or side group carbonyl functionalities. α,β-unsaturated ketones $\sim$CH=CH-CO$\sim$. Photolysis of -OOH and -O-O- groups from processing or from oxidation. Structural defects, pigments, and plasticizers.	[88–94]
Polystyrene	Direct photoexcitation/photoxidation of phenyl rings. Charge-transfer complex with oxygen. -C=O and -OOH groups from processing or from oxidation. Interactions with singlet oxygen.	[32,95–101]
Polymethacrylates	-C=O groups via Norrish I reactions. Direct photolysis of ester or methyl side groups. Photolysis of -O-O- groups from processing or from oxidation.	[102–107]
Polycarbonates	-O-C=O group in the main chain. Photo-Fries rearrangement.	[108, 109]
Aromatic Polyester (thermoplastic)	Light absorption by ester functionality, followed by main chain or side group scission. Norrish I and II reactions.	[110–113]
Polyamides	α,β -unsaturated carbonyl group impurities. Photolysis of OOH groups. H-bonding - mediated photoreactions of CONH group. Photolysis of C-N bond in main chain.	[90,114–117]

[a]Polyethylene and (ethylene-carbon monoxide) copolymer: Carbonyl photolysis in the early stages of photooxidation is via Norrish II process which occurs with a quantum efficiency $\phi. = 0.067$ in the presence or absence of oxygen [68,69]. Norrish I process can occur at a lower efficiency ($\phi. = 0.01$) but does not yield radicals [69]. Carbonyl moieties may also yield radicals by a primary process; intermolecular hydrogen - abstraction from polymer chains [70,71]. Photolysis of hydroperoxides is a key initiation pathway in early photodegradation of polythylenes; in spite of their low absorbance, the quantum yield of radicals is high ($\phi. = 1$) [70]. Hydroperoxides produced in thermal processing is believed to be the most important initiating species, followed by carbonyl groups, and then the charge transfer complexes with oxygen [68].

[b]Polypropylene: Initiation process in polypropylene (and in polyolefins in general) is still controversial. While many possible initiating species have been identified, the relative importance of these is as yet unresolved. In the case of polypropylene Carlsson [70] ranked the candidate species in the following decreasing order of importance; peroxides, titanium catalyst residues, polynuclear aromatic pollutants, carbonyl compounds, and charge-transfer complexes with oxygen. Singlet oxygen and polynuclear aromatic compounds (PNA) [72], have also been proposed as possible initiators of photodegradation and photooxidative degradation in polyolefins. Water, oxygen, and compounding ingredients commonly present in polyolefins can readily react with singlet oxygen, making it unavailable for slower-reacting unsaturated centers in the polymer. PNAs are not present in the polymer but sorbed from air where the compounds may exist as pollutants.

[c]Poly(vinyl chloride): Unsaturated centers (generally 1–3 per 1000 repeat units) are believed to be the most important initiating species [73]. Conjugated polyene sequences in the polymer have very high extinction coefficients in the UV. Depending on the initial concentration in the polymer, carbonyl groups are the next important initiator. Not only can these undergo Norrish reactions, but excited carbonyl groups can also transfer energy to unsaturated centers [74]. Hydroperoxides and peroxides formed during autooxidation of the polymer also contributes to initiation process. Photolysis of hydroperoxide yields alkoxy radicals with a quantum yield of about unity [18].

TABLE 51.5. *Consequences of exposure of polymers to ultraviolet radiation.*

Polymer	Degradation	Mechanism	Published data	Reference
Polyethylene	a) Product yield	Basic autoxidation scheme and secondary oxidations of products.	Percentages of major products formed.	[118–121]
			Same for (ethylene-ketone) copolymers.	
	b) Carbonyl group formation	Photo-reactions of hydroperoxide.	Empirical equations for [C═O] build-up in natural and artificial exposures.	[48,49,122]
			Change in [C═O] on irradiation for LDPE including those of different crystallinity.	[61,123]
	c) Change in tensile properties	Chain scission and crosslinking.	Correlation between the extensibility and [C═O] of films.	[34,79,118]
	d) Change in hardness	Chain scission and crosslinking reactions.	Correlation between Vicker's Hardness and [C═O].	[24]
	e) Decrease in average molecular weight	Chain scission reactions.	GPC data correlated with extensibility of weathered LDPE films.	[49]
	f) Gel formation	Crosslinking reactions.	Gel formation in LDPE.	[118,124]
	g) Other properties		Change in density and dynamic modulus.	[125]
Polypropylene	a) Product yield	Same as for polyethylene.	Product yield as a function of the atactic content.	[126–128]
			FTIR study of products.	
	b) Carbonyl group formation	Same as for polyethylene.	Data for samples of different tacticity.	[48,129]
	c) Change in hardness	Chain scission and crosslinking reactions.	Changes in brittleness, tensile properties, and FTIR, on irradiation. Surface changes.	[126,130]
Poly(vinyl chloride), (PVC)	a) HCl yield	Photodehydrochlorination yielding conjugated polyenes.	a) Kinetics of HCl evolution $E_a = 14\,\mathrm{KJ/mol}$.	[131–133]
			b) For exposure of film to $\lambda > 254\,nm$.	
			c) Rate is unaffected by light intensity. At 20–90°C, in N_2, $E_a = 8.3\,\mathrm{KJ/mol}$.	
			d) Effect of radiation wavelength.	
	b) Carbonyl and hydroperoxide yield	Photooxidation reactions.	The E_a for carbonyl build-up for photo-oxidation in O_2, $E_a = 21\,\mathrm{KJ/mol}$.	[118,134,135]
			Spectroscopic study of [C═O] and [ROOH] for PVC film. Effect of tacticity.	
	c) Gel formation	Crosslinking.	For crosslinking of PVC film, $E_a = 1.4 \times 10^{-3}$ (air) and $3.1 \times 10^{-3}\,\mathrm{KJ/mole}(N_2)$.	[136]
	d) Discoloration	Yellowing due to formation of conjugated polyene sequences.	Yellowing of extruded PVC compounds.	[14,129,138]
			Photobleaching of PVC yellowness at $\lambda > 514\,\mathrm{nm}$.	
	e) Decrease in average molecular weight	Oxidative chain-scission.	Change in molecular weight distribution during weathering.	[132,139,140]
			For chain scission, $E_a = 1.7 \times 10^{-4}\,\mathrm{KJ/mole}$.	
			Correlation between chain scission and [C═O].	

TABLE 51.5. *Continued.*

Polymer	Degradation	Mechanism	Published data	Reference
	f) Change in tensile properties	Chain scission and crosslinking.	Linear dependence of tensile strength on reciprocal molecular weight.	[141]
Polystyrene	a) Discoloration	Yellowing due to formation of unidentified chromophores.	Yellowing on exposure to solar UV radiation and to a filtered - xenon source radiation.	[142–144]
	b) Carbonyl and/or hydroperoxide yield	Photo-oxidation reactions.	[C═O] as a function of irradiation time at different temperatures.	[61,145]
	c) Decrease in molecular weight	Oxidative chain scission.	Random scission on photolysis in solution. Changes in molecular weight at different depths.	[12,146–147]
	d) Gel formation	Crosslinking.	Gel formation on irradiation in air at different temperatures.	[12,61,143]
Polymethacrylate	a) Decrease in average molecular weight	Oxidative chain scission.	Reduction in average molecular weight (depending on residual monomer concentration), on exposure to a filtered xenon source.	[148]
Polycarbonate	a) Discoloration	Yellowing due to photo-fries and oxidative processes.	Yellowing on exposure to solar UV radiation.	[15,149–152]
	b) Decrease in average molecular weight	Oxidative chain scission.	Change in molecular weight due to photo-degradation.	[149,153]
	c) Change in tensile properties	Chain scission and crosslinking.	Change in extensibility with exposure time in natural weathering.	[149]
Polyester (Polyethylene terephthalate)	a) Product yield	Photooxidative reactions and direct cleavage via Norrish reactions:	Quantum yields, ϕ., for CO, CO_2, -OH and -COOH products fored on photolysis of PE.	[110,154] [166]
Polyamide	a) Change in mechanical properties	Chain scission and crosslinking.	Changes in tenacity, yield strength and flexural strength of nylons on exposure to solar UV and to xenon source.	[42,155]
	b) Changes in average molecular weight	Oxidative chain scission.	Change in molecular weight on exposure to a filtered-xenon source, at different pH values.	[156]

strength or extensibility, changes in impact strength of the polymer, and changes in physical properties such as solubility. A large fraction of the reported literature is devoted to effects of solar UV radiation on polymers. With the practical lifetimes of polymers used outdoors being routinely determined by photodegradation rates, this interest in solar UV-B is not surprising. With recent observations of global stratospheric ozone depletion and the concomitant increase in UV-B fractions in the terrestrial solar spectrum, there is renewed interest in weatherability and stabilization of polymers used in outdoor applications.

A wide range of analytical approaches is available to study the effects of UV exposure on polymers. Table 51.4 summarizes the more common of these techniques and illustrates their use with selected examples. Table 51.5 attempts to summarize some of the published data on various effects of UV exposure on common polymers. Typical data are cited to illustrate the main types of physical and chemical changes obtained with different polymers. Data include those pertaining to exposure to solar radiation (solar UV-B effects), exposure to laboratory-filtered xenon sources or other UV-visible sources, and exposure to monochromatic UV wavelengths. Table 51.5 is not intended to be a comprehensive review but a set of selected examples to indicate the diversity of changes brought about by exposure to UV radiation.

EPDM rubber	Carbonyl absorption	Oxidative chain scission	Effect of crosslinking	[158]
Epoxy resin	(a) Indentation for hardness (b) Spectroscopy (ATR-FTIR)			
	(c) Differential scanning calorimetry	Chain scission	Presence of nanofiller $_{TiO2}$ in the compound improved photostability	[163]
Polyurethane acrylate	(a) FTIR spectroscopy	Urethane linkage was found to be most susceptible	Weathering resistance of the coating was established	[164]
Softwood and hardwood pulps	(a) Brightness measurements	Yellowing and brightness changes	Effectiveness of stabilizers against brightness reversion established	[165]

REFERENCES

1. D. J. Carlsson and D. M. Wiles, in *Encyclopedia of Polymer Science and Engineering*, Vol. 4, edited by H. F. Mark, N. M. Bikales, C. G. Overberger, and G. Menges (John Wiley & Sons, New York, 1986a), p. 665.
2. A. L. Andrady, M. B. Amin, S. H. Hamid *et al*., in *Environmental Effects Panel Report. 1991 Update* (United Nations Environmental Program, Nov. 1991b), p. 45.
3. W. Schnabel, in *Polymer Degradation. Principles and Practical Applications* (Hanser Publishers, 1981), p. 98.
4. N. S. Hon, J. Polymer Sci., A1 **13**, 1347 (1975).
5. A. Sakakibara, in *Wood and Cellulosic Chemistry*, edited by D. N.-S. Hon, and N. Shiraishi (Marcel Dekker, New York, 1991), p. 114.
6. F. G. Lennox, M. G. King, I. H. Leaver *et al*., Appl. Polym. Symp., No. **18**, 353 (1971).
7. R. A. A. Muzzarelli and R. Rocchetti, *Chitin in Nature and Technology*, edited by R. Muzzarelli, C. Jeuniaux, and G. W. Gooday (Plenum Press, New York, 1986), p. 385.
8. C. Decker and M. Balandier, J. Photochem. **15**, 213 (1981b).
9. G. Geuskens, M. Borsu, and C. David, Europ. Polym. J. **8**, 883 (1972); *ibid*. 1347 (1972).
10. D. David, M. Borsu, and G. Gueskins, Eur. Polym. J. **6**, 959 (1970).
11. G. Gueskins, G. Delaunois, D. Baeyens-Volant *et al*., Eur. Polym. J. **14**, 291 (1978).
12. C. David, D. Baeyens-Volant, G. Delaunois *et al*., Europ. Polym. J. **14**, 501 (1978).
13. F. B. Marcotte, D. Campbell, J. A. Cleaveland *et al*., J. Polymer Sci., A1 **5**, 481 (1967).
14. A. L. Andrady and N. D. Searle, J. Appl. Polym. Sci. **37**, 2789 (1989).
15. A. L. Andrady, N. D. Searle, L. F. E. Crewdson, Polym. Deg. Stab. **35**, 235–247 (1992).
16. A. L. Andrady, K. Fueki, and A. Torikai, J. Polym. Sci. **42**, 2105 (1991).
17. A. Blaga and R. S. Yamasaki, Durability Building Mater. **4**, 21 (1986).
18. D. J. Carlsson and D. M. Wiles, in *Ultraviolet Light Induced Reactions in Polymers*, ACS Symposium Ser. 25 (American Chemical Society, Washington DC, 1976), p. 321.
19. K. Esumi, K. Meguro, A. M. Schwartz *et al*., Bull. Chem. Soc. Jpn. **55**, 1649 (1982).
20. R. B. Fox and T. R. Price, J. Polym. Sci. A1 **3**, 2303 (1965).
21. W. V. Titow, in *PVC Technology* (Elsevier Applied Science Publishers, New York, 1984), p. 473.
22. A. Davis, Polym. Deg. Stab. **3**, 187 (1981).
23. J. H. Cornell, A. M. Kaplan, and M. R. Rogers, J. Appl. Polym. Sci. **29**, 2581 (1984).
24. Y. Watanabe and T. Shirota, Kenkyu Hokoku Kogyo Gijutsuin **2**, 141 (1981).
25. A. L. Andrady, J. E. Pegram, and S. Nakatsuka, J. Environ. Polym. Degradn. **0**, 00 (1994).
26. P. Mercea, T. Virag, D. Silipas *et al*., Polym. Comm. **28**, 31 (1987).
27. S. G. Croll, Prog. Org. Coat. **15**, 223 (1987).
28. R. Gooden, D. D. Davis, M. Y. Hellman *et al*., Macromolecules **21**, 1212 (1988).
29. A. Dilks, J. Polym. Sci., A1 **19**, 1319 (1981).
30. D. T. Clark and H. S. Munro, Polym. Deg. Stab. **8**, 195 (1984); **8**, 213 (1984).
31. M. M. Quayyum and J. R. White, Arabian Journal for Science and Engineering **13**, 547 (1988).
32. G. Geuskens, G. Delaunois, Q. Lu-Vinh *et al*., Eur. Polym. J. **18**, 387 (1982).
33. A. Torikai, H. Shirakawa, S. Nagaya *et al*., J. Appl. Polym. Sci. **40**, 1637 (1990).
34. A. L. Andrady, J. E. Pegram, and S. Nakatsuka, J. Environ. Polym. Degradn. **1**, 31 (1993).
35. C. S. Schollenberg and H. D. F. Meijer, Polymer **32**, 438 (1991).
36. M. Raab, L. Kotulak, J. Kolarik *et al*., J. Appl. Polym. Sci. **27**, 2457 (1982).
37. G. Geuskens, P. Bastin, Q. Lu-Vinh *et al*., Polym. Deg. Stab. **3**, 295 (1980).
38. G. Scott and M. Tahan, Europ. Polym. J. **13**, 997 (1977).
39. A. Kaminska and H. Kaczmarek, Angew. Makromol. Chem. **139**, 63 (1986); **144**, 139 (1986).
40. G. A. George and M. S. O'Shea, Polym. Deg. Stab. **28**, 289 (1990).
41. Y. W. Mai and B. Cotterell, J. Appl. Polym. Sci. **27**, 4885 (1982).
42. A. Davis and D. Sims, in *Weathering of Polymers* (Applied Science Publishers, London, 1983), p. 139.
43. C. M. Carr and I. H. Leaver, J. Appl. Polym. Sci. **33**, 2087 (1987).
44. N. S. Allen, Polym. Deg. Stab. **6**, 193 (1984); N. S. Allen, Polym. Deg. Stab. **8**, 55 (1984).
45. C. Decker, J. Appl. Polym. Sci. **28**, 97 (1983).
46. R. Sastre, G. Martinez, F. Castllo *et al*., Makromol. Chem. Rapid Commun. **5**, 541 (1984).
47. J. Lacoste, R. Arnaud, and J. Lemaire, J. Appl. Polym. Sci. A-1 **22**, 3855 (1984).
48. F. Gugumus, Die Angew. Makromol. Chem. **182**, 85 (1990a).
49. A. L. Andrady, J. E. Pegram, and Y. Tropsha, J. Env. Polym. Deg., 117–126 (1993a).
50. J. L. Gardette and J. Lemaire, Polym. Deg. Stab. **16**, 147 (1986); *ibid*. **25**, 293 (1989).
51. P. Blais, M. Day, and D. M. Wiles, J. Appl. Polym. Sci. **17**, 1895 (1973).
52. R. A. Costa, L. Coltro, and F. Galembeck, Angew. Makromol. Chem. **180**, 85 (1990).
53. R. O. Carter, P. M. Paputa, and D. J. Bauer, Polym. Deg. Stab. **23**, 121 (1989).
54. H. C. Pendey and A. K. Kulshreshtha, Eur. Polym. J. **24**, 599 (1988).
55. L. W. Jelinski, J. J. Dumais, J. P. Luongo *et al*., Macromolecules **17**, 1650 (1984).
56. F. Mori, M. Koyama, and Y. Oki, Angew. Makromol. Chem. **68**, 137 (1979); *ibid*. **64**, 89 (1977).
57. H. C. Beachell and L. H. Smiley, J. Polym. Sci., A1 **5**, 1635 (1967).
58. M. A. Golub, M. L. Rosenberg, and R. V. Gemmer, Rubber Chem. Technol. **50**, 704 (1977).
59. H. Kubota and M. Kimura, Polym. Deg. Stab. **38**, 1 (1992).
60. H. Kubota, K. Takahashi, and Y. Ogiwara, Polym. Deg. Stab. **33**, 115 (1990).
61. A. Torikai, A. Takeuchi, and K. Fueki, Polym. Deg. Stab. **14**, 367 (1986).
62. J. F. Rabek, T. A. Skowronsky, and B. Ranby, Polymer **21**, 226 (1980).
63. G. A. George and M. Gahemy, Polym. Deg. Stab. **33**, 411 (1991).
64. F. P. La Mantia and R. Schifani, Polym. Deg. Stab. **10**, 67 (1985).
65. N. A. Weir, Dev. Polym. Deg. **1**, 67 (1977).
66. I. Mita, T. Takagi, K. Horrie *et al*., Macromolecules **17**, 2256 (1984).
67. R. M. Ikeda, F. F. Rogers, S. Tocker *et al*., in *Ultraviolet Light Induced Reactions in Polymers*, edited by S. S. Labana, ACS Symposium Series **25**, 76 (1976).
68. G. Scott, in *Ultraviolet Light Induced Reactions with Polymers*, edited by S. S. Labana, ACS Symp. Ser. No. 25 (ACS, Washington, DC, 1976), p. 340.

69. G. H. Hartley and J. E. Guillet, Macromolecules **1**, 165 (1968).
70. D. J. Carlsson, A. Garton, and D. M. Wiles, Macromolecules **9**, 695 (1976).
71. N. S. Allen and J. F. McKellar, Chem. Soc. Revs. **4**, 533 (1965).
72. G. Scott, in *Singlet Oxygen*, edited by B. Ranby and J. F. Rabek (Wiley Interscience, London, 1978).
73. C. Decker, in *Degradation and Stabilization of PVC*, edited by E. D. Owen (Elsevier Applied Science Publishers, London, 1984), p. 95.
74. E. D. Owen, in *Developments in Polymer Photochemistry*, edited by N. S. Allen (Applied Science Publishers Ltd., London, 1982), p. 165.
75. S. Al-Malaika and G. Scott, Europ. Polym. J. **16**, 709 (1980).
76. D. J. Carlsson, K. H. Chan, A. Garton *et al*., Pure Appl. Chem. **52**, 289 (1980).
77. A. Garton, D. J. Carlsson, and D. M. Wiles, Makromol. Chem. **181**, 1841 (1980).
78. C. H. Chew, L. M. Gan, and G. Scott, Europ. Polym. J. **13**, 361 (1977).
79. F. Gugumus, Die Angew. Makromol. Chem. **176/177**, 27 (1990).
80. N. S. Allen, K. O. Fatinikun, J. Luc-Gardette *et al*., Polym. Deg. Stab. **4**, 95 (1982).
81. F. M. Rugg, J. J. Smith, and L. H. Waterman, J. Polym. Sci. **11**, 1 (1953).
82. D. J. Carlsson and D. M. Wiles, J. Macromol. Sci. Rev. Macromol. Chem. C **14**, 65 (1976).
83. J. Buil and J. Verdu, Europ. Polym. J. **15**, 389 (1979).
84. F. Gugumus, Makromol. Chem., Macromol. Symp. **27**, 25 (1989).
85. D. J. Carlsson and D. M. Wiles, Macromolecules **2**, 597 (1969).
86. D. C. Mellor, A. B. Moir, and G. Scott, Europ. Polym. J. **9**, 219 (1973).
87. N. S. Allen, K. O. Fatinikun, J. Luc-Gardette, and J. Lemaire, Polym. Deg. Stab. **4**, 95 (1982).
88. N. S. Allen, J. F. McKellar, and G. O. Phillips, J. Polym. Sci., A1 **12**, 1233 (1974).
89. L. Ackerman and W. J. McGill, South Afr. Chem. Inst. **26**, 82 (1973).
90. N. S. Allen, J. F. McKellar, and D. Wilson, J. Photochem. **6**, 337 (1976).
91. N. S. Allen, in *Degradation and Stabilization of Polyolefins* (Applied Science Publishers, Ltd., London, 1993).
92. N. S. Allen, A. Chirinois-Padron, and J. H. Appleyard, Polym. Deg. Stab. **6**, 149 (1984).
93. L. Ratti, F. Visani, and M. Ragazzani, Eur. Polym. J. **9**, 429 (1973).
94. A. Caraculacu, E. C. Buruiana, and G. Robila, J. Polymer Sci., Polym. Chem. Ed. **16**, 2741 (1978).
95. G. Geuskens, D. Baeyens-Volant, G. Delaunois *et al*., Europ. Polym. J. **14**, 299 (1978).
96. J. F. Rabek and B. Ranby, J. Polymer Sci., A1 **12**, 295 (1974).
97. M. Nowakowska, J. Najbar, and B. Waligor, Europ. Polym. J. **12**, 387 (1975).
98. J. R. MacCallum and D. A. Ramsey, Eur. Polym. J. **13**, 945 (1977).
99. N. Yamamoto, S. Akaishi, and H. Subomura, Chem. Phys. Lett. **15**, 458 (1972).
100. N. A. Weir, Dev. Polym. Deg. **4**, 143 (1982).
101. B. Rándy and J. Lucki, Pure Appl. Chem. **52**, 295 (1980).
102. B. Dickens, J. W. Martin, and D. Waksman, Polymer **25**, 706 (1984).
103. S. G. Bond and J. R. Ebdon, Polym. Commun. **32**, 290 (1991).
104. D. Panke and W. J. Wunderlich, J. Appl. Polym. Sci., Appl. Polym. Symp. **35**, 321 (1979).
105. A. Torikai and K. Fueki, J. Polym. Photochem. Photobiol. **2**, 297 (1982).
106. F. R. Mayo and A. A. Miller, J. Am. Chem. Soc. **80**, 2493 (1958).
107. N. S. Hon, J. Polymer Sci., A1 **14**, 2497 (1976).
108. J. S. Humphrey, A. R. Schultz, and D. B. G. Jaquiss, Macromolecules **6**, 305 (1973).
109. A. Rivaton, D. Sallet, and J. Lemaire, Polym. Photochem. **3**, 463 (1983).
110. M. Day and D. M. Wiles, J. Appl. Polym. Sci. **16**, 203 (1972a).
111. P. S. R. Cheung, C. W. Roberts, and K. B. Wagner, J. Appl. Polym. Sci. **24**, 1809 (1979).
112. M. Day and D. M. Wiles, J. Appl. Polym. Sci. **16**, 175 (1972b).
113. C. V. Stephenson, J. C. Lacey, and W. S. Wilcox, J. Polym. Sci. **55**, 177 (1961).
114. N. S. Allen, J. F. McKellar, and D. Wilson, J. Polym. Sci., A1 **15**, 2973 (1977).
115. C. H. Do, E. M. Pearce, B. J. Bulkin *et al*., J. Polym. Sci., A1 **25**, 2301 (1987).
116. A. Roger, D. Sallet, and J. Lemaire, Macromolecules **19**, 579 (1986).
117. J. F. McKellar and N. S. Allen, in *Photochemistry of Man-Made Materials* (Applied Science Publishers Ltd., London, 1979), p. 128.
118. G. Scott and M. Tahan, Europ. Polym. J. **11**, 535 (1975).
119. J. H. Adams, J. Polymer Sci., A1, **8**, 1279 (1970).
120. S. K. L. Li and J. E. Guillet, J. Polym. Sci., A1 **18**, 2221 (1980).
121. M. U. Amin, G. Scott, L. M. K. Tillerkeratne, Europ. Polym. J. **11**, 85 (1975).
122. K. Tsuji and H. Nagata, Rep. Prog. Polym. Phys. Jpn. **18**, 517 (1975).
123. P. Vink, in *Degradation and Stabilization of Polyolefins*, edited by N. S. Allen (Applied Science Publishers, London, England, 1983), p. 228.
124. R. Geetha, A. Torikai, S. Nagaya *et al*., Polym. Deg. Stab. **19**, 279 (1987).
125. G. Scott, J. Polym. Sci., Polym. Symp. **57**, 357 (1976a).
126. J. H. Adams and J. E. Goodrich, J. Polymer Sci., A1 **8**, 1279 (1970).
127. Y. Kato, D. J. Carlsson, and D. M. Wiles, J. Appl. Polym. Sci. **13**, 1447 (1969).
128. G. Geuskens and M. S. Kabamba, Polym. Deg. Stab. **5**, 399 (1983).
129. C. Decker and M. Balandier, Polym. Photochem. **1**, 221 (1981).
130. D. J. Carlsson and D. M. Wiles, Macromolecules **4**, 174, 179 (1971).
131. W. H. Gibb and J. R. MacCallum, Europ. Polym. J. **8**, 1233 (1972).
132. C. Decker and M. Balandier, J. Photochem. **15**, 221 (1981a).
133. D. Braun and S. Kull, Angew. Makromol. Chem. **85**, 79 (1980).
134. D. Braun and S. Kull, Angew. Makromol. Chem. **86**, 171 (1980).
135. G. Martinez, C. Mijangos, and J. Millan, J. Appl. Polym. Sci. **29**, 1735 (1984).
136. C. Decker and M. Balandier, Europ. Polym. J. **18**, 1085 (1982).
137. A. L. Andrady, A. Torikai, and K. Fueki, J. Appl. Polym. Sci. **37**, 935 (1989).
138. J. F. Rabek, B. Ranby, B. Ostenson *et al*., J. Appl. Polym. Sci. **24**, 2407 (1979).
139. S. Matsumoto, H. Ohshima, Y. Hosuda, J. Polym. Sci., Polym. Chem. Ed. **22**, 869 (1984).
140. F. Mori, M. Koyama, and Y. Oki, Angew. Makromol. Chem. **64**, 89 (1977).
141. G. Geuskens and C. David, Pure Appl. Chem. **51**, 2385 (1979).
142. A. L. Andrady and J. E. Pegram, J. Appl. Polym. Sci. **42**, 1589 (1991).
143. N. A. Weir, Dev. Polym. Deg. **4**, 143 (1982).
144. F. Gugumus, Dev. Polym. Stab. **1**, 8 (1978).
145. A. Ghaffer, A. Scott, and G. Scott, Eur. Polym. J. **12**, 615 (1976).
146. T. R. Price and R. B. Fox, J. Polym. Sci. **4**, 771 (1966).
147. Z. Osawa, F. Konomo, S. Wu *et al*., Polym. Photochem. **7**, 337 (1986).
148. M. Day and D. M. Wiles, Can. Text. J. **6**, 69 (1972).
149. A. Ram, O. Zilber, and S. Kenig, Polym. Eng. Sci. **25**, 535 (1985).
150. Andrady, 1991a.
151. A. Davis and J. H. Golden, J. Macromol. Sci., Rev. Macromol. Chem. C **3**, 49 (1969).
152. A. Factor and M. L. Chu, Polym. Deg. Stabil. **2**, 203 (1980).
153. J. D. Webb and A. W. Czanderna, Sol. Energy Mater. **15**, (1987).
154. M. H. Tabankia and J.-L. Gardette, Polym. Deg. Stab. **14**, 351 (1986).
155. A. Anton, J. Appl. Polym. Sci. **9**, 1631 (1965).
156. K. E. Kyllo and C. M. Ladish, ACS Symposium Series **318**, 343 (1986).
157. K. E. Kyllo and C. M. Ladisch, ACS Symposium Ser. **318**, 343 (1986).
158. C. Xudong, W. Jiasheng, and J. Shen, Polym. Degrad. Stab. **87**(3), 527 (2005).
159. E.A. Snijders, A. Boersma, B. van Baarle, and P. Gijsman, Polym. Degrad. Stab. **89**(3), 484 (2005).
160. E.A. Snijders, A. Boersma, B. van Baarle, and P. Gijsman, Polym. Degrad. Stab. **89**(2), 200 (2005).
161. K. Antos, and J. Sedlar, Polym. Degrad. Stab. **90**(1), 180 (2005).
162. P. Katangur, S. B. Warner, P. K. Patra, Y. K. Kim, S. K. Mhetre, and A. Dhanote, Continuous Nanophase and Nanostructured Materials). In *Materials Research Society Symposium Proceedings*. Materials Research Society. 589–594 (2003).
163. S. Scierka, P. L. Drzal, A. L. Forster, and S. Svetlik, Mater. Res. Soc. Symp. Proc. 217–222 (2005).
164. C. Decker, F. Masson, and R. Schwalm, Polym. Degrad. Stab. **83**(2), 309 (2004).
165. C. Li, D. Kim, and A. J. Ragauskas, J. Wood Chem. Technol. **24**(1), 39 (2004).
166. G. J. M. Fechine, M. S. Rabello, R. M. S. Maior, and L. H. Catalani, Polym. Degrad. Stab. **45**(7), 2303 (2004).

CHAPTER 52

The Effects of Electron Beam and γ-Irradiation on Polymeric Materials

K. Dawes*, L. C . Glover†, and D. A. Vroom†

*Department of Materials Science and Engineering, North Carolina State University
Campus Box 7907 Raleigh, NC, 27695-7907;
†Tyco Electronics 305 Constitution Dr Menlo Park, CA 94025

52.1 INTRODUCTION

The effect of high-energy irradiation on polymeric materials has been intensely studied over the past 60 years. These studies parallel the growth in the types and usage of polymeric materials and the availability of electrically generated radiation sources. The electron beam has been a commercially acceptable processing technique for the last 50 years and is the preferred radiation source for polymer modification. Several books are available that cover the high-energy irradiation of polymeric materials [1–6].

The effect of radiation on materials has importance in the areas of wire and cable insulation, heat-shrinkable articles, curing of elastomers, plastics, paints and inks, electron beam lithography, medical sterilization, polymer property control, and outer space applications.

In general, the effects of exposure of polymers to high-energy radiation will lead to some change in the properties of the polymer. Its interaction with a high-energy electron is a complex and random process. The energies involved are much greater than the electron binding energy of any electron to an atomic nucleus. In this respect it differs from ultraviolet (UV) irradiation in which the energy carried per particle (photon) is lower than the ionization energy of an atom or molecule. Ultraviolet irradiation is therefore very selective, whereas high-energy irradiation is nonselective. The changes are primarily a consequence of:

1. Electron linear energy transfer (LET) to a molecule, followed by bond cleavage to give radicals.
2. Radical combination leading to the formation of crosslinks and end-links or disproportionation to give scission.
3. Gas evolution is mainly a consequence of (2) and direct formation of gaseous molecules.

52.1.1 Radiation Sources

The sources of high-energy ionizing radiation are [7]:

1. Cobalt-60 sources of γ-rays (1.17–1.33 MeV) [8,9];
2. Cesium-137 sources of γ-rays (0.66 MeV) [10];
3. Electron accelerators (0.1–12 MeV) [11];
4. Bremstrahlung X-rays from accelerators (3–10 MeV) [12].

The International System unit of absorbed dose is the Gray (Gy), which is equal to the energy imparted by ionizing radiation to a mass of matter corresponding to 1 joule per kilogram. The other unit of radiation dose is a special unit, the rad, which is equal to the energy absorption of 0.01 joule per kilogram, that is, 0.01 Gray. Until recently the most common unit of dose used to be the

Megarad (Mrad). The Gray is now the most commonly used unit in the literature:

$$1\text{Mrad} = 10^4\text{Gy} = 10\,\text{kGy}$$

$$1\text{Gy} = 6.25 \times 10^8\,\text{eVKg}^{-1}.$$

γ-Ray sources give a deeper penetration into a material, (sometimes an order of magnitude deeper) but at a much slower dose rate for example, kGy per hour when compared to electron accelerators which have a much lower penetration but have a much higher dose rate, for example, kGy per second. This difference becomes important for irradiation in air or oxygen.

The amount of radiation absorbed can be measured either directly or indirectly using a variety of dosimeters. Several reviews of dosimeters are available [13–15].

52.2 GENERAL EFFECTS OF ELECTRON BEAM AND γ-IRRADIATION ON POLYMERIC MATERIALS

52.2.1 *G*-Factors

The common way to investigate the effects of irradiation by either electron beam or γ-rays is to determine the yield of an event. An event change may involve the measurement of the changes in, for example, molecular weight, solution viscosity or gel content, or the measurement of the amounts of specific gaseous materials evolved during exposure.

The standard measurement of the yield for an event resulting from the irradiation process is expressed as the G factor. This factor is universally accepted [16] and is defined as the event yield per 100 eV of energy deposited in the material. The SI unit for G is $\mu\text{mol}\,J^{-1}$. For the purposes of this review events per 100 eV will be used throughout. The most commonly quoted G factors are for crosslinking, chain scission, and gas evolution, G(X), G(S), and G(Gas), respectively. There may be several different values for the G-factor in the literature since several different methods of measurement may be used to determine the event yield. If different methods or standards are used to determine molecular weights, they can lead to widely different G-factors. For example, in the case of a low density polyethylene values for G(X) of 0.9 or 1.7 are obtained using the hydrogenated polybutadiene or polystyrene calibrations, respectively [17].

52.2.2 Changes in Molecular Weight Distribution

As stated above one of the main effects of exposure of polymeric materials to high energy radiation is that the material undergoes scission of the main chain and the creation of free radicals, unsaturation (double bonds), crosslinks, and end-links. Change in the molecular size distribution will be a consequence of main chain scission, crosslinking, and end linking. Much of the early theoretical expressions relating to the effect of radiation processes on molecular weight distribution were derived by Charlesby [18–20] and Saito [21–24].

Main Chain Scission

In deriving the basic equation for main chain scission, the following assumptions are made: (1) all polymer molecules are linear; (2) every structural unit is fractured with equal probability; (3) average molecular weight is sufficiently large; and (4) the total number of main chain scissions is sufficiently smaller than the total number of structural units.

The basic equation, derived by Saito [25], which expresses the change in molecular size distribution of linear polymer molecules undergoing main chain scission is

$$\frac{\partial w(p,y)}{\partial y} = -pw(p,y) + 2p\int_p^\infty \frac{w(l,y)}{l}\mathrm{d}l,$$

where

$$y = \int_0^t r\mathrm{d}t$$

and

$$G(S) = \frac{100N_\mathrm{A}y}{D}$$

where t is the time, p is the degree of polymerization of the polymer molecule, r is the probability that a structural unit undergoes scission in unit time, and $w(p,y)$ is the weight fraction of polymer molecules having p structural units, N_A is Avogadro's number, D is the radiation dose, and G(S) is the yield of main chain scissions. The first term, $-pw(p,y)$, corresponds to the decrease of the molecules having p structural units due to main chain scission, and the last term corresponds to the increase of the molecules having p structural units due to the scissions of those molecules having l units. The number of main chain scissions per structural unit is y, and since r is usually independent of t then y is equal to rt. Solution of the above equation leads to

$$w(p,y) = \left[w(p,0) + py\int_p^\infty \frac{(2+yl-yp)}{l}\,w(l,0)\,\mathrm{d}l\right]\exp(-py),$$

where $w(p,0)$ is the initial weight fraction. Calculation of the average molecular weight can be obtained from the following expression.

$$f_j(y) = \int_0^\infty p^{j-1}w(p,y)\,\mathrm{d}p, \quad j = 0, 1, 2, 3, \ldots.$$

The change in the average molecular weights due to main chain scission can be calculated from the last two equations. The number average degree of polymerization P_n in the absence of any crosslinking is given by

$$\frac{1}{P_n} = \frac{1}{u_n} + y,$$

where u_n is the number average degree of polymerization prior to irradiation. This relationship holds for any initial molecular size distribution. If M_n^0 and M_n are the number average molecular weight before and after irradiation, respectively, then

$$uy = \frac{[M_n^0 - M_n]}{M_n}.$$

Therefore the changes in the number average molecular weight depend only on M_n^0 and the number of chain scission per structural unit and not on the initial molecular weight distribution.

The changes in the weight average molecular weight after irradiation are dependent on the initial molecular weight distribution.

For initial uniform distribution then

$$\frac{\frac{M_w}{M_w^0} = 2(u_n - 1 + e^{u_n y})}{(u_n y)^2.}$$

For initial random distribution then

$$\frac{M_w}{M_w^0} = \frac{1}{(1 + u_n y)}.$$

For an initial Schulz–Zimm distribution then

$$\frac{M_w}{M_w^0} = \left[u_n y - 1 + \left(\frac{1 + u_n y}{\sigma}\right)^{-\sigma}\right] \frac{2\sigma}{(1+\sigma)(u_n y)^2},$$

where

$$\sigma = \frac{M_n}{M_w - M_n}.$$

When only degradation occurs with a polymer the molecular weight distribution will always approach the random case, that is

$$\frac{M_w}{M_n} = 2.$$

Simultaneous Crosslinking and Scission

For crosslinking, the basic equation which expresses the change in molecular size distribution of linear polymer molecules is

$$\frac{1}{p}\frac{\partial w(p,x)}{\partial x} = -2w(p,x)\int_0^\infty w(l,x)\mathrm{d}l + \int_0^p w(l,x)w(p-1,x)\mathrm{d}l,$$

where x is the number of crosslinks per structural unit, or the density of crosslinks. The assumptions made for this equation are as follows: (1) Crosslinks are produced at random; (2) every structural unit crosslinks with the same probability regardless of its position in the polymer molecule; (3) the number of crosslinks is sufficiently small in comparison to the total number of structural units; and (4) intramolecular linkings in molecules of finite size are negligible. $G(X)$ is the yield of crosslinks:

$$G(X) = \frac{100 N_A x}{D}.$$

When crosslinks and main chain scissions are produced simultaneously by irradiation it is assumed that they are independent of each other. The change in molecular size distribution can be obtained by first calculating the effect of all the scission on the initial distribution and then calculating the effect of all the crosslinking on the resultant distribution. This assumes that crosslinking occurs after all the main chain scissions have taken place. When crosslinking and scission occur simultaneously, the number average degree of polymerization $P_n(x,y)$, for any arbitrary shape of the initial molecular weight distribution, is given

$$\frac{1}{P_n(x,y)} = \frac{1}{u} + y - x$$

and

$$\frac{M_n}{M_n^0} = \frac{1}{1 + u_n(y - x)}.$$

The number average molecular weight resulting from simultaneous chain scission and crosslinking is independent of the initial molecular weight distribution, whereas the weight average molecular weight is not. The weight average degree of polymerization $P_w(x,y)$ for an initial random distribution is given by

$$\frac{1}{P_w(x,y)} = \frac{1}{2u} + \frac{y}{2} - 2x$$

and

$$\frac{M_w}{M_w^0} = \frac{1}{[1 + u_n(y - 4x)]}.$$

If the initial distribution is uniform then

$$\frac{M_w}{M_w^0} = \frac{2(e^{-u_n y} + u_{ny} - 1)}{[u_n y^2 - 4u_n x(e^{-u_n y} + u_n y - 1)]}$$

and the initial Schulz–Zimm distribution

$$\frac{M_w}{M_w^0} = \frac{2\left\{u_n y - 1 + \left[1 + \left(\frac{u_n y}{\sigma}\right)\right]^{-\sigma}\right\}}{(u_n x)^2 - 4\left\{u_n y - 1 + \left[1 + \left(\frac{u_n y}{\sigma}\right)\right]^{-\sigma}\right\} u_n x}.$$

Gelation

When a polymeric material undergoes radiation crosslinking the weight average molecular weight and intrinsic viscosity increase with radiation dose, until they finally tend to infinitely large values. A part which is insoluble in any solvent grows within the polymeric substance as the radiation level is increased. The phenomenon is called gelation and the insoluble part is the gel. The instance when an incipient gel is formed is the gel point. The density of crosslinks at the gel point, x_g, is given by

$$x_g = \frac{1}{2P_w^0}.$$

The number of crosslinks at the gel point is equal to half the ratio of the total number of structural units to the weight average degree of polymerization, P_w^0, prior to undergoing crosslinking.

When crosslinking and main chain scission occurs simultaneously, for an initial random distribution then

$$x_g = \frac{y}{4} + \frac{1}{2P_w^0}.$$

52.2.3 Determination of G Factors

Charlesby–Pinner Equation

In a paper published in 1959 [26] Charlesby and Pinner developed the Charlesby–Pinner equation which allows the experimentalist to determine the $G(S)$ and $G(X)$ ratios. The derivation of the equation is based on an initial random molecular weight distribution and relates to the sol fraction, s, to the crosslinking index, γ', when both main chain scission and crosslinking occur.

$$s + \sqrt{s} = \frac{1}{\gamma'}.$$

The basic equation, which is a slight modification of an earlier equation [18,19] is expressed as follows:

$$s + \sqrt{s} = \frac{p_0}{q_0} + \frac{1}{q_0 u_1 D},$$

where p_0 is the probability of main chain scission per monomer unit per unit dose, q_0, the probability of crosslinking per monomer unit per unit dose, u_1, the number average degree of polymerization, and, D, the radiation dose in Mrads.

The expression relates the sol fraction to the crosslinking and scission processes. The expression can also be written in terms of the ratio of $G(S)$ to $G(X)$ and the initial number average molecular weight, M_n^0, as follows:

$$s + \sqrt{s} = \frac{G(S)}{2G(X)} + \frac{9.6 \times 10^5}{2G(X)M_n^0 D}.$$

A plot of $s + \sqrt{s}$ against $1/D$ should yield a straight line with the intercept giving the ratio of scission to crosslinking. The plot is only linear for initial random molecular weight distribution and deviations occur when $M_w/M_n \neq 2$. For an initial distribution, which is either very broad or very narrow and for a moderate value of the ratio of the scission rate to crosslinking rate, considerable deviations from the Charlesby-Pinner relationship occur [27]. At high radiation doses, the assumptions for the Charlesby–Pinner relationship that there is no intramolecular crosslinking and that endlinking is negligible may not be valid since both these processes would be expected to occur at high doses. With polyethylene, extrapolation of the Charlesby–Pinner relation at higher doses yields a value for p_0/q_0 of zero [28], a decrease in the main chain scission rate with increasing dose suggesting that scission then becomes a minor component. Also, when $G(S) > 4G(X)$ [29] the polymer will remain completely soluble even though the polymer is still undergoing considerable modification; therefore, the Charlesby–Pinner relationship would not be applicable in this case since no gel would be formed.

Several modifications to the Charlesby–Pinner relationship that deal with deviation from the initial random distribution have been published [30–32]. In some cases a plot of $s + \sqrt{s}$ against D^{-k}, where k can vary from 0.42 to 0.55 leads to a better linear relationship for polyethylenes [28]. Vinyl group endlinking can also be taken into account with the following relationship [33]:

$$\ln \phi = (q_0 u_1 + k)D,$$

where $\ln \phi$ is the ratio of number of molecules before and after irradiation and, k The probability of one molecule of the ith species being removed through vinyl endlinking.

The Charlesby–Pinner equation can also be expressed in dimensionless quantities as

$$s + \sqrt{s} = \frac{G(S)}{2G(X)} + \left(2 - \frac{G(S)}{2G(X)}\right)\left(\frac{D_g}{D}\right),$$

where D_g is the dose to the gel point. The initial slope of the $s + \sqrt{s}$ vs D_g/D curve is more helpful in many cases in determining the ratio of $G(S)$ to $G(X)$ [34].

Other Methods

The yield of scission can be determined by the change in the number average molecular weight of the polymer using the equation [35]:

$$\frac{1}{M_n} = \frac{1}{M_n^0} + 1.04 \times 10^7 G(S)D.$$

The yield of crosslinking can be determined using the equation [36]:

$$G(X) = \frac{0.48 \times 10^6}{M_w D_g}$$

52.2.4 Polymeric Structure

The chemical structure of the polymer can determine the type of change that a polymer will undergo upon high energy irradiation. In very general terms, polymers of structure I will undergo crosslinking upon irradiation and those of structure II will undergo scission.

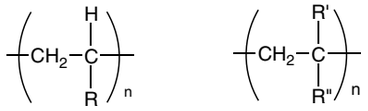

STRUCTURE I STRUCTURE II

An example of this is the case of poly(methyl acrylate), which has structure I ($R = COOCH_3$) and readily crosslinks, G(crosslinking) $\approx$ 0.5 [37]. In contrast, poly(methyl methacrylate), PMMA, which has structure II ($R' = CH_3$, $R'' = COOCH_3$) readily degrades via chain scission, G(scission) 2.28 [38]. Table 52.1 gives a list of the types of polymers that are prone to either crosslinking or scission.

The presence of unsaturation in the polymer chain can enhance the effects and increase the yields of crosslinking. Purified natural rubber (*cis*-1,4-polyisoprene) is highly unsaturated and is readily crosslinked upon irradiation in vacuo with either γ-rays or electron beam [39], giving a yield for physical crosslinking, $G(X)$, of 3.5. Some polymers that contain high levels of unsaturation also undergo a high yield for loss of unsaturation upon irradiation. For example synthetic polyisoprenes composed of 1,2 and 3,4 isomers give a G(loss of unsaturation) of $\approx$130 [40,41], whereas $G(X)$ is $\approx$ 2. Intramolecular cyclization upon irradiation appears to be a dominant process in this case.

If in structure I, R = X, that is a halogen atom, the carbon–halide bond is broken upon irradiation and dehydrohalogenation, loss of hydrogen halide gas can be the dominant process. The relative ease of loss of the halogen will depend on the carbon–halogen bond strength, following the order I > Br > Cl > F. Polyvinylchloride, PVC, although often cited [42] as a crosslinking polymer upon irradiation, readily and rapidly dehydrochlorinates on exposure to either electron beam or γ-irradiation. The yield for production of hydrogen chloride gas, G(HCl), is 13 at 30 °C [43].

The structural type of R, R′, and R″ can also influence reaction yields. In general, the larger the amount of aromaticity that is present, the lower the yield of any reaction occurring as a consequence of irradiation. The yields of aromatic-containing polymers can often be an order of magnitude lower than the corresponding hydrocarbon. In fact, some of the highly aromatic polymers are very resistant to the effects of irradiation. The aromatic unit has a protective effect, the resonant structure of the aromatic ring enabling a considerable amount of energy to be absorbed without any rupture of the bonds. An example of the protective effect of aromatic rings on the yield for crosslinking, $G(X)$, is the case of polystyrene, R = phenyl, where $G(X)$ is around 0.05, compared to polyethylene, structure I, R′ = H, and $G(X)$ is > 1 [44].

52.2.5 Effect of Atmosphere During Irradiation

A major effect of irradiation of polymeric materials is the atmosphere in which the material is exposed. As mentioned earlier, the irradiation process produces radical species, and depending on the relative stability of these species, several competing reactions can happen:

1. The radical can remain as a stable species within the polymeric matrix. In an inert atmosphere radicals can exist for extensive periods of time (up to many days or weeks).
2. The radical undergoes some reaction either with another radical to form a crosslink or undergoes disproportionation that leads to scission and the development of unsaturated groups in the polymer.

TABLE 52.1. *Generic types of polymers that either undergo crosslinking or scission.*

Prone to crosslinking	Prone to scission
Polyacrylates	Polyisobutylene
Polyvinylchloride	Poly α-methylstyrene
Polysiloxanes	Polymethacrylates
Polyamides	Polymethacrylamides
Polystyrene	Poly(vinylidene chloride)
Polyacrylamides	Polytetrafluoroethylene(PTFE)
Polyethylene copolymers such as EVA, EEA, EMA, EBA	Polytrifluorochloroethylene
Unsaturated elastomers	Polypropylene ether
Ethylene propylene elastomers	Cellulose and derivatives
Polyacrolein	
Polyethylene	

3. In the presence of oxygen, either already present in the polymeric material or by diffusion into the polymer, there are processes that compete with (1) and (2). Oxygen will react with radicals to form peroxides or hydroperoxides. Inevitably the presence of oxygen will lead to an increase in the extent or rate of the scission process and degradation of the polymer.

A good example of the effect of oxygen is the case of polypropylene which degrades when irradiated in oxygen, whereas crosslinking occurs when the irradiation takes place in vacuo. Another example is poly(tetrafluoroethylene) (PTFE) which readily degrades in air upon irradiation, whereas irradiation in the absence of air has much less of an effect on properties [45]. However in the case of poly(methyl methacrylate), which is very prone to degradation, the rate of degradation is lower in air than in vacuo [38].

As mentioned earlier, the dose rate can affect the choice of atmosphere used. For example, in the case of γ-irradiation the dose rate is of the order of kGy per hour. At this rate oxygen can readily diffuse into the polymer, react with radicals and lead to degradation. In general, irradiation with γ-rays is usually done in an inert atmosphere, unless you want to intentionally degrade the material. With an electron beam the dose rate is much higher at kGy per second; therefore, the competition with oxygen is reduced as it cannot diffuse into the material at a rate equal to the radiation induced reaction, although not totally eliminated.

52.2.6 Trapped Electrons/Radicals

If the polymeric material is in the glassy state, that is, below the glass transition temperature (T_g) or has some crystallinity, trapped electrons and trapped radicals can be produced upon irradiation with either electron beam or γ-irradiation. Phenomena such as thermoluminescence, electrical conductivity, color changes in the polymer, and imperfections within crystals have attributed to ionic species. Trapped electrons have been identified in γ-irradiated polyethylene [46].

In general, amorphous materials do not have the tendency to produce trapped electrons. Table 52.2 shows the yield of trapped electrons, $G(e_t^-)$ for a range of hydrocarbon polymers with different crystalline content that have been γ irradiated at 77 K [47,48]. The initial $G(e_t^-)$ was determined from ESR experiments by comparison with (e^-) in 2-methyltetrahydrofuran (MTHF) and based on a value of $G(e^-)$ of 2.6 for MTHF. All the polymers were free of antioxidants and stabilizers.

The materials with trapped electrons undergo photobleaching when exposed to near-infrared light ($\lambda > 1,000nm$).

52.2.7 Effect of the Temperature During Irradiation

Any effect of irradiation, in general, is increased with increasing temperature. At temperatures below T_g, a significant number of stable radicals are formed (radicals trapped in the glassy state) and, in general, crosslinking is reduced due to immobility in the glassy state. At temperatures above T_g the tendency to crosslink is usually increased, although scission processes will also increase.

An example of the change above T_g is illustrated for the case of the fluorocopolymer, FEP. Irradiation of FEP with high energy radiation above T_g (80 °C for 14% hexafluoropropylene) leads to crosslinking with maximum efficiency being at temperatures between 300 °C and 320 °C. Above 320 °C thermal degradation becomes a major factor [49,50]. On the other hand, polystyrene shifts from crosslinking below T_g (approximately 100 °C) to scission above T_g [44].

52.2.8 Effects in Semicrystalline Polymers

Semicrystalline polymers are polymers that contain both crystalline and amorphous states. In general, the major effect of irradiation, either electron beam or γ-rays, on the crystalline region is to cause some imperfections. At high levels of irradiation the original crystalline structure tends to be progressively destroyed and is nearly always accompanied by a drop in the crystalline melting point, T_m. An example is that of poly(ethylene terephthalate), which shows a decrease in melting point of approximately 25 °C after irradiation (20 MGy) [51].

On the other hand, some polymers show an initial increase in crystallinity, demonstrated by an increase in density. At relatively low doses (< 200 kGy), ultra high molecular weight polyethylene (UHMWPE) appears to show an increase in crystallinity. Since UHMWPE has a

TABLE 52.2. *Effect of crystallinity on trapped electrons yields in γ-irradiated hydrocarbon polymers.*

Polymer	Crystallinity (%)	Initial $G(e_t^-)$ (electrons/100 eV)
HDPE (Marlex 6050)	≈ 82	0.46
LDPE (Alathon 1414)	≈ 45	0.12
Isotactic PP (Phillips Petroleum Co.)	≈ 70	0.17
Atactic PP (Hercules Inc.)	0	<0.02
Isotactic Poly(4-methylpentene-1) (Mitsui)	≈ 40	0.08
Polyisobutylene (Exxon)	0	0

relatively low amount of crystallinity but a very high molecular weight, the effect is best explained by a scission process thereby reducing the molecular weight and reducing entanglements. Both these effects will increase mobility of the polymer chains and allow more crystallization [52]. Similar effects are seen with poly(tetrafluoroethylene) PTFE and poly(vinylidenefluoride) PVDF.

52.3 SPECIFIC EFFECTS ON POLYMERIC GROUPS

52.3.1 Elastomers

An excellent review on the radiation chemistry of elastomers up to 1980 has been published [53].

Elastomers such as *cis*-1,4-polyisoprene (natural rubber), polybutadiene, polybutadiene-styrene (SBR), and polychloroprene have large amounts of unsaturation in the polymer backbone and all undergo crosslinking upon irradiation with either electron beam or γ-irradiation. Table 52.3 gives some values for $G(X)$ and the ratio of scission to crosslinking $G(S)/G(X)$ for several elastomers. The protective effect of the aromatic ring is shown by the decrease in yield as the percentage of styrene is increased for the SBR series.

Polychloroprene also undergoes loss of the chlorine atom, which leads to a high yield of hydrogen chloride gas, $G(HCl)$ is 3.3 [54], as well as crosslinking. For a crystallizable polychloroprene both crosslinking and scission occur in the amorphous region [55].

The radiation effects on ethylene–propylene rubber (EPR) are modestly dependent on the ethylene content [63]. As the ethylene content is increased a shift to a larger yield for crosslinking occurs and the polymer is less prone to scission, the relationship is not linear since similar results for yields are found at 42 and 69% ethylene.

The irradiation of ethylene–propylene–diene–monomer (EPDM) elastomers, which contain some specific side chain unsaturation, leads to an increase in both crosslinking and scission. The type of diene monomer can affect the yield of crosslinking (curing) with 1,4-hexadiene being more effective than 5-ethylidene-2-norbornene (EN) [65] and EN more effective than dicyclopentadiene (DCP) [64]. The higher the levels of diene content the faster the crosslinking rate but this is also accompanied by an increase in the scission yield [64,66]. The properties of radiation cured EPDM are superior when compared to the more common sulfur cured material (conventional cure), with greatly improved compression set and oil resistance [65].

The block copolymer elastomeric materials such as styrene–butadiene–styrene (SBS) and styrene–isoprene–styrene (SIS) are readily crosslinked by an electron beam [67]. The increase in the properties such as dynamic and static moduli is consistent with crosslinking.

Polyphosphazene elastomers undergo crosslinking when γ-irradiation is performed in a vacuum. The yield of crosslinking, $G(X)$, varies from about 1 to 12 depending on the percentage of allyl groups in the polymer chain [68].

52.3.2 Polyethylene and Copolymers

Polyethylene (PE) is the most widely studied and commercially irradiated polymer class, with studies ranging from *n*-alkane waxes [69,70] as model compounds to UHMWPE [52,71–73].

The types of polyethylene can vary depending on the method of manufacture, the amount of comonomer and the type of comonomer, that is, whether hydrocarbon or polar. Polyethylene manufactured by the older high pressure process leads to the production of highly branched and long branched low density polyethylene (LDPE). With modern polymerization technology, which uses much lower pressures, polyethylenes are more linear in nature. They can be made with random short chain branches such as methyl, ethyl, butyl, and hexyl which arise from copolymerization

TABLE 52.3. *G(X) and G(S)/G(X) values for some common elastomers.*

Elastomer	$G(X)$	$G(S)/G(X)$
Purified natural rubber (in vacuo)	3.5 [39]	0.14, 0.11 [56], 0.18, 0.03 [57]
Natural rubber (in air)	1.05 [58]	
Polybutadiene (*cis*-1,4) [59]	5.3	0.1
Polybutadiene (90% vinyl 1,2) (in vacuo) [60]	≈ 10	
SBR (16% styrene) [61]	2.9	–
SBR (28% styrene) [61]	1.5	–
SBR (85% styrene) [61]	0.3	–
Polychloroprene [62]	3.2–4.8	–
EPR(≈ 4% ethylene) [63]		0.44
EPR(42% ethylene) [63]	0.46	0.21
EPR(69% ethylene) [63]	0.50	0.23
EPR(60 mole% ethylene) [64]	0.26	0.61
EPDM(56 mole% ethylene +1.9 mole% DCP) [64]	0.91	0.32
EPDM(57 mole% ethylene +2.0 mole% EN) [64]	2.18	0.26

with the corresponding alkene monomer. Linear low density PE (LLDPE) and high density PE (HDPE) are made using a low pressure technique in either liquid or gas phase.

The backbone structural feature of two hydrogen atoms per carbon leads to several unique responses to irradiation including hydrogen gas evolution, formation of *trans* vinylene unsaturation, the decay of vinyl end groups and extremely high crosslinking efficiency.

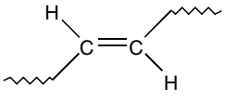

Trans Vinylene

The formation of the *trans* vinylene unsaturation is not molecular weight dependent, is linear over a substantial dose range and is used as a dosimeter [15]. From numerous investigations [15,74,75], the formation of *trans* vinylene unsaturation appears to be a primary process of irradiation with the detachment of a hydrogen molecule being a one step process. The $G(H_2)$ value is relatively high, 3–4 at room temperature and 3–6 at elevated temperatures (130 °C). The G values for some of the other processes are shown in Table 52.4. The values all show a relatively wide variation, due to the complexity of the polyethylene materials studied. Table 52.5 gives some values for the yield of crosslinking for a wide range of polyethylenes [33]. The materials cover a wide range of initial molecular weight distribution, density and initial vinyl content. However, the average measured $G(X)$ for LDPE, LLDPE, and HDPE is about 1. Chain scission in polyethylenes appears to be low with $G(S)$ values <0.1 [28].

Linear polyethylene (low pressure process) has been most widely studied where the effects of molecular weight, polydispersity, temperature, crystallinity, the presence or absence of terminal unsaturation, branching and postirradiation treatment have been shown to effect the previously mentioned main irradiation consequences. The consequences have been thoroughly reviewed [15,79–81].

Since polyethylene mainly crosslinks, the effect of irradiation is to generally enhance the physical properties. For example, for HDPE an increase in both the yield stress and secant modulus at 0.5% strain is observed [52]. The effect on the properties above the melting point have been extensively studied [82] and there is a direct relationship of the elastic modulus measured at 160 °C to the dose. For irradiated polyethylenes, the elastic modulus measured at 160 °C shows a growth rate of 3.8 and 3.9 Pa Gy^{-1} for LDPE and HDPE, respectively.

The effect of irradiation on the crystallinity of UHMWPE has already been described. Irradiation of UHMWPE in the melt leads to a high yield of crosslinks with effectively no chain scission occurring, and with increasing crosslink density a change from lamellar to micellar-like crystallization was found [83]. More recent thorough studies of UHMWPE often at sterilizing doses of around 25–50 kGy, show both scission and crosslinking as well as a ''transition'' zone within and below the polymer mass [84–87].

Polar copolymers of ethylene, such as ethylene-vinyl acetate (EVA) and ethylene-ethyl acrylate (EEA), are readily crosslinked upon exposure to high energy irradiation [88]. In fact, the melt index of EVA can be controlled by the use of low doses (<50 kGy) of irradiation [89]. The presence in polar ethylene copolymers of comonomer units such as vinyl acetate or alkyl acrylates (methyl, ethyl and *n*-butyl) proportionately reduces the level of crystallinity, and since the majority of radiation responses of interest take place in the amorphous phase, the responses are more uniform throughout the polymer mass. When the irradiation is done at room temperature, the physical properties after irradiation follow the same trend as polyethylene [90].

52.3.3 Polypropylene

Polypropylenes can be a semicrystalline polymer (atactic/isotactic), (atactic/syndiotactic) or a purely amorphous polymer (atactic). The effect of crystallinity on the yield of trapped electrons (Table 52.2) has already been discussed.

Although polypropylene is classed as a crosslinking type polymer, the initial studies on polypropylene [91,92] showed that the polymer, in the early stages of irradiation, undergoes scission, but at around 500 kGy a gel point was reached indicating the formation of crosslinks; $G(X)$ was found to be around 0.6. Irradiation at >500 kGy leads to further degradation. In fact polypropylene undergoes both scission and crosslinking at about equal amounts.

The mechanical degradation that arises after irradiation with γ-rays has been shown to be independent of the conditions of irradiation (air or vacuum) [93]. The post-irradiation effects of oxygen dominate, which will lead to a drop in both the tensile strength, modulus of elasticity, and elongation over time. Table 52.6 gives some changes for isotactic

TABLE 52.4. *G values for the generation of alkyl[G(alkyl)], allyl[G(allyl)], and dienyl[G(dienyl)] radicals, and trans vinylene [G(V_t)] for irradiated polyethylenes.*

Polymer	G(alkyl)	G(allyl)	G(dienyl)	G(V_t)	$G(X)$
HDPE	1.3–3.0 [76]	0.2–0.4	0.015 [77]	2.0+/−0.3 [78]	0.1–1.34 [79]
LLDPE	–	–	–	–	0.7–1.09
LDPE	–	–	–	1.7	0.8–1.25

TABLE 52.5. *Yields for crosslinking for a range of polyethylenes [33].*

Resin	Density	*G*(X)
LDPE	0.920	1.09
LDPE	0.935	0.8
LDPE	0.930	1.09
HDPE	0.962	1.0
HDPE	0.950	0.70
HDPE	0.945	0.50
HDPE	0.962	1.1
LLDPE	0.937	1.0
LLDPE	0.924	0.96
LLDPE	0.919	0.99

polypropylene after γ irradiation [94]. An increase in temperature will accelerate the process. For isotactic polypropylene the drop in elongation follows first order kinetics with an activation energy of 9 kcal/mole^{-1} [95].

The major gases evolved during irradiation under a vacuum are hydrogen and methane. In the presence of oxygen, carbon dioxide and carbon monoxide are also produced. Table 52.7 gives the yields for gas evolution for powdered isotactic polypropylene; similar values are found for polypropylene film [95].

Some values for the yields of crosslinking and scission are given in Table 52.8 for atactic and isotactic polypropylenes.

The $G(S)/G(X)$ ratio also tends to be a function of dose, with the value decreasing with increasing dose [97].

The irradiation will also show an effect on the level of crystallinity and melting point. For example, after a dose of 6 MGy the crystallinity was 73% of the original value and the melting point changed from 160°C to 105°C [98].

52.3.4 Fluoropolymers

General Trends in Fluoropolymers

A review of the effects of high energy radiation on fluoropolymers has recently been published [99] and provides a wealth of information. There is a relationship between the effect of high energy irradiation on a fluoropolymer and the amount of hydrogen atoms in the fluoropolymer. The trend can be approximately expressed as follows:

For *crosslinking*
PVF > PVDF > ETFE > FEP > PFA > PTFE

and for *degradation*
PTFE > PFA ≈ FEP>ETFE > PVDF > PVF

In general, the higher the hydrogen content the higher the tendency of the fluoropolymer to crosslink. The presence of hydrogen does lead to dehyrohalogenation (loss of hydrogen fluoride, HF) upon irradiation. The use of crosslinking promoters are advantageous since relatively high levels of crosslinking can be achieved without compromising the thermal stability of the polymer [99]. Recent work has reinforced the difference in radiation response between perfluoropolymers and those containing hydrogen with a study of the influence of low doses (10–200 kGy) of gamma irradiation on PVF, PVDF, ETFE, FEP, and PFA [100]. Also, gamma irradiated PVF has been shown to have much better UV stability than gamma irradiated PVDF [101].

52.3.5 Perfluoropolymers

Poly(tetrafluoroethylene) (PTFE) is very sensitive to irradiation with either an electron beam or γ source. It predominately undergoes degradation when irradiated [102,103] in fact high energy irradiation is used commercially to induce degradation to reduce and control the molecular weight of PTFE. The effect of irradiation on the high temperature (380 °C) viscosity measurements and the number average molecular weight are shown in Table 52.9.

The effect of gamma irradiation on the physical properties of PTFE film are shown in Table 52.10. The falloff in physical properties is dramatic, even after irradiation in vacuo followed by exposure to air. The radicals produced by irradiation have been shown to have a long lifetime even after heating to 300 °C [103]. By looking at the electron spin resonance spectrum, radical I is detected for irradiation in vacuo and peroxy radical II is detected after exposure to air [105].

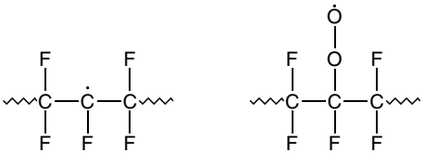

Radical I Radical II

TABLE 52.6. *Variation in the tensile strength, modulus of elasticity, elongation, and some electrical properties with irradiation dose in polypropylenes.*

Dose (kGy)	0	1,000	280	800	1,200	1,600
Tensile strength (MN m^{-2})	37.5	35.1	30.0	17.1	18.0	16.5
Modulus of elasticity (MN m^{-2})	1.45	1.35	1.30	1.20	1.15	
Elongation (%)	≈900	≈200	≈90	≈50	≈40	≈20
Dielectric rigidity (MV m^{-1})	168	165	150	100	99	98
Electrical permittivity (@ 50 Hz)	2.19	2.16	2.20	2.17	2.20	2.34

TABLE 52.7. *Yields for gas evolution for γ-irradiation (300 kGy) of powdered isotactic polypropylene in a vacuum or in air [95].*

Condition	$G(H_2)$	$G(CH_4)$	$G(CO)$	$G(CO_2)$
Vacuum	2.9	0.09	–	–
Air	2.5	0.17	1.2	2.1

TABLE 52.8. *G-factors for crosslinking and scission for polypropylenes.*

Polymer	$G(X)$	$G(S)$	$G(S)/G(X)$
Atactic PP [96]	0.27	0.22	0.8
Isotactic PP [96]	0.16	0.24	1.5

TABLE 52.9. *Molecular weights and high temperature viscosity of vacuum irradiated PTFE [104].*

Dose (kGy)	$M_n(\times 10^6)$	Viscosity at 380 °C (poise)
0	>10	3.2×10^{11}
150	2.5	2.8×10^{9}
750	2.1	1.4×10^{8}
750*	0.9	8.0×10^{6}

*Air sintered material, other materials were vacuum sintered.

An interesting, and somewhat surprising effect of high energy irradiation on PTFE is an increase in the level of crystallinity at relatively modest doses (<1 MGy) [106–108]. The changes in crystallinity with increasing dose are shown in Table 52.11 [107]. By studying the change in specific volume for PTFE it has been shown that when the irradiation dose is increased beyond 1 MGy, the trend is reversed and the crystallinity level starts to decrease; that is, the specific volume will start to increase [108].

The explanation for the increase in crystallinity at relatively low irradiation doses is chain scission when irradiated in the presence of oxygen. Scission will relieve stresses or entanglements within the polymer, leading to a lower molecular weight, more mobility, and further crystallization. It is well established that for PTFE the lower the molecular weight, the higher the density and correspondingly, the higher the crystallinity.

Recently, irradiation of PTFE in vacuo has shown evidence of crosslinking when the temperature during irradiation is above 200 °C. There is a significant increase in the tensile strength and elongation, measured at 200 °C, for PTFE that had been irradiated (2 kGy) above the melting point of 327 °C (330–340 °C), in vacuo [109,110]. Radical I may well be the source of crosslinking for in vacuo irradiation at high temperature.

The electron beam irradiation of a series of perfluoro copolymers of PTFE shows that the copolymers with hexafluoropropylene (HFP), octafluorobutylene, and perfluoroheptene-1 undergo crosslinking when irradiated at a temperature of between 200 – 250 °C [111]. On the other hand, irradiation of poly(hexafluoropropylene) and a copolymer of HFP and perfluoroheptene-1 underwent scission. The crosslinking of FEP at above the T_g has been mentioned earlier [49,50]. All these evaluations involved the determination of a change in the melt viscosity. For a series of FEP polymers with levels of HFP, from 4.7% to 29.8%, the higher the level of HFP the larger the increase in melt viscosity after irradiation at 250 °C in nitrogen [111].

The yields of volatile gases evolved after the irradiation of PTFE and FEP in vacuo and air [112] are given in Table 52.12. The results show relatively low yields in vacuo, but in oxygen the gas yield is high and almost entirely comprises carbonyl fluoride (COF_2).

Irradiation of the copolymers of PTFE at ambient temperature will generally lead to degradation of the polymer. Both FEP and poly(tetrafluoroethylene-*co*-perfluoropropylvinylether) PFA undergo predominantly chain scission which is also accompanied with a reduction of the mechanical properties [113]. However, with PFA, when the percentage of the comonomer is at a relatively high level, ca. 30% of perfluoro (methyl vinyl ether), there is some evidence of crosslinking [102]. The crosslinking may be due to the more ''rubbery'' nature of this copolymer at ambient temperature.

Poly(perfluoroethers) is another class of polymers that undergoes chain scission when subjected to high energy irradiation [114,115]. There appears to be no evidence for any crosslinking. The main products of degradation are the gaseous products COF_2 and CF_4; the G Factors for these gases are given in Table 52.13 [116,117].

52.3.6 ETFE and ECTFE Copolymers

These polymers are fluorocopolymers that have alternating units of ethylene and, respectively, TFE or CTFE. They are sometimes additionally modified with a third perfluoro monomer.

An increase in the high temperature (200 °C) tensile properties of the ethylene–tetrafluoroethylene copolymer, ETFE, after irradiation in nitrogen at room temperature followed by heat treatment at 162 °C in nitrogen for 20 min indicates some crosslinking [118]. On the other hand, irradiation carried out in air showed very little crosslinking [119]. ETFE behaves in some ways similar to polyvinylidene fluoride (PVDF) in that there is competition between crosslinking and scission. Some of the tensile properties, measured at 200 °C, of irradiated ETFE are shown in Table 52.14 [119].

ECTFE, the copolymer of ethylene and chlorotrifluoroethylene, has been shown to undergo some crosslinking

TABLE 52.10. *Tensile strength and elongation properties for γ-irradiated PTFE film [105].*

Condition	Dose (kGy)	Tensile strength (kg cm_{-2})	Elongation at break (%)	Sample thickness (mm)
Untreated	0	175	104	0.1
Irradiated in vacuo*	10	154	98	0.1
Irradiated in air	10	110	15	0.1
Untreated	0	269	129	0.04
Irradiated in vacuo*	104	136	10	0.04
Irradiated in air	104	0	0	0.04

*Tensile properties were measured in air.

TABLE 52.11. *Effect of dose on crystallinity levels of PTFE after γ-irradiation [106].*

Irradiation dose (KGy)	Density (g/cc)	Crystallinity (%)
0	2.17	59
250	2.23	79
500	2.24	83
750	2.24	83
1,000	2.24	83

TABLE 52.12. *Yields of volatile gases from the γ-irradiation of PTFE and FEP in vacuo and oxygen [112].*

	G(CO)	*G*(CF_4)	*G*(CO_2)	*G*(total gas)
PTFE (Vacuo)	0.03	0.006	0.08	0.43
FEP(Vacuo)	0.02	0.03	0.10	0.18
PTFE (Oxygen)	–	n. d.**	–	3.5*
FEP (Oxygen)	–	–	–	6.2*

*The main component of the total gas was almost entirely COF_2.
**Not detected within the limits of experimentation.

after irradiation with γ-rays [120], although there is competition between crosslinking and scission. Table 52.15 gives some data for high temperature (200 °C) tensile properties. The increase in both tensile strength and elongation is indicative of crosslinking, although at the higher doses the elongation starts to fall. The room temperature properties, Table 52.16, show a maintenance of tensile strength even up to 700 kGy, but they are accompanied by a steady decrease in elongation.

52.3.7 Vinylidene Fluoride Polymers

For the major polymer in this series, polyvinylidene fluoride (PVDF), the effects of high energy irradiation have been studied [99,119]. PVDF is a polymer that undergoes both crosslinking and scission with relatively high yields for both processes [121–124].

The radicals formed from electron and proton irradiation (50–5000 kGy) have been characterized by electron paramagnetic resonance (EPR). The radicals decay when exposed to normal light; however, when kept in the dark, no

TABLE 52.13. *Yields for gas evolution for the electron beam irradiation of a series of poly(perfluoroethers).*

Polymer	*G*(COF_2)	*G*(CF_4)	*G*(CF_3CFO)
$-(CF_2-O-)_x-(CF_2CF_2-O-)_y$	7.7	0.35	–
$HO-CH_2CF_2-O-(CF_2-O-)_x-(CF_2CF_2-O-)_y-CF_2CH_2-OH$	6.2	–	–
$-(CF_2-O-)_x-(CF(CF_3)CF_2-O-)_y$	1.7	1.1	0.3
$-(CF_2CF_2CF_2-O-)_x$	1.2	0.22	
$-(CF(CF_3)CF_2-O-)_x$	1.0	0.7	0.1

TABLE 52.14. *Tensile properties measured at 200 °C, of irradiated ETFE.*

Dose (kGy)	Temperature of irradiation (°C)	Tensile yield strength (psi)	Tensile strength (psi)	Ultimate elongation (%)
0	–	347	347	12
7	r. t.*	541	840	545
7	150–198	541	813	421
10	220–245	471	701	340

*Irradiation followed by heat treatment at about 160 °C for 20 min.

TABLE 52.15. *Mechanical properties measured at 200 °C of an ECTFE polymer after γ-irradiation.*

Dose (kGy)	Tensile strength (kg/cm^2)	Elongation (%)
0	13	37
40	33	679
70	44	660
100	43	377
700	85	132

TABLE 52.16. *Mechanical properties measured at room temperature of an ECTFE polymer after γ-irradiation.*

Dose (kGy)	Tensile strength (kg/cm^{-2})	Elongation (%)
0	486	309
40	453	298
70	430	268
100	452	224
700	479	72

decay was observed after 180 days [125]. The radical types identified are:

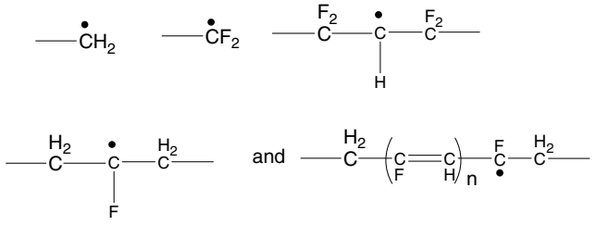

Radical III

Previous work had identified the five peaks in the spectra [126–128]. Radical III is a singlet and is long lived.

The thermal stability of the polymer after irradiation varies inversely with the radiation dose [129]. The yields for crosslinking and scission for several PVDF grades and its copolymers are given in Table 52.17. No substantial differences have been found for the radiation induced crosslinking of the α-, β-, and γ-crystalline forms of PVDF [130].

At relatively low doses, < 300 kGy, there is virtually no change in the room temperature tensile properties of PVDF when irradiated with an electron beam. For higher doses, > 300 kGy, there is an increase in the Young's modulus and a decrease in both tensile strength and elongation at break [124]. A recent study of the dependence of irradiation dose on the physical, chemical, and thermal properties of PVDF has been carried out [133].

The crystallinity of PVDF films has been shown to increase after irradiation with an electron beam followed by: (1) aging at ambient temperature for various periods and (2) uniaxial orientation [134]. The other observation from this work shows that in addition to the increase in crystallinity upon orientation there was a change in the crystalline form with a shift from the α form to the β form. The ratio of α to β after an irradiation dose of 200 kGy followed by aging and orientation was 32:68, and the degree of crystallinity increased from 0.40 to 0.66. The explanation for increasing crystallinity may be similar to that for PTFE, but may also be due to the effect of orientation.

A study of the irradiation of PVDF in vacuo has demonstrated the increase in crystallinity at low doses. However, the crystalline melting point decreased rapidly at approximately 3 °C/100 kGy between 100 and 300 kGy dose [135].

PVDF is known to exhibit a strong piezoelectric effect [136] with the Phase I (β form) being the most effective crystalline form for piezoelectric activity. Since molecular relaxation modes also contribute to overall piezoelectricity, high energy irradiation will affect the piezoelectric activity. This is due mainly to the effect of crosslinking which will increase the mechanical strength and change the molecular mobility of the polymer chains. A restriction in chain mobility will reduce reorientation of the molecular electric

TABLE 52.17. *Yields of crosslinking and scission for PVDF and copolymers after irradiation.*

Polymer	*G*(X)	*G*(S)	*G*(S)/*G*(X)	Remarks
PVDF [121]	1.0	0.3	0.30	
PVDF [122]	0.78	0.37	0.47	Solef 1010 Homopolymer
PVDF [131]	0.78	0.8	1.03	KF 1,000 irradiation at 61 °C
PVDF [128]	0.75	0.77	1.03	KF 1100 irradiation at 61 °C
PVDF [128]	0.90	0.85	0.94	Kynar 200 irradiation at 61 °C
PVDF [128]	0.70	0.57	0.81	Kynar 450 irradiation at 61 °C
VDF + HFP [121]	1.7	1.3	0.76	FluoroelastomerViton A
VDF + CTFE [121]	0.9	1.4	1.56	Fluoroelastomer Kel-F 3,700
PVDF [113]	0.60	0.29	0.48	Copolymer 3.5% tetrafluoroethylene
PVDF-HFP [122]	1.5	0.58	0.39	Solef 11010 Copolymer 6% (HFP)
PVDF-HFP [121,132]	3.4	1.3	0.4	

moments at the interphase. High energy irradiation of mainly β form PVDF leads to a lowering of the piezoelectric constant [137] and leads to improvement in the thermal stability of the β form and a slower piezoelectric decay [138].

An interesting comparison of the effect of electron beam irradiation on PVDF and ETFE, which differ only in chemical structure and have the same chemical composition, has shown that the irradiation has a more detrimental effect on tensile strength for ETFE than PVDF [139]. In fact, PVDF shows an increase in tensile strength compared to ETFE which shows a decease. In both cases, the elongation at break dropped with increasing dose, indicating crosslinking.

The copolymers of PVDF with trifluoroethylene and tetrafluoroethylene generally crystallize into the β form [140]. Irradiation with either electron beam or γ-radiation has been shown to induce solid-state ferroelectric to paraelectric transition in these copolymers as well as a decrease in their Curie temperature [141].

52.3.8 Other Fluoropolymers

Poly(vinylfluoride) (PVF) undergoes predominantly crosslinking when exposed to high energy irradiation [142] with a $G(X)$ of 3.4 to 5.7 $G(S)$ of 0.95 to 1.6 and $G(S)/G(X)$ of 0.28. The tensile strength of PVF almost doubles upon gamma irradiation of 10 kGy indicating the predominance of crosslinking [113].

Poly(trifluoroethylene) undergoes both crosslinking and chain scission with the former dominating. The $G(X)$ and $G(S)$ values are 1.1 and 0.4, respectively [121].

Poly(chlorotrifluoroethylene) (PCTFE) only degrades on exposure to high energy radiation. The $G(S)$ value is 0.67 from number average molecular weight determination [132]. The tensile properties degrade with relatively low doses of irradiation [143,144], Table 52.18, but slightly less rapid than PTFE. Irradiation in air will eventually give a yellow powder, as the critical dose for electrical breakdown is approached [145].

TABLE 52.18. *Mechanical properties of irradiated PCTFE [144].*

Dose (kGy)	Tensile strength(psi)	Shear strength (psi)	Elongation (%)
0	2,550	3,410	264
10	2,400	3,650	230
100	1,670	1,850	73
1,000	Failed	Failed	Failed

52.3.9 Polyvinylchloride

Polyvinylchloride (PVC) is one of the most reactive plastics when irradiated with either an electron beam or γ-rays. The major process is degradation via the loss of hydrogen chloride gas (dehydrochlorination). The dehydrochlorination is accompanied by a severe color change to a dark brown material [146], the color is due to the production of highly conjugated double bonds [147]. The degradation process is more pronounced in the presence of air and occurs after the irradiation has stopped (postirradiation effect) [43]. The dehydrochlorination process is dependent on temperature and increases with increasing temperature, as does the postirradiation effect [148]. At 90°C, that is, above T_g, gelation is observed at relatively low doses (120 kGy). For irradiation under nitrogen and at 150°C gelation occurs at $<$ 50 kGy [43], although at temperatures above T_g thermal dehydrochlorination will also be a major factor. Some yields for gas evolution under a variety of conditions are given in Table 52.19.

The physical properties of PVC film show an increase in elongation at low dose ($>$0.1 MGy) and then a dramatic fall off in elongation at 0.3 MGy Above doses of 0.3 MGy the material becomes brittle and has no elasticity.

When PVC is irradiated at very high doses (20 MGy), a material is formed that appears to have a structure that is mainly composed of carbon and in some cases is crystalline in nature [150,151].

52.3.10 Polyacrylates and Polymethacrylates

These are an interesting group of materials since they are clear examples of how the structure of the polymer can dramatically affect the changes that occur with either γ or electron beam irradiation. The poly(alkyl acrylates) undergo radiation crosslinking, whereas the poly(alkyl methacrylates) degrade so rapidly that they are used as positive-working electron beam resists [152]. Tables 52.20 and 52.21 give the yields for crosslinking and scission

TABLE 52.19. *G-Factors for degradation of PVC under vacuum and in the presence of oxygen.*

Condition	G(HCl)	$G(H_2)$	$G(CH_4)$	$G(CO_2)$	G(CO)	Dose (kGy)
Vacuum [149]	2.38	0.19	0.0013	0.007	0.001	300
Oxygen [110]	3.02	0.2	0.0063	0.115	0.1	300
−145 to −90°C [19]	5.6	–	–	–	–	–
30°C [19]	13	–	–	–	–	–
70°C [19]	23	–	–	–	–	–

TABLE 52.20. *The yields for crosslinking G(X), scission G(S) and the ratio G(S)/G(X) for a series of poly(alkyl acrylates).*

Polymer	*G*(X)	*G*(S)	*G*(S)/*G*(X)
Poly (methyl acrylate) [37]	0.5	–	0.07
Poly (ethyl acrylate) [153]	0.07	0.07	0.23
Poly (*n*-butyl acrylate)	0.21 [153]	–	0.07 [37], 0.14 [153]
Poly (iso-butyl acrylate) [37]	–	–	0.07
Poly (sec-butyl acrylate) [37]	–	–	0.10
Poly (tert-butyl acrylate) [37]	–	–	0.3–0.35

TABLE 52.21. *The yields for crosslinking G(X), scission G(S) and the ratio G(S)/G(X) for a series of poly(methacrylates).*

Polymer	G(X)	G(S)	G(S)/G(X)
Poly methyl methacrylate	–	1.63 (vacuo)	–
Poly methyl methacrylate	–	0.77 (air) [154]	–
Poly phenyl methacrylate	–	0.44 [155]	–
Poly benzyl methacrylate	–	0.14 [155]	–
Poly (1-naphthyl methacrylate)	–	0.14 [155]	–
Poly (2-naphthyl methacrylate)	–	0.19 [155]	–
Poly (Si methyl methacrylate) [156]	0.11	0.25	2.3
Poly (Si ethyl methacrylate) [156]	0.14	0.21	1.5
Poly (Si propyl methacrylate) [156]	0.54	0.58	1.07
Poly (Si Butyl methacrylate) [156]	0.99	0.77	0.78

for a series of poly(acrylates) and poly(methacrylates), respectively.

Modification of the alkyl methacrylate with a silicone group can cause a shift to a polymer that is more prone to crosslinking poly(Si butyl methacrylate) [156].

52.3.11 Polyesters

The dominant effect of high energy irradiation on a polyester is chain scission, although both crosslinking and scission occur. With the aromatic polyesters such as polyethylene terephthalate (PET) and polybutylene terephthalate (PBT) the aromatic groups will act as protection, and the yields of any process will have a tendency to be low.

Upon irradiation with an electron beam the aliphatic polyester, poly(butylene adipate)diol (PBAD) undergoes predominantly scission at low doses ($<$ 50 kGy) along with an increase in the level of crystallinity, whereas above 100 kGy both crosslinking and scission occur and the level of crystallinity decreases [157].

Although PET is regarded as relatively radiation resistant polymer, irradiation at relatively high dose ($>$1 MGy) with an electron beam in vacuo yields both crosslinking and scission with crosslinking predominating [158]. The initially semicrystalline material also becomes completely amorphous after high doses. Poly-1,6-hexamethylene terephthalate (PHT) behaves in a similar manner to PET but has higher yield of crosslinking. There is some evidence that both polymers undergo some crosslinking in the crystalline region as well as the amorphous region [159]. The radical produced from PET is shown as radical IV; there is evidence for the radical in both the amorphous and crystalline states. Two different decay rates are observed, the fast decay being attributed to the amorphous region and the slower decay to the crystalline region [160].

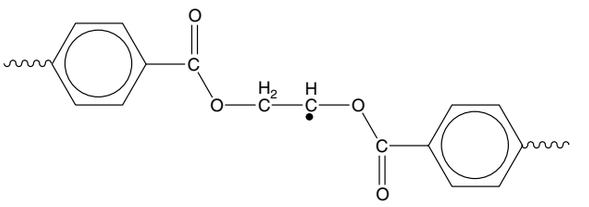

Radical IV

Irradiation of PET, in vacuo, is dose rate dependent [161] with γ-irradiation resulting in more degradation, leading to the production of acid groups, –COOH and evolution of the gases CO_2, CO, H_2 and CH_4 [162]. The yields of these products are shown in Table 52.22.

There appears to be some relationship between the number of methylene ($-CH_2-$) groups in poly(alkylene terephthalates), structure III, and irradiation, with even number of methylenes having a different effect in magnitude to the odd number of methylenes [164,165].

TABLE 52.22. *Yields for the products of electron beam and γ-irradiation of PET in vacuo [163].*

	$G(H_2)$	$G(CO)$	$G(CO_2)$	$G(X)$	$G(S)$	$G(CH_4)$
γ-rays	0.016	0.11	0.17	–	>0.8	0.003
E. beam	0.016	–	0. 08	0.08	0.16	–

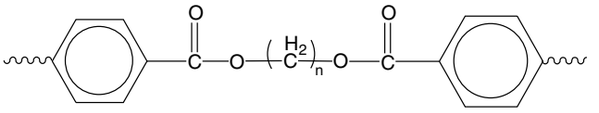

Structure III

52.3.12 Polyamides

Polyamides are classed in the family of crosslinking polymers when irradiated with either electron beam or γ-rays. Both crosslinking and scission occur, the yields for both processes $G(X)$ and $G(S)$ have been shown to be independent of the irradiation dose [166] but have been shown to be dependent on the number of hydrogen atoms or methylene groups in the amine residue [167]. Table 52.23 gives the yields of crosslinking and scission for a series of dry polyamides.

The yield of crosslinking correlates well with the number of methylene groups ($-CH_2-$) present in the polyamide structure. Absorbed water in the polyamide enhances crosslinking at higher concentration, and inhibits the process at low concentration. The presence of water does not appear to significantly affect the scission process.

Polyamides show a color change upon irradiation with either electron beam or γ-rays; the change is a consequence of radical formation. The radical is generally formed on the α-carbon, adjacent to the amide nitrogen [168], (radical V). Blocking of the hydrogen atom on the α-carbon with, for example, phenyl groups (Nylon MPD10) leads to a large reduction in the yields of both crosslinking and scission.

TABLE 52.23. *Yields of crosslinking and scission for a series of polyamides [131].*

Polyamide	$G(X)$	$G(S)$
Nylon 6	0.67	0.68
Nylon 6,6	0.50	0.70
Nylon 6,10	0.62	0.76
Nylon 11	0.92	0.85
Nylon 12	0.92	0.85
Nylon 10,10	1.12	1.10
Nylon 12,10	1.14	1.10
Nylon MPD10	0.07	0.07

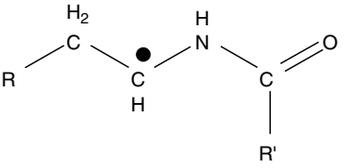

Radical V

As with many other polymers, the effects of irradiation on the physical properties of polyamides are highly dependent on the atmosphere during irradiation. For example, irradiation of a high tenacity Nylon 6,6 with an electron beam in an atmosphere free of oxygen showed only a 4% loss of tensile strength after 200 kGy and 35% loss after 2,000 kGy; the elongation to break showed little change. However, under similar irradiation conditions in air, after 2,000 kGy the tensile strength retention was 19% and the elongation to break was about a third of the original value [169].

Aromatic polyamides are much more resistant to irradiation than aliphatic polyamides, much of the effect is due to the protective effect of the aromatic groups. The highly aromatic polyamide, Nomex®, can retain about 80% of its tensile strength after a 6,000 kGy dose in air [170].

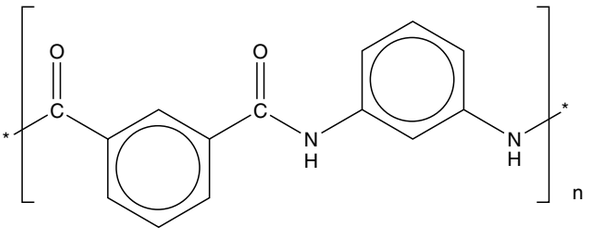

NOMEX

52.3.13 Polystyrene

Polystyrene is relatively resistant to the effects of high energy irradiation due to the "protective" effect of the aromatic groups. It does undergo crosslinking as the dominant process [171,172] with yields for crosslinking $G(X)$ being in the range, 0.019 to 0.051, depending on the method of determination. The effect of the irradiation temperature has already been discussed [44] in section 52.2.7.

The main volatile material evolved during the irradiation of polystyrene is hydrogen, the yield for hydrogen $G(H_2)$ is in the range, 0.022–0.026 with γ-irradiation [38,173,174]. Small amounts of benzene and methane have also been detected after irradiation with $G(C_6H_6)$ and $G(CH_4)$ being 0.008 and 10^{-5}, respectively [38].

The closely related polymer poly(α-methylstyrene) undergoes scission when irradiated with high energy [175] illustrating the importance of polymer structure. Polystyrene has structure I whereas poly(α-methylstyrene) has structure II and readily degrades [173]. Table 52.24 gives some crosslinking and scission yields for a variety of polystyrenes. The *p*-bromostyrene undergoes a high level of crosslinking, whereas the *p*-cyano and *p*-nitro show relatively high stability after irradiation [44].

The physical properties of polystyrene remain relatively stable even after high doses of irradiation. The hardness, tensile strength, and shear strength are all within 75% of the original values up to doses of 10^2 MGy [177]. The glass transition temperature is reported to increase by about 10 °C and the crystalline melting point increases to 150 °C after the irradiation of crystalline isotactic polystyrene to 40 MGy [178].

52.3.14 Polysiloxanes

Polysiloxanes readily undergo crosslinking when irradiated with high energy irradiation. Table 52.25 gives some *G* values for crosslinking for a series of polysiloxanes, poly (dimethyl siloxane) (PDMS), poly(phenylmethylsiloxane) (PPMS), and poly(diphenylsiloxane) (PDPS) and copolymers of dimethylsiloxane with phenylmethylsiloxane and diphenylsiloxane. As the percentage of aromaticity increases, the protective effect of the aromatic group leads to more radiation resistant polysiloxanes.

The gases evolved upon irradiation of PDMS comprise hydrogen, methane, and ethane. The total yield of gases is relatively high; *G*(Total gas) is 3.0 for PDMS [179].

There is a positive temperature effect, in that increasing temperature leads to increasing yield for crosslinking. For example, irradiation of a 1,000 centistokes dimethylsiloxane fluid gave *G*(X) values of 2.6, 2.8, 3.1, and 4.7 at −78 °C, 0 °C, 20 °C, and 150 °C, respectively [182].

The curing of silicone elastomers by irradiation leads to the typical properties of a cured elastomer, that is, an increase in hardness and tensile strength. Interestingly, the curing of PDMS using a peroxide cure system is very inefficient [183].

52.3.15 Highly Aromatic Polymers

All of the highly aromatic polymers are resistant, relative to the nonaromatic polymers, to irradiation with either electron beam or γ-rays. When irradiated in a vacuum many of these polymers are very stable and can show no change in physical properties even after high beam doses. For example, Kapton™ and Vespel™ aromatic polyimides have been shown to have resistance to both γ-rays and electron beams up to doses of 100 MGy of irradiation [184]. In the presence of oxygen, the physical properties of the aromatic polymers can be dramatically changed. For example, an aromatic polysulfone showed no change in the flexural strength after irradiation with γ-rays to 6 MGy, in vacuo. On the other hand, when the irradiation is carried out in the

TABLE 52.24. *Crosslinking and scission yields for a series of polystyrenes.*

Polymer	*G*(X)	*G*(S)
Polystyrene [176]	0.019 – 0.051	0.0094 – 0.019
Poly (α-methylstyrene) [174]	–	0.25
Poly (*p*-Methylstyrene) [44]	0.061	–
Poly (*p*-Methoxystyrene) [44]	0.074	–
Poly (*p*-Bromostyrene) [44]	3.1	–
Poly (*p*-Chlorostyrene) [44]	0.30	–
Poly (*p*-Cyanostyrene) [44]	No change in viscosity (200 kGy)	–
Poly (*p*-Nitrostyrene) [44]	No change in viscosity (1500 kGy)	–

TABLE 52.25. *Yields of crosslinking for a series of polysiloxanes.*

Polysiloxane	% Phenyl Groups	*G*(X)
PDMS	0	2.3 [180]
PPMS	50	0.25 [180,181]
PDPS	100	0.07 [180], 0.13 [181]
Dimethyl-/phenyl siloxane copolymer [180]	4.4	2.05
Dimethyl-/phenyl siloxane copolymer [180]	8.7	1.73
Dimethyl-/phenyl siloxane copolymer [180]	21.5	1.09
Dimethyl-/phenyl siloxane copolymer [180]	36	0.53
Dimethyl-/diphenyl siloxane copolymer [180]	17	1.44
Dimethyl-/diphenyl siloxane copolymer [181]	42	0.87

presence of air, the flexural strength dropped to about half its initial value at relatively low doses of between 0.2 and 4 MGy [185].

The radiation resistance for a series of polyimides(PI), poly(aryl ether ether ketone) (PEEK), poly(aryl ether sulphone) (PES), bisphenol A type Udel™ poly(aryl sulphone) (U-PS), and a poly(aryl ester) (U-Polymer) is shown to be excellent when compared to the related aliphatic polymers. *G* values for the evolution of gases were lower by factors of between 0.01 and 0.001 of the *G* values for the corresponding aliphatic polymers. From the study of gas evolution, the order of radiation resistance to γ-irradiation is [186]:

Upilex™-R(PI) > Kapton™ (PI) > PEEK > PES > Upilex™-S(PI) {≫} U-PS > U-Polymer

The order of resistance for electron beam irradiation is slightly different [187]:

Upilex™-R(PI) = Upilex™-S(PI) > Kapton™ (PI) > PEEK > PES {≫} U-PS > U-Polymer

The polyimides and PEEK show high radiation resistance to attenuation of physical properties.

The major component gases are: H_2 and N_2 for polyimides; CO_2 and CO for PEEK; CO_2, CO, and SO_2 for polysulphones; and CO_2 and CO for U-Polymer. The yields for gaseous evolution are very low and are given in Table 52.26 for electron beam and Table 52.27 for γ-irradiation.

An increase in the glass transition temperature T_g occurs when PEEK, either in the crystalline form PEEK-c or the amorphous form PEEK-a, is irradiated with γ-irradiation. This is indicative that a crosslinking process is occurring [188].

The irradiation of both amorphous and semicrystalline poly(phenylene sulfide) (PPS) with an electron beam in the presence of nitrogen shows no noticeable change in the mechanical or thermal properties at least to 10^4 kGy [189]. On the other hand, irradiation in air instead of nitrogen showed a change in both mechanical and thermal properties. At very high doses, 4×10^4 kGy, the amorphous PPS loses about 62% of its original tensile strength while the semicrystalline PPS loses about 57%. The T_m also changes, decreasing by about 10–271°C.

52.3.16 Other Polymers

Table 52.28 gives the *G*(X) and the *G*(S) values for a list of different polymers which will not be discussed in detail. The polyoxymethylene, cellulose, and polyisobutylene are all readily degraded upon irradiation.

The irradiation of some composite materials such as epoxy/graphite, polyimide/graphite, and polysulfone/graphite fibers have shown that the effects for irradiation up to 5×10^4kGy for electron radiation and up to 3,500 kGy for γ-radiation are negligible provided the irradiation is carried out in the absence of oxygen [196,197].

Polycarbonates, although they tend to strongly discolor for unstabilized grades, are relatively resistant to irradiation showing retention of elongation at yield and tensile modulus after irradiation up to 1,000 kGy [198].

Polymer Blends

The effect of electron beam irradiation on the miscible poly(styrene) and poly(vinyl methyl ether) (PVME) blend has been studied. The poly(styrene), being much more resistant to effects of irradiation, does not offer any protection to the poly(vinyl methyl ether). Gel content studies indicated significant crosslinking [199]. Further studies of this

TABLE 52.26. *Yields for gas evolution G(Gas)*(10^{-4}) *for electron beam irradiation.*

Polymer	$G(H_2)$	$G(N_2)$	G(CO)	$G(CO_2)$	$G(CH_4)$	Dose (MGy)
Kapton™	4.8	0.15	3.5	11	0.89	6.0
PEEK-c	7.5	–	3.4	11.3	0.16	5.8
PEEK-a	12	–	5.2	16	0.22	6.0
Upilex™-R	1.3	0.10	2.1	3.4	0.07	5.0
Upilex™-S	2.3	2.9	1.9	8.2	0.27	5.0

TABLE 52.27. *Yields for gas evolution G(Gas)*(10^{-4}) *for γ- irradiation under vacuum.*

Polymer	$G(H_2)$	$G(N_2)$	G(CO)	$G(CO_2)$	$G(CH_4)$	Dose (MGy)
Kapton™	2.1	3.6	3.9	7.4	0.89	7.4
PEEK-c	6.3	–	12	5.5	0.14	8.1
PEEK-a	12	–	6.5	12	0.20	7.4
Upilex™-R	0.38	9.8	2.5	5.2	0.08	5.7
Upilex™-S	8.4	13	1.8	15	0.30	8.1

TABLE 52.28. *Yields of crosslinking G(X) and scission G(S) for polymeric materials.*

Polymer	*G*(X)	*G*(S)	Reference
Polyoxymethylene	6.5	11.1	[190]
Polyisobutylene	–	5	[191]
Cellulose	–	11	[192]
Polyvinylacetate (O_2)	0.3	0.07	[26]
Polyvinylacetate (N_2)	0.15	0.06	[193]
Poly(vinyl ether)	5.8	–	[194]
Polypropylene oxide (atactic)	0.15	0.22	[195]
Polypropylene oxide (isotactic)	0.31	0.51	[195]

polymer blend with gamma irradiation and deuterated PS showed that a significant amount of grafting between the blend components occurred [200].

The gamma irradiation of a PS and PMMA blends showed that the polystyrene did not offer radiation protection for the PMMA. However, in the copolymer, poly(styrene- *co*-methylmethacrylate), a protective effect from the polystyrene was observed [201]. Some radiation(electron beam and gamma) crosslinking in PS/PMMA has also been reported [202]. A more recent study has shown the effect of gamma irradiation on the glass transition temperature (T_g) of the miscible blend [203].

Gamma irradiation of the highly miscible poly(vinyl alcohol)/polyacrylamide blends up to 100 kGy has been show to increase the thermal stability of the blend [204].

Recent irradiation studies with blends of PVC and modifiers such as flexible polymers (EVA [205] or ENR –epoxidized natural rubber [206]) or PFMs (polyfunctional monomers) have shown that the irradiation achieves more crosslinking and less degradation (chlorine loss) at lower doses. Seven PFMs, used at 10 parts per hundred rubber (phr), were compared for effectiveness for increasing softening temperature, gel yield and swelling ratio in PVC wire formulations [207].

EVA blends with PE (usually LDPE) have been studied and found to be more sensitive in achieving property improvements at lower doses [208,209]. In one case, a thermoplastic elastomer (TPE) with lower set was formed at < 50 kGy [210,211].

52.4 ADDITIVES

The above review of the effects of high energy irradiation on polymeric materials has covered the effects on the ''pure'' polymer, that is, the materials without the addition of additives except the ones added by the manufacturer, such as antioxidants.

With many of the materials discussed above, the effect of high energy irradiation can be dramatically changed by the addition of additives. For example, more efficient crosslinking can be induced in irradiated polyvinyl chloride by the addition of polyfunctional materials [212]; atactic polypropylene crosslinking is enhanced when irradiated, in vacuo, in the presence of nitrous oxide [213]. Many of the materials can be readily crosslinked at relatively low irradiation doses using crosslinking promoters, ''prorads'' [214–216]. The use of prorads, as well as increasing the crosslinking efficiency can reduce the other effects of irradiation, such as oxidation or gas evolution, because of the low doses that are used. In some cases, the need to retard crosslinking may be required. For example, with a highly efficient crosslinking polymer such as natural rubber the addition of ''antirads'' can reduce the yield of crosslinking [217,218].

The addition of fillers to a polymer will increase the back scattering of the incident radiation if the filler has a higher electron density than the polymer. The deposition of energy will in this case increase and will lead to an increase in crosslinking or scission, depending on which is the more dominant process.

All the processes of irradiation lead to the production of radicals. In the presence of monomers these radicals can initiate grafting on to the polymer chain. This review will not cover this aspect but an excellent introductory review is available [219].

52.5 SUMMARY

The effect of high energy irradiation on the properties of polymeric materials is complex and is dependent on the polymer structure, molecular weight, polymeric state, and the crystallinity level. The rate of irradiation and atmosphere during irradiation are major factors. Crosslinking, degradation, and evolution of gases are the major processes. These processes will lead to property changes in the polymer.

REFERENCES

1. A. Chapiro, ''Radiation Chemistry of Polymeric Systems,'' Interscience, New York, 1962.
2. A. Charlesby, ''Atomic Radiation and Polymers,'' Pergamon Press, London, 1960.
3. ''The Radiation Chemistry of Macromolecules. Volume I,'' edited by M. Dole, Academic Press, New York, 1972.
4. ''The Radiation Chemistry of Macromolecules. Volume II,'' edited by M. Dole, Academic Press, New York, 1973.
5. ''Radiation Processing of Polymers,'' edited by A. Singh and J. Silverman, Hanser, Munich, 1992.
6. ''Irradiation of Polymeric Materials,'' edited by E. Reichmanis, C. W. Frank and J. H. O'Donnell, American Chemical Society, 1993.
7. W. L. McLaughlin, Conference on National and International Standardization of Radiation Dosimetry Part I, p. 89, (1978).
8. R. A. Harrod, *Radiat. Phys. Chem.* **9**, 91, (1977).
9. A. Brynjolfsson, ''Sterilization By Ionizing Radiation,'' p. 145, Multiscience, Montreal, 1974.
10. R. Eymery, ''Sterilization by Ionizing Radiation,'' p. 84, Multiscience, Montreal, 1974.
11. M. R. Cleland, ''Radiation Processing of Polymers,'' Chapter 3, edited by A. Singh and J. Silverman, 1992.
12. K. Tomita and S. Sugimoto, *Radiat. Phys. Chem.* **9**, 576, (1977).

13. A. Charlesby, "Atomic Radiation and Polymers," Chapter 6, p. 96, Pergamon Press, London, 1960.
14. P. W. Moore, "Irradiation of Polymeric Materials," Chapter 2, p. 9, edited by E. Reichmanis, C. W. Frank and J. H. O'Donnell, American Chemical Society, 1993.
15. B. J. Lyons and W. C. Johnson, "Irradiation of Polymeric Materials," Chapter 5, p. 62, edited by E. Reichmanis, C. W. Frank and J. H. O'Donnell, American Chemical Society, 1993.
16. M. Burton, *Discuss. Faraday Soc*. **12**, 317, (1952).
17. B. J. Lyons and A. S. Fox, *J. Polym. Sci.: Part C*, **21**, 159, (1968).
18. A. Charlesby, *Proc. R. Soc. London,* **A222**, 60, (1954).
19. A. Charlesby, *Proc. R. Soc. London,* **A222**, 542, (1954).
20. A. Charlesby, *Proc. R. Soc. London,* **A224**, 120, (1954).
21. O. Saito, *J. Phys. Soc. Jpn*. **13**, 198, (1958).
22. O. Saito, *J. Phys. Soc. Jpn*. **13**, 1451, (1958).
23. O. Saito, *J. Phys. Soc. Jpn*. **13**, 1465, (1958).
24. O. Saito, *J. Phys. Soc. Jpn*. **13**, 798, (1959).
25. O. Saito, "The Radiation Chemistry of Macromolecules. Volume I," Chapter 11, p.223, edited by M. Dole, Academic Press, New York, 1972.
26. A. Charlesby and S. H. Pinner, *Proc. R. Soc*. **A249**, 367, (1959).
27. M. Inokuti, *J. Chem. Phys*. **18**, 2999, (1963).
28. B. J. Lyons, *J. Polym. Sci.: Part A*, **3**, 777, (1965).
29. A. Charlesby, "Atomic Radiation and Polymers," Chapter 9, p. 147, Pergamon Press, London, 1960.
30. D. I. C. Kells and J. E. Guillet, *J. Polym. Sci.: Part A-2,* **7**, 1895, (1969).
31. J. H. O'Donnell, N. P. Rahman, C. A. Smith and D. J. Winzor, *Macromolecules*, **12**, 113, (1979).
32. J. H. O'Donnell, N. P. Rahman, C. A. Smith and D. J. Winzor, *J. Polym. Sci.: Polym. Phys. Ed*. **16**, 1515, (1978).
33. B. J. Lyons, *Radiat. Phys. Chem*. **22**, 135, (1983).
34. O. Saito, H. Y. Kang and M. Dole, *J. Chem. Phys*. **46**, 3607, (1967).
35. A. Charlesby, in "Irradiation Effects on Polymers", p. 39, editors D. W. Clegg and A. A. Collyer, Elsevier Applied Science, Amsterdam, 1991.
36. A. Charlesby, "Atomic Radiation and Polymers," Chapter 9, p.142, Pergamon Press, London, 1960.
37. A. R. Shultz and F. A. Bovey, *J. Polym. Sci*. **22**, 485, (1956).
38. L. A. Wall and D. W. Brown, *J. Phys. Chem*. **61**, 129, (1957).
39. D. T. Turner, *J. Polym. Sci*. **35**, 541, (1959).
40. H. Kaufmann and H. Heusinger, *Makromol. Chem*. **177**, 871, (1976).
41. H. Katzer and H. Heusinger, *Makromol. Chem.* **163**, 195, (1973).
42. A. Charlesby, *Plastics*, **18**, 142, (1953).
43. A. A. Miller, *J. Phys. Chem.* **63**, 1755, (1959).
44. W. Burlant, J. Neerman and V. Serment, *J. Polym. Sci*. **58**, 491, (1962).
45. L. A. Wall and R. E. Florin, *J. Appl. Polym. Sci*. **2**, 251, (1959).
46. R. M. Keyser K. Tsuji and F. Williams, *Macromolecules*, **1**, 289, (1968).
47. R. M. Keyser and F. Williams, *J. Phys. Chem.* **73**, 1623, (1969).
48. R. M. Keyser, K. Tsuji and F. Williams, "The Radiation Chemistry of Macromolecules. Volume I," Chapter 9, p. 145, edited by M. Dole, Academic Press, New York, 1972.
49. G. H. Bowers and E. R. Lovejoy, *Ind. Eng. Chem. Prod. Res. Dev*. **1**, 89, (1962).
50. E. R. Lovejoy, M. I. Bro and G. H. Bowers, *J. Appl. Polym. Sci.* **9**, 401, (1965).
51. R. P. Kusy and D. T. Turner, *Macromolecules,* **4**, 337, (1971).
52. S. K. Bhateja, E. H. Andrews and R. J. Young, *J. Polym. Sci.:Polym. Phys. Ed.* **21**, 523, (1983).
53. G. G. A. Bohm and J. O. Tveekrem, *Rubber Chem. Technol*. **55**, 575, (1982).
54. K. Arakawa, T. Seguchi and K. Yoshida, *Radiat. Phys. Chem.* **27**, 157, (1986).
55. F. A. Makhlis, L. Y. Nikitin, A. K. Volkova and M. N. Tikhonova, *Vysokomol. Soedin*. **A13**, 596, (1971).
56. L. Mullins and D. T. Turner, *Nature*, **183**, 1547, (1959).
57. L. Mullins and D. T. Turner, *J. Polym. Sci*. **43**, 35, (1960).
58. A. Charlesby and E. von Arnim, *J. Polym. Sci*. **25**, 151, (1957).
59. V. T. Kozlov, A. G. Yevseyev and P. I. Zubov, *Vysokomol. Soed*. **A11**, 2230, (1969).
60. A. Von Raven and H. Heusinger, *J. Polym. Sci.: Polym. Chem. Ed*. **12**, 2255, (1974).
61. E. Witt, *J. Polym. Sci*. **41**, 507, (1959).
62. D. J. T. Hill, J. H. O'Donnell, M. C. S. Perera and P. J. Pomery, *ACS Symp. Ser*. **527**, "Irradiation of Polymeric Materials," Chapter 6, p. 74, edited by E. Reichmanis, C. W. Frank and J. H. O'Donnell, American Chemical Society, 1993.
63. G. Odian, D. Lamparella and J. Canamare, *J. Polym. Sci.: Part C,* **16**, 3619, (1968).
64. W. Geissler, H. Zott and H. Heusinger, *Makromol. Chem*. **179**, 697, (1978).
65. R. J. Elred, *Rubber Chem. Technol*. **47**, 924, (1974).
66. M. Aoshima, T. Jinno and T. Sassa, *Cell. Polym*. **10**, 359, (1991).
67. H. Kanbara, S. J. Huang and J. F. Johnson, *Polym. Eng. Sci*. **34**, 691, (1994).
68. G. L. Grune, V. T. Stannett, R. T. Chern and J. Harada, *Polym. Adv. Technol*. **4**, 341, (1993).
69. B. J. Lyons, *Nature,* **195**, 690, (1962).
70. L. Mandelkern, "The Radiation Chemistry of Macromolecules. Volume II," Chapter 13, p. 302, edited by M. Dole, Academic Press, New York, 1973.
71. Y. Sakai, K. Umetsu and K. Miyasaka, *Polymer,* **34**, 3362, (1993).
72. D. J. Dijkstra, W. Hoogsteen and A. J. Pennings, *Polymer,* **30**, 866, (1989).
73. S. K. Bhateja, *J. Appl. Polym. Sci.* **28**, 861, (1983).
74. M. Dole, D. C. Milner and T. F. Williams, *J. Am. Chem. Soc*. **80**, 1580, (1958).
75. B. J. Lyons and M. A. Crook, *Trans. F. Soc*. **59**, 2334, (1963).
76. M. Dole, "The Radiation Chemistry of Macromolecules. Volume II," Chapter 14, p. 339, edited by M. Dole, Academic Press, New York, 1973.
77. D. C. Waterman and M. Dole, *J. Phys. Chem.* **74**, 1906, (1970).
78. L. Mandelkern, "The Radiation Chemistry of Macromolecules. Volume II," Chapter 13, p. 322, edited by M. Dole, Academic Press, New York, 1973.
79. B. J. Lyons, *Radiat. Phys. Chem*. **28**, 149, (1986).
80. L. Mandelkern, "The Radiation Chemistry of Macromolecules. Volume II," Chapter 13, edited by M. Dole, Academic Press, New York, 1973.
81. M. Dole, "The Radiation Chemistry of Macromolecules. Volume II," Chapter 14, edited by M. Dole, Academic Press, New York, 1973.
82. B. J. Lyons and F. E. Weir, "The Radiation Chemistry of Macromolecules. Volume II," Chapter 7, edited by M. Dole, Academic Press, New York, 1973.
83. D. J. Dijkstra, W. Hoogsteen and A. J. Pennings, *Polymer,* **30**, 866, (1989).
84. G. Heirich *et al*., *Kunstoffe*, **57**, 156, (2004).
85. C. F. Coote, J. V. Hamilton, W. G. McGimpsey and R. W. Thompson, *J. Appl. Polym. Sci*. **77**, 2525, (2000).
86. E. A. Reeeves, D. C. Barton, D. P. Fitzpatrick and J. Fisher, *Proc. Inst. Mach. Eng., Part H: J. Eng. Med*. **214**, 249, (2000).
87. Y. Luisetto, B. Wesslen, F. Maurer and L. Lidgren, *J. Med. Mater. Res. Part A*, **67**, 908, (2000).
88. N. M. Burns, *Radiat. Phys. Chem.* **14**, 797, (1979).
89. P. E. Jacobs, *Polym.-Plast. Technol. Eng*. **17**, 69, (1981).
90. B. J. Lyons and C. R. Vaughn, in "Irradiation of Polymers", *Adv. Chem. Ser*. **66**, 139, (1967), American Chemical Society Publications.
91. R. M. Black and B. J. Lyons, *Nature,* **180**, 55, (1957).
92. R. M. Black and B. J. Lyons, *Proc. R. Soc*. **A253**, 322, (1959).
93. T. S. Dunn, B. J. Epperson, H. W. Sugg, V. T. Stannett and J. L. Williams, *Radiat. Phys. Chem*. **14**, 625, (1979).
94. D. E. Gavrila and B. Gosse, *J. Radioanal. Nucl. Chem. Art*. **185**, 311, (1994).
95. E. A. Hegazy, T. Seguchi, K. Arakawa and S. Machi, *J. Appl. Polym. Sci*. **26**, 1361, (1981).
96. W. Snabel and M. Dole, *J. Phys. Chem*. **67**, 295, (1963).
97. B. J. Lyons, *J. Polym. Sci*. **A3**, 777, (1965).
98. J. N. Tomlinson and D. E. Kline, *J. Appl. Polym. Sci*. **11**, 1931, (1967).
99. B. J. Lyons, *Radiat. Phys. Chem*. **45**, 159, (1995).
100. Y. Rosenberg, A. Siegmann, M. Narkis and S. Shkolnik, *J. Appl. Polym. Sci*. **45**, 783, (1992).
101. E. Katan, M. Narkis and A. Siegmann, *J. Appl. Polym. Sci*. **70**, 1471, (1998).
102. R. E. Uscold, *J. Appl. Polym. Sci*. **29**, 1335, (1984).
103. L. A. Wall and R. E. Florin, *J. Appl. Polym. Sci*. **2,** 251, (1959).

104. R. E. Florin, "Fluoropolymers", Chapter 11, p. 321, edited by L. A. Wall, Wiley Interscience, New York, 1972.
105. P. Hedvig, *J. Polym. Sci., Part A-1,* **7**, 1145, (1969).
106. A. Nishioka, A. K. Matsumae, M. Watanabe, M. Tajima and M. Owaki, *J. Appl. Polym. Sci.* **2,** 114, (1959).
107. D. E. Kline and J. A. Sauer, *J. Polym. Sci. Part A,* **1**, 1621, (1963).
108. W. R. Licht and D. E. Kline, *J. Polym. Sci. Part A,* **2**, 4673, (1964).
109. J. Sun, Y. Zhang, X. Zhong and X. Zhu, *Radiat. Phys. Chem.* **44**, 655, (1994).
110. J. Sun, Y. Zhang and X. Zhong, *Polymer*, **35**, 2881, (1994).
111. E. R. Lovejoy, M. I. Bro and G. H. Bowers, *J. Appl. Polym. Sci.* **9**, 401, (1965).
112. D. M. Pinkerton and B. T. Sach, *Austal. J. Chem.* **23**, 1947, (1970).
113. Y. Rosenberg, A. Siegmann, M. Narkis and S. Shkolnik, *J. Appl. Polym. Sci.* **45**, 783, (1992).
114. P. Barnaba, D. Cordischi, A. Dell Site and A. Mele, *J. Chem. Phys.* **44**, 3672, (1966).
115. J. Pacansky and R. J. Waltman, *J. Chem. Phys.* **95**, 1512, (1991).
116. J. Pacansky and R. J. Waltman, *Chem. Mater.* **5**, 486 and 1526, (1993).
117. J. Pacansky, R. J. Waltman and G. Pacansky, *Chem. Mater.* **5**, 1526, (1993).
118. D. P. Carlson and N. E. West, *US Patent No.* 3, 378, 923, (1973).
119. B. J. Lyons, *Rad. Proc. Plastics Rubber II,* University of Kent at Canterbury, The Chameleon Press, London, (1984).
120. Y. X. Luo, F. C. Pang and J. X. Sun, *Radiat. Phys. Chem.* **18**, 445, (1981).
121. T. Yoshida, R. E. Florin and L. A. Wall, *J. Polym. Sci.*: Part A, **3**, 1685, (1965).
122. I. Klier and A. Vokal, *Radiat. Phys. Chem.* **38**, 457, (1991).
123. V. S. Ivanov, I. I. Migunova and A. I. Mikhailov, *Radiat. Phys. Chem.* **37**, 119, (1991).
124. J. L. Suther and J. R. Laghari, *J. Mater. Sci. Lett.* **10**, 786, (1991).
125. E. Adem, G. Burillo, E. Munoz, J. Rickards, L. Cota and M. Avalos-Borja, *Polym. Degrad. Stab.* **81**, 75, (2003).
126. N. Betz, E. Petersohn and A. le Moël, *Radiat. Phys. Chem.* **46**, 411, (1996).
127. A. le Moël, J. P. Duraud, I. Lemaire, E. Balanzat, J. M. Ramillon and C. Darnez, *NUC. Instr. Methods Phys. Res.* **B105,** 71, (1987).
128. T. Seguchi, K. Makuuchi, T. Suwa, N. Tamura, T. Abe and M. Takehisa, *Nippon Kagaku Kaishi*, **7**, 686, (1975).
129. L. A. Wall, S. Straus and R. E. Florin, *J. Polym. Sci.: Part A-1*, **4**, 349, (1966).
130. A. J. Lovinger, *Macromolecules,* **18**, 910,(1985).
131. K. Makucchi, M. Asano and T. Abe, *Nippon Kagaku Kaishi*, 686, (1976).
132. R. E. Florin and L. A. Wall, *J. Res. NBS,* **65A**, 375, (1961).
133. M. M. Nasef, H. Saidi and Z. M. Dahlen, *Polym. Degrad. Stab.* **75**, 85, (2002).
134. K. D. Pae, S. K. Bhateja and J. R. Gilbert, *J. Polym. Sci.: Part B: Polym. Phys.* **25**, 717, (1987).
135. Z. Zhao, X. Chen and W. Yu, *Radiat. Phys. Chem.* **65**, 173, (2002).
136. H. Kawai, *Jpn. J. Appl. Phys.* **8**, 975, (1969).
137. P. Harnischfeger and B. J. Jungnickel, *Appl. Phys.* **A 50**, 523, (1990).
138. T. T. Wang, *Ferroelectrics,* **41**, 213, (1982).
139. M. M. Nasef and Z. M. Dahlen, *Nuclear Inst. Methods Phys. Res.; Section B,* **201**, 604, (2003).
140. A. J. Lovinger, T. Furukawa, G. T. Davies and M. G. Broadhurst, *Polymer,* **24**, 1225 and 1233, (1983).
141. A. J. Lovinger, *ACS Symp. Ser.* **475**, "Radiation Effects on Polymers", edited by R. Clough and S. W. Shalaby, American Chemical Society, 1991.
142. R. Timmerman and W. Greyson, *J. Appl. Polym. Sci.* **22**, 456, (1962).
143. J. Byrne, T. W. Costikyan, C. B. Hanford, D. L. Johnson and W. L. Mann, *Ind. Eng. Chem.* **45**, 2549, (1953).
144. J. C. Bresee, J. R. Flanary, J. H. Goode, C. D. Watson and J. S. Watson, *Nucleonics,* **14**, 75, (1956).
145. J. Goodman and J. H. Coleman, *J. Polym. Sci.* **25**, 253, (1957).
146. G. J. Atchison, *J. Polym. Sci.* **49**, 385, (1961).
147. G. J. Atchison, *J. Appl. Polym. Sci.* **7**, 1471, (1963).
148. B. R. Joy, *J. Polym. Sci.* **50**, 245, (1961).
149. A. H. Zahran, E. A. Hegazy and F. M. Ezz Eldin, *Radiat. Phys. Chem.* **26,** 25, (1985).
150. L. Cota, M. Avalos-Borja, E. Adem and G. Burillo, *Radiat. Phys. Chem.* **44**, 579, (1994).
151. E. Adem, M. Avalos-Borja, L. Cota and G. Borillo, *Radiat. Phys. Chem.* **39**, 397, (1992).
152. K. Harada, O. Kogure and K. Murase, *IEEE Trans. Elect on. Dev.* **29**, 518, (1982).
153. W. Burlant, J. Hinsch and C. Taylor, *J. Polym. Sci.: Part A,* **2**, 57, (1964).
154. K. Ishigure, S. Egusa, S. Tagawa and Y. Tabata, *Radiat. Phys. Chem.* **14**, 585, (1979).
155. I. Gitsov and O. G. Todorova, *J. Appl. Polym. Sci.* **46**, 1631, (1992).
156. R. G. Jones, R. H. Cragg, R. D. P. Davies and D. R. Brambley, *J. Mater. Sci.* **2**, 371, (1992).
157. A. Masayuki and U. Toshiyuki, *Radiat. Phys. Chem.* **33**, 461, (1989).
158. N. A. Slovokhotova, G. K. Sadovskaya and V. A. Kargin, *J. Polym. Sci.* **58**, 1293, (1962).
159. Z. Yiquin, J. Danliang, C. Xinfang, C. Zhanchen, L. Yuxia and L. S. Hua, *Radiat. Phys. Chem.* **43**, 459, (1994).
160. T. Memetea and V. Stannett, *Polym. Prepr.* **18**, 777, (1977).
161. V. H. Ritz, *Radiat. Res.* **15**, 460, (1961).
162. S. D. Burow, D. T. Turner, G. F. Pezdirtz and G. D. Sands, *J. Polym. Sci. Part A-1,* **4**, 613, (1966).
163. D. T. Turner, "The Radiation Chemistry of Macromolecules. Volume II," Chapter 8, p. 137, edited by M. Dole, Academic Press, New York, 1973.
164. J. Kroh and M. Pietrzak, *Khim. Vys. Energ.* **4**, 246, (1970).
165. M. Pietrzak, *Radiochem. Radioanal. Lett.* **54**, 67, (1982).
166. B. J. Lyons and L. C. Glover, *Radiat. Phys. Chem.* **35**, 139, (1990).
167. B. J. Lyons and L. C. Glover, *Radiat. Phys. Chem.* **37**, 93, (1991).
168. J. Zimmerman, *J. Appl. Poly. Sci.* **2**, 181, (1959).
169. J. Zimmerman "The Radiation Chemistry of Macromolecules. Volume II," Chapter 7, p. 129, edited by M. Dole, Academic Press, New York, 1973.
170. L. K. McCune, *Textile Res.* **32**, 262, (1962).
171. A. Charlesby, *J. Polym. Sci.* **11**, 513 and 521, (1953).
172. J. C. Spiro and C. A. Winkler, *J. Appl. Polym. Sci.* **8**, 1709, (1964).
173. J. Wilske and H. Heusinger, *J. Polym. Sci. Part A-1,* **7**, 995, (1969).
174. R. M. Keyser, W. K. Kirkland and W. W. Parkinson, *Oak Ridge Nat. Lab. Reactor Chem. Div. Ann. Prog. Rep. ORNL-3591,* 224, (1964).
175. A. M. Kotliar, *J. Appl. Polym. Sci.* **2**, 134, (1959).
176. W. W. Parkinson and R. M. Keyser, "The Radiation Chemistry of Macromolecules. Volume II," Chapter 5, p. 72, edited by M. Dole, Academic Press, New York, 1973
177. O. Sisman and C. D. Bopp, *Physical Properties of Irradiated Plastics, ORNL-928, Nat. Tech. Info. Ser., Operations Div.* Springfield, Virginia, (1951).
178. M. Baccaredda, E. Butta and V. Frosini, *J. Appl. Polym. Sci.* **10**, 399, (1966).
179. A. A. Miller, *J. Amer. Chem. Soc.* **82**, 3519, (1960).
180. W. Schnabel, *Makromol. Chem.* **104**, 1, (1967).
181. A. A. Miller, *Ind. Eng. Chem. (Prod. Res. Dev.),* **3**, 252, (1964).
182. A. Charlesby, "Atomic Radiation and Polymers," Chapter 16, p. 307, Pergamon Press, London, 1960.
183. A. A. Miller, *J. Polym. Sci.* **42**, 441, (1960).
184. C. L. Hanks and D. J. Hamman " Radiation Effects Design Handbook", NASA-CR-1787, Sec 3, (1971).
185. J. R. Brown, J. H. O'Donnell, *J. Appl. Polym. Sci.* **23**, 2763, (1979).
186. E. A. Hegazy, T. Sasuga, M. Nishii and T. Seguchi, *Polymer*, **33**, 2897, (1992).
187. E. A. Hegazy, T. Sasuga, M. Nishii and T. Seguchi, *Polymer*, **33**, 2904, (1992).
188. E. A. Hegazy, T. Sasuga and T. Seguchi, *Polymer*, **33**, 2911, (1992).
189. A. M. El-Naggar, H. C. Kim, L. C. Lopez and G. L. Wilkes, *J. Appl. Polym. Sci.* **37**, 1655, (1989).
190. H. Fischer and W. Langbein, *Kolloid-Z.* **216–217**, 329, (1967).
191. P. Alxander, R. M. Black and A. Charlesby, *Proc. R. Soc.* **A232**, 31, (1955).
192. A. Charlesby, *J. Polym. Sci.* **15**, 263, (1955).
193. S. Miller, M. W. Spindler and R. L. Vale, *Polym. Sci. Part A,* **1**, 2537, (1963).
194. X. Liu, R. M. Briber and B. J. Bauer, *J. Polym. Sci.: Part B: Polym. Phys.* **32**, 811, (1994).

195. G. P. Roberts, M. Budzol and M. Dole, *J. Polym. Sci. Part A-2,* **9**, 1729, (1971).
196. R. E. Fornes, J. D. Memory and N. Naranong, *J. Appl. Polym. Sci*. **26**, 2061, (1981).
197. J. D. Memory, R. E. Fornes and R. D. Gilbert, *J. Reinf. Plast. Compos.* **7**, 33, (1988).
198. R. E. Weyers, P. R. Blankenhorn, L. R. Stover and D. E. Kline, *J. Appl. Polym. Sci*. **22**, 2019, (1978).
199. D. C. McHerron and G. L. Wilkes, *Polymer,* **34**, 3976, (1993).
200. R. M. Briber and B. J. Baure, *Macromolecules*, **21**, 3296, (1988).
201. T. Ayoko, H. Ken-ichi, H. Nobutomo and M. Takuya, *Radiat. Phys. Chem.* **43**, 493, (1994).
202. R. Katare, R. Bajpai and S. C. Datt, *Polym. Testing*, **13**, 107, (1994).
203. K. El-Salmawi, M. M. Abu Zeid, A. M. El-Naggar and M. Mamdouh, *J. Appl. Polym. Sci*. **72**, 509, (1999).
204. H. M. N. El-din, A. M. El-Naggar and F. I. Ali, *Polym. Int.* **52**, 225, (2003).
205. S. Wang, Y. Zhang, C. Zhang and E. Li, *J. Appl. Polym. Sci*. **91**, 1571, (2004).
206. C. T. Ratnam, M. Nasir, A. Baharin and K. Zaman, *J. Appl. Polym. Sci*. **81,** 1926, (2001).
207. H. A. Youssef, Z. I. Ali and A. H. Zahran, *Polym. Degrad. Stab.* **74,** 213, (2001).
208. J. Sharif, S. H. S. A. Aziz and K. Hashim , *Radiat. Phys. Chem.* **58**, 191 (2000).
209. S. M. A. Salehi, G. Mirjalili and J. Amrollahi, *J. Appl. Polym. Sci*. **92**, 1049, (2004).
210. S. Chattopadhyay, T. K. Chaki and A. K. Bhowmick, *J. Appl. Polym. Sci*. **79**, 1877, (2001).
211. S. Chattopadhyay, T. K. Chaki and A. K. Bhowmick, *J. Appl. Polym. Sci.* **81**, 1936, (2001).
212. K. Posselt, *Kolloid-Z. Z. Polym.* **223**, 104, (1968).
213. Y. Okada, *Adv. Chem. Ser*. **66**, 44, (1967).
214. B. J. Lyons, *Nature*, **185**, 604, (1960).
215. A. A. Miller, *J. Appl. Polym. Sci*. **5**, 388, (1961).
216. B. J. Lyons and P. E. Cross, *Trans. F. Soc*. **59**, 2350, (1963).
217. R. G. Bauman, *J. Appl. Polym. Sci*. **2**, 328, (1959).
218. R. G. Bauman and J. W. Born, *J. Appl. Polym. Sci*. **1**, 351, (1959).
219. A. Chapiro, "Radiation Chemistry of Polymeric Systems," Chapter 12, p. 596, Interscience, New York, 1962.

CHAPTER 53

Flammability

Archibald Tewarson

FM Global Research, 1151 Boston-Providence Turnpike, Norwood, MA 02062

53.1 INTRODUCTION

The flammability of a polymer is an interaction of pyrolysis, ignition, combustion, flame propagation, and flame extinction processes. The processes are brought about by the heat exposure of the polymer. Pyrolysis is an endothermic process and involves softening, melting, discoloration, cracking, decomposition, vaporization, etc. of the polymer and release of pyrolysis products. The boundary of the pyrolysis process on the surface of the polymer is defined as the pyrolysis front. Pyrolysis process is also defined as the gasification of the polymer.

Ignition is a process in which the gasified polymer mixes with air, forms a combustible mixture and the mixture ignites by itself (auto-ignition) or is ignited by a flame, a hot object, an electrical spark, etc., (piloted-ignition).

Combustion is a process in which the solid surface of the polymer or the gasified polymer reacts with the oxygen from air with a visible flame (flaming combustion) or without a visible flame (nonflaming combustion).

Flame propagation is a process in which the pyrolysis front accompanied by flaming- or nonflaming combustion moves with time beyond the point of origin.

Flame extinction is a process where the pyrolysis, ignition, combustion, and fire propagation processes are interrupted by applying agents such as water, inert or chemically active gases, liquids or solids, or reducing the oxygen concentration.

Heat and products are generated in pyrolysis, ignition, combustion, and flame propagation processes, presenting hazards to life and property. Hazard due to release of heat (high temperature and radiation) is defined as thermal hazard [1]. Hazard due to release of products is defined as

nonthermal hazard [2]. Nonthermal hazard is due to toxic and corrosive products which interfere in light transmission (reducing visibility) and in electrical operations of delicate electrical components and equipment, and impart discolor and malodor.

For the assessment of thermal and nonthermal hazards, fire prevention and protection, several types of models have been developed. All these models use fire properties of polymers associated with pyrolysis, ignition, combustion, and flame propagation as inputs [2,3]. These properties are listed in Table 53.1 and are discussed in this chapter.

53.2 FIRE PROPERTIES ASSOCIATED WITH THE PYROLYSIS OF THE POLYMER: HEAT OF GASIFICATION AND SURFACE RE-RADIATION LOSS

The steady state polymer gasification rate is expressed as [2,3]:

$$\dot{m}_f'' = \frac{\dot{q}_e'' - \dot{q}_{rr}''}{\Delta H_g}, \tag{53.1}$$

where $\dot{m}_f''$ is the polymer gasification rate or the mass loss rate in pyrolysis ($kg/m^2 - s$), $\dot{q}_e''$ is the external heat flux

TABLE 53.1. *Fire properties associated with pyrolysis, ignition, combustion, and fire propagation processes.*

Fire property	Fire property description
Pyrolysis process	
Heat of gasification (ΔH_g) in MJ/kg	Energy required to vaporize a unit mass of the polymer originally at ambient temperature.
Surface re-radiation Loss ($\dot{q}_{rr}''$) in kW/m^2	Heat lost to the environment from the hot surface of the polymer.
Yield of a product (y_j) in kg/kg	Amount of a product generated per unit mass of the polymer gasified.
Product generation parameter (PGP)	Defines product generation rate in non-flaming combustion for a specified heat flux exposure.
Ignition process	
Critical Heat Flux, CHF, ($\dot{q}_{cr}''$) in kW/m^2	Minimum heat flux at or below which a flammable vapor-air mixture is not created. It is related to the fire point or ignition temperature.
Thermal Response Parameter (TRP) in kJ/m^2 for thermally thin polymer and in kW-$s^{1/2}m^2$ for thermally thick polymer	Resistance to ignition and fire propagation.
Combustion process	
Flame heat flux ($\dot{q}_f''$) in kW/m^2	Heat flux transferred from the flame back to the surface of the burning polymer.
Net Heat of Complete Combustion (ΔH_T) in MJ/kg	Amount of energy released in the complete combustion of a unit mass of the polymer with water as a gas.
Chemical Heat of Combustion (ΔH_{ch}) in MJ/kg	Amount of energy actually released in the flaming combustion of a unit mass of the polymer.
Convective heat of combustion (ΔH_{con}) in MJ/kg	Component of the chemical heat of combustion carried away from the flame by combustion product-air mixture.
Radiative heat of combustion (ΔH_{rad}) in MJ/kg	Component of the chemical heat of combustion transmitted away from the flame by radiation.
Yield of a product (y_j) in kg/kg	Amount of a product generated per unit mass of the polymer gasified.
Heat release parameter (HRP)	Defines heat release rate in the combustion process for a specified heat flux exposure.
Product generation parameter (PGP)	Defines product generation rate in the combustion process for a specified heat flux exposure.
Fire propagation	
Limiting oxygen index (LOI) Flame propagation rate Fire propagation index (FPI)	Defines propagating and non-propagating fire behavior.

(kW/m^2), $\dot{q}''_{rr}$ is the surface re-radiation loss (kW/m^2), and ΔH_g is the heat of gasification (MJ/kg). Pyrolysis experiments are performed where the polymer is heated in an inert environment and various measurements are made. The most widely used techniques are: (1) differential scanning calorimetry, and (2) mass pyrolysis technique.

In the differential scanning calorimetry, measurements are made for the specific heat, heats of melting, vaporization, decomposition, etc., in a differential scanning calorimeter and the data are used in the following equation to calculate the heat of gasification, such as for a melting polymer [2]:

$$\Delta H_g = \int_{T_a}^{T_m} c_{p,a} dT + \Delta H_m + \int_{T_m}^{T_v} c_{p,l} dT + \Delta H_v, \quad (53.2)$$

where ΔH_m and ΔH_v are the heats of melting and vaporization at the respective melting and vaporization temperatures in MJ/kg, $c_{p,\,s}$ and $c_{p,\,l}$ are the specific heats of the polymer in the solid and molten states in MJ/kg respectively, and T_a, T_m, and T_v are the ambient, melting, and vaporization temperatures in K, respectively. For polymers which do not melt, but sublime, decompose or char, Eq. (53.2) is modified accordingly. The values of the heat of gasification calculated from the differential scanning calorimetry in our laboratory are listed in Table 53.2 [4].

In the mass pyrolysis technique, the mass loss rate is measured as a function of external heat flux in the presence of co-flowing nitrogen or air with an oxygen concentration of 10% by volume, and the data are used in Eq. (53.1). The heat of gasification is determined from the linear regression

TABLE 53.2. *Surface re-radiation loss and heat of gasification of polymers.*[a]

Polymer[b]	Surface reradiation loss (kW/m^2)	Heat of gasification (MJ/kg)	
		ASTM E 2058 FPA	DSC
Natural polymers			
Filter paper	10	3.6	—
Corrugated paper	10	2.2	—
Wood (Douglas fir)	10	1.8	—
Plywood/FR	10	1.0	—
Particle board	—	3.9	—
Synthetic polymers			
Epoxy resin	—	2.4	—
Polypropylene	15	2.0	2.0
Polyethylene (low density)	15	1.8	1.9
Polyethylene (high density)	15	2.3	2.2
Polyethylene foams	12	1.4–1.7	—
Polyethylene/25% Chlorine	12	2.1	—
Polyethylene/36% Chlorine	12	3.0	—
Polyethylene/48% Chlorine	10	3.1	—
Rigid polyvinylchloride (PVC)	15	2.5	—
PVC/plasticizer	10	1.7	—
Plasticized PVC, LOI = 0.20	10	2.5	—
Plasticized PVC, LOI = 0.25	—	2.4	—
Plasticized PVC, LOI = 0.30	—	2.1	2.1
Plasticized PVC, LOI = 0.35	—	2.4	2.4
Rigid PVC, LOI = 0.50	—	2.3	2.3
Polyisoprene	10	2.0	—
PVC panel	17	3.1	—
Nylon 6/6	15	2.4	—
Polyoxymethylene	13	2.4	2.4
Polymethylmethacrylate	11	1.6	1.6
Polycarbonate	11	2.1	—
Polycarbonate panel	16	2.3	—
Isophthalic polyester	—	3.4	—
Polyvinyl ester	—	1.7	—
Acrylonitrile-Butadiene-Styrene	10	3.2	—
Styrene-Butadiene	10	2.7	—
Expanded Polystyrene	10–13	1.3–1.9	—
Polystyrene (granular)	13	1.7	1.8

TABLE 53.2. *Continued.*

Polymer[b]	Surface reradiation loss (kW/m^2)	Heat of gasification (MJ/kg)	
		ASTM E 2058 FPA	DSC
Expanded polyurethane (flexible)	16–19	1.2–2.7	1.4
Expanded polyurethane (Rigid)	14–22	1.2–5.3	—
Expanded polyisocyanurate	14–37	1.2–6.4	—
Expanded phenolic	20	1.6	—
Expanded phenolic/FR	20	3.7	—
Tefzel® (ETFE)	27	0.9	—
Teflon® (FEP)	38	2.4	—
Teflon® (TFE)	48	0.8;1.8	—
Teflon® (PFA)	37	1.0	—
PEEK-30% fiber glass	—	7.9	—
Polyethersulfone-30% fiber glass	—	1.8	—
Polyester1-fiber glass	—	2.5	—
Polyester2-fiber glass	10	1.4	—
Polyester3-fiber glass	10	6.4	—
Polyester4-fiber glass	15	5.1	—
Polyester5-fiber glass	10	2.9	—
Phenolic-fiber glass (thick sheet)	20	7.3	—
Phenolic-Kevlar (thick sheet)	15	7.8	—

[a]Data are from the Flammability Laboratory of the FM Global using the ASTM E 2058 FPA shown in Fig. 53.1 and a differential scanning calorimeter.
[b]Abbreviations listed in the nomenclature.

analysis of the data. An external heat flux value at which there is no measurable mass loss rate for 15 min of heat flux exposure is taken as the value for the surface re-radiation loss. The mass pyrolysis technique is used in the ASTM E 2058 FPA, shown in Fig. 53.1, originally designed in our laboratory for this application [4]. Table 53.2 lists the values of the heat of gasification and surface re-radiation loss using the mass pyrolysis technique in our laboratory [4].

The interruption of pyrolysis by passive and/or active fire protection techniques would prevent fires to propagate beyond the ignition zone resulting in reduced fire hazards. The passive fire protection technique involves changes in the polymer to increase the values of the surface re-radiation loss and heat of gasification.

53.3 FIRE PROPERTIES ASSOCIATED WITH IGNITION OF THE POLYMER: CRITICAL HEAT FLUX AND THERMAL RESPONSE PARAMETER

Ignition of a polymer involves formation of a flammable vapor air mixture and initiation of combustion on its own (auto-ignition) or assisted by a small heat source (piloted ignition). Minimum heat flux at or below which there is no ignition is defined as the critical heat flux (CHF).

The surface of a polymer exposed to heat flux is at a higher temperature than the interior. A polymer with a steep temperature gradient between the surface and the interior is defined as thermally thick. If there is no temperature gradient between the surface and the interior, the polymer is defined as thermally thin. Thermally thick and thin conditions depend on the actual thickness of the polymer, heating rates, chemical structures of the polymers and additives. The time to ignition and external heat flux satisfy the following relationships [2,3]:

$$\frac{1}{t_{ig}} = \frac{\pi}{4}\frac{\dot{q}''_e}{K_{\text{thin}}}, \tag{53.3}$$

for thermally thin polymers where $K_{\text{thin}} = \rho c_p \delta \Delta T_{ig}$ is defined as the thermal response parameter (TRP) for thermally thin polymers (kJ/m^2), ρ is the density of the polymer (kg/m^3), c_p is the specific heat of the polymer (MJ/kg-K), δ is the actual thickness of the polymer (m), and T_{ig} is the ignition temperature above ambient (K); and

$$\sqrt{\frac{1}{t_{ig}}} = \sqrt{\frac{\pi}{4}}\frac{\dot{q}''_e}{K_{\text{thick}}}, \tag{53.4}$$

for thermally thick polymers where $K_{\text{thick}} = \Delta T_{ig}\sqrt{k\rho c_p}$ is the defined as the TRP for thermally thick polymers (kW $-$ s$^{1/2}$/m^2), and k is the thermal conductivity of the polymer (kW.m-K).

The TRP represents resistance of a polymer to generate flammable vapor-air mixture. The CHF and TRP values of the polymers are obtained by using the ignition technique [3,4]. External heat flux at which there is no ignition for 15 min is taken as the CHF. The CHF value is generally close to the value for the surface re-radiation loss. In the ignition technique, time to ignition is measured at various external

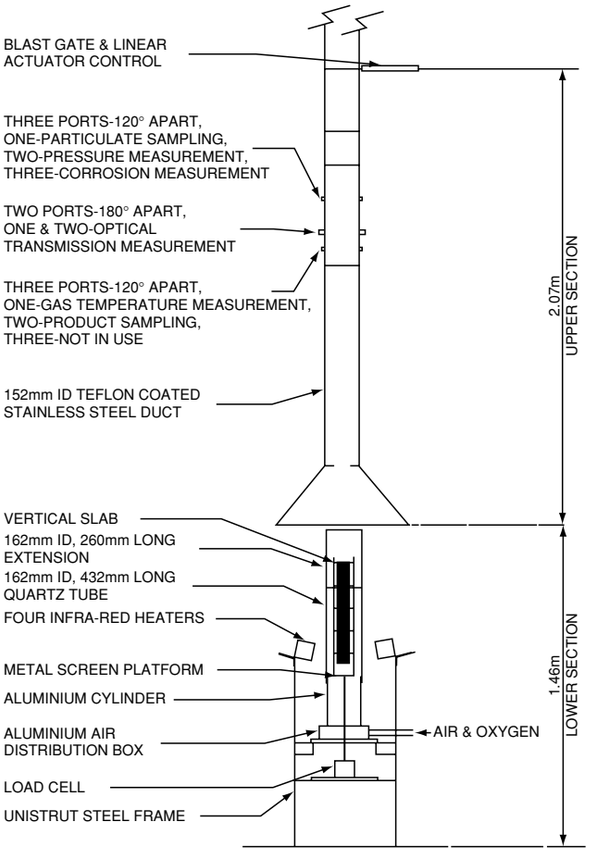

FIGURE 53.1. The ASTM E 2058 Fire Propagation Apparatus (FPA).

heat flux values and the data are used in Eqs. 53.3 and 53.4. A linear relationship between the time to ignition or square root of time to ignition and external heat flux, away from the CHF value [Eqs. (53.3) or (53.4), respectively], is indicative of the thermally thin or thick behavior, such as shown in Fig. 53.2 for a silicone polymer, which behaves as a thermally thick polymer. The TRP value is obtained from the linear regression analysis of the data in the linear portion of the curve, away from the CHF value.

The ASTM E 2058 FPA, shown in Fig. 53.1, has been designed to use this technique. The TRP values from the ignition technique are listed in Table 53.3. The values of the ignition temperature, thermal conductivity, and specific heat, which are individual components of TRP, taken from Tewason *et al*. [7,8] are listed in Table 53.4.

The CHF and TRP values depend on the physical and chemical characteristics of the polymers. Increasing the CHF and TRP values of the polymers by various passive protection techniques would delay initiation of combustion and flame would propagate at lower rate or there would be no fire propagation beyond the ignition zone.

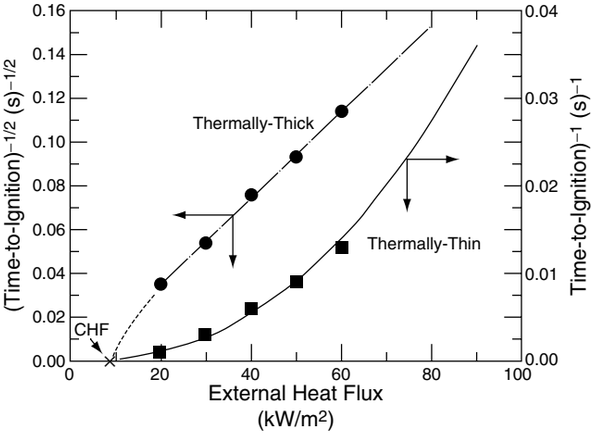

FIGURE 53.2. Time to ignition versus external heat flux for a 100×100 mm×10 mm thick silicone based polymer. Data were measured in the ASTM E 2058 FPA. Data satisfy the thermally-thick behavior away from the critical heat flux value.

53.4 FIRE PROPERTIES ASSOCIATED WITH COMBUSTION OF THE POLYMER: FLAME HEAT FLUX, HEAT OF GASIFICATION, AND SURFACE RE-RADIATION LOSS

The steady state relationship for polymer gasification rate or mass loss rate is similar to the relationship for the pyrolysis condition [Eq. (53.1)], except for an additional term for the flame heat flux [2,3]:

$$\dot{m}_f'' = \frac{\dot{q}_e'' + \dot{q}_f'' - \dot{q}_{rr}''}{\Delta H_g}, \tag{53.5}$$

where $\dot{m}_f''$ is the mass loss rate in combustion ($kg/m^2 - s$) and $\dot{q}_f''$ is the flame heat flux transferred back.

The values of the heat of gasification and surface re-radiation loss determined in pyrolysis are used. The flame heat flux is determined from the flame radiation scaling technique [2,3,13]. This technique utilizes the knowledge that in small-scale fires, flame radiative heat flux increases with increase in the oxygen mass fraction (Y_0) [2,3,13]. For $Y_0 \geq 0.30$, the flame radiative heat flux reaches an asymptotic limit comparable to the limit for large-scale fires burning in the open [2,3,13].

In the flame radiation scaling technique, mass loss rate is measured with co-flowing air having various oxygen mass fractions. Flame heat flux is calculated by using the mass loss rate data in Eq. (53.5), along with the values of the heat of gasification and surface radiation loss measured in pyrolysis [13]. The convective component of the flame heat flux is determined from the combustion of methanol dominated by convective heat transfer [13]. The flammability

TABLE 53.3. *Critical heat flux and thermal response parameter.*[a]

Polymer	Critical heat flux (kW/m^2)	Thermal response parameter	
		Thermally thick ($kW\text{-}s^{1/2}/m^2$)	Thermally thin (kJ/m^2)
Natural polymers			
100% cellulose	13	—	159
Tissue paper	13	—	130
News paper	11	—	175
Wood (red oak)	10	134	—
Wood (Douglas fir)	10	138	—
Wood (Douglas fir/FR)	10	251	—
Wood (hemlock)	—	175	—
Corrugated paper	13	—	385
Wool 100%	—	252	—
Nonhalogenated synthetic polymers			
Epoxy resin	15	457	—
Polystyrene	13	162	—
Polypropylene	15	193	—
Styrene-butadiene	10	198	—
Crosslinked polyethylenes	15	224–301	—
Polyvinyl ester	—	263	—
Polyoxymethylene	13	269	—
Nylon	15	270	—
Polymethylmethacrylate	11	274	—
Isophthalic polyester	—	296	—
Acrylonitrile-butadiene -styrene	13	317	—
Polyethylene (high density)	15	321	—
Polyethylene/NH- FR	15	652–705	—
Polycarbonate	15	331	—
Halogenated synthetic polymers			
Isoprene	10	174	—
Plasticized PVC, LOI = 0.20	10	285	—
Plasticized PVC, LOI = 0.25	10	401	—
Plasticized PVC, LOI = 0.30	10	397	—
Plasticized PVC, LOI = 0.35	10	345	—
Rigid PVC, LOI = 0.50	10	388	—
Rigic PVC	15	406	—
Tefzel® (ETFE)	27	356	—
Teflon® (FEP)	38	682	—
Composite systems			
Polyester-0% fiber glass	—	296	—
Polyester1-30% fiber glass	—	256	—
Polyester2-70% fiber glass	10	275	—
Polyester3-70% fiber glass	10	382	—
Polyester4-70% fiber glass	15	406	—
Polyester5-70% fiber glass	10	338	—
Polyester-77% fiber glass	—	426	—
Epoxy-0% fiber glass	—	257	—
Epoxy-fiber glass (thin sheet)	10	156	—
Epoxy-65% fiber glass	10	420	—
Epoxy-76% fiber glass	15	667	—
Vinyl ester-0% fiber glass	—	263	—
Vinyl ester-62% fiber glass	—	312	—
Vinyl ester-69% fiber glass	—	444	—
Polyimide-fiber glass	—	833	—
PPS-fiber glass	—	588	—
PPS-84% fiber glass	20	909	—
Bismaleimide-fiber glass	—	625	—

TABLE 53.3. *Continued.*

Polymer	Critical heat flux (kW/m^2)	Thermal response parameter	
		Thermally thick ($kW\text{-}s^{1/2}/m^2$)	Thermally thin (kJ/m^2)
Phenolic-fiber glass (thin sheet)	33	105	—
Phenolic-80% fiber glass	20	610	—
Phenolic-fiber glass	—	345–769	—
Epoxy/phenolic-fiber glass	20	1250	—
PEEK-30% fiber glass	—	301	—
Polyethersulfone-30% FG	—	256	—
Phenolic-kevlar (thin sheet)	20	185	—
Phenolic-84% kevlar	15	403	—
Cyanate-73% graphite	20	1000	—
Epoxy-71% graphite	24	667	—
Epoxy-graphite	—	476–667	—
Bismaleimide-graphite	—	526–588	—
PPS-graphite	—	333	—
PEEK-graphite	—	526	—
Phenolic-graphite	—	400–714	—
Expanded synthetic polymers			
Polyurethanes	13–40	55–221	—
Polystyrenes	10–15	111–317	—
Phenolics	20	610	—
Neoprenes	16	113–172	—
Polymers with fiberweb, net-like and multiplex structures			
Polypropylenes	8–15	—	278–385
Polyester-polypropylene	10	—	139
Wood pulp-polypropylene	8	—	130
Polyesters	8–18	—	161–303
Rayon	14–17	—	161–227
Polyester-rayon	13–17	—	119–286
Wool-nylon	15	—	293
Nylon	15	—	264
Cellulose	13	—	159
Cellulose/polyester	13–16	—	149–217
Polymers as electrical power cable insulation and jackets			
PVC/PVC	13–25	156–341	—
PE/PVC	15	221–244	—
Silicone/PVC	19	212	—
Silicone/XLPO	25–30	435–457	—
EPR/EPR	20–23	467–567	—
EPR,FR/EPR,FR	14–28	289–448	—
XLPE/XLPE	20–25	273–386	—
XLPE/EVA	12–22	442–503	—
XLPE/Neoprene	15	291	—
XLPO/XLPO	16–25	461–535	—
XLPO,PVF/XLPO	14–17	413–639	—
EPR/CLS-PE	14–19	283–416	—
Polymers as communications cable insulation and jackets			
PVC/PVC	15	131	—
PE/PVC	20	183	—
XLPE/XLPO	20	461–535	—
Si/XLPO	20	457	—
EPR-FR	19	295	—
Chlorinated PE	12	217	—
ETFE/EVA	22	454	—
PVC/PVF	30	264	—

[a]Data from the ASTM E 2058 FPA at FMRC [2,3,5–8] or calculated from the data reported in Refs. 9 and 10.

TABLE 53.4. *Ignition temperature, thermal conductivity, and specific heats of polymers.*[a]

Polymers	Ignition temperature (K)[b]	Specific heat (kJ/kg-K)	Thermal conductivity (kW/m-K) $\times 10^4$
Natural polymers			
Cotton	527	—	—
News paper	503	—	—
White pine, shavings	533	—	—
Nonhalogenated synthetic polymers			
ABS	527	1.26–1.67	1.88–3.35
Acetal homopolymer	—	1.46	2.30
Acrylics	—	1.46	1.67–2.51
Cellulose acetate	—	1.26–2.09	1.67–3.35
Epoxy	—	1.05	1.67–2.09
Epoxy/silica	—	0.84–1.13	4.18–8.37
Nylon 6/6	785	1.67	2.43
Nylon 6/6/33% glass	—	1.26	2.13
Nylon 6	—	1.67	2.43
Nylon 6/30–35% glass	—	2.09	2.43
Polymethylmethacrylate	651	2.09	2.68
Polyethylene			
Low density	622	2.30	3.35
Medium density	—	2.30	3.35–4.18
High density	—	2.30	4.60–5.19
Polypropylene	736	1.92	1.17
Polystyrene	675	1.34	1.00–1.38
Polycarbonate	651	1.17–1.26	1.92
Polyester	—	1.17–2.30	1.76–2.89
Polyester/premix chopped glass	—	1.05	4.18–6.69
Polyaryl ether	—	1.46	2.98
Polyether sulfone	—	1.09	1.34–1.84
Phenol-formaldehyde	—	1.59–1.76	1.26–2.51
Polyphenylene oxide	—	1.34	1.88
Polyurethane	—	1.67–1.88	0.63–3.10
Styrene-acrylonitrile (SAN)	—	1.34–1.42	1.21–1.26
Styrene-butadiene (SB)	645	1.88–2.09	1.51
Halogenated synthetic polymers			
PVC	675	1.34	1.25–2.93
PVC_2	—	1.34	1.26
PTFE	767	1.05	2.51
FEP	900	1.17	2.51
PVF_2	—	1.38	1.26
PCTFE	—	0.92	1.97–2.22
Inert fibers for composite systems			
Kevlar	—	—	2.00
Glass	—	—	10.5
Quartz	—	—	17.2
Graphite	—	—	50.2
Sapphire (aluminum oxide)	—	—	240
Silicone carbide	—	—	850

[a]Data taken from Refs. 11 and 12.
[b]Estimated from the CHF value in Table 53.3.

apparatus, shown in Fig. 53.1, has been designed to use this technique.

The asymptotic values for the mass loss rate in combustion and flame heat flux determined from the radiation scaling technique in the ASTM E 2058 FPA are listed in Table 53.5. The measured asymptotic values of the mass loss rate in combustion in large-scale fires reported in the literature are also listed in Table 53.5. The asymptotic flame

TABLE 53.5. *Asymptotic mass loss rate and flame heat flux.*

Polymers/Liquids[a]	Mass loss rate $(kg/m^2\text{-}s) \times 10^3$		Flame heat flux (kW/m^2)	
	Flame rad. Scaling tech[b]	Largescale	Flame rad. scaling tech[b]	Largescale
Aliphatic carbon-hydrogen atoms				
Polyethylene	26	—	61	—
Polypropylene	24	—	67	—
Heavy fuel oil (2.6–23 m)	—	36[c]	—	29
Kerosene (30–80 m)	—	65[c]	—	29
Crude oil (6.5–31 m)	—	56[c]	—	44
n-Dodecane (0.94 m)	—	36[c]	—	30
Gasoline (1.5–223 m)	—	62[c]	—	30
JP-4 (1.0–5.3 m)	—	67[c]	—	40
JP-5 (0.60–17 m)	—	55[c]	—	39
n-Heptane (1.2–10 m)	~66	75[c]	32	37
n-Hexane (0.75–10 m)	—	77[c]	—	37
Transformer fluids (2.37 m)	27–30	25–29	23–25	22–25
Aromatic carbon-hydrogen atoms				
Polystyrene (0.93 m)	36	34	75	71
Xylene (1.22 m)	—	67[c]	—	37
Benzene (0.75–6.0 m)	—	81[c]	—	44
Aliphatic carbon-hydrogen-oxygen atoms				
Polyoxymethylene	16	—	50	—
Polymethylmethacrylate (2.37 m)	28	30	57	60
Methanol (1.2–2.4 m)	20	25	22	27
Acetone (1.52 m)	—	38[c]	—	24
Aliphatic carbon-hydrogen-oxygen-nitrogen atoms				
Expanded Polyurethanes (flexible)	21–27	—	64–76	
Expanded Polyurethanes Rigid	22–25	—	49–53	—
Aliphatic carbon-hydrogen-halogen atoms				
Polyvinylchloride	16	—	50	
Tefzel® (ETFE)	14	—	50	
Teflon® (FEP)	7	—	52	

[a]Numbers in parentheses are the pool diameters in meters.
[b]Flame radiation scaling technique: pool diameter fixed at 0.10 m, $Y_0 \geq 0.30$. ASTM E 2058 FPA.
[c]Taken from various references in the literature.

heat flux values, determined in the ASTM E 2058 FPA are in good agreement with the values derived from the mass loss rate in large-scale fires.

The asymptotic flame heat flux values vary from 22 to 77 kW/m^2, dependent primarily on the pyrolysis mode rather than on the chemical structures. For examples, for the liquids, which vaporize primarily as monomers or as very low molecular weight oligomer, the asymptotic flame heat flux values are in the range of 22–44 kW/m^2, irrespective of their chemical structures. For polymers, which vaporize as high molecular weight oligomer, the asymptotic flame heat flux values increase substantially to the range of 49 to 71 kW/m^2, irrespective of their chemical structures. The independence of the asymptotic flame heat value from the chemical structure is consistent with the dependence of the flame radiation on optical thickness, soot concentration and flame temperature.

Decrease in the flame heat flux and increase in the heat of gasification and surface re-radiation loss through various passive fire protection techniques would prevent the fire to grow and propagate beyond the ignition zone and the thermal and nonthermal hazards would be reduced and/or eliminated.

53.5 FIRE PROPERTIES ASSOCIATED WITH FLAME PROPAGATION: LIMITING OXYGEN INDEX AND FIRE PROPAGATION INDEX

Flame propagation is a process where the pyrolysis front moves beyond the ignition zone over the polymer surface,

accompanied by the sustained combustion process. The rate of the movement of the pyrolysis front, accompanied by the sustained combustion process, is defined as the flame propagation rate. For a sustained fire propagation process, flame or external heat sources need to transfer heat flux ahead of the pyrolysis front to satisfy the CHF and TRP values. Flame propagation can occur in the downward, upward, and horizontal directions.

Three test apparatuses and methods have been developed to determine the fire properties associated with flame propagation: (1) the ASTM D 2863 oxygen index test method for downward flame propagation for small samples [14]; (2) the ASTM E 1321-90 lateral ignition and flame spread (LIFT) test method for horizontal and lateral flame propagation [15,16]; and (3) the fire propagation index (FPI) test method for vertical flame propagation [2,3,17,18].

In the LIFT and FPI test methods, the following definition of the flame propagation velocity for thermally thick polymers is utilized [2,3,7,15]:

$$u = \frac{\text{funct}(\dot{q}''_f)}{[\Delta T_{\text{ig}}^2 k\rho c_P]}, \tag{53.6}$$

where u is the flame propagation rate in m/s, funct $(\dot{q}''_r)$ is a function representing the flame heat flux transferred to the surface of the polymer ahead of the pyrolysis front (kW^2/m^3), ρ is the density of the polymer (kg/m^3), c_p is the specific heat of the polymer (MJ/kg-K), k is the thermal conductivity of the polymer (kW/m-K) and ΔT_{ig} is the ignition temperature above ambient (K) [see the definition of the TRP for thermally thick polymer in Eq. (53.4)].

53.6 TESTING METHODS FOR FLAME PROPAGATION

53.6.1 The ASTM D 2863 Oxygen Index Test

In this test, downward flame propagation for small vertical sheets (6.5-mm wide, 70–150-mm long, 3-mm thick) is examined, in air flowing in the opposite direction with variable oxygen concentration [14]. Minimum oxygen concentration (volume percent) at or below which the downward flame propagation cannot be sustained, defined as the limiting oxygen index (LOI), is determined [14]. The LOI values reported in the literature [8,19] are compiled in Table 53.6.

For PMMA, LOI=17.3 in Table 53.6 which is higher than the oxygen concentration of 16.0% required for flame extinction for larger PMMA slabs [6]. The difference is probably due to differences in the flame radiation and flow characteristics. For example, for larger PMMA slabs exposed to external heat flux values of 40, 60, and $65\,\text{kW}/\text{m}^2$ in the ASTM E 2058 FPA, flame extinction occurs at oxygen concentrations of 13.0%, 12.0%, and 11.5%, respectively [6]. The LOI value decreases with increase in the gas temperature as indicated by the LOI values of the composite systems in Table 53.6.

The oxygen index test utilizes the flame radiation scaling technique for small samples and indirectly assesses heat flux from the flame through LOI. At or below the LOI value of a polymer, the heat flux requirements for CHF and TRP values for fire propagation are not satisfied. The higher is the LOI of a polymer, higher are its CHF and TRP values and/or lower is the heat flux provided by its flame, and the polymer is considered as fire hardened.

The oxygen index test is used for molded polymers, fabrics, expanded polymers, thin films, polymers which form char, drip, or soften, and for liquids. The data are reproducible. The test is used to study polymer combustion chemistry, fire retardant treatment of the polymers and for screening the polymers. No relationships have been established between LOI and the flame heat flux, CHF, TRP, and fire propagation rate. The application of the oxygen index test data to predict the fire propagation behavior of polymers expected in actual fires is thus uncertain.

53.6.2 The ASTM E 1321-90 Lateral Ignition and Flame Spread (LIFT) Test

Equation (53.6) is expressed as [15]:

$$u = \frac{\Psi}{\text{TRP}^2}, \tag{53.7}$$

where Ψ is defined as the flame heating parameter (kW^2/m^3). The ignition and flame spread tests are performed in normal air at various external heat flux values [15,16]. In the ignition tests, 155-×155-mm samples are exposed to various external heat flux values and times to flame attachment are measured [15,16]. The values of k, ρ, c_p, ΔT_{ig} are determined from the relationship between the time to flame attachment and external heat flux [15,16]. These values can be used to calculate the TRP value [Eq. (53.4)].

In the flame spread tests, 155-mm wide and 800-mm long horizontal samples in a lateral configuration are used [15,16]. The samples are exposed to an external heat flux which is $5\,\text{kW}/\text{m}^2$ higher than the CHF value in the ignition zone [15,16]. Beyond the ignition zone, the external heat flux decreases gradually and is significantly lower than the CHF value at the end of the sample [15,16]. The sample is preheated to thermal equilibrium and ignited with a pilot flame in the ignition zone. The pyrolysis front is tracked as a function of time and is used to determine the flame heating parameter and used in Eq. (53.7) along with the TRP value to calculate the flame propagation rate. The flame propagation rate calculated from the data reported in Refs. 15 and 19 are listed in Table 53.7. The relative flame propagation rate is also listed in Table 53.7.

In the LIFT Apparatus, most of the common polymers and carpets have faster lateral flame propagation than

TABLE 53.6. *Limiting oxygen indices for polymers.*[a]

Polymer	LOI	Polymer	LOI
Cotton	16–17	Polyethylene1	17.4
Cotton (loosely woven)	18.5	Polyethylene2	17.4
Filter paper	18.2	Polyethylene-50% Al_2O_3	19.6
Wood (birch)	20.5	Polypropylene	17.4
Wood (red oak)	23.0	Polypropylene-30% FG	18.5
Wood (plywood)	23.0	Polystyrene1	17.8
Cellulose	19.0	Polystyrene2	17.6–18.3
Cellulose acetate (dry)	16.8	Polymethylmethacrylate(Plexiglas®)	17.3
Cellulose acetate (4.9% water)	18.1	Polycarbonate1	22.5
Cellulose butyrate (0.06% water)	18.8	Polycarbonate2	24.9
Cellulose butyrate (2.8% water)	19.9	Polycarbonate3	26.0–28.0
Cellulose acetate-butyrate	19.6	ABS-1	18.3–18.8
Rayon	18.7–18.9	ABS-2	18.8
Wool (loosely woven)	23.8	ABS-20% FG	21.6
Wool fiber (dry cleaned)	25.2	SBR foam	16.9
Leather (chrome based)	34.8	Nylon fiber	20.1
Natural rubber foam	17.2	Nylon-6,6	24.3
Polyacetal (Celcon®)	14.9	Nylon-6,6	24.0–29.0
Polyacetal-30% FG	15.6	Nylon-6,12	25.0
Polyformaldehyde	15.0	Nylon-6	25.0–26.0
Poly(ethylene oxide)	15.0	Polyacrylonitrile	18.0
Polyoxymethylene (Delrin®)	14.9	Polyimide (Kapton®)	36.5
Polyphenylene oxide	29.9	Silicon rubber	30.0
Polyurethane foam	16.5	Polyester2–70% fiber glass, °C	
Polyvinyl alcohol	22.5	25	28.0
Polysulfone	30.0–32.0	100	28.0
PVC fiber	37.1	200	13.0
PVC (rigid)	45.0–49.0	300	<10
PVC (chlorinated)	45.0–60.0	Polyester3–70% fiber glass, °C	
Poly(vinyl fluoride) (Tedlar®)	22.6	25	52.0
Polyethylene (20% chlorine)	24.5	100	95.0
Neoprene	40.0	200	77.0
Neoprene rubber	26.3	300	41.0
Polyisoprene	18.5	Epoxy resin	19.8
Poly(vinylidene chloride) (Saran®)	60.0	Epoxy1–65% fiber glass, °C	
Polytrichlorofluoroethylene	95.0	25	38.0
Teflon® (TFE)	95.0	100	43.0
Nomex®	28.5	200	34.0
Polyester fabric	20.6	300	16.0
Polyester	41.5	Epoxy2–65% fiber glass, °C	
Polyester-70% fiber glass; (heated to °C)		25	50.0
25	23.0	100	59.0
100	23.0	200	49.0
200	<10	300	24.0
300	<10		
Epoxy3–65% fiber glass, (heated to °C)		Phenolic-80% fiber glass, °C	
25	43.0	200	94.0
100	54.0	300	80.0
200	47.0	Phenolic-84% Kevlar, °C	
300	27.0	25	28.0
Phenolic resin	21.0	100	30.0
Phenol-formaldehyde resin	35.0	200	29.0
Phenolic-80% fiber glass, (heated to °C)		300	26.0
25	53.0		
100	98.0		

[a]Data taken from Refs. 8 and 19.

TABLE 53.7. *Lateral flame propagation rate in the LIFT apparatus.*[a]

Polymers	Thickness (mm)	Flame propagation rate (mm/s)	Relative flame propagation rate
Natural polymers			
Hardboard	3	10	1.0
Hardboard (gloss paint)	3	5	0.5
Hardboard	6	6	0.6
Plywood plain	6	11	1.1
Plywood plain	13	13	1.3
Particle board	13	5	0.5
Douglas fir particle board	12	10	1.0
Fiber insulation board	—	7	0.7
Gypsum board, wall paper	—	3	0.3
Gypsum board	13	10	1.0
Asphalt shingle	—	9	0.9
Fiberglass shingle	—	10	1.0
Synthetic polymers			
Polyisocyanurate foam	51	37	3.7
Rigid polyurethane foam	25	28	2.8
Flexible polyurethane foam	25	16	1.6
Polymethylmethacrylate	2	11	1.1
Polymethylmethacrylate	13	11	1.1
Polycarbonate	2	7	0.7
Carpets			
Acrylic	—	17	1.7
Nylon/wool blend	—	15	1.5
Wool, Untreated	—	13	1.3
Wool, Treated	—	4	0.4
Aircraft panel materials			
Phenolic fiberglass	—	14	1.4
Phenolic kevlar	—	13	1.3
Epoxy kevlar	—	11	1.1
Phenolic graphite	—	9	0.9
Epoxy fiberglass	—	6	0.6

[a]Calculated from the data reported in Refs. 15 and 20.

Douglas fir. Three out of five aircraft panel materials also have faster lateral flame propagation than a Douglas fir. For most of the ordinary polymers, the lateral flame propagation rate is either comparable to or lower than the rate for a Douglas fir.

53.6.3 The Fire Propagation Index (FPI) Test for Vertical Flame Propagation

The fire propagation test is performed in the ASTM E 2058 FPA (Fig. 53.1) using the flame radiation scaling technique with the TRP value determined from the ignition test. The test can be considered as a larger version of the ASTM D 2863 oxygen index test, with an ignition zone provided by four external heaters. In the test, upward fire propagation is examined under co-flowing air with an oxygen concentration of 40% [2,3]. Polymers as vertical slabs and cylinders of up to 600 mm in length and up to about 25 mm in thickness, 100 mm in width or diameter are used. The chemical heat release rate is measured during flame propagation and is used in the following relationship [modified Eq. (53.6)]:

$$\sqrt{u} \propto \frac{(0.42\dot{Q}'_{ch})^{1/3}}{[\Delta T_{ig}(k\rho c_p)^{1/2}]}. \tag{53.8}$$

where $\dot{Q}'_{ch}$ is the chemical heat release rate per unit width or circumference (kW/m). The fire propagation index (FPI) is calculated from Eq. (53.8) with a proportionality constant of $1000\,\mathrm{kW^{2/3} - s^{1/2}/m^{5/3}}$ and TRP from Eq. (53.4):

$$\mathrm{FPI} = 1000\frac{(0.42\dot{Q}'_{\mathrm{ch}})^{1/3}}{\mathrm{TRP}}. \tag{53.9}$$

The FPI values determined in this fashion are listed in Table 53.8 for selected polymers and shown in Fig. 53.3 for a fire

TABLE 53.8. *Fire propagation index for polymers.*

Polymers	Diameter/ thickness (mm)	FPI	Group	Fire propagation[a]
Synthetic polymers				
PMMA	25	30	3	P
PP-FR	25	$\gg 10$	3	P
Polymers as electrical cable insulation and jacket				
PVC/PVC (power)	4–13	11–28	2–3	P
PVC/PVC (communications)	4	36	3	P
PE/PVC (power)	11	16–23	3	P
PE/PVC (communications)	4	28	3	P
PVC/PE (power)	34	13	2	P
PVC/PVF (communications)	5	7	1	NP
Silicone/PVC (power)	16	17	2	P
Silicone/XLPO (power)	55	6–8	1	NP; DP
Si/XLPO (communications)	28	8	1	DP
EP/EP (power)	10–25	6–8	1	NP; DP
XLPE/XLPE (power)	10–12	9–17	1–2	DP; P
XLPE/XLPO (communications)	22–23	6–9	1	NP; DP
XLPE/EVA (power)	12–22	8–9	1	DP
XLPE/Neoprene (power)	15	9	1	DP
XLPO/XLPO (power)	16–25	8–9	1	DP
XLPO, PVF/XLPO (power)	14–17	6–8	1	NP; DP
EP/CLP (power)	4–19	8–13	1–2	DP; P
EP, FR/None (power)	4–28	9	1	DP
EP-FR/none (communications)	28	12	2	P
ETFE/EVA (communications)	10	8	1	DP
FEP/FEP (communications)	8–10	4–5	1	NP
Composite systems				
Polyester1-70% fiber glass	4.8	13	2	P
Polyester2-70% fiber glass	4.8	10	2	P
	19	8	1	DP
	45	7	1	NP
Epoxy1-65% fiber glass	4.4	9	1	DP
Epoxy2-65% fiber glass	4.8	11	2	P
Epoxy3-65% fiber glass	4.4	10	2	P
Epoxy4-76% fiber glass	4.4	5	1	NP
Phenolic-80% fiber glass	3.2	3	1	NP
Epoxy-82% fiber glass-phenolic	—	2	1	NP
Phenolic-84% kevlar	4.8	8	1	DP
Cyanate-73% graphite	4.4	4	1	NP
PPS-84% fiber glass	4.4	2	1	NP
Epoxy-71% fiber glass	4.4	5	1	NP
Polymers as conveyor belts[b]				
SBR	—	8–11	1–2	DP; P
CR	—	5	1	NP
CR/SBR	—	8	1	DP
PVC		4–10	1–2	NP; DP

[a]P: propagating; DP: decelerating propagation; NP: nonpropagating.
[b]3–25 mm thick.

retarded polypropylene slab. The FPI values show the following flame propagation behavior in large-scale fires:

1. FPI$\leq$7: there is no flame propagation beyond the ignition zone, defined as nonpropagating (NP). Polymers showing this type of behavior are defined as Group 1-*NP* polymers. Flame is at a critical extinction condition.
2. 7<FPI<10: there is decelerating flame propagation beyond the ignition zone, defined as decelerating

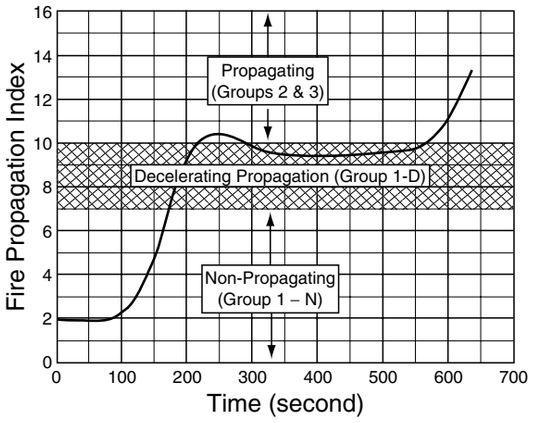

FIGURE 53.3. Fire propagation index versus time for a 10 mm thick, 100 mm wide, and 600 mm long vertical slab of fire retarded polypropylene in co-flowing air with 40% oxygen concentration. The sides and back of the slab were covered tightly with ceramic paper and heavy duty aluminum foil. The data were measured in the ASTM E 2058 FPA.

propagation (DP). Flame propagation beyond the ignition zone is limited. Polymers showing this type of behavior are defined as Group 1-*DP* polymers.

3. 10≤FPI<20: there is slow flame propagation beyond the ignition zone. Polymers showing this type of behavior are defined as Group 2 polymers.
4. FPI≥20: there is a rapid flame propagation beyond the ignition zone. Polymers showing this type of behavior are defined as Group 3 polymers.

The FPI is one of the most important fire properties to assess fire hazard and protection requirements. Increasing the TRP value and decreasing the heat release rate for polymers by various passive fire protection techniques would decrease the FPI value and change the fire propagation behavior from propagating to decelerating to non-propagating. Passive fire protection techniques could involve modifications of chemical structures, incorporation of fire retardants, and changes in the shape, size, and arrangements of the polymers, use of coatings, and inert barriers. The heat release rate could also be reduced by the application of active fire protection agents such as water, Halon and alternates, etc.

53.7 FIRE PROPERTIES ASSOCIATED WITH THE GENERATION OF PRODUCTS: YIELDS OF PRODUCTS

The mass generation rate of a product is directly proportional to the mass loss rate, the proportionality constant is defined as the yield of the product [3,4]:

$$\dot{G}''_j = y_j \dot{m}''_f, \tag{53.10}$$

where $\dot{G}''_j$ is the mass generation rate of product j ($kg/m^2 - s$) and y_j is the yield of product j (kg/kg). The average yield of a product is determined from the ratio of the total mass of the product generated, W_j, obtained by the summation of the mass generation rate of the products to the total mass of the polymer gasified, W_f, obtained by the summation of the mass loss rate:

$$y_j = \frac{W_j}{W_f}. \tag{53.11}$$

The average yields of products obtained in this fashion are listed in Table 53.9.

53.7.1 Generation Rates of Products at Various Heat Fluxes

The generation rates of products can be predicted at various heat flux values from the following relationship obtained from Eqs. (53.5) and (53.10):

$$\dot{G}''_j = \left(\frac{y_j}{\Delta H_g}\right)(\dot{q}''_e + \dot{q}''_f - \dot{q}''_{rr}), \tag{53.12}$$

where $y_j/\Delta H_g$ is defined as the product generation parameter (PGP) (kg/kJ). PGP values of the products are independent of the fire size, but depend on the ventilation and can be calculated from the data such as listed in Tables 53.2, 53.5, and 53.9, from the slopes of the lines obtained by plotting the generation rates of the products against the external heat flux for various fire scenarios with specified external and flame heat flux values.

53.7.2 Generation of Products and Ventilation

The concentrations of products generated at various ventilation conditions are predicted by the following equations [21]:

$$c_{j,v} = (y_{j,\infty}/S)(\rho_a/\rho_j)[1 + \{\alpha/\exp(\beta\Phi^{-\xi})\}]\Phi, \tag{53.13}$$

where $c_{j,v}$ is the concentration for the ventilation controlled combustion; $y_{j,\infty}/S$ is the yield of product j per unit mass of air consumed (kg/kg) for well-ventilated combustion (values are listed in Table 53.10), ρ_a and ρ_j are the densities of air and product j respectively (kg/m^3) (ρ_a/ρ_j values for O_2, CO, CO_2, hydrocarbons (methane) and smoke (carbon) are 0.905, 0.654, 1.034, 1.804, and 2.333, respectively); Φ is the equivalence ratio (ratio of the amount of gasified polymer (fuel) to the amount of air, normalized by the stoichiometric air-to-fuel ratio; for well-ventilated combustion, $\Phi < 1.0$ and for ventilation controlled combustion, $\Phi > 1.0$); α, β, and ξ are the ventilation correlation coefficients. Values for the coefficients for CO, hydrocarbons, and smoke listed in Table 53.11. For O_2 and CO_2, the values of the coefficients are same and are independent of the chemical structures within the halogenated and nonhalogenated polymers (for

TABLE 53.9. *Yields of products and heats of combustion for well ventilated combustion.*[a]

Polymers[b]	Yield (kg/kg)				Heat of Combustion (MJ/kg)[d]			
	CO_2	CO	Hyd[c]	Smoke	Comp	Chem	Con	Rad
Natural polymers								
Tissue paper	1.05	—	—	—	—	11.4	6.7	4.7
News paper	1.32	—	—	—	—	14.4	—	—
Wood (red oak)	1.27	0.004	0.001	0.015	17.1	12.4	7.8	4.6
Wood (Douglas fir)	1.31	0.004	0.001	—	16.4	13.0	8.1	4.9
Wood (pine)	1.33	0.005	0.001	—	17.9	12.4	8.7	3.7
Corrugated paper	1.22	—	—	—	—	13.2	—	—
Wood (hemlock)[e]	1.22	—	—	0.015	—	13.3	—	—
Wool 100%[e]	1.79	—	—	0.008	—	19.5	—	—
Synthetic polymers								
ABS[e]	—	—	—	0.105	—	30.0	—	—
POM	1.40	0.001	0.001	—	15.4	14.4	11.2	3.2
PMMA	2.12	0.010	0.001	0.022	25.2	24.2	16.6	7.6
PE	2.76	0.024	0.007	0.060	43.6	38.4	21.8	16.6
PP	2.79	0.024	0.006	0.059	43.4	38.6	22.6	16.0
PS	2.33	0.060	0.014	0.164	39.2	27.0	11.0	16.0
Silicon	0.96	0.021	0.006	0.065	21.7	10.6	7.3	3.3
Polyester-1	1.65	0.070	0.020	0.091	32.5	20.6	10.8	9.8
Polyester-2	1.56	0.080	0.029	0.089	32.5	19.5	—	—
Epoxy-1	1.59	0.080	0.030	—	28.8	17.1	8.5	8.6
Epoxy-2	1.16	0.086	0.026	0.098	28.8	12.3	—	—
Nylon	2.06	0.038	0.016	0.075	30.8	27.1	16.3	10.8
Polyamide-6[e]	2.64	—	—	0.011	—	28.8	—	—
Silicon	0.96	0.21	0.005	0.078	21.7	10.9	—	—
Expanded polyurethanes (flexible)								
GM21	1.55	0.010	0.002	0.131	26.2	17.8	8.6	9.2
GM23	1.51	0.031	0.005	0.227	27.2	19.0	10.3	8.7
GM25	1.50	0.028	0.005	0.194	24.6	17.0	7.2	9.8
GM27	1.57	0.042	0.004	0.198	23.2	16.4	7.6	8.8
Expanded polyurethanes (rigid)								
GM29	1.52	0.031	0.003	0.130	26.0	16.4	6.8	9.6
GM31	1.53	0.038	0.002	0.125	25.0	15.8	7.1	8.8
GM35	1.58	0.025	0.001	0.104	28.0	17.6	7.8	9.8
GM37	1.63	0.024	0.001	0.113	28.0	17.9	8.7	9.2
GM41	1.18	0.046	0.004	—	26.2	15.7	5.7	10.0
GM43	1.11	0.051	0.004	—	22.2	14.8	6.4	8.4
Expanded polystyrenes								
GM47	2.30	0.060	0.014	0.180	38.1	25.9	11.4	14.5
GM49	2.30	0.065	0.016	0.210	38.2	25.6	9.9	15.7
GM51	2.34	0.058	0.013	0.185	35.6	24.6	10.4	14.2
GM53	2.34	0.060	0.015	0.200	37.6	25.9	11.2	14.7
Expanded polyethylenes								
1	2.62	0.020	0.004	0.056	41.2	34.4	20.2	14.2
2	2.78	0.026	0.008	0.102	40.8	36.1	20.6	15.5
3	2.60	0.020	0.004	0.076	40.8	33.8	18.2	15.6
4	2.51	0.015	0.005	0.071	40.8	32.6	19.1	13.5
Expanded phenolics								
1[e]	0.92	—	—	0.002	—	10.0	—	—
2[e]	0.92	—	—	—	—	10.0	—	—
Halogenated polymers								
PE + 25% chlorine	1.71	0.042	0.016	0.115	31.6	22.6	10.0	12.6
PE + 36% chlorine	0.83	0.051	0.017	0.139	26.3	10.6	6.4	4.2
PE + 48% chlorine	0.59	0.049	0.015	0.134	20.6	7.2	3.9	3.3

TABLE 53.9. *Continued.*

Polymers[b]	Yield (kg/kg)				Heat of Combustion (MJ/kg)[d]			
	CO_2	CO	Hyd[c]	Smoke	Comp	Chem	Con	Rad
PVC	0.46	0.063	0.023	0.172	16.4	5.7	3.1	2.6
PVC-1[e] (LOI = 0.50)	0.64	—	—	0.098	—	7.7	—	—
PVC-2[e] (LOI = 0.50)	0.69	—	—	0.076	—	8.3	—	—
PVC[e] (LOI = 0.20)	0.93	—	—	0.099	—	11.3	—	—
PVC[e] (LOI = 0.25)	0.81	—	—	0.078	—	9.8	—	—
PVC[e] (LOI = 0.30)	0.85	—	—	0.098	—	10.3	—	—
PVC[e] (LOI = 0.35)	0.89	—	—	0.088	—	10.8	—	—
ETFE	0.54	0.060	0.020	0.042	12.6	5.4	—	—
PFA	0.37	0.097	—	0.002	5.0	4.7	—	—
FEP	0.25	0.116	—	0.003	4.8	4.1	—	—
TFE	0.38	0.092	—	0.003	6.2	4.2	—	—
Polymers as building products[e]								
Particle board (PB)	1.28	0.004	—	—	—	14.0	—	—
Fiber board (FB)	1.28	0.015	—	—	—	14.0	—	—
Medium density FB	1.28	0.002	—	—	—	14.0	—	—
Wood panel	1.38	0.002	—	—	—	15.0	—	—
Melamine faced	0.98	0.025	—	—	—	10.7	—	—
Gypsum board (GB)	0.39	0.027	—	—	—	4.3	—	—
Paper on GB	0.49	0.028	—	—	—	5.6	—	—
Plastic on GB	1.31	0.028	—	—	—	14.3	—	—
Textile on GB	1.19	0.025	—	—	—	13.0	—	—
Textile on rock wool	2.29	0.091	—	—	—	25.0	—	—
Paper on PB	1.15	0.003	—	—	—	12.5	—	—
Rigid polyurethane	1.19	0.200	—	—	—	13.0	—	—
Expanded PS	2.60	1.9	0.054	—	—	28.0	—	—
Composite systems								
PEEK-fiber glass[e]	1.88	—	—	0.042	—	20.5	—	—
IPST-fiber glass[e]	2.48	—	—	0.032	—	27.0	—	—
Polyester1-fiber glass[e]	2.52	—	—	0.049	—	27.5	—	—
Polyester2-fiber glass[e]	1.47	—	—	—	—	16.0	—	—
Polyester3-fiber glass[e]	1.18	—	—	—	—	12.9	—	—
Polyester4-fiber glass	1.74	—	—	—	—	19.0	—	—
Polyester5-fiber glass	1.28	—	—	—	—	13.9	—	—
Polyester6-fiber glass	1.47	0.055	0.007	0.070	—	17.9	10.7	7.2
Polyester7-fiber glass	1.24	0.039	0.004	0.054	—	16.0	9.9	6.1
Polyester8-fiber glass	0.71	0.102	0.019	0.068	—	9.3	6.5	2.8
Epoxy1-fiber glass[e]	2.52	—	—	0.056	—	27.5	—	—
Epoxy2-fiber glass	1.10	0.166	—	0.128	—	11.9	—	—
Epoxy3-fiber glass	0.92	0.113	—	0.188	—	10.0	—	—
Epoxy4-fiber glass	0.94	0.132	—	0.094	—	10.2	—	—
Epoxy5-fiber glass	1.71	0.052	—	0.121	—	18.6	—	—
Epoxy-fiber glass-paint	0.83	0.114	0.016	0.166	—	11.3	6.2	5.1
Phenolic1-fiber glass	0.98	0.066	0.003	0.023	—	11.9	—	—
Phenolic2-fiber glass[e]	2.02	—	—	0.016	—	22.0	—	—
Phenolic-fiber glass-paint	1.49	0.027	0.002	0.059	—	22.9	11.5	11.4
Epoxy-fiberglass-phenolic	1.06	0.134	—	0.089	—	11.5	—	—
Vinylester-fiber glass	2.39	—	—	0.079	—	26.0	—	—
PPS-fiber glass	1.56	0.133	—	0.098	—	17.0	—	—
Phenolic-kevlar	1.27	0.025	0.002	0.041	—	14.8	11.1	3.7
Epoxy-kevlar-paint	0.873	0.091	0.016	0.126	—	11.4	6.3	5.1
Phenolic-kevlar-paint	1.67	0.026	0.003	0.062	—	24.6	14.0	10.6
Cyanate-graphite	1.73	0.058	—	0.102	—	18.9	—	—
Epoxy-graphite	1.63	0.046	—	0.107	—	17.8	—	—
Phenolic-graphite-paint	1.67	0.026	0.003	0.062	—	24.6	14.0	10.6

TABLE 53.9. *Continued.*

Polymers[b]	Yield (kg/kg)				Heat of Combustion (MJ/kg)[d]			
	CO_2	CO	Hyd[c]	Smoke	Comp	Chem	Con	Rad
Polymers as electrical cable insulation and jackets								
Polyethylene/polyvinylchloride cable								
1	2.08	0.100	0.021	0.076	—	31.3	11.6	19.7
2	1.75	0.050	0.013	0.115	—	25.1	11.1	14.0
3	1.67	0.048	0.012	—	—	24.0	13.0	11.0
4	1.39	0.166	0.038	—	—	22.0	14.0	8.1
5	1.29	0.147	0.042	0.136	—	20.9	10.7	10.2
Polyethylene-polypropylene copolymer/chlorosulfonated polyethylene cable								
1	1.95	0.072	0.014	—	—	29.6	15.8	13.9
2	1.74	0.076	0.022	—	—	26.8	17.0	9.8
3	1.21	0.072	0.014	—	—	19.0	12.3	6.7
4	0.99	0.090	0.085	0.082	—	17.4	6.6	10.8
5	0.95	0.122	0.024	—	—	17.3	7.5	9.8
6	0.89	0.121	0.022	0.164	—	13.9	9.2	4.7
Silicone/silicone cable								
1	1.65	0.011	0.001	—	—	25.0	17.5	7.3
2	1.47	0.029	0.001	—	—	24.0	20.0	4.0
Crosslinked polyethylene/crosslinked polyethylene cable								
1	1.78	0.114	0.029	0.120	—	28.3	12.3	16.0
2	0.83	0.110	0.024	0.120	—	12.5	7.5	5.0
Crosslinked polyethylene/neoprene cable								
1	0.68	0.122	0.031	—	—	12.6	5.9	6.7
2	0.63	0.082	0.014	0.175	—	10.3	4.9	5.5
Silicone/PVC cable								
1	0.76	0.110	0.015	0.111	—	10.0	—	—
2	1.19	0.065	0.005	0.119	—	15.6	—	—
PVC-nylon/PVC-nylon cable								
1	0.63	0.084	0.024	—	—	10.2	5.0	5.2
2	0.49	0.082	0.032	0.115	—	9.2	4.8	4.4
Polytetrafluoroethylene/polytetrafluoroethylene cable								
1	0.180	0.091	0.012	0.011	—	3.2	2.7	0.4
2	0.383	0.103	—	0.005	—	5.7	—	—
Polymers with fiberweb, net-like and multiplex structures								
Olefin	1.49	0.006	—	—	—	16.5	13.3	3.2
PP-1	1.25	0.0029	—	—	—	14.0	10.8	3.2
PP-2	1.56	0.0048	—	—	—	17.2	10.5	6.7
Polyester-1	2.21	0.015	—	—	—	24.6	8.9	15.7
Polyester-2	1.51	0.0079	—	—	—	16.8	9.1	7.7
Polyester-3	2.55	0.020	—	—	—	28.5	22.6	5.9
Polyester-4	1.92	0.014	—	—	—	21.4	12.4	9.0
Rayon-1	1.80	0.043	—	—	—	20.3	14.1	6.2
Rayon-2	1.91	0.043	0.002	—	—	21.5	13.3	8.2
Rayon-3	1.18	0.047	—	—	—	13.5	8.3	5.2
Polyester-Rayon	1.52	0.005	—	—	—	16.8	9.1	7.7
Polyester-polyamide	1.82	0.008	—	—	—	20.2	10.4	9.8
Rayon-PE	1.50	0.027	—	—	—	16.9	8.72	8.2

[a]Data from the ASTM E 2058 FPA (Fig. 53.1). Some of the data are corrected to reflect well-ventilated combustion. All the data are reported for turbulent fires, i.e., polymers exposed to higher external heat flux values. -: either not measured or are less than 0.001.
[b]Abbreviations are listed in the nomenclature.
[c]Hyd: mixture of low molecular weight gaseous hydrocarbons.
[d]Comp: net complete heat of combustion; chem: chemical heat of combustion; con: convective heat of combustion; rad: radiative heat of combustion.
[e]Calculated from the data in Refs. 9, 10 and 23.

TABLE 53.10. *Mass of O_2 consumed per unit mass of air and mass of products generated per unit mass of air consumed in mg/g.*

Polymer	O_2	CO_2	CO	Hydrocarbons	Smoke
Polystyrene	200	177	4.55	1.06	12.4
Polypropylene	210	190	1.63	0.408	4.01
Polyethylene	208	188	1.63	0.476	4.08
Nylon	213	184	3.39	1.43	6.70
Polymethylmethacrylate	226	257	1.21	0.121	2.67
Wood	220	219	0.691	0.173	2.59
Polyvinylchloride	92	76	10.3	3.78	28.2

TABLE 53.11. *Ventilation correlation coefficients for CO, hydrocarbons, and smoke for well ventilated combustion.*[a]

	CO			Hydrocarbons			Smoke		
Polymer	α	β	ξ	α	β	ξ	α	β	ξ
Polystyrene	2	2.5	2.5	25	5.0	1.8	2.8	2.5	1.3
Polypropylene	10	2.5	2.8	220	5.0	2.5	2.2	2.5	1.0
Polyethylene	10	2.5	2.8	220	5.0	2.5	2.2	2.5	1.0
Nylon	36	2.5	3.0	1200	5.0	3.2	1.7	2.5	0.8
Polymethylmethacrylate	43	2.5	3.2	1800	5.0	3.5	1.6	2.5	0.6
Wood	44	2.5	3.5	200	5.0	1.9	2.5	2.5	1.2
Polyvinylchloride	6.5	0.001	8.0	0.38	0.001	8.0	0.38	0.001	8.0

[a]From Ref. 21 and the ASTM E 2058 FPA in our laboratory.

the nonhalogenated polymers: $\alpha = -1$, $\beta = 2.5$, and $\xi = 1.2$; for the halogenated polymers, $\alpha = -0.30$, $\beta = 0.001$, and $\xi = 11.0$).

The concentrations of products can be calculated from Eq. (53.13), such as shown in Fig. 53.4 for CO. The predicted concentrations are in good agreement with the concentrations measured in larger-scale fires [22].

For nonhalogenated polymers, the concentration predictions show three regions: (1) flaming combustion region for well ventilated combustion ($\Phi < 1.0$), where a sufficient amount of oxygen is present and the concentrations of products of incomplete combustion are small; (2) transition combustion region for Φ values between 1.0 and 3.5, where oxygen concentration is close to zero and concentrations of products of incomplete combustion are high; and (3) nonflaming combustion region for $\Phi \geq 3.5$, where pyrolysis becomes the dominant process. For halogenated polymers, only flaming combustion region ($\Phi < 1.0$) and nonflaming combustion region ($\Phi \geq 1.0$) are present.

The concentration variations with the equivalence ratio depends on the generic nature of the polymer. The increase in the concentration of hydrocarbons with the equivalence ratio follows the order:

1. Hydrocarbon: nylon>PMMA>PE and PP>wood and PS>PVC,
2. CO_2: the concentrations for polymers with oxygen atom in the structure (PMMA and wood) are higher than the concentrations for polymers with only carbon and hydrogen atoms (PS, PE, PE, and natural gas).
3. CO: the concentrations are high for oxygen containing polymers (PMMA, wood, and PU) and lower for non-

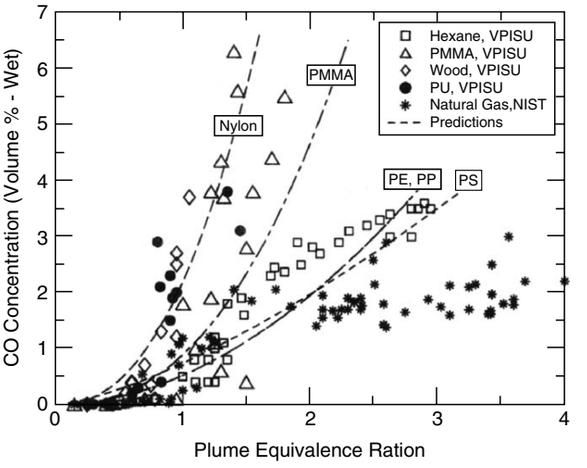

FIGURE 53.4. Carbon monoxide concentration versus the equivalence ratio. Symbols are the experimental concentrations measured in larger-scale fires by the Virginia Polytechnic Institute and State University (VPISU) and by the National Institute of Standards and Technology (NIST) [22]. Lines are the predicted concentrations from Eq. (53.13) using the data from Tables 53.10 and 53.11 and density ratio of 0.654.

oxygenated polymers (PE, PP, PS). The CO concentration increases with the molecular weight as predicted [2]. For example, within the carbon-hydrogen atom containing materials (PE, PP, PS, hexane, and natural gas), the CO concentration is lower for the lower molecular weight natural gas (mostly methane) than for the higher molecular weight hexane, PP, PE, and PS.

4. Smoke: the smoke concentration follows the order: PS (carbon-hydrogen atom aromatic bonds)>nylon (car bon-hydrogen-oxygen-nitrogen atom aliphatic bonds)>PE and PP (carbon-hydrogen atom aliphatic bonds)>wood (carbon-hydrogen-oxygen atom aliphatic bonds)>PMMA (carbon-hydrogen-oxygen atom aliphatic bonds). This order is opposite to the order for CO, but is expected on the basis of the fundamental understanding of the smoke formation in the combustion of the polymeric materials.

The concentration predictions can be used to define the experimental conditions in various toxicity, corrosion, and smoke damage evaluation tests. The correlations for the concentration predictions can be combined with various toxicity, corrosion, and smoke damage relationships, as inputs to the hazard assessment models.

53.8 FIRE PROPERTIES ASSOCIATED WITH THE GENERATION OF HEAT

The heat release rate is directly proportional to the mass loss rate and the proportionality constant is defined as the heat of combustion:

$$\dot{Q}_i'' = \Delta H_i \dot{m}_f'', \tag{53.14}$$

where $\dot{G}_i''$ is the heat release rate (kW/m^2), ΔH_i is the heat of combustion (kJ/kg), and $\dot{m}_f''$ is the mass loss rate (kg/m^2-s). The rate of heat release in a combustion process, within the flame, is defined as the chemical heat release rate. The chemical heat released within the flame is carried away from the flame by flowing product-air mixture and is emitted to the environment as radiation. The component of the chemical heat release rate carried away by the flowing products-air mixture is defined as the convective heat release rate. The component of the chemical heat release rate emitted to the environment is defined as the radiative heat release rate. The heat of combustion is defined respectively as the chemical, convective, and radiative heat of combustion.

The chemical heat release rate is determined from the carbon dioxide generation (CDG) and oxygen consumption (OC) calorimetries [2,3]. In the CDG calorimetry, the chemical heat release rate is determined from the mass generation rate of CO_2 corrected for CO [2,3]. In the OC calorimetry, the chemical heat release rate is determined from the mass consumption rate of O_2 [2,3,24]. The convective heat release rate is determined from the gas temperature rise (GTR) calorimetry [2,3,25]. The radiative heat release rate is determined from the difference between the chemical and convective heat release rates [2,3].

53.8.1 The CDG Calorimetry

The chemical heat release rate is determined from the following relationships:

$$\dot{Q}_{\text{ch}}'' = \Delta H_{\text{co}_2}^* \dot{G}_{\text{co}_2}'' + \Delta H_{\text{co}}^* \dot{G}_{\text{co}}'', \tag{53.15}$$

$$\Delta H_{\text{co}_2}^* = \frac{\Delta H_T}{\Psi_{\text{co}_2}}, \tag{53.16}$$

$$\Delta H_{\text{co}}^* = \left[\frac{\Delta H_T - \Delta H_{\text{co}} \Psi_{\text{co}}}{\Psi_{\text{co}}}\right], \tag{53.17}$$

where $\dot{Q}_{\text{ch}}''$ is the chemical heat release rate (kW/m^2), ΔH_{co2}^* is the net heat of complete combustion per unit mass of CO_2 generated (MJ/kg), ΔH_{co}^* is the net heat of complete combustion per unit mass of CO generated (MJ/kg), ΔH_T is the net heat of complete combustion per unit mass of fuel consumed (kJ/g), Ψ_{co2} is the stoichiometric yield of CO_2 (kg/kg), Ψ_{co} is the stoichiometric yield of CO (kg/kg), $\dot{G}_{\text{co}_2}''$ is the generation rate of CO_2(kg/m^2-s) and $\dot{G}_{\text{co}}''$ is the generation rate of CO (kg/m^2-s).

The values of ΔH_{co2}^* and ΔH_{co}^* for over 200 fuels are tabulated in Tewarson [2]. The values depend on the chemical structures of the fuels. With some exceptions, the values remain approximately constant within each generic group of fuels. For approximate calculations, the average values can be used, which are: $\Delta H_{\text{co2}}^* = 13.3\ \text{kJ/g} \pm 11\%$, and $\Delta H_{\text{co}}^* = 11.1\ \text{kJ/g} \pm 18\%$.

In the CDG calorimetry, the CO correction for well-ventilated combustion is very small, because of the small amounts of the CO generated. The variations of 11% and 18% in the ΔH_{co2}^* and ΔH_{co}^* values, respectively, would reduce significantly if values for low molecular weight hydrocarbons with small amounts of O, N, and halogen were used in averaging.

For the determination of the chemical heat release rate, mass generation rates of CO_2 and CO are measured and actual values of ΔH_{co2}^* and ΔH_{co}^* are used for accuracy or the average values for approximate results. The CO_2 and CO measurement details are described in Tewarson [2].

53.8.2 The OC Calorimetry

The chemical heat release rate is determined from the following relationship:

$$\dot{Q}_{\text{ch}}'' = \Delta H_0^* \dot{C}_0'', \tag{53.18}$$

$$\Delta H_0^* = \frac{\Delta H_T}{\Psi_0}, \tag{53.19}$$

where ΔH_0^* is the net heat of complete combustion per unit mass of oxygen consumed (MJ/kg), $\dot{C}_0''$ is the mass consumption rate of oxygen (kg/m^2-s) and Ψ_0 is the stoichiometric mass-oxygen-to-fuel ratio (kg/kg).

The values of ΔH_0^* for over 200 fuels are tabulated in Tewarson [2]. The values depend on the chemical structures of the fuels. With some exceptions, the values remain approximately constant within each generic group of fuels. For approximate calculations, the average value can be used, which is: $\Delta H_0^* = 12.8$ kJ/g $\pm$ 7%. The variation of $\pm$ 7% would reduce significantly if values for low molecular weight hydrocarbons with small amounts of O, N, and halogen were used in averaging.

For the determination of the chemical heat release rate, mass consumption rate of O_2 is measured and the actual value of ΔH_0^* is used for accuracy or the average value for approximate results. The O_2 measurement details are described in Tewarson [2].

The chemical heat release rates determined from the CDG and OC calorimetries are very similar.

53.8.3 The GTR Calorimetry

The convective heat release rate is determined from the following relationship:

$$\dot{Q}''_{\text{con}} = \frac{\dot{W} c_p (T_g - T_a)}{A}, \tag{53.20}$$

where $\dot{Q}''_{\text{con}}$ is the convective heat release rate (kW/m^2), c_p is the specific heat of the combustion product-air mixture at the gas temperature (MJ/kg-K), T_g is the gas temperature (K), T_g is ambient temperature (K), $\dot{\mathbf{W}}$ is the total mass flow rate of the fire product-air mixture (kg/s), and A is the total exposed surface (m^2).

For the determination of the convective heat release rate, temperature and total mass flow rate of the fire-products air mixture are measured. The literature value of the specific heat of air at the gas temperature is used as the fire products are diluted by fresh air by about 20 times their volume. The temperature and mass flow rate measurement details are described in Tewarson [2].

53.8.4 Heat of Combustion

The average heat of combustion is determined from the ratio of the energy, E_i, obtained from the summation of the chemical, convective, and radiative heat release rates and the total mass of gasified polymer, W_f, obtained from the summation of the mass loss rate:

$$\Delta H_i = \frac{E_j}{W_f}, \tag{53.21}$$

where ΔH_i is the average chemical, convective, or radiative heat of combustion (MJ/kg). The values of the average heat of combustion obtained in this fashion are listed in Table 53.9. The radiative heat of combustion is obtained from the difference between the chemical and convective heats of combustion, as heat losses are negligibly small in the ASTM E 2058 FPA.

53.8.5 Heat Release Rate at Various Heat Fluxes

The heat release rate can be predicted at various heat flux values from the following relationship obtained from Eqs. (53.5) and (53.14):

$$\dot{Q}''_i = \left(\frac{\Delta H_i}{\Delta H_g}\right)(\dot{q}''_e + \dot{q}''_f - \dot{q}''_{rr}), \tag{53.22}$$

where $\Delta H_i/\Delta H_g$ is defined as the heat release parameter (HRP) (kJ/kJ). HRP values are independent of the fire size, but depend on the ventilation and can be calculated from the data such as listed in Tables 53.2 and 53.9 or from the slopes of the lines obtained by plotting the heat release rates against the external heat flux. The heat release rate can be calculated from the HRP and $\dot{q}''_{rr}$ values for the fire scenario for specified external and flame heat flux values.

53.8.6 Generation of Heat and Ventilation

The relationship between heat release rate or heat of combustion and the equivalence ratio is expressed as [21]:

$$\dot{Q}''_{i,v} = \dot{Q}''_{i,\infty}\left[1 - \frac{\alpha}{\exp\ \beta\Phi^{-\xi}}\right], \tag{53.23}$$

$$\Delta H_{i,v} = \Delta H_{i,\infty}\left[1 - \frac{\alpha}{\exp\ \beta\Phi^{-\xi}}\right], \tag{53.24}$$

$$\chi_v = \chi_\infty\left[1 - \frac{\alpha}{\exp\ \beta\Phi^{-\xi}}\right], \tag{53.25}$$

where $\dot{Q}''_{i,v}$ is the heat release rate, $\Delta H_{i,v}$ is the heat of combustion, and χ_v is the combustion efficiency for the ventilation-controlled combustion (kW/m^2), $\dot{Q}''_{i,\infty}$ is the heat release, $\Delta H_{i,\infty}$ is the heat of combustion, and χ_∞ is the combustion efficiency for the well-ventilated combustion (kW/m^2), and α, β and ξ are the ventilation correlation coefficients. Combustion efficiency is the ratio of the chemical heat release rate or chemical heat of combustion to the heat release rate for complete combustion or net heat of complete combustion. For the nonhalogenated polymers, $\alpha = 0.97$, $\beta = 2.5$, and $\xi = 1.2$ for the chemical heat release rate or the chemical heat of combustion and $\alpha = 1.0$, $\beta = 2.5$, and $\xi = 2.8$ for the convective heat release rate or the convective heat of combustion. For the halogenated polymers, $\alpha = 0.30$, $\beta = 0.001$, and $\xi = 11$ for the chemical heat release rate or the chemical heat of combustion. Chemical heat release rate, chemical heat

of combustion, and combustion efficiency decrease with ventilation restriction or increase in the equivalence ratio.

Figure 53.5 shows the combustion efficiency calculated from Eq. (53.25). As expected, combustion efficiency decreases with increase in the equivalence ratio due to limitation in the availability of air. For the nonhalogenated polymers, flame extinction occurs for combustion efficiency between about 0.20 and 0.40. The halogenated polymer burns with a low combustion efficiency; a slight decrease in the combustion efficiency (below about 0.30) results in flame extinction, although combustion remains well ventilated. The combustion efficiency decreases rapidly with increase in the equivalence ratio for the low molecular fuel (natural gas, methane) compared to the polymers, which gasify as higher molecular weight oligomer.

53.9 FIRE PROPERTIES ASSOCIATED WITH CORROSION AND SMOKE DAMAGE

53.9.1 Corrosion Damage

The fire property associated with corrosion damage is defined as corrosion index (CI), which is the corrosion rate per unit mass concentration of the products [(Å/min)/(g of polymer gasified products/m^3 of air flow)] [2,3]:

$$\mathrm{CI} = \{\delta_{\mathrm{loss}}/\Delta t_{\mathrm{exposure}}\}/\{W_f/\dot{V}_T \Delta t_{\mathrm{test}}\}, \qquad (53.26)$$

where CI is in (Å/min)/(mg/g), δ_{loss} is the metal loss due to corrosion (Å), $\Delta t_{\mathrm{exposure}}$ is the time the corrosive product deposit is left on the surface of the metal (min), W_{f} is the total mass of the polymer lost in the experiment (g), $\dot{V}_T$ is the total volumetric flow rate of the mixture of fire products and air (m^3/s) and Δt_{test} is the combustion duration (s).

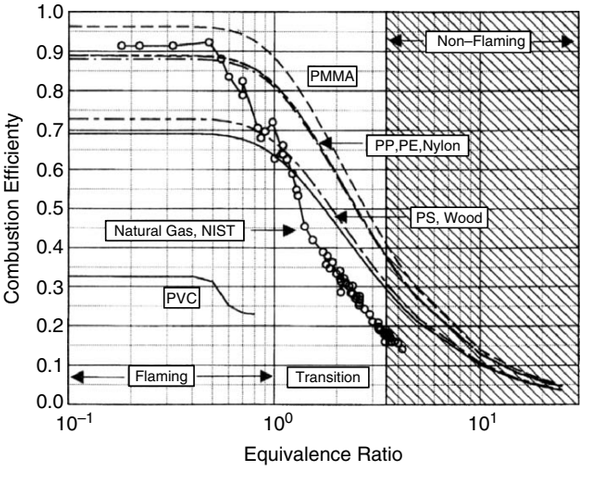

FIGURE 53.5. Calculated combustion efficiency versus the equivalence ratio. For the calculations, Eq. (53.25) and data from Table 53.9 and [2] were used. For natural gas, the data measured at the National Institute of Standards and Technology (NIST) as reported in [22] were used.

Corrosion is measured by exposing metal surfaces to the flowing fire products in the sampling duct of the ASTM E 2058 FPA. The change in resistance due to corrosion is measured as a function of time such as shown in Fig. 53.6. The slopes of the lines represent corrosion rates, (Å/min). In Fig. 53.6, corrosion rate is faster for the polyester-PVC-fiber glass sample than it is for the fire-retarded (FR) polypropylene (PP) sample. PP polymer sample shows negligible corrosion as it does not contain halogen atoms.

The total mass loss of the polymer lost (g), total volumetric flow rate of the mixture of fire products and air mixture (m^3/s) and combustion duration (s) are measured in the experiments.

The CI values for various polymers have been determined in the flammability apparatus; Table 53.12 lists values for some selected polymers, as examples. The CI values for nonhalogenated polypropylene and wood are negligibly small. For the highly halogenated polymers, the CI value is

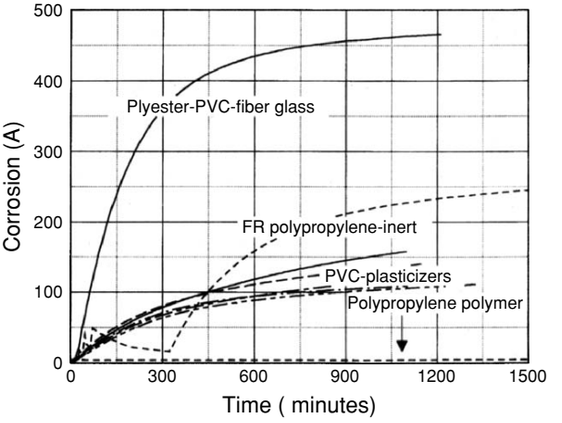

FIGURE 53.6. Corrosion of thin copper strip on a fiber glass polyester plate by the flowing combustion products -air mixture in the sampling duct of the ASTM E 2058 FPA.

TABLE 53.12. *Corrosion index for selected polymers.*[a]

Materials	Corrosion index [(Å/min)/(*g* polymer gasified/m^3 of air)]
Polyvinylchloride (PVC)[b]-*1*	1.8
PVC-2	0.78
PVC-3	0.60
PVC-4	0.36
Polypropylene	0.074
Polypropylene/fire retardant	1.7
Teflon® (TFE)	0.28
Wood	0.088

[a]Determined in the ASTM E 2058 FPA at the Factory Mutual Research Corporation.
[b]Amount of nonhalogenated additive increasing from 1 to 4.

high if hydrogen atoms are present in the structure (PVC) or halogenated fire-retardant additive is present (PP/FR), and is low if there are no hydrogen atoms in the structure (Teflon® TFE). The difference in the CI values indicate the importance of water as a combustion product to generation acids for PVC and PP/FR. Teflon® (TFE) does not generate water as a product of combustion and thus the formation of an acid (HF) would depend on the efficiency of the hydrolysis process between the ambient water from air and Teflon® (TFE) vapors. The hydrolysis process appears to be inefficient. The CI value decreases with increase in the amount of non-halogenated additive (PVC-1 to -4).

53.9.2 Smoke Damage

The fire property associated with smoke damage is the ratio of the yield of smoke-to-the yield of CO_2. The ratio increases with increase in the equivalence ratio or ventilation restriction. The yield of smoke is proportional to the smoke generation rate and the yield of CO_2 is proportional to the chemical heat release rate. The higher the ratio of the yield of smoke to the yield of CO_2, higher the damage due to smoke relative to the damage due to heat.

Smoke is a mixture of black carbon (soot) and aerosol [26,27]. It has been suggested that soot nucleation and growth occur near the highly ionized regions of the flames in combustion processes, and that some of the charges are transferred to smoke particles. Multimodal distributions show that the soot particle radii belong to three ''modes'' [26]:

1. ''Nuclei mode'' has a geometric mean radius between 0.0025 and 0.020 μ and probably results from the condensation of gaseous carbon moieties.
2. ''Accumulation mode'' encompasses particles in the size range 0.075–0.25 μ and apparently results from the coagulation and condensation of the ''nuclei mode'' particles.
3. ''Coarse mode'' at several microns that is attributed to the precipitation of fine particles on the walls of vehicle exhaust systems and a subsequent entrainment in the issuing gases.

In fires, large variations in smoke particle size are due to coagulation and condensation. Data from various fires show that initially the smoke particles are in the coarse mode. As the smoke moves away from the fire origin, large particles settle down to the floor, leaving small particles having radii of 0.04–0.09 μ (accumulation mode). It thus appears that smoke damage in the room of fire origin is expected to be due to particles of several microns in radius in the coarse mode, whereas smoke damage downstream of the fire is expected to be due to particles with radius less than 0.1 μ in the lower end of the accumulation mode. Soot is an efficient absorber of HCl. In the combustion of 79.5% PVC-20.5% PE, 19 mg of HCl/g of smoke is loosely bound and 27 mg of HCl/gm of smoke is tightly bound to soot [28].

Smoke damage in industrial and commercial occupancies is considered in terms of discoloration and odor of the property exposed to smoke, interference in the electric conduction path and corrosion of the parts exposed to smoke is a carrier of the corrosive products.

53.10 FIRE PROPERTIES ASSOCIATED WITH FIRE SUPPRESSION/EXTINGUISHMENT

Several fire properties are associated with fire suppression/extinguishment by active and passive fire protection techniques. Changes in the values of the properties are used to assess the effectiveness of the techniques. Passive fire protection techniques enhance resistance to: (1) pyrolysis, ignition, combustion, and fire propagation processes, and (2) generation of heat and products. Active fire protection techniques provide hinderance to the growth of the fire by: (1) interacting with the burning polymer in the solid phase (mainly removal of heat) [29]; (2) reducing the availability of the oxygen to the fire (creation of nonflammable mixture); and (3) removal of heat from the flame and interference with the chemical reactions within the flame [30].

53.10.1 Passive Fire Protection

Passive fire protection is provided by various chemical and physical means.

Increasing the Resistance to Ignition and Fire Propagation by Increasing the Values of CHF and TRP

The CHF and TRP values can be increased by modifying the pertinent parameters such as the chemical bond dissociation energy and thermal diffusion (combination of the density, specific heat and thermal conductivity).

Decreasing the Values of the HRP and the Flame Heat Flux

The heat release rate is equal to the Heat Release Parameter (HRP) times the net heat flux [Eq. (53.22)]. Decrease in the HRP value would decrease the heat release rate. The HRP value can be decreased by decreasing the heat of combustion and/or increasing the heat of gasification by various chemical and physical means. An examination of the data in Table 53.9 for heat of combustion show that introduction of oxygen, nitrogen, sulfur, halogen, and other atoms into the chemical structures of the polymers reduces the heat of combustion. For example, the heat of combustion decreases when the hydrogen atoms attached to

carbon atoms in polyethylene are replaced by the halogen atoms, such as by fluorine in TFE. The chemical heat of combustion decreases from 38.4 MJ/kg to 4.2 MJ/kg and the HRP value decreases from 17 to 2 (Table 53.9).

The HRP values can also be reduced by increasing the heat of gasification and decreasing the heat of combustion by retaining the major fraction of the carbon atoms in the solid phase, a process defined as charring. Several passive fire protection agents are commercially available to enhance the charring characteristics of materials.

The effect on flame heat flux by passive fire protection is determined by using the radiation scaling technique, where combustion experiments are performed in oxygen concentration higher than the ambient values. As discussed previously, liquids which vaporize primarily as monomers or as very low molecular weight oligomer, the flame heat flux values are in the range of $22–44\,kW/m^2$, irrespective of their chemical structures. For solid polymers, which vaporize as high molecular weight oligomer, the flame heat flux values increase substantially to the range of $49–71\,kW/m^2$, irrespective of their chemical structures. Passive fire protection agents which can reduce the molecular weight of the pyrolysis products of the polymers would be effective in reducing the flame heat flux and complement the active fire protection agents.

Changing the Melting Behavior of Materials

The chemical heat release rate increases very rapidly as a polymer changes from a solid to a boiling liquid pool, creating dangerous conditions and presenting a serious challenge to the active fire protection agents. Inert passive fire protection agents added to the polymer which would eliminate the boiling liquid pool would be effective in complementing the active fire protection agents.

Decreasing the Value of the Product Generation Parameter (PGP)

Nonhalogenated passive fire protection agents which reduce or eliminate the release of halogenated and highly aromatic products and enhance release of aliphatic products, rich in hydrogen and oxygen atoms but poor in carbon atoms, would be effective in reducing the nonthermal damage due to smoke and corrosion. Some of the passive fire protection agents, available commercially, interact with the polymers in the solid as well as in the gas phase during pyrolysis and combustion.

The critical parameter that needs to be examined in the presence and absence of the passive fire protection agents is the ratio of PGP (smoke, CO, corrosive and toxic products) to HRP. The effectiveness of the passive fire protection agent would be reflected in the small values of the ratios at fire control, suppression, and/or extinguishment stage.

53.10.2 Active Fire Protection

Active fire protection is provided by applying agents as liquids, gases, solid powders, or foams to the flame and/or to the surface of the burning polymers.

Flame Suppression/Extinguishment by Liquid Vapors and Gaseous Agents

A flame will extinguish when the time required for the chain reaction which sustains the combustion process exceeds the time it takes to replenish the necessary heat and reactants [30]. The most commonly used liquid and gaseous chemical inhibition agents at the present time are: Halon[1] - 1211 ($CBrClF_2$), 1301 ($CBrF_3$), and 2402 ($CBrF_2CBrF_2$). Because of the contribution of Halons to depletion of the stratospheric ozone layer, they will, however, not be used in the future [30]. There is thus an intense effort underway to develop alternative fire suppressants to replace ozone layer depleting Halons. The Halon alternatives belong to one of the following classes: (1) Hydrobromofluorocarbons (HBFC); (2) Chlorofluorocarbons (CFC); (3) Hydrochlorofluorocarbons (HCFC); (4) Perfluorocarbons (FC); (5) Hydrofluorocarbons (HFC); and (6) Inert gases and vapors.

The most common test to screen the Halon alternates is the ''cup burner'' test, where concentration of Halons or alternates required for extinction of a small laminar diffusion flame are determined. Table 53.13 lists the concentrations of Halon 1301 and alternates required for heptane flame extinction in the ''cup burner'' test. Acceptable total flooding agents in normally occupied areas are indicated by bold letters and numbers.

When the amount of an agent applied to a burning polymer is close to the amount required for flame extinction, first flame instability sets in, followed by flame liftoff from the surface and finally the flame is extinguished, as indicated in Fig. 53.7 for the flame extinction of PMMA by Halon 1301. Initially there is a rapid decrease in the chemical heat release rate as Halon is added to the flame. There is a gradual increase in the chemical heat release rate between 5.40% and 6.25% of Halon unto flame extinction. The increase in the chemical heat release rate appears to be due to increase in the flame luminosity (increase in the flame radiative heat flux transferred back to the fuel surface).

Figure 53.8 shows that the generation efficiencies of CO, mixture of hydrocarbons, and smoke increase significantly with increase in the Halon concentration. The effect of Halon on the generation efficiencies is strong for CO and the mixture of hydrocarbons and weak for smoke. This type of combustion behavior of PMMA is similar to one found with the ventilation controlled combustion, i.e., increasing preference of fuel carbon atom to convert to CO and the mixture of hydrocarbons rather than to smoke. It thus appears that the chemical interruption processes for flame extinction by Halon and reduced oxygen are very similar.

TABLE 53.13. *Concentrations of halon 1301 and alternates required for flame extinction in the heptane "cup burner" test.*[a]

Agent Name	Formula	Concentration (volume %)	Relative concentration
	Inert Agents		
Nitrogen	N_2	32	11.0
Carbon dioxide	CO_2	23	7.9
Helium	He	31	10.7
Argon	Ar	41	14.1
Silicone Containing Agent			
Silicone tetrafluoride	SiF_4	36	12.4
Sodium Containing Agent			
Sodium bicarbonate (10–20 μm)	$NaHCO_3$	3.0*b*	—
Halon			
Halon 1301	CF_3Br	2.9	1.0
HFC			
HCFC-22 (Du Pont FE 232)	$CHClF_2$	11.6	4.00[b]
HBFC-22B1 (Great Lakes FM 100)	$CHBrF_2$	4.4	1.52
HFC-23 (Du Pont FE13)	CHF_3	12.4	4.28
HFC-32	CH_2F_2	8.8	3.03
HCFC-124	$CHClFCF_3$	8.2	2.83
HBFC-124B1	CF_3CHFBr_3	2.8	0.97
HFC-125 (Du Pont FE 25)	CF_3CHF_2	9.40	3.24
HFC-134	CHF_2CHF_2	11.2	3.86
HFC-134a	CF_3CH_2F	10.5	3.62
HFC-142b	$CClF_2CH_3$	11.0 (calc)	3.79
HFC-152a	CHF_2CH_3	27.0 (calc)	9.31
HFC-218	$CF_3CF_2CF_3$	6.1	2.10
HFC-227ea (Great Lakes FM 200)	CF_3CHFCF_3	6.1	2.10[b]
Trifluoromethyl Iodide 1311	CF_3I	3.0	1.03
FC-14	CF_4	13.8	4.76
FC-116	CF_3CF_3	7.8	2.69
C318	C_4F_8	7.3	2.52
FC-5-1-14 (3M PFC 614)	C_4F_{10}	5.5	1.90[b]

[a]From Refs. 30 and 31.
[b]Acceptable total flooding agents in normally occupied areas [32].

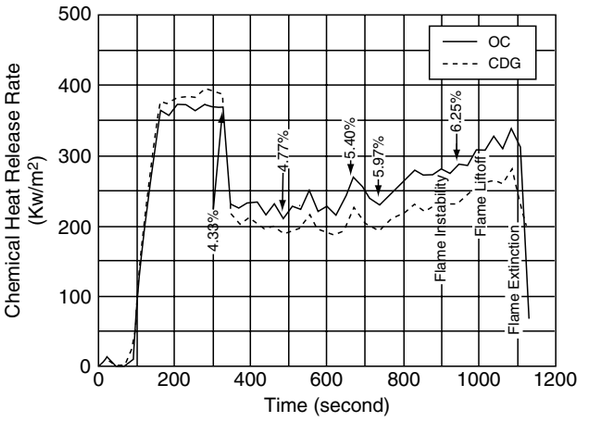

FIGURE 53.7. Chemical heat release rate versus time for the combustion of 100 mm $\times$ 100 mm $\times$ 25 mm thick horizontal slab of polymethylmethacrylate exposed to 40 kw/m^2 in co-air flow with varying Halon 1301 concentration at a velocity of 90 mm/s in the ASTM E 2058 FPA. Numbers and their locations represent Halon 1301 concentrations in volume percents and application times. Times for flame instability, liftoff, and extinction are also indicated.

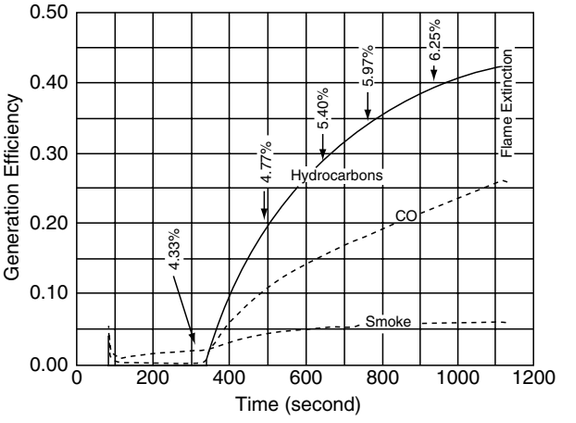

FIGURE 53.8. Generation efficiencies of CO, mixture of hydrocarbons, and smoke versus time for the combustion of 100 mm $\times$ 100 mm $\times$ 25 mm thick horizontal slab of polymethylmethacrylate exposed to 40 kw/m^2 in co-air flow with varying Halon 1301 concentration at a velocity of 90 mm/s in the ASTM E 2058 FPA. Numbers and their locations represent Halon 1301 concentrations in volume percents and application times. Times for flame instability, liftoff, and extinction are also indicated.

This experimental finding is consistent with the concept that a critical value of the Damkohler number for flame extinction [30].

The existence of the critical conditions at flame extinction has also been postulated by the "Fire Point Theory" [29] and supported by the experimental data for the critical mass pyrolysis and heat release rates [2].

The fire property associated with flame extinction by gaseous agents thus would be the critical value of the HRP.

Flame Suppression/Extinguishment by Liquids

At the flame extinction condition, the critical mass pyrolysis and heat release rates can be expressed as:

$$\dot{m}''_{cr} = \frac{\dot{q}''_e + \dot{q}''_f - \dot{q}''_{rr} - \dot{q}''_w}{\Delta H_g}, \tag{53.27}$$

$$\dot{Q}''_{cr} = \left[\frac{\Delta H_{ch}}{\Delta H_g}\right](\dot{q}''_e + \dot{q}''_f - \dot{q}''_{rr} - \dot{q}''_w), \tag{53.28}$$

where $\dot{m}''_{cr}$ is the critical mass pyrolysis rate for flame extinction (kg/m^2-s), $\dot{q}''_e$ is the external heat flux (kW/m^2), $\dot{q}''_f$ is the flame heat flux transferred back to the surface (kW/m^2), $\dot{q}''_{rr}$ is the surface re-radiation loss (kW/m^2), ΔH_g is the heat of gasification (kJ/kg), $\dot{Q}''_{cr}$ is the critical value of the chemical heat release rate for flame extinction (kW/m^2), ΔH_{ch} is the chemical heat of combustion (kJ/kg), $\Delta H_{ch}/\Delta H_g$ is the HRP, and $\dot{q}''_w$ is the heat flux removed from the surface of a burning polymer by a liquid such as water, as a result of vaporization expressed as:

$$\dot{q}''_w = \varepsilon_w \dot{m}''_w \Delta H_w, \tag{53.29}$$

where ε_w is the water application efficiency, $\dot{m}''_w$ is the water application rate per unit surface area of the polymer (kg/m^2-s), and ΔH_w is the heat of gasification of water (2.58 MJ/kg). If only part of the water applied to a hot surface evaporates and the other part forms a puddle, such as on a horizontal surface, blockage of flame heat flux to the surface and escape of the fuel from the polymer surface are expected. Eq. 53.27 thus is modified as:

$$\dot{q}''_w = \dot{m}''_w(\varepsilon_w \Delta H_w + \delta_w), \tag{53.30}$$

where δ_w is the energy associated with the blockage of flame heat flux to the surface and escape of the fuel vapors per unit mass of the fuel (MJ/kg).

From Eqs. 53.27 and 53.30, with no external heat flux:

$$\dot{m}''_w = \frac{\dot{q}''_f - \dot{q}''_{rr}}{\varepsilon_w \Delta H_w + \delta_w} - \frac{\dot{m}''_{cr} \Delta H_g}{\varepsilon_w \Delta H_w + \delta_w}. \tag{53.31}$$

The first term on the right-hand side takes into account the effects of the physical differences on flame extinction such as the fire size and polymer shape, size, and arrangement. The second term on the right-hand side takes into account the effects of the chemical differences on flame extinction such as the chemical structures of the polymers and additives. In large-scale fires, the second term is negligibly small and water application rate required for flame extinction depends mainly on the flame heat flux, surface re-radiation loss, and mode of water application.

The critical values of the mass pyrolysis rate, heat release rates, and water application rates for flame extinction for polymers, are listed in Table 53.14. For the polymers listed in the table, the critical values of the heat release rates do not depend on the generic natures of the polymers. The average critical values of the chemical, convective, and radiative heat release rates are 100 ± 7, 53 ± 9, and 47 ± 10 kW/m^2, respectively. The critical water application rate required for flame extinction is: polyoxymethylene, polymethylmethacrylate and polyethylene with 25% chlorine (2.1–2.5 g/m^2-s)<polyethylene and polypropylene (3.5–4.1 g/m^2-s)<polystyrene (5.1 g/m^2-s).

53.11 STANDARDS AND TESTING OF POLYMER PRODUCTS AND MATERIALS

Polymer products are used in a variety of applications in residential, private, government, industrial, transportation, and manufacturing occupancies. Consequently, for the assessment of the fire hazards of polymer products large numbers of fire scenarios need to be considered for testing. To avoid this problem of large number of fire scenarios to be considered for testing, two types of standard test methods have been developed:

1. *Test methods to comply with specific regulations or voluntary agreements*: these types of test methods are usually larger than laboratory-scale tests and are included in the prescriptive (specification)-based fire codes[1]. Generally, products in their end-use configurations are tested under a defined fire condition.
2. *Small-scale standard test methods*: these types of test methods have been developed based on qualitative experiences as well as on the understanding of fire stages and associated hazards. Relatively simple types of measurements are made for various fire properties of the polymeric materials for each fire stage. These types of standard test methods are useful for the performance-based fires codes which are being considered to augment or replace the prescriptive-based fire codes[2] [33–35].

Both types of standard test methods for products in their end-use configurations and polymeric materials used for the construction of products are promulgated by various

[1] The codes reflect expectations for the level of fire protection.

[2] An example of the prescriptive-based code for passive fire protection is the specified fire resistance rating for an interior wall, whereas for the performance-based code it would be a prediction for the desired passive fire protection based on the engineering standards, practices, tools, and methodologies.

TABLE 53.14. *Critical mass pyrolysis, heat release, and water application rate.*[a]

Polymers	Critical values for flame extinction				
	$\dot{m}''_{cr}$(kg/m^2-s) $\times 10^3$	$\dot{Q}''_{ch}$(kW/m^2)	$\dot{Q}''_{con}$(kW/m^2)	$\dot{Q}''_{rad}$(kW/m^2)	$\dot{W}''_{w}$(kg/m^2-s) $\times 10^3$
Polyoxymethylene	4.5	(65)	50	(14)	2.3
Polymethylmethacrylate	3.2	77	53	24	2.5
Polyethylene	2.5	96	55	42	3.8
Polypropylene	2.7	104	61	43	3.0
Polystyrene	4.0	108	44	64	5.1
Polyethylene foams					
1	2.6	—	—	—	—
2	2.6	—	—	—	—
3	2.5	—	—	—	—
4	2.6	—	—	—	—
Average	2.6	88	51	38	3.8
Chlorinated polyethylenes					
25% chlorine	6.6	95	48	47	2.1
36% chlorine	7.5	—	—	—	—
48% chlorine	7.6	—	—	—	—
Expanded polystyrene					
GM47	6.3	—	—	—	—
GM49	4.9	—	—	—	—
GM51	6.3	—	—	—	—
GM53	5.7	—	—	—	—
Average	5.8	108	44	64	5.1
Polyurethane foams (flexible)					
GM21	5.6	—	—	—	—
GM23	5.3	—	—	—	—
GM25	5.7	—	—	—	—
GM27	6.5	—	—	—	—
1/$CaCO_3$	7.2	—	—	—	—
Average	6.1	101	48	53	—
Polyurethane foams (rigid)					
GM29	7.9	—	—	—	—
GM31	8.4	—	—	—	—
GM35	6.9	—	—	—	—
Average	7.7	102	44	58	—
Polyisocyanurate foams (rigid)					
GM41	6.8	—	—	—	—
GM43	5.5	—	—	—	—
Phenolic foam	5.5	—	—	—	—

[a]From the data measured in the ASTM E 2058 FPA at FMRC; -: no data or considered in the average data.

national and international standards organizations and government and private agencies, for example the following [36,37].

1. Australia (Standards Australia, SA);
2. Canada (Canadian General Standards Board, CGSB);
3. China-People's Republic (China Standards Information Center, CSIC);
4. China-Republic of China-Taiwan-(Bureau of Standards, Metrology and Inspection, BSMI);
5. Europe (International Electrotechnical Commission, IEC; European Committee for Electrotechnical Standardization, CENELEC; European Committee for Standardization, CEN, International Standards Organization, ISO);
6. Finland (Finnish Standards Association, SFS);
7. France (Association Europeene Des Constructeurs De Materiel Aerospatial, AECMA; Association Francaise De Normalisation, AFNOR);

8. Germany (Deutsches Institut Fur Normung, DIN);
9. India (Indian Standards Institution, ISI);
10. Israel (Standards Institution of Israel, SII);
11. Italy (Ente Nazionale Italiano Di Unifacazione, UNI);
12. Japan (Japanese Standards Association, JSA);
13. Korea (Korean Standards Association, KSA);
14. New Zealand (Standards New Zealand, SNZ);
15. Nordic Countries (Nordtest: Denmark, Finland, Greenland, Iceland, Norway, and Sweden);
16. Russia (Gosudarstvennye Standarty State Standard, GOST);
17. South Africa (South African Bureau of Standards, SABS);
18. United Kingdom (British Standards Institution, BSI; Civil Aviation Authority, CAA);
19. USA (examples of government agencies: department of transportation, DOT; military-MIL; National Aeronautical and Space Administration, NASA. Examples of private agencies: American National Standards Institute, ANSI, American Society for Testing and Materials, ASTM; Building Officials & Code Administrators International Inc., BOCA; Electronic Industries Alliance, EIA; FM Approvals; Institute of Electrical and Electronics Engineers, IEEE; National Fire Protection Association, NFPA; Underwriters Laboratories, UL).

Each national and international standards organization, government, and private industries from each country, listed above and others, use their own standard test methods for the evaluation of the products and materials. Consequently, there are literally thousands of standard test methods used on a worldwide basis [37–41]. The national and international standards organizations list their test methods in catalogues for standards such as: the European Committee for Standardization, CEN [42], FM Approvals [43], Underwriter's Laboratories (UL) [44], International Standards Organization (ISO) [45], American Society of Testing and Materials (ASTM) [46] and others.

Because of the use of thousands of standard testing methods, products accepted in one country may be unacceptable in the other, creating confusion and serious problems for the manufacturers and fire safety regulator. Vigorous efforts are thus being made, especially in Europe, to harmonize the standard test methods[3]. Recently the European Commission's, single burning item (SBI) and reaction to fire classification [42] is the best example of harmonizing hundreds of European standard testing methods for building products into a single standard test method. The single burning item test method (EN 13823) for testing the fire safety of construction products will be widely used by the manufacturers to allow for the affixing of ''C'' marking that will indicate compliance with the ''Essential Requirements of the Union Directive 89/106/EEC''. In addition, new regulations, Euroclasses[4], and test methods designated EN ISO, are in a process of being introduced that will be used throughout Europe [47,48].

Further harmonization is expected as many regulatory agencies are considering augmenting or replacing the prescriptive-based fire codes (currently in use) by the performance-based fire codes. In the performance-based fire codes, engineering methods are used that need data for the fire properties [33–35]. The data for the fire properties can be obtained from many standard test methods currently in use worldwide by modifying the test procedures and data acquisition methodology. Since fire properties will be measured quantitatively, the standard test methods will be automatically harmonized worldwide and the assessment for the fire resistance of materials and products will become reliable, as it will be subject to quantitative verification. Following sections describe some commonly used standard test methods:

53.11.1 Standard Tests for the Ignition Behavior of Polymer Materials

Standard test methods have been developed for examining the ignition behavior of polymeric materials. Some test methods provide qualitative data, while others provide partial or complete quantitative data for the ignition resistance of materials (Section 53.3, Tables 53.3 and 53.4). The following are examples of the common standard test methods used for examining the ignition resistance of materials:

1. ISO 871 (T_{ig}, ignition temperature in the hot oven) [45];
2. ASTM D 1929 (T_{flash}, flash ignition temperature) and T_{ig} (spontaneous) [46];
3. ASTM E 1352 (qualitative-cigarette ignition of upholstered furniture) [46];
4. ASTM E 1353 (qualitative-cigarette ignition resistance of components of upholstered furniture) [46];
5. ASTM F 1358 (qualitative-effects of flame impingement on materials used in protective clothing not designed primarily for flame resistance) [46];
6. ASTM C 1485 (CHF value of exposed attic floor insulation using an electric radiant heat energy source) [46];

[3] ISO, IEC, Nordtest, CEN, US Federal Aviation Administration's (FAA) standards criteria are internationally acceptable for regulations, and others.

[4] There are seven main Euroclasses for building materials for walls, ceiling, and floors: A1, A2, B, C, D, E, and F [47,48]. A1 and A2 represent different degrees of limited combustibility. B to E represent products that may go to flashover in a room within certain times [47,48]. F means that no performance is determined [47,48]. Thus there are seven classes for linings and seven class for floor coverings [47,48]. There are additional classes of smoke and any occurrence of burning droplets [47,48].

7. ASTM E 648 (CHF value of floor covering systems using a radiant heat energy source) [46];
8. ASTM E 1321 and ISO 5658 (CHF and TRP values) [45,46];
9. ASTM E 1354 and ISO 5660 (CHF and TRP values) [45,46];
10. ASTM D 1929 (T_{ig} values) [46];
11. ASTM E 2058 (CHF and TRP values) [46].

Tests performed in the apparatuses specified in the three standards listed above, i.e., ASTM E 1321/ISO 5658 (LIFT apparatus), ASTM E 1354/ISO 5660 (cone calorimeter), and ASTM E 2058 (fire propagation apparatus) provide complete set of fire properties for the assessment of ignition behavior of polymer products. These apparatuses also provide data in a format that is useful for the engineering methods in the performance-based fire codes.

Examples of the data for CHF and TRP values are listed in Table 53.3. Polymer products with high CHF and TRP values have high resistance to ignition.

53.11.2 Standard Tests for the Combustion Behavior of Polymer Materials

The burning behaviors of polymeric materials are examined by measuring the release rates of material vapors, heat, and chemical compounds including smoke in the apparatuses specified in the standard test methods. From these measurements, the following fire properties are derived:

1. Heat of gasification and heat losses (Table 53.2);
2. Chemical, convective, and radiative heats of combustion (ratio of the summation of the heat release rate to the summation of the release rate of material vapors) (Table 53.9);
3. Yields of various chemical compounds (ratio of the summation of the release rate of each compound to the summation of the release rate of material vapors, Table 53.9).
4. Combustion efficiency (ratio of the heat of combustion to the net heat of complete combustion);
5. Generation efficiency of chemical compounds (ratio of the yield of a compound to the maximum possible stoichiometric yield of the compounds based on the elemental composition of the material).

The heat of complete combustion is measured according to ASTM D 5865/ISO 1716 test methods [45,46]. The release rates of material vapors, heat, and various chemical compounds (including smoke) are measured according to ASTM E 906 (the Ohio State University Heat Release Rate, OSU-HRR, Apparatus), ASTM E 2058 (fire propagation apparatus) and ASTM E 1354/ISO 5660 (cone calorimeter) [45,46]. Smoke released in flaming and nonflaming fires of materials is also characterized following these standard test methods as well by the ASTM E 662 (smoke density Chamber) [46].

ASTM D 5865/ISO 1716: Test Method for Gross Heat of Complete Combustion [45,46]

This standard test method incorporates the fundamental principles for the energy associated with the complete combustion of materials and thus is independent of fire scenarios [49]. Gross and net of complete combustion of materials are used in the performance-based fire codes for the assessment of fire hazards associated with the use of products and protection needs. The gross heat of complete combustion is measured in the oxygen bomb calorimeter.

In Europe, gross heat of complete combustion (gross calorific potential, PCS), measured by following the ISO 1716 standard test method is used for the classification of reaction to fire performance for construction products (prEN 13501-1) [42]:

1. *Construction products excluding floorings*:
   - *Class A1*: PCS $\leq$ 1.4–2.0 MJ/kg.
   - *Class A2*: PCS $\leq$ 3.0–4.0 MJ/kg.
2. *Floorings*:
   - *Class*$A1_{fl}$: PCS $\leq$ 1.4–2.0 MJ/kg.
   - *Class*$A2_{fl}$: PCS $\leq$ 3.0–4.0 MJ/kg.

The gross heat of complete combustion is used to determine the net heat of complete combustion[5] defined as the quantity of energy released when a unit mass of specimen is burned at constant pressure, with all the combustion products, including water, being gaseous.

ASTM E 136/ISO 1182: Standard Test Method for Behavior of Materials in a Vertical Tube Furnace at 750 °C [45,46]

This standard test method specifies the use of a small-scale apparatus to assess the noncombustibility behavior of building construction materials under the test conditions. The standard test apparatus consists of two concentric, vertical refractory tubes, 76-mm and 102-mm (3 and 4-in.) in inside diameter and 210 to 250-mm (8.5–10-in.) in length. Electric heating coils outside the larger tube are used to apply heat. A controlled flow of air is admitted tangentially near the top of the annular space between the tubes and passes to the bottom of the inner tube. The top of the inner tube is covered. Temperatures are measured by thermocouples at the center: (1) between the two concentric tubes, (2) close to specimen location, and (3) sample surface.

[5] If the percentage of hydrogen atoms in the sample is known: net heat of complete combustion in kJ/g = gross heat of complete combustion in kJ/g − 0.2122 × mass percent of hydrogen atoms, where heats of combustion are in kJ/g [46]. If the percentage of hydrogen atoms is not known: net heat complete of complete combustion in kJ/g = 10. 025 + (0.7195) gross heat of combustion in kJ/g [46].

Test specimens are used in granular or powdered form contained in a 38-mm × 38-mm × 51-mm holder. The specimen in the holder is placed in the center of the inside vertical refractory tube after the temperature at the specimen location is maintained at 750 ± 5.5°C for 15 min. The test is continued until all the temperatures have reached their maximum values. Visual observations are made throughout the test on the specimen behavior, combustion intensity, smoke formation, melting, charring, etc. The specimen is weighed before and after the test. The data measured in the test are used to assess the following specimen behaviors:

1. Weight loss, $\Delta m \leq 50\%$;
2. Surface and interior temperature, $\Delta T \leq 30\ ^\circ C$;
3. There is either no flaming, i.e., flaming duration, $t_f = 0$, or there is no flaming after the first 20 seconds, $t_f \leq 20$ s.

In Europe, data from ISO 1182 are used for the classification of reaction to fire performance for construction products (prEN 13501-1) [42]:

1. *Construction products excluding floorings:*
   - *Class A1*: $\Delta T \leq 30\ ^\circ C$, $\Delta m \leq 50\ \%$, and $t_f = 0$.
   - *Class A2*: $\Delta T \leq 30\ ^\circ C$, $\Delta m \leq 50\ \%$, and $t_f \leq 20$ s.
2. *Floorings*:
   - *Class* $A1_{fl}$: $\Delta T \leq 30\ ^\circ C$, $\Delta m \leq 50\ \%$, and $t_f = 0$.
   - *Class* $A2_{fl}$: $\Delta T \leq 30\ ^\circ C$, $\Delta m \leq 50\ \%$, and $t_f \leq 20$ s.

ASTM E 906, ASTM E 2058, and ASTM E 1354/ISO 5660: Standard Test Methods for Release Rates of Material Vapors, Heat, and Chemical Compounds [45,46]

These standard test methods specify the use of small-scale apparatus to quantify the fire properties of materials. The apparatuses specified are:

1. ASTM E 906 (the OSU-HRR Apparatus);
2. ASTM E 2058 (the fire propagation apparatus, FPA);
3. ASTM E 1354/ISO 5660 (cone calorimeter).

One of the standard test apparatuses (the FPA is shown in Figs. 53.1).

ASTM E 119: Standard Test Methods for Fire Tests of Building Construction and Materials-The Fire Endurance Test [46]

This standard test method specifies use of large-scale furnace for testing of walls, columns, floors, and other building members, under high fire exposure conditions. Fire resistance is expressed in terms of time to reach critical point, i.e., "1/2-h (hour)", "2-h", "6-h", and other ratings of building materials and assemblies as they are exposed to heat. The building materials and assemblies are exposed to heat in a natural gas or propane fueled furnace with temperature increasing in the following fashion:

5 min	538 °C	10 min	704 °C	30 min	843 °C
1 h	927 °C	2 h	1,010 °C	4 h	1,093 °C
≥ 8 h	1,260 °C				

The standard test method has been designed to test the following building materials and assemblies in the furnace[6]:

1. *Bearing and nonbearing walls and partitions*: the area exposed to fire is ≥ 9-m^2(100-ft^2) with neither dimension less than 2.7-m (9-ft);
2. *Columns*: the length of the column exposed to fire is ≥ 2.7-m (9-ft);
3. *Protection for structural steel columns:* the length of the protected column is ≥ 2.4-m (8-ft) held in a vertical orientation. The column is exposed to heat on all sides;
4. *Floors and roofs*: the area exposed to fire is ≥ 16-m^2(180-ft^2) with neither dimension ≥ 3.7-m (12-ft);
5. *Loaded restrained and unstrained beams:* the length of the beam exposed to fire ≥ 3.7-m (12-ft) and tested in a horizontal position;
6. *Protection for solid structural steel beams and girders*: the length of beam or girder exposed to the fire is ≥ 3.7-m (12-ft) tested in a horizontal position;
7. *Protective members in walls, partition, floor, or roof assemblies*: the sizes used are same as above for the respective specimens.

Various criteria are used for the acceptance of the specimens:

1. Sustains itself or with the applied load without passage of flame or gases hot enough to ignite cotton waste or the hose assembly for a period equal to that for which classification is desired;
2. There is no opening that projects water from the stream beyond the unexposed surface during the time of water hose stream test;
3. Rise in the temperature on the unexposed surface remains ≤ 139 °C above its initial temperature;
4. Transmission of heat through the protection during the period of fire exposure for which classification is desired maintains the average steel temperature ≤ 538 °C (measured temperature ≤ 649 °C);
5. For steel structural members (beams, open-web steel joists, etc), spaced more than 1.2-m (4-ft), the average temperature of steel ≤ 593 °C (measured temperature ≤ 704 °C) during the classification period.

[6] As needed, load is applied to the specimens throughout the test to simulate a maximum load condition in their end use application.

ASTM E 1529: Standard Test Methods for Determining Effects of Large Hydrocarbon Pool Fires[7] on Structural Members and Assemblies [46]

The standard test method specifies large-scale test, similar to ASTM E 119, except that exposure of specimens consist of rapidly increasing heat flux. In the test, specimen surface is exposed to an average heat flux exposure of $158\,kW/m^2 \pm 8\,kW/m^2$ attained within the first 5-min and maintained for the duration of the test. The temperature of the environment reaches $\geq 815\ ^\circ C$ after the first 3-min of the test and remains between 1010 °C and 1180 °C at all times after the first 5-min.

This standard test method is used to determine the response of columns, girders, beams or structural members, and fire-containment walls, or either homogeneous or complete construction exposed to rapidly increasing heat flux. In this standard test method, combination of heat flux and temperature for the control is specified compared to ASTM E 119, where only temperature is specified. Performance is defined as the period during which structural members or assemblies will continue to perform their intended function when subjected to fire exposure. The results are reported in terms of time increments such as 1/2-h (hour), 3/4-h, 1-h, 1.5-h, and others.

The tests are performed in a fashion similar to that in the ASTM E 119, except for the heat flux and temperature profiles. For example, in this standard test method, a heat flux exposure of $158\,kW/m^2$ to the specimen surface is specified within first 5-min of the test. In the ASTM E 119, a heat flux exposure of $35\,kW/m^2$ at 5-min and $118\,kW/m^2$ at 60-min to the specimen surface is specified.

In this standard test method, conditions are simulated to test the performance of structural members and assemblies exposed to fire conditions resulting from large, free-burning (outdoors), fluid-hydrocarbon-fueled pool fires. This information is needed for the design of facilities for the hydrocarbon processing industry (oil refineries, petrochemical plants, offshore oil production platforms, and others) and chemical plants. In the future, this information may also be used in the design of high rise buildings because of the extreme terrorist act that occurred in New York City on September 11, 2001. There was a complete collapse of the World Trade Center Towers due to exposure to very hot pool fires from the large spillage of aviation gasoline.

[7] A large pool fire is defined as that resulting from hundreds (or thousands) of gallons of liquid hydrocarbon fuel burning over a large area (several hundred to thousand square meters) with relatively unrestricted airflow and release of chemical compounds. A range of temperatures, velocities, heat fluxes, and chemical conditions exist and vary dramatically with time and spatial location.

53.11.3 Standard Tests for the Flame Spread Behavior of Polymer Materials

In the standard test methods, specifications are made for making visual observations for movement of flame and char during the test and measurements for the surface temperature and release rates of material vapors, heat, and chemical compounds, including smoke. Both small-scale and large-scale flame spread and fire growth tests are performed using materials and products. Following are some of the popular standard test methods for characterizing flame spread and fire growth behaviors of materials and products. The following are some of the popular standard test methods for the flame spread behaviors of the polymeric materials.

prEN ISO/FDIS 11925-2: Reaction to Fire Tests for Building Products-Part 2: Ignitability When Subjected to Direct Impingement of Flame [42,45]

The apparatus consists of a stainless steel 800-mm high, 700-mm long, and 400-mm wide chamber with an exhaust duct attached at the top of the chamber. In the test, 250-mm long and 180-mm wide specimen with thickness $\leq$ 60-mm is used. The specimen is placed in a holder consisting of a double U-shaped frame made from 15-mm wide and 5-mm thick stainless steel sheets hanging vertically inside the stainless steel chamber. The holder is 370-mm long and 110-mm wide with a 80-mm wide open mouth.

The specimen is placed between two halves of the holder that are held together by screws or clamps. The holder can move closer to or away from a 45°-propane gas burner (similar to a Bunsen burner). A 100-mm $\times$ 50-mm $\times$ 10-mm deep aluminum foil tray containing filter paper is placed beneath the specimen holder and replaced between the tests.

The flame from the burner is applied for 15 or 30 s and the burner is retracted smoothly. For 15 s flame application, the test duration is 20 s after flame application. For 30 s flame application time, the test duration is 60 s after flame application. The following observations are made in the test:

1. Ignition of the specimen;
2. F_s: Flame spread up to150-mm and time taken;
3. Presence of flaming droplets;
4. Ignition of the filter paper below the specimen.

In Europe, data from ISO 11925-2 are used for the classification of reaction to fire performance for construction products (prEN 13501-1) [42]:

1. *Construction products excluding floorings:*
   - *Class B*: $F_s \leq$ 150-mm within 60 s for 30-s exposure.
   - *Class C*: $F_s \leq$ 150-mm within 60 s for 30-s exposure.

– *Class D*: $F_s \leq$ 150-mm within 60 s for 30-second exposure.
– *Class E*: $F_s \leq$ 150-mm within 20 s for 15-s exposure

2. *Floorings*

– *Class* B_{fl}: $F_s \leq$ 150-mm within 20 s for 15-s exposure.
– *Class* C_{fl}: $F_s \leq$ 150-mm within 20 s for 15-s exposure.
– *Class* D_{fl}: $F_s \leq$ 150-mm within 20 s for 15-s exposure.
– *Class* E_{fl}: $F_s \leq$150-mm within 20 s for 15-s exposure.

UL 94: Standard Test Methodology for Flammability of Plastic Materials for Parts in Devices and Appliances [44]

This standard test method is similar to prEN ISO/FDIS 11925-2 test. In the test, both horizontal burning (HB) and vertical burning (V) behaviors of 127-mm (5-in) long, 13-mm (0.5-in) wide, and up to 13-mm (0.5-in) thick material samples are examined. Horizontal burning test is performed for 94HB classification of materials. The sample used is placed on top of a wire gauge and ignited by a 30-s exposure to a Bunsen burner at one end.

The material is classified as 94HB if over 76-mm (3.0-in) length of sample: (1) flame spread rate $<$ 38.1 mm/min for 3–13-mm thick sample and $<$ 76-mm/min for 3-mm thick sample or flame spread is $<$ 102-mm (4.0-in.).

Vertical burning test is performed for the 94V-0, 94V-1, or 94V-2 classification of materials. The bottom edge of the sample is ignited by a 5-s exposure to a Bunsen burner with a 5-s delay and repeated five times until the sample ignites. The 94V-0, 94V-1, and 94V-2 material classification criteria are listed in Table 53.10.

The relative resistance of materials to flame spread and burning according to UL94 is HB $<$ V-2 $<$ V-1 $<$ V-0. The ordinary polymeric materials, which generally have low fire resistance, are classified as HB. Most of the high temperature and halogenated polymeric materials, that generally have high fire resistance, are classified as V-0.

ASTM D 2863 (ISO 4589): Test Methodology for Limited Oxygen Index [46]

The test is described in Section 53.6.1. The LOI values and UL 94 classification of materials are interrelated. The LOI values for V-0 materials are $\geq$ 35, whereas the LOI values are $<$ 30 for materials classified as V-1, V-2, and HB.

The standard test method has not been developed to predict the fire behavior of materials expected in actual fires, bur rather to screen materials for low and high resistance to fire propagation. For the majority of high temperature and highly halogenated materials, the LOI values are $\geq$ 40. These polymers have high resistance to ignition, combustion, as well as fire spread, independent of fire size and ignition source strength.

ASTM E 162 (D 3675): Standard Test Method for Surface Flammability Using a Radiant Energy Source [46]

In this small-scale test method, 460-mm (18-in.) $\times$ 150-mm (6-in.) wide and up to 25-mm (1-in.) thick vertical sample is used. The sample is exposed to a temperature of 670 $\pm$ 4 °C at the top from a 300-mm (18-in.) $\times$ 300-mm (12-in.) inclined radiant heater with top of the heater closest to and the bottom farthest away from the sample surface. The sample is ignited at the top and flame spreads in the downward direction. In the test, measurements are made for the arrival time of flame at each of the 75-mm (3-in.) marks on the sample holder and the maximum temperature rise of the stack thermocouples. The test is completed when the flame reaches the full length of the sample or after an exposure time of 15-min, whichever occurs earlier, provided the maximum temperature of the stack thermocouples is reached. Flame spread index (I_s) is calculated from the measured data, defined as the product of flame spread factor, F_s, and the heat evolution factor, Q.

Many polymeric materials and products have been tested using this standard test method. The I_s values vary from 0 to 2,220, suggesting large variations in the fire spread behavior of materials.

Many regulations and codes specify the I_s value as an acceptance criterion of materials and products. For example, for structural composites inside naval submarines and for passenger cars and locomotive cabs [50,51], the following I_s values are specified for the acceptance of the materials:

1. $I_s < 20$ for structural composites inside naval submarines;
2. $I_s \leq 25$ for cushions, mattresses, and vehicle components made of flexible cellular foams for passenger cars and locomotive cabs and thermal and acoustic insulation for buses and vans;
3. $I_s \leq 35$ for all vehicle components in passenger cars and locomotive cabs and for seating frame, seating shroud, panel walls, ceiling, partition, windscreen, HVAC ducting, light diffuser, and exterior shells in buses and vans;
4. $I_s \leq 100$ for vehicle light transmitting polymers in passenger cars and locomotive cabs.

The above listed criteria for the I_s values (< 20) suggest that structural composites for inside naval submarines are expected to have high resistance to flame spread and heat release if exposed to heat flux values similar to those used in the ASTM E 162. Also, materials used in passenger cars, locomotive cabs, buses, and vans with I_s values ≤ 25 as well as ≤ 35 are expected to have relatively higher resistance to fire spread and heat release rate compared to the ordinary materials with I_s values ≤ 100 under low heat exposure conditions.

ASTM E 1321 (ISO 5658): Standard Test Method for Determining Material Ignition and Flame Spread Properties (Lateral Ignition and Flame Spread Test, LIFT) [45,46]

This standard test method is discussed in Section 53.6.2. The test has been developed to provide pertinent data needed by the prescriptive-based and performance-based fire codes for the fire hazard analyses and protection needs for residential, private, government and industrial occupancies, transport and manufacturing, and others.

ASTM E 648 (ISO 9239-1): Standard Test Method for Critical Radiant Flux of Floor-Covering Systems Using a Radiant Heat Energy Source [45,46]

This standard test method specifies the use of an intermediate-scale test method for testing, similar in principle to ASTM E 1321 (ISO 5658). A 1.0-m (39.4-in.) long and 0.20-m (7.9-in.) wide horizontal sample is exposed to radiant heat flux in the range of 1–11 kW/m^2 from a 30°-inclined radiant panel all contained inside a chamber. The heat flux is at 11 kW/m^2 at the sample surface that is closer to the radiant heater. The radiant flux decreases as the distance between the sample surface and the radiant heater increases to the lowest value of 1 kW/m^2.

A pilot flame ignites the sample surface exposed to 11 kW/m^2, and flame spread is observed until the flame is extinguished at some downstream distance due to decrease in the radiant flux. The radiant flux at this distance is defined as the critical radiant flux (CRF) of the sample:

$$\text{CRF} = \dot{q}''_{\text{cr}} - \dot{q}''_{\text{f}}(x) \tag{53.32}$$

where $\dot{q}''_{\text{f}}(x)$ is the flame heat flux at distance x where flame is extinguished (kW/m^2). Thus, materials and products for which radiant fraction of the flame heat flux is higher would have lower CRF values. Materials with higher radiant fraction of the flame heat flux have lower resistance to flame spread due to efficient heat transfer ahead of the flame front.

This test method was developed as a result of need for flammability standard for carpets and rugs to protect the public against fire hazards [52]. Consequently, several carpet systems were tested by this standard [52–54]. This standard test method (ASTM E 648) is specified for the classification of the interior floor finish in buildings in the NFPA 101 Life Safety Code [55]:

1. *Class I*: interior floor finish: CRF $>$ 4.5 kW/m^2;
2. *Class II*: interior floor finish: 2.2 kW/m^2 $<$ CRF $<$ 4.5 kW/m^2.

And ISO 9293-1 with a test duration of 30-min is specified in Europe for the Euroclasses for flooring in prEN 13501-1 [42]:

1. *Class* $A2_{\text{fl}}$: CRF $\geq$ 8 kW/m^2
2. *Class* B_{fl}: CRF $\geq$ 8 kW/m^2
3. *Class* C_{fl}: CRF $\geq$ 4.5 kW/m^2
4. *Class* D_{fl}: CRF $\geq$ 3 kW/m^2

ASTM E 84: Standard Test Method for Surface Burning Characteristics of Building Materials [46]

This standard test method specifies the use of a larger-scale apparatus for testing. It is one of the most widely specified methods. In this 10-min test, a 7.3-m (24-ft) long and 0.51-m (20-in.) wide horizontal sample is used inside a 7.6-m (25-ft) long, 0.45-m (17-in.) wide and 0.31-m (12-in.) deep tunnel. Two gas burners, located 0.19-m (7-in.) below the specimen surface and 0.31-m (12-in.) from one end of the tunnel are used as ignition sources. The two burners release 88 kW of heat creating a gas temperature of 900 °C near the specimen surface. The flames from the burners cover 1.37-m (4.5-ft) of the length and entire width or 0.63-m^2 (7-ft^2) area of the specimen. Air enters the tunnel at 1.4-m (54-in.) upstream of the burner at a velocity of 73-m (240-ft)/min. The test conditions are set such that for red oak flooring control material, flame spreads to the end of the 7.3-m (24-ft) long sample in 5.5 min or a flame spread rate is 22 mm/s.

In the test, measurements are made for the percent light obscuration by smoke flowing through the exhaust duct, gas temperature (7.0-m/23-ft from the burner) and location of the leading edge of the flame (visual measurement) as functions of time. The measured data are used to calculate the flame spread index (FSI) and smoke developed index (SDI) from the flame spread distance-time and percent light absorption-time areas, respectively. Some typical FSI values are listed in Table 53.16 taken from Ref. 46.

The NFPA 101 Life Safety Code uses the ASTM E 84 test data for the following classification of building products (Table 53.17 lists the interior finish classification limitations) [55]:

1. *Class A interior wall and ceiling finish:* FSI- 0 to 25, SDI- 0 to 450;
2. *Class B interior wall and ceiling finish:* FSI- 26 to 75, SDI- 0 to 450;
3. *Class C interior wall and ceiling finish*: FSI- 76 to 200, SDI- 0 to 450.

FM Global Approval Class 4910 [43] (NFPA 318 [56]): Standard Test Methods for Clean Room Materials for the Semiconductor Industry

This standard test method is discussed in Section 53.6.3.

ASTM E 603: Standard Guide for Room Fire Experiments [46]

One major reason for performing room fire tests is to learn about various fire stages in the room so that results of standard fire test methods can be related to the performance of the products in full-scale room fires. In addition, some of the tests or their reduced versions are used for the acceptance of building products as they are specified in the prescriptive-based fire codes.

The ASTM E 603 is a guide written to assist in conducting full-scale compartment fire tests dealing with any or all stages of fire in a compartment. Whether it is a single- or multi-room test, observations can be made from ignition to flashover or beyond full-room involvement. Examples of the full-scale room fire tests are:

1. FM approval class no. 4880 for building wall and ceiling panels and coatings and interior finish materials [43];
2. ISO 9705: full scale fire test for surface products [45];
3. EN 13823: single burning item (SBI) [42,47,48].

FM Approval Class No. 4880: Test for Building Wall and Ceiling Panels and Coatings and Interior Finish Materials [43]

This standard test method specifies use of a larger-scale test, identified as the ''25-ft Corner Test'', to evaluate flame spread characteristics of building walls and ceiling panels and coatings. The test is performed in a 7.6-m (25-ft) high, 15.2-m (50-ft) long, and 11.6-m (38-ft) wide walls and ceiling forming a corner of a building. The products tested are typically panels with a metal skin over the insulation core material. The panels installed on the walls and ceiling are subjected to a growing exposure fire at the base of the corner. The growing exposure fire consists of a burning 340 kg (750 lb.), 1.2-m (4-ft) × 1.2-m (4-ft) oak crib pallets, stacked 1-5-m (5-ft) high with a peak heat release rate of about 3 MW.

In the test, measurements are made for the surface temperatures (at 100 equidistant locations on the walls and ceiling) and length of flame on the wall (under the ceiling) visually. After the test, visual measurements are made for the flame spread by the extent of charring on the walls and ceiling. The product is considered to have failed the test if within 15 min either:

1. Flame spread on the wall and ceiling extends to the limits of the structure or
2. Flame extends outside the limits of the structure through the ceiling smoke layer.

The fire environment within the ''25-ft Corner Test'' has been characterized by heat flux and temperature measurements [57]. It has been shown that the flame spread boundary (measured visually by the extent of surface charring) is very close to the CHF boundary for the material, very similar to the flame spread behavior in the ASTM E 1321 (ISO 5658). A good correlation has been developed between the extent of flame spread and the ratio of the convective heat release rate to $\Delta T_{ig}\sqrt{k\rho c}$, measured in the ASTM E 2058 apparatus.

This test has been instrumental in encouraging the development of other larger-scale and intermediate-scale standard corner tests such as ISO 9705 [45] and prEN 13823 (single burning item) [42].

ISO 9705: Room/Corner Test Method for Surface Products [45]

This standard test method specifies the use of a larger-scale test to simulate a well-ventilated fire, starting at the corner of a 3.6-m long, 2.4-m high, and 2.4-m wide room with a 0.8-m wide and 2.0-m high doorway. Figure 53.12 shows the sketch of the room. The walls and ceiling with a total surface area of 32 m^2 (344 ft^2) are covered with the specimen. The ignition source, located in the corner of the room, consists of a propane-fuelled 0.17-m square sandbox burner set to produce a heat release rate of 100-kW[8] for the first 10 min. If the flashover does not occur, then the sandbox burner output is increased to produce a heat release rate of 300-kW[16] for another 10 min. The test is ended after 20 min or as soon as the flashover is observed.

A hood attached to a sampling duct is used to capture heat and chemical compounds that are released during the test. In the sampling duct measurements are made for gas temperature, concentrations of chemical compounds released in the fire and oxygen, light obscuration by smoke, total flow of the mixture of air and chemical compounds and heat flux values at various locations in the room. Two parameters are used for ranking the products [47,48,58]:

1. *FIGRA index* (*fire growth rate index*): defined as the peak heat release rate in kW during the period from ignition to flashover (excluding the contribution from the ignition source) divided by the time at which the peak occurs (kW/s);
2. *SMOGRA index* (*smoke release index):* defined as the 60 s average of the peak smoke production rate (SPR in m^2/s) divided by the time at which this occurs and the value is multiplied by 1,000 (m^2/s^2). SPR is defined as $[\ln(I_0/I)/\ell]\dot{V}$, where I/I_0 is the fraction of light transmitted through smoke, ℓ is the optical path length (m), and $\dot{V}$ is the volumetric flow rate of the mixture of smoke and other compounds and air (m^3/s). SPR can

[8] 100 kW diffusion flame is used to simulate a burning large waste paper basket and the 300 kW diffusion flame is used to simulate a burning small upholstered chair [47,48].

also be expressed in terms of gm of smoke released per second as $[\ln(I_0/I)/\ell]\dot{V}(\lambda\rho_s \times 10^{-6}/\Omega)$, where λ is the wavelength of light (0.6328 μm used in the Cone), ρ_s is the density of smoke ($1.1 \times 10^6 g/m^3$[59]), and Ω is the coefficient of particulate extinction (7.0 [59]). Thus, SPR in m^2/s multiplied by 0.0994 changes the unit to g/s (for $\lambda = 0.6328\,\mu m$).

Numerous products have been tested during the last 10 years following the ISO 9705 Room/Corner test method [58,60].

Under similar burning conditions, the combustion chemistry responsible for release of heat and smoke are conserved and thus release rates of heat and smoke are interrelated:

$$\text{SMOGRA}/\text{FIGRA} = y_s/\Delta H_{ch}. \tag{53.33}$$

This interrelationship was found to be satisfied by the data from the ISO 9705 tests.

prEN 13823: The Single Burning Item [42]

This standard test method specifies use of an intermediate-scale apparatus. The apparatus consists of a trolley with two 1.5-m high, 1.0-m wide, and 0.5-m wide vertical noncombustible boards mounted at 90° to each other. The test specimen (wall and ceiling materials) are mounted and fixed onto the noncombustible boards in a manner representative of ''end-use''. The ignition source consists of a 31 kW propane right-angled triangular sandbox burner (each side: 250-mm and 80-mm high), placed at the bottom of the vertical corner. The test is performed inside a 2.4-m high and 3.0-m square room with top attached to a hood connected to a sampling duct to exhaust heat and chemical compounds released during the fire test. Evenly distributed airflow along the floor of the test room is achieved by introduced the air under the floor of the trolley through perforated plates.

In the sampling duct measurements are made for the gas temperature, concentrations of chemical compounds released in the fire and oxygen, light obscuration by smoke, and total flow of the mixture of air and chemical compounds. The parameters used for the assessment of fire performance of specimens are:

1. Heat release rate obtained from the measurements for oxygen depletion in the sampling duct;
2. Smoke release from the light obscuration by smoke in the sampling duct;
3. Horizontal flame spread observed visually, i.e., time taken to reach the extreme edge of the main 1.5-m × 1.0-m sample panel;
4. Falling molten droplets and particles.

The performance of the specimen is evaluated over a period of 20 min. However, the test is terminated earlier if any of the following conditions occur:

1. Heat release rate >350 kW at any instant or >280 kW over a period of 30 s;
2. Sampling duct temperature >400 °C at any instant or >300 °C over a period of 30 s;
3. Material falling onto the sandbox burner substantially disturbs the flame of the burner or extinguishes the burner by choking.

The test data are used to obtain the following parameters to rank the fire performance of the specimens:

1. FIGRA index,
2. SMOGRA index[9],
3. THR_{600s}: total heat released within 600 s,
4. TSP_{600s}: total smoke released within 600 s,
5. LFS: lateral flame spread,
6. Flaming/nonflaming droplets/particles and ignition of the paper[10] (prEN ISO 11925–2).

In Europe, data from prEN 13823 are used for the classification of reaction to fire performance for construction products (prEN 13501–1) [42]:

1. *Construction products excluding floorings:*
   - *Class A2*: FIGRA ≤ 120 W/s; LFS < edge of specimen, $THR_{600s} \le 7.5$ MJ, smoke production and melting/burning drops.
   - *Class B*: FIGRA ≤ 120 W/s; LFS < edge of specimen, $THR_{600s} \le 7.5$ MJ, smoke production and melting/burning drops.
   - *Class C*: FIGRA ≤ 250 W/s; LFS < edge of specimen, $THR_{600s} \le 15$ MJ, smoke production and melting/burning drops
   - *Class D*: FIGRA ≤ 750 W/s, smoke production and melting/burning drops.

The use of this standard test method for regulatory purposes is very similar to that of the ASTM E 84 standard test method. The intent of this standard test method is to separate materials and products with higher flame spread resistance from those with lower resistance. It has not been designed to predict the flame spread behavior of materials and products in actual fires.

---

[9] s1 = SMOGRA ≤ $30\,m^2/s^2$ and $TSP_{600s} \le 50\,m^2$; s2 = SMOGRA ≤ $180\,m^2/s^2$ and $TSP_{600s} \le 200\,m^2$: s3: neither s1 nor s2.

[10] d0 = no flaming droplets/particles in prEN 13823 within 600s; d1 = no flaming droplets/particles persisting longer than 10 s in prEN 13823 within 600 s; d2 = neither d0 nor d1 (ignition of paper in prEN ISO 11925–2 results in a d2 classification).

53.12 APPENDIX

53.12.1 Nomenclature

A	total exposed surface area of the material (m^2)
CHF	critical heat flux (kW/m^2)
CI	corrosion index (Å/min)/(g/m^3)
c_p	specific heat (MJ/kg-K)
CDG	carbon dioxide generation calorimetry
FPI	fire propagation index $[1000\ (0.42\dot{Q}'_{ch})^{1/3}/\{\Delta T_{ig}(kpc_p)^{1/2}\}]$
$\dot{G}''_j$	mass generation rate of product j (kg/m^2-s)
GTR	gas temperature rise calorimetry
ΔH_i	heat of combustion per unit mass of fuel pyrolyzed (MJ/kg)
ΔH_{co}	heat of complete combustion of CO (MJ/kg)
ΔH_g	heat of gasification of the polymer (MJ/kg)
ΔH_w	heat of gasification of water (2.58 MJ/kg)
ΔH^*_{co}	net heat of complete combustion per unit mass of CO generated (MJ/kg)
ΔH^*_{co2}	net heat of complete combustion per unit mass of CO_2 generated (MJ/kg)
ΔH^*_o	net heat of complete combustion per unit mass of oxygen consumed (MJ/kg)
HRP	heat release parameter ($\Delta H_{ch}/\Delta H_g$)
K_{thick}	thermal response parameter for thermally thick polymers ($kW\text{-}s^{1/2}/m^2$)
K_{thin}	thermal response parameter for thermally thin polymers (kJ/m^2)
$\dot{m}_a$	mass flow rate of air (kg/s)
$\dot{m}''_f$	gasification rate of the polymer or the mass loss rate (kg/m^2-s)
$\dot{m}''_w$	water application rate per unit surface area of the material (kg/m^2-s)
OC	oxygen consumption calorimetry
PGP	product generation parameter $\{y_j/\Delta H_g\}$ (kg/MJ)
$\dot{q}''_e$	external heat flux (kW/m^2)
$\dot{q}''_f$	flame heat flux (kW/m^2)
$\dot{q}''_{rr}$	surface re-radiation loss (kW/m^2)
$\dot{Q}''_i$	heat release rate per unit sample surface area ($\dot{m}''\Delta H_{ch}$) (kW/m^2)
$\dot{Q}'_i$	heat release rate per unit sample width (kW/m)
S	stoichiometric mass air-to-fuel ratio (−)
ΔT_{ig}	ignition temperature above ambient (K)
TRP	Thermal Response Parameter
u	fire propagation rate (mm/s)
$\dot{V}_T$	total mass flow rate of the fire product-air mixture (m^3/s) volumetric
W_f	total mass pyrolyzed in the pyrolysis or combustion of the polymer (kg)
W_j	total mass of product j generated in the pyrolysis or combustion of the polymer (kg)
y_j	yield of product $j(W_j/W_f)$ (kg/kg)
Y_o	mass fraction of oxygen (−)

Greek

α	ventilation correlation coefficient for nonflaming region (−)
β	ventilation correlation coefficient for transition region (−)
ξ	ventilation correlation coefficient for the equivalence ratio (−)
Φ	equivalence ratio ($S\dot{m}''_p\ A/\dot{m}_{air}$)
δ	thickness or depth (m)
δ_w	energy associated with the blockage of flame heat flux to the surface and escape of the fuel vapors per unit mass of the fuel (MJ/kg)
ε_w	water application efficiency (−)
χ	combustion efficiency $[\dot{Q}''_{ch}/\dot{m}''\Delta H_T]$
ρ	density (kg/m^3)
ψ_j	stoichiometric yield for the maximum conversion of fuel to product j (−)

Subscript

a	air or ambient
ch	chemical
con	convective
corr	corrosion
cr	critical
e	external
ex	flame extinction
f	flame or fuel
fc	flame convective
fr	flame radiative
g	gas or gasification
i	chemical, convective, radiative
ig	ignition
j	fire product
m	melting
n	net
o	initial
rad	radiation
stoich	stoichiometric for the maximum possible conversion of the fuel to the product
rr	surface re-radiation
s	surface
v	ventilation-controlled fire
w	water
∞	well-ventilated

Superscripts

.	per unit time (s^{-1})
′	per unit width (m^{-1})
″	per unit area (m^{-2})

Abbreviations

ABS	acrylonitrile-butadiene-styrene
CPVC	chlorinated polyvinylchloride

CR	neoprene or chloroprene rubber
CSP, CSM, CLS-PE	chlorosulfonated polyethylene rubber (Hypalon)
CTFE	chlorotrifluoroethylene (Kel-F)®
E-CTFE	ethylene-chlorotrifluoroethylene (Halar)®
EPR	ethylene propylene rubber
ETFE	ethylenetetrafluoroethylene (Tefzel)®
EVA	ethylvinyl acetate
FG	fiber glass reinforced
FR	fire retarded
FEP	fluorinated polyethylene-polypropylene (Teflon®)
IPST	isophthalic polyester
PAN	polyacrylonitrile
PC	polycarbonate
PE	polyethylene
PEEK	polyether ether ketone
PES	polyethersulphone
PEST	polyester
PET	polyethyleneterephthalate (Melinex®, Mylar®)
PFA	perfluoroalkoxy (Teflon®)
PMMA	polymethylmethacrylate
PO	polyolefin
PP	polypropylene
PPS	polyphenylene sulfide
PS	polystyrene
PTFE	polytetrafluoroethylene (Teflon®)
PU	polyurethane
PVEST	polyvinylester
$PVCl_2$	polyvinylidene chloride (Saran®)
PVF	polyvinyl fluoride (Tedlar®)
PVF_2	polyvinylidene fluoride (Kynar®, Dyflor®)
PVC	polyvinylchloride
Si	silicone
SBR	styrene-butadiene rubber
TFE	tetrafluoroethylene (Teflon®)
XLPE	crosslinked polyethylene
XLPO	crosslinked polyolefin

Related information can be found in Chapter 43.

REFERENCES

1. A. Tewarson, J. Fire Science **10**, 188 (1992).
2. A. Tewarson, *SFPE Handbook of Fire Protection Engineering*. (The National Fire Protection Association Press, Quincy, MA, 1995) pp. 3-53–3-124.
3. A. Tewarson, J. Fire Science **12**, 329 (1994).
4. A. Tewarson and R. F. Pion, Combustion and Flame, **26**, 85 (1976).
5. A. Tewarson, "Fire Hardening Assessment (FHA) Technology for Composite Systems", Technical Report ARL-CR-178, Contract DAAL01-93-M-S403, prepared by the Factory Mutual Research Corporation, Norwood, MA for the U.S. Army Research Laboratory, Watertown, MA., November 1994.
6. A. Tewarson and S. D. Ogden, Combustion and Flame, **89**, 237 (1992).
7. A. Tewarson and M. M. Khan, "Flame Propagation for Polymers in Cylindrical Configuration and Vertical Orientation," Twenty-Second Symposium (International) on Combustion, (The Combustion Institute, Pittsburgh, PA, 1988) pp. 1231–1240.
8. A. Tewarson and D. Macaione, J. Fire Sciences, **11**, 421 (1993).
9. M. J. Scudamore, P. J. Briggs, and F. H. Prager, Fire and Materials, **15**, 65 (1991).
10. M. M. Hirschler, J. Fire Sciences, **5**, 289 (1987).
11. *Handbook of Plastics and Elastomers*, edited by C. A. Harper (McGraw-Hill, New York, 1975).
12. C. J. Hilado, *Flammability Handbook for Plastics*, (Technomic Publications, Stamford, CT, 1969).
13. A. Tewarson, J. L. Lee, and R. F. Pion, "The Influence of Oxygen Concentration on Fuel Parameters for Fire Modeling," Eighteenth Symposium (International) on Combustion, (The Combustion Institute, Pittsburgh, PA, 1981) pp. 563–570.
14. ASTM D 2863–70, *Flammability of Plastics Using the Oxygen Index Method*, (The American Society for Testing and Materials, Philadelphia, PA, 1970).
15. J. G. Quintiere, *The SFPE Handbook of Fire Protection Engineering*, (The National Fire Protection Association Press, Quincy, MA, 1988) pp. 1-360–1-367.
16. ASTM E 1321-90 "Standard Test Method for Determining Material Ignition and Flame Spread Properties" (The American Society for Testing and Materials, Philadelphia, PA., 1990).
17. *Specification Standard for Cable Fire Propagation*, Class No. 3972, (Factory Mutual Research Corporation, Norwood, MA, 1989).
18. Approval Standard Class I for Conveyor Belting, Class No. 4998, (Factory Mutual Research Corporation, Norwood, MA, 1995).
19. C. F. Cullis and M. M. Hirschler, *The Combustion of Organic Polymers*, (Clarendon Press, Oxford, U.K., 1981).
20. J. G. Quintiere, V. Barbrauskas, L. Cooper, *et al*. "The Role of Aircraft Panel Materials in Cabin Fires and Their Properties", Final Report DOT/FAA/CT-84/30, (The Federal Aviation Administration, Atlantic City Airport, NJ, 1985).
21. A. Tewarson, F. H. Jiang, and T. Morikawa, Combustion and Flame, **95**, 151 (1993).
22. W. M. Pitts, "The Global Equivalence Ratio Concept and the Prediction of Carbon Monoxide Formation in Enclosure Fires", Monograph 179, (National Institute of Standards and Technology, Gaithersburgh, MD, 1994).
23. L. Tsantarides and B. Ostman, "Smoke, Gas, and Heat Release Data for Building Products in the Cone Calorimeter", Technical Report I 8903013, (Swedish Institute for Wood Technology Research, Stockholm, Sweden, 1989).
24. ASTM E 1354-90, "Standard Test Method for Heat and Visible Smoke Release Rates for Materials and Products Using Oxygen Consumption Calorimeter", (The American Society for Testing and Materials, Philadelphia, PA, 1990).
25. ASTM E 906-83, "Standard Test Method for Heat and Visible Smoke Release Rates for Materials and Products" (The American Society for Testing and Materials, Philadelphia, PA., 1984).
26. E. D. Goldberg, "Black Carbon in the Environment-Properties and Distribution", (John Wiley & Sons, New York, 1985).
27. *Particulate Carbon Formation During Combustion*, edited by D. C. Siegla and G. W. Smith, (Plenum Press, New York, 1981).
28. J. P. Stone, R. N. Hazlett, J. E. Johnson, *et al*. J. Fire and Flammability, **4**, 42 (1973).
29. D. J. Rasbash, "The Extinction of Fire with Plain Water: A Review", Fire Safety Science-Proceedings of the First International Symposium, (Hemisphere Publishing Co., New York, 1986) pp. 1145–1163.
30. "Evaluation of Alternative In-Flight Fire Suppressants for Full-Scale Testing in Simulated Aircraft Engine Nacelles and Dry Bays", edited by W. L. Grosshandler, R. G. Gann, W. M. Pitt, (National Institute of Standard and Technology, Gaithersburgh, MD., 1994), Superintendent of Documents, U.S. Government Printing Office, Washington, D.C.
31. E. W. Heinonen and S. R. Skaggs, "Fire Suppression and Inertion Testing of Halon 1301 Replacement Agents", Proceedings -Halon Alternates Technical Working Conference 1992, pp. 213–223. The University of New Mexico, New Mexico Engineering Research Institute, (Center for Global Environmental Technologies, Albuquerque, NM, 1992).
32. K. Metchis, "The Regulation of Halon and Halon Substitutes", Proceedings of the Halon Options Technical Working Conference 1994, pp. 7–30, The University of New Mexico, New Mexico Engineering

Research Institute, (Center for Global Environmental Technologies, Albuquerque, NM, 1994).
33. V. Beck, "Performance-Based Fire Engineering Design and Its Application in Australia", *Fire Safety Science, Fifth International Symposium*, pp. 23–40, International Association for Fire Safety Science, edited by Y. Hasemi, Japan, 1997.
34. B.J. Meacham, "Concepts of a Performance-Based Building Regulatory System for the United States", *Fifth International Symposium*, pp. 701–712, International Association for Fire Safety Science, edited by Y. Hasemi, Japan, 1997.
35. ASTM's Role in Performance-Based Fire Codes and Standards, edited by J.R. Hall, ASTM STP 1377, The American Society for Testing and Materials, West Conshohocken, PA. 1999.
36. Worldwide Standards Service for Windows, HIS, Englewood, CO, 2002.
37. J. Troitzsch, "International Plastics Flammability Handbook--Principles, Regulations, Testing and Approval", (Macmillan Publishing Co., Inc., New York, NY 1983).
38. A.H. Landrock, "Handbook of Plastics Flammability and Combustion Toxicology-Principles, Materials, Testing, Safety, and Smoke Inhalation Effects", (Noyes Publications, Park Ridge, NJ, 1983).
39. "Flammability Testing of Building Materials-An International Survey", Document NO. TH 42126, British Standards Institution, London, UK, 2000.
40. A.D. Makower, "Fire Tests-Buildings Products, and Materials", British Standards Institution, London, UK.
41. C.J. Hilado, "Flammability Test Methods Handbook", Technomic Publication, Westport, Conn, 1973.
42. European Committee for Standardization (CEN) (http://www.cenorm.be/).
43. FM Approval Standards (http://www.fmglobal.com/research_standard_testing/product_certification /approval_standards.html).
44. UL Standards (http://ulstandardsinfonet. ul.com/catalog/).
45. ISO Standards (http://www.iso.ch/iso/en/isoonline.frontpage).
46. ASTM Standards (http://www.astm.org).
47. B. Sundstrom, "European Classification of Building Products", Interflam′99, 8th International, Fire Science & Engineering Conference, **2**, pp. 769- Interscience Communications, London, UK, 1999.
48. B. Sundstrom, and S.D. Christian, "What are the New Regulations, Euroclasses, and Test Methods Shortly to be Used Throughout Europe", Conference Papers, Fire and Materials, pp. 117–127, January 22–24, 2001, Interscience Communications, London, UK, 1999.
49. F.B. Clarke, "Issues Associated with Combustibility Classification: Alternate Test Concepts", *Fire Safety Science, Proceedings of the Fifth International Symposium*, pp. 165–175, International Association for Fire Safety Science, edited by Y. Hasemi, Japan, 1997.
50. "Test Procedures and Performance Criteria for the Flammability and Smoke Emission Characteristics of Materials Used in Passenger Cars and Locomotive Cabs", Federal Register, Rules and Regulations, **64**(91), Wednesday, May 12, 1999.
51. Department of Transportation, Federal Transit Administration, Docket 90-A "Recommended Fire Safety Practices for Transit Bus and Van Materials Selection", Federal Register, **58**(201), Wednesday, October 20, 1993.
52. I.A. Benjamin, and C.H. Adams, "The Flooring Radiant Panel Test and Proposed Criteria", *Fire Journal*, **70** (2), 63–70, March 1976.
53. S. Davis, J.R. Lawson, and W.J. Parker, "Examination of the Variability of the ASTM E 648 Standard with Respect to Carpets", Technical Report NISTIR 89–4191, National Institute of Standards and Technology, Gaithersburg, MD, October 1989.
54. K. Tu, and S. Davis, "Flame Spread of Carpet Systems Involved in Room Fires", Technical Report NBSIR 76–1013, National B.
55. NFPA 101 Life Safety Code, Chapter 10 Annex, National Fire Codes-A Compilation of NFPA Codes, Standards, Recommended Practices and Guides, **5**, pp. 101–306 to 101–307, National Fire Protection Association, Quincy, MA 2000.
56. NFPA 318 "Standard for the Protection of Cleanrooms", National Fire Codes, **6**, pp. 318–1 to 318–22, National Fire Protection Association, Quincy, MA, 2000;
57. J.S. Newman, and A. Tewarson, "Flame Spread Behavior of Char-Forming Wall/Ceiling Insulation", *Fire Safety Science, Third International Symposium*, pp. 679–688, International Association for Fire Safety Science, edited by G. Cox and B. Langford, (Elsevier Applied Science, New York, NY, 1991).
58. B. Sundstrom, P.V. Hees, and P. Thureson, "Results and Analysis from Fire Tests of Building Products in ISO 9705, the Room/Corner Test; The SBI Research Program", Technical report SP-RAPP, 1998:11, Swedish National Testing and Research Institute, Fire Technology, Boras, Sweden 1998.
59. J.S. Newman, and J. Steciak, "Characterization of Particulates from Diffusion Flames", *Combustion and Flame*, **67**, 55–64, 1987.
60. S.E. Dillon, "Analysis of the ISO 9705 Room/Corner Test: Simulation, Correlations, and Heat Flux Measurements", NIST-GCR-98–756, National Institute of Standards and Technology, Gaithersburg, MD, August 1998.

CHAPTER 54

Thermal-Oxidative Stability and Degradation of Polymers

Vladyslav Kholodovych and William J. Welsh

Department of Pharmacology, University of Medicine & Dentistry of New Jersey (UMDNJ) – Robert Wood Johnson Medical School (RWJMS) and the UMDNJ Informatics Institute, Piscataway, NJ 08854

54.1 BASIC DEFINITIONS AND MODES OF DEGRADATION

Thermal stability refers to the ability of a material to maintain desirable mechanical properties such as strength, toughness, or elasticity at a given temperature. At the other extreme, thermal degradation can be defined functionally as the deterioration of those properties of polymers which make them useful commercially as rubbers, plastics, and fibers. Degradation reactions are most important in two phases of the life of a synthetic polymer: (1) during fabrication when both thermal and oxidative reactions can occur, and (2) during service life under prolonged exposure to light and oxidation. Symptoms of polymer degradation include hardening, brittleness, softening, cracking, discoloration, as well as alteration of specific polymer properties, e.g., mechanical and thermodynamic properties. In cases where molecular weight decreases, such molecular weight-sensitive properties as mechanical strength, elasticity, solution viscosity, and softening point will suffer most dramatically. Thermal degradation of organic polymers typically begins around 150–200 °C, and the rate of degradation increases as the temperature increases. The types of polymer degradation can be divided into three general categories: chain depolymerization, random scission, and substituent reactions [1–11].

In chain depolymerization (also known as chain depropagation or ''unzipping''), a given main chain is reduced in length by the sequential removal of monomer units from chain termini or at ''weak links''. A ''weak link'' may be a chain defect, such as an initiator fragment, peroxide, or an ether linkage arising as impurities from polymerization in the presence of oxygen. The slightly higher activity of a tertiary H atom may also provide a site for the initiation of the degradation process. Chain depolymerization exhibits three characteristic features: (1) the major product (volatile or not) is monomer, (2) the decrease in bulk-polymer molecular weight is initially negligible, and (3) the rate of conversion gradually decreases. Chain depolymerization can be regarded as the opposite of addition (chain-growth) polymerization. A specific example is poly(methyl methacrylate) (PMMA).

In random scission, chain breaking occurs at random points along the chain. Random scission exhibits the following characteristic features: (1) the major products are typically fragments of monomer, dimer, trimer, etc., up to molecular weights of several hundred; (2) the decrease in molecular weight is initially appreciable; and (3) the rate of degradation is initially rapid and approaches a maximum. Random scission, as exemplified by polyethylene (PE) and polypropylene (PP), can be viewed as the reverse of

condensation (step-growth) polymerization. In random scission, the polymer radical is both highly reactive and surrounded by an abundance of secondary hydrogens. This type of thermal degradation will therefore be favored if transfer is significant. Transfer reactions, in which a long-chain radical attacks another chain (intermolecular) or itself (intramolecular), produce fragments larger than monomer and promote random chain scission.

In both chain depolymerization and random scission, thermal degradation is a free-radical chain reaction. Initiation, which is the splitting of the chain to form radicals, may occur at chain ends, at ''weak links'', or at random points along the chain structure. Radical degradation often leads to crosslinking which can be visualized as resulting from the combination of radical sites on adjacent chains. Chain cleavage can occur either by primary homolytic skeletal cleavage or by an intramolecular attack by a terminal radical unit on its own chain. It is possible to differentiate between chain depolymerization and random scission in some cases by following the molecular weight of the residue as a function of the extent of reaction. Specifically, the ultimate product of random scission is likely to be a disperse mixture of fragments of molecular weight up to several hundred, whereas chain depolymerization yields large quantities of monomer.

In degradation by substituent reactions, the substituents attached to the polymer-chain backbone are modified or eliminated. Any volatile products evolved will therefore be chemically unlike monomer. The most prominent example of degradation via substituent reaction is poly(vinyl chloride) (PVC). Like all thermoplastics, PVC is processed at about 200 °C at which temperature it loses HC1 quite rapidly and is converted to a deeply colored polyene polymer, i.e.,

$$-CH_2-CHCl-CH_2-CHC1 \rightarrow -CH=CH-CH=CH-+ 2HCl.$$

The actual degradation mechanism is more complex than implied by this simple reaction. If substituents reactions occur, they generally ensue at temperatures ($T < 150$ °C) below that of degradation reactions in which the backbone bonds are broken. Consequently, the reactivity of the substituents relative to that of the polymer backbone will largely dictate whether a particular polymer undergoes thermal degradation by substituent reactions or by reactions involving the backbone (e.g., chain depolymerization and random scission) [1–11].

54.2 STRUCTURE–PROPERTY RELATIONSHIPS

Polymers decompose at significantly lower temperatures than model compounds, perhaps by as much as 200 °C. The main reasons are twofold: (1) polymer molecules often incorporate reactive structural abnormalities (''weak links'') absent in the model compound; and (2) polymer degradation can lead to chain processes, not accessible to model compounds, which accelerate the degradation reaction. The limited thermal stability of organic high polymers is due to several factors, including: (1) C–C bonds are relatively weak and oxidatively unstable; (2) fragmentation of the polymer during degradation is entropy favored; and (3) the presence of terminal catalytic sites, reactive atoms (e.g., tertiary H atoms), and ''weak links'' (e.g., branch points) along the chain which initiate decomposition [1–11].

The thermal stability and mode of decomposition of a polymer are determined by both physical and chemical factors [1–11]. In many cases, the maximum service temperature of polymers is limited not by the breaking of chemical bonds but rather by changes in physical characteristics at elevated temperatures. While retaining their chemical structures, they become weak, soft, and eventually fluid. The physical requirement of a thermally stable polymer is that it has high melting or softening temperature. The same factors that raise T_g and T_m, namely, chain rigidity and strong interchain forces, also raise thermal stability. Chain rigidity can be conferred by ring structures linked by collinear or *para* chain-extending bonds, while strong interchain attractions are attained by (intermolecular) dipolar and hydrogen-bonding interactions. The introduction of polar groups (e.g., CN, Cl, F) and hydrogen-bonding groups (e.g., –OH, –C(O)NH–) will often raise the melting and softening points appreciably. Stereoregularity in a vinyl-type polymer can produce a dramatic positive effect on thermal stability. For example, atactic polystyrene is amorphous with a T_g of about 80 °C while isotactic polystyrene is crystalline with a T_m of about 230 °C. The regular structure of the latter fits more readily into a crystalline lattice, and intermolecular forces are more difficult to overcome. Short bulky sidegroups (e.g., $-CH_3$ in polypropylene) can actually increase the melting point by reducing chain mobility, but long bulky sidegroups tend to reduce the melting point by disrupting the efficiency of chain packing. Crystalline forms of polymers are more resistant to oxidation than amorphous forms due to oxygen-permeability differences. For amorphous polymers, polymers oxidize more rapidly above than below their T_g due to the faster rate of diffusion of oxygen. Surface regions are particularly susceptible to oxidative degradation.

The chemical factors which influence thermal stability are more diverse than the physical factors. Of primary importance, heat-resistant polymers require bonds of high dissociation energy. For example, poly(tetrafluoroethylene) (PTFE) is superior to PE and many other polymers in terms of thermal stability. The stability conferred by fluorine substitution is clearly associated with the relatively high value for the dissociation energy of C–F bonds. In fact, PTFE [$-CF_2CF_2-$] is the most stable and most widely applied of the fluorinated polymers. Since the strong C–F bond renders transfer unlikely, chain depolymerization of PTFE gives high yields of monomer.

Van Krevelen [12] found a reasonably linear correlation between the half-decomposition temperature $T_{1/2}$ and the

TABLE 54.1. *Typical bond dissociation energies (kJ/mol).*

Bond	Aromatic or heterocyclic	Aliphatic	Reference
C–C	410	284–368	[1,22,23]
C=C	—	615	[22]
C≡C	—	812	[22]
C–H	427–435	381–410	[1,22,23]
C–Cl	—	326	[22]
C–F	—	452	[23]
C–O	448	350–389	[22]
C–N	460	293–343	[22]
C=N	—	615	[22]
N–H	—	390	[22]
ROO–H	—	377	[1]
$CH_3C(O)-H$	—	368	[1]

bond dissociation energy E_{diss} of vinyl polymers, i.e., $T_{1/2} = 1.6E_{diss}$ (in kJ/mol)+140. The bond dissociation energy (Table 54.1) of the bond in question depends on its bond order (i.e., single, double, triple), on resonance effects, on steric strain induced by bulky neighboring groups, and on the rigidity of their own or adjacent valence structures. Steric strain from crowded methyl groups, for example, makes polyisobutylene less stable to heat than PE. Most heat-resistant polymers, other than some inorganic and fluorinated polymers, have wholly aromatic chains like poly(*p*-phenylene). A rigid crosslinked network will also improve thermal stability. Crosslinked thermosets, such as phenolic, melamine, and epoxy plastics, are more resistant to heat than general purpose thermoplastics. Whereas thermoplastics are limited in use by the temperatures at which they soften, thermoset materials are limited by temperatures at which bonds begin to break [13].

Two additional chemical factors that are important in determining thermal stability are the reactivity of the depropagating radical and the availability of reactive hydrogen atoms for transfer. Reactive tertiary H atoms are important for the production of oligomers, whereas methylene or benzene H atoms are relatively inert. In 1,1-disubstituted vinyl polymers (e.g., poly (vinylidene cyanide): $[-CH_2- C(CN)_2-]$), the degrading radical is relatively unreactive by virtue of being trisubstituted. Since there are no reactive hydrogen atoms, transfer is suppressed and monomer production is dominant. The influence of radical stability is emphasized by a comparison of the behaviors of PE and PP with the polydienes $[-CH_2-CR=CH-]$. While PE and PP engage overwhelmingly in transfer (i.e., random scission) due to high radical reactivity, the polydienes engage in chain depolymerization due to the high relative stability the allylic radical. The relative reactivity of C–H bonds in polymers follows the order: allylic > tertiary > secondary > primary. Polystyrene and polyisobutylene are exceptions to this rule in that the benzylic and secondary H atoms, respectively, are shielded by relatively inert phenyl and methyl groups [1–13].

Degradation rates of polymers in air at temperatures below 150 °C depend on the reactivities of the peroxy radicals formed. In polymers most resistant to oxidation, H atoms are either totally absent or appear in unreactive methyl and phenyl groups. Polymers containing unsaturated linkages, such as polyisoprene or polybutadiene rubbers, can be attacked by atmospheric ozone as well as by oxygen. Polarity effects usually dominate in polymers containing heteroatoms, hence the rate of oxidation decreases along the series: $CH_2 > CHC1 > C(H)COOCH_3 > C(CH_3)COOCH_3 > CH(CN) > CF_2-CF_2$. Heteroatoms affect the strength of neighboring C–H bonds mainly by modifying the polar properties of transition states. Since the peroxy radical is electrophilic, the oxidation of ethers, aldehydes, amines, and sulfides occurs through abstraction of H atoms on carbons adjacent to the unshared electron pair on the heteroatom. Conversely, electron-deficient groups tend to stabilize neighboring H atoms.

Few polymers can withstand temperatures above 200 °C in air. Exceptions include aromatic, heterocyclic, and so-called ladder polymers (Fig. 54.1) [13,14–19]. Appropriately named, ladder polymers will degrade into fragments only if two parallel main-chain bonds (the "rungs" of the ladder) break [13]. Since this event is unlikely, ladder polymers like the two benzimidazobenzophenanthrolines designated BBB and BBL [17] (Fig. 54.1) possess exceptional thermal-oxidative stability. Moreover, recombination ("healing") of the broken bond is facilitated by the remaining intact bond which holds the severed bond in close proximity for recombination. These rigid aromatic and ladder polymers can be "articulated" by linking the rigid units together by ether [–O–], ester [–C(O)O–], amide [–C(O)NH–], or sulfone $[-SO_2-]$ groups. The insertion of these flexible units between the rings imparts added flexibility but at the cost of reduced thermal stability [13].

In summary, the basic requirements for heat-resistant polymers are: (1) high bond-dissociation energies (i.e., strong primary bonds); (2) chain rigidity supplemented by resonance stabilization; (3) high melting or softening points (i.e., strong secondary bonds); (4) structures resistant to free-radical chain processes; (5) low permeability and chemical reactivity (especially to oxygen) by virtue of crystallinity, crosslinking, and efficient chain packing; and (6) elimination (during synthesis and processing) of "weak links" in the chain where free-radical degradation often initiates.

54.3 DEGRADATION REACTION MECHANISMS

The oxidative degradation of polymers involves free-radical chain reactions. For example, degradation of polyolefins such as PE is commonly initiated by hydroperoxide impurities incorporated during synthesis and processing.

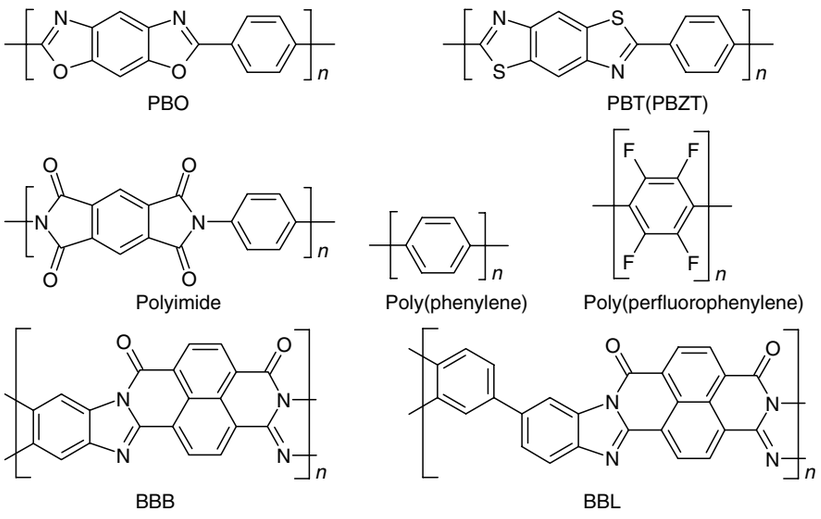

FIGURE 54.1. Examples of aromatic, heterocyclic, and ladder polymers.

Polymers may be attacked by molecular oxygen, ozone, or by indigenous free radicals in the polymer. Thermal-oxidative degradation of polyolefins in air is autocatalytic, i.e., the rate is slow at first but gradually accelerates to a constant value. According to the three-step mechanism outlined below, the $RO_2^{\cdot}$ peroxy radicals formed (Step 1) are sufficiently reactive to attack some primary CH bonds of the chain R′H (Step 2). The peroxy radical $RO_2^{\cdot}$ is thus reformed (Step 3) and can attack another CH bond. This chain reaction continues until termination occurs (Step 4) [1–11].

	Step 1: polymer	$\rightarrow$	$RO_2^{\cdot}$ (Initiation)
(slow)	Step 2: $RO_2^{\cdot} + R'H$	$\rightarrow$	$ROOH + R'^{\cdot}$ (Propagation)
(fast)	Step 3: $R^{\cdot} + O_2$	$\rightarrow$	$RO_2^{\cdot}$
	Step 4: $2RO_2^{\cdot}$	$\rightarrow$	unreactive products (Termination)

Step 3 is accelerated by the decomposition of the hydroperoxide products ROOH to form additional free radicals, i.e., $ROOH \rightarrow RO^{\cdot} + OH$. Degradation is also accelerated by the presence of even a small number of reactive tertiary H atoms but sometimes secondary H atoms. Evidence indicates that a plethora of free-radicals including peroxy $RO_2^{\cdot}$, hydroperoxy $HO_2^{\cdot}$, oxyradicals $RO^{\cdot}$, hydroxy $HO^{\cdot}$, and alkyl $R^{\cdot}$ are capable of formation and thereby initiating thermal-oxidative degradation of the polymer [1–11].

54.4 SPECIFIC EXAMPLES

An exhaustive survey of the thermal stabilities and degradation processes of the multitude of polymer families is beyond the scope of this work. Instead, the polymers selected for discussion below are both familiar and representative of the wide range of thermal-oxidative behavior exhibited by polymers [1–13].

54.4.1 Polyethylene (PE)

PE is thermally stable to about 290 °C, above which it undergoes a decrease in molecular weight with little volatilization. Above 360 °C, volatilization is rapid. The polymer also undergoes some crosslinking when heated at elevated temperatures. The rate of oxidation is related to the degree of chain branching since this gives rise to susceptible tertiary hydrogens. Small concentrations of C═C and C═O double bonds or peroxides along the chain will activate H atoms on neighboring bonds, thus complete saturation (no double bonds) improves oxidation resistance. The volatile products consist of a continuous spectrum of hydrocarbons ranging from C_1 to C_{70} or higher. This suggests a random-scission degradation mechanism initiated at the weak links followed by inter- and intramolecular chain transfer. Low-density polyethylene (LDPE) contains more chain branching than high-density polyethylene (HDPE). Therefore, the order of increasing oxidation is HDPE < LDPE. Few additives to impart thermal stability are compatible with PE in amounts larger than 1 % or so.

54.4.2 Polypropylene (PP)

Thermal degradation of PP starts at about 230 °C by a random scission process which yields virtually no monomer up to about 300 °C. Similar to PE, the degradation products of PP span a range of unsaturated hydrocarbons up to C_{70} and higher. PP is much more susceptible than PE to oxidation because PP has branch points on alternate carbon atoms. The greater availability of reactive tertiary H atoms explains why the temperature at which degradation initiates is lower for PP (230 °C) than for PE (290 °C).

54.4.3 Polystyrene (PS)

PS exhibits a maximum in the rate of degradation and a rapid decrease in molecular weight, both of which are characteristic of a random scission process. Evidence suggests that the decrease in molecular weight is the result of scission of a limited number of ''weak links'' in the polymer structure. The volatile products of thermal degradation of PS are monomer (42%) with progressively decreasing amounts of dimer, trimer, tetramer, and pentamer. Thermal degradation initiates along the chain at weak links, which might be unsaturated bonds or perhaps CH_2–CHPh–CHPh–CH_2– (Ph = C_6H_5) sequences resulting from head-to-head addition of monomer units during polymerization.

54.4.4 Poly(vinylchloride) (PVC)

PVC is relatively unstable to heat above 250 °C, even in the absence of oxygen. The substituent reaction is initiated by scission of the weakest C–Cl bonds, which are characteristically located at the chain ends since double bonds are formed as a result of disproportionation or transfer to monomer during polymerization. The chlorine radical $Cl^{\cdot}$ so formed abstracts an H atom to form HC1. The resulting chain radical then reacts to form a double bond with regeneration of a chlorine radical. The reaction is accompanied by embrittlement and dramatic discoloration of the material, arising from light absorption by the conjugated backbone (C–C=C–). The polymer yellows when there are seven conjugated double bonds and discolors through brown to black with increasing extension of the conjugated double-bond system. Stabilizers which are invariably added to improve the heat and light stability include inorganic and organic derivatives of lead as well as organic derivatives of barium, cadmium, zinc, and tin.

54.4.5 Poly(acrylonitrile) (PAN)

Like PVC, PAN discolors thermally at 175 °C due to the linking of nitrile groups to form conjugated carbon–nitrogen sequences. Consistent with degradation by substituent reaction, the color of degrading polymer progresses through the spectrum from yellow to red and the decrease in molecular weight is initially negligible.

54.4.6 Poly(tetrafluoroethylene) (PTFE)

PTFE is a highly crystalline polymer that is devoid of crosslinks and branching. PTFE undergoes nearly 100% conversion to monomer at elevated temperatures. Thermal degradation by chain depolymerization at the chain ends probably starts at low temperatures (250–350 °C), while random-scission cleavage likely becomes more pronounced at higher temperatures. Although PTFE is the most stable of the vinyl polymers, it cannot withstand prolonged exposure to temperatures above about 350–400 °C. The much greater strength of the C–F bond over the C–H bond explains why transfer processes, which largely control the thermal degradation of PE, are virtually absent in the thermal decomposition of PTFE. The degradation process is more complicated in the presence of air than in vacuum.

54.4.7 Polyamides (PAs)

Degradation of PAs can occur at melt-spinning and molding temperatures. Residual water plays an important role, initiating hydrolysis of peptide linkages followed by decarboxylation of the resulting carboxyl groups. The principal volatile products of thermal degradation are carbon dioxide and water.

54.4.8 Heat-Resistant Polymers

Many of the emerging technologies, particularly in the realm of electronics and aerospace science, require processable polymers endowed with superior mechanical properties and thermal-oxidative stability [13,16]. The structural feature common to such high-performance polymers is an aromatic backbone associated with high-bond dissociation energies, rigidity, and resonance stabilization. The mechanism of polymer degradation is principally oxidative in nature, hence incorporation of heterocyclic units further improves the thermal stability by increasing the char yield at very high temperature. The most successful of the new high-temperature polymers are those containing aromatic units in the chain backbone. For example, the polypyromellitimides (more commonly known as polyimides) (Fig. 54.1) show considerable promise as temperature-resistant plastics. The commercial polyimide Kapton is extremely heat stable, retaining more than 50% of its original tensile strength after 1,000 hours in air at 300 °C. The fluorination of aromatic structures provides additional thermal-oxidative stability. The parent structure, polytetrafluorophenylene, is stable to 500 °C in vacuum [1–11].

The aromatic heterocyclic rodlike polymers poly(*p*-phenylenebenzobisoxazole) (PBO) and poly(*p*-phenylenebenzobisthiazole) (PBZT or PBT) [14–20] possess rigid rodlike structures which provide superior tensile properties and excellent thermal stability. Thermal analysis of PBO and PBT reveals minimal weight loss in air at 316 °C. Thermal decomposition of both polymers begins at 600 °C and reaches a maximum between 660 and 700 °C. The total weight loss for both PBO and PBT is about 28% at 1,000 °C [16].

Unfortunately, wholly aromatic and/or heterocyclic polymers are notoriously difficult to process because they: (1) exhibit low solubilities in common organic solvents and (2) typically start to decompose at a lower temperature than they melt. Attempts to improve the processing characteristics of

these polymers have focused on inserting flexible ''spacer'' groups (e.g., amides, esters, ethers, sulfones) into the otherwise rigid chain backbone. The incorporation of even a small number of such spacer groups will increase the polymer's conformational flexibility and entropy and thus improve its tractability by allowing mutual rotation of adjacent chain elements about the flexible moieties. At the same time, these spacer groups will often alter the colinearity of the otherwise rigid chain thereby lowering the melt temperature. In general, the thermal-oxidative stability of these polymers diminishes as the ratio of flexible-to-rigid moieties increases [13].

The so-called ''articulated'' PBO and PBT, in which 3,3′-biphenyl or 4,4′-(2,2′-bipyridyl) moieties have been incorporated into the otherwise rodlike backbone, are appreciably more stable than those containing diphenoxybenzene (Ph–O–Ph) segments (Fig. 54.2). While PBO and PBT articulated with diphenoxybenzene units experience significant weight losses at 316 °C, those articulated with biphenyl and bipyridyl units are largely unaffected at that temperature and display thermo-oxidative stability comparable to the parent PBO and PBT polymers. While the biphenyl unit appears to give better stability than the dipyridyl unit, the stability of the articulated PBO and PBT polymers decreases with increased content of the flexible unit in the backbone [14].

A number of techniques, including addition of stabilizers and crosslinking, are used to extend thermal stability. Some polymers, for example PEEK (polyaryletherether ketone) and poly(phenylene sulfide), gain their thermal stability by virtue of their high degree of crystallinity. Other temperature-resistant polymers contain wholly inorganic backbones with high bond energies, such as the polyphosphazenes [–P(RR′)═N–] and the polysiloxanes [SiRR′–O] [9]. Some polyorganosilanes [–SiRR′–] are thermally stable to temperatures above 250 °C (>350 °C under inert conditions). This thermal stability is consistent with the strengths of silicon–silicon (80 kcal/mol) and carbon–silicon (90 kcal/mol) bonds [20].

A clever strategy for imparting thermal-oxidative stability in a polymer is exemplified by the so-called ''ladder polymer'' (Fig. 54.1) [13,17]. As the name implies, the chain of a ladder polymer can be broken only if at least two bonds on the same ring are severed. The likelihood that this will happen is low. Moreover, the broken bond has a high probability of reconnecting since the other ''rung'' of the ladder will hold the atoms of the severed bond in close proximity for bond reformation. Owing to these design features, the thermal stability of ladder polymers is often superior to the usual single-stranded types.

Based on the extensive experimental analysis of numerous heat-resistant polymers, Arnold [13] proposed a set of generalizations regarding correlations between polymer structure and thermal stability. Summarizing the more notable points, the highest stabilities were found for ladder-type polymers (e.g., BBB and BBL) and those containing heterocyclic or aromatic conjugated rings (e.g., polyimides, polyphenylenes, perfluoropolyphenylenes, PBO, PBT) (Fig. 54.1). The stability of polymers containing fused rings decreases as the number of fused chain segments increases. With few exceptions, most high-temperature polymers start to decompose at nearly the same temperatures

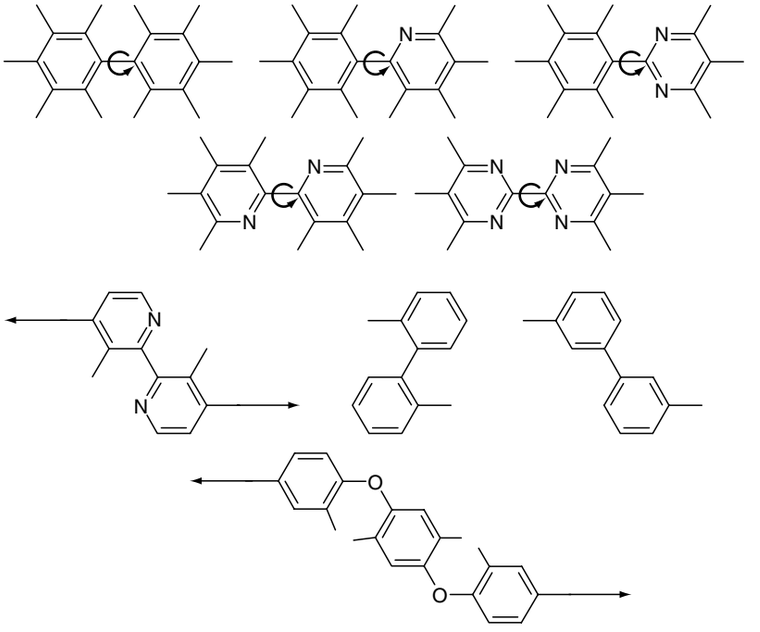

FIGURE 54.2. Examples of flexible spacer groups.

in both air and nitrogen. For polymers containing phenylene groups, the order of stability is *para* > *meta* > *ortho*. Crosslinking generally results in enhanced stability. Copolymerization can yield enhanced thermo-oxidative stability as, for example, imide copolymers of various heterocyclics are oxidatively more stable than the imide homopolymer. In terms of flexible spacer groups, the most stable are perfluoroaliphatics like $-CF_2-$ followed by –O–, –S–, –CONH–, and –CO–. The least stable were alkylene linkages, $-SO_2-$, –NH–, Cl-containing groups, and alkylene groups. However, any flexible spacer unit inserted into the backbone of aromatic or heterocyclic polymers can be expected to diminish both short-term and long-term stability.

54.5 ADDITIVES FOR ENHANCED THERMAL-OXIDATIVE STABILITY

Oxidative degradation of polymers typically follows a free-radical mechanism involving crosslinking and/or chain scission initiated by free radicals from peroxides formed during the initial oxidation step [1–11]. Enhanced stability has been achieved by the use of additives which are frequently called antioxidants or heat stabilizers. One approach employed to reduce the oxidation of polyolefins like PE and PP is to terminate the chain reaction by introducing an antioxidant with a greater affinity than a polyolefin for the peroxy radical $RO_2^{\cdot}$. Such antioxidants (AH) function by reacting with $RO_2^{\cdot}$ to form a relatively inactive radical $A^{\cdot}$, i.e.,

$$RO_2^{\cdot} + AH \rightarrow ROOH + A^{\cdot}$$

While amines and some annular hydrocarbons are suitable chain terminators, hindered phenols such as di-*t*-butyl-*p*-cresol (alias butylated hydroxytoluene or BHT) are most popular because they avoid discolorization and they eliminate two free radicals per BHT molecule (Fig. 54.3). The resonance-stabilized aryloxy radical is protected by the bulky electron-releasing *t*-butyl groups in the 2 and 6 positions, so the hindered phenol can combine with a second peroxy radical but cannot combine readily with molecular oxygen or with another aryloxy radical nor abstract H atoms from the polymer to initiate a new free-radical chain reaction.

Oxidative free-radical degradation by hydroperoxides can be catalyzed by certain transition metal ions, especially those of copper, cobalt, and manganese. To reduce the rate of free radical formation, two classes of additives are used: (1) organic phosphines, amines, and sulfides which catalyze the decomposition of the hydroperoxides to nonradical products, and (2) metal-ion chelators (e.g., Ph–CH═NNH–CO–CO–NHN═CH–Ph). Tertiary phosphines are thus oxidized to phosphine oxides, tertiary amines to amine oxides, and sulfides to sulfoxides, e.g.,

$$R_3P + ROOH \rightarrow R_3PO + ROH \text{ (tertiaryphosphine)}.$$

The inclusion of very small quantities of ethylene or propylene (1–3%) in poly(vinyl chloride) has resulted in copolymers of greatly improved heat stability relative to the parent PVC. Since degradation of PVC involves loss of HC1, compounds that react with the HC1 to form stable products, such as metal oxides, are used as stabilizers.

54.6 EXPERIMENTAL METHODS OF ANALYSIS

Polymer degradation can be monitored by measurement of molecular weight using viscometry, osmometry, light scattering, ultracentrifuge, and gel-permeation chromatography (GPC). GPC (more generally called size-exclusion chromatography) can be used in estimating the effect of degradation on molecular-weight distribution (MWD). Spectroscopic probes of thermal degradation include UV spectroscopy, IR spectroscopy, NMR spectroscopy, electron-spin resonance spectroscopy (ESR, EPR), and mass spectrometry (MS). Multiple internal reflectance infrared spectroscopy (MIRS) allows a very thin surface layer to be examined. Another method is flash pyrolysis in which the polymer's temperature is raised very rapidly to 500 °C or more at which the molecules are broken down into small fragments. The fragment pattern can be analyzed by gas chromatography (pyrolysis-GC) and mass spectrometry (pyrolysis-MS), either separately or in combination (pyrolysis-GC/MS) [2–6,13].

Several thermal techniques are commonly employed to monitor the thermal stabilities of polymers [2–6,13]. In thermogravimetric analysis (TGA), a sensitive balance is used to follow the weight change of the sample in a specified environment (vacuum, air, or inert atmosphere)

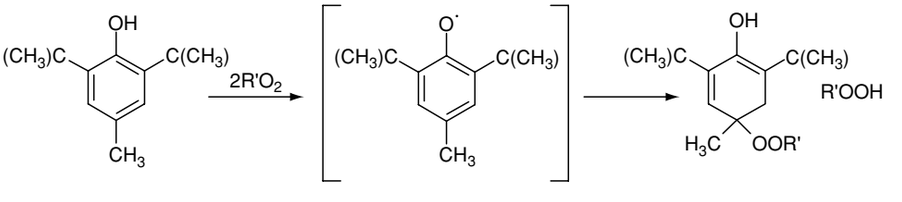

FIGURE 54.3. Illustration of the function of the hindered phenol di-*tert*-butyl-*p*- cresol (BHT).

as a function of time or temperature. Thermomechanical analysis (TMA) measures the mechanical responses of a polymer as a function of temperature. Typical measurements include: expansion properties, tension properties (elastic modulus), dilatometric properties (specific volume), single-fiber properties (single-fiber modulus), and compression properties. In isothermogravimetric analysis (IGA), weight loss as a function of time is recorded at a specified temperature. At lower temperatures, IGA is a valuable supplement to TGA in obtaining data on long-term stability. Thermal volatilization analysis (TVA) records the evolution of volatile products by measuring the pressure of volatile degradation products continuously in an evacuated system. According to Arnold [13], the preferred method of determining the relative short-term thermal or thermo-oxidative stability of high-temperature polymers is dynamic TGA. Longer-term stabilities are most conveniently defined by IGA if the temperature is properly chosen. Combination of these tests with TMA, which provides data on the T_g and softening behavior, gives a complete picture of the thermal limitations of most polymers.

Accelerated aging tests, such as the familiar ''air-oven test'', have aided the investigation of thermal-oxidative degradation. The air-oven test involves subjecting a polymer sample to temperatures ranging from 70 °C to 150 °C with air flowing over the surface of the sample. The change in stress–strain behavior (e.g., tensile modulus, tensile strength, elongation at break) is measured on samples removed from the oven at intervals until the point of failure is reached. The rationale behind accelerated testing is basically that the results can be extrapolated in time to simulate actual service conditions. In reality, most accelerated aging tests are therefore a compromise between convenience and reliability [2].

In organic polymers, the progress of oxidation reactions can be followed using infrared (IR) spectroscopy. IR absorption bands of interest in PE and related polymers are C–H stretching (3.4 μm), C–H bending of CH_2 groups (6.8 μm) and CH_3 groups (shoulder at 7.25 μm on an amorphous band at 7.30 μm), and CH_2 rocking in sequences of methylene groups (13.9 μm). Other key absorption bands include C═C in natural rubber (6.1 μm), C═O and ether in PMMA (5.8 and 8.9 μm, respectively), aromatic structures in PS (6.2, 6.7, 13.3, and 14.4 μm), C–Cl in PVC (14.5 μm), peptide groups in nylon (3.0, 6.1, and 6.5 μm), and CF_2 in PTFE (8.2–8.3 μm) [1–11].

54.7 TABULATED DATA

There seems to be no accepted standard way of quantifying the thermal-oxidative stability and/or degradation of polymers. Therefore, different sources of data will often provide different criteria for describing the absolute or relative stability of polymers. Tables 54.2–54.5 summarize thermal-stability data extracted from a variety of sources

TABLE 54.2. *Half-decomposition temperature* $T_{1/2}$[a] *and monomer yield for selected polymers.*

Polymer	$T_{1/2}$(°C)[b]	Monomer yield (%)
Poly(tetrafluoroethylene) (PTFE)	509	> 95
Poly(*p*-phenylene methylene)	430	0
Polymethylene	414	< 0.1
Polybutadiene	407	< 1
Polyethylene (PE) (branched)	404	< 0.025
Polypropylene	387	< 0.2
Polystyrene (PS)	364	40
Polyisobutylene	348	20
Poly(ethylene oxide)	345	4
Poly(methyl acrylate)	328	0
Poly(methyl methacrylate) (PMMA)	327	> 95
Poly(propylene oxide) (isotactic)	313	1
Poly(propylene oxide) (atactic)	295	1
Poly(vinyl acetate)	269	0
Poly(vinyl alcohol)	268	0
Poly(vinyl chloride) (PVC)	260	0

[a]Data taken from [12].
[b]Temperature at which the polymer loses 50% of its weight, if heated in vacuum for 30 min.

TABLE 54.3. *Typical values of the upper use temperature (°C) for several familiar and commercial polymers.*

Polymer	Upper use temperature (°C)	Reference
Natural rubber	80	[11]
SBR	110	[11]
Acrylate	150	[11]
Butyl	100	[11]
Chlorosulfonated polyethylene	120	[11]
EPDM	150	[11]
Epichlorohydrin	120	[11]
Fluorinated rubbers	230	[11]
Neoprene	100	[11]
Nitrile	120	[11]
Polybutadiene (*cis*-1,4)	100	[11]
Polyisoprene (*cis*-1,4)	60–80	[11,12]
Polysulfide	80	[11]
Silicone	230	[11]
Poly(vinyl chloride) (PVC)	60	[12]
Polystyrene (PS)	60	[12]
Polymethacrylates	60–80	[12]
Polyolefins	60–90	[12]
Polyamides	80–100	[12]
Epoxy resins	80–110	[12]
Polycarbonate	100–135	[12]
Poly(phenylene oxide) (PPO)	130–150	[12]
Polysulfone	130–150	[12]
Polyfluorocarbons	150–220	[12]
Aromatic polyamides	180–230	[12]
Polyimides	180–250	[12]
Poly(tetrafluoroethylene)	180–250	[12]
Polybenzimidazole (PTFE)	250–300	[12]
Polyurethanes	70–110	[11]

TABLE 54.4. *Thermal stability of selected heat-resistant aromatic, heterocyclic, and ladder-type polymers in an inert atmosphere.*

Polymer	PDT (°C)[a]	Reference
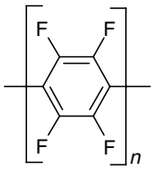	720	[13]
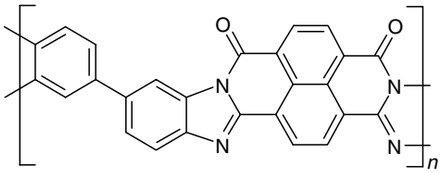	690–710	[13]
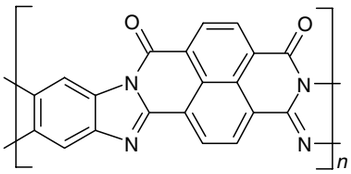	690–710	[13]
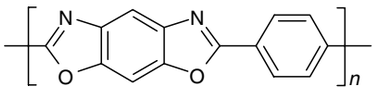	660–700	[b]
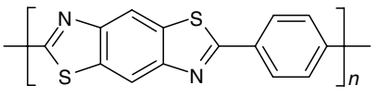	700	[b]
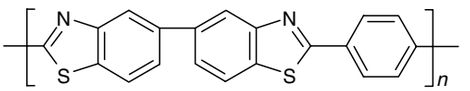	685–700	[13]
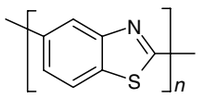	685–700	[13]
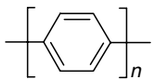	660	[13]
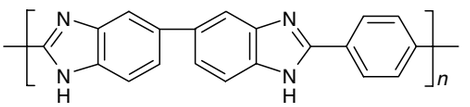	650	[13]
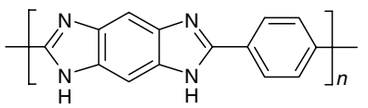	650	[13]
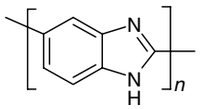	650	[13]
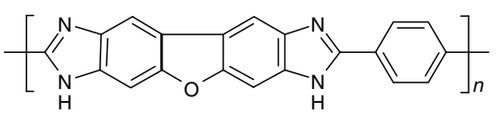	650	[13]

[a] Polymer decomposition temperature.
[b] A number of relevant articles on PBO and PBT and related rodlike polymers can be found in Macromolecules, 14, 891 (1981) and in the Dec. 1980 and March 1981 special issues of the Brit. Polym. J.

TABLE 54.5. *Initial temperature reported for thermal decomposition of selected common polymers.*

Polymer	Initial decomposition temperature[a] (°C)
Poly(acetylene)	650
Poly(butadiene)	325
Poly(chloroprene)	170
Natural rubber	287
Poly(ethylene)	264
Poly(propylene)	120
Poly(acrylonrtrile)	235
Poly(methacrylic acid)	200
Poly(vinyl acetate)	213
Poly(vinyl alcohol)	240
Poly(vinyl chloride)	200
Poly(styrene)	300
Phenol-formaldehyde resin	250
Cellulose	250
Cellulose triacetate	250
Ethyl cellulose	306

[a]Data taken from [21]. Value given for each polymer represents the lowest decomposition temperature for which decomposition products are given in [21].

in the literature on selected familiar and commercial polymers. Table 54.6 compares the relative stability of several flexible linking groups. For a comprehensive listing of polymers, including a description of the products of thermal degradation, the reader is directed to Grassie [21].

Related information can be found in Chapter 53.

TABLE 54.6. *Thermal and thermal-oxidative stability of some simple flexible linking groups[a].*

Group	Thermal stability[b] (°C)	Thermal-oxidative stability[c] (°C)
–CO–	500	389
–CONH–	500	431
$-(CF_2)_3-$	469	—[d]
–COO–	457	447
–S–	436	418
$-CH_2CH_2-$	429	383
$-CH_2-$	408	—[d]
–O–	—[d]	368

[a]Data taken from [13].
[b]Temperature for 25% weight loss in 2 hours in inert environment.
[c]Temperature for 25% weight loss in 2 hours in air (oxygen).
[d]Data not available.

54.8 MATERIAL SCIENCE TOOLS ON THE WORLD WIDE WEB

Today more and more information is taken from on-line resources. The World Wide Web has become a popular and reliable tool for research in many disciplines including polymer science. Rather than an exhaustive overview of the available web-based resources for polymer scientists, this section is interned to point the scientist to a few notable Internet portals that were useful in preparing this chapter.

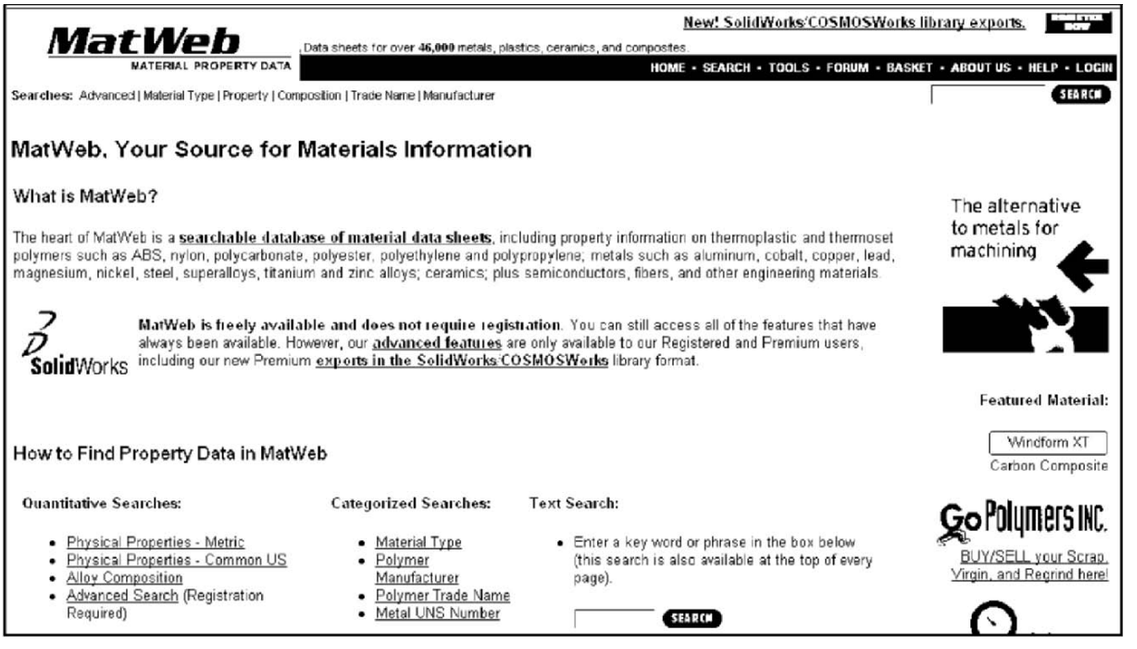

FIGURE 54.4. A screenshot of the main page of the MatWeb portal. Reprinted with permission © (1996-2006) by Automation Creations, Inc.

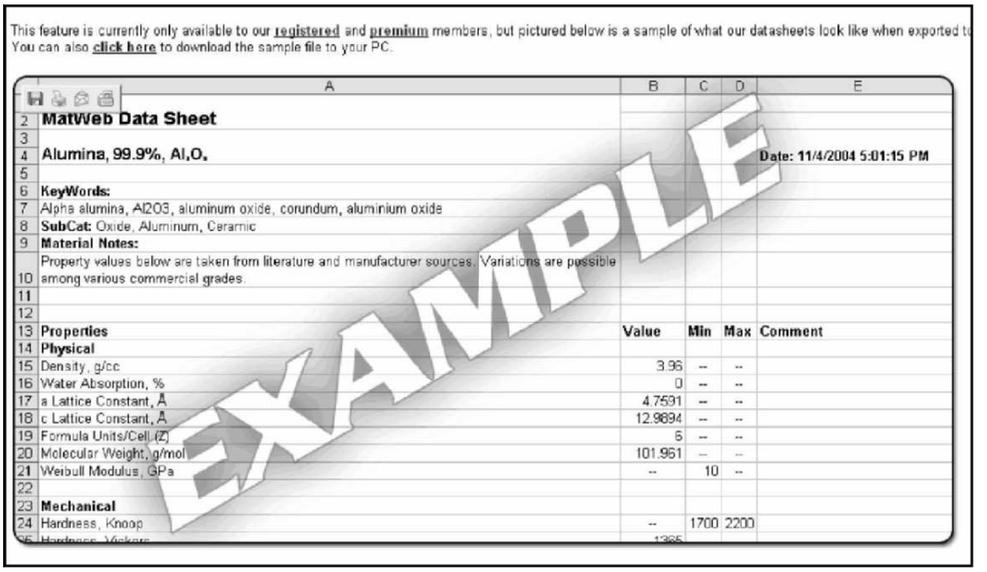

FIGURE 54.5. Example of the Excel spreadsheet generated after MatWeb search. Reprinted with permission © (1996–2006) by Automation Creations, Inc.

MatWeb, http://www.matweb.com, is a searchable database of over 46,000 metals, plastics, ceramics, and composite materials. It allows search by material type, trade name, range of values, composition, UNS number (Unified Numbering System for Metals and Alloys) and even system of units (metric, common US units). An example of searchable materials includes thermoplastic and thermoset polymers such as ABS, nylon, polycarbonate, polyester, polyethylene, and polypropylene; metals such as aluminum, cobalt, copper, lead, magnesium, nickel, steel, superalloys, titanium, and zinc alloys; ceramics; plus semiconductors, fibers, and other engineering materials.

For registered users, all data retrieved from searches can be exported to an Excel spreadsheet for further analysis (Fig. 54.4, 54.5).

Another web resource, Omnexus can be found at the following address: http://www.omnexus.com/index.aspx (Fig. 54.6).

FIGURE 54.6. A screenshot taken of the front page of the Omnexus website. Reprinted with permission from Omnexus.com.

This site contains very useful information, such as current news in polymer science, information about on-line seminars and scientific conferences, and numerous material databases. Databases are searchable by various criteria, such as physical and chemical properties, molecular weight or density. The search output also contains information about manufacturer and on-line vendors. This site requires registration for full access, but registration is free.

REFERENCES

1. L. D. Loan and F. H. Winslow, in *Macromolecules: An Introduction to Polymer Science,* edited by F. A. Bovey and F. H. Winslow, (Elsevier Science & Technology, Amsterdam, 1982) p. 576.
2. N. Grassie and G. Scott, *Polymer Degradation & Stabilisation* (Cambridge University Press, Cambridge, 1988) p. 222.
3. L. Reich and S. S. Stivala, *Elements of Polymer Degradation,* (McGraw-Hill Book Company, New York, 1971) p. 361.
4. N. Grassie, in *Encyclopedia of Polymer Science and Technology,* vol.4, (Interscience Publishers, New York, 1966) p. 647.
5. L. I. Nass, in *Encyclopedia of Polymer Science and Technology,* vol.12, (Interscience Publishers, New York, 1966) p. 725.
6. J. E. Mulvaney, in *Encyclopedia of Polymer Science and Technology,* vol. 7, (Interscience Publishers, New York, 1966) p. 478.
7. R. B. Seymour and C. E. Carraher, Jr., *Structure-Property Relationships in Polymers,* (Plenum Press, New York, 1984) p. 246.
8. C. Hall, *Polymer Materials,* (Halsted Press: John Wiley & Sons, New York, 1989) p. 243.
9. H. R. Allcock and F. W. Lampe, *Contemporary Polymer Chemistry,* third edition, (Prentice-Hall, Inc., Upper Saddle River, NJ, 2003) p. 832.
10. H.-G. Elias, *Macromolecules,* second edition, (Plenum Press, New York, 1984), p. 564.
11. F. W. Billmeyer, Jr., *Textbook of Polymer Science,* third edition (Wiley-Interscience: John Wiley & Sons, New York, 1990) p. 578.
12. D. W. van Krevelen, *Properties of Polymers: Their Correlation with Chemical Structure: Their Numerical Estimation and Prediction from Additive Group Contributions,* third edition, (Elsevier Scientific, Amsterdam, 1997), p. 875.
13. C. Arnold, Jr., *J. Polym. Sci.: Macromolecular Rev*. 14, 265 (1979).
14. W. J. Welsh, D. Bhaumik, H. H. Jaffe, *et al*. *Polym. Eng. Sci*. 24, 218 (1984).
15. R. C. Evers and G. J. Moore, *J. Polym. Sci.: Part A: Polym. Chem*. 24, 1863 (1986).
16. W. J. Welsh, in *Current Topics in Polymer Science*, vol. I, edited by R.M. Ottenbrite, L. A. Utracki, and S. Inoue, (Hanser Publishers, Munich, 1987) p. 217.
17. F. E. Arnold and R. L. Van Deusen, Macromolecules, 2, 497 (1969); R.L. Van Deusen, O. K. Goins, and A. J. Sicree, *J. Polym. Sci*. A-l, 6, 1777 (1968).
18. W. J. Welsh, D. Bhaumik, and J. E. Mark, *J. Macromol. Sci. Phys*. 20, 59 (1981).
19. W. J. Welsh and J. E. Mark, in *Computational Modeling of Polymers,* edited by J. Bicerano, (Marcel Dekker, Inc., New York, 1992) p. 648.
20. R. D. Miller and J. Michl, *Chem. Rev*. 89, 1359 (1989).
21. N. Grassie, in the *Polymer Handbook,* fourth ed., edited by J. Brandrup (Editor), Edmund H. Immergut, Eric A. Grulke, Akihiro Abe, Daniel R. Bloch, (Wiley-Interscience: John Wiley & Sons, New York, 2003) p. 2336.
22. J. H. Noggle, *Physical Chemistry,* third ed., (Pearson Education, New York, 2002), p. 1108.
23. B. E. Douglas, D. H. McDaniel, and J. J. Alexander, *Inorganic Chemistry,* 2nd ed., (John Wiley & Sons, Inc., New York, 1993) p. 78.

CHAPTER 55

Synthetic Biodegradable Polymers for Medical Applications

Laura J. Suggs*, Sheila A. Moore†, and Antonios G. Mikos†

*Department Biomedical Engineering, University of Texas at Austin, Austin, TX 78712
†Department of Bioengineering, Rice University, PO Box 1892, MS-142, Houston, TX 77251-1892

55.1 INTRODUCTION

Biodegradability has been the primary consideration in the development of biomedical materials due to problems associated with the biocompatibility of long-term, nondegradable polymer implants. Biodegradable polymers have been formulated for uses such as sutures, drug delivery devices, scaffolds for tissue regeneration, vascular grafts and stents, artificial skin, orthopedic implants, and others. The purpose of this overview is to elucidate the characteristics of several synthetic biodegradable polymers for medical applications, which include degradation modes and rates and their relationship to physicochemical, thermal, and mechanical properties. Polymers mentioned in the chapter are poly (α-hydroxy esters), poly(ε-caprolactone), poly (*ortho* esters), polyanhydrides, poly(3-hydroxybutyrate) polyphosphazenes, polydioxanones, fumarate-based polymer, polyoxalates, poly(amino acids), and pseudopoly (amino acids). The synthesis, medical uses, and processing techniques of these polymers are not discussed in detail, but additional references are given for each polymer as well as several comprehensive review articles [1–8].

55.2 BIODEGRADABLE POLYMERS

55.2.1 Poly(α-Hydroxy Esters)

Poly(Glycolic Acid)

Poly(glycolic acid) (PGA) is a highly crystalline, hydrophilic, linear aliphatic polyester (Structure 1). As such, it has a high melting point and a relatively low solubility in most common organic solvents. At room temperature, PGA is soluble in hexafluoroisopropanol, a highly toxic solvent. It degrades primarily by bulk erosion through random hydrolysis of its ester bonds. Reed and Gilding [9] report that the degradation kinetics is biphasic, with the first phase of degradation occurring by diffusion of water to the amorphous regions and subsequent hydrolysis. The second phase begins as water penetrates and hydrolyzes the more crystalline regions. The molecular weight distributions, which show two degradation phases, are given in Fig. 55.1 [9]. For PGA surgical sutures, mass loss occurs primarily during the second phase, completing the entire process between weeks 4 and 12. The rate of hydrolysis can be controlled

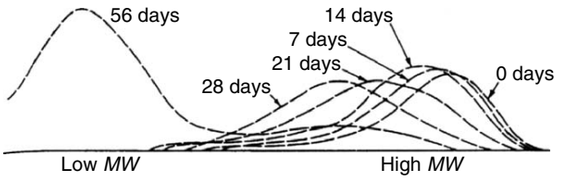

FIGURE 55.1. Molecular weight distributions as a function of degradation time for PGA sutures at pH 7 and 37 °C. The formation of a bimodal distribution is evident at large times due to the biphasic degradation of PGA. (Reprinted with permission from [9].)

in vitro by varying the pH [10]. Any large deviation from neutral pH drives hydrolytic cleavage. In addition, the degradation rate can be affected by the degree of crystallinity or ''curing time'' of PGA, as shown in in vivo studies [11].

The crystallinity of PGA is typically between 46% and 52% [9], the maximum crystallinity during degradation occurring in the time between the two degradation phases. The values of crystallinity are not only influenced by the quenching or ''curing'' process but also the molecular weight of the polymer [12].

PGA (crystallinity 50%) loses most of its mechanical strength over the first 2–4 weeks of degradation [9]. This is asynchronous with the mass loss which begins at approximately week 4. This is due to the bimodal degradation distribution. The amorphous regions are hydrolyzed first which results in loss of mechanical strength, while the degradation and diffusion of low molecular weight chains later result in significant mass loss. The stress/strain curves showing the effect of degradation on mechanical strength are given in Fig. 55.2 [9].

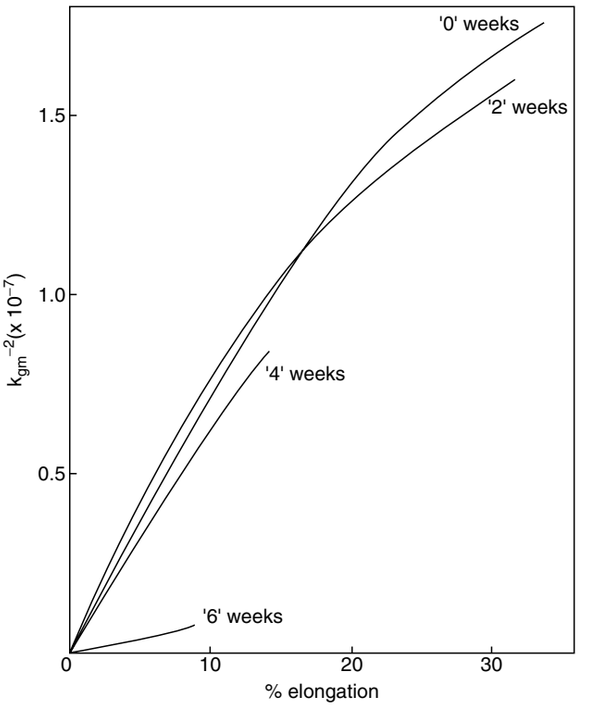

FIGURE 55.2. Stress/strain curves showing the loss of mechanical strength with degradation time for PGA sutures at pH 7 and 37 °C. (Reprinted with permission from [9].)

Poly(Lactic Acid)

Poly(lactic acid) (PLA) (Structure 2) is also a linear polyester, but the presence of an extra methyl group makes it more hydrophobic than PGA. Its water uptake in thin films is approximately 2% [13]. The methyl group contributes to a more amorphous character as well as increasing its solubility in organic solvents. In addition, this group creates a chiral center which results in two different enantiomeric forms of the polymer, P(D)LA and P(L)LA. The racemic mixture of the two is abbreviated as P(D,L)LA. The most commonly used form is P(L)LA which, like all poly(lactic acids), releases lactic acid upon degradation. PLA is frequently cast from common solvents. These include: chloroform, methylene chloride, methanol, ethanol, benzene, acetone, dioxane, dimethylformamide, and tetrahydrofuran [14–16]. PLA has also been shown to degrade by a homogeneous, hydrolytic erosion [17–19]. For example, P(D,L)LA degrades in a conventional two-stage process where the majority of molecular weight loss occurs in the first stage, and the subsequent loss in mass and tensile strength begins in the second stage at a number average molecular weight of 15,000 [9]. P(L)LA of molecular weight 95,000 degraded in vivo by 56% in 6 months based on peak molecular weight (M_p) [20]. For P(D,L)LA between 58,000 and 87,000, 49% degraded in vivo in 1 month, also based on M_p. A half-life of 6.6 months by mass was reported [11] for P(L)LA of molecular weight 85,000. In vitro studies [9] showed a 50% loss in weight average molecular weight (M_w) in 16 weeks with a concurrent loss of 10–15% by mass. The degradation rate of PLA also varies with varying pH [21,22]. The amount of lactic acid released during the course of PLA degradation is very small but increases rapidly as PLA is broken down to low molecular weight oligomers. A sudden rise in the lactic acid concentration in vivo can render the local environment acidic and induce an inflammatory reaction or even tissue necrosis. The use of polydispersed PLA can result in distribution of the lactic acid production over time [23].

Thermal and mechanical properties of both P(L)LA and P(D,L)LA of various molecular weights are given in Table 55.1. Additional thermal properties of PLA are found in Lu *et al*. [24].

Poly(Lactic-co-Glycolic Acid) Copolymers

The advantage of copolymerizing poly(α-hydroxy esters) is the ability to control physical and mechanical properties;

TABLE 55.1. *Thermal and mechanical properties of respective synthetic biodegradable polymers [4,24,48,74,75,95,96].*

Polymer	Weight average molecular weight	Glass transition temp. (°C)	Melting temp.[a] (°C)	Decomposition temp. (°C)	Heat of fusion[a] (Jg^{-1})	Tensile strength (MPa)	Tensile modulus (MPa)	Flexural modulus (MPa)	Elongation at yield (%)	Elongation at break (%)
Poly(α-Hydroxy Ester)										
PLGA	50,000	35	210	254	71	—	—	—	—	—
P(L)LA	50,000	54	170	242	41	28	1,200	1,400	3.7	6
P(L)LA	100,000	58	159	235	20	50	2,700	3,000	2.6	3.3
P(L)LA	300,000	59	178	255	39	48	3,000	3,250	1.8	2
P(D,L)LA	21,000	50	A	255	A	—	—	—	—	—
P(D,L)LA	107,000	51	A	254	A	29	1,900	1,950	4.0	6
P(D,L)LA	550,000	53	A	255	A	35	2,400	2,350	3.5	5
Poly(ε-Caprolactone)	44,000	−62	57	350	34	16	400	500	7.0	80
Poly(Ortho Esters)										
P(CDM-*co*-HD) 35:65	99,700	55	A	358	A	20	820	950	4.1	220
P(CDM-*co*-HD) 70:30	101,000	84	A	362	A	19	800	1,000	4.1	180
P(CDM-*co*-HD) 90:10	131,000	95	A	338	A	27	1,150	1,250	3.4	7
Polyanhydrides										
PSA	—	60	86	—	153	—	—	—	—	—
P(CPP-*co*-SA) 22:78	—	47	66	—	64	—	—	—	—	—
P(CPP-*co*-SA) 41:59	—	4	178	—	8	—	—	—	—	—
P(CPP-*co*-SA) 60:40	—	0	200	—	25	—	—	—	—	—
P(CPP-*co*-SA) 80:20	—	15	205	—	34	—	—	—	—	—
PCPP	—	96	240	—	111	—	—	—	—	—
Poly(3-Hydroxybutyrates) Copolymers										
PHB	370,000	1	171	252	51	36	2,500	2,850	2.2	2.5
P(HB-*co*-HV) 93:7	450,000	−1	160	243	32	24	1,400	1,600	2.3	2.8
P(HB-*co*-HV) 89:11	529,000	2	145	235	12	20	1,100	1,300	5.5	17
P(HB-*co*-HV) 78:22	227,000	−5	137	251	7	16	620	750	8.5	36
Polydioxanones										
PTMC	48,000	−15	A	261	A	0.5	3	—	20	160
Pseudopoly(Amino Acids)										
PBPA	105,000	69	A	135	A	50	2,150	2,400	3.5	4
PDTH	101,000	55	A	138	A	40	1,630	—	3.5	7
Poly(Fumarates)										
PPF:PPF-DA 1:2[b]	2,600	11.2	A	—	A	61	857	3,124	5.6	10.8
PPF:PPF-DA 1:1	2,600	11.2	A	—	A	70	923	2,644	4.3	11.3
PPF:PPF-DA 2:1	2,600	11.2	A	—	A	64	806	2,206	4.3	12.9
P(PF-*co*-EG)[c] 33:66	8,200	−54.1	26.5	—	17.5	0.23	2.16	0.87	—	—
P(PF-*co*-EG) 33:66	14,200	−44.6	39.7	—	20.1	0.32	1.9	3.87	—	—
P(PF-*co*-EG) 66:33	8,050	−43.5	25.0	—	0.2	1.06	11.02	1.69	—	—
P(PF-*co*-EG) 66:33	13,090	−46.1	27.7	—	9.9	0.91	5.05	2.39	—	—

[a] The symbol A designates amorphous polymer.
[b] PPF:PPF-DA 1:2 refers to the ratio of double bonds present in each monomer.
[c] P(PF-*co*-EG) was crosslinked with poly(*N*-vinyl pyrrolidinone).

however, there is no linear relationship between the physical properties of the constituent homopolymers and their copolymers. Most of these copolymers are amorphous (between approximately 24 and 67 mol% glycolic acid) [13], and therefore, degradation rates are highly dependent on the relative amount of each comonomer. Copolymers with high or low comonomer ratios are less sensitive to hydrolysis than copolymers with a more equimolar ratio, due to their greater crystallinity. Half-lives for various PLA and PGA ratios are depicted graphically in Fig. 55.3 [11].

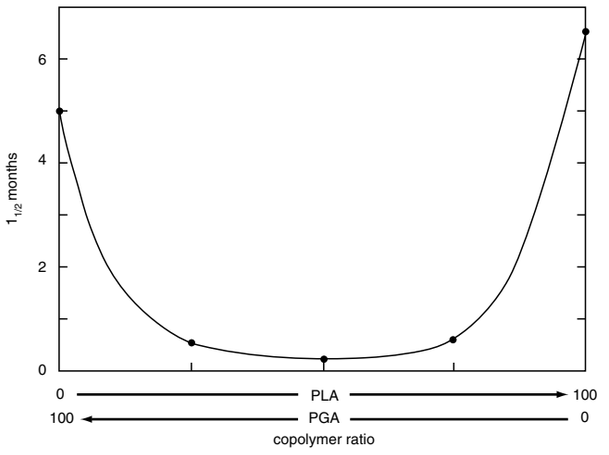

FIGURE 55.3. Variation of half-life of PLGA copolymers with the lactic acid and glycolic acid copolymer ratio in vivo. (Reprinted with permission from [11].)

Due to the dependence of the degradation rate of poly (lactic-*co*-glycolic acid) (PLGA) copolymers on pH, a phenomenon known as autocatalysis occurs where the carboxylic acid monomers released during degradation reduce the pH and further induce degradation [22–25]. For large-scale polymers, autocatalysis causes a heterogeneous degradation where the pH decreases in the center of the polymer, and a differential in the degradation rate is created [26].

Multiple uses of poly(lactic acid), poly(glycolic acid), and their copolymers have been described including sutures [27], vascular grafts [28], drug carriers [29,30], and scaffolds for tissue engineering [31,32]. This is due in part to the FDA approval of these polymers for certain medical applications.

55.2.2 Poly(ε-Caprolactone)

Poly(ε-caprolactone) (PCL) is a semicrystalline, aliphatic polyester (Structure 3). It is soluble in tetrahydrofuran, chloroform, methylene chloride, carbon tetrachloride, benzene, toluene, cyclohexanone dihydropyran, and 2-nitropropane; and only partially soluble in acetone, 2-butanone, ethyl acetate, acetonitrile, and dimethyl fumarate [33]. PCL is also capable of forming blends as well as useful copolymers with a wide range of polymers [34].

PCL has been shown to degrade by random hydrolytic scission of its ester groups, and under certain circumstances, by enzymatic degradation [33]. It is similar to P(D,L)LA, in that it degrades in a two-phase process with the molecular weight loss occurring primarily in the first phase, and the major mass and strength loss at the onset of the second at a number average molecular weight of 5,000 [35]. However, PCL degrades almost three times slower than P(D,L)LA [4]. A graph of molecular weight versus time showing the degradation of PCL capsules in vivo is given in Fig. 55.4 [35]. The crystallinity of PCL increases with decreasing molecular weight with polymers of molecular weight above 100,000 being about 40% crystalline. This value increases to about 80% for molecular weights of 5,000 [35]. As a result, PCL behaves like PGA in that the residual crystallinity increases

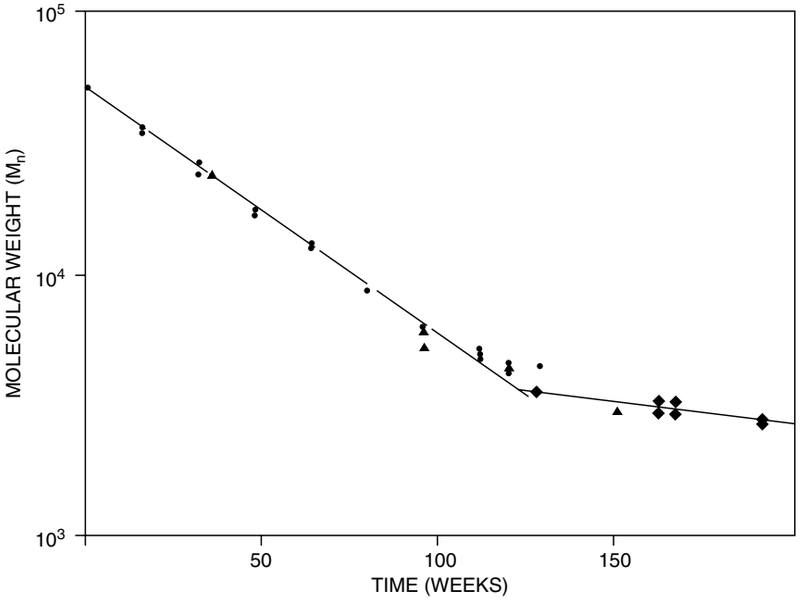

FIGURE 55.4. Decrease of molecular weight of PCL with the degradation time for PCL capsules loaded with various drugs in vivo. (Reprinted with permission from [35].)

as the polymer degrades. The degradation rate of PCL can be increased by forming a copolymer with DL-lactide [36]. In addition, PCL is affected by acidic conditions consistent with an autocatalytic degradation mechanism, and it is also influenced by the addition of small molecules such as ethanol, pentanol, oleic acid, decylamine, and tributyiamine [37].

PCL has a low glass transition temperature of $-62\ ^{\circ}C$, existing always in a rubbery state at room temperature, and a melting temperature of 57 °C. It has been postulated that these properties lead to a high permeability of PCL for controlled release agents. Other thermal and mechanical properties are listed in Table 55.1.

55.2.3 Poly(*Ortho* Esters)

Poly(*ortho* esters) are amorphous, hydrophobic polymers containing hydrolytically labile, acid-sensitive, backbone linkages (Structures 4, 5, 6). Due to their hydrophobicity, they can easily dissolve in organic solvents including: chloroform, methylene chloride, and dioxane. However, it can be difficult to remove the solvent in a situation such as a solvent casting [38]. In addition, these polymers are not inherently susceptible to degradation in the presence of water, although they can be if anhydrides (acid excipients), glycolic acid, or lactic acid are incorporated. They are susceptible to thermal degradation and must be processed accordingly.

Poly(*ortho* esters) are a class of polymers which can degrade heterogeneously by surface erosion [39]. These polymers lose material from the surface only, while retaining their original geometry. As such, their primary use is in drug delivery [40]. The first class of poly(*ortho* esters), as shown in Structure 4, generates a carboxylic acid upon hydrolysis which then further catalyzes the acid-sensitive cleavage. A basic salt such as Na_2CO_3 or $Mg(OH)_2$ is usually incorporated to neutralize the acid product, however, this creates a diffusion-limited system which exhibits nonzero-order drug release characteristics.

The second class, represented by Structures 5 and 6, does not produce acidic hydrolysis products, and its degradation can be controlled by the incorporation of either acidic or basic excipients. In the case of acid addition, water penetrates, ionizes the acid, and reduces the pH. This then catalyzes the hydrolysis, resulting in a hydration front and an erosion front. For a basic excipient, water must penetrate, elute, or neutralize the base, and then allow erosion to occur, decreasing the rate of hydrolysis [41]. According to the choice of additive, degradation rates can be varied from several days to years. Acid excipients can also be incorporated into the polymer itself as pendant chains which are solubilized upon cleavage [42]. For example, the degradation rates are enhanced for polymers containing *trans*-cyclohexanedimethanol (CDM) and 1,6-hexanediol (HD) when acidic functionalities, 9,10-dihydroxy-stearic acid (DHSA) [43], are incorporated, as shown in Fig. 55.5. The polymer can also be crosslinked at temperatures as low as 40 °C with an excipient stabilized interior [44].

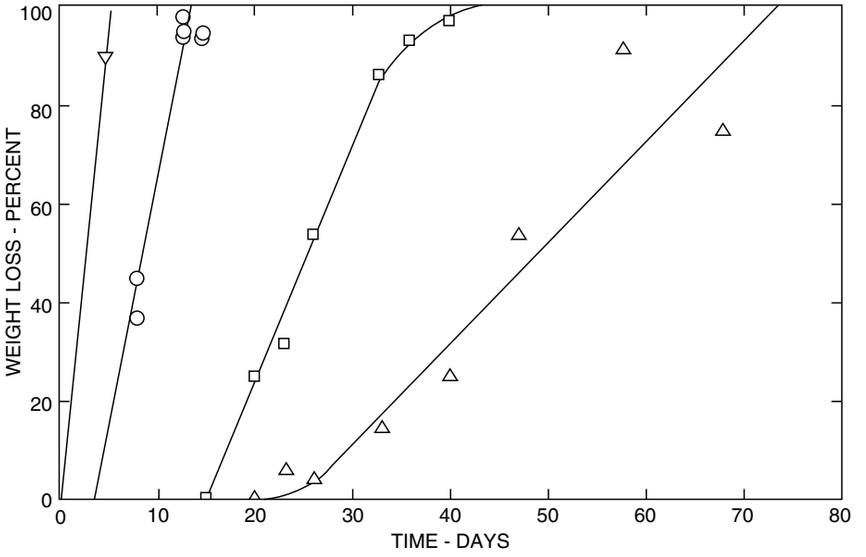

FIGURE 55.5. Variation of cumulative weight loss with time for poly(*ortho* esters) containing *trans*-cyclohexanedimethanol (CDM), 1,6-hexanediol (HD), and 9,10-dihydroxy-stearic acid (DHSA) (in the form of 6 × 0.5 mm disks at pH 7 and 37 °C). *S* = 58% CDM, 38% HD, 4% DHSA; *E* = 59% CDM, 39% HD, 2% DHSA; *G* = 59.5% CDM, 39.5% HD, 1% DHSA; *C* = 59.7% CDM, 39.75% HD, 0.5% DHSA. (Reprinted with permission from J. Heller, D. W. H. Penhale, and S. Y. Ng. in Long-Acting Contraceptive Delivery Systems, edited by G. I. Zatuchni, A. Goldsmith, J. D. Shelton, and J. J. Sciarra, (Harper and Row, New York, 1984), p. 127.)

Functionalizing the third class with lactic acid or glycolic acid produces an autocatalytic polymer [45,46]. Degradation is mediated by surface and bulk erosion, which is controlled by the concentration of the α-hydroxy acid segments [47]. There is a linear relationship between weight loss and lactic acid release suggesting surface erosion, also molecular weight decreases signifying bulk erosion. Unlike PLGA and PLA the bulk of the material does not become acidic; the acid products from hydrolysis are concentrated at the surfaces and are easily diffused away [47].

The mechanical and thermal properties of these polymers can also be varied over a wide range by the selection of starting materials with differing compositions and molecular weights. The tripolymerization of 3,9-*bis*(ethylidene 2,4,8,10-tetraoxaspiro[5,5]undecane) with mixtures of the rigid diol CDM and the flexible diol HD allows preparation of polymers with controlled glass transition temperature [40] (Fig. 55.6). Other thermal and mechanical properties for P(CDM-*co*-HD) copolymers are listed in Table 55.1.

55.2.4 Polyanhydrides

Polyanhydrides are a class of hydrolytically unstable polymers that are usually either aliphatic, aromatic, or a combination of the two. Two general representations are given in Structures 7 and 8. These polymers dissolve in common organic solvents including chloroform and methylene chloride and are extremely sensitive to aqueous environments. In addition, they are very reactive and can react with amine or other nucleophilic groups that are present in drugs intended for controlled release. This is true especially at elevated temperatures, for example, as occurs during polymer processing [48].

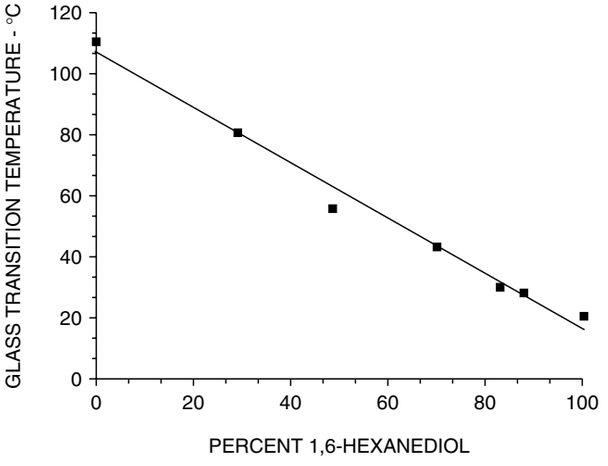

FIGURE 55.6. Glass transition temperatures of poly(*ortho* esters) consisting of 3,9-*bis*(ethylidene 2,4,8,10 tetraoxaspiro [5,5]undecane) with *trans*-cyclohexanedimethanol and 1,6-hexanediol as a function of the 1,6-hexanediol content. (Reprinted with permission from [40].)

The degradation of polyanhydrides can be varied from days to years depending on the choice or combination of choices of backbone structure [49,50]. The degradation rate of several different combinations of the aliphatic monomer, sebacic acid (SA), and the aromatic monomer, *bis*-(*p*-carboxyphenoxy)propane (CPP), is given in Fig. 55.7. The polymer primarily degrades by surface erosion [51–53]. As such, it is a candidate for drug delivery, eliminating the need for additional excipients. Its degradation rate is also sensitive to changes in pH, typically increasing with increasing pH as shown in Fig. 55.8 [50].

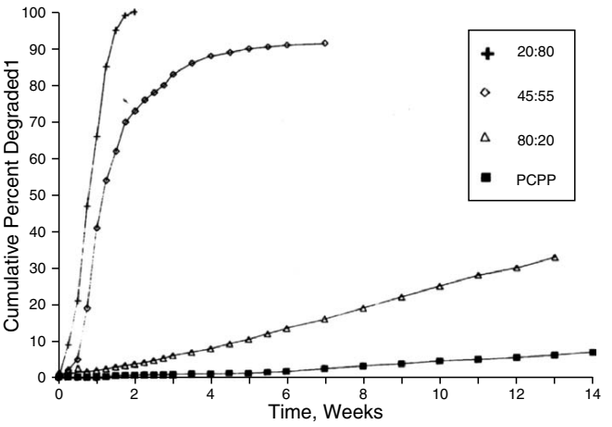

FIGURE 55.7. Change of cumulative percent of polymer degraded with degradation time for P(CPP-*co*-SA) copolymers in the form of compression-molded disks of 1.4 cm diameter and 1 mm thickness at pH 7.4 and 37 °C. (Reprinted with permission from K. W. Leong, B. G. Brott, and R. Langer, J. Biomed. Mater. Res. 19, 941 (1985).)

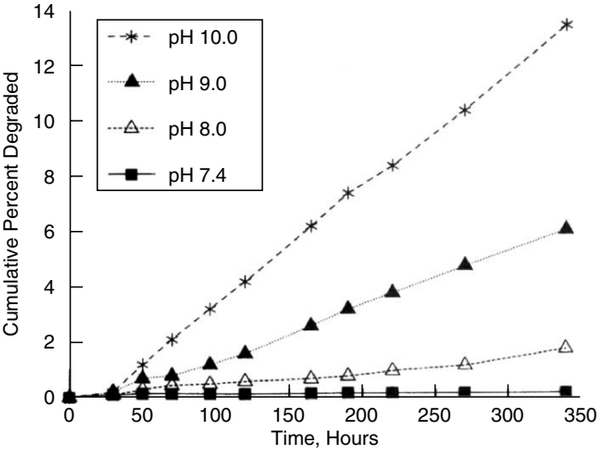

FIGURE 55.8. Change of cumulative percent of polymer degraded with degradation time at varying pH levels for PCPP in the form of compression-molded disks of 1.4 cm diameter and 1 mm thickness at 37 °C. (Reprinted with permission from K. W. Leong, B. G. Brott, and R. Langer, J. Biomed. Mater. Res. 19, 941 (1985).)

There are a wide variety of processing techniques available for forming polyanhydrides, however, care must be taken in incorporating controlled release agents at high temperatures because of the reactivity of the polymer with the drug and the instability of the polymer itself. The mechanical properties of polyanhydrides are generally poor, tending to be brittle with minimal fiber-forming abilities. Forming copolymers of polyanhydrides increases the mechanical properties, while maintaining their degradation characteristics [54,55]. Copolymers of methacrylated sebacic acid (MSA) and 1,6-*bis*(carboxyphenoxy) hexane (MCPH) have been shown to have similar mechanical properties of cortical and trabecular bone [56]. These copolymers degrade by surface erosion allowing the scaffold to maintain its structural integrity [56].

In addition, polyanhydrides have been shown to have excellent in vivo biocompatibility [57]. The thermal properties of representative P(CPP-*co*-SA) copolymers are given in Table 55.1. A detailed presentation of thermal properties is given in Domb *et al*. and Tamada and Langer [48,58].

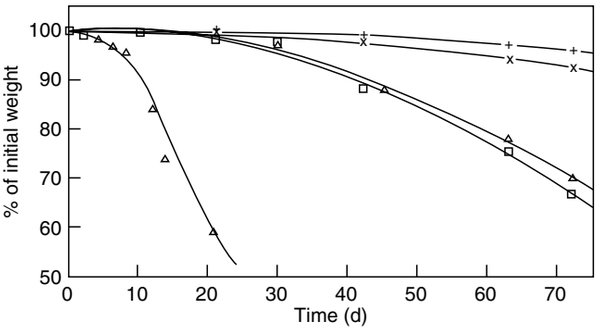

FIGURE 55.9. Kinetics of percent of initial weight loss for P(HB-*co*-HV) copolymers of different copolymer ratios and molecular weights in the form of solvent-cast disks of 2 cm diameter and 0.15 mm thickness at 70 °C and pH 7.4. D = 10% HV, $M_w = 750{,}000$; I = 20% HV, $M_w = 300{,}000$; C = 12% HV, $M_w = 170{,}000$; G = 12% HV, $M_w = 100{,}000$; C = 20% HV, $M_w = 36{,}000$. (Reprinted with permission from [60].)

55.2.5 Poly(3-Hydroxybutyrate) Copolymer

Poly(3-hydroxybutyrate) (PHB) is crystalline, thermoplastic polyester made by micro-organisms as an energy storage molecule (Structure 9). As such, it can be enzymatically degraded by certain bacteria. It is often copolymerized with hydroxyvaleric acid (Structure 10) to create poly(3-hydroxybutyrate-*co*-3-hydroxyvalerate), P(HB-*co*-HV). Solvent casting has been described from solution in chloroform, methylene chloride, and tetrahydrofuran [59,60].

The degradation of PHB produces D-3-hydroxy butyric acid, normally found in human blood, which may contribute to its low toxicity. There is evidence for both enzymatic and hydrolytic degradation in vivo [61]. In vitro studies [59, 60] suggest that PHB and P(HB-*co*-HV) copolymers degrade by hydrolysis in a multistage process where the majority of the molecular weight loss occurs before any significant mass loss. A graph of weight loss for various P(HB-*co*-HV) copolymers is given in Fig. 55.9 [60]. The copolymerization of hydroxybutyric acid with hydroxyvaleric acid increases the percentage of amorphous regions compared to PHB, which are readily attacked by hydrolytic degradation thereby increasing degradation rates. In addition, elevated temperatures and alkaline conditions have been shown to increase degradation rates.

The crystallinity and mechanical properties of the P(HB-*co*-HV) copolymer can be varied by modification of the percentages of the respective monomers. The higher the percentage of hydroxyvalerate, the less crystalline and the more elastic the polymer becomes. Some thermal and mechanical properties are presented in Table 55.1. A study of thermal characteristics in vivo is given in Gogolewski et al. [61], and a mechanical evaluation in vivo and in vitro is found in Miller and Williams [62].

55.2.6 Polyphosphazenes

Polyphosphazenes consist of a backbone of alternating nitrogen and phosphorus atoms (Structure 11). The R and R′ groups on either side of the phosphorus can be widely varied depending on the route of synthesis. The choice of functional groups determines the physical and chemical properties of the polymer [63,64]. Some important types of polyphosphazenes that have been synthesized are nonhydrolyzable, hydrophobic polymers; nonhydrolyzable, hydrophilic polymers; and hydrolyzable polymers. Those in the first class include polymers with side fluoroalkoxy, aryloxy, or organosilicon hybrid groups. These polymers are usually elastomers with water contact angles on the order of poly (tetrafluoroethylene) [65]. The second class consists of polymers with alkylamino, alkylether, alcohol, carboxylic acid, glyceryl, or glucosyi functionalities. These can be quite hydrophilic and are often crosslinked to form hydrogels. The third class of polymers includes those that can be hydrolyzed to form phosphate and ammonia derivatives. Some important side groups include: amino acid esters, steroidal groups, imidazolyl groups, and other bioactive molecules. In addition, the surface can also be activated for use in controlled release.

55.2.7 Fumarate-Based Polymers

The following polyesters are based on fumaric acid, a naturally occurring substance found in the Krebs cycle [8]. Three types of fumarate-based polymers are discussed: poly(propylene fumarate) (PPF), poly(propylene fumarate-*co*-ethylene glycol) (P(PF-*co*-EG)), and oligo(poly(ethylene glycol) fumarate) (OPF).

Poly(Propylene Fumarate)

Poly(Propylene Fumarate) (PPF) is a linear, unsaturated, hydrophobic polyester (Structure 12) containing hydrolyzable ester bonds along its backbone. PPF is highly viscous at room temperature and is soluble in chloroform, methylene chloride, tetrahydrofuran, acetone, alcohol, and ethyl acetate [66]. The double bonds of PPF can form chemical crosslinks with various monomers, such as *N*-vinyl pyrrolidone, poly(ethylene glycol)-dimethacrylate, PPF-diacrylate (PPF-DA), and diethyl fumarate [67,68]. The choice of monomer and radical initiator directly influence the degradative and mechanical properties of the crosslinked polymer. Once crosslinked, PPF forms a solid material with mechanical properties suitable for a range of bone engineering applications.

PPF crosslinked with either thermal- or photo-initiators exhibits a biphasic degradation at 37 °C. During the initial phase of degradation, PPF's mechanical strength increases, whereas the mechanical strength diminishes in the second phase [69,70]. This phenomenon can be explained by the fact that, at 37 °C, enough energy is provided for the entrapped initiators to sustain the crosslinking reaction [70,71]. To produce a crosslinked polymer of composition similar to that of the uncrosslinked polyester, diethyl fumarate or a derivative of PPF, PPF-diacrylate (PPF-DA) is used as a crosslinker [71,72].

Particulate ceramics such as β-tricalcium phosphate (β-TCP) can also be incorporated within the network to modify the crosslinked polymer's mechanical properties [67]. Hybrid alumoxane nanoparticles can also be incorporated in PPF to provide mechanical reinforcement [73].

Poly(Propylene Fumarate-co-Ethylene Glycol)

Poly(propylene fumarate-*co*-ethylene glycol) (P(PF-*co*-EG)), (Structure 13), is an amphiphilic block copolymer of PPF and poly(ethylene glycol) (PEG). P(PF-*co*-EG) is soluble in toluene, *N*, *N*-dimethylformamide, tetrahydrofuran, and acetone [74]. Similar to PPF, P(PF-*co*-EG) degrades via hydrolysis of the ester bonds found along its backbone [74]. Unlike PPF, the crosslinked P(PF-*co*-EG) forms hydrogels. Increasing the amount of PEG within the copolymer increases its hydrophilicity, thus encouraging an influx of water within the network and inducing the material to swell [75]. Similarly, increasing the concentration and/or molecular weight of the PPF block reduces the degree of swelling [75].

The relative amount of the PPF block also affects the mechanical properties of the crosslinked P(PF-*co*-EG). PPF is the only portion of the copolymer that can form covalent bonds for crosslinking, so more PPF block result in more possible crosslinks, yielding a stronger material [75]. Additionally the hydrophobic PPF moieties can interact with each other, forming secondary interactions that further strengthen the material. A compilation of thermal and mechanical properties for P(PF-*co*-EG) are listed in Table 55.1.

Oligo (Poly(Ethylene Glycol) Fumarate)

The final type of fumarate-based polymer discussed, oligo (poly(ethylene glycol) fumarate) (OPF) (Structure 14), is a highly hydrophilic, linear, unsaturated polymer, composed of alternating PEG and fumarate moieties [76]. OPF is soluble in aqueous and organic solvents [76]. Like all fumarate-based polymers, crosslinking occurs through the fumarate groups and degradation is mediated by hydrolysis of the ester bonds. Similar to P(PF-*co*-EG), the PEG block gives OPF its hydrophilicity. In addition, OPF's properties are controlled by the ratio of fumarate to PEG and the molecular weight of the PEG. Increasing the molecular weight of the PEG produces a less crosslinked, and more swollen hydrogel [76,77]. Moreover, increasing the fumarate to PEG ratio increases the number of crosslinks within the network and decreases the swelling of the hydrogel [76]. Due to their high hydrophilicity, OPF hydrogels have been used to encapsulate mesenchymal stem cells for bone engineering applications [78,79].

55.2.8 Polydioxanones and Polyoxalates

Four important classes of polymers from dioxane-diones and oxalates are poly(l,4-dioxane-2,5-diones), polyoxalates, poly(l,3-dioxane-2-one) and poly(l,4-dioxane-2,3-dione), and poly(*p*-dioxanone). Representative diagrams are given in structures 15, 16, 17, and 18, respectively.

The first class has been produced with an alternating glycolide/lactide sequence. Both PGA and PLA have been mentioned previously, and the physical properties of the alternating copolymer are a weighted average of the two homopolymers.

Secondly, a polyoxalate has been reported [80] with an ester backbone, which can be hydrolytically cleaved to produce propylene glycol and oxalic acid. The predicted degradation rate is faster than PGA owing to its lower degree of crystallinity and less hydrophobic character.

The third class primarily consists of polymers of 1,3-dioxane-2-one otherwise known as trimethylene carbonate (TMC) and its copolymers with glycolide and lactide. PTMC degrades at a much slower rate than PGA. In addition, it softens between 40 °C and 60 °C, has low mechanical strength [5], and is reported to improve handling properties in copolymers with PGA [4]. Some thermal and mechanical properties of PTMC are shown in Table 55.1.

Lastly, poly(*p*-dioxanone) is thought to degrade by a mechanism similar to PGA [81]. The backbone is hydrolytically cleaved in a bulk erosion process with the major weight loss occurring between weeks 12 and 18 [82]. It has superior strength characteristics compared to PGA as well as high crystallinity up to 37%.

55.2.9 Poly(Amino Acids)

Poly(amino acids) as shown in Structure 19 are synthetically derived polymers which can be prepared from a variety of amino acids. The physical and chemical properties depend, in large part, on the functionalities of their respective side chains, however, poly(amino acids) have some common features. Most are highly insoluble in organic solvents, and they tend to swell in aqueous solution. They have poor mechanical properties and are difficult to process. In addition, the hydrolysis of the amide bond has an enzymatic contribution that is difficult to predict or control in vivo. The degradation products, amino acids, are natural components of proteins and should not cause a toxic response upon degradation, however, polymers containing three or more amino acids can elicit a strong immunologic response [83]. Additional properties for specific combinations of amino acids are given in Banera et al. [84]. Certain side chain modifications have been made in order to avoid some of these limitations. Poly(L-lysine) [85,86] and poly (L-glutamic acid) [87] have both been modified through their chemically reactive side chains to produce hybrids with bioactive molecules.

55.2.10 Pseudopoly(Amino Acids)

Pseudopoly(amino acids) are polymers derived from amino acids with nonamide linkages; these are represented by the wavy line in Structures 20, 21, and 22. This is usually done by the polymerization of trifunctional amino acids by reaction with side chain functional groups. Three important categories include: serine derived polyesters [88] hydroxyproline derived polyesters, and tyrosine-derived polymers. The first has not been widely used as a biomaterial [89]. The second group consists of poly(*N*-acyl-hydroxyproline esters) from *N*-protected hydroxyproline. These polyesters are soluble in benzene, toluene, chloroform, dichloromethane, carbon tetrachloride, tetrahydrofuran, and dimethylformamide. They are thermally stable up to 300 °C, have glass transition temperatures ranging from 71 °C to 157 °C, and are easily processed [89].

The third group consisting primarily of modified polycarbonates [90] can be derived from diphenols such as hydroquinone or Bisphenol A [91] (BPA), or a tyrosine dipeptide such as desaminotyrosyl-tyrosine hexyl ester (DTH). PDTH was found to be relatively strong with good biocompatibility [89,92,91]. The degradation of the tyrosine-derived polycarbonates is controlled by the hydrolysis of the ester and carbonate bonds [93]. Carbonate bonds will hydrolyze at a faster rate than the ester bonds, which leads to an initial reduction of molecular weight without mass loss [93,94]. Its reported half-life is 26 weeks, but it can take up to 4 years before the polymer is completely resorbed [91,93]. Additional thermal and mechanical data is given in Table 55.1

55.3 SUMMARY

While the previous list summarizes most of the currently used biodegradable polymers as well as some new materials, and while it describes the state-of-the-art at this time, it is certainly not exhaustive. There are many new products being developed as well as novel modifications of the polymers described with in the chapter. Ideally, polymers can be chosen and tailored for a specific application based on their physical and chemical properties. We have shown properties that are crucial to the function of the polymer in question and also give sources where additional information can be found.

55.4 ACKNOWLEDGMENTS

We acknowledge support by the National Institutes of Health and the Alliances for Graduate Education and the Professoriate related to synthetic biodegradable polymers for medical applications.

55.5 APPENDIX

Abbreviations

β-TCP	β-tricalcium phosphate
BPA	Bisphenol A
CDM	*trans*-cyclohexanedimethanol
CPP	*bis*-(*p*-carboxyphenoxy)propane
DHSA	9,10-dihydroxy-stearic acid
DTH	desaminotyrosyl-tyrosine hexyl ester
HD	1,6-hexanediol
M_p	peak molecular weight
M_w	weight average molecular weight
OPF	oligo(poly(ethylene glycol) fumarate)
PBPA	poly(Bisphenol A)
P(CDM-*co*-HD)	poly(*trans*-cyclohexanedimethanol-*co*-1,6-hexanediol)
PCL	poly(ε-caprolactone)
PCPP	poly(*bis*-(*p*-carboxyphenoxy)propane)
P(CPP-*co*-SA)	poly(*bis*-(*p*-carboxyphenoxy)propane-*co*-sebacic acid)
P(D)LA	D enantiomer of poly (lactic acid)
P(D,L)LA	racemic mixture of D and L enantiomers of poly(lactic acid)
PDTH	poly(desaminotyrosyl-tyrosine hexyl ester)
PEG	poly(ethylene glycol)
PGA	poly(glycolic acid)
PHB	poly(3-hydroxybutyrate)
P(HB-*co*-HV)	poly(3-hydroxybutyrate-*co*-3-hydroxyvalerate)
PLA	poly(lactic acid)
PLGA	poly(lactic-*co*-glycolic acid)
P(L)LA	L enantiomer of poly(lactic acid)
PPF	poly(propylene fumarate)
PPF-DA	PPF-diacrylate

P(PF-*co*-EG)	poly(propylene fumarate-*co*-ethylene glycol)
PSA	poly(sebacic acid)
PTMC	poly(trimethylene carbonate)
SA	sebacic acid
TMC	trimethylene carbonate

56.6 CHEMICAL STRUCTURES

Structure 1: Poly(glycolic acid)

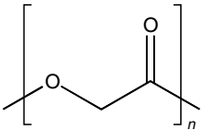

Structure 2: Poly(lactic acid)

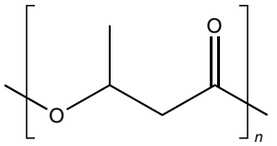

Structure 3: Poly(ε-caprolactone)

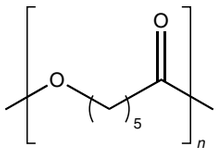

Structure 4: Poly(*ortho* ester)

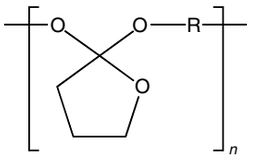

Structure 5: Poly(*ortho* ester)

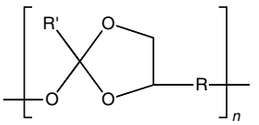

Structure 6: Poly(*ortho* ester)

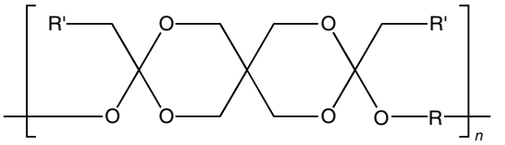

Structure 7: Polyanhydride

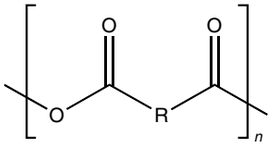

Structure 8: Polyanhydride

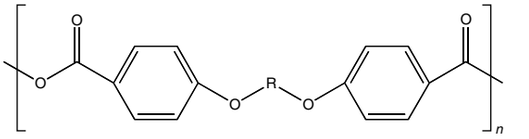

Structure 9: Poly(3-hydroxybutyrate)

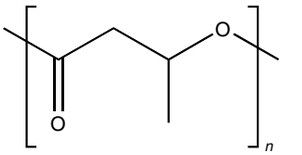

Structure 10: Poly(3-hydroxybutyrate)

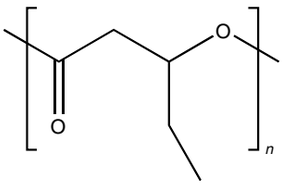

Structure 11: Polyphosphazenes

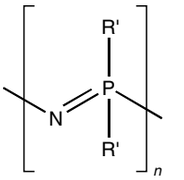

Structure 12: Poly(propylene fumarate)

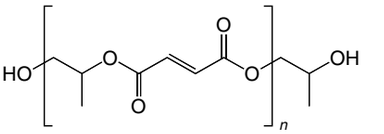

Structure 13: Poly(propylene fumarate-*co*-ethylene glycol)

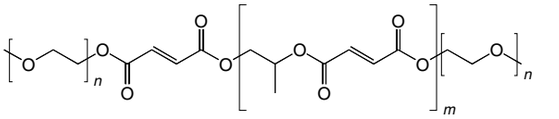

Structure 14: Oligo (poly(ethylene glycol) fumarate)

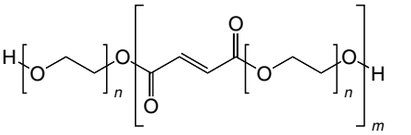

Structure 15: Poly(1,4-dioxane)

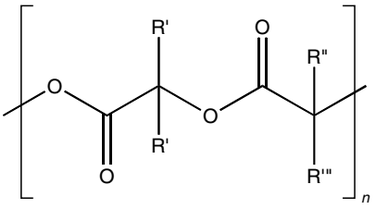

Structure 16: Polyoxalate

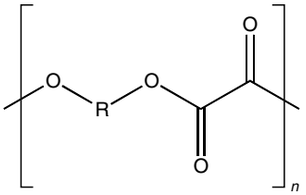

Structure 17: Poly(1,3-dioxane-2-one)

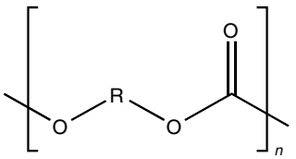

Structure 18: Poly(*p*-dioxanone)

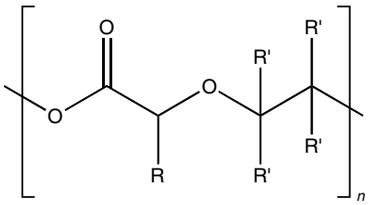

Structure 19: Poly(amino acid)

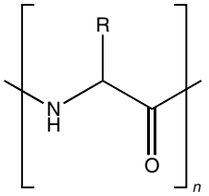

Structure 20: Pseudopoly(amino acid)

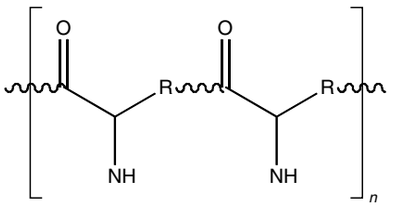

Structure 21: Pseudopoly(amino acid)

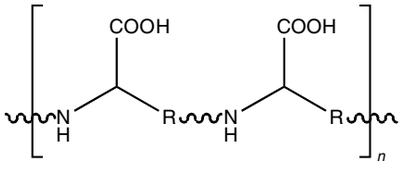

Structure 22: Pseudopoly(amino acid)

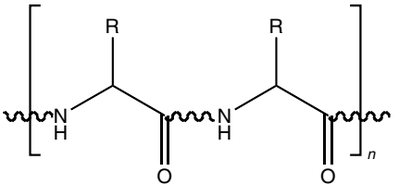

REFERENCES

1. R. C. Thomson, S. L. Ishaug, A. G. Mikos, "Polymer for biological systems," in *Encyclopedia of Molecular Biology: Fundamentals and Applications,* edited by R. A. Meyers (VCH Publishers, New York, 1996) pp 31–44.
2. R. C. Thomson, M. C. Wake, M. J. Yaszemski, A. G. Mikos, Adv. Polym. Sci. 122, *245* (1995).
3. S. Pulapura and J. Kohn, J. Biomater. Appl. 6, *216* (1992).
4. I. Engelberg and J. Kohn, Biomaterials 12, *292* (1991).
5. S. J. Holland, B. J. Tighe, P. L. Gould, J. Control. Release 4, *155* (1986).
6. P. A. Gunatillake and R. Adhikari, Eur. Cell Mater. 5, *1* (2003).
7. A. Atala and D. J. Mooney, *Synthetic Biodegradable Polymer Scaffolds*. (Birkhauser, Boston, 1997).
8. J. S. Temenoff and A. G. Mikos, "Fumarate-based macromers as scaffolds for tissue engineering applications," in *Polymeric Materials Encyclopedia*, edited by J. C. Salamone (CRC Presss, Boca Raton, in press).
9. A. M. Reed and D. K. Gilding, Polymer 22, *494* (1981).
10. C. C. Chu, J. Biomed. Mater. Res. 15, *19* (1981).
11. R. A. Miller, J. M. Brady, D. E. Cutright, J. Biomed. Mater. Res. 11, *711* (1977).
12. D. Cohn, H. Younes, G. Marom, Polymer 28, *2018* (1987).
13. D. K. Gilding and A. M. Reed, Polymer 20, *1459* (1979).
14. H. Younes and D. Cohn, J. Biomed. Mater. Res. 21, *1301* (1987).
15. S. Gogolewski and A. J. Pennings, Colloid Polym. Sci. 261, *477* (1983).
16. S. Gogolewski and A. J. Pennings, Makromol. Chem. Rapid Commun. 3, *839* (1982).
17. A. S. Chawla and T. M. S. Chang, Biomater. Med. Dev. Art. Org. 13, *153* (1985).
18. H. Pistner, D. R. Bendix, J. Mühling, J. F. Reuther, Biomaterials 14, *291* (1993).
19. R. K. Kulkarni, E. G. Moore, A. F. Hegyeli, F. Leonard, J. Biomed. Mater. Res. 5, *169* (1971).
20. G. Spenlehauer, M. Vert, J. P. Benoit, A. Boddaert, Biomaterials 10, *557* (1989).
21. C. C. Chu, Ann. Surg. 195, *55* (1982).
22. M. Vert, S. Li, H. Garreau, J. Control. Release. 16, *15* (1991).
23. H. A. Von Recum, R. L. Cleek, S. G. Eskin, A. G. Mikos, Biomaterials 16, *441* (1995).
24. L. Lu and A. G. Mikos, "Poly(lactic acid)," in *Polymer Data Handbook*, edited by J. E. Mark (Oxford University Press, NewYork, 1999).
25. M. Vert, J. Mauduit, S. Li, Biomaterials 15, *1209* (1994).
26. M. Vert, S. M. Li, H. Garreau, J. Biomater. Sci. Polym. Ed. 6, *639* (1994).
27. E. Frazza and E. Schmitt, J. Biomed. Mater. Res. 5, *43* (1971).
28. C. M. Agrawal, K. F. Haas, D. A. Leopold, H. G. Clark, Biomaterials 13, *176* (1992).
29. L. Lu, M. J. Yaszemski, A. G. Mikos, J. Bone Joint Surg. Am. 83-A Suppl 1, *S82* (2001).
30. D. H. Lewis, "Controlled release of bioactive agents from lactide/glycolide polymer," in *Biodegradable Polymers As Drug Delivery Systems,* edited by M. Chasin, R. Langer (Marcel Dekker, New York, 1990) pp 1–42.
31. A. G. Mikos, A. J. Thorsen, L. A. Czerwonka, Y. Bao, R. Langer, D. N. Winslow, J. P. Vacanti, Polymer 35, *1068* (1994).
32. L. Lu, S. J. Peter, M. D. Lyman, H. L. Lai, S. M. Leite, J. A. Tamada, S. Uyama, J. P. Vacanti, R. Langer, A. G. Mikos, Biomaterials 21, *1837* (2000).
33. C. G. Pitt, "Poly-ε-caprolactone and its copolymers," in *Biodegradable Polymers As Drug Delivery Systems*, edited by M. Chasin, R. Langer (Marcel Dekker, New York, 1990) pp 71–120.

34. J. R. Koleske, "Blend containing poly(ε-caprolactone) and related polymers," in *Polymer Blends,* vol 2 edited by D. R. Paul, S. Newman (Academic Press, New York, 1978) pp 369–338.
35. C. G. Pitt, F. I. Chasalow, Y. M. Hibionada, D. M. Kilmas, A. Schindler, J. Appl. Polym. Sci. 26, *3779* (1981).
36. J. C. Middleton and A. J. Tipton, Biomaterials 21, *2335* (2000).
37. C. G. Pitt and G. Zhong-Wei, J. Control. Release 4, *283* (1987).
38. J. Heller, R. V. Sparer, G. M. Zentner, "Poly(ortho esters)," in *Biodegradable Polymers As Drug Delivery Systems,* edited by M. Chasin, R. Langer (Marcel Dekker, New York, 1990) pp 121–161.
39. J. Heller, Adv. Polym. Sci. 107, *41* (1993).
40. J. Heller, D. W. Penhale, B. K. Fritzinger, J. E. Rose, R. F. Helwing, Contracept. Deliv. Syst. 4, *43* (1983).
41. J. Heller, Biomaterials 11, *659* (1990).
42. C. Shih, T. Higuchi, K. J. Himmelstein, Biomaterials 5, *237* (1984).
43. J. Heller, J. Control. Release 2, *167* (1985).
44. J. Heller, B. K. Fritzinger, S. Y. Ng, D. W. H. Pennale, J. Control. Release 1, *233* (1985).
45. K. Schwach-Abdellaoui, J. Heller, R. Gurn, Macromolecules 32, *301* (1999).
46. S. Ng, T. Vandamme, M. Taylor, J. Heller, Macromolecules 30, *770* (1997).
47. J. Heller, J. Barr, S. Y. Ng, K. S. Abdellauoi, R. Gurny, Adv. Drug Deliv. Rev. 54, *1015* (2002).
48. A. Domb, S. Amselem, J. Shah, M. Maniar, Adv. Polym. Sci. 107, *93* (1993).
49. A. Gopferich, Biomaterials 17, (1996).
50. M. Chasin, A. Domb, E. Ron, E. Mathiowitz, K. Leong, C. Laurencin, H. Brem, B. Grossman, R. Langer, "Polyanhydrides as drug delivery systems," in B*iodegradable Polymers As Drug Delivery Systems,* edited by M. Chasin, R. Langer (Marcel Dekker, New York, 1990) pp 43–70.
51. A. Gopferich, R. Langer, J. Polym. Sci. [A1]. 31, *2445* (1993).
52. H. B. Rosen, J. Chang, G. E. Wnek, R. J. Linhardt, R. Langer, Biomaterials 4, *131* (1983).
53. J. A. Tamada and R. Langer, Proc. Natl. Acad. Sci. USA 90, *552* (1993).
54. K. E. Uhrich, A. Gupta, T. Thomas, C. Laurencin, R. Langer, Macromolecules 28, *2184* (1995).
55. K. S. Anseth, V. R. Shastri, R. Langer, Nat. Biotechnol. 17, *156* (1999).
56. D. S. Muggli, A. K. Burkoth, K. S. Anseth, J. Biomed. Mater. Res. 46, *271* (1999).
57. C. Laurencin, A. Domb, C. Morris, V. Brown, M. Chasin, R. Mcconnell, N. Lange, R. Langer, J. Biomed. Mater. Res. 24, *1463* (1990).
58. J. Tamada and R. Langer, J. Biomater. Sci. Polym. Ed. 3, *315* (1992).
59. H. T. Wang, H. Palmer, R. J. Linhardt, D. R. Flanagan, E. Schmitt, Biomaterials 11, *679* (1990).
60. S. J. Holland, A. M. Jolly, M. Yasin, B. J. Tighe, Biomaterials 8, *289* (1987).
61. S. Gogolewski, M. Jovanovic, S. M. Perren, J. G. Dillon, M. K. Hughes, J. Biomed. Mater. Res. 27, *1135* (1993).
62. N. D. Miller and D. F. Williams, Biomaterials 8, *129* (1987).
63. C. T. Laurencin, M. E. Norman, H. M. Elgendy, S. F. El-Amin, H. R. Allcock, S. R. Pucher, A. A. Ambrosio, J. Biomed. Mater. Res. 27, *963* (1993).
64. S. Cohen, M. C. Bano, K. B. Visscher, M. Chow, H. R. Allcock, R. Langer, J. Am. Chem. Soc. 112, *7832* (1990).
65. H. R. Allcock, "Polyphosphazenes as new biomedical and bioactive materials," in *Biodegradable Polymers As Drug Delivery Systems*, edited by M. Chasin, R. Langer (Marcel Dekker, New York, 1990) pp 163–194.
66. A. J. Domb, "Poly(propylene glycol fumarate) compositions for biomedical applications." US Patent 4, 888, 413 (1988).
67. S. Peter, P. Kim, A. Yasko, M. J. Yaszemski, A. G. Mikos, J. Biomed. Mater. Res. 44, *314* (1999).
68. S. He, M. J. Yaszemski, A. W. Yasko, P. S. Engel, A. G. Mikos, Biomaterials 21, *2389* (2000).
69. M. J. Yaszemski, R. G. Payne, W. C. Hayes, R. Langer, A. G. Mikos, Biomaterials 17, *2127* (1996).
70. M. D. Timmer, C. G. Ambrose, A. G. Mikos, Biomaterials 24, *571* (2003).
71. M. D. Timmer, C. G. Ambrose, A. G. Mikos, J. Biomed. Mater. Res. 66A, *811* (2003).
72. J. Fisher, D. Dean, A. G. Mikos, Biomaterials 23, *4333* (2002).
73. R. A. Horch, N. Shahid, A. S. Mistry, M. D. Timmer, A. G. Mikos, A. R. Barron, Biomacromolecules 5, *1990* (2004).
74. L. J. Suggs, R. G. Payne, M. J. Yaszemski, L. B. Alemany, A. G. Mikos, Macromolecules 30, *4318* (1997).
75. L. J. Suggs, E. Y. Kao, L. L. Palombo, R. S. Krishnan, M. S. Widmer, A. G. Mikos, J. Biomater. Sci. Polym. Ed. 9, *653* (1998).
76. S. Jo, H. Shin, A. K. Shung, J. P. Fisher, A. Mikos, Macromolecules 34, *2839* (2001).
77. J. S. Temenoff, K. A. Athanasiou, R. G. Lebaron, A. G. Mikos, J. Biomed. Mater. Res. 59, *429* (2002).
78. J. S. Temenoff, H. Park, E. Jabbari, D. E. Conway, T. L. Sheffield, C. G. Ambrose, A. G. Mikos, Biomacromolecules 5, *5* (2004).
79. J. Temenoff, H. Park, E. Jabbari, T. L. Sheffield, R. G. Lebaron, C. G. Ambrose, A. G. Mikos, J. Biomed. Mater. Res. 70A, *235* (2004).
80. D. K. Gilding, Biocomp. Clin. Implant Mater. 2, *209* (1981).
81. N. Doddi, C. C. Versfelt, D. Wasserman, "Synthetic Absorbable Surgical Devices of Poly-Dioxanone." US Patent 4,052,988. (1976).
82. J. A. Ray, N. Doddi, D. Regula, J. A. Williams, A. Melveger, Surg. Gynecol. Obstet. 153, *497* (1981).
83. J. M. Anderson, K. L. Spilizewski, A. Hiltner, "Poly-alpha-amino acids as biomedical polymers," in *Biocompatibility of Tissue Analogs* (CRC Press, Boca Raton, 1985) pp 67–88.
84. D. A. Barrera, E. Zylstra, P. T. Lansbury, R. Langer, Macromolecules 28, *425* (1995).
85. P. Campbell, G. I. Glover, J. M. Gunn, Arch. Biochem. Biophys. 203, *676* (1980).
86. D. A. Barrera, E. Zylstra, P. T. Lansbury, R. Langer, J. Am. Chem. Soc. 115, *11010* (1993).
87. K. R. Sidman, A. D. Schwope, W. D. Steber, S. E. Rudolph, S. B. Poulin, J. Membr. Biol. 7, *277* (1980).
88. Q. X. Zhou and J. Kohn, Macromolecules 23, *3399* (1990).
89. J. Kohn, "Pseudopoly(amino acids)," in *Biodegradable Polymers As Drug Delivery Systems*, edited by M. Chasin, R. Langer (Marcel Dekker, New York, 1990) pp 195–230.
90. S. L. Bourke, J. Kohn, Adv. Drug. Deliv. Rev. 55, *447* (2003).
91. A. J. Domb, Biomaterials 11, *686* (1990).
92. J. Kohn and R. Langer, Biomaterials 7, *176* (1986).
93. V. Tangpasuthadol, S. M. Pendharkar, R. C. Peterson, J. Kohn, Biomaterials 21, *2379* (2000).
94. V. Tangpasuthadol, S. M. Pendharkar, J. Kohn, Biomaterials 21, *2371* (2000).
95. M. D. Timmer, C. Carter, C. G. Ambrose, A. G. Mikos, Biomaterials 24, *4707* (2003).
96. X. Shi and A. G. Mikos, "Poly(propylene fumarate)," in *An Introduction to Biomaterials*, edited by S. A. Guelcher, E. J. Beckman, J. O. Hollinger (Boca Raton, FL, 2005).

CHAPTER 56

Biodegradability of Polymers

Anthony L. Andrady

Engineering & Technology Dirsian, RTI International, Research Triangle Park, NC 27709

56.1 INTRODUCTION

Biodegradation might be conveniently defined as "a chemical change in polymer facilitated by living organisms, usually micro-organisms" [1]. This definition is somewhat restricted, however, in that it excludes chemical breakdown processes on polymer substrates mediated by manmade enzymes. Inspite of its emphasis on microbial processes, the definition covers both key areas of interest: environmental biodegradability of polymers, and in vivo biodegradability of polymers in mammalian systems. The present discussion is limited to the environmental biodegradation of polymers.

Adopting a definition for practical purposes, particularly to delimit those polymers that are "environmentally biodegradable," is more complicated and several definitions have been proposed [2]. There is renewed interest in the use of such polymers in disposable packaging materials to ensure their degradation in post-consumer litter and waste streams. All organic materials must invariably biodegrade (despite the extremely slow kinetics in the case of most synthetic polymers) in the environment; however, to be of practical benefit a readily biodegradable polymer must break down due to biotic causes in a reasonable timescale. With no agreed benchmark available to indicate what such a "reasonable" rate of biodegradation might be, the use of natural biopolymers as standard biodegradable materials [3] is a common trend reported in the literature. Because of their rapid breakdown, regenerated cellulose or filter paper [4], wood pulp [5], and even whole leaves might be used as reference materials in biodegradation studies.

In general, biodegradation of polymers occurs as an extracellular process (because macromolecular dimensions do not permit their transport across cell membranes), catalyzed by enzymes. A number of such enzymes are known and are classified on the basis of the degradation reaction step they catalyze. Thus, hydrolases, esterases, isomerases (or transferases), oxido-reductases, hydrogenases, and ligases can increase the rates of respective reactions by 6–20 orders of magnitude even under ambient temperatures [6]. Enzymes that specifically catalyze the breakdown of naturally occurring polymers such as cellulose, lignin, chitin, and proteins are readily available in nature. For synthetic polymers, with a much shorter history of less than half a century of use, appropriate enzymes are more difficult to find in nature. Given the impressive diversity of microbiota, as yet unknown enzyme systems for synthetic polymers might very well exist. Exceptions to the rule of recalcitrance of synthetic polymers include aliphatic polyesters, polyethers, some polyamides, and poly(vinyl alcohol).

As most of the readily biodegradable polymers are water-insoluble, the degradation reaction must be heterogeneous, initially localized at the surface of the polymer. Close contact between the biota and polymer is generally a prerequisite to ensure the high concentration of enzymes to enable these reactions. With biopolymers, the general process involves both exo- and endo-enzymes. The former yields fragments from chain ends, while the latter causes random

main-chain scission. The fragments, such as cellobiose in the case of cellulose, might then be further biodegraded by specific enzymes.

A distinction needs to be made between true biodegradation and biologically mediated disintegration or volume reduction of polymers, which does not amount to biodegradation. The attack of polyethylene by insects [7,8] for instance, belongs to this latter category. In spite of the 'damage' suffered by the polymer, the predominant change is physical, and the indigestible polymer is merely reduced in particle size at the end of process. The blends of a biologically inert thermoplastic, such as polyethylene, and a readily biodegradable substance, such as starch, also belong to the same class of biodeteriorable materials. On biodegradation of surface starch, a thin film of the composite material disintegrates into small particulates without substantial chemical breakdown of the polymer.

A second class of biodegradable polymers of interest are those used in the human (or animal) body. These polymers include those used in artificial organs, other implants, and controlled release devices for delivery of pharmaceuticals. Being placed in contact with the tissue environment, they can potentially biodegrade. In products such as biodegradable sutures and bioerodible drug-delivery matrices, such breakdown in the body may be undesirable.

Experimental data reported on biodegradation of polymers are somewhat limited. However, from a consideration of the available data and the characteristics of the biodegradation process, several factors that affect the environmental biodegradability of polymers might be identified.

56.1.1 Molecular Weight

Long chain-like molecular geometry and high molecular weights do not necessarily preclude biodegradation. Both biopolymers (cellulose, chitin), as well as some synthetic polymers (i.e., polycaprolactone) are readily biodegradable. However, a general relationship does exist between the average molecular weight of polymers and their amenability to biodegradation: the shorter the chains, the higher the likelihood of biodegradation [9–11]. Not only does a lower degree of polymerization yield a higher concentration of chain end groups, but it also discourages the formation of crystalline domains that are generally difficult to biodegrade. High chain-end concentrations [12] promote exotype reactions, and noncrystalline regions are known to be preferentially biodegraded in synthetic polymers [13–16] as well as in the biopolymer lignocellulose [17].

Even with polyethylenes generally regarded as being bioinert, the lower molecular weight fractions biodegrade and yield carbon dioxide product at a measurable rate. Gel permeation chromatography (GPC) was recently used to demonstrate the biodegradability of polyethylene wax exposed to bacteria and fungi. The beta oxidation rates for the low-molecular weight polyethylene exposed to bacterial consortia were 36 times higher compared to that exposed to Aspergillus sp. isolated from soil [150]. Several researchers [151,152] reported the average molecular weight of polyethylenes exposed to biotic environments to slightly increase compared to those incubated in sterile media. The observation is likely a result of the lower molecular weight fraction of the sample with a higher concentration of chain ends being selectively biodegraded. (However, the alternative explanation of the formation of a surface biofilm that limits oxygen availability to the polymer has also been proposed [153].) Even with LDPE exposed to biotic environments (cultured compost microorganisms were used at 95 °C) it is the short chain branches on the chains that are preferentially biodegraded [154]. Observations on common plastics (LDPE, PVC, PS, and urea formaldehyde) subjected to long-term (32 years) soil-burial studies show only the LDPE films to be surface-degraded to any significant extent. The surface molecular weight of these samples decreased to almost 50% of that of the bulk [155,156].

Partially photodegraded polymers contain low-molecular weight fraction of degradation products and therefore biodegrade at a faster rate compared to the virgin material [157,158]. Similarly prethermal degradation of biodegradable polymers such as PHB, PHBV, and PCL copolymer also was reported to increase the rate of biodegradability under compost conditions [159]. The same was also reported for starch/LDPE blends [160]. Degradation of the polymer yields hydrophilic carboxylic acids, susceptible to easy biodegradation, as a major degradation product. These functional groups appear to be preferentially biodegraded under biotic exposure. Unlike with the thermo-oxidative degradation of LDPE where the concentration of carbonyl groups increase with exposure, biodegradation results in a decrease of these hydrophilic groups with the duration of exposure [161,162].

56.1.2 Structural Complexity

In most cases, the biodegradability implies the existence of a set of micro-organisms able to utilize the polymer substrate as a carbon and energy source. Since this has to be accomplished with minimum expenditure of energy by the organism, complex polymers requiring numerous enzyme-mediated steps for their breakdown represent a poor substrate [18]. Often, the required ensemble of enzymes is not available from a single species of micro-organism, and the substrate requires several different organisms to act in concert to effect biodegradation. Increased structural complexity of a substrate generally leads to recalcitrance in the environment. Persistence of soil humic acids, naturally occurring biopolymers in soil, are attributed to their structural complexity [19,20].

This assumes that biologically mediated breakdown of organic compounds always involves the use of substrate as a source of energy. Co-metabolism is an important exception in which the biodegradation does not yield any energy

for use by the organism contributing the enzyme. Nevertheless, co-metabolism is common in nature, and is a true biodegradation process to the extent that it depletes the substrate polymer.

56.1.3 Hydrophilicity

Water-soluble synthetic polymers such as poly(vinyl alcohol) [21], poly(acrylic acid) [6], and polyethers tend to be more biodegradable than water-insoluble polymers of comparable molecular weight. Increasing the hydrophilicity of a polymer by chemical modification also increases its biodegradability [22]. The functional groups that impart water-solubility may also contribute to ready biodegradability of these systems. From a microbiological standpoint, the presence of a dissolved substrate may induce the production of necessary enzymes within the micro-organisms.

56.2 ENVIRONMENTAL BIODEGRADABILITY OF BIOPOLYMERS

Unlike xenobiotic substrates, biopolymers such as cellulose have been in the eco-system for a very long time, allowing the evolution of efficient enzymatic pathways specific for the breakdown of these substrates. Common biopolymers therefore readily undergo biodegradation in a wide variety of environmental conditions ranging from aerobic compost heaps to anoxic deep-sea marine sediments.

56.2.1 Cellulose

The average degree of polymerization (DP) of cellulose depends upon the source; values of 153 300 for California cotton [23] and 2000–6000 for Valonia sp. [24], have been reported. Pulp and viscose (cellophane) are processed celluloses with drastically reduced DP ranging in the low thousands at best. The lower-DP polymer is generally more readily biodegraded. The common micro-organisms involved in cellulose biodegradation are summarized in Table 56.1. These include both bacteria and fungi; the deleterious effect of white-rot and brown-rot fungi on lignocellulose is well known.

Several enzymes act synergistically in the breakdown of cellulose in a series of hydrolysis reactions [25,26]. Endocellulases attacking the amorphous regions of the celluloses cause random chain scission. The exo-cellulases act at terminals of chains splitting off cellobiose units that, in turn, are hydrolyzed by β-glucosidase. Lignin component, often found associated with cellulose, also can biodegrade via oxidative pathways. Relevant enzymes (such as lignases, laccase, alcohol oxidase) have been reported [27,28].

Cellulose fillers [172,173] including some types of wood fibers [174] have been used as a filler with thermoplastics to obtain biodegradable materials with improved film quality. Crude cellulose in the form of surface-modified flax fibers reinforce biodegradable polyesters [175]. Particularly interesting are cellulose filled composites of biodegradable resins such as poly(propylene carbonate) filled with short lignocellulosic fibers. Cellulose being less hydrophilic compared to biodegradable additives such as starch, yields materials of good mechanical properties [176].

Cellulose is often found in close association with lignin fibers (hence is strictly lignocellulose) in mechanical pulps or flax fiber material. In these, the cellulose component is rapidly biodegradable in the environment while lignin biodegrades but at a much slower rate. However, lignin has also been used in plastic materials to impart some degree of biodegradability. Lignin grafted to PVAc, and PVA enhanced the biodegradability of these materials while that grafted to the readily biodegradable PLC decreased the materials overall its biodegradability [177]. The effect of compatibilizers on cellulose acetate – organoclay was recently reported [178].

56.2.2 Chitin and Chitosan

Chitin that occurs in the exoskeleton of invertebrates (such as mollusks and arthropods) is composed of N-acetyl-D-glucosamine residues linked by 1,4 β-linkages. A partially deacetylated chitin also occurs naturally as chitosan. Microbial species responsible for the breakdown of chitin and chitosan have not been comprehensively studied. Micro-organisms found in a variety of environments (for instance, in fresh water [29], marine sediment [30], garden soil [31], and even anaerobic environments [32]) are known to produce chitinases and/or chitosanases. Table 56.1 shows a listing of some reported species of bacteria and fungi that yield these enzymes and are therefore, able to biodegrade these polysaccharides.

56.2.3 Starch

A polysaccharide made of linear amylose chains and branched amylopectins, starch is well known to be readily biodegradable [33]. The α 1–4 linkages in both components are easily hydrolyzed by amylases while the α 1–6 links at branch points in amylopectin are attacked by glucosidases.

Biodegradable multiphase systems that include starch as one of the phases has been reviewed [163]. (Interestingly, proteins such as crosslinked furfural-soy protein concentrates have also been used in place of carbohydrate polymers for biodegradable polymers [164] or as biodegradable fillers in polyesters [165]. It is important to note that it is only the starch content of the composite that is biodegradable. The biodegradable systems typically include a pro-oxidant additive to facilitate rapid thermooxidative breakdown of the synthetic polymer [166]). To that extent, these systems display not only biodegradation of the starch but concurrent thermooxidative degradation of the synthetic polymer.

Systems where the synthetic polymer matrix is also biodegradable have been reported in recent literature. The morphology and interface properties [167] as well as the biodegradation [168] of starch with poly(lactic acid) was recently reported. A silica filled crosslinked starch/polyacrylamide composite showed superabsorbancy as well as enhanced biodegradability by sewage sludge inoculum as well as specific microorganisms (*Bacillus cereus* and *E. coli*), (note, however, that polyacrylamide is not an enhanced biodegradable polymer). Starch–poly (propylene carbonate) composites not only yielded a fully biodegradable composite material, but also a composite with improved the mechanical properties [169]. PVA–starch composites were processed into a foam with biodegradable as well as good mechanical properties [170]. PVA is biodegradable, but at a much slower rate compared to PCL or

TABLE 56.1. *Microbial biodegradation of cellulose and chitin.*

Substrate	Class	Micro-organism	Reference
Cellulose	Bacteria	*Cellvibro gilvus*	[53]
		Clostridium thermocellum	[54]
		Bacteroides succinogenus	[55]
		Ruminococcus albus	[56]
		Psudomonas fluorescence var cellulosa	[57]
		Sporocytophaga myxococcides	[58]
	Fungi	*Coriolus vesicolor* [W][a]	[59,60]
		Phanerochaete chrysosprium [W][a]	[61]
		Irpex lacteus [W][a]	[62]
		Schizophyllum commune [W][a]	[63]
		Fomes annosus [W][a]	[64]
		Stereum sanguinolentum [W][a]	[65]
		Peurotus ostreatus [W][a]	[66]
		Polyporus schweinitzii [B][a]	[67]
		Poria Placenta [B][a]	[68,69]
		Poria Vailantii [B][a]	[70]
		Coniophora cerebella [B][a]	[71]
		Tyromyces palustris	[71,72]
		Serpula lacrymans [B][a]	[73]
		Lentinus lepideus [B][a]	[74]
	Ascomycetes and fungi imperfecti	*Chaetomium globosum*	[75]
		Chaetomium thermophile	[76]
		Trichoderma viride	[77,78]
		Trichoderma reesei	[77,78]
		Trichoderma koningii	[77,78]
		Penicillium funiculosum	[79]
		Fusarium solani	[80]
		Aspergillus aculeatus	[81]
		Aspergillus niger	[82]
		Sporotrichum thermophile	[83]
		Myrothecium verrucaria	[84]
Chitin	Bacteria and fungi	*Myxobacteria spp.*	[85]
		Psudomonas spp.	
		Serratia spp.	[86,87]
		Bacillus spp. Pseudmonas spp.	[88]
		Flavobacterium spp.	
		Streptomyces antibioticus	[89]
		Streptomyces griseus	[90]
		Penicillium oxalicum	[91]
		Streptomyces erythaeus	[92]
		Trichoderma harzianum	[93]
		Streptomyces orientalis	[94]
		Aspergilus niger	
Chitosan		*Myxobacter*	[95]
		Streptomyces griseus	[96]
		Streptomyces spp.	[97]

[a][W] and [B] refer to white-rot and brown-rot fungi, after [98].

cellulose. Lactide fillers have also been successfully used in place of starch with a biodegradable polymer matrix (copolymers of 1,3,trimethylene carbonate) to obtain environmentally biodegradable materials [171].

56.2.4 Polyhydroxyalkanoates (Bacterial polyesters)

These polymers are produced as intracellular storage materials in a variety of bacteria grown under physiologically stressed conditions. Specific species, such as *Alcagenes eutrophus* (cultured under ammonium-limited growth conditions), and *Rhodobacter sphaeroides* (cultured under phosphate or sulfate-limited growth conditions) can yield as much as 80% dry weight of the polyester. The use of mixed organic carbon sources during bacterial fermentation allows the production of a variety of polymers and copolymers of this class. Poly-(hydroxybutyrate), PHB, and the random copolymer of poly(hydroxybutyrate-co-valerate), PHBV, have been the most studied of this class of biopolymers [34]. The structure of the 100% isotactic polymer is given below [6].

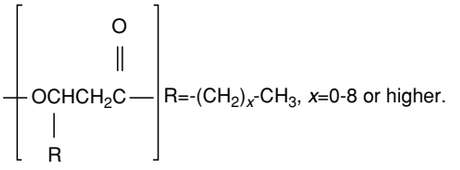

Thermal and mechanical properties of several of the copolymers have been reported [35,36]. Biodegradation of these polymers by bacterial esterases yield monomers, dimers and trimers split off from the hydroxyl-terminal of the polymer chain.

45.2.5 Other Filler Materials

A variety of fillers are used with biodegradable polymer materials to obtain the mechanical properties needed for specific applications. As reported in the literature these additives do not generally alter the biodegradability of the polymer matrix. The effect of the new nanosized filler materials in this regard, however, is interesting and has not been extensively studied. Because of their superior reinforcing characteristics [179] nanofillers such as montmorillonite (nanoclays) and hectile silicates are likely to be a popular additive and its impact on biodegradability needs to be studied. With silica fillers in a range of biodegradable polymers (layered nanocomposites), the general trend was toward increased biodegradability [180]. With nanoclays as well, the same trend was observed for both photo- and biodegradation [181].

56.3 PROBLEM OF ASSESSING BIODEGRADABILITY OF SYNTHETIC POLYMERS

Synthetic polymers generally biodegrade very slowly, but several exceptions exist. These exceptions undergo biodegradation in the environment at a measurable rate and are commonly referred to as "biodegradable plastics." Several experimental approaches to establishing the rates and extents of their biodegradation under specific exposure conditions are available. To quantify the rates of breakdown, it is important to define a criterion for assessment of polymer biodegradability.

With a hypothetical polymer, it is convenient to represent the biodegradation process by the following generalized sequence [1].

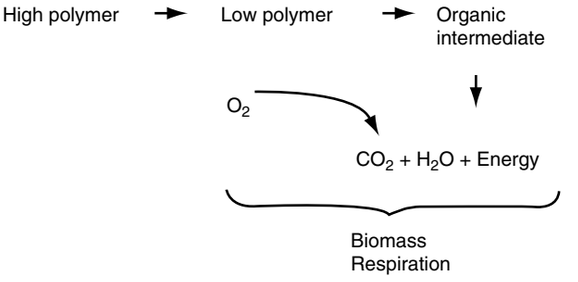

The sequence suggests that the criterion for assessment of biodegradation depends upon the particular definition of biodegradation adopted. For instance, the rate of depletion of the polymer substrate might be adopted as the approach; alternatively, the rate of carbon dioxide generation might be used in its place. Under identical conditions, the rates of biodegradation of the same substrate, obtained using these two approaches, will be quite different. The choices of tests available are listed in Table 56.2, along with references on their use to determine the environmental biodegradability of polymers (or organic substrates). Each approach focuses on a different stage of the biodegradation process [37]. Consequently, the results from different tests on the same substrate are not comparable. This is demonstrated in a comparison of the test data on aliphatic polyesters. Lenz [6] compared the data by Potts *et al*. [38] for surface colonization of polymers by micro-organisms (i.e., biomass yield) with data on weight loss in soil burial and on hydrolysis by fungal lipases, for the same polymers. As expected, the rankings of five polyesters in terms of their biodegradability, estimated using two different criteria, were quite different. Recent work by Yakabe *et al*. [39] showed that for PHBV, cellulosics and poly(caprolactone) substrates biodegradability as measured by the MITI standard test, and fresh sewage sludge exposure test, showed poor agreement. However, they noted the half-lifetimes for the substrates in sewage sludge exposure, and soil burial exposure to show a moderate degree of correlation.

TABLE 56.2. *Summary details for six biodegradability tests based on OECD guidelines.*

Test method (OECD)	[S]	Units	[I]	Units	Cells/l	Analysis	pH/T °C
Die-away (301 A)	10–40	mg DOC/l	<100	ml/l	10^7–10^8	Dissolved organic carbon	7.4/22
CO_2 Evolution (301 B)	10–20	mg/l	<100	ml/l	10^7–10^8	Carbon dioxide evolution	7.4/22
Respirometry (301 F)	100	mg/l	<100	ml/l	10^7–10^8	Oxygen consumption	7.4/22
Modified screening test (301 E)	10–40	mg DOC/l	0.5	ml/l	10^5	Dissolved organic carbon	7.4/22
Closed bottle (301 D)	2–10	mg/l	<5	ml/l	10^4–10^6	Dissolved oxygen	7.4/22
MITI (1) (301 C)	100	mg/l	30	mg/l[a]	10^7–10^8	Oxygen consumption	7.0/25

[a]mg of suspended solids per liter. DOC = dissolved organic carbon; [S] = substrate concentration; [I] = inoculum concentration. Based on [1, 39].

Biodegradability of a given polymer can, therefore, be discussed only in relation to the criterion adopted in its assessment and to the nature of microbial environment used for the purpose. Generalization of experimental data (particularly the description of a polymer as being ''biodegradable'' without qualification) can be misleading and contribute to confusion in the literature.

Several standard test protocols for measurement of polymer biodegradation are presently available. Organizations which have published such tests include the American Society for Testing and Materials (ASTM), Ministry of International Trade and Industry (MITI) (Japan) [40] and the Organization for Economic Cooperation and Development (OECD) [41]. They are, however, for the most part deficient to the extent that they have no control over the nature of microbial inoculum used, or the possible preadaptation of the mixed populations to specific substrates, and over the adequate control of particle size of the substrate. The relevance of these factors to laboratory assessment of the biodegradability of synthetic polymers has been recently discussed [1]. Most of these test methods have been derived from tests first used with detergents [42], and are not always well-suited for solid polymer substrates.

The test methods recently published by the ASTM relating to biodegradability of polymers are as follows.

D 5209-91 Standard Test Method for Determining the Aerobic Biodegradation of Plastic Materials in the Presence of Municipal Sewer Sludge.

D 5210-92 Standard Test Method for Determining the Anaerobic Biodegradation of Plastic Materials in the Presence of Municipal Sewer Sludge.

D 5271-92 Standard Test Method for Assessing Aerobic Biodegradation of Plastic Materials in an Activated Sludge - Waste Water System.

D 5338-93 Standard Test Method for Determining the Aerobic Biodegradation of Plastic Materials Under Controlled Composting Conditions.

D 5247-92 Standard Test Method for Determining the Aerobic Biodegradability of Degradable Plastics by Specific Micro-organisms.

G21-90 Standard Practice for Determining the Resistance of Synthetic Polymeric Materials to Fungi.

G22-76 Standard Practice for Determining the Resistance of Synthetic Polymeric Materials to Bacteria.

G29-30 Standard Practice for Determining the Resistance of Synthetic Polymeric Materials to Algae.

OECD, an international organization with 24 member countries, developed guidelines for establishing biodegradability through their Chemical Testing Program [41,43]. Their approach identifies three levels of biodegradability; ready biodegradability, inherent biodegradability, and simulation of environmental compartments. Of these, ready biodegradability or stringent tests that provide limited opportunity for biodegradation and acclimatization to occur are considered screening tests. Yakabe *et al*. [39] recently summarized the test parameters for the six tests used for the purpose. Basic features of the tests are shown in Table 56.2.

56.4 BIODEGRADABILITY OF SYNTHETIC POLYMERS

Results from biodegradation studies on numerous synthetic polymers, polymer blends, modified natural polymers and biopolymers have been reported. However, as pointed out earlier, biodegradability of a polymer is a function of several variables, including, but not limited to, the following.

Material characteristics: molecular weight, crystallinity, crosslink density, solubility, likelihood of yielding toxic biodegradation products;

Substrate form: film, molded specimen, powder, solubility in test medium, swelling in water;

Biodegradation conditions: inoculum type, pre-adaptation of organisms, use of single species versus mixed consortia, use of naturally-occurring consortia, use of nutrients or minerals in cultures, aeration levels;

Test parameters: concentration of substrate, [substrate]: [inoculum] ratio, test pH, test temperature, agitation, aeration rate; and

Measurements: Biochemical oxygen demand, substrate depletion, carbon dioxide generation, biomass estimate, properties of the polymer.

The importance of chain branching and crystallinity of polymer in controlling its biodegradability was already mentioned earlier in the chapter. Substrate geometry affects the surface area available for biotic interaction and is therefore an important factor in controlling biodegradability. During some stage or the other of the biodegradation process shape (specially film versus powder) of the substrate (PLLA, PCL, PBS, PBSA, and PP control) was shown to significantly affect rate of biodegradation [182]. The nature of the inocula is another critical factor in determining the rate of biodegradability. Industrial and municipal sewage inocula were found to be significantly different in this regard when used to biodegrade PCL and cellulose [183]. Test parameters such as temperature also influence the rate of the process and needs to be carefully controlled in biodegradation experiments. PCL and PHB incubated with soil compost inocula the biodegration rate was found to be higher at 46 °C compared to that at 24 °C [184].

The test method employed to assess biodegradation is a crucial consideration in establishing biodegradability, as different techniques measure different aspects of the degradation process. New test methods are being developed continuously and some of these are later incorporated into standards documents. For instance, Japanese researchers have used the weight gain of CO_2 sorbed in a column charged with sodalime as a modified method for evaluating biodegradability of materials [185]. Under the composting conditions used to demonstrate the method it was found to be a good screening test. Korean workers have reported the biodegradation of plastic-paper laminated or coated composites, by enzymes. Higher degradability compared to the polymer powder was observed for PCL, PLA, PHB, and PBS polymers [186]. A similar result, but using regenerated cellulose films in place of paper, has also been reported recently [187]. The limitations of each test method in quantifying the relevant aspect of the process needs to be taken into account in interpreting test data on polymer biodegradability.

The potential toxicity to soil biota from any products of biodegradation has also received attention in the literature. The presence of deteriorated plastic residue generally does not impair the growth of higher plants; this is an important consideration in using plastic mulch material in agriculture. In the case of water-soluble polymers such as PVA, however, the situation is less clear. Lee *et. al.* [188] found a significant reduction in the yield of red pepper and tomato cultivars when PVA was blended in with the soil at levels as low as 0.05%. In the cases of lactic acid polymers, however, the oligomers and degradation products were claimed to have a positive effect on plant growth [189].

Thus, biodegradability of a polymer can be discussed only in terms of alone characteristics. At the very least, it is necessary to specify the molecular weight of the polymer, composition in case of a copolymer or a blend, the origin of inoculum, and the criterion (and specific measurements) used to establish biodegradation. Composition of the biotic environment (in the case of laboratory tests, the inoculum) is a key factor in all biodegradation tests; however, there is no convenient way to adequately describe a consortium of micro-organisms in even semi-quantitative terms, for this purpose. Data in Table 56.3 attempt to summarize the recently reported results from various studies on biodegradation of polymers. Unfortunately, not all such reports provide the necessary information. The summarized data is limited to reported polymer biodegradation studies using live cultures or micro-organisms as opposed to those using extracted enzymes.

It is crucial to appreciate that biodegradability under a specific set of conditions as shown in Table 56.3 (particularly where only a single species of micro-organism is involved), does not necessarily imply biodegradability under a different set of conditions. Even when the study used a naturally occurring consortium, the results cannot always be readily extrapolated to natural environments. Even the mere isolation, or ''bottling,'' of a natural consortium is well known to affect its composition in a relatively short time [44,45].

Published data can rarely be used to compare the ''biodegradability'' of two materials, except in instances in which both materials were tested under identical conditions. Even in the latter instance, the ranking obtained is solely applicable to biodegradation under that particular test condition. The result cannot be extrapolated to field conditions, to other test conditions, or even to experiments carried out under identical conditions but using a different criterion for biodegradability.

56.5 CHEMICAL MODIFICATIONS TO ENHANCE BIODEGRADABILITY OF POLYMERS

High molecular weight polyethylene is virtually nonbiodegradable. Being a commodity thermoplastic widely used in disposable packaging and consequently a very visible component of urban litter, there is interest in rendering the material environmentally biodegradable.

Early attempts to address the problem included the use of biodegradable starch fillers in either polyethylenes,

TABLE 56.3. *Selected studies on biodegradation of polymeric materials.*

Substrate	Example	Method	Inoculum	Reference
Polyethylene/ starch blends	LDPE/EAA/Starch blends	Weight loss FTIR Tensile properties	Mixed culture	[99]
		CO_2 evolution	Soil culture	[100]
	LDPE or HDPE+starch 0–20%	Weight loss and FTIR	Compost culture	[101]
	LDPE+starch (67%, 52%, 29%)	Weight loss and FTIR	Soil culture (three types)	[48]
	LLDPE+starch (~6%)	Molecular weight	Soil culture, landfill soil culture, and activated sludge	[46]
		Elongation at break, and CO_2 evolution		
	LDPE+starch (0, 29, 52, 67%)	Weight loss and FTIR	Soil culture Marine sediment	[8]
	LDPE+starch (0, 3, 5.5, 6, 9%)	Starch analysis, elongation at break, and molecular weight	Soil culture, refuse culture, and anaerobic digester culture	[47]
	LDPE+starch (3.85, 5.77, 7.70%)	CO_2 radiotracer studies, chemiluminescence, calorimetry and molecular weight	*Verticillum lecanii* *Verticillum nigrescens*	[102]
	LDPE/starch blends	Tensile properties, SEM, spectroscopy	Soil microbes	[160]
Polyethers	Poly(propylene glycol) ($M_n = 2000$–4000)	HPLC Analysis	Soil-*Corynebacterium sp.*	[103]
		Optical density	*Alcaligenes denitrificans*	
	Poly(ethylene glycol) ($M_n = 600$–20000)	Biomass and analysis	*Sphingomonas parapegl-ytica*+ *Pseudomonas* (symbiotic)	[104][a]
	Poly(tetramethylene glycol) ($M_n = 200$ and 265)	Analysis	*Alcaligenes denitrificans and Xanthomonas maltophilia*	[105][a]
Poly(carboxylic acid)	Poly(acrylic acid salt)-co-(vinyl alcohol)-($M_n = 7300$–12000).	BOD measurements	Activated sludge	[106]
		Optical density and analysis	*Pseudomonas sp.* and *Trichoderma sp.*	
Acrylamide polymers	Crosslinked starch graftpolyacrylamide composite	SEM and CO_2 release	Sewage sludge *Bacillus cereus* and *E. coli*	[193]
Polyesters	Poly(ethylene adipate) (M_n) = 3000)	Biomass and analysis	*Penicillium sp.* (soil isolate)	[107]
	Polycaprolactone ($M_n = 25{,}000$)	Biomass and TOC		
	Polycaprolacton ($M_n = 2000$ and 7000, 19,000, and 35,000)	Molecular weight measurements	*Cryptococcus laurenti* *Acinetobacter calcoaceticus*	[108]
	Polycaprolactone ($M_w = 40{,}000$)	Visual and microscopy	Soil culture.	[109]
	Polycaprolactone, PCL. $M_n = 80{,}000$. Blends of PCL/LDPE (10%, 80% PCL)	Tensile properties, FTIR spectroscopy, and molecular weight	A mixed culture of: *Aspergillus niger* *Penicillium funiculosum* *Chaetomium globosum* *Gliocladium virens* *Aureobasidium pullulans*	[110]
	Polycaprolactone	CO_2 evolution	*Aspergillus flavus, soil*	[49]
	Copolymer (styrene and cyclic ketene acetal) ($M_n = 13{,}000$–$25{,}000$)	CO_2 evolution	*Aspergillus flavus, soil*	
	Polycaprolactone ($M_n = 4000$ and 37,000). Methoxy and hydroxy terminated polymer chains	CO_2 evolution, weight loss, and molecular weight	Compost inoculum Actinomycetes species isolated from compost	[111]

TABLE 56.3. *Continued.*

Substrate	Example	Method	Inoculum	Reference
	Polycaprolactone	Weight loss, tensile properties and mol. weight	Soil (20 sites) and water (2 marine, 1 fresh water)	[112]
	Polycaprolactone $M_n = 40{,}000$ and 70,000	Visual substrate loss (clear zone)	Soil culture	[113]
	Polycaprolactone $M_n \sim 25{,}000$	Weight loss	*Penicillium sp.*	[114]
Bacterial Polyester	Poly(3 hydroxybutyrate-co-3 hydroxyvalerate) blends with cellulose acetate (25, 50 and 75% CA)	Dynamic mechanical properties, NMR, and FTIR spectroscopy	Activated sludge	[115]
	Poly(3 hydroxy butyrate), PHB, and copolymers	Molecular weight Tensile Strength	Soil culture (several types) Compost culture	[116][a]
	PHB, and 3 hydroxy valeric acid, HV. (10% and 20% HV)	Weight loss	Freshwater/sea water	
	Poly(3 hydroxybutyrate-co-3 hydroxyvalerate) 7% HV, plasticized	Weight loss	Compost culture	[117]
	Poly(3 hydroxybutyrate-co-3 hydroxyvalerate) 20% HV	Visual substrate loss (clear zone) CO_2 evolution	Bacterial strains (pure culture)	[118]
	Poly(3 hydroxybutyrate-co-3 hydroxyvalerate) HV = 22% $M_w = 400{,}000$–$700{,}000$	BOD and weight loss	Activated sludge Soil culture	[39]
		Weight loss and microscopy	Soil culture and compost culture	[119]
	Poly(3 hydroxybutyrate-co-3 hydroxyvalerate) 12.5%, 8.4% HV	Visual substrate loss (clear zone)	Soil culture	[113]
	Poly(3 hydroxybutyrate), $M_w = 230{,}000$. Poly(3 hydroxyvalerate), PHA $M_w = 820\ 000$. Copolymer 11% HV $M_w = 150{,}000$	Visual substrate loss (clear zone)	Soil suspension culture	[120]
	Poly(3 hydroxybutyrate), $M_w = 220{,}000$. Crystalline samples	Microscopy and crystallinity	*Alcaligenes paradoxus* *Pseudomonas testosteroni* Soil culture isolate	[121]
	Poly(3 hydroxybutyrate) PHB $M_w = 539{,}000$ blended with cellulose acetate butyrate $M_w = 130{,}000$ 20, 40, 60, and 80% PHB	Weight loss, differential scanning calorimetry, and wide angle xray scattering	Activated sludge	[122]
	Poly(3 hydroxybutyrate-co-3 hydroxyvalerate) $M_w = 330{,}000$ 26.5% HV	Tensile properties and molecular weight	Activated sludge	[123]
	Blends of PHBV and PHEMA	CO_2 evolution, mass loss	Penicillium funiculosum and other fungi	[194]
Polyurethane	Polyether-urethane	FTIR or UV spectroscopy	Aspergillus niger and Cladosporium herbarium	[124]
	Polyester-urethane poly-D, L-lactic acid polyurethane	FTIR spectroscopy	Soil culture	[125]
		Weight loss and biochemical oxygen demand	Mixed fungal spore inoculum	[126]
	Polyester-urethane ($M_n = \sim 40{,}000$)	Molecular weight measurements	*Aspergillus fumigatus* *Frusarium solanii* *Cryptococcus laurenti*	[127,128]
Polyethylenes	(Ethylene-carbon monoxide) copolymer	CO_2 radiotracer studies	Soil culture and sewage sludge	[129]

TABLE 56.3. *Continued.*

Substrate	Example	Method	Inoculum	Reference
	LDPE	CO_2 radiotracer studies	Soil culture	[130]
	HDPE ($M_w = 300{,}000$)	CO_2 radiotracer studies	Soil, mixed fungal culture *Fusarium redolens*	[131,132]
	LDPE ($M_w = 18{,}000$)	CO_2 radiotracer studies	*Fusarium redolens*	[133]
	HDPE and LDPE 1.5 and 2 mils.	Biomass	Mixed fungal inoculum as per ASTM G21, with *Aspergillus versicolor*	[134]
	Photo-degraded (partly cross-linked) $M_n = 10{,}980$ (undegraded)		*Aspergillus flavus*	
	Polyethylene LDPE and HDPE with and without prooxidant	CO_2, wt. loss, tensile strength, and IR spectroscopy	Municipal solid waste compost	[195]
	LDPE and PP	Tensile properties, turbidity, and BOD changes	*Pseudomonas stutzeri*	[196]
Nonionic Ethoxylates Polyalcohols	Poly(vinyl alcohol) and PVA	CO_2 radiotracer studies	Activated sludge	[135]
		Weight loss, tensile props, and molecular weight	Soil (20 sites) and water (2 marine, 1 fresh water)	[112]
	Block copolymer of PVA and 1,1 dicarboxylated malonate copolymer. $M_n = 9000$–$24{,}000$ VA block content 8–72%	Biochemical oxygen demand, molecular weight, CO_2 evolution, organic carbon analysis	River water culture isolates (aerobic) River sediment or anaerobic activated sludge (anaerobic)	[136]
Cellulose	Cellophane (regenerated cellulose)	Tensile properties and water vapor permeability	Soil culture isolate	[137]
	Cellophane	Crystallinity	Soil culture isolate	[138]
	Cellophane	Weight loss and CO_2 evolution	*Aspergillus niger* *Trichoderma viridi* *Pseudomonas fluorescens* *Bacillus subtilis*	[4]
	Lignocellulose (plant material from several species)	CO_2 and CH_4 radiotracer studies	Soil sulture (swamp soil) for anaerobic species	[139]
	Cellulose acetate. DS = 1.7 and 2.5	Visual, weight loss, and CO_2 evolution	Compost inoculum 1%	[140,141]
	Cellulose acetates with DS = 1.74, 1.86, 2.06, 2.21, 2.52, and 2.97	Weight loss and changes in molecular weight	Simulated compost	[142]
	Cellulose acetate. DS = 1.6, 1.7, 1.85, and 2.5	Analysis for DS, CO_2 radiotracer studies, and molecular weight	Activated sludge	[143]
	Cellulose fabric	XRD, microscopy	Soil microbes Sewage sludge microbes	[178]
	Cellulose acetates	Weight loss and mechanical properties	Soil microorganism	[197]
	Chemically modified flax fiber	CO_2 evolution, weight loss	Soil microorganisms *Cellvibrio fibrovorans*	[198]
Polyuronides	Partially dicarboxylated pectic acid $M_n = 11{,}900$ 67% carboxylated	Biological oxygen demand	Activated sludge	[144]
Polybutadiene	Cis 1,4 polybutadiene $M_n = 650$ (liquid)	Molecular weight measurements and Biomass	*Acenitobacter spp*	[145]
Polystyrene	Styrene oligomer $M_n \sim 400$ (liquid)	Molecular weight measurements and Biomass	*Alcaligens spp*	[146]
Polyisoprene	$M_n = 990$, 1500, 2500 (liquid)	Molecular weight measurements and Biomass	Soil culture isolates	[147]
Ethylene Copolymer	EVA copolymers and poly (vinyl acetate)	Weight loss	Activated sludge	[148]
	EVA 40/60 copolymer $M_w = 70{,}000$ EVA: starch = 1:1	Weight loss and FTIR	Soil culture and activated sludge	[149]

polyethylene-containing blends, or copolymers of ethylene. Although several technologies that could blend from about 6%–60% of starch into an extrusion-blown thin film were developed, their biodeteriorability characteristics fell short of expectations. In low-starch formulations, limited accessibility of the starch granules by microbial flora restricted biodegradation, limiting it to only about 10% of the available starch [8,46,47]. In high-starch formulations, the starch domains were sufficiently interconnected to allow a more complete degradation of the starch, but such films often exhibited poor mechanical properties. Adequate connectivity between starch domains to allow biodegradation is expected only at high levels of the additive, around 30 weight percent of starch in the blend [48]. At low starch levels below the percolation threshold only the surface starch can be reasonably be expected to degrade. LDPE with 29 wt% starch, for instance, showed degradation of only about 25% of the starch that was in the surface layers [190]. In starch polyethylene composite materials it is only the starch that biodegrades [191] the same is true in the case of PP [192]. The biodegradation of the starch itself cannot of course, be expected to lead to any significant biodegradation of the polymer matrix.

Copolymerization of ethylene (or other vinyl monomers such as styrene) with a vinyl monomer that undergoes ring-opening to yield a main-chain aliphatic ester group has been reported. For instance, 1,3 dioxepane can be used as a comonomer with styrene, or a ketene acetal might be used with styrene. This approach was shown to increase the biodegradability of polyethylene [49]. The lower molecular weight polyethylenes generated during biodegradation are more likely to undergo faster biodegradation compared to virgin polyethylene.

Biodegradable polymer sequences such as polysaccharides can be block copolymerized with synthetic polymers to obtain a partially biodegradable polymer material. Using a preformed macromolecular block, a ring-opening polymerization of *N*-carboxy anhydride was used to prepare an amylose-poly(α-benzyl-*L*-glutamate) block copolymer. Alternatively, a segmented block copolymer can be made by reacting low molecular weight amylose or cellulose blocks with terminal hydroxy groups with a synthetic prepolymer (such as a polyether) with reactive end groups using an appropriate diisocyanate. Gilbert *et al*. used a five step reaction sequence to produce several such block copolymers [50–52].

56.6 CONCLUSIONS

While naturally occurring polymers are readily biodegradable in the environment, most synthetic high polymers biodegrade only very slowly under comparable exposure conditions. There are, however, exceptions to this observation, and several classes of synthetic polymers that undergo ready environmental biodegradation are known. The ease of biodegradability of these polymers depend on their structural, macromolecular, and morphological characteristics.

Assessment of biodegradability is a key consideration in the development of biodegradable polymers. No strict definitions exist of what constitutes an appropriate biotic environment to carry out such testing and of what criterion is best suited to establish biodegradability of a polymer in the laboratory. The test results are sensitive to a variety of factors, particularly the consortia of micro-organisms used. It is, therefore, often difficult to appreciate the full significance of the reported data and to understand how different test results relate to each other. As more detailed reports of biodegradation assessments are reported, as seen in recent publications, some of these uncertainties and inconsistencies in the reported biodegradability of polymers will be removed.

REFERENCES

1. A. L. Andrady, J. Macromol. Sci. Rev. Macromol. Chem. Phys. **C34**, 25 (1994).
2. R. M. Ottenbrite and A. C. Albertsson, in *Biodegradable Polymers and Plastics*, edited by M. Vert, J. Feijen, A. Albertsson, *et al*. (Royal Soc. Chemistry, Cambridge, England, 1992) p. 73.
3. A. L. Andrady, ASTM Standardization News, p. 46, Oct. 1988.
4. V. Coma, Y. Couturier, B. Pascat, *et al*. in *Biodegradable Polymers and Plastics*, edited by M. Vert, J. Feijen, A. Albertsson, G. Scott, and E. Chellini (Royal Society of Chemistry, Cambridge, England, 1992), p. 242.
5. A. L. Andrady, V. R. Parthasarathy, and Ye Song, Tappi **75**, April, (1992).
6. R. W. Lenz, Adv. in Polym. Sci. **107**, 28 (1993).
7. R. A. Connolly, in *Biodeterioration of Materials*, edited by H. Walters and E. H. Huech-van der Plas (Applied Science Publishers, London, 1972), p. 168.
8. R. P. Wool, J. S. Peanasky, J. M. Long, *et al*. in *Degradable Materials, Perspectives, Issues, and Opportunities*, edited by S. A. Barenberg, J. L. Brash, R. Narayan, *et al*. (CRC Press, Boca Raton, FL 1990), p. 515.
9. Y. Toikawa and T. Suzuki, Agric. Biol. Chem. **42**, 1071 (1978).
10. R. D. Fields, F. Rodriguez, and R. K. Finn, J. Appl. Polym. Sci. **18**, 3571 (1974).
11. R. D. Fields and F. Rodriguez, in *Proceedings of the Third International Biodegradation Symposium*, edited by J. M. Sharpley and A. M. Kaplan (Applied Science, Barking, England, 1976), p. 775.
12. E. Kuhlwein and F. Demmer, Kunstoffe **57**, 183 (1967).
13. L. Kravetz, in *Agricultural and Synthetic Polymers. Biodegradability and Utilization*, Vol. 433, edited by J. E. Glass and G. Swift (ACS Symposium Series, Washington, DC, 1990), p. 96.
14. W. J. Cook, J. A. Cameron, J. T. Bell, *et al*. J. Polym. Sci., Polym. Lett. Ed. **19**, 159 (1981).
15. Y. Doi, Y. Kumagai, N. Tanahashi, *et al*. in *Biodegradable Polymers and Plastics*, edited by M. Vert, J. Feijen, A. Albertsson, *et al*. (Royal Society of Chemistry, Cambridge, England, 1992), p. 139.
16. P. Jarrett, C. V. Benedict, J. P. Bell, J. A. Cameron, and S. J. Huang, in *Polmers as Biomaterials*, edited by S. W. Shalaby, A. S. Hoffmann, B. D. Ratner, and T. A. Hobart (Plenum Publishers, New York, 1983), p. 3.
17. K. K. Y. Wong, K. F. Deverell, K. L. Mackie, *et al*., Biotechnol Bioeng. **24**, 447 (1988).
18. R. L. Tate, in *Soil Organic Matter—Biological and Ecological Effects* (John Wiley and Sons, New York, 1987), p. 158.
19. J. P. G. Ballesta and M. Alexander, J. Bacteriology **106**, 938 (1971).

20. R. J. Swaby and J. N. Ladd, in *The Use of Isotopes in Soil Organic Matter Studies*, edited by R. A. Silow (Pergamon Press, Oxford, England, 1966), p. 153.
21. M. Shimao and N. Kato, in *International Symposium on Biodegradable Polymers*, Abstracts (Biodegradable Plastics Society, Tokyo, Japan, 1990), p. 80.
22. K. W. March, C. R. Widevuur, W. L. Sederel, *et al*., Biomed. Mater. Res. **11**, 405 (1977).
23. D. A. I. Goring and T. E. Timell, Tappi **45**, 454, (1969).
24. M. Marx-Figini, Biochim. Biophys. Acta. **177**, 27 (1969).
25. G. Halliwell and M. Griffin, Biochem. J. **128**, 1183 (1973).
26. L. E. R. Berghem and L. G. Petterson, Eur. J. Biochem. **37**, 21 (1973).
27. M. Tien and T. K. Kirk, Science **221**, 661 (1983).
28. M. Shimada and T. Higuchi, in *Wood and Cellulosic Chemistry*, D. N.-S. Hon and N. Shiraishi (Marcel Dekker, Inc., New York, 1992), p. 557.
29. L. G. Willoughby, Hydrobiologica **34**, 465 (1969).
30. H. Seki and N. Taga, J. Oceanog. Soc. Japan **19**, 27 (1963a).
31. N. Okafor, J. Gen. Microbiol. **44**, 311 (1966).
32. J. N. Boyer and R. S. Wolfe, Biological Bull. **165.N2**, 505, (1983).
33. J. J. Marshall, editor *Mechanism of Saccharide Polymerization and Depolymerization* (Academic Press, New York, 1980), p. 55.
34. Y. Doi, in *Microbial Polyesters* (VCH Publisher, 1990).
35. Zeneca, in *Biopol, Natures Plastic: Properties and Processing* (Zeneca, Billingham, United Kingdom, 1993).
36. A. Schirmer, D. Jendrossek, and H. G Schlegel, Appl. Env. Microbiol. **59**, 1222 (1993).
37. P. Gerike and W. K. Fischer, Ecotoxicol. Environ. Safety **3**, 159 (1979).
38. J. E. Potts, in *Encyclopedia of Chemical Technology*, 2nd edition. Suool. Vol. (Wiley Interscience, New York, 1984), p. 626.
39. Y. Yakabe and M. Kitano, in *Biodegradable Plastics and Polymers*, edited by Y. Doi and K. Fukuda (Elsevier Science, 1994), p. 331.
40. Ministry of Trade and Industry, Japan. *The Biodegradability and Bioaccumulation of New and Existing Chemical Substances*, 1983.
41. *OECD Guidelines for Testing Chemicals* (Organization of Economic Corporation and Development, Paris, 1981).
42. Soap and Detergent Association, J. Am. Oil Chem. Soc. **42**, 3 (1965).
43. *OECD Expert Group, Determination of the Biodegradability of Anionic Synthetic Surface Active Agents* (Organization for Economic Cooperation and Development, Paris, 1971).
44. R. T. Wright, A. W. Bourquin, and P. H. Pritchards, editors *Microbial Degradation of Pollutants in the Marine Environment* (USEPA, Gulf Breeze, FL, 1979), p. 119.
45. L. H. Stevenson, Microbiol. Ecol. **4**, 127 (1978).
46. R. G. Austin, in *Degradable Materials: Perspectives, Issues and Opportunities*, edited by S. A. Barenberg, J. L. Brash, R. Narayan, and A. E. Redpath (CRC Press, Boca Ration, FL, 1990), p. 237.
47. G. Iannotti, N. Fair, M. Tempesta, *et al.* in *Degradable Materials; Perspectives, Issues and Opportunities*, edited by S. A. Barenberg, J. L. Brash, R. Narayan, *et al*. (CRC Press, Boca Raton, FL, 1990), p. 425.
48. S. M. Goheen and R. P. Wool, J. Appl. Polym. Sci. **42**, 2691–2701 (1991).
49. W. J. Bailey, V. Kuruganti, and J. S. Angle, in *Agricultural and Synthetic Polymers. Biodegradability and Utilization*, vol. 433, edited by J. E. Glass and G. Swift (ACS Symposium Series, Washington, DC, 1990), p. 149.
50. K.-S. Lee and R. D. Gilbert, Carbohydr. Res. **88**, 162 (1981).
51. M. M. Lynn, V. T. Stannett, and R. D. Gilbert, J. Polym. Sci., Polym. Chem. Ed. **18**, 1967 (1980).
52. S. L. Kim, V. T. Stannett, and R. D. Gilbert, J. Macromol. Sci. **7**, 101 (1979).
53. K. W. King and M. I. Vessal, Adv. Chem. Ser. **95**, 7 (1969).
54. T. K. Ng, A. ben-Bessat, and J. G. Zeikus, Appl. Environ. Microbiol. **41**, 1337 (1981).
55. D. Groleau and C. W. Forsberg, Can. J. Microbiol. **27**, 517 (1981).
56. K. Omiya, K. Nokura, and S. Shimizu, J. Ferment. Technol. **61**, 25 (1983).
57. K. Yamane, H. Suzuki, and K. Nisizawa, J. Biochem. **67**, 19 (1970).
58. K. Osmundsvag and J. Goksor, Eur. J. Biochem. **57**, 405 (1975).
59. D. S. Chahal and W. D. Gray, in *Biodeterioration of Materials*, edited by A. H. Walters and J. J. Elphick (Elsevier, New York, 1968), p. 584.
60. M. P. Levi and E. B. Cowling, in *Biodeterioration of Materials*, edited by A. H. Walters and J. J. Elphick (Elsevier, New York, 1968), p. 575.
61. M. Streamer, K. E. Eriksson, and B. Pettersson, Eur. J. Biochem. **51**, 607 (1975).
62. T. Kanda, K. Wakabayashi, and K. Nisizawa, J. Biochem. **79**, 977 (1976).
63. M. Paice, M. Desrochers, D. Roh, *et al*. Biotechnology **2**, 535 (1984).
64. A. Hutterman and A. Noelle, Holzforsch. **36**, 283 (1982).
65. B. Bucht and K. E. Eriksson, Arch. Biochem. Biophys. **129**, 416 (1969).
66. T. Hiroi, Mokuzai Gakkaishi **27**, 684 (1981).
67. G. Keilich, P. J. Bailey, E. G. Afting, *et al*., Biochim. Biophys. Acta. **185**, 392 (1970).
68. E. B. Cowling and W. Brown, Adv. Chem. Ser. **95**, 152 (1969).
69. T. L. Highley, Wood and Fiber **5**, 50 (1973).
70. B. C. Sison, W. J. Schubert, and F. F. Nord, Arch. Biochem. Biophys. **68**, 502 (1957).
71. N. J. King, in *Biodeterioration of Materials*, edited by A. H. Walters and J. J. Elphick (Elsevier, NY, 1968), p. 558.
72. M. Ishihara and K. Shimizu, Mokuzai Gakkaishi **30**, 79 (1984).
73. S. Doi, Mokuzai Gakkaishi **31**, 843 (1985).
74. H. Shimazono, Arch. Biochem. Biophys. **83**, 206 (1959).
75. G. Keilich, P. Bailey, and W. Liese, Wood Sci. Technol. **4**, 273 (1973).
76. J. Eriksen and J. Goksor, Eur. J. Biochem. **77**, 445 (1977).
77. T. M. Wood and S. I. McCrae, Adv. Chem. Ser. **181**, 181 (1979).
78. R. D. Brown, Jr. and L. Jurasek, Adv. Chem. Ser. **181**, 399 (1979).
79. T. M. Wood, S. I. McCrae, and C. C. MacFarlane, Biochem. J. **198**, 51 (1980).
80. T. M. Wood and S. I. McCrae, Carbohydrate Res. **57**, 117 (1977).
81. S. Murao and R. Sakamoto, Agric. Biol. Chem. **43**, 1791 (1979).
82. A. Ikeda, T. Yamamoto, and M. Funatsu, Agric. Biol. Chem. **37**, 1169 (1973).
83. M. R. Coudray, G. Canevascini, and H. Meier, Biochem. J. **203**, 277 (1982).
84. D. R. Whitaker, Arch. Biochem. Biophys. **43**, 253 (1953).
85. C. E. Warnes and C. I. Randles, Ohio J. Sci. **77**, 224 (1983).
86. N. G. Aumen, Microb. Ecol. **6**, 317, (1981).
87. E. Young, R. L. Bell, and P. A. Carroad, Biotechnol. and Bioeng. **27**, 769 (1985).
88. M. Srikantiah and K. C. Mohankumar, Indian J. Microbiol. **20**, 216 (1981).
89. C. Jeuniaux, J. C. Bussers, M. F. Voss-Foucart, and M. Poulicek, in *Chitin in Nature and Technology* edited by R. A. Muzarelli, C. Jeuniaux, and G. W. Gooday (Plenum Press, New York, 1986), p. 516.
90. R. A. Smucker, in *Chitin in Nature and Technology*, edited by R. A. Muzarelli, C. Jeuniaux and G. W. Gooday (Plenum Press, New York, 1986), p. 254.
91. J. Rodriguez, M. I. Perez-Leblic, and F. Laborda, in *Chitin in Nature and Technology*, edited by R. A. Muzarelli, C. Jeuniaux, and G. W. Gooday (Plenum Press, New York, 1986), p. 102.
92. S. Hara, Y. Yamamura, Y. Fuji, *et al*., in *Proc. 2nd Int. Conf. on Chitin and Chitosan*, edited by S. Hirano and S. Tokura, July 12–14, 1982, Sapporo, Japan. The Japanese Soc. of Chitin and Chitosan, p. 125.
93. I. Chet, E. Cohen and I. Elster, in *Chitin in Nature and Technology*, edited by R. A. Muzarelli, C. Jeuniaux, and G. W. Gooday (Plenum Press, New York, 1986), p. 237.
94. A. Ohtakara, H. Ogata, Y. Taketomi, and M. Mitsutomi, in *Chitin, Chitosan, and Related Enzymes*, edited by J. P. Zikakis (Academic Press, Orlando, 1984), p. 147.
95. A. Hedges and R. S. Wolf, J. Bacteriology **120–2**, 844 (1974).
96. A. Ohtakara, H. Ogata, Y. Taketomi, *et al*. in *Chitin, Chitosan and Related Enzymes*, edited by J. P. Zikakis (Academic Press, Orlando, 1984), p. 147.
97. J. S. Price and R. Storck, J. Bacteriology **124–3**, 1574 (1975).
98. M. Shimada and M. Takahashi, in *Wood and Cellulosic Chemistry*, edited by D. N.-S. Hon and N. Shiraishi (Marcel Dekker, Inc., New York, 1992), p. 625.
99. J. M. Gould, S. H. Gordon, L. B. Dexter, *et al*. in *Agricultural and Synthetic Polymers Biodegradability and Utilization*, vol. 433, edited by J. E. Glass and G. Swift (ACS Symposium Series, Washington, DC, 1990), p. 65.

100. M. A. Cole, in *Agricultural and Synthetic Polymers. Biodegradability and Utilization*, edited by J. E. Glass and G. Swift (ACS Symposium Series 433. American Chemical Society, Washington DC, 1990), p. 76.
101. A. Corti, G. Vallini, A. Pera, *et al*. in *Biodegradable Polymers and Plastics*, edited by M. Vert, J. Feijen, A. Albertsson, *et al*. (Royal Soc. Chemistry, Cambridge, England, 1992), p. 245.
102. A. C. Albertsson, C. Barnstedt, and S. Karlsson, J. Environ. Polym. Deg. **1**, 241 (1993).
103. F. Kawai, in *Agricultural and Synthetic Polymers. Biodegradability and Utilization*, vol. 433, edited by J. E. Glass and G. Swift (ACS Symposium Series, 1989), p. 110.
104. F. Kawai and H. Yamanaka, Arch. Microbiol. **146**, 125 (1986).
105. F. Kawai, Japanese patent 208289 (1987a).
106. S. Matsumara, S. Maeda, J. Takahashi, *et al*., Kobunshi Ronbunshu, **45**, 317 (1988).
107. Y. Toikawa, T. Ando, T. Suzuki, *et al*., in *Agricultural and Synthetic Polymers. Biodegradability and Utilization*, vol. 433, edited by J. E. Glass and G. Swift (ACS Symposium Series, Washington, DC, 1989), p. 136.
108. C. V. Benedict, W. J. Cook, P. Jarrett, *et al*., J. Appl. Polym. Sci. **28**, 327 (1983).
109. M. Kimura, K. Toyota, M. Iwatsuki, *et al*., in *Biodegradable Plastics and Polymers*, edited by Y. Doi and K. Fukuda (Elsevier Science, New York, 1994), p. 92, 237.
110. L. Tilstra and D. Johnsonbaugh, J. Environ. Polym. Deg. **1**, 257 (1993).
111. F. Lefebvre, A. Daro, and C. David, Macromol. Sci., Pure Appl. Chem. **A32**, 867 (1995).
112. H. Sawada, in *Biodegradable Plastics and Polymers*, edited by Y. Doi and K. Fukuda (Elsevier Science, New York, 1994), p. 298.
113. M. Tsuji and Y. Omoda, in *Biodegradable Plastics and Polymers*, edited by Y. Doi and K. Fukuda (Elsevier Science, New York, 1994), p. 345; Engl. **31**, 1200 (1992).
114. Y. Toikawa, T. Ando, T. Suzuki, and K. Takeda, in *Agricultural and Synthetic Polymers. Biodegradability and Utilization*, Vol. 433, edited by J. E. Glass and G. Swift (ACS Symposium Series, Washington, DC, 1989), p. 136.
115. D. F. Gilmore, R. C. Fuller, B. Schneider, *et al*., J. Environ. Polym. Deg. **2**, 49 (1994).
116. J. Mergaert, A. Wouters, J. Swings, *et al*., in *Biodegradable Polymers and Plastics*, edited by M. Vert, J. Feijen, A. Albertsson *et al*. (Royal Soc. Chemistry, Cambridge, England, 1992), p. 267.
117. M. Gada, R. A. Gross, and S. P. McCarthy, *Biodegradable Plastics and Polymers*, edited by Y. Doi and K. Fukuda (Elsevier Science, New York, 1994), p. 177; C. Bastioli, V. Bellotti, M. Camia, Del Giudice, and A. Rallis, *ibid*., p. 204.
118. R. J. Muller, J. Augusta, T. Walter, *et al*. in *Biodegradable Polymers and Plastics*, edited by M. Vert, J. Feijen, A. Albertsson (Royal Soc. Chemistry, Cambridge, England, 1992), p. 149.
119. H. Eya, N. Iwaki, and Y. Otsuji, in *Biodegradable Plastics and Polymers*, edited by Y. Doi and K. Fukuda (Elsevier Science, New York, 1994), p. 337.
120. D. Jendrossek, I. Knoke, R. B. Habibian, *et al*., J. Environ. Polym. Deg. **1**, 53 (1993).
121. H. Nishida and Y. Tokiwa, J. Environ. Polym. Deg. **1**, 65 (1993).
122. G. Tomasi and M. Scandola, J. Macromol. Sci., Pure Appl. Chem. **A32**, 671 (1995).
123. D. F. Gilmore, S. Antoun, R. W. Lenz, *et al*., J. Environ. Polym. Deg. **1**, 269 (1993).
124. Z. Fillip, Europ. J. Appl. Microbiol. Biotechnol. **7**, 277 (1979).
125. Z. Fillip, Europ. J. Appl. Microbiol. Biotechnol. **5**, 225 (1978).
126. S. Owen, M. Masaoka, R. Kawamura, *et al*., J. Macromol. Sci., Pure Appl. Chem. **A32**, 843 (1995).
127. S. J. Huang, M. S. Roby, C. A. Macri, *et al*. in *Biodegradable Polymers and Plastics*, edited by M. Vert, J. Feijen, A. Albertsson, *et al*. (Royal Soc. Chemistry, Cambridge, England, 1992), p. 149.
128. S. J. Huang, C. Marci, M. Roby, *et al*., ACS Symp. Ser. **172**, 471 (1981).
129. J. E. Guillet, Adv. Chem. Ser. **169**, 1 (1978).
130. N. B. Nykvist, in *Proc. of Degradability of Polymers and Plastics Conference* (Inst. Electrical Engineering, London, England, 1973), p. 18.
131. A. C. Albertsson, Z. G. Banhidi, and L. L. Beyer-Ericcsson, J. Appl. Polym. Sci. **22**, 3434 (1978).
132. A. C. Albertsson and Z. G. Banhidi, J. Appl. Polym. Sci. **25**, 1655 (1980).
133. A. C. Albertsson and S. Karlsson, J. Appl. Polym. Sci. **35**, 1289 (1988).
134. J. H. Cornell, A. M. Kaplan, and M. R. Rogers, J. Appl. Polym. Sci. **29**, 2581 (1984).
135. L. Kravetz, in *Agricultural and Synthetic Polymers. Biodegradability and Utilization*, vol. 433, edited by J. E. Glass and G. Swift (ACS Symposium Series, Washington, DC, 1989), p. 96.
136. S. Matsumara and T. Tanaka, J. Environ. Polym. Deg. **2**, 89 (1994).
137. P. Engler and S. H. Carr, J. Polym. Sci., Polym. Phys. Ed. **11**, 313 (1973).
138. S. A. Bradley, S. H. Engler, and S. H. Carr, *Polymeric Materials for Unusual Service Conditions*, edited by M. A. Golub and J. A. Parker (Wiley, New York, 1973), p. 269.
139. R. Benner, A. E. Macubbin, and R. E. Hodson, Appl. Envir. Microbiol. **47**, 998 (1984).
140. J. Gu, D. Eberiel, S. P. McCarthy, and R. A. Gross, J. Environ. Polym. Deg. **1**, 281 (1993).
141. R. A. Gross, J. Gu, D. Eberiel, and S. McCarthy, J. Macromol. Sci., Pure Appl. Chem. A **32**, 613 (1995).
142. C. M. Buchanan, D. Dorschel, R. M. Gardner, R. J. Komarek, and A. W. White, J. Macromol. Sci. Pure Appl. Chem. A **32**, 683 (1995).
143. C. M. Buchanan, R. M. Gardner, and R. J. Komarek, J. Appl. Polym. Sci. **47**, 1709 (1993).
144. S. Matsumara, K. Amaya, and S. Yoshikawa, J. Environ. Polym. Deg. **1**, 23 (1993).
145. A. Tsuchii, T. Suzuki, and Y. Takahara, Agri. Biol. Chem. **42**, 1217 (1978).
146. A. Tsuchii, T. Suzuki, and Y. Takahara, Agri. Biol. Chem. **41**, 2417 (1977).
147. A. Tsuchii, T. Suzuki, and Y. Takahara, Agri. Biol. Chem. **43**, 2441 (1979).
148. R. T. Darby and A. M. Kaplan, Appl. Microbiol. **6**, 900 (1968).
149. C. Bastioli, V. Bellotti, M. Camia, L. Del'Giudice, and A. Rallis, in *Biodegradable Plastics and Polymers*, edited by Y. Dio and K. Fukuda (Elsevier Science, New York, 1994), p. 201.
150 F. Kawai, M. Watanabe, Polymer Degradation and Stability **86,** 105–114 (2003).
151 A. L. Pometto, K. E. Johnson, M. Kim, J. Environ. Polym. Degrad. **1,** 213 (1993)
152 B. Erlandsson, A.-C. Albertsson. *Acta Polym*. **49,** 363 (1998).
153 A. L. Pometto, K. E. Johnson, J. Environ. Polym. Degrad. **1,** 213 (1993).
154 M. Hakkarainen, A. Albertsson, Adv. Polym. Sci., **169**(177) (2004).
155 Y. Otake, T. Kobayashi, J. Appld. Polym. Sci., **56,** 1789 (1995).
156 Y. Otake, T. Kobayashi, J. Appld. Polym. Sci., **70,** 1643 (1998).
157 A.-C. Albertsson, B. Erlandsson, M. Hakkarainen, S. Karlsson, J. Environ. Polym. Degrad. **6,** 187 (1998).
158 J. H. Cornell, A. M. Kaplan, J. Appl. Polym. Sci., **29,** 2581 (1984).
159 R. Derval dos Santa, M. R. Callil, C. D. G. F. Guedes, T. C. Rodriguez, J. Polymers and Environment **12(4)**, 239 (2004).
160 H. A. Abd El-REhim, E. A. Hegazy, J. Photochem. Photobiol. **163(3)**, 547 (2004).
161 M. Weiland, C. David, Polymer Degradation and Stability **48**, 275 (1995).
162 T. Volke-Sepulveda, E. Favela-Torres, J. Appld. Polym. Sci. **73,** 1435 (1999).
163 L. Averous, J. Macromolecular Science, Polymer Reviews **C44(3)**, 231 (2004).
164 D. Graiver, L. H. Waikul, J. Appld. Polym. Sci. **92(5)**, 3231 (2004).
165 S. N. Swain, K. K. Rao, P. L Nayak, J. Appld. Polym. Sci., **93(6),** 2590, (2004).
166 G. Vallini, A. Corti, A. Pera, R. Solaro, F. Cioni, E. Chellini, Gen. Appl. Microbiol., **40,** 445 (1994).
167 E. Schwach, L. Averous, Polymer International, **53(12)**, 2115 (2004).
168 A. Copinet, C. Bertrand, J. Polym. Environ. **11(4)**, 169 (2003).
169 X. C. Ge, X. H. Li, Q. Zhu, L. Li, Y. Z. Meng, Polymer Eng. Sci., **44(11)**, 2134 (2004).
170 D. Preechawong, M. Peesan, Macromolecular Symposia **216**, 217 (2004).
171 Z. Zhang, D. W. Grijpma, Macromolecular Chemistry and Physics, **205(7)**, 867 (2004).

172 A. Barclay, 9th Plastics Additives and Modifiers Conference, Vienna, Austria, RAPRA Technologies Ltd., Shrewsbury, UK (2003).
173 M. Shibata, S. Oyamada, *J. Appld. Polym. Sci.* **92(6)**, 3857 (2004).
174 S. Lee, T. Ohkita, J. Appld. Polym. Sci. **90(7)**, 1900 (2003).
175 E. Zini, M. Baiardo, Macromolecular Bioscience **4(3),** 286 (2004).
176 X. H. Li, Y. Z. Meng, J. Polym. Sci., Part B: Polymer Physics **42(4),** 666 (2004).
177 A. Corti, F. Cristiano, 7th World Conference on Biodegradable Polymers and Plastics, Terrenia, Ital, Kluwer Academic/Plenum Publishers (2002).
178 H. Park, X. Liang, K. Amar, M. Misra, L. T. Drzai, Macromolecules, **37(24),** 9076 (2004).
179 R. Hiroi, S. Suprakas, Macromolucular Rapid Communications **25(15),** 1359 (2004).
180 M. J. Okamoto, Ind. Eng. Chem (Korea) **10(7),** 1156 (2004).
181 H. Park, X. Liang, K. Amar, M. Misra, L. T. Drzai, Macromolecules, **37(24),** 9076 (2004).
182 H. Yang, J. Yoon, Polymer Degradation and Stability **87(1)**, 131 (2005).
183 V. Mezanotte, R. Bertani, Polymer Degradation and Stability **87(1)**, 51 (2004).
184 N. T. Lotto, M. R. Calil, Material Sciience and Engineering **C24(5)**, 659 (2004).
185 A. Hoshino, M. Tsuji, 7th World Conference on Biodegradable Polymers & Plastics, Terrenia, Italy, Kluwer Academic/Plenum Publishers, New York, NY (2002).
186 H. Lim, T. Raku, Macromolecular Bioscience **4(9)**, 875 (2004).
187 Y. Lu, L. Zhang, Polymer Degradation and Stability, **86**(1), 51 (2004).
188 J.-A. Lee, M.-N. Kim, J. Polym. Environ., **9,** 91 (2001).
189 A. M. Kinnersley, T. C. Scott III, Plant Growth Regul., 137 (1990).
190 S. M. Goheen, R. P. Wool J. Appld. Polym. Sci., **42,** 2691 (1991).
191 D. F. Gilmore, S. Antoun, Ind. Microbiol., **10,** 199 (1992).
192 X. Ramis, A. Cadenato, Polymer Degradation and Stability, **86,** 483–491 (2004).
193 P. K. Sahoo, P. K. Rana, A. Sahoo, Polymer and Polymer Composites, **12(7),** 627 (2004).
194 J. Gracida, J. Alba, J. Cardoso, F. Perez-Guvera, Polymer Degradation and Stability, **83(2)**, 247 (2004).
195 Y. Orhan, J. Hrenovic, H. Bueyuekguengier, Acta Chemica Slovenica, **513,** 579 (2004).
196 A. Sharma, J. Sci. Ind. Res., **63(3)**, 293 (2004).
197 K. H. Guruprasad, G. M. Shashidara, J. Appld. Polym. Sci., **91(3),** 1716 (2004).
198 A. Modelli, G. Rondinelli, M. Scandola, J. Mergaert, M. Cnockaert, Biomacromolecules, **5(2)**, 596 (2004).

CHAPTER 57

Properties of Photoresist Polymers

Qinghuang Lin

IBM Thomas J. Watson Research Center, 1101 Kitchawan Rd, Route 134 / P.O. Box 218, Yorktown Heights, NY 10598

57.1 INTRODUCTION

The explosive growth of semiconductor industry has been fueled by the relentless pursuit for miniaturization of semiconductor devices. The minimal feature sizes or critical dimensions (CDs) of semiconductor devices in mass production have shrunk from 10μm more than 30 years ago to less than 100 nm in 2005. According to the International Technology Roadmap for Semiconductors, this miniaturization trend is expected to continue unabated with the production of sub-25 nm generations of devices later next decade [1]. The miniaturization of semiconductor devices has made it possible to offer a host of sophisticated devices and equipment, from super computers, personal computers, personal digital assistants, cellular phones to medical devices and household appliances, with ever increasing performance at steadily reduced prices per transistor or bit.

This miniaturization trend has been made possible by advances in a critical device patterning process called photolithography, including constantly improved photosensitive polymeric materials called photoresists, advances in optical lenses, and the use of shorter wavelengths of light for patterning. In 2004, the semiconductor industry quietly ushered in the Nanoelectronics Age with the mass production of sub-100 nm node devices. The current leading-edge semiconductor devices in mass production—the so called 90 nm node devices—have a transistor gate length of less than 50 nm. These leading-edge devices are fabricated using photoresists based on alicyclic polymers at 193 nm wavelength, as well as Novolak-based mid-ultra violet (MUV) photoresists or poly(4-hydroxystyrene)-based deep UV (DUV) photoresists at wavelengths of 365 and 248 nm, respectively.

57.2 PHOTORESIST MATERIALS AND LITHOGRAPHIC PATTERNING PROCESS

In a typical photolithography process, a UV light is projected by a set of sophisticated lenses onto a silicon wafer coated with a thin layer of photoresist through a mask that defines a particular circuitry. Exposure to the UV light, coupled with a subsequent baking, induces photochemical reactions that change the solubility of the exposed regions of the photoresist film. Subsequently an appropriate developer, usually an aqueous base solution, is used to selectively remove the photoresist either in the exposed regions (positive-tone photoresists) or in the unexposed regions (negative-tone photoresists). The pattern thus defined is then imprinted on the wafer by etching away the regions that are not protected by the photoresist with reactive ion (plasma) etching (RIE). Figures 57.1 and 57.2 depict schematic of a typical photolithographic system and a typical device patterning process. Excellent reviews on photoresist materials have been published [2–6].

Advanced photoresists, such as 193 and 248 nm photoresists, are based on chemical amplification concept [7,8]. These chemically amplified photoresists generally consist of a base polymer, a photo-sensitive compound called photoacid generator (PAG), and sometimes a cross-linking

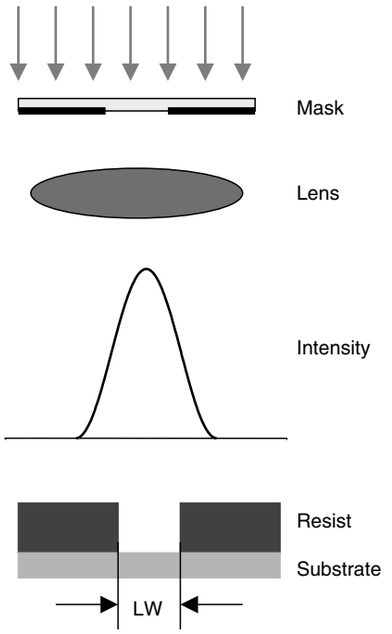

FIGURE 57.1. Schematic of a typical photolithographic system.

agent for negative-tone photoresists. When these resists are exposed to UV irradiation, a strong acid is generated in the exposed regions as a result of the photochemistry of the PAG. This strong catalytic acid then induces a cascade of subsequent chemical transformations of the photoresist that alter the solubility of the exposed regions. Thus the quantum efficiency of the photochemistry is amplified by hundreds or even thousands of times through the catalytic chain reactions. This catalytic effects of the chemical amplified resists greatly enhance the sensitivity of a photoresist, thus the efficiency of photolithographic processes. The chemical amplification process of a positive-tone resist is illustrated in Scheme 57.1. The most popular chemical amplification involves the acid catalyzed deprotection poly(4-hydroxystyrene) or poly(acrylic acid) protected by various acid sensitive protecting groups for positive-tone photoresists using a photoacid generator (PAG) [9].

The key figures of merit for a photoresist are resolution, process latitudes (dose and focus), and reactive ion etch resistance. Other important performance parameters include sensitivity, compatibility with industrial standard developer (0.263N aqueous tetramethylamoniumhydroxide (TMAH) solution), adhesion to substrates, environmental stability, and shelf life. These performance characteristics are mainly determined by the base polymer in the photoresist. It should be pointed out, however, that some of these performance parameters, such as resolution, process latitudes and etch resistance, are also tool and process condition dependent.

Polymers for advanced photoresists, therefore, need to meet the following requirements in order to deliver the performance necessary for device fabrication: good transparency at the imaging wavelength, etch resistance, optimal dissolution properties, high sensitivity, compatibility with the industrial standard 0.263N TMAH developer, as well as thermal and mechanical properties and shelf life requirements. These stringent requirements led to the design and synthesis of distinct polymer platforms for the evolving lithographic exposure technologies. Table 57.1 summarizes the major polymer platforms for the various exposure technologies.

Photoresists can be classified into three categories based on the lithographic processes: single layer photoresists (SLRs), bilayer photoresists (BLRs), and top surface imaged (TSI) photoresists [5]. Single layer photoresists have traditionally been the work horse for patterning semiconductor devices due to its process simplicity as compared with the bilayer and the TSI processes.

Properties of photoresist polymers were surveyed and reviewed by Kunz [10]. This present chapter is intended to complement, not replace, the review chapter by Kunz. Emphasis in this chapter has been placed on physical property data of photoresist polymers published after Kunz's review.

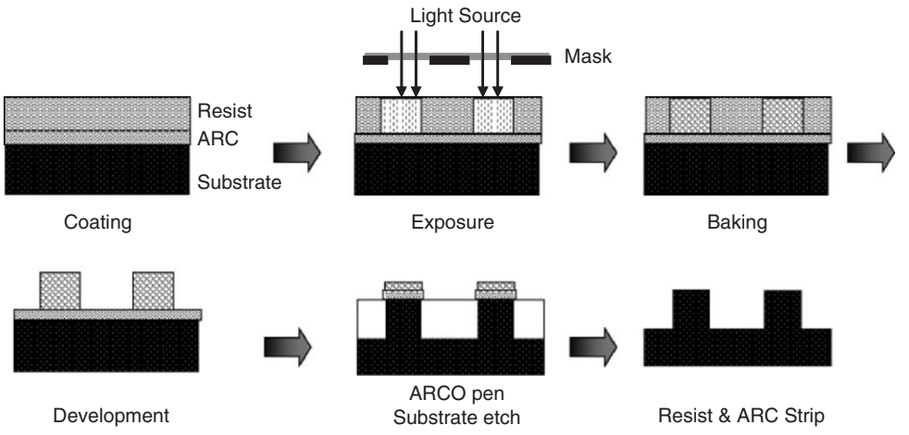

FIGURE 57.2. Schematic of a typical photolithographic patterning process using a positive-tone resist. ARC=antireflective coating.

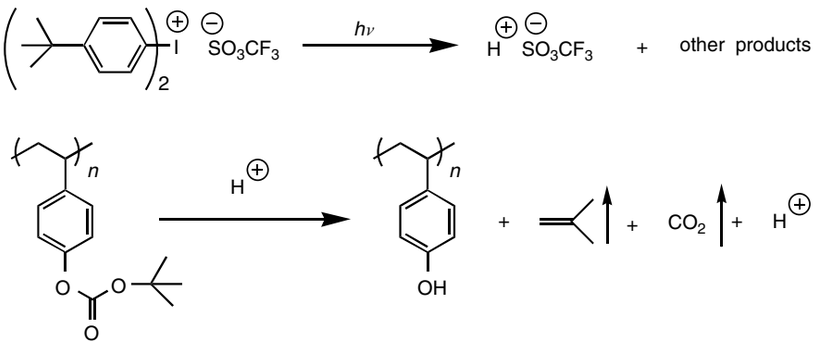

SCHEME 57.1. Chemical amplification in a positive-tone photoresist.

57.3 OPTICAL PROPERTIES OF LITHOGRAPHIC POLYMERS AND PHOTORESISTS

Polymers for photoresists must meet stringent transparency requirements at the imaging wavelength in order to deliver superior resolution and image quality. Suitable polymer platforms have been identified for I-line (365 nm) and 248 nm DUV lithography. They are *meta*-cresol novolak and poly(4-hydroxystyrene), respectively. Novolak and poly(4-hydroxystyrene), however, are not suitable for 193 nm single layer lithography because of their high absorption at 193 nm wavelength as a result of the $\pi-\pi^*$ transition of the double bonds in these polymers.

The transparency requirements, along with plasma etch resistant requirements, have led to a strategy for designing new polymers for 193 nm lithography, namely, the

TABLE 57.1. *Major polymer platforms for the evolving exposure technologies.*

Technology node	Exposure technology	Polymer platform
0.8–0.35μm	I-Line (365 nm)	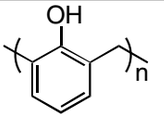
0.25–0.15μm	DUV (248 nm)	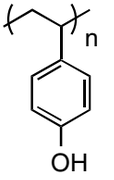
130–65 nm	DUV (193 nm)	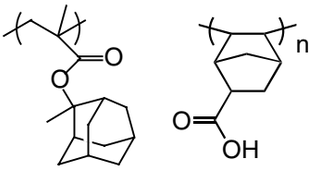
45–32 nm	DUV (157 nm)	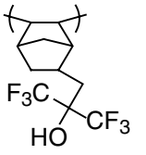
≤ 25 nm	EUV (13 nm)	?

incorporation of saturated aliphatic rings to form cycloaliphatic polymers. These saturated aliphatic rings can be incorporated into the polymer side chain [11–14] or in the polymer main chain [15,16], or a combination of both. Some of the most popular alicylic 193 nm photoresist polymers are depicted below:

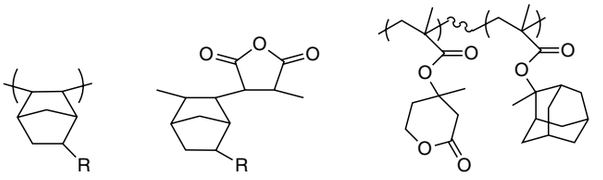

SCHEME 57.2. Alicyclic polymers for 193 nm lithography.

The absorption of organic polymers at 157 nm is dominated by the C (2p) electrons. An early audition of a large number of both organic and inorganic polymers indicated that fluorinated hydrocarbon polymers and siloxane polymers were the most promising polymer platforms to achieve adequate transparency and plasma etch resistance [17]. This pioneering work has spurred tremendous efforts to develop transparent and etch resistant fluoropolymers for 157 nm lithography.

Tables 57.2–57.4 list the optical constants of some polymers at 157 nm. In these tables, M_w and T_g are weight average molecular weight and glass transition temperature, respectively. Both the real (n) and imaginary (k) parts of the complex refractive indices ($n+ik$) are listed. The absorption coefficient (α) is correlated to the imaginary (k) part of the refractive index via the following equation:

$$\alpha = 4\pi k/\lambda,$$

where λ is the imaging wavelength.

As can be seen in Tables 57.2–57.4, many of the traditional polymers used for 248 and 193 nm lithography have prohibitively high absorbance at the 157 nm imaging wavelength. So are some of the key functional groups, such as phenol and carboxylic acid employed for solubility in aqueous base solutions. New polymer platforms and functional groups, therefore, must be designed/discovered for the 157 nm lithography.

The world-wide efforts to search for 157 nm transparent and etch resistant polymers for 157 nm lithography have resulted in several promising polymer platforms. They include highly fluorinated polymers as well as aromatic and aliphatic alcohols bearing highly electron withdrawing groups such as hexafluoroisopropanol. These polymers and their copolymers and terpolymers have been explored as possible polymer platforms for 157 nm lithography as well as lithography at longer wavelengths of 193 and 248 nm. Table 57.5 shows the absorbance of some of these polymers and some reference polymers.

Optical properties of a photoresist are determined by its base polymer as well as additives in the photoresist system, such as photoactive compounds, dissolution inhibitors, etc. Tables 57.6 and 57.7 list optical properties of some commercial I-line (365 nm) and DUV (248 nm) resists.

57.4 DISSOLUTION PROPERTIES OF PHOTORESIST POLYMERS

Proper dissolution of photoresist polymers in aqueous base solutions, usually 0.263N aqueous tetramethylamoniumhydroxide (TMAH) solution, is critical to achieving good resist performance. The dissolution rate of photoresist polymers depends on various parameters, including polymer type, molecular weight, copolymer composition, interactions with additives in the polymers, as well as temperature and base strength.

The dissolution rate of a photoresist polymer, like many other physical properties, depends heavily on the molecular weight of the polymer. The dissolution rate generally decreases with increasing molecular weight of the polymer. Figure 57.3 shows the dependence of dissolution rate of novolak with nearly monodisperse molecular weight distribution on its molecular weight [31]. The nearly monodisperse molecular weight distribution was achieved by fractionation with supercritical CO_2 fluids.

Similar dependence of dissolution of poly(4-hydroxystyrene)—the key polymer for 248 nm lithography—have been observed [32] (Fig. 57.4). Again the dissolution rate of poly(4-hydroxystyrene) decreases with increasing molecular weight of the polymer. The relatively narrow molecular weight distribution of poly(4-hydroxystyrene) was achieved by ''living'' free radical polymerization (Table 57.8).

The dissolution rates (DR) of poly(4-hydroxystyrene) in 0.14N TMAH were found to correlate well with its weight average molecular weight (M_w) as described by the following equation [33]:

$$\mathrm{DR} = K_1(M_w)^{-1/m}$$

where DR=dissolution rate in Å/s in 0.14N TMAH at room temperature and M_w = Weight average molecular weight. For poly(4-hydroxystyrene) with a molecular weight range of 3,500–240,000, K_1 = 19,100 and m=1.98

The dissolution rates of photoresist and polymers can also be regulated by making miscible blends of two or more polymers. Tables 57.9 and 57.10 list dissolution rates of binary blends of poly(4-hydroxystyrene) as well as poly(4-hydroxystyrene) and a silicon-containing copolymer [32,34]. This blending method is a convenient way to optimize the dissolution rates of photoresist polymers.

TABLE 57.2. *Optical constants and other properties of polymers for 157 nm lithography.*

Polymer	M_w	$n_{157\,nm}$	$k_{157\,nm}$	$\alpha_{157\,nm}$ (μm^{-1})	λ_{max}(nm)	α_{max} (μm^{-1})	T_g(°C)	Reference
Poly(methyl methacrylate)				5.69				[17]
Poly(acrylic acid)				11.00				[17]
Poly(norbornene)				6.1				[17]
Poly(vinyl naphthalene)				10.60				[17]
Poly(norbornyl methacrylate)				6.7				[18]
Poly(norbornene-*alt*-maleic anhydride)				8–9				[18]
Poly(tetrafluoroethylene/ norbornene) (49/51)	1,700(M_n)	1.6		1.3			151	[18]
Poly(methyl α-trifluoromethylacrylate)				2.68–3.0				[19–21]
Poly(styrene)	∼50,000			6.6	193.0	22.7	∼100	[22]
Poly(4-fluorostyrene)	17,500	1.35	0.199	7.0	189.0	24.0	110	[22]
Poly(3-fluorostyrene)	16,000	1.24	0.205	7.08	189.5	29.7		[22]
Poly(pentafluorostyrene)				5.8	177.0	14.4		[22]
Poly(4-trifluoromethyl styrene)	24,900	1.36	0.130	4.33	189.0	14.7	115	[22]
Poly(3,5-bis(trifluoromethy) styrene)	22,600	1.29	0.096	3.63	185.0	17.2	119	[22]
Poly(4-*tert*-butyl styrene)	19,600	1.42	0.162	5.67	193.5	22.7	151	[22]
Poly(2-hexafluoroisopropanol styrene)	3,100	1.48	0.094	3.40	191.5	17.8		[22]
Poly(3-hexafluoroisopropanol styrene)	36,700	1.29	0.107	3.80	190.0	17.9	81	[22]
Poly(4-hexafluoroisopropanol styrene)	26,300	1.39	0.099	3.44	190.5	20.5	129	[22]
Poly(4-*t*-BOC-hexafluoroisopropanol styrene)	6,700	1.52	0.087	2.95	191.0	9.6	62	[22]
Poly(4-*t*-butylacetate-hexafluoroisopropanol styrene)		1.48	0.111	4.29	191.5	11.2		[22]
Poly(*t*-butyl acrylate)		1.70	0.147	5.43				[22]
Poly(4-hydroxystyrene)		1.49	0.204	6.70	194.5	28.5		[22]
Poly(norbornene methylene hexafluoro isopropanol)	9,300	13,500		1.67, 1.80	<150	>3.0		[19,23]
Poly(norbornene hexafluoro alcohol-*co*-norbornene hexafluoro alcohol *t*-butoxycarbonyl) (20:80)				1.90				[24,25]
Poly(norbornene hexafluoro alcohol-*co*-norbornene hexafluoro alcohol acetal) (20:80)				1.78				[24,25]
Poly(1,1,2,3,3-pentafluoro, 4-trifluoromethyl-4-hydroxy-1,6-heptadiene) (PFOP)				0.4			152	[26]
Poly(*tert*-butyl[2,2,2-trifluoro-1-trifluoromethyl-1-(4-vinyl-phenyl) ethoxy]-acetate)	14,500			4.29			55	[27]
Poly(1-(2,2,2-trifluoro-1-methoxymethoxy-1-trifluoromethyl-ethyl)-4-vinyl benzene)	16,200			2.60			69	[27]
Poly(1-[1-(*tert*-butoxymethoxy)-2,2,2-trifluoro-1-trifluoro-methylethyl]-4-vinylbenzene)	16,600						63	[27]
Poly(1-[1-(*tert*-butoxycarbonyl)-2,2,2-trifluoro-1-trifluoro-methylethyl]- 4-vinylbenzene)	6,700			2.95			93	[27]
Poly(2-[4-(2-hydroxyhexafluoro isopropyl) cyclohexane] hexafluoroisopropyl acrylate)				1.93				[28]

TABLE 57.3. *Optical constants and other properties of fluorinated copolymers for 157 nm lithography.*

Monomer 1	Monomer 2	Ratio (M_1/M_2)	M_n	$n_{157\ nm}$	$k_{157\ nm}$	$\alpha_{157\ nm}(\mu m^{-1})$	T_g(°C)	Reference
4-HFIPS	*t*-BMA	60/40		1.454	0.112	3.99		[22]
4-HFIPS	*t*-BMA	50/50		1.496	0.112	4.05		[22]
4-HFIPS	*t*-BMA	70/30				3.74		[22]
3-HFIPS	*t*-BMA	60/40		1.476	0.105	3.92		[22]
4-HFIPS	α-CF3-*t*-BMA	75/25		1.382	0.104	3.71		[22]
4-HFIPS	*t*BOC-pHFIPS	70/30		1.398	0.102	3.58		[22]
4-HFIPS	*t*BOC-pHFIPS	60/40		1.378	0.097	3.44		[22]
4-HFIPS	*t*BAcetHFIPS	60/40	61,600	2.354	0.117	3.80	93	[22,27]
4-HS	*t*BA	50/50				6.5	155	[29]
4-HFIPS	*t*BA	50/50				3.7	120	[29]
4-HFIPS	*t*-BMA	50/50				4.0	154	[29]
3-HFIPS	*t*-BMA	50/50				3.9	111	[29]
4-HFIPS	*t*BA	60/40	17,600			3.74	124	[27]
4-HFIPS	*t*BAcetHFIPS	70/30	4,500			3.71	107	[27]
4-HFIPS	*t*BOC-HFIPS	50/50	16,900			3.39	69	[27]
4-HFIPS	*t*BOC-HFIPS	60/40	21,800			3.44	73	[27]
4-HFIPS	*t*BOC-HFIPS	70/30	25,800			5.57	73	[27]
4-HFIPS	MOM-HFIPS	60/40	25,500			3.08	107	[27]
4-HFIPS	MOM-HFIPS	70/30	26,900			3.27	117	[27]
4-HFIPS	BOM-HFIPS	60/40	26,300			2.82	97	[27]
4-HFIPS	BOM-HFIPS	70/30	26,300			3.16	106	[27]
PFOP	MOMPFOP	100/0				0.4	152	[26]
PFOP	MOMPFOP	82/17				0.5	145	[26]
PFOP	MOMPFOP	70/30				0.6	140	[26]
PFOP	MOMPFOP	54/46				0.8	137	[26]
NBHFA	NBC	60/40				2.99		[20]
NBHFA	NBC	80/20				2.28		[20]
NBHFA	TBTFMA	33/67	8,300			2.7		[23]

Note: 4-HFIPS, 4-hexafluoroisopropanol styrene; 3-HFIPS, 3-hexafluoroisopropanol styrene; *t*-BMA, *t*-butyl methacrylate; *t*BA, *t*-butyl acrylate; α-CF3-t-BMA, α-trifluoromethyl *t*-butyl methacrylate; *t*BOC-pHFIPS, *t*-butoxycarbonyl protected 4-hexafluoroisopropanol styrene; *t*BAcetHFIPS, *t*-butyl acetate protected 4-hexafluoroisopropanol styrene; 4-HS, 4-hydroxystyrene; *t*-BuAc HFIPS, *t*-butylacetate protected 4-hexafluoroisopropanol styrene; MOM HFIPS, methoxymethyl proected 4-hexafluoroisopropanol styrene; BOM HFIPS, butoxymethyl protected 4-hexafluoroisopropanol styrene; PFOP, 1,1,2,3,3-pentafluoro, 4-trifluoromethyl-4-hydroxy-1,6-heptadiene; MOMPFOP, methyoxymethyl protected 1,1,2,3,3-pentafluoro, 4-trifluoromethyl-4-hydroxy-1,6-heptadiene; NBHFA, norbornene-5-methylenehexafluoroisopropanol; BNC, butylnorbornene carboxylate; TBTFMA, methyl 2-trifluoromethylmethylacrylate.

Another very effective way to regulate the dissolution rate of photoresist polymers is copolymerization. Table 57.11 lists the physical properties of poly(4-hydroxystyrene-*co*-styrene) [35].

The copolymer architecture of poly(4-hydroxystyrene-*co*-styrene) was found to have insignificant effect on its dissolution rate (Fig. 57.5; Table 57.12) [36]. On the other hand, incorporation of inert styrene unit into poly(4-hydroxystyrene) drastically reduces dissolution rate. This method of incorporating inert unit has been employed to optimize the dissolution of base polymers for advanced DUV photoresists.

The dissolution rates of photoresist polymers can be further modulated by additives, such as photoacid generators or dissolution inhibitors. The photoacid generators are generally hydrophobic due to their usually bulky chromophores. Therefore, they generally act as to slow down the dissolution of photoresist polymers in aqueous base solutions, a phenomenon called dissolution inhibition. Figure 57.6 exhibits the effect of a photoacid generator on the dissolution rates of another key 248 nm photoresist polymer, poly(4-hydroxystyrene- *co*-*t*-butyl acrylate) [37]. It can also be seen that the level of protection, i.e., the fraction of *t*-butyl acrylate monomer in the copolymer, has an even more prominent effect on the dissolution rates. Increasing the protection level sharply reduces dissolution rates in 0.26N TMAH.

Similar dissolution inhibition effect by photoacid generators has also been observed in poly(norbornene-methylenehexafluoroisopropanol) (poly(NBHFA)) system [38]. Table 57.13 lists dissolution rates of poly(NBHFA) in 0.26N TMAH at room temperature with various photoacid

TABLE 57.4. *Optical constants and other properties of fluorinated terpolymers for 157 nm lithography.*

Monomer 1	Monomer 2	Monomer 3	Ratio ($M_1/M_2/M_3$)	M_n	$n_{157\,nm}$	$k_{157\,nm}$	$\alpha_{157\,nm}(\mu m^{-1})$	T_g(°C)	Reference
4-HFIPS	*t*-BMA	3,5-DiCF3-S	60/20/20		1.378	0.112	3.99		[22]
4-HFIPS	*t*-BMA	4-FHIPyp-S	60/20/20		1.330	0.113	3.89		[22]
4-HFIPS	*t*-BMA	4-C3F7CO-S	60/20/20		1.350	0.115	4.03		[22]
3-HFIPS	*t*-BMA	Acrylonitrile	70/20/10		1.397	0.106	3.80		[22]
4-HFIPS	*t*-BMA	Methacrylonitrile	70/20/10		1.408	0.102	3.72		[22]
PFOP	MOMPFOP	*t*-BMA	71.5/23.5/5	10,000			0.7	150	[26]
PFOP	MOMPFOP	*t*-BMA	73/10/17	6,700			1.0	154	[26]
PFOP	MOMPFOP	*t*-BMA	67/0/33	5,800			1.2	154	[26]
PFOP	MOMPFOP	VP	68/19/13	9,600			0.8	144	[26]
PFOP	MOMPFOP	MA	30/50/20	9,300			1.3		[26]
PFOP	MOMPFOP	PFVE	40/10/50	10,200			0.4		[26]

Note: 4-HFIPS, 4-hexafluoroisopropanol styrene; 3-HFIPS, 3-hexafluoroisopropanol styrene; *t*-BMA, *t*-butyl methacrylate; *t*BA, *t*-butyl acrylate; α-CF3-*t*BMA, α-trifluoromethyl *t*-butyl methacrylate; *t*BOC-pHFIPS, *t*-butoxycarbonyl protected 4-hexafluoroisopropanol styrene; *t*BAcetHFIPS, *t*-butyl acetate protected 4-hexafluoroisopropanol styrene; 4-HS, 4-hydroxystyrene; *t*-BuAc HFIPS, *t*-butylacetate protected 4-hexafluoroisopropanol styrene; MOM HFIPS, methoxymethyl proected 4-hexafluoroisopropanol styrene; BOM HFIPS, butoxymethyl protected 4-hexafluoroisopropanol styrene; PFOP, 1,1,2,3,3-pentafluoro, 4-trifluoromethyl-4-hydroxy-1,6-heptadiene; MOMPFOP, methyoxymethyl protected 1,1,2,3,3-pentafluoro, 4-trifluoromethyl-4-hydroxy-1,6-heptadiene; VP, vinyl pivalate; V4*t*BB, Vinyl-4-*tert*-butyl benzoate; MA, maleic andydride; PFVE, perfluoro vinyl ether.

TABLE 57.5. *Absorbance of some cycloolefin polymers, copolymers, and reference polymers [30].*

Polymer	$\alpha_{248\,nm}(\mu m^{-1})$	$\alpha_{193\,nm}(\mu m^{-1})$	$\alpha_{157\,nm}(\mu m^{-1})$
Poly(NBHFA)	0.00	0.38	1.76
Poly(BNC)	0.11	0.48	6.41
Poly(BNC-*co*-MCA) (2:1)	0.04	0.23	5.05
Poly(BNC-*co*-MCA) (1:1)	0.02	0.38	5.20
Poly(NBHFA-*co*-MCA) (2:1)	0.10	0.28	3.29
Poly(NB-*co*-MCA) (2:1)	0.03	0.11	4.98
Poly (MMA)	0.00	0.05	5.60
Poly(MTFA)	0.00	0.00	2.90
Poly(ECA)	0.00	0.00	3.90

Note: NB, norbornene; NBHFA, norbornene-methylenehexafluoroisopropanol; MCA, methyl cyanoacrylate; BNC, butyl norbornene carboxylate; MA, methylacrylate; MMA, methyl methylacrylate; MTFA, methyl trifluoromethyl acrylate; ECA, ethyl cyanoacrylate.

TABLE 57.6. *Optical constants of commercial I-line (365 nm) photoresists*[a].

Resist	Supplier	Type	$n_{365\,nm}$	$k_{365\,nm}$	$a_{365\,nm}(\mu m^{-1})$	$n_{633\,nm}$
IBM7500	IBM	Positive tone	1.701	0.0190	0.65	1.641
IBM7518	IBM	Positive tone	1.694	0.0216	0.74	1.627
Spectralith 5105	IBM	Positive tone	1.693	0.0298	1.03	1.628
Spectralith 5108	IBM	Positive tone	1.683	0.0284	0.98	1.620
IX300	JSR	Positive tone	1.690	0.0177	0.61	1.626
JSR 1010	JSR	Positive tone	1.690	0.0178	0.61	1.622
TMHR 2600	TOK	Positive tone	1.685	0.0209	0.72	1.618
TMHR 3250	TOK	Positive tone	1.687	0.0242	0.83	1.620
THMR 3720	TOK	Positive tone	1.697	0.0277	0.95	1.628
THMR 3780	TOK	Positive tone	1.694	0.0294	1.01	1.625
THMR NP4S	TOK	negative tone	1.654	0.0106	0.36	1.587
TSMR IN008	TOK	negative tone	1.652	0.0063	0.22	1.587
TSMR IN011	TOK	negative tone	1.660	0.0183	0.63	1.588
TSMR IN-TR12	TOK	negative tone	1.641	0.0043	0.15	1.584

[a]Courtesy of Dr. James Bruce, IBM, 2005.

TABLE 57.7. *Optical constants of commercial DUV (248 nm) photoresists*[a].

Resist	Supplier	Type	$n_{248\,nm}$	$k_{248\,nm}$	$a_{248\,nm}(\mu m^{-1})$	$n_{365\,nm}$	$k_{365\,nm}$	$a_{365\,nm}(\mu m^{-1})$	$n_{633\,nm}$
APEX-M	IBM/ Shipley	Positive tone	1.780	0.0076	0.39	1.614	0.0000	0.00	1.562
UVII-HS	Shipley/Rohm Hass	Positive tone	1.730	0.0113	0.57	1.590	0.0000	0.00	1.545
UV4	Shipley/Rohm Hass	Positive tone	1.802	0.0129	0.65	1.631	0.0000	0.00	1.575
UV5	Shipley/Rohm Hass	Positive tone	1.804	0.0109	0.55	1.631	0.0019	0.07	1.577
UV82	Shipley/Rohm Hass	Positive tone	1.762	0.0122	0.62	1.611	0.0000	0.00	1.561
UV110	Shipley/Rohm Hass	Positive tone	1.787	0.0121	0.61	1.626	0.0057	0.20	1.577
UV-113	Shipley/Rohm Hass	Positive tone	1.785	0.0125	0.63	1.628	0.0061	0.21	1.577
UV-N	Shipley/Rohm Hass	Negative tone	1.803	0.0101	0.51	1.640	0.0053	0.18	1.587
CGR 248	Shipley/Rohm Hass	Negative tone	1.813	0.0100	0.51	1.643	0.0003	0.01	1.589
CGR CE	Shipley/Rohm Hass	Negative tone	1.773	0.0077	0.39	1.617	0.0005	0.02	1.567
M20G	JSR	Positive tone	1.779	0.0100	0.51	1.616	0.0002	0.01	1.564
M22G	JSR	Positive tone	1.775	0.0120	0.61	1.616	0.0059	0.20	1.565
M60G	JSR	Positive tone	1.772	0.0133	0.67	1.621	0.0028	0.10	1.574
M92Y	JSR	Positive tone	1.775	0.0074	0.37	1.622	0.0040	0.14	1.574
P015	TOK	Positive tone	1.816	0.0093	0.47	1.641	0.0041	0.14	1.591

[a]Courtesy of Dr. James Bruce, IBM, 2005.

generators and photoacid generator concentrations. As expected, more bulky, hydrophobic photoacid generators effect better dissolution inhibition.

The effects on dissolution inhibitors on the dissolution of a 193 nm terpolymers poly(norbornene-*alt*-melaic anhydride-*co*-acrylic acid) (p(NB/MA-20%AA) are shown in Figure 57.7 [39]. Again the dissolution rate of this 193 nm terpolymer is significantly reduced with the addition of the dissolution inhibitors. The effects of various dissolution inhibitors were attributed to the varied degree of the interactions between the base polymer and the dissolution inhibitors. In these cycloolefin-maleic anhydride terpolymer systems, the position of the base soluble carboxylic group appeared to have no significant effect on the dissolution of the base polymers. The dissolution rates were very similar whether the carboxylic group is part of norbornene or part of the acrylate [40].

As the resist film thickness shrinks, the interactions of photoresist polymers and substrates become increasingly important. Dissolution rates of photoresist polymers were found to change as the film thickness decreases. Figure 57.8 shows variation of the dissolution rates of poly(4-hydroxystyrene) and poly(norbornene-methylene-hexafluoroisopropanol) as a function film thickness. The dissolution rates of both polymers increase with decreasing initial film thickness [41].

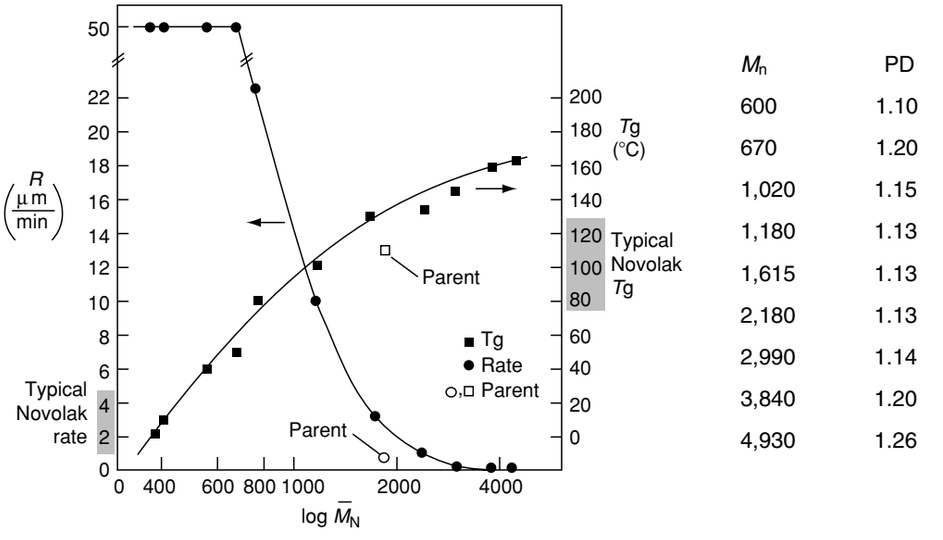

FIGURE 57.3. Glass transition temperature and dissolution rate of fractionated novolak in 0.263N TMAH at room temperature [31].

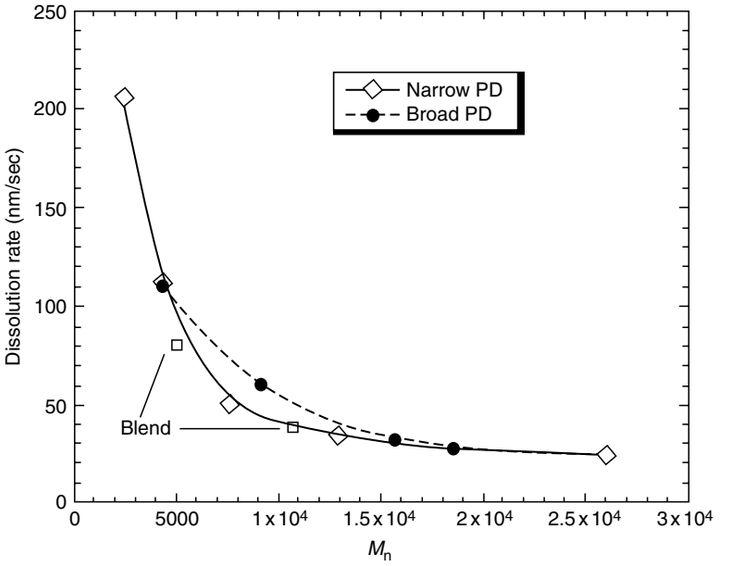

FIGURE 57.4. Dissolution rates of narrow polydispersity poly(4-hydroxystyrene) in 0.21 TMAH aqueous solution at room temperature [32].

TABLE 57.8. *Glass transition temperature of narrow PD of poly(4-hydroxystyrene) synthesized by "living" free radical polymerization [32].*

PHOST	M_n	M_w/M_n	T_g (°C)
PHOST-1	2,304	1.19	149
PHOST-2	3,874	1,18	172
PHOST-3	6,528	1.42	177
PHOST-4	12,726	1.38	185
PHOST-5	24,298	1.43	186

TABLE 57.9. *Dissolution rates of binary blends of poly (4-hydroxystyrene) in 0.21N TMAH at room temperature [32].*

Binary blend (wt/wt)	M_n	M_w/M_n	Dissolution rate (nm/s)
100/0	2,304	1.19	206
68/32	3,500	4.94	121
50/50	4,400	5.46	81
40/60	4,900	5.49	67
0/100	24,298	1.43	25

TABLE 57.10. *Dissolution rates of binary blends of P (4-hydroxystyrene) and poly(4-hydroxybenzylsilsesquioxane-co-4-methoxybenzylsilsesquioxane) in 0.26N TMAH at room temperature [34].*

PHS wt%	Si conc. (wt%)	Dissolution rate (A/s)	T_g (°C)	Etch selectivity
0	17	5,011	106.8	27.8
10	15.3	4,128	—	—
20	13.6	3,601	115.4	21.6
30	11.9	3,230	121.0	19.0
40	10.2	3,115	130.5	15.6
60	6.8	2,829	139.8	6.6
80	3.4	2,748	150.0	2.5
100	0	2,483	162.4	0.9

Note: etch rate of O_2-based plasma chemistries vs novolak.

TABLE 57.11. *Physical properties of poly(4-hydroxystyrene-co-styrene) [35].*

Styrene (mol%)	M_w	PD	$a_{248\,nm}$ (μm^{-1})	T_g (°C)
0	19,400	1.67	0.172	178
5	19,180	1.87	0.165	168
10	11,540	1.56	0.164	166
15	13,650	1.76	0.152	161
20	11,040	1.95	0.156	160
25	14,500	2.00	0.155	158
30	12,570	1.90	0.154	155

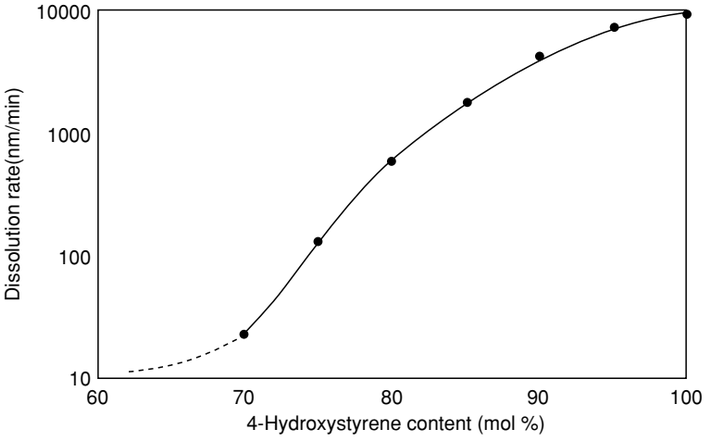

FIGURE 57.5. Effect of copolymer composition on the dissolution rates of poly(4-hydroxystyrene -*co*-styrene) in 0.26N TMAH at room temperature [36].

TABLE 57.12. *Effect of copolymer architecture and composition on the dissolution rates of poly(4-hydroxystyrene- co-styrene) in 0.26N TMAH at room temperature [36].*

4-HOST	Styrene	Architecture	M_w	M_n	PD	DR (Å/s)
100	0	Homo	9,550	7,958	1.20	2,050
90	10	Random	8,297	6,533	1.27	677
80	20	Random	9,908	8,188	1.21	34
70	30	Random	8,197	7,190	1.14	3
55	45	Random	8,559	6,793	1.26	1
90	10	Block	10,155	8,324	1.22	330
80	20	Block	8,854	7,568	1.17	94
70	30	Block	6,856	6,121	1.12	7
55	45	Block	10,020	8,564	1.17	1

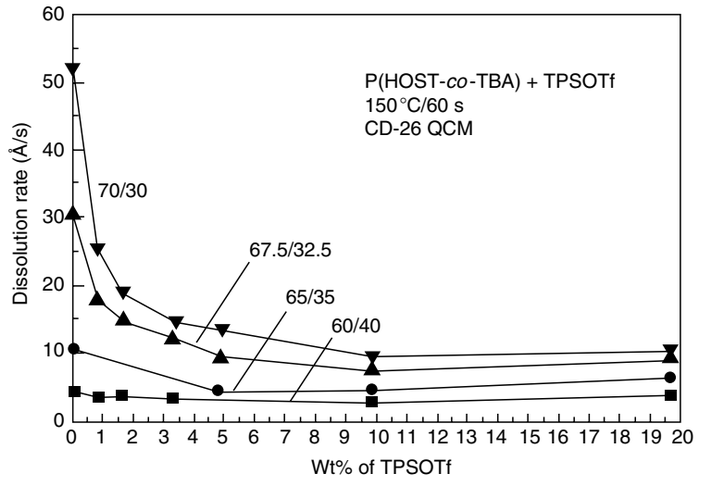

FIGURE 57.6. Effects of protection level and photoacid generator on the dissolution of poly(4-hydroxystyrene- *co-t*-butyl acrylate) (P(HOST-*co-t*BA) in 0.26N TMAH at 150 °C. The photoacid generator used is triphenylsulfonium triflate (TPSOTf). The developer is a 0.26N TMAH aqueous solution (CD-26) [37].

TABLE 57.13. *Effects of photoacid generators (PAGs) on the dissolution rates of poly(NBHFA) in 0.26N TMAH at room temperature [38].*

PAG	Wt% of PAG	Mol % of PAG	Dissolution rate (Å/s)
None			3,162.3
1	9.72	4.99	121.4
1	20.50	11.16	44.0
2	7.31	4.98	69.4
3	12.67	4.96	60.3
4	10.06	8.92	400.0
5	2.33	1.24	20.6
5	5.22	2.81	1.5
5	5.94	3.22	0.91
5	10.72	5.95	<0.05
6	8.34	3.60	0.70
7	4.16	1.87	4.84
7	8.00	3.68	0.86
8	4.08	1.73	6.61
8	7.94	3.45	0.64
9	3.13	2.84	503.2

Note: PAG 1, triphenylsulfonium nonaflate; PAG 2, triphenylsulfonium triflate; PAG 3, triphenylsulfonium perfluorooctylsulfonate; PAG 4, *N*-Trifluoromethylsulfonyloxy- 1,8-naphthalimide; PAG 5, diphenyl(4-thiophenylphenyl)-sulfonium triflate; PAG 6, diphenyl(4-thiopheny lphenyl) -sulfonium nonaflate; PAG 7,4-methoxy-1-naththalenyldiphenysulfonium nonaflate; PAG 8, diphenyliodium triflate; PAG 9, di-1-naphthalenylphenylsulfonium nonaflate.

57.5 PROPERTIES OF PHOTOACID GENERATORS

Photoacid generator (PAG) is a critical component of modern chemically amplified resists. It not only determines the sensitivity but also influences the dissolution and the stability of a chemically amplified photoresist. Major requirements for photoacid generators are sufficient absorption at the imaging wavelength, production of a strong acid to catalyze chemical transformation of the base photoresist polymer. Other considerations include effects on the dissolution of the base photoresist polymer, solubility in

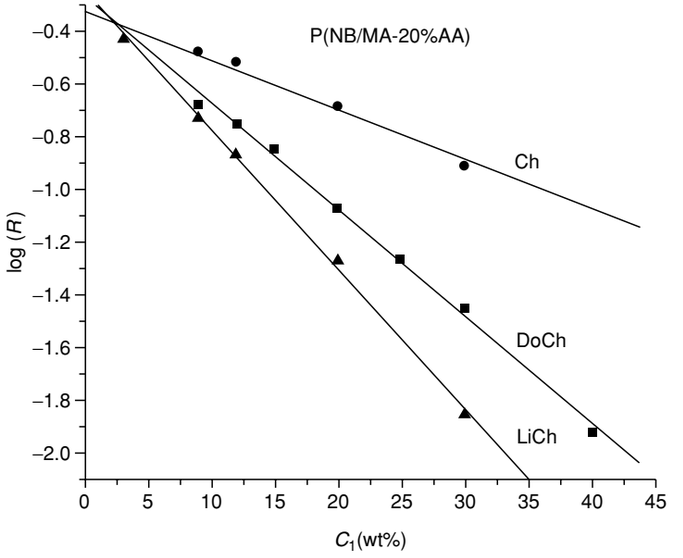

FIGURE 57.7. The effects on dissolution inhibitors on the dissolution rate (R) of a 193 nm terpolymers poly(norbornene-*alt*-melaic anhydride-*co*-acrylic acid) (p(NB/MA-20%AA) in 0.26N TMAH at room temperature [39]. Ch=*t*-butylcholate, DoCH=*t*-butyldeoxycholate, LiCH=*t*-butyllithocholate.

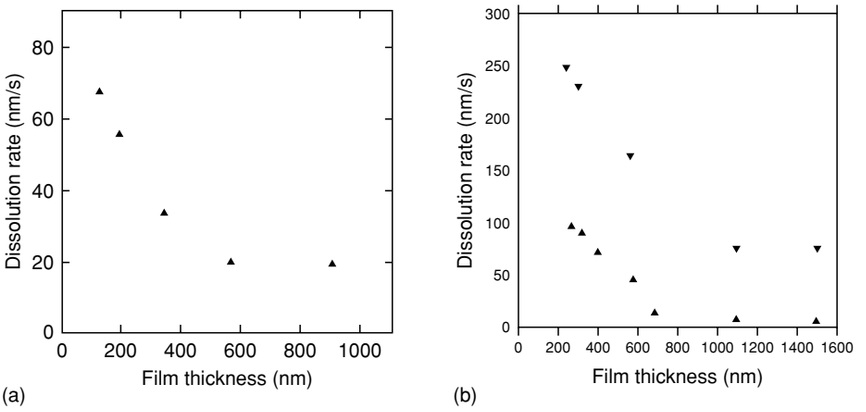

FIGURE 57.8. Dissolution rates of poly(norbornene-methylenehexafluoroisopropanol) (poly(NBHFA) (a) in 0.165N TMAH at room temperature and poly(4-hydroxystyrene) (b) in 0.12 and 0.165N TMAH at room temperature [41].

photoresist solvents, stability of the photoacid generator before exposure to a light source, miscibility with the base photoresist polymer, toxicity, etc. The most popular and efficient photoacid generators are onium salts, such as aryl iodonium and sulfonium salts [42] although some nonionic photoacid generators have also been used in chemically amplified resists. The synthesis, photochemistry, photosensitization of onium salts are reviewed elsewhere [42].

Key performance parameters of photoacid generators are absorbance, quantum efficiency, dissolution inhibition effect, etc. Table 57.14 shows quantum yields for the photolysis of some aryl iodonium and sulfonium salts.

The metal-containing onium salts are generally not preferred in modern photoresists as they will contaminate the device fabrication processes. Instead organic onium salts are preferred in chemically amplified photoresist formulations. Table 57.15 shows extinction coefficients at 248 nm, 254 nm, and the absorption maxima as well as thermal stability of some organic onium salts [43].

Table 57.16 lists the quantum yields of some organic photoacid generators obtained from actual photoresist systems.

57.6 REACTIVE ION (PLASMA) ETCH RESISTANCE OF PHOTORESIST POLYMERS

Superior reactive ion (plasma) etch resistance of photoresist polymers is crucial to ensuring faithful transfer of the photoresist images into the appropriate substrates. In general, two types of etch chemistries are of particular interest: One is the CF_x type of chemistry for patterning silicon oxide type of dielectrics. The other is halogen type of etch chemistry for patterning polysilicon. Phenomenological parameters have been proposed to correlate the etch rates of a photoresist polymer to its composition. One such empirical parameter is Ohnishi parameter [46], the other is ring parameter [47] as expressed below.

$$\text{Ohnishi parameter} = N/(N_c - N_o),$$
$$\text{Ring parameter} = M_{cr}/M_{tot},$$

where N, N_c, N_o are the total number of atoms, number of carbon atoms, and number of oxygen atoms in a polymer repeat unit. M_{cr}, M_{tot} are the mass of the resist existing as

TABLE 57.14. *Quantum yields for the photolysis of some aryl iodonium and sulfonium salts [42]*[a].

Onium salt	Products	Excitation wavelength (nm)	
		313	254
$(C_6H_5)_2I^+AsF_6^-$	C_6H_5I	0.34	0.39
	$HAsF_6$	0.7	0.65
(4-*t*-Butyl-$C_6H_4)_2I^+AsF_6^-$	4-*t*-Butyl-C_6H_4I	0.2	—
(4-*t*-Butyl-$C_6H_4)_2I^+PF_6^-$	4-*t*-Butyl-C_6H_4I	0.22	—
(4-*t*-Butyl-$C_6H_4)_2I^+SbF_6^-$	4-*t*-Butyl-C_6H_4I	0.22	—
$(C_6H_5)_3S^+AsF_6^-$	$(C_6H_5)_2S$	0.06	0.26
	$HAsF_6$	0.11	0.74
(4-CH_3O-$C_6H_5)_3S^+AsF_6^-$	(4-CH_3O-$C_6H_5)_2S$	0.17	—

[a]Determined in acetonitrile.

TABLE 57.15. *Optical properties of sulfonium triflate photoacid generators [43].*[a]

PAG	$\varepsilon_{248\ nm}$	$\varepsilon_{254\ nm}$	$\varepsilon_{max}(\lambda_{nm})$	Thermal stability (°C)
TPSOTf	13,302	8,665	3,925 (267), 2,772 (275)	406
SPTOTf	8,314	6,269	5,042 (265), 5,940 (308)	378
DTSOTf	10,075	8,209	19,832 (302)	408
BDSOTf	24,469	17,080	16,023 (271), 18,077 (278), 18,171 (290), 17,779 (319.5)	406
TASOTf	12,416	9,176	10,801 (9,299)	398

[a]In methanol.
Note: TPSOTf, triphenylsulfonium triflate; SPTOTf, *S*-phenylthioanthrylsulfonium triflate; DTSOTf, diphenyl-4-thiophenoxyphenylsulfonium triflate; BDSOTf, bis[4-(diphenylsulfonio)phenyl]sulfide triflate; TASOTf, triarylsulfonium triflate.

TABLE 57.16. *Quantum yields of photoacid generation in resist systems [44,45].*

PAG	Polymer matrix	Base additive	Quantum yields	Reference
DTBPICSA	ESCAP	Yes	0.211	[45]
DTBPICSA	ESCAP	No	0.277	[45]
TPSCSA	ESCAP	Yes	0.237	[45]
Methyl-SP	Novolak	No	0.11	[44]
Ethyl-SP	Novolak	No	0.075	[44]
Propyl-SP	Novolak	No	0.071	[44]
Phenyl-SP	Novolak	No	0.035	[44]
Tolyl-SP	Novolak	No	0.029	[44]
Naphthyl-SP	Novolak	No	0.020	[44]

Note: DTBPICSA, di-(4-*tert*-butylphenyl)iodonium camphoresulfonate; TPSCSA, triphenylsulfonium camphoresulfonate; Methyl-SP, methylesulfonic acid ester of 1,2,3-trihydroxybenzene (pyrogallol); Ethyl-SP, ethylsulfonic acid ester of 1,2,3-trihydroxybenzene (pyrogallol); Propyl-SP, propylsulfonic acid ester of 1,2,3-trihydroxybenzene (pyrogallol); Methyl-SP, phenylesulfonic acid ester of 1,2,3-trihydroxybenzene (pyrogallol); Tolyl-SP, tolulenesulfonic acid ester of 1,2,3-trihydroxybenzene (pyrogallol); Naphthyl-SP, naphthalenesulfonic acid ester of 1,2,3-trihydroxybenzene (pyrogallol).

TABLE 57.17. *Relative etch rates of selected cyclic olefin-based 193 nm photoresist polymers [48].*

Polymer	LD Psi	HD PSi	Oxide
IBM V2 Methacrylate	1.98	1.71	2.33
IBM V3 Methacrylate	1.45	1.3	1.94
IBM Cyclic olefin polymer 1	1.48	1.62	1.15
IBM Cyclic olefin polymer 2	1.33	1.46	1.02
IBM Apex-E 248 nm resist	1.35	1.23	1.36
SPR-510L i-Line resist	1	1	1

Note: LD PSi, low-density polysilicon etch, Cl_2/HBr etch chemistry (158 m Torr); HD PSi, high-density polysilicon etch, Cl_2/HBr etch chemistry (10 mTorr); Oxide, high-density oxide etch, C_2F_6 etch chemistry (5 mTorr).

carbon atoms contained in a ring and total resist mass, respectively. Correlations of these parameters with experiment results suggest that incorporating more carbon atoms, particularly in a ring form, would enhance etch resistance. In Tables 57.17–57.19, the etch rates of photoresist polymers are expressed as ratios to reference polymers/photoresists. The lower the ratio, the higher the etch resistance of the photoresist polymer (Tables 57.20 and 57.21).

TABLE 57.18. *Relative etch rates of methacrylate-based 193 nm photoresist polymers [49].*

Polymer	CF_4	Ar	Cl_2	Cl_2/HBr
Novolak	1	1	1	1
PMMA	1.4	2	2.5	—
MLMA-MAdMA	1.1	1.2	1.3	1.4

Note: MLMA-MAdMA=mevalonic lactone methacrylate (MLMA), 2-methyl-2-adamantane methacrylate (2-MAdMA) copolymer, (51:49).

TABLE 57.19. *Relative etch rates of 193 nm cyclic olefin-maleic anhydride copolymer [50].*

Polymer	Oxide etch (CHF_3)	Polysilicon etch (Cl_2)	Metal etch (SF_6)
I-line resist	1.00	1.00	1.00
248 nm resist	1.13	1.33	1.71
Poly(HNC/BNC/NC/MA)	1.00	1.35	1.07

Note: Poly (HNC/BNC/NC/MA)=copolymer of 2-hydroxyethyl- 5-norbornene-2-Carboxylate (HNC), *t*-butyl- 5-norbornene-2-Carboxylate (BNC) 5-norbornene-2-carboxylic acid (NC), maleic anhydride (MA).

TABLE 57.20. *Reactive ion etch rates and selectivity of 157 nm photoresist polymers [27].*

Polymer	Oxide etch rate (nm/s)	Oxide etch selectivity	Polysilicon etch rate (nm/s)	Polysilicon etch selectivity
60:40 HOST/TBA	0.86	7.1	0.71	4.0
60:40 HFIP/TBA	1.34	4.5	1.01	2.6
70:30 HFIP/MOM	1.11	5.5	0.72	4.0
70:30 HFIP/BOM	0.89	6.8	0.62	4.6
Thermal oxide	6.05	1.0	0.13	22.6
Amouphous silicon	0.60	10.2	2.85	1.0

TABLE 57.21. *Relative etch rate of fluorinated polymers [51].*

Polymer	$\alpha_{157\,nm}(\mu m^{-1})$	Cl_2 Etch rate (nm/min)	CF_x Etch Rate (nm/min)
p(STHFA)	3.6	147	89
ESCAP (69:31)	6.9	132	54
PF-ESCAP	4.0–4.2	165	76
PF2-ESCAP	3.2–3.6	183	75
PF-APEX (50:50)	4.3	—	—
PHOST	—	100	49
SiO_2	—	22	287

REFERENCES

1. SIA *International Technology Roadmap for Semiconductors*; International Sematech: Austin, Texas, 2004.
2. Dammel, R. *Diazonaphthoquinone-Based Resists*; SPIE Press: Bellingham, Washington, USA, 1993.
3. Macdonald, S. A.; Willson, C. G.; Frechet, J. M. J. *Accounts of Chemical Research* **1994**, *27*, 151.
4. Reichmanis, E.; Thompson, L. F. *Chem. Rev*. **1989**, *89*, 1273.
5. Willson, C. G. In *Introduction to Microlithography, 2nd ed*, Thompson, L. F., Willson, C. G., Bowden, M. J., Eds.; American Chemical Society: Washington, DC, 1994, pp. 139–258.
6. Ito, H. *Adv. Polym. Sci*. **2005**, *172*, 37–245.
7. Frechet, J. M. J.; Willson, C. G.; Ito, H. *Proceedings of Microcircuit Engineering* **1982**, 260.
8. Ito, H.; Willson, C. G.; Frechet, J. M. J. *Digest of Technical Papers of 1982 Symposium on VLSI Technology* **1982**, P86.
9. Ito, H. *Advances in Polymer Science* **2005**, *172*, 37–245.
10. Kunz, R. In *Physical Properties of Polymers*; Mark, J. E., Ed.; Springer: New York 1995, pp. 637–642.
11. Allen, R. D.; Wallraff, G. M.; Hinsberg, W. D.; Conley, W. E.; Kunz, R. R. *Solid State Technology* **1993**, *36*, 53.
12. Nozaki, K.; Kaimoto, Y.; Takahashi, M.; Takechi, S.; Abe, N. *Chemistry of Materials* **1994**, *6*, 1492–1498.
13. Nozaki, K.; Watanabe, K.; Namiki, T.; Igarashi, M.; Kuramitsu, Y.; Yano, E. *Japanese Journal of Applied Physics Part 2-Letters* **1996**, *35*, L528–L530.
14. Nozaki, K.; Yano, E. *Journal of Photopolymer Science and Technology* **1998**, *11(3)*, 493–498.
15. Okoroanyanwu, U.; Shimokawa, T.; Byers, J.; Medeiros, D.; Willson, C. G.; Niu, Q. J.; Frechet, J. M. J.; Allen, R. *Proceedings of the SPIE—The International Society for Optical Engineering* **1997**, *3049*, 92–103.
16. Wallow, T. I.; Houlihan, F. M.; Nalamasu, O.; Chandross, E. A.; Neenan, T. X.; Reichmanis, E. *Proceedings of the SPIE—The International Society for Optical Engineering* **1996**, *2724*, 355–364.
17. Kunz, R. R.; Bloomstein, T. M.; Hardy, D. E.; Goodman, R. B.; Downs, D. K.; Curtin, J. E. *Journal of Vacuum Science and Technology B* **1999**, *17*, 3267–3272.
18. Crawford, M. K.; Feiring, A. E.; Feldman, J.; French, R.; Periyasamy, M.; Schadt, F. L.; Smalley, R. J.; Zumsteg, F. C.; Kunz, R.; Rao, V.; Liao, L.; Holl, S. In *Proceedings of the SPIE—The International Society for Optical Engineering: Advances in Resist Technology and Processing XVii*; Houle, F., Ed.; SPIE: 2000; Vol. 3999, p. 357.
19. Chiba, T.; Hung, R. J.; Yamada, S.; Trinque, B.; Yamachika, M.; Brodsky, C.; Patterson, K.; Vander Heyden, A.; Jamison, A.; Shang-Ho, L.; Somervell, M.; Byers, J.; Conley, W.; Willson, C. G. *Journal of Photopolymer Science and Technology* **2000**, *13(4)*, 657–664.
20. Dammel, R. R.; Sakamuri, R.; Romano, A.; Vicari, R.; Hacker, C.; Conley, W.; Miller, D. *Proceedings of the SPIE—The International Society for Optical Engineering* **2001**, *4345, pt.1–2*, 350–360.
21. Ito, H.; Wallraff, G. M.; Brock, P.; Fender, N.; Truong, H.; Breyta, G.; Miller, D. C.; Sherwood, M. H.; Allen, R. D. *Proceedings of the SPIE—The International Society for Optical Engineering* **2001**, *4345, pt.1–2*, 273–284.
22. Kunz, R. R.; Sinta, R.; Sworin, M.; Mowers, W. A.; Fedynyshyn, T. H.; Liberman, V.; Curtin, J. E. *Proceedings of the SPIE—The International Society for Optical Engineering* **2001**, *4345, pt.1–2*, 285–295.
23. Ito, H.; Truong, H. D.; Okazaki, M.; Miller, D. C.; Fender, N.; Breyta, G.; Brock, P. J.; Wallraff, G. M.; Larson, C. E.; Allen, R. D. *Proceedings of the SPIE—The International Society for Optical Engineering* **2002**, *4690*, 18–28.
24. Trinque, B. C.; Chiba, T.; Hung, R. J.; Chambers, C. R.; Pinnow, M. J.; Osburn, B. P.; Tran, H. V.; Wunderlich, J.; Hsieh, Y. T.; Thomas, B. H.; Shafer, G.; DesMarteau, D. D.; Conley, W.; Willson, C. G. *Journal Of Vacuum Science and Technology B* **2002**, *20*, 531–536.
25. Trinque, B. C.; Osborn, B. P.; Chambers, C. R.; Yu-Tsai, H.; Corry, S. B.; Chiba, T.; Hung, R. J.; Tran, H. V.; Zimmerman, P.; Miller, D.; Conley, W.; Willson, C. G. *Proceedings of the SPIE—The International Society for Optical Engineering* **2002**, *4690*, 58–68.
26. Kodama, S.; Kaneko, I.; Takebe, Y.; Okada, S.; Kawaguchi, Y.; Shida, N.; Ishikawa, S.; Toriumi, M.; Itani, T. *Proceedings of the SPIE—The International Society for Optical Engineering* **2002**, *4690*, 76–83.
27. Fedynyshyn, T. H.; Mowers, W. A.; Kunz, R.; Sinta, R.; Sworin, M.; Cabral, A.; Curtin, J. E. In *Polymers fir Microelectronics and Nanoelectronics*; Lin, Q., Pearson, R. A., Hedrick, J. C., Eds.; American Chemical Society: Washington, DC, 2004; vol. 784, pp. 54–71.
28. Bae, Y. C.; Douki, K.; Yu, T. Y.; Dai, J. Y.; Schmaljohann, D.; Koerner, H.; Ober, C. K. *Chemistry of Materials* **2002**, *14*, 1306–1313.

29. Fedynyshyn, T. H.; Kunz, R. R.; Sinta, R. F.; Sworin, M.; Mowers, W. A.; Goodman, R. B.; Doran, S. P. *Proceedings of the SPIE—The International Society for Optical Engineering* **2001**, *4345, pt. 1–2*, 296–307.
30. Dammel, R. R.; Sakamuri, R.; Sang-Ho, L.; Rahman, M. D.; Kudo, T.; Romano, A. R.; Rhodes, L. F.; Lipian, J.; Hacker, C.; Barnes, D. A. *Proceedings of the SPIE—The International Society for Optical Engineering* **2002**, *4690*, 101–109.
31. Allen, R. D.; Chen, K. J. R.; Gallagher-Wetmore, P. M. *Proceedings of the SPIE—The International Society for Optical Engineering* **1995**, *2438*, 250–260.
32. Barclay, G. G.; Hawker, C. J.; Ito, H.; Orellana, A.; Malenfant, P. R. L.; Sinta, R. F. *Macromolecules* **1998**, *31*, 1024–1031.
33. Thackeray, J. W.; Orsula, G. W.; Denison, M. *Proceedings of the SPIE—The International Society for Optical Engineering* **1994**, *2195*, 152–163.
34. Lin, Q.; Simons, J. P.; Angelopoulos, M.; Sooriyakumaran, R. *Proceedings of the SPIE—The International Society for Optical Engineering* **2002**, *4690*, 410–418.
35. Padmanaban, M.; Kinoshita, Y.; Kudo, T.; Lynch, T.; Masuda, S.; Nozaki, Y.; Okazaki, H.; Pawlowski, G.; Przybilla, K. J.; Roeschert, H.; Spiess, W.; Suehiro, N.; Wengenroth, H. *Proceedings of the SPIE—The International Society for Optical Engineering* **1994**, *2195*, 61–73.
36. Barclay, G. G.; King, M.; Orellana, A.; Malenfant, P. R. L.; Sinta, R.; Malmstrom, E.; Ito, H.; Hawker, C. J. In *Organic Thin Films* 1998; vol. 695, pp. 360–370.
37. Ito, H. *IBM Journal of Research and Development* **2001**, *45*, 683–695.
38. Toukhy, M. A.; Oberlander, J.; Rahman, D.; Houlihan, F. M. *Proceedings of the SPIE—The International Society for Optical Engineering* **2004**, *5376 (1)*, 384–391.
39. Dabbagh, G.; Houlihan, F. M.; Ruskin, I.; Hutton, R. S.; Nalamasu, O.; Reichmanis, E.; Gabor, A. H.; Medina, A. N. *Proceedings of the SPIE—The International Society for Optical Engineering* **1999**, *3678, pt. 1–2*, 86–93.
40. Rushkin, I. L.; Houlihan, F. M.; Kometani, J. M.; Hutton, R. S.; Timko, A. G.; Reichmanis, E.; Nalamasu, O.; Gabor, A. H.; Medina, A. N.; Slater, S. G.; Neisser, M. *Proceedings of the SPIE—The International Society for Optical Engineering* **1999**, *3678, pt. 1–2*, 44–50.
41. Singh, L.; Ludovice, P. J.; Henderson, C. L. *Proceedings of the SPIE—The International Society for Optical Engineering* **2005**, *5753*, 319.
42. Crivello, J. V. *Advances in Polymer Science* **1984**, *62*, 2–48.
43. Cameron, J. F.; Adams, T.; Orellana, A. J.; Rajaratnam, M. M.; Sinta, R. F. *Proceedings of the SPIE—The International Society for Optical Engineering* **1997**, *3049*, 473–484.
44. Ueno, T.; Schlegel, L.; Hayashi, N.; Shiraishi, H.; Iwayanagi, T. *Polymer Engineering and Science* **1992**, *32*, 1511–1515.
45. Cameron, J.; Fradkin, L.; Moore, K.; Pohlers, G. In *Proceedings of the SPIE—The International Society for Optical Engineering*; Houlihan, F., Ed., 2000; vol. 3999, pt.1–2, pp. 190–203.
46. Gokan, H.; Esho, S.; Ohnishi, Y. J. *Electrochem. Soc*. **1983**, *130*, 143.
47. Kunz, R.; Palmateer, S. C.; Forte, A. R.; Allen, R.; Wallraff, G.; DiPietro, P. A.; Hofer, D. *Proceedings of the SPIE—The International Society for Optical Engineering* **1996**, *2724*, 365–376.
48. Wallow, T.; Brock, P.; DiPietro, R.; Allen, R.; Opitz, J.; Sooriyakumaran, R.; Hofer, D.; Meute, J.; Byers, J.; Rich, G.; McCallum, M.; Schuetze, S.; Jayaraman, S.; Hullihen, K.; Vicari, R.; Rhodes, L.; Goodall, B.; Shick, R. *Proceedings of the SPIE—The International Society for Optical Engineering* **1998**, *3333, pt. 1–2*, 92–101.
49. Dammel, R. R.; Ficner, S.; Oberlander, J.; Klauck-Jacobs, A.; Padmanaban, M.; Khanna, D. N.; Durham, D. L. *Proceedings of the SPIE—The International Society for Optical Engineering* **1998**, *3333, pt. 1–2*, 144–151.
50. Jung, J. C.; Bok, C. K.; Baik, K. H. *Proceedings of the SPIE—The International Society for Optical Engineering* **1998**, *vol. 3333, pt. 1–2*, 11–25.
51. Fender, N.; Brock, P. J.; Chau, W.; Bangsaruntip, S.; Mahorowala, A.; Wallraff, G. M.; Hinsberg, W. D.; Larson, C. E.; Ito, H.; Breyta, G.; Burnham, K.; Truong, H.; Lawson, P.; Allen, R. D. *Proceedings of the SPIE—The International Society for Optical Engineering* **2001**, *vol. 4345, pt.1–2*, 417–427.

CHAPTER 58

Pyrolyzability of Preceramic Polymers

Yi Pang[†], Ke Feng[‡], and Yitbarek H. Mariam

Department of Chemistry & Center for High Performance Polymers and Composites, Clark Atlanta University, Atlanta, GA 30314

58.1 INTRODUCTION

Ceramic materials encompass a range of compounds such as silicates, carbides, nitrides, borides, oxides, sulfides, etc. Some of these materials have excellent mechanical properties under heavy stress, outstanding electrical properties, and exceptional resistance to high temperatures and corrosive environments. Such materials are generally known as high-technology ceramics/materials materials and it is because of their potential uses as engineering and structural materials that high-technology ceramics had gained intense interest in industry, government, and academia since early 1970s [1].

The potential uses cannot be fully realized, however, if the methods of preparation and/or fabrication of the materials have shortcomings and/or defects and are not economically feasible. This indeed had been true in the case of traditional methods of preparing ceramics which almost invariably required extremely high temperatures [2]. Fortunately, new and unconventional preparative methods have been developed since the mid-1970s as the result of Yajima *et al.'s* work, which led to the fabrication of silicon carbide (SiC) fibers based on the polysilane to polycarbosilane (PCS) transformation technology [3]. In such a transformalion, a metalorganic polymer may be converted to a ceramic, and the transformation is not unlike that for the preparation of carbon fibers, which can be summarized as shown below [4,5]

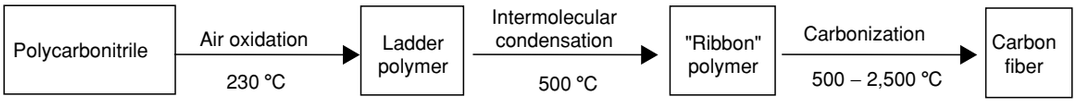

[†]Department of Chemistry, The University of Akron, Akron, OH 44325. [‡]Ticona, 8040 Dixie Highway, Florence, KY 41042

whereas the Yajirna *et al*. technology can be represented as [5]

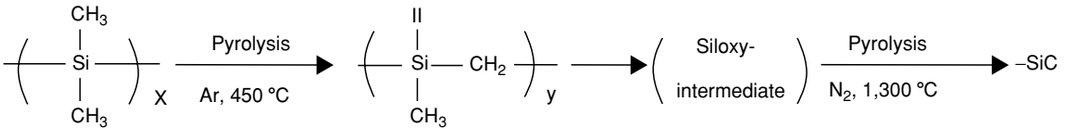

The Yajima *et al*. process [3] possesses general applicability to the preparation of ceramic materials from polymeric and oligomeric precursors via pyrolysis. In some cases even monomeric units can be used as precursors. Thus, the invention of the Yajima *et al*. process [3] has generated tremendous research activities in the synthesis of precursors and their pyrolytic conversion to ceramic powders and/or fibers, leading to the fields of what generally are known now as ''preceramic polymer chemistry'' and ''polymer pyrolysis technology'' [1,6].

The polymer pyrolysis technology has several advantages over the conventional methods and some of these include the ability to purify precursors at low cost; lower processing temperature; versatility of precursors to form complex shapes, films, fibers, etc; the opportunity to prepare novel materials such as ceramic–ceramic and ceramic–metal composites and modify chemical, physical, optical, mechanical, and electrical properties; and at least some ability to control grain size, microstructure, and crystallinity, thereby allowing densification at temperature lower than traditional processing temperatures.

Early work in the polymer pyrolysis technology area focused on the synthesis of preceramic polymers [7] with various elemental compositions and their pyrolytic conversion to ceramics. More recent work has, however, focused on the detailed studies of the precursor-to-ceramic conversion processes including amorphous to crystal transitions by several techniques. Despite the tremendous amount of work that has been accomplished in this area, the scope of this review will focus on pyrolyzability of precursors that lead to SiC and Si_3N_4 ceramics as judged primarily by the amount of ceramic product, but consideration of the extent of impurity such as free carbon, free silicon, and oxygen is also made.

58.2 PYROLYZABILITY

For the purposes of this review, pyrolyzability is defined as mineralizability, and the mineralization (from metalorganic to inorganic) can be in one of the three general ways (the term metalorganic will be used in this review as opposed to organometallic, since the latter is usually used to mean M–C (metal–carbon) bond [8]) presented below schematically (Scheme 58.1).

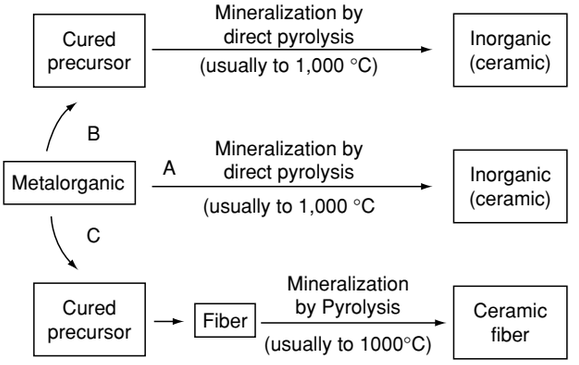

Whatever route is used, one of these three or any other similar ones, the transformation from metalorganic precursors to the final inorganic product can be roughly divided into three major stages spanning temperature ranges of a few hundred degrees each as shown in the following scheme (Scheme 58.2).

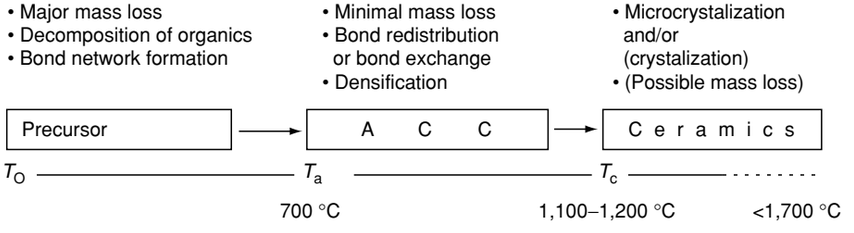

The first stage ($T_o - T_a$) can generally be up to 700 °C. This is a stage where a major mass loss occurs and can roughly be divided into two regions: below 400 °C and 400–700 °C. Below about 400 °C, cleavage of weak bonds such as Si–H, vinylic; Si–Si, N–H, and accompanying reactions will take place. In the range 400–700 °C, strong bonds such as C–C, C–N, Si–N, Si–C, and C–H will be affected. The exact nature of the reaction will depend on the type of functional group constituting the precursors and the method and/or approach of curing used. Typically, oxidative, thermal, and UV curing are undertaken. In some cases catalysts and free-radical initiators are used. Depending on which approach is taken, the type of reaction that is effected may be rather complex. Overall, what takes place in the first stage of the pyrolysis will include, but not be limited to, bond breaking and formation, cross-linking reaction, skeletal bond network formation and bond rearrangement, decomposition/fragmentation, and volatilization of organics. Significant changes in the atomic ratio of the starting material and density changes should also take place.

The second stage ($T_a - T_c$) can cover from roughly 700 °C to about 1,100–1,200 °C. This is a region of minimal mass loss and the material can be described as a disordered solid. Soraru, Babonneau, and Mackenzie [9] have described the materials in this temperature range as a ''new family of noncrystalline solids'' and have coined the term ''amorphous covalent ceramics (ACC)'' to describe the high degree of covalency of carbides and nitrides. As alluded to before, there is minimal mass loss in the range $T_a - T_c$. Figure 58.1 shows the thermogravimetric analysis (TGA) curve for a precursor prepared from dichloromethylvinylsilane and ethylenediamine (vide infra, Section 58.5.3). In the TGA experiment, the material was heated to 700 °C, held at 700 °C for 1 h, and then further heated to 1,000 °C (Fig. 58.1). There was only about 2 wt% loss between 700 and 1,000 °C compared to 31 wt% between 400 and 700 °C and about 8 wt% below 400 °C (at least some of which can be accounted for by loss of solvent and low-molecular-weight products) for a total of 39 wt%. The solid-state ^{29}SiNMR spectra of three samples of the precursor pyrolyzed in a furnace at 400, 700, and 900 °C for 1 h in N_2 are also shown in the inset. The chemical shifts, assignments, and the percentage composition of each component (determined by NMR) are indicated in Fig. 58.1.

The spectral data clearly show that even though the weight loss is minimal in the 700–1,000 °C range, there

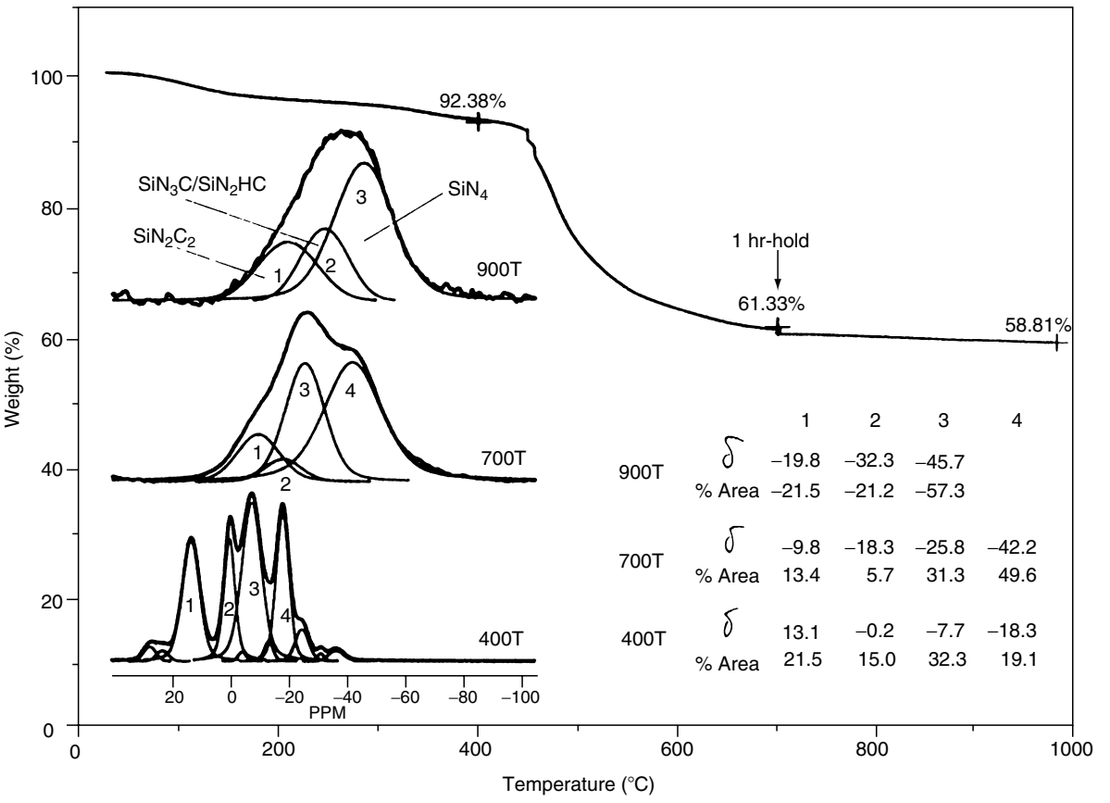

FIGURE 58.1. (A) TGA profile (5 °C/min, N_2 of poly(methylvinyisily)ethylenediamine (see Ref. [194] for structure). (B) 39.7 MHz ^{29}SI CP/MAS spectra with simulations of samples 400T, 700T, and 900T. [Heating schedules for samples 400T, 700T, and 900T were 5 °C/min (in N_2) from room termperature (RT) to 400, 700, and 900 °C, respectively, a 1 h-hold at the respective temperature, and furnace cooling (at approx. 100 °C/h) to RT]. δ (chemical shift) is in ppm relative to external tetramethylsilane.

are clear indications for chemical transformations such as Si–C– N→Si–N–C taking place. While there are not enough data in the literature to ascertain that this kind of chemical trans-formation does take place in every case, it can be generally assumed that the weight loss is minimal, in most cases, in the $T_a - T_c$ range.

Finally, above T_c, a given ceramic product may remain amorphous or in microcrystalline form. In some, and perhaps most, cases crystallization will take place. The final product and its physical characteristics will differ and depend on the nature of the starting material as well as on the processing atmosphere and temperature. For example, Nicalon, which is nearly amorphous, contains 61% SiC, 28% SiO_2, and 10% free carbon [10]. Some precursors give excess free carbon or free silicon. Such impurities usually hinder crystallization and may bring problems of oxidation at high temperature in wet air [lla], e.g., $Si_3N_4 + O_2 \rightarrow SiO_2 + N_2$. Additionally, decomposition reactions are possible in some cases. For example, if Si_3N_4 is formed along with free carbon, the reaction $Si_3N_4 + 3C \rightarrow 43SiC + 2N_2(gas)$ has been observed above 1,450 °C in Ar [1lb]. Similarly, the presence of SiO_2 and excess Si and C along with SiC may lead to reactions such as [12] (i) $3Si + 2N_2 \rightarrow Si_3N_4$; (ii) $3SiO_2 + 6C + 2N_2 \rightarrow Si_3N_4$; (iii) $SiC + CO \rightarrow SiO + 2C$; and maybe even (iv) $2CO \rightarrow CO_2 + C$.

Oxygen impurities are sometimes introduced by inadvertent hydrolysis or during oxidative curing. The presence of oxygen has be shown, experimentally, to lower thermal stability especially when the weight% content of oxygen is greater than about 1.4 [13].

58.3 LATENT REACTIVITY, CERAMIC YIELD, AND DENSITY CHANGES

Most Si-containing ceramics have densities between 2.5 and 3.5 g ml^{-1}, which are significantly higher than their precursors ($\sim$ 1 g ml^{-1}). For a pyrolytic process of no mass loss (100% ceramic yield), transformation from a precursor to the densified ceramics will bring about 70% volume change. In reality, the pyrolytic conversion of precursors to ceramic materials involves additional volume changes as extraneous organic ligands are removed as gaseous products. This process may, and often does, create porosity/voids and densification-induced stress [14]. If problems associated with porosity/voids and densification are to be minimized the ceramic yield (=weight of ceramic residue $\times$ 100/weight of pyrolysis charge) should be in an acceptable range of 60–75% or greater. The lower the quantity of gases evolved, the higher the ceramic yield [15]. Cracking and/or rupture of the ceramic product can happen especially if the gases are released in a narrow range of temperatures [15]. The pyrolyzability of a given precursor should then be considered from a practical point view of whether the precursor gives the desired composition and with reasonably high yield (low yield can sometimes be tolerated if the ceramic product is pure and the porosity generated during pyrolysis has open porosity so that the pyrolysis gases can escape [15]). A precursor should, therefore, have at least two inherent characteristics: latent reactivity and branched structures. The latent reactivity can provide the opportunity for cross-linking and thereby provide for both maintaining appropriate shape during processing and high ceramic yield. Linear polymers generally give low ceramic yield due to backbone reactions, which lead to volatiles. Branched structures can, however, slow backbone reactions by sterically hindered structures that require multiple bond ruptures [8,15]. The branching should not, however, be too extensive so as to restrict chain mobility that may lead to poor mechanical property. In the case of linear structures, linkages such as Si–Si can lead to cross-linking after UV radiation treatment. The capacity of a given precursor to give the desired product in reasonable yield also depends on the molecular weight of the precursor [16] (at least in some cases), the curing and pyrolysis condition [temperature and atmosphere (inert versus reactive gas)], heating rate, etc.

58.4 SILICON CARBIDE (SIC) AND SILICON NITRIDE (Si_3N_4)

SiC and Si_3N_4 are two of the most studied nonoxide ceramic materials derived from metalorganic precursors (others include BN, B_4C_3, and AlN). The conventional methods of preparation of Si_3N_4 powder are [2(a)] (a) nitridation of silicon (at 1,200–1,450 °C), $3Si + 2N_2 \rightarrow Si_3N_4$; (b) carbothermic reduction of silica (at 1,200–1,450 °C), $3SiO_2 + 6C + 2N_2 \rightarrow Si_3N_4 + 6CO$; (c) gas-phase ammonolysis of silicon tetrachloride, $3SiC1_4 + 4NH_3 \rightarrow Si_3N_4 + 12HCl$; (d) thermal decomposition of silicon diimide, $3Si(NH)_2 \rightarrow Si_3N_4 + 2NH_3$. On the other hand, SiC can be prepared by the high-temperature (2,600 °C) reaction between silicon dioxide and graphite [17], $SiO_2 + C \rightarrow SiC + CO$. Both Si_3N_4 and SiC prepared by the conventional methods are expected to be infusible, intractable, and not applicable for the preparation of fibers and films. The structure of SiC is based on the diamond structure with both Si and C tetrahedral and with alternating Si and C atoms [18]. The basic structural types (polymorphs) are thus hexagonal α-SiC and cubic β-SiC. As opposed to diamond, SiC has many crystalline α-SiC modifications called polytypes, and approximately 200 polytypes have been determined [18]. Similarly, Si_3N_4 is found to have two crystalline forms (α and β forms), and in both structures each silicon atom is tetrahedrally bonded to four nitrogens [19]. Both SiC [20] and Si_3N_4 [21] can be used as tough and refractory materials.

58.5 PYROLYSIS DATA ON SiC AND Si_3N_4 PRECURSORS

The pyrolyzability of a fair number of SiC, Si_3N_4, and Si_3N_4/SiC precursors are examined in various tables below. Data included in the tables are the approximate structures/representations of the precursors, the pyrolysis conditions, and the compositions of the residues. The precursors are grouped together so that direct comparisons can easily be made. Thus, the tables should be, to some extent at least, self-explanatory. In some selected cases, specific curing, and/or other treatments are also indicated in the tables to illustrate the effects of those treatments. In those cases where curing and/or other treatments, ceramic yields, and pyrolysis conditions are not indicated, it generally means either none was done or the relevant information was not available. In all the tables P and Y denote, respectively, pyrolysis conditions (temperature/atmosphere) and ceramic yield (as in Table 58.1). In a number of cases, the compositions of the residues are not given in detail. This is either indicated by NDG (no details given) or left blank and the original publication can be consulted for additional information.

58.5.1 SiC Precursors

Metalorganic precursors for SiC include polysilanes, polycarbosilanes, silicon–acetylene and silicon–olefin polymers, polysiloxanes, polysilsesquioxanes, and polydisilylazanes. Polysilanes are generally converted to a polycarbosilane by thermal, oxidative, and UV radiation curing. UV radiation curing is used sometimes to convert polysilanes to SiC directly. Lack of space here does not allow us to cover all the synthetic aspects of SiC precursors. These are, however, excellent reviews that deal with the synthetic aspects, uses, and applications as well as characterization in some cases [1,7,14,22–31]. These and the original publications can thus be consulted for further details. In some cases, the precursors have been modified to incorporate metals such as titanium to prepare precursors such as polytitanocarbosilane [32,33]. These are also not covered here in any detail. There are a number of elegant works dealing with the direct synthesis of polycarbosilanes for which the reviews cited and the original publications can be consulted.

Polysilanes

Entries (1)–(6) in Table 58.1 compare polydimethylsilane (PDMS) [5,34,35] with other polysilanes. West and coworkers [35] have actually reported a fairly large number of polysilanes although thermal analysis data are not always reported on them. Abu-eid, King, and Kotliar [41] have investigated polyorganosilanes of the type $[R_1R_2Si]_,$, where $R_1 = CH_3$ and $R_2 = H$, C_2H_5, etc. The yields were $<25\%$ (at 750 °C), except for the case $R_2 = H$

TABLE 58.1. *Pyrolysis data on polysllane precursors: Comparison of PDMS with other polysilanes.*

Precursors	Pyrolysis condition, yield, and composition			References
	P[a]	Y[b]	Residue and impurities	
(1) Polydimethylsilane (PDMS): —$Si(Me)_2$— (T=400 °C)[c]	a		SiC; NDG	[5,34,35]
(2) Polysilastyrene (UV)[d]	a	30	SiC; NDG	[35–37]
(3) Polysilastyrene (T=500 °C)[c]	b	68	SiC; C (30°)	[36,37]
(4) —(SiM_2)—	c	1	SiC; C	[38,39]
(5) —(PhSiMe)—	c	24.6	SiC; C	[39]
(6) —[(C_6H_{13})SiMe]—	c	5.8	SiC; C	[39]
(7) PDMS + $B(OR)_3$(cat., 380–400 °C)[e]	d	63–80		[40]
(8) PDMS+PBDBS (cat., 340 °C)[e]			NDG	[44]
(9) PDMS→"SiC" fiber			SiC; <2%O	[46]
(10) PDMS→PCS fiber→SiC fiber	e	60–65	SiC	[47]
(11) PDMS→PCS	e	58–87	SiC, O	[48]
(12) PDMS (T=4000 °C)[c]	e	60	β-SiC; C, O?	[34]
(13) Yajima *et al.*'s PCS	f	42	SiC (83%);C (14.5%), SiO_2 (2%)	[49]
(14) Yajima *et al.*' PCS	g	54	Si_3N_4; C (4.5%), SiO_2 (8.4%),	[49]
(15) Nicalon SiC-based fibers, NG 100		NI[f]	SiC, SiC_2O_2,SiO_4C_{graph}[g] (35%)	[50]
(16) Nicalon SiC-based fibers, NG 200		NI	SiC, SiC_2O_2,$SiCO_3$,SiO_4,C_{graph}. (19%)	[50]
(17) Polytitanocarbosllance	h	75	SiC/TiC, C, O ($SiC_{4-x}O_x$)	[32,33]

[a]Pyrolitic conditions: a, >800 °C; b, 1,500 °C/Ar; c, 1,000 °C/Ar;, d, 900 °C; e, 1,300 °C/Ar or vacuum; f, 1,350 °C/Ar; g, 1,350 °C/(Ar/NH_3: 70/30); h, 840 °C.
[b]Yield in wt% of residue recovered at the pyrolysis condition.
[c]Precursors were heat-treated at the temperatures Indicated before being pyrolized.
[d] Precursors were UV irradiated before being pyrolized.
[e]Precursors were treated with a catalyst at the indicated temperatures before being pyrolized.
[f]NI denotes "not indicated."
[g]C_{graph} denotes graphite.

(yield = 60%) [41]. A report by Sinclair [5] on polysilastyrene indicated a ceramic yield of 63% at 500 °C when UV cured. Copolymers and terpolymers reported by Carlesson and coworkers [39] are not included here because of space limitation. Unlike PDMS, which requires some sort of curing, conversion to an intermediate carbosilane polymer is unnecessary in the case of polysilastyrene [42] and vinylic silane, $Me_3Si-(MeSiH)_x-(MeSiVi)-SiMe_3$ (Vi denotes vinyl), which gives mostly SiC in 72% yield (1,000 °C/inert gas) after cross-linking with 6% dicumyl peroxide at 250 °C [43]. Entries (7)–(17) are also based on PDMS. As the examples shown here indicate, PDMS is probably the most studied metalorganic precursor. Entries (7) and (8) are examples of use of catalysts for the conversion of PDMS to PCS without the use of autoclave [40,44]. Catalysts used other than $B(OR)_3$ and PBDPS (polyborodiphenylsiloxane [44,45]) are $MeBN(SiMe_3)_2$ [40] and $B(NEt_2)_3$ [40]. Entries (9)–(16) deal with fibers [45–50]. The difference between precursors (15) and (16) is the oxygen content [16% (mass) for NG100 and 11% for NG200 [50]]. The percentage composition of SiC_4(=SiC), Si_2O_2, $SiCO_3$, SiO_4, and C_{graph}. was 64/65, 9, 12, 15, and 35 for (15) and 78/81, 7, 7, 7, and 19 for (16), respectively, as determined by NMR studies [50].

Several other studies on Nicalon-based ceramic fibers have also been conducted in addition to the investigation of oxidation curing of PCS fibers and effect of oxygen in tensile strength of SiC fibers [51]. Similarly, studies dealing with the chemistry, characterization, modification, use, and applications of polysilanes and polycarbosilane are also available [52].

Data on various other polysilanes are presented in Table 58.2. The vinylic polysilane in entry (1) is that of Schilling's sodium-derived vinylic polysilane [54], the pyrolysis of which had been investigated by Schmidt and coworkers [53]. Fibers were prepared (and investigated [13]) from entries (2)–(4). In the case of entry (4), 1 wt% of PBDPS was added and the oxygen content in the residue was 1.4 wt%. The tensile strength and Young's moduli determination showed that when the oxygen content is > 1.4 or so, the heat resistance property was poor (at about 1,600 and 1,800 °C [13]). DMCS (dodecamethylcyclohexasilane) has also been investigated before for fiber production [58]. The system in entry (5) represents a family of polysilanes

TABLE 58.2. *Pyrolysis data on polysilane precursors with various structures.*

Precursors	Pyrolysis condition, yield, and composition			References
	P[a]	Y	Residue and impurities	
(1) Vinylic polysilane (Schilling's system)	a	57	SiC; C (17%)0	[53]
(2) HO–($(Me)_2Si$)–OH (AC, 470 °C)[b]	Fiber		SiC; 0 (0.35%); Si/C=1.35	[13]
(3) $[(Me)_2Si]_6$ (DMCS) (AC, 480 °C)[b]	Fiber		SiC; 0(0.2%); Si/C=1.41–1.35	[13]
(4) HO–((Me_2)Si–)–OH+PBDPS (cat., 420 °C)[c]	Fiber		SiC; O(1.4%);	[13]
(5) $\{RR'Si[(CH_2)_r]_s\}_n$	b	18–65	SiC;NDG	[54]
(6) H–(SiMeH)–H	a	77	SiC; O, H,=($Si_1C_{0.9}H<0.2O_{0.1}$)	[55]
(7) $[(MeSiH)_x(CH_3Si)_y]_n$	c	12–27	SiC (77%); C (23%)	[56]
(8) $[(MeSiH)_x(CH_3Si)_y]_n$ (ca.)[b]		71–85	SiC (95%); Si(5%), ZrC/TC (<2%)	56
(9) $[(MeSiH)_x(CH_3Si)_y]_n$ (XL)[d]		60	SiC; Si (25.6%)	[56]
(10) Methyloplysilane	d	97[e]	SiC;81%; SiO_2: 12%; C: 7%; 0: 2%	[57]
(11) Commercial Si–C–O fiber (Nicalon)	d	82	SiC; O (11%)	[57]
(12) $-(Si(Me)_2-C_6H_4)_n-$, n=28		58	SiC; NDG	[59]
(13) Methylpolysiane $(MeSi)_x(RSi)_y(R'Si)_z$	b	40–60	SiC; O impurity present	[60]
(14) $(MeSiH)_{0.35}(MeSiPh)_{0.4}(MeSi)_{0.25}$		30[f]	SiC; O impurity present	[61]
(15) $(MeSiH)_{0.3}(Me_2Si)_{0.3}(MeSi)_{0.4}$	f	20[g]	SiC; O impurity present	[61]
(16)$(MeSiH)_{0.3}(MeSiPh)_{0.7}$	f	10[e]	SiC; O impurity present	[61]
(17) Hydropolysilane	g	19–53	SiC; C (4–40%)	[62]
(18) $[(MeSiH)_{30}(PhSiMe)_{70}]_n$(I)	f	8.2–13.8	NDG	[63]
(19) $[(MeSiH)_{25}(PhSiMe)_{40}(MeSi)_{35}]_n$(II)	f	8.2–13.8	NDG	[63]
(20) PPMCHS[h]		31	SiC; NDG	[64(a)]
(21) PPMCHS[d]		41	SiC; NDG	[64(a)]
(22) $(MeSiH)_x(CH_2=CH-SiH)_y$	g		SiC	[64(b)]

[a]Pyrolitic conditions: a, 1,000 °C/N_2; b, 1,200 °C; c, 950 °C/A; d, 540 °C/He; e, 600–900 °C/N_2; f, 900 °C/N_2; g, 1,400 °C/N_2.
[b]Autoclave (AC) used at temperatures specified.
[c]Catalyst (group-IV metal complexes) used at temperatures specified.
[d]Cross-linked.
[e]Data are for fiber.
[f]When pyrolized in air at 900 °C, yield was 100%.
[g]When pyrolized in air at 900 °C, yield was 70%.
[h]PPMCHS= poly(permethylcyclohexasilane).
[i]When pyrolized in air at 900 °C, yield was 50%.

synthesized and investigated by Schilling [54]. Of the 15 polysilanes studied, the preferred R is Me or H while the preferred R' is vinyl. The polymers that gave the highest ceramic yields (64.5% and 56.6%) were prepared from a mixture of, respectively, $Me_3SiCl/MeSiHC1_2/CH_2 = CHSiMeC1_2$ and $Me_2SiC1_2/CH_2{=}CHSiMeC1_2$ in 1.0/0.3/1.0 and 1/1 ratios, respectively [54]. The presence of microcrystalline β-SiC was confirmed by x-ray diffraction for the former system. The precursors can be directly converted to SiC, and impurities in the residue were not reported. The poly(methylsilane) (MPS) of entry (6) is reported [55] to produce near-stoichometric (with minor H and O impurities), noncrystalline SiC at temperatures that are lower than some cases [55]. Polysilanes of entries (7)–(9) where $(x + y = 1)$ gave a substantial amount of elemental Si when pyrolyzed. However, use of catalytic quantities of group-IV–metal–organometallic complexes or borate (such as $B(OSiMe_3)_3$) resulted in cross-linking processes such that pyrolysis of these polysilanes gave close to stoichiometric SiC (>95 wt%) and only very little elemental Si. Fibers prepared from MPS [57] of entry (10) can be compared to that of entry (11) (with its higher oxygen content). The composition reported was determined using rule of mixtures calculation from elemental analysis data. Ceramic fibers with 2 wt% oxygen contain 80 wt% noncrystalline SiC having 2 nm crystallite size in a continuous glassy silicon oxycarbide phase. The excess carbon is thought to be in the form of microcrystalline, terbostratic pyrolytic carbon [57]. MPS fibers with low oxygen content (<1%) are expected to have more β-SiC polycrystallinity, improved thermal stability, and higher elastic modulus. The ceramic yields of entry (12) were 15% and 32% for n = 5 and 13, respectively [59]. No additional compositional information was provided for these systems. The organic substituents of MPS entry (13) were methyl, phenyl, and *n*-octyl and various ratios (five different cases) of these were used. T_g values [by Dupont TMA (thermomechanical analyzer)] ranged from 53 to 155 °C while the oxygen content ranged from 0.42 to 2 wt%. The authors reported that modification of a branched polymethylsilane by substitution with higher alkyl or aryl groups allows control of preceramic polymer rheology and ceramic char composition (for melt spinning of fibers and production of stoichiometric SiC). The thermal sensitivity and degradation of linear and branched hydropolysilane [61,62] and evaluation of crosslinking of hydropolysilanes [63] have been investigated by Sawan and coworkers [61–63]. For entries (14)–(16), the ceramic yields were 100%, 70%, and 50% (at 900 °C) when pyrolyzed in air [61]. About 14 hydropolysilanes [copolymers with methyl and phenyl substitutes in various combinations, entry (17)] were investigated by Shieh, Sawan, and Milstein [62]. The C/Si ratios ranged from 3.2 to 11.3 with one exception for which the ratio was 1.3. The residue of only four systems had free carbon greater than about 10% and the free carbon was indiscernible for several cases. The one with the highest yield [52.6%, prepared from a mixture of $PhSiHC1_2/(CH_3)_2SiC1_2/CH_3SiC1_3 = 50/25/15$] had a C/Si ratio of 5 and 5.7% free carbon. The work by Shieh and Sawan used different cross-linking agents [63]. The yields for I and II [entries (18) and (19)] were 8.2 and 38.6% before cross-linking. Using $C1CH_2C1$, tetravinylsilane, and trivinylmethylsilane as cross-linking agents, the yields were 9.2%, 21.6%, and 13.8% for I and 38.3%, 53.5%, and 47.5% for II, respectively.

Polycarbosilanes: Directly Synthesized Precursors

The synthesis of poly[(methylchlorosilylene)methylene] (PMCS-Cl) [65(a)] and poly(silapropylene) (PSP) [65(b)] have been reported by Bacque and coworkers [65,66]. Derivatives of PMCS–Cl where Cl has been replaced by H, D, –Si,–NH–Si,–NHMe,–NMe_2, etc. has been accomplished [67]. It was shown in further work by the same group [67] that derivatives prepared from PMCS–Cl by reacting the Si–Cl functionality with Na, K, Me_2NH, $MeNH_2$, NH_3, and H_2O and the Si–H functionality with 1,3-butadiene and divinylbenzene gave, upon pyrolysis (1,000 °C/Ar), relatively low ceramic yields which ranged from 11.4 to 77.6%. Of these the four highest yields were the Na, K, $MeNH_2$, and H_2O derivatives with yields, respectively, 77.6%, 59.3%, 53%, and 54.3%. The yields for the K, Na, $MeNH_2$ derivatives were for insoluble and unmeltable fractions of the product. All samples pyrolyzed at 1,200 °C were reported to contain O impurities (14–24 at.%) [67(b)]. Poly[(dimethylsilylene)methylene] [=poly(silabutylene)] has been converted to PSP [PSP-1, entry (1), Table 58.3]. The low ceramic yield for PSP-1 was attributed to the linearity of the polymers. PMCS-Cl and PSP were also synthesized by Wu and Interrante [68] by ring-opening polymerization of 1,3-dichloro-1,3-dimethyl- 1,3-disilacyclobutane, which was in turn prepared from $C1_2(Me)SiCH_2C1$. The PSP prepared this way is designed as PSP-2 in entry (2). The thermal properties of entries (1)–(6) should be evident from Table 58.3. Related work has dealt with the structural elucidation of a PCS [70] derived from $C1_3SiCH_2C1$ and the ceramic evolution of PCS [71] prepared by the Yajima *et al*. process [48(d)]. The effect of thermal cross-linking is demonstrated by the data in entries (7) and (8). Interrante *et al*. [72] have also investigated Schilling's VPS [73,74] of entries (9) and (10). The approximate composition of the VPS was determined by NMR to be $\{[Si(Me)_3]_{0.32}[Si(CH{=}CH_2)Me]_{0.35}[Si(H)Me]_{0.18}[SiMe_2]_{0.7}[CH_2SiMe]_{0.08}\}_n$. The ceramic composition of entry (11) is close to $Si_4C_5O_2$ and can be described as a continuum of SiC_4 and/or $SiC_{4-x}O_x$ tetrahedral species (and possibly contains free carbon) with homogeneity domain size less than 1 nm. Although details are not given here, SiC/AlN ceramics have been prepared by using polycarbosilane and appropriate polymers [77(a–c)]. Photoirradiation of poly[(methylsilylene)methylene can rapidly lead to a crosslinked structure, which is then pyrolyzed at 1,200 °C to give a β-SiC ceramics (C:Si = 1.79:1) in 70% yield [77(d)].

TABLE 58.3. *Pyrolysis data on poly(silapropylenes) (PSPs).*

Precursors	Pyrolysis condition, yield, and composition			References
	P[a]	Y	Residue and impurities	
(1) $\{Me_2Si-CH_2\} \rightarrow$ PSP-1(linear)	a	5	SiC; NDG	[65,66]
(2) $Cl_2MeSi-CH_2Cl \rightarrow$ PSP-2	b	10	SiC; NDG	[68]
(3) PSP-2a$\{CH_3SiH-CH_2\}$[b]	b	20	SiC; NDG	[68]
(4) PSP-2(TXL , 400 °C)[c]	c	66	β-SiC (at 1,600 °C); NDG	[68]
(5) $\{SiH_2-CH_2\}$	b	80	SiC, NDG	[69]
(6) $\{(Me)_2Si-CH_2\}$	b	0		[69]
(7) $\{SiH_{2-x}Et_x-CH_2\}_{x=0.15}$	b	58–76	NDG	[72]
(8) $\{SiH_{2-x}Et_x-CH_2\}$ (TXL, 80–200 °C)[c]	b	80	β-SiC[d]; low C[e]	[72]
(9) VPS (Union Carbide Y-12044)	b	55	β-SiC[d]; C-rich	[72]
(10) VPS (Union Carbide Y-12044)	d	40	α-Si_3N_4; C (1.8%)	[72,75]
(11) $\{HSiCH_3-CH_2\}$(OX)[f, g]	e	85	SiC; $SiC_{4-x}O_x$; C(?)	[76]

[a]Pyrolitic conditions: a, 1,000 °C/Ar; b, 1,000 °C/N_2, c, 1,200 °C/N_2; d, 1,000 °C/NH_3; e, 1,200 °C inert gas.
[b]PSP-2a has a higher molecular weight than PSP-2 for entries 1 and 2, the yields are for PSP-1 and PSP-2.
[c]Thermal cross-linking at the temperatures indicated.
[d]Partially crystalline.
[e]Compare to VPS No. 9.
[f]Oxidative curing.
[g]Yajima *et al.* PCS.

Entries (1)–(4) in Table 58.4 are for polysilmethylene or polysilaethylene (PSM or PSE, respectively). PSM was synthesized by ring-opening polymerization of 1,3-disilacy-clobutane [78] and the PSE's [entries (2)–(4)] from 1,1,3,3-tetrachloro-1,3-disilacyclobutane [79,80]. PSM is believed to be linear and can be used to make fibers or molded and shaped in various forms. The SiC obtained from PSM had amorphous and crystalline components at 900 °C [78]. The ceramic yield difference between PSE-I and PSE-II is attributed to a difference in molecular-weight distribution ($M_n = 10\ 762$ and $M_w = 32\ 823$ for PSE-I; $M_n = 7,480$ and $M_w = 25\ 600$ for PSE-II [79]). NMR data on PSE ($M_n = 12\ 300$ and $M_w = 33,\ 000$) was consistent with the expected structure, $(-SiH_2-CH_2-)_n$, and gave α-SiC (at 1,000 °C/N_2) with average crystallite size of 2.5 nm, indicating a high level of purity for the results that an initially cross-linked structure is by no means a requirement for high ceramic yields [80].

Entries (5)–(7) compare PCS (Dow Corning X9-6348, $\{[-(Me)_2Si-CH_2-]_{1.00}[-(Me)_2Si-CH_2-]_{0.8}\}$ and poly-(ethynyl)carbosilane prepared by chemical modification of PCS to provide a precursor with high solubility and latent reactivity [81]. The data in entry (5) are for the original PCS. Pyrolysis to 1,000 °C gave –SiC with small crystal-lites [by x-ray diffraction (XRD)] [81]. In entries (8) and (9), data for poly(vinylsilane) (=polysilylethylene) and poly(dimethylsi-lylethylene) are provided [82,83]. The former was synthe-sized from $ViSiHC1_2$ and the latter from $ViSiHMe_2$ (Vi=vinyl).

The data provided in entries (10)–(26) should be pretty self-explanatory. For entries (13)–(15), the structures given are only approximate (as are probably for many other cases, in general) and NMR results have shown (13)–(15) to be composed of a mixture of PCS (74%) and polysilane (26%) [86]. The use of 10 mol% of the potential cross-linking agent 1,2-disilylethene ($H_3SiCH_2CH_2SiH_3$) BSE during polymerization did not significantly increase the polymer molecular weight of the vinylsilane polymer in contrast to what was observed for methylsilane polymerization [86]. In the case of entry (21), when polysiltrimethylene was pre-pared from allyldiphenylsilane ($H_2C=CH-CH_2SiHPh_2$) [88], the ceramic yield was 30%.

Overall the data presented here attempt to bring out the influence of $Si-CH=CH_2$ and $Si-H$ functional groups and the comparison of precursors with $-SiCH_2-$, $-SiCH_2CH_2-$, and $-SiCH_2CH_2CH_2-$ unit in the main chain. UV-irradiation of $[-(CH_2=CH)_2SiCH_2-]_n$ can lead to a crosslinked material, which then pyrolyzed at 1,000 °C to give SiC ceramics in 58% yield [80(c)].

Table 58.5 deals with several PCS precursors to SiC investigated by Schilling and coworkers. Those in entries (1)–(5) were based on K metal dechlorination of mixtures of vinylmethylchlorosilanes or methyltrichlosilane [91]. This is a one-step preparation of branched PCS. For entries (3) and (5), the starting monomers are indicated since the struc-tures of the PCS's were not provided. Those in entries (6)–(8) and (11) are K-derived while (9) and (10) were Na-derived [73,91(c)]. Precursor (6) was prepared from $Me_3Cl/MeSiC1_2/CH_2=CHSiMeC1_2 = 0.85/0.3/1$. When Me_2SiC1_2 was changed to $MeSiHC1_2$, the $=Si-H$ modified PCS gave a ''SiC'' yield of 50% (1,200 °C). Precursor (7) was prepared by reaction of $H-C\equiv C-Na$ with $\{-[Si(Cl)MeCH_2]_x-[SiMe_2CH_2]_{1.0}-[SiHMeCH_2]_{0.8-x}-\}_n$, while precursor (8) was obtained by self hydosilylation of $CH_2=CH-SiHCl_2$ followed by reduction with $LiAlH_4$. Precursor (9) was prepared using the same ratio as in (6)

TABLE 58.4. *Pyrolysis data on various PCSs.*

Precursors	Pyrolysis condition, yield, and composition			References
	P[a]	Y	Residue and impurities	
(1) Polysilmethylene (PSM)	a	85	SiC; NDG	[78]
(2) Polysilaethylene (PSE-I)	b	80	SiC; NDG	[79]
(3) Polysilaethylene (PSE-II)	b	60	SiC; NDG	[79]
(4) Polysilaethylene	c	87	β-SiC (at 1,000 °C); NDG	[80]
(5) PCS (Dow Corning X9-6348)	d	63[b]	SiC; NDG	[82]
(6) Poly(ethylnyl)carbosilane	d	74[b]	SiC; NDG	[81]
(7) Poly(ethylnyl)carbosilane (UV)[c]	d	85[b]	SiC; no surface oxide contamination	[81]
(8) $+Si(H)_2-CH_2CH_2+$	b	30–40	SiC; slight excess C, H, O	[82,83]
(9) $+Si(Me)_2-CH_2CH_2+$	e	0	NDG	[84]
(10) PCS-I[d]	f	32	β-SiC; O (0.3–3%)	[84,85]
(11) PCS-II[e]	f	12	β-SiC; O (0.3–3%)	[84]
(12) PCS-III[f]	f	52	β-SiC; O (0.3–3%)	[84]
(13) $ViSiH_2-SiViH-H_2SiVi$	g	60	SiC; C-rich, 3% Ti (from catalyst)	[86]
(14) $MeSiH_2-SiMeH-SiH_2Me$	g	65	SiC; NDG	[86]
(15) Copolymer[g]	g	73	SiC (CSi = 1.3); NDG	[86]
(16) $SiH_3-(C_2H_4SiH_2)_n-H$(A)	g	12	NDG	[87]
(17) $H_3Si-(C_2H_4SiH_2)_n-Vi$	g	30	SiC; 0.19 C, 0.01 SiO_2	[87]
(18) $H_2ViSi-(C_2H_4SiH_2)_n-Vi$	g	56	NDG	[87]
(19) $+SiViH-C_2H_4+_n$(B)	g	60	SiC; 2.21 C, 0.03 SiO_2	[87]
(20) 2.5(A) + 1.0(B)	g	62	SiC; 1.41 C, 0.07 SiO_2	[87]
(21) $+SiH_2-CH_2CH_2CH_2+_n$	h	45–50	SiC; NDG	[88]
(22) $H-[SiH(C_2H_4SiH_2Me)]_n-H$ + Ti(*cat.*)	b	73	Si/C=1.01/1, −SiC (at 1,400 °C)	[89]
(23) $-[SiH(C_2H_4SiHMe)]_n-$ + Ti (cat.)	b	73	Si/C=1.01/1, −SiC (at 1,400 °C)	[89]
(24) $-[SiH(C_2H_4SiHMe)]_n-$ + no Ti	b	30	NDG	[89]
(25) $[(Cl_2Si)_{1.5}SiCl(CH_2)_3]_x$	b	22.6	NDG	[90]
(26) $[(H_2Si)_{1.5}SiH(CH_2)_3]_x$	b	30.9	NDG	[90]

[a]Pyrolitic conditions: a, 900 °C/Ar; b, 1,200 °C/(N_2orAr);c, > 600 °C/N_2; d, 950 °C/Ar; e, 550 °C/Ar; f, 1,000 °C; g, 1,400 °C/N_2; h, 1,300 °C.
[b]Fibers.
[c]UV radiation.
[d]PCS-I=$ViSiH_2-[C_2H_4-SiH_2]-[CH(Me)-SiH_2]-SiH_3$.
[e]PCS-II=$H_3Si-[C_2H_4-SiH_2]-[CH(Me)-SiH_2]-SiMe_3$.
[f]PCS-III=$ViSiH_2-[C_2H_4-SiH_2]-[CH(Me)-SiH_2]-SiH_2Vi$.
[g]30% vinylsilane/70% methylsilane.

TABLE 58.5. *Pyrolysis data on PCSs prepared mostly by K and Na dechlorination of chlorisllanes.*

Precursors	Pyrolysis condition, yield, and composition			References
	P[a]	Y	Residue and impurities	
(1) $(Me_3Si)_{0.5}(CH_2-CH(-SiMe)-)_{1.0}(SiMe_2)_{1.0}$	a	18–43		[91]
(2) $+CH_2-SiMe_2+$	a	Nil		[91]
(3) $ClCH_2SiMe_2Cl + MeSiCl_3 \rightarrow$ PCS	a	30.8		[91]
(4) $+CH_2CH(SiMe_3)-Si(Me)_2+_x$	a	Nil		[91]
(5) $MeSiCl_2 + ViSiMe_3 \rightarrow$ PCS		40.9		[91]
(6) $(Me_3-Si)_{0.85}(SiMe_2)_{0.3}(CH_2-CH(-)-SiMe)_{1.0}$	b	32		[74]
(7) $+Me-Si-CH_2-CH(Ph)+$	a	28		[74]
(8) $+Me-Si-CH_2-C(Me)=CHCH_2+$	a	25		[73,74]
(9) $Me_3Si(SiMe_2)_x(SiViMe)_ySiMe_3$	a	49.5	SiC; C and O	[74]
(10) $Me_3Si(HSiMe)_x(SiViMe)_ySiMe_3$	a	57.2	SiC; C and O	[74]
(11) $Me_3SiCH_2CH(SiMe_3)_y$		77.4	SiC; C and O	[74]
(12) BHMPCS[b]	a	11.1–53	SiC	[92,93]

[a]Pyrolytic conditions: a, 1,200 °C/Ar, b, 700 °C/N_2.
[b]BHMPCS = branched hydrosilyl-modified polycarbosilanes.

but Na/solvent was used. Precursor (10) was a modification of (9) where $MeSiHC1_2$ was used instead of Me_2SiC1_2. Precursor (11) was prepared from Me_3SiC1 and $CH_2{=}CHSiMe_3$ using K/THE. When Na/solvent was used, there was no reaction. Entry (12) concerns hydrosilyl-modified polysilane precursors for SiC [92,93]. About ten different various cases were examined with ceramic yields in the range 11.1–53%.

Seyferth, Sobon, and Bonn have investigated photochemical and thermal reactions of small amounts (0.25–2 wt%) of polynuclear metal carbonyls for the purpose of cross-linking Si—H containing silicon polymers [95]. In entries (1)–(6) (Table 58.6), the effect on ceramic yield and composition are demonstrated, particularly in entry (6). Seyferth and Lang [96] have also demonstrated that *n*-BuLi/*t*-BuOK can be a most effective reagent for metallization of CH_2 groups in a $SiCH_2Si$ [e.g., in poly(dimethylsilylenemethylene), (Me_2SiCH_2)] environment and some results are demonstrated in entries (7)–(10). Seyferth *et al*. [97] also investigated pyrolysis of hybrid polymers by reactions of precursors E and F [entries (11) and (12)] with various E/F ratios. An AIBN free radical initiator was used. The NMR-determined structure of $PVSiH_3$ [(14)–(16)] was more complicated than the simplified representation as $[CH_2CH(SiH_3)]_n$. The effect on the compositions can easily be discerned from the data in Table 58.6. Similar and related work by Seyferth and coworkers involving modifications and cross-linking of preformed precursors by using metal carbonyls, alkali-metal amide, and silylamides can be found in the literature [98,99]. Additionally, Seyferth and coworkers have demonstrated that multiple-phase ceramics can be prepared by pyrolysis of preceramic polymer/metal powder composites. The metal powders were oxides of Si and early transition metals [100]. This approach was particularly useful to convert excess and/or unbound Si and C into metal silicides and carbides.

Work by several groups of investigators dealing with PCSs with regard to conversion and processing [101], NMR characterization [102], curing of PCS fibers [103], fabrication of C/SiC composites [104], mechanical properties [105], and other similar studies on PCS [106] are available but not reviewed here. Also not reviewed are publications on polysilanes [107] and polyhydridosilanes [108].

Polysilylacetylenes

Table 58.7 lists some silicon–acetylene, silicon–olefin, silylene–diacetylene, and silylene–vinylene polymers. In the case of entry (6), R=Me, Et, *i*-Pr, *n*-Bu, *c*-Hx, *n*-Hx and Ph were investigated. Of these, the R=*c*-Hx and *n*-Hx cases gave higher ceramic yields of 76% and 72%, respectively [112]. In the case of entry (7), the three cases reported were with R=R′=Me, R=R′=Ph, and R=Ph and R′=Me with yields of 85%, 96%, and 95%, respectively [112].

Polysiloxanes

Several polysiloxane systems that have been investigated as precursors to SiC are given in Table 58.8 and brief comments are made here only for a few cases. For entries (5) and (6), about 11 systems were investigated by Burns *et al*. [118]. They found formation of amorphous SiCO at 1,200 °C that continued to undergo Si–O to Si–C bond distribution as the temperature increased to 1,400 °C and a small amount of oxygen remained even at 1,800 °C. Trace amounts of β-SiC

TABLE 58.6. *Pyrolysis data on various PCSs: Effect of modification and/or cross-linking of preformed precursors.*

Precursors	Pyrolysis condition, yield, and composition			References
	P[a]	Y	Residue and impurities	
(1) Nicalon PCS (A)	a	55–60	SiC; C (15%)	[94,95]
(2) Nicalon PCS + metal carbonyls (cat., e.g., Ru)		83–88		[95]
(3) $[(MeSiH)_x(MeSi)_y]_n$	b	Low	1 SiC + 0.5Si	[95]
(4) $[(MeSiH)_{0.65}(MeSi)_{0.35}]_n$(B)		12		[95]
(5) (B) + 2%$Ru_3(CO)_{12}$(cat.)	b	55		[95]
(6) (A) + (B) + 2%$Ru_3(CO)_{12}$(cat.)	b	68	SiC (99%); C (1%)	[95]
(7) $-(Me_2SiCH_2)_n-$	c	0		[96]
(8) $\{[Me_2SiCH_2]_3[Me_2SiCH(SiMe_2Vi)]\}_n$(C)	d	0–2		[96]
(9) $[(MeSiH)_{0.8}(MeSi)_{0.2}]_n$(D)	d	15–20	SiC (74%); Si (25%)	[96]
(10) 1(C) + 4(D) + AIBN(cat.)	d	68	SiC (91–94%); C (6–9%)	[96]
(11) $[(MeSiH)_{0.4}(MeSi)_{0.6}]_n$(E)	b	60	SiC (76%); C (24%)	[56,97,98]
(12) $[MeViSi{-}C{\equiv}C]_n$(F)	b	83	SiC (50%); C (50%)	[97]
(13) Various ratios of (E)/(F)=1.5–8	b	79–84	SiC (82–99%); C (1–18%)	[97]
(14) $[CH_2CH(SiH_3)]_n$ or $PVSiH_3$	e	39–47	NDG	[97]
(15) $PVSiH_3$ + Zr-metallocene(cat.), UV		80	β-SiC (88.7%), C (0.7%), ZrC (0.6%)	[97]
(16) $PVSiH_3$ (bulk pyrolysis)	f	39	β-SiC (94%), C (6%)	[97]

[a]Pyrolitic conditions: a, 1,200 °C/Ar; b, 1,000 °C/Ar; c, 600 °C/Ar; d, 900 °C/Ar; e, 960 °C/Ar; f, 1,500 °C.

TABLE 58.7. *Pyrolysis data on polysilylacetylene and related precursors.*

Precursors	Pyrolysis condition, yield, and composition			References
	P[a]	Y	Residue and impurities	
(1) $+Me_2Si-C\equiv C-SiMe_2-CH=CH+_n$	a	50,55	β-SiC; excess C	[109]
(2) $+Si(Me)_2-C\equiv C+_n$	b	80	SiC (59.6%); C (40.4%)	[110]
(3) $+Si(Ph)_2-C\equiv C+_n$	b	81	SiC (29%); C (71%)	[110]
(4) $+PhSiMe-C\equiv C+_n$	b	77	SiC (35.5%); C (64.5%)	[110]
(5) $+Si(Me_2)-Si(Me_2)-C\equiv C+_n$	b	59	SiC (70.9%); C (29.1%)	[110, 111]
(6) $+R_2Si-C\equiv C+_n$	c	20–76	SiC; excess C	[112]
(7) $+RR' Si-C\equiv C+$	c	85–95	SiC; excess C	[112]
(8) $+Me(Ch_2=CH)Si-C\equiv C+_n$	d	83	SiC (50%); C (50%)	[113]
(9) $+(Me)_2Si-(Me)_2Si-C\equiv C-C\equiv C+$	b	82	β-SiC (59%); C (41%)	[114]
(10) $+Me_2Si-C\equiv C-C\equiv C+$	b	82	β-SiC (40%); C (60%)	[114]
(11) $+Ph_2Si-C\equiv C-C\equiv C+$	b	80	β-SiC (23.4%); C (76.6%)	[114]
(12) $+Ph(Me)Si-C\equiv C-C\equiv C+$	b	79	β-Si (33.7%); C (66.3%)	[114]
(13) $+(Me)_2Si-CH=CH+$	b	27	SiC; NDG	[115]
(14) $+(Et)_2Si-CH=CH+$	b	16.7	SiC; NDG	[115]
(15) $-[-Ph(Me)Si-CH=CH+$	b	40	SiC; NDG	[115]

[a]Pyrolitic conditions: a, 1,200 °C/He; b, 1,000 °C/He; c, 1,100 °C/He; d, 1,000 °C/Ar.

TABLE 58.8. *Pyrolysis data on polysiloxane SiC precursors.*

Precursors	Pyrolysis condition, yield, and composition			References
	P[a]	Y	Residue and impurity	
(1) (DEDMS[b] + TEOS[c])/H_2O/EtOH	a	85	Si–C–O	[116]
(2) (DEDMS + TEOS)/H_2O/EtOH	b	50	SiC[d]; SiO_2, C	[116]
(3) Polysiloxane[e]	c	76.9	$Si_1O_{1.36}C_{2.7}$ (β-SiC, trace)	[117]
(4) Polysiloxane	d	49.5	$Si_1O_{0.18}C_{1.67}$ (β-SiC, 90%)	[117]
(5) Polysiloxane	e	44.5	$Si_1O_{0.1}C_{1.47}$(−SiC, 97%)	[117]
(6) $(PhSiO_x)_r(MeSiO_y)_s(Me_2ViSi_z)_t$	f	67–77	Si–C–O with O (13.35–18.03 wt%)	[118]
(7) $(PhSiO_x)_r(MeSiO_y)_s(Me_2ViSi_z)_t$	e	35–49	SiC (68–100%), C[f] (0–31.6%)	[118]
(8) Polymethylsilsesquioxane (A)	c	77	Silicon oxycarbide and glassy C at 1,000 °C.	[119]
(9) Polyphenylsilsesquioxane (B)	c	63	Between 1,200 and 1,400 °C, amorphous silica, amorphous SiC, some crystalline	[119]
(10) 50(A)/50(B) copolymer	c	70	SiC, graphitic C found	[119]

[a]Pyrolitic conditions: a, 1,000 °C/Ar; b, firing at low temperature (e.g., 700 °C) and then at 1,550 °C; c, 1,400 °C/[Ar for entries (8)–(10)]; d, 1,600 °C; e, 1,800 °C/Ar; f, 1,100 °C/Ar.
[b]DEDMS = dimethyldiethoxysilane.
[c]TEOS = tetraethoxysilane.
[d]Partially amorphous, partially crystalline.
[e]Polysiloxane = $(MeSiO_{1.5})_{0.75-x}(PhSiO_{1.5})_x(MeViSiO_{0.5})_{0.25}$.
[f]Turbostratic graphite.

were seen at 1,400 °C. By 1,600 °C, the carbothermic reduction was well underway and only a small percentage of oxygen remained in the material. At 1,800 °C, the pyrolysis is complete with the final product containing a substantial amount of β-SiC and excess C. The conversion process can be summarized as $(RSiO_{1.5})_n \rightarrow C_xSi_yO_z \rightarrow ySiC + (x-y-z)C + zCO$. If insufficient C is present, SiO is given off. As reported by Chen *et al*. [116(b)] the conversion can be envisioned to take place by polymer/copolymer$\rightarrow SiO_2 + C \rightarrow$ β-SiC with the carbotherrnic reduction being represented by $SiO_2 + 3C \rightarrow SiC + 2CO$, which occurs at 1,550 °C. Overall, the conversion to SiC of the various systems investigated are expected to have general commonality with the brief discussion above, and the original publications can be consulted for details. Other cases studied included redistribution reactions in polysiloxanes [120] and silsesquioxanes [121], arylsilsesquioxane gels, and related materials [122]. Additional examples can be found in a recent review [118(c)].

Polydisilylazanes

Some representative polydisilylazanes [123−126] are presented in Table 58.9. The composition of a fiber of

TABLE 58.9. *Pyrolysis data on polydisilylazane precursors.*

Precursors	Pyrolytic condition, yield, and composition			References
	P[a]	Y	Residue and impurity	
(1) Methylpolydisilylazane		53	$Si_1C_{0.8}N_{0.7}O_{0.5}$	[123]
(2) $[Me_{2.6}(Si_2)_1NH_{1.5}]_{11}$(A)	a	60	NDG	[124]
(3) (A) (1200)[b]	b	51	NDG	[124]
(4) (A) + additives[c]	a	51	$Si_1C_{0.8}N_{0.2}O_{0.03}$	[124]
(5) (A) (fiber)—aid cured	a		$Si_1C_{0.9}N_{0.2}O_{0.6}$	[124]
(6) (B)[d]	c	61	$Si_1C_{0.92}N_{0.22}O_{0.59}$ (at 1,200 °C)	[125]
(7) PhVi-modified MPDZ resin (C)	a		SiC with residue containing O (11%), and N (13.3%)	[126]
(8) PhVi-modified MPDZ resin (C)	b	62	SiC[e]; O (0.4%), N (13.3%)	[126]
(9) (C)+boron (BBr_3)	a		Residue contained B (1.2%), O (30.1%)	[126]
(10) (C)+ boron (BBr_3)	d		Residue contained B (1.2%), O (0.13%).	[126]

[a]Pyrolitic conditions: a, 1,200 °C/Ar; b, 1,600 °C/Ar; c, 1,000 °C; d, 2,100 °C/Ar.
[b]Further pyrolysis of char from (A).
[c]When additives are used α-Si_3N_4 and β-Si_3N_4 were observed at temperatures as low as 1000 °C
[d](B)={$[(Me)_2Si_2]_{0.6}[(Me)_3Si_2]_{0.4}\{(Me)_4Si_2]_{0.1}[NHSi(Me)_3]_{0.4}$}.
[e]α-SiC (35%) and β-Sic (65%).

phenylvinyl-modified methylpolydisilylazane (MDPZ PhVi) [127] is also compared with other systems in Table 58.10 and in other related work [128].

Methylchloropolysilanes

Baney and coworkers [125,130,131] have prepared a class of polyfunctional polysilanes from catalyzed Si–Si/Si–Cl bond redistribution of methylchlorodisilane, which gave polycyclic structures with approximately seven rings per molecule (for the reaction carried out at 250 °C). The proposed structure of this polymer designated as PCP-Cl-250 is shown below (Fig. 58.2). Pyrolysis of PCP-C1-250 gave 80% yield (TGA, 1,200 °C) [125]. Using the Si—Cl reactive group, derivatives of PCP-Cl-250 have been made and references to the original works can be found in the reviews by Baney and Chandra [23(a)] and Laine and Babonneau [14]. The composition of the ceramics (at 1,200 °C) obtained for the oxygen (PCP-O-250) and methyl (PCP-M-250) derivatives are included in Fig. 58.2 [125]. The compositions of PCP-O-250 and PCP-Me-250 at 1,600 °C were reported to be $SiC_{0.74}O_{0.004}$ and $SiC_{0.63}O_{0.02}$, respectively.

58.5.2 Si_3N_4 Precursors

As opposed to the conventional methods of the preparation of Si_3N_4, which generally produced infusible and intractable products, the preparation of Si_3N_4 from metalorganic precursors stemmed from the work of Verbeek and coworkers, who synthesized polysilazanes precursors for

TABLE 58.10. *Composition calculated using the rule of mixture [127,129].*

Fiber[a]	Composition (wt%)				
	SiO_2	Si_3N_4	SiC	C	Si
MPDZ-PhVi	14.3	37.1	27.2	21.3	0
HPZ	5.8	71.3	18.5	4.4	0
SGN	26.8	0	61.6	11.6	0
CGN	19.1	0	90.9	10	0
MPS	1	0	94	0	4.3

[a]Fibers were prepared from phenylvinyl-modified methylpolydisilylazane (MPDZ-PhVi), hydridopolysilazane (HPZ), Nicalon fiber with 15% oxygen (SGN), Nicalon fiber with 10%. oxygen (CGN), and methylpolysilane (MPS).

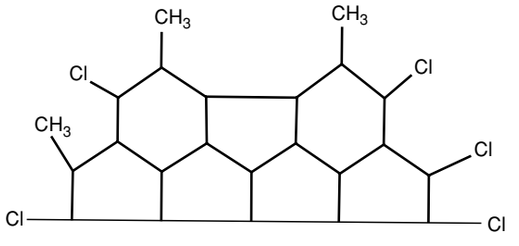

$(Me_2Si)_3(MeSi)_{1.7}Cl_5$

Derivatives	Compositions
PCP-Cl-250	$Si_1C_1O_{0.05}$
PCP-O-250	$Si_1C_{0.62}O_{0.42}$
PCP-Me-250	$Si_1C_{0.53}O_{0.15}$
Yajima's PCS	$Si_1C_{1.1}O_{0.6}$

FIGURE 58.2. Proposed structure of PCP-Cl-250 and some related data.

Si_3N_4 [132]. There are several synthetic routes that are used nowadays for the preparation of Si_3N_4 polymeric/ oligomeric precursors [22,133,134]. The reactions listed below and further manipulations of the same provide for the preparation of appropriate precursor [22,133]:

(i) Ammonolysis and aminolysis:

$$RR'SiCl_2 + 3xR'NH_2 \rightarrow \text{+}R'RSi{-}NR'\text{+}_n + 2xR'NH_3^+C1^-$$

$$RSiC1_3 + 6xNH_3 \rightarrow RSi(NH)_{3/2} + 3xNH_4C1,$$

$$RSiC1_3 + 6R'NH_2 \rightarrow RSi(NHR')_3 + 3xR'NH_3^+C1,$$

where R′ and R are usually H and Me but can also be Et, Vi, Ph, etc.

(ii) Ring-opening polymerization:

$$NH_3 + \overline{[Me_2Si{-}NH_3]_3} \longrightarrow NH_2\text{+}Me_2Si{-}NH\text{+}_xH$$

or

$$(Me_3Si)_2NH + \overline{[Me_2Si{-}NH]_4} \rightarrow Me_3Si - NH\text{+}Me_2Si{-}NH\text{+}_xSiMe_3$$

using transition metals such $Ru_3(CO)_{12}/135\ ^\circ C/1h/H_2$ as catalyst for the latter.

(iii) Deamination/condensation polymerization:

$$R_2Si(NHMe)_2 \xrightarrow{200\text{–}800\ ^\circ C} MeNH_2 + \overline{[R_2SiNMe]_3} + \text{polymer.}$$

(iv) Si—Cl/Si—N redistribution polymerization:

$MeSiC1_3 + (Me_3Si)_2NH \rightarrow Me_3SiCl + \text{polymer},$

$MeC1_2SiSiMeC1_2 + (Me_3Si)_2NH \rightarrow MeSiCl + \text{polymer}.$

(v) Catalytic dehydrocoupling–dehydrocyclization reactions:

$$H_2NRNH_2 + 2R_2SiH_2 \rightarrow H_2 - [RN(H - R_2Si)_2N-]_x.$$

(vi) Transition-metal catalyzed dehydrocoupling polymerization reactions:

$$R_2SiH_2 + R'NH_2 \xrightarrow{\text{catalyst}} H_2 + [-R_2SiNR'-]_n$$

An example of strong base is KH for reaction (v) and $Ru_3(CO)_{12}$ is an example of a catalyst for (vi). If the substituents on the Si of the silane and amine monomers are different from H, SiC and C are usually obtained along with Si_3N_4. In a few cases Si can also be obtained. The SiC and the free and/or unbound C can be, in some cases, the major constituents. C-rich composites are particularly common where vinyl (Vi) and phenyl (Ph) groups are present and more C seems to be present with Ph than with Vi. It is, however, easy to reduce the C content to <1 wt% by carrying out the pyrolysis in NH_3 gas at temperatures >500 °C. Both the excess Si and C can also be converted to metal silicides and carbides if such multiphase composites are desired [100]. As the result of the lability of the Si–N bond due to the reaction $\equiv Si{-}N + H_2O \rightarrow \equiv Si{-}OH + =N{-}H$, oxygen can also be present in the form of SiO_2, SiN_2O_2, etc. Although most organopolysilazanes give Si_3N_4, SiC, and C, there are several cases in which >95% Si_3N_4 has been obtained [135–138] with at least two cases with >99% Si_3N_4 (with-out using NH_3 during the pyrolysis) [135,137].

Pyrolysis of Si_3N_4 Precursors

A variety of monomeric, oligomeric, and polymeric silazane systems including polydisilacyclobutasilazanes [139], cyclodisilazanes [140], and alkyl and arylsilsequiazanes [22,141] have been investigated as Si_3N_4 precursors. In the tables that follow, some of these are examined in some details.

Results of pyrolysis of perhydropolysilazanes, polyorganosilazanes, and $Si(NHEt)_4$ (after polymerization) are shown in Table 58.11. Seyferth and coworkers [138,142] has also investigated reactions of H_2SiC1_2 and CH_3SiHC1_2 with CH_3NH_2 and NH_3, respectively, the products of which gave ceramic yields of 38% and 20%, respectively [142]. Other cases of reactions of $RSiHC1_2$ and NH_3 with $R{=}(CH_3)_2CH$, $(CH_3)_3C$, Ph, and $C_6H_5CH_2$ have also been reported. Where a catalyst for ring-opening polymerization (ROP) was used, the ceramic yield for $(CH_3SiHNH)_x$ was 39%. Use of $Ru_3(CO)_{12}$ and a mixture of $[CH_3SiHNH]_x$ and $(Me_3Si)_2NH$ gave 74% ceramic yield. Work on the $H_2SiC1_2 + NH_3$ system by Shimizu *et al*. [143] has demonstrated an increase of the molecular weight of the product from about 100 to about 100,000 by reacting the oligosilazane with various organic reagents, and the Si/N ratio changed from 1.01 to 1.0−1.03. Related work on the same system and treatment of the product with various amounts of pyridine in an autoclave at 120−150 °C increased the molecular weight, and the ceramic residue at 1,400 °C/N_2 (TGA) was 79.6% [144]. The residue contained Si (63.8%), N (28.7%), C (0.36%), 0 (2.7%), and H (0.11%). The OCMTS [entry (6)] was polymerized in the presence of KOMe. Similar work in which $MeSiC1_3$ was used for ROP of OCMTS and hexamethylcyclotrisilazane (HMCTS) and a mixture of OCMTS and HMCTS resulted in 70−80% ceramic yield (TGA 1,400 °C inert atmosphere), and the material contained Si, N, and C (no composition details were reported) [145].

Optimal candidate precursors for Si_3N_4 can be —$(H_2Si{-}NH)$—, —$(H_2Si{-}NHNH)$—, —$(MeSiH{-}NH)$—, and —$(SiH_2{-}NMe)$— because they can be converted to Si_3N_4 upon pyrolysis by losing H_2 and/or CH_4 [153]. The precursors can be prepared from ammonolysis of H_2SiC1_2 and $MeHSiC1_2$, as an example:

$$H_2SiC1_2 + NH_3 \xrightarrow{0\ ^\circ C/Et_2O} -(H_2Si{-}NH)_x- + [H_2Si{-}NH]_x.$$

But such systems are unstable and/or of low molecular weight to be directly useful. $-(H_2Si{-}NMe)_n-$ is more stable in the absence of air and moisture but gives only 38–40% yield because of its low molecular weight [153]. Two approaches that have been undertaken to address such problems were developed by Laine and Blum [154] and Seyferth and coworkers [155]. Some results of work of

TABLE 58.11. *Pyrolysis data on some silazane/polysilazane systems.*

Precursors	Pyrolysis condition, yield, and composition			References
	P[a]	Y	Residue and impurities	
(1) Perhydropolysilazane $+H_2Si-NH+_n$[b]	a	70	$\alpha\beta$-Si_3N_4; Si (trace)	[138,142]
(2) $(SiH_2NH)_a(SiH_2N)_b(SiH_3)_c$	b	80	α-Si_3N_4; Si, O	[146]
(3) $(H_2SiNH)_n$[c]	c	82–93[c]	Si_3N_4; Si	[147]
(4) $Si(NH)_2/NH_4Cl$ (coprecipitate)	d	20	α-Si_3N_4 (93%, 1,400 °C); Cl>1%	[137]
(5) $+(Me)_2Si-NH-Si(Me)_2+_nOSZ1$	e	57	Si_3N_4; SiC	[148]
(6) OCMTS + KOMe (cat.)[d]	e	76–79	SiCN; high C content	[149]
(7) OCMTS + KOMe (cat.)	f	69	α-Si_3N_4; <0.2% C	[149(a)]
(8) PBSZ Fiber[e]	f	90	Amorphous Si–B–O–N fiber	[150]
(9) $SiC_{1.07}N_{1.17}O_{0.07}H_{3.63}$ (at 500 °C)[f]	g	83	Si_3N_4; SiC, Si (O)	[151]
(10) $Si(NHEt)_4 \rightarrow$ precursor	c	55	Si_3N_4; C	[152]
(11) $Si(NHEt)_4 \rightarrow$ precursor	h		α,β-Si_3N_4; $C_{graph.}$	[152]
(12) $Si(NHEt)_4 \rightarrow$ precursor	i		α-Si_3N_4; $C_{graph.}$	[152]

[a]Pyrolitic conditions: a, 1,150 °C/N_2; b, 1,100–1,300 °C/N_2; c, 1,000 °C/N_2; d, >400 °C/N_2; e, 1,200 °C/N_2; f, 1,200 °C/NH_3; g, 1,600 °C/He; h, 1,500 °C/Ar; i, 1,600 °C/N_2.
[b]n= 7–8.
[c]Depending on the preparation method.
[d]OCMTS=octamethylcyclotetrasilazane.
[e]Perhydropolysilazane + $B(OME)_3 \rightarrow$ polyborosilazane(PBSZ).
[f]Composition is for polymer after being heated at 500 °C.

Laine and coworkers [136,156] are given in Table 58.12. Comparison of the data in entries (5), (8), and (9) can serve to illustrate the advantage gained by the use of transition-metal catalyst [the data in entry (5) were obtained by catalytic polymerization whereas that in (9) was not]. The effect of increase in molecular weight, at least in these types of systems was illustrated by the pyrolysis studies on $MeNH-[H_2Si-NMe-]_x-H$ oligomers and polymers [157]. By increasing the molecular weight from 600–700 to 2300, the ceramic yield increased from 40% to 60–65%,

TABLE 58.12. *Pyrolysis and compositional data on some polysilazane systems.*

Precursors	Yield[a]	Composition				
		Si_3N_4	SiC	C	N	O
(1) $(MeHSi-NH)_x(MeSiN)_y$[b]	85	65	29	4		
(2) $[H_2Si-NMe-]_x[H(NMe)Si-NMe]_y$[b, c]	63	75		18	6	
(3) [Me(H or NH)Si–NH][b]	57	64	25	10		
(4) [Ph(H)Si–NH–][b]	61	29	12	42		
(5) $[H_2Si-NMe]_x-H$[d]	>80	97				
(6) $[HSi(NH)_{1.5}]_x[SiNH(NHSiMe_3]_y$[d]	50	96		2		2

Precursors	Yield[a]	Precursor[e]	Yield[a]
(7) $[C_6H_{13}$(H or NH)Si–NH][b]	35	(12) Poly(Si-phenylsilazane)[f]	75[g]
(8) –[Me(H)SiNH]–[b]	19–57	(13) Poly(Si-hexylsilazane)[f]	45[g]
(9) $-[H_2Si-NMe]-$[b]	40–63	(14) Poly(N-methyl§ilazane)[f]	61[g]; 49[h]
(10) Poly(dimethylsilazane)[f]	Negligible	(15) Oligo(N-methylsilazane)[f]	48[g]; 41[h]
(11) Oligo (Si-diethylsilazane)[f]	Negligible	(16) $(SiViHNH)_x-(SiMeH-NH)_y$	71–84[i]

[a]Residue wt% at 900 °C/N_2.
[b]Reference [156(a)].
[c]Reference [153].
[d]Reference [136(a)].
[e]The composition of the residue from precursors (12)–(14) consisted of Si_3N_4, SiC, and C (impurity).
[f]Reference [156(b)].
[g]To 800 °C.
[h]To 1,600 °C.
[i]Reference [220(h and i)].

while at the same time the viscosity increased from 1–3 to 100 P (the attainment of appropriate viscosity is also necessary for the purposes of preparing fibers and for use in coating [157]).

Methylhydridopolysilazane (MHPS) was prepared from CH_3SiHCl_2 and NH_3 [155], which gives $[—CH_3SiH—NH—]_x$ (MHPS1), containing both cyalic and linear structures.

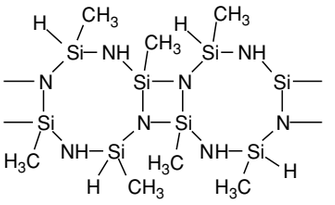

MHPS3

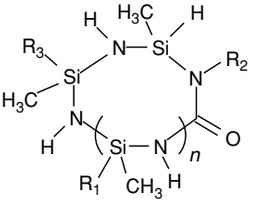

Poly(ureasilazanes): PUSZ (R_1=R_2=R_3=H)

PUMVS (R_1=H, CH=CH_2; R_2=alkyl; R_3=vinyl)

TABLE 58.13. *Pyrolysis data on some polysilazanes, polysilsesquizanes, polyvinylsilazanes and polycarbosilazanes.*

	Pyrolysis condition, yield, and composition				(A)	Pyrolysis condition, yield, and composition			
Polymers	P[a]	Y	Residue and impurity	References	Polymers	P[a]	Y	Residue and impurity	References
(1) ONMS[b]	a	48	α,β-Si_3N_4;C	[161,162(a)]	(12) PCSZ-I[c]	e	50	SiCN	[163]
(2) ONMS	b	40	Si_3N_4;C(< 1%)	[161]	(13) PCSZ-II	e	70	SiCN	[163]
(3) PNMS[d]	c	63	α,β-Si_3N_4;C	[153,161]	(14) PCSZ-III	e	90	SiCN	[163]
(4) PNMS	b	65	α,β-Si_3N_4;C	[153,161]	(15)PCSZ(I-III)	f		β-SiC;C	[163,164]
(5) APNMS[e]	c	80–85	α,β-Si_3N_4;C	[162]	(16) TNMAPS[f]	g	Fiber[g]	SiC	[165]
(6) APNMS	b	72		[162]	(17) TNMAMS[h]	g	Fiber[g]	SiC	[165]
(7) CMS[i]		20		[162(b)]	(18) HSZ1[j, k]	h	53	α-Si_3N_4[l]; Si (62%)	[166]
(8) PCMS[m]	c	65–85	α,β-Si_3N_4; SiC,C	[162]	(19) HSZ2[n]	h	48	α-Si_3N_4;α-SiC,Si (62%)	[166]
(9) PCMS	d	80		[162]	(20) HSZ3[o]	l	54	SiC, NDG	[167]
(10) APCMS[p]	e	95	α,β-Si_3N_4; SiC,C	[162]	(21) HSZ4[q]	g	60	SiC, NDG	[168]
(11) APNES[r]	a	72–84	α,β-Si_3N_4	[161,162]	(22) HSZ5[c]	g	74	SiNC,[s]C(< 3%), lowO	[136b,169]

[a]Pyrolitic conditions: a, 800 °/C/N_2; b, 800 °C/NH_3; c, 1200 °C/N_2; d, 1200 °C/N_2; e, 950 °C/Ar; f, 1600 °C/Ar; g, 1000 °C/N_2; h, 1600 °C/He; l, 1000 °C/inert gas;
[b]*ONMS* = Oligo (N-methyl) silazane, H_2N┼SiH_2—NMe┼H.
[c]PCSZ-(I to III)=PSSZ heat-treated, respectively, at 335, 372, and 470 °C (in autoclave);
PSSZ = $[SiMe_2][Si(Me)_2—NH—Si(Me)_2]_x$.
[d]PNMS = poly(N-methyl) silazane, $—[SiH_2—NMe]_x[SiH—(NMe)_{1.5}]_y$.
[e]APNMS = aminated PNMS.
[f]TNMAPS = tris (N-methylamino)phenylsilane.
[g]Weight loss insignificant up to 1000 °C.
[h]TNMAMS = tris (N-methylamino)methylsilane.
[i]CMS = cyclicmethylsilazane, $(MeSiH—NH)_n$.
[j]HSZ1 and HSZ5 were both obtained from $(Me_3Si)_2NH + HSiCl_3$.
[k]Related work to systems (18)–(22) can also be found in Refs. [170] and [171].
[l]No β-SiC detected.
[m]PCMS = polycyclicmethylsilazane obtained from CMS + KH.
[n]HSZ2 from $(Me_2SiH)_2NH + HSiCl_3$.
[o]HSZ3 = $[Me_{2.6}Si_2(NH)_{1.5}(NHSiMe_3)_{0.4}Cl_{0.15}]_{13}$.
[p]APCMS = aminated PCMS.
[q]HSZ4 = $(Me)_{2.6}(Si)_1(NH)_{1.5}(NHSiMe_3)_{0.4}$.
[r]APNES = aminated poly(N-ethyl)silazane, $[H_2Si—NEt]_{nw}[HSi(NH)_{0.5}—NEt]_x[HSi(NH_2)—NEt]_y[HSi(NEtH)—NH]_z$.
[s]Amorphous fiber.

TABLE 58.13. *Continued.*

Polymers	Pyrolysis condition, yield, and composition P[a]	Y	Residue and impurity	Refs.	(B) Polymers	Pyrolysis condition, yield, and composition P[a]	Y	Residue and impurity	Refs.
(1) VMHZ[b]	a	67	Si_3N_4, C, β-SiC (1,400 °C)	[172]	(12) VSA[c] (XL)[d]	f	83–85	Si_3N_4, SiC, C, Si	[177]
(2) VPS-I[e]	a	55	SiC	[173]	(13) VSA	f	59	Si_3N_4, SiC, C, Si	[177]
(3) VPS-I	b	47	amorph−Si_3N_4, < 2%C	[173]	(14) OVS[f]	f	83	SiCN, C	[178]
(4) VPS-II[g]	b		α-Si_3N_4	[174]	(15) OVNMS[h]	f	66	SiCN,C	[178,179]
(5) MPS-673[i]	c	88	Si_3N_4;	[175]	(16) OMS	f	46	SiCN,C	[178]
(6) HPZ-673[j]	c	72	C: <0.4%	[175]	(17) VS/DMS[k]	f	63	SiCN,C	[178]
(7) PCS-823[l]	c	81	O: 2.3–2.3%	[175]	(18) VS/MS[m]	f	77	SiCN,C	[178]
(8) MPS-673	d	52	SiC,Si-rich	[175]	(19) VS/MS[n]	g	72–87	Si_3N_4, SiC, C, SiO_2 (8.5%)	[179,180]
(9) HPZ-673	d	64	Si_3N_4, C	[175]	(20) PVSZ[o] (TXL)[p]	h	83	Si_3N_4, SiC, C, SiO_2	[181]
(10) PCS-823	d	55	SiC, C rich	[175]	(21) PVSZ (UV)[q]	h	76	Si_3N_4, SiC, C, SiO_2	[181]
(11) (A)[r]	e	40	Si_3N_4	[176]	(22) PMSZ[s]	h	81	Si_3N_4, SiC, C (7.5%), SiO_2	[179]
					(23) PSSZ[t]	h	61	Si_3N_4, SiC, C, SiO_2 (8.4%)	[181]

[a]

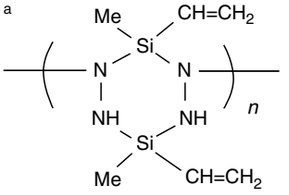

[b]VMHZ

[b]Pyrolitic conditions: a, 1,000 °C/N_2; b, 1,000 °C/NH_3; c, 1,500 °C/NH_3; d, 1,200 °C/Ar; e, 1,400 °C/NH_3; f, 1,000 °C/Ar, g, 1,400 °C/N_2; h, 1, 350 °C/Ar.
[c]VSA=$\{$ViHSi−NH$\}_x$.
[d]Cross-linked.
[e]VPS = vinylic polysllane; VPS-I=$\{[(SiMe_3)_{0.32}][SiViMe]_{0.36}[SiHMe]_{0.18}[SiMe_2][CH_2SiMe_3]_{0.18}\}$
[f]OVS=oligovinylsilazane, $\{$ViHSi-NH$\}$.
[g]VPS-II=$[(MeSi_w(ViSiMe)_x(HSiMe)_y(SiMe_2)_z]$.
[h]OVNMS = oligovinyl (N-methyl) silazane, $\{$ViHSi−NMe$\}$.
[i] MPS-673 = methylchloropolysilane heat-treated at 400 °C.
[j]HPZ- 673 = hydridopolysilazane heat-treated at 400 °C.
[k]VS/DMS=−$(ViHSi\text{-}NH)_x(Me_2Si{-}NH)_y$.
[l]PCS-823 = polycarbosilane heat-treated at 550 °C.
[m]VS/MS=$(ViHSi{-}NH)_x(MeHSi{-}NH\}_y$.
[n]Cross-linked and yield depended on heating rate (TGA).
[o]PVSZ=$\{$ViHSi−NH$\}$.
[p]Thermally cross-linked.
[q]UV radiation.
[r](A)=$Si_1C_{1.93}H_{4.7}O_{0.01}N_0$.
[s]PMSZ=poly(methyisilazane).
[t]PSSZ=phenylsilsesquizane.

The cyclic product, $[CH_3SiH{-}NH]_x$ can undergo ammonium-salt-induced polymerization to give a product (MHPS2). Dehydrocyclodimerization (DHCD) reaction of MHPS1 by using KH gives MHPS3 whose approximate structure can be expressed as $(CH_3SiH{-}NH)_{0.39}(CH_3SiH{-}NCH_3)_{0.04}(CH_3SiN)_{0.57}$. MHPS3 has been demonstrated to consist of the structure shown below. The ceramic yields (TGA, 1,000 °C/N_2) of MHPS1, MHPS2, and MHPS3 were found to be 20%, 36%, and 80–85%, respectively, thus illustrating the advantage gained by the DHCD reaction [the composition for MHPS3 consisted of Si_3N_4, SiC with some C and SiO_2(?)]. Equallyimportant other studies to increase molecular weight and/or yield by modifying preformed precursors have also been undertaken by

TABLE 58.13. *Continued.*

Precursors	(C) Pyrolysis condition, yield, and composition			References
	P[a]	Y	Residue and impurities	
(1) ⊣SiViH–NH⊢	a		Si_3N_4 (30%); SiCN (26%), C (44%)	[182]
(2) ⊣SiViH–NMe⊢	a		Si_3N_4; SiC (9.7%), C, SiO_2 (5%)	[179]
(3) —⊣MeSiVi–NH⊢$_x$—(XL)[b]	b		$\alpha\beta$-Si_3N_4	[183]
(4) —⊣MeSiVi–NH⊢$_x$—	c		α,β-SiC	[183]
(5) ⊣MeSiVi–NH⊢$_x$	d	64–67	NDG	[184]
(6) ⊣Me_2Si–NH⊢	e	5–10	Si_3N_4 (30–40%), NDG	[185]
(7) ⊣MeSiH–NMe⊢	e	15–20	Si_3N_4 (50–60%), NDG	[185]
(8) ⊣MeSiH–NMe⊢$_{n/2}$⊣MeSiH–NH⊢$_{n/2}$	e	50–55	Si_3N_4 (80–85%), NDG	[185]
(9) [MeSiH–NH⊢$_{0.8}$(MeSiVi–NH)$_{0.2}$]$_x$	f	54	NDG	[186][c]
(10) [MeSiH–NH⊢$_{0.8}$(MeSiVi–NH)$_{0.2}$]$_x$ (CD)[d]	f	84	NDG	[186]
(11) [MeSiH–NH⊢$_{0.8}$(MeSiVi–NH)$_{0.2}$]$_x$	g		α,β-Si_3N_4	[186]
(12) [MeSiH–NH⊢$_{0.8}$(MeSiVi–NH)$_{0.2}$]$_x$	h		β-SiC; Si (8%), N (1%)	[186]
(13) Polymethyisilzane	i	84	SiCN	[187]
(14) [(NH_2)SiH–N(CH_3)]$_x$	j		Si_3N_4 (82%?)	[12b]
(15) [(CH_3NH)SiH–N(CH_3)]$_x$	j		Si_3N_4 (69%?); SiC[d]	[12b]
(16) ⊣(NH_2)SiVi–NH⊢$_x$	j		Si_3N_4 (74%?) + SiC + C[e]	[12b]
(17) [$(NHCH_3)$SiVi–N(CH_3)]$_x$	k		Si_3N_4 (70%?) + SiC + C[e]	[12b]
(18) Me (Me) ⊣$Si_2N_2Me_2$⊢Vi(Me) + AIBN	l	42	$Si_1N_{0.9}C_{1.59}O_{0.12}H_{0.32}$	[140]

[a]Pyrolitic conditions: a, 1400 °C/Ar; b, 1500 °C; c, 1650 °C; d, 1000 °C/Ar; e, 800 °C/N_2; f, 950 °C/N_2; g, 1000\degC/NH_3 then 1600 °C/Ar; h, 1600 °C/Ar; i, 1300 °C/?; j, 1000 °C/N_2;$k_1$1500 °C/N_2;l,1000 °C/He.
[b]Crosslinked.
[c]Related work can also be found in Ref. 188.
[d]Cured.
[e]Minor product.

several groups of scientists although these works are not discussed here in any detail [156–160].

In Table 58.13 [153,161–187] various polysilazanes, polysilsequizanes, polyvinylsilazanes, polycarbosilazanes, and some isocyanate modified systems [186,187] are presented. The data should be fairly self-explanatory and the original publications can be consulted for additional information.

The influence of pyrolysis atmospheres (inert versus oxidative and reactive), heating rates, duration of pyrolysis on ceramic yield, and composition can be gleaned from the various tables. There is, thus, a need to pay attention to the effects of pyrolysis conditions. As an example, work by Bahloul, Pereira, and Goursat [179,180] summarized in Table 58.14 can illustrate the point. While there was only very little change in the composition of VS/MS [entry (19), Table 58.13(b)] pyrolyzed at 1,200 and 1,400 °C in N_2 and Ar (for 1 h), the pyrolysis at 1,450 °C, 24 h in Ar, drastically changed the composition for VS/MS. For the purpose of comparison, compositional data are also included for VMSZ [—(ViSiH—NMe)—]. The theoretical formula for VMSZ is SiC_3NH_7 and that for VS/MS $SiC_{1.5}NH_5$. The former precursor has a higher carbon content and led to about half as much SiC and about twice as much excess C although the compositions of Si_3N_4 were comparable (at 1,400 °C).

Pyrolysis of poly(ureasilanes) (PUSZ) to 1,000 °C under an argon flow gives silicon carbonitride ceramics in 61–76% yield [189], which is significantly higher than that form the linear silazane oligomers [—CH_3(H)Si—NH—]$_n$ of similar mass. The observed improvement may be a combined contribution from inclusion of urea bond linkage (—NH—CO—NH—) and formation of a cyclic structure. Poly (ureamethylvinyl)silazane (PUMVS) can also be thermally converted to an infusible solid at $T>250$ °C. Subsequent pyrolysis of the cross-linked products at ~1,000 °C yields amorphous silicon carbonitride (Si/C/N) ceramics

TABLE 58.14. *Composition of residue from VS/MS and VMSZ [179,180].*

Pyrolysis conditions	Composition (wt%)			
	Si_3N_4	SiC	SiO_2	C
1,200 °C/Ar, 1 h	55.3	21.6	5.3	17.8
1,400 °C/Ar, 1 h	55.9	21.1	5.7	17.3
1,400 °C/N_2, 1 h	54.3	20.2	8.5	17.0
1,400 °C/Ar, 1 h (VMSZ)	54.4	9.7	4.8	31.1
1,450 °C/Ar, 24 h	5.7	86.4	2.6	5.3

in ~70% yield with an empirical composition of $SiN_{0.82}C_{0.86}$ [190].

58.5.3 Other Systems

There are at least three structurally related polysilazanes that contain cyclic disilazane structures in the main backbone that have been synthesized. The proposed structures of these systems are presented below (I, II, and III).

System I has been investigated as a precursor for Si_3N_4 and SiC fiber [191]. Pyrolysis of system I at 1,000 °C in N_2 and NH_3 gave ceramic yields of 82% and 68%, respectively. The elemental composition (see below)

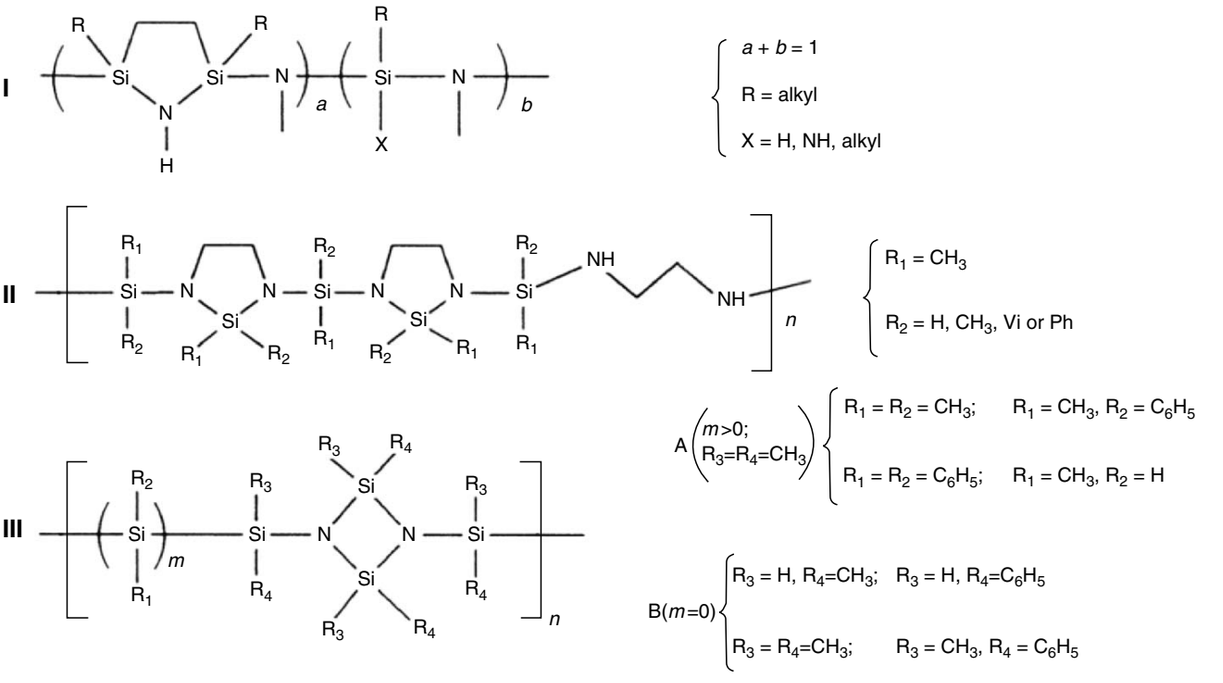

(wt%) of the Si_3N_4 residue was Si (57), N (37.9), C. (0.3), H (0.2), and O (3.1), while that for the silicon carbonitride was Si (55.4), N (33.3), C (7.0), H (0.3), and 0 (1.0). System II with R_1=CH_3 and R_2 being H, CH_3, Ph, and vinyl groups have been investigated [192–194]. As an example, the ceramic residue at 1, 000 °C/N_2 (TGA, 10 °C/min) for the R_1=CH_3 and R_2= vinyl case was found to be 64% with an elemental composition of $Si_1N_{1.07}C_{1.73}O_{0.13}$. No pyrolysis data was reported for system III**A** [195,196]. Pyrolysis of III**B** (at 900 °C in N_2) shows that the polymers with reactable Si–H group give higher ceramic yield (~69% when R_3=H and R_4=CH_3) [197]. Upon heating to >1,500 °C, the pyrolyzed residues are crystallized to give Si_3N_4 (~74 wt%) and SiC (~25%).

Furthermore, work by Baldus *et al*. [198] indicated that the novel compound $SiPN_3$ has been prepared by reacting $C1_3Si$–N=$PC1_3$ with liquid ammonia, giving $SiPN(NH)(NH_2)_4$ (system IV) as a precursor. Pyrolysis of system IV is reported to proceed according to IV → $SiPN_3 + 3NH_3$ with a ceramic yield of 72% (900 °C/NH_3). Crystalline $SiPN_3$ is, in turn, reported to decompose between 900 and 1,000 °C, giving Si_3N_4 according to $12SiPN_3 \rightarrow 4Si_3N_4$ (amorphous) $+3P_4 + 10N_2 \xrightarrow{1,\ 000\ ^\circ C} \alpha\text{-}Si_3N_4$ with a yield of 42.4%. The phosphorous and oxygen content was reported to be extremely low (200 and 200–400 ppm, respectively).

As seen in Table 58.12, pyrolysis of polysilazanes typically give silicon nitride/silicon carbide-based composites with chemical compositions at $Si_xC_yN_z (z < 4/3x)$. As a result of mismatched ratio among ceramic elements, the obtained ceramic residues often contain ''free'' carbon impurity, which may ultimately weaken the oxidatitative stability at elevated temperature. Polysilazanes of formula $[(SiH_2{-}NH)_3(MeSiH{-}NH)]_n$ and $[(SiH_2{-}NH)_3(SiH_2{-}NMe)]_n$ [199], which are designed specifically to release Si_3N_4/SiC composites, are shown to be pyrolyzed into ceramics in 77 and 83% yields, respectively. Crosslinking of the polymer samples significantly improves their ceramic yield to ~94%. Neutron wide angle scattering proved the absence of ''free'' carbon phase in the Si_3N_4/SiC composites. Additional examples of polysilazanes can be found in reviews [200,201].

58.6 PYROLYSIS ON SOME BORON-CONTAINING PRECURSORS

Recent studies have shown that incorporation of boron element into silicon-based ceramics increases their thermal stability and retard crystallization [202–204]. For example, the materials of the binary system Si—N start to crystallize at T=1,000 °C forming α-Si_3N_4, while metastable solid solutions of the ternary and quaternary systems Si—C—N and Si—B—C—N withstand crystallization up to 1,450 and 1,700 °C, respectively [205]. In order to form an amorphous uniform phase in the final multinary ceramics, the ceramic elements are preferably distributed homogeneously in the preceramic polymers. The general consensus in the ceramics community is that the quaternary system Si—B—C—N as well as the ternary systems Si—B—N and Si—B—C would be particularly suitable for producing amorphous ceramics that resist the microstructural changes even at top loads.

Some representative examples are listed in Table 58.15. Thermal condensation of borazine ($B_3N_3H_6$) with silazanes produces copolymers with highly branched structures (entry 1 and 2). Pyrolysis of the borazine-containing polymer in the entry 1 yields B/N/Si ceramics with trace carbon contamination, while that in the entry 2 gives B/N/Si/C ceramics. Both ceramic products are amorphous up to 1,400 °C [206]. Hydroboration of 2,4,6-trimethyl- 2,4,6-trivinylcyclotrisilaza (TMTVS) with borazine affords the polymer in the entry 4, which leads to B/N/Si/C ceramics upon pyrolysis at 1,000 °C [208]. In comparison with the borazine-containing polymers in the entry 1 and 2, the polymer in the entry 4 gives a higher ceramic yield, as hydroboration in the latter maintains the structural integrity of cyclosilazane ring. In the entry 5, hydroboration of TMTVS with borane in dry toluene gives polymers **A** (a colorless liquid), **B** (a hard glassy solid), and **C** (a white powder) [209]. Polymers **B** and **C** can not be redissolved once the solvent is removed, indicating a relatively high degree of branching or cross-linking and a higher content of boron (than polymer **A**). The relative contents of boron element in the ceramic products are in the same order found in the polymer precursors: **A**<**B**<**C** (the empirical formula for precursors **A**,

TABLE 58.15. *Pyrolysis data on boron-containing precursors with various structures.*

Polymer precursors	Pyrolysis condition, yield, and composition				References
	Pyrolytic condition	Yield (%)	System	Composition	
(1) 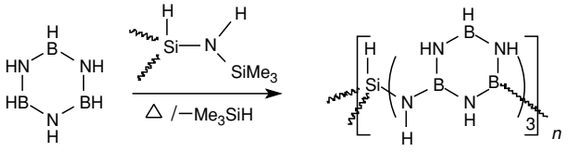	1,400 °C (Ar)	38–42	B/N/Si	From $B_{1.00}N_{1.05}Si_{0.17}C_{0.01}$ to $B_{1.00}N_{1.17}Si_{0.19}C_{0.05}$	[206]
(2) 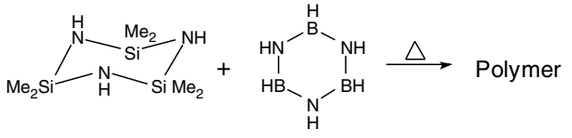	1,400 °C (Ar)	43–58	B/N/Si/C	From $B_{1.00}N_{1.40}Si_{0.35}C_{0.21}$ to $B_{1.00}N_{1.48}Si_{0.37}C_{0.23}$	[206]
(3) 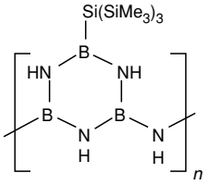	1,400°C (N_2)	47%	B/N/Si/C	$B_{1.00}N_{1.28}Si_{0.29}C_{0.10}$	[207]
(4) 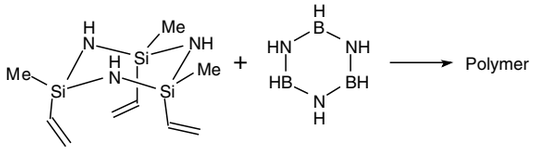	1,000 °C (Ar)	73–77	B/N/Si/C	—	[208]

TABLE 58.15. *Continued.*

Polymer precursors	Pyrolysis condition, yield, and composition				References
	Pyrolytic condition	Yield (%)	System	Composition	
(5) 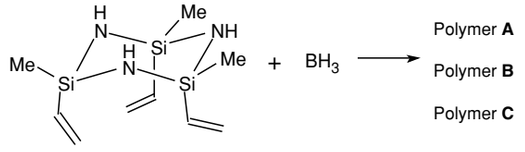 Polymer **A** Polymer **B** Polymer **C**	1,000 °C (N_2)	40–55	B/N/Si/C	$B_{0.29}N_{2.13}Si_{3.0}C_{4.18}$ $B_{0.82}N_{2.58}Si_{3.0}C_{5.03}$ $B_{1.93}N_{2.40}Si_{3.0}C_{5.83}$	[209]
(6) 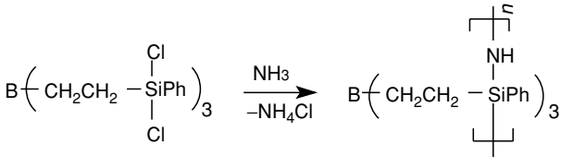	1,050 °C (Ar)	75	B/N/Si/C	From $B_{1.0}N_{2.8}Si_{2.9}C_{4.5}$ to $B_{1.0}N_{2.8}Si_{3.0}C_{4.4}$	[210]
(7) 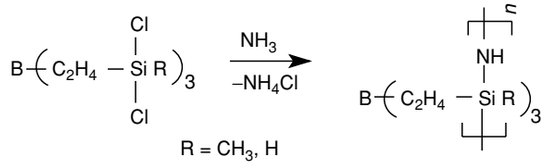 R = CH_3, H	1,000 °C (Ar)	83 (R=H) 52–55 (R=CH_3)	B/N/Si/C	—	[211–212]
(8)  R1=H,CH3,vinyl	1,100°C (Ar)	53 (R_1=H) 63(R_1=CH_3) 70–75[a]	B/N/Si/C	—	[211, 215, 216]
(9) 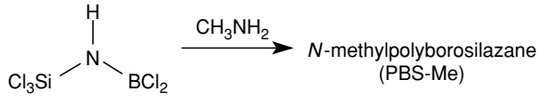	1,200 °C (N_2)		B/N/Si or B/N/Si/C	$B_{1.0}N_{2.3}Si_{1.0}C_{0.8}$	[216, 217]
(10) 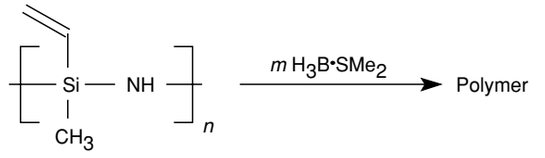 molar ratio (*m*:*n*) = 0, 1:8, 1:5, 1:4, and 1:3.	1,400 °C (Ar)		*m*/*n*= 0 1:8 1:5 1:4 1:3	**D**: $SiC_{1.6}N_{1.0}$ **E**: $SiC_{1.5}N_{1.0}B_{0.15}$ **F**: $SiC_{1.6}N_{1.0}B_{0.22}$ **G**: $SiC_{1.7}N_{1.0}B_{0.28}$ **H**: $SiC_{1.7}N_{1.0}B_{0.37}$	[218]

[a] R_1=vinyl, R_2=$-C_2H_4B$=.

B, and **C** are $Si_{3.0}N_{3.0}B_{0.33}C_{9.0}H_{22.0}$, $Si_{3.0}N_{3.0}B_{1.0}C_{9.0}H_{24.0}$, $Si_{3.0}N_{3.0}B_{3.0}C_{9.0}H_{30.0}$, respectively).

Pyrolysis of poly(organoborosilazane) (entry 6) under argon at 1,050 °C gives an amorphous ceramics, which resist crystallization up to 1,700 °C and thermally degradation up to 2,200 °C [210]. It should be noticed that the ratio of ceramic elements (B:Si:N) in the ceramic chars is about the same as that in the polymer precursors, illustrating the importance to control the ratio of ceramic elements in the preceramic polymers. Ceramic fibers can be obtained from this type of polymer for high temperature application [212]. Boron-containing polysilylcarbodi-imides (entry 8) also give amorphous ceramics upon pyrolysis to 1,100–1,400 °C, whose compositions as thermolyzed ceramics are located in or close to the phase fields $BN + Si_3N_4 + C$, $BN + Si_3N_4 + SiC + C$, $BN + SiC + C$, or $BN + B_{4+\delta}C + SiC + C$. Comparison of ceramics from five different samples at 1,600–2,000 °C shows that the SiC-poor (Si_3N_4-rich) materials are not high-temperature stable, whereas SiC-rich (Si_3N_4-poor) materials are mass stable up to 2,000 °C [215(b)]. Pyrolysis of N-methylpolyborosilazane (entry 9) produces amorphous $SiBN_3C$ ceram-

ics, which is stable up to 1,800 °C with respect to weight loss and microstructure changes [217]. The polymer precursor can be processed to a green fiber by melt-spinning, which then undergoes an intermediate curing step and successive pyrolysis into ceramic fiber.

Controlled hydroboration of $[—MeSi(Vi)—NH—]_n$ with BH_3 leads to precursors with different content of boron (entry 10), which are then converted to ceramics at 1,400 °C [218]. The thermal stability of the obtained amorphous ceramics is strongly dependent on the boron content. The boron-free ceramics (sample **D**), which is obtained from the pyrolysis of the parent polymer $[—MeSi(Vi)—NH—]_n$, decomposes at about 1,500 °C. The decomposition temperatures of the boron-modified ceramics **E** and **F** are raised to 1,650 °C and 1,900 °C, respectively, showing that boron not only retards the crystallization of SiC and Si_3N_4 but also protects the thermodynamically not stable Si_3N_4 against decomposition at elevated temperature.

58.7 CONVERSION STUDIES, USES, AND APPLICATIONS

Conversion of a precursor to its respective ceramics involves numerous reactions. During the pyrolysis process, volatile organic species are generated and eliminated, which may drastically lower the ceramic yield. Cross-linking of the preceramic polymers before pyrolysis is often necessary to help retention of the ceramic elements in the solid states, thereby improving the desirable ceramic yields. As an additional example, pyrolysis of linear poly(vinylsilane), $[—CH_2—CH(SiH_3)—]_n$, in argon to 1,500 °C gives only about 40% ceramic yield. The crosslinked (but still soluble) poly(vinylsilane), however, substantially improves the ceramic yield to 70–80% [219].

In order to control the chemical composition and microstructure of the final ceramic produce, it is of great value to understand the nature, rates, and mechanisms of the gaseous product evolution at various stages of the thermal conversion process. Mass spectrometry (MS) in conjunction with TGA provides useful suggestions about the reaction mechanisms responsible for the mass loss. XRD and solid state NMR (^{11}B, ^{13}C, ^{15}N, and ^{29}Si) becomes a powerful tool to reveal chemical environmental changes in the ceramic residues during the pyrolysis conversion. There are several cases of studies dealing with conversions processes as studied by NMR [220] other than those already cited and with uses and/or applications as fibers, films, coatings, binders, etc. For example, the pyrolytic conversion of polysilazane precursors $[(ViSiH–NH)_{0.5}–(MeSiH–NH)_{0.5}]$ to ceramics is studied by means of TGA, MS, solid-state NMR, and X-ray diffraction [220(f,g)]. Mass losses of ~3% and ~11% were observed at 200–400 °C (releasing ammonia) and 400–800 °C (releasing methane, hydrogen, and to a lesser extent, ethene and propene), respectively, producing a ceramic char in about 80% yield. Although the major chemical composition change of the ceramics occurs within the temperature range of 400–800 °C, the amorphorous silicon carbonitride was formed in 800–1,400 °C (by ^{29}Si and ^{13}C NMR data), and crystallization in the ceramics can only be observed after heating the ceramics to above 1,450 °C.

Currently, preceramic polymers are successfully used to produce ceramic fibers, coatings, joints, porous materials, nanotubes, and ceramic composites. For further appraisal of the efforts in uses and/or applications of SiC and Si_3N_4 precursors, the references in the Ref. [1,7,14] and other reviews [221−227], as well as in some of the recent work [228] pertaining to fiber processing and property thereof, uses and/or applications can be consulted. Thermal stability of the ceramic composite products has been constantly improved for high-temperature engine applications [229,228(l)], which will enable high-efficiency use of energy resources and reduce burden on the environment. Precursor-derived sintered SiC fibers are stable at 2,200 °C [230]. Smooth continuous SiC films have been recently demonstrated through pyrolysis of polymethylsilyne $[SiMe]_n$ [231]. Porous ceramic foams with variable cell sizes (100–600 μm) [232–240] and ceramic microtubes [241−243] can be obtained via pyrolysis of a preceramic polymer. Blend of different preceramic polymers can lead to a phase-separated mixture in nanosized domain. Direct pyrolytic conversion of such phase-separated mixture to ceramics [244] could retain the microstructure developed in the polymer blend, thereby offering an attractive route to nano ceramic composites. The composition of the $SiC–Si_3N_4$ composites can be controlled by adjusting the ratio of polymer precursors (e.g., polysilanes and polycyclodisilazanes) in the blends [245].

58.8 SUMMARY

Preceramic polymers offer an exciting alternative route to fabricate ceramics. In principle, these polymers can be fabricated into any desirable shapes, and then converted through pyrolysis to ceramics. Over the past two and half decades, research activities in this field have led to the development of many useful materials, which include commercial transformation of polycarbosilane into silicon carbide fiber (NICALON). Pyrolytic conversion of a preceramic polymer to its ceramics products typically accompanies a high level of volume shrinkage, which remains to be a barrier for the full development of preceramic polymer technology. The volume shrinkage can be minimized by choosing the polymer of high ceramic yields and using a controllable pyrolytic degradation condition, which allows cross-linking prior to the ceramic conversion. Conversion of molecular precursors into hybrid materials with desirable nanostructures remains to be a challenge [246,247].

This review has attempted to focus on ceramic yields and compositions of residues obtained from a host of SiC and

Si_3N_4/SiC precursors, and the presence of deleterious impurity elements is very apparent in most cases. The impurities in the form of SiO_2, excess Si and C, etc. can lead to decomposition reactions as well as affect crystallization, thermodynamic, and kinetic reactions, particularly at high temperatures. Combined interests in energy conservation and nano science will continue to foster activities in the multicomponent ceramic products of suitable microstructures, which exhibit superior thermal stability for the fuel-efficient high-temperature engine and other applications. Protective defect-free ceramic coatings, which are covalently bond to carbon fibers or light metal surfaces to extend their service life, will enable advanced technology in various industries such as automobile [248], if cost effective ceramic composites is realized.

ACKNOWLEDGMENTS

Support from NASA through Center for High Performance Polymers and Composites is acknowledged.

REFERENCES

1. (a) K. J. Wynne and R. W. Rice, Annu. Rev. Mater. Sci. **14,** 297 (1984); (b) M. Birot, J.-P. Pillot, and J. Dunogues, Chem. Rev. **95**, 1443 (1995); (c) A. R. Bunsell and M.-H. Berger, J. Eur. Ceram. Soc. **20**, 2249 (2000).
2. (a) D. L. Segal, Br. Ceram. Trans. J. **85**, 184 (**1986**); (b) K. Komeya, Am. Ceram. Soc. Bull. **63,** 1158 (**1984**); (c) N. N. Ault and S. D. Hartline, Am. Ceram. Soc. Bull. **5,** 773 (1987); (d) S. B. Hanna, N. A. L. Mansour, A. S. Tails, and H. M. A. Abd-allah, Br. Ceram. Trans. J. **84**, 18 (1985).
3. S. Yajima, K. Okamura, J. Hayashi, and M. Omori, J. Am. Ceram. Soc. **59,** 324 (1976).
4. J. P. Riggs, Encycl. Polym. Sci. Eng. **2**, 640 (1988);
5. R. A. Sinclair, in *Ultrastructure Processing of Ceramics, Glasses and Composites,* edited by L. L. Hench and D. R. Ulrich (Wiley-Interscience, New York, 1984), p. 256.
6. (a) R. W. Rice, Am. Ceram. Soc. Bull. **62**, 889 (1983); (b) B. E. Walker, Jr., R. W. Rice, P.F. Becker, B. A. Bender, and W. S. Coblenz, Am. Ceram. Soc. Bull. **62**, 619 (1983); (c) R. Baney and G. Chandra, in *Concise Encyclopedia of Polymer Science and Engineering*, edited by J. I. Kroschwitz and P. M. Siegel (Wiley-Interscience, New York, 1990), p. 899; (c) D. Segal, *Chemical Synthesis of Advanced Ceramic Materials* (Cambridge University Press, New York, 1989).
7. For an overview see: (a) D. Seyferth, Adv. Chem. Ser. **245**, 131 (1995); (b) R. M. Laine and A. Sellinger, Si-containing ceramic precursors. In *The Chemistry of Organic Silicon Compounds*, vol. 2, chapter 39, edited by Z. Rappoport and Y. Apeloig (John Wiley & Sons Ltd., 1996), pp. 2245–2315; (c) J. Livage, C. Sanchez and F. Babonneau, Molecular precursor routes to inorganic solid. In *Chemistry of Advanced Materials: An Overview,* chapter 9, edited by L. V. Interrante and M. J. Hampden-Smith (Wiley-VCH, 1998), pp. 389–448; (d) R. Richter, G. Roewer, U. Böhme, K. Busch, F. Babonneau, H. P. Martin, and E. Müller, Appl. Organomet. Chem. **11**, 71 (1997).
8. G. Pouskouleli, Ceram. Int. **15**, 213 (1989).
9. G. D. Soraru, F. Babonneau, and J. D. Mackenzie, J. Non-Cryst. Solids **106**, 256 (1988).
10. (a) C. H. Anderson and R. Warren, Composites **15,** 16 (1984); (b) C. H. Anderson and R. Warren, Composites. **15**, 101 (1984).
11. (a) A. Zangvil, Y-W. Chang, N. Finnegan, and J. Lipowitz, Ceram. Int. **18**, 271 (1992); (b) A. Kato, H. Mizumoto, and Y. Fukushige, Ceram. Int. **10**, 37 (1984).
12. (a) O. Devverdier, M. Monthioux, D. Mocaer, and R. Pallier, J. Eur. Ceram. Soc. **12,** 27 (1993); (b) B. Kanner and R. E. King III, in *Silicon-Based Polymer Science: A Comprehensive Resource,* edited by J. M. Zeigler and F. W. G. Fearon (American Chemical Society, Washington, D.C. 1990), p. 607; (c) G. S. Bibbo, P. M. Benson, and C. G. Pantano, J. Mater. Sci. **26**, 5075 (1991).
13. K. Okamura, H. Ichikawa, M. Takeda, T. Sefachi, N. Kaoai, and M. Nishii, U.S. Patent No. 5,283,044 (February 1, 1994).
14. R. M. Laine and F. Babonneau, Chem. Mater. **5**, 260 (1993).
15. D. Seyferth, C. Strohmann, H. J. Tracy, and J. L. Robinson, Mater. Res. Soc. Symp. Proc. **249**, 3 (1992).
16. R. M. Laine, Y. D. Blum, R. D. Hamlin, and A. Chow, National Technology Information Service Technical Report No. 5, Order No. AD-A178136, 1987.
17. M. C. Parche, in *Kirk–Othmer Encyclopedia of Chemical Technology,* vol. 4, edited by H. F. Mark, J. J. Meketta, Jr., and D. F. Othmer, 2nd edition (Interscience, John Wiley, New York, 1964), pp. 114–132.
18. (a) A.R. Verma and P. Krishna, in *Polymorphism and Polytypism in Crystals* (Wiley, New York, 1966); (b) *Gmelin Handbook of Inorganic Chemistry,* 8th ed., edited by J. Schlichting, G. Czack, E. Koch-Bienemann, P. Kuhn, and F. Schroder (Springer, New York, 1984), Suppl. vol. B2, Si-Silicon; (c) P. T. B. Shaffer, Acta Crystallogr. **B 25**, 477 (1969).
19. (a) R. Marchand, Y. Laurent, and J. Lang, Acta Crystallogr. **B 25**, 2157 (1969); (b) K. Kato, Z. Inoue, K. Kijima, and J. Kawada, J. Am. Ceram. Soc. **58,** 90 (1975); (c) R. Gran, Acta Crystallogr. B **35,** 800 (1979).
20. (a) *Silicon Carbide–1973*, edited by R. C. Marshall, J. W. Faust, Jr., and C. E. Ryan (University of South Carolina Press, Columbia, 1974); (b) *Silicon Carbide Ceramics,* edited by S. Somiya and Y. Inomata (Elsevier Applied Science, London, 1991).
21. (a) G. R. Terwillinger, J. Am. Chem. Soc. **57,** 48 (1974); (b) T. Ekstrom, Mater. Forum **17**(1), 62 (1993); (c) R. N. Katz, Ind. Ceram. **17**(3), 158 (1997).
22. R. West, J. Organomet. Chem. **300**, 327 (1986).
23. (a) R. Baney and G. Chandra, in *Encyclopedia of Polymer Science and Engineering*, edited by H. F. Mark, N. M. Bikales, C. G. Overberger, G. Menges, and J. I. Kroschwitz (Wiley-Interscience, New York, 1988), Vol. 13, p. 312, and references therein; (b) P. Trefonas, in *Encyclopedia of Polymer Science and Engineering*, edited by H. F. Mark, N. M. Bikales, C. G. Overberger, G. Menges, and J. I. Kroschwitz (Wiley-Interscience, New York, 1988), vol. 13, p. 162.
24. R. R. Wills, R. A. Markle, and S. P. Mukherjee, Am. Ceram. Soc. Bull. **62**, 904 (1983).
25. R. D. Miller and J. Michl, Chem. Rev. **89**, 1359 (1989).
26. Z. F. Zhang, Y. Mu, F. Babonneau, R. M. Laine, J. E. Harrod, and J. A. Rahn, in *Inorganic and Organometallic Oligomers and Polymers,* edited by J. F. Harrod and R. M. Laine (Kluwer Academic, Boston, 1991), p. 127.
27. H. R. Allcock, in *Chemical Processing of Advanced Materials*, edited by L. L. Hench and J. K. West (Wiley, New York, 1992), p. 699.
28. G. Soula, in *Inorganic and Organometallic Polymers* with *Special Properties,* edited by R. M. Laine (Kluwer Academic, Boston, 1992), p. 31.
29. R. West, in *Inorganic Polymers,* edited by J. E. Mark, H. R. Allcock, and R. West (Prentice Hall, Englewood Cliffs, NJ, 1992), p. 186.
30. R. Richter, G. Roewer, K. Leo, and B. Thomas, Frieberg. Forschungsh. A. **A 832**, 99 (1993).
31. (a) *Silicon-Based Polymer Science: A Comprehensive Resource*, edited by J. M. Zeigler and F. W. G. Fearon (American Chemical Society, Washington, D.C., 1990), Chaps. 31–34; (b) P. Kochs In *Silicon in Polymer Synthesis*, edited by H. R. Kricheldorf (Springer, Berlin 1996), pp.223–287.
32. T. Yamamura, Polym. Prepr. (Am. Chem. Soc. Div. Polym. Chem.) **25,** 8 (1984).
33. F. Babonneau, J. Livage, G. D. Soraru, G. Carturan, and J. D. Mackenzie, New J. Chem. **14**, 539 (1990).
34. S. Yajima, J. Hayashi, M. Omori, and K. Okamura, Nature **261,** 683 (1976).
35. R. West, L Nozue, X.-H. Zhang, and P. Trefonas, Polym. Prepr. (Am. Chem. Soc. Div. Polym. Chem.) **25**, 4 (1984).
36. R. West, L. D. David, P. I. Djurovich, H. Yu, and R. Sinclair, Am. Ceram. Soc. Bull. **62,** 899 (1983).

37. R. West, L. D. David, P. L. Djurovich, K. L. Stearley, K. S. V. Srinivasan, and H. Yu, J. Am. Chem. Soc. **103,** 7352 (1981).
38. R. Riedel, K. Strecker, and G. Petzow, J. Am. Chem. Soc. **72,** 2071 (1989).
39. D. J. Carlsson, J. D. Cooney, S. Gauthier, and D. J. Worsfold, J. Am. Ceram. Soc. **73**, 237 (1990).
40. F. Duboudin, M. Birot, O. Babot, J. Dunogues, and R. Galas, J. Organomet. Chem. **341**, 125 (1988).
41. M. A. Abu-eid, R. B. King, and A. M. Kotliar, Eur. Polym. J. **28,** 315 (1992).
42. B. I. Lee and L. L. Hench, in *Science of Ceramic Chemical Processing,* edited by L. L. Hench and D. R. Ulrich (Wiley, New York, 1986), p. 345.
43. B. L Lee and L. L. Hench, Mater. Res. Soc. Symp. Proc. **73,** 815 (1986).
44. T. Ishikawa, M. Shibuya, and T. Yamamura, J. Mater. Sci. **25,** 2809 (1990).
45. (a) S. Yajima, Y. Hasegawa, K. Okamura, and T. Matsuzawa, Nature, **273,** 525 (1978); (b) S. Yajima, Philos. Trans. R. Soc. London Ser. A. **294,** 419 (1980).
46. W. Toreki, C. D. Batich, M. D. Sacks, M. Salaam, and G. J. Choi, Mater. Res. Soc. Symp. Proc. **271**, 761 (1992).
47. S. Yajima, K. Okamura, J. Hayashi, and M. Omori, J. Am. Ceram. Soc. **59,** 324 (1976).
48. (a) Y. Hasegawa, M. Iimura, and S. Yajima, J. Mater. Sci. **15**, 720 (1980); (b) S. Yajima, Y. Hasegawa, J. Hayashi, and M. Kimura, J. Mater. Sci. **13,** 2569 (1978); (c) Y. Hasegawa and K. Okamura, J. Mater. Sci. **21**, 321 (1986); (d) H. Ichikawa, F. Machino, S. Mitsuno, T. Ishikawa, K. Okamura, and Y. Hasegawa, J. Mater. Sci. **21**, 4352 (1986); (e) Y. Hasegawa, J. Mater. Sci. **24**, 1177 (1989).
49. R. J. P. Corriu, D. Leclercq, P. H. Mutin, and A. Vioux, Chem. Mater. **4,** 711 (1992).
50. (a) P. H. Hommel, J. L. Miquel, and A. P. Legrand, Industrie Ceramique **849,** 344 (1990); (b) M. Takeda, J.-I. Sakamoto, Y. Imai, and H. Ichikawa, Compos. Sci. Technol. **59**, 813 (1999).
51. (a) R. A. Petrisko and G. L. Stark, 33rd International SAMPE (The Society for the Advancement of Materials Process Engineering) Symposium, edited by G. Carrillo, E. D. Newell, W. D. Brown, and P. Phelan, Anaheim, CA, March 7–10, 1988; (b) K. Okamura, M. Sato, T. Matsuzawa, and Y. Hasegawa, Polym. Prepr. (Am. Chem. Soc. Div. Polym. Chem.) **25**, 6 (1984); (c) T. Taki, S. Maeda, K. Okamura, M. Sato, and T. Mutsuzawa, J. Mater. Sci. Lett. **6**, 826 (1987); (d) T. Mah, N. L. Hecht, D. E. McCullum, J. R. Hoenigman, H. M. Kim, A. P. Katz, and H. A. Lipsitt, J. Mater. Sci. **19**, 1191 (1984); (e) C. Laffon *et al*., J. Mater. Sci. **24**, 1503 (1989).
52. (a) R. H. Baney and J. H. Gaul, Jr., U.S. Patent No. 4,310,651 (January 12, 1982); (b) D. Reyx, J. M. N. Martins, and I. Campistron, Makromol. Chem. **194,** 87 (1993); (c) R. D. Miller, Polym. News **12,** 326 (1987); (d) R. West, in *Ultrastructure Processing of Ceramics, Glasses and Composites,* edited by L. L. Hench and D. R. Ulrich (Wiley-Interscience, New York, 1984), p. 235; (e) F. Yenca, Y. L. Chen, and K. Matyjaszewski, Polym. Prepr. (Am. Chem. Soc. Div. Polym. Chem.) **28,** 222 (1987); (f) S. M. Bushnell-Watson and J. H. Sharp, J. Therm. Anal. **40,** 189 (1993).
53. W. R. Schmidt, L. V. Interrante, R. H. Doremus, T. K. Trout, P. S. Marchetti, and G. E. Maciel, Chem. Mater. **3**, 257 (1991).
54. C. L. Schilling, Jr., U.S. Patent No. 4,783,516 (November 8, 1988).
55. (a) Z. F. Zhang, F. Babonneau, R. M. Laine, Y. Mu, J. P. Harrod, and J. A. Rahn, J. Am. Ceram. Soc. **74,** 670 (1991); (b) M. F. Gozzi, M. D. C. Goncalves, and I. V. P. Yoshida, J. Mater. Sci. **34**, 155 (1999); (c) B. Boury, N. Bryson and G. Soula, Appl. Organomet. Chem. **13**, 419 (1999).
56. (a) D. Seyferth, T. G. Wood, H. J. Tracy, and J. L. Robison, J. Am. Ceram. Soc. **75,** 1300 (1992); (b) M. F. Gozzi and I. V. P. Yoshida, Macromolecules **28**, 7235 (1995); (c) B. Boury, N. Bryson, and G. Soula, Chem. Mater. **10**, 297 (1998).
57. J. Lipowitz, G. E. LeGrow, T. F. Lim, and N. Langley, Ceram. Eng. Sci. Proc. **9**, 931 (1988).
58. (a) S. Yajima, J. Hayashi, and M. Omori, Chem. Lett. September (9), 931 (1975); (b) S. Yajima, K. Okamura, and J. Hayashi, Chem. December (12), 1209 (1975); (c) S. Yajima, M. Mori, J. Hayashi and K. Okamura, Lett. June (6), 551 (1976).
59. J. G. Noltes, in *Transformation of Organometallics into Common and Exotic Materials: Design and Activation,* edited by R. M. Laine, (Martinus Nijhoff, Amsterdam, 1988), p. 97.
60. D. R. Bujalski, G. E. LeGrow, and T. F. Lim, Polym. Prepr. (Am. Chem. Soc. Div. Polym. Chem.) **28,** 396 (1987).
61. T. M. Hsu and S. P. Sawan, Polym. Prepr. (Am. Chem. Soc. Div. Polym. Chem.) **33,** 1034 (1992).
62. (a) Y. T. Shieh, S. P. Sawan, and J. B. Milstein, Polym. Prepr. (Am. Chem. Soc. Div. Polym. Chem.) **33,** 1044 (1992); (b) Y. T. Shieh and S. P. Sawan, J. Polym. Res. **1**(4), 367 (1994); (c) Y. T. Shieh and S. P. Sawan, J. Appl. Polym. Sci. **58**, 2013 (1995).
63. Y. T. Shieh and S. P. Sawan, Polym. Prepr. (Am. Chem. Soc. Div. Polym. Chem.) **31,** 1042 (1992).
64. (a) K. Kumar, J. Polym. Sci. C **26,** 25 (1988); (b) F. I. Hurwitz, T. A. Kacik, X.-Y. Bu, J. Masnovi, P. J. Heimann, and K. Beyene, J. Mater. Sci. **30**, 3130 (1995).
65. (a) E. Bacque, J. P. Pillot, M. Birot, and J. Dunogues, Macromolecules **21**, 30 (1988); (b) **21**, 34 (1988).
66. E. Bacque, J. P. Pillot, M. Birot, and J. Dunogues, in *Transformation of Organometallics into Common and Exotic Materials: Design and Activation,* edited by R. M. Laine, (Martinus Nijhoff, Amsterdam, 1988), p. 116.
67. (a) E. Bacque, J. P. Pillot, M. Birot, J. Dunogues, P. Lapouyade, E. Bouillon, and R. Pailler, Chem. Mater. **3**, 348 (1991); (b) E. Bouillon, R. Pallier, R. Naslain, E. Bacques, J. P. Pillot, M. Birrot, I. Dunogues, and P. V. Huong, Chem. Mater. **3**, 356 (1991).
68. H. J. Wu and L. V. Interrante, Chem. Mater. **1**, 564 (1989).
69. (a) H. J. Wu and L. V. Interrante, Polym. Prepr. (Am. Chem. Soc. Div. Polym. Chem.) **33**, 210 (1992); (b) L. V. Interrante, C. W. Whitmarsh, W. Sherwood, H.-J. Wu, R. Lewis, and G. Maciel, NATO ASI Ser., Ser. E: Appl. Sci. **297** (Appl. Organomet. Chem. Prepar. Process. Adv. Mater.), 173 (1995); (c) Q. Liu, H.-J. Wu, R. Lewis, G. E. Maciel, and L. V. Interrante, Chem. Mater. **11**, 2038 (1999).
70. C. K. Whitmarsh and L. V. Interrante, Organometallics **10**, 1336 (1991).
71. C. Laffon, A. M. Flank, P. Lagarde, and E. Bouillon, Physica B **158**, 229 (1989).
72. L. V. Interrante, C. K. Whitmarsh, T. K. Trout, and W. R. Schmidt, in *Inorganic and Organometallic Polymers with Special Properties,* edited by R. M. Laine (Kluwer Academic, Netherlands, 1992), p. 243.
73. C. L. Schilling, Jr. and T. C. Williams, Polym. Prepr. (Am. Chem. Soc. Div. Polym. Chem.) **25**, 1 (1984).
74. C. L. Schilling, Jr., Brit. Polym. J. **18**, 355 (1986).
75. W. R. Schmidt, V. Sukumar, W. J. Hurley, R. Garcia, L. V. Interrante, R. H. Doremus, and G. M. Renlund, J. Am. Ceram. Soc. **73**, 2412 (1990).
76. E. Bouillon, D. Mocaer, J. F. Villeneuve, R. Pailler, R. Naslain, M. Monthioux, A. Oberlin, C. Guimon, and G. Pfister, J. Mater. Sci. **26,** 1517 (1991).
77. (a) C. L. Czekaj, M. L. J. Hackney, W. J. Hurley Jr., L. V. Interrante, G. A. Sigel, P. J. Schields, and G. A. Slack, J. Am. Ceram. Soc. **73**, 352 (1990); (b) L. V. Interrante, W. R. Schmidt, S. N. Shaikh, R. Garcia, P. S. Marchetti, and G. E. Maciel, in *Chemical Processing of Advanced Materials,* L. L. Hench and J. R. West, eds. (Wiley, New York, 1992), p. 777; (c) J. A. Jensen, U.S. Patent No. 5,229,468 (July 20, 1993); (c) B. E. Fry, A. Guo, and D. C. Neckers, J. Organomet. Chem. **538**, 151 (1997).
78. (a) T. L. Smith, Jr., U.S. Patent No. 4,631,179 (December 23, 1986); (b) Q. Liu, H.-J. Wu, R. Lewis, G. E. Maciel, and L. V. Interrante, Chem. Mater. **11**, 2038 (1999).
79. H.-J. Wu and L. V. Interrante, Polym. Prepr. (Am. Chem. Soc. Div. Polym. Chem.) **32**, 588 (1991).
80. (a) H.-J. Wu and L. V. Interrante, Macromolecules **25**, 1840 (1992); (b) L. V. Interrante, Q. Liu, I. Rushkin, and Q. Shen, J. Organomet. Chem. **521**, 1 (1996); (c) W. Habel, A. Oelschläger, and P. Sartori, J. Organomet. Chem. **486**, 267 (1995).
81. K. J. Thorne, S. E. Johnson, H. Zheng, J. D. Mackenzie, and M. F. Hawthorne, Chem. Mater. **6**, 110 (1994).
82. B. Boury, R. J. P. Corriu, D. Leclerq, P. H. Mutin, J. M. Planeix, and A. Moux, Organometallics **10**, 1457 (1991).
83. R. J. P. Corriu, D. Leclerq, P. H. Mutin, J. M. Planeix, and A. Vioux, Organometallics **12**, 454 (1993).
84. B. Boury, R J. P. Corriu, D. Leclerq, H. Mutin, J. M. Planeix, and A. Vioux, in *Inorganic and Organometallic Polymers with Special*

Properties, edited by R. M. Laine (Kluwer Academic, Netherlands, 1992), p. 255.
85. V. B. Boury, L. Carpenter, and R J. P. Corriu, Angew. Chem. Int. Ed. Engl. **29,** 785 (1990).
86. (a) J. Masnovi, X. Y. Bu, K. Beyene, P. Heimann, T..Kacilc, A. H. Andrist, and F. I. Hurwitz, Mater. Res. Soc. Symp. Proc. **271**, 771 (1992); (b) J. Masnovi, X. Y. Bu, P. Conroy, A. H. Andrist, F. I. Hurwitz and D Miller, Mater. Res. Soc. Symp. Proc. **180**, 779 (1988).
87. B. Boury, R. J. P. Corriu, and W. E. Douglas, Chem. Mater. **3**, 487 (1991).
88. B. Boury, L. Carpenter, R. Corriu, and H. Mutin, New J. Chem. **14**, 535 (1990).
89. R. J. P. Corriu, M. Enders, S. Huille, and J. E. Moreau, Chem. Mater. **6**, 15 (1994).
90. (a) W. Habel, B. Hamack, C. Hover, and P. Sartori, J. Organomet. Chem. **467**, 13 (1994); (b) P. Sartori, W. Habel, B. V. Aefferden, and L. Mayer, Chem. Ind. **12**, 54 (1990).
91. (a) C. L. Schilling, Jr., J. P. Wesson, and T. C. Williams, J. Polym. Sci. Polym. Symp. **70**, 121 (1983); (b) C. L. Schilling, Jr., J. P. Wesson, and T. C. Williams, Am. Ceram. Soc. Bull. **62,** 912 (1983); (c) C. L. Schilling, Jr. NTIS Technical Report 83–3, Order No. AD-A141649, 1983; (d) C. L. Schilling, Jr. and T. C. Williams, NTIS Technical Report 83–2, Order No. AD-A141558, 1983.
92. C. L. Schilling, Jr., U.S. Patent No. 4,472,591 (September 18, 1984).
93. C. L. Schilling, Jr., NTIS Technical Report 83–1 Order No. AD-A141546, 1983.
94. S. Yajima, Am. Ceram. Soc. Bull. **62**, 893 (1983).
95. (a) D. Seyferth, C. A. Sobon, and J. Boren, New J. Chem. **14**, 545 (1990); (b) D. Seyferth, T. G. Wood, H. J. Tracy, and J. L. Robison, J. Am. Ceram. Soc. **75**, 1300 (1992).
96. (a) D. Seyferth and H. Lang, Organometallics **10**, 551 (1991); (b) D. Seyferth and H. Lang, in *Ultrastructure Processing of Advanced Materials,* edited by D. R. Uhlmann and D. R. Ulrich (Wiley, New York, 1992), p. 667.
97. D. Seyferth, G. E. Koppetsch, T. G. Woods, H. J. Tracy, J. L. Robinson, P. Czubarow, M. Tasi, and H. G. Woo, Polym. Prepr (Am. Chem. Soc. Div. Polym. Chem.) **34**, 223 (1993).
98. T. G. Wood, Ph.D. Thesis, Massachusetts Institute of Technology, Cambridge, MA., 1984.
99. D. Seyferth, N. Bryson, D. P. Workman, and C. A. Sobon, J. Am. Ceram. Soc. **74**, 2687 (1991).
100. D. Seyferth, H. Lang, C. A. Sobon, J. Borm, H. J. Tracy, and N. Bryson, J. Inorg. Organomet. Polym. **2**, 59 (1992).
101. (a) E. Bouillon *et al.,* J. Mater. Sci. **26**, 1331 (1991); (b) D. M. Kalyon and S. Kovenklioglu, Adv. Polym. Tech. **7**, 191 (1987).
102. (a) C. Gerardin, F. Taulelle, J. Livage, M. Birot, and J. Dunogues, Bull. Magn. Reson. **12**, 84 (1988); (b) T. Taki, J. Inorg. Organomet. Polym. **2**, 269 (1992).
103. (a) K. Okamura, T. Matsuzawa, and Y. Hasegawa, J. Mater. Sci. Lett. **4**, 55 (1985); (b) K. Okamura, M. Sato, and Y. Hasegawa, J. Mater. Sci. **2**, 769 (1983); (c) K. Okamura and T. Seguchi, J. Inorg. Organomet. Polym. **2**, 171 (1992); (d) D. W. Matson, R. C. Petersen, and R. D. Smith, Mater. Lett. **4**, 429 (1986); (e) M. Takeda, Y. Imai, H. Ickikawa, T. Ishikawa, and K. Okamura, Ceram. Eng. Sci. Proc. **13**, 209 (1992); (f) Y. Hasegawa, J. Inorg. Organomet. Polym. **2**, 161 (1992).
104. X: J. Wang, F. R. Liu, and C. R. Zhang, in *Material Research Society International Symposium Proceedings,* edited by Y. Han (North-Holland, Amsterdam, 1991), vol. 2, p. 93.
105. K. Okamura, T. Mutsuzawa, M. Sato, Y. Higashiguchi, S. Morozumi, and A. Kohyama, J. Nucl. Mater. **141–143,** 102 (1986).
106. (a) J. J: Poupeau, D. Abbe, and J. Jamet, Mater. Res. Soc. Symp. Proc. **17**, 287 (1984); (b) M. J. Morris, V. E. McGrath, S. Norris, W. G. Stibbs, R. J. P. Emsley, and J. H. Sharp, Proc. Eur. Conf. Adv. Mater. Process. 2nd. vol. 3. 259 (1991); (c) W. P. Weber and S. Q. Zhou, U.S. Patent No. 5,171,810 (December 15, 1992); (d) M. J. Michalczyk, U.S. Patent No. 5,270,429 (December 14, 1993); (e) C. K. Whitmarsh and L. V. Inerrante, U.S. Patent No. 5,153,295 (October 6, 1992); Whitmarsh and L. V. Inerrante; (f) M. Yazdi, D. Dollimore, and D. Agar, Thermochim. Acta **144**, 159 (1989); (g) T. Seguchi and K. Okamura, Keobunshi Kakeo **42**, 163 (1993).
107. (a) D. Seyferth and Y.-F. Yu, U.S. Patent No. 4,639,501 (January 27, 1987); (b) R. A. Sinclair and R. West, Meet Res. Soc. Symp. Proc. **32**, 387 (1984); (c) K. Koga, S. Nagano, S. Mizuta, and M. Nakayama, U.S. Patent No. 4,374,793 (February 22, 1983); (d) T. D. Tilley, U.S. Patent No. 5,229,481 (July 20, 1993); (e) H.-G. Woo and T. D. Tilley, in *Ultrastructure Processing of Advanced Materials,* edited by D. R. Uhlmann and D. R. Ulrich (Wiley, New York, 1992), p. 651; (f) R. C. West and L. D. David, U.S. Patent No. 4,324,901 (April 13, 1982) (g) R. C. West, U.S. Patent No. 4,260,780 (April 7, 1981).
108. K. A. Brown-Wensley and R. A. Sinclair, U.S. Patent No. 4,537,942 (August 27, 1985)
109. (a) T. J. Barton, S. Ijadi-Maghsoodi, and Y. Pang, U.S. Patent No. 5,241,029 (August 31, 1993); (b) N. I. Baklanova, V. N. Kulyukin, N. Z. Lyakhov, G. Y. Turkina, O. G. Yarosh and M. G. Voronkov, J. Mater. Synth. Proc. **5**, 443 (1997).
110. S. Ijada-Maghsoodi, Y. Pang, and T. J. Barton, J. Polym. Sci. **28**, 955 (1990).
111. M. Ishikawa, Y. Hasegawa, T. Hatano, and A. Kunai, Organometallics **8**, 2741 (1989).
112. S. Ijadi-Maghsoodi, X. P. Zhang, Y. Pang, M. Meyer, M. Akinc, and T. J. Barton, Polym. Prepr. (Am. Chem. Soc. Div. Polym. Chem.) **32**, 577 (1991).
113. (a) D. Seyferth, Y.-F. Yu, and G. H. Wiseman, U.S. Patent No. 4,719,273 (January 12, 1988); (b) D. Seyferth, G. H. Wiseman, Y.-F. Yu, T. S. Targos, C. A. Sobon, T. G. Wood, and G. E. Koppetsch, in *Silicon Chemistry,* edited by J. Y. Corey, E. R. Corey, and P. P. Gaspar (Ellis Harwood, Chichester, UK, 1988), p. 415.
114. (a) S. Ijadi-Maghsoodi and T. J. Barton, Macromolecules **23,** 4485 (1990); (b) R. J. P. Corriu, P. Gerbier, C. Guérin, and B. Henner, J. Mater. Chem. **10**, 2173 (2000).
115. Y. Pang, S. Ijadi-Maghsoodi, and T. J. Barton, Macromolecules **26**, 5671 (1993).
116. (a) F. Babonneau, K. Thorne, and J. D. Mackenzie, Chem. Mater. **1**, 554 (1989); (b) K. C. Chen, K. J. Thorne, A. Chemseddine, F. Babonneau, and J. D. Mackenzie, Mater. Res. Soc. Symp. Proc. **121**, 571 (1988).
117. R. B. Taylor and G. A. Zank, Polym. Prepr. (Am. Chem. Soc. Div. Polym. Chem.) **32**, 586 (1991).
118. (a) G. T. Burns, R. B. Taylor, Y. Xu, A. Zangvil, and G. A. Zank, Chem. Mater. **4**, 1313 (1992); (b) D. R. Bujalski, S. Grigoras, W.-L. Lee, G. M. Wieber, and G. A. Zank, J. Mater. Chem. **8**, 1427 (1998); (c) G. A. Zank, in *Silicon-Containing Polymers*, edited by R. G. Jones, W. Ando, and J. Chrojnowski (Kluwer Academic Publishers, Dordrecht, 2000), pp. 697–726.
119. F. I. Hurwitz, P. Heimann, S. C. Farmer, and D. M. Hembree, Jr., J. Mater. Sci. **28**, 6622 (1993).
120. (a) V. Belot, R. J. P. Corriu, D. Leclercq, P. H. Mutin, and A. Vioux, J. Polym. Sci. A Polym. Chem. **30**, 613 (1992); (b) J. R. Fox, D. A. White, S. M. Oleff, R. D. Boyer, and P. A. Budinger, Mater. Res. Soc. Syrup. Proc. **73**, 395 (1986); (c) P. H. Mutin, J. Am. Ceram. Soc. **85**, 1185 (2002).
121. V. Belot, R. J. P. Corriu, D. Leclercq, P. H. Mutin, and A. Vioux, J. Mater. Sci. Lett. **9**, 1052 (1990).
122. K. J. Shea, D. A. Loy, and O. Webster, J. Am. Chem. Soc. **114**, 6700 (1992).
123. R. H. Baney, G. T. Burns, J. P. Cannady, and T. K. Hilty, in *Organosilicon and Bio-organosilicon Chemistry,* edited by H. Sakurai (Ellis Harwood, Chichester, 1985), p. 269.
124. R. H. Baney, in *Ultrastructure Processing of Ceramics, Glasses and Composites,* edited by L. L. Hench and D. R. Ulrich (Wiley-Interscience, New York, 1984), p. 245.
125. R. H. Baney, J. H. Gaul, Jr., and T. K. Hilty, Mater. Res. Soc. Syrup. Proc. **17**, 253 (1984).
126. D. C. Deleeuw, J. Lipowitz, and J. A. Rabe, U.S. Patent No. 5,268,336 (December 7, 1993).
127. J. Lipowitz and G. L. Turner, Polym. Prepr. (Am. Chem. Soc. Div. Polym. Chem.) **29**, 74 (1988).
128. (a) J. Lipowitz, H. A. Freeman, R. T. Chen, and E. R. Prack, Adv. Ceram. Mater. **2**, 121 (1987); (b) R. M. Salinger, T. D. Barnard, C. T. Li, and L. G. Mahone, Soc. Adv. Mater. Process Eng. Q. **19**, 27 (1988).
129. D. R. Stull and H. Prophet, *JANAF Thermochemical Tables,* 2nd ed., NSRDS-NBS Publication No. 37 (National Bureau of Standards, Washington, D.C., 1971).
130. R. H. Baney, J. H. Gaul, Jr., and T. K. Hilty, Organometallics **2**, 859 (1983).
131. R. H. Baney, Chemtech **18** (12), 738 (1988).

132. (a) G. Winter, W. Verbeek, and M. Mansmann, U.S. Patent No. 3,892,583 (July 1, 1975); (b) W. Verbeek, U.S. Patent No. 3,853,567 (December 10, 1974).
133. R. M. Laine, Y. D. Blum, D. Tse, and R. Glaser, in *Inorganic and Organometallic Polymers,* ACS Syrup. Series No. 360, edited by M. Zeldin, K. J. Wynne, and H.. R. Allcock (American Chemistry Society, Washington, D.C., 1988), p. 124, and references therein.
134. Y. Nakaido, Research Institute for Special Inorganic Materials Report No. 9 (1991), p. 139.
135. D. L. Delaet, Patent Cooperation Treaty International Publication No. WO 91/19688 (December 26, 1991).
136. (a) R. M. Laine, Y. D. Blum, A. Chow, R. Hamlin, K. B. Schwartz, and D. J. Rowecliffe, Polym. Prepr. (Am. Chem. Soc. Div. Polym. Chem.) **28**, 393 (1987); (b) G. E. Legrow, T. F. Lim, J. Lipowitz, and R. S. Reaoch, Am. Ceram Soc. Bull. **66,** 363 (1987).
137. (a) S. Ampuero, P. Bowen, and T. A. Ring, Mater. Res. Soc. Symp. Proc. **287**, 227 (1993); (b) T. Yamada, T. Kawahito, and T. Iwai, J. Mater. Sci. Lett. **2,** 275 (1983); (c) K. S. Mazdiyasni and C. M. Cooke, J. Am. Ceram. Soc. **56**, 628 (1973).
138. D. Seyferth, C. C. Prud'Homme, and G. H. Wiseman, U.S. Patent No. 4,397,828 (August 9, 1983).
139. (a) G. T. Burns, C. K. Saha, G. A. Zank, and H. A. Freeman, J. Mater. Sci. **27**, 2131 (1992); (b) C. K. Saha and H. A. Freeman, J. Mater. Sci. *27,* 4651 (1992); (c) G. T. Burns, European Patent Application No. EP 295062 A2 (June 8, 1988); (d) G. T. Burns, U.S. Patent No. 4,774,312 (September 27, 1988).
140. E. Duguet and M. Schappacher, Pct. Int. Application No. WO 92/ 17527 (October 15, 1992).
141. (a) G. T. Burns and G. A. Zank, Polym Prepr. (Am. Chem. Soc. Div. Polym. Chem.) **34**, 343 (1993); (b) G. T. Burns, T. P. Angellotti, L. F. Hanneman, G. Chandra, and J. A. Moore, J. Mater. Sci. **22**, 2609 (1987).
142. (a) D. Seyferth and G. H. Wiseman, Polym. Prepr. (Am. Chem. Soc. Div. Polym. Chem.) **25**, 10 (1984); (b) D. Seyferth, G. H. Wiseman, and C. Prud'Homme, J. Am. Ceram. Soc. **66** (1) C-13 (1983) (c) D. Seyferth, G. H. Wiseman, and C. Prud'Homme, Mater. Res. Soc. Symp. Proc. **17**, 263 (1984).
143. Y. Shimizu, Y. Tashiro, H. Aoki, M. Ichiyama, H. Nishii, T. Kishi, K. Okuda, and T. Isoda, European Patent Application No. EP 544959A1 (December 30, 1991).
144. O. Funayama, M. Aral, and T. Isoda, European Patent Application No. EP 303498A1 (August 12, 1988).
145. (a) Y. Nakaido and N. Kozakai, Nippon Kagaku Kaishi **7**, 1080 (1989); (b) Y. Nakaido, T. Matsuura, D. Yamashita, M. Okabe, and S. Ishikita, Nippon Kagaku Kaishi **5,** 487 (1990).
146. M. Arai, S. Sakurada, T. Isoda, and T. Tomizawa, Polym. Prepr. (Am. Chem. Soc. Div. Polym. Chem.) **28**, 407 (1987).
147. O. Funayama, T. Isoda, H. Kaya, T. Suzuki, and Y. Tashiro, Polym. Prepr. (Am. Chem. Soc. Div. Polym. Chem.) **32**, 542 (1991).
148. A. A. Gallo, U.S. Patent No. 4,778,907 (October 18, 1988).
149. (a) D. Bahloul, M. Pereira, and P. Goursat, Ceram. Int. **18**, 1 (1992); (b) F. Sirieix, P. Goursat, A. Lecomte, and A. Dauger, Compos. Sci. Technol. **37**, 7 (1990).
150. O. Funayama, H. Nakahara, A. Tezuka, T. Ishii, and T. Isoda, J. Mater. Sci. **29**, 2238 (1994).
151. M. G. Salvetti, M. Pijolat, M. Soustelle, and E. Chassagneux, Solid State Ionics **63–65**, 332 (1993).
152. D. M. Narsavage, L. V. Interrante, P. S. Marchetti, and G. E. Maciel, Chem. Mater. **3**, 721 (1991).
153. R. M. Laine, Platinum Met. Rev. **32**, 64 (1988).
154. (a) Y. Blum and R. M. Laine, Organometallics **5**, 2081 (1986); (b) R. M. Laine and Y. Blum, U.S. Patent No. 4,612,383 (September 16, 1986).
155. (a) D. Seyferth and G. H. Wiseman, J. Am. Ceram. Soc. **C-132** (1984); (b) D. Seyferth, G. H. Wiseman, J. M. Schwark, Y.-F. Yu, and C. A. Poutasse, in *Inorganic and Organometallic Polymers* (ACS Symp Proc. No. 360), edited by M. Zeldin, K. J. Wynne, and H. R. Allcock (American Chemistry Society, Washington, D.C., 1988), p. 144; (c) D. Seyferth and G. H. Wiseman, in *Science of Ceramic Chemical Processing,* edited by L. L. Hench and D. R. Ulrich (Wiley, New York, 1986), p. 354; (d) D. Seyferth and G. H. Wiseman, U.S. Patent No. 4,482,669 (November 13, 1984); (e) D. Seyferth, in *Transformation of Organometallics into Common and Exotic Materials: Design and Activation,* edited by R. M. Laine (Nijhoff, Dordrecht, 1988), p. 133; (f) R. M. Stewart, N. K. Dando, D. Seyferth, and A. J. Perrotta, Polym. Prepr. (Am. Chem. Soc. Div. Polym. Chem.) **32**, 569 (1991); (g) H. N. Han, D. A. Lindquist, J. S. Haggerty, and D. Seyferth, Chem. Mater. **4**, 705 (1992); (h) N. R. Dando and A. J. Perrotta, Chem. Mater. **5**, 1624 (1993); (i) D. Seyferth and R. M. Stewart, Appl. Organomet. Chem. **11**, 813 (1997).
156. (a) K. A. Youngdahl, R. M. Laine, R. A. Kennish, T. R. Cronin, and G. G. A. Balavoine, Mater. Res. Soc. Symp. Proc. **121**, 489 (1988); (b) Y. D. Blum, K. B. Schwartz, and R. M. Laine, J. Mater. Sci. **24**(5), 1707 (1989).
157. R. M. Laine, Y. D. Blum, R. D. Hamlin, and A. Chow, in *Ultrastructure Processing of Advanced Ceramics,* edited by J. D. Mackenzie and D. R. Ulrich (Wiley, New York, 1988), p. 761.
158. (a) J. D. Bolt and F. N. Tebbe, U.S. Patent No. 4,730,026 (March 8, 1988); (b) J: J. Lebrun and H. Porte, U.S. Patent No. 4,689,832 (August 25, 1987); (c) J. M. Schwark, Polym. Prepr. (Am. Chem. Soc. Div. Polym. Chem.) **34**, 294 (1993).
159. (a) M. Matsumoto, K. Niwada, and S. Tanaka, Jpn. Kokai Tokkyo Koho JP 61072607 A2 (April 14, 1986); (b) M. Balasubramanian and P. Choudhury, U.S. Patent No. 5,010,157 (December 9, 1988) (c) Y. Takeda, M. Takamizawa, T. Takeno and A. Hayashida, European Patent Application EP 323062 (December 9, 1988).
160. (a) D. Seyferth, H. Lang, H. J. Tracy, C. Sobon, and J. Borm, Polym. Prepr. (Am. Chem. Soc. Div. Polym Chem.) **32,** 581 (1991); (b) D. Seyferth, J. M. Schwark, and Y. F. Yu, U.S. Patent No. 4,767,876 (August 30, 1988); (c) D. Serferth, Y. F. Yu, and T. S. Targos, U.S. Patent No. 4,705,837 (November 10, 1987); (d) D. Seyferth and Y. F. Yu, U.S. Patent No. 4,650,837 (March 17, 1987); (e) D. Seyferth, T. G. Wood, and Y. F. Yu, U.S. Patent No. 4,645,807 (February 24, 1987) (f) D. Seyferth and J. M. Schwark, U.S. Patent No. 4,720,532 (January 19, 1988).
161. Y. D. Blum, K. B. Schwartz, E. J. Crawford, and R. M. Laine, Mater. Res. Soc. Symp. Proc. **121**, 565 (1988).
162. (a) Y. D. Blum, G. A. McDermott, and A. S. Hirschon, in *Inorganic and Organometallic Oligmers and Polymers,* edited by J. F. Harrod and R. M. Laine (Kluwer Academic, Netherlands, 1991), p. 161; (b) Y. D. Blum, G. A. McDermott, R. B. Wilson, and A. S. Hirschon, Polym. Prepr. (Am. Chem. Soc. Div. Polym. Chem.) **32**, 548 (1991).
163. D. Mocaer, R. Pailler, R. Naslaih, C. Richard, J. P. Pillot, J. Dunogues, C. Gerardin, and F. Taulelle, J. Mater. Sci. **28**, 2615 (1993).
164. (a) D. Mocaer, R. Pailler, R. Naslain, C. Richard, J. P. Pillot, and I. Dunogues, J. Mater. Sci. **28**, 2632 (1993); (b) D. Mocaer, R. Pallier, R. Naslain, C. Richard, J. P. Pillot, J. Dunogues, O. Delverdier, and M. Monthioux, J. Mater. Sci. **28,** 2639 (1993); (c) D. Mocaer, R. Pailler, R. Naslain, C. Richard, J. P. Pillot, J. Dunogues, C. Darnez, M. Chambon, and M. Lahaye, J. Mater. Sci. **28,** 3049 (1993); (d) D. Mocaer, G. Chollon, R. Pailler, L. Filipuzzi, and R. Naslain, J. Mater. Sci. **28,** 3059 (1993).
165. B. G. Penn, J. G. Daniels, F. E. Ledbetter III, and J. M. Clemons, Polym. Eng. Sci. **26**, 1191 (1986).
166. (a) J. P. Cannady, U.S. Patent No. 4,543,344 (September 24, 1985); (b) J. P. Cannady, U.S. Patent No. 4,540,803 (September 10, 1985).
167. (a) J. Lipowitz, J. A. Rabe, and T. M. Carr, Polym. Prepr. (Am. Chem. Soc. Div. Polym. Chem.) **28,** 411 (1987); (b) J. Lipowitz, J. A. Rabe, and T. M. Carr, in *Inorganic and Organometallic Polymers* (ACS Symposium Series 360), edited by M. Zeldin, K. J. Wynne, and H. R. Allcock (American Chemical Society, Washington, D.C., 1988), p. 156; (c) J. H. Gaul, Jr., U.S. Patent No. 4,340,619 (July 20, 1982).
168. R. H. Baney, Polym. Prepr. (Am. Chem. Soc. Div. Polym. Chem.) **25**, 2 (1984).
169. G. E. Legrow, T. F. Lim, J. Lipowitz, and R. S. Reaoch, Mater. Res. Soc. Symp. Proc. **73**, 553 (1986).
170. J. H. Gaul, Jr., U.S. Patent No. 4,312,470 (January 26, 1982).
171. J. P. Cannady, U.S. Patent No. 4,535,007 (August 13, 1985).
172. N. Brodie, J: P. Majoral, and J.-P. Disson, Inorg. Chem. **32**, 4646 (1993).
173. W. R. Schmidt, P. S. Marchetti, L. V. Interrante, W. J. Hurley, Jr., R. H. Lewis, R. H. Doremus, and G. E. Maciel, Chem. Mater. **4**, 937 (1992).
174. W. R. Schmidt: V. Sukumar, W. J. Hurley, Jr., R. Garcia, R. H. Doremus, L. V. Interrante, and G. M. Renlund, J. Am. Ceram. Soc. **73**, 2412 (1990).
175. G. T. Burns and G. Chandra, J. Am. Ceram. Soc. **72**, 333 (1989).
176. K. Okamura, M. Sato, and Y. Hasegawa, Ceram. Int. **13,** 55 (1987).

177. N. S. C. K. Yive, R. Corriu, D. Leclercq. P. H. Mutin, and A. Vioux, New J. Chem. **15**, 85 (1991).
178. N. S. C. K. Yive, R. J. P. Corriu, D. Leclercq. P. H. Mutin, and A. Vioux, Chem. Mater. **4,** 141 (1992).
179. D. Bahloul, M. Pereira, and P. Goursat, J. Am. Ceram. Soc. **76**, 1163 (1993).
180. D. Bahloul, M. Pereira, and P. Goursat, J. Am. Ceram. Soc. **76**, 1156 (1993).
181. (a) N. S. C. K. Yive, R. J. P. Corriu, D. Leclercq, P. H. Mutin, and A. Vioux, Chem. Mater. **4**, 1263 (1992); (b)J. Bill, J. Seita, G. Thurn, J. Dürr, J, Canel, B. Z. Janos, A. Jalowiecki, D. Sauter, S. Schempp, H. P. Lamparter, J. Mayer, and F. Aldinger, Phys. Status Solidi A **166**, 269 (1998).
182. (a) C. M. Gerardin, F. Taulelle, and J. Livage, Mater. Res. Soc. Symp. Proc. **287**, 233 (1993); (b) C. Gerardin, F. Taulelle, and J. Livage, J. Chim. Phys. **89,** 461 (1992); (c) D. Bahloul, P. Goursat, and A. Lavedrine, J. Eur. Ceram. Soc. **11**, 63 (1993).
183. (a) W. Toreki, C. D. Batich, M. D. Sacks, and A. A. Morrone, Ceram. Eng. Sci. Proc. **11**, 1371 (1990); (b) W. Toreki, N. A. Creed, and C. D. Batich, Polym. Prepr. (Am. Chem. Soc. Div. Polym. Chem.) **31**, 611 (1990); (c) A. A. Morrone, W. Toreki, and C. D. Batich, Mater. Lett. **11**, 19 (1991).
184. (a) A. Lavedrine, D. Bahloul, P. Goursat, N. C. K. The, R. Corriu, D. Leclerq, H. Mutin, and A. Viola, J. Eur. Ceram. Soc. **8**, 221 (1991); (b) J. Lücke, J. Hacker, D. Suttor and G. Ziegler, Appl. Organomet. Chem. **11**, 181 (1997).
185. B. Arkles, J. Electrochem. Soc. **133** (1), 233 (1986).
186. (a) J. M. Schwark, U.S. Patent No. 4,929,704 (May 29, 1990); (b) J. M. Schwark and M. J. Sullivan, Mater. Res. Soc. Symp. Proc. **271**, 807 (1992); (c) J. M. Schwark, Polym. Prepr. (Am. Chem. Soc. Div. Polym. Chem.) **32**, 567 (1991); (d) A. Kojima, S. Hoshii, and T. Muto, J. Mater. Sci. Lett. **21**, 757 (2002).
187. Y. Abe, T. Ozai, Y. Kuno, Y. Nagao, and T. Misono, J. Inorg. Organomet. Polym. **2**, 143 (1992).
188. (a) J. M. Schwark, U.S. Patent No. 5,155,181 (October 13, 1992); (b) J. M. Schwark, U.S. Patent No. 5,021,533 (June 4, 1991); (c) J. M. Schwark, U.S. Patent No. 5,032,649 (July 16, 1991); (d) U.S. Pat. 5,001,090 (Mar. 19, 1991), J. M. Schwark, U.S. Patent No. 5,001,090 (March 19, 1991).
189. D. Seyferth, C. Strohmann, N. D. Dando, and A. J. Perrotta, Chem Mater. **7**, 2058 (1995).
190. Y. L. Li, E. Kroke, R. Riedel, C. Fasel, C. Gervais, and F. Babonneau, Appl. Organomet. Chem. **15**, 820 (2001).
191. T. Vaahs, M. Bruck, and W. D. G. Boker, Adv. Mater. **4**, 224 (1992).
192. K. Feng, A. Rodriguez, and Y. H. Mariam, Polym. Mater. Sci. Eng. (ACS) **69,** 337 (1993).
193. K. Feng and Y. H. Mariam, Appl. Organomet. Chem. **7**, 253 (1993).
194. (a) K. Feng and Y. H. Mariam, Macromolecules **24**, 4729 (1991); (b) K. Feng and Y. H. Mariam (Figure 47.1 are unpublished results).
195. Z. Du, J. Chen, and T. Han, Chin. J. Polym. Sci. **7**, 31 (1989).
196. H. Qiu, S. Yu, H. Ren, and Z. Du, Polym. Bull. **27**, 607 (1992).
197. X. Bao and M. J. Edirisinghe, J. Mater. Chem. **10**, 395 (2000).
198. H.-P. Baldus, W. Schnick, J. Lucke, U. Wannagat, and G. Bogedain, Chem. Mater. **5**, 845 (1993).
199. M. Hörz, A. Zern, F. Berger, J. Haug, K. Müller, F. Aldinger, and M. Weinmann, J. Eur. Ceram. Soc. **25**, 99 (2005).
200. A. Soum In *Silicon-Containing Polymers,* edited by R. G. Jones, W. Ando, and J. Chojnowski (Kluwer Academic Publishers, Dordrecht, 2000), pp. 323–349.
201. E. Kroke, Y. L. Li, C. Konetschny, E. Lecomte, C. Fasel, and R. Riedel, Mater. Sci. Eng. **R 26**, 97 (2000).
202. R. Riedel, A. Kienzle, W. Dressler, L. Ruwisch, J. Bill, and F. Aldinger, Nature **382**, 796 (1996).
203. B. Jaschke, U. Klingebiel, R. Riedel, N. Doslik, and D. Gadow, Appl. Organomet. Chem. **14**, 671 (2000).
204. H.-P. Baldus and M. Jansen, Angew. Chem. Int. Ed. Engl. **36**, 328 (1997).
205. R. Riedel and W. Dressler, Ceram. Int. **22**, 233(1996).
206. T. Wideman, K. Su, E. E. Remsen, G. A. Zank, and L. G. Sneddon, Chem. Mater. **7**, 2203 (1995).
207. D. Srivastava, E. N. Duesler, and R. T. Paine, Eur. J. Inorg. Chem. 855 (1998).
208. Q. D. Nghiem, J.-K. Jeon, L.-Y. Hong, and D.-P. Kim, J. Organomet. Chem. **688**, 27 (2003).
209. W. R. Schmidt, D. M. Narsavage-Heald, D. M. Jones, P. S. Marchetti, D. Raker, and G. E. Maciel, Chem. Mater. **11**, 1455 (1999).
210. (a) Z.-C. Wang, F. Aldinger, and R. Riedel, J. Am. Ceram. Soc. **84**, 2179 (2001); (b) J. Bill, T. W. Kamphowe, A. Müller, T. Wichmann, A. Zern, A. Jalowieki, J. Mayer, M. Weinmann, J. Schuhmacher, K. Müller, J. Peng, H. J. Seifert, and F. Aldinger, Appl. Organomet. Chem. **15**, 777 (2001).
211. F. Aldinger, M. Weinmann, and J. Bill, Pure Appl. Chem. **70**, 439 (1998).
212. R. Riedel, J. Bill, and A. Kienzle, Appl. Organomet. Chem. **10**, 241 (1996).
213. S. Bernard, M. Weinmann, D. Cornu, P. Miele, and F. Aldinger, J. Eur. Ceram. Soc. **25**, 251 (2005).
214. M. Weinmann, R. Haug, J. Bill, F. Aldinger, J. Schuhmacher, and K. Müller, J. Organomet. Chem. **541**, 345 (1997).
215. (a) A. Müller, P. Gerstel, M. Weinmann, J. Bill, and F. Aldinger, Chem. Mater. **14**, 3398 (2002); (b) A. Müller, J. Peng, H. J. Seifert, J. Bill, and F. Aldinger, Chem. Mater. **14**, 3406 (2002).
216. H. P. Baldus, O. Wagner, and M. Jansen, Key Eng. Mater. **89**, 75 (1994).
217. P. Baldus, M. Jansen, and D. Sporn, Science **285**, 699 (1999).
218. A. Müller, P. Gerstel, M. Weinmann, J. Bill, and F. Aldinger, J. Eur. Ceram. Soc. **20**, 2655 (2000).
219. D. Seyferth, M. Tasi, and H. G. Woo, Chem. Mater. **7**, 236 (1995).
220. S. J. Ting, C. J. Chu, and J. D. Mackenzie, J. Mater. Res. **7**, 164 (1992); (b) G. D. Soraru, F. Babonneau, and J. D. Mackenzie, J. Mater. Sci. **25,** 3886 (1990); (c) G. R. Hatfield and K. R. Carduner, J. Mater. Sci. **24,** 4209 (1989); (d) F. Babonneau, J. Livage, and R. M. Laine, Polym. Prepr. (Am. Chem. Soc. Div. Polym. Chem.) **32**, 579 (1991); (e) J. Lipowitz, J. A. Rabe, and T. M. Carr, Spectrosc. Lett. **20**, 53 (1987); (f) D. Bahloul, M. Pereira and C. Gerardin, J. Mater. Chem. **7**, 109 (1997); (g) D. Bahloul, M. Pereira and C. Gerardin, J. Mater. Chem. **7**, 117 (1997); (h) H. Q. Ly, R. Taylor, R. J. Day, and F. M. Heatley, J. Mater. Sci. **36**, 4037 (2001); (i) C. Gervais, F. Babonneau, L. Ruwisch, R. Hauser, and R. Riedel, Can. J. Chem. **81**, 1359 (2003).
221. T. F. Cooke, J. Am. Ceram. Soc. **74**, 2959 (1991).
222. K. Okamura, Composites **18**, 107 (1987).
223. J. Lipowitz, Am. Ceram. Soc. Bull. **70**, 1888 (1991).
224. W. Wade Adams and S. Kumar, in *Ultrastructure Processing of Advanced Materials,* edited by D. R. Uhlmann and D. R. Ulrich (Wiley, New York, 1992), p. 343.
225. N. R. Langley, G. E. LeGrow, and J. Lipowitz, in *Reinforced Ceramic Composites,* edited by K. S. Mazdiyasni (Noyes, Park Ridge, NJ, 1989), p. 63.
226. W. H. Atwell, P. Foley, W. E. Hauth, R. E. Jones, N. R. Langley, and R. M. Salinger, Final Report No. AFWAL-TR-86-4146 (1989).
227. (a) D. J. Pysher, K. C. Goretta, R S. Hodder, Jr., and R. E. Tressler, J. Am. Ceram. Soc. **72**, 284 (1988); (b) B. Jaschke, U. Klingebiel, R. Riedel, N. Doslik, and D. Gadow, Appl. Organomet. Chem. **14**, 671 (2000).
228. (a) T. Shimoo, H. Chen, and K. Okamura, J. Mater. Sci. **29**, 456 (1994); (b) W. Habel, B. Hamack, C. Nover, and P. Sartori, J. Organomet. Chem. **467**, 13 (1994); (c) D. R. Bujalski, G. A. Zank, and T. D. Barnard, U.S. Patent No. 5,262,553 (November 16, 1993) (d) Y. Yokoyamo, T. Nanba, I. Yasui, H. Kays, T. Maeshima, and T. Isoda, J. Am. Ceram. Soc. **74,** 654 (1991); (e) T. Ishikawa, T. Yamamura, and K. Okamura, J. Mater. Sci. **27**, 6627 (1992); (f) K. E. Gonsalves, T. D. Xiao, and P. R. Strutt, Ind. J. Technol. **31**, 436 (1993); (g) S. T. Schwab *et al.,* Polym. Prepr. (Am. Chem. Soc. Div. Polym. Chem.) **34**, 296 (1993); (h) G. Passing, H. Schonfelder, R. Riedel, and R. J. Brook, Br. Ceram. Trans. **92,** 21 (1993); (i) W. Toreki, G. J. Choi, C. D. Batich, M. D. Sacks, and M. Saleem, Ceram. Eng. Sci. Proc. **13**, 198 (1992); (j) A. Herzog and U. Vogt, Adv. Eng. Mater. **4**, 877 (2002); (k) F. Cao, X.-D. Li, J.-H. Ryu, and D.-P. Kim, J. Mater. Chem. **13**, 1914 (2003); (l) L. Macdonald, Ceramic Transactions, 144 (Advanced SiC/SiC Ceramic Composites: Developments and Applications in Energy Systems), 87–95 (2002); (m) A. Herzog and U. Vogt, Adv. Eng. Mater. **4**, 877 (2002); (n) A. Herzog and U. Vogt, Ceram. Eng. Sci. Proc. **23**, 19 (2002); (o) J. Clade, E. Seider, and D. Sporn, J. Eur. Ceram. Soc. **25**, 123 (2005).
229. P. Baldus, M. Jansen, and D. Sporn, Science **285**, 699 (1999).
230. T. Ishikawa, Y. Kohtoku, K. Kumagawa, T. Yamamura, and T. Nagasawa, Nature (London) **391**, 773 (1998).

231. M. W. Pitcher, S. J. Joray, and P. A. Bianconi, Adv. Mater. **16**, 706 (2004).
232. P. Colombo and M. Modesti, J. Am. Ceram. Soc. **82**, 573 (1999).
233. P. Colombo and M. Modesti, J. Sol–Gel Sci. Technol. **14**, 103 (1999).
234. P. Colombo and J. R. Hellmann, Mat. Res. Innovat. **6**, 260 (2002).
235. I.-K. Sung, S.-B. Yoon, J.-S. Yu, and D. P. Kim, Chem. Commun. 1480 (2002).
236. M. R. Nangrejo and M. J. Edirisinghe, J. Porous Mater. **8**, 131 (2002).
237. P. Colombo, J. R. Hellmann, and D. L. Shellman, J. Am. Ceram. Soc. **85**, 2306 (2002).
238. P. Colombo and E. Bernardo, Compos. Sci. Technol. **63**, 2353 (2003).
239. T. Takahashi and P. Colombo, J. Porous Mater. **10**, 113 (2003).
240. Y. W. Kim, S. H. Kim, H. D. Kim, and C. B. Park, J. Mater. Sci. **39**, 5647 (2004).
241. R. Melcher, P. Cromme, M. Scheffler, and P. Greil, J. Am. Ceram. Soc. **86**, 1211 (2003).
242. P. Colombo, K. Perini, G. Bernardo, T. Capelletti, and G. Maccagnan, J. Am. Ceram. Soc. **86**, 1025 (2003).
243. Q.-M. Cheng, L. V. Interrante, M. Lienhard, Q. Shen, and Z. Wu, J. Eur. Ceram. Soc. **25**, 233 (2005).
244. (a) L. V. Interrante, K. Moraes, Q. Liu, A. Puerta, and L. G. Sneddon, Pure Appl. Chem. **74**, 2111 (2002); (b) K. Moraes, J. Vosburg, D. Wark, L. V. Interrante, A. R. Puerta, L. G. Sneddon, and M. Narisawa, Chem. Mater. **16**, 125 (2004).
245. X. Bao and M. J. Edirisinghe, Mater. Technol. (Poulton-le-Fylde, United Kingdom) **15**(2), 137 (2000).
246. M. Sternitzke, J. Eur. Ceram. Soc. **17**, 1061 (1997).
247. R. J. P. Curriu, Angew. Chem. Int. Ed. **39**, 1376 (2000).
248. (a) C. K. Narula, A. Varshney, M. P. Everson, P. Schmitz, L. F. Allard, A. Gandopadhyay, T. S. Lewkbandara, C. H. Winter, P. Czubarow, and D. Seyferth, Mater. Res. Soc. Symp. Proc. **495**, 287 (1998); (b) M. Buchmann, R. Gadow, E. Scherer, and M. Speicher, Ceram. Trans. **139**, 3 (2002).

CHAPTER 59

Surface and Interfacial Properties

Afshin Falsafi*, and Subu Mangipudi†, and Michael J. Owen‡

*3M Company, 3M Center, 260-2B-12, St. Paul, MN 55144
†Medtronic Corporation, 6800 Shingle Creek Parkway, Brooklyn Center, MN 55430
‡Dow Coming Corporation, Midland, MI, 48686-0994

59.1 INTRODUCTION

Quantitative surface and interfacial tension data for polymers are crucial to many aspects of the production and application of elastomers, plastics, textiles, films and coatings, foams, polymer blends, adhesives, and sealants. Although interface is the inclusive term for the region in space where two phases meet, if one of the phases is gaseous it is usually called a surface [1]. Thus we refer here to the surface tension of a polymer in air but to the interfacial tension between a polymer and a condensed phase such as water or another polymer.

A further nomenclature choice must be made between surface tension and surface free energy. The fundamental surface properties in capillarity can be thought of as the surface tension, i.e., force per unit length, and the surface free energy, i.e., free energy per unit area, which are numerically and dimensionally identical [2]. This is true for liquid surfaces that can assume an equilibrium shape but is not the case for solids where elastic forces complicate the issue and the surface state after measurement may be far from equilibrium. The surface tensions of liquids and solids are necessarily obtained in different manners. Liquid surface tensions are directly measured [3] and values are usually independent of the specific technique used, provided equilibrium is established, whereas solid surface tensions are generally derived from contact-angle measurements using semiempirical equations, yielding values dependent on the choice of liquids and equations.

The term *surface free energy* is more appropriate for a solid surface than surface tension, and we use it for the solid surface properties in this compilation with the exception of the earliest and most familiar contact-angle approach to polymer surface characterization, the Zisman critical surface tension of wetting [4]. The word *tension* is properly applied here as it refers to the liquid that just wets (zero contact angle) the solid. The contact-angle approaches only infer the surface free energy of solids; they do not measure it directly. To avoid confusion, note that some other polymer surface data compilations [5,6] use solid surface tension where we use surface free energy. We use the symbol γ in units of mN/m for liquid surface tension and critical surface tension of wetting and in units of mJ/m^2 for solid surface free energies. Note that the symbol σ is also used instead of γ, particularly in Europe.

Surface tension is the result of the imbalance of attractive forces between molecules at a surface. These may be very similar for a liquid and solid polymer of the same chemical constitution but, because they are derived differently, liquid surface tension and solid surface free energy need not have the same values for a particular polymer. For this reason separate tables of directly measured liquid

and contact angle-derived solid polymer surface properties are given. These two approaches account for most of the data available. There are a variety of other less exploited methods such as inverse gas chromatography that have been applied to polymers. The only one included here is that based on direct work of adhesion measurement by the Johnson, Kendall, and Roberts (JKR) equation [7].

59.2 LIQUID SURFACE TENSION

Liquid surface tensions γ_{LV} of selected homopolymers at 20 °C are given in Table 59.1. γ_{LV} is defined as the surface tension of the liquid in equilibrium with the saturated vapor pressure of the liquid. The table is not comprehensive. It is limited to the more important polymers, and where a datum

TABLE 59.1. *Liquid surface tension.*

Polymer	M_W	γ_{LV} at 20 °C (mN/m)	$-d\gamma/dT$[mN/(mK)]	References
Poly(oxyhexafluoropropylene)	∞	18.4 (25 °C)	0.059 (M_n − 7,000)	[17,10]
Poly[(heptadecafluorodecyl) methylsiloxane]	$M_n \sim$ 19,600	18.5 (25 °C)	—	[31]
Poly(dimethylsiloxane)	∞	21.3 (20 °C)	0.048 (10^6 cS)	[8,32]
Poly[methyl(trifluoropropyl)siloxane]	∞	24.4 (25 °C)	—	[31]
Poly(tetrafluoroethylene)	∞	25.6	0.053(M_n = 1,038)	[9]
Poly(oxyisobutylene)	M∼30,000	27.5	0.066	[6]
Poly(vinyl octanoate)	—	28.7	0.061	[33]
Polypropylene, atactic	Melt index ∼1,000	29.4	0.056	[32]
Paraffin wax	—	30.0 (20 °C)	∼0.06	[34]
Poly(1,2-butadiene)	$M_n \sim$ 1,000	30.4 (25 °C)	—	[35]
Poly(*t*-butyl methacrylate)	$M_v \sim$ 6,000	30.5	0.059	[23]
Poly(oxypropylene)	$M_n \sim$ 4,100	30.7 (25 °C)	0.073	[11]
Poly(*i*-butyl methacrylate)	$M_v \sim$ 35,000	30.9	0.060	[23]
Poly(chlorotrifluoroethylene)	$M_n \sim$ 1,280	30.9	0.067	[36]
Poly(vinyl hexadecanoate)	—	30.9	0.066	[33]
Poly(*n*-butyl methacrylate)	$M_v \sim$ 37,000	31.2	0.059	[37]
Poly(oxytetramethylene)	$M_n \sim$ 32,000	31.8	0.060	[38]
Poly(methoxyethylene)	$M_n \sim$ 46,500	31.8	0.075	[6]
Poly(*n*-butyl acrylate)	*M*∼32,000	33.7	0.070	[39]
Polyethylene, branched	$M_n \sim$ 7,000	34.3	0.060	[40]
Poly(isobutylene)	∞	35.6 (24 °C)	0.064 ($M_n \sim$ 2,700)	[8,41]
Polyethylene, linear	$M_w \sim$ 67,000	35.7	0.057	[41]
Poly(oxydecamethylene)	—	36.1	0.068	[42]
Poly(vinyl acetate)	$M_w \sim$ 120,000	36.5	0.066	[41]
Poly(2-methylstyrene)	$M_n \sim$ 3,000	38.7	0.058	[6]
Poly(oxydodecamethyleneoxyisophthaloyl)	—	40.0	0.070	[30]
Polystyrene	$M_v \sim$ 44,000	40.7	0.072	[37]
Poly(methyl acrylate)	$M_n \sim$ 25,000	41.0	0.070	[6]
Poly(methyl methacrylate)	$M_v \sim$ 3,000	41.1	0.076	[37]
Poly(epichlorohydrin)	$M_n \sim$ 1,500	43.2 (25 °C)	—	[43]
Polychloroprene	$M_v \sim$ 30,000	43.6	0.086	[23]
Poly(oxyethyleneoxyterephthaloyl)	$M_n \sim$ 16,000	44.5	0.064	[44]
Poly(oxyethylene)	∞	45.0 (24 °C)	0.076 (M_n − 6,000)	[45,32]
Poly(hexamethylene adipamide)	$M_n \sim$ 17,000	46.4	0.064	[44]
Poly(oxyisophthaloyloxypropylene)	—	49.3	0.083	[30]

Structural note regarding fluoropolymers in Tables 59.1 *and* 59.3: Rigorous application of nomenclature rules can lead to fluoropolymer names of excessive length for tabulations. There are few generally agreed abbreviations or acronyms for such polymers so rather than add to this problem we have dropped precise descriptions of substituent positions in the names in the tables. To avoid any confusion, the full names of these polymers are given below:
poly[(heptadecafluorodecyl)methylsiloxane] is poly[(1*H*, 1*H*, 2*H*, 2*H*-heptadecafluorodecyl)methylsiloxane], poly[methyl(trifluoropropyl)siloxane] is poly[methyl(1*H*, 1*H*, 2*H*, 2*H*-trifluoropropyl)siloxane], poly(heptadecafluorodecyloxymethylstyrene) is poly(1*H*, 1*H*, 2*H*, 2*H*-heptadecafluorodecyloxymethylstyrene), poly(pentadecafluorooctyl acrylate) is poly(1*H*, 1*H*-pentadecafluorooctyl acrylate), poly(pentadecafluorooctyl methacrylate) is poly(1*H*, 1*H*-pentadecafluorooctyl methacrylate), poly[heptadecafluorooctylsulfonamido(propyl)ethyl acrylate] is poly[2-(*N*-propyl-*N*-heptadecafluorooctylsulfonamido)ethyl acrylate], and poly[methyl(nonafluorohexyl)siloxane] is poly[methyl(1*H*, 1*H*, 2*H*, 2*H*-nonafluorohexyl)siloxane].

choice is possible only one reliable value has been chosen. The selection is guided by a preference for numerical rather than graphical data, studies of purified polymers, true equilibrium measurement techniques with a minimum of assumptions such as zero contact angle of the polymer with the material of construction of the measuring device, data on polymers of reported molecular weight, and original citations rather than subsequent compilations. Surprisingly some of the often quoted key values are in rather obscure sources. On occasion, for sufficiently important polymers, each of these preferences has been compromised in the preparation of Table 59.1 and the other tables.

The molecular-weight criterion is important since polymer liquid surface tension is a function of molecular weight. This is a density and end-group effect and is most apparent at low molecular weight. For this reason, either the highest-molecular-weight study is selected, in which case the actual molecular weight is given (MW column), or, if sufficient data are available, an extrapolated value to infinite molecular weight is given. This is shown in the MW column of Table 59.1 as ∞. All but one of these extrapolated selections use the LeGrand and Gaines equation [8]

$$\gamma_{LV} = \gamma_{\infty} - \boldsymbol{K}/\boldsymbol{M}_n^{2/3}, \tag{59.1}$$

where γ_{LV} is the surface tension at number average molecular weight M_n and K is a constant. The exception in Table 59.1 is the polytetrafluoroethylene γ_{∞} value which comes from extrapolation of γ_{LV}^{-1} vs n^{-1}, where n is the number of carbon atoms in the chain [9]. Wu [5] has given another alternative to Eq. (59.1). Equation (59.1) is used because most of the available data are presented in this manner. Sauer and Dee [10] have shown that theoretical predictions follow the $M_n^{-2/3}$ dependence for lower molecular weights and the M_n^{-1} dependence for high molecular weight. The difference between the surface tension of a polymer at $M_n \sim$ 3,000 and γ_{∞} is usually less than 1 mN/m.

If the polymer is a liquid at room temperature, the γ_{LV} at 20 °C column of Table 59.1 contains the actual data available nearest to 20 °C (the precise temperature of measurement is shown in parentheses). Other figures in this column are from extrapolation from higher temperature studies of polymer melts. The surface tension should change discontinuously at the crystal–melt transition and continuously at the glass transition with discontinuous $d\gamma/dT$, where T is the temperature in degrees Centigrade. Wu [5] has shown that extrapolation is usually adequate as semicrystalline polymers generally have amorphous surface when prepared by cooling from the melt, and the effect of glass transition temperature is small.

$d\gamma/dT$ data are not available at infinite molecular weight. Thus the highest-molecular-weight studies have been chosen in these instances and the molecular weight given in parentheses. When it is a separate study to the γ_{LV} at 20 °C data, a second citation is given in the reference column. Surface tensions of polymers vary linearly with temperature with $-d\gamma/dT$ typically being from 0.05 to 0.08; increasing γ_{LV} weakly correlates with larger values of $-d\gamma/dT$. This is somewhat less than the temperature coefficient for nonpolymeric liquids and is attributed to conformational restrictions of long-chain molecules, $-d_{\gamma}/dT$ being the surface entropy [5].

Table 59.1 is arranged, like all the tables in this compilation, in order of increasing surface tension so the familiar effect of polar constituent groups raising the surface tension is readily apparent. Most polymer chemists are familiar with Zisman's critical surface tension of the wetting [4] constituent effect (see Table 59.3) where the order of increasing surface tension is

$$CF_3 \rightarrow CF_2 \rightarrow CH_3 \rightarrow CH_2$$

A surprising aspect of Table 59.1 is the higher γ_{LV} at 20 °C (∞) value for CF_2 (polytetrafluoroethylene) than CH_3 (in the polydimethylsiloxane case).

No copolymer data are included in these tables. Random copolymers sometimes follow simple mixing expectations, e.g., random copolymers of ethylene oxide and propylene oxide show a linear dependence of liquid surface tension with mole fraction of propylene oxide over most of the composition range [11], but there are many deviations from this behavior [12]. This is probably due to development of significant sequence lengths of the lower-surface-tension component as block polymers can show marked preferential adsorption of the lower-surface-tension block [11,13].

No data on solutions are included either. Although there is considerable information in the literature on certain polymers, it is dependent on the particular choice of solvent and not amenable to systematic tabulation. The same is true of the wealth of adsorption from solution onto solids and spread film Langmuir trough data. Equations are available for calculating the surface tension of simple liquid mixtures that could be applied to polymers [14] and for calculating polymer solvent solution [15] surface tensions.

59.3 INTERFACIAL TENSION

Selected values of the interfacial tension at 20 °C between homopolymers γ_{12} are given in Table 59.2. Since these are studies of liquid polymers the table is constructed in a similar manner to Table 59.1 inasmuch as γ_{12} at 20 °C is extrapolated from higher-temperature studies except when an actual temperature is given in parentheses. Table 59.2 does not contain molecular-weight information. There are insufficient data available to make any predictions at infinite molecular weight. In large part these interfacial tension values are derived from the same materials that were used to obtain the temperature coefficient data in Table 59.1 and in these cases molecular-weight information can be obtained from that table.

TABLE 59.2. *Interfacial tension.*

Polymer pair	γ_{12} at 20 °C (mN/m)	$-d\gamma/dT$ [mN/(m K)]	References
Polychloroprene/polystyrene	0.5 (140 °C)	—	[23]
Polychloroprene/poly(*n*-butyl methacrylate)	1.6 (140 °C)	—	[23]
Poly(methyl methacrylate)/poly(*t*-butyl methacrylate)	3.0	0.005	[23]
Poly(methyl methacrylate)/polystyrene	3.2	0.013	[37]
Poly(dimethylsiloxane)/polypropylene	3.2	0.002	[6]
Poly(methyl methacrylate)/poly(*n*-butyl methacrylate)	3.4	0.012	[37]
Poly(dimethylsiloxane)/poly(*t*-butyl methacrylate)	3.6	0.003	[23]
Polybutadiene/poly(dimethylsiloxane)	4.0	0.009	[46]
Poly(methyl acrylate)/poly(*n*-butyl acrylate)	4.0	0.008	[6]
Poly(dimethylsiloxane)/poly(isobutylene)	4.0	0.016	[47]
Poly(*n*-butyl methacrylate)/poly(vinyl acetate)	4.2	0.011	[37]
Poly(dimethylsiloxane)/poly(*n*-butyl methacrylate)	4.2	0.004	[23]
Polystyrene/poly(vinyl acetate)	4.2	0.004	[23]
Polyethylene/polystyrene	4.4 (200 °C)	—	[48]
Poly(oxyethylene)/poly(oxtetramethylene)	4.5	0. 005	[38]
Polychloroprene/polyethylene, branched	4.6	0.008	[23]
Polyethylene, linear/poly(*n*-butyl acrylate)	5.0	0.014	[6]
Polyethylene, branched/poly(oxytetramethylene)	5.0	0.007	[38]
Poly(dimethylsiloxane)/polyethylene, branched	5.3	0.002	[38]
Poly(oxytetramethylene)/poly(vinyl acetate)	5.5	0.008	[38]
Polyethylene, branched/poly(*i*-butyl methacrylate)	5.5	0.010	[23]
Polyethylene, branched/poly (oxydodecamethyleneoxyisophthaloyl)	5.9	0.011	[30]
Polyethylene, branched/poly(*t*-butyl methacrylate)	5.9	0.016	[23]
Poly(dimethylsiloxane)/polystyrene	6.1	~0	[6]
Poly(dimethylsiloxane)/poly(oxytetramethylene)	6.4	0.001	[23]
Poly(dimethylsiloxane)/polychloroprene	7.1	0.005	[23]
Polyethylene, linear/poly(*n*-butyl methacrylate)	7.1	0.015	[37]
Polyethylene, linear/polystyrene	8.3	0.020	[37]
Poly(dimentylsiloxane)/poly(vinyl acetate)	8.4	0.008	[23]
Poly(isobutylene)/poly(vinyl acetate)	9.9	0.020	[41]
Polyethylene, linear/poly(methyl acrylate)	10.6	0.018	[6]
Polyethylene/poly(caprolactam)	10.7 (250 °C)	—	[48]
Poly(dimethylsiloxane)/poly(oxyethylene)	10.9	0.008	[38]
Polyethylene, branched/poly(oxyethylene)	11.6	0.016	[38]
Polyethylene, linear/poly(methyl methacrylate)	11.9	0.018	[37]
Polyethylene, linear/poly(vinyl acetate)	14.5	0.027	[41]
Polyethylene, linear/poly(hexamethylene adipamide)	14.9	0.018	[6]
Polyethylene, branched/poly(oxyisophthaloyloxypropylene)	15.4	0.030	[30]

Two points stand out when Tables 59.1 and 59.2 are compared; the temperature coefficients for interfacial tension are lower than those for surface tension, and there is no correlation between the interfacial tension of a polymer pair and the difference in their surface tensions. The former effect arises because the variation with temperature is a density effect.

The smaller magnitude of $-d\gamma_{12}/dT$ is due to the fact that $d(\rho_1 - \rho_2)/dT$ is less than $d\rho_1/dT$ or $d\rho_2/dT$, where ρ_i is the density of phase i. The latter effect shows that the interface between polymers is not simple. Equality of γ_{12} with $\gamma_1 - \gamma_2$ is Antonow's rule [16], the oldest such relationship. Clearly, few polymer pairs obey the rule. More complex relationships of this type are discussed in the following section.

There are also a few reports of interfacial tension of polymers with simpler liquids. Water is the most important of these liquids, e.g., the interfacial tension between water and poly(oxyhexafluoropropylene) is 53.1 mN/m at 25°C (Krytox AX, 300 cS viscosity [17]) and between water and poly(dimethylsiloxane) is 42.7 mN/m at 24°C at ($M_n \sim 1{,}000$[18]). Interfacial tensions with liquids can also be calculated from the equations discussed in Section 59.4 [Eqs. (59.6), (59.7), or (59.8)]. For example, King *et al.* [19] have calculated using the harmonic mean equation [Eq. (59.8)] that the interfacial tension with water of poly

(methyl methacrylate) is 24 mN/m while that for poly (hydroxyethyl methacrylate) is 0.1 mN/m.

59.4 SOLID SURFACE PROPERTIES

Solid surface properties based on contact-angle data for selected homopolymers are shown in Tables 59.3 and 59.4. The γ_c column of Table 59.3 is the Zisman critical surface tension of wetting [4] obtained from the quasistatic, advancing contact angles θ of a series of liquids of surface tension γ_{LV} by the empirical equation:

$$\cos\theta = 1 - b(\gamma_{LV} - \gamma_c), \tag{59.2}$$

where b is a constant. For nonpolar polymers the *n*-alkanes are a preferred set of homologous liquids to use and such data are indicated by footnote indicator *a* in the γ_c column.

Young's equation for the contact of a liquid (L) with a solid (S) is

$$\gamma_{LV}\cos\theta = \gamma_{SV} - \gamma_{SL}, \tag{59.3}$$

where γ_{LV} and γ_{SV} are defined as being in equilibrium with the saturated vapor (V) pressure of the liquid. From Eqs. (59.2) and (59.3) it follows that

$$\gamma_c = \gamma_{SV} - \gamma_{SL} \tag{59.4}$$

and other approaches to obtaining solid surface free energy from contact-angle data are essentially ways to calculate the usually unknown interfacial tension γ_{SL} between the polymer solid and the test liquid. These equations are of the form

$$\gamma_{SL} = \gamma_{SV} + \gamma_{LV} - F, \tag{59.5}$$

where F is given in a variety of ways, including

$$F = 2\left(\gamma_{LV}^{d}\gamma_{SV}^{d}\right)^{1/2}, \tag{59.6}$$

$$F = 2\left(\gamma_{LV}^{d}\gamma_{SV}^{d}\right)^{1/2} + 2\left(\gamma_{LV}^{p}\gamma_{SV}^{p}\right)^{1/2}, \tag{59.7}$$

$$F = 4\left(\gamma_{LV}^{d}\gamma_{SV}^{d}\right)/\left(\gamma_{LV}^{d} + \gamma_{SV}^{d}\right) + 4\left(\gamma_{LV}^{p}\gamma_{SV}^{p}\right)/\left(\gamma_{LV}^{p} + \gamma_{SV}^{p}\right). \tag{59.8}$$

In these equations γ^d is the dispersion force component and γ^p the other polar force components of surface free energy ($\gamma = \gamma^d + \gamma^p$). Equation (59.6) was introduced by Good and Girifalco [20] and Fowkes [21], Eq. (59.7) was introduced by Owens and Wendt [22], and Eq. (59.8) was introduced by Wu [23]. Data in Table 59.3 are mostly derived via Eq. (59.7) using water and methylene iodide; exceptions are noted by footnotes. Actual contact-angle data are usually, but not always, available in the references cited. As water is the ubiquitous liquid and used in many studies, a column for such data is included in Table 59.3. Where possible only quasistatic advancing contact-angle values were chosen.

Table 59.3 is based primarily on the Zisman critical surface tension of wetting and Owens and Wendt approaches because most of the polymer data available is in these forms. The inadequacies of equations such as Eq. (59.7) have been known for a decade, and newer, more refined approaches are becoming established, notably these of van Oss and coworkers [24]. A more limited number of polymers have been examined in this way and the data (at 20 °C) are summarized in Table 59.4. γ^{LW} is the component of surface free energy due to the Lifshitz–van der Waals (LW) interactions that includes the London (dispersion, γ^d), Debye (induction), and Keesom (dipolar) forces. These are the forces that can correctly be treated by a simple geometric mean relationship such as Eq. (59.6). γ^{AB} is the component of surface free energy due to Lewis acid–base (AB) polar interactions. As with γ^d and γ^p the sum of γ^{LW} and γ^{AB} is the total solid surface free energy. γ^{AB} is obtained from

$$\gamma^{AB} = 2(\gamma^{+}\gamma^{-})^{1/2}, \tag{59.9}$$

where γ^+ stands for the electron-acceptor parameter and γ^- for the electron-donor parameter of the surface free energy.

One of the problems of simple geometric and other combining rules is that none accounts for the occurrence of a zero polar surface free energy component between quite polar solids or liquids. If γ^+ is zero, i.e., for a monopolar material, then so will be γ^{AB}, however, large the value of γ^-. Moreover, the interfacial free energy equation that follows from Eq. (59.9) is a double asymmetrical interaction that allows the possibility of a negative interfacial free energy in certain cases. No absolute values of γ^+ and γ^- are known; the values in Table 59.4 are based on assumed values for reference liquids such as water, but note that the values of γ^{AB} are based only on the polarity ratios of γ^+ and γ^- relative to the reference liquid values and these polarity ratios can be precisely established. Table 59.4 is constructed from Tables XIII-5 and XIII-8A in van Oss's book [24]. These contain other copolymer and biopolymer surface-free-energy data (van Oss uses the term *surface tension* rather than *surface free energy*).

59.5 DIRECTLY MEASURED SOLID SURFACE FREE ENERGY

Surface free energies can be obtained from direct work of adhesion measurements using the Johnson, Kendall, and Roberts (JKR) [7] approach. According to the JKR theory, the contact radius a between two elastic bodies of radii of curvature R_1 and R_2, Young's moduli of E_1 and E_2, and Poisson ratios of ν_1 and ν_2, under an applied load P is given by

$$a^3 = \frac{R}{K}\left[P + 3\pi WR + \sqrt{6\pi WRP + (3\pi WR)^2}\right], \tag{59.10}$$

TABLE 59.3. *Solid surface properties,* γ_c, γ^d, γ^p.

Polymer	γ_c (mN/m)	Reference	γ^d (mJ/m^2)	γ^p (mJ/m^2)	Reference	$\theta(H_2O)$ (deg)	Reference
Poly(heptadecafluorodecyl oxymethylstyrene)	6[a]	[49]	9[b]	—	[49]	—	
Poly(pentadecafluorooctyl acrylate)	10.4[a]	[50]	—	—		—	
Poly(pentadecafluorooctyl methacrylate)	10.6[a]	[51]	9.1	0.3	[22]	119	[51]
Poly[heptadecafluorooctyl sulfonamido(propyl) ethylacrylate]	11.1[a]	[51]	10.3	0.4	[52]	118	[51]
Poly(hexafluoropropylene)	16.2[a]	[53]	11.7	0.7	[52]	—	
Poly[methyl(nonafluorohexyl) siloxane]	16.3[a]	[54]	8.4	1.1	[54]	115	[54]
Poly(tetrafluoroethylene)	18.3[a]	[55]	18.6	0.5	[22]	108	[22]
Poly[methyl(trifluoro)siloxane]	21.4[a]	[56]	10.8	2.8	[56]	104	[56]
Poly(trifluoroethylene)	22	[57]	19.9	4.0	[22]	92	[57]
Paraffin wax	23	[22]	25.4	0	[22]	112	[58]
Poly(dimethylsiloxane)	24	[59]	21.7	1.1	[22]	101	[22]
Poly(vinylidene fluoride)	25	[57]	23.2	7.1	[22]	82	[57]
Poly(1,2-butadiene)	25	[60]	—	—		—	
Poly(isobutylene)	27	[60]	—	—		—	
Poly(vinyl butyral)	28	[60]	—	—		—	
Poly(vinyl fluoride)	28	[57]	31.3	5.4	[22]	80	[57]
Polypropylene	29	[61]	28.6	0.4	[35]	116	[35]
Poly(chlorotrifluoroethylene)	31	[62]	23.9	3.6	[23]	90	[62]
Polyisoprene, *cis*	31	[63]	—	—		106	[63]
Poly(oxypropylene)	32	[60]	—	—		—	
Poly(*n*-butyl methacrylate)	32	[64]	31.3	2.0	[23]	91	[23]
Polystyrene	32.8	[65]	41.4	0.6	[22]	91	[65]
Polyethylene, branched	33	[66]	32.0	1.1	[22]	94	[66]
Poly(undecanoamide)	33	[67]	—	—		89	[67]
Poly(epichlorohydrin)	35	[63]	—	—		87	[63]
Poly(vinyl alcohol)	37	[68]	—	—		—	
Poly(vinyl acetate)	37	[60]	—	—		—	
Polychloroprene	38	[63]	—	—		—	
Poly(vinyl chloride)	39	[57]	40.0	1.5	[22]	87	[57]
Cellulose acetate	39	[69]	—	—		65	[69]
Poly(methyl methacrylate)	39	[70]	35.9	4.3	[22]	80	[70]
Poly(vinylidene chloride)	40	[57]	42.0	3.0	[22]	80	[57]
Poly(oxyphenylene)	41	[60]	—	—		—	
Polycaprolactam	42	[64]	—	—		70	[64]
Poly(hexamethylene adipamide)	42.5	[65]	40.8	6.2	[22]	72	[22]
Poly(oxyethyleneoxyterephthaloyl)	43	[65]	43.2	4.1	[22]	76	[22]
Poly(ethylene oxide)	43	[60]	—	—		—	
Poly(acrylonitrile)	44	[60]	—	—		—	
Polyglycine	44	[71]	—	—		49	[71]
Cellulose, regenerated	44	[68]	—	—		—	
Poly(ether ketone ketone)	—		41.7	6.5	[35]	85	[35]
Poly(2-hydroxyethyl methacrylate)	52	[72]	34.1[c]	24.3[c]	[72]	—	
Poly(acrylamide)	52.3	[73]	—	—		—	
Urea–formaldehyde resin	61	[74]	—	—		—	

[a]Determined using *n*-alkane contact-angle test liquids.
[b]Determined by use of Eq. (59.6).
[c]Determined by use of Eq. (59.7) but using methylene iodide and glycerol (not water).

TABLE 59.4. *Solid surface properties* γ^{LW},γ^{AB}.

Polymer	γ^{LW} (mJ/m^2)	γ^{AB} (mJ/m^2)	γ^+ (mJ/m^2)	γ^- (mJ/m^2)	Reference
Poly(tetrafluoroethylene)	18.5	0	0	0	[75]
Poly(isobutylene)	25.0	0	0	0	[76]
Poly(propylene)	25.7	0	0	0	[76]
Polyethylene	33.0	0	0	0	[77]
Poly(hexamethylene adipamide)	36.4	1.3	0.02	21.6	[78]
Poly(methyl methacrylate)	41.4	0	0	12.2	[78]
Poly(oxytetramethylene)	41.4	2.6	0.06	27.6	[24]
Polystyrene	42	0	0	1.1	[24]
Poly(vinyl alcohol)	42	0	0	17–57	[79]
Poly(vinyl chloride)	43	0.75	0.04	3.5	[76]
Poly(vinyl pyrrolidone)	43.4	0	0	29.7	[24]
Cellulose	44.0	10.5	1.6	17.2	[24]
Cellulose nitrate	44.7	0.4	0.003	13.9	[80]
Cellulose acetate	44.9	7.7	0.8	18.5	[24]
Poly(oxyethylene)	45.9	0	0	58.5	[24]

where

$$\frac{1}{R} = \frac{1}{R_1} + \frac{1}{R_2}, \tag{59.11}$$

$$\frac{1}{K} = \frac{3}{4}\left[\frac{1-\nu_1^2}{E_1} + \frac{1-\nu_2^2}{E_2}\right] \tag{59.12}$$

and W is the *thermodynamic work of adhesion*. For two identical surfaces in contact:

$$W = 2\gamma \tag{59.13}$$

and, for two dissimilar surfaces in contact:

$$W = \gamma_1 + \gamma_2 - \gamma_{12} \tag{59.14}$$

γ_1,γ_2 are the surface energies of materials 1 and 2, and γ_{12} is the interfacial energy between 1 and 2.

Equation (59.10) may be rearranged as

$$W = \frac{\left(P - \frac{a^3 K}{R}\right)^2}{6\pi K a^3}. \tag{59.15}$$

When the surfaces are in contact due to the action of the attractive interfacial forces, a finite tensile load is required to separate the bodies from adhesive contact. This tensile load is called the ''pull-off'' force (P_s). According to the JKR theory, the pull-off force is related to the thermodynamic work of adhesion (W) and the radius of curvature (R).

$$P_s = \frac{3}{2}\pi W R. \tag{59.16}$$

γ_{JKR} values are presently not extensive in number but offer instructive comparisons with contact angle studies. This is done in Table 59.5. The references cited are to the JKR values, γ_{JKR}. Other data for the four polymers come from Tables 59.1 and 59.3. The poly(oxyethyleneoxyterephthaloyl) (PET) and polyethylene (PE) JKR studies of Tirrell and coworkers [25,26] are on samples biaxially stretched during sample preparation, so these surfaces should be semicrystalline in contrast to the amorphous surfaces used for most contact-angle studies. Despite this, their contact angle studies on the same samples used in the JKR studies gave values similar to other contact angle studies such as those listed in Table 59.3. This implies little difference between amorphous and semicrystalline surfaces in these two instances; another explanation is needed for the unexpectedly high JKR surface-free-energy values for poly(oxyethyleneoxyterephthaloyl).

Also included in Table 59.5 are data for various self-assembled silane monolayers formed on plasma-oxidized polydimethylsiloxane (PDMS) surfaces [27] that offer a measure of the effect of changing the outermost groups on a polymer surface. The γ^d_{SV} data come from Eq. (59.7) using water and methylene iodide, except for the perfluoromethyl surface for which the contact angle of perfluorodecalin was used. The comparative γ_c and γ_{LV} figures come from Shafrin and Zisman [28] and Wu [6], respectively. A more extensive compilation of γ_c and $\gamma^d{}_{SV}$ and $\gamma^p{}_{SV}$ for functional silane layers is available [29] but comparative γ_{JKR} data are currently lacking.

To understand the reasons for different predictions of different methods, Li *et al*. [83] measured the adhesion between a variety of polymers with well-controlled backbone chemistry These polymers include: poly(4-methyl 1-pentene) [TPX], poly(vinyl cyclohexane) [PVCH], polystyrene [PS], poly(methyl methacrylate) [PMMA], and poly(2-vinyl pyridine) [PVP], poly(4-*tert*-butyl styrene) [PtBS], poly(acrylonitrile) [PAN], poly(*p*-phenyl styrene) [PPPS], poly(vinyl benzyl chloride) [PVCB]. It may be noted that, among the polymers listed above, TPX and PVCH are purely dispersive in nature. PS is predominantly dispersive with some dipole-induced dipole interactions.

TABLE 59.5. *Surface free energy comparisons.*

Polymer or terminal surface functionality	$\gamma_{JKR}(mJ/m^2)$	Reference	$\gamma_C(mN/m)$	$\gamma_{LV}(mN/m)$	$\gamma^d{}_{SV}(mN/m)$
Poly(dimethylsiloxane) [PDMS]	22.6	[27]	24	21.3	22.8
Natural rubber (*cis* 1,4 polyisoprene)	35	[7]	31	—	—
Poly(oxyethyleneoxyterephthaloyl)	61.4	[25]	43	44.5	47.3
Polyethylene	33	[26]	32	34.3	32.0
Corona-treated polyethylene	52	[83,84]	34	—	—
Poly(4-methyl 1-pentene)	27	[83,84]	22	—	—
Poly(vinyl cyclohexane)	28	[83,84]	29	—	—
PS polystyrene	44	[83,84]	30	—	—
Poly(2-vinyl pyridine)	63	[83,84]	50	—	—
Poly(methyl methacrylate)	53	[83,84]	40	—	—
$-CF_3$	16.0	[27]	6	15	15.0
$-CH_3$	20.8	[27]	22	30	20.6
$-OCH_3$	26.8	[27]	—	—	30.8
$-CO_2CH_3$	33.0	[27]	—	—	36.0
$-Br$	36.8	[27]	—	—	37.9

In the case of PMMA and PVP, just as in the case of poly(ethyleneterephthalate) [PET] and corona-treated polyethylene [PE] surfaces, the nondispersive interactions are dominant. These polymers essentially form a set with increasing degrees of polar interactions. The values of surface energies of these polymers obtained from contact mechanics measurements are listed in Tables 59.5 and 59.6. Examination of the data in these two tables shows the curious effect that all of the polymers which are dominated by dispersive force intermolecular bonding (PE, TPX, PVCH, PtBS) show relatively good agreement between the contact mechanics determined surface energy and the contact angle inferred surface energy (depending upon the model chosen for inferring the surface energy). However, the contact mechanics determined surface energy is markedly higher for those polymers which have a substantial component of nondispersive intermolecular bonding (PET, PVP, PMMA, PS, corona treated PE). The greater the nondispersive character, the greater the discrepancy between contact angle and contact mechanics determined surface energy. Lee *et al*. conjecture that the reason for the discrepancy between these two methods of determination of polymer surface energy is that the intermolecular energetics of the liquids used to determine contact angles are not the same as those in the polymer surfaces. In addition, contact angle liquids can induce changes in the substrate surface (such as rearrangement, crystallization, etc.) which would not occur for a material in contact with itself. In contact mechanics measurements, the probe of surface energy is just the material itself, thus having identical intermolecular bonding on both sides of the interface in question. However, contact mechanics measurements may cause the surface to respond by rearrangement, but possibly in a different fashion from liquid contact.

In a separate study using the JKR technique, Chaudhury and Owen [81,82] attempted to understand the correlation between the *contact adhesion hysteresis* and the phase state of the monolayers films. In these studies, Chaudhury and Owen prepared self-assembled layers of hydrolyzed hexadecyltrichlorosilane (HTS) on oxidized PDMS surfaces at varying degrees of coverage by vapor phase adsorption. The phase state of the monolayers changes from crystalline (solid-like) to amorphous (liquid-like) as the surface coverage (ϕ_s) decreases. The authors attributed the hysteresis in the case of compact monolayers to line defects and point defects formed during the vapor phase adsorption of the monolayers. The authors ruled out stress-induced rearrangement or interdigitation as a possible cause of hysteresis in these systems. It should be pointed out that the exact origins of the contact adhesion hysteresis are not well understood.

Table 59.6 gives a few interfacial-free-energy measurements against poly(dimethylsiloxane) using the JKR approach. Johnson, Kendall, and Roberts [7] give a value of 3.4 mJ/m^2 between rubber and water and Mangipudi, Tirell, and Pocius [26] give a value of 17.1 mJ/m^2 between polyethylene and poly(oxyethyleneoxyterephthaloyl). This is somewhat higher than an unattributed extrapolated melt value of 9.4 mN/m quoted by Wu [6] but in line with the value from Kasemura, Kondo, and Hata [30] of 15.4 mN/m for polyethylene/poly(oxyisophthaloyloxypropylene).

Related information can be found in Chapter 27.

TABLE 59.6. *Surface and Interfacial energies determined by JKR contact mechanics method and comparison to surface energies inferred from contact angle measurements.*

Polymer	γ_{JKR} (mJ/m^2)	γ_{SV}[a] (mN/m)	$\gamma_{PDMS\text{-}polymer}$ (from JKR technique) (mJ/m^2)	References
Poly(dimethylsiloxane) [PDMS]	21	26	0	[83]
Poly(vinyl cyclohexane)	30	32	3	[83]
Poly(4-ter-butyl styrene)	33	35	9	[83]
Polystyrene	38	39	10	[83]
Poly(*p*-phenyl styrene)	42	40	11	[83]
Poly(vinyl benzyl chloride)	43	40	12	[83]
Poly(acrylonitrile)	54	54	20	[83]
Poly(ethylenepropylene)	30	—	—	[85,86]
Poly(ethylethylene)	25	—	—	[86]
Poly(isoprene)	28	—	—	[86]

[a]Calculated from contact angle data based on Van Krevelen Group Contribution method [87].

REFERENCES AND NOTES

1. A. Couper, in Vol. IXA *of Physical Methods of Chemistry*, edited by B. W. Rossiter and R. C. Baetzold, *Investigations of Surfaces and Interfaces-Part* A (Wiley, New York, 1993), p. 1.
2. A. W. Adamson, *Physical Chemistry of Surfaces*, 4th ed. (Wiley, New York, 1982), p. 4.
3. Reference [1] is a good introduction to techniques of liquid surface tension measurement; Ref. [5] deals specifically with polymers.
4. W. A. Zisman, in *Contact Angle, Wettability, and Adhesion*, Advances in Chemistry Series No. 43, edited by F. M. Fowkes (American Chemical Society, Washington, D.C., 1964), p. 1.
5. S. Wu, *Polymer Interface and Adhesion* (Dekker, New York, 1982).
6. S. Wu, in *Polymer Handbook, 3rd* ed., edited by J. Brandrup and E. H. Immergut (Wiley, New York, 1989), p. VI/411.
7. K. L. Johnson, K. Kendall, and A. D. Roberts, Proc. R. Soc. Lond. Ser. A 324, 301 (1971).
8. D. G. LeGrand and G. L. Gaines, Jr., J. Colloid Interf. Sci. 31, 162 (1969).
9. R. H. Dettre and R. E. Johnson, Jr, J. Colloid Interf. Sci. 31, 568 (1969).
10. B. B. Sauer and G. T. Dee, J. Colloid Interf. Sci. 162, 25 (1994).
11. A. K. Rastogi and L. E. St. Pierre, J. Colloid Interf. Sci. 35, 16 (1971).
12. T. Hata and T. Kasemura, in *Adhesion and Adsorption of Polymers*, Vol. 12A *of Polymer Science and Technology*, edited by L. -H. Lee (Plenum, New York, 1980), p. 15.
13. T. C. Kendrick, B. M. Kingston, N. C. Lloyd, and M. J. Owen, J. Colloid Interf. Sci. 24, 135 (1967).
14. J. W. Belton and M. G. Evans, Trans. Faraday Soc. 41, 1 (1945).
15. G. L. Gaines Jr., J. Phys. Chem. 73, 3143 (1969).
16. G. N. Antonow, J. Chim. Phys. 5, 372 (1907).
17. M. K. Bernett and W. A. Zisman, J. Phys. Chem. 77, 2324 (1973).
18. A. G. Kanellopoulos and M. J. Owen, Trans. Faraday Soc. 67, 3127 (1971).
19. R. N. King, J. D. Andrade, S. M. Ma, D. E. Gregonis, and L. R. Brostrom, J. Colloid Interf. Sci. 103, 62 (1985).
20. R. J. Good and L. A. Girifalco, J. Phys. Chem. 64, 561 (1960).
21. F. M. Fowkes, J. Phys. Chem. 66, 382 (1962).
22. D. K. Owens and R. C. Wendt, J. Appl. Polym. Sci. 13. 1741 (1969).
23. S. Wu, J. Polym. Sci. Part C 34, 19 (1971).
24. C. J. van Oss, *Interfacial Forces in Aqueous Media* (Dekker, New York, 1994).
25. W. W. Merrill, A. V. Pocius, B. V. Thakker, and M. Tirrell, Langmuir 7, 1975 (1991).
26. V. Mangipudi, M. Tirrell, and A. V. Pocius, J. Adhes. Sci. Technol. 8, 1251 (1994).
27. M. K. Chaudhury, J. Adhes. Sci. Technol. 7, 669 (1993).
28. E. G. Shafrin and W. A. Zisman, J. Phys. Chem. 64, 519 (1960).
29. M. J. Owen, in *Silicon-Based Polymer Science*, Advances in Chemistry Series No. 224, edited by J. M. Zeigler and F. W. G. Fearon (American Chemical Society, Washington, D.C., 1990), p. 705.
30. T. Kasemura, T. Kondo, and T. Hata, Kobunshi Ronbunshu 36, 815 (1979).
31. H. Kobayashi and M. J. Owen, Makromol Chem. 194, 1785 (1993).
32. R. J. Roe, J. Phys. Chem. 72, 2013 (1968).
33. T. Kasemura, F. Uzi, T. Kondo, and T. Hata, Kobunshi Ronbunshu 36, 337 (1979).
34. J. F. Padday, in Proceedings of the 2nd International Congress on Surface Activity, Vol. 3, 1957, p. 136.
35. B. B. Sauer and N. V. Diapaolo, J. Colloid Interf. Sci. 144, 527 (1991).
36. H. Schonhorn, F. W. Ryan, and L. H. Sharpe, J. Polym. Sci. A-2 4, 538 (1966).
37. S. Wu, J. Phys. Chem. 74, 632 (1970).
38. R. J. Roe, J. Colloid Interf. Sci. 31, 228 (1969).
39. S. Wu, Org. Coat. Plast. Chem. 31(2), 27 (1971).
40. R. H. Dettre and R. E. Johnson, Jr., J. Colloid Interf. Sci. 21, 367 (1966).
41. S. Wu, J. Colloid Interf. Sci. 31, 153 (1969).
42. T. Kasemura, N. Yamashita, K. Suzuki, T. Kondo, and T. Hata, Kobunshi Ronbunshu 35, 215 (1978).
43. A. K. Rastogi and L. E. St. Pierre, J. Colloid Interf. Sci. 31, 168 (1969).
44. S. Wu, Polym. Eng. Sci. 27, 335 (1987).
45. G. W. Bender, D. G. LeGrand, and G. L. Gaines Jr., Macromolecules 2, 681 (1969).
46. S. H. Anastasiadis, J. K. Chen, J. T. Koberstein, J. E. Soho, and J. A. Emerson, Polym. Eng. Sci. 26, 1410 (1986).
47. M. Wagner and B. A. Wolf, Macromolecules 26, 6498 (1993).
48. J. J. Elmendorp and G. De Vos, Polym. Eng. Sci. 26, 415 (1986).
49. J. Hopken and M. Moller, Macromolecules 25, 1461 (1992).
50. A. G. Pittman, D. L. Sharp, and B. A. Ludwig, J. Polym. Sci. A-I 6, 1729 (1968).
51. M. K. Bernett and W. A. Zisman, J. Phys. Chem. 66, 1207 (1962).
52. D. H. Kaelble, J. Adhes. 2(4), 66 (1970).
53. M. K. Bernett and W. A. Zisman, J. Phys. Chem. 65, 2266 (1961).
54. H. Kobayashi and M. J. Owen, Macromolecules 23, 4929 (1990).
55. H. W. Fox and W. A. Zisman, J. Colloid Sci. 5, 514 (1950).
56. M. J. Owen, J. Appl. Polym. Sci. 35, 895 (1988).
57. A. H. Ellison and W. A. Zisman, J. Phys. Chem. 58, 260 (1954).
58. B. R. Ray and F. E. Bartell, J. Colloid Sci. 8, 214 (1953).
59. E. G. Shafrin and W. A. Zisman, in *Contact Angle. Wettability, and Adhesion*, Advances in Chemistry Series No. 43, edited by F. M. Fowkes (American Chemical Society, Washington, D.C., 1964), p. 145.
60. L. -H. Lee, in *Interaction of Liquids at Solid Substrates,* Advances in Chemistry Series No. 87 (American Chemical Society, Washington, D.C., 1968), p. 106.
61. H. Schonhorn and L. H. Sharpe, J. Polym. Sci. B 3, 235 (1965).

62. H. W. Fox and W. A. Zisman, J. Colloid Sci. 7, 109 (1952).
63. L. -H. Lee, J. Polym. Sci. A-2 5, 1103 (1967).
64. S. Wu, J. Phys. Chem. 72, 3332 (1968).
65. A. H. Ellison and W. A. Zisman, J. Phys. Chem. 58, 503 (1954).
66. H. W. Fox and W. A. Zisman, J. Colloid Sci. 7, 428 (1952).
67. T. Fort, Jr., in *Contact Angle, Wettability, and Adhesion,* Advances in Chemistry Series No. 43, edited by F. M. Fowkes (American Chemical Society, Washington D.C., 1964), p. 302.
68. B. R. Ray, J. R. Anderson, and J. J. Scholz, J. Phys. Chem. 62, 1220 (1958).
69. D. A. Olsen and A. J. Osteraas, J. Appl. Polym. Sci. 13, 1523 (1969).
70. N. L. Jarvis, R. B. Fox, and W. A. Zisman, in *Contact Angle, Wettability, and Adhesion,* Advances in Chemistry Series No. 43 (American Chemical Society, Washington, D.C., 1964), p. 317.
71. R. E. Baier and W. A. Zisman, Macromolecules 3, 70 (1970).
72. Y. C. Ko, B. D. Ratner, and A. S. Hoffman, J. Colloid Interf. Sci. 82, 25 (1981).
73. Y. Kitazaki and T. Hata, J. Adhes. Soc. Jpn 8, 131 (1972).
74. H. D. Feltman and J. R. McPhee, Text. Res. J. 34, 634 (1964).
75. C. J. van Oss, R. J. Good, and M. K. Chaudhury, J. Colloid Interf. Sci. 111, 378 (1986).
76. C. J. van Oss, M. K. Chaudhury, and R. J. Good, Sep. Sci. Technol. 24, 15 (1989).
77. From methylene iodide contact angle data in F. M. Fowkes, J. Adhes. Sci. Technol. 1, 7 (1987).
78. C. J. van Oss, R. J. Good, and H. J. Busscher, J. Dispers. Sci. Technol. 11, 75 (1990).
79. C. J. van Oss, M. K. Chaudhury, and R. J. Good, Adv. Colloid Interf. Sci. 28, 35 (1987).
80. From contact-angle data in C. J. van Oss, R. J. Good, and M. K. Chaudhury, J. Chromatogr. 391, 53 (1987). Note that this article quotes different calculated surface-free-energy parameters for cellulose acetate and cellulose nitrate to those in Ref. [24].
81. M. K. Chaudhury and M. J. Owen, Langmuir 9, 29 (1993).
82. M. K. Chaudhury and M. J. Owen, J. Phys. Chem. 97, 5722 (1993).
83. L. Li, V. S. Mangipudi, M. Tirrell, A. V. Pocius, NATO Science Series, II: Mathematics, Physics and Chemistry, 10 (Fundamentals of Tribology and Bridging the Gap Between the Macro- and Micro/Nanoscales), 305–329 (2001).
84. V. S. Mangipudi, and A. Falsafi in *Direct Estimation of the Adhesion of Solid Polymers*, edited by A. V. Pocius and M. Chaudhury, *Adhesion Science and Engineering, Vol. II: Surface Science* (Elsevier, Amsterdam, 2002).
85. A. Falsafi, P. Deprez, F. S. Bates, and M. Tirrell, J. Rheol. 41, 1349 (1997).
86. A. Falsafi, Ph.D. Thesis, University of Minnesota (1998).
87. D. W. Van Krevelen in *Properties of Polymers*, 3rd ed., Chapter 8 (Elsevier, Amsterdam, 1990), p. 227.

CHAPTER 60

Acoustic Properties of Polymers

Moitreyee Sinha and Donald J. Buckley

General Electric Global Research Center, One Research Circle, Niskayuna, NY 12309

60.1 INTRODUCTION

The measurement of acoustic properties of polymers, longitudinal and shear sound speeds and absorption, probe the molecular structure of polymers as well as provide a source of engineering design properties for various applications [1]. The term *acoustic* refers to a periodic pressure wave. The term includes waves in the audio frequency range (those that can be heard by the human ear) as well as those above the audio range (ultrasonic and hypersonic) and below the audio range. Acoustic waves are characterized by their sound speed and sound absorption. The sound speed C is the scalar magnitude of the sound velocity vector and has units of m/s. Sound absorption α is a measure of the energy removed from the sound wave by conversion to heat as the wave propagates through a given thickness of material. Absorption has units of dB/cm, where a dB (decibel) is a unit based on ten times the common logarithm of the ratio of two acoustic energies. Alternatively, the natural logarithm can be used, in which case the units are Np/cm, where 1 Np (neper) is equal to 8.686 dB. It is sometimes convenient to consider the amount of absorption in a thickness equal to one wavelength, λ. The quantity $\alpha\lambda$ then has units of dB (or Np). Absorption is a material property, in contrast to attenuation, which includes energy loss due to scattering and reflection as well as absorption and depends on sample size and experimental configuration.

In an unbounded isotropic solid, two types of waves can be propagated. In one case, the chain segments vibrate along the direction of propagation. This is called a longitudinal wave. In the other case, the motion of the segments is perpendicular to the direction of propagation and is called a shear wave. Longitudinal waves are also sometimes referred to as dilatational, compressional, or irrotational waves. Shear waves are also called distortional, isovoluminous, or transverse waves. These two types of waves propagate independently of one another and are the only two types possible in an unbounded, isotropic solid. The longitudinal and transverse sound speeds are related to the elastic constants by the relations

$$\begin{aligned} v_{\mathrm{l}} &= \sqrt{\frac{K + 4G/3}{\rho}}, \\ v_{\mathrm{s}} &= \sqrt{\frac{G}{\rho}}, \end{aligned} \tag{60.1}$$

where K is the bulk modulus (equal to the reciprocal of compression), G the shear modulus, and ρ the density.

For a sample whose lateral dimensions are much less than a wavelength, an extensional wave is propagated. For such a wave, the sound speed is

$$v_{\mathrm{EXT}} = \sqrt{E/\rho}, \tag{60.2}$$

where E is Young's modulus. As mentioned earlier, there are only two independent sound speeds, and the extensional sound speed can be expressed in terms of the longitudinal and shear sound speeds. It is common to express Young's modulus as a complex quantity, $E^* = E' + \mathrm{i}E''$. The ratio of the imaginary part of the modulus (Young's shear of bulk) to

the real part is the tangent of the phase angle between the two components and is called the loss factor, $\tan\delta$. The loss factor is approximately related to absorption per wavelength by the equation

$$\tan\delta = E''/E' = \alpha\lambda/\pi \tag{60.3}$$

in units of Nepers (Np). Other types of waves include surface waves and bulk waves but such waves will not be discussed here.

In viscoelastic materials such as polymers the moduli depend on frequency. Physically, the amount of deformation that is produced in a polymer by a given stress depends on the length of time that the stress is applied. In typical high frequency measurements (ultrasonic or Brillouin), during the short time that the stress of a sound wave is applied in one direction, only relatively small portions of the polymer can move; hence not as much strain is induced as in typical static or low frequency measurements, and the high frequency modulus is higher than the static modulus. Another way of looking at it is that for high frequency measurements, the time scales are so short that the distances over which the chains can relax are very short. For ultrasonic measurements, this effect is not too pronounced for the bulk modulus (on the order of 20%), but can be significant for shear and Young's modulus (a factor of 10 or more).

Because of the above dependence on frequency, sound waves represent a mechanical probe for particular wave motions, namely, motion that can occur in the period of the sound wave. Viewed as one technique for making mechanical measurements on polymers, sound wave measurements using ultrasonic or Brillouin scattering probe motions of the polymer on short length scales while methods such as audio or low frequency DMA measurements probe large-scale motions.

The different experimental methods for sound wave propagation and for measuring the mechanical response or elastic constants of polymers are summarized below with an attempt to give an idea of the different time scales involved.

Audio or ultralow frequency DMA (dynamic mechanical analysis) measurements:

1 Hz–20 kHz.

Ultrasonic experiments: 1 kHz–1 GHz.

Brillouin light scattering at hypersonic frequencies: 0.1–100 GHz.

At high frequencies (higher than 1 MHz), there is no direct way to measure the modulus by applying known values of stress and measuring the strain. At these frequencies, the elastic constants for polymers are calculated from sound velocity measurements using ultrasonic or Brillouin light scattering experiments. In this review, we will largely focus on measurements at ultrasonic frequencies. For elastomeric networks we will briefly review sound wave measurements reported at very low frequencies and at very high (GHz) frequencies.

The propagation of a sound wave is fundamentally a molecular process, and the interaction between elastic wave propagation and molecular behavior has a significant effect on sound dispersion and attenuation, particularly at ultrasonic frequencies. If a sound wave in a fluid disturbs any particular equilibrium molecular aggregation, it takes a certain time t, called the relaxation time, for the original state to be restored after the passage of the crest of the wave. The process is usually called thermal relaxation.

As is well known for viscoelastic materials, the frequency and temperature dependencies of polymer properties are related. For groups of relaxation processes that encompass a very broad time range, it often happens that the experimentally limited frequency range is not large enough to obtain a complete curve. Using the time–temperature superposition principle, measurements carried out at a sequence of different temperatures can provide the missing information to generate the frequency-dependent curve as shown in Fig. 60.1 [2].

60.2 LOW FREQUENCIES

At the lower frequency end (less than 20 kHz), there have been some earlier studies on sound or pulse propagation in rubbery polymers. Some related work on natural and butyl rubber is discussed below.

Witte *et al*. reported velocity and attenuation measurements in thin strips of butyl rubber from 0.5 to 5 kHz (audio frequency) at different temperatures [3]. They found the speed of sound to increase with decreasing temperature and increasing frequency. The attenuation showed a peak with temperature. The experimental procedure made use of a signal generator for driving a crystal, setting up longitudinal waves which were transmitted through the sample and picked up by a crystal receiving element. Thus it was possible to determine the phase difference between the driven end and the pickup for any point along the sample. By

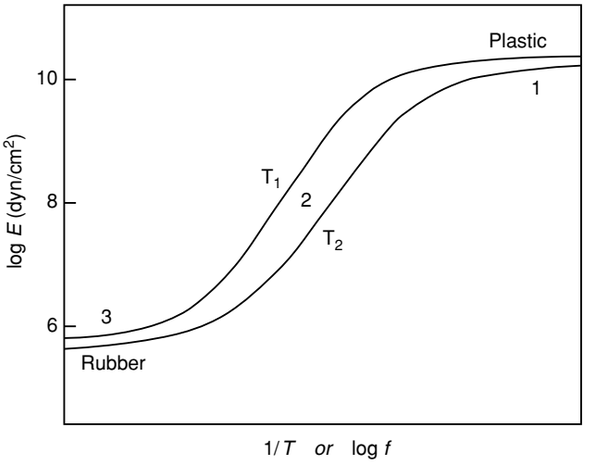

FIGURE 60.1. Rubber to glass transition at two temperatures ($T_1 < T_2$) [2]. Reprinted with permission from J. D. Ferry, Viscoelastic Properties of Polymers, 3rd ed. (1980). Copyright 1980, Wiley.

moving the pickup along the sample, the distance between two adjacent points in the same phase of motion were measured, and thus the wavelength of the sound wave in the sample could be determined. Knowing the frequency of the driving oscillator, the velocity was directly obtained. The attenuation was obtained by moving the pickup along the sample and reading on the wave analyzer, the amplitude of the received signal as a function of distance. This method of measurement is limited to a definite frequency range; an upper limit to the frequency range is determined by the fact that the largest cross-sectional dimension of the sample had to be kept small in comparison with the wavelength of the propagated wave. At sufficiently low frequencies, the sample length became smaller than the half-wavelength of the transmitted sound wave making velocity measurements impossible.

Figure 60.2 shows the velocity curves of butyl rubber as a function of frequency at different temperatures. The velocity increases very slowly with frequency at high temperatures where the values of the velocity are of the order of 40 m/s. The increase in velocity with frequency is much more rapid as the temperature is lowered, and at 0 °C the velocity is about 300 m/s. The corresponding modulus curves derived from the velocity curves is shown in Fig. 60.2. At all temperatures the modulus was seen to increase with frequency. From ultrasonic experiments on the same polymers, the data obtained at frequencies in the MHz range indicated a continuous rise in the modulus with frequency (measured up to 15 MHz). The dispersion over a limited frequency range can be attributed to a mechanism involving relaxation times of the order of $1/\omega$, whereas the entire dispersion range would have to be explained on the assumption of a wide distribution of relaxation times. The relaxation mechanism for these low frequency measurements responsible for the dispersion would involve the assumption of a number of relaxation times of the order of 10^{-3}s. Also from their results they found that an increase in temperature produced the same effect as a decrease in frequency. This supports the time–temperature superposition principle for viscoelastic materials.

Gent and Marteny [4] measured the difference in time for loading and unloading pulses to reach two phonograph pickups, placed a known distance apart, to determine the velocity of sound as a function of strain in filled and unfilled natural rubber. For both cases they found a marked increase in the speed of sound with imposed strain. For the unfilled rubber, the sound velocity increased from about 60 m/s at zero strain up to about 600 m/s at high strains (about four times the original length) (Fig. 60.3). For the filled rubber, the speed was about 160 m/s at zero strain and reached about 800 m/s at high strains.

Although wave propagation techniques have been used extensively to study the bulk properties of polymers, their application in understanding the microscopic structure of networks has been limited. Most of the studies have been directed toward studying the change in sound velocity with temperature and frequency, or toward the determination of various bulk properties such as the modulus, hysteresis, absorption, etc. of networks. The nonlinear nature of the elastic material carrying the disturbance has been treated in a phenomenological manner. Sinha *et al*. measured the speeds of longitudinal and transverse pulses in uniaxially stretched siloxane (PDMS) networks as a function of the extension ratio, the degree of crosslinking and the amount of swelling [5]. They used a theoretical framework combining the theory of elastic wave propagation and molecular models for the networks to determine network parameters from measurements of the wave velocity in deformed

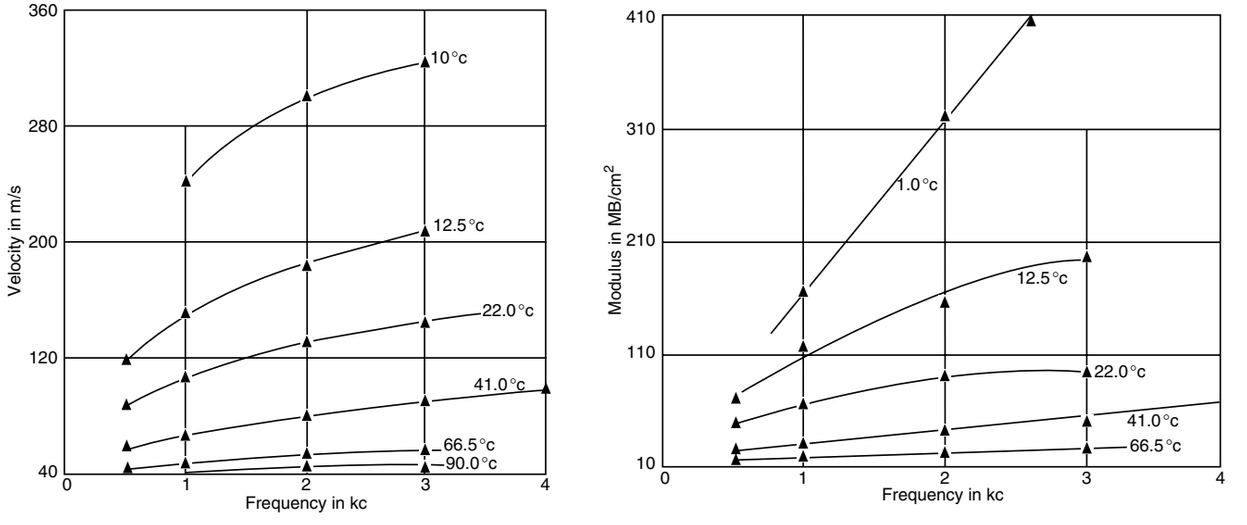

FIGURE 60.2. Velocity versus frequency for butyl rubber. The dynamic Young's modulus as a function of frequency for butyl rubber [3]. Reprinted with permission from R.S. Witte, B.A. Mrowca, and E. Guth, Journal of Applied Physics, 20, 481 (1949). Copyright 1949, American Institute of Physics.

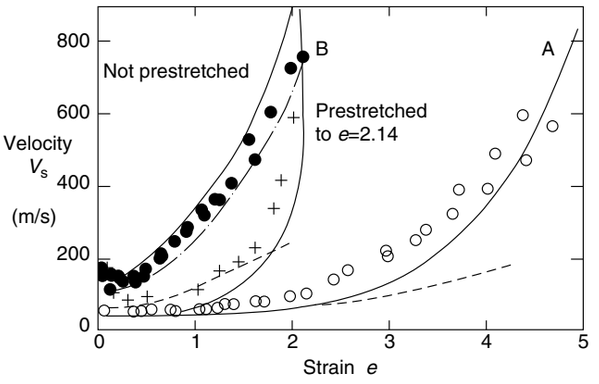

FIGURE 60.3. Velocity of sound for unfilled rubber (open circles) and in carbon-black filled rubber (filled circles); Velocity in filled rubber after prestretching to a strain value of 2.14 (crosses). Full curves: calculated from values of the instantaneous modulus obtained from unloading stress–strain relations. Broken curves: calculated using loading stress–strain relations. Chain curve: calculated using loading-after-resting stress–strain relations [4]. Reprinted with permission from A.N. Gent and P. Marteny, Journal of Applied Physics, 53, 6069 (1982). Copyright 1982, American Institute of Physics.

networks. From ultrasonic measurements on PDMS [6], the values reported for the longitudinal speed is 1,020 m/s using an immersion measurement technique based on measuring the differences between acoustic paths with and without the specimen. This corresponds to a longitudinal elastic modulus of 1.087 GPa, about 10^4 times higher than the equilibrium modulus.

60.3 ULTRASONIC FREQUENCIES

60.3.1 Ultrasonic Material Properties

The term ultrasound in its broadest sense covers all sound with frequencies greater than the audible range. In general use, however, the term is restricted to frequencies of 1 MHz and greater, up to the point where phonon processes, such as Brillouin scattering, become important.

Ultrasonic investigations are often performed using the immersion technique where the sample and transducer (a combined transmitter and receiver of ultrasonic radiation) are immersed in a liquid, typically water, although other fluids such as silicone oil may be used. The fluid supplies efficient coupling of ultrasonic energy between the output lens of the transducer, which is typically a hard thermoplastic such as polystyrene, and the sample. In another arrangement, energy is coupled directly to the sample in that a pulse propagates from the transducer through a thin layer of coupling medium (usually soapy water to assure good wetting of the polymer surface) into a plane polymer sample.

Both methods use the pulse–echo technique. A pulse is sent into the sample, where it is reflected by the front and back surfaces of the material and returned at reduced amplitude to the transducer, while the waveforms are monitored on a recording oscilloscope. From the timing and amplitude of the reflected waves the sound speed and attenuation of the material may be determined. Successive reflections provide additional information on both these properties. A typical ultrasound pattern obtained using the direct-coupled transducer method is shown in Fig. 60.4.

Normal Incidence

The longitudinal sound speed in the polymer can be determined by measuring the time required for a pulse propagated normally into the sample to reflect from its far surface (usually a polymer/air interface where the impedance mismatch generates a reflected wave), and dividing the sample's thickness by twice this time. The time is determined by the interval between the initial pulse and the successive reflections, which result as the wave bounces

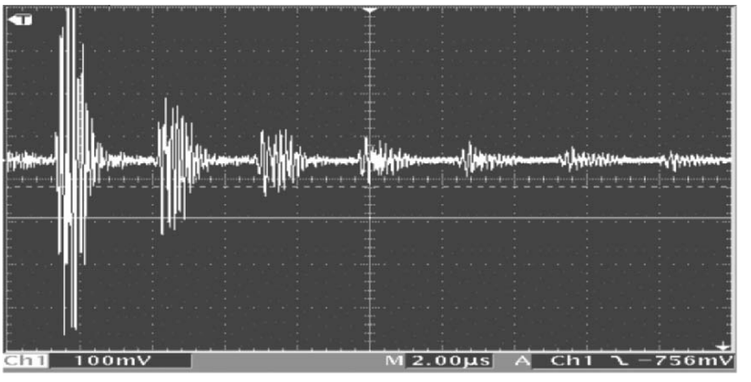

FIGURE 60.4. Ultrasound pulse–echo pattern obtained at 10 MHz in a polystyrene disk 3 mm thick. The interval between successive reflections indicates the velocity of the longitudinal wave, and the ratio of intensity of any two successive reflections the attenuation. The horizontal scale is 2.00 μs/division. In this material the (longitudinal) speed of sound is 2.14 km/s, the acoustic impedance is 2.25 MRayls (units of 10^6 kg/(cm^2-s) and the attenuation coefficient is ca. 12 db/cm. See text below for the calculation [57].

off the water/plastic interface repeatedly. The velocity is then

$$C_L = 2d/t. \tag{60.4}$$

In the example in Fig. 60.4, $d = 3$ mm, $t = 2.8$ μs, and C_L is 2.14 mm/μs or 2.14 km/s.

From the same trace, the longitudinal absorption coefficient can be determined by observing the peak height in successive reflected pulses. The attenuation per unit length is usually expressed on a logarithmic scale in units of decibels/cm (abbreviated dB/cm), where the decibel represents a reduction in power of 1.258 times. The attenuation is then:

$$\alpha(\text{dB/cm}) = 10/L \log (I_{\text{initial}}/I_{\text{final}}) \tag{60.5}$$

or, in terms of the voltages (signal amplitudes) displayed on an oscilloscope,

$$\alpha = 20/L \log (V_{\text{initial}}/V_{\text{final}}), \tag{60.6}$$

where V_{initial} is the pulse height going in, V_{final} the height coming out, and L the path length in the sample, equal to twice the thickness.

In addition to attenuation within the sample, there are losses from reflection at the sample/air and sample/coupling medium interfaces, and losses in transversing the coupling. The latter are small in the direct-coupled technique, but can be significant in the immersion tank method. The former can be significant to the extent of mismatch of the acoustic impedances of the two media. The acoustic impedance Z, a quantity analogous to the electrical impedance, is the product of the sound velocity and the density, expressed in units of megaRayls, MRayls or 10^6 kg/(s m^2). For example, the impedance mismatch of polystyrene (Z=2.5 and a material often used for transducer lensing) with water (Z=1.5) results in a portion of the incident beam being reflected, that portion having amplitude:

$$\begin{aligned} R_{\text{PS-Water}} &= [(Z_{\text{PS}} - Z_{\text{Water}})/(Z_{\text{PS}} + Z_{\text{Water}})] \\ &= [(2.5 - 1.5)/(2.5 + 1.5)] = 0.25 \end{aligned} \tag{60.7}$$

and the reflected intensity is

$$R^2_{\text{PS-Water}} = [0.25]^2 = .064. \tag{60.8}$$

The equivalent calculation for the air/polystyrene interface gives

$$R^2_{\text{PS-Air}} = 0.186. \tag{60.9}$$

Generally, sound velocities are much more readily and accurately measured than absorption coefficients, since only time differences are required for the former, while measurement of the latter are influenced by many artifacts, such as the reproducibility of the coupling, beam spread and dispersion.

Oblique Incidence

When the transducer beam is not normal to the sample surface, both longitudinal and shear waves are generated. The longitudinal wave may be eliminated by increasing the incident angle until total internal reflection of this component occurs, at the critical angle given by Snell's law,

$$\sin \theta_P / C_P = \sin \theta_m / C_m, \tag{60.10}$$

where the medium (m) of the incident wave is often a prism of polystyrene or polymethylmethacrylate (PMMA). For a polystyrene prism with $C_P = 2.4$ m/s, propagating into a PMMA slab with $C_P = 2.7$ m/s the critical angle is approximately 51 °.

Owing to the non-normal incidence, measurement of the shear wave velocity C_s requires a separate transmitter and receiver. The path length in the specimen is given by [43]:

$$x = L[1 - [C_s \sin \theta C_m^2]^{-1/2} \tag{60.11}$$

and the shear velocity C_s by [43]:

$$C_s = C_m\{[\cos \tilde{\theta} C_m \Delta t/L]^2 + \sin^2 \theta\}^{-1/2}. \tag{60.12}$$

Shear and Bulk Moduli

Ultrasound can also be used to determine the elastic moduli of materials, with the modulus of interest determined by the mode of propagation: longitudinal (sound waves producing motion of sample's atoms parallel to the direction propagation), shear (excitation at right angles to the direction of propagation) and extensional (longitudinal excitation in the sample with lateral dimensions small compared to the ultrasonic wavelength).

The speed of sound C for a given propagation mode is related to the corresponding modulus M and the density ρ by the general relation [2]

$$\rho C^2 = M. \tag{60.13}$$

For a longitudinal and shear waves, respectively, the relations are [43]:

$$\begin{aligned} \text{Longitudinal: } \rho C^2_{\text{Longitudinal}} &= K + 4/3G, \text{ Shear:} \\ \rho C^2_{\text{Shear}} &= G, \end{aligned} \tag{60.14}$$

where K and G are the bulk and shear moduli, respectively. At low frequencies, where the wavelength can be greater than the lateral dimension of the sample, there is a third mode, extension, where the relation is

$$\rho C^2_{\text{Extensional}} = E \tag{60.15}$$

with E being the Young's modulus. Typical sound velocities in materials are or order 2–5 × 10^2 for gases, 1–3 × 10^3 for organic solids, and 3–6 × 10^3 for dense crystalline solids. The frequencies of interest for applied ultrasound are in the range 1–100 MHz, corresponding to wavelengths of 2–0.02 mm when propagating in polystyrene. The shear velocities are typically (1/3)–(1/2) those in the longitudinal mode.

Longitudinal waves may be generated using a piezoelectric transducer activated by an RF pulse train of the

appropriate frequency, with the transducer coupled at normal incidence to the sample surface. Shear and longitudinal waves can be generated in a sample using the same equipment but with the transducer face oriented at angle from normal using a plastic coupling wedge.

Tables 60.1 and 60.2 list values of the longitudinal and shear velocities at 1 MHz, and attenuations at 2 MHz at room temperature for some common polymers [2].

Temperature, Frequency and Pressure Dependence of Ultrasonic Properties

The largest change in acoustic properties of a polymer occurs across T_g, when the material transitions from a hard glassy solid to the rubbery plateau. Above this temperature the moduli and sound speeds drop (a rule of thumb for the latter is that it decreases by a factor of 2) while the absorption increases by an order of magnitude or more, with a maximum some distance above T_g. The temperature derivatives are maximum around T_g and are of order 25 m/s/K [2].

Since there is a time–temperature superposition for polymers, the frequency and temperature dependences of the acoustic properties are inversely related, so that decrease in temperature correspond to the effect of increases in frequency. This behavior is illustrated by comparing Fig. 60.5(a) and (b) which display the temperature and frequency sensitivity for two polymers [1]. Since measurements over a wide temperature range are more readily made than those over a corresponding frequency range, the combination of the data from measurements over a wide temperature range and a modest frequency range usually serve to define the entire spectrum. The frequency sensitivity of ultrasound velocities is weak, of order 5–10 m/s/decade [2]. The attenuation, however, is strongly dependent, increasing at least linearly and often as the square of frequency, and is of order 20–100 dB/cm/decade. For example, over the range 4–6 MHz, the speed of longitudinal sound in PMMA changes by only 1%, [52] while the attenuation increases from 40 to 60 Nps/m. Both velocity and attenuation are sensitive functions of temperature, with velocity decreasing across T_g to ca. 1/2 its low temperature plateau value, while attenuation peaks at or near T_g.

The pressure derivative of the sound speeds are inversely related to temperature since a pressure change results in a change in free volume. Few pressure derivatives have been measured; typical values are of 0.5–0.9 GPa^{-1}.

49.3.2 Applications of Ultrasound for Polymers

Acoustic Dynamic Mechanical Analysis (DMA)

At acoustic frequencies, the attenuation goes through a maximum determined by the spectrum of relaxation times in the polymer; hence dynamical mechanical analysis can be performed by scanning over a wide frequency range, typically $10^3 - 10^{12}$ Hz. An example of the technique is sonic DMA of PVC [54] which shows that the shear modulus increase monotonically with frequency, while the longitudinal or extensional modulus displays the transition associated with T_β. The ratio of the loss and storage moduli, or tan delta obtained via DMA can be related to the absorption coefficient through the equation [2]:

$$\alpha = \Pi\lambda \tan\delta = \Pi\lambda E''/E'. \qquad (60.16)$$

TABLE 60.1. *Longitudinal and shear velocities for common polymers at 25 °C and 1 MHz [1].*

Acronym	Poly-	Density (g/cm^3)	C_L (m/s)	C_s (m/s)	References
ABS	acrylonitrile–butadiene–styrene	1.041	2,160	930	[30]
Epoxy	DGEBA/PDA	1.184	2,890	1,290	[34]
Nylon	hexamethylene adipamide	1.147	2,710	1,120	[6]
PC	carbonate	1.194	2,220	909	[28]
PE	ethylene	0.957	2,430	950	[6]
PEO	ethylene oxide	1.208	2,250	—	[6]
PES	ether sulfone	1.373	2,260	—	[29]
Phenolic		1.220	2,840	1,320	[25]
PMMA	methylmethacrylate	1.191	2,690	1,340	[6]
PMP	methyl pentene	0.835	2,180	1,080	[30]
POM	oxymethylene	1.425	2,440	1,000	[6]
PP	propylene	0.913	2,650	1,300	[6]
PPO	phenylene oxide	1.073	2,220	1,000	[28]
PS	styrene	1.052	2,400	1,150	[6]
PSU	sulfone	1.236	2,260	920	[28]
PVC	vinyl chloride	1.386	2,330	1,070	[29]
PVDF	vinylidene fluoride	1.779	1,930	775	[6]
Silicone	dimethylsiloxane	1.045	1,020	—	[6]
Teflon	tetrafluoroethylene	2.180	1,410	730	[33]
Urethane	polyol/TDI/ TMAB	1.118	1,750	—	[39]

TABLE 60.2. *Longitudinal and shear absorption coefficients for polymers at 25 °C & 2 MHz[1].*

Acronym	Polymer	ρ (g/cm^3)	α_L (dB/cm)	α_S (dB/cm)	References
ABS	Poly(acrylonitrile–butadiene–styrene)	1.02	1.8	15	[30]
Epoxy	DGEBA/PDA	1.1844	6.3	36.1	[34]
Epoxy	BGDE/PDA	1.179	21.0	—	[37]
Nylon 6	Polycaprolactam	—	13	—	[41]
PC	Polycarbonate	1.19	9.4	—	[29]
PMMA	Poly(methylmethacrylate)	1.19	1.4	4.3	[42]
PE	Polyethylene	0.96	3.3	25	[42]
PE	Polyethylene	—	13	—	[41]
PEO	Poly(ethyleneoxide)	1.21	7.1	—	[42]
PES	Poly(ethersulfone)	1.37	5	—	[29]
Phenolic		1.22	4.1	19	[25]
PIB	Polyisobutylene	0.91	67	—	[32]
PMP	Poly(4-methyl-1-pentene)	0.84	1.4	6.7	[30]
PS	Polystyrene	1.40	—	—	[41]
PS	Polysulfone	1.24	4	—	[29]
PU	Polyurethane, polyether based	1.104	7.5	—	[43]
PU	Polyurethane, polybutadiene based	1.008	9.1	—	[43]
PVC	Poly(vinylchloride)	—	8.1	—	[41]

Polymers for Medical Ultrasonic Devices

The optimal polymer material for use in ultrasound medical devices would have an impedance matching that of human tissue, 1.5 MRayls, and minimal attenuation at the frequencies of interest, which are typical between 5 and 10 MHz. Use of a material with a large impedance mismatch against tissue results in reflection of energy at the tissue/transducer interface, or more likely, the interface between the coupling gel, which is often silicone or a hydrogel, and the device lens. A polymer with an impedance mismatch and low attenuation can result in multiple reflections within the subject and consequent reduction of signal-to-noise in the image.

Hard, glassy, brittle thermoplastics such as polystyrene (PS) and polymethylmethacrylate (PMMA) have low attenuations, of order 6–10 dB/cm at 10 MHz, and in the case of PS, a low acoustic impedance. Ductile polymers such as polycarbonate (PC), many polyolefins and impact-modified thermoplastics generally have high absorption coefficients, in the range 20–40 dB/cm. The same molecular structures and mobility, which contribute to ductility, may also contribute to absorption of ultrasonic energy. Not surprisingly, rubbers and, by extension, any polymer above its

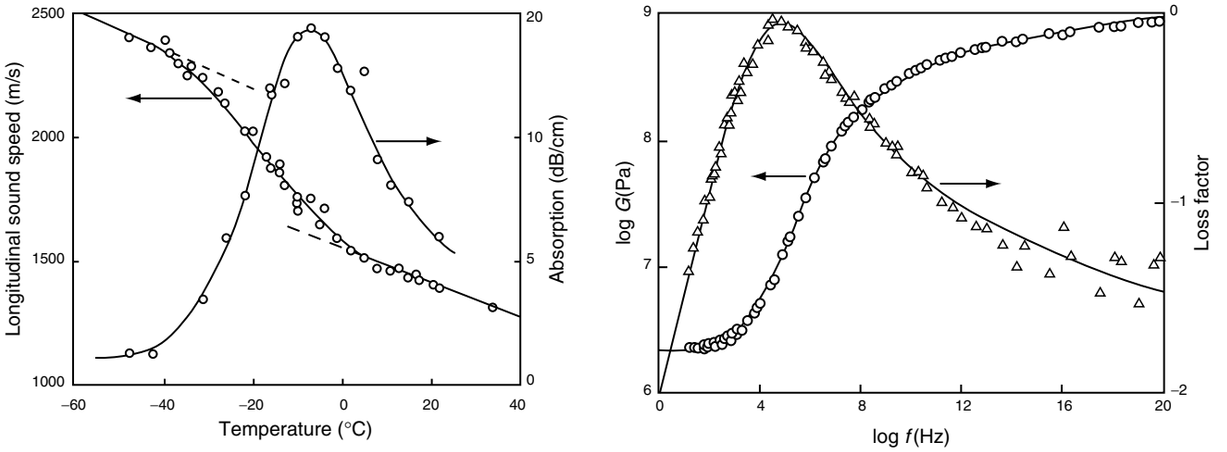

FIGURE 60.5. (a) Sound speed and absorption vs. temperature for poly (carborane siloxane) and (b) log plot of shear modulus and loss factor vs. frequency for polyurethane [1]. Reprinted from [1] Copyright 1996, with permission of Springer Science + Business Media.

glass transition temperature, are highly attenuating materials at all frequencies. The requirement of impedance match, low attenuation and reasonable mechanical properties (strength, toughness, etc.) limits the choice of available polymers for ultrasonic uses such as mammography compression paddles. In this application polymethylpenetane, a low-density polyolefin, has proven useful. This material has impedance of 1.7 MRayls and an absorption coefficient of 6 dB/cm at 10 MHz, and is a good compromise mechanically between brittle materials used in ultrasonic lenses, such as PS, and more ductile but highly absorbing polymers such as PC.

Acoustic Emission

When subjected to stresses sufficient to initate and propagate cracks, polymers emit sound waves with frequencies ranging from the upper acoustic limit (ca. 10 kHz) to 10 MHz that may be detected with suitable transducers. A well-isolated acoustic emission (AE) system may used to detect deformation events including the slow to fast brittle crack transition in PMMA, fatigue in SEN samples, and crack propagation under high hydrostatic pressure [53].

Sono-Chemistry

Ultrasound has also been employed to accelerate chemical reactions, including breakdown of polymers in solution, and catalytic reactions [55]. Ultrasound is capable of producing high local temperatures and pressures unlike any other apparatus, and can drive unique chemistries as a result. The principle mechanism is cavitation of the sonic agitated fluid and the resulting bubbles collapse/explode at surfaces, which in turn produce high velocity microjets of liquid. This produces both physical and chemical changes.

An example of sono-chemistry is degradation of high molecular weight PS and reaction of the low molecular weight block with MMA monomer to produce a PS-PMMA block copolymer [55]. Another example is surface modification of Polyethylene using moderate oxidizing agents to improve adhesion and wetability [55].

Ultrasonic Shear Rheology

Ultrasound can also be used to explore the viscoelastic properties of polymers in film form. Alig *et al*. [56] describe a shear rheometer operating in the range 1–40 MHz. on the shear reflection principle. A shear wave is sent through a quartz bar toward the interface between the bar and a polymer film. The film alters both the amplitude and phase of the reflected wave. The values of G' and G'' obtained when plotted against offset temperature from T_g (i.e., $T - T_g$), show broader transitions at higher temperatures than those obtained with low frequency mechanical DMA. One advantage of the ultrasound method is that it allows DMA of materials, which would be unsuitable for conventional DMA, such as latex dispersions, gels, and mechanically fragile films.

60.4 HYPERSONIC (GHZ) FREQUENCIES

Brillouin scattering measurements provide the velocity and attenuation of acoustic phonons having frequencies in the range of GHz and wavelengths of the order of 10^3Å [7]. Laser light of frequency ω_i and wave vector $\bar{k}_i$ is incident on the sample; the light interacts with the medium and is scattered through an angle θ. Phonons are absorbed or emitted in the inelastic light scattering process governed by the following energy and momentum conservation equations

$$\begin{aligned} \omega_s &= \omega_i \pm \Delta\omega, \\ \bar{k}_s &= \bar{k}_i \pm \bar{k}, \end{aligned} \tag{60.17}$$

where $\bar{k}_s$ and $\bar{k}$ are the wave vectors of the scattered laser light and the phonon, respectively. Likewise ω_i and $\Delta\cdot\omega$ are the frequencies of the scattered light and the phonon.

The basic experiment consists of measuring the spectrum of the scattered light. It consists of a strong elastic peak at one frequency with additional components whose frequency has been shifted by the inelastic scattering processes. The frequencies of these much weaker phonon peaks are measured relative to the elastic peak. From observation of the shifted Brillouin peak with respect to the central elastic peak, the longitudinal Brillouin splitting, $\Delta\omega_l$ is given by

$$\Delta\omega_l = kv_l, \tag{60.18}$$

where v_l is the longitudinal phonon velocity with wave vector $k = (4\pi n/\lambda_i)\sin(\theta/2)$, n is the refractive index of the material, λ_i is the wavelength of the incident light in vacuum. The longitudinal sound velocity, v_l depends on the real part of the longitudinal viscoelastic modulus. It can be expressed in terms of the longitudinal elastic modulus, M as shown

$$v_l = \sqrt{M/\rho} = \sqrt{(K + 4G/3)/\rho}, \tag{60.19}$$

where K is the bulk modulus and G is the shear modulus [8]. The line-width of the Brillouin peak measures the attenuation of the acoustic phonon. The Brillouin peaks are predicted to have a half-width at half-maximum, Γ given by

$$\Gamma = \frac{2}{3}\frac{q^2\eta}{\rho}, \tag{60.20}$$

where η is the longitudinal viscosity and Γ is measured in hertz.

For linear PDMS, Brillouin scattering measurements on two molecular weights of PDMS (3,800 and 68,000) by Patterson *et al*. exhibited no measurable difference in the phonon speed [9]. It was concluded that the asymptotic

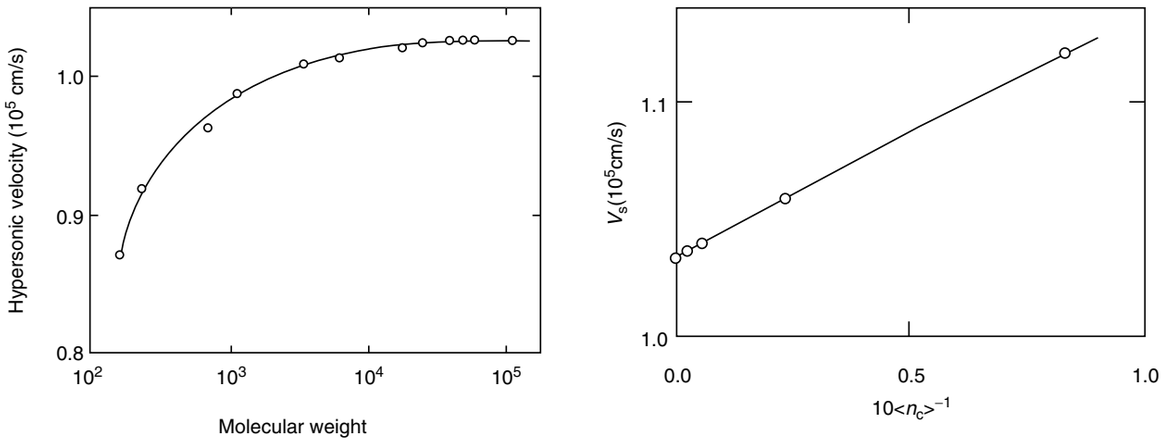

FIGURE 60.6. (a) Phonon velocity in linear polydimethylsiloxane as a function of the molecular weight. (b) Phonon velocity in rubbery PDMS as a function of cross-link density. Here n_c is the average number of monomer units between cross-links and is directly proportional to M_c [11]. Reprinted with permission from Shingo Kondo and Takashi Igarashi, Journal of Applied Physics, 51, 1514 (1980). Copyright 1980, American Institute of Physics.

leveling of the phonon speed happened below the lower number-averaged molecular weight of 3,800 g/mol. The samples used in this case were highly polydisperse. Kumar [10] and Kondo *et al*. [11] reported that the phonon velocity in linear PDMS increased with increasing molecular weight and had a tendency to level off in the region of higher molecular weight of around 7,000 g/mol (Fig. 60.6 (a)). For cross-linked networks, Lindsay *et al*. found the elastic modulus M to increase linearly with increasing cross-link density [12]. These were reported as preliminary results carried out on networks formed by random cross-linking using γ irradiation. Kondo and Igarashi reported the phonon velocity and modulus to increase linearly with cross-link density for networks with four molecular weights prepared by an addition reaction (Fig. 60.6 (b)) [11]. Kondo *et al*. also reported measurements on end-linked networks that were highly cross-linked and had much higher phonon speeds [13]. Delides *et al*. [14] measured average values of 1,040 $\pm$ 20 m/s, while Kondo and Igarashi reported values from 1,240 to 1,280 m/s. Wang *et al*. examined the effect of the relaxation of longitudinal stress modulus on the propagation behavior of the thermally driven acoustic wave in siloxanes [17]. Patterson reported the hypersonic attenuation in amorphous PDMS was studied as a function of temperature and pressure [7]. Kondo *et al*. investigated Brillouin scattering from networks of end-linked dimethylsiloxanes to study the hypersonic loss processes [13]. Figure 60.7 summarizes their findings. Here the attenuation $\alpha\lambda_s$ is defined as

$$\alpha\lambda_s = \pi\frac{2\Gamma}{\nu_p}, \tag{60.21}$$

where α is the attenuation per wavelength. The x-axis has been chosen as inverse of the number of skeletal elements $(2n + 5)$ with $n = 1, 2, 3, 4, 5$, and 6. This corresponds to extremely highly cross-linked networks with $M_c = 274$–644 g/mol. The hypersonic attenuation attained a maximum at $n = 4$–6. The hypersonic frequency shows a steep decrease with increasing chain length and decreases by about 45%. Since the refractive index changes only by about 2% for the different molecular weight samples, this would imply a very dramatic change in the phonon velocity.

Brillouin spectroscopy can also be used to study the change of sound velocity with deformation. Anders *et al*. reported the longitudinal sound velocity in stretched poly (urethane) and poly (diethylsiloxane) (PDES, Figure 60.8) networks [15]. They used the lattice-model to determine the force constants [11]. The samples showed different deformation-dependent behavior of the force constants. For the

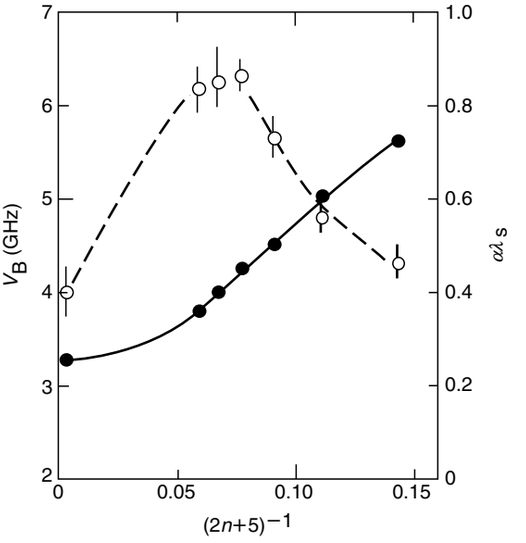

FIGURE 60.7. Phonon frequency (filled circle) and attenuation (empty circle) in highly cross-linked rubbery PDMS as a function of the number of skeletal elements. The hypersonic attenuation attains a peak for $n = 4$–6 [13].

diol-extended polyurethanes, the longitudinal sound velocity increased in the direction of stress and decreased in the direction perpendicular to it. The diamine-extended polyurethanes showed anomalous behavior. While the sound velocity increased parallel to the stress direction as expected, it also increased along the direction perpendicular to the stress. For the PDES samples, they found in some cases no significant variation of the sound velocity while in the other cases they found the same anomalous behavior as observed in the polyurethanes. Sinha *et al*. reported the molecular weight dependence of the phonon speed for a series of nearly monodisperse PDMS networks [16]. They showed that, at sufficiently low cross-link densities, the longitudinal phonon speed in these networks approaches the speed in uncross-linked high molecular weight PDMS liquids.

In comparing elastic constants measured ultrasonically or from Brillouin scattering with those observed in a "static" (very low frequency measurement), it is important to note that the ultrasonic/Brillouin values are adiabatic while static values are isothermal. In elastomers, the acoustic response is largely determined by the network structure introduced by chemical cross-linking. The mechanical behavior at higher frequencies (in the GHz regime) may have a very small molecular dependence, depending on the frequency at which the rubber–glass transition occurs for PDMS (Fig. 60.1). For PDMS networks [16], the change in modulus as a function of cross-link density in equilibrium measurements is considerably higher than that observed in Brillouin scattering measurements (about 90% decrease in modulus for $M_c = 4{,}000$–$40{,}000\,\mathrm{g/mol}$ in equilibrium measurements). The decrease in speed for the same range of molecular weights was found to be about 75% using the low frequency sound waves [5] compared to the 10% decrease at the GHz frequencies [16]. At GHz frequencies, when a stress is exerted in a particular place in the sample, the distance over which relaxations can occur is very short. The dependence of the modulus on the chain length between cross-links is therefore much less compared to low frequency measurements where there the time scales are much larger and therefore the chains can relax over longer length scales. At these frequencies, in Brillouin scattering experiments, the sound wave propagation of a polymer therefore depend primarily on the intermolecular potential, which is a function of intermolecular separation and hence volume. Thus there will be a change in the phonon velocity whenever there is a change in any physical property that affects volume, such as crystallinity, cross-linking, and plasticization.

60.5 CONCLUDING REMARKS

In order to have a more complete understanding of the acoustic properties of polymers, it is desirable to probe the response over as wide a range in frequency as possible. In the low frequency range (kHz), the propagation of an externally generated mechanical disturbance is used to measure the acoustic properties. In the high frequency hypersonic range (GHz), intrinsic thermal phonons using Brillouin scattering are used to measure the acoustic properties. In the ultrasonic (MHz) frequency range, which lies in between these two limits, propagation of externally excited sound waves is used to study amorphous polymeric medium. Collectively, results from these different measurement techniques can provide information about the mechanical behavior of polymers over a wide range of time scales.

ACKNOWLEDGMENTS

The authors would like to acknowledgment the contribution of Dr. Bruce Hartmann, now deceased, who was the author of the chapter on acoustical properties published in the previous edition of this handbook. Dr Hartmann's comprehensive work provided the starting point for this article.

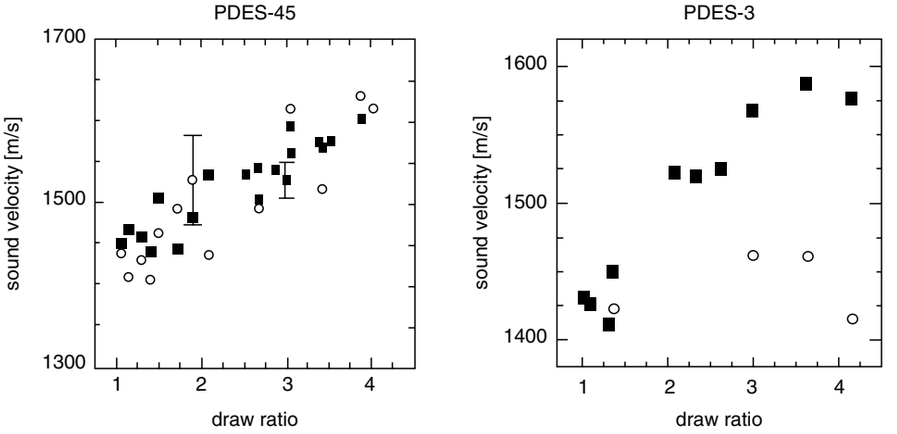

FIGURE 60.8. Sound velocity of the longitudinal polarized phonon measured parallel (filled squares) and perpendicular (empty circles) to the draw direction measured by Brillouin scattering. The samples are polydiethylsiloxanes with $M_n = 45{,}000$ and 43,000 labeled as PDES-45 and PDES-3, respectively [15]. Reprinted from S.H. Anders, H.H. Krbecek, and M. Pietralla, J. Polym. Sci., Polym. Phys. Ed. 35, 1661-1676 (1997). Copyright 1997, with permission of Wiley-VCH.

REFERENCES

1. B. Hartmann, *Physical Properties of Polymers Handbook*, ed. J. E. Mark, Chapter 49 (American Institute of Physics Press, 1996).
2. J. D. Ferry, Viscoelastic Properties of Polymers, 3rd. ed. (Wiley, New York, 1980).
3. R. S. Witte, B. A. Mrowca, and E. Guth, J. Appl. Phys. 20 (6), 481 (1949).
4. A. N. Gent and P. Marteny, J. Appl. Phys. 53(9), 6069–6075 (1982).
5. M. Sinha, J. E. Mark, B. Erman, T. H. Ridgway, and H. E. Jackson, Macromolecules 36, 6127–6134 (2003).
6. B. Hartmann and J. Jarzynski, J. Acoust. Soc. Am. 56, 1469 (1974).
7. G. D. Patterson in *Methods of Experimental Physics*, vol. 16, Part A, p. 170, ed. R. A. Fava (Academic Press, New York, 1980).
8. G. D. Patterson, J. Polym. Sci., Polym. Phys. Ed. 15, 455 (1977).
9. G. D. Patterson, Macromolecules 17, 885–888 (1984).
10. A. Kumar, Univ. Microfilms, Ann Arbor, Mich., Order No. 74–13, 926; through Diss. Abstr. Int. B 34 (no. 12), 6033 (1974).
11. S. Kondo and T. Igarashi, J. Appl. Phys. 51(3), 1514–1519 (1980).
12. S. M. Lindsay, A. J. Hartley, and I. W. Shepherd, Polymer 17, 501 (1976).
13. S. Kondo and T. Igarashi, Polymer 24 (Commun.), 221 (1983).
14. C. G. Delides and A. C. Stergiou, Polymer 26 (Commun.), 168 (1985).
15. S. H. Anders, H. H. Krbecek, and M. Pietralla, J. Polym. Sci., Polym. Phys. Ed. 35, 1661–1676 (1997).
16. M. Sinha, J. E. Mark, H. E. Jackson, and D. Walton, J. Chem. Phys. 117(6), 2968 (2002).
17. C. H. Wang, Q. L. Liu, and B. Y. Li, J. Polym. Sci., Polym. Phys. Ed. 25, 485 (1987).
18. H. H. Krbecek and M. Pietralla, J. Polym. Mater. 22, 177 (1993).
19. P. D. Davidse, H. Waterman, and J. B. Westerdijk, J. Polym. Sci. 59, 389–400 (1962).
20. B. Hartmann and J. Jarzynski, J. Polym. Sci. Part A-2, 9, 763–765 (1971).
21. R. K. Eby, J. Acoust. Soc. Am. 36, 1485–1487 (1964).
22. B. Hartmann, G. F. Lee, and J. D. Lee, J. Acoust. Soc. Am. 95, 226–233 (1994).
23. S. Havriliak and S. Negarni, J. Polym. Sci. Part C, No. 14, ed. R. F. Boyer (Interscience, New York, 1966), pp. 99–117.
24. I. I. Pavlinov, I. B. Rabinovich, V. Z. Pogorelko, and A. V. Ryabov, Polym. Sci. USSR AIO, 1471–1480 (1968).
25. B. Hartmann, J. Appl. Polym. Sci. 19, 3241–3255 (1975).
26. B. Hartmann and J. Jarzynski, J. Acoust. Soc. Am. 56, 1469–1477 (1974).
27. K. Shimizu, O. Yano, Y. Wada, and Y. Kawamura, J. Polym. Sci.: Phys. 11, 1641–1652 (1973).
28. N. Lagakos, J. Jarzynski, J. H. Cole, and J. A. Bucaro, J. Appl. Phys. 59, 4017–4031 (1986).
29. D. W. Phillips, A. M. North, and R. A. Pethrick, J. Appl. Polym. Sci. 21, 1859–1867 (1977).
30. B. Hartmann, J. Appl. Phys. 51, 310–314 (1980).
31. E. Morita, R. Kono, and H. Yoshizaki, Jpn. J. Appl. Phys. 7, 451–461 (1968).
32. H. Singh and A. W. Nolle, J. Appl. Phys. 30, 337–341 (1959).
33. I. I. Perepechko and V. E. Sorokin, Sov. Phys. Acoust. 18, 485–489 (1973).
34. B. Hartmann and G. Lee, J. Polym. Sci.: Phys. Ed. 20, 1269–1278 (1982).
35. E. Montgomery, F. J. Weber, D. F. White, and C. M. Thompson, J. Acoust. Soc. Am. 71, 735–741 (1982).
36. J. Sutherland, J. Appl. Phys. 49, 3941–3945 (1978).
37. B. Hartmann, Polymer 22, 736–739 (1981).
38. H. J. Sutherland and R. Lingle, J. Appl. Phys. 43, 4022–4026 (1972).
39. C. M. Thompson and W. L. Heimer, II, J. Acoust. Soc. Am. 77, 1229–1238 (1985).
40. N. V. Karyakin, I. B. Rabinovich, and V. A. Ulyanov, Polym. Sci. USSR 11, 3159–3164 (1969).
41. Y. Wada and K. Yamamoto, J. Phys. Soc. Jpn 11, 887–892 (1956).
42. B. Hartmann and J. Jarzynski, J. Appl. Phys. 43, 4304–4312 (1972).
43. B. Hartmann, "Ultrasonic Measurements", in *Methods of Experimental Physics,* Vol. 16c, ed. R. A. Fava, (Academic Press, New York, 1980), pp. 59–90.
44. D. L. Lamberson, J. R. Asay, and A. H. Guenther, "Polystyrene and Polymethylmethacrylate from Ultrasonic Measurements at Moderate Pressures", J. Appl. Phys. 43, 976–985 (1972).
45. J. R. Asay, D. L. Lamberson, and A. H. Guenther, J. Appl. Phys. 40, 1768–1783 (1969).
46. A. Lukashov, V. Feofanov, J. D. Schultze, M. Boehning, and J. Springer, Polymer 33, 2227–2228 (1992).
47. S. de Petris, V. Frosini, E. Butta, and M. Baccaredda, Makromol. Chemie. 109, 54–61, (1967).
48. I. I. Perepechko and V. A. Grechishkin, Polym. Sci. USSR A15, 1139–1148 (1973).
49. 13. Hartmann and G. F. Lee, J. Non-Cryst. Solids 131–133, 887–890 (1991).
50. J. V. Duffy, G. F. Lee, J. D. Lee, and B. Hartmann, in *Sound and Vibration Damping with Polymers,* eds. R. D. Corsaro and L. H. Sperling, ACS Symposium Series 424 (ACS Press, Washington, DC, 1990), pp. 281–300.
51. B. Hartmann, J. V. Duffy, G. F. Lee, and E. Balizer, J. Appl. Polym. Sci. 35, 1829–1852 (1988).
52. J.E. Carlson, J. van Deveneter, A. Scolan and C. Carlander, 2003 IEEE Ultrasonics Symposium, Honolulu, 5–8 Oct 2003, eds. D.E. Yuhas, and S.C. Schneider, IEEE, Piscataway, NJ, USA, pp. 885–888.
53. K. Matsushige, in *High Performance Polymers* (Hanser, New York, 1991), pp. 103–131.
54. H. Y. Guney, T. Oskay and H. S. Ozkan, J. Polym. Sci. B: Polym. Phys. 33, 985–991, (1995).
55. K.J. Suslick and G.J. Price, Annu. Rev. Mater. Sci. 29, 295–326, (1999).
56. I. Alig and D. Lellinger, Chem. Innovat. 30, 12–18, (2000).
57. D. Buckley, unpublished data.

CHAPTER 61

Permeability of Polymers to Gases and Vapors

S. A. Stern* and J. R. Fried†

*Department of Biomedical and Chemical Engineering, Syracuse University, Syracuse, NY 13244
†Department of Chemical and Materials Engineering, University of Cincinnati, Cincinnati, OH 45221

61.1 INTRODUCTION

All polymers are permeable to gases and vapors to different extents. Permeability is a physical property of great importance in a variety of industrial and biomedical applications of polymers. Examples of these applications include: the separation of gas and liquid mixtures, water desalination, food packaging, protective coatings (e.g., paints and varnishes), controlled drug release, and biomedical devices. Polymers are commonly used in these applications in the form of *nonporous* membranes (e.g., films or sheets, hollow fibers, or capillaries). The following discussion and accompanying references are based largely on studies made with such membranes. A *vapor* is defined in this chapter as a gas at a temperature below its critical temperature, i.e., as a condensable gas. Consequently, the term ''gas'' is used hereafter to designate both supercritical gases and vapors.

A large number of polymers have been synthesized for various applications that depend on gas permeability, but in particular for potential uses as membrane materials for gas separation processes. The permeability of these polymers to various gases has been measured at different temperatures and in some cases over a range of pressures. The objective of this chapter is to complement and update the compilations of gas permeability data already published in Chapter 50 of the first edition of this Handbook. Since, due to limitations of space, it was not possible to list gas permeability data at all the various temperatures and pressures at which these data have been determined, and since different readers have different interests, only references to permeability data have been given. However, all the gases used and the temperatures and pressures at which the referenced permeability measurements were made are listed. The references to gas permeabilities reported in this chapter are not comprehensive, but are representative of selected classes of homopolymers. References to some earlier gas permeability studies are included. This chapter also includes a brief review of the permeation mechanisms as well as a mention of the use of computer simulations of gas permeation in and through nonporous polymer membranes.

61.2 MECHANISMS OF GAS PERMEATION

61.2.1 Basic Relations and Definitions

Gases permeate through polymer membranes when a pressure differential is established at opposite membrane interfaces. The permeation of gases through *nonporous* polymer membranes is generally described in terms of a ''solution-diffusion'' mechanism [1–9]. According to this mechanism, gas permeation is a complex process consisting of the following sequence of events: (1) solution (absorption) of the gas into the membrane at its interface exposed to the higher pressure; (2) molecular (''random walk'') diffusion of the gas in and through the membrane; and (3) release of the gas from solution (desorption) at the opposite interface exposed to a lower pressure. The term *permeation* is accordingly used here to describe the overall mass transport of the penetrant gas across the membrane, whereas the term *diffusion* refers only to the movement of the penetrant molecules inside the polymer matrix.

In most practical applications, molecular diffusion is the slowest and, hence, the rate-determining step in the permeation process. By comparison, the absorption and desorption steps are very fast, so that solution equilibrium is assumed to be established between the gas phase in contact with the two membrane interfaces and the gas dissolved at these interfaces.

The diffusion of gas molecules in and through polymer membranes can in many cases of practical interest be described by Fick's two laws. Thus, for isothermal diffusion of a gas through a ν-dimensional hyperspherical membrane of sufficiently large area ($\nu = 1$ for a planar membrane or slab, $\nu = 2$ for a hollow cylinder, and $\nu = 3$ for a spherical shell), these laws are described by the following equations [1]:

$$J = -\omega_\nu r^{\nu-1} D(c) \frac{\partial c(r,t)}{\partial r} \tag{61.1}$$

and

$$\frac{\partial c}{\partial t} = \frac{1}{r^{\nu-1}} \frac{\partial}{\partial r} \left[r^{\nu-1} D(c) \frac{\partial c}{\partial r} \right] \quad R_1 < r < R_2, \tag{61.2}$$

where J is the local rate of penetrant gas diffusion (the local flux); $c(r,t)$ is the local penetrant concentration at a position coordinate r and at time t; $D(c)$ is the local mutual diffusion coefficient; $\omega_1 = 1$ for a planar membrane or slab; $\omega_2 = 2\pi$ for a hollow cylinder; and $\omega_3 = 4\pi$ for a spherical shell. The flux, J, is taken through unit area of slab, unit length of cylinder, and the whole area of the spherical shell. The diffusion coefficient, D, depends on temperature and the nature of the penetrant/polymer system and can be constant or a function of penetrant concentration.

Integration of Eq. (61.1) for the desired geometry and boundary conditions yields the total rate of permeation of the penetrant gas through the polymer membrane. Integration of Eq. (61.2) yields information on the temporal evolution of the penetrant concentration profile in the polymer. Equation (61.2) requires the specification of the initial and boundary conditions of interest. The above relations apply to homogeneous and isotropic polymers. Crank [3] has described various techniques of solving Fick's equations for different membrane geometries and boundary conditions, for constant and variable diffusion coefficients, and for both transient and steady-state transport.

The equilibrium concentration (solubility), c, of a penetrant gas dissolved in a polymer can be related to the pressure, p, of the penetrant by the isothermal relation

$$c = S(c) \cdot p, \tag{61.3}$$

where $S(c)$ [or $S(p)$] is a solubility coefficient. When the concentration of the penetrant in the polymer is very low, Eq. (61.3) reduces to a form of Henry's law; the solubility coefficient is then independent of c (or p). In the case of gas permeation Eq. (61.3) is applicable to the conditions prevailing at the membrane interfaces.

In practical applications it is often of interest to determine the rate of gas permeation under steady-state conditions. Steady state is achieved if, at a given temperature, the constant pressures p_h and $p_l (< p_h)$ are maintained at opposing membrane interfaces, respectively. For example, the following relation can be derived from Fick's first law, cf. Eq. (61.1), for the steady-state rate of gas permeation J_s through unit area of a planar, isotropic, and homogeneous membrane of effective thickness δ, i.e., when $\nu = 1$ and $\omega = 1$:

$$J_s = \overline{P}(p_h - p_l)/\delta, \tag{61.4}$$

where $\overline{P}$ is a mean "permeability coefficient" or "permeability"; Eq. (61.4) refers to a specified temperature and unit area of membrane. The ratio $\overline{P}/\delta$ is a mass-transfer coefficient.

Similarly, the steady-state rate of gas permeation through a tubular membrane, such as a capillary or hollow fiber, is given by the relation

$$J_s = \overline{P} \frac{2\pi L(p_h - p_l)}{\ln(R_o - R_i)}, \tag{61.5}$$

where R_o and R_i are the effective outer and inner radii of the tube, respectively, and L is the length of the tube. The mean permeability coefficient, $\overline{P}$, depends on the nature of the penetrant gas and polymer membrane, on the temperature, and, in the most general case, on both p_h and p_l. The rate of gas permeation of a component of a gas mixture is also given by Eqs. (61.4) and (61.5), but p_h and p_l are then the *partial* pressures of that component at opposite membrane interfaces and $\overline{P}$ may also be a function of composition.

61.2.2 Relations between Permeability, Diffusion, and Solubility Coefficients

It can be shown that the mean permeability coefficient $\overline{P}$ is a product of a mean diffusion coefficient, $\overline{D}$, and a function $\overline{S}$ related to the solubility of the penetrant gas in the polymer [1–9]:

$$\overline{P} \equiv \overline{D} \cdot \overline{S}, \tag{61.6}$$

where $\overline{D}$ is a mean diffusion coefficient

$$\overline{D} = \int_{c_l}^{c_h} [D(c)/(c_h - c_l)] dc \tag{61.7}$$

and $\overline{S}$ is a function defined by the relation

$$\overline{S} = \frac{(c_h - c_l)}{(p_h - p_l)}, \tag{61.8}$$

where c_h and $c_l (< c_h)$ are the equilibrium concentrations of the penetrant dissolved at the membrane interfaces at pressures p_h and p_l, respectively. When $p_h \gg p_l$, and therefore $c_h \gg c_l$ as is often the case, $\overline{S}$ reduces to

$$\overline{S} = S_h = c/p|_h, \tag{61.9}$$

where S_h is the solubility coefficient evaluated at the "upstream" pressure p_h, cf. Eq. (61.3).

When the solubility of a penetrant gas in a polymer is sufficiently low to be within the Henry's law limit, then $S(c) = S_o$, a constant at a given temperature, cf. Eq. (61.3). The mutual diffusion coefficient is then often also a constant, $D(c) = D_o$; this is the case for supercritical gases in "rubbery" polymers over wide ranges of pressure. Equation (61.6) then reduces to

$$P_o = D_o \cdot S_o, \tag{61.10}$$

where P_o depends only on the nature of the penetrant/polymer system and the temperature. This relation has been widely used in the literature, sometimes without qualification and sufficient justification. Equation (61.10) shows that P_o is a product of a diffusion coefficient, D_o (a kinetic factor), and of a solubility coefficient, S_o (a thermodynamic factor).

The problem of gas diffusion in, and permeation through, *inhomogeneous* polymers is more complex, but has been considered by a number of investigators [3,5,6,10]. The diffusion coefficient is then also a function of position. When the polymer is highly plasticized (i.e., swelled) by the penetrant, the diffusion coefficient may also become a function of time and of sample "history." Such "non-Fickian" diffusion has also been studied [3,5,11–16].

61.2.3 Gas Selectivity of Polymers

The overall *selectivity* of a polymer membrane toward two different penetrant gases A and B is commonly expressed in terms of an "ideal" separation factor, $\alpha^*(A/B)$, which is defined by the relation, cf., Eq. (61.6)

$$\alpha^*(A/B) \equiv \frac{\overline{P}(A)}{\overline{P}(B)} = \frac{\overline{D}(A)}{\overline{D}(B)} \cdot \frac{\overline{S}(A)}{\overline{S}(B)}, \tag{61.11}$$

where the ratios $\bar{D}(A)/\bar{D}(B)$ and $\bar{S}(A)/\bar{S}(B)$ are known, respectively, as the "diffusivity (or mobility) selectivity" and the "solubility selectivity." These ratios represent contributions to the overall selectivity due to the differences in the diffusivities and solubilities of gases A and B in a polymer.

61.2.4 Dependence on Temperature

In cases where the permeability coefficient for a gas/polymer system is independent of pressure, i.e., $\overline{P} = P_o$, the temperature dependence of P_o can be represented over small ranges of temperature by the Arrhenius-type relation

$$P_o = P_o^o \exp(-E_p/RT), \tag{61.12}$$

where P_o^o is a constant; E_p is the apparent energy of activation of the permeation process, R is the universal gas constant, and T is the absolute temperature. As mentioned above, P_o is independent of pressure when the mutual diffusion coefficient, D_o, is a constant (at constant temperature) and the solubility is within the Henry's law limit, i.e., the solubility coefficient, S_o, is a constant, cf., Eq. (61.10). In such cases, the temperature dependence of D_o can also be represented by the Arrhenius-type relation

$$D_o = D_o^o \exp(-E_d/RT), \tag{61.13}$$

whereas the temperature dependence of S_o is expressed by the van't Hoff-type relation

$$S_o = S_o^o \exp(-\Delta H_s/RT). \tag{61.14}$$

In equations (61.13) and (61.14) D_o^o and S_o^o are constants, E_d is an apparent activation energy of diffusion, and ΔH_s is the molar heat (enthalpy) of solution.

Equations (61.10), (61.12), (61.13), and (61.14) yield the following relations:

$$P_o^o = D_o^o \cdot S_o^o \tag{61.15}$$

and

$$E_p = E_d + \Delta H_s. \tag{61.16}$$

It follows from Eq. (61.16) that the sign and magnitude of E_p depend on the signs and relative values of E_d and ΔH_s. Since the value of E_d is always positive, D_o always increases with increasing temperature; ΔH_s can be either positive or negative, depending on the nature of the penetrant/polymer system, for the following reasons. The solution of a gas in a polymer can be visualized as occurring in two stages [1], namely, condensation of the gas to a liquid, followed by the mixing of the condensed gas with the polymer, i.e., solution in the polymer. Hence, the heat of solution, ΔH_s, can be expressed by the relation

$$\Delta H_s = \Delta H_{cond} + \Delta \bar{H}_1, \tag{61.17}$$

where ΔH_{cond} is the molar heat of condensation of the penetrant gas and $\Delta \bar{H}_1$ is the partial molar heat of mixing of the condensed gas with the polymer.

The molar heat of condensation, ΔH_{cond}, is a hypothetical quantity for supercritical gases, such as the helium-group gases, H_2, O_2, N_2, etc., at ambient temperature. It is assumed that ΔH_{cond} for such gases is very small. The value of ΔH_s then depends largely on that of $\Delta \bar{H}_1$, which is small and positive (i.e., the mixing process is endothermic). Therefore, ΔH_s for supercritical gases is commonly also small and positive, and the solubility coefficients S_o increases slightly as the temperature is raised, cf., Eq. (61.14). Equations (61.12) and (61.16) show that the permeability coefficient, P_o, then also increases with increasing temperature.

By contrast, for subcritical gases (vapors) ΔH_{cond} is the predominant term in Eq. (61.17). Since condensation is an exothermic process, ΔH_{cond} is negative. Therefore, the heat of solution, ΔH_s, of subcritical gases, such as organic vapors, is also negative and their solubility in polymers decreases with increasing temperature. In such cases, E_p may be either positive or negative depending on the relative values of E_d (which is always positive) and ΔH_s. Hence,

P_o for subcritical gases may increase, decrease, or change very little as the temperature is raised.

According to Eqs. (61.12), (61.13), and (61.14), plots of $\ln P_o$, $\ln D_o$, and $\ln S_o$ versus the reciprocal absolute temperature, $1/T$, should be linear over limited ranges of temperature in which E_p, E_d, and ΔH_s are constant. This is found to be the case for supercritical gases that exhibit a low solubility in polymers even at elevated pressures, provided that the polymers are not significantly plasticized (swelled) by the penetrant gases. The same linear plots are obtained with subcritical gases (which are more highly soluble in polymers) at very low penetrant gas concentrations, e.g., in the Henry's law limit. The plots of $\ln P_o$, $\ln D_o$, and $\ln S_o$ versus $1/T$ for different gases in rubbery and glassy polymers may exhibit single or double discontinuities (breaks), or no discontinuities at all, at or near the glass-transition temperature, T_g, of the polymers.

Equations (61.12), (61.13), and (61.14) can be applied over wider ranges of temperature if the dependence of E_p, E_d, and ΔH_s on temperature is known. For example, if E_p and E_d decrease with increasing temperature, plots of $\ln P_o$ and $\ln D_o$ versus $1/T$ are then curves with decreasing slopes.

When the permeability, diffusion, and solubility coefficients are functions of pressure their experimental values are mean values ($\overline{P}, \overline{D}$, and $\overline{S}$) for the pressures applied at the membrane interfaces, cf., eqs. (61.6–61.8). Equations (61.12–61.14) are applicable also to $\overline{P}, \overline{D}$, and $\overline{S}$ over a limited range of temperatures. The activation energies E_p and E_d commonly decrease with increasing pressure.

61.2.5 Dependence on Gas Pressure

The dependence of permeability, diffusion, and solubility coefficients on penetrant gas pressure (or concentration in polymers) is very different at temperatures above and below the glass transition temperature, T_g, of the polymers, i.e., for "rubbery" and "glassy" polymers, respectively. Thus, when the polymers are in the *rubbery* state the pressure dependence of these coefficients depends, in turn, on the gas solubility in polymers. For example, as mentioned in Section 61.2.4, if the penetrant gases are very sparsely soluble and do not significantly plasticize the polymers, the permeability coefficients as well as the diffusion and solubility coefficients are independent of penetrant pressure. This is the case for supercritical gases with very low critical temperatures (compared to ambient temperature), such as the helium-group gases, H_2, O_2, N_2, CH_4, etc., whose concentration in rubbery polymers is within the Henry's law limit even at elevated pressures.

Subcritical gases, such as organic vapors, are much more highly soluble in polymers, and, consequently, the above behavior is observed only at very low pressures (or concentrations in polymers). As the penetrant pressure is raised, and the polymers are increasingly plasticized by the penetrant gas, the permeability, diffusion, and solubility coefficients increase rapidly, in some cases exponentially, with increasing pressure.

By contrast, the permeability, diffusion, and solubility coefficients for gases in *glassy* polymers are strongly nonlinear functions of the penetrant gas pressure. Such a nonlinear behavior is observed even when the polymer is not significantly plasticized by the penetrant gas. This behavior is described satisfactorily by the "dual-mode" sorption model [3–7,9,17], which attributes it to the heterogeneity of glassy polymers. According to this model, the permeability and solubility coefficients decrease and the diffusion coefficients increase as the gas pressure is raised; all three coefficients reach asymptotic values at sufficiently high pressures. The dual-mode sorption model also shows that the permeability, diffusion, and solubility coefficients must become independent of pressure at sufficiently low pressures. Dual-mode sorption behavior has been observed experimentally with a variety of gases in many glassy polymers.

When the concentration of penetrant gases in glassy polymers becomes sufficiently high to plasticize the polymers, the permeability, diffusion, and solubility coefficients will deviate from dual-mode sorption behavior and increase as the pressure is raised.

61.2.6 Molecular Mechanisms and Computer Simulations

It has been shown in a previous section that, in most cases of practical interest, the rate of gas permeation through nonporous polymer membranes is controlled by the diffusion of the penetrant gas in the polymer matrix. Many theoretical models have been proposed in the literature to describe the mechanisms of gas diffusion in polymers on a *molecular* level. Such models provide expressions for gas diffusion coefficients, and sometimes also for permeability coefficients, derived from free volume, statistical–mechanical, energetic, structural, or other considerations. The formulation of these coefficients is complicated by the fact that gas transport occurs by markedly different mechanisms in rubbery and glassy polymers.

As a result, the mechanisms of gas transport in polymers are still incompletely understood, particularly below T_g, when considered on a microscopic level. Therefore, almost all transport models proposed in the literature are phenomenological and contain one or more adjustable parameters that must be determined experimentally. Moreover, most of these models have been found to be applicable only to a limited number of gas/polymer systems.

Clearly, a better understanding of the gas transport mechanisms in polymers would greatly facilitate the development of polymer membranes that exhibit both a higher selectivity and a higher (or lower) permeability to specified gases. It is beyond the scope of the present chapter to review this area of research, particularly since a number of extensive reviews are available [1,3–9,11–15,17,18].

It must be noted, however, that the development of very fast computers and recent advances in the computer simulation of polymer microstructures will make possible the formulation of much more realistic molecular models of gas transport in and through polymers. Information concerning self-diffusion and solubility, fractional free volume, *d*-spacing, and chain and substituent group mobility now can be obtained with good confidence by a variety of methods including molecular dynamics and Monte Carlo simulations using extensively parameterized polymer force fields such as COMPASS [19,20]. Several excellent reviews are available [21–24]. Recent developments in the applications of nonequilibrium molecular dynamics and Grand Canonical Monte Carlo methods following the work of Heffelfinger and Thompson [25,26] have extended the application of simulation methods to investigate transport through nonporous ''dense'' membrane as well as through membrane pores under a concentration gradient.

61.3 GAS PERMEABILITY DATA

A very large body of data on the gas permeability of many rubbery and glassy polymers has been published in the literature. These data were obtained with homopolymers as well as with copolymers and polymer blends in the form of nonporous ''dense'' (homogeneous) membranes and, to a much lesser extent, with asymmetric or ''composite'' membranes. The results of gas permeability measurements are commonly reported for ''dense'' membranes as permeability coefficients, and for asymmetric or composite membranes as ''permeances'' (permeability coefficients not normalized for the effective membrane thickness). Most permeability data have been obtained with pure gases, but information on the permeability of polymer membranes to a variety of gas mixtures has also become available in recent years. Many of the earlier gas permeability measurements were made at ambient temperature and at atmospheric pressure. In recent years, however, permeability coefficients as well as solubility and diffusion coefficients for many gas/polymer systems have been determined also at different temperatures and at elevated pressures. Values of permeability coefficients for selected gases and polymers, usually at a single temperature and pressure, have been published in a number of compilations and review articles [27–35].

It should be noted that the gas and vapor permeability of polymer membranes could be affected by pretreatment, ageing, plasticization, crosslinking and/or crystallinity of the polymer and, in some cases, by the experimental conditions and measurement techniques employed. For example, the type of solvent(s) used in the casting of membranes may affect their permeability.

Tables 61.2–61.17 list references to many recent and some earlier permeability measurements made with various pure gases and membranes cast from different classes of rubbery and glassy polymers, but mainly homopolymers. The ranges of experimental pressure and temperature reported in these references are also listed. Values of permeability coefficients for some gas/polymer systems can also been obtained from a number of correlations mostly based on group contribution methods [36–41].

The permeability of different polymers to a given gas can vary by many orders of magnitude. The permeability of a given polymer to different gases, i.e., its gas selectivity, can also vary significantly. Glassy polymers commonly exhibit a low permeability but high gas selectivity. By contrast, rubbery polymers exhibit a higher permeability but a much lower selectivity than glassy polymers under comparable conditions. Glassy polymers are commonly much more permeable to light gases, such as He, H_2, N_2, O_2, and CO_2 than to organic vapors whereas the opposite is true for rubbery polymers. The separation of gases by selective permeation through rubbery polymer membranes is due mainly to differences in the gas solubility whereas separation by glassy polymer membranes is caused mainly by differences in the gas diffusivity.

Some exceptions to the above behavior are known, such as in the case of poly(1-trimethylsilyl-1-propyne), PTMSP, a glassy polymer at ambient temperature. PTMSP has the highest gas permeability of all known synthetic polymers but a low gas selectivity due to its very large free volume. Although in the glassy state, this polymer is more permeable to organic vapors than to light gases.

The permeability coefficients of gases in rubbery polymers can also be used in calculations involving gas mixtures if the gas solubility in the polymers is sufficiently low, e.g., in the Henry's law limit. This is due to the fact that under such conditions the components of gas mixtures commonly permeate through a polymer membrane independently of each other. By contrast, the permeation of the components of gas mixtures in and through glassy polymers is ''coupled,'' i.e., each component affects the permeation behavior of the other component(s). Commonly, the permeation rate of the ''faster'' component(s) of a gas mixture is decreased while that of the ''slower'' component(s) is increased, thus decreasing the polymer selectivity. This behavior is quantitatively described by the ''dual-mode sorption'' model and its extensions [5–9,12,17].

The following tables also list values of T_g in order to facilitate the identification of polymers with high or low gas permeabilities and high or low gas selectivities. The T_gs were either stated in the listed references or, in some cases, obtained from other sources; values of T_g reported by different investigators for a given polymer sometimes may differ by 10 °C or more, depending on the method and time frame of the measurements and on other factors.

61.4 GAS PERMEABILITY UNITS

The permeability coefficient $\overline{P}$ for pure gases is defined by Eq. (61.4) in the form

$$\overline{P} = \frac{J_s \cdot \delta}{(p_h - p_l)}$$

where J_s is the *mass* of penetrant gas permeating per unit time through unit area of a membrane of effective thickness δ under a pressure differential $(p_h - p_l)$. Consequently, $\overline{P}$ has the following dimensions:

$$\overline{P}\left[\frac{\text{(mass of permeating gas)(effective membrane thickness)}}{\text{(time)(membrane area)(pressure difference across membrane)}}\right].$$

The effective thickness of ''asymmetric'' or ''composite'' membranes is much smaller than their actual thickness [6,9] and may not be known. Therefore, the permeability to gases of such membranes is often characterized by their ''permeance,'' $\overline{P}/\delta$.

A variety of units for $\overline{P}$ have been used by different investigators. Some of these units and their conversion factors are listed in Table 61.1.

The standard temperature and pressure (STP) are, respectively, 273.15 K and 1 atm. $(1.013 \times 10^5\,\text{Pa})$; $1\text{mil} = 1 \times 10^{-3}$ in. $= 2.540 \times 10^{-3}$cm; $1\text{in.}^2 = 6.4516\,\text{cm}^2$. The unit [in.^{3}(STP)·mil/(day·100 in.^{2} atm.)] has been used mainly in packaging applications. The quantity 1×10^{-10} $\left[\frac{\text{cm}^3\text{(STP)}\cdot\text{cm}}{\text{s}\cdot\text{cm}^2\cdot\text{cmHg}}\right]$ is designated by some investigators as ''1 Barrer''.

ACKNOWLEDGMENTS

This chapter is a revised and updated version of Chapter 50, ''Permeability of Polymers to Gases and Vapors'' by S. A. Stern, B. Krishnakumar, and S. M. Nadakatii, published in the first edition of ''Physical Properties of Polymers Handbook'', J. E. Mark, Editor, AIP Press, Woodbury, NY, 1996, pp. 687–700.

TABLE 61.1. *Various units of $\overline{p}$ used by different investigators.*

Unit	Multiplication factor		
	$\frac{\text{cm}^3\text{(STP)}\cdot\text{cm}}{\text{s}\cdot\text{cm}^2\cdot\text{cmHg}}$	$\frac{\text{cm}^3\text{(STP)}\cdot\text{cm}}{\text{s}\cdot\text{cm}^2\cdot\text{Pa}}$	$\frac{\text{in}^3\text{(STP)}\cdot\text{mil}}{\text{day}\cdot 100\,\text{in.}^2\cdot\text{atm.}}$
$\frac{\text{cm}^3\text{(STP)}\cdot\text{cm}}{\text{s}\cdot\text{cm}^2\cdot\text{cmHg}}$	1	7.5×10^{-4}	1.02×10^{11}
$\frac{\text{cm}^3\text{(STP)}\cdot\text{cm}}{\text{s}\cdot\text{cm}^2\cdot\text{Pa}}$	1.33×10^{3}	1	1.36×10^{14}
$\frac{\text{in}^3\text{(STP)}\cdot\text{mil}}{\text{day}\cdot 100\,\text{in.}^2\cdot\text{atm.}}$	9.82×10^{-12}	7.37×10^{-15}	1

TABLE 61.2. *Polyolefins.*

Polymer	Gases and vapors	T_g(°C)	Temperature (°C)	Pressure (atm.)	Ref.
Polyethylene	He, Ar, N_2, O_2, CO, CO_2, CH_4, C_2H_6, C_3H_4, C_3H_6, C_3H_8, SF_6	−20[a]	5–55	NR	[42]
	Ar, CF_4, $C_2H_2F_2$, SF_6	NR	5–50	1–15	[43]
	He, N_2, CO_2, CH_4, C_2H_4, C_2H_6, N_2O	NR	−10 to 60	1–60	[44]
	N_2, O_2, CO_2	NR	30	≤1	[45]
	He, Ne, Ar, Kr, H_2, N_2, O_2, CO_2, CH_4, N_2O	NR	25	1–130	[46]
	He, CO_2, CH_4	NR	35	1	[47]
Polyisobutene	He, H_2, N_2, O_2, CO_2, CH_4	−76[a]	17–50	1	[48]
Poly(4-methyl pentene-1)	N_2, O_2	29[a]	25	1.36	[49]
Polypropylene	He, Ne, Ar, Kr, H_2, N_2, O_2, CO_2, CH_4, N_2O	−1 to −13[a]	25	1–130	[46]
	O_2	NR	NR	NR	[50]

NR, not reported in cited reference.
[a]Value of T_g not from cited reference.

TABLE 61.3. *Vinyl and vinylidene polymers.*

Polymer	Gases and vapors	T_g (°C)	Temperature (°C)	Pressure (atm.)	Ref.
Poly(vinyl chloride)	CO_2	76	40–55	≤1	[51]
	He, Ne, Ar, Kr, H_2, N_2, O_2, CO_2, CH_4, H_2O	75	25	NR	[52]
Poly(vinyl alcohol)	O_2	85[a]	25	NR	[53]
	O_2, H_2O	NR	25	NR	[54]
Poly(vinyl acetate)	Ar, CO_2	32	8–45	≤1	[55]
Polystyrene	CO_2	NR	35	1–23	[56]
	CO_2	98	25–40	≤1	[51]
	CH_4, C_3H_8, *n*-C_4H_10, *iso*-C_4H_10	101	25–50	NR	[57]
	He, H_2, N_2, O_2, CO_2	NR	25	NR	[58]
	N_2, O_2, CO_2, H_2O	NR	25–30	NR	[59]
Poly(vinylidene chloride)	O_2	−18	35	NR	[60]
	N_2, O_2, CO_2, H_2O	NR	25–30	NR	[59]
	H_2O	NR	25	NR	[61]
	N_2, O_2, CO_2	NR	30	≤1	[45]
Poly(vinylidene fluoride)	He, CO_2, CH_4	−40[a]	35	1	[47]
Poly(vinyl benzoate)	He, N_2, CO_2, CH_4	74[a]	20–80	0.1–100	[62]

NR, not reported in cited reference.
[a]Value of T_g not from cited reference.

TABLE 61.4. *Natural and synthetic rubbers.*

Polymer	Gases and vapors	T_g(°C)	Temperature (°C)	Pressure (atm.)	Ref.
1,4-Polybutadiene	Ne, H_2, N_2, CO_2	−7[a]	15–65	NR	[63]
	H_2, N_2, O_2, CO_2, CH_4	NR	17–50	1	[48]
Poly(dimethyl butadiene)	He, H_2, N_2, O_2, CO_2, CH_4	−11[a]	17–50	1	[48]
cis-Polyisoprene	He, H_2, N_2, O_2, CO_2, CH_4	−73[a]	17–50	1	[48]
	Ar, N_2, O_2, CO, CO_2, CH_4, C_3H_6, C_3H_8, SF_6	NR	15–55	NR	[42]
trans-Polyisoprene	C_3H_8	−65	50	NR	[64]
	H_2	−58[a]	17	NR	[65]
Polychloroprene	He, H_2, N_2, O_2, CO_2, CH_4	NR	17–50	1	[48]

NR, not reported in cited reference.
[a]Value of T_g not from cited reference.

TABLE 61.5. *Polyesters and polycarbonates.*

Polymer	Gases and vapors	T_g(°C)	Temperature (°C)	Pressure (atm.)	Ref.
Poly(ethylene terephthalate)	CO_2	60–86[a]	25–115	2–20	[66]
	CO_2	69	25–40	≤1	[51]
	He, Ar, H_2, N_2, CO_2	NR	50	NR	[67]
Poly(ethylene terephthalate) (Mylar A™)	N_2, O_2, CO_2	NR	30	≤1	[45]
Bisphenol-A polycarbonate	CO_2	144[a]	35	1–20	[68]
	He, N_2, O_2, CO_2, CH_4	150	35	≤60	[69]
Bisphenol-A polyarylate	CO_2, CH_4	184	35	≤16	[70]
Tetramethylbisphenol-A PC[b]	He, N_2, O_2, CO_2, CH_4	193	35	≤60	[69]
Hexafluorobisphenol-A PC[b]	He, N_2, O_2, CO_2, CH_4	176	35	≤60	[69]
Tetramethylhexafluoro-bisphenol-A PC[b]	He, N_2, O_2, CO_2, CH_4	208	35	≤60	[69]

NR, not reported in cited reference.
[a]Value of T_g not from cited reference.
[b]PC, polycarbonate.

TABLE 61.6. *Cellulose and cellulose derivatives.*

Polymer	Gases and vapors	T_g(°C)	Temperature (°C)	Pressure (atm.)	Ref.
Cellulose	H_2, N_2, O_2, CO_2, SO_2, H_2S, NH_3	− 30 to 160[a]	25	NR	[71]
Cellulose acetate	Ar, Kr, Xe, N_2, O_2, CO_2	NR	−5 to 85	≤1	[72]
Cellulose acetate	N_2, O_2, CO_2	NR	30	≤ 1	[45]
Cellulose acetate	He, N_2, CO_2, CH_4	NR	20–80	≤ 100	[62]
Cellulose acetate (DS = 1.75)[b]	He, H_2, N_2, O_2, CO_2, CH_4	205–212	35	≤30	[73]
Cellulose acetate (DS = 2.45)[b]	He, H_2, N_2, O_2, CO_2, CH_4	187, 198	35	≤30	[73]
Cellulose acetate (DS = 2.84)[b]	He, H_2, N_2, O_2, CO_2, CH_4	185, 187	35	≤30	[73]
Cellulose nitrate	Ar, N_2, O_2, CO_2, SO_2	53[a], 66[a]	25	NR	[71]
Ethyl cellulose	N_2, O_2, CO_2	43[a]	30	≤1	[45]
Ethyl cellulose (DS = 2.3–2.4)[b]	He, N_2, O_2, CO_2, CH_4	113–115	35	4–13.6	[74]
Ethyl cellulose (DS = 2.41–2.51)[b]	He, N_2, O_2, CO_2, CH_4	113–115	35	4–13.6	[74]
Ethyl cellulose (DS = 2.55+)[b]	He, N_2, O_2, CO_2, CH_4	128–133	35	4–13.6	[74]
Trifluoroacetylated ethyl cellulose	N_2, O_2	≅ 135	20	1.58–2.37	[75]

NR, not reported in cited reference.
[a]Value of T_g not from cited reference.
[b]DS, degree of substitution.

TABLE 61.7. *Fluoropolymers.*

Polymer	Gases and vapors	T_g(°C)	Temperature (°C)	Pressure (atm.)	Ref.
Polytetrafluoroethylene	H_2, N_2, O_2, CO_2, NO_2, N_2O_4	−73[a]	25	1	[76]
Poly(tetrafluoroethylene-*co*-hexafluoropropylene) (Teflon-FEP)™	CH_4, C_2H_6, C_3H_8, C_4H_10	NR	90	NR	[77]
Poly(trifluorochloroethylene)	N_2, O_2, CO_2, CH_4, C_2H_4, C_2H_6, C_3H_8	NR	25	1	[78]
(Kel-F)™	N_2, O_2, CO_2, H_2O	NR	25–30	NR	[59]

NR, not reported in cited reference.
[a]Value of T_g not from cited reference.

TABLE 61.8. *Polyorganosiloxanes.*

Polymer	Gases and vapors	T_g(°C)	Temperature (°C)	Pressure (atm.)	Ref.
Polydimethylsiloxane	He, Ar, Ne, Kr, Xe,H_2, N_2, O_2, *n*-C_4H_10	−123[a]	−78 to 0	NR	[79]
	He, N_2, O_2, CO_2, CH_4, C_2H_4, C_2H_6, C_3H_8	−123	10–55	1–9	[80]
	N_2, O_2	−123	30	NR	[81]
	NH_3	−123	10–55	1–7.8	[82]
	H_2	−123	10–55	1–6.8	[83]
Poly(methylethylsiloxane)	He, N_2, O_2, CO_2, CH_4, C_2H_4, C_2H_6, C_3H_8	−135	10–55	1–9	[80]
	N_2, O_2	−135	30	NR	[81]
	NH_3	−135	10–55	1–7.8	[82]
	H_2	−135	10–55	1–6.8	[83]
Poly(methylpropylsiloxane)	He, N_2, O_2, CO_2, CH_4, C_2H_4, C_2H_6, C_3H_8	−120	10–55	1–9	[80]
	N_2, O_2	−120	30	NR	[81]
	NH_3	−120	10–55	1–7.8	[82]
	H_2	−120	10–55	1–6.8	[83]
Poly(methyloctylsiloxane)	He, N_2, O_2, CO_2, CH_4, C_2H_4, C_2H_6, C_3H_8	−92	10–55	1–9	[80]
	N_2, O_2	−92	30	NR	[81]
	NH_3	−92	10–55	1–7.8	[82]
	H_2	−92	10–55	1–6.8	[83]
Poly(trifluoropropylmethylsiloxane)	He, N_2, O_2, CO_2, CH_4, C_2H_4, C_2H_6, C_3H_8	−70	10–55	1–9	[80]
	N_2, O_2	−70	30	NR	[81]
	NH_3	−70	10–55	1–7.8	[82]
	H_2	−70	10–55	1–6.8	[83]

TABLE 61.8. *Continued.*

Polymer	Gases and vapors	T_g(°C)	Temperature (°C)	Pressure (atm.)	Ref.
Poly(phenylmethylsiloxane)	He, N_2, O_2, CO_2, CH_4, C_2H_4, C_2H_6, C_3H_8	−28	10–55	1–9	[80]
	N_2, O_2	−28	30	NR	[81]
	NH_3	−28	10–55	1–7.8	[82]
	H_2	−28	10–55	1–6.8	[83]
Poly(dimethylsilmethylene)	He, N_2, O_2, CO_2, CH_4, C_2H_4, C_2H_6, C_3H_8	−92	10–55	1–9	[80]
	N_2, O_2	−92	30	NR	[81]
	NH_3	−92	10–55	1–7.8	[82]
	H_2	−92	10–55	1–6.8	[83]
Poly(silethylenesiloxane)	He, N_2, O_2, CO_2, CH_4, C_2H_4, C_2H_6, C_3H_8	−88	10–55	1–9	[80]
	N_2, O_2	−88	30	NR	[81]
	NH_3	−88	10–55	1–7.8	[82]
	H_2	−88	10–55	1–6.8	[83]
Poly(silhexylenesiloxane)	He, N_2, O_2, CO_2, CH_4, C_2H_4, C_2H_6, C_3H_8	−90	10–55	1–9	[80]
	N_2, O_2	−90	30	NR	[81]
	NH_3	−90	10–55	1–7.8	[82]
	H_2	−90	10–55	1–6.8	[83]
Poly(siloctylenesiloxane)	He, N_2, O_2, CO_2, CH_4, C_2H_4, C_2H_6, C_3H_8	−88	10–55	1–9	[80]
	N_2, O_2	−88	30	NR	[81]
Poly(*m*-silphenylenesiloxane)	He, N_2, O_2, CO_2, CH_4, C_2H_4, C_2H_6, C_3H_8	−48	10–55	1–9	[80]
	N_2, O_2	−48	30	NR	[81]
	NH_3	−48	10–55	1–7.8	[82]
	H_2	−48	10–55	1–6.8	[83]
Poly(*p*-silphenylenesiloxane)	He, N_2, O_2, CO_2, CH_4, C_2H_4, C_3H_8	−18	10–55	1–9	[80]
	N_2, O_2	−18	30	NR	[81]
	NH_3	−18	10–55	1–7.8	[82]

NR, not reported in cited reference.
[a]Value of T_g not from cited reference.

TABLE 61.9. *Polynitriles.*

Polymer	Gases and vapors	T_g(°C)	Temperature (°C)	Pressure (atm.)	Ref.
Polyacrylonitrile	He, Ne, Ar, Kr, N_2, Kr, N_2, O_2,CO_2	95	25–135	NR	[84]
	CO_2	95	35–55	5–13	[85]
	H_2O	NR	15–45	0–0.8[b]	[86]
Polyacrylonitrile (Barex™)	O_2, CO_2, H_2O	NR	25–38	NR	[54]
Poly(methacrylonitrile)	O_2,H_2O	120[a]	25	NR	[53]
	O_2, CO_2, H_2O	NR	25–38	NR	[54]

NR, not reported in cited reference.
[a]Value of T_g not from cited reference.
[b]Relative vapor pressure.

TABLE 61.10. *Polyamides.*

Polymer	Gases and vapors	T_g (°C)	Temperature (°C)	Pressure (atm.)	Ref.
Nylon 6	N_2, O_2, CO_2	40[a]	0–90	NR	[87]
	N_2, O_2, CO_2, H_2O	NR	25–30	NR	[59]
	H_2S	NR	0–80	0.25–1	[88]
Nylon 6,6	H_2O	42 (at 0.0% RH)	25–45	30–90% RH	[89]
	CO_2	50[a]	25	NR	[90]
	H_2O	NR	10–100	10–90% RH	[61]
Nylon 11	He, Ne, Ar, H_2, N_2, CO_2	42–92[a]	≤60	0.04–0.2	[91]
Pendent phenyl-substituted aromatic polyamides	He, H_2, N_2, O_2, CO_2, CH_4	297–328	35	≤20	[92]

NR, not reported in cited reference.
[a]RH, relative humidity.
Value of T_g not from cited references.

TABLE 61.11. *Polyimides.*

Polymer	Gases and vapors	T_g (°C)	Temperature (°C)	Pressure (atm.)	Ref.
PMDA-ODA	N_2, O_2	410	25	NR	[93]
	CO_2	420	35–80	10–20	[94]
	He, N_2, O_2, CO_2, CH_4	NR	35	2–10	[95]
	CO_2	NR	60	2.7–16.3	[96]
	N_2, O_2	410	25–40	NR	[93]
PMDA-MDA	He, N_2, O_2, CO_2, CH_4	338	35	2–10	[95]
PMDA-IPDA	He, N_2, O_2, CO_2, CH_4	NR	35	2–10	[95]
PMDA-3-BDAF	H_2, N_2, O_2, CO_2, CH_4	235	35	2–9	[97]
PMDA-4-BDAF	H_2, N_2, O_2, CO_2, CH_4	310	35	2–9	[97]
BPDA-ODA	H_2, N_2, O_2, CO, CO_2, CH_4	270	35	2–10	[98]
	CO_2	270	80	2–28	[99]
	H_2, CO, CO_2, CH_4	270	50	10	[100]
	H_2, CO, CO_2, CH_4	270	50	10	[101]
BPDA-MDA	H_2, CO, CO_2, CH_4	300	35	10	[98]
	H_2, CO, CO_2, CH_4	300	≦120	10	[101]
BTDA-ODA	H_2, N_2, O_2, CO, CO_2, CH_4	266	35	2–10	[98]
BTDA-DATPA	H_2, N_2, O_2, CO, CO_2, CH_4	292	35	2–10	[98]
6FDA-*p*-ODA	H_2, N_2, CO_2, CH_4	299	25	1	[98]
	CO_2, CH_4	293	25	4.87	[102]
	H_2, N_2, O_2, CO_2, CH_4	288	35	2–9	[97]
6FDA-*m*-PDA	H_2, N_2, O_2, CO, CO_2, CH_4	298	35–80	2–10	[103]
	H_2, N_2, O_2, CO_2, CH_4	285	35	1.4–8.2	[104]
6FDA-*m*-ODA	H_2, N_2, O_2, CO_2, CH_4	244	35	2–9	[97]
6FDA-*p*-PDA	H_2, N_2, O_2, CO, CO_2, CH_4	351	35–80	2–10	[103]
	CO_2, CH_4	342	25	4.87	[102]
	H_2, N_2, O_2, CO_2, CH_4	305	35	2–9	[97]
6FDA-3,4′-ODA	CO_2, CH_4	248	25	4.87	[102]
6FDA-IPDA	CO_2, CH_4	298	25	4.87	[102]
6FDA-4-BDAF	H_2, N_2, O_2, CO_2, CH_4	262	35	2–9	[97]
6FDA-2,4-DATr	H_2, N_2, O_2, CO_2, CH_4	342	35	1–7	[104]
6FDA-2,6-DATr	H_2, N_2, O_2, CO_2, CH_4	372	35	1–7	[104]
6FDA-3,5-DBTF	H_2, N_2, O_2, CO_2, CH_4	284	35	1–7	[104]
6FDA-3-BDAF	H_2, N_2, O_2, CO_2, CH_4	224	35	2–9	[97]
6FDA-based polyimides	C_2H_4, C_2H_6, C_3H_6, C_3H_8	305–320	35	17	[105]
	C_3H_6, C_3H_8	217–406	25	1.12–10.3	[106]
	1,3-butadiene, *n*-butane	237–376	25	1.1–2	[107]
Indan-containing	H_2, N_2, O_2, CO_2	232–274	22.5	1.23	[108]
polyimides	N_2, O_2, CO_2, CH_4	NR	35	10	[109]
Aromatic polyimides	He, N_2, O_2, CO_2, CH_4	253–265	30	3	[110]
	H_2O	262–452	85–135	0.197–0.622	[111]
Aromatic polyimides (contains also references to other polyimides)	N_2, O_2	246–304	35	NR	[112]
6FDA-Durene polyimides	He, H_2, N_2, O_2, CO_2, CH_4	NR	35	2–10	[113]
Fluorinated 6FDA-based polyimides	C_3H_6	300–406	25	2–10	[114]
Polyimides with fluorinated side-groups	N_2, O_2, CO_2, CH_4	200–301	25	5	[115]
6FDA-based polyimide	He, N_2, O_2, CO_2, CH_4	NR	30–50	3.5–20	[116]
	C_2H_4, C_2H_6, C_3H_6, C_3H_8	NR	35	C_2's: 2.5–16 C_3's: 2.0–8.4	[117]
	N_2, O_2, CO_2, CH_4	336	30–50	3.5–20	[118]
	He, H_2, N_2, O_2, CO_2, CH_4	NR	35	10	[119]
Thianthrene-5,5,10,10-tetraoxide-containing polyimides	H_2, N_2, O_2, CO_2, CH_4	NR	35	2[a]	[120]
Hyperbranched polyimides	He, H_2, O_2, CO_2, CH_4	339[b]	35	1	[121]
Poly(amide imide)s	N_2, O_2, CO_2, CH_4	237–350	35–75	1–20	[122]
PMDA-, BPDA-, and DSDA-based polyimides	H_2O	NR	85	0.395	[123]
Poly(phenylene thioether imide)s	N_2, O_2, CO_2, CH_4	216–292	35	1–10	[124]

NR, not reported in cited reference.
[a] TADATO/DSDA (1/1)-DDBT; N_2, CO_2, CH_4: 1–10 atm.
[b] Uncrosslinked 6FDA-TAPA.

TABLE 61.12. *Polyurethanes.*

Polymer	Gases and vapors	T_g (°C)	Temperature (°C)	Pressure (atm.)	Ref.
Polyurethane	N_2, O_2	−22 to −64[a]	25	NR	[125]
	N_2, O_2	−0.7 to −64[a]	25	NR	[126]
Amine-containing polyurethane and poly(urethane urea)	He, H_2, N_2, O_2, CO_2, CH_4	−18 to 27	35	10	[127]

NR, not reported in cited reference.
[a]Value of T_g not from cited reference.

TABLE 61.13. *Polyoxides.*

Polymer	Gases and vapors	T_g (°C)	Temperature (°C)	Pressure (atm.)	Ref.
Poly(ethylene oxide)	He, H_2, N_2, O_2, CO_2, C_2H_4, C_2H_6, C_3H_6, C_3H_8	−50[a]	25–45	4.4–14.6	[128]
Poly(phenylene oxide)	CH_4, C_2H_4, C_2H_6	NR	25	4.93	[129]
	CO_2	NR	35	1–25	[56]
	N_2, O_2, CO_2, CH_4	214	35	1	[130]
Sulfonated poly(phenylene oxide)	H_2, N_2, O_2, CO_2	NR	23–24	6.58	[131]
2,6-Dimethyl-1,4-poly(phenylene oxide)	CO_2, CH_4	210	35	1–25	[132]
2,6-Dimethyl-1,4-poly(phenylene oxide) bromide (36% Br)	CO_2, CH_4	233	35	1–25	[132]
2,6-Dimethyl-1,4-poly(phenylene oxide) bromide (bromide-91%)	CO_2, CH_4	262	35	1–25	[132]

NR, not reported in cited reference.
[a]Value of T_g not from cited reference.

TABLE 61.14. *Polysulfones.*

Polymer	Gases and vapors	T_g (°C)	Temperature (°C)	Pressure (atm.)	Ref.
Polysulfone	H_2	190	40	4–27	[133]
	He, N_2, O_2, CO_2, CH_4	186	35	1–20	[134]
Bisphenol-A polysulfone	He, Ar, CO_2, CH_4	185	35	1–20	[135]
	CO_2, CH_4	186	35	1–14	[70]
Polyethersulfone	N_2, O_2, CO_2	225	30	≤30	[136]
Polyarylether sulfone	H_2, He, Ar, N_2, O_2, CO, CO_2, CH_4	260	25–160	NR	[137]
Tetramethyl bisphenol-A polysulfone	He, N_2, O_2, CO_2, CH_4	230	35	1–20	[134]
Polysulfone[a] and polysulfones with pendent groups	N_2, O_2, CO_2	188.1[a]	35	1	[138]
Polysulfones with trimethylsilyl groups	N_2, O_2	155–165	35	1	[139]
Silyl-modified polysulfones and poly(phenyl sulfones)	N_2, O_2, CO_2	149–280	35	1	[140]
	H_2, N_2, O_2, CO_2, CH_4	117–225	35	1	[141]

NR, not reported in cited reference.
[a]Value of T_g not from cited reference.

TABLE 61.15. *Polyacetylenes.*

Polymer	Gases and vapors	T_g (°C)	Temperature (°C)	Pressure (atm.)	Ref.
Poly(1-trimethylsilyl-1-propyne) (PTMSP)	H_2, Xe, N_2, O_2, H_2O, SF_6, N_2O, CH_3OH, CH_4, C_2H_2, C_2H_6, C_3H_8, *n*-C_4H_{10}, *i*-C_4H_{10}	230	22	0–1	[142]
	N_2, O_2, CO_2, CH_4	200	35	1–27	[143]
	N_2, O_2, CO_2, CH_4, H_2O, CH_2Cl_2, dimethylketone, toluene	NR	Gases: 20–70 Vapors: 40–65	Gases: 0.987 Vapor activity: 0.02–0.1	[144]
	H_2, N_2, O_2, CO_2, CH_4, C_2H_6, C_3H_8, CF_4, C_2F_6, C_3F_8	NR	35	2–17; $C_3H_8 \leq 4.5$; $C_3F_8 \leq 9$	[145]
	Ethylbenzene	NR	35–55	VP: 1.64–4.40 cmHg	[146]
Poly(1-trimethylgermyl-1-propyne) (PTMGP)	H_2, N_2, O_2, CO_2, CH_4, C_3H_8,*n*-C_4H_{10}	>250	35	4.4 *n*-C_4H_{10}: 1.7	[147]
Poly(*tert*-butylacetylene)	He, H_2, N_2, O_2, CO_2, CH_4	>200	25	1	[148]
Poly(1-chloro-2-phenylacetylene)	He, H_2, N_2, O_2, CO_2, CH_4	>200	25	1	[148]
Substituted polyacetylenes	He, N_2, O_2, CO_2, CH_4	NR	25	NR	[149]
Highly branched substituted polyacetylenes	He, H_2, N_2, O_2, CO_2, CH_4, C_2H_6, C_3H_8, n-C_4H_{10}	>270 to >430	35	4.4 *n*-C_4H_{10}: 1.7	[150]
Poly(diphenylacetylene)s	He, N_2, O_2, CO_2, CH_4	NR	25	NR	[66]
Poly[1-phenyl-2-[*p*-(triisopropylsilyl) phenyl acetylene]	He, H_2, N_2, O_2, CO_2, CH_4, C_2H_6, C_3H_8, n-C_4H_{10}	NR	35	4.4 *n*-C_4H_{10}: 1.7	[151]

NR, not reported in cited references
VP, vapor pressure.

TABLE 61.16. *Polyacrylics.*

Polymer	Gases and vapors	T_g (°C)	Temperature (°C)	Pressure (atm.)	Ref.
Poly(methyl methacrylate)	He, Ar, H_2, N_2, O_2, CO_2, CH_4	106	35	1	[152]
Poly(ethyl methacrylate)	He, Ne, Ar, Kr, N_2, O_2, CO_2, H_2S, H_2O	66[a]	25–85	NR	[153]
	Ar, N_2, O_2, CO_2, CH_4	69	35	0–35	[154]

NR, not reported in cited reference.
[a]Value of T_g not from cited reference.

TABLE 61.17. *Miscellaneous polymers.*

Polymer	Gases and vapors	T_g (°C)	Temperature (°C)	Pressure (atm.)	Ref.
Poly(ether ketone)s with indan groups in main chain	H_2, N_2, O_2, CO_2	218–255	22.5	1.23	[155]
Poly(3-dodecylthiophene)	N_2, O_2, CO_2	−20	35–37	1.45	[156]
Polyphosphazenes	H_2, N_2, O_2, CO_2, CH_4, C_2H_6, C_3H_8	−82 to −66	35	13.6 C_3H_8: 2.72	[157]
Poly(lactic acid)	He, H_2, N_2, O_2, CO_2, CH_4	−81 to 4	30	2.04	[158]
	N_2, O_2, CO_2, CH_4	58	30	2.63[a]	[159]
Polyarylates	H_2O	183–261	40	Vapor activity: 0–0.8	[160]
Poly(arylene ether)s	H_2, N_2, O_2, CO_2, CH_4	119–155	30–75	1	[161]
Poly(aryl ether ketone)s	He, N_2, O_2, CO_2, CH_4	175–203	30	3	[162]
Bis(phenyl)fluorene-based cardo polymers	N_2, CO_2	150–492	25	1	[163]
Cardo poly(arylether)s	H_2, N_2, O_2, CO_2, CH_4	218–289	30–100	NR	[164]
Oxyalkylenes with alkylsulfonylmethyl side chains	O_2	37–126	30	3.26	[165]

TABLE 61.17. *Continued.*

Polymer	Gases and vapors	T_g(°C)	Temperature (°C)	Pressure (atm.)	Ref.
Poly(arylene ether ketone)s	He, N_2, O_2, CO_2, CH_4	159–260	35	1.70–13.6	[166]
Polynorbornenes with aliphatic pendant groups	He, H_2, N_2, O_2, CO_2, CH_4	150–>380	35	10	[167]
ROMP polymers from silyl-substituted norbornadienes and norbornenes	He, H_2, N_2, O_2, CO_2, CH_4, C_2H_6	85–167	22	0.1–1	[168]
Alkyl-substituted poly(norbornene)	H_2O, Methanol	150–380	30	Vapor activity: 1	[169]
Polypyrrolones	He, N_2, O_2, CO_2, CH_4	NR	35–80	He, N_2, CO_2, CH_4: 3–10; O_2: 3–7	[170]
Poly(4-vinylpyridine)	He, H_2, N_2, O_2, CO_2, CH_4	158–162	35	3.3–10.5	[171]
Poly(ethylene-2,6-naphtalene dicarboxylate) (PEN)	H_2, CO_2	≈ 124 (Amorphous PEN)	20	2.96	[172]
Poly(oxyethylene)s with (alkylsulfonyl)methyl side chains	O_2	37–57	30	2.96[b]	[173]
Cardo poly(aryl ether ketone)s with pendent groups	H_2, N_2, O_2, CO_2, CH_4	239–266	25–100	5	[174]
Ladder polymer BBL and some semiladder polymers	He, N_2, O_2, CO_2, CH_4	NR	35–80	10	[175]
PIM-1, PIM-7 (Polymers of intrinsic porosity)	He, Ar, Xe, H_2, N_2, O_2, CO_2, CH_4	≥ 350	30	0.14–0.89	[176]

NR, not reported in cited reference; RH, relative humidity.
[a]Partial pressure difference.
[b]Pressure difference.

REFERENCES

1. R. M. Barrer, in *Permeability of Plastic Films and Coating to Gases, Vapors, and Liquids*, edited by H. P. Hopfenberg (Plenum Press, New York, 1974), p. 113.
2. W. R. Vieth, *Diffusion in and Through Polymers* (Hanser, Munich, 1991).
3. J. Crank, *The Mathematics of Diffusion* (Clarendon Press, Oxford, 1975).
4. S. A. Stern and H. L. Frisch, Annu. Rev. Mater. Sci. 11, 523 (1981).
5. H. L. Frisch and S. A. Stern, Crit. Rev. Solid State Mater. Sci. 11, 123 (1983).
6. W. J. Koros and R. T. Chern, in *Handbook of Separation Processes*, edited by R. W. Rousseau (Wiley-Interscience, New York, 1987), p. 862.
7. S. A. Stern and S. Trohalaki, in *Barrier Polymers and Structures*, edited by W. J. Koros, ACS Symposium Series No. 423 (American Chemical Society, Washington, DC, 1990), p. 22.
8. S. Kimura and T. Hirose, in *Polymers for Gas Separation*, edited by N. Toshma (VCH, New York, 1992), p. 15.
9. S. A. Stern, J. Membr. Sci. 94, 1 (1994).
10. R. M. Barrer, in *Diffusion in Polymers*, edited by J. Crank and G. S. Park (Academic Press, New York, 1968), p. 165.
11. G. S. Park, in *Diffusion in Polymers*, edited by J. Crank and G. S. Park (Academic Press, New York, 1968), p. 141.
12. V. Stannett, H. B. Hopfenberg, and J. H. Petropoulos, in *Macromolecular Science NTP International Review*, edited by C. E. H. Bawn (Butterworth, London, 1972), vol. 8, p. 329.
13. H. B. Hopfenberg and V. T. Stannett, in *The Physics of Glassy Polymers*, edited by R. N. Haward (Wiley, New York, 1973), p. 504.
14. J. H. Petropoulos and P. P. Roussis, in *Permeability of Plastic Films and Coatings to Gases, Vapors and Liquids*, edited by H. B. Hopfenberg (Plenum Press, New York, 1974), p. 219.
15. H. L. Frisch, J. Polym. Eng. 20, 2 (1980).
16. C. J. Durning, J. Polym. Sci., Polym. Phys. 23, 1831 (1985).
17. J. H. Petropoulos, in *Polymeric Gas Separation Membranes*, edited by D. R. Paul and Y. P. Yamkpol'skii (CRC Press, Boca Raton, 1994), p. 17.
18. C. A. Kumins and T. K. Kwei, in *Diffusion in Polymers*, edited by J. Crank and G. S. Park (Academic Press, New York, 1968), p. 108.
19. H. Sun, J. Phys. Chem. B 38, 7338 (1998).
20. H. Sun, P. Ren, and J. R. Fried, Comput. Theor. Polym. Sci. 8, 229 (1998).
21. A. S. Gusev, F. Müller-Plathe, and W. F. van Gunsteren, Adv. Polym. Sci. 116, 207 (1994).
22. F. Müller-Plathe, Acta Polym. 45, 259 (1994).
23. D. N. Theodorou, in *Diffusion in Polymers*, edited by P. Neogi (Marcel Dekker, Inc., New York, 1996).
24. J. R. Fried, in *Materials Science of Membranes for Gas and Vapor Separations*, edited by Y. Yampolskii, I. Pinnau, and B. D. Freeman (John Wiley & Sons, Ltd, West Sussex, UK, 2006), p. 93.
25. G. S. Heffelfinger and F. von Swol, J. Chem. Phys. 100, 7548 (1994).
26. A. Thompson and G. S. Heffelfinger, J. Chem. Phys. 110, 10693 (1999).
27. S. Pauly, in *Polymer Handbook*, edited by J. Brandrup and E. H. Immergut (Wiley-Interscience, New York, 1968), p. VI/435.
28. S. T. Hwang, C. K. Choi, and K. Kammermeyer, Sep. Sci. 9, 461 (1974).
29. V. T. Stannett, W. J. Koros, D. R. Paul, *et al*., Polym. Sci. 32, 69 (1979).
30. W. J. Koros, ed. *Barrier Polymers and Structures*. ACS Symposium Series. No. 423 (American Chemical Society, Washington, DC, 1990).
31. *Permeability Data for Aerospace Applications*, NAS1-388 (IIT Research Institute, Chicago, IL, March, 1968).
32. W. J. Koros, M. R. Coleman, and D. R. B. Walker, Annu. Rev. Mater. Sci. 22, 47 (1992).
33. W. J. Koros, G. K. Fleming, S. M. Jordan, *et al*., Prog. Polym. Sci. 13, 339 (1988).

34. R. R. Zolandz and G. K. Fleming, in *Membrane Handbook*, edited by W. S. W. Ho and K. K. Sirkar (Nostrand Reinhold, New York, 1992), p. 25.
35. M. Salame, in *The Wiley Encyclopedia of Packaging Technology*, edited by M. Bakker (Wiley, New York, 1986), p. 48.
36. G. S. Patil, M. Bora, and N. N. Dutta, J. Membr. Sci. 101, 145 (1995).
37. J. Y. Park and D. R. Paul, J. Membr. Sci. 125, 23 (1997).
38. L. M. Robeson, C. D. Smith, and M. Langsam, J. Membr. Sci. 132, 33 (1997).
39. Y. Yampol'skii, S. Shishatskii, A. Alientiev, *et al*., J. Membr. Sci. 148, 59 (1998).
40. Y. Yampol'skii, S. Shishatskii, A. Alientiev, *et al*., J. Membr. Sci. 149, 203 (1998).
41. A. Alentiev, K. A. Loza, and Y. P. Yampol'skii, J. Membr. Sci. 167, 91 (2000).
42. A. S. Michaels and A. J. Bixler, J. Polym. Sci. 50, 413 (1961).
43. S. A. Stern, S. R. Sampat, and S. S. Kulkarni, J. Polym. Sci., Part B: Polym. Phys. 24, 2149 (1986).
44. S. A. Stern, S. M. Fang, and R. M. Jobbins, J. Macromol. Sci. B5, 41 (1971).
45. A. W. Myers, C. E. Rogers, V. Stannett, *et al*., in *Proceedings of the 13th Annual Technical Conference, Society of Plastics Engineers*, St. Louis, Missouri, 1957.
46. Y. Naito, K. Mizoguchi, K. Terada, *et al*., J. Polym. Sci., Part B: Polym. Phys. 29, 457 (1991).
47. C. L. Kiplinger, D. F. Persico, R. J. Lagow, *et al*., J. Appl. Polym. Sci. 31, 2617 (1986).
48. G. J. van Amerongen, J. Appl. Phys. 17, 972 (1946).
49. J. Y. Lai and G. J. Wu, J. Appl. Polym. Sci. 34, 559 (1987).
50. A. K. Taraiya, G. A. Orchard, and I. M. Ward, J. Appl. Polym. Sci. 41, 1659 (1990).
51. K. Toi, Polym. Eng. Sci. 20, 30 (1980).
52. B. P. Tikhomorov, H. B. Hopfenberg, V. Stannett, *et al*., Makromol. Chem. 118, 177 (1968).
53. M. Salame, in *Proceedings of the Polymers, Laminations, and Coatings Conference*, Nashville, TN, 1986, p. 363.
54. M. Salame, in *Proceedings of the ACS 164th Meeting*, 1972, p. 113.
55. K. Toi, Y. Maeda, and T. Tokuda, J. Membr. Sci. 13, 15 (1983).
56. G. Morel and D. R. Paul, J. Membr. Sci. 10, 273 (1982).
57. J. A. Barrie and K. Munday, J. Membr. Sci. 13, 175 (1983).
58. H. Yasuda and K. Rosengren, J. Appl. Polym. Sci. 14, 2839 (1970).
59. A. W. Myers, V. Tammela, V. Stannett, *et al*., Mod. Plast. 37, 139 (1960).
60. J. M. Mohr and D. R. Paul, J. Appl. Polym. Sci. 42, 1711 (1991).
61. A. W. Myers, J. A. Meyer, C. E. Rogers, *et al*., TAPPI 44, 58 (1961).
62. N. Choji, W. Pusch, M. Satoh, *et al*., Desalination 53, 347 (1985).
63. R. Cowling and G. S. Park, J. Membr. Sci. 5, 199 (1979).
64. J. A. Barrie, P. Sagoo, and A. J. Thomas, J. Membr. Sci. 43, 229 (1989).
65. G. J. van Amerongen, J. Polym. Sci. 2, 381 (1987).
66. W. J. Koros and D. R. Paul, J. Polym. Sci., Polym. Phys. 16, 2171 (1978).
67. P. Mercea, T. Virag, and D. Silipas, Polym. Commun. 28, 31 (1987).
68. A. G. Wonders and D. R. Paul, J. Membr. Sci. 5, 63 (1979).
69. M. W. Hellums, W. J. Koros, G. R. Husk, *et al*., J. Membr. Sci. 46, 93 (1989).
70. T. A. Barbari, W. J. Koros, and D. R. Paul, J. Membr. Sci. 42, 69 (1989).
71. V. L. Simril and A. Hershberger, Mod. Plast. 27, 95 (1950).
72. S. A. Stern, S. K. Sen, and A. K. Rao, J. Macromol. Sci.—Phys. B10, 507 (1974).
73. A. C. Puleo, D. R. Paul, and S. S. Kelley, J. Membr. Sci. 47, 301 (1989).
74. A. Y. Houde and S. A. Stern, J. Membr. Sci. 92, 95 (1994).
75. Y. Wang and A. J. Easteal, J. Membr. Sci. 157, 53 (1999).
76. R. A. Pasternak, M. V. Christensen, and J. Heller, Macromolecules 3, 366 (1970).
77. N. Y. Yan, R. M. Felder, and W. J. Koros, J. Appl. Polym. Sci. 25, 1755 (1980).
78. R. A. Pasternak, G. L. Burns, and J. Heller, Macromolecules 4, 470 (1971).
79. R. M. Barrer and H. T. Choi, J. Polym. Sci., Part C: Polym. Symp. 10, 111 (1965).
80. S. A. Stern, V. M. Shah, and B. J. Hardy, J. Polym. Sci., Part B: Polym. Phys. 25, 1263 (1987).
81. C. Lee, H. L. Chapman, M. E. Cifuentes, *et al*., J. Membr. Sci. 38, 55 (1988).
82. S. A. Stern and B. D. Bhide, J. Appl. Polym. Sci. 38, 2131 (1989).
83. B. D. Bhide and S. A. Stern, J. Appl. Polym. Sci. 42, 2397 (1991).
84. S. M. Allen, M. Fuji, V. M. Stannett, *et al*., J. Membr. Sci. 2, 153 (1977).
85. G. S. Huvard, V. T. Stannett, W. J. Koros, *et al*., J. Membr. Sci. 6, 185 (1980).
86. V. T. Stannett, G. R. Ranade, and W. J. Koros, J. Membr. Sci. 10, 219 (1982).
87. R. Waack, N. H. Alex, H. L. Frisch, *et al*., Ind. Eng. Chem. 47, 2524 (1955).
88. W. Heilman, V. Tammela, J. A. Meyer, *et al*., Ind. Eng. Chem. 48, 821 (1956).
89. L.-T. Liu, I. J. Britt, and M. A. Tung, J. Appl. Polym. Sci. 71, 197 (1999).
90. W. W. Brandt, J. Polym. Sci. 41, 415 (1959).
91. R. Ash, R. M. Barrer, and D. G. Palmer, Polymer 11, 421 (1970).
92. A. Singh, K. Ghosal, B. D. Freeman, *et al*., Polymer 40, 5715 (1999).
93. H. Hachisuka, Y. Tsujita, A. Takizawa, *et al*., J. Polym. Sci., Part B: Polym. Phys. 29, 11 (1991).
94. K. J. Okamoto, K. Tanaka, and H. Kita, J. Polym. Sci., Part B: Polym. Phys. 27, 2621 (1989).
95. T. H. Kim, W. J. Koros, G. R. Husk, *et al*., J. Membr. Sci. 37, 45 (1988).
96. R. T. Chern, W. J. Koros, E. S. Sanders, *et al*., J. Membr. Sci. 15, 157 (1983).
97. S. A. Stern, Y. Mi, and H. Yamamoto, J. Polym. Sci., Part B: Polym. Phys. 27, 1887 (1989).
98. K. Okamoto, K. Tanaka, H. Kita, *et al*., Polym. J. 24, 451 (1992).
99. K. Okamoto, K. Tanaka, H. Kita, *et al*., J. Polym. Sci., Part B: Polym. Phys. 27, 1221 (1989).
100. K. Tanaka, H. Kita, K. Okamoto, *et al*., Polym. J. 21, 127 (1989).
101. K. Tanaka, H. Kita, K. Okamoto, *et al*., J. Membr. Sci. 47, 203 (1989).
102. K. Matsumoto and P. Xu, J. Membr. Sci. 81, 23 (1993).
103. K. Tanaka, M. Okano, H. Toshino, *et al*., J. Polym. Sci., Part B: Polym. Phys. 30, 907 (1992).
104. H. Yamamoto, Y. Mi, S. A. Stern, *et al*., J. Polym. Sci., Part B: Polym. Phys. 28, 2291 (1990).
105. C. Staudt-Bickel and W. J. Koros, J. Membr. Sci. 170, 205 (2000).
106. A. Shimazu, T. Miyazaki, M. Maeda, *et al*., J. Polym. Sci., Part B: Polym. Phys. 38, 2525 (2000).
107. A. Shimazu, T. Miyazaki, T. Matsushita, *et al*., J. Polym. Sci., Part B: Polym. Phys. 37, 2941 (1999).
108. G. Maier, M. Wolf, M. Bleha, *et al*., J. Membr. Sci. 143, 115 (1998).
109. S. L. Liu, M. L. Chng, T. S. Chung, *et al*., J. Polym. Sci., Part B: Polym. Phys. 42, 2769 (2004).
110. D. Ayala, A. E. Lozano, J. D. Abajo, *et al*., J. Membr. Sci. 215, 61 (2003).
111. J. Huang, R. J. Cranford, T. Matsuura, *et al*., J. Membr. Sci. 215, 129 (2003).
112. Y.-C. Wang, S.-H. Huang, C.-C. Hu, *et al*., J. Membr. Sci. 248, 15 (2005).
113. W.-H. Lin and T.-S. Chung, J. Membr. Sci. 186, 183 (2001).
114. A. Shimazu, T. Miyazaki, S. Katayama, *et al*., J. Polym. Sci., Part B: Polym. Phys. 41, 308 (2003).
115. J.-H. Kim, S.-B. Lee, and S. Y. Kim, J. Appl. Polym. Sci. 77, 2756 (2000).
116. R. Wang, S. S. Chan, Y. Liu, *et al*., J. Membr. Sci. 199, 191 (2002).
117. S. S. Chan, R. Wang, T.-S. Chung, *et al*., J. Membr. Sci. 210, 55 (2002).
118. T.-S. Chung, C. Cao, and R. Wang, J. Polym. Sci., Part B: Polym. Phys. 42, 354 (2004).
119. J. W. Xu, M. L. Chng, and T. S. Chung, Polymer 44, 4715 (2003).
120. L. Yang, J. Fang, and N. Meichin, Polymer 42, 2001 (2001).
121. J. Fang, H. Kita, and K.-i. Okamoto, J. Membr. Sci. 182, 245 (2001).
122. I. Kresse, A. Usenko, J. Springer, *et al*., J. Polym. Sci., Part B: Polym. Phys. 37, 2183 (1999).

123. J. Huang, R. J. Cranford, T. Matsuura, *et al*., J. Appl. Polym. Sci. 87, 2306 (2003).
124. Z.-K. Xu, M. Bohning, J. D. Schultze, *et al*., Polymer 38, 1573 (1997).
125. K. H. Hsieh, C. C. Tsai, and S. M. Tseng, J. Membr. Sci. 49, 341 (1990).
126. K. H. Hsieh, C. C. Tsai, and D. M. Chang, J. Membr. Sci. 56, 279 (1991).
127. L.-S. Teo, C.-Y. Chen, and J.-F. Kuo, J. Membr. Sci. 141, 91 (1998).
128. H. Liu and B. D. Freeman, J. Membr. Sci. 239, 105 (2004).
129. A. A. Lapkin, O. P. Roschupkina, and O. M. Ilinitch, J. Membr. Sci. 141, 223 (1998).
130. G. Perego, A. Roggero, R. Sisto, *et al*., J. Membr. Sci. 55, 325 (1991).
131. B. Kruczek and T. Matsuura, J. Membr. Sci. 146, 263 (1998).
132. R. T. Chern, F. R. Sheu, L. Jia, *et al*., J. Membr. Sci. 35, 103 (1987).
133. E. Sada, H. Kumazawa, P. Xu, *et al*., J. Appl. Polym. Sci. 38, 687 (1989).
134. C. L. Aitken, W. J. Koros, and D. R. Paul, Macromolecules 25, 3424 (1992).
135. A. J. Erb and D. R. Paul, J. Membr. Sci. 8, 11 (1981).
136. H. Kumazawa, J. S. Wang, and E. Sada, J. Polym. Sci., Part B: Polym. Phys. 31, 881 (1993).
137. W. Liu, T. Chen, and J. Xu, J. Membr. Sci. 53, 203 (1990).
138. Y. Dai, M. D. Guiver, G. P. Robertson, *et al*., Macromolecules 36, 6807 (2003).
139. K. J. Lee, J. Y. Jho, Y. S. Kang, *et al*., J. Membr. Sci. 212, 147 (2003).
140. K. J. Lee, J. Y. Jho, Y. S. Kang, *et al*., J. Membr. Sci. 223, 1 (2003).
141. I.-W. Kim, K. J. Lee, J. Y. Jho, *et al*., Macromolecules 34, 2908 (2001).
142. N. A. Platé, A. K. Bokarev, N. E. Kaliuzhnyi, *et al*., J. Membr. Sci. 60, 13 (1991).
143. Y. Ichiraku, S. A. Stern, and T. Nakagawa, J. Membr. Sci. 34, 5 (1987).
144. V. V. Teplyakov, D. Roizard, E. Favre, *et al*., J. Membr. Sci. 220, 165 (2003).
145. T. C. Merkel, V. Bondar, K. Nagai, *et al*., J. Polym. Sci., Part B: Polym. Phys. 38, 273 (2000).
146. S. V. Dixon-Garrett, K. Nagai, and B. D. Freeman, J. Polym. Sci., Part B: Polym. Phys. 38, 1078 (2000).
147. K. Nagai, L. G. Toy, B. D. Freeman, *et al*., J. Polym. Sci., Part B: Polym. Phys. 40, 2228 (2002).
148. K. Takada, H. Matsuya, T. Masuda, *et al*., J. Appl. Polym. Sci. 30, 1605 (1985).
149. M. Teraguchi and T. Masuda, Macromolecules 35, 1149 (2002).
150. T. Kanaya, I. Tsukishi, K. Kaji, *et al*., Macromolecules 35, 5559 (2002).
151. K. Nagai, L. G. Toy, B. D. Freeman, *et al*., J. Polym. Sci., Part B: Polym. Phys. 38, 1474 (2000).
152. K. E. Min and D. R. Paul, J. Polym. Sci., Part B: Polym. Phys. 26, 1021 (1988).
153. V. Stannett and J. L. Williams, J. Polym. Sci., Part C: Polym. Symp. 10, 45 (1965).
154. J. S. Chiou and D. R. Paul, J. Membr. Sci. 45, 167 (1989).
155. G. Maier, M. Wolf, M. Bleha, *et al*., J. Membr. Sci. 143, 105 (1998).
156. I. H. Musselman, L. Li, L. Washmon, *et al*., J. Membr. Sci. 152, 1 (1999).
157. K. Nagai, B. D. Freeman, A. Cannon, *et al*., J. Membr. Sci. 172, 167 (2000).
158. C. J. Orme, M. K. Harrup, T. A. Luther, *et al*., J. Membr. Sci. 186, 249 (2001).
159. H. J. Lehermeier, J. R. Dorgan, and J. D. Way, J. Membr. Sci. 190, 243 (2001).
160. A. J. Kelkar and D. R. Paul, J. Membr. Sci. 181, 199 (2001).
161. Z.-K. Xu, C. Dannenberg, J. Springer, *et al*., J. Membr. Sci. 205, 23 (2002).
162. C. Garcia, P. Tiemblo, A. E. Lozano, *et al*., J. Membr. Sci. 205, 73 (2002).
163. S. Kazama, T. Teramoto, and K. Haraya, J. Membr. Sci. 207, 91 (2002).
164. Z. Wang, T. Chen, and J. Xu, J. Appl. Polym. Sci. 83, 791 (2002).
165. J.-C. Lee, M. H. Litt, and C. E. Rogers, J. Polym. Sci., Part B: Polym. Phys. 36, 75 (1998).
166. Z. Y. Wang, P. R. Moulinie, and Y. P. Handa, J. Polym. Sci., Part B: Polym. Phys. 36, 425 (1998).
167. K. D. Dorkenoo, P. H. Pfromm, and M. E. Rezac, J. Polym. Sci., Part B: Polym. Phys. 36, 797 (1998).
168. E. S. Finkelshtein, M. L. Gringolts, N. V. Ushakov, *et al*., Polymer 44, 2843 (2003).
169. S. R. Thrasher and M. E. Rezac, Polymer 45, 2641 (2004).
170. C. M. Zimmerman and W. J. Koros, J. Polym. Sci., Part B: Polym. Phys. 37, 1235 (1999).
171. J.-J. Shieh and T. S. Chung, J. Polym. Sci., Part B: Polym. Phys. 37, 2851 (1999).
172. L. Hardy, E. Espuche, G. Seytre, *et al*., J. Appl. Polym. Sci. 89, 1849 (2003).
173. S.-Y. Kwak and J.-C. Lee, Macromolecules 33, 8466 (2000).
174. Z. Wang, T. Chen, and J. Xu, Macromolecules 33, 5672 (2000).
175. C. M. Zimmerman and W. J. Koros, Polymer 40, 5655 (1999).
176. P. M. Budd, K. J. Msayib, C. E. Tattershall, *et al*., J. Membr. Sci. 251, 263 (2005).

CHAPTER 62

Definitions

Ping Xu

W. L. Gore & Associates, Inc., Cherry Hill Division, 2401 Singerly Road, P.O. 1220, Elkton, MD 21922–1220

Adherend A body that is held to another body by adhesion.

Adhesion The state in which two surfaces are held together by interfacial forces of attraction.

Adhesive An adhesive is a linear or branched amorphous polymer applied in a fluid state. It must contain molecular moieties that are attracted to each of two surfaces being joined together.

Aging A long-term deleterious change in properties of a polymer composition during its service life.

Amorphous Orientation Oriented amorphous regions in a polymeric material where shear, etc., have caused elongational flow.

Amorphous Polymer A polymer in which the molecular chains exist in the random coil conformation since there is no regular three-dimensional arrangement of molecules or subunits of molecules extending over distances that are large compared to atomic dimensions, i.e., there is no long-range order. There is no crystallinity in an amorphous polymer.

Amorphous Region A region in a material or a portion of a property versus temperature curve in which the polymer chains exist in the random coil conformation.

Anelastic Mechanical behavior in which the stress and strain are not single-valued functions of each other. This occurs particularly when a periodic stress is applied due to internal friction in a viscoelastic material.

Anisotropy The dependence of the properties of a material on the direction in which they are being observed. In polymers, anisotropy occurs when the polymer molecules are oriented or when anisotropically shaped and oriented fillers are present.

Annealing The improvement of crystallinity by heating to temperatures below the melting temperature due to a certain amount of molecular rearrangement. A molecular process that allows relaxation of frozen-in stresses and strains in a bulk material.

Beta Transition A subsidiary glass transition occurring at a temperature, T_β, lower than that of the α-transition.

Biaxial Birefringence Birefringence resulting from biaxial orientation.

Bimodal Distribution A molecular-weight distribution in which the differential weight distribution function has two maxima.

Biodegradation Degradation induced by the physiological environment.

Biopolymers Biopolymers include all naturally occurring, large, polymeric molecules, such as polypeptides and proteins, nucleic acids, and polysaccharides.

Biplanar Fracture Fracture in which crack propagation takes place on two parallel planes.

Birefringence The difference between the refractive indices of two perpendicular directions as measured with polarized light along these directions.

Branched Polymer A branched polymer has side chains, or branches, of significant length, which are bonded to the main chain at branch points.

Brittle–Ductile Transition The temperature at which the mode of fracture changes from brittle to ductile fracture.

Brittle Fracture Fracture that occurs without significant plastic deformation of the material at the crack tip.

Cellular Polymer A polymer whose apparent density is decreased substantially by the presence of numerous cells dispersed throughout its mass.

Cellulose The most abundant natural polymer. It is composed of glucose, being the major cell-wall material in land plants and their main structural component.

Chain Flexibility The ability of polymer chain molecules to assume a variety of configurations, arising from freedom of segments to rotate around C–C bonds. Polar side groups generally hinder rotation, making chain stiffer, while alkyl side chains tend to increase flexibility.

Characteristic Ratio A measure of the expansion of a polymer chain due to steric interactions and valence-bond angle restrictions. It is defined as

$$C_\infty = \langle r^2 \rangle_0 / nl^2,$$

where $\langle r^2 \rangle_0$ is the unperturbed mean square end-to-end distance and n is the number of links of length l in the chain.

Chemical Cross-link The existence of a retaining force between polymer chains, brought about by covalent bonding.

Chemical Degradation Degradation induced by chemical attack on polymers.

Chemisorption Adsorption, especially when irreversible, by means of chemical, rather than physical, forces.

Circular Birefringence Birefringence due to the different velocities of propagation of light polarized circularly in the clockwise and anticlockwise directions in an optically active material.

Contact Angle The angle between the edge of a liquid drop and the solid surface with which it is in contact.

Complex Modulus A representation of the dynamic mechanical properties of viscoelastic materials. The real part of the complex modulus, the component in phase with the measuring frequency, is called the storage modulus and the imaginary part, the component out of phase with the measuring or driving frequency, is called the loss modulus.

Composite Material A material that consists of a combination of two or more materials and in which the individual components retain their separate identities. Usually one component is drastically more rigid than the other. If both components are similar, it is referred to as a blend.

Conducting Polymer A polymer that exhibits electrical conductivity, i.e., greater than about 10^{-10}S cm^{-1}.

Configuration Configuration denotes the stereochemical arrangements of the atoms in the polymer chain. The configuration of a polymer chain cannot be altered without breaking and reforming chemical bonds.

Conformation Conformation of a polymer molecule describes the geometrical arrangements of the atoms in the polymer chain achieved through rotations about or stretching of its chemical bonds and bending of its valence angles.

Constitutive Equation Any equation relating stress, stress rate, and strain rate.

Contour Length The length of a fully extended polymer chain along its backbone.

Controlled Release The systems that can provide some control, whether this be of a temporal or spatial nature, or both, of drug release in the body.

Copolymer A polymer that is derived from more than one species of monomer. There are several categories of copolymers, each being characterized by a particular form of arrangement of the repeat units along the polymer chain. A *random* copolymer is a special type of statistical polymer in which the distribution of repeat units is truly random. An *alternating* copolymer has only two different types of repeat units, which are arranged alternatively along the polymer chain. A *block* copolymer is a linear copolymer in which the repeat units exist only in long sequences, or blocks, of the same type. A *graft* copolymer is a branched polymer in which the branches have a different chemical structure from that of the main chain.

Coupling Agent A material applied as a thin layer to the surface of a reinforcing filler to improve the adhesion between the filler and a polymer matrix in a filler–polymer composite.

Crazing A localized form of plastic deformation due to internal stresses or solvents modifying a chemical structure.

Creep The progressively increasing strain over a period of time of a viscoelastic material when subject to a continuously applied stress.

Cross-link A structure chemically or physically bonding two or more chains together.

Crystal–Crystal Transition The transformation of one crystal structure of a polymer to a different crystal structure, for example, below 19 °C Teflon is triclinic and above 19 °C the packing is hexagonal.

Crystalline Orientation The component of the overall orientation due to the crystalline regions of a crystalline polymer.

Crystallinity The long-range regular ordering of atoms or molecules in unit cells on a three-dimensional crystalline lattice.

Crystallization The process of formation of a crystalline (ordered) material from a disordered aggregate of molecules.

Degree of Polymerization The number of repeat units in a polymer chain.

Dielectric Constant The ratio of the capacitance of the capacitor with the material in place to its capacitance with vacuum between the plates.

Dielectric Spectroscopy The determination of dielectric properties such as the loss factor and the dielectric constant as a function of frequency at different fixed temperatures.

Differential Scanning Calorimetry A thermal analysis technique that measures the energy required to maintain the temperature of the sample equal to that of an inert reference material.

Domain A region in a material that has homogeneous properties, e.g., a phase-separated block copolymer where aggregates of blocks of one type are incompatible with blocks of the second type.

Ductile Fracture Fracture in which significant plastic deformation occurs before fracture.

Dynamic Mechanical Behavior The stress–strain behavior of a material when subject to an applied sinusoidally varying stress or strain.

Dynamic Mechanical Spectroscopy The determination of dynamic mechanical behavior over a range of frequency or temperature.

Elasticity The reversible stress–strain behavior by which a body resists and recovers from deformation produced by a force.

Elastic Modulus A constant of proportionality in the generalized Hooke's law relationship between stress and strain.

Elastic–Plastic Transition The change from recoverable elastic behavior to nonrecoverable plastic strain, which occurs on stressing a material beyond its yield point.

Elastic Scattering The scattering of radiation by a medium in which the scattered radiation has the same wavelength as the incident radiation. There is conservation of energy and momentum.

Elastomers Elastomers are chemically or physically cross-linked rubbery polymers (i.e., rubbery networks) that can be easily stretched to high extensions and rapidly recover their original dimensions when the applied stress is released. Use temperatures are above T_g in the rubbery plateau region.

End-To-End Distance The distance separating the two ends of a polymer chain.

Engineering Polymer A processable polymeric material, capable of being formed to precise and stable dimensions, exhibiting high performance at the continuous use temperature above 100 °C and having tensile strength in excess of 40 MPa.

Environmental Stress Cracking A type of cracking in which the polymer fails by breaking when subject to mechanical stress in the presence of an organic liquid or an aqueous solution of a soap or other wetting agent.

Excluded Volume The volume in a solution, in addition to the volume physically necessarily occupied by the solute molecules, from which other molecules are excluded due to the fact that the distance between two molecules cannot be less than the sum of their radii.

Fatigue In general, the progressive weakening of a material component with increasing time under load, such that the load that would not produce failure at short times does produce failure at long times.

Fiber A solid material in the form of a piece whose length is very much greater than its diameter (typically a micron), and characterized by its fineness and flexibility. Often called a filament.

Filler A relatively inert additive for a polymer composition to modify the physical properties of a polymer, thus forming a composite.

Flory–Huggins Interaction Parameter A measure of polymer–solvent interaction energy.

Fractal Geometry Fractal geometry is concerned about the quantitative description of complex structures and the ways in which these structures transform under a change of length scales.

Fracture A stress-biased material disintegration through the formation of new surfaces within a body.

Free Volume The volume of the vacant sites or holes present in a amorphous solid, not occupied by the molecules of the polymer.

Freely Jointed Chain A simple model of a polymer chain consists of n links of length l joined in a linear sequence with no restrictions on the angles between successive bonds.

Gaussian Chain A chain whose statistical distribution of chain end-to-end distances is a Gaussian distribution.

Gel A polymer network that contains solvent.

Gelation Any process in which a gel is formed.

Glass Transition Temperature The temperature at which polymers transform abruptly from the glassy state (hard) to the rubbery state (soft), symbolized as T_g. This transform corresponds to the onset of chain motion. Below the glass transition temperature, the thermal energy available for chain motion is inadequate to allow much relative motion between chains.

Head-to-Head Structure A structure in a vinyl or related polymer that has the form $\sim CH_2{-}CHR{-}CHR{-}CH_2 \sim$, R being designated the head.

Head-to-Tail Structure A structure in a vinyl or related polymer that has the form $\sim CHR{-}CH_2{-}CHR{-}CH_2 \sim$, R being designated the head.

Heterogeneous Nucleation Primary nucleation in the presence of a foreign surface that enhances nucleation by reducing the critical size needed for crystal growth.

Homogeneous Nucleation Primary nucleation without the presence of preformed nuclei or crystalline surfaces.

Homopolymer A polymer whose structure can be represented by multiple repetition of a single type of repeat unit.

Hydrogel A slightly cross-linked polymer that is highly swollen by water.

Ideal Solution A mixture of molecules that are identical in size and for which the energies of like and unlike molecular interactions are equal.

Impact Resistance A measure of the ability of a material or structure to withstand the application of a sudden load.

Interface A surface separating dissimilar materials in intimate contact.

Interpenetrating Polymer Network An intimate combination of two polymer networks, not chemically bonded to each other, at least one of which is synthesized and/or cross-linked in the immediate presence of the other.

Ionic Polymer A polymer that carries electrostatic charges.

Ionomer A generic term for a class of thermoplastics containing ionizable carboxyl groups that can create ionic cross-links between chains.

Kinetic Chain Length The number of monomers consumed per active center.

Lamella The platelike crystal or crystallite that is the characteristic crystal habit of most crystalline polymers and polymer single crystals.

Linear Polymer A polymer in which the molecules consist of single unbranched chains of atoms.

Liquid-Crystalline Polymer A polymer that is capable of forming a liquid-crystalline phase (a mesophase).

Living Polymer A polymer in which the active centers of the polymerization are retained even if all the monomer has been consumed.

Mechanochemical Degradation A chain scission type of degradation induced by mechanical shear.

Melting Temperature The temperature at which the thermal energy in a solid material is just sufficient to overcome the intermolecular forces of attraction in the

crystalline lattice so that the lattice breaks down and the material becomes a liquid, i.e., it melts.

Membrane A thin barrier that permits selective mass transport.

Molecular-Weight Average Several different averages, all ratios of the moments of the distribution, are used. They are given by

$$M = \sum N_i M_i^{n+1} \Big/ \sum N_i M_i^n,$$

where there are N_i molecules of molecular weight M_i for each molecular species i. In the number-average weight (M_n), $n = 1$; in the weight-average molecular weight (M_w), $n = 2$; in the Z-average molecular weight (M_z), $n = 3$.

Molecular-Weight Distribution The distribution of molecular sizes in a polydisperse polymer.

Monolithic Device A device in which the drug of interest is uniformly dispersed within a polymeric matrix.

Monomers Small molecules that combine with each other to form polymers.

Nanotechnology The technology that creates functional materials, devices, and systems with novel properties and phenomena through control of matter on the scale of 1–100 nm

Neutron Scattering The interaction of neutrons with a material such that they are deflected.

Nonlinear Optics Nonlinear optics is basically concerned about the interaction of optical frequency electromagnetic fields with materials, resulting in the alteration of the phase, frequency, or other propagation characteristics of the incident light.

Nucleating Agent An additive that provides nuclei for heterogeneous crystallization, raising the crystallization rate and temperature. More and smaller spherulites are consequently produced.

Permeability The proportionality constant in the general equation for mass transport of a penetrant across the barrier, i.e., the product of permeance and thickness.

Permeation The rate at which a gas or vapor passes through a barrier material.

Photoconductive Polymer A polymer that exhibits a relatively high electrical conductivity when irradiated with visible or ultraviolet light.

Photodegradation Degradation induced by exposure to ultraviolet radiation.

Photoresist A photosensitive polymer system, which, when applied as a coating to a substrate, after interaction with ultraviolet or visible light undergoes a change in solubility.

Physical Cross-Link The existence of a retaining force between polymer chains, brought about by noncovalent bonding.

Piezoelectric Polymer A polymer whose polarization changes under strain, due either to a change in dimensions or to electrostriction.

Polymer A polymer is a large molecule built up by the repetition of small, simple units, which are linked to each other through primary covalent bonds.

Polymer Alloy Polymer blend having a modified interface and/or morphology.

Polymer Blend An intimate combination of two or more polymer chains of constitutionally or configurationally different features that are not bonded to each other.

Polymerization A process by which monomer molecules are linked to form polymers.

Pyroelectric Polymer A polymer whose polarization changes on heating.

Radius of Gyration A parameter characterizing the size of a polymer random coil. It is given by

$$R_G^2 = \sum m s_i^2 \Big/ \sum m = \sum s_i^2 / n,$$

where the polymer chain consists of n segments, each of mass m, located at distance s from the center of gravity of the coil.

Raman Scattering An inelastic process with a shift in wavelength due to chemical absorption or emission.

Rayleigh Scattering Elastically scattered light, usually measured as a function of scattering angle.

Relaxation Time The time required to respond to a change in temperature or pressure.

Repeat Unit The smallest structural unit of a polymer chain.

Reservoir Device A device in which the drug to be released is surrounded by an appropriate polymer membrane.

Rheo-Optics The use of optical methods to study flow and deformation in materials.

Second Virial Coefficient The coefficient of the most important term of the virial equation that accounts for the nonideality of behavior of a system, in particular of the colligative and other properties of dilute solutions. Generally, the virial equation is of the form.

$$P = RT(c_2/M_2 + A_2 c_2^2 + \dots),$$

where P is the colligative property, c_2 is the concentration of solute, M_2 is the molecular weight of solute, and A_2 is the second virial coefficient.

Self-Assembly A method of integration in which the components spontaneously assemble, typically by bouncing around in a solution or gas phase until a stable structure with minimum energy is reached.

Semiconducting Polymer A polymer having an electrical conductivity in the range 10^{-10}–10^{2}S cm^{-1}.

Semicrystalline Polymer A polymer that has both crystalline and amorphous regions.

Semi-Interpenetrating Polymer Network A combination of two polymers, not chemically linked to each other, one cross-linked and one linear, at least one of which is synthesized and/or cross-linked in the immediate presence of the other.

Sequence Length The number of repeat units of a specific type joined to each other contiguously in a polymer chain.

Solubility A measure of the extent to which two pure components can be mixed homogeneously.

Spherulite An aggregation of crystallites as a spherical cluster, consisting of fibrillar crystalline lamellae radiating from the center of the spherulite.

Spinodal The line on a temperature versus composition phase diagram of a mixture of two components that separates the two phase region from a metastable single phase region between the binodal and spinodal.

Spinodal Decomposition A process of phase separation that occurs when the temperature of a homogeneous mixture of two components is rapidly changed, so that the system is brought to a state in which both the spinodal and binodal have been crossed.

Star Polymer Three or more chains linked at one end through a central moiety.

Stress Intensity Factor A factor relating the magnitude of the stress components in the vicinity of a crack tip to the crack and specimen geometry and the overall stress.

Stress Relaxation The relatively slow decay of the stress when a viscoelastic material is held at a constant strain after being rapidly stressed initially.

Supercooling The temperature difference between the equilibrium melting temperature and the temperature of crystallization.

Supermolecular Structure Polymer structure features observable at a level above that of individual polymer molecules. These include crystal structure, crystallite, multilayer, crystalline, fibrillar, spherulitic, and fibrous morphologies.

Surface Tension The force per unit length acting in the surface of a liquid that opposes spreading.

Sustained Release The systems that only prolong therapeutic blood or tissue levels of the drug for an extended period of time.

Swelling The first step in the solubilization of a polymer. The degree of swelling depends on the polymer–solvent interaction parameter and the molecular weight of the polymer. In the case of a cross-linked polymer, solubilization cannot take place, and an equilibrium degree of swelling is attained.

Tacticity The tacticity of the polymer is concerned with the different possible spatial arrangements. In *isotactic* polymers, all the repeat units have the same configuration, whereas in *syndiotactic* polymers, the configuration alternates from one repeat unit to the next. *Atactic* polymers have a random placement of the two configurations. For example, in a vinyl polymer, $\sim [CH_2CHR]_n \sim$, where R is a substituent group, three distinct configurational arrangements of the repeat unit exist as follows:

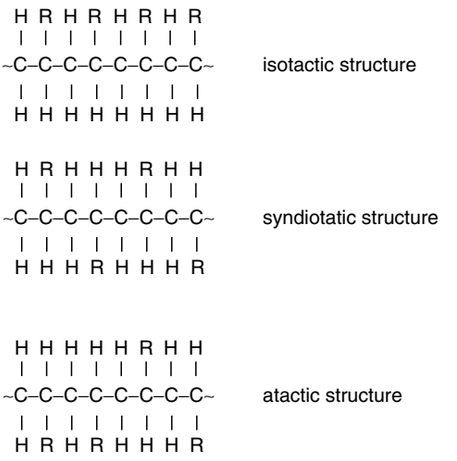

Terpolymer A polymer consisting of three different monomers.

Thermal Conductivity The ratio of the heat flow across unit area of a surface to the negative of the temperature gradient in the direction of flow.

Thermal Degradation Degradation induced by exposure to an elevated temperature.

Thermogravimetric Analysis A dynamic thermal analysis technique in which the weight loss of a sample is measured continuously while its temperature is increased at a constant rate.

Thermoplastic Elastomers Polymers capable of behaving as elastomers with the domains having physical cross-links. They are thermoformable, i.e., moldable and remoldable.

Thermoplastics Thermoplastics are linear or branched polymers that can be melted upon the application of heat. They can be molded and remolded into virtually any shape.

Thermosets Thermosets are rigid materials having short network polymers in which chain motion is greatly restricted by a high degree of cross-linking. They are intractable once formed and degrade rather than melt upon the application of heat.

Theta (Θ) Solvent A solvent for a polymer system that exhibits a theta temperature.

Theta (Θ) Temperature (Flory Temperature) The temperature at which, for a given polymer–solvent pair, the polymer exists in its unperturbed dimensions. Under these conditions, the long-range forces between polymer molecular segments that cause contraction are just balanced by the polymer–solvent interactions that cause the polymer molecular coil to expand.

Tie Molecule The intervening section in a polymer molecule that has started to crystallize independently in two different crystals.

Toughness The ability of a material to withstand fracture.

Unit Cell The basic unit for describing the ordered arrangement of atoms in a crystal.

Unperturbed Dimensions The dimension of a polymer coil in dilute solution at the θ temperature.

Viscoelasticity The ability for a material to exhibit viscous and elastic responses to deformation simultaneously.

Viscosity The ability of a fluid to resist flow.

Wetting The process in which a liquid spontaneously adheres to and spreads on a solid surface.

CHAPTER 63

Units and Conversion Factors

Shuhong Wang

DuPont Dow Elastomers L.L.C., One Innovation Way, Suite 400, Newark, DE 19711

TABLE 63.1. *SI prefixes.*

Multiplication factor			Prefix	Symbol
1 000 000 000 000 000 000 000 000	=	10^{24}	yotta	Y
1 000 000 000 000 000 000 000	=	10^{21}	zetta	Z
1 000 000 000 000 000 000	=	10^{18}	exa	E
1 000 000 000 000 000	=	10^{15}	peta	P
1 000 000 000 000	=	10^{12}	tera	T
1 000 000 000	=	10^{9}	giga	G
1 000 000	=	10^{6}	mega	M
1 000	=	10^{3}	kilo	k
100	=	10^{2}	hecto	h
10	=	10^{1}	deca	da
0.1	=	10^{-1}	deci	d
0.01	=	10^{-2}	centi	c
0.001	=	10^{-3}	milli	m
0.000 001	=	10^{-6}	micro	μ
0.000 000 001	=	10^{-6}	nano	n
0.000 000 000 001	=	10^{-9}	pico	p
0.000 000 000 000 001	=	10^{-15}	femto	f
0.000 000 000 000 000 001	=	10^{-18}	atto	a
0.000 000 000 000 000 000 001	=	10^{-21}	zepto	z
0.000 000 000 000 000 000 000 001	=	10^{-24}	yocto	y

TABLE 63.2. *SI base and supplementary units.*

Quantity	SI unit	SI symbol
Length	meter	m
Mass	kilogram	kg
Time	second	s
Electric current	ampere	A
Thermodynamic temperature	kelvin	K
Amount of substance	mole	mol
Luminous intensity	candela	cd
Plane angle	radian	rad
Solid angle	steradian	sr

TABLE 63.3. *Derived units of SI that have special names.*

Quantity	Unit	Symbol	Formula
Absorbed dose	gray	Gy	J/kg
Conductance	siemens	S	A/V
Electric capacitance	farad	F	C/V
Electric charge	coulomb	C	A s
Electric potential	volt	V	W/A
Electric resistance	ohm	Ω	V/A
Energy, work, heat	joule	J	N m
Force	newton	N	$(\text{kg m})/\text{s}^2$
Frequency	hertz	Hz	1/s

TABLE 63.3. *Continued.*

Quantity	Unit	Symbol	Formula
Illuminance	lux	lx	lm/m^2
Inductance	henry	H	Wb/A
Luminous flux	lumen	lm	cd sr
Magnetic flux	weber	Wb	V s
Magnetic-flux density	tesla	T	Wb/m^2
Pressure, stress, vacuum	pascal	Pa	N/m^2
Power, radiant flux	watt	W	J/s

TABLE 63.4. *Additional commonly derived SI units.*

Quantity	Unit	Symbol
Acceleration (linear)	meter per second squared	m/s^2
Acceleration (angular)	radian per second squared	rad/s^2
Area	square meter	m^2
Concentration	mole per cubic meter	mol/m^3
Current density	ampere per square meter	A/m^2
Density (mass)	kilogram per cubic meter	kg/m^3
Electric-charge density	coulomb per cubic meter	C/m^3
Electric-field strength	volt per meter	V/m
Energy density	joule per cubic meter	J/m^3
Entropy	joule per kelvin	J/K

TABLE 63.4. *Continued.*

Quantity	Unit	Symbol
Heat capacity	joule per kelvin	J/K
Luminance	candela per square meter	cd/m^2
Magnetic-field strength	ampere per meter	A/m
Molar energy	joule per mole	J/mol
Molar entropy	joule per mole-kelvin	J/(mol K)
Molar heat capacity	joule per mole-kelvin	J/(mol K)
Moment of force	newton-meter	N m
Permeability	henry per meter	H/m
Permittivity	farad per meter	F/m
Radiance	watt per sq. meter-steradian	$W/(m^2 sr)$
Radiant intensity	watt per steradian	W/sr
Specific-heat capacity	joule per kilogram-kelvin	J/(kg K)
Specific energy	joule per kilogram	J/kg
Specific entropy	joule per kilogram-kelvin	J/(kg K)
Specific volume	cubic meter per kilogram	m^3/kg
Surface tension	newton per meter	N/m
Thermal conductivity	watt per meter-kelvin	W/(m K)
Velocity (angular)	radian per second	rad/s
Velocity (linear)	meter per second	m/s
Viscosity (dynamic)	pascal-second	Pa s
Viscosity (kinematic)	sq. meter per second	m^2/s
Volume	cubic meter	m^3

TABLE 63.5. *Some quantities and units commonly used in polymer science.*

Quantity	Notation	Commonly used unit
Second and third virial coefficient	A_2, A_3	$mol\ cm^3/g^2$
Chain transfer constant for monomer	C_m	—
Chain transfer constant for solvent	C_s	—
Chain transfer constant for polymer	C_p	—
Characteristic ratio	C_∞	—
Diffusion coefficient	D	1/s
Tensile storage compliance	D'	1/Pa
Tensile loss compliance	D''	1/Pa
Complex tensile compliance	D^*	1/Pa
Young's modulus	E	Pa
Tensile storage modulus	E'	Pa
Tensile loss modulus	E''	Pa
Complex tensile modulus	E^*	Pa
Shear modulus	G	Pa
Shear storage modulus	G'	Pa
Shear loss modulus	G''	Pa
Complex shear modulus	G^*	Pa
Free energy of mixing	ΔG_m	kJ/mol
Enthalpy of mixing	ΔH_m	kJ/mol

TABLE 63.5. *Continued.*

Quantity	Notation	Commonly used unit
Shear compliance	J	1/Pa
Shear storage compliance	J'	1/Pa
Shear loss compliance	J''	1/Pa
Complex shear compliance	J^*	1/Pa
Molecular weight per cross-linked unit	M_c	g/mol
Number average molecular weight	M_n	g/mol
Molecular weight of a polymer chain unit	M_o	g/mol
Viscosity average molecular weight	M_v	g/mol
Weight average molecular weight	M_w	g/mol
z-average molecular weight	M_z	g/mol
Refractive index	n	—
Reactivity ratio of monomer A	r_A	—
Permeability coefficient	P	$cm^3 cm/(cm^2$ s Pa)
Mean-square end-to-end distance	$< r^2 >$	A^2
Unperturbed mean-square end-to-end distance	$< r^2 >_0$	A^2
Radius of gyration	s	A
Sedimentation coefficient	S	1/s
Solubility coefficient	S	$cm^3/(cm^3$ Pa)
Configurational entropy	S_{conf}	kJ/(mol K)
Entropy of mixing	ΔS_m	kJ/(mol K)
Brittleness temperature	T_B	°C
Crystallization temperature	T_c	°C
Temperature of fusion	T_f	°C
Glass transition temperature	T_g	°C
Melting temperature	T_m	°C
Supercooling	ΔT	°C
Molar volume	v	cm^3/mol
Volume fraction of species *i*	v_i	—
Weight fraction of species *i*	w_i	—
Mole fraction of species *i*	x_i	—
Number average degree of polymerization	x_n	—
Weight average degree of polymerization	x_w	—
z-average degree of polymerization	x_z	—
Elongation, linear deformation	α	—
Shear strain	γ	—
Birefringence	Δ	—
Solubility parameter	δ	$(MPa)^{1/2}$
Loss angle	δ	rad
Tensor strain	ε	—
Apparent viscosity, dynamic viscosity	η'	Pa s
Complex viscosity	η^*	Pa s
Intrinsic viscosity	$[\eta]$	ml/g
Theta temperature	θ	°C
Thermal conductivity	κ	W/(m K)
Deformation ratio	λ	—
Poisson ratio	υ	—
Osmotic pressure	π,Π	Pa
Stress	σ	Pa
Shear stress	τ	Pa
Relaxation time	τ	s
Retardation time	τ'	s
Flory–Huggins parameter	χ,ξ	—

TABLE 63.6. *Conversion factors for commonly used qualities.*

Acceleration (linear)	m/s^2	km/(hr s)	mil/(hr s)	ft/s^2	cm/s^2	
	1	3.600	2.237	3.281	1.000×10^2	
Acceleration (rotational)	rad/s^2	rad/min^2	$revol/s^2$	revol/(min s)	$revol/min^2$	
	1	3.600×10^3	1.592×10^{-1}	9.549	5.730×10^2	
Area	m^2	sq. in.	sq. ft	sq. yd	area	
	1	1.550×10^3	1.076×10	1.196	1.000×10^{-2}	
Coefficient of expansion	$kg/(m^3\ K)$	$kg/(m^3\ ^\circ C)$	$kg/(cm^3\ ^\circ C)$	$g/(cm^3\ ^\circ C)$	lb/(cu. ft °F)	
	1	1.000	1.000×10^{-6}	1.000×10^{-3}	3.468×10^{-2}	
Concentration (mass/volume)	kg/m^3(or g/l)	grains/gal(US)	grains/gal(UK)	ppm	lb/gal(US)	
	1	5.842×10^1	7.016×10^1	1.001×10^3	8.345×10^{-4}	
Concentration (mole/volume)	mol/m^3	$kmol/m^3$	(lb mol)/gal(US)		(lb mol)/gal(UK)	
	1	1.001×10^{-3}	8.345×10^{-3}		1.002×10^{-2}	
Density (mass)	kg/m^3	lb/cu. ft	lb/cu. in.	lb/gal(UK)	lb/gal(US)	
	1	6.243×10^{-2}	3.613×10^{-5}	1.002×10^{-2}	8.345×10^{-3}	
Electric charge	C (or A s)	Electronic charge		Statcoulomb		
	1	6.241×10^{18}		2.998×10^9		
Energy, heat, work	J (or N m)	kcal	Btu	kgf m	erg	
	1	2.388×10^{-4}	9.478×10^{-4}	1.020×10^{-1}	1.000×10^7	
Force	N	kgf	lbf	dyn	tonf(US)	
	1	1.020×10^{-1}	2.248×10^{-1}	1.000×10^5	1.124×10^{-4}	
Luminous intensity	cd	candle(UK)	carcel unit	hefner unit	lumen/steradian	
	1	9.600×10^{-1}	1.041×10^{-1}	1.111	1.000	
Length	m	in.	ft	yd	mil	angstrom
	1	3.937×10^1	3.281	1.094	3.937×10^4	1.000×10^{10}
Mass	kg	lb	ton(UK)	ton(US)	once	
	1	2.205	9.842×10^{-4}	1.102×10^{-3}	3.527×10^1	
Power	W (or J/s)	Btu/h	HP(UK)	erg/s	kcal/hr	
	1	3.412	1.341×10^{-3}	1.0×10^7	8.598×10^{-1}	
Pressure, vacuum, stress	Pa (or N/m^2)	bar	atm	torr (or mmHg)	psi (or lbf/sq. in)	
	1	1.0×10^{-5}	9.869×10^{-6}	7.501×10^{-3}	1.450×10^{-4}	
Surface tension	N/m	lbf/in.	kgf/m	dyn/cm		
	1	5.710×10^{-3}	1.020×10^{-1}	1.0×10^3		
Temperature	K	$^\circ C + 273.15$	$^\circ F + 459.67$	R		
	1	1.000	1.800	1.800		
Thermal conductivity	W/(m K)	kcal/(m h °C)	Btu/(ft h °F)	Btu/(in. h °F)	Btu in./(sq. ft h °F)	
	1	8.598×10^{-1}	5.778×10^{-1}	4.815×10^{-2}	6.933	
Time	s	min	h (or hour)	day	year (365day)	
	1	1.667×10^{-2}	2.778×10^{-4}	1.157×10^{-5}	3.171×10^{-8}	
Torque	N m	N cm	dyne cm	kgf m	in. lbf	
	1	1.000×10^2	1.000×10^7	1.02×10^{-1}	8.851	
Velocity (linear)	m/s	km/h	mile/h	ft/min	ft/s	
	1	3.600	2.237	1.969×10^2	3.281	
Viscosity (dynamic)	Pa s (or $N\ s/m^2$)	poise	centipoise	dyne s/cm^2	g/(cm s)	
	1	1.000×10^1	1.000×10^3	1.000×10^1	1.000×10^1	
Viscosity (kinematic)	m^2/s	cm^2/s	stoke	sq. ft/s	sq. ft/hr	
	1	1.000×10^4	1.000×10^4	1.076×10^1	3.875×10^4	
Volume	m^3	l(or litre)	cu. in.	gal(US)	gal(UK)	
	1	1.000×10^3	6.102×10^4	2.642×10^2	2.200×10^2	

TABLE 63.7. *General data and constants.*

Quantity	Symbol and equation	Value	
Atomic mass unit	$1u = 10^{-3}$ kg mol^{-1} L^{-1}	1.66057×10^{-27}	kg
Avogadro's number	L, N_a	6.02204×10^{23}	mole^{-1}
Bohr magneton	$\mu_B = eh/2m_e$	9.27408×10^{-24}	J T^{-1}
Bohr radius	$a_0 = \alpha/4\pi R_\infty$	5.29177×10^{-11}	m
Boltzmann constant	$k = R/L$	1.38066×10^{-23}	J K^{-1}
Electronic charge	e	1.60219×10^{-19}	C
Electron magnetic moment	μ_e	9.284832×10^{-24}	J T^{-1}
Electron mass	m_e	9.10953×10^{-31}	kg
Electronvolt	eV	1.60219×10^{-19}	J
Faraday constant	$F = Le$	9.64846×10^{4}	C mole^{-1}
Gravitational constant	G	6.6720×10^{-11}	N m^2 kg^{-2}
Gyromagnetic ratio of proton	γ_p	2.67520×10^{8}	s^{-1} T^{-1}
Neutron mass	m_n	1.67495×10^{-27}	kg
Nuclear magneton	$\mu_N = eh/2m_p$	5.05082×10^{-27}	J T^{-1}
Permeability of vacuum	μ_0	$4\pi \times 10^{-7}$	H m^{-1}
Permittivity of vacuum	$\varepsilon_N = (\mu_0 c^2)^{-1}$	$8.85418782 \times 10^{-12}$	F m^{-1}
Planck constant	h	6.62618×10^{-34}	J s
	$\bar{h} = h/2\pi$	$1.0545887 \times 10^{-34}$	J s
Proton mass	m_p	1.67265×10^{-27}	kg
Rydberg constant	$R_\infty = \mu_0^2 m_e e^4 c^3/8h^3$	1.09737×10^{7}	m^{-1}
Speed of light in vacuum	c	2.99792×10^{8}	m s^{-1}
Universal/molar gas constant	R	8.31441	J K^{-1} mol^{-1}
		1.98717	cal K^{-1} mol^{-1}
Standard molar volume of ideal gas	$V_0 = RT_0/P_0$	2.241383×10^{-2}	m^3 mol^{-1}

TABLE 63.8. *Greek alphabet.*

A	α	alpha	N	ν	nu
B	β	beta	Ξ	ξ	xi
Γ	γ	gamma	O	o	omicron
Δ	δ	delta	Π	π	pi
E	ε	epsilon	P	ρ	rho
Z	ζ	zeta	Σ	σ	sigma
H	η	eta	T	τ	tau
Θ	θ	theta	Υ	υ	upsilon
I	ι	iota	Φ	ϕ	phi
K	κ	kappa	X	χ	chi
Λ	λ	lambda	Ψ	ψ	psi
M	μ	mu	Ω	ω	omega

Subject Index

D

E

F

G

H

Q

R

S

T

U

V

W

X

Y

Z